Virchows Arch (2004) 445:1–8
DOI 10.1007/s00428-004-1021-5

REVIEW ARTICLE

Günter Klöppel · Sönke Detlefsen · Bernd Feyerabend

Fibrosis of the pancreas: the initial tissue damage and the resulting pattern

Received: 16 February 2004 / Accepted: 23 March 2004 / Published online: 8 May 2004
© Springer-Verlag 2004

Abstract Fibrosis in the pancreas is caused by such processes as necrosis/apoptosis, inflammation or duct obstruction. The initial event that induces fibrogenesis in the pancreas is an injury that may involve the interstitial mesenchymal cells, the duct cells and/or the acinar cells. Damage to any one of these tissue compartments of the pancreas is associated with cytokine-triggered transformation of resident fibroblasts/pancreatic stellate cells into myofibroblasts and the subsequent production and deposition of extracellular matrix. Depending on the site of injury in the pancreas and the involved tissue compartment, predominantly inter(peri)lobular fibrosis (as in alcoholic chronic pancreatitis), periductal fibrosis (as in hereditary pancreatitis), periductal and interlobular fibrosis (as in autoimmune pancreatitis) or diffuse inter- and intralobular fibrosis (as in obstructive chronic pancreatitis) develops.

Keywords Pancreatic fibrosis · Tissue damage · Cytokines · Pancreatic stellate cells · Fibrosis pattern

Introduction

Fibrosis in the pancreas is caused by such processes as necrosis/apoptosis, inflammation or duct obstruction. They result in the formation of extracellular matrix (ECM) in the interstitial spaces and in the areas where acinar cells disappear or duct cells are injured. This eventually leads to a loss of the lobular architecture of the pancreas, grotesque distortion of the large ducts and severe changes in the arrangement and composition of the islets. Functionally, the end-stage changes are associated with exocrine and endocrine insufficiency (diabetes).

G. Klöppel (✉) · S. Detlefsen · B. Feyerabend
Department of Pathology,
University of Kiel,
Michaelisstrasse 11, 24105 Kiel, Germany
e-mail: gkloeppel@path.uni-kiel.de
Tel.: +49-431-5973400
Fax: +49-431-5973462

The initial event that induces fibrogenesis in the pancreas is an injury, which may involve the interstitial mesenchymal cells, the duct cells and/or the acinar cells. Which of these elements is affected depends on the etiological factor. Damage to any one of these tissue compartments of the pancreas is associated with transformation of resident fibroblasts/pancreatic stellate cells (PSC) into myofibroblasts and the subsequent production and deposition of ECM, consisting mainly of collagen types I and III and fibronectin [4, 5, 10, 13, 26]. The exact mechanisms initiating and maintaining the development of fibrosis in the pancreas are poorly understood, but may be viewed as a stepwise process, similar to that observed in liver fibrosis [7]. The initial event is damage to one or all of the various tissue compartments or cell types of the pancreas, leading to cell necrosis and/or apoptosis and subsequent release of cytokines/growth factors [e.g., tumor growth factor β1 (TGFβ1), platelet-derived growth factor (PDGF)] and C-C or C-X-C chemokines, either from immigrating inflammatory cells, especially macrophages, and/or nearby preexistent epithelial or mesenchymal cells [3, 8, 28, 30, 32]. In a second step, the damaged cells are phagocytosed by macrophages, and the released cytokines cause activation and proliferation of resident fibroblasts/PSC in the immediate vicinity of the original site of damage and induce them to transform into myofibroblast cells [14, 34] (Fig. 1). As an alternative hypothesis, it has been suggested that the first two steps are bypassed, and the initiating etiological factor (for instance, ethanol consumption) directly activates resident fibroblasts [6]. In the last phase, myofibroblasts produce and deposit ECM, which replaces the inflammatory infiltrate and affects the architecture and function of the surviving pancreatic tissues [17] (Table 1). In order to facilitate the deposition of the newly formed ECM, myofibroblasts are also capable of producing specialized enzymes, such as metalloproteinases, which are able to destroy the normal pericellular ECM. If the ECM production is not maintained (because of withdrawal of the initiating factor), myofibroblasts may disappear via apoptosis or retransformation into fibroblasts [35].

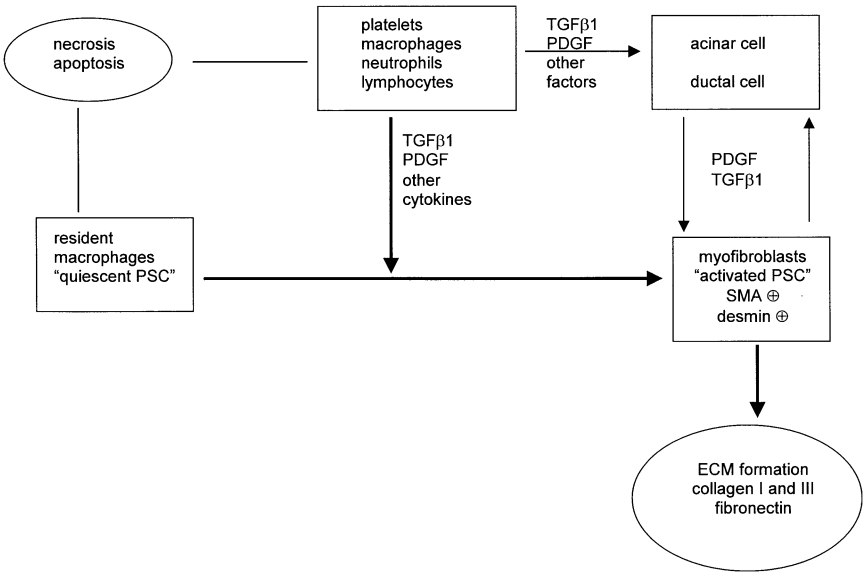


Fig. 1 Mechanisms of fibrogenesis in the pancreas. *PSC* pancreatic stellate cell, *TGFβ1* tumor growth factor β1, *PDGF* platelet-derived growth factor, *SMA* smooth-muscle actin, ECM extracellular matrix

Table 1 Pathogenesis of pancreatic fibrosis

1. Disease: chronic pancreatitis, duct obstruction
2. Causative factors: alcohol and other toxins, autoactivation of pancreatic enzymes, immune-mediated damage, intraductal pressure
3. Cell necrosis/apoptosis of mesenchymal and/or epithelial cells
4. Resorption of necrotic/apoptotic cells by macrophages
5. Induction of fibrosis by cytokines released by macrophages, platelets and epithelial cells
6. Production of extracellular matrix by fibroblasts/stellate cells/myofibroblasts

Although the basic processes leading to pancreatic fibrosis are probably the same, no matter what the etiology, the resulting phenotype of fibrosis, i.e., the pattern of fibrosis, differs. The main patterns are inter(peri)lobular, periductal and intralobular [2, 24, 29, 36] (Fig. 2). This article presents a working hypothesis that connects the etiological type of chronic pancreatitis (i.e., alcoholic, hereditary, autoimmune) with the initial site of damage in the pancreas and the resulting pattern of fibrosis.

Type of pancreatitis, initial damage in the pancreas and fibrosis pattern

The etiological classification of human chronic pancreatitis distinguishes between alcoholic, hereditary, autoimmune, idiopathic, tropical and other rare types [11, 20] (Table 2). Here, the mechanisms that may lead to certain patterns of fibrosis in the pancreas will be discussed for alcoholic chronic pancreatitis, hereditary pancreatitis, auto-immune pancreatitis and such types of chronic pancreatitis as obstructive chronic pancreatitis.

Alcoholic chronic pancreatitis

The first histologically recognizable lesion in alcoholic pancreatitis is focal autodigestive necrosis of interstitial fat cells, which usually also involves small vessels, preferably veins, and neighboring acinar tissue of the pancreas [21]. The inflammatory reaction and the hemorrhaging that follow this tissue necrosis initiate fibrosis [23] (Fig. 1). As discussed above, the most important known mediators of fibrosis are cytokines and growth factors. The cells from which fibrogenic cytokines, such as TGFβ1 and PDGF, may be released [8, 28] consist especially of infiltrating macrophages (among other inflammatory cells) and probably also platelets in areas of hemorrhagic necrosis. The cytokines generated by these cells may have autocrine and paracrine effects. The paracrine effects mainly target the neighboring resident fibroblasts/PSC. In addition, they also seem to stimulate the surrounding ductal and acinar cells to produce and release cytokines. The latter assumption is supported by immunocytochemical studies demonstrating that TGFβ1, fibroblast growth factor-1 and -2 and other factors are not only produced by fibroblasts, but also by epithelial cells of the pancreas [8, 12, 14]. This process of massive focal cytokine release triggers the transformation of fibroblastic cells/PSC to myofibroblastic cells expressing smooth muscle actin [36] and producing various ECM proteins. The concerted action then leads to the development of fibrous tissue at the initial site of necrosis (Fig. 2). Because the foci of autodigestive necrosis lie in the interstitial spaces surrounding the acinar lobules and the interlobular ducts, the expanding fibrous tissue forms an inter(peri)lobular pattern [21, 24] (Fig. 3). If the interlobular fibrosis involves interlobular ducts, it gradually causes duct sacculations and strictures. Ducts whose lumens are severely altered, however, very likely have difficulties allowing a normal flow of pancreatic secretions. Since pancreatic secretions are supersaturated by

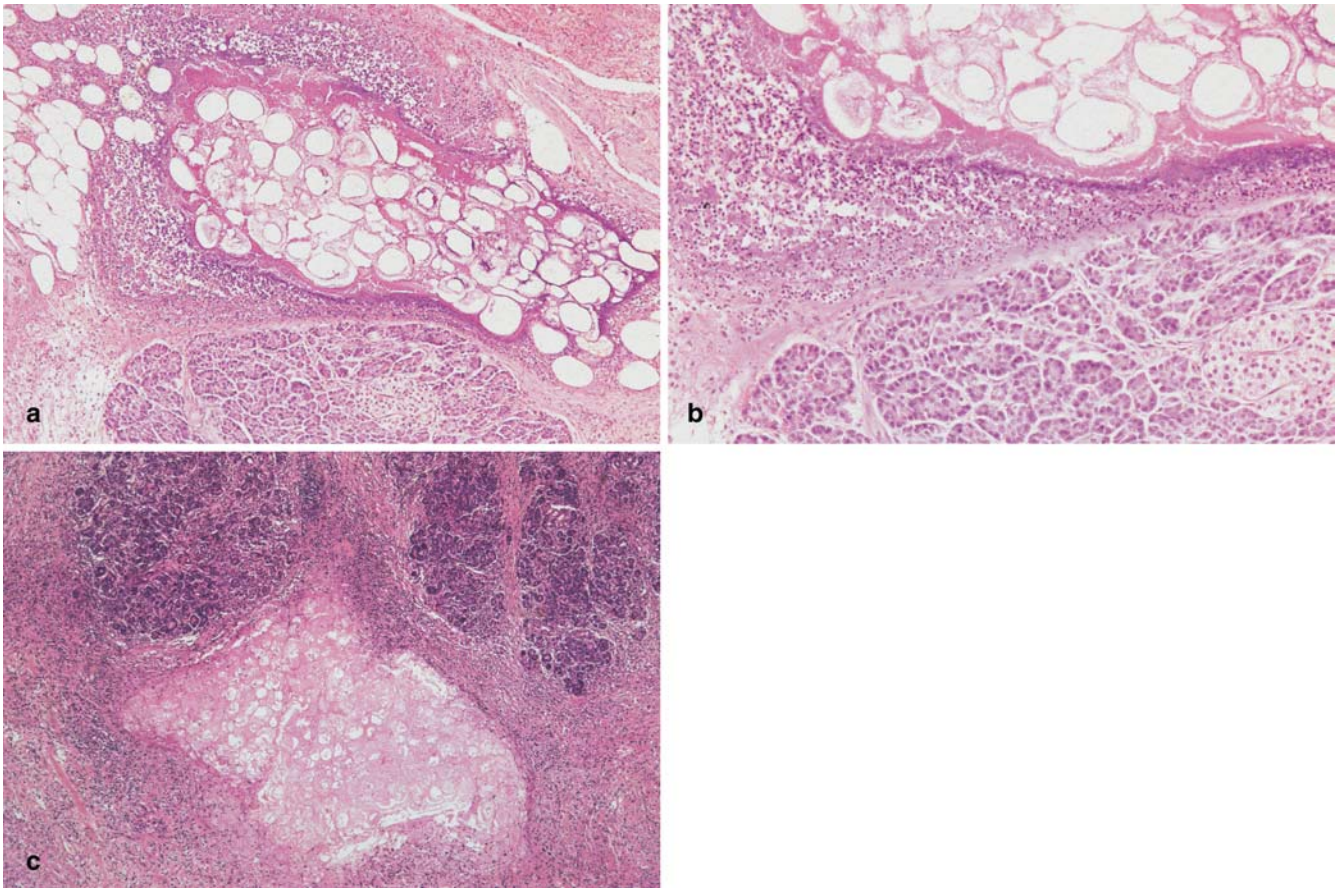


Fig. 2 Development of fibrosis in relapsing severe acute pancreatitis caused by alcohol abuse. Hematoxylin & eosin. **a** Interlobular fatty tissue necrosis demarcated from the adjacent preserved acinar tissue by inflammatory cells. **b** Margin of an area of autodigestive fatty tissue necrosis showing lipid-filled macrophages (foam cells) and newly formed fibrotic tissue infiltrated by inflammatory cells. **c** Cellular interlobular fibrosis developing adjacent to an area of old autodigestive fatty tissue necrosis

Table 2 Etiological classification of chronic pancreatitis and pancreatic fibrosis (modified from [20])

Chronic pancreatitis[a]
Alcoholic
Nonalcoholic
Hereditary
Metabolic (hypercalcemia, hyperlipidemia)
Autoimmune
Idiopathic
Tropical
Obstructive chronic pancreatitis[b]
Periampullary duodenal wall cysts
Pancreas divisum
Posttraumatic pancreatic scars
Pancreatic fibrosis not associated with chronic pancreatitis[a]
Pancreatic fibrosis in the elderly
Cystic fibrosis[b]
Hemochromatosis

[a] Clinically defined by the occurrence of symptoms such as pain, pancreatic exocrine deficiency and diabetes
[b] Usually only associated with pancreatic insufficiency

proteins and electrolytes, such as calcium, their impeded flow promotes precipitation of proteins, with eventual calcification and formation of calculi, as was experimentally demonstrated in dogs by partial pancreatic duct ligation for 4 months and longer [25]. Another effect of duct obstruction (see also below) is the induction of acinar atrophy and intralobular fibrosis in the incompletely drained regions. When this occurs, the interlobular fibrosis expands to the lobular area, resulting in fibrosis that diffusely affects a few or multiple lobules. These areas finally consist of sclerotic tissue containing only remnants of irregularly distributed ducts, islets, nerves and vessels (Fig. 4).

Hereditary chronic pancreatitis

It has recently been shown that the genetic alterations in hereditary chronic pancreatitis involve the cationic trypsinogen gene (*PRSS1*) or a serine protease inhibitor gene (*SPINK1*) [38, 39, 40]. Mutations in these two genes seem to trigger the autoactivation of trypsinogen in the pancreas, which in turn results in the early inappropriate activation of the other pancreatic enzymes with subsequent autodigestive necrosis and inflammation. This may occur either in the acinar cells or, more likely, in the ducts. In our series of pancreatic resection, specimens from six patients with hereditary chronic pancreatitis

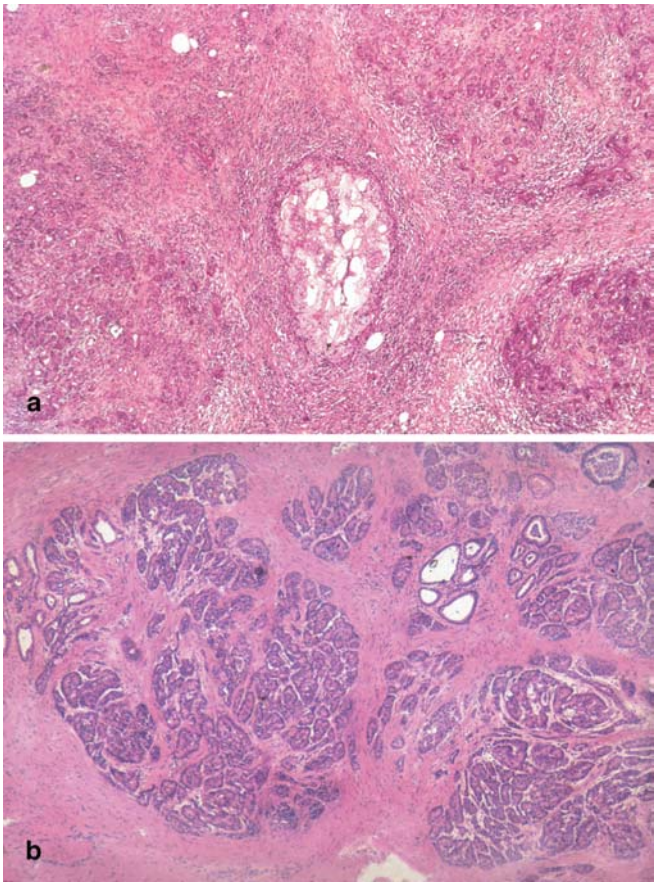


Fig. 3 Interlobular fibrosis pattern in alcoholic chronic pancreatitis. Hematoxylin & eosin. **a** Early stage of developing interlobular fibrosis in the vicinity of fatty tissue necrosis. **b** Late stage of interlobular fibrosis involving the ducts

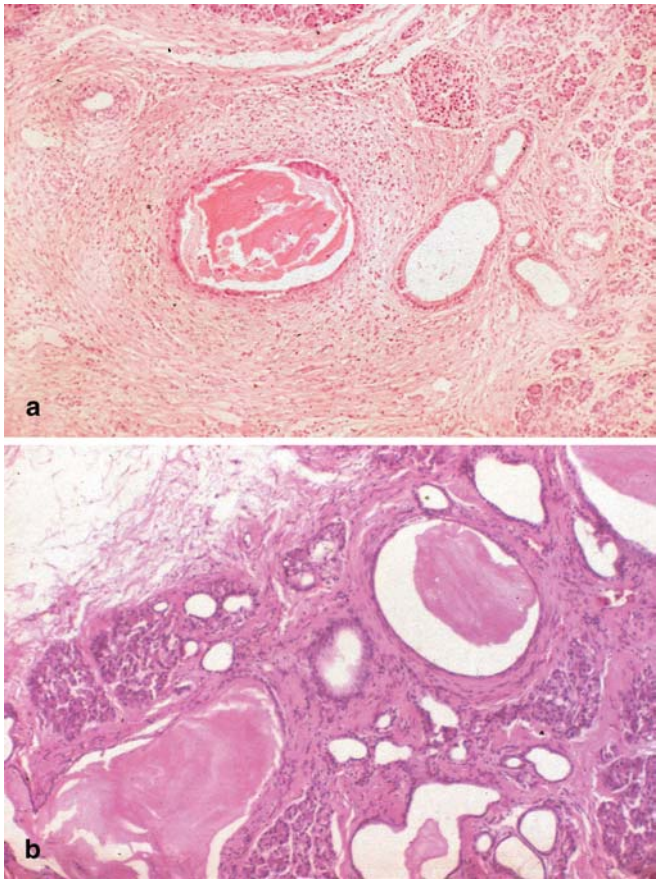


Fig. 5 Hereditary pancreatitis. Hematoxylin & eosin. **a** Interlobular duct showing granulocytes, epithelial destruction and inflammatory infiltration of the duct wall. **b** Dilated interlobular ducts with calculi and periductal fibrosis

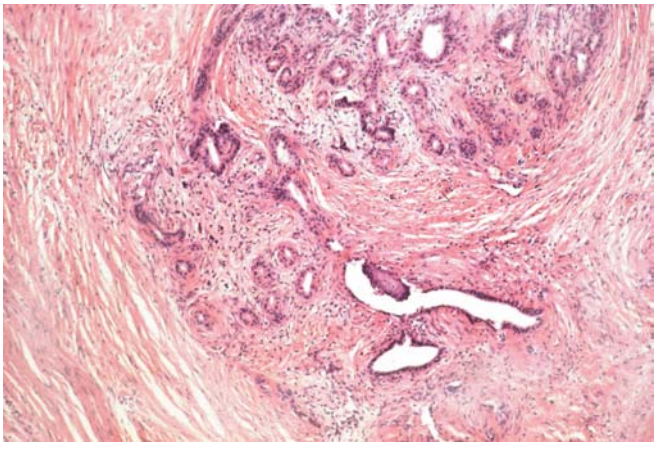


Fig. 4 Advanced inter- and intralobular fibrosis in alcoholic chronic pancreatitis. Hematoxylin & eosin

(G.K., unpublished observations), we found advanced chronic pancreatitis with severe periductal fibrosis and massively dilated ducts containing protein plugs and calculi staining for pancreatic stone protein. In one case, there was ductal necrosis in a number of medium-sized interlobular ducts that destroyed the duct epithelium and also involved the periductal area (Fig. 5A). This ductal and periductal necrosis, which we have also seen in a small number of rare cases of acute pancreatitis in patients after prolonged shock [19], suggests that the autodigestive process in hereditary pancreatitis may occur in the duct lumen, resulting initially in necrosis of the duct-lining cells and subsequently affecting the surrounding interstitial tissue. If we hypothesize that the relapsing autodigestive processes remain focused on the larger ducts and their surroundings, they may gradually induce dilatation of the involved duct segments, periductal fibrosis and, to a lesser extent, intralobular fibrosis (Fig. 5B). In addition, the dilated ducts may also contain calculi, since the duct changes probably create similar conditions for the flow of pancreatic secretions to those in alcoholic chronic pancreatitis.

Autoimmune (duct-destructive) chronic pancreatitis

Recent studies have suggested that there is a special type of chronic pancreatitis characterized by lymphoplasmacellular infiltration of the pancreas with conspicuous in-

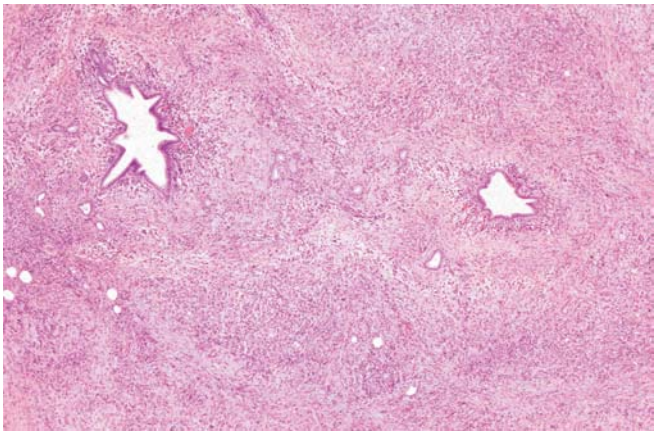


Fig. 6 Autoimmune (duct-destructive) chronic pancreatitis: interlobular ducts narrowed by a fibroinflammatory process that also involved the surrounding parenchyma. Hematoxylin & eosin

volvement of the ducts and with autoimmune features [1, 9, 18, 22, 31, 37]. Patients with this type of pancreatitis usually present with jaundice and/or abdominal pain, enlargement of the pancreas (usually the pancreas head) and an irregular narrowing of the main pancreatic duct and/or the bile duct. Most patients lack the symptoms of attacks of acute pancreatitis and fail to show calcifications or pseudocysts. Histologically, the pancreatic tissue displays lymphoplasmacytic infiltration and fibrosis, which focus on medium-sized ducts, causing duct narrowing and/or occasionally also destruction (Fig. 6). In addition to pancreatitis, autoimmune disorders, such as Sjögren's syndrome or ulcerative colitis, may occur synchronously or metachronously. The pattern of inflammation in the pancreas in patients with autoimmune pancreatitis is so unique that it can be clearly distinguished from other types of chronic pancreatitis, such as alcoholic chronic pancreatitis [9] or hereditary chronic pancreatitis. Apart from the ducts, probably in a second step, the chronic inflammation also affects the acinar tissue, leading to the disappearance of acinar cells. During the course of this progressive inflammation, periductal and later also interlobular fibrosis develops, which soon expands to the intralobular areas (Fig. 6). At the end of this process, the affected region of the pancreas shows diffuse fibrosis (Fig. 6). In some cases, the fibrosis may exhibit a myofibroblastic storiform pattern, characterized by the presence of myofibroblasts, scattered lymphocytes and plasma cells and dense collagen bundles. If such a fibrotic lesion is large, but still restricted to a portion of the pancreas, it acquires a tumorous appearance and may present as an inflammatory pseudotumor. Such lesions have been reported in the pancreatic head, but no connection with autoimmune pancreatitis was discussed. However, judging from the descriptions and illustrations of these cases [41], the lesions appear to be compatible with those seen in autoimmune pancreatitis [22]. Therefore, it is conceivable that the reported inflammatory pseudotumors of the pancreas represent an advanced stage of autoimmune pancreatitis in which the fibrotic changes predominate.

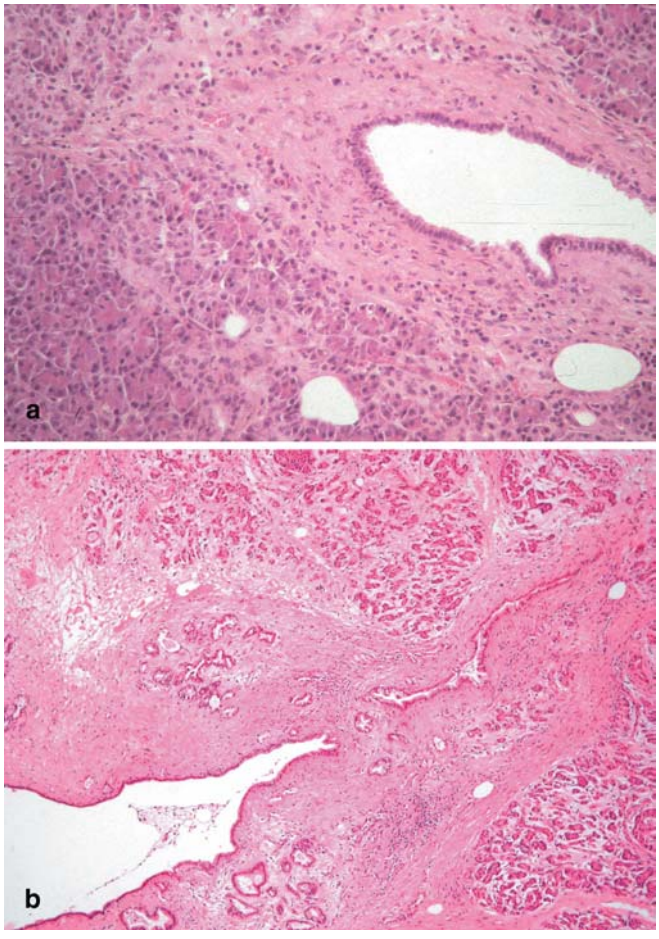


Fig. 7 Obstructive chronic pancreatitis. Hematoxylin & eosin. **a** Early stage showing dilated duct and beginning interlobular fibrosis. **b** Advanced interlobular fibrosis and beginning intralobular fibrosis

Obstructive chronic pancreatitis

As shown in Table 1, other types of pancreatitis include obstructive chronic pancreatitis, idiopathic chronic pancreatitis, tropical pancreatitis, chronic pancreatitis due to pancreas divisum or duodenal-wall pancreatitis [20]. With the exception of obstructive chronic pancreatitis, the morphological substrate of the other types of pancreatitis has not yet been systematically studied.

In obstructive chronic pancreatitis, there is a focal obstruction of the main pancreatic duct or one of the secondary ducts that lie in the interlobular spaces, leading to ductal dilation proximal (upstream) to the stenosis and to atrophy of the acinar cells and replacement by fibrous tissue (Fig. 7). There are various possible causes for a duct obstruction, but the most important and common cause is the narrowing and eventual occlusion of the main pancreatic duct in the head of the pancreas due to a ductal adenocarcinoma. As the head portion of the main pancreatic duct is affected, the fibrogenic process involves the body and tail of the gland and leads to the gradual development of interlobular fibrosis combined with in-

tralobular fibrosis. Other causes for an obstruction of the main pancreatic duct include intraductal papillary-mucinous neoplasms, some cystic and endocrine neoplasms and acquired fibrous strictures. In the smaller pancreatic ducts, ductal papillary hyperplasia is a common cause of narrowing of the duct lumen. Finally, the viscous mucin that is produced in cystic fibrosis may block the duct lumen and cause duct obstruction.

The effects of all the listed duct-obstructing mechanisms can be compared with those of duct ligation in the pancreas [15, 16]. In the early phase after duct ligation, the acini are transformed into small ductal (tubular) complexes. In a next step, the acinar cells disappear, probably due to apoptosis. These changes are associated with an inflammatory and fibrotic reaction involving numerous macrophages. The macrophages are the potential source of cytokines, which stimulate fibrogenesis by fibroblasts that acquire the properties of myofibroblasts. Because the inflammatory reaction takes place in all of the interlobular and intralobular areas of the pancreatic tissue that were once drained by the occluded duct, fibrosis develops at the same pace in these regions, producing interlobular and intralobular fibrosis in equal distribution.

Other types of pancreatic fibrosis

A special situation of fibrosis is encountered in cystic fibrosis of the pancreas and in pancreatic lobular fibrosis, which is frequently observed in post-mortem specimens from elderly persons without any known pancreatic disease. Whereas the first condition causes duct obstruction due to clogging by viscous mucin, the second condition leads to narrowing of the duct lumen by papillary hyperplasia of the duct epithelium. In cystic fibrosis, complete or almost complete (inter- and intralobular) fibrosis develops slowly after birth [33] (Fig. 8). After many years, this is more and more replaced by fatty tissue [27], a process that is not understood so far, but is of great interest for the regression of fibrosis. In the pancreas of elderly persons with obstructing ductal papillary hyperplasia in medium-sized ducts, the fibrosis that develops is mainly of the intralobular type and affects those lobes that are drained by ducts showing hyperplastic papillary changes (Fig. 9). The lobular fibrosis of the pancreas, therefore, has a patchy pattern. Its degree varies from person to person; the most severe form and the highest incidence (up to 50%) are found in persons older than 60 years (Detlefsen, Feyerabend and Klöppel, unpublished observations).

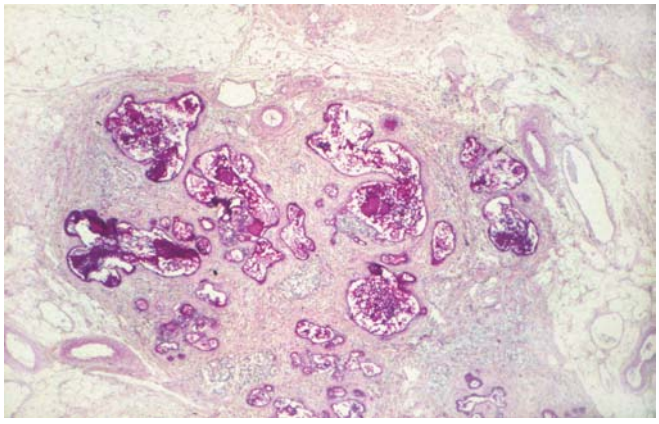


Fig. 8 Advanced cystic fibrosis: diffuse fibrosis of the pancreas alternating with fatty tissue cords. Dilated mucin-filled ducts. Periodic-acid Schiff

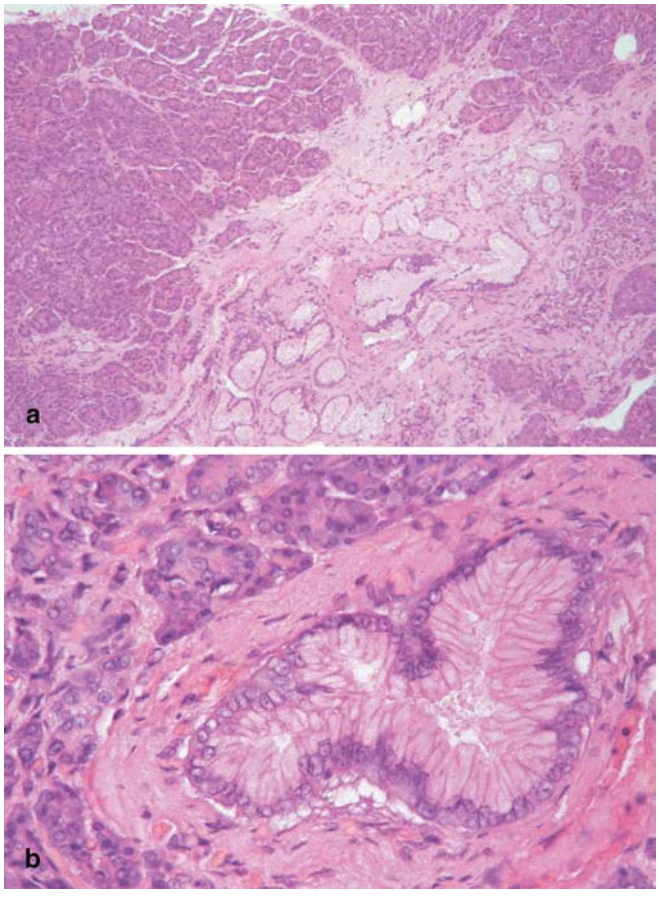


Fig. 9 Lobular fibrosis of the pancreas. Hematoxylin & eosin. **a** Interlobular duct showing mucinous hypertrophy of the epithelium and surrounded by fibrotic tissue containing islets and small ducts. **b** Ductal papillary hyperplasia of a duct with narrowing of the lumen

Conclusion

Fibrosis of the pancreas is observed in primary chronic pancreatitis or duct-obstructing processes. At its beginning, there is a tissue injury that induces a process of fibrogenesis similar to the development of fibrosis in other organs. The site where the process of fibrogenesis is initiated most likely determines the resulting pattern of fibrosis that develops in the pancreas. It is our working hypothesis that the initial site of tissue injury depends on

the etiological factors that cause necrosis and/or apoptosis. If the interstitial mesenchymal cells are primarily injured, as in alcoholic pancreatitis, mainly inter(peri)-lobular fibrosis develops. If the duct epithelium and the duct wall are injured, as in hereditary pancreatitis and autoimmune pancreatitis, the fibrosis initially affects the periductal area. If the acinar cells are injured, as in duct-obstructing processes, mainly diffuse (inter- and intra-lobular) fibrosis results.

References

1. Abraham SC, Leach S, Yeo CJ, Cameron JL, Murakata LA, Boitnott JK, Albores-Saavedra J, Hruban RH (2003) Eosinophilic pancreatitis and increased eosinophils in the pancreas. Am J Surg Pathol 27:334–342
2. Ammann RW, Heitz PU, Klöppel G (1996) Course of alcoholic chronic pancreatitis: a prospective clinicomorphological long-term study. Gastroenterology 111:224–231
3. Andoh A, Takaya H, Saotome T, Shimada M, Hata K, Araki Y, Nakamura F, Shintani Y, Fujiyama Y, Bamba T (2000) Cytokine regulation of chemokine (IL-8, MCP-1, and RANTES) gene expression in human pancreatic periacinar myofibroblasts. Gastroenterology 119:211–219
4. Apte MV, Haber PS, Applegate TL, Norton ID, McCaughan GW, Korsten MA, Pirola RC, Wilson JS (1998) Periacinar stellate-shaped cells in rat pancreas: identification, isolation, and culture. Gut 43:128–133
5. Apte MV, Haber PS, Darby SJ, Rodgers SC, McCaughan GW, Korsten MA, Pirola RC, Wilson JS (1999) Pancreatic stellate cells are activated by proinflammatory cytokines: implications for pancreatic fibrogenesis. Gut 44:534–541
6. Apte MV, Phillips PA, Fahmy RG, Darby SJ, Rodgers SC, McCaughan GW, Korsten MA, Pirola RC, Naidoo D, Wilson JS (2000) Does alcohol directly stimulate pancreatic fibrogenesis? Studies with rat pancreatic stellate cells. Gastroenterology 118:780–794
7. Bedossa P, Paradis V (2003) Liver extracellular matrix in health and disease. J Pathol 200:504–515
8. Ebert M, Kasper HU, Hernberg S, Friess H, Büchler MW, Roessner A, Korc M, Malfertheiner P (1998) Overexpression of platelet-derived growth factor (PDGF) B chain and type β PDGF receptor in human chronic pancreatitis. Dig Dis Sci 43:567–574
9. Ectors N, Maillet B, Aerts R, Geboes K, Donner A, Borchard F, Lankisch P, Stolte M, Lüttges J, Kremer B, Klöppel G (1997) Non-alcoholic duct destructive chronic pancreatitis. Gut 41:263–268
10. Elsässer HP, Adler G, Kern HF (1989) Fibroblast structure and function during regeneration from hormone-induced acute pancreatitis in the rat. Pancreas 4:169–178
11. Etemad B, Whitcomb DC (2001) Chronic pancreatitis: diagnosis, classification, and new genetic developments. Gastroenterology 120:682–707
12. Friess H, Yamanaka Y, Büchler M, Beger HG, Do DA, Kobrin MS, Korc M (1994) Increased expression of acidic and basic fibroblast growth factors in chronic pancreatitis. Am J Pathol 144:117–128
13. Gabbiani G (2003) The myofibroblast in wound healing and fibrocontractive diseases. J Pathol 200:500–503
14. Haber PS, Keogh GW, Apte MV, Moran CS, Stewart NL, Crawford DHG, Pirola RC, McCaughan GW, Ramm GA, Wilson JS (1999) Activation of pancreatic stellate cells in human and experimental pancreatic fibrosis. Am J Pathol 155:1087–1095
15. Hultquist GT, Jönsson LE (1965) Ligation of the pancreatic duct in rats. Acta Soc Med Upsal 70:82–88
16. Isaksson G, Ihse I, Lundquist I (1983) Influence of pancreatic duct ligation on endocrine and exocrine rat pancreas. Acta Physiol Scand 117:281–286
17. Izumi M, Suda K, Torii A, Inadama E (2001) Pancreatic ductal myofibroblasts. Proliferative patterns in various pathologic situations. Virchows Arch 438:442–450
18. Kawaguchi K, Koike M, Tsuruta K, Okamoto A, Tabata I, Fujita N (1991) Lymphoplasmacytic sclerosing pancreatitis with cholangitis: variant of primary sclerosing cholangitis extensively involving pancreas. Hum Pathol 22:387–395
19. Klöppel G (1997) Morphology of acute pancreatitis in relation to etiology and pathogenesis. In: Malfertheiner P, Domínguez-Muńoz JE, Schulz HU, Lippert H (eds) Diagnostic procedures in pancreatic disease. Springer, Berlin Heidelberg New York, pp 13–20
20. Klöppel G (1998) Chronic pancreatitis. Etiology, pathophysiology, and pathology. In: Howard J , Idezuki Y, Ihse I, Prinz R (eds) Surgical diseases of the pancreas, 3rd edn. Williams & Wilkins, Baltimore, pp 321–328
21. Klöppel G (1999) Progression from acute to chronic pancreatitis. A pathologist's view. Surg Clin North Am 79:801–814
22. Klöppel G, Lüttges J, Löhr M, Zamboni G, Longnecker D (2003) Autoimmune pancreatitis: pathological, clinical, and immunological features. Pancreas 27:14–19
23. Klöppel G, Maillet B (1991) Chronic pancreatitis: evolution of the disease. Hepatogastroenterology 38:408–412
24. Klöppel G, Maillet B (1992) The morphological basis for the evolution of acute pancreatitis into chronic pancreatitis. Virchows Arch [A] Pathol Anat 420:1–4
25. Konishi K, Izumi T, Kato O, Yamaguchi A, Miyazaki I (1981) Experimental pancreatolithiasis in the dog. Surgery 89:687–691
26. Kuroda J, Suda K, Hosokawa Y (1998) Periacinar collagenization in patients with chronic alcoholism. Pathol Int 48:857–868
27. Lack EE (2003) Cystic fibrosis and selected disorders with pancreatic insufficiency. In: Lack EE (ed) Pathology of the pancreas, gallbladder, extrahepatic biliary tract, and ampullary region. Oxford University Press, Oxford, pp 63–80
28. Luttenberger T, Schmid-Kotsas A, Menke A, Siech M, Beger H, Adler G, Grünert A, Bachem MG (2000) Platelet-derived growth factors stimulate proliferation and extracellular matrix synthesis of pancreatic stellate cells: implication in pathogenesis of pancreas fibrosis. Lab Invest 80:47–55
29. Martin ED (1984) Different pathomorphological aspects of pancreatic fibrosis, correlated with etiology: anatomical study of 300 cases. In: Gyr KE, Singer MV, Sarles H (eds) Pancreatitis: concepts and classification. Elsevier, Amsterdam, pp 77–82
30. Masi L, Malentacchi C, Campanacci D, Franchi A (2002) Transforming growth factor-beta isoform and receptor expression in chondrosarcoma of bone. Virchows Arch 440:491–497
31. Notohara K, Burgart LJ, Yadav D, Chari S, Smyrk TC (2003) Idiopathic chronic pancreatitis with periductal lymphoplasmacytic infiltration: clinicopathologic features of 35 cases. Am J Surg Pathol 27:1119–1127
32. Saurer L, Reber P, Schaffner T, Büchler MW, Buri C, Kappeler A, Walz A, Friess H, Mueller C (2000) Differential expression of chemokines in normal pancreas and in chronic pancreatitis. Gastroenterology 118:356–367
33. Seifert G (1984) Cystic fibrosis and haemochromatosis. In: Klöppel G, Heitz PU (eds) Pancreatic pathology. Churchill Livingstone, Edinburgh, pp 32–43
34. Shek FWT, Benyon RC, Walker FM, McCrudden PR, Pender SLF, Williams EJ, Johnson PA, Johnson CD, Bateman AC, Fine DR, Iredale JP (2002) Expression of transforming growth factor-β1 by pancreatic stellate cells and its implications for matrix secretion and turnover in chronic pancreatitis. Am J Pathol 160:1787–1798
35. Stamenkovic I (2003) Extracellular matrix remodelling: the role of matrix metalloproteinases. J Pathol 200:448–464
36. Suda K, Takase M, Takei K, Kumasaka T, Suzuki F (2000) Histopathologic and immunohistochemical studies on the

mechanism of interlobular fibrosis of the pancreas. Arch Pathol Lab Med 124:1302–1305
37. Weber SM, Cubukcu-Dimopulo O, Palesty JA, Suriawinata A, Klimstra D, Brennan MF, Conlon K (2003) Lymphoplasmacytic sclerosing pancreatitis: inflammatory mimic of pancreatic carcinoma. J Gastrointest Surg 7:129–139
38. Whitcomb DC, Gorry MC, Preston RA, Furey W, Sossenheimer MJ, Ulrich CD, Martin SP, Gates LK Jr, Amann ST, Toskes PP, Liddle R, McGrath K, Uomo G, Post JC, Ehrlich GD (1996) Hereditary pancreatitis is caused by a mutation in the cationic trypsinogen gene. Nat Genet 14:141–145
39. Witt H, Becker M (2002) Genetics of chronic pancreatitis. J Pediatr Gastroenterol Nutr 34:125–136
40. Witt H, Luck W, Hennies HC, Classen M, Kage A, Lass U, Landt O, Becker M (2000) Mutations in the gene encoding the serine protease inhibitor, Kazal type 1 are associated with chronic pancreatitis. Nat Genet 25:213–216
41. Wreesmann V, van Eijck CHJ, Naus DCWH, van Velthuysen MLF, Jeekel J, Mooi WJ (2001) Inflammatory pseudotumour (inflammatory myofibroblastic tumour) of the pancreas: a report of six cases associated with obliterative phlebitis. Histopathology 38:105–110

Virchows Arch (2004) 445:9–16
DOI 10.1007/s00428-004-1032-2

REVIEW ARTICLE

Thomas Stallmach · Gundula Hebisch

Placental pathology: its impact on explaining prenatal and perinatal death

Received: 27 November 2003 / Accepted: 15 April 2004 / Published online: 11 May 2004
© Springer-Verlag 2004

Abstract This review considers six main situations in which pathologists are expected to report and interpret placental messages for obstetricians, neonatologists and, indirectly, parents: (1) abortion is the body's corrective response to the embryonic defect suggested by malformed chorionic villi; (2) infection causing chorionic villous inflammation is specific and haematogenous; pathogen identification is mandatory, in contrast to chorioamnionitis caused by increased local immunosuppression allowing indiscriminate bacterial entry; (3) prematurity and (4) intrauterine growth restriction are often associated with pregnancy-specific disease (pre-eclampsia) or pre-existing maternal conditions (systemic lupus); parental studies may improve outcome in subsequent pregnancies; (5) intrauterine death near term is often due to placental dysmaturity featuring a severely reduced number of syncytiocapillary membranes; it accounts for the death in utero of 3 in 1000 pregnancies; detection helps to minimise recurrence in subsequent pregnancies; (6) twins are best confirmed as monozygous by the absence of chorionic tissue in the dividing membranes; most monochorionic twins have vascular connections whose detailed analysis is requested only if there are inter-twin differences in growth and colour. From a formal point of view, many more bits of pathology than discussed in this review can be found in placentas and, with the advances in ultrasonography, might even be seen prior to birth. The extent of such a disturbance might ultimately affect fetal growth, which is amenable to prenatal detection offering the chances for an appropriate management. In contrast, dysmaturity is a great challenge as no predictive tests are as yet available.

Keywords Placenta · Pathology · Abortion · Infection · Intrauterine growth restriction

T. Stallmach (✉)
Department of Pathology,
Zurich University Hospital,
Schmelzbergstrasse 12, 8091 Zurich, Switzerland
e-mail: thomas.stallmach@usz.ch
Tel.: +41-1-2552101
Fax: +41-1-2554416

G. Hebisch
Department of Obstetrics and Gynecology,
Zurich University Hospital,
Schmelzbergstrasse 12, 8091 Zurich, Switzerland

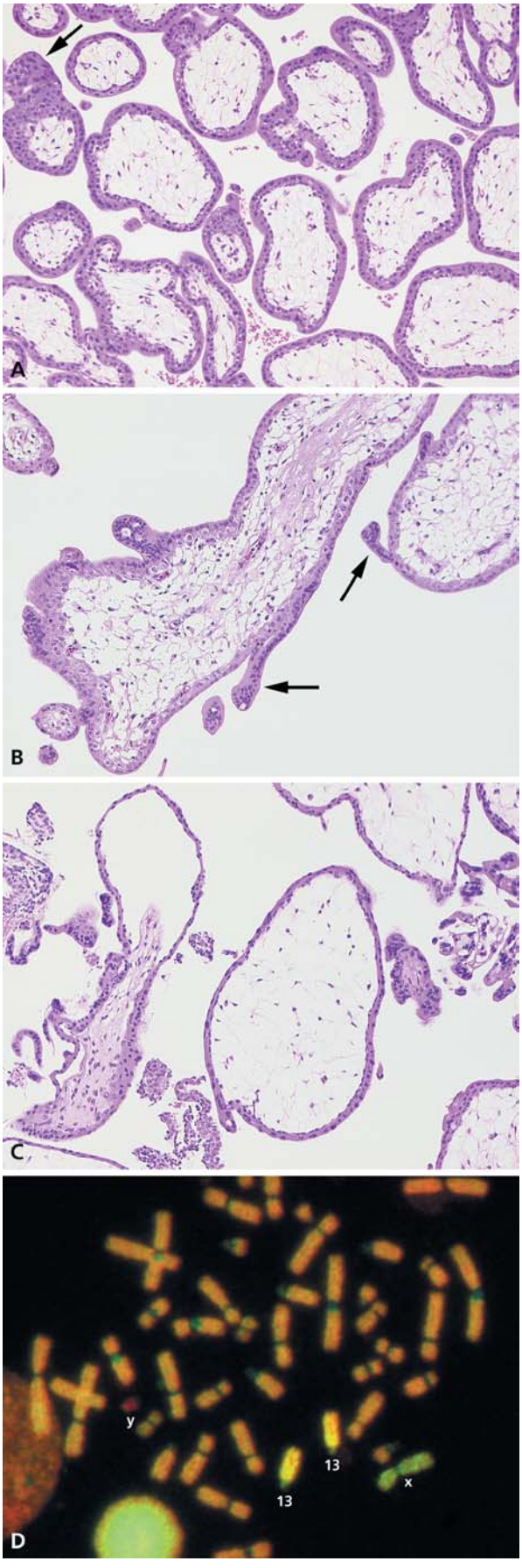
Introduction

Examination of the placenta by the pathologist is mandatory in cases of abortion, fetal malformation, infection, growth restriction, pre-eclampsia, late intrauterine death, intra-partum hypoxia (documented deterioration of the cardiotocogram or low pH immediately post-partum) and complicated twin pregnancy (feto-fetal transfusion syndrome, differences in body weight, zygosity). The pathologist needs a written request from the clinician, with information to include (at a minimum) the week of gestation, fetal weight, maternal health during pregnancy and the indications for referral (ideally in the form of the questions that the clinician would like to have answered).

Abortion (miscarriage)

Some 50% of all conceptions are thought to end in early abortion, many unnoticed. Timing life from the sperm's entry into the egg, John Opitz [17] said: "Most men die before birth, not after birth". Human reproductive failure is characterised less by resorption (as in mice) than by the expulsion of the products of conception. For the pathologist who receives the decidua with a line of demarcation and placenta, the single most important question is: are the chorionic villi normal? If 'No', it can be assumed that abortion has corrected an earlier mistake.

Chromosomal analysis of early and very early abortion tissue reveals a high proportion of pathological karyotypes [4, 12, 26], including tetraploidy, triploidy and trisomy of all chromosomes (with the sole exception to date of trisomy 1). Via an unknown mechanism, the maternal



organism detects and aborts these chromosomal pathologies. Although such karyotypes are compatible with limited trophoblastic and chorionic development, the architecture of the resulting chorionic villi, stratification of trophoblast layers, vascularisation and stromal density are abnormal (Fig. 1). Generally speaking, abnormal chorionic villi are mostly due to an abnormal karyotype, i.e. a genetic abnormality that—with very rare exceptions—is sporadic. Prolongation of such a pregnancy is neither desirable nor feasible. Precise characterisation of the chromosomal abnormality, e.g. trisomy of which chromosome, requires living cells for fibroblast culture and karyotype analysis. Alternatively, formalin-fixed, paraffin-embedded material can be subjected to comparative genomic hybridisation to detect the surplus DNA derived from the extra chromosome [5, 7] (Fig. 1d). Both methods are laborious and expensive, and the information retrieved is not required by the individual patient. If the parents wish for another child, there is no clearly defined need for a period of contraception.

If the chorionic villi are normal, on the other hand, this is bad news for the mother, since the assumption must be that she has aborted a potentially normal child. The reasons are not usually evident from the histology. Recurrence can be common. Many clinicians consider further exploration or a period of contraception helpful [25]. Recurrent abortion is defined by three consecutive early abortions of identical type, ideally with the chorionic villi showing the same disturbed architecture. Only then is parental karyotype analysis indicated. It occasionally detects a balanced chromosomal abnormality in one parent as the repeated cause of imbalance in the conceptus [1].

Infection

Irrespective of the cause of pregnancy failure, abortion material reveals inflammation as part of the desquamation process of devitalised tissues. In contrast, inflammation

Fig. 1 Early chorionic villus morphology and karyotype. **A** Normal chorionic villi show uniform branching architecture, trophoblast layering and stromal density. Polar proliferations of cytotrophoblast (*arrow*) are normal in early pregnancy. Haematoxylin and eosin (H&E), ×80. **B** Malformed villi are often large with irregular contours and syncytiotrophoblast piling (*arrow*). H&E, ×80. **C** The great diversity of abortifacient abnormal karyotypes is reflected in a variety of patterns of chorionic villus malformation. In this example, the dominant feature is stromal heterogeneity. H&E, ×80. **D** Ideogram of comparative genomic hybridisation analysis of DNA from a paraffin block with malformed chorionic villi (probe). The extracted DNA has a female karyotype and is hybridised on a normal male metaphase preparation: the Y chromosome is *red* because no corresponding DNA is present in the probe DNA (*green*). The X chromosome is *green* because of a surplus of X-derived DNA in the probe (ratio 2:1). Both chromosomes 13 are *bright yellow* compared with all other chromosomes because of a surplus of chromosome 13-derived probe DNA (ratio 3:2). The technology establishes the karyotype in different areas of the placenta with different morphology in cases of suspected mosaicism, but is not recommended for routine use. (Source: Scharpf P, doctoral thesis, Zurich 2002)

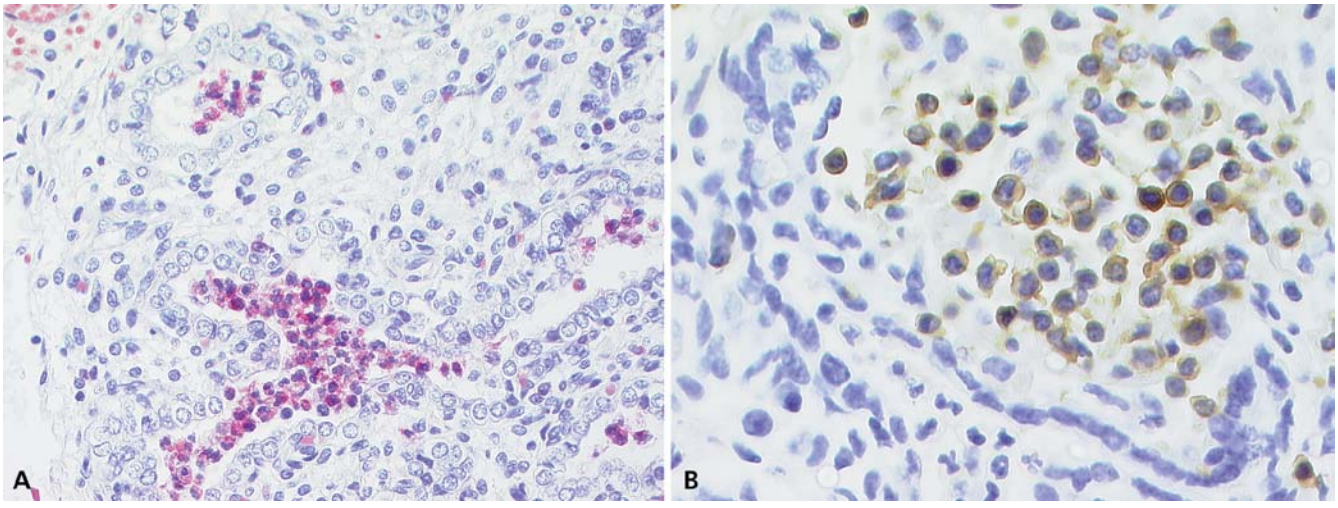


Fig. 2 Fetal lung with amniotic infection syndrome (chorioamnionitis). **A** Segmented maternal granulocytes aspirated into the alveoli from amniotic fluid. This should not be diagnosed as 'pneumonia'. The absence of aspirated granulocytes in otherwise unequivocal chorioamnionitis indicates oligohydramnios. Chloroacetate esterase stain, ×250. **B** Longstanding chorioamnionitis produces bronchus-associated lymphatic tissue. Lymphocytes labelled with CD45 antibody, ×400

due to infection becomes more prevalent from 16 weeks of pregnancy onwards.

There are two main scenarios. The first is that of so-called ascending amniotic infection [19], which is recognised by neutrophilic infiltrates in the membranes, chorionic plate and umbilical cord. At autopsy, the fetus—even when submitted without the placenta—readily reveals the diagnosis by increased hepatic granulopoiesis, ingested and aspirated granulocytes and the formation of bronchus-associated lymphatic tissue in the lungs (Fig. 2). The most sensitive finding is the presence of segmented neutrophilic (maternal) granulocytes within the fetal alveoli. However, care should be taken to discriminate apoptotic fetal cells from the alveolar lining. Furthermore, granulocyte aspiration and ingestion can be completely missing following oligohydramnios (preceding premature rupture of the membranes). Increased granulopoiesis within the fetal liver sinusoids, i.e. more than 15 granulopoietic cells per high power field (excluding the portal tract, where brisk granulopoiesis is physiological) visualised with a chloracetate esterase stain, is, thus, a more reliable indicator [22]. The formation of bronchus-associated lymphatic tissue can be most striking, however, and is seen in fetuses exposed to chorioamnionitis for several days [9]. Organism culture and special stains are not required. However, if the cord shows macroscopic yellow spots or histological evidence of superficial necrotising inflammation, there is a high suspicion of fungal infection, and periodic acid-Schiff staining for Candida is indicated.

The alternative scenario is haematogenous infection of the fetus, indicated by inflammation within the chorionic villi. In bacterial infections, granulocytes predominate while lympho-plasmocytic infiltration usually signifies cytomegalovirus (CMV) infection in developed countries. Whereas most viral infections can only access the fetus after primary infection of the mother during pregnancy [parvovirus infection, varicella (chickenpox), rubella (German measles) and toxoplasmosis], reactivation of latent maternal CMV infection can severely damage the fetus.

Haematogenous infection of the fetus is a mandatory indication for pathogen identification [3, 15]. It is the example *par excellence* of infectious disease. Chorioamnionitis, however, is not, since its most likely primary cause is an imbalance between fetal trophoblast invasion and maternal adaptation. Presumably, this results in a surplus of local immunosuppression and facilitates the ascension of bacteria from the vagina. Infection, then, can be caused by any of the bacteria present in the urogenital and intestinal tract, obviating in general the need to identify them as "pathogens".

Prematurity

Very immature newborns (24–28 weeks of gestation) are often the product of medical intervention designed to rescue either the fetus from adverse in utero conditions or the mother from the consequences of pre-eclampsia. Pregnancy is usually terminated by caesarean section timed by risk-factor assessment following the induction of fetal lung maturation using cortisone given to the mother.

Placentas should be sent for examination to document the antenatal diagnosis. Amniotic infection (see above), at some stage, induces labour, which cannot be stopped. Maternal inflammatory parameters (fever, C-reactive protein) and contraction intensity often correlate quite well with the intensity of placental inflammation, provided that at least two strips of extraplacental membranes, two to three segments of umbilical cord and three blocks from the placenta are examined [14, 29].

In contrast, pre-eclampsia does not induce uterine contractions. Termination is usually indicated on maternal

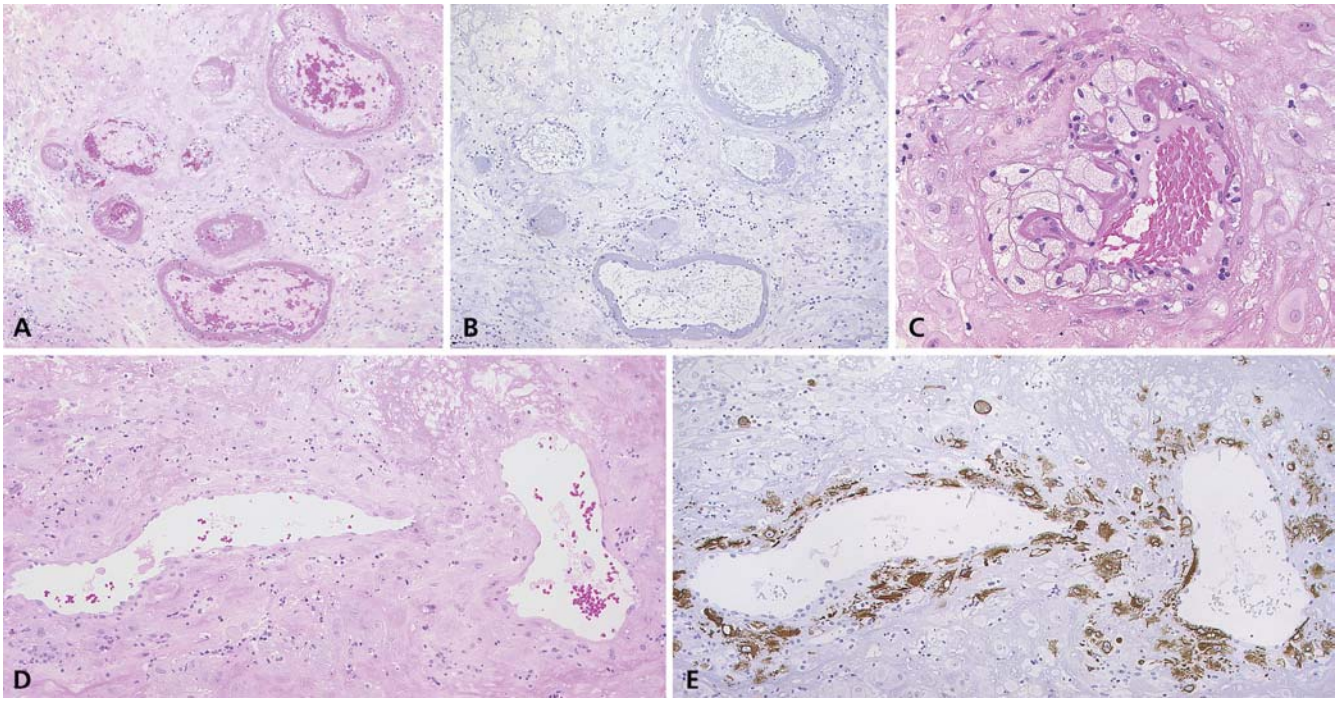


Fig. 3 Spiral artery pathology. **A** Acute atherosis is characterised by greater arterial density and a narrower arterial lumen on cross-section (compare the physiological transformation in **D**) and distinctive, strongly eosinophilic, hyaline replacement of the media. Haematoxylin and eosin (H&E), ×100. **B** In acute atherosis, the vessel wall is devoid of trophoblast cells (compare with **E**). Multinucleated trophoblast cells (none shown) may sometimes be present at a distance from the pathological vessels. Pancytokeratin, ×100. **C** High-power cross-sections in acute atherosis revealing segments with intimal foam cells. H&E, ×250. **D** Physiologically transformed spiral arteries are less coiled (fewer aggregated cross-sections); the muscle coat is replaced by (less eosinophilic) fibrinoid material (compare with acute atherosis in **A**). H&E, ×100. **E** Physiologically transformed spiral artery containing fetal trophoblast cells labelled with pancytokeratin antibody, ×100

grounds (oedema, proteinuria, hypertension and coagulation abnormalities). Pre-eclamptic placentas are usually below the fifth percentile for weight and size and display circulatory abnormalities in the intervillous space (infarcts of different age and size, thromboses). Very characteristic findings are seen in the underlying decidua, which is often inadequately represented in the usual placental blocks. When more of the basal plate tissue is retained, or the tissue submitted derives from curettage of the placental bed, a lack of trophoblast invasion can be seen [23]. Sometimes this goes along with a relative increase of multinucleated trophoblast cells clustered, albeit at some distance, around spiral arteries. These arteries themselves are narrow and show acute atherosis (Fig. 3). Similar placental findings can be present in mothers after organ (mostly kidney) transplantation and mothers with underlying autoimmune disease (lupus erythematosus).

Pre-eclampsia seems to be an aetiologically heterogeneous disorder. Late onset disease, greater than 34 weeks [30], usually does not restrict fetal growth [18], and, in most cases, the characteristic findings within and around spiral arteries are missing. There may be signs of intervillous circulatory disturbance; however, this increases anyway, to some extent, towards term. Meaningful research in this field has to take into account that clinical pre-eclampsia comprises at least two different conditions.

Intrauterine growth restriction

Serial fetal ultrasonography can now detect deviations from a growth curve that is initially unremarkable. Although this usually indicates a placental problem, there are multiple conditions that can restrict fetal growth (Table 1). The fetal growth curve evidences placental malfunction in the nutritional supply line and—as in children and adults—some time is required before death ensues. Given proper monitoring, fetal starvation is usually only fatal if it starts very early in pregnancy, when the risks of extreme prematurity put severe restrictions on caesarean section. The placenta of a growth-restricted child is almost always small (below the fifth percentile). However, if small size is the only placental abnormality, the term "placental insufficiency" is inappropriate, as the placenta will be small like any other fetal organ if the child is small for a non-placental reason. Thus, any genetic condition (e.g. uniparental disomy) or toxin (e.g. heavy smoking) that restricts fetal growth will also cause a small placenta. To identify a small placenta as a primary cause of fetal growth restriction, additional findings are required, e.g. impaired maternal blood flow through the intervillous space (infarcts) or impaired fetal blood flow through the cord and allantoic vessels or chorionic villi (fetal thrombotic vasculopathy) [13, 20]. Rarely, the combination of impaired maternal and fetal circulation

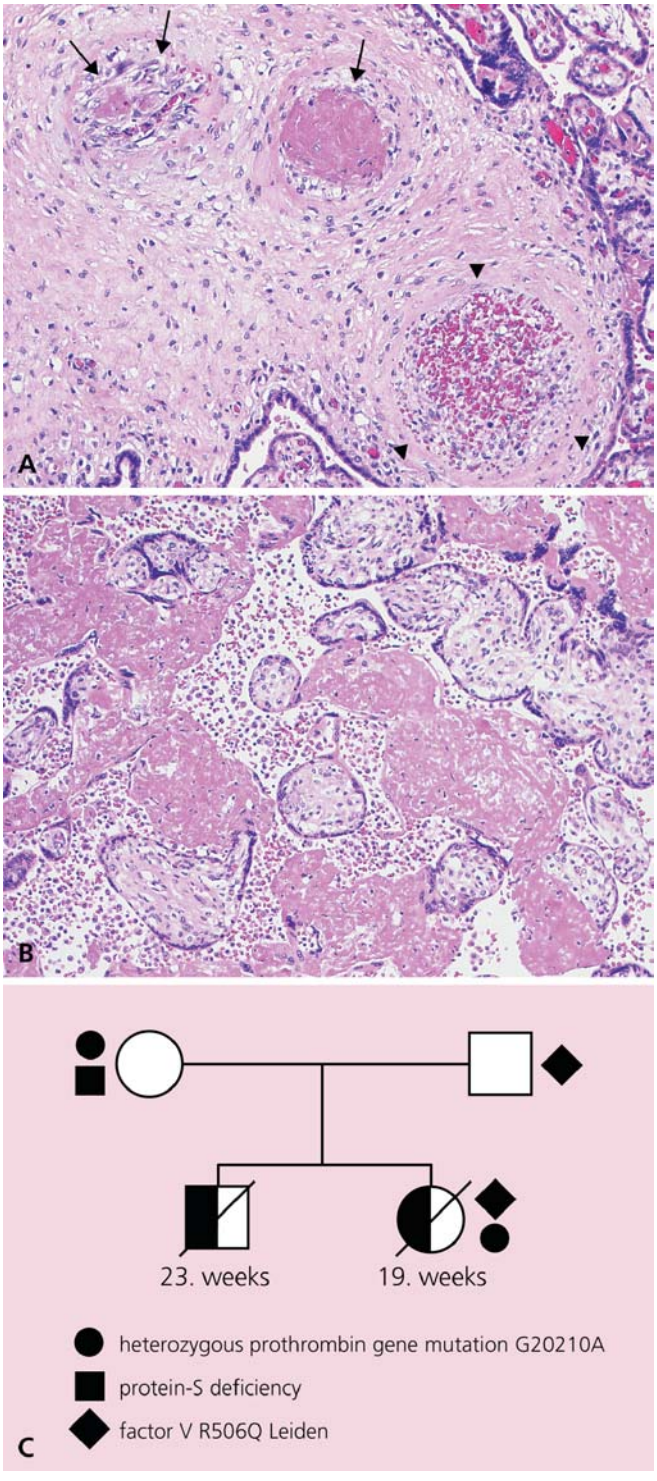


Fig. 4 Impaired fetomaternal circulation in the placenta. **A** Fetal thrombotic vasculopathy in a stem villus with two patterns: fresh thrombosis (*arrow*) followed by obliterating intimal proliferation (*two arrows*) and so-called haemorrhagic endovasculitis (*arrowheads*). **B** Obliteration of the maternal intervillous blood space by fibrin. Intervillous granulocytes and monocytes accompany the florid thrombotic process (haematogenous infection may show the same infiltrate but within the chorionic villi). **C** Genetic analysis of the female fetus fed by the above placenta and of the parents. Semi-shaded symbols denote two fetuses affected by a severely impaired placental circulation. No genetic analysis was performed of the first death at 23 weeks in 1981. *Small symbols* denote the genes analysed. The 19-week fetus is the double heterozygote infant of a family segregating a prothrombin gene mutation, factor V (Leiden) and protein S deficiency

Table 1 Possible causes of intrauterine growth restriction

(A)	Physical environment, mind, drugs
	Poor maternal nutritional status (low pre-pregnancy weight, vegetarians)
	Residence at high altitude (>5000 m above sea level)
	Stress factors (mental, physical, emotional)
	Drugs (nicotine, alcohol, medical and illegal drugs)
(B)	Pre-existing disease
	Cardiovascular (heart defects, heart insufficiency)
	Respiratory diseases (asthma)
	Haematological diseases (chronic anaemia, haemoglobinopathies)
	Gastrointestinal disorders (M. Crohn, ulcerative colitis)
	Renal transplantation, haemodialysis
	Chronic infections
	Immunological disorders (systemic lupus erythematodes, anti-phospholipid-antibody syndrome)
(C)	Pregnancy-specific disorders
	Hypertensive disorders of pregnancy (pre-eclampsia, HELLP syndrome)
	Chronic vaginal haemorrhage, retroplacental haematoma
	Multiple pregnancy
(D)	Fetal cause
	Fetal malformation (aneuploidy, single gene disorders, sporadic)
	Fetal infections (toxoplasmosis, CMV, others)
	Placental mosaicism and uniparental disomy

may reveal a combination of different—and perhaps as yet unknown—thrombophilic traits inherited by the fetus [6, 10, 28] (Fig. 4).

The functional reserve capacity of the placenta is usually given as 30%. However, live-born severely growth-restricted children are occasionally observed with placentas containing barely 30% of functional tissue. This makes it difficult to ascribe the in utero death of a severely dystrophic fetus merely to loss of functional placental tissue and starvation. The cause of death is rather a sudden additional pathology, e.g. focal abruptio from the decidua. Hence, the need for meticulous inspection to identify and report abruptio, even if focal and discrete.

Autopsy organ dimensions and weights in a small, non-malformed fetus can reveal two patterns. If all measures are similarly small, the placenta is a most unlikely cause. If the brain and feet are of normal size while the heart and kidney are small, and organs such as liver, spleen and thymus are very small, the asymmetry suggests insufficiency of the placental supply line. The risk of recurrence depends on the underlying condition causing the placental growth retardation and circulatory deficit. Even if unexplained, recurrence is readily detected by monitoring fetal growth during the next pregnancy. Some centres give prophylactic anticoagulation using heparin or aspirin alone or in combination [2, 11].

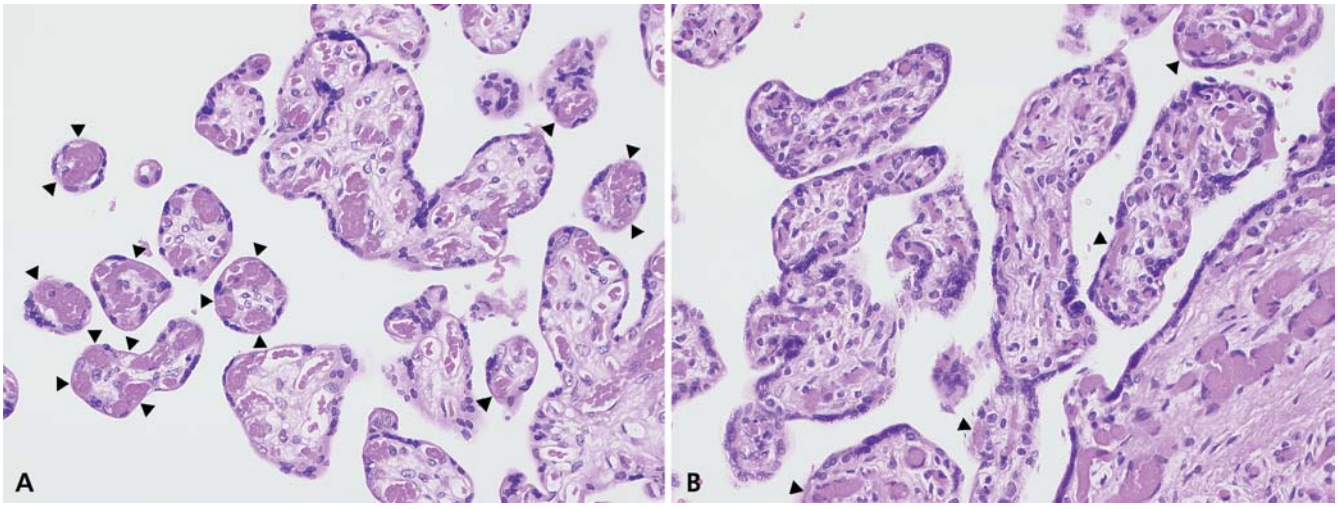


Fig. 5 Chorionic villus maturation in late pregnancy. **A** Normal maturation leads to a dominance of terminal villi with several syncytiocapillary membranes (*arrowheads*) per cross-section from 36 weeks onwards. Haematoxylin and eosin (H&E), ×250. **B** A dysmature term placenta has many fewer syncytiocapillary membranes (*arrowheads*); chorionic villi may be plumper. H&E, ×250

Intrauterine death near term

Of 1000 pregnancies that have progressed uneventfully to fetal viability, 3–4 will result in the catastrophe of sudden and silent in utero death. This represents one-half of perinatal mortality in highly developed countries. "Sudden" means the absence of warning, even in retrospect, from either maternal symptoms or fetal measurements. Given these circumstances, it is conceivable that the fetus has died from hypoxia, as either a single or repeated event. This makes it clear that the placental delivery of oxygen is not coupled to that of nutrients. A well-accepted cause is sudden premature abruptio; however, this produces symptoms in the mother and is, thus, not silent. In most other cases, mothers only present days after the child has died in utero because they have noticed the lack of fetal movements. Labour has to be induced to deliver the macerated child. At autopsy, so-called hypoxic haemorrhages are seen in the pleura, pericardium and meninges, and the approximate interval between death in utero and delivery can be estimated from the histology of the heart and lung [8].

The most common cause is placental dysmaturity or placental maturation defect [24]. Such placentas are of normal size or even large, but with a pale cut surface. In some cases of dysmaturity, the indication for examination by the pathologist is the midwife's observation that the placenta is pale. The pallor is due to defective formation of both the sinusoidal vessels in the terminal villi and the syncytiocapillary membranes. Sinusoidal vessels with broad contact and a short diffusion distance to maternal blood have been equated with impaired placental respiratory function and, thus, the risk of asphyxia. In its smallest and most mature terminal villi, a normal late pregnancy placenta ($\geq$35 weeks) has an average of three sinusoidal contacts with the surrounding maternal blood (Fig. 5). A dysmature placenta has an average of one such structure per terminal villus. About 5% of unselected placentas examined without indication reveal this pattern, and, up to now, there is no clue as to its cause. Although only 2% of fetuses with a dysmature placenta will actually die, this risk is 70-fold that of a fetus with a normal placenta [24]. A mother who has lost a child due to placental dysmaturity has a tenfold higher risk of recurrence compared with baseline. No predictive markers are presently available: placental dysfunction is manifested only as a terminal acute event. To minimise recurrence in a subsequent pregnancy, one option is to induce labour at completed 37 weeks, although this must be balanced against the risks of premature birth.

The concept of dysmaturity as a cause of fetal death is not yet widely accepted. A counter-argument is that fetuses dying from this supposed hypoxia are a minority. The answer is very simple: most fetuses are rescued by birth, as their placenta is required to function for only a few weeks more. Pathologists know how difficult it is to predict final decompensation in a diseased organ. For example, severely glomerulonephritic kidneys can force haemodialysis within a few weeks, but they can also stay functional for another couple of years.

Twin pregnancy

With very rare exceptions [21], a monochorionic twin pregnancy identifies the newborns as "identical" (monozygous). Thus, the fusion of placental tissues is considered an indication for histological examination of the dividing membrane. If the membrane contains chorionic tissue, it means that the twins lived in separate chorionic cavities. They still might be "identical". However, the rate of complications is low. In contrast, lack of chorionic tissue in the dividing membrane signifies a monochorionic cavity, which in most cases goes along with feto-

fetal vascular connections. If both twins are alive and similar in weight and colour (haemoglobin, haematocrit), there is no need for elaborate study of vessel connections. Intrauterine death and discrepancies of weight and colour, on the other hand, indicate the need to examine the chorionic plate for large connections. This can usually be performed within a few minutes by insufflation of the artery and vein of either umbilical cord using an air-filled syringe. Arteriovenous fistulas in the depths of the cotyledons are betrayed by small branches of arteries or veins coming from disparate sides and leading into the same area of the chorionic plate. These fistulas are usually multiple, although unbalanced in net blood flow [16, 27]. The imbalance is rescued by large connections, mostly arterio-arterial anastomoses, within the chorionic plate. However, these have their own intrinsic risk. If due to other causes, the condition of one twin deteriorates (eventually going along with a drop in its blood pressure), its circulation is overtransfused by the stronger pumping action (effecting a higher blood pressure) of the co-twin's heart.

Feto-fetal vascular connections are sometimes destroyed by laser coagulation. If this therapy is incomplete, it risks destabilising a previously labile balance in reciprocal transfusion. Some clinicians are, therefore, concerned to confirm successful coagulation of all connecting vessels after birth by examination of the placenta.

Conclusion

Examination of a placenta is clearly indicated in every pregnancy failure, as it can reveal underlying systemic causes and/or the risk of recurrence. Placentas should also be examined from children who survive birth but have an unexplained low Apgar score, infection or growth retardation. The routine storage of all placentas for at least 3 days is recommended, should the need for examination be dictated by subsequent deterioration in the newborn. From a formal point of view, many more bits of pathology than discussed in this review can be found in placentas and, with the advances in ultrasonography, might even be seen prior to birth, e.g. a "cyst" representing a subchorial haematoma. The extent of such a disturbance might ultimately affect fetal growth, which is amenable to prenatal detection offering the chances for an appropriate management. More to be feared is sudden deterioration, mostly by abruptio of the placenta. Dysmaturity causing sudden death due to hypoxia is the greatest challenge, as there are no premonitory signs and no predictive tests as yet available.

References

1. Badawy SZA, Westpfal EM (2000) Frequency of etiological factors and cost effectiveness of the work up for patients with history of recurrent pregnancy loss. Early Pregnancy 4:253–260
2. Bar J, Mashiah R, Cohen-Sacher B, Hod M, Orvieto R, Ben-Rafael Z, Lahav J (2001) Effect of thrombophylaxis on uterine and fetal circulation in pregnant women with a history of pregnancy complications. Thromb Res 101:235–241
3. Bruder E, Ersch J, Hebisch G, Ehrbar T, Klimkait T, Stallmach T (2000) Fetal varicella syndrome: disruption of neural development and persistent inflammation of non-neural tissues. Virchows Arch 437:440–444
4. Creasy MR, Crolla JA, Alberman ED (1976) A cytogenetic study of human spontaneous abortions using banding techniques. Hum Genet 31:177–196
5. Daniely M, Aviram-Goldring A, Barkai G, Goldman B (1998) Detection of chromosomal aberration in fetuses arising from recurrent spontaneous abortion by comparative genomic hybridization. Hum Reprod 13:805–809
6. Formstone CJ, Hallam PJ, Tuddenham EGD, Voke J, Layton M, Nicolaides K, Hann IM, Cooper DN (1996) Severe perinatal thrombosis in double and triple heterozygous offspring of a family segregating two independent protein S mutations and a protein C mutation. Blood 87:3731–3737
7. Fritz B, Hallermann C, Olert J, Fuchs B, Bruns M, Aslan M, Schmidt S, Coerdt W, Müntefering H, Rehder H (2001) Cytogenetic analyses of culture failures by comparative genomic hybridization (CGH)—re-evaluation of chromosome aberration rates in early spontaneous abortions. Eur J Hum Genet 9:539–547
8. Genest DR, Williams MA, Green MF (1992) Estimating the time of death in stillborn fetuses: I. Histologic evaluation of fetal organs; an autopsy study of 150 stillborns. Obstet Gynecol 80:575–584
9. Gould SJ, Isaacson PG (1993) Bronchus-associated lymphoid tissue (BALT) in human fetal and infant lung. J Pathol 169:229–234
10. Hebisch G, Bernasconi MT, Gmuer J, Huch A, Stallmach T (2001) Pregnancy-associated recurrent hemolytic uremic syndrome with fetal thrombotic vasculopathy in the placenta. Am J Obstet Gynecol 185:1265–1266
11. Heilmann L, von Tempelhoff GF, Pollow K (2003) Antiphospholipid syndrome in obstetrics. Clin Appl Thromb Hemost 9:143–150
12. Kajii T, Ferrier A, Niikawa N, Takahara H, Ohama K, Avirachan S (1980) Anatomical and chromosomal anomalies in 639 spontaneous abortuses. Hum Genet 55:87
13. Kraus FT, Acheen VI (1999) Fetal thrombotic vasculopathy in the placenta: cerebral thrombi and infarcts, coagulopathies, and cerebral palsy. Hum Pathol 30:759–769
14. Langston C, Kaplan C, Macpherson T, Manci E, Peevy K, Clark B, Murtagh C, Cox S, Glenn G (1997) Practice guideline for examination of the placenta: developed by the Placental Pathology Practice Guideline Development Task Force of the College of American Pathologists. Arch Pathol Lab Med 121:449–476
15. Meyer A, Stallmach T, Goldenberger D, Altwegg M (1997) Lethal maternal sepsis caused by Campylobacter jejuni: pathogen preserved in placenta and identified by molecular methods. Mod Pathol 10:1253–1256
16. Nikkels PG, van Gemert MJ, Sollie-Szarynska KM, Molendijk H, Timmer B, Machin GA (2002) Rapid onset of severe twin–twin transfusion syndrome caused by placental venous thrombosis. Pediatr Dev Pathol 5:310–314
17. Opitz JM (1987) The Farber lecture. Prenatal and perinatal death: the future of developmental pathology. Pediatr Pathol 7:363–394
18. Rasmussen S, Irgens LM (2003) Fetal growth and body proportion in preeclampsia. Obstet Gynecol 101:575–83
19. Redline RW, Faye-Petersen O, Heller D, Qureshi F, Savell V, Vogler C (2003) Amniotic infection syndrome: nosology and

reproducibility of placental reaction patterns. Pediatr Dev Pathol 6:435–448
20. Sander CM, Gilliland D, Akers C, McGrath A, Bismar TA, Swart-Hills LA (2002) Live births with placental hemorrhagic endovasculitis. Interledional relationships and perinatal outcomes. Arch Pathol Lab Med 126:157–164
21. Souter VL, Kapur RP, Nyholt DR, Skogerboe K, Myerson D, Ton CC, Opheim KE, Easterling TR, Shields LE, Montgomery GW, Glass IA (2003) A Report of dizygous monochorionic twins. N Engl J Med 349:154–158
22. Stallmach T, Károlyi L (1994) Augmentation of fetal granulopoiesis with chorioamnionitis during the second trimester of gestation. Hum Pathol 25:244–247
23. Stallmach T, Hebisch G, Orban P, Lü X (1999) Aberrant positioning of trophoblast and lymphocytes in the feto-maternal interface of growth-retarded fetuses. Virchows Arch 434:207–211
24. Stallmach T, Hebisch G, Meier K, Dudenhausen JW, Vogel M (2001) Rescue by birth: defective placental maturation and late fetal mortality. Obstet Gynecol 97:505–509
25. Stephansson O, Dickman PW, Cnattingius (2003) The influence of interpregnancy interval on the subsequent risk of stillbirth and early neonatal death. Obstet Gynecol 102:101–108
26. Stern JJ, Dorfmann AD, Gutierrez-Najar AJ, Cerrillo M, Coulam CB (1996) Frequency of abnormal karyotypes among abortuses from women with and without a history of recurrent spontaneous abortion. Fertil Steril 65:250–253
27. Umur A, van Gemert MJ, Nikkels PG, Ross MG (2002) Monochorionic twins and twin–twin transfusion syndrome: the protective role of arterio-arterial anastomoses. Phys Med Biol 49:57–64
28. Vern TZ, Alles AJ, Kowal-Vern A, Longtine J, Roberts DJ (2000) Frequency of factor V (Leiden) and prothrombin G20210A in placentas and their relationship with placental lesions. Hum Pathol 31:1036–1043
29. Vogel M (1996) Atlas der morphologischen Plazentadiagnostik. 2. Auflage. Springer, Berlin Heidelberg New York
30. von Dadelszen P, Magee LA, Roberts JM (2003) Subclassification of preeclampsia. Hypertens Pregnancy 22:143–148

Virchows Arch (2004) 445:17–21
DOI 10.1007/s00428-004-1034-0

ORIGINAL ARTICLE

Axel Glaessgen · Hans Hamberg · Carl-Gustaf Pihl · Birgitta Sundelin · Bo Nilsson · Lars Egevad

Interobserver reproducibility of modified Gleason score in radical prostatectomy specimens

Received: 16 February 2004 / Accepted: 20 April 2004 / Published online: 20 May 2004
© Springer-Verlag 2004

Abstract The Gleason score (GS) of prostate cancer is calculated by adding primary and secondary Gleason grades with patterns occupying less than 5% of the tumour often not included despite their probable prognostic significance. A modified Gleason score (mGS) comprising primary and tertiary patterns of higher grade has been proposed, but its interobserver variability has yet to be elucidated. Slides from 69 consecutive prostatectomy specimens were circulated among four genitourinary pathologists. GS and mGS were assessed, and results were compared in pairs. Mean weighted kappa for GS and mGS were 0.56 (range 0.52–0.66) and 0.58 (range 0.49–0.74), respectively. The difference between GS and mGS was 0, 1 and 2 score units in 66%, 26% and 8%, respectively, mean 0.41 score units (range 0.24–0.51). The increment was greater for transition-zone tumours than for peripheral-zone tumours (0.63 and 0.35 score units, respectively, P=0.002). An odd mGS (5, 7 or 9) was more often given than an odd GS (77% and 62%, respectively, P<0.001). Disagreement between observers greater than 1 score unit was more common with mGS than GS (18% and 4%, respectively, P<0.001). In conclusion, overall mean weighted kappa for interobserver reproducibility of mGS is at least as high as that of GS. However, there is a clustering of mGS in odd scores, and severe disagreement is more commonly observed than with GS. Training of mGS assessment would possibly improve agreement. Tertiary Gleason patterns need to be better defined.

Keywords Prostatic neoplasms/pathology · Prostatic neoplasms/Gleason grading · Prostatic neoplasms/classification · Prostatectomy, human

The study was approved by the ethics committee of The Karolinska Institute (01–443).

A. Glaessgen · H. Hamberg · B. Sundelin · L. Egevad (✉)
Department of Pathology and Cytology,
Karolinska Hospital,
Stockholm, Sweden
e-mail: Lars.Egevad@onkpat.ki.se
Tel.: +46-8-51775492
Fax: +46-8-331909

C.-G. Pihl
Department of Pathology,
Sahlgrenska University Hospital,
Gothenburg, Sweden

B. Nilsson
Department of Oncology and Pathology,
Karolinska Institute,
Stockholm, Sweden

Introduction

Few tumours display such remarkable morphological heterogeneity as prostate cancer. Usually more than one histological pattern is present in prostatectomy specimens, and cancer of a single grade is less common [1, 20]. The Gleason grading system is designed to take into account this complexity by including both the primary and secondary pattern (i.e. the most prevalent and the second most prevalent pattern) in the Gleason score (GS). However, in addition to the primary and secondary patterns, a tertiary pattern may be present. In a study from 1994, Aihara et al. found that over 50% of prostatectomy specimens contained cancer of at least three different Gleason patterns [1]. For convenience, the term tertiary pattern will be used in this article to designate only a grade that is higher than the primary and secondary patterns. Patterns occupying less than 5% of the tumour are often ignored when the GS is assessed [6]. Hence, if more than 95% of the tumour is occupied by a single pattern, GS is obtained by doubling that pattern. In those cases, the predominant pattern will be considered both primary and secondary, and a higher grade occupying less than 5% of the tumour will be referred to as tertiary.

Pan et al. showed that a tertiary grade has an adverse impact on prognosis after prostatectomy [19]. Men with a tertiary pattern 4 or 5 in a GS 5 or 6 tumour had a prognosis similar to those with a GS 7. The authors proposed that a tertiary component is reported together with the GS. However, it was also suggested that if future

studies would corroborate their findings, a modified Gleason score (mGS) calculated by adding primary and tertiary patterns might replace the GS. In a recent study on natural history of transurethral resection of the prostate (TURP)-detected prostate cancers, we demonstrated that mGS was a stronger predictor of disease-specific survival than GS and that both were independently significant prognosticators [8].

Before recommending mGS for general use, several issues have to be clarified, among them the reproducibility of this measure. Several studies on interobserver variability of Gleason grading have been published [3, 4, 7, 16], and, recently, we have shown that reproducibility of percentage Gleason grade 4/5 in prostatectomy specimens and prostate needle biopsies is at least as good as that of the GS [11, 12]. However, to our knowledge, reproducibility of the mGS has not been reported previously. In this study, interobserver reproducibility of this measure is investigated on a consecutive series of prostatectomy specimens.

Materials and methods

This study was based on a consecutive series of 69 radical prostatectomy specimens received from January 2000 to December 2000 at the Department of Pathology and Cytology at the Karolinska Hospital. The same set of slides was used in our recent study on reproducibility of percentage Gleason grade 4/5 [11].

The prostatectomy specimens were handled according to a standardised protocol previously described [11]. Briefly, the prostate was fixed overnight in 10% buffered formalin, inked and sliced horizontally at 4-mm intervals. The slices were cut in 2–6 segments, and the entire prostate was subsequently blocked in standard cassettes, sectioned at 4 μm and stained with haematoxylin and eosin. Cancer was outlined on the slides. The tumour originated from the peripheral zone in 54 cases and from the transition zone in 15 cases. Seminal vesicle invasion, extraprostatic extension and positive margins were present in 13 (19%), 41 (59%) and 33 (48%) cases, respectively.

Similar to our previous study, a single slide from the main tumour focus of each prostatectomy specimen was selected by one of the authors (L.E.) [11]. One of the slides with the greatest amount of cancer was chosen. When multiple slides with a substantial amount of cancer were available, the slide that most closely represented the GS of the main tumour was used. The glass slides were circulated among four pathologists who specialised in genitourinary pathology (L.E., H.H., C.G.P. and B.S.) for a total of 276 responses. No consensus training preceded the study. Slides were reviewed, and a mGS was calculated by adding primary (dominating) Gleason grade and tertiary Gleason pattern of higher grade when present. When no tertiary component was found, mGS was identical to conventional GS. The GS and percentage Gleason grade 4/5 given in our previous study were used [11]. Slides were circulated twice for the two studies, but GS and percentage Gleason grade 4/5 were only assessed at the first slide review, and mGS only at the second. By comparing the responses of each of the four participants with those of the other three, six pairwise comparisons were obtained for each of the 69 cases, for a total of 414 comparisons. Results were compared in pairs, and weighted kappa values were calculated for GS and mGS.

Results

The GSs given by the four observers ranged from 5 to 9 (mean 6.35–6.88, overall mean 6.68, Table 1). A GS of 6 or 7 was assigned to 81–90% of cases (mean 86%). Average GS was higher in peripheral-zone than in transition-zone tumours (6.83 and 6.13, respectively, $P<0.001$).

The mGSs given by the observers ranged from 5 to 9 (mean 6.86–7.35, overall mean 7.09, Table 1). The mean difference between mGS and GS was 0.24–0.51 (overall mean 0.41). A mGS of 6 or 7 was assigned to 70–90% of cases (mean 78%). Average mGS was higher in peripheral-zone than in transition-zone tumours (7.18 and 6.77, respectively, $P=0.015$).

The score distribution of GS and mGS differed significantly ($P<0.001$, Fig. 1). Of all responses, 6%, 32%, 54%, 6% and 3% were GSs 5, 6, 7, 8 and 9, respectively. For mGS, this distribution was 3%, 15%, 63%, 8% and 11%, respectively.

In 183 (66%) of the responses, GS and mGS were identical (Table 2). There was an increment from GS to mGS of 1 or 2 units in 72 (26%) and 21 (8%) responses, respectively. The increment was greater for transition-zone tumours than for peripheral-zone tumours (0.63 and 0.35, respectively, $P=0.002$). Of GSs 5, 6, 7 and 8 tumours, 56% (9 of 16 tumours), 56% (49 of 88), 20% (29 of 148) and 47% (8 of 17), respectively, had a tertiary pattern and, thus, a higher mGS than GS. Tertiary patterns 4 and 5 were reported 56 (20%) and 37 (13%) times, respectively. In peripheral-zone tumours, tertiary patterns 4 and 5 were reported in 17% and 13%, respectively, and in transition-zone tumours, these patterns were reported in 33% and 13%, respectively. When the increment from GS

Table 1 Distribution of Gleason scores and modified Gleason scores

Observer no.	5	6	7	8	9	Average
Gleason score						
1	6	15	41	3	4	6.77
2	5	15	45	3	1	6.71
3	4	42	20	1	2	6.35
4	1	16	42	10	0	6.88
No. of tumours (%)	16 (6)	88 (32)	148 (54)	17 (6)	7 (3)	276
Modified Gleason score						
1	5	11	39	6	8	7.01
2	1	9	45	7	7	7.14
3	2	14	48	2	3	6.86
4	1	7	41	7	13	7.35
No. of tumours (%)	9 (3)	41 (15)	173 (63)	22 (8)	31 (11)	276

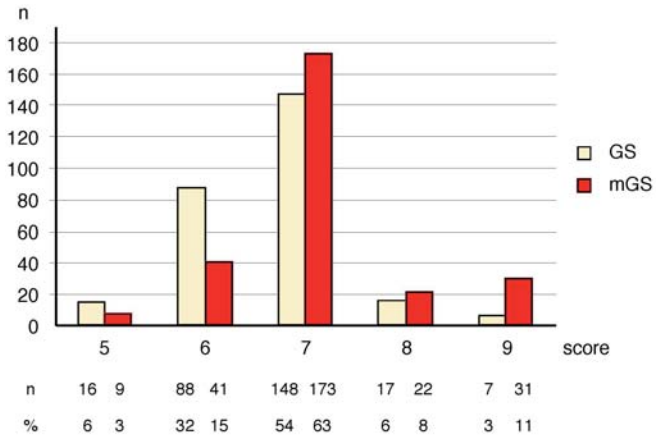


Fig. 1 Distribution of Gleason scores (GS) and modified Gleason scores (mGS)

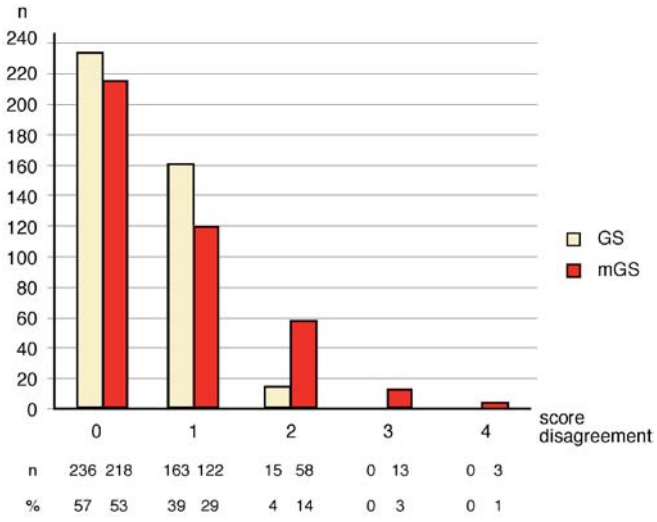


Fig. 2 Score disagreement in pairwise comparison of Gleason scores (GS) and modified Gleason scores (mGS)

Table 2 Gleason scores compared with modified Gleason scores

		Modified Gleason score					
		5	6	7	8	9	Totals
Gleason score	5	9	2	5	0	0	16
	6	0	39	49	0	0	88
	7	0	0	119	13	16	148
	8	0	0	0	9	8	17
	9	0	0	0	0	7	7
	Totals	9	41	173	22	31	276

to mGS was two units, a tertiary pattern 5 was more often responsible for the score shift than a tertiary pattern 4 (76% and 24%, respectively), while tertiary patterns 5 were less commonly seen in cases with one unit increment from GS to mGS (29% and 71%, respectively, $P<0.001$). A difference of more than one grade unit between the two patterns included in the score was more common with mGS than GS (6% and 0.7%, respectively, $P<0.001$, Table 3).

An odd mGS (5, 7 or 9) was more often given than an odd GS (77% and 62%, respectively, $P<0.001$). Of 93 changed scores, 57 (61%) were shifted from an even GS to an odd mGS (from 3+3=6 to 3+4=7 or from 4+4=8 to 4+5=9), 15 (16%) from an odd GS to an even mGS (from 2+3=5 to 2+4=6 or from 3+4=7 to 3+5=8) and 21 (23%) from an odd GS to another odd GS (from 3+2=5 to 3+4=7 or from 4+3=7 to 4+5=9) (Table 3).

All responses were compared in pairs, and differences in mGS were calculated. In 218 (53%) of the 414 pairs, agreement was exact. The disagreement between paired responses was one, two, three and four score units in 30%, 14%, 3% and 1%, respectively (Fig. 2). Disagreement of

Table 3 Score changes from Gleason scores to modified Gleason scores

Gleason score	Modified Gleason score	Totals	Peripheral-zone tumours	Transition-zone tumours	Unchanged	Changed
2+3	2+3	1	0	1	1	
2+3	2+4	2	0	2		2
2+3	2+5	0	0	0		0
3+2	3+2	8	0	8	8	
3+2	3+4	5	0	5		5
3+2	3+5	0	0	0		0
3+3	3+3	37	32	5	37	
3+3	3+4	49	36	13		49
3+3	3+5	0	0	0		0
2+4	2+4	1	0	1	1	
4+2	4+2	1	0	1	1	
3+4	3+4	93	78	15	93	
3+4	3+5	13	10	3		13
4+3	4+3	26	25	1	26	
4+3	4+5	16	11	5		16
4+4	4+4	9	9	0	9	
4+4	4+5	8	8	0		8
4+5	4+5	5	5	0	5	
5+4	5+4	2	2	0	2	
		276	216	60	183	93

Table 4 Weighted kappa values for Gleason scores and modified Gleason scores of the four observers

	Weighted kappa values				Totals
Observer no.	1	2	3	4	
Gleason score					
1		0.67	0.627	0.669	
2	0.670		0.507	0.496	
3	0.627	0.507		0.412	
4	0.669	0.496	0.412		
Average	0.655	0.558	0.515	0.526	0.563
Modified Gleason score					
1		0.735	0.668	0.501	
2	0.735		0.586	0.514	
3	0.668	0.586		0.487	
4	0.501	0.514	0.487		
Average	0.635	0.612	0.580	0.501	0.582

more than one score unit was more common with mGS than GS (18% and 4%, respectively, $P<0.001$).

The mean-weighted kappa value for GS and for mGS rendered by each observer and compared with each of the other three observers was 0.52–0.66 (overall mean 0.56) and 0.49–0.74 (overall mean 0.58), respectively (Table 4). The observer concordance was lower for transition-zone tumours than for peripheral-zone tumours, both with GS (weighted kappa 0.43 and 0.54, respectively) and with mGS (weighted kappa 0.52 and 0.59, respectively).

Discussion

The GS is a well-established prognostic parameter for prostate cancer [2, 5, 18]. The value of this grading as a predictor of recurrence after prostatectomy [10, 15] or radiotherapy [13] and as determinant of disease-specific survival in patients on deferred treatment [9] has been shown in several studies. The GS is calculated by adding primary and secondary Gleason grade and patterns occupying less than 5% of the tumour are often not included [6]. Hence, Gleason grading differs from many other grading systems in that the GS does not necessarily include the highest grade present in the tumour. Several authors have demonstrated the prognostic significance of a high-grade prostate cancer component [8, 9, 17, 19, 21]. The Stanford group has shown that the percentage of the tumour that is occupied by Gleason grades 4 or 5 (percentage Gleason grade 4/5) predicts lymph-node metastases [17] and recurrence [21] after radical prostatectomy. In a Swedish study of TURP-detected prostate cancer managed by watchful waiting, percentage Gleason grade 4/5 was a better predictor of disease-specific survival than the GS [8]. Furthermore, men with GS 6 tumours with a focal component of Gleason pattern 4 suffered a significantly higher risk of cancer-specific death than men with pure GS 6 tumours. A mGS calculated by adding the primary and tertiary pattern was also a better predictor of prognosis than the GS. In another study, Pan et al. showed that likelihood of recurrence after radical prostatectomy increased if a tertiary pattern of higher grade was found [19].

To be practically useful, a grading system must have satisfactory reproducibility. Numerous studies on interobserver reproducibility of the GS have been published in recent decades [3, 4, 7, 16]. Allsbrook et al. provided a detailed review [4]. The results of reproducibility studies are often difficult to compare, because the number of observers as well as number and type of specimens have not been the same. Some of the studies have been preceded by a tutorial, and others include selected sets of specimens rather than consecutive series. In the present study, we used the same consecutive series of prostatectomy slides as in a recent study on reproducibility of percentage Gleason grade 4/5 [11]. The same group of specialists in genitourinary pathology reviewed the slides. This gave us the opportunity to compare our results from three different grading systems, i.e. GS, percentage Gleason grade 4/5 and mGS.

We have previously shown that interobserver reproducibility of percentage Gleason grade 4/5 in prostatectomy specimens and needle biopsies is at least as good as that of the GS [11, 12]. In the present study, according to kappa analysis, interobserver reproducibility of mGS in prostatectomy specimens was at least as good as that of the GS. However, severe disagreement was more common with mGS than with GS, possibly because tertiary patterns are not sufficiently defined. The minimum amount of a pattern that is required for being identified at all is not clear. Occasional incomplete, fused or branching glands may be interpreted either as cutting artefacts or as a focal pattern 4. Similarly, occasional small solid epithelial structures may be interpreted either as cutting artefacts or as a focal pattern 5. It remains unclear whether pattern 5 requires clusters of individual cells, solid strands or solid nests seen at lower than ×40 magnification or whether this pattern also may be diagnosed when such structures are found interspersed among cancerous glands. Thus, to improve reproducibility of mGS, the definition of focal high-grade components has to be clarified.

Although weighted kappa for mGS was lower for transition-zone tumours than for peripheral-zone tumours (0.519 and 0.594, respectively), the zonal difference was less than that previously reported for GS (0.433 and 0.540, respectively) [11]. In tumours with three or more Gleason patterns, the proportion of the tumour occupied by the patterns is decisive for the GS. In tumours of transition-zone origin, Gleason patterns 2, 3 and 4 are often simultaneously present in the same tumour, resulting in GSs 5, 6 or 7, depending on the amount of each grade, and this may explain the lower weighted kappa for GS of transition-zone tumours compared with peripheral-zone tumours [11]. With mGS, this source of interobserver variability is to some extent avoided because a tertiary pattern is included in the score regardless of its proportion of the tumour.

The score distribution of GS and mGS differed significantly. The overall mean difference between mGS and

GS was 0.41, and in only 66% of the responses were GS and mGS identical. We believe that it must be clearly stated which of these scores is used. Redefining GS as the sum of primary and tertiary patterns is potentially confusing, and comparison with results from previous studies using the old definition of GS will turn out to be difficult. It is preferable that a new term is introduced to designate the sum of primary and tertiary patterns, tentatively mGS, a term that also was used by Pan et al. [19].

In this series, an odd mGS was more often given than an odd GS, leading to an increased clustering in a few scores. Although the Gleason system was originally designed as a nine-tier system (score 2–10), few of these scores are actually used. A reason to ignore minor components is that relatively few cases would otherwise be assigned an even score (such as GS 3+3=6), especially in radical prostatectomy specimens [1, 20]. A disadvantage of the mGS is that its value as predictor of aggressive behaviour may be questioned when a majority of cases are lumped into a single score.

For several reasons, we believe that it is too early to abandon the conventional GS. Before recommending a general use of mGS, previous results on its prognostic value need to be corroborated. The limited number of studies that have addressed the prognostic value of a mGS [8, 19, 21, 22] are as yet insufficient to support the introduction of a new grading system. Furthermore, the ability of preoperative core biopsies to predict mGS in prostatectomy specimens needs to be investigated. Theoretically, a minimal component of tertiary pattern would easily go undetected by needle biopsies, decreasing the practical utility of a mGS. Additionally, reproducibility of a mGS has to be improved, and consensus must be reached on the definition of tertiary Gleason patterns. No systematic training preceded the present study, but Kronz et al. [14] and Egevad [7] described that the use of reference images or web-based tutorials improves reproducibility of Gleason grading. Similar techniques would possibly improve interobserver reproducibility of mGS.

References

1. Aihara M, Wheeler TM, Ohori M, Scardino PT (1994) Heterogeneity of prostate cancer in radical prostatectomy specimens. Urology 43:60–66
2. Allsbrook WC Jr, Mangold KA, Yang X, Epstein JI (1999) The Gleason grading system: an overview. J Urol Pathol 10:141–157
3. Allsbrook WC Jr, Mangold KA, Johnson MH, Lane RB, Lane CG, Amin MB, Bostwick DG, Humphrey PA, Jones EC, Reuter VE, Sakr W, Sesterhenn IA, Troncoso P, Wheeler TM, Epstein JI (2001) Interobserver reproducibility of Gleason grading of prostatic carcinoma: urologic pathologists. Hum Pathol 32:74–80
4. Allsbrook WC Jr, Mangold KA, Johnson MH, Lane RB, Lane CG, Epstein JI (2001) Interobserver reproducibility of Gleason grading of prostatic carcinoma: general pathologists. Hum Pathol 32:81–88
5. Bostwick DG, Grignon DJ, Hammond ME, Amin MB, Cohen M, Crawford D, Gospadarowicz M, Kaplan RS, Miller DS, Montironi R, Pajak TF, Pollack A, Srigley JR, Yarbro JW (2000) Prognostic factors in prostate cancer. College of American Pathologists Consensus Statement 1999. Arch Pathol Lab Med 124:995–1000
6. Deshmukh N, Foster CS (1998) Grading prostate cancer. In Foster CS, Bostwick DG (eds) Pathology of the prostate. Saunders, Philadelphia, pp 191–227
7. Egevad L (2001) Reproducibility of Gleason grading of prostate cancer can be improved by the use of reference images. Urology 57:291–295
8. Egevad L, Granfors T, Karlberg L, Bergh A, Stattin P (2002) Percent Gleason grade 4/5 as prognostic factor in prostate cancer diagnosed at transurethral resection. J Urol 168:509–513
9. Egevad L, Granfors T, Karlberg L, Bergh A, Stattin P (2002) Prognostic value of the Gleason score in prostate cancer. BJU Int 89:538–542
10. Epstein JI, Partin AW, Sauvageot J, Walsh PC (1996) Prediction of progression following radical prostatectomy. A multivariate analysis of 721 men with long-term follow-up. Am J Surg Pathol 20:286–292
11. Glaessgen A, Hamberg H, Pihl CG, Sundelin B, Nilsson B, Egevad L (2002) Interobserver reproducibility of percent Gleason grade 4/5 in total prostatectomy specimens. J Urol 168:2006–2010
12. Glaessgen A, Hamberg H, Pihl CG, Sundelin B, Nilsson B, Egevad L (2003) Interobserver reproducibility of percent Gleason grade 4/5 in prostate biopsies. J Urol 171:664–667
13. Green GA, Hanlon AL, Al-Saleem T, Hanks GE (1998) A Gleason score of 7 predicts a worse outcome for prostate carcinoma patients treated with radiotherapy. Cancer 83:971–976
14. Kronz JD, Silberman MA, Allsbrook WC, Epstein JI (2000) A web-based tutorial improves practising pathologists' Gleason grading of images of prostate carcinoma specimens obtained by needle biopsy: validation of a new medical education paradigm. Cancer 89:1818–1823
15. Lerner SE, Blute ML, Bergstralh EJ, Bostwick DG, Eickholt JT, Zincke H (1996) Analysis of risk factors for progression in patients with pathologically confined prostate cancers after radical retropubic prostatectomy. J Urol 156:137–143
16. Lessells AM, Burnett RA, Howatson SR, Lang S, Lee FD, McLaren KM, Nairn ER, Ogston SA, Robertson AJ, Simpson JG, Smith GD, Tavadia HB, Walker F (1997) Observer variability in the histopathological reporting of needle biopsy specimens of the prostate. Hum Pathol 28:646–649
17. McNeal JE, Villers AA, Redwine EA, Freiha FS, Stamey TA (1990) Histologic differentiation, cancer volume, and pelvic lymph node metastasis in adenocarcinoma of the prostate. Cancer 66:1225–1233
18. Montironi R, Mazzucchelli R, Kwast T (2003) Morphological assessment of radical prostatectomy specimens. A protocol with clinical relevance. Virchows Arch 442:211–217
19. Pan CC, Potter SR, Partin AW, Epstein JI (2000) The prognostic significance of tertiary Gleason patterns of higher grade in radical prostatectomy specimens: a proposal to modify the Gleason grading system. Am J Surg Pathol 24:563–569
20. Ruijter ET, van de Kaa CA, Schalken JA, Debruyne FM, Ruiter DJ (1996) Histological grade heterogeneity in multifocal prostate cancer. Biological and clinical implications. J Pathol 180:295–299
21. Stamey TA, McNeal JE, Yemoto CM, Sigal BM, Johnstone IM (1999) Biological determinants of cancer progression in men with prostate cancer. JAMA 281:1395–1400
22. Stamey TA, Yemoto CM, McNeal JE, Sigal BM, Johnstone IM (2000) Prostate cancer is highly predictable: a prognostic equation based on all morphological variables in radical prostatectomy specimens. J Urol 163:1155–1160

Virchows Arch (2004) 445:22–26
DOI 10.1007/s00428-004-1036-y

ORIGINAL ARTICLE

Richard E. Tracy · Parvene Walia

Lipid fixation for fat staining in paraffin sections applied to lesions of atherosclerosis

Received: 12 February 2004 / Accepted: 21 April 2004 / Published online: 2 June 2004
© Springer-Verlag 2004

Abstract A new method to fix lipids for staining in paraffin sections was applied here to early lesions of atherosclerosis to test comparability with similar results using frozen-section fat stains. Small blocks of formalin-fixed human coronary artery were exposed to an emulsion of linoleic acid and lecithin in 70% ethylene glycol at 56°C for 3 days. The unsaturated fatty acids partitioned into the tissue lipids for later fixation by chromic acid and could then be processed through paraffin-section for fat staining. Blocks of tissue from the same specimens were also processed for standard frozen-section fat staining. The types of early atherosclerotic lesions described by the American Heart Association Lesions Committee—types I, II, III, and IV—were demonstrated equally well using the two methods. Additional newly described patterns of lipid deposits were also revealed by both methods. The paraffin method showed no indication of omitting or adding anything compared with frozen sections. The surprising finding of unexpected patterns of lipid distribution in human coronary artery suggests that the method may prove to be useful. Those novel patterns were first observed with the more flexible paraffin method and later confirmed by the more tedious and demanding frozen-section method.

Keywords Coronary artery · Human

Introduction

A novel method to fix lipids for demonstration in paraffin sections was recently reported from this laboratory [7]. In that report, the method was used to explore fat embolism in the lung and brain. The objective of this report was to extend the method to lesions of atherosclerosis. A major concern of this and other applications is the agreement of the findings using traditional stains of frozen sections.

A system for classifying early stages of human atherosclerotic lesions as types I, II, III, and IV was described by the influential publication from the Committee on Vascular Lesions of the Council on Arteriosclerosis of the American Heart Association [1], cited henceforth as the AHA Committee. The intention here is to compare the lesions of types I–IV as revealed by frozen- and paraffin-section methods.

In the course of carrying out the study, we encountered additional patterns of fat staining not described by the AHA Committee and having no place in that system. These newly described patterns therefore receive emphasis here.

R. E. Tracy (✉) · P. Walia
Department of Pathology,
Louisiana State University Health Sciences Center,
1901 Perdido Street, New Orleans, LA 70112, USA
e-mail: rtracy@lsuhsc.edu
Tel.: +1-504-5686072
Fax: +1-504-5686037

Methods

Specimens

Forensic autopsies of men and women over age 34 years provided samples of right coronary artery. Subjects who died of coronary heart disease or related conditions were omitted from the study. The first 9 cm of the right coronary artery was opened longitudinally upon the heart, removed from the heart using scissors, flattened under a soft rubber sponge, fixed in acetate-buffered 4% formaldehyde for at least 1 day (storing these for as much as 3 months), and cut into 3-cm-long segments. Each of the segments was split into two portions, cut along the longitudinal planes perpendicular to the luminal surface. One portion in each instance was preserved for later frozen sectioning and the other was processed for fat staining of paraffin sections as described next. From a series of 30 arteries examined by paraffin sections, 5 were chosen as showing lesions of interest (as shown in the photographs); these were processed for frozen-section fat stains. Having found the objects of particular concern by use of the flexible paraffin method, confirmation of those findings was subsequently sought using the more laborious frozen-section method.

Paraffin-section fat stain

The method, as previously published [7], is described here for the reader's convenience. The procedure requires 5–7 days, although

Table 1 Classification of atherosclerotic lesions proposed by the American Heart Association Lesions Committee [1]

Type 1	Small, isolated groups of macrophages containing lipid droplets
Type 2	Abundant smooth muscle cell and macrophage foam cells stratified in adjacent layers
Type 3	Type 2 features colocalized with adaptive thickening with extracellular lipid pools situated below the zone of foam cells
Type 4	Dense accumulation of extracellular lipid forming a lipid core (atheroma) in a well defined region of the intima

this is almost entirely waiting time with only a few minutes of active effort in those days; the greatest effort is still in the routine embedding, sectioning, and staining.

Solutions

All solutions are stable for indefinite intervals of at least several weeks, although the separation of solution 1 by funnel should be repeated if this step is delayed and an oil layer floats to the surface.

Solution 1. To 500 ml 70% ethylene glycol, add 20 ml linoleic acid (60% practical grade) and 2 g lecithin (Nature's Life dietary supplement); spin on a magnetic mixer for 4 h; allow to stand for 4 h, draw off the lower phase in a separatory funnel.

Solution 2. Chromium trioxide 2 g per 100 ml water.

Solution 3. Sodium bicarbonate 5 g per 100 ml water.

Procedure

Tissue samples of 1–2 mm thickness are taken from storage in formalin, rinsed for 1–2 hours in water, and placed into solution 1 for 3 days at 56°C. Rinse for at least 8 h in several changes of 70% ethanol followed by several changes of distilled water. Immerse in solution 2 for 24 h at 4°C. Rinse in several changes of distilled water for 24 h. Place in solution 3 for 24 h. Rinse in water for at least 8 h. Cut paraffin sections as usual and stain these with a standard oil-soluble dye such as Oil red O with hematoxylin counterstain.

Comments

Most of the steps are flexible. Ethylene glycol can be 60–80%, linoleic acid 20–40 ml, and lecithin 1–2 g. Exposure to solution 1 can be 2–5 days, solution 2 from 16 h to 36 h, and solution 3 from 1 day to 3 days. The emulsion in solution 1, however, must be critically controlled. The 500 ml of fluid should be placed into a 1000-ml Erlenmeyer flask and stirred briskly for 2–4 h. After draining from the separatory funnel, the emulsion subsequently separates slowly to form an oil layer on the surface; tissues should not be exposed directly to the oil layer. If tissues are handled within plastic cassettes, then those cassettes should not be crowded; the cassettes take up lipid and degrade the emulsion. A surplus of 5:1 fluid to cassette is recommended. Optimal results occur when the emulsion remains nearly opaque after 3 days at 56°C.

Results

Figure 1 illustrates the four types of early atherosclerotic lesions described by the AHA Committee (Table 1), as seen with paraffin- and frozen-section fat stains. These paired views seen using two methods are not cut from the same block of tissue, although they are from the same specimen in each instance.

Type I, initial lesion, is recognized by the scattered presence of fat-filled, elongated, narrow cells that are taken to be macrophages with perhaps some smooth muscle cells (SMCs), in keeping with published authorities. This type of intracellular lipid seems more darkly stained in the frozen section (Fig. 1B) than in the paraffin section (Fig. 1A), and this may relate to the thickness of sections that were cut at 15 μm and 5 μm, respectively (the thinnest practical settings for ordinary use of these two methods). The anatomic relationships of the lipid are not conspicuously different using the two methods.

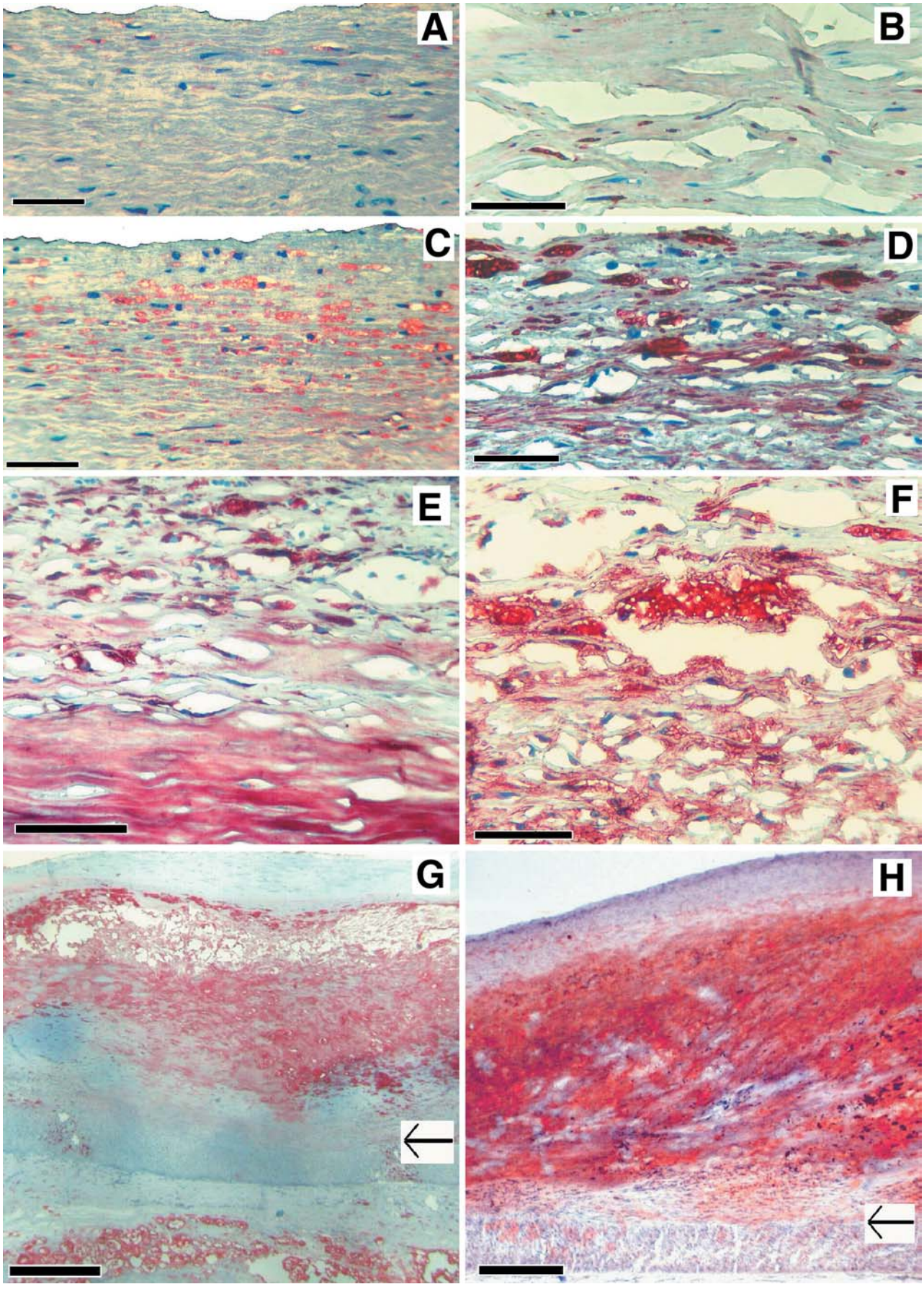
Type II, fatty streak lesion, is marked by numerous adjacent layers of closely spaced "foam cells" that are bloated by copious cytoplasmic lipid; authoritative sources refer to these as a mixture of SMCs and macrophages that are often accompanied by scattered lymphocytes. Here, again, the paraffin section (Fig. 1C) reveals architectural relationships of the lipid similar to those seen with frozen section (Fig. 1D).

Type III, intermediate lesion, has fully developed features of type-II lesions, but with thicker intima having abundant interstitial lipid in deeper intimal layers between the foam cell collections and the media. The extent and intensity of fat stain seems similar by paraffin (Fig. 1E) and by frozen section (Fig. 1F), as does their anatomic relationships.

Type IV, atheroma, expands the type-III deep core of interstitial lipid into ever-broadening regions marked by the absence of cells, eventuating in outright necrosis and dissolution of tissue into semisolid plaque gruel. Again the patterns of lipid staining seem similar using paraffin- and frozen-section methods (Fig. 1G and H, respectively). In these examples, a lipid-poor fibrous base is seen between the necrotic core and the media, and this feature is commonplace although not universal. Figure 1G also includes a view of adventitial adipose tissue to demonstrate its staining using the paraffin-section method.

Figure 2 offers some views of features not described by the AHA Committee or recently by other authors. Near the "A" in Fig. 2A is a type-II lesion. By scanning leftward from "A", lipid can be seen increasingly as isolated to interstitial locations, and dispersed through the deep intima and adjacent media as if centering on the internal elastic lamella. The contrast is striking between the patterns seen in the rightmost and the leftmost regions of Fig. 2A, one of which fits into conventional classifica-

Fig. 1 The newly introduced fat stain applied to paraffin sections (**A**, **C**, **E**, and **G**) is compared with fat stains of frozen sections (**B**, **D**, **F**, and **H**) in four exemplary specimens. These examples were chosen to illustrate AHA Committee lesion types I (**A** and **B**), II (**C** and **D**), III (**E** and **F**), and IV (**G** and **H**). Arrows mark intima-media boundaries. Oil red O—hematoxylin. (**A**–**F** are 240–320× and bar = 50 μm; **G**&**H** are 80× and bar = 200 μm) ▶


A
B
C
D
E
F
G
H

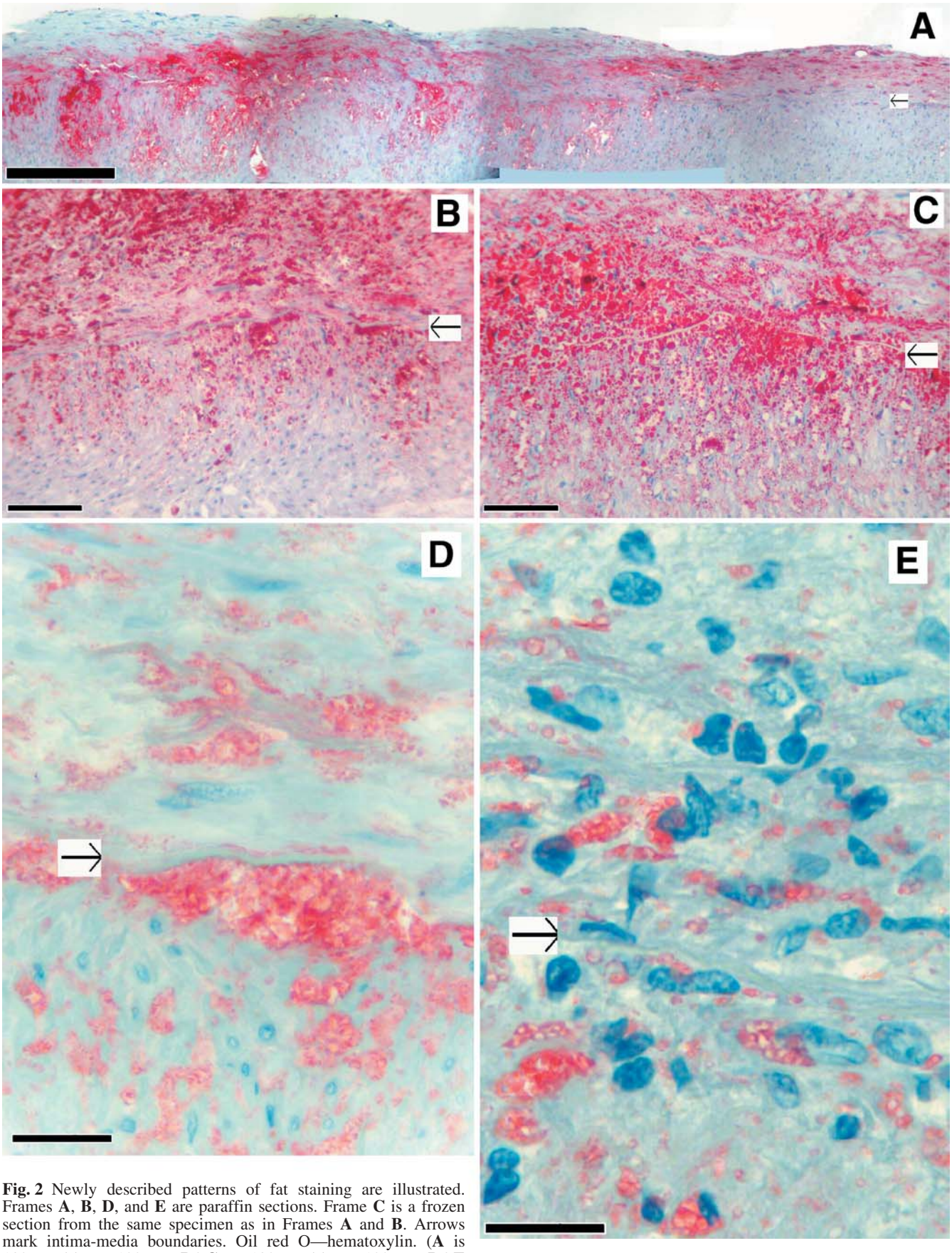


Fig. 2 Newly described patterns of fat staining are illustrated. Frames **A**, **B**, **D**, and **E** are paraffin sections. Frame **C** is a frozen section from the same specimen as in Frames **A** and **B**. Arrows mark intima-media boundaries. Oil red O—hematoxylin. (**A** is 180× and bar = 100 μm; **B**&**C** are 130× and bar = 100 μm; **D**&**E** are 1600× and bar = 10 μm)

tions and the other of which does not. Frames B and C show these features to be equally well demonstrated by the paraffin (B) and frozen (C) methods. Pools of isolated interstitial lipid are shown at higher power on the paraffin section in Fig. 2D. In that photograph, the blue-stained cytoplasm of numerous cells is clearly poor in lipid or perhaps free of lipid, and the pools of intensely staining lipid are isolated to interstitial locations; these features are visible in the media and the adjacent intima (below and above the arrow, respectively). The deposits do not greatly alter the usual architecture, but simply push the resident SMCs apart by filling the expanded interstitial spaces, leaving intact the medial SMCs and their nuclei seen as tiny rings when cut across, as shown in Fig. 2D.

By contrast, when lipid-laden cells are present, the lesion takes on a greatly different appearance (Fig. 2E). The usual architecture is obscured by numerous closely spaced cells of alien types, which are thought to be mainly macrophages and SMCs in a proliferative phase (Fig. 2E). These intrusive cell types often accompany lipid-laden cells, and they themselves usually become lipid laden, as seen in Fig. 2E.

Discussion

The method explored here for revealing tissue lipids in paraffin sections appears to be appropriate for studies of atherosclerosis. Features found by this method resemble those also found by frozen-section fat stains. The paraffin method shows no indication of omitting or adding anything compared with the conventional technique. The method is in routine use in this laboratory and has recently yielded some published findings [6].

The patterns represented by the examples in Fig. 2 appear to be newly described here for the first time. It is well known, of course, that lesion types III, IV, and greater can eventually expand into the media, as seen in the type-III example in the rightward regions of Fig. 2A. What is novel in the findings reported here is the presence of lipid confined to the media and deep layers of intima when features of type-I or -II lesions are absent in the superficial intima, as seen in the leftmost region of Fig. 2A. Figure 2D illustrates this kind of isolated interstitial lipid without perceptible occurrence of lipid within cells.

The recent literature rarely mentions the medial component or the isolated interstitial lipid component of atherosclerosis, in keeping with scarcity of such commentary in the AHA Committee reports. Some prior publications dealt with these topics, as exemplified by Duguid in 1926 [4], Duff in 1935 [2], Duff and McMillan in 1951 [3], and Haust in 1981 [5]. Those authors all mentioned finding occasional deposits of isolated interstitial lipid, but they never described the kinds of appearance illustrated in Fig. 2A, B, C, and D. The interaction of arterial proteoglycans with blood lipoproteins in the presence of bivalent metal ions is an intensively studied branch of histochemistry [8]. Whether such interactions have relevance to the kinds of appearance described here will call for further studies specifically addressing those issues.

In conclusion, the specimens examined in this study display the well-known lesion types I–IV and also often show extensive regions of tissue resembling the newly described examples in Fig. 2. These appearances are all demonstrated with exceptional ease and clarity by the new staining method and can subsequently be confirmed using the more laborious frozen-section method. The method now opens the way for systematic study of these newly described aspects of atherosclerosis.

References

1. Committee on Vascular Lesions of the Council on Arteriosclerosis, American Heart Association (1995) A definition of advanced types of atherosclerotic lesions and a histological classification of atherosclerosis. Circulation 92:1–20
2. Duff GL (1935) Experimental cholesterol arteriosclerosis and its relationship to human arteriosclerosis. Arch Pathol 20:81–304
3. Duff GL, McMillan GC (1951) Pathology of atherosclerosis. Am J Med 11:92–108
4. Duguid JB (1926) Atheroma of the aorta. J Pathol Bact 29:371–387
5. Haust MD (1981) The natural history of human atherosclerotic lesions. Chapter 1. In: Sean Moore (ed) Vascular injury and atherosclerosis. Marcel Dekker Inc., New York
6. Tracy RE (2003) Local sequestration of lipid from place to place within an artery. Chapter 11. In: RE Tracy (ed) The role of aging in atherosclerosis. Kluwer Academic Publishers, Dordrecht Netherlands
7. Tracy RE, Walia P (2002) A method to fix lipids for staining fat embolism in paraffin sections. Histopathol 41:75–79
8. Williams KJ, Taas I (1995) The response-to-retention hypothesis of early atherogenesis. Arterioscler Thromb Vasc Biol 15: 551–561

Virchows Arch (2004) 445:27–35
DOI 10.1007/s00428-004-1028-y

ORIGINAL ARTICLE

H. R. De Raeve · P. B. Vermeulen · K. Vanderkerken · A. L. Harris · E. Van Marck

Microvessel density, endothelial-cell proliferation and carbonic anhydrase IX expression in haematological malignancies, bone-marrow metastases and monoclonal gammopathy of undetermined significance

Received: 3 February 2004 / Accepted: 1 April 2004 / Published online: 28 May 2004
© Springer-Verlag 2004

Abstract The aim of the study was to compare the angiogenic status, potential qualitative differences in microvessels and carbonic anhydrase IX expression in bone-marrow (BM) metastases and different haematological tumours at time of diagnosis. The microvessel density (MVD), endothelial-cell proliferation (ECP) and carbonic anhydrase IX (CA IX) immunoreactivity were determined on 210 trephine biopsies from 57 patients with multiple myeloma (MM), 13 with acute myeloid leukaemia (AML), 48 with chronic myeloproliferative syndrome (CMPS), 26 with chronic lymphocytic leukaemia (CLL), 25 with epithelial BM metastases, 18 with monoclonal gammopathy of undetermined significance (MGUS) and from a control group composed of 23 patients without haematological neoplasm. There was an increased MVD and ECP in epithelial BM metastases, MM, AML, CMPS and in a part of CLL. While an ECP greater than 0 was detected in 72% of MM, 75% of CMPS and 92% of AML, it was invariably observed (100%) in the BM metastases. The absence of ECP together with a MVD comparable with the control group in our MGUS cases supports the view that MGUS is a pre-angiogenic condition. Qualitative differences in microvessels were associated with growth patterns in MM and CLL and were observed between the different entities of CMPS. In one-third of the epithelial BM metastases, there was a focal CA IX immunoreactivity, which was never observed in the haematological diseases.

Keywords Cancer angiogenesis · Haematological malignancies · Bone-marrow pathology · Bone metastasis · MGUS

H. R. De Raeve (✉) · P. B. Vermeulen · E. Van Marck
University Hospital Antwerp,
Department of Pathology,
Wilrijkstraat 10, 2650 Edegem, Belgium
e-mail: Hendrik.De.Raeve@uza.be
Tel.: +32-3-8213731
Fax: +32-3-8214753

K. Vanderkerken
Department of Haematology and Immunology,
Vrije Universiteit Brussel,
Laarbeeklaan 103, 1090 Brussels, Belgium

A. L. Harris
Weatherall Institute of Molecular Medicine,
John Radcliffe Hospital,
Oxford, OX39DS, UK

Introduction

There is strong evidence that not only solid tumour growth but also haematological tumour growth is accompanied by new vessel formation (angiogenesis) [21]. This vasculature is responsible for the appropriate oxygen and nutrient supply and the removal of waste products. It provides a route for homing and metastasis, and, last but not least, the bone-marrow endothelial cells (BMEC) secrete growth factors for haematological malignant cells [5, 9, 11].

The microvessel density (MVD) has been demonstrated to have a prognostic value in a wide range of solid cancers as well as in multiple myeloma (MM) [29]. The assumption that the MVD may reveal the degree of angiogenic activity of the tumour at the time of biopsy is a misconception [14]. Rather, the MVD is the integration in time of past and ongoing vascular remodelling. In this study, the endothelial-cell proliferation (ECP) was, in addition to the MVD, determined in trephine biopsies to have a better estimation of the ongoing angiogenesis at the time of diagnosis. Trephine biopsies from patients with several types of haematological tumours, from patients with epithelial BM metastases, from patients with monoclonal gammopathy of undetermined significance and from a control group of patients without haematological neoplasm were selected at the time of diagnosis. Qualitative differences based on morphology and CD34-staining intensity of microvessels were scored.

Carbonic anhydrase isoenzyme IX (CA IX) is a transmembrane glycoprotein, which is involved in the acid–base homeostasis by reversibly converting carbon dioxide and water to carbonic acid. The transcription is activated by hypoxia and suppressed in normoxia [18, 33]. In solid tumours, hypoxia is one of the major driving forces of angiogenesis [12]. In a study of ductal carcinoma in situ of the breast, CA IX expression was found in 50% of the cases and was associated with necrosis and with high histological grade [34]. In breast carcinomas, the CA IX positivity was observed in both tumour cells and stromal cells [8]. In non-Hodgkin's lymphoma, CA IX expression was only observed in 8% of the lymphoma cases [27]. Here, the expression of the CA IX was examined using immunohistochemistry in the haematological malignancies and in the metastases.

Materials and methods

Patients

The 210 cases were retrieved from the files of the pathology department of the University Hospital of Antwerp in a consecutive way in a period from 1998 to 2003, starting in 2003 and going backwards until we obtained a sufficient number of cases of each disease entity. Approval by the ethics committee of the University of Antwerp was observed. Only those cases with an unambiguous diagnosis and a representative trephine biopsy were withheld. A trephine biopsy was considered representative if the length of the biopsy was at least 1 cm and if at least three BM cavities contained haematopoietic marrow. Except for the BM metastases, all selected trephine biopsies were taken at the time of diagnosis prior to any oncological treatment. The diagnostic groups investigated are shown in Table 1.

Tissue processing

All trephine biopsies were fixed in AFA (8.5 l alcohol, 0.5 l acetic acid 80%, 1 l formalin 40%) for 2 h, decalcified for 24 h in FE10 [100 g ethylene diaminetetraacetate (EDTA), 12 g NaOH, 100 ml formalin 40%, add H_2O to 1 l] and embedded in paraffin. Haematoxylin and eosin (5 μm), Giemsa (3 μm) and Gordon–Sweets (5 μm) stains were made.

For the MM and chronic lymphocytic leukaemia (CLL) cases, the growth pattern was determined on these sections. Three growth patterns were distinguished: the interstitial, the nodular ± interstitial and the diffuse growth pattern. On the Giemsa stain, the plasma cells (PC) in MM were cytologically classified [4]. The following PC types were distinguished: mature (Marschalko), polymorphous, asynchronous and blastic type.

Table 1 Diagnostic groups included in the study with the median age and age range

Disease entity	Number of patients included	Median age (years)	Age range (years)
Multiple myeloma	57	66	37–95
Interstitial growth pattern	23		
Nodular ± interstitial	23		
Diffuse	11		
Monoclonal gammopathy of undetermined significance	18	57	45–73
Chronic myeloproliferative syndrome	48	61	18–81
Chronic myeloid leukaemia	12		
Idiopathic myelofibrosis	12		
Polycythaemia vera	11		
Essential thrombocythaemia	13		
Acute myeloid leukaemia (CD34-negative acute myeloid leukaemia)	13	64	20–83
Chronic lymphocytic leukaemia	26	62	39–88
Interstitial growth pattern	11		
Nodular ± interstitial	10		
Diffuse	5		
Epithelial metastases	25	62	26–85
Breast adenocarcinoma	10		
Prostate adenocarcinoma	3		
Adenocarcinoma of unknown origin	5		
Urothelial carcinoma	3		
Carcinoid tumour	1		
Renal-cell carcinoma	1		
Colonic adenocarcinoma	1		
Endometrial adenocarcinoma	1		
Control group	23	50	18–82
Anaemia	9		
Chronic fatigue syndrome	3		
Rheumatoid arthritis	2		
Fever of unknown origin	2		
Human immunodeficiency virus	1		
Thrombopenia	2		
Leukopenia	2		
Lyme disease	1		
Inflammation of unknown origin	1		

Immunohistochemistry

The slides were dewaxed and rehydrated. Antigen retrieval was performed using microwave for 30 min at 95°C in Tris/EDTA buffer pH 9 (PR20–0226, Prosan n.v., Merelbeke, Belgium). Endogenous peroxidase was blocked by 0.5% hydrogen peroxide for 20 min. Non-specific binding was blocked with normal goat serum. The primary antibodies were incubated overnight at room temperature. As negative control, the primary antibody was omitted.

The following immunohistochemical stainings were applied: anti-CD34 (clone QBEnd 10, 1/50, M7165; DakoCytomation A/S, Glostrup, Denmark), anti-Ki-67 (polyclonal, 1/2, N1574; DakoCytomation A/S), anti-CD138 (clone MI15, 1/25, M7228; DakoCytomation A/S), overnight incubation and anti-CA IX (clone M75, 1/50). The ability of this antibody to specifically detect CA IX expression in tissue sections was previously confirmed using direct correlation with Western-blot analysis in human breast-tumour specimens [34]. The CA IX staining was performed at the Weatherall Institute of Molecular Medicine, John Radcliffe Hospital, Oxford.

For the visualisation, the Envision+ detection systems (K4007, Envision+ kit, HRP. Mouse DAB+; DakoCytomation A/S, K4011, Envision+ kit, HRP, Rabbit DAB+; DakoCytomation A/S and K4018, Envision kit, AP, Rabbit/Mouse and K0625, Fuchsin+; DakoCytomation A/S) were used, respectively, for the single stains of monoclonal and polyclonal antibodies and for the CD34/Ki-67 and CD138/Ki-67 double stainings. The slides were counterstained with haematoxylin.

Immunohistochemical evaluation and counts

All immunostainings were performed by the same technician under the same experimental conditions (batch processed). All observations (except the CA IX scoring) were performed by the same observer.

Qualitative difference of the BM microvessels

The BM microvessels were scored as follows:

Score-1. All vessels are straight sinusoids with open lumen and an endothelial lining with a faint and partial staining for CD34
Score-2. The vessels are partly composed of straight sinusoids, partly of small and tortuous capillaries
Score-3. The majority of the vessels consist of small and tortuous microvessels with a strong endothelial CD34 staining

Microvessel density

An anti-CD34 antibody was selected because it has been most widely used for endothelial-cell identification. As a consequence of the choice of CD34 for highlighting the microvessels, we had to restrict the study of acute myeloid leukaemia (AML) cases to those with CD34-negative myeloblasts, since the presence of the CD34-positive blasts in the BM would interfere with the recognition of microvessels, especially the newly formed sprouting microvessels.

We used the most accredited method for evaluating MVD on sections by counting the number of microvessels at high magnification in an area with the impression of the highest vessel density ("hot spot") [32] at low magnification. The hot spots were identified by scanning the entire marrow section under a microscope at low power (×40). The microvessel density is subsequently determined in the hot spot by counting the number of cross-sections of microvessels (including endothelial sprouts) in an area defined by an eye-piece graticule in a Jenamed2 microscope (Zeiss, Germany) at ×200 magnification (0.20 mm^2).

Endothelial-cell proliferation

On a CD34/Ki-67 double immunostain, the endothelial lining of the blood vessels was stained with a red chromogen, and the Ki-67-positive nuclei were stained with a brown chromogen. At least 200 BMEC nuclei were counted, and the percentage of Ki-67-positive endothelial cells (co-localisation of a Ki-67 brown staining nucleus and the CD34 red cell membrane) was determined.

Tumour load

For MM, the tumour load was determined by counting the number of CD138-positive cells on the total number of nucleated haematological cells in a representative area of the marrow. At least 400 cells were counted.

Plasma-cell proliferation

Using a double staining of CD138/Ki-67, the percentage of CD138/Ki-67-positive cells was determined by one investigator. At least 400 nuclei were counted.

Carbonic anhydrase IX

The immunostaining was quantified by semi-quantitative scoring as previously described [7]. In brief, a score of 0 to 3 was given for the intensity of membrane staining in the bulk of the tumour deposit (0: no staining, 1: weak staining, 2: moderate staining, 3: strong staining). The percentage of immunostained tumour cells was estimated. The product of the intensity score and the percentage of tumour yielded a final score of 0 to 300. The scoring was performed by two observers, and the result was obtained by consensus.

Statistical analysis

For the multiple comparisons, the nonparametric unpaired Kruskal-Wallis and the Dunn's multiple comparison post-test was applied. For the correlation, the Spearman correlation statistical significant level was at 5%. For the qualitative differences in BM microvessels, a χ^2 test was used. Statistical calculations were performed using the Graph PadPrism version 4-software (San Diego, CA, USA).

Results

Microvessel density

The MVD (number of microvessels per 0.20 mm^2) was significantly higher in MM (mean ± standard deviation) (23.3±12.5) (P<0.001), chronic myeloproliferative syndrome (CMPS) (19.8±7.0) (P<0.001), AML (21.2±6.6) (P<0.01) and epithelial bone marrow metastasis (META) (24.1±7.6) (P<0.001) than in the control (8.1±2.6) (Fig. 1). The MVD was not statistically significantly increased in monoclonal gammopathy of undetermined significance (MGUS) (7.7±1.8) and CLL (10.8±3.9) compared with the control (8.2±2.6). Only the subgroup of CLL cases with a diffuse growth pattern (five cases) had an increased MVD (16.4±2.5) (P<0.001).

Within the MM, there was a strong variation in the MVD. The MM with a nodular ± interstitial (23 cases) (28.9±10.7) and diffuse growth pattern (11 cases) (32.6±

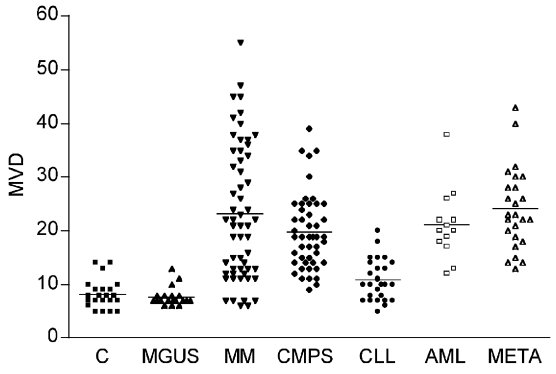


Fig. 1 Microvessel density, number of microvessels per 0.20 mm^2 area measured at the site with the highest density of microvessels (*hot spot*), in the control group (*C*) and in several haematological malignancies and in bone-marrow metastases of epithelial tumours

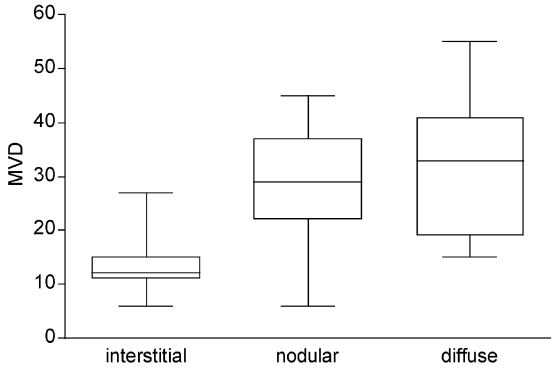


Fig. 2 Microvessel density (number of microvessels per 0.2 mm^2 area) in multiple myeloma with respectively interstitial, nodular ± interstitial and diffuse growth pattern

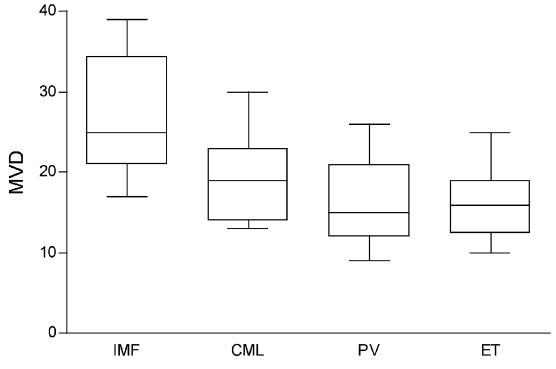


Fig. 3 Microvessel density (number of microvessels per 0.2 mm^2 area) in the different entities of chronic myeloproliferative syndrome

12.7) had a higher (P<0.001) MVD than the MM with a pure interstitial growth pattern (23 cases) (13.2±5.4) (Fig. 2).

Of MM, 23 were composed of mature (Marschalko) PC, 5 of pleomorphic PC, 23 asynchronous PC and 6 of plasmablasts. Only the plasmablastic MM (33.8±6.6) had

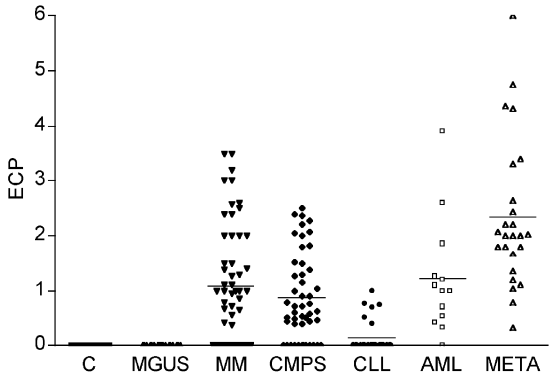


Fig. 4 Endothelial-cell proliferation in the control group (*C*), the haematological diseases and in bone-marrow metastases of epithelial tumours

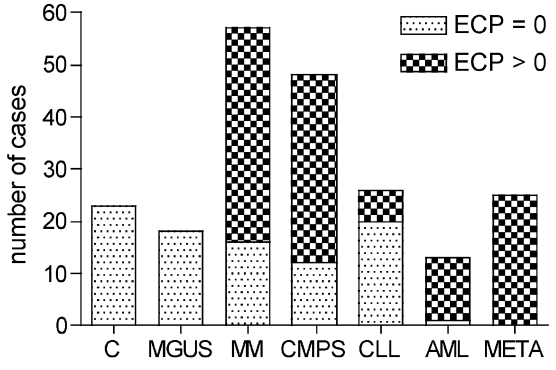


Fig. 5 Ratio of cases with an endothelial-cell proliferation (ECP) equal to 0 and an ECP greater than 0 in all diseases

a higher (P<0.05) MVD than the MM with Marschalko PC (18.0±10.1).

For MM, the MVD correlated moderately with ECP (r^2=0.52, P<0.0001), plasma cell proliferation (PCP) (r^2=0.45, P<0.0001) and tumour load (r^2=0.37, P<0.0001). Within the CMPS group, idiopathic myelofibrosis (IMF) (26.6±7.4), chronic myeloid leukaemia (CML) (19.5±5.3), polycythaemia vera (PV) (16.6±5.7) and essential thrombocythaemia (ET) (16.3±4.4) had a significant increase in MVD compared with the control. The MVD in IMF was higher than the MVD in ET (P<0.05) (Fig. 3).

Endothelial-cell proliferation

No ECP (number of Ki-67-positive BMEC nuclei per 100 endothelial-cell nuclei) was observed in the control group and the MGUS. There was a higher ECP (mean ± standard deviation) in MM (1.1±1.1) (P<0.01), in CMPS (0.9±0.8) (P<0.05), AML (1.2±1.1) (P<0.05) and the metastatic cases (2.3±1.3) (P<0.001) than in the control group (0.0±0.0) (Fig. 4). In, respectively, 28% and 25% of the MM and CMPS, no ECP was observed, while this was only 8% in AML (Fig. 5). In all cases with BM metastases, the ECP was increased. For the total CLL group,

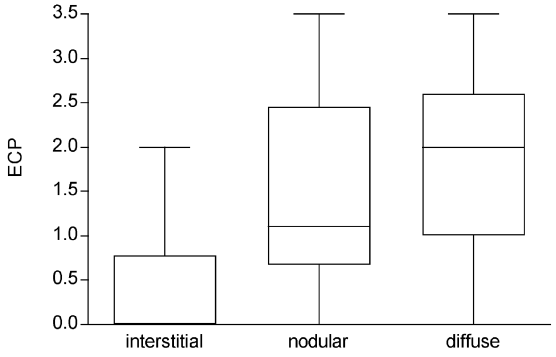


Fig. 6 Endothelial-cell proliferation in multiple myeloma with respectively interstitial, nodular ± interstitial and diffuse growth pattern

Table 2 Qualitative differences of microvessels in multiple myeloma with interstitial, nodular ± interstitial and diffuse growth patterns

	Score 1	Score 2	Score 3
Interstitial	20	3	0
Nodular ± interstitial	3	13	7
Diffuse	0	0	11

there was no significantly increased ECP (0.6±0.3), but in the CLL subgroup with diffuse growth pattern, all cases had ECP greater than 0 (0.7±0.2) (P<0.001). The MM with a nodular ± interstitial (1.4±1.0) and diffuse growth pattern (1.9±1.0) had a higher (P<0.001) ECP than the MM with a pure interstitial growth pattern (0.4±0.6) (Fig. 6).

Within the CMPS, only the CML (1.0±0.6) (P<0.001) and IMF (1.6±0.7) (P<0.01) cases had a higher ECP than the control group. In MM, the ECP correlated moderately with MVD (r^2=0.52, P<0.0001), PC proliferation (r^2=0.45, P<0,0001) and tumour load (r^2=0.37, P<0.0001).

Qualitative differences in blood vessels

In BM of the control group and in the BM of MGUS patients, the blood vessels were sinusoidal with patent lumen. These sinusoids had a thin endothelial lining, and the CD34 stain was weak and even sometimes partially failed to stain (score 1). These weakly CD34-stained sinusoids were readily recognisable because of their wide-open lumen (Fig. 7A). For the MM cases, the type of vessel was dependent on the growth pattern (Table 2). The interstitial pattern was invariably associated with a score-1 staining (20 of 23 cases); in the diffuse pattern there was a score-3 staining (11 cases; Fig. 7B, C, D) and in the nodular ± interstitial growth pattern, the majority (13 of 23 cases) had a mix of vessel types (score-2), with score-3 staining frequently observed within the nodules and score-1 staining confined to the internodular area (P<0.001, χ^2).

Table 3 Qualitative differences of microvessels in chronic lymphocytic leukaemia with interstitial, nodular ± interstitial and diffuse growth patterns

	Score 1	Score 2	Score 3
Interstitial	8	3	0
Nodular ± interstitial	4	6	0
Diffuse	0	5	0

Table 4 Qualitative differences of microvessels in the different entities of chronic myeloproliferative syndrome

	Score 1	Score 2	Score 3
Chronic myeloid leukaemia	1	9	2
Essential thrombocythaemia	6	7	0
Idiopathic myelofibrosis	0	3	9
Polycythaemia vera	4	7	0

The majority of the CLL cases with an interstitial growth pattern (8 of 11 cases) had a score-1, and all cases with a diffuse growth pattern (5 cases) had a score-2 (Fig. 7F). The nodular ± interstitial growth pattern had either a score-1 (4 of 10 cases) or a score-2 (6 of 10 cases) (P=0.001, χ^2) (Table 3).

In CMPS, there were qualitative blood vessel differences (P<0.0001) between CML, IMF, PV and ET (Table 4). While the majority of the IMF cases (9 of 12 cases) had a score-3 (Fig. 7E), this was only observed in 2 of the 12 CML cases and never observed in PV (0 of 11 cases) and ET (0 of 13 cases). In AML, 4 of 13 cases had score-1, -2 of 13 cases had score-2 (Fig. 7G) and 7 of 13 cases had score-3.

In the epithelial BM metastases, the majority had a score-3 (20 of 25 cases) and a few cases score-2 (3 of 25 cases) and score-1 (2 of 25 cases). The majority of the metastases elicited a desmoplastic stromal reaction (23 of 25 cases).

CA IX expression

In 6 of the 25 BM metastases, at least a focal membranous expression of CA IX in the tumour cells was present (Fig. 7H). The respective scores were 5, 10, 20, 20, 30, 300. In two cases, there was also expression of CA IX by the BM stromal cells. All haematological cases, including the control group, were totally negative for CA IX in the neoplastic cells as well as in the stromal cells.

Discussion

In this study, we determined the MVD within the “hot spots” and found a significant increase for MM, AML and CMPS, which is in agreement with previous studies [10, 15, 19, 23, 24, 29, 35].

Within the CMPS cases, the IMF had a higher MVD than the ET. This observation confirms the results of Mesa et al. [20], who found in 70% of the IMF a sub-

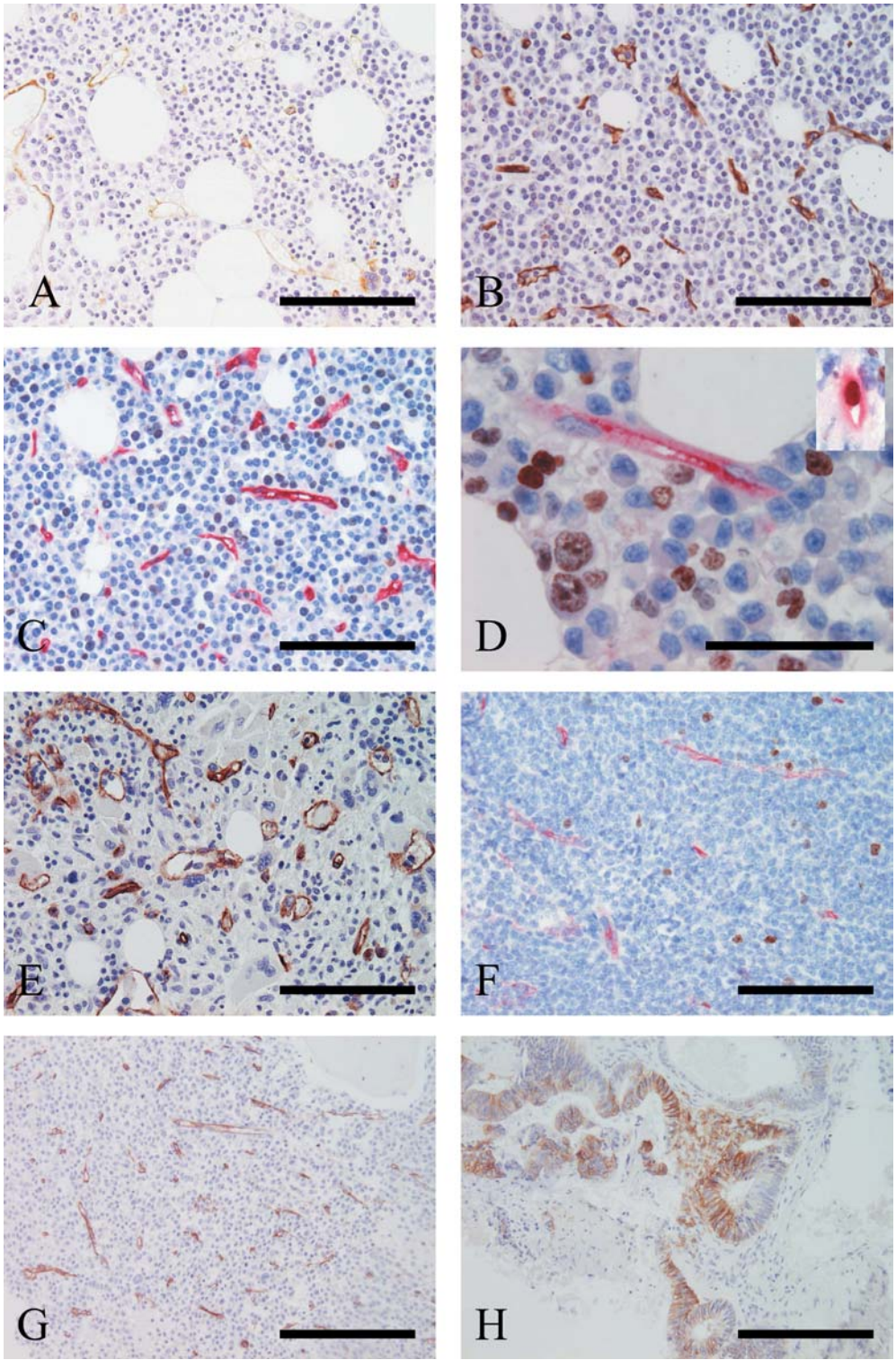


Fig. 7 Single CD34 and carbonic anhydrase IX (CA IX) immunostainings and double CD34/Ki-67 immunostainings (scale bar=50 μm in **D**, 100 μm in **A**, **B**, **C**, **E**, **F** and 200 μm in **G**, **H**) of bone-marrow trephine biopsies. **A** CD34 immunostaining of a monoclonal gammopathy of undetermined significance. The microvessel density (MVD) is not increased in contrast to multiple myeloma (MM). The microvessels are sinsoidal, and the endothelial lining is weakly positive for CD34 (score-1) **B** CD34 immunostaining of a MM with diffuse growth pattern. The MVD is increased. The microvessels are small, with slit-like lumina and intensely staining for CD34 (score-3) **C** Double CD34/Ki-67 immunostainings in the same case as **B**. The CD34 immunoreactivity is red; the Ki-67 nuclear immunoreactivity is brown. **D** Double CD34/Ki-67 immunostainings in a MM, high magnification. The microvessel in the centre has two non-proliferating endothelial cells. *Insert* microvessel with proliferating endothelial cell. **E** CD34 immunostaining of an idiopathic myelofibrosis (IMF), cellular phase. The MVD is increased. The large megakaryocytes are in close contact with the microvessels. **F** Double CD34/Ki-67 immunostainings in a chronic lymphocytic leukaemia (CLL). The

stantial increase of MVD, which was more pronounced than PV and ET. The MVD in epithelial BM metastases was in the same range as the MVD in the haematological malignancies. Only the CLL cases with a diffuse growth pattern had a higher MVD than the control group. Previous studies have shown conflicting results. Aguayo et al. [1] used the FVIII-RA immunostaining and found no increase in BM angiogenesis. Kini et al. [16] used the CD34 monoclonal antibody and found that the MVD correlated with the cellularity and the stage. Molica et al. [22] measured a microvessel area and could distinguish two subpopulations within the CLL: those with a microvessel area greater than or equal to 0.90 $mm^2 \times 10^{-2}$ had a significantly shorter survival than those with a microvessel area less than 0.90 $mm^2 \times 10^{-2}$. These data could be interpreted as pointing to a threshold of BM neovascularisation, above which the risk of progression increases. It seems that not all CLL cases are angiogenic, and the conflicting results observed in previous studies could probably be attributed to a different proportion of angiogenic and non-angiogenic cases.

Although the MVD has proven to have a prognostic value in a wide range of tumours, one should realise that the MVD is the net result of cumulative phases of angiogenesis and angioregression [14, 31]. To gain a better insight in the angiogenesis at the time of BM trephine biopsy, the ECP was quantified in all above-mentioned diseases. Like for the MVD, there was a wide variation for the ECP within each category. The ECP was increased in MM, CMPS, AML and all the metastases. Only in those CLL cases with a diffuse growth pattern could a significant increase be observed. This finding of an increased ECP in some cases of CLL together with the recent observation [6] that CLL cells express vascular endothelial growth factor (VEGF) mRNA and produce VEGF-protein are additional arguments in favour of the angiogenic potential of at least some CLL cells. It has been shown [28] that IL 8, an angiogenic factor, also stimulates motility of the CLL cells. This migratory potential determines the spread within the lymphoreticular tissue and the growth pattern. Therefore, we hypothesise that IL 8 is one of the factors involved in the regulation of the growth pattern and the angiogenesis in CLL.

The ECP was increased in all cases with BM metastases. In respectively 28% of the MM, 8% of the AML, 25% of the CMPS and 77% of the CLL cases, no ECP could be detected, implicating that, in these patients, the pro-angiogenic factors were balanced by the angiogenic inhibitors at the time of diagnosis. The increased MVD in these patients was due to angiogenesis that had taken place prior to the time of biopsy, a moment when the pro-angiogenic factors outweighed the angiogenic inhibitors. In all MGUS, such as in the control group, there was no ECP. The combination of a normal MVD without ECP indicates that MGUS is a pre-angiogenic condition within the PC dyscrasias. The ECP determination cannot be used as a diagnostic tool for separating MGUS from MM, since at the time of diagnosis, no ECP was observed in 28% of the MM patients.

Our results are in line with those of Vacca et al. [29], who showed that BM angiogenesis is increased in newly diagnosed MM compared with MGUS. Rajkumar et al. [26] determined the MVD in 42 normal control BM samples, 76 MGUS patients, 112 cases with (early) smouldering MM and 99 patients with newly diagnosed active MM. They observed a slight increase in BM angiogenesis in a small subset of patients with MGUS compared with controls. The number of patients with MGUS who had increased angiogenesis was too small to determine whether there was a greater likelyhood of progression to newly diagnosed MM. Angiogenesis was significantly increased in smouldering MM compared with MGUS and in active MM compared with the smouldering MM. It could be that the number of MGUS cases in our study was too small to distinguish the small subset of MGUS cases with a slight increase in MVD, but the overall results of previous studies, strengthened by the absence of ECP we observed, indicate that at least the majority of the MGUS cases are in a pre-angiogenic phase.

In MGUS and the initial phases of (smouldering) MM, when the neoplastic cells are intermingled with the normal haematopoietic cells, the nutrients and oxygen supply can be fulfilled by the original vasculature (co-option). The release of pro-angiogenic factors, without the tight control by angiogenesis inhibitors as observed under physiological conditions, results in an angiogenic switch once the MM clone is expanding. We recently had the opportunity to study angiogenesis during preclinical stages of MM in the murine 5T2MM model [2]. The BM MVD of 5T2MM-inoculated mice was analysed at weekly intervals until the end stage of the disease. We observed a pre-angiogenic stage where the MM cells were organised in small aggregates, followed by an angiogenic switch and an angiogenic stage once the MM cells formed confluent aggregates.

The observation that all the epithelial metastases showed ECP suggests that selection for the angiogenic phenotype is important in the establishment of distant metastases as well as growth of primary disease and systemic spread. This has not been shown in clinical samples previously and indicates that adjuvant anti-angiogenic treatment may be of value for this metastatic site.

We also investigated qualitative differences in microvessels. In MM, the prognostic value of the growth pattern has been shown [3]: MM with diffuse or nodular ± interstitial pattern [13] do worse than MM with purely interstitial pattern. These different growth patterns were

microvessel density is only marginally increased. There are some small intensely staining microvessels. As expected, only a limited number of CLL cells are proliferating. **G** CD34 immunostaining in an acute myeloid leukaemia. The MVD is increased and there are score-3 microvessels. **H** CA IX immunostaining in a bone-marrow metastasis of a colon carcinoma. There is a focal membranous positivity for CA IX, indicating that these tumour cells are hypoxic. In haematological malignancies, CA IX immunoreactivity was not observed

also associated with qualitatively different vessels. While the interstitial pattern frequently had straight sinusoidal vessels with open lumen and faint staining for CD34 (score-1), the diffuse MM contained almost exclusively small vessels with slit-like lumina and intense staining for CD34 (score-3). In the nodular ± interstitial pattern, the latter vessel morphology was confined to the nodules. CLL cases with an interstitial type of infiltration invariably presented with sinusoidal-type vessels (score-1), while the diffusely infiltrated cases partially had small strongly CD34-staining vessels (score-2). Like in MM, the smaller vessels were recognised in the nodules in the case of nodular ± interstitial infiltration. Different types of vessels were also observed in the CMPS entities. The idiopathic myelofibrosis cases generally had a majority of small strongly CD34-staining microvessels (score-3) in contrast with the ET cases, where most microvessels were sinusoidal (scores-1 and -2). In AML, the vessel pattern was variable. In all metastatic foci, score-3 vessels were observed. In the majority of the metastases, a desmoplastic growth reaction was present. The morphological difference of the small-tumour-associated vessels compared with normal sinusoidal vessels is in line with several observations by Perez-Atayde et al. [25]. They used a computer-aided three-dimensional reconstruction model of BM vascularity in BM biopsies of newly diagnosed cases of acute lymphoblastic leukaemia and found a complex, arborising branching of microvessels in the leukaemic specimens compared with single, straight microvessels without branching in controls. BMEC of active MM has been shown to be in an activated state [30], which can explain the stronger CD34 staining intensity we observed in the endothelial cells of the microvessels in the MM cases with nodular and diffuse growth pattern compared with the microvessels in the control group and the MGUS cases.

Since in some haematological tumours at least part of the BM microvessels were small with a slit-like lumen and because of the heterogeneous distribution of the microvessels, we wondered if this would not interfere with the transport capacity of the microvessels, resulting in hypoxia. We, therefore, investigated the CA IX expression using immunohistochemistry. CA IX is involved in the acid-base homeostasis of the cell, and its expression is under the control of the transcription factor hypoxia-inducible factor [12]. A focal expression of CA IX was present in one-third of the epithelial BM metastases, but no expression was observed in the malignant as well as in the stromal cells of all haematological malignancies. These findings suggest that untreated haematological diseases are either not hypoxic tumours and/or that the regulatory pathways involved in CA IX expression are not activated in haematological malignancies. It is possible that other carbonic anhydrases, e.g. CA II, which are normally expressed in the haematopoietic system [17], can substitute for CA IX.

In conclusion, this study confirmed an increased MVD and ECP in MM, AML, CMPS and in a part of CLL, but not in MGUS. The metastatic cases invariably had an increased ECP, which suggests that selection for the angiogenic phenotype is important in the establishment of distant metastases. Qualitative differences in microvessels were associated with growth patterns in MM, CLL and between the different entities in CMPS. Finally, in one-third of the epithelial BM metastases, there was a focal CA IX immunoreactivity, which was never observed in the haematological diseases.

Acknowledgements We thank Hilde Hellemans for helping with the immunostainings and Dr. Kewal Asosingh for his advice and encouragement. This work was supported by the Fund for Scientific Research—Flanders (Belgium) (F.W.O.-Vlaanderen) nr. G.0330.02. H.D.R. has a Clinical Doctoral Grant of F.W.O.-Vlaanderen and K.V. is a postdoctoral fellow of F.W.O.-Vlaanderen.

References

1. Aguayo A, Kantarjian H, Manshouri T, Gidel C, Estey E, Thomas D, Koller C, Estrov Z, O'Brien S, Keating M, Freireich E, Albitar M (2000) Angiogenesis in acute and chronic leukemias and myelodysplastic syndromes. Blood 96:2240–2245
2. Asosingh K, De Raeve H, Menu E, Van Riet I, Van Marck E, Van Camp B, Vanderkerken K (2004) Angiogenic switch during 5T2MM murine myeloma tumorigenesis, role of CD45 heterogeneity. Blood 103:3131–3137
3. Bartl R, Frisch B (1995) Diagnostic morphology in multiple myeloma. Current Diagn Pathol 2:222–235
4. Bartl R, Frisch B, Fatheh-Moghadam A, Kettner G, Jaeger K, Sommerfeld W (1987) Histologic classification and staging of multiple myeloma. A retrospective and prospective study of 674 cases. Am J Clin Pathol 2:222–235
5. Bertolini F, Mancuso P, Gobbi A, Pruneri G (2000) The thin red line: angiogenesis in normal and malignant hematopoiesis. Exp Hematol 28:993–1000
6. Chen J, Treweeke AT, West DC, Till KJ, Cawley JC, Zuzel M, Toh CH (2003) In vitro and in vivo production of vascular endothelial growth factor by chronic lymphocytic leukemia cells. Blood 96:3181–3187
7. Chia SK, Wykoff CC, Watson PH, Han C, Leek RD, Pastorek J, Gatter KC, Ratcliffe P, Harris AL (2001) Prognostic significance of a novel hypoxia-regulated marker, carbonic anhydrase IX, in invasive breast carcinoma. J Clin Oncol 19:3660–3668
8. Colpaert CG, Vermeulen PB, Fox SB, Harris AL, Dirix LY, Van Marck EA (2003) The presence of a fibrotic focus in invasive breast carcinoma correlates with the expression of carbonic anhydrase IX and is a marker of hypoxia and poor prognosis. Breast Cancer Res Treatment 81:137–147
9. Dankbar B, Padro T, Leo R, Feldmann B, Kropff M, Mesters RM, Serve H, Berdel WE, Kienast J (2000) Vascular endothelial growth factor and interleukin-6 in paracrine tumor-stromal cell interactions in multiple myeloma. Blood 95:2630–2636
10. Dickson DJ, Shami PJ (2001) Angiogenesis in acute and chronic leukemias. Leuk Lymph 42:847–853
11. Friedler W, Graeven U, Ergün S, Verago S, Kilic N, Stockschläder M, Hossfeld D (1997) Vascular endothelial growth factor, a possible paracrine growth factor in human acute myeloid leukemia. Blood 89:1870–1875
12. Harris AL (2002) Hypoxia—a key regulatory factor in tumour growth. Nature Rev 2:38–47
13. Hashimotto N, Kurihara K (1982) A histological study on the developmental process of myeloma nodules. J Kyushu Hematol Soc 30:1–8
14. Hlatky L, Hahnfeldt P, Folkman J (2002) Clinical application of antiangiogenic therapy: microvessel density, what it does and doesn't tell us. J Natl Cancer Inst 94:883–893

15. Hussong JW, Rodgers GM, Shami PJ (2000) Evidence of increased angiogenesis in patients with acute myeloid leukemia. Blood 95:309–313
16. Kini AR, Day NE, Peterson LC (2000) Increased bone marrow angiogenesis in B-cell chronic lymphocytic leukemia. Leukemia 14:1414–1418
17. Leppilampi M, Koistinen P, Savolainen ER, Hannuksela J, Parkkila AK, Niemelä O, Pastorekova S, Pastorek J, Waheed A, Sly WS, Parkkila S, Rajaniemi H (2002) The expression of carbonic anhydrase II in hematologic malignancies. Clin Cancer Res 8:2240–2245
18. Loncaster JA, Harris AL, Davidson SE, Longue JP, Hunter RD, Wykoff CC, Pastorek J, Ratcliffe PJ, Stratford IJ, West CM (2001) Carbonic anhydrase (CA IX) expression, a potential new intrinsic marker of hypoxia: correlations with tumor oxygen measurements and prognosis in locally advanced carcinoma of the cervix. Cancer Res 61:6394–6399
19. Lundberg LG, Lerner R, Sundelin P, Rogers R, Folkman J, Palmblad J (2000) Bone marrow in polycythemia vera, chronic myelocytic leukemia, and myelofibrosis has an increased vascularity. Am J Pathol 157:15–19
20. Mesa RA, Hanson CA, Li C, Yoon SY, Schroeder GS, Tefferi A (2000) Bone marrow immunohistochemical features complement histology in distinguishing essential thrombocythemia from reactive thrombocytosis. Blood 96[Suppl]:S3214
21. Moehler TM, Neben K, Ho AD, Goldschmidt H (2001) Angiogenesis in hematologic malignancies. Ann Hematol 80:695–705
22. Molica S, Vacca A, Ribatti D, Cuneo A, Cavazzini F, Levato D, Vitelli G, Tucci L, Roccaro AM, Dammacco F (2002) Prognostic value of enhanced bone marrow angiogenesis in early B-cell chronic lymphocytic leukemia. Blood 100:3344–3351
23. Munshi NC, Wilson C (2001) Increased bone marrow microvessel density in newly diagnosed multiple myeloma carries a poor prognosis. Semin Oncol 28:565–569
24. Padrò T, Ruiz S, Bieker R, Bürger H, Steins M, Kienast J, Büchner T, Berdel WE, Mesters RM (2002) Increased angiogenesis in the bone marrow of patients with acute myeloid leukemia. Blood 95:2637–2644
25. Perez-Atayde AR, Sallan SE, Tedrow U, Connors S, Allred E, Folkman J (1997) Spectrum of tumor angiogenesis in the bone marrow of children with acute lymphoblastic leukemia. Am J Pathol 150:815–821
26. Rajkumar SV, Mesa RA, Fonseca R, Schroeder G, Plevak MF, Dispenzieri A, Lacy MQ, Lust JA, Witzig TE, Gertz MA, Kyle RA, Russell SJ, Greipp PR (2002) Bone marrow angiogenesis in 400 patients with monoclonal gammopathy of undetermined significance, multiple myeloma, and primary amyloidosis. Clin Cancer Res 8:2210–2216
27. Stewart M, Talks K, Leek R, Turley H, Pezella F, Harris AL, Gatter K (2002) Expression of angiogenic factors and hypoxia factors HIF 1, HIF 2 and CA IX in non-Hodgkin's lymphoma. Histopathology 40:253–260
28. Till KJ, Zuzel M, Cawley JC (1999) The role of hyaluronan and interleukin 8 in the migration of chronic lymphocytic leukemia cells with lymphoreticular tissues. Cancer Res 59:4419–4426
29. Vacca A, Ribatti D, Roncali L, Ranieri G, Serio G, Silvestris F, Dammacco F (1994) Bone marrow angiogenesis and progression in multiple myeloma. Br J Haematol 87:503–508
30. Vacca A, Ria R, Semeraro F, Merchionne F, Coluccia M, Boccarelli A, Scavelli C, Nico G, Gernone A, Battelli F, Tabilio A, Guidolin D, Petrucci T, Ribatti D, Dammacco F (2003) Endothelial cells in the bone marrow of multiple myeloma. Blood 102:3340–3348
31. Vermeulen PB, Gasparini G, Fox SB, Colpaert C, Marson LP, Gion M, Beliën JAM, de Waal RMW, Van Marck E, Magnani E, Weidner N, Harris AL, Dirix LY (2002) Second international consensus on the methodology and criteria of evaluation of angiogenesis quantification in solid human tumours. Eur J Cancer 38:1564–1579
32. Weidner N, Semple JP, Welch WR, Folkman J (1991) Tumor angiogenesis and metastasis-correlation in invasive breast carcinoma. New Engl J Med 324:1–8
33. Wykoff CC, Beasley NJ, Watson PH, Turner KJ, Pastorek J, Sibtain A, Wilson GD, Turley H, Talks KL, Maxwell PH, Pugh CW, Ratcliffe PJ, Harris AL (2000) Hypoxia-inducible expression of tumor-associated carbonic anhydrases. Cancer Res 60:7075–7083
34. Wykoff CC, Beasley NJ, Watson PH, Campo L, Chia SK, English R, Pastorek J, Sly WS, Ratcliffe P, Harris AL (2001) Expression of the hypoxia-inducible and tumor-associated carbonic anhydrases in ductal carcinoma in situ of the breast. Am J Pathol 158:1011–1019
35. Xu JL, Lai R, Kinoshita T, Nakashima N, Nagasaka T (2002) Proliferation, apoptosis, and intratumoral vascularity in multiple myeloma: correlation with the clinical stage and cytological grade. J Clin Pathol 55:530–534

Virchows Arch (2004) 445:36–44
DOI 10.1007/s00428-004-1044-y

ORIGINAL ARTICLE

Arno van Heijst · Remco Haasdijk · Freek Groenman · Frans van der Staak · Christina Hulsbergen-van de Kaa · Ronald de Krijger · Dick Tibboel

Morphometric analysis of the lung vasculature after extracorporeal membrane oxygenation treatment for pulmonary hypertension in newborns

Received: 15 January 2004 / Accepted: 26 April 2004 / Published online: 3 June 2004
© Springer-Verlag 2004

Abstract Persistent pulmonary hypertension in the newborn (PPHN) is characterised by increased medial and adventitial thickness in the lung vasculature. This study describes morphometry of lung vasculature after extracorporeal membrane oxygenation (ECMO) in newborns with PPHN, due to meconium aspiration syndrome, sepsis or idiopathic persistent pulmonary hypertension of the newborn (i-PPHN). Three groups were studied: newborns with PPHN treated with ECMO (n=9), newborns with PPHN not treated with ECMO (n=12) and age-matched controls without PPHN (n=11). In pulmonary arteries with an external diameter of less than 150 μm, arterial media, adventitia and total wall thickness, expressed as a percentage of the external diameter, and their cross-sectional areas were calculated. Newborns with PPHN, compared with controls, demonstrated increased percentage of media thickness, adventitia thickness and total wall thickness, and increased medial, adventitial and total wall cross-sectional area. Newborns treated with ECMO, compared with those not treated so, showed a decreased percentage of media thickness and medial cross-sectional area in arteries with an external diameter less than 75 μm, and decreased percentage of media thickness and decreased medial, adventitial and total wall cross-sectional area in arteries with an external diameter of 75–150 μm. ECMO for persistent PPHN, due to meconium aspiration syndrome, sepsis or i-PPHN, reduces the abnormal morphometry of small pulmonary arteries. The underlying mechanisms contributing to this improved morphometry are yet unknown.

Keywords Morphometry · Medial thickness · Adventitial thickness · ECMO · Newborn

A. van Heijst · R. Haasdijk
Departments of Neonatology,
University Medical Centre Nijmegen,
Nijmegen, The Netherlands

F. Groenman · D. Tibboel
Department of Paediatric Surgery,
Erasmus Medical Centre-Sophia Children's Hospital,
Rotterdam, The Netherlands

F. van der Staak
Department of Paediatric Surgery,
University Medical Centre Nijmegen,
Nijmegen, The Netherlands

C. Hulsbergen-van de Kaa
Department of Pathology,
University Medical Centre Nijmegen,
Nijmegen, The Netherlands

R. de Krijger
Department of Pathology,
Erasmus Medical Centre-Sophia Children's Hospital,
Rotterdam, The Netherlands

A. van Heijst (✉)
Department of Pediatrics,
University Medical Centre Nijmegen,
PO Box 9101, 6500 HB Nijmegen, The Netherlands
e-mail: a.vanheijst@cukz.umcn.nl
Tel.: +31-24-3613936
Fax: +31-24-3619123

Introduction

The clinical syndrome of persistent pulmonary hypertension of the newborn (PPHN) is characterised by central cyanosis due to right-to-left shunting through the oval foramen and/or ductus arteriosus [14]. Right-to-left shunting develops as a consequence of persistence of a high pulmonary vascular resistance. Classically, and mainly based on morphological data, three different anatomical types of lung vascular abnormalities have been documented in cases of PPHN: underdevelopment, maldevelopment and maladaptation [12, 24, 39]. First, underdevelopment of the lung vasculature in combination with hypoplasia of the lung occurs in congenital diaphragmatic hernia. The second type of pulmonary vascular abnor-

mality is present in maldevelopment of pulmonary vessels in utero, such as in meconium aspiration syndrome and idiopathic persistent pulmonary hypertension of the newborn (i-PPHN). Finally, vascular abnormalities can be present in maladaptation of the pulmonary arteries to postnatal life, where there is a failure to decrease pulmonary vascular resistance after birth, such as in sepsis and pneumonia [12, 21, 26].

Despite the different aetiologies, the lung vascular morphology in all three forms of pulmonary hypertension in newborns is similar, showing an increased medial and adventitial thickness [16, 21, 22, 24, 26, 30]. In meconium aspiration syndrome, i-PPHN and sepsis, the number of intra-acinar arteries is normal, and the vessels have a normal external diameter. There is, however, extension of the muscle coat into normally non-muscular arteries [20, 21, 22]. However, in congenital diaphragmatic hernia, the situation is far more complicated because of lung hypoplasia with a decreased number of bronchial generations in which the vasculature is also hypoplastic with a decreased number of intra-acinar arteries. These intra-acinar arteries have a decreased external diameter in which the medial-wall thickness is increased. Extension of the muscle coat in the smaller arteries can either be normal or increased to distal into normally non-muscular arteries [12].

The treatment of PPHN currently consists of a combination of different therapies, including artificial ventilation, either conventional or high-frequency oscillatory ventilation, inhalation of nitric oxide and, recently, the use of phosphodiesterase inhibitors such as sildenafil [7, 27, 39, 41].

Extracorporeal membrane oxygenation (ECMO) can be used as a rescue treatment for PPHN when conservative therapy fails [37]. Generally, the effect of ECMO is described as "lung rest" [2, 11, 38]. Although the beneficial effect of ECMO with regard to changes in the pulmonary vasculature is unclear, it is thought that ECMO therapy "breaks" the circle of increasing pulmonary hypertension and right-to-left shunting [3].

In a series of congenital diaphragmatic hernia-case patients who, following successful decannulation from ECMO, died 12–48 h later because of therapy-resistant or recurrent pulmonary hypertension, our group formerly found a decrease in adventitial thickness of small pulmonary arteries after ECMO treatment. The medial smooth-muscle-cell hyperplasia was, however, not altered [26]. As described, the vascular changes in congenital diaphragmatic hernia patients can be different from those in patients with meconium aspiration syndrome, sepsis or i-PPHN. To our knowledge, the effect of ECMO treatment in newborns with pulmonary hypertension due to meconium aspiration syndrome, sepsis or i-PPHN has not been documented in a systematic way previously. We hypothesised that ECMO has an effect on the abnormal morphology of the vascular wall in patients with pulmonary hypertension [12, 21, 24]. We studied the morphology of the lung vasculature after ECMO treatment in patients with PPHN due to meconium aspiration syndrome, sepsis or i-PPHN and compared this with patients with PPHN who were not treated with ECMO and control patients without PPHN.

Materials and methods

Study group

We studied 32 consecutive lung autopsy specimens of newborns. Materials were retrieved from the archives of the Institute of Pathology, University Medical Centre Nijmegen, Nijmegen, and the Department of Pathology, Josephine Nefkens Institute Erasmus MC, Rotterdam. Tissue specimens were obtained from patients after parental consent for autopsy during the period of 1991–2001. All newborns had a gestational age above 34 weeks and a birth weight of at least 2000 g.

Patients were separated into three groups: (a) patients suffering from pulmonary hypertension due to meconium aspiration syndrome (n=3), sepsis (n=5) or i-PPHN (n=1) treated with ECMO after conservative treatment had failed (ECMO group, n=9); (b) patients suffering from pulmonary hypertension due to meconium aspiration syndrome (n=6), sepsis (n=3) or i-PPHN (n=3) treated with conservative therapy only (non-ECMO group, n=12); (c) a control group of patients (n=11) who died shortly after birth from asphyxia due to placental abruption and did not receive intensive therapy.

In all patients of the ECMO group and the non-ECMO group, the presence of pulmonary hypertension was confirmed using cardiac ultrasonography with right-to-left shunting together with the existence of a difference of 10% or more between pre-ductal and post-ductal transcutaneous oxygen saturation [26].

In four patients of the ECMO group, ECMO was withdrawn because of cerebral complications; the other five patients all were early post-ECMO deaths, median value 9 days, range 1–17 days after decannulation. The patients in the non-ECMO group all suffered from severe pulmonary hypertension but were not treated with ECMO because of the presence of a contra-indication for ECMO treatment: intracranial haemorrhage (n=7) or asphyxia with resulting brain damage (n=5). The patients in the control group showed no clinical features of pulmonary hypertension and had no lung abnormalities on histological examination. In these patients, therapy was withdrawn at the median age of 2 days (range 1–4 days) because of the severe neurological abnormalities and poor prognosis.

The entry criteria for ECMO treatment were: gestational age of at least 34 weeks, birth weight at least 2000 g, artificial ventilation for less than 10 days, $AaDO_2$ greater than 600 mmHg for more than 8 h.

Ventilation modes in the non-ECMO group and ECMO group were either conventional ventilation (peak inspiratory pressures of 30–38 mbar, positive end-expiratory pressures of 4–8 mbar, frequency 45–85/min, FiO_2 1.0) or high-frequency oscillation ventilation (mean airway pressure 16–22 mbar, amplitude 30–60 cm H_2O, frequency 10 Hz, FiO_2 1.0). The control group was ventilated with mild conventional ventilation; peak inspiratory pressure of 12–16 mbar, positive end-expiratory pressure of 3–5 mbar, frequency 20–40/min, FiO_2 0.21–0.40. Inhalation of nitric oxide became available as a treatment mode for pulmonary hypertension in 1996 and was used in five patients of the ECMO group and in seven patients of the non-ECMO group.

All autopsy lung specimens, obtained within 24 h after death, were routinely fixed using immersion in 4% buffered formalin and embedded in paraffin. Serial 4-μm sections were processed for histopathological and immunohistochemical examination. As our study material was routinely harvested at the time of autopsy, no predetermined protocol, including inflation fixation, was used [17, 18, 25, 40]. All slides were evaluated for diagnosis by an independent investigator, blinded for the clinical history of the individual patients.

Histological staining

Serial sections were mounted on polylysine-coated glass slides and stained with Masson trichrome staining, which stains elastic fibres dark blue/black, collagen fibres green and smooth muscle red, or Elastic von Giesson's staining, which stains elastic fibres dark violet, collagen fibres red and smooth muscle brownish yellow.

Immunohistochemistry

Formalin-fixed, paraffin-embedded sections of lung tissues were mounted on super-frost glass slides. Immunohistochemistry was performed using a standard avidin-biotin complex method. Deparaffinised slides were treated with 3% hydrogen peroxide in phosphate buffered saline (PBS, 30 min) to block the endogenous peroxidase activity, followed by rinsing with PBS. Slides were then placed in a Sequenza Immunostaining Workstation (Shandon Scientific Ltd, Astmoor, Runcorn, USA). Slides were pre-incubated for 10 min with 20% normal horse serum to block non-specific binding, then incubated for 60 min at room temperature with mouse monoclonal anti-human α-smooth-muscle actin antibodies (clone 1A4; Sigma, St. Louis, MO, USA) as a primary antiserum in dilution of 1:15,000 in monoclonal diluent (DPC, Los Angeles, USA). After rinsing with PBS, slides were incubated for 30 min with biotinylated horse-anti-mouse antibody 1:200 (Vector Laboratories) in polyclonal diluent (PLD-100; DPC, Los Angeles, USA). After further rinsing with PBS, slides were incubated for 45 min with peroxidase-conjugated avidin-biotin complex 1:50 (Vector Laboratories) in PLD-100 (DPC, Los Angeles, USA) and visualised with diaminobenzidine in PBS (5 min) as the chromogen. Slides were counter-stained with Mayer's haematoxylin for 20 s. Negative controls were prepared using omission of the primary antiserum.

Masson trichrome staining or Elastic von Giesson's staining and α-smooth-muscle actin immunostaining were compared on serial sections to check that the media is co-localised with α-smooth-muscle actin in pulmonary arteries prior to starting the morphometric measurements.

Morphometry

Pulmonary arteries were identified based on their position and structure. They mainly run along the terminal and respiratory bronchioles and at the alveolar duct level and are characterised by a distinct inner and outer elastic lamina [1, 30]. Arteries fulfilling these criteria, as well as having an external diameter measured between the external elastic laminae of up to 150 μm and a complete muscular coat, were measured. The diameter of less than 150 μm was chosen because these arteries are considered to be the pressure-regulating arteries [12]. Only arteries that were cut at approximately right angles, so that the maximal external diameter exceeded the minimal external diameter by less than 50%, were analysed using a calibrated eyepiece. Measurements of the arterial-wall layers in microns were done on Masson trichrome- or elastic von Gieson's-stained sections. Medial thickness in microns was calculated as the distance from the external elastic lamina to the internal elastic lamina along the shortest diameter of the artery. Adventitial thickness in microns was calculated along the shortest arterial diameter. Total wall thickness in microns consisted of medial thickness plus adventitial thickness, since the thickness of the intima was minimal in all cases. The thickness of the arterial media, of the adventitia and of the total vessel wall were expressed as a percentage of the external diameter to relate them to the arterial vessel size [17, 18, 25, 40]. To exclude the effect of vasoconstriction on medial, adventitial and total wall thickness, the cross-sectional areas of medial, adventitial and total wall thickness were, therefore, also calculated (expressed as μm^2) [33, 40]. The measured variables are demonstrated in Fig. 1.

Because in previous studies the most dramatic vascular-wall changes were demonstrated in arteries with an external diameter less than 75 μm, the small arteries were separated into two groups: a group of arteries with an external diameter less than 75 μm and a group with an external diameter between 75 μm and 150 μm [12, 21, 40].

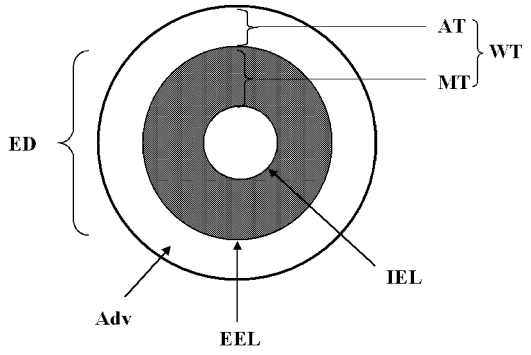


Fig. 1 Diagram of the measured morphometric variables. *IEL* internal elastic lamina, *EEL* external elastic lamina, *WT* total wall thickness in μm, *MT* medial thickness in μm, *AT* adventitial thickness in μm, *ED* external arterial diameter. In this study, MT, AT and WT are expressed as (1) percentage (%) of the ED, where MT%=[MT×2×100]/ED, AT%=[AT×2×100]/ED and WT%=[WT×2×100]/ED and (2) cross-sectional area in μm^2. The medial cross-sectional area is defined as the area contained by the EEL minus the area contained by the IEL. The adventitial cross-sectional area is defined as the area contained by the entire artery minus the area contained by the EEL. The wall-thickness cross-sectional area is defined by the area contained by the entire artery minus the area contained by the IEL

Statistical analysis

Study groups were compared for gender, gestational age and birth weight with Chi-square test and unpaired Student's *t*-test, respectively. Furthermore, the age at the moment of death in the non-ECMO group was compared with the age at the start of ECMO treatment in the ECMO group (unpaired Student's *t*-test).

Values of the thickness of the arterial media, of the adventitia and of the total vessel wall expressed as percentage of the external diameter and total wall cross-sectional area, medial cross-sectional area, and adventitial cross-sectional area from the three study groups were calculated and presented as mean (±standard deviation). Data from the three study groups were compared using the unpaired Student's *t*-test. P values less than or equal to 0.05 were considered statistically significant.

Results

There were no significant differences in demographic data among the studied groups, as they were comparable for gender, gestational age and birth weight (Table 1). Mean (±SD) ECMO treatment duration was 182±114 h. The non-ECMO group was ventilated for 7±8 days and the control group for 1±1 day. There was no significant difference in post-natal age at the moment of death in the non-ECMO group (7±8 days) and the moment of start of ECMO treatment in the ECMO group (4±4 days).

The mean number of investigated arteries per case was 34. The mean values (±SD) for thickness of the arterial media, of the adventitia and of the total vessel wall expressed as percentage of the external diameter, total wall

Table 1 Gender, gestational age and birth weight for the three study groups. Values for gestational age and birth weight are mean±standard deviation. *ECMO* extracorporeal-membrane oxygenation

	Gender (female:male)	Gestational age (days)	Birth weight (g)
Control group	4:7	277±18	3284±486
Non-ECMO group	4:8	273±15	2978±558
ECMO group	3:6	275±16	3248±520

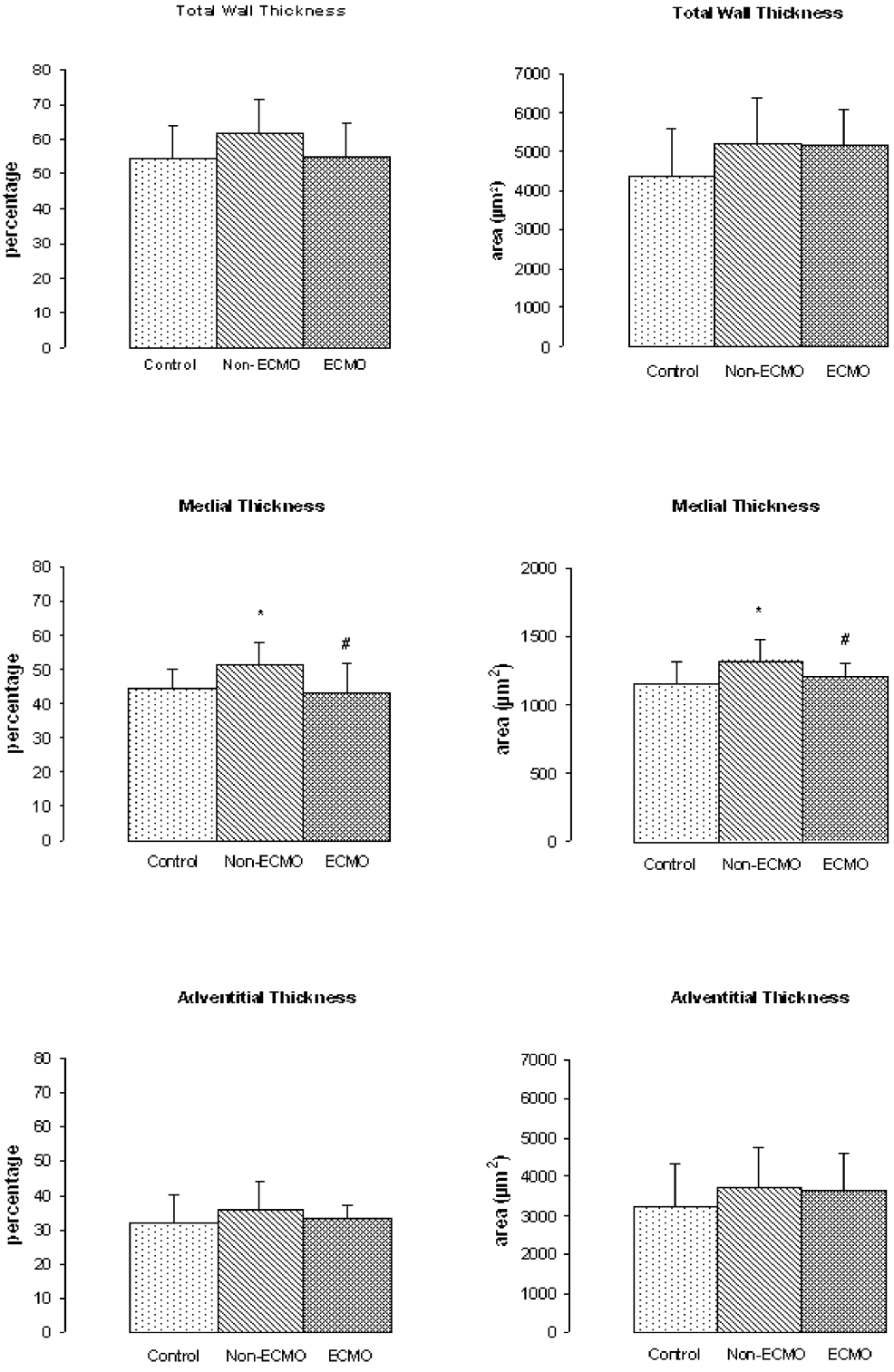


Fig. 2 Morphometric parameters in pulmonary arteries with external diameters of less than 75 μm. *Bars* represent mean values, *error bars* represent standard deviation. *Percentage* variable expressed as percentage of the external diameter, *control* control group, *non-extracorporeal membrane oxygenation (ECMO)* patients with pulmonary hypertension, not treated with ECMO, *ECMO* patients with pulmonary hypertension, treated with ECMO. **P*<0.05, non-ECMO group versus control group. #*P*<0.05 ECMO group versus non-ECMO group

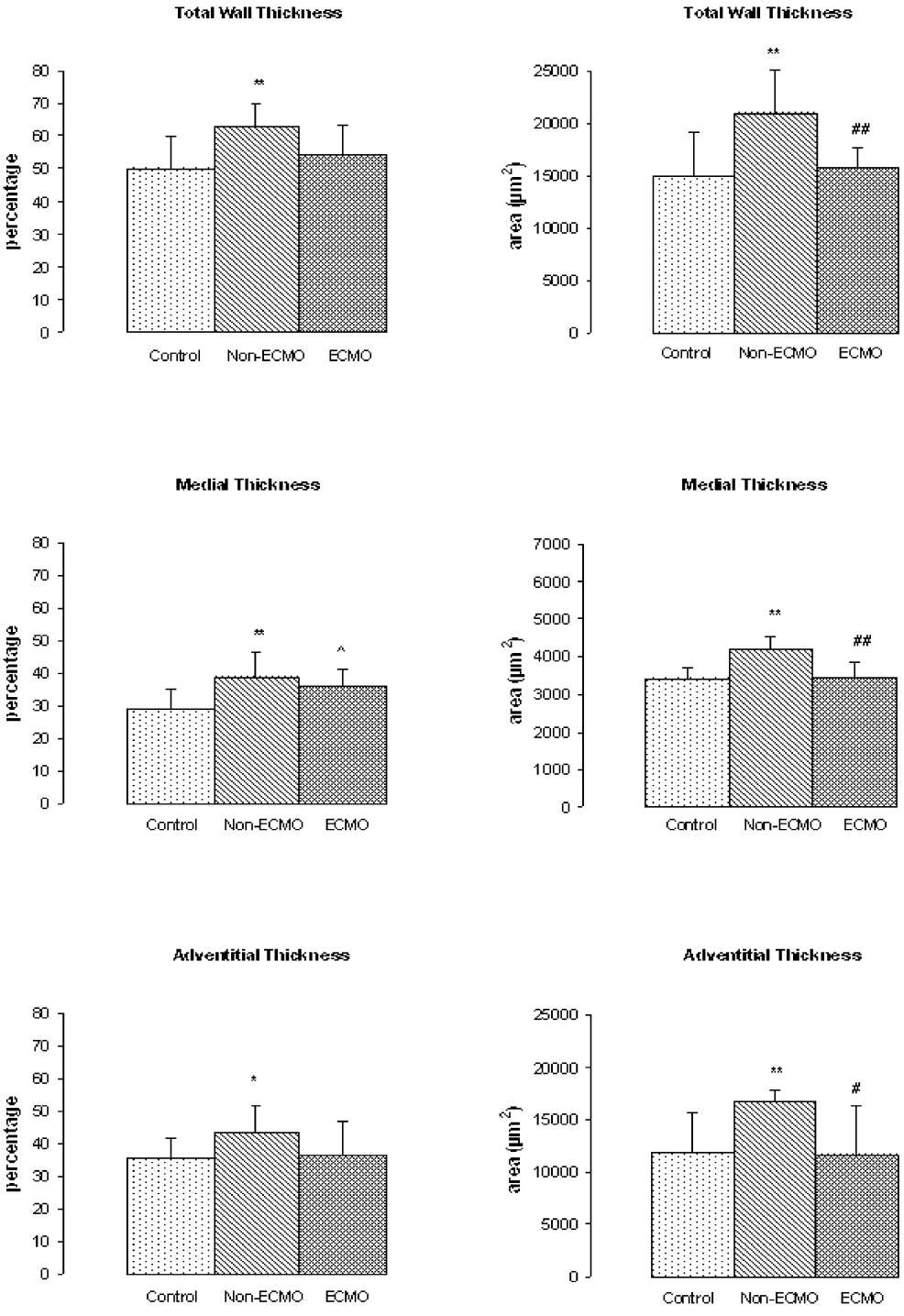


Fig. 3 Morphometric parameters in pulmonary arteries with external diameter between 75 μm and 150 μm. *Bars* represent mean values. *Error bars* represent standard deviation. *Percentage* variable expressed as percentage of external diameter, *control* control group, *non-extracorporeal membrane oxygenation (ECMO)* patients with pulmonary hypertension, not treated with ECMO, *ECMO* patients with pulmonary hypertension, treated with ECMO. **P*<0.05 non-ECMO group versus control group, ***P*<0.01 non-ECMO group versus control group, #*P*<0.05 ECMO group versus non-ECMO group, ##*P*<0.01 ECMO group versus non-ECMO group, ^*P*<0.05 ECMO group versus control group

cross-sectional area and medial and adventitial cross-sectional area of the small pulmonary arteries with an external diameter less than 75 μm and an external diameter between 75 μm and 150 μm are presented in Fig. 2 and Fig. 3. Figure 4 demonstrates the vascular changes in the three patient groups.

In pulmonary arteries with an external diameter less than 75 μm, there were differences in percentage of the total vessel-wall thickness, wall thickness cross-sectional areas, percentage of adventitial thickness and adventitial cross-sectional areas between the studied groups. The highest values were found in the pulmonary arteries of infants in the non-ECMO group, and the lowest values were found in the control group. However, these differences were not statistically significant.

The percentage of medial thickness and the medial cross-sectional area in the non-ECMO group were significantly increased compared with the control group. In the ECMO group, the percentage of medial thickness

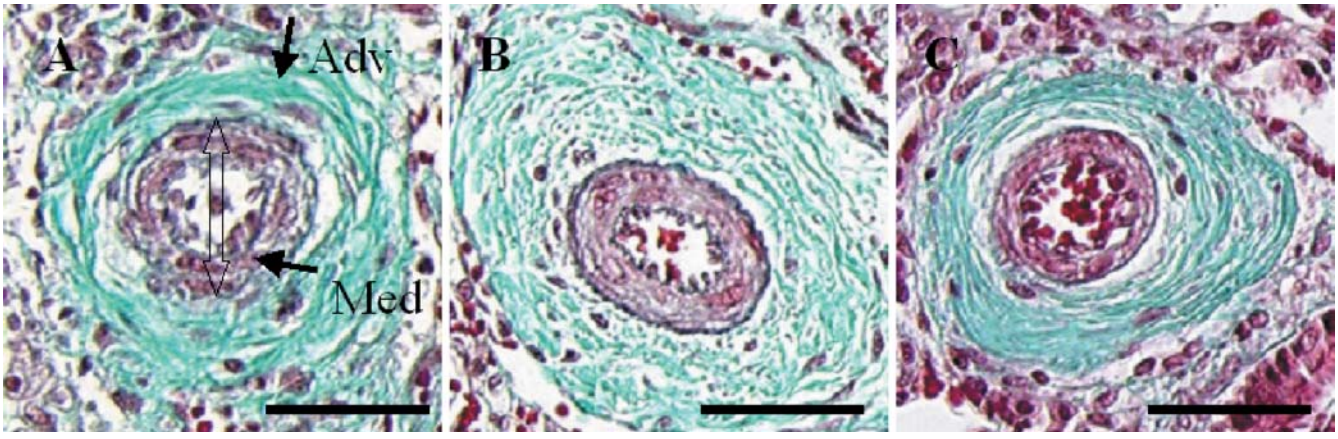


Fig. 4 Micrograph of the intraacinar arteries with Masson trichrome staining in the studied human lungs. *Panel A* control patient with thin media and thin adventitia. *Adv* adventitia, *Med* media. *Open arrow* external diameter. *Panel B* patient with PPHN not treated with extracorporeal membrane oxygenation (ECMO) (non-ECMO group). Increased media and adventitia. *Panel C* patient with persistent pulmonary hypertension in the newborn after ECMO treatment (ECMO group). Decreased media and adventitia compared with patient in *panel B*. (*Bar*=100 μm)

and the medial cross-sectional area were significantly decreased compared with the non-ECMO group ($P<0.05$).

In pulmonary arteries with an external diameter between 75 μm and 150 μm in the non-ECMO group, all studied variables were increased significantly compared with the control group ($P<0.01$), except for the percentage of adventitia thickness ($P<0.05$). The ECMO group demonstrated a decreased percentage of media thickness and wall thickness cross-sectional area compared with the non-ECMO group, where the decrease in wall thickness cross-sectional area was significant ($P<0.01$). The percentage of media thickness in the ECMO group was not significantly different from that in the control group.

The percentage of media thickness in the ECMO group was decreased compared with the non-ECMO group, but not significantly, and was still increased compared with the control group ($P<0.05$). The medial thickness cross-sectional area in the ECMO group was significantly decreased compared with the non-ECMO group ($P<0.01$).

Finally, the percentage of adventitia thickness in the ECMO group was comparable with that of the control group, but did not demonstrate a difference with the non-ECMO group. However, the adventitial cross-sectional area in the ECMO group was significantly decreased compared with the non-ECMO group ($P<0.05$).

Discussion

In this study, we demonstrated that, in patients with severe pulmonary hypertension, either idiopathic or secondary to meconium aspiration syndrome or sepsis, there were significant changes in pulmonary arterial-wall morphology compared with controls with the same postconceptional age. The percentage of total vessel-wall thickness and cross-sectional area, the percentage of me-dia thickness and cross-sectional area and the percentage of adventitia thickness and cross-sectional area in pulmonary arteries with an external diameter between 75 μm and 150 μm, as well as the percentage of media thickness and cross-sectional area in pulmonary arteries with an external diameter less than 75 μm were significantly increased.

When looking at the vascular-wall morphology in these patients after ECMO treatment, there was a significant decrease in the percentage of media thickness and cross-sectional area in pulmonary arteries with external diameters less than75 μm and a significant decrease in total wall-thickness cross-sectional area, medial cross-sectional area and adventitial cross-sectional area in arteries with an external diameter between 75 μm and 150 μm. In uninjected fixated arteries, the media cross-sectional area is thought to be a better measurement than the percentage of media thickness, because medial area does not vary with the degree of distension of the artery, whereas the percentage of media thickness does [6, 8, 36].

The observed changes suggest a beneficial effect of ECMO therapy on disturbed lung vascular morphology in newborns with severe pulmonary hypertension. The decreased vascular-wall thickness in ECMO-treated patients compared with non-ECMO-treated patients results in an increased arterial lumen in vessels with a comparable external diameter [20]. Since vascular resistance is inversely related to the fourth power of the intraluminal radius, even a small decrease in the medial diameter, causing a small increase in vascular lumen, may have an important effect on arterial resistance and pressure [12, 21]. Also, decreases in adventitial thickness are suggested to increase the compliance in small pulmonary arteries [12].

In both this study and that of Shehata et al. in patients with congenital diaphragmatic hernia, adventitial and wall thickness thinning was found in infants after ECMO treatment. Shehata et al. also suggested that adventitial thinning, which is followed by an increase of vascular compliance of the pressure regulating small pulmonary arteries, is a possible mechanism for a temporary decrease

of the vascular resistance in patients with congenital diaphragmatic hernia [26].

However, this study reveals an important difference between patients with and without congenital diaphragmatic hernia. We demonstrated a decrease in medial thickness and cross-sectional area after ECMO treatment in pulmonary arteries of patients with meconium aspiration syndrome, sepsis and i-PPHN. Both Shehata et al. and Thibeault and Haney, who only evaluated patients who died, could not demonstrate an effect of ECMO on medial thickness in patients with congenital diaphragmatic hernia [26, 34]. An explanation for differences between our study and these studies could be that pulmonary hypertension in congenital diaphragmatic hernia has a different pathogenesis than non-congenital diaphragmatic hernia causes of pulmonary hypertension. Congenital diaphragmatic hernia is a developmental disorder with antenatal anatomical abnormalities. Meconium aspiration syndrome, sepsis and i-PPHN are considered as maldevelopment or maladaptation, occurring in the transitional circulation around birth. In congenital diaphragmatic hernia as well as in meconium aspiration syndrome, sepsis and i-PPHN, an increase in medial and adventitial thickness is documented. However, in meconium aspiration syndrome, sepsis and i-PPHN, there is a normal external diameter and a normal number of intra-acinar arteries in contrast to patients with congenital diaphragmatic hernia, where there is a decrease in external diameter and number of intra-acinar arteries [12, 24]. The difference in timing of the occurrence of the vascular abnormalities in patients with and without congenital diaphragmatic hernia with pulmonary hypertension may determine the differences between these groups. Lung hypoplasia in congenital diaphragmatic hernia is generally considered to start in the first trimester of pregnancy. As a consequence, the vascular pathology is considered to be the result of an early foetal developmental anomaly [15, 19]. Although it is suggested that the vascular changes in meconium aspiration syndrome and i-PPHN do already occur before birth, it is unlikely that they develop in the first trimester [12, 22, 24]. The differences in underlying diseases for PPHN in the study groups may, however, be a limitation of this study.

Most likely, these differences in lung vasculature and timing influence the reaction to ECMO treatment and explain why, in congenital diaphragmatic hernia, no decrease in medial thickness was seen after ECMO treatment. In some congenital diaphragmatic hernia cases, the absence of changes of the pulmonary vasculature probably refers to an already fixed and irreversible pathology of the media. This is supported by the lack of response on inhaled nitric oxide therapy in congenital diaphragmatic hernia patients [23].

Our results may represent an underestimation of the real effect of ECMO on lung vascular morphology, as 9 of 12 patients of the non-ECMO group did not yet fulfil criteria for ECMO treatment at the moment of death. This suggests a milder amount of pulmonary hypertension in these patients than in patients of the ECMO group when ECMO was started. Therefore, lung vascular morphological abnormalities could be less pronounced at the moment of death in these patients than in the patients of the ECMO group at the moment of start of ECMO treatment. If all patients in the non-ECMO group would have fulfilled the ECMO criteria, the differences found between the non-ECMO group and ECMO group might have been more significant. Another possibility for underestimation of the effect of ECMO treatment may be that the patients in the ECMO group died and, therefore, did not completely "recover" from their abnormal vascular morphology. It is impossible to correlate our findings with lung vascular morphology in patients after successful ECMO treatment and survival, since all cases studied were autopsy cases. There are no data showing the median time on ECMO necessary to reverse abnormal vascular morphology in newborns with pulmonary hypertension towards a normal pulmonary vascular architecture. Laberge and Wilson, discussing the results found by Shehata et al., suggested that reversal of the abnormal vascular morphology in pulmonary hypertension is not an effect of ECMO, but rather of postnatal age. These arguments are speculative, as Shehata et al. found the same morphometric results in congenital diaphragmatic hernia patients after a short period of ECMO treatment as after a prolonged period [26]. We also found no differences in the studied morphometric parameters between newborns that died after a short (119±88 h) or long (287±57 h) ECMO run time, but conclusions are difficult to draw because the groups were relatively small.

From the results in this study, it could be argued that ECMO does not cause a reversal of abnormal lung vascular morphology, but only prevents a further deterioration when ECMO treatment is not started, as could have occurred in the non-ECMO group. As stated above, it seems unlikely that the vascular abnormalities in patients of the non-ECMO group were more severe than in patients of the ECMO group. Therefore, it is likely that ECMO influenced the medial and adventitial abnormalities in patients with pulmonary hypertension due to meconium aspiration syndrome, sepsis or i-PPHN.

The regression of the abnormal vascular morphology after ECMO treatment points to a mechanism that explains the beneficial effect of ECMO in patients with severe pulmonary hypertension. Further studies are needed to unravel the underlying processes involved in this regression. To study the exact effects of ECMO on lung vascular morphology, lung biopsies are needed before and after ECMO treatment, which is, however, not possible for obvious ethical reasons [5]. We speculate that in patients with pulmonary hypertension, sustained hypoxia may be the mechanism for abnormal vascular remodelling, as persistent ongoing hypoxia is a trigger for cell proliferation [29, 32]. Experimental models suggest an important role of both smooth-muscle cells and adventitial fibroblasts during the natural history of vascular remodelling in pulmonary hypertension [29, 31]. Detailed molecular analysis focusing on maturational changes of

the medial smooth-muscle cell population of the arterial media is warranted.

An adequate animal model for pulmonary hypertension in which the animals can be subjected to ECMO is necessary to obtain a better insight into reversal of the pathological vascular remodelling that exists in pulmonary hypertension [28]. An alternative way of evaluating the molecular background of the abnormal lung vascular morphology might include laser capture micro-array in combination with RNA protein isolation to quantify changes in gene products known to be involved in muscle-cell proliferation and vascular remodelling [13].

Again speculative, genes regulating, for instance, matrix metalloproteinases might not be switched on or off or at an abnormal time point. In animal models, matrix metalloproteinases are involved in vascular remodelling during pulmonary hypertension by influencing collagen deposition, smooth-muscle cell proliferation and apoptosis [9, 35]. To determine differences in matrix metalloproteinase effect between patients in the non-ECMO and ECMO group, extracellular-matrix composition may be studied [4, 9, 10]. Alternatively, in PPHN, there might be an imbalance between proliferation and apoptosis, a usual occurring feature in preparation for the ability to dilate at the transition for postnatal life. Geraci et al. showed an imbalance between genes regulating cell growth and genes regulating apoptosis in patients with primary pulmonary hypertension [13].

In summary, we demonstrated that ECMO therapy caused a reduction in abnormal vascular morphology in small pulmonary arteries of patients suffering from meconium aspiration syndrome, sepsis or iPPHN. The effect of ECMO therapy in these patients with pulmonary hypertension, often described as lung rest, can be "translated" into a documented reversal of the vascular-wall abnormalities that are present in pulmonary hypertension. The molecular mechanisms underlying this process are currently under investigation in our laboratory.

References

1. Allen K, Haworth SG (1988) Human postnatal pulmonary arterial remodeling. Ultrastructural studies of smooth muscle cell and connective tissue maturation. Lab Invest 59:702–709
2. Antunes MJ, Greenspan JS, Cullen JA, Holt WJ, Baumgart S, Spitzer AR (1995) Prognosis with preoperative pulmonary function and lung volume assessment in infants with congenital diaphragmatic hernia. Pediatrics 96:1117–1122
3. Bartlett RH, Andrews AF, Toomasian JM, Haiduc NJ, Gazzaniga AB (1982) Extracorporeal membrane oxygenation for newborn respiratory failure: forty-five cases. Surgery 92:425–433
4. Berger P, Lavallee J, Rouiller R, Laurent F, Marthan R, Tunon-de-Lara JM (1999) Assessment of bronchial inflammation using an automated cell recognition system based on colour analysis. Eur Respir J 14:1394–1402
5. Bond SJ, Lee DJ, Stewart DL, Buchino JJ (1996) Open lung biopsy in pediatric patients on extracorporeal membrane oxygenation. J Pediatr Surg 31:1376–1378
6. Bratu I, Flageole H, Laberge JM, Chen MF, Piedboeuf B (2001) Pulmonary structural maturation and pulmonary artery remodeling after reversible fetal ovine tracheal occlusion in diaphragmatic hernia. J Pediatr Surg 36:739–744
7. Clark RH, Kueser TJ, Walker MW, Southgate WM, Huckaby JL, Perez JA, Roy BJ, Keszler M, Kinsella JP (2000) Low-dose nitric oxide therapy for persistent pulmonary hypertension of the newborn. Clinical Inhaled Nitric Oxide Research Group. N Engl J Med 342:469–474
8. Colpaert C, Hogan J, Stark AR, Genest DR, Roberts D, Reid L, Kozakewich H (1995) Increased muscularization of small pulmonary arteries in preterm infants of diabetic mothers: a morphometric study in noninflated, noninjected, routinely fixed lungs. Pediatr Pathol Lab Med 15:689–705
9. Cowan KN, Jones PL, Rabinovitch M (1999) Regression of hypertrophied rat pulmonary arteries in organ culture is associated with suppression of proteolytic activity, inhibition of tenascin-C, and smooth muscle cell apoptosis. Circ Res 84: 1223–1233
10. Cowan KN, Jones PL, Rabinovitch M (2000) Elastase and matrix metalloproteinase inhibitors induce regression, and tenascin-C antisense prevents progression, of vascular disease. J Clin Invest 105:21–34
11. Frenckner B, Ehren H, Granholm T, Linden V, Palmer K (1997) Improved results in patients who have congenital diaphragmatic hernia using preoperative stabilization, extracorporeal membrane oxygenation, and delayed surgery. J Pediatr Surg 32:1185–1189
12. Geggel RL, Reid LM (1984) The structural basis of PPHN. Clin Perinatol 11:525–549
13. Geraci MW, Moore M, Gesell T, Yeager ME, Alger L, Golpon H, Gao B, Loyd JE, Tuder RM, Voelkel NF (2001) Gene expression patterns in the lungs of patients with primary pulmonary hypertension: a gene microarray analysis. Circ Res 88:555–562
14. Gersony WM (1984) Neonatal pulmonary hypertension: pathophysiology, classification, and etiology. Clin Perinatol 11:517–524
15. Harrison MR, Adzick NS, Nakayama DK, deLorimier AA (1986) Fetal diaphragmatic hernia: pathophysiology, natural history, and outcome. Clin Obstet Gynecol 29:490–501
16. Haworth SG, Reid L (1976) Persistent fetal circulation: newly recognized structural features. J Pediatr 88:614–620
17. Haworth SG, Hislop AA (1983) Pulmonary vascular development: normal values of peripheral vascular structure. Am J Cardiol 52:578–583
18. Hosoda Y (1994) Pathology of pulmonary hypertension: a human and experimental study. Pathol Int 44:241–267
19. Keijzer R, Liu J, Deimling J, Tibboel D, Post M (2000) Dual-hit hypothesis explains pulmonary hypoplasia in the nitrofen model of congenital diaphragmatic hernia. Am J Pathol 156:1299–1306
20. Meyrick B, Reid L (1983) Pulmonary hypertension. Anatomic and physiologic correlates. Clin Chest Med 4:199–217
21. Murphy JD, Rabinovitch M, Goldstein JD, Reid LM (1981) The structural basis of persistent pulmonary hypertension of the newborn infant. J Pediatr 98:962–967
22. Murphy JD, Vawter GF, Reid LM (1984) Pulmonary vascular disease in fatal meconium aspiration. J Pediatr 104:758–762
23. Neonatal Inhaled Nitric Oxide Study Group (NINOS) (1997) Inhaled nitric oxide and hypoxic respiratory failure in infants with congenital diaphragmatic hernia. Pediatrics 99:838–845
24. Rabinovitch M (1985) Morphology of the developing pulmonary bed: pharmacologic implications. Pediatr Pharmacol 5:31–48
25. Shehata SM, Tibboel D, Sharma HS, Mooi WJ (1999) Impaired structural remodelling of pulmonary arteries in newborns with congenital diaphragmatic hernia: a histological study of 29 cases. J Pathol 189:112–118
26. Shehata SM, Sharma HS, van der Staak FH, Kaa-Hulsbergen C, Mooi WJ, Tibboel D (2000) Remodeling of pulmonary arteries in human congenital diaphragmatic hernia with or without extracorporeal membrane oxygenation. J Pediatr Surg 35:208–215

27. Shekerdemian LS, Ravn HB, Penny DJ (2002) Intravenous sildenafil lowers pulmonary vascular resistance in a model of neonatal pulmonary hypertension. Am J Respir Crit Care Med 165:1098–1102
28. Steinhorn RH, Morin FC III, Fineman JR (1997) Models of persistent pulmonary hypertension of the newborn (PPHN) and the role of cyclic guanosine monophosphate (GMP) in pulmonary vasorelaxation. Semin Perinatol 21:393–408
29. Stenmark KR, Mecham RP (1997) Cellular and molecular mechanisms of pulmonary vascular remodeling. Annu Rev Physiol 59:89–144
30. Stenmark KR, Fasules J, Hyde DM, Voelkel NF, Henson J, Tucker A, Wilson H, Reeves JT (1987) Severe pulmonary hypertension and arterial adventitial changes in newborn calves at 4,300 m. J Appl Physiol 62:821–830
31. Stenmark KR, Bouchey D, Nemenoff R, Dempsey EC, Das M (2000) Hypoxia-induced pulmonary vascular remodeling: contribution of the adventitial fibroblasts. Physiol Res 49:503–517
32. Stenmark KR, Gerasimovskaya E, Nemenoff RA, Das M (2002) Hypoxic activation of adventitial fibroblasts: role in vascular remodeling. Chest 122:326–334
33. Taira Y, Yamataka T, Miyazaki E, Puri P (1998) Adventitial changes in pulmonary vasculature in congenital diaphragmatic hernia complicated by pulmonary hypertension. J Pediatr Surg 33:382–387
34. Thibeault DW, Haney B (1998) Lung volume, pulmonary vasculature, and factors affecting survival in congenital diaphragmatic hernia. Pediatrics 101:289–295
35. Vieillard-Baron A, Frisdal E, Eddahibi S, Deprez I, Baker AH, Newby AC, Berger P, Levame M, Raffestin B, Adnot S, D'Ortho MP (2000) Inhibition of matrix metalloproteinases by lung TIMP-1 gene transfer or doxycycline aggravates pulmonary hypertension in rats. Circ Res 87:418–425
36. Wagenvoort CA, Neufeld HN, Edwards JE (1961) The structure of the pulmonary arterial tree in fetal and early postnatal life. Lab Invest 10:751–762
37. Walsh MC, Stork EK (2001) Persistent pulmonary hypertension of the newborn. Rational therapy based on pathophysiology. Clin Perinatol 28:609–627
38. Weber TR, Kountzman B, Dillon PA, Silen ML (1998) Improved survival in congenital diaphragmatic hernia with evolving therapeutic strategies. Arch Surg 133:498–502
39. Weinberger B, Weiss K, Heck DE, Laskin DL, Laskin JD (2001) Pharmacologic therapy of persistent pulmonary hypertension of the newborn. Pharmacol Ther 89:67–79
40. Yamataka T, Puri P (1997) Pulmonary artery structural changes in pulmonary hypertension complicating congenital diaphragmatic hernia. J Pediatr Surg 32:387–390
41. Zhao L, Mason NA, Morrell NW, Kojonazarov B, Sadykov A, Maripov A, Aldashev A, Wilkins MR (2001) Sildenafil inhibits hypoxia-induced pulmonary hypertension. Circulation 104:424–428

Virchows Arch (2004) 445:45–53
DOI 10.1007/s00428-004-1023-3

ORIGINAL ARTICLE

Kazuto Yamazaki

Type-II pneumocyte differentiation in pulmonary sclerosing hemangioma: ultrastructural differentiation and immunohistochemical distribution of lineage-specific transcription factors (TTF-1, HNF-3 alpha, and HNF-3 beta) and surfactant proteins

Received: 8 December 2003 / Accepted: 24 March 2004 / Published online: 11 May 2004
© Springer-Verlag 2004

Abstract Sclerosing hemangioma (PSH) is a rare pulmonary tumor, in which two types of tumor cells could be histologically discerned—surface and stromal tumor cells. Nine tumor-tissue specimens from six female Japanese patients were studied, focusing on the distribution of several transcription factors related to lung epithelial development and surfactant proteins and comparing the ultrastructural features of the tumor cells. The immunohistochemical analysis revealed that the surfactant proteins of surfactant apoprotein A, surfactant protein B, and prosurfactant protein C were distributed in many of the surface-lining cells and in a small number of stromal-tumor cells. In addition, the nuclei of the tumor cells stained positive for thyroid transcription factor 1 (TTF)-1, hepatocyte nuclear factor (HNF)-3 alpha, and HNF-3 beta. In situ hybridization staining for TTF-1 showed similar positive signals. Ultrastructurally, two types of tu-mor cells showed similar features, but stromal tumor cells lost the definitive apico-lateral differentiation compared with the surface tumor cells and showed restricted surface differentiation between the adjacent tumor cells, forming small lumina accompanied by microvilli and occasional multi-vesicle or multi-lamellar bodies. Conclusively, the real tumoral population being undifferentiated stromal cells, the lining cells are fully differentiated type-II pneumonocytes. PSH is a proliferation of rather fetal type-II pneumonocytes (pneumocytoma or pneumoblastoma?).

Keywords Type-II pneumocyte · In situ hybridization · Pulmonary adenocarcinoma · Multi-vesicular bodies · Multi-lamellar bodies

K. Yamazaki (✉)
Department of Pathology,
Saiseikai Central Hospital,
l-4-17 Mita, Minatoku, 108-0073 Tokyo, Japan
e-mail: KazutoYamazaki@aol.com
Tel.: +81-3-34518211
Fax: +81-3-34516102

Introduction

Sclerosing hemangioma (PSH) is a rare pulmonary tumor, in which two types of tumor cells could be discerned—surface-lining cuboidal cells and more deeply positioned pale tumor cells in the stroma. Their cell lineage and morphological nature had been controversial [1, 2, 3, 5, 6, 8, 10, 13, 15, 16, 20, 22]. At the present time, for the histogenesis of PSH, it might be said that there is little controversy, since older theories of endothelial, mesothelial, and even neuroendocrine origin have been largely disproved. Recently, Niho et al. demonstrated the monoclonality of both types of PSH cells [16]. Many investigators have provided evidence that the tumor is derived from alveolar or bronchiolar epithelium [3, 5], while Xu et al. reported neuroendocrine differentiation of the tumor [20].

Recently, the immunohistochemical distribution of thyroid transcription factor 1 (TTF-1, Nkx2.1)—a kind of lung-relating transcriptional factor in the tumor cells of PSH—has been reported [2, 6]. In the present study, the author focuses on the important roles of transcription factors in normal lung morphogenesis and cell differentiation. These lung-related transcription factors include TTF-1, hepatocyte nuclear factor 3 alpha and hepatocyte nuclear factor 3 beta (HNF-3 alpha and HNF-3 beta/forkhead homologue 4, winged-helix protein) [9], the zinc finger GLI 1 (a transcription factor possibly having important roles in regulating the mesenchymal–epithelial interaction during lung development), and GATA 6 transcription factors [4, 9, 11, 14, 18, 21]. It has recently been shown that TTF-1, HNF-3 alpha, HNF-3 beta, and GATA 6 interact with each other and have essential roles in the morphogenesis of lung epithelial cells and the expression of significant molecules of surfactant proteins. To date, TTF-1, together with GATA 6, HNF-3 alpha, and HNF-3 beta, are assumed to be the master genes in normal lung development and are positioned high up in the hierarchy, since all three factors are thought to be essential for morphogenesis and lung epithelial-cell differentiation [4,

9, 11, 14, 18, 21]. The roles of these transcription factors in pulmonary disease states, including tumors and cancers, remain entirely unknown.

At an ultrastructural level, normal human airway lung-epithelial cells of type-II pneumocytes are assumed to be exocrine secretory elements [17, 19], and, in whose cytoplasm, vacuoles are characteristically included, known as cytosomes, multi-vesicular bodies, and multi-lamellar bodies [5, 7, 17, 19]. It is clear that the multi-vesicular bodies are the source of surfactant proteins in the lung. Compared with these ultrastructural characters of normal human type-II pneumocytes, PSH tumor cells should be defined ultrastructurally as tumor cells with the differentiation of putative surfactant protein-producing cells of type-II pneumocytes [5, 7, 17, 19].

Although this study is restricted to only six cases, the present study focused on the distribution of several transcription factors and surfactant proteins in PSH, comparing the ultrastructural features of both types of tumor cells and examining the similarities to or distortions from the characteristics of normal human lung-epithelial cells of type-II pneumocytes.

Materials and methods

Patients

As shown in Table 1, a total number of nine tumors from six cases were filed in the archive of the Department of Pathology. All patients were females and were asymptomatic before the excisional surgery or postmortem autopsy, and many of the tumors were incidentally found on X-ray images at routine health check-ups as abnormal small-mass lesions in the lung. Five were surgical cases, and one was an autopsy case. Case 3 had three tumors, measuring 3×2, 1×1, and 3×3 mm each, and they had been found during the post-excisional clinical 3-year follow-up by the periodic detailed check using chest X-ray, computed tomography, and nuclear magnetic resonance studies at the outpatient clinic. After the small nodular lesions had been found, their size was checked every time at the clinic. The smallest nodule of 1×1 mm was found at the incidental findings of the through-resected segments containing larger nodules. Histopathological diagnosis of these tiny growths was also made as PSH after the similar histological studies of the tumors.

Tissue samples

Tumor tissue specimens from the six patients were fixed in 10% neutral formalin and embedded in paraffin. They were histologically diagnosed PSH. Sets of the tumor tissue samples were subjected to conventional light microscopy, immunohistochemistry, transmission electron microscopy, and light microscopic in situ hybridization studies.

Light microscopy and immunohistochemistry

Tissue specimens were fixed in 15% formalin, embedded in paraffin wax, and processed according to conventional histological techniques for subsequent sectioning and staining in hematoxylin and eosin. For the immunohistochemical analysis, the following antibodies were used. Transcription factors: TTF-1 (Dako, Glostrup, Denmark), GATA 6, GLI 1, HNF-3, and HNF-3 beta (all four from Santa Cruz Biotechnology, Santa Cruz, CA); surfactant

Table 1 Patients, clinical features, and the analytical methods for tissue specimens of pulmonary sclerosing hemangioma, *TEM* transmission electron microscopy, *IHC* immunohistochemistry, *ISH* in situ hybridization

Case number	Age/sex at surgery or autopsy	Number and size	Location	Clinical features	Dominant histological pattern	Analytical methods
Case 1	75 years, female	Single, 20×17 mm	Left, S7	Incidental mass lesion during the excisional surgery of left lung (S1+2, adenocarcinoma, 3×2.8 cm in size, p-T1NoMo)	Solid and papillary	TEM, IHC, ISH
Case 2	52 years, female	Single, 2×1 cm	Right, S7	Slowly growing tumor, enucleation	Solid and hemangiomatous	TEM, IHC, ISH
Case 3	42 years, female	Sidle, 1.5×1 cm	Right, S8	Abnormal shadow at health check, suspected as being a benign hamartoma	Papillary	TEM, IHC, ISH
Case 3	45 years, female	Triple, 3×2 mm, 1×1 mm, 3×3 mm	Right, S1, Right, S1, Right, S3	Post-operative follow up for 3 years	Papillary and solid	IHC, ISH
Case 4	40 years, female	Single, 6×5 mm	Right, S9	Abnormal shadow, excisional biopsy	Sclerotic and solid	IHC, ISH
Case 5	73 years, female	Single, 7×5 mm	Left, S5	Incidental mass lesion in an autopsy case who died of renal failure with diabetes mellitus	Papillary	IHC
Case 6	53 years, female	Single, 10×12 mm	Left, S8	Abnormal shadow at health check	Hemangiomatous and solid	TEM, IHC, ISH

apoproteins: SPA, (surfactant apoprotein A, Dako), SPB (surfactant protein B, Calbiochem), SPC (prosurfactant protein C, Research Diagnostics), and CC10 (Clara cell 10 10-kDa protein, Santa Cruz Biotechnology, Santa Cruz, CA), SC (secretory component, Dako), EMA (epithelial membrane antigen, Dako), Laminin (Dako), type-IV collagen (Dako), Calretinin (NICHIREI; Zaimed), BerEP4 (Dako), CEA (carcinoembryonic antigen, Mochida), and keratins—AE1–AE3 (pankeratin, Dako), CAM5.2 (Becton Dickinson), 34bE12 (Enzo), KL-1 (Immunotech), CD10 (Novocastra), CD15 (Dako), crystallin (Novocastra), CD34 (Dako), Factor VIII (Dako), vimentin (Dako), Factor XIIIa (Calbiochem), ER (estrogen receptor, Dako), PGR (progesterone receptor, Dako), c-kit (Calbiochem), c-erbB2 (Dako), Kp-1 (CD68, Dako), CD56 (Novocastra), synaptophysin (Dako), and chromogranin A (Dako). Immunostains were examined using an ENVISION kit (Dako, Denmark). Immunostaining was done with or without antigen-retrieval techniques [12, 21].

In situ hybridization

The TTF-1-specific antisense oligonucleotide probe (5′-GTC AGA CAC TGA GAA CGG AGT CGT CTG CTT TGG ACT), the corresponding sense probe, and GATA 6-specific antisense (5′-AGT GGT CTG GGC ACC CCA TGG AGT TTC ATG TAG AGT) and sense oligonucleotide probes were synthesized and labeled with biotin at the 5′ ends [12]. The sense probe was used as the negative control. Hybridization was performed on formalin-fixed paraffin sections using a GenPoint System (Dako, Glostrup, Denmark) as previously described [12]. Briefly, 5-mm tumor sections were deparaffinized, incubated in Target Retrieval Solution (Dako) for 40 min at 95°C, followed by pretreatment with proteinase K at a dilution of 1:4000. After blocking endogenous peroxidase activity, the sections were incubated with the biotin-conjugated probe (1 mg/ml). Hybridization was carried out at 37°C overnight. Sections were then washed with Stringent Wash Solution for 20 min at 45°C before incubation with horseradish peroxidase-conjugated streptavidin (1:100). Each section was incubated with biotinylated tyramide (Dako), followed by incubation with streptavidin-biotin-peroxidase complex (Dako) at a dilution of 1:100; immunoreactive signals were visualized using diaminobenzidine [12].

Electron microscopy

Samples of the tumor tissue were fixed in phosphate-buffered 2.5% glutaraldehyde, then osmium tetroxide, and embedded in epoxy resin according to conventional procedures. Ultrathin sections were stained with uranyl acetate and lead citrate and examined in a JEOL 1200EXII electron microscope [12, 21].

Results

Light microscopy

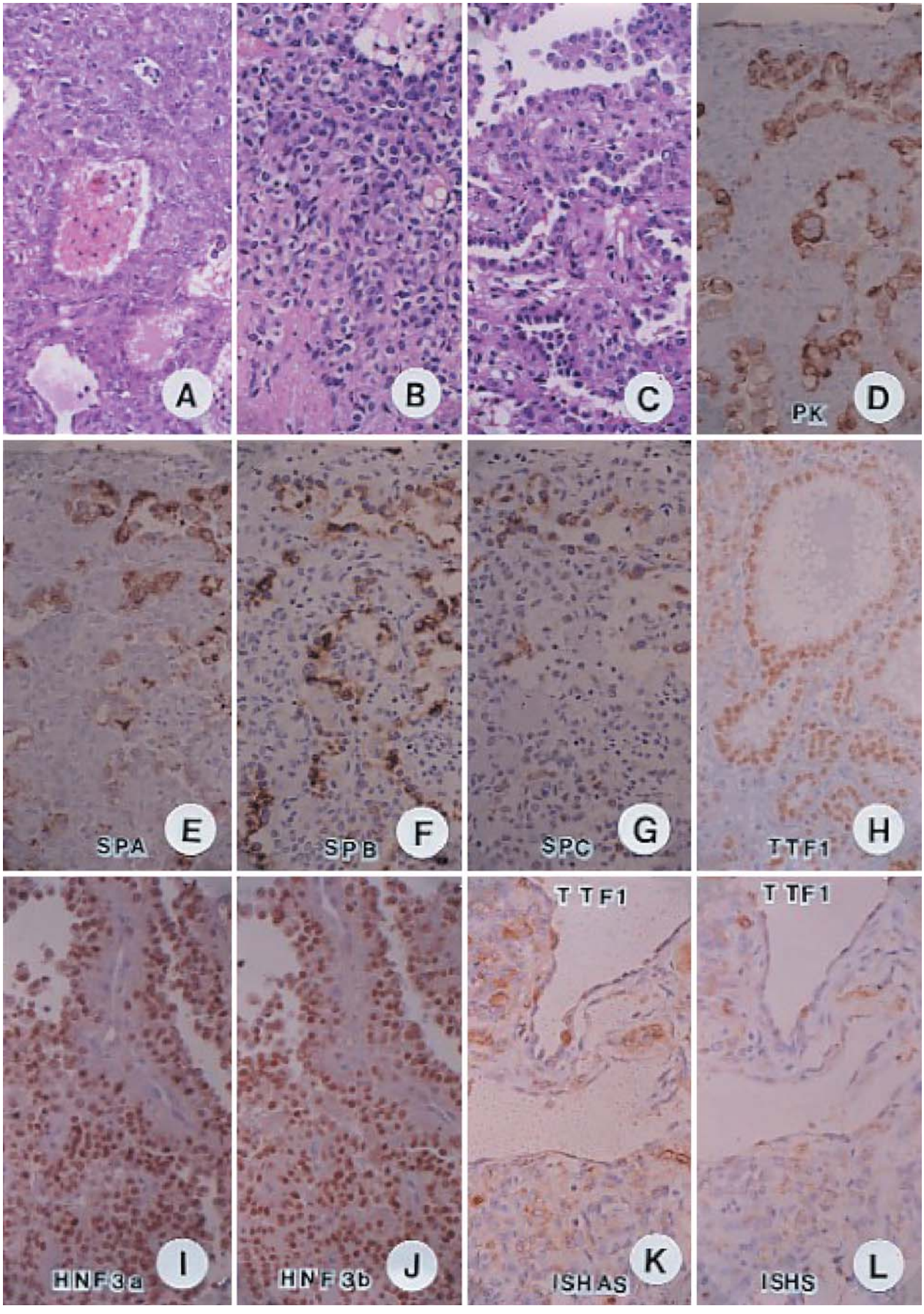
In the present series of tumor tissues, although seen in various combinations in single tumor tissue specimens, four major histological patterns emerged: (1) solid (Fig. 1A), (2) papillary (Fig. 1C), (3) sclerotic, and (4) hemorrhagic or hemangiomatous. Although some mixture of patterns was usually seen, many of the specimens had commonly both sclerotic and solid patterns (Table 1, Fig. 1A, B, C). In all histological patterns, the epithelioid round tumor cells were uniform and bland-appearing, with round-to-oval nuclei, distinct cytoplasmic borders, and fine chromatin with inconspicuous nucleoli. Cells lining the surface of the papillary structures were cuboid or large, with a voluminous eosinophilic cytoplasm and prominent nuclei (Fig. 1A, B, C). The papillary structures contained epithelioid tumor cells within the cores and had a prominent cuboidal epithelial lining along the surface. Tumor cells with a clear cytoplasm were also seen—stromal or pale cells (Fig. 1B, C). In the hemorrhagic or hemangiomatous pattern, collections of red blood cells within the lumina of these cystic spaces gave a hemorrhagic or vascular appearance (Fig. 1A). Cuboidal epithelial cells lined the cystic spaces that were present within the solid proliferation of the epithelioid tumor cells (Fig. 1A, B). Mast cells were numerous. Tumor cells lacked the organoid, trabecular, rosette, or spindle-cell histological patterns.

Immunohistochemistry

Keratins of AE1–AE3 (pankeratin) and CAM5.2 revealed a similar positive staining pattern (Fig. 1D) in the surface-lining cells and a small number of stromal-pale tumor cells. The EMA and SC revealed similar positive staining patterns (Fig. 1D). However, antibodies against other keratin-specific antibodies, 34bE12 and KL-1, did not stain positively. Some or many of the surface-lining cells and a very small number of stromal-pale tumor cells stained positively for the antibody against the surfactant apoproteins of SPA, (Fig. 1E), SPB (Fig. 1F), and SPC (Fig. 1G). The tumor cells failed to reveal any positive staining for CC10. A variable amount of the tumor cells stained positively for the antibody against vimentin. Basal lamina among the tumor tissue revealed positive staining for the antibody against laminin and type-IV collagen.

Immunostaining for c-erbB2, crystallin, CD15, CD10, Calretinin and BerEP4 revealed no positive stains in the tumor cells. The endothelial cells in the tumor tissue stained positive for the antibodies against CD34 and Factor VIII, but the tumor cells did not. Using Factor XIIIa, tumor cells were not stained, but some mixed short spindle-shaped possibly dendritic cells were positively stained. ER and PGR were occasionally positive in the nuclei of the tumor cells. Using the antibody against c-kit, only the intermingled mast cells were positively stained; the tumor cells were not. Using Kp-1(CD68), no positive stains were observed in the tumor cells, but intermingled macrophages stained positive. In all the tumor cells, both the surface lining and stromal-pale tumor cells, positive staining was not seen for the neuroendocrine cell markers of CD56, synaptophysin, and chromogranin A.

The nuclei of the tumor cells stained definitively positive for TTF-1 (Fig. 1H), as did many of the surface-lining tumor cells. Some stromal-pale tumor cells also stained positively (Fig. 1H). HNF-3 alpha and HNF-3 beta showed similarly positive signals in the nuclei of many of surface tumor cells and some stromal cells (Fig. 1I, J). Other transcriptional factors (GATA 6 and GLI 1) did not reveal definitive stains.


A
B
C
PK
D
SPA
E
SPB
F
SPC
G
TTF1
H
HNF3a
I
HNF3b
J
TTF1
ISHAS
K
TTF1
ISHS
L

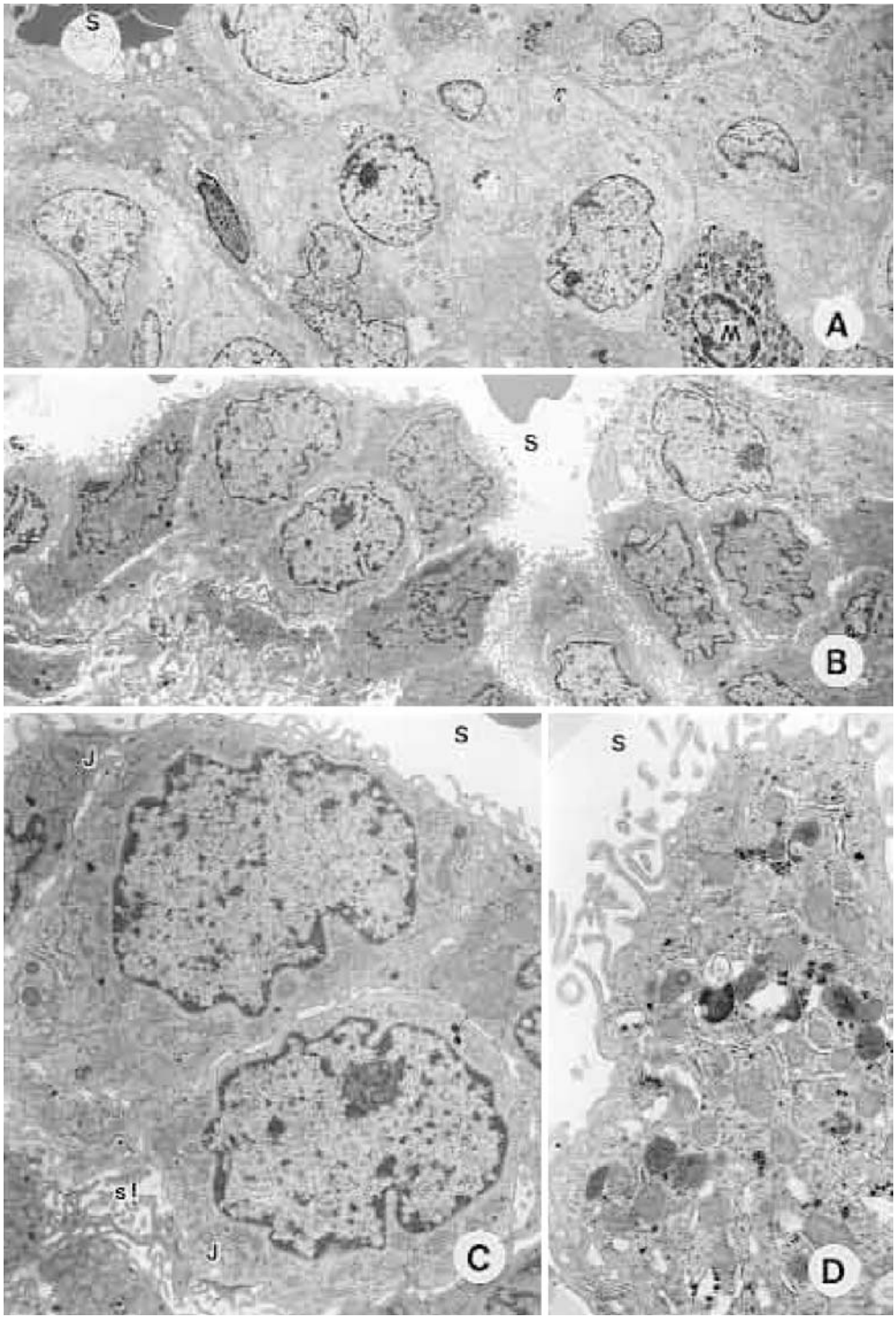


Fig. 2 Transmission electron photomicrographs of the tumor cells of pulmonary sclerosing hemangioma from case 1 and case 2. *S* apical surface of the differentiated tumor cells, *M* mast cell, *J* well-developed cell junctions of possibly tight junctions, *sl* small lumina formed between adjacent stromal tumor cells, *B* basal lamina around the tumor cells, *MY* myelinosome, *MV* multivesicular body. **A** Proliferation of stromal tumor cells and a mast cell. In the *upper left corner*, cystic space filled with red blood cells surrounded by surface-lining tumor cells with apical microvilli. Case 2. ×3500. **B** Papillary surface tumor cells. Case 1. ×3500. **C** Medium-power view of surface-lining tumor cells in the papillary pattern in **B** with apical microvilli and small granules. Case 1. ×8800. **D** High-power view of a surface=lining tumor cell in the papillary pattern with apical microvilli and small granules. Case 1. ×17,500

Fig. 1 Light photomicrographs of the tumor cells of pulmonary sclerosing hemangioma. **A–C** Hematoxylin and eosin stain. **A–L** ×190. **D–J** Immunostain. **K–L** In situ hybridization stain. **A** Erythrocytes in a lumen formed in the tumor tissue mimicking a vasculature. Case 2. **B** Sclerosing and solid pattern with many stromal-pale tumor cells. Case 4. Stain. **C** Solid with papillary histological pattern. Case 3. **D** *PK* pankeratin. Case 4. **E** *SPA* surfactant apoprotein A. Case 4. **F** *SPB* surfactant apoprotein B. Case 4. **G** *SPC* surfactant apoprotein C. Case 4. **H** *TTF-1* thyroid transcription factor 1. Immunostain. Case 2. **I** *HNF3a* HNF-3 alpha. Case 3. **J** *HNF3b* HNF-3 beta. Case 3. **K** Using TTF-1-specific antisense oligonucleotide probe. Case 1. **L** Using TTF-1-specific sense oligonucleotide probe. Case 1

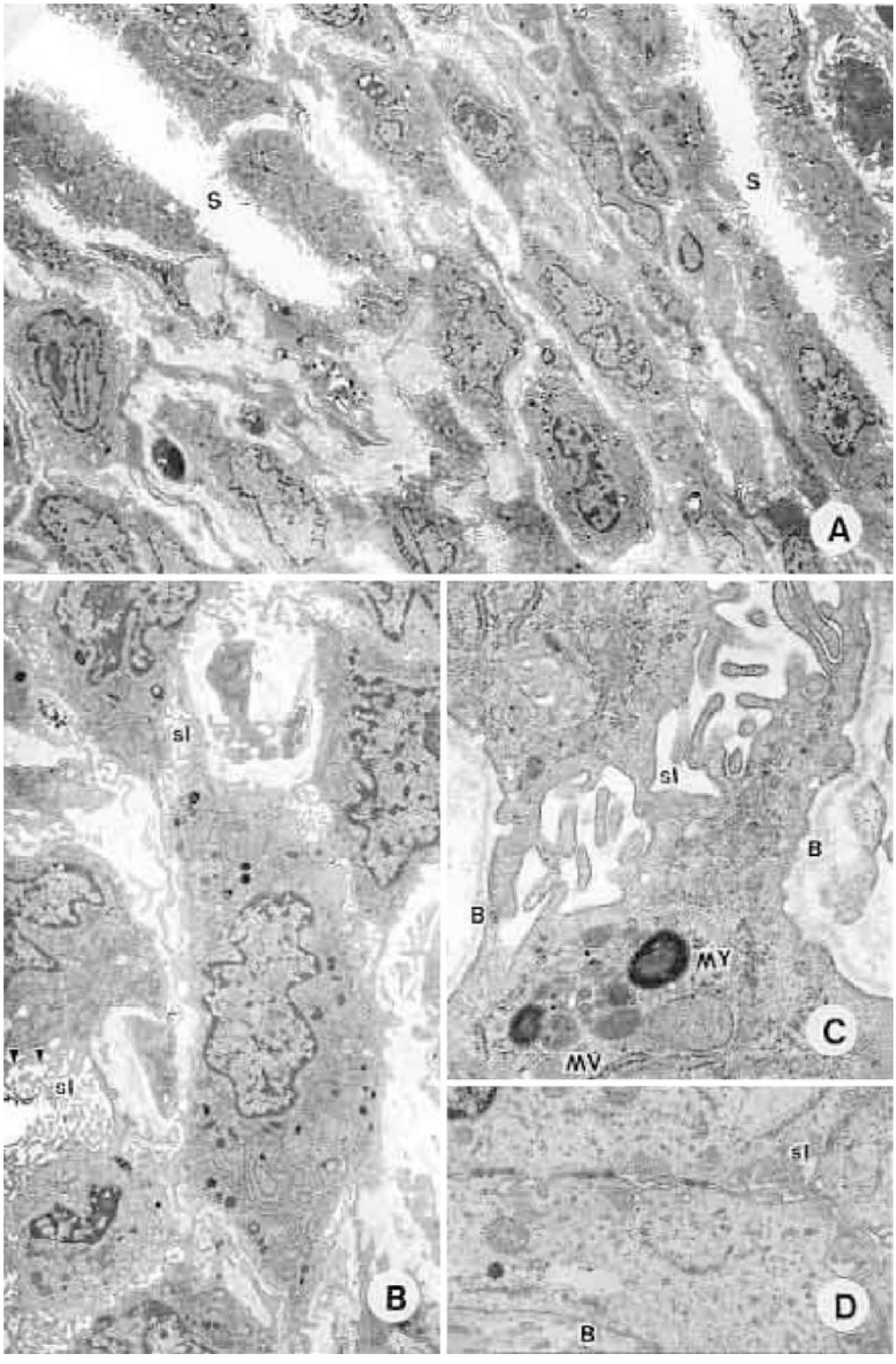


Fig. 3 **A** Surface lining tumor cells with apical differentiation. Stromal tumor cells embedded in the rich extracellular matrix containing fibrous collagen fibers, basal lamina, and a loose amorphous matrix. Case 1. ×3500. **B** Stromal tumor cells. *Arrowheads* indicating the small lumina with microvillous cytoplasm projections and a lipid-rich myelinoid body whose contents were extracted during processing of the tissue specimen. Case 1. ×7000. **C** High-power view of **C**. Case 1. ×35,000. **D** Between the adjacent tumor cells, primitive cellular junctions were seen. Case 2. ×17,500

In situ hybridization

In situ hybridization staining with the TTF-1-specific antisense oligonucleotide probe revealed many positive signals in the nuclei and also definitively in the cytoplasm of both some of the surface-lining cells and some of the stromal-pale tumor cells (Fig. 1K, L). The corresponding sense probe and GATA 6-specific antisense oligonucleotide probe revealed no definitive signal stains.

Electron microscopy

The electron microscopic characteristics of the tumor tissues showed similar histological subtypes as the char-

acteristics seen using light microscopy, and in a similar manner as using the light microscopy, namely hemangiomatous/hemorrhagic (Fig. 2A), papillary (Fig 2B, Fig 3A), solid (Fig. 2A, Fig. 3A, B), and sclerotic. The main constituents of non-tumorous cells were stromal fibroblasts, granulocytes, and mast cells (Fig. 2A).

Using electron microscopy, two types of tumor cells could be discerned—surface-lining cuboidal cells and more deeply positioned tumor cells in the stroma—mainly consistent with the pale cells seen using light microscopy. The surface tumor cells revealed microvillous cytoplasmic projections of the apical-cell membrane, lamellar inclusions similar to these seen in type-II pneumocytes, and apico-lateral cellular junctions facing the surface lumina in the tumor tissue (Fig. 2B, C). They showed the definitive apico-lateral polarity of cellular differentiation. In the apical region in particular, the observed characteristics included well-developed microvillous cytoplasmic folding and small granules of approximately around or over 300–500 nm in diameter, with high or medium electron-dense finely granular contents (Fig. 2D).

However, the other type of more deeply positioned tumor cells were embedded in a medium amount of extracellular matrix consisting of well-developed basal lamina around the tumor cells, a rich amorphous loose extracellular matrix, and some fibrous periodic collagenous fibers (Fig. 3A, B, C). Primitive cellular junctions were formed between the adjacent tumor cells of this type (Fig. 3B, D) and also small lumina, into which projected microvillous cytoplasmic foldings (Fig. 3B, C, D). Facing the small lumen, multivesicular bodies, myelinosomes, and small granules of approximately the same diameter as the high- or medium-electron-dense finely granular contents were formed, in a similar manner to the apical differentiation of the surface-lining cells. Occasionally in the small lumina, lipid-rich myelinoid bodies could be seen, the contents of which were extracted during the processing of the tissue specimens (Fig. 3B).

Although small intracytoplasmic granules of approximately 300–500 nm in diameter could be seen scattered in both cell types, the electron microscopy failed to reveal in either of the tumor cell types the definitive cored or empty smaller granules with neuroendocrine features at the smaller diameter of 100–300 nm. Although both the surface and deeper types of tumor cells could be discerned under electron microscopy, the latter showed various transitional features toward the former. They lost the definitive apico-lateral differentiation seen in the former and showed a somewhat distorted, abortive, or premature surface differentiation between the adjacent tumor cells forming the small lumina (Fig. 2C, Fig. 3B, C, D). No mucous-type or large apical intracytoplasmic granules of the Clara-cell type were seen.

Discussion

The histopathological diagnosis of PSH might be confused with other types of pulmonary tumors, such as papillary adenoma, well-differentiated adenocarcinoma, or even carcinoid tumors [3, 5]. However, the histopathological diagnosis could be confirmed by the presence of the mixture of the four major histological patterns (solid, papillary, sclerotic, and hemorrhagic or hemangiomatous) and also the distinctive cellular components (surface-lining cuboidal and stromal-pale tumor cells) within in the single tumor [3, 5]. PSH is usually considered a benign tumor because of its slow-growing and self-limiting characteristics. On rare occasions, PSH may be multiple [3, 5], as similar to the present case 3. There are some cases in which metastases to regional lymph nodes are observed. These results suggest that the nature of the tumor appears to exist somewhere between benign and malignant. The examples of PSH in the present study with multiple foci differed from papillary carcinomas by the presence of the distinct stromal round cells within the papillary stalks as well as the characteristic solid, hemorrhagic/hemangiomatous, or sclerotic patterns. In a similar manner, papillary adenoma or other lung tumors are also interpreted as related disease entities, but can be differentiated from PSH [3, 5].

Two types of tumor cells in PSH were discerned in the present study as had been shown in previous studies. Most of the recent immunohistochemical and ultrastructural data seen in the literature support the concept that PSH is an epithelial neoplasm derived from type-II pneumocytes and/or bronchiolar epithelial (Clara) cells [2, 3, 5, 6, 15, 22]. PSH has been reported to stain for a variety of antibodies against epithelial markers, including surfactant apoprotein, cytokeratin, EMA, CEA, and Clara-cell antigen (CC10) [3]. The surface cells lining the papillary structures tended to stain well for these epithelial antibodies, while the epithelioid cells of the solid areas did not [3]. In the present study, similar results could be obtained, but with minor variations in the immunohistochemical, ER, PGR, and even Clara-cell antigen (CC10) results.

Xu et al. [20] reported staining for neuroendocrine markers in the stromal-pale tumor cells of PSH and simultaneously demonstrated ultrastructurally neurosecretory granules; however, in the present study, all tumor cells, both the surface-lining cells and stromal-pale tumor cells, were not stained by the neuroendocrine cell markers of CD56, synaptophysin, and chromogranin A. In the present study, the ultrastructural findings revealed that the tumor cells did not have the definitive cored or empty 100–300 nm diameter granules associated with neuroendocrine features [7, 19, 20]. The explanation for the lack of neuroendocrine differentiation in the present study was not evident, but the present study does not substantiate their hypothesis.

In the present study, the transcriptional factor of TTF-1 was definitively positive as shown in the previous literature [2, 6]. Compared with the in situ hybridization study of TTF-1, there was a discrepancy between the extensive staining for TTF-I protein and the mRNA. There was not only nuclear staining, but also the definitive stains of mRNA in the cytoplasm. This might be related to the fact that mRNA stains generally give endoplasmic reticulum staining in the cytoplasm. HNF-3 alpha and HNF-3 beta

showed similarly positive signals in the nuclei of many of the surface and some of the stromal tumor cells. Many of the surface-lining tumor cells were immunohistochemically positively stained by the many epithelial markers, the SC (secretory component), and surfactant apoproteins, actually mimicking type-II pneumocytes. Compared with the distribution of to these lung epithelial-cell markers, the transcriptional factors (TTF-1, HNF-3 alpha, HNF-3 beta, GATA 6, and GLI 1) were very interesting [4, 9, 11, 14, 18, 21]. This study is the first immunohistochemical demonstration of HNF-3 alpha and HNF-3 beta among tumor cells in PSH, which could be interpreted as showing that the tumor cells in PSH reveal a similar or somewhat distorted differentiation toward the normal lung epithelial cells (most likely type-II pneumocytes) under the regulation of these lineage-specific transcription factors [4, 9, 11, 14, 18, 21].

In the ultrastructural study, both types of tumor cells in PSH frequently showed cellular junctions, small granules, occasional multi-lamellar bodies, and multi-vesicular bodies in a similar manner to the description of type-II pneumocytes in the literature [5, 7, 17, 19]. In the present study, part of those structures could be seen at the surface of some tumor cells, but the low frequency and small scale of their appearance would reflect the state of cellular differentiation. Ultrastructurally, the surface-lining tumor cells could be interpreted as more differentiated or revealing the correct morphological polarity with apicolateral differentiation when compared with the stromal tumor cells.

In conclusion, two types of tumor cells in PSH, the surface-lining cuboidal cells and the more deeply positioned stromal cells, showed variations in their characteristics. To some extent, both cell types had characteristics common to the differentiation of lung-epithelial cells, possibly type-II pneumocyte [2, 3, 5, 6, 15, 22]. In the present study, the surface-lining cells and the interstitial cells of sclerosing hemangiomas stained somehow differently for some antigens and showed some different ultrastructures. The single clonal nature of these tumor cells has been confirmed by a recent genetic study [16] and concluded that both cells are part of the tumor [16]. While, on the basis of present study, another or a new interpretation that might be more plausible is that the surface cells represent entrapped non-neoplastic alveolar epithelium, while the interstitial cells are true tumor cells. Using the distribution of different transcription factors specific for type-II cell lining (TTF-I, HNF-3 alpha, HNF-3 beta), this study could clearly show the different levels of differentiation of these two cell types, in good agreement with ultrastructural demonstration of specialized exocrine epithelial structures in these two kinds of type-II pneumonocytes in PSH. It might be summarized that the original part of this study is the more detailed description of the two cell types: both are in the type-II pneumocytes lineage. The stromal type is less differentiated toward an exocrine function. That is in accordance with the poor expression of surfactant proteins in this cell type, as similarly shown in the expression of TTF-1 and first description of HNF-3s in PSH. Since no definitive difference exists between normal type-II pneumonocytes and the lining cells of PSH, the author hereby would propose that the surface cells represent entrapped non-neoplastic type-II pneumonocytes, while interstitial cells are the real tumor cells. Namely, PSH is a composition of two types of differentiated type-II pneumonocytes, the real tumoral population is that of undifferentiated "stromal type-II cells." The surface-lining cells are fully differentiated type-II pneumonocytes. Subsequently, PSH might be assumed as a proliferation of rather fetal type-II pneumonocytes (pneumocytoma? being pneumoblastoma?). This possibility should be more precisely studied in the future. The methods used for the analysis in this study, especially of studying the expression of lineage-specific transcription factors, may well be applicable to the detection of the differentiated stage and biological behavior of cell types in other lung tumors or cancers and may also be applicable to the analysis of the physiological function of transcription factors [12, 21].

Acknowledgements The author would like to acknowledge the technical assistance of T. Nagai and K. Fujita with the electron microscopy, M. Furihata, T. Kohno, Y. Yamamoto, K. Nagawatari, A. Furusawa, and T. Oyama for the light microscopic histology and immunohistochemistry, Dr. K. Kitagawa for the in situ hybridization technique, and also the valuable discussion and help offered by Drs. H. Orikasa, H. Kayano, J. Shiraishi, Y. Mori, and H. Okita, T. Aoki, Y. Kishida, and K. Yakumaru.

References

1. Carstens P, Schrodt GR (1974) Ultrastructure of sclerosing hemangioma. Am J Pathol 77:377–386
2. Chan A, Chan JKC (2000) Pulmonary sclerosing hemangioma consistently express thyroid transcription factor-1 (TTF-1). A new clue to its histogenesis. Am J Surg Pathol 24:1531–1536
3. Colby T, Koss MN, Travis WD (1995) Atlas of tumor pathology. 21 Tumors of the lower respiratory tract. Armed Forces Institute of Pathology, Washington
4. Costa R, Kalinichenko VV, Lim L (2001) Transcription factors in mouse lung development and function. Am J Physiol Lung Cell Mol Physiol 280:L823–L838
5. Dail D, Hammar SP (1993) Pulmonary pathology. Springer, Berlin Heidelberg New York
6. Devouassoux-Shisheboran M, Hayashi T, Linnoila RI et al (2000) A clinicopathologic study of 100 cases of pulmonary sclerosing hemangioma with immunohistochemical studies. TTF-1 is expressed in both round and surface cells, suggesting an origin from primitive respiratory epithelium. Am J Surg Pathol 24:906–916
7. Ghadially F (1997) Ultrastructural pathology of the cell and matrix. Butterworth-Heinemann, Boston
8. Haas J, Unnis EJ, Totten RS (1972) Ultrastructure of a sclerosing hemangioma of the lung. Cancer 30:1092–1106
9. Ikeda K, Shaw-White JR, Wert SE et al (1996) Hepatocyte nuclear factor 3 activates transcription of thyroid transcription factor 1 in respiratory epithelial cells. Mol Cell Biol 16:3626–3636
10. Katzenstein A-L, Weise DL, Fulling K et al (1983) So-called sclerosing hemangioma of the lung: evidence for mesothelial origin. Am J Surg Pathol 7:3–14
11. Keijzer R, van Tuly M, Meijers C et al (2001) The transcription factor GATA6 is essential for branching morphogenesis and

epithelial cell differentiation during fetal pulmonary development. Development 128:503–511
12. Kodama H, Hirotani T, Suzuki Y et al (2002) Cardiomyogenic differentiation in cardiac myxoma expressing lineage-specific transcription factors. Am J Pathol 161:381–389
13. Liebow A, Hubbell B (1956) Sclerosing hemangioma (histiocytoma, xanthoma) of the lung. Cancer 9:53–75
14. Liu C, Glasser SW, Wan H et al (2002) GATA-6 and thyroid transcription factor-1 directly interact and regulate surfactant protein-C gene expression. J Biol Chem 277:4519–4525
15. Nagata N, Dairaku M, Ishida T et al (1985) Sclerosing hemangioma of the lung: immunohistochemical characterization of its origin as related to surfactant apoprotein. Cancer 55:116–123
16. Niho S, Suzuki K, Yokose T, et al (1998) Monoclonality of both pale cells and cuboidal cells of sclerosing hemangioma of the lung. Am J Pathol 152:1065–1069
17. Ochs M, Johnen G, Muller K-M et al (2002) Intracellular and intraalveolar localization of surfactant protein A (SP-A) in the parenchymal region of the human lung. Am J Respir Cell Biol 26:91–98
18. Warburton D, Schwarz M, Tefft D et al (2000) The molecular basis of lung morphogenesis. Mech Dev 92:55–81
19. Weiss L (1983) Histology. Cell and Tissue Biology. Macmillan Press, London
20. Xu H-M, Li W-H, Hou N et al (1997) Neuroendocrine differentiation in 32 cases of so-called sclerosing hemangioma of the lung: identified by immunohistochemical and ultrastructural study. Am J Surg Pathol 21:1013–1022
21. Yamazaki K (2003) Pulmonary well-differentiated fetal adenocarcinoma expressing lineage-specific transcription factors (TTF-1 and GATA-6) to respiratory epithelial differentiation: an immunohistochemical and ultrastructural study. Virchows Arch 442:393–399
22. Yousem S, Wick MR, Singh G et al (1988) So-called sclerosing hemangioma of lung. An immunohistochemical study supporting a respiratory epithelial origin. Am J Surg Pathol 12: 582–590

Virchows Arch (2004) 445:54–62
DOI 10.1007/s00428-004-1015-3

ORIGINAL ARTICLE

Shuji Misumi · Ken-ichi Iyama · Yumi Honda · Takao Kitano · Yoshikazu Sado · Yoshifumi Ninomiya · Masanori Shinohara

Differential expression of basement membrane type-IV collagen α1, α2, α5 and α6 chains among the histological subtypes of adenoid cystic carcinoma

Received: 30 October 2003 / Accepted: 17 March 2004 / Published online: 5 May 2004
© Springer-Verlag 2004

Abstract Six distinct α(IV) chains in the basement membrane (BM) of adenoid cystic carcinoma (ACC) of the salivary gland were immunohistochemically examined by anti-α(IV) chain-specific antibodies, and their expressions were compared with the histological subtypes and the expressions of cytokeratin 19 (CK19), cytokeratin 14 (CK14) and α-smooth muscle actin (α-SMA) and Ki-67. In the BM of normal salivary ducts, α1(IV), α2(IV), α5(IV) and α6(IV) chains were continuously stained, but α3(IV) and α4(IV) chains were negative. In the tubular and cribriform subtypes of ACC, tubules with continuous staining of α5(IV) and α6(IV) chains showed the biphasic-staining pattern among the expressions of CK19, CK14 and α-SMA. However, in cancer-cell nests with discontinuous or negative staining of α5(IV) and α6(IV) chains, the biphasic pattern was ambiguous. In the solid subtype, the staining of α1(IV) and α2(IV) chains was discontinuous, the staining of α5(IV) and α6(IV) chains was negative and the biphasic-staining pattern was unclear. The mitotic activity of cancer cells analyzed by the Ki-67 labeling index was significantly related to the expression of α5(IV) and α6(IV) chains in the cribriform subtype. These results suggest that BM irregularity with the differential expression of α(IV) chains in ACC closely relates to cell proliferation, cell differentiation and histological structure.

Keywords Adenoid cystic carcinoma · Basement membrane · Type-IV collagen · Cytokeratin · Ki-67

S. Misumi · K.-i. Iyama (✉) · Y. Honda
Department of Surgical Pathology,
Kumamoto University School of Medicine,
1-1-1 Honjo, 860-8556 Kumamoto, Japan
e-mail: iyama@kaiju.medic.kumamoto-u.ac.jp
Tel.: +81-96-3735795
Fax: +81-96-3735795

S. Misumi · M. Shinohara
Department of Oral and Maxillofacial Surgery,
Kumamoto University School of Medicine,
1-1-1 Honjo, 860-8556 Kumamoto, Japan

T. Kitano
Department of Public Health,
Kumamoto University School of Medicine,
1-1-1 Honjo, 860-8556 Kumamoto, Japan

Y. Sado
Division of Immunology,
Shigei Medical Research Institute,
Yamada, 701-0202 Okayama, Japan

Y. Ninomiya
Department of Molecular Biology and Biochemistry,
Okayama University Medical School,
2-5-1 Shikatamachi, 700-0082 Okayama, Japan

Introduction

Adenoid cystic carcinoma (ACC) is a rather rare malignant neoplasm arising from the salivary glands. Although the growth rate of the tumor is slow, the rate of invasiveness into adjacent tissue is very high. It has been reported that ACC cells often invade the tissue far from the primary site. Three well-known histological subtypes of ACC are the tubular, cribriform and solid subtypes. These histological subtypes are often confirmed simultaneously in the same nest of ACC [4].

In addition to the histological subtype, one of the diagnostic features of ACC is the eosinophilic basement membrane (BM)-like material produced by the cancer-cell nests [4]. The BM separates epithelial cells from the underlying stroma, and BM plays important roles both in biological functions, such as cell adhesion, cell differentiation and tissue repair, and in pathological events, such as cancer-cell invasion and metastasis [9].

Type-IV collagen is known to be a major component of the BM and to have six genetically different α(IV) chains: α1(IV)–α6(IV). Immunohistochemical studies have shown that α3(IV)–α6(IV) chains are localized in BMs of organs in a tissue-specific manner. For example, α3(IV)/α4(IV)/α5(IV) chains distribute in the BM of glomerulus of the kidney and in the BM of the alveoli of the lung [13], while α5(IV) and α6(IV) chains localize in

the BM of epidermis [22], smooth muscle cells [21], mammary gland [15] and epithelium of the alimentary tract [6]. Recently, differential expressions of type-IV collagen α(IV) chain have been reported in neoplasms (breast cancer [15], basal cell carcinoma [22], colorectal carcinoma [6], bronchioloalveolar carcinoma [13], prostate carcinoma [3], renal-cell carcinoma [10] and odontogenic tumors [12, 13]). However, the expression of α1(IV)–α6(IV) chains of the normal salivary gland and ACC have not been analyzed.

In this study, we examined the immunohistochemical localization of type-IV collagen α1(IV)–α6(IV) chains, cytokeratin 19 (CK19), cytokeratin 14 (CK14), α-smooth muscle actin (α-SMA) and Ki-67 in normal salivary gland and ACC. In addition, the relationship between these immunohistochemical results and the three histological subtypes of ACC was discussed.

Materials and methods

Tissue materials

The tissue materials of 20 cases of ACC were obtained using surgical resection after informed consent for histopathological studies and were examined at the Department of Surgical Pathology, Kumamoto University School of Medicine (between 1990 and 2002), as summarized in Table 1.

Resected tissues were fixed immediately in 15% buffered formalin (pH 7.0) and embedded in paraffin, and 4-μm-thick serial sections were prepared. For histopathological diagnosis, one of these serial sections was stained with hematoxylin-eosin (H&E). The others were used for immunohistochemistry. Normal salivary glands included in ten cases of ACC (three parotoid, two submandibular and five minor salivary glands) were also examined. When there were two or three histological subtypes in an ACC specimen, we investigated each subtype in 36 sample numbers, as summarized in Table 1 and Table 3, for immunohistochemistry.

Antibodies

The monoclonal antibodies to the six different α chains of human type-IV collagen used in this study are shown in Table 2. Antibodies against six different α(IV) chains, recognizing the sequences of each C-terminal non-collagenous (NC1) domain (H11, H21, H31, H43, H63) or helical domain (H53), were produced using the rat lymph-node method [20]. CK19 (Dako, Glostrup, Denmark),

Table 1 Clinical and histological features of adenoid cystic carcinoma

Case no.	Age (years)	Gender	Site	Histological subtype (Sample no. of Table 3)		
				Tubular	Cribriform	Solid
1	63	Female	Gum	◯(9)	×	×
2	70	Male	Parotid gland	◯(4)	◯(13)	×
3	35	Female	Abdominal muscle (metastasis)	◯(5)	◯(22)	×
4	56	Male	Lymph node (metastasis)	◯(1, 8)	◯(10, 24)	×
5	70	Female	Palatine gland	◯(2, 7)	◯(12, 25)	×
6	73	Male	Paranasal cavity	◯(3, 6)	◯(11, 16)	×
7	71	Male	Gum	×	◯(17)	×
8	64	Female	Palatine gland	×	◯(19)	×
9	53	Female	Oral mucosa	×	◯(23)	×
10	77	Female	External auditory duct	×	◯(26)	×
11	43	Female	Nasal cavity	×	◯(28)	×
12	42	Male	Palatine gland	×	◯(30)	×
13	57	Male	Submandibular gland	×	◯(14, 21)	×
14	66	Male	Paranasal cavity	×	◯(15, 31)	×
15	60	Female	Submandibular gland	×	◯(18, 29)	×
16	47	Female	Oral mucosa	×	◯(20)	◯(33)
17	51	Female	Palatine gland	×	◯(27)	◯(32)
18	52	Male	Lung (metastasis)	×	×	◯(34)
19	62	Male	Lymph node (metastasis)	×	×	◯(35)
20	46	Female	Brain (metastasis)	×	×	◯(36)

Table 2 Monoclonal antibodies used in this study. *AC* autoclave heating, *HA* hyaluronidase

Specificity	Clone	Epitope	Dilution	Source	Pretreatment
α1(IV)NC1	H11	KKPTPSTL	1:300	Rat IgG	AC+HA
α2(IV)NC1	H21	DTLKAGLIR	1:150	Rat IgG	AC+HA
α3(IV)NC1	H31	IPSTVKA	1:200	Rat IgG	AC+HA
α4(IV)NC1	H43	PAPDTLKE	1:7	Rat IgG	AC+HA
α5(IV)helix	H53	IDVEF	1:200	Rat IgG	AC+HA
α6(IV)NC1	H63	GELP	1:50	Rat IgG	AC+HA
CK14	LL002		1:200	Mouse IgG	AC
CK19	RCK108		1:100	Mouse IgG	Proteinase K
α-SMA	1A4		1:250	Mouse IgG	None
Ki-67	MIB-1		1:50	Mouse IgG	AC

Table 3 Immunohistochemical findings of ACC and Ki-67 L.I. + positive with continuous linear staining pattern, ± discontinuously positive staining pattern, – negative staining pattern, *P* positive in luminal cells, *N* negative staining *L* positive staining with lining the tumor nests, *D* disarrayed staining pattern (include negative staining pattern)

Sample no.	Histological subtype	α1(IV) and α2(IV)	α5(IV) and α6(IV)	CK19	CK14	α-SMA	Ki-67 L.I.
1	Tubular	+	+	P	L	L	1.80
2	Tubular	+	+	P	L	L	2.43
3	Tubular	+	+	P	L	L	2.94
4	Tubular	+	+	P	L	D	1.67
5	Tubular	+	±	P	L	L	4.24
6	Tubular	+	±	P	L	L	4.80
7	Tubular	+	±	P	L	D	6.21
8	Tubular	±	-	P	L	L	6.66
9	Tubular	±	-	N	D	L	6.01
10	Cribriform	+	+	P	L	L	3.41
11	Cribriform	+	+	P	L	L	6.40
12	Cribriform	+	+	P	L	D	7.11
13	Cribriform	+	+	P	D	L	3.39
14	Cribriform	+	+	P	D	D	3.62
15	Cribriform	+	+	N	D	D	2.98
16	Cribriform	+	±	P	L	L	11.23
17	Cribriform	+	±	P	D	L	11.98
18	Cribriform	+	±	P	D	L	7.56
19	Cribriform	+	±	P	D	D	7.76
20	Cribriform	+	±	N	D	D	7.40
21	Cribriform	+	±	N	D	D	8.85
22	Cribriform	+	-	P	L	L	12.54
23	Cribriform	+	-	P	D	L	12.27
24	Cribriform	+	-	P	D	D	14.32
25	Cribriform	+	-	P	D	D	15.88
26	Cribriform	+	-	N	L	L	6.03
27	Cribriform	+	-	N	D	L	7.03
28	Cribriform	+	–	N	D	L	6.16
29	Cribriform	±	–	N	D	L	7.56
30	Cribriform	±	–	N	D	D	12.04
31	Cribriform	±	–	N	D	D	14.33
32	Solid	±	–	N	D	D	16.35
33	Solid	±	–	N	D	D	14.98
34	Solid	±	–	N	D	D	21.37
35	Solid	–	–	N	D	D	15.67
36	Solid	–	–	N	D	D	27.71

CK14 (Biomeda, Foster City, CA, USA), α-SMA (Dako, Glostrup, Denmark) and Ki-67 (Dako, Glostrup, Denmark) are commercially available.

Immunohistochemistry

For immunostaining of α1(IV)–α6(IV) chains, deparaffinized sections were pretreated for antigen retrieval using autoclave heating (132°C, 303 kPa) in 10 mmol/l citrate buffer (pH 3.6) for 5 min. After autoclave heating, the sections were pretreated with hyaluronidase (Sigma, St. Louis, MO, USA) [1 mg/ml in phosphate-buffered saline (PBS), for 20 min at 37°C]. These sections were blocked for endogenous peroxidase activity with 3% H_2O_2 in methanol for 60 min and then washed in PBS. Thereafter, sections were immersed in 5% normal rabbit serum in PBS for 30 min, covered with primary rat monoclonal antibodies and incubated overnight at 4°C. Immunoreactions were performed using a Vectastain peroxidase aviditin-biotin peroxidase complex (ABC) kit (Vector Laboratories, Burlingame, CA, USA). The antigenic sites were demonstrated by reacting the sections with a mixture of 0.05% 3, 3′-diaminobenzidine tetrahydrochloride (Dojin Chemicals, Tokyo, Japan) in 0.05 mol/l Tris-HCl buffer, pH 7.6, containing 0.01% H_2O_2 for 7 min. The nuclei were stained with hematoxylin.

For immunostaining of CK19, deparaffinized sections were pretreated with proteinase K (Dako, Glostrup, Denmark) for 5 min at room temperature. For immunostaining of CK14 and Ki-67, deparaffinized sections were pretreated for antigen retrieval using autoclave heating (132°C, 303 kPa) in 10 mmol/l citrate buffer (pH 6.0) for 5 min. For immunostaining of α-SMA, no pretreatment was done. Immunodetection of immunostaining of CK19, CK14, α-SMA and Ki-67 were performed according to the same protocol for α(IV) chains.

The optimal dilution of each primary antibody is shown in Table 2. Negative controls for immunostaining were performed by substituting the primary antibodies with PBS or non-immune rat or mouse IgG.

Evaluation of Ki-67 and statistical analysis

The Ki-67 immunostaining result was evaluated by counting more than 200 tumor cells at ×200 magnifications in each of five representative areas, and by calculating the percentage of positive cells with nuclear staining as the labeling index (L.I.).

Statistical analyses were performed using two-way analysis of variance (ANOVA) and Stat View 4.0(J) software packages (Abicus Concepts Inc, Berkeley, CA, USA).

Results

Normal salivary gland

In the BM of normal salivary duct, including intercalated, striated and excretory ducts, α(IV), α2(IV), α5(IV) and

α6(IV) chains were stained continuously (Fig. 1a, b, c, d). In the BM of acinus, α1(IV) and α2(IV) chains were stained continuously (Fig. 1a, b). However, α5(IV) and α6(IV) chains were stained discontinuously (Fig. 1c, d). There was no expression of α3(IV) and α4(IV) chains in the BM of both salivary duct and acinus (data not shown). Both luminal and basal cells of salivary ducts mainly expressed CK19 in their cytoplasm (Fig. 1e). CK14 was positive in the myoepithelial cells of acini and intercalated ducts and in the basal cells of striated and excretory ducts (Fig. 1e). α-SMA-positive cells were confirmed as myoepithelial cells in acini and intercalated ducts (data not shown).

Adenoid cystic carcinoma

Tubular subtype

Six cases with the tubular subtype of ACC were examined (Table 1). Two immunostaining patterns of α(IV) chains were confirmed in the BM of the tumor nests. One was the continuous-staining pattern of α1(IV), α2(IV), α5(IV) and α6(IV) chains (Fig. 1f, g, h, i). Another was the mixed pattern with the continuous or discontinuous staining of α1(IV) and α2(IV) chains and the discontinuous or negative staining of α5(IV) and α6(IV)chains (Fig. 1k, l, m, n). The former was observed in four samples (sample nos. 1–4 in Table 3) and the latter in five samples (sample nos. 5–9 in Table 3). There was no staining of α3(IV) and α4(IV) chains in either group (data not shown).

In the area where all of α1(IV), α2(IV), α5(IV) and α6(IV) chains were expressed continuously in the BM of the tumor nests, CK19 was specifically expressed in the luminal epithelium, and CK14 was expressed in outer epithelium. The biphasic-staining pattern between CK19 and CK14 expression was confirmed (Fig. 1j). A few α-SMA-positive cells were located in the outer layer of the tubules (data not shown). In contrast, in the tumor nests with the BM of the discontinuous staining of α1(IV) and α2(IV) chains and the negative staining of α5(IV) and α6(IV) chains, CK19 was negative, and CK14 was intensely expressed in the inner epithelium and weakly expressed in the outer epithelium of the ductal structure. No evidence of the biphasic-staining pattern between CK19 and CK14 was observed (Fig. 1o). α-SMA-positive cells were located in the outer area of tubules and in the outer boundary of tumor islands (data not shown).

Cribriform subtype

We examined 16 cases with the cribriform subtype (Table 1). Two immunostaining patterns of α(IV) chains were observed. Six samples (sample nos. 10–15 in Table 3) with continuous staining of all α1(IV), α2(IV), α5(IV) and α6(IV) chains in the BM of tumor nests were included. The number of samples with continuous or discontinuous staining of α1(IV) and α2(IV) chains and discontinuous or negative staining of α5(IV) and α6(IV) chains was sixteen (sample nos. 16–31 in Table 3). There was no staining of α3(IV) and α4(IV) chains in either group (data not shown).

In the cribriform subtype with continuous staining of α1(IV), α2(IV), α5(IV) and α6(IV) chains, CK19-positive cells were frequently confined in the tumor nests as the true luminal epithelium (Fig. 2a, b, c, d, e). And in these samples, CK14-positive cells were partly located in the outer layer of the tumor nests and in the cells lining pseudocysts (Fig. 2e). α-SMA-positive cells surrounded the tumor nests and localized partially in pseudocysts (data not shown). The inside surface of the pseudocyst was linearly positive for α1(IV), α2(IV), α5(IV) and α6(IV) chains, while the luminal surface was negative for all of them (Fig. 2a, b, c, d). Meanwhile, in the areas of the continuous staining of α1(IV), α2(IV) chains and discontinuous or negative staining for α5(IV) and α6(IV) chains, CK19 expression tended to disappear, and CK14 was randomly expressed in the tumor nests (Fig. 2f, g, h, i, j). α-SMA-positive cells tended to disappear or be distributed randomly in the tumor nests (data not shown).

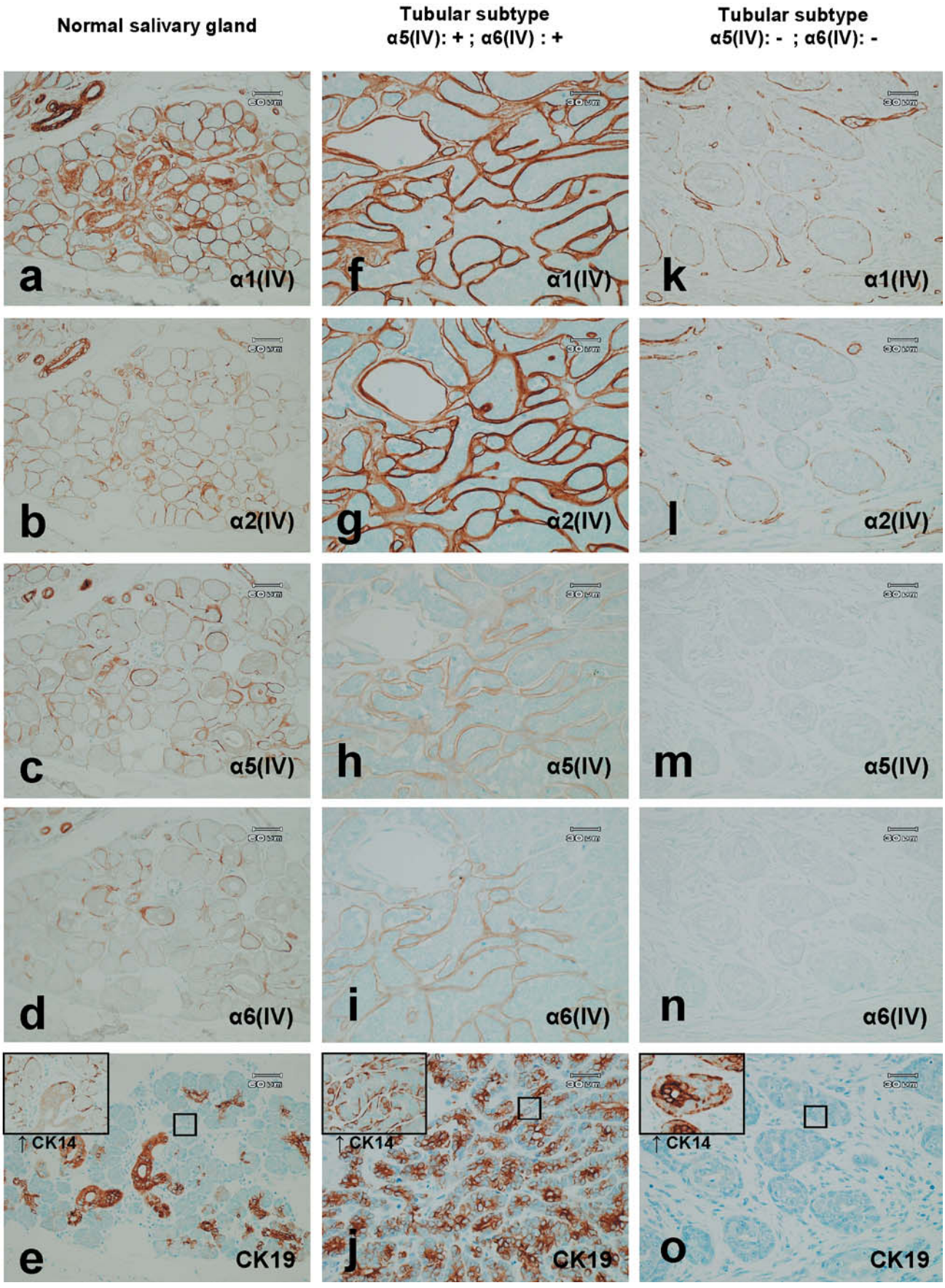
Solid subtype

Solid subtype was seen in five cases (Table 1). α1(IV) and α2(IV) chains were expressed discontinuously (sample nos. 32–34 in Table 3) or negatively (sample nos. 35, 36 in Table 3) in the BM of tumor nests, and the negative staining of α5(IV) and α6(IV) chains was confirmed in all samples. CK19 expression was negative in the tumor nests, while CK14 was randomly expressed in all cases of solid subtype (Fig. 2k, l, m, n, o). α-SMA-positive cells were also distributed randomly (data not shown). The biphasic-staining pattern between CK19 and CK14 was not observed in all samples (Table 3).

Ki-67 immunostaining and labeling index

Ki-67 L.I. in the tubular subtype with continuous staining of α1(IV), α2(IV), α5(IV) and α6(IV) chains was 2.21±0.59% (mean±standard deviation), and Ki-67 L.I. in the tubular subtype with the continuous or discontinuous staining of α1(IV), α2(IV) chains and the discontinuous or negative staining of α5(IV) and α6(IV) chains was 5.58±1.02%. In the same way, Ki-67 L.I. in the cribriform subtype with continuous staining of α1(IV), α2(IV), α5(IV) and α6(IV) chains was 4.49±1.78%, and the cribriform subtype with continuous or discontinuous staining of α1(IV), α2(IV) chains and discontinuous or negative staining of α5(IV) and α6(IV) chains was 10.18±3.24%. In the solid subtype, Ki-67 L.I. was 19.22±5.37%. As the solid subtype showed no expression of α5(IV) and α6(IV) chains in the tumor nests, statistical analysis of the solid subtype was excluded.

Two-way ANOVA showed that both the histological subtype (tubular and cribriform subtype) and the expres-


Normal salivary gland
Tubular subtype
α5(IV): + ; α6(IV) : +
Tubular subtype
α5(IV): - ; α6(IV): -
a
α1(IV)
f
α1(IV)
k
α1(IV)
b
α2(IV)
g
α2(IV)
l
α2(IV)
c
α5(IV)
h
α5(IV)
m
α5(IV)
d
α6(IV)
i
α6(IV)
n
α6(IV)
↑ CK14
e
CK19
↑ CK14
j
CK19
↑ CK14
o
CK19

sion of α5(IV) and α6(IV) chains had a significant effect on Ki-67 L.I. (P<0.05). There was no significant interaction (P=0.282) between the histological subtype and the expression of α5(IV) and α6(IV) chains.

In the Scheffé test, Ki-67 L.I. was significantly related to the staining of α5(IV) and α6(IV) chains in the cribriform subtype, and no significance was confirmed between Ki-67 L.I. and the staining pattern of α5(IV) and α6(IV) chains of the tubular subtype (Fig. 3).

Discussion

Many studies on the cellular characteristics as well as the histogenesis of ACC have been reported [1, 2, 18, 19]. However, the expression of extracellular matrix of ACC, in particular the BM components of ACC and their biological functions, is not known. In the present study, we examined for the first time the differential immunohistochemical distributions of six phenotypes of collagen α(IV) chains in the BMs of normal salivary glands and ACC. In addition, we compared these α(IV) chain expressions to the cellular expressions of cytoskeletal filaments (CK14 and CK19), α-SMA and Ki-67 as a marker of the mitotic activity of ACC cells.

In the BM of normal salivary ducts, including intercalated, striated and excretory ducts, α1(IV), α2(IV), α5(IV) and α6(IV) chains were stained continuously. There was no staining of α3(IV) and α4(IV) chains in the BM of salivary ducts. In the intercalated duct, differential localization among CK19, CK14 and α-SMA was confirmed as previously described [7, 8, 11, 18]. CK19 is expressed in luminal surface epithelium. α-SMA is expressed in myoepithelial cells of acini and intercalated ducts. CK14 is expressed in myoepithelial cells and ductal basal cells of excretory ducts. The biphasic-staining pattern between CK19 and CK14 is evident in normal salivary ducts with stable BM, composed of α1(IV), α2(IV), α5(IV) and α6(IV) chains.

In most of the tubular and some cribriform subtypes of ACC, composed of possibly well-differentiated structures with the biphasic-staining pattern between CK19 and CK 14, the BM of the tumor nests expressed all of α1(IV), α2(IV), α5(IV) and α6(IV) chains. In the cribriform subtype of ACC with the discontinuous or negative staining of α5(IV) and α6(IV) chains, neoplastic luminal cells seemed to be poorly differentiated, and the biphasic-staining pattern was ambiguous. In the solid subtype of ACC, tumor nests were mainly composed of CK14-positive immature neoplastic luminal cells or neoplastic myoepithelial cells with a severe loss of the α(IV) chains in the BM of the tumor nests.

Ki-67 L.I. of the cribriform subtype with the continuous staining of α5(IV) and α6(IV) chains was significantly lower than that of the discontinuous or negative staining of α5(IV) and α6(IV) chains. This result suggested that the remodeling of the BM was related to the increase of mitotic activity. However, no significance was confirmed between Ki-67 L.I. and the staining pattern for α5(IV) and α6(IV) chains of the tubular subtype. We suppose that these results could be due to the rarity of only two samples of the tubular type of ACC with the BM of the negative staining pattern of α5(IV) and α6(IV) chains compared with the cribriform subtype.

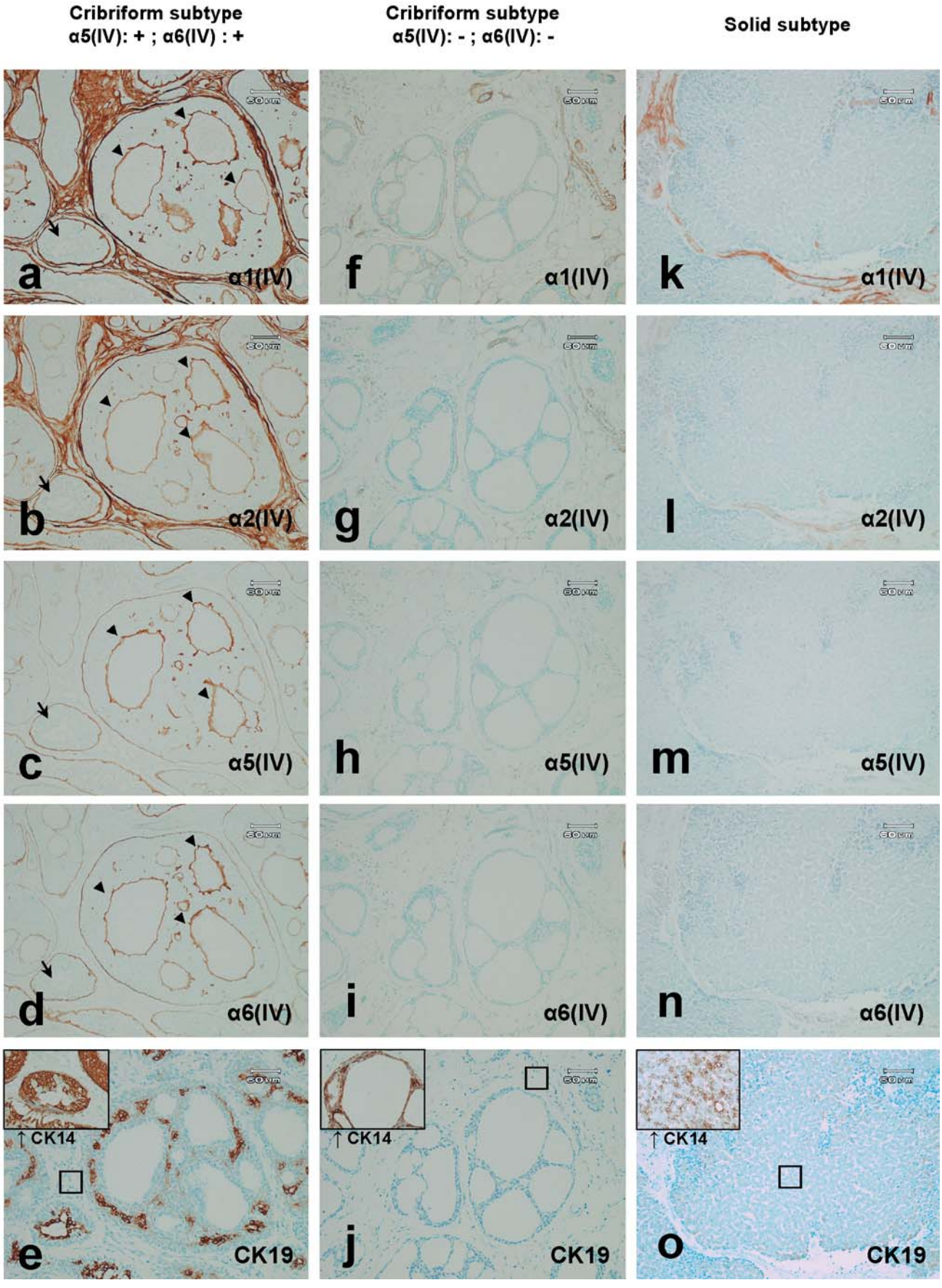
The solid subtype with continuous staining of α5(IV) and α6(IV) chains was not observed in this study. The result that Ki-67 L.I. was very high in the solid subtype may be in agreement previous reports [17].

In our previous study, we proved that the differential loss of the molecular form of α(IV) chains was closely related to cancer-cell growth and invasion [6, 13, 15, 22]. In the normal mammary epithelial duct, BM is composed of α1(IV) and α2(IV) chains and α5(IV) and α6(IV) chains, similar to salivary gland ducts. The BM remodeling of α(IV) chains from α1/α2(IV), α5/α6(IV) to α1/α2(IV) occurs during the progression of invasiveness of mammary cancer [15].

In our present study, the solid subtype of ACC had a tendency toward loss of immunoreactivity for α1(IV) and α2(IV) chains and showed negative staining of α5(IV) and α6(IV) chains. These seem to be the same features as the advanced invasive cancer, similar to those of mammary cancer. In the solid subtype of ACC, prognosis is poor [5, 16]. In contrast, many tubular and some cribriform subtypes with continuous-staining patterns of α1(IV), α2(IV), α5(IV) and α6(IV) chains are thought to be more differentiated phenotypes. In H&E staining, the eosinophilic BM-like material was seen abundantly in these subtypes of ACC. These subtypes of ACC may actively degrade and produce BM materials during invasion.

Developmentally, it is supposed that there are two cell lineages in developing normal salivary glands [18]. One is the luminal cell lineage, and the other is the myoepithelial cell lineage. According to previous reports [11, 18], as the luminal lineage cells mature, CK14-positive cells appear

Fig. 1 Immunohistochemical localization of α1(IV), α2(IV), α5(IV) and α6(IV) chains, cytokeratin 19 (CK19) and cytokeratin 14 (CK14) in the normal salivary gland (**a**–**e**), the tubular subtype of adenoid cystic carcinoma (ACC) with continuous staining of α5(IV) and α6(IV) chains (**f**–**j**) and the tubular subtype of ACC with discontinuous or negative staining of α5(IV) and α6(IV) chains (**k**–**o**). In normal salivary glands, α1(IV) and α2(IV) chains were continuously stained in the basement membrane (BM) of intercalated, striated and excretory ducts and acinus (**a**, **b**). α5(IV) and α6(IV) chains were also continuously stained in the BM of striated and excretory ducts, but discontinuously around acinus (**c**, **d**). Both luminal and basal cells predominantly express CK19 (**e**) and CK14 localized in basal cells and myoepithelial cell of acini and ducts (**e**, *inset*). In many cases of the tubular subtype of ACC with continuous staining of α1(IV) and α2(IV) chains (**f**, **g**), α5(IV) and α6(IV) chains were continuously stained (**h**, **i**). CK19 localized specifically in luminal cells (**j**) and CK14 localized in the outer boundary of the tumor nests (**j**, *inset*). In some cases of the tubular subtype of ACC with discontinuous staining of α1(IV) and α2(IV) chains (**k**, **l**), α5(IV) and α6(IV) chains and CK19 were negative (**m**, **n**, **o**), while CK14 was intensely localized in the luminal side and randomly in the outer side (**o**, *inset*). Scale: indicated (*upper right*)


Cribriform subtype
α5(IV): + ; α6(IV) : +
Cribriform subtype
α5(IV): - ; α6(IV): -
Solid subtype
a
α1(IV)
f
α1(IV)
k
α1(IV)
b
α2(IV)
g
α2(IV)
l
α2(IV)
c
α5(IV)
h
α5(IV)
m
α5(IV)
d
α6(IV)
i
α6(IV)
n
α6(IV)
↑ CK14
e
CK19
↑ CK14
j
CK19
↑ CK14
o
CK19

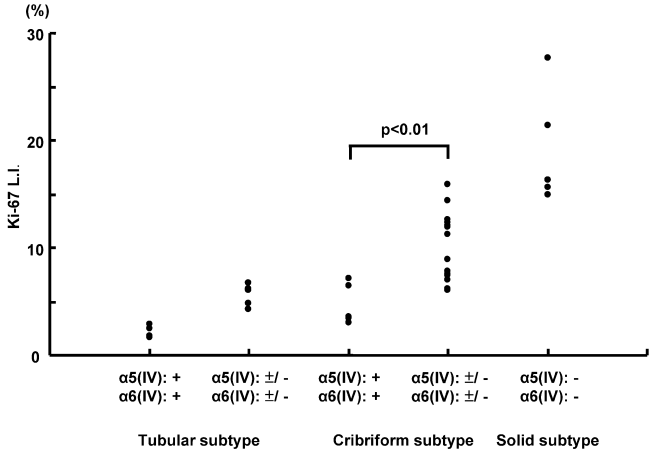


Fig. 3 The Ki-67 labeling index (L.I.) was significantly related to the expression for α5(IV) and α6(IV) chains of the cribriform subtype. No significance was demonstrated between Ki-67 L.I. and the staining pattern of α5(IV) and α6(IV) chains of tubular subtype. The solid subtype was excluded from the statistical analysis (as described in results)

first in the immature salivary duct. Thereafter, these cells differentiate to coexpress CK14 and CK19. However, in the myoepithelial lineage, the expression of α-SMA precedes the expression of CK14 during the differentiation of the acini and the intercalated duct. We consider that neoplastic luminal cells lining the true lumen with expression of only CK19 are the well-differentiated epithelial phenotype, and neoplastic solid nests with CK14-positive cells are the undifferentiated type. Similarly, we speculate that neoplastic myoepithelial cells with only α-SMA are the undifferentiated phenotype, and that neoplastic myoepithelial cells with coexpression of α-SMA and CK14 are the more differentiated phenotype. Therefore, these three monoclonal antibodies could differentiate neoplastic luminal cells from neoplastic myoepithelial cells, and demonstrate the biphasic-staining pattern between CK19 and CK14, as a marker of the well-differentiated structure.

The tubular subtype of ACC with the BM composed of α1(IV), α2(IV), α5(IV) and α6(IV) chains, reveals the biphasic-staining pattern of CK14 and CK19, and the low value of Ki-67 L.I. Many cribriform subtypes of ACC, compared with tubular subtypes, have unstable BM and reveal the ambiguous biphasic-staining pattern, in addition to the high value of Ki-67 L.I. The solid subtype of ACC has a tendency to lose BM, and shows complete loss of biphasic-staining pattern and the highest value of Ki-67 L.I. among these three subtypes.

As a conclusion, our results suggest that the BM irregularity with the differential expression of α(IV) chains of ACC is closely related to cell proliferation, cell differentiation and the biphasic architecture.

Fig. 2 Immunohistochemical localization of the cribriform subtype of adenoid cystic carcinoma (ACC) with continuous staining of α1(IV), α2(IV), α5(IV) and α6(IV) chains (**a**–**e**) and with discontinuous or negative staining of α5(IV) and α6(IV) chains (**f**–**j**) and of the solid subtype of ACC (**k**–**o**). In the cribriform subtype with continuous staining of α1(IV) and α2(IV) chains, both α5(IV) and α6(IV) chains were expressed in the basement membrane (BM) of the tumor nests, in addition to the BM of pseudocyst (**a**, **b**, **c**, **d** *arrowhead*), while there was no expression for any α(IV) chains in the true luminal surface (**a**, **b**, **c**, **d** *arrow*). Cytokeratin 19 (CK19) was expressed in luminal cells (**e**), and cytokeratin 14 (CK14) was expressed in the outer layer of the tumor nests (**e** *inset*). In some cribriform subtypes with the discontinuous staining of α1(IV) and α2(IV) chains, α5(IV) and α6(IV) chains were negatively stained (**f**, **g**, **h**, **i**). In this area, CK19 showed the negative staining (**j**), and CK14 was expressed outer layer of the tumor nests (**j** *inset*). The solid subtype of ACC had a tendency to loss of immunoreactivity for α1 (IV) and α2 (IV) chains (**k**, **l**) and showed negative staining for α5(IV) and α6(IV) chains (**m**, **n**). In this area, CK19 was negative (**o**) and CK14-positive cells were scattered randomly in the tumor nests (**o**, *inset*). Scale: indicated (*upper right*)

References

1. Araujo VC, Loducca SVL, Sousa SOM, Williams DM, Araujo NS (2001) The cribriform features of adenoid cystic carcinoma and polymorphous low-grade adenocarcinoma: cytokeratin and integrin expression. Ann Diagn Pathol 5:330–334
2. Darling MR, Schneider JW, Phillips VM (2002) Polymorphous low-grade adenocarcinoma and adenoid cystic carcinoma: a review and comparison of immunohistochemical markers. Oral Oncol 38:641–645
3. Dehan P, Waltregny D, Beschin A, Noel A, Castronovo V, Tryggvason K, De Leval J, Foidart JM (1997) Loss of type IV collagen α5 and α6 chains in human invasive prostate carcinomas. Am J Pathol 151:1097–1104
4. Ellis GL, Auclair PL (1996) Adenoid cystic carcinoma. In: Ellis GL, Auclair PL (eds) Atlas of tumor pathology: tumors of the salivary glands. Armed Forces Institute of Pathology, Washington, DC, pp 203–216
5. Hamper K, Lazar F, Dietel M, Caselitz J, Berger J, Arps H, Falkmer U, Auer G, Seifert G (1990) Prognostic factors for adenoid cystic carcinoma of the head and neck: a retrospective evaluation of 96 cases. J Oral Pathol Med 19:101–107
6. Hiki Y, Iyama K, Tsuruta J, Egami H, Kamio T, Suko S, Naito I, Sado Y, Ninomiya Y, Ogawa M (2002) Differential distribution of basement membrane type IV collagen α(IV), α2(IV), α5(IV) and α6(IV) chains in colorectal epithelial tumors. Pathol Int 52:224–233
7. Ihrler S, Zietz C, Sendelhofert A, Riederer A, Lohrs U (1999) Lymphoepithelial duct lesions in Sjögren-type sialadenitis. Virchows Arch 434:315–323
8. Ihrler S, Zietz C, Sendelhofert A, Lang S, Blasenbreu-Vogt S, L öhrs U (2002) A morphogenetic concept of salivary duct regeneration and metaplasia. Virchows Arch 440:519–526
9. Liotta LA, Stetler-Stevenson WG. (1991) Tumor invasion and metastasis: an imbalance of positive and negative regulation. Cancer Res 51[Suppl]:5054s–5059s
10. Lohi J, Korhonen M, Leivo I, Kangas L, Tani T, Kalluri R, Miner JH, Lehto VP, Virtanen I (1997) Expression of type IV collagen α1(IV)-α6(IV) polypeptides in normal and developing human kidney and in renal cell carcinomas and oncocytomas. Int J Cancer 72:43–49
11. Martins MD, Araujo VC, Raitz R, Araujo NS (2002) Expression of cytoskeletal proteins in developing human minor salivary glands. Eur J Oral Sci 110:316–321
12. Nagatsuka H, Siar CH, Nakano K, Tsujigiwa H, Gunduz M, Choufuku H, Lee Y-J, Naito I, Sado Y, Nagai N (2002) Differential expression of collagen IV α1 to α6 chains in basement membranes of benign and malignant odontogenic tumors. Virchows Arch 441:392–399

13. Nakano K, Iyama I, Mori T, Yoshioka M, Hiraoka T, Sado Y, Ninomiya Y (2001) Loss of alveolar basement membrane type IV collagen $\alpha 3$, $\alpha 4$, and $\alpha 5$ chains in bronchioloalveolar carcinoma of the lung. J Pathol 194:420–427
14. Nakano K, Siar CH, Nagai N, Naito I, Sado Y, Nagatsuka H, Hoh C, Kurada K, Tsujigiwa H, Gunduz M (2002) Distribution of basement membrane type IV collagen α chains in ameloblastoma: an immunofluorescence study. J Oral Pathol Med 31:494–499
15. Nakano S, Iyama K, Ogawa M, Yoshioka H, Sado Y, Oohashi T, Ninomiya Y (1999) Differential tissular expression and localization of type IV collagen $\alpha 1$(IV), $\alpha 2$(IV), $\alpha 5$(IV), and $\alpha 6$(IV) chains and their mRNA in normal breast and in benign and malignant breast tumors. Lab Invest 79:281–292
16. Nascimento AG, Amaral AL, Prado LA, Kligerman J, Silveira TR (1986) Adenoid cystic carcinoma of salivary glands. A study of 61 cases with clinicopathologic correlation. Cancer 57:312–319
17. Nordgard S, Franzen G, Boysen M, Halvorsen TB (1997) Ki-67 as a prognostic marker in adenoid cystic carcinoma assessed with the monoclonal antibody MIB1 in paraffin sections. Laryngoscope 107:531–536
18. Ogawa Y, Toyosawa S, Ishida T, Ijuhin N (2000) Keratin 14 immunoreactive cells in pleomorphic adenomas and adenoid cystic carcinomas of salivary glands. Virchows Arch 437:58–68
19. Raitz R, Martins MD, Araujo VC (2003) A study of the extracellular matrix in salivary gland tumors. J Oral Pathol Med 32:290–296
20. Sado Y, Kagawa M, Kishiro Y, Sugihara K, Naito I, Seyer JM, Sugimoto M, Oohashi T, Ninomiya Y (1995) Establishment by the rat lymph node method of epitope-defined monoclonal antibodies recognizing the six different α chains of human type IV collagen. Histochem Cell Biol 104:267–275
21. Seki T, Naito I, Oohashi T, Sado Y, Ninomiya Y (1998) Differential expression of type IV collagen isoforms, $\alpha 5$(IV) and $\alpha 6$(IV) chains, in basement membranes surrounding smooth muscle cells. Histochem Cell Biol 110:359–366
22. Tanaka K, Iyama K, Kitaoka M, Ninomiya Y, Oohashi T, Sado Y, Ono T (1997) Differential expression of $\alpha 1$(IV), $\alpha 2$(IV), $\alpha 5$(IV) and $\alpha 6$(IV) collagen chains in the basement membrane of basal cell carcinoma. Histochem J 29:563–570

Virchows Arch (2004) 445:63–67
DOI 10.1007/s00428-004-1030-4

ORIGINAL ARTICLE

A. Franchi · D. Massi · A. Palomba · M. Biancalani · M. Santucci

CDX-2, cytokeratin 7 and cytokeratin 20 immunohistochemical expression in the differential diagnosis of primary adenocarcinomas of the sinonasal tract

Received: 5 March 2004 / Accepted: 16 April 2004 / Published online: 3 June 2004
© Springer-Verlag 2004

Abstract Because the histopathological features of some primary adenocarcinomas of the sinonasal tract may show considerable overlap, we assessed the diagnostic value of a panel of immunohistochemical markers in the distinction between these malignancies. Paraffin-embedded tumour tissue sections from a series of 39 primary adenocarcinomas of the sinonasal tract, including 25 cases of intestinal-type adenocarcinoma (ITAC), 10 cases of salivary gland-type carcinoma and 4 cases of tubulopapillary low-grade adenocarcinoma were immunostained for CDX-2, cytokeratin 7 and cytokeratin 20. Diffuse nuclear staining for CDX-2 was identified in 80% of ITACs, while all non-ITACs were negative. Staining for cytokeratin 20 was positive in 84% of ITACs, including all cases negative for CDX-2, but negative in all other adenocarcinomas. Cytokeratin 7 was consistently positive in 88% of ITACs and in 100% of non-ITACs. Normal sinonasal epithelia expressed cytokeratin 7, but not CDX-2 and cytokeratin 20. Staining for CDX-2 and cytokeratin 20 has potential use in separating ITACs from other primary malignant glandular neoplasms of the nasal cavities and paranasal sinuses.

Keywords Nasal cavity · Paranasal sinuses · Intestinal-type adenocarcinoma · Salivary gland-type carcinoma · Low-grade adenocarcinoma

A. Franchi · D. Massi · M. Santucci
Department of Human Pathology and Oncology,
University of Florence, Italy

A. Palomba · M. Biancalani
Division of Anatomic Pathology,
Department of Laboratory Medicine,
"S. Giuseppe" Hospital,
Empoli, Italy

A. Franchi (✉)
Department of Human Pathology and Oncology,
University of Florence Medical School,
Viale G.B. Morgagni 85, 50134 Florence, Italy
e-mail: franchi@unifi.it
Tel.: +39-055-4478102
Fax: +39-055-4379868

Introduction

Sinonasal adenocarcinomas account for 10–40% of sinonasal epithelial malignancies [5, 13, 17, 20, 22]. This is a heterogeneous group of neoplasms, with different epidemiological features and variable clinical behaviour, which is rather poorly characterised from the histopathological point of view, also due to the rarity of these malignancies. A significant proportion of sinonasal adenocarcinomas show histological features reminiscent of colonic adenomas and adenocarcinomas and have therefore been termed intestinal-type adenocarcinomas (ITACs) [3]. Another major group of malignant glandular tumours of the nasal cavities and paranasal sinuses are histologically identical to major and minor salivary gland carcinomas and can be further classified according to salivary gland tumour classification schemes. Finally, there are reports concerning a rather ill-defined group of low-grade adenocarcinomas, most of which show papillary–tubular structures formed by bland cuboidal and columnar neoplastic cells [14, 19].

The differential diagnosis between these entities is clinically relevant, because ITACs are characteristically associated with occupational exposure to wood and leather dusts, and have an aggressive behaviour characterised by repeated local recurrences and ominous outcome [3, 9, 12]. Conversely, low-grade adenocarcinomas and salivary gland-type carcinomas tend to have a more indolent clinical course [19, 20]. However, due to their rarity and, in some instances, to the considerable overlap of their histological features, the distinction between sinonasal ITACs and non-ITACs may be difficult, especially in small biopsy material. In addition, there are only a few systematic immunohistochemical studies of sinonasal adenocarcinomas aimed at identifying potentially useful diagnostic markers to distinguish between these entities.

In a preliminary report, we analysed the expression of a marker of intestinal differentiation, the CDX-2 homeobox gene, and of cytokeratin 7 and 20 in a group of sinonasal ITACs [11]. The aim of the present study was to

Table 1 Antibodies used in this study

Antibody	Dilution	Pretreatment	Source
CDX-2	1:100	Citrate buffer pH 6, microwave (30 min)	Bio Genex, San Ramon, CA, USA
Cytokeratin 7	1:800	0.5% Protease XIV 20°C (15 min)	Bio Genex, San Ramon, CA, USA
Cytokeratin 20	1:60	0.5% Protease XIV 20°C (15 min)	Bio Genex, San Ramon, CA, USA

verify the possible use of these markers in the differential diagnosis of primary adenocarcinomas of the sinonasal tract.

Materials and methods

Sinonasal adenocarcinoma samples were obtained from tissue archives of the Department of Human Pathology and Oncology of the University of Florence, and from the Unit of Anatomic Pathology, Department of Laboratory Medicine, Empoli Hospital (Italy). The series included 25 cases of ITAC, 10 cases of salivary gland-type carcinoma and 4 cases of tubulopapillary low-grade adenocarcinoma. Paraffin-embedded tumour tissue sections were immunostained for CDX-2, cytokeratin 7 and cytokeratin 20 using an automated labelled streptavidin-biotin-peroxidase method on the GenoMX i6000 immunostainer (Biogenex). Table 1 reports the antibody source, dilution and antigen retrieval protocols used. Fragments of colorectal mucosa and colorectal adenocarcinomas were used as positive controls for CDX-2 and cytokeratin 20. Non-neoplastic sinonasal mucosa served as internal positive control for cytokeratin 7. Negative controls were performed by substituting primary antibody with non-immune mouse serum.

Cases were considered positive if more than 10% of neoplastic cells showed nuclear (CDX-2) or cytoplasmic (cytokeratin 7 and 20) immunoreactivity.

Results

The results of the immunohistochemical studies are summarised in Table 2. The group of ITACs included 6 well-differentiated, 9 moderately differentiated, 5 poorly differentiated, and 5 mucinous adenocarcinomas [9]. Nuclear immunostaining of neoplastic cells for CDX-2 was observed in all cases. In 5 adenocarcinomas (20%; 1 well differentiated, 2 moderately differentiated, 1 poorly differentiated and 1 mucinous) the immunoreactivity was focal (<10% of neoplastic cells); while, in the other cases, there was strong and diffuse (>50%) nuclear staining (Fig. 1D and G). Surface and glandular epithelia of the sinonasal mucosa were always negative for CDX-2 (Fig. 1A). Twenty-two ITACs (88%) showed cytoplasmic staining for cytokeratin 7 in the majority of neoplastic cells (Fig. 1E and H). Two mucinous adenocarcinomas and one moderately differentiated adenocarcinoma were negative or showed only focal immunoreactivity. Strong immunostaining for cytokeratin 7 was also observed in surface and glandular epithelia of normal sinonasal mucosa (Fig. 1B). Cytokeratin 20 expression was detected in 21 ITACs (84%), including 6 of 6 well differentiated, 7 of 9 moderately differentiated, 4 of 5 poorly differentiated and 4 of 5 mucinous adenocarcinomas (Fig. 1F and I). The 5 adenocarcinomas showing focal staining for CDX-2 were positive for cytokeratin 20. No cytokeratin 20 immunostaining was identified in normal sinonasal epithelia (Fig. 1C).

The group of non-intestinal-type adenocarcinomas was characterised by a uniform immunoprofile. All cases were strongly and diffusely positive for cytokeratin 7 (Fig. 1M and P), while no immunoreactivity for cytokeratin 20 and CDX-2 was observed (Fig. 1L, N, O and Q).

Table 2 Results of the immunohistochemical analysis of 39 primary adenocarcinomas of the sinonasal tract (cases showing positive staining, >10% of neoplastic cells)

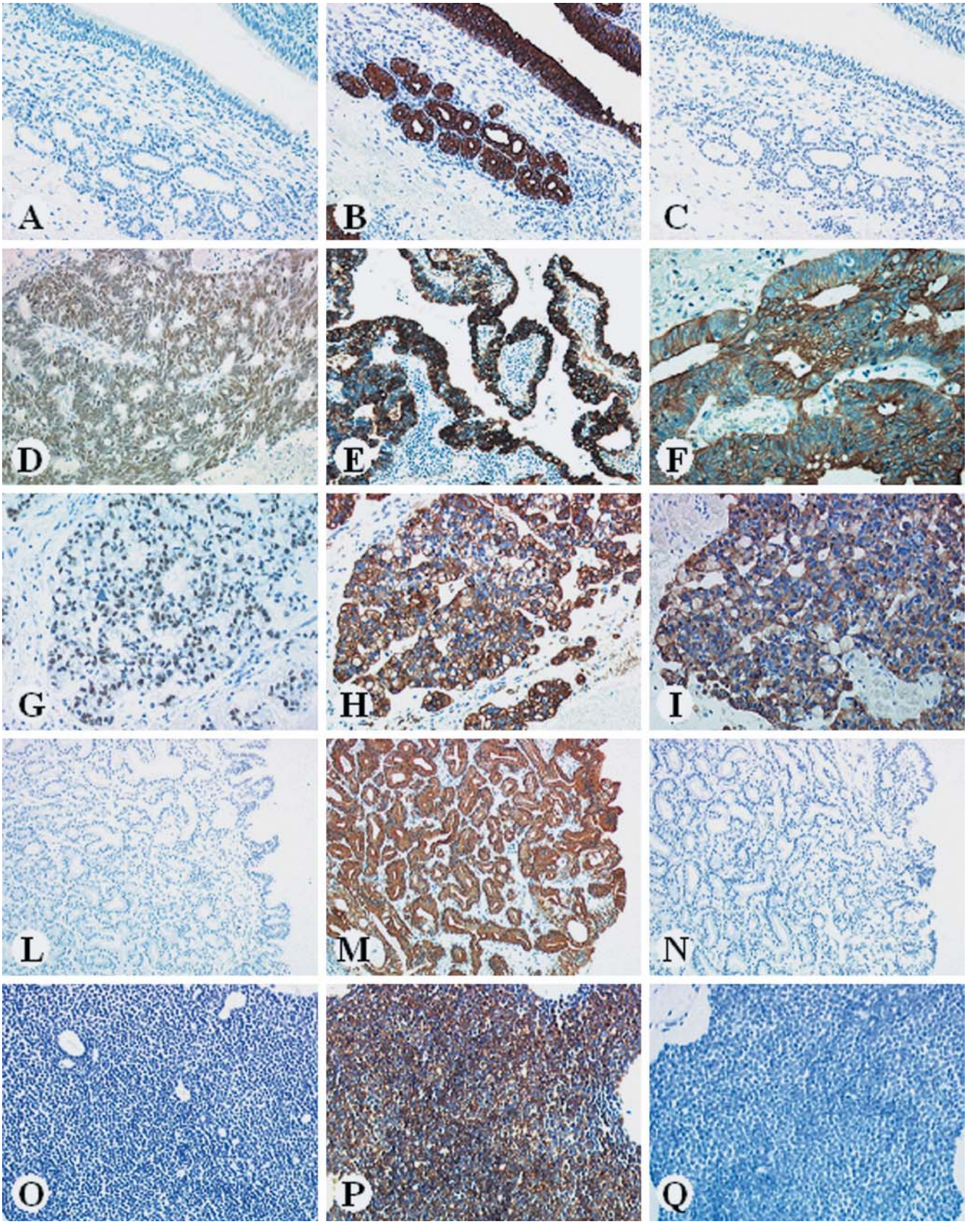
Tumor type	Cytokeratin 7	Cytokeratin 20	CDX-2
ITAC			
Well differentiated	6/6	6/6	5/6
Moderately differentiated	8/9	7/9	7/9
Poorly differentiated	5/5	4/5	4/5
Mucinous	3/5	4/5	4/5
Non-ITAC			
Salivary gland-type	10/10	0/10	0/10
Tubulopapillary	4/4	0/4	0/4

Discussion

Our analysis indicates that primary glandular epithelial malignancies of the sinonasal tract show a different immunoprofile. On the one hand ITAC is characterised by an immunophenotype resembling that of colonic adenocarcinoma, with the expression of CDX-2 and cytokeratin 20; on the other non-ITACs are characterised by the expression of cytokeratin 7 only, with consistent negative staining for CDX-2 and cytokeratin 20.

CDX-2 is a caudal-related homeobox transcription factor involved in the regulation of proliferation and differentiation of intestinal cells. In normal adult tissues its expression is restricted to the intestinal epithelium and to portions of the pancreatic duct system [16]. Immuno-

Fig. 1 Representative images of the immunohistochemical characterisation of sinonasal adenocarcinomas. *First column* CDX-2, *second column* cytokeratin 7, *third column* cytokeratin 20. *First row* normal sinonasal mucosa, *second row* moderately differentiated intestinal-type adenocarcinoma, *third row* mucinous intestinal-type adenocarcinoma, *fourth row* low-grade tubulopapillary adenocarcinoma, *fifth row* adenoid cystic carcinoma. Normal sinonasal mucosa and non-intestinal-type adenocarcinomas (salivary gland type and low-grade tubulopapillary adenocarcinomas) were characterised by expression of cytokeratin 7 only, whereas intestinal-type adenocarcinomas consistently expressed CDX-2 and both cytokeratins tested


A
B
C
D
E
F
G
H
I
L
M
N
O
P
Q

histochemical surveys in tumour tissues have demonstrated that this marker is significantly expressed by colonic adenocarcinomas and by a subset of gastric, oesophageal, bilio-pancreatic and ovarian carcinomas [1, 2, 16, 23]. Overall, CDX-2 appears to be a marker of intestinal differentiation in tumours, and its presence in ITACs of the sinonasal tract reinforces the notion that these neoplasms exhibit a high degree of overlap with normal intestinal epithelial cells and intestinal neoplasms. Moreover, it is conceivable that the acquisition of CDX-2 expression is a key event in the pathogenesis of ITAC, considering that the CDX-2 gene may regulate several genes involved in the acquisition of the mature intestinal phenotype.

The acquisition of cytokeratin 20 expression appears to be another aspect of the intestinal differentiation that characterizes ITAC. Indeed, this marker is absent in normal sinonasal epithelia, whereas, according to our study and to other reports [7, 15, 18], it is expressed by the majority of ITACs of the nasal cavities and paranasal sinuses, regardless the histologic subtype. Other immunohistochemical markers shared by ITAC and colorectal adenocarcinoma are CEA, MUC2 and sialosyl-Tn-antigen [8, 10, 15, 18, 21]. Interestingly, CK20 expression has also been evidenced in areas of intestinal metaplasia present in nasal respiratory type mucosa adjacent to ITAC, which may represent a precursor of these tumours [8].

The data presented in this study indicate that strong and diffuse CDX-2 and cytokeratin 20 immunostaining is very common in sinonasal ITACs, while no expression is detectable in non-ITACs. Such differential expression of CDX-2 protein and cytokeratin 20 in primary sinonasal adenocarcinomas may be of diagnostic aid in selected cases. Well-differentiated ITAC showing a predominance of tubulopapillary architecture and little or no cellular atypia should be differentiated from tubulopapillary low-grade adenocarcinoma, which is also characterised by formation of tubular structures and papillae [19]. This distinction is clinically relevant, because ITAC tends to pursue a more aggressive clinical course than tubulopapillary low-grade adenocarcinoma. Therefore, positivity for CDX-2 and/or cytokeratin 20 in a papillary–tubular adenocarcinoma of the sinonasal tract supports a diagnosis of ITAC.

Another setting in which immunostaining for CDX-2 and cytokeratin 20 may be of diagnostic aid is in the distinction of poorly differentiated ITAC, which shows minimal gland formation, from other primary epithelial neoplasms of the sinonasal tract, including poorly differentiated carcinomas of salivary gland origin, such as adenoid cystic carcinoma with predominantly solid pattern. Again, positivity for CDX-2 and/or cytokeratin 20 is in favour of a diagnosis of ITAC.

Both ITAC and non-ITAC groups showed expression of cytokeratin 7, a marker of normal sinonasal epithelia, which is also found in other sinonasal epithelial malignancies [10]. In our series, cytokeratin 7 was identified in 88% of ITAC, a level of expression which is comparable to the 100% expression detected in a previous report [15]. At variance, Sandison et al. found a positive rate of only 59% in a series of 22 primary sinonasal ITACs arising in woodworkers [18], similar to the 50% rate observed by Choi et al. in a study of 6 cases [7]. Despite these variable results, cytokeratin 7 immunostaining may be useful in the differential diagnosis between sinonasal ITAC and metastasis from a colorectal adenocarcinoma. Metastatic adenocarcinoma to the nasal cavity and paranasal sinuses from a primary adenocarcinoma of the gastrointestinal tract is a very uncommon occurrence [4, 7]. However, cases of gastrointestinal adenocarcinoma presenting with metastasis to the head and neck region have been reported [6], and it seems prudent to exclude this possibility before making a diagnosis of ITAC. Considering the overlap in the histological appearance between ITACs and metastatic lesions, immunohistochemistry may be of help in the differential diagnosis. In this setting, although sensitivity may not be high, positive staining for cytokeratin 7 supports the diagnosis of sinonasal ITAC.

References

1. Almeida R, Silva E, Santos-Silva F, Silberg DG, Wang J, De Bolos C, David L (2003) Expression of intestine-specific transcription factors, CDX1 and CDX2, in intestinal metaplasia and gastric carcinomas. J Pathol 199:36–40
2. Barbareschi M, Murer B, Colby TV, Chilosi M, Macri E, Loda M, Doglioni C (2003) CDX-2 homeobox gene expression is a reliable marker of colorectal adenocarcinoma metastases to the lungs. Am J Surg Pathol 27:141–149
3. Barnes L(1986) Intestinal-type adenocarcinoma of the nasal cavity and paranasal sinuses. Am J Surg Pathol 10:192–202
4. Bernstein JM, Montgomery WW, Balogh K Jr (1966) Metastatic tumors to the maxilla, nose, and paranasal sinuses. Laryngoscope 76:621–650
5. Bridger MW, Beale FA, Bryce DP (1978) Carcinoma of the paranasal sinusesla review of 158 cases. J Otolaryngol 7:379–388
6. Cama E, Agostino S, Ricci R, Scarano E (2002). A rare case of metastases to the maxillary sinus from sigmoid colon adenocarcinoma. ORL J Otorhinolaryngol Relat Spec 64:364–367
7. Choi HR, Sturgis EM, Rashid A, DeMonte F, Luna MA, Batsakis JG, El-Naggar AK (2003) Sinonasal adenocarcinoma: evidence for histogenetic divergence of the enteric and non-enteric phenotypes. Hum Pathol 34:1101–1107
8. Franchi A, Gallo O (1996) Prognostic implication of syalosil-Tn antigen expression in sinonasal intestinal type adenocarcinoma. Eur J Cancer 32B:123–127
9. Franchi A, Gallo O, Santucci M (1999). Clinical relevance of the histological classification of sinonasal intestinal-type adenocarcinomas. Hum Pathol 30:1140–1145
10. Franchi A, Moroni M, Massi D, Paglierani M, Santucci M (2002) Sinonasal undifferentiated carcinoma, nasopharyngeal-type undifferentiated carcinoma, and keratinizing and non-keratinizing squamous cell carcinoma express different cytokeratin patterns. Am J Surg Pathol 26:1597–1604
11. Franchi A, Massi D, Baroni G, Santucci M (2003). CDX-2 Homeobox Gene Expression. Am J Surg Pathol 27:1390–1391
12. Franquemont DW, Fechner RE, Mills SE (1991). Histologic classification of sinonasal intestinal-type adenocarcinoma. Am J Surg Pathol 15:368–375
13. Katz TS, Mendenhall WM, Morris CG, Amdur RJ, Hinerman RW, Villaret DB (2002) Malignant tumors of the nasal cavity and paranasal sinuses. Head Neck 24:821–829

14. Kleinsasser O (1985) Terminal tubulus adenocarcinoma of the nasal seromucous glands. A specific entity. Arch Otorhinolaryngol 241:183–193
15. Krane JF, O'Connel JT, Pilch BZ, Faquin WC (2000) Cytokeratin and mucin expression in intestinal-type sinonasal adenocarcinomas. Mod Pathol 80:139A
16. Moskaluk CA, Zhang H, Powell SM, Cerilli LA, Hampton GM, Frierson HF Jr (2003) Cdx2 protein expression in normal and malignant human tissues: an immunohistochemical survey using tissue microarrays. Mod Pathol 16:913–919
17. Robin PE, Powell DJ, Stansbie JM (1979) Carcinoma of the nasal cavity and paranasal sinuses: incidence and presentation of different histological types. Clin Otolaryngol 4:431–456
18. Sandison A, Lale A, Capper J, Peston D, Michaels L (2003). Immunohistochemical characterisation of adenocarcinoma of the nose and paranasal sinuses in woodworkers (abstract). Virchows Arch 443:259–260
19. Skalova A, Cardesa A, Leivo I, Pfaltz M, Ryska A, Simpson R, Michal M (2003) Sinonasal tubulopapillary low-grade adenocarcinoma. Histopathological, immunohistochemical and ultrastructural features of poorly recognised entity. Virchows Arch 443:152–158
20. Tran L, Sidrys J, Horton D, Sadeghi A, Parker RG (1989). Malignant salivary gland tumors of the paranasal sinuses and nasal cavity. The UCLA experience. Am J Clin Oncol 12:387–392
21. Urso C, Ninu MB, Franchi A, Paglierani M, Bondi R (1993) Intestinal-type adenocarcinoma of the sinonasal tract: a clinicopathologic study of 18 cases. Tumori 79:205–210
22. Weber AL, Stanton AC (1984) Malignant tumors of the paranasal sinuses: radiologic, clinical, and histopathologic evaluation of 200 cases. Head Neck Surg 6:761–776
23. Werling RW, Yaziji H, Bacchi CE, Gown AM (2003) CDX2, a highly sensitive and specific marker of adenocarcinomas of intestinal origin: an immunohistochemical survey of 476 primary and metastatic carcinomas. Am J Surg Pathol 27:303–310

Virchows Arch (2004) 445:68–73
DOI 10.1007/s00428-004-1019-z

ORIGINAL ARTICLE

Naomi Kaku · Kenji Kashima · Tsutomu Daa · Iwao Nakayama · Shigeo Yokoyama

Herpes simplex infection in urothelial carcinoma

Received: 28 January 2004 / Accepted: 23 March 2004 / Published online: 20 May 2004
© Springer-Verlag 2004

Abstract Herpes simplex virus (HSV), a member of the Herpesviridae family, is a very common pathogen that can infect any site in the body. Urothelial carcinoma (UC) is a common malignancy of the urinary tract. The possibility of HSV infection in cases of UC has attracted little attention. In this study, we investigated the possible presence of HSV in UC and non-neoplastic urothelium. We examined the incidence of HSV infection in 100 samples of UC from 78 patients and 50 samples of non-neoplastic urothelium from 50 autopsy cases using immunohistochemical staining and amplification of DNA using polymerase chain reaction (PCR). Infection by HSV was detected in 39 of the 100 samples of UC (35 of 78 patients) using immunohistochemical staining and/or PCR analysis, in marked contrast with 1 of 50 samples of non-neoplastic urothelium. There was no significant relationship between infection by HSV and anatomical site, growth pattern or depth of invasion of UC, but the frequency of HSV infection was significantly higher in females than in males. Our findings indicate that UCs become infected with HSV much more easily than non-neoplastic urothelium.

Keywords Herpes simplex virus · Urothelial carcinoma · Non-neoplastic urothelium · Immunohistochemical staining · Polymerase chain reaction

Introduction

Herpes simplex virus (HSV), a member of the Herpesviridae family, is one of the most serious human pathogens. It can infect any site in the body, but infection of the skin, genitalia, oral mucosa, eyes, anus, rectum and central nervous system is of particular concern. It has been generally accepted that HSV-1 is transmitted non-sexually, while HSV-2 is transmitted by sexual contact. The genome of HSV contains regions that endow the virus with the ability to transform cells in vitro, an observation that suggests the possible oncogenic potential of HSV in vivo [2, 6]. Indeed, HSV-2 had been suggested as a co-factor in the development of cancer of the uterine cervix [8, 12].

Urothelial carcinoma (UC) accounts for approximately 90% of malignant neoplasms in the urinary bladder. Risk factors for UC include viral infection, as well as cigarette smoking, exposure to certain chemicals and ingestion of certain artificial sweeteners [10]. Several DNA viruses, such as HSV, human papilloma virus (HPV), Epstein–Barr virus, cytomegalovirus and polyomavirus, have been reported to infect the urinary tract but possible infection by HSV in cases of UC has received little attention. Until now, there were no immunohistochemical reports demonstrating the infection by HSV in UC.

In this study, we investigated the possible presence of HSV in UC and non-neoplastic urothelium using immunohistochemical staining and using amplification of DNA using polymerase chain reaction (PCR).

N. Kaku (✉) · K. Kashima · T. Daa · I. Nakayama · S. Yokoyama
Department of Pathology,
Faculty of Medicine, Oita University,
Hasama-machi, 879-5593 Oita, Japan
e-mail: naokaku@med.oita-u.ac.jp
Tel.: +81-97-5865683
Fax: +81-97-5865686

Materials and methods

Samples

Samples (n=100) of archival formalin-fixed and paraffin-embedded tissue from UCs of 78 patients and samples (n=50) of non-neoplastic urothelium from 50 autopsy cases were examined in this study. All samples had been prepared at Oita Medical University Hospital between 1990 and 2001, and all (both UC and non-neoplastic urothelium) had been placed in formalin immediately after resection and had been fixed in formalin for 3–7 days. Paraffin blocks representative of each lesion were selected for immunohistochemical staining and for amplification of DNA using PCR. As a positive control for the presence of HSV-2 in analyses using immunohistochemical staining and PCR, we used a paraffin-embedded section of ulcerated vulval skin that had been infected with HSV-2. We also used a sample of plantar wart (myrmecia), which is known to be caused by HPV, to examine the possibility that an

antibody against HSV might cross react with HPV and that primers designed to amplify HSV-1 and HSV-2 DNA might also amplify HPV DNA. As a positive control for the analysis of HSV-1 by PCR, we used a commercially produced positive control (HSV-1; Maxim Biotech, Inc., San Francisco, CA, USA).

Immunohistochemical staining

As primary antibodies, we used polyclonal antibody against HSV-2 (1:100 dilution) and monoclonal antibody against HPV (clone K1H8; 1:50 dilution) from Dako (Carpinteria, CA, USA). We did not use antibody against HSV-1 in our immunohistochemical study because it is well known that polyclonal antibody against HSV-2 cross reacts with HSV-1. Immunopositive staining of HSV indicates the detection of the lytic protein of HSV.

After deparaffinization of samples in xylene and rehydration in a descending ethanol series, endogenous peroxidase activity was quenched by incubation in 3% H_2O_2 for 20 min at room temperature (RT). Then sections of UCs for immunostaining of HPV were autoclaved in 10 mM citric acid buffer (pH 6.0) at 121°C for 15 min for retrieval of antigens. Next, after 10% normal goat serum had been applied for 10 min at RT, sections of UCs and non-neoplastic urothelium were incubated with antibody against HSV-2 for 30 min or with sections of UCs antibody against HPV for 2 h. The products of immunoreactions were detected with the EnVision System (Dako) with 3,3′-diaminobenzidine as the chromogenic substrate. Finally, nuclei were counterstained for 1 min with Mayer's hematoxylin. Cells with apparent nuclear immunostaining, but not cytoplasmic, were judged to be positive for HSV and HPV to evaluate immunostaining strictly.

Amplification using PCR

We examined the presence of HSV-1 and HSV-2 genes using PCR. Genomic DNA was extracted from three to five 5-μm-thick paraffin-embedded sections of each sample with Takara DEXPAT (Takara Shuzo Co. Ltd., Tokyo, Japan). Then, 200 μl of each extract were supplemented successively with 6.6 μl of 3 M sodium acetate, 2.0 μl of Ethathinmate (Wako-Nippon Gene, Tokyo, Japan) and 420 μl of 99% ethanol. After centrifugation of the mixture at 12,000 rpm for 5 min, the precipitate was collected and re-suspended in 50 μl of distilled water. For detection of the presence of HSV-1 and HSV-2 genes, we used general primer sets for each viral DNA polymerase (Maxim Biotech, Inc.). The sequences of primers were as follows: HSV-1 forward, TAC GAC GGC CAG CAG ATC CGC GTC and HSV-1 reverse, CCC CCC CGG CGC CCC TAA ATC G; HSV-2 forward, TAC GAC GGC CAG CAG ATC CGC GTC and HSV-2 reverse, CCT TGT CGA GGC CCC GAA ACC G. Then, 5 μl of the solution of DNA were added to 50 μl of a reaction mixture that contained 5 μM of primers, 2.5 mM dNTP mixture, PCR buffer (Maxim Biotech, Inc.) and 1.25 U of *Taq* polymerase (Perkin-Elmer, Norwalk, CT, USA). The conditions for amplification of HSV-1 and HSV-2 genes were as follows: denaturation at 94°C for 1 min, annealing at 60°C for 1 min and primer extension at 72°C for 1 min. The final extension was allowed to proceed for an additional 10 min. Amplification was allowed to proceed for 30 cycles in a thermal cycler (Gene Amp PCR System 2400; Perkin Elmer). The products of PCR were analyzed using electrophoresis on a polyacrylamide gel and staining with a DNA silver-staining kit (Phast System; Pharmacia Biotech, Uppsala, Sweden). In cases that appeared to be HSV negative using PCR, we examined the integrity of the extracted DNA by amplifying exon 3 of the gene for β-catenin using PCR, since the product of amplification of this is longer than the products expected after the amplifications of HSV-1 and HSV-2. The primers and conditions for PCR were the same as those described by Kitaeva et al. [7]. The possible statistical dependence of the nature of each group of samples on any single variable and on multiple variables was tested using the chi-squared test.

Results

The results of the present study and the clinicopathological features of patients with UC are summarized in Table 1 and Table 2.

Clinicopathological data

The patients with UC consisted of 52 men and 26 women, aged 42–89 years, with a mean age of 69.5 years at presentation. Of the 100 samples from these 78 patients, 50 were from UC in the urinary bladder, 22 were from UC in the ureter and 28 were from UC in the renal pelvis. Of patients, 17 had multiple lesions at different sites. There were triple lesions in 5 patients (three men and two women) and double lesions in 12 patients (eight men and four women). The autopsy specimens from non-neoplastic urothelium came from 33 men and 17 women, aged 44–83 years, with a mean age of 66.1 years.

The histological grade, growth pattern and depth of invasion (pT) of representative specimens of the 100 UCs were evaluated according to the classification of the World Health Organization [11]. Of the 100 samples, 24 were classified histologically as grade 1, 51 as grade 2 and 25 as grade 3. With respect to growth pattern, 81 lesions were papillary, and 19 were non-papillary. In terms of the pT, 2 lesions were pTis (carcinoma in situ), 43 were pTa (non-invasive papillary carcinoma), 22 were pT1 (tumor invades subepithelial connective tissue), 8 were pT2 (tumor invades muscle), 21 were pT3 (tumor invades perivesical tissue) and 4 were pT4 (tumor extending into the prostate or other neighboring organs).

Table 1 Infection with herpes simplex virus (HSV) of non-neoplastic urothelium and urothelial carcinoma. *IHC* immunohistochemical staining, *PCR* polymerase chain reaction, *HSV-1/-2 PCR* positive for HSV-1 and/or HSV-2 using PCR, *HSV IHC/PCR* positive for HSV using IHC and/or PCR. Note: one sample of non-neoplastic urothelium that gave positive result using PCR was obtained at autopsy from a case of HSV-associated hemophagocytic syndrome

	Number of cases	HSV IHC	HSV-1/-2 PCR	HSV IHC/PCR
		(%)	(%)	(%)
Non-neoplastic urothelium	50	0 (0)	1 (2.0)	1 (2.0)
Urothelial carcinoma	100	11 (11.0)	33 (33.0)	39 (39.0)

Table 2 Clinicopathological features and results of immunohistochemical staining and analysis using polymerase chain reaction (PCR). *HSV* herpes simplex virus, *IHC* immunohistochemical staining, *pT* depth of invasion, *UC* urothelial carcinoma

	Number of cases	HSV IHC	HSV-1/-2 PCR	HSV IHC/PCR
		(%)	(%)	(%)
Gender				
Male	52	4 (7.7)	17 (32.7)	19 (36.5)
Female	26	7(26.9)	12 (46.2)	16 (61.5)*
Total under each heading	78 patients	11 patients	29 patients	35 patients
Anatomical site				
Urinary bladder	50	3 (6.0)	19 (38.0)	20 (40.0)
Ureter	22	2 (9.1)	8 (36.4)	10 (45.5)
Renal pelvis	28	6 (21.4)	6 (21.4)	9 (32.1)
Histological grade				
Grade 1	24	2 (8.3)	9 (37.5)	10 (41.6)
Grade 2	51	5 (9.8)	18 (35.3)	21 (41.2)
Grade 3	25	4 (16.0)	6 (24.0)	8 (32.0)
Growth pattern				
Papillary UC	81	8 (9.9)	28 (34.6)	31 (38.3)
Non-papillary UC	19	3 (15.8)	5 (16.3)	8 (42.1)
Depth of invasion (pT)				
pTis	2	0 (0)	1 (50.0)	1 (50.0)
pTa	43	3 (7.0)	15 (34.9)	17 (39.5)
pT1	22	2 (9.1)	5 (22.7)	6 (27.3)
pT2	8	0 (0)	4 (50.0)	4 (50.0)
pT3	21	6 (28.6)	8 (38.1)	11 (52.4)
pT4	4	0 (0)	0 (0)	0 (0)
Total for each subheading	100 samples	11 samples	33 samples	39 samples

*, Significant difference from the value for males ($p<0.05$) by the chi-square test

Immunohistochemical staining of HSV and HPV

Among the 100 samples of UC, 11 were immunopositive for HSV. In contrast, all 50 samples of non-neoplastic urothelium were immunonegative. In only one sample were typical HSV-infected cells detected on hematoxylin and eosin section, showing mononuclear and some multinucleate, with steel-gray homogeneous nuclei (Fig. 1A), whereas these were not detectable histologically in the remaining 99 samples. Immunoreaction products for HSV were strong mainly in the nuclei and weak in the cytoplasm (Fig. 1B, C). Characteristically, HSV-immunopositive cells were thickly clustered on the surface of tumors or grouped in small nests within tumors (Fig. 1B, C). HSV was detected more frequently in females than in males, but there was no significant relationship between immunopositivity for HSV, site, histological grade, growth pattern and pT. All samples of UC were immunonegative for HPV.

Detection of HSV using PCR

The predicted product of PCR specific for HSV-1 was 105 bp long, and the product specific for HSV-2 was 106 bp long. Among the 100 samples of UC, HSV-1 was detected using PCR in 5 samples, and HSV-2 was detected in 31 (Fig. 2). Three samples were positive for both HSV-1 and HSV-2. Neither HSV-1 nor HSV-2 was detected in the plantar wart, even though the integrity of the isolated DNA was confirmed using appropriate amplification using PCR of the gene for β-catenin (Fig. 2). No statistically significant relationship was found between HSV infection, as revealed using PCR, and clinicopathological features. HSV-1 was not detected in any of the 50 samples of non-neoplastic urothelium, while HSV-2 was detected in only 1 sample. The patient from whom non-neoplastic but HSV-2-positive urothelium was isolated had been diagnosed with virus-associated hemophagocytic syndrome caused by systemic infection with HSV-2.

Detection of HSV in UCs using immunohistochemical analysis and/or PCR

In 11 samples that were HSV positive using immunohistochemical staining, 5 samples were PCR positive and 6 samples were PCR negative. In 33 samples that were HSV positive using PCR, 5 samples were immunopositive and 28 samples were immunonegative. Therefore, infection by HSV was detected in 39 of the 100 samples of UC (35 of 78 patients) using immunohistochemical staining and/or PCR analysis. No correlation was found between HSV infection and the site, histological grade, growth pattern or pT, but the rate of infection was significantly higher in females than in males. Of the 17 patients with multiple lesions, 4 patients had evidence of HSV infection in each lesion. In 2 of these 4 patients, multiple infections by HSV were synchronous, and, in the other 2 patients, they were metachronous.

Amplification of the gene for β-catenin using PCR

In this study, 67 samples of UC and 49 samples of non-neoplastic urothelium were negative for HSV in the analysis using PCR. We successfully amplified exon 3 of

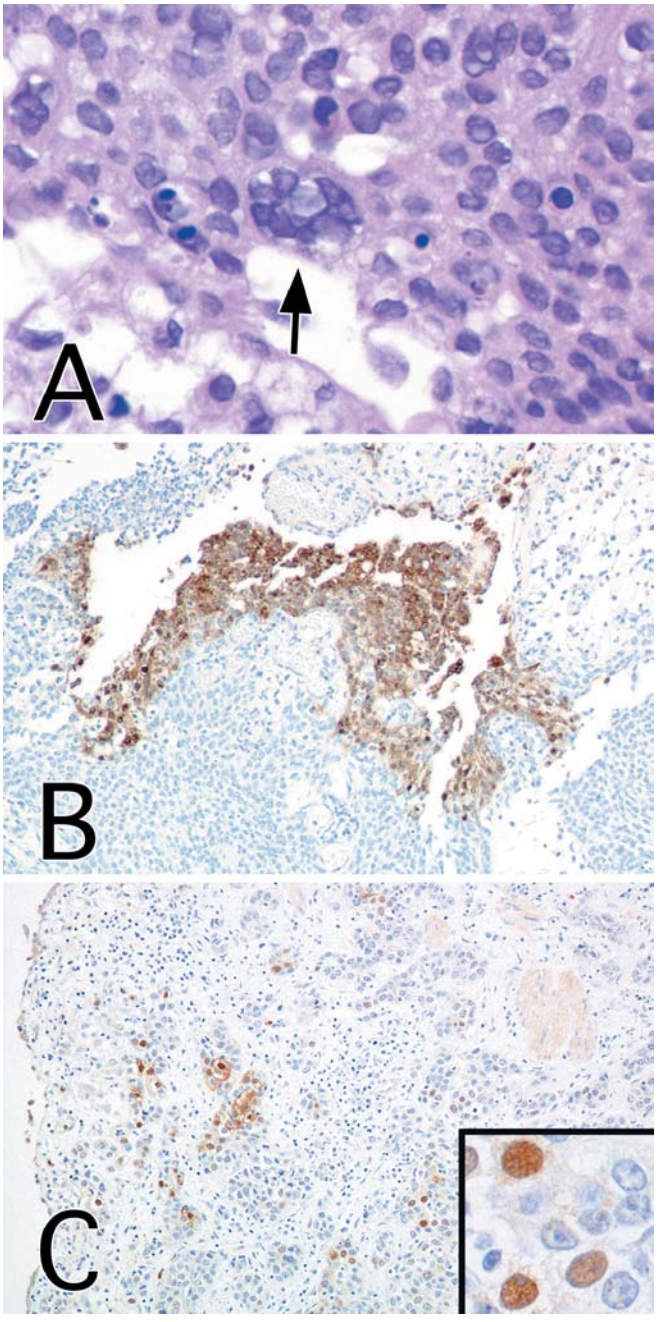


Fig. 1 **A, B** Detection of infection by herpes simplex virus (HSV) in a case of urothelial carcinoma. HSV-infected cells are multinucleate (*arrow*) or mononuclear, with steel-gray nuclei, in an hematoxylin and eosin-stained specimen. HSV-positive cells are seen on the surface of a tumor, and immunoreaction for HSV is found in the nuclei and cytoplasm. This case is also PCR positive for HSV-2. **C** HSV-positive cells are clustered in small nests within a tumor. Immunoreaction for HSV is found in the nuclei (*inset*). Original magnification ×400 (**A**), ×100 (**B** and **C**)

the gene for β-catenin from 64 of the 67 samples in UC and 47 of the 49 samples in non-neoplastic urothelium, demonstrating that we had successfully extracted appropriate DNA templates from most of the paraffin-embedded tissues (Fig. 2). In these 67 samples of UC, positive results using immunostaining for HSV were observed in 6

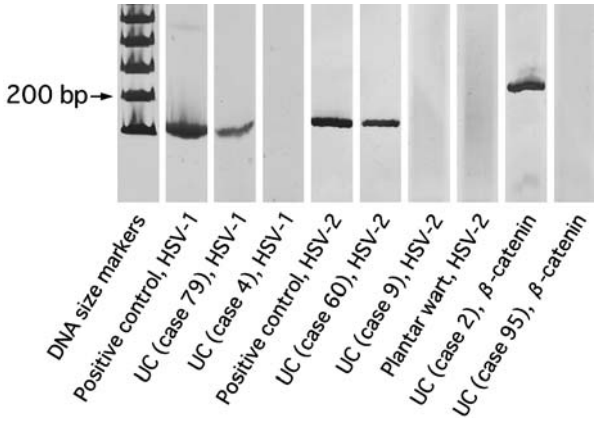


Fig. 2 Representative results of polymerase chain reaction for amplification of herpes simplex virus (HSV)-1 DNA, HSV-2 DNA and exon 3 of the gene for β-catenin

samples, in which exon 3 of the gene for β-catenin was amplified from all samples.

Discussion

Many viruses, such as HSV, HPV, polyomavirus, cytomegalovirus and Epstein–Barr virus, have been reported as causative agents of urinary tract infection. In the urothelial system, HSV-2 has been recognized as a cause of urethritis and cystitis [1, 9]. There have been only a few reports of HSV infection in UC. Tarro et al. [14] reported that 6 of 20 patients (30%) with UC were seropositive for HSV-2. Gazzaniga et al. [3] reported the detection of HSV-2 DNA in 3 of 35 biopsy specimens (9%) of UC using PCR, while Haid et al. [4] demonstrated the presence of HSV-2 particles using an immunofluorescence technique in 7 of 27 lesions (26%) of prostatic carcinoma. Strangely, to our knowledge, there has been no report that HSV-infected cells in UC were detected on HE sections. The only 1 of the 100 samples that demonstrated typical HSV-infected cells on HE (Fig. 1A) section seems to be exceptional.

In the present study, we analyzed 100 samples of UC in the urinary bladder, ureter and renal pelvis from 78 patients using immunohistochemical staining and PCR. We found evidence of HSV infection in 39 of 100 samples (35 of 78 patients) by one or other of the two methods. Our results revealed a higher rate of infection with HSV in UC than those found in previous studies, and this high rate was unexpected. Superti et al. noted the apparently elevated susceptibility of human bladder-derived cells to infection by HSV-2 in vitro [13]. Moreover, the mucosa in cases of UC might have been infected more easily. However, the discrepancy between the results in some previous reports and ours might also be due to differences in technique. The combination of immunohistochemical staining and amplification using PCR that we used might be more sensitive than amplification using PCR alone and might allow detection of small numbers of

virus particles that do not generate antibodies in the patient's serum.

Although there were no significant relationships between the rate of HSV infection and anatomical site, histological grade, growth pattern or pT, the rate of infection was significantly higher in females than in males. The short length of the female urethra is likely to be a predisposing factor in such infection. In our analysis using PCR, we detected HSV-1 DNA in only 5 samples and HSV-2 DNA in 31 samples. This result is consistent with the fact that HSV-1 infection is generally orofacial, while HSV-2 infection is genital [15]. Our observations also suggest that HSV gains access to UC in a retrograde manner through the urethra.

We also investigated the possible presence of HSV in 50 autopsy samples of non-neoplastic urothelium. We found only one case of HSV-2 infection using PCR analysis. This case had been diagnosed as virus-associated hemophagocytic syndrome caused by HSV-2 infection. In this study, we also examined other organs from the patient for the presence of HSV-1 and HSV-2 using PCR with the same method as described above. The examination using PCR of DNA from archival formalin-fixed and paraffin-embedded tissue from pulmonary hilar lymph nodes, liver, lumbar vertebra and sternum revealed the presence of HSV-2. Although the number of urothelial cells in the autopsy samples was generally lower than that in samples of UC, we can assume that amplification using PCR was effective, regardless of the number of cells, whenever HSV was present. Our results suggest that analysis using PCR might be a more sensitive method for detecting HSV infection than immunohistochemical staining.

In the literature on cervical cancer, many authors have discussed the role of HSV in carcinogenesis. Hamsíková et al. [5] excluded the possibility that HSV might be a carcinogen by showing that patients with invasive cervical cancer became seropositive for HSV-2 only after radiotherapy for cancer. They suggested that HSV-2 infection might follow, rather than precede, the development of cervical cancer. In our immunohistochemical study, we found that, in most cases, HSV-infected cells were distributed superficially or focally within the tumor. These findings also suggest that HSV infection might be a late event after the development of UC, rather than an early carcinogenic event.

Among the 39 samples of UC with evidence of HSV infection, only 5 gave positive results both using immunohistochemical analysis and using PCR analysis. Six samples were immunopositive but PCR negative. Possible reasons for this discrepancy are as follows: the extracted DNA might have been degraded during fixation of tissue in formalin. Alternatively, there might have been an insufficient level of the target HSV gene in the sample. To examine the condition of the DNA in the six PCR negative samples, we amplified exon 3 of the gene for β-catenin using PCR, which should yield a longer product of PCR than that predicted for HSV. Amplification was successful for these six samples, suggesting that the amount of HSV DNA had been too low for amplification using PCR. Indeed, in these six samples, HSV-immunopositive cells were a few in number. In contrast, 28 samples were PCR positive but immunonegative. In these samples, it is conceivable that HSV was present only in the sections from which DNA had been isolated for PCR and not in those subjected to immunohistochemical staining. Alternatively, the antigenicity of HSV might have been lost, or the level might have been too low for detection. There is a small possibility of false-positive immunostaining. However, samples of non-neoplastic urothelium were all completely immunonegative for HSV.

In the present study, we detected HSV infection in far more cases of UC than we had expected and found almost no evidence of HSV infection in non-neoplastic urothelium; that is, UC appears to be more easily infected with HSV than the non-neoplastic urothelium. The positive results (33% of examined samples) of PCR analysis seem to be reliable, but it is possible that some HSV-infected samples might give negative results in analysis using PCR, containing viruses that can only be detected using immunostaining. Thus, we interpret our results as indicating that the frequency of infection of UC by HSV is at least 33% using PCR and at most 39% using both immunostaining and PCR.

Acknowledgements The authors thank Mr. S. Yano and Ms. T. Nakamatsu for their skilled technical assistance.

References

1. Cleator GM, Klapper PE (1994) Herpes simplex. In: Zuckerman AJ, Banatvala JE, Pattison JR (eds) Principles and practice of clinical virology, 3rd edn. Wiley, Chichester, pp 5–36
2. Di Paolo JA, Woodworth CD, Popescu NC, Koval DL, Lopez JV, Doniger J (1990) HSV-2-induced tumorigenicity in HPV-16 immortalized human genital keratinocytes. Virology 177: 777–779
3. Gazzaniga P, Vercillo R, Gradilone A, Silvestri I, Gandini O, Napolitano M, Giuliani L, Fioravanti A, Gallucci M, Aglianò AM (1998) Prevalence of papillomavirus, Epstein–Barr virus, cytomegalovirus, and herpes simplex virus type 2 in urinary bladder cancer. J Med Virol 55:262–267
4. Haid M, Sharon N (1984) Immunofluorescent evidence of prior herpes simplex virus type-2 infection in prostate carcinoma. Urology 113:623–625
5. Hamsíková E, Ludvíková V, Tachezy R, Kovarík J, Brousková L, Vonka V (2000) Longitudinal follow-up of antibody response to selected antigens of human papillomaviruses and herpesviruses in patients with invasive cervical carcinoma. Int J Cancer 86:351–355
6. Hildesheim A, Mann V, Brinton LA, Szklo M, Reeves WC, Rawls WE (1991) Herpes simplex virus type 2: a possible interaction with human papilloma virus types 16/18 in the development of invasive cervical cancer. Int J Cancer 49:335–340
7. Kitaeva MN, Grogan L, Williams JP, Dimond E, Nakahara K, Hausner P, Denobile JW, Soballe PW, Kirsch IR (1997) Mutations in β-catenin are uncommon in colorectal cancer occurring in occasional replication error-positive tumors. Cancer Res 57:4478–4481
8. Kjaer SK, De Villiers E-M, Çaglayan H, Svare E, Haugaard BJ, Engholm G, Christensen RB, Moller KA, Poll P, Jensen H, Vestergaard BF, Lynge E, Jensen OM (1993) Human papillomavirus, herpes simplex virus and other potential risk factors

for cervical cancer in a high-risk area (Greenland) and a low-risk area (Denmark)—a second look. Br J Cancer 67:830–837
9. McClanahan C, Grimes MM, Callaghan E, Stewart J (1994) Hemorrhagic cystitis associated with herpes simplex virus. J Urol 151:152–153
10. Messing EM, Catalona W (1996) In: Walsh PC, Retik AB, Vaughan ED Jr, Wein AJ (eds) Urothelial tumors of the urinary tract. Campbell's Urology, 7th edn. Saunders, Philadelphia, p 2335
11. Mostofi FK (1999) Histological typing of urinary bladder tumors. In: Davis CJ, Sesterhenn IA (eds) World Health Organization International Histological Classification of Tumors, 2nd edn. Springer-Verlag, Berlin Heidelberg New York, p 9
12. Schmauz R, Okong P, De Villiers E-M, Dennin R, Brade L, Lwanga SK, Owor R (1989) Multiple infections in cases of cervical cancer from a high-incidence area in tropical Africa. Int J Cancer 43:805–809
13. Superti F, Longhi C, Di Biase AM, Tinari A, Marchetti M, Pisani S, Gallinelli C, Chiarini F, Seganti L (2001) Herpes simplex virus type 2 modulates the susceptibility of human bladder cells to uropathogenic bacteria. Med Microbiol Immunol 189:201–208
14. Tarro G, Flaminio G, Maturo S, Esposito C, Cocchira R (1982) Further studies on an immunoenzymatic assay for herpes simplex virus tumor-associated antigen. Clin Immunol Immunopathol 25:126–132
15. Whitley RJ, Roizman B (2001) Herpes simplex virus infections. Lancet 357:1513–1518

Virchows Arch (2004) 445:74–78
DOI 10.1007/s00428-004-1024-2

ORIGINAL ARTICLE

Henryk Wiktor · Marta Kankofer · Ivo Schmerold · Agnes Dadak · Maciej Lopucki · Hans Niedermüller

Oxidative DNA damage in placentas from normal and pre-eclamptic pregnancies

Received: 17 February 2004 / Accepted: 25 March 2004 / Published online: 5 May 2004
© Springer-Verlag 2004

Abstract Placental oxidative stress was suggested to play a role in the pathogenesis of pre-eclampsia (PE). In this study, levels of 8-hydroxy-2′-deoxyguanosine (8-OH-dG), a well-established marker of oxidative DNA damage, were analysed in placental cellular DNA from normal (group NP) and pre-eclamptic (group PE) pregnancies as well as from PE pregnancies complicated by intrauterine growth restriction (group PE-IUGR). Placental samples obtained immediately after delivery were frozen at −80°C until analysis. Cellular DNA was isolated, hydrolysed and analysed using high-performance liquid chromatography. Native nucleosides were monitored at 254 nm and 8-OH-dG using electrochemical detection. Concentrations of 8-OH-dG were expressed as μmol/mol 2′-deoxyguanosine. In group NP, mean concentration of 8-OH-dG reached 179.97±80.58 (±SEM; μmol/mol dG). 8-OH-dG levels were higher in group PE (273.44± 110.14 μmol/mol), but the difference was not significant in comparison with group NP. Highest concentrations of 8-OH-dG were found in group PE-IUGR (428.97± 141.40 μmol/mol), with levels significantly higher than in group NP, but not group PE. The results indicate a positive correlation between the severity of PE and the degree of oxidative stress and corroborate previous studies suggesting reactive oxygen species to be involved in the pathophysiology of PE.

Keywords Human placental DNA · Oxidative stress · 8-Hydroxy-2′-deoxyguanosine · Pre-eclampsia · Intrauterine growth restriction

H. Wiktor · M. Lopucki
Department of Obstetrics and Gynaecology,
Medical University School,
Lublin, Poland

M. Kankofer (✉)
Department of Biochemistry, Faculty of Veterinary Medicine,
Agricultural University,
Lubartowska 58a, 20-123 Lublin, Poland
e-mail: kankofer@agros.ar.lublin.pl
Tel.: +48-81-7474023
Fax: +48-81-4456006

I. Schmerold · A. Dadak
Institute of Pharmacology and Toxicology,
Veterinary University of Vienna, Austria

H. Niedermüller
Institute of Physiology and Ludwig Boltzmann Institute
for Aging Research,
Veterinary University of Vienna, Austria

Introduction

Pre-eclampsia (PE) is a pregnancy-specific disorder and is considered one of the most significant health problems in human pregnancy. It complicates approximately 5–10% of pregnancies, and there is no evidence that this has changed substantially during the last decade. PE is characterised by proteinuria, oedema, vasoconstriction and increased vascular resistance, leading to maternal hypertension, reduced organ perfusion, reduced uteroplacental blood flow and foetal growth restriction. At present, PE is a leading cause of maternal mortality and of indicated premature delivery; it is associated with a five-fold increase in perinatal mortality. Thus, PE adversely affects the mother by vascular dysfunction and the foetus by intrauterine growth restriction (IUGR) [5, 20].

The pathogenic mechanisms involved in the initiation and progression of PE are not clear as of yet. The only intervention that effectively reverses the syndrome is delivery of the placenta, which indicates that this tissue plays a key role in PE pathogenesis [20, 21].

There is increasing evidence indicating that placental oxidative stress is involved in the development of PE [9, 27, 28]. Previous studies suggest that placental oxidative stress is more intensive in PE cases complicated by IUGR than in PE without IUGR [26]. Wiktor and Kankofer [31, 32] have shown an increase in lipid peroxidation and a decrease in superoxide dismutase (SOD) activity in placentas of women with severe PE without IUGR in comparison with normal placentas. These authors also demonstrated further increase in lipid peroxidation [32] and

further decrease in SOD activity [31] and, in addition, a decrease in glutathione peroxidase [34] and catalase (CAT) activity [33] in severe PE cases complicated by IUGR. In other studies, Wiktor has reported elevated DNA adduct levels in placentas from pregnancies complicated by severe PE with IUGR [30].

Increased oxidative stress can lead to free-radical attack on physiologically important molecules, such as lipids, proteins, including enzymes, and DNA [10, 18, 21]. As a consequence, damage to purines and pyrimidines, yielding oxidative DNA modifications, occurs. Among the oxidised bases, 8-hydroxy-2′-deoxyguanosine (8-OH-dG) is the most abundant [1, 14] and is considered to be an important biomarker of oxidative DNA damage in tissues [13]. Therefore, 8-OH-dG was used in this study to quantify the extent of oxidative DNA damage in placentas. The aim was to compare the concentration of 8-OH-dG in placental tissue from normal and pre-eclamptic pregnancies with and without complication by IUGR.

Materials and methods

Patients

All of the 53 patients studied delivered by Caesarean section at the Department of Obstetrics and Gynaecology, Medical University School in Lublin, Poland. For Caesarean section, bupivacain (0.5%) was used for epidural anaesthesia.

Placental tissue samples were obtained: (i) from 18 deliveries in normal pregnancy cases (group NP), (ii) from 17 deliveries in pregnancies complicated by severe PE without IUGR and (iii) from 18 deliveries in pregnancies complicated by severe PE and IUGR (Table 1).

PE was defined using the criteria established by the Working Group of the National High Blood Pressure Education Program in the U.S.A. [19]. The severity of PE was established according to the criteria described by Steegers and van der Post [25]. All patients underwent clinical examination, including analysis of clinical blood and urine parameters. Only patients without chronic hypertension, renal or metabolic diseases were included in this study. Control patients of group NP had uncomplicated pregnancies, were normotensive throughout gestation and had no proteinuria. Exclusion criteria comprised hypertensive disorders, haemorrhage, intrauterine infection, foetal distress, abnormal placentation, oligohydramnios, polyhydramnios, diabetes mellitus, collagen vascular disease and alcohol or illicit substance use. Only non-smokers without other previous exposition known to lead to 8-OH-dG formation [16] were included. IUGR was diagnosed when foetal birth weight was below the tenth percentile.

Placental sampling

All samples (approximately 1 g) were taken from the mid-disc region of the chorionic plate (the middle between the edge of the placenta and the origin of the umbilical cord) from non-infarcted areas. Immediately after delivery, all specimens were frozen in liquid nitrogen and stored at −80°C until analysis.

DNA isolation and chromatography

Following rinsing of placental samples (sample weight approximately 100 mg) with physiological sodium chloride solution, cellular DNA was extracted using a Qiagen genomic DNA purification kit, following the standard protocol as given by the manufacturer (Qiagen Blood and Cell Culture DNA Midi Kit, No. 13343, Qiagen GmbH, 40724 Hilden, Germany). Isolated DNA pellets were dried under a stream of N_2, dissolved overnight in 200 μl 20 mmol/l sodium acetate buffer, pH 4.8, and digested with 20 μg nuclease P1 (Sigma N8630; 30 min, 37°C); then 20 μl Tris buffer (1 mol/l, pH 7.4) containing 1.3 U alkaline phosphatase (Boehringer-Mannheim, No. 713023) was added, followed by a further incubation for 60 min at 37°C. The DNA hydrolysate was directly applied onto a high-performance liquid chromatography (HPLC) column [7].

The HPLC system employed comprised a Waters station with a 600S controller, a 626 pump, a 717 plus autosampler, a 996 photodiode array detector and a serially connected 464 pulsed electrochemical detector equipped with a glassy carbon working electrode set at 0.6 V and a $Ag/AgCl_2$ reference electrode. Samples were injected into a Merck Superspher HPLC column (100 RP18e, 4 μm, 4.6×250 mm) and were isocratically eluted (50 mmol/l KH_2PO_4, 5% acetonitrile, pH 4.1; flow 0.5 ml/min; oven temp 44°C). Ultrapure water produced by a MILLI-Q 185 plus system was used in this study [23].

Native nucleosides were monitored at 254 nm and 8-OH-dG using electrochemical detection. Authentic marker substances purchased from Sigma and Merck were used as standards (8-OH-dG Sigma, No. H-5653). Peak areas served as integration parameters. Concentrations of 8-OH-dG were expressed as micromoles per mole 2′-deoxyguanosine (dG). Concentrations of DNA were determined using comparison of the dG-peak areas of tissue samples with the dG-peak areas of known amounts of calf thymus DNA. The calibration curves for all native nucleosides and 8-OH-dG were linear within the relevant concentration ranges measured in tissue DNA samples.

Statistical evaluation

Comparative analysis of the results was performed using the Wilcoxon test (for non-parametric values). A P value (two-sided) <0.05 was considered as significant.

Results

Samples collected from group NP showed 8-OH-dG levels ranging from 4.28 μmol/mol dG to 1413.96 μmol/mol dG with a mean value of 179.97 μmol/mol dG; this group had the lowest concentrations of 8-OH-dG, followed by group PE (mean 273.44 μmol /mol dG) and group PE-IUGR (mean 428.97 μmol/mol dG), with values ranging from 5.3 μmol/mol dG to 1828.57 μmol/mol dG and 7.92 μmol/mol dG to 1909.88 μmol/mol dG, re-

Table 1 Selected clinical data of groups of patients studied. Numbers are given as mean±standard deviation. *NP* normal pregnancy group, *PE* pre-eclampsia group, *PE-IUGR* pre-eclampsia complicated by intrauterine growth restriction

Group	Age (years)	Gestation age (weeks)	Mean arterial pressure (mmHg)	New-born weight (g)
NP	26.5±5.9	39.0±1.1	87.3±8.2	3608±505
PE	28.6±5.8	38.0±1.5	131.5±6.1	3283±512
PE-IUGR	26.9±5.9	36.3±2.7	138.0±23.2	1876±619

Table 2 Concentrations of 8-hydroxy-2′-deoxyguanosine (μmol/mol deoxyguanosine) in placental cellular DNA from groups NP (normal pregnancy group), PE (pre-eclampsia group), and PE-IUGR (pre-eclampsia complicated by intrauterine growth restriction)

Group	*n*	Mean	SEM
NP	18	179.97	80.58
PE	17	273.44	110.14
PE-IUGR	18	428.97	141.40
Group comparison		**Level of significance**	
NP		*P*=0.79	
PE			
NP		*P*=0.0085	
PE-IUGR			
PE		*P*=0.38	
PE-IUGR			

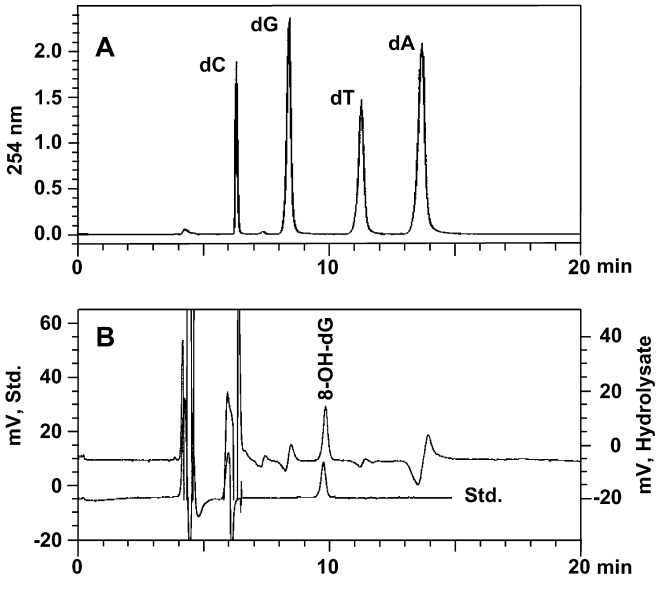


Fig 1 Ultraviolet and electrochemical chromatograms of a DNA hydrolysate (50 μl). DNA was isolated from 100 mg placental tissue using a commercial Quiagen DNA extraction kit, digested with nuclease P1 and alkaline phosphatase and subjected to reversed-phase high-performance liquid chromatography (HPLC). The nucleosides deoxycytosine (*dC*) (6.22 min), deoxyguanosine (*dG*) (8.34 min), deoxythymidine (*dT*) (11.24 min), and deoxyadenosine (*dA*) (13.66 min) were monitored at 254 nm (**A**), 8-hydroxy-2′-deoxyguanosine (8-OH-dG) (9.87 min) using electrochemical detection (**B**) during the same chromatographic run. Included is a chromatogram with 2 pmol 8-OH-dG standard (std.; 9.78 min) dissolved in 20 μl distilled water

spectively. Thus, mean values of 8-OH-dG concentrations in group PE were found to be increased by 52% and in group PE-IUGR by 138% when compared with group NP.

Differences in 8-OH-dG levels were statistically significant between group NP and PE-IUGR, but not between group NP and PE as well as PE and PE-IUGR (Table 2). Figure 1 shows typical chromatograms of a placental DNA hydrolysate (Fig. 1A, B). Figure 1A depicts the ultraviolet absorbance peaks of the normal nucleosides deoxycytosine (dC), deoxyguanosine (dG), deoxythymidine (dT) and deoxyadenosine (dA). The minor peaks also observed most probably represent hydrolysis products from residual RNA within the DNA isolates, since their retention times resemble those of RNA nucleoside standards.

Figure 1B shows the corresponding electrochemical 8-OH-dG chromatogram. A chromatogram of an 8-OH-dG standard run is also included. Following a number of high initial signals, 8-OH-dG elutes at approximately 9.8 min as a peak clearly separated from adjacent signals.

Discussion

There are only a few reports on profiles of oxidative DNA adducts in human placentas. This study revealed a mean concentration of 179.97 μmol 8-OH-dG/mol dG in placental cellular DNA in normal pregnancy cases. The mean concentration was higher than reported by Daube and co-workers [4], who found mean levels close to 10 per 10^6 dG in placentas of non-smoking women. Similar to the results of these authors, in the present study, high inter-individual variations in 8-OH-dG content were noticed. The comparatively high mean level of 8-OH-dG calculated in this study in group NP is mainly due to a single elevated concentration of 1413.36 μmol 8-OH-dG/mol dG found in the placental sample of one individual. In addition to this, the reason for the difference in the mean 8-OH-dG levels can presently not be interpreted. However, in this study, efforts were made to analyse placental specimens always taken from the same part of the placenta, i.e. the mid-disc region of the chorionic plate.

It was reported that the activity of anti-oxidative enzymes and levels of pro-oxidative metal ions, such as iron, are changing in different parts of the same human placenta [12, 15]. For example, it was established that CAT activity was 75% lower in the periphery of the placental plate than in peri-insertion and mid-disc regions, but glutathione reductase and glucose-6-phosphate dehydrogenase activity in the mid-disc region was lower than in the central peri-insertion region [12]. Manci and Blackburn [15] revealed that calcium levels were highest in the periphery of the placental disc, but levels of iron known to participate in the generation of reactive oxygen species (ROS) were highest in the mid-disc region. These heterogenic metabolic patterns must be considered to contribute to the variations of 8-OH-dG levels published for placental tissues.

Concentrations of 8-OH-dG in DNA extracted from tissues can be considered as momentary steady-state levels of this DNA lesion, which is sustained by several factors: the nature and concentrations of the ROS and oxygen, the metabolic rate, the overall efficiency of the anti-oxidant defence systems, the efficiency of the DNA repair system directed against 8-OH-dG and the rate of cell proliferation [2, 6, 7, 8]. Acute or continual alterations of one or more of these parameters in normal

placental tissues may physiologically affect the 8-OH-dG steady-state level.

To minimise the influence of possible factors with known impact on the generation of 8-OH-dG, only patients without smoking habits and free from other characteristic expositions leading to 8-OH-dG formation in tissue DNA were included in our study.

This study demonstrates that the concentrations of 8-OH-dG are significantly higher in placental DNA from pregnancies complicated by PE with IUGR than that extracted from normal placentas. Taking into account the elevated mean concentration of 8-OH-dG in placentas of group PE and, the most evident, of group PE-IUGR, the results suggest a correlation between the intensity of oxidative stress and the severity of the PE cases. Thus, these results corroborate recent immunohistochemical studies on placental oxidative stress [26], which revealed higher concentrations of 8-OH-dG in placental samples from PE-IUGR cases when compared with normal pregnancies.

Scholl and Stein [24] reported significant increases in urinary 8-OH-dG excretion in women giving pre-term birth (<37 completed weeks) or giving birth to a child with a body weight below 2500 g or growth-restriction (<10th percentile). Interestingly, Matsubasa and co-workers [17] observed a decrease in urinary 8-OH-dG excretion in very low-birth-weight infants, which was related to body-weight gain.

The biochemical mechanisms by which oxidative stress is induced in PE pathogenesis are far from being understood; however, ROS might be involved [9, 27, 28]. PE pathogenesis may be related to poor placentation and acute atherosis, which result in spiral arteries insufficiency, leading to trophoblast ischaemia and hypoxia [21]. These alterations may induce an imbalance between production and neutralisation of ROS associated with placental oxidative stress. It is known that ischaemia or hypoxia alone as well as posthypoxic reperfusion can initiate an overproduction of ROS, leading to oxidative tissue damage [11, 29].

Human placenta secretes intermediary lipid peroxidation products, both to the maternal side of the placenta and toward the foetal side [27]. Lipid peroxides stimulate the prostaglandin H synthase to increase thromboxane production and inhibit prostacyclin synthase. Thus, they may cause an increase in vasoconstriction in placental and maternal circulation, leading to the primary symptoms of PE, i.e. decreased placental blood flow and maternal hypertension [28, 29].

Ness and Roberts [20] described a two-stage model for the development of PE. During the initial stage, placental perfusion is reduced due to abnormal implantation or other disorders, such as diabetes and hypertension, which may further reduce placental perfusion by a microvascular disease or intervillous thrombosis. The second stage (maternal syndrome) is a consequence of the maternal response to the reduced placental perfusion. As Roberts and Hubel [22] hypothesised, oxidative stress can be the link in this two-stage model of PE.

Our study supports this view. Placental oxidative stress appears to be a key process and comes into view as a biological endpoint for the understanding of PE development. Chappell and co-workers [3] have already shown that supplementation with anti-oxidants (vitamins C and E) can be beneficial in the prevention of PE in patients at increased risk of this disease. For instance, it is known that 8-OH-dG levels in placental DNA are inversely correlated with the plasma vitamin E concentration, and it was suggested that vitamin E may have a protective effect on placental 8-OH-dG formation [4]. In an experimental study, pre-treatment of rats with ROS scavengers (SOD and CAT) significantly inhibited the formation of placental lipid peroxides and prevented IUGR [11].

Our study suggests involvement of oxidative stress in the pathophysiology of human IUGR in pre-eclamptic pregnancies. Further studies on the biochemical mechanisms underlying PE development will reveal whether anti-oxidative treatment would be an efficient measure to prevent this disease.

Acknowledgements The authors highly appreciate the expert technical assistance of Harald Kühnel and Michael Balka.

References

1. Ames BN (1989) Endogenous oxidative DNA damage, aging, and cancer. Free Radic Res Commun 7:121–128
2. Ames BN, Shigenaga MK, Hagen TM (1993) Oxidants, antioxidants and the degenerative diseases of aging. Proc Natl Acad Sci U S A 90:7915–7922
3. Chappell LC, Seed PT, Briley AL, Annette L, Kelly FJ, Lee R, Hunt BJ, Parmar K, Bewley SJ, Shennan AH, Steer PJ, Poston L (1999) Effect of antioxidants on the occurrence of pre-eclampsia in women at increased risk: a randomised trial. Lancet 354:810–816
4. Daube H, Scherer G, Riedel K, Ruppert T, Tricker AR, Rosenbaum P, Adlkofer F (1997) DNA adducts in human placenta in relation to tobacco smoke and plasma antioxidant status. J Cancer Res Clin Oncol 123:141–151
5. Dekker GA, Sibai BM (1999) Etiology and pathogenesis of preeclampsia: current concepts. Am J Obstet Gynecol 179:1359–1375
6. Demple B, Harrison L (1994) Repair of oxidative damage to DNA: enzymology and biology. Ann Rev Biochem 63:915–948
7. Fraga CG, Shigenaga MK, Park JW, Degan P, Ames BN (1990) Oxidative damage to DNA during aging: 8-hydroxy-2′-deoxyguanosine in rat organ DNA and urine. Proc Natl Acad Sci U S A 87:4533–4537
8. Greenberg JA, Wei H, Ward K, Boozer CN (2000) Whole-body metabolic rate appears to determine the rate of DNA oxidative damage and glycation involved in aging. Mech Ageing Dev 81:107–117
9. Gűlmezoglu AM, Oosthuizen MMJ, Hofmeyr GJ (1996) Placental malondialdehyde and glutathione levels in a controlled trial of antioxidant treatment in severe preeclampsia. Hypertens Pregn 15:287–295
10. Halliwell B, Gutteridge JMC (1990) Role of free radicals and catalytic metal ions in human disease: an overview. Methods Enzymol 186:1–85
11. Hitoshi I, Michiya N, Mamoru T, Toyohiko M, Toshifumi K, Yasunori Y (1997) Role of oxygen-derived free radicals in fetal growth retardation induced by ischemia-reperfusion in rats. Am J Physiol 41:H701–H705

12. Jendryczko A, Dróżdż M, Wójcik A (1991) Regional variation in the activities of antioxidant enzymes in the term human placenta. Zentralbl Gynäkol 113:1059–1066
13. Kakimoto M, Inoguchi S, Sonta T, Yu HY, Imamura M, Etoh T, Hashimoto T, Nawata H (2002) Accumulation of 8-hydroxy-2′-deoxyguanosine and mitochondrial DNA deletion in kidney of diabetic rats. Diabetes 51:1588–1595
14. Kuchino Y, Mori F, Kasai H, Inoue H, Iwai S, Miura K, Ohtsuki E, Mishimura S (1987) Misreading of DNA templates containing 8-hydroxydeoxyguanosine at the modified base and at adjacent residues. Nature 327:77–79
15. Manci EA, Blackburn WR (1987) Regional variations in the levels of zinc, iron, copper, and calcium in the term human placenta. Placenta 8:497–502
16. Marnett LJ (2000) Oxyradicals and DNA damage. Carcinogenesis 21:361–370
17. Matsubasa T, Uchino T, Karashima S, Tanimura M, Endo F (2002) Oxidative stress in very low birth weight infants as measured by urinary 8-OHdG. Free Rad Res 36:189–193
18. McCord JM (2000) The evolution of free radicals and oxidative stress. Am J Med 108:652–659
19. National High Blood Pressure Education Program Coordinating Committee. National High Blood Pressure Education Program (NHBPEP) Working Group. (1996) Report on high blood pressure in pregnancy. High Blood Press 5:33–60
20. Ness RB, Roberts JM (1996) Heterogeneous causes constituting the single syndrome of preeclampsia: a hypothesis and its implications. Am J Obstet Gynecol 175:1365–1370
21. Redman CWG, Sargent IL (2000) Placental debris, oxidative stress and pre-eclampsia. Placenta 21:597–602
22. Roberts JM, Hubel CA (1999) Is oxidative stress the link in two-stage model of pre-eclampsia? Lancet 354:788–789
23. Schmerold I, Niedermüller H (2001) Levels of 8-hydroxy-2′-deoxyguanosine in cellular DNA from 12 tissues of young and old Sprague-Dawley rats. Exp Gerontol 36:1375–1386
24. Scholl TO, Stein TP (2001) Oxidant damage to DNA and pregnancy outcome. J Maternal Fetal Med 10:182–185
25. Steegers EAP, van der Post B (1998) Hypertension in pregnancy. In: Kurjak A (ed) Textbook of perinatal medicine. The Parthenon Publishing Group, London, New York, pp 1889–1911
26. Takagi Y, Nikaido T, Toki T, Kita N, Kanai M, Ashida T, Ohira S, Konishi I (2004) Levels of oxidative stress and redox-related molecules in the placenta in preeclampsia and fetal growth restriction. Virchows Archiv 444:49–55
27. Walsh SW, Wang Y (1993) Secretion of lipid peroxides by the human placenta. Am J Obstet Gynecol 169:1462–1466
28. Walsh SW, Wang Y, Jesse R (1996) Placental production of lipid peroxides, thromboxane, and prostacyclin in preeclampsia. Hypertens Pregn 15:101–111
29. Wang Y, Walsh SW, Kay HH (1992) Placental lipid peroxides and thromboxane are increased and prostacyclin is decreased in women with preeclampsia. Am J Obstet Gynecol 167:946–949
30. Wiktor H (2001) DNA adducts level in placentas from normal and preeclamptic pregnancies. Gin Pol 72:1240–1246
31. Wiktor H, Kankofer M (1998) Superoxide dismutase activity in normal and preeclamptic placentas. Gin Pol 69:915–918
32. Wiktor H, Kankofer M (2001) Assessment of lipid peroxidation enhancement in placentas from normal and preeclamptic pregnancies. Gin Pol 72:1217–1221
33. Wiktor H, Kankofer M (2001) Catalase activity in placentas from normal and preeclamptic pregnancy. Gin Pol 72:1228–1232
34. Wiktor H, Kankofer M, Źrubek H, Kotarski J (2000) Glutathione peroxidase activity in normal and preeclamptic placentas. Gin Pol 71:799–803

Virchows Arch (2004) 445:79–82
DOI 10.1007/s00428-004-1011-7

CASE REPORT

Marc-Antoine Rousseau · Adriana Handra-Luca · Jean-Yves Lazennec · Yves Catonné · Gérard Saillant

Metachronous multicentric giant-cell tumor of the bone in the lower limb. Case report and Ki-67 immunohistochemistry study

Received: 17 September 2003 / Accepted: 3 March 2004 / Published online: 5 May 2004
© Springer-Verlag 2004

Abstract Multicentric giant-cell tumors of the bone (GCTs) are rare. Little is known about the mechanisms by which these tumors spread and how 1% of GCT turn out to be multicentric. We report the case of a 19-year-old woman with metachronous multiple and recurrent GCTs that were unusual in their pattern of progression along the right lower limb over a 23-year period. Histology showed no evidence of malignant transformation. The treatment was repeated curettage and packing with cement. This did not permit a wide surgical margin, but avoided amputation and preserved full limb function. We tested the proliferation index marker Ki-67 in the tumor specimens. Ki-67 expression was limited to the mononuclear cell component of the tumors. The proliferation index was similar in each new tumor and higher in recurrences for each location. In this case, proliferation was initially low in the new tumor location, despite the time difference and independent from the initial clone evolution. Proliferation index increased in recurrent GCTs after marginal margin resection.

Keywords Giant-cell tumor · Bone · Multicentric · Ki-67 · Immunohistochemistry

Introduction

Giant-cell tumors (GCTs) are benign epiphyseal osteolytic tumors that are encountered in young adults and account for 5–10% of all bone tumors [32, 34]. Multicentric GCTs are extremely rare and represent less than 1% of GCTs [32]. Fewer than 60 cases have been reported in the literature [2, 3, 7, 8, 9, 10, 11, 12, 13, 14, 15, 16, 17, 19, 20, 21, 22, 23, 24, 25, 26, 27, 29, 30, 31, 33, 35, 36]. Therefore, the pathogenesis of multiple benign lesions is still a matter of debate [22]. Multicentric GCT is considered to be either a genuine multifocal disease [4] or the result of local or distant spread of a solitary initial lesion [6, 32].

We report a very unusual case of multicentric and recurrent benign GCTs in a lower limb, which was a unique opportunity to investigate the natural histological course in multiple GCTs by retrospectively labeling the tumors with Ki-67 in new locations and recurrences over a period of 23 years in the same patient.

M.-A. Rousseau · J.-Y. Lazennec (✉) · Y. Catonné · G. Saillant
Service de Chirurgie Orthopédique et Traumatologique,
Hôpital La Pitié Salpêtrière, Université de Paris VI,
47 bd de l'Hôpital, 75013 Paris, France
e-mail: laurence.thomas@psl.ap-hp.fr
Tel.: +33-1-42177061
Fax: +33-1-42177062

A. Handra-Luca
Department of Pathology,
Hôpital La Pitié Salpêtrière, Université de Paris VI,
47 bd de l'Hôpital, 75013 Paris, France

Clinical history

A 19-year-old female patient was hospitalized for knee pain in 1980. Plain radiographs showed an osteolytic lesion in the distal right femur. This lesion was shown to be a benign GCT. The treatment was curettage and autologous trabecular bone grafting.

In 1984, a second tumor developed in the proximal right tibia. It was treated by the same procedure, and histology showed the same tumor type. In 1996, a third and a fourth tumor arose in the distal right tibia and the distal fibula (Fig. 1A). In addition, the previous femoral and tibial lesions had recurred (Fig. 1B). These tumors were grade 1 in the Campanacci roentgenographic classification scale/scheme [6], with well-defined margins and a thin rim of mature bone. Biopsy specimens again showed benign GCT. Treatment was curettage and packing with cement (Palacos, Biomet Inc., Warsaw, IN, USA). The benign nature of the lesions was confirmed by histological examination of the entire curettage specimen.

In 2000, 20 years after the diagnosis of the first tumor, the patient was admitted for a second recurrence in the proximal right tibia associated with a recurrence in the distal right fibula (Campanacci grade 2: no radioopaque rim). The treatment was curettage and packing with cement. Histology showed the same features of benign GCT.

In 2001, a third recurrence in the proximal right tibia was diagnosed. Spread into the soft tissues was noted (Campanacci grade 3), without evidence of blood-vessel involvement. The lesion was benign and was again treated by curettage and cement packing.

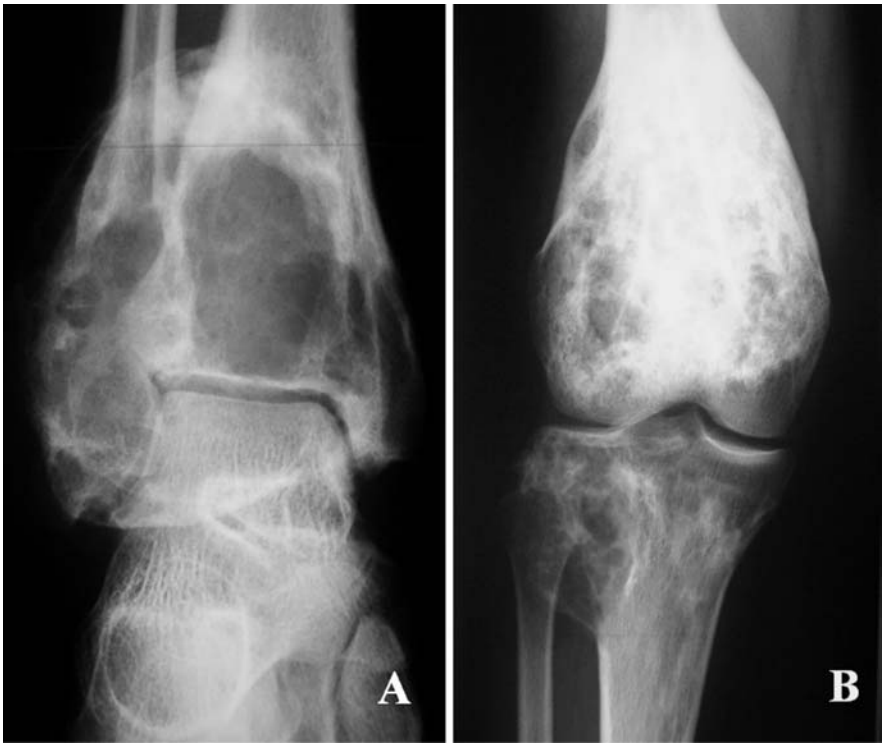


Fig. 1 Anteroposterior radiographs of the right ankle (**A**) and the right knee (**B**), showing new locations of giant cell tumor in the distal tibia and fibula and recurrences in the distal femur and proximal tibia (1996)

At last follow-up in 2003, the patient was able to walk alone and had full range of motion in her knee and ankle. A computed tomography scan showed no evidence of recurrence or new tumors.

At no point during the course in this patient did the laboratory tests show evidence of hyperparathyroidism. Imaging studies found no lung metastatic lesions. Neither radiation therapy nor chemotherapy was used in this patient.

Materials and methods

The nine tumor specimens were fixed in 10% formaldehyde solution and embedded in paraffin. Serial tissue sections 5-μm thick were cut and stained with hematoxylin and eosin. Immunohistochemical techniques were carried out using the avidin-biotin peroxidase complex method using an LSAB2 kit (Dako, Glostrup, Denmark). The primary antibody used in this study was Ki-67 (MIB-1 clone, dilution 1:25; Dako).

Histological grade [34], amount of spindle-cell transformation, presence of intercellular collagen, osteoid formation, necrosis and hemorrhage were noted.

Expression of the proliferation index marker Ki-67 in the nuclear area of the tumor cells was examined using immunohistochemistry. The labeled-cell count (Ki-67 proliferation index) was determined in ten high-power fields (×40 magnification) by a blinded observer. Ki-67 proliferation index was defined as the ratio of labeled cells to total cells.

Repeated measures of the Ki-67 proliferation index were compared between groups using a one-way analysis of variance. *P* values of 0.05 or less were considered significant. StatView 4.0 (Abacus Concepts Inc., Berkeley, CA, USA) was used to run the statistical tests.

Results

All tumor specimens showed a benign appearance with standard staining, rated histological grade 1 or 2 according to the proportion of mononuclear cells and multinuclear giant cells (Table 1). The mononuclear cells were round to oval or spindle shaped, with nuclei showing rare mitotic figures and no atypical features. Spindle-shape aspect of mononuclear cells was noted in all tumors, both primary and recurrent. It represented 25–50% of the tumoral tissue and was more frequent in recurrent GCTs (Fig. 2). The multinucleated giant cells contained 10–50

Table 1 Histology grade and Ki-67 proliferation index at each tumor site over time (average in ten high-power fields; range is listed in parentheses). Proliferation index is similar in each new tumor (P=0.1) and higher in recurrences for each location (P<0.001)

	1980	1984	1996	2000	2001
Distal femur	Histological grade: 1 Ki-67: 0.2 (0–1)	-	Histological grade: 2 Ki-67: 12 (5–19)	-	-
Proximal tibia	-	Histological grade: 1 Ki-67: 0.9 (0–4)	Histological grade: 1 Ki-67: 0.2 (0–1)	Histological grade: 1 Ki-67: 11.1 (5–21)	Histological grade: 2 Ki-67: 10.7 (2–25)
Distal tibia	-	-	Histological grade: 1 Ki-67: 0.2 (0–1)	-	-
Distal fibula	-	-	Histological grade: 1 Ki-67: 0.2 (0–1)	Histological grade: 1 Ki-67: 10.1 (2–22)	-

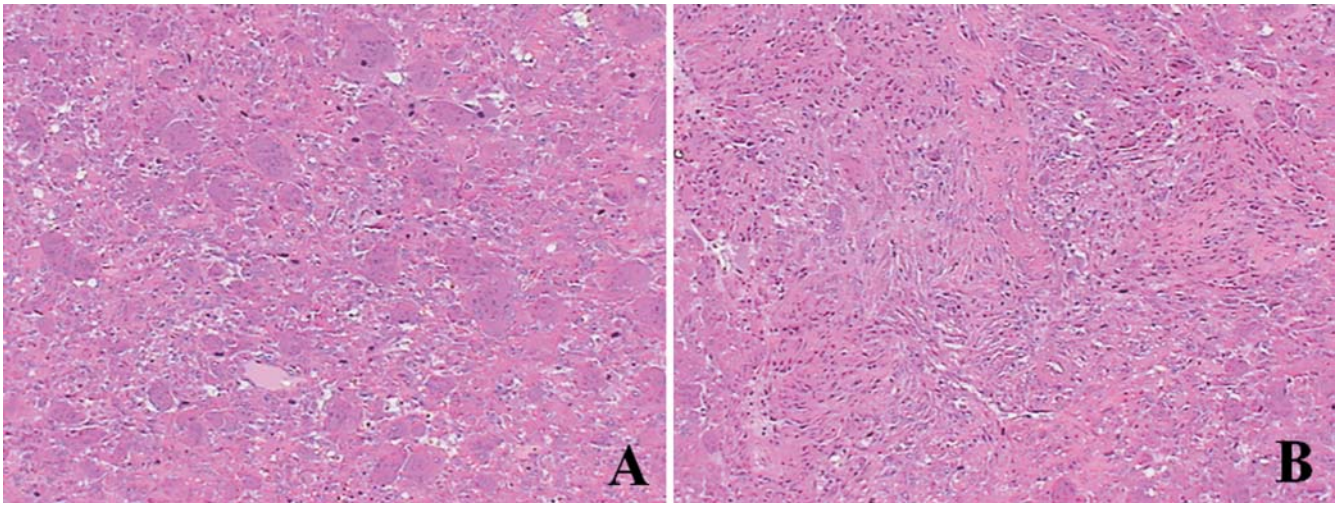


Fig. 2 Hematoxylin and eosin stain, original magnification ×10. **A** Primitive giant-cell tumor (GCT) of the distal femur (giant cells plentiful: histological grade 1). **B** Recurrent GCT in the distal femur (stroma prominent: histological grade 2). The recurrent tumor shows large zones of spindle-cell transformation after 16 years

nuclei each. Intercellular collagen was noted to a similar extent in both primary and recurrent tumors. Necrosis and osteoid formation were focal and seen only in GCTs of distal tibia and fibula. Intratumoral hemorrhage, without aneurismal cyst formation, was noted in all tumor specimens.

Ki-67 immunohistochemistry labeling was confined to the nuclei of the mononuclear cells. None of the multinucleated giant cells were labeled (Fig. 2). The Ki-67 proliferation index was not significantly different for each new tumor (P=0.10) despite the 16-year difference between the first and the most recent location. The Ki-67 proliferation index increased significantly (P<0.001) in the case of recurrence for a given location (Table 1).

Discussion

Multiple GCT cases are rare. This rich case was an exceptional opportunity to study changes of the Ki-67 proliferation index in benign multicentric and recurrent GCT over time. Comparisons were paired, since all data came from the same patient. This study demonstrated that the Ki-67 proliferation index was similar for each metachronous new location and increased in case of recurrence. The small mononuclear cells were confirmed to be the proliferating component in the GCTs.

Since the histologically benign aspect and the Ki-67 proliferation index were not significantly different in new tumors, the mechanism for GCT spread in this observation does not seem to correspond to the accumulation of tumor transformations. Each metachronous tumor evolved separately in a similar way, starting with the same proliferation profile. While little is known about the mechanism by which GCT spread, various hypotheses have been suggested from several patterns reported in the literature. Bipolar tumors (e.g., both sides of the knee or wrist) seem more common, and cases with tumors at distant sites have been described, which may involve both the right and the left sides [23] or both an upper and a lower limb [36]. Therefore, contiguous spread through a joint [26], skip metastasis within a given bone [22] and occurrence of several primary tumors at different sites [21, 26] have all been suggested, but no specific immunohistochemical characterization has been performed previously in multiple GCTs to investigate tumor filiation.

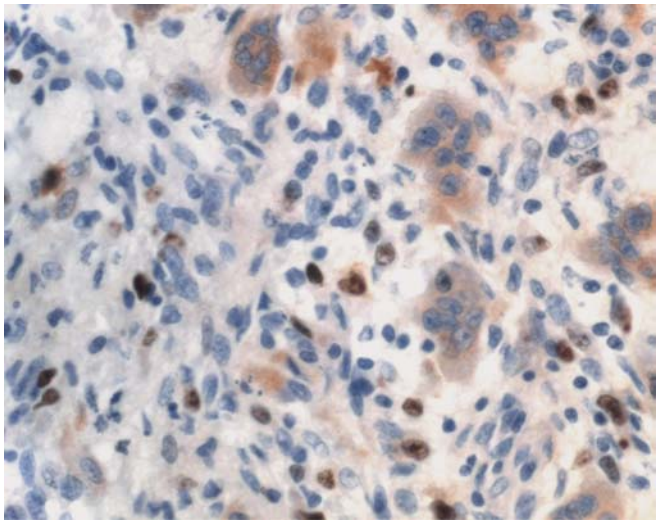


Fig. 3 Ki-67 immunohistochemistry, original magnification ×40. Ki-67 labeling (*in brown*) is limited to the nuclei of mononuclear cells

However, Ki-67 immunohistochemistry has been studied in single [18] and recurrent GCT [1, 28]. Our observation that Ki-67 labeling was confined to the mononuclear cells (Fig 3) is consistent with the literature [18] and confirms that GCTs result in the proliferation of

mononuclear cells as suggested previously [5]. The tumor heterogeneity in Ki-67 labeling that we observed in our study has also been reported in a single GCT [28]. The increase in Ki-67 proliferation index in the recurrent tumor for a given location in the case reported here shows that recurrent tissue may be more aggressive than primary tumors. This may be related to increasing Campanacci grade over time on the radiographs, as in the proximal tibia in this case. Ki-67 proliferation index increase in recurrent GCTs has been suggested by Antal et al. [1], but was not significant. Suhl et al. [28] concluded that Ki-67 was not predictive of GCT recurrence, but comparisons between recurrent and primary groups were not paired since tissue samples were from two different groups of patients.

The Ki-67 index in some of our GCT samples was lower than values reported in the literature, which may have been due to different fixation techniques over 23 years. However, since control labeling of endothelial cells was positive, low proliferation indexes were reliable, and comparisons between specimens were possible.

Acknowledgement The authors thank Dr. M. Landau-Ossondo (Centre Hospitalier Universitaire de Fort de France) for helping collect data.

References

1. Antal I, Sapi Z, Szendroi M (1999) The prognostic significance of DNA cytophotometry and proliferation index (Ki-67) in giant cell tumors of bone. Int Orthop 23:315–319
2. Averill RM, Smith RJ, Campbell CJ (1980) Giant-cell tumors of the bones of the hand. J Hand Surg 5:39–50
3. Bacchini P, Bertoni F, Ruggieri P, Campanacci M (1995) Multicentric giant cell tumor of skeleton. Skeletal Radiol 24:371–374
4. Bertoni F, Present D, Enneking W (1985) Giant cell tumor of bone with pulmonary metastases. J Bone Joint Surg Am 67:890–900
5. Bouropoulou V, Kontogeorgos G, Manika Z (1985) A histological and immunoenzymatic study on the histogenesis of "giant cell tumor of the bone". Path Res Pract 180:61–67
6. Campanacci M, Baldini N, Boriani S (1987) Giant cell tumor of bone. J Bone Joint Surg Am 69:106–114
7. Cannova J (1998) Multiple giant cell tumors in a patient with gulf war syndrome. Mil Med 163:184–185
8. Cummins CA, Scarborough MT, Enneking WF (1996) Multicentric giant cell tumor of bone. Clin Orthop 245–252
9. De Smedt M, Copin G, Boeri C, Dosch J, Dupuis M, Marcellin L (1999) A propos d'un cas de tumeur à cellules géantes d'évolution rapide avec métastases osseuses multiples. Rev Chir Orthop Reparatrice Appar Mot 85:293–296
10. Duan CX (1985) Multicentric giant-cell tumor of bone (a report of 5 cases). Zhonghua Fang She Xue Za Zhi 19:76–78
11. Dumford K, Moore TE, Walker CW, Jaksha J (2003) Multifocal, metachronous, giant cell tumor of the lower limb. Skeletal Radiol 32:147–150
12. Feldman F (1980) Case report 115. Skeletal Radiol 5:119–126
13. Goldenberg R, Campbell C, Bonfiglio M (1970) Giant cell tumor of the bone. An analysis of two hundred and eighteen cases. J Bone Joint Surg Am 52:619–663
14. Haskell A, Wodowoz O, Johnston JO (2003) Metachronous multicentric giant cell tumor: a case report and literature review. Clin Orthop 162–168
15. Hindman BW, Seeger LL, Stanley P, Forrester DM, Schwinn CP, Tan SZ (1994) Multicentric giant cell tumor: report of five new cases. Skeletal Radiol 23:187–190
16. Kadir S, Hudson TM (1978) Multicentric giant cell tumors of bone. ROFO Fortschr Geb Rontgenstr Nuklearmed 128:769–770
17. Kaufman S, Isaac P (1977) Multicentric giant-cell tumors. South Med J 70:105–107
18. Kauzman A, Li S, Bradley G, Bell R, Wunder J, Kandel R (2003) Cyclin alterations in giant cell tumor of bone. Mod Pathol 16:210–218
19. Macdonald D, Fornasier V, Cameron J (2001) Multicentric giant cell tumour involving the patella. Can J Surg 44:222–223
20. Madhuri V, Sundararaj GD, Babu NV, Ponnaiya J, Korula RJ (1993) Multicentric giant cell tumour of bone—a report of two cases. Indian J Cancer 30:135–139
21. Park IH, Jeon IH (2003) Multicentric giant cell tumor of bone: ten lesions at presentation. Skeletal Radiol 32:526–529
22. Park YK, Ryu KN, Han CS, Bae DK (1999) Multifocal, metachronous giant-cell tumor of the ulna. A case report. J Bone Joint Surg Am 81:409–413
23. Peimer CA, Schiller AL, Mankin HJ, Smith RJ (1980) Multicentric giant-cell tumor of bone. J Bone Joint Surg Am 62:652–656
24. Sadat-Ali M (1997) Metachronous multicentric giant-cell tumour: a case report. Indian J Cancer 34:169–76
25. Sanghvi V, Lala M, Desai S, Chaturvedi P, Rodrigues G (1999) Synchronous multicentric giant cell tumour: a case report with review of literature. Eur J Surg Oncol 25:636–637
26. Sim FH, Dahlin DC, Beabout JW (1977) Multicentric giant-cell tumor of bone. J Bone Joint Surg Am 59:1052–1060
27. Singson R, Feldman F (1983) Case report 229: multiple (multicentric) giant cell tumors of bone. Skeletal Radiol 9:276–281
28. Sulh M, Greco M, Jiang T, Goswami S, Present D, Steiner G (1996) Proliferation index and vascular density of giant cell tumors of bone: are they prognostic markers? Cancer 77:2044–2051
29. Sybrandy S, DeLaFuent A (1973) Multiple giant-cell tumor of bone. Report of a case. J Bone Joint Surg Br 55:350–358
30. Taraporvala JC, Goyal DR, Hire D (1997) Multicentric giant cell tumor of bone—a case report and comprehensive review of literature. Indian J Cancer 34:128–135
31. Taylor KF, Yingsakmongkol W, Conard KA, Stanton RP (2003) Multicentric giant cell tumor of bone: a case report and review of the literature. Clin Orthop 267–273
32. Tomeno B, Forest M (1990) Tumeurs à cellules géantes. In: Conférence d'enseignement de la SOFCOT. E. Scientifique, Paris, pp 31–50
33. Tornberg DN, Dick HM, Johnston AD (1975) Multicentric giant-cell tumors in the long bones. A case report. J Bone Joint Surg Am 57:420–422
34. Unni K (1996) Chapter 19: giant cell tumor. In: Dahlin's bone tumors. Lippincott-Raven, Philadelphia, pp 263–282
35. Williams HT (1989) Multicentric giant cell tumor of bone. Clin Nucl Med 14:631–633
36. Wu KK, Ross PM, Mitchell DC, Sprague HH (1986) Evolution of a case of multicentric giant cell tumor over a 23-year period. Clin Orthop 279–288

Virchows Arch (2004) 445:83–89
DOI 10.1007/s00428-004-1031-3

CASE REPORT

Bolesław Papla · Paweł Spólnik · Ewa Rzenno · Andrzej Zduńczyk · Zbigniew Rudzki · Krzysztof Okoń · Wojciech Szczepański · Wojciech Dąbroś · Jerzy Stachura

Generalized crystal-storing histiocytosis as a presentation of multiple myeloma: a case with a possible pro-aggregation defect in the immunoglobulin heavy chain

Received: 21 October 2003 / Accepted: 22 February 2004 / Published online: 12 May 2004
© Springer-Verlag 2004

Abstract Crystal-storing histiocytosis (CSH) with massive accumulation of particulate immunoglobulins is a rare phenomenon accompanying B-cell dyscrasias. In the reported case (M51), the disease presented as systemic CSH and later was proved to be a frank multiple myeloma. The aggregates of crystal-laden histiocytes were demonstrated in the bone marrow, lungs, kidney, and liver. Additionally, the crystalline immunoglobulin particles were identified in renal stromal cells and in hepatocytes. The patient developed lung adenocarcinoma and died 12 months after the presentation, shortly after the lobectomy. In this paper, we report the results of morphological (including electron microscopy), immunohistochemical, and biochemical analysis. The tendency for aggregation of the IgG kappa monoclonal protein was due to the abnormal physicochemical properties of its heavy chain. Massive accumulation of crystal-storing histiocytes surpassed the myeloma tumor burden and markedly contributed to the severity of the disease.

Keywords Plasma-cell myeloma · Crystal-storing histiocytosis · Trephine bone-marrow biopsy · Electron microscopy

B. Papla · Z. Rudzki · K. Okoń · W. Szczepański · W. Dąbroś · J. Stachura (✉)
Department of Pathomorphology, Collegium Medicum, Jagiellonian University,
Grzegórzecka 16, 31-531 Kraków, Poland
e-mail: mpstachu@cyf-kr.edu.pl
Tel.: +48-12-4211564
Fax: +48-12-4119725

P. Spólnik
Institute of Medical Biochemistry, Collegium Medicum, Jagiellonian University,
Kraków, Poland

E. Rzenno · A. Zduńczyk
Department of Hematology,
Ludwik Rydygier Memorial Hospital,
Kraków, Poland

Introduction

Intrahistiocytic accumulation of crystallized immunoglobulins is a rare manifestation of monoclonal gammapathies/plasma-cell dyscrasias [6]. Large histiocytes filled with crystalline particles are usually found in ample quantities in the biopsied organs, and their exact nature may be unclear until special immunohistochemical or biochemical studies are performed. In an extensive review, Schaefer called these histiocytes "pseudo-pseudo-Gaucher cells," to distinguish them from morphologically similar pseudo-Gaucher cells, found usually in the context of increased myeloid cell turnover, typically in chronic myelogenous leukemia [15]. Recently, Lebeau et al. reported a case of monoclonal gammapathy evolving into multiple myeloma, presenting initially as a systemic crystal-storing histiocytosis (CSH), and provided detailed proteome analysis of the pathological immunoglobulin [9]. We describe the morphology of involved organs and physicochemical properties of the protein in another case, presenting initially as a systemic CSH, and only later revealed to be secondary to multiple myeloma.

Case report

A 51-year-old male, diabetic for 3 years, presented with a 6-month history of progressive fatigue, episodic fevers, back pains without radiological lesions, slight anemia (Hb=12.9 g/dl), and minimal hepatosplenomegaly. Chest X-ray was normal. Serum protein analysis revealed total protein 83 g/l, albumin 41.8 g/l, globulin alpha-1 2.49 g/l, alpha-2 9.55 g/l, beta 7.06 g/l, gamma 22.16 g/l (IgG 21.3 g/l, IgA 0.36 g/l, IgM 0.25 g/l), kappa light chains 30.5 g/l, lambda 2.88 g/l (kappa/lambda=10.6). The urine sample contained Bence–Jones protein of the kappa type (1540 mg/l, kappa/lambda=51.7).

Multiple myeloma was suspected, but a trephine bone marrow biopsy revealed only fibrotic bone marrow occupied almost exclusively by histiocytes laden with discrete eosinophilic particles. The number of plasma cells was negligible, and they did not manifest signs of atypia or monoclonality using immunohistochemistry. Since the whole clinico-laboratory picture did not strictly fulfill the

Table 1 Antibodies used for immunohistochemistry in paraffin-embedded tissue sections

Antibody specificity	Supplier	Titer	Antigen retrieval
CD138	Dako	1:100	Citrate, pH 6.0
CD68/PGM1	Dako	1:50	Citrate, pH 6.0
Kappa	Dako	1:1600	-
Lambda	Dako	1:200	-
IgA	Dako	1:300	Proteinase K
IgG	Dako	1:500	-
IgM	Dako	1:300	-
AL amyloid	Dako	1:50	-
CD56	Novocastra	1:50	Ethylenediaminetetra-acetate pH 8.0

criteria to diagnose multiple myeloma, the patient was initially observed without any anti-neoplastic treatment.

Rapid weight loss and constant high fever 7 months later prompted the second trephine bone-marrow biopsy, diagnostic of multiple myeloma associated with CSH. At the time of the diagnosis, his anemia worsened (Hb=10.5 g/dl), the spleen measured 146×64 mm, the liver increased, and the platelets dropped to 140×10^9/l.

Due to the concomitant signs of progressive liver and renal insufficiency, both organs were biopsied using a thick-needle technique. Control chest X-ray showed a 25-mm tumor within the upper lobe of the left lung. Bronchoscopic biopsy was diagnostic of adenocarcinoma. Anti-myeloma cytostatic treatment was deferred, and the patient was subjected to lobectomy. Shortly after the surgery, he developed multi-organ failure and died 1 year after the initial presentation. Autopsy was not performed.

Materials and methods

Decalcified trephine bone-marrow biopsies were stained with hematoxylin/eosin, Giemsa, Gomori, and periodic acid-Schiff (PAS) methods. Immunohistochemical studies were performed using antibodies listed in Table 1. The thick-needle kidney and liver biopsies were divided into two parts for optical and electron microscopy studies. The lobectomy specimen was fixed in buffered formaldehyde and processed routinely.

For the serum protein studies, the small shreds found in the serum were incubated on a microscope slide at room temperature for 30 min with fluorescein isothiocyanate(FITC)-labeled anti-IgG antibodies and then carefully rinsed. The tendency of the paraprotein to crystallize was tested using a standard vapor diffusion experiment—"hanging drop technique." Crystals were searched in a pepsin-digested (1 mg/ml) sample of isolated myeloma protein (17 mg/ml) in acetate buffer (pH 4.0). Pepsin digestion was performed at 37°C with an enzyme:substrate ratio of 1:100 (wt:wt). Protein studies also involved controls composed of normal immunoglobulin samples.

The protein molecular weight was determined using sodium dodecyl sulfate-polyacrylamide gel electrophoresis (SDS-PAGE) on a 12.5% gel, using SIGMA molecular weight markers as standards.

Results

Morphology and immunohistochemistry

The first trephine biopsy visualized the bone marrow severely depleted of normal hemopoiesis and occupied by aggregates of large, CD68-PGM1-positive histiocytes with oval or round cytoplasm and small unremarkable nuclei (Fig. 1A, B, C). Their cytoplasm was filled with crescentic crystalline PAS-positive inclusions, somewhat reminiscent of inclusions found in the Gaucher cells, but shorter and more irregular. These cells were negative for lambda immunoglobulin light chain. The staining for the kappa chain was ambiguous and finally interpreted as negative. At this time, no heavy-chain staining was performed. The biopsy did not reveal any abnormal plasma cells or lymphocytes, and the few scattered typical plasmacytes visualized with the anti-CD138 antibody did not raise a suspicion of multiple myeloma.

On the second trephine performed 7 months later, the bone marrow contained identical abnormal histiocytes, but now intermingled with atypical plasma cells (Fig. 1D). The plasma cells formed an interstitial and diffuse infiltrate, constituting approximately 60% of hemopoiesis. The plasma cells were strongly immunopositive for CD138+, kappa light chain, and IgG and negative for lambda light chain, IgA, IgM, and CD56. In the second biopsy, the intrahistiocytic particles were weakly positive for the kappa light chain. Weak IgG staining in the histiocytes contrasted with the strong staining pattern of plasma cells (Fig. 1E). The histiocytes were negative for lambda chain, AL amyloid, IgA, and IgM. Few large plasma cells contained similar intracytoplasmic particles in quantities much lower than the histiocytes.

Kidney biopsy showed only nonspecific changes at the level of optical microscopy. Electron microscopy revealed electron dense, cristaloid intracytoplasmic inclusions in podocytes, glomerular endothelial cells, mesangial cells, and in the tubular epithelium (Fig. 2A). At higher magnification, the inclusions showed a multilayered structure with periodicity of about 10 nm.

The liver biopsy revealed small, dispersed clusters of macrophages located both in the periportal areas and within the lobules (Fig. 2B). Cytoplasm of some hepatocytes contained small particles, gray–blue in Masson trichrome. Both macrophages and hepatocytes showed positive immunoexpression of kappa chains, being negative for lambda, IgA, IgG, and IgM; however, the reaction was stronger in hepatocytes. Crystaloids similar to these found in the kidney were visualized in transmission electron microscopy in hepatocytes and macrophages. The crystaloids located within hepatocytes were less numerous, but more frequently formed discrete clusters (Fig. 2C).

The lobectomy specimen contained a 2.5-cm peribronchial tumor. Part of the tumor represented a well-differentiated adenocarcinoma, whereas the remaining part was either necrotic or occupied exclusively by storage histiocytes, identical to those found in other organs (Fig. 2D). Additionally, clumps of the histiocytes were seen both within the neoplastic glands and within bronchi and alveoli outside the tumor (Fig. 2E). Some storage histiocytes resided within the fibrotic pulmonary stroma. The lobectomy specimen was not infiltrated by atypical plasma cells. None of the examined tissues contained

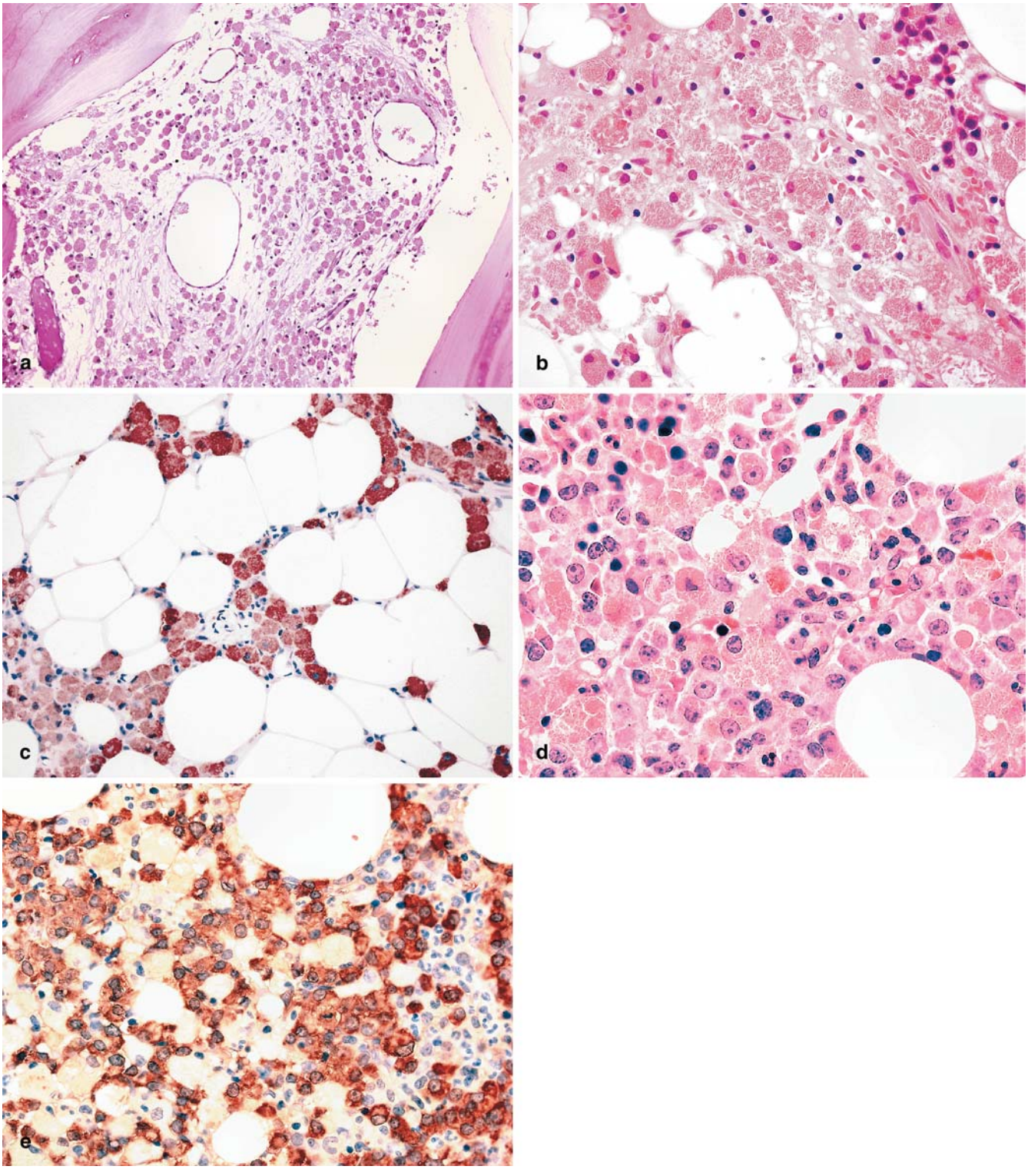


Fig. 1 Trephine bone-marrow biopsies in crystal-storing histiocytosis secondary to multiple myeloma. **A** At presentation, numerous histiocytes ("pseudo-pseudo-Gaucher cells") replace the major hematopoietic lineages. No plasma-cell infiltrate is evident (periodic acid-Schiff, lens ×20). **B** The histiocytes contain short, needle-like crystalline inclusions [hematoxylin/eosin (HE), lens ×60]. **C** Strong immunoreactivity for CD68-PGM1 in the crystal-storing histiocytes [alkaline phosphatase–antialkaline phosphatase (APAAP) technique, HE lens ×40]. **D** After 3 months, the crystal-storing histiocytes are mixed with a large number of atypical plasma cells (HE, lens ×60). **E** The plasma cells are strongly IgG positive, in contrast to the large histiocytes, showing only very weak IgG immunoreactivity (APAPP technique, lens ×60)

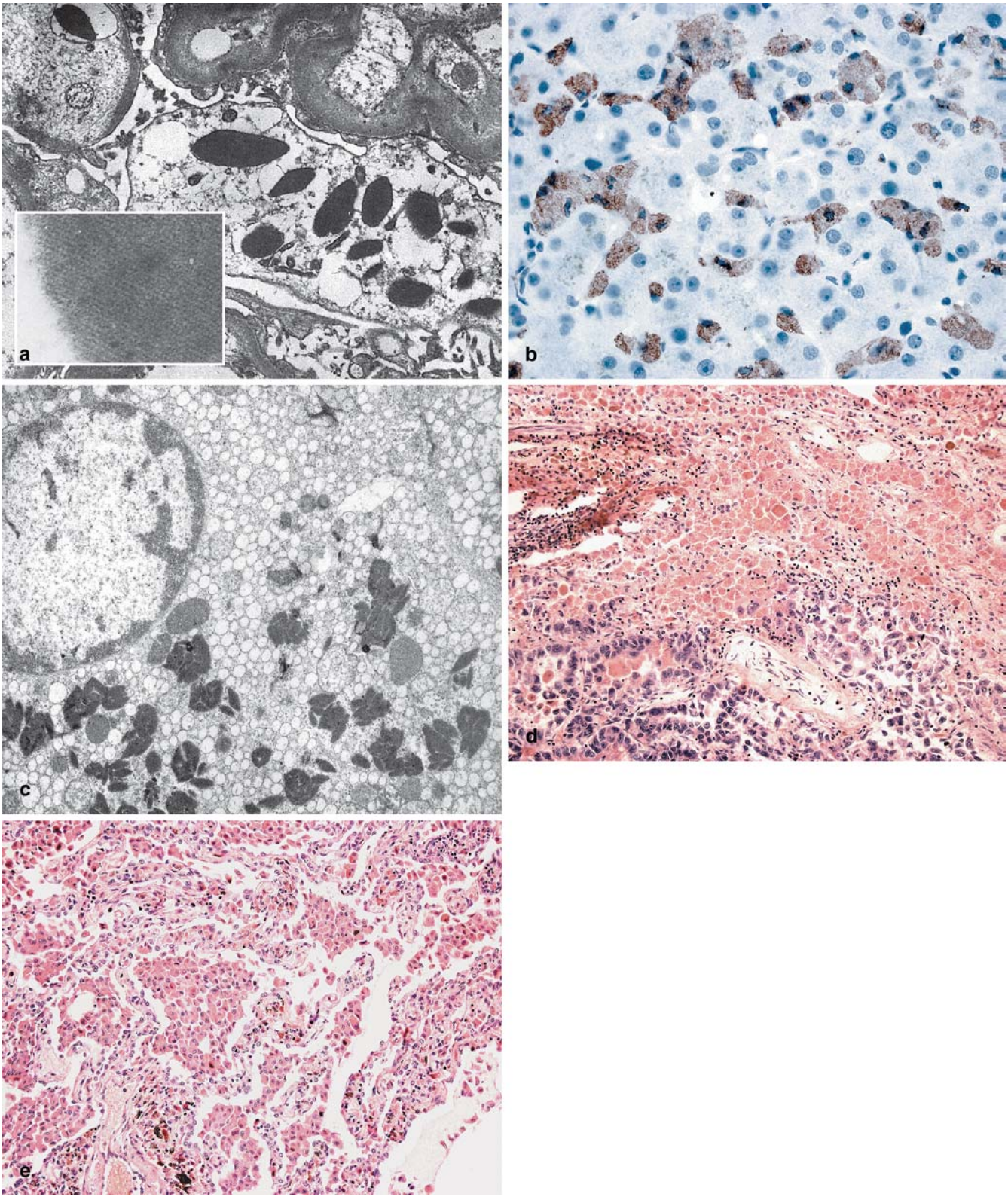


Fig. 2 Solid organ pathology in the course of crystal-storing histiocytosis. **A** Kidney biopsy. Transmission electron microscopy reveals rhomboid electron-dense particles also stored in the podocytes (original magnification ×7000). *Inset* periodical linear ultrastructure of the inclusions (original magnification ×50,000). **B** Liver biopsy immunostained with CD68, highlighting the histiocytes with ample cytoplasm [alkaline phosphatase–antialkaline phosphatase (APAAP) technique, lens ×60]. **C** Ultrastructure of a hepatocyte containing crystalline intracytoplasmic inclusions (original magnification ×4400). **D** Lobectomy specimen. Solid accumulation of storage histiocytes (*upper*) contributes to the formation of the tumor, also composed of well-differentiated pulmonary adenocarcinoma (*lower*) [hematoxylin/eosin (HE), lens ×20]. **E** Desquamative interstitial pneumonia-like reaction in the lung at the periphery of the resected lobe. The alveoli are filled with the crystal-storing histiocytes (HE, lens ×20)

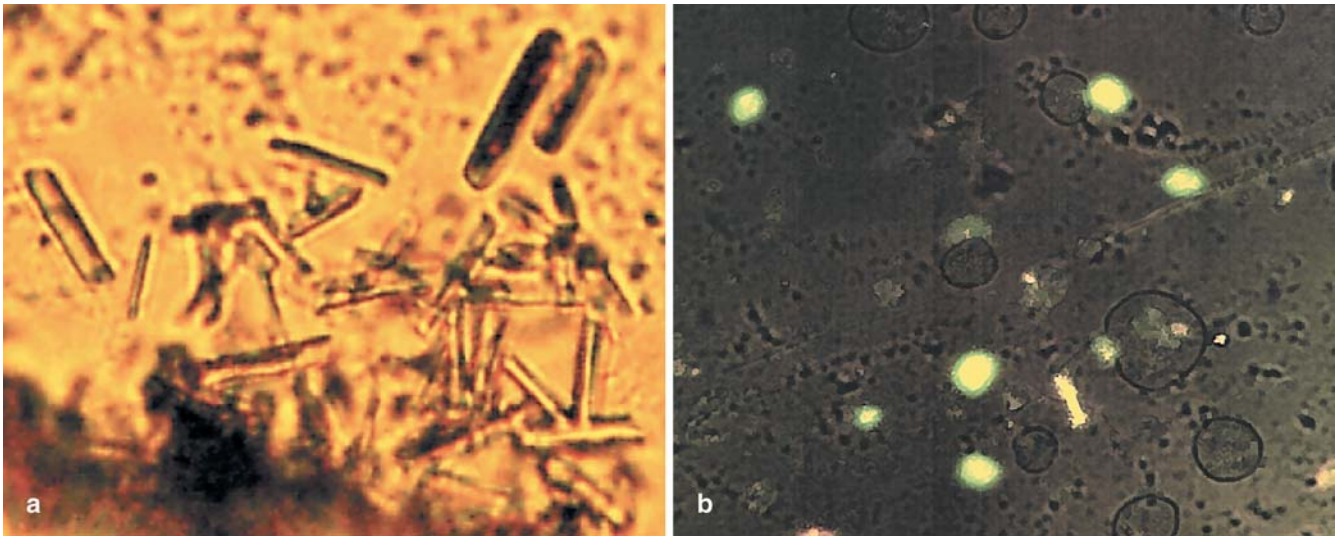


Fig. 3 Abnormal biochemical properties of the serum monoclonal protein. **A** The pathological protein aggregates spontaneously forming in the serum in vivo, demonstrated with fluorescein isothiocyanate-labeled anti-IgG antibody. **B** Protein crystals formation in vitro. This phenomenon constitutes a model of abnormal crystallization in histiocytes and other cells (the "hanging drop" technique)

intravascular crystals, typically characterizing cryocrystaglobulinemia [1, 3].

Protein studies

Serum did not contain cryoglobulins or free immunoglobulin light chains. The level of polyclonal immunoglobulins was low. A serum monoclonal protein fraction represented immunoglobulin of the IgG kappa class. It complexed efficiently with Congo red and demonstrated an abnormally high proteolytic susceptibility, surpassing that of normal IgG—a phenomenon attributed to the low-packing stability [12, 16]. The appearance of gamma heavy chain-derived proteolytic products upon brief trypsin digestion and the relatively high molecular weight of the heavy chain (56,000 Da) observed in SDS-PAGE provided the evidence that the structural abnormality was within the heavy chain rather than the light chain. The increased aggregation tendency of this protein likely resulted from its low structural stability [2, 8, 19]. This contributed to the formation of amorphous microaggregates present in the serum, visualized directly in the serum samples using the FITC-labeled anti-IgG antibodies (Fig. 3A). The expected high crystallization tendency of proteolytic products was confirmed in vitro using the hanging-drop technique applied to the pepsin-digested sample (Fig. 3B).

Discussion

A biopsy showing crystal-storing histiocytes presents a diagnostic dilemma. The obvious differential diagnosis includes metabolic storage disorders and accumulation of the pseudo-Gaucher cells. Thesaurysmoses may be usually eliminated upon a review of clinical data and morphology of the histiocytes, whereas the pseudo-Gaucher cells are, in practice, usually found in small numbers in association with a pathognomonic histological picture of chronic myeloid leukemia. The clinical information about the presence of monoclonal serum protein plays a pivotal role in the identification of the particle material as immunoglobulins, especially taking into account the possible faint or even negative staining for immunoglobulins in the histiocytes. In our case, the immunostaining both for the monoclonal light chain (kappa) and the heavy chain (gamma) gave very weak results, the kappa staining having been actually interpreted as negative in the first biopsy. This contrasted with a very strong staining of atypical plasma cells. A similar phenomenon was reported by Jones et al. in their series of 12 cases of CSH secondary to immune-cell dyscrasia [6]. These authors suggested that the discrepancy between the faint immunoglobulin staining in histiocytes and strong immunoreaction in monoclonal B-cells resulted from inaccessibility of histiocytic crystalline deposits to the staining reagents. This cannot be ruled out, although the fact that histological immunostains are performed on cross-sections through cells should theoretically overcome the problem of limited reagent accessibility into some intracytoplasmic compartments. Alternatively, it is possible that the histiocytes stored partially digested protein deposits whose weak immunogenecity was due to destruction of epitopes crucial for efficient immunostaining. Interestingly, a reverse phenomenon (i.e., strong reaction in the histiocytes and weak in the monoclonal plasma cells) was noted in another recently reported case [9]. A selective digestion of immunoglobulins within histiocytes leading

to unmasking of detectable epitopes could also account for this discrepancy.

CSH may complicate multiple myeloma, isolated plasma cell tumors, other lymphoid neoplasms (particularly lymphoplasmacytic lymphoma), transient polyclonal plasma-cell hyperplasia after bone-marrow transplantation, and finally monoclonal gammapathy [6, 9]. CSH is a systemic process, whereas its initiating condition may be confined to one organ or tissue compartment. In the cases suspected for multiple myeloma and negative upon the first bone marrow biopsy, control trephines performed in short time intervals might be diagnostic.

Apart from the underlying neoplasia, the systemic nature of the reactive histiocytosis causes significant clinical problems. CSH is typically associated with a poor prognosis, regardless of its origin [9]. In our case, the severe histiocytic infiltration of the liver and kidneys, not accompanied by myeloma invasion, likely contributed to the insufficiency of these organs. The storage of particulate immunoglobulins within the liver was previously described in the Kupffer cells [9] and within the hepatocytes [7, 9]. Hepatocytes express the receptors for the Fc portion of the immunoglobulin molecules and, in some circumstances, efficiently bind immune complexes or aggregates of immunoglobulins, especially heat-aggregated IgG [5, 14, 18]. The immunoglobulins can also enter the hepatocytes from plasma via passive fluid-phase endocytosis to be later secreted to bile ducts [10].

Interstitial lung disease, possibly provoked by the presence of abnormal histiocytes, could account for the rapidly fatal outcome after the surgery. The desquamative interstitial pneumonia-like pattern with relative sparing of the draining lymph nodes observed in our case may be characteristic for pulmonary CSH, as was already reported by other authors [13].

Among the 12 reviewed cases of CSH, only 1 case was secondary to the isolated heavy-chain disease, and the authors suggested that the light chain multimerization underlies most cases of the abnormal immunoglobulin storage [6]. Thus far, the detailed insight into the protein pathology was offered only in one case, in which microsequencing using mass-spectrometry analysis revealed unusual residues, partially homologous to known amyloidogenic proteins within the kappa light chain [9]. In our case, the abnormal physicochemical properties characterized the heavy chain; hence, it is possible that the pathology of both components of the immunoglobulin molecule can contribute to the formation of abnormal particles in different cases. Not only did the biochemical analysis of the monoclonal protein indicate its abnormal structure, but it also explained its high tendency to aggregate. It is conceivable that the observed immunoglobulin aggregates circulating in serum provoked abnormally increased phagocytic activity of the histiocytes. Suggestions of such mechanisms were previously raised [4, 11, 17]. Abnormal crystallization may adversely influence the immunostaining properties of the heavy chain, as it was seen in our case in the liver cells.

Our clinical, morphological, and biochemical data prove that the formation of immunoglobulin crystals in CSH secondary to multiple myeloma takes place in histiocytes, liver cells, interstitial cells of the kidney, and within serum. The crystallization results probably from the abnormal protein structure and significantly contributes to the severity of the clinical picture. The degree of organ infiltration with crystal-storing macrophages surpasses that of neoplastic plasma cells and may likely result in multi-organ failure.

Acknowledgements We thank Mrs. Renata Kornecka for performing the immunostains, Mrs. Beata Koźmińska, and Mrs. Barbara Regulska for processing the trephine bone-marrow biopsies, Dr. Jacek Czopek for electronic photography support, and Ms. Małgorzata Mulawka for the English language revision.

References

1. Ball NJ, Wickert W, Marx LH, Thaell JF (1993) Crystalglobulinemia syndrome. Cancer 71:1231–1234
2. Dobson CM (2001) The structural basis of protein folding and its links with human disease. Philos Trans R Soc Lond B Biol Sci 356:133–145
3. Dotten DA, Pruzanski W, Olin J, Brown TC (1976) Cryocrystalglobulinemia. Can Med Assoc J 114:909–913
4. Hashimoto N, Kurihara K, Sakai H (1983) Extramedullary plasmacytoma with crystal inclusions arising from the palatal tonsil. J Oral Pathol 12:309–318
5. Hopf U, Meyer zum Buschenfelde KH, Dietrich MP (1976) Demonstration of binding sites for IgG Fc and the third complement component (C3) on isolated hepatocytes. J Immunol 117:639–645
6. Jones D, Bhatia VK, Krausz T, Pinkus GS (1999) Crystal-storing histiocytosis: a disorder occurring in plasmacytic tumors expressing immunoglobulin kappa light chain. Hum Pathol 30:1441–1448
7. Kjeldsberg CR, Eyre HJ, Totzke H (1977) Evidence for intracellular amyloid formation in myeloma. Blood 50:493–503
8. Landsbury PT (1999) Evolution of amyloid: what normal protein folding may tell us about fibrillogenesis and disease. Proc Natl Acad Sci U S A 96:3342–3344
9. Lebeau A, Zeindl-Eberhart E, Müller EC, Müller-Höcker J, Jungblut PR, Emmerich B, Löhrs U (2002) Generalized crystal-storing histiocytosis associated with monoclonal gammopathy: molecular analysis of a disorder with rapid clinical course and review of the literature. Blood 100:1817–1827
10. MacSween RNM, Burt AD, Portmann BC, Ishak KG, Scheuer PJ, Anthony PP (eds) (2002) Pathology of the liver. Churchill Livingstone, London, pp 32–33
11. Mullen B, Chalvardjian A (1981) Crystalline tissue deposits in a case of multiple myeloma. Arch Pathol Lab Med 105:94–97
12. Piekarska B, Skowronek M, Rybarska J, Stopa B, Roterman I, Konieczny L (1996) Congo red-stabilized intermediates in the λ light chain transition from native to molten state. Biochimie 78:183–189
13. Prasad ML, Charney DA, Sarlin J, Keller SM (1998) Pulmonary immunocytoma with massive crystal storing histiocytosis. A case report with review of literature. Am J Surg Pathol 22:1148–1153
14. Sancho J, Gonzales E, Escanero JF, Egido J (1984) Binding kinetics of monomeric and aggregated IgG to Kupffer cells and hepatocytes of mice. Immunology 53:283–289
15. Schaefer HE (1996) Gammopathy-related crystal-storing histiocytosis, pseudo- and pseudo-pseudo-Gaucher cells. Critical commentary and mini-review. Pathol Res Pract 192:1152–1162

16. Spólnik P, Piekarska B, Stopa B, Konieczny L, Zemanek G, Rybarska J, Król M, Nowak M, Roterman I (2003) The structural abnormality of myeloma immunoglobulins tested by Congo red binding. Med Sci Mon 9:145–153
17. Takahashi K, Naito M, Takatsuki K, Kono F, Chitose M, Ooshima S, Mori N, Sakuma H, Uchino F (1987) Multiple myeloma IgA κ type, accompanying crystal-storing histiocytosis and amyloidosis. Acta Pathol Jpn 37:141–154
18. Van der Laan-Klamer SM, Harms G, Atmosoerodjo JE, Meijer DKF, Hardonk MJ, Hoedemaeker PJ (1986) Studies on the mechanism of binding and uptake of immune complexes by various cell types of rat liver in vivo. Scand J Immunol 23:127–133
19. Wetzel R (1997) Domain stability in immunoglobulin light chain deposition disorders. Adv Protein Chem 50:183–242

Virchows Arch (2004) 445:90–92
DOI 10.1007/s00428-004-0992-6

LETTER TO THE EDITOR

Günther Bayer · Johannes Pammer · Reinhard Horvat · Peter Birner

Clear-cell adenoma of the fallopian tube, a rare tumor of the tubal mucosa

Received: 15 January 2004 / Accepted: 6 February 2004 / Published online: 13 May 2004
© Springer-Verlag 2004

Sir,

Tumors of the fallopian tube are rare [1, 2, 3, 4, 5, 6, 7]. Benign tumors are mostly of mesodermal origin (e.g., Walthard nests, adenomatoid tumor), while, in most cases, malignant tumors (adenocarcinoma and mixed tumors) originate from the epithelium. In this case report, we present a benign tumor of the fallopian tube, which, based on its morphology and immunohistochemical profile, we have classified as clear-cell adenoma.

A 58-year-old woman underwent simple hysterectomy due to uterine leiomyomas. Both ovaries and fallopian tubes were left in situ. The patient was admitted to our hospital 2 years later due to the accidental finding of a cystic tumor in the lower pelvis at a routine sonographic examination; all serological parameters (including tumor markers) were within normal range. The patient underwent laparoscopy with bilateral adnexectomy. This tumor resembled a hydrosalpinx of the left fallopian tube. Both ovaries were normal, but we found a tumor with a diameter of 0.6 cm in the distal third of the right fallopian tube. This tumor had a smooth surface, was of gray-white color and was connected to the tubal wall with a short pedicule. Since this adnexectomy, 3 years have passed, and the patient is without any health problems.

The specimen was fixed in formalin, completely embedded in paraffin and 4-μm sections were cut. Routine hematoxylin and eosin staining and special stainings (Table 1) were performed. Immunohistochemistry was performed according to standard protocols using commercially available antibodies (Table 1) with adequate positive and negative controls.

The tumor consisted of cubic to cylindrical cells with only sparse connective stroma and was connected to the original mucosa by a thin pedicule, which was also covered by normal epithelium (Fig. 1A+B). The tumor cells showed a clear, in only a minor part, finely eosinophilic–granular cytoplasm with distinct cell borders. The nuclei were relatively small, cytologically normal and were located basally in most cells. Tumor cells formed a tubuloalveolar pattern in wide areas. In the lumen, we observed a homogeneous eosinophilic substance. This substance shows weak staining with Muzicarmin, but is negative for alcian and periodic acid-Schiff. A continuous transition of normal tubal mucosa to the described clear cells was seen at the pedicule (Fig. 1C). Tumor cells showed distinct positive reactions with antibodies against cytokeratins (AE1/AE3 and Lu-5), while no positive reactions were found with any other antibody (Table 1).

Due to the exclusion of all other benign tubal tumors and the documented transition from the normal epithelium, the only possible remaining origin is that of the Muellerian epithelium. Based on our findings, we, therefore, came to the conclusive diagnosis of a clear-cell adenoma of the fallopian tube.

Benign tumors of the fallopian tube are most often of mesodermal origin, and adenomatoid tumor (benign mesothelioma) is the most frequent type. Other tumors are serosal inclusion cysts and Walthard nests, epithelial papilloma, leiomyoma and adenomyoma, teratoma and other benign mesenchymal and mixed epithelial–mesenchymal tumors (e.g., hemangiomas, lipomas, angiomyolipomas, adenofibromas and neural tumors) [7]. The fallopian tube, the uterus and parts of the vagina originate from the Muellerian epithelium. The primitive Muellerian epithelium might physiologically and/or pathologically differentiate into several distinct histological types, i.e., serous, mucinous, endometrioid and clear-cell type, with the pathological differentiation resembling adenomas, tumors of low malignant potential and carcinomas. Since serous, endometrioid and mucinous tumors (benign and malignant) and malignant clear-cell tumors are rarely also found in the fallopian tube, a clear-cell differentiation of a benign tumor should also be possible, but to our knowledge has not been described previously.

G. Bayer · J. Pammer · R. Horvat · P. Birner (✉)
Medical University of Vienna,
Institute of Pathology,
Währinger Gürtel 18-20, 1090 Vienna, Austria
e-mail: peter.birner@meduniwien.ac.at
Tel.: +43-140-4003650
Fax: +43-140-4003707

Table 1 Immunohistological findings

Antibody		**Tumor cells**	**Normal tubal epithelium**
Cytokeratin (AE1/AE3)	(Dako, Glostrup, Denmark)	80%	100%
Cytokeratin (Lu-5)	(BMA, Angst, Schweiz)	70%	100%
Estrogen receptor	(Dako, Glostrup, Denmark)	-	-
Progesterone receptor	(Dako, Glostrup, Denmark)	-	-
S 100 protein	(Dako, Glostrup, Denmark)	-	-
Neuron-specific enolase	(Dako, Glostrup, Denmark)	-	-
Chromogranin A	(Biogenex, San Remon, CA)	-	-
Thyroglobulin	(Dako, Glostrup, Denmark)	-	-
Immunoglobulin G1 (control)	(Dako, Glostrup, Denmark)	-	-
Thyroid transcription factor	(BIOCARE, Walnut Creek, CA)	-	-
Calcitonin	(CHEMICON, Temecula, CA)	-	-
HMB-45	(Dako, Glostrup, Denmark)	-	-
Carcinoembryonic antigen	(Dako, Glostrup, Denmark)	-	-
Epithelial-membrane antigen	(Dako, Glostrup, Denmark)	-	-
Vimentin	(Immunotech, Marseille, France)	-	-
Desmin	(Monosan, Am Uden, Netherlands)	-	-
Anti-muscle-specific actin HHF-35	(Enzo, New York, NY)	-	-
Factor-VIII-related antigen	(Dako, Glostrup, Denmark)	-	-
PgM-1	(Dako, Glostrup, Denmark)	-	-
Calponin	(Dako, Glostrup, Denmark)	-	-
B 72.3	(Biogenex, San Remon, CA)	-	-
CA 125	(Histocis, Cedex, France)	-	-
CD 15 (Leu M1)	(Becton-Dick., CA)	-	-
Ki-67 (MIB-1)	(Novocastra, Newcastle, U.K.)	<5%	0%
Special staining		**Tumor epithelium**	**Luminal substance**
Muzicarmin		–	+
PAS		–	–
Alcian		–	–
Best		–	–

As differential diagnoses in our case, adenomatoid tumor, teratoma, steroid cell tumors (such as Luteoma, Leydig cell tumor, adrenocortical rests) or endometriosis with Arias–Stella phenomenon might also be possible. However, in our opinion, these entities could be excluded using histological, cytological and immunomorphological criteria. The tubulo-alveolar pattern, reminiscent of thyroid follicles, might also indicate disseminated thyroid tissue (Struma salpingii or teratoma) or the metastasis of a well-differentiated primary follicular thyroid carcinoma. This suspicion has been excluded immunohistologically, since no reaction was found for thyroglobulin, TTF-1, calcitonin and vimentin. A metastasis of a clear-cell renal carcinoma appears highly unlikely due to the negative immunoreaction for vimentin, the absence of sonographic changes as well as the clinical history and follow-up of the patient.

In summary, to the best of our knowledge, we present here the first case of a clear-cell adenoma of the fallopian tube.

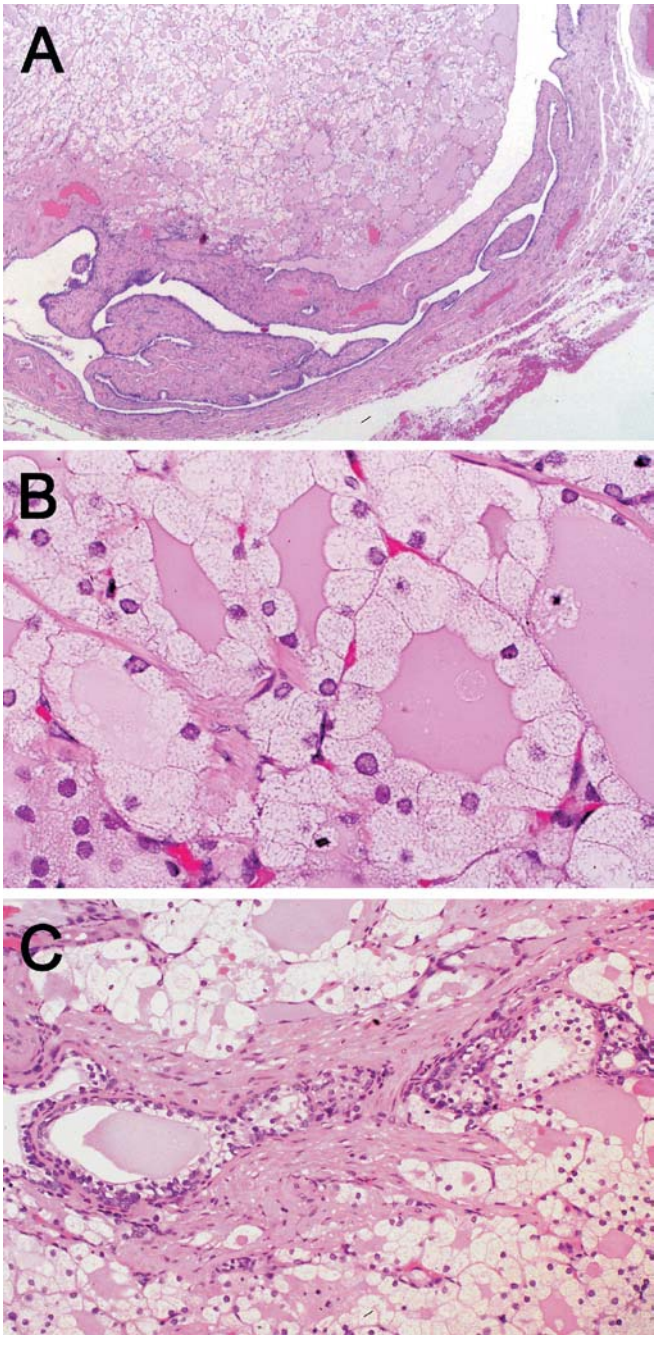


Fig. 1 **A** Overview of the tumor. Note the connecting pedicule. Hematoxylin and eosin (H&E) stain, original magnification ×40. **B** Details of tumor cells. H&E stain, original magnification ×400. **C** Transition from more tubal-like epithelium to clear cells. H&E stain, original magnification ×200

References

1. Alvarado-Cabrero I, Navani SS, Young RH, Scully RE (1997) Tumors of the fimbriated end of the fallopian tube: a clinicopathologic analysis of 20 cases, including nine carcinomas. Int J Gynecol Pathol 16:189–196
2. Baekelandt M, Jorunn NA, Kristensen GB, Trope CG, Abeler VM (2000) Carcinoma of the fallopian tube. Cancer 89:2076–2084
3. Devouassoux-Shisheboran M, Silver SA, Tavassoli FA (1999) Wolffian adnexal tumor, so called female adnexal tumor of probable Wolffian origin (FATWO): immunohistochemical evidence in support of a Wolffian origin. Hum Pathol 30:856–863
4. de la Torre FJ, Rojo F, Garcia A (2002) Clear cells carcinoma of fallopian tubes associated with tubal endometriosis. Case report and review. Arch Gynecol Obstet 266:172–174
5. Tziortziotis DV, Bouros AC, Ziogas VS, Young RH (1997) Clear cell hyperplasia of the fallopian tube epithelium associated with ectopic pregnancy: report of a case. Int J Gynecol Pathol 16:79–80
6. Voet RL, Lifshitz S (1982) Primary clear cell adenocarcinoma of the fallopian tube: light microscopic and ultrastructural findings. Int J Gynecol Pathol 1:292–298
7. Wheeler JE (2002) Diseases of the fallopian tube. In: Kurman RJ (ed) Blaustein's pathology of the female genital tract, 5th edn. Springer Verlag, Berlin Heidelberg New York, pp 617–648

Virchows Arch (2004) 445:93–95
DOI 10.1007/s00428-004-1005-5

LETTER TO THE EDITOR

Ana Saiz · Miguel A. Martinez · Carlos Grande · Francisco Vanaclocha

Langerhans' cell histiocytosis in an adult with acute myelogenous leukaemia

Received: 10 December 2003 / Accepted: 26 February 2004 / Published online: 22 April 2004
© Springer-Verlag 2004

Sir,
We have had the opportunity to study a case of localised Langerhans' cell histiocytosis (LCH) in a patient with a 10-year history of acute myelogenous leukaemia (AML). To the best of our knowledge, there is no other similar case in the literature.

The patient was a 57-year-old woman who consulted her primary care physician to complain of acute upper airway ache and a constitutional syndrome in October 1991. Her blood test revealed a leukocyte count of 9.5×10^9/l with 81% of blast cells, 8.3 g/dl of haemoglobin and a 115×10^9/l platelet count. Bone marrow biopsy and aspirate contained 85% blast cells with no significant maturation (Fig. 1). The blast cells occasionally exhibited Auer rods (Fig. 1) and were oxidase positive, chloroacetate esterase and non-specific esterases were negative and cytogenetic studies revealed no abnormalities. A diagnosis of AML-M1 was given. A later immunohistochemical study revealed the neoplastic cells to be strongly positive for myeloperoxidase (polyclonal, dilution 1/5000) and weakly positive for CD68 (monoclonal, clone KP1, 1/100) and lysozyme (polyclonal, 1/4); immunostaining for CD3 (monoclonal, 1/50), CD79α (monoclonal, 1/100), CD10 (monoclonal, 1/20), terminal deoxynucleotidyl transferase (polyclonal, 1/30), CD34 (monoclonal, 1/50), CD68 (monoclonal, clone PG-M1, 1/50), CD61 (monoclonal, 1/50), factor VIII (polyclonal, 1/500), factor XIIIa (polyclonal, 1/2000) and CD1a (monoclonal, predilute) were all negative (CD10 was manufactured by Novocastra, Newcastle, UK, lysozyme by Biomeda, Foster City, USA, factor XIIIa by Berhing, Marburg, GFR, CD1a by Master

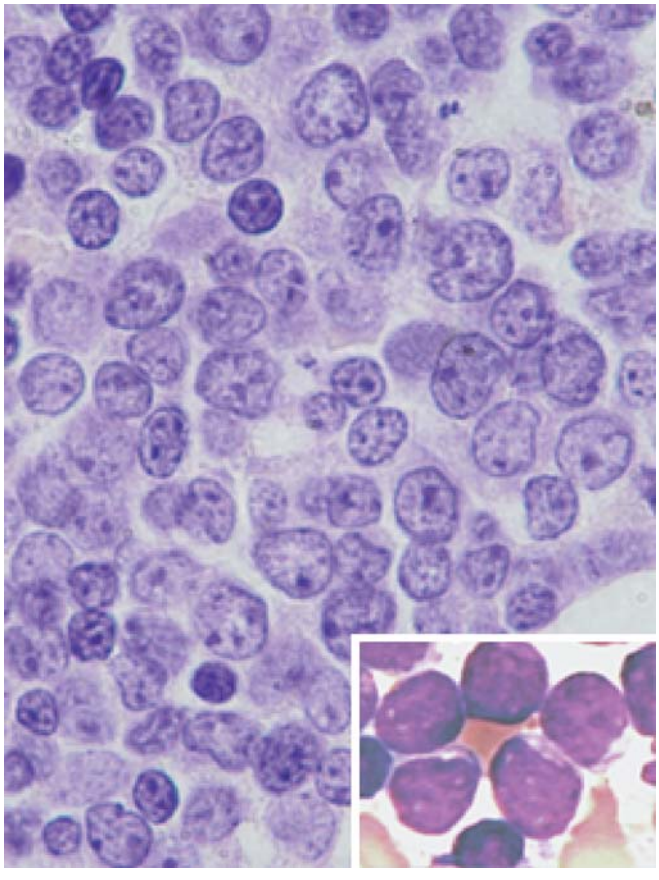


Fig. 1 Initial bone-marrow biopsy showing diffuse blast involvement. Haematoxylin and eosin ×1000. *Inset* Detail of the initial aspirate demonstrating medium size cells; one Auer rod may be seen. May-Grünwald-Giemsa ×1000

A. Saiz · M. A. Martinez (✉)
Departmento de Anatomía patológica,
Hospital 12 de Octubre,
Crta de Andalucía km 5400, 28041 Madrid, Spain
e-mail: mmartinezg.hdoc@salud.madrid.org
Tel.: +34-91-3908275
Fax: +34-91-3808462

C. Grande
Service of Haematology,
Hospital 12 de Octubre,
Madrid, Spain

F. Vanaclocha
Service of Dermatology,
Hospital 12 de Octubre,
Madrid, Spain

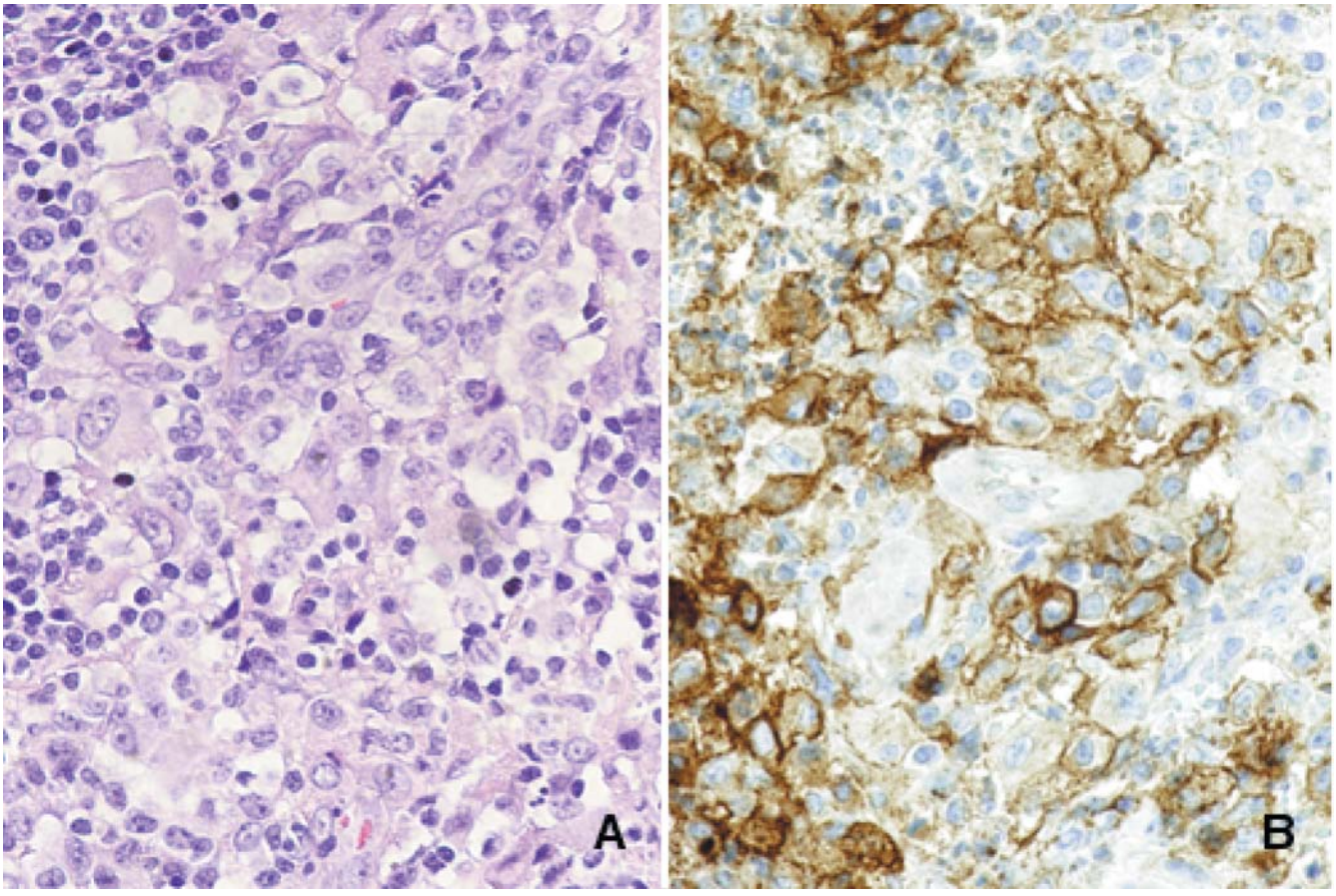


Fig. 2 **A** Detail of the lymph-node biopsy showing large cells with ample cytoplasm and irregular nuclei. Haematoxylin and eosin ×400. **B** Infiltrating cells were CD1a positive. Immunoperoxidase ×1000

Diagnostic, Granada, Spain and the remaining antisera by Dako, Glostrup, Denmark). A regimen of daunorubicin and cytosine arabinoside (ara-c) (3+7) obtained complete clinicocytological remission; consolidation treatment was based on high doses of daunorubicin and ara-c.

A recurrence was treated with idarubicin and ara-c (3+7), and the new remission was consolidated with medium doses of idarubicin and ara-c 5 years after the initial diagnosis. While in the second complete remission, the patient underwent an autologous bone marrow transplant in April 1997; her blood count was acceptable on day 21 post-transplant.

In October 2001, the patient presented with a hard, deep-tissue-adhering, 3×2-cm nodule in her left supraclavicular fossa. Histological study identified the nodule as a lymph node that was focally affected by an infiltrating proliferation of large cells with ample cytoplasm and convoluted nuclei with deep indentations and disperse chromatin (Fig. 2). These cells were positive for CD1a, S-100 protein (dilution 1/2000, Dako) and CD68 (clone KP1). The rest of the node showed preserved architecture, and neither haematoxylin eosin histological examination nor myeloperoxidase immunostaining revealed atypical cells. A diagnosis of LCH was made. At that time, there were no signs of recurrence of the leukaemia, and a staging study found no other sites of involvement.

The patient suffered a new recurrence of the leukaemia 1 year after the diagnosis of the LCH, and she died from acute respiratory insufficiency before any treatment could be initiated. Necropsy was not performed.

LCH is a rare condition, most commonly occurring in children under 5 years old. The clinical picture is variable, with localised, multifocal and disseminated forms. The aetiology is uncertain, but most cases studied have proved to be clonal proliferations. LCH has been reported in association with a large variety of lesions, including neonatal infection, solvent exposures, lack of vaccination in children and thyroid diseases [5], as well as a large number of tumours, including solid tumours, lymphomas and chronic as well as acute leukaemias [1, 3, 5].

The lymph nodes may be involved in both the disseminated and localised variants of LCH. Nodal involvement may be “primary” or associated with tumours, primarily Hodgkin’s lymphoma. In contrast to “primary” nodal LCH, lymph-node involvement in tumour-associated LCH is focal with an infiltrating margin and a necrotic eosinophilic central core, rather than sinusoidal and expansive [5].

LCH and acute leukaemia occurring in the same patient is unusual, and most cases have been described in paediatric patients, with two major clinical patterns: first, acute lymphoblastic leukaemia may precede LCH, which may be either localised or disseminated and may persist after the treatment of the leukaemia; the cause of this association remains uncertain. Second, AML may appear months or years after etoposide treatment of LCH, and, in these cases, leukaemic proliferation is attributed to the leukaemogenic effect of the drug.

In our case, the patient developed a localised nodal LCH 10 years after the initial diagnosis of AML-M1, which was treated with daunorubicin, ara-c, idarubicin and autologous bone marrow transplant. To explain this association, we suggest three possibilities.

First, we could hypothesise that both LCH and AML have their origin in a common progenitor. The reports of in vitro differentiation of human myeloid leukaemia-derived cell lines to Langerhans' cells, acute monocytic leukaemias expressing CD1a [4] and chronic myelomonocytic leukaemia associated with Langerhans' cell proliferation [3] all suggest a common origin for monocytic cells and Langerhans' cells. However, in our case, the hypothesis of a common origin for AML and LCH is improbable, since the retrospective CD1a staining of the leukaemic cells was negative, LCH was localised, and the Langerhans' cell proliferation she developed did not appear in the setting of a recurrence of her leukaemia.

Second, LCH could have resulted from an immunological surveillance deficiency, as has been suggested in some Langerhans' cell proliferations [1]. Although, at the time of the diagnosis of LCH, our patient did not show features of being immunodepressed, we must admit that in an aggressively treated patient, immune disregulation could be, at least, another factor in the pathogenesis of LCH.

Finally, a third and more attractive hypothesis is that LCH could be the result of anomalous cytokine production. The World Health Organization's Committee on Histiocytic/Reticulum Cell Proliferations [2] believes that tobacco-associated pulmonary Langerhans' cell proliferation is probably a cytokine-mediated reactive lesion. Although there are no clonality studies, the same committee classifies tumour-associated LCH under the heading of Secondary Dendritic Processes, suggesting that it would also correspond to a reactive lesion. In our patient, the fact that the lesion involved only one lymph node and was cured by surgical resection alone with no other treatment also suggests a reactive process.

In summary, we present the case of an adult woman who suffered from a localised nodal LCH after a 10-year history of recurrent AML-M1 treated with anti-neoplastic antibiotics, ara-c and autologous bone marrow transplant. To the best of our knowledge, this association has not been reported before and it should be kept in mind in the differential diagnosis of lumps arising in the course of AML.

References

1. Egeler RM, Neglia JP, Arico M et al (1998) The relation of Langerhans cell histiocytosis to acute leukaemia, lymphomas and other solid tumors. Hematol Oncol Clin North Am 12:369–378
2. Favara BE, Feller AC, Pauli M et al (1997) Contemporary classification of histiocytic disorders. Med Pediatr Oncol 29:157–166
3. Kaiserling E, Horny HP (1988) Dermal Langerhans' cell tumor in chronic myelomonocytic leukemia. Ultrastruct Pathol 12: 209–219
4. Srivastava BI, Srivastava A, Srivastava MD (1994) Phenotype, genotype and cytokine production in acute leukemia involving progenitors of dendritic Langerhans' cells. Leuk Res 18:499–511
5. Weiss LM (2001) Histiocytic and dendritic cells proliferations. Knowles DM (ed) Neoplastic hematopathology, 2nd edn. Lippincott Williams and Wilkins, Philadelphia, pp 1815–1846

Virchows Arch (2004) 445:96–97
DOI 10.1007/s00428-004-1022-4

LETTER TO THE EDITOR

Stefania Damiani

Pulmonary papillary adenoma-like tumour arising in ovarian teratoma

Received: 20 January 2004 / Accepted: 15 March 2004 / Published online: 13 May 2004
© Springer-Verlag 2004

Sir,
Papillary adenoma of the lung is a rare benign neoplasm composed of cuboidal cells with features of type-II pneumocytes or Clara cells [1]. Here, we report a pulmonary papillary adenoma (PPA) arising in a mature cystic teratoma of the ovary.

The patient, a 59-year-old woman, was found to have a cystic tumour in the right ovary. The patient had a family history (mother and one sibling) of ovarian cancer, and a bilateral ovariectomy was performed. Grossly, the right ovary was 3 cm in major axis. On cut section, it appeared completely transformed in a multi-cystic tumour. The cysts had a smooth inner surface and a mucoid content. The tissue between the cystic walls was thick and fibrous in appearance. The left ovary was unremarkable. Histologically, the cystic tumour had typical features of mature teratoma. Most of the cysts were lined by colonic-type epithelium (Fig. 1a), and, in limited tracts, by squamous and respiratory epithelium. A focus of solid nests composed of ovoid cells with coffee-bean nuclei, consistent with a small Brenner tumour, was also present adjacent to a cyst (Fig. 1b). In addition, one of the cysts showed a papillary proliferation abutting within the lumen. The lesion was 0.4 cm in its major axis and was constituted by anastomosing papillae bordered by cuboidal cells investing a fibrovascular core containing lymphoplasmacytic elements (Fig. 2a). The cells lining the papillae had a moderate amount of cytoplasm and regular ovoid nuclei, with occasional nuclear eosinophilic inclusions (Fig. 2b). Focally, the lining cells were columnar ciliated cells reminiscent of respiratory epithelium. Anti-surfactant, anti-cytokeratin 7 and anti-TTF1 antisera stained most of the cells lining the papillary structures (Fig. 2c), indicating a type-II pneumocyte differentiation. Anti-thyroglobulin antibody was negative, while CDX2 and cytokeratin 20 antisera stained the columnar cells showing colonic differentiation. Therefore, it appears that the papillary structure of the lesion, together with the epithelium showing histological and immunocytochemical features of type-II

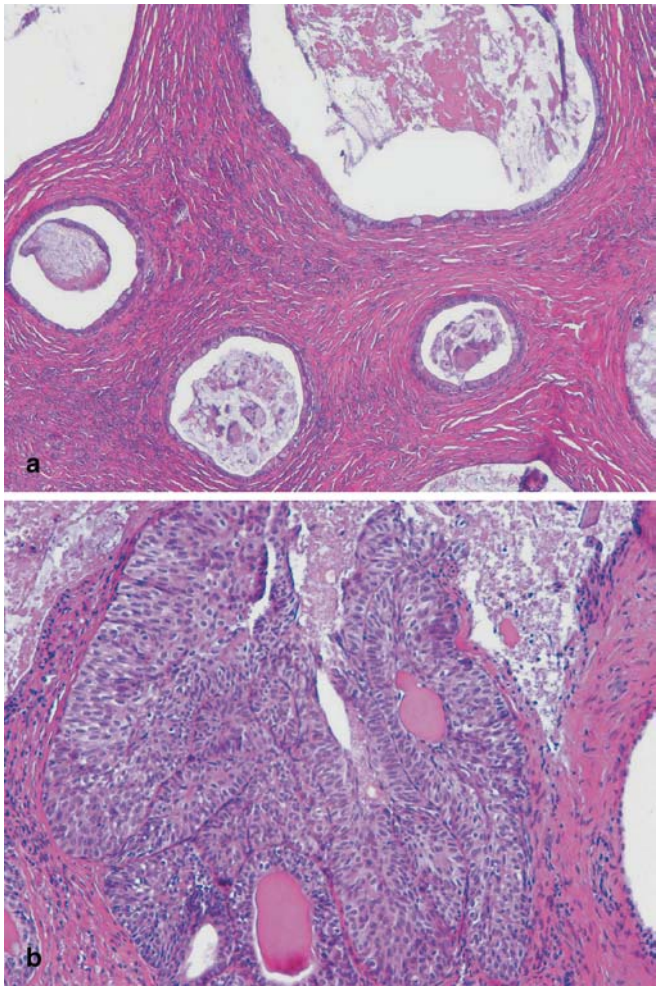


Fig. 1 **A** Most of the tumour was composed of cysts lined by colonic-type epithelium. **B** A small focus with features of Brenner tumour was also present

S. Damiani (✉)
Anatomia Patologica, University of Bologna,
Ospedale Bellaria,
Via Altura 3, 40139 Bologna, Italy
e-mail: Stefania.damiani@ausl.bo.it

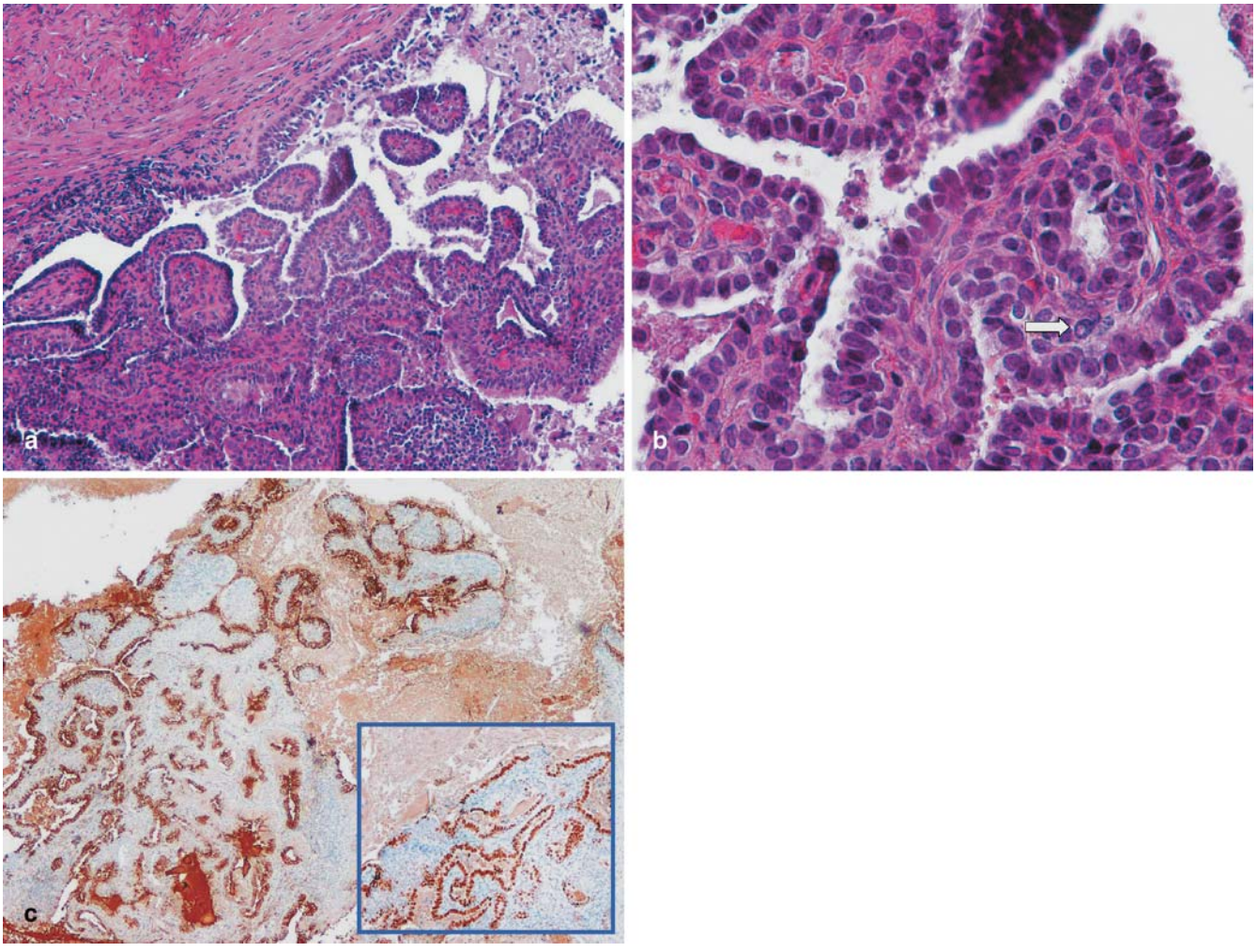


Fig. 2 **A** One of the cysts was lined by respiratory epithelium. A papillary proliferation was seen abutting within the lumen. This was composed of anastomosing papillae with a fibrovascular core showing focally a lymphoplasmacytic infiltrate. **B** The papillae were covered by a single layer of cuboidal cells with monomorphic nuclei and rare nuclear inclusions (*arrow*). **C** Anti-surfactant antiserum stained most of the cells in the papillary proliferation. These same cells were also TTF1 positive (*inset*)

pneumocytes, are consistent with a PPA arising in a mature ovarian teratoma.

To the best of our knowledge, there are no similar cases reported in literature. Papillary lesions arising in ovarian teratomas are mainly represented by struma ovarii with foci of papillary thyroid carcinoma [2], which is histologically similar to PPA. However, PPA usually lacks optically clear nuclei and atypia, and, finally, its positivity for surfactant antibody can easily ameliorate any doubt, as this is not expressed in thyroid lesions.

References

1. Colby TV, Koss MN, Travis WD (1995) Tumors of the lower respiratory tract. Fascicle 13 in atlas of tumor pathology. Armed Forces Institute of Pathology, Washington DC, pp 57–59
2. Kostoglou-Athanassiou I, Lekka-Katsouli I, Gogou L, Papagrigoriou L, Chatonides I, Kaldrymides P (2002) Malignant struma ovarii: report of a case and review of the literature. Hormone Res 58:34–38

Virchows Arch (2004) 445:98
DOI 10.1007/s00428-004-1026-0

LETTER TO THE EDITOR

João Magalhães · Manuel Sobrinho-Simões

Hyalinizing trabecular tumor of the thyroid displaying neuroendocrine differentiation

Received: 31 March 2004 / Accepted: 1 April 2004 / Published online: 11 May 2004
© Springer-Verlag 2004

Dear Sir,
Shikama and colleagues [3] reported recently an interesting case of a hyalinizing trabecular tumor of the thyroid (HTT) displaying neuroendocrine differentiation. We agree with the authors' assumption that their finding suggests HTT can differentiate into both follicular cells and neuroendocrine cells [3].

The prevalence of such dual differentiation in HTT is not known, but it is likely to be more frequent than suspected by Shikama and colleagues, who claimed that "In the world literature to date, only two cases of HTT with endocrine cells, including the current case, have been reported" [3]. Shikama and colleagues did not take into account the two cases reported by our group [1, 2]. In one of these cases, we had the opportunity of performing electron microscopy but, at variance with Shikama and colleagues, we did not detect typical neurosecretory granules.

The putative relationship between HTT and papillary thyroid carcinoma (PTC) is thoroughly reviewed by Shikama and colleagues, who pointed out similarities regarding CK19 and galectin immunoexpression and RET/PTC rearrangement in both tumor types [3]. Recently, we have shown that regarding the occurrence of BRAFV599E mutation, HTT differs from conventional PTC and resembles the follicular variant of PTC [4, 5]. It remains to be seen whether the aforementioned dual differentiation may occur in any type of HTT regardless of its association to PTC.

One of the cases of HTT without dual difference we studied gave rise to nodal metastases, thus showing that these tumors may be malignant [2]. As Shikama and colleagues stress in their study, it remains to be clarified whether the dual differentiation in HTT may have some clinical significance [3].

References

1. Sambade C, Sarabando F, Nesland JM, Sobrinho-Simões M (1989) Hyalinizing trabecular adenoma of the thyroid gland. Ultrastruct Pathol 13:275–280
2. Sambade C, Franssila KO, Cameselle-Teijeiro J, Nesland JM, Sobrinho-Simões M (1991) Hyalinizing trabecular adenoma. A misnomer for a peculiar tumor of the thyroid gland Endocr Pathol 2:83–291
3. Shikama Y, Osawa T, Yagihashi N, Kurotaki H, Yagihashi S (2003) Neuroendocrine differentiation in hyalinizing trabecular tumor of the thyroid. Virchows Arch 443:792–296
4. Soares P, Trovisco V, Rocha AS, Lima J, Castro P, Preto A, Maximo V, Botelho T, Seruca R, Sobrinho-Simões M (2003) BRAF mutations and RET/PTC rearrangements are alternative events in the etiopathogenesis of PTC. Oncogene 22:4578–4580
5. Trovisco V, Vieira de Castro I, Soares P, Maximo V, Silva P, Magalhaes J, Abrosimov A, Guiu XM, Sobrinho-Simões M (2004) BRAF mutations are associated with some histological types of papillary thyroid carcinoma. J Pathol 202:247–251

J. Magalhães · M. Sobrinho-Simões
Department of Pathology of Medical Faculty of Porto
and Hospital S. João,
Porto, Portugal

M. Sobrinho-Simões (✉)
Institute of Molecular Pathology and Immunology
of the University of Porto,
Rua Roberto Frias S/N, 4200-465 Porto, Portugal
e-mail: ssimoes@ipatimup.pt
Tel.: +351-2-25570700
Fax: +351-2-25570799

Virchows Arch (2004) 445:99–100
DOI 10.1007/s00428-004-1027-z

LETTER TO THE EDITOR

Pavlína Plevová · Eva Sedláková · Martina Papežová · Jana Zapletalová · Romuald Čuřik · Zdeněk Kolář · Anna Křepelová

Epidermal growth factor receptor expression in colorectal tumors with and without microsatellite instability

Received: 24 February 2004 / Accepted: 6 April 2004 / Published online: 11 May 2004
© Springer-Verlag 2004

Dear Editor, epidermal growth factor receptor (EGFR) is expressed in a proportion of colon cancers. High grades of EGFR expression have been described to be associated with worsened survival [1, 4]. We have studied EGFR expression in colon cancer specimens with respect to their status of microsatellite stability or instability. Included in the study were 31 specimens with high-frequency microsatellite instability (MSI-H) and 39 specimens with stable microsatellites (MSS). Of the specimens, 20 MSI-H cancers were from patients with a germline mutation in the hMLH1 or hMSH2 genes; 11 were sporadic MSI-H cancers. EGFR expression was detected via indirect immunohistochemistry [4] using mouse monoclonal anti-EGFR antibody (NeoMarkers, CA, USA). Antigen retrieval with trypsin was used. Membrane and/or cytoplasmic expression of EGFR was evaluated semiquantitatively as 0, negative; 1+, slight; 2+, moderate; and 3+, intense [1]. A sample of lung cancer with 3+ intensity was used as a positive control. Nerve fibers served as an internal positive control. Results were statistically analyzed using chi-square test. The EGFR protein was expressed in 5 of 31 MSI-H (16.1%) cancers [4 at 1+ level (12.9%) and 1 at 2+ level (3.2%)] and in 17 of 39 MSS (43.6%) cancers [11 at 1+ level (28.2%), 4 at 2+ level (10.3%), 2 at 3+ level (5.1%)]. The difference was statistically significant (P= 0.014), using chi-square test. EGFR expression did not correlate with age, grade and localization of the tumor. EGFR expression was usually not observed in adjacent normal colonic mucosa. In a few specimens, EGFR was expressed in enterocytes of superficial parts of colon mucosa. The percentage of EGFR-positive MSS tumors is in accord with two studies that reported 49% and 46% of EGFR-positive colorectal tumors, respectively [3, 4]. Goldstein and Armin found EGFR reactivity in 75.5% of cases [1].

The pathogeneses of MSS and MSI-H colorectal cancers are different. For instance, aneuploidy, 18q loss of heterozygosity and p53 mutations are predominantly present in MSS tumors [5]. Tumors with microsatellite instability are associated with unique pathological attri-butes [5] and better prognosis [2]. The significantly lower EGFR expression might correspond to the less aggressive behavior of MSI-H tumors.

Acknowledgement This work was supported by IGA Ministry of Health Care of the Czech Republic, grant No NC/6741–3/2001.

P. Plevová · E. Sedláková · Z. Kolář
Institute of Pathology and Laboratory of Molecular Pathology,
Medical Faculty of the Palacký University,
Hněvotinská 3, 775 15 Olomouc, Czech Republic

P. Plevová
Department of Radiotherapy,
Faculty Hospital,
Tř. 17. listopadu 1790, 708 52 Ostrava, Czech Republic

P. Plevová (✉)
Předvrši 560, 725 26 Ostrava-26, Czech Republic
e-mail: pavlina.plevova@volny.cz
Tel.: +420-59-6942580
Fax: +420-59-7375364

M. Papežová · A. Křepelová
Institute of Biology and Genetics,
1st Medical Faculty of Charles University,
Albertov 4, 128 00 Prague 2, Czech Republic

J. Zapletalová
Institute of Biophysics,
Medical Faculty of the Palacký University,
Hněvotinská 3, 775 15 Olomouc, Czech Republic

R. Čuřik
Department of Pathology,
Faculty Hospital,
Tř. 17. listopadu 1790,
708 52 Ostrava, Czech Republic

References

1. Goldstein NS, Armin M (2001) Epidermal growth factor receptor immunohistochemical reactivity in patients with American Joint Committee on cancer stage IV colon adenocarcinoma. Implications for a standardized scoring system. Cancer 92:1331–1346
2. Gryfe R, Kim H, Hsieh ETK, Aronson MA, Holowaty EJ, Bull SB, Redston M, Gallinger S (2000) Tumor microsatellite in-

stability and patient survival in a population-based series of young colorectal cancer patients. N Engl J Med 342:69–77
3. Kaklamanis L, Gatter KC, Mortensen N, Harris AL (1992) Interleukin-4 receptor and epidermal growth factor receptor expression in colorectal cancer. Br J Cancer 66:712–716
4. Khorana AA, Ryan CK, Cox C, Eberly S, Sahasrabudhe DM (2003) Vascular endothelial growth factor, CD68, and epidermal growth factor receptor expression and survival in patients with stage II and stage III colon carcinoma. Cancer 97:960–968
5. Redston M (2001) Carcinogenesis in the GI tract: from morphology to genetics and back again. Mod Pathol 14:236–245

Virchows Arch (2004) 445:101
DOI 10.1007/s00428-004-1067-4
© Springer-Verlag 2004

ANNOUNCEMENTS

9 September 2004
One day course on Advanced Ultrasound of the Breast
Nottingham, UK

For further information contact:
The Blamey Education Centre
Nottingham Breast Institute
City Hospital, Nottingham, NG5 1PB, UK
Tel.: 00 44 (115) 969 1689
E-mail: sbury@ncht.trent.nhs.uk

23–24 September 2004 **(Change of date)**
Thyroid Pathology for the Practicing Pathologist
15 rue de l'Ecole de Médecine, Paris, France

A 2-day course will take place in Paris under the auspices of the French Division of the I.A.P. This course will be given in English by Prof. M. Sobrinho-Simoes (Porto) and Prof. R. Heimann (Brussels).

It will consist of lectures alternating with slide reviews and a slide seminar over a multihead microscope. The cases of this seminar will be sent (on CD) before the meeting. The audience will be limited to 22 participants.

Course fee: 390 euros (320 euros for members of any IAP division). The fees include registration, hand-out, CD of the slide seminar and coffee breaks.

For further information, please contact:
Mrs. M. Fontanière
Administrative Secretary
French Division of the I.A.P. 32 Cours Albert Thomas
69008, Lyon, France
Fax: 33478754311
E-mail: academie.pathologie@wanadoo.fr

11 October 2004
Continuing Medical Education
Nottingham, UK

For further information contact:
The Blamey Education Centre
Nottingham Breast Institute
City Hospital, Nottingham, NG5 1PB, UK
Tel.: 00 44 (115) 969 1689
E-mail: sbury@ncht.trent.nhs.uk

22–24 November 2004
41st Nottingham Multi-disciplinary Course on breast disease
Nottingham, UK

For further information contact:
The Blamey Education Centre
Nottingham Breast Institute
City Hospital, Nottingham, NG5 1PB, UK
Tel.: 00 44 (115) 969 1689
E-mail: sbury@ncht.trent.nhs.uk

Virchows Arch (2004) 445:103–110
DOI 10.1007/s00428-004-1039-8

REVIEW ARTICLE

Antonio Lopez-Beltran · Pier Francesco Bassi · Michele Pavone-Macaluso · Rodolfo Montironi

Handling and pathology reporting of specimens with carcinoma of the urinary bladder, ureter, and renal pelvis. A joint proposal of the European Society of Uropathology and the Uropathology Working Group

Received: 21 January 2004 / Accepted: 22 April 2004 / Published online: 8 June 2004
© Springer-Verlag 2004

Abstract Pathologists play a pivotal role in the diagnosis and in the report of the pathological features related to prognosis. To meet these endpoints, the following issues must be addressed: adequate information about the patient history, proper handling of the specimens, identification of the reliable histopathological techniques necessary to reach the more detailed diagnostic information and evaluation of the prognostic variables, and standardized pathological reporting. In this review we discuss a proposal for standardization of sampling and reporting of the urothelial tissues achieved within uropathology. The urologists have a great role in assisting pathologists in the proper examination by providing them with clinical information.

Keywords Bladder · Ureter · Pelvis · Neoplasms · Transitional cell · Squamous carcinoma · Adenocarcinoma · Pathology report · Sampling · Standardization

A. Lopez-Beltran (✉)
Unit of Anatomic Pathology, Faculty of Medicine,
Avda. Menendez-Pidal S/N, 14004 Cordoba, Spain
e-mail: em1lobea@uco.es
Tel.: +34-957-218993
Fax: +34-957-218229

P. F. Bassi
Department of Urology, University of Padova Medical School,
Padova, Italy

M. Pavone-Macaluso
Clinica Urologica, Universitá di Palermo,
Palermo, Italy

R. Montironi
Institute of Pathological Anatomy,
Polytechnic University of the Marche Region (Ancona),
Ancona, Italy

Introduction

The urothelium covers the urinary tract from the kidney calyces, renal pelvis, ureter, urinary bladder, and a variable portion of the urethra. Most carcinomas of these organs are histologically similar [3]. Surgical procedures of these organs provide an important number of specimens in clinical practice [20]. An appropriate assessment of the specimens and reporting of pathological findings may assist urologists in the appropriate management of patients [20].

The most common bladder specimens are obtained from endoscopic biopsies and transurethral resections of the bladder (TURB), both of which sample subepithelial tissue of varying depth [12]. Other specimens can be obtained from a cystectomy (partial/total), cystoprostatectomy, pelvic exanteration ("en block" resection), and resection of diverticula [12]. Surgical excision of an urachal carcinoma usually includes the bladder dome, urachus, and umbilicus [12].

A bladder biopsy provides information to assess risk factors for recurrence, progression, and response to treatment [2, 16, 17, 18, 23, 28] (Table 1). Small, noninvasive papillary neoplasms are often excised using biopsy with cold-cup forceps, diathermy forceps, or a small diathermy loop. To avoid tissue distortion, these specimens should be

Table 1 Current prognostic factors in bladder cancer specimens

Number of tumors
Cancer size >5 cm in diameter
Tumor extent (stage)
Histological grade
Coexistent dysplasia or carcinoma in situ
Tumor growth pattern
Vascular/lymphatic invasion
Lymph-node involvement
Recurrence at 3 month follow-up cystoscopy
Molecular markers (p53, RB, cadherins)
Others: DNA ploidy, Ki67-MIB1

Table 2 Role of the urologist in handling urological specimens with tumor

To provide with appropriate clinical information, mainly:
Urological and non-urological disease
Previous treatments
To handle the biopsies/surgical specimens in a way to allow an overall assessment of the neoplasia and resection margins
To provide adequate tissue samples for pathological evaluation:
To resect a tumor superficially
To resect more deeply (including suburothelial connective tissues and superficial detrusor muscle)
Random biopsies of endoscopically normal urothelium and the prostatic urethra in case of a multifocal tumor
For small and single primary tumor, the random biopsies are not routinely recommended if urine cytology is negative
To submit all of the pieces of tissue for processing and multiple sectioning
To avoid unnecessary delay in bladder fixation in specific situations, the urologist himself can open the bladder from the urethra to the bladder dome using scissors and then fix it in formalin

Table 3 Handling and reporting of bladder biopsy and transurethral resections of the bladder (TURB) specimens

Specimens vary from single and minute to numerous and large, and orientation is generally difficult. Record the number, size, and epithelial proliferations when present. Report intraepithelial lesions, and, if present, report "denuded biopsy" (most probably related to carcinoma in situ)
Avoid the "common mistake" of overfilling specimen cassettes
Transurethral resections should be weighted in aggregate, and each submitted specimen should receive separate diagnosis
The presence or absence of detrusor muscle in the sample should be stated in the final report. Care must be taken to distinguish the muscularis mucosae bundles within the subepithelial connective tissue from the detrusor muscle. Immunohistochemical staining can help in selected cases
Provide the tumor node metastasis staging system. In TURB specimens showing muscularis propria invasion, the only reasonable statement is "stage T2 at least". Fat tissue in biopsy specimens is not an indication of extravesical extension, since fat may be present within the bladder wall
In TURB specimens, embedding all the resected tissue chips may be necessary in selected cases

transferred to fixative with minimal handling [12, 20]. Larger neoplasms are often sampled using TURB with a diathermy loop that produces strips of tissue 6 mm in diameter and of variable length [14]. Additional resection of the bladder base after a previous TURB provides additional information on tumor extension. All hyperemic or velvety areas of urothelium are sampled to exclude carcinoma in situ (CIS); random biopsies are commonly taken from macroscopically normal urothelium distant from the tumor site to determine the extent of involvement [25, 32]. Ideally, random samples should be obtained from predetermined sites in four vesical quadrants [25]. Some urologists also submit biopsy specimens of the urethra to assess other areas of the urothelium, particularly in patients with high-grade papillary urothelial carcinoma or CIS [1]. Nephroureterectomy or ureterectomy specimens are the result of cancer in these organs. This article reviews the handling and pathology reporting of bladder, ureter and renal pelvis specimens with tumor.

Role of the urologist

Urologists play a capital role in uropathology practice [25, 28], since they are responsible for providing the pathologist with adequate tissue samples for pathological evaluation and handling the biopsies in a way that will enable the pathologist to give the urologist an overall assessment of the neoplasia and the resections margins [30, 31]. Also, it is of great importance to provide the pathologist with all useful clinical information (Table 2).

Role of the pathologist

Handling of specimens

Routine protocol-based tissue sampling ensures consistent and thorough examination by trainees and consultants. The issue has been addressed in the last few years by different groups and societies, among which are the Association of Directors of Anatomic Pathology and the College of American Pathologists [2, 30, 31]. The conclusions of each of these contemporary statements have been incorporated to create a standardized approach to examination of tumor specimens obtained from the bladder, ureter, and renal pelvis [20]. The recommendations are related to the nature of specimens, that is: bladder biopsy and TURB [1, 5, 9, 10, 14, 18, 20, 21, 22, 25, 27, 33, 36] (Table 3); total cystectomy, radical cystoprostatectomy, pelvic exanteration, and partial cystectomy [1, 3, 8, 12, 18, 19, 20, 21, 23, 24, 26, 30, 31] (Table 4) (see also Appendix no. 1, Appendix no. 2, and Appendix no. 3); and ureterectomy or nephroureterectomy specimens [12] (Table 5).

Diagnostic reporting of pathological findings

The pathology report should include clinically relevant information as well as provide clinically useful information derived from the macroscopic examination and microscopic evaluation.

Table 4 Handling and reporting of total cystectomy, radical cystoprostatectomy, pelvic exanteration and partial cystectomy specimens

Orientation of the specimen
The peritoneum can be used as reliable anatomic landmark. It descends further along the posterior wall of the bladder than it does along the anterior wall. Other pelvic organs can also be used if present. Locate both ureters (lateral perivesical fatty connective tissues) and, when present, the vasa deferentia
Fixation of the specimen
Fixation of the bladder must be performed as soon as possible; formalin is widely used but other fixatives should be considered in specific situations (i.e., molecular studies)
Dissection of the specimen (see also Appendix no. 1)
Once the specimen is open, the bladder mucosal surface is examined for ulcerations or tumors. Size, gross morphology (flat, papillary, nodular, or ulcerated), and location (e.g., dome, trigone, free walls, and so on) of any lesion in the bladder are noted
Photograph(s) of the opened specimen are taken, if necessary. Fresh tissue may be collected for special studies by the urologist or, preferably by the pathologist, but this must be stated in the pathological report
Then shave the margins from each of the ureters and the urethra. When the specimen includes the prostate, this distal urethral margin should be taken from the distal end of the prostate
Next, beginning at their trigone orifices open the ureters on both sides using a small pair of scissors. Look for ureteral strictures and dilatations. Examine the mucosa for ulcerations, diverticula or exophytic lesions and document these findings. Submit transverse sections of the ureters
If a tumor is identified in the bladder, make a full-thickness cut through the tumor and bladder wall. See whether or not the tumor appears to infiltrate the muscularis propria and, if so, whether it extends into the perivesical fat or other anatomic structures. Take sections of the tumor to demonstrate its relationship to the adjacent urothelium and its maximal depth of invasion. In large exophytic tumors, sections will be more informative when they are taken from the base of the tumor
Carefully inspect and sample the normal appearing bladder mucosa. Be sure to search for lymph nodes, which are sometimes present in the perivesical fat (see Appendix no. 2)
Prostate examination will be performed according to the standard rules for pathological evaluation and reporting for radical prostatectomy. Similarly, uterus, rectum, and vagina will be evaluated according to standardized criteria. Section these structures to document their presence and demonstrate the relationship between the tumor and each of these structures. Evaluate the resection margins for each organ and record other primary diseases (see Appendix no. 3)
Partial cystectomy specimen
Partial cystectomy specimens (including resections of diverticula) should be fixed and dissected according to the guidelines given for complete bladder specimens. The edges of the specimen represent the surgical margins of the bladder wall
Ink the edges and assess these margins for tumor involvement by taking perpendicular sections from all edges of the specimen at regular intervals. Remember to include mucosa as well as the bladder wall
A variation of the partial cystectomy is seen in resections of neoplasms arising from the urachal tract. These specimens consist of the dome of the bladder in continuity with the urachal tract up to and including the umbilicus. In particular:
Sections should be taken at right angles to the long axis of the urachal tract. Submit a number of these cross sections from the urachal tract for histology as well as the standard sections for the bladder portion
Remember to sample the two additional margins introduced by this resection: the soft tissue margin surrounding the urachus and the skin margin around the umbilicus

Table 5 Handling and reporting of nephro-ureterectomy or ureterectomy specimens with tumor

Nephro-ureterectomy
Begin the dissection at the kidney hilum and identify the ureter, renal artery, and renal vein
Bivalve the kidney so that the relationship of the tumor of the renal pelvis or the calyces of the upper and lower poles can be easily visualized. In general, it will be a sagittal cut that begins at the hilum and exits laterally trough the perinephric fat
Obtain enough tissue sections to show the tumor and its relationship with renal parenchyma and peri-pelvic soft tissues
Record size of the tumor and if papillary or solid. At histology, describe type, grade, and stage. Submit sections that include the tumor, the adjacent non-neoplastic kidney and distal ureter
Ureterectomy specimen
Submit both margins for separate evaluation and then open the entire ureter with a pair of scissors. Carefully inspect the mucosa and wall
Report the gross characteristics of the ureter and of the tumor
Record the size of the tumor and if it is papillary or solid, invasive or non-invasive, and if the surgical margin or peri-ureteric soft tissues are affected

Histological tumor type

More than 95% of carcinomas of the urinary bladder, ureter, and renal pelvis are urothelial. Focal squamous and/or glandular differentiation may be present in the tumor (mixed differentiation), an aspect that must be clearly reported. Pure squamous or adenocarcinomas may also arise in these organs, as well as other unusual histological variants of urothelial carcinoma [7, 22] (Table 6).

Histological grade

There is significant controversy over the classification and grading of these tumors [4, 6, 28]. Papillary and invasive lesions are graded separately. Due to the different classification systems available and the need for a universally acceptable system, in 1998, the World Health Organization (WHO) and the International Society of Urological Pathology (ISUP) proposed a consensus clas-

Table 6 Histological type of tumors of the urinary bladder, ureter, and renal pelvis (World Health Organization, 2004) [22, 37]

Urothelial neoplasia
Benign
Urothelial papilloma
Inverted papilloma
Papillary urothelial neoplasia of low malignant potential
Malignant papillary
Papillary carcinoma, low grade
Papillary carcinoma, high grade
Papillary carcinoma with squamous or glandular differentiation
Malignant non-papillary
Flat carcinoma in situ
Invasive carcinoma
Variants of invasive carcinoma
Nested pattern
Small tubular patter
Microcystic pattern
Inverted pattern
With squamous differentiation
With glandular differentiation
Micropapillary
Sarcomatoid carcinoma
Clear-cell urothelial carcinoma
Plasmocytoid
With syncitiotrophoblasts
With unusual stromal reactions
Pseudosarcomatous stroma
Stromal osseous or cartilaginous metaplasia
Osteoclast-type giant cells
With prominent lymphoid infiltrate
Squamous-cell carcinoma
Usual type
Variant
Verrucous
Basaloid
With sarcomatoid features
Adenocarcinoma (from bladder mucosa, urachal, with extrophy)
Usual intestinal type
Mucinous (including colloid)
Signet-ring cell
Clear cell
Hepatoid
Mixture of above patterns
Adenocarcinoma not otherwise specified
Tumors of mixed cell types
*Undifferentiated carcinomas
Small-cell carcinoma
Large-cell neuroendocrine carcinoma
Lymphoepithelioma-like carcinoma
Giant-cell carcinoma
Undifferentiated carcinoma not otherwise specified
Metastatic carcinoma

* Refers to tumors that are undifferentiated by light microscopy

sification known as the WHO/ISUP classification [9]. This has recently been recognized as the WHO 2004 histological classification of non-invasive papillary urothelial tumors [37] (Table 6). Until the WHO 2004 system is clinically and prognostically validated, tumor grade according to both the WHO 2004 system and the previous WHO (1973) [29] system should be used, for instance, papillary urothelial neoplasm of low malignant potential (WHO 2004)/transitional-cell (urothelial) carcinoma, grade I (WHO, 1973).

Tumor-growth pattern

The most important morphology-based prognostic factors in patients with advanced bladder cancer are tumor stage and lymph-node status. With regard to tumor grade, recent studies have failed to demonstrate a significant prognostic impact in muscle-invasive bladder cancer. In an attempt to identify new parameters allowing one to assess prognosis in bladder cancer patients more accurately, Jimenez et al. have recently introduced a new morphological classification, distinguishing three patterns of growth (nodular, trabecular, and infiltrative type) [13]. Tumors with an infiltrative growth pattern are associated with worse prognosis in comparison with a tumor displaying a non-infiltrative growth pattern. Morphologically, the three patterns are as follows.

- Nodular pattern. Tumor is growing as well-demarcated, round nests of cells. The nests vary in diameter, but display a tendency toward roundness. Desmoplasia is usually inconspicuous. Necrosis is uncommon.
- Trabecular pattern. Tumor is composed of infiltrating broad trabeculae usually anastomosing with each other. The trabeculae are at least three cell layers thick and are sometimes associated with extensive necrosis and desmoplastic stroma.
- Infiltrative pattern. Tumor composed of infiltrating narrow cords or single cells. Desmoplasia and necrosis are common. The cells are highly pleomorphic or small and morphologically undifferentiated.

Tumor extent

The definition of the tumor extent requires knowledge of the components of the organ and its relationship with the adjacent structures. For instance, the urinary bladder consists of three layers.

- Epithelium and sub-epithelial connective tissue that is the lamina propria or submucosa when muscularis mucosae is present (up to 94% of bladders).
- Muscularis propria (or detrusor muscle).
- The peri-vesical fat (peritoneum covering the superior surface and upper part). The bladder is located extraperitoneally.

A critical role of the pathologist is to diagnose the depth and extent of invasion breaking down a distinction between bladder mucosa (Ta), suburothelial connective tissue (T1), detrusor muscle (T2), or beyond (T3 or T4). The TNM (tumor node metastasis) Staging System, 2002 revision, for carcinomas of the urinary bladder, ureter, and renal pelvis of the American Joint Committee on Cancer (AJCC)/International Union Against Cancer (UICC) is recommended [10] (Table 7). The corresponding pT (pathological tumor stage) category must be applied only to the surgical (cystectomy) specimens.

Table 7 TNM (tumor node metastasis) staging system (AJCC/UICC, 2002) of the urinary bladder, renal pelvis, and ureter [10]

Primary tumor (T): urinary bladder	
TX	Primary tumor can not be assessed
T0	No evidence of primary tumor
Ta	Papillary non-invasive carcinoma
Tis	Carcinoma in situ: "flat tumor"
T1	Tumor invades sub-epithelial connective tissue
T2	Tumor invades muscle
T2a	Tumor invades superficial muscle (inner half)
T2b	Tumor invades deep muscle (outer half)
T3	Tumor invades perivesical tissue
T3a	Microscopically
T3b	Macroscopically (extra-vesical mass)
T4	Tumor invades any of the following: prostate, uterus, vagina, pelvic wall, and abdominal wall
T4a	Tumor invades prostate or uterus or vagina
T4b	Tumor invades pelvic wall or abdominal wall
Primary tumor (T): renal pelvis and ureter	
TX	Primary tumor cannot be assessed
T0	No evidence of primary tumor
Ta	Papillary noninvasive carcinoma
Tis	Carcinoma in situ
T1	Tumor invades subepithelial connective tissue
T2	Tumor invades the muscularis
T3	For renal pelvis only: tumor invades beyond muscularis into peripelvic fat or the renal parenchyma
T3	For ureter only: tumor invades beyond muscularis into periureteric fat
T4	Tumor invades adjacent organs, or through the kidney into the perinephric fat
The suffix "m" should be added to the appropriate T category to indicate multiple tumors. The suffix "is" may be added to any T to indicate the presence of associated carcinoma in situ	
Regional lymph nodes (N)	
NX	Regional lymph nodes cannot be assessed
N0	No regional lymph node metastasis
N1	Metastases in a single lymph node, 2 cm or less in greatest dimension
N2	Metastases in a single lymph node, more than 2 cm but not more than 5 cm in greatest dimension, or multiple lymph nodes, none more than 5 cm in greatest dimension
N3	Metastasis in a lymph node more than 5 cm in greatest dimension
Distant metastasis (M)	
MX	Distant metastasis cannot be assessed
M0	No distant metastasis
M1	Distant metastasis

The pathologist must pay attention to diagnose tumor infiltrating the sub-epithelial connective tissue (T1); this diagnosis should be supported in uncertain cases using immunohistochemical studies [14, 15, 27]. T1 substaging based on the relationship of the tumor with the muscularis mucosae is not universally accepted, even though evidence seems to support its clinical value.

Designation of a tumor as merely muscle invasive is inappropriate: the type of muscle invasion, i.e., muscularis mucosae (T1 tumors) versus detrusor muscle (T2 tumors) invasion, needs to be clearly stated [14]. Descriptive terminology, such as "urothelial carcinoma with muscle invasion, indeterminate for type of muscle invasion," may be used when it is not possible to assess the type of muscle invaded by the tumor (muscularis mucosae or detrusor muscle). A comment on thermocoagulation effect may be reported if it makes diagnostic evaluation difficult.

Tumor size and multicentricity

In surgical specimens, the pathology report has to include the size of the tumor and information on its multicentricity, especially when dealing with bladder specimens. Tumor size affects tumor invasiveness. Of lesions that are larger than 5 cm, 35% will progress to muscularis propria invasion, whereas only 9% of tumors smaller than 5 cm progress similarly. In some studies, the presence of multiple tumors affects recurrence rates but does not affect the likelihood for invasion, whereas other studies have shown an association with progression of disease [18].

Margins

Tumors involving the resection margin on pathological examination may be assumed to correspond to residual tumor in the patient and may be classified as macroscopic or microscopic according to the findings at the specimen margin(s). The resection margin status should be carefully specified. In particular:

- Statements about deep soft tissue margins should specify whether peritoneal surfaces are involved with the tumor
- In cases of urachal adenocarcinoma in which partial cystectomy with excision of the urachal tract and umbilicus is performed, the margins of the urachal tract, i.e., the soft tissue surrounding the urachus and the skin around the umbilical margin, should be specified
- In renal pelvis, ureter, and nephroureterectomy specimens, the margins may include radial hilar soft tissue margin, bladder cuff, ureteral, renal parenchyma, and Gerota's fascia margins, depending on the type of surgical specimen

Venous/lymphatic vascular invasion

Urothelial carcinoma may invade blood vessels or lymphatic channels. In suspicious cases, blood vessels can be highlighted using immunohistochemical staining for factor-VIII-related antigen, CD31, or CD34 [35]. Staining will not resolve the problem of differentiating lymphatic versus artifactual space entrapment by tumor cells in some cases. Retraction artifact is also prominent in the "micropapillary variant" of urothelial carcinoma.

Urothelial carcinoma in situ

The evaluation of urothelium in patients who have superficial (stage Ta or T1) tumors is important because those patients who have associated CIS are at higher risk of tumor recurrence and disease progression [14].

Additional information

Additional information (epidemiological, morphological, and molecular or genetic abnormalities) can be reported by the pathologist (Table 8). For instance, urothelial carcinoma has been studied extensively on a biological (molecular or genetic) basis. Prognostic factors identified from such studies have been proposed and include blood-group antigen expression in tumor cells, measurement of proliferative activity by DNA content analysis and S-phase fraction, and proliferation markers. Immunohistochemical analysis has been used to detect abnormal gene products. Multiple genetic changes are associated with bladder carcinoma and are detected by karyotyping, fluorescent in situ hybridization, restriction-fragment-length polymorphisms, and microsatellite analysis. There is no consensus in the current literature about the definitive role and value of such prognostic factors [11, 15, 34].

Acknowledgements This publication is made under the auspices of the European Society of Uropathology (a full section office member of the European Association of Urology, EAU) and the Uropathology Working Group (European Society of Pathology, ESP). It is based on the Uropathology Workshop held in Sesto Fiorentino (Ely Lilly Italia Headquarter), Florence, Italy, 15 June 2003.

Appendix no. 1

Sections for microscopic evaluation
(with special reference to bladder)

In transurethral resections of the bladder specimens, submit one section per centimeter of tumor diameter (up to ten cassettes). If the tumor is noninvasive by the initial sampling, additional submission of tissue (including possibly submitting all tissue) is necessary to diagnose or rule out the presence of invasion. If tumor is invasive into the lamina propria in the initial sampling, additional sections (including possibly submitting the entire specimen) may be necessary to diagnose or rule out the possibility of muscularis propria invasion.

In cystectomy specimens, several representative sections of the tumor, including the macroscopically deepest penetration, should be sampled. Submit several sections of the mucosa remote from the carcinoma, especially if abnormal, including the lateral wall(s), dome, and trigone.

Submit one section of ureteral margin, unless submitted separately as frozen section specimens, and one section of urethral margin. If a long segment of the ureter(s) is present, then additional sections from the midportion may be necessary, as urothelial cancer often is multifocal. For additional information see: ftp://ftp.cap.org/cancerprotocols/Blad03_p.pdf.

Appendix no. 2

Lymph nodes and distant spread

The regional lymph nodes are the nodes of the pelvis, which essentially are the pelvic nodes below the bifurcation of the common iliac arteries. The significance of the regional lymph-node metastasis in staging bladder cancer lies in the number and size, not in whether metastasis is unilateral or bilateral. One of the major prognostic determinants of ultimate cure is whether the tumor is confined to the bladder, and a major adverse prognostic feature is the presence of any lymph-node metastasis.

Regional lymph nodes include: hypo-gastric, obturator, iliac (internal, external, not otherwise specified), perivesical, pelvic (not otherwise specified), sacral (lateral, sacral promontory), pre-sacral. The common iliac nodes are considered sites of distant metastasis and should be coded as M1.

It is recommended that the number of lymph nodes submitted by the urologist should be reported. All the nodes should be widely sampled and evaluated. In particular, submit one section from each grossly positive lymph node. All other lymph nodes should be entirely submitted, as presence of nodal disease may be used as an

Table 8 Practice parameters for handling and reporting bladder, ureter, and renal pelvis specimens (checklist). *TURB* transurethral resections of the bladder, *CIS* carcinoma in situ, *PIN* prostatic intraepithelial neoplasia, *WHO* World Health Organization, *TNM/AJCC* Tumor Node Metastasis/American Joint Committee on Cancer

I.	General information
	Pertinent clinical information: name, medical record number, data, referring physician, relevant clinical history past and present
II.	Gross description
	Fresh or fixed specimen
	Nature of the specimens: biopsy, chips (TURB), partial cystectomy, radical cystectomy, cysto prostatectomy, "en bloc" resection, nephroureterectomy, ureterectomy
	Total weight of resected tissue fragments (TURB); three dimensional measurements of recognizable anatomic structures and tumors or other recognizable lesions
	Site of involvement, gross fat extension
III.	Diagnostic and prognostic information
	Histological tumor type: urothelial, squamous, adenocarcinoma, other
	Tumor grade: use current grading schemes (WHO 2004, WHO 1973, or both)
	Extent of tumor in bladder (degree of invasion)*
	No invasion
	Invasion of the suburothelial connective tissue, muscularis propria, perivesical tissue
	Presence or absence of lymphatic/vascular invasion
	Tumor arising in a diverticulum (state whether muscularis propria is present)
	Intraepithelial abnormalities (dysplasia, CIS)
	Report focality or multifocality
	Report presence of pagetoid spread of CIS (this finding is not dysplasia)
	Extent of tumor in organs attached to the bladder
	Prostate: direct extension to the prostate, involvement of prostatic urethra, involvement of prostatic ducts with or without stromal involvement
	Ureter, renal pelvis, and urethra: report any dysplastic/neoplastic change of the mucosa, and report any invasion into adjacent suburothelial connective tissue or muscularis propria
	Seminal vesicles: report spread of carcinoma in these organs either through epithelium or by direct extension of an infiltrative tumor
	Vagina/uterus: report direct extension or metastasis to either organ
	Surgical margins: report status of ureteral/urethral margins. Report perivesical margin involvement
	Report important associated conditions such PIN and adenocarcinoma of the prostate
	Lymph nodes: report presence or absence of metastasis. If metastasis are present state number and size of the largest one (<2.0 cm, 2.1 to 5 cm, >5 cm)
IV.	Features considered optional in the final report
	Invasion of the muscularis mucosa, if present; T1 substaging with micrometer, or just focal/wide suburothelial connective tissue invasion
	Genetic abnormalities
	Cytometric examination
	Morphometric examination
	p53, ki-67
	Other immunohistochemical markers
	Stage: use TNM/AJCC 2002 revision (T1–T4, N, and M)

* Immunohistochemistry may be useful in selected cases using either cytokeratin for suburothelial connective tissue invasion or vascular endothelial markers for vascular invasion

indication for adjuvant therapy. Lymph nodes may also be grossly or microscopically detected in the perivesical fat. In case of positive node(s), the size must be reported in order to fulfill tumor node metastasis requirements for staging [10] (Table 7). Distant spread is most commonly to liver, bone, lung, and lymph nodes.

Appendix no. 3

Sampling criteria for the definition of T4

In the male, the bladder adjoins the rectum and seminal vesicle posteriorly, the prostate inferiorly, and the pubis and peritoneum anteriorly. In the female, the vagina is located posteriorly, and the uterus is located superiorly.

As far as the prostate and prostatic urethra are concerned, prostatic urethral involvement should be carefully investigated in cystectomy specimens [24, 25, 26] (Table 8). In particular, sections should include the prostatic urethra, including at the margin and with the surrounding prostatic parenchyma. Representative sections of the peripheral zone, central zone, and seminal vesicles should be included. It must be noted that there is a higher incidence of prostatic adenocarcinoma in cystoprostatectomy specimens of bladder carcinoma. Close gross examination may help target sampling of selective abnormal-appearing areas.

As far as other tissues are concerned, the following is recommended: submit one or more sections of uterus as indicated and one or more sections of vagina, seminal vesicles, and other organs as indicated. If the tumor grossly appears to invade the prostate, uterus, or vagina, sections should be targeted, such that the relationship of the infiltrating tumor in the bladder wall and the adjacent viscera is clearly demonstrable.

References

1. Amin MB, Young RH (1997) Intraepithelial lesions of the urinary bladder with a discussion of the histogenesis of urothelial neoplasia. Semin Diagn Pathol 14:84–97
2. Amin MB, Srigley JR, Grignon DJ, Reuter VE, Humphrey PA, Cohen MB, Hammond ME (2003) Updated protocol for the examination of specimens from patients with carcinoma of the urinary bladder, ureter, and renal pelvis. Arch Pathol Lab Med 127:1263–1279
3. Bostwick DG, Lopez-Beltran A (1999) Bladder biopsy interpretation. UPP, New York
4. Bostwick DG, Mikuz G (2002) Urothelial papillary (exophytic) neoplasms. Virchows Arch 441:109–116
5. Bostwick DG, Ramnani D, Cheng L (1999) Diagnosis and grading of bladder cancer and associated lesions. Urol Clin North Am 26:493–507
6. Busch C, Algaba F (2002) The WHO/ISUP 1998 and WHO 1999 systems for malignancy grading of bladder cancer. Scientific foundation and translation to one another and previous systems. Virchows Arch 441:105–108
7. Eble JN, Young RH (1997) Carcinoma of the urinary bladder: a review of its diverse morphology. Semin Diagn Pathol 14:98–108
8. Eble JN, Amin MB (2001) Practice protocol for examination of cystectomy and cystoprostatectomy specimens: proposal of a standardized reporting form. Adv Anat Pathol 8:360–361
9. Epstein JI, Amin MB, Reuter VR, Mostofi FK (1998) The World Health Organization/International Society of Urological Pathology consensus classification of urothelial (transitional cell) neoplasms of the urinary bladder. Bladder Consensus Conference Committee. Am J Surg Pathol 22:1435–1448
10. Greene FL, Page DL, Fleming ID, Fritz AG, Balch CM, Haller DG, Morrow M (2002). AJCC cancer staging manual, 6th edn. Springer, Berlin Heidelberg New York
11. Helpap B, Schmitz-Drager BJ, Hamilton PW, Muzzonigro G, Galosi AB, Kurth KH, Lubaroff D, Waters DJ, Droller MJ (2003) Molecular pathology of non-invasive urothelial carcinomas (part I). Virchows Arch 442:309–316
12. Hruban RH, Wetra WH, Phelps TH, Isacson C (1996) Surgical pathology dissection. An illustrated guide. Springer, Berlin Heidelberg New York
13. Jimenez RE, Gheiler E, Oskanian P, Tiguert R, Sakr W, Wood DP Jr, Pontes JE, Grignon DJ (2000) Grading the invasive component of urothelial carcinoma of the bladder and its relationship with progression-free survival. Am J Surg Pathol 24:980–987
14. Jimenez RE, Keane TE, Hardy HT, Amin MB (2000) pT1 urothelial carcinoma of the bladder: criteria for diagnosis, pitfalls, and clinical implications. Adv Anat Pathol 7:13–25
15. Kausch I, Bohle A (2002) Molecular aspects of bladder cancer III. Prognostic markers of bladder cancer. Eur Urol 41:15–29
16. Kurth K, Schroeder FH, Debruyne F, Senge T, Pavone-Macaluso M, de Pauw M, ten Kate F, Sylvester R (1989) Long-term follow-up in superficial transitional cell carcinoma of the bladder: prognostic factors for time to first recurrence, recurrence rate, and survival. Final results of a randomized trial comparing doxorubicin hydrochloride, ethoglucid, and transurethral resection alone. EORTC Genitourinary Tract Cancer Cooperative Group. Prog Clin Biol Res 303:481–490
17. Kurth KH, Denis L, Bouffioux C, Sylvester R, Debruyne FM, Pavone-Macaluso M, Oosterlinck W (1995) Factors affecting recurrence and progression in superficial bladder tumours. Eur J Cancer 31:1840–1846
18. Lapham RL, Grignon D, Ro JY (1997) Pathologic prognostic parameters in bladder urothelial biopsy, transurethral resection, and cystectomy specimens. Semin Diagn Pathol 14:109–122
19. Lesourd A, Billerey C (2000) Protocol for the pathologic examination of cystectomy and cystoprostatectomy specimens. Proposal for a standardized form. Ann Pathol 20:85–90
20. Lopez-Beltran A, Bollito E, Luque RJ, Montironi R (2001) A practical approach to bladder sampling and diagnostic reporting of pathological findings. Pathologica 93:688–692
21. Lopez-Beltran A, Cheng L, Andersson L, Brausi M, de Matteis A, Montironi R, Sesterhenn I, van det Kwast KT, Mazerolles C (2002) Preneoplastic non-papillary lesions and conditions of the urinary bladder: an update based on the Ancona International Consultation. Virchows Arch 440:3–11
22. Lopez-Beltran A, Sauter G, Gasser T, Hartmann A, Schmitz-Dräger BJ, Helpap B, Ayala AG, Tamboli P, Knowles MA, Sidransky D (2004) Urothelial tumors: infiltrating urothelial carcinoma. In: Eble JN, Sauter G, Epstein JI, Sesterhenn I (eds) World Health Organization classification of tumors. Pathology and gentics of tumors of the urinary system and male genital organs. IARC Press, Lyon
23. Maffezzini M, Audisio R, Pavone-Macaluso M, Hall RR (1998) Bladder cancer. Crit Rev Oncol Hematol 27:151–153
24. Mahadevia PS, Koss LG, Tar IJ (1986) Prostatic involvement in bladder cancer. Prostate mapping in 20 cystoprostatectomy specimens. Cancer 58:2096–2102
25. May F, Treiber U, Hartung R, Schwaibold H (2003) Significance of random bladder biopsies in superficial bladder cancer. Eur Urol 44:47–50
26. Mazzucchelli R, Santinelli A, Lopez-Beltran A, Scarpelli M, Montironi R (2002) Evaluation of prognostic factors in radical prostatectomy specimens with cancer. Urol Int 68:209–215
27. Mhawech P, Iselin C, Pelte MF (2002) Value of immunohistochemistry in staging T1 urothelial bladder carcinoma. Eur Urol 42:459–463
28. Montironi R, Lopez-Beltran A, Mazzucchelli R, Bostwick DG (2003) Classification and grading of the non-invasive urothelial neoplasms: recent advances and controversies. J Clin Pathol 56:91–95
29. Mostofi FK, Sobin LH, Torloni H (1973) Histological typing of urinary bladder tumors. World Health Organization, Geneva
30. Murphy WM (1994) ASCP survey on anatomic pathology examination of the urinary bladder. Am J Clin Pathol 102:715–723
31. Murphy WM, Crissman JD, Johanssson SL, Ayala AG (1996) Association of directors of anatomic and surgical pathology recommendations for reporting of urinary bladder specimens containing bladder neoplasms. Hum Pathol 27:751–753
32. Pagano F, Garbeglio A, Milani C, Bassi P, Pegoraro V (1987) Prognosis of bladder cancer. I. Risk factors in superficial transitional cell carcinoma. Eur Urol 13:145–149
33. Philip AT, Amin MB, Tamboli P, Lee TJ, Hill CE, Ro JY (2000) Intravesical adipose tissue: a quantitative study of its presence and location with implications for therapy and prognosis. Am J Surg Pathol 24:1286–1290
34. Quek ML, Quinn DI, Daneshmand S, Stein JP (2003) Molecular prognostication in bladder cancer-a current perspective. Eur J Cancer 39:1501–1510
35. Ramani P, Birch BR, Harland SJ, Parkinson MC (1991) Evaluation of endothelial markers in detecting blood and lymphatic channel invasion in pT1 transitional carcinoma of bladder. Histopathology 19:551–554
36. Ro JY, Ayala AG, el-Naggar A (1987) Muscularis mucosa of urinary bladder. Importance for staging and treatment. Am J Surg Pathol 11:668–673
37. Sauter G, Algaba F, Amin MB, Busch C, Cheville J, Gasser T, Grignon D, Hofstaedter F, Lopez-Beltran A, Epstein JI (2004) Non invasive urothelial neoplasias: WHO classification of non-invasive papillary urothelial tumors. In: Eble JN, Sauter G, Epstein JI, Sesterhenn I (eds) World Health Organization classification of tumors. Pathology and gentics of tumors of the urinary system and male genital organs. IARCC Press, Lyon

Virchows Arch (2004) 445:111–118
DOI 10.1007/s00428-004-1047-8

REVIEW ARTICLE

Cord Langner · Helmut Denk

Wilson disease

Received: 19 December 2003 / Accepted: 3 May 2004 / Published online: 17 June 2004
© Springer-Verlag 2004

Abstract Wilson disease (WD) is an autosomal recessive disorder of copper metabolism. Since daily copper intake exceeds the body's requirements, effective means of excreting excess copper are essential. These are accomplished by ATP7B, a new member of the cation-transporting p-type ATPase family, which is mainly expressed in the liver and mediates both copper secretion into plasma (coupled with ceruloplasmin synthesis) and its excretion into bile. Thus far, more than 200 mutations of the WD gene have been detected, causing impairment of ATP7B function and, ultimately, copper accumulation. Excess copper, however, induces free-radical reactions and lipid peroxidation. Resultant liver damage leads to steatosis, inflammation, cirrhosis, and, occasionally, fulminant liver failure. The diagnosis of WD is commonly made on the basis of typical clinical and laboratory findings, including low serum ceruloplasmin, increased urinary copper excretion, and increased hepatic copper content. Since liver morphology is non-specific, and copper histochemistry may lead to both false-negative and false-positive results, the pathologist usually only suspects the disease or assists in its confirmation. Although the value of molecular genetic testing is limited due to the high number of possible gene mutations, polymerase chain reaction may be useful for the evaluation of family members of homozygous index patients.

Keywords Wilson disease · ATP7B · Lipid peroxidation · Liver pathology

Dedicated to Prof. Dr. med. O. Klinge, Kassel, Germany, on the occasion of his 70th birthday.

C. Langner (✉) · H. Denk
Institute of Pathology,
Medical University of Graz,
Auenbruggerplatz 25, 8036 Graz, Austria
e-mail: cord.langner@meduni-graz.at
Tel.: +43-316-38583665
Fax: +43-316-384329

Introduction

In 1912, the British neurologist Samuel Alexander Kinnier Wilson [63] reported on seven patients with a familial form of a primary neurological disorder associated with liver cirrhosis, which he referred to as progressive lenticular degeneration. In the same year, Fleischer [17] described patients with a combination of corneal pigmentation, neuropsychiatric symptoms, and liver cirrhosis. These were the primary reports dealing with a peculiar disorder now recognized as Wilson disease (Wilson's disease, WD). In 1948, Cumings [9] identified the role of copper in the pathogenesis of WD, detecting huge amounts of this metal in liver and brain tissue of affected patients. Scheinberg and Gitlin [54] reported serum ceruloplasmin deficiency in WD patients 4 years later, providing the basis for a diagnostic test still widely used today. In 1960, Bearn [1] demonstrated the autosomal recessive nature of WD, and, in 1985, Frydman et al. [18] established linkage of the WD gene to the esterase D locus on chromosome 13q14.3. Finally, in 1993, the WD gene was cloned and shown to encode a new member of the cation-transporting p-type ATPase family [5, 60].

Copper metabolism

Copper is a trace element that plays a fundamental metabolic role. It serves as an essential cofactor for a number of (cupro-) enzymes that mediate various cellular processes, including mitochondrial energy generation (cytochrome-*c*-oxidase), iron homeostasis (ferroxidase), free-radical detoxification (Mn^{2+}/Cu^{2+} superoxide dismutase), melanin formation (tyrosinase), neurotransmitter synthesis (dopamine-b-hydroxylase), and connective tissue cross-linking (lysyl oxidase) [33, 45]. The adult human body contains approximately 100 mg of copper, the balance of this metal being maintained almost entirely by gastrointestinal absorption and biliary excretion [35]. Dietary sources of copper include shellfish, liver, mushrooms, nuts, soy products, gelatin, and chocolate. After absorption

from the gastrointestinal tract, copper rapidly appears in the portal circulation, bound to albumin and amino acids such as histidine. In the liver, hepatocytes are thought to extract copper from sinusoidal blood via basolateral surface transporters called hCTR1 (for high-affinity transport) and hCTR2 (for low-affinity transport) [23, 65]. Intracellular copper then interacts with certain proteins, i.e., copper chaperones, which are essential for the delivery of copper to specific intracellular targets. Since the average daily copper intake exceeds the body's requirements, effective means of excreting excess copper are essential. Hepatocytes are able to sense the copper status in their cytoplasm and regulate copper excretion depending on the intracellular concentration of the metal. The regulation is accomplished by the copper-transporting ATPase encoded at the WD gene locus. This ATPase is now called ATP7B and shares 65% homology with ATP7A, the Menkes disease protein [23]. ATP7B contains eight transmembrane segments, six copper-binding regions, an ATP-binding domain, a transmembrane cation channel, a phosphorylation region, and a transduction domain responsible for the conversion of energy of ATP hydrolysis to cation transport [23]. The proper function of ATP7B in copper homeostasis depends on its intracellular localization: at low copper levels, the transporter is located in the trans-Golgi network, where it is responsible for the incorporation of copper into apoceruloplasmin to form ceruloplasmin, the main copper-binding serum glycoprotein, constituting a pathway for ceruloplasmin and other cuproenzymes from the Golgi complex to the sinusoidal plasma membrane. In contrast, cellular exposure to high copper levels results in intracellular trafficking of ATP7B from the trans-Golgi network to a post-Golgi vesicular compartment, which is involved in biliary copper excretion and is localized in close vicinity to the biliary canalicular membrane. Once copper is removed from the cytosol, ATP7B recycles back to the trans-Golgi network [26, 50, 52, 53].

Pathophysiology and molecular pathogenesis of WD

WD is an autosomal recessive disease with a worldwide prevalence of approximately 1 in 30,000 individuals. The gene frequency varies between 0.3% and 0.7%, corresponding to an asymptomatic heterozygous carrier rate of 1 in 90 [20]. The risk of WD in siblings and parents or children of an index patient is 25% and 0.5%, respectively [39]. Until now, more than 200 disease-specific mutations in the *ATP7B* gene have been detected, including single base insertions and deletions, frame-shifts, missense, nonsense, and splice-site mutations [23, 49]. Most WD patients are compound heterozygotes, possessing alleles with two different mutations. Recent studies have shown that some mutations of the *ATP7B* gene show a particular geographic distribution. Thus, the most common mutation, His1069Gln (H1069Q), is present in over 70% of Polish [11] and over 60% of Austrian and East German [6, 39] WD patients and accounts for between 10% and 40% of all mutations identified in patients of other European and North American origin. In contrast, the same mutation has only rarely, if at all, been documented in WD patients from India and other parts of Asia. Finally, over half of all known mutations are known to occur only rarely in any given population and have been documented in single patients only [49].

The mutation of the *ATP7B* gene results in functional impairment of the ATP7B protein. However, during recent years, increasing evidence has been provided that different mutations are related to different degrees of functional ATP7B deficiency and that such variability may contribute to the diverse clinical manifestations of WD [49]. Hence, large efforts are currently being made to elucidate possible genotype–phenotype correlations [49]. A recent study by Huster et al. [26] was the first to demonstrate that mutations of the WD gene lead to incorrect intracellular localization of ATP7B to distinct subcellular compartments, thereby causing disruption of the intracellular copper balance in hepatic cells. The impairment of ATP7B-mediated intracellular copper transport results in accumulation of hepatic copper due to both reduced biliary copper excretion and abrogation of ceruloplasmin synthesis. The latter, however, seems to be of minor importance in copper homeostasis, since patients with aceruloplasminemia were shown to have normal copper metabolism [24]. Finally, it is important to realize that ceruloplasmin deficiency is not the primary gene defect or abnormality, but rather represents an associated phenomenon.

Although copper is an essential trace element, the intrahepatic excess of this metal results in severe hepatocellular injury and, ultimately, in the deposition of copper in non-hepatic tissues. According to Britton [3], copper may play a catalytic role in the initiation of free-radical reactions. The resulting reactive oxygen/nitrogen species and unsaturated aldehydes have the potential to deplete cellular stores of antioxidants and finally damage cellular lipids, nucleic acids, proteins, and carbohydrates, resulting in impairment of cellular function and integrity. During the last years, evidence has accumulated that copper overload can indeed induce peroxidative lipid damage in vivo and consecutive impairment of membrane-dependent functions of both mitochondria and lysosomes. Moreover, damage of hepatic mitochondrial DNA has been documented in WD patients [40]. In mice, which are homozygous (null) mutants for the *ATP7B* gene, intracellular copper accumulation, and development of liver cirrhosis resembling human WD has been shown [4]. Oxidative stress has additionally been linked to an increased risk of liver cancer; reactive oxygen and nitrogen species are able to cause mutations in cancer-related genes, such as the p53 tumor-suppressor gene [62]. In a recent study by Hussain et al. [25], 60% of WD cases showed high expression of inducible nitric oxide synthase in the liver, suggesting nitric oxide as a source of increased oxidative stress. Moreover, the frequency of p53-mutated alleles was increased when compared with liver tissue from normal controls, and p53 mutations could be experimen-

tally attributed to the generation of reactive oxygen/nitrogen species and unsaturated aldehydes. These data link metal overload directly to the development of hepatocellular carcinoma.

Pathology of WD

The earliest signs of liver cell injury are evident at the ultrastructural level. According to Dickersin [13], diagnostic criteria in the early asymptomatic stage of WD are: (i) enlarged, pleomorphic mitochondria with increased matrix density, (ii) increased number, size, and pleomorphism of peroxisomes, (iii) vesiculation of smooth endoplasmic reticulum, and (iv) increase of triglyceride vacuoles. In the later, symptomatic stage (v), lipofuscin and (vi) copper deposits within lysosomes, characterized as multivesiculated densities, are found. These abnormalities, however, are not specific for WD. Hence, additional element analyses with transmission electron microscopy with electron energy-loss spectroscopy and with scanning electron microscopy with energy dispersive x-ray analysis have been applied to show copper-specific signals inside hepatocellular lysosomes of affected patients, thus, strongly supporting the diagnosis of WD [30].

The ultrastructural changes along with reduced mitochondrial enzyme activity are thought to be linked to a pathogenetic chain of events responsible for diminished lipid oxidation and consequent triglyceride accumulation in the hepatocytes, which, together with glycogen deposition in the nuclei of periportal hepatocytes, represent the earliest changes detectable at light microscopy [57]. The lipid droplets progressively increase in number and size and may, in some cases, resemble the steatosis induced by ethanol (Fig. 1A). The rate of progression from steatosis to cirrhosis is variable, showing no relationship between age and likelihood of cirrhosis [21]. Progression tends to involve processes with or without hepatic inflammation [20, 58]. Thus, some patients may develop mild hepatocellular damage with slight to moderate anisocytosis and anisonucleosis of hepatocytes as well as slight ballooning of disseminated hepatocytes. Acidophilic bodies are scarce, and foci of necrosis are usually absent. Peripheral hepatocytes may contain an atypical form of lipofuscin, appearing as large, irregular, and sometimes vacuolated deposits [58]. Portal inflammation, when present, is generally slight, but varying degrees of fibrosis may be encountered. Other patients may show histological changes, resembling autoimmune or chronic active viral hepatitis with slight to moderate degeneration and necrosis of peripheral (periportal) hepatocytes along with predominant-ly lymphocytic portal inflammation with irregular extension beyond the limiting plate (interface hepatitis) (Fig. 1B). These cases generally display larger amounts of portal, periportal, or bridging fibrosis and may, if untreated, rapidly progress to liver cirrhosis [58]. Multilobular (submassive) necrosis may also be seen, particularly in fulminant WD [12], but these patients are only rarely biopsied. In the cirrhotic stage, patients usually exhibit macronodular or mixed macro-/micronodular cirrhosis. Anisocytosis and anisonucleosis of hepatocytes are moderate or marked, and focal necroses and hepatocytic degeneration are present, but are quite variable in degree. Interface hepatitis is regarded as a constant finding [58]. Classical Mallory bodies can be found in about 25% of cirrhotic cases [29], either predominantly at the periphery of the parenchymal nodules or dispersed (Fig. 1D, E). Usually, they are associated with cells showing marked ballooning degeneration or necrosis with or without neutrophilic satellitosis. Additionally, clusters of large hepatocytes with eosinophilic granular cytoplasm due to an increased number of mitochondria (oncocytic or oxyphil cells), cholestasis, inflammatory changes, or fibrosis of residual central or sublobular veins, as well as foci of regenerative liver cells, may be found. Each of the morphological findings pointed out above is non-specific, but their combination suggests the possibility of WD [58]. In our personal experience, the diagnosis of WD should be considered in the presence of steatosis and periportal glycogenated nuclei along with hepatocyte ballooning and varying degrees of portal and periportal inflammation (interface hepatitis), particularly in children or young adults.

The suspicion of WD should prompt the pathologist to perform histochemical stains for the detection of copper or copper-binding protein in the liver biopsy. The various methods have been reviewed previously [27, 34, 46]. The stains reveal copper itself (e.g., rhodanine, rubeanic acid, Timm's silver stain) or copper-binding protein, which is believed to represent polymerized metallothionein sequestered in lysosomes (e.g., Victoria blue, orcein). From a practical point of view, the application of several staining methods is recommended to increase the diagnostic utility of copper histochemistry. Nevertheless, in the early stage of WD (steatosis and slender fibrosis) intrahepatic copper accumulation may be undetectable in more than 50% of patients [46], since copper is diffusely distributed in the cytoplasm and highly soluble, particularly in poorly buffered formalin. Hence, it must be pointed out that a negative staining result does not rule out increased hepatic copper content and should not be considered sufficient for the exclusion of WD. In the advanced stage, however, copper is sequestered within lysosomes and is usually (sensitivity >80%) detectable as pericanalicular granules [37, 46, 58]. In pre-cirrhotic livers, histochemically demonstrable copper appears to be confined to periportal hepatocytes (Fig. 1C), whereas in cirrhotic livers, it is generally diffusely distributed in the parenchymal nodules (Fig. 1F), although the copper content may vary significantly from nodule to nodule, with some of the nodules even containing little or no stainable material [37, 58]. Moreover, hepatic copper has been shown to be unevenly distributed throughout the whole organ [15, 41]. Therefore, hepatic copper accumulation may entirely be missed, especially when the biopsy cylinder is small, inadequately fixed, or mainly contains regenerative parenchymal foci or nodules that usually lack specific staining [37, 58]. In contrast, stainable

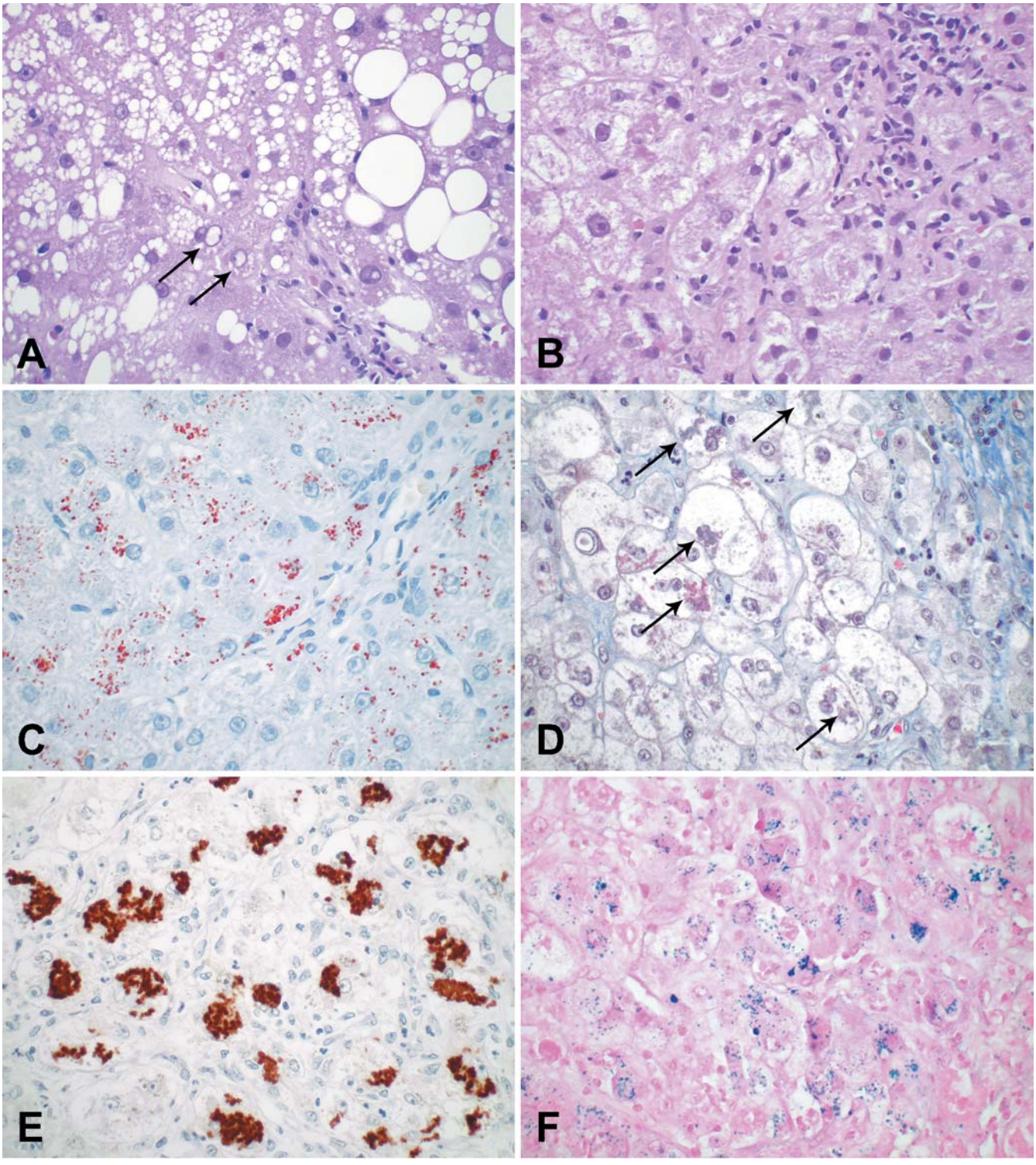


Fig. 1 Marked micro- and macrovesicular steatosis with glycogen nuclei (*arrows*, **A**) and non-specific portal lymphohistiocytic inflammation, including foci of interface hepatitis (**B**) in a case of non-cirrhotic Wilson disease. Periportal deposition of copper as red granules is shown in the rhodanine-stained section (**C**). Wilsonian liver cirrhosis with marked ballooning of hepatocytes containing classical Mallory bodies (**D** CAB, *arrows*; **E** ubiquitin immunostaining). In this case, large amounts of copper-binding protein are detected throughout the parenchymal nodules in the Victoria blue-stained section (**F**). Originals ×150

amounts of copper may sometimes be even more conspicuous in chronic cholestatic liver diseases, such as primary biliary cirrhosis [28] and primary sclerosing cholangitis [22]; usually, however, they are confined to zone I or to the periphery of parenchymal nodules. The only other non-cholestatic and non-WD liver disorders with high intrahepatic copper levels are Indian childhood cirrhosis and endemic Tyrolean infantile cirrhosis (idiopathic copper toxicosis), both of which are extremely rare conditions, show a specific geographic distribution, and have to be distinguished from WD on both clinical and morphological grounds [43, 44, 59].

In summary, hepatic histological findings alone are not diagnostic for WD and may be similar to those in a broad spectrum of other acute and chronic liver disorders. Moreover, the pathologist must be aware that WD may be encountered together with other liver diseases, such as viral hepatitis [32], autoimmune hepatitis [42], or hereditary hemochromatosis [36], which may blur morphological features suggestive of WD.

As already pointed out, intrahepatic copper accumulation may be directly related to the development of hepatocellular carcinoma. However, hepatocellular carcinoma is uncommon in WD in contrast to hemochromatosis [8, 48]. The reason for the apparently low cancer risk is unclear and has been attributed to the relatively poor inflammatory component in the pathogenesis of Wilsonian cirrhosis and to a putative protective effect of chelation therapy [20, 49, 57].

Clinical background and diagnosis of WD

The biochemical defect that leads to the accumulation of copper in WD is already present at birth. However, clinical symptoms are rarely observed before the age of 5 years [20]. The initial signs of WD are generally detected in older children, adolescents, and young adults, but presentation can occasionally be delayed until the sixth decade [10, 47, 51]. WD may present under a variety of clinical conditions. In a large series of patients, the initial clinical manifestations were hepatic in 42%, neurological in 34%, hematological in 12%, psychiatric in 10%, and renal in 1% [cited in 20]. Interestingly, the way the disease emerges appears to be related to the age of the first clinical presentation: over 80% of presentations within the first decade of life and 40–70% of presentations overall are related to liver involvement, whereas 75% of patients presenting after the age of 20 years have developed neuropsychiatric disturbances at time of diagnosis [23]. Liver disease ranges from mild elevation of serum aminotransferases in asymptomatic individuals to cirrhosis with all its complications or occasionally to fulminant hepatic failure, which is often accompanied by the sudden release of excess copper into the bloodstream with resultant hemolytic anemia. In fulminant hepatic failure, relatively mild elevations of serum aminotransferases are seen despite massive hepatic necrosis, which is responsible for the deleterious clinical course, with survival generally no longer than days to weeks unless hepatic transplantation is performed (see below). The disease prevails in women, suggesting that hormonal factors may in some way be involved [20, 49]. Regarding neurological disturbances, Parkinsonian symptoms predominate, but pseudosclerotic, dystonic, and choreic symptoms can also be found, often associated with a change in personality [35, 49]. As expected, these clinical features mirror the underlying pathological alterations with cavitary degeneration in the basal ganglia, extensive gliosis, and neuronal loss in association with a marked increase of the copper content in this region of the brain [35]. The most common ocular finding in WD is the presence of asymptomatic copper deposition in the limbus of the cornea, which can be detected using slit-lamp examination and is referred to as a Kayser–Fleischer ring. Kayser–Fleischer rings are present in nearly all patients with WD complicated by neurological symptoms, whereas they occur in only 55–70% of patients with hepatic disease [19]. Although the rings are considered pathognomonic for WD, they may, although rarely, be encountered also in conditions of prolonged cholestasis [19]. In addition to these common presentations, signs and symptoms of WD may arise as a result of dysfunction of any organ in which excess copper is deposited. Clinical manifestations may, thus, include endocrine abnormalities, cardiac arrhythmias, arthritis, and arthralgias, as well as secondary amenorrhea. Because of this tremendous variability in clinical presentation, correct clinical diagnosis is often difficult and sometimes delayed.

Traditionally, the diagnosis of WD is based on Sternlieb's criteria, two or more of which have be present: (i) Kayser–Fleischer ring, (ii) typical neurological symptoms, (iii) low serum ceruloplasmin level (<20 mg/dl), and (iv) increased hepatic copper content (>250 μg/g dry weight) [19]. Ceruloplasmin is an acute-phase protein, the serum levels of which are increased due to infection or inflammation, including active liver involvement. Therefore, ceruloplasmin levels will be in a normal range in 5–15% of WD patients [20]. Moreover, screening for WD in unselected patients with liver disease by serum ceruloplasmin determination is neither feasible nor cost-effective, showing a positive predictive value of only about 5% [7]. WD patients are known to exhibit increased urinary copper excretion (>100 μg/24 h), and this was recently shown to be the most sensitive clinical diagnostic test, at least in children [64]. However, according to Steindl et al. [56], only about two-thirds of patients presenting with liver disease can be diagnosed by these typical findings, and the authors concluded that the commonly used clinical and laboratory parameters are not sufficient to exclude the diagnosis of WD in patients with liver disease of unknown origin. Often, morphological studies of the liver in WD fail to identify specific changes. Therefore, histology may only permit one to suspect the disease or to assist in its confirmation by recognition of more or less typical histological features, histochemical demonstration of copper accumulation, evaluation of liver architecture for the staging of the disease, and finally by the exclusion

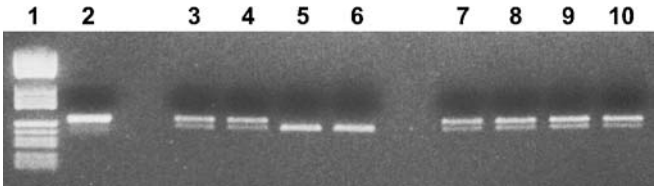


Fig. 2 Molecular analysis of the His1069Gln (H1069Q) mutation of the *ATP7B* gene: *lane 1* molecular weight standards, *lane 2* uncut polymerase chain reaction product, *lanes 3* and *4* positive control, *lanes 5* and *6* negative control, and *lanes 7–10* Wilson patient

of concurrent liver disorders. Although the value of molecular genetic testing is limited due to the large number of possible mutations, polymerase chain reaction is useful for screening of asymptomatic family members of homozygous index patients (Fig. 2). However, can limited genetic screening for WD in patients with liver disease not completely fulfilling the clinical and laboratory criteria mentioned above be recommended? Since data in the literature are currently lacking, future studies are needed to answer this question.

Once the diagnosis of WD is established, lifelong treatment with chelating agents (D-penicillamine, trientine) and/or with zinc is necessary and usually sufficient to stabilize the patient and to achieve clinical remission in most cases. Chelating agents prevent the formation and promote the solubilization of copper-rich particles in lysosomes, thus facilitating urinary copper excretion [31]. Zinc administration inhibits lipid peroxidation by increasing glutathione availability [16]. Patients with acute hepatic failure or advanced chronic liver disease have been reported to benefit from orthotopic liver transplantation, which corrects the underlying metabolic defect and may, thus, improve neurological and/or psychiatric symptoms [2, 14, 55]. Recurrence of copper-associated liver damage in a transplanted liver has not been reported in a WD patient thus far. Finally, the introduction of functional ATP7B protein by recombinant adenovirus-mediated gene delivery will be a potential approach for the correction of WD in the future [61].

Conclusions

Since patients with WD may present with a variety of clinical symptoms and laboratory alterations, and morphology alone is not diagnostic, a multidisciplinary approach is required. This may facilitate early diagnosis, which should be the primary goal, since effective management of the disease is best achieved by its recognition before damage of liver, brain, and other organs is advanced. Although molecular testing has been proven to be beneficial in some patients, the value of this approach appears to be limited in daily practice due to the high number of possible gene mutations.

References

1. Bearn AG (1960) A genetical analysis of 30 families with Wilson's disease (hepatolenticular degeneration). Ann Hum Genet 24:33–43
2. Bellary S, Hassanein T, van Thiel DH (1995) Liver transplantation for Wilson's disease. J Hepatol 23:373–381
3. Britton RS (1996) Metal-induced hepatotoxicity. Semin Liver Dis 16:3–12
4. Buiakova OI, Xu J, Lutsenko S, Zeitlin S, Das K, Das S, Ross BM, Mekios C, Scheinberg IH, Gilliam TC (1999) Null mutation of the murine ATP7B (Wilson disease) gene results in intracellular copper accumulation and late-onset hepatic nodular transformation. Hum Mol Genet 8:1665–1671
5. Bull PC, Thomas GR, Rommens JM, Forbes JR, Cox DW (1993) The Wilson's disease gene is a putative copper transporting P-type ATPase similar to the Menkes gene. Nat Genet 5:327–337
6. Caca K, Ferenci P, Kühn HJ, Polli C, Willgerodt H, Kunath B, Hermann W, Mössner J, Berr F (2001) High prevalence of the H1069Q mutation in East German patients with Wilson disease: rapid detection of mutations by limited sequencing and phenotype-genotype analysis. J Hepatol 35:575–581
7. Cauza E, Maier-Dobersberger T, Polli C, Kaserer K, Kramer L, Ferenci P (1997) Screening for Wilson's disease in patients with liver diseases by serum ceruloplasmin. J Hepatol 27:358–362
8. Cheng WS, Govindarajan S, Redeker AG (1992) Hepatocellular carcinoma in a case of Wilson's disease. Liver 12:42–45
9. Cumings JN (1948) Copper and iron content of brain and liver in normal and in hepatolenticular degeneration. Brain 71:410–415
10. Czlonkowska A, Rodo M (1981) Late onset of Wilson's disease. Report of a family. Arch Neurol 38:729–730
11. Czlonkowska A, Rodo M, Gajda J, Ploos van Amstel HK, Juyn J, Houwen RH (1997) Very high frequency of the His1069Gln mutation in Polish Wilson disease patients. J Neurol 244:591–592
12. Davies SE, Williams R, Portmann B (1989) Hepatic morphology and histochemistry of Wilson's disease presenting as fulminant hepatic failure: a study of 11 cases. Histopathology 15:385–394
13. Dickersin GR (2000) Diagnostic electron microscopy. A text and atlas. Springer, Berlin Heidelberg New York, pp 747–756
14. Emre S, Atillasoy EO, Ozdemir S, Schilsky M, Rathna Varma CV, Thung SN, Sternlieb I, Guy SR, Sheiner PA, Schwartz ME, Miller CM (2001) Orthotopic liver transplantation for Wilson's disease: a single-center experience. Transplantation 72:1232–1236
15. Faa G, Nurchi V, Demelia L, Ambu R, Parodo G, Congiu T, Sciot R, van Eyken P, Silvagni R, Crisponi G (1995) Uneven hepatic copper distribution in Wilson's disease. J Hepatol 22:303–308
16. Farinati F, Cardin R, D'Inca R, Naccarato R, Sturniolo GC (2003) Zinc treatment prevents lipid peroxidation and increases glutathione availability in Wilson's disease. J Lab Clin Med 141:372–377
17. Fleischer B (1912) Über eine der "Pseudosclerose" nahestehende bisher unbekannte Krankheit. Dtsch Z Nervenheilk 44:179–201
18. Frydman M, Bonne-Tamir B, Farrer LA, Conneally PM, Magazanik A, Ashbel S, Goldwitch Z (1985) Assignment of the gene for Wilson's disease to chromosome 13: linkage to the esterase D locus. Proc Natl Acad Sci U S A 82:1819–1821
19. Gitlin N (1998) Wilson's disease: the scourge of copper. J Hepatol 28:734–739
20. Gollan JL, Gollan TJ (1998) Wilson disease in 1998: genetic, diagnostic, and therapeutic aspects. J Hepatol 28:28–36
21. Gow PJ, Smallwood RA, Angus PW, Smith AL, Wall AJ, Sewell RB (2000) Diagnosis of Wilson's disease. An experience over three decades. Gut 46:415–419

22. Gross JB Jr., Ludwig J, Wiesner RH, McCall JT, LaRusso NF (1985) Abnormalities in tests of copper metabolism in primary sclerosing cholangitis. Gastroenterology 89:272–278
23. Harada M (2002) Wilson disease. Med Electron Microsc 35:61–66
24. Harris ZL, Takahashi Y, Miyajima H, Serizawa M, MacGillivray RTA, Gitlin JD (1995) Acerulopasminemia: molecular characterization of this disorder of iron metabolism. Proc Natl Acad Sci U S A 92:2539–2543
25. Hussain SP, Raja K, Amstad PA, Sawyer M, Trudel LJ, Wogan GN, Hofseth LJ, Shields PG, Billiar TR, Trautwein C, Höhler C, Galle PR, Phillips DH, Markin R, Marrogi AJ, Harris CC (2000) Increased p53 mutation load in nontumorous human liver of Wilson disease and hemochromatosis: oxyradical overload diseases. Proc Natl Acad Sci U S A 97:12770–12775
26. Huster D, Hoppert M, Lutsenko S, Zinke J, Lehmann C, Mössner J, Berr F, Caca K (2003) Defective cellular localization of mutant ATP7B in Wilson's disease patients and hepatoma cell lines. Gastroenterology 124:335–345
27. Irons RD, Schenk EA, Lee JCK (1977) Cytochemical methods for copper. Semiquantitative screening procedure for identification of abnormal copper levels in liver. Arch Pathol Lab Med 101:298–301
28. Janssens AR, van Noord MJ, van Hoek CJ, Ruiter DJ, Mauw BJ, van den Hamer CJ (1984) The lysosomal copper concentration in the liver in primary biliary cirrhosis. Liver 4:396–401
29. Jensen K, Gluud C (1994) The Mallory body: morphological, clinical and experimental studies (part 1 of a literature survey). Hepatology 20:1061–1077
30. Jonas L, Fulda G, Salameh T, Schmidt W, Kröning G, Hopt UT, Nizze H (2001) Electron microscopic detection of copper in the liver of two patients with Morbus Wilson by EELS and EDX. Ultrastruct Pathol 25:111–118
31. Klein D, Lichtmannegger J, Heinzmann U, Summer KH (2000) Dissolution of copper-rich granules in hepatic lysosomes by D-penicillamine prevents the development of fulminant hepatitis in Long-Evans cinnamon rats. J Hepatol 32:193–201
32. Lembowicz K, Kryczka W, Walewska-Zielecka B, Kubicka J (1999) Wilson's disease coexisting with viral hepatitis type C: a case report with histological and ultrastructural studies of the liver. Ultrastruct Pathol 23:39–44
33. Linder MC, Hazegh-Azam M (1996) Copper biochemistry and molecular biology. Am J Clin Nutr 63:797–811
34. Lindquist RR (1969) Studies on the pathogenesis of hepatolenticular degeneration. II. Cytochemical methods for the localization of copper. Arch Pathol 87:370–379
35. Loudianos G, Gitlin JG (2000) Wilson's disease. Semin Liver Dis 20:353–364
36. Luca P, Demila L, Lecca S, Ambu R, Faa G (2000) Massive hepatic hemochromatosis in Wilson's disease. Histopathology 37:187–189
37. Ludwig J, Moyer TP, Rakela J (1994) The liver biopsy diagnosis of Wilson's disease. Methods in pathology. Am J Clin Pathol 102:443–446
38. Maier-Dobersberger T, Mannhalter C, Rack S, Granditsch G, Kaserer K, Korninger L, Steindl P, Gangl A, Ferenci P (1995) Diagnosis of Wilson's disease in an asymptomatic sibling by DNA linkage analysis. Gastroenterology 109:2015–2018
39. Maier-Dobersberger T, Ferenci P, Polli C, Balac P, Dienes HP, Kaserer K, Datz C, Vogel W, Gangl A (1997) Detection of the His1069Gln mutation in Wilson disease by rapid polymerase chain reaction. Ann Int Med 127:21–26
40. Mansouri A, Gaou I, Fromenty B, Berson A, Letteron P, Degitt C, Erlinger S, Pessayre D (1997) Premature oxidative aging of hepatic mitochondrial DNA in Wilson's disease. Gastroenterology 113:599–605
41. McDonald JA, Snitch P, Painter D, Hensley W, Gallagher ND, McCaughan GW (1992) Striking variability of hepatic copper levels in fulminant hepatic failure. J Gastroenterol Hepatol 7:396–398
42. Milkiewicz P, Saksena S, Hubscher SG, Elias E (2000) Wilson's disease with superimposed autoimmune features: report of two cases and review. J Gastroenterol Hepatol 15:570–574
43. Müller T, Müller W, Feichtinger H (1998) Idiopathic copper toxicosis. Am J Clin Nutr 67:1082–1086
44. Müller T, Langner C, Fuchsbichler A, Heinz-Erian P, Ellemunter H, Schlenck B, Bavdekar AR, Pradhan AM, Pandit A, Müller-Hocker J, Melter M, Kobayashi K, Nagasaka H, Kikuta H, Müller W, Tanner MS, Sternlieb I, Zatloukal K, Denk H (2004) Immunohistochemical analysis of Mallory bodies in Wilsonian and non-Wilsonian hepatic copper toxicosis. Hepatology 39:963–969
45. Pena MM, Lee J, Thiele DJ (1999) A delicate balance: homeostatic control of copper uptake and distribution. J Nutr 129:1251–1260
46. Pilloni L, Lecca S, Van Eyken P, Flore C, Demelia L, Pilleri G, Nurchi AM, Farci AM, Ambu R, Callea F, Faa G (1998) Value of histochemical stains for copper in the diagnosis of Wilson's disease. Histopathology 33:28–33
47. Pilloni L, Lecca S, Coni P, Demelia L, Pilleri G, Spiga E, Faa G, Ambu R (2000) Wilson's disease with late onset. Dig Liver Dis 32:180
48. Polio J, Enriquez RE, Chow A, Wood WM, Atterbury CE (1989) Hepatocellular carcinoma in Wilson's disease. Case report and review of the literature. J Clin Gastroenterol 11:220–224
49. Riordan SM, Williams R (2001) The Wilson's disease gene and phenotypic diversity. J Hepatol 34:165–171
50. Roelofsen H, Wolters H, Van Luyn MJA, Miura N, Kuipers F, Vonk RJ (2000) Copper-induced apical trafficking of ATP7B in polarized hepatoma cells provides a mechanism for biliary copper excretion. Gastroenterology 119:782–793
51. Ross ME, Jacobsen IM, Dienstag JL, Martin JB (1985) Late-onset Wilson's disease with neurological involvement in the absence of Kayser-Fleischer rings. Ann Neurol 17:411–413
52. Schaefer M, Hopkins RG, Failla ML, Gitlin JD (1999) Hepatocyte-specific localization and copper-dependent trafficking of the Wilson's disease protein in the liver. Am J Physiol 276:639–646
53. Schaefer M, Roelofsen H, Wolters H, Hofmann WJ, Muller M, Kuipers F, Stremmel W, Vonk RJ (1999) Localization of the Wilson's disease protein in human liver. Gastroenterology 117:1380–1385
54. Scheinberg IH, Gitlin D (1952) Deficiency of ceruloplasmin in patients with hepatolenticular degeneration (Wilson's disease). Science 116:484–485
55. Schilsky ML, Scheinberg IH, Sternlieb I (1994) Liver transplantation for Wilson's disease: indications and outcome. Hepatology 19:583–587
56. Steindl P, Ferenci P, Dienes HP, Grimm G, Pabinger I, Madl C, Maier-Dobersberger T, Herneth A, Dragosics B, Meryn S, Knoflach P, Granditsch G, Gangl A (1997) Wilson's disease in patients presenting with liver disease: a diagnostic challenge. Gastroenterology 113:212–218
57. Sternlieb I (1990) Perspectives on Wilson's disease. Hepatology 12:1234–1239
58. Stromeyer FW, Ishak KG (1980) Histology of the liver in Wilson's disease. A study of 34 cases. Am J Clin Pathol 73:12–24
59. Tanner MS (1998) Role of copper in Indian childhood cirrhosis. Am J Clin Nutr 67:1074–1081
60. Tanzi RE, Petrukhin K, Chernov I, Pellequer JL, Wasco W, Ross B, Romano DM, Parano E, Pavone L, Brzustowitz LM, Devoto M, Peppercorn J, Bush AI, Sternlieb I, Pirastu M, Gusella JF, Evgrafov O, Pechaszadeh GK, Honig B, Edelman IS, Soares MB, Scheinberg IH, Gilliam TC (1993) The Wilson's disease gene is a copper transporting ATPase with homology to the Menkes disease gene. Nat Genet 5:344–350
61. Terada K, Schilsky ML, Miura N, Sugiyama T (1998) ATP7B (WND) protein. Int J Biochem Cell Biol 30:1063–1067

62. Wang XW, Hussain SP, Huo TI, Wu CG, Forgues M, Hofseth LJ, Brechot C, Harris CC (2002) Molecular pathogenesis of human hepatocellular carcinoma. Toxicology 181–182:43–47
63. Wilson SAK (1912) Progressive lenticular degeneration: a familial nervous disease associated with cirrhosis of the liver. Brain 34:295–507
64. Yuce A, Kocak N, Demir H, Gurakan F, Ozen H, Saltik IN, Ozcay F (2003) Evaluation of diagnostic parameters of Wilson's disease in childhood. Indian J Gastroenterol 22:4–6
65. Zhou B, Gitschier J (1997) hCTR: a human gene for copper uptake identified by complementation in yeast. Proc Natl Acad Sci U S A 94:7481–7486

Virchows Arch (2004) 445:119–128
DOI 10.1007/s00428-004-1063-8

ORIGINAL ARTICLE

C. A. Wells · J. P. Sloane · D. Coleman · C. Munt · I. Amendoeira · N. Apostolikas · J. P. Bellocq · S. Bianchi · W. Boecker · G. Bussolati · C. E. Connolly · P. Dervan · M. Drijkoningen · I. O. Ellis · C. W. Elston · V. Eusebi · D. Faverly · P. Heikkila · R. Holland · J. Jacquemier · M. Lacerda · J. Martinez-Penuela · C. De Miguel · J. L. Peterse · F. Rank · A. Reiner · E. Saksela · B. Sigal-Zafrani · M. Sylvan · B. Borisch · G. Cserni · T. Decker · H. Kerner · J. Kulka · P. Regitnig · A. Sapino · A. M. Tanous · S. Thorstenson · E. Zozaya
The European Working Group for Breast Screening Pathology

Consistency of staining and reporting of oestrogen receptor immunocytochemistry within the European Union—an inter-laboratory study

Received: 7 April 2004 / Accepted: 28 May 2004 / Published online: 24 June 2004
© Springer-Verlag 2004

The European Working Group for Breast Screening Pathology is supported by the European Commission through the European Breast Cancer Network

C. A. Wells (✉)
Department of Histopathology,
St. Bartholomew's Hospital Medical School,
West Smithfield, London, EC1A 7BE, United Kingdom
e-mail: c.a.wells@qmul.ac.uk
Tel.: +44-20-76018451
Fax: +44-20-76018543

J. P. Sloane
Department of Pathology,
Liverpool, United Kingdom

D. Coleman · C. Munt
Cancer Screening Evaluation Unit,
Institute of Cancer Research,
Sutton Surrey, United Kingdom

I. Amendoeira
Department of Pathology,
Instituto de Patologia & Imunologia Molecular
da Universidade do Porto,
Porto, Portugal

N. Apostolikas
Department of Pathology, Saint Savvas Hospital,
Athens, Greece

J. P. Bellocq
Service d'Anatomie Pathologique,
Hopital de Hautepierre, Strasbourg, France

S. Bianchi
Department of Human Pathology and Oncology,
University of Florence, Italy

W. Boecker
Gerhard-Domagk Institut fur Pathologie,
Universitat et Munster,
Munster, Germany

G. Bussolati · A. Sapino
Istituto di Anatomia e Istologia Patologica,
Torino, Italy

C. E. Connolly
Department of Pathology,
Clinical Sciences Institute, University College Hospital,
Galway, Ireland

P. Dervan
Pathology Department,
Mater Hospital, University College,
Dublin, Ireland

M. Drijkoningen
Pathologische Ontleedkunde, University Hospital,
Leuven, Belgium

I. O. Ellis · C. W. Elston
Department of Histopathology, City Hospital,
Nottingham, United Kingdom

V. Eusebi
Sezione Anatomia Patologica M. Malpigni,
Universita di Bologna,
Ospedale Bellaria, Bologna, Italy

D. Faverly
CMP Laboratory, Bruxelles, Belgium

P. Heikkila · E. Saksela
Haartman Institute, University of Helsinki,
Helsinki, Finland

R. Holland
National Expert & Training Centre for Breast Cancer Screening,
Academisch Ziekenhuis Nijmegen,
Nijmegen, The Netherlands

J. Jacquemier
Institut Paoli Calmettes, Marseille, France

M. Lacerda
Laboratorio De Histopatologica,
Centro Regional De Oncologia De Coimbra,
Coimbra, Portugal

J. Martinez-Penuela · E. Zozaya
Department of Pathology, Hospital de Navarra,
Pamplona, Spain

C. De Miguel
Department of Pathology, Hospital Virgen del Camino,
Pamplona, Spain

J. L. Peterse
Department of Pathology,
The Netherlands Cancer Institute,
Amsterdam, The Netherlands

F. Rank
Center of Laboratory Medicine and Pathology,
Department of Pathology,
Rigshospitalet, Copenhagen University Hospital,
Copenhagen, Denmark

A. Reiner
Institute of Pathology, Donauspital,
Wien, Austria

B. Sigal-Zafrani
Institut Curie, Section Medicale et Hospitaliere,
Paris, France

M. Sylvan
Department of Clinical Pathology and Cytology,
Huddinge University Hospital,
Stockholm, Sweden

B. Borisch
Centre Médicale Universitaire,
Genève, Switzerland

G. Cserni
Department of Pathology,
Bács-Kiskun County Teaching Hospital,
Kecskemét, Hungary

T. Decker
Department of Pathology,
The Breast Unit, HELIOS Medical Centre,
Berlin, Germany

H. Kerner
Department of Pathology,
Rambam Hospital,
Haifa, Israel

J. Kulka
2nd Institute of Pathology, Semmelweis University,
Budapest, Hungary

P. Regitnig
Institut fur Pathologie der Karl-Franzens Universitat Graz,
Graz, Austria

A. M. Tanous
Division d'Anatomie Pathologique,
Laboratoire National de Santé,
Luxembourg

S. Thorstenson
Kalmar County Hospital,
Kalmar, Sweden

Abstract To assess the variability of oestrogen receptor (ER) testing using immunocytochemistry, centrally stained and unstained slides from breast cancers were circulated to the members of the European Working Group for Breast Screening Pathology, who were asked to report on both slides. The results showed that there was almost complete concordance among readers (kappa=0.95) in ER-negative tumours on the stained slide and excellent concordance among readers (kappa=0.82) on the slides stained in each individual laboratory. Tumours showing strong positivity were reasonably well assessed (kappa=0.57 and 0.4, respectively), but there was less concordance in tumours with moderate and low levels of ER, especially when these were heterogeneous in their staining. Because of the variation, the Working Group recommends that laboratories performing these stains should take part in a external quality assurance scheme for immunocytochemistry, should include a tumour with low ER levels as a weak positive control and should audit the percentage positive tumours in their laboratory against the accepted norms annually. The Quick score method of receptor assessment may also have too many categories for good concordance, and grouping of these into fewer categories may remove some of the variation among laboratories.

Keywords Oestrogen receptor · Immunohistochemistry · Quality assessment · Variability

Introduction

Since the advent of breast screening and detection of breast cancers using mammography, tumours in general are being detected at a smaller size. The necessity to obtain oestrogen receptor (ER) status on these very small tumours has led to the measurement of receptor status using immunocytochemistry. The older biochemical methods of dextran-coated charcoal and enzyme-linked immunoassay are unable to provide results on these small tumours which often require the entire tumour to be sampled for accurate diagnosis. Even in the sampling of larger tumours for biochemical assay, the problems of

sampling error, with benign areas having a low level of oestrogen positivity being included with a negative tumour in the homogenate, led to certain ER-negative tumours being falsely classified as low expressers of ER. Conversely, areas of tumour from high ER-expressing tumours composed predominantly of the fibro-elastotic core could be falsely classified as ER poor. Older publications based on the biochemical methods put the level of response to anti-oestrogens at approximately 60% of those tumours that were ER rich, but also acknowledged a response rate of about 8% in totally ER-negative tumours. For these reasons, coupled with the availability of high-quality antibodies, the assessment of receptors using the biochemical methods has largely been superseded by immunocytochemistry on tissue sections [1, 4, 17]. This has the following advantage: direct visualisation of the cells expressing the receptor enables an assessment of whether these are tumour cells or are associated benign tissue. More recent publications seem to agree that totally ER-negative tumours identified using immunocytochemistry do not respond to hormonal therapy [6] and that these should be preferentially treated with other therapeutic modalities, although some debate persists about women with tumours expressing very low levels of receptor.

Most workers are now agreed that immunocytochemistry for ER is the method of choice [1, 4, 5, 17], and a number of scoring systems have been developed in an attempt to semi-quantify the test. The most complex of these is the H-score, which is still used by a number of laboratories [7]. More recently, the recommended method by the European Organization for the Research and Treatment of Cancer (EORTC) working group has been the modified Quick score [6, 9], which has been adopted by some national guidelines [12]. This has the advantage that it is somewhat quicker to perform than the H-score and still correlates well with clinical response [1]. Some laboratories have used 10% ER positivity of any type as the threshold for considering breast cancers as ER positive. However, with the Quick score, a score above two (e.g., above 1% of weakly positive cells) has been reported to predict responsiveness to endocrine treatment [6]. One of the strengths of the old biochemical methods, however, was that the technical aspects of the methodology were rigorously quality controlled through the EORTC and biochemical networks using a vial of known oestrodiol content. Quality control of the immunocytochemical test is not so well developed, and there is some concern that tumours having low levels of ER may be scored as negative in some laboratories, leading to the possibility that these women will not benefit from anti-oestrogen therapy. Previous publications have concentrated on the variation in technical methods among laboratories [11, 14] but have not investigated the inter-observer variation in scoring.

Materials and methods

Slides from 30 cases of breast carcinoma were cut from the paraffin block. One set of slides was stained with haematoxylin and eosin (H&E) for grading, another set of slides from the same tissue blocks was stained using immunocytochemistry for ER in the University of Liverpool laboratory and a final set of unstained slides was also prepared.

One slide stained with H&E, one stained for ER and one unstained slide were sent to each laboratory participating in the European Working Group. For each tumour, members of the group were asked the following.

a. To score the Liverpool-stained slides of the tumours for the percentage of positive cells in 10% bands (0, 1–10, 11–20, 21–30, 31–40, 41–50, 51–60, 61–70, 71–80, 81–90 and 91–100) and to assess the intensity of staining on a four-point scale of negative, weakly positive, moderately positive and strongly positive, assessing also whether the staining is homogeneous or heterogeneous. Only nuclear staining was assessed.
b. To stain the unstained sections in their own laboratory using their standard routine method and to score these slides in the same way.
c. To grade the tumour on the H&E section.

Although the Liverpool-stained slides were there at the same time, the members of the Working Group were asked to score them independently. They were blinded to the original Liverpool reports of the cases.

Readers, all members of the Working Group because of their recognised expertise in breast pathology, submitted their assessment of the staining on standard forms designed for the purpose to the Cancer Screening Evaluation Unit (CSEU) in Sutton, Surrey. The results of the submitted forms were analysed anonymously. The CSEU then calculated the variation in assessment of the staining both on the slides stained in Liverpool and on the slides stained in the individual reader's laboratory using kappa statistics. Due to the large number of classes involved in the assessment using 10% bands, the bands were amalgamated into the groups used in the recommendations for the modified Quick score [1]. The reason for the analysis using this method was that the Quick score method was adopted as the recommended method after the circulations were performed. Kappa scores were calculated for the variation in percentage positivity for each case and for positive versus negative using a 10% positive cell staining cut-off for staining intensity and for the presence or absence of tumour heterogeneity. The scores were calculated according to the recommended method using the modified Quick score [6], and kappa statistics were performed on the scores 0–8.

Results

The results for the percentage of positive cells are given in Table 1; not all cases were reported by all pathologists; cases with less than 10 assessments were excluded.

While the results for the Liverpool-stained slide (i.e. interpretation only—line B) showed excellent correlation on kappa statistics for receptor negativity (0.95), the slides stained in the participant's own laboratories (line A) were a little more variable but still extremely good (kappa=0.82). When the variation in assessment of percentages was taken into account, there was reasonable correlation on assessment with a kappa score of 0.57 on the Liverpool-stained slide (Fig. 1 and Fig. 2), while this drops to only moderate correlation (kappa=0.4) when the inter-laboratory variation is taken into account. This in-

Table 1 Oestrogen receptor—percentage of positive cells. *A* own laboratory slide, *B* Liverpool slide

Slide		0	10–30	40–60	70–90	100	Majority opinion	% Of readers in agreement with majority
11595/97	A	11	0	0	0	0	0	100
	B	10	1	0	0	0	0	91
13955/97	A	1	0	1	9	0	70–90	82
	B	0	0	1	11	0	70–90	92
22338/97	A	1	0	1	9	0	70–90	82
	B	0	0	0	9	3	70–90	75
26342/97	A	2	2	4	4	0	Tie 40–60/70–90	-
	B	0	4	5	4	0	40–60	56
1/98	A	1	1	4	11	2	70–90	58
	B	0	0	0	15	5	70–90	75
4/98	A	0	0	3	6	12	100	57
	B	0	0	0	3	17	100	85
5/98	A	0	0	2	12	7	70–90	57
	B	0	0	0	4	16	100	80
7/98	A	0	1	0	10	9	70–90	50
	B	0	0	0	6	14	100	70
8/98	A	0	0	3	6	12	100	57
	B	0	0	0	5	15	100	75
9/98	A	0	0	1	4	15	100	75
	B	0	0	0	3	17	100	85
10/98	A	0	1	4	14	1	70–90	70
	B	0	0	2	15	3	70–90	75
11/98	A	0	1	4	13	3	70–90	62
	B	0	0	1	18	1	70–90	90
12/98	A	15	5	0	0	0	0	75
	B	17	2	1	0	0	0	85
13/98	A	0	1	5	13	2	70–90	62
	B	0	0	1	16	3	70–90	80
15/98	A	1	4	8	6	1	40–60	40
	B	0	2	10	8	0	40–60	50
16/98	A	0	0	2	6	13	100	62
	B	0	0	0	7	13	100	65
17/98	A	21	0	0	0	0	0	100
	B	20	0	0	0	0	0	100
18/98	A	0	0	2	12	7	70–90	57
	B	0	0	0	15	5	70–90	75
19/98	A	0	2	2	11	4	70–90	58
	B	0	0	0	16	4	70–90	80
20/98	A	0	2	5	9	4	70–90	45
	B	0	0	3	16	1	70–90	80
21/98	A	21	0	0	0	0	0	100
	B	20	0	0	0	0	0	100
22/98	A	19	2	0	0	0	0	90
	B	20	0	0	0	0	0	100
23/98	A	21	0	0	0	0	0	100
	B	20	0	0	0	0	0	100
24/98	A	19	0	0	0	0	0	100
	B	22	0	0	0	0	0	100
25/98	A	3	12	4	1	0	10–30	60
	B	0	11	10	1	0	10–30	50
26/98	A	4	6	3	7	0	70–90	35
	B	1	7	7	7	0	Tie10–30/40–60/70–90	-
Total	A	140	40	58	163	92	Grand total	493
	B	130	27	41	179	117		494
Kappa	A	0.82	0.20	0.06	0.27	0.33	Overall kappa	0.40
	B	0.95	0.27	0.26	0.45	0.52		0.57
Total $\leq$10%	A	163		Kappa	0.80			
	B	142		Kappa	0.91			
Total >10%	A	330		Kappa	0.80			
	B	352		Kappa	0.91			

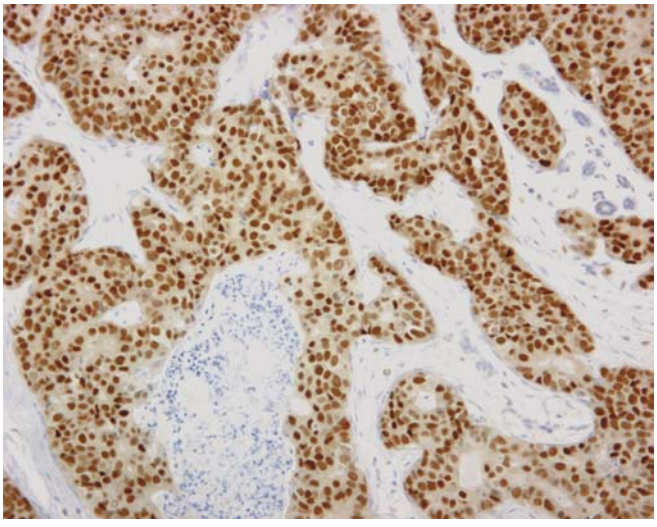


Fig. 1 Medium-power view of a Liverpool-stained oestrogen-receptor-positive slide (case 11/98), which had one of the best scores for inter-observer concordance in reporting (×200)

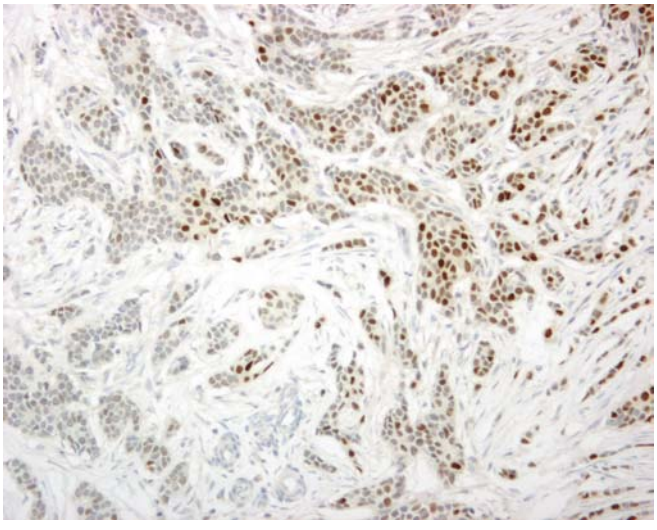


Fig. 2 Medium-power view of a Liverpool-stained oestrogen-receptor-positive slide (case 26342/97), which had the worst inter-observer concordance in reporting (×200)

creased variability must be interpreted as due to technical variability among methods used in each laboratory.

When the cut-off point for ER-positive tumours was based on the >10% value used in some laboratories, the correlation between laboratories was excellent (kappa=0.80) and even better for interpretation only (kappa=0.91).

The results for intensity are given in Table 2. Variation of the intensity reading by the pathologists is only assessed on tumours with positive staining, and, hence, the kappa statistics are lower than if negative staining was included. As in any three-way classification, the middle grade (i.e. intermediate in this case) shows poorer correlation than the two other grades. A similar result is found for intensity as with percentage positive cells in that the overall kappa value is 0.35 for interpretation only, which falls to 0.23 when inter-laboratory technical variation is also taken into account. These figures are low, as they exclude those cases with no staining, but could clearly be improved by closer quality assurance.

The results of the assessment of homogeneity or heterogeneity are given in Table 3. Again, the results show moderate agreement for the Liverpool-stained slide with a kappa value of 0.48, but this also excludes those cases with no staining. The level of agreement falls significantly when inter-laboratory variation is taken into account and is poor at 0.28.

The results of the analysis recalculating the results to give a Quick score are given in Table 4 for slides stained in each laboratory and Table 5 for the Liverpool-stained slide. For interpretation alone (Table 5), the results are excellent for lack of staining (0.95) and good for the highest Quick score of 8 (0.62). Kappas in the intermediate groups QS 3–7 are, however, not so good, with poor correlation within the groups. The results with inter-laboratory variation included show increased variability as before, still with an excellent score for negative tumours (0.82) but a slightly lower score of 0.45 for a Quick score of 8. Looking at the original results for each tumour, one can see that a small number of cases appear to be responsible for the majority of the variation. The cases with the most variation (23642/97, 15/98, 25/98 and 26/98) all scored highly for heterogeneity of staining, and this may well be an area where counting systems may be less consistent, as the area chosen for counting will vary from observer to observer.

Discussion

ER and progesterone-receptor analyses are now mandatory tests on breast cancer to determine appropriate therapy. There is now good evidence that tumours negative for ER are highly unlikely to respond to endocrine manipulation unless they happen to fall into the small proportion of tumours (approximately 2–5%) that are ER negative, progesterone-receptor positive. The older biochemical methods of assessment of tumour positivity have largely been superseded by the immunocytochemical method. This has gained favour due to the ready availability of good specific antibodies to the receptor proteins and due to the decreasing size of tumours detected using mammography. This latter problem has made it impossible to persist with the older biochemical methods, as there is insufficient tumour for analysis without compromising diagnosis.

ER status using immunocytochemistry is now crucial to therapy, especially in pre-menopausal women, where the side-effects of unnecessary Tamoxifen may be severe. Even in post-menopausal women, the side-effects are not negligible, and the rationale for giving irrelevant therapy in receptor-negative tumours is, at best, dubious.

The variation in general immunocytochemical staining is assessed by external quality assessment schemes run by

Table 2 Oestrogen receptor—intensity of stain. *A* own laboratory slide, *B* Liverpool slide

Slide		Weak	Moderate	Strong	Majority opinion	% Of readers in agreement with majority
11595/97	A	0	0	0	Negative	100
	B	1	0	0	Negative	95
13955/97	A	1	6	3	Moderate	60
	B	1	7	4	Moderate	58
22338/97	A	1	3	6	Strong	60
	B	0	3	9	Strong	75
26342/97	A	0	7	3	Moderate	70
	B	1	8	4	Moderate	62
1/98	A	6	11	2	Moderate	58
	B	1	13	6	Moderate	65
4/98	A	0	4	16	Strong	80
	B	0	0	20	Strong	100
5/98	A	1	3	17	Strong	81
	B	0	2	18	Strong	90
7/98	A	1	3	17	Strong	81
	B	0	2	18	Strong	90
8/98	A	1	1	19	Strong	90
	B	0	0	19	Strong	100
9/98	A	1	3	16	Strong	80
	B	0	2	18	Strong	90
10/98	A	3	12	5	Moderate	60
	B	1	9	10	Strong	50
11/98	A	2	6	13	Strong	62
	B	0	8	12	Strong	60
12/98	A	5	0	0	Negative	75
	B	3	0	0	Negative	85
13/98	A	3	8	9	Strong	45
	B	0	9	11	Strong	55
15/98	A	10	7	2	Weak	53
	B	5	14	1	Moderate	70
16/98	A	2	2	17	Strong	81
	B	0	0	20	Strong	100
17/98	A	0	0	0	Negative	100
	B	0	0	0	Negative	100
18/98	A	2	5	14	Strong	67
	B	0	6	14	Strong	70
19/98	A	3	5	11	Strong	58
	B	0	6	14	Strong	70
20/98	A	5	10	5	Moderate	50
	B	4	12	4	Moderate	60
21/98	A	0	0	0	Negative	100
	B	0	0	0	Negative	100
22/98	A	2	0	0	Negative	90
	B	0	0	0	Negative	100
23/98	A	0	0	0	Negative	100
	B	0	0	0	Negative	100
24/98	A	0	0	0	Negative	100
	B	0	0	0	Negative	100
25/98	A	11	5	1	Weak	65
	B	9	13	0	Moderate	59
26/98	A	10	6	0	Weak	62
	B	14	7	0	Weak	67
Total	A	70	107	176	Grand total	353
	B	40	121	202		363
Kappa	A	0.26	0.10	0.33	Overall kappa	0.23
	B	0.38	0.21	0.47		0.35

the National External Quality Assessment Scheme for Immunocytochemistry (NEQAS) scheme in the UK [14]. In other European countries, similar initiatives have been successfully established [11]. Although ER staining has been included in the UK scheme recently [16], the scheme does not assess the variation in reading the slides and in determining the variation in positivity and negativity of the test. Many laboratories are still using the simple method of counting the percentage of positive cells, although the intensity of staining appears also to be important. In this regard, there is a necessity to standardise the quality of the staining technique and the assessment to ensure that the level of the receptors is consistently estimated. Indeed, it is entirely possible that the response of some tumours with low Quick scores reported in the lit-

Table 3 Oestrogen receptor—distribution of positive cells. *A* own laboratory slide, *B* Liverpool slide

Slide		Homogeneous	Heterogeneous		% Of readers in agreement with majority opinion
11595/97	A	0	0		-
	B	0	1		100
13955/97	A	4	4		Tie
	B	6	4		60
22338/97	A	4	2		67
	B	6	2		75
26342/97	A	0	8		100
	B	0	9		100
1/98	A	12	6		67
	B	18	1		95
2/98	A	0	0		-
	B	0	0		-
3/98	A	0	0		-
	B	0	0		-
4/98	A	17	4		81
	B	19	1		95
5/98	A	12	8		60
	B	16	3		84
6/98	A	0	0		-
	B	0	0		-
7/98	A	18	3		86
	B	18	0		100
8/98	A	18	3		86
	B	20	0		100
9/98	A	17	3		85
	B	19	1		95
10/98	A	13	7		65
	B	10	10		Tie
11/98	A	8	12		60
	B	6	13		68
12/98	A	1	5		83
	B	2	3		60
13/98	A	13	7		65
	B	15	4		79
14/98	A	0	0		-
	B	0	0		-
15/98	A	5	14		74
	B	6	14		70
16/98	A	21	0		100
	B	19	1		95
17/98	A	1	0		100
	B	1	0		100
18/98	A	18	3		86
	B	18	2		90
19/98	A	12	7		63
	B	17	3		85
20/98	A	10	10		Tie
	B	7	12		63
21/98	A	1	0		100
	B	1	0		100
22/98	A	1	2		67
	B	1	0		100
23/98	A	1	0		100
	B	1	0		100
24/98	A	1	0		100
	B	1	0		100
25/98	A	0	17		100
	B	0	22		100
26/98	A	4	12		75
	B	4	17		81
Total	A	212	137	Grand total	349
	B	231	123		354
Kappa	A	0.28	0.28	Overall kappa	0.28
	B	0.48	0.48		0.48

Table 4 Oestrogen receptor—Quick score calculated from original submitted results of intensity and percentage positivity (own laboratory slide)

Case	Score of own laboratory slide						
	0	3	4	5	6	7	8
11595/97	11	0	0	0	0	0	0
13955/97	1	0	0	1	0	6	3
22338/97	1	0	0	0	2	2	6
26342/97	2	0	0	2	3	3	2
1/98	1	1	0	2	4	9	2
4/98	0	0	0	0	2	2	16
5/98	0	0	0	0	1	5	15
7/98	0	0	0	1	1	2	16
8/98	0	0	0	0	2	2	17
9/98	0	0	0	0	2	2	16
10/98	0	0	1	2	2	10	5
11/98	0	0	0	3	2	3	13
12/98	15	5	0	0	0	0	0
13/98	0	1	0	1	5	4	9
15/98	1	2	2	5	4	4	2
16/98	0	0	0	1	2	1	17
17/98	21	0	0	0	0	0	0
18/98	0	0	0	0	3	5	13
19/98	0	2	0	0	2	5	10
20/98	0	1	1	1	6	6	5
21/98	21	0	0	0	0	0	0
22/98	19	2	0	0	0	0	0
23/98	21	0	0	0	0	0	0
24/98	19	0	0	0	0	0	0
25/98	3	6	4	2	5	0	0
26/98	4	2	4	1	5	4	0
Kappa	0.82	0.10	0.09	0.04	0.04	0.13	0.45
					Overall kappa		0.39

Table 5 Oestrogen receptor—Quick score calculated from original submitted results of intensity and percentage positivity (Liverpool slide)

Case	Score of Liverpool slide						
	0	3	4	5	6	7	8
11595/97	10	1	0	0	0	0	0
13955/97	0	0	0	1	0	7	4
22338/97	0	0	0	0	0	3	9
26342/97	0	0	0	3	6	3	1
1/98	0	0	0	0	1	13	6
4/98	0	0	0	0	0	0	20
5/98	0	0	0	0	0	2	18
7/98	0	0	0	0	0	2	18
8/98	0	0	0	0	0	0	19
9/98	0	0	0	0	0	2	18
10/98	0	0	0	0	2	9	9
11/98	0	0	0	0	1	7	12
12/98	17	2	0	1	0	0	0
13/98	0	0	0	0	0	10	10
15/98	0	0	2	1	11	5	1
16/98	0	0	0	0	0	0	20
17/98	20	0	0	0	0	0	0
18/98	0	0	0	0	0	6	14
19/98	0	0	0	0	0	6	14
20/98	0	0	0	0	7	9	4
21/98	20	0	0	0	0	0	0
22/98	20	0	0	0	0	0	0
23/98	20	0	0	0	0	0	0
24/98	22	0	0	0	0	0	0
25/98	0	2	5	7	8	0	0
26/98	1	4	2	7	3	5	0
Kappa	0.95	0.07	0.11	0.19	0.29	0.23	0.62
					Overall kappa		0.55

erature is due to the technical differences in the quality of the immunocytochemical staining [11, 15].

The results of this circulation demonstrate that there is some variation in reporting of the level of ER positivity, but encouragingly the variation, on the whole, is very small for completely negative tumours, even when inter-laboratory variation is taken into account. This means that a negative result may be generally relied upon for therapy, unlike some of the older biochemical results. Similar reliability for ER-negative and also for progesterone-receptor-negative results have also been demonstrated in a study performed in a number of pathology departments in Austria [11]. Tumours with a high degree of tumour heterogeneity may cause problems in arriving at a consistent level of positivity, but this heterogeneity would also give rise to difficulties with biochemical methods, depending on which bit of the tumour is submitted for biochemical analysis.

The results do, however, indicate the need for some quality control of the technical aspects of immunocytochemical staining as well as guidance in the aspects of reporting of the stains. As Table 1 shows, there were a few "false-negative" cases reported, coming from 11 different laboratories, but there was one laboratory responsible for five of these false negatives. To reduce and avoid such discrepancies, the Working Group recommends that laboratories performing ER and progesterone-receptor tests for therapeutic reasons take part in one of the circulations of quality assurance of immunocytochemistry, such as the NEQAS scheme in the UK [2, 11, 13, 14]. It is also helpful to include a composite block with a known positive, a known negative and a very weakly positive tumour as a control with each run. The assessment of the strength of staining of internal controls in each slide can also help to remove variations. Comparison of the strength of staining with the strongest cell in the normal tissue allows a rather more objective assessment of the staining intensity. It is also recommended that the percentage of tumours positive and negative per year be calculated and that variation from the normally accepted distribution be investigated [8].

Variation in the assessment of the Quick score is interesting in that there is poor concordance between observers in allocating a specific Quick score to tumours except in very strongly positive or completely negative tumours, and this suggests that the eight-point score may have too many categories for good inter-laboratory concordance. It may be more consistent to stratify tumours into those that are completely negative (Quick score=0), negative with low receptor levels (Quick score=1 or 2), weakly positive (Quick score=3 or 4), moderately positive (Quick score=5 or 6), or strongly positive (Quick score=7 or 8). This is consistent with the known response rates to therapy and may remove some insignificant variation among laboratories in assessment of receptor levels [3]. When this was done in the present study (Table 6), the kappa statistics were clearly shown to be better and excellent for strongly positive (Quick score 7&8) cases and for negative cases (Quick score=0). Where assessment was made on the previously stained slide, the concordance of the moderately positive cases was also reasonable (kappa=0.43). This concordance disappears when the same cases are stained in individual laboratories, suggesting a technical variation, which needs to be addressed [10, 13].

Table 6 Oestrogen receptor—kappa scores calculated by broad bands from the above table

Score	Own slide	Liverpool slide
0	0.82	0.95
3.4	0.19	0.17
5.6	0.10	0.43
7.8	0.55	0.82
Overall kappa	0.51	0.76

In summary, the variation in assessment of receptor status among laboratories has two components, a technical variation and an interpretative variation. These variations are less pronounced in negative tumours and in strongly positive tumours, but significant variation is seen in tumours that express low or moderate levels of receptor. Technical external quality assessment schemes and inclusion of a weakly positive control may help reduce technical variation, and guidelines on assessment of receptors may also help to reduce the interpretative variation.

References

1. Barnes DM, Hanby AM (2001) Oestrogen and progesterone receptors in breast cancer: past, present and future. Histopathology 38:271–274
2. Barnes DM, Millis RR, Beex LVAAM, Thorpe SM, Leake RE (1998) Increased use of immunohistochemistry for oestrogen receptor measurement in mammary carcinoma: the need for quality assurance. Eur J Cancer 34:1677–1682
3. Early Breast Cancer Trialists Collaborative Group (1998) Tamoxifen for early breast cancer: an overview of randomised trials. Lancet 351:1451–1467
4. Elledge RM, Green S, Pugh R, Allred DC, Clark GM, Hill J, Ravdin P, Martino S, Osborne CK (2000) Estrogen receptor (ER) and progesterone receptor (PgR), by ligand-binding assay compared with ER, PgR and pS2, by immuno-histochemistry in predicting response to tamoxifen in metastatic breast cancer: a Southwest Oncology Group Study. Int J Cancer 89:111–117
5. Ferrero-Pous M, Trassard M, Le Doussal V, Hacene K, Tubiana-Hulin M, Spyratos F (2001) Comparison of enzyme immunoassay and immunohistochemical measurements of estrogen and progesterone receptors in breast cancer patients. Appl Immunohistochem Mol Morphol 9:267–275
6. Harvey JM, Clark GM, Osborne CK, Allred DC (1999) Oestrogen receptor status by immunohistochemistry is superior to the ligand-binding assays for predicting response to adjuvant therapy in breast cancer. J Clin Oncol 17:1474–1485
7. Lacroix M, Querton G, Hennebert P, Larsimont D, Leclercq G (2001) Estrogen receptor analysis in primary breast tumors by ligand-binding assay, immunocytochemical assay, and northern blot: a comparison. Breast Cancer Res Treat 67:263–271
8. Leake R (2000) Detection of the oestrogen receptor (ER). Immunohistochemical versus cytosol measurements. Eur J Cancer 36[Suppl 4]:S18–S19
9. Leake R, Barnes D, Pinder S, Ellis I, Anderson L, Anderson T, Adamson R, Rhodes T, Miller K, Walker R (2000) Immuno-

histochemical detection of steroid receptors in breast cancer: a working protocol. UK Receptor Group, UK NEQAS, The Scottish Breast Cancer Pathology Group, and The Receptor and Biomarker Study Group of the EORTC. J Clin Pathol 53:634–635
10. Lee H, Douglas-Jones AG, Morgan JM, Jasani B (2002) The effect of fixation and processing on the sensitivity of oestrogen receptor assay by immunohistochemistry in breast carcinoma. J Clin Pathol 55:236–238
11. Regitnig P, Reiner A, Dinges HP, Hoefler G, Mueller-Holzner E, Lax SF, Obrist P, Rudas M, Quehenberger F (2002) Quality assurance for estrogen and progesterone receptors by immunohistochemistry in Austrian pathology laboratories. Virchows Arch 441:328–334
12. Rhodes A, Jasani B, Balaton AJ, Barnes DM, Miller KD (2000) Frequency of oestrogen and progesterone receptor positivity by immunohistochemical analysis in 7016 breast carcinomas: correlation with patient age, assay sensitivity, threshold value, and mammographic screening. J Clin Pathol 53:688–696
13. Rhodes A, Jasani B, Balaton AJ, Miller KD (2000) Immunohistochemical demonstration of oestrogen and progesterone receptors: correlation of standards achieved on in house tumours with that achieved on external quality assessment material in over 150 laboratories from 26 countries. J Clin Pathol 53:292–301
14. Rhodes A, Jasani B, Barnes DM, Bobrow LG, Miller KD (2000) Reliability of immunohistochemical demonstration of oestrogen receptors in routine practice: interlaboratory variance in the sensitivity of detection and evaluation of scoring systems. J Clin Pathol 53:125–130
15. Thike AA, Chng MJ, Fook-Chong S, Tan PH (2001) Immunohistochemical expression of hormone receptors in invasive breast carcinoma: correlation of results of H-score with pathological parameters. Pathology 33:21–25
16. United Kingdom National Coordinating Group for Breast Screening Pathology (2001). Guidelines for non-operative diagnostic procedures and reporting in breast cancer screening. NHSBSP Publication, Sheffield
17. Zafrani B, Aubriot MH, Mouret E, De Cremoux P, De Rycke Y, Nicolas A, Boudou E, Vincent-Salomon A, Magdelenat H, Sastre-Garau X (2000) High sensitivity and specificity of immunohistochemistry for the detection of hormone receptors in breast carcinoma: comparison with biochemical determination in a prospective study of 793 cases. Histopathology 37:536–545

Virchows Arch (2004) 445:129–134
DOI 10.1007/s00428-004-1059-4

ORIGINAL ARTICLE

Lina Ghabreau · Jean Paul Roux · Alain Niveleau · Bernard Fontanière · Cédric Mahe · Moncef Mokni · Lucien Frappart

Correlation between the DNA global methylation status and progesterone receptor expression in normal endometrium, endometrioid adenocarcinoma and precursors

Received: 11 March 2004 / Accepted: 18 May 2004 / Published online: 19 June 2004
© Springer-Verlag 2004

Abstract Endometrial carcinomas are the most common malignancy of the female genital tract and the third most common cancer in women. Progesterone and oestrogen receptors (PRs, ERs) are the most widely documented prognostic and predictive factors in endometrioid adenocarcinoma. Besides the hormonal pathway involved in the progression of preneoplastic and neoplastic lesions, alterations of the DNA methylation status have been shown to be an early signal of tumorigenesis. In this study, we show that in normal endometrium, during the proliferative phase, DNA methylation and PR expression are high, with a significant decline towards the end of the secretory phase and a gradual increase in non-atypical and atypical endometrial hyperplasia; they reach their highest level in grade I, then decrease significantly in grade-II and grade-III endometrioid adenocarcinomas. During each stage, a significant positive correlation is observed between DNA methylation and PR ($P<0.0001$). The strong parallelism between DNA methylation and PR expression precludes establishing a precise determination regarding the timing of these events, clearly involved in the genesis of endometrioid adenocarcinoma.

Keywords DNA methylation · Progesterone receptor · Endometrium · Cancer

L. Frappart (✉)
Department of Pathology,
Bat 10, Edouard Herriot Hospital,
69437 Lyon Cedex 03, France
e-mail: frappart@wanadoo.fr
Tel.: +33-4-72110746
Fax: +33-4-72116891

L. Ghabreau · L. Frappart
Anatomie Pathologique,
Bat 10, Hôpital Edouard Herriot,
69003 Lyon, France

J. P. Roux · L. Frappart
Unité Inserm U 403,
Faculté de Médecine Laennec,
69008 Lyon, France

A. Niveleau
LVMS EA 2939,
Faculté de Médecine, Université Joseph Fourier,
38700 Grenoble, France

B. Fontanière
Anatomie Pathologique,
Centre Léon Bérard,
Lyon, France

C. Mahe
International Agency for Research on Cancer,
Lyon, France

M. Mokni
Anatomie Pathologique,
CHU Farhat. Hached,
4000 Sousse, Tunisie

Introduction

Endometrial carcinoma is the most common malignant tumour of the female genital system in developed countries [49]. Endometrial hyperplasia encompasses conditions that range from benign oestrogen-dependent proliferation to atypical hyperplasia and well- to poorly differentiated adenocarcinoma [42]. In this course, atypical hyperplasia is considered the most likely precursor of invasive carcinoma, and approximately 23% of women with endometrial hyperplasia will progress to having adenocarcinoma [26]. Few attempts have been made to identify the most significant prognostic and predictive factors for endometrioid adenocarcinoma. The identification of high-risk groups, especially among women with localised disease, would make it possible to avoid the over-treatment of patients with a good prognosis and reserve the most intensive therapy for those with aggressive tumours [50].

The proliferation and the secretory activity of the endometrium are controlled by ovarian steroid hormones—oestrogen and progesterone—through their nuclear re-

ceptor signalling pathways. Progesterone counteracts the growth-stimulatory effects of oestrogen by inducing glandular and stromal differentiation of the endometrium. Progesterone receptors (PRs) are ligand-activated nuclear transcription factors, which are involved in the development and the terminal differentiation of female target tissues, such as endometrium. They bind specifically to DNA at progesterone response elements [47]. Binding of the receptors to progesterone response elements occurs through a molecular DNA binding domain. High levels of PRs are associated with a better disease-free survival and constitute one of the most powerful predictive and prognostic factors [16].

Besides the hormonal pathways, the role of DNA methylation is currently being investigated in carcinogenesis and is suspected to participate in the establishment of the malignant phenotype. This link between tumorigenesis and the alterations of DNA methylation patterns has now been firmly established [4, 6, 23, 27, 29]. DNA methylation is a post-replicative event that affects the modelling of chromatin and the expression of genes [3, 13]. A global hypomethylation was first discovered in tumour tissues relative to their normal counterparts [15, 45]. Then it was shown that this general modification could be accompanied by the occurrence of local hypermethylated sites [12, 32]. It was then reasonable to postulate that hypomethylation might trigger the expression of oncogenes, whereas hypermethylation was responsible for the silencing of tumour suppressor genes [5, 8, 11, 18, 31] and rapidly the alteration of DNA methylation pattern was shown to be an early event in colon cancer [7, 21, 22, 24].

The demonstration that DNA methyltransferase activity was associated with the replication machinery [28] and then that the acetylation/deacetylation of histones could be related to alterations of the DNA methylation pattern highlighted the importance of chromatin organisation, giving birth to a global model for the control of gene expression and carcinogenesis [3, 12]. The immunohistochemical approach we developed had illustrated this particular relationship between DNA methylation, poly (ADP-ribosyl)ation and chromatin compaction [9]. Our results also showed that a low immunohistochemical signal for 5-methyl cytidine (5-MeCyd) was associated with a change of chromatin condensation in tumour cells and tissues [19].

The current study was undertaken to examine a possible relationship between PR expression and the extent of DNA methylation in endometrioid adenocarcinomas and precursors

Material and methods

Case selection and morphological classification

Seventy cases of normal, precancerous and cancerous lesions of endometrium were retrieved from the surgical pathology files of the Department of Pathology and Gynaecology at Edouard Herriot Hospital, Lyon. The cases studied were distributed into the following groups according to the World Health Organisation (WHO) Classification of Tumours of the Breast and Female Genital Organs [49]: normal proliferative phase (10), normal secretory phase (10), non-atypical hyperplasia (10), atypical hyperplasia (10), endometrioid carcinomas (10 grade I, 10 grade II, and 10 grade III). The slides were reviewed by two pathologists (L.F., L.G.). These cases were randomly selected, except for the 20 cases of normal endometrium which were selected mainly among women in the reproductive years and who were scheduled for hysterectomy because of benign gynaecological abnormalities; none of them had any history of exogenous hormonal therapy. The histological type, tumour grade and clinical stage were assessed in accordance with the Federation International of Gynecology and Obstetrics system [46].

Immunohistochemistry

One to two paraffin blocks containing representative portions of the tumours were selected for each case, and 4-μm thick serial sections were obtained and mounted on silanised glass slides. The sections were deparaffinized in xylene then rehydrated through a decreasing ethanol series (100%, 95%, 80%) and washed in phosphate-buffered saline (PBS) for 10 min. Endogenous peroxidase activity was blocked with 3% hydrogen peroxide for 15 min. Antigen retrieval was performed using a 700-W microwave oven for 15 min (5-MeCyd), 10 min (PR). The immunostaining procedure (PAP method) was then carried out. Sections were incubated for 60 min with primary monoclonal antibodies against 5-MeCyd dilution 1:20 as already described for other tissues [20, 37, 41], or PR antibodies (PgR 636; dilution 1:50, Dako, Trappes, France). Negative control staining was carried out using non-specific IgG in the primary reaction. As previously described in previous work, these antibodies do not bind to non-methylated DNA [34]. The remaining part of the procedure was performed as previously published [17].

Quantification

The results were quantified using an automatic image analyser (Visiolab 2000, Biocom, La Rochelle, France) and a Zeiss microscope with a 20× objective lens and 0.5× magnification module, equipped with a tri-CCD colour camera. An automatic memorised colour threshold was used to detect positive immunoreactivity of stained cells. The number of labelled cells was assessed by quantifying the ratio between the positive-cell area and the total tissue area, as described previously [17].

Statistical analysis

Descriptive statistics were summarised by calculating mean values, standard deviations and ranges. The comparison of 5-MeCyd and PR expression between tissues groups was based on a non-parametric Mann-Whitney U test and a test for trend (GI, GII, GIII endometrioid adenocarcinomas). Data for 5-MeCyd and PR were normally distributed (Kolmogorof-Smirnof test). A linear regression analysis was performed between 5-MeCyd and PR expression. Statistical tests were performed using software STATA V.8.0 (College Station, TX).

Results

DNA methylation

Normal menstrual cycle

In normal endometrial tissue, the immunostaining of interphase nuclei is strong during the proliferative phase. The DNA methylation significantly decreases towards the

secretory phase (P=0.0004), it is marked in glandular cells, but it increases in the stromal component as illustrated in Fig. 1A.

Endometrioid adenocarcinoma precursors

5-MeCyd immunolabelling increases progressively from endometrial hyperplasia without atypia to atypical endometrial hyperplasia (P=0.0002). It is marked in epithelial cells and less evident in the stroma as illustrated in Fig. 1B.

Endometrioid adenocarcinoma progression

The 5-MeCyd immunolabelling showed a significant correlation with the degree of differentiation; it is high in grade I and markedly decreases in grade-II and grade-III endometrioid adenocarcinomas (P<0.01) (Fig. 1C).

PR expression

Normal menstrual cycle

During the proliferative phase, PR is strongly expressed in both the epithelial and stromal components, reaching a maximum in the late proliferative phase. There is a significant decline in PR expression, near the end of the secretory phase (P=0.0007), which is marked in glandular cells but increases in the stromal component (Fig. 1A).

Endometrioid adenocarcinoma precursors

PR expression increases progressively from non-atypical hyperplasia to atypical endometrial hyperplasia (P= 0.0002). This progression is marked in epithelial cells and less evident in the stroma as illustrated in Fig. 1B.

Endometrioid adenocarcinoma progression

PR expression in endometrioid carcinomas varies according to the tumour grade**.** Although the PR was expressed at a high level in grade I, it decreased in grade II and grade III (P<0.01), as illustrated in Fig. 1C. These results are summarised in Table 1.

Correlations between DNA methylation and PR expression

There is a significant positive linear correlation between DNA methylation and PR expression in normal endometrium, endometrioid adenocarcinomas and precursors (R2=0.73, P<0.0001), as shown in Fig. 2.

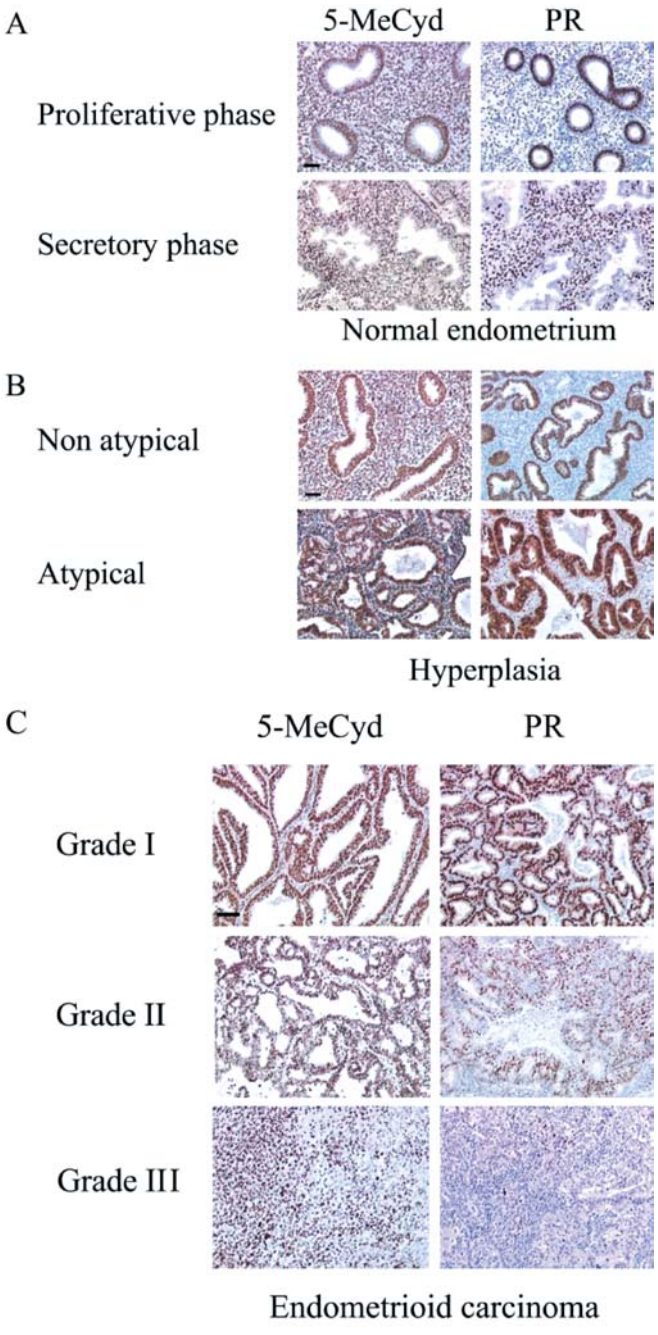


Fig. 1 DNA methylation and progesterone receptor (PR) expression in normal endometrium, endometrioid carcinomas and precursors. **A** A strong labelling of the cell nuclei with 5-MeCyd and PR antibodies in both glandular and stromal components is observed during the proliferative phase. There is a strong decline of DNA methylation and PR expression during the secretory phase. There is little or no expression in glandular epithelial cells, in contrast to the stromal cells where the expression is still high. **B** The immunolabelling of 5-MeCyd and PRs in atypical hyperplasia is more intense than in simple hyperplasia and more marked in epithelial cells. **C** Well-differentiated endometrioid carcinoma (grade I) shows a strong immunostaining for 5-MeCyd and PRs that decreases progressively towards grade-II and grade-III endometrioid carcinomas. All pictures are at original magnification (×25)

Table 1 Quantification of progesterone receptor (PR) expression and DNA methylation in normal endometrium, endometrioid carcinomas and precursors

	5-MeCyd immunolabelling			PR immunolabelling		
Tissues	*Mean±SD	Range	*P* value	*Mean±SD	Range	*P* value
Proliferative phase	17.08±3.73	10.15–22.93	0.0004[1]	16.59±3.8	9.75–22.92	0.0007[1]
Secretory phase	8.51±2.65	5.18–12.98		9.81±2.79	5.07–13.84	
Non-atypical hyperplasia	15.39±3.17	10.87–19.34	0.0002[1]	16.93±2.76	11.23–19.7	0.0002[1]
Atypical hyperplasia	25.84±3.77	19.87–29.68		26.69±2.78	22.2–30.71	
Endometrioid carcinoma						
Grade I	28.82±4.63	23.43–36.19	<0.01[2]	31.61±5.28	23.84–39.7	<0.01[2]
Grade II	14.4±2.65	10.73–19.75		13.41±6.29	3.09–22.74	
Grade III	3.75±2.15	0–6.36		2.55±3.42	0–9.08	

[1] Mann-Whitney U test
[2] Test for trend
* The ratio (%) between positive-cell area and total tissue area

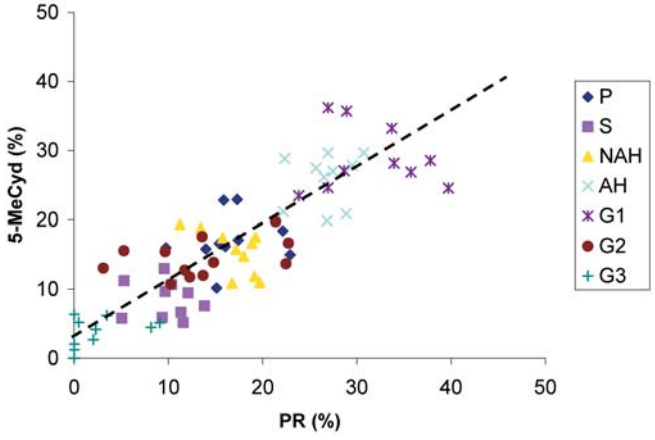


Fig. 2 Significant positive correlation between DNA methylation and progesterone receptor expression in normal endometrium, endometrioid carcinomas and precursors (linear regression analysis, R2=0,73, *P*<0.0001)

Discussion

The alteration of the DNA methylation is frequently observed in numerous human tumours. The link between this post-replicative modification and the control of gene expression as well as the detection of frequent C→T mutations have lead authors to build a genetic model of carcinogenesis and tumour progression, especially for colorectal cancer for which a DNA global hypomethylation is an early event [7, 15]. These biochemical changes are paralleled by modifications of the histopathological patterns of colorectal tumours and precursors, which include successive steps progressing from adenomas to carcinomas. In our study, similar alterations are observed in endometrioid carcinomas and precursors.

We had previously evaluated the global methylation status of DNA in human tumour tissues using the immunohistochemical approach [20, 37, 40]. These studies indicated that anti-5-MeCyd antibodies reached the nucleus and bound only methylated DNA [34]. Previously published competition experiments also demonstrated the specificity of these antibodies [36]. Finally, by comparing the results obtained using radiolabelled methyl incorporation with those observed after immunohistochemical labelling of the same tissue sections, the validity of the latter approach [39] was clearly established.

In this study, a significant difference of the methylation intensity between the normal proliferative and secretory phases of the endometrium was observed. A progressive increase of the signal accompanied the progression among non-atypical and atypical hyperplasia and endometrioid adenocarcinoma grade I. This moderate but constant abnormal hypermethylation was regularly observed in grade-I carcinomas followed by a progressive decrease of the signal from grade I to grade III, suggesting a massive loss of methyl groups in high-grade lesions. The question then arose as to whether this hypermethylation might highlight an increased DNA methylation of numerous genes. Gene-specific analysis has revealed that, in addition to a genome-wide hypomethylation, local hypermethylated sites can be identified in tumours [2, 12, 32] in concert with an increased DNA methyltransferase activity [10, 21, 22, 35]. For several years, most studies in this field aimed at the detection of altered methylation patterns of oncogenes [5, 45, 48] or tumour suppressor genes [8, 11, 13, 31, 32, 38]. It has recently been shown that DNA hypermethylation can be an important mechanism of gene silencing or tumour progression [3] and may cause progressive epigenetic inactivation of tumour suppressor genes or genes involved in DNA repair, such as poly (ADP-ribose) polymerase (PARP-1) [17]. The demonstration of MLH-1 promoter hypermethylation in endometrial carcinomas suggested that abnormal methylation is the first step in endometrial carcinogenesis [33]. Microsatellite instability in sporadic endometrial adenocarcinomas is also probably related to the epigenetic silencing of DNA mismatch repair genes [14], it seems to occur late in the transition from complex hyperplasia to carcinoma, but it is preceded by the progressive inactivation of MLH-1 by promoter hypermethylation [33]. The same observation is made for the inactivation of the multiple promoters of catechol-O-methyltransferase (COMT), which plays an important role in oestrogen-induced cancers: COMT inactivates catechol estrogens that have cancer-promoting activities [44].

It is intriguing to speculate that some of the earliest events of carcinogenesis may not be mutations detectable through standard DNA sequence analysis but rather consisting of a more subtle epigenetic modulation of gene expression. The increase of the methyl-specific signal in GI endometrioid adenocarcinomas followed by a marked decrease in the GII and GIII groups might reflect this process. This progressive decrease has been reported for other malignancies, such as breast carcinoma [45] and lung squamous cell carcinoma [40, 41]. Then a genome-wide hypomethylation following hypermethylation of numerous chromatin regions, as clearly demonstrated here, can be accepted as the hallmark of the progression of the disease.

Expression of high levels of PR is associated with a better disease-free overall survival and is an independent predictor of endometrial carcinoma outcome. Although the alteration of PRs in the progression of endometrioid carcinoma has been well documented, the mechanisms of PR downregulation in endometrioid carcinogenesis have not been characterised**.** DNA methylation participates in the organisation of the chromatin through the specific binding of proteins to methyl-rich regions. Heterochromatin is silent, whereas euchromatin is actively transcribed. Recently, we have shown that the DNA strand break-sensing molecule (PARP-1), thought to stabilise the genome, associated with the DNA binding domain of PR is substantially involved in the regulation of progesterone action in the development of endometrioid carcinomas [17]. The synergy of these two phenomena—DNA methylation and PARP-1 expression—seems to play a key role in the expression of PR. Moreover, it has been shown that the downregulation of the PR isoform B in poorly differentiated human endometrial cancer cells [1, 25] is linked to a selective hypermethylation [30, 43]. Such methylation may be functionally equivalent to an inactivating mutation for the silencing of these genes**.**

The strong parallelism between DNA methylation and PR expression precludes establishing a precise determination with regards to the timing of these events, clearly involved in the genesis of endometrioid adenocarcinoma.

Acknowledgments We thank Mrs N. Lyandrat and Eric Lucas for their technical assistance and Mrs Evelyn Bayle for reviewing the manuscript. This work was supported in part by grants from the Ligue contre le Cancer de la Drôme, France (LF) and the Institut National de Santé et de Recherche Médicale, France (LF).

References

1. Arnett-Mansfield RB, deFazio A, Wain GV, Richard CJ, Byth K, Mote PA, Clark CL (2001) Relative expression of progesterone receptors A and B in endometrioid cancers of the endometrium. Cancer Res 61:4576–4582
2. Baldwin RL, Nemeth E, Tran H, Shvartsman H, Cass I, Narod S, Karlan BY (2000) BRCA1 promoter region hypermethylation in ovarian carcinoma: a population-based study. Cancer Res 60:5329–5333
3. Baylin SB, Esteller M, Rountree MR, Bachman KE, Schuebel K, Herman JG (2001) Aberrant patterns of DNA methylation, chromatin formation and gene expression in cancer. Hum Mol Genet 10:687–692
4. Bird A (1996) CpG-rich islands and function of DNA methylation. Nature 321:209–213
5. Cheah MS, Wallace CD, Hoffman RM (1984) Hypomethylation of DNA in cancer cells: a site-specific change in the c-myc oncogene. J Natl Cancer Inst 73:1057–1065
6. Costello JF, Fruhwald MC, Smiraglia DJ, Rush LJ, Robertson GP, Gao X, Wright FA, Feramiqco JD, Peltomäki P, Lang JC, Schuller DE, Yu L, Bloomfield CD, Caligiuri MA, Yates A, Nishikawa R, Su-Huang H-J, Petrelli NJ, Zhang X, O'Dorisio MS, Held WA, Cavenee WK, Plass C (2000) Aberrant CpG-island methylation has non-random and tumour-type-specific patterns. Nat Genet 24:132–138
7. Cravo M, Pinto R, Fidalgo P, Chaves P, Gloria L, Nobre-Leitao C, Mira FC (1996) Global DNA hypomethylation occurs in the early stages of intestinal type gastric carcinoma. Gut 39:434–438
8. Dammann R, Yang G, Pfeifer GP (2001) Hypermethylation of the CpG island of Ras association domain family 1A(RASSF1A), a putative tumor suppressor gene from the 3p21.3 locus occurs in a large percentage of human breast cancers. Cancer Res 61:3105–3109
9. de Capoa A, Romana Febbo F, Giovanelli F, Niveleau A, Zardo G, Marenzi S, Caiafa P (1999) Reduced levels of poly(ADP)-ribosylation result in chromatin compaction and hypermethylation as shown by a cell-by-cell computer-assisted quantitative analysis. FASEB J 13:89–93
10. el-Deiry WS, Nelkin BD, Celano P, Yen RW, Falco JP, Hamilton SR, Baylin SB (1991) High expression of the DNA methyltransferase gene characterizes human neoplastic cells and progression stages of colon cancer. Proc Natl Acad Sci U S A 88:3470–3474
11. Esteller M, Sanchez-Cespedes M, Rosell R, Sidransky D, Baylin SB, Herman JG (1999) Detection of aberrant promoter hypermethylation of tumor suppressor genes in serum DNA from non-small cell lung cancer patients. Cancer Res 59:67–70
12. Esteller M, Corn PG, Baylin SB, Herman JG (2001) A gene hypermethylation profile of human cancer. Cancer Res 61:3225–3229
13. Esteller M, Herman JG (2002) Cancer as an epigenetic disease: DNA methylation and chromatin alterations in human tumours. J Pathol 196:1–7
14. Faquin WC, Fitzgerald JT, Lin MC, Boynton KA, Muto MG, Mutter GL (2000) Sporadic microsatellite instability is specific to neoplastic and preneoplastic endometrial tissues. Am J Clin Pathol 113:576–582
15. Feinberg AP, Gehrke CW, Kuo KC, Ehrlich M (1988) Reduced genomic 5-methylcytosine in human colonic neoplasia. Cancer Res 48:1159–1161
16. Fukuda K, Mori M, Uchiyama M, Iwai K, Iwasaka T, Sugimori H (1998) Prognostic significance of progesterone receptor immunohistochemistry in endometrial carcinoma. Gynecol Oncol 69:220–225
17. Ghabreau L, Roux JP, Frappart PO, Mathevet P, Patricot LM, Mokni M, Wang ZQ, Tong ZM, Frappart L (2004) Poly(ADP-ribose) polymerase1, a novel partner of nuclear steroid receptors in endometrial cancer and its precursors. Int J Cancer 109:317–321
18. Gonzalez-Zuleta M, Bender CM, Yang AS, Nguyen T, Beart RW, Van Tornout JM (1995) Methylation of the 5′ CpG island of the p16/CDKN2 tumor-suppressor gene in normal and transformed human tissues correlates with gene silencing. Cancer Res 55:4531–4535
19. Habib M, Fares F, Bella C, Bourgeois CA, Bernardino J, Blazquez-Hernandez F, de Capoa A, Niveleau A (1999) DNA global hypomethylation in EBV-transformed interphase nuclei. Exp Cell Res 249:46–53
20. Hernandez-Blazquez FJ, Habib M, Dumollard J-M, Barthelemy C, Benchaib M, de Capoa A, Niveleau A (2000) Evaluation of global DNA hypomethylation in human colon cancer tissues by immunohistochemistry and image analysis. Gut 47:689–693

21. Issa J-P, Vertino PM, Wu J (1993) Increased cytosine DNA-methyltransferase activity during colon cancer progression. J Natl Cancer Inst 85:1235–1240
22. Jakob CA, Guldenschuh I, Mullhaupt B, Muller A, Ammann R, Fried M, Roth J (1999) 5'-Cytosine DNA-methyltransferase mRNA levels in hereditary colon carcinoma. Virchows Archiv 434:57–62
23. Jones PA (1996) DNA methylation errors and cancer. Cancer Res 56:2463–2467
24. Kang GH, Shim YH, Jung HY, Kim WH, Ro JY, Rhyu M (2001) CpG island methylation in premalignant stages of gastric carcinoma. Cancer Res 61:2847–2851
25. Kumar NS, Richer J, Owen G, Litman E, horwitz KB, Leslie KK (1998) selective dowen-regulation of progesterone receptor isoform B in poorly differentiated human endometrial cancer: implication for unopposed estrogen action. 58:1860–1865
26. Kurman RJ, Kaminski PF, Norris HJ (1995) The behaviour of endometrial hyperplasia a long-term study of untreated hyperplasia in 170 patients. Cancer 56:403–412
27. Laird PW, Jaenisch R (1996) The role of DNA methylation in cancer genetics and epigenetics. Annu Rev Genet 30:441–464
28. Leonhardt H, Page AW, Weier HU, Bestor TH (1992) A targeting sequence directs DNA methyltransferase to sites of DNA replication in mammalian nuclei. Cell 71:865–873
29. Leonhardt H, Cardoso MC (2000) DNA methylation, nuclear structure, gene expression and cancer. J Cell Biochem Suppl 35:78–83
30. Liu ZJ, Maekawa M, Horii T, Morita M (2003) The multiple promoter methylation profile of PR gene and ER alpha gene in tumor cell lines. Life Sci 73:1963–1972
31. Magewu AN, Jones PA (1994) Ubiquitous and tenacious methylation of the CpG site in codon 248 of the p53 gene may explain *ist* frequent appearance as a mutational hot spot in human cancer. Mol Cell Biol 14:4225–4232
32. Makos M, Nelkin BD, Lerman MI, Latif F, Zbar B, Baylin SB (1992) Distinct hypermethylation patterns occur at altered chromosome loci in human lung and colon cancer. Proc Natl Acad Sci U S A 89:1929–1933
33. Matias-Guiu X, Ctasus L, Bussaglia, E, Lagarda H, Garcia A, Pons C, Munoz J, Arguelles R, Macin P, Prat J (2001) Molecular pathology of endometrial hyperplasia and carcinoma. Hum Pathol 32:569–577
34. Mayer W, Niveleau A, Walter J, Fundele R, Haaf T (2000) Active demethylation of the zygotic paternal genome. Nature 403:501–502
35. Melki JR, Warnecke P, Vincent PC, Clark SJ (1998) Increased DNA methyltransferase expression in leukaemia. Leukemia 12:311–316
36. Montpellier C, Bourgeois C, Kokalj-Vokac N, Muleris M, Niveleau A, Gibault A, Malfoy B, Dutrillaux B (1994) Detection of methylcytosine rich heterochromatin on banded chromosomes. Application to cells with various status of DNA methylation. Cancer Genet Cytogenet 78:87–93
37. Niveleau A, Piyathilake C, de Capoa A, Grappelli C, Dumollard J-M, Frappart L, Drouet E (2003) The loss of methyl groups in DNA of tumour cells and tissues: the immunochemical approach. In: Szyf M (ed) DNA methylation and cancer therapy. Landers Biosciences, Georgetown
38. Nuovo GJ, Plaia TW, Belinsky SA,Baylin SB, Herman JG (1999) In situ detection of the hypermethylation-induced inactivation of the p16 gene as an early event in oncogenesis.Proc Natl Acad Sci U S A 96:12754–12759
39. Piyathilake CJ, Johanning GL, Frost AR, Whiteside MA, Manne U, Grizzle WE, Heimburger DC, Niveleau A (2000) Immunohistochemical evaluation of global DNA methylation: comparison with in vitro radiolabeled methyl incorporation assay. Biotech Histochem 75:251–258
40. Piyathilake CJ, Frost AR, Bell WC, Oelschlager D, Weiss H, Johanning GL, Niveleau A, Heimburger DC, Grizzle WE (2001) Altered global methylation of DNA: An epigenetic difference in susceptibility for lung cancer is associated with its progression. Hum Pathol 32:856–862
41. Piyathilake CJ, Henao O, Frost AR, Maccaluso M, Bell WC, Johanning GL, Heimburger DC, Niveleau A, Grizzle WE (2003) Race and age dependent alterations in global methylation of DNA in squamous cell carcinoma of the lung. Cancer Causes Control 14:37–42
42. Salvesen HB, Iversen OE, Akslen LA (1998) Prognostic impact of morphometric nuclear grade of endometrial carcinoma. Cancer 83:956–964
43. Sasaki M, Dahria A, Oh BR, Tanaka Y, Fujimoto S, Dahya R (2001) Progesterone receptor β gene inactivation and CpG hypermethylation in human uterine endometrial cancer. Cancer Res 61:97–102
44. Sasaki M, Kaneuci M, Sakuragi N, Dahiya R (2003) Multiple promoters of catechol-O-methyltransferase gene are selectively inactivated by CpG hypermethylation in endometrial cancer. Cancer Res 63:3101–3106
45. Soares J, Pinto AE, Cunha CV, Andres S, Barao I, Sousa JM, Cravo M (1999) Global DNA hypomethylation in breast carcinoma: correlation with prognostic factors and tumor progression. Cancer 85:112–118
46. Sobin LH, Wittekind Ch (eds) (2002) TNM classification of malignant tumours, 6th edn. International Union Against Cancer, Wiley & Sons, New York
47. Tasi MJ, O'Malley BW (1994) Molecular mechanisms of action of steroid/thyroid receptor superfamily members. Annu Rev Biochem 63:451–486
48. Tao L, Yang S, Xie M, Kramer PM, Pereira MA (2000) Hypermethylation and overexpression of c-*jun* and c-*myc* protooncogenes and increased DNA methyltransferase activity in dichloroacetic and trichloroacetic acid-promoted mouse liver tumors. Cancer Lett 158:185–193
49. Tavassoli FA, Devilee P (eds) (2003) Tumours of the breast and female genital organs. IARC Press, Lyon
50. Zaino RJ, Kurman RJ, Diana KL, Morrow CP (1996) Pathologic models to predict outcome for women with endometrial adenocarcinoma: the importance of the distinction between surgical stage and clinical stage-a Gynecologic Oncology Group study. Cancer 77:1115–1121

Virchows Arch (2004) 445:135–141
DOI 10.1007/s00428-004-1042-0

ORIGINAL ARTICLE

Michael Vieth · Regine Schneider-Stock · Knut Röhrich · Andrea May · Christian Ell · Anett Markwarth · Albert Roessner · Manfred Stolte · Andrea Tannapfel

INK4a-ARF alterations in Barrett's epithelium, intraepithelial neoplasia and Barrett's adenocarcinoma

Received: 12 January 2004 / Accepted: 28 February 2004 / Published online: 8 June 2004
© Springer-Verlag 2004

Abstract *Introduction:* The INK4a-ARF [CDKN2A]-locus on chromosome 9p21 encodes for two tumour suppressor proteins, $p16^{INK4a}$ and $p14^{ARF}$, which act as upstream regulators of the Rb-CDK4 and p53 pathways. To study the contribution of each pathway to the carcinogenesis of Barrett's adenocarcinoma, we analysed the alterations of $p14^{ARF}$and $p16^{INK4a}$ in preneoplastic and neoplastic lesions of this disease. *Materials and methods:* After microdissection, DNA of 15 Barrett's adenocarcinomas, 40 Barrett's intraepithelial neoplasms (*n*=20 low- and *n*=20 high-grade) and 15 Barrett's mucosa without neoplasia was analysed for INK4-ARF inactivation using DNA sequence and loss of heterozygosity (LOH) analysis, methylation-specific polymerase chain reaction, restriction-enzyme-related polymerase chain reaction and immunohistochemistry. *Results:* We detected 9p21 LOH, $p16^{INK4a}$ methylation and $p16^{INK4a}$ mutations in Barrett's adenocarcinomas in 5 of 15 (33%), 8 of 15 (53%) and 1 of 15 (7%) patients, respectively. $P14^{ARF}$ was methylated in 3 of 15 (20%) adenocarcinomas. In Barrett's intraepithelial neoplasia, $p16^{INK4a}$ was altered in 12 of 20 (60%) high-grade and in 4 of 20 (20%) low-grade intraepithelial neoplasms. In Barrett's mucosa without intraepithelial neoplasia $p16^{INK4a}$ was methylated in one case (7%). $P14^{ARF}$ was intact in Barrett's mucosa without intraepithelial neoplasia. *Conclusions:* We conclude that most Barrett's intraepithelial neoplasms contain genetic and/or epigenetic INK4a-ARF alterations. Methylation of $p16^{INK4a}$ appears to be the most frequent epigenetic defect in the neoplastic progression of Barrett's tumourigenesis.

Keywords Barrett · Neoplasia · Methylation · $p16^{INK4a}$ · $p14^{ARF}$

M. Vieth (✉) · R. Schneider-Stock · A. Roessner
Institute of Pathology,
Otto-von-Guericke University Magdeburg,
Leipziger Strasse 44, 39120 Magdeburg, Germany
e-mail: Michael.Vieth@medizin.uni-magdeburg.de
Tel.: +49-391-6715817
Fax: +49-391-6715818

K. Röhrich · A. Markwarth · A. Tannapfel
Institute of Pathology, University of Leipzig,
04103 Leipzig, Germany

A. May · C. Ell
Clinic of Internal Medicine II,
HSK-Clinics Wiesbaden,
65199 Wiesbaden, Germany

M. Stolte
Institute of Pathology, Klinikum Bayreuth,
95445 Bayreuth, Germany

Introduction

Barrett's epithelium is a columnar-cell metaplasia (specialised intestinal metaplasia) in the distal oesophagus, occurring in patients with gastro-oesophageal reflux disease [7, 18]. The clinical diagnosis of Barrett's epithelium is important because of potential neoplastic transformation [36, 41] and is, therefore, considered a precancerous condition. The incidence of Barrett's adenocarcinoma is increasing [9, 10, 34, 40]. Novel endoscopic techniques designed for detection of minute lesions and for local treatment have been developed [4, 13, 15, 29, 33, 38].

Still problematic is the fair histological inter- and intra-observer agreement of neoplastic lesions in Barrett's epithelium [30], which doesn't substantially improve on subsequent re-evaluation following establishment of uniform histological criteria [32]. Some molecular markers [11, 44] that could support the gold standard of histological diagnosis of neoplasia are available, but these cannot be applied to all cases at all stages [31].

To date, the exact cellular and molecular mechanisms leading to neoplastic progression in Barrett's epithelium have not yet been fully understood [31]. Deep insights could possibly be gained by understanding signals of different pathways interfering with cell-cycle regulation and proliferation [43, 45] in detail. There is evidence that alterations in the INK4a-ARF locus, which maps to chromosome 9p21, contribute to the development of Barrett's neoplasia and clonal expansion [2, 46]. The

INK4a-ARF or CDKN2A locus codes for two different proteins, $p16^{INK4a}$ and $p14^{ARF}$, both involved in cell-cycle regulation; at least, $p16^{INK4a}$ is involved in the progression of neoplasia in Barrett's epithelium [12, 26].

Methylation of the CDKN2A promoter is the predominant mechanism that triggers $p16^{INK4a}$ inactivation. This hypermethylation is a very common event in oesophageal adenocarcinoma and occurs as early as metaplasia [6]. Compared with $p16^{INK4a}$, $p14^{ARF}$ is generated through an alternative splicing process, thus resulting in a different reading frame. $P14^{ARF}$ has been demonstrated to be a growth suppressor [39] that specifically activates the p53 pathway via stabilisation of p53 by inhibiting MDM 2-dependent p53 degradation. This leads to cell-cycle arrest or apoptosis, which is a stimulus-dependent pathway [25]. The aim of this study was to specify the role of $p16^{INK4a}$ and $p14^{ARF}$ alterations in the progression of tumourigenesis of Barrett's adenocarcinomas.

Materials and methods

Patients and tissue samples

Between February 2000 and September 2001, 15 patients with well-differentiated mucosal Barrett's adenocarcinoma, 40 patients with Barrett's epithelium and intraepithelial neoplasia (n=20 with low- and n=20 with high-grade intraepithelial neoplasia) and 15 patients with Barrett's mucosa without neoplasia were included in this retrospective study (Fig. 1). All specimens obtained from patients with Barrett's neoplasia were taken from endoscopic resections. Barrett's mucosa without neoplasia was obtained from biopsies of patients without neoplasia.

The present study was in accordance with the ethics standards of the Committee on Human Experimentation of the University of Leipzig. All samples were taken during treatment procedures under curative intent.

Each tumour was re-evaluated with regard to typing and grading (World Health Organization, 2002) [19] and diagnosed according to recent guidelines [14]. In all cases, haematoxylin-eosin-stained slides were re-examined independently by three experienced gastrointestinal pathologists (AT, MS, MV) without any knowledge of clinical data. In case of conflicting results of grading intraepithelial neoplasia, microscopic re-evaluation was obtained until concordance was achieved.

DNA samples

For each tumour sample, the histopathological lesions of interest were first identified on routinely stained sections, as described previously [42]. Sections 12-μm thick were cut from tissue blocks and were mounted on glass slides with a thickness of 0.17 mm (very thin glass slides are needed to prevent laser energy from being dispersed before reaching the tissue section). An ultraviolet (UV) laser microscope system was then used to isolate particular cell populations (UV-laser microbeam; PALM, Bernried, Germany). The pulsed UV laser of high-beam quality (nitrogen laser, wavelength 337 nm, maximum frequency 20 pulses/s, pulse duration 3 ns) was combined with an inverse microscope and focused through an objective of high numerical aperture into the tissue plane. Beam-spot diameter measured approximately 0.3–0.5 μm. Because of the extremely high energy density within the focal point (laser energy at object plane approximately 5 μJ), all biological material is completely destroyed. Using the UV laser beam at a high repetition rate (approximately 20 pulses/s), a circle was cut around the target cells. This resulted in complete separation of the target population from neighbouring tissues (Fig. 2). The approximate number of cells was estimated to be at least 1000 per sample for polymerase chain reaction (PCR) analysis. After microdissection, the tissue samples were placed into Eppendorf tubes and were incubated with proteinase K at 37°C overnight. Proteinase K activity was inactivated by heating to 95°C for 10 min. For DNA extraction, standard methods were used: after incubation with proteinase K at 37°C overnight, the tissue was extracted twice in phenol and twice in chloroform, followed by ethanol precipitation.

Methylation status of INK4a-ARF locus

The CpG WIZ p16 Methylation Assay Kit was used (Oncor Inc, Gaithersburg, MD, USA) according to the manufacturer's instructions. After an initial bisulphite reaction to modify the DNA, PCR amplification with specific primers was performed to distinguish methylated from unmethylated DNA. Primers specific for unmethylated $p16^{INK4a}$ 5′-TTATTAGAGGGTGGGGTGGATTGT-3′ (sense), 5′-CAACCCCAAACCACAACCATAA-3′ (antisense) or methylated $p16^{INK4a}$ 5′-TTATTAGAGGGTGGGGCGGATCGC-3′ (sense), 5′-GACCCCGAACCGCGACCGTAA-3′ (antisense) were used. Next, 7 μg/100 μl DNA was denatured by 2 M NaOH for 10 min at room temperature. DNA Modification Reagent I was added, incubated for 24 h at 50°C and subsequently purified using DNA Modification Reagents II and III in the presence of 50 μl water. The bisulphite modification of DNA was completed with 3 M NaOH treatment for 5 min, followed by ethanol precipitation. For hot-start PCR, the PCR mixture contained Universal PCR Buffers [1×9, 4dNTP's (1.25 nM)], unmethylated or methylated primers (300 ng each per reaction). The PCR product was directly electrophoresed on a 3% agarose gel, stained with ethidium bromide and visualised under UV illumination. Bisulphite-converted DNA from corresponding squamous epithelium from each patient

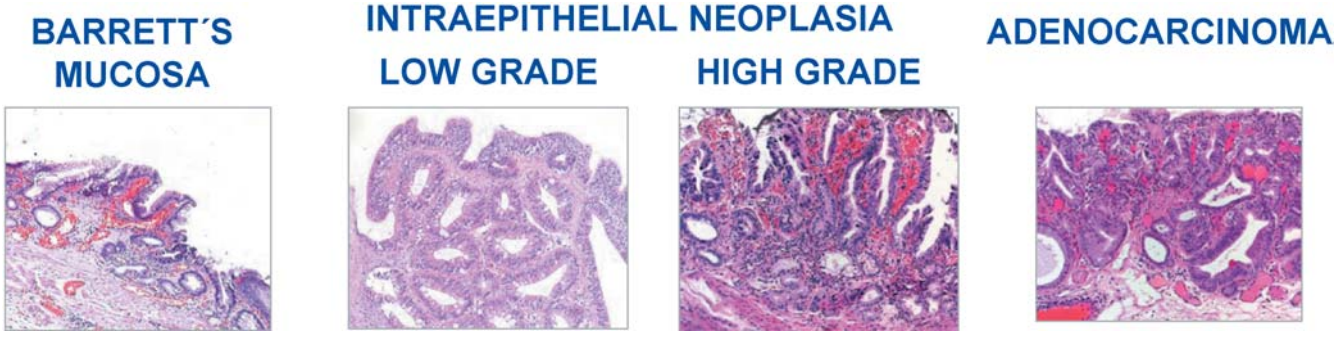


Fig. 1 Histological samples of Barrett's mucosa without intraepithelial neoplasia, with low- and high-grade intraepithelial neoplasia and well-differentiated mucosal Barrett's adenocarcinoma. (haematoxilyn-eosin stain, ×100)

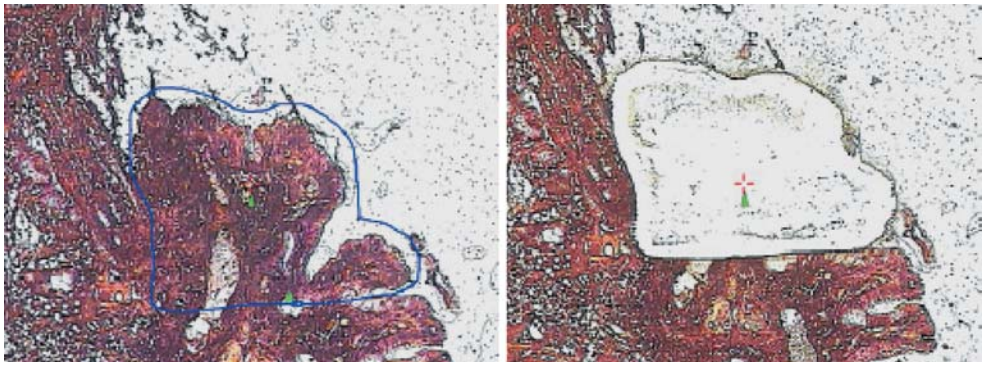


Fig. 2 Barrett's mucosa without neoplasia before and after microdissection of representative areas

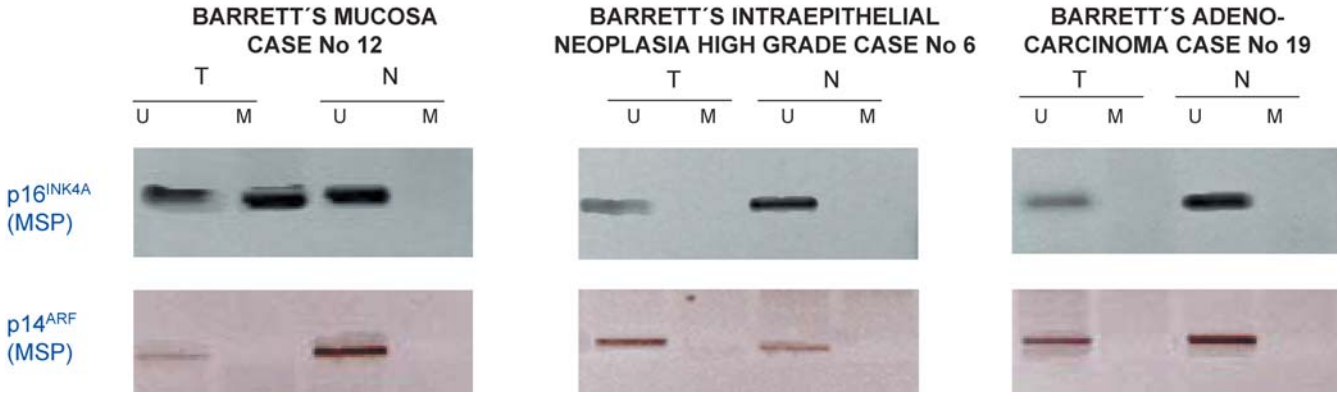


Fig. 3 Methylation status of p14 and p16 (*u* unmethylated, *m* methylated) in selected patients with Barrett's mucosa without neoplasia, with high-grade intraepithelial neoplasia and well-differentiated adenocarcinoma showing unexpected methylation of Barrett's epithelium without neoplasia and unmethylated protein in cases with neoplasia. *T* area from which histological diagnosis was made, *N* adjacent squamous epithelium from oesophagus serving as control tissue, *MSP* methylation-specific polymerase chain reaction

served as a negative control as indicated by the presence of the unmethylated but not the methylated band. To control the efficacy of bisulphite treatment, a primer set used for unmodified or wild type was used 5′-CAGAGGGTGGGGCGGACCGA-3′ (sense) and 5′-CGGGCCGCGGCCGTGG-3′ (antisense). In case of insufficient bisulphite modification of the DNA, the wild-type primers should have been amplified.

The methylation pattern in the CpG islands of the $p14^{ARF}$ was determined using primers designed for either methylated or unmethylated DNA [27]. The primers spanned six CpG sites within the 5′ regions of the gene. The 5′ position of the sense unmethylated and methylated primer corresponds to 195 bp and 201 bp of GenBank sequence number LA1934. The primer sequences for the unmethylated reaction were 5′TTTTTGGTGTTAAAGGGTGGTGTGGTGTAGT-3′ (sense) and 5′-CACAAAAACCCTCACTCACAACAA-3′ (antisense), yielding a PCR product of 132 bp. The primer sequences for the methylated reaction were 5′-GTGTTAAAGGGCGGCGTAGC-3′ (sense) and 5′-AAAACCCTCACTCGCGACGA-3′ (antisense), which amplify a 122 bp product [25].

Placental DNA treated with methyltransferase (Oncor Inc, Gaithersburg, MD, USA) was used as a positive control for methylated alleles. Of the PCR products, 15 μl were electrophoresed on an 8% polyacrylamide gel, stained and directly visualised.

In addition to methylation-specific PCR, a second approach was used to determine the methylation status of both $p14^{ARF}$ and $p16^{INK4a}$—the restriction enzyme-related polymerase chain reaction (RE-PCR), as described by Chaubert et al. [8]. Genomic DNA was digested with four methyl-sensitive (*Hpa*II, *Nae*I, *Eag*lI and *Ksp*1) and with one non-methyl-sensitive (*Msp*I) restriction enzymes, as described in detail previously [42].

Undigested placental and tumour DNA was used as a control. Cases were considered positive using RE-PCR when PCR amplification was obtained after digestion with one of the methyl-sensitive restriction enzymes used (Fig. 3). Both methods revealed concordant results for the methylation status.

LOH DNA sequencing for INK4a-ARF (CDKN2A) locus

Microsatellite analysis using six microsatellites of chromosome 9p21 was performed, as described previously [42]. The markers used were D9S156, D9S157, D9S162, D9S171, D9S126 and IFNA and were obtained from Research Genetics (Huntsville AL, USA) (Fig. 4). These markers were chosen empirically for their robustness in fresh-frozen and in formalin-fixed DNA specimens. Comparative PCR assays for paired tumour and normal samples were done simultaneously. PCR products from paired normal and tumour reactions were electrophoresed. Visual assessment of band intensities were confirmed and quantified in most cases densitometrically.

Band intensities of normal alleles were used for baseline comparison values. A hemizygous allele loss was regarded as present in the tumour when a band was diminished in expected intensity by at least 50% on at least two separate PCR runs, as according to the literature [31, 38].

Coding sequences and flanking intronic sequences of exons 1α, β and 2 of the INK4a-ARF gene were analysed using PCR single-stranded conformation polymorphism (PCR-SSCP). Primer sequences for exons 1 α, 1β and 2 have been described previously [21]. Exon 1β was analysed using two overlapping PCR products generated with the primer pairs P14F1 5′-TCAGGGAAGGG-

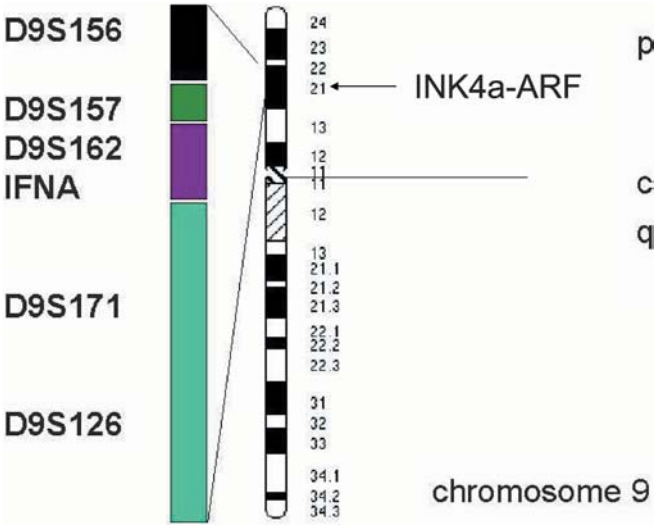


Fig. 4 Schematic representation of the 9p21 locus with the microsatellite markers used

CGGGTGCG-3′ (sense) and P14R1 5′-GCCGCGGGATGTGAACCA-3′ (antisense), which generated a 245-bp product. PCR and PCR primers were used as previously described [42]. After purification of the PCR products, sequencing analysis was performed using the DNA-Sequenase-Kit (Amersham, Germany) and an automatic sequencing analyser (ABI 373; Applied Biosystems-Perkin-Elmer, Germany).

Immunohistochemical analysis and assessment

The immunohistochemical analysis was performed as described recently [42]. The following antibodies were used: p16 (polyclonal, rabbit, dilution 1:500; Pharmingen, San Diego, CA) and p14 (polyclonal, rabbit, dilution: 1:100; Zymed Laboratories, South San Francisco, CA, USA).

Sections known to stain positively were included in each batch, and negative controls were also performed by replacing the primary antibody with mouse or goat ascites fluid (Sigma-Aldrich Biochemicals, St. Louis, MO, USA) (Fig. 5).

Results

Methylation status of $p14^{ARF}$ and $p16^{INK4a}$

Promoter methylation of $p16^{INK4a}$ revealed that 8 of 15 carcinomas (53%) examined showed aberrant methylation at the 5′CpG island. Samples of Barrett's mucosa with low- and high-grade intraepithelial neoplasia exhibited methylated $p16^{INK4a}$ in 4 of 20 (20%) and 12 of 20 (60%) cases, respectively. Barrett's mucosa without evidence of neoplasia had methylated $p16^{INK4a}$ in 1 of 15 cases (7%). In corresponding non-tumourous normal squamous-cell epithelium, methylated templates were not amplified.

All cases with aberrant methylation of the $p16^{INK4a}$ gene showed a complete loss of immunoreactivity within the tumour tissue. In the cases exhibiting neither methylation nor allelic loss, nuclear staining of $p16^{INK4a}$ protein was observed in nearly all tumour cells with a moderate to strong intensity of immunoreactivity. In normal squamous-cell epithelium, $p16^{INK4a}$ protein was detected in all cases. The analysis of the methylation status of the adjacent gene $p14^{ARF}$ was present in 3 of 15 cases with mucosal Barrett's adenocarcinoma (20%). In all patients, corresponding non-neoplastic tissue was also analysed; no $p14^{ARF}$-promoter methylation was observed in any case. In normal Barrett's mucosa, we failed to detect $p14^{ARF}$ alterations. All three cases with a methylated $p14^{ARF}$

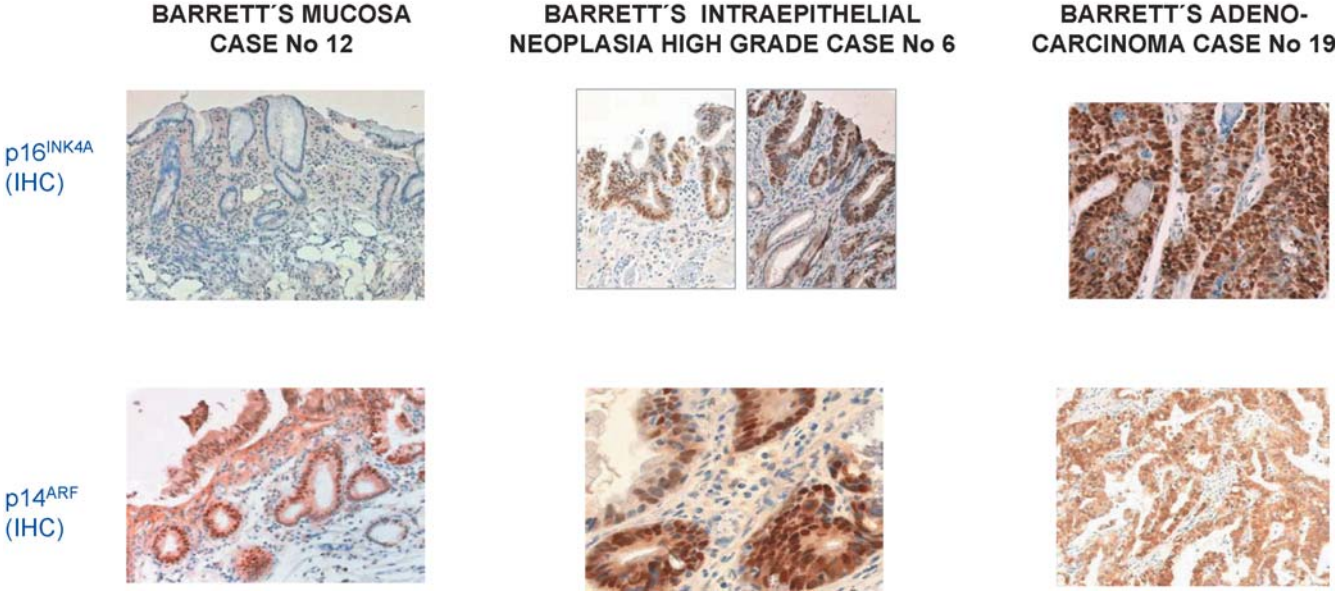


Fig. 5 Immunohistochemistry of p16 and p14 in selected patients corresponding to Fig. 3 with Barrett's mucosa without intraepithelial neoplasia, high-grade intraepithelial neoplasia and well-differentiated Barrett's adenocarcinoma (*IHC* immunohistochemistry) (×40–100)

Table 1 $p16^{INK4a}$ and $p14^{ARF}$ alterations in Barrett's mucosa, intraepithelial neoplasia and adenocarcinoma. *LOH* loss of heterozygosity

	$p16^{INK4a}$				$p14^{ARF}$		
	No. of patients	LOH	Methylation	Mutation	LOH	Methylation	Mutation
Barrett's mucosa	15	-	1/15	-	-	-	-
Intraepithelial neoplasia							
Low grade	20	-	4/20	-	-	-	-
High grade	20	-	12/20	-	-	-	-
Adenocarcinoma (pT1m)	15	5/15	8/15	1/15	-	3/15	-

promoter lacked specific $p14^{ARF}$ protein staining. In non-neoplastic tissue, $p14^{ARF}$ was detected in the nuclear or nucleolar compartment of the cells (Fig. 5).

The three adenocarcinomas with methylated $p14^{ARF}$ had an unmethylated $p16^{INK4a}$ promoter. Thus, the methylation status of $p16^{INK4a}$ and $p14^{ARF}$ promoters seems not to be related. One can assume a negative association, but no significant correlation can be calculated due to the sample size of only 3 of 15 cases with methylated $p14^{ARF}$ (Table 1).

All samples of normal squamous-cell epithelium, obtained from the resection margins of the patients with adenocarcinoma, exhibited an unmethylated INK4-ARF status.

$P16^{INK4a}$ and $p14^{ARF}$ methylation was found more frequently in high-grade intraepithelial neoplasia and invasive carcinoma compared with low-grade intraepithelial neoplasia and Barrett's epithelium without pathological changes. Patients' age or gender was not related to the frequency of inactivated $p16^{INK4a}$ or $p14^{ARF}$.

LOH on chromosome 9p21 and homozygous deletion

Using microsatellite marker flanking the INK4a-ARF region, LOH was detected in 5 of 15 adenocarcinomas (33%). No patient showed homozygous deletion spanning the D9S156 and D9S126 markers, indicating the loss of both $p16^{INK4a}$ and $p14^{ARF}$ genes. LOH was not observed in Barrett's intraepithelial neoplasia or Barrett's mucosa without neoplasia. Three patients with high-grade intraepithelial neoplasia exhibited apparent retention of marker D9S157 but not IFNA or D9S171, suggesting that the deletion excludes the exon 1β or p16INK4 gene.

Mutations of exons 1 and 2 were analysed using PCR-SSCP followed by direct sequencing of the cases with anomalous migrating bands. We detected a specific mutation (c.305G>A: G102 V) in one case of Barrett's adenocarcinoma, affecting the 1β exon. All of these tumours had an unmethylated INK4a status.

Discussion

Aberrant methylation of the $p16^{INK4a}$ promoter has been reported in carcinomas as well as in early preneoplastic lesions in the lung, stomach, oesophagus and pancreas [1, 28]. We examined the status of $p14^{ARF}$ and $p16^{INK4a}$ simultaneously to analyse whether alterations in these genes may function as co-operative or alternative mechanisms in the pathogenesis of neoplastic transformation of Barrett's epithelium.

Our study shows that inactivation of $p16^{INK4a}$ using methylation was observed in 53% of Barrett's adenocarcinomas. Additionally, one patient was shown to have undergone a p16 mutation. Methylated protein was seen in 60% of Barrett's epithelium with high-grade intraepithelial neoplasia, in 20% of low-grade intraepithelial neoplasia and in one patient without neoplasia. Due to the missing detection of simultaneous methylation of both genes, we concluded that $p14^{ARF}$ methylation is independent of $p16^{INK4a}$ methylation. At this point it must be noted that we did not analyse a large group of patients; however, the size of our study is still large enough to interpret the results accordingly.

The neighbouring gene, $p14^{ARF}$ promoter was inactivated in 20% of pT1 (m-type)-Barrett's adenocaricnomas but not at all in Barrett's epithelium with or without intraepithelial neoplasia.

Thus, the $p16^{INK4a}$ promoter demonstrates selective epigenetic silencing compared with $p14^{ARF}$ in Barrett's epithelium with and without neoplasia. The findings of the present study indicate that aberrant methylation is a major mechanism of selective inactivation of the INK4a-ARF locus in patients with Barrett's neoplasia. Specific mutations of $p16^{INK4a}$ and $p14^{ARF}$ are rare and have been described in very few patients with glioma, pancreatic cancer and melanoma [3, 20, 24, 37]. Sole $p14^{ARF}$ mutations or homozygous deletions that spare the remainder $p16^{INK4a}$ have been described only in a melanoma-cell line and glioma xenograft [23].

Our data are comparable with that of Rashid et al. [35], who described methylation of $p16^{INK4a}$ in approximately 73% of tubulovillous adenoma of the colorectum. These lesions are precancerous conditions, as is Barrett's epithelium. Nevertheless, we found a lesser frequency of methylation in Barrett's epithelium than reported in the literature [6, 26, 46]. This may be due to the very early stages of Barrett's neoplasia that were all limited to the mucosa. Conversely, the study of Doak et al. [11] as well as ours showed that $p16^{INK4a}$ was inactivated in Barrett's mucosa without neoplasia in approximately 7%. Some data published in the literature show that, theoretically, it cannot be excluded that methylation is a phenomenon of increased cellular proliferation and immortalisation and not an initial sign of neoplastic transformation. Findings

from non-tumourous tissue in gastric cancer cases and lung tumours in animal studies [5, 23] do not support this; whereas, findings in ulcerative colitis [22] do support this hypothesis. In our study, we detected hypermethylation of $p16^{INK4a}$ in Barrett's epithelium without neoplasia in one case, thus indicating that hypermethylation can be an early event in precancerous conditions [16] compared with other epithelia. In the literature, this is regarded as an explanation for the high malignant potential of Barrett's epithelium [17].

In conclusion, our data suggest that promoter methylation appears to be the main cause of inactivation of the INK-ARF locus in Barrett's epithelium and adenocarcinoma. Therefore, silencing of INK4a-ARF gene products—coding for critical regulators of cell-cycle progression—is one of the most frequent genetic defects in Barrett's adenocarcinoma and precursor lesions.

References

1. Ahrendt SA, Eisenberger CF, Yip L, Rashid A, Chow JT, Pitt HA, Sidransky D (1999) Chromosome 9p21 loss and p16 inactivation in primary sclerosing cholangitis-associated cholangiocarcinoma. J Surg Res 84:88–93
2. Barrett MT, Sanchez CA, Galipeau PC, Neshat K, Emond M, Reid BJ (1996) Allelic loss of 9p21 and mutation of the CDKN2/p16 gene develop as early lesions during neoplastic progression in Barrett's esophagus. Oncogene 13:1867–1873
3. Bartsch DK, Sina-Frey M, Lang S, Wild A, Gerdes B, Barth P, Kress R, Grutzmann R, Colombo-Benkmann M, Ziegler A, Hahn SA, Rothmund M, Rieder H (2002) CDKN2A germline mutations in familial pancreatic cancer. Ann Surg 236:730–737
4. Basu KK, Pick B, Bale R, West KP, de Caestecker JS (2002) Efficacy and one year follow up of argon plasma coagulation therapy for ablation of Barrett's oesophagus: factors determining persistence and recurrence of Barrett's epithelium. Gut 51:776–780
5. Belinsky SA, Snow SS, Nikula KJ, Finch GL, Tellez CS, Palmisano WA (2002) Aberrant CpG island methylation of the p16(INK4a) and estrogen receptor genes in rat lung tumors induced by particulate carcinogens. Carcinogenesis 23:335–339
6. Bian YS, Osterheld MC, Fontolliet C, Bosman FT, Benhattar J (2002) P16 inactivation by methylation of the CDKN2A promoter occurs early during neoplastic progression in Barrett's esophagus. Gastroenterology 122:1113–1121
7. Cameron AJ, Ott BJ, Payne WS (1985) The incidence of adenocarcinoma in columnar-lined (Barrett's) esophagus. N Engl J Med 313:857–859
8. Chaubert P, Gayer R, Zimmermann A, Fontolliet C, Stamm B, Bosman F, Shaw P (1997) Germ-line mutations of the p16INK4(MTS1) gene occur in a subset of patients with hepatocellular carcinoma. Hepatology 25:1376–1381
9. Conio M, Cameron AJ, Romero Y, Branch CD, Schleck CD, Burgart LJ, Zinsmeister AR, Melton LJ 3rd, Locke GR 3rd (2001) Secular trends in the epidemiology and outcome of Barrett's oesophagus in Olmsted County, Minnesota. Gut 48: 304–309
10. Devesa SS, Blot WJ, Fraumeni JF Jr (1998) Changing patterns in the incidence of esophageal and gastric carcinoma in the United States. Cancer 83:2049–2053
11. Doak SH, Jenkins GJ, Parry EM, D'Souza FR, Griffiths AP, Toffazal N, Shah V, Baxter JN, Parry JM (2003) Chromosome 4 hyperploidy represents an early aberration in premalignant Barrett's oesophagus. Gut 52:623–628
12. Eads CA, Lord RV, Wickramasinghe K, Long TI, Kurumboor SK, Bernstein L, Peters JH, DeMeester SR, DeMeester TR, Skinner KA, Laird PW (2001) Epigenetic patterns in the progression of esophageal adenocarcinoma. Cancer Res 61:3410–3418
13. Egger K, Werner M, Meining A, Ott R, Allescher HD, Höfler H, Classen M, Rösch T (2003) Biopsy surveillance is still necessary in patients with Barrett's oesophagus despite new endoscopic imaging techniques. Gut 52:18–23
14. Faller G, Borchard F, Ell C, Seitz G, Stolte M, Walch A, Rüschoff J, Working Group for Gastroenterological Pathology of the German Society for Pathology (2003) Histopathological diagnosis of Barrett's mucosa and associated neoplasias: results of a consensus conference of the Working Group for Gastroenterological Pathology of the German Society for Pathology on 22 September 2001 in Erlangen. Virchows Arch 443:597–601
15. Fitzgerald RC (2003) Ablative mucosectomy is the procedure of choice to prevent Barrett's cancer. Gut 52:16–17
16. Fitzgerald RC, Abdalla S, Onwuegbusi BA, Sirieix P, Saeed IT, Burnham WR, Farthing MJ (2002) Inflammatory gradient in Barrett's oesophagus: implications for disease complications. Gut 51:316–322
17. Fujii T, Nakagawa S, Hanzawa M, Sueyoshi S, Fujita H, Shirouzu K, Yamana H (2003) Immunohistological study of cell-cycle-related factors, oncogene expression, and cell proliferation in adenocarcinoma development in Barrett's esophagus. Oncol Rep 10:427–431
18. Haggitt RC (1994) Barrett's esophagus, dysplasia, and adenocarcinoma. Hum Pathol 25:982–993
19. Hamilton SR, Aaltonen LA (eds) (2000) WHO Pathology and genetics. IARC Press, Lyon, pp 173–200
20. Hearle N, Damato BE, Humphreys J, Wixey J, Green H, Stone J, Easton DF, Houlston RS (2003) Contribution of germline mutations in BRCA2, P16(INK4A), P14(ARF) and P15 to uveal melanoma. Invest Ophthalmol Vis Sci 44:458–462
21. Hussussian CJ, Struewing JP, Goldstein AM, Higgins PA, Ally DS, Sheahan MD, Clark WH Jr, Tucker MA, Dracopoli NC (1994) Germline p16 mutations in familial melanoma. Nat Genet 8:15–21
22. Issa JP, Ahuja N, Toyota M, Bronner MP, Brentnall TA (2001) Accelerated age-related CpG island methylation in ulcerative colitis. Cancer Res 61:3573–3577
23. Jang TJ, Kim DI, Shin YM, Chang HK, Yang CH (2001) p16(INK4a) Promoter hypermethylation of non-tumorous tissue adjacent to gastric cancer is correlated with glandular atrophy and chronic inflammation. Int J Cancer 93:629–634
24. Jen J, Harper JW, Bigner SH, Bigner DD, Papadopoulos N, Markowitz S, Willson JK, Kinzler KW, Vogelstein B (1994) Deletion of p16 and p15 genes in brain tumors. Cancer Res 54:6353–6358
25. Karayan L, Riou JF, Seite P, Migeon J, Cantereau A, Larsen CJ (2001) Human ARF protein interacts with topoisomerase I and stimulates its activity. Oncogene 20:836–848
26. Klump B, Hsieh CJ, Nehls O, Dette S, Holzmann K, Kiesslich R, Jung M, Sinn U, Ortner M, Porschen R, Gregor M (1998) Hypermethylation of the CDKN2/p16 promoter during neoplastic progression in Barrett's esophagus. Gastroenterology 115:1381–1386
27. Lo DYM, Wong IHN, Zhang J, Tein MS, Ng MH, Hjelm NM (1999) Quantitative analysis of aberrant p16 methylation using real-time quantitative methylation-specific polymerase chain reaction. Cancer Res 59:3899–3903
28. Martin A, Baran-Marzak F, El Mansouri S, Legendre C, Leblond V, Charlotte F, Davi F, Canioni D, Raphael M (2000) Expression of p16/INK4a in posttransplantation lymphoproliferative disorders. Am J Pathol 156:1573–1579
29. May A, Gossner L, Pech O, Fritz A, Günter E, Mayer G, Müller H, Seitz G, Vieth M, Stolte M, Ell C (2002) Local endoscopic therapy for intraepithelial high-grade neoplasia and early adenocarcinoma in Barrett's oesophagus: acute-phase and intermediate results of a new treatment approach. Eur J Gastroenterol Hepatol 14:1085–1091

30. Montgomery E, Bronner MP, Goldblum J, Greenson JK, Haber MM, Hart J, Lamps LW, Lauwers GY, Lazenby AJ, Lewin DN, Robert ME, Toledano AY, Shyr Y, Washington K (2001) Reproducibility of the diagnosis of dysplasia in Barrett esophagus: a reaffirmation. Hum Pathol 32:368–378
31. Morales CP, Souza RF, Spechler SJ (2002) Hallmarks of cancer progression in Barrett's oesophagus. Lancet 360:1587–1589
32. Ormsby AH, Petras RE, Henricks WH, Rice TW, Rybicki LA, Richter JE, Goldblum JR (2002) Observer variation in the diagnosis of superficial oesophageal adenocarcinoma. Gut 51: 671–676
33. Ortner MA, Ebert B, Hein E, Zumbusch K, Nolte D, Sukowski U, Weber-Eibel J, Fleige B, Dietel M, Stolte M, Oberhuber G, Porschen R, Klump B, Hortnagl H, Lochs H, Rinneberg H (2003) Time gated fluorescence spectroscopy in Barrett's oesophagus. Gut 52:28–33
34. Pera M (2000) Epidemiology of esophageal cancer, especially adenocarcinoma of the esophagus and esophagogastric junction. Recent Results Cancer Res 155:1–14
35. Rashid A, Shen L, Morris JS, Issa JP, Hamilton SR (2001) CpG island methylation in colorectal adenomas. Am J Pathol 159:1129–1135
36. Reid BJ (1991) Barrett's esophagus and esophageal adenocarcinoma. Gastroenterol Clin North Am 20:817–834
37. Rutter JL, Goldstein AM, Dávila MR, Tucker MA, Struewing JP (2003) CDKN2A point mutations D153spl(c.457G>T) and IVS2+1G>T result in aberrant splice products affecting both p16INK4a and p14ARF. Oncogene 44:4444–4448
38. Sharma P, Weston AP, Topalovski M, Cherian R, Bhattacharyya A, Sampliner RE (2003) Magnification chromoendoscopy for the detection of intestinal metaplasia and dysplasia in Barrett's oesophagus. Gut 52:24–27
39. Sherr CJ (2001) The INK4a/ARF network in tumour suppression. Nat Rev Mol Cell Biol 2:731–737
40. Spechler SJ (1994) Barrett's esophagus. Semin Oncol 21:431–437
41. Spechler SJ (2002) Barrett's esophagus. N Engl J Med 346: 836–842
42. Tannapfel A, Benicke M, Katalinic A, Uhlmann D, Köckerling F, Hauss J, Wittekind C (2000) Frequency of p16INK4A alterations and k-ras mutations in intrahepatic cholangiocarcinoma of the liver. Gut 47:721–727
43. Tannapfel A, Busse C, Geißler F, Witzigmann H, Hauss J, Wittekind C (2002) INK4a-ARF alterations in liver cell adenoma. Gut 51:253–258
44. Tselepis C, Morris CD, Wakelin D, Hardy R, Perry I, Luong QT, Harper E, Harrison R, Attwood SE, Jankowski JA (2003) Upregulation of oncogene c-myc in Barrett's adenocarcinoma: induction of c-myc by acidified bile acid in vitro. Gut 52:174–180
45. Wheeler JM, Bodmer WF, Mortensen NJ (2000) DNA mismatch repair genes and colorectal cancer. Gut 47:148–153
46. Wong DJ, Paulson TG, Prevo LJ, Galipeau C, Longton G, Blount PL, Reid BJ (2001) $P16^{INK4a}$ lesions are common, early abnormalities that undergo clonal expansion in Barrett's metaplastic epithelium. Cancer Res 61:8284–8289

Virchows Arch (2004) 445:142–150
DOI 10.1007/s00428-004-1055-8

ORIGINAL ARTICLE

Umio Yamaguchi · Tadashi Hasegawa · Taizo Masuda · Shigeki Sekine · Akira Kawai · Hirokazu Chuman · Tadakazu Shimoda

Differential diagnosis of gastrointestinal stromal tumor and other spindle cell tumors in the gastrointestinal tract based on immunohistochemical analysis

Received: 6 April 2004 / Accepted: 19 May 2004 / Published online: 30 June 2004
© Springer-Verlag 2004

Abstract To confirm the usefulness of an immunohistochemical panel of antibodies for KIT (c-kit/CD117), CD34, desmin, smooth-muscle actin (SMA), h-caldesmon (HCD), S-100 protein, neuron-specific enolase (NSE), and beta-catenin, 297 mesenchymal and peripheral nerve-sheath tumors of the gastrointestinal tract and intra-abdominal locations including 211 gastrointestinal stromal tumors (GISTs), 12 leiomyomas, 18 leiomyosarcomas, 17 solitary fibrous tumors (SFTs), 14 schwannomas, and 25 desmoid-type fibromatoses (DTFs) were analyzed immunohistochemically. Consistent (100%) immunoreactivity for KIT, CD34, desmin and S-100, and nuclear accumulation of beta-catenin were detected in GISTs, SFTs, smooth-muscle tumors, schwannomas, and DTFs, respectively. Immunoreactivity for SMA, HCD, and NSE was observed in a wide range of these tumors. In addition, 418 bone and soft tissue tumors were enrolled in this study for KIT immunostaining. As a result, a limited number of these tumors were KIT positive, including synovial sarcoma that showed morphological similarity to GISTs. These findings suggest that KIT, CD34, desmin, S-100, and beta-catenin are key markers for clinical diagnosis of GISTs and other spindle cell tumors that may involve the gastrointestinal tract, whereas SMA, HCD, and NSE have only limited value.

U. Yamaguchi · T. Hasegawa · T. Masuda · S. Sekine · A. Kawai · H. Chuman · T. Shimoda
Divisions of Orthopaedic Oncology,
Pathology and Clinical Laboratory,
National Cancer Centre Hospital and Research Institute,
Tokyo, Japan

T. Hasegawa (✉)
Pathology Division,
National Cancer Centre Research Institute,
5-1-1 Tsukiji, Chuo-ku, 104-0045 Tokyo, Japan
e-mail: tdhasega@ncc.go.jp
Tel.: +81-3-35422511
Fax: +81-3-32482463

Keywords Gastrointestinal stromal tumor (GIST) · Spindle cell tumor · KIT · Beta-catenin · S-100 · Soft tissue sarcoma

Introduction

The primary mesenchymal and peripheral nerve sheath tumors arising in the gastrointestinal tract of adults form a large, diverse group that differ in their histological features and clinical behavior, but sometimes pose diagnostic problems. Gastrointestinal stromal tumors (GISTs) comprise the majority of this tumor group. GIST is an entity that was defined recently on the basis of its ultrastructural and immunohistochemical similarity to the interstitial cells of Cajal [22, 27, 46]. Immunohistochemically, most GISTs are KIT (c-kit proto-oncogene protein) positive, and c-kit tyrosine kinase is rendered constitutively active by mutations [17, 23, 25, 26, 31, 44, 47]. Application of c-kit tyrosine kinase inhibitor STI-571 (Glivec, imatinib) to the treatment of GISTs has proved to be promising for clinical management [21, 56]. Accordingly, it has become more important for pathologists to diagnose GISTs accurately.

Although numerous studies have evaluated various pathological and immunohistochemical parameters in an attempt to identify GISTs specifically [10, 11, 35, 36, 37, 40, 41, 43, 58, 59], there have been no systematic studies that attempt to distinguish GISTs from other spindle cell tumors arising in the gastrointestinal tract and intra-abdominal locations. The present study was conducted to confirm the usefulness of an immunohistochemical panel of antibodies for KIT, CD34, desmin, smooth-muscle actin (SMA), h-caldesmon (HCD), S-100 protein, neuron-specific enolase (NSE), and beta-catenin, which might be used to clinically diagnose GISTs and other spindle cell tumors that can arise in the gastrointestinal tract. In addition, as relatively little is known about expression of KIT in other mesenchymal tumors, we studied its ex-

pression pattern in a large number of bone and soft tissue tumors.

Materials and methods

Tumor selection

The medical records of 297 adult patients with mesenchymal and peripheral nerve-sheath tumors, mainly of the gastrointestinal tract, mesentery, retroperitoneum, and pelvis, were selected from the pathology files of the National Cancer Center, Tokyo (Table 1). Tumors used in this study included 211 GISTs (stomach 177, small intestine 22, rectum 8, esophagus 3, omentum 1), 12 leiomyomas (stomach 9, esophagus 3), 18 leiomyosarcomas (gastrointestinal 3, retroperitoneum and pelvis 15), 14 schwannomas (stomach 13, colon 1), 17 solitary fibrous tumors (SFTs) (all from the retroperitoneum and pelvis), and 25 desmoid-type fibromatoses (DTFs) (mesentery 3, other locations 22).

We also selected 418 cases of other bone and soft tissue sarcomas, mainly of the extremities and trunk, for KIT immunostaining, which included 11 fibrosarcomas, 11 leiomyosarcomas, 52 myxoid liposarcomas, 50 well-differentiated liposarcomas, 53 myxofibrosarcomas, 18 malignant peripheral nerve-sheath tumors (MPNSTs), 44 pleomorphic malignant fibrous histiocytomas, 42 synovial sarcomas, 20 Ewing sarcoma/primitive neuroectodermal tumors (ES/PNETs), 6 desmoplastic small round cell tumors, 11 neuroblastomas, 15 clear cell sarcomas, 30 angiosarcomas, 20 osteosarcomas, and 35 rhabdomyosarcomas (Table 2).

For light microscopic review, all specimens were fixed in 10% formalin and processed routinely for paraffin embedding. Sections 4-μm thick were stained with hematoxylin and eosin. A GIST in this study was defined as a mesenchymal spindle or epithelioid cell lesion arising in the wall of the gastrointestinal tract (Fig. 1A, B) that exhibited consistent immunoreactivity for KIT. As a result, 158 (75%) GISTs were shown to be the spindle cell type, 39 (18%) the mixed (combination of spindle and epithelioid cell) type, and 14 (7%) the epithelioid cell type. Smooth-muscle tumors were classified primarily on the basis of morphological appearance and strong immunoreactivity for SMA and desmin. Leiomyomas were paucicellular and composed of elongated spindle cells with abundant eosinophilic, fibrillary cytoplasm. Leiomyosarcoma were characterized by long fascicles of eosinophilic spindle cells with elongated nuclei with rounded ends (Fig. 2A). Focal pleomorphism was common. Schwannomas were characterized microscopically by the presence of peripheral lymphoid cuffs and short fascicles of spindle cells and bizarre cells (Fig. 3A) and strong immunoreac-

Table 1 Frequency of immunostaining for each antibody in gastrointestinal stromal tumors (GISTs) and other spindle cell tumors of gastrointestinal tract. Note: 70 cases of GIST (stomach 50, non-stomach 20) were studied for neuron-specific enolase (NSE) and beta-catenin immunostaining. *KIT* c-kit/CD117, *SMA* smooth-muscle actin, *HCD* h-caldesmon

Tumor type	KIT (%)	CD34 (%)	Desmin (%)	SMA (%)	HCD (%)	S-100 (%)	NSE (%)	Beta-catenin (%)
GIST (*n*=211)	211 (100)	192 (91)	8 (4)	65 (31)	167 (79)	16 (8)	57 (81)	0*
Stomach (*n*=177)	177 (100)	173 (98)	8 (5)	42 (24)	147 (83)	6 (3)	40 (80)	0*
Non-stomach (*n*=34)	34 (100)	19 (56)	0	23 (68)	20 (59)	10 (29)	17 (85)	0*
Smooth-muscle tumor								
Leiomyoma (*n*=12)	0	0	12 (100)	12 (100)	12 (100)	0	0	0
Leiomyosarcoma (*n*=18)	0	0	18 (100)	18 (100)	18 (100)	0	0	0
Peripheral nerve-sheath tumor								
Schwannoma (*n*=14)	0	7 (50)	0	0	0	14 (100)	3 (21)	0*
Fibrous tumor								
Solitary fibrous tumor (*n*=17)	0	17 (100)	0	0	0	4 (24)	3 (18)	4 (24)**
Desmoid-type fibromatosis (*n*=25)	0*	0	5 (20)	21 (84)	0	0	25 (64)	10 (100)**

* Some of cases showed weak (1+) cytoplasmic staining (see text)
** Nuclear accumulation

Table 2 KIT (c-kit/CD117) immunoreactivity in other 418 bone and soft-tissue sarcomas. *MPNST* malignant peripheral nerve sheeth tumor, *PMFH* pleomorphic malignant fibrous histiocytoma, *ES/PNET* Ewing sarcoma/primitive neuroectodermal tumor, *DSRCT* desmoplastic small round cell tumor

Tumor type	Number	KIT/c-kit protein				Negative	Positive
		0	1+	2+	3+	(0/1+)	(2+/3+)
Fibrosarcoma	11	11	0	0	0	11 (100%)	0
Leiomyosarcoma	11	8	3	0	0	11 (100%)	0
Myxoid lipsarcoma	52	52	0	0	0	52 (100%)	0
Well-differentiated liposarcoma	50	50	0	0	0	50 (100%)	0
Myxofibrosarcoma	53	52	1	0	0	53 (100%)	0
MPNST	18	17	1	0	0	18 (100%)	0
PMFH	44	44	0	0	0	44 (100%)	0
Synovial sarcoma	42	40	0	2	0	40 (95%)	2 (5%)
ES/PNET	20	8	7	4	1	15 (75%)	5 (25%)
DSRCT	6	6	0	0	0	6 (100%)	0
Neuroblastoma	11	10	0	0	1	10 (91%)	1 (9%)
Clear cell sarcoma	15	14	0	0	1	14 (93%)	1 (7%)
Angiosarcoma	30	26	0	4	0	26 (87%)	4 (13%)
Osteosarcoma	20	20	0	0	0	20 (100%)	0
Rhabdomyosarcoma	35	35	0	0	0	35 (100%)	0
Total	418	-	-	-	-	405 (97%)	13 (3%)

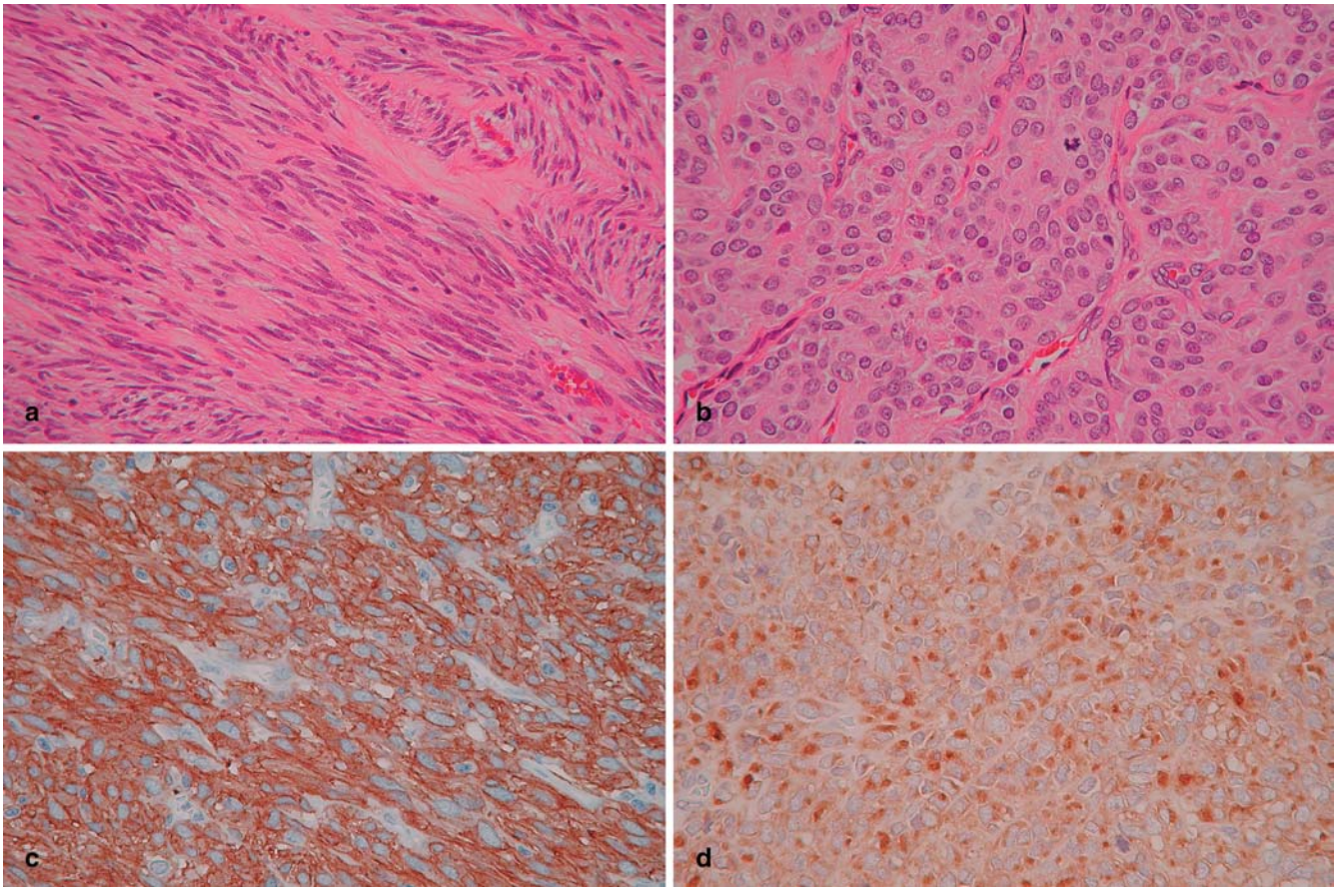


Fig. 1 Gastrointestinal stromal tumors. A gastric stromal tumor of spindle cell type is composed of uniform eosinophilic cells arranged in short fascicles (**A**). A small intestinal stromal tumor of epithelioid type shows a nested paraganglioma-like appearance (**B**). Diffuse and strong membrane and cytoplasmic staining for KIT (c-kit/CD117) in a majority of tumor cells (**C**). Dot-like immunoreactivity for KIT in the tumor cytoplasm (**D**)

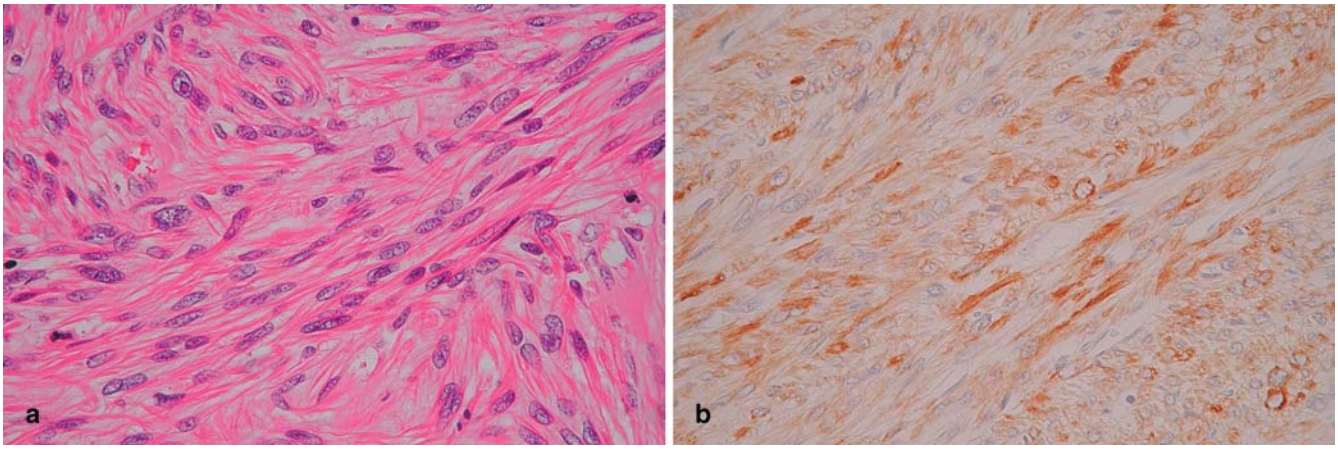


Fig. 2 Smooth-muscle tumors. A rectal leiomyosarcoma consists of long fascicles of eosinophilic spindle cells (**A**). Focal and strong positivity for desmin in tumor cells (**B**)

tivity for S-100. SFTs were microscopically defined as neoplasms showing "patternless" growth, with a haphazard arrangement of bland-looking short spindle or polygonal cells, alternating hypercellular and hypocellular sclerotic foci, keloid-like stromal hyalinization, and a prominent branching vasculature (Fig. 4A). Immunohistochemically, SFTs were always CD34 positive. DTFs were infiltrative and locally aggressive, characterized by a loose fascicular arrangement of spindle cells in a predominantly collagenous background (Fig. 4C).

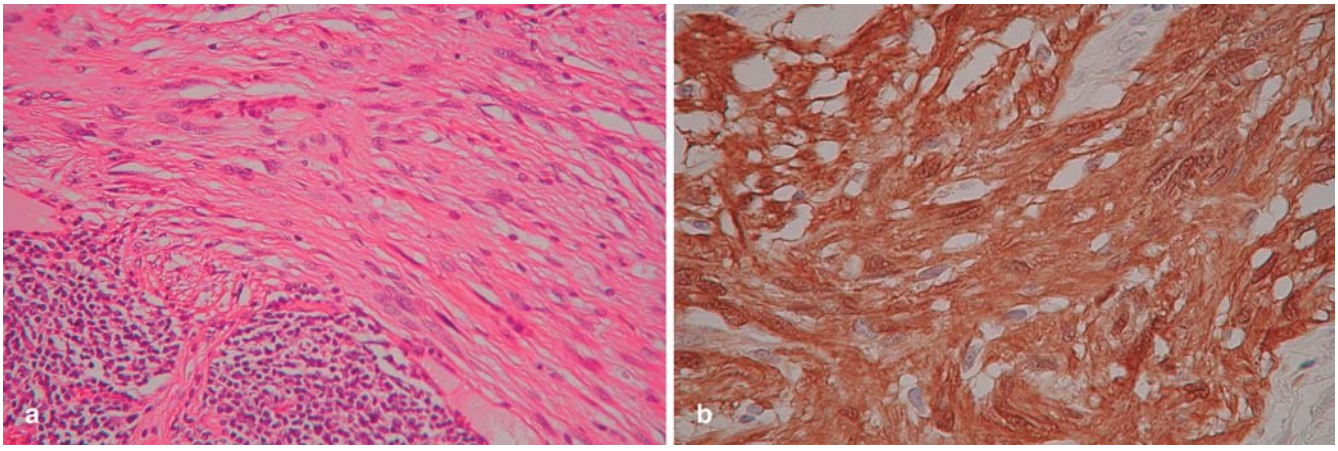


Fig. 3 Peripheral nerve-sheath tumors. A gastric schwannoma is composed of short fascicles of spindle cells and bizarre cells with peripheral lymphoid cuffs (**A**). Many tumor cells show diffuse and strong staining for S-100 (**B**)

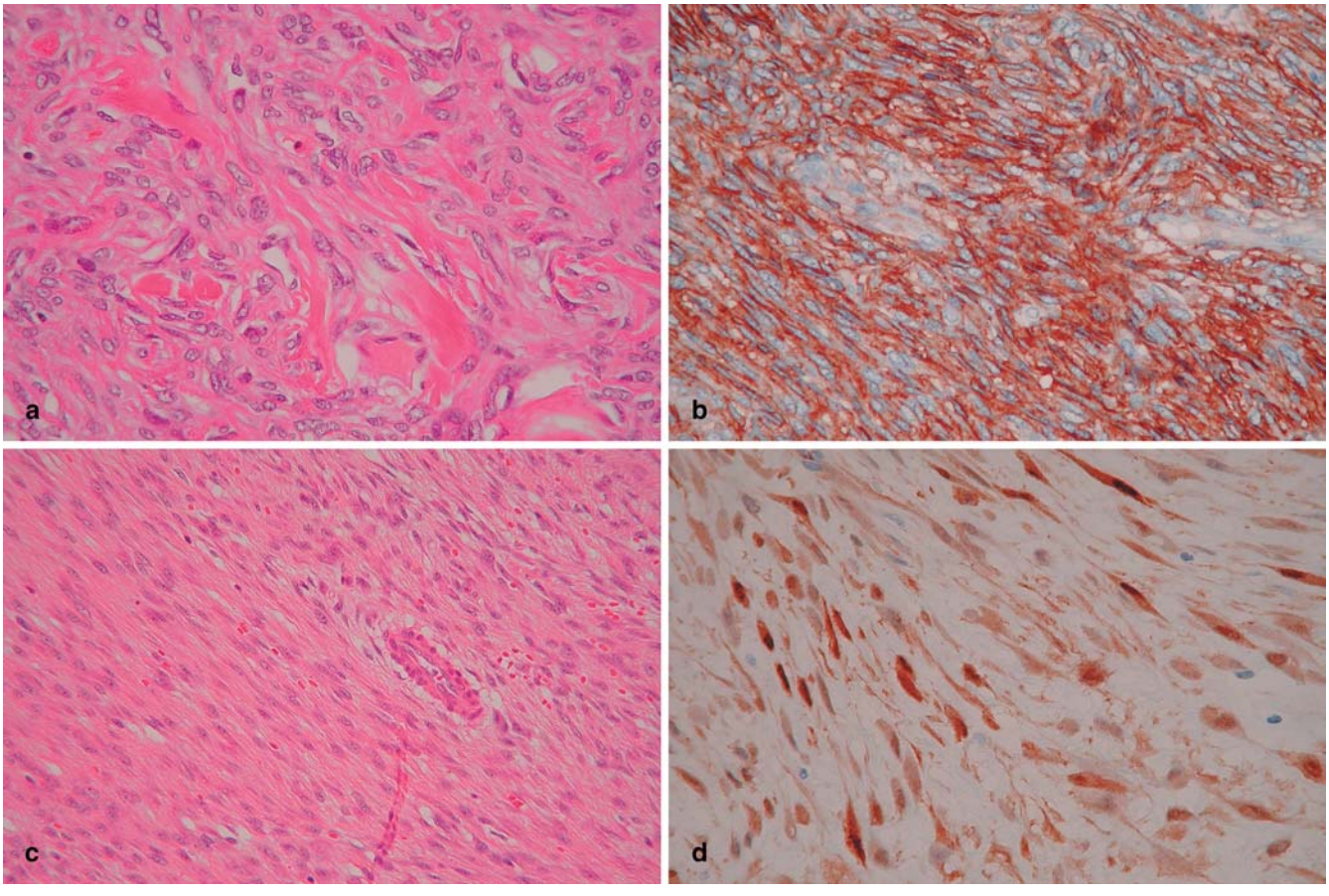


Fig. 4 Fibrous tumors. A pelvic solitary fibrous tumor shows a haphazard arrangement of spindle cells with hyalinized bands of collagen (**A**). Many tumor cells show strong immunoreactivity for CD34 (**B**). A mesenteric desmoid-type fibromatosis involving gastric wall shows a loose fascicular arrangement of spindle cells around vessels (**C**). Strong nuclear accumulation of beta-catenin in many spindle cells (**D**)

Immunohistochemical analysis

Immunohistochemical analysis was performed on tissue sections from paraffin blocks by the labeled streptavidin-biotin method. The sections were dewaxed, rehydrated, and moistened with phosphate-buffered saline (PBS; pH 7.4). They were then pretreated in an autoclave at 121°C for 10 min in 10 mmol/l citrate buffer (pH 6.0), before being incubated with antibodies against the following antigens on an automated immunostaining system (i6000; BioGenex, San Ramon, CA) for 30 min: KIT (polyclonal antibody, 1/50 dilution; DakoCytomation, Glostrup, Denmark), CD34 (clone My 10, 1/100 dilution; Becton Dickinson, San Jose, CA), desmin (clone

D33, 1/200 dilution; DakoCytomation), alpha-SMA (clone 1A4, 1/100 dilution; DakoCytomation), HCD (clone h-CD, 1/100 dilution; DakoCytomation), S-100 protein (polyclonal, 1/2000 dilution; DakoCytomation), NSE (clone BBS/NC/VI-H14, 1/200 dilution; DakoCytomation), and beta-catenin (clone 14, 1/500 dilution; Transduction Laboratories, Lexington, KY). Heat-induced epitope retrieval was not used for sections stained with antibodies against NSE and S-100 protein.

Immunohistochemical results were judged by all investigators using a multiheaded microscope. A consensus judgment was adopted as the proper immunohistochemical score of the tumor based on strength: 0, negative; 1+, weak staining; 2+, moderate staining; 3+, strong staining. Tissue mast cells, which stain 2+ or 3+, were used as internal positive controls for KIT. The distribution of positive cells was also recorded in an effort to impart the diffuse or focal nature of the positive cells: sporadic (positive cells <10%); focal (10% ≥positive cells<50%); diffuse (positive cells ≥50%). The immunohistochemical scores of 2+ and 3+ with focal to diffuse distribution were considered to be positive for all markers.

Results

The immunohistochemical results are summarized in Table 1 and Table 2.

Gastrointestinal stromal tumor

All 211 GISTs were positive for KIT, and the reactivity was typically diffuse and strong in the cytoplasm and membrane of most tumor cells (Fig. 1C). The pattern of KIT immunostaining was cytoplasmic reactivity in 113 (54%) and cytoplasmic dot-like reactivity in 98 (46%) tumors (Fig. 1D). In 16 (mixed type 9, epithelioid cell type 7) tumors, KIT immunoreactivity for epithelioid cells was weaker than in spindle cells in the same tissue sections or other tumors. CD34 positivity was observed in almost all of the tumors (98%) of the stomach and in more than half of non-gastric tumors (56%). Immunoreactivity for desmin and S-100 was usually focal (4% for desmin and 8% for S-100). Positivity for SMA and HCD was variably expressed, 65 (31%) and 167 (79%) of 211 GISTs being positive, respectively. The frequency of positive desmin tended to be higher in epithelioid cell (21%, 3/14) than that in spindle cell (2.5%, 4/158) and mixed-type GIST (2.6%, 1/39). In this study, 70 GISTs were available for immunohistochemical evaluation of NSE and beta-catenin, and 57 of 70 (81%) GISTs were found to show moderate to strong NSE immunoreactivity, whereas 59 of 70 (84%) were positive for beta-catenin, the staining showing a cytoplasmic pattern.

Smooth-muscle tumor

Immunostaining for desmin, SMA, and HCD was positive in all leiomyomas and leiomyosarcomas (Fig. 2A, B). The staining was diffuse and strong in leiomyomas but tended to be less intense and heterogeneous in leiomyosarcomas. KIT, CD34, S-100, NSE, and beta-catenin were negative in all tumors.

Peripheral nerve-sheath tumor

All schwannomas showed strong nuclear and cytoplasmic staining for S-100 (Fig. 3A, B). Of 14 schwannomas, 13 (93%) showed staining for beta-catenin, but it was weak and cytoplasmic. Of cases, 7 (50%) and 3 (21%) were focally CD34 and NSE positive, respectively. Staining for KIT, desmin, SMA, and HCD was negative.

Fibrous tumor

All SFTs stained positively for CD34 but not for KIT; the staining for CD34 was generally strong and diffuse in the cytoplasm of spindle cells (Fig. 4A, B). None of the 25 DTFs were CD34 positive; 15 (60%) DTFs showed weak (1+) coarsely granular cytoplasmic immunostaining for KIT (Fig. 5A), which was eliminated without heat-induced antigen retrieval. In all cases of DTF, immunore-

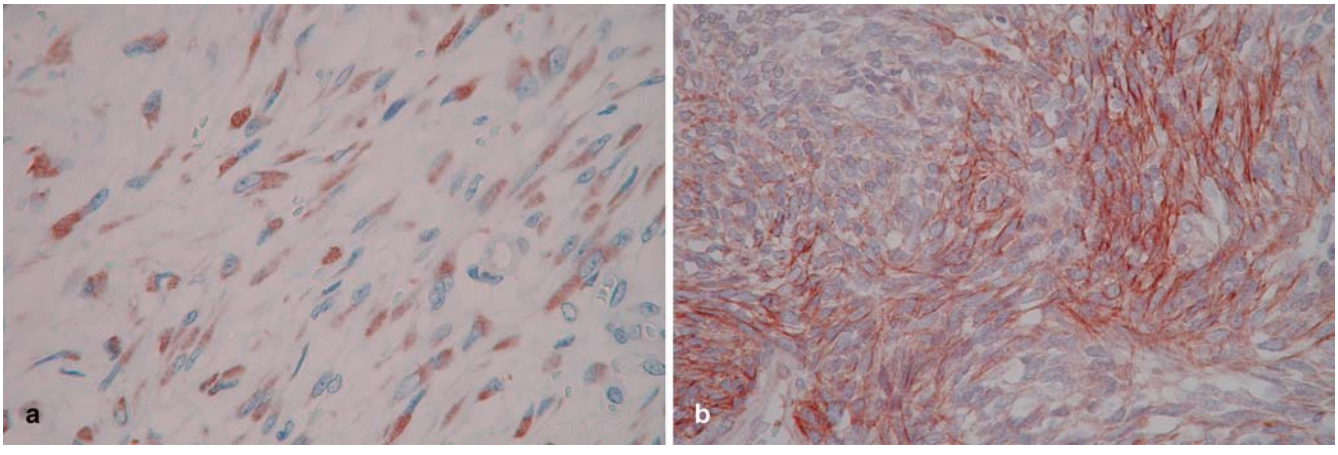


Fig. 5 A desmoid-type fibromatosis shows weak (1+) coarsely granular cytoplasmic immunostaining for KIT(c-kit/CD117) (**A**). A monophasic synovial sarcoma shows focal and moderate (2+) membranous immunoreactivity for KIT (**B**)

activity for beta-catenin was recognized in the nuclei, and the staining was uniformly distributed throughout the sections despite variable proportions of positive cells (Fig. 4C, D). As for SFT, 4 cases (24%) were noted to show nuclear accumulation of beta-catenin. Of DTF cases, 21 (84%) showed moderate to strong positivity for SMA, but all SFTs were negative. In addition, scattered desmin immunoreactivity was detected in 5 (20%) DTFs. S-100 positivity was detected in 4 SFTs (24%) but not in any of the DTFs. Immunostaining for NSE was varied. Three SFTs (18%) were NSE positive, whereas the staining tended to be more frequent in DTFs, 64% (16 cases) being moderately to strongly positive. Staining for HCD was negative in both types of tumor.

KIT immunoreactivity in other bone and soft tissue sarcomas

Staining of KIT in other bone and soft tissue sarcomas was limited (Table 2). Moderate (2+) to strong (3+) staining of KIT was observed in 2 synovial sarcomas (Fig. 5B), 5 ES/PNETs, 1 neuroblastoma, 1 clear cell sarcoma, and 4 angiosarcomas, while weak (1+) staining was identified in 3 leiomyosarcomas, 1 myxofibrosarcoma, 1 MPNST, and 7 ES/PNETs.

Discussion

GISTs have a wide spectrum of clinicopathological features, ranging from benign to evidently malignant. Most of them are predominantly spindle cell, whereas others are epithelioid and, rarely, pleomorphic cell tumors. In the earlier literature, GISTs were described as unusual tumors of smooth-muscle origin [33], designated as leiomyoblastomas [53], leiomyomas, cellular leiomyomas, and leiomyosarcomas [3]. During that time, the term stromal tumor was first used to describe tumor lacking smooth-muscle differentiation immunohistochemically and ultrastructurally [34].

Recent molecular pathology studies have revealed that most GISTs are immunoreactive for KIT and CD34 [13, 17, 20, 32, 35, 38, 49, 55]. The 211 GISTs selected for the present study were all KIT positive. We carefully evaluated the variability in the subcellular localization of KIT staining and found that over half of the GISTs had cytoplasmic immunostaining, whereas the others showed a combination of both cytoplasmic and dot-like immunostaining. No example of a pure dot-like staining pattern was observed among our materials. In 16 tumors (8%), however, immunoreactivity in epithelioid cells was weaker than that in spindle cells in the same tissue sections or other tumors. The significance of this heterogeneity of KIT staining in GISTs remains to be investigated, but it is necessary to be aware of these patterns when carrying out immunostaining in suspected cases of GIST. There is a possibility that these varied staining patterns are associated with different KIT mutations [8].

It is known that a small number of GISTs are KIT negative. Over the past year, mutations of platelet-derived growth factor alpha (PDGFRA) gene encoding the PDGFRA have been reported in some of these tumors, suggesting that instead of KIT, PDGFRA appears to play an important role in development of GISTs without KIT mutations [14, 18]. We analyzed PDGFRA gene mutation using polymerase chain reaction (PCR) techniques in 27 cases of KIT-weak or -negative GIST, including the above 16 tumors. As a result, the PDGFRA gene mutation was observed in 17 of 27 cases (63%) (unpublished data).

Although the results of KIT immunostaining in other bone and soft tissue sarcomas are at times conflicting [4, 19, 48, 52], at least a small number of these tumors are KIT positive from weak, focal staining to occasionally strong staining. These findings suggest the possibility that KIT immunostaining would lead to diagnostic confusion because KIT positivity was detected in other morphological similar tumors, including intra-abdominal desmoid fibromatoses [30, 59] and other mesenchymal tumors, such as leiomyosarcoma, fibrosarcoma, and synovial sarcoma [48, 52]. In our 25 cases of DTF, KIT staining was frequent (60%) using heat-induced antigen retrieval, but it was eliminated without the antigen retrieval. Further PCR analysis revealed that neither mutations of c-kit exon 11 nor PDGRA exon 12 or 18 were detected in these tumor samples (data not shown). False positives for KIT in other non-GIST tumors may occur due to the inappropriate staining technique used. Moreover, KIT-positive non-GIST tumors, in the absence of any accompanying mutation such as KIT and PDGFRA gene mutation, have no therapeutic significance with Glivec.

The present study revealed variable immunoreactivity for desmin, SMA, HCD, and S-100 in the GISTs we examined. As discussed in a previous study [13], a large percentage of GISTs are HCD positive, and SMA positivity was present in approximately 30% of the present cases, indicating possible traits of smooth-muscle differentiation in these tumors. Although staining for desmin was very rare in GISTs, the frequency of positive desmin tended to be higher in epithelioid cell (21%) than that in spindle cell (2.5%) and mixed-type GIST (2.6%). There was no significant difference observed among these three types of GIST in immunostaining pattern for the remaining markers (data not shown).

Information on NSE reactivity in GISTs is limited [7]. We found that over 80% of GISTs were NSE positive and that approximately 30% of non-gastric tumors were S-100 positive, suggesting the possibility of neural differentiation. Gastrointestinal autonomic nerve tumors (GANTs) are described as distinctive entities that differ from other mesenchymal tumors of the gastrointestinal tract [2, 57], and most have been reported as immunoreactive for vimentin, NSE, and occasionally S-100 [7]. However, recent studies have suggested that GANTs are not a separate entity because they share a molecular genetic identity with conventional spindle and epithelioid cell forms of GIST [28].

Leiomyomas and leiomyosarcomas are the main tumors of the gastrointestinal tract that are often confused with GISTs. Their well-differentiated smooth-muscle cells are negative for KIT and CD34 and positive for SMA and, usually, for desmin [25, 36, 37, 38, 39, 41, 58]. Our findings are similar to those of previous studies and confirm that all leiomyomas and leiomyosarcomas were immunoreactive for desmin, SMA, and HCD.

Schwannomas rarely occur in the gastrointestinal tract and are characterized microscopically by the presence of peripheral lymphoid cuffs and short fascicles of spindle cells and bizarre cells. Unlike conventional soft tissue schwannomas, they usually have regular whorls or a storiform pattern and lack distinct palisading [6]. Positive CD34 immunostaining was detected not only in tumors located in the stomach, as in our findings, but also detected in tumors that occurred in other locations [16]. Positivity for S-100 and negativity for smooth-muscle markers and KIT can separate schwannomas from GISTs.

SFTs may occur in the gastrointestinal tract, mesentery, or retroperitoneum and become a diagnostic problem because they mimic GISTs to some extent histologically. Microscopically, SFTs have been described as showing "patternless" growth, with a haphazard arrangement of bland-looking short spindle or polygonal cells, alternating hypercellular and hypocellular sclerotic foci, keloid-like stromal hyalinization, and a prominent branching vasculature. Immunohistochemically, all of the SFTs were CD34 positive and KIT negative, in agreement with previous studies [38, 49, 50], and none of the SFTs showed immunostaining for smooth-muscle markers (desmin, SMA, HCD). These findings suggest that the combination of immunostaining for KIT, CD34, and smooth-muscle markers might be helpful for differentiating GISTs from SFTs.

Beta-catenin is an important multifunctional protein involved in the Wingless/Wnt signal transduction pathway and also acts as a cell–cell adhesion regulator when binding to E-cadherin adhesion molecules [5, 15]. Constitutional activation of the Wingless/Wnt signaling pathway by stabilization and accumulation of beta-catenin in the nucleus and cytoplasm, caused mainly by inactivating mutations in the adenomatous polyposis coli (APC) gene, has been revealed to be important in the development of human colon cancers and other carcinomas [45] and also in deep fibromatosis [1, 54] and some sarcomas [12, 24]. Reports on the expression of beta-catenin in GISTs, however, are very limited. Previous authors reported that no nuclear accumulation was detected in GISTs [43]. Our present study showed that none of 70 GISTs had nuclear immunostaining, although more than 80% of them had weak cytoplasmic immunostaining. A large percentage of schwannomas also showed weak cytoplasmic immunoreactivity for beta-catenin, the extent and pattern of the staining being quite similar as those in GISTs.

Intra-abdominal DTFs are uncommon tumors that primarily affect the mesentery or retroperitoneum and often invade the wall of the gastrointestinal tract. They are infiltrative and locally aggressive, characterized by florid fibroblastic proliferation. It is well known that DTFs typically have APC gene and beta-catenin gene mutations [9, 42, 51, 54] and that APC-truncating mutations confer a proliferative advantage on aggressive fibromatosis cells through beta-catenin [29]. In our series, nuclear accumulation was detected in all DTFs, suggesting the usefulness of beta-catenin for distinguishing this tumor from GISTs, as reported previously [43]. However, careful evaluation should be done, because there is an overlap in the nuclear accumulation of beta-catenin in DTFs and SFTs. In this situation, additional CD34 immunostaining might be helpful for separating SFTs from DTFs.

Metastatic melanoma and primary clear cell sarcoma may occur in the walls of the intestines or stomach and should be separated from GIST due to the histological resemblance. Positivity for melanocytic markers (tyrosinase, melan-A, and HMB-45) with the combinations of other markers such as KIT, CD34, and S-100, or using molecular cytogenetic methods to detect the chromosomal translocation t(12;22)(q13;q12) or the EWS-ATF1 fusion transcript are diagnostic [60].

The extent and patterns of KIT immunostaining in GISTs are varied, and KIT immunostaining, although in a limited number, is also detected in other mesenchymal tumors that may involve the gastrointestinal tract and abdominal cavity. Thus, it is inevitable for the diagnosis of GISTs to use an immunohistochemical panel along with appropriate morphological evaluation. In this context, the findings that consistent (100%) immunoreactivity for KIT, CD34, desmin, and S-100 and nuclear accumulation of beta-catenin in GISTs, SFTs, smooth-muscle tumors, schwannomas, and DTF each suggest that these are key markers for clinical diagnosis of GISTs and other spindle cell tumors that can arise in the gastrointestinal tract; whereas, SMA, HCD, and NSE are of only limited value, because immunoreactivity for these tumors was observed in a wide range of these tumors.

References

1. Alman BA, Li C, Pajerski ME, Diaz-Cano S, Wolfe HJ (1997) Increased beta-catenin protein and somatic APC mutations in sporadic aggressive fibromatoses (desmoid tumor). Am J Pathol 151:329–334
2. Antonioli DA (1989) Gastrointestinal autonomic nerve tumors. Expanding the spectrum of gastrointestinal tumors. Arch Pathol Lab Med 113:831–833
3. Appelman HD (1990) Mesenchymal tumors of the gut: histological perspectives, new approaches, new results, and does it make any difference. Monogr Pathol 31:220–246
4. Barisella M, Andreola S, Rosai J (2002) CD117 in soft tissue sarcomas. Am J Clin Pathol 118:470–471
5. Brabletz T, Herrmann K, Jung A, Faller G, Kirchner T (2000) Expression of nuclear beta-catenin and c-myc is correlated with tumor size but not with proliferative activity of colorectal adenomas. Am J Pathol 156:865–870
6. Daimaru Y, Kido H, Hashimoto H, Enjoji M (1988) Benign schwannoma of the gastrointestinal tract: a clinicopathologic and immunohistochemical study. Hum Pathol 19:257–264

7. Dhimes P, Lopez-Carreira M, Ortega-Serrano MP, Garcia-Munoz H, Martinez-Gonzalez MA, Ballestin C (1995) Gastrointestinal autonomic nerve tumors and their separation from other gastrointestinal stromal tumors: an ultrastructural and immunohistochemical study of seven cases. Virchows Arch 426:27–35
8. Fletcher CDM, Berman JJ, Corless C, Gorstein F, Lasota J, Longley BJ, Miettinen M, O'Leary TJ, Remotti H, Rubin BP, Shmookler B, Sobin LH, Weiss SW (2002) Diagnosis of gastrointestinal stromal tumors: a consensus approach. Hum Pathol 33:459–465
9. Giarola M, Wells D, Mondini P, Pilotti S, Sala P, Azzarelli A, Bertario L, Pierotti MA, Delhanty JD, Radice P (1998) Mutations of adenomatous polyposis coli (APC) gene are uncommon in sporadic desmoid tumors. Br J Cancer 78:582–587
10. Graadt van Roggen JF, van Velthuysen MLF, Hogendoorn PCW (2001) The histopathological differential diagnosis of gastrointestinal stromal tumors. J Clin Pathol 54:96–103
11. Greenson JK (2003) Gastrointestinal stromal tumors and other mesenchymal lesions of the gut. Mod Pathol 16:366–375
12. Hasegawa T, Yokoyama R, Matsuno Y, Shimoda T, Hirohashi S (2001) Prognostic significance of histologic grade and nuclear expression of beta-catenin in synovial sarcoma. Hum Pathol 32:257–263
13. Hasegawa T, Matsuno Y, Shimoda T, Hirohashi S (2002) Gastrointestinal stromal tumor: consistent CD117 immunostaining for diagnosis, and prognostic classification based on tumor size and MIB-1 grade. Hum Pathol 33:669–676
14. Heinrich MC, Corless CL, Duensing A, McGreevey L, Chen CJ, Joseph N, Singer S, Griffith DJ, Haley A, Town A, Demetri GD, Fletcher CD, Fletcher JA (2003) PDGFRA activating mutations in gastrointestinal stromal tumors. Science 299:708–710
15. Hirohashi S (1998) Inactivation of the E-cadherin-mediated cell adhesion system in human cancers. Am J Pathol 153:333–339
16. Hirose T, Tani T, Shimada T, Ishizawa K, Shimada S, Sano T (2003) Immunohistochemical demonstration of EMA/Glut1-positive perineurial cells and CD34-positive fibroblastic cells in peripheral nerve sheath tumors. Mod Pathol 16:293–298
17. Hirota S, Isozaki k, Moriyama Y, Hashimoto K, Nishida T, Ishiguro S, Kawano K, Hanada M, Kurata A, Takeda M, Muhammad Tunio G, Matsuzawa Y, Kanakura Y, Shinomura Y, Kitamura Y (1998) Gain-of-function mutations of c-kit in human gastrointestinal stromal tumors. Science 279:577–580
18. Hirota S, Ohashi A, Nishida T, Isozaki K, Kinoshita K, Shinomura Y, Kitamura Y (2003) Gain-of-function mutations of platelet-derived growth factor receptor alpha gene in gastrointestinal stromal tumors. Gastroenterology 125:660–667
19. Hornick JL, Fletcher CDM (2002) Immunohistochemical staining for KIT (CD117) in soft tissue sarcomas is very limited in distribution. Am J Clin Pathol 117:188–193
20. Hurlimann J, Gardiol D (1991) Gastrointestinal stromal tumors. An immunohistochemical study of 165 cases. Histopathology 19:311–320
21. Joensuu H, Roberts PJ, Sarlomo-Rikara M, Andersson LC, Tervahartiala P, Tuveson D, Silberman SL, Capdeville R, Dimitrijevic S, Druker B, Demetri GD (2001) Effect of tyrosine kinase inhibitor STI-571 in a patient with a metastatic gastrointestinal stromal tumor. N Engl J Med 344:1052–1056
22. Kindblom L, Remotti HE, Aldenborg F, Meis-Kindblom JM (1998) Gastrointestinal pacemaker cell tumor (GIPACT): gastrointestinal stromal tumors show phenotypic characteristics of the interstitial cells of Cajal. Am J Pathol 152:1259–1269
23. Kitamura Y, Hirota S, Nishita T (1998) Molecular pathology of c-kit proto-oncogene and development of gastrointestinal stromal tumors. Ann Chir Gynaecol 87:282–286
24. Kuhnen C, Herter P, Muller O, Muehlberger T, Krause L, Homann H, Steinau HU, Muller KM (2000) Beta-catenin in soft tissue sarcomas: expression is related to proliferative activity in high-grade sarcomas. Mod Pathol 13:1005–1013
25. Lasota J, Jasinski M, Sarlomo-Rikara M, Miettinen M (1999) C-kit mutations occur preferentially in malignant versus benign GISTs and do not occur in leiomyomas and leiomyosarcomas. Am J Pathol 154:53–60
26. Lasota J, Wozniak A, Sarlomo-Rikara M, Rys J, Kordek R, Nassar A, Sobin LH, Miettinen M (2000) Mutations in exons 9 and 13 of KIT gene are rare events in gastrointestinal stromal tumors: a study of two hundred cases. Am J Pathol 157:1091–1095
27. Lauwers GY, Erlandson RA, Casper ES, Brennan MF, Woodruff JM (1993) Gastrointestinal autonomic nerve tumors. A clinicopathological, immunohistochemical, and ultrastructural study of 12 cases. Am J Surg Pathol 17:887–897
28. Lee JR, Joshi V, Griffin JW Jr, Lasota J, Miettinen M (2001) Gastrointestinal autonomic tumors: immunohistochemical and molecular identity with gastrointestinal stromal tumor. Am J Surg Pathol 25:979–987
29. Li C, Bapat B, Alman BA (1998) Adenomatous polyposis coli gene mutation alters proliferation through its beta-catenin-regulatory function in aggressive fibromatosis (desmoid tumor). Am J Pathol 153:709–714
30. Lucas DR, Al-Abbadi M, Tabaczka P, Hamre MR, Weaver DW, Mott MJ (2003) c-Kit expression in desmoid fibromatosis. Am J Clin Pathol 119:339–345
31. Lux M, Rubin BP, Biase TL, Chen CJ, Maclure T, Demetri G, Xiao S, Singer S, Fletcher CD, Fletcher JA (2000) KIT extracellular and kinase domain mutations in gastrointestinal stromal tumors. Am J Pathol 156:791–795
32. Ma CK, Amin MB, Kintanar E, Linden MD, Zarbo RJ (1993) Immunohistologic characterization of gastrointestinal stromal tumors: a study of 82 cases compared with 11 cases of leiomyomas. Mod Pathol 6:139–144
33. Martin JF, Bazin P, Feroldi J (1960) Tumeurs myoides intramurales de lestomac; consideration microscopiques a propos de 6 cas. Ann Anat Pathol 5:484–497
34. Mazur MT, Clark HB (1983) Gastric stromal tumors: reappraisal of histogenesis. Am J Surg Pathol 7:507–519
35. Miettinen M, Lasota J (2001) Gastrointestinal stromal tumors: definition, clinical, histological, immunohistochemical, and molecular genetic features and differential diagnosis. Virchows Arch 438:1–12
36. Miettinen M, Virolainen M, Sarlomo-Rikara M (1995) Gastrointestinal stromal tumors: value of CD34 antigen in their identification and separation from true leiomyomas and schwannomas. Am J Surg Pathol 19:207–216
37. Miettinen M, Sarlomo-Rikara M, Sobin LH, Lasota J (2000) Gastrointestinal stromal tumors and leiomyosarcomas in the colon: a clinicopathologic, immunohistochemical, and molecular genetic study of 44 cases. Am J Surg Pathol 24:1339–1352
38. Miettinen M, Sobin LH, Sarlomo-Rikara M (2000) Immunohistochemical spectrum of GISTs at different sites and their differential diagnosis with a reference to CD117 (KIT). Mod Pathol 13:1134–1142
39. Miettinen M, Furlong M, Sarlomo-Rikala M, Burke A, Sobin LH, Lasota J (2001) Gastrointestinal tumors, intramural leiomyomas, and leiomyosarcomas in the rectum and anus: a clinicopathologic, immunohistochemical, and molecular genetic study of 144 cases. Am J Surg Pathol 25:1121–1133
40. Miettinen M, Majidi M, Lasota J (2002) Pathology and diagnostic criteria of gastrointestinal stromal tumors (GISTs): a review. Eur J Cancer 38[Suppl]:S39–S51
41. Miettinen M, Kopczynski J, Makhiouf HR, Sarlomo-Rkala M, Gyorffy H, Burke A, Sobin LH, Lasota J (2003) Gastrointestinal stromal tumors, intramural leiomyomas, and leiomyosarcomas in the duodenum: a clinicopathologic, immunohistochemical, and molecular genetic study of 167 cases. Am J Surg Pathol 27:625–641
42. Miyoshi K, Iwao K, Nawa G, Yoshikawa H, Ochi T, Nakamura Y (1998) Frequent mutation in the beta-catenin gene in desmoid tumors from patients without familial adenomatous polyposis. Oncol Res 10:591–594
43. Montgomery E, Torbenson MS, Kaushal M, Fisher C, Abraham SC (2002) Beta-catenin immunohistochemistry separates me-

senteric fibromatosis from gastrointestinal stromal tumor and sclerosing mesenteritis. Am J Surg Pathol 26:1296–1301
44. Moskaluk CR, Tian Q, Marshall CR, Rumpel CA, Franquemont DW, Frierson HF Jr (1999) Mutation of c-kit JM domain are found in a minority of human gastrointestinal stromal tumors. Oncogene 18:1897–1902
45. Polakis P (1999) The oncogenetic activation of beta-catenin. Curr Opin Genet Dev 9:15–21
46. Rubin BP, Fletcher JA, Fletcher CD (2000) Molecular insights into the histogenesis and pathogenesis of gastrointestinal tumors. Int J Surg Pathol 8:5–10
47. Rubin BP, Singer S, Tsao C, Duensing A, Lux ML, Ruiz R, Hibbard MK, Chen CJ, Xiao S, Tuveson DA, Demetri GD, Fletcher CD, Fletcher JA (2001) KIT activation is a ubiquitous feature of gastrointestinal stromal tumors. Cancer Res 61:8118–8121
48. Sabah M, Leader M, Kay E (2003) The problem with KIT: clinical implications and practical difficulties with CD117 immunostaining. Appl Immunohistochem Mol Morphol 11:56–61
49. Sarlomo-Rikala M, Kovatich AJ, Barusevicius A, Miettinen M (1998) CD117: a sensitive marker for gastrointestinal stromal tumors that is more specific than CD34. Mod Pathol 11:728–734
50. Shidham VB, Chivukula M, Gupta D, Rao RN, Komorowski R (2002) Immunohistochemical comparison of gastrointestinal stromal tumor and solitary fibrous tumor. Arch Pathol Lab Med 126:1189–1192
51. Shitoh K, Konishi F, Iijima T, Ohdaira T, Sakai K, Kanazawa K, Miyaki M (1999) A novel case of a sporadic desmoid tumor with mutation of the beta-catenin gene. J Clin Pathol 52:695–696
52. Smithey BE, Pappo AS, Hill DA (2002) c-kit expression in pediatric solid tumor: a comparative immunohistochemical study. Am J Surg Pathol 26:486–492
53. Stout AP (1962) Bizarre smooth muscle tumors of the stomach. Cancer 15:400–409
54. Tejpar S, Nollet F, Li C, Wunder JS, Michils G, dal Cin P, Van Cutsem E, Bapat B, van Roy F, Cassiman JJ, Alman BA (1999) Predominance of beta-catenin mutations and beta-catenin dysregulation in sporadic aggressive fibromatosis (desmoid tumor). Oncogene 18:6615–6620
55. Ueyama T, Guo KJ, Hashimoto H, Daimaru Y, Enjoji M (1992) A clinicopathologic and immunohistochemical study of gastrointestinal stromal tumors. Cancer 69:947–955
56. van Oosterom AT, Judson I, Verweij J, Stroobants S, Donato di Paola E, Dimitrijevic S, Martens M, Webb A, Sciot R, Van Glabbeke M, Silverman S, Nielsen OS (2001) Safety and efficacy of imatinib (STI-571) in metastatic gastrointestinal stromal tumors: a phase I study. Lancet 358:1421–1423
57. Walker P, Dvorak AM (1986) Gastrointestinal autonomic nerve (GAN) tumor: ultrastructural evidence for a newly recognized entity. Arch Pathol Lab Med 110:309–316
58. Wieczorek TJ, Faquin WC, Rubin BP, Cibas ES (2001) Cytologic diagnosis of gastrointestinal stromal tumor with emphasis on the differential diagnosis with leiomyosarcoma. Cancer (Cancer Cytopathol) 93:276–287
59. Yantiss RK, Spiro IJ, Compton CC, Rosenberg AE (2000) Gastrointestinal stromal tumor versus intra-abdominal fibromatosis of the bowel wall: a clinically important differential diagnosis. Am J Surg Pathol 24:947–957
60. Zambrano E, Reyes-Mugica M, Franchi A, Rosai J (2003) An osteoclast-rich tumor of the gastrointestinal tract with features resembling clear cell sarcoma of soft parts: reports of 6 cases of a GIST simulator. Int J Surg Pathol 11:75–81

Virchows Arch (2004) 445:151–159
DOI 10.1007/s00428-004-1052-y

ORIGINAL ARTICLE

Susanna Petzmann · Reinhard Ullmann · Iris Halbwedl · Helmut H. Popper

Analysis of chromosome-11 aberrations in pulmonary and gastrointestinal carcinoids: an array comparative genomic hybridization-based study

Received: 3 February 2004 / Accepted: 17 May 2004 / Published online: 3 July 2004
© Springer-Verlag 2004

Abstract Carcinoid tumors are a heterogeneous group of neoplasms arising from the diffuse neuroendocrine system. Pulmonary as well as gastrointestinal carcinoids can be separated into those with low malignant and intermediate malignant potential. DNA losses of chromosome arm 11q are commonly seen in pulmonary neuroendocrine tumors. Conflicting results have been published comparing atypical with typical lung carcinoids with respect to imbalances of chromosome 11. In the present study, a DNA microarray with genomic clones mapped to chromosome 11 was created, and array comparative genomic hybridization (CGH) with DNA derived from formalin-fixed, paraffin-embedded tissue was performed. We investigated 4 typical and 12 atypical carcinoids of the lung and, for comparison, 9 gastrointestinal carcinoids and 6 endocrine pancreatic tumors. We have shown that formalin-fixed, paraffin-derived DNA can be successfully used for array CGH. Alterations of 11q were rarely detected not only in typical carcinoids of the lung but also in gastrointestinal carcinoids. Atypical lung carcinoids that comprised extensive DNA losses also presented retained fragments in between these deleted regions. The array CGH data were consistent with the data of a previously published classical CGH study and were additionally confirmed using fluorescence in situ hybridization in the present investigation.

Keywords Array CGH · Neuroendocrine tumor · Carcinoid tumor · Chromosome-11 aberration

S. Petzmann · R. Ullmann · I. Halbwedl · H. H. Popper
Institute of Pathology,
Medical School Graz,
Austria

H. H. Popper (✉)
Institute of Pathology,
Auenbruggerplatz 25, 8036 Graz, Austria
e-mail: popper@uni-graz.at
Tel.: +43-316-3804405
Fax: +43-316-384329

Introduction

Sporadic bronchopulmonary carcinoids are rare neuroendocrine lung tumors. They can be separated into typical carcinoids (TCs) and atypical carcinoids (ATCs) based on their mitotic counts (0–1/2 mm^2 versus 2–10/2 mm^2) and the absence or presence of necrosis. This reasonably separates most of them. However, those with 1–3 mitoses per 2 mm^2 form a borderline group for which prognosis can hardly be predicted. Overall, TCs have a good prognosis, whereas the prognosis for ATCs is intermediate between TCs and the high-grade neuroendocrine carcinomas. Several groups have tried to improve the separation of TCs from ATCs using cytogenetic and molecular genetic methods [5, 11, 32, 33, 35, 38].

Chromosome-11 alterations are commonly seen in carcinoids [32, 35] and other tumors of the lung [16, 20]. Deletions of 11q are the most frequent chromosomal aberrations in ATCs. However, conflicting results have been published on the distribution of 11q in TCs and ATCs. No changes—simple numerical changes or even complex structural abnormalities—were detected (Table 1). The application of different classification schemes and reproducibility of neuroendocrine lung tumor classification are the most probable causes for these contrary results [31].

Loss of heterozygosity (LOH) within chromosomal regions 11p12–15, 11q13 and 11q14–24 was reported in several lung cancer studies, suggesting putative tumor-suppressor genes in these areas [3, 5, 8, 10, 17, 18, 23, 36]. In a previously published study, we used ten polymorphic markers scattered along the long arm of chromosome 11 to detect allelic losses in bronchopulmonary carcinoids. The region 11q13 was more often affected in ATCs (7/11) than in TCs (2/9). LOH of 11q13 combined with LOH at distal parts of 11q in ATCs was associated with a bad prognosis, defined by high mitotic counts, vascular invasion and/or organ metastasis [21].

In carcinoid tumors of the gastrointestinal (GI) tract, DNA losses on chromosome 11 were reported more often than DNA gains, using CGH analysis (Table 1). Deletions

Table 1 Published data of cytogenetic and comparative genomic hybridization (CGH) analysis of carcinoids with special emphasis on chromosome 11

Author	Method	Number of samples studied	Percentage of cases with 11q alterations	Description of altered regions (number of affected cases given in parentheses)
Lung: typical carcinoid				
Whang-Peng et al., 1991 [38]	Cell lines/cytogenetics	1	100	der(11)t(3;11) and +11 (1)
Johansson et al., 1993 [11]	Short-term culturing/cytogenetics	4	0	0
Ullmann et al., 1998 [32]	CGH	3	0	0
Walch et al., 1998 [35]	CGH	17	48	Losses: −11 (3), 11q- (1), 11q13-qter (2), 11q13–22 (1), 11q21–22 (1)
Zhao et al., 2000 [41]	CGH	11	36	Losses: 11q13-qter (2), 11cen-p14 and 11q13-qter (1), 11p15 and 11q13.2-qter (1)
Ullmann et al., 2002 [33]	CGH	15	13	Losses:11q11–14 and 11q24-qter (1), 11q12-q23 (1)
Lung: aypical carcinoid				
Whang-Peng et al., 1991 [38]	Cell lines/cytogenetics	3	67	der(11)t(11;20) (1), −11 and der(11)t((2;11) and der(11)t(5;11) and der(11)t(6;11) (1)
Johansson et al., 1993 [11]	Short-term culture/cytogenetics	2	50	+11
Ullmann et al., 1998 [32]	CGH	4	50	Losses:11p- and 11q- (1), 11q- (1)
Walch et al., 1998 [35]	CGH	6	67	Losses: −11 (1), 11q13-qter (2), 11q22-qter (1)
Ullmann et al., 2002 [33]	CGH	20	55	Losses: −11 (1), 11p11-pter and 11q13-q14 and 11q23-qter (1), 11p11.2–11p14 and 11q13–11qter (1), 11p11.2-pter and 11q13-qter (1), 11p12-pter and 11q14-qter (1), 11q- (4), 11q13-qter (1), 11q14-qter (1)
Endocrine pancreas				
Terris et al., 1998 [30]	CGH	12	33	Gains:11p (1), 11q (1); losses:11q (1), 11q11-q21 (1)
Speel et al., 1999 [28]	CGH	44	36	Gains:11q (1); losses:11p and 11q (13), 11q (2)
Stumpf et al., 2000 [29]	CGH	25	48	Gains: +11 (2), 11cen-q14 (1), 11q11-q13 (1), 11q12-q13 losses of 11p13-p15 and 11q14-q22 (1), 11q14-q23 (1); losses: −11 (4), 11p13-pter and 11q14-q23 (1), 11q21-q23 (1)
Other gastrointestinal carcinoids				
Terris et al., 1998 [30]	CGH	8	50	Five ileal, two duodenal, one gastric; losses: −11 (1), 11q11-q13 (2), 11q21-q23 (1)
Zhao et al., 2000 [41]	CGH	21	5	Four appendical, nine ileal, two colon, four duodenal, two gastric: loss of 11q (1)
Kytölä et al., 2001 [13]	CGH	18	33	Midgut carcinoids; losses:11q14-qter (3), 11q21-qter (1), 11q22-q23 (1), 11q22-qter (1)

of 11q were frequently detected in endocrine pancreatic tumors (EPTs) [29, 30], whereas 18q losses were most commonly found in other neuroendocrine tumors of the GI tract [13, 41]. A genome-wide LOH screening in eight classical midgut carcinoids presented allelic losses on chromosome 18 in seven cases (88%) but found no LOH of chromosome 11 [15].

In this study, we aimed to test the feasibility of formalin-fixed, paraffin-embedded tissue for array CGH. We tried to figure out common patterns of chromosome-11 aberrations in pulmonary and GI carcinoids that may point to a similar mechanism of tumorigenesis. Further, we expected a better characterization of structural chromosome changes using array CGH.

Materials and methods

Materials

TC (n=4) and ATC (n=12) of the lung, as well as EPTs (n=6), midgut carcinoids (n=7) and gastric carcinoids (n=2), were available as formalin-fixed tissues. All relevant data are given in Table 2. In all these cases, sufficient normal tissue from the same patients was archived to serve as a reference. In the case of metastatic carcinoids, the metastases were included in the investigation if enough tissue was available (Table 2). TCs and ATCs were separated applying the criteria of the World Health Organization (WHO) [39]: TCs were characterized by mitotic counts of less than 2 per 2 mm^2, ATCs by 2–10 mitotic counts per 2 mm^2 and/or the presence of necrosis. Neuroendocrine tumors of the GI tract were diagnosed according to the WHO classification criteria [40]. Tissue sections were prepared on glass slides, and tumor and non-tumor areas were separated under an inverted microscope to avoid normal cell contamination. Genomic DNA was isolated using proteinase K digestion [the lysis buffer contained 10% 10× polymerase chain reaction (PCR) Buffer II, Applied Biosystems, Foster City, CA; 1% Tween 20, Merck, Darmstadt, Germany; 1 mg/ml Proteinase K, Sigma-Aldrich Corporation, St. Louis, MO; all diluted in Aqua bidest], phenol-chloroform extraction and ethanol precipitation [1].

Table 2 Data of patients. Given is the tumor-node metastasis classification. *WDNCa* well-differentiated neuroendocrine carcinoma

No.	Diagnosis	Age (years)	Male/ Female	Staging	Mitosis/ 2 mm^2	Lymphatic invasion	Blood vessel invasion	Organ	Classification	Metastases and other related diseases
1	1997	56	Female	T2N0M0	0	-	-	Lung	Typical carcinoid	
2	2001	72	Male	N0	1	-	-	Lung	Typical carcinoid	
3	1984	52	Male	T1N0M0	1	-	-	Lung	Typical carcinoid	Emphysema
4	1991	52	Male	T1N0M0	1	+	+	Lung	Typical carcinoid	
5	2000	73	Female	T1N2M0	9	+	+	Lung	Atypical carcinoid	Lymph-node metastases
6	1991	69	Male	T2N0M0	3	+	-	Lung	Atypical carcinoid	
7	1996	37	Female	T2N1	2	+	-	Lung	Atypical carcinoid	Lymph-node metastases
8	1998	44	Male	T1N0M0	9	-	+	Lung	Atypical carcinoid	
9	1998	55	Male	N1/2	5	+	+	Lung	Atypical carcinoid	Lymph-node metastases*
10	1985	74	Female	T3N2M1	10	+	+	Lung	Atypical carcinoid	Lymph-node metastases*
11	1991	47	Male	T1N1	10	+	+	Lung	Atypical carcinoid	Lymph-node metastases
12	1997	37	Female	T2N2M0	3	+	+	Lung	Atypical carcinoid	Lymph-node metastases
13	2000	62	Male	T1N1M1	3	+	+	Lung	Atypical carcinoid	Lymph-node* and organ metastases
14	1998	24	Female	T1N0M0	2	+	-	Lung	Atypical carcinoid	
15	1991	78	Male	T1N2		+	+	Lung	Atypical carcinoid	Lymph-node metastases*
16	1993	32	Female	T1N1M1	3	+	+	Lung	Atypical carcinoid	Metastases
17	1996	64	Female			+	-	Pancreas	WDNCa	Invasion of capsule
18	1996	56	Male			+	+	Pancreas	WDNCa	Lymph-node metastases*
19	1997	59	Male			-	+	Pancreas	WDNCa	Lymph-node metastases*
20	2000	45	Male			-	-	Pancreas	WDNCa	Infiltration of the duodenal wall
21	2000	13	Female			-	-	Pancreas	Neuroendocrine tumor	
22	2000	63	Female			-	-	Pancreas	Neuroendocrine tumor	Additional ductal carcinoma of exocrine pancreas
23	1993	66	Female			+	+	Midgut	Carcinoid of ileum	Lymph-node* and mesenterial metastases, nerve-sheath invasion
24	1995	69	Male			+	-	Midgut	Mixed adenocarcinoma/ malignant carcinoid	Adenocarcinoma with neuroendocrine differentiation, lymph-node metastases
25	1996	74	Female			+	+	Midgut	Malignant carcinoid	
26	1998	71	Male			-	-	Midgut	Meckel Diverticel with typical carcinoid	Adenoma of hindgut
27	1999	63	Male			+	+	Midgut	Malignant carcinoid of ileum	Hepatic metastases
28	1998	67	Male			+	+	Midgut	Malignant carcinoid	Mesenterial metastases
29	1999	78	Female			+	+	Midgut	Neuroendocrine carcinoma	Peritoneal* and lymph metastases, organ metastases, (foregut, hindgut, appendix), nerve-sheath invasion
30	2000	54	Male			+	-	Stomach	Malignant carcinoid	Lymph-node metastases
31	2000	54	Male			+	-	Stomach	Malignant carcinoid	Lymph-node metastases

* These metastases were included in the present investigation

Array CGH

DNA from BAC or PAC clones was isolated using standard alkaline lysis and exonuclease digestion (Qiagen, Hilden, Germany). We amplified DNA using linker adapter PCR according to the protocol of Snijders et al. [26] (Webnote A) using the primer described by Klein et al. [12]. Two alternative arrays were used: one small, consisting of 67 chromosome-11 clones, 12 clones of chromosome 1 and 8 clones of chromosome X, as well as 3 Drosophila clones as a negative control. Close to the end of the study, more clones of chromosome 11 were available, and a second array, consisting of the first array and 136 additional clones of chromosome 11, was prepared. Genomic clones of chromosome 19 and chromosome 8 were added for the purpose of intensity normalization. The BAC/PAC clones were obtained from Resources for Molecular Cytogenetics (Bari, Italy) and the Sanger Institute (Hinxton, GB) [7]. All clone data and links to genome databases are available on their homepages: http://www.biologia.uniba.it/rmc/; http://www.sanger.ac.uk/.

DNA spotting was done using a Genetic Microsystems robot (Affymetrix, Santa Clara, CA) and the Microgrid II (BioRobotics, Cambridge, UK), respectively. We printed each clone in triplicate on the small and in duplicate on the large DNA chip to create an array of 1 cm^2 or 2 cm^2 in size on homemade poly-L-lysine-coated glass slides (Sigma-Aldrich Corporation, St. Louis, MO).

The formalin concentration and its incubation time for tissue fixation have a big impact on DNA quality. The size of DNA fragments was evaluated using gel-electrophoresis; quality and quantity of DNA was determined using photometric measurements. Tumor and normal DNA of each patient was labeled with Cy3-dUTP and Cy5-dUTP (Amersham Biosciences, Piscataway, NJ) using nick translation (long DNA fragments), chemical linking (Nucleotide Labeling Kit, Kreatech Diagnostics, Amsterdam, NL) or random priming (short DNA fragments) (Bioprime Labeling Kit, Invitrogen, Carlsbad, CA), respectively. Unincorporated nucleotides were removed using Probe Quant G50 Columns (Amersham Biosciences). We set up test hybridizations on our microarrays with alternatively labeled male/female DNA and tumor/normal DNA of samples with known aberrations on chromosome 11 to verify the feasibility of the various labeling techniques. We used 1 μg of each test and reference DNA and 80 μg Cot-1 DNA per 1-cm^2 hybridization area in a buffer containing 50% formamide, 10% dextran sulfate, 2× sodium saline citrate (SSC). Slides were hybridized at 37°C for 3 days in an open-well format with agitation and washed according to the protocol of Snijders et al. [26] with minor modifications: we washed the slides 3×5 min in 50% formamide/1× SSC (pH=7–7.5) at 37°C subsequent to the rinsing with PN buffer (0.1 M sodium phosphate, 0.1% nonidet P40, pH 8).

After scanning (GMS 418, Genetic MicroSystems, Woburn, MA), image analyses were done with the IMAGene 4.1 software (BioDiscovery, Marina Del Rey, CA). The clones of chromosomes 1, 8 and 19 were used for data normalization (Microsoft, Excel). According to chip validation experiments with male and female normal DNA derived from formalin-fixed, paraffin-embedded tissue, the thresholds for aberrations were set to −0.32 and 0.26 (log2 ratios).

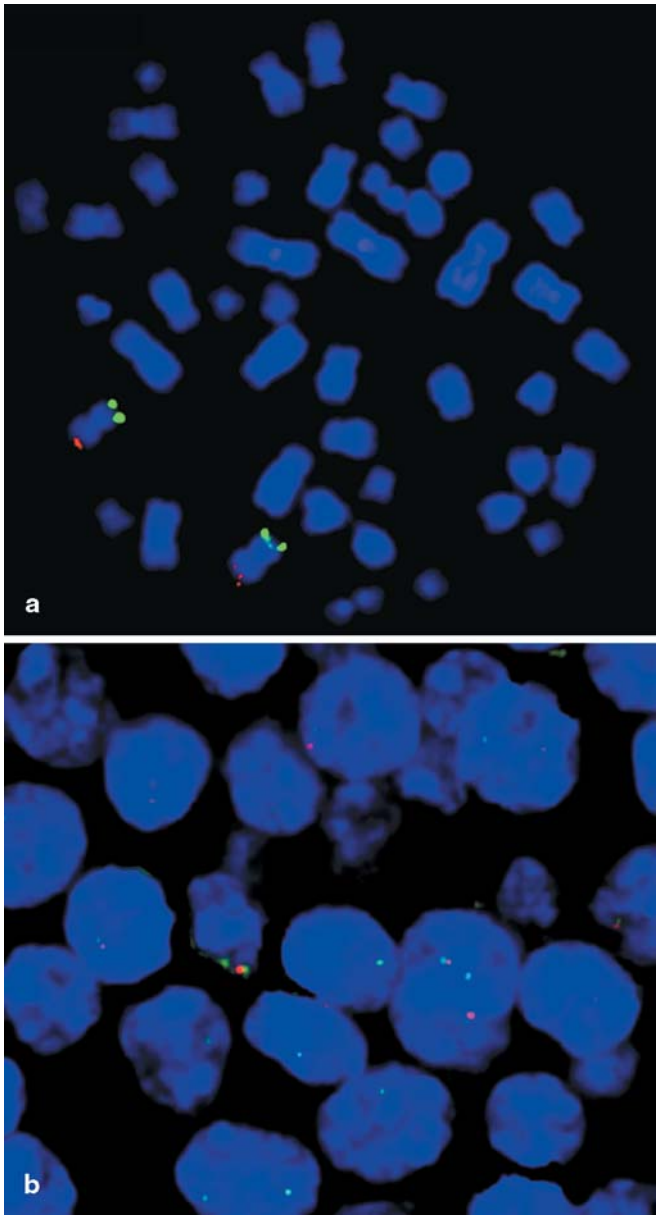


Fig. 1 a Fluorescence in situ hybridization (FISH) on metaphase spreads. BAC clone bA534I22 (11p15.5) in *green* (fluorescein) and BAC clone bA29L13 (11q25) in *red* (tetramethylrhodamine). **b** FISH on tissue sections of case 7. The *red* signals represent BAC bA150D18, the *green* represent BAC bA12C11. We compared the number of signals of each clone of a total of 125 nuclei: red 114/green 169

Fluorescence in situ hybridization

We mapped six pairs of randomly selected BAC/PAC clones on metaphase spreads by means of fluorescence in situ hybridization (FISH) using the product of the linker–adapter PCR (Fig. 1A). To confirm array results, FISH analyses on paraffin sections were done as well (Fig. 1B). Tumor sections 5-µm thick were prepared on slides and pretreated with the Paraffin Pretreatment Kit (Vysis Inc., Downers Groove, IL) according to the manufacturer's recommendations. Ten pairs of adjacent clones were selected, alternatively labeled with biotin-16-dUTP/digoxigenin-11-dUTP (Roche Diagnostics, Basel, Switzerland) using nick translation, and each pair was hybridized simultaneously according to standard FISH protocols. After hybridization, we rinsed the slides three times in 1× SSC/formamide (50%) at 37°C for 3 min and three times in 0.1× SSC at 60°C for 2–3 min. Next, 10 min of blocking (4× SSC/0.1% Tween 20/bovine albumin; Merck, Sigma-Aldrich) and 30 min of antibody incubation (fluorescin-avidin, Vector, Burlingeme, CA/anti-digoxipenin-rhodamine, Roche Diagnostics) were done at 37°C. Then we washed the slides three times in 4× SSC/Tween 20 (0.1%) for 3 min and counterstained the nuclei 5 min in 2× SSC/4′-6′-diamidino-2-phenylindole. Finally, slides were rinsed in 2× SSC/Tween 20 (0.05%), drained and embedded in 1,4-diazabicyclo-(2.2.2)octane (DABCO; Sigma-Aldrich).

Results

Control hybridizations of male versus female DNA extracted from formalin-fixed and paraffin-embedded tissue resulted in clear losses of all clones from chromosome X. In our experiments, the average ratio of signals to stringency controls (Drosophila genes) was 9.3 in Cy5 and 8.4 in Cy3. The signal-to-background ratio came to 9.6 in Cy5 and 8.8 in Cy3 on average.

A summary of all chromosome-11 alterations in pulmonary and GI carcinoids derived from the small array is given in Fig. 2. Metastasis shared similar aberration patterns as the corresponding primary tumor, but minor deviations were observed. Five ATCs of the lung were hybridized on the small and on the large array (cases 6–10) (Fig. 3). We found a concordance of 96% of the results of corresponding clones of the two arrays. The data of a previously reported CGH study [33] correlated well with the data of the present array-CGH study (Fig. 3).

Amplifications of chromosome X were seen in five of six EPTs. Four of them (cases 17, 18, 19, 21) showed DNA gains on both chromosome arms; case 20 presented gains on Xq22 only. We found similar amplification patterns of chromosome X in the primary tumors and the metastasis of cases 18 and 19. Further DNA gains of chromosome 1 were detected in case 17 and case 20 (data not shown).

A summary of FISH results and their comparison with the data of the array CGH is given in Table 3. The FISH findings confirmed the array-CGH results with the exception of two clones.

Discussion

Since the first description of array CGH with manual evaluation techniques [25, 27], this approach has been extended and modified with regard to target numbers and technical procedure [22, 34, 37]. Recently, DNA isolated from formalin-fixed and paraffin-embedded tissue samples was used for array-CGH analysis [4, 19]. In contrast to these studies, in the present investigation, normal DNA derived from formalin-fixed, paraffin-embedded tissue of each patient served as reference for the corresponding tumor DNA. The idea was to reduce hybridization artifacts by applying same quality DNA from the same resection with the advantage of analyzing DNA with a comparable grade of DNA degradation and labeling efficiencies on the microarray. This implied that chromosomal aberrations occurring in the normal as well as in the tumor cells were not detectable. A hierarchical clustering experiment of CGH data of lung tumors and GI tumors showed that pulmonary carcinoids are closely related to GI carcinoids [33]. Nevertheless, chromosome 11 might play a different role in the development of the two groups of neuroendocrine tumors. The array-CGH results of the present study demonstrated frequent losses on chromosome arm 11q in atypical bronchopulmonary carcinoids, which represent characteristic genomic alterations involved in this tumor type. Only small aberrations were found in typical lung carcinoids. In GI carcinoids, we rarely found 11q deletions. Conversely, deletions of chromosome arm 18q were frequently shown in midgut (67%) [13] and other GI carcinoids (38%) but not in TCs of the lung [41]. This will be discussed later on in more detail.

We detected DNA gains in four of six EPTs on chromosome band 11q14-q23.1 and DNA losses in two of six EPTs affecting small regions on 11q. These findings are in good concordance with several CGH studies reporting gains of 11q in 2–20% and losses of 11q in 30–36% of EPTs [28, 29, 30]. However, aberrations of chromosome 11 do not present the most frequent events in EPTs, and, therefore, we suggest that their tumorigenesis may be driven by other genetic abnormalities or deregulations at the post-transcriptional level [9], e.g., activation of the p38/MAPK (mitogen-activated protein kinase) and Akt pathways but downregulation of the ERK (extracellular signal-regulated kinase) pathway in cyclin D1 (11q13) overexpressing EPTs.

Although the chromosomal regions involved in ATCs comprise several hundred genes, we would like to focus on one interesting aspect. NCAM (neural cell adhesion molecule, 11q23.1) is represented by the clones bA87N22 and bA100J10 (http://genome.ucsc.edu/), which were commonly deleted in pulmonary carcinoids in the present study. NCAM is found in different neuroendocrine tissues, and changes of the expression level are associated with tumorigenesis and poor prognosis [14]. The sequence and structure of NCAM is similar to that of the tumor suppressor gene DCC (deleted in colorectal carcinoma) [6], which recently was associated with tumor progression of gastric carcinoma [2]. DCC was mapped to chromosomal region 18q21.3, a common region of 18q deletions in GI carcinoids. Both NCAM and DCC are important adhesion molecules, which also function as tumor suppressor genes [24]. If NCAM is one of the genes playing a fundamental role in the progression of pulmonary carcinoids, its homolog DCC might act similarly in GI carcinoids.

With respect to corresponding cases, we compared the present data with the results of a previously published conventional CGH investigation dealing with carcinoids of the lung [33]. The array data were consistent with the classical CGH data (Fig. 3). Certainly, the use of a larger number of clones resulted in a better resolution. Small areas with alterations that were not detected using classical CGH were identified using array CGH. Five pulmonary ATCs with extensive DNA losses of chromosome 11 were additionally hybridized on the large array. On both arrays, we recognized a retainment of isolated clones in between the deleted regions. With two exceptions, we could confirm the retention of those clones using FISH. In one case, the FISH result confirmed the result of the large array, but we had a divergence to the data of the small array, pointing to an array artifact. In the second example, the array-CGH results could not be confirmed using FISH

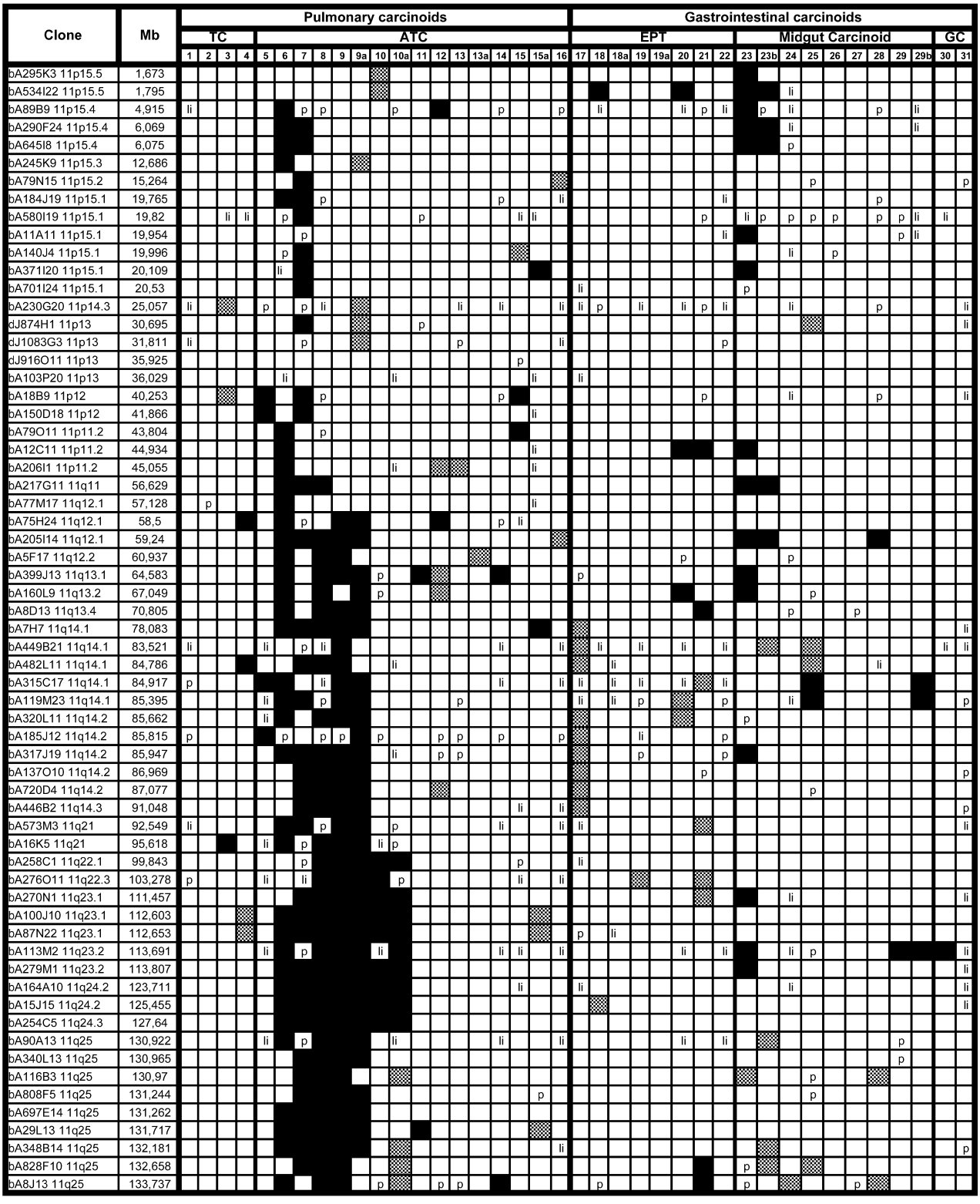


Fig. 2 Summary of array comparative genomic hybridization data of chromosome 11 of pulmonary and gastrointestinal carcinoids derived from the small array. *1–4* typical carcinoid of the lung. *5–16* atypical carcinoid of the lung. *17–22* endocrine pancreatic tumor. *23–29* midgut carcinoid. *30–31* gastric carcinoid. Lymph-node metastases are given under a (for example, primary atypical carcinoids 9 and corresponding metastasis 9a), peritoneal or mesenterial metastases under b. *Black square* DNA loss. *Checked square* DNA gain. *White square* retention. *li* low signal intensity. *p* poor spot

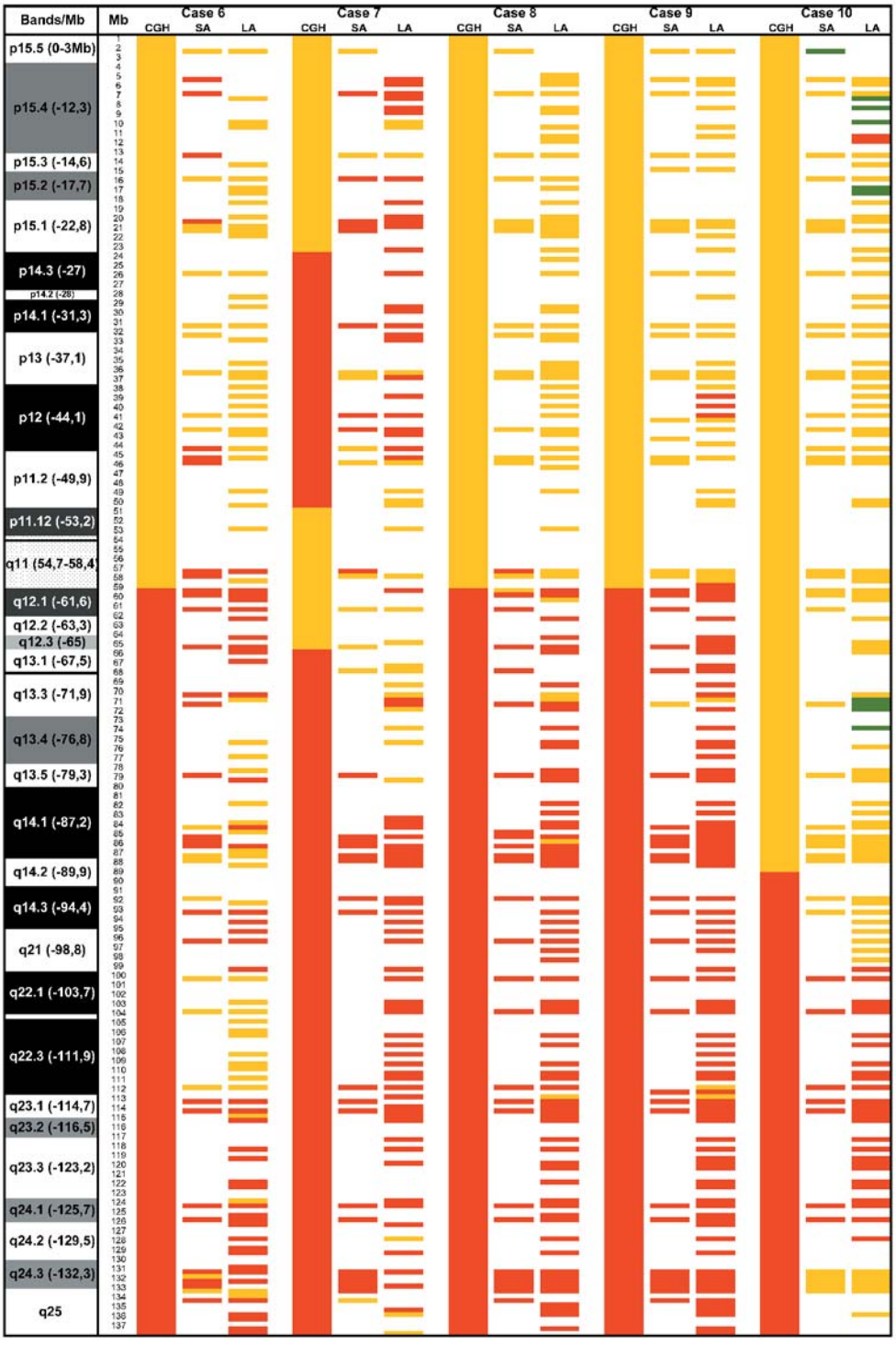


Fig. 3 Comparison of chromosome-11 aberrations between chromosome comparative genomic hybridization (CGH) and array CGH of five atypical carcinoids of the lung. Clones with spaces lower than 0.5 Mb in between are not visible as separate lines. *Red* DNA-loss. *Green* DNA-gain. *Yellow* retention/retained clones. *SA* small array. *LA* large array

analysis. Intratumoral heterogeneity may have contributed to this discrepancy.

There is a striking resemblance of our array-CGH results as shown in Fig. 2 and Fig. 3 and several reports of LOH dealing with various lung cancers: allelic losses alternate with retained DNA fragments [10, 17, 21, 36]. This opens up an interesting question for a subsequent investigation: are these alternating patterns of loss and retention the result of several independent deletions, or do they reflect the loss of an already rearranged chromosome?

In conclusion, we have shown that array CGH can be performed with formalin-fixed, paraffin-embedded tissue. Atypical pulmonary carcinoids do present large deletions on chromosome arm 11q, although small pieces of the chromosome are retained. The altered tumor suppressor gene NCAM in pulmonary carcinoids is probably mirrored in function by DCC alteration in GI-tract carcinoids.

Table 3 Fluorescence in situ hybridization (FISH) results compared with the array data. Nuclei without any signal were not counted

Tumor	BAC/PAC	Chromosomal position/Mb	Small array	Large array	Counted nuclei	Signal ratio	FISH ratio fits to array
6	bA7H7	11q14.1/78,083	Loss	Loss	50	0.67	Yes
6	bA482L11	11q14.1/84,786	No loss	No loss			
6	bA90A13	11q25/130,922	Loss	Loss	70	0.69	Yes
6	bA828F10	11q25/132,658	No loss	No result			
7	bA150D18	11p12/41,866	Loss	Loss	125	0.67	Yes
7	bA12C11	11p11.2/44,934	No loss	No loss			
7	bA18B9	11p12/40,253	Loss	Loss	100	0.69	Yes
7	dJ916O11	11p13/35,925	No loss	No loss			
7	bA217G11	11q11/56,629	Loss	No result	100	0.66	Yes
7	bA5F17	11q12.2/60,937	No loss	No loss			
8	bA205I14	11q12.1/59,24	Loss	Loss	110	0.62	Yes
8	bA77M17	11q12.1/57,128	No loss	No loss			
8	bA399J13	11q13.1/64,583	Loss	Loss	115	0.99	Yes/no[b]
8	bA75H24[a]	11q12.1/58,5	No loss	Loss			
9	bA399J13	11q13.1/64,583	Loss	Loss	120	0.61	Yes
9	bA160L9	11q13.2/67,049	No loss	No loss			
9	bA205I14[a]	11q12.1/59,24	Loss	Loss	100	0.95	No
9	bA77M17	11q12.1/57,128	No loss	No loss			
10	bA254C5	11q24.3/127,64	Loss	No result	115	0.76	Yes
10	bA90A13	11q25/130,922	No loss	No loss			

[a] Disconcordant results
[b] Clear interpretation of results is not possible

Acknowledgments We thank Dr. Mariano Rocchi, Resources for Molecular Cytogenetics, for providing us with BAC/PAC clones of chromosome 11. We would like to thank the Mapping Core and Map Finishing groups of the Wellcome Trust Sanger Institute for initial clone supply and verification. We thank Margit Gogg-Kammerer for her technical assistance. This work was supported by the Austrian National Bank Jubilee Fund, Project 8454 and the Austrian Research Fund, Project P14759.

References

1. Ausubel FM, Brent R, Kingston RE, Moore DD, Seidman JG, Smith JA, Struhl K (1998) Current protocols in molecular biology. John Wiley & Sons Inc., New York, pp 2.1.1–2.1.2
2. Bamias AT, Bai MC, Agnantis NJ, Michael MC, Alamanos YP, Stefanaki SV, Razi ED, Skarlos DV, Kappas AM, Pavlidis NA (2003) Prognostic significance of the deleted in colorectal cancer gene protein expression in high-risk resected gastric carcinoma. Cancer Invest 21:333–340
3. Chakrabarti R, Srivatsan ES, Wood TF, Eubanks PJ, Ebrahimi SA, Gatti RA, Passaro E Jr, Sawicki MP (1998) Deletion mapping of endocrine tumors localizes a second tumor suppressor gene on chromosome band 11q13. Genes Chromosomes Cancer 22:130–137
4. Daigo Y, Chin SF, Gorringe KL, Bobrow LG, Ponder BA, Pharoah PD, Caldas C (2001) Degenerate oligonucleotide primed-polymerase chain reaction-based array comparative genomic hybridization for extensive amplicon profiling of breast cancers: a new approach for the molecular analysis of paraffin-embedded cancer tissue. Am J Pathol 158:1623–1631
5. Debelenko LV, Brambilla E, Agarwal SK, Swalwell JI, Kester MB, Lubensky IA, Zhuang Z, Guru SC, Manickam P, Olufemi SE, Chandrasekharappa SC, Crabtree JS, Kim YS, Heppner C, Burns AL, Spiegel AM, Marx SJ, Liotta LA, Collins FS, Travis WD, Emmert-Buck MR (1997) Identification of MEN1 gene mutations in sporadic carcinoid tumors of the lung. Hum Mol Genet 6:2285–2290
6. Fearon ER, Pierceall WE (1995) The deleted in colorectal cancer (DCC) gene: a candidate tumour suppressor gene encoding a cell surface protein with similarity to neural cell adhesion molecules. Cancer Surv 24:3–17
7. Fiegler H, Carr P, Douglas EJ, Burford DC, Hunt S, Scott CE, Smith J, Vetrie D, Gorman P, Tomlinson IP, Carter NP (2003) DNA microarrays for comparative genomic hybridization based on DOP-PCR amplification of BAC and PAC clones. Genes Chromosomes Cancer 36:361–374
8. Fong KM, Kida Y, Zimmerman PV, Ikenaga M, Smith PJ (1995) Loss of heterozygosity frequently affects chromosome 17q in non-small cell lung cancer. Cancer Res 55:4268–4272
9. Guo SS, Wu X, Shimoide AT, Wong J, Moatamed F, Sawicki MP (2003) Frequent overexpression of cyclin D1 in sporadic pancreatic endocrine tumours. J Endocrinol 179:73–79
10. Iizuka M, Sugiyama Y, Shiraishi M, Jones C, Sekiya T (1995) Allelic losses in human chromosome 11 in lung cancers. Genes Chromosomes Cancer 13:40–46
11. Johansson M, Heim S, Mandahl N, Hambraeus G, Johansson L, Mitelman F (1993) Cytogenetic analysis of six bronchial carcinoids. Cancer Genet Cytogenet 66:33–38
12. Klein CA, Schmidt-Kittler O, Schardt JA, Pantel K, Speicher MR, Riethmuller G (1999) Comparative genomic hybridization, loss of heterozygosity, and DNA sequence analysis of single cells. Proc Natl Acad Sci U S A 96:4494–4499
13. Kytola S, Hoog A, Nord B, Cedermark B, Frisk T, Larsson C, Kjellman M (2001) Comparative genomic hybridization identifies loss of 18q22-qter as an early and specific event in tumorigenesis of midgut carcinoids. Am J Pathol 158:1803–1808
14. Lantuejoul S, Moro D, Michalides RJ, Brambilla C, Brambilla E (1998) Neural cell adhesion molecules (NCAM) and NCAM-PSA expression in neuroendocrine lung tumors. Am J Surg Pathol 22:1267–1276
15. Lollgen RM, Hessman O, Szabo E, Westin G, Akerstrom G (2001) Chromosome 18 deletions are common events in classical midgut carcinoid tumors. Int J Cancer 92:812–815
16. Mertens F, Johansson B, Hoglund M, Mitelman F (1997) Chromosomal imbalance maps of malignant solid tumors: a cytogenetic survey of 3185 neoplasms. Cancer Res 57:2765–2780
17. O'Briant KC, Bepler G (1997) Delineation of the centromeric and telomeric chromosome segment 11p15.5 lung cancer suppressor regions LOH11A and LOH11B. Genes Chromosomes Cancer 18:111–114
18. Onuki N, Wistuba, II, Travis WD, Virmani AK, Yashima K, Brambilla E, Hasleton P, Gazdar AF (1999) Genetic changes in the spectrum of neuroendocrine lung tumors. Cancer 85:600–607

19. Paris PL, Albertson DG, Alers JC, Andaya A, Carroll P, Fridlyand J, Jain AN, Kamkar S, Kowbel D, Krijtenburg PJ, Pinkel D, Schroder FH, Vissers KJ, Watson VJ, Wildhagen MF, Collins C, Van Dekken H (2003) High-resolution analysis of paraffin-embedded and formalin-fixed prostate tumors using comparative genomic hybridization to genomic microarrays. Am J Pathol 162:763–770
20. Petersen I, Langreck H, Wolf G, Schwendel A, Psille R, Vogt P, Reichel MB, Ried T, Dietel M (1997) Small-cell lung cancer is characterized by a high incidence of deletions on chromosomes 3p, 4q, 5q, 10q, 13q and 17p. Br J Cancer 75:79–86
21. Petzmann S, Ullmann R, Klemen H, Renner H, Popper HH (2001) Loss of heterozygosity on chromosome arm 11q in lung carcinoids. Hum Pathol 32:333–338
22. Pinkel D, Segraves R, Sudar D, Clark S, Poole I, Kowbel D, Collins C, Kuo WL, Chen C, Zhai Y, Dairkee SH, Ljung BM, Gray JW, Albertson DG (1998) High resolution analysis of DNA copy number variation using comparative genomic hybridization to microarrays. Nat Genet 20:207–211
23. Rasio D, Negrini M, Manenti G, Dragani TA, Croce CM (1995) Loss of heterozygosity at chromosome 11q in lung adenocarcinoma: identification of three independent regions. Cancer Res 55:3988–3991
24. Roesler J, Srivatsan E, Moatamed F, Peters J, Livingston EH (1997) Tumor suppressor activity of neural cell adhesion molecule in colon carcinoma. Am J Surg 174:251–257
25. Shalon D, Smith SJ, Brown PO (1996) A DNA microarray system for analyzing complex DNA samples using two-color fluorescent probe hybridization. Genome Res 6:639–645
26. Snijders AM, Nowak N, Segraves R, Blackwood S, Brown N, Conroy J, Hamilton G, Hindle AK, Huey B, Kimura K, Law S, Myambo K, Palmer J, Ylstra B, Yue JP, Gray JW, Jain AN, Pinkel D, Albertson DG (2001) Assembly of microarrays for genome-wide measurement of DNA copy number. Nat Genet 29:263–264
27. Solinas-Toldo S, Lampel S, Stilgenbauer S, Nickolenko J, Benner A, Dohner H, Cremer T, Lichter P (1997) Matrix-based comparative genomic hybridization: biochips to screen for genomic imbalances. Genes Chromosomes Cancer 20:399–407
28. Speel EJ, Richter J, Moch H, Egenter C, Saremaslani P, Rutimann K, Zhao J, Barghorn A, Roth J, Heitz PU, Komminoth P (1999) Genetic differences in endocrine pancreatic tumor subtypes detected by comparative genomic hybridization. Am J Pathol 155:1787–1794
29. Stumpf E, Aalto Y, Hoog A, Kjellman M, Otonkoski T, Knuutila S, Andersson LC (2000) Chromosomal alterations in human pancreatic endocrine tumors. Genes Chromosomes Cancer 29:83–87
30. Terris B, Meddeb M, Marchio A, Danglot G, Flejou JF, Belghiti J, Ruszniewski P, Bernheim A (1998) Comparative genomic hybridization analysis of sporadic neuroendocrine tumors of the digestive system. Genes Chromosomes Cancer 22:50–56
31. Travis WD, Gal AA, Colby TV, Klimstra DS, Falk R, Koss MN (1998) Reproducibility of neuroendocrine lung tumor classification. Hum Pathol 29:272–279
32. Ullmann R, Schwendel A, Klemen H, Wolf G, Petersen I, Popper HH (1998) Unbalanced chromosomal aberrations in neuroendocrine lung tumors as detected by comparative genomic hybridization. Hum Pathol 29:1145–1149
33. Ullmann R, Petzmann S, Klemen H, Fraire AE, Hasleton P, Popper HH (2002) The position of pulmonary carcinoids within the spectrum of neuroendocrine tumors of the lung and other tissues. Genes Chromosomes Cancer 34:78–85
34. Veltman JA, Schoenmakers EF, Eussen BH, Janssen I, Merkx G, van Cleef B, van Ravenswaaij CM, Brunner HG, Smeets D, van Kessel AG (2002) High-throughput analysis of subtelomeric chromosome rearrangements by use of array-based comparative genomic hybridization. Am J Hum Genet 70:1269–1276
35. Walch AK, Zitzelsberger HF, Aubele MM, Mattis AE, Bauchinger M, Candidus S, Prauer HW, Werner M, Hofler H (1998) Typical and atypical carcinoid tumors of the lung are characterized by 11q deletions as detected by comparative genomic hybridization. Am J Pathol 153:1089–1098
36. Wang SS, Virmani A, Gazdar AF, Minna JD, Evans GA (1999) Refined mapping of two regions of loss of heterozygosity on chromosome band 11q23 in lung cancer. Genes Chromosomes Cancer 25:154–159
37. Wessendorf S, Fritz B, Wrobel G, Nessling M, Lampel S, Goettel D, Kuepper M, Joos S, Hopman T, Kokocinski F, Dohner H, Bentz M, Schwaenen C, Lichter P (2002) Automated screening for genomic imbalances using matrix-based comparative genomic hybridization. Lab Invest 82:47–60
38. Whang-Peng J, Knutsen T, Gazdar A, Steinberg SM, Oie H, Linnoila I, Mulshine J, Nau M, Minna JD (1991) Nonrandom structural and numerical chromosome changes in non-small-cell lung cancer. Genes Chromosomes Cancer 3:168–188
39. World Health Organization (1999) World Health Organization: histological typing of lung and pleural tumors, 3rd edn. Springer, Berlin Heidelberg New York
40. World Health Organization (2000) World Health Organization: histological typing of endocrine tumors, 2nd edn. Springer, Berlin Heidelberg New York
41. Zhao J, de Krijger RR, Meier D, Speel EJ, Saremaslani P, Muletta-Feurer S, Matter C, Roth J, Heitz PU, Komminoth P (2000) Genomic alterations in well-differentiated gastrointestinal and bronchial neuroendocrine tumors (carcinoids): marked differences indicating diversity in molecular pathogenesis. Am J Pathol 157:1431–1438

Virchows Arch (2004) 445:160–167
DOI 10.1007/s00428-004-1051-z

ORIGINAL ARTICLE

C. Lackner · Z. Jukic · O. Tsybrovskyy · G. Jatzko · V. Wette · G. Hoefler · M. Klimpfinger · H. Denk · K. Zatloukal

Prognostic relevance of tumour-associated macrophages and von Willebrand factor-positive microvessels in colorectal cancer

Received: 18 May 2004 / Accepted: 18 May 2004 / Published online: 30 June 2004
© Springer-Verlag 2004

Abstract Tumour-associated macrophages (TAM) are involved in tumour angiogenesis and anti-tumour immune response. In colorectal cancer (CRC), an association of high microvascular density (MVD) and unfavourable prognosis has been reported by some investigators. However, heterogeneous patient groups were studied. We, therefore, analysed the correlation between TAM and MVD and the prognostic relevance of MVD, TAM and T lymphocyte infiltration for long-term survival in a homogeneous group of 70 patients with moderately differentiated cancers of the International Union Against Cancer (UICC) stages II and III, who did not receive chemotherapy. MVD was evaluated using immunohistochemistry with antibodies against CD34 and von Willebrand factor (vWF). TAM and T lymphocytes were visualised with antibodies against CD68 and CD3, respectively. Statistical analysis did not reveal a significant correlation between TAM and T lymphocyte numbers and MVD. Multivariate analysis of immunohistochemical data from all CRC patients and the subgroup of patients with UICC stage-II CRC identified TAM- and vWF-positive microvessel numbers as prognostically relevant markers. Low numbers of TAM- and high numbers of vWF-positive microvessels were associated with an unfavourable prognosis. In conclusion, TAM- and vWF-positive microvessel numbers may serve as independent prognostic markers for patients with UICC stage-II and -III CRC and may help to identify patients with an unfavourable prognosis.

Keywords Colorectal cancer · Microvascular density · Macrophages · Prognosis

C. Lackner · O. Tsybrovskyy · G. Hoefler · H. Denk · K. Zatloukal (✉)
Institute of Pathology,
Medical University Graz,
Auenbruggerplatz 25, 8036 Graz, Austria
e-mail: kurt.zatloukal@meduni-graz.at
Tel.: +43-316-3804404
Fax: +43-316-384329

Z. Jukic
Institute of Pathology,
St. Veiterstraße 47, 9020 Klagenfurt, Austria

G. Jatzko · V. Wette
Barmherzige Brüder Hospital,
Spitalgasse 26, 9300 Sankt Veit/Glan, Austria

M. Klimpfinger
Pathologisch-Bakteriologisches Institut,
Kaiser-Franz-Josef-Spital der Stadt Wien,
Kundratstraße 3, 1100 Wien, Austria

Introduction

Colorectal cancer (CRC) is among the most frequent cancers in the Western world [48]. Depending on the local extension of the disease and the number of lymph nodes involved, there are different options of adjuvant treatment after surgical removal. Consensus has been reached concerning the benefit of adjuvant chemotherapy for patients with advanced colon cancer with lymph-node metastases [International Union Against Cancer (UICC) stage III: T1–4, N1–3, M0]; adjuvant treatment is also recommended for advanced rectal cancer with and without lymph-node metastases (UICC stage II: T3–4, N0, M0 and stage III: T1–4, N1–3, M0) [47, 49]. However, for patients with advanced colon cancer without lymph-node metastases (UICC stage II: T2–4, N0, M0), the benefit of adjuvant therapy is still under debate [9, 32, 61]. Additional prognostic parameters, which help to identify subsets of patients who will benefit from adjuvant treatment, are, therefore, of clinical interest, particularly for UICC stage-II CRC.

It was not until the first reports by Folkman et al. [20], who showed that tumour growth beyond a certain size critically depends on the formation of a tumour-supporting vasculature, that angiogenesis has attracted considerable interest in tumour biology. Now, many pathways in the pathophysiology of tumour-related angiogenesis have been elucidated [8, 17, 19, 22, 28, 41, 43, 46, 50, 62], and its prognostic relevance has been described for many

human cancers [5, 10, 15, 21, 27, 30, 33, 37, 45, 51, 55, 56]. However, the prognostic relevance of tumour-related angiogenesis in CRC remains controversial. In many reports, an association between tumour angiogenesis, reflected by MVD in so-called "hot spots" of angiogenesis in the tumour tissue, and prognosis has been described. MVD has been shown to increase with progression from colonic adenoma to invasive carcinoma and has been associated with tumour size, lymphatic and venous blood vessel invasion and metastasis. Thus, MVD was regarded as an important prognostic factor by some investigators [3, 11, 23, 25, 34, 53, 54, 57] but not by others [4, 6, 40, 44].

Angiogenesis depends on the combined action of various cytokines and growth factors secreted by tumour cells, cells of the tumour stroma and infiltrating inflammatory cells. Among inflammatory cells, macrophages are believed to play an important role in tumour-related angiogenesis. Macrophages have been shown to be recruited by the tumour (i.e. tumour-associated macrophages, TAM) and to secrete angiogenic as well as angioinhibiting factors [17, 38]. Besides the involvement in tumour-associated angiogenesis, TAM may also play an important role in mediating a specific anti-tumour immune response. Furthermore, macrophages can act as non-specific effector cells and directly destroy tumour cells [2]. Regarding CRC, a few reports suggest that dense macrophage and lymphocytic infiltration of the tumour tissue is associated with a favourable prognosis [26, 35, 42, 44, 58].

Therefore, the aims of the present study were: (1) to investigate the correlation between the density of TAM and MVD and its prognostic significance and (2) to analyse whether the density of infiltration of the tumour by TAM and T lymphocytes is of prognostic significance for long-term survival (>5 years) in patients with advanced CRC with and without lymph-node metastasis (UICC stage II and III). Because other factors, such as tumour differentiation and adjuvant chemotherapy, can influence prognosis, we selected patients with moderately differentiated CRC who were treated by surgery between 1987 and 1989 without adjuvant chemotherapy.

Materials and methods

Patients

To ensure a homogeneous group of patients with regard to treatment and follow-up, 70 patients with pT3, pN0 and pN1–2, M0 CRC who underwent surgery at the Barmherzige Brüder Hospital, St. Veit/Glan, Austria, were studied. Patient history and follow-up was complete for all patients included in the study. The follow-up for patients with UICC stage-II CRC was 81.9±31.3 months. Paraffin-embedded tumour tissues were retrieved from the archives of the Institute of Pathology, Medical University of Graz, Austria. Patient characteristics are compiled in Table 1.

Table 1 Patient characteristics. *UICC* International Union Against Cancer

Age	69±11 years
Male	39
Female	31
UICC stages	
UICC stage II	36
UICC stage III	34
pN1	25
pN2	9
Tumor location	
Colon ascendens	22
Colon transversum	5
Colon sigmoideum	22
Rectum	21
Disease free	33
Dead of disease	37

Immunohistochemistry

Sections 5-μm thick of formalin-fixed, paraffin-embedded tumour tissue were deparaffinised and pre-treated with pronase in Ventana buffer (Ventana, Tuscon, AZ). Endogenous peroxidase was blocked with 2% H_20_2 in methanol. Two different endothelial markers, CD34 and vWF, were used to identify tumour microvessels [60]. Immunohistochemical staining was performed using antibodies against CD34 antigen (clone HPCA-1, dilution 1:200; Becton Dickinson, San Jose, CA) and vWF (clone F8/86, dilution 1:100; Dako, Copenhagen, Denmark) to detect endothelial cells. CD68 antibodies (clone KP-1, dilution 1:300; Dako) were used to identify macrophages; T lymphocytes were identified with CD3 antibodies (dilution 1:300; Dako). Sections were processed using a VENTANA ES automatic stainer. Sections were incubated with the primary antibody for 1 h, washed, blocked with 2% H_20_2 in methanol, washed and then incubated with biotinylated goat anti-mouse immunoglobulin secondary antibodies (dilution 1:1000; Dako), followed by incubation with streptavidin-coupled horseradish peroxidase (Ventana) for 8 min. For colour development, diaminobenzidine (8 min) and copper sulfate (4 min) were used as substrate and enhancer, respectively. Sections were counterstained with Gill's hematoxylin, dehydrated and mounted with Permount. For negative control, primary antibodies were replaced by buffer- or isotype-matched immunoglobulins.

Semi-quantitative analysis of MVD, TAM and T cells in CRC

MVD of highly vascularised tumour areas, so-called "hot spots of tumour neovascularisation", were evaluated as suggested by Folkman et al. [19]. To allow comparison of the different histological parameters, consecutive serial sections were stained. In contrast to tumour-associated vasculature in breast cancer, where hot spots of angiogenesis are distributed throughout the tumour, in CRC, tumour angiogenesis showed the highest intensity at the invasive front. Most of the CD34- and vWF-positive microvessels were identified in this area, which thus resembled an "extended hot spot" of angiogenesis. After identification of areas with the highest MVD, using a microscopic magnification of ×40, microvessels reactive with vWF and CD34 antibodies were counted at a magnification of ×400 in 20 microscopic fields (corresponding to an investigated area of 2.4 mm^2). Positively stained blood vessels with lumina as well as cell clusters without a lumen and single cells were considered as individual microvessels for two reasons: first, a single cell or cell cluster may represent the tip of a capillary sprout [19], and second, microvessels may collapse due to increased interstitial fluid pressure and decreased microvascular hydrostatic pressure in tumour tissue after intraoperative ligation of major blood vessels [7].

In order to analyse the correlation between angiogenesis and immune response of the host, TAM and T lymphocytes were also counted in 20 microscopic fields at a magnification of ×400 within the area of highest MVD at the invasive tumour front. Because the CRC tissues investigated displayed differences regarding TAM and T lymphocytes densities at the invasive tumour front and in the central areas of the tumour, TAM and T lymphocytes were also counted in 20 microscopic fields at ×400 magnification in the tumour centres.

The numbers of TAM, T lymphocytes and microvessels were assessed using a 6-grade score, using the Nikon-Laborphot-2 microscope with a ×40 objective and a ×10 eye piece in the following manner: 0, no positive cells or microvessels; 1, less than 4 positive cells or microvessels; 2, 4–20 positive cells or microvessels; 3, 21–100 positive cells or microvessels; 4, 101–500 positive cells or microvessels; and 5, more than 500 positive cells or microvessels. Necrotic or haemorrhagic tumour areas were excluded from the analysis.

Statistics

Statistical analysis was performed using SPSS for Windows 10.0.7 program. To investigate correlations between immunohistochemical variables, non-parametric hierarchical cluster analysis (nearest-neighbour clustering) and pairwise Spearman's correlation coefficients were used. Prognostic relevance of the variables was determined by a logistic regression analysis (both uni- and multivariate). In the case of multivariate analysis, a limited backward selection of variables was adopted. For the pN0 group, survival curves were plotted using the Kaplan-Meier method, with log-rank test being used to test differences in survival. Results were considered significant at P levels below 0.05 and marginally significant at levels between 0.05 and 0.1.

Results

Evaluation of MVD at "hot spots" of tumour angiogenesis

Adopting the methodology for evaluation of MVD as described by Folkman et al. [19], we evaluated MVD in hot spots of angiogenesis of CRC. In all CRC investigated, areas with the highest density of CD34- and vWF-positive microvessels were preferentially located at the invasive tumour front, whereas angiogenesis was much less pronounced in central tumour areas. Evaluation of CD34- and vWF-positive microvessels yielded microvessel counts between 0 and 500 per hot-spot area (corresponding to CD34 and vWF scores 0 to 4). However, in general we observed a higher score of CD34- than vWF-positive microvessels. Of 70 patients, 16 exhibited a high density of CD34-positive microvessels, corresponding to CD34 score 4, whereas in only 4 of 70 patients was a vWF score of 4 found at the invasive tumour front. VWF antigen was more prominently expressed in microvessels with larger lumina (e.g. venules) than in microvessels recognised by CD34 antibodies (Fig. 1).

Correlation between MVD and host anti-tumour inflammatory response

To analyse the correlation between tumour angiogenesis and the host inflammatory response, TAM and T cells were counted and scored in the hot-spot angiogenesis areas at the invasive tumour front and in the tumour centres (Fig. 2). In 45 of 70 cases, we found a very dense TAM infiltration, amounting to 101–500 or even more positive cells (CD68 scores 4 and 5). In 41 of 70 patients, the number of TAM was higher at the invasive tumour front than in the central portion of the tumour. In 24 of 70 cases, TAM infiltration was similar in central and peripheral invasive tumour areas. Only in 5 of 70 patients was a higher concentration of TAM observed in the centre of the tumour.

In 58 of 70 cases, T lymphocyte numbers at the invasive tumour front varied between 21 and more than 500 cells (CD3 scores 3–5). In 12 patients, a scant T lymphocytic infiltration between less than 4 and 20 cells at the invasive tumour front was observed (CD3 scores 1–2). In contrast to TAM, no differences between the density of T lymphocytic infiltration at the invasive front and central areas of the tumour were observed (data not shown).

To study the correlation between the density of the inflammatory infiltrate and tumour-related angiogenesis, non-hierarchical cluster analysis (Fig. 3) and pairwise Spearman's correlation coefficients were used. Both statistical tests did not reveal a correlation between the density of the inflammatory infiltrate (i.e. the density of TAM or T lymphocytes) and the density of CD34- or vWF-positive microvessels (Spearman's rho<0.25). However, there was a positive correlation between the numbers of TAM at the invasive tumour front and in the tumour centre (Spearman's rho=0.509) and between the number of T lymphocytes at the invasive tumour front and the number of TAM in the tumour centre (Spearman's rho=0.303), indicating that these parameters are interrelated.

Prognostic relevance of MVD and host anti-tumour inflammatory response

Univariate and multivariate logistic regression analysis was performed to test the prognostic relevance of the immunohistochemical results obtained from all patients included in the study (pT3, pN0/N1–2 group). Statistical analysis identified the number of TAM at the invasive tumour front (CD68 score) and number of vWF-positive microvessels (vWF score) as independent prognostic markers, whereas lymph-node status reached marginal statistical significance (P=0.043, P=0.001 and P=0.084, respectively). The correlation between the number of TAM in the tumour centre and location (colon versus rectum) of cancer failed to reach statistical significance (P=0.63 and P=0.27, respectively). Age only reached marginal significance with respect to long-term survival (P=0.088). Unfavourable prognosis was associated with a lower CD68 score, higher vWF score, higher lymph-node status and older age.

To focus our investigation on the prognostic relevance of MVD and the inflammatory infiltrate of patients with stage-II CRC, the pT3, pN0 patient group was analysed separately. Multivariate analysis revealed the vWF score

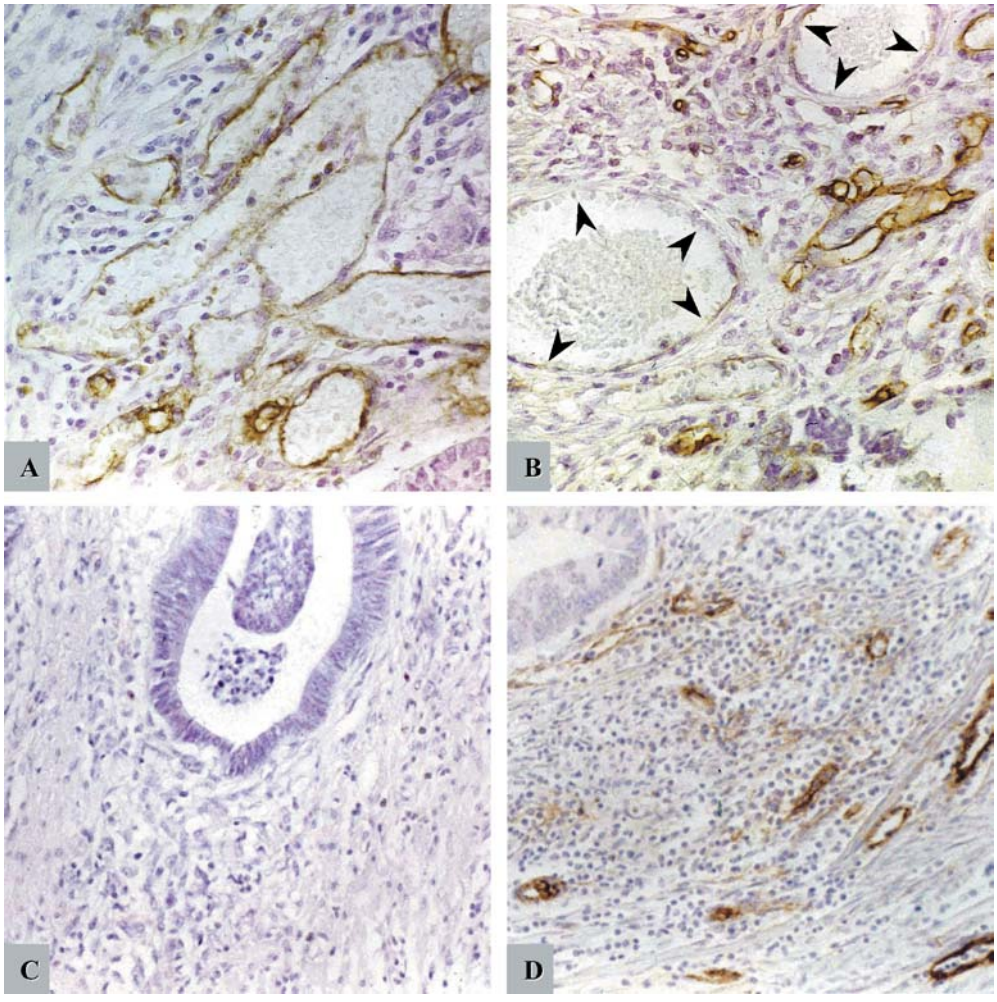


Fig. 1 Immunohistochemical detection of tumour angiogenesis at the invasive front of colorectal cancer (CRC) tissues. **A** Microvessels at the invasive front of a CRC immunostained with antibodies against von Willebrand factor (vWF). Vessels with larger lumina are predominantly stained (×400). **B** Similar area of the tumour as shown in **A** with microvessels recognised by CD34 antibodies. *Arrowheads* microvessels with larger lumina remain unstained (×400). **C** Invasive front of a CRC with areas without microvessels reactive with vWF antibodies of a patient who survived a 5-year observation period (×400) (see also Fig. 2: photomicrographs **A** and **B** are from the same tumour). **D** Microvessels at the invasive front of a CRC of a patient who died of recurrent cancer within 11 months after initial surgery, decorated by vWF antibodies (×400)

and CD68 score at the invasive tumour front as independent prognostic markers ($P<0.0005$, respectively). An unfavourable prognosis was associated with a higher vWF and lower CD68 score at the invasive tumour front. Based on these findings, an index of CD68 score minus vWF score was determined. All patients with an index of less than 2 ($n=11$) died of disease within 5 years of follow-up, whereas all patients with an index of greater than 2 ($n=12$) remained disease free within this period. Patients with an index of 2 ($n=13$) seemed to be at intermediate risk for tumour-related death. Six patients died of disease and seven patients remained disease free (Fig. 4). Thus, patients with an index of greater than 2 belonged to a "low risk" group, and patients with an index of less than 2 to a "high risk" group, as indicated by highly significant differences in long-term survival (log-rank test $P=0.0003$). The Kaplan-Meier survival curves are shown in Fig. 5.

We also investigated whether the immunohistochemical parameters in our study could be used to predict the presence of lymph-node metastases at the time of surgery. However, none of these parameters showed a significant correlation with lymph-node status, which further underlines that these parameters are independent.

Discussion

The aim of this study was to evaluate the prognostic relevance of MVD and TAM and T lymphocyte infiltration for long-term survival of patients with advanced (pT3) CRC with and without lymph-node metastases and without systemic metastases (UICC stages II and III).

Recently published results suggest an association of high MVD with poor prognosis in patients with different types of malignant tumours, such as cancers of the endometrium [37], uterine cervix [10], breast [27, 30], liver [51], lung [15, 33, 45], prostate [5], oesophagus [56], stomach [55] and thyroid medullary cancer [21]. Such an association was also reported for CRC by some investigators [3, 11, 23, 25, 29, 34, 53, 54, 57], but not confirmed by others [4, 6, 40, 44]. The reason for this discrepancy is unclear; however, several factors may be responsible: for example, counting procedures for assessment of MVD were not standardised, different antibodies were used for immunohistochemistry and different numbers of microscopic fields, ranging from one to five fields per area of hot-spot angiogenesis of the tumours, were evaluated at different magnifications. In addition, patient groups studied differed regarding treatment regimens and

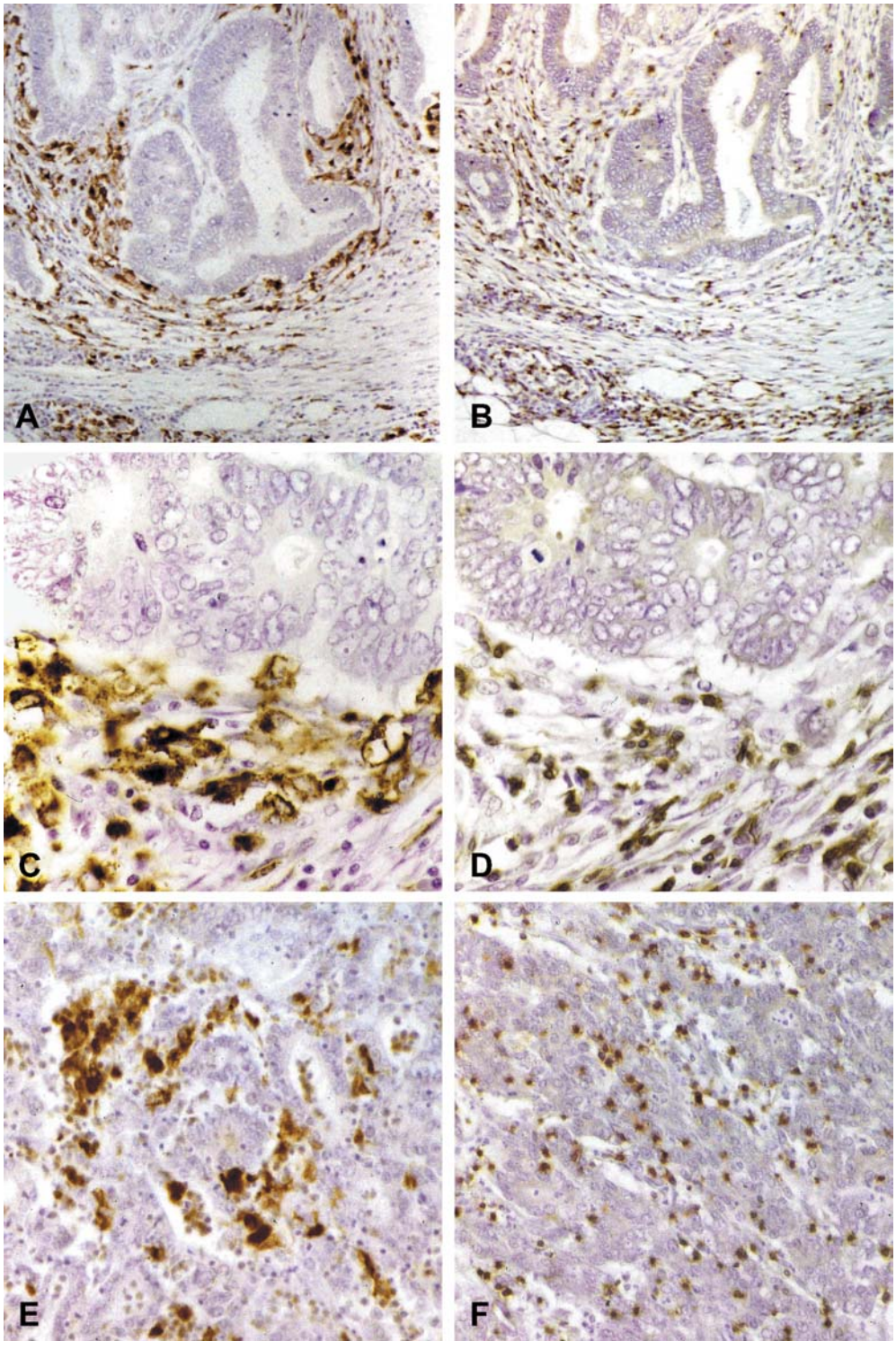


Fig. 2 Immunohistochemical detection of tumour-associated macrophages (TAM) and T cells at the invasive front of colorectal cancer (CRC) tissues. **A** High density of TAM at the invasive front of a CRC decorated by CD68 antibodies. This patient survived a 5-year observation period (the tumour of the same patient is also shown in Fig. 1C) (×100). **B** T lymphocytes in the same region as shown in **A** identified by CD3 antibodies (×100). **C** Higher magnification of **A** (×400). **D** Higher magnification of **B** (×400). **E** TAM infiltration in the tumour centre identified by CD68 antibodies (×200). **F** T cell infiltration in the tumour centre decorated by CD3 antibodies (×200)

length of follow-up. Another possibility could also be that the effect of MVD is modulated by additional parameters not evaluated in these studies. In our study, we observed differences in prognostic relevance of the densities of CD34- versus vWF-positive microvessels: whereas density of CD34-positive microvessels was not prognostically relevant regarding long-term survival, in patients with pT3, pN0/N1–2 cancers and in the subgroup of pT3, pN0 patients, a low number of vWF-positive microvessels was associated with a favourable prognosis.

Tumour location, i.e. proximal versus distal to the peritoneal colonic reflection, is regarded a prognostic factor by some investigators [47]. The influence of tumour location on prognosis was not statistically significant in our study. However, sample size in our study may have been too low to reveal prognostic relevance for a

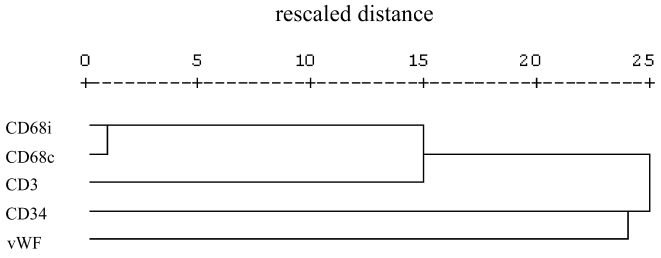


Fig. 3 Non-hierarchical cluster analysis of variables of the inflammatory infiltrate and microvascular density (MVD) in colorectal cancer (CRC) tissues of stage-II and -III CRC patients. The correlation between the density of the inflammatory infiltrate and MVD at "hot spots" of angiogenesis at the invasive tumour front and in the tumour centre was analysed by non-hierarchical cluster analysis. The dendrogram represents steps of hierarchical clustering of variables. No correlation existed between the density of tumour-associated macrophages (TAM) or T lymphocytes (represented by CD68i and CD3 scores, respectively) and the density of CD34- or von Willebrand factor (vWF)-positive microvessels (represented by CD34 and vWF scores, respectively) at the invasive tumour front. However, a correlation between the TAM numbers at the invasive tumour front (represented by the CD68i score) and the tumour centre (represented by the CD68c score) was found, indicating that these two parameters are interrelated

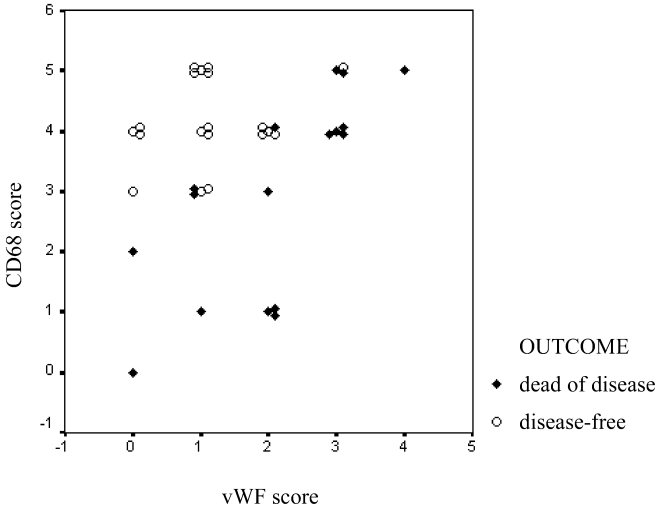


Fig. 4 Scatter blot analysis of tumour-associated macrophages (TAM) and von Willebrand factor (vWF)-positive microvessel scores at the invasive tumour front and survival of patients with UICC stage-II colorectal cancer (CRC). The survival of patients with stage-II CRC was analysed in correlation with their respective CD68 and vWF scores at the invasive tumour front. Patients with a lower CD68 score and higher vWF score (n=11), which corresponds to an CD68 score minus vWF score index of less than 2 died of recurrent cancer within 5 years of follow-up (*diamond*), whereas all patients with a higher CD68 score and lower vWF score (n=12), which corresponds to an CD68 score minus vWF score index of greater than 2 remained disease free within this time period (*circle*). Patients with an CD68 score minus vWF score index of 2 (n=13) seemed to be at intermediate risk for tumour-related death. Six patients died of recurrent cancer and seven patients remained disease free

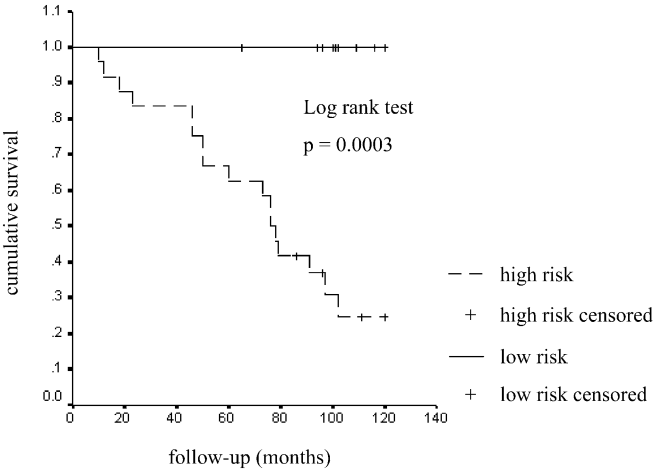


Fig. 5 Kaplan-Meier survival plot of stage-II colorectal cancer (CRC) patients. On the basis of the index of CD68 score minus von Willebrand factor (vWF) score, the patients with stage-II CRC could be separated into a "low-risk" and a "high-risk" group with respect to tumour-related death. Patients with an CD68-vWF score index of greater than 2 belonged to a "low-risk" group, and patients with an index of greater than 2 to a "high-risk" group as indicated by highly significant differences in long-term survival (log-rank test P=0.0003)

marker weaker than, for example, lymph-node status [18], CD68 score or vWF score.

In the CRC tissues studied by us, the number of CD34-positive microvessels was higher than that of vWF-positive microvessels, which may indicate the presence of newly formed endothelial cells in ongoing angiogenesis, since CD34 and vWF differ with respect to their expression patterns on endothelial cells. For example, during wound healing, CD34 is expressed in activated endothelial cells and in capillary sprouts, whereas vWF is associated with endothelial cells of larger arteries and veins [60].

Macrophages fulfil a variety of functions in tumour biology. They produce and secrete pro- as well as anti-angiogenic factors [17]. The angiogenic effect of TAM is supported by the positive correlation between TAM and MVD found in different human tumours [14, 24, 31, 34, 36, 38, 39, 52, 59]. In CRC, the association of TAM and MVD was not investigated directly, but studies exist dealing with mediators of angiogenesis produced by TAM. The results are controversial. Matsumura et al. [34] showed that the angiogenic platelet-derived endothelial cell growth factor (PD-ECGF) is expressed by tumour cells and also by TAM. PD-ECGF expression in CRC correlated with TAM infiltration and MVD. In contrast, Saito et al. [44] reported that PD-ECGF was mainly expressed by TAM, but PD-ECGF expression did not correlate with MVD. Results of another study [16] suggested that angiogenin is expressed by CRC cells in response to pro-inflammatory cytokines derived from TAM. The amount of angiogenin expression correlated with the density of TAM infiltration and MVD. In our study, we did not find an association between TAM numbers and CD34- or vWF-positive microvessels. These results and

the observation that macrophage infiltration is associated with a favourable outcome in CRC [44, 58] support the hypothesis that TAM play a role in mediating an anti-tumour immune response.

In some malignancies, such as certain types of melanoma, breast cancer and also in CRC, the presence of a dense lymphocytic infiltrate is associated with a better prognosis [1, 12, 13, 26, 42]. However, Naito et al. [35] showed that only infiltration by $CD8^+$ T lymphocytes within so-called "cancer cell nests" was associated with favourable prognosis, whereas T lymphocytic infiltration of the tumour stroma and the invasive tumour front was not. This is in line with our observation of lack of correlation between the number of CD3-positive T lymphocytes at the invasive tumour front and prognosis or MVD.

Our data suggest that there is a prognostically favourable subset of patients with pT3, pN0, M0 (UICC stage II) CRC whose tumours are characterised by a low number of vWF-positive microvessels and a high number of TAM at the invasive tumour front. We propose that the assessment of TAM and vWF at the invasive tumour front in patients with stage-II CRC is useful to identify patients with an unfavourable prognosis for whom additional therapeutic regimens should be considered.

Acknowledgements The authors thank Karl Pfeiffer, Ph.D., University Innsbruck, Austria, for statistical analysis as well as Monika Herzog and Sabine Mair for their excellent technical assistance.

References

1. Aaltomaa S, Lipponen PK, Eskelinen MJ, Kosma VM, Marin S, Alhava E, Syrjanen K Lymphocyte infiltrates as a prognostic variable in female breast cancer. Eur J Cancer 28:859–864
2. Abbas AK, Lichtmann AH, Pober JS (2000) Immunity to tumours. In: Abbas AK, Lichtman AH, Pober JS (eds) Cellular and molecular immunology. W.B. Saunders Company, Philadelphia, pp 384–403
3. Aotake T, Lu C, Chiba Y, Muraoka R, Tanigawa N (1999) Changes of angiogenesis and tumour cell apoptosis during colorectal carcinogenesis. Clin Cancer Res 5:135–142
4. Banner BF, Whitehouse R, Baker SP, Swanson RS (1998) Tumour angiogenesis in stage II colorectal carcinoma. Association with survival. Am J Clin Pathol 109:733–737
5. Bettencourt MC, Bauer JJ, Sesterhenn IA, Connelly RR, Moul JW (1998) CD34 immunohistochemical assessment of angiogenesis as a prognostic marker for prostate cancer recurrence after radical prostatectomy. J Urol 160:459–465
6. Bossi P, Viale G, Lee AKC, Alfano RM, Coggi G, Bossari S (1995) Angiogenesis in colorectal tumours: microvessel quantitation in adenomas and carcinomas with clinicopathological correlations. Cancer Res 55:5049–5053
7. Boucher Y, Rakesh KJ (1992) Microvascular pressure is the principal driving force for interstitial hypertension in solid tumours: implications for vascular collapse. Cancer Res 52:5110–5114
8. Breier G, Risau W (1996) The role of vascular endothelial growth factor in blood vessel formation. Trends Cell Biol 6:454–456
9. Buyse M, Piedbois P (2001) Should Dukes' B patients receive adjuvant therapy? A statistical perspective. Semin Oncol 28:20–24
10. Cheng WF, Lee CN, Chu JS, Chen CA, Chen TM, Shau WY, Hsieh CY, Hsieh FJ (1999) Vascularity index as a novel parameter for the in vivo assessment of angiogenesis in patients with cervical carcinoma. Cancer 85:651–657
11. Choi HJ, Hyun MS, Jung GJ, Kim SS, Hong SH (1998) Tumour angiogenesis as a prognostic predictor in colorectal carcinoma with special reference to mode of metastasis and recurrence. Oncology 55:575–581
12. Clark WH Jr, Elder DE, Guerry D IV, Braitman LE, Trock BJ, Schultz D, Synnestvedt M, Halpern AC (1989) Model predicting survival in stage I melanoma based on tumour progression. J Natl Cancer Inst 81:1893–1904
13. Clemente C, Mihm M, Bufalino R, Zurrida S, Collini P, Cascinelli N (1996) Prognostic value of tumour infiltrating lymphocytes in the vertical growth phase of primary cutaneous melanoma. Cancer 7:1303–1310
14. Davidson B, Goldberg I, Gotlieb WH, Lerner-Geva L, Ben-Baruch G, Agulansky L, Novikov I, Kopolovic J (1999) Macrophage infiltration and angiogenesis in cervical squamous cell carcinoma. Clinicopathologic correlation. Acta Obstet Gynecol Scand 78:240–244
15. Dazzi C, Cariello A, Maioli P, Solaini L, Scarpi E, Rosti G, Lanzanova G, Marangolo M (1999) Prognostic and predictive value of intratumoural microvessel density in operable non-small-cell lung cancer. Lung Cancer 24:81–88
16. Etoh T, Shibuta K, Barnard GF, Kitano S, Mori M (2000) Angiogenin expression in human colorectal cancer: the role of focal macrophage infiltration. Clin Cancer Res 6:3545–3551
17. Fidler J, Kerbel RS, Ellis LM (2001) Biology of cancer: angiogenesis. In: DeVita Jr VT, Hellman S, Rosenberg SA (eds) Cancer. Principles and practice of oncology. Lippincott Williams and Wilkins, Philadelphia, pp 137–148
18. Fielding LP, Phillips RK, Fry JS, Hittinger R (1986) Prediction of outcome after curative resection for large bowel cancer. Lancet 2:904–907
19. Folkman J (1995) Tumour angiogenesis. In: Mendelsohn J, Howley, PM, Israel MA, Liotta LA (eds) The molecular basis of cancer. Saunders, Philadelphia, pp 206–232
20. Folkman J, Long DM, Becker FF (1963) Growth and metastasis of tumour in organ culture. Cancer 16:453
21. Fontanini G, Vignati S, Pacini F, Pollina L, Basolo F (1996) Microvessel count: an indicator of poor outcome in medullary thyroid carcinoma but not in other types of thyroid carcinoma. Mod Pathol 9:636–641
22. Fox SB, Gatter KC, Harris AL (1996) Tumour angiogenesis. J Pathol 179:232–237
23. Frank RE, Saclarides TJ, Leurgans S, Speziale NJ, Drab EA, Rubin DB (1995) Tumour angiogenesis as a predictor of recurrence and survival in patients with node-negative colon cancer. Ann Surg 222:695–699
24. Fujimoto J, Sakaguchi H, Aoki I, Tamaya T (2000) Clinical implications of expression of interleukin 8 related to angiogenesis in uterine cervical cancers. Cancer Res 60:2632–2635
25. Giatromanolaki A, Stathopoulos GP, Tsiobanou E, Papadimitriou C, Georgoulias V, Gatter KC (1999) Combined role of tumour angiogenesis, bcl2, and p53 expression in the prognosis of patients with colorectal carcinoma. Cancer 86:1421–1430
26. Guidoboni M, Gafa R, Viel A, Doglioni C, Russo A, Santini A, Del Tin L, Macri E, Lanza G, Boiocchi M, Dolcetti R (2001) Microsatellite instability and high content of activated cytotoxic lymphocytes identify colon cancer patients with a favorable prognosis. Am J Pathol159:297–304
27. Heimann R, Ferguson D, Powers C, Recant WM, Weichselbaum RR, Hellman S (1996) Angiogenesis as a predictor of long-term survival for patients with node-negative breast cancer. J Natl Cancer Inst 88:1764–1769
28. Jones N, Iljin K, Dumont DJ, Alitalo K (2001) TIE receptors: new modulators of angiogenic and lymphangiogenic responses. Nat Rev Mol Cell Biol 2:257–267
29. Kimura T, Tanaka S, Haruma K, Sumii K, Kajiyama G, Shimamoto F, Kohno N (2000) Clinical significance of MUC1 and E-cadherin expression, cellular proliferation, and angiogenesis at the deepest invasive portion of colorectal cancer. Int J Oncol 16:55–64

30. Kumar S, Ghellal A, Li C, Bryne G, Haboubi N, Wang JM, Bundred N (1999) Breast carcinoma: vascular density determined using CD105 antibody correlates with tumour prognosis. Cancer Res 59:856–861
31. Leek RD, Hunt NC, Landers RJ, Lewis CE, Royds JA, Harris AL (2000) Macrophage infiltration is associated with VEGF and EGFR expression in breast cancer. J Pathol 190:430–436
32. Marsoni S (2001) Efficiacy of adjuvant fluorouracil and leucovorin in stage B2 and C colon cancer. International multicenter pooled analysis of colon cancer trials investigators. Semin Oncol 28:14–19
33. Matsuyama K, Chiba Y, Sasaki M, Tanaka H, Muraoka R, Tanigawa N (1998) Tumour angiogenesis as a prognostic marker in operable non-small cell lung cancer. Ann Thorac Surg 65:1405–1409
34. Matsumura M, Chiba Y, Lu C, Amaya H, Shimomatsuya T, Horiuchi T, Muraoka R, Tanigawa N (1998) Platelet-derived endothelial cell growth factor/thymidine phosphorylase expression correlated with tumour angiogenesis and macrophage infiltration in colorectal cancer. Cancer Lett 128:55–63
35. Naito Y, Saito K, Shiiba K, Ohuchi A, Saigenji K, Nagura H, Ohtani H (1998) $CD8^+$ T cells infiltrated within cancer cell nests as a prognostic factor in human colorectal cancer. Cancer Res 58:3491–3494
36. Nishie A, Ono M, Shono T, Fukushi J, Otsubo M, Onoue H, Ito Y, Inamura T, Ikezaki K, Fukui M, Iwaki T, Kuwano M (1999) Macrophage infiltration and heme-oxygenase 1 expression correlate with angiogenesis in human gliomas. Clin Cancer Res 5:1107–1113
37. Obermair A, Tempfer C, Wasicky R, Kaider A, Hefler L, Kainz C (1999) Prognostic significance of tumour angiogenesis in endometrial cancer. Obstet Gynecol 93:367–371
38. Ono M, Torisu H, Fukushi J, Nishie A, Kuwano M (1999) Biological implications of macrophage infiltration in human tumour angiogenesis. Cancer Chemother Pharmacol 43[Suppl]: S69–S71
39. Orre M, Rogers PA (1999) Macrophages and microvessel density in tumours of the ovary. Gynecol Oncol 73:47–50
40. Pavlopoulos PM, Konstantinidou AE, Agapitos E, Kavantzas N, Nikolopoulou P, Davaris P (1998) A morphometric study of neovascularization in colorectal carcinoma. Cancer 83:2067–2075
41. Risau W (1997) Mechanisms of angiogenesis. Nature 386:671–674
42. Ropponen KM, Eskelinen MJ, Lipponen PK, Alhava E, Kosma VM (1997) Prognostic value of tumour-infiltrating lymphocytes (TILs) in colorectal cancer. J Pathol 182:318–324
43. Sage EH (1998) Pieces of eight: bioactive fragments of extracellular proteins as regulators of angiogenesis. Trends Cell Biol 7:182–186
44. Saito S, Tsuno N, Nagawa H, Sunami E, Zhengxi J, Osada T, Kitayama J, Shibata Y, Tsuruo T, Muto T (2000) Expression of platelet-derived endothelial cell growth factor correlates with good prognosis in patients with colorectal carcinoma. Cancer 88:42–49
45. Shibusa T, Shijubo N, Abe S (1998) Tumour angiogenesis and vascular endothelial growth factor in stage I lung adenocarcinoma. Clin Cancer Res 4:1483–1487
46. Sim BK, MacDonald NJ, Gubish ER (2000) Angiostatin and endostatin: endogenous inhibitors of tumour growth. Cancer Metastasis Rev 19:181–190
47. Skibber JM, Hoff PM, Minsky BD (2001) Cancer of the rectum. Radical surgery and adjuvant postoperative combined modality therapy for resectable rectal cancer. In: DeVita VT Jr, Hellman S, Rosenberg SA (eds) Cancer. Principles and practice of oncology. Lippincott Williams and Wilkins, Philadelphia, pp 1296–1298
48. Skibber JM, Minsky BD, Hoff PM (2001) Cancer of the colon. In: DeVita VT Jr, Hellman S, Rosenberg SA (eds) Cancer. Principles and practice of oncology. Lippincott Williams and Wilkins, Philadelphia, pp 1217–1218
49. Skibber JM, Minsky BD, Hoff PM (2001) Cancer of the colon. Adjuvant therapies. In: DeVita VT Jr, Hellman S, Rosenberg SA (eds) Cancer. Principles and practice of oncology. Lippincott Williams and Wilkins, Philadelphia, pp 1245–1254
50. Strömblad S, Cheresh DA (1996) Cell adhesion and angiogenesis. Trends Cell Biol 6:462–467
51. Sun HC, Tang ZY, Li XM, Zhou YN, Sun BR, Ma ZC (1999) Microvessel density of hepatocellular carcinoma: its relationship with prognosis. J Cancer Res Clin Oncol 125:419–426
52. Takanami I, Takeuchi K, Kodaira S (1999) Tumour-associated macrophage infiltration in pulmonary adenocarcinoma: association with angiogenesis and poor prognosis. Oncology 57: 138–142
53. Takebayashi Y, Aklyama S, Yamada K, Akiba S, Aikou T (1996) Angiogenesis as an unfavourable prognostic factor in human colorectal carcinoma. Cancer 78:226–231
54. Tanigawa N, Amaya H, Matsumura M, Lu C, Kitaoka A, Matsuyama K, Muraoka R (1997) Tumour angiogenesis and mode of metastasis in patients with colorectal cancer. Cancer Res 57:1043–1046
55. Tanigawa N, Amaya H, Matsumura M, Shimomatsuya T (1997) Correlation between expression of vascular endothelial growth factor and tumour vascularity, and patient outcome in human gastric carcinoma. J Clin Oncol15:826–832
56. Tanigawa N, Matsumura M, Amaya H, Kitaoka A, Shimomatsuya T, Lu C, Muraoka R, Tanaka T (1997) Tumour vascularity correlates with the prognosis of patients with oesophageal squamous cell carcinoma. Cancer 79:220–225
57. Tomisaki S, Ohno S, Ichiyoshi Y, Kuwano H, Maehara Y, Sugimachi K (1996) Microvessel quantification and its possible relation with liver metastasis in colorectal cancer. Cancer 77:1722–1728
58. Toomey D, Harmey J, Condron C, Kay E, Bouchier-Hayes D (1999) Phenotyping of immune cell infiltrates in breast and colorectal tumours. Immunol Invest 28:29–41
59. Torisu H, Ono M, Kiryu H, Furue M, Ohmoto Y, Nakayama J, Nishioka Y, Sone S, Kuwano M (2000) Macrophage infiltration correlates with tumour stage and angiogenesis in human malignant melanoma: possible involvement of TNFalpha and IL-1alpha. Int J Cancer 85:182–188
60. Van de Rijn M, Rouse RV (1994) CD34 a review. Appl Immunohistochem 2:71–80
61. Wein A, Hahn EG, Merkel S, Hohenberger W (2000) Adjuvant chemotherapy for stages II (Dukes' B) colon cancer: too early for routine. Eur J Surg Oncol 26:730–732
62. Zetter BR (1998) Angiogenesis and tumour metastasis. Annu Rev Med 49:407–427

Virchows Arch (2004) 445:168–178
DOI 10.1007/s00428-004-1043-z

ORIGINAL ARTICLE

M. Kosmahl · U. Pauser · K. Peters · B. Sipos · J. Lüttges · B. Kremer · G. Klöppel

Cystic neoplasms of the pancreas and tumor-like lesions with cystic features: a review of 418 cases and a classification proposal

Received: 19 February 2004 / Accepted: 8 April 2004 / Published online: 8 June 2004
© Springer-Verlag 2004

Abstract Although cystic neoplasms and lesions of the pancreas are rare, they have attracted a great deal of attention because of their potential curability. Since, in recent years, several new entities have been identified, the relative frequency of the tumors and their classification need to be reevaluated. In a series of 1454 tumorous lesions of the pancreas collected between 1971 and 2003 in our surgical pathology files and consultation files, all cystic pancreatic neoplasms and tumor-like lesions were identified and typed both histologically and immunohistochemically. There were 418 cases (29%) showing cysts with a diameter ranging between 0.5 cm and 27 cm. Most common were solid pseudopapillary neoplasms (21%) and intraductal papillary-mucinous neoplasms (18%). When only the cystic neoplasms and lesions that had been resected in a single institution were considered, intraductal papillary mucinous neoplasms were the most frequent cystic neoplasms, while solid pseudopapillary neoplasms took fifth place behind ductal adenocarcinomas with cystic features, serous cystic neoplasms and mucinous cystic neoplasms. The most frequent cystic tumor-like lesions were pancreatitis-associated pseudocysts. New and rare entities that have recently been identified are mucinous nonneoplastic cysts, acinar cell cystadenomas and cystic hamartomas. Bearing in mind that figures from referral centers such as ours may be biased regarding the relative frequency of lesions, we concluded from our data that intraductal papillary-mucinous neoplasms are the most frequently occurring pancreatic cystic neoplasms, rather than solid pseudopapillary neoplasms. It was possible to classify all cystic lesions encountered in our files or described in the literature in a new system that distinguishes between neoplastic and nonneoplastic lesions, with further subdivisions into epithelial (adenomas, borderline neoplasms and carcinomas) and nonepithelial tumors. This classification is easy to handle and enables a distinction on the basis of clinical behavior and prognosis.

Keywords Pancreatic tumors · Cystic neoplasms · Frequency · Classification · Differential diagnosis

M. Kosmahl · U. Pauser · K. Peters · B. Sipos · J. Lüttges · G. Klöppel
Department of Pathology, University of Kiel, Germany

B. Kremer
Department of Surgery, University of Kiel, Germany

M. Kosmahl (✉)
Department of Pathology, University of Kiel, Michaelisstrasse 11, 24105 Kiel, Germany
e-mail: mkosmahl@path.uni-kiel.de
Tel.: +49-431-5973440
Fax: +49-431-5973462

Introduction

Cystic tumors of the pancreas are rare compared with the solid tumors of this gland. The interest that they have received, however, is disproportional to their incidence, mainly for three reasons. First, if appropriately treated, cystic tumors of the pancreas are usually cured by resection, in contrast to ductal adenocarcinoma (DAC), the predominant solid tumor [29]. Second, modern imaging techniques allow more precise recognition of cystic lesions, even if small and asymptomatic. Third, the decreasing risk of pancreatic surgery has led to an increase in the number of resected cystic lesions of the pancreas, which in turn has conspicuously furthered our knowledge of these special lesions.

The broad spectrum of pancreatic neoplasms and tumor-like lesions with cystic features has recently been reviewed [5, 26]. These reviews revealed that cystic tumors of the pancreas are very variable in their morphology, clinical behavior and pathogenesis. Because there has been no systematic study in a large series of cases comparing the incidence and biology of these tumors, we reviewed all cystic processes of the pancreas collected in our files over a period of 30 years. Also included were tumors and lesions whose cystic structures were not lined by epithelial cells but represented necrotic and usually

also hemorrhagic areas that had been transformed into cystic cavities by resorption of the necrotic tissue. Typical examples of such cystic degenerative lesions are solid pseudopapillary neoplasms (SPNs) [16, 24, 27] and pseudocysts [25]. Most of the neoplasms that we encountered in our series are well known and were included in the most recent World Health Organization (WHO) classification. However, recently a few new tumors (i.e., acinar cell cystadenoma, mucinous nonneoplastic cyst and cystic hamartoma) have been described. Because for practical purposes the cystic neoplasms and lesions of the pancreas need to have a classification system of their own, we attempted to develop a classification that is of morphological and biological relevance and can easily incorporate all new entities.

Materials and methods

The cases were retrieved from the surgical pathology files and consultation files of the Department of Pathology of the University of Kiel. They were collected during the period from 1971 to 2003. The diagnosis of the neoplasms was based on the WHO classification [18]. Clinical information was obtained from the patients' records and, in many cases, from the clinicians in charge. In most patients, the tumors had been removed surgically. All specimens were fixed in 4% formaldehyde solution and embedded in paraffin. Deparaffinized sections were stained with hematoxylin and eosin and periodic acid-Schiff. Where appropriate, additional immunohistochemical staining was performed, using several or all of the primary antisera listed in Table 1. Immunohistochemical analysis was carried out on serial sections cut from the cystic epithelial neoplasms and tumor-like lesions using the avidin-biotin-peroxidase technique (ABC ELITE, Vector Laboratories, Burlingame, CA, USA). Endogenous phosphatase activity was blocked with 1 mM levamisole in the substrate solution. The slides were either directly immunostained or first pretreated by incubation with protease or boiling in citrate-buffered saline for 3.5 min. The tumor-free adjacent pancreatic parenchyma and tissue from colon carcinomas, granulosa cell tumors of the ovary, breast carcinomas and stomach mucosa served as controls.

Results

Frequency

A total of 1454 pancreatic neoplasms and tumor-like lesions, such as pancreatitis-associated pseudocysts, were retrieved. The most frequent pancreatic neoplasms were DACs (483 cases), followed by endocrine tumors (ETs) (339 cases) and various other neoplasms (286 cases). Tumor-like lesions accounted for 269 cases (18%). Of these 1454 pancreatic neoplasms and tumor-like lesions, 418 cases (29%) showed cystic features (Table 2). Most numerous were SPNs (89 cases), followed by intraductal papillary-mucinous neoplasms (IPMNs) (77 cases), pancreatitis-associated pseudocysts (73 cases), serous cystic neoplasms (46 cases), mucinous cystic neoplasms (MCNs) (32 cases), DACs with cystic features (30 cases), cystic endocrine neoplasms (18 cases), retention cysts (12 cases), mucinous nonneoplastic cysts (9 cases), para-ampullary duodenal wall cysts (7 cases), acinar cell cystadenocarcinomas (5 cases), acinar cell cystadenomas (4 cases), lymphoepithelial cysts (3 cases), cystic metastases of a renal cell carcinoma (2 cases) and cystic hamartomas (2 cases). In addition, there were a number of individual cases with other diagnoses (for details see Table 2). Among the 418 cases, there were 325 neoplasms (78%), including such tumors as acinar cell cystadenomas and cystic hamartomas. These cystic neoplasms accounted for 28% (330/1186) of all primary neoplasms of the pancreas.

To establish the relative frequency of cystic neoplasms and lesions encountered in a single institution, the pancreatic neoplasms and tumor-like lesions resected in the Department of Surgery, University Kiel, during the period between 1995 and 2003 were evaluated separately. This series comprised 248 cases, including 129 DACs (13 with cystic features), 23 endocrine neoplasms (none with cystic features), 28 cystic neoplasms, 13 ampullary carcino-

Table 1 Antibodies used for immunostaining of cystic neoplasms of the pancreas. *CK* cytokeratin

Antigen/antibody	Host species	Source	Working dilution
CK7	Mouse	Dako	1:100[p]
Cam5.2 (CK8,18)	Mouse	Becton Dickinson (San Jose, CA, USA)	1:10[p]
CK5/6	Mouse	Zymed	1:100[b]
Vimentin	Mouse	Dako	1:200[b]
β-Catenin	Mouse	Zymed	1:250[b]
Calretinin	Rabbit	Chemicon Int. (Temecula, CA, USA)	1:100[p]
α-Inhibin	Mouse	Serotec (Oxford, UK)	1:10[b]
Carcinoembryonic antigen	Mouse	Dako	1:100[b]
Chromogranin A	Mouse	Linaris (Wertheim-Bettingen, Germany)	1:2
Synaptophysin	Rabbit	Biometra (Göttingen, Germany)	1:1500[b]
Neuron-specific enolase	Mouse	Dako	1:500[b]
Glucagon	Rabbit	Biogenex	1:60
Trypsin	Rabbit	Our laboratory	1:500[b]
Estrogen receptor	Mouse	Dako	1:30[b]
Progesterone receptor	Mouse	Dako	1:30[b]
MUC1	Mouse	Novo-Castra (Newcastle, UK)	1:100[b]
MUC2	Mouse	Novo-Castra	1:100[b]
MUC5AC	Mouse	Chemicon	1:500[b]
MUC6	Mouse	Novo-Castra	1:100[b]

[b] Antigen retrieval: boiling
[p] Antigen retrieval: protease treatment

Table 2 Number and relative frequency (%) of neoplasms and tumor-like cystic lesions retrieved from the files of the Department of Pathology, University Kiel, 1971–2003

Diagnosis	*n* (%)
Solid pseudopapillary neoplasm	89 (21.2)
Intraductal papillary-mucinous neoplasm	77 (18.3)
Pancreatitis-associated pseudocyst	73 (17.5)
Serous microcystic adenoma	24 (5.7)
Serous oligocystic ill-demarcated adenoma	16 (3.8)
Solid variant of serous cystic adenoma	1 (0.2)
Von Hippel–Lindau-associated serous cystic neoplasm	2 (0.4)
Serous cystadenocarcinoma	3 (0.7)
Mucinous cystic neoplasm	32 (7.6)
Ductal adenocarcinoma with cystic features	30 (7.2)
Cystic endocrine tumor	18 (4.3)
Retention cyst	12 (2.8)
Mucinous nonneoplastic cyst	9 (2.1)
Paraampullary duodenal wall cyst	7 (1.7)
Acinar cell cystadenocarcinoma	5 (1.2)
Acinar cell cystadenoma	4 (1.0)
Lymphoepithelial cyst	3 (0.7)
Cystic hamartoma	2 (0.4)
Cystic metastatic renal cell carcinoma	2 (0.4)
Endometrial cyst	1 (0.3)
Cystic pancreatoblastoma	1 (0.2)
Cystic paraganglioma	1 (0.2)
Lymphangioma	1 (0.2)
Malignant peripheral nerve sheath tumor with cystic features	1 (0.2)
Malignant peripheral neuroectodermal tumor with cystic features	1 (0.2)
Malignant epitheloid mesothelioma with cystic features	1 (0.2)
Leiomyosarcoma with cystic features	1 (0.2)
Gastrointestinal stromal tumor with cystic features	1 (0.2)
Total	418

mas that had infiltrated the pancreas, 3 carcinomas of the stomach and 1 carcinoma of the colon that had infiltrated the pancreas, 4 nonepithelial tumors and 2 metastases of renal cell carcinomas. In addition, there were 44 tumor-like lesions (all from patients with chronic pancreatitis), 21 of which showed pancreatitis-associated pseudocysts. Altogether, this series from one department comprised 62 cystic neoplasms and tumor-like lesions, which accounted for 25% (62/248) of all cases. If only the cystic neoplasms were considered, they accounted for 15% (28/184) of all primary neoplasms of the pancreas. This percentage increased to 22% (41/184), if DACs with cystic features were included among the cystic neoplasms. Table 3 lists all neoplasms and tumor-like lesions with cystic features in order of their relative frequency. It reveals that IPMNs (24%) were the most common entity in this series.

Clinicopathological data

Table 4 summarizes the data on age, gender, size, localization and communication with the duct system of the common cystic epithelial neoplasms of the pancreas.

Table 3 Cystic pancreatic neoplasms and lesions resected at the Department of Surgery, University of Kiel, 1995–2003

Type	*n* (%)
Pancreatitis-associated pseudocyst	21 (34)
Intraductal papillary-mucinous neoplasm	15 (24)
Ductal adenocarcinoma with cystic features	13 (21)
Serous cystic neoplasm	6* (10)
Mucinous cystic neoplasm	5 (8)
Solid pseudopapillary neoplasm	2 (3)
Total	62 (100)

* Two serous microcystic adenomas and four serous oligocystic ill-demarcated adenomas

Intraductal papillary-mucinous neoplasms

The series of 77 IPMNs comprised 19 adenomas, 13 borderline tumors and 45 intraductal carcinomas, 32 of which were invasive. In one case, a metastasis was found in the liver; in another case, there was a peritoneal metastasis. The majority of these neoplasms occurred in the main pancreatic duct in the head and body region (49 tumors). The tumors' cystic changes were caused by a dilatation of the duct from which the tumor originated (Fig. 1a). The cystic structures varied in size from 1 cm to 13 cm. Microscopically, the normal ductal epithelium was replaced by mucin-producing columnar cells showing papillary proliferations and variable degrees of cellular atypia. Of the IPMNs, 64 were classified as intestinal type (MUC1−/MUC2+ immunophenotype) (Fig. 1b), 6 as pancreatobiliary type (MUC1+/MUC2− immunophenotype) and 7 as oncocytic type (focally positive for MUC1 and MUC2). Of the IPMNs, 32 had an invasive component, showing the features of either a mucinous (colloid) carcinoma or a ductal carcinoma. The MUC profiles of the mucinous and ductal carcinoma component corresponded to the intestinal or pancreatobiliary type, respectively, of IPMN. All IPMNs stained for carcinoembryonic antigen (CEA), CKs (7, 8, 18, 19) and β-catenin (membranous pattern) and were negative for α-inhibin, neuron-specific enolase (NSE) and trypsin.

Serous cystic neoplasms

This group of 46 tumors encompassed the entities serous microcystic adenoma (SMA), serous oligocystic and ill-demarcated adenoma (SOIA), Von Hippel–Lindau-associated cystic neoplasm (VHL-CN) and serous cystadenocarcinoma. All these tumors were composed of the same cell type. It was a cuboidal or flattened epithelial cell with pale to clear cytoplasm and a small oval nucleus. A single layer of these cells lined the cyst and produced serous fluid. Immunohistochemically, these cells were found to stain for CKs (7, 8, 18, 19), α-inhibin, MUC6 and usually also for NSE [32] and were negative for trypsin. Staining for β-catenin revealed a membranous reaction. One solid tumor that showed the same cytological features as the serous cystic neoplasms was considered a solid variant of the serous cystic neoplasms

Table 4 Clinicopathological data on the most common cystic tumors of the pancreas encountered in a series of 1454 pancreatic neoplasms and tumor-like lesions collected between 1971–2003. *SPN* solid pseudopapillary neoplasm, *IPMN* intraductal papillary-mucinous neoplasm, *MCN* mucinous cystic neoplasm, *DAC* ductal adenocarcinoma, *SMA* serous microcystic adenoma, *ET* endocrine tumor, *SOIA* serous oligocystic ill-demarcated adenoma

Entity	*n*	Age in years (range)	Male	Female	Size in cm (mean)	Head	Body	Tail	Pancreas	Extrapan-creatic	Duct communication
SPN	89	30 (11–73)	13%	87%	2–17 (7)	25 (28%)	12 (13%)	27 (30%)	21 (24%)	4 (4%)	No
IPMN	77	64 (35–85)	60%	40%	1–13 (5)	58 (75%)	4 (5%)	6 (8%)	9 (12%)	-	Yes
MCN	32	47 (23–78)	-	100%	2.7–23 (9.8)	2 (6%)	4 (13%)	23 (72%)	3 (9%)	-	No
DAC, cystic	30	63 (43–78)	40%	60%	1–19 (5.6)	12 (40%)	4 (13%)	7 (23%)	7 (23%)	-	No
SMA	24	71 (45–91)	12%	88%	2.5–16 (6.4)	5 (21%)	2 (8%)	15 (63%)	2 (8%)	-	No
ET, cystic	18	53 (28–81)	28%	72%	1.2–15 (5.8)	6 (22%)	2 (33%)	6 (33%)	4 (22%)	-	No
SOIA	16	63 (38–85)	62%	38%	3–14 (7.2)	11 (69%)	-	4 (25%)	1 (6%)	-	No

[51]. Although histologically the serous cystic neoplasms looked alike, they differed in their localization, sex distribution, biology and genetic alterations [11, 32].

Among the serous cystic neoplasms, the most common subtype was SMA. The 24 SMAs in our series presented as single, well-circumscribed tumors, consisting of numerous small cysts with diameters between 0.1 cm and 0.5 cm. These small cysts were arranged around a central stellate scar that occasionally contained small calcifications.

The SOIAs showed a few relatively large cysts (diameter from 0.2 cm to 2.5 cm) and lacked the central stellate scar and sharp demarcation of the SMAs. One patient had a synchronous metastasis of a renal cell carcinoma in the body/tail region of the pancreas.

The two VHL-CNs in our series occurred in a 29-year-old woman and a 36-year-old man. The first patient had a history of cerebellar angiomas. The pancreatic resection specimen showed multiple serous cysts in the body/tail region of the pancreas. In a subsequent resection 2 years later, pancreatic tissue with additional pancreatic cysts was removed. The second patient had multiple cysts in the head region of the pancreas that had caused jaundice. The patient also had a cyst in the kidney and had an operation for a cerebellar hemangioblastoma. The patient's mother was known to suffer from VHL disease.

Three serous cystadenocarcinomas were among the serous cystic neoplasms. The first patient, a 60-year-old woman, had a cystic tumor 9.5 cm in diameter in the pancreas tail infiltrating the colon and the liver. The second patient, a 71-year-old man, had a tumor 4 cm in diameter in the head of the pancreas with metastases in regional lymph nodes [61]. The third patient, a 70-year-old man, had a large cystic mass with a diameter of 11 cm that involved the tail of the pancreas, the spleen and the stomach wall. In the liver, there were numerous small metastases with a maximum diameter of 1.5 cm [17]. With the exception of occasional mild nuclear polymorphism, the histological and immunohistochemical features of the serous cystadenocarcinomas and their metastases resembled those of SMAs.

The solid variant of serous cystic adenoma occurred in a 50-year-old man. It was a well-demarcated tumor with a diameter of 2.5 cm in the immediate vicinity of an invasive DAC. The clear tumor cells stained immunohistochemically for α-inhibin and were negative for vimentin.

Mucinous cystic neoplasms

The series of MCNs consisted of 32 tumors. The tumors presented as large round cystic masses with a unilocular or multilocular cut surface. Microscopically, the cysts were lined by mucin-producing epithelial cells with varying degrees of dysplasia, supported by an ovarian-like stroma. Of the MCNs, 10 were classified as adenomas (mean age, 42 years), 8 as borderline tumors (mean age, 39 years) and 14 as carcinomas (mean age, 56 years). One patient simultaneously had a lymphoepithelial cyst [8]. Of

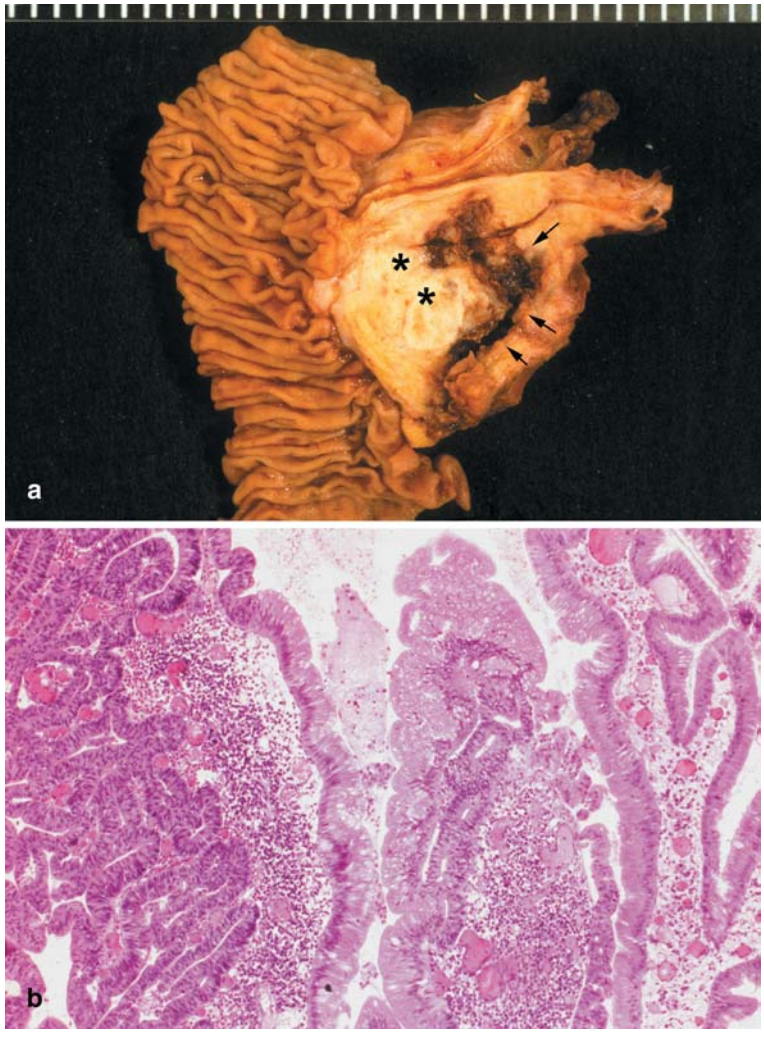


Fig. 1 Intraductal papillary-mucinous neoplasm with an invasive component. **A** Resection specimen showing a cystic dilation of part of the head of the pancreas that communicates with the main pancreatic duct (*arrows*). Invading tumor (*asterisks*). **B** The papillary proliferations of the intraductal component of the tumor show an intestinal cellular phenotype. Hematoxylin and eosin, ×120

the 14 carcinomas, 11 had an invasive component that usually showed the pattern of a DAC. One case each showed the features of an undifferentiated carcinoma with or without osteoclast-like giant cells, an adenosquamous carcinoma or a sarcoma. Immunohistochemically, the epithelial component of MCNs stained for CK7, 8, 18 and 19, CEA and MUC5A/C. MUC1 was additionally expressed in the invasive component [43]. Cells of the stromal component stained for α-inhibin, calretinin and estrogen and progesterone receptors.

Solid pseudopapillary neoplasms

Our series of 95 SPNs included 89 tumors with cystic features. Grossly, the remaining tumors had a solid appearance. The extent of the cystic changes varied from tumor to tumor, affecting either parts of the tumor or almost the entire tumor tissue (Fig. 2a). The cystic structures contained hemorrhagic debris and were usually surrounded by necrotic-hemorrhagic tissue (Fig. 2b). The six SPNs without cystic changes, which were excluded from this study, were smaller than the SPNs with cystic changes (mean size 4.7 cm versus 7 cm). Microscopically, the cystic SPNs showed pseudopapillary tissue structures next to areas with fresh hemorrhage between pseudopapillary elements and cystic areas containing blood and debris. The uniform tumor cells showed diffuse and strong positivity for vimentin, NSE and the progesterone receptor and occasionally faint staining for synaptophysin and CKs 8 and 18. In addition, they showed nuclear positivity for β-catenin. They were negative for CEA and trypsin. Of the SPNs, 10% (nine cases) were malignant, with metastases to the peritoneum and/or liver.

Ductal adenocarcinomas

The series of DACs with cystic structures consisted of 30 tumors. The majority of the carcinomas (19 cases, 18 well to moderately differentiated and 1 with adenosquamous differentiation) contained a varying amount of multiple small cystic structures that did not exceed 0.7 cm in diameter. The size of the tumors ranged from 2 cm to 15 cm (mean size 4.5 cm). Immunohistochemically, the cells lining the cystic structures showed the same staining

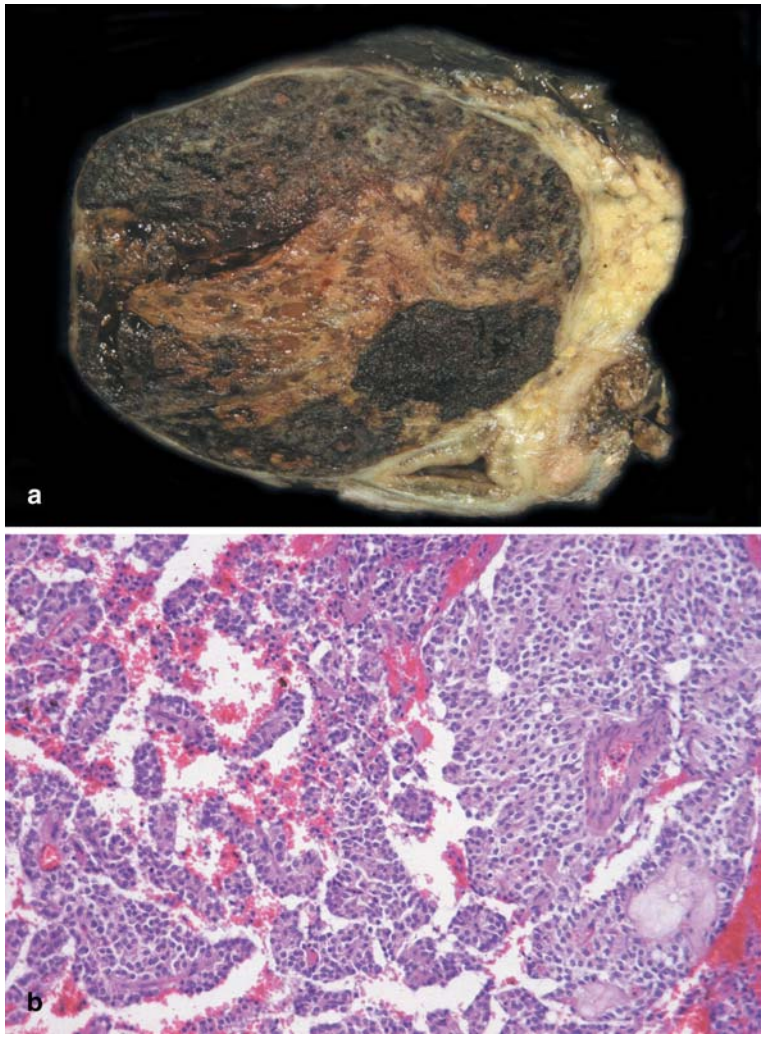


Fig. 2 Solid pseudopapillary neoplasm of the pancreas. **A** Resection specimen showing a well-demarcated tumor with cystic hemorrhagic degeneration. **B** Between pseudopapillary structures blood-filled spaces

pattern as the cells forming the small neoplastic ductal structures, i.e., positivity for MUC1 and CEA. Of the tumors, 11 (mean size 7.4 cm, range 4–19 cm) showed a central area of necrosis with cystic transformation. Most of these tumors were moderately to poorly differentiated DACs, but they also included two adenosquamous carcinomas, one medullary carcinoma and three undifferentiated carcinomas, one with osteoclast-like giant cells and a small DAC component [48].

Endocrine tumors

The series of cystic neuroendocrine neoplasms consisted of 18 tumors. Most tumors were solitary and exhibited either a unilocular cyst (6 cases) or a multilocular microcystic pattern (12 cases; mean size 5 cm). The microcystic tumors were lined by tumor cells that were positive for CKs 8 and 18, synaptophysin, chromogranin and commonly also glucagon. Six large malignant ETs (mean size 7.8 cm) displayed a central area of necrosis with cystic transformation. Two patients suffered from multiple endocrine neoplasia type 1 (MEN-1). In the first patient, one of the two ETs in the pancreas was cystic. The other patient showed a cystic ET among multiple ETs in the pancreas and duodenum. One additional patient had a solitary cystic ET in addition to multiple ETs without evidence of MEN-1.

Acinar cell cystadenoma

The series consisted of four cases, occurring in three women and one man (mean age, 38 years). One of the patients was an 8-year-old girl who showed a multicystic transformation of the pancreas with a diameter of 20 cm. The other three patients have been described previously [64]. The cyst-lining cells expressed trypsin, CKs (7, 8 and 18) and β-catenin (membranous pattern), but were negative for α-inhibin, NSE, CEA, synaptophysin and vimentin.

Acinar cell cystadenocarcinoma

The series consisted of five tumors, occurring in four men and one woman (mean age, 46 years; range 16–48 years).

In two tumors (5 cm and 11 cm in diameter), the cystic structures were composed of neoplastic acinar cells positive for trypsin, CKs (mainly 8 and 18) and β-catenin (membranous pattern), but negative for α-inhibin, NSE, vimentin and synaptophysin. In three other tumors (12, 20 and 21.5 cm in diameter), the cystic changes were caused by necrosis.

Rare epithelial neoplasms with cystic changes

This series consisted of four tumors with cystic changes caused by hemorrhagic necrotic alterations and two tumors with cysts with an epithelial lining. Cystic hemorrhagic changes were observed in a large pancreatoblastoma (10 cm in diameter) occurring in a 6-year-old boy, two metastases of renal clear cell carcinomas (occurring in a 59-year-old woman and an 80-year-old woman) and a cystic paraganglioma in the pancreatic head region (8 cm in maximum diameter) occurring in a 76-year-old woman. Epithelial cysts were observed in two hamartomas, both occurring in the head of the pancreas, one in a 25-year-old man (3 cm in diameter) and one in a 36-year-old female (10 cm). The cysts in the hamartomas showed flattened ductal epithelium and were embedded in fibrotic tissue that contained distorted and haphazardly organized small ducts, acini and single endocrine cells. Immunohistochemically, the pancreatoblastoma was characterized by the expression of CKs (mainly 8 and 18) and trypsin, the renal clear cell carcinomas by the co-expression of CK7 and vimentin and the hamartomas by the expression of CK7, 8 and 18 in the cystic and ductal structures.

Nonepithelial neoplasms

The series of nonepithelial neoplasms with cystic features consisted of a lymphangioma, a malignant epithelioid mesothelioma involving the pancreas, a malignant peripheral neuroectodermal tumor (PNET), a malignant gastrointestinal stromal tumor (GIST), a leiomyosarcoma and a malignant peripheral nerve sheath tumor (PNST). Their marker profiles corresponded to that typical for these tumors (data not shown).

The lymphangioma formed a microcystic mass (6 cm in diameter) occurring in the head of the pancreas of a 61-year-old woman. The malignant epithelioid mesothelioma was a large tumor (12 cm in diameter) showing prominent cystic degenerative changes in its center. It occurred in a 70-year-old man, was localized in the tail of the pancreas and invaded the wall of stomach and colon transversum [41]. The PNET was also a large tumor (22 cm in diameter) in the body/tail region of the pancreas containing cystic necrotic foci. It occurred in a 13-year-old girl [41]. The GIST presented as a partially cystic tumor (17 cm in diameter) involving the body and tail of the pancreas of a 36-year-old woman. The partially cystic leiomyosarcoma (11 cm in diameter) occurred in a 69-year-old woman and extended from the pancreas into the retroperitoneum. The PNST (19 cm in diameter) occurred in a 75-year-old man and contained multiple cystic foci [41].

Epithelial nonneoplastic tumor-like lesions

This series included retention cysts, lymphoepithelial cysts, mucinous nonneoplastic cysts, paraampullary duodenal wall cysts and endometrial cysts. Retention cysts, which result from duct obstruction, were observed in 12 cases, either associated with chronic pancreatitis or DAC. The patients with chronic pancreatitis (four men and two women; mean age, 43 years) had a single cyst (mean diameter, 4 cm) that occurred more frequently in the head of the pancreas than in the body or tail. The patients with a DAC (four women and two men; mean age, 65 years) had multiple small cysts (0.5–1.8 cm in maximum diameter), all localized at the tumor periphery in the head of the pancreas. Histologically, the retention cysts were lined by normal duct epithelium showing focal mucinous metaplasia. It stained for CKs (7, 8, 18, 19), but was negative for CEA and MUC1.

The three lymphoepithelial cysts (diameters from 1.5 cm to 5 cm) occurred in two men and one woman (mean age, 65 years; age range, 38–82 years) (two cases have been previously described) [6]. Microscopically, the lymphoepithelial cysts were lined by stratified squamous epithelium staining positively for CK5/6.

Mucinous nonneoplastic cysts of the pancreas affected nine patients (five of whom were previously described) [31]. These lesions occurred in five men and four women (mean age 58 years, range 20–88 years). Three patients showed obstructive jaundice, which occurred because the cystic lesion compressed and dislocated the common bile duct. The sizes of the cysts varied from 3 cm to 12 cm, and they were localized in the head (five), head/tail (one) and head/body (two) regions. One patient showed multiple cysts in the pancreas (maximum diameter 1 cm) with a large cyst (5 cm) in the head of the pancreas. Microscopically, the cysts were lined by mucin-producing cells without atypia. Immunohistochemically, they were positive for CKs (7, 8, 18, 19, 20), Ca 19–9 and MUC5AC. There was no malignant transformation (mean follow-up period 2 years).

The paraampullary duodenal wall cysts occurring in the duodenal wall and next to it caused jaundice, thereby imitating the symptoms of a DAC in the head of the pancreas. All of the seven patients were men (mean age 51 years, range 37–50 years). The size of the cysts varied from 2 cm to 17 cm. They showed a paraampullary localization in the wall of the duodenum (four cases) or next to it (three cases). Microscopically, the cysts in the duodenal wall showed mucin-producing duct epithelium, which was positive for the CKs 7, 8 and 18 and MUC5AC, and were surrounded by heterotopic pancreatic tissue. The cysts outside the duodenal wall had the features of small pseudocysts. In all cases, there was associated chronic inflammation and fibrosis surrounding the cysts and extending into the adjacent pancreatic tissue.

There was one endometrial cyst. It occurred in a 31-year-old woman who had multiple cysts (5 cm in diameter) in the tail of the pancreas connected to the spleen. Microscopically, the cysts showed endometrial glands and stroma as well as areas of epithelial denudation and hemorrhage.

Nonepithelial nonneoplastic tumor-like lesions

Most common were pseudocysts (Table 2 and Table 3). They usually occurred in alcohol-induced chronic pancreatitis. In five cases, the cause was duct obstruction due to a solid pancreatic neoplasm (three ETs, two DACs). One patient had a pancreas divisum, another a pancreas annulare. Four patients had acute pancreatitis, and three had hereditary pancreatitis. Most of the patients were men (51 men/22 women). The patients' age ranged from 3 years to 71 years. All of the patients with hereditary pancreatitis were girls (3, 5 and 17 years). The size of the pseudocysts varied from 0.5 cm to 9 cm in maximum diameter. The pseudocysts were found outside (27 cases) or within the pancreas (27 cases). In the remaining cases, the exact localization was not known. Histologically, the cysts were lined by granulation tissue and filled with hemorrhagic debris.

Discussion

The first description of a cystic tumor of the pancreas is probably that by Becourt in 1824: of a tumor "the size of a child's head and composed of a very strong fibrous wall" [14]. Because of the description and the fact that this "cystic tumor" occurred in a child, it is possible that it was a cystic pancreatoblastoma, but a pseudocyst cannot be fully excluded. An increasing number of cystic pancreatic tumors were observed at the end of the 19th century, when surgeons started to remove these lesions [59]. The first study on cystic epithelial neoplasms of the pancreas was probably that by Roux (cited in [59]), who reviewed cystic lesions reported by Riedel, Martin, Ménétrier and Hartmann prior to 1891. The oldest classification of pancreatic cysts that we are aware of is that of Yamane and Wegelin [60, 62], who distinguished congenital cysts, retention cysts, pseudocysts and cystadenomas. Subsequently, a number of case reports were published, which fell into the established classification system and did not expand it. An important step forward was the differentiation of serous cystic from MCNs by Compagno and Oertel [12] and Hodgkinson et al. [19]. Then followed the descriptions of the cystic variants of acinar cell carcinoma [10, 20, 56] and the cystic (ductectatic), mucin-producing, intraductal neoplasms [47, 49, 52] that were finally termed intraductal papillary-mucinous tumors [21, 28, 39, 54] and clearly distinguished from MCNs [55, 63]. Recently, the IPMNs have been subdivided into an intestinal, MUC2-positive type [which appears to be the precursor of mucinous noncystic (colloid) carcinoma] [42], a pancreatobiliary, MUC1-positive type and an oncocytic type [3]. Further new entities that have been described include serous oligocystic and ill-defined tumors [15] and lymphoepithelial cysts [6, 40]. SOIAs probably correspond to the serous macrocystic tumors described by Lewandrowski et al. [36] and have to be distinguished from SMAs [11, 32]. More recently, it was emphasized that the SPNs of the pancreas may often display cystic features [1] and that pancreatic DACs and endocrine neoplasms can also acquire cystic changes [1, 37].

Our series of 418 cystic neoplasms and tumor-like lesions of the pancreas includes all of the above-mentioned entities and also contains the most recently described entities (Table 2 and Table 3). These are mucinous nonneoplastic cysts [31], acinar cell cystadenoma [7, 64] and cystic hamartomas. Rare cystic lesions that have been described but were not observed in our series are parasitic cysts [23], congenital cysts, including those arising in inherited polycystic kidney disease [45, 46, 50], enterogenous cysts [22, 33, 44], dermoid cysts (cystic mature teratoma) [4], epidermoid cyst in intrapancreatic accessory spleen [4] and a few case reports, such as for cystic schwannoma [9, 35, 58] and cystic inflammatory tumor of the pancreas [38].

From daily practice, it is obvious that cystic changes of the pancreas are rare. In our files, however, they account for 29% of all pancreatic neoplasms and tumor-like lesions. If we consider only the cystic neoplasms and calculate their relative frequency among the primary neoplasms of the pancreas, the figure is 36%. This high percentage might reflect an increase in the resection rate of these tumors. However, despite the possibility that the number of cystic tumors observed in the pancreas has indeed increased because of their improved recognition and resectability, the most likely explanation is that our files contain a disproportionately large number of rare pancreatic tumors because of the department's function as a referral center for these diseases. To get more realistic figures on the frequency of cystic neoplasms and tumor-like lesions, we considered only the cases resected in the Department of Surgery of the University of Kiel between 1995 and 2003. In this series, cystic neoplasms and tumor-like lesions accounted for 25%, a figure that is also not entirely unbiased, because this department also acts as a referral center, but is certainly closer to reality than the 36% of the total series. This also holds for the relative frequency of the individual entities listed in the total series and in the one-institution series. While in the total series SPNs are the most common cystic change of the pancreas—followed by pancreatitis-associated pseudocysts—in the institutional series, pancreatitis-associated pseudocysts are most frequent (34%), followed by IPMNs (24%), DCAs with cystic features (21%), SCNs (10%) and MCNs (8%). SPNs (3%) rank only fifth, which seems to reflect the reality, because the first position for SPNs in our total series is most likely due to the special interest we are known to have in this peculiar neoplasm [28, 30]. When we compare our figures with those of other series [5, 34,

Table 5 Classification of cystic neoplasms and lesions of the pancreas

Neoplastic epithelial	Nonneoplastic epithelial
Benign	Congenital cyst (in malformation syndromes)
Intraductal papillary-mucinous adenoma	Lymphoepithelial cyst
Mucinous cystic adenoma	Mucinous nonneoplastic cyst
Serous microcystic adenoma	Enterogeneous cyst
Serous oligocystic ill-demarcated adenoma	Retention cyst
Von Hippel–Lindau associated cystic neoplasm	Paraampullary duodenal wall cyst
Benign neuroendocrine tumors, cystic	Endometrial cyst
Acinar cell cystadenoma	
Cystic teratoma (dermoid cyst)	
Accessory splenic epidermoid cyst	
Cystic hamartoma	
Borderline	
Intraductal papillary-mucinous neoplasm borderline	
Mucinous cystic neoplasm borderline	
Solid pseudopapillary neoplasm	
Malignant	
Intraductal papillary-mucinous carcinoma	
Mucinous cystic carcinoma	
Ductal adenocarcinoma, cystic	
Serous cystadenocarcinoma	
Pancreatoblastoma, cystic	
Cystic metastatic epithelial neoplasm	
Neuroendocrine carcinoma, cystic	
Neoplastic nonepithelial	**Nonneoplastic nonepithelial**
Benign nonepithelial neoplasm (e.g. lymphangioma)	Pancreatitis-associated pseudocyst
Malignant nonepithelial neoplasms (e.g. sarcomas)	Parasitic cyst

53] there are some differences. IPMNs and DACs with cystic features were most common in our series, while SCNs, MCNs and SPNs prevailed in the other series. Since 5–10 years ago IPMNs were often misdiagnosed as MCNs, their relative frequency has long been underestimated. We, therefore, believe that IPMNs, as recognized in our one-institution series, are indeed the most common cystic neoplasm of the pancreas, far surpassing MCNs and SCNs. The fact that DACs with cystic features are also frequent in our series but nonexistent in other studies, may be explained by the assumption that cystic features in DACs have not attracted much attention and have, therefore, probably been neglected. The only study on cystic tumors of the pancreas that also dealt with DACs with cystic features was that by Talamini et al. [57], who observed 6 of these tumors in a series of 50 cystic neoplasms.

The above-mentioned classification of Wegelin and Yamane [60, 62] was modified in the first fascicle of the Armed Forces Institute of Pathology (AFIP) on pancreatic tumors [16], in which Frantz distinguished cysts (traumatic, retention, congenital and parasitic) from cystic neoplasms (cystadenoma, teratoma and vascular tumors). In the AFIP fascicle on pancreatic tumors in the second series [13], Cubilla and Fitzgerald subdivided four groups (congenital cysts, retention cysts, pseudocysts and cystic neoplasms). The third series AFIP fascicle by Solcia, Capella and Klöppel distinguished cystic tumors of the pancreas on the basis of their biology (benign, borderline and malignant) from cysts. These tumors were then separated from tumor-like lesions.

As our knowledge of the cystic neoplasms and tumor-like lesions of the pancreas increases, it has become apparent that there is a need for a classification that incorporates all cystic lesions described thus far and that is easy to handle and may also facilitate the preoperative diagnosis. The classification that we are proposing here attempts to consider the basic biology and morphology of the cystic changes of the pancreas. Thus, we first separated the cystic processes into neoplastic and nonneoplastic cysts. In a second step, the cysts were then separated into those with and without an epithelial lining. This classification then results in four groups: neoplastic epithelial or nonepithelial and nonneoplastic epithelial or nonepithelial (Table 5). The most important and largest group is that of the neoplastic epithelial neoplasms. It contains the most common cystic neoplasms, such as IPMNs, MCNs, SCNs and SPNs, but also DACs and ETs with cystic features. We further subdivided this group according to the WHO classification [18] into benign, borderline and malignant tumors. The nonneoplastic nonepithelial group with its benign course includes the pseudocysts that are frequently associated with pancreatitis.

The differential diagnosis of many pancreatic cystic changes seems to be straightforward, because in addition to the morphological features, there are clinical criteria, such as age and sex, which help to establish the diagnosis. Nevertheless, it is quite common for uncertainties to remain in the preoperative work-up of these lesions, particularly if only a small biopsy specimen is available. In this situation, immunohistochemical stainings may be helpful. Our analysis revealed that many cystic neoplasms

Table 6 Immunohistochemical markers of the common cystic pancreatic neoplasms. *IPMN* intraductal papillary-mucinous neoplasm, *MCN* mucinous cystic neoplasm, *CK* cytokeratin, *SYN* synaptophysin, *TRYP* trypsin, *CEA* carcinoembryonic antigen, *NSE* neuron-specific enolase, *A-IN* α-inhibin, *VIM* vimentin, *β-CAT* β-catenin (nuclear staining), *CG* chromogranin A, *AAT* α-1-antitrypsin

Tumor type	CK7	CK8/18	MUC1	MUC2	SYN	TRYP	Other markers
IPMN, intestinal type	+	+	–	+	–**	–	CEA
IPMN, pancreaticobiliary type	+*	+	+	–	–**	–	CEA
IPMN, oncocytic type	+*	+	+	+	–	–	-
MCN, noninvasive	+	+	–	–	–**	–	CEA
MCN, invasive	+	+	+	–	–	–	CEA
Serous cystic neoplasm	+	+	–	–	–	–	NSE, A-IN, MUC6
Solid pseudopapillary neoplasm	–	–***	–	–	–***	–	NSE, VIM, β-CAT, AAT
Acinar cystadenocarcinoma	–	+	–	–	–	+	-
Ductal adenocarcinoma, cystic	+	+	+	–	–	–	CEA
Endocrine tumor, cystic	–**	+	–	–	+	–	CG, NSE, glucagon

* Occasionally negative
** Occasional positivity in single cells
*** Faint positivity in 25–50% of the cases

of the pancreas have a special distinguishing immunoprofile (Table 6). Markers that play a particular role in recognizing the various cystic lesions are the various MUCs, trypsin, α-inhibin, NSE and β-catenin. Using a set of these markers, it should be possible to identify most of the cystic lesions summarized in Table 6.

In summary, the exact morphological identification of cystic neoplasms and lesions of the pancreas in recent years has broadened our understanding of the diverse spectrum of these changes and now allows us to propose a classification system that distinguishes the lesions on the basis of their basic biology and morphology. The detailed knowledge of these special pancreatic changes, including their immunoprofiles, may help to improve the preoperative diagnosis and to assess the biology of these tumors more accurately than before. Despite the great advances in the recognition of the cystic neoplasms and tumor-like lesions of the pancreas, it is notable that only little is known about the etiology and pathogenesis of these tumors.

References

1. Adsay NV, Klimstra DS (2000) Cystic forms of typically solid pancreatic tumors. Semin Diagn Pathol 17:81–88
2. Adsay NV, Klimstra DS (2000) Cystic lesions of the pancreas. Saunders, Philadelphia
3. Adsay NV, Adair CF, Heffess CS, Klimstra DS (1996) Intraductal oncocytic papillary neoplasms of the pancreas. Am J Surg Pathol 20:980–994
4. Adsay NV, Hasteh F, Cheng JD, Klimstra DS (2000) Squamous-lined cysts of the pancreas: lymphoepithelial cysts, dermoid cysts (teratomas) and accessory-splenic epidermoid cysts. Semin Diagn Pathol 17:56–65
5. Adsay NV, Klimstra DS, Compton CC (2000) Cystic lesions of the pancreas. Introduction. Semin Diagn Pathol 17:1–6
6. Adsay NV, Hasteh F, Cheng JD, Bejarano PA, Lauwers GY, Batts KP, Klöppel G, Klimstra DS (2002) Lymphoepithelial cysts of the pancreas: a report of 12 cases and a review of the literature. Mod Pathol 15:492–501
7. Albores-Saavedra J (2002) Acinar cystadenoma of the pancreas: a previously undescribed tumor. Ann Diagn Pathol 6:113–115
8. Bernd HW, Burmester E, Horny HP (2002) Unusual coincidence of lymphoepithelial cyst and mucinous cystadenoma of the pancreas. Virchows Arch 441:303–305
9. Brown SZ, Owen DA, O'Connell JX, Scudamore CH (1998) Schwannoma of the pancreas: a report of two cases and a review of the literature. Mod Pathol 11:1178–1182
10. Cantrell BB, Cubilla AL, Erlandson RA, Fortner J, Fitzgerald PJ (1981) Acinar cell cystadenocarcinoma of human pancreas. Cancer 47:410–416
11. Capella C, Solcia E, Klöppel G, Hruban RH (2000) Serous cystic neoplasms of the pancreas. In: Hamilton SR, Aaltonen LA (eds) Pathology and genetics of tumours of the digestive system. WHO classification of tumours. IARC Press, Lyon, pp 231–233
12. Compagno J, Oertel JE (1978) Mucinous cystic neoplasms of the pancreas with overt and latent malignancy (cystadenocarcinoma and cystadenoma). A clinicopathologic study of 41 cases. Am J Clin Pathol 69:573–580
13. Cubilla AL, Fitzgerald PJ (1984) Tumors of the exocrine pancreas. AFIP atlas of tumor pathology, 2nd series, fascicle 19. Armed Forces Institute of Pathology, Washington, DC
14. de Lima JE, Javitt MC, Mathur SC (1999) Mucinous cystic neoplasm of the pancreas. Radiographics 19:807–811
15. Egawa N, Maillet B, Schröder S, Foulis A, Mukai K, Klöppel G (1994) Serous oligocystic and ill-demarcated adenoma of the pancreas: a variant of serous cystic adenoma. Virchows Arch 424:13–17
16. Frantz VK (1959) Tumors of the pancreas. AFIP atlas of tumor pathology, 1st series, section 7, fascicles 27 and 28. Armed Forces Institute of Pathology, Washington, DC
17. George DH, Murphy F, Michalski R, Ulmer BG (1989) Serous cystadenocarcinoma of the pancreas: a new entity? Am J Surg Pathol 13:61–66
18. Hamilton SR, Aaltonen LA (2000) Pathology and genetics of tumours of the digestive system. WHO classification of tumours. IARC Press, Lyon
19. Hodgkinson DJ, ReMine WH, Weiland LH (1978) A clinicopathologic study of 21 cases of pancreatic cystadenocarcinoma. Ann Surg 188:679–684
20. Hoorens A, Lemoine NR, McLellan E, Morohoshi T, Kamisawa T, Heitz PU, Stamm B, Rüschoff J, Wiedenmann B, Klöppel G (1993) Pancreatic acinar cell carcinoma. An analysis of cell lineage markers, p53 expression, and Ki-*ras* mutation. Am J Pathol 143:685–698
21. Hruban RH, Takaori K, Klimstra DS, Adsay NV, Albores-Saavedra J, Biankin AV, Biankin SA, Compton C, Fukushima N, Furukawa T, Goggins M, Kato Y, Klöppel G, Longnecker DS, Lüttges J, Maitra A, Offerhaus GJA, Shimizu M, Yonezawa S (2004) An illustrated consensus on the classification of pancreatic intraepithelial neoplasia (PanIN) and intraductal

papillary mucinous neoplasms (IPMNs). Am J Surg Pathol (in press)
22. Jaffe R (1992) The pancreas. In: Stocker JT, Dehner LP (eds) Pediatric pathology, Vol. 2. Lippincott, Philadelphia, PA, pp 791–823
23. Kattan YB (1975) Hydatid cysts in pancreas. BMJ 4:729–730
24. Klimstra DS, Wenig BM, Heffess CS (2000) Solid-pseudopapillary tumor of the pancreas: a typically cystic carcinoma of low malignant potential. Semin Diagn Pathol 17:66–80
25. Klöppel G (2000) Pseudocysts and other non-neoplastic cysts of the pancreas. Semin Diagn Pathol 17:7–15
26. Klöppel G, Kosmahl M (2001) Cystic lesions and neoplasms of the pancreas. The features are becoming clearer. Pancreatology 1:648–655
27. Klöppel G, Morohoshi T, John HD, Oehmichen W, Opitz K, Angelkort A, Lietz H, Rückert K (1981) Solid and cystic acinar cell tumour of the pancreas. A tumour in young women with favourable prognosis. Virchows Arch 392:171–183
28. Klöppel G, Solcia E, Longnecker DS, Capella C, Sobin LH (1996) Histological typing of tumours of the exocrine pancreas, 2nd edn. WHO International histological classification of tumours. Springer, Berlin Heidelberg New York
29. Klöppel G, Hruban RH, Longnecker DS, Adler G, Kern SE, Partanen TJ (2000) Ductal adenocarcinoma of the pancreas. In: Hamilton SR, Aaltonen LA (eds) Pathology and genetics of tumours of the digestive system. WHO classification of tumours. IARC Press, Lyon, pp 221–230
30. Kosmahl M, Seada LS, Jänig U, Harms D, Klöppel G (2000) Solid-pseudopapillary tumor of the pancreas: its origin revisited. Virchows Arch 436:473–480
31. Kosmahl M, Egawa N, Schröder S, Carneiro F, Lüttges J, Klöppel G (2002) Mucinous nonneoplastic cyst of the pancreas: a novel nonneoplastic cystic change? Mod Pathol 15:154–158
32. Kosmahl M, Wagner J, Peters K, Sipos B, Klöppel G (2004) Serous cystic neoplasms of the pancreas: an immunohistochemical analysis revealing alpha-inhibin, neuron-specific enolase and MUC6 as new markers. Am J Surg Pathol 28:339–346
33. Lavine JE, Harrison M, Heyman MB (1989) Gastrointestinal duplications causing relapsing pancreatitis in children. Gastroenterology 97:1556–1558
34. le Borgne J, de Calan L, Partensky C, French Surgical Association (1999) Cystadenomas and cystadenocarcinomas of the pancreas: a multiinstitutional retrospective study of 398 cases. Ann Surg 230:152–161
35. Lee JS, Kim HS, Jung JJ, Han SW, Kim YB (2001) Ancient schwannoma of the pancreas mimicking a cystic tumor. Virchows Arch 439:697–699
36. Lewandrowski K, Warshaw A, Compton C (1992) Macrocystic serous cystadenoma of the pancreas: a morphologic variant differing from microcystic adenoma. Hum Pathol 23:871–875
37. Ligneau B, Lombard-Bohas C, Partensky C, Valette PJ, Calender A, Dumortier J, Gouysse G, Boulez J, Napoleon B, Berger F, Chayvialle JA, Scoazec JY (2001) Cystic endocrine tumors of the pancreas: clinical, radiologic, and histopathologic features in 13 cases. Am J Surg Pathol 25:760
38. Liu TH, Consorti ET (2000) Inflammatory pseudotumor presenting as a cystic tumor of the pancreas. Am Surg 66:993–997
39. Longnecker DS, Adler G, Hruban RH, Klöppel G (2000) Intraductal papillary-mucinous neoplasms of the pancreas. In: Hamilton SR, Aaltonen LA (eds) Pathology and genetics of tumours of the digestive system. WHO classification of tumours. IARC Press, Lyon, pp 237–240
40. Luchtrath H, Schriefers KH (1985) A pancreatic cyst with features of a so-called branchiogenic cyst (in German). Pathologe 6:217–219
41. Lüttges J, Pierré E, Zamboni G, Weh G, Lietz H, Kussmann J, Klöppel G (1997) Maligne nicht-epitheliale Tumoren des Pankreas. Pathologe 18:233–237
42. Lüttges J, Zamboni G, Longnecker D, Klöppel G (2001) The immunohistochemical mucin expression pattern distinguishes different types of intraductal papillary mucinous neoplasms of the pancreas and determines their relationship to mucinous noncystic carcinoma and ductal adenocarcinoma. Am J Surg Pathol 25:942–948
43. Lüttges J, Feyerabend B, Buchelt T, Pacena M, Klöppel G (2002) The mucin profile of noninvasive and invasive mucinous cystic neoplasms of the pancreas. Am J Surg Pathol 26:466–471
44. Mahmood K, Butt MM, Haleem A (1989) Duplication of the duodenum exhibiting heterotopia in the pancreas: report of a case. Ann Saudi Med 9:602–604
45. Mares AJ, Hirsch M (1977) Congenital cysts of the head of the pancreas. J Pediatr Surg 12:547–552
46. Miles RM (1959) Pancreatic cyst in the newborn. Ann Surg 149:576–581
47. Morohoshi T, Kanda M, Asanuma K, Klöppel G (1989) Intraductal papillary neoplasms of the pancreas. A clinicopathologic study of six patients. Cancer 64:1329–1335
48. Oehler U, Jurs M, Klöppel G, Helpap B (1997) Osteoclast-like giant cell tumour of the pancreas presenting as a pseudocyst-like lesion. Virchows Arch 431:215–218
49. Ohhashi K, Murakami F, Takekoshi T et al (1982) Four cases of "mucin-producing" cancer of the pancreas on specific findings of the papilla of Vater (in Japanese). Proc Dig Endosc 20:348
50. Pasternack A, Hjelt L (1961) Cystic disease of the kidneys, liver, and pancreas. Ann Paediatr Finnlandiae 7:138–145
51. Perez-Ordonez B, Naseem A, Lieberman PH, Klimstra DS (1996) Solid serous adenoma of the pancreas. The solid variant of serous cystadenoma? Am J Surg Pathol 20:1401–1405
52. Rickaert F, Cremer M, Devière J, Tavares L, Lambilliotte JP, Schröder S, Wurbs D, Klöppel G (1991) Intraductal mucin-hypersecreting neoplasms of the pancreas. A clinicopathologic study of eight patients. Gastroenterology 101:512–519
53. Schmidt-Rohlfing B, Siech M, Mattfeldt T, Schoenberg MH, Beger HG (1998) Zystische Neoplasien des Pankreas: operative Therapie und Heilungschancen. Z Gastroenterol 36:939–945
54. Sessa F, Solcia E, Capella C, Bonato M, Scarpa A, Zamboni G, Pellegata NS, Ranzani GN, Rickaert F, Klöppel G (1994) Intraductal papillary-mucinous tumours represent a distinct group of pancreatic neoplasms: an investigation of tumour cell differentiation and K-*ras*, p53, and *c-erb*B-2 abnormalities in 26 patients. Virchows Arch 425:357–367
55. Solcia E, Capella C, Klöppel G (1997) Tumors of the pancreas. AFIP atlas of tumor pathology, third series, fascicle 20. Armed Forces Institute of Pathology, Washington, DC
56. Stamm B, Burger H, Hollinger A (1987) Acinar cell cystadenocarcinoma of the pancreas. Cancer 60:2542–2547
57. Talamini MA, Pitt HA, Hruban RH, Boitnott JK, Coleman J, Cameron JL (1992) Spectrum of cystic tumors of the pancreas. Am J Surg 163:117–123
58. Tan G, Vitellas K, Morrison C, Frankel WL (2003) Cystic schwannoma of the pancreas. Ann Diagn Pathol 7:285–291
59. Tilger A (1894) Beitrag zur pathologischen Anatomie und Aetiologie der Pankreas-Cysten. Arch Pathol Anat Physiol Klin Med 137:348–375
60. Wegelin C (1921) Zur Genese und Einteilung der Pankreaszysten. Verh Dtsch Pathol Ges 169–173
61. Widmaier J, Mattfeldt T, Siech M, Beger HG (1996) Serous cystadenocarcinoma of the pancreas. Int J Pancreatol 20:135–139
62. Yamane M (1921) Beiträge zur Kenntnis der Pankreaszysten. Akad. Buchhandl. Bern: Paul Haupt, Bern
63. Zamboni G, Scarpa A, Bogina G, Iacono C, Bassi C, Talamini G, Sessa F, Capella C, Solcia E, Rickaert F, Mariuzzi GM, Klöppel G (1999) Mucinous cystic tumors of the pancreas. Clinicopathological features, prognosis and relationship to other mucinous cystic tumors. Am J Surg Pathol 23:410–422
64. Zamboni G, Terris B, Scarpa A, Kosmahl M, Capelli P, Klimstra DS, Lam PWY, Klöppel G (2002) Acinar cell cystadenoma of the pancreas. A new entity? Am J Surg Pathol 26:698–704

Virchows Arch (2004) 445:179–182
DOI 10.1007/s00428-004-1046-9

ORIGINAL ARTICLE

Angelica A. Saetta · Pollyanthi Papanastasiou · Nikolaos V. Michalopoulos · Fanie Gigelou · Penelope Korkolopoulou · Thaleia Bei · Efstratios Patsouris

Mutational analysis of *BRAF* in gallbladder carcinomas in association with *K-ras* and *p53* mutations and microsatellite instability

Received: 26 January 2004 / Accepted: 1 April 2004 / Published online: 19 June 2004
© Springer-Verlag 2004

Abstract *Background:* Little is known about the genetic changes involved in the pathogenesis of gallbladder cancer. The aim of this study was to examine the presence of mutations in exon 15 of the *B-raf* gene to investigate its role in gallbladder carcinogenesis. *Materials and methods.* We examined the mutational status in exon 15 of *B-raf* gene in 21 gallbladder carcinoma specimens and investigated its association with the presence of *K-ras* and *p53* alterations, microsatellite instability and the clinicopathological features of tumors. *Results: B-raf* mutations were observed in 7 of 21 (33%) gallbladder carcinomas examined, and all were located at the hot spot codon 599 of exon 15. *K-ras* and *B-raf* mutations were never in the same specimens. *Conclusions: B-raf* gene mutations seem to be a quite common event in gallbladder carcinomas, implying that *B-raf* may play an important role in the pathogenesis of this tumor.

Keywords *B-raf* · Gallbladder cancer · *K-ras*

Introduction

Gallbladder carcinoma is rather uncommon in Western communities, yet it is the fifth most common malignancy of the gastrointestinal tract [8]. The molecular basis of gallbladder cancer has not been well defined. Nevertheless, it has been suggested that carcinoma of the gallbladder occurs via two distinct pathways: either *de novo*, showing a predominant *p53* alteration associated with a low *K-ras* mutation percentage, or via adenoma–carcinoma sequence, in the absence of *p53*, *K-ras* or *APC* gene mutations [4].

Activated *ras* genes are known to be involved in multiple downstream signaling pathways, of which the best characterized to date is the RAS/RAF/MEK/ERK growth signal transduction system. This pathway is organized as a cascade in which RAF proteins are activated in a RAS-dependent manner [7]. It has been proposed that the RAS/RAF/MEK/ERK pathway can be activated by mutation at various levels [3].

The *raf* family consists of three genes, which encode highly conserved serine/threonine cytoplasmic kinases, playing an important role in proliferation, differentiation and programmed cell death. The *B-raf* gene has been recently reported to be mutated in a variety of tumors. The highest frequency of somatic *B-raf* mutations has been detected in malignant melanoma and melanoma cell lines [3]. It is also associated with mismatch repair (MMR)-deficient colon cancers, in which it is commonly mutated [9].

As mutations of the *ras* genes have been observed in 10–57% of gallbladder carcinomas [10], the constitutive activation of this growth-promoting signal transduction pathway may be of critical importance for the development of gallbladder cancer. A mutation of *raf* or other kinases of this cascade would be expected in cases without *K-ras* mutation.

It has been suggested that *B-raf* mutations are equivalent to those in *ras* genes, at least as far as colon cancer is concerned. They arise at an early stage of adenoma–carcinoma sequence and are infrequent in adenomas from familial adenomatous polyposis cases. Moreover, both *B-raf* and *K-ras* mutations are strongly associated with villous architecture [15]. However, a trend toward the occurrence of *B-raf* mutations in cancer types that harbor

A. A. Saetta · P. Papanastasiou · N. V. Michalopoulos · F. Gigelou · P. Korkolopoulou · E. Patsouris
Department of Pathology,
Medical School, National and Kapodistrian University of Athens,
75 Mikras Asias Str, 11527 Goudi Athens, Greece

T. Bei
Section on Endocrinology and Genetics,
Developmental Endocrinology Branch,
National Institute of Child Health and Human Development,
National Institutes of Health,
Bethesda, MD 20892-1862, USA

A. A. Saetta (✉)
10 Pirrou Str, 145 64 Kifisia Athens, Greece
e-mail: asaetta@med.uoa.gr
Tel.: +30-210-7462168
Fax: +30-210-7462157

frequent *ras* mutations has been observed, although they rarely coexist in the same cancers. This has been taken as evidence that the inappropriate regulation of the downstream extracellular signal-regulated kinases [ERKs—the p42/p44 mitogen-activated protein (MAP) kinases] is a major contributing factor in the development of these cancers. *B-raf* is a far stronger activator of ERKs than its better-studied Raf-1 homologue.

The aim of this study was to screen gallbladder carcinomas for the presence of mutations in exon 15 of the *B-raf* to investigate the involvement of this gene in gallbladder carcinogenesis in parallel with *K-ras*, *p53* mutations and microsatellite instability (MSI) status. Additionally, we investigated the associations of the molecular alterations with the clinicopathological features of the examined carcinomas.

Materials and methods

Tumor specimens

Archiac tissue from 21 cholecystectomy specimens with gallbladder carcinomas was retrieved from the files of the Pathology Department of Athens University Medical School. Information regarding the gender (males=9, females=12) and age (range 42–96 years, median age 71 years) of the patients and Nevin tumor stage was obtained from hospital records. All cases were histologically diagnosed and classified according to grade (well differentiated=9, papillary=6, poorly differentiated=6) and stage (stage I=2, stage II=2, stage III=5, stage IV=6, stage V=6). Blocks consisting of more than 70% of tumor were selected, and non-neoplastic tissue was trimmed away as much as possible. The study has been performed in compliance with the appropriate ethics standards, and all patients gave their informed consent prior to their inclusion in this study.

Genomic DNA isolation

DNA from formalin-fixed paraffin-embedded tissues was extracted from 20-μm-thick sections. After deparaffinization with xylene, the samples were digested overnight at 55°C using 200 μl of digestion buffer consisting of 50 mM Tris, 1 mM ethylenediaminetetraacetate (EDTA), 0.5% sodium dodecyl sulfate and 200 μg/ml proteinase K. Genomic DNA was extracted with phenol-chloroform and precipitated in ice-cold ethanol. The DNA was redissolved in distilled water and quantified by means of spectrophotometry at 260 nm under ultraviolet light.

Polymerase chain reaction

A total of 500 ng of DNA was amplified in a 25-μl reaction mixture containing 25 pmoles of each primer, 25 mM each dNTP, 1.5 mM $MgCl_2$, 1 mM KCl, 0.1% gelatin and 1.5 U *Taq* DNA polymerase (Clontech Laboratories Inc, California, USA). The profile used in the Progene Techne thermal cycler was: 2 min at 94°C once; 45 s at 94°C, 45 s at 58°C, 50 s at 72°C for 40 cycles; 7 min at 72°C once. Sequences of the primers: *B-raf* exon 15 (forward primer): 5′ TCA TAA TGC TTG CTC TGA TAG GA 3′, *B-raf* exon 15 (reverse primer): 5′ GGC CAA AAA TTT AAT CAG TGG A 3′. Primers for amplification of *K-ras* and *p53* genes were described elsewhere [11, 12].

Single-strand conformation polymorphism analysis

Polymerase chain reaction (PCR) products were screened for mutations in exon 15 of the *B-raf* gene and in the conserved domains IV and V of the p53 gene. First, PCR products were diluted in 10 μl of formamide-dye solution (95% formamide, 20 mM EDTA, 0.05% bromophenol blue, 0.05% xylene cyanol), denatured at 95°C for 7 min and kept on ice until loaded onto a 0.5X MDE gel (BMA, USA). Electrophoresis was carried out at the following conditions: 4 W for 20–22 h at 7°C and 3–5 W for 16–19 h at 4°C for *B-raf* and *p53* genes, respectively. Following electrophoresis, the gel was silver stained and examined for abnormal band patterns.

Sequencing

Samples showing abnormal single-strand conformation polymorphism (SSCP) bands were further analyzed by sequencing. For sequencing, the Big Dye terminator sequencing kit was used. The products were analyzed on an ABI prism 310 Genetic analyzer (Perkin-Elmer, California, USA). *B-raf* PCR primers were also used for sequencing analysis to confirm the presence of mutations.

Restriction fragment-length polymorphism analysis

Next, 10- to 25-μl aliquots of the PCR product were digested with the appropriate restriction enzyme to reveal existence of mutations. Restriction-enzyme analysis of the PCR products was performed using the following enzymes: BstNI for codon 12 of the *K-ras* gene and MspI for codon 248, HaeIII for codon 249 and BstUI for codon 273 of the *p53* gene.

Results

Genomic DNA from 21 gallbladder carcinomas was screened for alterations in exon 15 of the *B-raf* gene using PCR-SSCP followed by sequencing in cases where abnormal bands were seen. The association of the mutational status with the presence of *K-ras* or *p53* mutations, MSI and the clinicopathological features (namely age, gender, histological type and stage of the tumor) was also examined (Table 1).

B-raf mutations were detected in 7 of 21 (33%) of the gallbladder carcinomas examined and were all located at the hot spot codon 599 of exon 15 (Fig. 1). *K-ras* mutations at codon 12 had been previously found in 4 of the 23 specimens examined (25%) and *p53* mutations in 5 of 21 cases (24%) [12]. Moreover, alterations of BAT26 indicating the presence of MSI were not observed in these specimens. No *K-ras* and *B-raf* mutations were identified simultaneously in the same samples. However, both *B-raf* and *p53* mutations were determined.

Statistical analysis revealed no statistically significant association between the presence of mutations in *B-raf* gene and the clinicopathological characteristics of the examined carcinomas, although the number of the carcinomas examined was not large enough to allow definite statistical correlations to be drawn.

Table 1 Clinicopathological characteristics of gallbladder carcinomas with alterations in *B-raf*, *K-RAS* and *p53* genes

No.	Age (years)	Gender	Histological classification	Stage	*B-raf*	*K-RAS*	*p53*
1	58	Male	Well differentiated	I	+	–	+ (exon 5)
2	76	Male	Well differentiated	III	+	–	–
3	96	Female	Papillary	V	+	–	–
4	62	Male	Poorly differentiated	IV	+	–	–
5	72	Male	Poorly differentiated	III	+	–	+ (exon 5)
6	81	Female	Well differentiated	II	+	–	–
7	61	Female	Well differentiated	III	+	–	–
8	80	Male	Well differentiated	V	–	+	–
9	75	Female	Papillary	III	–	–	+ (exon 7)
10	76	Female	Papillary	III	–	+	–
11	42	Male	Poorly differentiated	V	–	+	–
12	72	Female	Well differentiated	V	–	–	+ (exon 8)
13	96	Female	Well differentiated	V	–	–	+ (exon 7)
14	79	Female	Well differentiated	II	–	+	

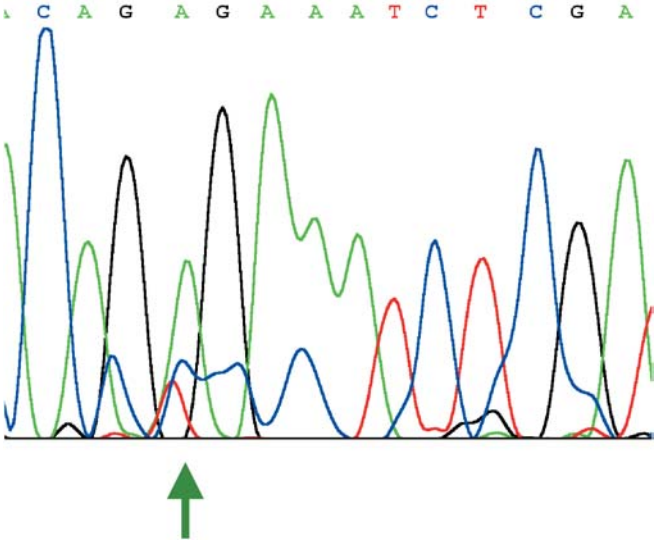


Fig. 1 Sequencing analysis of *B-raf* gene. The *arrow* indicates the T1796A nucleotide substitution

Discussion

To date, little is known about the molecular mechanisms underlying the development and progression of gallbladder cancer, which is a very aggressive disease with an overall 5-year survival rate of less than 5%. Thus, the identification of potentially useful prognostic markers is an interesting, yet unresolved issue. Certain pathways involved in the carcinogenesis of the gastrointestinal tract, such as MSI, do not seem to play an important role in gallbladder tumorigenesis [13]. However, it can be hypothesized that abnormal or constitutional activation of the RAS/RAF/MEK/ERK kinase cascade, which transduces various growth signals from the cell surface to the nucleus, is implicated in the pathogenesis of gallbladder neoplasms, since *K-ras* mutations have been identified in a proportion of such tumors.

Recently, *B-raf* mutations have been reported to occur in a variety of human malignancies, including colorectal cancer, in which they are considered to exert, at least partly, similar effects to *ras* mutations in tumorigenesis, both arising at approximately the same stage of the adenoma–carcinoma sequence. *B-raf* mutations, independently of RAS activation, lead to the synthesis of a dominant transforming protein, resulting in cancer [3].

B-raf mutations are currently under investigation in many tumor types. Whereas *K-ras* mutations have been extensively investigated in a variety of tumors of the gastrointestinal tract, including those of the gallbladder, this is the first study of the mutational status of *B-raf* in gallbladder carcinomas. We have screened for mutations in exon 15 of the *B-raf* gene and investigated the association with other genetic alterations observed in gallbladder carcinogenesis, such as *K-ras* and *p53* mutations, as well as the presence of MSI. The analysis of mutations in exon 15 of *B-raf* seems adequate, given that mutations are clustered in only two exons of the gene, approximately 80% of which occur at a hot spot codon of exon 15. This is a T→A substitution at nucleotide 1796, leading to the conversion of valine to glutamic acid at codon 599, which represents the most common amino acid substitution in tumors such as malignant melanoma (80%), cholangiocarcinomas (73%), thyroid (69%) and colon cancer (50%) [2, 3, 5, 14, 15]. This was the only alteration identified in our samples.

In the present study, *B-raf* mutations at codon 599 of exon 15 were observed in 33% of the gallbladder carcinomas examined, whereas *K-ras* mutations at codon 12 were found in 25% of our specimens [11]. This is in contrast to results from studies of colon adenocarcinomas, in which a higher incidence of *K-ras* mutations than *B-raf* mutations has been reported [15]. It is noteworthy that in two of the *B-raf* mutated samples, *p53* mutations have been also found [12], whereas none of the gallbladder carcinomas with the V599E *B-raf* mutation carried a *K-ras* mutation. This observation is concordant with previous results showing that *B-raf* mutations and, specifically, the V599E amino acid substitution occur more frequently in tumors that do not carry mutations in *K-ras* gene [1, 9, 6, 15]. It can be hypothesized that activation at various points of the RAS/RAF/MEK/ERK pathway may constitute a key event in gallbladder carcinogenesis. *K-ras* and *B-raf* mutations may independently activate the same intracellular signal-transduction system linked to cellular growth.

The association between MSI and mutations of *B-raf* gene has not yet been examined in gallbladder cancer. It is known that, at least in colorectal carcinomas, a higher incidence of *B-raf* mutations and a lower incidence of *K-ras* mutations are present in MMR-deficient tumors than in MMR-proficient tumors [9]. MSI, as estimated by alterations in markers such as BAT26, transforming growth factor-βRII and bax, has not been found in our samples, although a quite high percentage of *B-raf* mutations has been observed [12]. Since the involvement of MSI in gallbladder carcinogenesis is still an unresolved issue, a definite association with *B-raf* mutations has to be determined.

The present results highlight the involvement of the RAS/RAF/MEK/ERK signal-transduction cascade in the pathogenesis of gallbladder cancer. Disruption of this pathway, according to the present investigation, occurs in about 65% of gallbladder carcinomas, and it may, therefore, be considered one of the most common defects in the pathogenesis of this tumor identified as of yet.

Since gallbladder carcinoma is an uncommon tumor in Western communities, only a small number of specimens was available for analysis in this study. Therefore, investigation of a larger number of cases is warranted to elucidate the possible effect and prognostic significance of both *K-ras* and *B-raf* genes. Nevertheless, our results strongly support the view that disruption of the MAP kinase cascade plays a significant role in gallbladder cancer development.

References

1. Brose MS, Volpe P, Feldman M, Kumar M, Rishi I, Gerrero R, Einhorn E, Herlyn M, Minna J, Nicholson A, Roth JA, Albelda SM, Davies H, Cox C, Brignell G, Stephens P, Futreal PA, Wooster R, Stratton MR, Weber BL (2002) BRAF and RAS mutations in human lung cancer and melanoma. Cancer Res 62:6997–7000
2. Cohen Y, Xing M, Mambo E, Guo Z, Wu G, Trink B, Beller U, Westra W, Ladenson P, Sidransky D (2003) BRAF mutation in papillary thyroid carcinoma. J Natl Cancer Inst 95:625–627
3. Davies H, Bignell GR, Cox C, Stephens P, Edkins S, Clegg S, Teague J, Woffendin H, Garnett MJ, Bottomley W, Davis N, Dicks E, Ewing R, Floyd Y, Gray K, Hall S, Hawes R, Hughes J, Kosmidou V, Menzies A, Mould C, Parker A, Stevens C, Watt S, Hooper S, Wilson R, Jayatilake H, Gusterson BA, Cooper C, Shipley J, Hargrave D, Pritchard-Jones K, Maitland N, Chenevix-Trench G, Riggins GJ, Bigner DD, Palmieri G, Cossu A, Flanagan A, Nicholson A, Ho JW, Leung SY, Yuen ST, Weber BL, Seigler HF, Darrow TL, Paterson H, Marais R, Marshall CJ, Wooster R, Stratton MR, Futreal PA (2002) Mutations of the BRAF gene in human cancer. Nature 417: 949–954
4. Itoi T, Watanabe H, Ajioka Y, Oohashi Y, Takel K, Nishikura K, Nakamura Y, Horil A, Saito T (1996) APC, K-ras codon 12 mutations and p53 gene expression in carcinoma and adenoma of the gall-bladder suggest two genetic pathways in gall-bladder carcinogenesis. Pathol Int 46:333–340
5. Mercer KE, Pitchard CA (2003) Raf proteins and cancer: B-Raf is identified as a mutational target. Biochim Biophys Acta 1653:25–40
6. Naoki K, Chen TH, Richards WG, Sugarbaker DJ, Meyerson M (2002) Missense mutations of the BRAF gene in human lung adenocarcinoma. Cancer Res 62:7001–7003
7. Peyssonaux C, Eychene A (2001) The Raf/MEK/ERK pathway: new concepts of activation. Biol Cell 93:53–62
8. Pitt HA, Dooley WC, Teo CJ, Cameron JL (1995) Malignancies of the biliary tree. Curr Prob Surg 32:1–90
9. Rajagopalan H, Bardelli A, Lengauer C, Kinzler K, Vogelstein B, Velculescu V (2002) RAF/RAS oncogenes and mismatch-repair status. Nature 418:934
10. Reeves ME, DeMatteo RP (2000) Genes and viruses in hepatobiliary neoplasia. Semin Surg Oncol 19:84–93
11. Saetta A, Lazaris Ch, Davaris PS (1996) Detection of Ras oncogenes point mutations and simultaneous proliferative fraction estimation in gallbladder cancer. Pathol Res Pract 192:532–540
12. Saetta A, Lazaris AC, Michalopoulos NV, Davaris PS (2001) Genetic alterations involved in the development of gallbladder carcinomas from Greek patients. Hepatogastroenterology 48: 1284–1288
13. Sessa F, Furlan D, Genasetti A, Billo P, Feltri M, Capella C (2003) Microsatellite instability and p53 expression in gallbladder carcinomas. Diagn Mol Pathol 12:96–102
14. Tannapfel A, Sommerer F, Benicke M, Katalinic A, Uhlmann D, Witzigmann H, Hauss J, Wittekind (2003) Mutations of the BRAF gene in cholangiocarcinoma but not in hepatocellular carcinoma. Gut 52:706–712
15. Yuen ST, Davies H, Chan TL, Ho JW, Bignell GR, Cox C, Stephens P, Edkins S, Tsui WW, Chan AS, Futreal PA, Stratton MR, Wooster R, Leung SY (2002) Similarity of the phenotypic patterns associated with BRAF and KRAS mutations in colorectal neoplasia. Cancer Res 62:6451–6455

Virchows Arch (2004) 445:183–188
DOI 10.1007/s00428-004-1074-5

ORIGINAL ARTICLE

Marco Volante · Francesca Bozzalla-Cassione · Roberta DePompa · Enrico Saggiorato · Armando Bartolazzi · Fabio Orlandi · Mauro Papotti

Galectin-3 and HBME-1 expression in oncocytic cell tumors of the thyroid

Received: 9 April 2004 / Accepted: 8 June 2004 / Published online: 14 July 2004
© Springer-Verlag 2004

Abstract Oncocytic cell tumors (OCTs) of the thyroid include oncocytic cell adenomas (OCAs) and oncocytic cell carcinomas (OCCs). Oncocytic variant of papillary carcinoma (OVPC) has also been described. These tumors may present similar diagnostic problems as their non-oncocytic counterparts, in both conventional histology and fine-needle aspiration biopsies. Several markers were shown able to distinguish benign from malignant thyroid follicular tumors, galectin-3 and HBME-1 being the most promising ones. Controversial data have been reported on their discriminatory potential in the small series of OCTs so far analyzed. We aimed to assess the role of galectin-3 and HBME-1 in a large series of 152 OCTs (including 50 OCAs, 70 OCCs and 32 OVPCs). The expression of PPARγ protein was also evaluated. Using a biotin-free detection system, the sensitivity of galectin-3 was 95.1%, while that for HBME-1 was nearly 53%. The combination of galectin-3 and HBME-1 increased the sensitivity up to 99%. However, for both markers, the specificity was 88%, lower than that reported for non-oncocytic follicular tumors. PPARγ protein overexpression was absent in all OCAs tested and present in only 10% of OCCs, confirming previous reports on the low prevalence of PAX8-PPARγ translocations in OCT and ruling out its role as a potential diagnostic marker of malignancy.

Keywords Thyroid · Tumors · Oncocytic · HBME-1 · Galectin-3

M. Volante · F. Bozzalla-Cassione
Department of Biomedical Sciences and Oncology,
University of Turin,
Turin, Italy

A. Bartolazzi
Division of Pathology, Sant'Andrea Hospital,
Rome, Italy

R. DePompa · E. Saggiorato · F. Orlandi · M. Papotti
Department of Clinical and Biological Sciences,
San Luigi Hospital, Orbassano—University of Turin,
Turin, Italy

M. Papotti (✉)
Department of Biological and Clinical Sciences,
University of Turin, San Luigi Hospital,
Regione Gonzole 10, 10043 Orbassano (TO), Italy
e-mail: mauro.papotti@unito.it
Tel.: +39-011-6705432
Fax: +39-011-6705432

Introduction

Oncocytic cell tumors (OCTs) of the thyroid include adenomas and carcinomas of follicular origin characterized by a predominant (usually more than 75% of the tumor area) population of eosinophilic mitochondrion-rich cells [18, 31]. They may be separated into oncocytic cell adenomas (OCAs) and oncocytic cell carcinomas (OCCs). An oncocytic variant of papillary carcinoma (OVPC) has also been described [13, 27]. Their biological behavior has been the matter of long-standing controversies. Originally, these tumors, also referred to as Hürthle cell or oxyphilic tumors, were all considered potentially malignant, based on the reported higher aggressive behavior than their conventional non-oncocytic follicular counterparts [3, 32]. More recently [6, 23], it became evident that the clinical outcome of OCTs was by no means different from that of the corresponding non-oncocytic tumors, irrespective of them being benign (adenomas) or malignant (well or poorly differentiated carcinomas). Nevertheless, their recognition is an important task for pathologists, since oncocytic cells may also be found in non-neoplastic conditions (goiter, thyroiditis). In addition, as in the case of non-oncocytic minimally invasive follicular carcinomas, the differential diagnosis of oncocytic adenomas from carcinomas may not be easily performed in all cases, and it is, in any case, impossible in cytological material from fine-needle aspiration (FNA) biopsies.

Several markers have been proposed, in both surgical and FNA cytological specimens, to distinguish follicular adenomas from carcinomas, including the oncocytic cell types. The most promising appeared to be galectin-3, cytokeratin 19, the mesothelial cell marker HBME-1 and

thyroperoxidase [1, 4, 5, 8, 10, 11, 12, 22, 24, 25, 26, 28, 29]. In all published series, however, the number of OCTs studied was generally low. For galectin-3 and HBME-1 in particular, controversial data have been reported, indicating that the discriminatory potential of such markers in OCT was of limited value [14, 17]. To this purpose, we aimed to validate the role of galectin-3 and HBME-1 in a large series of 152 OCT, which included 50 OCAs, 70 OCCs and 32 OVPCs. In addition, we searched for PPARγ protein overexpression in all cases of OCA and OCC. PPARγ protein was found to be expressed by follicular carcinoma nuclei but not by adenomas [20], as a consequence of the PAX8-PPARγ translocation t(2;3)(q13;p25). This finding was not confirmed in subsequent reports and the specificity of this marker is rather poor [15]. Moreover, a very low rate of overexpression in OCC has been described in previous reports [20], thus excluding an involvement of PAX8-PPARγ translocation in the pathogenesis of this tumor type.

We here show that using a biotin-free detection system, galectin-3 alone is capable of correctly identifying 95% of malignant OCTs, and the association of galectin-3 and HBME-1 increases the sensitivity up to 99%.

Materials and methods

Case selection

We retrospectively analyzed 152 thyroid OCTs (including 50 OCAs, 70 OCCs and 32 OVPCs) and 34 non-neoplastic, oncocytic, cell-rich control cases (including 19 cases of nodular goiter with oncocytic changes and 15 cases of Hashimoto's thyroiditis). Tumor samples were collected from the pathology files of the Department of Pathology, University of Turin, from 1974 to 2003. All tumors were classified according to widely accepted histological criteria [13, 27], and a diagnosis of oncocytic cell neoplasm was made when more than 75% of the cells had oncocytic features. Diagnostic criteria of malignancy discriminating OCC from OCA were complete capsular penetration and/or invasion of blood vessels within the capsule or external to it. OVPC were diagnosed in the presence of the characteristic nuclear features of papillary carcinoma, irrespective of their growth pattern (either papillary or follicular).

Immunohistochemical analysis

Immunohistochemistry was performed on paraffin-embedded sections using a standard manual biotin-free immunoperoxidase procedure with monoclonal antibodies against human galectin-3 (clone 9C4, diluted 1:200; Novocastra, Newcastle, UK), HBME-1 (clone HBME-1, diluted 1:50, DakoCytomation, Glostrup, Denmark), and PPARγ (clone E-8, 1:300; Santa Cruz Biotechnology, Santa Cruz, CA). For all antibodies tested, antigen-retrieval treatment (three 3-min passages in citrate buffer, pH 6.0) was performed, and then immune complexes were detected with the EnVision system (DakoCytomation) to prevent endogenous biotin activity, and visualized by diaminobenzidine precipitation. Slides were then counterstained with Mayer's hematoxylin and mounted.

Scoring of staining and statistical data

All cases were evaluated by three independent investigators, blind with respect to the histological diagnosis. Cytoplasmic galectin-3 and HBME-1-positive cases were scored as + ($\leq$10%), ++ (11–50%) and +++ (>50%), as previously reported [1, 14]. Nuclear staining for PPARγ was scored as weak (+), moderate (++), or strong (+++), and as focal (<50% of the tumor cells positive) or diffuse (>50% of tumor cells), as proposed by Nikiforova et al. [20]. According to these latter authors, in the final interpretation of the results, only cases with diffuse (>50% of tumor cells) and strong (+++) staining were considered positive (being correlated to the presence of the translocation at a molecular level).

Sensitivity, specificity, and diagnostic accuracy were assessed for each antibody tested, considered separately or in combination. Sensitivity was defined as true positive/(true positive+false negative) and specificity as true negative/(true negative+false positive). Diagnostic accuracy was defined as (true positive+true negative)/(true positive+false positive+true negative+false negative).

Results

The immunohistochemical expression of galectin-3 and HBME-1 is summarized in Table 1. Among 50 cases of OCA, 44 were negative for galectin-3. In 6 cases (12%), a focal reactivity (score +) was observed. Accurate histological revision failed to detect in these latter cases the presence of capsular penetration or vascular invasion, or nuclear features suggestive of a follicular variant of papillary carcinoma. Cytoplasmic galectin-3 immunostaining was restricted to small clusters of tumor cells located beneath the tumor capsule. Cytoplasmic galectin-3 was expressed in 66 of 70 (94.3%) OCCs (Fig. 1) and in 31 of 32 (96.9%) OVPCs (Fig. 2). The immunoreactivity was typically strong and diffuse in cases of OVPC; while, in cases of OCC, it was mostly located at the periphery of the nodule and particularly in areas of capsular or vascular invasion, although some diffusely positive cases have been observed.

HBME-1 reactivity was detected in 6 of 50 OCAs (12%), 26 of 70 OCCs (37.1%) (Fig. 1) and 28 of 32 (87.5%) OVPCs. HBME-1 pattern of immunostaining

Table 1 Immunohistochemical results of galectin-3, HBME-1 and PPARγ in a series of 152 oncocytic cell tumors

Diagnosis	Galectin-3[a]	HBME-1[a]	PPARγ[b]
Oncocytic cell adenoma	6[c]/50 (12%)	6[c]/50 (12%)	0/50 (0%)
Oncocytic cell carcinoma	66/70 (94.3%)	26/70 (37.1%)	7/70 (10%)
Oncocytic variant of papillary carcinoma	31/32 (96.9%)	28/32 (87.5%)	ND

[a] Positive cases included scores + to +++, as detailed in the Materials and methods (see references [1, 14])
[b] Positive cases included only strong (+++) and diffuse (>50% of tumor cells) immunohistochemical features [20]
[c] All cases with + score

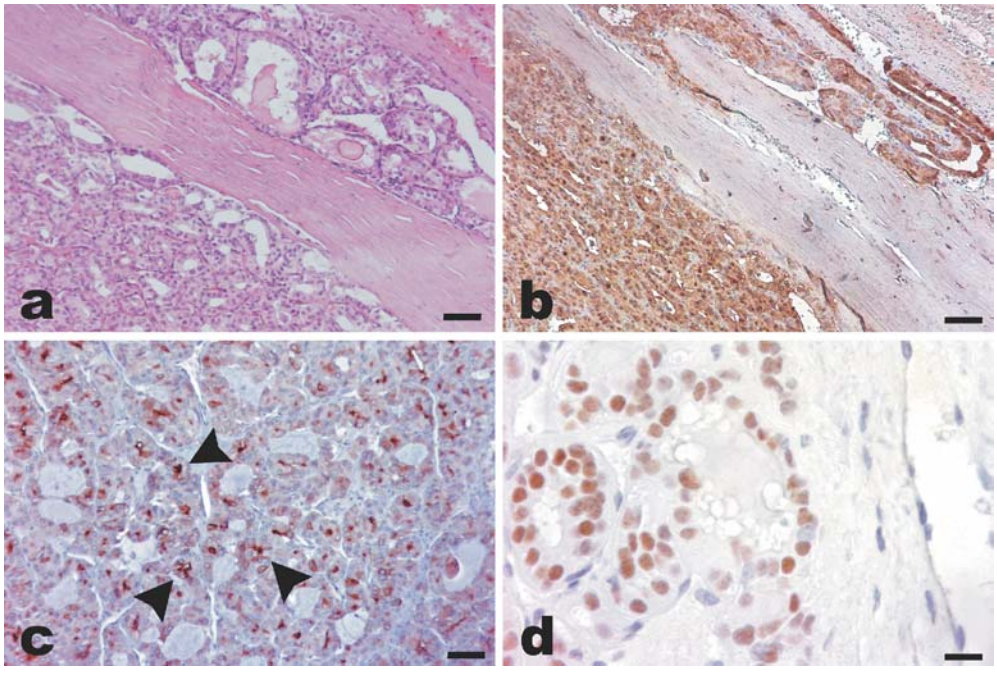


Fig. 1 A case of oncocytic cell carcinoma (**a**), angioinvasive (*top right*) diffusely expressing cytoplasmic and nuclear galectin-3 in tumor cells and also in a blood vessel (*top right*; **b**). Tumor cells also co-express HBME-1 (**c**), with the typical endoluminal reinforcement (*arrowheads*) and PPARγ proteins (**d**). **a** Hematoxylin and Eosin, ×100, *bar* 100 μm. **b** Immunoperoxidase, ×100, *bar* 100 μm. **c** Immunoperoxidase, ×200, *bar* 50 μm. **d** Immunoperoxidase ×400, *bar* 25 μm

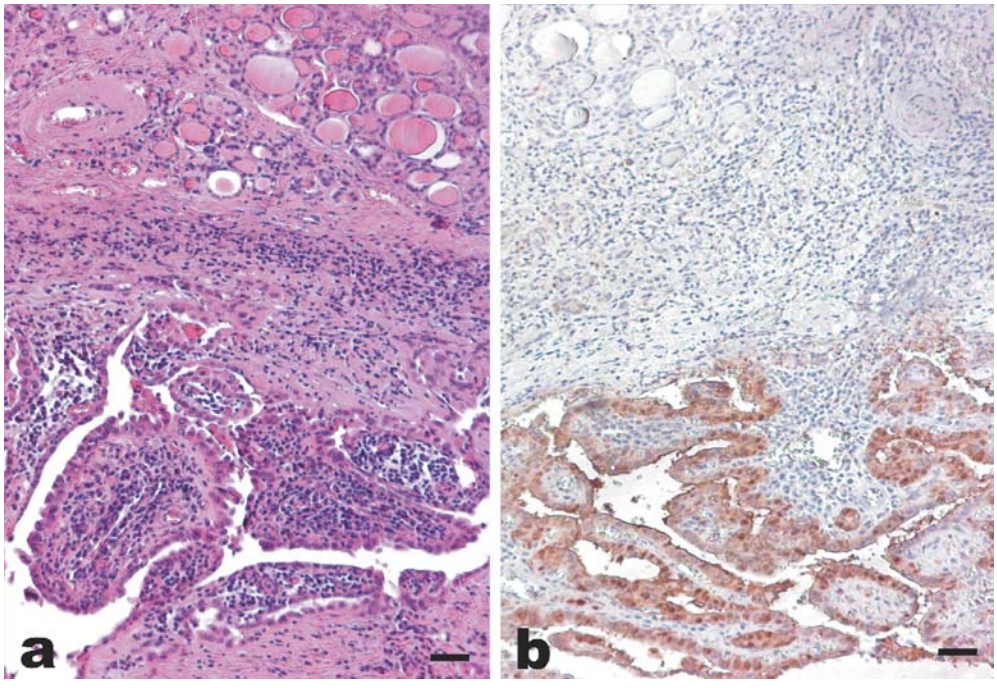


Fig. 2 A case of oncocytic variant of papillary carcinoma (**a**), strongly expressing cytoplasmic and nuclear galectin-3 (**b**). Normal peritumoral thyroid follicles show no reactivity for galectin-3 (*top*). **a** Hematoxylin and eosin, ×100. **b** Immunoperoxidase, ×100. **a**, **b** *Bar* 100 μm

was diffuse in most cases, while in some cases a clustered reactivity was observed either in the center or in the periphery of the nodule (in contrast with that of galectin-3). With respect to "false-positive" OCAs, 4 cases were reactive for both galectin-3 and HBME-1 (Fig. 3). Concerning "false-negative" OCCs, interestingly, 3 of the 4 galectin-3-negative cases were positive for HBME-1. All cases of hyperplastic nodular goiters with oncocytic changes were unreactive for both galectin 3 and HBME-1. Of 15 cases of Hashimoto's thyroiditis, 14 showed a moderate (score ++) to strong (score +++) immunoreactivity for both galectin-3 and HBME-1 in clusters of oncocytic epithelial cells within lymphocytic infiltrates.

Immunostaining with PPARγ antibody was performed on 120 oncocytic thyroid tumors, comprising 50 OCA and 70 OCC (Table 1). Seven carcinomas (10%), being all but one minimally invasive, showed a strong and diffuse nuclear staining. In 6 cases (5 OCCs and 1 OCA), a weak to moderate nuclear staining (either focal or diffuse) was observed; since, according to the literature data [9, 20], only the strong diffuse nuclear staining is correlated with the presence of the PAX8-PPARγ rearrangement detected

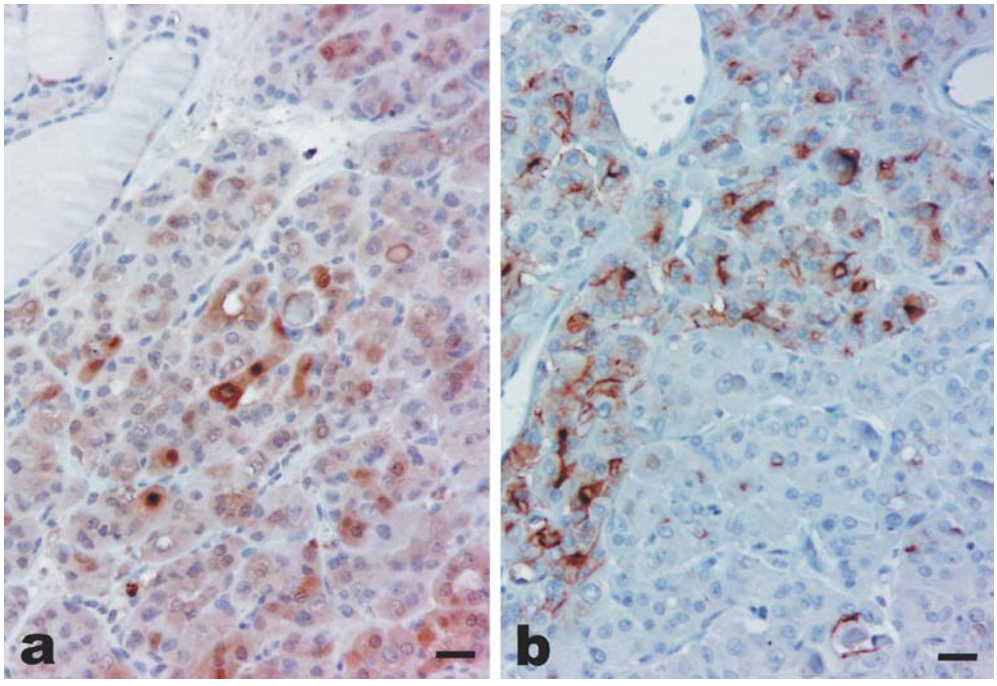


Fig. 3 A case of oncocytic cell adenoma expressing both galectin-3 (in the cytoplasms and nuclei of tumor cells; **a**) and HBME-1 proteins (**b**). In both cases, the reactivity is restricted to single cells or small clusters of tumor cells. **a**, **b** Immunoperoxidase ×400, *bar* 25 μm

Table 2 Sensitivity, specificity and diagnostic accuracy of galectin-3, HBME-1 and PPARγ, used alone or in combination

Immunohistochemical marker	Number of cases	Sensitivity (%)	Specificity (%)	Diagnostic accuracy (%)
GAL-3	152	95.1	88	92.8
HBME-1	152	52.9	88	64.5
PPARγ	120	10	100	47.5
GAL-3 + HBME-1	152	99	80	92.8
GAL-3 + HBME-1 + PPARγ	120	98.6	80	90.8

by RT-PCR, these latter cases were considered as negative.

Data on sensitivity, specificity and diagnostic accuracy of the three antibodies tested are reported in Table 2. Sensitivity ranged from 10% for PPARγ antibody to 95.1% for galectin-3. Although sensitivity for HBME-1 was very low (52.9%) in the present series of OCTs, the combination of galectin-3 and HBME-1 was shown to increase the general sensitivity up to 99%. Specificity was 88% for both galectin-3 and HBME-1, and slightly decreased using a combination of the two. A strong and diffuse PPARγ reactivity confirmed to be 100% specific of carcinomas. Finally, galectin-3 gained the highest diagnostic accuracy (92.8%) used alone or in combination with HBME-1, while HBME-1 alone showed a diagnostic accuracy of 64.5%, due to its low sensitivity.

Discussion

In this study, we have shown that galectin-3 is a useful marker of oncocytic carcinomas, having a sensitivity of 95.1%. Its combined use with HBME-1, however, increased sensitivity to 99%, suggesting that their association in a panel of markers is optimal for better characterizing OCCs in histological and, possibly, cytological specimens. These findings confirm the reported role of galectin-3 and HBME-1 when employed separately in conventional non-oncocytic tumors [1, 22] and also expand their usefulness for OCTs. Actually, the potential role of galectin-3 as a marker of malignancy in OCT as been questioned by some authors. In fact, a few recent papers suggested that galectin-3 immunodetection is not restricted to malignant tumors, but is also observed in adenomas [16, 17, 19].

A possible explanation for such reported discrepancies in OCT comes from the knowledge that oncocytic cells are rich in endogenous biotin and galectin-3 immunocytochemistry (as well as HBME-1) and may provide false-positive results in OCT using biotin-based detection systems, especially when heat-induced antigen retrieval methods (required in the case of galectin-3 immunocytochemistry) are employed. Therefore, as correctly pointed out by some authors [12, 30], galectin-3 immunodetection may be a useful adjunct to distinguish benign from malignant thyroid tumors, only if used in a biotin-free detection system.

Moreover, different technical procedures used to reveal galectin-3 may also explain controversial data from the literature. In some recent reports based on real-time reverse-transcription polymerase chain reaction (RT-PCR) methods [7], high levels of galectin-3 mRNA were de-

tected also in benign thyroid nodules. In our opinion, methods aimed to localize the molecule in the tissue, such as immunohistochemistry, seem to be more reliable in interpreting the final results, the cytoplasmic fraction of galectin-3 being the only specific sign of malignant transformation [2]. PCR-based techniques and in situ hybridization, although highly sensitive, can distinguish neither the cytoplasmic from the nuclear galectin-3 localization nor (with regard to PCR) the cell type expressing galectin-3 mRNA [4]. Since it is well known that macrophages and endothelial cells produce relatively large amounts of galectin-3 in physiological conditions, such cell types are probably present in the tissue submitted to PCR analysis, irrespective of the benign or malignant nature [2]. In addition, although the immunohistochemical expression of galectin-3 was found to correlate with mRNA expression [10], it is not completely understood how mRNA transcription is regulated in benign conditions.

Our data on 152 cases of OCTs, under strictly controlled technical conditions, showed a galectin-3 immunoreactivity in 95.1% malignant OCTs (including OCC and OVPC cases) and in 12% of OCAs, values that are consistent with those observed in non-oncocytic follicular and papillary tumors. Conversely, lower sensitivity, specificity and, therefore, diagnostic accuracy (52.9%, 88% and 64.5%, respectively) were observed for HBME-1, as also pointed out by other authors [14] with special reference to OVPC cases. Our data suggest a limited diagnostic role of HBME-1 used alone in the diagnosis of OCC (since only 37.1% of cases were positive), its sensitivity in OVPC being slightly below that of galectin-3 used alone. Nevertheless, HBME-1 was able to recognize three of the four galectin-3-negative OCCs. Although this result has poor diagnostic utility due to the low HBME-1 specificity (being positive in 12% of OCAs), it suggests that an alternative phenotype is probably present in this small group of tumors. The presence of two alternative and non-overlapping pathogenetic pathways of tumorigenesis in follicular carcinoma have already been postulated by some authors [21], the presence of the PAX8-PPARgamma translocation being most frequently associated with a galectin-3-positive/HBME-1-negative immunophenotype and the presence of RAS mutations associated with a galectin-3-negative/HBME-1-positive immunophenotype. These data indirectly indicate that, in the diagnosis of follicular tumors in general, a panel of markers including at least galectin-3 and HMBE-1 would probably increase the sensitivity of an immunohistochemical approach up to nearly 100%.

A separate comment is deserved for "false-positive" OCAs, i.e., four cases positive for both galectin-3 and HBME-1 and two cases positive for one of the two markers, each. They may represent, on the one hand, true false-positive cases by immunohistochemistry, but on the other may reflect lesions having a biologically malignant potential in the absence of morphological signs of invasive growth (as already described in conventional follicular adenomas) [1]. As opposed to molecular markers (such as PAX8-PPARγ gene fusion product), which possess oncogenic implications and therefore are an early event in malignant transformation, galectin-3 and HBME-1 regulation in morphologically benign tumors, in tumors of uncertain malignant potential, as well as in early malignant lesions is poorly understood. In this respect, we were able to confirm the presence of immunoreactivity for both galectin-3 and HBME-1 in clusters of epithelial follicular cells with oncocytic changes in the setting of Hashimoto's thyroiditis. These markers may be upregulated due to reactive processes rather than neoplastic transformation. The exact interactions between lymphoid and follicular epithelial cells, as well as the processes leading to oncocytic transformation in Hashimoto's thyroiditis, are far to be understood. However, the positive cells often present a mild to moderate degree of atypia, with nuclear features resembling those of papillary carcinoma, although clear molecular markers of oncogenic transformation, typical of papillary carcinoma, such as RET/PTC translocation, have not been definitely identified. Therefore, further studies are required to better understand the biological significance of such morphological and immunophenotypical features.

With regard to PAX8-PPARγ gene fusion protein, we have investigated a large series of 120 cases by means of immunohistochemistry, to validate previous reports, based on small number of cases, which failed to detect PPARγ abnormalities in OCT (either by RT-PCR or immunohistochemistry). Since a good correlation has been reported between the molecular detection of PAX8-PPARγ translocation and a strong and diffuse PPARγ protein overexpression, only immunohistochemistry was employed (also to check the possible applications of PPARγ as a diagnostic marker of OCC). Our data confirmed that PPARγ protein over-expression occurred in a very small number of OCCs, all being OCA negative. These results support the hypothesis that OCCs may follow distinct molecular pathways from those of non-oncocytic follicular carcinomas [20].

In conclusion, the present data confirm a high sensitivity and diagnostic accuracy of galectin-3 immunohistochemistry in the diagnosis of malignant OCT, at variance with HBME-1, which had a much lower sensitivity and specificity in OCT than that reported for non-oncocytic follicular tumors (an exception being OVPC). However, the combined use of these two markers was able to improve the sensitivity up to 99%, and therefore a panel including galectin-3 and HBME-1 is recommended in the diagnosis of OCT, although the low specificity of HBME-1 has to be considered when dealing with galectin-3-negative/HBME-1-positive OCT cases. Such a panel of markers is probably the best choice in FNA cytological diagnosis of OCT, to obtain the highest sensitivity in selecting presumably malignant cases to be sent to the surgeon.

Acknowledgements The work was supported by grants from the Italian Ministry of University and Education (ex 60% to M.P.), from the Regione Piemonte (D.D. no.173 dated October 30, 2003,

to F.O.), and The Compagnia di San Paolo "Progetto Speciale Oncologia".

References

1. Bartolazzi A, Gasbarri A, Papotti M, Bussolati G, Lucante T, Khan A, Inohara H, Marandino F, Orlandi F, Nardi F, Vecchione A, Tecce R, Larsson O, Thyroid Cancer Study Group (2001) Application of an immunodiagnostic method for improving preoperative diagnosis of nodular thyroid lesions. Lancet 357:1644–1650
2. Bartolazzi A, Papotti M, Orlandi F (2003) Methodological considerations regarding the use of galectin-3 expression analysis in preoperative evaluation of thyroid nodules. J Clin Endocrinol Metab 88:950
3. Carcangiu ML, Bianchi S, Savino D, Voynick IM, Rosai J (1991) Follicular Hurthle cell tumors of the thyroid gland. Cancer 68:1944–1953
4. Cheung CC, Ezzat S, Freeman JL, Rosen IB, Asa SL (2001) Immunohistochemical diagnosis of papillary thyroid carcinoma. Mod Pathol 14:338–342
5. De Micco C, Ruf J, Chrestian MA, Gros N, Henry JF, Carayon P (1991) Immunohistochemical study of thyroid peroxidase in normal, hyperplastic, and neoplastic human thyroid tissues. Cancer 67:3036–3041
6. Evans HL, Vassilopoulou-Sellin R (1998) Follicular and Hurthle cell carcinomas of the thyroid: a comparative study. Am J Surg Pathol 22:1512–1520
7. Feilchenfeldt J, Totsch M, Sheu SY, Robert J, Spiliopoulos A, Frilling A, Schmid KW, Meier CA (2003) Expression of galectin-3 in normal and malignant thyroid tissue by quantitative PCR and immunohistochemistry. Mod Pathol 16:1117–1123
8. Fonseca E, Nesland JM, Hoie J, Sobrinho-Simoes M (1997) Pattern of expression of intermediate cytokeratin filaments in the thyroid gland: an immunohistochemical study of simple and stratified epithelial-type cytokeratins. Virchows Arch 430:239–245
9. French CA, Alexander EK, Cibas ES, Nose V, Laguette J, Faquin W, Garber J, Moore F Jr, Fletcher JA, Larsen PR, Kroll TG (2003) Genetic and biological subgroups of low-stage follicular thyroid cancer. Am J Pathol 162:1053–1060
10. Gasbarri A, Martegani MP, Del Prete F, Lucante T, Natali PG, Bartolazzi A (1999) Galectin-3 and CD44v6 isoforms in the preoperative evaluation of thyroid nodules. J Clin Oncol 17: 3494–3502
11. Henry JF, Denizot A, Porcelli A, Villafane M, Zoro P, Garcia S, De Micco C (1994) Thyroperoxidase immunodetection for the diagnosis of malignancy on fine-needle aspiration of thyroid nodules. World J Surg 18:529–534
12. Herrmann ME, LiVolsi VA, Pasha TL, Roberts SA, Wojcik EM, Baloch ZW (2002) Immunohistochemical expression of galectin-3 in benign and malignant thyroid lesions. Arch Pathol Lab Med 126:710–713
13. LiVolsi VA (1990) Surgical pathology of the thyroid. Saunders, Philadelphia
14. Mai KT, Bokhary R, Yazdi HM, Thomas J, Commons AS (2002) Reduced HBME-1 immunoreactivity of papillary thyroid carcinoma and papillary thyroid carcinoma-related neoplastic lesions with Hurthle cell and/or apocrine-like changes. Histopathology 40:133–142
15. Marques AR, Espadinha C, Catarino AL, Moniz S, Pereira T, Sobrinho LG, Leite V (2002) Expression of PAX8-PPAR gamma 1 rearrangements in both follicular thyroid carcinomas and adenomas. J Clin Endocrinol Metab 87:3947–3952
16. Martins L, Matsuo SE, Ebina KN, Kulcsar MA, Friguglietti CU, Kimura ET (2002) Galectin-3 messenger ribonucleic acid and protein are expressed in benign thyroid tumors. J Clin Endocrinol Metab 87:4806–4810
17. Nascimento MC, Bisi H, Alves VA, Longatto-Filho A, Kanamura CT, Medeiros-Neto G (2001) Differential reactivity for galectin-3 in Hürthle cell adenomas and carcinomas. Endocr Pathol 12:275–279
18. Nesland JM, Sobrinho Simoes M, Holm R, Sambade MC, Johannessen JV (1985) Hurthle-cell lesions of the thyroid: a combined study using transmission electron microscopy, scanning electron microscopy, and immunohistochemistry. Ultrastruct Pathol 8:269–290
19. Niedziela M, Maceluch J, Korman E (2002) Galectin-3 is not an universal marker of malignancy in thyroid nodular disease in children and adolescents. J Clin Endocrinol Metab 87:4411–4415
20. Nikiforova MN, Biddinger PW, Caudill CM, Kroll TG, Nikiforov YE (2002) PAX8-PPARgamma rearrangement in thyroid tumors: RT-PCR and immunohistochemical analyses. Am J Surg Pathol 26:1016–1023
21. Nikiforova MN, Lynch RA, Biddinger PW, Alexander EK, Dorn GW 2nd, Tallini G, Kroll TG, Nikiforov YE (2003) RAS point mutations and PAX8-PPAR gamma rearrangement in thyroid tumors: evidence for distinct molecular pathways in thyroid follicular carcinoma. J Clin Endocrinol Metab 88:2318–2326
22. Orlandi F, Saggiorato E, Pivano G, Puligheddu B, Termine A, Cappia S, De Giuli P, Angeli A (1998) Galectin-3 is a presurgical marker of human thyroid carcinoma. Cancer Res 58:3015–3020
23. Papotti M, Torchio B, Grassi L, Favero A, Bussolati G (1996) Poorly differentiated oxyphilic (Hurthle cell) carcinomas of the thyroid. Am J Surg Pathol 20:686–694
24. Papotti M, Volante M, Saggiorato E, Deandreis D, Veltri A, Orlandi F (2002) Role of galectin-3 immunodetection in the cytological diagnosis of thyroid cystic papillary carcinoma. Eur J Endocrinol 147:515–521
25. Raphael SJ, McKeown-Eyssen G, Asa SL (1994) High-molecular-weight cytokeratin and cytokeratin-19 in the diagnosis of thyroid tumors. Mod Pathol 7:295–300
26. Raphael SJ (2002) The meanings of markers: ancillary techniques in diagnosis of thyroid neoplasia. Endocr Pathol 13:301–311
27. Rosai J, Carcangiu ML, De Lellis RA (1992) Tumors of the thyroid gland. In: Atlas of tumor pathology. Armed Forces Institute of Pathology, Washington, pp 161–182
28. Sack MJ, Astengo-Osuna C, Lin BT, Battifora H, LiVolsi VA (1997) HBME-1 immunostaining in thyroid fine-needle aspirations: a useful marker in the diagnosis of carcinoma. Mod Pathol 10:668–674
29. Saggiorato E, Cappia S, De Giuli P, Mussa A, Pancani G, Caraci P, Angeli A, Orlandi F (2001) Galectin-3 as a presurgical immunocytodiagnostic marker of minimally invasive follicular thyroid carcinoma. J Clin Endocrinol Metab 86:5152–5158
30. Saggiorato E, Aversa S, Deandreis D, Arecco F, Mussa A, Puligheddu B, Cappia S, Conticello S, Papotti M, Orlandi F (2004) Galectin-3: presurgical marker of thyroid follicular epithelial cell-derived carcinomas. J Endocrinol Invest (in press)
31. Tallini G (1998) Oncocytic tumors. Virchows Arch 433:5–12
32. Watson RG, Brennan MD, GoellnerJR, van Heerden JA, McConahey WM, Taylor WF (1984) Invasive Hurthle cell carcinoma of the thyroid: natural history and management. Mayo Clinic Proc 59:851–855

Virchows Arch (2004) 445:189–198
DOI 10.1007/s00428-004-1035-z

ORIGINAL ARTICLE

Maria P. Foschini · Mauro Papotti · Alfredo Parmeggiani · Giovanni Tallini · Luciano Castaldini · Domenico Meringolo · Vincenzo Eusebi

Three-dimensional reconstruction of vessel distribution in benign and malignant lesions of thyroid

Received: 3 February 2004 / Accepted: 21 April 2004 / Published online: 8 June 2004
© Springer-Verlag 2004

Abstract In order to better understand the spatial distribution of thyroid vessels, a series of benign and malignant thyroid lesions were studied with three-dimensional (3D) histological stereomicroscopic reconstruction. Cases consisted of normal autoptic thyroids (*n*=6), colloid goitres (*n*=6), Basedow's disease (*n*=2), follicular adenoma (FA) (*n*=4) one of which with Hurthle cells (HC), minimally invasive, well-differentiated follicular carcinoma (FTC) (*n*=1), well-differentiated FTC with HC (*n*=1), poorly differentiated FTC (*n*=13) with extensive angioinvasion, papillary carcinoma (PTC) (*n*=8) and medullary carcinoma (MTC) (*n*=1). From each selected nodule, parallel sections were obtained for 3D reconstruction and for histological and immunohistochemical studies. In normal thyroid, large vessels were located at the periphery of the gland with smaller branches present within the thyroid parenchyma that encircled follicles. The same pattern of vascularisation is maintained in lesions showing a follicular architecture as colloid goitre, Basedow's disease, FA, well-differentiated FTC and the follicular variant of PTC. Neoplastic lesions, at variance with non-neoplastic lesions, contained rare anastomoses. Poorly differentiated FTC and MTC contained large intratumoural vessels surrounding avascular areas corresponding to solid neoplastic cellular sheets with necrosis. PTC were more vascularised and contained numerous vascular anastomoses. In conclusion, the present data indicate that the vascular distribution is related to the follicular, papillary or solid type of growth. Vascular anastomoses and intratumoural vessels surrounding solid avascular areas are signs of malignancy.

Keywords Thyroid · Vessels · Papillary thyroid carcinoma · Follicular thyroid carcinoma · Thyroid nodule

M. P. Foschini · G. Tallini · V. Eusebi
Department of Anatomic Pathology,
University of Bologna Ospedale Bellaria,
Bologna, Italy

M. Papotti
Department of Anatomic Pathology,
University of Turin and San Luigi Hospital,
Turin, Italy

A. Parmeggiani
Department of Otolaryngology,
General Hospital,
Budrio, Bologna, Italy

L. Castaldini
Department of Radiology,
Ospedale Bellaria,
Bologna, Italy

D. Meringolo
Department of Endocrinology,
General Hospital,
Bentivoglio, Bologna, Italy

M. P. Foschini (✉)
Anatomia Patologica,
Ospedale Bellaria,
Via Altura 3, 40139 Bologna, Italy
e-mail: Mariapia.foschini@ausl.bologna.it
Tel.: +39-051-6225523
Fax: +39-051-6225759

Introduction

Thyroid is supplied by a rich vascular network that undergoes noticeable changes in most benign and malignant lesions [15]. Vascular modifications are well evident in cases of hyperthyroidism, as Basedow's disease, in cases of chronic thyroiditis, as Hashimoto's thyroiditis as well as in carcinomas [15]. Vascular changes are used to assist in preoperative diagnosis when visualised by flow colour Doppler sonography, which identifies several different vascular patterns in thyroid nodules. Nodules characterised by rare or absent vessels are more probably benign lesions, while nodules rich in vessels are more likely malignant lesions. Unfortunately, colour Doppler sonography is still hampered by a high rate of false-negative cases [8, 14], and cases of avascular malignant lesions are on record [8, 14].

Table 1 Antibodies used. *M* monoclonal, *P* pretreatment consisted of submitting sections at high pressure for 6 min at 100°C in citrate buffer. Slides were then cooled at room temperature. *ND* not done

Antibody	M	Manufacturer	Clone	Dilution	Pretreatment
CD 31	M	Dako Glostrup Denmark	JC70A	1:20	P
Collagen IV	M	Dako Glostrup Denmark	CIV 22	1:100	P
Smooth-muscle actin	M	Dako Glostrup Denmark	1A4	1:100	ND

To date, three-dimensional (3D) histological examination of tissues, using a stereomicroscope, has been mainly applied to the breast, where it provides information about the site of origin of carcinomas, the type of growth, the extension of neoplasm and margin assessment in cases of in situ and invasive carcinomas [3, 4, 6, 12, 16]. Recently, a modification of the 3D histological technique led to the direct visualisation of the vascular tree in twin placentas [7], giving noticeable insights to the understanding of the mechanism of twin-to-twin cytomegalovirus infection [10]. The same modified method, applied to benign and malignant thyroid nodules, gave a direct visualisation of their vessels [2]. These preliminary results prompted us to study a larger series of benign and malignant thyroid nodules with 3D histological stereomicroscopic reconstruction to better understand the spatial distribution of thyroid vessels.

Materials and methods

Cases consisted of 36 surgical specimens from total thyroidectomies and 6 normal autoptic thyroids obtained from the Departments of Anatomic Pathology of the Universities of Bologna and Turin (Italy). Cases were collected along a 23-year life span, and all cases had been kept in buffered formalin. Thyroidectomies had been performed in patients having severe clinical impairments in large goitres or in cases having a preoperative cytological diagnosis of malignancy (cases 36 to 41) or suspicious of follicular neoplasia (cases 14 and 15). Part of the specimens were from the pre-FNA (fine-needle aspiration) era. FNA was performed in 18 patients only. Of patients, 10 were male, and 26 patients were female, ranging in age from 24 years to 90 years (mean 54 years).

All thyroids were serially cross-sectioned perpendicularly to the longitudinal axis to examine all the nodules present. One nodule was selected for the present study. From each selected nodule, parallel sections were obtained and alternatively processed for 3D examination and for routine histology (RH). Care was taken to avoid areas of haemorrhage or areas of post-FNA artefacts

Accordingly, in addition to the 6 cases of normal autoptic thyroids, 6 large nodules from colloid goitres were retained, as well as 2 cases of Basedow's disease, 4 cases of follicular adenoma (FA), of which 1 case included Hurthle cell (HC) differentiation, 1 case of minimally invasive, well-differentiated follicular carcinoma (FTC), 1 case of well-differentiated FTC with HC differentiation, 13 cases of poorly differentiated FTC, 8 cases of papillary carcinoma (PTC) and 1 case of medullary carcinoma (MTC).

The 3D histological method is similar to that introduced in 1973 by Wellings et al. [16] to study breast tissue. Minimal changes to this method were recently introduced to study placental vessels [7]. These changes allowed direct visualisation of blood vessels together with red blood cells present in their lumina.

Cross-sections (3 mm) were obtained from each selected lesion. Sections were washed overnight in distilled water, dehydrated for 2 h in 70% alcohol followed by three passages in absolute alcohol, where an equal volume of xylene was added in the last change, and the specimen finally cleared in xylene for 1 h. Sections were then immersed in methyl salicylate for 3D examination using a stereomicroscope (Nikon, Tokyo, Japan).

From the RH block, serial 3-μm-thick sections were obtained and stained with haematoxylin-eosin and immunohistochemistry, applying the antibodies reported in Table 1. Immunohistochemical procedure was performed in an automatic stainer (Autostainer Dako, Carpintera, CA, USA) using biotinylated goat antiserum and streptavidin peroxidase (LabVision Corporation, Fremont, CA, USA). Dako Liquid DAB (diaminobenzidine) substrate–Chromogen system (Dako, Carpintera, CA, USA) was used to reveal peroxidase activity.

Results

The clinico-pathological data of the present case series are summarised in Table 2.

Normal thyroid

There were six cases of individuals with normal thyroid (Fig. 1A, B, C, D, E). In 3D, stereomicroscopic examination revealed large vessels mainly located in the capsular and subcapsular region (Fig. 1A). Vessels were also observed in the thyroid parenchyma, branching along the fibrous septa of the lobules. The smallest visible vessels encircled spheroidal structures corresponding to follicles (Fig. 1B).

In the corresponding RH sections, large arteries and veins in the capsular–subcapsular region were retraced. These branched into smaller vessels when located within the glandular parenchyma (Fig. 1C), and each follicle was encircled by thin capillaries as shown using CD31 (Fig. 1D) and collagen-IV immunostainings. These same capillaries were devoid of actin-rich cells along their walls.

Colloid goitre

There were six cases of colloid goitre (Fig. 2A, B, C, D, E). In the 3D examination, the vascular pattern was very similar to that observed in normal thyroid. Large vessels were mainly located in the capsular and subcapsular region as in normal gland. In addition, large vessels were retraced in the thyroid parenchyma, running along fibrous septa and branching into smaller channels that encircled nodules formed by expanded and/or cystic follicles. Within the nodules, rare thin vessels were observed. These lacked anastomotic connections (Fig. 2A, B).

In RH, the nodules were classically constituted by large follicles or cystic spaces lined by cuboidal to flat epithelium. Nodules were surrounded by a fibrous capsule of variable thickness from case to case. Medium-sized

Table 2 Clinical data. *HC* hurtle cell, *PD* poorly differentiated, *R* right lobe, *L* left lobe, *FNA* previous fine needle aspiration, *(x months)* interval between FNA procedure and thyroidectomy, *B* bilateral, *N* FNA not done, *Y* FNA preformed, *NK* laterality was not known

Case no.	Sex/age (years)	FNA	Laterality/size (cm)	Histological diagnosis
1	Male/69			Normal thyroid
2	Male/72			Normal thyroid
3	Male/80			Normal thyroid.
4	Male/62			Normal thyroid
5	Female/79			Normal thyroid
6	Male/79			Normal thyroid
7	Male/42	N	R/6	Colloid goiter
8	Female/50	Y (36 months)	L/5	Colloid goiter
9	Female/46	N	L/7	Colloid goiter
10	Female/79	Y (12 months)	R/8	Colloid goiter
11	Female/52	Y (72 months)	R/10	Colloid goiter
12	Female/48	Y (24 months)	L/5	Colloid goiter
13	Female/24	N	L/5	Basedow's disease
14	Female/33	N	R/5	Basedow's disease
15	Female/43	Y (3 months)	R/2.5	Follicular adenoma
16	Female/31	Y (2 months)	R/2	Follicular adenoma
17	Female/57	N	L/3, 5	Follicular adenoma
18	Female/46	N	R/2.1	Oncocytic follicular adenoma
19	Female/29	Y (5 months)	L/1	Minimally invasive, well-differentiated follicular carcinoma
20	Female/31	N	NK/7	Follicular carcinoma, PD
21	Female/50	N	NK/5	Follicular carcinoma, PD
22	Male/30	Y (2 months)	NK/5	Follicular carcinoma, PD
23	Male/38	Y (2 months)	NK/12	Follicular carcinoma, PD
24	Female/71	N	NK/8	Follicular carcinoma, PD
25	Female/70	N	R/6, 5	Follicular carcinoma, PD
26	Female/57	N	NK/9	Follicular carcinoma, PD
27	Male/81	N	NK/6	Follicular carcinoma, PD
28	Female/72	N	NK/7	Follicular carcinoma, PD
29	Female/41	Y (1 month)	R/5	Follicular carcinoma, PD
30	Male/82	N	R/6	Follicular carcinoma, PD
31	Male/65	Y (2 month)	NK/9	Follicular carcinoma, PD
32	Female/55	N	NK/7	Follicular carcinoma, PD, HC
33	Male/90	N	NK/10	Follicular carcinoma, well-differentiated HC
34	Male/70	N	R/12	Papillary carcinoma, follicular variant
35	Female/66	Y (1 month)	L/6	Papillary carcinoma, follicular variant
36	Female/39	Y (3 month)	R/1	Papillary carcinoma, tall-cell variant
37	Female/73	Y (5 days)	B/7	Papillary carcinoma, tall-cell variant
38	Female/51	Y(3 months)	R/1.5	Papillary carcinoma, classic variant
39	Male/28	Y (1 month)	R/1.4	Papillary carcinoma, follicular variant
40	Female/56	Y (20 days)	L/1.3	Papillary carcinoma, tall-cell variant
41	Female/63	Y (1 month)	R/3.5	Papillary carcinoma, classic variant
42	Male/77	N	L/8	Medullary carcinoma

* Normal thyroid. Autoptic thyroids were obtained from patients who died from unrelated causes, namely diffuse alveolar damage (cases 1 and 6), intestinal infarction (case2), renal-cell carcinoma (case 3), myocardial infarct (case 4) and sepsis (case 5)

arteries and veins were running into the capsule (Fig. 2C). The follicular part of the nodules contained small capillaries located between follicles. Capillaries were outlined by CD31 (Fig. 2D) and collagen-IV immunostainings, but lacked smooth-muscle actin cells.

Basedow's disease

There were two cases of Basedow's disease (Fig. 3A, B, C, D, E). In 3D examination, these two cases showed the same vascular pattern observed in those with normal thyroid, with large vessels located in the capsular and subcapsular region and their branches surrounding follicles. Vessels appeared somehow larger than those of normal thyroid. No vascular anastomoses were observed (Fig. 3A, B).

In RH, all follicles were encircled by capillary vessels. Papillary formations when present within the follicles had a fibrovascular core containing capillaries. All these surrounded follicles and were observed within the core of the papillae whenever present (Fig. 3C, D). The capillaries, at a variance with colloid goitre, contained smooth-muscle, actin-positive elements in their walls, in addition to endothelial CD 31-positive cells.

Follicular adenoma

There were four cases of FA (Fig. 4A, B, C, D). In 3D examination, large vessels surrounded the adenomatous

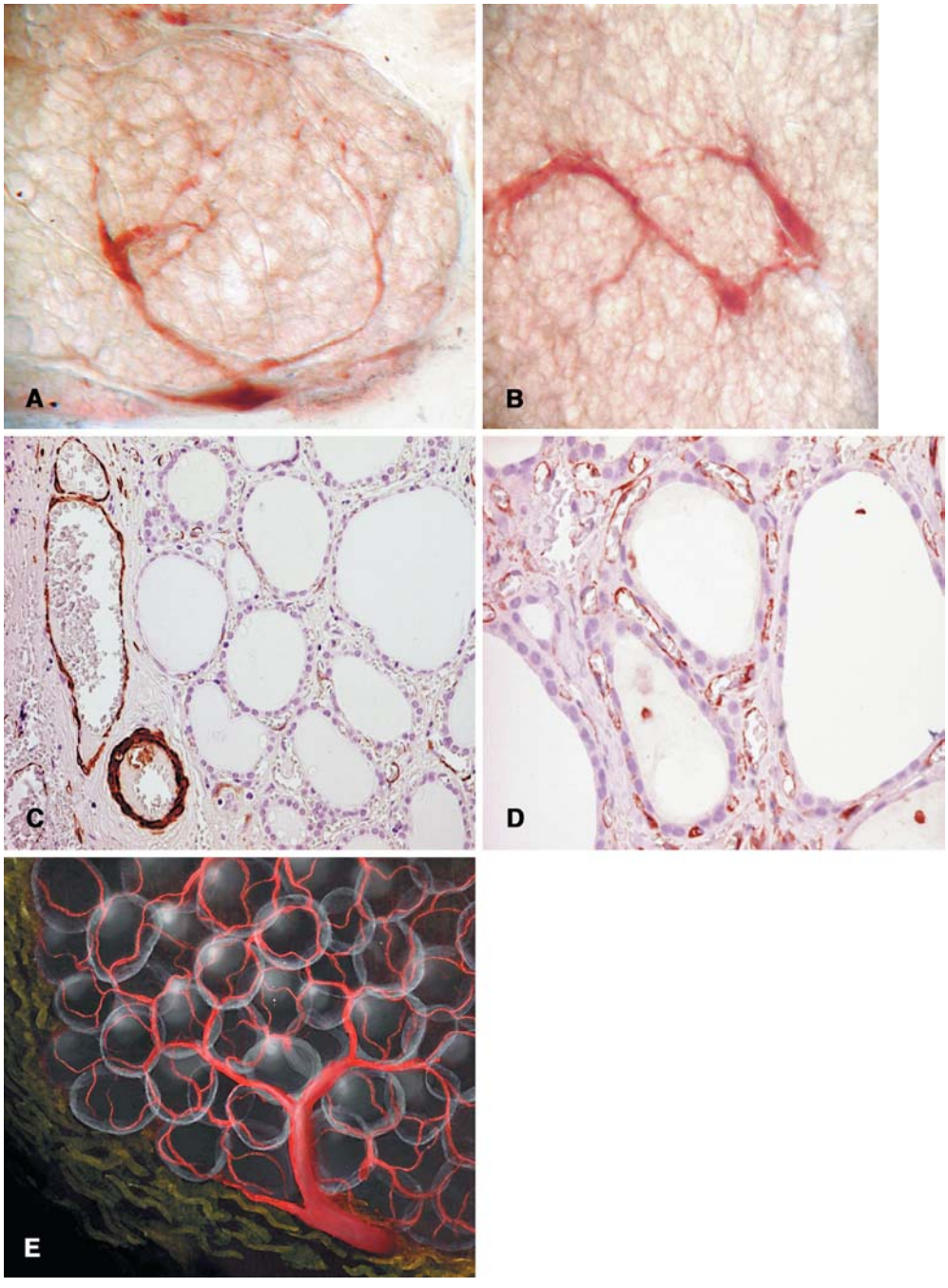


Fig. 1 Normal thyroid. **A** On three-dimensional examination, large vessels are mainly observed in the capsular and subcapsular regions. **B** Intraparenchymal vessels subdivide into smaller vessels that encircle follicles. **C** Smooth-muscle actin highlights arteries and veins in the intraparenchymal fibrous septa. **D** Capillaries around follicles are lined by CD31-positive endothelial cells. **E** Representation of vessels in normal tissue

nodules and were present along the capsule of the nodule (Fig. 4A). Their branches were seen mainly at the periphery of the nodular parenchyma. Focally, rare groups of anastomosing vessels similar to those seen in PTC were also observed (see below), but these were rare (Fig. 4B).

In RH, each single adenomatous follicle was encircled by capillaries, resulting in a noticeable vascular network. Capillary vessels, evidenced by CD31 and collagen-IV immunostaining, only focally contained smooth-muscle actin cells (Fig. 4C).

Follicular carcinoma

There were two cases cases of minimally invasive, well-differentiated FTC. In 3D examination, a vascular pattern similar to that observed in FA was found. Large vessels surrounded the neoplastic nodules and branched into the nodule. Intratumoural vessels only focally gave rise to the interanastomosing groups of vessel. The neoplastic angioinvasion was not visualised, as the technique is based on the observation of red blood cells within the vessels.

In RH, the vascular pattern was very similar to that of FA, characterised by a rich network of capillaries, which focally contained smooth-muscle cells in their wall.

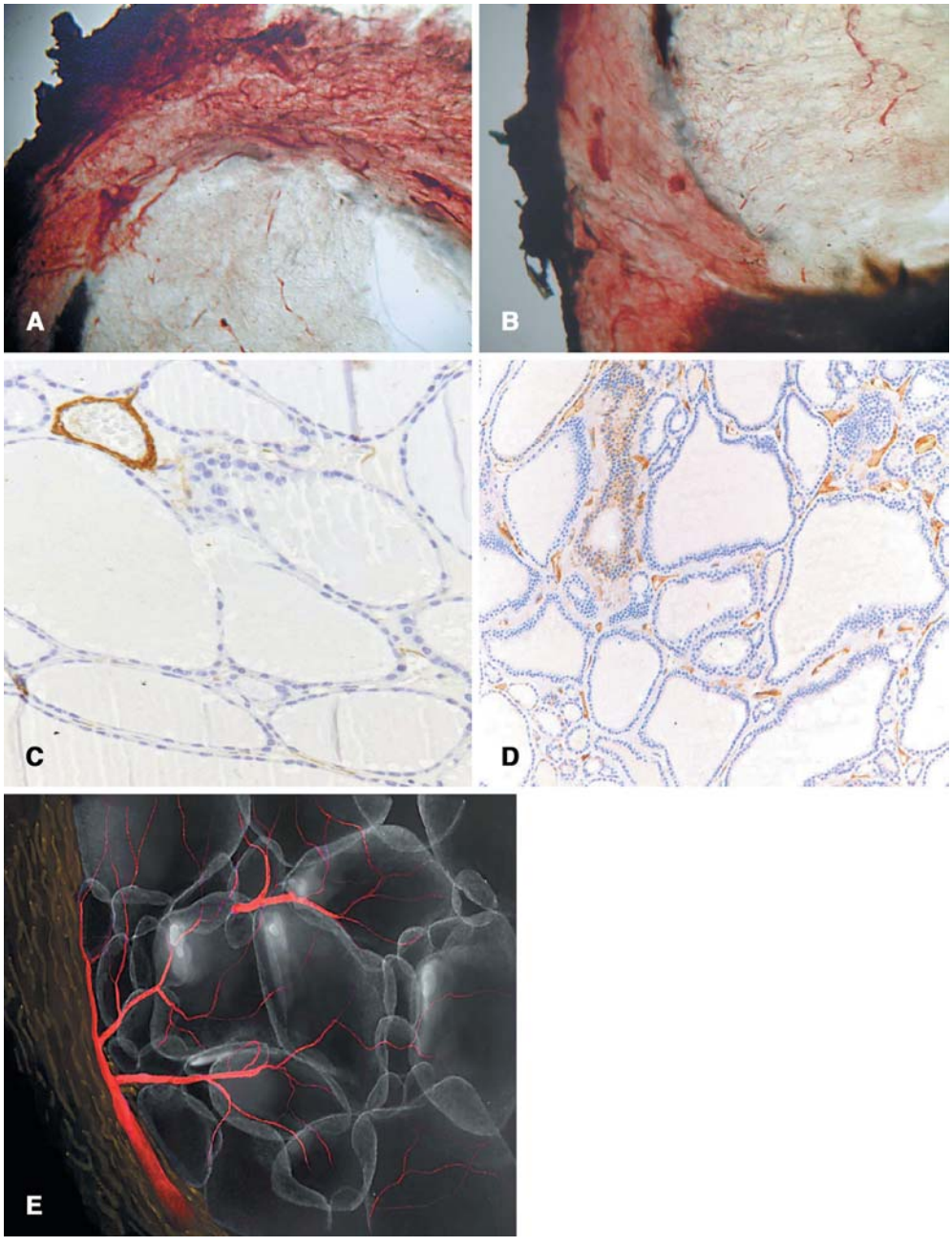


Fig. 2 Colloid goitre. **A**, **B** On three-dimensional examination, large vessels are mainly located at the periphery of the nodules, while the parenchyma contains only rare thin vessels. **C** Smooth-muscle actin is evident in cells located in the walls of the rare vessels. **D** Perifollicular capillaries are surrounded by capillaries with CD31-positive endothelial cells. **E** Representation of colloid vessels

Poorly differentiated FTC

There were 13 cases of poorly differentiated FTC (Fig. 5A, B, C, D, E, F, G). In 3D examination, the 13 cases studied showed large peritumoural (Fig. 5A, B) vessels, the branches of which were present within the neoplastic area and surrounded avascular tumoural areas. Intratumoural vessels were rare, single, large and curved (Fig. 5C). Anastomosing vessels were very rare.

In RH, typical solid-trabecular-insular areas were seen. These often had central necrosis and were surrounded by large vessels of venule type with an incomplete muscular wall. Capillaries were almost absent (Fig. 5D, E, F, G).

Follicular neoplasms, both adenomas and carcinomas with oncocitic features (HC) showed the same type of vessels as the conventional follicular types.

Papillary carcinoma

There were eight cases of PTC (Fig. 6A, B, C, D, E, F). In 3D examination, PTC appeared more rich in vessels than normal thyroid and benign goitres. Large vessels surrounded the neoplastic nodules (Fig. 6A, B, C). Intranodular vessels were numerous and were connected to each other by "glomeruloid" clusters of small vessels (Fig. 6D). These were constituted by variously anasto-

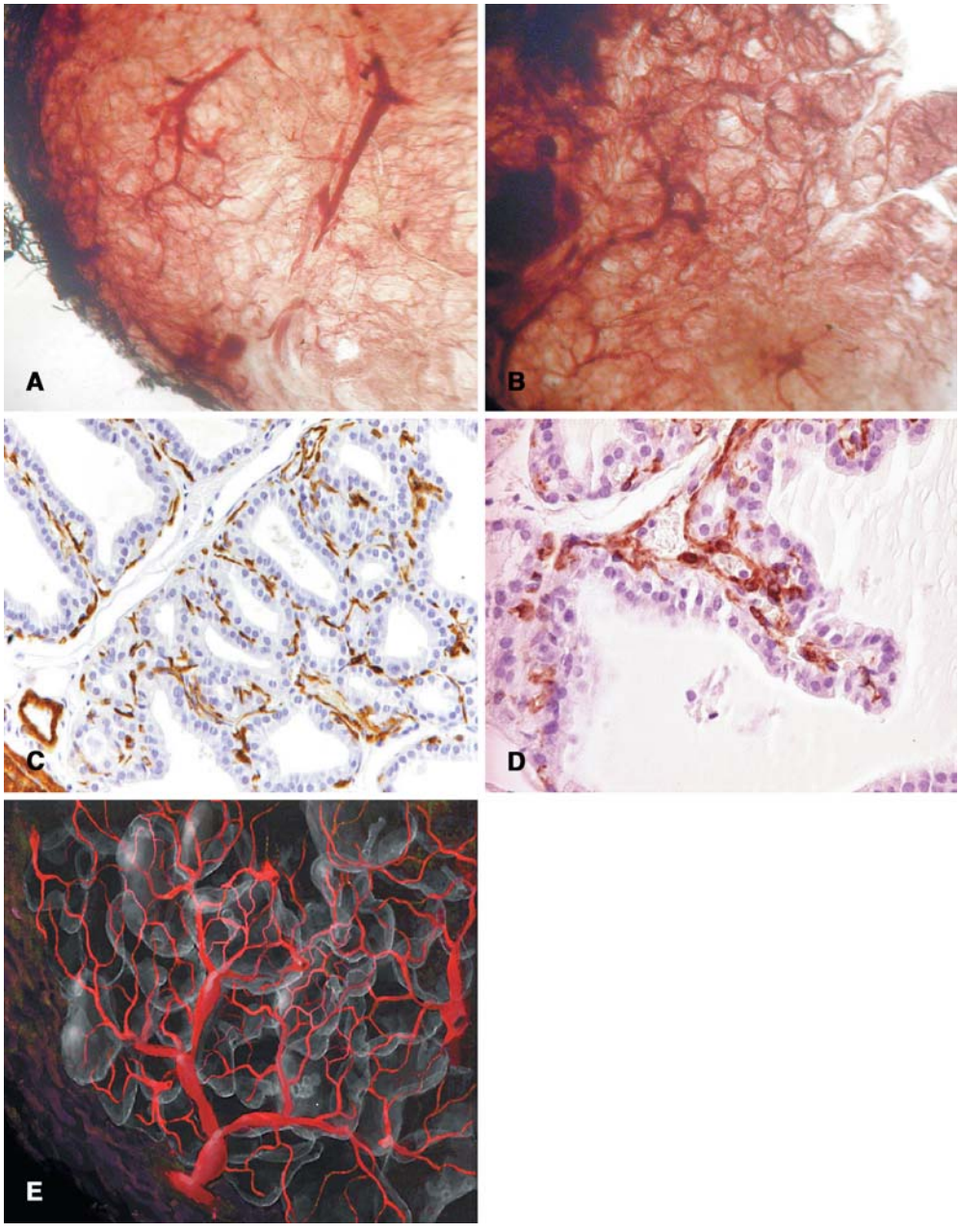


Fig. 3 Basedow's disease. **A**, **B** On three-dimensional examination, the vascular distribution is similar to that of normal thyroid, but vessels appear larger. **C**, **D** On histology, small capillaries located between follicles and in hyperplastic papillae are lined by smooth-muscle, actin-positive cells. **E** Representation of vessels in Basedow's disease

mosing small vessels, seen both in the classical and tall-cell variants. Three cases of the follicular variant of PTC were included in the study. In these latter cases, intratumoural vessels were similar to those seen in benign and well-differentiated follicular lesions and were characterised by larger linear vessels with rare anastomoses.

In RH, each papillary structure contained small capillaries lined by smooth-muscle, actin-rich cells (Fig. 6E).

Medullary carcinoma

There was one case of MTC. In 3D examination, the single MTC case showed features similar to those of benign lesions or poorly differentiated carcinomas, with rare large vessels observed within the tumour.

In RH, neoplastic vessels were irregular and only focally surrounded by smooth-muscle actin cells in a fashion reminiscent of that of poorly differentiated FTC.

Discussion

Increase of vascularity in thyroid nodules has been observed by radiologists who attempt, in colour Doppler sonography, to establish the benign or malignant nature of thyroid lesions based on the number and distribution of the vessels [8, 14]. Count and distribution of vessels have been used to search for prognostic parameters on thyroid

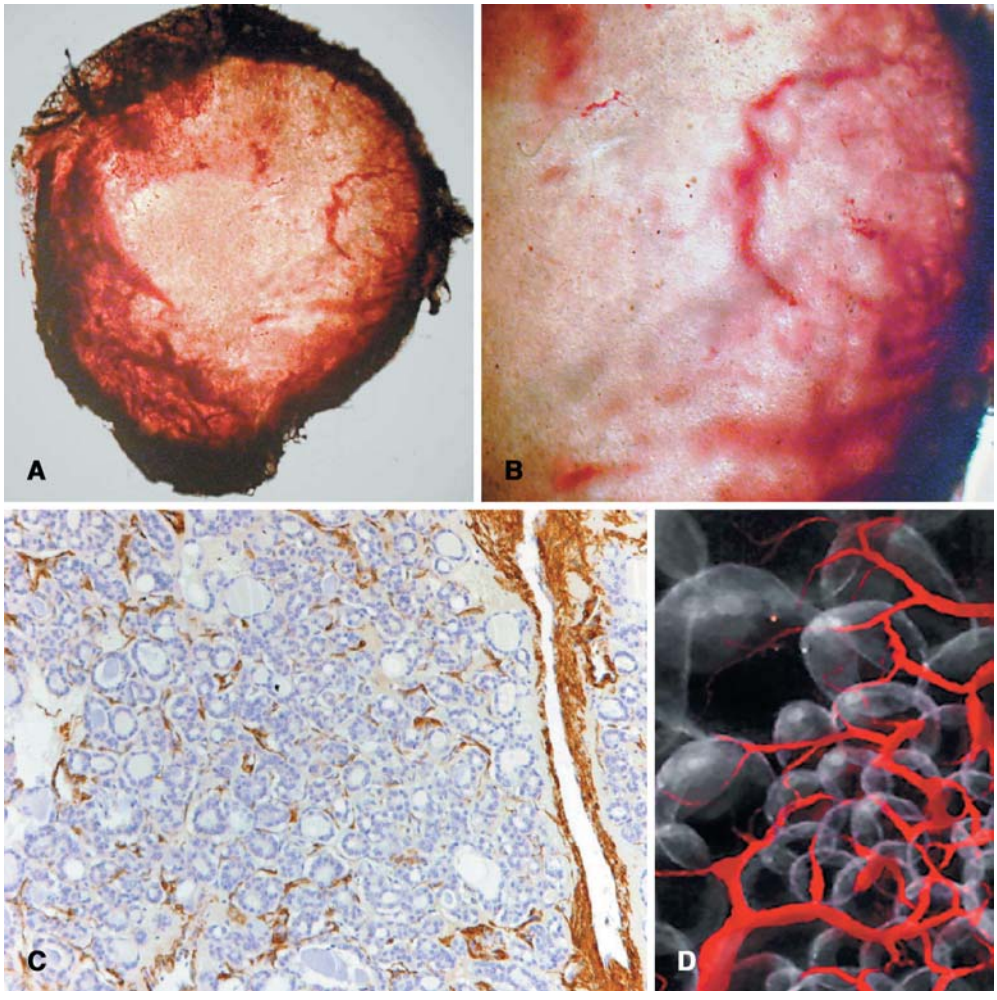


Fig. 4 Follicular adenoma. **A** On three-dimensional examination, large vessels are mainly located at the periphery of proliferating nodules. **B** Rare vessels are present within the nodular parenchyma. **C** Smooth-muscle actin immunostaining evidences intranodular vessels, and it is also focally positive in small capillaries that encircle follicles. **D** Representation of the adenomatous vessels

tumours [5, 17]. Nevertheless, no definite criteria are available to date, as there are no sufficient data on the vascularisation of thyroid.

In the present study, the vascular network was directly examined in cases of normal thyroid, and benign and malignant thyroid lesions using a stereomicroscope that allowed 3D visualisation. Data obtained by 3D analysis were compared with those of conventional histological and immunohistochemical evaluation. At the 3D level, vessels were traced up to small size (venules and arterioles), but capillaries were visualised only with routine histology and immunohistochemistry.

In the normal thyroid, large vessels were mainly located at the periphery of the gland, and small branches only were present within the thyroid parenchyma, running along the interlobular fibrous septa. Each follicle was encircled by capillary vessels that showed CD 31-positive endothelial cells, but were devoid of smooth-muscle, actin-positive elements.

Basically the same pattern of vascularisation, characterised by capillaries surrounding each follicle, was maintained in the lesions showing a follicular architecture, such as colloid goitres, adenomas, well-differentiated follicular carcinomas and the follicular variants of papillary carcinoma. At variance with the normal parenchyma, in colloid goitre, large vessels were located within the fibrous septa that surround nodules. The latter appeared on 3D examination as almost avascular. This was probably the consequence of the large and irregular dimensions reached by the follicles, which cause compression of the vessels.

Neoplastic (adenomas and well-differentiated FTC) follicular lesions showed a higher number of vessels than colloid goitres, both at 3D and histological levels. These vessels were also large, encircled the nodule and were seen among follicular structures, within fibrous septa. Vessels within the nodules were more frequently single and linear. Vascular anastomoses were rarely present. On histology, capillaries were seen surrounding the neoplastic follicles and occasionally displayed smooth-muscle fibres in their walls. Poorly differentiated FTC and MTC showed large peritumoural vessels, as observed in the well-differentiated counterpart, but showed large tumoural areas that on 3D examination appeared almost avascular. Intratumoural vessels were present and surrounded the avascular areas. The latter corresponded, on RH, to areas of solid neoplastic cellular sheets also containing necrotic patches.

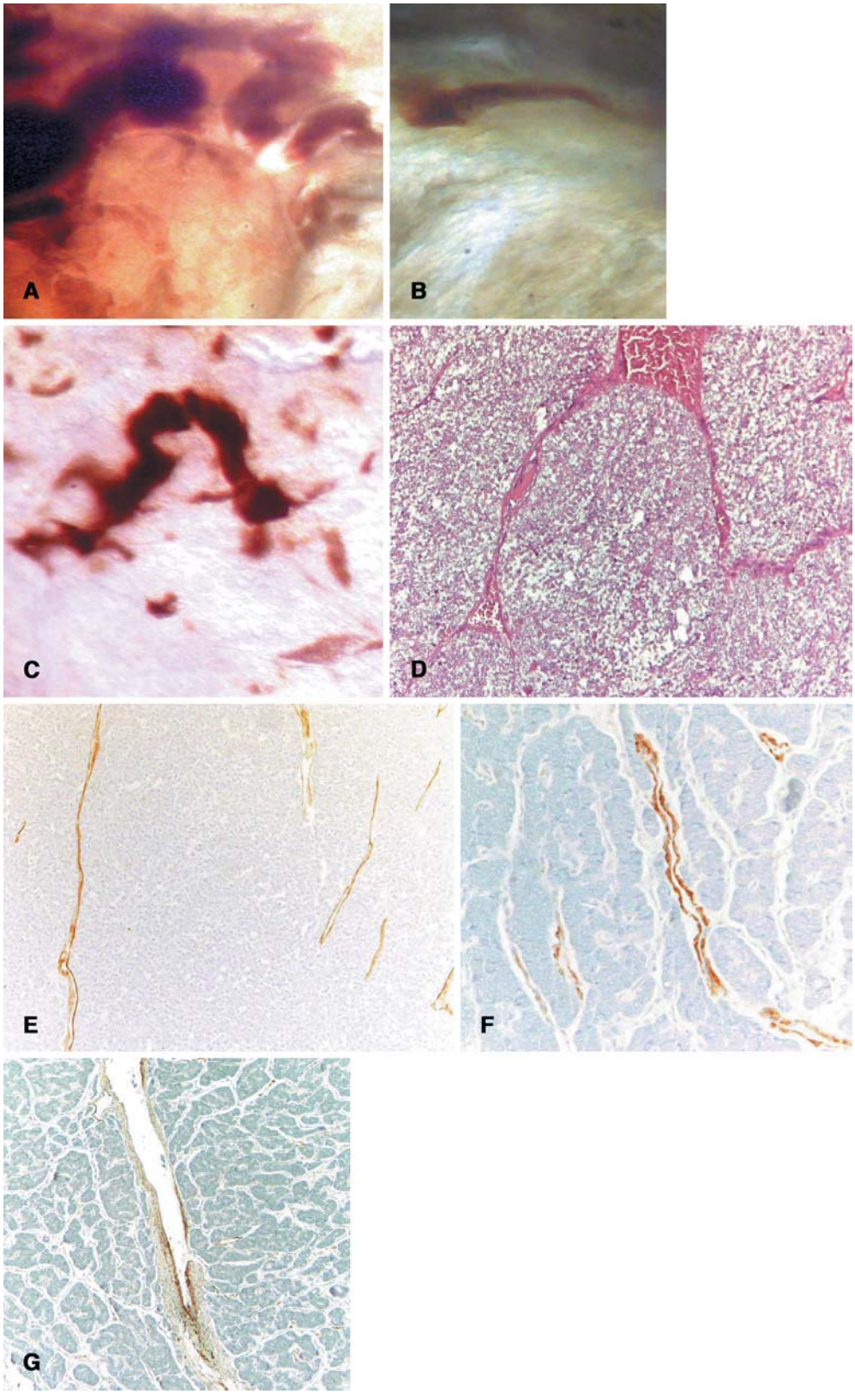


Fig. 5 Poorly differentiated follicular carcinoma. **A**, **B** On three-dimensional examination, large peritumoural vessels are seen. **C** Intratumoural vessels are rare, are single and often are arch shaped. **D** On histology, areas of poorly differentiated cells are surrounded by rare arch-shaped vessels. **E** CD31 immunostaining better evidences the rare intratumoural vessels. **F**, **G** Smooth-muscle actin stains the walls of rare intratumoural vessels

In contrast, papillary carcinomas appeared more vascularised, rich in vascular anastomoses as highlighted using 3D examination. On RH, neoplastic papillae contained capillaries rich in smooth-muscle fibres in their walls.

The two cases of Basedow's disease showed a vascular pattern with features common to the follicular and the papillary lesions. On 3D examination, the vessel distribution was similar to that of normal thyroid and colloid

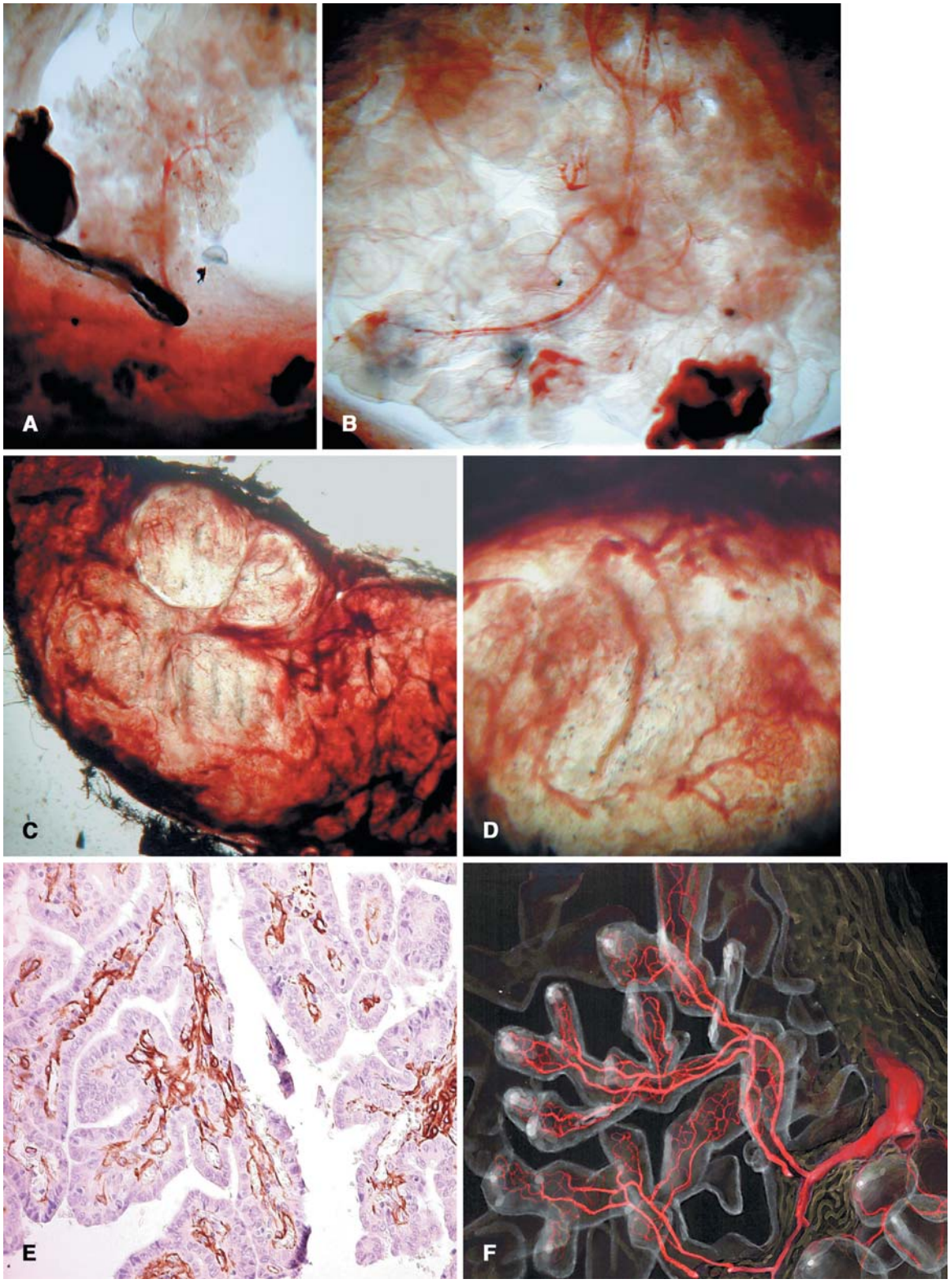


Fig. 6 Papillary carcinoma. **A**, **B** Three-dimensional (3D) images of cystic papillary carcinoma. **C** 3D image of solid papillary carcinoma. Papillary carcinoma appears rich in vessels. **D** Intranodular vessels are numerous. The glomeruloid pattern of anastomoses is self evident. **E** Smooth-muscle actin is positive in the intrapapillary vessels. **F** Schematic representation of vessels in papillary carcinoma

goitre, but vessels were larger. On histology, capillaries were numerous among hyperplastic follicles and were also seen in papillae when formed. These same capillaries display actin-rich cells in their walls.

On 3D examination, the main difference between neoplastic and non-neoplastic lesions concerned the anastomoses. These were composed of aggregates of small vessels variously anastomosing each other and probably indicate newly formed vessels as the result of neoangiogenetic factor, as seen in other carcinomas.

Anastomoses are occasionally observed in adenomatous lesions, but are easily recognisable in PTC. Katoh et al. [13], in a study using confocal laser microscopy, described "glomerular-like" vascular structures as well as tortuous, densely packed vascular complexes in five of seven PTC, a finding very similar to the presently described vascular findings, including vascular anastomoses. At variance with the study by Katoh et al. [13], in the present series, vascular anastomoses were occasionally also observed in benign tumours.

These data suggest that thyroid papillary neoplasms, in addition to a high number of vessels, harbour anastomosing vessels, which, when numerous, are indicative of PTC.

Vascular anastomoses are a well-known feature in several malignant tumours. They are particularly evident in glioblastoma multiforme [1] or endocrine tumours such as Merkel-cell carcinoma [9, 11]. Their radiological demonstration in glial tumours is considered diagnostic of malignancy [1].

Poorly differentiated FTC shows 3D characteristically large intratumoural vessels surrounding avascular areas. The 3D finding corresponds, at RH, to sheets of carcinomatous areas with necrosis.

In conclusion, the data here shown indicate that the angioarchitecture of the thyroidal neoplasms is related to the follicular, papillary or solid type of neoplastic growth. Nevertheless, there are signs of malignancy, such as numerous anastomoses in PTC and avascular sheets in poorly differentiated FTC separated by large intratumoural vessels that might be very useful diagnostic findings once available techniques, such as colour Doppler, become sensitive enough to reveal them.

Acknowledgements I would like to acknowledge Mr. Massimo Romagnoli for his artwork and Mrs. Luciana Muzzi for technical help. This study was supported by grants from the Ministry of University, Scientific and Technological Research (Rome) and University of Bologna.

References

1. Burger PC, Scheithauer BW (eds) (1994) Tumors of the central nervous system. Fascicle 10, Third series Atlas of Tumor Pathology, Armed Forces Institute of Pathology, Bethesda, MD
2. Dorji T, Foschini MP, Eusebi V (2002) Three dimensional images in thyroid pathology. 17th International Meeting of the Adriatic Society of Pathology, Brjuni (Croatia) 27–29 June
3. Faverly D, Holland R, Burgers L (1992) An original stereomicroscopic analysis of the mammary glandular tree. Virchows Archiv 421:115–119
4. Faverly D, Burgers L, Bult P, Holland R (1994) Three dimensional imaging of mammary ductal carcinoma in situ: clinical implications. Semin Diagn Pathol 11:193–198
5. Fontanini G, Vignati S, Pacini F, Pollina L, Basolo F (1996) Microvessel count: an indicator of poor outcome in medullary thyroid carcinoma, but not in other types of thyroid carcinomas. Mod Pathol 9:636–640
6. Foschini MP, Tot T, Eusebi V (2002) Large section (macrosection) histologic slides. In: Silverstein MJ (ed) Ductal carcinoma in situ of the breast, 2nd edn. Lippincott Williams & Wilkins, Philadelphia
7. Foschini MP, Gabrielli L, Dorji T, Kos M, Lazzarotto T, Lanari M, Landini MP (2003) Vascular anastomoses in dichorionic diamniotic fused placentas: a three dimensional (3D) reconstruction. Int J Gynecol Pathol 22:359–361
8. Frates MC, Benson CB, Doubilet PM, Cibas ES, Marqusee E (2003) Can color Doppler sonography aid the prediction of malignancy in thyroid nodules? J Ultrasound Med 22:127–133
9. Frigerio B, Capella C, Eusebi V, Tenti P, Azzopardi JG (1983) Merkel cell carcinoma of the skin: the structure and origin of normal Merkel cells. Histopathology 7:229–249
10. Gabrielli L, Lazzarotto T, Foschini MP, Lanari M, Guerra B, Eusebi V, Landini MP (2003) Horizontal in utero acquisition of a viral infection. J Clin Microbiol 41:1329–1331
11. Gaudin PB, Rosai J (1995) Florid vascular proliferation associated with neural and neuroendocrine neoplasms. A diagnostic clue and potential pitfall. Am J Surg Pathol 19: 642–652
12. Jackson PA, Merchant W, McCormick CJ et al (1994) A comparison of large block macrosectioning and conventional techniques in breast pathology. Virchows Archiv 425:243–248
13. Katoh R, Hemmi A, Komiyama A, Kawaoi A (1999) Confocal laser scanning microscopic observation in angioarchitectures in human thyroid neoplasms. Hum Pathol 301226–1231
14. Rago T, Vitti P, Chiovato L, Mazzeo S, De Liberi A, Miccoli P, Vacava P, Martino E, Pinchera A (1998) Role of conventional ultrasonography and color flow Doppler sonography in predicting malignancy in "cold" thyroid nodules. Eur J Endocrinol 138:41–46
15. Ramsed JD (2000) Angiogenesis in the thyroid gland. J Endocrinol 166:475–480
16. Wellings SR, Jensen HM (1973) On the origin and progression of ductal carcinoma in the human breast. J Natl Cancer Inst 50:1111–1118
17. Wong NACS, Willott J, Kendall MJ, Sheffield EA (1999) Measurement of vascularity as a diagnostic tool for well differentiated thyroid tumours: comparison of different methods of assessing vascularity. J Clin Pathol 52:593–597

Virchows Arch (2004) 445:199–202
DOI 10.1007/s00428-004-1050-0

CASE REPORT

Yasunori Takeda · Masanobu Satoh · Shin-ichi Nakamura

Pigmented pleomorphic adenoma, a novel melanin-pigmented benign salivary gland tumor

Received: 17 March 2004 / Accepted: 21 May 2004 / Published online: 30 June 2004
© Springer-Verlag 2004

Abstract This paper reports a pleomorphic adenoma with grossly visible pigmentation resulting in the macroscopic appearance of melanotic lesion in a 33-year-old Japanese male. In addition to the characteristic histopathological features of a benign pleomorphic adenoma, variously formed and -sized cells, many of which were considered to be melanocytes, containing melanin pigment in their cytoplasm, were distributed in the epithelial component. In addition, melanin pigment was deposited in tumor cells of duct structures. Furthermore, condensed secretory substances with marked pigmentation were frequently seen in the tubular lumina. Perusal of the English language literature revealed only two cases of parenchymal pigmentation of salivary gland tumors: both were mucoepidermoid carcinoma. The possible histogenesis of melanocytes in the salivary gland lesions is discussed, though no firm conclusion could be drawn.

Keywords Melanocyte · Melanin pigment · Pleomorphic adenoma · Salivary gland tumor

Introduction

Melanocytes are derived from the neural crest, from where most of their precursors travel during early embryonal life to the epidermis and hair follicles in mammals, while small numbers reach other locations such as the dermis, the sebaceous glands and lactiferous ducts of the nipple, the mucous membranes of the upper aerodigestive tract, the genital organs and anus, the orbital cavity, leptomeninges, inner ear, and occasionally some visceral organs [11]. It is well known that pre-existent melanocytes are stimulated to produce excess amounts of melanin and/or to proliferate to form nevus-like hyperplasia not only in some epithelial tumor of mucocutaneous origin but also in a few extra-mucocutaneous epithelial tumors. The examples of the former are basal cell carcinoma and squamous cell carcinoma [3, 8], hair follicle tumors [22], eccrine gland tumors [21], and mammary and extramammary Paget disease [9, 12]. Examples of the latter, which are rare, are ovarian adenocarcinoma [20], thymic carcinoma [7, 10], prostatic carcinoma [2, 6, 13], and various types of intraosseous odontogenic tumors [18].

A review of the literature yielded only two documented cases of salivary gland tumors containing melanocytes in their parenchyma; both are mucoepidermoid carcinoma [1, 19]. The authors have studied the occurrence and distribution of melanocytes in normal salivary glands and salivary gland tumors from Japanese patients and discussed their possible histogenesis and pathological significance [15, 16, 17]. The present paper reports a case of benign pleomorphic adenoma with grossly visible pigmentation, resulting in the macroscopic appearance of a melanotic lesion, in the belief that this represents a previously undescribed component within the spectrum of benign salivary gland tumors.

Y. Takeda (✉) · M. Satoh
Department of Oral Pathology,
School of Dentistry, Iwate Medical University,
Uchimaru 19-1, 020-8505 Morioka, Iwate, Japan
e-mail: ytakeda@iwate-med.ac.jp
Tel.: +81-19-6515111
Fax: +81-19-6213321

S.-i. Nakamura
Division of Clinical Pathology,
Central Clinical Laboratory,
Iwate, Japan

Case report

A 33-year-old Japanese male was referred to an oral surgeon by his dentist because of a swelling of the soft palate. He had no past or familial history of any diseases of the head and neck regions. The patient stated that the swelling was asymptomatic and had been first noticed as a soybean-sized nodule without pain in the soft palate approximately 5 years previously, after which it had gradually increased in size. The patient was examined and found to have a well-circumscribed tumor mass, measuring 28 mm in diameter, in the left area of the soft palate. The tumor was movable and firm, but slightly compressible on palpation. The covering and neighboring mucosa was normal in color. The rest of the physical examination

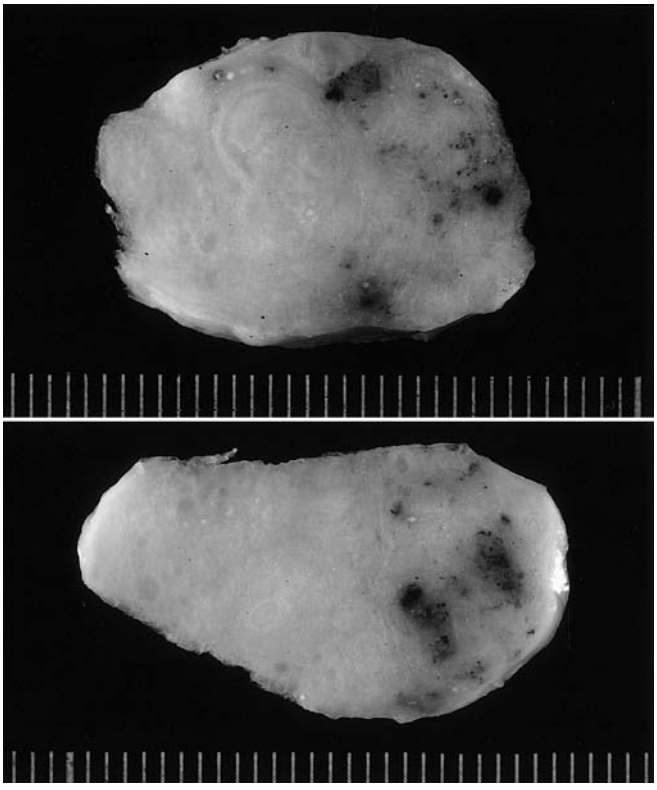


Fig. 1 Cut sections of a surgically resected specimen show a solid tumor with focal and/or diffuse black pigmentation in approximately one-half of the tumor, ×2.5

of the patient's intra- and extra-oral regions revealed normal findings. A clinical diagnosis of benign salivary gland tumor was made, and the tumor was surgically excised along with a clinically normal margin under general anesthesia. The postoperative course was uneventful, and no signs of recurrence have been noted at the time of writing, 10 months later.

Pathological findings

The surgical specimen was a 27×25×17 mm soft-tissue mass. Macroscopically, the cut surfaces revealed a solid, grayish-white-colored tumor, but focal and/or diffuse black pigmentation was found in approximately one-half of the tumor (Fig. 1).

Microscopically, the tumor was a pleomorphic adenoma with a typical histological appearance (Fig. 2), i.e., some areas contained cuboidal tumor cells arranged in tubular structures and proliferating tumor cells in strands or sheets around these tubular structures, whereas in other areas, the tumor cells showed stellate, polyhedral, or spindle form, mucoid and fibrous tissues constituted approximately one-half of the tumor, and areas of chondroid or mixed mucoid–chondroid tissue were also seen.

An unusual histological feature was the presence of numerous, variously formed and -sized cells with intracytoplasmic brownish-black pigment. Histochemistry indicated that the brownish-black pigment was melanin, with strong positivity with Masson–Fontana's staining for melanin and bleaching with hydrogen peroxide and potassium permanganate solution. The pigmented cells, some of which were dendritic and spindle in shape, were intermingled with tumor cells forming tubular structures (Fig. 3a, b). Brownish-black pigment granules were also in the cytoplasm of tumor cells, and marked pigmentation was seen in condensed secretory substances in the tubular lumina.

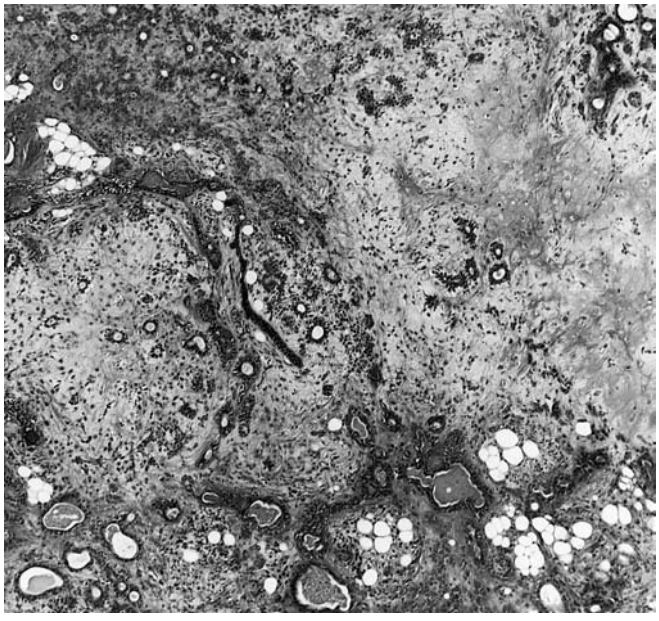


Fig. 2 Microscopic finding of the tumor showing a pleomorphic adenoma with a typical histological appearance, i.e., tubular structures, peritubular proliferation of cells, myxomatous area containing stellate and polyhedral cells, mucoid-chondroid tissue, and lipo-fibrous tissue. ×50

Other histochemistry of the brownish-black pigment showed that it was positive for melanin by the Lillie's ferrous iron method, but periodic acid-Schiff and stains for iron were negative. Immunohistochemistry using bleached sections showed positivity for S-100 protein (1:100 dilution, Dako, Japan), not only in variously shaped and -sized cells corresponding to melanocytes, but also in neoplastic myoepithelial cells (juxtatubular myoepithelial cells and modified myoepithelial cells in a loose arrangement). Therefore, true distribution of melanocytes with positivity for S-100 protein could not be demonstrated. Variously shaped and -sized pigmented cells were not reactive or were partially weakly positive for HMB-45 (1:50 dilution; Dako, Denmark) and not reactive for vimentin (1:50 dilution; Dako, Japan).

Discussion

A few carcinomas of major and minor salivary gland origin, containing numerous melanocytes and melanin pigmentin in the parenchyma and/or stroma, have been documented [1, 15, 19]. However, a review of the literature has yielded no convincing examples of the pre-existence of melanocytes in the salivary glands. To this point, we recently published two papers documenting the existence of melanocytes in the normal salivary glands [16, 17]. In one paper [16], melanocytes were found in the interlobular duct of the parotid gland in only 1 of over 400 autopsy cases using routine histopathological examination. In that case, melanocytes with long cytoplasmic processes were distributed in the basal and suprabasal layers of hyperplastic duct epithelium, and melanin pigment was seen in the duct epithelial cells. In another paper [17], melanocytes in labial minor salivary glands were found in 8 of 445 autopsies and biopsies (the overall

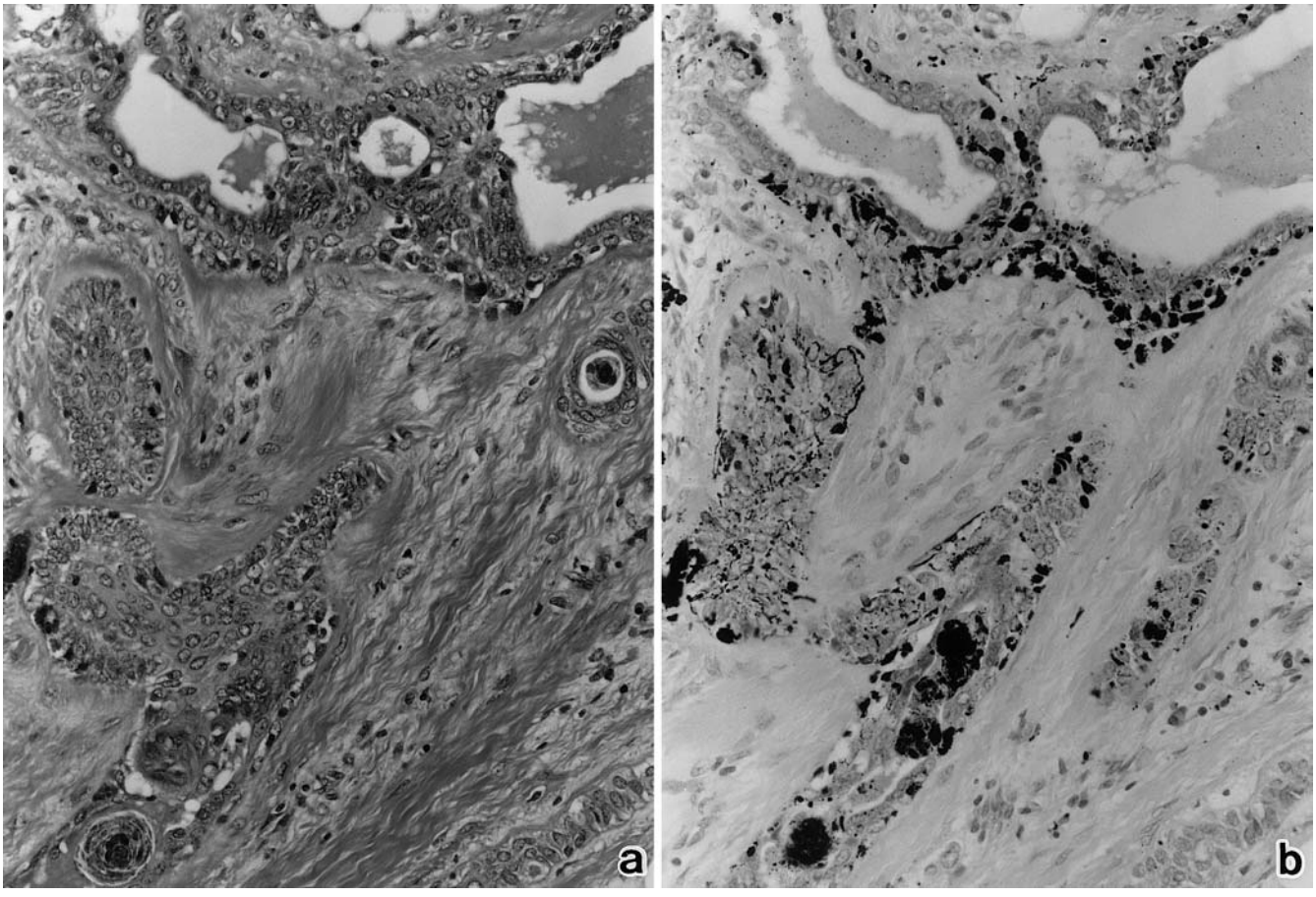


Fig. 3 Serial sections stained with hematoxylin and eosin (**a**) and Masson–Fontana's method for melanin (**b**). Numerous variously formed and -sized pigmented cells intermingled with tumor cells forming tubular structures. Dendritic and/or spindle forms are evident in some of the pigmented cells. Marked pigmentation in condensed secretory substances in the tubular lumina. ×200

incidence being 1.8%) using serial thin sections. Melanocytes were scattered in periductal and periacinar regions, varied in number, and were frequently seen around the duct system. Such evidences suggest that: (1) inactive melanocytes are occasionally present in salivary glands, similar to inactive melanocytes normally present in clinically non-pigmented oral mucosa, and (2) melanocytes in the salivary glands become activated to their proliferation and production of melanin pigment under certain conditions of tumorigenic transformation of salivary gland epithelia or tumor growth.

The present case of pleomorphic adenoma with macroscopically visible pigmentation showed histologically that vast numbers of variously shaped and -sized cells with intracytoplasmic brownish-black pigment were intermingled with tumor cells, forming tubular structures. Histochemistry indicated that the intracytoplasmic pigment was melanin using Fontana-Masson's method and Lillie's ferrous iron method. Of these pigmented cells, cells with dendritic and spindle appearance were regarded as melanocytes. Immunohistochemically, not only pigmented cells but also neoplastic myoepithelial cells were reactive for S-100 protein; true distribution of melanocytes could not be demonstrated in the tumor. HMB-45 is a well-known, diagnostically useful antibody that is a specific marker of immature and neoplastic melanocytes in paraffin sections, but it seldom reacts with melanocytes in normal tissue and nevus cells [11]. The lack of strong reactivity with HMB-45 with the spindle and dendritic pigmented cells in the present case does not disprove a melanocytic origin for these cells.

To our knowledge, the present paper is the first document of the existence of melanocytes and melanin pigment in the pleomorphic adenoma, which is the most common benign salivary gland tumor and constitutes 60–70% of parotid gland tumors, 40–60% of submandibular gland tumors, and 40–70% of all minor salivary gland tumors [4, 5, 14].

Apart from the distinctive presence of melanocytes and melanin pigment in the tumor parenchyma, the present case is histologically and biologically identical to that of common pleomorphic adenoma of the minor salivary gland origin. However, it is a very interesting phenomenon in the field of diagnostic pathology.

References

1. Aufdemorte TB, van Sickels E, Glass BJ (1985) Melanin pigmentation in a mucoepidermoid tumor of a minor salivary gland. J Oral Maxillofac Surg 43:876–879
2. Augilar M, Gaffney EF, Finnerty DP (1982) Prostatic melanosis with involvement of benign and malignant epithelium. J Urol 128:825–827
3. Bleehen SS (1975) Pigmented basal cell epithelioma: light and electron microscopic studies on tumors and cell cultures. Br J Dermatol 93:361–370
4. Ellis GL, Auclair PL (1996) Atlas of tumor pathology: tumor of the salivary glands, 3rd edn. Armed Forces Institute of Pathology, Washington DC
5. Eveson JW, Cawson RA (1985) Salivary gland tumors: a review of 2410 cases with particular reference to histologic types, site, age and sex distribution. J Pathol 146:51–58
6. Furusato M, Matsumoto I, Kato H (1989) Prostatic carcinoma with melanosis. Prostate 15:65–69
7. Ho FCS, Ho JCI (1977) Pigmented carcinoid tumour of the thymus. Histopathology 1:363–369
8. James MP, Wells GC, Whimster IW (1978) Spreading pigmented actinic keratoses. Br J Dermatol 99:373–379
9. Jones RE, Austin C, Ackerman AB (1979) Extramammary Paget's disease: a critical re-examination. Am J Dermatopathol 1:101–132
10. Lagrange W, Dahm HH, Karstens J, Feichtinger J, Mittermayer C (1987) Melanocytic neuroendocrine carcinoma of the thymus. Cancer 59:484–488
11. Mooi WJ, Krausz T (1992) Biopsy pathology of melanocytic disorders. Chapman Hall Med, London
12. Neubecker RD, Bradshaw RP (1961) Mucin, melanin and glycogen in Paget's disease of the breast. Am J Clin Pathol 36:49–53
13. Rios CN, Wright J (1976) Melanosis of the prostatic gland: report of a case with neoplastic epithelium involvement. J Urol 115:616–617
14. Seifert G (1991) World Health Organization international classification of tumors: histological typing of salivary gland tumours, 2nd edn. Springer, Berlin Heidelberg New York
15. Takeda Y (1996) Stromal melanocytosis of an adenoid cystic carcinoma arising from the palatal minor salivary gland. Pathol Int 46:467–470
16. Takeda Y (1997) Melanocytes in the human parotid gland. Pathol Int 47:581–583
17. Takeda Y (2000) Existence and distribution of melanocytes and HMB-45-positive cells in the human minor salivary glands. Pathol Int 50:15–19
18. Takeda Y, Satoh M, Nakamura S, Yamamoto H (2000) Pigmented ameloblastic fibrodentinoma: a novel melanin-pigmented intraosseous odontogenic lesion. Virchows Arch 437:454–458
19. Thomas KM, Hutt MSR, Borgstein J (1980) Salivary gland tumors in Malawi. Cancer 46:2328–2334
20. Waxman M, Vuletin JC, Rosenblatt, Herzberg FP (1986) Melanocytes colonization of adenocarcinoma arising in an ovarian dermoid. Histopathology 10:207–215
21. Wilson-Jones E (1971) Pigmented nodular hidradenoma. Arch Dermatol 104:117–123
22. Zaim MT (1987) Pilomatricoma with melanotic hyperplasia: an uncommon occurrence and a diagnostic pitfall. Arch Dermatol 123:865–866

Virchows Arch (2004) 445:203–205
DOI 10.1007/s00428-004-1058-5

CASE REPORT

Adriana Handra-Luca · Anne Couvelard · Alain Sauvanet · Jean-François Fléjou · Claude Degott

Mucinous cystadenoma with mesenchymal over-growth: a new variant among pancreatic mucinous cystadenomas?

Received: 22 January 2004 / Accepted: 18 May 2004 / Published online: 19 June 2004
© Springer-Verlag 2004

Abstract We report an unusual type of mucinous cystadenoma of the pancreas, characterised by a predominantly solid gross appearance due to the presence of an abundant ovarian-type stroma. The tumour, located in the body of the pancreas, was discovered after episodes of acute pancreatitis. It was composed of several mucus-secreting benign cysts placed within a highly cellular ovarian-type stroma, composed of undifferentiated spindle cells with mild atypia but without any increase of mitotic activity and with a low proliferative index. These cells expressed oestrogen and progesterone receptors, but they did not express CD34, CD117, p53 protein or bcl-2. Recognition of this peculiar mainly solid mucinous cystadenoma containing an abundant ovarian-type stroma is difficult. It is conceivable that the mesenchymal component described in our case could represent an early stage in the development of sarcoma in mucinous cystadenoma of the pancreas.

Keywords Pancreas · Mucinous cystadenoma · Sarcoma

A. Handra-Luca · A. Couvelard · C. Degott
Service d'Anatomie Pathologique,
Hôpital Beaujon, Clichy, France

A. Handra-Luca (✉)
Service d'Anatomie Pathologique,
Assistance Publique-Hôpitaux de Paris, Hôpital Jean Verdier,
Avenue du 14 Juillet, 93143 Bondy Cedex, France
e-mail: adriana.handra-luca@jvr.ap-hop-paris.fr
Tel.: +30-48-026676
Fax: +30-48-026877

A. Sauvanet
Service de Chirurgie Digestive,
Hôpital Beaujon, Clichy, France

J.-F. Fléjou
Service d'Anatomie Pathologique,
Hôpital Saint-Antoine, Assistance Publique-Hôpitaux de Paris,
Paris, France

Introduction

Mucinous cystadenomas of the pancreas are defined as cystic tumours lined by a benign mucus-secreting epithelium and underlined by a band-like ovarian-type mesenchymal stroma [1]. Malignant transformation occurs in these neoplasms and is traditionally considered as developing from the epithelial lining of the cyst into adenocarcinoma. Sarcomatous differentiation of the mesenchymal tissue surrounding the cyst has been reported, to our knowledge, in only four cases [4, 5].

We report here a case of a pancreatic mucinous cystadenoma, peculiar because of the presence of an abundant, highly cellular, ovarian-type mesenchymal stroma, but without sarcomatous transformation. The "diagnosis" of pancreatic mucinous cystadenoma with mesenchymal over-growth is proposed for this neoplasm.

Case report

Clinical history

A 30-year-old Caucasian woman was admitted for recurrent episodes of acute pancreatitis. Abdominal ultrasound and computed tomography scan showed a partially solid lesion located in the posterior part of the body of the pancreas and containing several small cysts. This lesion measured 15 mm. No abnormality of the main pancreatic duct was noted, and no communication between the lesion and the duct system was detected. The duct of Wirsung was compressed by this lesion. No fine-needle aspiration was performed. Treatment consisted of a splenopancreatectomy. The postoperative course was uneventful.

Materials and methods

The specimen was fixed in 10% neutral buffered formalin and embedded in paraffin. Serial sections (4 μm) were processed for routine staining, including hematoxylin and eosin, periodic acid–Schiff (PAS) and Alcian blue stains. Immunohistochemical staining was carried out using an avitin–biotin–peroxidase complex method. The following primary antibodies were used: cytokeratin (clone KL1, 1:25, Immunotech, Marseille, France), Ki67 (clone Mib1, 1:25, Immunotech), progesterone receptor (clone 1A6, 1:40, Immunotech), oestrogen receptor (clone ER105, 1:40, Immunotech),

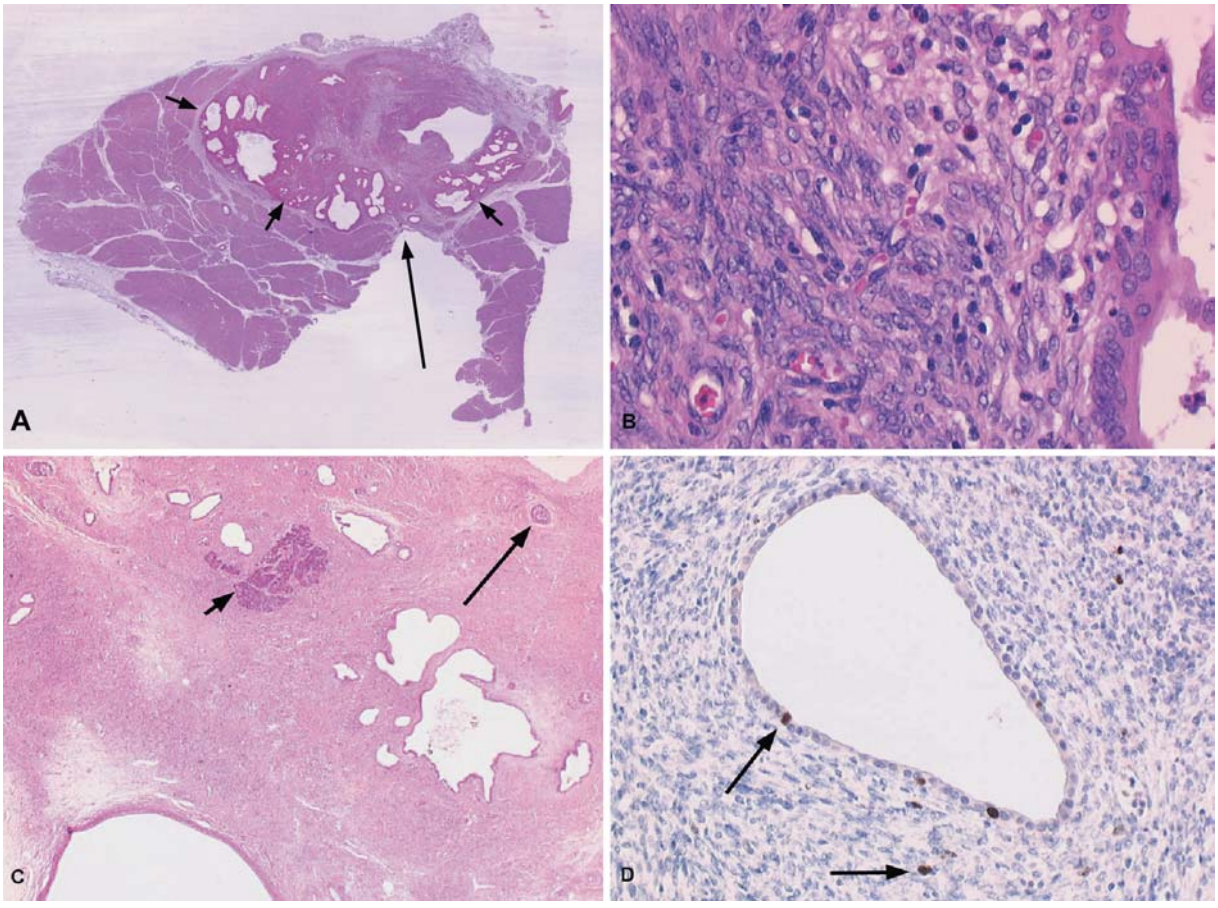


Fig. 1 **A** Predominantly solid lesion, containing small cysts (*long arrow* main pancreatic duct opened by dissection; *small arrows* well-delimited, partially surrounded by a fibrous capsule). **B** Ovarian-like stroma composed of a highly cellular proliferation of spindle cells around cysts lined by a benign appearing epithelium (hematoxylin and eosin stain). **C** Pancreatic normal structures (*short arrow* acinus, *long arrow* endocrine islets) entrapped in the ovarian-type stroma (hematoxylin and eosin stain). **D** Mib1 expression in rare nuclei of both epithelial and mesenchymal cells (*arrows*)

CD34 (clone Qbend10, 1:100, Dako, Glostrup, Denmark), CD117 (polyclonal, 1:40, Dako), p53 protein (clone DO7, 1:40, Dako) and bcl-2 (clone 124, 1:10, Dako).

Pathological findings

Grossly, the resected pancreas contained in the body a well-delimited, predominantly solid mass measuring 15 mm. This tumour contained numerous small cysts, which were disposed around a larger one measuring 7 mm. The cysts were filled with mucinous material. The internal surface of the cysts was smooth and glistening, without papillary projections. There was no communication with the main pancreatic duct, but it was slightly compressed by the lesion. Pancreatic parenchyma surrounding the lesion was normal.

Microscopically, the lesion consisted of a solid spindle-cell proliferation containing several small cysts (Fig. 1A) lined by a benign-appearing epithelium, either tall-columnar or flattened, containing intracellular mucin PAS and Alcian blue positive.

The solid part of the lesion was predominant and consisted of an ovarian-type stroma with large zones of a highly cellular proliferation of spindle-shaped, undifferentiated cells arranged in a fascicular pattern (Fig. 1B). The nuclei were irregular in size with atypia and showed rare mitotic figures (1 mitosis per 10 high-power fields). No necrosis was observed. Normal pancreatic tissue structures such as ducts, acini and endocrine islets were intermingled with the mesenchymal component (Fig. 1C).

Cytokeratin was strongly expressed in the epithelial lining of the cysts, but was negative in the mesenchymal cells. Rare spindle cells showed positive nuclei for Ki67 (Ki67 index calculated at 1%, Fig. 1D). Progesterone and oestrogen receptors were expressed in almost all mesenchymal cells. CD34, CD117, p53 protein and bcl-2 were not expressed by the mucus-secreting cells lining the cysts or by the mesenchymal cells.

Discussion

Mucinous cystadenomas are characterised by the presence of an ovarian-type mesenchymal stroma associated with a cystic epithelial neoplasm. This stroma may show variate morphologies: either it can become fibrotic and hypocellular in cases associated with large cysts or it can show large hypercellular areas. It is only recently, due to the reports of van den Berg et al. [4] and Wenig et al. [5], that attention was drawn to the possibility of malignant change of the ovarian-type stroma in mucinous cystadenoma, and a new type of mucinous cystadenoma showing an abundant sarcomatous stroma has been described. Such malignant transformation is infrequent since only four cases have been mentioned in the literature [3, 4, 5]. In these

cases several histological features altogether, such as nuclear atypia, mitosis, high cellularity, vascular invasion and the presence of metastases, have been considered as defining the sarcomatous nature of the mesenchymal component. Van de Berg et al. [4] demonstrated similar genetic changes involving the *p53* and the *K-ras* genes in both the epithelial and mesenchymal components in two of the above-mentioned cases. This supports the hypothesis that similar pathways are involved in the pathogenesis of both tumour components and suggests that the sarcomatous component may be, in some of the cases, the result of spindle-cell malignant transformation of the epithelial component, as is usually seen in sarcomatoid carcinomas.

The present case is different from previously reported cases because, despite the high cellularity and mild nuclear atypia, the spindle cells of the ovarian-type stroma did not show any feature of malignancy. The extension of the cellular stroma around non-neoplastic pancreatic parenchyma should not be regarded as a feature of malignancy, since this finding is relatively common in conventional mucinous cystadenomas. Moreover, the *p53* gene pathway was not altered as immunohistochemistry did not show aberrant expression of this protein. Therefore, we propose the term "mesenchymal over-growth" to define this highly cellular stroma, showing some, but not all, features of malignancy. A primary benign mesenchymal pancreatic tumour, such as a gastrointestinal stromal tumour or a solitary fibrous tumour entrapping pancreatic ducts [1, 2], were excluded because of the lack of CD117, CD34 and bcl2 expression.

The histogenesis of pancreatic mucinous cystadenoma of the pancreas is still debated, and special interest is shown to the pathogenesis of the ovarian-type mesenchymal stroma. One of the proposed hypotheses suggests that this mesenchymal component derives from the ovarian primordium, which is incorporated during embryogenesis in the pancreas. These cells may release hormones and growth factors that can cause proliferation of the nearby epithelium to form mucus-secreting cysts [1, 6]. The hormone and growth factors may act also on the mesenchymal cells of the stroma, which are hormonosensitive as they express hormone receptors. Such an interaction may result in the proliferation and development/evolution to the highly cellular mesenchymal stroma observed in our case. Additional genetic events like *p53* and/or *K-Ras* mutations are probably needed in order for this stroma to transform to a sarcomatous one.

In summary, we describe a pancreatic mucinous cystadenoma, peculiar because of the presence of an abundant ovarian-type mesenchymal stroma that results in a mainly solid lesion containing small mucus-secreting benign cysts. We believe that it may represent a distinctive type of pancreatic mucinous cystadenoma.

Acknowledgement The authors thank Nathalie Colnot for technical assistance.

References

1. Hamilton SR, Aaltonen LA (eds) (2000) Pathology and genetics of tumours of the digestive system. IARC Press, Lyon
2. Lüttges J, Mentzel T, Hübner G, Klöppel G (1999) Solitary fibrous tumours of the pancreas: a new member of the small group of mesenchymal pancreatic tumours. Virchows Arch 435: 37–42
3. Thompson LDR, Becker RC, Przygodzki RM, Adair CF, Hefess CS (1999) Mucinous cystic neoplasm (mucinous cystadenoma of low-grade malignant potential) of the pancreas. A clinicopathologic study of 130 cases. Am J Surg Pathol 23:1–16
4. Van den Berg W, Tascilar M, Offerhaus JA, Albores-Saavedra J, Wenig BM, Hruban RH, Gabrielson E (2000) Pancreatic mucinous cystic neoplasm with sarcomatous stroma: molecular evidence for monoclonal origin with subsequent divergence of the epithelial and sarcomatous components. Mod Pathol 13:86–91
5. Wenig BM, Albores-Saavedra J, Buetow PC, Hefess CS (1997) Pancreatic mucinous cystic neoplasm with sarcomatous stroma: a report of three cases. Am J Surg Pathol 21:70–80
6. Zamboni G, Scarpa A, Bogina G, Iacono C, Bassi C, Talamini G, Sessa F, Capella C, Solcia E, Rickaert F, Mariuzzi GM, Klöppel G (1999) Mucinous cystic tumours of the pancreas. Clinicopathologic features, prognosis, and relationship to other mucinous cystic tumours. Am J Surg Pathol 23:410–422

Virchows Arch (2004) 445:206–209
DOI 10.1007/s00428-004-1062-9

CASE REPORT

Sofia Asioli · Giulia Dal Piaz · Stefania Damiani

Localised pleural malignant mesothelioma. Report of two cases simulating pulmonary carcinoma and review of the literature

Published online: 30 June 2004
© Springer-Verlag 2004

Abstract

Aims To describe two cases of localised malignant mesothelioma with a predominantly intrapulmonary growth which led to a pre-operative diagnosis of pulmonary carcinoma. *Materials and methods:* Both cases presented as intrapulmonary masses, while at computed tomography scan the pleura appeared not significantly thickened. In one patient, the main bronchus was diffusely infiltrated by the tumour. In both cases, a preoperative biopsy showed a proliferation of large cells leading to a diagnosis of non-small-cell lung carcinoma. Histological examination of the surgical specimens revealed features consistent with epithelioid mesothelioma with deciduoid features in one case and with biphasic mesothelioma in the other. Both cases were diffusely positive with anti-calretinin antibody, while anti-TTF1, anti-surfactant and anti-CEA antisera were negative. *Conclusions:* Localised malignant mesotheliomas are unusual and predominantly intrapulmonary growth is rare. Pathologists should be aware of this possibility to avoid misdiagnosis, particularly in small biopsies.

Keywords Pleura · Localised mesothelioma · Intrapulmonary growth

S. Asioli · G. Dal Piaz · S. Damiani (✉)
Section of Anatomic Pathology "M. Malpighi"
Department of Oncologic Sciences,
University of Bologna, Bellaria Hospital,
Via Altura 3, 40139 Bologna, Italy
e-mail: stefania.damiani@ausl.bo.it
Fax: +39-051-6225759

G. Dal Piaz
Service of Radiology,
General Hospital,
S.Giovanni in Persiceto, Bologna, Italy

Introduction

Pleural mesotheliomas, defined as neoplasms derived from mesothelial lining cells, are uniformly malignant and nearly always present either as multiple nodules or as a diffuse tumour encasing a portion of the lung [1]. The finding of malignant mesothelioma as a localised tumour mass is extremely rare and may cause problems of differential diagnosis with other non-mesothelial tumours. We describe two cases of localised malignant mesothelioma presenting as lung tumours because of a predominantly intrapulmonary growth. The clinical and pathological features of the patients are described, and the literature on similar cases is reviewed.

Clinical histories

Case 1

A 69-year-old man presented with severe chest pain. He had no history of smoking and no known exposure to asbestos. Chest radiographic examination revealed a solitary, intrapulmonary mass in the left upper lung field. Computed tomography (CT) of the chest showed a 7-cm solitary mass in the upper lobe of the left lung, with involvement of the main bronchus and the chest wall (Fig. 1). The remaining pleura, far from the infiltration of the chest, was apparently unremarkable.

No pleural effusion was present. The patient underwent endoscopic biopsy, and the diagnosis was poorly differentiated non-small-cell carcinoma. CT total body scan failed to reveal any other tumoural localisation.

Left pneumonectomy was performed, together with resection of four ribs which were grossly involved by tumour. Mediastinal and hilar lymph nodes were also excised. Grossly, the mass was 8.5 cm in its major axis and composed of whitish-grey tissue, soft in consistency, with large areas of necrosis.

Seven months after surgery the patient died with severe respiratory failure. No autopsy was requested.

Case 2

The patient was a 62-year-old man, ex-smoker, with no history of exposure to asbestos. During the follow-up program after bronchopneumonia, a radiological chest examination revealed an intrapulmonary mass.

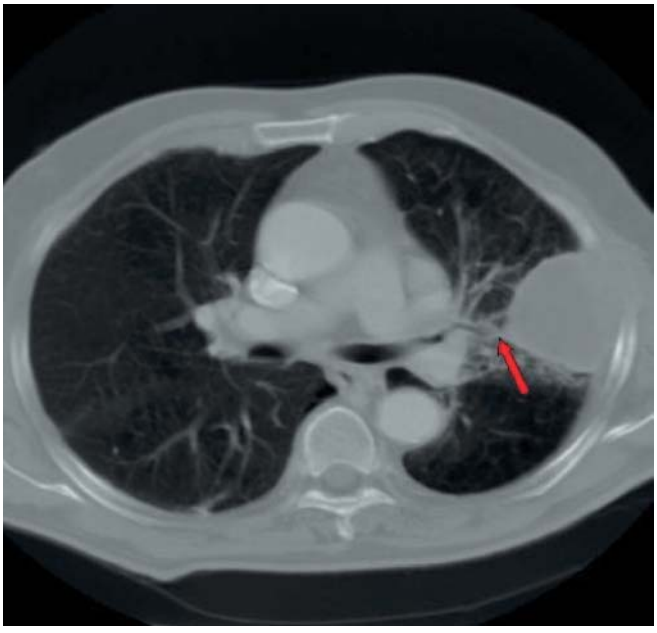


Fig. 1 Computed tomography of case 1: the tumoural mass has a predominantly intrapulmonary growth with involvement of the main bronchus (*arrow*)

Table 1 Antibodies employed for immunohistochemistry. *pc* pressure cooking, *Ed* enzymatic digestion, *Ck* cytokeratin, *Sma* smooth muscle actin, *Ttf-1* thyroid trascriptor factor-1

Antibody	Source	Dilution	Antigen retrival
Calretinin	Dba	1:1500	Ed
Ck-7	Dako	1:100	Ed
Ttf-1	Neomarkers	1:1000	pc
Vimentin	Dako	1:100	pc
Sma	Dako	1:100	-
Surfactant	Dako	1:150	pc

CT confirmed the presence of a 4-cm mass in the left upper lobe and revealed that the mass partly involved the chest wall. No associated pleural effusion was evident. The patient underwent transthoracic fine-needle aspiration, and the diagnosis was poorly differentiated adenocarcinoma. CT total body scan failed to reveal any other tumoural localization.

Upper left lobectomy was performed, together with the resection of three ribs which were grossly involved by the tumour. Mediastinal and hilar lymph nodes were also dissected. Grossly, the tumour was 4 cm in its major axis, whitish in colour and firm in consistency. The tumoural growth was predominantly intrapulmonary, while the pleura was involved just for a small area of 3 cm.

The patient is well without evidence of disease 20 months after surgery.

Materials and methods

Tissues were fixed in buffered formalin, paraffin embedded and routinely processed for histological diagnosis. For immunohistochemistry, the avidin-biotin peroxidase complex method was used. The antisera employed are listed in Table 1, together with their source, dilution and antigen retrieval method.

Results

In case 1, microscopically, the neoplasm diffusely infiltrated the main bronchus (Fig. 2) and large hilar vessels. It was mainly composed of closely packed spindle cells arranged in short fascicles variably oriented. The cells had abundant cytoplasm and pleomorphic nuclei with vesicular chromatin and prominent nucleoli (Fig. 3). Focally, areas with a papillary architecture and glandular differentiation were evident (Fig. 3 inset). Mitoses were frequent, and large areas of necrosis were also present. Metastases were found in two hilar lymph nodes. The anti-calretinin antibody stained most of the neoplastic cells strongly (Fig. 4).

In case 2, the neoplasm showed extruding borders (Fig. 5) and was composed entirely of polygonal epithe-

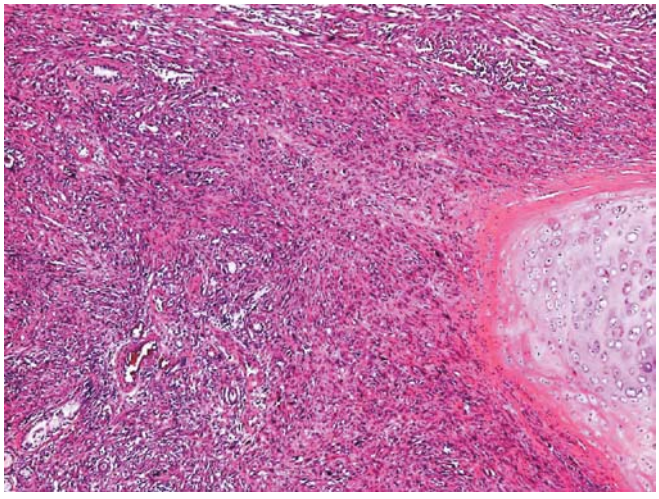


Fig. 2 Case 1: neoplastic spindle cells infiltrating the bronchial wall

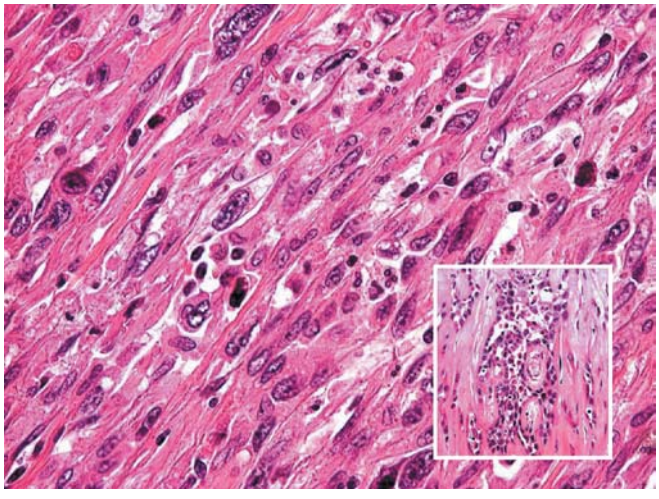


Fig. 3 Case 1: neoplastic cells have abundant eosinophilic spindled cytoplasm and pleomorphic nuclei with coarse chromatin. Focal glandular and papillary differentiation was also present in the tumour (*inset*)

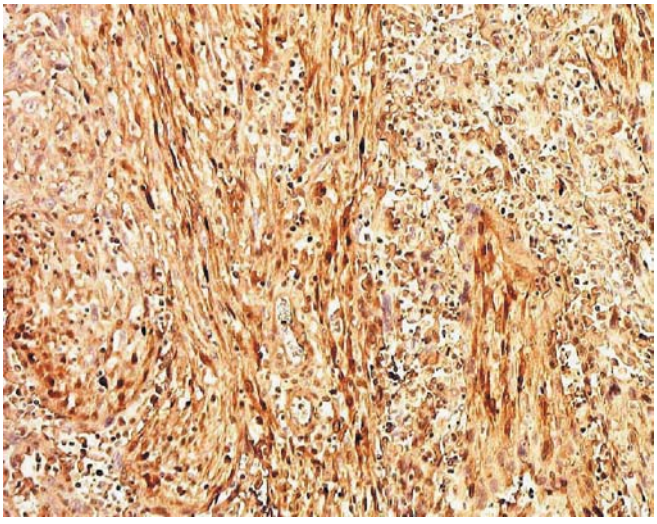


Fig. 4 Case 1: anti-calretinin antibody stains strongly most of the neoplastic cells. Note that positivity is nuclear and cytoplasmic

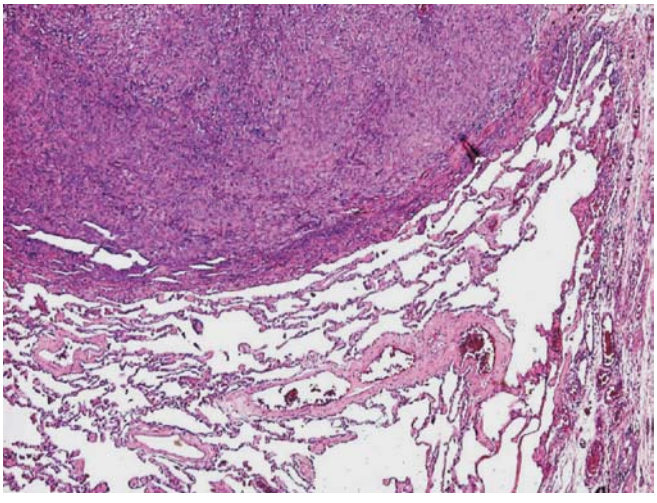


Fig. 5 Case 2: the intrapulmonary tumour shows well-defined, pushing borders

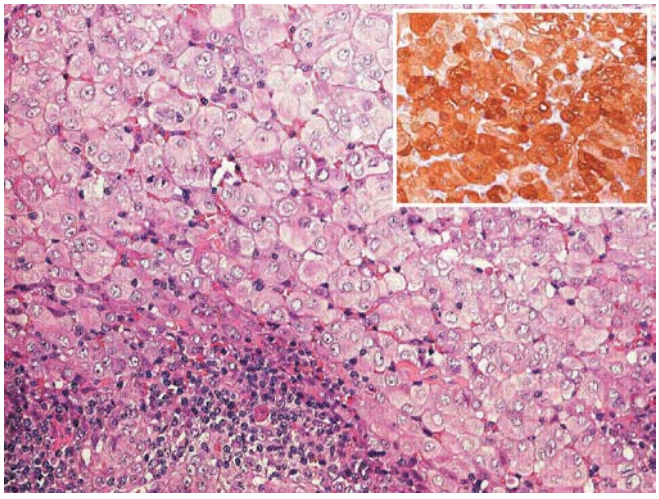


Fig. 6 Case 2: neoplastic cells have a deciduoid appearance. They have large round-to-polygonal eosinophilic cytoplasm and vesicular nuclei with prominent nucleoli. Anti-calretinin antibody stains most of the neoplastic cells (*inset*)

lioid cells with abundant cytoplasm and vesicular nuclei with prominent nucleoli. They were arranged in nests and sheets. In some areas, the cytoplasm was particularly abundant and pale eosinophilic, giving the neoplastic cells a "deciduoid" appearance (Fig. 6). A few binucleated cells were present. No metastases were found in mediastinal and hilar lymph nodes.

The neoplastic cells of case 2, as of case 1, showed diffuse immunoreactivity for calretinin (Fig. 4 and Fig. 6 inset), vimentin and cytokeratin 7. All the other antisera were negative.

Discussion

The present cases show morphological and immunohistochemical features consistent with malignant mesotheliomas. In case 1, the presence of areas with sarcomatoid appearance (spindle cells) intermingled with areas with papillary architecture and epithelioid cytology is in keeping with biphasic mesothelioma, while case 2 had the features of epithelioid "deciduoid" mesothelioma. Both cases were consistently positive with anti-calretinin antibody and negative with anti- surfactant and anti-TTF1 antisera [4, 11].

Localised intrapulmonary growth is very unusual in malignant mesotheliomas. Most of the cases previously reported in the literature as localised mesotheliomas actually belong to the category of solitary fibrous tumour (benign or malignant), now known as of fibroblastic (submesothelial) origin [5]. Solitary fibrous tumours are composed entirely of spindle cells without epithelial elements and histologically mimic sarcomatoid mesotheliomas. Although, a few examples of solitary fibrous tumour with cytokeratin positive cells have been reported [2], most cases are usually negative and, in addition, immunohistochemical evidence of CD 34 expression is found in about 80% of these neoplasms [7, 12].

The rarity of localised malignant mesothelioma of the pleura is emphasised by the fact that only 12 cases have been fully documented to date in the English literature, with histology and immunohistochemistry consistent with mesothelioma (Table 2) [3, 6, 8, 9, 10, 13].

True localised mesotheliomas are histologically, imunophenotypically and ultrastructurally indistinguishable from the diffuse type. However, localised mesotheliomas do not usually present with haemorrhagic pleural effusion (only 1 out of 12 cases had minimal exudative, non-haemmorrhagic, effusion [8]) and are seldom associated with asbestos exponsure (3 of 12 cases [3, 8]). Most localised mesotheliomas are sessile or peduncolated polyps. However, our 2 cases presented as tumours with a predominantly intrapulmonary growth. This type of growth was partly present in only 2 of the previously

Table 2 Clinico-pathological features in localised malignant mesotheliomas. *IP* intrapulmonary, *NA* data not available, *DOD* died of disease, *AW* alive and well, *REC* recurrence

Case	Presentation (asbestos exposure)	Pre-operative diagnosis	Gross features	IP growth	Histology	Follow-up
1 [10]	NA	NA	Polypoid	No	Epithelioid	DOD (2 years)
2 [10]	NA	NA	Polypoid	No	Epithelioid	DOD (2 years)
3 [3]	Solitary mass, no effusion (no)	NA	Peduncolated 10 cm	No	Epithelioid	DOD (6 months)
4 [3]	Solitary mass, no pleural effusion (yes)	No	Sessile	No	Epithelioid	REC (8 months)
5 [3]	Solitary mass, no pleural effusion (no)	No	Sessile	No	Epithelioid	AW (8 years)
6 [3]	Solitary mass	No	Peduncolated	No	Diphasic	AW (8 months)
7 [3]	Solitary mass, no pleural effusion (no)	No	Sessile	No	Diphasic	AW (2 years)
8 [3]	Lobulated mass, no pleural effusion (yes)	Adenocarcinoma	Sessile	Partial	Biphasic	DOD (8 months)
9 [9]	Solitary extrapulmonary mass (no)	NA	Sessile	No	Biphasic	DOD (16 months)
10 [6]	Solitary mass, no pleural effusion (no)	NA	Sessile	Yes	Epithelioid	REC (5 months)
11 [8]	Solitary mass, minimal pleural effusion (yes)	Malignant cells	NA	No	NA	NA
12 [13]	Solitary mass, no pleural effusion (no)	Metastatic adenocarcinoma	Polypoid	Yes	Epithelioid	REC (2 years)
Present case 1	Solitary mass, no pleural effusion(no)	Differentiated non small cell carcinoma	Sessile	Yes	Biphasic	DOD (7 months)
Present case 2	Solitary mass, no pleural effusion(no)	Poorly differentiated adenocarcinoma	Sessile	Yes	Epithelioid	AW (15 months)

reported cases [3, 13]. It is noteworthy that, in all cases with intrapulmonary growth, a pre-operative diagnosis of lung carcinoma (primary or metastatic) was reached, without taking into consideration the use of immunohistochemistry to exclude a mesothelial origin (Table 2).

Therefore, when dealing with a localised thoracic mass with no or minimal pleural effusion and no history of asbestos exposure, the problem is not to do the correct immunohistochemical panel and recognise the immunophenotype of mesothelioma, but to entertain the possibility of a localised mesothelioma in a case with clinical and radiological features suggesting a lung tumour.

In conclusion, localised mesotheliomas are rare, and predominantly intrapulmonary growth as in the present cases rarer still. In diagnosing small biopsies from thoracic masses, the clinical and radiological correlations are necessary, but not sufficient to avoid misdiagnosis. The lesson to be learned from these cases is that any thoracic tumour should be investigated using immunohistochemistry to exclude a mesothelioma, even in cases with predominant intrapulmonary growth.

Acknowledgement This work was partly financed by grants from MIUR, University of Bologna (60%).

References

1. Battifora H, McCaughey WTE (1994) Atlas of tumor pathology: tumors of the serosal membranes. Armed Forces Institute of Pathology, Washington DC
2. Cavazza A, Rossi G, Agostini L, Roncella S, Ferro P, Fedeli F (2003) Cytokeratin-positive malignant solitary fibrous tumour of the pleura: an unusual pitfall in the diagnosis of pleural spindle cell neoplasms. Histopathology 43:606–608
3. Crotty TB, Myers JL, Katzenstein AA, Tazelaar HD, Swcnsen SJ, Churg A (1994) Localized malignant mesothelioma: a clinicopathologic and flow cytometric study. Am J Pathol 51:357–363
4. Doglioni C, Tos AP, Laurino L et al (1996) Calretinin: a novel immunocytochemical marker for mesothelioma. Am J Surg Pathol 20:1037–1046
5. England DM, Hochholzer L, McCarthy MJ (1989) Localized benign and malignant fibrous tumors of the pleura: a clinicopathologic review of 223 cases. Am J Surg Pathol 13:640–658
6. Erkllç S, Sari I, Tunçözgür B (2001) Localized pleural malignant mesothelioma. Pahol Int 51:812–815
7. Flint A, Weiss SW (1995) CD-34 and keratin expression distinguishes solitary fibrous tumor (fibrous mesothelioma) of pleura from desmoplastic mesothelioma. Hum Pathol 26:428–431
8. Ojeda HF, Mech KJr, Hicken WJ (1998) Localized malignant mesothelioma: a case report. Am Surg 51:881–885
9. Okamura H, Kamei T, Mitsuno A, Hongo H, Sakuma N, Ishihara T (2001) Localized malignant mesothelioma of the pleura. Pathol Int 51:654–660
10. Okike N, Bematz PE, Woolner LB (1978) Localized mesothelioma of the pleural: benign and malignant variants. J Thorac Cardiovasc Surg 51:363–372
11. Ordonez NG (2002) Immunohistochemical diagnosis of epithelioid mesotheliomas: a critical review of old markers, new markers. Hum Pathol 33:953–967
12. Renshaw AA, Pinkus GS, Corson JM (1994) CD34 and AE1/AE3: diagnostic discriminants in the distinction of solitary fibrous tumor of the pleura from sarcomatoid mesothelioma. Appl Immunohistochem 2:94–102
13. Umezu H, Kuwata K, Ebe Y et al (2002) Microcystic variant of localized malignant mesothelioma accompanying an adenomatoid tumor-like lesion. Pathol Int 52:416–422

Virchows Arch (2004) 445:210–213
DOI 10.1007/s00428-004-1073-6

CASE REPORT

Ji Shin Lee · Yoo Duk Choi · Chan Choi

Primary testicular osteosarcoma with hydrocele

Received: 23 March 2004 / Accepted: 7 June 2004 / Published online: 1 July 2004
© Springer-Verlag 2004

Abstract Primary testicular osteosarcoma is an extremely rare malignancy. To date, only two cases have been reported. Here, we report a third case of primary testicular osteosarcoma complicated with hydrocele. A 78-year-old man presented with right scrotal swelling. Ultrasonography revealed hydrocele and a testicular heterogeneous solid mass with focal calcification in the right testis. Right inguinal orchiectomy revealed a pure intratesticular osteosarcoma. Retroperitoneal lymph-node dissection revealed no metastasis. Thorough sampling of the tumor failed to show any additional histological components. It is unlikely that our case arose from teratoma or mixed sex-cord/stromal tumor, because no other neoplastic elements were identified in whole sampling of the tumor. He remained well without evidence of disease 44 months after operation. This case illustrates that primary pure testicular osteosarcoma may be associated with a favorable prognosis.

Keywords Testis · Osteosarcoma · Primary · Hydrocele

Introduction

Extraskeletal osteosarcoma is a rare form of osteosarcoma arising in tissues without any connection to skeletal structures [2]. Although the majority of these cases arise in the soft tissues of the extremities, rare examples have been reported arising from parenchymal organs [5]. Even rarer are pure osteosarcomas arising from the testis without other germ cell components; only two such cases have been reported in the world literature [8, 19]. Little information exists about its natural history due to its rarity.

J. S. Lee (✉) · Y. D. Choi · C. Choi
Department of Pathology,
Chonnam National University Medical School and Hospital,
5 Hakdong, Dongku, 501-746 Gwangju, Korea
e-mail: jshinlee@hanmail.net
Tel.: +82-62-2321246
Fax: +82-62-2273429

Hydrocele may be an expression of other disease processes involving paratesticular region such as infection, inflammation, or tumors [6]. Intratesticular tumors may be associated with hydrocele [1, 13]. The previous two cases of primary testicular osteosarcoma were not complicated with hydrocele.

We report a third case of primary pure osteosarcoma in a 78-year-old man. The tumor was discovered by an ultrasound evaluation for hydrocele. The natural history of primary testicular osteosarcoma is briefly reviewed and the origin of this sarcoma is discussed.

Clinical history

A 78-year-old man presented with a 2-week history of painful swelling of the right scrotum. There was no history of trauma. Ultrasonography showed hydrocele and a heterogeneous solid mass with a moderate calcification in the right testis suggestive of testicular tumor. Serum α-fetoprotein and β-human chorionic gonadotropin levels were normal. Aspiration cytology of the hydrocele fluid showed no neoplastic cells. Right inguinal orchiectomy with retroperitoneal lymph-node dissection was performed. Histologically, the tumor was a pure osteosarcoma. Submitted three lymph nodes were free from tumor cell invasion. After the diagnosis was established, the patient underwent further work-up to find other possible primary tumors including a bone scan. No primary osseous tumor was found. After 44 months of follow-up, the patient remains free of disease.

Materials and methods

The excised tissue was fixed in 10% buffered formalin, embedded in paraffin, and stained with hematoxylin and eosin. Immunohistochemical stains were performed on 4-μm-thick sections using the avidin-biotin immunoperoxidase method for pankeratin (AE1/AE3, Dako, California, USA), epithelial membrane antigen (EMA; Dako), vimentin (Dako), α-smooth muscle actin (Dako), desmin (Zymed, California, USA), CD34 (Novocastra, Newcastle, UK), CD68 (Dako), inhibin (Dako), Ki-67 (Dako), p53 protein (Dako), and retinoblastoma gene product (Rb; Dako).



Fig. 1 Sectioned surface of testicular tumor shows a well-circumscribed mass displacing testicular tissue

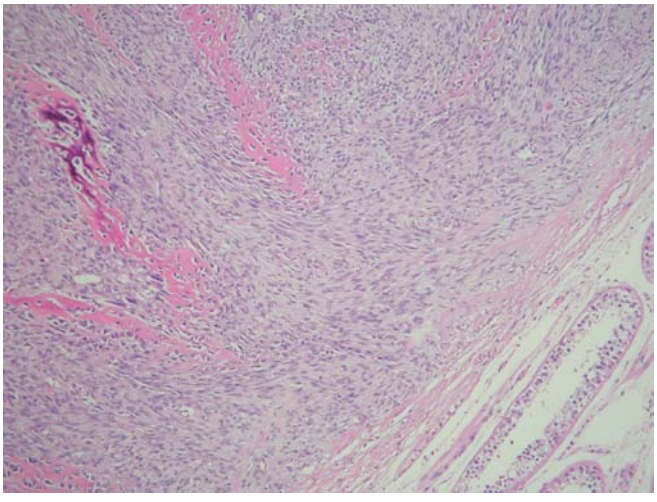


Fig. 2 The tumor is surrounded by normal testicular tissue. This tumor is composed of a compact growth of spindle cells with osteoid formation (hematoxylin-eosin, original magnification ×100)

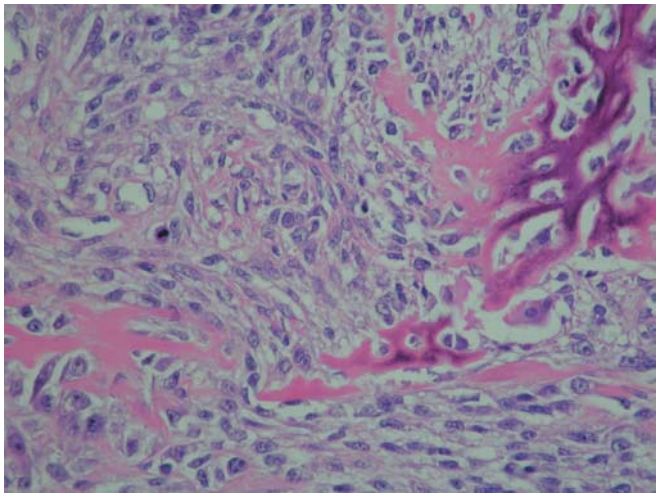


Fig. 3 Anastomosing trabeculae of neoplastic osteoid within sarcomatous areas and osteoclasts are identified (hematoxylin-eosin, original magnification ×200)

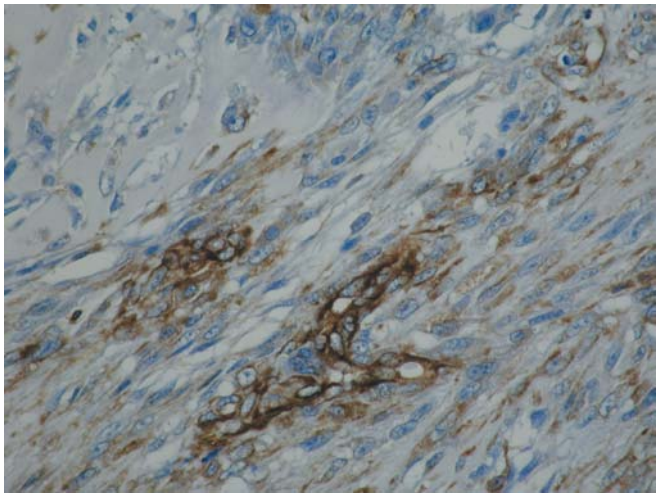


Fig. 4 The tumor cells are strongly immunoreactive to vimentin (original magnification ×200)

Results

Pathological findings

Gross examination of the resected specimen revealed a 17×9×7-cm hydrocele containing an enlarged testis. A cut surface of the testis revealed a well-circumscribed mass, 4.0 cm in diameter (Fig. 1). The surrounding testicular tissue was compressed by the expansile mass. The tumor was solid and firm with white-tan cut-surface. There were few small cysts. The tunica albuginea was intact. The epididymis and spermatic cord appeared normal. Histological examination revealed a well-demarcated, nonencapsulated lesion (Fig. 2). Normal testicular tissues were seen adjacent to the lesion. The tumor consisted of sheets of round to spindle cells with marked nuclear pleomorphism and prominent nucleoli. Intermingled with the tumor cells were irregular areas of neoplastic osteoid with scattered foci of mineralization (Fig. 3). Mitotic activity was high, with three to four mitoses per high-power field and atypical mitoses were frequently seen. Osteoclasts were seen along the area of osteoid formation. Despite whole sampling of the tumor, no other components were identified.

Immunohistochemistry

The tumor cells stained strongly for vimentin (Fig. 4). CD68 showed a focal immunoreactivity limited to osteoclasts. Stains for pankeratin, EMA, actin, CD34, desmin, and inhibin were uniformly negative in both osteoid-forming and sarcomatous areas. Ki-67-positive cancer cells were frequently observed. No overexpression of p53 and Rb was observed in the tumor cells.

Discussion

Extraosseous osteosarcomas are diagnosed on the basis of the following: presence of poorly differentiated sarcoma elements, formation of malignant osteoid, and no apparent skeletal origin [2]. In the present case, the tumor was confined entirely within the tunica albuginea, and no paratesticular mass was present. The tumor was composed of pure osteoid-forming malignant cells without any other germ cell component consistent with the diagnosis of pure osteosarcoma arising from the testis. The possibility of metastatic tumor was excluded by the absence of other skeletal osteosarcoma. In the literature, we have found that only two pure testicular osteosarcomas have been reported [8, 19]. The patients were age 30 years and 63 years. Each presented initially with a testicular mass. The tumors measured 13 cm and 6 cm in greatest dimension. The patients were treated with orchiectomy and high ligation of the spermatic cord. None received any post-operative therapy. Both of them were alive and well with no evidence of disease 9 weeks and 5.5 years, respectively, after orchiectomy. Our patient was a 78-year-old man who presented with scrotal swelling. He was treated with orchiectomy and retroperitoneal lymph-node dissection and received no further treatment. He remained well 44 months after the orchiectomy. No recurrence in our patient and in patients reported from previous cases illustrates that primary pure testicular osteosarcoma may be associated with a favorable prognosis.

Hydrocele is the most common cause of scrotal swelling [9]. Intratesticular tumors may be associated with hydrocele [1, 13]. However, the previous two cases of primary testicular osteosarcoma were not complicated with hydrocele [8, 19]. The testicular tumor in our patient was discovered by an ultrasound evaluation for hydrocele. To the best our knowledge, this is the first case of primary testicular osteosarcoma complicated with hydrocele.

Immunohistochemical staining of p53 and Rb in osteosarcoma of the bone has been fully described in the literature. Overexpression of p53 protein varies from 27% to 67% of patients [7, 15]. Staining for Rb has been reported in 40–50% of patients with skeletal osteosarcomas [3, 17]. No p53 and Rb immunostaining was observed in our patient. Our findings suggest that neither *Rb* nor *p53* may be essential for the development of a testicular osteosarcoma. Similar findings have also been reported in a malignant stromal tumor of the testis with osteosarcomatous components [12].

Primary intrascrotal sarcomas are rare. The most common sarcomas of the scrotum in adults are liposarcoma and leiomyosarcoma [4]. Primary testicular sarcomas that are neither associated with germ cell elements nor retroperitoneal metastases are extremely rare. Rhabdomyosarcoma, spindle cell sarcoma, leiomyosarcoma, fibrosarcoma, chondrosarcoma, and osteosarcoma have been described [18, 19].

The origin of primary testicular osteosarcoma is not known and remains speculative. They may originate from (1) a bone of mixed sex-cord/stromal tumor or teratoma, (2) primitive testicular stromal cells, or (3) metaplastic stromal cells [8, 19]. The majority of intratesticular sarcomas are usually associated with a germ cell tumor [14, 18, 19]. Testicular osteosarcomas may also occur as a component of malignant mixed sex-cord/stromal tumor [11] or as a part of testicular teratoma [10]. In the present case, extensive sampling of the entire tumor yielded only undifferentiated and osteosarcomatous tissues. It is unlikely that our case arose from teratoma or mixed sex-cord/stromal tumor.

The differential diagnosis of primary testicular osteosarcoma includes sarcomatous transformation of germ cell tumors and undifferentiated sex-cord/stromal tumors and Leydig cell tumors with unusual features [4, 9, 10, 16]. The tumor of the present case was composed of pure osteoid-forming malignant cells without any other neoplastic component in whole sampling of the tumor. Leydig cell tumors with unusual features can have a histopathological resemblance to unclassified sarcoma. Tumor cells of the present case were negative for inhibin, ruling out Leydig cell tumor.

In conclusion, this case calls attention to rare primary testicular osteosarcoma complicated with hydrocele and illustrates that primary pure testicular osteosarcoma may be associated with a favorable prognosis.

References

1. Ali Y, Kehinde EO, Makar R, Al-Awadi KA, Anim JT (2002) Leiomyosarcoma complicating chronic inflammation of the testis. Med Princ Pract 11:157–160
2. Allan CJ, Soule EH (1971) Osteogenic sarcoma of the somatic soft tissues. Clinicopathologic study of 26 cases and review of literature. Cancer 27:1121–1133
3. Benassi MS, Molendini L, Gamberi G, Sollazzo MR, Ragazzini P, Merli M, Magagnoli G, Sangiorgi L, Bacchini P, Bertoni F, Picci P (1997) Altered G1 phase regulation in osteosarcoma. Int J Cancer 74:518–522
4. Eble JN, Sauter G, Epstein JI, Sesterhenn IA (eds) (2004) (2004) Word Health Organization Classification of tumors. Pathology and genetics of tumors of the urinary system and male genital organs. IARC Press, Lyon
5. Goorin AM, Abelson HT, Frei E (1985) Osteosarcoma: fifteen years later. N Engl J Med 313:1637–1643
6. Lioe TF, Biggart JD (1993) Tumours of the spermatic cord and paratesticular tissue. A clinicopathological study. Br J Urol 71:600–606
7. Lonardo F, Ueda T, Huvos AG, Healey J, Ladanyi M (1997) p53 and MDM 2 alterations in osteosarcomas: correlation with clinicopathologic features and proliferative rate. Cancer 79:1541–1547
8. Mathew T, Prabhakaran K (1981) Osteosarcoma of the testis. Arch Pathol Lab Med 105:38–39
9. Micallef M, Torreggiani WC, Hurley M, Dinsmore WW, Hogan B (2000) The ultrasound investigation of scrotal swelling. Int J STD AIDS 11:297–302
10. Motzer RJ, Amsterdam A, Prieto V, Sheinfeld J, Murty VV, Mazumdar M, Bosl GJ, Chaganti RS, Reuter VE (1998) Teratoma with malignant transformation: diverse malignant histologies arising in men with germ cell tumors. J Urol 159:133–138
11. Oosterhuis JW, Castedo SM, de Jong B, Seruca R, Dam A, Vos A, de Koning J, Schraffordt Koops H, Sleijfer DT (1989) A malignant mixed gonadal stromal tumor of the testis with het-

erologous components and i(12p) in one of its metastases. Cancer Genet Cytogenet 41:105–114
12. Reuvekamp PT, Stulp RP, Schraffordt Koops H, Oosterhuis JW, Scheffer H, Buys CH (1992) Analysis of a metastasizing testicular mixed gonadal stromal tumor with osteosarcoma components suggests that a malignant tumor with the histology of osteosarcoma may develop without primary involvement of RB1 and TP53. Cancer Res 52:6705–6707
13. Suzuki K, Shioji Y, Morita T, Tokue A (2001) Primary testicular plasmacytoma with hydrocele of the testis. Int J Urol 8:139–140
14. Terrier-Lacombe MJ, Martinez-Madrigal F, Porta W, Rahal J, Droz JP (1990) Embryonal rhabdomyosarcoma arising in a mature teratoma of the testis: a case report. J Urol 143:1232–1234
15. Ueda Y, Dockhorn-Dworniczak B, Blasius S, Mellin W, Wuisman P, Bocker W, Roessner A (1993) Analysis of mutant P53 protein in osteosarcomas and other malignant and benign lesions of bone. J Cancer Res Clin Oncol 119:172–178
16. Ulbright TM, Srigley JR, Hatzianastassiou DK, Young RH (2002) Leydig cell tumors of the testis with unusual features; adipose differentiation, calcification with ossification, and spindle-shaped tumor cells. Am J Surg Pathol 26:1424–1433
17. Wadayama B, Toguchida J, Shimizu T, Ishizaki K, Sasaki MS, Kotoura Y, Yamamuro T (1994) Mutation spectrum of the retinoblastoma gene in osteosarcomas. Cancer Res 54:3042–3048
18. Washecka RM, Mariani AJ, Zuna RE, Honda SA, Chong CD (1996) Primary intratesticular sarcoma. Immunohistochemical ultrastructural and DNA flow cytometric study of three cases with a review of the literature. Cancer 77:1524–1528
19. Zukerberg LR, Young RH (1990) Primary testicular sarcoma: a report of two cases. Hum Pathol 21:932–935

Virchows Arch (2004) 445:214
DOI 10.1007/s00428-004-1101-6
© Springer-Verlag 2004

ANNOUNCEMENTS

9 September 2004
One day course on Advanced Ultrasound of the Breast
Nottingham, UK

For further information contact:
The Blamey Education Centre
Nottingham Breast Institute
City Hospital, Nottingham, NG5 1PB, UK
Tel.: 00 44 (115) 969 1689
E-mail: sbury@ncht.trent.nhs.uk

23–24 September 2004 **(Change of date)**
Thyroid Pathology for the Practicing Pathologist
15 rue de l'Ecole de Médecine, Paris, France

A 2-day course will take place in Paris under the auspices of the French Division of the I.A.P. This course will be given in English by Prof. M. Sobrinho-Simoes (Porto) and Prof. R. Heimann (Brussels).

It will consist of lectures alternating with slide reviews and a slide seminar over a multihead microscope. The cases of this seminar will be sent (on CD) before the meeting. The audience will be limited to 22 participants.

Course fee: 390 euros (320 euros for members of any IAP division). The fees include registration, hand-out, CD of the slide seminar and coffee breaks.

For further information, please contact:
Mrs. M. Fontanière
Administrative Secretary
French Division of the I.A.P. 32 Cours Albert Thomas
69008, Lyon, France
Fax: 33478754311
E-mail: academie.pathologie@wanadoo.fr

11 October 2004
Continuing Medical Education
Nottingham, UK

For further information contact:
The Blamey Education Centre
Nottingham Breast Institute
City Hospital, Nottingham, NG5 1PB, UK
Tel.: 00 44 (115) 969 1689
E-mail: sbury@ncht.trent.nhs.uk

22–24 November 2004
41st Nottingham Multi-disciplinary Course on breast disease
Nottingham, UK

For further information contact:
The Blamey Education Centre
Nottingham Breast Institute
City Hospital, Nottingham, NG5 1PB, UK
Tel.: 00 44 (115) 969 1689
E-mail: sbury@ncht.trent.nhs.uk

8–10 November 2004
Practical Adult Cardiovascular Pathology Course
Course organisers: Dr MN Sheppard/Dr Yen Ho

This particular "Hands On" course approaches in detail the problems that face the diagnostic pathologist when dealing with cardiovascular pathology both congenital and adult. The approach to a cardiac autopsy and sudden death will be emphasized. Cardiac specimens will be made available for analysis and practical demonstrations as well as video demonstrations will be highlighted. Organ retention will also be covered and minimal database for reporting cardiovascular specimens. A slide seminar with slides is included. The course is aimed at trainees studying for the MRCPATH and also senior pathologists who wish to update their knowledge.

Course fee: £ 400.00 (includes daily coffee, tea and lunch)
A special fee of £ 300.00 for juniors in training

For further information, please contact:
Short Course Office
National Heart and Lung Institute
Dovehouse Street
London SW3 6LY
Tel.: +44(0)20 7351 8172
Fax: +44(0)20 7351 8246
E-mail: shortcourse.NHLI@IC.AC.UK

8–10 December 2004
Combined Adult & Congenital Cardiovascular Pathology Course
Course Organisers: Dr MN Sheppard/Dr Yen Ho

This particular "Hands On" course approaches in detail the problems that face the diagnostic pathologist when dealing with cardiovascular pathology both congenital and adult. The approach to a cardiac autopsy and sudden death will be emphasized. Cardiac specimens will be made available for analysis and practical demonstrations as well as video demonstrations will be highlighted. Organ retention will also be covered and minimal database for reporting cardiovascular specimens. A slide seminar with slides is included. The course is aimed at trainees studying for the MRCPATH and also senior pathologists who wish to update their knowledge.

Course fee: £ 400.00 (includes daily coffee, tea and lunch)
A special fee of £ 300.00 for juniors in training

For further information, please contact:
Short Course Office
National Heart and Lung Institute
Dovehouse Street
London SW3 6LY
Tel.: +44(0)20 7351 8172
Fax: +44(0)20 7351 8246
E-mail: shortcourse.NHLI@IC.AC.UK

Virchows Arch (2004) 445:215–223
DOI 10.1007/s00428-004-1038-9

REVIEW ARTICLE

Cyril Fisher

Myofibrosarcoma

Received: 12 February 2004 / Accepted: 21 April 2004 / Published online: 2 June 2004
© Springer-Verlag 2004

Abstract Myofibrosarcomas are malignant tumours of myofibroblasts, which have been recognised for many years, but have become clearly defined only recently. They are low- or high-grade sarcomas that arise in soft tissue or bone in adults or children. Low-grade myofibrosarcomas are infiltrative tumours, usually in deep soft tissue, with a predilection for the head and neck region, which display a range of microscopic appearances from fasciitis-like to fibrosarcoma-like; all cases at least focally display nuclear pleomorphism. They express smooth-muscle actin and calponin, and some express desmin, but most lack h-caldesmon. Low-grade myofibrosarcomas can recur but rarely metastasise. Their differential diagnosis is from benign myofibroblastic proliferations, such as fasciitis and fibromatosis, as well as from fibrosarcoma and leiomyosarcoma. Pleomorphic myofibrosarcomas are high-grade pleomorphic sarcomas (malignant fibrous histiocytoma), which show ultrastructural evidence of myofibroblastic differentiation. They closely resemble malignant fibrous histiocytoma clinically and morphologically, but are more frequently actin positive. This article describes the low- and high-grade variants of myofibrosarcoma and other malignant tumours with myofibroblastic differentiation.

Keywords Myofibrosarcoma · Myofibroblast · Sarcoma · Soft tissue

Introduction

Malignant tumours of myofibroblasts, termed myofibrosarcomas by analogy with fibrosarcoma [41], are rare neoplasms, which have recently become better defined. Myofibrosarcomas display a range of histological differentiation, from fasciitis-like to frankly sarcomatous. Low- and intermediate-grade myofibrosarcomas are distinct from pleomorphic myofibrosarcomas, which are malignant fibrous histiocytoma (MFH)-like tumours. Other low-grade malignant tumours with myofibroblastic differentiation include inflammatory myofibroblastic tumour (IMT) and infantile fibrosarcoma (IFS). These tumours, which have characteristic and consistent genetic abnormalities, are not usually categorised as myofibrosarcomas, but are described briefly below.

C. Fisher (✉)
Royal Marsden Hospital,
Fulham Road, London, SW3 6JJ, UK
e-mail: cyril.fisher@rmh.nthames.nhs.uk
Tel.: +44-207-8082631
Fax: +44-207-3515376

Myofibroblasts

Myofibroblasts are modified fibroblasts, which occur in the stroma in some normal tissues [21, 32] (notably testicular peritubular stroma and the periodontal ligament), in inflammatory and reparative granulation tissue and as the principal cell type in some reactive and neoplastic soft-tissue lesions. In granulation tissue, in which they were first described and have been most intensively investigated, myofibroblasts are probably derived from local fibroblasts [40] in response to mechanical stress, and their functions, appearance and immunoprofile vary in relation to the phase of activity [75]. This variation is seen in the differing stages of reactive lesions, such as nodular fasciitis, and is reflected in the range of appearances seen in other pathological conditions. It has also been suggested that myofibroblast-like cells are sometimes derived from vascular smooth-muscle cells, from pericytes [32] or by metaplasia, as in spindled carcinomas [1], but these phenomena are less well documented. A number of fibroblastic lesions have a component of myofibroblasts, and it is possible that cells can modulate between the two morphological and functional states. There is no evidence that myofibroblasts differentiate to smooth-muscle cells; in wound healing, as epithelialisation is completed, the myofibroblasts are presumed to disappear by apoptosis [20, 38, 39].

Myofibroblasts are short, spindled, bi- or tripolar spindle-shaped or stellate cells, with wavy or ovoid pale-

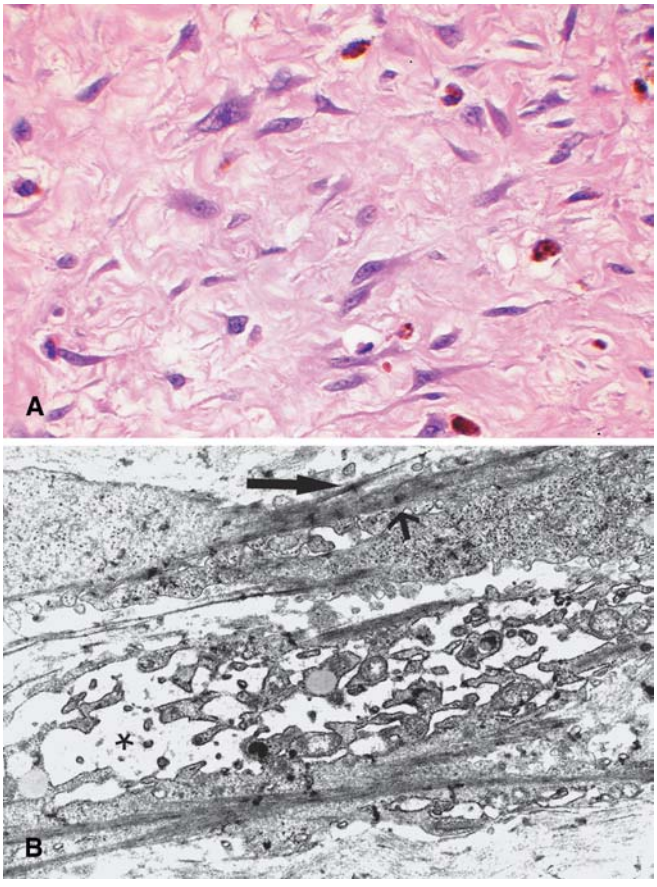


Fig. 1 Myofibroblasts in organising granulation tissue, showing spindle and stellate cells with small nucleoli. **b** Electron micrograph of a part of a myofibroblast, illustrating abundant rough endoplasmic reticulum (*asterisk*), fibronexus fibril (*large arrow*) and intracytoplasmic stress fibre (*small arrow*)

staining nuclei, each of which has a single, small nucleolus (Fig. 1). The cytoplasm is sparse to moderate in amount and sometimes amphophilic, and there are indistinct cell margins, which can appear to blend with the stroma. In addition to their ability to synthesise collagens and other stromal components, including fibronectin and laminin, myofibroblasts acquire contractile elements [22, 38, 39, 47, 75]. Using electron microscopy (Fig. 1), the cytoplasm has abundant rough endoplasmic reticulum (RER) and peripheral or subplasmalemmal bundles of thin cytoplasmic filaments with dense foci, termed stress fibres. This differs from smooth-muscle cells, in which myofilament bundles with focal dense bodies are distributed throughout the cytoplasm and where there are also cell-membrane vesicles and plaques, as well as external lamina. In myofibroblasts, the intracellular microfilament bundles are in continuity through the cell membrane with extracellular fibronectin fibrils forming the fibronexus adhesion complex. The fibronexus is a distinctive cell-stromal attachment that is seen in cells in reactive and other myofibroblastic lesions [25]. It is very rarely found in smooth-muscle cells, but has been identified in foetal endothelial cells, in spindle-cell carcinoma [27] and in fibrosarcoma [25]. Other features of myofibroblasts include a prominent Golgi complex and collagen secretion granules in Golgi-derived vesicles. Fibroblasts have variable amounts of RER, which can become distended with secretory products, but lack external lamina, pinocytotic vesicles and organised cytoplasmic filaments. Fibroblasts express only vimentin, whereas myofibroblasts display various combinations of vimentin, actin isoforms [especially alpha-smooth-muscle actin (SMA)], desmin and myosin [67, 69]. Desmin is expressed much less frequently in myofibroblastic neoplasms than in smooth-muscle tumours [26]. Nonetheless, both types of neoplasms can, on occasion, have detectable desmin, muscle-specific actin and SMA. Calponin is a sensitive, but not specific, marker of myofibroblasts, which are usually negative for h-caldesmon (a marker of smooth-muscle differentiation) [8]. Fibronectin positivity can be demonstrated on the cell surface [25]. Other diagnostic markers, including anaplastic lymphoma kinase (ALK)-1, are largely absent, but myofibroblasts can show cytoplasmic positivity for CD117 under some technical conditions, especially using the Dako antibody with antigen retrieval [60].

Low-grade myofibrosarcoma

Some 47 examples of low-grade myofibrosarcoma have been reported, although only half of these have electron microscopic confirmation. They occur at any age (range 9–75 years, mean 40 years) with a slight male predominance and with tumour size ranging from 1.5 cm to 17 cm. Tumours can arise in extremities and trunk (including breast or retroperitoneum), but there is a predilection (up to one-third of cases) for the head and neck region in both soft tissue (including oral cavity and especially tongue, face and neck) and bone (notably maxilla and mandible) [2, 3, 18, 19, 30, 31, 42, 55, 58, 62, 70, 74, 77].

Low-grade myofibrosarcomas can arise in subcutaneous tissue or in submucosa, but the majority are deep soft-tissue lesions, and some are intraosseous. They are unencapsulated tumours, which are sometimes circumscribed, but which more often infiltrate adjacent fibrous tissue, fat or skeletal muscle (Fig. 2). The usual microscopic pattern is of a rather cellular fibrosarcoma-like tumour composed of fascicles or broad sheets of cells, with or without focal herringbone arrangement or storiform whorls (Fig. 3, Fig. 4, Fig. 5). The cells are generally uniform, relatively long and spindle-shaped, with tapered nuclei and small nucleoli and scanty or moderate amounts of cytoplasm. There is a variably collagenous stroma (Fig. 3) and usually scanty inflammation, and occasionally there are osteoclast-like giant cells. Some tumours are focally myxoid (Fig. 4), and the patterns can closely resemble those of nodular fasciitis (Fig. 5). Unlike fasciitis, however, myofibrosarcomas display nuclear atypia. This is usually mild, with scattered enlarged hyperchromatic nuclei, but larger atypical cells and foci of polygonal cells

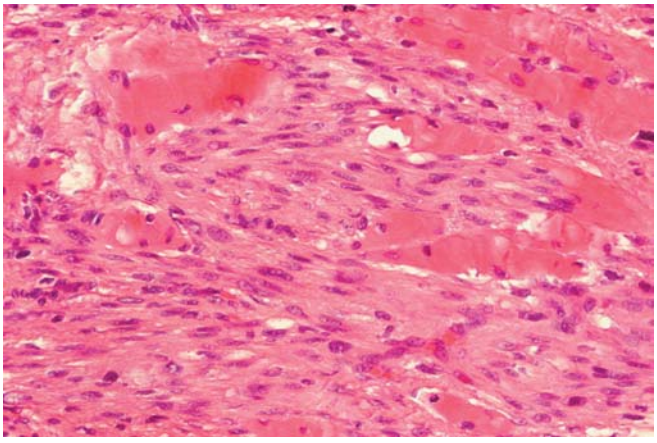


Fig. 2 Low-grade myofibrosarcoma infiltrating skeletal muscle. Note separation of muscle bundles

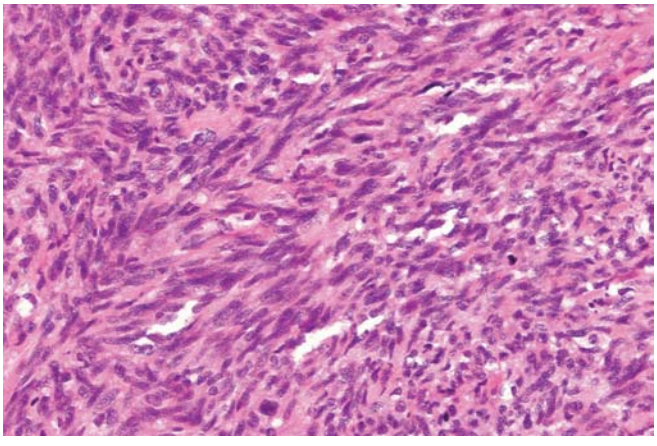


Fig. 3 Low-grade myofibrosarcoma. The cells are arranged in fascicles with intercellular collagen

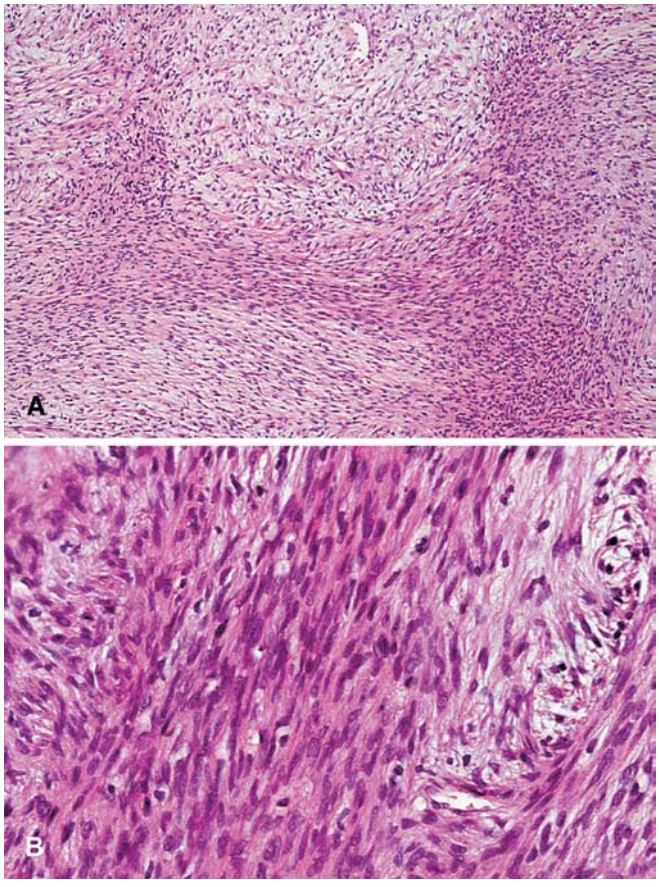


Fig. 4 Low-grade myofibrosarcoma with cellular and myxoid areas. **a** Low magnification showing variable cellularity and superficial resemblance to myxofibrosarcoma. **b** Cells have tapered nuclei and scanty cytoplasm

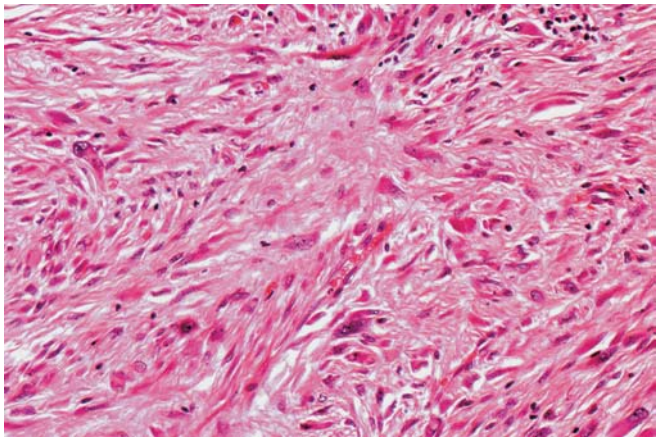


Fig. 5 Low-grade myofibrosarcoma. This tumour resembles nodular fasciitis, but there is focal nuclear pleomorphism. In spite of the latter, the infrequent mitoses and absence of necrosis indicate that this is a low-grade sarcoma

are sometimes seen; the changes can be very focal and sometimes are found only after searching several microscopic fields. Mitotic activity is variable, but abnormal mitotic figures are typically absent, and necrosis is rare and more often a feature of higher grades of malignancy. However, using a three-step grading system, such as that of the French Cancer Centres Sarcoma Group [45], grade-1 (low-grade) and grade-2 (intermediate-grade) myofibrosarcomas (Fig. 6) can be distinguished. Recurrent tumours can display areas of higher-grade malignancy [52, 62], but we have seen a pulmonary metastasis from an intermediate-grade myofibrosarcoma that was bland and fasciitis-like [62].

Most low-grade myofibrosarcomas are immunoreactive for SMA, and up to one half express desmin, usually more focally [58, 62]. Either or both of these antigens can be expressed, resulting in either a desmin-positive/SMA-negative or desmin-negative/SMA-positive immunophenotype [58]. Reflecting the microanatomy, the SMA staining can sometimes be seen in a peripheral linear distribution (Fig. 7). Calponin is diffusely positive in most cases, whereas h-caldesmon is detected with only focal expression in rare cases [35]. These findings are helpful in excluding leiomyosarcoma, which usually displays both h-caldesmon and calponin. Some myofibrosarcomas dis-

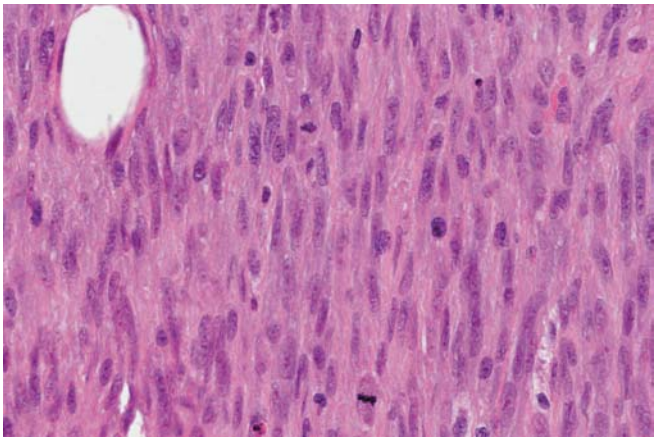


Fig. 6 Myofibrosarcoma, grade 2 (intermediate-grade), infiltrating fat. There are frequent mitoses. This tumour also had focal necrosis

play fibronectin [28, 58], but not collagen IV or laminin. This is potentially useful for diagnosis, but fibronectin is also positive in extracellular matrix [25] (rendering interpretation difficult, as the stain is not always "clean") [58] and, to some extent, in leiomyosarcoma [28]. Expression of cytokeratin, epithelial membrane antigen or CD34 is seen sporadically [58], and, very rarely, there is focal S100 protein positivity [30]. Ultrastructurally, the neoplastic cells have variable RER and peripheral filament bundles resembling stress fibres, collagen secretion granules and, rarely, fibronectin fibrils and a fibronexus junction (Fig. 7). Since neoplastic cells differ from their non-neoplastic counterparts by incomplete or abnormal development of morphological features, the fully developed fibronexus is not required for diagnosis by most observers. Some published accounts, however, illustrate fibronexus components, but do not describe them, so they may be more common than what has actually been reported [26].

Myofibrosarcomas are slowly growing, infiltrative tumours that are prone to local recurrence and can rarely relapse and metastasise, even after many years. In two large series [58, 62], the recurrence rate was 18% and 54%, respectively, but the latter study included intermediate-grade tumours, which recurred more frequently; in the 15 remaining published examples of low-grade myofibrosarcoma, the overall recurrence rate was 27%. Metastasis to lung occurred in one case in each of the large series and in two other published examples [52, 77].

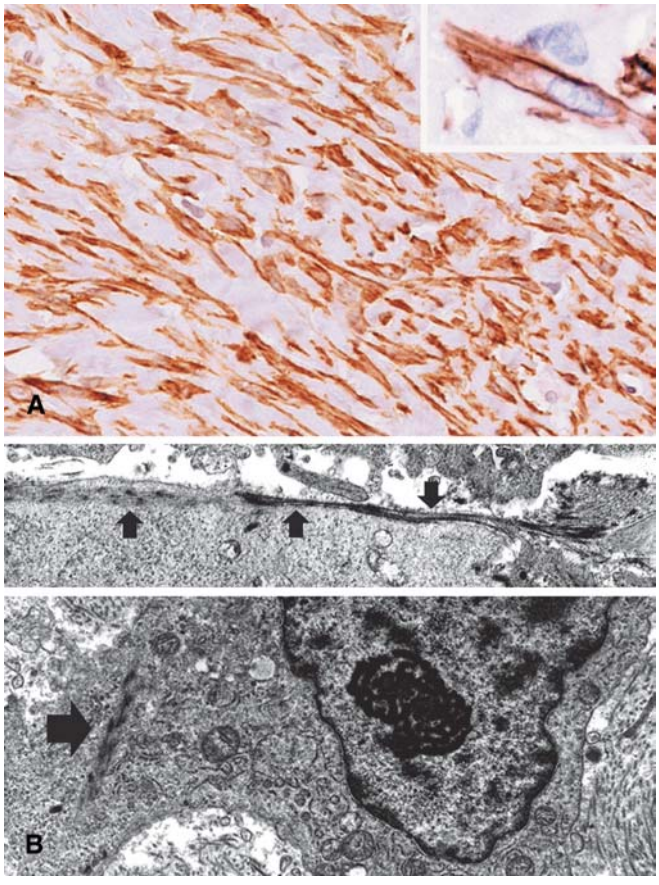


Fig. 7 Low-grade myofibrosarcoma. **a** Immunoperoxidase stain for smooth-muscle actin, showing peripheral accentuation. **b** *Upper* cell with fibronexus fibril and stress fibre (*arrows*); *lower* another cell in the same tumour showing a portion of stress fibre (*arrow*) in cytoplasm

The differential diagnosis includes benign myofibroblastic lesions, especially nodular fasciitis and fibromatosis, and other types of low-grade spindle-cell sarcoma, notably fibrosarcoma and leiomyosarcoma. The diagnosis can require both clinical and morphological data; immunohistochemistry is of limited use in distinguishing myofibroblastic lesions, but an extended immunohistochemical panel can be helpful in excluding leiomyosarcoma and fibrosarcoma (Table 1).

Nodular fasciitis is a rapidly growing lesion, which is usually subcutaneous and does not reach a large size. Histologically, there is a range of appearances within the same lesion, with variable cellularity and myxoid mi-

Table 1 Immunohistochemistry of smooth muscle and fibro/myofibroblastic tumours. + positive, ± sometimes found, − absent, *des* desmin, *SMA* smooth-muscle actin, *MSA* muscle−specific actin, *EMA* epithelial membrane antigen, *CK* cytokeratin, *Calp* calponin, *hCald* heavy caldesmon

	Des	SMA	MSA	S100	EMA	CK	CD34	Calp	hCald
Leiomyosarcoma	+	+	+	±	±	±	−	+	+
Myofibrosarcoma	±	+	±	−	−	rare	−*	+	−
Fibrosarcoma	−	−	−	−	−	−	±	−	−

* Very occasional positive

crocysts containing lymphocytes and erythrocytes. Nodular fasciitis is less cellular and uniform than myofibrosarcoma and does not infiltrate into skeletal muscle or bone. Unlike in myofibrosarcoma, nuclear atypia and necrosis are not seen. Fibromatosis, a collagen-producing myofibroblastic tumour, has aligned uniform myofibroblasts without nuclear pleomorphism, dispersed in dense collagen with characteristic blood vessels and mast cells. When fibromatosis infiltrates skeletal muscle, the muscle fibres become atrophic rather than separated by tumour as in myofibrosarcoma.

IMT has a distinct clinical picture, a wider range of histological patterns than myofibrosarcoma, a marked plasmacytic infiltrate and can be ALK positive. Adult-type fibrosarcoma is composed of cells with scanty cytoplasm and elongated tapered nuclei arranged in a distinctive fascicular or herringbone architecture, and there is usually more intercellular collagen than in myofibrosarcoma. Immunohistochemical markers other than vimentin are absent. Leiomyosarcoma typically has alternating fascicles of cells that are less tapered than myofibroblasts and that more frequently have blunt-ended nuclei with scattered paranuclear vacuoles. Moreover, there is diffuse h-caldesmon expression. The differential diagnosis can occasionally include other spindle-cell sarcomas, such as synovial sarcoma or malignant peripheral nerve sheath tumour, as well as some examples of angiosarcoma and spindle-cell rhabdomyosarcoma. Each of these can be recognised by its microscopic features and specific immunophenotype, as well as its ultrastructural and molecular genetic examination where indicated. In some locations, particularly head, neck and breast, spindle-cell carcinoma requires exclusion using a panel of anticytokeratin antibodies.

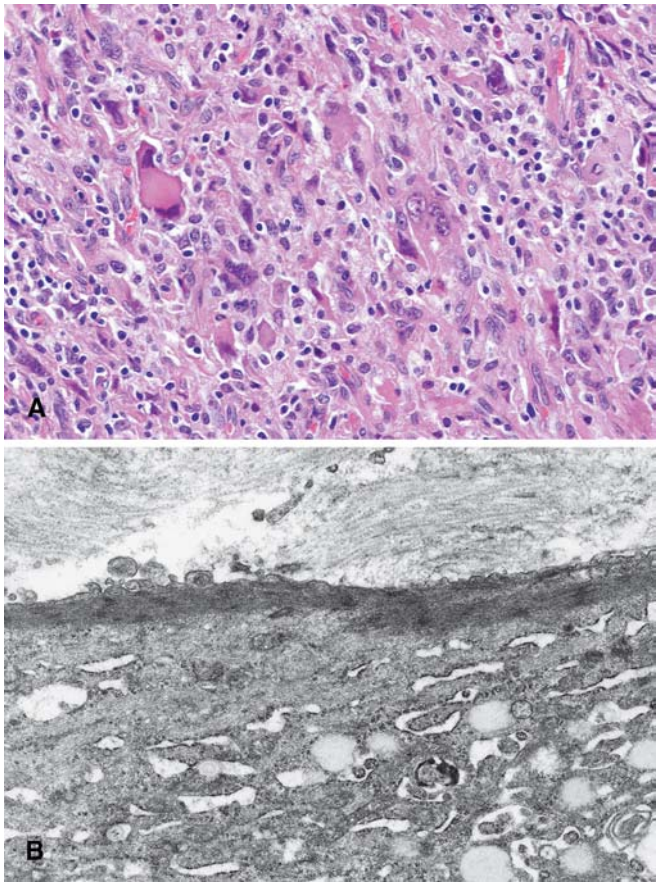


Fig. 8 Pleomorphic myofibrosarcoma. **a** Pleomorphic spindle and polygonal cells including some with abundant cytoplasm. **b** Peripheral cytoplasmic filaments resembling stress fibres

Pleomorphic myofibrosarcoma

Pleomorphic myofibrosarcoma is a pleomorphic high-grade sarcoma in which there is ultrastructural evidence of myofibroblastic, as well as fibroblastic, differentiation. Pleomorphic sarcomas of MFH type, for many years considered to be the most common type of adult soft-tissue sarcoma, have been defined as fascicular or storiform neoplasms composed of atypical spindle and polygonal cells, which do not show a specific line of differentiation. Myofibroblastic differentiation has, in fact, been observed since electron microscopy was first employed on examples of MFH [12, 34, 36, 48]. In these sarcomas, many of the atypical cells, whether fusiform or plump and histiocyte-like, have the ultrastructure of fibroblasts, with much RER. Additionally, some show myofibroblastic features, typically with subplasmalemmal aggregates of cytoplasmic filaments, and a neoplastic cell with a fibronexus has been recorded in a pleomorphic myofibrosarcoma of bone [76]. The proportion of pleomorphic sarcomas that display myofibroblastic differentiation increases with sample size and length of search. In one study, 56% of MFH of all types had detectable myofibroblasts, with a mean of 3% (range 0–22%) of myofibroblasts per case [37]. Some low- or intermediate-grade myofibrosarcomas have recurred as pleomorphic tumours [62, 70].

Notwithstanding the extensive literature on MFH, there have been few well-documented clinicopathological reports of pleomorphic myofibrosarcoma [3, 12, 28, 30, 61, 70, 76]. A subset has been described in the head and neck region in children [70], but the tumours predominantly involve deep soft tissues of extremities in adults. Myxofibrosarcoma, a more superficial tumour of which the higher grades overlap with MFH, typically lacks myofibroblastic differentiation. Histologically, most pleomorphic myofibrosarcomas are composed of spindle and polygonal cells arranged at least focally in a storiform pattern, with occasional fascicular areas. Large polygonal cells with abundant cytoplasm, which mimic rhabdomyoblasts, are seen (Fig. 8). Stromal changes of fibrosis, myxoid change, necrosis and inflammation are variable. In a recent study, pleomorphic myofibrosarcoma and pleomorphic undifferentiated sarcomas were found to be clinically and morphologically indistinguishable [61].

Immunohistochemically, both SMA and desmin have been described in pleomorphic sarcomas with ultrastruc-

turally confirmed myofibroblastic differentiation [46, 48]. In one series, just over half of pleomorphic myofibrosarcomas (57%) focally expressed SMA, and a smaller proportion (43%) had desmin positivity [61]. None of the pleomorphic myofibrosarcomas examined expressed h-caldesmon [35], which implies that they are not merely poorly differentiated leiomyosarcomas. However, both actin and desmin have been demonstrated in pleomorphic sarcomas without ultrastructural features of myofibroblastic or smooth-muscle differentiation [54, 66]. Montgomery et al. found SMA and desmin, respectively, in 33% and 27% of undifferentiated pleomorphic sarcomas [61]. In addition, calponin was expressed in 43% of these cases, and h-caldesmon was expressed in only a few cells, suggesting that myofibroblastic differentiation is more easily detected using immunohistochemistry than electron microscopy [35]. Ultrastructural examination reveals variable myofibroblastic differentiation (Fig. 8).

Pleomorphic myofibrosarcoma is a fully malignant tumour. We found that 29% of seven pleomorphic myofibrosarcomas recurred, 71% metastasised and 43% of patients died of disease [61]. These were compared with pleomorphic undifferentiated sarcomas, of which, in a similar period, 35% recurred, 59% metastasised and 41% of patients died of disease. Of the 15 other published examples defined using electron microscopy, 5 (33%) recurred and 10 (67%) metastasised [3, 12, 28, 30, 70, 76]. Thus, myofibroblastic differentiation in pleomorphic sarcomas cannot be used as a favourable prognostic indicator.

The differential diagnosis is from other pleomorphic sarcomas, including MFH, to which pleomorphic myofibrosarcoma is histologically identical. Using immunohistochemistry, myofibroblastic differentiation in a pleomorphic sarcoma can be inferred from the presence of SMA positivity in large polygonal or pleomorphic spindle cells, particularly if the staining is accentuated beneath the cell membrane. Pleomorphic rhabdomyosarcoma has large round cells with eosinophilic cytoplasm, and occasionally there are strap cells with cytoplasmic cross-striations. However, rhabdomyoblastic differentiation is more readily identified immunohistochemically by diffuse reactivity for desmin in the cytoplasm and nuclear positivity for myogenin, with lack of SMA. Pleomorphic leiomyosarcoma has, at least focally, a typical fascicular architecture as well as expression of myoid markers [63], while pleomorphic liposarcoma is defined by the presence of pleomorphic lipoblasts in an otherwise featureless pleomorphic MFH-like sarcoma [24] and can also have epithelioid areas [59]. Non-mesenchymal tumours presenting in soft-tissue locations, such as melanoma and sarcomatoid carcinoma, are usually recognised by demonstration of the appropriate immunophenotype.

Other sarcomas of myofibroblasts

Two further tumour types are generally included in the category of low-grade myofibroblastic malignancies. These are distinct clinicopathological entities, but are also characterised by specific genetic abnormalities.

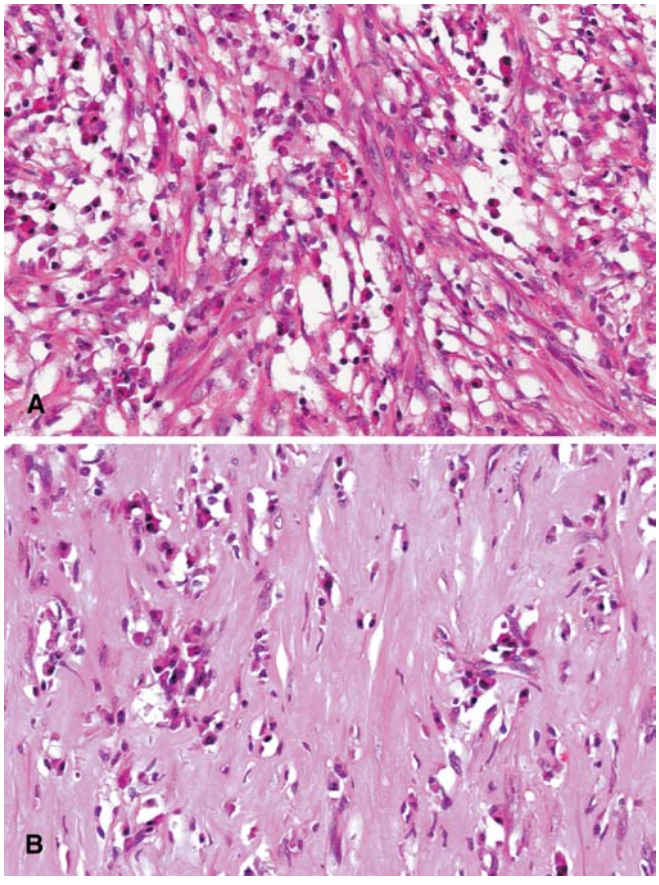


Fig. 9 Inflammatory myofibroblastic tumour. **a** Fascicular and fasciitis-like areas with marked plasma-cell infiltrate. **b** Sparsely cellular sclerosing area, again with abundant plasma cells

Inflammatory myofibroblastic tumour

IMT usually arises in lung or within the abdomen (retroperitoneum or mesentery) and occasionally in visceral or other soft tissue sites, as a solitary or multicentric mass, with a peak incidence in childhood or adolescence [15, 16]. Similar cases have also been termed inflammatory fibrosarcoma [56], but this and IMT are considered to represent a single entity within a morphological and behavioural spectrum [15]. Microscopically, there are fasciitis-like, fascicular and sclerosing areas, with a prominent chronic inflammatory infiltrate, including an abundance of plasma cells (Fig. 9). Pleomorphism is rare, although atypical cells can sometimes be seen. Most cases are positive for SMA, and a smaller number for desmin; some cases are cytokeratin positive. Overall, 30–40% of IMT stain for ALK using ALK-1 or p80 [9, 10, 17], especially abdominal and pulmonary IMT in the first decade. Ultrastructural examination shows a mixture of cells with fibroblastic and myofibroblastic features [14, 56, 57].

Many IMT have clonal abnormalities involving 2p22–24 [44, 73]. Fusion of the ALK gene, located on 2p23, which encodes a receptor tyrosine kinase, with the gene for tropomyosin 3 (TPM3-ALK) or tropomyosin 4 (TPM4-ALK) is seen in some of the tumours [53]. A novel transcript involving ALK and CLTC (clathrin heavy-chain gene, localised to 17q23) has also been described in two cases [7].

About one-third of IMT recur locally, and a small proportion, for which there are no histological predictive factors, progress to frank sarcoma [4, 23, 49]. The differential diagnosis includes sclerosing fibro-inflammatory lesions, such as retroperitoneal fibrosis, fibromatosis, low-grade myofibrosarcoma, inflammatory leiomyosarcoma and follicular dendritic-cell sarcoma.

Infantile fibrosarcoma

IFS is an additional tumour of borderline malignancy, occurring predominantly in the first 4 years of life. Up to 30% of IFSs recur, but metastases are rare, with a frequency of 5% or less in published series [11, 71]. However, local complications of the tumour can be fatal [13]. IFS is a cellular tumour with parallel or herringbone fascicles of fairly uniform, darkly staining ovoid spindle cells with mitotic activity but without cytological atypia or pleomorphism. A small subset of tumours contain immature small round cells. Ultrastructurally, IFSs are composed of fibroblasts and myofibroblasts, while immunohistochemistry shows SMA in about one-third of cases and desmin in one-quarter. CD34 and S100 protein expression are occasionally seen.

Chromosomal abnormalities described in IFS include trisomy 11, random gains of chromosomes 8, 11, 17 and 20 [65], deletion of the long arm of 17 [43] and a t(12;13) translocation [72]. More recently, a specific translocation t(12;15)(p13;q25), resulting in fusion of ETV6 and NTRK3 genes, has been identified in IFS [6, 51, 68]. This abnormality has also been identified in cellular variants of congenital mesoblastic nephroma, a spindle-cell tumour of the kidney histologically resembling IFS [50, 64].

In addition, myofibroblastic differentiation has been observed in tumours showing predominantly epithelial differentiation, notably epithelioid sarcoma [5, 29, 33] and sarcomatoid carcinomas [1]. In both, there appears to be progression or transition from cells with epithelioid features to those of myofibroblasts, with immunophenotypical and ultrastructural changes accompanying the change in cell shape. Clearly, at least the morphological features of myofibroblasts can appear in a variety of different malignant neoplasms. Further genetic studies, including gene expression profiling, might be contributory to an understanding of the mechanisms involved and whether these cells indeed represent true myofibroblasts.

References

1. Balercia G, Bhan AK, Dickersin GR (1995) Sarcomatoid carcinoma: an ultrastructural study with light microscopic and immunohistochemical correlation of 10 cases from various anatomic sites. Ultrastruct Pathol 19:249–263
2. Bisceglia M, Magro G (1999) Low-grade myofibroblastic sarcoma of the salivary gland. Am J Surg Pathol 23:1435–1436
3. Bisceglia M, Tricarico N, Minenna P, Magro G, Pasquinelli G (2001) Myofibrosarcoma of the upper jawbones: a clinicopathologic and ultrastructural study of two cases. Ultrastruct Pathol 25:385–397
4. Biselli R, Boldrini R, Ferlini C, Boglino C, Inserra A, Bosman C (1999) Myofibroblastic tumours: neoplasias with divergent behaviour. Ultrastructural and flow cytometric analysis. Pathol Res Pract 195:619–632
5. Blewitt RW, Aparicio SG, Bird CC (1983) Epithelioid sarcoma: a tumour of myofibroblasts. Histopathology 7:573–584
6. Bourgeois JM, Knezevich SR, Mathers JA, Sorensen PH (2000) Molecular detection of the ETV6-NTRK3 gene fusion differentiates congenital fibrosarcoma from other childhood spindle cell tumors. Am J Surg Pathol 24:937–946
7. Bridge JA, Kanamori M, Ma Z, Pickering D, Hill DA, Lydiatt W, Lui MY, Colleoni GW, Antonescu CR, Ladanyi M, Morris SW (2001) Fusion of the ALK gene to the clathrin heavy chain gene, CLTC, in inflammatory myofibroblastic tumor. Am J Pathol 159:411–415
8. Ceballos KM, Nielsen GP, Selig MK, O'Connell JX (2000) Is anti-h-caldesmon useful for distinguishing smooth muscle and myofibroblastic tumors? An immunohistochemical study. Am J Clin Pathol 114:746–753
9. Cessna MH, Zhou H, Sanger WG, Perkins SL, Tripp S, Pickering D, Daines C, Coffin CM (2002) Expression of ALK1 and p80 in inflammatory myofibroblastic tumor and its mesenchymal mimics: a study of 135 cases. Mod Pathol 15:931–938
10. Chan JK, Cheuk W, Shimizu M (2001) Anaplastic lymphoma kinase expression in inflammatory pseudotumors. Am J Surg Pathol 25:761–768
11. Chung EB, Enzinger FM (1976) Infantile fibrosarcoma. Cancer 38:729–739
12. Churg AM, Kahn LB (1977) Myofibroblasts and related cells in malignant fibrous and fibrohistiocytic tumors. Hum Pathol 8:205–218
13. Coffin CM, Jaszcz W, O'Shea PA, Dehner LP (1994) So-called congenital-infantile fibrosarcoma: does it exist and what is it? Pediatr Pathol 14:133–150
14. Coffin CM, Watterson J, Priest JR, Dehner LP (1995) Extrapulmonary inflammatory myofibroblastic tumor (inflammatory pseudotumor)—a clinicopathologic and immunohistochemical study of 84 cases. Am J Surg Pathol 19:859–872
15. Coffin CM, Dehner LP, Meis-Kindblom JM (1998) Inflammatory myofibroblastic tumor, inflammatory fibrosarcoma, and related lesions: an historical review with differential diagnostic considerations. Semin Diagn Pathol 15:102–110
16. Coffin CM, Humphrey PA, Dehner LP (1998) Extrapulmonary inflammatory myofibroblastic tumor: a clinical and pathological survey. Semin Diagn Pathol 15:85–101
17. Coffin CM, Patel A, Perkins S, Elenitoba-Johnson KS, Perlman E, Griffin CA (2001) ALK1 and p80 expression and chromosomal rearrangements involving 2p23 in inflammatory myofibroblastic tumor. Mod Pathol 14:569–576
18. Crocker DJ, Murad TM (1969) Ultrastructure of fibrosarcoma in a male breast. Cancer 23:891–899
19. d'Andiran G, Gabbiani G (1980) A metastasizing sarcoma of the pleura composed of myofibroblasts. Prog Surg Pathol 2:31–40
20. Darby I, Skalli O, Gabbiani G (1990) α-smooth muscle actin is transiently expressed by myofibroblasts during experimental wound healing. Lab Invest 63:21–29
21. Desmouliere A, Gabbiani G (1996) The role of the myofibroblast in wound healing and fibrocontractive diseases. In: Clark

RAF (ed) The molecular and cellular biology of wound repair, 2nd edn. Pentum Press, New York, pp 391–423
22. Desmouliere A, Geinoz A, Gabbiani F, Gabbiani G (1993) Transforming growth factor-beta 1 induces alpha-smooth muscle actin expression in granulation tissue myofibroblasts and in quiescent and growing cultured fibroblasts. J Cell Biol 122:103–111
23. Donner LR, Trompler RA, White RR (1996) Progression of inflammatory myofibroblastic tumor (inflammatory pseudotumor) of soft tissue into sarcoma after several recurrences. Hum Pathol 27:1095–1098
24. Downes KA, Goldblum JR, Montgomery EA, Fisher C (2001) Pleomorphic liposarcoma: a clinicopathologic analysis of 19 cases. Mod Pathol 14:179–184
25. Eyden B (2001) The fibronexus in reactive and tumoral myofibroblasts: further characterisation by electron microscopy. Histol Histopathol 16:57–70
26. Eyden B (2001) The myofibroblast: an assessment of controversial issues and a definition useful in diagnosis and research. Ultrastruct Pathol 25:39–50
27. Eyden BP (1993) Brief review of the fibronexus and its significance for myofibroblastic differentiation and tumor diagnosis. Ultrastruct Pathol 17:611–622
28. Eyden BP, Christensen L (1993) Leiomyosarcoma versus myofibrosarcoma: observations and terminology. Ultrastruct Pathol 17:231–239
29. Eyden BP, Harris M, Banerjee SS, McClure J (1989) The ultrastructure of epithelioid sarcoma. J Submicrosc Cytol Pathol 21:281–293
30. Eyden BP, Banerjee SS, Harris M, Mene A (1991) A study of spindle cell sarcomas showing myofibroblastic differentiation. Ultrastruct Pathol 15:367–378
31. Eyden BP, Christensen L, Tagore V, Harris M (1992) Myofibrosarcoma of subcutaneous soft tissue of the cheek. J Submicrosc Cytol Pathol 24:307–313
32. Eyden BP, Ponting J, Davies H, Bartley C, Torgersen E (1994) Defining the myofibroblast: normal tissues, with special reference to the stromal cells of Wharton's jelly in human umbilical cord. J Submicrosc Cytol Pathol 26:347–355
33. Fisher C (1988) Epithelioid sarcoma: the spectrum of ultrastructural differentiation in seven immunohistochemically defined cases. Hum Pathol 19:265–275
34. Fisher C (1990) The value of electronmicroscopy and immunohistochemistry in the diagnosis of soft tissue sarcomas: a study of 200 cases. Histopathology 16:441–454
35. Fisher C, Goldblum JR, Montgomery E (2003) Calponin and h-caldesmon in sarcomas of myofibroblasts. Mod Pathol 16:11A
36. Fu Y-S, Gabbiani G, Kaye GI, Lattes R (1975) Malignant soft tissue tumours of probable histiocytic origin (malignant fibrous histiocytomas): general considerations and electron microscopic and tissue culture studies. Cancer 35:176–198
37. Fukuda T, Tsuneyoshi M, Enjoji M (1988) Malignant fibrous histiocytoma of soft parts: an ultrastructural quantitative study. Ultrastructural Pathol 12:117–129
38. Gabbiani G (1996) The cellular derivation and the life span of the myofibroblast. Pathol Res Pract 192:708–711
39. Gabbiani G (2003) The myofibroblast in wound healing and fibrocontractive diseases. J Pathol 200:500–503
40. Gabbiani G, Ryan GB, Majno G (1971) Presence of modified fibroblasts in granulation tissue and their possible role in wound contraction. Experientia 27:549–550
41. Ghadially FN (1980) Diagnostic electron microscopy of tumours. Butterworths, London
42. Gocht A, Bosmuller HC, Bassler R, Tavassoli FA, Moinfar F, Katenkamp D, Schirrmacher K, Luders P, Saeger W (1999) Breast tumors with myofibroblastic differentiation: clinicopathological observations in myofibroblastoma and myofibrosarcoma. Pathol Res Pract 195:1–10
43. Gorman PA, Malone M, Pritchard J, Sheer D (1990) Deletion of part of the short arm chromosome 17 in a congenital fibrosarcoma. Cancer Gent Cytogenet 48:193–198
44. Griffin CA, Hawkins AL, Dvorak C, Henkle C, Ellingham T, Perlman EJ (1999) Recurrent involvement of 2p23 in inflammatory myofibroblastic tumors. Cancer Res 59:2776–2780
45. Guillou L, Coindre JM, Bonichon F, Bui NB, Terrier P, Collin F, Vilain MO, Mandard AM, LeDoussal V, Leroux A, Jacquemier J, Duplay H, SastreGarau X, Costa J (1997) Comparative study of the National Cancer Institute and French Federation of Cancer Centers Sarcoma Group grading systems in a population of 410 adult patients with soft tissue sarcoma. J Clin Oncol 15:350–362
46. Hasegawa T, Hasegawa F, Hirose T, Sano T, Matsuno Y (2003) Expression of smooth muscle markers in so-called malignant fibrous hisitocytoma. J Clin Pathol 56:666–671
47. Hinz B, Mastrangelo D, Iselin CE, Chaponnier C, Gabbiani G (2001) Mechanical tension controls granulation tissue contractile activity and myofibroblast differentiation. Am J Pathol 159:1009–1020
48. Hirose T, Kudo E, Hasegawa T, Abe J, Hizawa K (1989) Expression of intermediate filaments in malignant fibrous histiocytomas. Hum Pathol 20:871–877
49. Hussong JW, Brown M, Perkins SL, Dehner LP, Coffin CM (1999) Comparison of DNA ploidy, histologic, and immunohistochemical findings with clinical outcome in inflammatory myofibroblastic tumors. Mod Pathol 12:279–286
50. Knezevich SR, Garnett MJ, Pysher TJ, Beckwith JB, Grundy PE, Sorensen PH (1998) ETV6-NTRK3 gene fusions and trisomy 11 establish a histogenetic link between mesoblastic nephroma and congenital fibrosarcoma. Cancer Res 58:5046–5048
51. Knezevich SR, McFadden DE, Tao W, Lim JF, Sorensen PH (1998) A novel ETV6-NTRK3 gene fusion in congenital fibrosarcoma. Nat Genet 18:184–187
52. Kuhnen C, Homann HH, Mentzel T (2003) Myofibroblastic sarcoma of the thoracic wall. Change in appearance in tumour recurrence. Pathologe 24:128–135
53. Lawrence B, Perez-Atayde A, Hibbard MK, Rubin BP, Dal Cin P, Pinkus JL, Pinkus GS, Xiao S, Yi ES, Fletcher CD, Fletcher JA (2000) TPM3-ALK and TPM4-ALK oncogenes in inflammatory myofibroblastic tumors. Am J Pathol 157:377–384
54. Lawson CW, Fisher C, Gatter K (1987) An immunohistochemical study of differentiation in malignant fibrous histiocytoma. Histopathology 11:375–383
55. Lucin K, Mustac E, Jonjic N (2003) Breast sarcoma showing myofibroblastic differentiation. Virchows Arch 443:222–224
56. Meis JM, Enzinger FM (1991) Inflammatory fibrosarcoma of the mesentery and retroperitoneum. A tumor closely simulating inflammatory pseudotumor. Am J Surg Pathol 15:1146–1156
57. Meis-Kindblom JM, Kjellstrom C, Kindblom LG (1998) Inflammatory fibrosarcoma: update, reappraisal, and perspective on its place in the spectrum of inflammatory myofibroblastic tumors. Semin Diagn Pathol 15:133–143
58. Mentzel T, Dry S, Katenkamp D, Fletcher CD (1998) Low-grade myofibroblastic sarcoma: analysis of 18 cases in the spectrum of myofibroblastic tumors. Am J Surg Pathol 22: 1228–1238
59. Miettinen M, Enzinger FM (1999) Epithelioid variant of pleomorphic liposarcoma: a study of 12 cases of a distinctive variant of high-grade liposarcoma. Mod Pathol 12:722–728
60. Miettinen M, Lasota J (2001) Gastrointestinal stromal tumors—definition, clinical, histological, immunohistochemical, and molecular genetic features and differential diagnosis. Virchows Arch 438:1–12
61. Montgomery E, Fisher C (2001) Myofibroblastic differentiation in malignant fibrous histiocytoma (pleomorphic myofibrosarcoma): a clinicopathological study. Histopathology 38:499–509
62. Montgomery E, Goldblum JR, Fisher C (2001) Myofibrosarcoma: a clinicopathologic study. Am J Surg Pathol 25:219–228
63. Oda Y, Miyajima K, Kawaguchi K, Tamiya S, Oshiro Y, Hachitanda Y, Oya M, Iwamoto Y, Tsuneyoshi M (2001) Pleomorphic leiomyosarcoma: clinicopathologic and immunohistochemical study with special emphasis on its distinction

from ordinary leiomyosarcoma and malignant fibrous histiocytoma. Am J Surg Pathol 25:1030–1038
64. Rubin BP, Chen CJ, Morgan TW, Xiao S, Grier HE, Kozakewich HP, Perez-Atayde AR, Fletcher JA (1998) Congenital mesoblastic nephroma t(12;15) is associated with ETV6-NTRK3 gene fusion: cytogenetic and molecular relationship to congenital (infantile) fibrosarcoma. Am J Pathol 153:1451–1458
65. Schofield DE, Fletcher JA, Grier HE, Yunis EJ (1994) Fibrosarcoma in infants and children. Application of new techniques. Am J Surg Pathol 18:14–24
66. Schürch W, Bégin LR, Seemayer TA, Lagace R, Boivin JC, Lamoureux C, Bluteau P, Piche J, Gabbiani G (1996) Pleomorphic soft tissue myogenic sarcomas of adulthood: a reappraisal in the mid-1990s. Am J Surg Pathol 20:131–147
67. Schürch W, Seemayer TA, Gabbiani G (1997) Myofibroblast. In: Sternberg SS (ed) Histology for pathologists, 2nd edn. Raven Press, New York, pp 129–165
68. Sheng WQ, Hisaoka M, Okamoto S, Tanaka A, Meis-Kindblom JM, Kindblom LG, Ishida T, Nojima T, Hashimoto H (2001) Congenital-infantile fibrosarcoma. A clinicopathologic study of 10 cases and molecular detection of the ETV6-NTRK3 fusion transcripts using paraffin-embedded tissues. Am J Clin Pathol 115:348–355
69. Skalli O, Gabbiani G, Babai F, Seemayer TA, Pizzolato G, Schürch W (1988) Intermediate filament proteins and actin isoforms as markers for soft tissue tumor differentiation and origin. II. Rhabdomyosarcomas. Am J Pathol 130:515–531
70. Smith DM, Mahmoud HH, Jenkins JJ, 3rd, Rao B, Hopkins KP, Parham DM (1995) Myofibrosarcoma of the head and neck in children. Pediatr Pathol Lab Med 15:403–418
71. Soule EH, Pritchard DJ (1977) Fibrosarcoma in infants and children. A review of 110 cases. Cancer 40:1711–1721
72. Strehl S, Ladenstein R, Wrba F, Salzer-Kuntschik M, Gadner H, Ambros PF (1993) Translocation (12;13) in a case of infantile fibrosarcoma. Cancer Genet Cytogenet 71:94–96
73. Su LD, Atayde-Perez A, Sheldon S, Fletcher JA, Weiss SW (1998) Inflammatory myofibroblastic tumor: cytogenetic evidence supporting clonal origin. Mod Pathol 11:364–368
74. Taccagni G, Rovere E, Masullo M, Christensen L, Eyden B (1997) Myofibrosarcoma of the breast: review of the literature on myofibroblastic tumors and criteria for defining myofibroblastic differentiation. Am J Surg Pathol 21:489–496
75. Tomasek JJ, Gabbiani G, Hinz B, Chaponnier C, Brown RA (2002) Myofibroblasts and mechano-regulation of connective tissue remodelling. Nat Rev Mol Cell Biol 3:349–363
76. Watanabe K, Ogura G (2002) Fibronexus in “malignant fibrous histiocytoma” of the bone: a case report of pleomorphic myofibrosarcoma. Ultrastruct Pathol 26:47–51
77. Watanabe K, Ogura G, Tajino T, Hoshi N, Suzuki T (2001) Myofibrosarcoma of the bone: a clinicopathologic study. Am J Surg Pathol 25:1501–1507

Virchows Arch (2004) 445:224–230
DOI 10.1007/s00428-004-1065-6

ORIGINAL ARTICLE

Jacob Engellau · Annette Persson · Pär-Ola Bendahl · Måns Åkerman · Henryk A. Domanski · Bodil Bjerkehagen · Peer Lilleng · Johan Weide · Anders Rydholm · Thor A. Alvegård · Mef Nilbert

Expression profiling using tissue microarray in 211 malignant fibrous histiocytomas confirms the prognostic value of Ki-67

Received: 23 March 2004 / Accepted: 30 May 2004 / Published online: 7 August 2004
© Springer-Verlag 2004

Abstract The tissue microarray technology is a high-throughput technique that allows studies of multiple markers in large tumor materials. We performed immunohistochemical profiling using tissue microarray and immunostaining for Ki-67, p53, bcl-2, CD44, cyclin A and Pgp in a series of 211 malignant fibrous histiocytomas (MFHs) with correlation to prognosis. Tissue from 50 local recurrences and 20 metastases was available for comparison with the primary tumors. In univariate analysis, Ki-67 was the only immunohistochemical marker significantly correlated with metastasis with a hazard ratio of 1.9. Multivariate analysis, with tumor size, depth, necrosis, vascular invasion, mitotic rate and Ki-67 expression, revealed an independent prognostic value of tumor size and Ki-67. Local recurrences did not differ from the corresponding primary tumors, whereas metastases showed a trend for upregulation of cyclin A and Pgp. In this large series of MFHs, a tumor size greater than 8 cm and a Ki-67 index of more than 20% were strong and independent prognostic factors for metastasis. In contrast, p53, bcl-2, CD44, cyclin A and Pgp, which have previously been suggested as prognostic factors in soft tissue sarcomas, did not show such correlations. Hence, we suggest that proliferation, as measured by Ki-67 index, should be considered as a prognostic marker in clinical management of pleomorphic soft tissue sarcomas.

Keywords Malignant fibrous histiocytoma · Tissue microarray · Ki-67 · Prognosis · Soft tissue sarcoma

J. Engellau (✉) · P.-O. Bendahl · T. A. Alvegård · M. Nilbert
Department of Oncology,
Jubileum Institution, Lund University,
221 85 Lund, Sweden
e-mail: Jacob.Engellau@onk.lu.se
Tel.: +46-46-177520
Fax: +46-46-176080

A. Persson · M. Åkerman · H. A. Domanski
Department of Pathology and Cytology,
Lund University Hospital,
221 85 Lund, Sweden

A. Rydholm
Department of Orthopedics,
Lund University Hospital,
221 85 Lund, Sweden

B. Bjerkehagen
Department of Pathology,
Norwegian Radium Hospital,
0310 Oslo, Norway

P. Lilleng
Department of Pathology,
Haukeland University Hospital,
5021 Bergen, Norway

J. Weide
Department of Pathology,
Karolinska University Hospital,
171 76 Stockholm, Sweden

Introduction

Malignant fibrous histiocytoma (MFH), not long ago the largest subgroup of soft tissue sarcomas (STSs), has been the focus of considerable debate regarding its specificity. The heterogeneous microscopic features, as well as prognosis related to the five recognized variants of MFH, has initiated a re-evaluation of MFH, and theories of an origin from undifferentiated mesenchymal stem-cells—from fibroblasts or dual fibroblastic–histiocytic origin—have been investigated and debated. In this search for a generally accepted histogenetic origin, thorough re-evaluation of microscopic features, combined with ancillary diagnostic procedures such as immunohistochemistry (IHC) and electron microscopy, has been able to identify a lineage of differentiation in many of these tumors [8, 9, 27, 34]. Based on current research, the five original variants of MFH (storiform-pleomorphic, myxoid, giant-cell, inflammatory and angiomatoid) have been re-appraised, and the angiomatoid variant has been universally considered as a separate tumor entity. It has also been proposed that the term myxofibrosarcoma should be used defining the myxoid variant of MFH. This change in

nomenclature has, however, not been universally accepted and, at present, the terms myxofibrosarcoma and myxoid MFH are used synonymously [29]. Most investigators consider the giant-cell and inflammatory subgroups as rare variants. The storiform-pleomorphic and myxoid MFHs are at present considered as essentially fibroblastic/myofibroblastic tumors, diagnosed by exclusion, ruling out other pleomorphic and myxoid sarcomas of specific lineage as well as carcinomas, melanomas and lymphomas [10, 22, 23, 29].

Most patients with STS of the extremities and trunk wall are elderly with a median age of about 70 years. One-third of the patients will die from their tumor, mainly because of metastatic disease [11]. Determination of prognostic factors, generally based on initial tumor-related factors, forms the basis for decisions on adjuvant therapy in STS. Many factors, e.g., tumor size, depth, malignancy grade, microscopic tumor necrosis, mitotic rate, DNA ploidy, proliferation and genetic aberrations have been suggested, and some of these are included in various prognostic systems [3, 12, 37]. Altered expression of tumor-associated proteins, such as Ki-67, p53, MDM 2, bcl-2, cyclin A, CD44 and Pgp, have also been suggested to represent prognostic markers in STS, although the findings are partly contradictory [2, 6, 15, 16, 20, 25, 31, 35, 42].

In the present study, we have used pathology-reviewed tumor tissue from MFHs treated at four centers (Lund and Stockholm in Sweden, Oslo and Bergen in Norway) in Scandinavia. We performed IHC expression profiling using tissue microarray (TMA) for the proliferation markers Ki-67 and cyclin A, the tumor suppressor p53, the oncoprotein bcl-2, the adhesion protein CD44 and the multidrug resistance gene product Pgp in 211 MFHs. The prognostic value of these markers was assessed and correlated to metastasis in 201 patients and compared with the previously established prognostic factors tumor size, tumor depth, microscopic tumor necrosis, vascular invasion and mitotic rate. Furthermore, the expression of these markers during tumor progression was assessed through analysis of primary tumors in relation to corresponding subsequent local recurrences and metastases.

Patients and methods

Patients and specimens

The study was approved by the Lund University ethics committee. From 1986 through 1994, 1470 patients with STS of the extremities and the trunk wall from Norway and Sweden were reported to the Scandinavian Sarcoma Group (SSG) register, which is estimated to contain 90% of all STSs diagnosed [1]. Of these, 682 cases had originally been diagnosed as MFHs, and 545 (80%) were histologically reviewed by the SSG Pathology Review Group, which consists of 10 Scandinavian pathologists. The diagnosis or exclusion of MFH was based on established microscopic criteria [41]. After thorough evaluation of all available sections, including the IHC stainings performed at the primary diagnosis, new sections were cut and additional IHC was performed when necessary. The antibody panel included muscle specific actin, smooth muscle actin, desmin, S-100 protein, epithelial membrane antigen (EMA), cytokeratins and the specific markers for melanoma and lymphoma HMB45, CD45, CD30, CD20 and CD3. The tumors diagnosed as MFH were subclassified as storiform-pleomorphic, myxoid (at least 10% of the examined area being myxoid [10]), giant-cell and inflammatory. The outcome for 338 of these patients has previously been presented in a study of the variability of the clinico-pathological prognostic factors over time [7], and 57 of the tumors have been included in a study of the prognostic relevance of Ki-67 in STS [2]. Malignancy grading was based on a IV-tiered grading system, including the following factors: cellularity, pleomorphism, nuclear atypia, tumor necrosis, and mitotic activity [27]. Grades III and IV correspond to grade III in the NCI-grading and FNCLCC-grading systems. Of the 545 reviewed tumors, 170 were excluded; 134 were reclassified (98 as another type of sarcoma, 3 as malignant non-sarcomatous tumors, and 33 as benign lesions), 30 tumors were excluded because of insufficient histological or non-representative material, 2 patients with cutaneous tumors, and 4 patients due to incomplete follow-up. From the remaining 375 patients, paraffin-embedded tumor tissue could be retrieved from 218. Primary tumors were available from 211 patients and 50 local recurrence and 20 metastases were also analyzed. In total, 288 tumors from 218 patients were retrieved and a median of 3 (range 1–7) representative tumor blocks were selected from each tumor by two of the authors (M.Å. and H.A.D.), resulting in a total of 717 tumor blocks.

Of the 218 tumors, 133 were storiform-pleomorphic, 83 were myxoid (at least 10% of the examined area being myxoid), one giant-cell type and one inflammatory. The myxoid tumors were subcutaneous in 35 of 83 (42%), 2 of which were low grade (II), and deep seated in 48 of 83 (58%), 3 of which were low grade (II). For the analyses of metastasis-free survival, 7 patients from whom no primary tumor was available and 10 patients with metastasis at diagnosis were excluded. The prognostic studies were thus based on 201 patients (Table 1). The patients were followed with clinical examination and conventional chest X-ray every 3 months for 2 years and thereafter twice yearly. Median follow-up for the metastasis-free survivors was 9 years (range 4–13 years). Of the 201 patients, 67 (33%) developed a local recurrence after a median follow-up of 1 year (range 45 days to 11 years), and metastasis occurred in 65 (32%) after a median time of 1 year (range 66 days to 7 years). Both a local recurrence and metastasis occurred in 27 of 201 (13%) of the patients.

Table 1 Patient and tumor characteristics in 201 malignant fibrous histiocytomas

Factor	*n* (%)
Sex	
Men	105 (52)
Women	96 (48)
Age	
Median (range) years	71 (19–96)
Site	
Trunk wall	24 (12)
Upper extremity	44 (22)
Lower extremity	133 (66)
Depth	
Subcutaneous	77 (38)
Deep seated	124 (62)
Size	
Median (range) cm	7 (1–30)
Malignancy grade	
I	0
II	6 (3)
III	57 (28)
IV	138 (69)
Local recurrence	67 (33)
Surgically treated	54 (81)
Metastasis	65 (32)
Surgically treated	25 (38)

Table 2 Immunohistochemical markers and evaluation criteria

Marker	Clone	Company	Dilution	Buffer	Control	Non-evaluable sections, *n* (%)	Evaluation of immunohistochemistry
Ki-67	MIB-1	Dako	1:1000	Citrate	Normal colon	121 (5)	High; >20% of nuclei
Cyclin A	6E6	Novocastra	1:100	Citrate	Normal colon	282 (12)	Positive; >5% of nuclei
P53	DO-7	Dako	1:300	Citrate	Normal colon	186 (7)	Positive; >20% of nuclei
Bcl-2	M0887	Dako	1:50	Citrate	Normal colon	132 (5)	Positive; >10% of cells
CD44	F10 44–2	Novocastra	1:500	Citrate	Tonsil	203 (8)	Positive; >25% of cells
Pgp	JSB-1	Novocastra	1:10	Citrate	Normal cerebrum	469 (19)	Positive; >10% of cells

Preparation of the TMA blocks

From each selected tumor block, a fresh section was made and stained with hematoxylin-erythrosin. One to four viable and representative areas were marked by one of the pathologists (M.Å. or H.A.D.). Tissue cylinders with a diameter of 0.6 mm were punched out from these areas in each donor tumor block and brought into a recipient paraffin block using a custom-made precision instrument (Beecher Instruments, Silver Spring, MD, USA) [21, 24]. The tissue biopsies were aligned and marked for identification. In total, 2410 core biopsies were obtained with a median of 9 (range 3–10) biopsies from each tumor.

Immunohistochemistry

Fresh 5-μm sections from the TMA blocks were transferred to glass slides (Dako Chem-Mate Capillary Gap Microscope slides, 57 mm; Dako A/S, Glostrup, Denmark). The sections were de-waxed and rehydrated. To achieve antigen retrieval, the sections were pretreated in 10 mM citrate buffer (pH 6.0) in a microwave at 900 W for 8 min followed by 15 min at 350 W. All primary antibodies used were commercially available mouse antibodies (Table 2). An automated immunostainer, TechMate 500Plus (Dako), was used for the staining procedure, with Dako Chem-Mate Kit peroxidase/3–3′ diaminobenzidine (Dako). After counterstaining with hematoxylin, the slides were dehydrated in ascending concentrations of ethanol to xylene and mounted.

Evaluation of IHC staining

The cut-off values for the evaluation of the IHC stainings as well as data on the loss of sections are listed in Table 2. Representative normal and aberrant staining patterns are shown in Fig. 1. The slides were evaluated independently by two of the investigators (J.E. and M.N.), whereafter 14% of the sections were re-evaluated by a pathologist (M.Å.). The TMA sections were scored according to cut-off levels for each IHC marker. Scoring was done in a high-power field (×40), with an area of 0.16 mm^2 almost entirely covering the area of a cylinder section. The score from the tumor block with the highest staining score was used for statistical analysis. A median of 7% (range 5–19%) for the different antibodies) of the array sections were damaged, but only 4% (range 3–4%) of the sections were not evaluable. In the Pgp staining two primary tumors lost all the sections. Discrepancies in the evaluation of the immunostainings were seen in 2–3% of the TMA sections. After joint evaluation of the discrepant cases, consensus was reached among the three reviewers.

Statistical methods

The correlations among the different IHC staining patterns were assessed using Pearson correlation. The IHC expression of the factors in the primary tumors, the local recurrences and the metastases were tested for trend using the nonparametric Wilcoxon matched pairs signed-rank test. Exact McNemar tests were used for sparse matched 2×2 tables. Univariate and multivariate analysis, with time to metastasis as endpoint, was done using Cox regression. A two-tailed *P* value of less than 0.05 was considered significant. All statistical calculations were performed using Stata 8.0 (StataCorp. 2003, College Station, TX, USA).

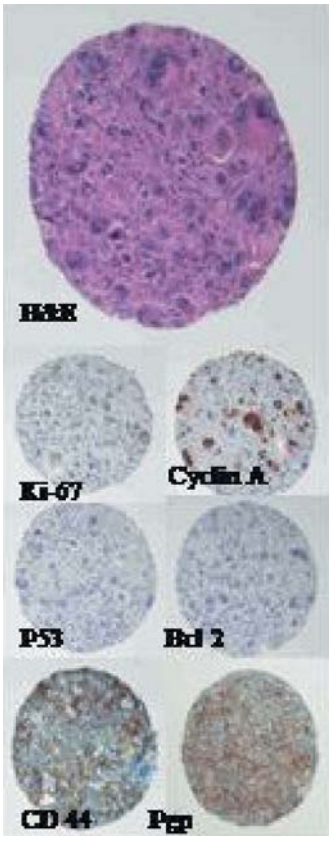


Fig. 1 A primary MFH stained with H&E and with immunohistochemistry for the markers Ki-67, p53, bcl-2, CD44, cyclin A and Pgp

Results

The staining patterns in the 211 primary tumors were a high Ki-67 index in 32%, p53 positivity in 37%, bcl-2 staining greater than 10% in 53%, CD44 expression greater than 25% in 61%, cyclin A greater than 5% in 55% and Pgp greater than 10% in 39% of the tumors. The corresponding figures for the local recurrences (*n*=50) were for Ki-67 42%, p53 28%, bcl-2 48%, CD44 74%,

Table 3 Univariate and multivariate analysis for metastasis-free survival in 201 malignant fibrous histiocytomas. *HR* hazard ratio, *CI* confidence interval

			Metastasis-free survival					
			Univariate analysis			Multivariate analysis		
Factor	*n*	(%)	HR	95% CI	*P* value	HR	95% CI	*P* value
Tumor size >8 cm	85	42	3.8	2.3-6.4	<0.001*	3.0	1.6–5.7	0.001*
Deep location	124	62	2.6	1.4-4.7	0.003*	1.4	0.7–2.8	0.29
Tumor necrosis	113	58	2.5	1.4-4.5	0.001*	1.2	0.6–2.4	0.54
Vascular invasion	21	11	1.8	0.9-3.6	0.11	1.0	0.5–2.0	0.94
High mitotic rate	140	70	2.3	1.2–4.3	0.01*	1.5	0.7–3.1	0.32
Ki-67>20%	60	30	1.9	1.2-3.2	0.009*	1.8	1.1–3.2	0.03*
Cyclin A >5%	108	54	1.3	0.8–2.0	0.37	-	-	-
p53>20%	71	35	1.1	0.7-1.9	0.63	-	-	-
bcl-2>10%	107	53	0.9	0.5–1.4	0.63	-	-	-
CD44>25%	121	60	1.0	0.6–1.6	0.97	-	-	-
Pgp >10%	80	40	0.9	0.5–1.4	0.59	-	-	-

* Statistically significant

cyclin A 64% and for Pgp 54%. The expression levels in the metastases (n=20) were for Ki-67 50%, p53 35%, bcl-2 60%, CD44 65%, cyclin A 70% and Pgp 53%.

In the primary tumors, a significant positive correlation was observed between Ki-67 and cyclin A (r=0.49; P<0.0001); 91% (61 of 67) of Ki-67-expressing tumors showed over-expression of cyclin A. An inverse correlation was found between p53 and cyclin A (r=–0.16; P=0.02); nuclear accumulation of p53 was correlated with a lower expression of cyclin A. The remaining expression patterns did not show significant correlations.

There were no significant differences in metastasis-free survival between myxoid tumors and non-myxoid tumors (data not shown). These subsets were therefore not further analyzed separately. When the IHC expression data from the primary tumors were correlated with metastasis-free survival, only Ki-67 was significantly correlated with outcome (Table 3). In the univariate analysis, a Ki-67 index greater than 20% gave a hazard ratio (HR) of 1.9 for development of metastases. In a multivariate analysis including the factors tumor size (greater than 8 cm), tumor depth (deep versus subcutaneous), microscopic tumor necrosis (+/–), vascular invasion (+/–) and mitotic rate (more than ten mitotic figures per high power field versus less than ten), independent prognostic value was seen for tumor size and high Ki-67 expression (Table 3).

When the staining patterns in the primary tumors were compared with those in the local recurrences and metastases, there was a weak, but non-significant trend, for an increased expression of all markers in the local recurrences compared with the primary tumors (data not shown). In the metastases, no marker showed significantly altered expression relative to the matched primary tumors. However, cyclin A and Pgp were consistently upregulated in metastases. For cyclin A, all five metastases that differed from the primary tumors showed increased expression (P=0.06) and the same trend was seen for Pgp where seven matched metastases showed increased expression (P=0.07).

Discussion

We applied the high-throughput TMA technology to study multiple tumor-associated markers in a large (n=211) series of MFHs. TMA data have been validated in several tumor types, including fibroblastic tumors, synovial sarcomas and MFHs, and have shown good reproducibility when compared with the results obtained using whole-tissue sections [7, 16, 32]. We experienced damage of mean 7% of the array sections and obtained good quality immunostainings. The IHC markers included were chosen since they have all been suggested to represent potential prognostic factors for metastasis in STS.

A high proliferative index as assessed by increased expression of Ki-67 has been the most consistent tumor biological marker reported as a prognostic factor in STS [2, 14, 15, 17, 19]. However, the majority of the previous studies constitutes series with different histopathological entities of STS, and the prognostic importance of Ki-67 has been questioned in cases of MFH and high-grade sarcomas. Jensen et al. [19] showed that Ki-67 had an independent prognostic value in a series of 216 mixed STSs, but could not demonstrate an independent value in the subset of MFH. In contrast, Hoos et al. [16] and Hasegawa et al. [14] have reported that analysis of Ki-67 can identify tumors with aggressive behavior also among tumors with other high-risk characteristics. We found that Ki-67 expression had an independent prognostic value in MFHs, although this tumor type represents a subtype with pronounced pleomorphism and a high fraction of highly malignant tumors (Fig. 2). Indeed Ki-67 did, together with tumor size, best predict development of metastasis with HRs of 1.8 and 3.0, respectively. Since Ki-67 expression has shown a prognostic value in independent studies, this marker can be regarded as well established and should be considered for clinical use in STS [14, 15, 16, 19]. Considering the independent prognostic importance conferred by Ki-67, it was notable that Ki-67 was not significantly upregulated in the local recurrences or the metastases relative to the primary tumors. This observation probably reflects that high Ki-67 expression does not correlate with tumor progression, but rather

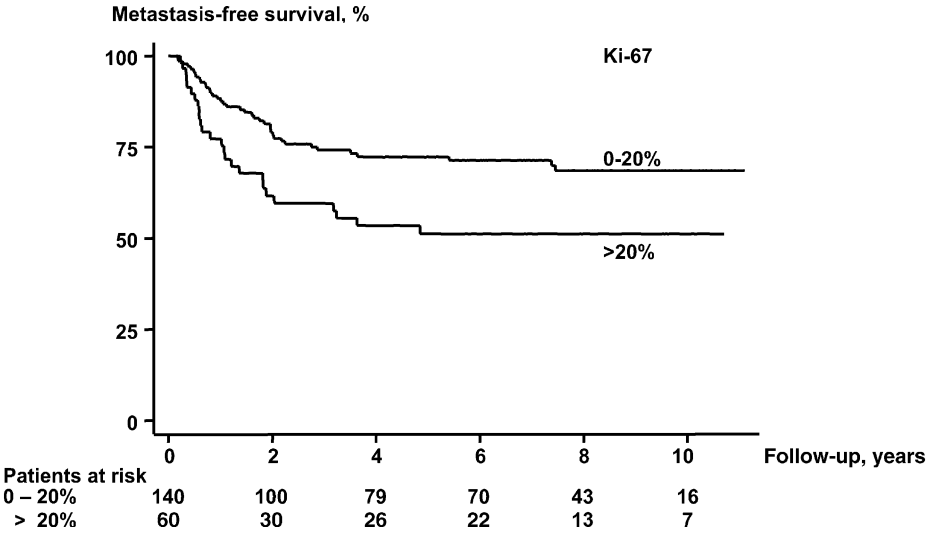


Fig. 2 Metastasis-free survival stratified by Ki-67 expression in 201 MFH

signifies specific tumor biology, i.e., highly proliferating and aggressive tumors.

The cell-cycle protein cyclin A has a dual role since it is required for DNA replication during S-phase and also plays a role for initiation of mitosis. Cyclin A has been suggested to represent a prognostic factor in STS [18, 33]. Huuhtanen et al. [18] linked high cyclin A expression in primary STS to a poor prognosis, but in multivariate analysis cyclin A did not show an independent prognostic value. Noguchi et al. [33] demonstrated a correlation between cyclin A expression and local recurrence and metastasis in leiomyosarcomas. In the present series, cyclin A showed a non-significant trend for upregulation in metastasis, but had no prognostic impact in primary tumors (Table 3).

The tumor suppressor p53 plays an important role in cell growth and differentiation. In STS, p53 function is in most cases abrogated through two alternative mechanisms; through inactivating mutations of the *TP53* gene or interaction between p53 and MDM 2. Both mechanisms may inhibit p53-dependent cell-cycle arrest and apoptosis and thereby promote tumorigenesis. Alterations of p53 have been suggested to be of prognostic value in STS [6, 38, 42], whereas other studies have not shown any such correlation [13, 15, 19, 43]. We found no correlation between p53 staining and local recurrence or metastasis. Increased immunostaining for p53 is unlikely to have a strong and independent prognostic importance in STS, although current data do not exclude a prognostic importance in the subset of tumors characterized by the IHC phenotype p53+/MDM 2+ or in tumors with *TP53* gene mutations [42].

Several genes, both inducers and anti-apoptotic suppressors, are involved in apoptosis. In STS, the prognostic role of impaired regulation of apoptosis is unclear. Increased expression of bcl-2 protein has been found in STS, with the highest expression levels detected in synovial sarcomas [4, 30]. The level of bcl-2 expression in the present series, comparable to those previously reported, was not upregulated in local recurrences or metastases and did not correlate with prognosis.

Alterations of adhesion molecules that take part in the cell–cell boundaries and cell–matrix interactions are a prerequisite for tumor invasion and dissemination. In STS, expression of the cell-surface antigen CD44 has been associated with local recurrence [26] and, in particular, the isoform CD44v6 has also been correlated with metastatic disease [20]. In the present series, we found no differences in the expression of CD44 in primary tumors, local recurrences or metastases; nor could we find any correlation between CD44 and prognosis, but it should be kept in mind that the CD44v isoform was not analyzed, which could possibly explain the lack of prognostic importance.

Metastasis occurred in 32% of the patients in our series, which is in agreement with other reports [3, 40, 44]. Subcutaneous myxoid MFHs of low-malignancy grade are commonly perceived as low-risk tumors for metastasis, but in our material only 6% of the sc tumors were grade II. This explains the overall rate of metastasis, despite the large proportion of myxoid tumors, as there was no difference between myxoid and non-myxoid tumors in metastasis-free survival. The rate of local recurrences was 33%, which is higher than previously reported in a large series of MFHs [36, 39]. This may be explained by almost all tumors being highly malignant and the long follow-up time, with a median of 9 years for the survivors, and the quite large proportion of myxoid tumors (38%), which are known to have a high rate of local recurrence [5, 28].

We assessed the differences in the IHC expression patterns between primary tumors, and local recurrences, and metastases from the same patient with the aim to identify IHC markers of importance for tumor progression. The IHC patterns partly differed between local recurrences and metastases; all markers except p53 showed a weak, albeit non-significant trend for upregulation in the local recurrences when compared with the primary tumors. In the metastases, p53, cyclin A and Pgp showed a consistent but non-significant trend for upregulation, with

higher expression in the metastases compared with the primary tumors. This observation may reflect the biological differences involved in these processes. Our data support a concept of local recurrences as a consequence of residual disease and metastasis rather reflecting manifest invasion and clonal tumor progression, although this needs to be confirmed in extended sample sets.

In conclusion, TMA-based IHC profiling in a series of 211 MFHs with long follow-up confirms that proliferation, as assessed by Ki-67 staining greater than 20%, represents an independent prognostic marker for metastasis. Ki-67 is as of today the strongest candidate marker for application in clinical routine analyses and incorporation into prognostic systems. In contrast, the other tumor biological markers studied—p53, bcl-2, CD44, cyclin A and Pgp –which have previously been suggested to have a prognostic importance in STS, did not show such correlations in this large series of MFHs.

Acknowledgements We would like to acknowledge the work performed by the SSG Pathology review committee, which apart from the authors consist of: Lars-Gunnar Kindblom[1], Tom Böhling[2], Tore B. Halvorsen[3], and Helena Willén[4]. ([1]Sahlgrenska University Hospital, Gothenburg, Sweden, [2]University of Helsinki, Helsinki, Finland, [3]St Olavs Hospital, Trondheim, Norway, [4]Uppsala University Hospital, Uppsala, Sweden). Evy Nilsson at the SSG office is acknowledged for efficient help administrating tissue blocks and with clinical data. The study was financially supported by the Swedish Cancer Society, the Children's Cancer Foundation, the G. Nilsson Cancer Foundation, the B. Kamprad Cancer Foundation and the Lund University Hospital Fund.

References

1. Bauer HC, Trovik CS, Alvegard TA, Berlin O, Erlanson M, Gustafson P, Klepp R, Moller TR, Rydholm A, Saeter G, Wahlstrom O, Wiklund T (2001) Monitoring referral and treatment in soft tissue sarcoma: study based on 1,851 patients from the Scandinavian Sarcoma Group Register. Acta Orthop Scand 72:150–159
2. Choong PF, Akerman M, Willen H, Andersson C, Gustafson P, Baldetorp B, Ferno M, Alvegard T, Rydholm A (1994) Prognostic value of Ki-67 expression in 182 soft tissue sarcomas. Proliferation—a marker of metastasis? APMIS 102:915–924
3. Coindre JM, Terrier P, Bui NB, Bonichon F, Collin F, Le Doussal V, Mandard AM, Vilain MO, Jacquemier J, Duplay H, Sastre X, Barlier C, Henry-Amar M, Mace-Lesech J, Contesso G (1996) Prognostic factors in adult patients with locally controlled soft tissue sarcoma. A study of 546 patients from the French Federation of Cancer Centers Sarcoma Group. J Clin Oncol 14:869–877
4. Dan'ura T, Kawai A, Morimoto Y, Naito N, Yoshida A,Inoue H (2002) Apoptosis and expression of its regulatory proteins in soft tissue sarcomas. Cancer Lett 178:167–174
5. Deyrup AT, Haydon RC, Huo D, Ishikawa A, Peabody TD, He TC,Montag AG (2003) Myoid differentiation and prognosis in adult pleomorphic sarcomas of the extremity: an analysis of 92 cases. Cancer 98:805–813
6. Drobnjak M, Latres E, Pollack D, Karpeh M, Dudas M, Woodruff JM, Brennan MF,Cordon-Cardo C (1994) Prognostic implications of p53 nuclear overexpression and high proliferation index of Ki-67 in adult soft-tissue sarcomas. J Natl Cancer Inst 86:549–554
7. Engellau J, Akerman M, Anderson H, Domanski HA, Rambech E, Alvegard TA, Nilbert M (2001) Tissue microarray technique in soft tissue sarcoma: immunohistochemical Ki-67 expression in malignant fibrous histiocytoma. Appl Immunohistochem Mol Morphol 9:358–363
8. Fletcher CD (1992) Pleomorphic malignant fibrous histiocytoma: fact or fiction? A critical reappraisal based on 159 tumors diagnosed as pleomorphic sarcoma. Am J Surg Pathol 16:213–228
9. Fletcher CD, Gustafson P, Rydholm A, Willen H, Akerman M (2001) Clinicopathologic re-evaluation of 100 malignant fibrous histiocytomas: prognostic relevance of subclassification. J Clin Oncol 19:3045–3050
10. Fletcher CDM, Unni KK, Mertens FE (2002) Pathology and genetics of tumours of soft tissue and bone. World Health Organisation classification of tumours. Fletcher CDM, Unni KK, Mertens F (ed) IARC Press, Lyon
11. Gustafson P (1994) Soft tissue sarcoma. Epidemiology and prognosis in 508 patients. Acta Orthop Scand Suppl 259:1–31
12. Gustafson P, Akerman M, Alvegard TA, Coindre JM, Fletcher CD, Rydholm A, Willen H (2003) Prognostic information in soft tissue sarcoma using tumour size, vascular invasion and microscopic tumour necrosis-the SIN-system. Eur J Cancer 39:1568–1576
13. Hasegawa T, Yokoyama R, Lee YH, Shimoda T, Beppu Y,Hirohashi S (2000) Prognostic relevance of a histological grading system using MIB-1 for adult soft-tissue sarcoma. Oncology 58:66–74
14. Hasegawa T, Yamamoto S, Yokoyama R, Umeda T, Matsuno Y, Hirohashi S (2002) Prognostic significance of grading and staging systems using MIB-1 score in adult patients with soft tissue sarcoma of the extremities and trunk. Cancer 95:843–851
15. Heslin MJ, Cordon-Cardo C, Lewis JJ, Woodruff JM, Brennan MF (1998) Ki-67 detected by MIB-1 predicts distant metastasis and tumor mortality in primary, high grade extremity soft tissue sarcoma. Cancer 83:490–497
16. Hoos A, Stojadinovic A, Mastorides S, Urist MJ, Polsky D, Di Como CJ, Brennan MF, Cordon-Cardo C (2001) High Ki-67 proliferative index predicts disease specific survival in patients with high-risk soft tissue sarcomas. Cancer 92:869–874
17. Hoos A, Urist MJ, Stojadinovic A, Mastorides S, Dudas ME, Leung DH, Kuo D, Brennan MF, Lewis JJ, Cordon-Cardo C (2001) Validation of tissue microarrays for immunohistochemical profiling of cancer specimens using the example of human fibroblastic tumors. Am J Pathol 158:1245–1251
18. Huuhtanen RL, Blomqvist CP, Bohling TO, Wiklund TA, Tukiainen EJ, Virolainen M, Tribukait B,Andersson LC (1999) Expression of cyclin A in soft tissue sarcomas correlates with tumor aggressiveness. Cancer Res 59:2885–2890
19. Jensen V, Sorensen FB, Bentzen SM, Ladekarl M, Nielsen OS, Keller J, Jensen OM (1998) Proliferative activity (MIB-1 index) is an independent prognostic parameter in patients with high-grade soft tissue sarcomas of subtypes other than malignant fibrous histiocytomas: a retrospective immunohistological study including 216 soft tissue sarcomas. Histopathology 32:536–546
20. Kahara N, Ozaki T, Doi T, Nishida K, Kawai A, Shibahara M,Inoue H (2000) CD44 expression in soft tissue sarcomas. Virchows Arch 436:574–578
21. Kallioniemi OP, Wagner U, Kononen J, Sauter G (2001) Tissue microarray technology for high-throughput molecular profiling of cancer. Hum Mol Genet 10:657–662
22. Kempson RL, Evans HL, Hendrickson MR, Sibley RK (2001) Tumors of the soft tissues. Vol. Third series. Armed Forces Institute of Pathology, Washington D.C.
23. Kindblom LG, Widehn S, Meis-Kindblom JM (2003) The role of electron microscopy in the diagnosis of pleomorphic sarcomas of soft tissue. Semin Diagn Pathol 20:72–81
24. Kononen J, Bubendorf L, Kallioniemi A, Barlund M, Schraml P, Leighton S, Torhorst J, Mihatsch MJ, Sauter G, Kallioniemi OP (1998) Tissue microarrays for high-throughput molecular profiling of tumor specimens. Nat Med 4:844–847
25. Levine EA, Holzmayer T, Bacus S, Mechetner E, Mera R, Bolliger C, Roninson IB, Das Gupta TK (1997) Evaluation of

newer prognostic markers for adult soft tissue sarcomas. J Clin Oncol 15:3249–3257
26. Maula S, Huuhtanen RL, Blomqvist CP, Wiklund TA, Laurila P, Ristamaki R (2001) The adhesion molecule CD44v6 is associated with a high risk for local recurrence in adult soft tissue sarcomas. Br J Cancer 84:244–252
27. Meis-Kindblom JM, Bjerkehage B, Bohling T, Domanski H, Halvorsen TB, Larsson O, Lilleng P, Myhre-Jensen O, Stenwig E, Virolainen M, Willen H, Akerman M, Kindblom LG (1999) Morphologic review of 1000 soft tissue sarcomas from the Scandinavian Sarcoma Group (SSG) Register. The peer-review committee experience. Acta Orthop Scand Suppl 285:18–26
28. Mentzel T, Calonje E, Wadden C, Camplejohn RS, Beham A, Smith MA, Fletcher CD (1996) Myxofibrosarcoma. Clinicopathologic analysis of 75 cases with emphasis on the low-grade variant. Am J Surg Pathol 20:391–405
29. Miettinen M (2003) Diagnostic soft tissue pathology, 1st edn. Churchill Livingstone, Philadelphia
30. Miettinen M, Sarlomo-Rikala M,Kovatich AJ (1998) Cell-type- and tumour-type-related patterns of bcl-2 reactivity in mesenchymal cells and soft tissue tumours. Virchows Arch 433:255–260
31. Nakanishi H, Myoui A, Ochi T,Aozasa K (1997) P-glycoprotein expression in soft-tissue sarcomas. J Cancer Res Clin Oncol 123:352–356
32. Nielsen TO, Hsu FD, O'Connell JX, Gilks CB, Sorensen PH, Linn S, West RB, Liu CL, Botstein D, Brown PO, van de Rijn M (2003) Tissue microarray validation of epidermal growth factor receptor and SALL2 in synovial sarcoma with comparison to tumors of similar histology. Am J Pathol 163:1449–1456
33. Noguchi T, Dobashi Y, Minehara H, Itoman M, Kameya T (2000) Involvement of cyclins in cell proliferation and their clinical implications in soft tissue smooth muscle tumors. Am J Pathol 156:2135–2147
34. Oda Y, Tamiya S, Oshiro Y, Hachitanda Y, Kinukawa N, Iwamoto Y, Tsuneyoshi M (2002) Reassessment and clinicopathological prognostic factors of malignant fibrous histiocytoma of soft parts. Pathol Int 52:595–606
35. Pakos EE, Ioannidis JP (2003) The association of P-glycoprotein with response to chemotherapy and clinical outcome in patients with osteosarcoma. A meta-analysis. Cancer 98:581–589
36. Pezzi CM, Rawlings MS Jr, Esgro JJ, Pollock RE, Romsdahl MM (1992) Prognostic factors in 227 patients with malignant fibrous histiocytoma. Cancer 69:2098–2103
37. Pisters PW, Pollock RE (1999) Staging and prognostic factors in soft tissue sarcoma. Semin Radiat Oncol 9:307–314
38. Reid AH, Tsai MM, Venzon DJ, Wright CF, Lack EE, O'Leary TJ (1996) MDM 2 amplification, P53 mutation, and accumulation of the P53 gene product in malignant fibrous histiocytoma. Diagn Mol Pathol 5:65–73
39. Salo JC, Lewis JJ, Woodruff JM, Leung DH, Brennan MF (1999) Malignant fibrous histiocytoma of the extremity. Cancer 85:1765–1772
40. Stojadinovic A, Leung DH, Allen P, Lewis JJ, Jaques DP, Brennan MF (2002) Primary adult soft tissue sarcoma: time-dependent influence of prognostic variables. J Clin Oncol 20:4344–4352
41. Weiss SW, et al. (2001) Enzinger and Weiss's soft tissue tumors, 4th edn. Strauss M. (ed) C.V. Mosby Co, St. Louis
42. Wurl P, Meye A, Lautenschlager C, Schmidt H, Bache M, Kalthoff H, Schonfelder M, Rath FW, Taubert H (1999) Clinical relevance of pRb and p53 co-overexpression in soft tissue sarcomas. Cancer Lett 139:159–165
43. Yang P, Hirose T, Hasegawa T, Seki K, Sano T, Hizawa K (1995) Prognostic implication of the p53 protein and Ki-67 antigen immunohistochemistry in malignant fibrous histiocytoma. Cancer 76:618–625
44. Zagars GK, Ballo MT, Pisters PW, Pollock RE, Patel SR, Benjamin RS, Evans HL (2003) Prognostic factors for patients with localized soft-tissue sarcoma treated with conservation surgery and radiation therapy: an analysis of 225 patients. Cancer 97:2530–2543

Virchows Arch (2004) 445:231–235
DOI 10.1007/s00428-004-1037-x

ORIGINAL ARTICLE

Nobuyuki Ohike · Markus Kosmahl · Günter Klöppel

Mixed acinar–endocrine carcinoma of the pancreas. A clinicopathological study and comparison with acinar-cell carcinoma

Received: 30 March 2004 / Accepted: 24 April 2004 / Published online: 29 July 2004
© Springer-Verlag 2004

Abstract We compared the clinicopathological features of acinar-cell carcinomas (ACCs) with those of mixed acinar–endocrine carcinomas (MAECs). Specimens from 37 patients with ACC and 6 patients with MAEC were examined histologically and immunohistochemically. The mean age of ACC and MAEC patients was similar (61.3 years versus 58.4 years), but the sex ratio differed (ACC, 29 males and 8 females; MAEC, 2 males and 4 females). The size of the tumor was large in both cases (ACC, 13.8 cm in diameter; MAEC, 8.2 cm). Immunohistochemically, more than half of the tumor cells in all tumors, whether ACC or MAEC, stained for trypsin. In 20 of the 37 ACCs (54%), scattered endocrine cells (SECs) were found, which stained positively for synaptophysin (SYN) and/or chromogranin A (CGA). Interestingly, there was also a difference in the sex ratio between ACC patients without SECs (16 males and 1 female) and ACC patients with SECs (13 males and 7 females). In MAECs, the cells staining for SYN were more common than those staining for CGA and made up more than one-third of the neoplastic-cell population. In all but one case (in which the endocrine component was arranged in islet-like cell clusters), the endocrine cells were intimately mixed with trypsin-positive tumor cells. The endocrine cells only rarely expressed one of the known pancreatic or gastrointestinal hormones. Both ACCs and MAECs had a high proliferation rate and lacked p53 overexpression or progesterone and estrogen receptors. This study revealed that ACCS and MAECs share most clinicopathological features and, therefore, may form a single tumor entity, though they differ in the number of endocrine cells. The frequent identification of endocrine cells in these tumors suggests the existence of a pluripotent cell of origin that is capable of differentiating into acinar and endocrine cells.

Keywords Pancreas · Acinar-cell carcinoma · Mixed acinar–endocrine carcinoma · Immunohistology

N. Ohike (✉)
First Department of Pathology,
Showa University School of Medicine,
1-5-8 Hatanodai, Shinagawa-ku, 42-8555 Tokyo, Japan
e-mail: ohike@med.showa-u.ac.jp
Tel.: +81-3-37848119
Fax: +81-3-37848249

M. Kosmahl · G. Klöppel
Department of Pathology,
University of Kiel,
Germany

Introduction

Acinar-cell carcinoma (ACC) constitutes a phenotypically and genotypically different entity from ductal adenocarcinomas and endocrine tumors [1, 2, 4, 11, 14], but it is well known that one-third of the tumors may express neuroendocrine markers [2, 4]. Though the endocrine component is usually limited to scattered cells, occasionally the endocrine cells constitute a significant proportion of the tumor tissue [5, 6, 7]. If they exceed 30% of the tumor, the neoplasm is called mixed acinar–endocrine carcinoma (MAEC). Because of its histological and biological similarity to ACC, MAEC is considered a variant of ACC [15], but it is so rare that we do not yet know whether it may have some features that are distinct from those of the usual ACCs. Another question is whether MAECs show a special hormonal expression profile. We therefore evaluated the clinicopathological features of a series of ACCs and contrasted them with six cases of MAEC.

Materials and methods

The cases were retrieved from the surgical files and the consultation files of the Department of Pathology of the University of Kiel, Germany. Tumor specimens from 43 patients, including 37 with ACC and 6 with MAEC, were examined. Of these patients, 18 had been investigated in a previous study [2]. All tumors but one occurred in the pancreas. This tumor was a MAEC that was localized in the stomach wall and probably originated from heterotopic pancreas tissue. The clinicopathological features that were studied included patient age and sex, tumor size and histological growth pattern (acinar, solid or glandular). Clinical information was ob-

tained from the patients' records, but follow-up information was not available. The tumor tissue was fixed in 10% formalin and routinely processed for paraffin embedding. The sections were stained with hematoxylin and eosin (H&E) and periodic acid-Schiff for microscopic study.

Immunohistochemistry

Depending on the amount of material available, immunostaining was performed with several or all of the following antibodies: anti-trypsin monoclonal antibody (Ventrex Laboratories, Portland, OR, USA; 1:500), anti-chromogranin A (CGA) monoclonal antibody (Ventana Medical Systems, Tucson, AZ, USA; 1:50), anti-synaptophysin (SYN) polyclonal antibody (Ventana; 1:50), anti-insulin monoclonal antibody (BioGenex, San Ramon, CA, USA; 1:40), anti-glucagon polyclonal antibody (BioGenex; 1:60), anti-somatostatin polyclonal antibody (Dako Cytomation, Glostrup, Denmark; 1:200), anti-pancreatic polypeptide (PP) polyclonal antibody (Dako Cytomation; 1:10,000), serotonin (Dako Cytomation; 1:20), anti-gastrin (Paesel, Frankfurt, Germany; 1:3000), anti-progesterone receptor (PgR) monoclonal antibody (Ventana; 1:50), anti-estrogen receptor (ER) monoclonal antibody (Ventana, 1:50), anti-Ki-S5 (which recognizes a formalin-resistant epitope of the Ki-67 proliferation antigen) [10] monoclonal antibody (Department of Hemapathology, University of Kiel, Germany) and anti-p53 monoclonal antibody (Oncogene Research Products, Boston, MA, USA; 1:20). The immunostaining was carried out using the avidin-biotin-peroxidase complex method. The tissue samples were subjected to pressure cooker treatment for 3.5 min prior to SYN, Ki-S5 and p53 immunostaining. The positivity of CGA and SYN immunostaining was interpreted on a three-point scale: negative, scattered (less than 30% of the neoplastic cell population was immunoreactive) and diffuse (greater than 30% of the neoplastic cell population). Tumors with scattered CGA or SYN positivity were designated as ACCs with scattered endocrine cells (SECs), and those with diffuse positivity were designated as MAECs. For PgR, ER and p53, we considered strong nuclear labeling in >30% of neoplastic cells as the cutoff for positivity. The Ki-S5 labeling index (LI) was calculated as percentage of positive cells in at least 1000 tumor cells and was scored as high when the Ki-S5 LI was higher than 5%.

All statistical evaluations were carried out using a χ^2 test (2×2 contingency table). Statistical significance was tested at a probability level of 0.05.

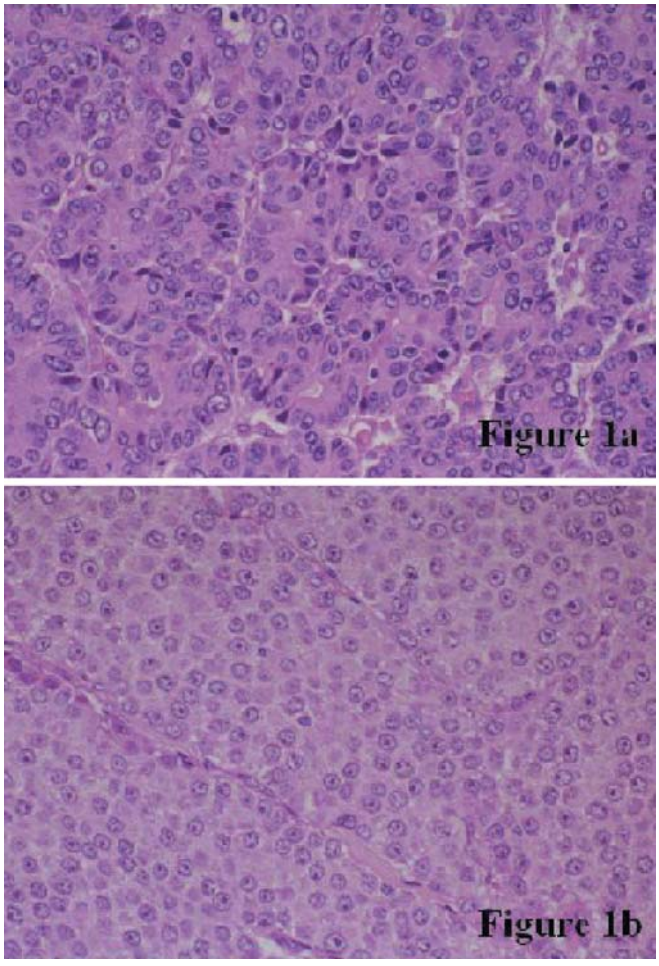


Fig. 1 The main histological patterns found in acinar cell carcinomas and mixed acinar–endocrine carcinomas: acinar pattern (**a**) and solid pattern (**b**). Hematoxylin and eosin, ×250

Results

ACC versus MAEC

Clinicopathological findings

The age of 35 patients with ACC ranged from 35 years to 79 years, with a mean of 61.3 years. There were two exceptions (a 13-year-old girl and a 19-year-old boy). The age of 5 patients with MAEC ranged from 49 years to 65 years (mean 58.4 years). The one exception was a 16-year-old girl. The patients with ACC included 29 males and 8 females, while among the patients with MAEC, females (4 patients) outnumbered males (2 patients). The mean tumor size of both ACCs and MAECs was large (13.8 cm and 8.2 cm in diameter). They showed no preferential localization in the pancreas. Histologically, both tumor types exhibited a nodular pattern at low power, with the nodules often separated by fibrous cords. In ACCs, the tumor cells showed an acinar growth pattern in 5 cases (Fig. 1a), a solid pattern in 10 cases (Fig. 1b) and a mixed pattern in 22 cases (acinar-glandular in 3 cases, acinar-solid in 17, acinar-glandular-solid in 2). MAECs showed a solid pattern in 2 cases and a mixed acinar-solid pattern in 3. There was one case with scattered cell clusters the size of islets composed of cells with pale cytoplasm (Fig. 2a) (Table 1).

Immunohistochemical findings

All tumors, whether ACC or MAEC, showed scattered to diffuse staining for trypsin. The reactivity was more intense than that of the endocrine markers SYN or CGA. Among 37 ACCs, SECs with SYN and occasional CGA positivity were found in 16 (43%) and 11 cases (30%), respectively. Of the 6 MAECs, 3 showed positivity for both SYN and CGA and 3 only for SYN. In the tumors with SYN and CGA positivity, there were more SYN-positive than CGA-positive cells. CGA and SYN positivity was found mainly in tumor cells growing in a solid pattern reminiscent of low-grade endocrine tumors. In 1

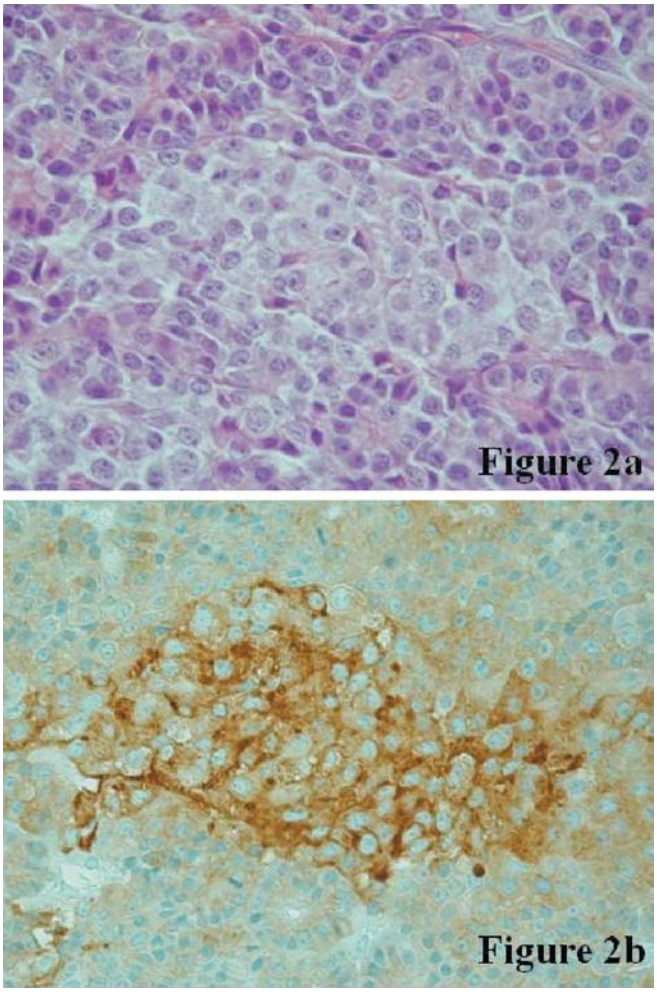


Fig. 2 Histological features of a mixed acinar–endocrine carcinoma showing a cluster of tumor cells with pale cytoplasm resembling an islet (**a**). The cell clusters stain with endocrine markers (synaptophysin) but not acinar markers (**b**). Hematoxylin and eosin, ×300 (**a**) and immunostaining for synaptophysin, ×250 (**b**)

of 6 MAEC, approximately 5% of the tumor cells stained for serotonin, and a few individual cells stained for somatostatin and glucagon. None of the MAECs stained for insulin, PP or gastrin. The endocrine cells were intimately mixed with trypsin-positive tumor cells in all but one tumor. In this tumor, clusters of cells with pale cytoplasm that had been recognized in the H&E sections were found to stain for endocrine markers (Fig. 2b) but not for trypsin. In the other tumors, there was a mixture of endocrine and acinar cells (Fig. 3). PgR and ER positivity was not found in either type of tumor cell. Of 21 ACCs, 14 showed high proliferative activity, as did 2 of 2 MAECs. p53 expression was detected in only 2 of 20 ACCs and in neither of the 2 MAECs investigated. Statistically, there was a significant difference between ACC and MAEC cases in the sex ratio but not in the other factors (Table 1).

ACC without SECs versus ACC with SECs

The mean age of 17 patients with ACC without SECs was 64.3 years, while that of 18 patients (excepting two pediatric patients) with ACC with SECs was 58.0 years. The patients with ACC without SECs included 16 males and 1 female, while there were 13 males and 7 females with ACC with SECs. There was a significant difference in the sex ratio between ACC without SECs and ACC with SECs. None of the pathological and biological factors investigated revealed a significant difference between the two tumors, as shown in Table 1.

Discussion

Our study revealed that the two groups of ACCs, i.e., those with or without SECs and those with a MAEC population share most clinicopathological features and may, therefore, be of similar origin. In addition, we found that MAECs, even when they contain many endocrine cells, only rarely express one of the known pancreatic or gastrointestinal hormones.

Table 1 Clinicopathological findings in 37 acinar-cell carcinomas and 6 mixed acinar–endocrine carcinomas. *NS* not significant

	Acinar cell carcinoma	Mixed acinar-endocrine carcinoma	*P* value	Acinar cell carcinoma		*P* value
				Endocrine component		
				Absent	Present	
No. of patients	37	6		17	20	
Mean age (years)	61.3*	58.4**	NS	64.3	58.0	NS
Sex (male:female)	29:8	2:4	0.03	16:1	13:7	0.04
Tumor size (cm)	13.8 (*n*=18)	8.2 (*n*=2)	NS	15.0 (*n*=6)	13.2 (*n*=12)	NS
Acinar pattern	27/37	4/6	NS	14/17	13/20	NS
Solid pattern	29/37	6/6	NS	14/17	15/20	NS
PgR positivity	0/19	0/2	NS	0/7	0/12	NS
ER positivity	0/19	0/2	NS	0/7	0/12	NS
Ki-S5 >5%	14/21	2/2	NS	4/8	10/13	NS
p53 positivity	2/20	0/2	NS	0/7	2/13	NS

* Excluding a 13-year-old girl and a 19-year-old boy
** Excluding a 16-year-old girl

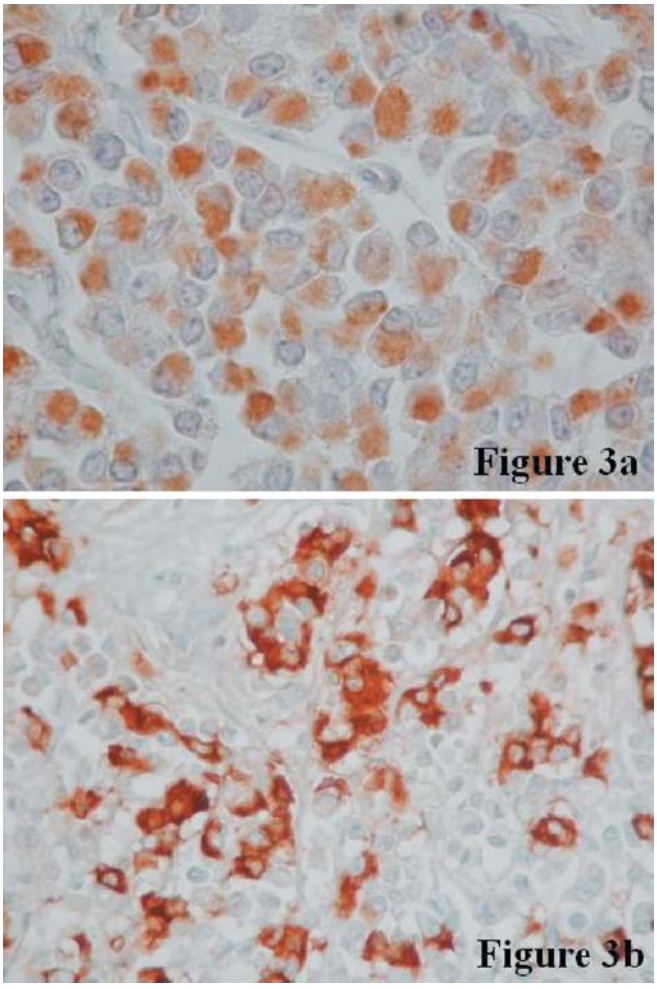


Fig. 3 Trypsin and chromogranin A-positive cells are intimately mixed in mixed acinar–endocrine carcinomas. Immunostaining for trypsin (**a**) and chromogranin A (**b**), ×400

It appears that the only difference between ACCs and MAECs is the number of endocrine cells. Most of the features, such as histological differentiation, tumor size and location and nuclear p53 expression, are similar. The only exception is the gender, since the ACCs in our series showed the well-known male preponderance of this tumor group, whereas MAECs were more common in women than men. Considering the small number of MAECs, this difference could be incidental. However, we noted that there was also a female predominance (three women and two men) among the five MAECs reported by Klimstra et al. [5], and there was again a similar sex distribution in our ACCs with SECs compared with those without SECs. The reason why MAECs occur predominantly in females is unclear. Among pancreatic tumors, the tumors with a strong female predominance include solid-pseudopapillary tumors, mucinous cystic neoplasms and serous microcystic adenomas [8]. It has been hypothesized that they might derive from genital ridge/ovarian anlage-related cells, which become attached to the pancreatic tissue during early embryogenesis [9]. Since MAECs, however, show a typical pancreatic acinar phenotype, they seem to have no relationship with the female genital tract. Moreover, MAECs did not show expression of PgR or ER, which might have an influence on the growth and prognosis of female-predominant tumors [16]. A clinicopathological study of a larger number of MAECs is necessary to clarify the reason for the female predominance.

The presence of SYN- and, to a minor degree, also CGA-expressing cells in MAECs and ACCs with SECs indicates that the cells giving rise to these tumors are pluripotent and may differentiate towards acinar and endocrine cells. The endocrine cells, however, seem to remain at a low differentiation level, since most of these tumors do not stain with antisera against the common gastroenteropancreatic hormones. There was only one MAEC in which a small number of cells expressed serotonin, somatostatin and glucagon. Among Klimstra's five MAECs, there were two tumors that contained a few hormone-positive cells staining for somatostatin, glucagon, PP, gastrin or vasoactive intestinal polypeptide. This scarcity of hormone expression in MAECs demonstrates that either these tumors produce immature hormone products or the hormone production in the tumor cells is generally so low that it escapes immunocytochemical detection. The fact that usually somatostatin, but never insulin, was among the hormones identified thus far in ACCs and MAECs might indicate that the neoplastic endocrine cells are comparable in their genetic equipment to the endocrine cells that occur early in the embryological development of the endocrine pancreas [13]. It is also of interest in this connection that the endocrine cells fail to express the receptor for progesterone, which normal islet cells and cells in pancreatic endocrine tumors constantly show [12]. Finally, MAECs, though equipped with many endocrine cells, differ from the typical well-differentiated neuroendocrine tumors of the pancreas in their much higher proliferation rate. This difference is also reflected in their poorer prognosis, which is identical to that of ACCs with or without SECs.

The endocrine cells that occur in ACCs with SECs and in MAECs might derive from a common progenitor cell with a potential for dual acinar–endocrine differentiation. A second possibility leading to endocrine cells in ACCs is a non-dysjunctional mitosis in which dual differentiation arises initially and concurrently from a single precursor cell [3]. MAECs with segregated areas showing only endocrine marker positivity may follow the latter pathway of differentiation. However, as we had only one MAEC that showed this pattern, it seems that this type is the exception, and a complete mixture is the usual case. The factors driving the pronounced endocrine differentiation that characterizes MAECs are not yet known.

In summary, we found no distinct differences between ACCs and MAECs, except for the sex ratio. This suggests that they may form a single tumor entity, though they differ in the number of endocrine cells, and that they have in common a progenitor cell that is able to give rise to acinar and endocrine cells. In the case of the endocrine

cells, it seems that these cells still have a precursor cell status, since most of them lack definite hormone production, as is usually seen in endocrine tumors of the pancreas.

References

1. Abraham SC, Wu TT, Hruban RH, Lee JH, Yeo CJ, Conlon K, Brennan M, Cameron JL, Klimstra DS (2002) Genetic and immunohistochemical analysis of pancreatic acinar cell carcinoma. Frequent loss on chromosome 11p and alterations in the APC/β-catenin pathway. Am J Pathol 160:953–962
2. Hoorens A, Lemoine NR, McLellan E, Morohoshi T, Kamisawa T, Heitz PU, Stamm B, Rüschoff J, Wiedenmann B, Klöppel G (1993) Pancreatic acinar cell carcinoma. An analysis of cell lineage markers, p53 expression, and Ki-*ras* mutation. Am J Pathol 143:685–698
3. Kim KM, Kim MJ, Cho BK, Choi SW, Rhyu MG (2002) Genetic evidence for the multi-step progression of mixed glandular-neuroendocrine gastric carcinomas. Virchows Arch 440:85–93
4. Klimstra DS, Heffess CS, Oertel JE, Rosai J (1992) Acinar cell carcinoma of the pancreas: a clinicopathologic study of 28 cases. Am J Surg Pathol 16:815–837
5. Klimstra DS, Rosai J, Heffess CS (1994) Mixed acinar-endocrine carcinomas of the pancreas. Am J Surg Pathol 18:765–778
6. Klöppel G (2000) Mixed exocrine-endocrine tumors of the pancreas. Semin Diagn Pathol 17:104–108
7. Klöppel G, Kosmahl M (2001) Cystic lesions and neoplasms of the pancreas. The features are becoming clearer. Pancreatology 1:648–655
8. Klöppel G, Hruban RH, Longnecker DS, Adler G, Kern SE, Partanen TJ (2000) Ductal adenocarcinoma of the pancreas. In: Hamilton SR, Aaltonen LA (eds) Pathology and genetics of tumours of the digestive system. WHO classification of tumours. IARC Press, Lyon, pp 221–230
9. Kosmahl M, Seada LS, Jänig U, Harms D, Klöppel G (2000) Solid-pseudopapillary tumor of the pancreas: its origin revisited. Virchows Arch 436:473–480
10. Kreipe H, Wacker HH, Heidebrecht HJ, Haas K, Hauberg M, Tiemann M, Parwaresch R (1993) Determination of the growth fraction in non-Hodgkin's lymphoma by monoclonal antibody Ki-S5 directed against a formalin-resistant epitope of the Ki-67 antigen. Am J Pathol 142:1689–1694
11. Morohoshi T, Kanda M, Horie A, Chott A, Dreyer T, Klöppel G, Heitz PU (1987) Immunocytochemical markers of uncommon pancreatic tumors. Acinar cell carcinoma, pancreatoblastoma, and solid cystic (papillary-cystic) tumor. Cancer 59:739–747
12. Pelosi G, Bresaola E, Bogina G, Pasini F, Rodella S, Castelli P, Iacono C, Serio G, Zamboni G (1996) Endocrine tumors of the pancreas: Ki-67 immunoreactivity on paraffin sections is an independent predictor for malignancy: a comparative study with proliferating-cell nuclear antigen and progesterone receptor protein immunostaining, mitotic index, and other clinicopathologic variables. Hum Pathol 27:1124–1134
13. Peters J, Jürgensen A, Klöppel G (2000) Ontogeny, differentiation and growth of the endocrine pancreas. Virchows Arch 436:527–538
14. Rigaud G, Moore PS, Zamboni G, Orlandini S, Taruscio D, Paradisi S, Lemoine NR, Klöppel G, Scarpa A (2000) Allelotype of pancreatic acinar cell carcinoma. Int J Cancer 88:772–777
15. Solcia E, Capella C, Klöppel G (1997) Tumors of the pancreas. Atlas of Tumor Pathology, third series, fascicle 20. Armed Forces Institute of Pathology, Washington, DC
16. Talley LI, Grizzle WE, Waterbor JW, Brown D, Weiss H, Frost AR (2002) Hormone receptors and proliferation in breast carcinomas of equivalent histologic grades in pre- and postmenopausal women. Int J Cancer 98:118–127

Virchows Arch (2004) 445:236–247
DOI 10.1007/s00428-004-1053-x

ORIGINAL ARTICLE

Paolo Monti · Federica Marchesi · Michele Reni · Alessia Mercalli · Valeria Sordi · Alessandro Zerbi · Giampaolo Balzano · Valerio Di Carlo · Paola Allavena · Lorenzo Piemonti

A comprehensive in vitro characterization of pancreatic ductal carcinoma cell line biological behavior and its correlation with the structural and genetic profile

Received: 3 March 2004 / Accepted: 15 May 2004 / Published online: 17 July 2004
© Springer-Verlag 2004

Abstract There are a large number of stable pancreatic ductal carcinoma cell lines (PDCL) that are used by researchers worldwide. Detailed data about their differentiation status and genetic alterations are present in the literature, but a systematic correlation with cell biological behavior is often lacking. PDCL (n=12) were clustered by source of tumor cell (ascites, primary tumor, metastasis), and the data of functional cell biology were correlated with the reported structural and genetic profiles. Major histocompatibility complex expression, chemosensitivity and aneuploidia appeared to be related to the source of PDCL, and proliferative capacity appeared to be related to the grade of differentiation. No correlation between genetic/structural features of PDCL and biological behavior was found. All the cell lines appeared generally insensitive to in vitro treatment with 5-fluorouracil and showed variable degrees of susceptibility to gemcitabine, raltitrexed and oxaliplatin. All the PDCL showed resistance to Fas-mediated apoptosis but were significantly sensitive to the pro-apoptotic effect of inflammatory cytokines [interleukin (IL)-1β, tumor necrosis factor (TNF)α and interferon γ]. PDCL were characterized for the secretion of several factors relevant to the tumor-immune cross talk. Vascular endothelial growth factor, CCL2, CCL5 and transforming growth factor β were the factors most frequently released; less frequent was the secretion of CXCL8, CCL22, IL-6 and sporadically CXCL12, IL-10 and hepatocyte growth factor. The cytokines IL-1β and TNFα were always undetectable. In conclusion, a clear correlation between structural/genetic features and function could not be detected, suggesting the weakness of a "morphological" classification for the in vitro studies of pancreatic cancer.

Keywords Pancreatic cancer · Cell lines · Chemo-sensitivity · Immunoescape · Apoptosis

P. Monti · A. Mercalli · V. Sordi · A. Zerbi · G. Balzano · V. Di Carlo · L. Piemonti (✉)
Laboratory of Experimental Surgery,
Department of Diabetes and Transplant Immunology,
S. Raffaele Scientific Institute,
Via Olgettina 60, 20132 Milan, Italy
e-mail: piemonti.lorenzo@hsr.it
Tel.: +39-2-26432706
Fax: +39-2-26432871

F. Marchesi · P. Allavena
Department Immunology and Cell Biology "Mario Negri" Institute,
Via Eritrea 62, 20157 Milan, Italy

M. Reni
Department of Oncology, S. Raffaele Scientific Institute,
Milan, Italy

Introduction

Human pancreatic cancer is a neoplasia primarily of ductal origin, which continues to represent a significant oncological challenge in the 21st century. Pancreatic carcinoma ranks as the eighth most frequent type of solid tumor arising worldwide, yet it represents the fourth most frequent cause of death [1, 2]. This discrepancy reflects the current lack of effective treatment available. Despite advances in surgical as well as non-surgical treatment efforts, it remains a tumor with poor prognosis and a 5-year survival rate of 3–8% [3, 4, 5]. From these data, it appears clear that a better understanding of the fundamental nature of pancreatic cancer is needed to improve the clinical outcome. Molecular pathology and cancer genetic studies have provided an outline of the cellular perturbations that are associated with pancreatic adenocarcinoma; however, the picture remains static, with only correlative links to its underlying biology at present [6]. The pathogenetic processes of pancreatic cancer progression consist of multiple and sequential steps in which, through a selection process, cancer cells develop into more malignant clones, able to evade immune recognition by several mechanisms, such as alteration and downreg-

ulation of both major histocompatibility complex (MHC) class I and co-stimulatory molecules [7], production of immunoregulatory cytokines [8, 9], loss or damage in signal transduction of death receptors and upregulation of anti-apoptotic molecules [10].

As in the case of other carcinomas, studies on the cell biology of ductal adenocarcinoma of the pancreas are largely based on in vitro investigations, employing various cell lines that are commonly available through cell-culture collections. The data produced in these studies are often used to make general statements regarding the biological features of ductal adenocarcinoma and their response to certain stimuli, even if only a few cell lines were examined. The various cell lines reveal a great deal of diversity, so that generalized interpretation of results needs to be viewed cautiously. To understand pancreatic cancer biology better, a few recent studies listing cell lines according to their morphological differentiation and main genetic changes were made [11, 12, 13]. As helpful as these studies were in providing structural and genetic profiles of pancreatic carcinoma cell lines, they did not correlate tumor features with functional cell biology. For example, insensitivity to growth-inhibitory and apoptotic signals as well as self-sufficiency of growth-promoting factors and natural chemoresistance, hallmarks of the pathogenesis of this malignancy [14, 15], were not reported.

In the present study, we systematically studied the functional cell biology of 12 pancreatic carcinoma cell lines (PDCL) in a monolayer culture system with particular interest in their expression of immunorelevant molecules, secretion of immunomodulatory cytokines, susceptibility to apoptosis and chemotherapeutic agents. The cell lines were clustered by source of tumor cell (ascites, primary tumor, metastasis), and the data of functional cell biology were correlated with the reported structural and genetic profiles [11, 12, 13].

Materials and methods

Cell lines

The origin, histological type, grade of differentiation and mutational status of the most frequent genetic changes (p53, K-ras, DPC4/smad4, p16) of PDCL investigated are reported in Table 1 [11, 12, 16, 17, 18, 19, 20, 21, 22, 23, 24, 25, 26, 27, 28, 29, 30, 31, 32, 33, 34, 35, 36, 37, 38]. All the cell lines were cultured as monolayers in RPMI 1640 (Biochrom, Berlin, Germany) supplemented with 10% heat-inactivated fetal calf serum (FCS) (Hyclone, Logan, UT), penicillin and streptomycin (100 μg/ml) under standard culture conditions (5% CO_2, 95% air in humidified chamber at 37°C). Pancreatic cancer cell lines were classified regarding the source: PANC-1, MiaPaCa-2, PaCa44, PT45 from primary cancer; Capan-1, HS766T, CFPAC, T3M4, Su8686 from metastases; ASPC-1, A818–4, HPAF from ascites.

Fluorescence-activated cell-sorter analysis of surface molecules

Cell staining was performed using mouse monoclonal antibodies followed by fluorescein isothiocyanate-conjugated affinity-purified, isotype-specific goat anti-mouse antibodies (Ancell, Bayport, MN, USA). The following monoclonal antibodies (mAbs) were used: L243 (IgG2a, anti-MHC class II) from ATCC (Rockville,

Table 1 Sex, age, source, histology, grade of differentiation, tumorigenicity, histology and grade of transplanted tumor, grading of ultrastructural features, doubling time, genetic aberration of pancreatic ductal adenocarcinoma (PDAC) cell lines. *Nt* not tested, *?* unknown, *p.m.* point mutation, *W.t.* wild type, *f.s.* frameshift, *meth* methylated, *h.d.* homozygous deletion

Cell line	Source	Established by	Sex, age (years)	Histology	Grade	In vitro grade [11]	Ultrastructure grading [11]	Doubling time [11]	Tumorigenic (nude mouse)	Transplanted tumor grade	Provided by	K-ras	p53	p16	DPC4/smad
Panc-1	Primary tumor	M. Lieber (USA) [17]	Male, 56	PDAC	G3	G3	14.5	25	Yes	G3	ATCC	Mut (p.m.) [11, 12]	Mut (p.m.) [11, 12]	Mut (h.d.) [11, 12]	W.t. [11, 12]
MIA Paca2		A. Yunis (USA) [18]	Male, 65	PDAC	G3	G3	13.5	18	Yes	G3 [11]	ATCC	Mut (p.m.) [11, 12]	Mut (p.m.) [11, 12]	Mut (h.d.) [11, 12]	W.t. [11, 12]
Paca44		H. Elsasser, H. Ker (Germany) [19]	?	PDAC	G2	Nt	Nt	Nt	Yes	G2/3	A. Scarpa	Mut (p.m) [11, 12]	Mut (p.m) [11, 12]	Mut (meth) [11, 12]	W.t. [11, 12]
Pt45P1		H. Kalthoff (Germany) [11]	?	PDAC	G3	G3	14.5	24	Yes	G3	A. Scarpa	Mut (p.m.) [11, 12]	Mut (p.m.) [11, 12]	Mut (h.d.) [11, 12]	W.t. [11, 12]
Su.86.86	Liver metastasis	W.D. Holder, Jr. (USA) [20]	Female, 57	PDAC	G2/3	Nt	Nt	Nt	Yes	?	ATCC	?	?	?	?
Capan-1		J. Fogh (USA) [21]	Male, 40	PDAC	G1	G1	7	60	Yes	G1 [22]	ATCC	Mut (p.m.) [23, 24]	Mut (p.m.) [23]	Mut [25]	Mut (p.m.) [26]
CFPAC-1		R.A. Schoumacher (USA) [27, 28]	Male, 26	PDAC	G1	Nt	Nt	Nt	Yes	?	ATCC	Mut (p.m) [11, 12]	Mut (p.m) [11, 12]	Mut (meth) [11, 12]	Mut (h.d) [11, 12]
Hs 766T	Lymph metastasis	R.B. Owens (USA) [29]	Male, 46	PDAC	G2	Nt	Nt	Nt	Yes	?	ATCC	?	Mut [23, 30]	?	Mut [31]
T3M-4		T. Okabe (Japan) [32, 33]	Male, 64	PDAC	G2	G3	9	25	Yes	G2/G3	A. Scarpa	W.t./Mut (p.m.) [11, 12, 24, 34]	Mut (p.m) [11, 12]	Mut (meth) [11, 12]	W.t. [11, 12]
AsPC-1	Ascites	M.H Tan (USA) [35, 36]	Female, 62	PDAC	G2	G2	10	26	Yes	G1/G2/G3 [35, 36]	ATCC	Mut (p.m.) [11, 12]	Mut (f.s.) [12]	Mut (f.s.) [11, 12]	W.t./Mut (p.m.) [11, 12, 26]
HPAF-II		Metzgar (Germany) [37]	Male, 44	PDAC	G1	G2	9	43	Yes	G1	ATCC	Mut (p.m.) [11, 12]	Mut (p.m.) [11, 12]	Mut (del)[11, 12]	W.t. [11, 12]
A8184		H. Kalthoff (Germany) [11]	?	PDAC	G2	G2	10	47	Yes	G2 [11]	A.Scarpa	Mut (p.m.) [11, 12]	Mut [11, 12]	Mut (h.d) [11, 12]	W.t. [11, 12]

MD, USA); W6/32 (IgG2a, anti-MHC class I), CY-90 (IgG2a, anti cytokeratin peptide 18) from Sigma (St. Louis, Missouri, USA); EA-5 (IgG1, anti CD40) from Ancell (Bayport, MN, USA); 4E3 [IgG2a, anti p-glycoprotein multidrug resistance-1 gene product (MDR1)], SM1/1 (IgG2a, anti CD95) from Alexis (Lausen, CH). Results are expressed as mean fluorescence intensity (MFI), calculated according to the formula: MFI=(mean fluorescence sample-mean florescence control)/mean fluorescence control.

Apoptosis, cell-cycle analysis and growth kinetics

PDCL were seeded at 1×10^5 cells/ml in a volume of 1.5 ml in 12-well Costar plates (Corning, Inc.). Cells were treated in duplicate with different stimuli: tumor necrosis factor (TNF)α (10 ng/ml), interleukin (IL)-1β (10 ng/ml), RPMI 1640 without FCS (starvation), 5-fluorouracil (FU) (1–100 μM), gemcitabine (GC) (1–100 nM), raltitrexed (RTX) (1–100 nM), oxaliplatin (OXA) (0.1–10 μM), anti-fas mAb (CH11, IgM, from Kamiya Biomedical Company; Seattle, WA, USA), and J558 cell lines transfected with human CD40L (ratio1/1). To evaluate the effects of monocytes on PDCL, monocytes (10^6/ml) were seeded in the upper chamber of 6-well Transwell plates with permeable membrane pores (0.2 μm) (Costar Corning Incorporated 3412; NY, USA). Tumor cell lines (1×10^5 cells/ml) were seeded in the lower chamber. After different time points (24, 48 and 72 h), cells were trypsinized, washed once with phosphate-buffered saline and fixed with 70% ethanol at –20°C for 24 h. Fixed cells were washed three times and incubated for 1 h with a propidium iodide (PI; Sigma Chemical Co.) solution (20 µg/ml) containing 0.1 mg/ml of RNase A (Sigma Chemical Co.). Cells were then subjected to cell-cycle analysis for determining DNA contents using flow cytometry. Data from 10,000 events were collected in the final gated histograms.

Proliferation was measured in vitro using assays for thymidine incorporation. Cells were plated in 96-well flat bottom tissue culture plates at a density of 0.5×10^5 cells per well. All experimental measurements were performed in triplicate. After 48 h, [^{3}H]thymidine was added at 1 μCi per well for 6 h, and the cells were harvested onto glass fiber filter membranes (Titertek). Radioactive uptake on the filter membranes was measured in a scintillation counter with automatic quench adjustment (Beckman).

Analysis of drug effect and synergism (chemosensitivity)

Dose–response curves were plotted, and 10–20–30% inducing apoptosis concentrations of drugs (AC_{10}; AC_{20}; AC_{30}) were calculated. Moreover, the highest percentage of apoptosis (A_{max}) induced by the drug in the range of tested concentrations was reported. For combination toxicity experiments, FU, GC, RTX and OXA were added, respectively, at 10 μM, 10 nM, 10 nM and 1 μM.

Cytokine measurement using enzyme-linked immunosorbent assay

PDCL were seeded at 1×10^6 cells/ml in a volume of 3 ml in six-well Costar plates (Corning, Inc.). Cytokine production by tumor cells was measured at 24 h and quantified. CCL2 and CXCL8 were detected using a sandwich enzyme-linked immunosorbent assay (ELISA) as described [39]. ELISA for CCL2 did not cross-react with closely related chemokines CCL7 and CCL8. Other cytokines and factors were quantified by ELISA: IL-10, IL-1β, IL-6, vascular endothelial growth factor (VEGF), CCL5, CCL22, hepatocyte growth factor (HGF), TNFα with commercial Kit by Pierce Endogen (Woburn, Ma, USA); transforming growth factor (TGF)β1 and CXCL12 with commercial Kit by R&D (Minneapolis, MN, USA).

In vitro model of DC differentiation and maturation in a pancreatic cancer microenvironment

Peripheral blood monocytes were obtained by density gradients, as described [40]. To evaluate the effects of pancreatic cancer cell lines on dendritic cells (DC), monocytes (10^6/ml) were seeded with granulocyte macrophage colony-stimulating factor (GM-CSF) (50 ng/ml) and IL-4 (10 ng/ml) in the lower chamber of six-well Transwell plates with permeable membrane pores (0.2 μm) (Costar Corning Incorporated 3412; NY, USA). Tumor cell lines (1×10^5 cells) were seeded in the upper chamber. At day 6 of culture, DC were induced to maturation by addition of a transfected CD40L cell line (J558LmCD40L). At day 8, DC were harvested, and MHC II/CD40 expression was analyzed using fluorescence-activated cell sorter (FACS).

Statistical analysis

Student's *t* test or analysis of variance test for unpaired data was used to compare mean values. Mann Whitney U or Krusckal-Wallis H test was used to compare data showing non-Gaussian distribution.

Results

Growth kinetic and chemosensitivity

We investigated, in vitro, the proliferative capacity, the growth kinetic and chemosensitivity of PDCL classified according to the tissue origin (Table 2). Cell lines derived from primary tumors tended to have higher proliferative capacity (median: 5552 cpm) than cell lines derived from ascites (median: 1332 cpm) and metastasis (median: 650 cpm). This difference in proliferative rate reflects the different distribution of grading between the cell lines (Fig. 1). In fact, primary tumor cell lines tended to have a higher grade (75% G_3, 25% G_2, 0% G_1) than metastatic (0% G_3, 40% G_2, 60% G_1) and ascitic cell lines (0% G_3, 66% G_2, 33% G_1) (Pearson Chi-Square: P=0.08).

To characterize the growth kinetics of the cell lines, we also performed a cell-cycle kinetics analysis. PDCL derived from primary tumor showed a higher percentage of cells in G_1 phase than cell lines derived from metastases and ascites. However, cell lines derived from metastases and ascites tended to be more aneuploid (iperploid) than cell lines derived from primary tumor (Table 2).

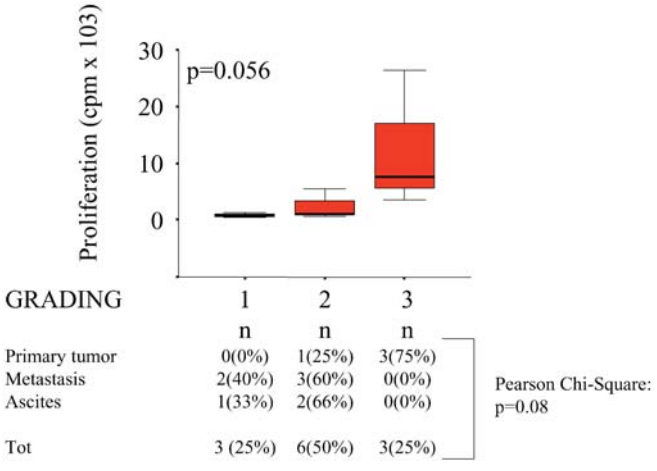


Fig. 1 Proliferative capacity of pancreatic cancer cell lines and its relationship with grading and source. The proliferative capacity of cell lines was assessed by thymidine incorporation

Table 2 Growth kinetics of pancreatic cancer cell lines. Data are expressed as medians of 12 experiments. *Nt* not tested

Cell line	Source	Proliferation (cpm)	SubG1	G1	S	G2	Iper-ploidia	G2/G1
Panc-1	Primary tumor	3545	11.00	52.00	16.00	16.00	4.00	0.31
Mia-Paca2	Primary tumor	26396	6.00	43.00	9.00	25.00	15.00	0.58
Paca44	Primary tumor	1073	12.00	37.00	11.00	26.00	14.00	0.70
PT45P1	Primary tumor	7560	4.00	48.00	11.00	22.00	15.00	0.46
Median		5552	8.5	45	11	23	14	0.51
Su 8686	Liver	Nt	Nt	Nt	Nt	Nt	Nt	Nt
Capan1	Liver	484	8.00	34.00	11.00	17.00	31.00	0.51
CFPAC	Liver	775	20.00	40.00	5.00	19.00	14.00	0.48
Hs766T	Lymph node	525	10.00	33.00	9.00	24.00	25.00	0.72
T3M4	Lymph node	3339	Nt	Nt	Nt	Nt	Nt	Nt
Median		650	10	34	9	19	25	0.51
AsPC1	Ascites	5492	4.00	36.00	15.00	30.00	17.00	0.83
HPAF II	Ascites	1332	10.00	26.00	3.00	14.00	45.00	0.54
A8184	Ascites	1000	3.00	20.00	10.00	31.00	35.00	1.55
Median		1332	4	26	10	30	35	0.83
*P** value		0.08	0.28	0.046	0.46	0.64	0.075	0.21

* Krusckal-Wallis H test

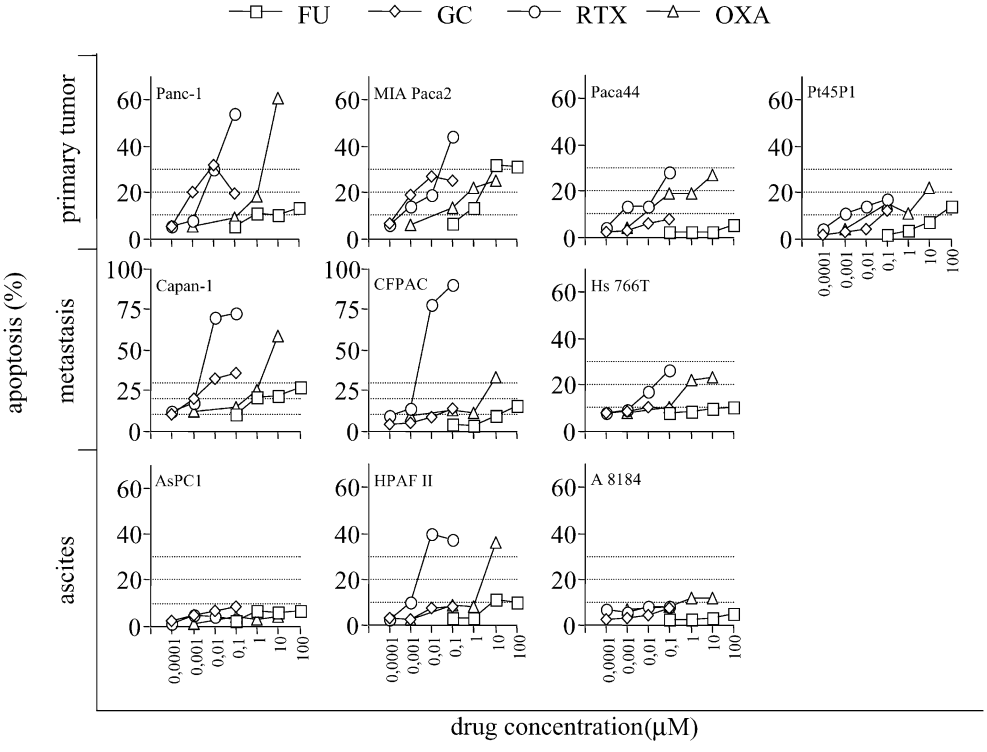


Fig. 2 Pancreatic cancer cell lines chemosensitivity. The cells were exposed to GC (Gemcitabine), FU (5-Fluoruracil), RTX (Raltitrexed) and OXA (Oxaliplatin) for 48 h and then apoptosis was assayed using DNA content analysis. From the dose–response curves, the 10–20–30% inducing apoptosis concentrations of drugs (AC_{10}; AC_{20}; AC_{30}) were calculated. Results represent the median value of three experiments

Inasmuch as most effects of chemotherapeutic agents are mediated via the activation of apoptosis, the effects of GC, FU, RTX and OXA—in correlation with apoptosis—were analyzed (Fig. 2 and Table 3). PDCL were generally resistant to FU. In fact, in only five of ten lines did FU induce more than 10% apoptosis (range of concentration tested: 0–100 μM). The median A_{max} was 11.6% (min–max: 5–31), and the medians of AC_{10}, AC_{20} and AC_{30} were, respectively, 74.7 μM (0.01–100 μM), 100 μM (0.91–100 μM) and 100 μM (9–100 μM).

Also, GC (range of concentration tested: 0–100 nM) did not show a relevant capacity to induce apoptosis on PDCL (six of ten lines showed more than 10% of apoptosis; A_{max} median: 10.32%, min–max 7.8–36; AC_{10}: 53 nM, 0.1–100 nM; AC_{20}: 100 nM, 1–100 nM; AC_{30}: 100 nM, 83–100 nM). The pancreatic cell lines derived from ascites appeared resistant to both FU and GC, while pancreatic cell lines from other sources displayed a wide range of responses.

PDCL were more sensitive to RTX and OXA. Of pancreatic cancer cell lines, eight of ten and nine of ten showed more than 10% of apoptosis after exposure respectively to RTX (range of concentration tested: 0–100 nM) and OXA (range of concentration tested: 0–

Table 3 In vitro chemosensitivity human pancreatic cancer cell line. The cells were exposed to gemcitabine (GC), 5-fluouracil (FU), raltitrexed (RTX) and oxaliplatin (OXA) for 48 h. From the dose–response curves the 10–20–30% inducing apoptosis concentrations of drugs (AC_{10}; AC_{20}; AC_{30}) were calculated. The highest percentage of apoptosis (A_{max}) induced by the drug in the range of tested concentrations was reported. The data represent the median of three experiments. *Nt* not tested

		FU (μM)			GC (nM)				OXA (μM)				RTX (nM)			
Cell line		AC_{10}	AC_{20}	AC_{30}	A_{max}	AC_{10}	AC_{20}	AC_{30}	A_{max}	AC_{10}	AC_{20}	AC_{30}	A_{max}	AC_{10}	AC_{20}	AC_{30}	A_{max}
Panc-1	Primary	0.83	>100	>100	13%	0.4	1	8.4	32%	0.18	1.37	3.5	61%	1.8	5.8	10	54%
MiaPaca2	tumor	0.58	4.25	9	31%	0.35	2	>100	25%	0.06	0.8	>10	25%	0.55	13	49.1	44%
Paca44		>100	>100	>100	5%	>100	>100	>100	8%	0.045	2.1	>10	27%	0.7	52	>100	28%
PT45P1		49.5	>100	>100	13%	76	>100	>100	11%	0.06	8.3	>10	22%	0.9	>100	>100	17%
Median		25	100	100	13%	38	51	100	18%	0.06	1.73	10	26%	0.8	32	74.5	36%
Su 8686	Liver	Nt	Nt	Nt	Nt	Nt	Nt	Nt	Nt	Nt	Nt	Nt	Nt	Nt	Nt	Nt	Nt
Capan1		<0.01	0.91	>100	27%	0.1	1	8.3	36%	0.01	0.54	2.26	59%	0.1	1.5	3.2	73%
CFPAC		23	>100	>100	15%	30	>100	>100	13%	0.03	4.6	8.8	33%	0.26	1.8	3.2	90%
Hs766T	Lymph	100	>100	>100	10%	10	>100	>100	10%	0.1	0.84	>10	23%	2.1	38	>100	22%
T3M4		Nt	Nt	Nt	Nt	Nt	Nt	Nt	Nt	Nt	Nt	Nt	Nt	Nt	Nt	Nt	Nt
Median		23	100	100	15%	10	100	100	13%	0.03	0.84	8.8	33%	0.6	1.8	3.2	73%
AsPC1	Ascites	>100	>100	>100	7%	>100	>100	>100	8.5%	>10	>10	>10	4%	>100	>100	>100	3%
HPAF II		100	>100	>100	10%	>100	>100	>100	8.3%	1.62	4.8	8	36%	1	3.9	7	37%
A8184		>100	>100	>100	5.3%	>100	>100	>100	7.8%	0.56	>10	>10	12%	>100	>100	>100	8%
Median		100	100	100	7%	100	100	100	8.3%	1.62	10	10	12%	100	100	100	8%
*P** value		0.19	0.56	0.47	0.19	0.08	0.78	0.56	0.14	0.042	0.047	0.58	0.44	0.15	0.09	0.40	0.16

* Krusckal-Wallis H test

10 μM). RTX A_{max} median was 32.5%, min–max 3–90 (AC_{10}: 0.95 nM, 0.01–10 nM; AC_{20}: 25.5 nM, 1.5–100 nM; AC_{30}: 74.5 nM, 3.2–100 nM). OXA A_{max} median was 26%, min–max 4–61 (AC_{10}: 0.08 μM, 0.01–10 μM; AC_{20}: 3.3 μM, 0.5–10 μM; AC_{30}: 10 μM, 2.2–10 μM). Also, for RTX and OXA, pancreatic cancer cell lines derived from ascites appeared more resistant than those from other sources.

We also studied the effects of drug combinations (Fig. 3). For combination toxicity experiments, FU, GC, RTX and OXA were added respectively at 10 μM, 10 nM, 10 nM and 1 μM. GC–FU combination showed increased toxicity in eight of nine pancreatic cancer cell lines. RTX–OXA combination generally did not increase toxicity of single drugs, with the exception of ASPC-1 line and, in some lines, induced an antagonistic effect (MIA Paca2, Capan-1, Hs766 t). Similar behavior was seen for the OXA–GC combination.

Susceptibility to apoptosis

Pancreatic cancer is an aggressive malignancy characterized by low responsiveness to pro-apoptotic signal. The sensitivity of PDCL to Fas activation (CH11), CD40, starvation (absence of FCS), monocyte co-culture, IL-1β and TNFα was investigated.

First, we studied in vitro the expression of CD95 and CD40 using FACS analysis. CD95 was expressed at a low level in three of four primary cancer cell lines (MFI 5.6), in three of three ascitic cancer cell lines (MFI 5.1) and in five of five metastatic cancer cell lines (MFI 3.0). Expression of CD40 was found with different intensity in four of four primary cancer cell lines (MFI 11.7), three of three ascitic cancer cell lines (MFI 10) and in four of five metastatic cancer cell lines (MFI 10.6). Both CD95 and CD40 expressions were not different in relation to the source (Table 4). We also investigated the expression of MHC class I and MHC class II. A constitutive expression of MHC class-I molecule was present in all cell lines tested. Bright expression of MHC class I was detected in cell lines derived from primary and ascitic tumor (MFI median, respectively, 283 and 183), while a significantly lower expression was observed in cell lines derived from metastases (MFI 29). A weak expression of MHC class II was found in six of ten PDCL without significant differences of intensity among primary, ascitic and metastatic cancer cell lines (MFI, respectively, 2.6, 4.0 and 1.9).

Cell lines were cultured for 48 h in the presence of different proapoptotic stimuli and then were subjected to cell-cycle analysis for determining DNA contents using flow cytometry. Apoptosis percentage was calculated as $SubG_1$ fraction. Responsiveness was defined as variation of more than 20% compared with control (untreated cell lines) (Table 5).

Four of ten cell lines were low responders to Fas activation, and cell lines from ascites tended to be more responsive than those from other sources. Six of ten cell lines were responsive to CD40 ligand with no differences

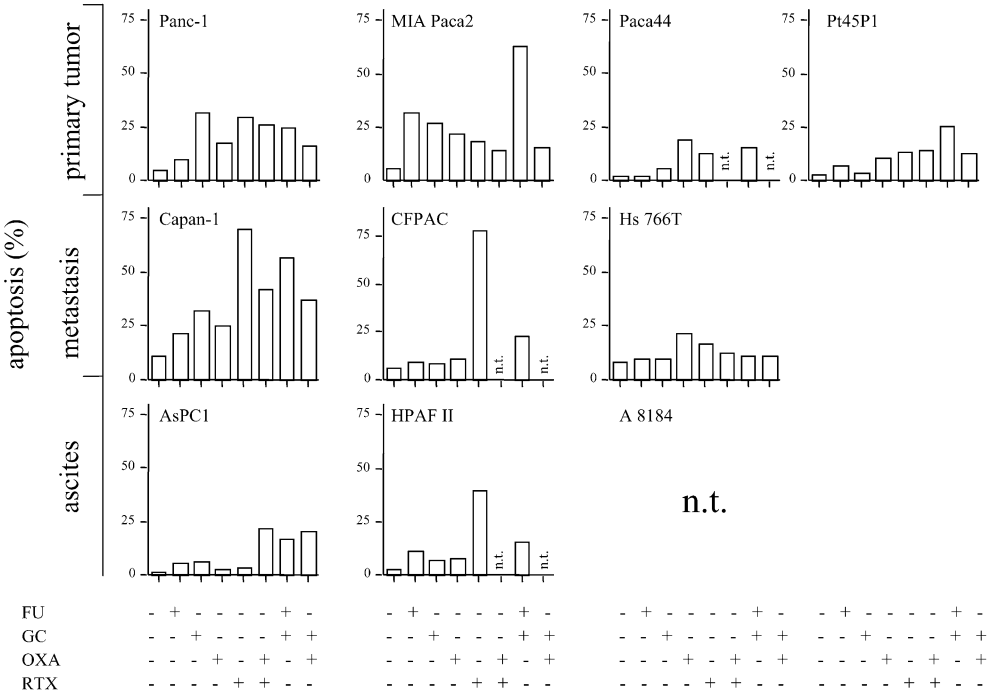


Fig. 3 Chemosensitivity of pancreatic cancer cell lines: effects of drugs combination. For combination toxicity experiments, 5-Fluoruracil, Gemcitabine, Raltitrexed and Oxaliplatin were added respectively at 10 μM, 10 nM, 10 nM, and 1 μM for 48 h, and then apoptosis was assayed using DNA content analysis. Data represent the median value of three experiments

Table 4 Pancreatic cancer cell lines phenotype. Data are expressed as mean fluorescence intensity. Medians of three different experiments were reported for each line. *Nt* not tested

Cell line	Source	MHCI	MHCII	CD95	CD40	MDR1	CK18
Panc-1	Primary tumor	327	64	6.5	16.9	2.4	115
MiaPaca2	Primary tumor	198	0.0	11	6.6	0	158
Paca44	Primary tumor	240	5	2.8	2.5	2.3	58
PT45P1	Primary tumor	327	0.0	0.0	26.1	0	12.3
Median		283	2.6	5.6	11.7	0.13	86.5
Su 8686	Liver	Nt	Nt	2.5	25	Nt	151.6
Capan1	Liver	31	40	6.7	10.6	0	141.0
CFPAC	Liver	11	19	22.5	7.8	0	110.9
Hs766T	Lymph node	67	0.0	2.3	38.9	0	47.9
T3M4	Lymph node	27	Nt	3	0	Nt	106.0
Median		29	19	3	10.6	0	110.8
AsPC1	Ascites	126	0.0	5.1	10	0	62.5
HPAF II	Ascites	347	4.0	10.3	7.1	4.6	80.3
A8184	Ascites	183	54	3	23.8	0	Nt
Median		183	4.0	5.1	10	2.3	71.4
*P** value		0.027	0.83	0.98	0.77	0.42	0.69

* Krusckal-Wallis H test

between the different sources. All the cell lines tested showed a significantly increasing apoptosis after co-culture with monocytes (six of six) and, with the exception of MIA Paca2, after exposure to TNFα, IL-1β or both. Three of five were also low responsive to starvation.

We also analyzed the ratio between the percentage of cells in G_2 and in G_1 phases (G_2/G_1). With the exception of Paca44, no relevant modifications of G_2/G_1 were present after exposure to CD40 ligand and CH11. However, a decreased G_2/G_1 was present in some cancer cell lines after starvation, monocyte co-culture and cytokine exposure with no differences between the different sources (Table 5).

Soluble-factor release

Insensitivity to growth-inhibitory and apoptotic signals as well as self-sufficiency of growth-promoting factors and release of immuno-modulatory and pro-angiogenetic factors are hallmarks of the pathogenesis of pancreatic cancer. Therefore, we characterized all the cell lines for their ability to release pro-angiogenetic factor and growth-promoting factors (VEGF, TGFβ, HGF), chemokines (CCL5, CCL2, CXCL8, CXCL12, CCL2) and cytokines (IL-6, IL-10, TNFα, IL-1β). Cell lines were cultured for 24 h under standardized conditions, and the supernatants were tested for measurement of soluble factors in ELISA. A summary of the data is reported in Table 6. VEGF, CCL2, CCL5 and TGFβ are the more frequent factors released by pancreatic cancer cell lines

Table 5 Apoptosis and G2/G1 ratio of pancreatic cancer cell lines after exposure to various stimuli. Data are expressed as fold increase of untreated cell line and are medians of three different experiments. *Gray cells* variation >20% of control, *Nt* not tested, *TNF* transforming growth factor, *IL* interleukin

Cell line	Source	Apoptosis							G_2/G_1						
		CD40	CH11	Monocytes	IL-1β	TNFα	IL-1β+TNFα	Starvation	CD40	CH11	Monocytes	IL-1β	TNFα	IL-1β+TNFα	Starvation
Panc-1	Primary tumor	0.8	1.2	1.7	3.2	2.8	1.9	1.5	1	1	1.02	1	1.03	1.05	1
MiaPaca2	Primary tumor	1.3	1.1	3.7	1.2	1.2	1.2	2	1	0.98	0.97	1.1	1.11	1.20	0.94
Paca44	Primary tumor	3.3	0.9	Nt	1.2	1.4	1.4	Nt	1.86	1.66	Nt	0.94	1	1.04	Nt
PT45P1	Primary tumor	2.2	1	2.8	Nt	Nt	Nt	Nt	1.06	0.84	0.9	Nt	Nt	Nt	Nt
Mean		1.9	1.0	2.7	1.9	1.8	1.5	1.7	1.21	1.12	0.96	1.01	1.04	1.09	0.97
Su 8686	Liver	Nt	Nt	Nt	Nt	Nt	Nt	Nt							
Capan1	Liver	2.4	1.3	4.2	1.6	1.5	1.8	1.0	1.19	1.13	0.71	0.89	0.94	0.59	1.07
CFPAC	Liver	1.8	0.9	Nt	Nt	Nt	Nt	Nt	0.96	1.02	Nt	Nt	Nt	Nt	Nt
Hs766T	Lymph node	1.2	0.8	4.3	1.6	1.5	1.6	1.1	1.14	0.91	0.89	1.02	1.09	0.91	0.67
T3M4	Lymph node	Nt	Nt	Nt	Nt	Nt	Nt	Nt	Nt	Nt	Nt	Nt	Nt	Nt	Nt
Median		1.8	1	4.2	1.6	1.5	1.7	1.0	1.09	1.02	0.79	0.95	1.01	0.74	0.86
AsPC1	Ascites	2.8	1.8	3.3	3.4	3.9	3.9	2.3	1.04	0.83	0.79	0.96	0.98	0.86	0.69
HPAF II	Ascites	1.2	2	Nt	Nt	Nt	Nt	Nt	0.94	1.20	Nt	Nt	Nt	Nt	Nt
A8184	Ascites	1.2	1.7	Nt	Nt	Nt	Nt	Nt	0.91	1.20	Nt	Nt	Nt	Nt	Nt
Median		1.73	1.8	3.3	3.4	3.9	3.9	2.3	0.96	1.08	0.79	0.96	0.98	0.86	0.69
*P value		0.99	0.15						0.71	0.43					

* Krusckal-Wallis H test

Table 6 Secretion of pro-angiogenetic factor [vascular endothelial growth factor (VEGF)], growth promoting factor [transforming growth factor β (TGFβ), hepatoctye growth factor (HGF)], chemokines (CCL5, CCL2, CXCL8, CXCL12, CCL2) and cytokines [interleukin (IL)-6, IL-10, tumor necrosis factor α (TNFα), IL-1β] by pancreatic cancer cell lines. Data are expressed as pg/ml/24 h/10^6 cell and are the median of three different experiments. *Nt* not tested, *DC* dendritic cells

Cell line	Source	CCL2	CCL5	CCL22	CXCL8	CXCL12	VEGF	HGF	TGFβ	IL-1β	IL-6	IL-10	TNFα	DC MHCII	DC CD40
Panc-1	Primary tumor	2290	107	0	0	0	140	0	40	0	0	0	0	−19	−45
MiaPaca2	Primary tumor	0	847	20	20	0	60	0	40	0	0	0	0	−45	−56
Paca44	Primary tumor	0	91	70	0	0	110	310	180	0	0	0	0	−54	−45
PT45P1	Primary tumor	2290	27	0	480	0	1070	0	90	0	530	0	0	−11	−46
Median		2290	99	10	20	0	125	0	65	0	0	0	0	−32	−45
Su 8686	Liver	270	Nt	0	240	Nt	0	0	0	0	0	0	0	Nt	Nt
Capan1	Liver	970	107	60	10	0	190	0	30	0	40	0	0	29	11
CFPAC	Liver	0	14	20	40	0	90	0	260	0	600	40	0	−34	−50
Hs766T	Lymph node	580	Nt	20	0	1326	0	0	0	0	0	80	0	29	16
T3M4	Lymph node	0	Nt	1200	130	0	90	0	0	Nt	90	0	0	−75	−81
Median		485	60	40	25	0	140	0	145	0	320	20	0	−9	−22
AsPC1	Ascites	0	Nt	20	0	59	70	0	0	0	0	0	0	−52	−62
HPAF II	Ascites	0	0	20	0	0	40	0	40	0	0	0	0	−88	−91
A8184	Ascites	Nt	42	Nt	Nt	0	Nt	Nt	Nt	Nt	Nt	Nt	Nt	Nt	Nt
Median		0	21	20	0	0	55	0	20	0	0	0	0	−70	−76
P		0.4	0.33	0.69	0.28	0.32	0.28	0.42	0.21	1	0.37	0.27	1	0.26	0.18

* Krusckal-Wallis H test

(respectively, 9/11, 8/11, 7/8, 7/11). Less frequent was the secretion of CXCL8, CCL2, IL-6 (6/11, 5/11, 4/11), and the secretion of CXCL12, IL-10 and HGF (2/11, 2/11, 1/11) appeared sporadic. IL-1β and TNFα were always undetectable. No correlation with source of cell lines was present for the release of soluble factors even if a trend in a low-production phenotype by ascites-derived pancreatic cancer cell lines was detected.

Some of these tumor-derived factors, including VEGF, TGF β, IL-10 and IL-6, were described to be able to alter differentiation or maturation of DC. To evaluate the effects of a tumor environment on DC, monocytes were differentiated to DC with GM-CSF and IL-4 in the presence or absence of 11 different pancreatic cancer cell lines in a Transwell system. At day 6 of culture, DC were induced to maturation by addition of a transfected CD40L cell line (J558LmCD40L), and, after 48 h, MHC II and CD40 expression as markers of DC maturation were analyzed using FACS. Of 11 cell lines, 9 inhibited DC maturation, and correlation with the source of cell lines was not present.

Relationship between morphological differentiation, main genetic changes and functional cell biology

Table 7 shows grading, ultrastructural grade, the mutational status of the cell lines for K-ras, p53, p16, DPCA4/smad and the biological behavior in vitro. The biological characteristics were profiled separately: growth kinetics (black cells 3°terzile, gray cells 2°terzile, light gray cells 1°terzile), soluble factors release (white cell not producers, light gray <50 pg/ml 24 h low producers, black cells >50 pg/ml 24 h high producers), phenotype (white cell undetectable; light gray cells low expression, 1°terzile; gray cells medium expression, 2°terzile; black cells high expression, 3°terzile), apoptosis susceptibility (white cell <20% apoptosis increase, unresponsive; light gray cells 20–100% apoptosis increase, low susceptibility; gray cells 100–200% apoptosis increase, medium susceptibility; black cells >200% apoptosis increase, high susceptibility), chemosensitivity (white cells A_{max} <10%, insensitive; light gray cells A_{max} 10–20%, low sensitivity; gray cells A_{max} 20–30%, medium sensitivity; black cells A_{max} >30%, high sensitivity).

There were no correlations between grading or main genetic changes and functional cell biology with the exception of proliferation (the higher the grading the higher the proliferation is).

Discussion

In this study, we analyzed the biological behavior of 12 established PDCL, and we tried to correlate it with grade of differentiation, source and genetic changes. In partic-

Table 7 Relationship between morphological differentiation, main genetic changes and functional cell biology (see text). *Nt* not tested, *GC* gemcitabine, *FU* 5-fluouracil, *RTX* raltitrexed, *OXA* oxaliplatin

Genetic and morphologic differentiation							Growth kinetics				Soluble factor release														Phenotype						Apotpsosis susceptibility							Chemo sensitivity			
Cell Line	Grade	Ultrastructure	K-ras	p53	p16	DPC4/smad	proliferation	SubG1	G2/g1	iperploide	VEGF	CCL5	TGFβ	CXCL12	CCL22	CCL2	CXCL8	IL-6	HGF	IL-10	TNFα	IL-1β	DC (MHCII)	DC (DC40)	CK18	MHCI	CD95	CD40	MHCII	MDR1	mono	CD40	starvation	IL-1β	TNF α	IL-1β + TNFα	CH11	5FU	GC	OXA	RTX
Panc-1	3	14	+	+	+	-																																			
PT45P1	3	14	+	+	+	-																											Nt	Nt	Nt	Nt	Nt					
Mia Paca2	3	13	+	+	+	-																																			
AsPC1	2	10	+	+	+	-						Nt																														
A8184	2	10	+	+	+	-					Nt		Nt		Nt	Nt	Nt	Nt	Nt	Nt	Nt	Nt	Nt	Nt	Nt							Nt	Nt	Nt	Nt	Nt	Nt				
T3M4	2	9	+	+	+	+		Nt	Nt	Nt		Nt										Nt							Nt	Nt	Nt	Nt	Nt	Nt	Nt	Nt	Nt	Nt	Nt	Nt	Nt	Nt
Su 8686	2/3	Nt	?	?	?	?	Nt	Nt	Nt	Nt		Nt		Nt									Nt	Nt					Nt	Nt	Nt	Nt	Nt	Nt	Nt	Nt	Nt	Nt	Nt	Nt	Nt
Hs766T	2	Nt	?	+	?	+						Nt																													
Paca44	2	Nt	+	+	+	-																									Nt										
HPAF II	1	9	+	+	+	+																									Nt	Nt	Nt	Nt	Nt	Nt					
Capan1	1	7	+	+	+	+																																			
CFPAC-1	1	Nt	+	+	+	+																									Nt		Nt	Nt	Nt	Nt					
p*							**0.05**	0.44	0.16	0.21	0.33	0.41	0.17	0.22	0.15	0.35	0.81	0.44	0.55	0.64	1	1	0.6	0.97	0.65	0.14	0.07	0.81	0.69	0.93	0.50	0.27	0.49	0.88	0.78	0.29	0.84	0.06	0.09	0.11	0.06

Nt= not tested ; * = Krusckal-Wallis H test

ular, we analyzed the hallmarks of the pathogenesis of this malignancy [14, 15], such as insensitivity to growth-inhibitory and apoptotic signals as well as self-sufficiency of growth-promoting factors, natural chemoresistance and ability to modulate immune response. The data obtained in our study seem to indicate that few features of PDCL biology may be related to the source of origin. PDCL obtained from primary tumor showed a high proliferative capacity, a low percentage of aneuploidia, a low grade of differentiation, a low sensitivity to FU and GC and a high sensitivity to OXA and RTX. PDCL obtained from metastasis showed a loss of MHCI expression, a very low proliferative capacity with a higher percentage of aneuploidia, a low sensitivity to FU and GC and a very high sensitivity to OXA and RTX. PDCL obtained from ascites showed a relative low proliferative capacity, a high percentage of aneuploidia, insensitivity to all the drugs tested and also tended to be low producers of soluble factors. All the other behaviors analyzed did not segregate with the sources. With the exception of the proliferative activity, the biological behaviors did not correlate with the main genetic changes and grades of differentiation. Even if a clear correlation between structural/genetic features and function could not be detected (suggesting the weakness of a "morphological" classification for the in vitro studies of pancreatic cancer), this study had increased our understanding of the fundamental nature of this tumor.

First, we systematically evaluated the chemosensitivity of PDCL. Three relevant aspects emerged: (I) the MDR1 product was practically absent in all the cell lines extending previous data on a limited number of lines [41]; (II) lines derived from ascites seem to be more resistant than primary and metastatic cell lines, and, since ascites are usually present in the late phases of the disease, this could reflect the selection of more malignant clones; and (III) PDCL appeared generally resistant to FU and, in part, GC and more sensitive toward RTX and OXA. Independently of the mechanisms of drug resistance phenotype, the higher susceptibility to RTX and OXA even in GC- and FU-resistant cells encourages the use of these two drugs in clinical experimental protocols as second-line treatment.

Second, a general consideration arising from this study is that pancreatic tumor cells express a variety of mechanisms described as relevant for the immune escape. Low MHC class-I expression as well as ectopic MHC class-II expression were present, confirming previous investigations [42, 43], and the evidence of lower levels of MHCI in cell lines derived from metastases suggests that this mechanism is relevant for the spreading of this tumor. All the PDCL showed a resistance to Fas-mediated apoptosis (extending previous analyses on a limited number of lines) [44, 45, 46], and all but two inhibited dendritic cell maturation. Collectively, these findings highlight the ability of pancreatic cancer to escape from specific immune response both by inhibiting the afferent arm presentation and by escaping the efferent arm recognition.

Third, PDCL showed a high susceptibility to inflammation-induced apoptosis. In fact, inflammatory cytokines and monocyte co-culture appeared to be powerful pro-apoptotic stimuli for this tumor. Independently of the mechanisms (direct induction of apoptosis and inhibition of cell growth [47, 48] or indirect action via nitric oxide induction [49, 50]), the susceptibility to inflammation appeared to be a feature of this tumor, and we recently confirmed the in vivo relevant role of inflammatory response in terms of prognosis for pancreatic cancer [51].

Fourth, we studied systematically the expression of CD40 and its ability to induce apoptosis in PDCL. CD40 is well expressed by a variety of human carcinomas, including bladder, breast and ovarian cancers as well as in melanoma cells [52, 53]. In contrast to leucocytes, where the role of the CD40–CD40L pair has been systematically investigated, its function in the biology of solid tumors remains surprisingly obscure, even despite the fact that CD40 was initially described on carcinomas [54]. It has been suggested that ligation of cell surface CD40 on certain tumor cells may convey a pro-apoptotic or inhibitory signal, while, on other tumor cell populations, CD40 ligation results in increased cell survival and activation [53]. CD40 was commonly expressed by PDCL with a wide range of intensity, and treatment with CD40L significantly inhibited proliferation and induced apoptosis. This finding extends to pancreatic cancer the observation that CD40 ligation may deliver signals that induce apoptosis and growth arrest in cancer and highlights the possible therapeutic potential of anti-CD40 antibody and/or soluble CD40L for this tumor.

Lastly, we have shown that PDCL have a characteristic ability to secrete soluble factors. VEGF, CCL2, CCL5 and TGFβ are the most frequent factors released. Less frequent was the secretion of CXCL8, CCL22 and IL-6, and the secretion of CXCL12, IL-10 and HGF sporadically appeared. IL-1β and TNFα were always undetectable. Many of these factors belong to the small molecule chemoattractive cytokine family denominated chemokines. Chemokines may influence the extent and phenotype of the leukocyte infiltrate in the cancer but also may have multiple effects on tumor growth, angiogenesis and metastasis. CCL22 and CCL5 release by pancreatic cancer was never been described before. The well-described activity of CCL2 in allergic inflammation [55] allows one to speculate a role in inducing a preferential Th_2 response against this tumor [56], and CCL5, increasing matrix metalloproteinase expression [57], could facilitate metastasis formation and disease progression. Both CCL2 and CXCL8 expression were previously described in pancreatic cancer [58, 59, 60, 61, 62]. CXCL8 expression correlates with its tumorigenic and metastatic potential, and multiple mechanisms are apparently involved in CXCL8 activity, including direct effects on tumor-cell proliferation and angiogenesis. However, the biological significance of CCL2 expression in pancreatic cancer microenvironment appears particularly complex and has not yet been definitively clarified [58]. Finally, CXCL12 has been demonstrated to play an important role in organ vascularization, and Koshyba [63] suggested that the CXCL12/CXCR4 receptor ligand system may have a

role in pancreatic cancer progression through tumor cell migration and angiogenesis.

As far as cytokines and growth factors are concerned, VEGF, TGFβ and IL-6 have been well described as relevant in pancreatic cancer progression, inducing angiogenesis, metastasization and stroma reaction [64, 65], and their frequency in PDCL confirms their potential relevant role in tumor progression and malignity. Both IL-10 and HGF could contribute to pancreatic cancer growth through inducing, respectively, a systemic Th2/Tregulatory immune phenotype [56, 66, 67] and stimulating proliferation, migration and morphogenesis of epithelial cells by specific binding to receptor c-met. The low frequency of IL-10 and HGF production by PDCL suggests that other sources in the tumor microenvironment, such as fibroblasts for HGF and leucocytes for IL-10, could be responsible for a higher level of these factors in the sera of pancreatic cancer patients. Finally, an autocrine mechanism involving IL-1β by which pancreatic carcinoma cells develop chemoresistance was recently described [68]. Since in our systematic study, IL-1β was undetectable in all cell lines tested, we probably have to consider this mechanism not a feature of pancreatic cancer.

In conclusion, our study shows that some features of pancreatic cancer cell line biology may be related to the source of origin (MHCI expression, chemosensitivity, aneuploidia) and grade of differentiation (proliferation). Other relevant in vitro biological characteristics did not show a clear correlation with structural/genetic features and sources. Moreover, the various cell lines revealed a great deal of diversity, so that generalized interpretation of results of in vitro studies need to be viewed cautiously. Since there are not valid animal models and it is difficult to obtain primary culture from the resected pancreatic cancer, the data obtained may be used to create a biological catalogue of pancreatic cancer cell lines, listing their specific characteristics, and may be helpful in interpreting the relevance of many biological observations.

Acknowledgements This work was supported by grants from the Ministry of Universities and Research (MURST) (Cofin. 2002) and Italian Association for Cancer Research (AIRC).

References

1. Parker SL, Tong T, Bolden S, Wingo PA (1997) Cancer statistics. CA Cancer J Clin 47:5–27
2. Wanebo HJ, Vezeridis MP (1996) Pancreatic carcinoma in perspective. A continuing challenge. Cancer 78[Suppl]:580–591
3. Hawes RH, Xiong Q, Waxman I, Chang KJ, Evans DB, Abbruzzese JL (2000) A multispecialty approach to the diagnosis and management of pancreatic cancer. Am J Gastroenterol 95:17–31
4. Wolff RA, Chiao P, Lenzi R, Pisters PW, Lee JE, Janjan NA et al (2000) Current approaches and future strategies for pancreatic carcinoma. Invest New Drugs 18:43–56
5. Abbruzzese JL (2002) New applications of gemcitabine and future directions in the management of pancreatic cancer. Cancer 95[Suppl]:941–945
6. Bardeesy N, DePinho RA (2002) Pancreatic cancer biology and genetics. Nat Rev Cancer 2:897–909
7. Ruiz-Cabello F, Garrido F (1998) HLA and cancer: from research to clinical impact. Immunol Today 19:539–542
8. Pardoll D (2003) Does the immune system see tumors as foreign or self? Annu Rev Immunol 21:807–839
9. Dunn GP, Bruce AT, Ikeda H, Old LJ, Schreiber RD (2002) Cancer immunoediting: from immunosurveillance to tumor escape. Nat Immunol 3:991–998
10. Chouaib S, Thiery J, Gati A, Guerra N, El Behi M, Dorothee G et al (2002) Tumor escape from killing: role of killer inhibitory receptors and acquisition of tumor resistance to cell death. Tissue Antigens 60:273–281
11. Sipos B, Moser S, Kalthoff H, Torok V, Lohr M, Kloppel G (2003) A comprehensive characterization of pancreatic ductal carcinoma cell lines: towards the establishment of an in vitro research platform. Virchows Arch 442:444–452
12. Moore PS, Sipos B, Orlandini S, Sorio C, Real FX, Lemoine NR et al (2001) Genetic profile of 22 pancreatic carcinoma cell lines. Analysis of K-ras, p53, p16 and DPC4/Smad4. Virchows Arch 439:798–802
13. Vila MR, Lloreta J, Schussler MH, Berrozpe G, Welt S, Real FX (1995) New pancreas cancers cell lines that represent distinct stages of ductal differentiation. Lab Invest 72:395–404
14. Ozawa F, Friess H, Tempia-Caliera A, Kleeff J, Buchler MW (2001) Growth factors and their receptors in pancreatic cancer. Teratog Carcinog Mutagen 21:27–44
15. Shi X, Friess H, Kleeff J, Ozawa F, Buchler MW (2001) Pancreatic cancer: factors regulating tumor development, maintenance and metastasis. Pancreatology 1:517–524
16. Kloppel G, Lingenthal G, von Bulow M, Kern HF (1985) Histological and fine structural features of pancreatic ductal adenocarcinomas in relation to growth and prognosis: studies in xenografted tumours and clinico-histopathological correlation in a series of 75 cases. Histopathology 9:841–856
17. Lieber M, Mazzetta J, Nelson-Rees W, Kaplan M, Todaro G (1975) Establishment of a continuous tumor-cell line (panc-1) from a human carcinoma of the exocrine pancreas. Int J Cancer 15:741–747
18. Yunis AA, Arimura GK, Russin DJ (1977) Human pancreatic carcinoma (MIA PaCa-2) in continuous culture: sensitivity to asparaginase. Int J Cancer 19:218–235
19. Elsasser HP, Lehr U, Agricola B, Kern HF (1993) Structural analysis of a new highly metastatic cell line PaTu 8902 from a primary human pancreatic adenocarcinoma. Virchows Arch 64:201–207
20. Drucker BJ, Marincola FM, Siao DY, Donlon TA, Bangs CD, Holder WD Jr (1988) A new human pancreatic carcinoma cell line developed for adoptive immunotherapy studies with lymphokine-activated killer cells in nude mice. In Vitro Cell Dev Biol 24:1179–1187
21. Fogh J, Wright WC, Loveless JD (1977) Absence of HeLa cell contamination in 169 cell lines derived from human tumors. J Natl Cancer Inst 58:209–214
22. Kyriazis AP, Kyriazis AA, Scarpelli DG, Fogh J, Rao MS, Lepera R (1982) Human pancreatic adenocarcinoma line Capan-1 in tissue culture and the nude mouse: morphologic, biologic, and biochemical characteristics. Am J Pathol 106:250–260
23. Berrozpe G, Schaeffer J, Peinado MA, Real FX, Perucho M (1994) Comparative analysis of mutations in the p53 and K-ras genes in pancreatic cancer. Int J Cancer 58:185–191
24. Kalthoff H, Schmiegel W, Roeder C, Kasche D, Schmidt A, Lauer G et al (1993) p53 and K-RAS alterations in pancreatic epithelial cell lesions. Oncogene 8:289–298
25. Naumann M, Savitskaia N, Eilert C, Schramm A, Kalthoff H, Schmiegel W (1996) Frequent codeletion of p16/MTS1 and p15/MTS2 and genetic alterations in p16/MTS1 in pancreatic tumors. Gastroenterology 110:1215–1224
26. Schutte M, Hruban RH, Hedrick L, Cho KR, Nadasdy GM, Weinstein CL et al (1996) DPC4 gene in various tumor types. Cancer Res 56:2527–2530

27. McIntosh JC, Schoumacher RA, Tiller RE (1988) Pancreatic adenocarcinoma in a patient with cystic fibrosis. Am J Med 85:592
28. Schoumacher RA, Ram J, Iannuzzi MC, Bradbury NA, Wallace RW, Hon CT et al (1990) A cystic fibrosis pancreatic adenocarcinoma cell line. Proc Natl Acad Sci U S A 87:4012–4016
29. Owens RB, Smith HS, Nelson-Rees WA, Springer EL (1976) Epithelial cell cultures from normal and cancerous human tissues. J Natl Cancer Inst 56:843–849
30. Sun C, Yamato T, Furukawa T, Ohnishi Y, Kijima H, Horii A (2001) Characterization of the mutations of the K-ras, p53, p16, and SMAD4 genes in 15 human pancreatic cancer cell lines. Oncol Rep 8:89–92
31. Fink SP, Mikkola D, Willson JK, Markowitz S (2003) TGF-beta-induced nuclear localization of Smad2 and Smad3 in Smad4 null cancer cell lines. Oncogene 22:1317–1323
32. Yamaguchi N, Uozumi G, Ikeuchi H, Morioka H, Machino M, Kawai K (1983) Establishment and characterization of a carcinoembryonic antigen producing cell line derived from human pancreatic exocrine cancer. Gastroenterol Jpn 18:585–592
33. Okabe T, Yamaguchi N, Ohsawa N (1983) Establishment and characterization of a carcinoembryonic antigen (CEA)-producing cell line from a human carcinoma of the exocrine pancreas. Cancer 51:662–668
34. Hirai H, Okabe T, Anraku Y, Fujisawa M, Urabe A, Takaku F (1985) Activation of the c-K-ras oncogene in a human pancreas carcinoma. Biochem Biophys Res Commun 127:168–174
35. Tan MH, Shimano T, Chu TM (1981) Differential localization of human pancreas cancer-associated antigen and carcinoembryonic antigen in homologous pancreatic tumoral xenograft. J Natl Cancer Inst 67:563–569
36. Chen WH, Horoszewicz JS, Leong SS, Shimano T, Penetrante R, Sanders WH et al (1982) Human pancreatic adenocarcinoma: in vitro and in vivo morphology of a new tumor line established from ascites. In Vitro 18:24–34
37. Metzgar RS, Gaillard MT, Levine SJ, Tuck FL, Bossen EH, Borowitz MJ (1982) Antigens of human pancreatic adenocarcinoma cells defined by murine monoclonal antibodies. Cancer Res 42:601–608
38. Barton CM, Staddon SL, Hughes CM, Hall PA, O'Sullivan C, Kloppel G et al (1991) Abnormalities of the p53 tumour suppressor gene in human pancreatic cancer. Br J Cancer 64:1076–1082
39. Peri G, Milanese C, Matteucci C, Ruco L, Zhou D, Sozzani S et al (1994) A new monoclonal antibody (5D3-F7) which recognizes human monocyte-chemotactic protein-1 but not related chemokines. Development of a sandwich ELISA and in situ detection of producing cells. J Immunol Methods 174:249–257
40. Piemonti L, Monti P, Sironi M, Fraticelli P, Leone BE, Dal Cin E et al (2000) Vitamin D3 affects differentiation, maturation, and function of human monocyte-derived dendritic cells. J Immunol 164:4443–4451
41. Miller DW, Fontain M, Kolar C, Lawson T (1996) The expression of multidrug resistance-associated protein (MRP) in pancreatic adenocarcinoma cell lines. Cancer Lett 107:301–306
42. Torres MJ, Ruiz-Cabello F, Skoudy A, Berrozpe G, Jimenez P, Serrano A et al (1996) Loss of an HLA haplotype in pancreas cancer tissue and its corresponding tumor derived cell line. Tissue Antigens 47:372–381
43. Scupoli MT, Sartoris S, Tosi G, Ennas MG, Nicolis M, Cestari T et al (1996) Expression of MHC class I and class II antigens in pancreatic adenocarcinomas. Tissue Antigens 48:301–311
44. Pernick NL, Sarkar FH, Tabaczka P, Kotcher G, Frank J, Adsay NV (2002) Fas and Fas ligand expression in pancreatic adenocarcinoma. Pancreas 25:36–41
45. Kornmann M, Ishiwata T, Kleeff J, Beger HG, Korc M (2000) Fas and Fas-ligand expression in human pancreatic cancer. Ann Surg 231:368–379
46. Ungefroren H, Voss M, Bernstorff WV, Schmid A, Kremer B, Kalthoff H (1999) Immunological escape mechanisms in pancreatic carcinoma. Ann N Y Acad Sci 880:243–251
47. Wright P, Braun R, Babiuk L, Littel-van den Hurk SD, Moyana T, Zheng C et al (1999) Adenovirus-mediated TNF-alpha gene transfer induces significant tumor regression in mice. Cancer Biother Radiopharm 14:49–57
48. Stoelcker B, Ruhland B, Hehlgans T, Bluethmann H, Luther T, Mannel DN (2000) Tumor necrosis factor induces tumor necrosis via tumor necrosis factor receptor type 1-expressing endothelial cells of the tumor vasculature. Am J Pathol 156:1171–1176
49. Thomas WJ, Thomas DL, Knezetic JA, Adrian TE (2002) The role of oxygen-derived free radicals and nitric oxide in cytokine-induced antiproliferation of pancreatic cancer cells. Pancreas 24:161–168
50. Gansauge S, Nussler AK, Beger HG, Gansauge F (1998) Nitric oxide-induced apoptosis in human pancreatic carcinoma cell lines is associated with a G1-arrest and an increase of the cyclin-dependent kinase inhibitor p21WAF1/CIP1. Cell Growth Differ 9:611–617
51. Monti P, Leone BE, Marchesi F, Balzano G, Zerbi A, Scaltrini F et al (2003) The CC chemokine MCP-1/CCL2 in pancreatic cancer progression: regulation of expression and potential mechanisms of antimalignant activity. Cancer Res 63:7451–7461
52. Alexandroff AB, Jackson AM, Paterson T, Haley JL, Ross JA, Longo DL et al (2000) Role for CD40–CD40 ligand interactions in the immune response to solid tumours. Mol Immunol 37:515–526
53. Young LS, Eliopoulos AG, Gallagher NJ, Dawson CW (1998) CD40 and epithelial cells: across the great divide. Immunol Today 19:502–506
54. Paulie S, Ehlin-Henriksson B, Mellstedt H, Koho H, Ben-Aissa H, Perlmann P (1985) A p50 surface antigen restricted to human urinary bladder carcinomas and B lymphocytes. Cancer Immunol Immunother 20:23–28
55. Romagnani S (2002) Cytokines and chemoattractants in allergic inflammation. Mol Immunol 38:881–885
56. Bellone G, Turletti A, Artusio E, Mareschi K, Carbone A, Tibaudi D et al (1999) Tumor-associated transforming growth factor-beta and interleukin-10 contribute to a systemic Th2 immune phenotype in pancreatic carcinoma patients. Am J Pathol 155:537–547
57. Azenshtein E, Luboshits G, Shina S, Neumark E, Shahbazian D, Weil M et al (2002) The CC chemokine RANTES in breast carcinoma progression: regulation of expression and potential mechanisms of promalignant activity. Cancer Res 62:1093–1102
58. Monti P, Leone BE, Marchesi F, Balzano G, Zerbi A, Scaltrini F et al (2003) The CC chemokine MCP-1/CCL2 in pancreatic cancer progression: regulation of expression and potential mechanisms of antimalignant activity. Cancer Res 63:7451–7461
59. Takaya H, Andoh A, Shimada M, Hata K, Fujiyama Y, Bamba T (2000) The expression of chemokine genes correlates with nuclear factor-kappaB activation in human pancreatic cancer cell lines. Pancreas 21:32–40
60. Shimada M, Andoh A, Araki Y, Fujiyama Y, Bamba T (2001) Ligation of the Fas antigen stimulates chemokine secretion in pancreatic cancer cell line PANC-1. J Gastroenterol Hepatol 16:1060–1067
61. Shi Q, Abbruzzese JL, Huang S, Fidler IJ, Xiong Q, Xie K (1999) Constitutive and inducible interleukin 8 expression by hypoxia and acidosis renders human pancreatic cancer cells more tumorigenic and metastatic. Clin Cancer Res 5:3711–3721
62. Miyamoto M, Shimizu Y, Okada K, Kashii Y, Higuchi K, Watanabe A (1998) Effect of interleukin-8 on production of tumor-associated substances and autocrine growth of human liver and pancreatic cancer cells. Cancer Immunol Immunother 47:47–57
63. Koshiba T, Hosotani R, Miyamoto Y, Ida J, Tsuji S, Nakajima S et al (2000) Expression of stromal cell-derived factor 1 and

CXCR4 ligand receptor system in pancreatic cancer: a possible role for tumor progression. Clin Cancer Res 6:3530–3535
64. Baker CH, Solorzano CC, Fidler IJ (2001) Angiogenesis and cancer metastasis: antiangiogenic therapy of human pancreatic adenocarcinoma. Int J Clin Oncol 6:59–65
65. Keleg S, Buchler P, Ludwig R, Buchler MW, Friess H (2003) Invasion and metastasis in pancreatic cancer. Mol Cancer 2:14
66. von Bernstorff W, Voss M, Freichel S, Schmid A, Vogel I, Johnk C et al (2001) Systemic and local immunosuppression in pancreatic cancer patients. Clin Cancer Res 7:925–932
67. Liyanage UK, Moore TT, Joo HG, Tanaka Y, Herrmann V, Doherty G et al (2002) Prevalence of regulatory T cells is increased in peripheral blood and tumor microenvironment of patients with pancreas or breast adenocarcinoma. J Immunol 169:2756–2761
68. Arlt A, Vorndamm J, Muerkoster S, Yu H, Schmidt WE, Folsch UR et al (2002) Autocrine production of interleukin 1beta confers constitutive nuclear factor kappaB activity and chemoresistance in pancreatic carcinoma cell lines. Cancer Res 62:910–916

Virchows Arch (2004) 445:248–254
DOI 10.1007/s00428-004-1080-7

ORIGINAL ARTICLE

Stefano La Rosa · Elena Rigoli · Silvia Uccella · Anna Maria Chiaravalli · Carlo Capella

CDX2 as a marker of intestinal EC-cells and related well-differentiated endocrine tumors

Received: 5 May 2004 / Accepted: 17 June 2004 / Published online: 29 July 2004
© Springer-Verlag 2004

Abstract Gastroenteropancreatic (GEP) endocrine tumors (ETs) are neoplasms showing different hormonal profiles and different clinical and prognostic features, which depend consistently on the site of origin. Histological features and general endocrine markers do not differentiate tumors in relation to their location, making it difficult to establish the site of origin of a GEP ET that has metastasized to the liver or lymph nodes. A site-specific marker would be particularly useful in the examination of small specimens where there is not sufficient material for an extensive study of the hormonal expression. CDX2 is a transcription factor that has been recently proposed as a marker of intestinal adenocarcinomas. Our aim was to evaluate the immunohistochemical expression of CDX2 in normal tissues and in 184 formalin-fixed and paraffin-embedded ETs to verify whether it could be used to identify intestinal ETs with a high degree of sensitivity and specificity. Of these cases, 154 were primary tumors (99 GEP and 55 non-GEP tumors), 101 were well-differentiated endocrine tumors, and 53 were poorly differentiated endocrine carcinomas (PDECs). Of the cases, 30 were metastases from differently located ETs. Nuclear CDX2 immunoreactivity was found in all EC-cells (serotonin-producing cells), in about 10% of G-cells (gastrin-producing cells), in about 30% of GIP-cells (gastric inhibitory peptide cells) and in a few motilin-positive cells of the normal intestinal mucosa, while other gastrointestinal endocrine cell types were CDX2 negative. All midgut EC-cell tumors, their metastases, and two of three pancreatic EC-cell ETs were diffusely and intensely CDX2 positive. The other GEP ETs, their metastases, as well as the non-GEP ETs, were all CDX2 negative, with the exception of four PDECs, five gastrinomas and one pheochromocytoma, which were only focally positive. We conclude that CDX2 may be considered a sensitive and specific marker of midgut EC-cells and EC-cell tumors, and its expression may be useful in the diagnosis of metastases from occult ETs.

Keywords CDX2 · Endocrine tumor · Gut · Pancreas · Immunohistochemistry

S. La Rosa · E. Rigoli · S. Uccella · A. M. Chiaravalli · C. Capella
Department of Pathology,
Ospedale di Circolo and University of Insubria,
Varese, Italy

S. La Rosa (✉)
Servizio di Anatomia Patologica,
Ospedale di Circolo,
Viale Borri 57, 21100 VareseItaly
e-mail: anapat@ospedale.varese.it
Tel.: +39-0332-264557
Fax: +39-0332-262313

Introduction

Cdx2 is a homeobox gene that has been recently found to play a role in the development and differentiation of mammalian intestine [8, 24, 25]. The gene codifies a transcription factor protein named CDX2 [5], which increases the expression of several gene products associated with mature intestinal epithelial cells [30]. This complex machinery of sequentially activated genes seems to decrease cellular replication and induce differentiation to mature intestinal epithelium [30].

All recent published papers regarding the role and expression of CDX2 in intestinal epithelium have focused their attention on the exocrine component of the bowel mucosa. However, it is well known that there are several scattered endocrine cell types along the gut that, together with those located in the pancreas, form a large endocrine organ, generally referred to as the gastroenteropancreatic (GEP) endocrine system [27]. This system is remarkably heterogeneous and is composed of as many as 15 highly specialized endocrine cells, which show different hormonal profiles, physiological functions and site distribution [13, 27]. To the best of our knowledge, it is not known whether various endocrine cell types of the gut and pancreas express the CDX2 protein.

GEP endocrine tumors (ETs) form a heterogeneous group of neoplasms showing different hormonal profiles and different morphological, clinical and prognostic fea-

tures, depending on the site of origin [13, 26]. According to the World Health Organization classification of ETs [27], pure endocrine neoplasms are separated into two main categories: well-differentiated endocrine tumors (WDETs) and poorly differentiated endocrine carcinomas (PDECs). In histological preparations, PDECs are easily distinguished from WDETs because they show solid sheets composed of cells with high-grade atypia, hyperchromatic nuclei, a high nuclear/cytoplasmic ratio, a high mitotic rate and extensive necrosis. In contrast, WDETs are generally formed by uniform small/medium-sized cells with regularly shaped nuclei, arranged in trabeculae or solid nests, with low or no mitotic activity and no necrosis. The histopathological features do not differentiate tumors in relation to the site of origin, with the only exception of duodenal somatostatin-producing D-cell neoplasms, which show a prevalent pseudoglandular pattern of growth [6]. In routine surgical pathology practice, GEP ETs are often first discovered as liver or lymph-node metastases coming from an occult primary neoplasm. The diagnosis is frequently made on a small specimen, such as a needle biopsy, and there is often insufficient material to perform a complete immunohistochemical hormonal profile, which may be "per se" a good indicator of the primary tumor site (e.g., insulin for a pancreatic tumor). The endocrine nature of neoplasms is confirmed by the expression of general endocrine markers, such as chromogranins, synaptophysin and neuron-specific enolase, which, however, are not useful for identifying the location of the primary tumor. The presence of a clinical endocrine syndrome may help to identify the site of origin of a GEP tumor [27]. However, several neoplasms are nonfunctioning at a clinical level, and their identification is, therefore, frequently difficult.

It has recently been suggested that CDX2 protein expression is an important marker of colorectal adenocarcinomas [2, 31], and it seems to be particularly useful for the differential diagnosis of primary lung adenocarcinomas and lung metastases from intestinal adenocarcinomas. As far as we aware, apart from GEP hormones, there is no other specific marker for intestinal endocrine tumors, and the expression of CDX2 protein in GEP endocrine neoplasms has only been investigated in preliminary studies [3, 14].

The aim of the present investigation was to evaluate the expression of CDX2 in normal GEP endocrine cells and in a large series of intestinal and extra-intestinal endocrine tumors to verify whether CDX2 may be used as a marker of tumors of intestinal origin.

Materials and methods

Cases

The material used in this study was obtained from the files of the Department of Pathology of the Ospedale di Circolo-University of Insubria in Varese. The material consisted of 184 endocrine tumors from different sites, which are listed in Table 1, Table 2 and Table 3. Of the cases, 154 were primary tumors, while 30 neoplasms represented metastases to the liver (6 cases), lymph nodes (22

Table 1 Main clinicopathological features and CDX2 expression in gastroenteropancreatic well-differentiated endocrine tumors. *WHO* World Health Organization, *B* benign behavior, *UB* uncertain behavior, *C* well-differentiated carcinoma, *type 1* gastric histamine-producing enterochromaffin-like (ECL)-cell tumor associated with chronic atrophic gastritis, *type 3* sporadic gastric ECL-cell tumor, *G-cell* gastrin-producing cell, *D-cell* somatostatin-producing cell, *GP* gangliocytic paraganglioma, *EC-cell* serotonin-producing cell, *L-cell* glicentin-producing cell, *A-cell* glucagon-producing cell, *PP-cell* pancreatic polypeptide-producing cell

Site	*n*	WHO classification			Tumor	Sex	Age (years)		Size (cm)		Metastases	CDX2	
		B	UB	C	Type	F/M	Mean	Range	Mean	Range		Primary	Metastases
Stomach	3	2	1		Type 1	3/0	71	64–78	1.5	0.5–2	0/3	0/3	
	3			3	Type 3	1/2	41	26–56	2.4	2–2.8	3/3	0/3	0/3
Duodenum	4	4			G-cell	1/3	54.5	46–63	0.7	0.5–1	0/4	3/4*	
	3	1	1	1	D-cell	3/0	46	38–54	1.5	0.5–2.5	1/3	0/3	0/1
	2	1		1	GP	0/2	57.5	36–79	3	2–4	1/2	0/2	
Ileum	12			12	EC-cell	5/7	56	40–72	2.4	0.9–3	12/12	12/12	6/6
Appendix	5	5			EC-cell	2/3	71	23–96	1.7	1–2.5	0/5	5/5	
Right colon	2			2	EC-cell	1/1	48	46–50	4.6	3–8	2/2	2/2	2/2
Rectum	8	6	1	1	L-cell	2/5	52	34–70	2.5	0.1–5	1/8	0/8	0/1
	2		1	1	L/EC-cell	0/2	56	42–70	1.2	0.2–2	1/2	0/2	
	3	2		1	Undefined	2/1	52	38–72	0.2	0.1–0.3	1/2	0/3	0/1
	1		1		EC-cell	0/1	45		2		0/1	0/1	
Pancreas	8	8			Insulinoma	4/4	59	33–85	1.3	1–1.7	0/8	0/8	
	2			2	Gastrinoma	2/0	55.5	40–71	2	2–2	2/2	2/2*	
	5	5			A-cell	3/2	58	25–66	1.6	1.2–2.1	0/5	0/5	
	3		1	2	PP-cell	1/1	57.5	28–59	4.9	1.8–8	2/3	1/3	
	1			1	A/D-cell	1/0	37		6		1/1	0/1	
	3	2		1	EC-cell	2/1	62.3	50–75	2.5	2–3	1/3	2/3	
	1		1		VIPoma	0/1	72		5.5		0/1	0/1	
	1			1	Undefined	0/1	57		3.5		1/1	0/1	
Total	72											27/72 (37.5%)	8/14

* Nuclear immunoreactivity was weak and focal

Table 2 Main clinicopathological features and CDX2 expression in non-gastroenteropancreatic well differentiated endocrine tumors. *MTC* medullary thyroid carcinoma

Site	*n*	Type	Sex	Age (years)		Size (cm)		Metastases	CDX2
				Mean	Range	Mean	Range		
Thyroid	10	MTC	8/2	40.8	26–62	3.6	2–5	2/10	0/10
Parathyroid	3	Hyperplasia	2/1	36	34–39	0.9	0.8–1.2	No	0/3
Carotid body	3	Paraganglioma	2/1	65.6	62–69	3.6	3–4.3	No	0/3
Ear	1	Carcinoid	1/0	57		[b]		No	0/1
Adrenal	5	Pheochromocytoma	2/3	54.7	32–71	6.6	5–9	1/5	1/5[a]
Lung	6	Typical carcinoid	2/4	55.5	37–63	1.9	1.2–3	0/6	0/6
	1	Atypical carcinoid	1/0			4		0/1	0/1
Total	29								1/29 (3.4%)

[a] Nuclear immunoreactivity was weak and focal
[b] Material examined was represented by bioptic tissues

Table 3 Main clinicopathological features and CDX2 expression in poorly differentiated endocrine carcinomas (PDECs) of different sites. *nk* not known

Site	*n*	Sex	Age (years)		Size (cm)		Metastases	CDX2	
		Female/male	Mean	Range	Mean	Range		Primary	Metastases
Skin	5	3/2	76.7	52–87	3	2.7–4	2/5	0/5	0/1
Lung	14[b]	1/13	60	41–75	5.4	1.5–7.8	14/14	1/14[c]	0/5
Oesophagus/cardias	8	1/7	60	45–73	3.6	2.3–5.5	8/8	1/8[a]	
Stomach	7	0/7	56	38–74	7.6	1.2–14	7/7	1/7[a]	1/3
Right colon	6	3/3	67.5	50–92	4	2.5–7	6/6	0/6	0/5
Rectum	4	0/4	61	56–67	3.7	1.3–7	3/4	1/4[a]	1/2
Pancreas	2	1/1	70	61–79	6.5	3–10	2/2	0/2	
Prostate	4	0/4	67.7	57–69	[d]		Nk	0/4	
Urinary bladder	3	2/1	82	79–86	[d]		Nk	0/3	
Total	53							4/53 (7.5%)	2/16 (12.5%)

[a] All these PDECs contained serotonin-immunoreactive cells
[b] Nine small cell and five large cell PDECs
[c] The positive case was a large cell PDEC
[d] Material examined was represented by bioptic tissues obtained from needle biopsy or transurethral resection

cases) or omentum (2 cases). Among the primary tumors, 101 were WDETs: 72 GEP (Table 1) and 29 non-GEP (Table 2) endocrine neoplasms. Of the tumors, 53 were PDECs, originating in the gut (25 cases), pancreas (2 cases) or non-GEP sites, including skin, lung, prostate and urinary bladder (Table 3). In addition, normal tissues from a variety of organs (gut, pancreas, thyroid, parathyroid, adrenal gland, skin, lung, prostate, urinary bladder) were also analyzed. All tissues were fixed in buffered formalin (formaldehyde 4% and acetate buffer 0.05 M) for 24 h and routinely embedded in paraffin wax. Sections 5-μm thick were stained with hematoxylin-eosin, alcian blue-periodic acid-Schiff and Grimelius' silver stain for the histopathological examination.

Immunohistochemistry

All tumors were characterized on the basis of their hormonal expression, evaluated using the antibodies listed in Table 4. CDX2 expression was detected with the monoclonal antibody CDX2–88 (Biogenex) raised against a full-length CDX2 recombinant protein. Immunohistochemistry was performed using the avidin-biotin complex procedure [10], while colocalization studies were performed using double-label immunostains according to Mason et al. [20] or Lan et al. [15]. Specificity controls consisted of absorption of antibodies and antisera with 10–20 nM of their related antigens, substitution of the primary antibody with non-immune serum of the same species at the same dilution and use of control tissues with or without the pertinent antigen.

The specificity and sensitivity of CDX2 immunostaining in detecting intestinal EC-cell (serotonin-producing cell) neoplasms was calculated as follows: specificity=true negatives/(true negatives+false positives); sensitivity=true positives/(true positives+false negatives) [2, 12]. For detecting intestinal well-differentiated EC-cell tumors, false positives were defined as intestinal non-EC-cell tumors or extraintestinal ETs showing CDX2 immunoreactivity, while false negatives were intestinal EC-cell neoplasms lacking CDX2. For detecting EC-cell tumors independent of the site of origin, false positives were defined as non-EC-cell tumors showing CDX2 immunoreactivity, while false negatives were EC-cell neoplasms lacking CDX2.

Results

Normal tissue

No CDX2 immunoreactivity was observed in normal lung, skin, prostate, urinary bladder, adrenal gland, thyroid gland, parathyroid glands, pancreas, esophagus or stomach, with the only exception being areas of intestinal metaplasia in gastric mucosa. Conversely, nuclear CDX2 immunoreactivity was found in epithelial cells of the small and large bowel. The staining was present in all exocrine cells of the villi and crypts, while cells of duodenal Brunner glands were negative or weakly stained. Double-label immunohistochemical stains revealed that

Table 4 Antibodies and antisera employed. *P/M* polyclonal/monoclonal

Antibodies/antisera	P/M(clone)	Dilution	Source
Synaptophysin	M(snp88)	1:100	BioGenex Laboratories, San Ramon, USA
Neuron-specific enolase	M(MIG.N3)	1:100	Monosan San Bio, Am Uden, The Netherlands
Chromogranin A	M(PHE5)	1:100	Enzo Diagnostic, New York, USA
Insulin	M(AE9D6)	1:200	BioGenex Laboratories
Glucagon	P	1:1250	Milab, Malmo, Sweden
Glucagon/glicentin	P	1:2500	Milab
Pancreatic polypeptide	P	1:4000	Cambridge Research Biochemicals, Cambridge, UK
Somatostatin	P	1:500	Dako, Copenhagen, Denmark
Serotonin	M(YC5)	1:50	Biogenesis, Bournemouth, UK
C-terminus gastrin-CCK-cerulein	M(B4)	1:10000	Farmitalia, Milan, Italy
Secretin	P	1:1000	Milab
Motilin	P	1:400	Biogenesis
Gastric inhibitory peptide	P	1:320	Milab
Vesicular monoamine transporter 2	P	1:500	Chemicon, Tamecula, CA, USA
Peptide YY (PYY)	P	1:1000	Biogenesis
CDX2	M(CDX2–88)	1:100	BioGenex

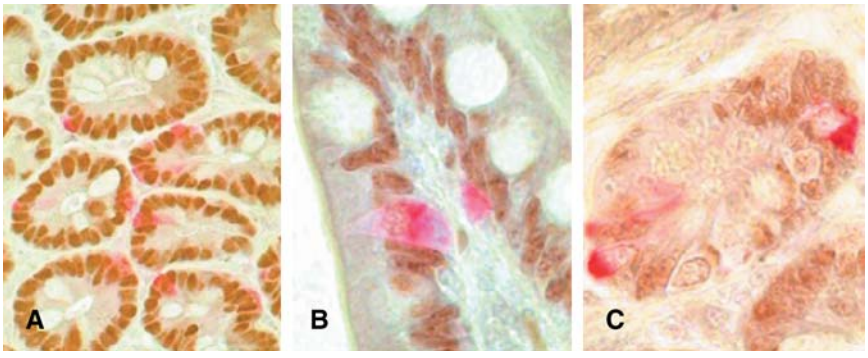


Fig. 1 Double-label immunostainings in duodenal mucosa show that nuclear CDX2 immunoreactivity (*brown*) co-localizes with serotonin in all EC-cells (serotonin-producing cells) (**A**) and also with gastrin in G-cells (gastrin-producing cells), although in the latter the reaction is weaker (**B**). It is worth noting that only about 10% of gastrin-producing G-cells are CDX2 positive (data not shown). Nuclei of somatostatin-producing D-cells (somatostatin-producing cells) are CDX2 negative (**C**). All hormones are stained in *red*, original magnification ×200 (**A**), ×400 (**B** and **C**)

only a fraction of chromogranin-A-positive intestinal endocrine cells were CDX2 positive. Using antibodies directed against specific hormones, it was possible to demonstrate that CDX2 nuclear staining was present in all serotonin-immunoreactive (IR) intestinal EC-cells (Fig. 1A), in about 30% of duodenal GIP (gastric inhibitory peptide)-IR cells, in a minority (about 10%) of duodenal gastrin-IR G-cells (gastrin-producing cells) (Fig. 1B) and motilin-IR cells. The CDX2 immunostaining was strong in EC-cells, while it was rather weak in G-, GIP-, and motilin-cells. No CDX2 nuclear staining was found in somatostatin- (Fig. 1C), cholecystokinin-, secretin- and glicentin-IR intestinal cells. All chromogranin-positive endocrine cells of the stomach, pancreas, lung, prostate, adrenal gland, thyroid, skin and paraganglia were CDX2 negative.

Endocrine tumors

The CDX2 expression in various endocrine GEP tumor types is summarized in Table 1. Nuclear CDX2 immunoreactivity was mainly restricted to midgut EC-cell tumors (19/19 positive cases), in which the majority of cells were strongly positive (Fig. 2A). A strong CDX2 expression was also noted in all eight metastases (three nodal, three liver, two omental) from intestinal EC-cell WDECs (Fig. 2B, C). In addition, two of three nonfunctioning pancreatic EC-cell tumors showed CDX2-positive cells, while the three rectal tumors composed of EC-cells were CDX2 negative. The other GEP WDETs studied (47 cases) were CDX2 negative (Fig. 3), except for one PP-cell (pancreatic polypeptide-producing cell) tumor and five gastrinomas, which had a few cells with a weak CDX2 immunoreactivity. Therefore, considering all non-midgut GEP tumors, only 8 of 53 (15%) cases showed CDX2-positive cells; in addition, in these cases, the nuclear CDX2 staining was weaker and more focal than that observed in midgut EC-cell tumors. The six metastases from non-EC-cell WDECs [three from type-III ECL-cell (enterochromaffin-like cell) gastric tumors, one from a duodenal D-cell neoplasm and two from rectal tumors], such as the primary neoplasms, were completely negative for nuclear CDX2 expression.

In addition to GEP cases, we investigated the expression of CDX2 in 29 WDETs and WDECs from different

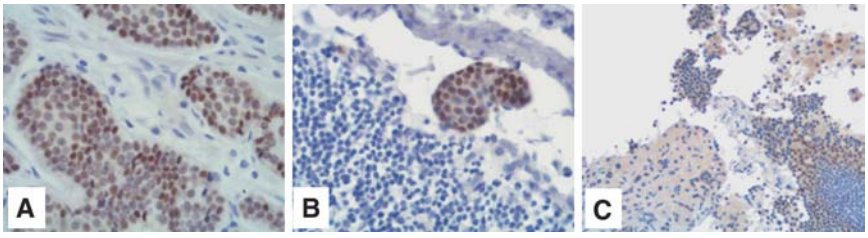


Fig. 2 Ileal EC-cell (serotonin-producing cell) tumor shows a diffuse and intense nuclear CDX2 immunoreactivity (**A**). The lymph-node (**B**) and liver (**C**) and metastases coming from this tumor show the same pattern of CDX2 expression (original magnification, ×200)

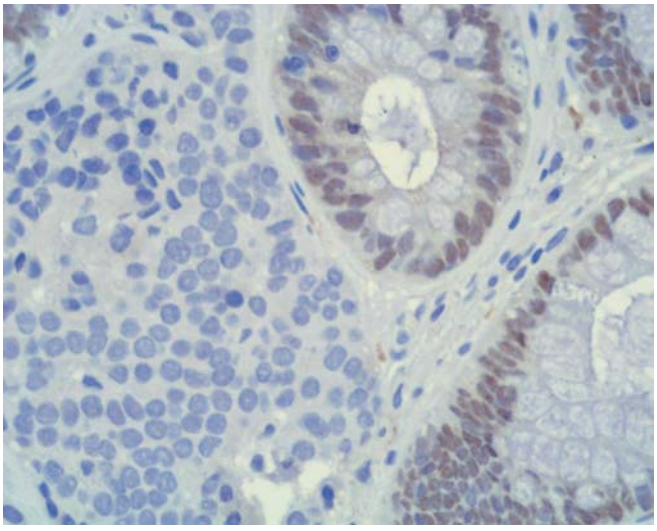


Fig. 3 Rectal L-cell (glicentin-producing cell) tumor completely CDX2 negative (on the *left side*). Note the internal positive control in normal epithelial cells of the adjacent mucosa (on the *right side*) (original magnification, ×400)

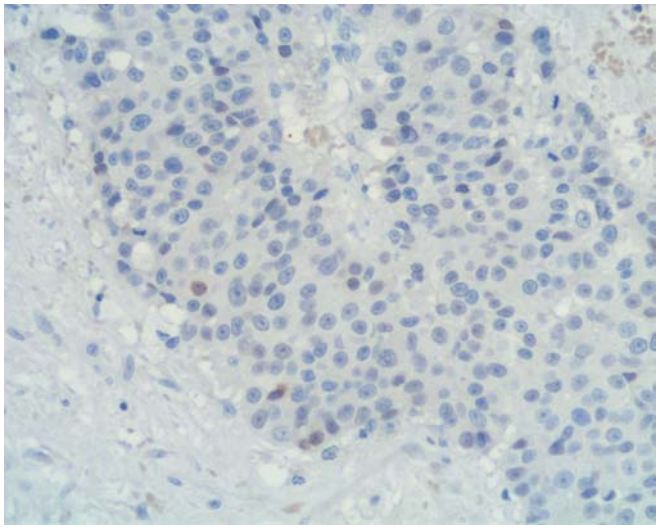


Fig. 4 Large cell neuroendocrine carcinoma of the lung showing a few weak CDX2-positive cells (original magnification ×400)

sites, including thyroid, parathyroid, carotid body, ear, adrenal gland and lung (Table 2). With the exception of one pheochromocytoma showing a few CDX2-positive nuclei, all tumors were negative.

The expression of CDX2 in 53 PDECs is summarized in Table 3. Only 3 of 27 (11%) GEP cases, located respectively in the stomach, right colon and rectum, showed a nuclear CDX2 immunoreactivity in a few cells of both primary and respective metastases. Among PDECs located in organs outside the digestive system, only one large cell neuroendocrine carcinoma of the lung showed a few weak CDX2 immunoreactive cells (Fig. 4). The three GEP tumors presented a component of serotonin-positive cells, which was lacking in the lung tumor. Metastases from CDX2-negative primary PDECs (14 cases) were completely CDX2 negative.

In this study, CDX2 had a specificity of 0.87 and a sensitivity of 0.90 in detecting intestinal well-differentiated EC-cell tumors. As for the identification of endocrine tumors expressing serotonin, apart from the tumor site and cell differentiation, CDX2 had a specificity of 0.93 and a sensitivity of 0.89.

Discussion

In the present study, we have investigated the immunohistochemical expression of CDX2 in normal tissues and in a large series of endocrine neoplasms from different sites, and we have proved that CDX2 is a good marker of intestinal EC-cells and related neoplasms.

CDX2 is a transcription factor, which is expressed by epithelial cells of the intestinal mucosa, playing a role in their differentiation both in fetal and adult tissues [30]. Although CDX2 expression in exocrine intestinal epithelial cells has been well documented, there are no previous studies that look at the localization of CDX2 protein in normal intestinal endocrine cells. Our results demonstrate that CDX2 is expressed in normal human intestinal endocrine cells and that it shows a specific distribution among the different intestinal endocrine cell types. In particular, CDX2 is expressed in all serotonin-producing intestinal EC-cells and in a small fraction of duodenal G-, GIP- and motilin-cells but not in other intestinal or extra-intestinal endocrine cell types. It is well known that other transcription factors show a specific distribution among GEP endocrine cells, and, for several of them, a role in endocrine cell differentiation has been

demonstrated. The factors that have been mostly considered include neurogenin 3 [11], pax4 and pax6 [16, 28, 29]. The findings of the present study raise the possibility that the CDX2 protein may play some roles in the regulation of the transcription of multiple intestinal genes, including those involved in EC-, G-, GIP- and motilin-cell differentiation.

An interesting approach to verify the role of CDX2 in the maturation and differentiation of serotonin-producing EC-cells would be the study of intestinal mucosa in null mutant *cdx2*$^{-/-}$ mice. Unfortunately, as far as we know, the endocrine population in *cdx2*$^{-/-}$ null mutant mice has been never investigated. This has been mainly due to the fact that the homozygous *cdx2*$^{-/-}$ phenotype is embryo lethal in the perimplantation period [7]. However, some studies have been performed in heterozygous *cdx2*$^{+/-}$ mice that develop polypoid lesions in the pericaecal region and proximal colon [4]. These polyps showed the histological features of gastric cardia and body mucosa and were completely negative for CDX2 expression. Endocrine cells in these lesions have not been examined.

After the initial hypothesis of the origin of GEP endocrine cells from the neural crest [22, 23], chimeric models have shown a common embryologic origin of gut endocrine epithelial cells from the endoderm layer [1, 17]. In this context, CDX2 expression in both normal endocrine and exocrine intestinal cells and related neoplasms lends additional support to the hypothesis of the endodermal origin of both these cell types, considering also that the expression of this transcription factor is restricted to endoderm-derived tissues.

Our study of the expression of CDX2 in 184 endocrine tumors has demonstrated that the nuclear immunoreactivity was mainly restricted to GEP WDETs and, in particular, to midgut EC-cell tumors and to a few gastrin-producing G-cell neoplasms. These findings are in concurrence with data reported in recent papers [2, 21, 31] and in abstracts presented at the 2004 Vancouver USCAP meeting [3, 14, 18, 19]. All these papers conclude that CDX2 is mainly expressed by midgut WDETs. Unlike other studies, in which the functional immunophenotype has not been fully defined, in the present investigation, we have clearly demonstrated that, among midgut WDETs, EC-cell neoplasms of the ileum, appendix and right colon strongly express CDX2, mirroring the distribution of CDX2 in normal endocrine cells of the gut. Similarly, we have proved that CDX2 expression by gastrin-producing G-cell tumors reflects a biological characteristic of normal intestinal G-cells but not of gastric G-cells.

We found CDX2 expression in 5 of 24 (20%) pancreatic WDETs, represented by 2 gastrinomas and 3 nonfunctioning (2 EC-cell and 1 PP-cell) tumors, with a correlation of tumor cell type and CDX2 expression similar to that of intestinal WDETs. Lin et al. [18] did not find CDX2 immunoreactivity in the 30 pancreatic endocrine tumors analyzed, while Barbareschi et al. [3] have reported CDX2 positivity in 14 of 48 (29%) nonfunctioning pancreatic WDETs, and, interestingly, CDX2-positive tumors were more frequently found among malignant cases. In our cases of pancreatic WDETs, we did not find a similar trend. In the 14 paired samples of primary and metastatic WDETs analyzed, CDX2 expression was equal in both sites.

In our cases, intense nuclear positivity was restricted to metastases from ileal EC-cell tumors. Therefore, CDX2 immunoreactivity in a metastasis from an occult WDEC should first suggest an ileal origin of the primary neoplasm. Considering also that appendiceal EC-cell tumors are very rarely malignant [6] and that right colon EC-cell neoplasms are much less frequent than ileal EC-cell tumors, CDX2 immunohistochemistry may, therefore, be recommended in the study of small specimens of liver or lymph-node metastases for which the pathologist does not have sufficient material for an extensive hormonal immunoprofile that, in most cases, could help to identify the primary site of the tumor. It is important to underline that among GEP tumors, five of six gastrinomas also presented a CDX2 immunoreactivity. However, the pattern of CDX2 positivity observed in G-cell tumors was different from that found in EC-cell neoplasms, being weaker and focal.

The fact that CDX2 may be used as a marker to identify intestinal EC-cell neoplasms is also corroborated by our finding that endocrine tumors that arise outside the digestive system are CDX2 negative, with the exception of only one pheochromocytoma showing a focal positivity. In fact, we did not find any CDX2 immunoreactivity in lung carcinoids (seven cases) or small cell PDECs (nine cases). Among five large cell neuroendocrine carcinomas of the lung, one showed a few weak positive cells. These findings are in concordance with previously reported data [2, 3, 18, 21, 31]. As far as we know, there are no reports of CDX2 expression in non-GEP WDETs other than the lung, so it is not possible to compare our findings, which represent the first description demonstrating that endocrine tumors located in tissues outside the digestive system lack CDX2 immunoreactivity.

Our results prove that CDX2 is a less important marker of PDECs, being expressed in only four (7.5%) of the cases examined. Three tumors were located in the digestive system and, as in the majority of WDETs, showed a component of serotonin-positive cells (Table 3). In previous studies, some authors [2, 31] investigated small cell lung carcinomas, and, interestingly, all but one cases were CDX2-negative. More recently, Barbareschi et al. [3] have found that 77% of intestinal and 42% of non-intestinal PDECs were CDX2 positive. The reason for these differing results is not clear. The low CDX2 expression that we observed in PDECs can be explained if one considers that CDX2 is a differentiation factor, important in maintaining the mature features of endocrine cells, and its loss may lead to an immature endocrine pattern. In this context, it is interesting to recall that CDX2 expression is inversely correlated with the grade of dysplasia in colorectal adenomas and with the grade of colorectal carcinomas, being less expressed in poorly differentiated adenocarcinomas [9].

In summary, this study demonstrates that CDX2 has a different expression among different endocrine cell types of the normal GEP system and among functionally well-characterized GEP endocrine tumors. CDX2 is expressed in normal EC-, G-, GIP- and motilin-cells of the intestinal tract, in all primary and metastatic well-differentiated EC-cell tumors of the ileum, appendix and right colon and in a subset of duodenal and pancreatic G-cell and EC-cell tumors. CDX2 is expressed only focally in PDECs of the GEP system and is not found in PDECs of other sites.

Acknowledgements Part of the work has been supported by a grant from the University of Insubria and Fondazione Cariplo, Varese, Italy.

References

1. Andrew A, Kramer B, Rawdon BB (1998) The origin of gut and pancreatic neuroendocrine (APUD) cells—the last word? J Pathol 186:117–118
2. Barbareschi M, Murer B, Colby TV, Chilosi M, Macri E, Loda M, Doglioni C (2003) CDX-2 homeobox gene expression is a reliable marker of colorectal adenocarcinoma metastases to the lungs. Am J Surg Pathol 27:141–149
3. Barbareschi M, Roldo C, Zamboni G, Capelli P, Cavazza A, Cangi MG, Chilosi M, Doglioni C (2004) CDX2 homeobox gene product expression in neuroendocrine tumors: its role as a marker of intestinal neuroendocrine tumors. Lab Invest 84[Suppl 1]:101A
4. Beck F, Chawengsaksophak K, Luckett J, Giblett S, Tucci J, Brown J, Poulsom R, Jeffery R, Wright NA (2003) A study of regional gut endoderm potency by analysis of cdx2 mutant chimeric mice. Dev Biol 255:399–406
5. Burglin TR (ed) (1994) A comprehensive classification of homeobox genes. Sambrook and Tooze, New York
6. Capella C, Solcia E, Sobin LH, Arnold R (2000) Endocrine tumours of the small intestine. In: Hamilton SR, Aaltonen LA (eds) Pathology and genetics of the digestive system. IARC Press, Lyon, pp 77–82
7. Chawengsaksophak K, James R, Hammond VE, Kontgen F, Beck F (1997) Homeosis and intestinal tumours in cdx2 mutant mice. Nature 386:84–87
8. Drummond F, Putt W, Fox M, Edwards YH (1997) Cloning and chromosome assignment of the human CDX2 gene. Ann Hum Genet 61:393–400
9. Ee HC, Erler T, Bhathal PS, Young GP, James RJ (1995) Cdx-2 homeodomain protein expression in human and rat colorectal adenoma and carcinoma. Am J Pathol 147:586–592
10. Hsu SM, Raine L, Fanger H (1981) Use of avidin-biotin-peroxidase complex (ABC) in immunoperoxidase technique. J Histochem Cytochem 25:577–589
11. Jenny M, Uhl C, Roche C, Duluc I, Guillermin V, Guillemont F, Jensen J, Kendinger M, Gradwohl G (2002) Neurogenin 3 is differentially required for endocrine cell fate specification in the intestinal and gastric epithelium. EMBO J 21:6338–6347
12. Kaufmann O, Dietel M (2000) Expression of thyroid transcription factor-1 in pulmonary and extrapulmonary small cell carcinomas and other neuroendocrine carcinomas of various primary sites. Histopathology 36:415–420
13. La Rosa S, Furlan D, Sessa F, Capella C (2003) The endocrine pancreas. In: Lloyd RV (ed) Endocrine pathology. Differential diagnosis and molecular advances. Humana Press, Totowa, pp 291–328
14. La Rosa S, Rigoli E, Uccella S, Capella C (2004) CDX2 is a marker of midgut EC-cell tumors and their metastases. Lab Invest 84[Suppl 1]:108A
15. Lan HY, Mu W, Nikolic-Paterson DJ, Atkins RC (1995) A novel, simple, reliable, and sensitive method for multiple immunoenzyme staining: use of microwave oven heating to block antibody cross-reactivity and retrieve antigens. J Histochem Cytochem 43:97–102
16. Larsson LI, St-Onge L, Hougaard DM, Sosa-Pineda B, Gruss P (1998) Pax 4 and 6 regulate gastrointestinal cell development. Mech Dev 79:153–159
17. Le Dourain N (1988) On the origin of pancreatic endocrine cells. Cell 53:169–171
18. Lin X, Luckasevic T, Silverman JF, Medich D, Keenan RJ, Tung MT, Liu YL (2004) Diagnostic value of CDX2 and TTF1 expression in separating metastatic neuroendocrine neoplasms of unknown origin. Lab Invest 84[Suppl 1]:106A
19. Luckasevic TM, Silverman JF, Medich D, Celebrezze J, Tung MT, Liu YL (2004) Diagnostic value of CDX2 expression in endocrine neoplasms of gastrointestinal origin. Lab Invest 84[Suppl 1]:106A
20. Mason DY, Abdulaziz B, Falini H, Stein H (1983) Double immunoenzymatic labelling. In: Polak JM, Van Noorden S (eds) Immunocytochemistry. Practical applications in pathology and biology. Bristol, Wright, pp 113–128
21. Moskaluk CA, Zhang H, Powell SM, Cerilli LA, Hampton GM, Frierson HF Jr (2003) Cdx2 protein expression in normal and malignant human tissues: an immunohistochemical survey using tissue microarrays. Mod Pathol 16:913–919
22. Pearse AGE, Polak JM (1971) Neural crest origin of the endocrine polypeptide (APUD) cells of the gastrointestinal tract and pancreas. Gut 12:783–788
23. Pearse AGE (1973) Cell migration and the alimentary system: endocrine contribution of the neural crest to the gut and its derivatives. Digestion 8:372–385
24. Qualtrough D, Hinoi T, Fearou E, Paraskeva C (2002) Expression of CDX2 in normal and neoplastic human colon tissue and during differentiation of an in vitro model system. Gut 51:184–190
25. Silberg DG, Swain GP, Suh ER, Traber PG (2000) Cdx1 and cdx2 expression during intestinal development. Gastroenterology 119:961–971
26. Solcia E, Capella C, Fiocca R, Sessa F, La Rosa S, Rindi G (1998) Disorders of the endocrine system. In: Ming S, Goldman H (eds) Pathology of the gastrointestinal tract, 2nd edn. Williams & Wilkins, Baltimore, pp 295–322
27. Solcia E, Kloppel G, Sobin LH (eds) (2000) Histological typing of endocrine tumours. Springer, Berlin Heidelberg New York
28. Sosa-Pineda B, Chowdhury K, Torres M, Oliver G, Gruss P (1997) The Pax 4 gene is essential for differentiation of insulin-producing beta cells in the mammalian pancreas. Nature 386:399–402
29. St-Onge L, Sosa-Pineda B, Chowdhury K et al (1997) Pax 6 is required for differentiation of glucagon-producing alpha-cells in mouse pancreas. Nature 387:406–409
30. Suh ER, Traber PG (1996) An intestine-specific homeobox gene regulates proliferation and differentiation. Mol Cell Biol 16:619–625
31. Werling RW, Yaziji H, Bacchi CE, Gown AM (2003) CDX2, a high sensitive and specific marker of adenocarcinomas of intestinal origin. An immunohistochemical survey of 476 primary and metastatic carcinomas. Am J Surg Pathol 27:303–310

Virchows Arch (2004) 445:255–262
DOI 10.1007/s00428-004-1048-7

ORIGINAL ARTICLE

Mikihiko Kimura · Hitoshi Tsuda · Daisaku Morita · Takashi Ichikura · Sho Ogata · Shinsuke Aida · Yutaka Yoshizumi · Tadaaki Maehara · Hidetaka Mochizuki · Osamu Matsubara

A proposal for diagnostically meaningful criteria to classify increased epidermal growth factor receptor and c-erbB-2 gene copy numbers in gastric carcinoma, based on correlation of fluorescence in situ hybridization and immunohistochemical measurements

Received: 28 January 2004 / Accepted: 3 May 2004 / Published online: 28 July 2004
© Springer-Verlag 2004

Abstract Amplification of the epidermal growth factor receptor (EGFR) and/or c-erbB-2 oncogenes and overexpression of their proteins are detected in 30% of gastric carcinomas, but there are few reports regarding the correlation between gene amplification and protein overexpression. We examined the correlation between amplification of the EGFR and c-erbB-2 genes, detected using fluorescence in situ hybridization, and overexpression of their proteins, detected using immunohistochemistry, in formalin-fixed tissue sections of 54 surgically resected gastric carcinomas. A mean EGFR copy number per nucleus of four or more and an EGFR/chromosome 7 centromere (CEP7) ratio of 1.7 or more were each detected in 4 specimens (7%). The sensitivity and specificity of both criteria for EGFR protein overexpression were 75% and 92%, respectively. A mean c-erbB-2 copy number per nucleus of 7.0 or more and a c-erbB-2/chromosome 17 centromere (CEP17) ratio of 2.0 or more were detected in six (11%) and eight (15%) specimens, respectively. The sensitivity and specificity of the former criterion to c-erbB-2 overexpression were 83% and 98%, respectively, while those of the latter were 63% and 98%. A mean EGFR gene copy number of 4.0 or more and/or an EGFR/CEP7 ratio of 1.7 and a mean c-erbB-2 gene copy number of 7.0 or more and/or a c-erbB-2/CEP17 ratio of 2.0 or more would be useful in defining increased EGFR and c-erbB-2 gene copy numbers, respectively, in gastric carcinomas.

Keywords Epidermal growth factor receptor · C-erbB-2(HER2) · Fluorescence in situ hybridization · Immunohistochemistry · Gastric carcinoma

M. Kimura · H. Tsuda (✉) · D. Morita · O. Matsubara
Department of Pathology II,
National Defense Medical College,
3-2 Namiki, Tokorozawa, 359-8513 Saitama, Japan
e-mail: htsuda@cc.ndmc.ac.jp
Tel.: +81-042-995-1507
Fax: +81-42-996-5193

T. Ichikura · H. Mochizuki
Department of Surgery I,
National Defense Medical College,
3-2 Namiki, Tokorozawa, 359-8513 Saitama, Japan

S. Ogata · S. Aida
Department of Laboratory Medicine,
National Defense Medical College,
3-2 Namiki, Tokorozawa, 359-8513 Saitama, Japan

Y. Yoshizumi · T. Maehara
Department of Surgery II,
National Defense Medical College,
3-2 Namiki, Tokorozawa, 359-8513 Saitama, Japan

Introduction

Both the epidermal growth factor receptor (EGFR, also known as c-erbB-1) and c-erbB-2 (also known as HER2/neu) are the products of a family of growth factor receptor oncogenes with tyrosine kinase activity [1, 28]. The EGFR and/or c-erbB-2 proteins are frequently overexpressed in human cancers of various types and have been shown to be indicators of a poorer prognosis in patients with cancers of the breast, stomach, and ovary [5, 26, 31]. Recently, a humanized monoclonal antibody against c-erbB-2, trastuzumab, was developed and entered clinical use for the treatment of patients with c-erbB-2-overexpressing and/or -amplifying metastatic breast cancers [20, 22, 25]. Patients with such breast cancers can be identified as candidates for trastuzumab therapy using an appropriate combination of immunohistochemistry (IHC) and fluorescence in situ hybridization (FISH) [13, 17, 19, 23].

With regard to the EGFR, inhibitors of EGFR tyrosine phosphorylation, e.g., gefitinib, have undergone phase-I

and -II clinical trials and have been shown to be effective in some patients with various types of cancer [3, 10]. Humanized monoclonal antibodies against the EGFR, e.g., cetuximab (IMC-C225), have also undergone phase-I and -II trials as part of a combined chemotherapy regimen for patients with squamous cell carcinoma of the head and neck, lung cancer, or pancreatic cancer [4, 11, 27]. However, tests for identifying patients in whom EGFR antibody therapies would be effective have not yet been established. It is not even known whether the copy number of the EGFR gene correlates with overexpression of the EGFR protein.

In gastric carcinoma, the incidences of EGFR and c-erbB-2 overexpression and/or amplification have been reported to be 18–28% [14, 29] and 6–30% [6, 12, 21, 30], respectively. Therefore, therapeutic strategies targeted against EGFR- and/or c-erbB-2-overexpressing gastric carcinomas seem reasonable. In the present study, we examined the correlations between amplification of the EGFR and c-erbB-2 genes (as detected using FISH) and overexpression of their proteins (as detected using IHC) in gastric carcinoma specimens from 54 patients to determine whether the FISH method would be useful in accurately identifying EGFR- or c-erbB-2-overexpressing gastric carcinomas. For this purpose, criteria for evaluating gene amplification were devised and compared with the IHC scores for protein expression.

Materials and methods

Specimens

This study was carried out after approval by the internal review board and after gaining the patients' consent to use their cancer specimens for research. Surgically resected gastric carcinoma tissue specimens were obtained from 54 patients who underwent gastrectomy at the National Defense Medical College Hospital, Tokorozawa, Japan, between October 2000 and September 2002. Immediately after resection, the specimens were fixed by placing them in 10% neutral buffered formalin at room temperature for 48 h, routinely dissected, embedded in paraffin, sliced into 5-μm-thick tissue sections, and mounted on silane-coated glass slides. The sections were stained with hematoxylin-eosin (HE) and subjected to routine histological diagnostic procedures. These showed that all of the patients had adenocarcinomas (well differentiated in 13, moderately differentiated in 16, and poorly differentiated in 25). Other clinicopathological features are shown in Table 1 and Table 2.

A representative tissue block containing many carcinoma cells was selected for each specimen, and additional 5-μm- and 4-μm-thick sections were prepared for FISH and IHC, respectively. Sections of the normal gastric mucosa surrounding the cancerous lesions from five patients were used as control non-neoplastic tissues.

Fluorescence in situ hybridization

Before deparaffinization, a 1×1-cm square, the major component of which was carcinoma cells, was cut from one of the serial sections by reference to the HE-stained section. The DNA probes used were EGFR SpectrumOrange/CEP7 SpectrumGreen, and c-erbB-2 SpectrumOrange/CEP17 SpectrumGreen (Vysis Inc., Downers Grove, IL, USA). FISH was carried out following the manufacturer's protocol, with minor modifications.

The 1×1-cm sections were deparaffinized, rehydrated, and dried. After treating with 0.2 N HCl for 20 min, followed by two washes in 2×sodium saline citrate (SSC), the sections were immersed in 1 M sodium thiocyanate for 30 min at 80°C, then washed once in distilled water and twice in 2×SSC. They were then treated with either proteinase K (50 μg/ml, Boehringer-Mannheim, Mannheim, Germany) for 10 min at 37°C for EGFR detection or with a protease solution (Vysis) for 30 min at 37°C for c-erbB-2 detection, washed twice in 2×SSC, and dried. Subsequently, the sections were refixed in 10% neutral buffered formalin for 10 min followed by two washes in 2×SSC and drying.

A 10-μl aliquot of the probe was denatured for 5 min at 80°C, then immediately cooled on ice. In parallel, the sections were denatured in 70% formamide/2×SSC at 80°C for 5 min, then dehydrated in 70%, 85%, and 100% ethanol at 4°C for 1 min each. After

Table 1 Correlation between the epidermal growth factor receptor (EGFR) gene status and clinicopathological parameters. *CEP7* centromere enumeration probe of chromosome 7, *TNM* tumor node metastasis

	Number of specimens (%)		
	Total	Mean EGFR copy number of ≥4.0	EGFR/CEP7 ratio of ≥1.7
Histological differentiation of adenocarcinoma			
Well	13	1 (8)	2 (15)
Moderately and poorly	41	3 (7)	2 (5)
TNM classification (6th Edition, 2002)			
Primary tumor			
pT1	14	0 (0)	0 (0)
pT2	23	4 (17)	4 (17)
pT3, pT4	17	0 (0)	0 (0)
Regional lymph-node metastasis			
pN0	19	0 (0)	1 (5)
pN1, pN2, pN3	35	4 (11)	3 (9)
Stage grouping			
I	19	0 (0)	1 (5)
II	11	2 (18)	1 (9)
III, IV	24	2 (8)	2 (8)
Lymphatic invasion			
Negative	8	0 (0)	0 (0)
Positive	46	4 (9)	4 (9)
Venous invasion			
Negative	13	0 (0)	0 (0)
Positive	41	4 (10)	4 (10)

Table 2 Correlation between the c-erbB-2 gene status and clinicopathological parameters. *CEP17* centromere enumeration probe of chromosome 17, *TNM* tumor node metastasis

	Number of specimens (%)		
	Total	Mean c-erbB-2 copy number of ≥7.0	C-erbB-2/CEP17 ratio of ≥2.0
Histological differentiation of adenocarcinoma			
Well	13	5 (38)*	5 (38)*
Moderately and poorly	41	1 (2)*	3 (7)*
TNM classification (6th Edition, 2002)			
Primary tumor			
pT1	14	1 (7)	2 (14)
pT2	23	5 (22)	5 (22)
pT3, pT4	17	0 (0)	1 (6)
Regional lymph node metastasis			
pN0	19	2 (11)	2 (11)
pN1, pN2, pN3	35	4 (11)	6 (17)
Stage grouping			
I	19	2 (11)	2 (11)
II	11	4 (36)	5 (45)
III, IV	24	0 (0)	1 (4)
Lymphatic invasion			
Negative	8	1 (13)	1 (13)
Positive	46	5 (11)	7 (15)
Venous invasion			
Negative	13	2 (15)	2 (15)
Positive	41	4 (10)	6 (15)

*$P<0.05$

air drying, the cooled, denatured probe was applied to the sections, and a coverslip was placed on the slide. Hybridization was carried out for 14–18 h at 37°C. After hybridization, the sections were immersed in 0.3% NP40/2×SSC to remove the coverslip gently, washed in 0.3% NP40/2×SSC at 73°C for 2 min, and then in 2×SSC at room temperature for 2 min and counterstained with 4′,6-diamidine-2′-phenylindole dihydrochloride (DAPI, Vysis).

A Leica DMR fluorescence microscope (Leica, Cambridge, UK) was used to detect the EGFR and c-erbB-2 signals. The red signals representing EGFR or c-erbB-2 were acquired through a TexasRed single-band-pass filter (excitation spectrum 596 nm, absorption spectrum 620 nm), and the green signals representing CEP7 or CEP17 were acquired through a fluorescein isothiocyanate (FITC) single-band-pass filter (excitation spectrum 490 nm, absorption spectrum 520 nm). A DAPI (excitation spectrum 372 nm, absorption spectrum 456 nm) filter was used to detect the cell nuclei. Images of each microscopic field were taken using a COHU CCD camera (Leica) and saved in a Q550CW computer. The images obtained through the TexasRed filter, the FITC filter, and the DAPI filter for each microscopic field were merged using QFISH software (Leica), and 60 individual carcinoma cell nuclei were examined.

For each specimen, the number of red EGFR signals was counted for the 60 nuclei, and the mean EGFR copy number was calculated by dividing the total number of EGFR signals by 60 [18]. The mean green CEP7 copy number was also calculated by dividing the total number of CEP7 signals by 60. The EGFR/CEP7 ratio was also calculated for each specimen by dividing the total number of red EGFR signals by the total number of green CEP7 signals. In the same way, the mean c-erbB-2 copy number, the mean CEP17 copy number, and the c-erbB-2/CEP17 ratio were calculated. Although there is no established definition of EGFR gene amplification, amplification of c-erbB-2 in breast cancer was defined as a mean c-erbB-2 copy number of more than ten, or as a c-erbB-2/CEP17 ratio of 2.0 or more in one study [16].

Immunohistochemistry

The primary antibodies used for IHC were a mouse anti-EGFR monoclonal antibody (clone 31G7, 1:100 dilution; Zymed Inc., South San Francisco, CA, USA) and a rabbit anti-c-erbB-2 polyclonal antibody (1:500 dilution; Nichirei Inc., Tokyo, Japan). This polyclonal antibody is widely used in Japan, and the judgment of c-erbB-2 status using this antibody is shown to be highly concordant with those detected using HercepTest [24]. After deparaffinization, the EGFR sections were treated with 0.1% type-XXIV protease (Sigma, St. Louis, MO, USA). The c-erbB-2 sections were not subjected to antigen retrieval. After internal blockade with 5% hydrogen peroxide for 5 min, the sections were incubated with the primary antibody overnight at 4°C, then incubated with a labeled polymer (Envision+, DakoCytomation, Glostrup, Denmark) for 2 h at room temperature, and treated with 3,3′-diaminobenzidine tetrahydrochloride/hydrogen peroxide.

EGFR and c-erbB-2 expression in the carcinoma cells was scored as 2+ if the entire circumference of the cell membrane was weakly to moderately stained and as 3+ if it was strongly stained in 10% or more of the constituent carcinoma cells. A score of 1+ was given if incomplete membrane staining was observed in 10% or more of the carcinoma cells. A score of 0 was given if there was membrane staining in less than 10% of the constituent cells or no membrane staining [24].

A431 vulvar squamous cell carcinoma cell line, which shows a high-level EGFR gene amplification, and MKN7 gastric adenocarcinoma cell line, which shows a high-level c-erbB-2 gene amplification, were used as positive controls. As negative controls, sections without loading the primary antibody were used in each assay.

Statistical analysis

The correlation between the EGFR gene or c-erbB-2 gene status and the corresponding immunohistochemical staining scores was analyzed using the Mann-Whitney U test. The correlation between the EGFR and c-erbB-2 status and the clinicopathological parameters was analyzed using the chi-squared test or Fisher's exact test.

Results

EGFR and c-erbB-2 gene statuses in normal gastric mucosa and gastric carcinoma

In the five normal gastric mucosal specimens, the mean numbers of EGFR copies were 1.48, 1.59, 1.78, 1.83, and 1.85, with an overall mean of 1.71 and a SD of 0.16. The mean numbers of CEP7 copies were 1.59, 1.62, 1.76, 1.81, and 1.73, with an overall mean of 1.70 and a SD of 0.09. The mean EGFR/CEP7 ratios in these tissues were 0.93, 0.98, 1.01, 1.01, and 1.07, with an overall mean of 1.00 and a SD of 0.05. The mean numbers of c-erbB-2 copies were 1.57, 1.71, 1.73, 1.78, and 1.85, with an overall mean of 1.73 and a SD of 0.10. The mean numbers of CEP17 copies were 1.73, 1.78, 1.77, 1.78, and 1.80, with an overall mean of 1.77 and a SD of 0.03. The c-erbB-2/CEP17 ratios were 0.91, 0.96, 0.98, 1.00, and 1.03, with an overall mean of 0.98 and a SD of 0.05.

The mean number of copies of both EGFR and c-erbB-2 should theoretically be 2.0 for normal tissues. However, a substantial number of normal cell nuclei were truncated in the process of preparing the 5-μm-thick sections, and only one or two EGFR or c-erbB-2 signals was often obtained from each section.

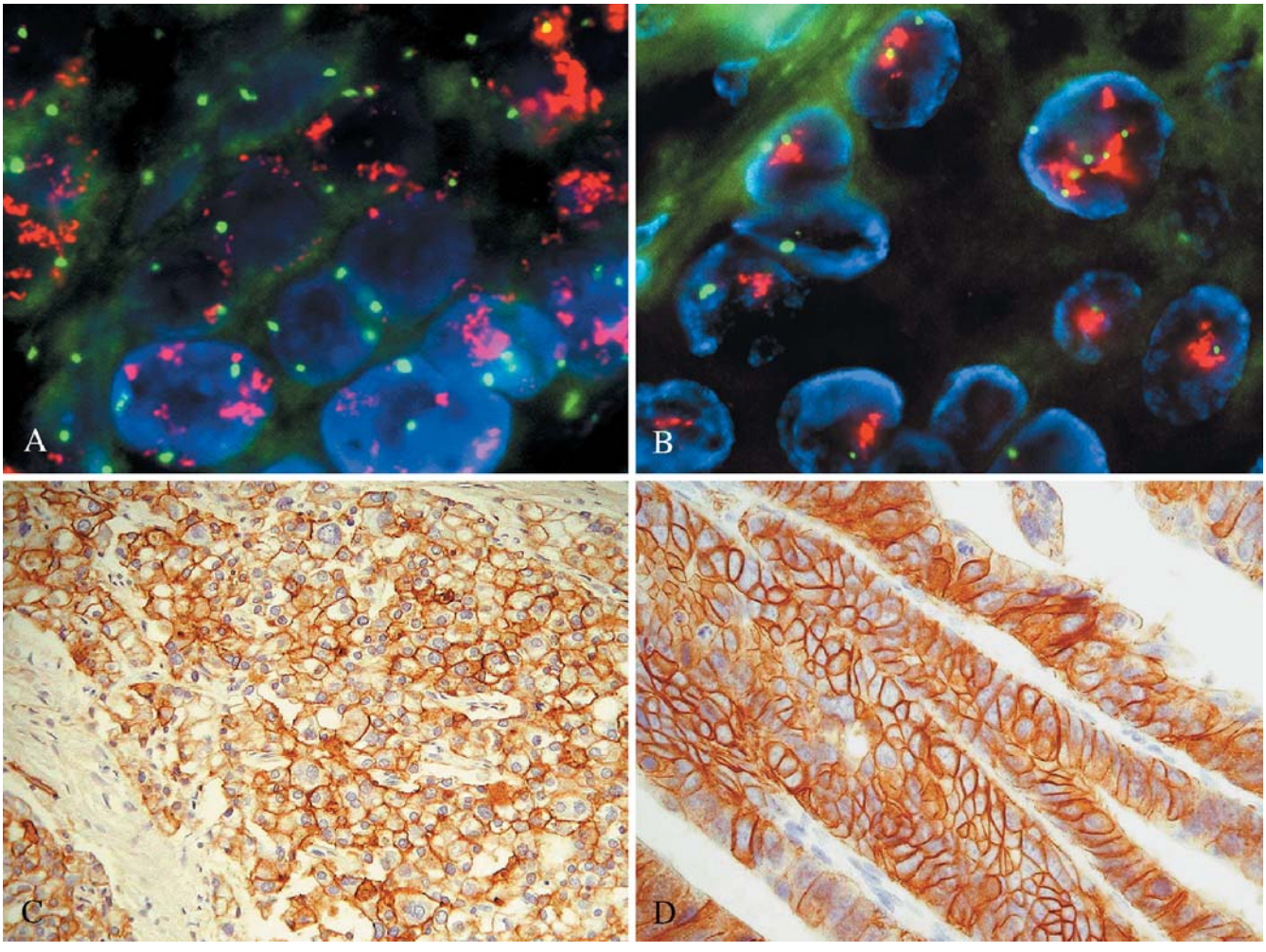


Fig. 1 Increased gene copies and protein overexpression of epidermal growth factor receptor (EGFR) and c-erbB-2 in gastric carcinomas. **A** A poorly differentiated adenocarcinoma with an increased EGFR copy number, detected using fluorescence in situ hybridization (FISH). Numerous EGFR signals (*red*) and three to five chromosome 7 centromere (CEP7) signals (*green*) are localized on the carcinoma cell nuclei (*blue*). The mean EGFR copy number was 8.2 and the EGFR/CEP7 ratio was 4.2. **B** A well-differentiated tubular adenocarcinoma with an increased c-erbB-2 copy number, detected using FISH. Numerous c-erbB-2 signals (*red*) and one to six chromosome 17 centromere (CEP17) signals (*green*) are localized on the carcinoma cell nuclei (*blue*). The mean c-erbB-2 copy number was ten, and the c-erbB-2/CEP17 ratio was 5.1. **C** Overexpression of EGFR protein, detected using immunohistochemistry (IHC), in the same specimen shown in **A**. The cell membranes of almost all the constituent carcinoma cells are strongly and entirely stained (score 3+). **D** Overexpression of c-erbB-2 protein, detected using IHC, in the same specimen shown in **B**. The cell membranes of all the constituent carcinoma cells are strongly and entirely stained (score 3+). **A** and **B** Images merged through a TexasRed filter, a fluorescein isothiocyanate filter and a 4′,6-diamidine-2′-phenylindole dihydrochloride filter, ×1000. **C** and **D** Immunoperoxidase stain, ×200

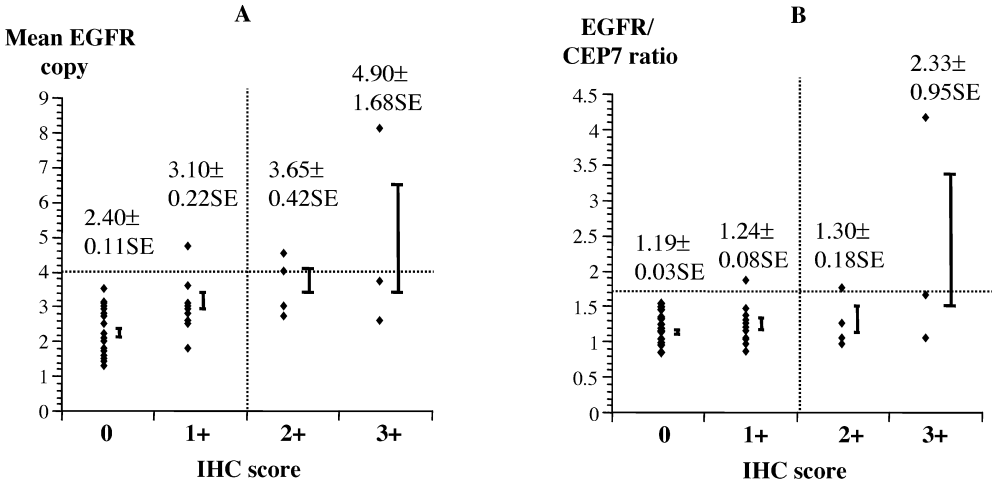


Fig. 2 Correlation between the epidermal growth factor receptor (EGFR) gene status, as detected using fluorescence in situ hybridization, and EGFR protein overexpression, as detected using immunohistochemistry (IHC). **A** The correlation between the IHC score and the mean EGFR copy number. **B** The correlation between the IHC score and the EGFR/chromosome 7 centromere (CEP7) ratio. Each *dot* indicates one specimen. The *vertical bars* indicate the range of standard errors (SE)

Regarding the 54 gastric carcinoma specimens, the mean EGFR copy number was less than 2.0 in 14, between 2.0 and 2.9 in 22, between 3.0 and 3.9 in 14, and between 4.0 and 4.9 in 3. One specimen had a mean EGFR copy number of 8.2 (Fig. 1A). The mean CEP7 copy number was less than 2.0 in 23, between 2.0 and 2.9 in 25, and between 3.0 and 3.9 in 6 specimens. The EGFR/CEP7 ratio was less than 1.0 in 4 specimens, between 1.0 and 1.6 in 46, between 1.7 and 1.9 in 3, and 2.0 or more in 1. For c-erbB-2, the mean copy number was less than 2.0 in 13 specimens, between 2.0 and 2.9 in 22, between 3.0 and 3.9 in 7, between 4.0 and 4.9 in 3, between 5.0 and 6.9 in 3, and 7.0 or more in 6. The mean CEP17 copy number was less than 2.0 in 20 specimens, between 2.0 and 2.9 in 24, between 3.0 and 3.9 in 9, and between 4.0 and 4.9 in 1. Of the 6 specimens with 7.0 or more copies, 3 had more than 10 (Fig. 1B). For all 54 specimens, the c-erbB-2/CEP17 ratio was less than 1.0 in 18, between 1.0 and 1.9 in 28, between 2.0 and 2.9 in 3, and higher than 3.0 in 5. The EGFR/CEP7 ratio of 1.7 or more and the c-erbB-2/CEP17 ratio of 2.0 or more were co-incident in two cases.

EGFR and c-erbB-2 protein scores in gastric carcinoma

In the 54 gastric carcinoma specimens, the IHC score for EGFR expression was 0 in 36 cases (67%), 1+ in 11 (20%), 2+ in 4 (7%), and 3+ in 3 (6%). A total of 7 specimens (13%) were classified as showing overexpression (Fig. 1C).

The IHC score for c-erbB-2 expression was 0 in 42 specimens (78%), 1+ in 6 (11%), 2+ in 2 (4%), and 3+ in 4 (7%). A total of 6 specimens (11%) were classified as showing overexpression (Fig. 1D).

When heterogeneity was defined as a tumor with EGFR or c-erbB-2 score of 2+/3+ in 10% or more but less than 90% of the tumor area, five and three cases were heterogeneous for the EGFR and c-erbB-2, respectively. Because we performed FISH analysis on the area of EGFR/c-erbB-2 score 2+ or 3+, we could not find clonal heterogeneity using FISH.

Correlation between FISH and IHC data for EGFR

With reference to the FISH and IHC data shown in Fig. 2, we tentatively set the criterion to define an increase in EGFR copies as a mean EGFR copy number of 4.0 or more and/or an EGFR/CEP7 ratio of 1.7 or more. With regard to the 4 specimens with a mean EGFR copy number of 4.0 or more, the sensitivity to an IHC score of 2+ or 3+ was 75% (3 of 4). In the 50 specimens with a mean EGFR copy number of less than 4.0, the specificity to an IHC score of 0 or 1+ was 92% (46 of 50).

The overall mean numbers of EGFR copies in the carcinoma groups with IHC scores of 0, 1+, 2+, and 3+ were 2.40 with a SE of 0.11, 3.10 with a SE of 0.22, 3.65 with a SE of 0.42, and 4.90 with a SE of 1.68, respectively (Fig. 2A). The overall mean number of EGFR copies differed between the carcinoma groups with IHC scores of 2+ or 3+ and those with IHC scores of 0 or 1+ ($P<0.01$).

With regard to the 6 specimens with a mean CEP7 copy number of 3.0 or more, the sensitivity to an IHC score of 2+ or 3+ was 33% (2 of 6). In the 48 specimens with a mean CEP7 copy number of less than 3.0, the specificity to an IHC score of 0 or 1+ was 90% (43 of 48).

With regard to the 4 specimens with an EGFR/CEP7 ratio of 1.7 or more, the sensitivity to an IHC score of 2+ or 3+ was 75% (3 of 4). For the 50 specimens with an EGFR/CEP7 ratio of less than 1.7, the specificity to an IHC score of 0 or 1+ was 92% (46 of 50). One specimen with an EGFR/CEP7 ratio of more than 2.0 had an IHC

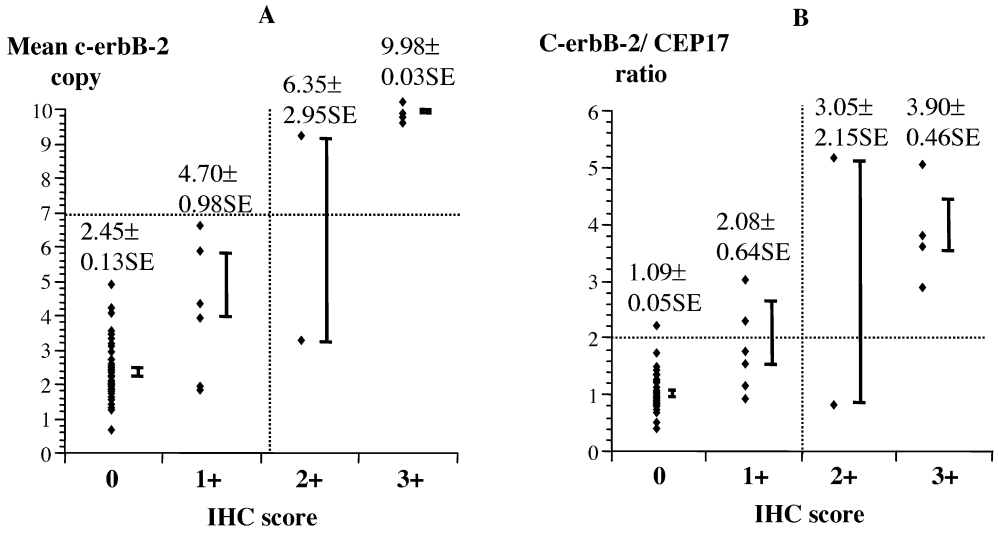


Fig. 3 Correlation between the c-erbB-2 gene status, as detected using fluorescence in situ hybridization, and c-erbB-2 protein overexpression, as detected using immunohistochemistry (IHC). **A** The correlation between the IHC score and the mean c-erbB-2 copy number. **B** The correlation between the IHC score and the c-erbB-2/chromosome 17 centromere (CEP17) ratio. Each *dot* indicates one specimen. The *vertical bars* indicate the range of standard errors (SEs)

score of 3+. The overall mean EGFR/CEP7 ratios in the carcinoma groups with IHC scores of 0, 1+, 2+, and 3+ were 1.19 with a SE of 0.03, 1.24 with a SE of 0.08, 1.30 with a SE of 0.18, and 2.33 with a SE of 0.95, respectively (Fig. 2B). The overall mean EGFR/CEP7 ratio did not differ significantly between the carcinoma groups with IHC scores of 2+ or 3+ and those with IHC scores of 0 or 1+.

Correlation of FISH and IHC data for c-erbB-2

With reference to the FISH and IHC data shown in Fig. 3, we tentatively set the criterion to define an increase in c-erbB-2 copies as a mean c-erbB-2 copy number of 7.0 or more and/or a c-erbB-2/CEP17 ratio of 2.0 or more. With regard to the 6 specimens with a mean c-erbB-2 copy number of 7.0 or more, the sensitivity to an IHC score of 2+ or 3+ was 83% (5 of 6). For the 48 specimens with a mean c-erbB-2 copy number of less than 7.0, the specificity to an IHC score of 0 or 1+ was 98% (47 of 48). The overall mean number of c-erbB-2 copies in the carcinoma groups with IHC scores of 0, 1+, 2+, and 3+ were 2.45 with a SE of 0.13, 4.70 with a SE of 0.98, 6.35 with a SE of 2.95, and 9.98 with a SE of 0.03, respectively (Fig. 3A). The overall mean c-erbB-2 copy number differed significantly between the carcinoma groups with IHC scores of 2+ or 3+ and those with IHC scores of 0 or 1+ ($P<0.01$).

With regard to the 10 specimens with a mean CEP17 copy number of 3.0 or more, the sensitivity to an IHC score of 2+ or 3+ was 20% (2 of 10). For the 44 specimens with a mean CEP17 copy number of less than 3.0, the specificity to an IHC score of 0 or 1+ was 91% (40 of 44).

With regard to the 8 specimens with a c-erbB-2/CEP17 ratio of 2.0 or more, the sensitivity to an IHC score of 2+ or 3+ was 63% (5 of 8). For the 46 specimens with a c-erbB-2/CEP17 ratio of less than 2.0, the specificity to an IHC score of 0 or 1+ was 98% (45 of 46). The overall mean c-erbB-2/CEP17 ratios in the carcinoma groups with IHC scores of 0, 1+, 2+, and 3+ were 1.09 with a SE of 0.05, 2.08 with a SE of 0.64, 3.05 with an SE of 2.15, and 3.90 with a SE of 0.46, respectively (Fig. 3B). The overall mean c-erbB-2/CEP17 ratio differed significantly between the carcinoma groups with IHC scores of 2+ or 3+ and those with IHC scores of 0 or 1+ ($P<0.01$).

Correlations between EGFR or c-erbB-2 statuses and clinicopathological parameters

The EGFR gene status, as detected using FISH, did not correlate with the degree of differentiation of the carcinoma cells (Table 1). A mean EGFR copy number of 4.0 or more or an EGFR/CEP7 ratio of 1.7 or more did not correlate with the depth of tumor invasion (pT-factor), regional lymph-node status (pN-factor), stage grouping by tumor node metastasis (TNM) classification, and presence of lymphatic or venous invasion. There was also no correlation between the IHC score for EGFR protein and the clinicopathological parameters (data not shown).

A mean c-erbB-2 copy number of 7.0 or more and a c-erbB-2/CEP17 ratio of 2.0 or more were detected in 38% and 38%, respectively, in the group of well-differentiated adenocarcinoma, whereas these were detected in 2% and 7%, respectively, in the group of moderately differentiated adenocarcinoma and poorly differentiated adenocarcinoma ($P<0.05$, Table 2). The increase in the c-erbB-2 copy numbers did not correlate with the pT-factor, pN-factor, stage grouping by TNM classification, and pres-

ence of lymphatic or venous invasion. There was also a correlation between the IHC score for c-erbB-2 protein and the degree of histological differentiation of the gastric carcinoma (data not shown).

Discussion

It would be difficult to define gene amplification, or a significant increase in the gene copy number, in carcinomas if gene amplification does not correlate with overexpression of the corresponding protein. Therefore, in the present study, we tried to determine diagnostically meaningful criteria to define increases in the EGFR and c-erbB-2 gene copy numbers that correlate with IHC scores of 2+ or 3+ in gastric carcinoma.

The EGFR gene is often amplified in esophageal carcinoma and glioblastoma, and this is associated with overexpression of its protein [2, 9]. However, EGFR gene amplification is infrequent in gastric cancer, and the correlation between amplification of the gene and overexpression of its protein has not been clearly shown. Lemoine et al. studied this correlation using Southern blotting and IHC [14]. They found EGFR overexpression not only in one of two gastric cancers with EGFR gene amplification, but also in six of seven cancers without EGFR gene amplification. However, their cut-off value for EGFR gene amplification using Southern blotting was more than five-fold per haploid, and this value might have been too high to allow detection of any correlation with protein overexpression.

In the present study, we set the criteria for defining an increase in the EGFR gene copy number as a mean EGFR gene copy number of 4.0 or more and/or an EGFR/CEP7 ratio of 1.7 after preliminary consideration of several tentative cut-off values. Although the correlation between an increased EGFR gene copy status and an IHC score of 2+ or 3+ was not perfect, the sensitivity and specificity appeared to be substantial. Although the level of increase in the EGFR gene copy number described by these criteria is so low that it would be difficult to define it specifically as gene amplification, there does seem to be some kind of "dose effect" of the EGFR gene on the overexpression of its protein. In breast cancer, a striking difference in the rate of c-erbB-2 gene amplification has been shown between specimens with an IHC score of 2+ and those with an IHC score of 3+ for the c-erbB-2 protein expression level [15, 23]. However, the degree of EGFR overexpression (2+ versus 3+) did not seem to differ according to an increase in the EGFR gene copy number in gastric carcinoma. At this stage, both examinations of gene amplification and protein overexpression would be necessary for the evaluation of EGFR status in individual gastric carcinomas.

IHC studies have reported the incidence of c-erbB-2 overexpression in gastric carcinoma to be 6–30% [6, 21, 30], whereas amplification of the c-erbB-2 gene has been reported to occur in 18% of specimens analyzed using FISH. Using this technique, Ishikawa et al. reported that, in their series, all gastric carcinoma specimens with c-erbB-2 amplification also showed overexpression of the protein [12]. In the present study, c-erbB-2 overexpression as defined by an IHC score of 2+ or 3+ was detected in six specimens (11%), whereas six specimens had a mean c-erbB-2 copy of 7.0 or more and eight had a c-erbB-2/CEP17 ratio of 2.0 or more, as detected using FISH. Based on these criteria, the FISH results correlated well with the IHC results. The criterion for c-erbB-2 amplification routinely used for metastatic breast cancer (a c-erbB-2/CEP17 ratio of $\geq$2.0) [7], thus, appears to be applicable to gastric cancer. In addition, we suggest that a mean c-erbB-2 copy number of seven or more per nucleus would also be useful in identifying c-erbB-2-overexpressing gastric carcinomas.

In previous immunohistochemical studies, both EGFR and c-erbB-2 were found to occur more frequently in differentiated-type adenocarcinomas than in undifferentiated-type adenocarcinomas of the stomach [8, 29]. However, there are no reports examining the correlation between EGFR gene amplification and the histological typing of gastric carcinomas. In the present study, neither a mean EGFR copy number of 4.0 or more nor an EGFR/CEP7 ratio of 1.7 or more correlated with the degree of differentiation of the adenocarcinoma. In contrast, c-erbB-2 gene amplification was confirmed to be correlated with well-differentiated-type adenocarcinoma. However, we could find no correlations between an increased EGFR or c-erbB-2 gene copy number and the extent of tumor invasion or the presence of lymph-node metastasis.

In summary, we showed that increased DNA copy numbers of both EGFR and c-erbB-2, as detected using FISH, correlated well with overexpression of their proteins, as detected using IHC, in gastric carcinoma. The cut-off values for defining increased copy numbers will, however, differ between the genes, according to the degree of correlation between the results of FISH and IHC. The FISH analysis could be a reliable test for the identification of gastric carcinomas with c-erbB-2 overexpression, and suitable candidates for antibody therapies targeted against the c-erbB-2 could be identified using IHC, FISH, or both. To date, it is not clear whether these cut-off values of the EGFR are relevant to therapy response in the same way as the case of the c-erbB-2.

Acknowledgements Supported in part by Grants-in-Aid from the Foundation for the Promotion of Cancer Research, Japan, the Chugai Pharmaceutical Co., Japan, the Fujisawa Pharmaceutical Co., Japan, and the Taiho Pharmaceutical Co., Japan, and a Grant-in-Aid to young researchers from the National Defense Medical College, Tokorozawa, Japan.

References

1. Akiyama T, Sudo C, Ogawara H, Toyoshima K, Yamamoto T (1986) The product of the human c-erbB-2 gene: a 185-kilodalton glycoprotein with tyrosine kinase activity. Science 232:1644–1646

2. al-Kasspooles M, Moore JH, Orringer MB, Beer DG (1993) Amplification and over-expression of the EGFR and erbB-2 genes in human esophageal adenocarcinomas. Int J Cancer 54:213–219
3. Baselga J, Rischin D, Ranson M, Calvert H, Raymond E, Kieback DG, Kaye SB, Gianni L, Harris A, Bjork T, Averbuch SD, Feyereislova A, Swaisland H, Rojo F, Albanell J (2002) Phase I safety, pharmacokinetic, and pharmacodynamic trial of ZD1839, a selective oral epidermal growth factor receptor tyrosine kinase inhibitor, in patients with five selected solid tumor types. J Clin Oncol 20:4292–4302
4. Bunn PA Jr, Franklin W (2002) Epidermal growth factor receptor expression, signal pathway, and inhibitors in non-small cell lung cancer. Semin Oncol 29:38–44
5. Costa MJ, Walls J (1996) Epidermal growth factor receptor and c-erbB-2 oncoprotein expression in female genital tract carcinosarcomas (malignant mixed mullerian tumors). Clinicopathologic study of 82 cases. Cancer 77:533–542
6. David L, Seruca R, Nesland JM, Soares P, Sansonetty F, Holm R, Borresen AL, Sobrinho-Simoes M (1992) c-erbB-2 expression in primary gastric carcinomas and their metastases. Mod Pathol 5:384–390
7. Ellis IO, Dowsett M, Bartlett J, Walker R, Cooke T, Gullick W, Gusterson B, Mallon E, Lee PB (2000) Recommendations for HER2 testing in the UK. J Clin Pathol 53:890–892
8. Falck VG, Gullick WJ (1989) c-erbB-2 oncogene product staining in gastric adenocarcinoma. An immunohistochemical study. J Pathol 159:107-111
9. Fleming TP, Saxena A, Clark WC, Robertson JT, Oldfield EH, Aaronson SA, Ali IU (1992) Amplification and/or overexpression of platelet-derived growth factor receptors and epidermal growth factor receptor in human glial tumors. Cancer Res 52:4550–4553
10. Fukuoka M, Yano S, Giaccone G, Tamura T, Nakagawa K, Douillard JY, Nishiwaki Y, Vansteenkiste J, Kudoh S, Rischin D, Eek R, Horai T, Noda K, Takata I, Smit E, Averbuch S, Macleod A, Feyereislova A, Dong RP, Baselga J (2003) Multi-institutional randomized phase II trial of gefitinib for previously treated patients with advanced non-small-cell lung cancer. J Clin Oncol 21:2237–2246
11. Herbst RS, Hong WK (2002) IMC-C225, an anti-epidermal growth factor receptor monoclonal antibody for treatment of head and neck cancer. Semin Oncol 29:18–30
12. Ishikawa T, Kobayashi M, Mai M, Suzuki T, Ooi A (1997) Amplification of the c-erbB-2 (HER-2/neu) gene in gastric cancer cells. Detection by fluorescence in situ hybridization. Am J Pathol 151:761–768
13. Jacobs TW, Gown AM, Yaziji H, Barnes MJ, Schnitt SJ (1999) Specificity of HercepTest in determining HER-2/neu status of breast cancers using the United States Food and Drug Administration-approved scoring system. J Clin Oncol 17:1983–1987
14. Lemoine NR, Jain S, Silvestre F, Lopes C, Hughes CM, McLelland E, Gullick WJ, Filipe MI (1991) Amplification and overexpression of the EGF receptor and c-erbB-2 proto-oncogenes in human stomach cancer. Br J Cancer 64:79–83
15. Mass RD, Sanders C, Kasian C, Johnson L, Everett T, Anderson S (2000) The concordance between the clinical trials assay (CTA) and fluorescence in situ hybridization (FISH) in the herceptin pivotal trials (abstract). Proc Am Soc Clin Oncol 18:75
16. Pauletti G, Godolphin W, Press MF, Slamon DJ (1996) Detection and quantitation of HER-2/neu gene amplification in human breast cancer archival material using fluorescence in situ hybridization. Oncogene 13:63–72
17. Pauletti G, Dandekar S, Rong H, Ramos L, Peng H, Seshadri R, Slamon DJ (2000) Assessment of methods for tissue-based detection of the HER-2/neu alteration in human breast cancer: a direct comparison of fluorescence in situ hybridization and immunohistochemistry. J Clin Oncol 18:3651–3664
18. Persons DL, Bui MM, Lowery MC, Mark HF, Yung JF, Birkmeier JM, Wong EY, Yang SJ, Masood S (2000) Fluorescence in situ hybridization (FISH) for detection of HER-2/neu amplification in breast cancer: a multicenter portability study. Ann Clin Lab Sci 30:41–48
19. Press MF, Slamon DJ, Flom KJ, Park J, Zhou JY, Bernstein L (2002) Evaluation of HER-2/neu gene amplification and overexpression: comparison of frequently used assay methods in a molecularly characterized cohort of breast cancer specimens. J Clin Oncol 20:3095–3105
20. Seidman AD, Fornier MN, Esteva FJ, Tan L, Kaptain S, Bach A, Panageas KS, Arroyo C, Valero V, Currie V, Gilewski T, Theodoulou M, Moynahan ME, Moasser M, Sklarin N, Dickler M, D'Andrea G, Cristofanilli M, Rivera E, Hortobagyi GN, Norton L, Hudis CA (2001) Weekly trastuzumab and paclitaxel therapy for metastatic breast cancer with analysis of efficacy by HER2 immunophenotype and gene amplification. J Clin Oncol 19:2587–2595
21. Shun CT, Wu MS, Lin JT, Chen SY, Wang HP, Lee WJ, Wang TH, Chuang SM (1997) Relationship of p53 and c-erbB-2 expression to histopathological features, Helicobacter pylori infection and prognosis in gastric cancer. Hepatogastroenterology 44:604–609
22. Slamon DJ, Leyland-Jones B, Shak S, Fuchs H, Paton V, Bajamonde A, Fleming T, Eiermann W, Wolter J, Pegram M, Baselga J, Norton L (2001) Use of chemotherapy plus a monoclonal antibody against HER2 for metastatic breast cancer that overexpresses HER2. N Engl J Med 344:783–792
23. Tsuda H, Akiyama F, Terasaki H, Hasegawa T, Kurosumi M, Shimadzu M, Yamamori S, Sakamoto G (2001) Detection of HER-2/neu (c-erb B-2) DNA amplification in primary breast carcinoma. Interobserver reproducibility and correlation with immunohistochemical HER-2 overexpression. Cancer 92: 2965–2974
24. Tsuda H, Tani Y, Hasegawa T, Fukutomi T (2001) Concordance in judgments among c-erbB-2 (HER2/neu) overexpression detected by two immunohistochemical tests and gene amplification detected by Southern blot hybridization in breast carcinoma. Pathol Int 51:26–32
25. Vogel CL, Cobleigh MA, Tripathy D, Gutheil JC, Harris LN, Fehrenbacher L, Slamon DJ, Murphy M, Novotny WF, Burchmore M, Shak S, Stewart SJ, Press M (2002) Efficacy and safety of trastuzumab as a single agent in first-line treatment of HER2-overexpressing metastatic breast cancer. J Clin Oncol 20:719–726
26. Wright C, Angus B, Nicholson S, Sainsbury JR, Cairns J, Gullick WJ, Kelly P, Harris AL, Horne CH (1989) Expression of c-erbB-2 oncoprotein: a prognostic indicator in human breast cancer. Cancer Res 49:2087–2090
27. Xiong HQ, Abbruzzese JL (2002) Epidermal growth factor receptor-targeted therapy for pancreatic cancer. Semin Oncol 29:31–37
28. Xu YH, Richert N, Ito S, Merlino GT, Pastan I (1984) Characterization of epidermal growth factor receptor gene expression in malignant and normal human cell lines. Proc Natl Acad Sci U S A 81:7308–7312
29. Yasui W, Sumiyoshi H, Hata J, Kameda T, Ochiai A, Ito H, Tahara E (1988) Expression of epidermal growth factor receptor in human gastric and colonic carcinomas. Cancer Res 48:137–141
30. Yonemura Y, Ninomiya I, Ohoyama S, Kimura H, Yamaguchi A, Fushida S, Kosaka T, Miwa K, Miyazaki I, Endou Y et al (1991) Expression of c-erbB-2 oncoprotein in gastric carcinoma. Immunoreactivity for c-erbB-2 protein is an independent indicator of poor short-term prognosis in patients with gastric carcinoma. Cancer 67:2914–2918
31. Yonemura Y, Sugiyama K, Fushida S, Kamata T, Ohoyama S, Kimura H, Yamaguchi A, Miyazaki I (1991) Tissue status of epidermal growth factor and its receptor as an indicator of poor prognosis in patients with gastric cancer. Anal Cell Pathol 3:343–350

Virchows Arch (2004) 445:263–270
DOI 10.1007/s00428-004-1033-1

ORIGINAL ARTICLE

Femke Vlems · Erik van der Worp · Jeroen van der Laak · Cornelis van de Velde · Iris Nagtegaal · Han van Krieken

A study into methodology and application of quantification of tumour vasculature in rectal cancer

Received: 16 December 2003 / Accepted: 1 April 2004 / Published online: 28 May 2004
© Springer-Verlag 2004

Abstract The application of new surgical techniques in combination with preoperative radiotherapy has minimised the risk of local recurrence in rectal cancer. However, distant metastasis is still a serious problem after seemingly curative resection in patients with rectal cancer. The present study aimed to evaluate the methodology for quantification and the characteristics of the tumour vasculature in relation to the development of metastasis in patients with rectal cancer. From a large multicentre trial, 88 patients were selected, ensuring a relatively high percentage of metastasis. This selection facilitates the study of tumour vasculature characteristics in relation to metastasis. Vessel number, perimeter and area were assessed at both the invasive front and intratumoural area. Hot-spot and random selections were performed simultaneously. The median of each vessel parameter in the study population was used to separate patients into a low- and high-vessel group. Differences in development of distant metastasis were studied between low- and high-vessel groups. The data of the present study show that only vascular perimeter randomly assessed at the invasive front was associated with distant metastasis. Patients with a high score had a lower distant metastasis rate than patients with a low score (37% and 62%, respectively). High-vessel perimeter was independent of tumor node metastasis staging, but was associated with an increased presence of immune cells, comprising T cells, mast cells, eosinophils and neutrophils. This methodological study on the biological relevance of various vessel characteristics showed that a large vascular endothelial surface, as reflected by a high perimeter, was the only vessel characteristic indicative of improved patient outcome. The underlying principle for this association may be the improved immune response.

Keywords Rectal cancer · Angiogenesis · Microvessel perimeter · Prognosis · Random spots · Invasive front · Computerised-image analysis

F. Vlems · E. van der Worp · J. van der Laak · I. Nagtegaal · H. van Krieken (✉)
Department of Pathology, UMC Nijmegen,
PO Box 9101, 6500 HB Nijmegen, The Netherlands
e-mail: j.vankrieken@pathol.umcn.nl
Tel.: +31-24-3614352
Fax: +31-24-3540520

C. van de Velde
Department of Surgery,
LUMC, PO Box 9600, 2300 RC Leiden, The Netherlands

Introduction

In rectal cancer, the only option for cure is complete resection of the tumour. However, local recurrence has been a major problem for a long time [13, 15]. The introduction of standardised total mesorectal resection (TME) substantially reduced the local recurrence rate, since adequate surgery is a prerequisite for local control in rectal cancer [1, 9, 20]. Recently, results of a large randomised trial have shown that short-term preoperative radiotherapy further reduces the risk of local recurrence in patients with rectal cancer to about 2.5 percent after 2 years of follow-up [16].

Now that the problem of local recurrence is better controlled, the most important threat after seemingly curative resection of rectal cancer is distant metastasis. In general, tumour node metastasis (TNM) staging at presentation is the most important prognostic factor. However, with the introduction of immunohistochemical and molecular techniques, the relevance of several tumour-related parameters have been evaluated to improve the TNM-based prognosis. Angiogenesis, which is one of these parameters intensively studied, is known to play an important role in tumour growth, invasion and metastasis [10, 19]. It is assumed that intratumoural microvessel density reflects the intensity of tumour angiogenesis. Several studies have found an association between high microvessel density and tumour aggressiveness and, thus, shorter (disease-free) survival in patients with colorectal cancer [27, 29, 30, 35]. However, the correlation between high microvessel density and worse prognosis is disputed. Some studies could not demonstrate any correlation [2, 4,

Table 1 Patients' characteristics. *n.s.* not significant, *TME* total mesorectal resection, *TNM* tumour node metastasis, *RT* radiotherapy

		RT+TME	TME	*P* value
Gender	Male	29	26	n.s.
	Female	12	21	
Age	Mean	64.7	63.2	n.s.
TNM stage	I	8	4	n.s.
	II	7	7	
	III	21	30	
	IV	5	6	
Tumour diameter	≤4 cm	25	22	n.s.
	>4 cm	13	24	
Tumour type	Adenocarcinoma	34	47	0.003
	Mucinous carcinoma	7		
Differentiation grade	Well/moderate	21	32	n.s.
	Poor/undifferentiated	20	15	
Growth pattern	Circumscribed	27	28	n.s.
	Diffuse	13	18	
Inflammatory infiltrate	None/few	40	39	0.024
	Moderate/extensive	1	8	

25], while others reported high microvessel density in patients with prolonged survival [18, 26].

Methodological differences between studies in microvessel staining and counting may, at least partly, explain the conflicting results [7, 8, 11, 21]. Most studies now use a protocol to quantify angiogenesis based on an international consensus method that was described by Vermeulen et al., which assesses intratumoural microvessel density in hot spots. However, even then, various difficulties will arise, including the low reproducibility of hot-spot determination [12, 34]. Moreover, some important matters are left unresolved when this consensus method is used. The number of vessels is simply counted, while other characteristics of the vessels, such as perimeter and area, may be more important, since they reflect the endothelial surface and volume of blood available for interaction with the tumour [11]. The vessel density is determined intratumoural, whereas the invasive front of the tumour, where the contact between tumour and surrounding stoma is maximal, may be more indicative for prognosis [5]. In addition, the make-up of the clinical study population varies between studies and makes comparisons between studies difficult.

The present study aimed to evaluate some of the important issues regarding tumour vasculature and prognosis. In a selected group of patients with rectal cancer, microvessels were assessed in hot spots and random spots. Tumour vasculature was quantitatively characterised on three different points: number, perimeter and area. A comparison was made between the intratumoural region and the invasive front. Finally, the association between vessel quantification and development of distant metastasis was studied.

Materials and methods

Patients

Patients were selected from a large multicentre trial for patients with rectal cancer [6]. In this randomised trial, the additional value of preoperative radiotherapy was studied when TME was applied. Radiotherapeutical, surgical and pathological procedures were standardised and quality controlled [23]. To study the relationship between the characteristics of the tumour vasculature and development of distant metastasis in patients with rectal cancer, 88 patients were artificially selected, ensuring a high rate of distant metastases. At the time of surgery, 11 of these patients had distant metastases. Of the remaining 77 patients, 9 patients developed local recurrence, 21 patients distant metastases and 8 patients both local recurrence and distant metastases at time of selection, after a median follow-up of 25 months (range 0.7–43.5 months). At the moment of selection, 39 patients were disease free. However, at the time of writing, after completion of the study, more recurrences had developed, and this was taken into account for the results. This selection of patients implies that survival percentages in this study cannot be extrapolated towards the general patient population. However, due to the increased tumour recurrence rate, the selection renders an outstanding circumstance to study the biological relevance of various vessel characteristics. Patients' characteristics are summarised in Table 1. Clinical and pathological characteristics were equally distributed among the randomisation groups, except that, as expected, there were more mucinous tumours, and there was less lymphocyte reaction in the irradiated group (Table 1). Distant and local recurrences were checked by a radiation oncologist using radiological and/or histological confirmation.

Microvessel staining

Tissue sections of 4 μm were cut from representative formalin-fixed and paraffin-embedded tissue blocks containing the invasive front of the primary tumour. Our blocks included the area of deepest invasive growth of the tumour in all cases. Sections were deparaffinised in xylene and rehydrated. Endogenous peroxidase was blocked with 1% hydrogen peroxide in phosphate buffered saline (PBS) for 30 min. Sections were pre-treated with 0.1% pronase in PBS to retrieve antigen expression. After overnight incubation at 4°C with the primary anti-endothelial antibody CD31 (1:400, Dako, Glostrup, Denmark) in PBS/1% bovine serum albumin, the slides were washed with PBS, and the secondary biotin-conjugated anti-mouse antibody (Vectastain Elite ABC kit; Vector Laboratories, Burlingame, California, USA) was applied for 30 min at room temperature. Then the slides were washed and incubated with the aviditin-biotin peroxidase complex complex (Vectastain Elite ABC kit) for 45 min at room temperature. The slides were washed once more, and the reactions were visualised with 3′,3′-diaminobenzidine. Finally, the sections were counterstained with Mayer's haematoxylin for 10 s and mounted with paramount. All incubations were performed in a humidified chamber.

Microvessel evaluation

The Vidas^{Plus} system (Kontron GmbH, Eching, Germany) was used to evaluate the CD31 expression. Conventional light microscope images (×10 objective, NA=0.3) were recorded by a three-chip CCD camera (DXC-325P, Sony). The computerised analysis classified image pixels as either object pixels, representing the brown colour of the stained endothelial cells, or background pixels. In each measured image, three different microvessel parameters were assessed, describing the microvessel number per mm^2, the microvessel perimeter per mm^2 and the microvessel area per mm^2.

In each tissue section, three images were analysed at the invasive front and three within the tumour mass using both hot-spot and random selection. Mean microvessel number, microvessel perimeter and microvessel area values were calculated for every three images. The invasive front was defined as the first layers of tumour cells invading the adjacent tissue resulting in a field containing 50% tumour and 50% adjacent tissue. Tumour mass images contained 100% tumour tissue, avoiding areas of ulceration and necrosis. Hot spots, which represent the area with the highest microvessel density [37], were identified by scanning the tissue section with a ×4 objective. Random spots were selected in the tissue outside the hot spots. The mean value of the different vessel characteristics (number, perimeter and area) was calculated of the three analysed images in each section. This was done at both the invasive front and intratumoural area using two different measuring methods (hot spot and random). The median of each vessel parameter in the study population was used to separate the patients into two categories: a low and a high group.

Immune-response evaluation

In a previous study, the inflammatory infiltrate of the tumours had been characterised in detail [24]. These results were used to examine the correlation between the vessel results and the immune response. This previous study has assessed the presence of various inflammatory cells using immunohistochemical investigation. The studied cell types comprise: T cells, CD4-positive T cells, CD8-positive T cells, eosinophils, neutrophils, mast cells, macrophages and NK cells.

Statistical analysis

Differences between groups were studied by (un)paired student's *t*-test, χ^2-test and Mann Whitney U test. Associations between parameters were analysed using the Pearsons' correlation. The Kaplan Meier method was used to perform univariate survival analysis of time to distant metastasis and death, with the time of randomisation as entry date. Log-rank tests were used to study the differences in observed survival between groups. Survival analyses were performed with and without stratification for the randomisation arm. Data were analysed using the SPSS software package (SPSS 10.0 for windows, SPSS Inc., Chicago, Illinois, USA). At $P<0.05$, differences were considered significant.

Results

Patients

At surgery, 11 patients had distant metastases and were not included in the follow-up analysis. At time of writing, the median follow-up of the remaining 77 patients was extended to 46 months (range 3–82 months), and new cases of local recurrence, distant metastasis and death had occurred: 6 patients had local recurrence, 27 patients had distant metastases, 12 patients had both and 43 patients died. Survival rates after 4 years of follow-up were 74%, 71%, 39% and 18% for TNM stage-I, -II, -III and -IV patients, respectively.

Microvessels

Table 2 gives an overview of the microvessel results. For all parameters studied, vessel results were significantly higher ($P<0.001$) in the hot spots than in their random counterpart (Table 2). Comparison of the results at the invasive front with the intratumoural results revealed that the hot spots within the tumour mass contained more vessels and had a higher perimeter ($P=0.004$ and $P<0.001$, respectively) (Table 2). The vessel area was larger at the invasive front ($P=0.008$) (Table 2). Therefore, vessels at the invasive front are larger, but less numerous than those that are intratumoural.

Vessel perimeter assessed in hot spots within the tumour mass was significantly lower in patients treated with preoperative radiotherapy (mean: 0.0196/mm^2) than in patients treated using surgery alone (mean: 0.0230/mm^2) ($P=0.038$). For the other vessel parameters, there was no difference between the two randomisation groups. However, vessel number assessed in hot spots within the tumour mass, vessel number assessed in random spots at the

Table 2 Vessel results

	Hot-spot measurements (/mm^2)		Random measurements (/mm^2)		*P* value[a]
	Mean	Range	Mean	Range	
Vessel number					
Invasive front	272[b]	66–518	179	28–468	<0.001
Intratumoral	314[b]	106–718	203	0–582	<0.001
Vessel perimeter					
Invasive front	0.0183[c]	0.01–0.04	0.0112	0.00–0.03	<0.001
Intratumoral	0.0214[c]	0.01–0.04	0.0116	0.00–0.04	<0.001
Vessel area					
Invasive front	5.6	1.9–12.5	3.0[d]	0.7–7.4	<0.001
Intratumoral	5.9	1.6–13.1	2.4[d]	0.0–7.4	<0.001

[a] *P* value for difference between hot-spot and random measurements, paired *t*-test
[b] The intratumoral vessel number was significantly higher, paired *t*-test, $P=0.004$
[c] The intratumoral vessel perimeter was significantly higher, paired *t*-test, $P<0.001$
[d] The vessel area at the invasive front was significantly higher, paired *t*-test, $P=0.008$

Table 3 Log-rank analyses for distant metastasis among M_0 patients according to vessel results. *n.s.* not significant

	Random		Hot spot	
	Low-high[a]	*P* value[b]	Low-high[a]	*P* value[b]
Invasive front				
Number	42–56%	n.s.	44–58%	n.s.
Perimeter	37–62%	0.003	50–51%	n.s.
Area	43–57%	n.s.	50–52%	n.s.
Intratumoral				
Number	51–51%	n.s.	44–59%	n.s.
Perimeter	54–48%	n.s.	47–56%	n.s.
Area	50–51%	n.s.	48–56%	n.s.

[a] Disease-free survival at 4 years for low- and high-vessel group
[b] *P* value for unstratified log rank analyses. Stratified analyses resulted in comparable results

invasive front and vessel perimeter assessed in random spots at the invasive front tended to be lower (although not significant) in the radiotherapy group (P=0.071, P=0.071, P=0.076, respectively). Thus, the influence of radiotherapy on vascular counts is limited, especially using random field selection.

Microvessels and prognosis

The median microvessel result was used as a cut-off point to separate the patients in a low- and a high-vessel group for each parameter. None of the vessel parameters was associated with the TNM stage, and our results are, therefore, independent of TNM stage. In the group of patients that had no metastasis at time of operation and that were considered for follow-up analysis, only the perimeter assessed in random spots at the invasive front was significantly associated with the development of distant metastasis (Table 3). High perimeter at the invasive front increased the chance of disease-free and overall survival (Fig. 1).

Random perimeter at the invasive front and clinicopathological parameters

We evaluated whether the vessel perimeter randomly assessed at the invasive front was linked to several clinicopathological parameters, such as tumour growth and tumour type. The level of vessel perimeter (low versus high) did not associate with any of the parameters studied (Table 4).

Random perimeter at the invasive front and immune response

High numbers of intratumoural T cells, intratumoural CD8+ cells, peritumoural eosinophils, peritumoural mast cells and intra and peritumoural neutrophils were significantly associated with high-vessel perimeter assessed in random spots at the invasive front (Table 5). Because

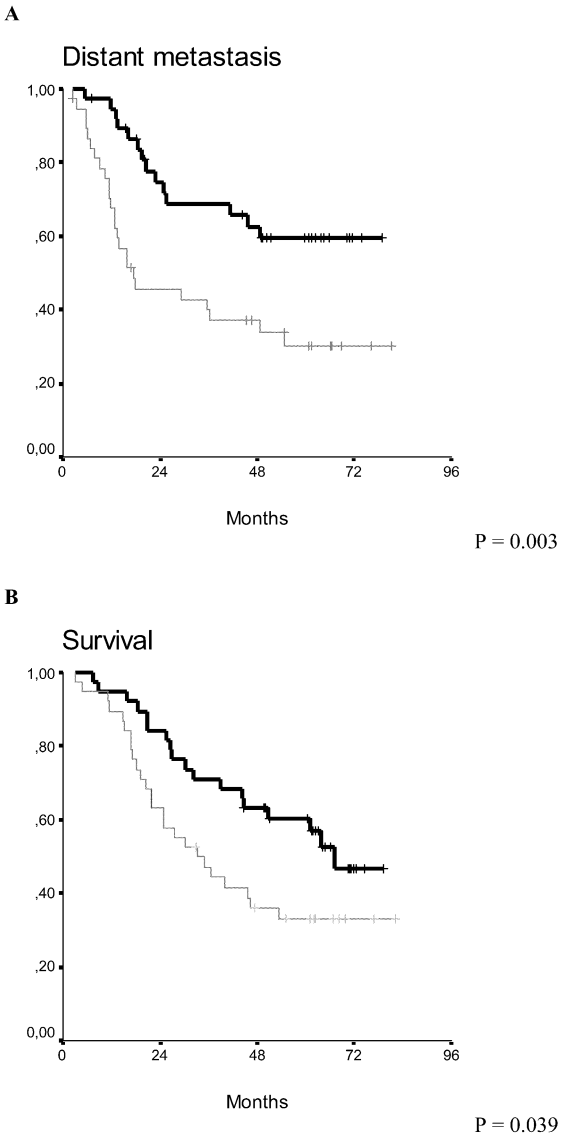


Fig. 1 Kaplan-Meier disease-free survival (**A**) and overall survival (**B**) curves according the results of random measurements of the perimeter at the invasive front separated into two groups of patients (only M0 patients): low (*grey line*) and high (*black line*) perimeter

differences in cell counts were observed between both randomisation groups [24], the analyses were also performed in both groups separately. The association between high-vessel perimeter and high numbers of intratumoural T cells and CD8+ cells tended to be present i n both randomisation groups, but was not statistically significant, probably due to the reduced number of patients. The association between high-vessel perimeter and high numbers of peritumoural eosinophils was statistically significant in the non-radiotherapy group (P=0.041), and, in the radiotherapy group, there was a strong trend towards significance (P=0.059). The association between high-vessel perimeter and high numbers of peritumoural mast cells and intratumoural neutrophils was only statistically significant in the non-radiotherapy group

Table 4 Clinicopathological parameters of patients in the low and high category of vessel perimeter randomly measured at the invasive front. *n.s.* not significant

	Perimeter		*P* value
	Low	High	
Depth of penetration			
T2	11	15	n.s.
T3	31	28	
T4	2		
Lymph metastasis			
N0	13	14	n.s.
N+	31	29	
Distant metastases			
M0	38	38	n.s.
M1	6	5	
Tumour diameter			
≤4 cm	38	38	n.s.
>4 cm	6	5	
Tumour type			
Adenocarcinoma	39	42	n.s.
Mucinous	5	1	
Differentiation grade			
Well/moderate	27	26	n.s.
Poor/undifferentiated	17	17	
Growth pattern			
Circumscribed	26	28	n.s.
Diffuse	17	14	
Inflammatory infiltrate			
None/few	42	36	n.s.
Moderate/extensive	2	7	
Radiotherapy			
Yes	22	18	n.s.
No	22	25	

(*P*=0.022 and *P*=0.011, respectively); whereas, in the radiotherapy group, there was only a very weak trend towards significance (*P*=0.12 and *P*=0.25). The presence of high numbers of peritumoural neutrophils was strongly associated with high-vessel perimeter in the radiotherapy group (*P*=0.002); whereas, this relationship was not observed in the non-radiotherapy group (*P*=0.89).

Discussion

The main purpose of this study was to evaluate the methodology for quantification and the characteristics of the tumour vasculature in relation to the development of metastasis in patients with rectal cancer. Assessment of intratumoural vascular density in hot spots, as performed in most studies [31, 35, 37] and which is put forward as consensus approach [33] was not indicative for prognosis in the present study. Our data show that only high-vascular perimeter randomly assessed at the invasive front was associated with low incidence of distant metastases and a longer disease-free survival. High-vessel perimeter was independent of TNM staging, but was associated with an increased number of several immune cells.

The literature on the role of tumour vasculature in prognosis of patients with colorectal cancer is by no means conclusive. The combined action between tumour cells, vascular endothelial cells, surrounding stromal cells and circulating blood cells is complex, and, therefore, it is not obvious whether high vessel count puts the tumour at a benefit [27, 29, 30, 35] or at a disadvantage [18, 26].

The finding that vascular perimeter is indicative for metastasis, as shown in the present study, points to an important role for endothelial cells. High vascular pe-

Table 5 Immune response in patients in the low and high category of vessel perimeter randomly measured at the invasive front. *n.s.* not significant

		Intratumoral			Peritumoral		
		Low[a]	High[a]	P	Low[a]	High[a]	*P* value
NK cells	None/few	13	13	n.s.	16	17	n.s.
	Many	29	29		19	19	
T cells	None/few	17	4	0.023	11	6	n.s.
	Moderate	11	20		16	24	
	Many	13	17		13	11	
CD4+ cells	None/few	17	13	n.s.	7	8	n.s.
	Moderate	14	11		22	12	
	Many	9	17		6	13	
CD8+ cells	None/few	14	9	0.047			
	Moderate	19	15		29	22	n.s.
	Many	9	18		5	8	
Eosinophils	None/few	16	14	n.s.	19	7	0.002
	Moderate	20	19		15	18	
	Many	6	9		5	13	
Macrophages	None/few	13	14	n.s.	28	23	n.s.
	Moderate	20	21				
	Many	9	7		11	15	
Mast cells	None/few	11	6	n.s.	15	3	0.005
	Moderate	20	24		21	27	
	Many	11	12		5	9	
Neutrophils	None/few	13	4	0.004	15	6	0.023
	Moderate	24	25				
	Many	5	13		26	35	

[a] Number of patients

rimeter reflects a large endothelial contact surface between circulating blood and the tumour. Consequently, this may give rise to an improved immune response, as host defence is dependent on blood supply [3]. Possibly, inflammatory cells can reach the tumour more easily and, thus, prevent tumour spread. Our data confirm this, since high vascular perimeter is associated with increased presence of T cells, mast cells, eosinophils and neutrophils [24]. This observation substantiates the thought that angiogenesis is in favour of the host because of the close interplay between the angiogenic process and inflammatory cell infiltrate.

The result that angiogenesis is linked to improved prog-nosis contradicts the most prevailing view, which proposes that highly vascularised tumours are more prone to metastasis [22, 36]. The theoretical basis for the latter view comprises the presence of a larger vascular window through which tumour cells can pass, an increased chance to seed highly angiogenic clones and the presence of more endothelial cells, which provide tumour-promoting factors. Part of the conflicting results may be explained by differences in the composition of the patient population studied [22, 36]. A group of well-characterised patients with rectal cancer was subject to the present study. The patient selection in this study, which ensured a relatively high percentage of metastasis, facilitates study of the association between tumour vasculature characteristics and metastasis.

In addition, the conflicting results may also be partly explained by differences in methods, such as choice of antibody [21] and vessel-assessing method [8, 11]. To overcome these differences, an international consensus protocol concerning the methodology and evaluation criteria to quantify angiogenesis has been proposed, which is based on intratumoural assessment of number of microvessels in hot spots [33]. In the present study, measurements according to this prescribed protocol showed, in contrast to most reports performed in line with this standard [31, 35, 37], no association between microvessel density and the development of metastasis. However, the microvessel perimeter randomly assessed at the invasive front was significantly associated with an improved prognosis. These findings indicate that sole assessment of intratumoural microvessel density may be too simple an approach to explain the association between tumour vasculature and tumour progression and metastasis. Therefore, the three principles of the consensus method comprising hot spots, number of microvessels and intratumoural area have to be discussed.

Due to substantial intratumoural heterogeneity, microvessel assessment in hot spots is prescribed by the consensus method [33]. Reproducible overall assessment would imply evaluation of large areas, and, thus, the analysis of selected areas is more practical. However, this practical rationale is subverted by the fact that the definition of vascular hot spots is subjective and is inclined to large observer variability [12, 34]. Eventually, for the quantification of angiogenesis to yield a reliable prognosticator, low intra- and inter-observer variations are required.

From a biological viewpoint, it is believed that the hot spots, rather than the random fields, are important [8] because these spots provide an optimal environment for tumour growth and metastasis, due to the direct and indirect interactions between tumour and endothelial cells. Then, however, assessing the vascular endothelial surface would be more biologically relevant than assessing the vascular density as recommended by the consensus method. The results of the present study confirm this, showing an association between vessel perimeter and prognosis. A computerised image analysis system, as used in the present study, allows measurement of several morphometric parameters, such as vessel perimeter and vessel area additional to the number of vessels [11]. An additional advantage of such a computerised system is the possibility to circumvent subjective hot-spot selection using whole-tumour-section scanning [6]. Unfortunately, the computerised methods are often time consuming, which may be solved using full automation of the system.

The consensus method commends the study of the intratumoural vasculature. However, there are several indications that the invasive front is more biologically relevant. The invasive front is defined as the side of interaction between the tumour cells and the microenvironment. Several processes that are important in metastasis take place at the invasive front of the tumour. Invasion and metastasis is often associated with loss of epithelial differentiation of tumour cells at the invasive front [17]. Additionally, the presence of more severe tumour "budding", defined as small clusters of undifferentiated cancer cells at the invasive front, indicates a worse survival in patients with colorectal cancer [14]. With respect to angiogenesis, it has been shown that the microvessel density at the in situ growth regions is approximately half of the microvessel density at the invasive front [32]. Furthermore, tumour cells that are strongly positive for vascular endothelial growth factor are more often located at the invasive front than in the centre of the tumour [28], indicating that the invasive front is, indeed, the most important region for angiogenesis. The results of the present study substantiate this view—that the invasive front is more biologically relevant than the intratumoural area. Moreover, assessment of vessel characteristics at the invasive front may be more reproducible than vessel assessment in intratumoural hot spots, because the invasive front is well defined.

It is beyond question that angiogenesis plays an important role in tumour progression and metastasis. Angiogenesis is mostly designated as a bad prognostic sign if the simple association between microvessel density, as a reflection of the angiogenesis, and prognosis is studied [27, 29, 30, 35]. However, because of the complex and often dualist interaction between all factors involved in tumour progression and metastasis, it is of utmost importance to study the biological relevance of the different vessel characteristics. The present study was performed in a selected group of patients with rectal cancer, which

renders outstanding circumstances to study the biological relevance of various vessel characteristics. We studied patients with and without short-term preoperative radiotherapy, thereby excluding this treatment as major factor. We have questioned the aim of the three principles of the consensus method and argue that the hot spot, microvessel density and intratumoural area may be better replaced by random spots, microvessel perimeter and invasive front. This statement is validated by the results of the present study, showing that the vascular endothelial surface, as reflected by the perimeter, randomly assessed at the invasive front, was the only vessel characteristic indicative of patient outcome. Perimeter count was independent of TNM staging, and high-vessel perimeter was accompanied by a lower rate of metastasis and a longer disease-free survival. Improved immune response probably underlies this association. Our data are based on a selected patient group and, therefore, need to be confirmed in prospective randomised clinical trial.

Acknowledgements This study was supported by a grant of the Dutch Digestive Disease Foundation.

References

1. Aitken RJ (1996) Mesorectal excision for rectal cancer. Br J Surg 83:214–216
2. Banner BF, Whitehouse R, Baker SP, Swanson RS (1998) Tumor angiogenesis in stage II colorectal carcinoma: association with survival. Am J Clin Pathol 109:733–737
3. Blood CH, Zetter BR (1990) Tumor interactions with the vasculature: angiogenesis and tumor metastasis. Biochim Biophys Acta 1032:89–118
4. Bossi P, Viale G, Lee AK, Alfano R, Coggi G, Bosari S (1995) Angiogenesis in colorectal tumors: microvessel quantitation in adenomas and carcinomas with clinicopathological correlations. Cancer Res 55:5049–5053
5. Bryne M, Boysen M, Alfsen CG, Abeler VM, Sudbo J, Nesland JM, Kristensen GB, Piffko J, Bankfalvi A (1998) The invasive front of carcinomas. The most important area for tumour prognosis? Anticancer Res 18:4757–4764
6. Chantrain CF, DeClerck YA, Groshen S, McNamara G (2003) Computerized quantification of tissue vascularization using high-resolution slide scanning of whole tumor sections. J Histochem Cytochem 51:151–158
7. de Jong JS, van Diest PJ, Baak JP (1995) Heterogeneity and reproducibility of microvessel counts in breast cancer. Lab Invest 73:922–926
8. de Jong JS, van Diest PJ, Baak JP (2000) Hot spot microvessel density and the mitotic activity index are strong additional prognostic indicators in invasive breast cancer. Histopathology 36:306–312
9. Enker WE, Thaler HT, Cranor ML, Polyak T (1995) Total mesorectal excision in the operative treatment of carcinoma of the rectum. J Am Coll Surg 181:335–346
10. Folkman J (1990) What is the evidence that tumors are angiogenesis dependent? J Natl Cancer Inst 82:4–6
11. Fox SB, Leek RD, Weekes MP, Whitehouse RM, Gatter KC, Harris AL (1995) Quantitation and prognostic value of breast cancer angiogenesis: comparison of microvessel density, Chalkley count, and computer image analysis. J Pathol 177: 275–283
12. Hansen S, Grabau DA, Rose C, Bak M, Sorensen FB (1998) Angiogenesis in breast cancer: a comparative study of the observer variability of methods for determining microvessel density. Lab Invest 78:1563–1573
13. Harnsberger JR, Vernava VM III, Longo WE (1994) Radical abdominopelvic lymphadenectomy: historic perspective and current role in the surgical management of rectal cancer. Dis Colon Rectum 37:73–87
14. Hase K, Shatney C, Johnson D, Trollope M, Vierra M (1993) Prognostic value of tumor "budding" in patients with colorectal cancer. Dis Colon Rectum 36:627–635
15. Kapiteijn E, Marijnen CA, Colenbrander AC, Klein KE, Steup WH, van Krieken JH, van Houwelingen JC, Leer JW, van de Velde CJ (1998) Local recurrence in patients with rectal cancer diagnosed between 1988 and 1992: a population-based study in the west Netherlands. Eur J Surg Oncol 24:528–535
16. Kapiteijn E, Marijnen CA, Nagtegaal ID, Putter H, Steup WH, Wiggers T, Rutten HJ, Pahlman L, Glimelius B, van Krieken JH, Leer JW, van de Velde CJ (2001) Preoperative radiotherapy combined with total mesorectal excision for resectable rectal cancer. N Engl J Med 345:638–646
17. Kirchner T, Brabletz T (2000) Patterning and nuclear beta-catenin expression in the colonic adenoma-carcinoma sequence. Analogies with embryonic gastrulation. Am J Pathol 157:1113–1121
18. Lindmark G, Gerdin B, Sundberg C, Pahlman L, Bergstrom R, Glimelius B (1996) Prognostic significance of the microvascular count in colorectal cancer. J Clin Oncol 14:461–466
19. Liotta LA, Kleinerman J, Saidel GM (1974) Quantitative relationships of intravascular tumor cells, tumor vessels, and pulmonary metastases following tumor implantation. Cancer Res 34:997–1004
20. MacFarlane JK, Ryall RD, Heald RJ (1993) Mesorectal excision for rectal cancer. Lancet 341:457–460
21. Martin L, Green B, Renshaw C, Lowe D, Rudland P, Leinster SJ, Winstanley J (1997) Examining the technique of angiogenesis assessment in invasive breast cancer. Br J Cancer 76:1046–1054
22. Meert AP, Paesmans M, Martin B, Delmotte P, Berghmans T, Verdebout JM, Lafitte JJ, Mascaux C, Sculier JP (2002) The role of microvessel density on the survival of patients with lung cancer: a systematic review of the literature with meta-analysis. Br J Cancer 87:694–701
23. Nagtegaal ID, Kranenbarg EK, Hermans J, van de Velde CJ, van Krieken JH (2000) Pathology data in the central databases of multicenter randomized trials need to be based on pathology reports and controlled by trained quality managers. J Clin Oncol 18:1771–1779
24. Nagtegaal ID, Marijnen CA, Kranenbarg EK, Mulder-Stapel A, Hermans J, van de Velde CJ, van Krieken JH (2001) Local and distant recurrences in rectal cancer patients are predicted by the nonspecific immune response; specific immune response has only a systemic effect—a histopathological and immunohistochemical study. BMC Cancer 1:7
25. Pietra N, Sarli L, Caruana P, Cabras A, Costi R, Gobbi S, Bordi C, Peracchia A (2000) Is tumour angiogenesis a prognostic factor in patients with colorectal cancer and no involved nodes? Eur J Surg 166:552–556
26. Qiu H, Sirivongs P, Rothenberger M, Rothenberger DA, Garcia-Aguilar J (2000) Molecular prognostic factors in rectal cancer treated by radiation and surgery. Dis Colon Rectum 43:451–459
27. Saclarides TJ, Speziale NJ, Drab E, Szeluga DJ, Rubin DB (1994) Tumor angiogenesis and rectal carcinoma. Dis Colon Rectum 37:921–926
28. Saito H, Tsujitani S, Oka S, Kondo A, Ikeguchi M, Maeta M, Kaibara N (1999) The expression of transforming growth factor-beta1 is significantly correlated with the expression of vascular endothelial growth factor and poor prognosis of patients with advanced gastric carcinoma. Cancer 86:1455–1462
29. Sokmen S, Sarioglu S, Fuzun M, Terzi C, Kupelioglu A, Aslan B (2001) Prognostic significance of angiogenesis in rectal cancer: a morphometric investigation. Anticancer Res 21:4341–4348

30. Takebayashi Y, Aklyama S, Yamada K, Akiba S, Aikou T (1996) Angiogenesis as an unfavorable prognostic factor in human colorectal carcinoma. Cancer 78:226–231
31. Tanigawa N, Amaya H, Matsumura M, Lu C, Kitaoka A, Matsuyama K, Muraoka R (1997) Tumor angiogenesis and mode of metastasis in patients with colorectal cancer. Cancer Res 57:1043–1046
32. Vermeulen PB, Verhoeven D, Fierens H, Hubens G, Goovaerts G, Van Marck E, De Bruijn EA, Van Oosterom AT, Dirix LY (1995) Microvessel quantification in primary colorectal carcinoma: an immunohistochemical study. Br J Cancer 71:340–343
33. Vermeulen PB, Gasparini G, Fox SB, Toi M, Martin L, McCulloch P, Pezzella F, Viale G, Weidner N, Harris AL, Dirix LY (1996) Quantification of angiogenesis in solid human tumours: an international consensus on the methodology and criteria of evaluation. Eur J Cancer 32:2474–2484
34. Vermeulen PB, Libura M, Libura J, O'Neill PJ, van Dam P, Van Marck E, Van Oosterom AT, Dirix LY (1997) Influence of investigator experience and microscopic field size on microvessel density in node-negative breast carcinoma. Breast Cancer Res Treat 42:165–172
35. Vermeulen PB, Van den Eynden GG, Huget P, Goovaerts G, Weyler J, Lardon F, Van Marck E, Hubens G, Dirix LY (1999) Prospective study of intratumoral microvessel density, p53 expression and survival in colorectal cancer. Br J Cancer 79:316–322
36. Weidner N (1998) Tumoural vascularity as a prognostic factor in cancer patients: the evidence continues to grow. J Pathol 184:119–122
37. Weidner N, Semple JP, Welch WR, Folkman J (1991) Tumor angiogenesis and metastasis—correlation in invasive breast carcinoma. N Engl J Med 324:1–8

Virchows Arch (2004) 445:271–278
DOI 10.1007/s00428-004-1029-x

ORIGINAL ARTICLE

Shinji Murai · Toshifumi Umemiya · Motoharu Seiki · Kenichi Harigaya

Expression and localization of membrane-type-1 matrix metalloproteinase, CD 44, and laminin-5γ2 chain during colorectal carcinoma tumor progression

Received: 3 March 2004 / Accepted: 16 April 2004 / Published online: 28 July 2004
© Springer-Verlag 2004

Abstract Membrane-type-1 matrix metalloproteinase (MT1-MMP) is overexpressed in many malignant tumor tissues and would be involved in tumor-cell migration. Using dual immunofluorescence of frozen sections, this study examined the expression and localization of MT1-MMP and its interacting molecules, CD44 and laminin-5γ2 chain (LN-5γ2) monomer, in 48 cases of colorectal tumors. Recent studies have shown that MT1-MMP, CD44 and LN-5γ2 are direct downstream targets in the adenomatosis polyposis coli (APC)/β-catenin (Wnt)-signaling pathway, which is upregulated in most colorectal epithelial tumors. MT1-MMP overexpression was observed in adenocarcinoma cases with moderate and/or less differentiation coinciding with CD44 downmodulation. Recent observations indicate that MT1-MMP overexpression disrupts tubulogenesis of MDCK cells in type-I collagen-rich tissues. Therefore, MT1-MMP overexpression might involve disturbances of neoplastic glandular structures during colorectal adenocarcinoma tumor progression. Intensity distribution analyses of images with dual immunofluorescence indicated that overexpressed MT1-MMP is closely associated with the enhanced expression of the LN-5γ2 monomers at the invasive front of dedifferentiated tumor cells. Additionally, the graded expression of nuclear active β-catenin was found in moderately differentiated and dedifferentiated areas of adenocarcinomas, where MT1-MMP overexpression was observed. Therefore, this study reveals that MT1-MMP might be a major effector of Wnt signaling in the late stage of colorectal carcinoma tumor progression.

S. Murai · T. Umemiya · K. Harigaya (✉)
Department of Molecular and Tumor Pathology,
Chiba University Graduate School of Medicine,
1-8-1 Inohana, Chuo-ku, 260-8670 Chiba, Japan
e-mail: harigaya@faculty.chiba-u.jp
Tel.: +81-43-2262053
Fax: +81-43-2262058

M. Seiki
Division of Cancer Cell Research,
Institute of Medical Science, University of Tokyo,
4-6-1 Shiroganedai, Minato-Ku, 108-869 Tokyo, Japan

Keywords MT1-MMP · CD44 · LN-5γ2 · β-Catenin · Colorectal carcinoma

Introduction

The invasion and metastasis of tumor cells requires cell-motility events, such as cell adhesion, spreading, and migration. It is possible that proteinases affect cell detachment, cell–cell adhesion, and receptor-matrix interactions, or perhaps the way a cell perceives its surrounding matrix, in addition to the removal of mechanical barriers [6, 20, 34]. Matrix metalloproteinases (MMPs) are a broad family of zinc-binding endopeptidases that degrade various components of the extracellular matrix (ECM). These enzymes are encoded by different genes and produced by a variety of cell types, including epithelial, mesenchymal, and inflammatory and neoplastic cells. Based on abundant data correlating invasive phenomena with the presence of MMPs [41], there is general agreement that MMPs are important in executing migration through the matrix and, likewise, invasion. Membrane-type-1 matrix metalloproteinase (MT1-MMP) is a prototypical member of the membrane-anchored MMP subclass. Whereas all secreted MMPs are normally released as proenzymes, the MT1-MMP prodomain can be removed and the active enzyme generated before or simultaneously with its delivery to the cell surface. Membrane-anchored MMPs (MT1-MMPs) are physiological activators of latent soluble forms of MMPs.

MT1-MMP and CD44 are overexpressed in many cancers, including colorectal carcinomas [13, 22, 25, 42], at least partly because they are target genes of the Wnt pathway [38, 42], which is upregulated in carcinomas mainly due to losses in adenomatosis polyposis coli (APC) gene function [18]. Recently, it was reported that CD44 is shed from the cell surface by the actions of metalloproteinases and stimulating cell motility [17, 28, 29]. Furthermore, MT1-MMP co-localizes with the CD44 standard form (CD44s) at the ruffling edges and facilitates shedding from the cell surface along with cell-motility

stimulation [17]. A previous study by the authors also revealed that hyaluronan (HA)-stimulation of CD44 induces cell adhesion and motility [5] (Tsuchiya et al., unpublished data). Accordingly, it is likely that associations between MT1-MMP and CD44 regulate both matrix degradation and cell motility in colorectal cancer cases, thereby facilitating direct cellular invasion.

The laminin-5γ2 chain (LN-5γ2) monomer is also one of target genes of the Wnt pathway—playing an important role in cell migration during tumor invasion and tissue remodeling [14]. Abnormally strong cytoplasmic expression of LN-5γ2 has been observed in dedifferentiated cells of colorectal carcinoma dissociated from neoplastic tubules [35]. A recent study confirmed that this increased immunoreactivity indicates the high invasive potential of the tumor cells [36]. It has also been shown that MT1-MMP triggers migration over LN-5 by cleaving LN-5γ2 [20].

The present study examines alterations in the expression and localization of MT1-MMP and its interacting molecules, CD44 and LN-5γ monomer, during colorectal epithelial neoplasm tumor progression using a dual immunofluorescence method on frozen tissue sections and subsequent intensity distribution analyses of the images.

Materials and methods

Cases

Fresh tissue samples were obtained from 48 operative specimens between 2000 and 2002—43 cases of colorectal carcinoma and 5 of adenoma. These samples were snap-frozen in liquid nitrogen within 10 min of arrival at the pathology facility and remained frozen until use. Some of the samples were used for immunohistochemical staining. Non-neoplastic tissues were obtained from specimens surgically resected for cancer treatment. Carcinoma histological findings were separated into four groups: (1) adenoma, (2) well-differentiated, (3) moderately differentiated, and (4) dedifferentiated (poorly differentiated), according to the classification of hematoxylin–eosin-stained sections.

Double immunofluorescence staining

Frozen sections 30 μm thick were obtained from the 48 colorectal tumor specimens and fixed with cold acetone. After washing three times with PBS (1/15 M phosphate buffer, pH 7.2, and 150 mM NaCl), samples were treated with 10 mg/ml bovine serum albumin, Fraction V (Sigma Chemical Co, St. Louis, MO), to inhibit nonspecific antibody binding and were then incubated with the primary antibody cocktails for 1 h. Antibodies used were as follows: murine monoclonal antibodies against MT1-MMP; 114–6G6 (Daiichi Fine Chem Co. LTD, Japan), CD44v4; BMS114 (Bender Med Sys, Viena, Austria) and active non-phosphorylated β-catenin; #05–665 (Upstate, Waltham, MA), rabbit polyclonal antibodies against CD44; CD44s; sc-7946 (Santa Cruz Biotech, Santa Cruz, CA), variant 6; AB2080, and variant 10; AB2082 (Chemicon International Inc., Temecula, CA), and goat polyclonal antibodies against CD44; sc-7051, and LN-5γ2; sc-7652 (Santa Cruz Biotech Inc.). The samples were then washed three times with PBS and incubated with either rhodamine-conjugated swine anti-rabbit IgG (R 0156) (DakoCytomation, Glostrup, Denmark), or fluorescein isothiocyanate (FITC)-conjugated rabbit anti-goat IgG (F 0479) (DakoCytomation, Glostrup, Denmark). After washing with PBS, the samples were incubated once more in FITC-conjugated rabbit anti-mouse IgG (F 0261) for 40 min. After further washing, fluorescein- and rhodamine-labeled samples were examined using a confocal laser-scanning microscope (Zeiss LSM 510 META). To detect nonspecific-antibody binding, control sections were incubated with fluorescein- and rhodamine-conjugated preimmune rabbit IgG. For CD44s staining, antibody-absorbed negative control sections were also examined using the available blocking peptide (sc-7051, Santa Cruz Biotech lab); no labeling was observed in these control samples. All procedures were performed at room temperature.

Profile display

Intensity distributions of the immunohistochemical images of each frozen tissue section were displayed with fluorescence-labeled antibody reactions along an appropriate straight line. Laser confocal microscopy (Zeiss LSM 510 META) was employed to produce images and intensity graphs according to the LSM 510 META Operating Manual (2001, Carl Zeiss, Jena, Germany). In each image, five different dissection lines were examined. Two markers were placed on the profile line to measure differences in intensity and distance on the XY plane.

Results

MT1-MMP, CD44, LN-5γ2 monomer, and active β-catenin expressions were observed in carcinoma cells obtained from fresh sections of 48 cases of colorectal tumors, including five cases of adenoma, using confocal microscopy with special reference to histological differentiation of adenocarcinoma: well-differentiated, moderately-differentiated, or poorly differentiated (dedifferentiated) tumors. As most cases included combined histology, well-differentiated, moderately differentiated, and poorly differentiated, each area of particular carcinoma histological differentiation was evaluated separately (79 areas, 43 cases) (Table 1).

Localization and intensity of active β-catenin expression are dynamically altered in accord with histological differentiation in colorectal tumors

Membranous active β-catenin expression was found in five cases of adenoma—with staining the strongest at the lateral side of tumor cells (Fig. 1, *3a*). Significant cytoplasmic reactions with intense membranous staining were demonstrated in the well-differentiated areas of the adenocarcinomas (Fig. 1, *3b*, *c*). In moderately differentiated areas of adenocarcinomas and central dedifferentiated areas at the invasive front, significant nuclear localization of active β-catenin in addition to strong membranous and cytoplasmic reaction was observed (Fig. 1, *3d*). The dedifferentiated cells at the periphery of the invasive front and in scattered cell clusters around the invasive front frequently showed intense nuclear reaction of active β-catenin that presumably occupied the whole nucleus, though their membranous and cytoplasmic reactions were feeble (Fig. 1, *3e*). The intensity of nuclear staining was graded according to the morphological invasive phenotype that reflected the late stage of tumor progression in colorectal adenocarcinomas. These results are comparable

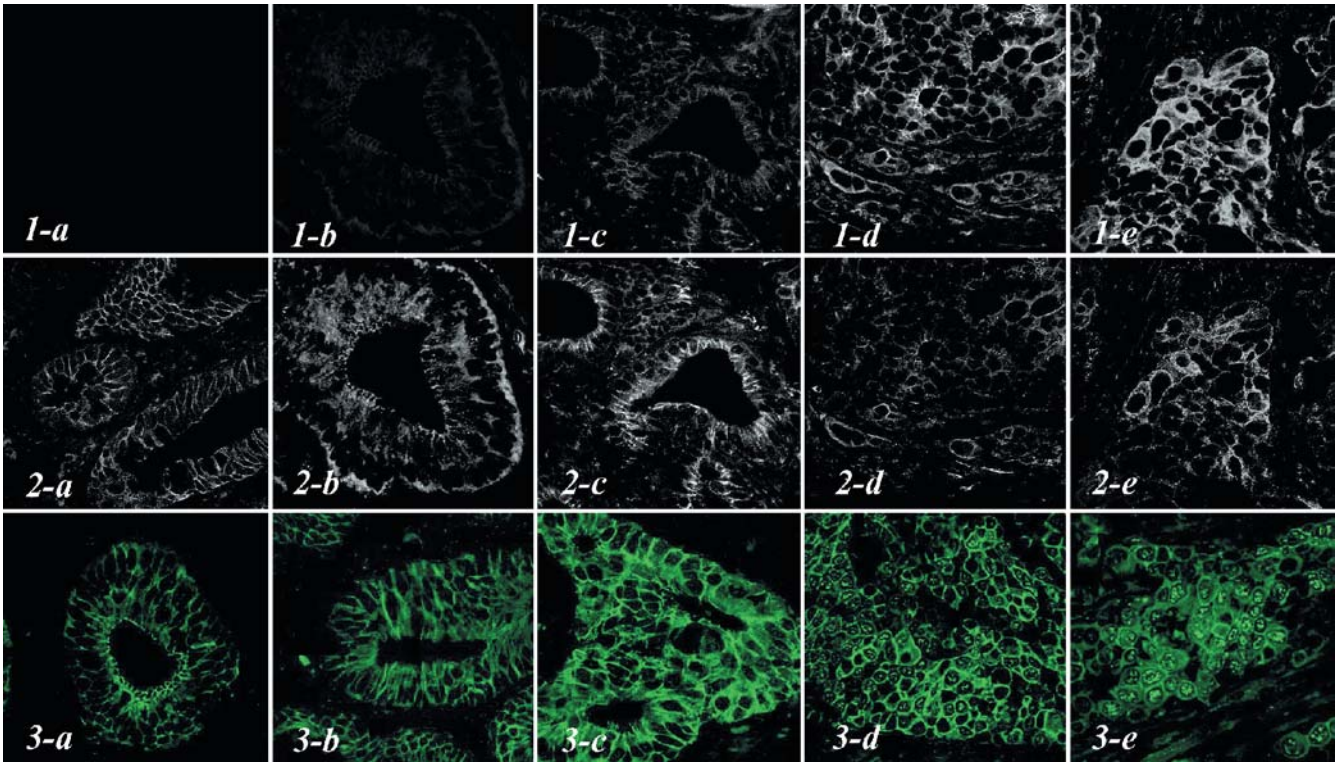


Fig. 1 Membrane-type-1 matrix metalloproteinase (MT1-MMP), CD44 and active β-catenin expression in colorectal tumors. *Panels 1a–e* MT1-MMP, *2a–e* CD44, *3a–e*: active β-catenin. **a** Adenoma. **b** Well-differentiated adenocarcinoma. **c** Moderately differentiated adenocarcinoma. **d** Dedifferentiated area of the adenocarcinoma. **e** Dedifferentiated cells at the invasive front

Table 1 Expression of membrane-type-1 matrix metalloproteinase (MT1-MMP) and CD44 in 79 different histological differentiation areas in 43 cases of colorectal carcinoma

Histological subtype	No. of areas/no. of cases examined	No. of MT1-MMP-positive areas			No. of CD44-positive areas		
Well differentiated	21 areas/11 cases	-	1+	3+	-	1+	3+
Well differentiated	11/11	11					11
Moderately differentiated	9/11	2		7	3	6	
Poorly differentiated	1/11			1		1	
Moderately differentiated	58 areas/32 cases						
Well differentiated	19/32	11	8		1		18
Moderately differentiated	32/32	4		28	11	21	
Poorly differentiated	7/32			7	1	6	

with observations that β-catenin/T-cell factor family of transcription factors (TCF) signaling inhibits lineage-specific differentiation and also confirm the functionally relevant intratumorous heterogeneity of β-catenin expression in colorectal epithelial cells [3, 19, 24]. Accordingly, it is likely that the localization and intensity of β-catenin is a useful monitor of colorectal adenocarcinoma tumor progression and correlates well with histological differentiation.

Overexpression of MT1-MMP during colorectal tumor progression

MT1-MMP staining was analyzed by obtaining a series of optical section images. The endogenous expression of MT1-MMP was not found to be sufficient for generating specifically detectable staining in normal absorptive epithelium, adenoma epithelia (0/5) (Fig. 1, *1a*), or well-differentiated areas of well-differentiated adenocarcinomas (0/11) and moderately differentiated adenocarcinomas (11/19) (Fig. 1, *1b*). Small amounts of reaction products were observed on the apical and/or basolateral cell surfaces of well-differentiated areas of moderately differentiated adenocarcinomas (8/19) (Fig. 1, *1c*), whereas intense reaction products without polarity were demonstrated on almost all whole-surface membranes of neoplastic epithelial cells in moderately differentiated areas of the well-differentiated and moderately differentiated adenocarcinomas (35/41) (Fig. 1, *1d*) and in dedifferentiated cell clusters of the invasive front where nuclear-activated β-catenin was frequently seen (8/8) (Fig. 1, *1e*). Intracellular staining was also observed in cells at the periphery of the invasive front of adenocarcinomas.

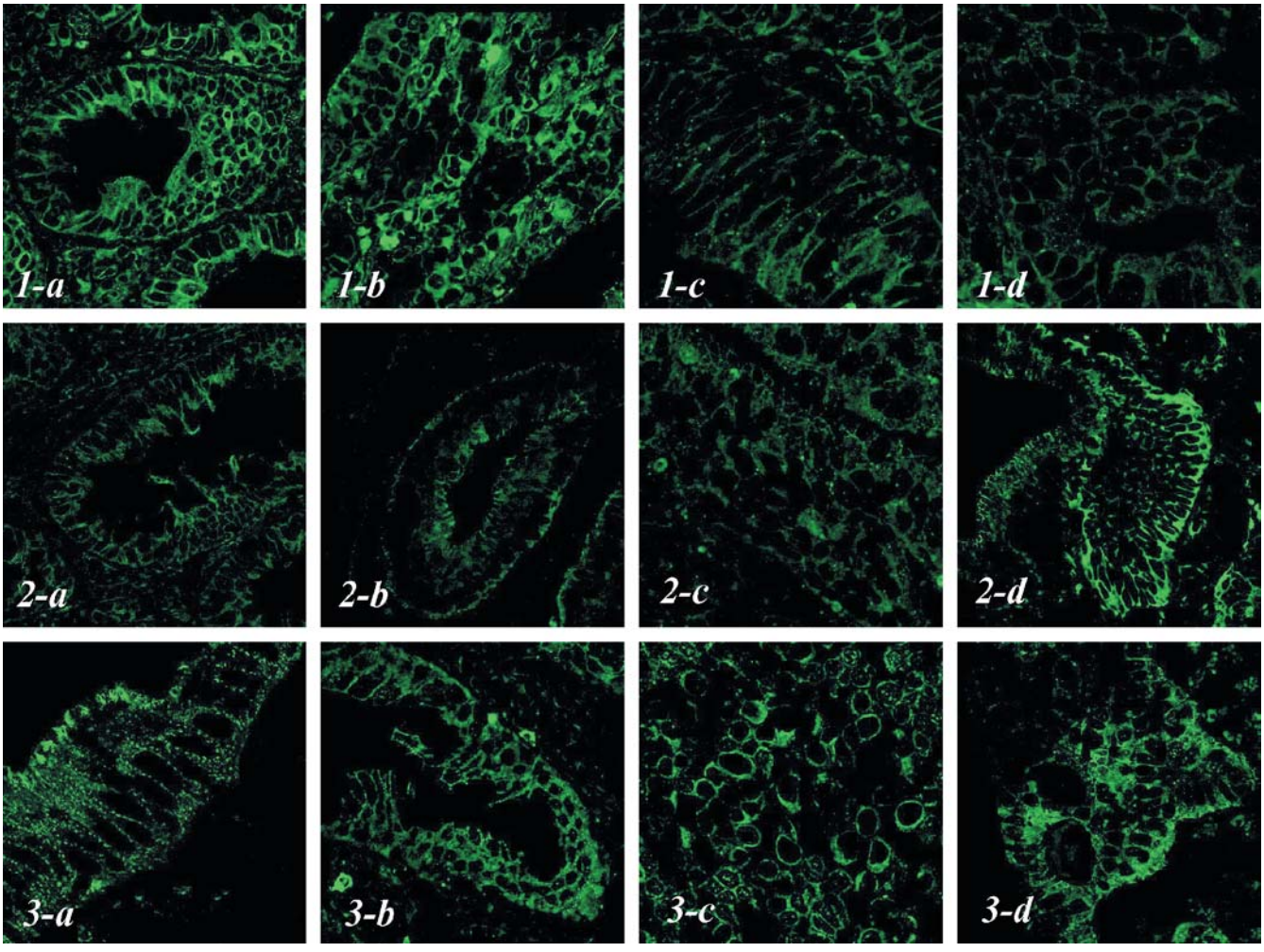


Fig. 2 Expression of CD44 variants in colorectal tumors. *Panels 1a–e* CD44v4, *panels 2a–e* CD44v6, *panels 3a–e* CD44v10. **a** Adenoma. **b** Well-differentiated adenocarcinoma. **c** Dedifferentiated area of the adenocarcinoma. **d** Dedifferentiated cells at the invasive front

Correlation between CD44 isoforms (s, v6, v10) and MT1-MMP expression in colorectal adenomas and carcinomas

Recently, it was reported that MT1-MMP is associated with CD44s at its platform on the plasma membrane and plays a critical role in cell migration in vitro [17]. Epithelia from cases of adenoma (5/5) and well-differentiated areas of adenocarcinomas (29/30) showed intense positive staining for CD44 common epitope in the apical and basolateral membrane (Fig. 1, *2a*, *b*). In contrast, CD44 reaction products significantly decreased in the plasma membrane of neoplastic cells from moderately differentiated areas of adenocarcinomas (27/41), and dedifferentiated cell clusters appeared at the invasive front (7/8) (Fig. 1, *2d*, *2e*). A dedifferentiated area and 14 moderately differentiated areas were negative for CD44 staining.

To test what isoform(s) localize in the plasma membranes of dedifferentiated cells at the invasive front, polyclonal antibodies (v4, v6, and v10) against various exons were used for indirect immunofluorescent staining (Table 2). Intense v4 and v10 reactions were demonstrated in cases of adenoma and well-differentiated adenocarcinoma. With moderately differentiated and dedifferentiated areas of moderately differentiated adenocarcinoma, v4 expression dramatically decreased according to the degree of histological dedifferentiation (Fig. 2, *1a*, *b*, *c* and *d*) as in the expression for CD44 common epitope (Fig. 1, *2a*, *b*, *c*, and *e*), while v10 expression remained strong (Fig. 2, *3a*, *b*, *c*, and *d*). An intense v6 variant reaction was observed in dedifferentiated cancer cells at the invasive front (Fig. 2, *2a*, *b*, *c*, and *d*). The v6 variant showed the most intense reactions at the border between dedifferentiated cells and the surrounding stroma at the invasive front of the double-immunofluorescent-strain sections (Fig. 2, *2d*), while the staining of v10 variant was evenly intense (Fig. 2, *3d*). Intensity distribution profiles confirmed the results (Fig. 3, *a*, *b*), which are reproducible in five different dissection lines in each image. These support previous reports that the v6 variant plays an important role in invasion and metastasis in neoplastic cells [1, 7, 37, 39].

Table 2 Relative intensity of reaction in CD44 variants (Cv4, v6, and v10) in 79 different areas of 43 colorectal carcinomas. *v4* CD44 variant4, *v6* CD44 variant6, *v10* CD44 variant10. The strongest reaction is considered as 3+ positivity in each CD44 variant staining

	No. of v4-positive area			No. of v6-positive areas			No. of v10-positive areas		
Well differentiated 21 areas/11 cases	-	1+	3+	-	1+	3+	-	1+	3+
Well differentiated 11/11		4	7	8	3		1	2	8
Moderately differentiated 9/11	4	5		6	3		3		6
Poorly differentiated 1/11	1					1			1
Moderately differentiated 58 areas/32 cases									
Well differentiated 19/32	2	11	6	15	4		2	1	16
Moderately differentiated 32/32	18	14		23	9		11	4	17
Poorly differentiated 7/32	7			1		6	1	1	5

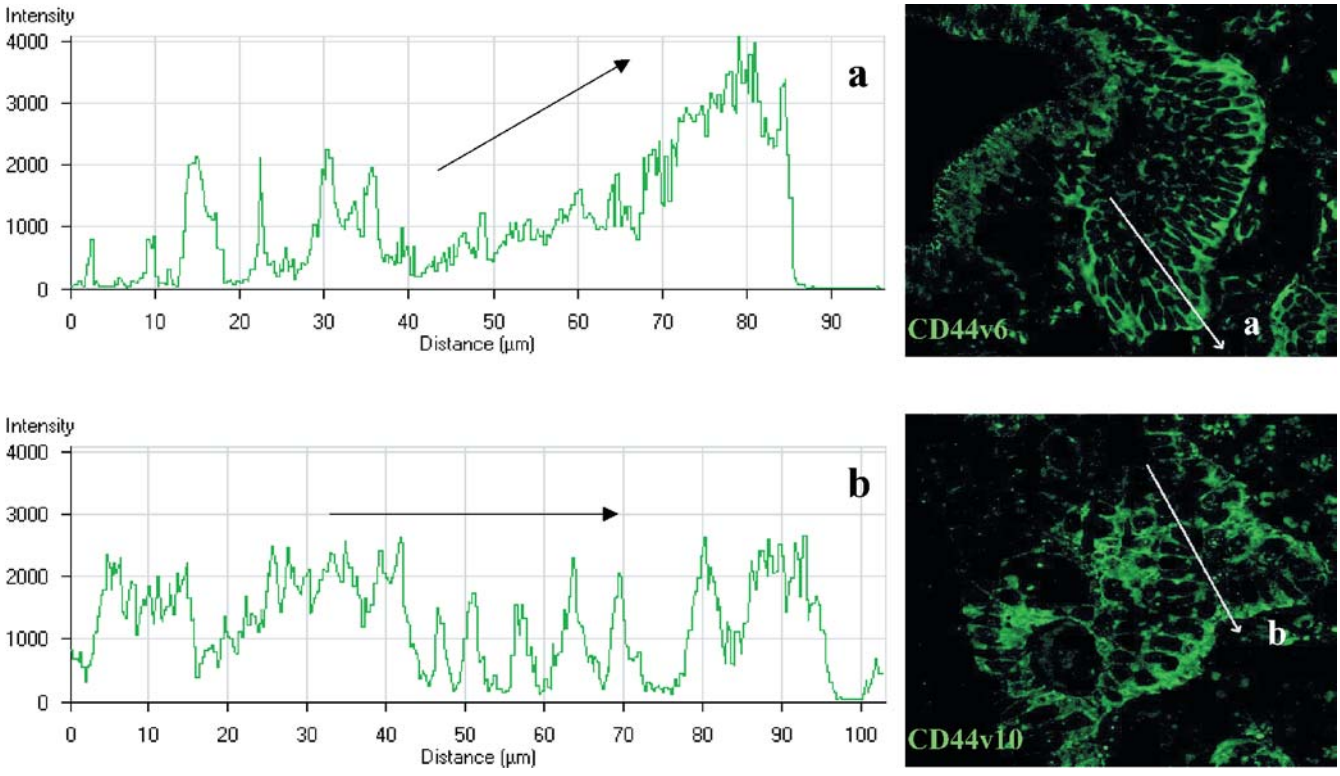


Fig. 3 Expression of CD44 v6 and v10 in invasive front of colorectal carcinoma. Profiles are representative of data from five different dissect lines in each image. Lines with an *arrowhead* represent the appropriate dissect lines (from the inside of each dedifferentiated cell cluster towards the stroma of the invasive front) for intensity distribution analysis. **a** CD44 v6, **b** CD44 v10

Dedifferentiated cells at the invasive front show MT1-MMP and LN-γ2 monomer co-localization

To examine the expression of LN-5γ2 monomer and its association with MT1-MMP, double immunofluorescence was performed in the tissue samples. LN-5γ2 monomers play an important role in cell migration during tumor invasion and tissue remodeling. LN-5, which consists of LN α3, β3 and γ2, is an LN isoform present in the basement membrane of the skin and various epithelial tissues [32]. In this study, positive membranous and cytoplasmic LN-5γ2 monomers were strongly expressed in dedifferentiated cells at the periphery of the invasive front (Fig. 4, *b*), whereas tumor cells in central dedifferentiated areas usually showed membranous expression of LN-5γ2 monomers as well as the expression profile of MT1-MMP. These staining patterns reflected well the graded intensity of nuclear active β-catenin reaction in the dedifferentiated cells at the invasive front. Furthermore, the density distributions of the immunohistochemical sections observed in this study confirm that MTI-MMP co-localizes well with LN-5γ2 monomers at the membrane and cytoplasm of cells in the dedifferentiated cancer-cell nests (Fig. 5, *a–c*). In the histogram profiles, narrow peaks of MT1-MMP and LN-5γ2 monomer reactions in the central dedifferentiated cells are seen to change to peaks with a broad base of dedifferentiated cells at the periphery of the invasive front (Fig. 5, *a–c*). Five different dissection lines in each image revealed relatively similar and reproducible histogram profiles.

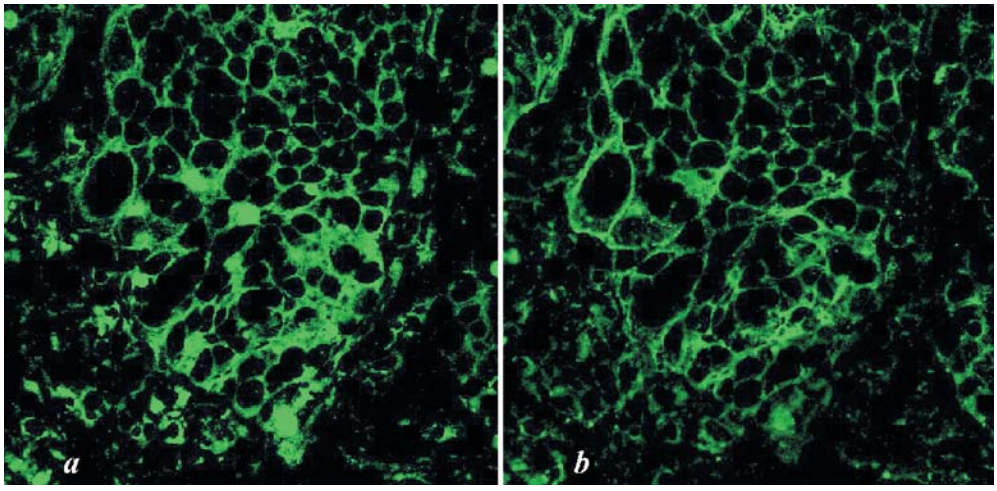


Fig. 4 Expression of membrane-type-1 matrix metalloproteinase (MT1-MMP) and LN-5 $\gamma 2$ in dedifferentiated cells at the invasive front of colorectal carcinoma. **a** MT1-MMP, **b** LN-5 $\gamma 2$. Positive nuclear staining of active β-catenin is visible in the dedifferentiated cells and aggregates of the invasive front, where intracellular LN-5 $\gamma 2$ monomers are strongly expressed (*panel b*)

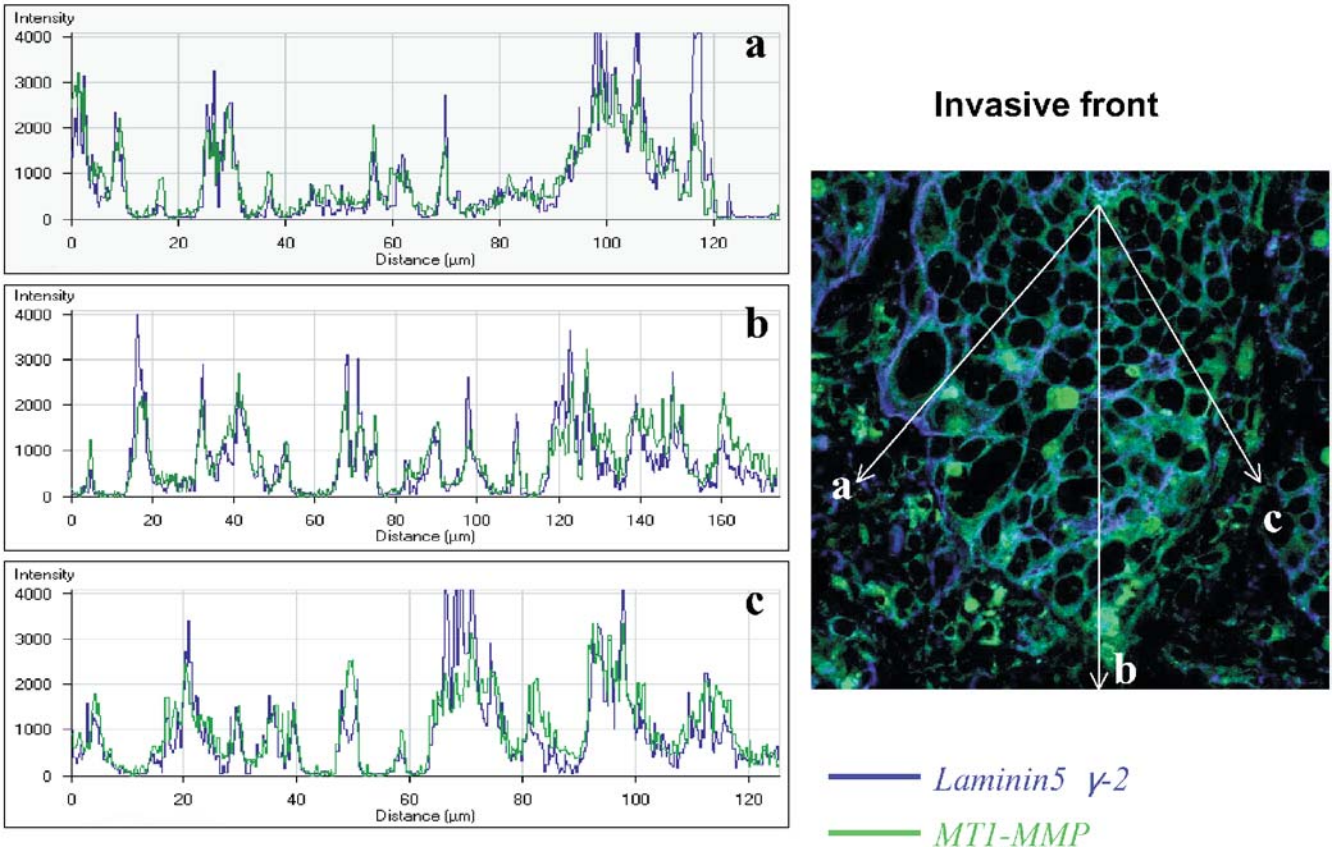


Fig. 5 Co-localization of membrane-type-1 matrix metalloproteinase (MT1-MMP) and LN-5 $\gamma 2$ in colorectal tumors. Profiles are representative of data from five different dissect lines in each image. **a**, **b**, and **c** Profiles of intensity distributions. Lines with an *arrowhead* represent the appropriate dissect lines (from the inside of each dedifferentiated cell cluster towards the stroma of the invasive front) for intensity distribution analysis. *Green line* LN-5 $\gamma 2$, *blue line* MT1-MMP

Discussion

Activation of the APC/β-catenin pathway plays an important role in colorectal tumorigenesis. The major activity attributed to APC is the ability to bind β-catenin and to promote its degradation [31]. When this process is abolished by most APC mutations of colorectal carcinomas, β-catenin increases in the cytosol, binds proteins of the T-cell factor family of transcription factors, and moves to the nucleus with its stable accumulation. Therefore, our results suggest that nuclear accumulation of active β-catenin may be sufficient for the constitutive activation of Wnt signal transduction pathways, resulting in the upregulation of TCF-β-catenin target genes.

These include a number of genes such as c-myc [11], cyclin D1 [40], MMP-7 [2], urokinase-type plasminogen activator receptor [23], CD44 [12, 42], AF17 [21], ENC1 [4], LN-5 γ2 [14], Claudin-1 [26], and MT1-MMP [38]. These molecular expressions might be important during tumorigenesis in the onset of the majority of colorectal tumors [33]. It should be noted that these molecular expressions do not necessarily occur simultaneously during colorectal tumorigenesis. Some upregulate from the adenoma stage: CD44s, v3, v4, v10, and MMP7, for example, while others upregulate from carcinomas with moderate differentiation. Increased MT1-MMP expression was also induced by the activation of several transcription factors, including Egr-1 [8], NFkB [10], and E1AF [9]. However, the molecular details of MT1-MMP expression remain unsolved, though it is known to upregulate at a relatively late stage of colorectal carcinoma tumor progression.

MT1-MMP degrades a wide variety of ECM proteins, including collagen types I, II, and III, fibronectin, laminin 1 and 5, vitronectin, and aggrecan, and also activates other MMPs, such as proMMP-2 and proMMP-13 [17]. This study showed that MT1-MMP overexpression is found in the non-polarized whole-cell membranes of histological subtypes of moderately differentiated and dedifferentiated areas of the carcinomas. Hoary et al. revealed that MT1-MMP overexpression disrupts the tubulogenesis of MDCK cells in type-I collagen-rich tissues [16]; this is comparable with the suggested notion that MT1-MMP overexpression might disturb the capability of colorectal carcinoma cells to form polarized glandular structures.

The downregulation of CD44 expression during colorectal neoplasm tumor progression is puzzling because different CD44 variant transcripts, including the standard form, generally increase with colorectal neoplasm tumor progression at the transcriptional level [13, 25, 42]. Recent reports indicate that CD44 is shed from cell surfaces through the actions of metalloproteinases such as MT1-MMP [17, 28, 29]. Additionally, it has also been reported that patients with colorectal cancer show significantly higher serum concentrations of CD44, including the standard form (CD44s), compared with healthy individuals, although these concentrations showed no correlation with tumor burden or CD44 expression level. Therefore, it is possible that this downregulation of CD44 expression partly indicates that the CD44 epitopes in these cases are masked as a result of ectodomain shedding by MT1-MMP. Recently, it was reported that CD44 molecules act as a platform for the assembly of multiple MMPs (MT1-MMP, MMP-7, and MMP-9) and their substrates [17, 43, 44]; but the partner proteinase(s) of CD44 v6 or v8–10 has(have) not yet been identified, even on an experimental level. CD44v6 variant can act as essential co-receptor for the activation of Met [27] and catalyze the formation of a complex with Met [30] and its ligand. This suggests that v6 variants might have a role that is distinct from the platforms for the proteinases.

This study shows that MT1-MMP overexpression might effect the histological differentiation of colorectal carcinomas due to disturbing neoplastic glandular structures. This overexpression also coincides with the downregulation of the CD44 protein expression. Further, the interactions between MT1-MMP and LN-5 γ2 monomers might induce tumor-cell motility of dedifferentiated cells at the periphery of the invasive front, as has been indicated [15, 20]. These morphological phenotypes of tumor progression appear to be well correlated with the localization and intensity of active β-catenin expression. Accordingly, our results suggest that MT1-MMP might be a major effector of β-catenin/TCF signaling in the late stage of colorectal carcinoma tumor progression. Additionally, this study indicates that various molecular interactions due to abnormal β-catenin/TCF signaling could define the biological behavior as well as the morphological phenotypes of colorectal carcinomas.

Acknowledgements This research was supported by a Grant-in Aid for Scientific Research Priority Area 12215018 from the Ministry of Education, Culture, Sports, Science and Technology, Japan (to K. Harigaya) and by a Grant-in Aid for Scientific Research 13670163 from the Japan Society for the Promotion of Science (to K. Harigaya). We would like to thank Ms. Sayuri Akiyama for her help in preparing this manuscript. All the experiments in this study comply with the current laws of Japan where they were performed.

References

1. Bartolazzi A, Peach R, Aruffo A, Stamenkovic I (1994) Interaction between CD44 and hyaluronate is directly implicated in the regulation of tumor development. J Exp Med 180:53–66
2. Brabletz T, Jung A, Dag S, Hlubek F, Kirchner T (1999) Beta-catenin regulates the expression of the matrix metalloproteinase-7 in human colorectal cancer. Am J Pathol 155:1033–1038
3. Brabletz T, Jung A, Reu S, Porzner M, Hlubek F, Kunz-Schughart LA, Knuechel R, Kirchner T (2001) Variable beta-catenin expression in colorectal cancers indicates tumor progression driven by the tumor environment. Proc Natl Acad Sci U S A 98:10356–10361
4. Fujita M, Furukawa Y, Tsunoda T, Tanaka T, Ogawa M, Nakamura Y (2001) Up-regulation of the ectodermal-neural cortex 1 (ENC1) gene, a downstream target of the beta-catenin/T-cell factor complex, in colorectal carcinomas. Cancer Res 61:7722–7726
5. Fujita Y, Kitagawa M, Nakamura S, Azuma K, Ishii G, Higashi M, Kishi H, Hiwasa T, Koda K, Nakajima N, Harigaya K (2002) CD44 signaling through focal adhesion kinase and its anti-apoptotic effect. FEBS Lett 528:101–108
6. Giannelli G, Falk-Marzillier J, Schiraldi O, Stetler-Stevenson WG, Quaranta V (1997) Induction of cell migration by matrix metalloprotease-2 cleavage of laminin-5. Science 277:225–228
7. Gunthert U, Hofmann M, Rudy W, Reber S, Zoller M, Haussmann I, Matzku S, Wenzel A, Ponta H, Herrlich P (1991) A new variant of glycoprotein CD44 confers metastatic potential to rat carcinoma cells. Cell 65:13–24
8. Haas TL, Stitelman D, Davis SJ, Apte SS, Madri JA (1999) Egr-1 mediates extracellular matrix-driven transcription of membrane type 1 matrix metalloproteinase in endothelium. J Biol Chem 274:22679–22685
9. Habelhah H, Okada F, Kobayashi M, Nakai K, Choi S, Hamada J, Moriuchi T, Kaya M, Yoshida K, Fujinaga K, Hosokawa M (1999) Increased E1AF expression in mouse fibrosarcoma promotes metastasis through induction of MT1-MMP expression. Oncogene 18:1771–1776
10. Han YP, Tuan TL, Wu H, Hughes M, Garner WL (2001) TNF-alpha stimulates activation of pro-MMP2 in human skin

through NF-(kappa)B mediated induction of MT1-MMP. J Cell Sci 114:131–139
11. He TC, Sparks AB, Rago C, Hermeking H, Zawel L, da Costa LT, Morin PJ, Vogelstein B, Kinzler KW (1998) Identification of c-MYC as a target of the APC pathway. Science 281:1509–1512
12. He TC, Chan TA, Vogelstein B, Kinzler KW (1999) PPARdelta is an APC-regulated target of nonsteroidal anti-inflammatory drugs. Cell 99:335–345
13. Heider KH, Hofmann M, Hors E, van den Berg F, Ponta H, Herrlich P, Pals ST (1993) A human homologue of the rat metastasis-associated variant of CD44 is expressed in colorectal carcinomas and adenomatous polyps. J Cell Biol 120:227–233
14. Hlubek F, Jung A, Kotzor N, Kirchner T, Brabletz T (2001) Expression of the invasion factor laminin gamma2 in colorectal carcinomas is regulated by beta-catenin. Cancer Res 61:8089–8093
15. Hlubek F, Spaderna S, Jung A, Kirchner T, Brabletz T (2004) Beta-catenin activates a coordinated expression of the proinvasive factors laminin-5 gamma2 chain and MT1-MMP in colorectal carcinomas. Int J Cancer 108:321–326
16. Hotary K, Allen E, Punturieri A, Yana I, Weiss SJ (2000) Regulation of cell invasion and morphogenesis in a three-dimensional type I collagen matrix by membrane-type matrix metalloproteinases 1, 2, and 3. J Cell Biol 149:1309–1323
17. Kajita M, Itoh Y, Chiba T, Mori H, Okada A, Kinoh H, Seiki M (2001) Membrane-type 1 matrix metalloproteinase cleaves CD44 and promotes cell migration. J Cell Biol 153:893–904
18. Kinzler KW, Vogelstein B (1996) Lessons from hereditary colorectal cancer. Cell 87:159–170
19. Kirchner T, Brabletz T (2000) Patterning and nuclear beta-catenin expression in the colonic adenoma-carcinoma sequence. Analogies with embryonic gastrulation. Am J Pathol 157:1113–1121
20. Koshikawa N, Giannelli G, Cirulli V, Miyazaki K, Quaranta V (2000) Role of cell surface metalloprotease MT1-MMP in epithelial cell migration over laminin-5. J Cell Biol 148:615–624
21. Lin YM, Ono K, Satoh S, Ishiguro H, Fujita M, Miwa N, Tanaka T, Tsunoda T, Yang KC, Nakamura Y, Furukawa Y (2001) Identification of AF17 as a downstream gene of the beta-catenin/T-cell factor pathway and its involvement in colorectal carcinogenesis. Cancer Res 61:6345–6349
22. Malhotra S, Newman E, Eisenberg D, Scholes J, Wieczorek R, Mignatti P, Shamamian P (2002) Increased membrane type 1 matrix metalloproteinase expression from adenoma to colon cancer: a possible mechanism of neoplastic progression. Dis Colon Rectum 45:537–543
23. Mann B, Gelos M, Siedow A, Hanski ML, Gratchev A, Ilyas M, Bodmer WF, Moyer MP, Riecken EO, Buhr HJ, Hanski C (1999) Target genes of beta-catenin-T cell-factor/lymphoid-enhancer-factor signaling in human colorectal carcinomas. Proc Natl Acad Sci U S A 96:1603–1608
24. Mariadason JM, Bordonaro M, Aslam F, Shi L, Kuraguchi M, Velcich A, Augenlicht LH (2001) Down-regulation of beta-catenin TCF signaling is linked to colonic epithelial cell differentiation. Cancer Res 61:3465–3471
25. Matsumura Y, Tarin D (1992) Significance of CD44 gene products for cancer diagnosis and disease evaluation. Lancet 340:1053–1058
26. Miwa N, Furuse M, Tsukita S, Niikawa N, Nakamura Y, Furukawa Y (2000) Involvement of claudin-1 in the beta-catenin/Tcf signaling pathway and its frequent up-regulation in human colorectal cancers. Oncol Res 12:469–476
27. Nestl A, Von Stein OD, Zatloukal K, Thies WG, Herrlich P, Hofmann M, Sleeman JP (2001) Gene expression patterns associated with the metastatic phenotype in rodent and human tumors. Cancer Res 61:1569–1577
28. Okamoto I, Kawano Y, Matsumoto M, Suga M, Kaibuchi K, Ando M, Saya H (1999) Regulated CD44 cleavage under the control of protein kinase C, calcium influx, and the Rho family of small G proteins. J Biol Chem 274:25525–25534
29. Okamoto I, Kawano Y, Tsuiki H, Sasaki J, Nakao M, Matsumoto M, Suga M, Ando M, Nakajima M, Saya H (1999) CD44 cleavage induced by a membrane-associated metalloprotease plays a critical role in tumor cell migration. Oncogene 18:1435–1446
30. Orian-Rousseau V, Chen L, Sleeman JP, Herrlich P, Ponta H (2002) CD44 is required for two consecutive steps in HGF/c-Met signaling. Genes Dev 16:3074–3086
31. Oving IM, Clevers HC (2002) Molecular causes of colon cancer. Eur J Clin Invest 32:448–457
32. Patarroyo M, Tryggvason K, Virtanen I (2002) Laminin isoforms in tumor invasion, angiogenesis and metastasis. Semin Cancer Biol 12:197–207
33. Powell SM, Zilz N, Beazer-Barclay Y, Bryan TM, Hamilton SR, Thibodeau SN, Vogelstein B, Kinzler KW (1992) APC mutations occur early during colorectal tumorigenesis. Nature 359:235–237
34. Pozzi A, Moberg PE, Miles LA, Wagner S, Soloway P, Gardner HA (2000) Elevated matrix metalloprotease and angiostatin levels in integrin alpha 1 knockout mice cause reduced tumor vascularization. Proc Natl Acad Sci U S A 97:2202–2207
35. Pyke C, Romer J, Kallunki P, Lund LR, Ralfkiaer E, Dano K, Tryggvason K (1994) The gamma 2 chain of kalinin/laminin 5 is preferentially expressed in invading malignant cells in human cancers. Am J Pathol 145:782–791
36. Sordat I, Bosman FT, Dorta G, Rousselle P, Aberdam D, Blum AL, Sordat B (1998) Differential expression of laminin-5 subunits and integrin receptors in human colorectal neoplasia. J Pathol 185:44–52
37. Sy MS, Guo YJ, Stamenkovic I (1991) Distinct effects of two CD44 isoforms on tumor growth in vivo. J Exp Med 174:859–866
38. Takahashi M, Tsunoda T, Seiki M, Nakamura Y, Furukawa Y (2002) Identification of membrane-type matrix metalloproteinase-1 as a target of the beta-catenin/Tcf4 complex in human colorectal cancers. Oncogene 21:5861–5867
39. Tanabe KK, Ellis LM, Saya H (1993) Expression of CD44R1 adhesion molecule in colon carcinomas and metastases. Lancet 341:725–726
40. Tetsu O, McCormick F (1999) Beta-catenin regulates expression of cyclin D1 in colon carcinoma cells. Nature 398:422–426
41. Werb Z (1997) ECM and cell surface proteolysis: regulating cellular ecology. Cell 91:439–442
42. Wielenga VJ, Heider KH, Offerhaus GJ, Adolf GR, van den Berg FM, Ponta H, Herrlich P, Pals ST (1993) Expression of CD44 variant proteins in human colorectal cancer is related to tumor progression. Cancer Res 53:4754–4756
43. Yu Q, Stamenkovic I (1999) Localization of matrix metalloproteinase 9 to the cell surface provides a mechanism for CD44-mediated tumor invasion. Genes Dev 13:35–48
44. Yu WH, Woessner JF Jr, McNeish JD, Stamenkovic I (2002) CD44 anchors the assembly of matrilysin/MMP-7 with heparin-binding epidermal growth factor precursor and ErbB4 and regulates female reproductive organ remodeling. Genes Dev 16:307–323

Virchows Arch (2004) 445:279–284
DOI 10.1007/s00428-004-1078-1

ORIGINAL ARTICLE

Anne Couvelard · François Paraf · Dominique Vidaud · Sylvie Dubois · Michel Vidaud · Jean-François Fléjou · Claude Degott

Human chorionic gonadotrophin beta expression in malignant Barrett's oesophagus

Received: 22 April 2004 / Accepted: 14 June 2004 / Published online: 10 August 2004
© Springer-Verlag 2004

Abstract *Background:* Human chorionic gonadotrophin beta (hCGβ) is expressed in several non-trophoblastic tumours, and this is usually associated with aggressive behaviour. Little is known about hCGβ expression in Barrett's adenocarcinoma. *Materials and methods:* We determined the hCGβ profile in a large series of surgically resected Barrett's adenocarcinoma (a) at mRNA level using real-time quantitative reverse-transcription polymerase chain reaction analysis and (b) at protein level using immunohistochemistry with a polyclonal antibody and with a monoclonal antibody specific for free hCGβ. We then sought links between the hCGβ protein expression pattern and clinical and pathological parameters, including patient outcome as well as vascular endothelial growth factor (VEGF) expression. *Results:* hCGβ protein expression was observed in 43 of 76 (57%) Barrett's adenocarcinomas. We showed a strong correlation between hCGβ protein abundance and CGB mRNA level. We observed a statistical link between hCGβ protein expression and infiltrative tumour type (P=0.023), perineural neoplastic invasion (P= 0.007) and VEGF protein expression (P=0.016). hCGβ expression tended to be associated with a poor outcome (16% versus 36% survival 8 years after resection). *Conclusion:* Expression of hCGβ correlates with specific infiltrative characteristics and is associated with higher VEGF expression. Both molecules may play a co-ordinated role in the development of Barrett's adenocarcinomas.

Keywords Barrett's adenocarcinoma · hCGβ · Immunohistochemistry · Real-time quantitative RT-PCR · VEGF

A. Couvelard (✉) · S. Dubois · C. Degott
Service d'Anatomie Pathologique,
Hôpital Beaujon,
92118 Clichy cedex, France
e-mail: anne.couvelard@bjn.ap-hop-paris.fr
Tel.: +33-1-40875462
Fax: +33-1-40870077

F. Paraf
Service d'Anatomie Pathologique,
Centre Hospitalier Universitaire Dupuytren,
Limoges, France

D. Vidaud · M. Vidaud
Laboratoire de Génétique Moléculaire—UPRES EA 3618,
Faculté des Sciences Pharmaceutiques et Biologiques,
Université Paris V,
Paris, France

J.-F. Fléjou
Service d'Anatomie Pathologique,
Hôpital Saint-Antoine,
Paris, France

Introduction

In the last decade, the incidence of oesophageal adenocarcinoma, developing almost exclusively in columnar-lined Barrett's oesophagus, has been steadily increasing [13]. These adenocarcinomas, most frequently diagnosed in elderly white men, have a poor prognosis, since metastases are often present at the time of diagnosis. Treatment is based on radical surgery, and tumour node metastasis (TNM) stage is the most important prognostic factor [8, 34]. However, the outcome is variable within a given stage, and response to therapy cannot be predicted on that base.

Human chorionic gonadotrophin β subunit (hCGβ) is a significant indicator of malignant transformation [1, 2]. It is not only detected in trophoblastic neoplasms [3], but also in carcinomas of breast [7], bladder [24], gynaecological [17], prostatic [36] and gastrointestinal origin [11, 12, 25, 42]. Its expression has been demonstrated to correlate with a more aggressive behaviour and a higher rate of metastasis in such tumours [7, 18, 36]. Factors that regulate hCGβ expression during malignancy are poorly known. However, it has been shown, mainly in the ovary, that vascular endothelial growth factor (VEGF) expression increases following gonadotrophin stimulation in vivo and in vitro [22, 31]. To date, no study concerning the expression of hCGβ has been reported in Barrett's adenocarcinomas.

The aims of our study were to examine the expression of hCGβ using immunohistochemistry and reverse-tran-

scription polymerase chain reaction (RT-PCR) analysis in a large surgical series of Barrett's adenocarcinoma, to compare hCGβ and VEGF expression and to correlate these results with clinico-pathological data and prognosis.

Materials and methods

Patients

A total of 76 patients with Barrett's adenocarcinoma underwent potentially curative surgical resection at Beaujon Hospital between 1976 and 1997. The patients were 73 men and 3 women, with a mean age of 62.2±12.9 years (range 19–84 years). None of the patients had neoadjuvant chemotherapy or radiation therapy before surgery. The medical history of each patient was collected.

Tumour samples

Surgical specimens were received fresh, fixed in 10% neutral formalin and embedded in paraffin wax. Samples for real-time RT-PCR analysis were, immediately after surgery, snap-frozen in liquid nitrogen and stored at −70°C until RNA extraction.

In all patients, the tumour was classified as an adenocarcinoma developed in Barrett's oesophagus by preoperative endoscopy and macroscopic examination of the surgical specimen: the tumour was regarded as having developed in Barrett's oesophagus when specialised metaplastic mucosa was observed between the tumour and the squamous oesophageal mucosa or the gastric mucosa. Samples of adenocarcinoma (76 cases) and Barrett's mucosa around the tumour (negative for dysplasia in 15 cases or with high-grade dysplasia in 15 cases) were selected for immunohistochemistry. For each tumour, the following features were recorded: tumour differentiation, depth of infiltration, perineural neoplastic invasion, vascular invasion, regional lymph-node metastasis, distant metastasis, pTNM (pathological TNM) stage according to the Union Internationale de Lutte Contre le Cancer, stage according to the Rosenberg's classification and tumour type in Lauren's and Ming's classifications of gastric adenocarcinoma [23, 29, 35, 40].

Immunohistochemistry

Immunohistochemistry was performed on formalin-fixed, paraffin-wax-embedded sections using a three-step indirect method for the monoclonal antibody free hCGβ (clone FBT11, kind gift from J-M Bidart, Institut Gustave Roussy, Villejuif, France) and a peroxidase anti-peroxidase method for polyclonal antibody [27] (hCGβ, polyclonal, Dako, Glostrup, Denmark). The VEGF staining had been previously reported in this series [14]. Sections 3 μm thick were cut from paraffin-embedded tissue, dried at 37°C, deparaffinised, heated in a microwave oven (3×5 min) in buffered citrate (citric acid and sodium citrate, pH 6.2) and treated with 0.1% hydrogen peroxide in methanol for 30 min. After staining with the three-step indirect or peroxidase anti-peroxidase method, the colour reaction was developed by adding 3′3-diaminobenzidine (Sigma, Saint Quentin Fallavier, France) in Tris-buffered saline (TBS) containing 0.05% hydrogen peroxide for 10 min. Sections were then counterstained with haematoxylin, dehydrated and mounted with permount. Negative control slides were obtained by omitting the primary antibody, replaced by TBS. Normal placental tissue was used as an external positive control for hCGβ.

hCGβ staining was scored semi-quantitatively for monoclonal and polyclonal antibodies. It was reported from 0 to 4 as follows: 0 negative (no cell positivity), 1 occasional (some isolated positive cells are identified), 2 focal (rare clusters of positive cells are detected), 3 moderate (some clusters of positive cells are detected) and 4 diffuse (isolated and clusters of positive cells found in most areas of the tumour).

hCGβ mRNA expression by real-time RT-PCR

Frozen tissue samples of 15 of the 76 Barrett's adenocarcinomas tested using immunohistochemistry were used for real-time RT-PCR analysis. Real-time quantitative RT-PCR using the ABI Prism 7700 Sequence Detection System (Perkin-Elmer Applied Biosystems) was performed according to a previously described method [7]. Briefly, total RNA extracted from frozen Barrett's adenocarcinoma tissues was reverse-transcribed before real-time PCR amplification. Quantitative values were obtained from the threshold cycle (Ct) number at which the increase in the signal associated with exponential growth of PCR products begins to be detected using PE Biosystems analysis software, according to the manufacturer's manuals. The precise amount of total RNA added to each reaction mix (based on optical density) and its quality (i.e. lack of extensive degradation) are both difficult to assess. We therefore also quantified transcripts of the *TBP* gene coding for the TATA box-binding protein (a component of the DNA-binding protein complex TFIID) as the endogenous RNA control, and each sample was normalised on the basis of its TBP content.

Results, expressed as N-fold differences in *CGB* gene expression relative to the TBP gene, termed "N*CGB*", were determined by the formula: N*CGB*=$2^{\Delta Ctsample}$, where ΔCt value of the sample was determined by subtracting the average Ct value of the *CGB* gene from the average Ct value of the *TBP* gene.

The N*CGB* values of the samples were subsequently normalised such that the N*CGB* value to the tumour sample among our tested series that contained the smallest amount of *CGB* mRNA would equal a value of 1.

The nucleotide sequences of the primers used for PCR amplification were the following: CGB-U (5′-GCTACTGCCCCACCATGACC-3′), CGB-L (5′-ATGGACTCGAAGCGCACATC-3′) and TaqMan fluorogenic probe CGB-P (5′-CCTGCCTCAGGTGGTGTGCAACTACC-3′), with a CGB-specific product size of 94 bp, and TBP-U (5′-CACGAACCACGGCACTGATT-3′), TBP-L (5′-TTTTCTTGCTGCCAGTCTGGAC-3′) and TaqMan fluorogenic probe TBP-P (5′-TGTGCACAGGAGCCAAGAGTGAAGA-3′), with a *TBP*-specific product size of 89 bp.

PCR was performed using the TaqMan PCR Core Reagents kit (Perkin-Elmer Applied Biosystems). The thermal cycling conditions comprised an initial denaturation step at 95°C for 10 min and 50 cycles at 95°C for 15 s and 65°C for 1 min. Experiments were performed with duplicates for each data point.

Statistical analysis

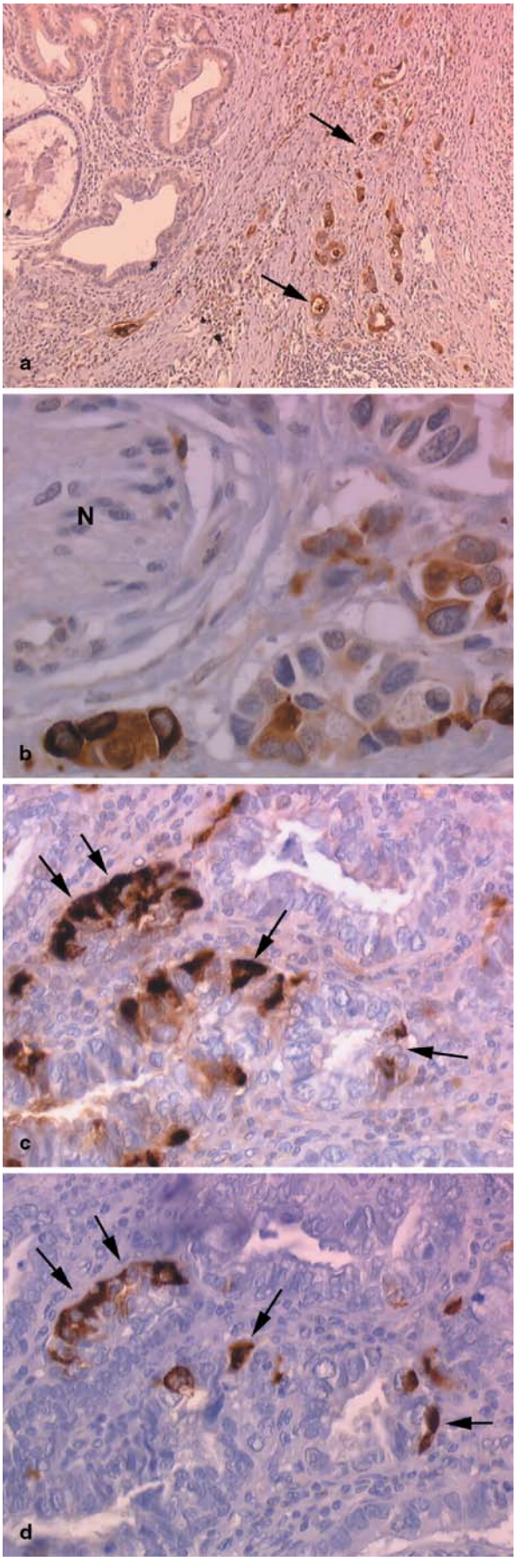
Qualitative data were compared using the chi square test with Yates correction when appropriate. Quantitative data were expressed as mean±SEM and compared by the non-parametric Mann-Whitney or Kruskal-Wallis tests. Survival rates were calculated by the Kaplan Meier method using the date of surgery as the starting point and compared by the log-rank test [20, 33]. All deaths were considered, including the postoperative deaths. The follow-up period ranged from 0.9 months to 189 months, with a mean of 36.7 months. At the time of analysis, 17 patients (22%) were alive, with a mean follow up of 93.5 months (range 41.1 months to 189.4 months). A two-tailed P value <0.05 was considered to indicate statistical significance.

Results

Immunohistochemistry

hCGβ expression

Staining pattern. hCGβ expression was detected in 57% (43/76) of the tumour samples and ranged from score 0 to score 4. No positivity was demonstrated in the normal or



metaplastic mucosa. All positive cases showed the same cytoplasmic staining pattern. The pattern of expression of the monoclonal antibody recognising the free beta subunit of hCG was similar to that observed with the polyclonal antibody. The two antibodies detected the same group of cells in the same areas of tumours; however, the monoclonal antibody stained less cells than the polyclonal one. hCGβ-positive cells were, for both antibodies, predominantly observed in deep infiltrative areas and in perineural neoplastic invasion (Fig. 1a, b). Often, hCGβ expression was detected in the same cells that showed immunoreactivity for VEGF, as shown in serial sections (Fig. 1c, d).

Correlation with pathological findings. The 76 patients were dichotomised into two subgroups: 43 patients with hCGβ expression (score>0) and 33 patients without hCGβ expression (score 0). A statistically significant relationship was observed between hCGβ expression and perineural neoplastic invasion (P=0.007) and infiltrative carcinomas according to Ming's classification (P=0.023). There was also a tendency between hCGβ immunoreactivity and tumour extension, with a higher rate of pT4 tumours (P=0.062), and pTNM stage-III and -IV cancers (P=0.086). There was no significant difference between the hCGβ-positive and -negative tumours regarding the other pathological features: tumour differentiation, vascular invasion, Lauren's classification, lymph-node status, distant metastasis, TNM and Rosenberg classifications (Table 1). Univariate analysis did not show a significant relationship between hCGβ expression and survival, although patients with hCGβ-positive tumours tended to have a worse prognosis, with 5-year and 8-year survival rates of 20% and 16% versus 39% and 36% (Fig. 2).

Relationship between hCGβ expression status and VEGF expression status

The 76 tumours studied for hCGβ expression had previously been tested for VEGF expression. The VEGF staining had been scored semi-quantitatively, and scores ranged from 1 to 11 [14]. The 76 patients were dichotomised into two groups: 64 patients with high VEGF expression (score greater than 3) and 12 patients with low VEGF expression (score 1–3). We found a significant

Fig. 1 Expression of vascular endothelial growth factor (VEGF) and human chorionic gonadotrophin beta (hCGβ) using immunohistochemistry. **a** hCGβ is strongly detected in invasive tumoral cells situated in the most infiltrating and deeper areas (*arrows*). Immunoperoxidase with nuclear counterstain using Mayer's haematoxylin. **b** hCGβ expression in a Barrett's adenocarcinoma with neoplastic perineural invasion showing a strong cytoplasmic staining pattern. *N* nerve section. Immunoperoxidase with nuclear counterstain using Mayer's haematoxylin. **c** and **d** VEGF (**a**) and hCGβ (**b**) expression in seriated sections demonstrating a strong cytoplasmic staining in the same glandular territories (*arrows*) of this well-differentiated Barrett's adenocarcinoma. Immunoperoxidase with nuclear counterstain by Mayer's haematoxylin

Table 1 Relationship between human chorionic gonadotrophin beta (hCGβ) expression and clinico-pathological data. All results are expressed as percentages except for age (years)

	hCGβ positive (n=43)	hCGβ negative (n=33)	P value
Age (years)	61.5±14.6	65.4±9.9	0.191
Tumour differentiation			0.225
Well and moderate	79	67	
Poor	21	33	
Vascular invasion	84	73	0.246
Perineural invasion	67	36	0.007
Ming classification			0.023
Expanding	47	75	
Infiltrative	53	25	
Lauren classification			0.374
Intestinal	79	83	
Diffuse	21	27	
Tumour infiltration			0.062
pT1, pT2, pT3	56	76	
pT4	44	24	
Regional lymph node invasion (N1)	65	55	0.350
Distant metastasis (M1)	12	12	0.947
TNM stage			0.086
Stage I–IIA–IIB	35	55	
Stage III–IV	65	45	
Rosenberg classification			0.311
Stage I–II	26	36	
Stage III–IV	74	64	
VEGF expression	95	75	0.016
Survival			0.252
2 years	37.2±7.4	45.5±8.7	
5 years	20.3±6.3	39.4±8.5	
8 years	16.3±6.2	36.1±8.4	

positive relationship between hCGβ and VEGF expression (P=0.016; Table 1).

RT-PCR analysis

CGB mRNA levels were analysed in 15 cases of the 78 Barrett's adenocarcinomas. Large differences in the amount of *CGB* mRNA were observed (N*CGB* from 1 to 118) in the 15 Barrett's adenocarcinomas. To better study the link between CGB mRNA level and hCGβ immunohistochemistry status, the 15 tumours were subdivided into three groups (6, 6 and 3 tumours, respectively), with tumours with negative (score 0), occasional or focal (score 1 to 3) and diffuse (scored 4) hCGβ immunoreactivity status. We observed a significant link between CGB mRNA level and hCGβ immunohistochemistry status (Table 2; Kruskal-Wallis test, P=0.023). Surprisingly, one tumour (T6) with high CGB mRNA level was hCGβ immunoreactive negative. However, tumour sampling was different in frozen and formalin-fixed tissue. This could be explained by the heterogeneous hCGβ immunostaining in most tumours.

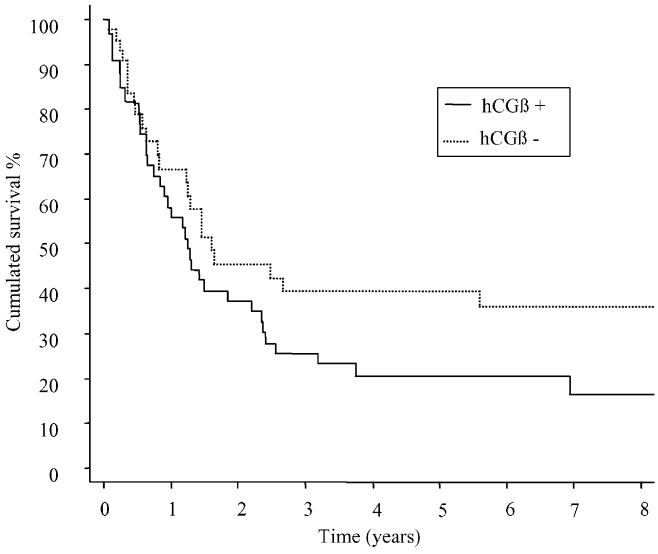


Fig. 2 Kaplan Meier survival curves according to human chorionic gonadotrophin beta expression for positive cases (n=43) and negative cases (n=33)

Table 2 Correlation between human chorionic gonadotrophin beta (hCGβ) subunit protein and CGB mRNA levels in Barrett's adenocarcinomas

Samples	Immunohistochemistry* (staining score)	RT-PCR (NCGB value)
Negative hCGβ immunoreactivity (score=0)		
T1	0	1
T2	0	1.2
T3	0	1.3
T4	0	2.2
T5	0	4.3
T6	0	9.2
Median		1.7
Occasional or focal hCGβ immunoreactivity (score=1 or 2)		
T7	1	2.1
T8	1	4.0
T9	2	4.0
T10	1	5.1
T11	1	6.6
T12	2	14.9
Median		4.5
Diffuse hCGβ immunoreactivity (score=4)		
T13	4	10.1
T14	4	11.4
T15	4	118.0
Median		11.4

* The staining score values (determined as described in Materials and methods) indicated in this column were obtained with the polyclonal antibody; identical staining scores were obtained by using the monoclonal antibody (FBT11)

Discussion

We demonstrated, in this series of Barrett's adenocarcinomas, that hCGβ expression was related to infiltrative tumours, high VEGF expression and tended to be associated with a poor outcome. hCGβ is a significant indicator of malignant transformation. It is not only detected in trophoblastic neoplasms for which it represents a

valuable tumour marker [3], but also in non-trophoblastic tumours, including carcinomas of breast, urinary bladder, gynaecological, prostatic and colonic origin [5, 7, 11, 12, 17, 24, 36, 42]. The role of hCGβ in the development of oesophageal adenocarcinoma has never been studied. In this work, we first evaluated the expression of hCGβ in Barrett's-related adenocarcinomas using immunohistochemistry with a polyclonal antibody that recognised antigenic regions of the hCGβ protein normally present in trophoblastic cells, as previously used in several studies [5, 26, 42]. However, this polyclonal antibody is not specific and cross-reacts with the beta subunit of human luteinizing hormone (LH). In addition, we therefore comparatively studied the expression of the monoclonal antibody specific for the free beta subunit of hCG specifically expressed by tumour tissues [6]. The immunostaining obtained by both antibodies showed similar cellular distribution in all 76 Barrett's adenocarcinomas tested. The two antibodies recognised the same group of cells in the same areas of tumours. We detected with the two antibodies the presence of hCGβ in 57% of Barrett's adenocarcinomas. The incidence of expression of hCGβ is similar to that reported in other immunohistochemical studies, in colonic and prostatic adenocarcinomas [11, 12, 36, 42]. Moreover, we showed that hCGβ expression was associated with an infiltrative tumour pattern (P=0.023) and with perineural neoplastic invasion (P=0.007). Our results also showed a tendency for a poor outcome associated with hCGβ expression in Barrett's adenocarcinoma, although it was not significant. Despite the absence of a significant association with standard prognostic parameters (such as tumour size, pTNM stage or presence of metastasis), expression of hCGβ probably reflects aggressive behaviour of Barrett's adenocarcinomas. These results are in accordance with previous studies in some other malignancies showing that hCGβ production, evaluated both at the RNA [7] and at the protein levels [15, 36, 42], is correlated with an unfavourable prognosis. Some recent studies also pointed out the interest of the hCGβ serum level as an independent prognostic variable in renal carcinoma [18] and gastrointestinal malignancies [25]. We interestingly found that hCGβ immunoreactivity was preferentially localised into the deeper invasive areas and around infiltrated nerves. This supports some previous studies suggesting that hCGβ may act as a growth factor with characteristics similar to nerve, platelet-derived and β-transforming growth factors [28].

We demonstrated a significant positive correlation between hCGβ and VEGF expression. Tumour cells that expressed hCGβ often showed immunoreactivity for VEGF, and the two markers were often co-localised in the same tumours. Our results show a positive link between hCGβ and VEGF expression in Barrett's adenocarcinoma, in agreement with previous studies in other cancers. VEGF is one of the most potent known tumour angiogenic factors [9, 10, 19, 21, 30, 32, 37, 38].

In vitro and in vivo experiments have shown that in the ovary, VEGF is chorionic gonadotrophin dependent [22, 31, 41]. hCGβ may play a significant role in tumour progression through upregulation of VEGF. Another possible pathway could involve the regulation of VEGF and hCGβ by the same factors. It is noteworthy that hypoxia influences the secretion of both of these molecules in trophoblastic-derived cell lines [39]. The above correlates well with the fact that placental cells have angiogenic and invasive properties, which are also characteristic features of malignant cells.

The significance of hCGβ production by non-trophoblastic tumours is still under investigation. Whereas the α subunit of hCG is encoded by a single gene (CGA) present on chromosome 6, the β subunit is potentially encoded by at least four genes (CGB 7, 3, 5 and 8), located in a cluster on chromosome 19q13.3 and physically linked to the LHB gene. Bellet et al. have shown that malignant transformation of non-trophoblastic cells was associated with the emergence of the three hCGβ genes normally transcribed at a high level in the placenta ("trophoblastic" CGB 3, 5 and 8) [4]. In breast cancer, the detection of these "trophoblastic" CGB genes is of prognostic significance [7]. Moreover, the emergence of these "trophoblastic" CGB genes in breast cancer is accompanied by an increase of the total CGB steady-state mRNA level [16]. In the present study, we report a strong correlation between CGB mRNA copy numbers and hCGβ protein abundance, suggesting that this gene is mainly dysregulated at the transcriptional level and points out a role of hCGβ in Barrett's adenocarcinoma tumorigenesis.

In conclusion, hCGβ and VEGF play a co-ordinated role in the tumorigenesis of Barrett's adenocarcinomas through their angiogenic and invasive properties. Our results may give new insights into the mechanisms of hCGβ regulation.

Acknowledgements We thank Jean-Michel Bidart (Institut Gustave Roussy, Villejuif) for generously providing the monoclonal antibody directed against free hCGβ, clone FTB11. This work was supported by a Grant for Clinical Research (Association pour la Recherche contre le Cancer).

References

1. Acevedo HF, Krichevsky A, Campbell-Acevedo EA, Galyon JC, Buffo MJ, Hartstsock RJ (1992) Expression of membrane associated human chorionic gonadotropin, its subunits, and fragments by cultured human cancer cells. Cancer 69:1829–1842
2. Acevedo HF, Tong JY, Hartsock RJ (1995) Human chorionic gonadotropin β subunit gene expression in cultured human fetal and cancer cells of different types and origins. Cancer 76:1306–1311
3. Bagshawe KD (1992) Choriocarcinoma: a model for tumor markers. Acta Oncol 31:99–106
4. Bellet D, Lazar V, Bieche I, Paradis V, Giovangrandi Y, Paterlini P, Lidereau R, Bedossa P, Bidart JM, Vidaud M (1997) Malignant transformation of nontrophoblastic cells is associated with the expression of chorionic gonadotropin beta genes normally transcribed in trophoblastic cells. Cancer Res 57:516–523
5. Bhalang K, Kafrawy AH, Miles DA (1999) Immunohistochemical study of the expression of human chorionic gonado-

tropin-beta in oral squamous cell carcinoma. Cancer 85:757–762
6. Bidart JM, Troalen F, Lazar V, Berger P, Marcillac I, Lhomme C, Droz JP, Bellet D (1992) Monoclonal antibodies to the free beta-subunit of human chorionic gonadotropin define three distinct antigenic domains and distinguish between intact and nicked molecules. Endocrinology 131:1832–1840
7. Bieche I, Lazar V, Nogues C, Poynard T, Giovangrandi Y, Bellet D, Lidereau R, Vidaud M (1998) Prognostic value of chorionic gonadotropin beta gene transcripts in human breast carcinoma. Clin Cancer Res 4:671–676
8. Bonavina L, Via A, Incarbone R, Saino G, Peracchia A (2003) Results of surgical therapy in patients with Barrett's adenocarcinoma. World J Surgery 27:1062–1066
9. Brown LF, Berse B, Jackman RW, Tognazzi K, Manseau EJ, Senger DR, Dvorak HF (1993) Expression of vascular permeability factor (vascular endothelial growth factor) and its receptors in adenocarcinomas of the gastrointestinal tract. Cancer Res 53:4727–4735
10. Brown LF, Berse B, Jackman RW, Tognazzi K, Guidi AJ, Dvorak HF, Senger DR, Connolly JL, Schnitt SJ (1995) Expression of vascular permeability factor (vascular endothelial growth factor) and its receptors in breast cancer. Hum Pathol 26:86–91
11. Buckley CH, Fox H (1979) An immunohistochemical study of the significance of HCG secretion by large bowel adenocarcinoma. J Clin Pathol 32:368–372
12. Campo E, Palacin A, Benasco C, Quesada E, Cardesa (1987) A human chorionic gonadotropin in colorectal carcinoma. An immunohistochemical study. Cancer 59:1611–1616
13. Cossentino MJ, Wong RK (2003) Barrett's esophagus and risk of esophageal adenocarcinoma. Semin Gastrointest Dis 14:128–135
14. Couvelard A, Paraf F, Gratio V, Scoazec J-Y, Henin D, Degott C, Flejou J-F (2000) Angiogenesis in the neoplastic sequence of Barrett's oesophagus. Correlation with VEGF expression. J Pathol 192:14–18
15. Dirnhofer S, Koessler P, Ensinger C, Feichtinger H, Madersbacher S, Berger P (1998) Production of trophoblastic hormones by transitional cell carcinoma of the bladder: association to tumor stage and grade. Hum Pathol 29:377–382
16. Giovangrandi Y, Parfait B, Asheur M, Olivi M, Lidereau R, Vidaud M, Bieche I (2001) Analysis of the human CGB/LHB gene cluster in breast tumors by real-time quantitative RT-PCR assays. Cancer Lett 168:93–100
17. Higashida T, Koizumi T, Yamagushi S, Ichimura T, Hasegawa K, Nishimura R (2001) Ovarian malignant mixed mesodermal tumor producing the free form of the beta-subunit of human chorionic gonadotropin. Int J Clin Oncol 6:97–100
18. Hotakainen K, Ljungberg B, Paju A, Rasmuson T, Alfthan H, Stenman UH (2002) The free beta-subunit of human chorionic gonadotropin as a prognostic factor in renal cell carcinoma. Br J Cancer 86:185–189
19. Inoue K, Ozeki Y, Suganuma T, Sugiura Y, Tanaka S (1997) Vascular endothelial growth factor expression in primary esophageal squamous cell carcinoma. Association with angiogenesis and tumor progression. Cancer 79:206–213
20. Kaplan EL, Meier P (1958) Nonparametric estimation from incomplete observations. J Am Stat Assoc 53:457–481
21. Kitadai Y, Haruma K, Tokutomi T, Tanaka S, Sumii K, Carvalho M, Kuwabara M, Yoshida K, Hirai T, Kajiyama G, Tahara E (1998) Significance of vessel count and vascular endothelial growth factor in human esophageal carcinomas. Clin Cancer Res 4:2195–2200
22. Koos RD (1995) Increased expression of vascular endothelial growth/permeability factor in the rat ovary following an ovulatory gonadotropin stimulus: potential roles in follicle rupture. Biol Reprod 52:1426–1435
23. Lauren P (1965) The two histological main types of gastric carcinoma diffuse and so-called intestinal type carcinoma. An attempt at a histo-clinical classification. Acta Pathol Microbiol Scand 64:31–49
24. Lazar V, Diez SG, Laurent A, Giovangrandi Y, Radvanyi F, Chopin D, Bidart JM, Bellet D, Vidaud M (1995) Expression of human chorionic gonadotropin beta subunit genes in superficial and invasive bladder carcinomas. Cancer Res 55:3735–3738
25. Luohimo J, Finne P, Alfthan H, Stenman UH, Haglund C (2002) Combination of HCGbeta, CA 1–9 and CEA with logistic regression improves accuracy in gastrointestinal malignancies. Anticancer Res 22:1759–1764
26. Marcillac I, Troalen F, Bidart JM, Ghillani P, Ribrag V, Escudier B, Malassagne B, Droz JP, Lhomme C, Rougier P (1992) Free human chorionic gonadotropin beta subunit in gonadal and nongonadal neoplasms. Cancer Res. 52:3901–3907
27. Mason DY, Summons RE (1979) The labeled antigen method of immuno-peroxidase staining. J Histochem Cytochem 27:832–840
28. Melmed S, Braunstein GD (1983) Human chorionic gonadotropin stimulates proliferation of Nb 2 rat lymphoma cells J Clin Endocrinol Metab 56:1068–1070
29. Ming S-C (1977) Gastric carcinoma: a pathobiological classification. Cancer 39:2475–2485
30. Mise M, Arii S, Higashituji H, Furutani M, Niwano M, Harada T, Ishigami S, Toda Y, Nakayama H, Fukumoto M, Fujita J, Imamura M (1996) Clinical significance of vascular endothelial growth factor and basic fibroblast growth factor gene expression in liver tumor. Hepatology 23:455–464
31. Neulen J, Raczek S, Pogorzelski M, Grunwald K, Yeo TK, Dvorak HF, Weich HA, Breckwoldt M (1998) Secretion of vascular endothelial growth factor/vascular permeability factor from human luteinized granulosa cells is human chorionic gonadotrophin dependent. Mol Hum Reprod 4:203–206
32. Niedergethmann M, Hildenbrand R, Wostbrock B, Hartel M, Sturm JW, Richter A, Post S (2002) High expression of vascular endothelial growth factor predicts early recurrence and poor prognosis after curative resection for ductal adenocarcinoma of the pancreas. Pancreas 25:122–129
33. Peto R, Pike MC, Armitage P (1977) Design and analysis of randomized clinical trials requiring prolonged observation of each patient. II. Analysis and examples. Br J Cancer 35:1–39
34. Reynolds JC, Rahimi P, Hirschl D (2002) Barrett's esophagus: clinical characteristics. Gastroenterol Clin North Am 31:441–60
35. Rosenberg JC, Budev H, Edwards RC, Singal S, Steiger Z, Sundareson AS (1985) Analysis of adenocarcinoma in Barrett's esophagus utilizing a staging system. Cancer 55:1353–1360
36. Sheaff MT, Martin JE, Badenoch DF, Baithun SI (1996) beta hCG as a prognostic marker in adenocarcinoma of the prostate. J Clin Pathol 49:329–332
37. Takahashi Y, Kitadai Y, Bucana CD, Cleary KR, Ellis LM (1995) Expression of vascular endothelial growth factor and its receptor, KDR, correlates with vascularity, metastasis, and proliferation of human colon cancer. Cancer Res 55:3964–3968
38. Takahashi Y, Cleary KR, Mai M, Kitadai Y, Bucana CD, Ellis LM (1996) Significance of vessel count and vascular endothelial growth factor and its receptor (KDR) in intestinal-type gastric cancer. Clin Cancer Res 2:1679–1684
39. Taylor CM, Stevens H, Anthony FW, Wheeler T (1997) Influence of hypoxia on vascular endothelial growth factor and chorionic gonadotrophin production in the trophoblast-derived cell lines: JEG, JAr and BeWo. Placenta 18:451–458
40. UICC (1987) TNM Classification of malignant tumors, 4th edition. Hermanek P, Sobin LH (eds) Springer, Berlin Heidelberg New York, pp 40–42
41. Wang TH, Horng SG, Chang CL, Wu HM, Tsai YJ, Wang HS, Soong YK (2002) Human chorionic gonadotropin-induced ovarian hyperstimulaion syndrome is associated with up-regulation of vascular endothelial growth factor. J Clin Endocrinol Metab 87:3300–3308
42. Webb A, Scott-Mackie P, Cunningham D, Norman A, Andreyev J, O'Brien M, Bensted J (1995) The prognostic value of CEA, beta HCG, AFP, CA125, CA19-9 and C-erbB-2, beta HCG immunohistochemistry in advanced colorectal cancer. Ann Oncol 6:581–587

Virchows Arch (2004) 445:285–291
DOI 10.1007/s00428-004-1083-4

ORIGINAL ARTICLE

Johannes J. P. M. Bogers · Shyama Chatterjee · Werner Jacobs · Padraic G. Fallon · David W. Dunne · Jan A. M. Langermans · Andre M. Deelder · Alan W. Thomas · Eric A. E. Van Marck

Juvenile rhesus monkeys have more colonic granulomas than adults after primary infection with *Schistosoma mansoni*

Received: 28 January 2004 / Accepted: 16 June 2004 / Published online: 30 July 2004
© Springer-Verlag 2004

Abstract Adults and children have differences in their susceptibility to schistosomiasis. Whether this age-dependent innate susceptibility influences parasite-caused granulomogenesis is difficult to assess in humans. Therefore, we exposed juvenile and adult female rhesus monkeys to primary infection with *Schistosoma mansoni*. Hepatic and intestinal granuloma formation was observed in both pre-pubescent and adult monkeys. Two distinct stages of granulomas were discerned, the exudative and the productive stage. In the intestine, more granulomas were generated in the colon than in the ileum. In contrast to the adult animals, the juvenile rhesus monkeys had higher numbers of colonic granulomas, these higher numbers being predominantly of the more advanced productive stage. Juvenile animals had a statistically non-significant increased worm burden. These results suggest that juvenile rhesus monkeys have a significantly more intense and advanced colonic response towards entrapped *S. mansoni* eggs after primary schistosome infections and, thereby, are more susceptible to parasite infection.

Keywords *Schistosoma mansoni* · Pathology · Granuloma · Rhesus · Age

Research protocols involving non-human primates received ethical clearance by the Institutional Animal Care and Use Committee of the Biomedical Primate Research Centre (Rijswijk, The Netherlands), according to Dutch Law.

J. J. P. M. Bogers · S. Chatterjee · W. Jacobs · E. A. E. Van Marck (✉)
Laboratory of Pathology,
University of Antwerp (UA),
Universiteitsplein 1, 2610 Antwerp (Wilrijk), Belgium
e-mail: eric.van.marck@uza.be
Tel.: +32-3-8213604
Fax: +32-3-8214753

P. G. Fallon · D. W. Dunne
Department of Pathology,
University of Cambridge,
Cambridge, UK

J. A. M. Langermans · A. W. Thomas
Department of Parasitology,
Biomedical Primate Research Centre,
Rijswijk, The Netherlands

A. M. Deelder
Leiden University Medical Center,
Leiden, The Netherlands

Introduction

Schistosomiasis affects more than 250 million people worldwide. This disease is caused by infection with trematode parasites of the *Schistosoma* species. Considerable hepatic morbidity in terms of fibrosis, variceal bleeding and host mortality are caused by the inflammatory granulomatous response to tissue entrapped *Schistosoma mansoni* eggs [36]. In addition, 85% of *S. mansoni*-infected individuals suffer from gastrointestinal manifestations caused by parasite egg-induced granulomas in the gastrointestinal tract, with symptoms such as bloody diarrhoea (frequently seen in children) [33], abdominal pain, nausea, dysentery, malnutrition, iron deficiency and anaemia [27, 31].

Extensive epidemiological studies on human populations in endemic countries have shown that adults generally have lower intensities of schistosome infection than children do [2]. Observation of the effects of host age, per se, on the susceptibility to human schistosomiasis is usually confounded by differences between adults and children with regard to: (1) water contact patterns, (2) development of acquired immunity due to previous infections and (3) age-related, neurohormonal influences. Much discussion has been prompted on this controversial issue [12, 13, 14, 15]. How this differential susceptibility pattern defines the egg-induced inflammatory response, how the dynamics of granulomogenesis differ with age and how this antigenic profile provides the prerequisite condition for the development of adult resistance to schistosomiasis are difficult to identify and quantify in human studies.

It is reported [9] that the peak of re-infection is coincident with puberty (about 12–14 years of age), suggesting that, after puberty, a mechanism may mediate the development of resistance to infection in adults. The corollary of this is that "juveniles" (i.e. those aged less than 12 years) may be innately more susceptible to schistosome infection than adults in terms of the inflammatory granulomatous response to parasite eggs and/or are unable to develop the acquired immunological responses that provide protection in adults.

In this study, we have used rhesus monkeys (*Macaca mulatta*), a widely used primate model for studies on primary infection with schistosomes [30], to investigate the morphology of the hepatic and intestinal granulomatous response and the nature of age-related differences in susceptibility to a primary infection with *S. mansoni*.

Materials and methods

Experimental animals and infection

Ten rhesus monkeys were used in this study. They were matched for sex (all females) and housed in the Biomedical Primate Research Center (Rijswijk, The Netherlands). The five adult monkeys were aged 13–19 years (mean age±SD, 16.1±3.1 years) and weighed 5.5±1.1 kg. Five juvenile monkeys were selected by age to be at the pre-pubertal to mid-pubertal stages of development (range, 1–3 years; mean±SD, 2.4±0.6 years) and weighed 3.0±0.9 kg. Before the start of the study, a veterinarian examined the animals. Levels of serum dehydroepiandrosterone (DHEA) were measured to ensure the correct categorisation of animals as juvenile or adult. Measurement of serum DHEA sulfate (DHEAS) was performed using standard methods in the clinical chemistry department of the district laboratory (SSDZ, Renier de Graaf Hospital, Delft, The Netherlands) [22]. DHEA levels confirmed pre-pubescent (DHEAS 0.9±1.7 μmol/l) versus adult (DHEAS <0.8 μmol/l) status of the animals [20, 21].

A Puerto Rican strain of *S. mansoni*, maintained at the Department of Parasitology (University of Leiden, The Netherlands) was used for infections. Animals were percutaneously exposed to 1000 *S. mansoni* cercariae on the shaved abdomen. After 30 min, the cercarial suspension was recovered, and the number of non-penetrating cercariae were counted. Both groups were sacrificed under anaesthesia after an infection period of 8 weeks. The animals were perfused with citrated saline, and worms were collected from the perfusion fluid and counted.

Morphological experiments

Histology

From each animal, a specimen of the liver, proximal and distal small bowel, proximal and distal colon and lung were investigated. A part of each organ was fixed in 4% buffered formalin, and another part was snap frozen in liquid nitrogen. The tissues fixed in buffered formalin were paraffin embedded, and 4-μm-thick sections were made. These sections were routinely stained using haematoxylin-eosin (HE), sirius-red-haematoxylin and Dominici-stain (for the detection of eosinophilic granulocytes) [3]. Cryostat sections were stained with toluidine-blue (for the detection of mast cells).

Cryostat sections were also used for immunohistochemistry, according to a routine procedure (indirect immunoperoxidase technique) using mouse anti-human antibodies against CD68 (clone KP-1, 1:80; Dako, Glostrup, Denmark), CD3 (clone F7.2.38, 1:50; Dako) and CD20 (clone L26, 1:80; Dako), respectively, for the detection of macrophages, T-lymphocytes and B-lymphocytes. These antibodies cross-react with rhesus monkey epitopes. The Peyer's patches showed strong immunoreactivity for CD20 and the lamina propria T-lymphocytes for CD3, serving as an internal control.

Morphometry

The number of granulomas was counted on the HE sections using a Zeiss light microscope (objective ×10/0.32; Zeiss Oberkochen, Germany), and the number was corrected for the amount of tissue investigated. At least ten sections per intestinal region were investigated with a total mean length of 4.5 cm tissue sampled per region. For the intestine, the number was expressed as mean number of granulomas per centimetre tissue±standard error of mean.

Statistical analysis

For basis statistical analysis, a Graph-Pad Prism Program was used. Continuous data were tested for normality. Normally distributed continuous data were compared by a Student's *t*-test for unpaired values (STT) and two-way analysis of variance followed by a Bonferroni post-hoc test where indicated. *P* values of less than 0.05 were considered significant.

Results

Macroscopy

In both age groups, the liver surface showed miliary patterns with 1–2 mm large, white nodules but with no fibrosis. The colon showed a diffuse punctate, mucosal haemorrhage. The hyperaemic mucosa was visible along the total length of the large bowel. No polyps or ulcerations were detected. Two animals (one adult, one pre-pubescent) had severe diarrhoea at the time of sacrifice.

Histopathology

Two distinct morphological stages in the granuloma formation were observed. One type showed a centrally located egg surrounded by lymphocytes, histiocytes (macrophages) and mainly eosinophilic granulocytes staining brightly red in the Dominici-stained sections. Among the eosinophilic granulocytes, rare neutrophilic granulocytes that stained faintly blue with Dominici stain were seen. This type of granuloma was termed the exudative-stage granuloma (ESG) (Fig. 1a).

The other granuloma type consisted of parts of eggshell surrounded by numerous foreign body-type giant cells, often partly engulfing the eggshell or eggshell remnants. Lymphocytes, eosinophilic granulocytes and acidophilic, eosinophilic rays of the Splendore–Hoeppli phenomenon were noted. This stage was termed the productive-stage granuloma (PSG), (Fig. 1b).

Both types of granulomas were found in the ileum, colon and liver of pre-pubescent and adult animals. In the intestinal wall, the granulomas were almost exclusively detected in the submucosa.

Both stages of granulomas were also present in the lungs of the animals. On an average, one pulmo-nary granuloma was noted per five ×10-magnification fields.

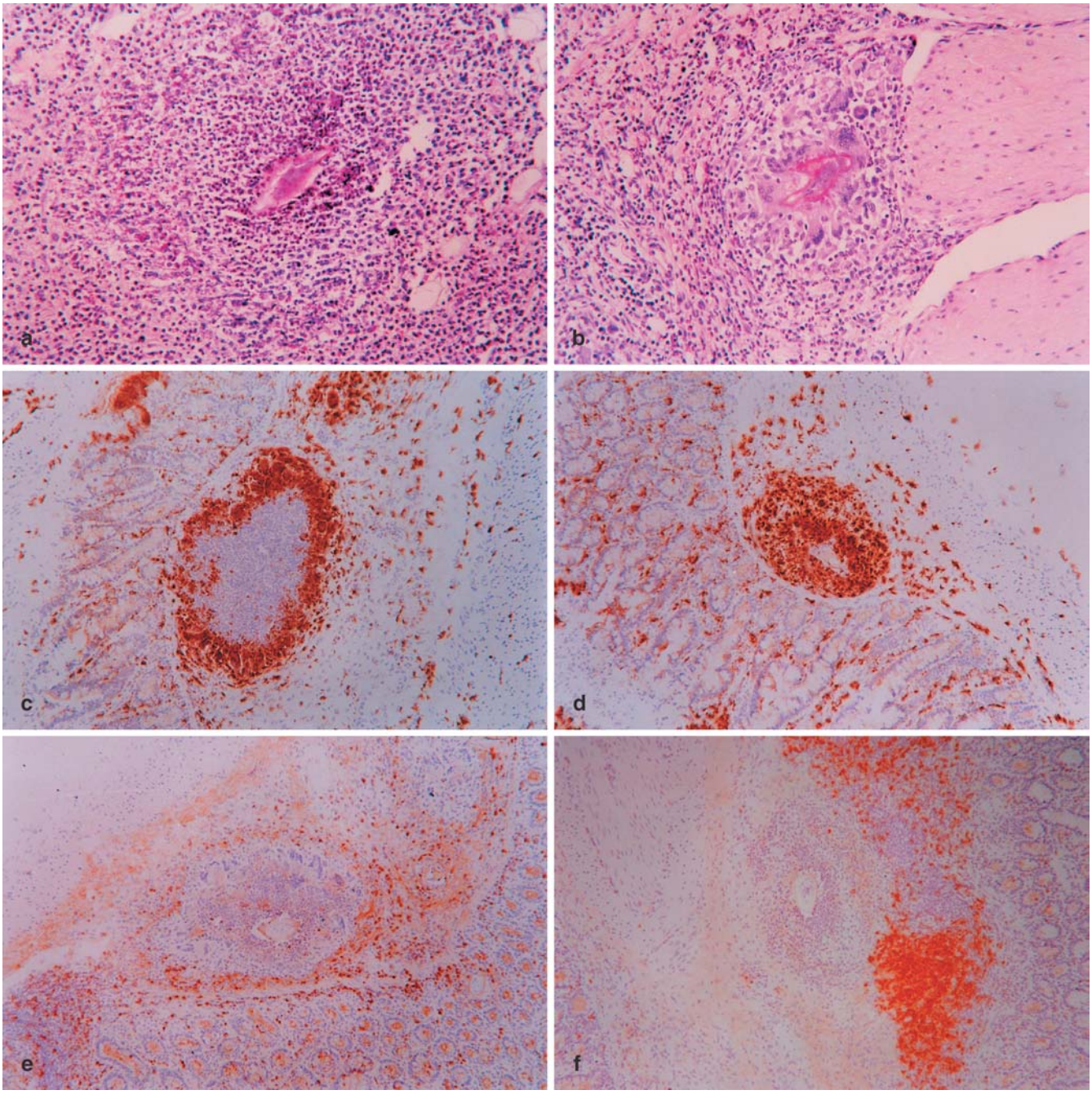


Fig. 1 Micrograph of the different types of intestinal granulomas detected in the *S. mansoni*-infected rhesus monkey. The exudative-stage granuloma (ESG; **a**) shows a centrally located egg surrounded by eosinophilic granulocytes. The outer rim is formed by lymphocytes and histiocytes. The productive-stage granuloma (PSG; **b**) containing an egg (*centre*) surrounded by histiocytes and foreign-body giant cells. The outer rim of the granuloma is mainly formed by lymphocytes. The eggshell is surrounded by eosinophilic rays of the Splendore–Hoeppli phenomenon as the result of an antigen–antibody reaction. Both (**a** and **b**) were treated with Dominici-stain. **c** and **d** ESG and PSG, respectively, using CD68 immunohistochemistry. The epithelioid histiocytes and the foreign-body giant cell show strong immunoreactivity. **e** The very small number of CD3-positive T lymphocytes, located at the boundary of the ESG. This is in contrast to *S. mansoni*-induced granulomas in rodents, which are mainly a T-cell-dependent reaction. There is no immunoreactivity for CD20 (B-cell marker) in the ESG. The location of B- and T-lymphocytes in PSG showed similar results (not shown). Final magnification ×200 (**a**, **b**); ×75 (**c**, **d**, **e**, **f**)

The Splendore–Hoeppli phenomenon was frequently observed in the lung specimens.

The fibrotic reaction in the liver and intestinal granulomas was minimal at 8 weeks post-infection in both age groups. In the small and large intestine, no mast cells were detected in the toluidine blue-stained cryostat sections, whereas the lamina propria showed a normal lymphoplasmocytic infiltrate.

Table 1 Total granuloma number in the ileum and the colon. The pre-pubescent animals showed significantly more colonic granulomas than the adult animals. The number of granulomas in the ileum was very small and showed considerable variation. Results are presented as number of granulomas per centimetre of intestinal tissue and expressed as mean±standard error of mean (n=5 for both groups)

	Pre-pubescent	Adult	P value
Ileum	1.05±1.9	0.14±0.37	>0.05
Colon	6.9±3.6	3.9±2.3	<0.05

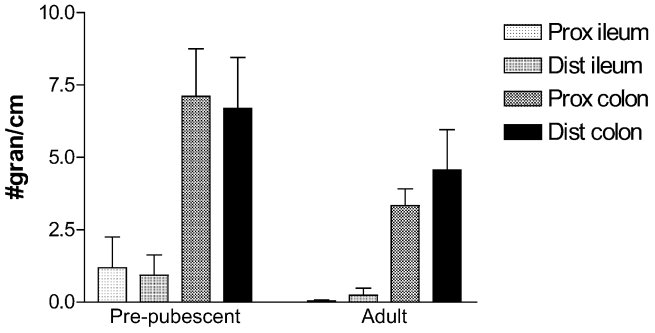


Fig. 2 *Bar graph* representing the number of granulomas in the different intestinal regions. The difference in the number of granulomas between the ileum and the colon, both in pre-pubescent as well as in adult animals, is statistically significant (two-way analysis of variance). Results are presented as number of granulomas per centimetre of intestinal tissue and are expressed as mean±standard error of mean (n=5 for both groups)

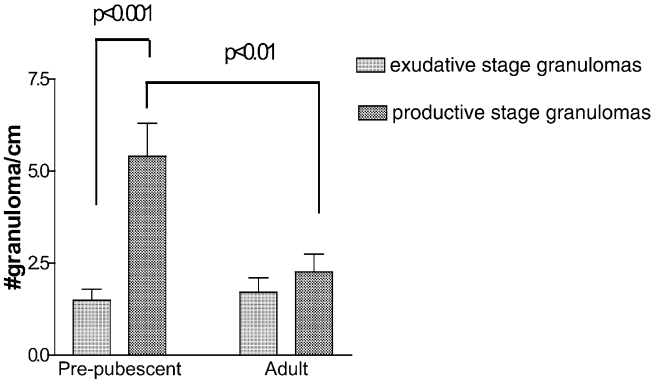


Fig. 3 *Bar graph* showing the number of granulomas in the colon of *S. mansoni*-infected rhesus monkeys divided by subtype. The difference of exudative-stage granuloma (ESG) versus productive-stage granuloma (PSG) in pre-pubescent animals is highly significant [P<0.001, student's t-test for unpaired values (STT)]. In the adult age group, there is no difference. The number of PSG between the pre-pubescent and the adult animals is also statistically significant (P<0.01, STT). Results are presented as number of granulomas per centimetre of intestinal tissue and expressed as mean±standard error of mean (n=5 for both groups)

Morphometry

Total granuloma number

The number of colonic granulomas was significantly higher in the pre-pubescent animals (Table 1, P<0.05, STT) than in the adult animals. When the granuloma numbers were compared between the ileum and colon, higher numbers were found in the colon, this difference being statistically significant (Fig. 2). There was no significant difference between the number of granulomas in the proximal and the distal colon (Fig. 2), nor between the numbers of granulomas in the liver of adult versus pre-pubescent monkeys (data not shown).

When the worms were recovered from the experimental animals by perfusion at the end of the study, there were 38% fewer female worms, as a measure of egg-producing worm pairs, in the adult than in pre-pubescent animals. However, this difference in the mean number of recovered female worms was not statistically significant. The number of granulomas per centimetre colonic tissue per worm couple was calculated and showed no significant difference between the two groups (0.17±0.009 and 0.25±0.03 granulomas per centimetre colonic tissue per female worm for pre-pubescent versus adult animals respectively; P=0.44, STT).

Stage of granuloma

When the dataset for the large intestine was divided on the basis of the two granuloma stages (ESG and PSG), there was a significant difference between the number of ESG and the number of PSG in the pre-pubescent animals (Fig. 3; P<0.001, STT); there was, however, no significant difference in the adult age group (Fig. 3). When the number of PSG was compared, pre-pubescent animals showed significantly more colonic granulomas (Fig. 3; P<0.01, STT) than the adult animals. In the liver, no significant difference was seen (data not shown).

Immunohistochemistry

The two granuloma stages detected in the morphological investigation could also be separated on immunohistochemical grounds. The ESG showed a centre of non-immunostained eosinophils surrounded by a rim of a small number of CD3-positive T-lymphocytes (Fig. 1e). CD20-positive B-lymphocytes were extremely rare (Fig. 1f). The outer rim was formed by CD68-positive macrophages (Fig. 1c).

The PSG showed a strong central immunoreactivity for CD68-positive cells, including the multinucleated giant cells (Fig. 1d). CD3-positive T-lymphocytes were detected mainly on the boundary and rarely mixed with the CD68-positive macrophages. The number of B-lymphocytes in or in the vicinity of the granulomas was very small. The T- and B-lymphocytes showed no quantitative difference between the two age groups.

Discussion

Rhesus monkeys (*Macaca mulatta*) have been extensively used in the past to study experimental *S. mansoni* infection [28]. Keeping in mind the implications of age-dependent susceptibility on schistosoma vaccine development and the implementation of control measures, our study delineated whether naive, pre-pubescent animals were innately more susceptible to infection with *S.mansoni* and whether age-related changes in enteric granulomogenesis were evident in these animals.

Previous experiments in small laboratory animals (mainly mice) have shown specific organ-dependent granulomatous patterns towards *S. mansoni* egg antigens [34, 35]. Colonic granulomas were comparable with the liver granulomas, whereas granulomas in the ileum were smaller and showed no down-modulation during the course of the infection [18]. A different cellular composition of the granulomas in the various organs has also been described [18, 34]. Granulomas were abundantly present in the murine ileum and were accompanied by a diffuse mucosal inflammation, a diffuse mast cell infiltrate—mainly in the muscularis propria—and specific ganglionitis [1].

In the present study, granulomogenesis induced by an acute, primary *S. mansoni* infection in adult versus pre-pubescent rhesus monkeys was almost exclusively located in the colon, in contrast with the results of Sadun et al. [28], who found entrapped eggs mainly in the small intestine of primates. Our observations are, however, confirmed by results from a large autopsy series on 197 human patients reported by Cheever [4]. In his study, Cheever found most of the granulomas in the sigmoid colon of a population of not heavily infected patients. When infected patients developed Symmer's fibrosis, etiologically linked with heavy infection and a worm load of at least 160 worm pairs [4], the eggs shifted from the sigmoid colon towards the small intestine. The predilection of the sigmoid colon, however, could not be corroborated in the present study, where there were no significant differences in the number of granulomas in the proximal versus the distal part of the colon. Investigating the difference of infection intensities, Cheever et al. [6] confirmed the shift of worms and eggs from the colonic towards the small intestinal venules in heavily infected rhesus monkeys (600 cercariae) but only after an infection period of 12–27 weeks. Although the infective dose in the present study was 1000 cercariae per animal, the animals were investigated after an infection period of 8 weeks. It, therefore, seems that the preferential habitat of worms shifts from the colonic towards the small intestinal circulation, both in man as well as in rhesus monkey, in cases of heavy infection and/or after an infection period of at least 10 weeks.

In the present study, two distinct stages in the development of granulomas were detected. The first stage (ESG) comprises a central, mainly eosinophilic reaction surrounded by a rim of lymphocytes and some macrophages. This granuloma resembles the experimentally induced *S. mansoni* granulomas seen in mice and smaller laboratory animals (e.g. hamsters).

The second stage (PSG) resembles foreign body-type granulomas as well as the granulomas often seen in *S. japonicum* infection in man and smaller animals [17]. PSG *S. mansoni* granulomas appear to be encountered more frequently in primate hosts [11]. In both granuloma types, the main polymorphonuclear cell is the eosinophilic granulocyte, a clear difference with *S. japonicum* granulomas, in which the granulomas mainly contain neutrophilic granulocytes [17].

The development of *S. mansoni*-induced granulomas is well studied and described by Hsu et al., who recognised five stages in the hepatic granuloma development in the rhesus monkey [16]. One of the earlier stages is the exudative stage, which is followed by the productive stage, via an intermediate, mixed stage, before complete healing without fibrosis. Indeed, both in our study as well as in the study by Hsu et al. and other studies [28], no clear fibrosis was detected [5]. Because the animals were all infected at the same time and sacrificed after the same infection period, the higher number of intestinal granulomas in the productive, more advanced stage in pre-pubescent animals suggests that the intestinal granulomogenic process in pre-pubescent animals is faster than in adult animals.

The two stages in the intestinal granulomatous inflammation presented in the present study are similar to the evolution of human colonic schistosomiasis [24], stressing the importance of data acquired in the rhesus model for human pathology. Smaller colonic lesions consisted mainly of eosinophilic granulocytes, while larger granulomas often contained multinucleated giant cells. Immunotyping of these cells showed the transition of a hypersensitivity granuloma to a foreign-body granuloma [10].

In the present work, the number of granulomas in the large intestine was significantly higher in the pre-pubescent group than in the adult group. Interestingly, the number of female worms also showed an increased trend, without reaching significance. These findings might be explained both by a higher susceptibility to infection in the younger age group as well as by a higher fecundity of the female worms. Although the total number of eggs produced by the worms could not be calculated from the present data, the number of granulomas per centimetre colonic tissue per worm showed no significant difference in the two age groups, suggesting a similar fecundity. These findings support the hypothesis of a higher degree of susceptibility in younger animals.

Ageing plays an important role in the efficacy of the gastrointestinal immune system. Taylor et al. [32] demonstrated a decrease of luminally secreted immunoglobulins with age, due to alterations in the process of maturation and homing of specific B-lymphocytes, while the total number of CD4+ T lymphocytes showed a senescence-associated decline [19]. These data, mainly on the mouse model, are in accordance with the present study, showing a more intense response in younger animals. The

total number of CD3+ T-lymphocytes, however, showed no difference. The mast cell response, which we detected in the mouse small intestine and the specific ganglionitis of the myenteric plexus, was not seen in the tissues investigated from the rhesus monkey [1].

On the same animals studied here, Fallon et al. [8] delineated the immune responses after primary *S. mansoni* infection. They showed that, in contrast with adults, juvenile (pre-pubescent) rhesus monkeys failed to develop type-2 cytokine responses [normally associated with high interleukin (IL)-4, IL-5 and low interferon (IFN)-gamma levels] and showed markedly reduced parasite-antigen-specific antibody responses and significantly limited overall IgE production. In their study, no differences were observed between adult and juveniles in the number of non-penetrating cercariae. They speculate, however, that a number of other physiological non-immunological responses could account for the differences in susceptibility between juvenile and adult, including age-associated changes in skin thickness, body fat or even size of the animal.

It has been hypothesised that the increased susceptibility to re-infection in young children is caused by an inability to induce appropriate—that is, protective—immune responses [26]. Our data indicate that juvenile monkeys elicit a higher colonic inflammatory response towards an increased number of entrapped *S. mansoni* eggs. It has yet to be elucidated whether the impaired immune responses in juveniles is a result of the differential granulomogenesis we observe, or whether senescence-related immunomodulation is involved. Yet other innate differences in susceptibility cannot be excluded as causes, including circulating putative schistosomicidal factors and age-associated hormones [7, 25] and neurohormones. In utero sensitisation to schistosomes could also be a significant factor in the subsequent susceptibility of children to schistosome infection [23].

There is ongoing debate whether the increased resistance of adult humans to schistosome infection is due to the age of the host, per se, or to previous experience of infection(s) [12, 37]. Recent evidence from a new focus of infection in Senegal showed that children were still at a higher risk of schistosoma infection with higher intensities of infection than adults [29]. Such studies stress that the changes associated with the age of the host determine susceptibility patterns to primary infection. Future research is required to give appropriate answers regarding the physiological differences between juveniles and adults with respect to susceptibility to schistosome infection and generation of anti-parasitic immune responses.

Acknowledgements We are grateful to the staff of animal caretakers at Biomedical Primate Research Centre (Rijswijk, The Netherlands). Financial support for this study was obtained from the European Commission (DG XII FP4 program under contracts CT96–0125 and ERB FMGE CT950024) and from the Interuniversity Poles of Attraction Programme (grants P4/16, P5/20) of the Services of the Prime Minister, Federal Agency for Scientific, Technical and Cultural Affairs (Belgium). The support of the technical staff at the laboratory of pathology, University of Antwerp, is kindly appreciated.

References

1. Bogers J, Moreels T, De Man J, Vrolix G, Jacobs W, Pelckmans P, Van Marck E (2000) Intestinal Schistosoma mansoni infection causing diffuse enteric inflammation and damage of the enteric nervous system in the mouse small intestine. Neurogastroenterol Motil 12:431–440
2. Butterworth AE (1994) Human immunity to schistosomes: some questions. Parasitol Today 10:378–380
3. Byram JE, Imohiosen EA, Von Lichtenberg F (1978) Tissue eosinophil proliferation and maturation in schistosome-infected mice and hamsters. Am J Trop Med Hyg 27:267–270
4. Cheever AW (1968) A quantitative post-mortem study of Schistosomiasis mansoni in man. Am J Trop Med Hyg 17:38–64
5. Cheever AW, Anderson LA (1971) Rate of destruction of *Schistosoma mansoni* eggs in the tissues of mice. Am J Trop Med Hyg 20:62–68
6. Cheever AW, Powers, KG (1972) *Schistosoma mansoni* infection in rhesus monkeys: comparison of the course of heavy and light infections. Bull World Health Organ 46:301–309
7. Fallon PG, Richardson EJ, Jones FM, Dunne DW (1998) Dehydroepiandrosterone sulfate treatment of mice modulates infection with *Schistosoma mansoni*. Clin Diagn Lab Immunol 5:251–253
8. Fallon PG, Gibbons J, Vervenne RA, Richardson EJ, Fulford AJC, Kiarie S, Sturrock RF, Coulson PS, Deelder AM, Langermans JAM, Thomas AW, Dunne DW (2003) Juvenile rhesus monkeys have lower type 2 cytokine responses than adults after primary infection with Schistosoma mansoni. J Infect Dis 187:939–945
9. Fulford AJC, Webster M, Ouma JH, Kimani G, Dunne DW (1998) Puberty and age-related changes in susceptibility to *Schistosoma infection*. Parasitol Today 14:23–26
10. Geboes K, el-Dosoky I, el-Wahab A, Abou Almagd K (1990) The immunopathology of *Schistosoma mansoni* granulomas in human colonic schistosomiasis. Virchows Arch 416:527–534
11. Ghandour AM, Zahid NZ, Banaja AA, Ghanem AM (1999) Histopathological and parasitological changes in baboons (*Papio hamadryas*) experimentally infected with baboon and human isolates of *S. mansoni* from Saudi Arabia: a comparative study. Ann Trop Med Parasitol 93:197–201
12. Gryseels B (1994) Human resistance to schistosoma infections: age or experience? Parasitol Today 10:380–384
13. Gryseels B, Polderman, AM (1992) Acquired immunity in schistosomiasis. Parasitol Today 8:271–272
14. Hagan P, Abath FG (1992) Recent advances in immunity to human schistosomiasis. Mem Inst Oswaldo Cruz 87[Suppl 4]: 95–98
15. Hagan P, Ndhlovu PD, Dunne DW (1998) Schistosome immunology: more questions than answers. Parasitol Today 14:407–412
16. Hsu SY, Hsu HF, Davis JR, Lust GL (1972) Comparative studies on the lesions caused by eggs of *Schistosoma japonicum* and *Schistosoma mansoni* in livers of albino mice and rhesus monkeys. Ann Trop Med Parasitol 66:89–97
17. Hsu SY, Hsu HF, Lust GL, Davis JR, Eveland LK (1973) Comparative studies on the lesions caused by eggs of *Schistosoma japonicum* and *Schistosoma mansoni* in the liver of hamsters, guinea pigs, and albino rats. Ann Trop Med Parasitol 67:349–356
18. Jacobs WJ, Bogers J, Timmermans JP, Deelder AM, Van Marck E (1998) Adhesion molecules in intestinal *Schistosoma mansoni* infection. Parasitol Res 84:276–280
19. Kawanishi H, Kiely J (1989) Immune-related alterations in aged gut-associated lymphoid tissues in mice. 34:175–184

20. Kemnitz JW, Roecker EB, Haffa AL et al (2000) Serum dehydroepiandrosterone sulfate concentrations across the life span of laboratory-housed rhesus monkeys. J Med Primatol 29:330–337
21. Lane MA, Ingram DK, Roth GS (1995) Effects of aging and long-term calorie restriction on DHEA and DHEA sulfate in rhesus monkeys. Ann N Y Acad Sci 774:319–322
22. Lane MA, Ingram DK, Ball SS, Roth GS (1997) Dehydroepiandrosterone sulphate: a biomarker of primate aging slowed by calorie restriction. J Clin Endocrinol Metab 82:2093–2096
23. Malhotra I, Mungai P, Wamachi A et al (1999) Helminth- and bacillus Calmette-Gue'rin–induced immunity in children sensitized in utero to filariasis and schistosomiasis. J Immunol 162:6843–6848
24. Mohamed AR, al Karawi M, Yasawy MI (1990) Schistosomal colonic disease. Gut 31:439–442
25. Nakazawa M, Fantappie MR, Freeman GL Jr et al (1997) *Schistosoma mansoni*: susceptibility differences between male and female mice can be mediated by testosterone during early infection. Exp Parasitol 85:233–240
26. Roberts M, Butterworth AE, Kimani G et al (1993) Immunity after treatment of human schistosomiasis: association between cellular responses and resistance to reinfection. Infect Immun 61:4984–4993
27. Rocha MO, Pedroso ER, Lambertucci JR, Greco DB, Rocha RL, Rezende DF, Neves J (1995) Gastro-intestinal manifestations of the initial phase of schistosomiasis mansoni. Ann Trop Med Parasitol 89:271–278
28. Sadun EH, Von Lichtenberg F, Bruce JI (1966) Susceptibility and comparative pathology of ten species of primates exposed to infection with Schistosoma mansoni. Am J Trop Med Hyg 15:705–718
29. Stelma FF, Talla I, Polman K et al (1993) Epidemiology of *Schistosoma mansoni* infection in a recently exposed community in northern Senegal. Am J Trop Med Hyg 49:701–706
30. Sturrock RF (1986) A review of the use of primates in studying human schistosomiasis. J Med Primatol 15:267–279
31. Tatala S, Svanberg U, Mduma B (1998) Low dietary iron availability is a major cause of anemia: a nutrition survey in the Lindi District of Tanzania. Am J Clin Nutr 68:171–178
32. Taylor LD, Daniels CK, Schmucker DL (1992) Ageing compromises gastrointestinal mucosal immune response in the rhesus monkey. Immunology 75:614–618
33. Utzinger J, N'Goran E, Esse Aya CM, Acka Adjoua C, Lohourignon KL, Tanner M, Lengeler C (1998) *Schistosoma mansoni*, intestinal parasites and perceived morbidity indicators in schoolchildren in a rural endemic area of western Cote d'Ivoire. Trop Med Int Health 3:711–720
34. Weinstock JV, Boros DL (1981) Heterogeneity of the granulomatous response in the liver, colon, ileum and ileal Peyer's patches to Schistosome eggs in murine schistosomiasis mansoni. J Immunol 127:1906–1909
35. Weinstock JV, Boros DL (1983) Organ-dependent differences in composition and function observed in hepatic and intestinal granulomas isolated from mice with Schistosomiasis mansoni. J Immunol 130:418–422
36. WHO Expert Committee (1993) The control of schistosomiasis. Second report of the WHO Expert Committee. World Health Organ Tech Rep Ser 830:1–86
37. Woolhouse ME, Hagan P (1999) Seeking the ghost of worms past. Nat Med 5:1225–1227

Virchows Arch (2004) 445:292–297
DOI 10.1007/s00428-004-1041-1

ORIGINAL ARTICLE

P. Soriano · S. Navarro · M. Gil · A. Llombart-Bosch

Small-cell carcinoma of the urinary bladder. A clinico-pathological study of ten cases

Received: 29 March 2004 / Accepted: 22 April 2004 / Published online: 10 July 2004
© Springer-Verlag 2004

Abstract Small-cell carcinoma (SCC) of the urinary bladder is an infrequent neoplasia accounting for 0.5% of all tumors located at this level. There is a predilection for males over females with a 4:1 proportion and a median age of 66 years. In most cases, the initial diagnosis is made at the metastatic or progressive stage of the disease. For this study, we collected ten cases of SCC of the urinary bladder, diagnosed over a period of 16 years, to describe the morphological and immunocytochemical characteristics of these infrequent neoplasia. In all cases, clinical data such as age at presentation, personal background, clinical symptoms, stage, treatment, clinical outcome and present status were available. Primary antibodies included chromogranin, neuron-specific enolase, synaptophysin, PGP 9.5, HNK-1, cytokeratin 34βE12, cytokeratin 20, thyroid transcription factor-1 (TTF-1), c-erbB2 (CB-11), p53 (DO7), and Ki67 (MIB-1). In addition to the expression of neural/neuroendocrine markers, immunostaining for p53 and c-erbB2 was found in 80% and 50% of cases, respectively. In this paper, we confirm the aggressive course of the neoplastic disease. The expression of c-erbB2 in 50% of cases opens up hypothetical new possibilities for the use of immunotherapy in such cases.

Keywords Small-cell carcinoma · Urinary bladder · Immunohistochemical · Oat-cell carcinoma · Survival · c-erbB2

Introduction

Small-cell carcinoma (SCC) of the urinary bladder is an infrequent neoplasia accounting for 0.5% of all tumors located at this level. A predilection for males over females with a 4:1 proportion and a median age of 66 years [4, 22] are characteristics of this neoplasia. The clinical presentation includes hematuria and is less often found with pain or obstructive symptoms. In most cases, the initial diagnosis is made at the metastatic or progressive stage of the disease. Exceptionally, paraneoplastic symptoms derived from adrenocorticotrophin secretion [22, 33], hypercalcemia [8, 12, 22, 34, 35] or hypophosphatemia are observed [12]. The main diagnosis is based upon the histopathological features, consisting of a diffuse growth pattern of small cells with a highly condensed chromatin, the immunodetection of neuroendocrine markers and the presence at the ultrastructural level of dense core neurosecretory granules [13]. In addition, several reports indicate the possibility of diagnosing this SCC in urinary cytology specimens [1, 3, 9, 25, 26].

From the molecular genetic point of view, several chromosomal abnormalities have been described. Terracciano et al. [41] reported deletions in 10(q), 4q, 5q and 13 q, as well as gains in 8q, 5p, 6p and 20q, and genetic amplification in 1p22–32, 3q26.3, 8q24 y 12q14–21 in ten tumors analyzed using comparative genomic hybridization. Leonard et al. [24] described a monosomy 9, homozygous deletion of P16 and trysomy 7 using conventional karyotyping and mutations of p53 as being event frequent.

The clinical behavior is very aggressive, with early lymph-node metastasis and liver, bone or peritoneal cavity deposits [8]. The prognosis is based upon the clinical staging and the therapeutic strategy, but a high percentage of deaths (68.7%) are seen within 2 years of follow-up [42]. The purpose of this paper is to communicate a number of new cases of this entity, supported with immunohistochemistry and focusing on possible therapeutic targets.

Materials and methods

For this study, we collected ten cases of SCC of the urinary bladder, diagnosed over a period of 16 years and retrieved from the files of the Department of Pathology of the University Clinic Hospital of

P. Soriano · S. Navarro · M. Gil · A. Llombart-Bosch (✉)
Departments of Pathology and Urology University of Valencia, University of Valencia,
Avda Blasco Ibáñez 17, 46010 Valencia, Spain
e-mail: antonio.llombart@uv.es
Tel.: +34-963-864646
Fax: +34-963-864173

Table 1 Clinical data, outcome and present status for all cases. *SURG* radical cystectomy, *TUR* transurethral resection, *CT* chemotherapy, *RT* radiotherapy, *DOD* died of disease, *A* alive, *Survival* minimal survival in the last control

Mean age/sex	Onset	Stage initial	Metastases	Treatment	Survival
70 Years/male	Hematuria	-	-	TUR	-/DOD
47 Years/male	Hematuria Polaquiuria Tenesm	PT3bN2M0	Bone	SURG+CT+RT	12 Months/DOD
72 Years/male	Hematuria	-	Liver Bone	SURG+CT+RT	16 Months/DOD
52 Years/male	Hematuria	pT3N3M0	Lymph nodes	SURG+CT	+16 Months/A
82 Years/male	Hematuria Dysuria Polaquiuria Incontinence	pTxN2M0	Lymph nodes	TUR	+2 Months/-
57 Years/male	Hematuria	pT4aN2M0	Lymph nodes	SURG+CT	+3 Months/-
82 Years/male	Urinary discomfort	-	-	TUR	3 Months/DOD
66 Years/male	Hematuria	-	Lung Liver Bone	SURG+CT+RT	15 Months/DOD
74 Years/female	Hematuria Hipogastric Slowness	-	Lymph nodes Liver Mediastinum Soft tissue	TUR+RT	6 Months/DOD
52 Years/male	Hematuria	pT3N0M0	-	SURG+CT	+16 Months/A

Valencia. The material was formalin fixed and paraffin embedded, and the sections were immunostained using the avidin-biotin peroxidase method. Antigen retrieval was obtained using heating in autoclave (1.5 ATM, 3 min.) and citrate buffer pH 6.0.

Primary antibodies included chromogranin A (Biomeda 1/50), neuron-specific enolase (Biogenex 1/50), synaptophysin (Boehringer Mannhein 1/20), PGP 9.5 (Biomeda 1/50), HNK-1 (ATCC 1/10), cytokeratin 34βE12 (Dako 1/50), cytokeratin 20 (Biogenex 1/50), thyroid transcription factor-1 (TTF-1) (Dako 1/50), c-erbB2 (CB-11, Novocastra 1/50), p53 (DO7, Dako 1/50) and Ki67 (MIB-1, Dako 1/50). In all cases, clinical data such as age at presentation, personal background, clinical symptoms, stage, treatment, clinical outcome and present status were available (Table 1).

Results

Clinical aspects

The mean age of the patients was 65 years (47–82 years). A clear predominance of males in a proportion 10:1 was observed. The existence of several types of antecedents, such as smoking (5/10), hypercholesterolemia (4/10), benign neoplasms (Warthin tumor, 1/10) and larynx epidermoid carcinoma (1/10) were identified. All but two patients presented metastatic disease on initial diagnosis at the following locations: lymph nodes (4/10), liver (3/10), bone (2/10) and soft tissue (1/10).

Pathological findings

Macroscopically, these tumors ranged in size from 2-cm polipoid lesions to 10-cm solid neoplasms (Fig. 1). The overlying mucosa was commonly ulcerated. Microscopically, the tumors displayed a uniform diffuse or organoid growth pattern and were constituted of solid nests of intermediate or small cells, showing scarce cytoplasm, round nuclei with granular dense chromatin and no evident nucleoli (Fig. 2). Less numerous intermediate cells displayed large visible cytoplasm and a voluminous nuclei with granulous dense core chromatin. Other common features found were extensive necrosis and numerous mitosis (more than 28 per 10 high-power field). Azzopardi artifact was also evident.



Fig. 1 Computed tomography scan showing a solid neoplasm invading the bladder cavity

The immunohistochemical analysis revealed the presence of two or more neuroendocrine markers in each case. Chromogranin was positive in 50% of cases (5/10) (Fig. 3), NSE in 100% (10/10), synaptophysin in 40% (4/

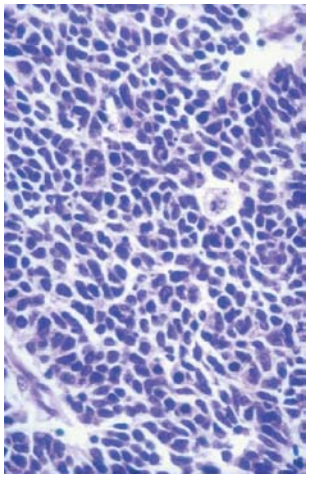


Fig. 2 Solid nest of small cells showing scarce cytoplasm, round nuclei with granular dense chromatin (hematoxylin and eosin ×40)

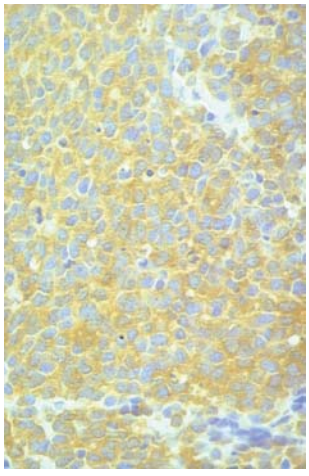


Fig. 3 Intense cytoplasmic expression of chromogranin (×40)

10), PGP 9.5 in 40% (4/10) and HNK in 50% (5/10). In addition, 34βE12 cytokeratin expression was observed in 40% of cases (4/10), whereas CK 20 was negative in all cases. Finally, 20% of cases (2/10) showed expression of TTF-1. The immunohistochemical results are summarized in Table 2.

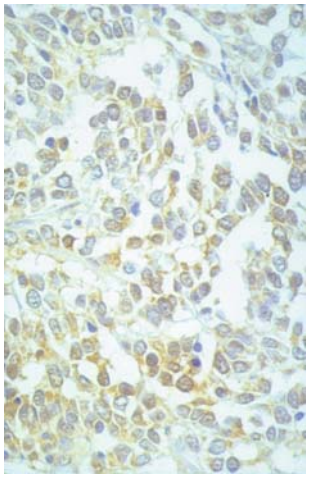


Fig. 4 A typical membranous c-erbB2 immunostaining pattern (×40)

Interestingly, c-erbB-2 immunostaining was observed in 50% of cases with a typical membranous pattern (Fig. 4). Moreover, p53 nuclear expression was found in 80% of cases (8/10). The proliferative index measured with Ki 67 (MIB 1) expression varied from 15% to 70%, with a mean of 33%.

Discussion

It is important that small-cell neuroendocrine carcinomas of urinary bladder be clearly distinguished from their non-neuroendocrine counterparts because of differences in treatment and prognosis [8]. The clinical outcome of this type of carcinoma is very poor, although a relatively better survival of patients has been reached in some series [8].

The present clinical records of our cases are similar with respect to age (65 years), and initial symptoms [17, 27] to those indicated in the literature [22, 42]. Metastatic spread to the lymph nodes, liver, bone and soft tissue as

Table 2 Immunohistochemical study. *CHROM* chromogranin, *NSE* neuron-specific enolase, *SYN* synaptophysin, *CK P* cytokeratin 34βE12, *CK 20* cytokeratin 20, *TTF-1* thyroid transcription factor-1, + <25% positive cells, ++ 25–75% positive cells, +++ >75% positive cells, *C-erbB-2 0/+* cases negatives, *++/+++* cases positives (Dako system)

Case	CHROM	NSE	SYN	PGP	HNK1	CK P	CK 20	TTF-1	C-erb	P53	Ki67
1	0	++	+	++	+++	0	0	0	+	90%	45%
2	++	+++	0	0	0	+++	0	0	+	0	15%
3	+++	+++	0	+++	+	0	0	0	0	50%	50%
4	0	++	+	0	++	0	0	0	0	60%	40%
5	0	+++	0	++	0	+	0	0	0	30%	30%
6	+++	+++	+	0	+	0	0	+++	0	70%	70%
7	0	+++	0	0	0	0	0	0	++	90%	20%
8	++	+++	+	+++	0	+++	0	0	++	90%	20%
9	+++	+++	+++	0	0	0	0	+	0	25%	30%
10	0	++	0	0	+	++	0	0	++	0	15%

the locations preferentially involved is also in agreement with previous reports [33].

Regarding treatment, 30% of patients (3/10) were treated exclusively using TUR (transurethral resection) , with a survival of 2–5 months (death due to obstructive uropathy). The survival improved up to 14 months in those cases (3/10) treated using cystectomy, CT (chemotherapy) and RT (radiotherapy) in combination. The mean survival of our patients was 8.77 months, lower than that reported in some series [7, 8, 18, 25] but consistent with other published survivals of 6 months [23, 30], 6.9 months [20] and 8 months, respectively [9]. In addition to the clinical aggressiveness, the major diagnosis came from histology and the immunohistochemical detection of neuroendocrine markers.

All cases except one presented at least two neuroendocrine markers confirming previous reports. Iczkowski et al. [43] demonstrated a high expression of chromogranin (65%), synaptophisin (76%) and NSE (93%). Additionally, Van Hoeven et al. [26] showed expression of NSE in 11 of 11 cases and synaptophisin in 2 of 11 cases, whereas chromogranin was detected in only 2 of 13 cases and Leu 7 in 2 of 7 cases, respectively. Grignon et al. [17] detected the following immunoprofile: NSE in 10 of 10, chromogranin in 8 of 9, serotonin in 7of 9 and s-100 in 4of 10 cases. Helpap and Kollermann [21] showed that the expression of chromogranin was highest in low-grade neuroendocrine tumors and lowest in high-grade small-cell neuroendocrine carcinomas. Cytokeratin immunostaining is a common feature in SCC [17, 43]. Moreover, 34βE12 cytokeratin expression has also been reported in these tumors [22, 32, 44]. In this study, we detected such expression in 40% of our cases. Controversial results regarding CK 20 expression in SCCs have been published. In our study, all the cases proved negative for CK 20 in agreement with the results published by Ordoñez et al. [11] and Helpap [20]. In contrast, Cheuk et al. [2] reported expression of CK 20 in 4% of extrapulmonary SCCs.

TTF-1 is a marker that has been described in extrapulmonary SCC [2, 11, 37]. In this study, we saw expression in two cases. This data limits the value of this marker for establishing the differential diagnosis between primary SCC of the bladder and possible bladder metastasis from a pulmonary SCC. The human epidermal-growth-factor receptor-2 (c-erbB-2) is overexpressed and amplified throughout a broad spectrum of tumor types in breast, bladder, ovarian, salivary gland, endometrium, pancreas and lung [37]. C-erbB-2 is implicated in disease initiation and progression, is associated with poor prognosis and may also predict the response to chemotherapy and hormonal therapy. Above all, its expression is considered to be a negative prognostic indicator in metastatic breast carcinoma. A relationship between high expression of c-erbB-2 and poor survival has been reported in breast cancer. In these cases, clinical phase-II and -III trials have demonstrated the efficacy of the humanized anti-c-erbB-2 Mab, Trastuzumab (Herceptin), both as a single agent and in combination with chemotherapy, in c-erbB-2-positive metastatic breast cancer patients [10, 29, 38]. The expression of c-erbB-2 in SCC of the bladder has not previously been reported. In our analysis, we demonstrated high expression of c-erbB-2 in 50% of the cases. This expression should be used as a prognostic indicator in bladder SCC (as already confirmed in transitional tumors) [5] and, moreover, opens up a new method of planning clinical trials and assessing the therapeutic role of Trastuzumab in SCC of the bladder. A recent study found an inverse relationship between c-erbB2 expression and survival in transitional-cell carcinoma of the urinary bladder [28]. The mean survival of our patients was 4 months in positive c-erbB-2 cases and 12.83 months in negative c-erbB-2 cases. Accordingly, we confirm an inverse relationship between c-erbB-2 expression and survival in SCC of the urinary bladder. Currently, fluorescence in situ hybridization analysis of c-erbB-2 gene amplification is in progress, and, although the results are not yet available, they will serve for a future publication.

Mutations of the tumor suppressor gene p53 of chromosome 17 have already been reported in bladder SCC [24, 28]. Among our cases, we described a high expression of p53 (63%), possibly representing a poor prognostic factor as well as an indicator of neoplastic progression. Mutations of the p53 suppressor gene have been found in urothelial carcinoma [6, 14, 16, 19, 31, 36, 39, 40, 45]: several studies have demonstrated a positive correlation between p53 abnormalities and higher tumor stage [14, 16, 40, 45]. Sarkis et al. [36] reported a higher risk of progression in patients with pT1 tumors with abnormal p53 protein expression than in those lacking the expression. Esriget et al. [15] observed that p53 overexpression correlated significantly with recurrence and crude survival, and, in multivariate regression analysis, it was a factor independent of pathological stage and histological grade. For muscle-invasive tumors (pT2 y pT3a) the 5-year survivals were 79% and 64% for p53 negative cases and 30% and 22% for p53 positive cases, respectively.

In conclusion, we believe that it is very important in bladder cancer to identify the neuroendocrine differentiation as a prognostic indicator to choose the appropriate therapy. Thus, the prognosis could then be improved with multidisciplinary treatment [17, 22]. Moreover, the overexpression of c-erbB-2 in cases of SCC opens up new methods for the application of immunotherapy in these infrequent and aggressive neoplasms.

Acknowledgement Supported by grant 01/0673 from FIS. MADRID, SPAIN.

References

1. Acs G, Gupta PK, Baloch ZW (2000) Cytomorphology of high-grade neuroendocrine carcinoma of the urinary tract. Diagn Cytopathol 23:92–96
2. Agoff SN, Lamps LW, Philip AT el al (2000) Thyroid transcription factor-1 is expressed in extrapulmonary small cell

carcinomas but not in other extrapulmonary neuroendocrine tumors. Mod Pathol 13:238–242
3. Ali SZ, Reuter VE, Zakowski MF (1997) Small cell neuroendocrine carcinoma of the urinary bladder. A clinicopathologic study with emphasis on cytologic features. Cancer 79:356–361
4. Angulo JC, Lopez JI, Sanchez-Chapado M et al (1996) Small cell carcinoma of the urinary bladder: a report of two cases with complete remission and a comprehensive literature review with emphasis on therapeutic decisions. J Urol Pathol 5:1–19
5. Atkin NB, Baker MC, Wilson GD (1995) Chromosome abnormalities and p53 expression in a small cell carcinoma of the bladder. Cancer Genet Cytogenet 79:111–114
6. Bartek J, Bartkova J, Vojtesek B et al (1991). Aberrant expression of the p53 oncoprotein is a common feature of wide spectrum of human malignancies. Oncogene 6:1699–1703
7. Bastus R, Caballero JM, Gonzalez G et al (1999) Small cell carcinoma of the urinary bladder treated with chemotherapy and radiotherapy: results in five cases. Eur Urol 35:323–326
8. Blomjous CEM, Vos W, De Voogt HJ et al (1989) Small cell carcinoma of the urinary bladder: a clinicopathologic, morphometric, inmunohistochemical, and ultrastructural study of 18 cases. Cancer 64:1347–1357
9. Borghi L, Bianchini E, Altavilla G (1995) Undifferentiated small-cell carcinoma of the urinary bladder: report of two cases with a primary urinary cytodiagnosis. Diagn Cytopathol 13:61–65
10. Charles V, Melody C, Debu T et al (2002) Efficacy and safety of Trastuzumab as a single agent in first-line treatment of HER2-overexpressing metastatic breast cancer. J Clin Oncol 20:719–726
11. Cheuk W, Kwan MY, Suster S et al (2001). Immunostaining for thyroid transcription factor-1 and cytokeratin 20 aids the distinction of small cell carcinoma from Merkel cell carcinoma, but not pulmonary from extrapulmonary small cell carcinomas. Arch Pathol Lab Met 125:228–231
12. Cramer SF, Aikawa M, Cebelin M (1981) Neurosecretory granules in small cell invasive carcinoma of the urinary bladder. Cancer 47:724–730
13. Davis BH, Ludwig ME, Cole SR et al (1983) Small cell neuroendocrine carcinoma of the urinary bladder: report of three cases with ultrastructural analysis. Ultrastruct Pathol 4:197–204
14. Esrig D, Spruck CH III, Nichols PW et al (1993) P53 nuclear protein accumulation correlates with mutations in the p53 gene, tumor grade, and stage in bladder cancer. Am J Pathol 143: 1389–1397
15. Esrig D, Elmajian D, Groshen S et al (1994) Accumulation of nuclear p53 and tumor progression in bladder cancer. N Engl J Med 331:1259–1264
16. Furihata M, Inoue K, Ohtsuki Y et al (1993) High risk human papilloma virus infections and overexpression of p53 protein as prognostic indicators in transitional cell carcinoma of the urinary bladder. Cancer Res 53:4823–4827
17. Grignon DJ, Ro JY, Ayala AG et al (1992) Small cell carcinoma of the bladder. A clinicopathologic analysis of 22 cases. Cancer 69:527–536
18. Grossl NA, Candel AG, Nordbock HA, Grossl AC (1992) Undifferentiated small cell carcinoma of the urinary bladder. South Med J 85:189–192
19. Habuchi T, Takahashi R, Yamada H et al (1993) Influence of cigarette smoking and schistosomiasis on p53 gene mutation in urothelial cancer. Cancer Res 53:3795–3799
20. Helpap B (2002) Morphology and therapeutic strategies for neuroendocrine tumors of the genitourinary tract. Cancer 95: 1415–1420
21. Helpap B, Kollermann J (2001) Immunohistochemical analysis of the proliferative activity neuroendocrine tumors from various organs. Are there indications for a neuroendocrine tumor-carcinoma sequence? Virchows Arch 438:86–91
22. Helpap B, Kloppel G (2002) Neuroendocrine carcinomas of the prostate and urinary bladder: a diagnostic and therapeutic challenge. Virchows Arch 440:241–248
23. Iczkowski KA, Shanks JH, Allsbrook WC (1999) Small-cell carcinoma of the urinary bladder is differentiated from urothelial carcinoma by chromogranin expression, absence of CD44 variant 6 expression, a unique pattern of cytokeratin expression, and more intense gamma-enolase expression. Histopathology 35:150–156
24. Leonard C, Huret JL, GFCO (2002) From cytogenetics to cytogenomics of bladder cancers (in French). Bull Cancer 89:166–173
25. Lopez JL, Angulo JC, Flores N et al (1994) Small cell carcinoma of the urinary bladder. A clinicopathological study of six cases. Br J Urol 73:43–49
26. McRae S, Garcia BM (1997) Cytologic diagnosis of a primary pure oat cell carcinoma of the bladder in voided urine. A case report. Acta Cytol 41:1279–1283
27. Mills SE, Wolfe JT, Weiss MA et al (1987) Small cell undifferentiated carcinoma of the urinary bladder. A light-microscopic, inmunocytochemical, and ultrastructural study of 12 cases. Am J Surg Pathol 11:606–617
28. Nguyen PL, Swanson PE, Jaszcz W et al (1994) Expression of epidermal growth factor receptor in invasive transitional cell carcinoma of the urinary bladder: a multivariate survival analysis. Am J Clin Pathol 101:166–176
29. Nicholson RI, Gee JM, Harper ME (2001) EGFR and cancer prognosis. Eur J Cancer 37:9–15
30. Oesterling JE, Brendler CB, Burgers JK et al (1990) Advanced small cell carcinoma of the bladder: successful treatment with combined radical cystoprostatectomy and adjuvant methotrexate, vinblastine, doxorubicin and cisplatin chemotherapy. Cancer 65:1928–1936
31. Oka K, Ishikawa J, Bruner JM et al (1991) Detection of loss of heterozygosity in the p53 gene in renal cell carcinoma and bladder cancer using the polymerase chain reaction. Mol Carcinog 4:10–13
32. Ordoñez NG (2000) Value of thyroid transcription factor-1 immunostaining in distinguishing small cell lung carcinomas from other small cell carcinomas. Am J Surg Pathol 24:1217–1223
33. Partanen S, Asikainen U (1985) Oat cell carcinoma of the urinary bladder with ectopic 3 adrenocorticotropic hormone production. Hum Pathol 16:313–315
34. Podesta AH, True LD (1989) Small cell carcinoma of the bladder: report of five cases with immunohistochemistry and review of the literature with evaluation of prognosis according to stage. Cancer 64:710–714
35. Reyes CV, Soneru I (1985) Small cell carcinoma of the urinary bladder with hypercalcemia. Cancer 56:2530–2533
36. Sarkis AS, Dalbagni G, Cordón-Cardo C et al (1993) Nuclear overexpression of p53 protein in transitional cell bladder carcinoma: a marker for disease progression. J Natl Cancer Inst 85:53–59
37. Scholl S, Beuzeboc P, Pouillart P (2001) Targeting HER2 in other tumor types. Ann Oncol 12[Suppl 1]:S81–S87
38. Seidman A, Fornier M, Esteva F et al (2001) Weekly Trastuzumab and Paclitaxel therapy for metastatic breast cancer with analysis of efficacy by HER2. Immunophenotype and gene amplification. J Clin Oncol 19:2587–2595
39. Sidransky D, Von Eschenbach A, Tsai YC et al (1991) Identification of p53 mutations in bladder cancers and urine samples. Science 25:705–709
40. Soini Y, Turpeenniemi Hujanen T, Kamel D et al (1993) P53 immunohistochemistry in transitional cell carcinoma and dysplasia of the urinary bladder correlates with disease progression. Br J Cancer 68:1029–1035
41. Terracciano L, Richter J, Tornillo L et al (1999) Chromosomal imbalances in small cell carcinoma of the urinary bladder. J Pathol 189:230–235
42. Trias I, Algaba F, Condom E, Espanol I et al (2001) Small cell carcinoma of the urinary bladder. Presentation of 23 cases and review of 134 published cases. Eur Urol 39:1385–1390

43. Van Hoeven KH, Artymyshyn RL (1996) Cytology of small cell carcinoma of the urinary bladder. Diagn Cytopathol 14: 292–297
44. Viverti L, Bongiovanni M, Groce S et al (2000) 34βE12 cytokeratin immunodetection in the differential diagnosis of small cell tumors of lung. Int J Surg Pathol 8:317–322
45. Wright C, Mellon K, Johnston P et al (1991) Expression of mutant p53, c-erbB-2 and the epidermal growth factor receptor in transitional cell carcinoma of the human urinary bladder. Br J Cancer 63:967–970

Virchows Arch (2004) 445:298–304
DOI 10.1007/s00428-004-1056-7

ORIGINAL ARTICLE

Alina Romanenko · Luisa Morell-Quadreny · Jose Antonio Lopez-Guerrero · Antonio Pellin · Valentin Nepomnyaschy · Alexander Vozianov · Antonio Llombart-Bosch

The INK4a/*ARF* locus: role in cell cycle control for renal cell epithelial tumor growth after the Chernobyl accident

Received: 25 November 2003 / Accepted: 19 May 2004 / Published online: 1 July 2004
© Springer-Verlag 2004

Abstract Previous studies have shown that during the period subsequent to the Chernobyl accident, increases in morbidity, aggressivity and proliferative activity of renal-cell carcinomas (RCCs) in Ukrainian patients were recognized. The present paper describes the molecular alterations of those tumor suppressor genes located on chromosome 9p21 (*INK4a/ARF* locus and $p15^{INK4B}$) in 26 primary renal-cell epithelial tumors from patients with different degrees of radiation exposure after the Chernobyl accident in Ukraine. Radiometric measurement of Cesium 137 (^{137}Cs) was conducted with 1-day urine from all patients before surgery. Our results demonstrate that RCCs from patients living in the radio-contaminated areas showed aberrant hypermethylation of $p14^{ARF}$ and $p16^{INK4A}$ genes, associated with increased p38MAPK, $p14^{ARF}$, mdm2, cyclinD1 and Ki67 protein expression levels. Present findings show the possibility that chronic long-term low-dose radiation activates the *INK4a/ARF* locus, targeted by activation of the p38MAPK cascade. These actions could lead to disruptions and loss of cell cycle checkpoints and, thereby, to cellular transformation.

Keywords Chernobyl accident · Renal-cell carcinogenesis · p38MAPK · *INK4a/ARF* locus

A. Romanenko · V. Nepomnyaschy · A. Vozianov
Departments of Pathology and Urology,
Institute of Urology, Academy of Medical Sciences of Ukraine,
9ª Yu. Kotzubinsky, 04053 Kiev, Ukraine

L. Morell-Quadreny · A. Pellin · A. Llombart-Bosch (✉)
Department of Pathology,
Medical School of Valencia,
Avda Blasco Ibañez 17, 46010 Valencia, Spain
e-mail: antonio.llombart@uv.es
Fax: +34-96-3864173

J. A. Lopez-Guerrero
Department of Pathology,
Fundacion Instituto Valenciano de Oncologia,
C/ Beltran Baguena 8-11, 46009 Valencia, Spain

Introduction

The understanding of molecular mechanisms controlling cell proliferation has undergone a revolution over the past decade with the discovery and description of the cell-cycle clock apparatus. This molecular machinery, operating in the cell nucleus, is composed of three core components: cyclin-dependent kinases (CDKs), the cyclins, and cyclin-dependent kinase inhibitors (CKIs). Two families of CKIs are known: KIP and INK4. A variety of specific cyclin–CDK complexes are formed during distinct phases of the cell cycle, each dedicated to the phosphorylation of a distinct set of target proteins, which are responsible for the progression of each cell-cycle phase [7, 12].

Cyclin D1, in association with its CDK4 and CDK6 partners, targets the retinoblastoma (*Rb*) gene product (pRb) for the phosphorylation required for cells to make the transition from G1 into S phase [9]. In tumorigenesis, loss of *Rb* function can occur by direct mutation, sequestration of the pRb by oncoproteins, promoter hypermethylation or by deregulation of the genes controlling pRb phosphorylation status [7, 12]. These latter alterations include *cyclinD1* and *CDK4* gene amplification, and also inactivation of CDK4 inhibitors, such as the INK4 family, composed of $p16^{INK4A}$, $p15^{INK4B}$, $p18^{INK4C}$ and $p19^{INK4D}$ genes [4, 9].

Recently, it was demonstrated that a portion of the $p16^{INK4A}$ gene has the capacity to encode a second product: murine $p19^{ARF}$ [16] or human $p14^{ARF}$, which has a unique first exon 1-β located approximately 20 kb centromeric to the first exon of $p16^{INK4A}$ (denoted as exon 1-α). Under the control of its own promoter, exon 1-β splices into exon 2 of INK4a in an alternative reading frame (ARF), producing a different protein than $p16^{INK4A}$ [19]. $p14^{ARF}$ antagonizes mdm2-dependent p53 degradation and induces G1- and G2-phase arrest through a $p16^{INK4A}$-independent mechanism [5, 25].

Radiation carcinogenesis can be modulated by a variety of factors, including the mitogen activated protein kinase (MAPK) cascade. Four groups of MAPKs have

been identified in mammalian cells. The p38 group of MAPKs (also termed CSBP) is a part of the early stress response pathways, activated by cellular stress including heat and osmotic shock, ultraviolet (UV), ionizing radiation (IR) and inflammatory cytokines, which mediate inhibition of cell proliferation and cause cell death [6, 27, 28].

It has been demonstrated that low-dose Cesium 137 (^{137}Cs) γ-rays intensify the oxidative stress and activate transcription factors for induction of several genes in the control of cell proliferation in human blood cells [15].

The Chernobyl accident introduced for the first time the problem of chronic persistent long-term, low-dose exposure to IR in humans [17]. Recent studies by our group have shown that during the period subsequent to the Chernobyl accident, increases in morbidity, aggressivity and proliferative activity of renal-cell carcinomas (RCCs) in Ukrainian patients were recognized. The development of "radiation sclerosing proliferative atypical nephropathy" in the peritumoral kidney tissue then followed and demonstrated a good correlation with the duration of radiation exposure [22]. In addition, the influence of chronic, regular and sustained low-dose IR on renal carcinogenesis in the population living in ^{137}Cs-contaminated areas of Ukraine was confirmed [21].

However, we have not elucidated until now the precise mechanisms and the significance of the effect of long-term (more than 15 years), low-dose exposure to ^{137}Cs, as well as the possible concomitant activation of signal transduction pathways in human kidneys, which are known to play a pivotal role in ^{137}Cs concentration and elimination through urinary excretion [18].

The present study was carried out in order to examine the frequency of the molecular alterations of those tumor suppressor genes located on chromosome 9p21 (*INK4A/ARF locus* and *p15^{INK4B}*) in 26 primary renal-cell epithelial tumors (RCETs) from patients with different radiation exposure following the Chernobyl accident in Ukraine. The pathway marker of MAPK signal transduction, the p38MAPK protein, was also analyzed. Additionally, we evaluated alterations of the *p53* tumor suppressor gene and genetic amplification of the *cyclinD1*, *CDK4* and *mdm2* in association with the immunohistochemical protein expression of the same genes in the same cases.

This is the first report of INK4a/ARF locus measurement in RCETs reflecting the effect of chronic persistent low-dose IR exposure in humans. Three groups of RCETs from Ukrainian patients with varying degrees of exposure to irradiation were therefore selected for comparison.

Materials and methods

Patients and tumor samples

From 26 patients with RCETs, who underwent surgery at the Institute of Urology in Kiev (Ukraine), 112 formalin-fixed, paraffin-embedded tissue blocks and frozen material were investigated. The control group I of patients were from the so-called "clean" area (without indicated radio-contamination); group II were from the less contaminated city of Kiev; and group III patients were from heavily contaminated areas. All patients resided in the same areas both before and after the Chernobyl accident. Radiometric measurement of ^{137}Cs was conducted using urine collected over a 24-h period from all patients before surgery and was performed using a Standard Y-Radiometer RUB-01.

Histopathology and immunohistochemistry

Sections of RCET tissue, 4- to 5-μm thick were stained with hematoxylin and eosin (H&E) and were rated in accordance with the Heidelberg Classification [2]. The number of slides retrieved per case ranged from 4 to 11, with an average of 7 slides per case. We included in our study, one sample from the interface between the tumor and the normal tissue, a block of normal kidney away from the tumor, as well as two blocks of the best representative areas of tumor. Immunohistochemistry (IHC) staining was performed using a standard avidin-biotin peroxidase complex (ABC) method with LSAB kit (Dako, Denmark). Serial sections were deparaffinized and endogenous peroxidase activity was blocked with 3% hydrogen peroxide in distilled water for 5 min. Sections were heated for 3–5 min in an autoclave (1–1.5 atmospheres) in citrate buffer, pH 6.1, for antigen retrieval. Non-specific binding was blocked with 5% normal horse serum at room temperature (for p53, Ki67, cyclin D1, mdm2, p16^{INK4A} and p38MAPK), goat serum (for p14^{ARF}) in PBS at 37°C for 30 min. Incubation was performed with anti-mouse human p53 monoclonal antibody (Mab DO-7, IgG2b; Dako, Glostrup, Denmark) at 1:300 dilution; anti-mouse Ki67 monoclonal antibody (Biomeda) at 1:50 dilution; anti-mouse cyclin D1 (NCL-cyclin D1-GM) monoclonal antibody (NOVOCASTRA) at 1:10 dilution; anti-mouse mdm2 (NCL-MDM 2) monoclonal antibody (NOVOCASTRA) at 1:50 dilution, anti-mouse p16^{INK4a} (F-12): sc–1661 monoclonal Ig G2a antibody JC8 (Santa Cruz Biotechnology, Santa Cruz, CA) at 1:200 dilution; anti-mouse p-p38 (D-8) monoclonal human antibody (Santa Cruz Biotechnology, Santa Cruz, CA) at 1:800 dilution; and anti-rabbit p14^{ARF} (FL-132): sc-8340 polyclonal antibody (Santa Cruz Biotechnology, Santa Cruz, CA) at 1:30 dilution for 1 h at room temperature.

As controls, known positive tissue sections were used, and for negative controls, exposure to the primary antibody was omitted. Color was developed using 3′,3′-diaminobenzidine, and counter staining with Mayer's hematoxylin for 1 min was applied. The IHC analysis was performed in a blind fashion without knowledge of the patient group. All specimens were evaluated independently by at least two pathologists.

DNA extraction

Fresh frozen tumor samples without macroscopic hemorrhage or necrosis were stored at −80°C until the molecular analysis was performed. At this moment, a control of the material was done by imprint and staining of samples with H&E. Moreover, DNA was isolated from frozen tissue samples. High-molecular-weight DNA was prepared according to standard phenol/chloroform protocol [23].

Status of *p16^{INK4A}*, *p15^{INK4B}*, and *p14^{ARF}* genes, amplification of *cyclin D1*, *CDK4*, and *mdm2* genes, and *p53* sequencing

DNA samples were analyzed for homozygous deletion of the *p16^{INK4A}*, *p15^{INK4B}* and *p14^{ARF}* genes by means of differential polymerase chain reaction (dPCR). In this assay, a simultaneous amplification of genomic DNA was carried out using two sets of primers, one to target the gene sequence under study, the other to target the β-globin gene, which was used as an internal control for DNA quality and loading. Homozygous deletion, hypermethylation of the 5′CpG island in the promoter region of the *p16^{INK4A}* and *p14^{ARF}* genes were also analyzed simultaneously using methyla-

tion-specific PCR (MSP) after alkali chemical modification of the DNA.

Gene amplification of the *MDM 2*, *CDK4* and *cyclin D1* genes was determined by means of dPCR employing two sets of primers, one corresponding to the target gene and the other to an internal gene sequence—the dopamine receptor (DR), the β-globin and the interferon γ (INFγ) genes for MDM, CDK4 and cyclin D1 analysis, respectively.

For *p53* sequencing, approximately 100 ng of genomic DNA was used in four different PCR-amplification reactions (exons 5–8). After 35 cycles, PCR products were purified using Centricon columns (Amicon, Beverly, MA, USA) and sequenced on an Applied Biosystem model 310 automated sequencer (Foster City, CA, USA) using the dRhodamine terminator cycle sequencing ready reaction kit (PE Applied Biosystem, Warrington, GB).

All these analyses were performed in accordance with the conditions referred to in the article by Lopez-Guerrero et al. [11].

Quantitative analysis

Histological analysis of RCETs was done using a semi-quantitative scale for the evaluation of variables. Each case was evaluated as 0, when the finding for the study was negative, and as 1, 2 or 3, when the same finding extended over a greater area and/or occurred with a higher intensity. IHC analysis for p53 and p38MAPK proteins was performed using a system for evaluation and grading of the immunostaining patterns with values for intensity, distribution and extent. The intensity of staining was scored using the following criteria: zero (no detectable staining), low, moderate and strong staining. The extent of the staining was scored as: zero; low (less than 10% scattered stained cells); moderate (more than 10% but less than 50% stained cells); and strong (staining in more than 50% of cells). The percentage of cells expressing cyclinD1, mdm2, Ki67, $p16^{INK4A}$ and $p14^{ARF}$ proteins was determined by counting 1000 cells per slide.

Statistical analysis

For analysis, each variable had a qualitative or quantitative connotation, depending on the possibility for evaluation. Patient's age, tumor size and cyclinD1, mdm2, Ki67, p38MAPK, $p16^{INK4A}$ and $p14^{ARF}$ protein expression as a percentage had a quantitative variable; the other histological and immunohistochemical variables had qualitative connotations. Statistical analysis was performed to determine whether pathological and immunohistochemical data were related to each other, as well as with the different groups of patients. We applied the χ^2 test for statistical analysis between qualitative variables; Fisher's test and Student's *t*-tests were used to assess the relationship between qualitative and quantitative variables, and the Pearson correlation test was used to assess the relationships between quantitative variables.

Results

Patients

Pathological and epidemiological data are summarized in Table 1. Samples for our study were obtained from 16 males and 10 females, with a mean age of 54 years and living in Ukraine with varying degrees of environmental ^{137}Cs contamination. Significant elevation of ^{137}Cs levels via urinary excretion occurred in patients from groups II and III when compared with group I. Patients from radio-contaminated areas with the highest levels of urinary ^{137}Cs excretion presented tumors with a larger size (P=0.02) and higher stage.

Histopathology

Predominant conventional RCCs were diagnosed in 18 (69%) of 26 cases with a similar distribution between groups. Comparative analysis between all groups showed more frequent incidences of high-grade RCCs in patients from radio-contaminated areas. Two poorly differentiated RCCs demonstrated sarcomatoid changes. Moreover, there were significant relationships between the poorly differentiated RCCs and the highest levels of ^{137}Cs urinary excretion (x=2.16; st=3.36) compared with the moderately (x=0.31; st=0.40) and well- (x=0.22; st=0.21) differentiated RCCs. Inflammation was seen in 12 tumors, being predominantly low (6 cases) or moderate (5 cases), with only one tumor showing severe inflammatory infiltration. Renal oncocytomas were diagnosed in 4 (15%) of

Table 1 Pathological and epidemiological data. *RCC* renal-cell carcinoma, *NC* non-contaminated

	Group I	Group II	Group III
Number of patients	7	10	9
Mean age (years)	54 (40–73)	55 (46–65)	52 (35–70)
Contamination (Ci/Km^2) (19)	NC	0.5–5	5–30
Mean ^{137}Cs urinary excretion/day	0.37 (0.32–0.41)	0.91 (0.54–1.27)	2.4 (0.64–3.64)
Mean tumor size (cm)	6.78 (3–14)	7.85 (5–12)	9.66 (4–18)
Tumor stage in RCCs			
I	4	3	1
II	2	1	4
III	-	3	4
Histological type			
Conventional	6	5	8
Papillary	-	1	-
Chromophobe	-	1	-
Collecting Ducts	-	-	1
Oncocytoma	1	3	-
Grade in RCCs			
Well differentiated	4	1	2
Moderately differentiated	2	5	3
Poorly differentiated	-	1	4

Table 2 Relationship between groups. Molecular and immunohistochemical data in renal-cell carcinomas (RCCs). *SD* standard deviation

	Group I	Group II	Group III
Number of patients	6	7	9
$p14^{ARF}$ Hypermethylation	-	3	1
$p14^{ARF}$ Protein mean (SD)	0.83 (1.1)	24.75 (35.82)	11.33 (12.40)
p53 >10% Stained	1	1	1
MDM 2 Mean (SD)	19.16 (18.19)	38.14 (15.23)	33.11 (34.48)
$p38^{MAPK}$ Strong intensity	-	4	5
$p38^{MAPK}$ >10% Stained	4	7	7
Ki67 mean (SD)	6.16 (10.81)	13 (8.28)	13 (18.26)
$p16^{INK4A}$ Hypermethylation	1	1	1
$p16^{INK4A}$ Protein mean (SD)	10.83 (12.56)	6 (6.42)	19.11 (32.30)
Cyclin D1 mean (SD)	2.33 (4.80)	3 (4.39)	10.66 (13.53)

26 cases, corresponding to 1 patient from group I and 3 patients from group II.

Immunohistochemistry and molecular biology

Data from IHC analysis and molecular biology in RCCs are summarized in Table 2, and some immunohistochemical findings are illustrated in Fig. 1.

The results from molecular analysis revealed no homozygous deletions of *p16*^{INK4A}, *p15*^{INK4B} or *p14*^{ARF} genes in any sample, no point mutations of *p53*, and also no genetic amplifications of *mdm2*, *cyclin D1* or *CDK4* genes. No association between any pathological or epidemiological parameters and hypermethylation of the *p15*^{INK4B} gene was found. Aberrant hypermethylation of the 5′CpG islands in the promoter region of the *p14*^{ARF} gene was observed in 4 (18%) cases in high-stage and -grade RCCs of group II and group III (Fig. 2).

P53 protein nuclear overexpression occurred in 3 (13%) conventional RCCs, having between 10% and 50% of stained nuclei and in 4 (18%) from 22 cases (one papillary, one Bellini, and two conventional RCCs) with less than 10% of stained nuclei, predominantly from groups II and III. RCCs from radio-contaminated areas expressed higher quantities of $p14^{ARF}$ protein in relation to tumors from "clean" regions. There was a direct relationship between $p14^{ARF}$ protein and mdm2 expression in RCCs from groups I to III with the increased overexpression of $p14^{ARF}$ and mdm2 in radio-contaminated areas.

Proliferative activity showed differences between groups with Ki67 stained nuclei, and was highest in groups II and III. The relationship between Ki67 immunostaining and histological variables demonstrated an increase in mean values of positive cells in high-grade RCCs, with significant differences.

Regular homogeneous or granular p38 MAPK cytoplasmic immunostaining in RCCs was detected in 100% and 78% of cases from group II and group III, respectively. RCCs from radio-contaminated areas showed the highest frequency of *p14*^{INK4A} gene hypermethylation and the strongest intensity of p38MAPK overexpression (P=0.003) when compared with RCCs from group I.

Furthermore, $p16^{INK4A}$ protein immunostaining showed an irregular tendency in relation to groups. A direct relationship was present between increased nuclear overexpression of cyclinD1 and cytoplasmic expression of p38MAPK in tumors from group II and group III. Moreover, we could not see a relationship between $p16^{INK4A}$ protein expression and cyclin D1 nuclear overexpression, although tumors from patients who live in contaminated areas showed high levels of $p16^{INK4A}$ and cyclin D1 nuclear expression. Interestingly, hypermethylation of *p16*^{INK4A} and *p14*^{ARF} genes were never observed simultaneously in the same sample.

No relationship was seen between cyclinD1, mdm2, $p16^{INK4A}$ and $p14^{ARF}$ protein expression, and histological variables of RCC stage and grade. Areas of $p16^{INK4A}$ and $p14^{ARF}$ protein overexpression were irregular with alternating negatively stained areas. Furthermore, the levels of urinary excretion of ^{137}Cs showed a direct correlation with IHC expression of $p14^{ARF}$ protein (P=0.005) and mdm2 (P=0.044).

Renal oncocytomas showed no molecular changes in *p14*^{INK4A}, *p16*^{INK4A} and *p15*^{INK4B} genes. p53 protein expression was also negative in all oncocytic tumors. Oncocytomas of group II presented positive immunostaining against mdm2 in 11, 15 and 30% of tumoral cells. Moreover, two cases from group II showed cyclin D1 positivity in 1% and 26% respectively. Ki67 immunostaining was positive in three tumors with levels of 0.3, 0.2 and 2% respectively. All oncocytomas were positive against p38MAPK with a cytoplasmic granular distribution, but the intensity of staining was strong in only one case.

Discussion

The present study represents the first finding of a specific lesion in the *INK4a/ARF* locus of chromosome 9q21 in primary human RCETs from patients chronically exposed to low doses of IR, living in the radio-contaminated areas of Ukraine, and a significant increase of ^{137}Cs in 1-day urine of these patients, as demonstrated by the radiometric study, so the long-term radiation exposure of the kidney tissue could be easily supposed. There is no dose–response relationship in the range 2–12 Gy, suggesting that an unstable phenotype may be induced by quite low radiation doses [10].

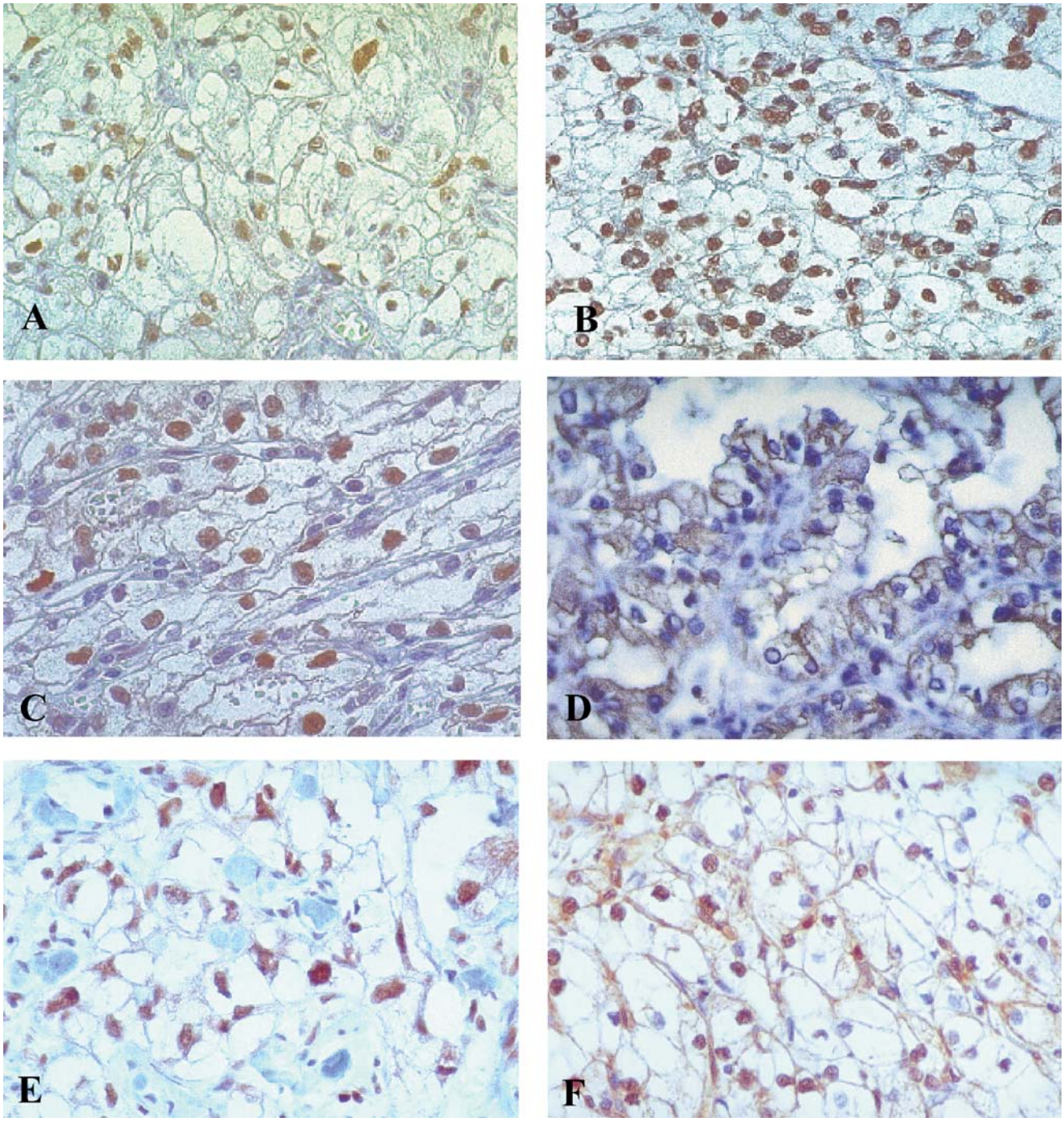


Fig. 1 Immunohistochemistry findings for conventional renal-cell carcinomas from radio-contaminated areas. **A** p53 expression. **B** mdm2 expression. **C** Cyclin D1 expression. **D** p38MAPK expression. Magnification ×400

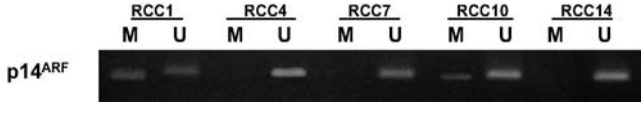


Fig. 2 Methylation-specific polymerase chain reaction showing cases with hypermethylation of the $p14^{ARF}$ gene

Moreover, the "bystander" or non-targeted effects of very low doses of IR were recently described as important genetic consequences of IR, which may arise in cells that in themselves received no direct nuclear exposure [10]. Thus, the actual target for radiation effect in a cell population may be much larger than the irradiated cell itself [28]. The data support our hypothesis that long-term (more than 15 years) persistent low-dose radiation exposure can lead to chronic DNA damage with disruption of

the molecular mechanisms that control cell proliferation—"the cell-cycle clock apparatus".

This study has documented the fact that RCCs from patients living in the radio-contaminated areas of Ukraine showed aberrant hypermethylation of the $p14^{ARF}$ gene associated with increased mdm2 and cyclin D1 protein levels. Moreover, $p14^{ARF}$ promoter hypermethylation occurs independently of the $p16^{INK4A}$ methylation status. Furthermore, the *p53* stable status is associated with increased levels of nuclear mdm2 and $p14^{ARF}$ proteins in the same tumors. Several studies have recently shown that $p14^{ARF}$ acts through mdm2 to inhibit *p53* tumor suppressor gene degradation and that exon 1-β is sufficient for $p14^{ARF}$-mediated stabilization of the *p53* function [24]. Furthermore, in RCCs, the coexpression of mdm-2 and p53 proteins has been related with poor prognosis [8]. However, although the mechanism of cyclin D1 expression is not well known, recent studies suggest that the von Hippel-Lindau (VHL) gene is required for the downregulation of cyclin D1 and, in some kidney cell types, pVHL may regulate a proliferative response to hypoxia, whereas the loss of VHL leads to elevated cyclin D1 abnormal proliferation under normal growth conditions [3]. The $p16^{INK4A}$ gene promoter hypermethylation in three cases was associated with immunohistochemical decrease, or loss of the $p16^{INK4A}$ protein. This protein is known to accumulate in response to low doses of UV in cultured cell lines and correlates with G1 phase cell-cycle arrest [14]. Furthermore, the loss of the $p16^{INK4A}$ function correlates with the loss of the UV-induced G1 arrest [20]. In the same RCCs, an increase of cyclinD1 expression occurred; although a relationship between groups was not seen. However, a high level of cyclinD1 was often found in many different human tumor types—breast, urinary bladder carcinomas and squamous cell carcinomas of the head and neck [13, 20].

In RCCs, $p16^{INK4A}$ promoter hypermethylation was never combined with $p14^{ARF}$ promoter hypermethylation. The most common situation was the simultaneous absence of methylation in both promoters; but, after this, the two possible scenarios ($p16^{INK4A}$ methylated alone, $p14^{ARF}$ methylated alone) were similarly represented. These data suggest the existence of multiple levels of "cross-talk" between the $p16^{INK4A}$/*pRb* and $p14^{ARF}$/*p53* pathways in RCCs. Moreover, they support the recent studies that have shown the potential to change $p16^{INK4A}$ status as a predominant tumor suppressor gene at this locus, since they imply that there may be genetic pressure for $p14^{ARF}$ loss, being independent of $p16^{INK4A}$ [19]. Usually it appears that $p16^{INK4A}$ and $p14^{ARF}$ tumor suppressor genes do not continuously inhibit proliferation under normal conditions, but in fact are "waiting" to be activated in response to the appropriate signals. These signals are now beginning to be identified as either oncogenic or the cause of some other stresses. Oxidative stress, induced by IR, usually involves production of reactive oxygen species (ROS) by activated mitochondria and also causes activation of MAP kinases; in addition, p38MAPK activities are known to be a critical component of ROS-mediated signaling [1, 26]. Long-term, low-dose exposure to IR on people living in radio-contaminated areas chronically induces the persistent activation of transcription factors via a p38MAPK cascade. There was a significant relationship between strong immunostaining against p38MAPK and RCCs of radio-contaminated areas.

Thus, our results demonstrate that long-term low doses of IR can possibly stimulate multiple signal transduction pathways (both, $p14^{ARF}$/*p53* and $p16^{INK4A}$/*pRb* pathways) simultaneously. Recent studies suggest that *INK4a/ARF* haploinsufficiency may have strong effects on tumorigenesis. Remarkably, findings in gliomas and melanomas show that different cell types have different sensitivities to changes in the genetic dose of *INK4a/ARF* [24].

To summarize, we have demonstrated that the tendency for inactivation of $p16^{INK4A}$ and $p14^{ARF}$ by promoter hypermethylation represents an important molecular pathogenesis in RCCs from radio-contaminated areas of Ukraine. Thus, the *INK4A/ARF* locus is a part of a "gate-keeper" mechanism that responds to persistent low-dose radiation stimuli. Chronic, but regular and sustained, long-term *INK4a/ARF* locus activation, targeted by oxidative stress via activation of the p38MAPK cascade, leads to disruptions and loss of cell-cycle checkpoints with subsequent deregulated mitotic cell-cycle control and, thereby, to cellular transformation. Further studies are necessary for a better understanding of the molecular pathology of RCETs developed under chronically affected low doses of IR, which could then provide the ability for more effective prognoses and treatment of these patients.

Acknowledgements The authors are grateful to Estela Pons and Alejo Sempere for their technical assistance. Source of support: GV01–532 from the Generalitat Valenciana and FIS 01/0702 from the Ministry of Health, Madrid, Spain.

References

1. Adler V, Yin Z, Tew KD, Ronai Z (1999) Role of redox potential and reactive oxygen species in stress signaling. Oncogene 18:6104–6111
2. Bostwick DG, Murphy GP (1998) Diagnosis and prognosis of renal cell carcinoma: highlights from an international consensus workshop. Semin Urol Oncol 16:46–52
3. Brinda RS, Vasselli JR, Stearman R, Linehan WM, Klauser RD (2002) VH-mediated hypoxia regulation of cyclin D1 in renal carcinoma cells. Cancer Res 62:3014–3019
4. Carnero A (2000) Cell cycle and cancer, rev. Oncologia 2:12–22
5. Esteller M, Tartola S, Toyota M, Capella G, Peinado MA, Baylin SB, Herman JG (2000) Hypermethylation—associated inactivation of $p14^{ARF}$ is independent of $p16^{INK4A}$ methylation and p53 mutation status. Cancer Res 60:129–133
6. Galibert MD, Carreira S, Goding CR (2001) The Usf-1 transcription factor is a novel target for the stress-responsive p38 kinase and mediates UV-induced tyrosinase expression. EMBO J 20:5022–5031
7. Gillett CE, Barnes DM (1998) Cell cycle. J Clin Pathol 51:310–316
8. Haitel A, Wiener HG, Baethge U, Marberger M, Susani M (2000) Mdm2 expression as a prognostic indicator in clear cell

carcinoma: comparison with p53 overexpression and clinicopathological parameters. Clin Cancer Res 6:1840–1844
9. Johnson DG, Walker CL (1999) Cyclins and cell cycle checkpoints. Annu Rev Pharmacol Toxicol 39:295–312
10. Little JB (2000) Radiation carcinogenesis. Carcinogenesis 21:397–404
11. Lopez-Guerrero JA, Pellin A, Noguera R, Carda C, Llombart-Bosch A (2001) Molecular analysis of the 9q21 locus and p53 gene in Ewing family tumors. Lab Invest 81:803–814
12. Lundberg AS, Weinberg RA (1999) Control of the cell cycle and apoptosis. Eur J Cancer 35:531–539
13. Martin JMC, Balkenende A, Verschoor T, Lallemand F, Michalides R (1999) CyclinD1 over-expression enhances radiation-induced apoptosis and radiosensitivity in a breast tumor cell line. Cancer Res 9:1134–1140
14. Parvey S, Conroy S, Rassell T, Gabrielli B (1999) Ultraviolet radiation induces p16CDKN2a expression in human skin. Cancer Res 59:4185–4189
15. Prasad AV, Mohan N, Chandrasekar B, Meltz ML (1994) Activation of nuclear factor kB in human lymphoblastoid cells by low-dose ionizing radiation. Radiat Res 138:367–372
16. Quelle DE, Zindy F, Roussel MF, Quelle DE, Downing JR, Ashmun RA, Grosveld G, Sherr CJ (1997) Tumor suppression at the mouse INK4a locus mediated by the alternative reading frame product $p19^{ARF}$. Cell 9:649–659
17. Raes F, De Cort M, Graziani G (1991) Multi-fractal nature of radioactivity deposition on soil after the Chernobyl accident. Health Phys 61:271–282
18. Richmond CR (1968) Accelerating the turnover of internally deposited radiocesium. In: Kornberg HA, Norwood WD (eds) Diagnosis and treatment of deposited radionuclides. Excerpta Medical Foundation, Richland, WA, pp 315–325
19. Rocco JW, Sidransky D (2001) p16(MTS-1/CDKN2/INK4a) in cancer progression. Exp Cell Res 264:42–55
20. Romanenko A, Lee CC, Yamamoto S, Hori TA, Wanibuchi H, Zaparin W, Vinnichenko W, Vozianov A, Fukushima S (1999) Urinary bladder lesions after the Chernobyl accident: immunohistochemical assessment of p53, proliferating cell nuclear antigen, cyclin D1 and $p21^{WAF1/Cip1}$. Jpn J Cancer Res 90:144–153
21. Romanenko A, Morell-Quadreny L, Nepomnyaschy V, Vozianov A, Llombart-Bosch A (2000) Pathology and proliferative activity of renal-cell carcinomas (RCCs) and renal oncocytomas in patients with different radiation exposure after the Chernobyl accident in Ukraine. Int J Cancer 87:880–883
22. Romanenko A, Morell-Quadreny L, Nepomnyaschy V, Vozianov A, Llombart-Bosch A (2001) Radiation sclerosing proliferative atypical nephropathy of peritumoral tissue of renal-cell carcinomas after the Chernobyl accident in Ukraine. Virchows Arch 438:146–153
23. Sambrook J, Fritsch EF, Maniatis T (1989) Molecular cloning. A laboratory manual. Cold Spring Harbor Laboratory Press, Cold Spring Harbor, pp 1–83
24. Serrano M (2000) The INK4a/ARF locus in murine tumorigenesis. Carcinogenesis 21:865–869
25. Sherr CJ, Weber JD (2000) The ARF/p53 pathway. Curr Opin Genet Dev 10:94–99
26. Suzuki K, Kodama S, Watanabe M (2001) Extremely low-dose ionizing radiation causes activation of mitogen-activated protein kinase pathway and enhances proliferation of normal human diploid cells. Cancer Res 61:5396–5401
27. Wang X, Martindale IL, Liu Y, Holbrook NJ (1998) The cellular response to oxidative stress: influences of mitogen-activated protein kinase signalling pathways on cell survival. Biochem J 333:291–300
28. Wu LJ, Randers-Pehrson G, Xu A, Waldren CA, Geard CR, Yu ZL, Hei TK(1999) Targeted cytoplasmic irradiation with alpha particles induces mutations in mammalian cells. Proc Natl Acad Sci U S A 96:4959–4964

Virchows Arch (2004) 445:305–314
DOI 10.1007/s00428-004-1069-2

ORIGINAL ARTICLE

An Hang Yang · Jinn Yang Chen · Be Fun Chen

The dysregulated glomerular cell growth in Denys–Drash syndrome

Received: 17 February 2004 / Accepted: 28 May 2004 / Published online: 1 July 2004
© Springer-Verlag 2004

Abstract While diffuse mesangial sclerosis is traditionally described as being the glomerulopathy of Denys–Drash syndrome (DDS), the podocyte proliferative lesions may be overlooked in these DDS cases. In the present study, an evolving process is extrapolated from a selected case of DDS that demonstrated glomerulopathy with conspicuous podocyte proliferation. The observation that podocytes express proliferation markers (Ki67, proliferating-cell nuclear antigen and topoisomerase IIα) in non-proliferative, mature-looking glomeruli suggests an initial pathogenic act to activate or to keep podocytes from quiescence. The subsequent proliferation of podocytes is in keeping with downregulation of WT1 and cyclin kinase inhibitors of p16 and p21. The emergence of cytokeratin-positive cells in glomeruli that show typical mesangial sclerosis implies elimination of podocytes and replacement with tubular and/or parietal epithelial cells. The final scene of evolving glomerulopathy displays apoptosis and expression of Fas-L and Bax in sclerotic mesangial lesions, which eventually end up with global sclerosis. This novel concept of DDS glomerulopathy implies complex molecular mechanisms involved in glomerular injury.

Keywords Denys–Drash syndrome · Glomerulopathy · Cyclin · Cyclin kinase inhibitor · Podocyte · Apoptosis · WT1

A. H. Yang (✉)
Ultrastructural and Molecular Pathology, Department of Pathology,
Taipei Veterans General Hospital,
Taipei, Taiwan
e-mail: ahyang@vghtpe.gov.tw
Fax: +886-2-28214330

J. Y. Chen
Department of Nephrology,
Taipei Veterans General Hospital,
Taipei, Taiwan

B. F. Chen
Department of Pathology,
McKay Memorial Hospital,
Taipei, Taiwan

A. H. Yang
Department of Pathology,
School of Medicine, National Yang-Ming University,
Taipei, Taiwan

Introduction

The renal involvement in the Denys–Drash syndrome (DDS) is manifested by Wilms' tumor and glomerulopathy. The latter eventually leads to end-stage renal failure and is the primary cause of death in this syndrome [19]. The investigation of genetic abnormality in nearly all patients of DDS reveals constitutionally heterozygous point mutations for WT1, a gene that encodes a transcription factor that functions in kidney and gonad proliferation and differentiation [2, 16, 33]. Incomplete DDS and isolated diffuse mesangial sclerosis (IDMS), which share similar glomerulopathy with the complete form of DDS, also demonstrate various *wt1* mutations [33]. It has been suggested that glomerulopathy results from debilitating transcriptional function of WT1 in a dominant negative fashion [2, 16, 17]. A mouse model of DDS, which was heterozygous for a target *wt1* allele, demonstrated truncated zinc finger 3 at amino acid 396 of WT1 protein and severe proliferative glomerulopathy with crescent formation [24]. In a human study, mild increase of cell proliferation was demonstrated by proliferating-cell nuclear antigen (PCNA)-positive podocytes in two-thirds of DDS patients; one case even showed abundant positive cells in up to 50% glomeruli [33]. Recent studies have revealed that some genes of the WT1 network may play pathogenic roles directly or indirectly linked to the growth control of glomerular cells. For example, PAX2, a transcriptional factor that is downregulated by WT1 during normal maturation of podocytes, is persistently expressed in podocytes of DDS and IDMS kidneys [4, 25, 33]. The PAX2 is speculated to be capable of stimulating cell proliferation by the observations that PAX2 induced

podocyte hypertrophy and increased PCNA nuclear labeling [33]. Another target gene of WT1, *novH*, whose expression in podocytes is also downregulated by WT1 during normal nephrogenesis [18, 22], is capable of stimulating cell proliferation in synergy with growth factors such as transforming growth factor-β and basic fibroblast growth factors [6]. These data imply that the basic pathology of glomerulopathy in DDS and related disorders may be associated with dysregulation of cell proliferation in glomeruli.

The major purpose of our study was to analyze the growth response of glomerular cells in DDS kidney. We assessed cellular proliferation activity, cell-cycle regulatory factors, WT1 protein expression, apoptosis and apoptotic modulation factors to explore the pathogenic mechanism of DDS glomerulopathy.

Materials and methods

Tissue

We selected a case of DDS from our autopsy archives for this study. The clinical and histopathological features are summarized in Table 1. The major presenting symptoms and signs of this patient were a renal mass at the left kidney, nephrotic syndrome and genital abnormalities. We also retrieved control tissues of patients of similar age with neither DDS nor Wilms' tumor or of patients with Wilms' tumor but without DDS from surgical or autopsy archives.

Morphological studies and immunohistochemical analyses

The kidney tissues subjected to histochemical and immunohistochemical examinations were paraffin embedded and cut into 3-μm-thick sections. Sections were stained for hematoxylin and eosin, periodic acid–Schiff and periodic acid silver methanamine for routine morphological examination. The paraffin sections for immunohistochemical analyses were deparaffinized in xylene substitute (Paraclean, Earthsafe Tech, USA), rehydrated and immersed in 3% H_20_2/methanol for 10 min. The primary antibodies used in this study are listed in Table 2. Before incubation with primary antibodies, sections were microwaved either in 0.01 M sodium citrate buffer (pH 6.0) for 10 min or with pressure cooker in 1.0 mM ethylenediaminetetraacetate buffer for 5 min and blocked with blocking serum in phosphate-buffered saline (PBS) for 20 min at room temperature. The sections were then subjected to incubation in primary antibody and peroxidase–antiperoxidase (PAP) reagents for 30 min, respectively. The sections were thoroughly washed between incubations. After the final wash in 1% Triton X-100/PBS, sections were stained using diaminobenzidine (DAB)–H_2O_2 as substrate. Negative controls included replacing primary antibodies with normal serum or omission of PAP reagents or both. Additional absorption control using specific blocking peptide (sc192 P, Santa Cruz) was applied to WT1 staining procedure. Appropriate tissue sections containing the specific antigen were prepared from the surgical specimen to serve as positive controls.

Assessment of apoptosis

Enzymatic in situ labeling of apoptosis induced DNA strand breaks [transferase–mediated dUTP nick end-labeling (TUNEL) assay] was assessed using the kit (#1684817 POD, Boehringer, Mannheim) as previously described with slight modification [32]. Deparaffinized sections were stained according to the instruction given by the manufacturer. Chromogenic reaction was carried out using DAB as substrate, and all sections were counterstained with

Table 1 Clinical and pathological features of the Denys–Drash syndrome patient. *BUN* serum BUN (mg/dl), *Cr* serum creatinine (mg/dl), *24UPt* 24 h urine protein (gm)

Age at first symptom	9 months
External genitalia	Micropenis, hypospadia and cryptorchidism
BUN/Cr/24UPt*	56/1.8/1.2
Karyotype	46,XY
Wilms' tumor	Unilateral, 2 cm in diameter
Proliferative glomerulopathy**	28%
WT1 genotype	Absence of mutation in exons 1 and 3–10
Outcome (months)	Dead (12)

* Renal function at first symptoms
** Average % proliferative glomeruli/5 low power fields (×10)

Table 2 Primary antibodies used for immunohistochemical analyses

Antibodies/hosts or clones	Dilution	Source (Cat. #)*
Actin/mouse clone 1A4	1/70	Dako (M0851)
Vimentin/mouse clone V9	1/50	Dako (M0725)
Cytokeratin/mouse clone AE1/AE3	1/200	Signet (464)
Topoisomerase IIα/mouse clone Ki-S1	1/75	Dako (M7186)
Ki67/mouse clone MIB-1	1/75	Immunotech (0505)
Proliferating-cell nuclear antigen/mouse clone PC-10	1/120	Dako (M0879)
Cyclin A/rabbit polyclone	1/20	Santa Cruz (sc-751)
P16/mouse monoclone	1/50	Santa Cruz (SC-1661)
P21/mouse clone SX118	1/25	PharMingen (65951A)
Bcl2/mouse monoclone	1/50	Santa Cruz (sc-7382)
Bax/rabbit polyclone	1/50	Santa Cruz (sc-526)
Fas-L/rabbit polyclone	1/100	Santa Cruz (sc-834)
WT1/rabbit polyclone	1/50	Santa Cruz (sc-192)

* Dako, Glostrup, Denmark; Signet Laboratories, Dedham, MA; Santa Cruz Biotechnology, Santa Cruz, CA; PharMingen, San Diego, CA; Immunotech, Cedex, France

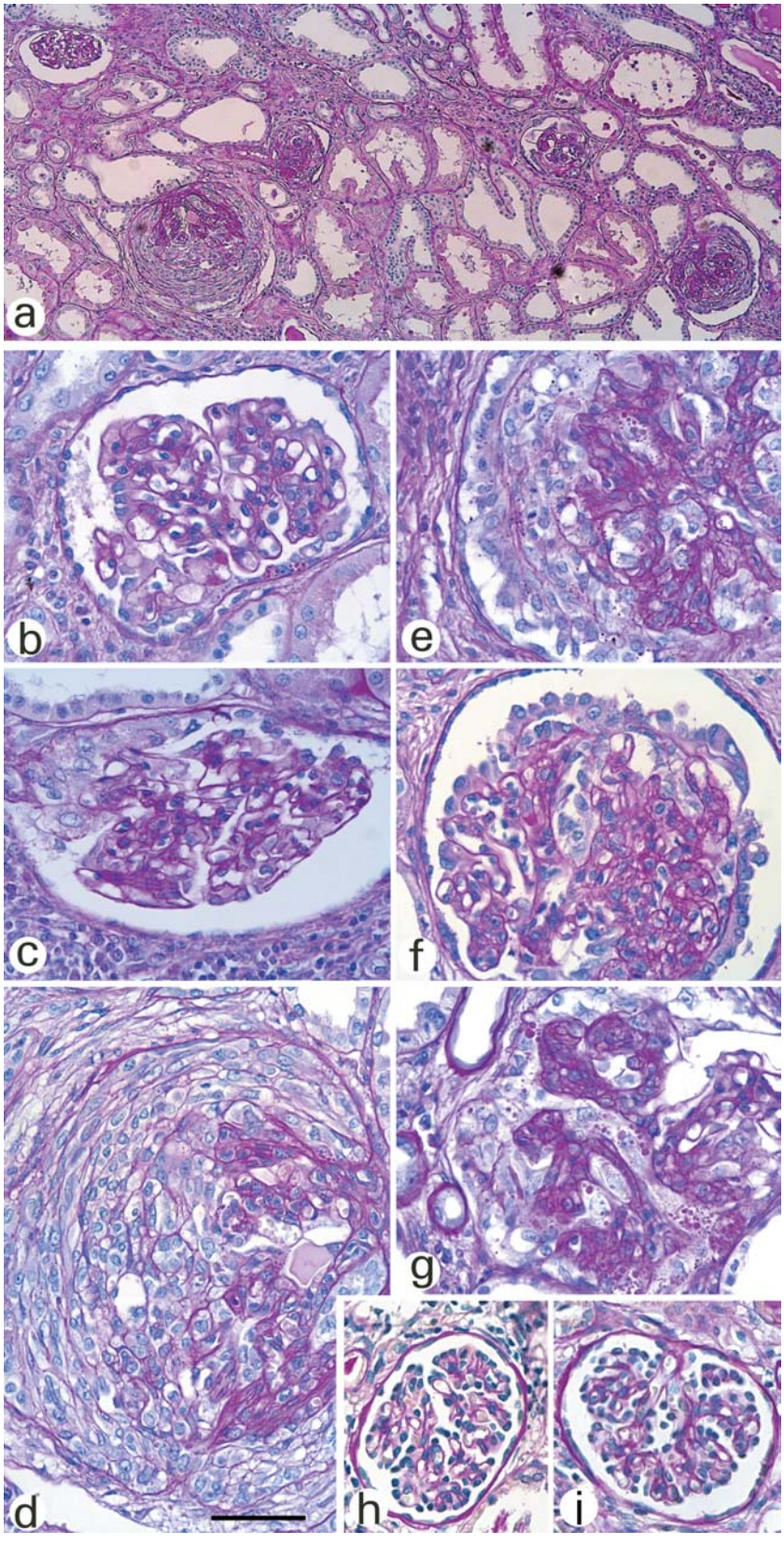


Fig. 1 Light microscopy of glomeruli in Denys–Drash syndrome (DDS) kidneys (**a**–**g**) and glomeruli in non-DDS kidney (**h**–**i**). Periodic acid–Schiff stain, *scale bar* 50 μm

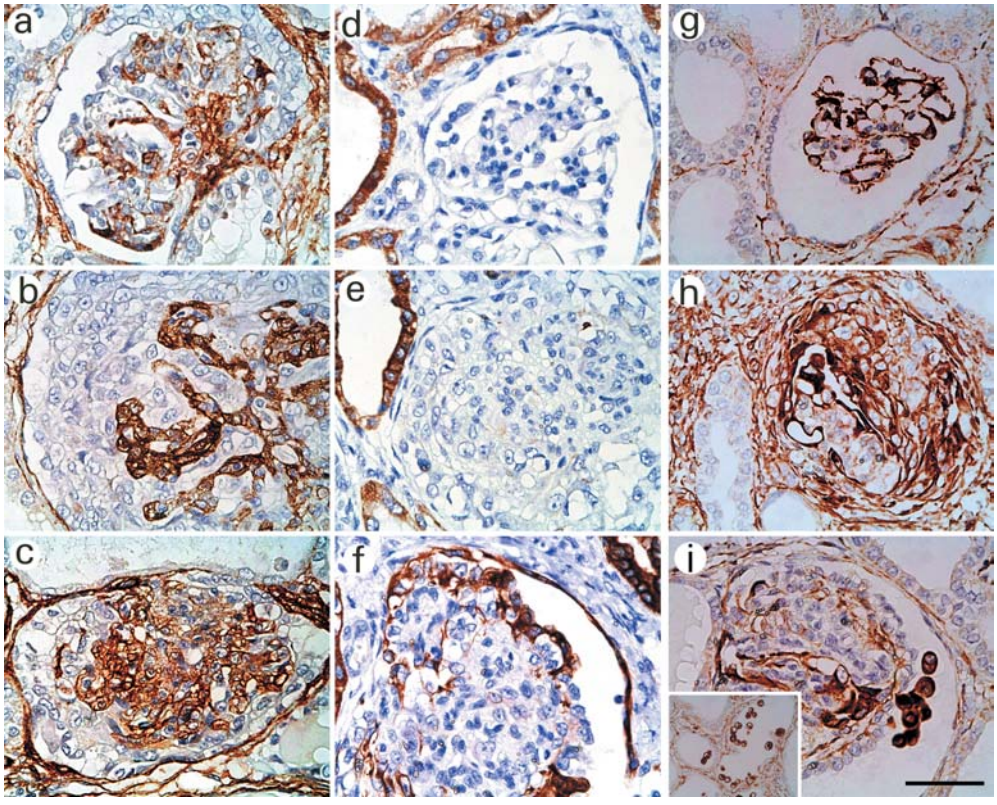


Fig. 2 Immunohistochemical staining patterns of actin (**a**–**c**), cytokeratin (**d**–**f**) and vimentin (**g**–**i**) in Denys–Drash syndrome kidney. Peroxidase–antiperoxidase stain, *scale bar* 50 μm

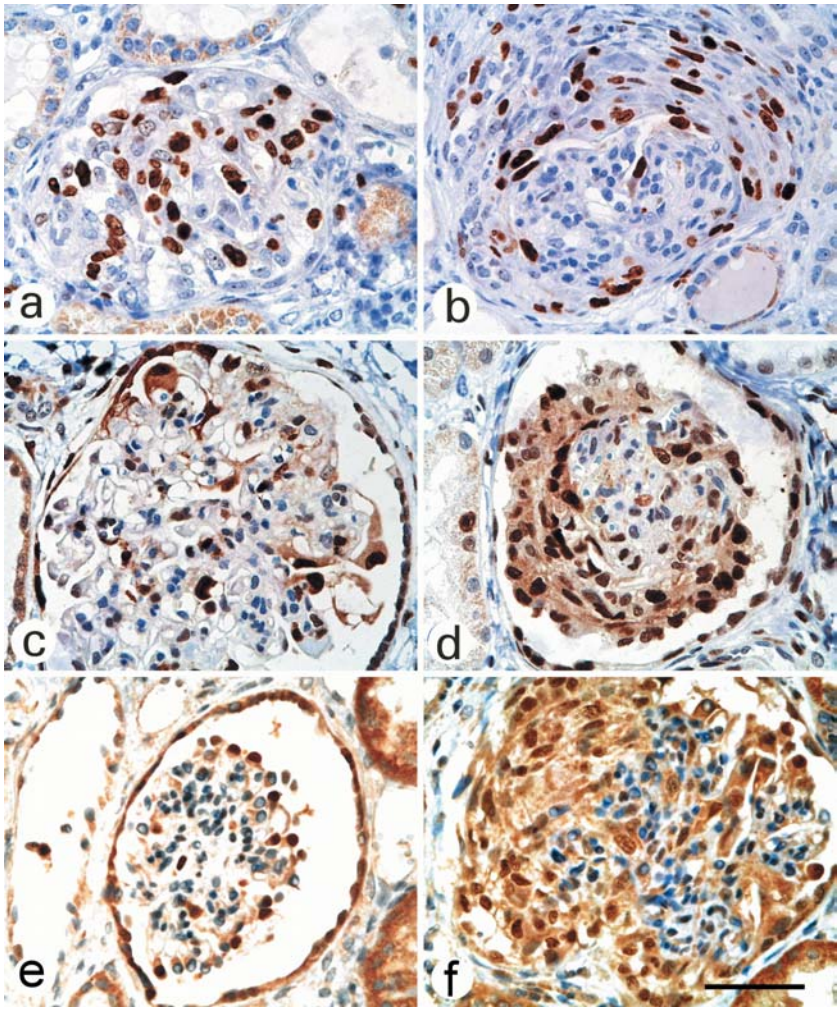


Fig. 3 Immunohistochemical staining patterns of cell proliferation markers: Ki67 (**a**, **b**), proliferating-cell nuclear antigen (**c**, **d**) and topoisomerase IIα (**e**, **f**) in glomeruli with early (**a**, **c**, **e**) and advanced (**b**, **d**, **f**) Denys–Drash syndrome glomerulopathy. Peroxidase–antiperoxidase stain, *scale bar* 50 μm

hematoxylin prior to analysis under light microscope. The negative controls used label solution without terminal transferase, while the positive controls received pre-treatment of DNase I (10 μg/ml, room temperature, 10 min) prior to TUNEL reaction.

DNA sequencing

Genomic DNA was retrieved from archived paraffin blocks. The WT-1 coding sequence (exon 1 to exon 10) and flanking intron–exon boundaries were amplified using polymerase chain reaction (PCR) with a set of 12 pairs of primers (exon 1: ex1.1f 5′CGG CCC CTC TTA TTT GAG CT3′ and ex1.1r 5′AAC GAC CCG TAA GCC GAA G3′; ex1.2f 5′TCC ACG TGT GTC CCG GA3′ and ex1.2r 5′GAA AAG TGG ACA GTG AAG GCG3′; ex1.3f 5′CGC CTC ACT CCT TCA GGC TCC TA3′ and ex1.3r 5′TGC GAA CAG TCA GGC TCC TA3′; exon 2: ex2f 5′CGA GAG CAC CGC TGA CAC T3′ and ex2r 5′CTT TGC CTA ATT TGC TGT GGG3′; exon 3: ex3f 5′CAC TCG CTC AGC TGT CTT CG3′ and ex3r 5′AAC ATA AGA ACA ACT CAG AGA CCA GG3′; exon 4: ex4f 5′TGT ATG AAG TGT ATA ACT GTG CAG CAG AGA TC3′ and ex4r 5′CCA GAT AGA AAC AAC CCA CAT TTA TG3′; exon 5: ex5f 5′AAG CTC TTT GCA GCC TCC G3′ and ex5r 5′GGG CAT GTT GAT GAG AAA TGC3′; exon 6: ex6f 5′TCT AAA GTG GCC CCA TGG AG3′ and ex6r 5′CCG CCT TAT CAG ACC CAG G3′; exon 7: ex7f 5′ACA TGT GGC TTA AAG CCT CCC3′ and ex7r 5′TGA GAG CCT GGA AAA GGA GC3′; exon 8: ex8f 5′CAG CGA AGT GCC TTA GGC ATT3′ and ex8r 5′ACG CTA CAA ATT GGA TTC CGC3′; exon 9: ex9f 5′CTC TGT GGT TAA GGA ATG GTT G3′ and ex9r 5′AAC TTT TAC ACT AGT CTT TTC CAA TCC C3′; exon 10: ex10f 5′CCC AAG AGG TGC TGC TGT TT3′ and ex10r 5′AGG GCA GAG ACC AAC TCT TCC3′). All amplified regions were sequenced on both strands by means of automatic fluorescent sequencing, using the sequencing kit (Bigdye Terminator) on an ABI sequencer (3100 Genetic Analyzer). Three randomly selected parallel tissue samples from non-DDS patients were used as control.

Results

Analyses of glomerular cell proliferation

The clinical and pathological features of the DDS patient are summarized in Table 1. In the DDS kidneys, focal glomeruli show typical glomerular lesions composed of sclerotic mesangial masses surrounded by a corona of epithelial cells (Fig. 1f). The epithelial corona is strongly positive for cytokeratin (Fig. 2f) but negative for vimentin (Fig. 2i). The cytokeratin is normally expressed in the tubular epithelial cells and, segmentally, in glomerular parietal epithelial cells (Fig. 2d). The rest of the glomeruli in the DDS kidneys show complex morphological changes (Fig. 1a), ranging from normal-appearing glomeruli (Fig. 1b) to gigantic proliferative (Fig. 1d) or sclerosed shrunken glomerular lesions (Fig. 1g). Intermediate spectrum of extracapillary proliferation is observed in glomeruli with or without mesangial sclerosis (Fig. 1c, e). It is worth noting that many shedding podocytes, which are strongly labeled by vimentin stain, are scattered in Bowman's space of glomeruli with mesangial sclerosis and in tubular lumens (Fig. 2i and insert). In contrast to DDS kidneys, the non-DDS kidneys, whether harboring Wilms' tumor (Fig. 1h) or not (Fig. 1i), show normal glomerular size without glomerular cell proliferation. Glomerular cell proliferation is demonstrated by the expression of nuclear proliferating antigens, including PCNA, Ki67 and topoisomerase IIα (TopIIα) (Fig. 3). The proliferative podocytes, which are characterized by negativity for actin (Fig. 2b) and cytokeratin (Fig. 2e) and positivity for vimentin (Fig. 2h), constantly express all proliferating antigens in hypertrophic or crescentic glomeruli in DDS kidneys (Fig. 3a, b, c, d, e, f). In contrast, endocapillary cells, which are specifically labeled by smooth-muscle actin (Fig. 2a, b, c), show little proliferative activity (Fig. 3a, b, c, d, e, f). Focal proliferation of endocapillary cells is observed only in glomeruli with advanced glomerulosclerosis (Fig. 3d, f). The assessments of cell-cycle regulatory proteins show no cyclin-A expression in either DDS or non-DDS kidneys (Fig. 4a, b). The positive cyclin-A expression in blastema cells of concurrent Wilms' tumors serves as an internal control of cyclin-A staining (Fig. 4c). The non-DDS kidneys show

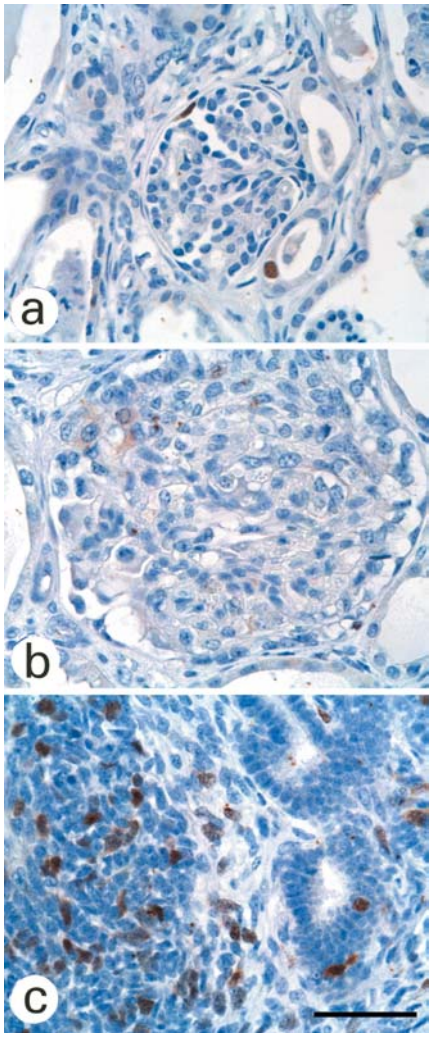


Fig. 4 Immunohistochemical staining patterns of cyclin A in glomerulus in non-Denys–Drash syndrome (DDS) kidney (**a**) and in DDS kidney (**b**). Positive control of cyclin-A expression in concurrent Wilms' tumor (**c**). Peroxidase–antiperoxidase stain, *scale bar* 50 μm

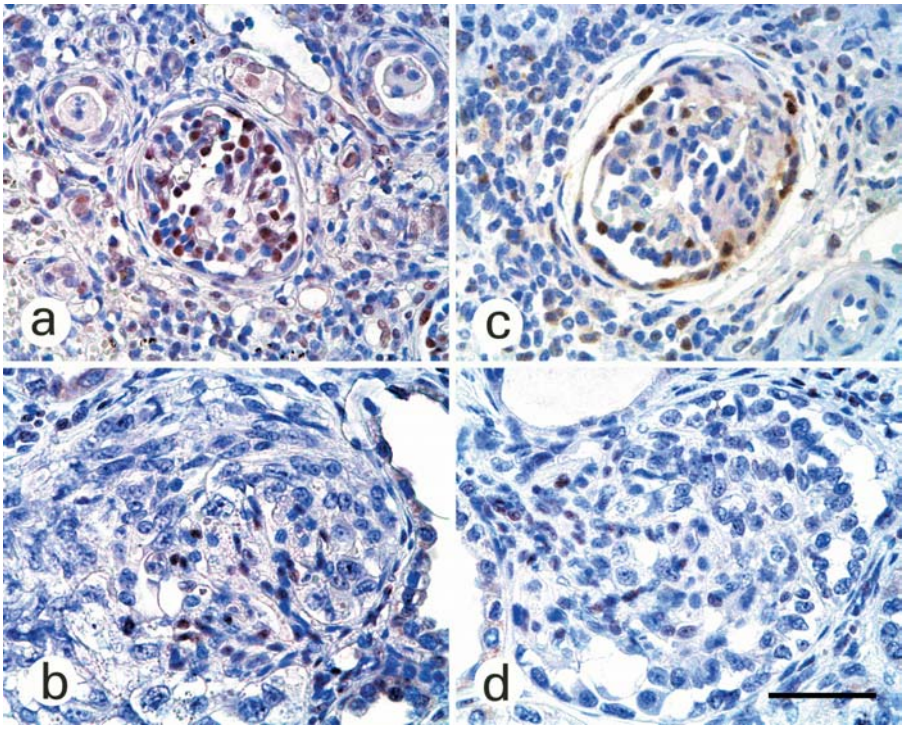


Fig. 5 Immunohistochemical staining patterns of p16 (**a**, **b**) and p21 (**c**, **d**) in glomeruli in non-Denys–Drash syndrome (DDS) kidney (**a**, **c**) and in DDS kidney (**b**, **d**). Peroxidase–anti-peroxidase stain, *scale bar* 50 μm

extensive expression of cyclin kinase inhibitor p16 in podocytes (Fig. 5a), while DDS kidneys show loss of p16 expression in these cells (Fig. 5b). There is only mild and scattered expression of p16 in glomerular endocapillary regions of DDS kidneys (Fig. 5b). The expression of p21 (Fig. 5d) is similar to that of p16 in DDS kidneys (Fig. 5b). However, p21 expression pattern in non-DDS kidneys (Fig. 5c) differs slightly from that of p16 (Fig. 5a) in a lower labeling rate of podocytes and a higher labeling rate in parietal epithelial cells.

Assessment of WT1 expression in glomerular cells

The non-DDS kidneys constantly show diffuse global expression of WT1 on the nuclei of podocytes (Fig. 6a). The WT1 expression in the non-proliferative or mild proliferative hypertrophic glomeruli in the DDS kidneys is similar to that of non-DDS kidneys in terms of its distribution and intensity (Fig. 6b). However, the labeling intensity of WT1 gradually decreases as podocytes proliferate (Fig. 6c). WT1 expression diminishes sharply in those glomeruli with advanced extracapillary proliferation (Fig. 6d). In glomeruli with typical mesangial sclerosis, no cell of epithelial corona expresses WT1 (Fig. 6e). The glomerular endocapillary cells are constantly negative for WT1 in both DDS and non-DDS kidneys.

Analysis of apoptosis in glomerular cells

The patterns of Fas ligand (Fas-L), Bax and Bcl-2 expression in the glomerular cells of the DDS kidneys and the non-DDS kidneys are depicted in Fig. 7. In the non-DDS kidneys, they are essentially absent from the cells of glomerular tufts (Fig. 7a, c, e), except for the low level of Bcl-2 expression in some glomerular parietal epithelial cells and tubular epithelial cells (Fig. 7c). Focal tubular epithelial cells also express Bax in the non-DDS kidneys (Fig. 7e). There is considerable increase of Bax (Fig. 7b) and Fas-L (Fig. 7f) expression in those glomeruli with advanced mesangial sclerosis in the DDS kidneys. The glomerular cells of both DDS and non-DDS kidneys do not express Bcl-2, except for the glomerular parietal epithelial cells (Fig. 7c, d).

The assessment of apoptosis using TUNEL assay reveals scattered labeling of the cells in the glomeruli that have advanced mesangial sclerosis in the DDS kidneys (Fig. 7h), whereas TUNEL-positive cells are not detected in the glomerular cells of the non-DDS kidneys (Fig. 7g). The cell origin of apoptotic cells is not readily discernible. They might be either residual podocytes or endocapillary cells. We did not observe apoptotic cells in the proliferating glomerular epithelial cells of the DDS kidneys.

Mutation analysis of WT-1

The DNA sequences of WT1 exons and exon–intron boundaries were derived from non-tumor kidney tissue of the DDS patient and the control specimens. We failed to amplify DNA of WT-1 exon 2 from the DDS patient, despite the fact that the primer set worked well on control specimens. Sequence analysis did not reveal any mutation in these DNA fragments (sequencing data not shown).

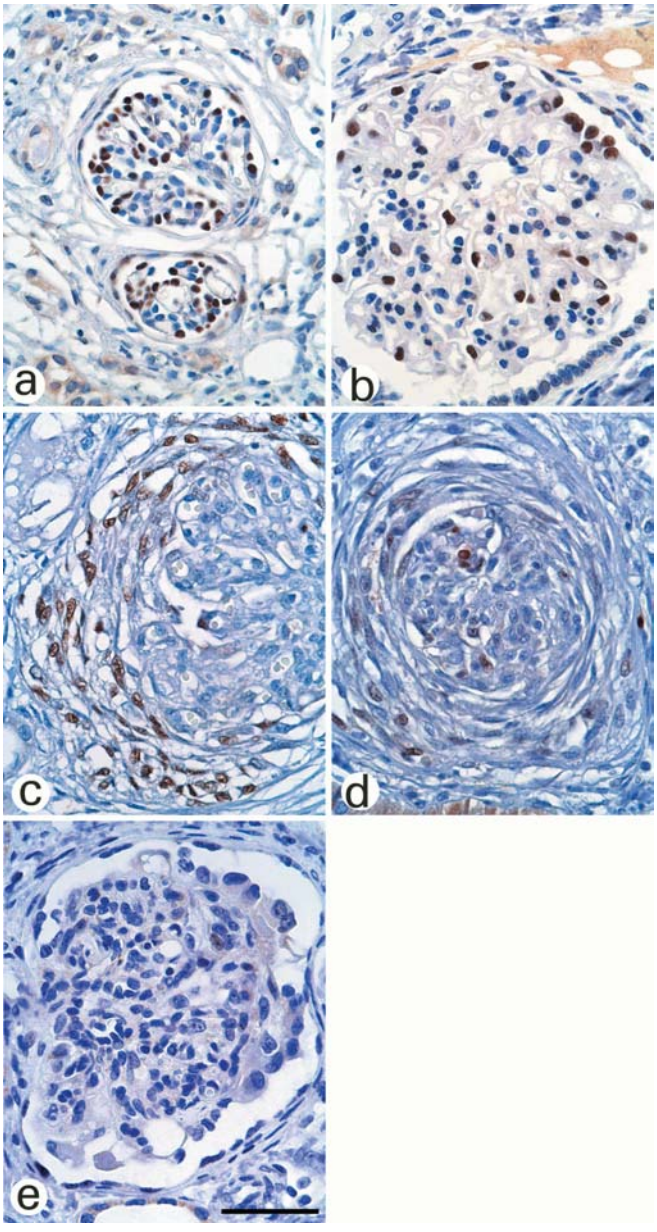


Fig. 6 Immunohistochemical staining patterns of WT1 in glomerulus in non-Denys–Drash syndrome (DDS) kidney (**a**) and in glomeruli in DDS kidney (**b**–**e**). Peroxidase–antiperoxidase stain, *scale bar* 50 μm

Neither was there mutation in the 3′ alternative splice donor site in intron 9. There was a 915C→T (Pro→Pro) polymorphism in WT-1 exon 1 of the DDS patient.

Discussion

The WT1 expression in glomerulopathy of DDS and IDMS kidney have been reported recently by Yang et al. [33]. They demonstrated marked decrease in WT1 nuclear staining of podocytes in glomeruli that looks to have typical mesangial sclerosis [33]. The low nuclear concentration of WT1 in glomerular cells was attributed to the dominant-negative effects of mutated protein. In our study, we also observed the diminishing of WT1 in the glomerulopathy of a DDS patient. In addition, we noticed that the degree of the loss of WT1 nuclear labeling intensity was in reverse to the degree of proliferative activity of podocytes, and once glomeruli progressed to advanced glomerulosclerosis, nearly all WT1 reactivity in glomerular epithelial cells disappeared. The complete loss of WT-1 protein in DDS glomeruli with typical mesangial sclerosis might reflect the complete loss (shedding) of podocytes in these glomeruli. We speculate that the initial nuclear concentrating or binding capability of wild-type WT1 protein is not hampered because the non-proliferative glomeruli in both DDS and non-DDS kidneys have similar WT1 staining intensity. However, *wt1* mutation is proposed to act in a dominant-negative manner, and a minor amount of mutant WT1 can have devastating effects [24]. Yet, it has been speculated that the loss of WT1 function in the DDS kidney might not be directly related to the effect of mutant WT1, since it has been reported that DNA binding by wild-type WT1 protein is not inhibited by an excess of mutant WT1 protein [26, 27]. This observation implies that, in addition to the alteration of DNA-binding zinc finger domain or the pertubation of WT1 isoform balance, other detrimental genetic effects might be responsible for the DDS phenotypical expression. This speculation is also supported by the fact that identical glomerulopathy can present in patients of IDMS without the evidence of mutation in all coding sequences of WT1 gene [11, 33]. In this report, we also demonstrated a DDS patient who had characteristic phenotypical manifestations of DDS but had neither Denys–Drash nor Frasier-type mutation in the *wt1* gene.

Mature podocytes are constantly positive for vimentin and WT1 but negative for cytokeratin and smooth-muscle actin [10, 21]. The total loss of vimentin/WT1-positive extracapillary cells on glomerular tufts implies the elimination of podocytes in advanced DDS glomerulopathy. The observation of free-floating vimentin-positive cells in Bowman's space and tubular lumens further suggests that shedding of podocytes from basement membrane might account, at least partly, for the loss of podocytes from DDS glomeruli. The wrapping of conglomerated glomerular tufts by cytokeratin-positive epithelial cells forms the "corona" of DMS and implicates the ingrowth of parietal or tubular epithelial cells to glomerular tufts. Whether apoptosis is responsible for the elimination of podocytes in our case of DDS remains to be determined, since we did not observe large-scale apoptosis in the glomeruli that had visceral epithelial proliferation (pictures not shown). However, several lines of evidence show that apoptosis of glomerular cells is indeed temporally and spatially related to the WT1 expression [14, 15]. Furthermore, our studies revealed some clues implicating apoptotic regulation in DDS glomerulopathy. The expression of apoptotic regulatory factors in DDS glomerulopathy depicts an apoptosis-permissive profile with increased Fas-L/Bax expression in lack of Bcl-2 activity. Both Bax, a pro-apoptotic factor, and Bcl-2, an

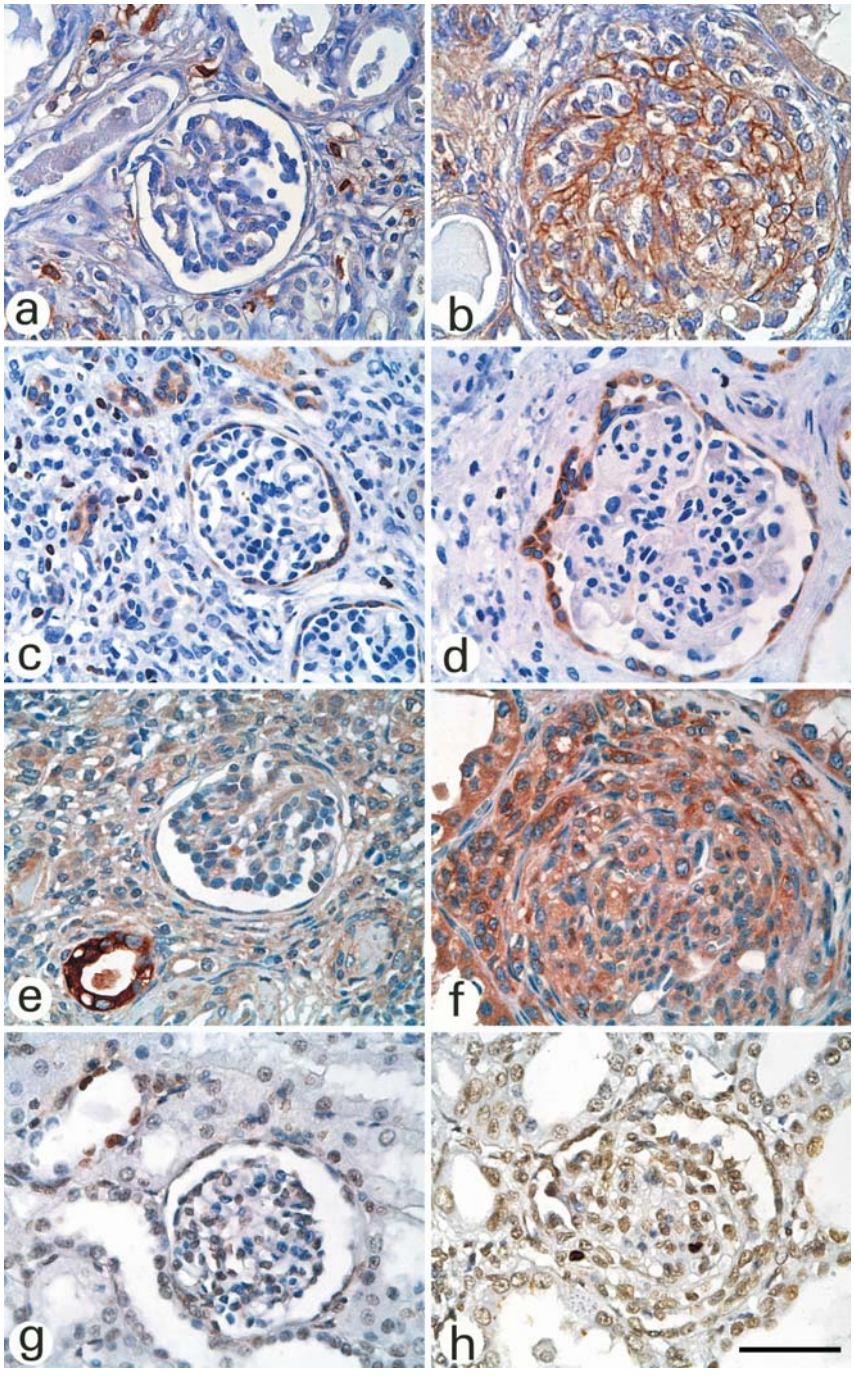


Fig. 7 Immunohistochemical staining patterns of Fas-L (**a**, **b**), Bcl-2 (**c**, **d**) and Bax (**e**, **f**) in glomeruli in non-Denys–Drash syndrome (DDS) kidney (**a**, **c**, **e**) and in DDS kidney (**b**, **d**, **f**). Peroxidase–antiperoxidase (PAP) stain, transferase-mediated dUTP nick end-labeling assay of apoptosis in glomerulus in non-DDS kidney (**g**) and in DDS glomerulus (**h**). PAP stain, *scale bar* 50 μm

anti-apoptotic factor, are normally absent in the podocytes of mature glomeruli [9, 13, 31]. It has been reported that Bcl-2 is a potential target of WT1 repression and spatially and temporally reverse to the WT1 expression during podocyte differentiation in the developing kidney [3, 7, 20]. However, the lack of this reciprocal correlation in DDS glomerulopathy implicates that proliferative podocytes are resistant to the induction of Bcl-2 expression and permissive for apoptosis. Since our study detected apoptotic cells only in advanced glomerulopathy of DDS, apoptosis should play a pathogenic role in advanced mesangial sclerosis and is probably initiated through Fas–L/Fas interaction in an autocrine fashion between mesangial cells or other endocapillary cells [9].

The demonstration of exaggerated podocyte proliferation in DDS glomerulopathy would address several key questions: (1) is it a common pathway to all causes of severe glomerular injury? (2) if the podocyte proliferation is a default process of DDS glomerulopathy, how does it link to WT1 mutation? The postnatal reentry of podocytes to cell cycle is definitely a pathological process, since in normal ontogenesis of human glomeruli, only immature podocytes at S-shape bodies are positive for proliferation markers Ki67 and PCNA [1, 23]. Podocytes rapidly be-

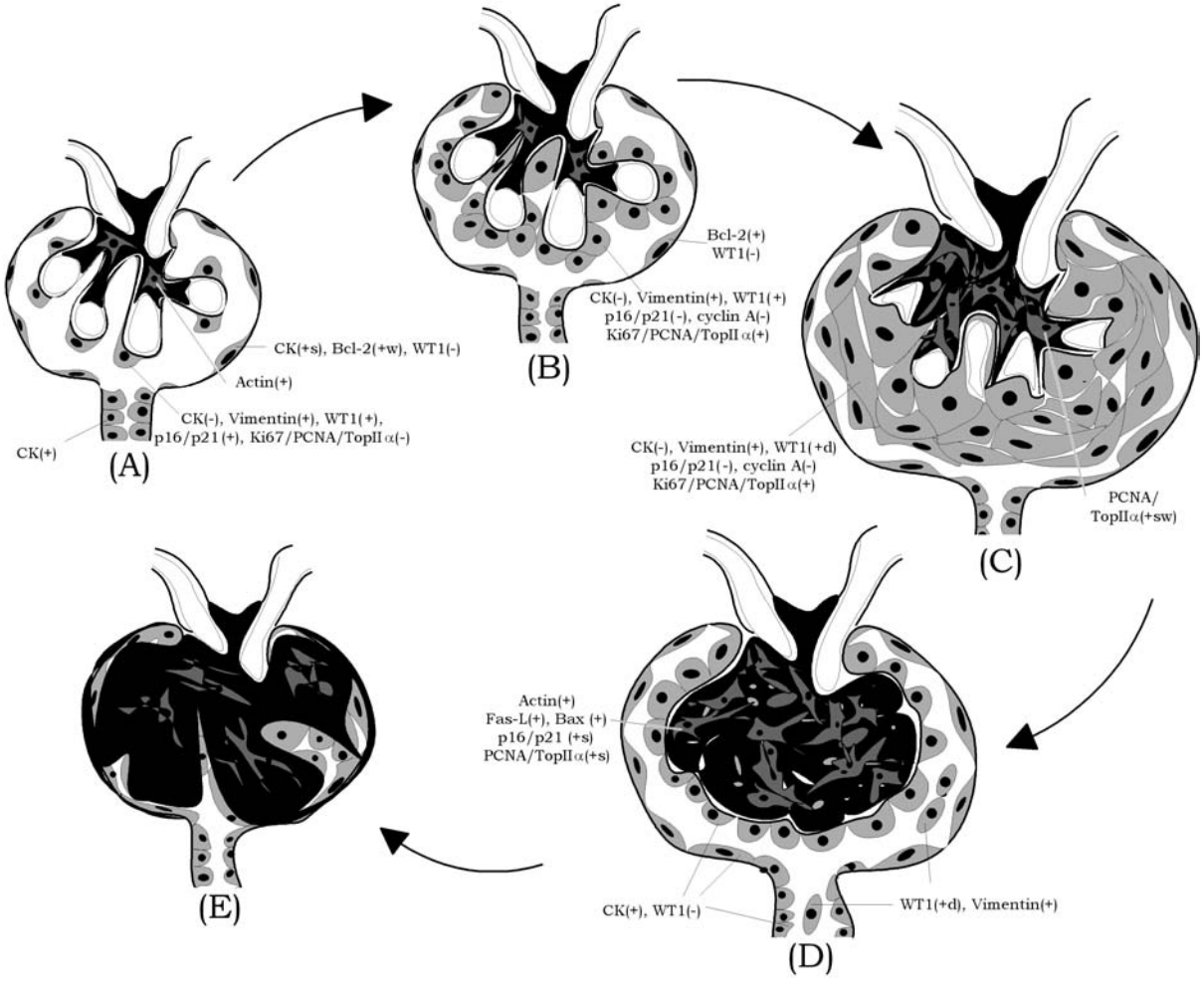


Fig. 8 Schematic representation of morphological and immunohistochemical evolving process of Denys–Drash syndrome glomerulopathy: normal glomerulus (**A**); hypertrophy of glomerulus with initial hyperplasia of podocytes (**B**); crescentic hyperplasia of podocytes and expansion of mesangium (**C**); mesangial sclerosis with tubulization of Bowman's spaces and shedding of visceral epithelial cells (**D**); global glomerulosclerosis (**E**). The following marks in parentheses indicate staining patterns: *(+)* positive, *(+s)* segmentally positive, *(+w)* weakly positive, *(+sw)* segmentally and weakly positive, *(+d)* positive but decrease in reactivity, *(−)* negative

come quiescent after the capillary-loop stage with loss of proliferation markers [23, 29]. In the present study, the podocytes in DDS glomerulopathy, regardless of proliferative or non-proliferative glomeruli, switched their cell-cycle machinery on and diffusely expressed proliferating markers, including Ki67, PCNA and topoisomerase IIα. This unique phenomenon of DDS glomerulopathy indicates that podocyte proliferation in DDS glomerulopathy is a genetic default process rather than a final result of a common pathway of non-specific glomerular injury, in which cell proliferation markers are segmentally expressed in crescentic or cellular glomerular lesions but not in mature, non-proliferating podocytes [1]. Our results also suggest that podocyte proliferation in DDS glomerulopathy may be mediated through the downregulation of both p16 and p21, which belong to the INK4 and Cip/Kip family of cyclin kinase inhibitors, respectively, and function mainly in the G1 or G1/S phase through interactions with the cyclin D-CDK complex [8, 28]. It has been reported that WT1 is able to induce p21 and is associated with G1-phase arrest and WT1-dependent differentiation pathways in the kidney [5, 21]. In experimental glomerulonephritis, the reentry of podocytes into the cell cycle is associated with the loss of WT1 and p21 expression [12]. Our results, as well as those mentioned previously, indicate the existence of an intimate relationship between WT1 and cell-cycle regulation [5, 6, 12, 32, 33]. Finally, our results also indicate that proliferation of podocytes in DDS glomerulopathy does not exactly recapture the podocyte proliferation during glomerular ontogenesis, since there is no upregulation of cyclin A [23, 29, 30].

In conclusion, the normal development and growth of glomeruli are the results of tightly controlled proliferation, differentiation and apoptosis of glomerular cells. Based on our observations, a morphological and immunohistochemical evolving process of DDS glomerulopathy is proposed (Fig. 8).

Acknowledgements The present study was supported by Taipei Veterans General Hospital, under research grant no. VGH-89-140 and also by the National Science Council, ROC, under grant no. NSC 89–2320-B-075–034.

References

1. Barisoni L, Kriz W, Mundel P, D'Agati V (1999) The dysregulated podocyte phenotype: a novel concept in the pathogenesis of collapsing idiopathic focal segmental glomerulosclerosis and HIV-associated nephropathy. J Am Soc Nephrol 10:51–61
2. Borel F, Barilla KC, Hamilton TB, Iskandar M, Romaniuk PJ (1996) Effects of Denys–Drash syndrome point mutations on the DNA binding activity of the Wilms' tumor suppressor protein WT1. Biochemistry 35:12070–12076
3. Chandler D, el-Naggar AK, Brisbay S, Redline RW, McDonnell TJ (1994) Apoptosis and expression of the bcl-2 protooncogene in the fetal and adult human kidney: evidence for the contribution of bcl-2 expression to renal carcinogenesis. Hum Pathol 25:789–796
4. Dressler GR, Douglass EC (1992) Pax-2 is a DNA-binding protein expressed in embryonic kidney and Wilms tumor. Proc Natl Acad Sci U S A 89:1179–1183
5. Englert C, Maheswaran S, Garvin AJ, Kreidberg J, Haber DA (1997) Induction of p21 by the Wilms' tumor suppressor gene WT1. Cancer Res 57:1429–1434
6. Grotendorst GR, Okochi H, Hayashi N (1996) A novel transforming growth factor beta response element controls the expression of the connective tissue growth factor gene. Cell Growth Differ 7:469–480
7. Grubb GR, Yun K, Williams BR, Eccles MR, Reeve AE (1994) Expression of WT1 protein in fetal kidneys and Wilms tumors. Lab Invest 71:472–479
8. Gu Y, Turck CW, Morgan DO (1993) Inhibition of CDK2 activity in vivo by an associated 20 K regulatory subunit. Nature 366:707–710
9. Hattori T, Shindo S, Kawamura H (1998) Apoptosis and expression of Bax protein and Fas antigen in glomeruli of a remnant-kidney model. Nephron 79:186–191
10. Holthofer H, Miettinen A, Lehto VP, Lehtonen E, Virtanen I (1984) Expression of vimentin and cytokeratin types of intermediate filament proteins in developing and adult human kidneys. Lab Invest 50:552–559
11. Jeanpierre C, Denamur E, Henry I, Cabanis MO, Luce S, Cecille A, Elion J, Peuchmaur M, Loirat C, Niaudet P, Gubler MC, Junien C (1998) Identification of constitutional WT1 mutations, in patients with isolated diffuse mesangial sclerosis, and analysis of genotype/phenotype correlations by use of a computerized mutation database. Am J Hum Genet 62:824–833
12. Kim YG, Alpers CE, Brugarolas J, Johnson RJ, Couser WG, Shankland SJ (1999) The cyclin kinase inhibitor p21CIP1/WAF1 limits glomerular epithelial cell proliferation in experimental glomerulonephritis. Kidney Int 55:2349–2361
13. Krajewski S, Krajewska M, Shabaik A, Miyashita T, Wang HG, Reed JC (1994) Immunohistochemical determination of in vivo distribution of Bax, a dominant inhibitor of Bcl-2. Am J Pathol 145:1323–1336
14. Kreidberg JA, Sariola H, Loring JM, Maeda M, Pelletier J, Housman D, Jaenisch R (1993) WT1 is required for early kidney development. Cell 74:679–691
15. Lipschutz JH (1998) Molecular development of the kidney: a review of the results of gene disruption studies. Am J Kidney Dis 31:383–397
16. Little M, Wells C (1997) A clinical overview of WT1 gene mutations. Hum Mutation 9:209–225
17. Little MH, Williamson KA, Mannens M, Kelsey A, Gosden C, Hastie ND, van Heyningen V (1993) Evidence that WT1 mutations in Denys–Drash syndrome patients may act in a dominant-negative fashion. Hum Mol Genet 2:259–264
18. Martinerie C, Chevalier G, Rauscher FJ 3rd, Perbal B (1996) Regulation of nov by WT1: a potential role for nov in nephrogenesis. Oncogene 12:1479–1492
19. Mueller RF (1994) The Denys–Drash syndrome. J Med Genet 31:471–477
20. Mugrauer G, Ekblom P (1991) Contrasting expression patterns of three members of the myc family of protooncogenes in the developing and adult mouse kidney. J Cell Biol 112:13–25
21. Mundel P, Reiser J, Kriz W (1997) Induction of differentiation in cultured rat and human podocytes. J Am Soc Nephrol 8:697–705
22. Mundlos S, Pelletier J, Darveau A, Bachmann M, Winterpacht A, Zabel B (1993) Nuclear localization of the protein encoded by the Wilms' tumor gene WT1 in embryonic and adult tissues. Development 119:1329–1341
23. Nagata M, Nakayama K, Terada Y, Hoshi S, Watanabe T (1998) Cell cycle regulation and differentiation in the human podocyte lineage. Am J Pathol 153:1511–1520
24. Patek CE, Little MH, Fleming S, Miles C, Charlieu JP, Clarke AR, Miyagawa K, Christie S, Doig J, Harrison DJ, Porteous DJ, Brookes AJ, Hooper ML, Hastie ND (1999) A zinc finger truncation of murine WT1 results in the characteristic urogenital abnormalities of Denys–Drash syndrome. Proc Natl Acad Sci U S A 16:2931–2936
25. Ryan G, Steele-Perkins V, Morris JF, Rauscher FJ 3rd, Dressler GR (1995) Repression of Pax-2 by WT1 during normal kidney development. Development 121:867–875
26. Scharnhorst V, Dekker P, van der Eb AJ, Jochemsen AG (1999) Internal translation initiation generates novel WT1 protein isoforms with distinct biological properties. J Biol Chem 274:23456–23462
27. Scharnhorst V, van der Eb AJ, Jochemsen AG (2001) WT1 proteins: functions in growth and differentiation. Gene 8:141–161
28. Serrano M, Hannon GJ, Beach D (1993) A new regulatory motif in cell-cycle control causing specific inhibition of cyclin D/CDK4. Nature 366:704–707
29. Shankland SJ, Al'Douahji M (1999) Cell cycle regulatory proteins in glomerular disease. Exp Nephrol 7:207–211
30. Shankland SJ, Floege J, Thomas SE, Nangaku M, Hugo C, Pippin J, Henne K, Hockenberry DM, Johnson RJ, Couser WG (1997) Cyclin kinase inhibitors are increased during experimental membranous nephropathy: potential role in limiting glomerular epithelial cell proliferation in vivo. Kidney Int 52:404–413
31. Takemura T, Murakami K, Miyazato H, Yagi K, Yoshioka K (1995) Expression of Fas antigen and Bcl-2 in human glomerulonephritis. Kidney Int 48:1886–1892
32. Yang AH, Chen JY, Lin YP, Huang TP, Wu CW (1977) Peritoneal dialysis solution induces apoptosis of mesothelial cells. Kidney Int 51:1280–1288
33. Yang Y, Jeanpierre C, Dressler GR, Lacoste M, Niaudet P, Gubler MC (1999) WT1 and PAX-2 podocyte expression in Denys–Drash syndrome and isolated diffuse mesangial sclerosis. Am J Pathol 154:181–192

Virchows Arch (2004) 445:315–319
DOI 10.1007/s00428-004-1066-5

CASE REPORT

T. Hansen · A. Gaumann · M. Ghalibafian · A. Höferlin · A. Heintz · C. J. Kirkpatrick

Haemangiopericytoma of the thyroid gland in combination with Hashimoto's disease

Received: 30 March 2004 / Accepted: 29 May 2004 / Published online: 9 July 2004
© Springer-Verlag 2004

Abstract We present a hitherto unique case of haemangiopericytoma (HP) of the thyroid gland in a 15-year-old female patient suffering from Hashimoto's disease for several months. Since angiogenesis has been discussed to play a major role in both diseases, we examined the expression of vascular endothelial growth factor (VEGF), VEGF receptors (VEGFRs) and platelet-derived growth factor receptors (PDGFRs). Most interestingly, strong expression of PDGFR α and β was found in spindle-shaped tumour cells and tumour vessels in HP, while VEGF and VEGFR type I and -II were negative in these regions. In contrast, VEGF was expressed in the lymphoid infiltrate of Hashimoto's disease. Since PDGFR-β is commonly expressed in pericytes, we suggest that the strong expression discovered in this study further supports the view that HP is derived from pericytes. The combination of HP and Hashimoto's disease is most probably a coincidental event. However, this case confirms previous reports demonstrating that in patients with Hashimoto's disease different neoplasias can occur.

Keywords Haemangiopericytoma · Hashimoto's disease · Pericyte · PDGF receptor · VEGF receptor

T. Hansen (✉) · M. Ghalibafian · C. J. Kirkpatrick
Institute of Pathology,
Johannes Gutenberg, University of Mainz,
Langenbeckstrasse 1, 55101 Mainz, Germany
e-mail: hansen@pathologie.klinik.uni-mainz.de
Tel.: +49-6131-177306
Fax: +49-6131-17477306

A. Gaumann
Institute of Pathology,
University of Regensburg,
Germany

A. Höferlin · A. Heintz
Department of Surgery,
St. Hildegardis Hospital,
Mainz, Germany

Introduction

Haemangiopericytoma (HP) is a mesenchymal neoplasm accounting for a minority of all vascular tumours. It mostly arises in the lower extremities and the retroperitoneum, while the head and neck area is the third most common site. In this localisation, HP mainly occurs in the soft tissues of the neck and mouth (Brandwein et al. 2001; Weiss and Goldblum 2001). In the thyroid gland, HP is exceedingly rare. So far, only eight reported cases exist (Table 2).

According to the recently published World Health Organization (WHO) classification of tumours of soft tissue and bone (2002), HP represents a group of lesions that closely resemble cellular areas of solitary fibrous tumour. The term haemangiopericytoma has been used to encompass a variety of tumours, which have in common the presence of a thin-walled branching vascular pattern. Histologically, the tumour is generally composed of tightly packed fusiform cells, which are arranged around medium-sized vessels. The vessels form a ramifying network with a prominent staghorn-like configuration. Pericytic origin has been suggested for the fusiform cells. Immunohistochemically, HP is characterised by strong positivity for vimentin and, to a lesser degree, for CD34 (Weis and Goldblum 2001). Furthermore, it has been demonstrated that tumour cells express bcl-2 (Miettinen et al. 1998), and partially factor XIIIa and HLA-DR (Nemes 1992). Current concepts concerning aetiology and pathogenesis of HP are based on the studies of Stout and Murray (1942), who suggested that the tumour develops from the pericytes surrounding small vessels. It has also been considered that angiogenetic factors could be of special importance for the pathogenesis of HP (Hatva et al. 1996; Dietzmann et al. 1997). We report on a hitherto unique case of a HP of the thyroid gland in combination with Hashimoto's disease. By examination of several angiogenetic factors, such as vascular endothelial growth factor (VEGF), and receptors for VEGF and platelet-derived growth factor (VEGFRs and PDGFRs), special emphasis is placed on possible pathomechanisms of both disorders.

Clinical history

A 15-year-old female patient suffered from Hashimoto's disease for several months [initial laboratory findings: anti-thyroperoxidase 3900 U/ml (normal: <600 U/ml); thyroid stimulating hormone basal 6.92 μU/ml (normal: 0.35–5 μU/ml)]. Despite long-term medical treatment with 100 μg thyroxine, the patient complained of increasing dyspnea and inspiratory stridor. Physical examination revealed an underweight woman (body mass index: 17.9 kg/m^2) with a pulse of 132 beats per minute and blood pressure of 140/90 mmHg. Furthermore, clinical examinations showed an enlarged thyroid gland involving the retrosternal area. On the left side of the thyroid gland, several hard and painful nodes were palpable. Radiological evaluation revealed conspicuous compression of the trachea and of the oesophagus. Blood tests including thyroid parameters ranged within normal levels. It was decided to perform a total thyroidectomy of the left side and a near-total resection of the right side.

Materials and methods

Specimens were fixed in 4% phosphate-buffered saline (PBS)-buffered formaldehyde and routinely processed according to standard protocols. For histological examination, multiple samples were taken, routinely processed and paraffin embedded. Sections, 4 μm to 5 μm thick, were cut and stained with hematoxylin and eosin and Gomori methanamine silver. In addition, tissue specimens were examined by immunohistochemistry using the avidin-biotin-peroxidase complex method according to previous protocols (Konerding et al. 2001). After pretreatment (Table 1), the sections were incubated with goat serum (for poyclonal rabbit antibodies) or horse serum (for monoclonal antibodies) for 30 minutes, followed by a 1-h incubation of primary antibodies. The primary antibodies (shown in Table 1) were applied according to standard recommendations. For negative control, primary antibody was omitted. Subsequently, the secondary antibodies and the ABC-horseradish-peroxidase-complex were incubated according to manufacturer's protocol (Vector Laboratories, Burlingame, USA). Finally, the sections were treated with either 3,3′-diaminobenzidine tetrahydrochloride (DAB; Sigma, St. Louis, USA) or 3-amino-9-ethyl-carbazole substrate (AEC; Vector) rinsed for 10 min in running tap water and counterstained with hematoxylin. In the case of immunohistochemistry with VEGF, VEGFRs and PDGFRs, tissue specimens of colon carcinoma or human umbilical cords served as positive controls.

Slides were examined under a Leica microscope (type Dialux, Leica Microsystems, Bensheim, Germany) and digitalised with a Nicon camera (Düsseldorf, Germany). For immunohistochemical analysis, the extent of binding was estimated by counting the number of positive cells per five high power fields (HPF). Results were classified as follows: – no expression, (+) less than 10% of cells positive, + more than 10% of cells positive, ++ more than 50% of cells positive.

Results

The surgical resection specimen of the left side of the thyroid contained several lesions measuring 5 cm at maximum, with a total weight of 18 g. On the cut surface, they appeared as grey-reddish masses, which were partially of nodular consistence. The near-total resection specimen of the right side contained a 10-g-weight part of the thyroid, measuring 3.5 cm at maximum, without any macroscopically suspicious areas.

Histological examination of both sides revealed thyroid follicles with infiltration and destruction by lymphocytes and plasma cells. Reactive lymphoid follicles were often present. The remaining thyroid epithelium exhibited extensive oncocytic change (Fig. 1). Furthermore, a mesenchymal tumour was found in the thyroid tissue of the left side. Histologically estimated, the tumour measured 4 cm at maximum. The tumour consisted of tightly packed fusiform or spindle-shaped cells (Fig. 1). Polymorphism of the nucleus as well as an increased mitotic rate (4–5 mitoses/10 HPF) was observed. These cells were arranged around a prominent vasculature, which formed a ramifying network, sometimes with a staghorn configuration. The vessels were lined by flat endothelial cells. The tumour was embedded in a dense stroma of intervening reticulin fibres (positive for Gomori's silver reaction). The results of the immunohistochemical evaluation are summarised in Table 1. The tumour cells displayed strong expression of CD34 (Fig. 2) and a moderate expression of vimentin. Cells were negative for desmin. The proliferation marker Ki-67 was only focally positive in up to 15% of the tumour cells. Taken together, HP of the left thyroid gland and Hashimoto's disease of both the right and left sides were diagnosed.

Most interestingly, VEGF was strongly expressed in the lymphoid follicles of the thyroid gland (Fig. 3); while, in the thyroid epithelium and in the tumour cells, staining was completely negative. VEGF staining mainly occurred in the cytoplasm of lymphocytes and endothelial cells. VEGFR-1 and -2 were found in numerous vessels of

Table 1 Results of immunostaining reactions. Suppliers of the antibodies (no. of the marker): Cymed, Berlin, Germany (7); Dako, Hamburg, Germany (3); Dianova, Hamburg, Germany (4); Immunotech, Marseille, France (1); Progen, Heidelberg, Germany (2); Santa Cruz Biotechnology, Grünberg, Germany (5, 6, 8, 9). *MW* microwave 600 W for 3×5 min, *T* trypsin 0.1% for 15 min

Marker			Haemangiopericytoma		Thyreoiditis	
Antibody		Pre-treatment	Endothelial cells	Tumor cells	Lymphoid infiltrate	Thyreocytes
1	CD34 [QBEND 10]	T	++	++	–	–
2	Vimentin [VIM 3B4]	T	++	++	–	–
3	Desmin [D33]	None	–	–	–	–
4	Ki-67 [MIB-1]	MW	–	(+)	(+)	(+)
5	PDGFR-α	MW	++	++	(+)	+
6	PDGFR-β	MW	++	++	(+)	+
7	VEGF	MW	++	-	++	(+)
8	VEGFR-1	MW	++	-	(+)	(+)
9	VEGFR-2	MW	++	-	(+)	(+)

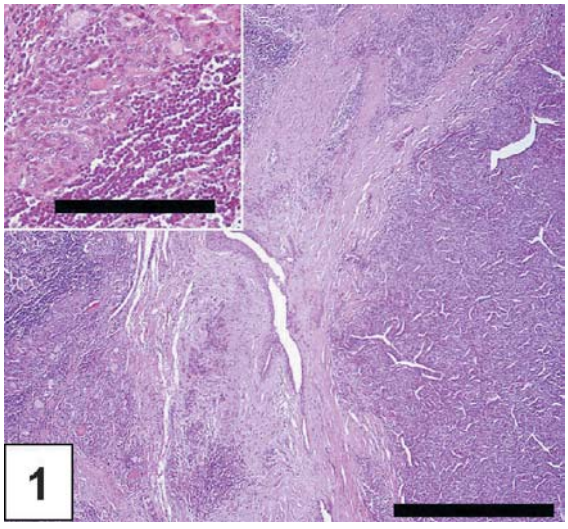


Fig. 1 Histological overview shows lymphoid follicles on the *left side* with oncocytic metaplasia of the follicles surrounded by numerous lymphocytes. On the *right side* mesenchymal tumour (*inset* oncocytic metaplasia of the follicles *Scale bar*—overview 1250 μm; *inset* 100 μm)

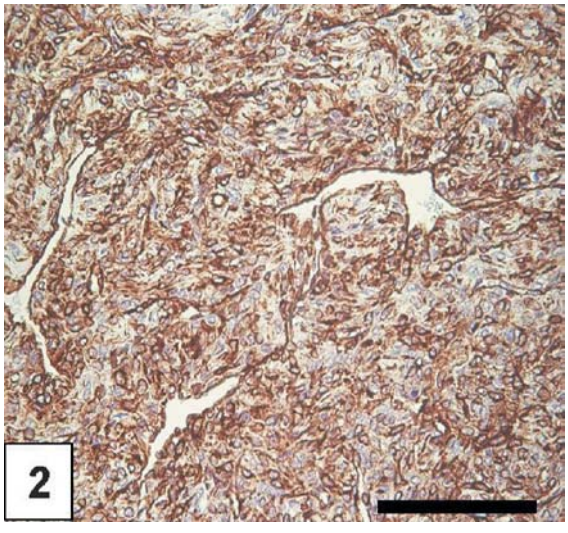


Fig. 2 Strong expression of CD34 in the tumour cells (*brown* ABC/DAB technique, *scale bar* 50 μm)

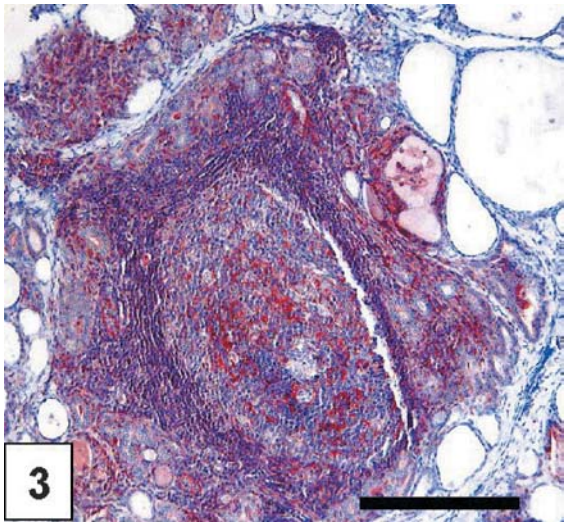


Fig. 3 Strong expression of vascular endothelial growth factor (*red*) in lymphocytes surrounding follicles (ABC/AEC method; *scale bar* 200 μm)

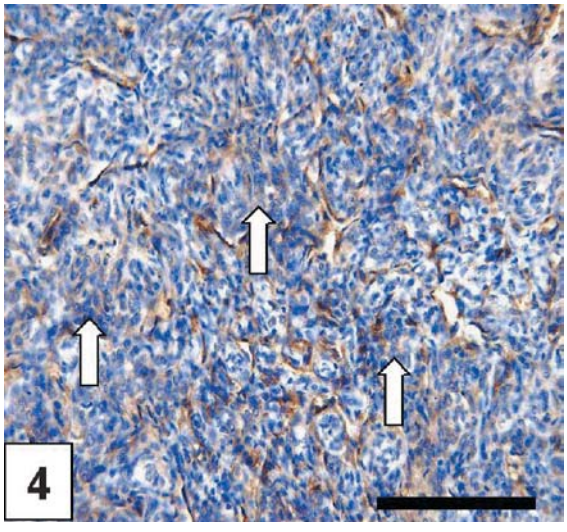


Fig. 4 Strong expression of platelet-derived growth factor receptor (PDGFR)-β (*brown*) in both ramifying vessels as well as spindle-shaped tumour cells of haemangiopericytoma (*arrows* ABC technique with DAB chromogen; *scale bar* 50 μm)

the thyroid gland as well as in a few cells of the lymphoid follicle. In HP, both receptors were detected only in the blood vessels at the tumour border. Conspicuously, PDGFR-α and -β were present in the majority of the tumour cells as well as in the tumour vessels (Fig. 4). Finally, both PDGFRs could be detected in thyroid epithelial cells as well as in some lymphocytes.

Discussion

HP is a rare mesenchymal tumour, which is composed of a ramifying network of medium-sized vessels and tightly packed spindle-shaped cells. In the head and neck area, HP occurs mainly in the cervical and oral soft tissue, while it is exceedingly rare in the thyroid gland (Brandwein et al. 2001; Weiss and Goldblum 2001). Our patient included, there are only nine reported cases of HP in the thyroid gland. The mean age of the patients is 45 years, with a female:male ratio of 3:1 (Table 2). This is the first report of a HP of the thyroid gland in combination with Hashimoto's disease. The clinical symptoms of HP are not characteristic, except for hypoglycaemia, which has been described mainly in retroperitoneal and pelvic localisation and is caused by production of insulin-like growth factor by the tumour (Weis and Goldblum 2001).

Table 2 Summary of the cases with haemangiopericytoma of the thyroid gland. *ND* no data, *Ø* no further disorder

References	Age	Sex	Further thyroid disorder
Prokš (1961) [18]	37	Female	Ø
Tano Assini et al. (1968) [21]	31	Female	ND
Kallenberg and Anagnostaki (1979) [14]	59	Male	Ø
Tytor and Olofsson (1986) [22]	79	Female	Ø
Justrabo et al. (1989) [13]	77	Female	Goiter
Geisinger et al. (1990) [9]	66	Female	ND
Dictor et al. (1992) [5]	5	Male	Ø
Cameselle-Teijero et al. (2003) [3]	36	Male	Goiter
Present case	15	Female	Hashimoto's disease

In the present case as well as in the previous reports of the thyroid gland, hypoglycaemia did not occur.

The pathogenesis of HP is poorly understood. Since the studies of Stout and Murray (1942), it has been suggested that the tumour is derived from pericytes. Pericytes are located within the basement membrane of the wall of microvessels. Pericytes express α-smooth muscle actin, desmin, and PDGFR-β (Hellström et al. 1999; Abramsson et al. 2003). PDGF-B and PDGFR-β play a critical role in the recruitment, proliferation and migration of pericytes. Cao et al. (2002) found positivity of this molecule in newly formed corneal blood vessels; however, they could not distinguish whether the receptor was localised on the endothelial cells or on the mural cells. In contrast, PDGF was demonstrated in HP, both in the vessels and the spindle-shaped cells (Dietzmann et al. 1997). Therefore, we investigated the expression of both PDGFR-α and -β in tissue specimens of the presented HP case. Most interestingly, we found a strong expression of both markers in the spindle-shaped tumour cells as well as in the vessels, suggesting that these cells produce significant amounts of these proteins. So far, expression of PDGFR-α in pericytes has not been described.

In addition, we found strong expression of VEGF in the lymphoid follicles of the inflammatory infiltrate, while in thyroid epithelium no staining could be detected. Interestingly, it has been demonstrated that serum levels of VEGF are significantly increased in patients with Hashimoto's disease compared with normal subjects (Iitaka et al. 1998). Previous studies showed that several different cell populations occurring in the lymphoid follicle such as endothelial cells and precursors of B-lymphocytes are able to produce VEGF (Foss et al. 1997; El-Obeid et al. 2004). Thus, it should be further investigated which subgroup of lymphocytes is involved in the synthesis of VEGF in Hashimoto's disease.

Numerous authors described patients with Hashimoto's disease in combination with several neoplasias, mainly presented as case reports. Moreover, several studies have revealed evidence for association between Hashimoto's disease and papillary or follicular thyroid cancer as well as between Hashimoto's disease and C-cell hyperplasia or medullary carcinoma (Segal et al. 1985; Guyetant et al. 1994; Unger et al. 2003). However, as mentioned above, combination of HP and Hashimoto's disease has not yet been reported. From our results, we suggest that the combination of these two disorders most probably is coincidental. However, this case report underlines that in patients with Hashimoto's disease many different disorders can occur, which may not be found by clinical examination, but by histological evaluation.

In summary, we have presented a hitherto unique case of a HP of the thyroid gland in combination with Hashimoto's disease. Most interestingly, we found strong expression of PDGFR-β in tumour cells. As this protein is commonly expressed in pericytes, we suggest that this result supports the concept of a pericyte origin for HP. According to the new WHO classification for soft-tissue tumours (2002), further investigation should elucidate whether these findings can be used in order to characterise those HPs with "real" pericytic differentiation. Finally, we conclude that the combination of Hashimoto's disease with HP is most probably a coincidental event. However, Hashimoto's disease can be associated with neoplasias, which are clinically asymptomatic, but can be evaluated by means of microscopy.

References

Abramsson A, Lindblom P, Betsholtz C (2003) Endothelial and nonendothelial sources of PDGF-B regulate pericyte recruitment and influence vascular pattern formation in tumors. J Clin Invest 112:1142–1151

Brandwein MS, Kapadia SB, Gnepp DR (2001) Nonsquamous pathology of the larynx, hypopharynx, and trachea. In: Gnepp DR (ed) Diagnostic surgical pathology of the head and neck. Saunders, Philadelphia, pp 304–305

Cameselle-Teijero J, Lopes JM, Villanueva JP, Gil-Gil P, Sobrinho-Simoes M (2003) Lipomatous haemangiopericytoma (adipocytic variant of solitary fibrous tumour) of the thyroid. Histopathology 43:406–408

Cao R, Bråkenheim E, Li X, Pietras K, Widenfalk J, Östman A, Eriksson U, Cao Y (2002) Angiogenesis stimulated by PDGF-CC, a novel member in the PDGF family, involves activation of PDGFR-$\alpha\alpha$ and -$\alpha\beta$ receptors. FASEB J 16:1575–1583

Dietzmann K, von Bossanyi P, Warich-Kirches M, Kirches E, Synowitz HJ, Firsching R (1997) Immunohistochemical detection of vascular growth factors in angiomatous and atypical meningiomas, as well as hemangiopericytomas. Pathol Res Pract 193:503-510.

Dictor M, Elner A, Andersson T, Ferno M (1992) Myofibromatosis-like hemangiopericytoma metastasizing as differentiated vascular smooth-muscle and myosarcoma. Myopericytes as a subset of "myofibroblasts". Am J Surg Pathol 16:1239–1247

El-Obeid A, Sunnuqrut N, Hussain A, Al-Hussein K, Gutierrez MI, Bhatia K (2004) Immature B cell malignancies synthesize VEGF, VEGFR-1 (Flt-1) and VEGFR-2 (KDR). Leuk Res 28: 133–137

Fletcher DM, Unni K, Mertens F (eds) (2002) World Health Organization classification of tumours. Tumours of soft tissue and bone. IARC Press, Lyon

Foss HD, Araujo I, Demel G, Klotzbach H, Hummel M, Stein H (1997) Expression of vascular endothelial growth factor in lymphomas and Castleman's disease. J Pathol 183:44–50

Geisinger KR, Silverman JF, Cappellari JO, Dabbs DJ (1990) Fine-needle aspiration cytology of malignant hemangiopericytomas with ultrastructural and flow cytometric analyses. Arch Pathol Lab Med 114:705–710

Guyetant S, Wion-Barbot N, Rousselet MC, Franc B, Bigorgne JC, Saint-Andre JP (1994) C-cell hyperplasia associated with chronic thyroiditis: a retrospective quantitative study of 112 cases. Hum Pathol 25:514–521

Hatva E, Bohling T, Jaaskelainen J, Persico MG, Haltia M, Alitalo K (1996) Vascular growth factors and receptors in capillary hemangioblastomas and hemangiopericytomas. Am J Pathol 148:763-775

Hellström M, Kalén M, Lindahl P, Abramsson A, Betsholtz C (1999) Role of PDGF-B and PDGFR-β in recruitment of vascular smooth muscle cells and pericytes during embryonic blood vessel formation in the mouse. Development 126:3047–3055

Iitaka M, Miura S, Yamanaka K, Kawasaki S, Kitahama S, Kawakami Y, Kakinuma S, Oosuga I, Wada S, Katayama S (1998) Increased serum vascular endothelial growth factor levels and intrathyroidal vascular area in patients with Grave's disease and Hashimoto's thyroiditis. J Clin Endocrinol Metab 83:3908–3912

Justrabo E, Michiels JF, Maire J, Jacquot JP, Levillain P (1989) Hémangiopéricytome de la gland thyroide. Ann Endocrinol 50:26–30

Kallenberg F, Anagnostaki L (1979) Hemangiopericytoma. Report of a case in the thyroid gland. Ugeskr Laeg 141:3530–3531

Konerding MA, Fait E, Gaumann A (2001) 3D microvascular architecture of pre-cancerous lesions and invasive carcinomas of the colon. Br J Cancer 18:1354–1362

Miettinen M, Sarlomo-Rikala M, Kovatich AJ (1998) Cell-type- and tumour-type-related patterns of bcl-2 reactivity in mesenchymal cells and soft tissue tumours. Virchows Arch 433:255–260

Nemes Z (1992) Differentiation markers in hemangiopericytoma. Cancer 69:133–140

Prokš (1961) Generalized hemangiopericytoma of the thyroid gland (report of a case). Neoplasma 8:219–224

Segal K, Ben-Bassat M, Avraham A, Har-El G, Sidi J (1985) Hashimoto's thyroiditis and carcinoma of the thyroid gland. Int Surg 70:205–209

Stout P, Murray M (1942) Hemangiopericytoma. A vascular tumor featuring Zimmerman's pericytes. Ann Surg 116:26–33

Tano-Assini MT, Oliva Otero G, Gomez SC (1968) Hemangiopericytoma visceral. Pren Med Argent 55:997–1000

Tytor M, Olofsson J (1986) Thyroid tumors invading the larynx and trachea. J Otolaryngol 15:74–79

Unger P, Ewart M, Wang BY, Gan L, Kohtz DS, Burnstein DE (2003) Expression of p63 in papillary thyroid carcinoma and in Hashimoto's thyroiditis: a pathobiologic link? Hum Pathol 34:764–769

Weis SW, Goldblum JR (eds) (2001) Soft tissue tumors. Mosby, St. Louis

Virchows Arch (2004) 445:320–322
DOI 10.1007/s00428-004-1061-x

LETTER TO THE EDITOR

Jean-Louis Dargent · Laurence Lespagnard · Jean-Marc Verdebout · Pierre Bourgeois · Denis Munck

Glomeruloid microvascular proliferation in angiomyomatous hamartoma of the lymph node

Received: 4 April 2004 / Accepted: 20 May 2004 / Published online: 19 June 2004
© Springer-Verlag 2004

Sir, angiomyomatous hamartoma (AH) of the lymph node is a benign vascular disorder of unknown etiology, first described by Chan et al. in 1992 [1]. This uncommon disease particularly affects lymph nodes of the inguinal area, but cases involving femoral or cervical lymph nodes have also been described [1, 2, 3, 4, 5]. A peculiar characteristic of this disorder is the association with lymphedema of the ipsilateral limb in some patients [1]. Microscopically, AH is characterized by a proliferation of abnormal blood vessels set in connective tissue that contains sparsely and haphazardly distributed smooth-muscle cells [1]. At times, some interspersed adipocytes may also be found [2]. This lesion usually involves the hilum of the affected lymph node and variably extends to its convex surface. Its precise pathogenesis is still undetermined, but the possibility of an acquired hamartomatous condition or that of an abnormal reparative reaction have been initially considered [1]. Herein, we report the case of a 29-year-old male who presented with an AH involving an inguinal lymph node. The clinical and pathological findings in this patient, which were quite similar to those described in previous studies, certainly support the specificity of this disorder. Moreover, the presence of vascular alterations resembling those classically found in primary pulmonary hypertension or in glioblastoma multiforme, which has never been described to our knowledge, also provides further evidence that AH actually represents a disordered angiogenic reaction involving the blood vessels of the lymph node.

J.-L. Dargent (✉) · L. Lespagnard
Service d'Anatomie Pathologique,
Institut Jules Bordet,
1 rue Héger-Bordet, 1000 Brussels, Belgium
e-mail: jean.dargent@bordet.be
Tel.: +32-2-5413124
Fax: +32-2-5413281

J.-M. Verdebout
Laboratoire d'Anatomie Pathologique,
Centre Hospitalier Etterbeek-Ixelles,
63 rue Jean Paquot, 1050 Brussels, Belgium

P. Bourgeois
Service de Médecine Nucléaire,
Institut Jules Bordet,
1 rue Héger-Bordet, 1000 Brussels, Belgium

D. Munck
Service de Chirurgie,
Centre Hospitalier Etterbeek-Ixelles,
63 rue Jean Paquot, 1050 Brussels, Belgium

The patient was admitted in the Department of Surgery because of a progressive lymphedema of the right leg. This lymphedema, which spontaneously appeared 12 months previously, first showed a fluctuating course. Later on, it became permanent and was associated with few episodes of erysipelas. Apart from a prominent swelling of the right leg, clinical examination did not reveal any abnormality. Peripheral blood analysis was within normal limits, and serum investigations for human immunodeficiency virus types 1 and 2, hepatitis B and C viruses and filariasis were negative. Although obstruction of the lymphatic drainage in the right inguinal area was demonstrated using radionuclide lymphoscintigraphy, ultrasonography or computed tomography scan could evidence no enlarged lymph node or tumor process. A surgical exploration of the right inguinal area revealed the presence of marked fibrous changes in the soft tissues surrounding the inguinal lymph nodes. A lymph node was excised, which allowed both pathological and bacteriological investigations to be performed.

The lymph node measured 1.7×1.2×0.5 cm. On cross-sections, it had a gray-white appearance. Microscopically, the nodal parenchyma was completely replaced by a fibrous tissue containing numerous irregular vessels, interspersed spindle cells and some fat lobules (Fig. 1). These changes gradually extended from the hilum to the convex surface of the lymph node, leaving a thin rim of cortical lymphoid tissue. The capsule was thickened, and no subcapsular or medullary sinuses were found. On further examination, the lesion appeared somewhat organized. The outer part, namely the adipose tissue surrounding the hilum, contained numerous small arteries and veins, whereas enlarged and thin-walled capillaries colonized the inner one. In this region, close to the cortex

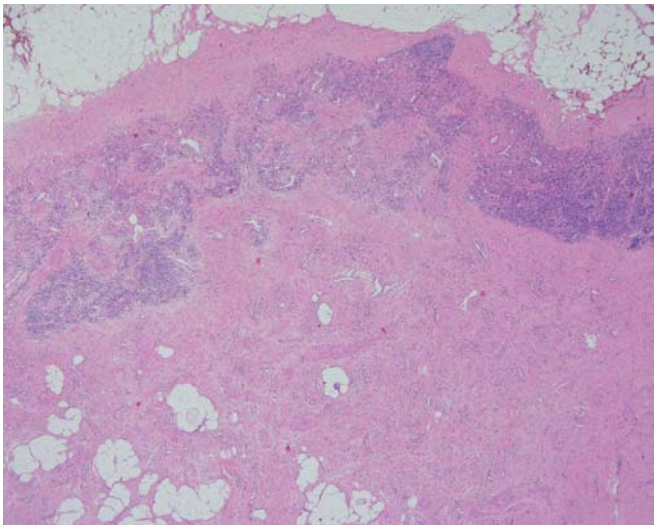


Fig. 1 Low-magnification appearance of the lesion. A fibrous tissue that contains numerous vessels and some entrapped fat lobules extensively replaces the nodal parenchyma. Note the thickened capsule and the absence of subcapsular sinuses

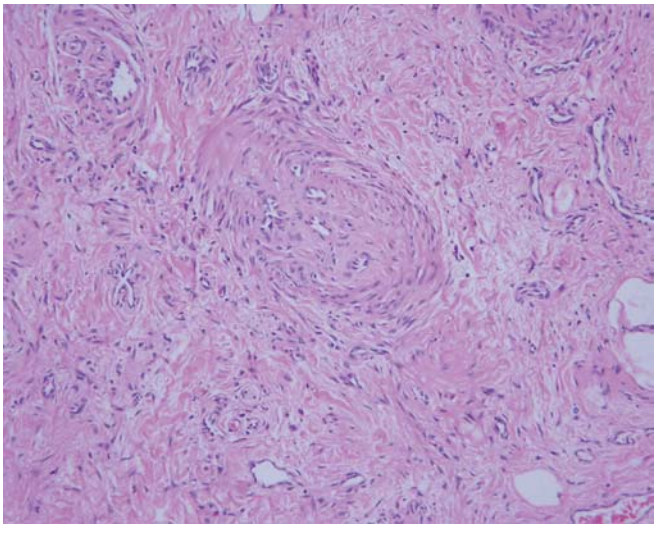


Fig. 2 Illustration of plexiform vessels. Note the enlarged endothelial cells and the presence of smooth-muscle cells in the nearby stroma

of the lymph node, the capillaries possessed few pericytes and merged into the surrounding connective tissue. Between these two areas, small-sized but thick-walled blood vessels featuring plexiform or glomeruloid changes were found (Fig. 2). These peculiar vessels occasionally displayed enlarged endothelial cell nuclei, which protruded into the lumen. No discernible thrombus or embolus was found. At times, inflammatory cells, such as lymphocytes or histiocytes, clustered around plexiform vessels or within their walls. However, there was no evidence of vasculitis. The surrounding connective tissue was rich in collagen and contained scattered spindle cells. These did not show any atypia or mitotic activity, and their morphology was strongly suggestive of smooth-muscle differentiation. Many of these cells also appeared to be detached from the outer part of the plexiform vessels and radiated into the fibrous background.

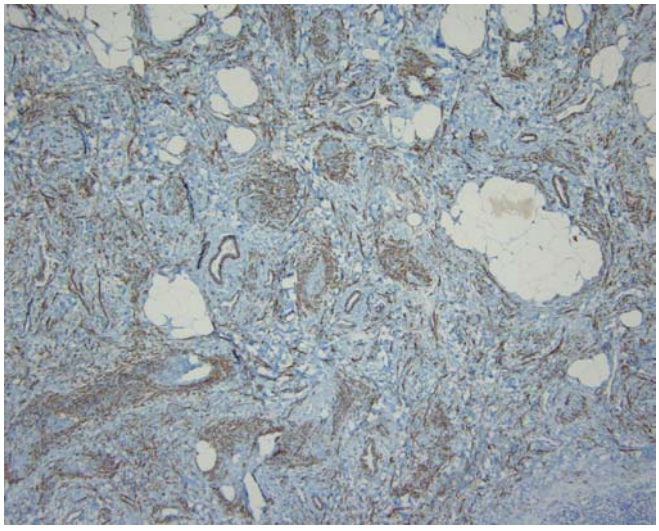


Fig. 3 Immunostaining with antibody directed against h-caldesmon revealed the presence of numerous smooth-muscle cells around and between the vessels

On immunohistochemical analysis, the spindle cells were found to be h-caldesmon, smooth-muscle actin- and desmin-positive, which confirmed their smooth-muscle origin (Fig. 3). In contrast, these cells did not show any immunoreactivity with the antibodies directed against S-100 protein, CD34, anaplastic lymphoma kinase or HMB45-related antigen. Immunostainings for CD34 and CD31 highlighted the rather well-developed vascular network and the enlarged appearance of some endothelial cells. The proliferative activity within this fibrovascular process was evaluated using the Ki-67 protein expression. Only a few endothelial or pericytic cells within the plexiform vessels were positive (Fig. 4). Lymphocytes in the residual lymphoid tissue expressed either CD3 or CD20. Additional immunostainings directed against CD4, CD8, CD68 or granzyme B showed that inflammatory cells clustered around or within plexiform vessels were mainly composed of T helper lymphocytes and histiocytes. In situ hybridization for Epstein–Barr virus-encoded RNA did not reveal the presence of such a virus. Lastly, bacteriological investigations were negative.

All the aforementioned clinical and pathological findings are consistent with the diagnosis of AH of the lymph node. In contrast with the cases previously reported, peculiar alterations of the lymph-node vascular supply were found in our patient. These included increased numbers of small blood vessels (mainly venules), thickening of their walls and formation of plexiform or glomeruloid structures, such as in primary pulmonary hypertension or glioblastoma multiforme. Interestingly, these vascular changes are very similar if not identical to those that have been described in experimental studies on the angiogenic response induced by vascular permeability factor/vascular endothelial growth factor (VPF/VEGF)

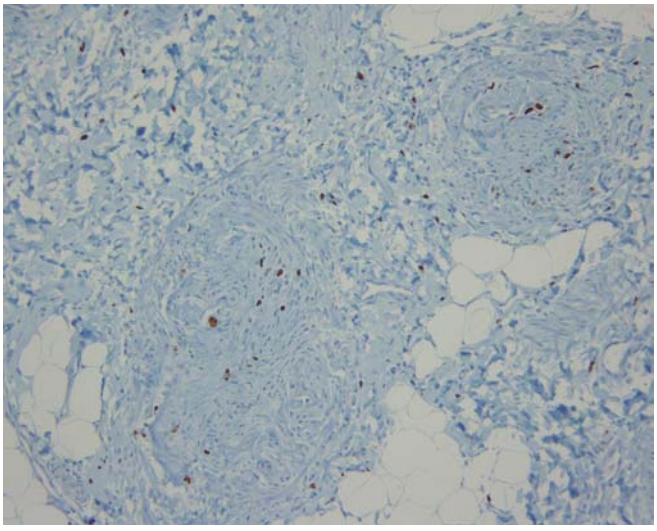


Fig. 4 Immunostaining with antibody directed against the proliferation antigen Ki-67. Several endothelial or pericytic cells are stained, which suggests active angiogenesis

gene expression [6, 7]. In our opinion, such similarities suggest that AH of the lymph node actually represents a disordered angiogenic process arising from blood vessels located in the hilum of the lymph node, presumably the hilar vein and its branches. Likewise, we think smooth-muscle cells making up the surrounding connective tissue arise from pericytic cells that are detached from the outer part of these plexiform vessels during the course of such disordered angiogenesis. Our assertion is based on the peculiar aspect of these cells on the periphery of plexiform vessels, the pattern of Ki-67 protein expression and the description of similar cells in the angiogenic response induced by VPF/VEGF gene expression [6, 7]. The strong association between the lymph node content in smooth-muscle cells and the number of muscular vessels within the hilum, which has been demonstrated in a previous study [8], also supports this point of view. As a result, the destruction of nodal sinuses by all these vascular and stromal alterations seriously impairs the lymphatic circulation across the affected lymph node.

The observation of fibrous changes in the soft tissues surrounding inguinal lymph nodes at the time of surgical operation also suggests that AH may simultaneously involve several lymph nodes and the soft tissues surrounding them. This finding, which has been noted in some studies [1, 5], is further illustrated in our patient using ultrasonographic evaluation of the right inguinal area. Indeed, this procedure demonstrated significant alterations within several lymph nodes as well as the presence of numerous venous structures in their vicinity. Further examination of the radionuclide lymphoscintigram also revealed abnormal lymphatic flow across lymph nodes of the right inguinal area and within pelvic lymph nodes of each side. Such a disease extension, therefore, explains the occurrence of lymphedema in some patients.

In conclusion, our case offers further evidence that AH of the lymph node certainly is a distinct clinicopathological entity. The presence of glomeruloid microvascular proliferation, a yet unreported feature, also indicates that this disease actually represents an exuberant angiogenic reaction arising from blood vessels located in the hilum of the lymph node and extending to the nearby tissues. The precise cause of such disordered angiogenesis remains, however, to be determined.

References

1. Chan JKC, Frizzera G, Fletcher CDM, Rosai J (1992) Primary vascular tumors of lymph nodes other than Kaposi's sarcoma. Analysis of 39 cases and delineation of two new entities. Am J Surg Pathol 16:335–350
2. Allen PW, Hoffman GJ (1993) Fat in angiomyomatous hamartoma of lymph node. Am J Surg Pathol 17:748–749
3. Laeng RH, Hotz MA, Borisch B (1996) Angiomyomatous hamartoma of a cervical lymph node combined with haemangiomatoids and vascular transformation of sinuses. Histopathology 29:80–84
4. Magro G, Grasso S (1997) Angiomyomatous hamartoma of the lymph node: case report with adipose tissue component. Gen Diagn Pathol 143:247–249
5. Sakurai Y, Shoji M, Matsubara T, Imazu H, Hasegawa S, Ochiai M, Funabiki T, Mizoguchi Y, Kuroda M, Kasahara M (2000) Angiomyomatous hamartoma and associated stromal lesions in the right inguinal lymph node: a case report. Pathol Int 50:655–659
6. Pettersson A, Nagy JA, Brown LF, Sundberg C, Morgan E, Jungles S, Carter R, Krieger JE, Manseau EJ, Harvey VS, Eckelhoefer IA, Feng D, Dvorak AM, Mulligan RC, Dvorak HF (2000) Heterogeneity of the angiogenic response induced in different normal adult tissues by vascular permeability factor/vascular endothelial growth factor. Lab Invest 80:99–115
7. Sundberg C, Nagy JA, Brown LF, Feng D, Eckelhoefer IA, Manseau EJ, Dvorak AM, Dvorak HF (2001) Glomeruloid microvascular proliferation follows adenoviral vascular permeability factor/vascular endothelial growth factor-164 gene delivery. Am J Pathol 158:1145–1160
8. Channer JL, Davies JD (1985) Smooth muscle proliferation in the hilum of superficial lymph nodes. Virchows Arch 406:261–270

Virchows Arch (2004) 445:323–325
DOI 10.1007/s00428-004-1076-3

LETTER TO THE EDITOR

Dimas Suárez-Vilela · Francisco Miguel Izquierdo-Garcia · Nieves Alonso-Orcajo

Epithelioid and rhabdoid rhabdomyosarcoma in an adult patient: a diagnostic pitfall

Received: 22 April 2004 / Accepted: 14 June 2004 / Published online: 29 July 2004
© Springer-Verlag 2004

Sir, adult rhabdomyosarcoma (RMS) constitutes a very small fraction of soft tissue sarcomas, estimated between 2% and 5% [1, 6]. These tumors present with different histological patterns [1, 6], the epithelioid RMSs [14] and the RMSs with rhabdoid cells being very uncommon [5, 7, 9, 12, 13]. We report a case of RMS in an adult patient, which was composed of cells with rhabdoid and epithelioid features. The histological appearance of this tumor was very unusual, and it raises differential diagnoses with neoplasms of other histogenetic origins.

A 70-year-old man was sent to our hospital for study of a retroauricular and submandibular right mass. It measured 4.5×5.5 cm in size. Around the tumor he had enlarged lymph nodes in supraclavicular fossas, accessories spinal chains and jugulo-digastric confluence. At the axial computed tomography study, it was found that the tumor, being well delimited, infiltrated the right posterior cervical muscles. Bone infiltration was not found. A fine-needle aspiration of the tumor showed numerous isolated medium and large cells, with abundant, amphophilic cytoplasm, vesicular nuclei and prominent nucleoli. Some of these cells presented paranuclear hyaline cytoplasmic inclusions (Fig. 1). The aspiration was diagnosed as a poorly differentiated tumor, probably carcinoma, with no other specific features. As the cytological findings were inconclusive, a right supraclavicular lymph-node biopsy was performed. Microscopically, most of the node was diffusely infiltrated by neoplastic cells of epithelioid appearance, wide eosinophilic cytoplasm, vesicular nuclei and prominent nucleoli (Fig. 2A). The mitotic count was higher than 15 mitoses per 10 high power fields (×400), and extensive necrosis was present. In some areas, the tumor was composed of cells of rhabdoid appearance with hyaline or eosinophilic inclusions that seemed to compress the nuclei (Fig. 2A). On the immunohistochemical study, the tumoral cells showed intense cytoplasmic staining with antibodies against vimentin (Novocastra, Newcastle, United Kingdom) and desmin (Dako, Glostrup, Denmark), with stronger intensity for both markers in the inclusions (Fig. 2B). Some isolated cells showed nuclear staining for myogenin (MYF-4) (Novocastra) (Fig. 2B) and cytoplasmic staining for smooth-muscle actin (Novocastra) and specific-muscle actin (Dako), the cytoplasmic inclusions for both actins being negative. Also, some isolated cells were positive with AE1–AE3 (Zymed, San Francisco, California, USA) and CAM5.2 (Becton Dickinson, San Jose, California, USA) anticytokeratin antibodies (Fig. 2B), antiCD 99 antibody (Dako) and for E-cadherin (Bio Genex, San Ramón, California, USA) (Fig. 2B) and myoglobin (Bio Genex). The antibody against epithelial membrane antigen (EMA) (Novocastra) presented a membranous and cytoplasmic pattern in 10% of the cells. The index of cellular proliferation was 80% with the MIB-1 (Dako) antibody. Of the nuclei, 7–10% stained for p53 (Dako) protein. The immunostainings for carcinoembryonic antigen (Zymed),

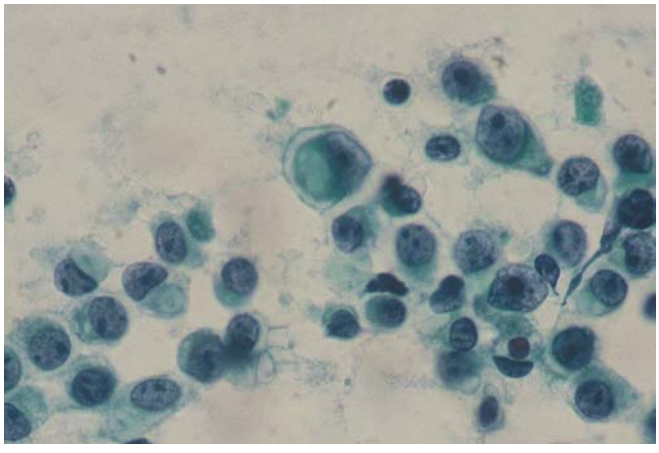


Fig. 1 At the fine-needle aspiration, round cells with vesicular nuclei and prominent nucleoli are present. Some of them show cytoplasmic hyaline inclusions

D. Suárez-Vilela (✉) · F. M. Izquierdo-Garcia · N. Alonso-Orcajo
Servicio de Anatomía Patológica,
Hospital de León,
Altos de la Nava s/n, 24008-León, Spain
e-mail: pacoizq20@hotmail.com
Tel.: +9-87-237400

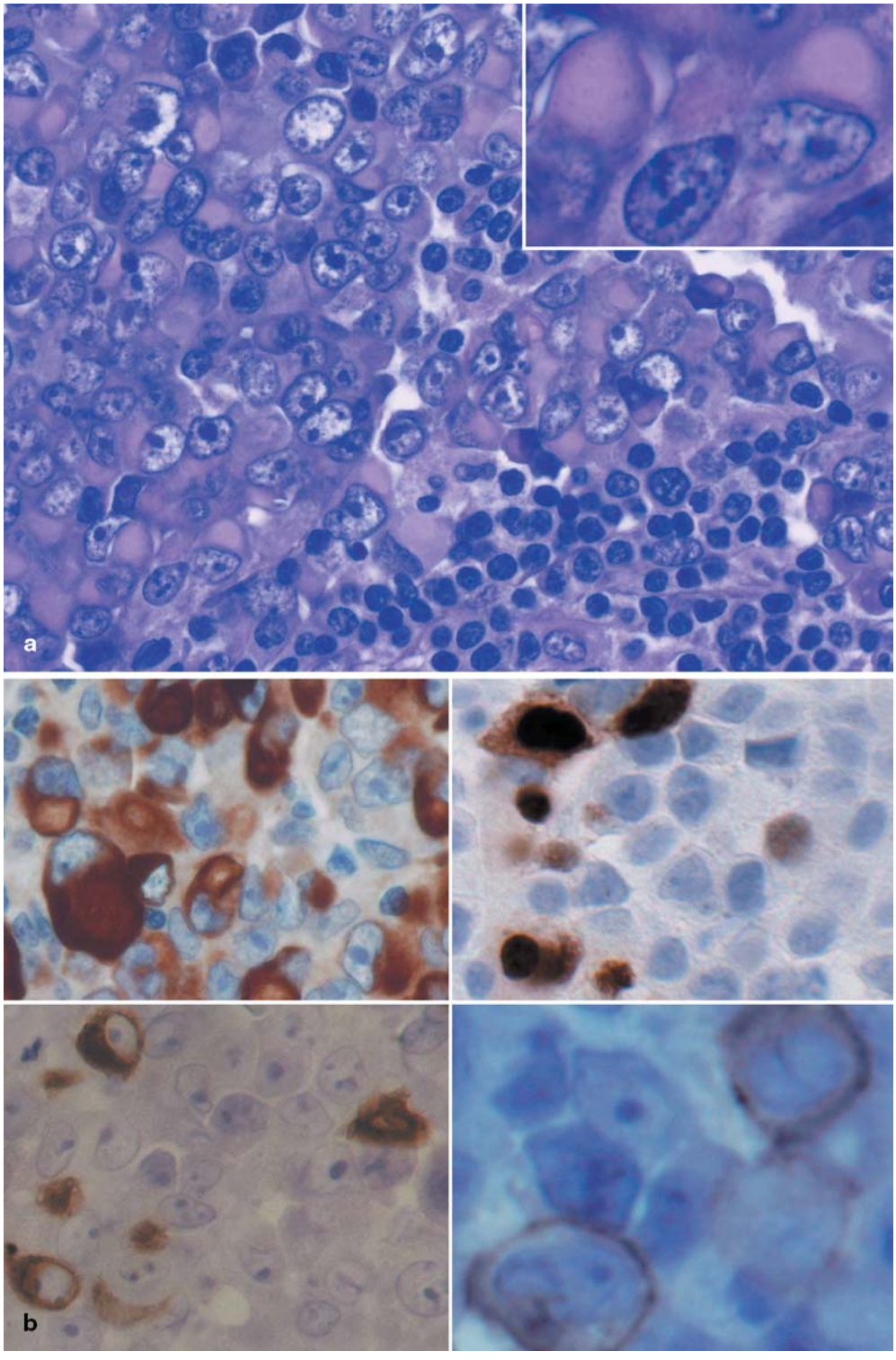


Fig. 2 A Malignant cells with epithelioid and rhabdoid morphology. *Inset* higher power of cells with rhabdoid phenotype. **B** *Upper left* globular cytoplasmic staining for desmin. *Upper right* nuclear positivity for myogenin. *Lower left* isolated cells stained with AE1–AE3 anticytokeratin antibody. *Lower right* membrane decoration of some cells for E-cadherin

placental alkaline phosphatase, collagen IV (Novocastra), neuron-specific enolase, heavy caldesmon, melan A, cytokeratin 7, cytokeratin 20, CD3, CD20, CD68 (Dako), CD23, CD34 and CD45 (Novocastra) were negative in the tumoral component.

The patient was treated with adriamycin, isophosphamide and mesna, without clinical response, and died 3 months later in another hospital. Autopsy was not performed.

The most common histological types of adult RMS are embryonal RMS and alveolar RMS; both types together comprise between 70% and 80% of the RMSs of an adult aged between 16 years and 40 years [1, 6]. However, in adults over 40 years old, 42% of the adult RMSs corre-

spond to the pleomorphic variant [1, 5, 6, 7, 13]. Other less frequent RMSs in adults are sclerosing RMS, epithelioid RMS and RMS with rhabdoid cells. Sclerosing RMS is a distinctive RMS in adults that closely mimics osteosarcoma or chondrosarcoma because of the extensive matrix production [2, 10]. Epithelioid RMS is an extremely unusual type of RMS. Seidal et al. [14] reported a tumor with this name in the pelvis minor of a 60-year-old woman. This case showed a histological appearance similar to ours, and it was composed of epithelioid cells arranged in narrow anastomosing rows. However, they did not find rhabdoid cells. RMS with rhabdoid-like features is uncommon in adults. Kodet et al. [9] reported 22 embryonal RMSs and 5 alveolar RMSs that included rhabdoid cells. Only two of these cases were adult patients. Since then, there have been very few reports of adult RMS with a rhabdoid component, and most of them correspond to the pleomorphic variant [5, 7, 13]. Pérez-Ordóñez et al. [12] described a case of rhabdoid RMS in a 35-year-old woman and suggest that since this tumor cannot be classified as one of the usual types of RMS, it may represent a new variant.

The microscopic appearance of our case with epithelioid and rhabdoid elements has not been previously described in adult RMS to our knowledge. On hematoxylin and eosin, it may be mistaken for other poorly differentiated neoplasms with rhabdoid phenotype, such as carcinomas, melanomas or different types of sarcomas (epithelioid angiosarcoma, epithelioid hemangioendothelioma, epithelioid malignant peripheral nerve-sheath tumor, epithelioid sarcoma, epithelioid leiomyosarcoma and sclerosing epithelioid fibrosarcoma), which are more common than RMSs in older patients [4, 8, 11]. In this case, the immunohistochemical study was essential to resolve the problem of the differential diagnosis, inasmuch as the expression of desmin, myogenin and actins is conclusive for the diagnosis of RMS [8]. Tumoral cells positive for cytokeratins, EMA, E-cadherin and S-100 protein have been frequently described in RMSs [3, 8], so in this context, the isolated finding of these antigens should not induce us to make an erroneous diagnosis of carcinoma or melanoma. This is important because although adult RMSs are very aggressive tumors with a poor prognosis, some cases may have therapeutic responses with protocols similar to those used in pediatric RMSs [1, 6].

This case may be placed in the heterogeneous group of composite rhabdoid tumors. Under this name, tumors of several histogenesis, in multiple anatomical locations and with different percentages of rhabdoid cells are included [4, 11]. These tumors do not seem related to renal and extrarenal true rhabdoid tumors that, in general, present in children younger than 2 years [4, 11] and are associated in 75% of the cases to inactivation of the hSNF5/INI1 tumor suppressor gene, which resides on the long arm of chromosome 22, whereas most of the composite rhabdoid tumors lack this genetic change [4, 11].

In summary, our case corresponds to a poorly differentiated neoplasm with epithelioid and rhabdoid phenotype. The immunohistochemical findings of this tumor are diagnostic of rhabdomyosarcoma, ruling out a true extrarenal rhabdoid tumor.

Acknowledgements We thank very sincerely Dr. CDM Fletcher of Brigham and Women's Hospital for reviewing the case and performing part of the immunohistochemical study.

References

1. Ferrari A, Dileo P, Casanova M. Bertulli R, Meazza C, Gandola L, Navarria P, Colini P, Gronchi A, Olmi P, Fossati-Bellani F, Casali PG (2003) Rhabdomyosarcoma in adults. A retrospective analysis of 171 patients treated at a single institution. Cancer 98:571–580
2. Folpe AL, McKenney JK, Brigde JA, Weiss SW (2002) Sclerosing rhabdomyosarcoma in adults. Report of four cases of a hyalinizing, matrix-rich variant of rhabdomyosarcoma that may be confused with osteosarcoma, chondrosarcoma or angiosarcoma. Am J Surg Pathol 26:1175–1183
3. Frisch SM (1994) E1a induces the expression of epithelial characteristics. J Cell Biol 124:619–626
4. Fuller CE, Pfeifer J, Humphrey P, Bruch LA, Dehner LP, Perry A (2001) Chromosome 22q dosage in composite extrarenal rhabdoid tumors: clonal evolution or a phenotypic mimic? Hum Pathol 32:1102–1108
5. Gaffney EF, Dervan PA, Fletcher CDM (1993) Pleomorphic rhabdomyosarcoma in adulthood. Analysis of 11 cases with definition of diagnostic criteria. Am J Surg Pathol 17:601–609
6. Hawkins WG, Hoos A, Antonescu CR, Urist MJ, Leung DHY, Gold JS, Woodruff JM, Lewis JJ, Brenna MF (2001) Clinicopathologic analysis of patients with adult rhabdomyosarcoma. Cancer 91:794–803
7. Hollowood K, Fletcher CDM (1994) Rhabdomyosarcoma in adults. Semin Diag Pathol 11:47–57
8. Kempson RL, Fletcher CDM, Evans HL, Hendrickson MR, Sibley RK (2001) In: Rosai J, Sobin LH (eds) Tumors of the soft tissues. Atlas of tumor pathology, 3rd series. Armed Forces Institute of Pathology, Washington, DC
9. Kodet R, Newton WA, Hamoudi AB, Asmar L (1991) Rhabdomyosarcomas with intermediate-filament inclusions and features of rhabdoid tumors. Light microscopic and immunohistochemical study. Am J Surg Pathol 15:257–267
10. Mentzel T, Katenkamp D (2000) Sclerosing, pseudovascular rhabdomyosarcoma in adults. Clinicopathological and immunohistochemical analysis of three cases. Virchows Arch 436:305–311
11. Ogino S, Ro JY, Redline RW (2000) Malignant rhabdoid tumor: a phenotype? an entity?—a controversy revisited. Adv Anat Pathol 7:181–190
12. Perez-Ordoñez B, Kandel RA, Bell R, Bédard YC (1998) Rhabdomyosarcoma with rhabdoid-like features. Pathol Res Pract 194:357–361
13. Schürch W, Bégin LR, Seemayer TA, Lagacé R, Boivin J-C, Lamoreux C, Bluteau P, Piché J, Gabbiani G (1996) Pleomorphic soft tissue myogenic sarcomas of adulthood. A reappraisal in the mid-1990s. Am J Surg Pathol 20:131–147
14. Seidal T, Kindblom L-G, Angervall L (1989) Rhabdomyosarcoma in middle-aged and elderly individuals. APMIS 97:236–248

Virchows Arch (2004) 445:326
DOI 10.1007/s00428-004-1119-9
© Springer-Verlag 2004

ANNOUNCEMENTS

11 October 2004
Continuing Medical Education
Nottingham, UK

For further information contact:
The Blamey Education Centre
Nottingham Breast Institute
City Hospital, Nottingham, NG5 1PB, UK
Tel.: 00 44 (115) 969 1689
E-mail: sbury@ncht.trent.nhs.uk

22–24 November 2004
41st Nottingham Multi-disciplinary Course on breast disease
Nottingham, UK

For further information contact:
The Blamey Education Centre
Nottingham Breast Institute
City Hospital, Nottingham, NG5 1PB, UK
Tel.: 00 44 (115) 969 1689
E-mail: sbury@ncht.trent.nhs.uk

8–10 November 2004
Practical Adult Cardiovascular Pathology Course
Course organisers: Dr MN Sheppard/Dr Yen Ho

This particular "Hands On" course approaches in detail the problems that face the diagnostic pathologist when dealing with cardiovascular pathology both congenital and adult. The approach to a cardiac autopsy and sudden death will be emphasized. Cardiac specimens will be made available for analysis and practical demonstrations as well as video demonstrations will be highlighted. Organ retention will also be covered and minimal database for reporting cardiovascular specimens. A slide seminar with slides is included. The course is aimed at trainees studying for the MRCPATH and also senior pathologists who wish to update their knowledge.

Course fee: £ 400.00 (includes daily coffee, tea and lunch)
A special fee of £ 300.00 for juniors in training

For further information, please contact:
Short Course Office
National Heart and Lung Institute
Dovehouse Street
London SW3 6LY
Tel.: +44(0)20 7351 8172
Fax: +44(0)20 7351 8246
E-mail: shortcourse.NHLI@IC.AC.UK

8–10 December 2004
Combined Adult & Congenital Cardiovascular Pathology Course
Course Organisers: Dr MN Sheppard/Dr Yen Ho

This particular "Hands On" course approaches in detail the problems that face the diagnostic pathologist when dealing with cardiovascular pathology both congenital and adult. The approach to a cardiac autopsy and sudden death will be emphasized. Cardiac specimens will be made available for analysis and practical demonstrations as well as video demonstrations will be highlighted. Organ retention will also be covered and minimal database for reporting cardiovascular specimens. A slide seminar with slides is included. The course is aimed at trainees studying for the MRCPATH and also senior pathologists who wish to update their knowledge.

Course fee: £ 400.00 (includes daily coffee, tea and lunch)
A special fee of £ 300.00 for juniors in training

For further information, please contact:
Short Course Office
National Heart and Lung Institute
Dovehouse Street
London SW3 6LY
Tel.: +44(0)20 7351 8172
Fax: +44(0)20 7351 8246
E-mail: shortcourse.NHLI@IC.AC.UK

Virchows Arch (2004) 445:327–333
DOI 10.1007/s00428-004-1105-2

REVIEW ARTICLE

Dominique Wendum · Joëlle Masliah · Germain Trugnan · Jean-François Fléjou

Cyclooxygenase-2 and its role in colorectal cancer development

Received: 30 June 2004 / Accepted: 12 July 2004 / Published online: 1 September 2004
© Springer-Verlag 2004

Abstract Cyclooxygenase 2 (COX-2), also called prostaglandin endoperoxide synthase 2, is involved in colorectal tumor development. This review deals with particular questions raised in this field such as the mechanisms of COX-2 related tumor promotion, the role of the different types of cells (epithelial and interstitial) expressing COX-2, the factors that trigger COX-2 induction, and the clinical potential of selective COX-2 inhibitors to treat or prevent colorectal tumors. Several mechanisms of COX-2 related tumor promotion have been identified. Some are dependent on prostaglandin E_2 production (such as induction of cell proliferation, angiogenenis or local immunosuppression, inhibition of apoptosis, increase in cell motility) and others are not (such as carcinogen activation or malondialdehyde production). COX-2 expression has been demonstrated in epithelial cells of colorectal cancers and adenomas and also in interstitial cells. These cells correspond to macrophages and/or fibroblasts and endothelial cells. COX-2 expression in these interstitial cells participates in tumor development. Factors or events that trigger COX-2 expression include oncogene activation, antioncogene inactivation, cytokines, growth factors, some fatty acids, bile salts, and mucins. Finally, selective COX-2 inhibitors may be effective in preventing or treating colorectal adenomas or carcinomas. However, their real efficiency and the cost/benefit balance are currently evaluated, and no definite conclusion can be made at the moment.

D. Wendum (✉) · J.-F. Fléjou
Service d'Anatomie Pathologique,
Hôpital Saint-Antoine, AP-HP,
184 rue du Faubourg Saint-Antoine, 75571 Paris Cedex 12, France
e-mail: dominique.wendum@sat.ap-hop-paris.fr
Tel.: +33-1-49282181
Fax: +33-1-49282878

D. Wendum · J. Masliah · G. Trugnan
Unité INSERM U538, Faculté de Médecine Saint-Antoine,
Université Pierre et Marie Curie,
27 rue Chaligny, 75012 Paris, France

Keywords Colorectal tumor · Cyclooxygenase 2 · Familial adenomatous polyposis · Prostaglandin · Selective COX-2 inhibitors

Introduction

It is now accepted that nonsteroidal anti-inflammatory drugs (NSAIDs) have antineoplastic effects, particularly in the gastrointestinal tract. NSAIDs have been shown to prevent colorectal adenomas and cancer in the general population and to induce polyp regression in familial adenomatous polyposis (FAP) [6, 23, 24, 25, 51, 74]. This protection against colorectal tumor development seems to be related particularly to cyclooxygenase-2 (COX-2) inhibition by NSAIDs, although this is probably not the only mechanism [29, 47]. Therefore selective COX-2 inhibitors such as celecoxib and rofecoxib, the use of which is safer than classical NSAIDs, might be effective for colorectal cancer prevention and treatment. However, COX-2 involvement in colorectal tumor development raises several questions for which answers are not always well established. For instance, how does COX-2 contribute to tumor development, what cells express COX-2 in tumors, and what triggers COX-2 induction in tumors? Finally, what is the clinical potential of selective COX-2 inhibitors for treatment and prevention of colorectal tumors?

Main characteristics of cyclooxygenases

COXs are key enzymes for prostaglandin production. COXs are also called prostaglandin endoperoxide synthase or prostaglandin (PG) G/H synthase. COX transforms arachidonic acid, which is released from membrane phospholipids by a phospholipase A_2 into PGG_2 (cyclooxygenase activity) and then rapidly into PGH_2 (peroxidase activity). These two activities occur at distinct sites in the protein. In vitro the peroxidase activity can operate independently or during on going of the

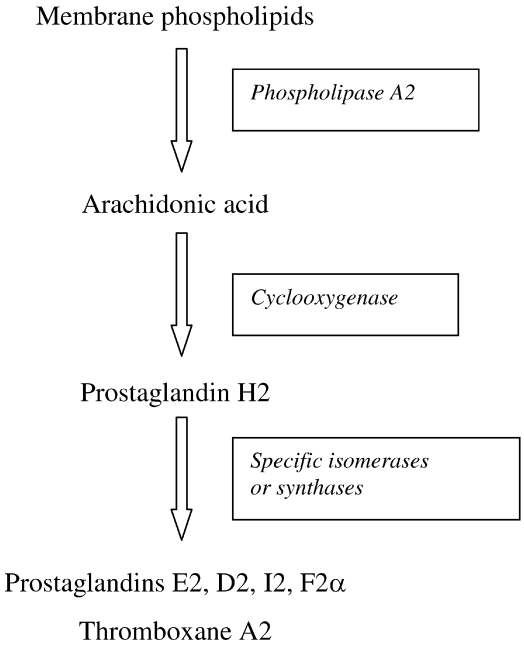


Fig. 1 COX and prostaglandin production

cyclooxygenase catalysis. Both the cyclooxygenase and the peroxidase activities are inactivated during catalysis, and these activities therefore fall to zero within 1–2 min (suicide inactivation) [64]. Finally, PGH2 is converted into a series of PGs (PGE_2, $PGF_{2\alpha}$, and PGI_2, or prostacyclin) and thromboxane A_2 by several synthases/isomerases (Fig. 1).

Three COX isoforms have been identified so far, termed COX-1, COX-2, and COX-3. COX-1 and COX-2 have a 60% amino acid sequence homology. In humans COX-1 and COX-2 genes are located on chromosomes 9 and 1, respectively [63]. COX-1 is expressed constitutively in most tissues and appears to be responsible for prostaglandin production in various physiological functions such as platelet aggregation and maintenance of gastric mucosa. In contrast, COX-2 is induced by several inflammatory cytokines and growth factors [35, 56]. However, asserting that COX-1 is a "good cyclooxygenase" and COX-2 a "bad one" may be an oversimplification. Indeed, COX-2 is involved in several physiological functions such as renal function or ovulation [15, 39, 42], and COX-1 can be involved in pathological processes such as inflammation and tumor development [11, 69, 75, 76]. COX-3 is a variant of COX-1 and is abundant in cerebral cortex. COX-3 seems to be especially sensitive to acetaminophen and related compounds [9].

How does COX-2 expression contribute to colorectal tumor development?

COX-2 is overexpressed in about 90% of colorectal adenocarcinomas and in 40–90% of colorectal adenomas, according to different studies [17, 19, 30]. In colorectal cancer the absence or a low COX-2 expression is related to microsatellite instability [36, 62, 77]. In adenomas COX-2 expression depends on size and seems to be unrelated to the degree of dysplasia or architecture [18, 19, 31].

COX-2 expression is thus observed early during colorectal tumor development and in most tumors, either benign or malignant. However, these findings do not confirm COX-2 expression as a central event in colorectal carcinogenesis. Direct evidence of COX-2 early and important contribution in colorectal tumor development has been found in animal models. Indeed, in animal models of FAP knockout of the COX-2 gene dramatically reduces the number of polyps [43]. Similarly, treatment with selective COX-2 inhibitors in these models also significantly reduced the number of polyps, although in a lesser extent [34, 44]. Selective COX-2 inhibitors also reduced tumor incidence and multiplicity in azoxymethane-treated rats [37]. Various mechanisms of COX-2 related tumor promotion have been identified. Some of these depend on PGE_2 production while others do not. The principal effects of COX-2 expression that may contribute to colorectal tumor development are the following:

- Effects independent of PGE_2 production
- Activation of carcinogens
- Production of malondialdehyde
- Reduction in free arachidonic acid levels

- Effects dependent on PGE_2 production
- Induction of cell proliferation
- Inhibition of apoptosis
- Induction of angiogenesis
- Increase in cell motility
- Increase in metastatic potential
- Induction of local immunosuppression

Mechanisms independent of PGE_2 production

First, COX-2 may play a role in colorectal carcinogenesis by directly activating carcinogens; indeed, COX-2 peroxidase activity can act on polycyclic hydrocarbons, aflatoxin, halogenated pesticides, and phenols [60]. Second, PGH_2 can be transformed into malondialdehyde, which is a direct mutagen that forms adducts with deoxynucleosides [48]. Finally, the level of free arachidonic acid, which is the main COX substrate and has a pro apoptotic action, is reduced by COX-2 activation [7, 8].

Mechanisms dependent on PGE_2 production

PGE_2 levels are elevated in colorectal cancer [50]. PGE_2 can promote tumor development by inducing cell proliferation [59] and by inhibiting apoptosis [57]. Cell proliferation may be secondary to epidermal growth factor receptor transactivation by PGE_2 [45] and inhibition of apoptosis could be related to an increased Bcl-2 expres-

sion [57]. In addition, PGE_2 increases the motility and metastatic potential of cancer cells [59, 72]. PGE_2 can also lead to a local immunosuppression that favors tumor development [3, 38]. Finally, COX-2 expression induces angiogenesis [73]. The latter effect of COX-2 expression seems to be very important since angiogenesis allows the tumors to grow and metastasize [49]. COX-2 has a key role in the release of proangiogenic factors such as vascular endothelial growth factor and basic fibroblast growth factor and in tumors COX-2 expression is correlated with vascular endothelial growth factor expression and with microvessel density [12]. COX-2 induced angiogenesis is related to PGE_2 production [53], although it is not the only mechanism [13].

What cells express COX-2 in colorectal tumors?

Early studies demonstrated COX-2 overexpression in colorectal tumors throughtout the whole tumor without defining precisely which cells overexpressed this enzyme [17]. Knowing the localization of COX-2 expression can help to understand how COX-2 promotes colorectal tumor development. Several studies using immunohistochemistry have demonstrated frequent COX-2 overexpression in epithelial cells in human colorectal adenomas and adenocarcinomas [19, 30, 52, 78]. However, several studies also demonstrate a noteworthy COX-2 overexpression in the stroma (Fig. 2). It appears quite difficult to identify precisely what interstitial cells overexpress COX-2 in these lesions. Indeed, almost every cell type present in the stroma of human colorectal adenocarcinomas has been described as overexpressing COX-2: fibroblasts, myofibroblasts, mononuclear inflammatory cells, and endothelial cells [52, 62, 79]. Moreover, for some authors COX-2 overexpression in interstitial cell seems to be located mainly in superficial macrophages [4, 10] while others report COX-2 expression principally in fibroblasts and endothelial cell in human adenomas [65]. This difficulty in defining precisely which mesenchymal cells in the stroma overexpress COX-2 is also seen in animal studies. Indeed, in animal models of FAP (Min or Δapc716 mice) COX-2 expressing interstitial cells are identified as fibroblasts and endothelial cells by some authors [55, 65] and as macrophages by others [32]. These discrepancies may be related to antibody specificity. Interstitial cells overexpressing COX-2 are most likely a heterogeneous population.

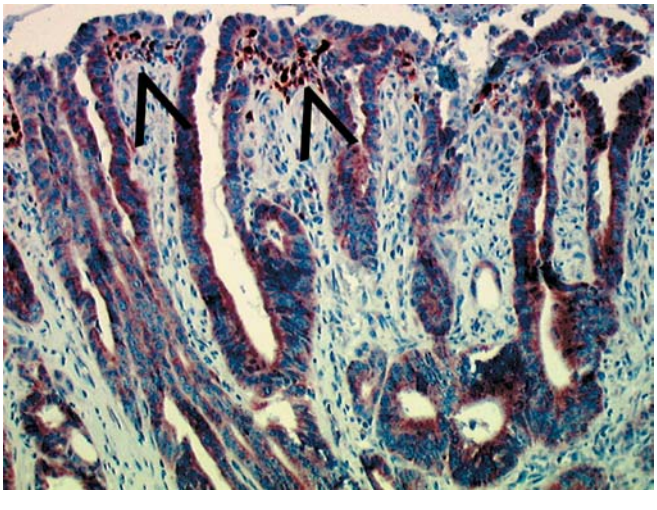


Fig. 2 COX-2 expression in tumoral cells and superficial interstitial cells (*arrows*) in a well differentiated colon adenocarcinoma. Immunohistochemistry, ×200

Role of COX-2 overexpressing interstitial cells in colorectal tumor development

To investigate the relationship between COX-2 expression and tumor promotion most authors have studied cancer cells. It has been shown that COX-2 expression in colorectal cancer cells modifies cell adhesion, increases metastatic potential, inhibits apoptosis, and induces angiogenesis for instance [71, 72, 73]. However, COX-2 expression in interstitial cells seems to be very important for tumor development as well in adenomas as in cancers. Animal studies provide some convincing arguments. First, in the Δapc 716 animal model of FAP there is no COX-2 expression in the dysplastic epithelial cells but only in interstitial cells (fibroblasts and endothelial cells) [43, 65]. Second, in a very elegant study Williams et al. [79] demonstrated that tumor growth of an implanted carcinoma is favored by COX-2 expression in the host: knock out of COX-2 gene or treatment with specific COX-2 inhibitors reduces tumor growth. This study suggests that host COX-2 expression in fibroblasts regulate intratumoral angiogenesis. Finally, the link between tumor angiogenesis and COX-2 expression in interstitial cells has been demonstrated in intestinal adenomas in Δapc 716 animal model and is related to PGE_2 production [53].

What triggers COX-2 expression in colorectal tumors?

Increased COX-2 expression is due to an increased gene transcription and to increased mRNA stability (transcriptional and posttranscriptional regulation) [16, 54]. Several pathways are involved in COX-2 regulation. The mitogen-activated extracellular signal regulated kinase activating kinase/extracellular signal regulated kinase pathway (MEK/ERK) regulates both transcriptional and posttranscriptional COX-2 expression. The Rho B signaling pathway regulates predominantly COX-2 expression at the transcriptional level whereas Akt/protein kinase B predominantly regulates COX-2 mRNA stability [54, 58]. In colorectal tumors little is known about the precise factors or events that triggers COX-2 induction.

COX-2 expression is very rapidly induced by a vast number of cytokines and growth factors as well as oncogenes, and all of these may be involved during colo-

rectal tumor development. COX-2 expression is induced particularly by mediators of inflammation (interleukin 1, tumor necrosis factor (TNF) α, lipopolysaccharide, interleukin 6, interferon γ), by growth factors such as epidermal growth factor, transforming growth factors α and β, basic fibroblast growth factor, and platelet-derived growth factor, and by some fatty acids, bile salts, and mucins secreted from colon cancer cells [26, 33, 35, 41, 64]. Moreover, COX-2 expression is regulated by activation of oncogenes and inactivation of antioncogenes known to be involved in colorectal tumor development. For instance, Ki-ras activation and Wnt pathway activation stimulate COX-2 expression [2]. Concerning Ki-ras, the ras/mitogen-activated extracellular signal regulated kinase activating kinase/extracellular signal regulated kinase (ras/MEK/ERK) pathway seems to be essential for COX-2 transcriptional induction whereas the ras/Akt/protein kinase B pathway predominantly modulates COX-2 mRNA stability [58]. Wild-type but not mutant p53 markedly inhibits COX-2 transcription [22, 67]. The respective role of each factor may differ depending on the cell type considered (epithelial cells or interstitial cell) or the stage of tumor development (e.g., early vs. late adenoma).

Clinical potential of selective COX-2 inhibitors

Numerous experiments including in vitro and animal studies have demonstrated a significant efficacy of selective COX-2 inhibitors for the treatment or prevention of colorectal tumors [20, 34, 37, 44, 70, 80]. Since these drugs are safer than classical NSAIDs, their use for the treatment or prevention of colorectal tumors seems very promising [61]. Moreover, whereas both NSAIDs and selective COX-2 inhibitors inhibit chemically induced colon tumors in rodents at the early stage of tumor development, only selective COX-2 inhibitors seem to be effective in established tumors [68]. Although numerous clinical trials are ongoing, at present only few results are available concerning selective COX-2 inhibitors efficiency in human colorectal tumor development. In addition, the cost/benefit balance must be precisely evaluated since they are expensive and not completely devoid of adverse effects [14, 27, 28].

Selective COX-2 inhibitors in familial adenomatous polyposis

Use of the COX-2 inhibitor celecoxib in FAP reduces the number of colorectal and duodenal adenomas. However, adenoma regression is incomplete since a significant number of polyps remain even under continuous therapy [46, 66]. Therefore it is very likely that COX-2 inhibitors, as with classical NSAIDs, are not completely protective against cancer development in these patients. It would be interesting to determine whether COX-2 inhibitors are able to inhibit the development of adenomas in young patients with a preclinical FAP.

Selective COX-2 inhibitors in sporadic colorectal cancers

It is not known yet if COX-2 inhibitors are effective for prevention or treatment of colorectal cancer. Double-blinded, placebo-controlled randomized trials are ongoing to evaluate COX-2 inhibitors for preventing colorectal adenomas. The use of COX-2 inhibitors is also being evaluated in conjunction with chemotherapy and radiotherapy in metastatic colorectal cancers. Some preliminary data suggest a possible beneficial effect, but contradictory results have also been reported [5, 21, 40]. Finally, although probably efficient in some patients, COX-2 inhibitors will certainly not be a miraculous anticancer therapy. This is suggested by the first results in clinical use of celecoxib and rofecoxib [5, 21, 46, 66] and also by experimental data. Indeed, whereas COX-2 expression contributes to colorectal tumor development, COX-1 may also be involved [11]. Moreover, colorectal cancers with microsatellite instability, which account for about 10% of sporadic colorectal cancers, have a less frequent COX-2 expression [1, 36]. Therefore COX-2 inhibitors to prevent or treat these cancers could be of limited use.

Conclusion

COX-2 involvement in colorectal tumor development is well demonstrated. However, the underlying mechanisms are numerous and complex. Many questions remain concerning, among others, COX-2 regulation and the respective role of epithelial and interstitial cells in tumor development. Selective COX-2 inhibitors may prove effective in preventing or treating adenomas or cancer. However, their real efficiency is currently evaluated in clinical trials and no definite conclusion can be made at the moment.

Note: Many works have been carried out regarding the role of COX-2 in colorectal tumor development, and extensive findings have been published. We have chosen to deal with only certain questions raised in this field, and therefore some works are not cited directly in this review; we apologize for this.

References

1. Aaltonen LA, Peltomaki P, Mecklin JP, Jarvinen H, Jass JR, Green JS, Lynch HT, Watson P, Tallqvist G, Juhola M et al. (1994) Replication errors in benign and malignant tumors from hereditary nonpolyposis colorectal cancer patients. Cancer Res 54:1645–1648
2. Araki Y, Okamura S, Hussain SP, Nagashima M, He P, Shiseki M, Miura K, Harris CC (2003) Regulation of cyclooxygenase-2 expression by the Wnt and ras pathways. Cancer Res 63:728–734
3. Arvind P, Papavassiliou ED, Tsioulias GJ, Qiao L, Lovelace CI, Duceman B, Rigas B (1995) Prostaglandin E2 down-regulates

the expression of HLA-DR antigen in human colon adenocarcinoma cell lines. Biochemistry 34:5604–5609
4. Bamba H, Ota S, Kato A, Adachi A, Itoyama S, Matsuzaki F (1999) High expression of cyclooxygenase-2 in macrophages of human colonic adenoma. Int J Cancer 83:470–475
5. Becerra CR, Frenkel EP, Ashfaq R, Gaynor RB (2003) Increased toxicity and lack of efficacy of Rofecoxib in combination with chemotherapy for treatment of metastatic colorectal cancer: a phase II study. Int J Cancer 105:868–872
6. Benamouzig R, Deyra J, Martin A, Girard B, Jullian E, Piednoir B, Couturier D, Coste T, Little J, Chaussade S (2003) Daily soluble aspirin and prevention of colorectal adenoma recurrence: one-year results of the APACC trial. Gastroenterology 125:328–336
7. Cao Y, Pearman AT, Zimmerman GA, McIntyre TM, Prescott SM (2000) Intracellular unesterified arachidonic acid signals apoptosis. Proc Natl Acad Sci U S A 97:11280–11285
8. Chan TA, Morin PJ, Vogelstein B, Kinzler KW (1998) Mechanisms underlying nonsteroidal antiinflammatory drug-mediated apoptosis. Proc Natl Acad Sci U S A 95:681–686
9. Chandrasekharan NV, Dai H, Roos KL, Evanson NK, Tomsik J, Elton TS, Simmons DL (2002) COX-3, a cyclooxygenase-1 variant inhibited by acetaminophen and other analgesic/antipyretic drugs: cloning, structure, and expression. Proc Natl Acad Sci U S A 99:13926–13931. Epub 12002 Sep 13919
10. Chapple KS, Cartwright EJ, Hawcroft G, Tisbury A, Bonifer C, Scott N, Windsor AC, Guillou PJ, Markham AF, Coletta PL, Hull MA (2000) Localization of cyclooxygenase-2 in human sporadic colorectal adenomas. Am J Pathol 156:545–553
11. Chulada PC, Thompson MB, Mahler JF, Doyle CM, Gaul BW, Lee C, Tiano HF, Morham SG, Smithies O, Langenbach R (2000) Genetic disruption of Ptgs-1, as well as Ptgs-2, reduces intestinal tumorigenesis in Min mice. Cancer Res 60:4705–4708
12. Cianchi F, Cortesini C, Bechi P, Fantappie O, Messerini L, Vannacci A, Sardi I, Baroni G, Boddi V, Mazzanti R, Masini E (2001) Up-regulation of cyclooxygenase 2 gene expression correlates with tumor angiogenesis in human colorectal cancer. Gastroenterology 121:1339–1347
13. Daniel TO, Liu H, Morrow JD, Crews BC, Marnett LJ (1999) Thromboxane A2 is a mediator of cyclooxygenase-2-dependent endothelial migration and angiogenesis. Cancer Res 59:4574–4577
14. Deviere J (2002) Do selective cyclo-oxygenase inhibitors eliminate the adverse events associated with nonsteroidal anti-inflammatory drug therapy? Eur J Gastroenterol Hepatol 14:S29–S33
15. Dinchuk JE, Car BD, Focht RJ, Johnston JJ, Jaffee BD, Covington MB, Contel NR, Eng VM, Collins RJ, Czerniak PM et al. (1995) Renal abnormalities and an altered inflammatory response in mice lacking cyclooxygenase II. Nature 378:406–409
16. Dixon DA, Tolley ND, King PH, Nabors LB, McIntyre TM, Zimmerman GA, Prescott SM (2001) Altered expression of the mRNA stability factor HuR promotes cyclooxygenase-2 expression in colon cancer cells. J Clin Invest 108:1657–1665
17. Eberhart CE, Coffey RJ, Radhika A, Giardiello FM, Ferrenbach S, DuBois RN (1994) Up-regulation of cyclooxygenase 2 gene expression in human colorectal adenomas and adenocarcinomas. Gastroenterology 107:1183–1188
18. Einspahr JG, Krouse RS, Yochim JM, Danenberg PV, Danenberg KD, Bhattacharyya AK, Martinez ME, Alberts DS (2003) Association between Cyclooxygenase expression and colorectal adenoma characteristics. Cancer Res 63:3891–3893
19. Elder DJ, Baker JA, Banu NA, Moorghen M, Paraskeva C (2002) Human colorectal adenomas demonstrate a size-dependent increase in epithelial cyclooxygenase-2 expression. J Pathol 198:428–434
20. Elder DJ, Halton DE, Crew TE, Paraskeva C (2000) Apoptosis induction and cyclooxygenase-2 regulation in human colorectal adenoma and carcinoma cell lines by the cyclooxygenase-2-selective non-steroidal anti-inflammatory drug NS-398. Int J Cancer 86:553–560
21. Fenwick SW, Toogood GJ, Lodge JP, Hull MA (2003) The effect of the selective cyclooxygenase-2 inhibitor rofecoxib on human colorectal cancer liver metastases. Gastroenterology 125:716–729
22. Gallo O, Schiavone N, Papucci L, Sardi I, Magnelli L, Franchi A, Masini E, Capaccioli S (2003) Down-regulation of nitric oxide synthase-2 and cyclooxygenase-2 pathways by p53 in squamous cell carcinoma. Am J Pathol 163:723–732
23. Giardiello FM, Hamilton SR, Krush AJ, Piantadosi S, Hylind LM, Celano P, Booker SV, Robinson CR, Offerhaus GJ (1993) Treatment of colonic and rectal adenomas with sulindac in familial adenomatous polyposis. N Engl J Med 328:1313–1316
24. Giovannucci E, Egan KM, Hunter DJ, Stampfer MJ, Colditz GA, Willett WC, Speizer FE (1995) Aspirin and the risk of colorectal cancer in women. N Engl J Med 333:609–614
25. Giovannucci E, Rimm EB, Stampfer MJ, Colditz GA, Ascherio A, Willett WC (1994) Aspirin use and the risk for colorectal cancer and adenoma in male health professionals. Ann Intern Med 121:241–246
26. Glinghammar B, Rafter J (2001) Colonic luminal contents induce cyclooxygenase 2 transcription in human colon carcinoma cells. Gastroenterology 120:401–410
27. Gomez Cerezo J, Lubomirov Hristov R, Carcas Sansuan AJ, Vazquez Rodriguez JJ (2003) Outcome trials of COX-2 selective inhibitors: global safety evaluation does not promise benefits. Eur J Clin Pharmacol 59:169–175
28. d'Halluin PN, Turlin B, Polard E, Dinasquet M, Pagenault M, Rioux N, Gosselin M, Bretagne JF, Heresbach D (2003) [Selective COX-2 inhibitor-associated colitis: two case reports]. Gastroenterol Clin Biol 27:932–935
29. Hanif R, Pittas A, Feng Y, Koutsos MI, Qiao L, Staiano-Coico L, Shiff SI, Rigas B (1996) Effects of nonsteroidal anti-inflammatory drugs on proliferation and on induction of apoptosis in colon cancer cells by a prostaglandin-independent pathway. Biochem Pharmacol 52:237–245
30. Hao X, Bishop AE, Wallace M, Wang H, Willcocks TC, Maclouf J, Polak JM, Knight S, Talbot IC (1999) Early expression of cyclo-oxygenase-2 during sporadic colorectal carcinogenesis. J Pathol 187:295–301
31. Hasegawa K, Ichikawa W, Fujita T, Ohno R, Okusa T, Yoshinaga K, Sugihara K (2001) Expression of cyclooxygenase-2 (COX-2) mRNA in human colorectal adenomas. Eur J Cancer 37:1469–1474
32. Hull MA, Booth JK, Tisbury A, Scott N, Bonifer C, Markham AF, Coletta PL (1999) Cyclooxygenase 2 is up-regulated and localized to macrophages in the intestine of Min mice. Br J Cancer 79:1399–1405
33. Inaba T, Sano H, Kawahito Y, Hla T, Akita K, Toda M, Yamashina I, Inoue M, Nakada H (2003) Induction of cyclooxygenase-2 in monocyte/macrophage by mucins secreted from colon cancer cells. Proc Natl Acad Sci U S A 100:2736–2741. Epub 2003 Feb 2721
34. Jacoby RF, Seibert K, Cole CE, Kelloff G, Lubet RA (2000) The cyclooxygenase-2 inhibitor celecoxib is a potent preventive and therapeutic agent in the min mouse model of adenomatous polyposis. Cancer Res 60:5040–5044
35. Jones DA, Carlton DP, McIntyre TM, Zimmerman GA, Prescott SM (1993) Molecular cloning of human prostaglandin endoperoxide synthase type II and demonstration of expression in response to cytokines. J Biol Chem 268:9049–9054
36. Karnes WE Jr, Shattuck-Brandt R, Burgart LJ, DuBois RN, Tester DJ, Cunningham JM, Kim CY, McDonnell SK, Schaid DJ, Thibodeau SN (1998) Reduced COX-2 protein in colorectal cancer with defective mismatch repair. Cancer Res 58:5473–5477
37. Kawamori T, Rao CV, Seibert K, Reddy BS (1998) Chemopreventive activity of celecoxib, a specific cyclooxygenase-2 inhibitor, against colon carcinogenesis. Cancer Res 58:409–412
38. Kojima M, Morisaki T, Uchiyama A, Doi F, Mibu R, Katano M, Tanaka M (2001) Association of enhanced cyclooxygenase-

2 expression with possible local immunosuppression in human colorectal carcinomas. Ann Surg Oncol 8:458–465
39. Lim H, Paria BC, Das SK, Dinchuk JE, Langenbach R, Trzaskos JM, Dey SK (1997) Multiple female reproductive failures in cyclooxygenase 2-deficient mice. Cell 91:197–208
40. Lin E, Morris JS, Ayers GD (2002) Effect of celecoxib on capecitabine-induced hand-foot syndrome and antitumor activity. Oncology (Huntingt) 16:31–37
41. Meade EA, McIntyre TM, Zimmerman GA, Prescott SM (1999) Peroxisome proliferators enhance cyclooxygenase-2 expression in epithelial cells. J Biol Chem 274:8328–8334
42. Morham SG, Langenbach R, Loftin CD, Tiano HF, Vouloumanos N, Jennette JC, Mahler JF, Kluckman KD, Ledford A, Lee CA et al. (1995) Prostaglandin synthase 2 gene disruption causes severe renal pathology in the mouse. Cell 83:473–482
43. Oshima M, Dinchuk JE, Kargman SL, Oshima H, Hancock B, Kwong E, Trzaskos JM, Evans JF, Taketo MM (1996) Suppression of intestinal polyposis in Apc delta716 knockout mice by inhibition of cyclooxygenase 2 (COX-2). Cell 87:803–809
44. Oshima M, Murai N, Kargman S, Arguello M, Luk P, Kwong E, Taketo MM, Evans JF (2001) Chemoprevention of intestinal polyposis in the Apcdelta716 mouse by rofecoxib, a specific cyclooxygenase-2 inhibitor. Cancer Res 61:1733–1740
45. Pai R, Soreghan B, Szabo IL, Pavelka M, Baatar D, Tarnawski AS (2002) Prostaglandin E2 transactivates EGF receptor: a novel mechanism for promoting colon cancer growth and gastrointestinal hypertrophy. Nat Med 8:289–293
46. Phillips RK, Wallace MH, Lynch PM, Hawk E, Gordon GB, Saunders BP, Wakabayashi N, Shen Y, Zimmerman S, Godio L, Rodrigues-Bigas M, Su LK, Sherman J, Kelloff G, Levin B, Steinbach G (2002) A randomised, double blind, placebo controlled study of celecoxib, a selective cyclooxygenase 2 inhibitor, on duodenal polyposis in familial adenomatous polyposis. Gut 50:857–860
47. Piazza GA, Alberts DS, Hixson LJ, Paranka NS, Li H, Finn T, Bogert C, Guillen JM, Brendel K, Gross PH, Sperl G, Ritchie J, Burt RW, Ellsworth L, Ahnen DJ, Pamukcu R (1997) Sulindac sulfone inhibits azoxymethane-induced colon carcinogenesis in rats without reducing prostaglandin levels. Cancer Res 57:2909–2915
48. Prescott SM, White RL (1996) Self-promotion? Intimate connections between APC and prostaglandin H synthase-2. Cell 87:783–786
49. Rao M, Yang W, Seifalian AM, Winslet MC (2004) Role of cyclooxygenase-2 in the angiogenesis of colorectal cancer. Int J Colorectal Dis 19:1–11
50. Rigas B, Goldman IS, Levine L (1993) Altered eicosanoid levels in human colon cancer. J Lab Clin Med 122:518–523
51. Sandler RS, Halabi S, Baron JA, Budinger S, Paskett E, Keresztes R, Petrelli N, Pipas JM, Karp DD, Loprinzi CL, Steinbach G, Schilsky R (2003) A randomized trial of aspirin to prevent colorectal adenomas in patients with previous colorectal cancer. N Engl J Med 348:883–890
52. Sano H, Kawahito Y, Wilder RL, Hashiramoto A, Mukai S, Asai K, Kimura S, Kato H, Kondo M, Hla T (1995) Expression of cyclooxygenase-1 and -2 in human colorectal cancer. Cancer Res 55:3785–3789
53. Seno H, Oshima M, Ishikawa TO, Oshima H, Takaku K, Chiba T, Narumiya S, Taketo MM (2002) Cyclooxygenase 2- and prostaglandin E (2) receptor EP (2)-dependent angiogenesis in Apc (Delta716) mouse intestinal polyps. Cancer Res 62:506–511
54. Shao J, Sheng H, Inoue H, Morrow JD, DuBois RN (2000) Regulation of constitutive cyclooxygenase-2 expression in colon carcinoma cells. J Biol Chem 275:33951–33956
55. Shattuck-Brandt RL, Varilek GW, Radhika A, Yang F, Washington MK, DuBois RN (2000) Cyclooxygenase 2 expression is increased in the stroma of colon carcinomas from IL-10 (-/-) mice. Gastroenterology 118:337–345
56. Sheng H, Shao J, Hooton EB, Tsujii M, DuBois RN, Beauchamp RD (1997) Cyclooxygenase-2 induction and transforming growth factor beta growth inhibition in rat intestinal epithelial cells. Cell Growth Differ 8:463–470
57. Sheng H, Shao J, Morrow JD, Beauchamp RD, DuBois RN (1998) Modulation of apoptosis and Bcl-2 expression by prostaglandin E2 in human colon cancer cells. Cancer Res 58:362–366
58. Sheng H, Shao J, Dubois RN (2001) K-Ras-mediated increase in cyclooxygenase 2 mRNA stability involves activation of the protein kinase B1. Cancer Res 61:2670–2675
59. Sheng H, Shao J, Washington MK, DuBois RN (2001) Prostaglandin E2 increases growth and motility of colorectal carcinoma cells. J Biol Chem 276:18075–18081
60. Shiff SJ, Rigas B (1997) Nonsteroidal anti-inflammatory drugs and colorectal cancer: evolving concepts of their chemopreventive actions. Gastroenterology 113:1992–1998
61. Silverstein FE, Faich G, Goldstein JL, Simon LS, Pincus T, Whelton A, Makuch R, Eisen G, Agrawal NM, Stenson WF, Burr AM, Zhao WW, Kent JD, Lefkowith JB, Verburg KM, Geis GS (2000) Gastrointestinal toxicity with celecoxib vs nonsteroidal anti-inflammatory drugs for osteoarthritis and rheumatoid arthritis: the CLASS study: a randomized controlled trial. Celecoxib Long-term Arthritis Safety Study. JAMA 284:1247–1255
62. Sinicrope FA, Lemoine M, Xi L, Lynch PM, Cleary KR, Shen Y, Frazier ML (1999) Reduced expression of cyclooxygenase 2 proteins in hereditary nonpolyposis colorectal cancers relative to sporadic cancers. Gastroenterology 117:350–358
63. Smith WL, Garavito RM, DeWitt DL (1996) Prostaglandin endoperoxide H synthases (cyclooxygenases)-1 and -2. J Biol Chem 271:33157–33160
64. Smith WL, DeWitt DL, Garavito RM (2000) Cyclooxygenases: structural, cellular, and molecular biology. Annu Rev Biochem 69:145–182
65. Sonoshita M, Takaku K, Oshima M, Sugihara K, Taketo MM (2002) Cyclooxygenase-2 expression in fibroblasts and endothelial cells of intestinal polyps. Cancer Res 62:6846–6849
66. Steinbach G, Lynch PM, Phillips RK, Wallace MH, Hawk E, Gordon GB, Wakabayashi N, Saunders B, Shen Y, Fujimura T, Su LK, Levin B (2000) The effect of celecoxib, a cyclooxygenase-2 inhibitor, in familial adenomatous polyposis. N Engl J Med 342:1946–1952
67. Subbaramaiah K, Altorki N, Chung WJ, Mestre JR, Sampat A, Dannenberg AJ (1999) Inhibition of cyclooxygenase-2 gene expression by p53. J Biol Chem 274:10911–10915
68. Thun MJ, Henley SJ, Patrono C (2002) Nonsteroidal anti-inflammatory drugs as anticancer agents: mechanistic, pharmacologic, and clinical issues. J Natl Cancer Inst 94:252–266
69. Tiano HF, Loftin CD, Akunda J, Lee CA, Spalding J, Sessoms A, Dunson DB, Rogan EG, Morham SG, Smart RC, Langenbach R (2002) Deficiency of Either Cyclooxygenase (COX)-1 or COX-2 Alters Epidermal Differentiation and Reduces Mouse Skin Tumorigenesis. Cancer Res 62:3395–3401
70. Tomozawa S, Nagawa H, Tsuno N, Hatano K, Osada T, Kitayama J, Sunami E, Nita ME, Ishihara S, Yano H, Tsuruo T, Shibata Y, Muto T (1999) Inhibition of haematogenous metastasis of colon cancer in mice by a selective COX-2 inhibitor, JTE-522. Br J Cancer 81:1274–1279
71. Tsujii M, DuBois RN (1995) Alterations in cellular adhesion and apoptosis in epithelial cells overexpressing prostaglandin endoperoxide synthase 2. Cell 83:493–501
72. Tsujii M, Kawano S, DuBois RN (1997) Cyclooxygenase-2 expression in human colon cancer cells increases metastatic potential. Proc Natl Acad Sci U S A 94:3336–3340
73. Tsujii M, Kawano S, Tsuji S, Sawaoka H, Hori M, DuBois RN (1998) Cyclooxygenase regulates angiogenesis induced by colon cancer cells. Cell 93:705–716
74. Waddell WR, Ganser GF, Cerise EJ, Loughry RW (1989) Sulindac for polyposis of the colon. Am J Surg 157:175–179
75. Wallace JL, Bak A, McKnight W, Asfaha S, Sharkey KA, MacNaughton WK (1998) Cyclooxygenase 1 contributes to inflammatory responses in rats and mice: implications for gastrointestinal toxicity. Gastroenterology 115:101–109

76. Wallace JL, Chapman K, McKnight W (1999) Limited anti-inflammatory efficacy of cyclo-oxygenase-2 inhibition in carrageenan-airpouch inflammation. Br J Pharmacol 126:1200–1204
77. Wendum D, Boelle PY, Rigau V, Sebbagh N, Olschwang S, Mourra N, Parc R, Trugnan G, Masliah J, Flejou JF (2003) Mucinous colon carcinomas with microsatellite instability have a lower microvessel density and lower vascular endothelial growth factor expression. Virchows Arch 442:111–117
78. Wendum D, Svrcek M, Rigau V, Boelle PY, Sebbagh N, Parc R, Masliah J, Trugnan G, Flejou JF (2003) COX-2, inflammatory secreted PLA2, and cytoplasmic PLA2 protein expression in small bowel adenocarcinomas compared with colorectal adenocarcinomas. Mod Pathol 16:130–136
79. Williams CS, Tsujii M, Reese J, Dey SK, DuBois RN (2000) Host cyclooxygenase-2 modulates carcinoma growth. J Clin Invest 105:1589–1594
80. Yao M, Kargman S, Lam EC, Kelly CR, Zheng Y, Luk P, Kwong E, Evans JF, Wolfe MM (2003) Inhibition of cyclooxygenase-2 by rofecoxib attenuates the growth and metastatic potential of colorectal carcinoma in mice. Cancer Res 63:586–592

Virchows Arch (2004) 445:334–343
DOI 10.1007/s00428-004-1077-2

ORIGINAL ARTICLE

Eva Geissinger · Tobias Odenwald · Seung-Sook Lee · Irina Bonzheim · Sabine Roth · Peter Reimer · Martin Wilhelm · Hans Konrad Müller-Hermelink · Thomas Rüdiger

Nodal peripheral T-cell lymphomas and, in particular, their lymphoepithelioid (Lennert's) variant are often derived from CD8$^+$ cytotoxic T-cells

Received: 2 April 2004 / Accepted: 14 June 2004 / Published online: 29 July 2004
© Springer-Verlag 2004

Abstract Nodal peripheral T-cell lymphomas are not well understood, and most of them are classified in the "not otherwise specified group" (PTCL-NOS). Data on their normal cellular derivation are ambiguous. Most peripheral T-cell lymphomas are composed of tumor cells and a (sometimes dominant) reactive background, which also includes resting and activated T-lymphocytes. We defined the phenotype of the tumor cells in 101 PTCL-NOS based on their cytological atypia and using immunohistochemical double stains on paraffin sections with CD4/Ki67 and CD8/Ki67. The results were correlated to clinical presentation and outcome. Lineage could be defined in 98 cases (97%). Tumor cells were CD4$^+$ in 43 cases and CD8$^+$ in 38. These presented at a younger age but a higher clinical stage compared with the CD4$^+$ lymphomas. In 15 cases, the atypical cells were CD4$^-$CD8$^-$; two cases were CD4$^+$CD8$^+$. Of 17 lymphoepithelioid (Lennert's) lymphomas, 15 expressed CD8, one each was CD4$^+$ and CD4$^-$CD8$^-$.

E. Geissinger · I. Bonzheim · S. Roth · H. K. Müller-Hermelink · T. Rüdiger (✉)
Institute of Pathology, University of Würzburg,
Josef-Schneider-Strasse 2, 97080 Würzburg, Germany
e-mail: thomas.ruediger@mail.uni-wuerzburg.de
Tel.: +49-931-20147783
Fax: +49-931-8887518

T. Odenwald
Pediatric Clinic, University of Heidelberg, Germany

S.-S. Lee
Department of Pathology,
Korea Cancer Center Hospital, Seoul, Korea

P. Reimer
Medizinische Poliklinik, University of Würzburg, Germany

M. Wilhelm
Medizinische Klinik 5, Klinikum Nürnberg, Germany

Keywords T-cell lymphoma · Lennert's lymphoma · Immunohistochemistry · Clinicopathological correlation · Phenotype

Introduction

Peripheral T-cell lymphomas (PTCL) comprise a heterogeneous group, and their classification is still debated. While the working formulation [1]—classifying malignant lymphomas on the basis of hematoxylin and eosin (H&E) sections alone—did not recognize PTCL as a separate group, the Kiel classification [44]—listing entities corresponding to a proposed normal counterpart [46]—distinguished PTCL from the more common B-cell lymphomas and defined various morphological subtypes. Despite their sound conceptual background, these categories were poorly reproducible [13, 18] and only vaguely correlated with clinical presentation and outcome [9, 38, 43]. While the Kiel classification comprises nodal lymphomas only, the extranodal PTCL could not be satisfactorily diagnosed in this scheme.

In the Revised European–American Classification of Lymphoid Neoplasms (REAL) [16] and World Health Organization (WHO) [21] classifications of malignant lymphoma, clinicopathological entities are defined by their morphological, immunophenotypical, genetic, and clinical characteristics. Applying these principles, the clinical presentation is an important feature and defines most extranodal PTCL [24, 38]. Among nodal PTCL, anaplastic large cell lymphoma and angioimmunoblastic T-cell lymphoma represent disease entities that are fairly frequent in the Western population. Other PTCL categories show considerable overlap in both their pathological and clinical characteristics [38]. These form the—admittedly heterogeneous—category of "not otherwise specified" PTCL (PTCL-NOS) [16], a category that comprises several morphological variants that correspond to entities defined in the Kiel classification: a medium-sized cell, a mixed

medium and large cell, and a large cell variant as well as T-zone and lymphoepithelioid (Lennert's) lymphoma (LeL). The international non-Hodgkin's lymphoma classification project [2, 38] proved that PTCL can be reliably diagnosed according to the REAL classification. Variants of PTCL-NOS were not clinically distinguishable and are all equally characterized by a poor prognosis when using currently available therapy.

Lacking reproducible criteria to subclassify PTCL-NOS morphologically, tumor cell immunophenotype has been suggested to be a good basis for their classification. This approach seems particularly tempting because peripheral post-thymic T-cells, with few exceptions [14], exclusively express the lineage-specific molecules CD4 or CD8. Functional subsets comprise helper and cytotoxic T-cells, as well as T/NK-cells. While subsets of helper T-cell lymphomas (T_{H1} and T_{H2}) cannot be defined in paraffin sections, cytotoxic granules and CD56 are easily detectable. However, phenotypical data on nodal PTCL are heterogeneous, regarding both tumor cell lineage and expression of cytotoxic granules [5, 7, 9, 30, 32, 33, 35, 39].

This heterogeneity might result from technical problems because, in addition to the neoplastic cells, PTCL also comprises varying numbers of reactive T-lymphocytes [16, 22, 27, 42]. Since most of these studies were performed, methods have become available to assess the morphology in immunostained slides and to double stain cells on paraffin sections. Applying these, we tried to define the phenotype of tumor cells in 101 PTCL-NOS and to correlate it to clinical presentation and follow-up.

Materials and methods

Altogether, we analyzed 101 cases of PTCL-NOS, including 18 LeLs. All cases were stained with H&E, Giemsa, periodic acid-Schiff, and silver impregnation (Gömöri) to assess morphology. Diagnoses were made according to the WHO classification [21]. Cases were included in this study as variants of PTCL-NOS after better-defined entities of PTCL had been ruled out. Cases with prominent CD30 expression and sinus infiltration in particular were diagnosed as anaplastic large cell lymphoma and excluded from the study. Angioimmunoblastic T-cell lymphomas were identified by their prominent proliferation of follicular dendritic cell networks and published separately [27].

Routine immunohistochemical stains were performed using mouse monoclonal antibodies against CD3, CD5, CD4, CD8, TIA-1, granzyme B, CD56, CD57, CD20, CD21, Ki-67, CD30, and latent membrane protein (LMP). T-cell receptor γ gene rearrangement [48] was studied if necessary to confirm the diagnosis.

Immunohistochemical double stains were performed for CD4/Ki67 and CD8/Ki67 to assess the proliferation of these subpopulations individually. For double stains, antibodies against CD4 or CD8 and Ki-67 were applied in consecutive steps and visualized with AEC (Zymed, Berlin, Germany) and Fast Blue (Zymed, Berlin, Germany), respectively. Prior to the application of the second antibody, free binding sites were blocked with Fab fragment goat anti-mouse IgG.

Tumor cell lineage was defined by assessing the staining of atypical T-cells in conventional stains and the proliferation rate in the double stains. Proliferation was assessed independently for the $CD4^+$ and $CD8^+$ population, counting Ki67 staining in 200 cells that stained positively for the respective antibody. In histiocyte-rich cases, morphology and staining intensity for CD4 were used as criteria to distinguish T-cells from histiocytes. Nuclear atypia was evaluated in additional single stains for CD4 and CD8. Tumors were regarded as positive for a particular antibody if more than 30% of morphologically identifiable tumor cells were clearly stained, regardless of their proliferation rate.

Clinical data could be obtained retrospectively for 66 patients from patient records. Estimates of overall survival distribution and failure-free survival were calculated using the method of Kaplan and Meier [23]; time-to-event distributions were compared using the log-rank test. The individual items for histological features, immunological, and clinical parameters, including international prognostic index (IPI) [40], were estimated in correlation with the other items and clinical outcome using χ^2 tests or t-tests as appropriate. Statistical significance was assumed if $P<0.05$.

Results

Our study included 101 patients with PTCL-NOS diagnosed from lymph-node biopsies. The majority of these lymphomas consisted of a mixed medium-sized and large cell population (56 cases), while predominantly medium-sized or large tumor cells occurred in 10 and 17 cases, respectively. LeL was diagnosed in 18 cases according to the WHO classification when clusters of epithelioid histiocytes were prominent in the infiltrate.

While most of the tumors infiltrated into the perinodal fat (43%) or infiltrated the lymph-node capsule (19%), 38% were confined to the lymph-node. In 32% of our cases, the lymph-node tissue was only partially effaced, and areas of pre-existing lymphatic tissue were still present. Within the infiltrated areas, remnant regressive networks of follicular dendritic cells, partially infiltrated by the tumor, were identified in 32% of the cases. The lymph-node sinuses were partially or completely obliterated by tumor cells in 52% of cases. Cytologically, the tumor cell nuclei were mildly (54%), moderately (32%), or markedly (14%) atypical. Clear cells were prominent in 43% of all cases and detectable in another 27% (Fig. 1).

Accompanying reactive changes comprised various degrees of eosinophilia, plasmacytosis, and blood vessel proliferation encountered in 44%, 51%, and 79% of our cases, respectively. Epithelioid cells formed granulomas that were infiltrated by tumor cells in the 18 cases of LeL. Histiocytes were prominent in 20 additional cases, but did not form granulomas and were not epithelioid. Tumors were partially necrotic in 14 of 101 cases, and necrosis was extensive in an additional 9 tumors. In 3 of these 23 cases, these necroses were accentuated in lymph-node sinuses.

Fig. 1 Morphological variability of peripheral T-cell lymphomas "not otherwise specified." **A** Spread: lymphoma confined to the lymph node (*left*), infiltrating the capsule (*middle*) or perinodal fat (*right*). **B** Remnant reactive uninvolved areas. **C** Remnant follicles in the infiltrated areas (CD3 and CD21). **D** Mild (*left*), moderate (*middle*), and severe (*right*) cellular atypia ▶

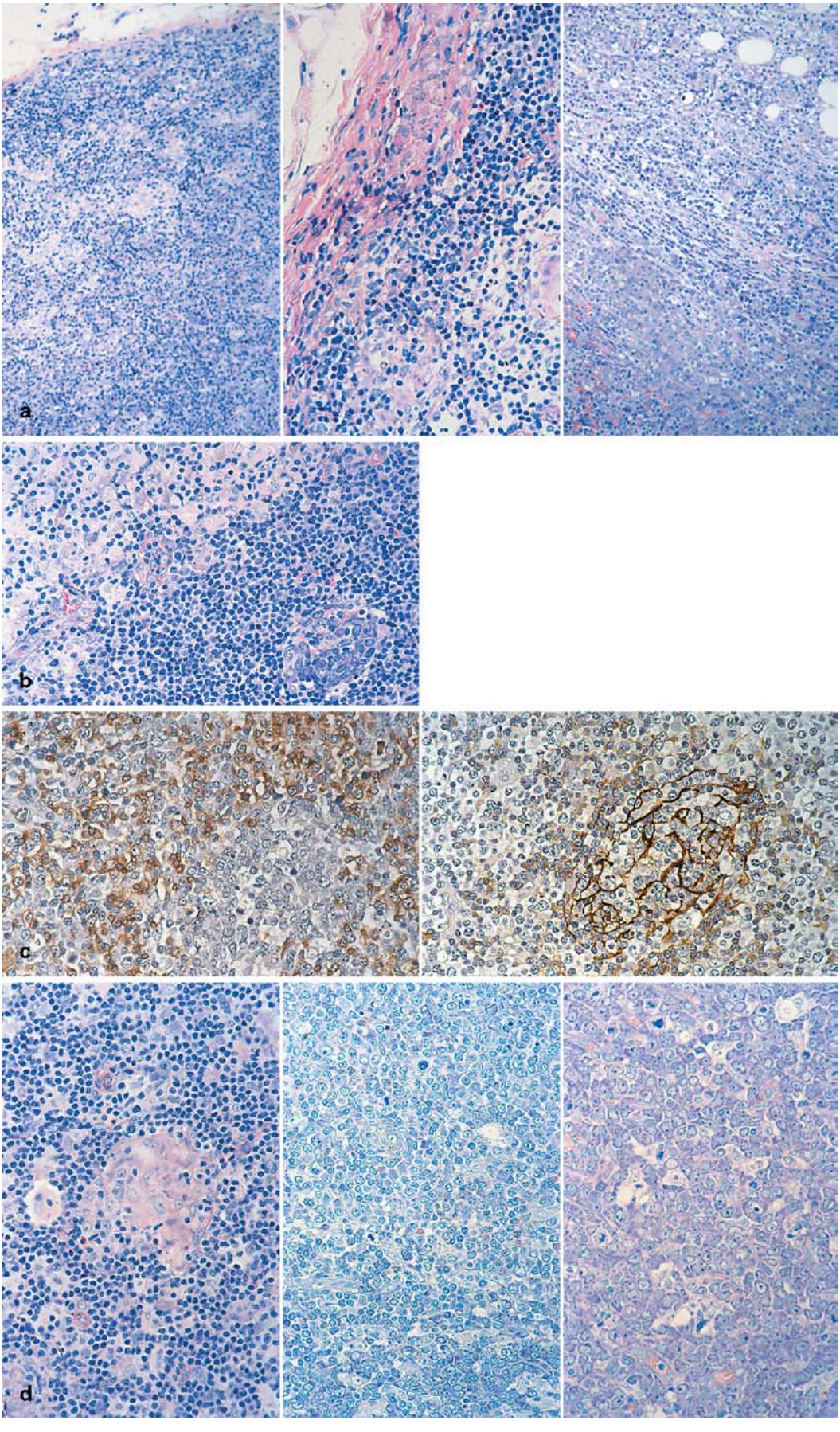

a
b
c
d

Table 1 Immunophenotypes of peripheral T-cell lymphomas "not otherwise specified" (PTCL-NOS) and comparison of Lennert's lymphoma to all other cases. *DN* double negative (CD4– CD8–), *DP* double positive ($CD4^+$ $CD8^+$), *ctx* $TIA1^+$ or GrB^+

	All PTCL-NOS	Lennert's lymphoma	PTCL-NOS (excluding Lennert's lymphoma)	*P* value
	(*n*=101)	(*n*=18)	(*n*=83)	
	%	%	%	
CD3	93%	100%	92%	0.21
CD5	78%	94%	75%	0.07
CD2	47%	56%	45%	0.41
CD4	44%	6%	54%	0.00
CD8	41%	88%	30%	
DN	14%	6%	15%	
DP	1%	0%	1%	
TIA	36%	53%	32%	0.11
GrB	20%	35%	17%	0.10
ctx	40%	64%	35%	0.03
CD56	3%	0%	4%	0.37
CD57	11%	27%	7%	0.01
CD30*	18%	12%	19%	0.48

* CD30 expression was weak and limited to individual cells in cases regarded as positive; anaplastic large cell lymphoma was excluded

Immunophenotypes

Our PTCL were positive for CD3 in almost all cases (93%), but only 78% and 13% expressed CD5 and CD7, respectively. Altogether, 29% of all cases exhibited an antigen loss, i.e., were negative for CD3, CD5, or both lineage markers (CD4 and CD8). Only three cases were negative for both CD3 and CD5, and two of these expressed CD56. Immunophenotypes are detailed in Table 1.

Based on nuclear atypia and proliferation of T-cell subsets, lineage could be defined in 98 cases (97%): tumor cells were $CD4^+$ in 43 cases and $CD8^+$ in 38 cases (Fig. 2). In 15 cases, the atypical cells were negative for both antigenes, and these were considered to be double negative (DN). Two cases expressing both CD4 and CD8 on the tumor cells (double positive, DP) showed the morphology of PTCL-NOS and were negative for both TdT and CD99.

Correlating tumor cell lineage to the results of the double stains (that could both be evaluated in 69 cases), the proliferation index of the neoplastic subpopulation exceeded that of the reactive one ($P<0.01$, Fig. 3) in all but 14 cases (11 $CD4^+$ and 3 $CD8^+$). In these latter cases, the nuclear atypia was clear cut, and tumor cell lineage definition was based on this.

Concerning the background infiltrate, histiocytes and/or epithelioid cells occurred more frequently in $CD8^+$ than in $CD4^+$ lymphomas ($P<0.001$). This association remained significant ($P=0.004$) after excluding the LeL, which, by definition, contain epithelioid cell granulomas. Among the $CD4^+$ lymphomas, epithelioid cell clusters

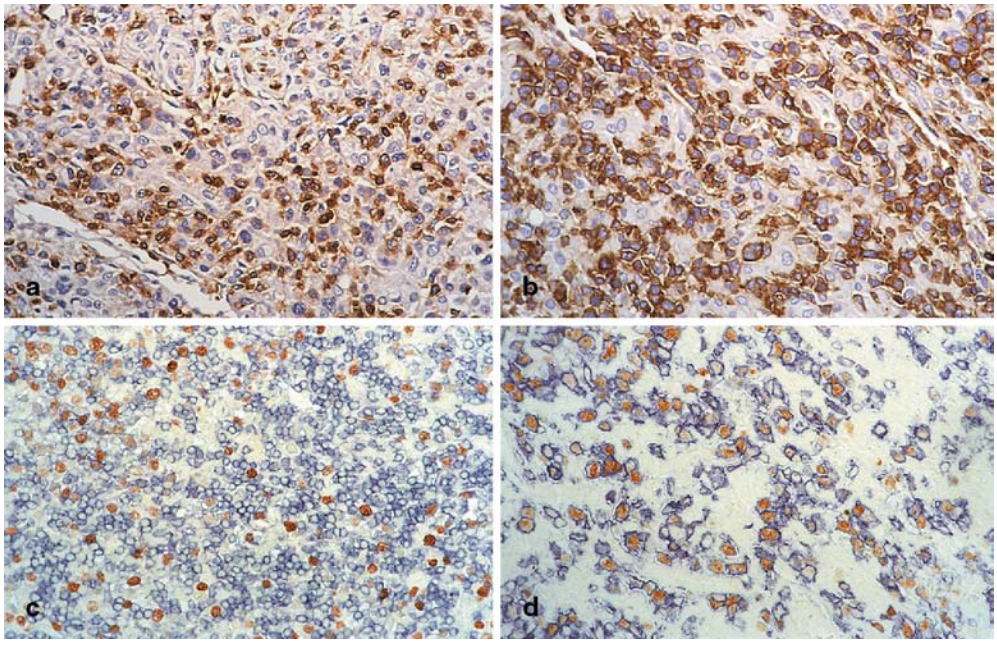


Fig. 2 Definition of tumor cell lineage in a $CD8^+$ peripheral T-cell lymphomas "not otherwise specified": CD3– (*upper left*), $CD5^+$ (*upper right*). Ki67 (*red*) labels $CD8^+$ cells (*blue, lower right*), but not $CD4^+$ cells (*blue, lower left*)

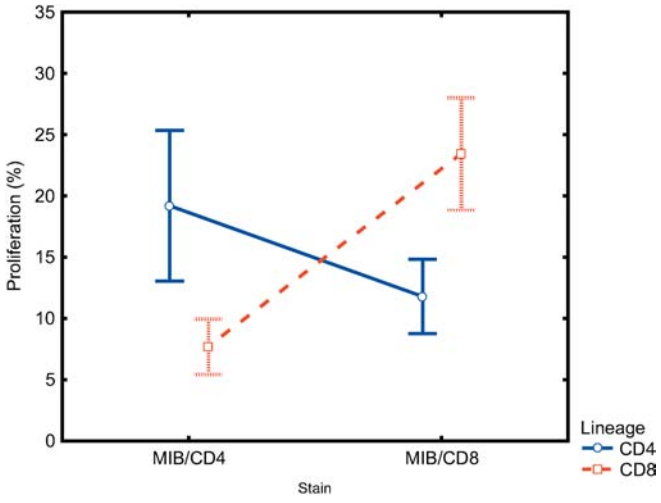


Fig. 3 Mean proliferation and 95% confidence interval for tumors with lineage defined as CD4 or CD8

were seen more often in those that coexpressed cytotoxic molecules than in others ($P<0.001$).

Cytotoxic molecules (either TIA1, granzyme B or both) were detected in 38 cases (38%) altogether. Their expression was strongly correlated with lineage ($P<0.01$): while 26 of 38 (68%) of the $CD8^+$ tumors were cytotoxic, only 7 of 43 (16%) $CD4^+$ lymphomas expressed cytotoxic granules. Additionally, 4 of 15 DN tumors and 1 of the 2 DP lymphomas expressed cytotoxic granules. As a group, cytotoxic lymphomas lacked CD5 more frequently (37%) than non-cytotoxic lymphomas (14%; $P=0.03$).

Compared with other patients, those with cytotoxic lymphoma presented at younger age (57 years versus 65 years; $P=0.024$) but more often at an advanced stage (stage 3/4: 85% versus 56%; $P=0.034$). However, their IPI scores and outcomes were similar to non-cytotoxic lymphoma.

CD30, an activation marker in T-cells, was detected in 18% of our cases in individual tumor cells. It was more frequently detected in tumors composed of large atypical cells; however, its expression was often weak and inconsistent among tumor cells in contrast to the strong membrane staining observed in anaplastic large cell lymphoma, LMP-positive B-cells were detected in the background of three cases.

Of the 101 nodal PTCL, 4 expressed CD56 (Table 2). None of them was associated with Epstein–Barr virus by LMP stain or by Epstein–Barr encoded RNA in situ hybridization. This group included two of the three $CD3^-CD5^-$ cases. In two cases, T-cell receptor (TCR)γ was clonally rearranged. In the other cases, the DNA quality did not allow the respective investigation. Three of these patients presented in their 80s, but one patient was only 21 years old. Follow-up was available for three of these patients. They had clinical stage 3, and no sites of extranodal involvement were detected; however, there was marked blood leukocytosis in two patients. The young patient died from the disease within 8 days of diagnosis, but the two elderly patients were alive after 5 months and 23 months, respectively.

Variants

The subdivision of our cases, according to their cell size, did not reveal any significant differences between the respective groups with regard to immunophenotype. By definition, tumor cell atypia was more pronounced in larger cell tumors.

Table 2 Detailed characteristics of CD56-positive nodal lymphoma. + positive, − negative, *CR* complete remission, *FFD* free from disease, *DOD* death of disease, *CHOP* cyclophosphamide, hydroxydaunomycin, vincristine (= Oncovin), predisone (regimen), *OAS* overall survival, *EBER* Epstein–Barr encoded RNA, *FFTF* freedom from treatment failure, *LMP* latent membrane protein

	Case 1	Case 2	Case 3	Case 4
CD2	+	−	+	+
CD3	−	−	+	+
CD5	−	−	+	+
CD7	−	−	−	−
CD4	−	+	−	−
CD8	−	−	−	+
CD30	−	−	+	−
CD57	−	+	−	−
LMP1	−	−	−	−
EBER	−	−	−	−
TIA1	+	+	+	−
Granzyme B	−	+	+	−
TCRγ rearrangement	Not done	mc	mc	Not done
Age (years)	21	76	76	74
Sex	Male	Female	Male	Female
Stage	3	3		3
Extranodal involvement	None	None		None
Performance status	Non-ambulatory	Ambulatory		Non-ambulatory
B-symptoms	Yes	None		None
Blood lymphocytes	16,000	6800		11,500
Lactic dehydrogenase (U/l)	758	234		588
Therapy		CHOP		CHOP
Remission		CR		None
FFTF (days)		382 (relapse)		151 (FFD)
OAS (days)	8 (DOD)	690 (alive)		151 (alive)

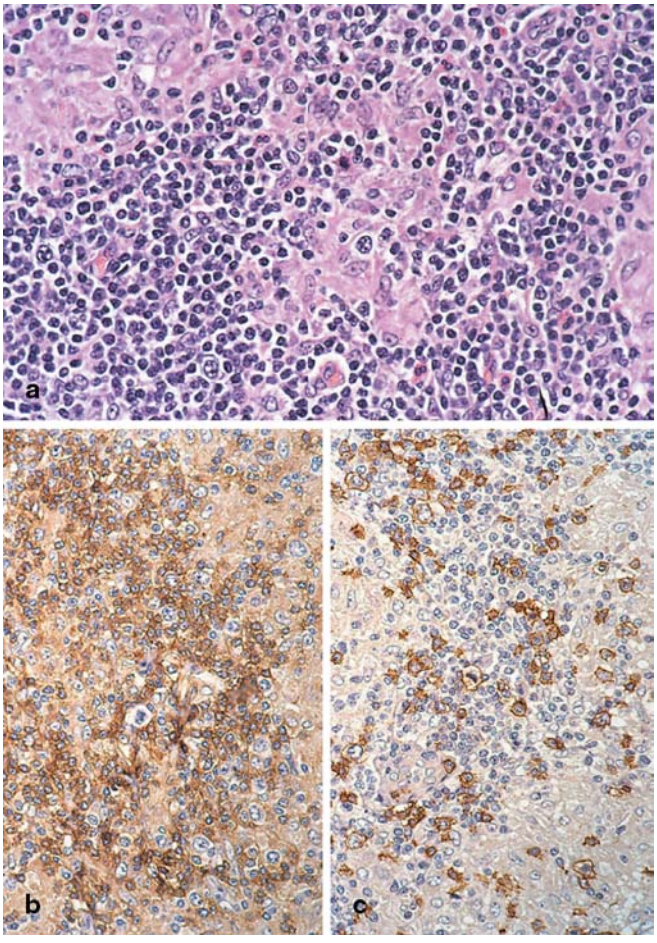


Fig. 4 Lennert's lymphoma. Hematoxylin and eosin (*top*), CD4– (*bottom left*), $CD8^+$ (*bottom right*)

Among the morphological variants, LeL exhibited a distinct phenotype; 15 cases (88%) were derived from $CD8^+$ cells. One case each was $CD4^+$ and DN, and, in the remaining case, lineage could not be defined due to poor preservation of the material. In the $CD8^+$ LeL, $CD4^+$ cells often predominated in the infiltrate (Fig. 4), which was composed of epithelioid histiocytes, small and activated T-cells. Morphologically, these T-cells did not exhibit nuclear atypia or atypical mitoses, features that were confined to the $CD8^+$ population. Therefore, the phenotype of LeL significantly differed from other PTCL-NOS ($P<0.001$) that were $CD4^+$ in 51%, $CD8^+$ in 28%, DN in 17%, and DP in 2% of the cases (Table 1). Cytotoxic molecules were detected in 11 of 18 LeL cases (61%), including the $CD4^+$ LeL, compared with 43% in the other group ($P=0.03$). LeL also contained significantly fewer plasma cells than the other PTCL-NOS. The clinical presentation, however, was not significantly different for LeL versus other PTCL-NOS.

Clinicopathological correlations

Detailed clinical data were available for 66 patients (Table 3) who were mostly elderly and presented at a high clinical stage but ambulatory performance status. Most reached remission after therapy, but the long-term outcome was poor (Fig. 5).

Treatment was variable: while 51 patients received an intense treatment, 15 patients were treated with less intense regimens. Intensely treated patients achieved higher remission rates ($P<0.01$) than others (81% versus 41% complete or partial remission; $P<0.01$), resulting in a significantly better overall survival (OAS) ($P=0.013$), but not freedom from treatment failure (FFTF).

As detailed in Table 4, survival could be predicted by patient characteristics and response to therapy, but indi-

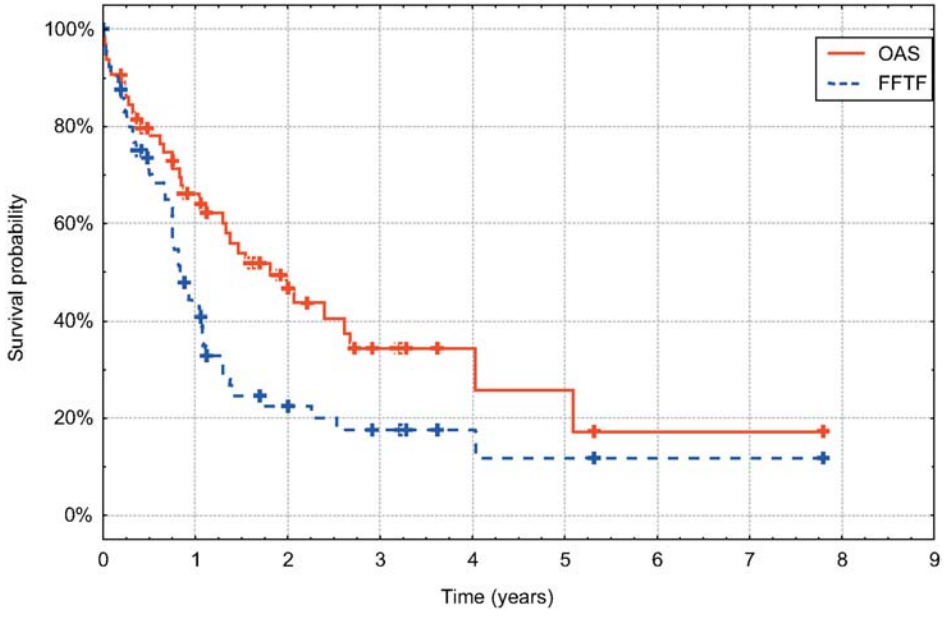


Fig. 5 Overall survival and freedom from treatment failure in 66 patients with available follow-up

Table 3 Detailed clinical characteristics of our patients. Numbers in parentheses indicate number of patients with available information. *CHOP* cyclophosphamide, hydroxydaunomycin, vincristine (= Oncovin), predisone (regimen), *FFTF* freedom from treatment failure, *OAS* overall survival

Median age (98)	62.5 years
Age range (98)	21–89 years
Male-to-female ratio (98)	1.04
Stage (60)	
I	15%
II	15%
III	40%
IV	30%
B symptoms (61)	51%
Elevated serum lactic dehydrogenase (53)	60%
Non-ambulatory performance status (59)	24%
International prognostic index scores (42)	
0–1	38%
2	29%
3	26%
4–5	7%
Presentation	
Nodal only	91%
Nodal + extranodal	9%
Primary treatment (66)	
High dose + stem cell transplant	14%
CHOP	56%
Other antharcyclin-containing therapy	8%
Other	22%
Treatment result (60)	
Complete remission	48%
Partial remission	25%
No response/progressive disease	27%
Survival	
FFTF (median)	10 months
OAS (median)	20 months

vidual morphological or immunophenotypical parameters failed to predict survival. Compared with other $CD8^+$ PTCL, patients with $CD8^+$ LeL ($CD8^+$ cases only) showed a significantly better FFTF (P=0.027) but not OAS.

Discussion

We studied 101 cases of nodal PTCL-NOS with special regard to the immunophenotype of the tumor cells. Nodal PTCL-NOS were derived from $CD8^+$ or cytotoxic cells in 38% of our cases. Although we used a meticulous approach to define tumor cell phenotype, it did not distinguish clinically different groups. The clinical presentation is, rather, correlated to the expression of cytotoxic granules than to derivation from $CD4^+$ or $CD8^+$ cells. Patients' outcome can be predicted using a morphological grading of PTCL-NOS. LeL is mainly derived from $CD8^+$ cytotoxic cells and has a better survival than other $CD8^+$ lymphomas.

Lineage of PTCL

The definition of the functional phenotype of the tumor cells of the 101 PTCL-NOS was a major goal of our study. Although some cases with large cell morphology are composed of an almost pure proliferation of tumor cells, most PTCL-NOS—in contrast to B-cell lymphomas—comprise a heterogeneous cellular population [16, 22, 42]. Apart from the tumor cells, there were abundant histiocytes, eosinophils, plasma cells, B-lymphocytes, and reactive T-lymphocytes. These reactive T-cells greatly complicate the study of PTCL. The mixed composition, comprising both neoplastic and reactive T-cells in varying proportions, may cause a lack of identifiable clonal TCR gene rearrangements in some cases of PTCL [50]. Reactive cells may exhibit a mild degree of nuclear atypia and, analogous to T-cell-rich B-cell lymphomas, may form the majority of the infiltrate in PTCL-NOS [37]. However, the neoplastic cells in PTCL cannot yet be specifically stained on histological sections and distinguished from infiltrating reactive T-cells. Therefore, studies attempting to define tumor cell lineage had to make various assumptions.

Some studies [12, 31, 47, 50] determined the proliferation fraction in immunohistochemical double stains and assumed the proliferating fraction to be neoplastic. However, proliferation alone is insufficient to define tumor cells, and the authors themselves found it difficult to associate their signals to morphology in frozen sections [50]. In such material, proliferating cells with their $Ki67^+$ nuclei may be completely surrounded by $CD4^+$ cells; this may easily give the impression that the $Ki67^+$ nuclei are

Table 4 *P*-values for the prediction of survival by different variables. (N1 and N2 are the numbers of patients in the respective groups). *DN* double negative, *CR* complete remission, *PR* partial remission, *FFTF* freedom from treatment failure, *OAS* overall survival, *PD* progressive disease

	N1 versus N2	N1	N2	OAS	FFTF
Diagnosis		55	11	0.489	0.135
Lineage	CD4 versus DN	29	10	0.289	0.048*
	CD8 versus DN	25	10	0.482	0.172
	CD4 versus CD8	29	25	0.617	0.445
Phenotype	ctx versus non-ctx	34	31	0.480	0.750
Age	≤60 years versus >60 years	31	35	0.006*	0.036*
Stage	1/2 versus 3/4	18	42	0.010*	0.076
Performance	Ambulatory versus non-ambulatory	45	14	0.005*	0.123
Lactic dehydrogenase	Normal versus elevated	19	29	0.021*	0.053
International prognostic index groups	1/2 versus 3/4	28	14	0.001*	0.027*
Therapy	Intensive versus non-intensive	51	6	0.021*	0.179
Remission	CR versus PR/PD	29	31	0.002*	0.100
	CR/PR versus PD	44	16	0.001*	0.010*

* Differences are statistically significant

located within $CD4^+$ cells. In LeL, atypical $CD8^+$ cells were often situated within granulomas that were mainly composed of such $CD4^+$ epithelioid cells.

In other studies, the proportion of T-cell subpopulations was compared, and the predominant population was regarded as neoplastic [9, 45]. However, the numbers of $CD4^+$ and $CD8^+$ T-lymphocytes in the infiltrate were often similar [26], and tumor lineage remained undetermined in 36% of 174 PTCL [32]. In a flow cytometry study, 6 of 31 PTCL did not show any subtype predominance [28]. Conceptually, a mere majority of a cell population in an infiltrate does not prove its clonality. For example, tumor cells are in the minority in Hodgkin's lymphoma, and predominant subpopulations may occur in reactive lesions.

To better distinguish the neoplastic from reactive T-cells, we assumed that tumor cells could be characterized morphologically by atypical mitoses, nuclear atypia, and proliferation. These features can all be assessed in immunostained paraffin sections. To correlate the immunophenotype to morphology, we analyzed double stains for Ki67 and CD4 or CD8, respectively. Although it cannot be ruled out with certainty that two phenotypically different neoplastic populations existed in those 14 cases that showed a higher proliferation in the non-atypical versus atypical cells, proliferation may be considerable in reactive T-cell populations as in infectious mononucleosis. Therefore, we considered clear-cut atypia as definitive proof of malignancy regardless of the proliferation.

This approach allowed us to define tumor cell lineage in 98 of 101 cases (97%). The tumor cells were $CD4^+$ in 43 cases, $CD8^+$ in 38 cases, DN in 15 cases, and DP in 2 cases. None of these phenotypes are actually new to the literature, but the proportion of $CD8^+$ tumors in our study is considerably higher than in previous ones [5, 7, 9, 30, 32, 33, 35, 39] that showed $CD8^+$ tumors in 4–18% only. Apart from the far possibility of a selection bias that we cannot rule out with certainty, these discrepancies most likely result from different approaches to define the tumor cells, as discussed previously. These results suggested that a reliable identification of tumor cells in PTCL-NOS is a prerequisite to classify PTCL successfully.

Lennert's lymphoma

LeL, with its typical prominent epithelioid cell reaction, was derived from $CD8^+$ cytotoxic T-cells in 15 of 18 cases. In the two remaining evaluable cases, one was $CD4^+$, and one was DN.

In contrast to our results of $CD8^+$ tumor cells in LeL, in the original description [12], the tumor cells in four cases investigated with double stains on frozen sections were $CD3^+CD4^+CD8^-$. In the early 1990s, $CD4^+$ cells were regarded as the predominant cell type in most LeL [31, 32, 47], but intermingled $CD8^+$ cells were reported. Proliferation seemed to be confined to the $CD4^+$ population, but the authors suggested that $CD4^+$ histiocytes may have distorted this result. While the percentage of $CD4^+Ki67^+$ cells was well correlated to clonal TCRβ gene rearrangements in both angioimmunoblastic lymphoma (AILT) and T-zone lymphoma, no such correlation could be established in LeL [47], probably because the clonal TCRβ rearrangement was correlated to the $CD4^+$ population, which should be regarded as reactive.

In our LeL, we also found a quantitative predominance of $CD4^+$ cells. However, using cytological criteria that were difficult to assess in frozen sections, the $CD8^+$ cells, although comprising a minor population, were atypical (Fig. 4), and we, therefore, regarded them as neoplastic. Recently, Kagami et al. investigated paraffin sections and found six of eight nodal cytotoxic PTCL to be LeLs [22]. Subsequently, they could show that five of ten LeLs were $CD8^+$, and TIA1 and/or granzyme B were expressed in seven of ten cases [51]. Adding our cases to these, evidence is accumulating that, based on the investigation of paraffin sections, LeL is possibly derived from a $CD8^+$ cytotoxic T-cell.

$CD8^+$ LeL also showed a significantly better OAS than other $CD8^+$ PTCL-NOS in our study. Together with the established morphological criteria, CD8 expression and cytotoxic phenotype may well allow us to delineate LeL more precisely.

Other phenotypes

Having identified the tumor cells, it was possible to define the expression of other antigens on the tumor cells (Table 1). Cytotoxic granules (TIA1 or granzyme B) were expressed in 9 of 42 $CD4^+$ tumors and in 32 of 38 $CD8^+$ tumors. Excluding LeL, 31% of the remaining PTCL-NOS were still derived from $CD8^+$ T-cells, and 30% of these expressed cytotoxic markers. This cytotoxic phenotype is well established for primary extranodal lymphomas; anaplastic large cell lymphomas also contain such granules, but they are derived from $CD4^+$ cells [4, 6]. The coexpression of CD4 and cytotoxic granules has been described in nodal PTCL-NOS, but has been thought to be rare [6, 10, 11, 50].

In addition to these major observations, some of our cases exhibited phenotypes that presently cannot be included easily in our understanding of malignant lymphoma mirroring normal T-cell development.

Four cases strongly expressed CD56. While most published $CD56^+$ lymphomas presented at extranodal sites, a few cases without extranodal involvement have been described [6, 7, 25, 34]. Extranodal sites were not involved in our cases; however, white blood cell counts in two patients suggested circulating tumor cells. Being confined to the lymph nodes, these tumors are distinct from $CD4^+CD56^+$ plasmacytoid dendritic cell precursor leukemia [8, 36].

Two other cases in our series of PTCL-NOS were positive for both CD4 and CD8. Six similar cases were described by Yamashita et al. [50]. Both morphologically and phenotypically, they represent a very rare and peculiar phenotype of PTCL-NOS.

Loss of any pan-T-cell antigen (CD3, CD5, CD4/8) has been proposed as a major criterion for the immunohistochemical diagnosis of PTCL [35], and it frequently concerns CD5 and CD7 [26]. In our series, CD7 was negative in 87% of cases, and at least one of the other pan-T-cell antigens was negative in 29% of our cases, similar to 31% in Chott's series [9].

Clinicopathological correlations

The clinical presentation and outcome of our patients was similar to other published studies [9, 38, 49], after 3 years, approximately 30% of the patients were still alive (Fig. 5). In prospective studies, survival reached a plateau at 43% after 3 years [41], and 41% of the patients, treated with an intensive regimen, were alive after 5 years [15]. The poorer outcome in our cohort was probably caused by the heterogeneous treatment, because patients receiving either CHOP [cyclophosphamide, hydroxydaunomycin, vincristine (= Oncovin), predisone (regimen)] or a high-dose regimen with autologous stem cell transplant had a significantly better survival rate than those treated with a less intense regimen. In contrast, in our series of AILT, there was no correlation between primary therapy and survival [27]. These differences between PTCL-NOS and AILT are in concordance with the philosophy of the WHO to define prognostic factors within entities [17, 19, 20].

Outcome in patients with aggressive lymphomas can be predicted by clinical characteristics combined with IPI score [40]. This is also applicable to PTCL as a group [3, 29, 38] and to our cohort. However, the IPI score does not include tumor biology and is probably not very specific for malignant lymphoma.

We, therefore, correlated the phenotypes of our tumors with clinical presentation and outcome. Interestingly, tumors derived from helper and suppressor cells showed virtually identical clinical characteristics, as did the DN cases. LeL, in contrast, had a survival superior to other $CD8^+$ lymphomas. The expression of cytotoxic markers was correlated with clinical presentation but not with outcome. Patients with cytotoxic lymphomas presented at younger age but with more advanced stages.

PTCL-NOS form a heterogeneous group of diseases, exhibiting a wide range of morphology and differentiating along both helper and suppressor lines. LeL is almost homogeneously CD8+, and its survival is different from other CD8+ PTCL-NOS. Immunophenotypical characteristics of the tumor cells cannot distinguish clinically relevant groups with available therapy, but for future studies, it will be crucial to reliably distinguish the tumor cells in PTCL-NOS from reactive T-lymphocytes.

Acknowledgement This work was partly supported by a grant from the Korea Science and Engineering Foundation.

References

1. (1982) National Cancer Institute sponsored study of classifications of non-Hodgkin's lymphomas: summary and description of a working formulation for clinical usage. The Non-Hodgkin's Lymphoma Pathologic Classification Project. Cancer 49:2112–2135
2. (1997) A clinical evaluation of the International Lymphoma Study Group classification of non-Hodgkin's lymphoma. The Non-Hodgkin's Lymphoma Classification Project. Blood 89:3909–3918
3. Ansell SM, Habermann TM, Kurtin PJ, Witzig TE, Chen MG, Li CY, Inwards DJ, Colgan JP (1997) Predictive capacity of the International Prognostic Factor Index in patients with peripheral T-cell lymphoma. J Clin Oncol 15:2296–2301
4. Benharroch D, Meguerian-Bedoyan Z, Lamant L, Amin C, Brugières L, Terrier-Lacombe M-J, Haralambieva E, Pulford K, Pileri S, Morris SW, Mason DY, Delsol G (1998) ALK-positive lymphoma. A single disease with a broad spectrum of morphology. Blood 91:2076–2084
5. Boulland ML, Kanavaros P, Wechsler J, Casiraghi O, Gaulard P (1997) Cytotoxic protein expression in natural killer cell lymphomas and in alpha beta and gamma delta peripheral T-cell lymphomas. J Pathol 183:432–439
6. Chan AC, Ho JW, Chiang AK, Srivastava G (1999) Phenotypic and cytotoxic characteristics of peripheral T-cell and NK-cell lymphomas in relation to Epstein–Barr virus association. Histopathology 34:16–24
7. Chan JK, Sin VC, Wong KF, Ng CS, Tsang WY, Chan CH, Cheung MM, Lau WH (1997) Nonnasal lymphoma expressing the natural killer cell marker CD56: a clinicopathologic study of 49 cases of an uncommon aggressive neoplasm. Blood 89:4501–4513
8. Chaperot L, Bendriss N, Manches O, Gressin R, Maynadie M, Trimoreau F, Orfeuvre H, Corront B, Feuillard J, Sotto JJ, Bensa JC, Briere F, Plumas J, Jacob MC (2001) Identification of a leukemic counterpart of the plasmacytoid dendritic cells. Blood 97:3210–3217
9. Chott A, Augustin I, Wrba F, Hanak H, Ohlinger W, Radaszkiewicz T (1990) Peripheral T-cell lymphomas: a clinicopathologic study of 75 cases. Hum Pathol 21:1117–1125
10. de Bruin PC, Kummer JA, van der Valk P, van Heerde P, Kluin PM, Willemze R, Ossenkoppele GJ, Radaszkiewicz T, Meijer CJ (1994) Granzyme B-expressing peripheral T-cell lymphomas: neoplastic equivalents of activated cytotoxic T cells with preference for mucosa- associated lymphoid tissue localization. Blood 84:3785–3791
11. Felgar RE, Macon WR, Kinney MC, Roberts S, Pasha T, Salhany KE (1997) TIA-1 expression in lymphoid neoplasms. Identification of subsets with cytotoxic T lymphocyte or natural killer cell differentiation. Am J Pathol 150:1893–1900
12. Feller AC, Griesser GH, Mak TW, Lennert K (1986) Lymphoepithelioid lymphoma (Lennert's lymphoma) is a monoclonal proliferation of helper/inducer T cells. Blood 68:663–667
13. Feller AC, Lennert K, Zwingers T (1991) Peripheral T-cell lymphomas. Histopathology 19:481–484
14. Flamand L, Crowley RW, Lusso P, Colombini-Hatch S, Margolis DM, Gallo RC (1998) Activation of CD8+ T lymphocytes through the T cell receptor turns on CD4 gene expression: implications for HIV pathogenesis. Proc Natl Acad Sci U S A 95:3111–3116
15. Gisselbrecht C, Gaulard P, Lepage E, Coiffier B, Briere J, Haioun C, Cazals-Hatem D, Bosly A, Xerri L, Tilly H, Berger F, Bouhabdallah R, Diebold J (1998) Prognostic significance of T-cell phenotype in aggressive non-Hodgkin's lymphomas. Groupe d'Etudes des Lymphomes de l'Adulte (GELA). Blood 92:76–82
16. Harris NL, Jaffe ES, Stein H, Banks PM, Chan JKC, Cleary ML, Delsol G, De Wolf Peeters C, Falini B, Gatter KC, Grogan TM, Isaacson PG, Knowles DM, Mason DY, Müller-Hermelink HK, Pileri SA, Piris MA, Ralfkiaer E, Warnke RA (1994) A revised European-American classification of lymphoid neo-

plasms: a proposal from the International Lymphoma Study Group. Blood 84:1361–1392
17. Harris NL, Jaffe ES, Diebold J, Flandrin G, Muller-Hermelink HK, Vardiman J, Lister TA, Bloomfield CD (1999) The World Health Organization classification of neoplastic diseases of the hematopoietic and lymphoid tissues. Report of the Clinical Advisory Committee meeting, Airlie House, Virginia, November, 1997. Ann Oncol 10:1419–1432
18. Hastrup N, Hamilton Dutoit S, Ralfkiaer E, Pallesen G (1991) Peripheral T-cell lymphomas: an evaluation of reproducibility of the updated Kiel classification. Histopathology 18:99–105
19. Jaffe ES (1999) Hematopathology: integration of morphologic features and biologic markers for diagnosis. Mod Pathol 12:109–115
20. Jaffe ES, Harris NL, Diebold J, Müller-Hermelink HK (1999) World Health Organization classification of neoplastic diseases of the hematopoietic and lymphoid tissues. A progress report. Am J Clin Pathol 111:8–12
21. Jaffe ES, Harris NL, Stein H, Vardiman JW (2001) World Health Organization classification of tumours. Pathology and genetics of tumours of haematopoietic and lymphoid tissues. IARC Press, Lyon
22. Kagami Y, Suzuki R, Taji H, Yatabe Y, Takeuchi T, Maeda S, Kondo E, Kojima M, Motoori T, Mizoguchi Y, Okamoto M, Ohnishi K, Yamabe H, Seto M, Ogura M, Koshikawa T, Takahashi T, Kurita S, Morishima Y, Suchi T, Nakamura S (1999) Nodal cytotoxic lymphoma spectrum: a clinicopathologic study of 66 patients. Am J Surg Pathol 23:1184–1200
23. Kaplan EL, Meier P (1958) Nonparametric estimation from incomplete observations. J Am Stat Assoc 53:457
24. Kluin PM, Feller A, Gaulard P, Jaffe ES, Meijer CJ, Muller-Hermelink HK, Pileri S (2001) Peripheral T/NK-cell lymphoma: a report of the IXth Workshop of the European Association for Haematopathology. Histopathology 38:250–270
25. Kobashi Y, Nakamura S, Sasajima Y, Koshikawa T, Yatabe Y, Kitoh K, Mori S, Ueda R, Yamabe H, Suchi T (1996) Inconsistent association of Epstein–Barr virus with CD56 (NCAM)-positive angiocentric lymphoma occurring in sites other than the upper and lower respiratory tract. Histopathology 28:111–120
26. Krajewski AS, Myskow MW, Cachia PG, Salter DM, Sheehan T, Dewar AE (1988) T-cell lymphoma: morphology, immunophenotype and clinical features. Histopathology 13:19–41
27. Lee SS, Rudiger T, Odenwald T, Roth S, Starostik P, Muller-Hermelink HK (2003) Angioimmunoblastic T cell lymphoma is derived from mature T-helper cells with varying expression and loss of detectable CD4. Int J Cancer 103:12–20
28. Macon WR, Salhany KE (1998) T-cell subset analysis of peripheral T-cell lymphomas by paraffin section immunohistology and correlation of CD4/CD8 results with flow cytometry. Am J Clin Pathol 109:610–617
29. Melnyk A, Rodriguez A, Pugh WC, Cabannillas F (1997) Evaluation of the Revised European–American Lymphoma classification confirms the clinical relevance of immunophenotype in 560 cases of aggressive non-Hodgkin's lymphoma. Blood 89:4514–4520
30. Montalban C, Obeso G, Gallego A, Castrillo JM, Bellas C, Rivas C (1993) Peripheral T-cell lymphoma: a clinicopathological study of 41 cases and evaluation of the prognostic significance of the updated Kiel classification. Histopathology 22:303–310
31. Nakamura S, Suchi T (1991) A clinicopathologic study of node-based, low-grade, peripheral T-cell lymphoma. Angioimmunoblastic lymphoma, T-zone lymphoma, and lymphoepithelioid lymphoma. Cancer 67:2566–2578
32. Nakamura S, Koshikawa T, Koike K, Kitoh K, Suzuki H, Oyama A, Motoori T, Kojima M, Ogura M, Kurita S et al (1993) Phenotypic analysis of peripheral T cell lymphoma among the Japanese. Acta Pathol Jpn 43:396–412
33. Ng CS, Lo ST, Chan JK (1999) Peripheral T and putative natural killer cell lymphomas commonly coexpress CD95 and CD95 ligand. Hum Pathol 30:48–53
34. Ohshima K, Suzumiya J, Sugihara M, Kanda M, Shimazaki K, Kawasaki C, Haraoka S, Kikuchi M (1999) Clinical, immunohistochemical and phenotypic features of aggressive nodal cytotoxic lymphomas, including alpha/beta, gamma/delta T-cell and natural killer cell types. Virchows Arch 435:92–100
35. Picker LJ, Weiss LM, Medeiros LJ, Wood GS, Warnke RA (1987) Immunophenotypic criteria for the diagnosis of non-Hodgkin's lymphoma. Am J Pathol 128:181–201
36. Reimer P, Rudiger T, Kraemer D, Kunzmann V, Weissinger F, Zettl A, Konrad Muller-Hermelink H, Wilhelm M (2003) What is CD4+CD56+ malignancy and how should it be treated? Bone Marrow Transplant 32:637–646
37. Rüdiger T, Jaffe ES, Delsol G, deWolf Peeters C, Gascoyne RD, Georgii A, Harris NL, Kadin ME, MacLennan KA, Poppema S, Stein H, Weiss LE, Müller-Hermelink HK (1998) Workshop report on Hodgkin's disease and related diseases ("grey zone" lymphoma). Ann Oncol 9[Suppl 5]:S31–S38
38. Rüdiger T, Weisenburger DD, Anderson JR, Armitage JO, Diebold J, MacLennan KA, Nathwani BN, Ullrich F, Müller-Hermelink HK (2002) Peripheral T-cell lymphoma. Results from the Non-Hodgkin's Lymphoma Classification Project. Ann Oncol 13:140–149
39. Shih LY, Kuo TT, Dunn P, Liaw SJ (1992) HTLV-I-positive and HTLV-I-negative peripheral T-cell lymphomas in Taiwan Chinese. Int J Cancer 50:186–191
40. Shipp MA (1994) Prognostic factors in aggressive non-Hodgkin's lymphoma: who has "high-risk" disease? Blood 83:1165–1173
41. Siegert W, Nerl C, Engelhard M, Brittinger G, Tiemann M, Parwaresch R, Heinz R, Huhn D (1994) Peripheral T-cell non-Hodgkin's lymphomas of low malignancy: prospective study of 25 patients with pleomorphic small cell lymphoma, lymphoepitheloid cell (Lennert's) lymphoma and T-zone lymphoma. The Kiel Lymphoma Study Group. Br J Haematol 87:529–534
42. Smith JL, Haegert DG, Hodges E, Stacey GN, Howell WM, Wright DH, Jones DB (1988) Phenotypic and genotypic heterogeneity of peripheral T-cell lymphoma. Br J Cancer 58:723–729
43. Sng I, Levin A, Jaffe ES, Ng HW, Sim CS, Blattner WB (1992) T-cell lymphoma in Singapore: pathology, clinical findings and association with HTLV-1 antibodies. Histopathology 21:101–113
44. Stansfeld AG, Diebold J, Noel H, Kapanci Y, Rilke F, Kelenyi G, Sundstrom C, Lennert K, van Unnik JAM, Mioduszewska O, Wright DH (1988) Updated Kiel classification for lymphomas. Lancet 1:292–293
45. Su IJ, Wang CH, Cheng AL, Chen YC, Hsieh HC, Chen CJ, Tien HF, Tsay W, Huang SS, Hu CY et al (1988) Characterization of the spectrum of postthymic T-cell malignancies in Taiwan. A clinicopathologic study of HTLV-1-positive and HTLV-1-negative cases. Cancer 61:2060–2070
46. Suchi T, Lennert K, Tu LY, Kikuchi M, Sato E, Stansfeld AG, Feller AC (1987) Histopathology and immunohistochemistry of peripheral T cell lymphomas: a proposal for their classification. J Clin Pathol 40:995–1015
47. Takagi N, Nakamura S, Ueda R, Osada H, Obata Y, Kitoh K, Suchi T, Takahashi T (1992) A phenotypic and genotypic study of three node-based, low-grade peripheral T-cell lymphomas: angioimmunoblastic lymphoma, T-zone lymphoma, and lymphoepithelioid lymphoma. Cancer 69:2571–2582
48. Trainor KJ, Brisco MJ, Wan JH, Neoh S, Grist S, Morley AA (1991) Gene rearrangement in B- and T-lymphoproliferative disease detected by the polymerase chain reaction Blood 78:192–196
49. Weisenburger DD, Linder J, Armitage JO (1987) Peripheral T-cell lymphoma: a clinicopathologic study of 42 cases. Hematol Oncol 5:175–187
50. Yamashita Y, Yatabe Y, Tsuzuki T, Nakayama A, Hasegawa Y, Kojima H, Nagasawa T, Mori N (1998) Perforin and granzyme expression in cytotoxic T-cell lymphomas. Mod Pathol 11:313–323
51. Yamashita Y, Nakamura S, Kagami Y, Hasegawa Y, Kojima H, Nagasawa T, Mori N (2000) Lennert's lymphoma: a variant of cytotoxic T-cell lymphoma? Am J Surg Pathol 24:1627–1633

Virchows Arch (2004) 445:344–346
DOI 10.1007/s00428-004-1057-6

ORIGINAL ARTICLE

Sophie Camilleri-Broët · Christophe Fermé · Françoise Berger · Eric Lepage · Serge Bain · Josette Brière · Béatrice Marmey · Philippe Gaulard · Josée Audouin

TiA1 in advanced-stage classical Hodgkin's lymphoma: no prognostic impact for positive tumour cells or number of cytotoxic cells

Received: 4 March 2004 / Accepted: 19 May 2004 / Published online: 19 June 2004
© Springer-Verlag 2004

Abstract No reliable marker still exists for predicting those patients with Hodgkin's lymphoma (HL) who may experience a fatal outcome. Among the factors tested in the literature, it has been suggested that the number of activated cytotoxic T cells may represent a prognostic marker in HL. In 244 samples from patients with stage-IIIB/IV HL issued from the GELA H89 trial, we have analysed TiA1 expression on Reed Sternberg (RS) cells as well as the percentage of positive reactive lymphocytes. There were 34 cases (13.7%) that showed TiA1 expression on tumour cells; whereas, in 32 cases (13.1%), TiA1-positive reactive lymphocytes represented more than 30% of the reactive lymphocytes. LMP-1 was found co-expressed with TiA1 in 10 of the 22 positive cases tested. Our study confirms that a subset of classical HL expresses cytotoxic proteins, with occasional co-expression of CD20. In stage-IIIB/IV disease, neither TiA1 expression by RS cells nor a high percentage of TiA1-positive reactive lymphocytes have a prognostic impact on outcome.

S. Camilleri-Broët (✉) · S. Bain · B. Marmey · J. Audouin
Service Central d'Anatomie et de Cytologie Pathologiques,
Hotel-Dieu 1, Place du Parvis Notre Dame, 75181 Paris Cedex 04, France
e-mail: sophie.camilleri-broet@htd.ap-hop-paris.fr
Tel.: +33-1-42348282
Fax: +33-1-42348641

C. Fermé
Institut Gustave Roussy,
Villejuif, France

F. Berger
Centre Hospitalier Lyon-Sud,
Lyon, France

E. Lepage · P. Gaulard
Hôpital Henri Mondor,
Créteil, France

J. Brière
Hôpital Saint Louis,
Paris, France

Keywords Immunohistochemistry · Lymphoma · Clinical pathology

Introduction

While the outcome of patients with Hodgkin's lymphoma (HL) has been dramatically improved, the disease still follows a fatal course for a minority of patients, and there is still no valuable marker for predicting those who may benefit from different therapeutic options. It has been suggested that a high percentage of activated cytotoxic T cells may represent a strong indicator for an unfavourable clinical outcome in HL [8], a disease characterised by the great number of reactive cells. In the present study, we have investigated TiA1 (T-cell-restricted intracellular antigen-1) expression in a large series of advanced stages of classical HL issued from the H89 protocol conducted by the GELA (Groupe d'étude des Lymphomes de l'Adulte) study group.

Materials and methods

Patients and tumour specimens

Between 1 July 1989 and 1 December 1996, 553 patients with stage-IIIB/IV HL were enrolled in the H89 trial [3]. After six cycles of MOPP/ABV hybrid or ABVPP regimens, patients in complete or partial remission of at least 75% were randomised for consolidation treatment (two more cycles of the same chemotherapy or radiotherapy). Any advantage of radiotherapy over chemotherapy as consolidation treatment was demonstrated. Histological slides from 93% underwent re-evaluation by a panel of haematopathologists.

For the present study, we analysed retrospectively TiA1 expression in 244 patients for whom histological slides were available for additional immunohistochemistry. This subpopulation was representative of the whole population (Table 1). Among this subgroup, 200 cases (82%) were classified as nodular sclerosis, 27 (11%) mixed cellularity and 2 cases (1%) as lymphocyte-depleted HL. The 15 remaining cases could not be subclassified because of inadequate material.

Table 1 Patient characteristics

	H89 Clinical trial (*n*=533)	Current study (*n*=244)
Male gender (%)	66	70
Age (% ≥45 years)	23	24
Stage		
IIIB (%)	40	41
IV (%)	60	59
Mediastinum		
Uninvolved (%)	22	21
Involved (%)	78	79
ECOG performance		
Statut ≥2 (%)	12	12
Tumor >10 cm (%)	24	17
Extranodal sites ≥2 (%)	27	26
Bone-marrow involvement (%)	20	16
International prognostic score (%)		
0	2	1
1	8	8
2	29	28
3	28	25
4	19	18
≥5	14	20
Histological subtype (%)		
Nodular sclerosis	77	82
BNLI grade I	64	66
BNLI grade II	36	34
Mixed cellularity	11	11
Lymphocyte depleted	2	1
Others	10	6

Immunohistochemistry

Two hours incubation at 1:20 dilution was performed with an antibody raised against TiA1 (IM2550, Immunotech, Marseille, France) on deparaffinised tissue sections [1]. A standard streptavidin-biotin-peroxidase complex (SABC) method was applied using a commercially available kit (BIOSPA, ABCYS GMR4–61, Milano, Italy).

Two pathologists (S.C.B., J.A.) interpreted slides at a double-headed microscope, without knowledge of clinical data. The quality of the technique was evaluated by the presence of bright reactive lymphocytes. TiA1 expression in tumour cells (none, <10%, ≥10%) and percentages of TiA1-positive reactive lymphocytes in comparison with the whole lymphocyte population (<10%, 10–30%, ≥30%) were scored semi-quantitatively.

Statistical analysis

The characteristics of the patients and their TiA1 immunohistochemical results were compared using the chi-square test. Event-free survival and overall survival intervals were calculated from the date of the first randomisation until death, progression stopping date or date of last follow-up evaluation, and were compared using the log-rank test [6]. *P* values ≤0.05 were considered significant.

Results

Expression of TiA1 on tumour cells and reactive lymphocytes

Of the 244 cases tested, cytoplasmic granular staining of tumour cells was found in 34 cases (14%), representing more than 10% of tumour cells in half of them (17 cases, Fig. 1). CD20 antigen was expressed by tumour cells in 5 of the 28 TiA1-positive cases tested and LMP-1 was detected in 10 of the 22 cases tested (45%) (data not shown).

Most of the cases contained less than 10% of TiA1-positive reactive lymphocytes (149 of 244 cases, 61.1%). In 63 cases (25.8%), TiA1-positive lymphocytes accounted for between 10% and 30%, and in 32 cases (13.1%) they represented more than 30% of the reactive lymphocytes.

Association with clinico-biological variables

No correlation was found between TiA1 expression by tumour cells as well as the percentage of TIA1-positive reactive lymphocytes and the following clinical or biological characteristics: age, stage, performance status,

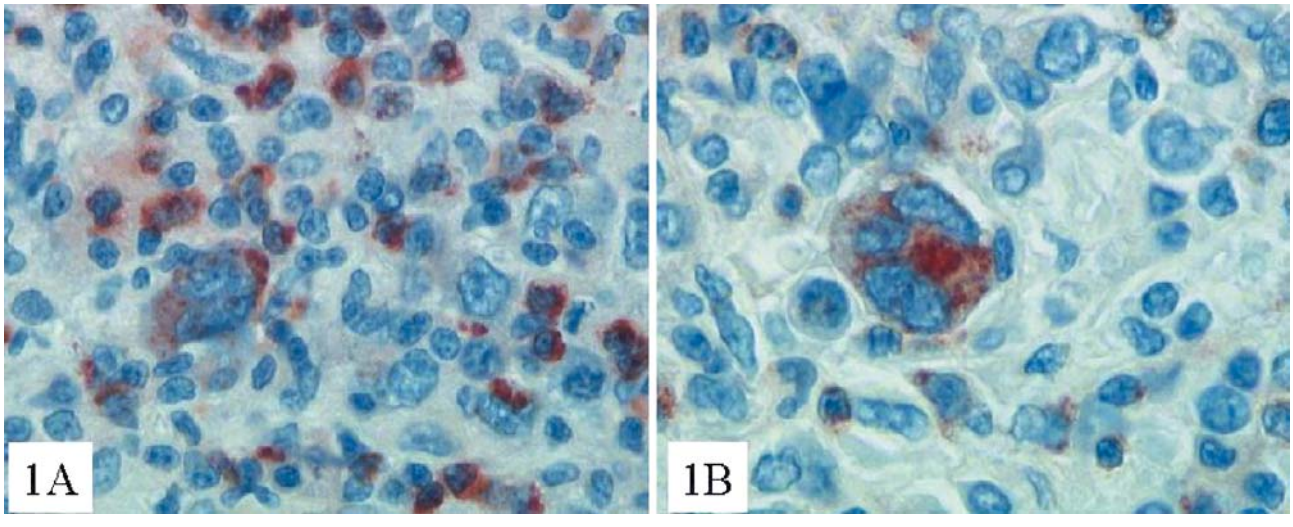


Fig. 1 TiA1 immunohistochemical detection in two cases of Hodgkin's lymphoma. Granular cytoplasmic expression of TiA1 in tumour cells with either numerous (**A**) or few (**B**) TiA1-positive reactive lymphocytes

extranodal site involvement, bone-marrow involvement, systemic symptoms, lactate dehydrogenase level, serum albumin and haemoglobin levels. In contrast, there was an inverse correlation between the white blood cell count and both TiA1 expression by tumour cells (P=0.02) and the percentage of TiA1-positive lymphocytes (P=0.007). Also, there was a positive correlation between TiA1-positive tumour cells and the presence of more than 30% of TiA1-positive reactive lymphocytes (P=0.0003).

Patient's outcome

In univariate analysis, no significant prognostic impact has been shown for TiA1 expression on tumour cells with respect to event-free survival or overall survival. The percentage of TiA1-positive reactive lymphocytes on both outcomes was not significant either.

Discussion

In accordance with previous studies [2, 4, 5, 8], we have shown that, in a subset of HL (14%), Reed-Sternberg (RS) cells contained cytotoxic granules. This result raises the question of the lineage of RS cells. Two main hypotheses exist: (1) a subset of HL is of T-cell lineage; (2) there is an aberrant expression of cytotoxic protein in RS cells of B origin. In a previous report, single-cell polymerase chain reaction from cytotoxic-expressing RS cells harboured either clonal TCR or IgH rearrangements [7]. In our series, five cases co-expressed CD20 and TiA1 on tumour cells, favouring B-cell derivation.

In this series, we did not evidence any prognostic impact regarding TiA1 expression by both RS cells as well as the percentage of positive reactive lymphocytes. Our result differs from the series published by Oudejans [8], who concluded that a high number of activated cytotoxic T cells were linked with an adverse prognosis. This discrepancy may be explained in part by the population studied, our study dealing only with stage-III/IV HL. Moreover, we have analysed expression of TiA1, whereas Oudejans et al. investigated granzyme B expression, which defines cytotoxic T-cells with activated status.

In conclusion, we have found that neither TiA1 expression by RS cells nor a high percentage of TiA1-positive reactive lymphocytes has a prognostic value in a large number of patients enrolled in randomised protocol with a long follow-up and retrospective slides review.

Acknowledgements The authors wish to thank J. Diebold for his helpful comments.

References

1. Anderson P, Nagler-Anderson C, O'Brien C et al (1990) A monoclonal antibody reactive with a 15-kDa cytoplasmic granule-associated protein defines a subpopulation of CD8+ T lymphocytes. J Immunol 144:574–582
2. Felgar RE, Macon WR, Kinney MC et al (1997) TIA-1 expression in lymphoid neoplasms. Identification of subsets with cytotoxic T lymphocyte or natural killer cell differentiation. Am J Pathol 150:1893–1900
3. Fermé C, Sebban C, Hennequin C et al (2000) Comparison of chemotherapy to radiotherapy as consolidation of complete or good partial response after six cycles of chemotherapy for patients with advanced Hodgkin's disease: results of the Groupe d'étude des Lymphomes de l'Adulte H89 trial. Blood 95:2246–2252
4. Kanavaros P, Vlychou M, Stefanaki K et al (1999) Cytotoxic protein expression in non-Hodgkin's lymphomas and Hodgkin's disease. Anticancer Res 19:1209–1216
5. Krenacs L, Wellmann A, Sorbara L et al (1997) Cytotoxic cell antigen expression in anaplastic large cell lymphomas of T- and null-cell type and Hodgkin's disease: evidence for distinct cellular origin. Blood 89:980–989
6. Mantel N (1966) Evaluation for survival data and two new rank order statistics arising in its consideration. Cancer Chemother Rep 50:163
7. Muschen M, Rajewsky K, Brauninger A et al (2000) Rare occurrence of classical Hodgkin's disease as a T cell lymphoma. J Exp Med 191:387–394
8. Oudejans JJ, Jiwa NM, Kummer JA et al (1997) Activated cytotoxic T cells as prognostic marker in Hodgkin's disease. Blood 89:1376–1382

Virchows Arch (2004) 445:347–353
DOI 10.1007/s00428-004-1102-5

ORIGINAL ARTICLE

Michal Michal · Dmitry V. Kazakov · Irena Belousova · Michele Bisceglia · Michal Zamecnik · Petr Mukensnabl

A benign neoplasm with histopathological features of both schwannoma and retiform perineurioma (benign schwannoma-perineurioma): a report of six cases of a distinctive soft tissue tumor with a predilection for the fingers

Received: 1 April 2004 / Accepted: 20 July 2004 / Published online: 20 August 2004
© Springer-Verlag 2004

Abstract We present six cases of a distinctive soft tissue tumor which occurred in five women and one man. None of the patients had signs of neurofibromatosis. All tumors occurred on the fingers (n=5) or the thenar eminence of the hand (n=1). The mean age of the patients was 33 years. The tumors were 1–2.5 cm in diameter (mean size 1.6 cm). Three patients with follow-up were without signs of recurrence or metastasis. Microscopically the lesions were nonencapsulated and featured a multilobular architecture and both myxoid and pseudocystic change. The lobules varied in size and shape and were separated by variably thickened, dense, sclerotic/collagenous septae. The lobules were composed of two components: schwannomatous and perineuriomatous. The schwannomatous component was immunohistochemically S-100 protein positive and CD34 and EMA negative, and the perineuriomatous component had the appearance of retiform perineurioma. The perineurial parts were mostly S-100 protein and CD34 negative and EMA positive. These two components either formed separate nodules or the schwannomatous tissue surrounded the perineurial parts located in the centers of the lobules. We interpreted the lesions as hybrid tumors with features of schwannoma and retiform perineurioma.

Keywords Retiform perineurioma · Reticular perineurioma · Benign schwannoma-perineurioma · Neurothekeoma

M. Michal (✉) · D. V. Kazakov · M. Zamecnik · P. Mukensnabl
Sikl's Department of Pathology,
Charles University, Medical Faculty Hospital,
Alej Svobody 80, 30460 Pilsen, Czech Republic
e-mail: michal@medima.cz
Tel.: +420-37-7104630
Fax: +420-37-7104650

I. Belousova
Department of Dermatology,
Medical Military Academy,
Saint Petersburg, Russia

M. Bisceglia
Department of Pathology,
IRCCS-Ospedale Casa Sollievo della Sofferenza,
San Giovanni Rotondo, Italy

Introduction

Peripheral nerve sheath tumors are traditionally divided into schwannomas, neurofibromas, and perineuriomas. Perineuriomas were described relatively recently [26], and with the help of immunohistochemical stains for epithelial membrane antigen (EMA) these tumors were defined in recent years [4, 7, 8, 10, 11, 19, 31, 35, 40, 41, 43]. The last distinctive type of perineurioma [35] was identified in small series in recent years, and it was variously named retiform [28] or reticular perineurioma [30]. We are aware of only a single case of hybrid tumor containing a component of retiform perineurioma and a schwannian component in the literature [42]. Here we report a small series of six neoplasms with retiform perineurioma/schwannoma features. Our report demonstrates that these hybrid tumors are distinctive lesions.

Materials and methods

All lesions coded as "perineurioma," "schwannoma," "neurothekeoma," and "nerve sheath myxoma" were retrieved from our consultation files. We looked for the cases which contained areas typical of perineuriomas and schwannomas. Six cases met the criteria of this unusual neoplasm. Clinical data were obtained from the hospital records and/or from contributing clinicians or pathologists. There were five women and one man (mean age 33 years, range 20–52). None of the patients had signs of neurofibromatosis. All patients presented with a solitary subcutaneous tumor. The main clinical data are summarized in Table 1. In three cases tissue blocks were available, in one case there was a large number of

Table 1 Main clinical data (*NED* no evidence of disease)

Case no.	Sex	Age (years)	Size (cm)	Location	Treatment	Follow-up
1	F	28	1.5	Thumb, left hand	Excision	4 years NED
2	F	50	2.5	Thenar eminence	Excision	Unknown
3	M	26	2.0	2nd finger, left hand	Excision	Recent case
4	F	24	1.5	5th finger, left hand	Excision	Recent case
5	F	20	2.5×2.0	2nd finger, left hand	Excision	1 year NED
6	F	52	1.0×0.5	2nd finger	Excision	7 years NED

Table 2 Antibodies used for immunohistochemical study (*EMA* epithelial membrane antigen, *ASMA* α-smooth muscle actin, *MSA* muscle-specific actin, *NFP* neurofilament protein)

Antibody specificity	Clone	Dilution	Source
EMA	E29	1:700	DakoCytomation
S-100 protein	Poly	1:4000	DakoCytomation
NFP	2F11	1:1000	DakoCytomation
CD34	QBEnd/10	1:25	Novocastra
Desmin	D33	1:3000	DakoCytomation
ASMA	1A4	1:200	DakoCytomation
MSA	HHF-35	1:4000	DakoCytomation
Melanosome	HMB45	1:200	DakoCytomation

unstained reserve slides available, and in two cases only limited number of unstained reserve slides were obtained for the study. Tissue samples were fixed in 4% formaldehyde and paraffin-embedded. Sections (5 μm thick) were stained with routine methods, and the Bodian histochemical method for detecting neuroaxons was performed.

In all cases examined by immunohistochemistry either newly cut sections from formaldehyde-fixed, paraffin-embedded material or unstained reserve slides were used. As a detection system we employed the avidin-biotin complex or streptavidin-biotin complex labeled with peroxidase or alkaline phosphatase. Microwave antigen pretreatment was performed prior to applying the primary antibodies. Automated immunostaining employing the Lab Vision autostainer was used. Table 2 lists primary antibodies used in the study. Appropriate positive and negative controls were applied.

For electron microscopic investigations wet formol-fixed tissue was available in one case. It was postfixed in 4% paraformaldehyde, contrasted in 1% osmium tetroxide, and embedded in epoxy resin (Durcupan-Epon). Sections were cut 1 μm thick, stained with toluidine blue, and examined by light microscopy. Appropriate areas were selected, and thin sections were cut and stained with uranyl acetate and lead citrate, and examined with a Philips (Eindhoven, Holland) EM 208S electron microscope.

Results

Clinical data

The lesions ranged in size from 1.0 to 2.5 cm (mean 1.6). In five patients the neoplasm was located on a finger. The thenar eminence was involved in one patient. Duration was indicated in one case (no. 6); the lesion was present for 15 years before the patient sought medical advice. All lesions were surgically excised. Three patients had a disease free follow-up 1, 4, and 7 years postoperatively. Two patients underwent the excision recently, and in one patient the follow-up was unknown.

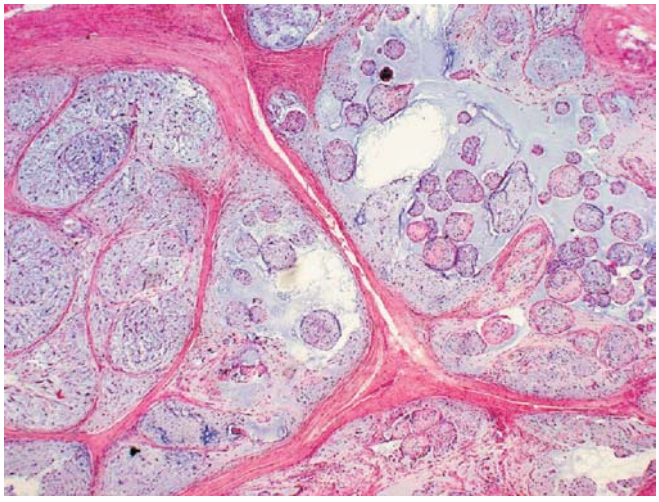


Fig. 1 The lobules vary in size and shape and are separated by variably thickened dense, sclerotic/collagenous septae

Histopathological findings

In all cases the lesions were nonencapsulated and featured a multilobular architecture and both myxoid and pseudocystic change. The latter three features seemed to correlate with the size of the lesions, being more prominent in larger ones. The lobules varied in size and shape and were separated by variably thickened dense, sclerotic/collagenous septae (Fig. 1). The lobules mainly presented perineuriomalike tissue that for the most part demonstrated elongated, spindled cells which often formed loops set in a myxoid matrix typical of retiform perineuriomas (Fig. 2). Occasional cells had multivacuolated cytoplasm and thus vaguely resembled lipoblasts. When myxoid degeneration was prominent, the retiform pattern of perineurioma in lobules was less apparent (Fig. 3). Such lobules contained spindled and occasional epithelioid cells disposed in a loose network in a mucin-rich matrix. Prominent myxoid change was also associated with the formation of peculiar "fibrohyaline balls" lying free in an abundant myxoid matrix in a destroyed lobule (Fig. 4). These balls were composed of a peripheral rim of spindled neoplastic cells and a central collagenous core with radiating delicate collagen fibrils that resembled a spider or a jellyfish. Rare fibrohyaline balls had undergone calcification.

The schwannomatous areas consisted of elongated cells with tapered, spindled nuclei, mostly arranged in a compact Antoni A pattern, but occasionally also formed

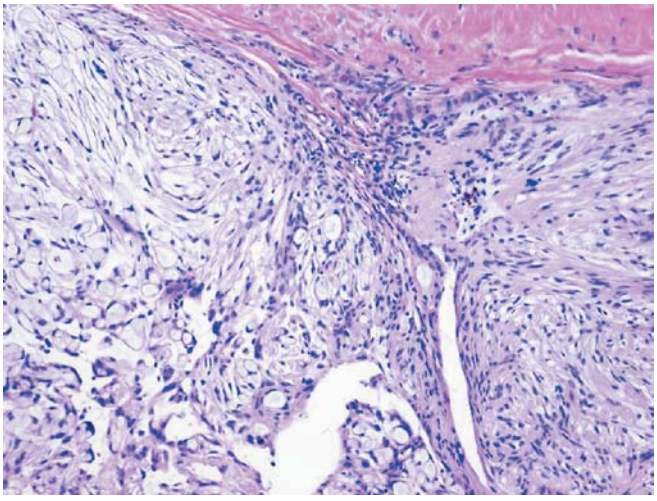


Fig. 2 The spindled cells, which often form loops set in a myxoid matrix typical of retiform perineuriomas are seen on the left side and the schwannomatous differentiation on the right

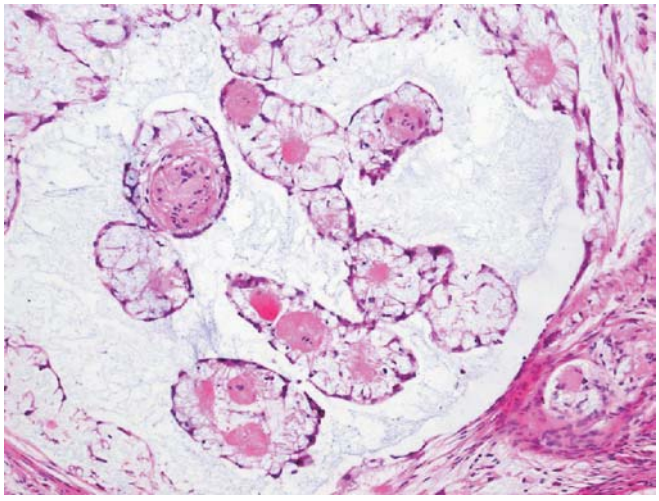


Fig. 4 Prominent myxoid change leading to the formation of peculiar "fibrohyaline balls" lying free in an abundant myxoid matrix in a destroyed lobule

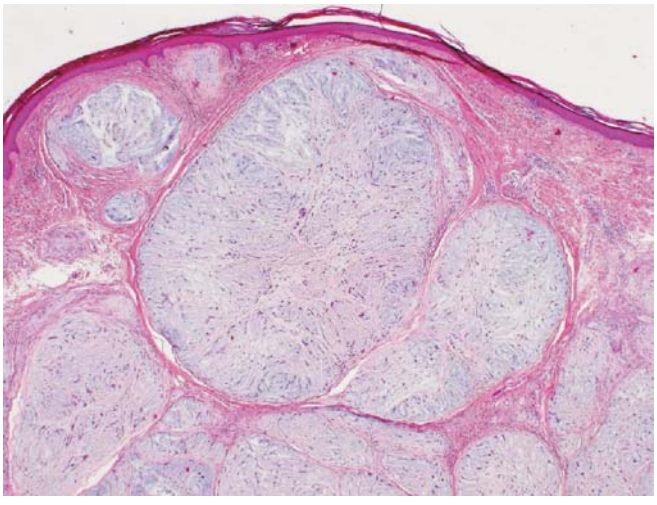


Fig. 3 The retiform pattern of perineurioma in lobules is less apparent when myxoid degeneration is prominent

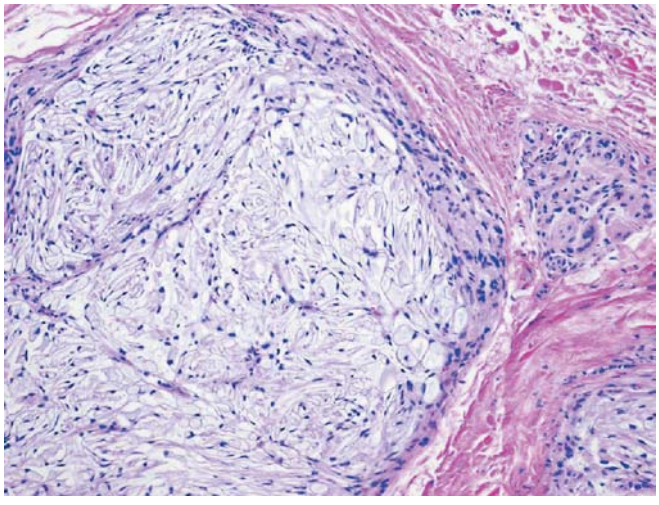


Fig. 5 The schwannomatous areas tend to be located at the periphery of a lobule that otherwise resembles perineurioma. The schwannomatous peripheral rim consists of cells with much more eosinophilic cytoplasm

arrangement vaguely resembling Verocay bodies. The cells of the schwannomatous component had deeply eosinophilic cytoplasm, by which they differed from the cells constituting the perineuriomatous component. The schwannoma cells were uniform, with only occasional cells possessing a large hyperchromatic nucleus probably representing degenerative atypia. Variously dense deposits of hemosiderin were frequently seen in the schwannomatous areas. These hemosiderin deposits were never seen in the perineuriomatous component of the tumors. Parent nerves were identified in one case. The schwannomatous areas tended to be located at the periphery of a lobule that otherwise represented perineurioma (Fig. 5). In some lobules schwannomatous tissue completely encircled the perineuriomatous tissue (Fig. 6). In three cases the perineuriomatous and schwannomatous lobules were sharply demarcated from each other (Fig. 7). Perineuriomatous areas usually dominated over schwannomatous areas. All tumors lacked mitoses, necroses, and signs of infiltrative growth pointing to the benign nature of the neoplasms.

Immunohistochemical findings

The neoplastic cells in the perineuriomatous areas were variously strongly positive for EMA and most of them were negative for S-100 protein (Fig. 8). The neoplastic cells in the schwannomatous areas stained positively with S-100 protein antibody (Fig. 9) and reacted negatively with EMA. In the areas where a cuff of schwannomatous cells encircled a perineuriomatous component located in the centers of the lobules S-100 protein

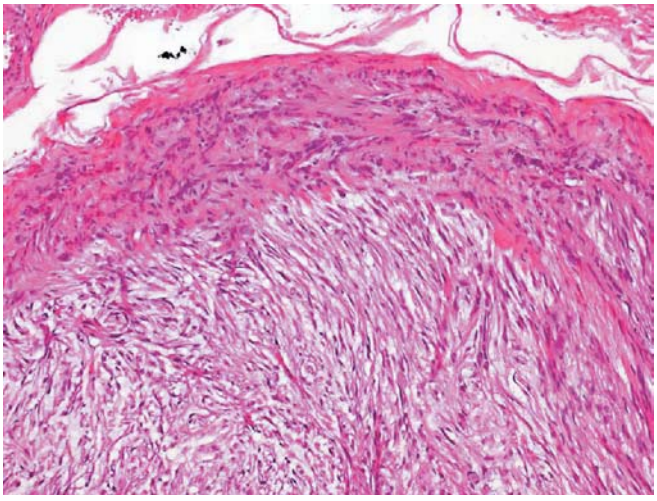


Fig. 6 In some lobules schwannomatous tissue completely encircles the perineuriomatous tissue

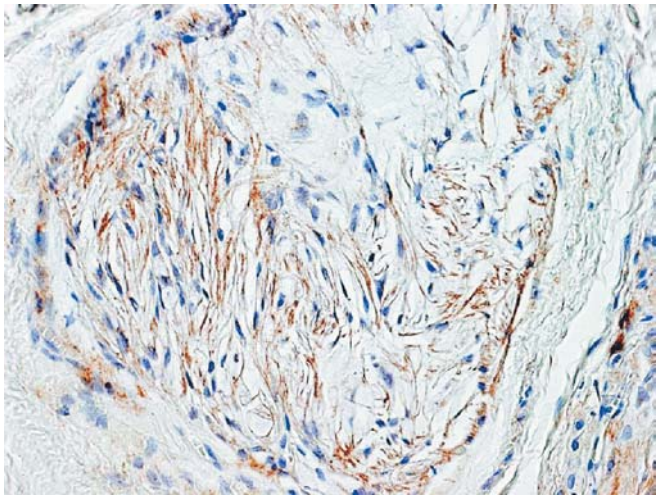


Fig. 8 The neoplastic cells in the perineuriomatous areas were variously strongly positive for EMA and most of them were negative for S-100 protein

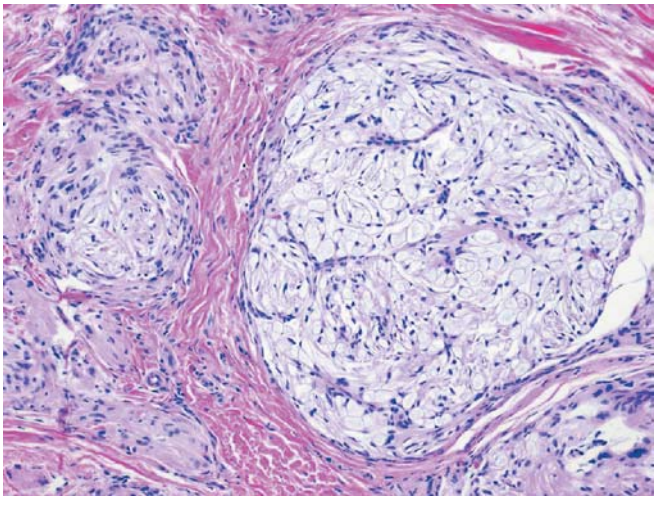


Fig. 7 In this case the schwannomatous (*left*) and perineuriomatous lobules (*right*) are sharply demarcated from each other

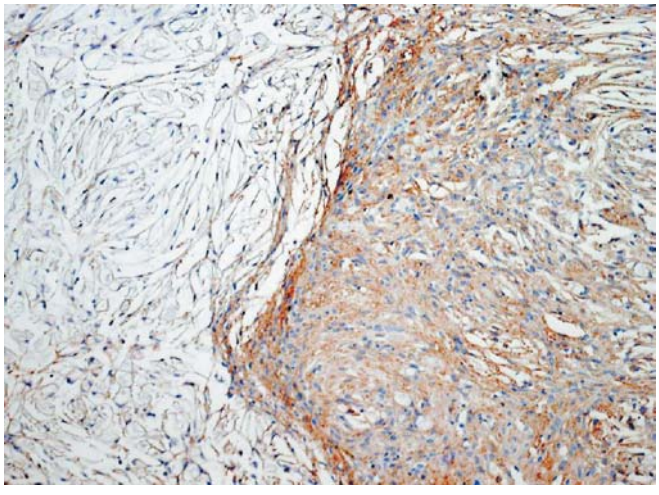


Fig. 9 The neoplastic cells in the schwannomatous areas tested positively with S-100 protein

stained exclusively the peripheral rim of the lobules (Fig. 10). In three cases there were areas with cellular populations which revealed both S-100 protein and EMA immunoreactivity. These cells with both S-100 protein and EMA positivity are probably cells with dual schwannoma/perineurioma features. There were no neurofilament protein positive axons. Absence of axons was also confirmed by the negativity of the tumors with Bodian staining. CD34 highlighted small blood vessels. The tumorous cells were CD34 negative. Smooth muscle actin and α-smooth muscle actin decorated pericytes around blood vessels. All the rest of the antibodies were negative in the tumors.

Ultrastructural findings

Six blocks were available from one case for ultrastructural examination. Unfortunately only a myxoid retiform perineurioma component was found in these six blocks. The schwannomatous component of the tumor was not sampled. Most of the cells examined ultrastructurally were cells with bipolar or multipolar slender cytoplasmic processes set in a myxoid extracellular matrix. Many nuclei were convoluted or deeply indented, with a thin rim of heterochromatin and occasional nucleoli. The cytoplasm contained a various amount of rough endoplasmic reticulum, a few mitochondria, some glycogen particles, and numerous intermediate filaments. The cell membranes showed occasional pinocytotic vesicles. The tumor cells formed many well developed attachment sites with numerous cytoplasmic processes of the neighboring cells. The cells were invested with external lamina (Fig. 11).

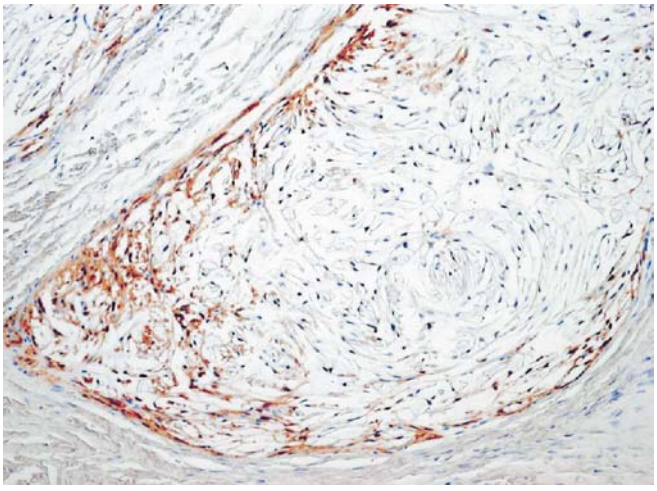


Fig. 10 In the areas where a cuff of schwannomatous cells encircles a perineuriomatous component located in the centers of the lobules, S-100 protein stained exclusively the peripheral rim of the lobules

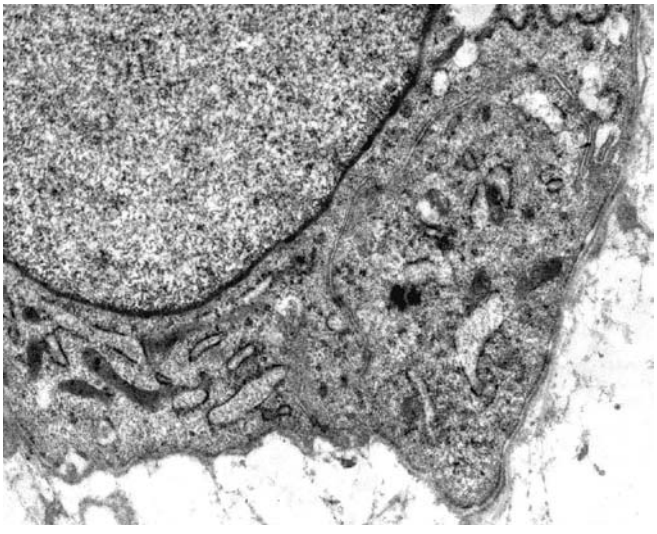


Fig. 11 The tumor cells were invested with external lamina, and they formed numerous attachment sites

Discussion

The connective tissue sheath of a peripheral nerve is composed of Schwann cells, perineurial cells, and fibroblasts. Tumors arising from a peripheral nerve sheath can contain these cells in various proportions, as found in many ultrastructural studies [9, 15, 18, 25, 32, 36, 37]. Moreover, some authors [9, 15] have also observed additional cells that had ultrastructural features interpretable as transitional stages among the three main cell types. Erlandson [9] has described the following cells in neurofibromas: (a) Schwann cells, (b) perineurial cells, (c) cells having features of Schwann cell and fibroblast, (d) fibroblasts, and (e) transitional Schwann-perineurial cells. Although ultrastructural studies of neurofibromas clearly showed that the perineurial cells are part of a cell population in neurofibromas, immunohistochemical studies using EMA as a marker for perineurial cell differentiation failed to demonstrate convincingly this differentiation [1, 18, 33]. EMA^+ cells were rarely found only in peripheral areas of some neurofibromas [1, 29, 34], and these were interpreted as remnants of the nerve sheath of the affected nerve.

The presence of perineurial cells was later confirmed by Zamecnik and Michal [42], who described them as a prominent histological feature in 8% of neurofibromas. The perineurial cells were most often present in pericapsular and perivascular areas. These perineurial cells in pericapsular and perivascular areas are most probably preexisting perineurial cells of the peripheral nerves from which the neurofibromas arose and are not, in contrast to the tumors that we describe, an integral part of the tumors. In addition, the authors presented an interesting tumor which had features of both neurofibroma and retiform perineurioma. This was the first published neoplasm having both perineuriomatous and peripheral nerve sheath differentiation. We again reviewed this case, which is included in our present series, and together with other five similar to identical cases they have now been studied immunohistochemically for the presence of neurofilaments and CD34, which label axons and fibroblasts in neurofibromas respectively [21, 24, 38]. The nonperineuriomatous parts of the tumor were immunohistochemically negative for the antibody to neurofilament proteins and histochemically negative with the Bodian method, findings which confirm that the lesions are devoid of axons. In addition, these parts of the tumors showed an absence of CD34 positive cells. Based upon these findings we think that these nonperineuriomatous parts of the lesions should be interpreted as schwannomatous rather than neurofibromatous component. Interestingly, only the S-100 protein positive schwannomatous parts but not EMA positive perineuriomatous parts of the tumors had sometimes heavy depositions of hemosiderin. The lobular architecture, frequent pseudocystic arrangement of the lobules, myxoid nature of the lesions, the retiform arrangement of the perineuriomatous parts of the lesions, which is identical to the retiform (reticular) perineurioma [28, 30] and predominant occurrence in the fingers highlight the uniqueness of the tumors in this report. We have seen examples of schwannoma-perineurioma hybrid tumors outside the soft tissues of the fingers. These tumors look different from our cases. They can be considerably larger, usually lack the pseudocystic lobular arrangement, the perineuriomatous and schwannomatous components are much more intermingled, and the retiform arrangement of the perineurial component is much less expressed [28, 30].

We reviewed the literature for similar lesions published in the past. Judging purely from a morphological point of view, several reports may have described identical neoplasms under the names of dermal nerve sheath myxoma, cutaneous lobular neuromyxoma, bizarre cutaneous neurofibromas, Pacinian neurofibroma, and neu-

rothekeoma [1, 5, 13, 16, 17, 22, 27]. These lesions had a similar lobular architecture and myxoid areas resembling retiform perineuriomas. In particular, the lesion pictured in Fig. 1 in the report of Argenyi et al. [3] on nerve sheath myxomas seems to show similarities to our cases. Their detailed Fig. 1B is highly suggestive of a retiform perineurioma arrangement. In addition, at least two of the cases in their report revealed both S-100 protein and EMA positivity. The rest of the reports that we reviewed, however, were published either before the era of immunohistochemistry or presented no information on EMA and/or S-100 protein staining. It is therefore impossible to judge these reports critically and objectively and compare them with our cases.

Owing to distinct histopathological features the differential diagnosis of this neoplasm should pose no problem provided a pathologist is familiar with the appearance of retiform perineurioma, a relatively rare neoplasm and that of schwannoma. However, retiform perineurioma is rare and less known lesion, and therefore we ourselves started to recognize these hybrid tumors only after having seen quite a number of retiform perineuriomas. When a myxoid change is prominent, this hybrid tumor may resemble nerve sheath myxoma (neurothekeoma) [24]. The combination of schwannomatous tissue and perineuriomatous tissue enables a clear distinction from any known neoplasm. In addition, staining for both EMA and S-100 protein assists in revealing the biphasic nature of the neoplasm. We have also recently seen an example of benign schwannoma in which peculiar multifocal myxoid degeneration resulted in an appearance simulating a retiform perineurioma. Microscopically this neoplasm was probably the closest mimic of the reported tumor we ever saw; however, immunohistochemistry facilitated the correct diagnosis.

Retiform perineurioma was first described by Ushigome et al. [35] and later defined in small series in recent years, and it was named as retiform perineurioma [28]. We use a descriptive name for the reported tumor: a neoplasm with histopathological features of both schwannoma and retiform perineurioma. Because the term "retiform" has been used in some tumors to connote the resemblance of rete testis other term, namely "reticular" was suggested for this tumor [30]. However, we think that there are other well established anatomical terms in which the word "rete" is used, for example, "rete carpi dorsale" [39], "rete mirabile" [20], and "rete pedis" [12] as well as other terms with histological connotations such as "choroid rete" [23] "rete ridges" in the skin [6], "rete ridges" in esophagus [14], and others [2]. We therefore believe that there is no need to compare the term "retiform" to the rete testis. In the case of perineurioma it was devised to describe the typical netlike arrangement of the tumor [28].

In conclusion, we describe clinicopathological features of distinctive benign hybrid neoplasm composed of schwannoma and retiform perineurioma. In contrast with other nerve sheath tumors, the lesion shows no association with neurofibromatosis or schwannomatosis.

References

1. Allen PW (2000) Myxoma is not a single entity: A reviewf of the concept of myxoma. Ann Diagn Pathol 4:99–123
2. Alper M, Kavak A, Parlak AH, Demirci R, Belenli I, Yesildal N (2004) Measurement of epidermal thickness in a patient with psoriasis by computer-supported image analysis. Braz J Med Biol Res 37:111–117
3. Argenyi Z, LeBoits PE, Santa Cruz D, Swanson PE, Kutzner H (1993) Nerve sheath myxoma (neurothekeoma) of the skin: light microscopic and immunohistochemical reappraisal of the cellular variant. J Cutan Pathol 20:294–303
4. Ariza A, Bilbao JM, Rosai J (1988) Immunohistochemical detection of epithelial membrane antigen in normal perineurial cells and perineurioma Am J Surg Pathol 12:678–683
5. Blumberg AK, Adelaar RS (1989) Nerve sheath myxoma of digital nerve. Cancer 63:1215–1218
6. Braun-Falco M, Ring J (2003) Enhanced cytoplasmic expression of desmocollin 3 in epidermal rete ridges of Dowling-Degos syndrome. Br J Dermatol 149:1293–1296
7. Burger PC, Scheithauer BW (1994) Atlas of tumor pathology. Tumors of the central nervous system, 3rd series, fascicle 10. AFIP, Washington, DC
8. Emory TS, Scheithauer BW, Hirose T, Wood M, Onofrio BM, Jenkins RB (1995) Intraneural perineurioma. A clonal neoplasm associated with abnormalities of chromosome 22. Am J Clin Pathol 103:696–703
9. Erlandson RA (1991) The enigmatic perineurial cell and its participation in tumors and in tumorlike entities. Ultrastruct Pathol 15:335–351
10. Fetsch JF, Miettinen M (1997) Sclerosing perineurioma: a clinicopathologic study of 19 cases of a distinctive soft tissue lesion with a predilection for the fingers and palms of young adults. Am J Surg Pathol 21:1433–1442
11. Fletcher CDM (1989) Solitary circumscribed neuroma of the skin (so-called palisaded, encapsulated neuroma). A clinicopathologic and immunohistochemical study. Am J Surg Pathol 13:574–580
12. Hamada N, Ikuta Y, Ikeda A (1994) Arteriographic study of the arterial supply of the foot in one hundred cadaver feet. Acta Anat (Basel) 151:198–206
13. Henmi A, Sato H, Wataya T, Inaniwa Y, Mori Y (1986) Neurothekeoma. Report of a case with immunohistochemical and ultrastructural features. Acta Pathol Jpn 36:1911–1919
14. Hirokawa M, Takenaka R, Takahashi A, Sugihara K, Wada H, Tashiro T, Horiguchi H, Wakatsuki S, Sano T (2003) Esophageal xanthoma: report of two cases and a review of the literature. J Gastroenterol Hepatol 18:1105–1108
15. Hirose T, Sano T, Hizawa K (1986) Ultrastructural localization of S100-protein in neurofibroma. Acta Neuropathol (Berl) 69:103–110
16. Holden CA, Wilson-Jones E, McDonald DM (1982) Cutaneous lobular neuromyxoma. Br J Dermatol 106:211–215
17. Husain S, Silvers DN, Halperin AJ, McNutt NS (1994) Histologic spectrum of neurothekeoma and the value of immunoperoxidase staining for S-100 protein in distinguishing it from melanoma. Am J Dermatol 16:496–503
18. Jurecka W (1987) Neurogenic tumors of the skin. Wien Klin Wochenschr 99 [Suppl 176]:3–16
19. Kahn DG, Duckett T, Bhuta SM (1993) Perineurioma of the kidney: report of a case with histologic, immunohistochemical and ultrastructural studies. Arch Pathol Lab Med 117:654–657
20. Karasawa J, Touho H, Ohnishi H, Kawaguchi M (1997) Rete mirabile in humans-case report. Neurol Med Chir (Tokyo) 37:188–192
21. Khalifa MA, Montgomery EA, Ismiil A, Azumi A (2000) What are the CD34+ cells in benign peripheral nerve sheath tumors? Double immunostaining study of CD34 and S100 protein. Am J Clin Pathol 114:123–126
22. King DT, Barr RJ (1980) Bizarre cutaneous neurofibromas. J Cutan Pathol 7:21–31

23. Koppang EO, Bjerkas E, Bjerkas I, Sveier H, Hordvik I (2003) Vaccination induces major histocompatibility complex class II expression in the Atlantic salmon eye. Scand J Immunol 58:9–14
24. Laskin WB, Fetsch JF, Miettinen M (2000) The "neurothekeoma": immunohistochemical analysis distinguishes the true nerve sheath myxoma from its mimics. Hum Pathol 31:1230–1241
25. Lassmann H, Jurecka W, Lassmann G, Gebhart W, Matras H, Watzek G (1997) Different types of nerve sheath tumors. Light microscopy, electron microscopy and autoradiography. Virchows Arch A Pathol Anat Histopathol 375:197–210
26. Lazarus SS, Trombetta LD (1978) Ultrastructural identification of benign perineurial cell tumor. Cancer 41:1823–1829
27. McDonnald DM, Wilson-Jones E (1977) Pacinian neurofibroma. Histopathology 1:247–255
28. Michal M (1999) Extraneural retiform perineuriomas. A report of four cases. Pathol Res Pract 195:759–763
29. Perentes E, Nakagawa Y, Ross GW, Stanton C, Rubinstein LJ (1987) Expression of epithelial membrane antigen in perineurial cells and their derivatives. An immunohistochemical study with multiple markers. Acta Neuropathol (Berl) 75:160–165
30. Roggen JFG van, McMenamin ME, Belchis D, Nielsen GP, Rosenberg AE, Fletcher CDM (2001) Reticular perineurioma. A distinctive variant of soft tissue perineurioma. Am J Surg Pathol 25:485–493
31. Scheithauer BW, Woodruff JM, Erlandson RA (1999) In: Atlas of tumor pathology. Tumors of the peripheral nervous system, 3rd series, fascicle 24. AFIP, Washington
32. Smith TW, Bhawan J (1980) Tactile-like structures in neurofibromas. An ultrastructural study. Acta Neuropathol (Berl) 50:233–236
33. Theaker JM, Gatter KC, Puddle J (1988) Epithelial membrane antigen expression by the perineurium of peripheral nerve and in peripheral nerve tumors. Histopathology 13:171–179
34. Tsang WYW (1996) Perineuriomas: perineurial cell neoplasms with distinctive extra- and intra-neural forms. Adv Anat Pathol 3:212–222
35. Ushigome S, TakakuwaT, Hyuga M, Tadokoro M, Shinagawa T (1986) Perineurial cell tumor and the significance of the perineurial cells in neurofibroma. Acta Pathol Jpn 36:973–987
36. Weiser G (1975) An electron microscopic study of "pacinian neurofibroma." Virchows Arch A Pathol Anat Histopathol 366:331–340
37. Weiser G (1978) Neurofibroma and perineurial cell. Electron optical examination of 9 neurofibromas. Virchows Arch A Pathol Anat Histopathol 379:73–83
38. Weiss SW, Nickoloff BJ (1993) CD-34 is expressed by a distinctive cell population in peripheral nerve, nerve sheath tumors, and related lesions Am J Surg Pathol 17:1039–1045
39. Yilmaz S, Aydin A, Dinc G (2001) The anatomy of the arterial supply of the thoracic limb of the porcupine (Hystrix cristata). Anat Histol Embryol 30:273–275
40. Zamecnik M, Gomolcak P (1997) A case of perineurioma. Gen Diagn Pathol 143:261
41. Zamecnik M, Gomolcak P (1997) Perineurioma (in Slovak). CS Patol 33:28–30
42. Zamecnik M, Michal M (2001) Perineurial cell differentiation in neurofibromas. Report of eight cases including a case with composite perineurioma-neurofibroma features. Pathol Res Pract 197:537–544
43. Zelger B, Weinlich G, Zelger B (2000) Perineuroma. A frequently unrecognized entity with emphasis on a plexiform variant. Adv Clin Pathol 4:25–33

Virchows Arch (2004) 445:354–358
DOI 10.1007/s00428-004-1085-2

ORIGINAL ARTICLE

Juan C. Tardío · José A. Aramburu · Carlos Santonja

Desmin expression in spindle cell lipomas: a potential diagnostic pitfall

Received: 3 February 2004 / Accepted: 6 July 2004 / Published online: 20 August 2004
© Springer-Verlag 2004

Abstract The immunohistochemical analysis of the spindle cell lipomas has been for the most part limited to the study of S-100 protein, CD34, and Bcl-2 reactivity. To evaluate the immunoexpression of desmin and actins in spindle cell lipomas of different histological subtypes a retrospective immunohistochemical study of 25 spindle cell lipomas using archival formalin-fixed, paraffin-embedded tissue was performed. Strong positivity of the spindle cell component for desmin was found in 4 of 25 cases (16%). The expression was diffuse in two cases and focal (in up to 25% of the spindle cells) in the other two. Two of these cases were of the classical type and the other two were angiomatous spindle cell lipomas. Desmin-positive and desmin-negative spindle cells showed no morphological differences. The spindle cell component expressed CD34 in all cases and Bcl-2 in 14 of the 25 cases. There was no immunoreactivity for smooth muscle actin, muscle-specific actin, or S-100 protein. We conclude that a significant proportion of spindle cell lipomas express desmin, and therefore that the immunoreactivity for this antigen does not exclude the diagnosis, even in lesions with nonclassical histological features and/or atypical locations.

Keywords Spindle cell lipoma · Desmin · Immunohistochemistry

J. C. Tardío (✉)
Servicio de Anatomía Patológica,
Hospital de Fuenlabrada,
Camino del Molino 2, 28942 Fuenlabrada Madrid, Spain
e-mail: jtardio.hflr@salud.madrid.org
Tel.: +34-91-6006054
Fax: +34-91-6006083

J. C. Tardío
Servicio de Anatomía Patológica,
Hospital El Escorial Carretera de Guadarrama,
28200 San Lorenzo de El Escorial, Madrid, Spain

J. A. Aramburu · C. Santonja
Servicio de Anatomía Patológica,
Hospital Universitario de Getafe,
Carretera de Toledo, kilómetro 12,5, 28905 Getafe Madrid, Spain

Introduction

Spindle cell lipoma was first described by Enzinger and Harvey [4] in 1975. Since then studies of several series have reported the morphological and immunophenotypical features of this tumor. Spindle cell lipomas are circumscribed lesions typically arising in the subcutaneous tissue of the posterior neck and upper back. The majority of the cases occur in men in the fifth to seventh decades. They are composed of a mixture of bland spindle cells and mature adipocytes in variable proportions together with bundles of ropy collagen and scattered mast cells. Most immunohistochemical analyses have been limited to the study of S-100 protein, CD34, and Bcl-2 protein expression, with only some reports including a small number of other antigens [1, 15, 16, 17]. This has hampered our knowledge of the complete immunophenotypical profile of spindle cell lipomas, which may induce to misdiagnosis when studying lesions with nonclassical histological features or those in unusual locations.

Prompted by our recent observation of desmin positivity in an angiomatous spindle cell lipoma and to elucidate the actual frequency of muscle antigens immunoreactivity in the spindle cell component of this lesion, we explored the expression of desmin and actins in a retrospective series of spindle cell lipomas of different histological subtypes.

Materials and methods

From the pathology files of our hospitals we retrieved 25 cases of spindle cell lipoma diagnosed between October 1996 and February 2003 (22 men, 3 women; mean age 55 years, median 54, range 21–82). The clinicopathological features of the cases are summarized in Table 1. The location of the lesions was as follows: posterior neck (n=5 cases), back (n=4 cases), scapular area and occipital region (n=3 each), shoulder (n=2), and retroauricular area, supraclavicular region, buttock, wrist, hand, thumb and oropharynx (n=1 each); the location was not available in one case. Twenty-two tumors arose in the subcutaneous tissue, two involved the dermis (with a plexiform pattern) and the subcutis, and another one was

Table 1 Spindle cell lipomas: clinicopathological features (*SMA* smooth muscle actin, *MSA* muscle-specific actin)

Case no.	Age (years)	Sex	Location	Size (mm)	Histological subtype	CD34	S-100	Desmin	SMA	MSA	Bcl-2
1	46	M	Shoulder	20	Angiomatous	+	–	+	–	–	–
2	57	M	Posterior neck	50	Angiomatous	+	–	+	–	–	+
3	47	M	Posterior neck	80	Classical	+	–	+ Focal	–	–	+
4	58	M	Oropharynx	30	Classical	+	–	+ Focal	–	–	+ Focal
5	42	M	Wrist	35	Classical	+	–	–	–	–	+
6	42	M	Posterior neck	16	Classical	+	–	–	–	–	+ Focal
7	41	M	Scapular region	70	Classical	+	–	–	–	–	+ Focal
8	44	M	Shoulder	20	Classical	+	–	–	–	–	–
9	55	M	Occipital region	70	Classical	+	–	–	–	–	–
10	48	M	Posterior neck	40	Classical	+	–	–	–	–	–
11	68	M	Occipital region	85	Classical	+	–	–	–	–	–
12	73	F	Hand	30	Classical	+	–	–	–	–	–
13	81	F	Occipital region	80	Classical	+	–	–	–	–	+
14	71	M	Back	75	Classical	+	–	–	–	–	+
15	68	M	Retroauricular region	25	Classical	+	–	–	–	–	+
16	50	M	Not available	30	Classical	+	–	–	–	–	–
17	76	M	Posterior neck	20	Classical	+	–	–	–	–	–
18	41	M	Scapular region	30	Classical	+	–	–	–	–	–
19	55	M	Thumb	20	Classical	+	–	–	–	–	+ Focal
20	82	M	Back	35	Classical	+	–	–	–	–	+ Weak
21	21	M	Buttock	45	Classical	+	–	–	–	–	–
22	65	M	Back	30	Classical	+	–	–	–	–	+ Focal
23	45	M	Back	110	Angiomatous	+	–	–	–	–	+
24	54	F	Supraclavicular	15	Plexiform	+	–	–	–	–	–
25	44	M	Scapular region	18	Plexiform	+	–	–	–	–	+ Focal

located in the submucosa of the oropharynx. The size of the lesions ranged between 15 and 110 mm (mean 44, median 30).

Each specimen had been fixed in formalin, routinely processed, and embedded in paraffin. Hematoxylin and eosin stained sections of 4 μm were reviewed, and representative paraffin blocks were selected for immunohistochemical analysis. Antibodies against the following antigens were used: desmin (clone D33, dilution 1/120, Dako, Denmark), smooth muscle actin (SMA; clone 1A4, dilution 1/120, Dako), muscle-specific actin (MSA; clone HHF35, dilution 1/120, Dako), CD34 (clone QBEnd10, dilution 1/120, Novocastra, UK), S-100 protein (polyclonal, prediluted, Dako), and Bcl-2 (clone 120, dilution 1/160, Dako). Immunohistochemistry was performed on deparaffinized sections by the streptavidin-biotin method (StreptABComplex/HPR, Dako), with diaminobenzidine as chromogen, following heat-induced epitope retrieval by pressure cooker in citric acid at pH 6.0 for 3 min. Sections were counterstained with hematoxylin.

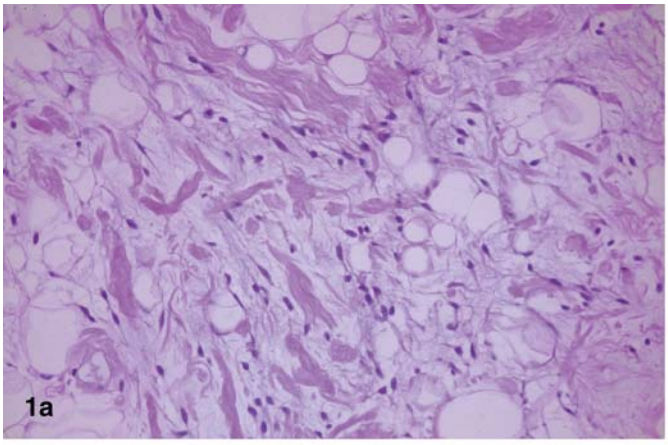
Results

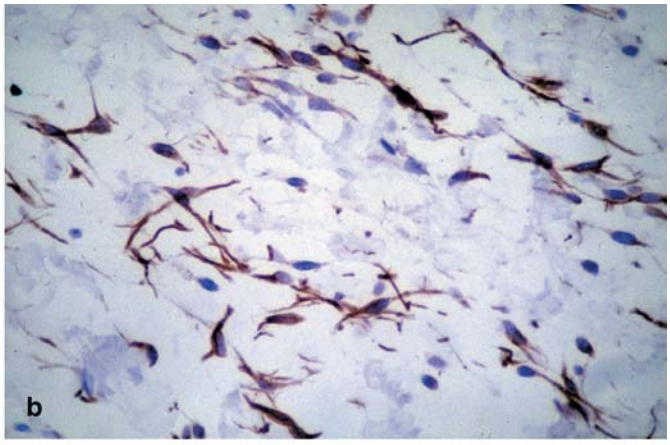
Pathological features

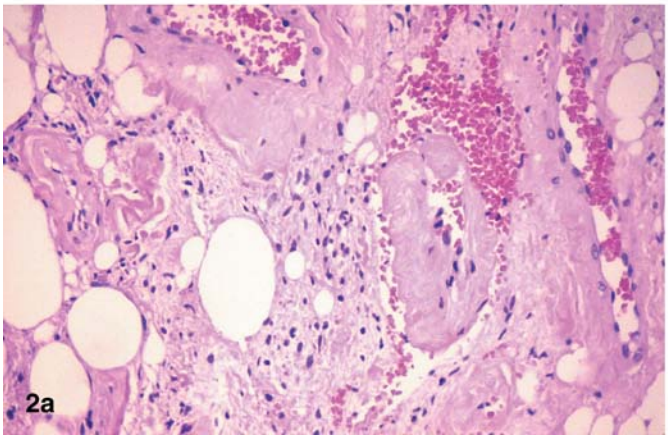
Grossly the lesions were yellow to whitish and well demarcated or encapsulated masses except for the dermal plexiform tumors that had ill defined margins. Twenty tumors were classical spindle cell lipomas (Fig. 1a), three had a clearly vascular component, and two were of the plexiform variant. Two of the three tumors with a prominent vascularity (cases 1 and 2) were composed of spindle cells similar to those of the classical type, very scarce mature adipocytes, and numerous blood vessels of hyalinized walls (Fig. 2a). The third angiomatous tumor (case 23) showed an area (amounting to 25% of its volume) with numerous closely apposed small vessels of capillary type and some interspersed spindle cells. The remainder of this tumor had features of classical spindle cell lipoma. One case of the classical type (case 17) and one case of the plexiform variant (case 25) were local recurrences. The original tumor in the latter had been incompletely excised 23 months before, while in the former it had been removed at another institution, and the sections were not available for review.

Immunohistochemical findings

The immunohistochemical study showed strong positivity of the spindle cell component for desmin in four of the 25 cases (16%). The expression was diffuse in two of the tumors (cases 1 and 2), both of them histologically corresponding to the angiomatous lesions featuring numerous hyalinized-walled blood vessels (Fig. 2b). Focal desmin expression (up to 25% of the spindle cells) was found in the other two tumors (cases 3 and 4), which were classical spindle cell lipomas (Fig. 1b). Desmin-positive spindle cells showed no morphological differences from the remaining spindle cells in our cases. The spindle cell component expressed CD34 in all cases, and Bcl-2 in 14 of the 25 cases, and was not immunoreactive for SMA, MSA or S-100 protein. The adipocytes expressed S-100 protein in all tumors.







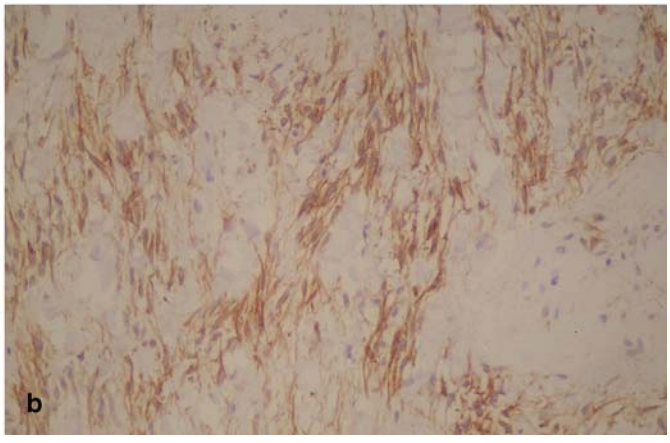


Fig. 1 Classical spindle cell lipoma (case 4) with focal areas of desmin reactivity, amounting to 25% of the spindle cells. **a** Hematoxylin and eosin, ×200. **b** Immunohistochemical staining for desmin, ×200

Fig. 2 Spindle cell lipoma with hyalinized vascular walls (case 1) featuring diffuse positivity of the spindle cell component for desmin. **a** Hematoxylin and eosin, ×200. **b** Immunohistochemical staining for desmin, ×200

Discussion

We present a series of spindle cell lipomas with clinicopathological characteristics similar to those previously reported in this type of tumors. An outstanding finding was the presence of a prominent vascular component in three cases. One of them (case 23) had features of classical spindle cell lipoma and an area containing closely apposed small blood vessels and some interspersed spindle cells. This tumor was similar to those previously reported as "vascular variant of spindle cell lipoma" [19]. The other two lesions (cases 1 and 2) had more peculiar features. They were spindle cell proliferations with very scarce mature fat cells and numerous blood vessels with a hyalinized wall. Their histological features were different from those reported either in the vascular or in the pseudoangiomatoid variants of spindle cell lipoma. The latter shows irregular and branching pseudovascular spaces, devoid of intraluminal red blood cells and endothelial lining [8]. Although infrequent, a vascular component such as that seen in our cases has been reported and illustrated in previous series of spindle cell lipomas [2].

The immunohistochemical study of spindle cell lipomas is said to yield only positive results for vimentin and CD34. According to standard textbooks, the absence of smooth muscle markers allows the differential diagnosis with look-alikes of spindle cell lipoma, such as the rare myolipoma, a variant of lipoma usually located in the deep soft tissues of the abdomen [20] and the soft tissue counterpart of mammary myofibroblastoma [11].

In this series we found four cases (16%) with desmin expression in the spindle cell component. To our knowledge, this has not been reported previously. Previous immunohistochemical studies of spindle cell lipomas have mainly been guided to determine the expression of CD34, S-100 protein, and Bcl-2 [1, 15, 16, 17]. We have not been able to find reports that include desmin. We are aware of only a single reference to desmin positivity in spindle cell lipomas, as a personal observation in a report of mammary-type myofibroblastomas of soft tissue by McMenamin and Fletcher [11]. When discussing the differential diagnosis between mammary-type myofibroblastoma and spindle cell lipoma, the authors state that spindle cell lipomas are positive for desmin in fewer than 2% of cases.

However, according to our findings, a higher number of spindle cell lipomas express desmin. Pathologists need to be aware of this fact because it is a potential diagnostic

pitfall, mainly when confronted with morphological variants and/or atypical locations of spindle cell lipomas. Two of our desmin-positive tumors were examples of the classical histological type, but the other two (cases 1 and 2) were spindle cell tumors with a minimal component of mature adipocytes and numerous blood vessels with hyalinized walls. They occurred in men in their fifth or sixth decade and were located in sites (shoulder and posterior neck) typical for spindle cell lipoma. These two lesions are histologically quite similar to the cellular angiofibroma, also known as "angiomyofibroblastoma-like tumor" [9, 13]. This is a neoplasm that consists of spindle cells in a fibromyxoid stroma and features a minor adipocytic component and numerous blood vessels, often with fibrotic walls. In contrast to spindle cell lipoma, cellular angiofibroma occurs in both men and women and appears to be restricted to the groin and pelvic areas (although one case has been reported in the subcutaneous tissue of the chest [6]). Furthermore, the expression of CD34 is not consistent in this tumor. Immunoreactivity for desmin has been reported in a minority of cellular angiofibromas, often with a focal and weak positivity. Some cases express estrogen and/or progesterone receptor proteins. One of our two cases with angiomatous pattern (case 1) was tested for estrogen and progesterone receptor proteins and was negative for both antigens.

Mammary-type myofibroblastoma of extrammamary location [11] must also be included in the differential diagnosis. This CD34 and desmin-positive spindle cell neoplasm shares with spindle cell lipoma its preference for adult men, the morphology of the spindle cells, an adipocytic component of variable extension, and numerous stromal mast cells. The blood vessels are generally not prominent, but when present, they can have hyalinized walls, such as those seen in our cases 1 and 2. However, both lesions can be distinguished by the presence of a hyalinized stroma with thick bands of collagen and a fascicular arrangement of the spindle cells in mammary-type myofibroblastoma. Moreover, this tumor has not yet been reported in locations typical of spindle cell lipoma (as posterior neck, upper back, or shoulder), and lacks ropy collagen, a consistent feature of the latter neoplasm. Nevertheless, they probably are two closely related neoplasms, as evidenced by their common chromosomal aberrations [14].

The desmin-positive spindle cells of our cases are morphologically indistinguishable from the remaining spindle cells in this series. The presence of desmin-positive cells has previously been reported in other fat tumors. Dei Tos et al. [3] reported two cases with expression of this antigen in their series of six spindle cell liposarcomas. Furthermore, desmin positivity has been sporadically found in myxoid liposarcomas [7, 10]. The reactivity for desmin was described as focal in all these cases. As in our series, desmin-positive and desmin-negative cells showed no morphological differences. Spindle cell liposarcomas were not immunoreactive with SMA. This phenotype was interpreted as a possible myofibroblastic differentiation [3]. A wholly unrelated condition is the presence of desmin-positive cells that show morphological and phenotypical distinct features of smooth muscle cells in fat tumors such as those in myolipomas [12] and lipoleiomyosarcomas [5]. It has been suggested that spindle cell lipomas could arise from immature mesenchymal cells capable of differentiating along several mesenchymal lines [18]. The existence of desmin-positive and SMA- and MSA-negative spindle cells in our cases suggests a myofibroblastic differentiation.

In conclusion, our findings show that a significant proportion of spindle cell lipomas express desmin, and therefore that the immunoreactivity for this antigen does not exclude the diagnosis, even in lesions with nonclassical histological features and/or atypical locations.

References

1. Beham A, Schmid C, Hodl S, Fletcher CD (1989) Spindle cell and pleomorphic lipoma: an immunohistochemical study and histogenetic analysis. J Pathol 158:219–222
2. Bolen JW, Thorning D (1981) Spindle-cell lipoma. A clinical, light-and electron-microscopical study. Am J Surg Pathol 5: 435–441
3. Dei Tos AP, Mentzel T, Newman PL, Fletcher CDM (1994) Spindle cell liposarcoma, a hitherto unrecognized variant of liposarcoma. Analysis of six cases. Am J Surg Pathol 18:913–921
4. Enzinger FM, Harvey DA (1975) Spindle cell lipoma. Cancer 36:1852–1859
5. Folpe AL, Weiss SW (2002) Lipoleiomyosarcoma (Well-differentiated liposarcoma with leiomyosarcomatous differentiation). A clinicopathologic study of nine cases including one with dedifferentiation. Am J Surg Pathol 26:742–749
6. Garijo MF, Val-Bernal JF (1998) Extravulvar subcutaneous cellular angiofibroma. J Cutan Pathol 25:327–332
7. Gibas Z, Miettinen M, Limon J, et al (1995) Cytogenetic and immunohistochemical profile of myxoid liposarcoma. Am J Clin Pathol 103:20–26
8. Hawley IC, Krausz T, Evans DJ, Fletcher CDM (1994) Spindle cell lipoma-a pseudoangiomatous variant. Histopathology 24: 565–569
9. Laskin WB, Fetsch JF, Mostofi FK (1998) Angiomyofibroblastomalike tumor of the male genital tract. Analysis of 11 cases with comparison to female angiomyofibroblastoma and spindle cell lipoma. Am J Surg Pathol 22:6–16
10. Leader M, Collins M, Patel J, Henry K (1987) Desmin: its value as a marker of muscle derived tumours using a commercial antibody. Virchows Arch A Pathol Anat Histopathol 411:345–349
11. McMenamin ME, Fletcher CDM (2001) Mammary-type myofibroblastoma of soft tissue. A tumor closely related to spindle cell lipoma. Am J Surg Pathol 25:1022–1029
12. Meis JM, Enzinger FM (1991) Myolipoma of soft tissue. Am J Surg Pathol 15:121–125
13. Nucci MR, Granter SR, Fletcher CDM (1997) Cellular angiofibroma: a benign neoplasm distinct from angiomyofibroblastoma and spindle cell lipoma. Am J Surg Pathol 21:636–644
14. Pauwels P, Sciot R, Croiset F, Rutten H, Van den Berghe H, Dal Cin P (2000) Myofibroblastoma of the breast: genetic link with spindle cell lipoma. J Pathol 191:282–285
15. Suster S, Fisher C (1997) Immunoreactivity for the human hematopoietic progenitor cell antigen (CD34) in lipomatous tumors. Am J Surg Pathol 21:195–200
16. Suster S, Fisher C, Moran CA (1998) Expression of bcl-2 oncoprotein in benign and malignant spindle cell tumors of soft

tissue, skin, serosal surfaces, and gastrointestinal tract. Am J Surg Pathol 22:863–872
17. Templeton SF, Solomon AR Jr (1996) Spindle cell lipoma is strongly CD34 positive. An immunohistochemical study. J Cutan Pathol 23:546–550
18. Toker C, Tang CK, Whitely JF, Berkheiser SW, Rachman R (1981) Benign spindle cell breast tumor. Cancer 48:1615–1622
19. Warkel RL, Rehme CG, Thompson WH (1982) Vascular spindle cell lipoma. J Cutan Pathol 9:113–118
20. Weiss SW, Goldblum JR (2001) Benign lipomatous tumors. In: Enzinger and Weiss's soft tissue tumors. Mosby, St. Louis, pp 586–587

Virchows Arch (2004) 445:359–367
DOI 10.1007/s00428-004-1060-y

ORIGINAL ARTICLE

Michal Michal · Ondrej Hes · Michele Bisceglia · Roderick H. W. Simpson · Dominic V. Spagnolo · Alberto Parma · Ludmila Boudova · Milan Hora · Roman Zachoval · Saul Suster

Mixed epithelial and stromal tumors of the kidney. A report of 22 cases

Received: 16 March 2004 / Accepted: 28 May 2004 / Published online: 20 August 2004
© Springer-Verlag 2004

Abstract Mixed epithelial and stromal tumor of the kidney (MESTK) is a recently described subset of renal neoplasm that tends to occur in middle-aged and older women and is characterized by a distinctive histological appearance. To further characterize this lesion, we report the clinicopathological and immunohistochemical features of 22 additional cases from our institutional files. Grossly, the tumors ranged in size from 1 cm to 14 cm (mean 6.7 cm), were well circumscribed but unencapsulated, and showed a cystic cut surface. The tumors were composed of a spindle cell proliferation that resembled ovarian stroma, as well as an epithelial component lining the cystic structures, which usually consisted of flat to hobnailed cells typical of collecting-duct epithelium. Areas displaying features of Müllerian differentiation were also documented in 6 cases, including epithelium of endometrioid, tubal, clear cell and squamous cell type as well as one case showing an architecture that closely resembled Müllerian adenofibroma and adenosarcoma. Follow-up in 14 patients (average 4.4 years) showed no evidence of recurrence or metastasis. We believe these tumors represent the renal counterpart of similar mixed epithelial and stromal neoplasms occurring in the biliary tract and pancreas, which is also characterized by cystic structures lined by epithelium, admixed with ovarian-type stroma. The differential diagnosis for these tumors includes cystic nephroma and cystic partially differentiated nephroblastoma, which we believe to represent clinically and morphologically distinct entities from MESTK. In particular, the distinction from cystic nephroma in adult male patients is emphasized, and two cases of this entity are included in the study for comparison.

Keywords Mixed epithelial and stromal tumors of the kidney · Müllerian differentiation · Müllerian adenosarcoma · Cystic nephroma

M. Michal (✉) · O. Hes · L. Boudova
Sikl's Department of Pathology, Laboratore Spec. Diagnostiky Medical Faculty Hospital,
Charles University Hospital,
Alej Svobody 80, 304 60 Pilsen, Czech Republic
e-mail: michal@medima.cz
Tel.: +420-37-7104630
Fax: +420-37-7104650

M. Bisceglia
Department of Pathology,
IRCCS-Ospedale "Casa Sollievo della Sofferenza"
Viale Cappuccini, San Giovanni Rotondo, Italy

R. H. W. Simpson
Department of Pathology, Royal Devon and Exeter Hospital,
Exeter, UK

D. V. Spagnolo
The Western Australian Centre for Pathology and Medical Research, Nedlands, Australia

A. Parma
Anatomic Pathology Unit, Ospedali Riuniti di Bergamo,
Bergamo, Italy

M. Hora
Department of Urology, Charles University Hospital,
Pilsen, Czech Republic

R. Zachoval
Department of Urology,
University Hospital Kralovske Vinohrady,
Prague, Czech Republic

S. Suster
Department of Pathology,
The Ohio State University Hospital, Columbus, OH, USA

Introduction

The first renal tumor described under the name "Mixed epithelial and stromal tumor of the kidney" (MESTK) was first published by Michal and Syrucek in 1998 [47]. In 2000, Michal suggested the concept of MESTK as an entity encompassing a group of renal tumors occurring usually in perimenopausal women, which are histologically composed of spindle cell stroma and variously sized gland-like structures ranging from small hardly luminized tubules to cystic cavities layered by a hobnail-shaped

epithelium typical of renal collecting ducts [48]. A few months later, Adsay et al. suggested almost the same concept [3]. These tumors which arise almost exclusively in adult females used to be mistakenly diagnosed as cystic nephromas in the past and therefore, for comparison, we also describe two cases of cystic nephroma in adult men.

Materials and methods

We reviewed more than 8000 renal tumors in the consultation and routine files of the Department of Pathology at Charles University Hospital in Pilsen and retrieved all cases diagnosed as cystic nephromas or MESTK. Similarly, we reviewed all cases diagnosed as cystic nephromas or MESTK from the archives of the Pathology Department of "Casa Sollievo della Sofferenza" Hospital in San Giovanni Rotondo (Italy), the Western Australian Centre for Pathology and Medical Research in Nedlands (Western Australia), Department of Pathology of the Ohio State University (USA), and the Department of Pathology of the Royal Devon and Exeter Hospital (UK). Tissue samples were fixed in 4% formaldehyde and paraffin-embedded. Sections (5-μm thick) were stained using routine methods. In all cases examined by means of immunohistochemistry, newly cut sections from either formaldehyde-fixed or paraffin-embedded material or unstained reserve slides were used. As a detection system, we employed the avidin-biotin complex or streptavidin-biotin complex labeled with peroxidase or alkaline phosphatase. Microwave antigen pretreatment was performed prior to applying the primary antibodies. Automated immunostaining employing the Lab Vision autostainer was used. The following primary antibodies were used: α-smooth muscle actin (1A4; DakoCytomation, Glostrup, Denmark), S-100 protein (polyclonal; DakoCytomation), cytokeratin (CAM 5.2; Becton Dickinson, Mountain View, CA, USA), cytokeratin (AE1/AE3; Boehringer, Mannheim, Germany), inhibin (R1; Serotec, Kidlington/Oxford, UK), desmin (D-33; DakoCytomation), melanosome (HMB-45; DakoCytomation), neurofilament protein (2F11; DakoCytomation), synaptophysin (polyclonal; DakoCytomation), and chromogranin A (DAK-A3; DakoCytomation).

Results

Altogether, from our files, we found 24 cases diagnosed as MESTK or cystic nephroma, in both men and women. The case published by Michal and Syrucek [47] and case 1 published by Bisceglia and Bacchi [11] are included in this series. Of 24 patients, 22 were women and 2 were men.

A. Female patients (22 cases)

The precise age was known in 20 of the 22 female patients. The mean age was 54 (ranging from 41 years to 75 years). The other two women were said to be "middle aged". Follow-up was available in 14 patients. The follow-up ranged from 3 years to 8 years, the average period being 4.4 years. No recurrence or metastasis was observed in any of the patients.

The size of the neoplasms was known in 21 of the 22 cases. The mean largest diameter was 6.7 cm (ranging from 1 cm to 14 cm). Grossly, the tumors were confined to the kidney, although in one third of the cases they bulged into the renal pelvis. They were non-encapsulated, but well circumscribed and delineated by compressed fibrous tissues. All tumors were single, localized and unilateral. All but one tumor were predominantly cystic: the cysts varied in size and shape from hardly perceivable microcysts to spaces of several centimeters (Fig. 1). The number of cysts in each case varied from few to innumerable, and the lining was smooth and glistening. The intervening septa were thin or they were expanded by the mural growth of the stromal component of the neoplasm. One lesion was described as mostly solid with microcysts imparting a sponge-like appearance to the lesion.

Histologically, the tumors consisted both of solid (Fig. 2) and of extensive multicystic areas, the latter generally predominating, and in which most of the tissue was concentrated within the intervening thin fibrous septa (Fig. 3). Both epithelial and stromal components were

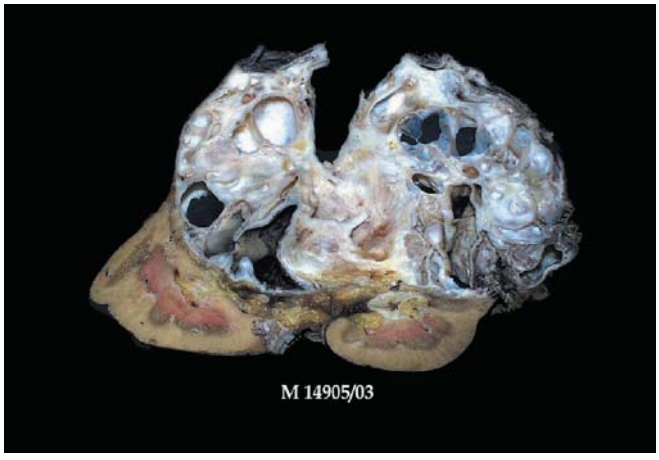


Fig. 1 Grossly, mixed epithelial and stromal tumor of the kidney (MESTK) usually appears as a multicystic lesion, unencapsulated yet well circumscribed

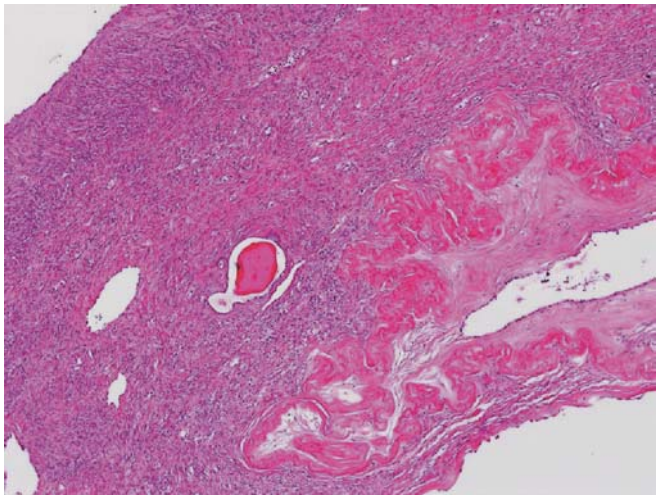


Fig. 2 A solid area of the tumor is illustrated; the ovarian-like stroma as well as a hyaline scar reminiscent of an ovarian hyalinized corpus albicans are well visible

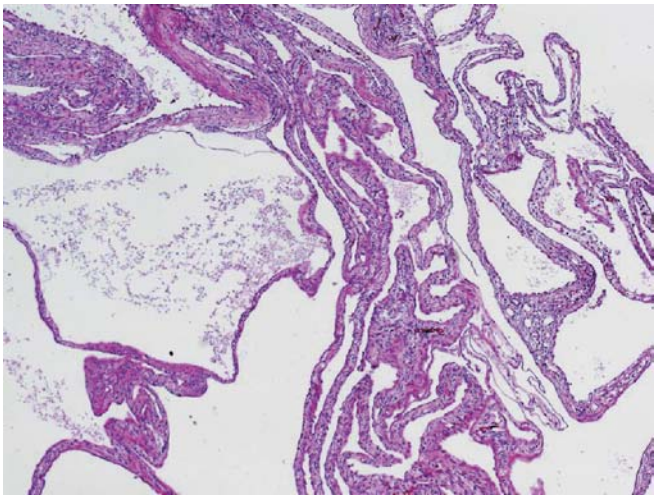


Fig. 3 Some cases consisted of large cysts bridged by thin fibrous septa containing benign-looking spindle cells

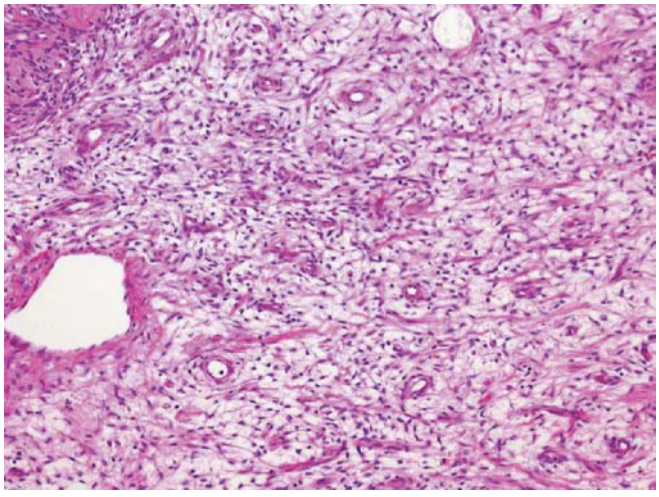


Fig. 4 In the parts where tumors underwent myxoid change, the stroma lost its similarity with ovarian stroma

seen, the latter consisting of spindle shaped cells, with an appearance usually indistinguishable from ovarian stroma. Only in the hyalinized or myxoid areas (Fig. 4) did the stroma lose its similarity to the ovary. Quite often the stroma underwent focal smooth muscle metaplasia, and, in one case, there was frank fibroleiomyomatous change forming large nodules of up to several centimeters (Fig. 5A). Microscopically, these areas had the appearance of leiomyomas (Fig. 5B).

In two cases, the stroma underwent distinctive forms of scarring that resembled the hyalinized scars left by ovarian corpora albicantia. These were well-circumscribed structures with convoluted borders and were almost entirely composed of densely packed collagen fibers with occasional admixed fibroblasts (Fig. 2). Focal calcification and ossification were seen in these densely fibrous corpora albicantia-like bodies in one case.

The epithelial component had various appearances depending on the size and shape of the tubulo-cystic structures. Mostly, it consisted of cystic cavities lined by flat to eosinophilic hobnail cells, which were similar to the epithelial cells of the collecting ducts (Fig. 6). In places, as a minor component of the tumor, there was an apparent vaguely lobular arrangement of groups of eosinophilic epithelial cells, sometimes lining barely luminized tubules, each surrounded by a thick basement membrane, set in a very cellular spindle cell stroma (Fig. 7). Such a miniaturized tubular pattern in one case comprised the predominant part of the tumor. In several other cases, there were sparse tubules composed of ciliated cells with basophilic cytoplasm resembling serous inclusion cysts of the ovarian medulla or cortex (Fig. 8).

A unique case showed a remarkable endometrioid differentiation. In addition to the cystic areas of typical

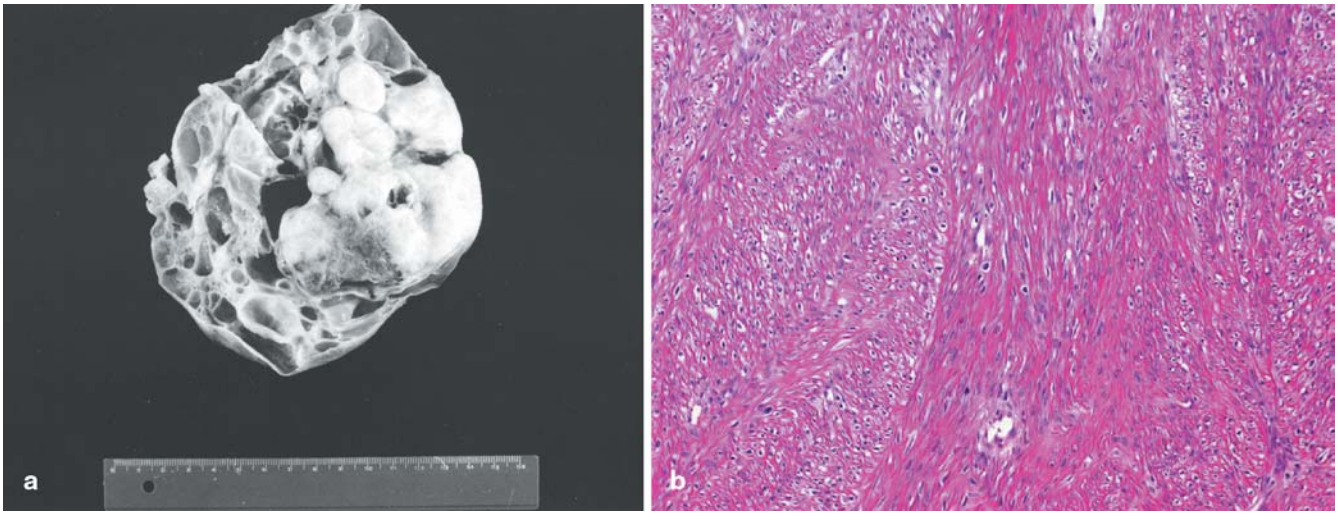


Fig. 5 On sectioning, the cut surface of this tumor—which was 14 cm in size—showed both a solid multinodular and multicystic aspect (**A**). Microscopically, the solid areas had the appearance of a leiomyoma (**B**)

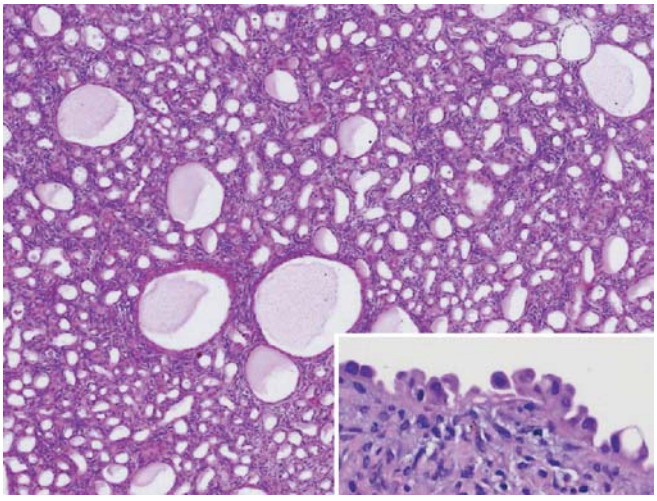


Fig. 6 The lining epithelium of the cystic cavities consisted of a monolayer of flat cells with eosinophilic cytoplasm. Some glands were lined by prominent hobnail epithelium (*inset*)

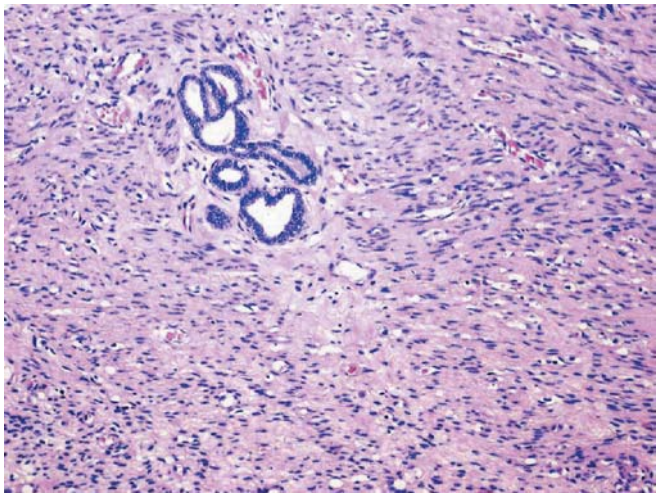


Fig. 8 In this case, sparse tubules composed of serous cells with basophilic nuclei and sparse ciliated cytoplasm were seen

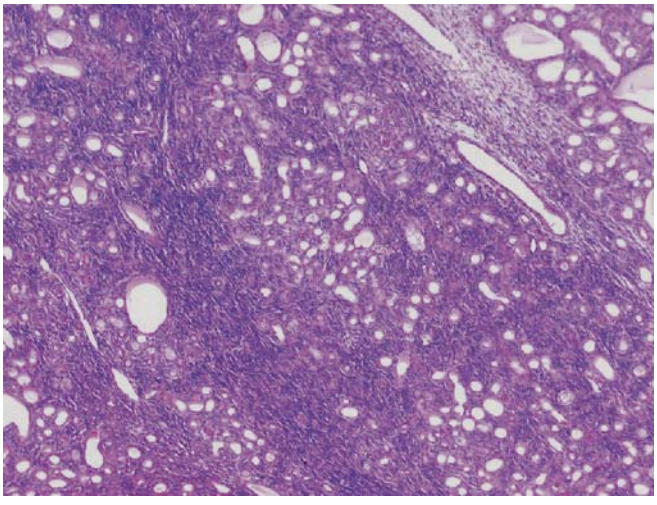


Fig. 7 In this case, the epithelial component of tumor comprised of minute eosinophilic tubules intimately admixed with a very cellular stromal component. The microscopic tubules were arranged in a vaguely lobular pattern

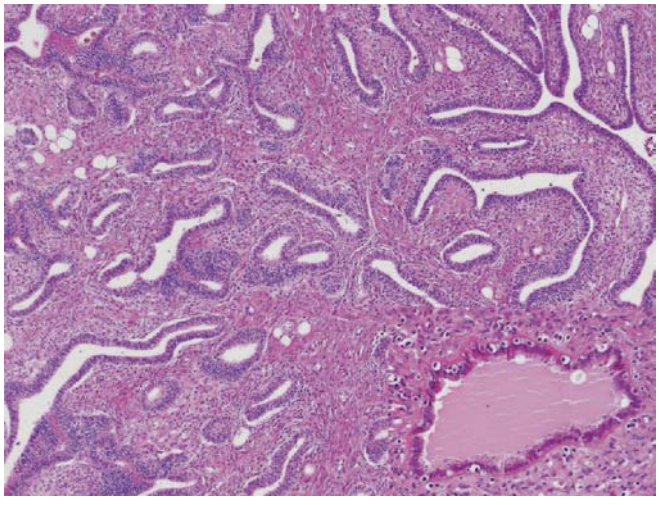


Fig. 9 In this case, glandular areas lined with distinct endometrioid or tubal epithelium (*right lower inset*) were seen within the tumor

MESTK, it contained multiple nodules composed of leaflet-like structures having glandular and stromal elements of a different appearance. The glandular structures in this case were lined partly by cells resembling endometrial epithelium (Fig. 9), and in some cells this similarity was even further enhanced by focal subnuclear vacuoliza- tion. Furthermore tubal metaplastic epithelium with ciliated and peg cells could also be seen in places (Fig. 9). The stroma within these leaflet-like structures was more cellular, resembling endometrial rather than ovarian stro-ma, thus creating an appearance very similar to Müllerian adenofibromas or adenosarcomas (Fig. 10). Also, the ovarian-like stroma close to the leaflet-like structures focally displayed lipomatous differentiation (Fig. 10). The endometrioid epithelium of this tumor often transformed into a clear cell epithelium partly endowed with a ciliated border. An epithelial clear cell change was also seen in three other cases (Fig. 11) and some minor foci of endometrioid differentiation were present in another. A transitional epithelium with an inner mucinous layer, as sometimes seen in cystic Brenner tumors, and squamous epithelium were also detected in one case each.

All cases analyzed using immunohistochemical methods were of female patients. Thirteen cases in which tissue blocks or unstained reserve slides were available were studied for their immunohistochemical profile. The spindle cells stained consistently with vimentin. Alpha-smooth muscle actin often marked large areas, especially those with smooth muscle metaplasia. In contrast, desmin was more patchy in distribution.

In nine cases, the stroma reacted with the antibody to estrogen receptor protein, and the epithelium in five

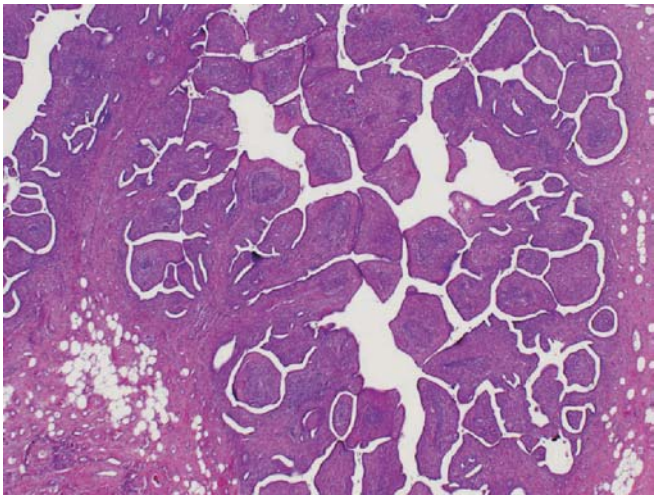


Fig. 10 A complex leaflet-like structure with stromal cores and outer luminal epithelial rim is depicted in the main area of the field. Small areas of fatty change are also present. The overall appearance closely resemble a Müllerian adenofibroma or adenosarcoma of various gynecological sites

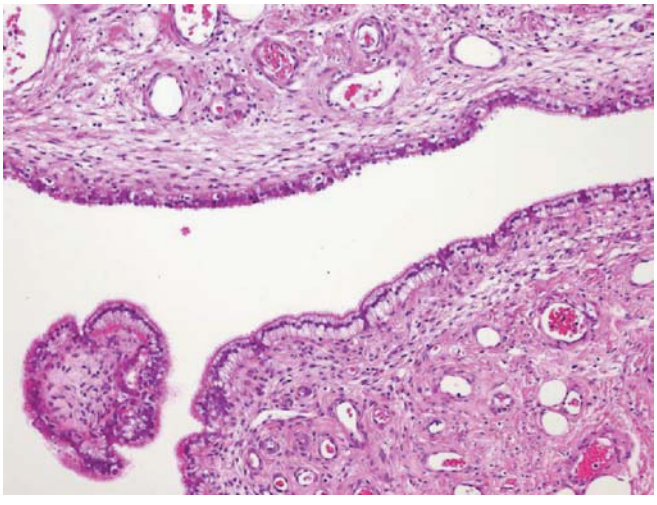


Fig. 11 Basophilic ciliated epithelium transforms into the clear cell ciliated epithelium

cases. Progesterone receptors were positive in the spindle cell component in five cases and in the epithelium in one.

The epithelium reacted positively with antibodies to cytokeratins. Glands and stroma in all cases failed to stain with S-100 protein, chromogranin A, neurofilament protein, synaptophysin, inhibin or HMB-45.

B. Male patients (2 patients)

Both tumors in the male patients were labeled as cystic nephromas. The patients were 58 years and 92 years old respectively. The tumors measured 1.5 cm and 8 cm in the largest diameter. Both were unencapsulated but well circumscribed. These neoplasms in the males were

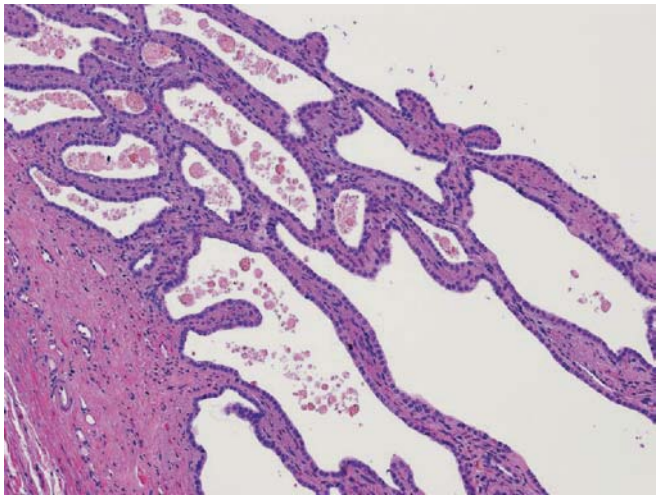


Fig. 12 Neoplasms filed as cystic nephromas in the males looked microscopically different from mixed epithelial and stromal tumor of the kidney (MESTK) in females. They were composed of thin-walled cysts filled with serous fluid and entirely devoid of the ovarian-like stroma. The lining of the cyst was composed of eosinophilic epithelium without hobnail appearance

histologically different from the MESTK in females. They were composed of thin-walled cysts filled with serous fluid and entirely devoid of the ovarian-like stroma. The luminal lining of the cysts was composed of an eosinophilic epithelium without any hobnail appearance (Fig. 12). No Müllerian-type epithelium was seen in the male tumors.

Discussion

A distinctive benign renal neoplasm was recently recognized by Michal and Syrucek [47]. The descriptive name MESTK suggested by these authors is currently the favored terminology [3, 9, 11, 22, 48, 54]. Several tumors reported under various names in the previous literature appear identical to MESTK. Despite the difficulty in assessing critically published illustrations and sometimes poorly documented histological features in previous case reports, it is our impression that MESTKs have been published under the following names in the older literature: leiomyomatous renal hamartoma [1], congenital type of mesoblastic nephroma in an adult [13, 15, 16, 23, 25, 26, 29, 30, 32, 36, 42, 43, 45, 51, 55, 59, 62, 64, 65, 66, 67], cystic hamartoma of renal pelvis (when they bulged into the renal pelvis) [34, 46, 52], solitary multilocular cyst of the kidney [10, 24], multilocular renal cyst with Müllerian-like stroma [60], and adult metanephric stromal tumor [14].

Grossly and histologically, MESTKs are dimorphic tumors composed of solid and cystic areas, consisting of a mesenchymal component in the form of a solid septal growth of spindle cell stroma, morphologically and immunohistochemically indistinguishable from ovarian stroma as well as an epithelial component composed of tu-

bules or cystically dilated glands which are often lined by hobnail eosinophilic cells. Besides the lack of the ETV6-NTK3 gene fusion, as found in the congenital mesoblastic nephroma [54], nothing is known about the molecular genetic profile of the MESTK.

MESTKs occur almost exclusively in middle-aged perimenopausal to older women. The age and sex of the patients points to the importance of hormonal factors in the pathogenesis. There is only one reported case of a MESTK in a male: case 9 in the series of Adsay et al. [3] was a 71-year-old man, with prostatic carcinoma treated hormonally with diethylstilbestrol for 7 years, followed by lupron therapy for 4 years, before an 11.5 cm MESTK was detected and surgically resected. Interestingly, the nuclei of the ovarian-like stroma in most of the MESTKs express estrogen receptors including that in the single male case [3].

MESTK usually displays a benign morphology and generally behaves in a benign fashion without recurrence or metastasis [3]. The only possible exception is a single recurrence occurring 21 years after the excision of a tumor reported as "mesoblastic nephroma", although the evidence suggests to us that it is more likely to have been a MESTK [43].

There are a few recorded cases developing a malignancy in the background of MESTK. Svec et al. recently described a MESTK that underwent malignant change in the stromal component, resembling a poorly differentiated variant of synovial sarcoma [61]. Another case of MESTK with malignant stroma was published by Bisceglia and Bacchi [11]. Other similar cases may have previously been reported under the designation of sarcomatous transformation of cystic nephromas in adults [5]. Therefore, it may be possible that at least some so-called primary synovial sarcomas of the kidney in females develop as a sarcomatous transformation in MESTK [6, 41].

The relationship of MESTK and cystic nephroma is interesting. Eble and Bonsib [27] suggested that cystic nephroma is not one but two diseases, and this position seems well substantiated. Cystic nephroma in adults is said to occur with an 8:1 predominance in women, while in children it occurs more often in boys [44]. Cystic nephroma in children forms a continuous spectrum with cystic partially differentiated nephroblastoma [39]. The adult type hardly occurs before the age of 30 years, whereas cystic partially differentiated nephroblastoma is exceptional beyond the age of 2 years. Furthermore, skeletal muscle fibers are common in cystic partially differentiated nephroblastoma but are not present in cystic nephroma. Therefore, if adult-type cystic nephroma were a terminally differentiated variant of cystic partially differentiated nephroblastoma, it would be remarkable that the skeletal muscle should disappear along with the immature elements.

In order to see what proportion of cystic nephromas diagnosed in the past might represent MESTKs, we searched for, and retrieved, all cases diagnosed as such in our files. Interestingly, all cases in females were more or less cystic, well-circumscribed, unencapsulated tumors with an ovarian-like stroma. We found only two cases diagnosed previously as cystic nephromas or MESTK in males in our joint files. Both of these lacked the ovarian-like stroma and the distinctive hobnail epithelium seen in the female cases. These two male tumors might therefore represent examples of true cystic nephromas. Most if not all cases diagnosed as cystic nephromas in the past arising in middle-aged to elderly females are probably examples of MESTKs. No case of cystic nephroma occurring in childhood was found in our files. This may be explained by the fact that childhood tumors are usually treated in specialized pediatric oncology centers, and none of our hospitals would routinely receive these tumors. We suspect, however, that most cases diagnosed as cystic nephromas in children represent examples of cystic partially differentiated nephroblastoma. Therefore, we suggest that cystic renal neoplasms diagnosed as cystic nephromas in the past contain at least three different entities: (1) most of the tumors in adult middle-aged to elderly females represent MESTK; (2) a minority of cystic tumors lacking ovarian-like stroma represent genuine cystic nephromas, and most of these probably occur in males; and (3) most benign-looking cystic tumors in children are probably examples of cystic partly differentiated nephroblastomas [39].

It is important to note that similar cystic tumors containing an ovarian-like stroma occur not only in the kidney, but are also described in the biliary tract and pancreas [17, 20, 21, 68, 71]. There is on record even one case of mucinous cystadenoma with ovarian-like stroma, which arose in pancreatic heterotopia in the spleen [49]. Similar to MESTK, these tumors arise almost exclusively in middle-aged and elderly females, and they represent a distinct entity. In the pancreas, tumors with a mesenchymal ovarian-like stroma are called "mucinous cystic tumors of pancreas" [4, 63, 73] and must be distinguished from pancreatic intraductal papillary mucinous neoplasms, because the latter are often accompanied by an invasive ductal component and, consequently, they have a much worse prognosis. In contrast, mucinous cystic tumors with ovarian-like stroma of the pancreas only rarely have a fatal outcome [2, 4, 69]. Like their renal counterparts, these biliary tract and pancreatic tumors show immunohistochemical expression of estrogen receptors, and the stroma reveals widespread smooth muscle actin and focally desmin positivity [68]. We therefore think that MESTKs represent the renal counterpart of the cystic tumors in the biliary tract and pancreas with an ovarian-like stroma [17, 20, 21, 68, 71]. Interestingly, the pancreatic tumor sometimes contains inhibin-positive luteinized cells in the ovarian-like stroma [37, 73], which are identical to similar cells of the ovarian medulla and cortex [19, 56]. However, no such steroidogenic cells could be demonstrated by inhibin immunostaining in our cases of MESTKs.

Müllerian differentiation has never been described in biliary and pancreatic tumors with ovarian-like stroma, and we are aware of only one case report briefly alluding to endometrioid differentiation in MESTK [9]. Beiko et

al. described a case of MESTK with columnar and ciliated serous epithelium. They hypothesized that their case may possibly have arisen from paramesonephric remnants, which may be closely related to the kidney and upper urothelial tract [9]. We can confirm such Müllerian differentiation in MESTK. Several cases in our series contained various types of Müllerian epithelium including endometrioid, tubal, squamous and clear cell epithelia. In addition, one MESTK contained large areas with leaflet-like structures rimmed by an endometrioid glandular epithelium bearing a remarkable similarity to Müllerian adenofibroma or adenosarcomas of the female genital tract [28, 38, 40]. Even the lipomatous differentiation seen around these leaflet-like structures is sometimes seen in Müllerian adenofibromas and adenosarcomas of the female genital tract [28, 35, 53, 72].

Typical stromal hyalinization resembling corpora albicantia is an interesting, but, nonspecific feature in our cases. We think that they are not real corpora albicantia, because we did not observe any primordial follicles in MESTKs, but rather that they represent a type of nonspecific pattern of scarring with hyalinization characteristic of ovarian stroma. Identical corpus albicans-like scarring was recently described by Cerilli in a mucinous tumor of the pancreas with ovarian stroma [18].

In the differential diagnosis, MESTK must be distinguished from several entities.

In the past MESTK was most often considered as an adult form of congenital mesoblastic nephroma (CMN) [13, 15, 16, 23, 25, 26, 29, 30, 32, 36, 42, 43, 45, 51, 55, 59, 62, 64, 65, 66, 67]. CMN is a rare pediatric renal tumor with a peak incidence in the first 3 months after birth [12]. The recent recognition of the metanephric stromal tumor and its distinction from CMN makes the oldest patient in the National Wilms' Tumor Pathology Center with a confirmed CMN 29 months of age [7]. In CMN, a spindle cell population of variable density predominates, and these cells can take on features of fibroblasts, myofibroblasts or smooth muscle cells. Wigger considered CMN to arise from secondary mesenchyme, which—in contrast to primary mesenchyme—lacks the capacity to form epithelial structures [70]. CMN thus differs from MESTK in several respects. It affects both sexes and occurs almost exclusively in early childhood. It is a purely mesenchymal tumor in which epithelial structures are not a component of the neoplasm [12], although quite often entrapped tubules and glomeruli are seen encased within the infiltrating spindle cells. Metaplastic changes may occur in the entrapped epithelial structures and adjacent epithelium [50], but only seldom is there cystic change [31]. In contrast, MESTK is characterized by an intimate relationship of epithelial and stromal elements, both of which appear neoplastic. The infiltrative pattern so typical of CMN is lacking in MESTK. Further, CMN is known to harbor the ETV6-NTK3 gene fusion similar to congenital (infantile) fibrosarcoma [57]. No such gene fusion was found in the seven cases of MESTK which have been so far investigated [54]. Based on these different clinical, morphological and molecular features, we believe that MESTK and CMN are two entirely different tumors. Thus, the term "adult type of mesoblastic nephroma" should be discarded.

MESTK can be easily distinguished from nephrogenic or metanephric adenofibroma, a rare biphasic neoplasm of the kidney, which—unlike MESTK—occurs in children and young adults [33, 58]. The epithelial component of metanephric adenofibroma has the typical appearance of metanephric adenoma. Cysts are uncommon and, if present, are only focal findings. The spindle cell component is usually negative for actin and desmin [8].

In conclusion, we have presented 22 cases of MESTK, the largest series of this newly delineated entity which we consider to be different from cystic nephromas, cystic partially differentiated nephroblastomas and mesoblastic nephromas. MESTK is often macroscopically cystically arranged. Microscopic examination shows a dimorphic tumor exhibiting a variable epithelial component lining the cysts, which can exhibit a range of Müllerian appearances, in addition to a stromal component morphologically and immunohistochemically identical to ovarian stroma. MESTK represents the renal counterpart of similar cystic tumors with ovarian-like stroma occurring in the biliary tract and pancreas. MESTK behaves in the benign way. It can be hypothesized that MESTK is induced by deranged hormonal milieu, because it usually occurs in middle-aged to elderly females, and in many patients a long-term history of estrogen use can be found [3].

Acknowledgements The authors thank Dr. P. Mukensnabl for the excellent photographic work. We are also most grateful to Richard Pocock and Mark Stott, Consultant Urologists in Exeter, for the extra clinical information on their patients.

References

1. Abaitua J, Val Bernal JF (1975) Hamartoma leiomyomatoso renal del adulto. Segundo caso de la literatura. Arch Es Urol 26:601–612
2. Adsay NV, Conlon KC, Zee SY, Brennan MF, Klimstra DS (2002) Intraductal papillary-mucinous neoplasms of the pancreas: an analysis of in situ and invasive carcinomas in 28 patients. Cancer 94:62–77
3. Adsay NV, Eble JN, Srigley JR, Jones EC, Grignon DJ (2000) Mixed epithelial and stromal tumor of the kidney. Am J Surg Pathol 24:958–970
4. Adsay NV, Longnecker DS, Klimstra DS (2000) Pancreatic tumors with cystic dilatation of the ducts: intraductal papillary mucinous neoplasms and intraductal oncocytic papillary neoplasms. Semin Diagn Pathol 17:16–30
5. Antonescu C, Bisceglia M, Reuter V, Rosai J (1997) Sarcomatous transformation of cystic nephromas. Mod Pathol 10: 391A
6. Argani P, Faria PA, Epstein JI, Reuter VE, Perlman EJ, Beckwith JB, Ladanyi M (2000) Primary renal synovial sarcoma. Molecular and morphologic delineation of an entity previously included among embryonal sarcomas of the kidney. Am J Surg Pathol 24:1087–1096
7. Argani P, Beckwith JB (2000) Metanephric stromal tumor. Report of 31 cases of a distinctive pediatric renal neoplasm. Am J Surg Pathol 24:917–926

8. Arroyo MR, Green DM, Perlman EJ, Beckwith JB, Argani P (2001) The spectrum of metanephric adenofibroma and related lesions. Clinicopathologic study of 25 cases from the National Wilms Tumor Study Group Pathology Center. Am J Surg Pathol 25:433–444
9. Beiko DT, Nickel JC, Boag AH, Srigley JR (2001) Benign mixed epithelial stromal tumor of the kidney of possible Müllerian origin. J Urol 166:1381–1382
10. Bennington JL, Beckwith JB (1983) Atlas of tumor pathology. Tumors of the kidney, renal pelvis, and ureter. Second series, Fascicle 12, 1975, Reprinted 1983. Armed Forces Institute of Pathology, Washington, D.C., pp 84–85
11. Bisceglia M, Bacchi CE (2003) Mixed epithelial-stromal tumor of the kidney in adults: two cases from the Arkadi M. Rywlin slide seminars. Adv Anat Pathol 10:223–233
12. Bisceglia M, Carosi I, Vairo M, Zaffarano L, Bisceglia M, Creti G (2000) Congenital mesoblastic nephroma: report of a case with review of the most significant literature. Pathol Res Pract 196:199–204
13. Block NL, Grabstald HG, Melamed MR (1973) Congenital mesoblastic nephroma (leiomyomatous hamartoma): first adult case. J Urol 110:380–383
14. Bluebond-Langner R, Pinto PA, Argani P, Chan TY, Halushka M, Jarrett TW (2002) Adult presentation of metanephric stromal tumor. J Urol 168:1482–1483
15. Bouvier R, Beurlet J, Roux MG (1996) Mesoblastic nephroma in adults. Apropos of a case and review of the literature. Arch Anat Cytol Pathol 44:37–41
16. Bruet A, Fingerhut A, Felsenheld C, Laffrat I, Mathe C, Fendler JP (1989) Le nephroma mésoblastique congenital de l'adulte. Ann Urol (Paris) 23:27–29
17. Caturelli E, Bisceglia M, Villani MR, de Maio G and Siena DA (1998) CA 19–9 production by a cystadenoma with mesenchymal stroma of the common hepatic duct: a case report. Liver 18:221–224
18. Cerilli LA (2003) Mucinous tumor of the pancreas: Corpora albicans-like structures within the ovarian stroma. Int J Surg Pathol 11:219
19. Clement PB (1987) Histology of the ovary. Am J Surg Pathol 11:277–303
20. Compagno J, Oertel JE (1978) Mucinous cystic neoplasms of the pancreas with overt and latent malignancy (cystadenocarcinoma and cystadenoma). A clinicopathologic study of 41 cases. Am J Clin Pathol 69:573–580
21. Devaney K, Goodman ZD, Ishak KG (1994) Hepatobiliary cystadenoma and cystadenocarcinoma. A light microscopic and immunohistochemical study of 70 patients. Am J Surg Pathol 18:1078–1091
22. Pierson CR, Schober MS, Wallis T, Sarkar FH, Sorensen PHB, Eble JN, Srigley JR, Jones EC, Grignon DJ, Adsay V (2002) Mixed epithelial and stromal tumor of the kidney lacks the genetic alterations of cellular congenital mesoblastic nephroma. Hum Pathol 32:513–520
23. Chandeck K, Cerrud L, Hernandez L (1992) Nefroma mesoblastico congenito en el adulto (primer caso de tumor en adulto mayor de 40 aňos). Rev Med Panama 17:50–56
24. Davila RM, Kissane JM, Crouch EC (1992) Multilocular renal cyst. Immunohistochemical and lectin-binding study. Am J Surg Pathol 16:508–514
25. Désligneres S, Flam T, Vacher-Lavenu MC, Debré B (1992) Le nephroma mésoblastique cellulaire ou atypique à forme partiellement kystique. A propos d'une observation chez une femme de 27 ans. J Urol 98:138–147
26. Durham JR, Bostwick DG, Farrow GM, Ohorodnik JM (1992) Mesoblastic nephroma of adulthood. Report of three cases. Am J Surg Pathol 17:1029–1038
27. Eble JN, Bonsib SM (1998) Extensively cystic renal neoplasms: cystic nephroma, cystic partially differentiated nephroblastoma, multilocular cystic renal cell carcinoma, and cystic hamartoma of renal pelvis. Semin Diagn Pathol 15:2–20
28. Eichhorn JH, Young RH, Clement PB, Scully RE (2002) Mesodermal (Müllerian) adenosarcoma of the ovary. A clinicopathologic analysis of 40 cases and a review of the literature. Am J Surg Pathol 26:1243–1258
29. el Mrini M, Debbagh A, Hafiani M, Aboutaieb R, Bennani S, Beljelloun S (1998) Tumeur de Bolande de l'adulte: à propos d'un cas. Prog Urol 8:95–98
30. Freeby JA, Fishman EK, Marshall FF, Henneberry JM (1997) Mesoblastic nephroma in an adult: spiral CT appearance. Abdom Imaging 22:439–440
31. Ganick DJ, Gilbert EF, Beckwith JB, Kiviat N (1981) Congenital cystic mesoblastic nephroma. Hum Pathol 12:1039–1043
32. Gonzales Moran MA, Salas Valien JS, Suarez Vilela D, Rodriguez Lopez JA, Garcia Diez F (1993) Nefroma mesoblastico congenito en el adulto: studio inmunohistoquimico. Arch Espanoles Urol 46:56–59
33. Hennigar RA, Beckwith JB (1992) Nephrogenic adenofibroma. A novel kidney tumor of young people. Am J Surg Pathol 16:325–334
34. Hirota S, Hase M, Matsumoto S, Fukuda T, Fujii M, Sugimoto K, Sugimura K, Hanioka K (2000) Cystic hamartoma of the renal pelvis: imaging features. Radiat Med 18:139–142
35. Horie Y, Ikawa S, Kadowaki K, Minagawa Y, Kigawa J, Terakawa N (1995) Lipoadenofibroma of the uterine corpus. Report of a new variant of adenofibroma (benign Müllerian mixed tumor). Arch Pathol Lab Med 119:274–276
36. Iraqi A, Meziane EM, Sqalli S, Morchid A, Gueraoui M (1984) Histogenetic aspects of mesoblastic nephroma. Apropos of a case in an adult. Arch Anat Cytol Pathol 32:249–252
37. Ishiguro H, Kato K, Kishimoto T, Nagai Y, Takahashi T, Sasano H, Ishikura H (2003) Expression of steroidogenic enzymes by luteinizing cells in the ovarian-type stroma of a mucin-producing cystic tumour of the pancreas. Histopathology 43:97–98
38. Jones MW, Lefkowitz M (1995) Adenosarcoma of the uterine cervix: A clinicopathological study of 12 cases. Int J Gynecol Pathol 14:223–229
39. Joshi VV, Beckwith JB (1989) Multilocular cyst of the kidney (cystic nephroma) and cystic, partially differentiated nephroblastoma. Cancer 64:466–479
40. Kerner H, Munichor M (1997) Papillary cystadenofibroma of the vagina. Histopathology 30:84–86
41. Kim DH, Sohn JH, Lee MC, Lee G, Yoon GS, Hashimoto H, Sonobe H, Ro JY (2000) Primary synovial sarcoma of the kidney. Am J Surg Pathol 24:1097–1104
42. Kleist B, Lorenz G, Dietrich H, Klebingat KJ (1998) Mesoblastic nephroma in adults. Pathologe 19:226–229
43. Levin NP, Damjanov I, Depilis VJ (1982) Mesoblastic nephroma in an adult patient: recurrence 21 years after removal of the primary lesion. Cancer 49:573–577
44. Madewell JE, Goldman SM, Davis CJ, Hartman DS, Feigin DS, Lichtenstein JE (1983) Multilocular cystic nephroma. A radiographic-pathologic correlation of 58 patients. Radiology 146:309–321
45. Mahalati K, Sahin A, Ozen H, Bozdogan O, Cila A, Ruacan S (1994) Mesoblastic nephroma in adults: a clinical case. Bull Cancer 81:928–930
46. Mensch LS, Trainer TD, Plante MK (1999) Cystic hamartoma of the pelvis: a rare pathologic entity. Mod Pathol 12:417–421
47. Michal M, Syrucek M (1998) Benign mixed epithelial and stromal tumour of the kidney. Pathol Res Pract 194:445–448
48. Michal M (2000) Benign mixed epithelial and stromal tumor of the kidney. Pathol Res Pract 196:275–276
49. Mourra N, Balladur P, Parc R, Flejou J-F (2003) Intrasplenic mucinous cystadenoma with mesenchymal stroma arising in pancreatic heterotopia. Histopathology 42:616–617
50. Murphy WM, Beckwith JB, Farrow GM (1994) Tumors of the kidney, bladder and related urinary structures. In: Rosai J, Sobin LH (eds) Atlas of tumor pathology, vol 11. Washington D.C.: Armed Forces Institute of Pathology, pp 55–67
51. Ogawa O, Okumura K, Taniguchi T, Nakagawa T (1989) A case of giant renal hamartoma considered as congenital mesoblastic nephroma of adult. Hinyokika Kio 35:1749–1753

52. Pawade J, Soosay GN, Delprado W, Parkinson MC, Rode J (1993) Cystic hamartoma of the renal pelvis. Am J Surg Pathol 17:1169–1175
53. Payne F, Rollandson TP, Sivridis E (1992) Adenomyolipoma of the endometrium: a hamartoma? Histopathology 20:357–359
54. Pierson CR, Schober MS, Wallis T, Sarkar FH, Sorensen PH, Eble JN, Srigley JR, Jones EC, Grignon DJ, Adsay V (2001) Mixed epithelial and stromal tumor of the kidney lacks the genetic alterations of cellular congenital mesoblastic nephroma. Hum Pathol 32:513–520
55. Prats Lopez J, Palou Redorta J, Morote Robles J, Martinez Perez E, Ruiz Marcellan C (1988) Leiomyomatous renal hamartoma in an adult. Eur Urol 14:80–82
56. Reeves G (2002) The ovarian cortex and medulla have their specific stromal component. A passionate review: 40 years of theory and practice. Patologia 40:7–25
57. Rubin BP, Chen CJ, Morgan TW, Xiao S, Grier HE, Kozakewich HP, Perez-Atayde AR, Fletcher JA (1998) Congenital mesoblastic nephroma t(12;15) is associated with ETV6-NTRK3 gene fusion: cytogenetic and molecular relationship to congenital (infantile) fibrosarcoma. Am J Pathol 154:1451–1458
58. Shek TWH, Luk ISC, Peh WCG, Chan KL (1999) Metanephric adenofibroma. Report of a case and review of the literature. Am J Surg Pathol 23:727–733
59. Smida L, Taief YL, Rebai T (1989) Mesoblastic nephroma. Unusual renal tumor in adults. Apropos of a case. J Urol 95:423–426
60. Steele R, Daroca PJ, Hill S, Reed RJ, Thomas R (1994) Multilocular renal cyst (cystic nephroma) with Müllerian-like stroma. Urology 43:549–553
61. Svec A, Hes O, Michal M, Zachoval R (2001) Malignant mixed epithelial and stromal tumor of the kidney. Virchows Arch 439:700–702
62. Terai A, Terachi T, Machida S (1985) Case of adult renal hamartoma resembling congenital mesoblastic nephroma. Hinyokika Kiyo 31:2219–2223
63. Thompson LD, Becker RC, Przygodzki RM, Adair CF, Heffess CS (1999) Mucinous cystic neoplasm (mucinous cystadenocarcinoma of low-grade malignant potential) of the pancreas: a clinicopathologic study of 130 cases. Am J Surg Pathol 23:1–16
64. Trillo A (1990) Adult variant of congenital mesoblastic nephroma. Arch Pathol Lab Med 114:533–555
65. Truong LD, Williams R, Ngo T, Cawood C, Chevez-Barrios P, Awalt HL, Brown RW, Younes M, Ro JY (1998) Adult mesoblastic nephroma. Expansion of the morphologic spectrum and review of literature. Am J Surg Pathol 22:827–839
66. Tulbach A, Kardar AH, Akhtar M (1997) Mesoblastic nephroma in an adult. J Urol Pathol 6:67–73
67. Van Velden DJ, Schneider JW, Allen FJ (1990) A case of adult mesoblastic nephroma: ultrastructure and discussion of histogenesis. J Urol 143:1216–1219
68. Weihing RR, Shintaku IP, Geller SA, Petrovic LM (1997) Hepatobiliary and pancreatic mucinous cystadenocarcinomas with mesenchymal stroma: analysis of estrogen receptors/progesterone receptors and expression of tumor-associated antigens. Mod Pathol 10:372–379
69. Wenig BM, Albores-Saavedra J, Buetow PC, Heffess CS (1997) Pancreatic mucinous cystic neoplasm with sarcomatous stroma: a report of three cases. Am J Surg Pathol 21:70–80
70. Wigger HG (1975) Fetal mesenchymal hamartoma of the kidney. A tumor of secondary mesenchyme. Cancer 36:1002–1008
71. Wong NA, Arnott ID, Pope I, Palmer KR, Garden OJ, Thomas JS, Piris J (2001) Hepatobiliary cystadenoma with mesenchymal stroma may mimic biliary smooth muscle neoplasms. Histopathology 39:34–36
72. Yavuz E, Tuzlali S, Iplikci A, Ilhan R (2001) Adenomyolipoma of the uterus: a case report. Pathology 33:96–100
73. Zamboni G, Scarpa A, Bogina G, Iacono C, Bassi C, Talamini G, Sessa F, Capella C, Solcia E, Rickaert F, Mariuzzi GM, Kloppel G (1999) Mucinous cystic tumors of the pancreas: clinicopathological features, prognosis, and relationship to other mucinous cystic tumors. Am J Surg Pathol 23:410–422

Virchows Arch (2004) 445:368–374
DOI 10.1007/s00428-004-1103-4

ORIGINAL ARTICLE

U. Zimmermann · C. Woenckhaus · S. Pietschmann · H. Junker · S. Maile · K. Schultz · C. Protzel · J. Giebel

Expression of annexin II in conventional renal cell carcinoma is correlated with Fuhrman grade and clinical outcome

Received: 4 May 2004 / Accepted: 19 July 2004 / Published online: 26 August 2004
© Springer-Verlag 2004

Abstract Conventional renal cell carcinomas (CRCCs) were investigated for the expression of annexin II (ANX II) to determine out whether this calcium-binding protein could serve as a useful prognostic marker. CRCCs and adjacent nonneoplastic tissue from 33 patients were investigated for ANX II by immunohistochemistry, RT-PCR, and western blot analysis. ANX II expression was correlated with tumor differentiation (Fuhrman grade) and to clinical outcome. Tumors were composed of ANX II positive and negative cells. In grade I tumors only a weak membranous staining was seen in immunopositive cells. In grade II and III tumors, however, ANX II was seen in the cytoplasm and at the cell membranes of tumor cells. On serial sections membranous and cytoplasmic immunoreactivity for ANX II occurred predominantly in eosinophilic cells whereas clear cells were mostly immunonegative. The ANX II expression in CRCCs was correlated with clinical outcome and Fuhrman grade. Since ANX II expression is correlated with Fuhrman grade and clinical outcome it may be a useful marker for prognosis in CRCC.

U. Zimmermann (✉) · C. Protzel
Department of Urology,
Ernst Moritz Arndt University,
Fleischmannstrasse 42–44, 17487 Greifswald, Germany
e-mail: ziuro@uni-greifswald.de
Tel.: +49-3834-865976
Fax: +49-3834-865978

C. Woenckhaus
Institute for Pathology,
Ernst Moritz Arndt University,
F.-Loeffler-Str. 23c, 17487 Greifswald, Germany

S. Pietschmann · S. Maile · K. Schultz · J. Giebel
Institute for Anatomy,
Ernst Moritz Arndt University,
F.-Loeffler-Str. 23c, 17487 Greifswald, Germany

H. Junker
Department of Medical Biochemistry and Molecular Biology,
Ernst Moritz Arndt University,
Sauerbruchstr., 17487 Greifswald, Germany

Keywords Annexin · Kidney · Cancer · Immunohistochemistry · Prognosis

Introduction

Renal epithelial neoplasms account for about 2% of adult malignancies and comprise different histopathological subtypes such as conventional renal cell carcinomas (CRCC), papillary, chromophobe, and unclassified types as well as oncocytomas [18]. The term CRCC, which differs from that of the World Health Organization, reflects to the fact that clear cell renal carcinomas are often composed of different cell types including clear cells, eosinophilic cells, and chromophilic cells and can even show sarcomatoid features. Interestingly, it was previously hypothesized that the amount of eosinophilic cells contribute to unfavorable prognosis [28]. CRCCs are characterized by solid, trabecular, alveolar, and acinar growth patterns with thin walled-blood vessels in the tumor stroma [16, 28, 33]. CRCC is the most common renal neoplasm, is often of low cytological grade, protrudes from the renal cortex, spreads by local invasion, and in advanced stages tends to invade the renal vein but rarely involves lymph nodes [8, 10, 20, 21, 27]. CRCCs share antigenic and ultrastructural characteristics with the proximal tubule cells, and thus they therefore probably originate from the proximal nephron epithelium [1, 34, 13]. However, contrary concepts favour the hypothesis that CRCCs develop from an uncommitted or primitive cell rather than from any particular portion of the nephron [4, 7].

In addition to their obscure histiogenesis, CRCCs have acquired a reputation for unpredictable clinical outcome [22]. This is due to the fact that CRCCs show spontaneous regression, long-term survival in the presence of metastases, and occasionally late recurrence [5, 17]. Although many parameters including tumor grade, abnormal DNA ploidy, nuclear morphometry, and proliferation have been employed, a reliable marker to predict the prognosis of CRCCs has yet not been established [31]. Promising

progress in the search for prognostic markers has been provided by recent studies showing that the prognosis of several carcinomas is correlated with the expression of annexin (ANX) II. ANX II belongs to a family of calcium and phospholipid proteins which are ubiquitous in most tissues [11]. Their molecular weight ranges from 34 to 36 kDa. Since transfection experiments with an antisense ANX II vector resulted in inhibition of cell division and proliferation, an important role for DNA synthesis is indicated [3, 11, 12, 14].

ANX II has previously been shown to be highly expressed in glioblastoma multiforme [26]. Furthermore, a strong association between ANX II staining and histological grade has been observed in astrocytic malignancies [29]. Moreover, ANX II over expression is seen in human gastric carcinomas that is correlated with poor prognosis [9]. Therefore since ANX II may represent a useful marker for tumor progression, we investigated the putative role of ANX II in CRCCs by immunohistochemistry. We also carried out reverse transcription polymerase chain reaction (RT-PCR) and western blot analysis to investigate the presence of ANX II mRNA and protein in homogenates of neoplastic and nonneoplastic tissues.

Materials and methods

Tissue samples

The study was based on 33 renal carcinoma patients (13 women, 20 men; age 36–75 years) diagnosed and treated at the Department of Urology, University of Greifswald. Tissue samples and patient data for this study were obtained and used after advice from the ethics committee of the University of Greifswald and in accordance with the Declaration of Helsinki. Follow-up data were collected from patient records. Representative tumor tissue samples with adjacent nonneoplastic tissue allowing proper classification and grading were obtained during radical nephrectomy and subjected to 4% buffered formalin. Furthermore, small samples of neoplastic and nonneoplastic tissue were snap frozen in liquid nitrogen for isolation of RNA and western blot analysis.

Histological methods and classification of tumors

Typing and classification were performed on specimens stained with hematoxylin and eosin. All specimens underwent additional independent histopathological review (C.W.). Tumors were classified (Table 1) as recommended by the latest TNM classification [32] and graded according to Fuhrman et al. [10]. The 33 CRCCs were composed of different cell types (clear cell, eosinophilic or chromophilic cells) to different extents. The proportion of eosinophilic cells was assessed by two independent observers (C.W., J.G.) and scored as E0 (<10%), E1 (10–30%), or E2 (>30%).

Immunohistochemistry

Immunohistochemistry was carried out on paraffin sections (4 μm). In detail, endogenous peroxidase activity was blocked prior to immunohistochemistry by incubation in 0.3% H_2O_2 in methanol for 40 min (22°C). Sections were subjected to heat antigen retrieval using 10 mM citrate buffer (pH 6.0). After cooling in citrate buffer and subsequent washings in a proteinaceous buffer (50% glycerol, 20 mM Na_2PO_4, 150 mM NaCl, 1.5 mM sodium azide, 1 mg/ml BSA; pH 7.5; 2×5 min), immunohistochemistry was performed using a staining kit (Vectastain, Santa Cruz Biotechnology, Santa Cruz, Calif., USA) employing the proteinaceous buffer: Blocking with goat serum (Vectastain kit, 20 min) was followed by incubation with monoclonal mouse anti-ANX II antibody (45 min, 22°C, Biotrend, Cologne, Germany) and two washes in buffer (2×5 min). Incubation with secondary antibody (30 min, 22°C) was followed by washing in buffer (2×5 min). Slides were subjected to aviditin-biotin peroxidase complex reagent (45 min). Visualization was performed after washing in buffer (2×5 min) with 0.1% diaminobenzidine in PBS/0.01% H_2O_2 followed by hematoxylin counterstaining and mounting in glycerol-gelatin (Merck, Darmstadt, Germany). Controls were established by (a) incubating slides with PBS alone, (b) using PBS instead of primary antibody, and (c) replacing the ANX II antibody with a monoclonal antibody (β_1 integrin, Biomol, Hamburg, Germany) not reactive in paraffin sections. Photographs were taken by an Olympus Bx50 microscope equipped with a Olympus DP10 digital camera. Immunohistochemical staining for ANX II in tumors was judged by two independent observes (C.W., J.G.) and intensity was scored as A0 (no reaction), as A1 (+) for membranous staining only, or as A2 (++) for membranous and cytoplasmic staining.

RNA isolation

Tissue samples (100 mg) were homogenized in 1 ml Trizol reagent (GibcoBRL, Berlin, Germany) for isolation of RNA. After incubation (5 min, 22°C) 0.2 ml chloroform was added, mixed carefully (15 s), incubated (3 min, 22°C), and centrifuged (10 min, 12,000 *g*, 4°C). The supernatant was supplemented with 0.2 ml isopropanol, incubated (5 min, 22°C), and centrifuged (10 min, 12,000 *g*, 4°C). The pellet was resuspended in 1 ml 75% ethanol (1 ml/1 ml Trizol) and centrifuged at 7,500 *g* (5 min, 4°C). The resulting pellet was dried and resuspended in diethylpyrocarbonate-H_2O.

RT-PCR

cDNA was generated according to the manufactures protocol (Amersham Biosciences, Freiburg, Germany) using 1 μg total RNA. After reverse transcription 95 μl H_2O was added to each probe and stored at −20°C. PCR was performed using the specific ANX II primer (forward: CCA AAG GTG TGG ATG AGG TC; reverse: TGA TCC ACT TGG GAA CAT CA) according to the following protocol: 37.5 μl H_2O, 5 μl 10× PCR buffer (Mg^{2+}), 1 μl 10 mM deoxyribonucleoside triphosphates, 2 μl forward primer, 2 μl reverse primer (20 pmol/μl), 1/10 cDNA (2.5 μl), 0.5 μl *Taq* polymerase (5 U/ul). PCR was run with 35 cycles. PCR products (20 μl) were separated using agarose gel electrophoresis (80 V, Tris-acetate EDTA buffer) and ethidium bromide stained bands were visualized by UV illumination.

Western blot

Tissue samples were subjected to lysis buffer (4.8 g urea, 1.52 g thiourea, 0.4 g 3-[(3-cholamidopropyl)dimethylammonio]-1-propanesulfonate, 0.2 g dithiothreitol, 0.096 g Tris ad 10 ml aqua bidest.) and homogenized with an ultra-turrax homogenizer (4°C) for western blot. Protein extracts (30 μg/lane) were separated by sodium dodecyl sulfate polyacrylamide gel electrophoresis using a gradient gel (12.5% separating gel; 5% stacking gel), constant current 120 V, 3 h. Proteins were transferred onto nitrocellulose-membranes using a semidry blot technique 15 V, 1 h. ANX II antibodies were used at a dilution of 1:2,500. Bands were visualized using secondary AP-conjugated antibody (Tropix, Bedford, Mass., USA) and bromo-4-indolyl-phosphate (25 mg/10 ml aqua dest. Sigma, Munich, Germany).

Table 1 Characterization of 33 CRCCs (*AAD* age at diagnosis, *E score* eosinophil score, *FG* Fuhrman grade, *pT* primary tumor stage, *pN* lymph node metastasis, *DM* distant metastases, *NED* no evidence of disease, *AWD* alive with disease, *DOD* dead of disease, *LTF* lost to follow-up. *Med* mediastinum, *SG* suprarenal gland, *LN* lymph node)

Case no.	Sex	AAD (years)	E score	FG	pT	pN	DM	ANX score	Follow-up status	Survival (months)
1	M	67	E0	G2	pT1a	pN0	–	A0	NED	42+
2	F	62	E0	G2	pT1b	pNx	–	A0	NED	40+
3	M	56	E1	G2	pT1b	pN0	–	A0	NED	40+
4	F	75	E0	G2	pT2	pN0	–	A0	LTF	–
5	F	69	E2	G3	pT3	pN0	–	A2	DOD	28
6	F	72	E1	G2	pT3a	pN0	Bone	A2	DOD	4
7	M	65	E2	G2	pT4	pN2	Bone	A2	DOD	28
8	F	58	E1	G2	pT3	pN0	Liver	A2	DOD	53
9	F	56	E0	G2	pT1b	PN0	–	A0	NED	42+
10	M	67	E0	G1	pT2	pN0	–	A0	NED	60+
11	M	62	E1	G2	pT2	pN0	Med	A2	AWD	84+
12	M	56	E2	G2	pT3b	pNx	–	A2	DOD	40
13	M	53	E0	G2	pT1a	pNx	–	A1	NED	16+
14	F	64	E0	G1	pT3b	pN0	Pleura	A0	DOD	8
15	M	59	E2	G2	pT3a	pN0	–	A1	NED	78+
16	F	60	E0	G1	pT2	pN0	–	A1	NED	64+
17	F	59	E0	G2	pT2	pN0	–	A1	LTF	–
18	M	62	E1	G2	pT2	pN0	–	A2	DOD	26
19	F	43	E0	G1	pT1a	pN0	–	A0	NED	57+
20	M	58	E1	G3	pT3b	pN0	Lung	A2	DOD	29
21	M	48	E0	G2	pT2	pN0	Brain	A1	AWD	129+
22	F	75	E2	G2	pT1b	pN0	–	A0	LTF	–
23	M	70	E0	G2	pT1b	pN0	SG	A0	DOD	33
24	M	65	E2	G2	pT4	pN2	SG	A0	DOD	6
25	F	59	E0	G2	pT3b	pN2	Bone	A2	AWD	132+
26	M	52	E0	G3	pT3	pN0	Liver	A2	DOD	40
27	F	58	E0	G2	pT3a	pN0	Lung	A0	AWD	30+
28	M	36	E2	G2	pT2	pN0	Skin	A2	DOD	40
29	M	61	E0	G2	pT3a	pN0	Liver	A0	AWD	64+
30	M	36	E1	G2	pT3a	pN2	LN	A1	AWD	44+
31	M	68	E1	G2	pT2	pN0	–	A0	DOD	27
32	M	70	E0	G1	pT1a	pN0	–	A0	NED	18+
33	M	65	E0	G1	pT1a	pN0	–	A0	NED	9+

Statistical analysis

Statistical analysis used Pearson's χ^2 analysis and Kendall's τ_c nonparametric coefficient to evaluate the relationship between (a) ANX II score and clinical outcome and (b) proportion of eosinophilic cells and clinical outcome. Follow-up data were available from 30 patients ranging from 4 months to 11 years. Further statistical analysis by Pearson's χ^2 and Kendall's τ_c correlation was performed to examine the correlation between (a) ANX II score and proportion of eosinophilic cells (eosinophil score) and (b) ANX II score and grade.

Results

Routine histology, grade, score of eosinophilic cells, and correlation with clinical outcome

Table 1 presents the pathological characterization of 33 CRCCs investigated in the present study. Six tumors were G1, 24 were G2, and 3 were G3. In hematoxylin and eosin stained sections CRCCs were seen to be composed of clear cells but often contained eosinophilic cells, however to varying extent (Fig. 1C). The eosinophil scores and follow-up status of the 33 patients were as follows (alive with disease, AWD; evidence of disease, NED; dead of disease DOD; lost to follow-up LTF):

- E0, n=18: 9 NED, 4 AWD, 3 DOD, 2 LTF
- E1, n=8: 1 NED, 2 AWD, 5 DOD, 0 LTF
- E2, n=7: 1 NED, 0 AWD, 5 DOD, 1 LTF

The correlation between eosinophil score and clinical outcome (alive vs. dead) was statistically significant (χ^2, P=0.012; τ_c=0.57, P=0.003).

Immunohistochemistry

In nonneoplastic tissue ANX II immunostaining was seen in Bowman's capsule, loop of Henle, distal convoluted tubule, and collecting tubules and ducts. Immunostaining was stronger at the basolateral membranes than the cytoplasm. The proximal tubules were immunonegative. Immunostaining was also seen in endothelial cells.

In CRCCs the immunoreactivity for ANX II was heterogeneous, and in most samples immunopositive cells formed foci. Tumor cells were immunonegative in 16 samples (score A0). In six samples judged as A1 immu-

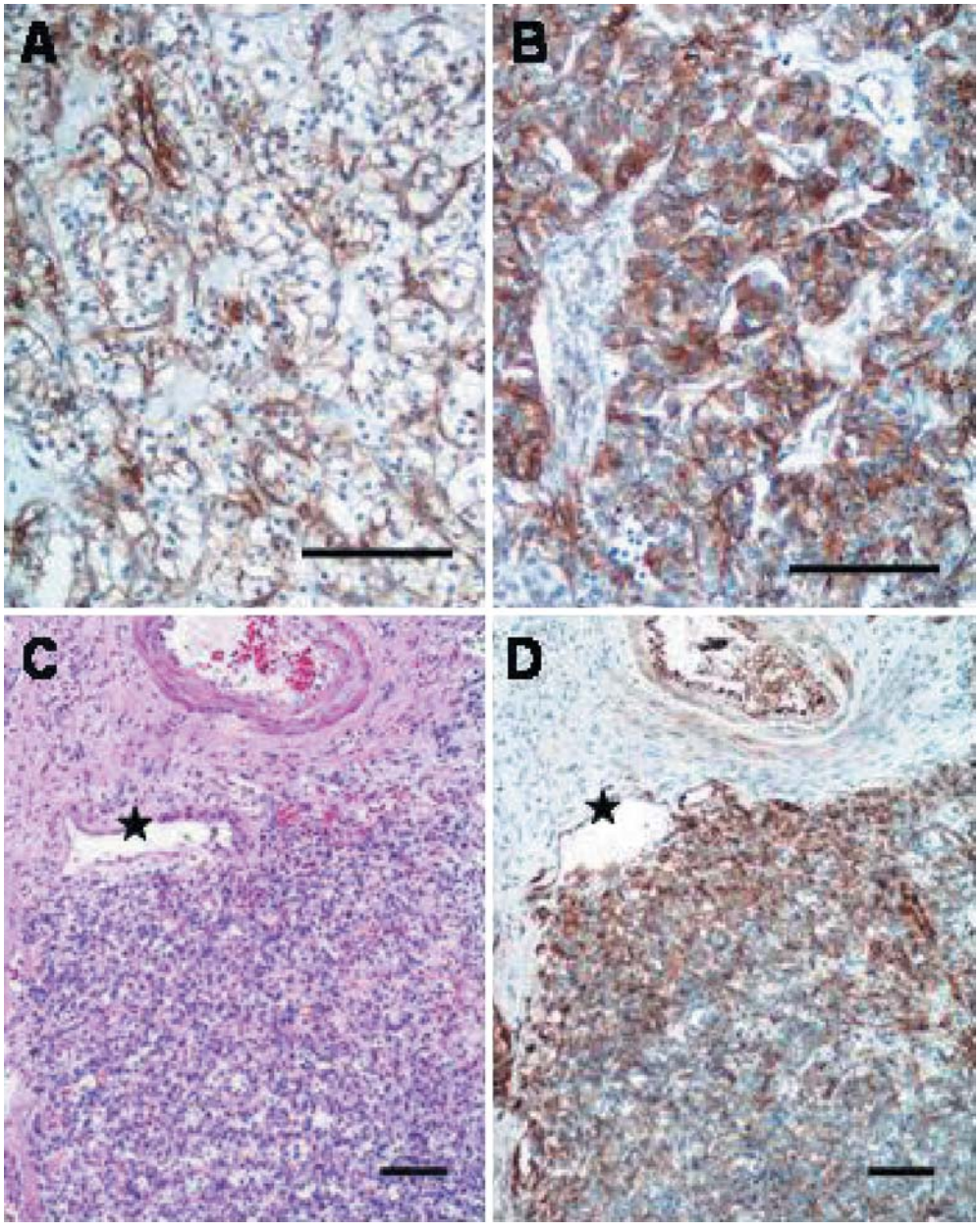


Fig. 1 **A** Immunolocalization of ANX II at the tumor cell membranes: score A1. **B** Intense immunostaining for ANX II in the cytoplasm and at the cytoplasma membranes of tumor cells: score A2. **C**, **D** Hematoxylin and eosin staining (**C**) and ANX II immunohistochemistry on a subsequent section (**D**). Tumor cells in close vicinity to a vein (*asterisk*) were strongly positive for ANX II (**D**). *Bars* 50 μm

noreactivity was strong at the cell membranes and occasionally appeared faintly in the cytoplasm of tumor cells (Fig. 1A). Eleven samples showed a strong immunreactivity both at the cell membranes and in the cytoplasm and were scored A2 (Fig. 1B, D; Table 1). In all samples investigated both endothelial cells and some connective tissue cells were immunopositive.

The distribution of patients by ANX II score and their respective follow-up status was found to be as follows:

- A0, *n*=16: 8 NED, 2 AWD, 4 DOD, 2 LTF
- A1, *n*=6: 3 NED, 2 AWD, 0 DOD, 1 LTF
- A2, *n*=11: 0 NED, 2 AWD, 9 DOD, 0 LTF

The correlation between ANX II score and clinical outcome (alive vs. dead) was statistically significant (χ^2, P=0.002; τ_c=0.48, P=0.015).

Examination by immunohistochemistry and conventional histology revealed following relationship between ANX II score and eosinophil score:

- A0, *n*=16: 12 E0, 2 E1, 2 E2
- A1, *n*=6: 4 E0, 1 E1, 1 E2
- A2, *n*=11: 2 E0, 5 E2, 4 E2

The correlation between ANX II score and eosinophil score was barely nonsignificant (χ^2, P=0.061; τ_c=0.38, P=0.009).

The following relationship was observed between ANX II score and Fuhrman grade:



Fig. 2 RT-PCR of neoplastic (*lanes 1, 2*) and nonneoplastic samples (*lanes 3, 4*) from two representative patients. Bands for ANX II are seen at 495 bp; *S* bp marker

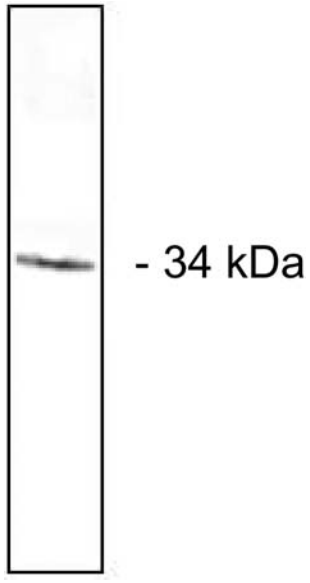


Fig. 3 Demonstration of ANX II in one neoplastic sample by western blot analysis. The band (34 kDa) is representative for nonneoplastic and neoplastic samples

– G1, n=6: 5 A0, 1 A1
– G2, n=24: 11 A0, 5 A1, 8 A2
– G3, n=3: 0 A0, 0 A1, 3 A3

The correlation between ANX II score and Fuhrman grade was statistically significant (χ^2, P=0.035; τ_c=0.35, P=0.005).

PCR and western blot

PCR revealed ANX II mRNA in both normal and tumor tissue (Fig. 2), and western blot analysis identified ANX II protein in both normal and tumor tissue. The molecular mass was 34 kDa (Fig. 3).

Discussion

This study investigated 33 CRCCs with adjacent nonneoplastic tissues regarding the proportion of eosinophilic cells and the expression of ANX II by immunohistochemistry. Western blot analysis and qualitative RT-PCR showed the presence of a 34-kDa protein ANX II mRNA in tissue homogenates. The purposes were (a) to obtain information of the ANX II expression in CRCCs vs. nonneoplastic tissue, (b) to analyze the correlation between immunohistochemical ANX II expression and Fuhrman grade, and (c) to examine whether ANX II can serve as a prognostic factor.

Previous studies localized ANX II immunoreactivity in nonneoplastic renal tissue in Bowman's capsule, loop of Henle, distal convoluted tubules, and the collecting tubules and ducts; these findings are in complete accordance with our own data [6]. However, to our knowledge, the expression of ANX II in CRCCs has not yet been reported. To avoid confusion this study classified CRCCs as in previous reports since clear cell carcinomas are often composed of different cell types (eosinophilic and chromophilic) to varying extent and may exhibit different growth patterns [28, 33]. In accordance, the tumor samples investigated in the present study contained different proportions of eosinophilic cells, as quantified by eosinophil score. Interestingly, the proportion of eosinophilic cells (score E2) increased in higher grade lesions (Fuhrman grades 2 and 3) and was significantly correlated with clinical outcome. These findings strongly support the earlier hypothesis that tumor cells with eosinophilic rather than clear cytoplasm entail a unfavorable prognosis [28].

The heterogeneity in CRCCs is reflected not only by hematoxylin and eosin staining but also by immunohistochemical stainings for vimentin or cytokeratin, as reported previously and in our study by ANX II staining [15, 19]. The different expression of antigens could be due to the fact that the tumor develops from various cell types. On the other hand, it is possible that different staining properties indicate that tumor cells exhibit varying degrees of differentiation [8, 28]. Eosinophilic cells in CRCCs have consistently been regarded as a dedifferentiated cell type originating from clear cells [28]. In this context one should note that the histiogenesis remains controversial although the origin of CRCCs has been the subject of intense interest. A previous view suggested that they arise from proximal tubule cells [24, 28, 34]. On the other hand, immunohistochemical studies indicate a variable antigenic composition, favoring the hypothesis that CRCCs develop from an uncommitted or primitive cell rather than from any particular portion of the nephron [4, 7].

The amount of eosinophilic cells was less than 10% (E1/E2) in 11 of 17 samples with ANX II score of A1 or A2, indicating a relationship between the expression of ANX II and eosinophilic differentiation. Although the statistical correlation between ANX II score and eosinophil score was barely not significant (P=0.061), we believe that the dedifferentiation of tumor cells results from increased ANX II expression. Thus the high expression of ANX II as seen in some specimens with low eosinophil scores (E0/A2) may characterize an early stage of dedifferentiation and underlines the above concepts [28].

As shown in our study eosinophilic cells at the invasive edge (Fig. 1C) exhibited both cytoplasmic and membranous ANX II immunoreactivity, while clear cells were stained at the membranes only. As ANX II is known to inhibit membrane aggregation, which may contribute to the shedding of cells, ANX II expression could reflect the malignant potential of CRCCs [35]. This is supported by investigations on several cell lines showing the differential expression of ANX subtypes on the cell surface depending on both histological cell type and the metastatic potential [35]. Furthermore, ANX II serves as a marker of malignancy in brain tumors, and overexpression of ANX II in gastric carcinomas is associated with a poor prognosis [9, 23]. Although we observed a significantly correlation between ANX score and clinical outcome, further studies must determine whether ANX II expression is related to the development of metastases in CRCCs. ANX II localization at the cell membranes may indicate an involvement in signal transduction since previous studies have shown that ANXs are targets for tyrosine kinases, and reversible tyrosine phosphorylation is a regulatory mechanism in cell growth [30]. Moreover ANX II is a major substrate of the epidermal growth factor receptor (EGFR) which has been localized in cultures of renal cell carcinoma cell lines. As EGFR is thought to facilitate deregulated proliferation in tumor cells, it may be speculated that ANX II is involved in this mechanism and possibly stimulates cancer growth [2, 25, 30]. Evaluation of the possible correlation between ANX II expression and EGFR would require colocalization studies and coexpression experiments in tumor tissues and in cell lines. On tissue homogenates we observed ANX II mRNA in all neoplastic and nonneoplastic tissues. However, the special cell type expressing ANX II mRNA and the role of ANX II expression remains to be elucidated in further investigations.

Taken together, our study shows that (a) CRCCs are composed of tumor cells of variable stages of differentiation as reflected by heterogeneous ANX II expression, (b) the proportion of eosinophilic cells is related to clinical outcome, (c) ANX II expression is correlated with Fuhrman grade, and (d) ANX II expression is correlated with clinical outcome. Therefore immunohistochemistry of ANX II can serve as an additional prognostic marker in CRCCs in the future.

References

1. Bander NH (1987) Monoclonal antibodies in urologic oncology. Cancer 60:658–667
2. Cheng YS, Chen LB (1981) Detection of phosphotyrosine-containing 34,000-dalton protein in the framework of cells transformed with Rous sarcoma virus. Proc Natl Acad Sci USA 78:2388–2392
3. Chiang Y, Rizzino A, Sibenaller ZA, Wold MS, Vishwanatha JK (1999) Specific down-regulation of annexin II expression in human cells interferes with cell proliferation. Mol Cell Biochem 199:139–147
4. Cohen C, McCue PA, Derose PB (1988) Histiogenesis of renal cell carcinoma and renal oncocytoma. An immunohistochemical study. Cancer 62:1946–1951
5. DeKernion JB, Ramming KP, Smith RB (1978) The natural history of metastatic renal cell carcinomas: a computer analysis. J Urol 120:148–152
6. Dreier R, Schmid KW, Gerke V, Riehemann K (1998) Differential expression of annexins I, II and IV in human tissues: an immunohistochemical study. Histochem Cell Biol 110:137–148
7. Droz D, Zachar D, Charbit L, Gogusev J, Chretien Y, Iris L (1990) Expression of the human nephrone differentiation molecules in renal cell carcinomas. Am J Pathol 137:895–905
8. Eker R, Nesland JM, Andersen A, Johannessen JV (1986) Prognostic factors in renal cell carcinoma. Histol Histopathol 1:255–270
9. Emoto K, Sawada H, Yamada Y, Fujimoto H, Takahama Y, Ueno M, Takayama T, Uchida H, Kamada K, Naito A Hirao S, Nakajima Y (2001) Annexin II overexpression is correlated with poor prognosis in human gastric carcinoma. Anticancer Res 21:1339–1345
10. Fuhrman SA, Lasky LC, Limas C (1982) Prognostic significance of morphologic parameters in renal cell carcinoma. Am J Surg Pathol 6:655–663
11. Gerke V, Moss SE (1997) Annexins and membrane dynamics. Biochim Biophys Acta 1357:129–154
12. Gerke V, Moss SE (2002) Annexins: from structure to function. Physiol Rev 82:331–371
13. Grone HJ, Weber K, Helmchen U Osborn M (1986) Villin—a marker of brush border differentiation and cellular origin in human renal cell carcinoma. Am J Pathol 124:294–302
14. Hawkins TE, Merrifield CJ, Moss SE (2000) Calcium signaling and annexins. Cell Biochem Biophys 33:275–296
15. Kanamaru H, Muranaka K, Mori H, Akino H, Arai Y, Okada K (1996) Analysis of histological heterogeneity in renal cell carcinoma: tumor size-related histological change and its prognostic significance. Int J Urol 3:256–260
16. Kovacs G, Akhtar M, Beckwith BJ, Bugert P, Cooper CS, Delahunt B, Eble JN, Fleming S, Ljungberg B, Medeiros LJ, Moch H, Reuter VE, Ritz E, Roos G, Schmidt D, Srigley JR, Storkel S, van den Berg E, Zbar B (1997) The Heidelberg classification of renal cell tumours. J Pathol 183:131–133
17. Kradjian RM, Bennington JL (1965) Renal carcinoma recurrent 31 years after nephrectomy. Arch Surg 90:192–195
18. Landis SH, Murray T, Bolden S, Wingo PA (1999) Cancer statistics, 1999. CA Cancer J Clin 49:8–31
19. Markovic-Lipkovski J, Brasanac D, Todorovic V, Müller CA, Müller GA (1995) Immunomorphological characteristics of renal cell carcinoma. Histol Histopathol 10:651–659
20. Medeiros LJ, Gelb AB, Weiss LM (1988) Renal cell carcinoma: prognostic significance of morphologic parameters in 121 cases. Cancer 61:1639–1651
21. Murphy GP, Mostofi FK (1965) The significance of cytoplasmic granularity in the prognosis of renal cell carcinoma. J Urol 94:48–54
22. Myers GH Jr, Fehrenbaker LG, Kelalis PP (1968) Prognostic significance of renal vein invasion by hypernephroma. J Urol 100:420–423
23. Nygaard SJ, Haugland HK, Kristoffersen EK, Lund-Johansen M, Laerum OD, Tysnes OB (1998) Expression of annexin II in glioma cell lines and in brain tumour biopsies. J Neurooncol 38:11–18
24. Oosterwijk E, Rutter DJ, Wakka JC (1986) Immunohistochemical analysis of monoclonal antibodies to renal antigens. Application in the diagnosis of renal cell carcinoma. Am J Pathol 123:301–309
25. Petrides PE, Bock S, Bovens J, Hofmann R, Jakse G (1990) Modulation of pro-epidermal growth factor, pro-transforming growth factor alpha and epidermal growth factor receptor gene expression in human renal carcinomas. Cancer Res 50:3934–3939

26. Reeves SA, Chavez-Kappel C, Davis R, Rosenblum M, Israel MA (1992) Developmental regulation of annexin II (Lipocortin 2) in human brain and expression in high grade glioma. Cancer Res 52:6871–6876
27. Reis M, Faria V (1988) Renal carcinomas: reevaluation of prognostic factors. Cancer 61:1192–1199
28. Reuter VE, Gaudin PB (1999) Adult renal tumors. In: Sternberg S (ed) Diagnostic surgical pathology, 3rd edn. Lippincott Williams & Wilkins, Philadelphia
29. Roseman BJ, Bollen A, Hsu J, Lamborn K, Israel MA (1994) Annexin II marks astrocytic brain tumors of high histologic grade. Oncol Res 6:561–567
30. Sawyer ST, Cohen S (1985) Epidermal growth factor stimulates the phosphorylation of the calcium-dependent 35,000-dalton substrate in intact A-431 cells. J Biol Chem 260:8233–8226
31. Slaton JW, Inoue K, Perrotte P, El-Naggar AK, Swanson DA, Fidler IJ, Dinney CPN (2001) Expression levels of genes that regulate metastasis and angiogenesis correlate with advanced pathological stage of renal cell carcinoma. Am J Pathol 158: 735–743
32. Sobin LH, Wittekind C (ed) (2002) TNM classification of malignant tumours, 6th edn. Wiley, New York
33. Störkel S, Eble JN, Adlakha K, Amin M, Blute ML, Bostwick DG, Darson M, Delahunt B, Iczkowski K (1997) Classification of renal cell carcinoma. Cancer 80:987–989
34. Wallace AC, Nairn RC (1972) Renal tubular antigens in kidney tumors. Cancer 29:977–981
35. Yeatman TJ, Updyke TV, Kaetzel MA, Dedman JR, Nicolson GL (1993) Expression of annexins on the surfaces of non-metastatic and metastatic human and rodent tumor cells. Clin Exp Metastasis 11:37–44

Virchows Arch (2004) 445:375–381
DOI 10.1007/s00428-004-1079-0

ORIGINAL ARTICLE

Iris Bittmann · Christian Müller · Jürgen Behr · Jan Groetzner · Lorenz Frey · Udo Löhrs

Fas/FasL and perforin/granzyme pathway in acute rejection and diffuse alveolar damage after allogeneic lung transplantation—a human biopsy study

Received: 22 April 2004 / Accepted: 14 June 2004 / Published online: 29 July 2004
© Springer-Verlag 2004

Abstract Acute rejection and diffuse alveolar damage are major problems during the early time after transplantation. Against this background, lung biopsies after allogeneic lung transplantation were studied using immunohistochemistry. Biopsies with acute rejection, diffuse alveolar damage and morphological inconspicuous biopsies were chosen. The objectives of this study were to ascertain: (a) if and how CD4 and CD8 T cells contribute to allograft rejection and diffuse alveolar damage, (b) whether there is a correlation of the chemoattractant regulated on activation normal T cells (RANTES) with the mononuclear infiltrate and (c) whether perforin/granzyme and Fas/FasL pathways contribute to lung injury after lung transplantation. Our results show that $CD4^+$ and $CD8^+$ T cells were increased in biopsies with acute rejection and, to a minor extent, also in biopsies with diffuse alveolar damage due to reperfusion injury. RANTES expression of T cells was increased in biopsies with acute rejection. Perforin seemed to have a dual role in the alloimmune response. In one regard, it had a cytolytic function in the acute rejection process, and, in contrast, it may be responsible for downregulating both CD4- and CD8-mediated alloimmune responses. The FasL/Fas pathway is not only important for induction of apoptosis during rejection but is also a mechanism of lung injury in the development of diffuse alveolar damage.

Keywords Lung transplantation · Rejection · Diffuse alveolar damage · T-lymphocytes

I. Bittmann (✉) · U. Löhrs
Ludwig-Maximilians University Munich,
Pathologisches Institut,
Thalkirchner Strasse 36, 80337 München, Germany
e-mail: Iris.Bittmann@patho.med.uni-muenchen.de
Tel.: +49-89-51604067
Fax: +49-89-51604043

C. Müller
Department of Surgery,
Klinikum of the University Munich,
Großhadern, Marchioninistrasse 15, 81377 Munich, Germany

J. Behr
Department of Internal Medicine I,
Klinikum of the University Munich,
Großhadern, Marchioninistrasse 15, 81377 Munich, Germany

J. Groetzner
Department of Cardiac Surgery,
Klinikum of the University Munich,
Großhadern, Marchioninistrasse 15, 81377 Munich, Germany

L. Frey
Clinic for Anesthesiology,
Klinikum of the University Munich,
Großhadern, Marchioninistrasse 15, 81377 Munich, Germany

Introduction

Lung transplantation has evolved from an experimental endeavour to the mainstay of therapy for many end-stage lung diseases. Despite the success of lung transplantation, rejection, infection and poor immediate graft function present persistent problems and contribute to a mortality rate of 20–30% at 1 year [16].

Acute rejection episodes most frequently occur during the first 3–6 months after transplantation [19] and are characterised by varying degrees of mononuclear cell infiltrates into the alveolar space and interstitium of the transplanted lung. During the early time after transplantation, the allografted lung is additionally mainly compromised by reperfusion injury and infectious disease. Reperfusion injury refers to non-cardiogenic pulmonary oedema resulting from capillary injury. The principal histological finding is diffuse alveolar damage (DAD) [7]. DAD occurring after the early post-transplantation period (more than 2 weeks post-transplantation) should raise the possibility of aetiological factors other than reperfusion injury, such as severe acute rejection, drug toxicity and cytomegalovirus pneumonia.

The mechanisms of allogeneic injury are only partially understood. Recognition of alloantigens expressed by donor tissues by recipient T cells initiates immune destruction of allogeneic transplants. However, there is

controversy concerning the relative contribution of $CD4^+$ and $CD8^+$ T cells to allograft rejection [4].

Although most of the work on leukocytes in reperfusion injury has focused on the role of neutrophils and macrophages, recent studies suggest that lymphocytes may also be involved in reperfusion injury [11].

Little is known how the influx of mononuclear cells is regulated. Regulated on activation normal T cells (RANTES), a member of the C-C chemokine family, is a potent chemotactic cytokine for macrophages, eosinophils and T cells. Several recent studies suggest that RANTES have an important role for the extravasation of mononuclear cells during allograft rejection [1].

Several groups have shown that $CD8^+$ T cells utilise two primary molecular mechanisms to induce target cell death: the perforin/granzyme-mediated pathway of cytolysis and the Fas ligand (FasL)-Fas (CD95) pathway of induction of target-cell apoptosis [11].

Against this background, lung biopsies after allogeneic lung transplantation were studied. Biopsies with acute rejection or DAD (most of the cases were interpreted as reperfusion injury) and inconspicuous biopsies without any evidence of rejection or infectious disease were chosen.

The objectives of this study were then to determine: (1) if and how CD4 and CD8 T cells contribute to acute allograft rejection and diffuse alveolar damage; (2) whether there are differences of expression of RANTES between biopsies with acute rejection and diffuse alveolar damage; (3) whether perforin/granzyme and Fas/FasL pathways contribute to lung injury in both conditions after lung transplantation; (4) whether immunohistochemical staining patterns exist that strengthen the diagnosis of acute cellular rejection.

Materials and methods

Patients

Lung tissue of patients (n=61; female=30; male=31) who underwent lung transplantation was studied. The transplantations were performed from 1992 until 2001 in the departments of surgery and cardiac surgery of the university hospital in Munich. Single lung transplantation (n=34), double lung transplantation (n=23) and heart and lung transplantation (n=4) were performed. Characteristics of recipients are presented in Table 1.

Table 1 Patient characteristics

Age	22–65 years (median 46 years)
Sex	30 Females
	31 Males
Diagnosis	Pulmonary fibrosis (n=21)
	Emphysema (n=20)
	Cystic fibrosis (n=9)
	Primary pulmonary hypertension (n=3)
	Lymphangioleiomyomatosis (n=2)
	Bronchiectasis (n=1)
	Sarcoidosis (n=1)
	Secondary pulmonary hypertension (n=1)
	Congenital heart defect (n=3)

Biopsies

Lung tissue (n=80; transbronchial biopsies=64, open lung biopsies=16) post-transplantation was studied. The biopsies were obtained from post transplantation day (PTD) 3 until PTD 289 (mean PTD 18). For most of the patients (n=47), only one biopsy was studied, and, for a minor number of patients, two (patients=12) and three biopsies (patients=3) were obtained during the time period after transplantation.

All biopsies were routinely fixed in 4% buffered formalin and stained with haematoxylin and eosin, Elastic van Gieson and Prussian blue according to standard procedures. The histological alterations were graded according to the revised working classification of the International Society of Heart and Lung Transplantation [41]. An additionally performed immunohistochemical staining reaction with an antibody against human cytomegalovirus antigen (Dako, Glostrup, Denmark, dilution 1:2000) showed no positive reaction in all studied tissue specimens. The biopsies were put together into three groups: (a) inconspicuous biopsies without any morphological evidence for rejection or infectious disease (n=22), (b) biopsies with different grades of acute rejection (n=36: minimal 13, mild 21, moderate 2) and (c) biopsies with different grades of DAD (n=22) but without any morphological signs of rejection or virus pneumonitis. The patient characteristics as well as the mean time post-transplantation were comparable among the three morphologically defined biopsy groups.

Immunohistochemistry

Consecutive 3-µm sections were cut and mounted on sialinised slides (Superfrost Plus; Menzel Gläser. Braunschweig, Germany). Sections were dewaxed in xylene and rehydrated. Immunohistochemistry was performed with antibodies against CD4, CD8, RANTES, granzyme B, perforin, Fas and FasL (Table 2). Incubation time was 60 min at room temperature for all used antibodies. Detection of bound primary antibodies was done using standard immunohistochemical streptavidin-biotin-peroxidase technique

Table 2 Antibodies and methods used for immunohistochemistry. *RANTES* regulated on activation normal T cells, *TUF* target unmasking fluid (Quartett, Berlin, Germany), *TRS6* target retrieval solution 6 (Dakopatts; Dako, Glostrup, Denmark), *MW* microwave, *APAAP* alkaline phosphatase anti-alkaline phosphatase, *LSAB* labelled streptavidin biotin, *ABC* avidin biotin complex. Source: Innovative Diagnostik Systeme, Hamburg, Germany

Antibody	Source of supply	Primary concentration	Dilution	Pretreatment	Technique
CD4	Novocastra (Newcastle, UK)	250 µg/ml	1:10	30 min MW TUF	APAAP
CD8	Dako (Hamburg, Germany)	250 mg/l	1:50	30 min MW TUF	APAAP
RANTES	Labgen (Frankfurt, Germany)	0.1 mg/ml	1:30	30 min MW TRS6	ABC
Granzyme B	Dako	70 mg/l	1:150	30 min MW TRS6	LSAB
Perforin	Dako	60 mg/l	1:100	30 min MW TRS6	ABC
FasL	Transduction Laboratory (Heidelberg, Germany)	250 µg/ml	1:800	30 min MW Glyka	APAAP
FasDx	Dako	823 µg/ml	1:100	30 min MW TRS6	APAAP

[18] and alkaline phosphatase anti-alkaline phosphatase method [10], respectively, using commercially available staining kits.

To prove staining specificity, the following controls were included in all experiments: for a negative control, the primary antibody was replaced with mouse isotype immunoglobulins or dilution medium. No immunohistochemical staining was observed in these controls. For every staining procedure, all 80 cases were processed simultaneously with the same standardised method. This allowed a highly reproducible comparative analysis of staining patterns.

Quantification of the immunohistochemical results and statistical analysis

The scoring was done as follows: the number of graft infiltrating CD4-, CD8-, RANTES-, granzyme B-, perforin- and Fas-positive T-lymphocytes was determined by evaluating ten randomly selected high-power fields (HPFs) of the lung biopsies. One HPF had a field diameter of 0.5 mm and a field area of 0.196 mm^2. For every case, the absolute number of positively reacting cells was counted.

The results of Fas and FasL immunohistochemistry were additionally classified on the percentage of positively stained cells. Results were expressed as mean±SD unless otherwise mentioned. Starting from the respective mean values of the morphological inconspicuous biopsies, two groups of biopsies were determined: (a) ≤mean value, (b) >mean value. Next, biopsies with rejection and DAD, respectively, were compared with inconspicuous biopsies and biopsies with rejection versus DAD using cross-classified tables. Comparison was done by Pearsons χ^2-test. A probability of $P \leq 0.05$ was considered statistically significant. All data were analysed utilising SPSS (Superior Performance Software System Version 10.0 for Windows, Chicago, IL).

Results

Based on the mean value of positively reacting cells of the collective of inconspicuous biopsies (Table 3), two groups of biopsies were determined for each immunohistochemical staining pattern. Table 4 shows the portion of biopsies with rejection and alveolar damage with values greater than the calculated median value for the different immunohistochemical staining reactions.

Table 4 Biopsy cases with acute rejection and diffuse alveolar damage which demonstrate after immunohistochemical evaluation values higher than the calculated median values of morphological inconspicuous biopsies. *RANTES* regulated on activation normal T cells, *AM* alveolar macrophage

Antibody/cell type	% Of biopsy cases with values greater than the median value	
	Rejection	Diffuse alveolar damage
$CD4^+$ T cells	80.0	59.1
$CD8^+$ T cells	72.2	63.6
$RANTES^+$ T cells	69.4	45.5
$RANTES^+$ AM	19.4	31.8
$Perforin^+$ T cells	52.7	50.0
Granzyme B^+ T cells	58.3	77.3
Fas^+ alveolar epithelium	61.6	100.0
Fas^+ bronchial epithelium	76.7	85.7
Fas^+ AM	79.4	81.8
Fas^+ T cells	67.6	63.6
$FasL^+$ AM	60.0	59.1
$FasL^+$ bronchial epithelium	25.0	57.1

CD4 and CD8

The number of $CD4^+$- and $CD8^+$ T-lymphocytes was increased in biopsies with rejection (CD4: P=0.018, CD8: P=0.088) compared with inconspicuous biopsies (Table 3) (Fig. 1A, B). The number of $CD4^+$- and $CD8^+$-lymphocytes was also slightly increased in biopsies with DAD but without reaching statistical significance. The differences between lung tissue with rejection and DAD were not statistically significant. The CD4/CD8 ratio did not vary significantly among the three morphologically defined groups.

RANTES

RANTES expression could be detected in lymphocytes and alveolar macrophages (AM) but not in epithelial or endothelial cells. The number of $RANTES^+$ lymphocytes was increased in biopsies with rejection (P=0.07) com-

Table 3 Immunohistochemical evaluation of morphological inconspicuous biopsies (n=22), biopsies with rejection (n=36) and diffuse alveolar damage (n=22). *RANTES* regulated on activation normal T cells, *AM* alveolar macrophage, *DAD* diffuse alveolar damage, *HPFs* high-power fields

	Inconspicuous	Rejection	DAD
	Minimum–maximum (mean; median) ±SD		
$CD4^+$ T cells/10 HPFs	11–255 (73.8; 60.5) ±49.3	19–206 (95.7; 86.0) ±47.7	11–190 (76.7; 69.0) ±46.7
$CD8^+$ T cells/10 HPFs	20–294 (104.5; 83.0) ±75.2	57–398 (135.9; 114.5) ±75.5	34–390 (145.3; 131.5) ±92.1
$Perforin^+$ T cells/10 HPFs	30–272 (120.9; 106.0) ±69.6	32–275 (118.5; 109.0) ±65.3	38–294 (129.9; 112.0) ±79.7
$Granzyme^+$ T cells/10HPFs	26–316 (108.4; 81.0) ±86.5	14–315 (104.7; 97.0) ±71.8)	10–314 (111.6; 108.5) ±72.4
$RANTES^+$ T cells/10 HPFs	8–218 (86.9; 85.0) ±66.5	16–344 (117.6; 102.5) ±68.3	13–264 (89.0; 82.5) ±56.3
$RANTES^+$ AM%	0–70 (16.1; 5.0) ±23.5	0–60 (6.4; 1.5) ±14.2	0–70 (10.4; 2.0) ±17.5
Fas^+ alveolar epithelium%	0–9 (2.0; 1.0) ±2.4	0–31 (6.4; 3.5) ±6.9	2–42 (7.9; 5.0) ±9.8
Fas^+ bronchial epithelium%	0–60 (21.9; 20.0) ±20.0	0–40 (15.8; 10.0) ±12.9	1–70 (16.6; 10.0) ±15.7
Fas^+ AM%	0–12 (2.9; 2.0) ±3.4	0–39 (8.5; 5.0) ±8.9	1–28 (10.8; 9.5) ±8.3
Fas^+ T cells/10 HPFs	0–10 (1.9; 1.0) ±2.7	0–21 (5.1; 3.5) ±5.5	0–45 (5.5; 2.0) ±10.2
$FasL^+$ bronchial epithelium%	0–50 (26.3; 30.0) ±14.6	0–70 (25.9; 29.0) ±17.9	0–50 (31.4; 30.0) ±13.5
$FasL^+$ AM%	0–30 (11.8; 13.0) ±9.1	0–95 (21.6; 17.0) ±19.7	0–86 (18.9; 17.0) ±17.9

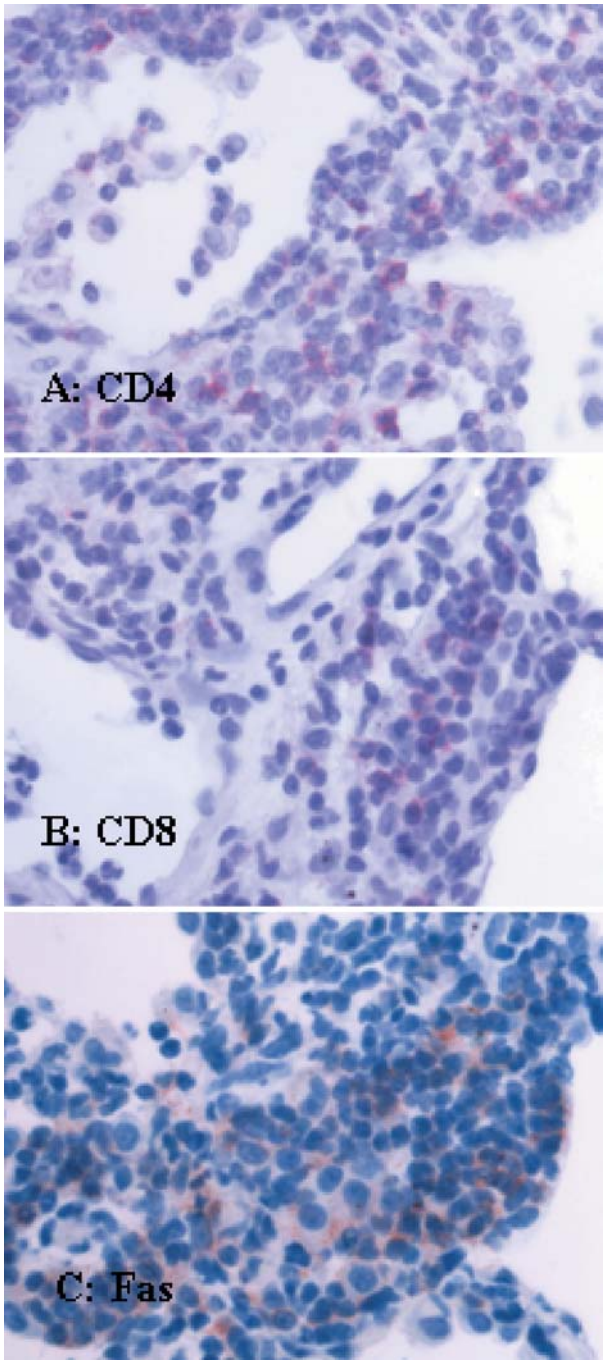


Fig. 1 Transbronchial biopsy obtained 23 days after transplantation with mild acute cellular rejection with perivascular infiltrates of lymphocytes. The mononuclear infiltrate is mainly composed of CD4- (**A**) and CD8- (**B**) positive lymphocytes. The lymphocytes additionally partly express Fas (**C**); a Fas expression of some intermingled macrophages is also recognisable

pared with inconspicuous biopsies and biopsies with DAD but did not reach statistical significance (Table 4) (Fig. 1C). There was a positive correlation of the increase of RANTES$^+$ lymphocytes and increase of CD4$^+$ and CD8$^+$ T cells (P<0.005). There was no increase of the portion of RANTES$^+$ AM in biopsies with rejection or DAD. In contrast, the portion of RANTES$^+$ macrophages seemed to be higher in morphologically inconspicuous biopsy tissue.

Perforin and granzyme B

No significant differences of the number of perforin$^+$ lymphocytes could be detected in the three morphologically defined biopsy groups. The number of granzyme$^+$ lymphocytes tended to increase in biopsies with DAD without reaching statistical significance (P=0.172) (Table 4).

Fas and FasL

Immunohistochemical expression of Fas could be detected in alveolar and bronchial epithelium, AM and lymphocytes and of FasL in alveolar and bronchial epithelium and AM (Table 3). FasL expression of the alveolar epithelium was so minimal that it was only graded as a positive or negative immunohistochemical staining reaction.

Fas expression of lymphocytes (P=0.005) and macrophages (P<0.005) was significantly increased in biopsies with rejection compared with inconspicuous biopsies. Biopsies with DAD showed a statistically significant increase of Fas expression of alveolar epithelium (P<0.005), AM (P<0.005) and lymphocytes (P=0.012) as compared with inconspicuous biopsies. The portion of FasL$^+$ AM was higher in biopsies with rejection and alveolar injury compared with inconspicuous lung biopsies, but without statistical significance (Table 4).

Summary

Our studies revealed an increase of CD4$^+$, CD8$^+$, RANTES$^+$ and Fas$^+$ T cells and Fas$^+$ AM in biopsies with acute rejection compared with inconspicuous biopsies. Biopsies with DAD showed an increase of Fas expression of alveolar epithelium and of Fas$^+$ AM and lymphocytes and a slight increase of granzyme B$^+$ lymphocytes compared with inconspicuous biopsies. The number of CD4$^+$ and CD8$^+$ T cells was higher in biopsies with DAD than in the inconspicuous lung tissue, but without statistical significance. There were no significant differences concerning the number of perforin$^+$ T cells between morphologically inconspicuous biopsies and biopsies with alveolar damage and rejection. No statistically significant differences were found comparing lung biopsies with acute rejection and DAD.

Discussion

Acute cell-mediated transplant rejection is represented by an interstitial mononuclear infiltrate consisting predominantly of CD4$^+$ and CD8$^+$ T cells and macrophages. However, there is controversy concerning the relative

contribution of $CD4^+$ and $CD8^+$ T cells to allograft rejection. Some animal models indicate that there is an absolute requirement for $CD4^+$ T cells in allogeneic rejection [38]; whereas, in others, CD4-depleted mice reject certain types of allografts [14]. The present study could demonstrate an increase of $CD4^+$ and $CD8^+$ T cells in biopsies with acute allograft rejection compared with inconspicuous lung tissue after transplantation. Studies investigating bronchoalveolar lavage (BAL) fluid of lung-transplanted patients found a decreased CD4/CD8 ratio mainly due to an increase of $CD8^+$ T cells [42]. The same results were found in animal models [17, 21]. These changes of the CD4/CD8 ratio could not be confirmed in the present study. This is probably due to the different distribution of lymphocyte subsets in the lung tissue. Clelland et al. [8] showed a broad increase of $CD8^+$ T cells only in BAL fluids but not in the referring lung biopsy. $CD4^+$ and primarily $CD8^+$ T cells were also increased in biopsies with different grades of DAD compared with inconspicuous tissue. DAD occurring during the early post-transplantation period is predominantly a manifestation of ischaemia–reperfusion (IR) injury, as in most biopsies of the present study. Although most of the work on leukocytes in IR has focused on the role of neutrophils and macrophages, recent studies suggest that lymphocytes may also be involved in reperfusion injury. Several studies applying a non-transplant model of warm ischaemia of the liver and the kidney in nude mice, in $CD4^+CD8^+$ knockout mice and in $CD4^+$ depleted mice revealed a reduction of the reperfusion injury after 2 h of reperfusion as compared with control non-immunodeficient mice in an ex vivo model of liver reperfusion [5, 35, 43]. Perrot et al. [11] showed in a rat lung transplant model that recipient T cells did not appear to be involved in the early phase of reperfusion injury. However, after 12 h of reperfusion, recipient T cells mediated reperfusion injury and were associated with significant release of interferon-γ in lung tissue. The findings of the present study on human biopsy material confirmed these animal models, suggesting a role of T cells in the pathogenesis of reperfusion injury after lung transplantation.

Acute allograft rejection is characterised by infiltration of mononuclear cells as shown in the present study, as well. However, the mediators that orchestrate the extravasation of leukocytes during lung allograft rejection have not been fully elucidated. Since RANTES is a potent chemoattractant for mononuclear cells [37], we studied whether a significant immunohistochemical expression of RANTES could be found during acute lung allograft rejection. RANTES can be expressed by a variety of cell types, including $CD8^+$ T cells [33], AM [1], endothelial cells [27] and lung epithelial cells [24]. In the present study, immunohistochemical RANTES expression was only detected in lymphocytes and AM. These results are similar to other studies evaluating human lung tissue [12, 34]. Epithelial or endothelial RANTES expression was particularly found in animal models [11, 39] and cell culture experiments [6], which probably do not reflect the human in vivo expression of RANTES protein. In addition, some of the studies failed to perform an exact cellular immunolocalisation of RANTES protein and described only a mucosal or submucosal RANTES expression [13]. Biopsies with acute rejection showed a tendential increase of RANTES-positive T cells, indicating its potential role as chemoattractant for mononuclear cells during acute rejection. Belperio et al. [1] demonstrated in a rat model of allogeneic lung transplantation that RANTES mRNA and protein levels increased in a time-dependent manner after transplantation with maximal expression and levels occurring on day 6 coincidental with maximal lung allograft rejection. The association between RANTES and acute lung allograft rejection is supported by other studies of solid organ allograft rejection [23, 29, 33]. RANTES mRNA was detected in infiltrating mononuclear cells and renal tubular epithelium during acute renal allograft rejection [33]. In addition, Kondo examined RANTES mRNA expression using three histoincompatible models of allogeneic skin graft in mice [22]. RANTES expression was found to coincide with maximal allograft rejection in all three skin allograft models on day 7. These results suggest an important relationship between augmented expression of RANTES and mononuclear cell infiltration during acute rejection.

The events that lead to allograft loss were partly clarified through the identification of the cytolytic proteins produced by cytotoxic T cells, NK cells and parenchymal cells. Two distinct cytolytic pathways have been described: (a) the pore-forming protein, perforin, and serine protease, granzyme B, which lead to DNA fragmentation and cell death and (b) the interaction between Fas antigen and the Fas ligand, which leads to apoptosis.

Granzyme B, the serine peptidase of the chymotrypsin family, is primarily expressed in activated cytotoxic cells and is the main component of the lytic machinery of cytotoxic cells [15]. Our results showed an increase of granzyme B-positive T cells in 50% of the biopsies with acute rejection and more clearly in biopsies with DAD that did not reach significance compared with morphological inconspicuous biopsies.

Perforin is a cytolytic protein synthesised by cytotoxic lymphocytes and NK cells that, after activation, induce cell death [40]. In the present study, no significant differences of the number of perforin-positive T cells could be observed in the biopsies with histological confirmed acute rejection, DAD or biopsies without any significant morphological alterations.

Several studies demonstrated a significant association between granzyme B and perforin expression and acute cellular rejection episodes after allogeneic kidney [25, 30] and heart [9] transplantation. The expression of granzyme and perforin was partly quantified in peripheral blood [30] and urinary samples [25]. However, when evaluating renal aspirates, the sensitivity of granzyme and perforin expression for the diagnosis of acute rejection episodes clearly decreased. An explanation for the findings of the present study could be given by recent observations of Bose et al. [3]. In their mouse model, perforin was not required for acute rejection but was essential for the in-

duction of long-term allograft survival. Their studies indicate that perforin has a dual role during alloimmune response. In one regard, it has an important but dispensable cytolytic function in the acute rejection process. In contrast, it is essential for downregulating both CD4- and CD8-mediated alloimmune responses by inducing the apoptosis of activated T cells.

The results of the present study showed an increase of granzyme B-positive T cells in 50% of lung biopsies with acute cellular rejection, emphasising the role of the cytotoxic pathway for lung injury during allograft rejection. Additionally, a more clear increase of granzyme B expression could be observed in biopsies with DAD. These observations underscore the role of T cells and T-cell mediated lung injury via granzyme B pathway in the development of DAD after transplantation, even in the absence of morphological signs of rejection or cytomegalovirus pneumonitis.

The calcium-dependent granule exocytosis is not the only cell-death pathway that is used by cytotoxic T cells (CTLs). CTLs can also kill through the Fas (CD95, a member of the tumour-necrosis factor receptor family of death receptors) pathway, which requires neither calcium nor perforin [36]. It seems, however, that CTLs use the granule pathway most often to destroy target cells in culture. Only if this pathway is compromised can significant levels of Fas-mediated cell killing be observed [2]. Fas is widely expressed in numerous different cell types throughout the body, whereas FasL expression appears to be more restricted [31].

In the present study, biopsies with acute rejection showed an increase of Fas^+ lymphocytes and $Fas^+/FasL^+$ AM compared with morphological inconspicuous biopsies. Binding of FasL to Fas antigen causes apoptosis in Fas antigen-bearing cells. Although the expression of FasL was originally thought to be limited to T cells, FasL can be found in a soluble form in the circulation and on the surface of other cells, such as activated neutrophils [26]. Oh et al. [32] could demonstrate in biopsies of human heart allografts that Fas was constitutively expressed both in biopsies with and without rejection. However, FasL expression was detected in 66% of samples with rejection and 40% of samples without rejection by cardiomyocytes as well as graft-infiltrating cells. These results indicate that the upregulation of FasL may be one possible mechanism of apoptosis in tissue damage due to rejection.

Lung biopsies with DAD had an increase of Fas expression of alveolar epithelium, AM and lymphocytes and an increase of $FasL^+$ AM. In a mice model of lipopolysaccharide (LPS)-induced lung injury, the authors [20] could demonstrate, similar to our study, that Fas was upregulated in alveolar and inflammatory cells and that FasL-positive inflammatory cells migrated into the air spaces in the LPS-instilled lungs. Matute-Bello et al. [28] showed that Fas activation in vivo results in acute alveolar epithelial injury and lung inflammation. Taken together, these findings and the results of the present study, it seems quite probable that the Fas/FasL pathway is common for several causing mechanisms of lung injury and is not only induced by an allogeneic immunological reaction.

In summary, the data show that $CD4^+$ and $CD8^+$ T cells were increased in biopsies with acute rejection and to a minor extent also in biopsies with DAD due to reperfusion injury, indicating that T cells were not only involved in the pathological mechanisms of rejection but also in that of DAD after lung transplantation. RANTES expression of T cells was increased in biopsies with acute rejection, indicating a relationship between augmented RANTES expression and mononuclear cell infiltration during acute rejection. There were no significant differences regarding the number of $perforin^+$ cells. This, perhaps, could be explained by recent findings, which demonstrated a dual role of perforin. In one regard, it has a cytolytic function in the acute rejection process, and, in contrast, it may be responsible for downregulating both CD4- and CD8-mediated alloimmune responses. The FasL/Fas pathway is not only important for induction of apoptosis during rejection but is also a mechanism of lung injury in the development of DAD.

Accordingly, the conventional evaluation of lung morphology remains the gold standard of diagnosis of lung rejection. The increase of CD4 and CD8 lymphocytes strengthen the suspicion of rejection, but there exists no typical immunohistochemical staining pattern that allows the diagnosis of acute allograft rejection without regarding the known morphological characteristics [41].

Acknowledgement The authors thank Andrea Sendelhofert for excellent technical skills.

References

1. Belperio JA, Burdick MD, Keane MP, Xue YY, Lynch JP III, Daugherty BL, Kunkel SL, Strieter RM (2000) The role of the CC chemokine, RANTES, in acute lung allograft rejection. J Immunol 165:461–472
2. Bennett WM, DeMattos A, Meyer MM, Andoh T, Barry JM (1996) Chronic cyclosporine nephropathy in renal transplantation. Transplant Proc 28:2100–2103
3. Bose A, Inoue Y, Kokko KE, Lakkis FG (2003) Cutting edge: perforin down-regulates CD4 and CD8 T cell-mediated immune responses to a transplanted organ. J Immunol 170:1611–1614
4. Bueno V, Pestana JO (2002) The role of CD8+ T cells during allograft rejection. Braz J Med Biol Res 35:1247–1258
5. Burne MJ, Elghandour A, Haq M, Saba SR, Norman J, Condon T, Bennett F, Rabb H (2001) IL-1 and TNF independent pathways mediate ICAM-1/VCAM-1 up-regulation in ischemia reperfusion injury. J Leukoc Biol 70:192–198
6. Casola M, Caulet T, Pluot M, Grimbert D, Ferrand O, Baehrel J (1983) [Pulmonary lymphangioleiomyomatosis and bronchiolo-alveolar carcinoma. Apropos of a case]. Arch Anat Cytol Pathol 31:237–240
7. Chaparro C, Chamberlain D, Maurer J, De Hoyos A, Winton T, Kesten S (1995) Acute lung injury in lung allografts. J Heart Lung Transplant 14:267–273
8. Clelland C, Higenbottam T, Stewart S, Otulana B, Wreghitt T, Gray J, Scott J, Wallwork J (1993) Bronchoalveolar lavage and transbronchial lung biopsy during acute rejection and infection in heart-lung transplant patients. Studies of cell counts, lymphocyte phenotypes, and expression of HLA-DR and interleukin-2 receptor. Am Rev Respir Dis 147:1386–1392
9. Clement MV, Legros-Maida S, Israel-Biet D, Carnot F, Soulie A, Reynaud P, Guillet J, Gandjbakch I, Sasportes M (1994) Perforin and granzyme B expression is associated with severe

acute rejection. Evidence for in situ localization in alveolar lymphocytes of lung-transplanted patients. Transplantation 57:322–326
10. Cordell JL, Falini B, Erber WN, Ghosh AK, Abdulaziz Z, MacDonald S, Pulford KA, Stein H, Mason DY (1984) Immunoenzymatic labeling of monoclonal antibodies using immune complexes of alkaline phosphatase and monoclonal anti-alkaline phosphatase (APAAP complexes). J Histochem Cytochem 32:219–229
11. De Perrot M, Sekine Y, Fischer S, Waddell TK, McRae K, Liu M, Wigle DA, Keshavjee S (2002) Interleukin-8 release during early reperfusion predicts graft function in human lung transplantation. Am J Respir Crit Care Med 165:211–215
12. Dorfmuller P, Zarka V, Durand-Gasselin I, Monti G, Balabanian K, Garcia G, Capron F, Coulomb-Lhermine A, Marfaing-Koka A, Simonneau G, Emilie D, Humbert M (2002) Chemokine RANTES in severe pulmonary arterial hypertension. Am J Respir Crit Care Med 165:534–539
13. Fahy JV, Figueroa DJ, Wong HH, Liu JT, Abrams JS (1997) Similar RANTES levels in healthy and asthmatic airways by immunoassay and in situ hybridization. Am J Respir Crit Care Med 155:1095–1100
14. Fishbein MP, Yun J, Laks H, Fishbein MC, Irie Y, Wortham C, Bonavida B, Ardehali A (2001) CD8+ lymphocytes participate in the development of chronic rejection. J Heart Lung Transplant 20:228–229
15. Goto S, Kamada N, Lord R, Kobayashi E, Enosawa S, Kim YL (1994) Induction of natural chimerism after retransplantation of the liver in rats. Transplantation 58:1230–1235
16. Hertz MI, Taylor DO, Trulock EP, Boucek MM, Mohacsi PJ, Edwards LB, Keck BM (2002) The registry of the international society for heart and lung transplantation: nineteenth official report—2002. J Heart Lung Transplant 21:950–970
17. Higashi K, Imura M, Yada I, Namikawa S, Yuasa H, Kusagawa M (1987) Experimental lung transplantation in the rat: study of rejection monitoring using monoclonal antibodies. Transplant Proc 19:1049–1051
18. Hsu SM, Raine L, Fanger H (1981) Use of avidin-biotin-peroxidase complex (ABC) in immunoperoxidase techniques: a comparison between ABC and unlabeled antibody (PAP) procedures. J Histochem Cytochem 29:577–580
19. Keenan RJ, Bruzzone P, Paradis IL, Yousem SA, Dauber JH, Stuart RS, Griffith BP (1991) Similarity of pulmonary rejection patterns among heart-lung and double-lung transplant recipients. Transplantation 51:176–180
20. Kitamura Y, Hashimoto S, Mizuta N, Kobayashi A, Kooguchi K, Fujiwara I, Nakajima H (2001) Fas/FasL-dependent apoptosis of alveolar cells after lipopolysaccharide-induced lung injury in mice. Am J Respir Crit Care Med 163:762–769
21. Kondo T, Wu GD, Saito R, Marchevsky AM, Prehn J, Matloff JM, Waters PF, Jordan SC (1993) Immunocytologic analysis of cells obtained from bronchoalveolar lavage in a model of rat lung allograft rejection. J Surg Res 55:351–356
22. Kondo T, Novick AC, Toma H, Fairchild RL (1996) Induction of chemokine gene expression during allogeneic skin graft rejection. Transplantation 61:1750–1757
23. Kondo T, Morita K, Watarai Y, Auerbach MB, Taub DD, Novick AC, Toma H, Fairchild RL (2000) Early increased chemokine expression and production in murine allogeneic skin grafts is mediated by natural killer cells. Transplantation 69:969–977
24. Kwon KY, Park CK, Park SB, Jeon YJ, Kim HC (1998) Early posttransplantation complication pathology in the experimentally induced allograft lung rejection. Transplant Proc 30:3351–3353
25. Li B, Hartono C, Ding R, Sharma VK, Kracker D, Dadhania D, Serur D, Mouradian J, Seshan S, Schwartz JE, Suthanthiran M (2001) Renal allograft surveillance by mRNA profiling of urinary cells. Transplant Proc 33:3280–3282
26. Liles WC, Kiener PA, Ledbetter JA, Aruffo A, Klebanoff SJ (1996) Differential expression of Fas (CD95) and Fas ligand on normal human phagocytes: implications for the regulation of apoptosis in neutrophils. J Exp Med 184:429–440
27. Lim KG, Wan HC, Resnick M, Wong DT, Cruikshank WW, Kornfeld H, Center DM, Weller PF (1995) Human eosinophils release the lymphocyte and eosinophil active cytokines, RANTES and lymphocyte chemoattractant factor. Int Arch Allergy Immunol 107:342
28. Matute-Bello G, Winn RK, Jonas M, Chi EY, Martin TR, Liles WC (2001) Fas (CD95) induces alveolar epithelial cell apoptosis in vivo: implications for acute pulmonary inflammation. Am J Pathol 158:153–161
29. Nadeau KC, Azuma H, Tilney NL (1995) Sequential cytokine dynamics in chronic rejection of rat renal allografts: roles for cytokines RANTES and MCP-1. Proc Natl Acad Sci U S A 92:8729–8733
30. Netto MV, Fonseca BA, Dantas M, Saber LT, Castro MC, Ferraz AS (2002) Granzyme B, FAS-ligand and perforin expression during acute cellular rejection episodes after kidney transplantation: comparison between blood and renal aspirates. Transplant Proc 34:476–478
31. O'Connell J, Houston A, Bennett MW, O'Sullivan GC, Shanahan F (2001) Immune privilege or inflammation? Insights into the Fas ligand enigma. Nat Med 7:271–274
32. Oh SI, Kim IW, Jung HC, Seo JW, Chae IH, Kim HS, Oh BH (2001) Correlation of Fas and Fas ligand expression with rejection status of transplanted heart in human. Transplantation 71:906–909
33. Pattison J, Nelson PJ, Huie P, von Leuttichau I, Farshid G, Sibley RK, Krensky AM (1994) RANTES chemokine expression in cell-mediated transplant rejection of the kidney. Lancet 343:209–211
34. Petrek M, Pantelidis P, Southcott AM, Lympany P, Safranek P, Black CM, Kolek V, Weigl E, du Bois RM (1997) The source and role of RANTES in interstitial lung disease. Eur Respir J 10:1207–1216
35. Rabb H, Daniels F, O'Donnell M, Haq M, Saba SR, Keane W, Tang WW (2000) Pathophysiological role of T lymphocytes in renal ischemia-reperfusion injury in mice. Am J Physiol Renal Physiol 279:525–531
36. Rouvier E, Luciani MF, Golstein P (1993) Fas involvement in Ca(2+)-independent T cell-mediated cytotoxicity. J Exp Med 177:195–200
37. Schall TJ, Bacon K, Toy KJ, Goeddel DV (1990) Selective attraction of monocytes and T lymphocytes of the memory phenotype by cytokine RANTES. Nature 347:669–671
38. Smith MA, Sundaresan S, Mohanakumar T, Trulock EP, Lynch JP, Phelan DL, Cooper JD, Patterson GA (1998) Effect of development of antibodies to HLA and cytomegalovirus mismatch on lung transplantation survival and development of bronchiolitis obliterans syndrome. J Thorac Cardiovasc Surg 116:812–820
39. Suga M, Maclean AA, Keshavjee S, Fischer S, Moreira JM, Liu M (2000) RANTES plays an important role in the evolution of allograft transplant-induced fibrous airway obliteration. Am J Respir Crit Care Med 162:1940–1948
40. Trapani JA, Browne KA, Smyth MJ, Jans DA (1996) Localization of granzyme B in the nucleus. A putative role in the mechanism of cytotoxic lymphocyte-mediated apoptosis. J Biol Chem 271:4127–4133
41. Yousem SA, Berry GJ, Cagle PT, Chamberlain D, Husain AN, Hruban RH, Marchevsky A, Ohori NP, Ritter J, Stewart S, Tazelaar HD (1996) Revision of the 1990 working formulation for the classification of pulmonary allograft rejection: Lung Rejection Study Group. J Heart Lung Transplant 15:1–15
42. Zeevi A, Rabinowich H, Paradis I, Gryzan S, Dauber JH, Hardesty RL, Kormos B, Griffith B, Duquesnoy RJ (1988) Lymphocyte activation in bronchoalveolar lavages from heart-lung transplant recipients. Transplant Proc 20:189–192
43. Zwacka RM, Zhang Y, Zhou W, Halldorson J, Engelhardt JF (1998) Ischemia/reperfusion injury in the liver of BALB/c mice activates AP-1 and nuclear factor kappaB independently of IkappaB degradation. Hepatology 28:1022–1030

Virchows Arch (2004) 445:382–388
DOI 10.1007/s00428-004-1081-6

ORIGINAL ARTICLE

Andrea Hartner · Timo Eifert · Christian S. Haas · Cigdem Tuysuz · Karl F. Hilgers · Dieter P. Reinhardt · Kerstin Amann

Characterization of the renal phenotype in a mouse model of Marfan syndrome

Received: 5 May 2004 / Accepted: 29 June 2004 / Published online: 29 July 2004
© Springer-Verlag 2004

Abstract The microfibrillar protein fibrillin-1 is expressed abundantly in the vasculature and the glomerulus of the kidney. Mutations in the fibrillin-1 gene lead to Marfan syndrome. The most common complication of this disease is aortic dilatation due to elastic deficiencies of the vascular wall. Several case reports describe glomerular disease in patients with Marfan syndrome, and fibrillin-1 has been implicated in nephrogenesis. To study the role of fibrillin-1 in renal development and function, we characterized the renal phenotype of fibrillin-1-underexpressing mice. Kidney histology was evaluated by means of morphometry and stereology. Relative kidney weights, daily urine excretion, urinary albumin excretion, serum and urinary creatinine, as well as serum urea were not different than wild-type mice. Glomerular number and renal capillarization were normal. The size of the renal filtration surface was comparable in wild-type and fibrillin-1-underexpressing mice. There was no indication for glomerular, renal vascular, or tubulointerstitial injury. However, glomerular volume and mesangial area were reduced. No changes in glomerular cell numbers were detected, but the cellular volume of mesangial cells was significantly lower in glomeruli of fibrillin-1-underexpressing mice. Thus, despite the high abundance of fibrillin-1 in glomeruli of wild-type animals, underexpression of fibrillin-1 did not lead to functional deficiencies of the glomerulus. Alterations in renal histology were only subtle with a reduced glomerular volume and mesangial area likely due to a reduced mesangial cell volume.

Keywords Fibrillin-1 · Marfan syndrome · Fibrillin-1-underexpressing mice · Renal phenotype · Vascular phenotype

A. Hartner (✉)
Department of Pediatrics,
University of Erlangen-Nürnberg,
Loschgestrasse 15, 91054 Erlangen, Germany
e-mail: andrea.hartner@rzmail.uni-erlangen.de
Tel.: +49-9131-8536873
Fax: +49-9131-8533113

C. S. Haas · K. F. Hilgers
Department of Medicine IV,
University of Erlangen-Nürnberg,
Erlangen, Germany

T. Eifert · C. Tuysuz · K. Amann
Department of Pathology,
University of Erlangen-Nürnberg,
Erlangen, Germany

D. P. Reinhardt
Institute for Medical Molecular Biology,
University of Lubeck,
Germany

Introduction

Fibrillin-1 is a microfibril-associated protein of the extracellular matrix which is abundantly present in elastic fibers in many organs. Mutations in the fibrillin-1 gene lead to Marfan syndrome [21]. Besides abnormalities of the skeleton or the eye, patients with Marfan syndrome suffer from severe dilatations of the aorta frequently leading to a rupture of the aorta, which is the most common cause of premature death in Marfan patients [21]. Recent studies revealed that fibrillin-1 is not only abundantly expressed in the walls of larger vessels and the vasculature of several organs including the kidney, but also in the mesangium of the glomerular capillary tuft [27]. Regarding its localization surrounding the glomerular capillaries, it seems likely that fibrillin-1 could contribute to the elastic strength and anchorage of the glomerular capillary tuft, a structure that is exposed to a high hydrostatic pressure to maintain a high ultrafiltration rate [28]. Several reports of different types of renal disease in Marfan patients have appeared [5, 12, 22, 24, 25], but it remains unknown whether these associations were coincidental or due to a systematic renal defect caused by the fibrillin-1 mutation. Studies have reported two models of fibrillin-1 gene-mutated mice [17, 18]. Depending on the precise gene defect, these mice die within the first few months after birth because of cardiovascular complications due to dissecting aneurysms of the aortic wall.

Whereas fibrillin-1-underexpressing mice showed other hallmarks of Marfan syndrome [18], no obviously abnormal renal phenotype was observed [18]. However, no detailed investigations of kidney structure and function were performed in these mice. A study by Kanwar et al. suggested an important role for fibrillin-1 in kidney development [13]. Therefore, we aimed to characterize the renal phenotype in mice with a fivefold underexpression of fibrillin-1 using morphometric and stereologic techniques and by evaluating glomerular function.

Methods

Fibrillin-underexpressing mice

Heterozygous fibrillin-1-underexpressing mice (strain mgR) were a generous gift of Dr. F. Ramirez (Mount Sinai School of Medicine, New York, USA), and maintained by heterozygous breeding pairs at our animal facilities. Mice were housed in a room maintained at 22±2°C, exposed to a 12-h dark/light cycle with free access to standard chow (#1320, Altromin, Lage, Germany) and tap water (or 1% saline, see below). All procedures performed on animals were done in accordance with guidelines of the American Physiological Society and were approved by the local government authorities (Regierung von Mittelfranken, AZ # 621-2531.31-1/01).

Homozygous fibrillin-1-underexpressing (R/R) mice and their wild-type (WT) siblings were included in the study. All animals were genotyped using polymerase chain reaction (PCR) primers for fibrillin-1 (left: 5′ CTC CGT GGG ACC TAC AAA TG 3′; right: 5′ CCA GGT GTG TTT CGA CAT TG 3′) and neomycin (left: 5′ GTG TTC CGG CTG TCA GCG CA 3′; right: 5′ GTC CTG ATA GCG GTC CGC CA 3′), detecting the native fibrillin-1 gene or the introduced neomycin cassette, respectively. R/R mice had a reduced life span of only a few weeks up to 6 months. The animals were followed using regular measurements of weight and conscious systolic blood pressure (Visitech Systems, Apex, N.C., USA).

At 8 weeks or 20 weeks after birth, the mice were put into metabolic cages, and urine was collected for 24 h for measurement of albuminuria and urinary creatinine. The urinary albumin content was measured using an enzyme immunosorbent assay kit (Cell-Trend, Luckenwalde, Germany). Blood samples were taken for determination of serum creatinine (Autoanalyzer, Hitachi Systems, Munich, Germany) and serum urea. Some animals (n=5 each group) were sacrificed by dissecting the abdominal artery and bleeding while under deep ketamine/xylazine anesthesia. After measuring kidney and heart weights, the kidneys were decapsulated. One kidney was put in methyl-Carnoy solution (60% methanol, 30% chloroform and 10% glacial acetic acid) for fixation and embedded in paraffin. Two-micron sections were cut with a Leitz SM 2000 R microtome (Leica Instruments, Nussloch, Germany). Half of the other kidney was immediately snap frozen in liquid nitrogen for mRNA analyses, and half of the kidney was embedded in TissueTek (Sakura, Zoeterwoude, The Netherlands) and frozen in liquid nitrogen for cryostat sections.

Additional animals (R/R 8 weeks, n=6; WT 8 weeks, n=8; R/R 20 weeks, n=5; WT 20 weeks, n=7) were perfusion fixed with glutaraldehyde/cacodylate buffer in deep anesthesia after cannulating the left ventricle as described elsewhere [3]. The kidneys were excised, and the right kidneys were embedded in Epon-Araldite. Semi-thin sections of 0.5 µm were prepared and stained with methylene blue and basic fuchsine. Left kidneys were embedded in paraffin; 2-µm sections were cut and stained with hematoxylin/eosin (HE) or periodic acid–Schiff's reagent (PAS). Thereafter, the kidney sections were investigated using morphometry and stereology [2, 3, 4].

Glomerular geometry

For glomerular geometry, PAS- and HE-stained paraffin sections were investigated using light microscopy. Briefly, glomerular geometry was analyzed as follows: volume density (V_V) of glomeruli and cortex were measured by a point-counting method according to the principle $P_P=A_A=V_V$ at magnifications of ×200 on HE sections [2] and corrected for tissue shrinkage. In addition, the number of glomeruli per cortex (N_A), was assessed using a model based approach according to Weibel/Gomez [29]. The number of glomeruli per volume (N_V) was calculated using the formula $N_V=k/\beta\times N_A^{1.5}/V_V^{0.5}$ with k=1.04 and β=1.38. The total number of glomeruli was derived from the total volume of the renal cortex and the number of glomeruli per cortex volume $N_{Glom}=N_V\times V_{Cortex}$. The total glomerular volume (V_{Glom}) was calculated with $V_{Glom}=V_{VGlom}\times V_{Cortex}$, and the mean glomerular tuft volume was determined according to $v_{glom}=V_{Glom}/N_{Glom}$ [2]. Mean glomerular volume (v_{glom}) was also determined on semi-thin sections using the formula $v_{glom}=\beta/\kappa\times A_T^{1.5}$ with β=1.382 and κ=1 [1, 3, 26]. (A_T, area of glomerular tuft, was determined by point counting on semi-thin sections).

Glomerular capillarization and cellularity

For investigating glomerular capillarization and cellularity, five semi-thin sections per animal were investigated using the point-counting method and a 121-point eyepiece (Zeiss Co., Oberkochen, Germany) at a magnification of ×1000 with oil immersion. Briefly, length density (L_V) of glomerular capillaries was determined according to the standard stereological formula $L_V=2xQ_A$ with Q_A being the number of capillaries transsects per area of the capillary tuft [16]. Total length of glomerular capillaries per one kidney (L_{total}) was then derived from L_V and the total glomerular volume (V_{Glom}) with $V_{Glom}=V_{Vglom}\times V_{cortex}$.

Glomerular cellularity was assessed using stereological techniques in at least 20 glomeruli per animal. Volume density of the various cell types (V_{Vcell}) and cell density per volume (N_{Vcell}) were determined according to $N_{Vcell}=k/\beta\times N_{Acell}^{1.5}/V_{VCell}^{0.5}$ with β=1.5 for podocytes, β=1.4 for mesangial and endothelial cells, and k=1 [4]. The number of cells per glomerulus was determined using the formula $N_{Cell}=N_{Vcell}\times v_{glom}$. The mean cell volume is derived from $v_{Cell}=V_{Vcell}\times V_{Glom}/N_{Glom}$.

Quantitative analysis of the renal vasculature

Staining for α-smooth muscle actin was used for counting myocytes in all cortical arteries at a magnification of ×1000 using oil immersion. Furthermore, length density (L_V) of renal cortical arteries was determined according to $L_V=c\times Q_A$ at a magnification of ×100. Briefly, Q_A was determined as the number of vessels per cortical area. The area and lumen of cortical vessels were determined using planimetry and a semi-automatic image analyzing system (Soft Imaging System, Muenster). In all αsm–actin-stained kidney sections, the minimal and maximal inner and outer vessel diameter were measured (D_{min} and D_{max}). c was determined as D_{min}/D_{max}; Vessel and lumen area were determined using $A_{vessel}=\pi\times(D_{outer}/2)^2$ and $A_{lumen}=\pi\times(D_{inner}/2)^2$. The lumen of the vessel was calculated from the difference of both [4].

Immunohistochemistry

Staining of cryostat sections was performed as described elsewhere [10]. The primary rabbit antibody to fibrillin-1 [20] was used at a dilution 1:500. CY3-labelled anti-rabbit IgG (Dako Diagnostica, Hamburg, Germany) was used as secondary antibody. Stained sections were evaluated in a Leitz Aristoplan microscope (Leica Instruments).

Real-time PCR

Renal cortical tissue was homogenized and isolated as described [11]. mRNA levels of fibrillin-1 were detected using RT–PCR with the TaqMan PCR system (Applied Biosystems, Weiterstadt, Germany) using 18S RNA as the reference and Cyber green as the staining agent. Primers were selected for mouse fibrillin-1: forward primer 5′ GGG-GCA-GCT-GCA-GCG-ATG 3′ and reverse primer 5′ GCC-CAC-GGT-GGC-ACA-GCA 3′. Real time PCR was carried out and relative mRNA levels were calculated according to the suppliers' protocols.

Indices of renal damage

The degree of sclerosis within the glomerular tuft as an index of progression was determined on PAS-stained paraffin sections adopting the semiquantitative scoring system proposed by el Nahas et al. [7]. Using light microscopy at a magnification of ×400, the glomerular score of each animal was derived as the mean of 100 glomeruli. The severity of glomerulosclerosis was expressed on an arbitrary scale from 0 to 4 [3, 7]. The glomerular score for individual glomeruli was: grade 0, normal glomerulus; grade 1, presence of mesangial expansion/thickening of the basement membrane; grade 2, mild/moderate segmental hyalinosis/sclerosis involving less than 50% of the glomerular tuft; grade 3, diffuse glomerulosclerosis with total tuft obliteration and collapse. The resulting index in each animal was expressed as a mean of all scores obtained.

Tubulointerstital and vascular damage was assessed on PAS-stained paraffin sections at a magnification of ×100 using similar semiquantitative scoring systems [3, 26]. For determination of the tubulointerstitial damage score, ten fields per kidney were randomly sampled and graded as follows: grade 0, no change; grade 1, lesions involving less than 25% of the area; grade 2, lesions affecting 25–50%; grade 3, lesions involving more than 50%; and grade 4, fibrinoid necrosis of the vascular wall.

Analysis of data

All data are expressed as means±standard deviation. After testing for normality distribution, one-way analysis of variance (ANOVA) was performed, followed by the least significant difference test to assess the differences between the groups. Results were considered significant when the probability of error (P) was less than 0.05.

Results

Expression of fibrillin-1

As expected, fibrillin-1 mRNA expression in kidneys of fibrillin-1-underexpressing mice (R/R) was significantly lower than in wild-type litters (Fig. 1A). The localization of fibrillin-1 protein, as detected using immunofluorescence, was comparable in renal tissue sections of R/R and wild-type animals: positive immunoreaction was detected in the tubulointerstitium, in the perivascular areas, and in the glomerular mesangium (Fig. 1B).

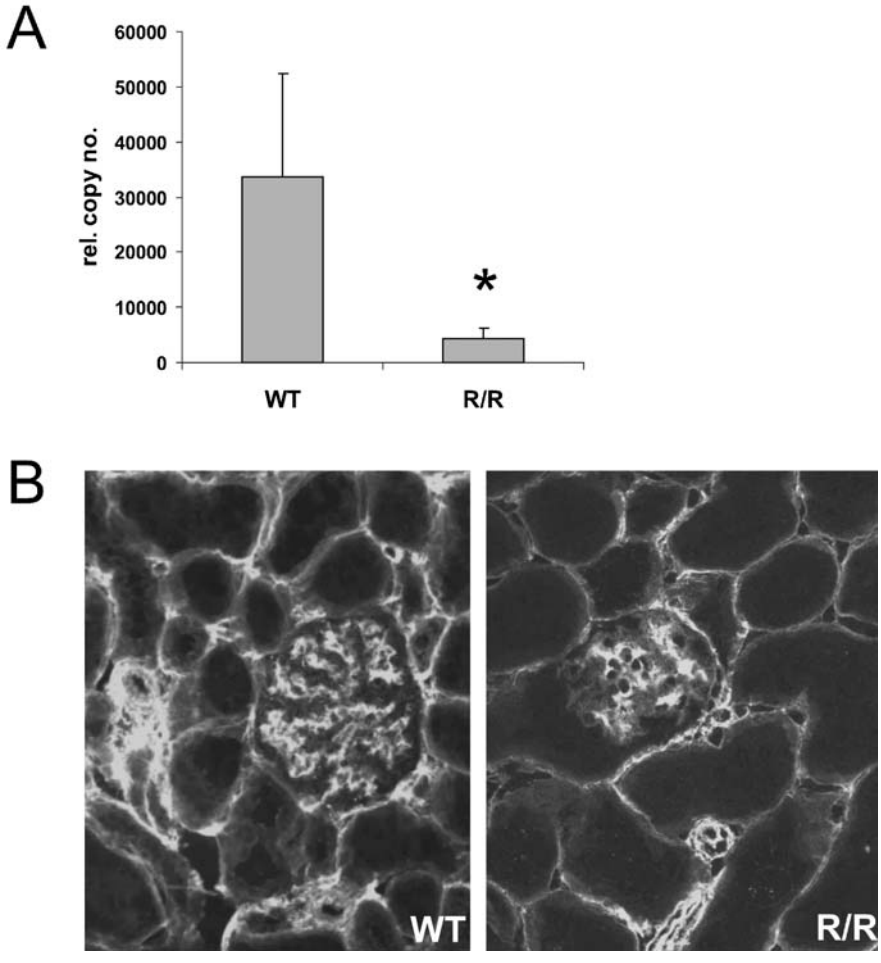


Fig. 1 Detection of fibrillin-1 in fibrillin-1-underexpressing (R/R) mice. **A** Fibrillin-1 mRNA expression levels as assessed by real-time PCR. **B** Immunofluorescence detection of fibrillin-1 in mesangial areas, renal vasculature and the interstitium of wild-type (WT) and R/R mice. Data are mean±SEM, * P<0.05 versus WT

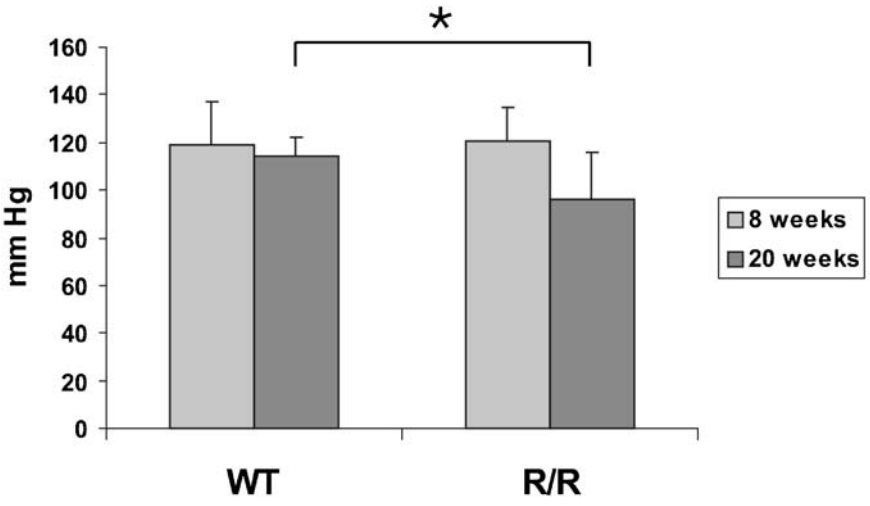


Fig. 2 Systolic blood pressure of 8-week and 20-week-old fibrillin-1-underexpressing (R/R) mice compared with wild types (WT). Data are mean±SD, * $P<0.05$ versus 8-week-old R/R

Animal data and physiological parameters

During the first weeks, R/R mice gained weight comparable with their wild-type littermates. At week 20, however, R/R mice had a significantly lower body weight than wild types (Table 1). Similarly, kidney weight was significantly lower in 20-week-old R/R than in wild types (122.0±25.2 mg versus 186.29±37.8 mg, $P<0.05$), which resulted in comparable relative kidney weights of R/R and wild types (5.9±0.5 mg/g versus 6.3±0.7 mg/g body weight, n.s.). Systolic blood pressure was not different between the genotypes (Fig. 2), but 20-week-old R/R had significantly lower blood pressure than 8-week-old R/R (Fig. 2). The relative heart weights of R/R mice at the age of 20 weeks were slightly higher than that of wild-type litters (7.8±0.9 mg/g versus 6.0±0.4 mg/g body weight, $P<0.05$). No significant differences between R/R and wild types were detected with respect to daily urine excretion, urinary albumin excretion, serum and urinary creatinine, or serum urea (Table 2).

Table 1 Development of body weight of fibrillin-1-underexpressing (RR) or wild-type mice. Data are expressed as mean±SD

Weeks of age	R/R	Wild type
4	13.2±4.2 g	11.7±2.2 g
10	16.0±0.1 g	18.7±1.9 g
13	18.7±0.5 g	22.0±3.6 g
20	21.2±1.0 g*	29.2±7.6 g

* $P<0.05$ versus wildtype

Table 2 Renal physiological parameters of 20-week-old fibrillin-1 underexpressing or wild-type mice. Data are expressed as mean±SD

	R/R	Wild type
Urine/day (ml)	0.65±0.40	0.90±0.12
Urinary albumin (μg/day)	32.7±11.4	39.9±11.6
Albumin/crea (μg/mg)	215.6±59.9	172.2±128.3
Serum creatinine (mg/dl)	0.28±0.27	0.29±0.76
Urinary creatinine (mg/day)	34.9±0.3	33.6±10.4
Serum urea (mg/dl)	53.5±13.3	56.9±17.3

Kidney histology

Morphometric and stereologic analyses revealed no differences in the total number of glomeruli per kidney (12830±1792 versus 12554±3411 in wild types, n.s.), neither at the age of 8 weeks nor 20 weeks. In contrast, mean glomerular volume of 20-week-old R/R mice was significantly reduced as assessed by measurements in paraffin ($740\pm113.2\times10^3$ μm^3 versus $1155.7\pm275\times10^3$ μm^3 in wild types, $P<0.05$) and semi-thin sections (Fig. 3A). Moreover, the mesangial area in semi-thin sections was smaller in R/R than in wild types (Fig. 3B).

Renal capillarization appeared normal in R/R both at the age of 8 weeks and 20 weeks. Total length and length density of capillaries was not significantly different in R/R and wild-type mice (Table 3). In addition, calculation

Table 3 Renal capillarization, glomerular cell number, and cell volume of 20-week-old fibrillin-1-underexpressing or wild-type mice. Data are expressed as mean±SD

	R/R	Wild type
Total length of renal capillaries/kidney (m)	63.5±30.1	106.6±40.4
Length density of capillaries/volume (1/mm^2)	8178.9±911.8	7483.1±1213.5
Filtration surface/kidney (mm^2)	13.4±6.7	17.5±7.4
Number of mesangial cells/glomerulus	56.4±32.9	87.0±23.6
Number of podocytes/glomerulus	48.7±22.1	63.4±15.0
Number of endothelial cells/glomerulus	84.1±25.7	74.8±12.5
Mean volume of podocytes (μm^3)	927.1±121.6	1143.1±223.3
Mean volume of endothelial cells (μm^3)	291.5±90.7	355.4±47.8

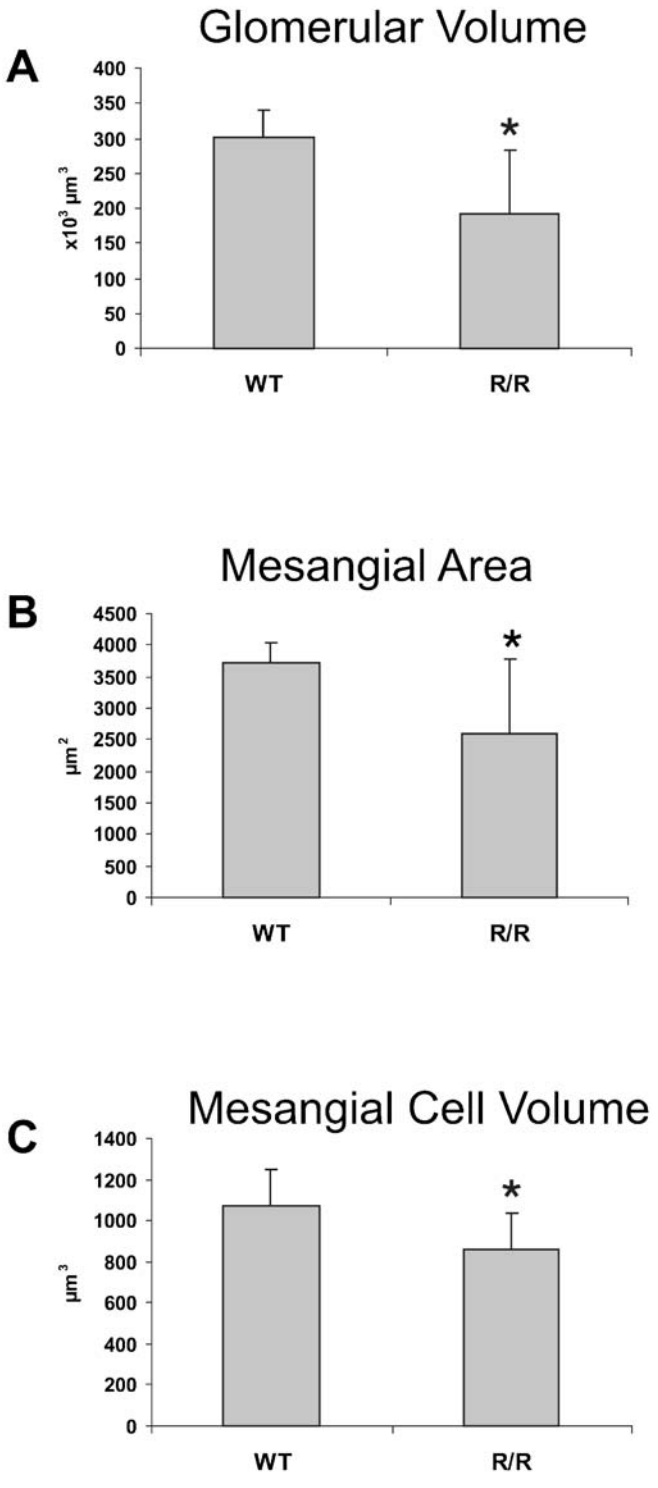


Fig. 3 Glomerular morphological changes of 20-week-old fibrillin-1-underexpressing (R/R) mice compared with wild types (WT). **A** Glomerular volume. **B** Mesangial area. **C** Mesangial cell volume. Data are mean±SD, * $P<0.05$ versus WT

of the filtration surface per kidney did not reveal any differences in R/R and wild-type mice (Table 3).

For each glomerular cell type the total number of cells per glomerulus was calculated. The number of mesangial cells, podocytes, and endothelial cells was not different in R/R and wild-type mice (Table 3). The mean volumes of podocytes and endothelial cells were the same in R/R and wild types (Table 3), but the mean volume of mesangial cells was significantly lower in R/R than in wild types (Fig. 3C).

Morphological indices of renal damage

There was no evidence of glomerulosclerosis (score 0.77±0.22 versus 1.23±0.49 in wild types, n.s.) or tubulointerstitial damage (score 0.48±0.15 versus 0.51±0.09 in wild types, n.s.) in kidneys of 8-week-old R/R mice (data not shown) or 20-week-old mice. No severe renal vascular lesions (i.e., fibrinoid necrosis) were detected (score 0.89±0.29 versus 0.74±0.25 in wild types, n.s.).

Discussion

Glomerular function in mice with a fivefold underexpression of fibrillin-1 was not different from that in wild types. Moreover, there were only subtle alterations in kidney histology with a reduced glomerular volume and mesangial area likely due to a reduced mesangial cell volume. No indications of glomerular, renal vascular, or tubulointerstitial injury were found. Thus, fibrillin-1 underexpression in mice does not seem to lead to defects in renal function, despite some reports of glomerular disease in patients with Marfan syndrome [12, 22, 24]. Sbar et al. [24] described four Marfan patients with microhematuria and proteinuria. Renal biopsies of these patients revealed segmental increase in mesangial matrix with some sclerotic lesions. The authors postulated that changes of microfibrillar arrangements could possibly lead to glomerular basement membrane alterations that might be the cause for microhematuria and proteinuria [24]. The reason that fibrillin-1-underexpressing mice do not show similar renal alterations to the Marfan patients might be that they still have enough normal fibrillin-1 to maintain glomerular structure and function; whereas, in Marfan syndrome, mutations in the fibrillin-1 gene generally lead to the expression of altered fibrillin-1 microfibrils and a lack of normal fibrillin-1 [21]. In contrast to our findings in the kidney, fibrillin-1-underexpressing mice show severe defects in the vasculature, such as aortic aneurysms or rupture some weeks after birth, which is very reminiscent of the lesions frequently seen in the aortas of Marfan patients [18]. Obviously, a mere underexpression of fibrillin-1 is sufficient to destroy the structural integrity of the vasculature. Underexpression of fibrillin-1 might also be compensated for in the kidney. There is a number of other components of microfibrils known to date, e.g., MAGP-1 and -2 [9, 15], fibrillin-2 [19], emilin [6], LTBP-1 [23], and collagen VI [8]. The regulation of these molecules in the glomerulus of fibrillin-1-underexpressing mice is not known. Besides fibrillin-1, MAGP-1 and -2, emilin and LTBP-1 can be detected in the mesangial

matrix [27]. Cultivated mesangial cells are able to express fibrillin-1, emilin, MAGP-1 and-2, and could thus be a source of mesangial microfibrillar proteins [28].

Given the fact that the glomerulus is exposed to relatively high expansile forces due to glomerular capillary blood pressure and glomerular filtration, it is conceivable that the fibrillar material detected by electron microscopy in the extracellular matrix of the glomerulus contributes to the elasticity of these structures [14, 28]. Interestingly, elastin was not detected in the mesangium, arguing for a role of microfibrils composed only of microfibrillar proteins in the elastic strength of the glomerular capillary tuft [28].

The importance of fibrillin-1 in the kidney was emphasized by Kanwar et al. [13], who showed that during renal development of rats fibrillin-1 is tightly regulated. At day 15 of gestation it is expressed in the metanephric mesenchyme, while at day 18 it is confined to nascent blood vessels and glomeruli [13]. Administration of fibrillin-1 antisense oligonucleotides to embryonic metanephroi revealed that fibrillin-1 is essential for metanephric development in organ culture, as sprouting of the ureteric bud was disturbed while the cells of the surrounding mesenchyme were atrophic [13]. These alterations possibly lead to disturbance of epithelial–mesenchymal interactions, which are important for the development of nephrons. Consequently, the number of nephrons was reduced in fibrillin-1 antisense oligonucleotide-treated organ cultures [13]. This is in contrast to the findings of the present study, revealing no differences in nephron number between wild-type and fibrillin-1-underexpressing mice. Again, the reason for the differences observed could be the incomplete lack/eradication of fibrillin-1 in the fibrillin-1-underexpressing mice, or, alternatively, compensatory mechanisms may be active in those mice, which did not have the chance do develop in the more acute model of fibrillin-1 blockade in the metanephric cultures.

Taken together, our data do not support the notion that underexpression of fibrillin-1 leads to severe alterations in renal structural and functional integrity. Pereira et al. also developed mice with a targeted deletion in the fibrillin-1 gene leading to the expression of a low amount of mutated fibrillin-1 (mgΔ) [17]. Unfortunately, homozygous mgΔ/mgΔ mice die shortly after birth, which makes it difficult to use them for determination of the renal phenotype. However, embryonic renal development was not significantly altered in these mice [17]. Further studies in mgR/mgR mice may define a role for fibrillin-1 in the development and/or resolution of experimental renal injury or the renal adaptation to mechanical strain.

Acknowledgements This study was supported by a grant from the Deutsche Forschungsgemeinschaft, Bonn, Germany (STE 196/4-1) and an ELAN grant from the Faculty of Medicine, University of Erlangen-Nürnberg. The authors thank Dr. Francesco Ramirez for kindly providing the fibrillin-1-underexpressing mice. We gratefully acknowledge the expert technical assistance of Monika Klewer, Hans Fees, and Miroslava Kupraszewicz-Hutzler.

References

1. Amann K, Irzyniec T, Mall G, Ritz E (1993) The effect of enalapril on glomerular growth and glomerular lesions after subtotal nephrectomy in the rat: a stereological analysis. J Hypertens 11:969–975
2. Amann K, Nichols C, Tornig J, Schwarz U, Zeier M, Mall G, Ritz E (1996) Effect of ramipril, nifedipine, and moxonidine on glomerular morphology and podocyte structure in experimental renal failure. Nephrol Dial Transplant 11:1003–1011
3. Amann K, Rump LC, Simonaviciene A, Oberhauser V, Wessels S, Orth SR, Gross ML, Koch A, Bielenberg GW, Van Kats JP et al (2000) Effects of low-dose sympathetic inhibition on glomerulosclerosis and albuminuria in subtotally nephrectomized rats. J Am Soc Nephrol 11:1469–1478
4. Amann K, Koch A, Hofstetter J, Gross ML, Haas C, Orth SR, Ehmke H, Rump LC, Ritz E (2001) Glomerulosclerosis and progression: effect of subantihypertensive doses of alpha and beta blockers. Kidney Int 60:1309–1323
5. Biermann CW, Rutishauser G (1994) Polycystic kidneys associated with Marfan syndrome in an adult. Scand J Urol Nephrol 28:295–296
6. Bressan GM, Daga-Gordini D, Colombatti A, Castellani I, Marigo V, Volpin D (1993) Emilin, a component of elastic fibers preferentially located at the elastin-microfibrils interface. J Cell Biol 121:201–212
7. el Nahas AM, Bassett AH, Cope GH, Le Carpentier JE (1991) Role of growth hormone in the development of experimental renal scarring. Kidney Int 40:29–34
8. Fauvel-Lafeve, F (1999) Microfibrils from the arterial subendothelium. Int Rev Cytol 188:1–40
9. Gibson MA, Finnis ML, Kumaratilake JS, Cleary EG (1998) Microfibril-associated glycoprotein-2 (MAGP-2) is specifically associated with fibrillin-containing microfibrils but exhibits more restricted patterns of tissue localization and developmental expression than its structural relative MAGP-1. J Histochem Cytochem 46:871–886
10. Hartner A, Schocklmann H, Prols F, Muller U, Sterzel, RB (1999) Alpha8 integrin in glomerular mesangial cells and in experimental glomerulonephritis. Kidney Int 56:1468–1480
11. Hartner A, Porst M, Gauer S, Prols F, Veelken R, Hilgers KF (2001) Glomerular osteopontin expression and macrophage infiltration in glomerulosclerosis of DOCA-salt rats. Am J Kidney Dis 38:153–164
12. Hsu HC, Churg J (1979) Glomerular microfibrils in renal disease: a comparative electron microscopic study. Kidney Int 16:497–504
13. Kanwar YS, Ota K, Yang Q, Kumar A, Wada J, Kashihara N, Peterson DR (1998) Isolation of rat fibrillin-1 cDNA and its relevance in metanephric development. Am J Physiol 275:F710–F723
14. Kriz W, Elger M, Lemley K, Sakai T (1990) Structure of the glomerular mesangium: a biomechanical interpretation. Kidney Int Suppl 30:S2–S9
15. Kumaratilake JS, Gibson MA, Fanning JC, Cleary EG (1989) The tissue distribution of microfibrils reacting with a monospecific antibody to MAGP, the major glycoprotein antigen of elastin-associated microfibrils. Eur J Cell Biol 50:117–127
16. Mattfeldt T, Mall G, Gharehbaghi H, Moller P (1990) Estimation of surface area and length with the orientator. J Microsc 159:301–317
17. Pereira L, Andrikopoulos K, Tian J, Lee SY, Keene DR, Ono R, Reinhardt DP, Sakai LY, Biery NJ, Bunton T et al (1997) Targeting of the gene encoding fibrillin-1 recapitulates the vascular aspect of Marfan syndrome. Nat Genet 17:218–222
18. Pereira L, Lee SY, Gayraud B, Andrikopoulos K, Shapiro SD, Bunton T, Biery NJ, Dietz HC, Sakai LY, Ramirez F (1999) Pathogenetic sequence for aneurysm revealed in mice underexpressing fibrillin-1. Proc Natl Acad Sci U S A 96:3819–3823
19. Ramirez F, Pereira L (1999) The fibrillins. Int J Biochem Cell Biol 31:255–259

20. Reinhardt DP, Sasaki T, Dzamba BJ, Keene DR, Chu ML, Gohring W, Timpl R, Sakai LY (1996) Fibrillin-1 and fibulin-2 interact and are colocalized in some tissues. J Biol Chem 271:19489–19496
21. Robinson PN, Booms P (2001) The molecular pathogenesis of the Marfan syndrome. Cell Mol Life Sci 58:1698–1707
22. Saborio P, Scheinman J (1998) Genetic renal disease. Curr Opin Pediatr 10:174–183
23. Saharinen J, Hyytiainen M, Taipale J, Keski-Oja J (1999) Latent transforming growth factor-beta binding proteins (LTBPs)—structural extracellular matrix proteins for targeting TGF-beta action. Cytokine Growth Factor Rev 10:99–117
24. Sbar GD, Venkataseshan VS, Huang Z, Marquet E, Brunswick JW, Churg J (1996) Renal disease in Marfan syndrome. Am J Nephrol 16:320–326
25. Schoeneman MJ, Plewinska M, Mucha M, Mieza M (1984) Marfan syndrome and medullary sponge kidney: case report and speculation on pathogenesis. Int J Pediatr Nephrol 5:103–104
26. Schwarz U, Amann K, Orth SR, Simonaviciene A, Wessels S, Ritz E (1998) Effect of 1,25 (OH)2 vitamin D3 on glomerulosclerosis in subtotally nephrectomized rats. Kidney Int 53:1696–1705
27. Sterzel RB, Hartner A, Schlotzer-Schrehardt U, Voit S, Hausknecht B, Doliana R, Colombatti A, Gibson MA, Braghetta P, Bressan GM (2000) Elastic fiber proteins in the glomerular mesangium in vivo and in cell culture. Kidney Int 58:1588–1602
28. Sterzel RB, Hartner A, Hilgers KF, Bressan GM (2001) Contribution of the mesangium to elastic strength and anchorage of the glomerular capillary tuft. Contrib Nephrol 132–141
29. Weibel ER (1979) Morphometry of the human lung: the state of the art after two decades. Bull Eur Physiopathol Respir 15:999–1013

Virchows Arch (2004) 445:389–395
DOI 10.1007/s00428-004-1064-7

ORIGINAL ARTICLE

Hendrik R. De Raeve · Kewal Asosingh · Eddie Wisse · Ben Van Camp · Eric Van Marck · Karin Vanderkerken

Part of the multiple myeloma-associated microvessels is functionally connected to the systemic circulation: a study in the murine 5T33MM model

Received: 21 April 2004 / Accepted: 26 May 2004 / Published online: 30 June 2004
© Springer-Verlag 2004

Abstract It is now well established that angiogenesis in multiple myeloma (MM) is associated with poor prognosis. The exact function of the newly formed vessels in MM is, however, a matter of debate. It is believed that, in contrast to solid tumor growth, the bone marrow (BM) is a sufficiently vascularized organ to support expansion of the MM clone with no need for additional blood vessels. From this point of view, it could be that MM-associated angiogenesis is rather an epiphenomenon and that the newly formed microvessels form a chaotic network that does not contribute to the blood flow. We investigated whether these newly formed microvessels in MM are connected to the blood circulation. The intravenously injected ferritin 30 min prior to sacrifice was detected in 100% of the BM vessels of control mice. In MM-bearing mice, the ferritin tracer was found in 31% of the MM-associated vessels, indicating a connection with the peripheral blood circulation in these vessels. We conclude that, comparable to the situation in solid tumors, at least part of the tumor-associated microvessels in MM is functionally connected to the blood circulation and, therefore, can participate in the transport of nutrients and in the dissemination of MM cells.

H. R. De Raeve (✉) · E. Van Marck
Department of Pathology,
University of Antwerp,
Wilrijkstraat 10, B-2650 Edegem, Belgium
e-mail: Hendrik.De.Raeve@uza.be
Tel.: +32-3-8213731
Fax: +32-3-8214753

K. Asosingh · B. Van Camp · K. Vanderkerken
Department of Hematology and Immunology,
Vrije Universiteit Brussel,
Belgium

E. Wisse
Laboratory of Cell Biology and Histology,
Vrije Universiteit Brussel,
Belgium

Keywords Angiogenesis · Multiple myeloma · Microvessel density · Delivery capacity · Ferritin

Introduction

In solid tumors, it is well recognized that an increase in microvasculature is needed to compensate for the increased nutritional and oxygen demand during expansive tumor growth. In multiple myeloma (MM) it is now well established that active disease is associated with an increase in bone marrow (BM) microvessel density (MVD) [16], which correlates with clinical stage [22], cytological grade [22] and poor prognosis [15].

BM microvessels are involved at different stages of MM development. Initially, MM cells are attracted by the BM endothelial cells (BMECs). Subsequently, the MM cells leave the vasculature (transendothelial migration). The BM environment provides the appropriate growth factors for the expansion of the MM clone. This expansion is accompanied by an angiogenic switch [2, 3]. The dissemination of the MM cells over the whole BM again requires transendothelial migration and in the fully developed stage there is a continuous recirculation of MM cells.

The exact role of the newly formed microvessels in MM biology is a subject of debate. It is believed that the BM itself is a sufficiently vascularized organ to support expansion of MM clone, with no need for additional blood vessels, in contrast to solid tumor growth. From this point of view, MM-associated angiogenesis is rather considered as an epiphenomenon. It could be that the newly formed MM-associated microvessels form a chaotic network that does not contribute to a better blood perfusion and merely functions, like the BM stromal cells, as a source of paracrine growth factors for the MM clone. However, the growing evidence of important similarities between angiogenesis in MM and angiogenesis in solid cancers raises the possibility that neovascularization in MM may be of functional importance for transport of

oxygen and nutrients and for the dissemination of MM cells. In this work, we put a first step in exploring the possibility of the functional importance of MM-associated blood vessels as a transport system. Adequate connection of the MM-associated vessels to the systemic blood circulation is a prerequisite for this involvement. For this purpose, we used the murine 5T33MM model [18]. In this model, we previously demonstrated an increased MVD in the end-stage of the disease [21]. Here, the MVD, and its association with tumor load and paraproteinemia were assessed during MM tumor development. Moreover, the size and the delivery capacity of the microvessels was analyzed at the overt disease of MM and compared with age-matched, non-tumor-bearing (control) mice. The presence of i.v.-injected ferritin was determined in the MM-associated microvessels. The presence of ferritin in the lumen as well as number of the ferritin aggregates in the BMECs was determined.

Materials and methods

The 5T33MM vivo model

5T33MM myeloma originally developed de novo spontaneously in elderly C57BL/KaLwRij mice [14]. This myeloma model has been initiated and is propagated by i.v. injection of diseased BM cells into 6- to 10-week-old syngeneic recipients (Harlan, Horst, The Nederlands). All mice were housed and treated following the rules approved by the ethics committee for Animal Experiments of the Vrije Universiteit Brussel (license no. LA1230281) and University of Antwerp. The animal ethics meet the standards required by the "Principles of laboratory animal care" and follow the Belgian law of 14/08/1986 and 14/11/1993 on the protection of animals. The mice were sacrificed by CO_2 asphyxiation.

Study design

Thirty-six control mice were i.v. injected with 0.5×10^6 5T33MM vivo cells. Six mice were sacrificed at day 7, 13, 16, 20, 23 and 26 after inoculation. Serum paraprotein levels were determined by means of standard electrophoresis [18]. One hind leg was fixed, decalcified and paraffin embedded. On a hematoxylin-and-eosin-stained section, the tumor growth pattern was scored while the MVD was determined by CD31 staining for immunohistochemical analysis. The BM of the other hind leg was flushed, and the tumor load was determined on the mononuclear cell fraction by fluorescence-activated cell-sorting (FACS) staining and analysis for 5T33MM-anti-idiotype positive cells [18].

At day 18 after tumor inoculation, six 5T33MM-bearing mice and six control animals were injected i.v. in the tail vein with 300 µl anionic ferritin (66 mg/ml, ferritin type I isolated from horse spleen, Sygma-Aldrich, Bornem, Belgium). The mice were sacrificed 30 min later (optimal time determined in preliminary experiments). One hind leg was processed for light microscopy and a combination of Perls iron stain and CD31 immunohistochemistry was performed. This light microscopy provided an overview of the whole limb regarding tumor infiltration and ferritin accumulation in the vascular and the extravascular compartment. The other hind leg was processed for transmission electron microscopy (TEM). On ultra-thin sections, the perimeter and the area of the cross-section of 25 microvessels was measured, the presence or absence of ferritin aggregates was assessed in the lumen and the number of aggregates in the EC were counted. For the 5T33MM-bearing mice, the analysis was restricted to areas of tumor infiltration.

Immunohistochemical staining

The anti-CD31 immunohistochemical staining was performed as previously described [21]. Briefly, one hind leg was fixed in zinc fixative for 48 h, decalcified for 2 days and embedded in paraffin. Using anti-CD31 (Mec 13.3, Becton Dickinson Pharmingen, LA, CA; dilution 1/10) and a biotin-conjugated goat anti-rat polyclonal immunoglobulin (Becton Dickinson Pharmingen, dilution 1/70), 5-µm sections were immunostained. The signal was enhanced with a Tyramide Signal Amplification kit (TSA, NEN Life Science Products, Boston, MA, USA). The sections of mice injected with ferritin were stained with a Perls iron stain, followed by CD31 immunostaining.

The combined Perls iron stain/CD31 immunostaining of BM samples from control and tumor-bearing mice not injected with ferritin did not show any ferritin accumulation in the endothelial lining or the lumen of the microvessels (Fig. 2F).

Assessment of the BM MVD

On CD31 immunostained sections of the hind leg, the area within the BM with the highest MVD (hot spot) was selected. In this hot spot, the number of blood vessels per 0.20 mm^2 was counted under a light microscope (200× magnification) by two observers using an eye-piece graticule. The results were obtained by consensus.

Utrastructural analysis of the microvessels

Within 1–2 min after sacrifice, the bones of hind legs were dissected, cut into fragments of 3 mm length, and immersed in 1.5% glutaraldehyde (Sigma-Aldrich) in cacodylate buffer (0.1 M, pH 7.4) for a minimum of 24 h, rinsed, decalcified for 5 days and post-fixed in 1% osmiumtetroxyde for 2 h at 4°C and en bloc stained with 2% uranylacetate for 15 min. After dehydration with ethanol, the tissues were embedded in EPON. Ultra-thin sections of the BM were made and stained with uranyl acetate and lead citrate. An ultra-thin section from the pellet obtained after centrifugation of the injected anionic ferritin was made (to have a morphological reference) (Fig. 4C, right panel). Slides were analyzed by means of TEM with a Philips F.E.I. Tecnai 10 at 80 kV.

Statistics

A mixed-effect general linear model analysis of variance (ANOVA) was used for the comparison between 5T33MM and control mice of perimeter, area and the number of ferritin aggregates per micron EC perimeter. A chi-square test was used for comparison of the presence or absence of ferritin aggregates in the microvessels between 5T33MM and control mice. The tests were performed using SPSS 11.0 software.

Results

To validate this model for the study of angiogenesis in MM, tumor load, serum paraproteinemia and MVD were determined at regular time intervals after i.v. tumor inoculation. At day 7, no MM cells could be identified by light microscopy, and the paraprotein levels were under the detection limit. At day 13, several small aggregates of MM cells were present, paraprotein levels were detectable and the MM population could be distinguished on FACS analysis. The MM cells formed confluent nodules at day 16; the BM was sub-totally infiltrated at day 23, followed by a massive diffuse infiltration at day 26. From

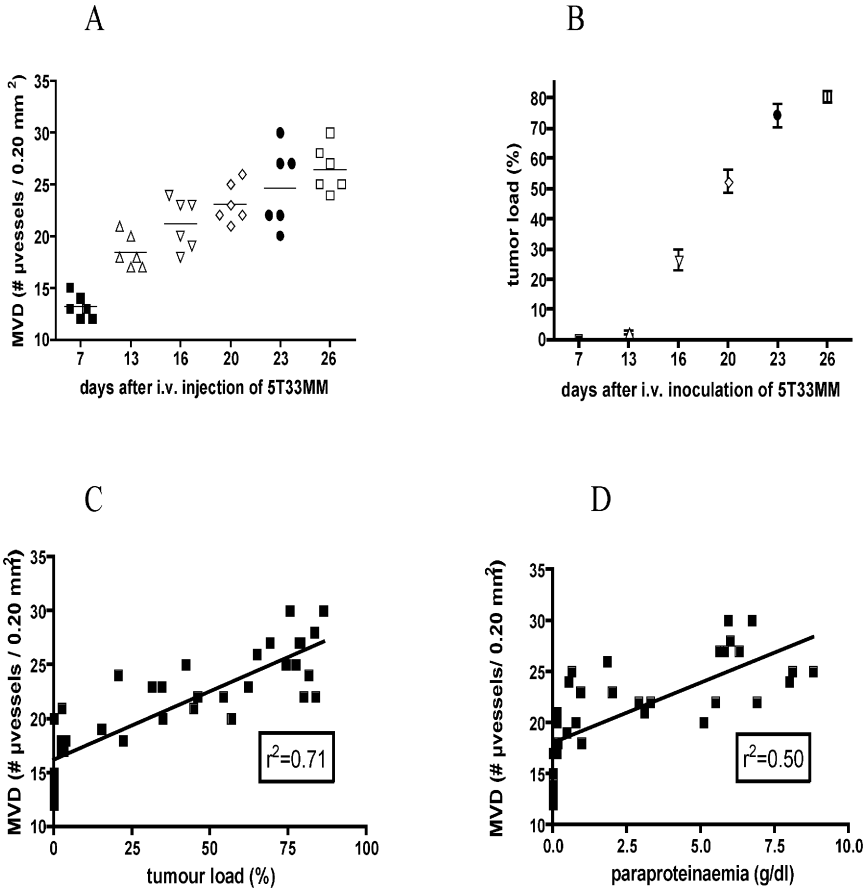


Fig. 1 A Microvessel density (MVD) at different time intervals after i.v. inoculation of 5T33MM cells. **B** Tumor load [percentage of 5T33MM idiotype positive cells of the bone marrow (BM) mononuclear cells] at different time intervals (days) after i.v. inoculation of 5T33MM cells. **C** Correlation between tumor load and MVD. **D** Correlation between paraproteinemia and MVD

day 7 until day 26 there was a steady increase in MVD (Fig. 1A) accompanied by a rise in tumor load and paraproteinemia (Fig. 1B). The MVD correlated with tumor load (r^2=0.71, P<0.0001) (Fig. 1C) and paraproteinemia (r^2=0.50, P<0.0001) (Fig. 1D). The paraproteinemia correlated with tumor load (r^2=0.83, P<0.0001).

At day 18, six 5T33MM-bearing mice and six control animals were injected i.v. with ferritin tracer. On light microscopic examination of the combined Perls iron-stained/CD31-immunostained sections, ferritin was present in all BM microvessels of the control mice (Fig. 2A, B). In tumor-bearing mice, all microvessels in areas of normal BM also contained ferritin, indicating that this tracer was able to reach the BM of diseased animals (Fig. 2E). Moreover, in the tumor-infiltrated areas, ferritin was also detected in at least part of the newly formed vessels (Fig. 2C, D). Besides uptake of ferritin in rare macrophages, there was no accumulation in the extravascular compartment of the BM in both control and 5T33MM mice, excluding the possibility that in the MM-associated microvessels ferritin could already have left the blood stream due to an increased permeability. To assess the presence of ferritin in more detail, TEM analyses were performed. On ultra-thin sections, the perimeter and area of the cross sections of microvessels (Fig. 3A) were significantly lower (P=0.001) in the 5T33MM-bearing mice (82.7±41.8 µm; 257.3±191.7 µm^2, respectively) than in the control mice (111.9±57.5 µm; 563.8±434.3 µm^2, respectively). The presence of ferritin was assessed in the lumen of the microvessels as well as in the cytoplasm of the EC (Fig. 4). While in control mice ferritin aggregates (mean diameter 0.78±0.28 µm) were invariably found in the cytoplasm of the EC of all (100%) 150 (=6×25) microvessels counted in six mice, in the six 5T33MM-bearing mice 47 of 150 (31.3%) of the newly formed BM microvessels (respectively 3, 14, 13, 7, 4, 6 of the 25 counted BM microvessels in each mouse) contained one or more ferritin aggregates in their ECs (P<0.001). The number of ferritin aggregates accumulated in the cytoplasm of the ECs was counted as a measure for the delivery capacity of the vasculature. This number was significantly lower (P<0.001) in tumor-bearing mice (mean±SD) (0.73±1.39) than in control mice (10.5±6.7). The ratio of ferritin aggregates per micron of endothelial lining was calculated in order to adjust for the differences in perimeter between MM-associated microvessels and the control group. This ratio was also significantly lower (P<0.001) in the tumor-bearing mice (0.009±0.018 granules/µm) than in control mice (0.10±0.05 granules/µm) (Fig. 3B). Ferritin was observed in the lumen of 73 of 150 (48.6%) microvessels in the control mice and in 14 of 150 (9.3%) of the myeloma-associated microvessels. Similar results were obtained in the 5T2MM murine model, which is a less aggressive in vivo MM model (results not shown).

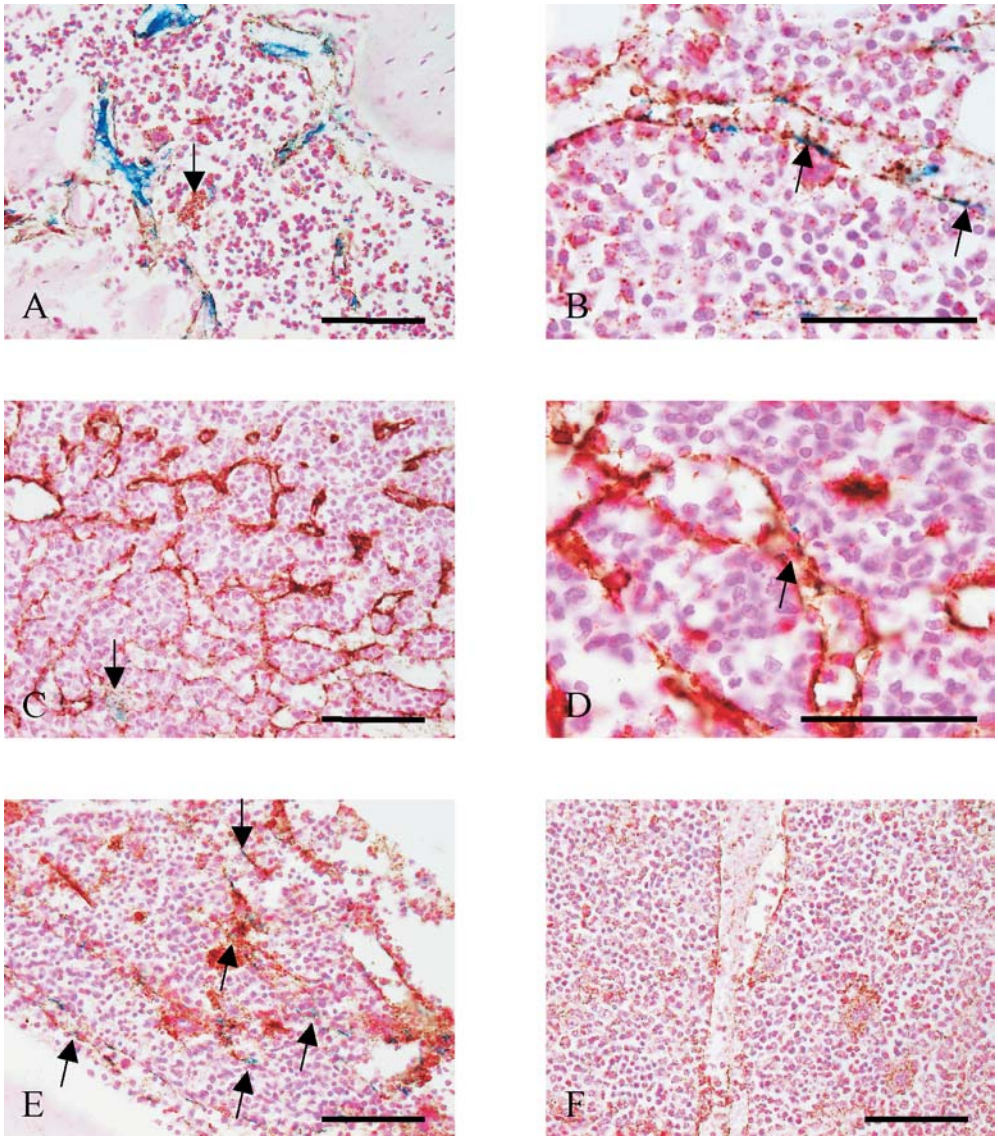


Fig. 2 Combined Perls iron stain/CD31 immunohistochemical stain of bone marrow (BM) of hind leg 30 min after i.v. inoculation of anionic ferritin. CD31-positive endothelial cells stain brown. Ferritin aggregates stain blue with Perls iron stain (*scale bar*=100 μm in **A**, **C**, **E** and **F**; *scale bar*=50 μm in **B** and **D**). **A** In non-tumor-bearing mice, ferritin aggregates are present in all microvessels. Megakaryocytes (*arrow*) also weakly express CD31. **B** At high magnification, ferritin can be observed in the lumen as well as within the endothelial cells (EC; *arrows*) of the microvessels in naive mice. **C** In part of the 5T33MM-associated microvessels, some ferritin aggregates were present (*arrow*), while others were totally devoid of ferritin. There is no ferritin accumulation in the interstitium of the BM. Some microvessels (*upper-right quadrant*) have slit-like lumina. **D** 5T33MM-associated microvessel with a few aggregates within the EC. **E** In less densely MM-infiltrated areas, ferritin granules (*arrows*) are readily found in the majority of the vessels, indicating that the tracer was able to reach the BM in diseased mice. **F** The same combined CD31/Perls staining of a BM from a non-tumor-bearing mouse that was not inoculated with ferritin (negative control). There is no detectable ferritin in the lumen and the EC lining. In the center is a straight sinusoid with open lumen in contrast to the small MM-associated microvessels. There are also few megakaryocytes with a weak CD31 expression. The microvessels (**C**, **D**) in the densely 5T33MM-infiltrated areas stain stronger for CD31 than the sinusoidal microvessels in non-tumor-bearing mice (**A**, **B** and **F**)

Discussion

To investigate whether the MM-associated microvessels are functionally connected to the systemic circulation, we selected the murine 5T33MM model, in which we previously demonstrated an increased angiogenesis at the stage of established disease [21]. The significant correlations between MVD and tumor load and between MVD and paraproteinemia are comparable to the human situation and further validate this model for the study of angiogenesis.

We selected anionic ferritin as a macromolecular tracer, because ferritin has been previously used for this purpose in solid tumors [10, 12]. It has the advantage of being an endogenous component and can be directly recognized in TEM. In addition, a Perls iron stain can be

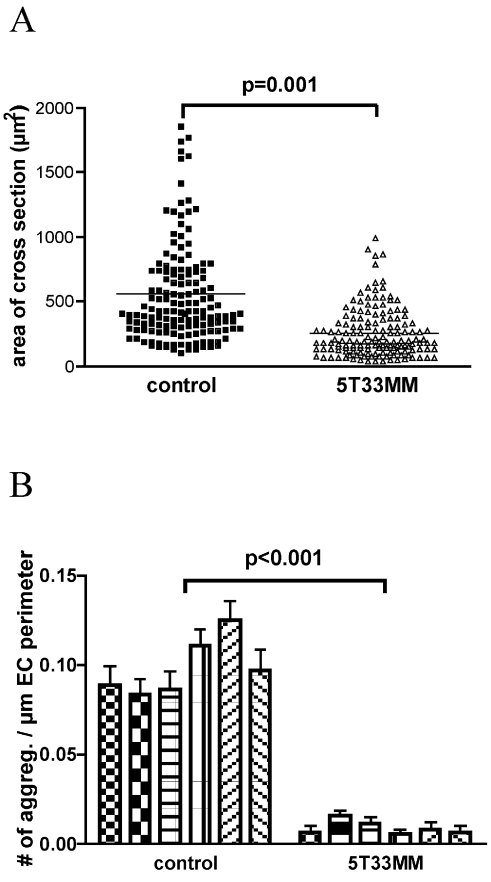


Fig. 3 **A** The area of the cross-sections of 6× 25 bone marrow (BM) microvessels was analyzed in six naive and six 5T33MM-bearing mice. The 5T33MM-associated microvessels are significantly smaller. **B** Ferritin accumulation in the endothelial cell (EC) lining of BM microvessels of, respectively, six naive and six 5T33MM-bearing mice after i.v. injection of ferritin. Shown are the mean and single SD of the number of cytoplasmic ferritin aggregates of ECs per micron perimeter measured along the EC bordering the lumen of microvessel

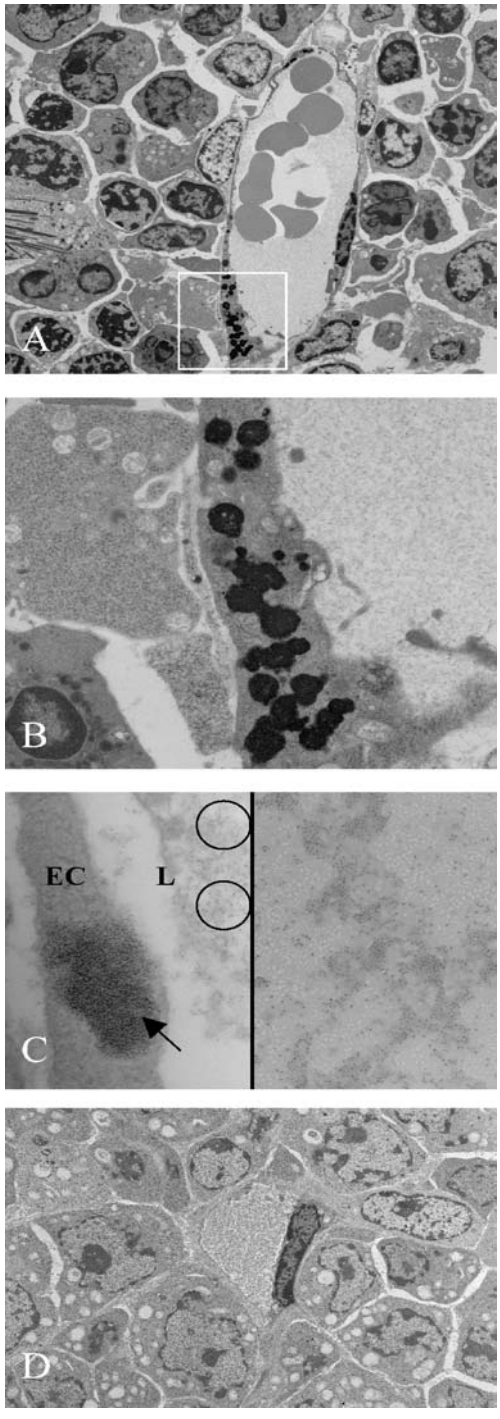


Fig. 4 Transmission electron microscopy (TEM) analysis of ferritin accumulation in endothelial cells (ECs) after i.v. injection of ferritin in naive mice (**A**, **B** and **C**) and 5T33MM-bearing mice (**D**). **A** Several electron-dense aggregates within the cytoplasm of the EC (*rectangle*) (magnification 1275×). **B** Higher magnification of the area limited by the rectangle in **A** (magnification 6130×). EC of normal microvessel with intracytoplasmic ferritin aggregates (*arrow*). **C** *Left panel* high magnification (55,000×) of a ferritin aggregate in the cytoplasm of an EC (*arrow*) and ferritin in the lumen (*circles*); *right panel* high magnification of a dried droplet of the anionic ferritin product used for i.v. injection. Similar ferritin aggregates as in the left panel are present. **D** 5T33MM-associated microvessel without ferritin accumulation (magnification 1275×). The lumen of this vessel contains proteinaceous material without ferritin aggregates

used for staining ferritin in sections for light microscopy. The optimal time between injection and sacrifice, when we could detect most of the injected tracer, was determined in preliminary experiments. The observation in control mice that, 30 min after i.v. injection, in half of the microvessels ferritin was only detected in the ECs but not any more in the lumen indicates that the clearing from the blood stream had already started. The ferritin tracer was found in 100% of the ECs of the microvessels of control mice and in 31% of the ECs in MM-associated vessels.

This observation clearly demonstrates that, in analogy to neovascularization of solid tumors [9], at least part of the newly formed microvessels in massively MM-infiltrated areas is functionally connected to the systemic blood circulation. This connection with the peripheral blood circulation raises the possibility that newly formed blood vessels in MM may participate in the spread of the tumor to anatomically distant BM sites and in the transport of nutrients and oxygen to the myeloma cells and clearance of waste products from the cancer cells. The

ferritin tracer was absent in part of the MM-associated microvessels in areas of massive infiltration. This indicates that either part of the blood vessels are not physically connected to the circulation and/or that there is a poor ferritin delivery brought about by a reduced blood flow. Several mechanical and anatomical factors can account for these findings: in this study, we observed that the newly formed microvessels were significantly smaller than the BM microvessels in control mice (according to Poiseuille's Equation, blood flow is proportional to the fourth power of the radius in a rigid tube). One can hypothesize that the expansion of the MM population within the confinement of the bone could lead to an increased pressure exerted on the microvessel wall. The appearance of slit-like lumina of MM-associated microvessels in densely infiltrated areas, as we [8] and others already observed [16] in human BM specimens, is compatible with this hypothesis. The overexpression of vascular endothelial growth factor by human MM [7] and by 5T33MM cells [21] leads to angiogenesis with a partially disorganized vascular tree composed of tortuous microvessels. In solid tumors, it has been demonstrated that the tortuosity of the vessels, the presence of shunts and vascular loops produces regions of locally flow-limited transport and reduces flow through the tumor as a whole [4, 5, 9, 11, 13]. Although the reduced ferritin delivery in the MM-associated microvessels is totally in line with the observations in solid tumors, further studies are needed to elucidate whether in MM similar factors as in solid tumors can account for this observation.

The MM-associated microvessels are, besides their transport function (recirculation of MM cells, delivery of oxygen and nutrients), involved in several other aspects of the MM pathophysiology [17]: murine BMECs produce monocyte chemoattractant protein-1 [19], which after binding on CC chemokine receptor 2, present on both the 5T2MM and 5T33MM cells, induced chemoattraction of the MM cells, and contact of 5T33MM cells with BMEC upregulates the expression of key molecules such as CD44v6, insulin-like growth factor 1 receptor and matrix metalloproteinase 9 by the MM cells [1, 20]. On stimulation by vascular endothelial growth factor secreted by the MM cells, BMECs produce interleukin 6 [6, 7], which is a major growth factor for MM.

In conclusion, we demonstrated in the 5T33MM model that, in analogy to solid tumors, at least part of the newly formed MM-associated microvessels is connected to the systemic blood circulation, and this raises the possibility that neovascularization in MM may be of functional importance.

Acknowledgements This work was supported by the Fund for Scientific Research—Flanders (Belgium), G.0330.02 (F.W.O.—Vlaanderen), Kom op tegen Kanker, Onderzoeksraad VUB, the International Myeloma Foundation Ashley Barit Research Grant (K.A.), and the Multiple Myeloma Research Foundation (K.V.). Hendrik De Raeve has a Clinical Doctoral Grant from F.W.O.—Vlaanderen, and Kewal Asosingh and Karin Vanderkerken are postdoctoral fellows of F.W.O.—Vlaanderen. We thank Professor Floris Wuyts for the statistical analysis and Dr. Ivan Van Riet for the critical reading of the manuscript. We thank Marijke Baekeland, Carine Seynaeve, Daniëlle Blijweert, Gunther Vrolix and Angelo Willems for skilled technical assistance.

References

1. Asosingh K, Gunthert U, Bakkus MHC, De Raeve H, Goes E, Van Riet I, Van Camp B, Vanderkerken K (2000) In vivo induction of insulin-like growth factor-I receptor and CD44v6 confers homing and adhesion to murine multiple myeloma cells. Cancer Res 60:3096–3104
2. Asosingh K, De Raeve H, Van Riet I, Van Camp B, Vanderkerken K (2003) Multiple myeloma tumor progression in the 5T2MM murine model is a multistage and dynamic process of differentiation, proliferation, invasion, and apoptosis. Blood 101:3136–3141
3. Asosingh K, De Raeve H, Menu E, Van Riet I, Van Marck E, Van Camp B, Vanderkerken K (2004) Angiogenic switch during 5T2MM murine myeloma tumorigenesis; role of CD45 heterogeneity. Blood 103:3131–3137
4. Baish JW, Gazit Y, Berk DA, Nozue M, Baxter LT, Jain RK (1996) Role of Tumor vascular architecture in nutrient and drug delivery: an invasion percolation-based network model. Microvasc Res 51:327–246
5. Baish JW, Jain RK (2000) Fractals and cancer. Cancer Res 60:3683–3688
6. Bellamy WT, Richter L, Frutiger Y, Grogan TM (1999) Expression of vascular endothelial growth factor and its receptors in hematopoietic malignancies. Cancer Res 59:728–733
7. Dankbar B, Padro T, Leo R, Feldmann B, Kropff M, Mesters RM, Serve H, Berdel WE, Kienast J (2000) Vascular endothelial growth factor and interleukin-6 in paracrine tumor-stromal cell interactions in multiple myeloma. Blood 95:2630–2636
8. De Raeve HR, Vermeulen PB, Vanderkerken K, Harris AL, Van Marck E (2004) Microvessel density, endothelial cell proliferation and carbonic anhydrase IX expression in haematological malignancies, bone marrow metastases and monoclonal gammopathy of undetermined significance. Virchows Arch (Published online 28 May 2004)
9. Eskey CJ, Koretsky AP, Domach MM, Jain RK (1992) H-Nuclear magnetic resonance imaging of tumour blood flow: spatial and temporal heterogeneity in tissue-isolated mammary adenocarcinoma. Cancer Res 52:6010–6019
10. Feng D, Nagy JA, Hipp J, Dvorak HF, Dvorak AM (1996) Vesiculo-vacuolar organelles and the regulation of venule permeability to macromolecules by vascular permeability factor, histamine, and serotonin. J Exp Med 183:1981–1986
11. Jain RK (1988) Determinants of tumor blood flow: a review. Cancer Res 48:2641–2658
12. Kohn S, Nagy JA, Dvorak HF, Dvorak AM (1992) Pathways of macromolecular tracer transport across venules and small veins. Lab Invest 67:596–607
13. Mollica F, Jain RK, Netti PA (2003) A model for temporal heterogeneities of tumor blood flow. Microvascular Res 65:56–60
14. Radl J, Croese JW, Zurcher C, Van den Enden-Vieveen MH, de Leeuw AM (1988) Animal model of human disease. Multiple myeloma. Am J Pathol 132:593–597
15. Rajkumar SV, Leong T, Roche PC, Fonseca R, Dispenzieri A, Lacy Q, Lust JA, Witzig TE, Kyle RA, Gertz MA, Greipp PR (2000) Prognostic value of bone marrow angiogenesis in multiple myeloma. Clin Cancer Res 6:3111–3116
16. Vacca A, Ribatti D, Roncali L, Ranieri G, Serio G, Silvestris F, Dammacco F (1994) Bone marrow angiogenesis and progression in multiple myeloma. Br J Haematol 87:503–508
17. Vacca A, Ria R, Semeraro F, Merchionne F, Coluccia M, Boccarelli A, Scavelli C, Nico G, Gernone A, Battelli F, Tabilio A, Guidolin D, Petrucci T, Ribatti D, Dammacco F (2003)

Endothelial cells in the bone marrow of multiple myeloma. Blood 102:3340–3348
18. Vanderkerken K, De Raeve H, Goes E, Van Meirvenne S, Radl J, Van Riet I, Thielemans K, Van Camp B (1997) Organ involvement and phenotypic adhesion profile of 5T2 and 5T33 myeloma cells in the C57BL/KaLwRij mouse. Br J Cancer 76:451–460
19. Vanderkerken K, Vande Broek I, Eizirik DL, Van Valckenborgh E, Asosingh K, Van Riet I, Van Camp B (2002) Monocyte chemoattractant protein-1 (MCP-1), secreted by bone marrow endothelial cells, induces chemoattraction of 5T multiple myeloma cells. Clin Exp Metastasis 19:87–90
20. Van Valckenborgh E, Bakkus M, Munaut C, Noel A, St Pierre Y, Asosingh K, Van Riet I, Van Camp B, Vanderkerken K (2002) Upregulation of matrix metalloproteinase-9 in murine 5T33 multiple myeloma cells by interaction with bone marrow endothelial cells. Int J Cancer 101:512–518
21. Van Valckenborgh E, De Raeve H, Devy L, Blacher S, Munaut C, Noel A, Van Marck E, Van Riet I, Van Camp B, Vanderkerken K (2002) Murine 5T multiple myeloma cells induce angiogenesis in vitro and in vivo. Br J Cancer 86:796–802
22. Xu JL, Lai R, Kinoshita T, Nakashima N, Nagasaka T (2002) Proliferation, apoptosis, and intratumoural vascularity in multiple myeloma: correlation with the clinical stage and cytological grade. J Clin Pathol 55:530–534

Virchows Arch (2004) 445:396–404
DOI 10.1007/s00428-004-1070-9

ORIGINAL ARTICLE

Stephen P. Finn · Paul Smyth · Esther O'Regan · Susanne Cahill · Richard Flavin · John O'Leary · Orla Sheils

Array comparative genomic hybridisation analysis of gamma-irradiated human thyrocytes

Received: 2 April 2004 / Accepted: 18 May 2004 / Published online: 17 July 2004
© Springer-Verlag 2004

Abstract The susceptibility of thyroid epithelium to radiation-induced carcinogenesis is well recognised. In this context, thyroid carcinogenesis is associated with specific somatic *ret*/papillary thyroid carcinoma (PTC) rearrangements and morphologically with the papillary phenotype. Previous studies have demonstrated the possibility of inducing *ret* rearrangements in vitro using X-rays. The purpose of our study was to assess whether gamma (γ) radiation using a Caesium 137 source can induce specific *ret* rearrangements in a human thyroid epithelial cell culture model. We further hypothesised that if radiation-induced thyroid carcinogenesis is associated with non-random rearrangement events, then DNA copy gain and loss induced by irradiation may also occur in a non-random manner. We irradiated SV40-immortalised human thyroid epithelial cells with incremental doses of γ-radiation and, using TaqMan reverse-transcription polymerase chain reaction, looked for the presence of the common *ret* rearrangements. Cohorts showing evidence of *ret*/PTC chimeric transcripts were further analysed using microarray comparative genomic hybridisation (CGH) to detect copy gain and loss associated with radiation. Four Grays of γ-radiation was sufficient to induce *ret*/PTC-3. In this model, transcripts of *ret*/PTC-1 were not detected, and we suggest that the type of radiation may influence the resulting rearrangement that occurs. Using array CGH, we have demonstrated a predominant pattern of subtelomeric deletions occurring in association with this radiation cohort and raise the possibility that chromosome 10 may be a hotspot for radiation-induced damage for as yet unknown reasons.

Keywords Thyroid carcinoma · Radiation · Array comparative genomic hybridisation · RET

S. P. Finn (✉) · P. Smyth · S. Cahill · R. Flavin · J. O'Leary · O. Sheils
Department of Histopathology Research,
University of Dublin, Trinity College, Room 35/72,
Institute of Molecular Medicine,
Trinity Centre for Health Sciences, St. James's Hospital,
James's Street, Dublin 8, Ireland
e-mail: sfinn@gofree.indigo.ie
Tel.: +353-1-6083289
Fax: +353-1-6083285

E. O'Regan
Department of Oral Pathology,
Dublin Dental School and Hospital,
Ireland

Introduction

The susceptibility of the thyroid gland to radiation-induced carcinogenesis is well recognised, particularly when radiation exposure occurs at a young age. This applies especially to papillary thyroid carcinoma (PTC) developing in children. The evidence from epidemiological and molecular studies carried out both before and particularly after the Chernobyl nuclear disaster is compelling [1]. The excess relative risk per Gray (Gy) delivered to the thyroid has been estimated to be 7.7 [2], and this has been confirmed in subsequent studies [3, 4]. Exposure to radioactive iodine isotopes has correlated with increased incidence of PTC in contaminated children as occurred in the Marshall Islands in 1954 [5] (BRAVO thermonuclear test) and in Belarus and the Ukraine (Chernobyl disaster 1986) [6, 7].

In PTC, molecular evidence now indicates a major role for somatic rearrangements involving the *ret* proto-oncogene (chromosome 10q11.2) [8] and, to a lesser extent, the *N-trk* gene (chromosome 1) in the pathogenesis of PTC. The emerging role of *BRAF* mutations is also currently being recognised [9, 10, 11], although no association between radiation-induced PTC and *BRAF* mutations has been described [12].

With regard to *ret* rearrangements, 15 fusion rearrangements [13] involving ten different donor genes leading to oncogenically activated forms of the *ret* proto-oncogene have been described. The 5′ domain of the activating gene acts as a promoter and constitutively activates the tyrosine kinase activity of *ret*, which is normally not active in thyroid follicular cells. The most

prevalent of these are *ret*/PTC-1 (fusion of *ret* tyrosine kinase domain with the 5′ domain of a gene known as *H4*) and *ret*/PTC-3 (fusion of *ret* tyrosine kinase domain with *ELE-1*, also known as *ret* fused gene (*RFG*). It has been suggested that *ret* rearrangements, particularly *ret*/PTC-3, represent a radiation signature because of their prevalence in PTC occurring in children after the Chernobyl disaster [14].

Comparative genomic hybridisation (CGH) is a technique that allows the detection of chromosomal copy number changes (gains and losses) across the entire genome. Array CGH in principle broadly conforms to traditional chromosomal CGH [15] but uses DNA target clones (P1, PAC or BAC clones) spotted onto a glass slide and, therefore, obviates the need for metaphase spreads and expert cytogenetic input [16, 17, 18]. Microarray CGH is more sensitive than conventional CGH and shows higher resolution with precise mapping of amplicon boundaries and simplified data analysis. The Genosensor array 300 system (Vysis, Downer's Grove, Illinois) is a recently developed system and consists of an array of 287 DNA clones (spotted in triplicate) representing genomic regions that are important in cytogenetics and oncology. The array provides a powerful tool for genome-wide evaluation of genomic instability manifested as copy gain and loss. However, as with conventional CGH, array CGH cannot detect structural chromosomal abnormalities not involving copy number changes, such as balanced translocations, inversions or ring chromosomes [19]. For conventional CGH, the resolution (minimal size of the DNA aberration that can be detected) may be between 5 MB and 10 MB and is homogeneous along the chromosomes (except around the centromeres).

For GenoSensor, the resolution can be as low as 100 KB, but it is not homogeneous along the chromosome. The targets used on the microarray have been selected for providing information on known regions of interest, and the approximate coverage for each chromosome is 40 MB. A fully annotated list of the targets is available at http://www.vysis.com.

Studies have demonstrated that previously non-neoplastic human thyroid cells can be transformed by single and fractionated doses of gamma (γ)-irradiation in the range of 0.5 Gy to 4.0 Gy and that these irradiated cells become tumourigenic in nude mice [20]. Chromosomal instability has been described in a similar model of radiation-induced thyroid tumourigenesis using conventional cytogenetics, spectral karyotyping and conventional CGH [21]. However, although these experiments demonstrated that previously non-tumourigenic thyroid cells became tumourigenic in nude mice after irradiation and also elegantly described the resulting cytogenetic profiles, the authors did not demonstrate the radiation signature of rearranged *ret* in the tumours examined. Work by Mizuno et al has demonstrated the possibility of inducing *ret* rearrangements in vitro using X-radiation [22, 23]. However, the type (X-irradiation) and dose (50 Gy) of radiation used in Mizuno's experiment does not approximate Chernobyl conditions, where the major sources of radiation comprised predominantly beta (β)-irradiation with a significant but smaller component of γ-radiation from various isotopes [24]. In addition, the average dose received was lower [25]. There is no previous report of γ-irradiation-induced *ret* rearrangements in vitro in the literature.

We wished to investigate whether γ-irradiation could induce either of the two common *ret* rearrangements. We used a source of Caesium 137 (^{137}Cs), a known persisting post-Chernobyl contaminant, as an appropriate source of γ-radiation. (^{137}Cs is the second most abundant of three major radioactive isotopes released as a result of the Chernobyl disaster, the other two being Iodine 131 and Strontium 90, both of which release β radiation). Furthermore, we wished to describe the pattern of DNA copy gain and loss in γ-irradiated cells using induction of rearranged *ret* as a surrogate endpoint.

Materials and methods

Cell culture

The human thyroid epithelial cell line (N thy-ori 3–1, ECACC number 90011609) is derived from the normal thyroid tissue of an adult. The cells have been immortalised by transfection with a plasmid encoding for the Simian Virus 40 (SV40) large T antigen [26]. It is of interest that SV40-like DNA sequences have previously been linked to PTC, although not in a causative role [27]. N thy-ori cells were grown in 75-cm^2 flasks in 15 ml of culture medium consisting of RPMI 1640 (2 mM Glutamine), 10% foetal calf serum (FCS) and 2% penicillin streptomycin at 37°C with 5% CO_2.

Passage

Cells were passaged when sub-confluent (defined as 70–80% area monolayer coverage of the T75 flask). Sub-confluent non-irradiated cell cultures split equally into four flasks required 4 days (mean) to reach sub-confluence again. The cells were washed with 5 ml of phosphate buffered saline (PBS), then were separated using 5 ml of trypsin/ethylenediaminetetraacetate (EDTA) (10% solution in PBS) for 3 min. The trypsin was neutralised using a further 5 ml of trypsin-neutralising solution consisting of RPMI 1640 (2 mM glutamine) with 20% FCS. The separated cells were removed to a 15-ml tube, and the flask was washed with a further 5 ml of PBS, which was subsequently added to the same 15-ml tube. The cells were centrifuged at 170 *g* for 4 min. The supernatant was decanted and retained, and the cells were re-suspended in 2 ml culture medium and split into three new flasks, each receiving 500 µl (25%) of cell suspension. The supernatant medium was decanted and retained for DNA/RNA co-extraction and subsequent TaqMan polymerase chain reaction (PCR) for *ret* rearrangements throughout the culture period. In addition, at each passage, an aliquot of cells (25% by volume) was taken for DNA/RNA extraction and *ret* rearrangement detection.

γ-Irradiation

Irradiation was performed using the Gammacell 3000 Elan (MDS Nordion, Ottawa, Canada), which uses a ^{137}Cs γ source. The cells were passaged and re-suspended briefly in PBS/10% FCS. Four irradiation cohorts were selected: 0 Gy (control), 2 Gy, 3 Gy and 4Gy. This range approximates the average doses received by children in the Belarus region of the Ukraine who received radiation doses within this range.

DNA/RNA extraction

Co-extraction of RNA and DNA was performed for each of the cell culture experiments. Extracted total RNA was subsequently used for One Step TaqMan reverse-transcription (RT)-PCR (Applied Biosystems, Foster City, CA) to detect chimeric transcripts of the two most common *ret* rearrangements (*ret*/PTC-1 and *ret*/PTC-3). A modification of the Puregene DNA isolation method (Gentra Systems Inc., MN) was used. The protocol is available from the manufacturer's website (http://www.gentra.com).

TaqMan RT-PCR

RT-PCR of extracted total RNA was performed using a TaqMan One Step Reverse Transcription Reagent kit (Applied Biosystems, Foster City, CA). A 25-μl reaction volume comprising TaqMan One Step RT Universal Mastermix, multiscribe reverse transcriptase, target-specific probe, forward and reverse primers for *ret*/PTC-1, *ret*/PTC-3 and glyceraldehyde-3-phosphate dehydrogenase (GAPDH), and extracted template RNA was used. The cycling parameters were as follows: hold at 48°C for 30 min (RT), hold at 95°C for 10 min (activation of Amplitaq Gold), followed by 40 cycles of 95°C for 15 s, 60°C for 1 min.

Target-specific primers and probes were designed using ABI Prism Primer Express 1.5 software (Applied Biosystems, Foster city, CA) as previously described. Sequences of primers and probes for *ret*/PTC-1, *ret*/PTC-3 and GAPDH have been published [28]. Probes were designed to span the fusion points of the chimeric transcripts of *ret*/PTC-1 and *ret*/PTC-3.

All probes used in the TaqMan reactions were designed to have non-fluorescent quenchers and minor groove binding (MGB) modifications. MGB probes have low background fluorescence and bind more tightly to their target. This raises the T_m of the probes and allows for a more flexible assay design. Six negatives were included in each TaqMan run. These included four no-template controls and two no-amplification controls. GAPDH was used to confirm the integrity of the extracted RNA. Two replicates were run for each assay. For *ret*/PTC-1 detection, RNA from the cell line TPC-1 was included as a positive control. For *ret*/PTC–3, plasmid-derived *ret*/PTC cRNA transcripts were used. Thermal cycling was performed on an ABI PRISM 7000 Sequence Detection system (Applied Biosystems, Foster City).

Array CGH

In classical CGH, the labelled test DNA is hybridised to the metaphase spreads in an equimolar quantity to competing differentially labelled normal reference DNA source. In the case of the Vysis array CGH (Vysis, Downer's Grove, Illinois), the manufacturer provides a sample of male or female reference DNA for this purpose. Array CGH was performed according to the manufacturer's instructions.

Briefly, after extraction, DNA was quantified by measuring absorbance at 260/280 nm. Working solutions of test and reference DNA at 25 ng/μl in 10 mM Tris, 1 mM EDTA pH 7.4–8.0 were made.

Labelling

DNA was labelled using random priming according to the manufacturer's protocol. Test DNA (irradiated N-thy-ori with *ret*/PTC3 transcripts demonstrated by RT-PCR) was labelled with Cy-3 dCTP (PE Lifesciences) and reference DNA (supplied by the manufacturer) with Cy-5 dCTP (PE Lifesciences). After labelling, the DNA was digested using DNAase Amp grade in order to obtain DNA fragments of between 200 base pairs and 500 base pairs in length. The resultant probes were purified by precipitation (sodium acetate) and ethanol extraction according to the Vysis protocol. DNA pellets were re-suspended in 4.0 μl of 10 mM Tris pH 8.0. Of this, 0.5 μl of test and reference DNA were run on a 1% agarose gel to ensure that DNAase digestion had been successful.

Hybridisation

Equal volumes of test and reference were combined (2.5 μl of each) with microarray hybridisation buffer (25 μl volume containing cot-1 DNA to block repetitive sequences). After denaturing the DNA (80°C for 10 min), the hybridisation mixture (volume 30 μl) was transferred to the array and coverslipped using the hybridisation coverslip supplied. Each array was hybridised at 37°C in darkness for 60–72 h in an airtight container, the atmosphere of which was saturated with 50% formamide/2× sodium saline citrate (SSC).

Washing the microarray

After removing the hybridisation coverslip, each microarray was washed sequentially in Coplin jars containing 50% formamide/2× SSC (3× 10-min washes at 40°C) followed by 1× SSC (4× 5-min washes at room temperature) and finally rinsed in distilled water (2 s). Array 4′, 6-diamidino-2-phenylindole (array DAPI 25 μl) was applied to the wet surface of the array, and the final coverslip was mounted. The arrays were stored in the dark for 45 min prior to visualising the hybridisation using the Genosensor reader software. The Genosensor Reader Software automatically captures three images of each microarray, specific for the DAPI counterstain (blue), the test DNA (Cy3 green) and the reference DNA (Cy5 red), respectively. The image analysis portion of this software uses the blue image to identify target spots and their location in the grid.

Having identified all spots, the program analysed each pixel within each spot for its intensity in each of the remaining colour planes (green and red). An algorithm was employed to determine the local background for each of these colours, which was then subtracted from the intensity of each colour. The background-corrected intensities were then used to determine the ratio of test intensity (green) to reference intensity (red) and, after further normalisation, were used to estimate the relative abundance of a specific target sequence in the test DNA. Normalised per-spot ratios were defined to be the unnormalised ratio divided by the median unnormalised ratio for all spots on the array.

Reports and statistical analysis

A report is generated for each array. This report tabulates, among other variables, the assigned target number, target clone name, cytogenetic location, the number of spots included and the normalised test to reference intensity. *P* values for non-modal copy number are computed for each target. With circa 300 targets on a chip, a *P* value of 0.01 can be expected to occur randomly for about three modal targets. For this reason, in our study, loci are only accepted as being reliably amplified or deleted on the following conditions: the *P* value for the null hypothesis was less than 0.005, all three spots were included and the mass ratio clearance volume was less than or equal to 7.0%.

Two cohorts were examined. We selected non-irradiated N-thy-ori cells as the control and demonstrated absence of *ret* rearrangements in this control group. N-thy-ori cells irradiated with 4 Gy γ-radiation, in which *ret* rearrangements that were demonstrable using RT-PCR were used to assess the effects of γ-irradiation. Both cohorts were of identical passage number. The normalised mass to mean ratio for each locus was tabulated for each of the two cohorts. Thresholds for gain of 1.2 and 0.8 for a loss have been validated by Vysis. A control experiment was run in tandem with the experiment using cell line DNA (CoSH mixture comprising three cell lines) provided by the manufacturer with known documented amplifications of a variety of oncogenes. Our results were exactly concordant with those described by Vysis.

Results

Immediately after irradiation, increased numbers of dead cells were noted in the irradiated flasks in comparison with control flasks. All of the irradiated cohorts suffered a lag period before achieving confluence again. During this post-irradiation lag period, the media was replaced at regular 3-day intervals. The period for the cells to become confluent varied in proportion to the dose of γ-radiation received, i.e. 0 Gy cohort first sub-confluent at 5 days, 2 Gy cohort first sub-confluent at 18 days, 3 Gy cohort first sub-confluent at 24 days and 4 Gy cohort first sub-confluent at 27 days. This phenomenon reflects the increasing numbers of cells killed at the outset of the experiment due to an incremental dose of radiation (with a resultant smaller pool for regeneration). After this first long passage period, the cells became sub-confluent more quickly and at the same rate as for non-irradiated cells (4–5 days). Each cohort of cells was grown for 50 days (ten passages each) after reaching their first post-radiation sub-confluence.

Striking morphological differences became apparent between the irradiated cells and their non-irradiated counterparts. Irradiated cells showed marked elongation (spindling) and concordant cytomegaly and nucleomegaly (without marked increase in nuclear: cytoplasmic ratio. This appearance is often seen by pathologists in the radiation phenotype of cells reacting to radiation damage). The nuclear membranes of the irradiated cells showed coarse irregularities, and each nucleus contained increased numbers of nucleoli (Fig. 1).

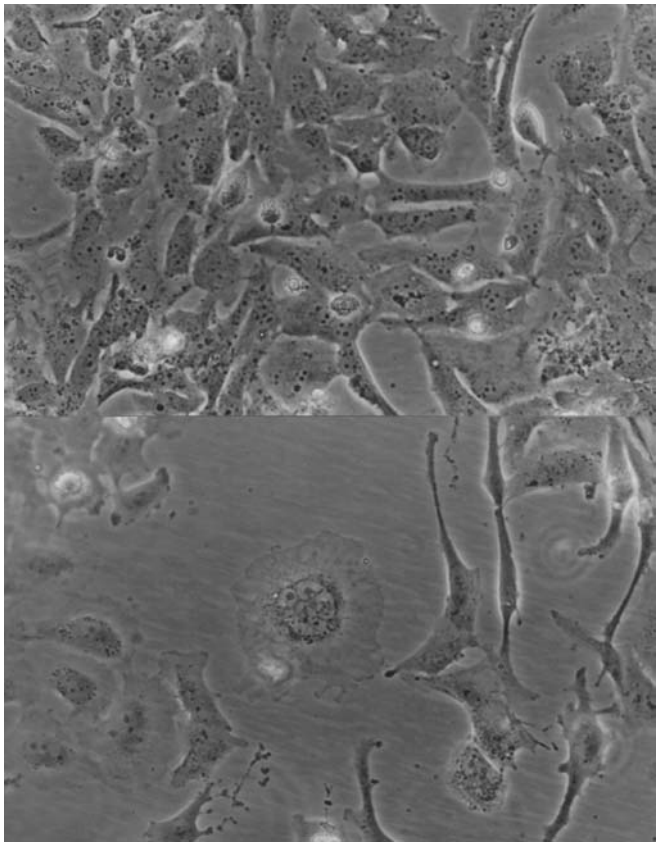


Fig. 1 Composite image of irradiated N thy-ori cells. *Upper pane* ×20, *lower pane* ×40

TaqMan RT-PCR for *ret*/PTC-1 and *ret*/PTC-3

Control n-thy-ori cells

Neither *ret*/PTC-1 nor *ret*/PTC-3 was demonstrated in the non-irradiated control cell group at any time before or after irradiation.

Irradiated N-thy-ori cells

Ret/PTC-1. We failed to demonstrate the presence of chimeric transcripts of *ret*/PTC-1 in any of the three irradiated cell cohorts examined at any time before or after irradiation using sensitive RT TaqMan PCR. This applied both to aliquots of the cultured cells and from supernatants of the cell culture.

Ret/PTC-3. Chimeric transcripts of *ret*/PTC-3 were detected exclusively in the cohort of cells, which received 4 Gy γ-irradiation. *Ret*/PTC-3 was detected in RNA extracted from cell aliquots and not from supernatants. Because rearranged *ret* is not expressed in normal cells, an end point plus/minus (presence or absence) TaqMan assay was utilised at 99.9% confidence intervals. Expression of *ret*/PTC-3 was detectable after the first passage and until the third passage but not thereafter.

CGH array analysis

The results of the array CGH experiments are seen in Table 1. The gains and losses seen in the unirradiated cells represent the effects of SV40-mediated transformation. All amplifications were at a low level (1.2 to 3.0). The cytogenetic consequences of the immortalising effect of SV40 are reflected in the striking concordance of gain and loss at numerous loci. Additional statistically significant gains and losses occurred only in the irradiated cells. The irradiated cells show prominent loss of DNA sequences with occasional gains. Of the 30 additional aberrations or presumed aberrations in the irradiated cell line, 83% (25 of 30) were deletions and 40% (10 of 25) of these deletions occurred distally on the chromosome at unique sub-telomeric loci.

Discussion

The predominant exposure occurring after the Chernobyl accident was to ^{131}I with emission of β-radiation. Ingestion of contaminated milk by children with actively

Table 1 Aberrations detected by array CGH in thyroid cells. The *P* value for the null hypothesis is <0.005; all three spots are included, and the mass ratio coefficiant of variation is less than or equal to 7.0%. Gain or loss in parentheses indicates a suggested gain or loss in comparison with the control cells

Target number and name	Non-irradiated N-thy-ori	Irradiated N-thy-ori	Cytogenetic locus
006 D1S2660	Normal	Loss[a]	1p36.32
038 D2S447	Loss[b]	Loss[b]	2q tel
039 3PTEL25	Loss[b]	Loss[b]	3p tel
040 3PTEL01,CHL1	Normal	Loss[a]	3p tel
046 FHIT	Loss[b]	Loss[b]	3p14.2
048 D3S1274, ROBO1	Loss[b]	Loss[b]	3p12–3p13
053 TP63	Loss[b]	Loss[b]	3q27–q29
058 D4S114	Normal	Loss[a]	4p16.3
064 PGRMC2	Loss[b]	Loss[b]	4q26
067 D4S2930	Loss[b]	Loss[b]	4q tel
071 DAB2	Normal	Loss[a]	5p13
076 NIB1408	Gain[c]	Gain[c]	5q tel
077 5QTEL70	Gain[c]	Gain[c]	5q tel
078 9PTEL48	Gain[c]	Gain[c]	6p tel
079 PIM1	Normal	Loss[a]	6p21.2
087 ESR1	Loss[b]	Loss[b]	6q25.1
089 G31341	Gain	Loss[a]	7p tel
093 RFC2, CYLN2	Gain[c]	Gain[c]	7q11.23
099 stSG48460	Gain[c]	Gain[c]	7q tel
100 7QTEL20	Gain[c]	Gain[c]	7q tel
116 MTAP	Normal	Loss[a]	9p21.3
126 10QTEL006	Gain	Normal (Loss)[a]	10p tel
127 SHGC-44253	Gain	Normal (Loss)[a]	10p tel
128 D10S249, D10S533	Gain	Normal (Loss)[a]	10p15
131 BMI1	Normal	Loss[a]	10p13
137 stSG27915	Gain[c]	Gain[c]	10q tel
138 10QTEL24	Gain	Normal (Loss)[a]	10q tel
139 11PTEL03	Normal	Loss[a]	11p tel
146 MEN1	Gain[c]	Gain[c]	11q13
154 MLL	Loss[b]	Loss[b]	11q23
155 WI-6509	Loss[b]	Loss[b]	11q tel
156 AF240622	Loss[b]	Loss[b]	11q tel
157 8M16/SP6	Gain[c]	Gain[c]	12p tel
158 SHGC-5557	Gain[c]	Gain[c]	12p tel
160 CDKN1B (p27)	Gain[c]	Gain[c]	12p13.1–p12
163 CDK2, ERBB3	Normal	Gain[d]	12q13
172 D13S319	Normal	Loss[a]	13q14.2
178 IGH (D14S308)	Gain[c]	Gain[c]	14q tel
182 UBE3A, D15S10	Loss[b]	Loss[b]	15q11–q13
185 FES	Normal	Loss[a]	15q26.1
187 PACE4C	Normal	Loss[a]	15q tel
189 16PTEL03	Gain	Normal (Loss)[a]	16p tel
190 stSG48414	Normal	Loss[a]	16p tel
200 stSG30213	Normal	Loss[a]	16q tel
209 D17S1296, D17S1523	Loss	Normal (Gain)[d]	17p12–p11.2
214 BRCA1	Normal	Gain[d]	17q21
241 AKT2	Normal	Loss[a]	19q13.1–q13.2
244 20PTEL18	Gain[c]	Gain[c]	20p tel
245 SOX22	Gain[c]	Gain[c]	20p tel
246 JAG1	Gain[c]	Gain[c]	20p12.1–p11.23
247 MKKS, SHGC-79896	Gain[c]	Gain[c]	20p12.1–p11.23
248 TOP1	Gain[c]	Gain[c]	20q12–q13.1
249 NCOA3 (AIB1)	Gain[c]	Gain[c]	20q12
250 MYBL2	Gain[c]	Gain[c]	20q13.1
251 CSE1L (CAS)	Gain[c]	Gain[c]	20q13
252 PTPN1	Gain[c]	Gain[c]	20q13.1–q13.2
253 STK6 (STK15)	Gain[c]	Gain[c]	20q13.2–q13.3
254 ZNF217(ZABC1)	Gain[c]	Gain[c]	20q13.2
255 CYP24	Gain[c]	Gain[c]	20q13.2
256 TNFRSF6B (DCR3)	Gain[c]	Gain[c]	20q13
257 TPD52L2, TOM	Gain[c]	Gain[c]	20q tel
258 20QTEL14	Gain[c]	Gain[c]	20q tel
260 RUNX1 (AML1)	Gain[c]	Gain[c]	21q22.3
261 DYRK1A	Normal	Gain[d]	21q22
263 PCNT2 (KEN)	Gain[c]	Gain[c]	21q tel
264 21QTEL08	Gain[c]	Gain[c]	21q tel
265 D22S543	Gain	Normal (Loss)[a]	22q11

Table 1 (continued)

Target number and name	Non-irradiated N-thy-ori	Irradiated N-thy-ori	Cytogenetic locus
266 GSCL	Normal	Gain[d]	22q11.21
268 TBX1	Normal	Gain[d]	22q11.2
273 ARSA	Loss[b]	Loss[b]	22q tel
274 22QTEL31	Gain[c]	Loss[a]	22q tel
275 DXYS129	Normal	Loss[a]	X/Yp tel
279 DMD exon 45–51	Loss[b]	Loss[b]	Xp21.1
280 DXS580	Loss[b]	Loss[b]	Xp11.2
281 DXS7132	Normal	Loss[a]	Xq12
286 SRY	Loss[b]	Loss[b]	Yp11.3
287 AZFa region	Loss[b]	Loss[b]	Yq11

[a] Losses exclusive to irradiated cells
[b] Losses common to both
[c] Gains common to both
[d] Gains exclusive to irradiated cells

growing thyroid glands in the context of moderate iodine deficiency is assumed to be the most likely reason for the marked increase in PTC that subsequently occurred [24]. However, a significant and somewhat overlooked source of irradiation resulted from exposure to ^{137}Cs with release of γ-irradiation. The aims of this study were twofold. First, we wished to assess whether γ-irradiation is capable of inducing *ret*-rearrangements at a dose corresponding to the dose received by children in the Belarus area after the Chernobyl disaster and using a source of γ radiation (^{137}Cs) known to have been released and to have persisted after the initial radio-iodine shock.

Second, although post-irradiation and sporadic PTC is strongly associated with chromosomal rearrangements, a number of other genome-wide biological consequences may result from exposure to ionising radiation [29]. We assessed the pattern of DNA copy gain and loss in irradiated immortalised thyroid cells showing evidence of *ret*/PTC-3 chimeric transcripts using RT-PCR, with the Genosensor array system. We used the detection of a radiation-specific rearrangement as the most appropriate available surrogate endpoint for an experiment investigating the effects of γ-irradiation on the genome of thyroid cells.

The present study shows for the first time that γ radiation can induce a *ret* rearrangement, namely *ret*/PTC-3. Induction of *ret* rearrangements using γ-irradiation has not been shown previously in vitro. Although Riches et al demonstrated the tumourigenicity of γ-irradiation [20, 21, 30], *ret* rearrangements were not described in the tumours that were derived. Previously, cell-culture models have shown that *ret*/PTC-1 could be induced in in-vitro X-ray-treated tumour cell lines not showing *ret* activation/rearrangement prior to irradiation [22]. Following this, the *ret*/PTC-3 rearrangement was induced in normal human thyroid tissue transplanted into SCID mice after 50 Gy of X-ray exposure [23]. However, in that study, *ret*/PTC-1 was observed more frequently and persisted throughout the observation period of up to 60 days. The reasonable conclusion drawn by these authors is that although *ret*/PTC-3 can be induced by X-irradiation, *ret*/PTC-1 rearrangement appears to be preferentially induced by X-ray irradiation.

Like Mizuno, our study demonstrates transient expression of *ret*/PTC-3. This may be explained either by selective loss of the cells bearing the *ret*/PTC-3 rearrangement or alternatively by transcriptional silencing of expression of the rearranged genes. Some have argued that *ret* rearrangements are merely needed to initiate thyroid malignancy but may not play a central role in tumour progression, and it is possible that silencing of expression may occur in this context.

Remarkably, we failed to demonstrate chimeric transcripts of *ret*/PTC-1 at any stage or in any cohort of γ-irradiated cells. It is clear that *ret* rearrangements are highly specific for thyroid carcinogenesis. *Ret*/PTC-3 is strongly associated with aggressive post-Chernobyl PTC with a specific solid morphology occurring in children [14] and with short latency [31]. Indeed, *ret*/PTC-3 may well be a radiation-specific signature, notwithstanding that it can be detected at a lower rate in sporadic PTC [28]. The matter is complicated, however, by the findings of another important study [32]. In this study, the authors assessed the *ret* status of thyroid tumours developing in patients who had received radiation therapy (most commonly X-ray irradiation) for benign or malignant conditions during childhood or young adulthood. The most frequent rearrangement detected in this series was *ret*/PTC-1 (63%), not *ret*/PTC-3 (10%). In another review paper, the question was begged as to why the types of *ret* rearrangement seen in PTC associated with accidental (Chernobyl) and therapeutic irradiation should be so different. These authors suggest that it may be explained as a consequence of the different types of radiation received [33], specifically X-irradiation related to therapeutic intervention and radioactive isotopes in relation to Chernobyl. Although the design and methodology of the current study and that of Mizuno et al. are different, both studies, when considered together, raise the possibility that the *ret*/PTC-3 rearrangement may be associated with γ-irradiation and/or β-irradiation and the *ret*/PTC-1 rearrangement with X-ray irradiation. This interpretation would allow us to rationalise the conflicting literature

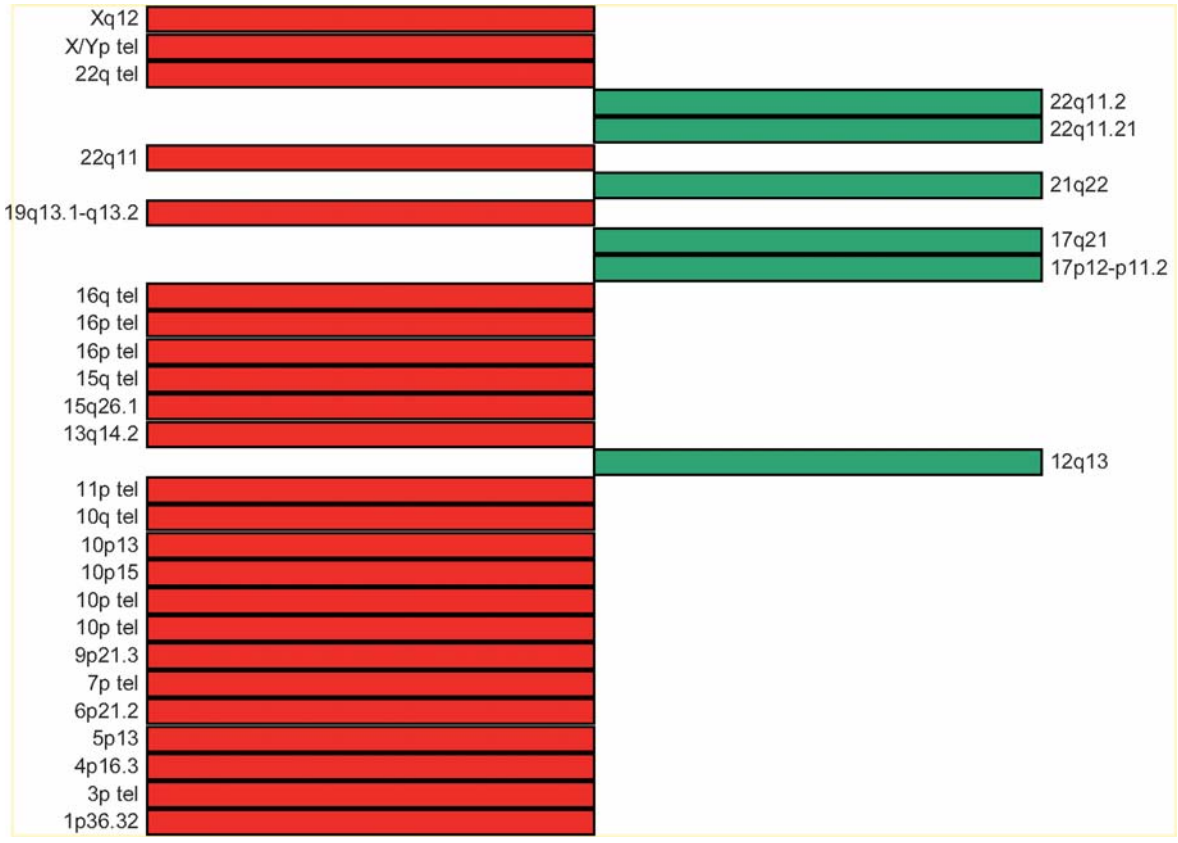


Fig. 2 Irradiated cells: distribution of statistically significant gains (*green*) and losses (*red*) according to locus

regarding which rearrangement is more commonly associated with radiation.

The results of the CGH microarray analysis have to be interpreted carefully, with due regard to the limitations of the experiment design. Our data provides a single snapshot of dominant gains and losses occurring in a cell-culture system using demonstration of expression of the *ret*/PTC-3 rearrangement as a marker of the appropriate dose of irradiation. It must be acknowledged that this in vitro model cannot reflect in vivo selection processes that may operate in PTC. Furthermore, the data from the irradiated cells almost certainly represents an overall view of multiple clones rather than a single clone, and patterns of gain and loss reflect the dominant profile in the cells examined. For these reasons, the pattern of gains and losses is likely to be more informative than specific loci involved.

The irradiated and non-irradiated cells are of equal passage number in order to allow for control of cell-culture-induced aberrations. The CGH profiles (Table 1) are identical at the majority of the loci examined, and this reflects genomic instability induced in the normal thyroid cells by SV40 large T antigen transfection. This SV40- and cell culture-mediated genomic stability is highlighted when comparison is made to Zitelsberger's conventional CGH data for the same cell line [21]. Although the CGH profiles and array CGH profiles are partially coincident (gains at chromosomes 5, 7, 10, 11q13, 12p, 16p, 20q13, 21, 22 and losses at 3p, 4q and X) at certain loci, mutually exclusive aberrations are noted in both data sets.

Figure 2 highlights the additional gains (green) and losses (red) seen in the irradiated cells in comparison with the non-irradiated cells. In this model, γ-irradiation appears to be predominantly associated with a pattern of loss of genetic material, which occurs relatively evenly, spread out across the genome. However, it is noteworthy that the loss of DNA occurred at sub-telomeric loci (40% of all losses). Although our clones are specific for unique regions, at telomeres the data is suggestive that the larger telomere itself may be susceptible to radiation damage. This is concordant with Zitelsberger's CGH study of tumours resulting from γ-irradiated thyroid epithelial cells [21]. Telomeres cap chromosome ends and prevent end-to-end fusions and subsequent chromosome instability. Latre et al have demonstrated that chromosomes with shortened telomeres fuse to radiation-induced DNA breaks and interfere with the correct rejoining of the broken ends [34]. It is possible that radiation-induced loss of telomeric DNA may explain the propensity for chromosomal rearrangements that occurs in PTC associated with radiation. It has also been shown that genomic instability occurs in successive generations of cells exposed to radiation. This instability preferentially affects telomeres and may play a role in radiation-induced carcinogenesis [35].

It is also noteworthy that chromosome 10 appears to represent a "susceptible" chromosome in this radiation model. Given the known tendency for chromosome 10 to become involved in illegitimate rearrangements in radiation-induced PTC and its strong representation as a site of deletions in this data, it may well be that chromosome 10 is, for as yet unknown reasons, a hotspot for radiation-induced thyroid carcinogenesis. Riches et al have shown high-level amplification of 10p11.2 associated with a deletion of the remaining short arm segment of chromosome 10 distal to 10p11.2 in epithelial cells exposed to low dose γ-radiation [20]. However, Zitelsberger's study [21] shows gains associated with chromosome 10p rather than losses, and it must be acknowledged that the occurrence of radiation-induced aberrations on chromosome 10 may be an entirely stochastic phenomenon, especially when one considers that the non-irradiated cells show overrepresentation of amplifications of DNA on chromosome 10, consequently presenting a higher probability of sustaining irradiation-induced damage.

In our data, amplifications are uncommon (five loci only). Although this may reflect sample heterogeneity, this is unlikely when one considers the abundance of deletions present. The detection of deletions is far more sensitive to sample heterogeneity than the detection of amplifications. Hence, it is reasonable to say that amplifications are uncommon in this model. Previous conventional CGH studies of thyroid carcinoma tumours demonstrated that DNA copy number changes were rare in papillary carcinoma [36] (12% in one series) and, when demonstrated, were all shown to be gains and occurred in elderly patients. Our experience using this array system in sporadic PTC (unpublished data) suggests that while copy number changes are low, both gains and losses occur. CGH data on radiation-associated PTC is limited. One conventional CGH study included two cases of papillary thyroid carcinoma associated with a history of radiation [37]. One of the two cases showed a gain on 17q, which correlates with the in vitro data seen in this experiment. A second study performed extensive karyotyping [38] of Chernobyl-related tumours using conventional cytogenetics; however, only one tumour had CGH and SKY performed, and there are no large studies providing CGH profiles of post-Chernobyl solid PTC associated with *ret*/PTC-3 rearrangement.

In conclusion, the current study demonstrates, for the first time, γ-irradiation induction of *ret*/PTC-3 in vitro. A true in vitro model of post-Chernobyl conditions is difficult to achieve, requiring a mixture of radiation including both β-irradiation from ^{131}I and γ-irradiation from ^{137}Cs. However, this model more closely approximates an ideal model than previous X-irradiation based models. The failure to detect *ret*/PTC-1 is remarkable and, taken in the context of the literature, suggests that the type of radiation influences the type of *ret* rearrangement that derives. By using array CGH, we have demonstrated a clear pattern of deletion of genomic DNA with subtelomeric deletions occurring prominently.

Acknowledgements This work was supported by a grant from the Health Research Board of Ireland. Thanks to Professor Sissy Jhiang for providing *ret*/PTC-3 plasmid used for positive control. Thanks to Professor Kingston Mills for providing irradiation facilities.

References

1. Rubino C, Cailleux AF, De Valthaire F, Schlumberger M (2002) Thyroid cancer after radiation exposure. Eur J Cancer 38:645–647
2. Ron E, Lubin JH, Shore RE, Mabuchi K, Modan B, Pottern LM, Schneider AB, Tucker MA, Boice JD Jr (1995) Thyroid cancer after exposure to external radiation: a pooled analysis of seven studies. Radiat Res 141:259–277
3. Lundell M, Hakulinen T, Holm LE (1994) Thyroid cancer after radiotherapy for skin hemangioma in infancy. Radiat Res 140:334–339
4. De Vathaire F, Hardiman C, Shamsaldin A, Campbell S, Grimaud E, Hawkins M, Raquin M, Oberlin O, Diallo I, Zucker JM, Panis X, Lagrange JL, Daly-Schveitzer N, Lemerle J, Chavaudra J, Schlumberger M, Bonaiti C (1999) Thyroid carcinomas after irradiation for a first cancer during childhood. Arch Int Med 159:2713–2720
5. Hamilton TE, Van Belle G, LoGerfo JP (1987) Thyroid carcinoma in Marshall Islanders exposed to nuclear fallout. JAMA 258:629–636
6. Kazakov VS, Demidchik EP, Astakhova LN (1992) Thyroid cancer after Chernobyl. Nature 359:21–22
7. Shibata Y, Yamashita S, Masyakin VB, Panasyuk GD, Nagataki S (2001) 15 years after Chernobyl: new evidence of thyroid cancer. Lancet 358:1965–1966
8. Santoro M, Carlomagno F, Hay ID, Herrmann MA, Grieco M, Melillo R, Pierotti MA, Bongarzone I, Della-Porta G, Berger N, Paulin C, Fabien N, Vecchio G, Jenkins RB, Fusco A (1992) Ret oncogene activation in human thyroid neoplasms is restricted to the papillary cancer subtype A. J Clin Invest 89:1517–1522
9. Kimura ET, Nikiforova MN, Zhaowen Z, Knauf J, Nikiforov YE, Fagin JA (2003) High prevalence of BRAF mutations in thyroid carcinoma: genetic evidence for constitutive activation of the RET/PTC-RASBRAF signaling pathway in papillary thyroid carcinoma. Cancer Res 63:1454–1457
10. Soares P, Trovisco V, Rocha AS, Lima J, Castro P, Preto A, Maimo V, Botelho T, Seruca R, Sobrinho-Simoes M (2003) BRAF mutations and RET/PTC rearrangements are alternative events in the etiopathogenesis of PTC. Oncogene 22:4578–4580
11. Xu X, Quiros RM, Gattuso P, Ain KB, Prinz RA (2003) High prevalence of BRAF gene mutations in papillary thyroid carcinoma and thyroid tumour cell lines. Cancer Res 63:4561–4567
12. Xing M, Vasko V, Tallini G, Larin A, Wu G, Udelsman R, Ringel MD, Ladenson PW, Sidransky D (2004) BRAF T1796A transversion mutation in various thyroid neoplasms. J Clin Endocrinol Metab 89:1365–1368
13. Tallini G, Asa SL (2001) Ret oncogene activation in papillary thyroid carcinoma. Adv Anat Pathol 8:345–354
14. Thomas GA, H. Bunnell, Cook HA, Williams ED, Nerovnya A, Cherstvoy ED, Tronko ND, Bogdanova TI, Chiappetta G, Viglietto G, Pentimalli F, Salvatore G, Fusco A, Santoro M, Vecchio G (2001) High prevalence of RET/PTC rearrangements in Ukrainian and Belarusian post-Chernobyl thyroid papillary carcinomas: a strong correlation between *RET*/PTC3 and the solid-follicular variant. J Clin Endocrinol Metab 84:4232–4238
15. Kallioniemi A, Kallioniemi OP, Sudar D, Rutovitz D, Gray JW, Waldman F, Pinkel D (1992) Comparative genomic hybridization for molecular cytogenetic analysis of solid tumours. Science 258:818–821

16. Hui AB, Lo KW, Yin XL, Poon WS, Ng HK (2001) Detection of multiple gene amplifications in glioblastoma multiforme using array based comparative genomic hybridization. Lab Invest 81:717–723
17. Pollack JR, Sørlie T, Perou CM, Rees CA, Jeffrey SS, Lonning PE, Tibshirani R, Botstein D, Børresen-Dale AL, Brown PO (2002) Microarray analysis revels a major direct role of DNA copy number alteration in the transcriptional program of human breast tumours. PNAS 99:12963–12968
18. Wilhelm M, Veltman JA, Osshen AB, Jain AN, Moore DH, Presti JC, Kocacs G, Waldman FM (2002) Array-based comparative genomic hybridization for the differential diagnosis of renal cell cancer. Cancer Res 62:957–960
19. Weiss M, Hermsen MAJA, Meijer GA, van Grieken NCT, Baak JPA, Kuipers EJ, van Diest PJ (1999) Demystified...comparative genomic hybridization. J Clin Pathol 52:243–251
20. Riches AC, Herceg Z, Bryant PE, Wynford-Thomas D (1994) Radiation-induced transformation of SV40-immortalized human thyroid epithelial cells by single and fractionated exposure to γ-irradiation in vitro. Int J Radiat Biol 66:757–765
21. Zitelsberger H, Bruch J, Smida J, Hieber L, Peddie CM, Bryant PE, Riches AC, Fung J, Weier HU, Bauchinger M (2001) Clonal chromosomal aberrations in Simian virus 40-transfected thyroid cells and in tumors developed after in vitro irradiation. Int J Cancer 96:166–177
22. Ito T, Seyama T, Iwamoto KS, Hayashi T, Mizuno T, Tsuyama N, Dohi K, Nakamura N, Akiyama M (1993) In vitro irradiation is able to cause RET oncogene rearrangement. Cancer Res 53:2940–2943
23. Mizuno T, Iwamoto KS, Kyoizumi S, Nagamura H, Shinohara T, Koyama K, Seyama T, Hamatani K (2000) Preferential induction of RET/PTC1 rearrangement by X-ray irradiation. Oncogene 19:438–443
24. Williams ED (2002) Cancer after nuclear fallout: lessons from the Chernobyl accident. Nature 2:543–549
25. Gavrilin YI, Khrouch VT, Shinkarev SM, Krysenko NA, Skryabin AM, Bouville A, Anspaugh LR (1999) Chernobyl accident: reconstruction of thyroid dose for inhabitants of the Republic of Belarus. Health Phys 76:105–119
26. Lemoine NR, Mayall ES, Jones T, Sheer D, McDermid S, Kendall-Taylor P, Wynford-Thomas D (1989) Characteristics of human thyroid epithelial cells immortalized in vitro by simian virus 40 DNA transfection. Br J Cancer 60:897–903
27. Pacini F, Vivaldi A, Santoro M, Fedele M, Fusco A, Romei C, Basolo F, Pinchera A (1998) Simian virus 40-like DNA sequences in human papillary thyroid carcinomas. Oncogene 16:665–669
28. Finn SP, Smyth P, O'Leary JJ, Sweeney EC, Sheils OM (2003) Ret/PTC chimeric transcripts in an Irish cohort of sporadic papillary thyroid carcinoma. J Clin Endocrinol Metab 88:938–941
29. Wright EG (1999) Inherited and inducible chromosomal instability: a fragile bridge between genome integrity mechanisms and tumourigenesis. J Pathol 187:19–27
30. Riches A, Peddie C, Rendell S, Bryant P, Zitzelsberger H, Bruch J, Smida J, Hieber L, Bauchinger M (2001) Neoplastic transformation and cytogenetic changes after Gamma irradiation of human epithelial cells expressing telomerase. Radiat Res 155:222–229
31. Smida J, Salassidis K, Hieber L, Zitzelsberger H, Kellerer AM, Demidchik EP, Negele T, Spelsberg F, Lengfelder E, Werner M, Bauchinger M (1999) Distinct frequency of ret rearrangements in papillary thyroid carcinomas of children and adults from Belarus. Int J Cancer 80:32–38
32. Bounacer A, Wicker R, Caillou B, Cailleux AF, Sarasin A, Schlumberger M, Suarez HG (1997) High prevalence of activating ret proto-oncogene rearrangements, in thyroid tumors from patients who had received external radiation. Oncogene 15:1263–1273
33. Sarasin A, Bounacer A, Lepage F, Schlumberger M, Suarez HG (1999) Mechanisms of mutagenesis in mammalian cells. Application to human thyroid tumours. C R Acad Sci III 322:143–149
34. Latre L, Tusell L, Martin M, Miro R, Egozcue J, Blasco MA, Genesca A (2003) Shortened telomeres join to DNA breaks interfering with their correct repair. Exp Cell Res 287:282–288
35. Sabatier L, Lebeau J, Dutrillaux B (1995) Radiation-induced carcinogenesis: individual sensitivity and genomic instability. Radiat Environ Biophys 34:229–232
36. Hemmer S, Wesenius VM, Knuutila S, Franssila K, Joensuu H (1999) DNA copy number changes in thyroid carcinoma. Am J Pathol 154:1539–1547
37. Kjellman P, Lagercrantz S, Hoog A, Wallin G, Larsson C, Zedenius J (2001) Gain of 1q and loss of 9q21.3-q32 are associated with a less favorable prognosis in papillary thyroid carcinoma. Genes Chromosomes Cancer 32:43–49
38. Zitelsberger H, Lehmann L, Hieber L, Weier HG, Janish C, Fung J, Negele T, Spelsberg F, Lengfelder E, Demidchik E, Salassidis K, Kellerer AM, Werner M, Bauchinger M (1999) Cytogenetic changes in radiation induced tumors of the thyroid. Cancer Res 59:135–140

Virchows Arch (2004) 445:405–409
DOI 10.1007/s00428-004-1007-3

CASE REPORT

V. P. Andrade · C. C. V. Nemer · A. N. L. Prezotti · W. S. L. Goulart

Erdheim–Chester disease of the breast associated with Langerhans-cell histiocytosis of the hard palate

Received: 30 July 2003 / Accepted: 8 February 2004 / Published online: 24 August 2004
© Springer-Verlag 2004

Abstract We report a patient with Langerhans-cell histiocytosis (LCH) localized to the hard palate that was later proven to be associated with Erdheim–Chester disease (ECD), involving the right breast, skeleton, retroperitoneum and left orbit. The diagnosis was based on the symmetric osteosclerosis of the long bones diaphyses (tibias and fibulas), breast lump histopathological/immunohistochemical findings and retroperitoneum and left orbit images in magnetic resonance. Mammary involvement by ECD is an extremely rare condition, which should be differentiated from some benign and malignant mimickers, especially the histiocytoid type of breast carcinoma. Characteristic histological features plus clinical and radiographic information are needed to achieve a correct diagnosis. The ECD, its relation to the LCH and details of the breast lesion are discussed.

Keywords Erdheim–Chester disease · Langerhans-cell histiocytosis · Breast lump

Introduction

Erdheim–Chester disease (ECD) is a rare, non-inherited lipid-storing systemic histiocytosis of unknown etiology, with distinct radiological and clinicopathological findings in absence of detectable serum lipid abnormalities, which was first described in 1930 by William Chester [9]. Whether this histiocytic proliferation represents a monoclonal neoplastic population or part of a polyclonal reactive process remains unclear [8, 39]. This disease is characterized by a distinct form of bilateral, symmetric, diaphyseal or metaphyseal sclerotic lesions of the long bones, mainly the femur, tibia and fibula, associated with a mononuclear xanthomatous histiocytic infiltrate. Radiographs of the spine, ribs, skull and pelvis are usually normal [39]. Extra-skeletal involvement can be observed in half of the cases anytime during the evolution of the disease, mainly affecting the skin (30%), orbit (27%), hypophysis (28%), retroperitoneum (28%), pericardium, lungs (15–33%) and central nervous system (36%) [1, 5, 24, 25, 31, 36, 38, 39, 40, 42, 45].

Initial symptoms are bone pain (50%), xanthelasmas, exophtalmos, heart failure and psychoneuroendocrine disturbances, especially diabetes insipidus [25, 31, 39, 42]. Respiratory failure is rare and develops in patients with advanced disease due to pulmonary fibrosis [10, 17, 32, 44]. Dyspnea and cough are the most frequent respiratory symptoms. The radiological evidence of pulmonary disease is a symmetric reticular interstitial pattern of lung disease that precedes clinical symptoms. The constellation of pulmonary radiological findings, although not pathognomonic, is strongly suggestive of ECD [44]. Intracranial involvement is mainly represented by retro-orbital and hypothalamic/selar masses leading to a partial or total pituitary deficiency [5, 25, 38, 42]. Cerebellar dysfunction, pyramidal signs, hemiparesis and paraplegia are less frequent [24]. The prognosis is greatly influenced by the extra-skeletal involvement, and there is no established treatment [6, 17, 32]. Patients' age range is between 21 years and 77 years (average 54 years) and the male/female ratio is approximately 1.3:1 [39].

Histologically, ECD lesions show a cell infiltrate of xanthomatous histiocytes of non-Langerhans-cell lineage (CD68 positive; S100 protein, CD1a and Birbeck granules negative) and fibrosis with an infiltrative pattern [9, 10, 19, 20, 23, 26]. Histiocytes have no nuclear atypia, and scattered lipid-laden multi-nucleated giant cells of the Touton-type can be found. In the sclerotic bone, xanthomatous cells are loosely grouped among collagen bundles, leading to an extensive substitution of the normal hematopoietic elements. In the lungs, histiocytes show a bronchovascular and subpleural predominant distribution [10, 30].

V. P. Andrade (✉) · C. C. V. Nemer · A. N. L. Prezotti · W. S. L. Goulart
Fleury, Centro de Medicina Diagnóstica,
Av. Gal Waldomiro de Lima, 508. Jabaquara, CEP 04344-070,
Saõ Paulo, Brazil
e-mail: victor.andrade@fleury.com.br
Tel.: +55-11-50147664
Fax: +55-11-50147651

Several cases of patients with ECD have been reported in association with Langerhans-cell histiocytosis (LCH), and some authors believe that this is not a fortuitous association [4, 18, 19, 26, 40]. We report here an additional case of the association of the two diseases in the same patient.

Case history

A 40-year-old Caucasian woman sought medical care in 1995 due to hard palate ulcerated lesions. The histopathological and immunohistochemical studies revealed a histiocytic cell infiltrate (S100 protein and CD1a positive) with scattered eosinophils consistent with LCH (Fig. 1). The patient underwent a ten-cycle radiotherapy scheme (total dosage 2000 cGy). During the radiographic staging, bilateral symmetric osteosclerotic lesions on diaphyseal region of the tibia and fibula were noted (Fig. 2), but this information was considered not relevant due to the absence of symptoms or lytic lesions.

After radiotherapy, the hard-palate lesions healed, and the patient became asymptomatic until 1998, when ulcerated lesions reappeared, and a palpable lump was noted in the right breast. There was no breast trauma antecedent. This was a soft lump localized to the external upper quadrant, 3-cm-sized in its greatest diameter. The mammographic and ultrasound images were unspecific. The incisional biopsy showed a cell infiltrate rich in xanthomatous histiocytes loosely grouped between a collagenized stroma. Even though the appearances of the histiocytes were not similar to those observed in the hard-palate ulcers, the first diagnosis was "consistent with Langerhans-cell histiocytosis." Then, a 50-mg/day steroid therapy was administered, and, by the 28th day, the hard-palate ulcers had healed again. The breast lump disappeared by the 65th day. The patient was submitted to steroid therapy until December 1999.

In February 2001, a slight left eye proptosis was noted, and the ophthalmological examination revealed some irregularity on perimacular choroids. The magnetic resonance image showed an 8-mm nodule adjacent to the lateral straight muscle. For staging purposes, an abdominal computed tomography scan (CT) was performed, and a retroperitoneal fibrosis leading to left ureter compression and renal pelvis dilatation was documented. In August 2001, both the hard-palate and right-breast lesions recurred when the bilateral sclerotic lesions of the long bones were reevaluated, and the association of LCH and ECD was suspected.



Fig. 2 Left leg, plain X-ray. The characteristic dyaphyseal osteosclerotic lesions of tibia and fibula. These lesions were bilateral and symmetric

On newly performed biopsies of both hard-palate ulcer and breast lump, the diagnosis of LCH was confirmed for the former whilst it was reversed to ECD for the latter. The breast lesion showed a parenchymal-cell infiltrate of xanthomatous histiocytes with scattered lymphocytes and a total absence of eosinophils and plasma cells (Fig. 3a, b, c). The histiocytes showed a nodular periductal and diffuse distribution. In some areas, the lesion was composed of single lines of cells mimicking the infiltrating lobular carcinoma, histiocytoid variant (Fig. 3d). The immunohistochemical profile for each lesion is summarized in Table 1.

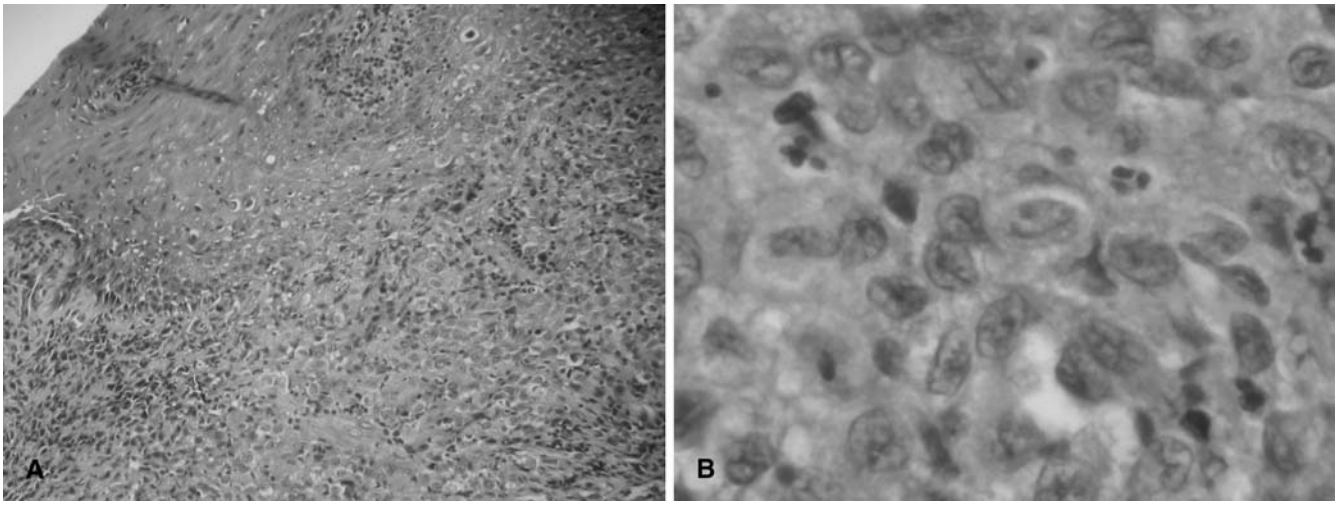


Fig. 1 Hard palate biopsy: histiocytic cell infiltrate showing nuclear grooving consistent with Langerhans-cell histiocytosis. **A** hematoxylin and eosin (H&E), ×40. **B** H&E, ×400

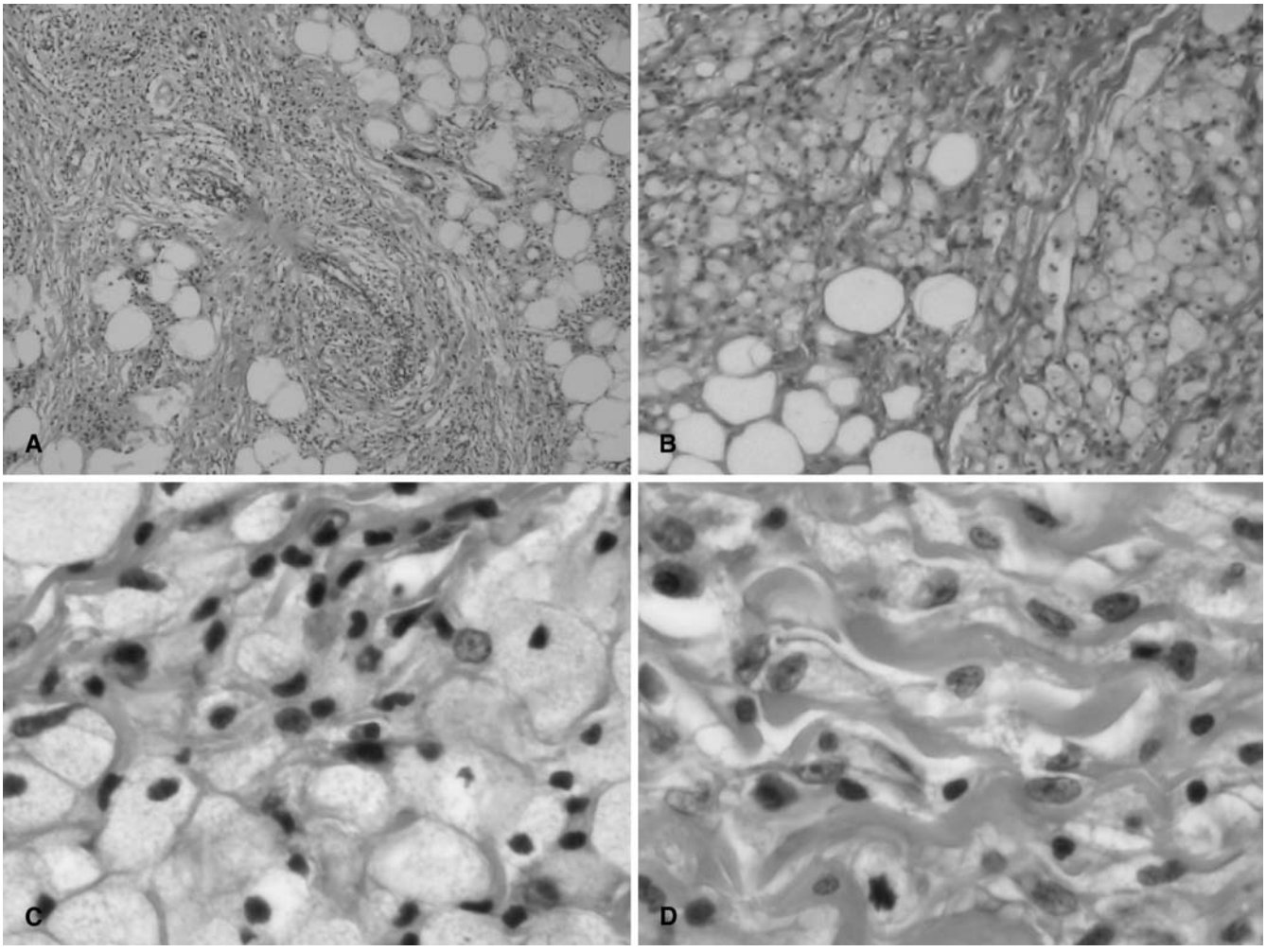


Fig. 3 Breast lump biopsy. **A** Loosely grouped histiocytes around mammary ducts (*arrows*). Hematoxylin and eosin (H&E), ×40. **B** and **C** Xanthomatous histiocytic infiltration among collagen bundles and fat cells with some lymphocytes. Histiocytes lack nuclear atypia. **B** H&E, ×100. **C** H&E, ×400. **D** Histiocytes in single line of cells mimicking histiocytoid variant of breast carcinoma. H&E, ×400

Table 1 Immunohistochemical profile of histiocytes in the hard palate and breast lump biopsies

	Hard palate	Breast lump
CD-68	Positive	Positive
S-100	Positive	Negative
CD1a	Positive	Negative

The patient was submitted to a third treatment protocol using steroids. Oral lesions healed, breast lump partially regressed, and the CT images confirmed the diffuse fibroinflammatory retroperitoneum lesion mass, leading to the functional exclusion of the left kidney and to a mild right hydroneprosis. No pulmonary involvement was documented. In the same year, the patient underwent an autologous hematopoietic stem-cell transplantation, and the clinical picture was stable by January 2004. A second autologous bone marrow transplantation is planned for this patient as suggested by Boissel et al. [6].

Discussion

The case presented is an example of ECD with its classical clinical, radiographic, morphological and immunohistochemical findings in association to LCH (localized to the hard palate), which has been consistently reported in the literature [4, 7, 17, 18, 19, 26, 28, 30, 34, 40, 41]. Based on both the immunohistochemical profile and electronic microscopy (LCH: CD68 and CD1a positive, S100 negative; ECD: CD68 positive, S100/CD1a/Birbeck granules negative), ECD is considered a disease of the monocyte/macrophage lineage, while LCH is a disease of the Langerhans-cell lineage [4, 12, 18, 26, 40]. The monocyte/macrophage and the Langerhans cell are both derived from the same CD34-positive marrow precursor, which has the in vitro capability to differentiate toward either lineage under the influence of different environmental conditions [21, 29].

Although breast involvement by ECD has been reported, we could not find histological illustrations in the

English literature [11, 35]. Breast ECD shows histological similarities with both benign and malignant breast lesions, such as fat necrosis, Rosai–Dorfman disease (RDD) and breast carcinoma of the histiocytoid variant. Fat necrosis can share some histological aspects, but there is architectural distortion and trauma antecedent. RDD is a rare histiocytic proliferation, primarily nodal-based but with extra-nodal involvement, including the breast [12, 15, 22]. It is represented by a histiocytic proliferation with pale acidophilic cytoplasm, mildly atypical round vesicular nuclei and so-called lymphocytophagocytosis. The histiocytes are strongly positive for S100-protein. The most relevant differential diagnosis is the histiocytoid variant of breast carcinoma [14, 16, 33, 37], which can additionally metastasize to cutaneous sites, such as eyelids [37], mimicking xanthelasmas, a cutaneous lesion evident in ECD patients. Helpful diagnostic features favoring ECD versus histiocytoid carcinoma both in the primary and metastatic depositories are the lack of nuclear atypia in the former as well as absence of the immunoreactivity for cytokeratins. In this case, the breast lump partially regressed after the steroid therapy. Nevertheless, a high grade of suspicion is needed to establish the correct diagnosis. It is important to keep in mind that patients harboring systemic illness and breast lumps should be carefully investigated to exclude a breast involvement by the generalized disease.

William Chester believed that the sclerosis was secondary to the infiltration with lipid-laden macrophages, but this issue remains to be explained [9]. Clearing this subject would be important to prognosis and treatment, since the major adverse effects of this disease are carried by multi-organ fibrosis, especially on the hypophysis, lungs and retroperitoneum. Chemotherapy, radiotherapy, steroids, immunotherapy and bone marrow transplantation have been tried with different and confusing successful rates. Thus far, there is no established treatment protocol available. The related mortality rates are higher in ECD than in LCH (57% versus 30%, respectively) after a mean follow-up of 32±30 months (range 3–120 months) [30, 39].

The association between ECD and LCH seen in this case is probably not fortuitous and has been consistently reported in the literature [4, 18, 19, 26, 40]. These diseases can share some aspects, and, a few years ago, some authors advocated that ECD was part of LCH morphological spectrum, perhaps as a dendritic-cell counterpart [31]. Nowadays, much more information is available, and this concept has been hardly challenged. Evidences favoring distinct entities are the age of presentation (children or young adults in LCH against adults or elderly in ECD), the characteristic osteosclerotic symmetrical lesions of ECD as opposed to the frequent osteolytic lesions of LCH, the proliferative index of ECD lesions consistently lower than 3% as opposed to the LCH range (2% to 60%; mean value 10.5% for cytologically typical cases and 22.5% for cytologically atypical cases) [18, 20, 23, 35]. Further, ECD histiocytes are uniformly negative for CD1a antigen, and no Birbeck granule has been demonstrated. Clonality analysis on LCH has proved its malignant character [43, 46]. Polymerase chain reaction-based analysis of clonality and human androgen receptor gene assay on ECD has showed puzzling results instead [2, 8]. The most significant clue to ECD diagnosis is the represented symmetric sclerotic lesion at the diaphyseal or metaphyseal regions of the long bones. This is a virtually pathognomonic finding and should guide the pathologist to the correct diagnosis when dealing with xanthomatous lesions of any site.

References

1. Adle-Biassette H, Chetritt J, Bergemer-Fouquet AM, Wechsler J, Mussini JM, Gray F (1997) Pathology of the central nervous system in Chester–Erdheim disease: report of three cases. J Neuropathol Exp Neurol 56:1207–1216
2. Al-Quran S, Reith J, Bradlei JBS, Rimsza L (2002) Erdheim–Chester disease: case report, PCR-based analysis of clonality and review of literature. Mod Pathol 15:666–672
3. Bisceglia M, Cammisa M, Suster S, Colby TV (2003) Erdheim–Chester disease: clinical and pathological spectrum of four cases from the Arkadi M Rywlin slide seminars. Adv Anat Pathol 10:160–171
4. Bisceglia M, Danza A, Sassano A, Filotico R, Gravante M (2003) La malattia di Chester-Erdheim e l'istiocitosi a cellule di Langerhans: un'associazione probabilmente non fortuita. Osservazione di um caso con coinvolgimento cutâneo. G Ital Dermatol Venereol 138:126–128
5. Bohlega S, Alwatban J, Tulbah A, Bakheet S, Powe J (1997) Cerebral manifestation of Erdheim–Chester disease: clinical and radiologic findings. Neurology 49:1702–1705
6. Boissel N, Wechsler B, Leblond V (2001) Treatment of refractory Erdheim–Chester disease with double autologous hematopoietic stem-cell transplantation (Letter). Ann Intern Med 135:844–845
7. Brower AC, Worsham GF, Dudley AH (1984) Erdheim–Chester disease: a distinct lipoidosis or part of the spectrum of histiocytosis? Radiology 151:35–38
8. Cherrit J, Paradis V, Dagere D, Adle-Biassette H, Maurage CA, Mussini JM (1999) Chester–Erdheim disease: a neoplastic disorder. Hum Pathol 30:1093–1096
9. Chester W (1930) Über Lipoidgranulomatose. Virchows Arch 279:561–602
10. Egan AJ (1999) Erdheim–Chester disease: clinical, radiologic and histopathologic findings in five patients with interstitial lung disease. Am J Surg Pathol 23:17–26
11. Ferrozi F, Bova D, Tognini G, Zuccoli G (2000) Pseudotumoral bilateral involvement of the breast in Erdheim–Chester disease: CT appearance. J Comput Assist Tomogr 24:281–283
12. Foucar E, Rosai J, Dorfman RF (1990) Sinus histiocytosis with massive lymphadenopathy (Rosai–Dorfman disease): review of the entity. Semin Diag Pathol 7:19–73
13. Green I, Dorfman RF, Rosai J (1997) Breast involvement by Rosai–Dorfman disease: report of seven cases. Am J Surg Pathol 21:664–668
14. Gupta D, Croitoru CM, Ayala AG, Sahin AA, Middleton LP (2002) E-cadherin immunohistochemical analysis of histiocytoid carcinoma of the breast. Ann Diagn Pathol 6:141–147
15. Hammond LA, Keh C, Rowlands DC (1996) Rosai–Dorfman disease in the breast. Histopathology 29:582–584
16. Hood CI, Font RL, Zimmerman LE (1973) Metastatic mammary carcinoma in the eyelid with histiocytoid appearance. Cancer 31:793–800
17. Kambouchner M, Colby TY, Domenge C, Battesti JP, Soler P, Tazi A (1997) Erdheim–Chester disease with prominent pulmonary involvement associated with eosinophilic granuloma of mandibular bone. Histopathology 30:353–358

18. Kenn W, Eck M, Allolio B, Jakob F, Illg A, Marx A, Mueller-Hermelink HK, Hahn D (2000) Erdheim–Chester disease: evidence for a disease entity different from Langerhans' cell histiocytosis? Three cases with detailed radiological and immunohistochemical analysis. Hum Pathol 31:734–739
19. Lieberman PH, Jones CR, Steinman TM, Erlandson TA, Smith J, Gee T, Huvos A, Garin-Chesa P, Filippa DA, Urmacher C, Gangi MD, Sperber M (1996) Langerhans cell (eosinophilic) granulomatosis. A clinicopathologic study encompassing 50 years. Am J Surg Pathol 20:519–552
20. Malpas JS (1998) Langerhans' cell histiocytosis in adults. Hematol Oncol Clin North Am 12:259–268
21. Moore MAS (2001) The hematopoietic system and hematopoiesis. In: Knowles DM (ed) Neoplastic hematopathology, 2nd edn. Lippincott Williams & Wilkins, Philadelphia, pp 1–42
22. Ng SB, Tan LH, Tan PH (2000) Rosai–Dorfman disease of the breast: a mimic of breast malignancy. Pathology 32:10–15
23. Ono K, Oshiro M, Katsuyama T (1996) Erdheim–Chester disease: a case report with immunohistochemical and biochemical examination. Hum Pathol 27:91–95
24. Pautas E, Chérin P, Pelletier S, Vidailhet M, Herson S (1998) Cerebral Erdheim–Chester disease: report of two cases with progressive cerebellar syndrome with dentate abnormalities on magnetic resonance imaging. J Neurol Neurosurg Psychiatry 65:597–599
25. Perras B, Petersen D, Lorch H, Fehm HL (2002) Psychoneuroendocrine disturbances in patient with a rare granulomatous disease. Exp Clin Endocrinol Diabetes 110:248–252
26. Pertuiset E, Laredo JD, Liote F, Wassef M, Jagueux M, Kuntz D (1993) Erdheim–Chester disease: report of a case, review of the literature, and discussion of relationships with Langerhans' cell histiocytosis. Rev Rheum Ed Fr 60:504–511
27. Pileri SA, Grogan TM, Harris NL, Banks P, Campo E, Chan JK, Favera RD, Delsol G, De Wolf Peeters C, Falini B, Gascoyne RD, Gaulard P, Gatter KC, Isaacson PG, Jaffe ES, Kluin P, Knowles DM, Mason DY, Mori S, Muller-Hermelink H-K, Piris MA, Ralfkiaer E, Stein H, Su I-J, Warnke RA, Weiss LM (2002) Tumors of histiocytes and accessory dendritic cell: an immunohistochemical approach to classification from the International Lymphoma Study Group based on 61 cases. Histopathology 41:1–29
28. Popolizio T, De Serio A, Scarabino T, Bisceglia M, Cammisa M. (1999) Mallatia di Erdheim–Chester: entità autonoma o espressioni di estiocitosi evoluta a cellule di Langerhans? Radiol Med 97:422–424
29. Reid CD, Stackpoole A, Meager A (1992) Interactions of tumor necrosis factor with granulocyte-macrophage colony-stimulating factor and other cytokines in the regulation of dendritic cell growth in vitro from early bipotent CD34+ progenitors in human bone marrow. J Immunol 149:2681–2688
30. Rush W, Andriko JW, Galateau F, Brambilla E, Brambilla C, Ziany-Bey I, Rosado-De-Christenson ML, Travis WD (2000) Pulmonary pathology of Erdheim–Chester disease. Mod Pathol 13:747–754
31. Rush WL, Lupton GP (2001) Cutaneous manifestations of Chester–Erdheim disease. Report of a patient and review of the literature. Dermatopathology: practical & conceptual 7:247–254
32. Shamburck RD, Brewer HB Jr, Gochuico BR (2001) Erdheim–Chester disease: a rare multisystem histiocytic disorder associated with interstitial lung disease. Am J Med Sci 321:66–71
33. Shimizu S, Kitamura H, Ito T, Nakamura T, Fujisawa J, Matsukawa H (1998) Histiocytoid breast carcinoma: histological, immunohistochemical, ultrastructural, cytological and clinicopathological studies. Pathol Int 48:549–556
34. Strouse PJ, Ellis BI, Shifrin LZ, Shah AR (1992) Case report 710. Skeletal Radiol 21:64–71
35. Tan AP, Tan LK, Choo IH (1995) Erdheim–Chester disease involving breast and muscle: image findings. AJR Am J Roentgenol 164:1115–1117
36. Tien RD, Brasch RC, Jackson DE, Dillon WP (1989) Cerebral Erdheim–Chester disease: persistent enhancement with Gd-DTPA on MR images. Radiology 172:791–792
37. Tomasini C, Soro E, Pippione M (2002) Eyelid swelling: think of metastasis of histiocytoid breast carcinoma. Dermatology 205:63–66
38. Tritus NA, Weinrib S, Kaye TB (1998) Endocrine manifestations of Erdheim–Chester disease (a distinct form of histiocytosis) J Int Med 244:529–535
39. Veyssier-Belot C, Cacoub P, Caparros-Lefebvre D, Wechsler J, Brun B, Remy M, Wallaert B, Petit H, Grimaldi A, Wechsler B, Godeau P (1996) Erdheim–Chester disease. Clinical and radiologic characteristics of 59 cases. Medicine 75:157–169
40. Vital C, Bioulac-Sage P, Tison F, Rivel J, Begueret H, Gomez C, Leaute-Labreze C, Diard F, Vital A (1999) Brain stem infiltration by mixed Langerhans cell histiocytosis and Chester–Erdheim disease: more than just an isolated case. Clin Exp Pathol 47:71–76
41. Waite RJ, Doherty PW, Liepman M, Woda B (1988) Langerhans cell histiocytosis with the radiographic findings of Erdheim–Chester disease. AJR AM J Roentgenol 150:869–871
42. Weidauer S, von Stuckrad-Barre S, Dettmann E, Zanella FE, Lanfermann H (2003) Cerebral Erdheim–Chester disease: case report and review of the literature. Neuroradiology 45:241–245
43. Willman CL, Busque L, Griffith BB, Favara BE, McClain KL, Duncan MH (1994) Langerhans' cell histiocytosis (histiocytosis X)—a clonal proliferative disease. N Engl J Med 331:154–160
44. Wittenberg KH, Swensen SJ, Myers JL (2000) Pulmonary involvement with Erdheim–Chester disease: radiographic and CT findings. AJR Am J Roentgenol 174:1327–1331
45. Wright AR, Hermann RC, Parisi JE (1999) Neurological manifestations of Erdheim–Chester disease. J Neurol Nerosurg Psychiatry 66:72–75
46. Yu RC, Chu C, Buluwela L, Chu AD (1994) Clonal proliferation of Langerhans' cell in Langerhans' cell histiocytosis. Lancet 343:767–768

Virchows Arch (2004) 445:410–413
DOI 10.1007/s00428-004-1068-3

CASE REPORT

Kazuo Watanabe · Toshimitsu Suzuki

Epithelioid fibrosarcoma of the ovary

Received: 22 February 2004 / Accepted: 27 May 2004 / Published online: 19 August 2004
© Springer-Verlag 2004

Abstract Recently, low-grade fibromyxoid sarcoma/hyalinizing spindle cell tumor with giant rosettes (LGMFS/HSCT) and sclerosing epithelioid fibrosarcoma (SEFS) have come to be recognized as distinctive types of fibrosarcoma. Because their pathological features seem to sometimes overlap, it may be that these tumors belong to a similar entity. We report an aggressive sarcoma with unusual histology arising from the right ovary of a 44-year-old woman. The tumor was 12 cm in size, and there were multiple distant metastases to lung, kidney, stomach and bones. Microscopically, the tumor was composed of broad sheets or variously sized nodules of polygonal epithelioid cells accompanied by hyalinous stroma, resembling SEFS. The hyalinous nodules surrounded by the palisading epithelioid cells, as seen in a rosette of HSCT, were scattered. Between these nodules, spindle cells arranged in fascicles or whorled bundles, mimicking LGMFS, proliferated. Immunohistochemical and ultrastructural analyses revealed fibroblastic differentiation of epithelioid cells and the myofibroblastic nature of the spindle tumor cells. We think the present tumor is a distinctive epithelioid fibrosarcoma with the combined features of SEFS and LGFMS/HSCT, suggesting their intimate relationship.

Keywords Fibrosarcoma · Epithelioid · Rosette · Low-grade · Ovary

Introduction

In the past, fibrosarcoma was one of the most common soft tissue malignancies, but it became rare to encounter a convincing case of fibrosarcoma, since many spindle cell sarcomas are now classified into specific entities according to their clinicopathological, immunohistochemical and ultrastructural characteristics [11]. In contrast, recently some tumors have been described as being a distinctive type of fibroblastic sarcoma, which include low-grade fibromyxoid sarcoma (LGFMS) [2, 3, 6], sclerosing epithelioid fibrosarcoma (SEFS) [1, 4, 8] and hyalinizing spindle cell tumor with giant rosettes (HSCT) [5, 7, 9]. Each tumor has characteristic clinicopathological features, but it has been pointed out that sometimes (to varying degrees) they have common histological components, suggesting their intimate relationship [5, 10]. We report a case of distinctive epithelioid fibrosarcoma with multiple distant metastases arising from the ovary. Although it predominantly had the features of SEFS, they were frequently intermingled with distinctive histological features resembling those of LGFMS and HSCT. Its immunohistochemical and ultrastructural characteristics are also described.

K. Watanabe (✉) · T. Suzuki
Pathology Division,
Fukushima Medical University School of Medicine Hospital,
1 Hikariga-oka, 960-1295 Fukushima City, Japan
e-mail: w-kazuo@fmu.ac.jp
Tel.: +81-24-5482111
Fax: +81-24-5481090

Clinical history

A 44-year-old woman was admitted to a gynecological hospital with a complaint of hypermenorrhea, and a uterine myoma-like pelvic tumor was found. She had been examined medically every year, and no abnormal changes were reported in her gynecological organs. The tumor grew rapidly for 3 months, and she was admitted to our hospital. Radiological examinations revealed an 11-cm pelvic tumor arising from her right ovary and multiple nodules, which appeared to be metastases in the lungs, left kidney and pelvic, femoral and vertebral bones. The pelvic lymph nodes were also involved. A small submucosal tumor was found by gastrointestinal endoscopy. Histological examinations of the kidney and stomach suggested SEFS. A simple hystero-oophorectomy was performed to make the diagnosis. Subsequently, she underwent irradiation of the rapidly growing bone metastases, and she survived for 4 months with disease. After the final pathological diagnosis, her whole body was re-examined, but no soft tissue or skin lesions were found. She had no previous history of tumor extirpation.

Materials and methods

Immunohistochemistry and electron microscopy

Immunohistochemical staining was performed on formalin-fixed, paraffin-embedded sections using the streptavidin-biotin-complex method (LSAB kit, Dako Japan, Kyoto, Japan). The primary antibodies and their final dilutions were: CD31 (1:25; Dako Japan), CD34 (NU-4A1, 1:100; Nichirei, Tokyo, Japan), CD57 (1:100; Becton Dickinson, CA, U.S.A.), high molecular weight caldesmon (h-CD, 1:50; Dako Japan), c-kit (polyclonal, 1:50; IBL, Gunma, Japan), cytokeratin (AE1/AE3, 1:50; Dako, Japan and CAM5.2, prediluted; Becton Dickinson), desmin (D33, 1:50; Dako), epithelial membrane antigen (EMA, E29, 1:50; Dako), neuron-specific enolase (polyclonal prediluted; Nichirei), α-smooth-muscle actin (1A4, 1:100; Dako), S-100 protein (polyclonal, 1:1,000; Dako) and vimentin (V9, 1:25; Dako). For electron microscopy, fresh tumor tissue was fixed in 2% glutaraldehyde and osmium tetroxide, processed into epoxy resin using conventional methods and examined with a JEM-1200EX transmission electron microscope (JOEL Ltd., Tokyo, Japan).

Results

Gross and microscopic findings

The right ovarian tumor had a 12.0-cm maximum diameter and was firm, well demarcated and tan-gray in color. Some cystic degenerative areas with hemorrhage were observed in the central area of the tumor. No macroscopic necrosis was present.

Microscopically, the tumor was composed of broad sheets or variously sized nodules of epithelioid cells, which were separated by various amounts of hypocellular and myxoid spindle cell area (Fig. 1). The epithelioid cells with polygonal clear or eosinophilic cytoplasm and round or ovoid vesicular nuclei, sometimes with prominent nucleoli, were arranged in cords and small nests in the fibrous and hyalinous stroma (Fig. 2). Although mild to moderate nuclear atypia was common, prominent atypia, cellular pleomorphism or multinucleated giant cells were not seen. Mitoses were present but not numerous. The tumor nodules were often accompanied by one or a few thin-walled venules. In addition, tumor cells occasionally palisaded in the periphery of the nodules and surrounded the hyalinous cores, resembling rosettes (Fig. 3). Epithelioid tumor cells in the periphery of the nodules were often degenerated and necrotic. Spindle tumor cells had eosinophilic fibrillary cytoplasm and were arranged in vague fascicles or whorls with myxoid stroma. They had uniform oval nuclei, and atypia was minimal. Coagulation necrosis of the tumor was seen focally.

Biopsy specimens of metastatic lesions of the stomach and kidney showed small nodules composed of epithelioid tumor cells in the hyalinous stroma similar to the primary site. Rosette-like structures were not found.

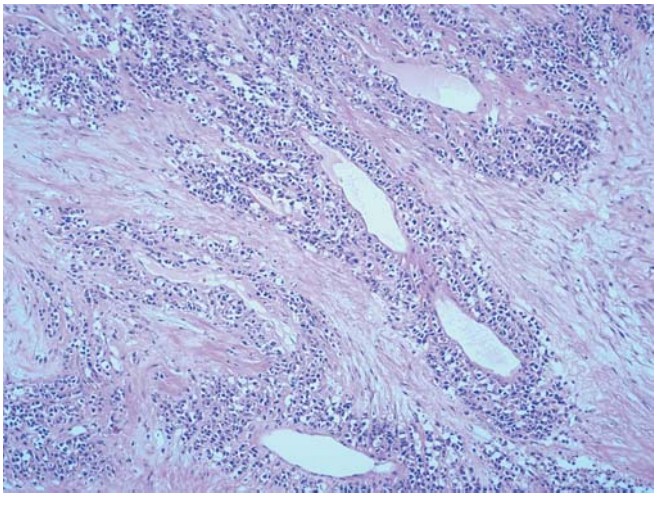


Fig. 1 Epithelioid nodules and hypocellular myxoid spindle cell area were intimately intermingled. Nodules were often accompanied by a central blood vessel

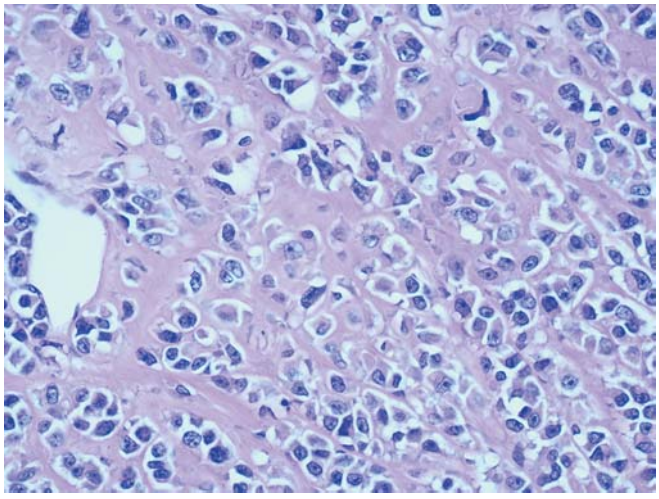


Fig. 2 Epithelioid tumor cells in the fibrous or hyalinous stroma

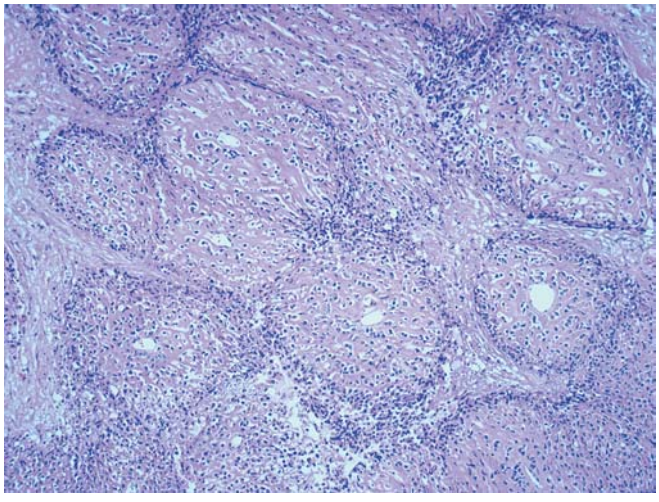


Fig. 3 Accumulation of many rosette-like hyalinous nodules. The tumor cells in the periphery of nodules often degenerated and tended to become necrotic

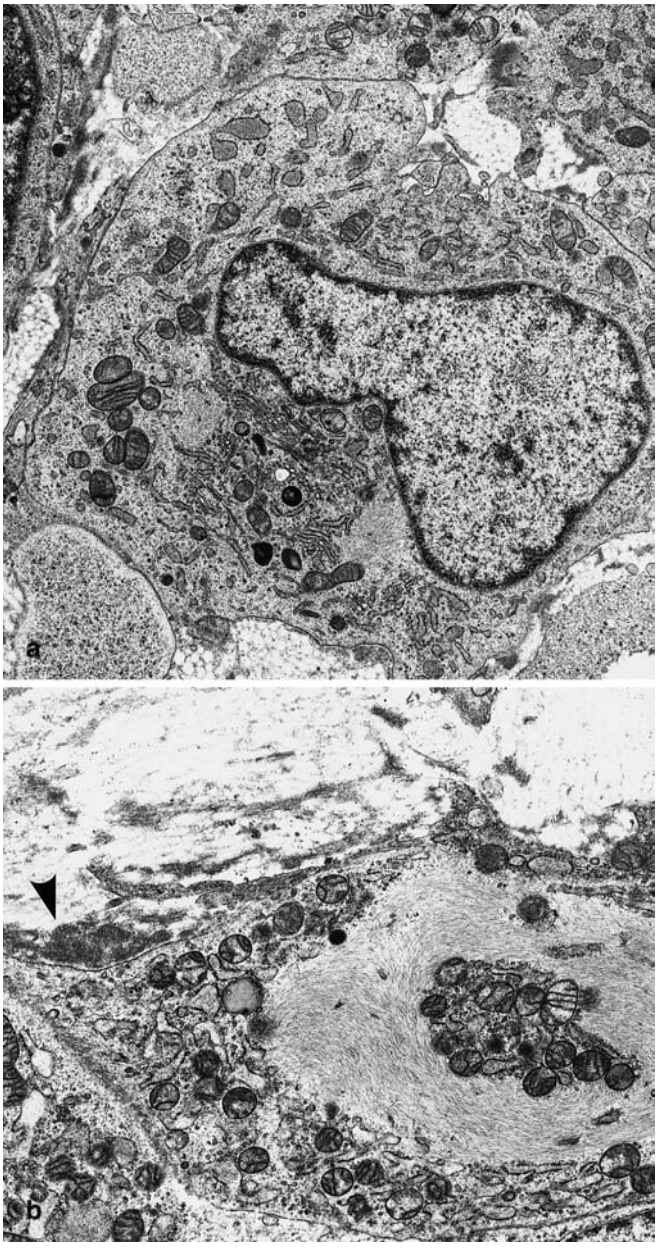


Fig. 4 The epithelioid tumor cell had much rough endoplasmic reticulum, numerous mitochondria and Golgi apparatus in the cytoplasm, ×6500 (**A**). A large number of vimentin-type intermediate filaments adjacent to the nucleus were also a common feature. External lamina-like material surrounded the epithelioid tumor cells (*arrowheads*), ×12,000 (**B**)

Immunohistochemistry

The tumor cells were positive for vimentin diffusely and neuron-specific enolase focally but were completely negative for cytokeratin (CAM5.2) and EMA. Although scattered epithelioid tumor cells were positive for keratin (AE1/AE3), the reactivities were often restricted to the perinuclear cytoplasm. Spindle cells were diffusely positive for α-smooth-muscle actin. The tumor cells were negative with all other antibodies.

Ultrastructure

The epithelioid cells had abundant and often dilated rough endoplasmic reticulum, numerous mitochondria and Golgi apparatus in their cytoplasm (Fig. 4A). A large number of intermediate filaments adjacent to the nuclei were also a common feature (Fig. 4B). Although epithelioid cells were intimately adjoined each other, no intercellular junctions were seen. Occasionally, external lamina-like material surrounded the epithelioid tumor cells. Spindle cells exhibited a distinct myofibroblastic differentiation, such as abundant actin filament with focal density, rough endoplasmic reticulum and well-developed fibronexus junctions. A few stellate fibroblastic cells surrounded by external lamina-like material were scattered around the nest of epithelioid cells.

Discussion

Since epithelioid fibrosarcoma has not been reported in the ovary and other internal organs [1, 4, 8], the differentiation from primary and metastatic carcinoma using light microscopy was problematic. Indeed, if epithelioid fibrosarcoma occurs in the internal organs, it would be easily misinterpreted as undifferentiated carcinoma unless immunohistochemical and ultrastructural analyses are performed. The epithelioid cells of the present tumor were immunohistochemically negative for epithelial markers, including cytokeratin (CAM5.2) and EMA, except for focal positivity of cytokeratin (AE1/AE3). Ultrastructural examination revealed a well-developed rough endoplasmic reticulum, absence of typical external lamina, lack of intercellular junctions and abundant vimentin-type intermediate filaments. These findings indicated fibroblastic differentiation of epithelioid tumor cells, and a diagnosis of fibrosarcoma was considered. The whole body radiological examinations failed to find a soft tissue mass, which is likely the primary lesion. In addition, the patient had no history of tumor extirpation. Thus, we think the present tumor is of ovarian origin.

Histologically, the present tumor showed a distinctive complex feature composed of a broad or nodular epithelioid cell component with sclerosing stroma, a hypocellular fibrous and myxoid area and many rosette-like lobules often accompanied by central vessels. These histological features resembled not only SEFS but also LGFMS or HSCT. SEFS was first reported by Meis-Kindblom et al. [8] as a variant of fibrosarcoma with relatively low-grade malignant potential and with characteristic epithelioid cells and strikingly hyalinized stroma. LGFMS and HSCT were first reported by Evans [2] in 1987 and by Lane et al. [7] in 1997, respectively, but they are now understood to be a single tumor entity of distinctive low-grade fibrosarcoma with or without characteristic rosettes [5, 7, 10]. In contrast, it has not been elucidated whether SEFS and LGFMS/HSCT belong to an analogous entity. Age and the primary site of SEFS and LGFMS/HSCT are almost identical, both tumors af-

fecting the deep soft tissues of young to middle-aged adults [1, 2, 3, 4, 5, 6, 7, 8, 9, 10]. The prognosis of SEFS was considered to be rather favorable at first [8], but a recent study by Antonescu et al. [1] demonstrated its high metastatic potential (86%) and mortality (57%) in contrast with the indolent low metastatic rate of LGFMS/HSCT [5]. Their light microscopy features seem to overlap occasionally, and SEFS-like areas can be found in LGFMS/HSCT [5, 10]. Additionally, hypocellular fibrous areas resembling fibroma or LGFMS have been described in SEFS [1], whereas giant rosettes characteristic of HSCT have not been reported to our knowledge. We believe the present tumor is a distinctive case, suggesting an intimate relationship between SEFS and LGFMS/HSCT. In the present case, rosette-like structures were composed of atypical epithelioid cells identical to the tumor cells in the SEFS area and often included central small vessels. A similar feature was described by Reid et al. [10] as an unusual HSCT. The biological nature of the present tumor appears to be closely related to that of SEFS rather than to LGFMS/HSCT because of its aggressive behavior with multiple distant metastases and the atypical feature of epithelioid cells.

Although spindle tumor cells of LGFMS have been reported to sometimes be positive for α-smooth-muscle actin, suggesting myofibroblasts [6], ultrastructural myofibroblastic differentiation has not been reported in the previous studies on LGFMS [6, 9, 12]. The present case study demonstrates well-developed thin actin filaments with focal densities and fibronexus junctions characteristic of myofibroblasts in the spindle tumor cells. This finding seems to be well correlated with intensive expression of α-smooth-muscle actin in spindle tumor cells. In addition, external lamina-like amorphous material surrounding epithelioid and fibroblastic stellate cells was frequently seen. Similar material was found in the previous cases of both SEFS and HSCT [1, 9]. Its meaning has been unclear, but it may be an ultrastructural characteristic, since usual fibrosarcomas do not include such material.

Epithelioid fibrosarcoma of the ovary should be differentiated from primary and secondary epithelioid tumors. Among these, distinguishing it from undifferentiated carcinoma is most difficult, and it seems impossible to differentiate on the basis of cellular morphology alone. Characteristic sclerosing collagenous stroma surrounding tumor cell is an important feature for differentiating the present tumor from carcinoma. Immunohistochemical examination using several epithelial markers is necessary for final diagnosis, but it should be remembered that epithelioid fibrosarcoma can exhibit focal immunoreactivity for epithelial markers, especially for EMA [1]. Because of its variable epithelioid feature, synovial sarcoma is included in the differential diagnosis. Although synovial sarcoma may have an extensive hyalinous stroma, a conventional epithelioid or spindle cell area is invariably intermingled. Finally, because the sclerosing stroma sometimes mimics an immature osteoid, epithelioid fibrosarcoma may be confused with osteosarcoma, including small cell type. However, osteosarcoma contains more matured osteoid or bone, at least focally, and malignant cartilaginous tissue frequently.

References

1. Antonescu CR, Rosenblum MK, Pereira P, Nascimento AG, Woodruff JM (2001) Sclerosing epithelioid fibrosarcoma. A study of 16 cases and confirmation of a clinicopathological distinct tumor. Am J Surg Pathol 25:699–709
2. Evans HL (1987) Low-grade fibromyxoid sarcoma. A report of two metastasizing neoplasms having a deceptively benign appearance. Am J Clin Pathol 88:615–619
3. Evans HL (1993) Low-grade fibromyxoid sarcoma. A report of 12 cases. Am J Surg Pathol 595–600
4. Eyden BP, Manson C, Banerjee SS, Roberts ISD, Harris M (1998) Sclerosing epithelioid fibrosarcoma: a study of five cases emphasizing diagnostic criteria. Histopathology 33:354–360
5. Folpe AL, Lane KL, Paull G, Weiss SW (2000) Low-grade fibromyxoid sarcoma and hyalinizing spindle cell tumor with giant rosettes. A clinicopathologic study of 73 cases supporting their identity and assessing the impact of high-grade area. Am J Surg Pathol 24:1353–1360
6. Goodlad JR, Mentzel T, Fletcher CDM (1995) Low grade fibromyxoid sarcoma: clinicopathological analysis of eleven cases in support of a distinct entity. Histopathology 26:229–237
7. Lane KL, Shannon RJ, Weiss SW (1997) Hyalinizing spindle cell tumor with giant rosettes. A distinctive tumor closely resembling fibromyxoid sarcoma. Am J Surg Pathol 21:1481–1488
8. Meis-Kindblom JM, Kindblom L-G, Enzinger FM (1995) Sclerosing epithelioid fibrosarcoma. A variant of fibrosarcoma simulating carcinoma. Am J Surg Pathol 19:979–993
9. Nielsen GP, Selig MK, O'Connell JX, Keel SB, Dickersin GR, Rosenberg AE (1999) Hyalinizing spindle cell tumor with giant rosettes. A report of three cases with ultrastructural analysis. Am J Surg Pathol 23:1227–1232
10. Reid R, Chandu de Silva MV, Paterson L, Ryan E, Fisher (2003) Low-grade fibromyxoid sarcoma and hyalinizing spindle cell tumor with giant rosettes share a common t(7;16)(q34;p11) translocation. Am J Surg Pathol 27:1229–1236
11. Scott SM, Reiman HM, Pritchard DJ, Ilstrup DM (1989) Soft tissue fibrosarcoma. A clincopathological study of 132 cases. Cancer 64:925–931
12. Woodruff LM, Antonescu CR, Erlandson RA, Boland PJ (1999) Low-grade fibrosarcoma with palisaded granulomalike bodies (giant rosettes). A report of a case that metastasized. Am J Surg Pathol 23:1423–1428

Virchows Arch (2004) 445:414–418
DOI 10.1007/s00428-004-1071-8

CASE REPORT

Enrico R. Bollito · Mauro Papotti · Francesco Porpiglia · Massimo Terzolo · Cecilia M. Cracco · Susanna Cappia · Luciano Gubetta · Gregor Mikuz

Myxoid adrenocortical adenoma with a pseudoglandular pattern

Received: 9 February 2004 / Accepted: 2 June 2004 / Published online: 3 July 2004
© Springer-Verlag 2004

Abstract Myxoid changes rarely occur in adrenocortical adenomas and carcinomas. Only eight benign tumours with such features have been described thus far, five of which also had a prominent pseudoglandular component. We report an additional pseudoglandular myxoid adenoma of the adrenal gland detected in a 58-year-old male patient who developed mild hypertension. At surgery, a 4-cm mass was resected and found to contain cords and tubules of polygonal cells in a myxoid background. Limited areas of classical adrenocortical adenoma were detected in less than 20% of the tumour area. Lack of atypias and absence of mucin markers, together with an immunophenotype consistent with adrenal tumours (focal cytokeratin, vimentin, synaptophysin and alpha-inhibin immunoreactivities), led to a diagnosis of primary adrenocortical adenoma with an extensive pseudoglandular myxoid pattern. However, the differential diagnosis from metastatic well-differentiated adenocarcinomas, chordomas and retroperitoneal myxoid mesenchymal tumours (e.g. liposarcoma) may be difficult in the absence of a complete clinical history and a reliable immunoprofile. We strongly recommend staining of any myxoid or glandular tumour of the adrenal gland for alpha-inhibin and synaptophysin (probably the currently best characterised markers of adrenocortical origin) before considering alternative (probably more common) diagnoses of metastatic adenocarcinoma or retroperitoneal tumours localised to the adrenal gland.

Keywords Adrenal gland · Adenoma · Myxoid · Glandular pattern · Differential diagnosis

E. R. Bollito · S. Cappia · L. Gubetta
Division of Pathology,
San Luigi Gonzaga Hospital,
Reg. Gonzole, 10-10043 Orbassano, Italy

M. Papotti (✉)
Department of Clinical and Biological Sciences,
University of Turin and San Luigi Gonzaga Hospital,
Reg. Gonzole, 10-10043 Orbassano (Turin), Italy
e-mail: mauro.papotti@unito.it
Tel.: +39-011-6705432
Fax: +39-011-6705432

F. Porpiglia
Department of Urology,
San Luigi Gonzaga Hospital,
Reg. Gonzole, 10-10043 Orbassano, Italy

M. Terzolo
Division of Internal Medicine,
San Luigi Gonzaga Hospital,
Italy

M. Terzolo
Department of Clinical and Biological Sciences,
University of Turin,
Reg. Gonzole, 10-10043 Orbassano, Italy

C. M. Cracco
Department of Urology,
San Luigi Gonzaga Hospital,
Reg. Gonzole, 10-10043 Orbassano, Italy

G. Mikuz
Department of Pathology,
University of Innsbruck,
Muellerstrasse 44, 6020 Innsbruck, Austria

Introduction

Myxoid changes in adrenocortical tumours are extremely rare. They were originally described in carcinomas [5, 10]. In a series from the Mayo Clinic [1], eight additional carcinomas were described, as well as six adenomas, thus extending the observation of a myxoid component to benign lesions, as well. Heterogeneous growth patterns were described in the reported tumours, including prominent pseudoglandular areas in approximately half (6/14) of Brown's series [1]. Two other myxoid adenomas, one with pseudoglandular areas, were recently described [4, 6], as well as the occurrence of lipomatous metaplasia in a myxoid cortical carcinoma [8]. The currently reported myxoid adrenocortical adenomas are, therefore, eight in number, five of which are characterised by pseudoglandular areas. We describe an additional case of myxoid

adrenocortical adenoma with a pseudoglandular component and discuss the differential diagnosis from metastatic adenocarcinomas of the adrenal gland.

Clinical history

A 58-year-old man was admitted to the Division of Internal Medicine of our hospital in September 2002 complaining of a recent and abrupt onset of hypertension. His past medical history was unremarkable, except for positive hepatitis C virus serology. The infection was probably due to a blood transfusion, which occurred many years earlier at the time of a juvenile abdominal trauma. On examination, the liver function was not impaired, and blood pressure levels were 150/95 on diuretic (chortalidone) treatment. Laboratory tests were all in the normal range with the exception of the urinary metanephrines and normetanephrines (520 μl and 620 μl/24 h, n.v. <440 μl/24 h) and the plasma cortisol levels, which were in the normal range during the day but slightly increased around midnight (5.5 μg/dl, n.v. 0–4.5 μg/dl). Ultrasound and computed tomography scan revealed a 4-cm solid, slightly unhomogeneous, hyperdense mass in the right adrenal gland. A pheochromocytoma was suspected, and a right retroperitoneoscopic adrenalectomy was performed. The follow-up was uneventful, the patient is currently free of disease 15 months after the operation and the blood pressure was normalised without medication.

Materials and methods

The surgical specimen was fixed in 10% formaldehyde and embedded in paraffin. Sections (4–5 μm) were obtained for conventional histopathological examination and special stains [(Alcian blue and periodic acid–Schiff (PAS)]. Immunohistochemistry was performed on serial sections of representative blocks collected onto charged slides. The following markers were analysed and revealed with a biotin-free detection system (EnVision, DakoCytomation, Glostrup, Denmark): low molecular weight cytokeratins (clones LP5 K/35βH11/CD10/b170, 1/100; DakoCytomation and Novocastra Laboratories Ltd., UK), high molecular weight cytokeratins (clones Ks1A3/LL02/E3/D5–16B4, 1/100; DakoCytomation/Novocastra), vimentin (clone V9, 1/200; DakoCytomation), synaptophysin (clone SY38, 1/100; DakoCytomation), alpha-inhibin (clone R1, 1/75; Serotec Ltd., UK), early membrane antigen (EMA) (clone E29, 1/350; DakoCytomation), S-100 protein (polyclonal, 1/1000; DakoCytomation), chromogranin A (clone LK2H10, 1/50; Novocastra), smooth-muscle actin (clone 1A4, 1/2000; Sigma, Missouri, USA), tyrosine hydroxylase (polyclonal, 1/50; Chemicon International Inc., California, USA), cytochrome P_{450}SCC (polyclonal, 1/500, Chemicon), MUC1 (clone Ma695, 1/200; Novocastra) and Ki67 (clone MIB-1, 1/150; DakoCytomation).

Results

Pathological findings

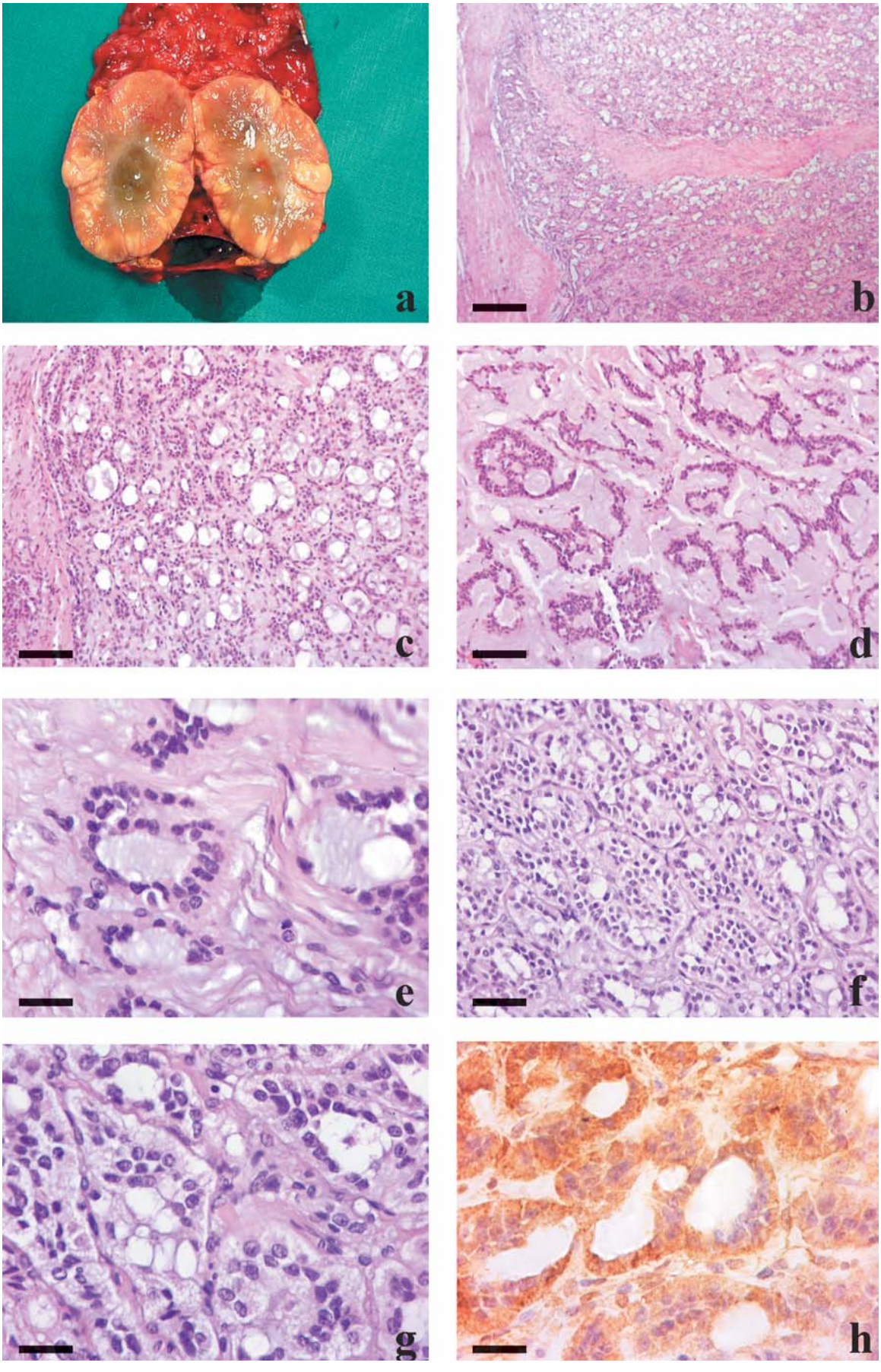
Grossly, the surgical specimen was roundish, apparently well demarcated, measured 5×4 cm and weighed 55 g. On cut surface, a rim of compressed adrenal tissue was present in the periphery of the mass, and the tumour had a yellow-greyish colour, with gelatinous myxoid areas admixed with areas of firm and fibrous consistency (Fig. 1a).

At light microscopy, the tumour was almost completely demarcated by a fibrous capsule, at the periphery of which partially atrophic adrenal gland parenchyma was found. The tumour was mostly (>75%) characterised by a myxoid background containing cords and tubules of medium-sized polygonal cells (Fig. 1b). The cords were irregularly anastomosing, while the tubular formations had occasional microcystic dilatations, as commonly observed in so-called "cylindromas" (Fig. 1c). The tubular formations contained finely granular weakly eosinophilic material, which was faintly stained by either Alcian blue or PAS. The morphological similarity with true glands was striking, but no dysplasia nor cell pleomorphism (as commonly seen in metastatic adenocarcinomas) was ever observed (Fig. 1d, e). Irrespective of the growth pattern, the cells had a variable amount of eosinophilic cytoplasm. In limited areas (less than 20%), cell clusters having an amphophilic or clear cytoplasm were observed. The latter features recalled the classical adrenocortical adenoma cells (Fig. 1f), but the myxoid background was still recognisable in these cytologically classical areas. The nuclei were usually centrally located and were round or oval. They had fine chromatin and generally lacked atypias, with the exception of an occasional single enlarged pleomorphic nuclei (Fig. 1g). The mitotic count was three per ten high power fields (HPFs). This finding was confirmed by a low proliferative index, as detected using Ki67 immunostaining (2.5%). No necrosis or signs of invasive growth were observed.

The immunophenotype of this tumour was consistent with that of primary adrenocortical adenomas. Vimentin was positive as well as cytokeratin (restricted to a focal reactivity of low molecular weight keratins). Alpha-inhibin, cytochrome P_{450}scc and synaptophysin were also positive (Fig. 1h). No immunoreactivity was found for EMA, S-100 protein, chromogranin A, smooth-muscle actin or tyrosine hydroxylase. The mucin marker MUC1 was also negative in the myxoid material. A diagnosis of myxoid adenoma with prominent pseudoglandular component, primarily of the adrenal cortex, was made.

Discussion

In this study, we have described an additional case of pseudoglandular myxoid adenoma of the adrenal gland. After the original description of six benign adrenocortical tumours having myxoid changes [1], only two other single cases have appeared in the English literature [4, 6]. The current case shared the histological features and the immunophenotype of the described cases. Grossly, gelatinous areas were observed, indicating an extensive myxoid transformation in the present tumour. This is not the rule in similar cases, as the occurrence of myxoid changes is limited to focal areas in some cases [1]. Microscopically, the tumour had prominent pseudoglandular areas characterised by a small tubular formation containing mucin-type material. The resemblance with epithelial glandular tumours was striking, and the differential diagnosis from metastatic adenocarcinomas is of paramount importance (see below). Other tumour fields contained myxoid ma-


a
b
c
d
e
f
g
h

terial and cords of eosinophilic tumour cells, occasionally admixed with areas of classical adrenocortical adenoma. While the latter finally addressed to a correct diagnosis, the former growth pattern is also shared by some myxoid high- or low-grade (i.e. liposarcomas) mesenchymal neoplasms.

Before entering into the differential diagnosis of pseudoglandular myxoid adenoma, a comment is warranted on the diagnostic criteria and immunophenotype. With regard to the former, once areas of classical adrenocortical tumour are identified, the same criteria apply to distinguish an adenoma from a carcinoma [12]. The size and the weight were in the expected range for adenomas, as well as the mitotic count (three per ten HPF). No necrosis or vascular invasion was observed in this case, while focal capsular penetration was seen in some cases of the Mayo Clinic series [1]. With regard to the immunophenotypical profile, the presently described case as well as those reported in the literature [1, 4, 6] expressed vimentin, synaptophysin and α-inhibin, as expected in adrenocortical adenomas [3, 9]. Chromogranin A was negative in the present tumour, as in most adrenocortical adenomas, although rare cases are on record [7] that are shown to contain adrenalin-type neurosecretory granules. This feature may mimic a pheochromocytoma and may be clinically responsible for a hypertensive syndrome. In our case, cytokeratins were focally and weakly expressed at variance with the findings of Brown [1], who failed to demonstrate cytokeratin expression in their tumours. The type of cytokeratin was glandular (low molecular weight) and was expressed by tumour cells in either the classical or the myxoid areas. The tumour cells were negative for EMA, a useful finding to exclude the diagnosis of chordoma. The myxoid material was faintly positive for PAS, Alcian blue, and MUC1, which recognises a mucin antigen, was negative. The observed staining of the myxoid material indicates that its origin is probably related to degenerative changes, rather than to production of mucosubstances by the tumour cells.

Ki67 proliferative index showed a fraction of 3% of positive tumour cells. This figure is intermediate between the reported values for adenomas and carcinomas [11]. The clinical outcome of the present case was uneventful after 1 year.

The major issue in the characterisation of this rare variant of adrenocortical tumour is the differential diagnosis from other more or less common neoplastic conditions affecting the adrenal gland and the retroperitoneal space. When pseudoglandular areas are prominent, a well-differentiated metastatic adenocarcinoma is to be taken into account first, since pulmonary, breast and, more rarely, other glandular carcinomas may spread to the adrenal gland. Strong cytokeratin expression is usually helpful to identify a metastatic carcinoma. In this context, the possibility of a chordoma is always to be considered, since this tumour expresses cytokeratin and EMA, as well. However, all mesenchymal tumours having myxoid features are potential mimickers of myxoid adrenal adenoma. Immunohistochemical markers are generally helpful to identify liposarcomas, chondrosarcomas and nerve-sheath tumours (all S-100 protein positive) or leiomyosarcomas (smooth-muscle actin and desmin positive) (Table 1).

Table 1 Differential diagnosis of myxoid adrenocortical tumours. *HMW* high molecular weight, *LMW* low molecular weight *EMA* early membrane antigen

Marker	Myxoid adrenal tumour	Metastatic adenocarcinoma	Chordoma	Myxoid sarcoma
Cytokeratin (HMW)	–	++	++	–
Cytokeratin (LMW)	+focal	++	+	–
Vimentin	+	–	–	++
Synaptophysin	+	–	–	–
Alpha-inhibin	++	–	–	–
EMA	–	+	++	–
S-100 protein	–	–	+	+[a]
MUC1	–	+	–	–
Smooth-muscle actin	–	–	–	+[b]
Cytochrome P_{450}scc	+	–	–	–
Chromogranin A	–	–	–	–

[a] Chondrosarcomas, liposarcomas, nerve-sheath tumors
[b] Leiomyosarcomas

In conclusion, the histological features of pseudoglandular myxoid adenoma are peculiar for a primary adrenocortical tumour and may superficially address a wrong interpretation of a metastatic adenocarcinoma. An immunophenotype similar to that of conventional adrenal adenomas (i.e. synaptophysin and α-inhibin reactivity) and possibly the recognition of classical steroidogenic cell areas are the clues to a correct diagnosis.

The pathogenesis of this tumour is not known. From the rare reported cases, no data are currently available on possible associations with genetic disorders. Among them, Carney complex may be a possible underlying hereditary disease, since it is known to affect the adrenal gland and, above all, to be associated with myxoid tumours elsewhere in the body [2].

Acknowledgements Work partially supported by grants from the Italian Ministry of University and Research (MIUR, Rome, to MP and MT).

Fig. 1 Pseudoglandular myxoid adrenocortical adenoma. A yellow-grey gelatinous appearance is evident on the cut surface of a 4-cm mass (**a**); the tumour is encapsulated (**b**) and characterised by polygonal regular cells arranged in cords and tubules in a myxoid or fibrous background (**c**, **d**, **e**). Limited areas of classical adrenocortical adenoma with large clear cells were occasionally found (**f**, **g**). Immunoreactivity for alpha-inhibin was present in the pseudoglandular areas (**h**). **b**–**g** Hematoxylin-eosin. **h** Immunoperoxidase. *Bar* 250 μm (**b**); 100 μm (**c**, **d**); 50 μm (**f**); 25 μm (**e**, **g**, **h**)

References

1. Brown FM, Gaffey TA, Wold LE, Lloyd RV (2000) Myxoid neoplasm of the adrenal cortex: a rare histologic variant. Am J Surg Pathol 24:396–401

2. Carney JA, Gordon H, Carpenter PC, Shenoy BV, Go VL (1985) The complex of myxomas, spotty pigmentation, and endocrine overactivity. Medicine (Baltimore) 64:270–283
3. Chivite A, Matias-Guiu X, Pons C, Algaba F, Prat J (1998) Inhibin A expression in adrenal neoplasms: a new immunohistochemical marker for adrenocortical tumors. Appl Immunohistochem 6:42–49
4. Dundr P, Novak K (2003) Pseudoglandular myxoid adenoma of the adrenal gland. Pathol Res Pract 199:493–496
5. Forsthoefel KF (1994) Myxoid adrenal cortical carcinoma. A case report with the differential diagnostic considerations. Arch Pathol Lab Med 118:1151–1153
6. Honda K, Kashima K, Daa T, Gamachi A, Nakayama I, Yokoyama S (2001) Myxoid adrenal cortical adenoma. Pathol Int 51:887–891
7. Ivsic T, Komorowski RA, Sudakoff GS, Wilson SD, Datta MW (2002) Adrenal cortical adenoma with adrenalin-type neurosecretory granules clinically mimicking a pheochromocytoma. Arch Pathol Lab Med 126:1530–1533
8. Izumi M, Serizwa H, Iwaya K, Takeda K, Sasano H, Mukai K (2003) A case of myxoid adrenocortical carcinoma with extensive lipomatous metaplasia. Arch Pathol Lab Med 177:227–230
9. McNicol AM (2002) The adrenal cortex. In: Li Volsi VA, Asa SL (eds) Endocrine pathology. Churchill Livingstone, New York, pp 171–204
10. Tang CK, Harriman BB, Toker C (1979) Myxoid adrenal cortical carcinoma: a light and electron microscopy study. Arch Pathol Lab Med 103:635–638
11. Terzolo M, Boccuzzi A, Bovio S, Cappia S, De Giuli P. Alì A, Paccotti P, Porpiglia F, Fontana D, Angeli A (2001) Immunohistochemical assessment of Ki-67 in the differential diagnosis of adrenocortical tumors. Urology 57:176–182
12. Weiss LM (1984) Comparative histologic study of 43 metastasizing and non-metastasizing adrenocortical tumors. Am J Surg Pathol 8:163–169

Virchows Arch (2004) 445:419–420
DOI 10.1007/s00428-004-1072-7

CASE REPORT

Karima Mrad · Ehsen Ben Brahim · Maha Driss · Imene Abbes · Mounir Marakchi · Khaled Ben Romdhane

Lymphoepithelioma-like carcinoma of the submandibular salivary gland associated with Epstein–Barr virus in a North African woman

Received: 19 January 2004 / Accepted: 2 June 2004 / Published online: 17 July 2004
© Springer-Verlag 2004

We report the first case of submandibular gland lymphoepithelioma-like carcinoma (LELC) associated with Epstein–Barr virus (EBV) infection in a North African woman. The patient is a 34-year-old woman with an 8-month history of a submandibular left mass. Physical examination revealed a firm, mobile and indolent submandibular gland mass, measuring 2×2 cm. The magnetic resonance imaging demonstrated a well-delineated tumor mass measuring 30 mm in antero-posterior diameter, with heterogeneous high-intensity signal on T2-weighted images and homogeneous enhancement after contrast product injection (Fig. 1). The contra lateral gland was normal. A submandibulectomy with excision of two lymph nodes was performed. Permanent sections established the diagnosis of LELC of the submandibular salivary gland with reactive lymph nodes. Further investigation consisted of negative random biopsies of the nasopharynx. No more therapy was added. The patient is well with a 40-month follow-up.

Histological analysis demonstrated a malignant proliferation growing in a nested and trabecular pattern, arranged in large lobules. Neoplastic cells exhibited syncytial appearance, with a large vesicular nucleus displaying one prominent nucleolus (Fig. 2). Tumor cells were closely intermingled with small aggregates of large pale histiocytes and abundant lymphoid cells, focally arranged in follicles. Some residual salivary gland ducts were present on the periphery of the tumor.

K. Mrad (✉) · E. Ben Brahim · M. Driss · I. Abbes · K. Ben Romdhane
Department of Pathology,
Salah Azaiez Institute,
1006 Bab Saadoun, Tunis, Tunisia
e-mail: karima.mrad@rns.tn
Tel.: +216-1-577847
Fax: +216-1-574725

M. Marakchi
Head and Neck Department,
Charles Nicole Hospital,
Tunis, Tunisia

Immunohistochemistry (Dako, Denmark; dilution: 1/50) demonstrated that neoplastic cells expressed cytokeratin (clone: MNF116) and epithelial membrane antigen (clone: E29) (Fig. 3) and were negative with EBV-latent membrane antigen LMP-1 antibody (clone: CS1–4). The background lymphoid infiltrate was mixed expressing both CD2O (clone: L26) and CD3 (clone: PC3/188A). CD68 (clone: KP1) staining enhanced the presence of numerous histiocytes.

In situ hybridization (ISH) showed that neoplastic cells were strongly and diffusely labeled by the EBV-encoded RNA probe (Dako, Denmark, alkaline phosphatase/anti-alkaline phosphatase technique) (Fig. 4). Residual normal glands as well as lymphoid and histiocytes were negative.

LELC of salivary glands is strongly related to racial factors, since it predominates in Eskimos and Asian pa-

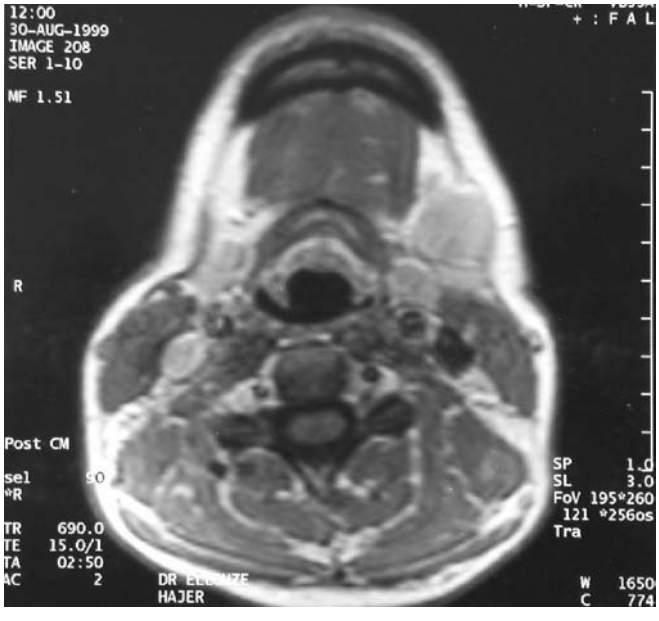


Fig. 1 Magnetic resonance imaging (T2-weighted images, after injection of contrast product) demonstrating swelling of the left submandibular gland

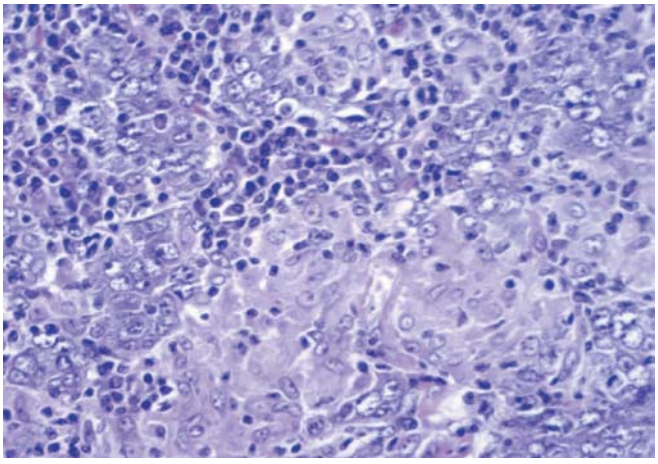


Fig. 2 Neoplastic cells with indistinct borders, vesicular nuclei and prominent nucleoli, surrounded by lymphocytes and histiocytes (hematoxylin and eosin, ×400)

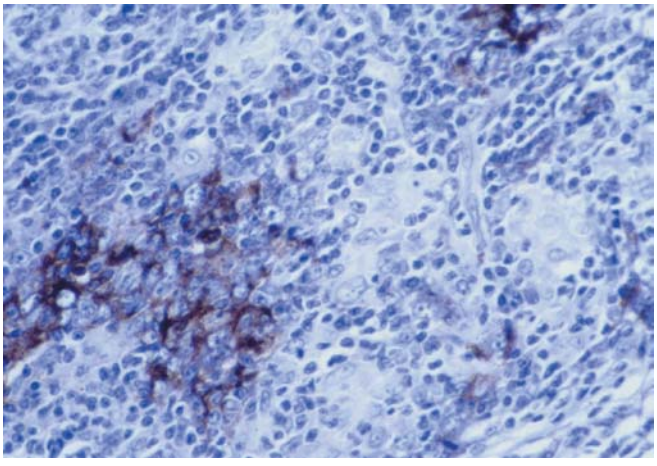


Fig. 3 Immunohistochemistry: neoplastic cells express epithelial membrane antigen (Dako, clone E29, diaminobenzidine, ×400)

tients [1]. The parotid glands were more often affected than the submandibular glands in the largest series [1]. The median age was 50 years [1]. The 4-year survival was 85% [1]. Of the cases in the literature, 47 were examined using ISH for EBV. All cases from Eskimo patients (11 cases) [2] and South-eastern Asians (36 cases) [1] were positive. In Western patients, two cases of LELC [3] and one case of undifferentiated carcinoma [4] were negative, while two cases were associated with EBV—one in a Greek [3] and the other in an Italian [5] man. The linkage of EBV with salivary gland neoplasia seems to be restricted to tumors of the LELC type. All tumor-like lesions of the salivary glands in Asian patients and benign lymphoepithelial lesions from Western patients studied

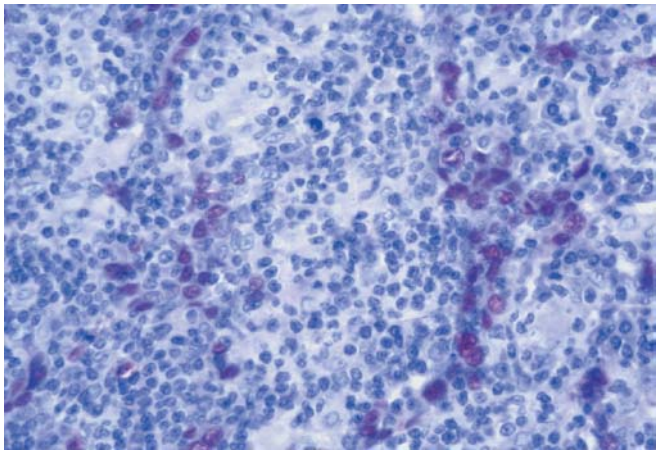


Fig. 4 In situ hybridization: EBER-1 antisense probe labeling in tumor cells. Reactive cells are negative (Dako, alkaline phosphatase–antialkaline phosphatase, ×400)

using ISH for EBV detection were negative [4]. Our case is the third case of EBV-associated salivary gland LELC in a patient who is neither Eskimo nor Chinese, but Mediterranean, as in the two previously reported cases [3, 5], and it is the first one described in a submandibular gland. Our findings suggest that predisposing genetic factors are less important than environmental factors, which include EBV infection in LELC.

Acknowledgements The authors wish to express their appreciation to Dr George Delsol for his precious help with the in situ hybridization study.

References

1. Kuo T, Hsueh C (1997) Lymphoepithelioma-like salivary gland carcinoma in Taiwan: a clinicopathological study of nine cases demonstrating a strong association with Epstein–Barr virus. Histopathology 31:75–82
2. Hamilton-Dutoit SJ, Therkildsen MH, Nielsen NH (1991) Undifferentiated carcinoma of the salivary gland in Greenlandic Eskimos: demonstration of Epstein–Barr virus DNA by in situ nucleic acid hybridization. Hum Pathol 22:811–815
3. Kotsianti A, Costopoulos J, Morgello S, Papadimitriou C (1996) Undifferentiated carcinoma of the parotid gland in a white patient: detection of Epstein–Barr virus by in situ hybridization. Hum Pathol 27:87–90
4. Pollock AM, Toner M, McMenamin M, Walker J, Timon CI (1999) Absence of Epstein-Barr virus encoded RNA and latent membrane protein (LMP1) in salivary gland neoplasms. J Laryngol Otol 113:906–908
5. Squillaci S, Bertalot G, Vago L, Berlotti F, Chiodera PL, Capitanio A (2000) Lymphoepithelioma-like carcinoma of the parotid gland. Description of a case with detection of EBV by in situ hybridization. Pathologica 92:189–194

Virchows Arch (2004) 445:421–424
DOI 10.1007/s00428-004-1082-5

CASE REPORT

Kyoji Okada · Tadashi Hasegawa · Ukihide Tateishi · Eiji Itoi

Second primary osteosarcoma with rosette-like structure in a patient with retinoblastoma

Received: 4 February 2004 / Accepted: 15 June 2004 / Published online: 28 July 2004
© Springer-Verlag 2004

Abstract A Japanese male patient developed bilateral retinoblastomas at the age of 1 year, but remained continuously disease-free after enucleation of the left eye and radiation therapy to the right eye. He noticed a painless hard mass around the right temporal bone when he was 25 years old. Biopsy specimen showed a small multinodular proliferation of tumor cells with prominent rosette-like structures. Eosinophilic material with focal mineralization was seen in the center of the rosettes. Immunostaining of the tumor cells showed positive reactions for epithelial membrane antigens CD 56 and CD 99. The patient was treated with systemic chemotherapy, and the tumor partially diminished. It is well known that a few osteosarcomas show a rosette-like appearance with production of osteoid in the center, but this is the first case of second primary osteosarcoma with prominent rosette-like features.

Keywords Second primary osteosarcoma · Retinoblastoma · Rosette · Diagnosis

Introduction

Retinoblastoma is a malignant neoplasm in childhood occurring in 1/15,000 to 1/30,000 live births. Improved treatment for retinoblastoma together with early diagnosis has resulted in the cure of an increasing number of patients [17]. It has long been established that children affected by retinoblastoma have a high risk for the development of second primary malignant lesions. The majority of these second primary malignancies are osteosarcomas and soft-tissue sarcomas [1, 11, 14].

Second primary sarcomas after retinoblastoma may be related to prior radiation therapy for the original retinoblastoma [5, 6, 12]. In patients previously irradiated for bilateral or familial unilateral retinoblastoma, 70% of second malignancies have occurred within the radiation field, while 30% occurred outside the field of radiation [1]. Differential diagnosis between these second primary sarcomas and recurrent retinoblastoma may be problematic [19].

Recently, we encountered a 25-year-old Japanese man with a second primary osteosarcoma within the prior radiation field. Peculiarly, this lesion showed rosette-like features that have not been described in previous literature in a second primary osteosarcoma. We, therefore, present here a case requiring special attention during the differential diagnosis of osteosarcoma with rosette-like features from recurrence of retinoblastoma.

K. Okada (✉) · E. Itoi
Department of Orthopedic Surgery,
Akita University School of Medicine,
Hondo 1-1-1, Akita 010-8543 Akita, Japan
e-mail: cshokada@med.akita-u.ac.jp
Tel.: +81-18-8846148
Fax: +81-18-8362617

T. Hasegawa
Pathology Division,
National Cancer Center Research Institute,
Tokyo, Japan

U. Tateishi
Diagnostic Radiology Division,
National Cancer Center Research Institute,
Tokyo, Japan

Clinical history

A Japanese male patient was diagnosed with bilateral retinoblastomas at the age of 1 year and underwent enucleation of the left eye and radiation therapy with 49 Gy to the right eye. He had remained continuously disease-free after the treatments. Both his father and mother had a history of retinoblastoma. When he was 25 years old, he noticed a painless hard mass around the right temporal bone. Axial computed tomography showed a well mineralized mass (arrow) on the temporal bone associated with focal subarachnoid hemorrhage (arrowheads, Fig. 1). Axial T1-weighted magnetic resonance (MR) images showed a mass of iso signal intensity relative to white matter. On T2-weighted MR images, the tumor showed heterogeneous and high signal intensity relative to white matter. Multiple fluid levels suggesting the presence of intratumoral hemorrhage were also observed (arrows, Fig. 2A, B). Laboratory data, including peripheral blood count, alkaline phosphatase, and C-reactive protein, were within the normal range. Clinical



Fig. 1 Axial cranial computed tomography showing a well-mineralized tumor (*arrow*) around the right temporal bone associated with focal subarachnoid hemorrhage (*arrowheads*)

and radiological diagnosis was second primary osteosarcoma after retinoblastoma. A biopsy was performed, and the diagnosis of second primary osteosarcoma with rosette-like features was established. The patient was treated with systemic chemotherapy of high-dose methotrexate, cisplatinum, and adriamycin in March 2001, and the tumor size partially decreased. A surgery of the tumor was not performed, since the tumor was still not resectable after the chemotherapy. The patient has been alive with disease for 43 months after the treatment without any sign of regrowth of the tumor or distant metastases.

Materials and methods

The biopsy specimen was fixed in 10% formalin, embedded in paraffin, and sectioned. One of the 4-mm-thick sections was stained with hematoxylin and eosin. The other serial sections were examined using the labeled streptavidin–biotin method with appropriate use of positive and negative controls throughout, after pretreatment with heat-induced epitope unmasking in a 10-mM citrate buffer, pH 6.0, in an autoclave at 121°C for 10 min. The primary antibodies were applied as follows: cytokeratin (clone AE 1/3, 1:100, Dako, Glostrup, Denmark), CD99 (clone O-13, 1:50, Signet, Dedham, MA), epithelial membrane antigen (EMA, clone E29, 1:100, Dako) and CD56 (clone N-CAM; NCC-Lu-243, 1:200, Nihonkayaku, Tokyo, Japan). In the evaluation of immunostaining for AE1/3, CD99, EMA, and CD56, when there was only homogeneous staining, along with staining of the cell membranes or cytoplasm at the same intensity and pattern as that in the adjacent normal epithelium, the finding was assessed as 2+ positive, while heterogeneous or focal staining was assessed as 1+.

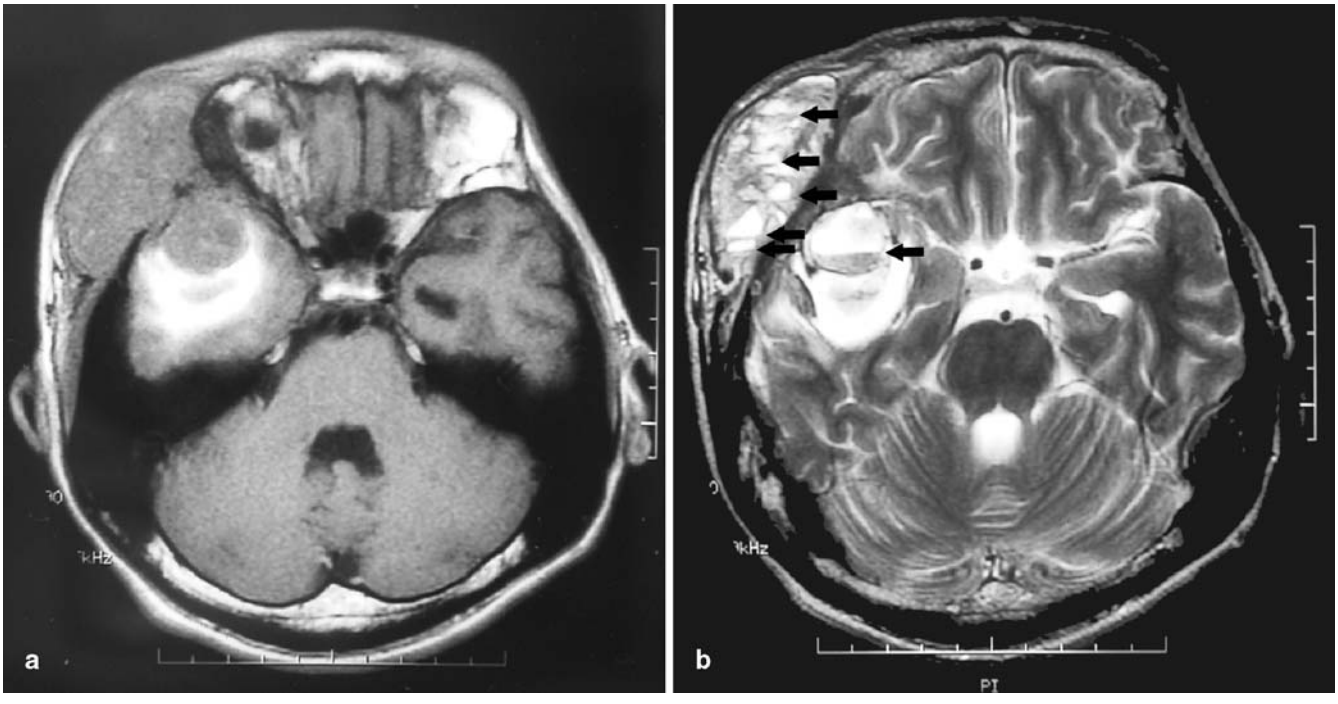


Fig. 2 **a** Axial T1-weighted magnetic resonance (MR) image (TR/TE: 440/7.3 ms) showed a mass of iso signal intensity relative to white matter. Focal subarachnoid hemorrhage corresponded to area of high signal intensity surrounding the tumor. **b** Axial T2-weighted MR image (TR/TE: 4000/118 ms) showed a mass of heterogeneous and high signal intensity relative to white matter. Also noted was the presence of multiple fluid levels within the tumor (*arrows*)

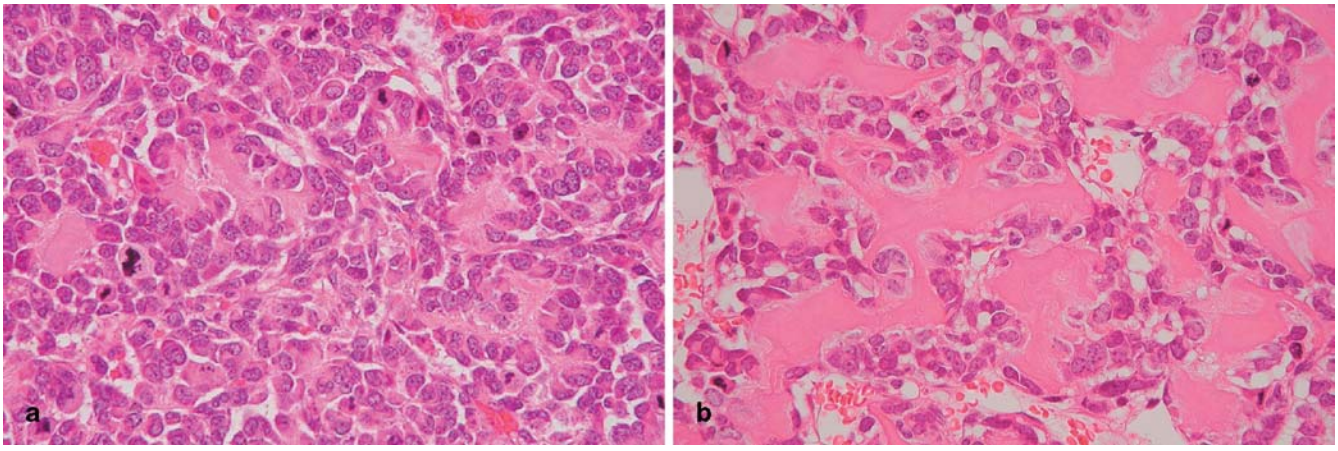


Fig. 3 **a** Microphotograph of the biopsy specimen showed a proliferation of tumor cells with prominent rosette-like structures. The tumor cells were generally small and round with abundant mitoses. Eosinophilic material was seen in the center of the rosette (×400). **b** Microphotograph showed conventional lace-like osteoid formation with partial mineralization (×400)

Results

Light microscopic findings

The biopsy showed a small multi-nodular proliferation of the tumor cells. These tumor cells formed a rosette-like structure, and eosinophilic material was seen in the center of the rosette. Focal mineralization was apparent in the eosinophilic material. Between the rosette-like structures, many small vessels proliferated, showing a hemangiopericytoma-like pattern. Under high power, tumor cells were generally small and round with abundant mitoses. In several areas, conventional lace-like osteoid was seen. The rosette-like structures were also observed around the conventional osteoid area. There was no typical Flexner-Wintersteiner rosette in the biopsied specimen (Fig. 3A, B).

Immunostainings

In immunohistochemical features, CD56 was 2+ positive, CD 99 and EMA were 1+ positive (Fig. 4), but cytokeratin was negative.

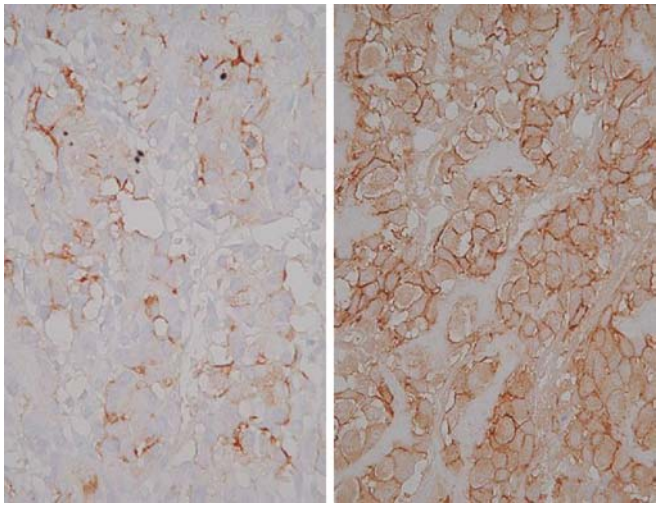


Fig. 4 Immunostaining of the tumor cells with EMA and CD56. The tumor cells showed a characteristic membrane-positive appearance for EMA (left, ×200) and for CD56 (right, ×200)

Discussion

Osteosarcoma is the most common type of second malignancy associated with hereditary retinoblastoma [11, 14]. Hawkins et al. reported that the incidence of osteosarcoma after heritable retinoblastoma is 300 times greater than the risk in the general population [8]. More than 100 cases of second primary osteosarcoma in the irradiated fields in patients with retinoblastoma have been reported in the literature [2, 3, 7, 14]. However, to our knowledge, there has not been any report describing second primary osteosarcoma having rosette-like structures. The rosette-like feature of osteosarcoma was first described in the textbook by Unni in 1996 [23]. In 2002, we reported that several primary osteosarcomas in the extremities showed a rosette-like structure with production of osteoid in the center. This special type of osteosarcoma usually showed a positive immunoreaction for EMA, CD56, and CD99 [15]. The histological and immunohistochemical features described in the literature were identical to those of the current case.

Second primary sarcomas often demonstrate both high-grade and undifferentiated features, making them difficult to distinguish from small, undifferentiated round cell tumors [19]. In addition, the rosette-like structure raises the possibility of recurrent retinoblastoma. However, the long interval (24 years) in the current case between the primary retinoblastoma and development of the second tumor suggests that a recurrence of retinoblastoma is less likely [22]. Furthermore, a definite tumor osteoid

in the center of a rosette-like structure and scattered typical lace-like osteoid, indicating osteosarcoma, and the absence of a typical Flexner-Wintersteiner rosette should be emphasized in the differential diagnosis between osteosarcoma with rosette-like features and recurrent retinoblastoma.

Careful immunohistochemical examinations were useful for distinguishing the current tumor from recurrent retinoblastoma or other small round cell tumors such as rhabdomyosarcoma, Ewing sarcoma/Primitive neuroectodermal tumor (ES/PNET), and metastatic cancer [9]. Positive immunoreactivity for EMA, CD56, CD99, but negativity for cytokeratin in the current case were consistent with those of osteosarcoma with rosette-like features [15]. Positive immunoreaction for EMA would suggest metastatic cancer, but the patient had no cancer history or visceral lesion. Furthermore, negative reaction for cytokeratin indicates that metastatic cancer would be an unlikely diagnosis. It is well known that CD 56 (N-CAM) and CD99 are expressed not only in neural neoplasms or ES/PNET but also in other several kinds of tumors [13, 18, 20]. Definite osteoid formation by tumor cells strongly favored the diagnosis of osteosarcoma.

Little is known in the literature regarding the relationship between treatment of the second primary osteosarcoma and prognosis [2, 4, 10, 16, 19]. Recently, encouraging results have been achieved with adjuvant chemotherapy and/or aggressive surgery [2, 21]. The current patient has remained alive with disease after effective treatment by systemic chemotherapy without any regrowth of the tumor or distant metastasis for 43 months. Similarly, in the review of the other four cases registered in the National Cancer Center in Tokyo (data not shown), three died of disease, but one patient was alive with disease for 99 months after systemic chemotherapy. However, our previous study showed that rosette-like feature in primary osteosarcoma is an adverse prognostic factor [15]. Further study is required with regard to prognosis of osteosarcoma with this specific background and histology.

References

1. Abramson DH, Ellsworth RM, Kitchin FD, Tung G (1984) Second non-ocular tumors in retinoblastoma survivors. Are they radiation-induced? Ophthalmology 91:1351–1355
2. Bielack SS, Kempf-Bielack B, Schwenzer D, Winkler K (1999) Combined modality treatment for osteosarcoma occurring as a second malignant disease. J Clin Oncol 17:1164–1174
3. Draper GJ, Sanders BM, Kingston JE (1986) Second primary neoplasms in patients with retinoblastoma. Br J Cancer 53:661–671
4. Dunkel IJ, Gerald WL, Rosenfield NS, Strong EW, Abramson DH, Ghavimi F (1998) Outcome of patients with a history of bilateral retinoblastoma treated for a second malignancy: the Memorial Sloan-Kettering experience. Med Pediatr Oncol 30:59–62
5. Folberg R, Cleasby G, Flanagan JA, Spencer WH, Zimmerman LE (1983) Orbital leiomyosarcoma after radiation therapy for bilateral retinoblastoma. Arch Ophthalmol 101:1562–1565
6. Font RL, Jurco S III, Brechner RJ (1983) Postradiation leiomyosarcoma of the orbit complicating bilateral retinoblastoma. Arch Opthalmol 101:1557–1561
7. Francois J (1977) Retinoblastoma and osteogenic sarcoma. Opthalmologica 175:185–191
8. Hawkins MM, Draper GJ, Kingston JE (1987) Incidence of second primary tumors among childhood cancer survivors. Br J Cancer 56:339–347
9. Hasegawa T, Matsuno Y, Niki T, Hirohashi S, Shimoda T, Takayama J, Watanabe C, Kaneko A, Sano T, Sato M, Suzuki J (1998) Second primary rhabdomyosarcomas in patients with bilateral retinoblastoma. A clinicopathologic and immunohistochemical study. Am J Surg Pathol 22:1351–1360
10. Maes P, Brichard B, Vermylen C, Cornu G, Ninane J (1998) Primary and secondary osteosarcoma of the face: a rare childhood malignancy. Med Pediatr Oncol 30:170–174
11. Meadow AT, Baum E, Fossati-Bellani F, Green D, Jenkin RD, Marsder B, Nesbit M, Newton W, Oberlin O, Sallan SG (1985) Second malignant neoplasms in children: an update from the Late Effects Study Group. J Clin Oncol 3:532–538
12. Mihara F, Gupta KL, Kartchner ZA, Kogutt MS, Robinson AE (1991) Leiomyosarcoma after retinoblastoma radiotherapy. Radiat Med 9:183–184
13. Molenaar WM, Muntinghe FL (1999) Expression of neural cell adhesion molecules and neurofilament protein isoforms in Ewing's sarcoma of bone and soft tissue sarcomas other than rhabdomyosarcoma. Hum Pathol 30:1207–1212
14. Newton WA, Meadows AT, Shimada H, Bunin GR, Vawter GF (1991) Bone sarcomas as second malignant neoplasms following childhood cancer. Cancer 67:193–201
15. Okada K, Hasegawa T, Yokoyama R (2001) Rosette-forming epithelioid osteosarcoma: a histologic subtype with highly aggressive clinical behavior. Hum Pathol 32:726–733
16. Pillay R, Graham-Pole J, Novak L, Kurczynski E, Yulish B (1983) Successful treatment of osteogenic sarcoma developing as a second cancer in childhood. Am J Pediatr Hemat Oncol 5:103–105
17. Schifter S, Vendelbo L, Jensen OM, Kaae S (1983) Ewing's tumor following bilateral retinoblastoma. Cancer 51:1746–1749
18. Sebire NJ, Ramsay AD, Levitt G, Malone M, Risdon RA (2002) Aberrant immunohistochemical expression in nonrhabdomyosarcoma soft tissue sarcomas of infancy: retrospective review of clinical material. Pediatr Dev Pathol 5:579–586
19. Smith LM, Donaldson SS, Egbert PR, Link MP, Bagshaw MA (1989) Aggressive management of second primary tumors in survivors of hereditary retinoblastoma. Int J Radia Oncol Biol Phys 17:499–505
20. Stevenson AJ, Chatten J, Bertoni F, Miettinen M (1994) CD99 ($p30/32^{MIC2}$) neuroectodermal/Ewing's sarcoma antigen as an immunohistochemical marker: review of more than 600 tumors and the literature experience. Appl Immunohistochem 2:231–240
21. Stine KC, Saylors RL, Saccente S, Becton DL (2003) Long-term survival in osteosarcoma patients following retinoblastoma using doxorubicin, cisplatin and methotrexate. Med Pediatr Oncol 41:77–78
22. Tateishi U, Hasegawa T, Miyakawa K, Sumi M, Moriyama N (2003) CT and MRI features of recurrent tumors and second primary neoplasms in pediatric patients with retinoblastoma. Am J Roentgenol 181:879–884
23. Unni KK (1996) Dahlin's bone tumors: general aspects and data on 11,087 cases, 5th edn. Lippincott-Raven, Philadelphia, pp 143–160

Virchows Arch (2004) 445:425–428
DOI 10.1007/s00428-004-1075-4

LETTER TO THE EDITOR

Simonetta Piana · Stefania Damiani · Silvia Asioli · Elisabetta Magrini · Werter Barbieri · Alberto Cavazza

Epstein–Barr-positive lymphoepithelial carcinoma and epi-myoepithelial cell carcinoma of the parotid gland: a hitherto unreported example of hybrid tumour

Received: 22 March 2004 / Accepted: 9 June 2004 / Published online: 29 July 2004
© Springer-Verlag 2004

Sir, the term "hybrid tumour" of the salivary glands has been proposed by Seifert and Donath [11] to define a tumour consisting of two histologically distinct entities that arise in the same nodule. Hybrid tumours of the salivary glands are rare, accounting for less than 0.1% of all the salivary gland neoplasms [3, 4, 7, 9, 11, 12, 15]. Several histological combinations are reported, including acinic cell carcinoma, salivary duct carcinoma, adenoid cystic carcinoma, epithelial–myoepithelial carcinoma, basal cell carcinoma, myoepithelial carcinoma, mucoepidermoid carcinoma and polymorphous low-grade adenocarcinoma [9].

We describe an Epstein–Barr virus (EBV)-positive hybrid tumour of the parotid gland composed of epi-myoepithelial carcinoma and lymphoepithelial carcinoma, arising in a Caucasian woman. The patient presented with a slowly growing mass in the right parotid gland. At physical examination, no signs of facial nerve paralysis or oropharyngeal lesions were noted. The patient underwent a right total parotidectomy with upper latero-cervical lymph-node dissection. Grossly, the resected specimen consisted of the right parotid gland, 7 cm in greatest axis, and the surrounding soft tissue. On cut surface, the gland contained a well-circumscribed, firm, greyish nodule measuring 4 cm in greatest axis. Several lymph nodes were identified in the adjacent adipose tissue.

Histologically, the tumour had a lobular appearance and was composed of nests and lobules of neoplastic cells immersed in a dense lymphoplasmacytic infiltrate, with germinal centre formation. At a higher power, it became evident that the tumour was constituted by two components intermingled without a clear-cut separation (Fig. 1).

The first component consisted of small nests and glands with a distinct pattern. Neoplastic cells were dis-

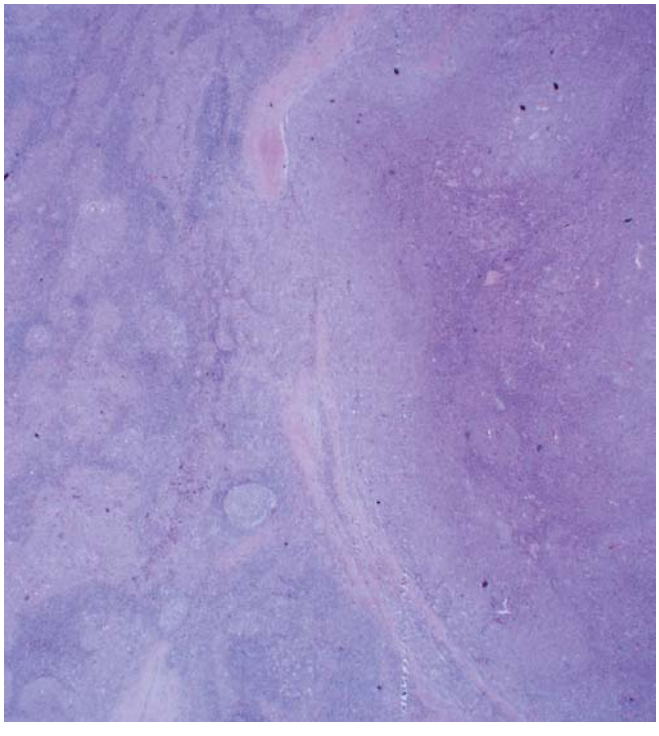


Fig. 1 The tumour is composed of nests and lobules of neoplastic cells immersed in a dense lymphoplasmacytic infiltrate, with germinal centre formation, with both a glandular (*right*) and a solid (*left*) pattern of growth. Haematoxylin and eosin, ×20

S. Piana (✉) · S. Asioli · A. Cavazza
Department of Pathology,
Arcispedale Santa Maria Nuova,
Viale Risorgimento 80, 42100 Reggio Emilia, Italy
e-mail: simonetta.piana@asmn.re.it
Tel.: +0039-522-295919
Fax: 0039-522.296945

S. Damiani · E. Magrini
Section of Anatomic Pathology "M. Malpighi",
University of Bologna, Bellaria Hospital,
Bologna, Italy

W. Barbieri
Department of Otorhinolaryngology,
Arcispedale Santa Maria Nuova,
Reggio Emilia, Italy

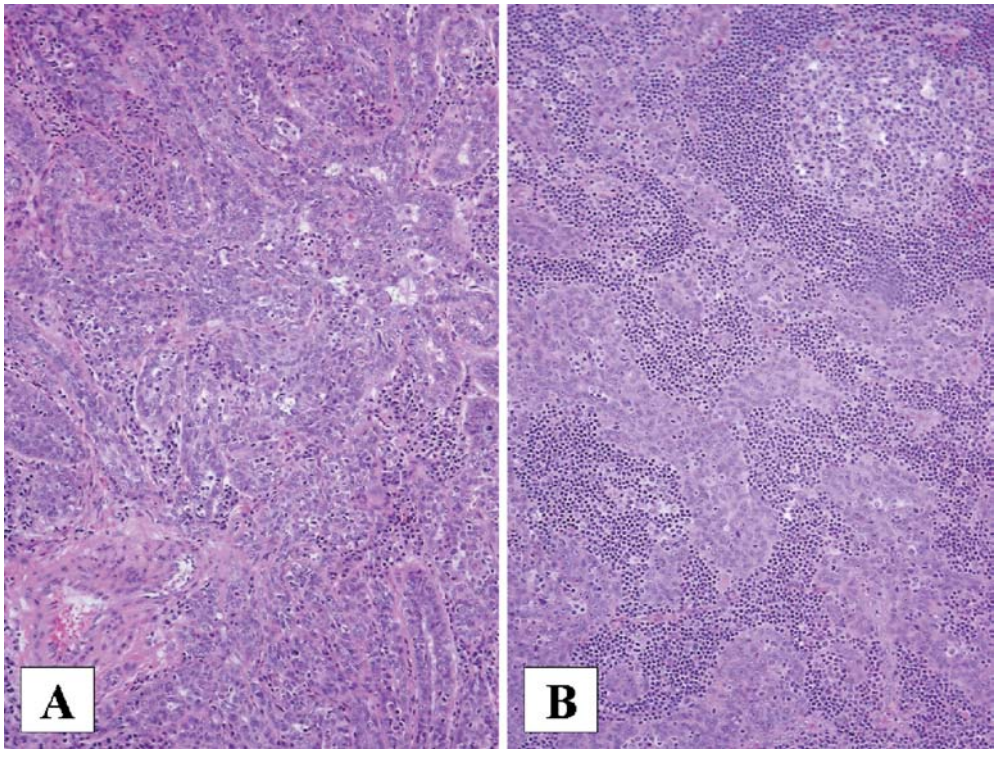


Fig. 2 At high magnification, small nests and glands (**A**) merge into irregular sheets and nests of large epithelial cells, with indistinct boundaries (**B**). Haematoxylin and eosin, ×100

posed in two layers: the outer layer was composed of cells with a small amount of cytoplasm and irregular, ovoid nuclei, while the inner (luminal) layer consisted of cuboidal cells with eosinophilic abundant cytoplasm and vesicular nuclei (Fig. 2A). Neoplastic glands and nests were closely packed, giving this component a solid appearance at low power. Mitoses were rare, and no areas of necrosis were evident.

The second component consisted of irregular, sometimes solid, sheets of large epithelial cells, with indistinct boundaries. Neoplastic cells were polygonal to spindle shaped and had abundant eosinophilic cytoplasm. Nuclei were large and vesicular, with prominent nucleoli (Fig. 2B), and mitoses were numerous. Single cell necrosis was evident.

The surrounding salivary tissue was compressed but unremarkable. There was no evidence of a pre-existing benign neoplasm, and no features of benign lymphoepithelial lesions were evident. Two regional lymph nodes contained metastatic deposits, entirely composed of the second component. Immunohistochemically, cytokeratin 14 stained neoplastic cells in both the components: in the glandular one, this antibody highlighted the bilayered pattern of the glands, as the staining was mainly localised to the outer layer (Fig. 3A, right). In the solid component, the same antibody stained approximately 20% of the cells without any specific pattern (Fig. 3A, left). Cytokeratins 7 and 19 selectively stained the inner luminal cells in the first component (Fig. 3C), while, in the second component, only rare cells were weakly stained. Smooth-muscle actin and the other myoepithelial markers (p63, myosin, calponin and S100 protein) stained the outer cell layer in the glandular component and a variable proportion of cells in the solid component (Fig. 3B). In situ hybridisation for Epstein–Barr encoded RNA revealed the presence of EBV in almost all tumour cells. The staining was more intense in the large cells of the solid component (Fig. 4A). However, both the inner (luminal) and the outer layer cells of the glandular component were stained (Fig. 4B). Adjuvant radiation therapy was administered. The patient is well without evidence of tumour 6 months after surgery.

The recognition of the most aggressive component in hybrid carcinomas is crucial, as several reports suggest that the clinical behaviour is determined by the higher grade component [4, 7, 11]. In the present case, a tumour with morphological and immunohistochemical features of epithelial–myoepithelial cell carcinoma merges with a poorly differentiated neoplasm consistent with lymphoepithelial carcinoma. Moreover, both the two components are positive for EBV with an in situ hybridisation technique.

Epithelial–myoepithelial carcinoma is an uncommon malignant tumour, which accounts for about 1% of salivary gland neoplasms [5]. In hybrid carcinomas, it has been reported in association with adenoid cystic carcinoma, salivary duct carcinoma and mucoepidermoid carcinoma [9]. Chetty et al. [3] correctly stated that adequate tissue sampling in a low-grade neoplasm, such as epithelial–myoepithelial carcinoma, may disclose a more aggressive component, and, therefore, the patient management has to be modified.

Lymphoepithelial carcinoma is an equally rare malignant neoplasia and accounts for approximately 0.4% of

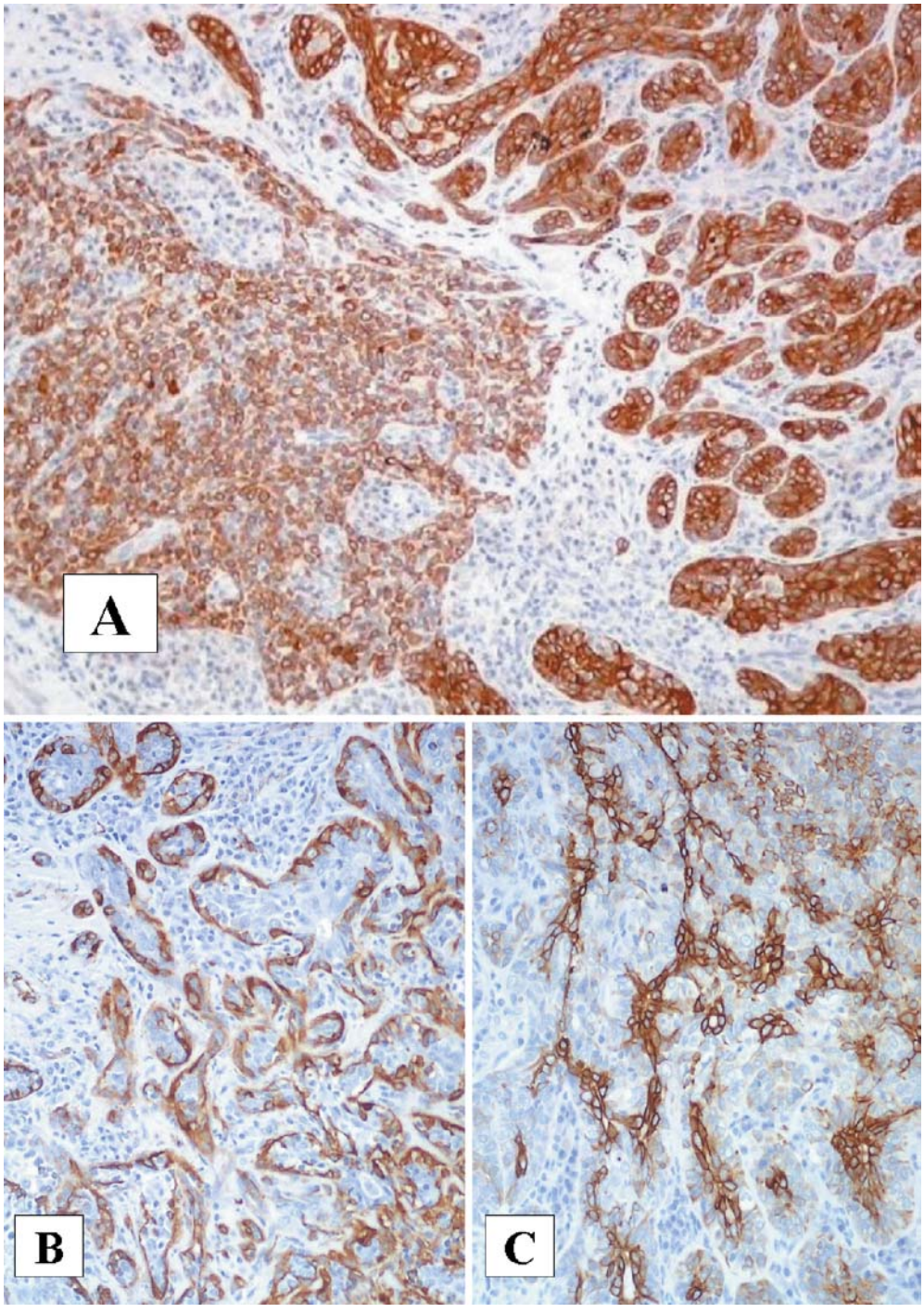


Fig. 3 A Cytokeratin 14 highlights the bilayered pattern of the glands (*right*) in the glandular component and the diffuse growth pattern in the solid component (*left*), ×100. **B** Smooth-muscle actin stains the outer cell layer of the glandular component, ×200. **C** Cytokeratin 7 stains selectively the inner, luminal cells, ×200

the salivary gland tumours [5]. It occurs almost exclusively in major salivary glands, with very few exceptions [13], and shows a higher incidence in the Eskimo and Southern Chinese population, while Caucasian patients represent less than 15% of the total cases [5]. EBV has been extensively studied as a possible causative agent, due to the striking morphological similarities with the lymphoepithelial carcinoma of the nasopharynx [1, 2, 6, 8, 10, 13, 14].

While it is common knowledge that nasopharyngeal lymphoepithelial carcinoma is very frequently associated with EBV infection in any site of the globe, with no racial preference, a consistent association with EBV in lymphoepithelial carcinoma arising in other sites, including salivary glands, has been demonstrated mainly in Eastern patients [2]. Nevertheless, some cases of EBV-positive lymphoepithelial carcinomas have also been reported in non-endemic areas [14].

The present case appears to be unique for several features: first, the finding of EBV mRNA in salivary gland tumours is quite rare in Caucasians and, to the best of our knowledge, has never been reported in a tu-

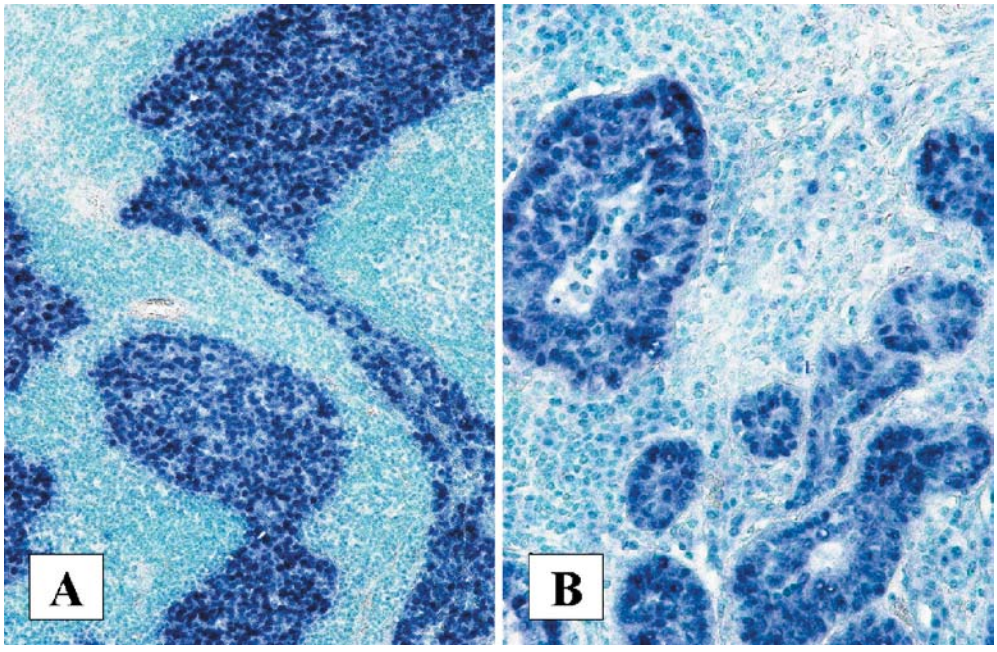


Fig. 4 In situ hybridisation for Epstein–Barr encoded RNA reveals the presence of Epstein–Barr virus either in the solid component (**A**) or in the glandular component (**B**), ×200

mour with myoepithelial differentiation. In addition, the association between lymphoepithelial carcinoma and a tumour with myoepithelial differentiation has never been recorded, and these findings open new possible pathways to the understanding of salivary gland malignancies. Finally, in our case, the lymphoepithelial carcinoma appears to be responsible for the clinical course of the disease, as lymph-node metastases were entirely composed of this tumour type. Therefore, the possible association between epithelial–myoepithelial carcinoma and lymphoepithelial carcinoma has to be kept in mind when dealing with a epimyoepithelial tumour, particularly if a lymphoplasmacytic stroma is present, in order to avoid erroneous diagnoses.

Acknowledgement The authors are grateful to Prof. Vincenzo Eusebi, Università di Bologna, for helpful suggestions.

References

1. Abdulla AK, Mian MY (1996) Lymphoepithelial carcinoma of salivary glands. Head Neck 18:577–581
2. Chan JKC, Yip TTC, Tsang WYW, Poon YF, Wong CSC, Ma VWS (1994) Specific association of Epstein–Barr virus with lymphoepithelial carcinoma among tumors and tumorlike lesions of the salivary gland. Arch Pathol Lab Med 118:994–997
3. Chetty R, Medley P, Essa A (2000) Hybrid carcinoma of salivary glands. Arch Pathol Lab Med 124:494–496
4. Croitoru CM, Suarez PA, Luna MA (1999) Hybrid carcinomas of salivary glands. Report of 4 cases and review of the literature. Arch Pathol Lab Med 123:698–702
5. Ellis GL, Auclair PL (1996) Tumors of the salivary glands. In: Atlas of tumor pathology, vol. 17, 3rd series, Armed Forces Institute of Pathology, Washington, DC
6. Jen KY, Cheng J, Li J, Wu L, Li Y, Yu S, Lin H, Chen Z, Gurtsevitich V, Saku T (2003) Mutational events in LMP1 gene of Epstein–Barr virus in salivary gland lymphoepithelial carcinomas. Int J Cancer 10:654–660
7. Kamio N, Tanaka Y, Mukai M, Ikeda E, Kuramochi S, Fujii M et al (1997) A hybrid carcinoma, adenoid cystic carcinoma and salivary duct carcinoma of the salivary gland: an immunohistochemical study. Virchows Arch 430:495–500
8. Nagao T, Ishida Y, Sugano I, Tajima Y, Matsuzaki O, Hino T, Kondo Y, Nagao K (1996) Epstein–Barr virus-associated undifferentiated carcinoma with lymphoid stroma of the salivary gland in Japanese patients. Comparison with benign lymphoepithelial lesion. Cancer 78:695–703
9. Nagao T, Sugano I, Ishida Y, Asoh A, Munakata K, Yamazaki K, Konno A, Iwaya k, Shimizu T, Serizawa H, Ebihara Y (2002) Hybrid carcinoma of the salivary glands: report of nine cases with a clinicopathologic, immunohistochemical, and p53 gene alteration analysis. Mod Pathol 15:724–733
10. Saw D, Lau WH, Ho JH, Chan JK, Ng CS (1986) Malignant lymphoepithelial lesion of the salivary gland. Hum Pathol 17:914–923
11. Seifert G, Donath K (1996) Hybrid tumours of salivary glands. Definition and classification of five rare cases. Eur J Cancer Oral Oncol 32:251–259
12. Snyder ML, Paulino AF (1999) Hybrid carcinoma of the salivary gland: salivary duct adenocarcinoma and adenoid cystic carcinoma. Histopathology 35:380–383
13. Worley NK, Daroca PJ Jr (1997) Lymphoepithelial carcinoma of the minor salivary gland. Arch Otolaryngol Head Neck Surg 123:638–640
14. Wu DL, Shemen L, Brady T, Saw D (2001) Malignant lymphoepithelial lesion of the parotid gland: a case report and review of the literature. Ear Nose Throat J 80:803–836
15. Zardawi IM (2000) Hybrid carcinoma of the salivary gland. Histopathology 37:283–284

Virchows Arch (2004) 445:429
DOI 10.1007/s00428-004-1133-y
© Springer-Verlag 2004

ANNOUNCEMENTS

22–24 November 2004
41st Nottingham Multi-disciplinary Course on breast disease
Nottingham, UK

For further information contact:
The Blamey Education Centre
Nottingham Breast Institute
City Hospital, Nottingham, NG5 1PB, UK
Tel.: 00 44 (115) 969 1689
E-mail: sbury@ncht.trent.nhs.uk

8–10 November 2004
Practical Adult Cardiovascular Pathology Course
Course organisers: Dr MN Sheppard/Dr Yen Ho

This particular "Hands On" course approaches in detail the problems that face the diagnostic pathologist when dealing with cardiovascular pathology both congenital and adult. The approach to a cardiac autopsy and sudden death will be emphasized. Cardiac specimens will be made available for analysis and practical demonstrations as well as video demonstrations will be highlighted. Organ retention will also be covered and minimal database for reporting cardiovascular specimens. A slide seminar with slides is included. The course is aimed at trainees studying for the MRCPATH and also senior pathologists who wish to update their knowledge.

Course fee: £ 400.00 (includes daily coffee, tea and lunch)
A special fee of £ 300.00 for juniors in training

For further information, please contact:
Short Course Office
National Heart and Lung Institute
Dovehouse Street
London SW3 6LY
Tel.: +44(0)20 7351 8172
Fax: +44(0)20 7351 8246
E-mail: shortcourse.NHLI@IC.AC.UK

8–10 December 2004
Combined Adult & Congenital Cardiovascular Pathology Course
Course Organisers: Dr MN Sheppard/Dr Yen Ho

This particular "Hands On" course approaches in detail the problems that face the diagnostic pathologist when dealing with cardiovascular pathology both congenital and adult. The approach to a cardiac autopsy and sudden death will be emphasized. Cardiac specimens will be made available for analysis and practical demonstrations as well as video demonstrations will be highlighted. Organ retention will also be covered and minimal database for reporting cardiovascular specimens. A slide seminar with slides is included. The course is aimed at trainees studying for the MRCPATH and also senior pathologists who wish to update their knowledge.

Course fee: £ 400.00 (includes daily coffee, tea and lunch)
A special fee of £ 300.00 for juniors in training

For further information, please contact:
Short Course Office
National Heart and Lung Institute
Dovehouse Street
London SW3 6LY
Tel.: +44(0)20 7351 8172
Fax: +44(0)20 7351 8246
E-mail: shortcourse.NHLI@IC.AC.UK

19–24 April 2005
10th International Congress on Oral Cancer
Crete, Greece

Creta Maris Conference Centre

- The 10th International Congress on Oral Cancer is supported by the World Health Organization, the International Union Against Cancer, the International Congress on Oral Cancer, the Hellenic Association for the Research and Treatment of Oral Cancer, and the Hellenic Cancer Society
- The Congress theme is *The Oral Cancer Patient: the anthropocentric approach to a multidisciplinary problem*
- A number of Keynote Lectures will be delivered by international leaders in their specialties
- Limited attendance Courses will be provided for interested participants
- Deadline for abstract submission: November 30th, 2004
- Accepted abstracts for oral and poster presentations will be published as a supplement to the journal Oral Oncology. Details at www.harcourt-international.com/journals/oron
- Social events include Presidents Reception, Cretan Night and Gala Dinner

Further details at www.icooc-2005.org or from the Congress President at rapidis@icooc-2005.org

13–24 June 2005
International course on Laboratory Animal Science
Utrecht, The Netherlands

A two week intensive course on laboratory animal science will be organized at the Division of Laboratory Animal Science – Utrecht, The Netherlands in June 2005. This course is organized once a year since 1993.
The objective of this course is to present basic facts and principles that are essential for the humane use and care of animals and for the quality of research.
The contents of the course are in line with recommendations of the Federation of European Laboratory Animal Science Associations (FELASA) regarding the training of the young scientist whose research involves the use of vertebrate animals.
The course may also be of interest for those who intend to set up a similar course at their location. For this purpose, during the course the acquisition of teaching materials can be discussed with the course committee.

For information and application forms please contact:
Mr. Stephan van Meulebrouck, MA
Division of Laboratory Animal Science
Faculty of Veterinary Medicine
P.O. Box 80.166
3508 TD Utrecht
The Netherlands
Tel.: +31-30-2532033
Fax: +31-30-2537997
E-mail: pdk@las.vet.uu.nl
Internet: http://las.vet.uu.nl>Education and Training>International Course

Virchows Arch (2004) 445:431–441
DOI 10.1007/s00428-004-1090-5

REVIEW ARTICLE

Jinru Shia · Nathan A. Ellis · David S. Klimstra

The utility of immunohistochemical detection of DNA mismatch repair gene proteins

Received: 28 June 2004 / Accepted: 12 July 2004 / Published online: 29 September 2004
© Springer-Verlag 2004

Abstract Since the development of monoclonal antibodies against the MSH2 protein by Leach et al. in 1996, a series of investigations has been undertaken to determine the utility of immunohistochemical detection of DNA mismatch repair (MMR) gene proteins in the identification of hereditary or sporadic colorectal tumors with microsatellite instability. These studies, however, have been performed with different aims and on different patient populations. Interpretation of these immunohistochemical data relies on a thorough understanding of the biological and technical factors that affect the detection of MMR proteins. In this review, we analyze the data from the published research studies, pointing out the various factors affecting immunohistochemical detection of MMR proteins and projecting the utility of immunohistochemistry in different clinical settings.

Keywords Microsatellite instability · DNA mismatch repair gene proteins · Immunohistochemistry

Introduction

The last decade saw a rapid advance in our understanding of colorectal carcinomas (CRCs) that harbor DNA mismatch repair (MMR) gene abnormalities [1]. It is now known that altered MMR gene function is associated with approximately 15% of all CRCs, which translates to around 20,000 cases per year in the United States. About one-third or fewer of these MMR-deficient CRCs arise in patients with the hereditary nonpolyposis colorectal cancer (HNPCC) syndrome, while the rest occur sporadically. It has been shown [2, 5, 36, 38, 63] that approximately 30–70% of patients with a clinical diagnosis of HNPCC have a germline mutation in one of the MMR genes, most commonly in *MLH1* or *MSH2*, less often in *PMS1*, *PMS2*, or *MSH6*. (A mutation database is available at http://www.nfdht.nl/database/mdbchoice.htm.) In those individuals with a germline mutation, inactivation of the second allele in a colonic crypt cell can result in the development of an HNPCC-type MMR-deficient tumor. Carriers of a mutation in *MLH1* or *MSH2* have up to a 70–80% lifetime risk of developing a CRC [3, 7, 59]. Hence, although HNPCC was originally defined based on clinical findings and family history, in a more strict sense, HNPCC is now molecularly defined as individuals carrying a disease-causing germline mutation in an MMR gene. In sporadic CRCs, MMR abnormality is largely but not exclusively caused by abnormal methylation of the promoter region of one MMR gene, *MLH1* [24, 29, 47, 63].

Irrespective of the underlying mechanisms, both hereditary and sporadic tumors with MMR abnormalities have a common molecular phenotype—microsatellite instability (MSI). This phenotype results from the fact that microsatellites, i.e., mono-, di-, tri-, or tetranucleotide repeat sequences within DNA, are hypersensitive to MMR dysfunction. These small repetitive sequences accumulate insertions or deletions of repeats during DNA replication. Failure of repair of mismatches immediately after replication because of MMR dysfunction causes contraction or expansion of repeat units, thereby exhibiting the genetic instability [32, 43].

The MSI status of a tumor can be detected using a polymerase chain reaction-based molecular assay. The National Cancer Institute [8] has recommended the use of a set of five microsatellite markers and defines the status of microsatellite stability as: high frequency MSI or MSI-H when one-third or more of the markers show a band shift in the tumor when compared with normal; low frequency MSI or MSI-L when less than one-third of the markers are abnormal; and microsatellite stable or MSS

J. Shia · D. S. Klimstra (✉)
Department of Pathology,
Memorial Sloan-Kettering Cancer Center,
1275 York Avenue, New York, NY 10021, USA
e-mail: klimstrd@mskcc.org
Tel.: +1-212-6392410
Fax: +1-212-7173203

N. A. Ellis
Department of Medicine,
Memorial Sloan-Kettering Cancer Center,
New York, NY, USA

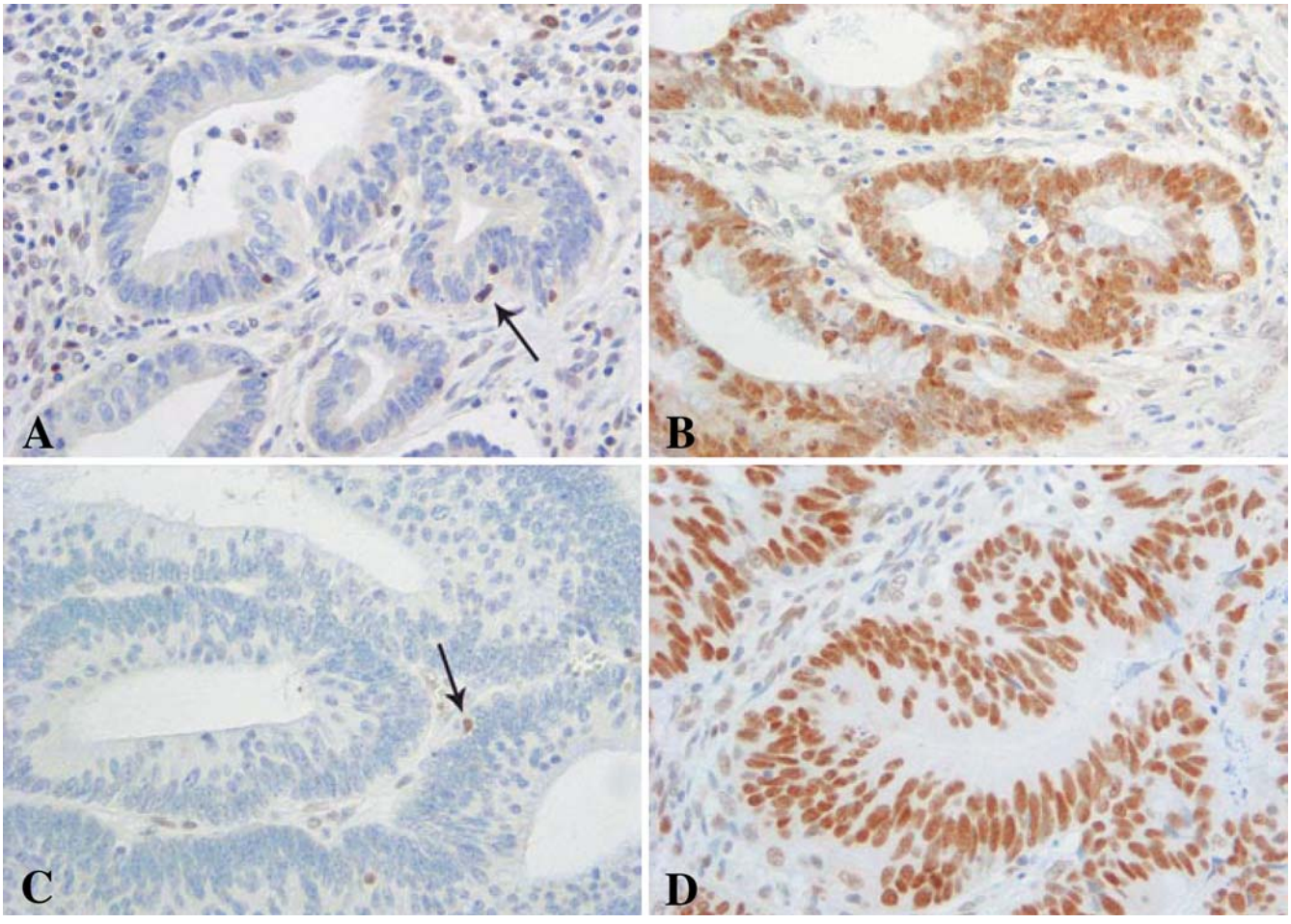


Fig. 1 Immunohistochemical staining demonstrating lack of expression of MLH1 (**A**) and MSH2 (**C**) in two adenocarcinomas (*arrow* indicating positively stained intraepithelial lymphocytes) and intact expression of these two proteins (**B** for MLH1, **D** for MSH2) in two other carcinomas

when no band shift is observed in any of the markers tested. This assay is now used as the gold standard to detect tumors with an abnormal MMR function [34, 40].

Because MSI testing is labor intensive, has a long turnaround time, and requires skilled molecular geneticists, with the development of monoclonal antibodies against MMR proteins, much research has been performed on the utility of immunohistochemistry (IHC) to predict MSI status. The research on IHC has been further promoted by our increasing understanding about the biology of CRCs that exhibit MSI. It has been shown that when compared with patients with MSS CRCs, patients with MSI tumors have a different clinical outcome and, most importantly, respond differently to certain treatment regimens [19, 48, 58]. As such, it is foreseeable that routine detection of the MSI phenotype will become important, and simple and universally available methods such as IHC will become valuable. Recent studies on validation of tissue microarray technology in immunohistochemical detection of MMR proteins [23, 28] have further expanded the field of investigation. Examples of immunohistochemical staining on MMR-proficient and -deficient CRCs are illustrated in Fig. 1. The numerous studies on IHC, however, have been performed with different aims, using different patient populations, and many biological, clinical, and technical issues may affect the assessment of IHC. Without a thorough literature review, it is difficult to extract answers to questions such as, what is the chance a tumor is MSI or has a germline mutation if tested abnormal by IHC or how best to incorporate IHC into the workup strategy for identifying HNPCC patients or sporadic MSI CRCs. Thus, the purpose of this review is to provide an objective appraisal of the utility of IHC, primarily in the detection of MLH1 and MSH2 proteins. We first analyzed data from various types of research studies, then identified issues affecting the interpretation of IHC, and, finally, projected its use in different clinical settings.

Review of the literature

The data in the literature on the utility of IHC are divided into two major categories: (1) quantitative—the sensitivity and specificity of IHC in predicting MSI or mutation

status in different patient populations and (2) qualitative—the staining adequacies and staining variabilities.

Sensitivity and specificity of IHC in predicting MSI or mutation status in different patient populations

The published studies can be divided into three major groups. Studies belonging to the first group aimed at analyzing the sensitivity and specificity of IHC in predicting MSI in general. The study subjects were composed of mixed familial and sporadic cases. The second group specifically assessed the sensitivity and specificity of IHC in predicting MSI in consecutive or sporadic CRC series. A few studies in this group also analyzed the association between IHC and abnormal methylation in the *MLH1* promoter region in sporadic cases. Finally, the third group assessed the utility of IHC in hereditary conditions by analyzing the ability of IHC in predicting disease-causing germline mutations in MMR genes.

A relatively large number of studies on IHC belongs to the first group [9, 12, 17, 18, 22, 37, 41, 50, 54]. These studies primarily assessed the sensitivity and specificity of immunohistochemical method in detecting MSI phenotype in colorectal tumors, irrespective of the clinical setting, i.e., hereditary or sporadic. The study subjects were often selected from patient series for which MSI testing had been performed for other purposes. MSI-positive cases were often derived from high-risk patient series (patients fulfilling Amsterdam Criteria or other clinical criteria for HNPCC, patients with synchronous or metachronous CRCs, or early onset CRCs). However, the group of tumors that did not exhibit MSI was often composed of consecutive or sporadic cases. A more detailed listing of patient composition of these studies is provided in Table 1. Overall, as shown in Table 1, the sensitivity of IHC in detecting MSI ranged from 77% to 100%, whereas the specificity has been greater than 99%.

Studies belonging to the second group or containing data belonging to this group are summarized in Table 2. The study subjects of these studies were either consecutive [13, 35, 49, 54, 56] or "sporadic" patients with colorectal cancers [11, 12, 16, 27, 30, 33, 62]. In most studies, the definition of "sporadic" was clinical (i.e., patients who do not fulfill Amsterdam Criteria) [11, 12, 14, 62] and, in one study, genetic (i.e., patients without germline mutation in *MLH1* or *MSH2* genes) [33]. Overall, as summarized in Table 2, the sensitivity of IHC in predicting MSI ranged from 75% to 100%, with an average of 90% (weighted for sample size). Its specificity was greater than 99%. Not surprisingly, in these consecutive and sporadic groups of patients, a large proportion of IHC-abnormal cases (79%) were due to lack of MLH1 protein expression.

A few studies specifically analyzed the association between IHC with the MLH1 antibody and abnormal methylation in the promoter region of the *MLH1* gene in sporadic cases (Table 3) [29, 31, 33, 51]. Although the numbers in these studies are small, there is a strong correlation between hypermethylation in the *MLH1* promoter and lack of MLH1 protein expression.

Finally, other studies have correlated immunohistochemical detection of MMR proteins with germline mutations using familial cases for which the mutational status was known. As summarized in Table 4, the sensitivity and specificity of IHC in predicting germline mutations in this group appear less favorable than that in consecutive or sporadic series, although the studies in this group are almost invariably limited by small sample sizes (Table 3) [14, 18, 21, 23, 25, 41, 51, 52, 54, 55, 61]. We have recently analyzed the performance of IHC in predicting *MLH1* and *MSH2* germline mutations in a group of 110 patients with strong family histories of colorectal cancer (data to be published) and found that IHC had an overall sensitivity of 78% in identifying tumors that had a disease-causing germline mutation in either one of these two genes. When we combine our data with that reported in the literature, IHC has an overall sensitivity of 82% in detecting disease-causing germline mutations in the two commonly affected genes. It becomes apparent upon analyzing the data that this relatively low sensitivity of IHC in detecting germline mutation largely stems from a lower detection rate of cases with *MLH1* germline mutations using IHC with the MLH1 antibody [14, 23, 61]. As summarized in Table 4, IHC with the MLH1 antibody detected only 74% (weighted for sample size) of cases that had a *MLH1* germline mutation, with a specificity of 81%. However, IHC with the MSH2 detected 91% (weighted for sample size) of the cases with an *MSH2* germline mutation, with a specificity of 90%.

The sensitivity of IHC in predicting *MLH1* or *MSH2* germline mutation in patients with known mutation status appears comparable with that of MSI testing as shown by one relatively large study [51]. In this study, the authors analyzed both IHC and MSI in 30 patients with known *MLH1* (n=22) or *MSH2* (n=8) germline mutations and found the sensitivity in predicting *MLH1* mutation to be 70% for IHC and 86% for MSI testing. Both methods detected 100% of *MSH2* mutation carriers in this study.

In summary, IHC has an overall sensitivity of approximately 90% and specificity of greater than 99% in detecting MSI colorectal tumors in consecutive and sporadic series. However, in pure hereditary cases, the sensitivity of IHC in predicting germline mutations in *MLH1* and *MSH2* genes drops to 82%, largely owing to its lower sensitivity in detecting *MLH1* mutation (74%). IHC detects 91% of the cases with disease-causing *MSH2* germline mutations. The specificity of IHC in detecting *MLH1* mutation and *MSH2* mutation was 81% and 90%, respectively. The data obtained from the first group of studies that used mixed patient populations confirm the overall utility of IHC in predicting MSI status. However, the heterogeneous composition of the study subjects limits their value in guiding the use of IHC in different clinical settings.

Table 1 Use of immunohistochemistry (IHC) in detecting microsatellite instability (MSI) in mixed study populations. *CRCs* colorectal carcinomas, *HNPCC* hereditary nonpolyposis colorectal cancer, *AC* Amsterdam Criteria, *ICG* International Collaborative Group

Reference	*n*	Patient composition	Sensitivity (abnormal IHC/MSI-H)			Specificity (normal IHC/non-MSI)
			Overall	MLH1	MSH2	
[37] Lindor 2002	1144	1. Cooperative familial cancer registry cases (*n*=753) 2. Consecutive series (*n*=391)	92% (323/350)	65% (228/350)	27% (95/350)	100% (794/794)
[9] Cawkwell 1999	275[a]	1. Early onset CRC (*n*=23) 2. Synchronous CRC (*n*=106) 3. Metachronous CRC (*n* =47) 4. Late onset CRC (*n*=99)	100% (82/82)	83% (68/82)	13% (14/82)	100% (54/54)
[12] Chiaravalli 2001	201[b]	1. Patients with CRCs fulfilling AC I or II (*n*=12) 2. Endometrial, gastric and ovarian, HNPCC or familial[b] (*n*=8) 3. Patients not fulfilling above criteria (sporadic) (*n*=60 for CRCs, *n*=121 for non-CRCs)	93% (51/55)	78% (43/55)	15% (8/55)	99.3% (145/146)
[50] Ruszkiewicz 2002	742[c]	1. Patients fulfilling modified Bethesda Criteria 2. Consecutive right hemicolectomies (*n*=204) 3. Consecutive resections for CRCs (*n*=135)	90% (168/187)[d]	68% (127/187)	22% (42/187)	99.8% (554/555)
[17] Dietmaier 1997	58	1. Patients fulfilling AC (*n*=4) 2. Patients fulfilling relaxed AC (*n*=5) 3. Patients with three metachronous cancers but not meeting AC (*n*=1) 4. Early onset CRC (<45 years) (*n*=5) 5. "Sporadic" CRC without any of the above features (*n*=43)	93% (14/15)	53% (8/15)	40% (6/15)	100% (43/43)
[41] Marcus 1999	72	1. Patients fulfilling AC or less stringent local criteria for HNPCC (*n*=33, 28 MSI[e]) 2. Patiens from a "population-based" study- family history not available (*n*=39, 10 MSI)	97% (37/38)[f]	59% (22/38)	42% (16/38)	100% (34/34)
[18] Dieumegard 2000	31	1. ICG HNPCC (*n*=10) 2. Incomplete HNPCC (*n*=7) 3. Clinic-based population prospectively selected solely on the criterion of age $\leq$50 years at diagnosis of CRC (*n*=17)	77% (10/13)	54% (7/13)	23% (3/13)	100% (18/18)
[54] Stone 2001	46	All early onset CRCs (<55 years)	96% (22/23)	74% (17/23)	22% (5/23)	100% (23/23)
[22] Halvarsson 2004	128	1. Patients fulfilling AC I or II (*n*=52) 2. Patients fulfilling less stringent AC (*n*=48) 3. CRC at young age (23–53 years, mean 38 years) (*n*=21) 4. Patients with metachronous HNPCC-type cancers (*n*=7)	84% (50/59)[g]	47% (28/59)	37% (22/59)	100% (69/69)
Total	2697		92% (757/822)	67% (548/822)	26% (211/822)	>99% (1734/1736)

[a] Included two additional series for "confirmation of immunohistochemical detection of RER positivity" and "prospective feasibility study". Data on these two series are not included in this table

[b] Included non-colonic, HNPCC-type tumors. "Endometrial, gastric and ovarian cancers classified as familial when at least two cases of the same malignant tumor observed in 1st degree relatives"

[c] Included 661 colorectal tumors and 81 extracolonic tumor belong to the HNPCC spectrum

[d] The study also reported three MSI tumors lacking MSH6 expression, one lacking PMS2 expression, data not included in the calculation in this table. Included in the calculation was one case showing concurrent loss of MLH1 and MSH2 expression

[e] Included 25 colorectal tumors and 3 endometrial carcinoma

[f] One case showed concurrent loss of MLH1 and MSH2

[g] The study also reported four MSI tumors lacking MSH6 expression alone. These four cases were not included in the calculation in this table

Table 2 Use of immunohistochemistry (IHC) in detecting microsatellite instability (MSI) in consecutive/sporadic patient populations. *CRCs* colorectal carcinomas, *HNPCC* hereditary nonpolyposis colorectal cancer, *AC* Amsterdam Criteria, *FAP* familial adenomatous polyposis, *IBD* Inflammatory bowel disease

Reference	*n*	Patient composition	Sensitivity (abnormal IHC/MSI-H)			Specificity (normal IHC/non-MSI-H)
			Overall	MLH1	MSH2	
[13] Cunningham 2001	257	Consecutive series	100% (51/51)	94% (48/51)	6% (3/51)	100% (206/206)
[56] Thibodeau 1998	188	Consecutive surgical cases	95% (40/42)	90% (38/42)	5% (2/42)	100% (146/146)
[35] Lanza 2002	305	CRC resected in one institution (1999–2000). Selection based solely on tissue availability. FAP and IBD excluded.	91% (120/132)	80% (106/132)	11% (14/132)	100% (173/173)
[49] Rigau 2003	204[a]	Consecutive series (9/204 fulfilled AC or Bethesda criteria.	94% (29/31)[b]	71% (22/31)	23% (7/31)	100% (173/173)
[62] Ward 2001	308	Sporadic by clinical criteria[c]	82% (27/33)	73% (24/33)	9% (3/33)	99.6% (274/275)
[11] Chaves 2000	76	Sporadic by clinical criteria[c]	75% (6/8)	62.5% (5/8)	12.5% (1/8)	95.6% (65/68)
[12] Chiaravalli 2001	60	Sporadic by clinical criteria[c]	85.7% (12/14)			100% (46/46)
[27] Jeong 2003	230	Sporadic by clinical criteria[c]	95.2% (20/21)	66.6% (14/21)	28.6% (6/21)	100% (209/209)
[30] Kim 1998	32	Sporadic by clinical criteria[c]	83.3% (5/6)[d]	33.3% (2/6)	66.7% (4/6)	100% (26/26)
[33] Kuismanen 2000	51[d]	Sporadic by genetic criteria[e]	80% (37/46)	78% (36/46)	15% (7/46)	–
[16] Deng 2002	63	Sporadic by clinical criteria[c]	75% (12/16)	56.3% (9/16)	18.7% (3/16)	100%(47/47)
Total	1774		90% (359/400)	79% (304/386)	13% (50/386)	>99% (1365/1369)

[a] Included a small percentage of HNPCC-related extra-colonic tumors
[b] The study also reported four tumors lacking PMS2 alone (all MSS) and two tumors lacking MSH6 alone (all MSI), data not included in the calculation in this table
[c] Clinical criteria imply lack of AC I or II
[d] One MSI case showed simultaneous loss of both MLH1 and MSH2 expression
[e] The case series was defined as "true" sporadic by virtue of lack of germline mutation in MLH1 or MSH2. Some of the abnormal IHC cases were defined as abnormal when there is reduced staining, i.e., staining in <25% of the tumor

Table 3 Correlation of abnormal methylation and MLH1 immunohistochemistry (IHC) in sporadic colorectal tumors

Reference	Patient composition	Methylation	
		Abnormal IHC/abnormal MLH1 methylation	Normal IHC/no methylation
[33] Kuismanen 2000	Sporadic[a]	30/36	
[29] Kane 1997	Sporadic by clinical criteria[b]	4/4	9/9
[31] Kim 2003	Sporadic by clinical criteria[b]	7/7	
[51] Salahshor 2001	Sporadic by clinical criteria[b]	7/7	
[16] Deng 2002	Sporadic by clinical criteria[b]	7/7[c]	

[a] The case series was defined as true sporadic by virtue of lack of germline mutation in MLH1 or MSH2. Some of the abnormal IHC cases were defined as abnormal when there is reduced staining, i.e., staining in <25% of the tumor
[b] Clinical criteria imply lack of Amsterdam Criteria I or II
[c] ndicates methylation at CpG sites in a proximal region of MLH1 promoter

Staining variability

Although IHC with MLH1 and MSH2 antibodies often yields satisfactory staining results, a number of studies have noted that staining variabilities or inadequacies do exist. There are three major types of staining variability noted in the literature. First, some cases show un-interpretable staining because of lack of definitive positive staining in normal cells in the same slide [14, 55, 62]. The reported frequency of this phenomenon varied from 0.6% (2 of 308 sporadic tumors) [62] to 13% (5 of 38 hereditary tumors) [55]. Such ambiguity has resulted in either elimination of questionable cases from the analysis [55] or inclusion as cases with probable absent of protein expression [14]. Second, there are tumors that show staining heterogeneity or only weak or focal staining [12, 15, 22, 26, 33, 50]. As many studies defined "loss of expression" as "absent nuclear staining in all malignant cells" [11, 13, 27, 31, 49, 51, 62], tumors with weak or focal staining usually have been regarded as having intact protein expression. However, a few more recent studies have investigated the possibility that weak or heterogeneous staining may be associated with gene defects in some cases [22, 33]. Third, aberrant cytoplasmic or membra-

Table 4 Use of IHC in predicting germline mutation in mismatch repair (MMR) genes in familial cases with known mutation status. *IHC* immunohistochemistry

Ref	Sensitivity (*n* with abnormal IHC/*n* with pathogenic mutation)			Specificity (*n* with normal IHC/*n* with no mutation detected)	
	Overall	MLH1	MSH2	MLH1	MSH2
[51] Salahshor 2001	22/28	14/20	8/8	–	–
[15] Debniak 2000	4/6	2/4	2/2	18/19	19/19
[52] Scartozzi 2002	3/4	2/2	1/2		
[23] Hendriks 2003	29/33	18/21	11/12	–	–
[41] Marcus 1999	16/16	5/5	11/11	–	–
[21] Furukawa 2002	8/8	3/3	5/5		
[54] Stone 2001	4/4	4/4		6/19[a]	14/19
[61] Wahlberg 2002	4/9	1/5	3/4	12/13	14/18
[55] Terdiman 2001	11/13	6/7	5/6		
[18] Dieumegard 2000	5/7	3/4	2/3	11/15	14/15
[25] Hoedema 2003	4/4	–	4/4		
Our series[a]	25/32	4/9	21/23	95% (41/43)	98% (41/42)
Total	82% (135/164)	74% (62/84)	91% (73/80)	81% (88/109)	90% (102/113)

[a] Data to be published

nous staining has also been noted in some studies [26, 50, 51]. The exact frequency of staining heterogeneity or cytoplasmic or membranous staining is unknown.

However, some groups have encountered no staining variability and found no difficulty in interpreting the stains [9, 54]. In one study, there was "clear cut staining quality," as none of the 502 carcinomas investigated showed heterogeneity of staining, i.e., "tumor cells in all cases were either totally positive or totally negative" [9].

What factors may affect the assessment of IHC

To best understand the value of IHC and the implications of data derived from different studies with different designs, it is important to analyze the variety of biological and technical factors, as well as the current gold standards in detecting MMR abnormality, which could potentially affect IHC or the assessment of IHC.

Biological factors

A variety of biological factors affect the expression of MMR gene proteins. In the hereditary setting, the first and foremost factor relates to the fact that different MMR gene mutations have different affects on protein expression. It is estimated that the distribution of disease-causing germline mutations is roughly equal between *MLH1* and *MSH2* genes [45, 57]. Most mutations in *MSH2* are protein truncating; consequently, most CRCs arising in *MSH2* mutation carriers are expected to show absent MSH2 protein expression using IHC. However, approximately half of the mutations in *MLH1* genes are missense mutations, which usually result in mutant proteins that are catalytically inactive but antigenically intact [39, 46, 51, 61]. Moreover, even protein truncating mutations in *MLH1* can result in a protein that reacts with the commonly used MLH1 antibody [61]. These observations can explain the lower sensitivity of IHC in predicting germline mutation in *MLH1*; it may also explain the focal or weak staining in some cases [22, 33].

In sporadic colorectal cancers, most cases (>90%) with MMR abnormalities acquire an MSI phenotype via hypermethylation of the promoter region of the *MLH1* gene. Such a defect most often results in complete silencing of transcription and loss of protein expression. Thus, a significantly higher percentage of sporadic MSI CRCs show negative MLH1 staining using IHC. However, there are data suggesting that the promoter of *MLH1* gene can be partially methylated [16, 20, 42], and partial methylation can result in decreased expression of MLH1, providing a possible explanation for the occurrence of staining heterogeneity.

Other biological factors explain why the extent of abnormalities detected using IHC is limited by the antibodies employed. Although the widely used MLH1 and MSH2 antibodies cover the two most commonly involved genes, defects in the expression of other genes have been detected. In hereditary cases, disease-causing mutations of *MSH6* and *PMS2* have been associated with MSI in CRCs. In sporadic cases, although those cases resulting from promoter hypermethylation may be identified using IHC, those that result from somatic mutations in one of the MMR genes other than *MLH1* or *MSH2* may be missed.

Last, interactions among MMR proteins may also affect the sensitivity of IHC in detecting individual proteins. For example, it is known that MSH2 forms heterodimers with both MSH3 and MSH6 [4, 6]. Negative staining for both MSH2 and MSH6 is common in tumors from *MSH2* mutation carriers[23]. It is speculated that deficiencies of MSH2 cause destabilization of MSH6. Alternatively, the defect in MMR caused by loss of MSH2 may result in selective mutation of the *MSH6* gene. Similarly, MLH1 forms heterdimers with PMS2 [65]. Thus, adding MSH6 and PMS2 antibodies to the staining panel may increase the overall sensitivity of IHC. Furthermore, the detection of MSH6 or PMS2 protein loss using IHC may help identify mutations in these genes, which are otherwise

less often tested for mutation by clinical molecular genetics laboratories.

Technical factors

The importance of technical protocol components to successful immunohistochemical staining of MMR proteins has been analyzed. Muller et al. [44] assembled a set of 20 colorectal carcinoma cases of known *MLH1* and *MSH2* mutation and expression status and distributed the tumors among multiple institutions to test the performance of IHC. Each institution used its own technical protocol. Staining for MSH2 was successful in most laboratories, while staining for MLH1 proved problematic in multiple laboratories. The major cause of misinterpretation and discordance was technically suboptimal preparations. However, 4 of 16 laboratories demonstrated excellent results, including high discriminatory power with both monoclonal antibodies. These laboratories appropriately identified *MLH1* or *MSH2* inactivation with high sensitivity and specificity. The key protocol point associated with successful staining was an antigen retrieval step involving heat treatment and either ethylenediaminetetraacetate or citrate buffer. This step is, however, integral to the staining protocol in the majority of the published studies [11, 51, 52, 62], including studies that had a high percentage of ambiguous staining [55]. It should be noted here that antigen retrieval may be technically less reliable for older tissue blocks, as pointed out by some investigators [11, 12].

The specific antibody clone used for a particular protein is also an important component to successful staining. For detection of MLH1 protein, the most commonly used antibody is a murine immunoglobulin G (IgG) monoclonal antibody raised against full-length MLH1 protein from BD PharMingen. Different clones of this antibody have been used in different studies. Chiaravalli et al. [12] pointed out that clone G168–15 may be more sensitive and reproducible than the clone G168–728. However, a clear advantage to this clone is not apparent upon review of the reported studies. The specific location of the epitope of this antibody is not known. A definitive localization of the epitope may help correlate a false-positive IHC and the type of *MLH1* mutation. For detection of MSH2 protein, the most commonly used antibody is a murine IgG monoclonal antibody against the carboxy-terminal fragment of MSH2 protein, clone FE11 from Calbiochem, Oncogene Research Products or Oncogene Sciences (all three companies are related to EMD Biosciences). Overall, the staining quality of MSH2 antibodies has been more satisfactory and may, at least in part, be related to the fact that MSH2 abnormality is mainly related to truncating mutations.

The importance of adequate tissue sampling for both immunohistochemical and MSI testing appears obvious. Identical samples will yield the most valid correlation between immunohistochemical and MSI results. Indeed, discordant tissue samples, such as fresh frozen tissue for MSI testing and paraffin block of different tumor areas for IHC, have been the reason for discordant results in certain cases [10, 62], and the highest correlation between immunohistochemical and MSI testing has been demonstrated when identical tissue samples were used for both methods using microdissection techniques [10].

Another clinical scenario where special attention to sampling is needed is with tumors that have been subjected to neoadjuvant therapy. Discrepant immunohistochemical and MSI results have indeed been shown to occur in post-neoadjuvant therapy tumors that had but a few residual tumor cells remaining [37]. It was postulated that the very few tumor cells in the specimen may not have been enough to yield an MSI-H phenotype due to stromal contamination but may have been sufficient to be detected as islands of MMR protein-deficient tumor cells using IHC [37].

The standards against which IHC has been evaluated

The utility of IHC has been tested mainly against MSI or mutational status. However, these two methods (MSI testing and mutation analysis) are subject to biological and technical variability as well.

Major factors affecting MSI testing include: (1) the markers used (some studies used the NCI-suggested set of five markers [10, 23, 25, 31]; others used more [11, 13, 21, 52] or less [12] markers); (2) the definition for MSI-H (some used 30% of the markers positive as the cutoff for MSI-H [10, 11, 13, 23, 31, 52], others used 40%[21]; still others relied solely on the status of BAT-25 and/or BAT-40 [12] or BAT-26 [27]); (3) the type of tissue used (fresh frozen tissue [21, 35, 62] or paraffin-embedded tissue [27, 52] or a combination of both [10, 11, 12, 13]); and (4) the precision involved in tissue dissection [10]. These factors may at least in part be the reasons that MSI status has not been consistently in perfect match with stringent Amsterdam criteria [21], mutational status [39, 51, 52], or the status of MMR gene promoter hypermethylation [33].

It has been pointed out that the commonly employed mutation detection methods do not detect all the pathogenic mutations in *MLH1* or *MSH2* [60]. Mutations may be present in sequences not subjected to analysis (e.g., promoter regions or deep intronic regions), or they may consist of large genetic rearrangements that are not detected by DNA sequence analysis. Other reasons for missing mutations by sequence analysis include insensitive technique (e.g., analysis using a pre-screening meth-od such as the single stranded conformation polymorphism technique or analysis of mRNA is not as sensitive when the mutation causes instability of the mRNA), faulty interpretation, and laboratory error (e.g., a mutation in a splice site that is not coding but can cause disease). Using other methods, such as haploid conversion technology, may increase the sensitivity of mutation detection [64]. However, haploid conversion is expensive; once a mutation is missed by standard methods, the investigation of a potential mutation-bearing family enters an intensive

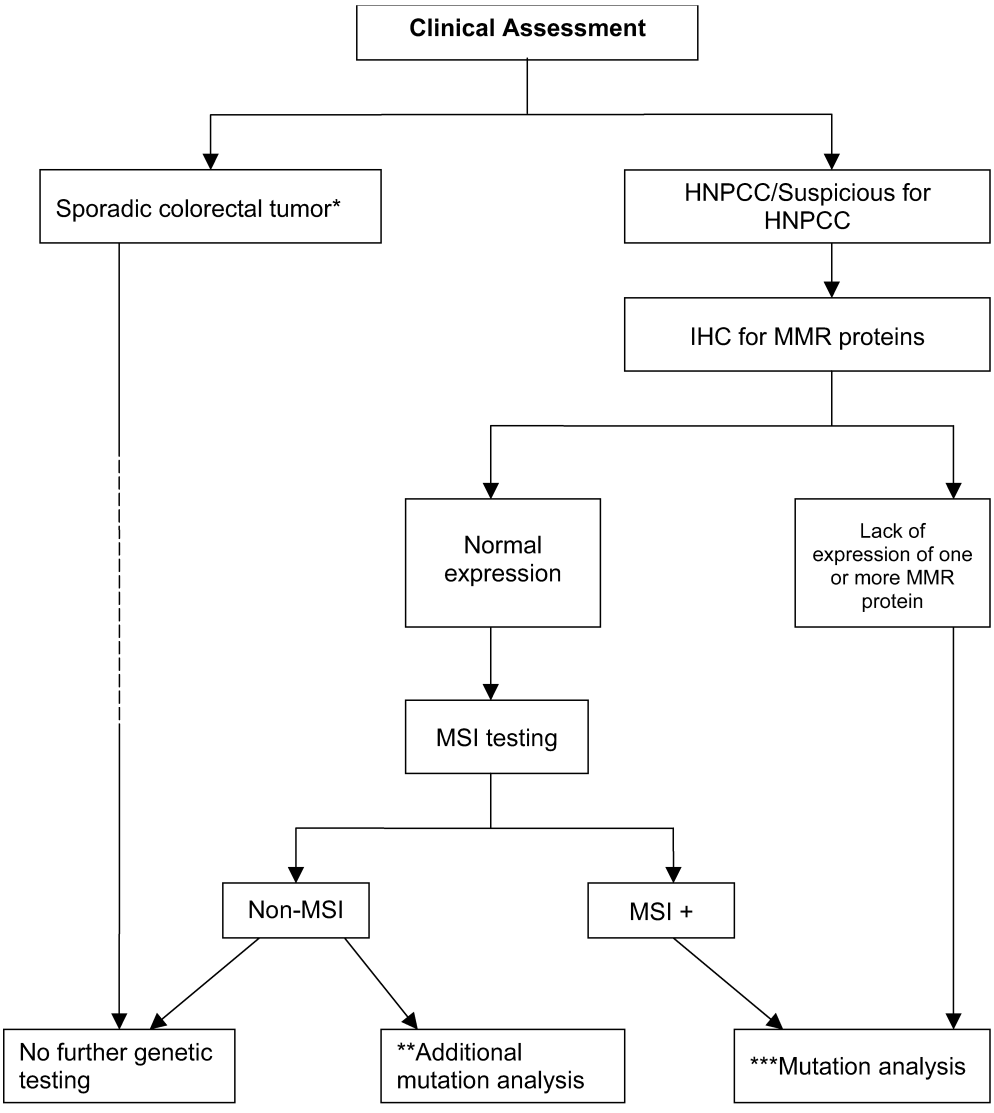


Fig. 2 Work-up algorithm for identification of colorectal tumors with MMR abnormality

* A subset of clinically sporadic cases maybe judged suspicious for MSI by tumor histology. We strongly recommend such cases be tested by IHC, particularly when the patient is young. This may help detect HNPCC probands. Currently, there is no pressing clinical need for genetic testing for MMR function for "true" sporadic CRCs.

** Additional mutation analysis may be pursued if clinically judged necessary.

*** In cases where an abnormality is detected by either IHC or MSI testing or both but no mutation is detected using commonly employed methods, additional analysis should be performed, including testing for additional defects such as deletion mutations or, testing of other MMR genes or linkage analysis.

phase. The relatively less than optimal sensitivity of commonly used mutation detection methods might have been part of the reason that IHC exhibited a reduced specificity in predicting the absence of a mutation, i.e., abnormal IHC has been noted in a small but definite number of cases in which a germline mutation in an MMR gene was not detected (Table 4).

Summary

The various biological and technical factors discussed above apparently are the main reasons that IHC fails to identify a certain proportion of tumors exhibiting MSI or carrying a disease-causing germline mutation. The higher false-negative rate of IHC in CRCs derived from *MLH1* germline mutation carriers is largely because of the nature of the commonly seen germline mutations in *MLH1* and the limitations of IHC. Similarly, a higher sensitivity of IHC in detecting MSI in sporadic or consecutive series is explained by the nature of the MMR abnormality involved in most of such cases, i.e., hypermethylation of the promoter region of the *MLH1* gene with loss of protein expression. The types of mutation as well as the possibility of partial methylation are also reasons for partial protein loss and IHC staining heterogeneity.

Staining variability, however, is an issue of concern, and it requires additional investigation. A small but definite number of cases that were either eliminated from analysis because of "poor quality" or considered "IHC normal" in some studies may, in fact, be tumors with MMR abnormalities. Better definition of "abnormal immunohistochemical expression" and better denotation of findings such as "heterogeneous staining" and "variation in staining intensity" may be enhanced by a better understanding of the underlying biology of MMR abnormalities. Improvement in immunohistochemical methodology is also highly desirable. Further efforts should be geared toward (1) refining the immunohistochemical antibodies, particularly the MLH1 antibody, (2) standardizing and optimizing the protocols for tissue fixation and for the immunohistochemical staining procedure, and (3) ensuring sufficient well-preserved tumor tissue in each sample.

The potential utility of IHC in different clinical settings

Although limitations to IHC do exist, owing to the various biological and technical factors, this methodology at the current stage is still very valuable, particularly taking into consideration its simplicity and easy availability. It should serve as a complementary test, which would reduce the number of cases to be tested by MSI. The potential utility of IHC in different clinical settings is outlined below and is also illustrated in Fig. 2.

IHC should be incorporated into the workup algorithm in detecting familial cases with MMR abnormalities. Such an algorithm starts with clinical assessment and pedigree investigation. IHC should be used as the first-line test for definitive or suspicious HNPCC patients as judged by clinical criteria (Amsterdam and Bethesda criteria). Should IHC indicate lack of expression of one or more MMR proteins, the patient can go directly to mutation analysis. If no immunohistochemical abnormality is detected, MSI testing would then be performed, and patients with positive MSI would then undergo mutation analysis. For patients with negative IHC and negative MSI, sequencing for mutations usually would not be recommended, although it may be pursued if clinically judged necessary, for example, in a person from a family in which tumor material is unavailable for testing. In cases where an abnormality is detected using either IHC or MSI testing, but no mutation is detected using commonly employed methods, additional analyses would be performed, including testing for additional genetic mutations, such as deletions and insertions, testing of other MMR genes, or linkage analysis.

The need to define the status of MMR function in a sporadic CRC that is clinically not suspicious for HNPCC is not as strong at the present time. However, there exists a group of patients about whom there may be no clinical suspicion for HNPCC, and yet on pathological examination, their tumors show morphological features suggesting an MSI phenotype [53], such as increased intraepithelial lymphocytes, a right-sided mucinous carcinoma, medullary type, poor differentiation, or marked morphological heterogeneity. It is likely a small subset of these patients may be probands of an HNPCC family, particularly if the patient is young. As such, we strongly recommend that tumors of this group be tested for MMR protein expression using IHC. Should IHC show abnormal expression of an MMR protein, further analysis should be performed to determine whether the case is caused by methylation of the *MLH1* promoter or by mutation in an MMR gene.

Although IHC for true sporadic CRCs is currently limited to research protocols and trials, it is foreseeable that as the prognosis of MMR-abnormal CRCs and the role of MMR function in tumor response to therapeutic agents become better defined [48] and specific treatment regimens become tailored to the MSI phenotype, IHC for detecting MMR abnormalities will become a routine test for every CRC in our practice. Should a tumor be tested abnormal in either MLH1 or MSH2 expression, the patient will then be managed according to new guidelines for MSI CRCs.

References

1. Aaltonen LA, Peltomaki P, Leach FS, Sistonen P, Pylkkanen L, Mecklin JP, Jarvinen H, Powell SM, Jen J, Hamilton SR et al (1993) Clues to the pathogenesis of familial colorectal cancer. Science 260:812–816
2. Aaltonen LA, Salovaara R, Kristo P, Canzian F, Hemminki A, Peltomaki P, Chadwick RB, Kaariainen H, Eskelinen M, Jarvinen H, Mecklin JP, de la Chapelle A (1998) Incidence of hereditary nonpolyposis colorectal cancer and the feasibility of molecular screening for the disease. N Engl J Med 338:1481–1487
3. Aarnio M, Sankila R, Pukkala E, Salovaara R, Aaltonen LA, de la Chapelle A, Peltomaki P, Mecklin JP, Jarvinen HJ (1999) Cancer risk in mutation carriers of DNA-mismatch-repair genes. Int J Cancer 81:214–218
4. Acharya S, Wilson T, Gradia S, Kane MF, Guerrette S, Marsischky GT, Kolodner R, Fishel R (1996) hMSH2 forms specific mispair-binding complexes with hMSH3 and hMSH6. Proc Natl Acad Sci U S A 93:13629–13634
5. Bapat BV, Madlensky L, Temple LK, Hiruki T, Redston M, Baron DL, Xia L, Marcus VA, Soravia C, Mitri A, Shen W, Gryfe R, Berk T, Chodirker BN, Cohen Z, Gallinger S (1999) Family history characteristics, tumor microsatellite instability and germline MSH2 and MLH1 mutations in hereditary colorectal cancer. Hum Genet 104:167–176
6. Berends MJ, Wu Y, Sijmons RH, Mensink RG, van der Sluis T, Hordijk-Hos JM, de Vries EG, Hollema H, Karrenbeld A, Buys CH, van der Zee AG, Hofstra RM, Kleibeuker JH (2002) Molecular and clinical characteristics of MSH6 variants: an analysis of 25 index carriers of a germline variant. Am J Hum Genet 70:26–37
7. Boland CR (2000) Molecular genetics of hereditary nonpolyposis colorectal cancer. Ann N Y Acad Sci 910:50–61
8. Boland CR, Thibodeau SN, Hamilton SR, Sidransky D, Eshleman JR, Burt RW, Meltzer SJ, Rodriguez-Bigas MA, Fodde R, Ranzani GN, Srivastava S (1998) A National Cancer Institute Workshop on Microsatellite Instability for cancer detection and familial predisposition: development of international criteria for the determination of microsatellite instability in colorectal cancer. Cancer Res 58:5248–5257

9. Cawkwell L, Gray S, Murgatroyd H, Sutherland F, Haine L, Longfellow M, O'Loughlin S, Cross D, Kronborg O, Fenger C, Mapstone N, Dixon M, Quirke P (1999) Choice of management strategy for colorectal cancer based on a diagnostic immunohistochemical test for defective mismatch repair. Gut 45:409–415
10. Chapusot C, Martin L, Bouvier AM, Bonithon-Kopp C, Ecarnot-Laubriet A, Rageot D, Ponnelle T, Laurent Puig P, Faivre J, Piard F (2002) Microsatellite instability and intratumoural heterogeneity in 100 right-sided sporadic colon carcinomas. Br J Cancer 87:400–404
11. Chaves P, Cruz C, Lage P, Claro I, Cravo M, Leitao CN, Soares J (2000) Immunohistochemical detection of mismatch repair gene proteins as a useful tool for the identification of colorectal carcinoma with the mutator phenotype. J Pathol 191:355–360
12. Chiaravalli AM, Furlan D, Facco C, Tibiletti MG, Dionigi A, Casati B, Albarello L, Riva C, Capella C (2001) Immunohistochemical pattern of hMSH2/hMLH1 in familial and sporadic colorectal, gastric, endometrial and ovarian carcinomas with instability in microsatellite sequences. Virchows Arch 438:39–48
13. Cunningham JM, Kim CY, Christensen ER, Tester DJ, Parc Y, Burgart LJ, Halling KC, McDonnell SK, Schaid DJ, Walsh Vockley C, Kubly V, Nelson H, Michels VV, Thibodeau SN (2001) The frequency of hereditary defective mismatch repair in a prospective series of unselected colorectal carcinomas. Am J Hum Genet 69:780–790
14. Debniak T, Kurzawski G, Gorski B, Kladny J, Domagala W, Lubinski J (2000) Value of pedigree/clinical data, immunohistochemistry and microsatellite instability analyses in reducing the cost of determining hMLH1 and hMSH2 gene mutations in patients with colorectal cancer. Eur J Cancer 36:49–54
15. Debniak T, Gorski B, Cybulski C, Jakubowska A, Kurzawski G, Kladny J, Lubinski J (2001) Comparison of Alu-PCR, microsatelite instability, and immunohistochemical analyses in finding features characteristic for hereditary nonpolyposis colorectal cancer. J Cancer Res Clin Oncol 127:565–569
16. Deng G, Peng E, Gum J, Terdiman J, Sleisenger M, Kim YS (2002) Methylation of hMLH1 promoter correlates with the gene silencing with a region-specific manner in colorectal cancer. Br J Cancer 86:574–579
17. Dietmaier W, Wallinger S, Bocker T, Kullmann F, Fishel R, Ruschoff J (1997) Diagnostic microsatellite instability: definition and correlation with mismatch repair protein expression. Cancer Res 57:4749–4756
18. Dieumegard B, Grandjouan S, Sabourin JC, Le Bihan ML, Lefrere I, Bellefqih, Pignon JP, Rougier P, Lasser P, Benard J, Couturier D, Bressac-de Paillerets B (2000) Extensive molecular screening for hereditary non-polyposis colorectal cancer. Br J Cancer 82:871–880
19. Elsaleh H, Joseph D, Grieu F, Zeps N, Spry N, Iacopetta B (2000) Association of tumour site and sex with survival benefit from adjuvant chemotherapy in colorectal cancer. Lancet 355:1745–1750
20. Furukawa T, Konishi F, Masubuchi S, Shitoh K, Nagai H, Tsukamoto T (2002) Densely methylated MLH1 promoter correlates with decreased mRNA expression in sporadic colorectal cancers. Genes Chromosomes Cancer 35:1–10
21. Furukawa T, Konishi F, Shitoh K, Kojima M, Nagai H, Tsukamoto T (2002) Evaluation of screening strategy for detecting hereditary nonpolyposis colorectal carcinoma. Cancer 94:911–920
22. Halvarsson B, Lindblom A, Rambech E, Lagerstedt K, Nilbert M (2004) Microsatellite instability analysis and/or immunostaining for the diagnosis of hereditary nonpolyposis colorectal cancer? Virchows Arch 444:135–141
23. Hendriks Y, Franken P, Dierssen JW, De Leeuw W, Wijnen J, Dreef E, Tops C, Breuning M, Brocker-Vriends A, Vasen H, Fodde R, Morreau H (2003) Conventional and tissue microarray immunohistochemical expression analysis of mismatch repair in hereditary colorectal tumors. Am J Pathol 162:469–477
24. Herman JG, Umar A, Polyak K, Graff JR, Ahuja N, Issa JP, Markowitz S, Willson JK, Hamilton SR, Kinzler KW, Kane MF, Kolodner RD, Vogelstein B, Kunkel TA, Baylin SB (1998) Incidence and functional consequences of hMLH1 promoter hypermethylation in colorectal carcinoma. Proc Natl Acad Sci U S A 95:6870–6875
25. Hoedema R, Monroe T, Bos C, Palmer S, Kim D, Marvin M, Luchtefeld M (2003) Genetic testing for hereditary nonpolyposis colorectal cancer. Am Surg 69:387–392
26. Jansson A, Arbman G, Zhang H, Sun XF (2003) Combined deficiency of hMLH1, hMSH2, hMSH3 and hMSH6 is an independent prognostic factor in colorectal cancer. Int J Oncol 22:41–49
27. Jeong SY, Shin KH, Shin JH, Ku JL, Shin YK, Park SY, Kim WH, Park JG (2003) Microsatellite instability and mutations in DNA mismatch repair genes in sporadic colorectal cancers. Dis Colon Rectum 46:1069–1077
28. Jourdan F, Sebbagh N, Comperat E, Mourra N, Flahault A, Olschwang S, Duval A, Hamelin R, Flejou JF (2003) Tissue microarray technology: validation in colorectal carcinoma and analysis of p53, hMLH1, and hMSH2 immunohistochemical expression. Virchows Arch 443:115–121
29. Kane MF, Loda M, Gaida GM, Lipman J, Mishra R, Goldman H, Jessup JM, Kolodner R (1997) Methylation of the hMLH1 promoter correlates with lack of expression of hMLH1 in sporadic colon tumors and mismatch repair-defective human tumor cell lines. Cancer Res 57:808–811
30. Kim H, Piao Z, Kim JW, Choi JS, Kim NK, Lee JM, Park JH (1998) Expression of hMSH2 and hMLH1 in colorectal carcinomas with microsatellite instability. Pathol Res Pract 194:3–9
31. Kim HC, Kim CN, Yu CS, Roh SA, Kim JC (2003) Methylation of the hMLH1 and hMSH2 promoter in early-onset sporadic colorectal carcinomas with microsatellite instability. Int J Colorectal Dis 18:196–202
32. Kolodner RD, Marsischky GT (1999) Eukaryotic DNA mismatch repair. Curr Opin Genet Dev 9:89–96
33. Kuismanen SA, Holmberg MT, Salovaara R, de la Chapelle A, Peltomaki P (2000) Genetic and epigenetic modification of MLH1 accounts for a major share of microsatellite-unstable colorectal cancers. Am J Pathol 156:1773–1779
34. Lamberti C, Kruse R, Ruelfs C, Caspari R, Wang Y, Jungck M, Mathiak M, Malayeri HR, Friedl W, Sauerbruch T, Propping P (1999) Microsatellite instability-a useful diagnostic tool to select patients at high risk for hereditary non-polyposis colorectal cancer: a study in different groups of patients with colorectal cancer. Gut 44:839–843
35. Lanza G, Gafa R, Maestri I, Santini A, Matteuzzi M, Cavazzini L (2002) Immunohistochemical pattern of MLH1/MSH2 expression is related to clinical and pathological features in colorectal adenocarcinomas with microsatellite instability. Mod Pathol 15:741–749
36. Leach FS, Nicolaides NC, Papadopoulos N, Liu B, Jen J, Parsons R, Peltomaki P, Sistonen P, Aaltonen LA, Nystrom-Lahti M et al (1993) Mutations of a mutS homolog in hereditary nonpolyposis colorectal cancer. Cell 75:1215–1225
37. Lindor NM, Burgart LJ, Leontovich O, Goldberg RM, Cunningham JM, Sargent DJ, Walsh-Vockley C, Petersen GM, Walsh MD, Leggett BA, Young JP, Barker MA, Jass JR, Hopper J, Gallinger S, Bapat B, Redston M, Thibodeau SN (2002) Immunohistochemistry versus microsatellite instability testing in phenotyping colorectal tumors. J Clin Oncol 20:1043–1048
38. Liu B, Parsons R, Papadopoulos N, Nicolaides NC, Lynch HT, Watson P, Jass JR, Dunlop M, Wyllie A, Peltomaki P, de la Chapelle A, Hamilton SR, Vogelstein B, Kinzler KW (1996) Analysis of mismatch repair genes in hereditary non-polyposis colorectal cancer patients. Nat Med 2:169–174
39. Liu T, Tannergard P, Hackman P, Rubio C, Kressner U, Lindmark G, Hellgren D, Lambert B, Lindblom A (1999) Missense mutations in hMLH1 associated with colorectal cancer. Hum Genet 105:437–441

40. Liu T, Wahlberg S, Burek E, Lindblom P, Rubio C, Lindblom A (2000) Microsatellite instability as a predictor of a mutation in a DNA mismatch repair gene in familial colorectal cancer. Genes Chromosomes Cancer 27:17–25
41. Marcus VA, Madlensky L, Gryfe R, Kim H, So K, Millar A, Temple LK, Hsieh E, Hiruki T, Narod S, Bapat BV, Gallinger S, Redston M (1999) Immunohistochemistry for hMLH1 and hMSH2: a practical test for DNA mismatch repair-deficient tumors. Am J Surg Pathol 23:1248–1255
42. Miyakura Y, Sugano K, Konishi F, Ichikawa A, Maekawa M, Shitoh K, Igarashi S, Kotake K, Koyama Y, Nagai H (2001) Extensive methylation of hMLH1 promoter region predominates in proximal colon cancer with microsatellite instability. Gastroenterology 121:1300–1309
43. Modrich P (1991) Mechanisms and biological effects of mismatch repair. Annu Rev Genet 25:229–253
44. Muller W, Burgart LJ, Krause-Paulus R, Thibodeau SN, Almeida M, Edmonston TB, Boland CR, Sutter C, Jass JR, Lindblom A, Lubinski J, MacDermot K, Sanders DS, Morreau H, Muller A, Oliani C, Orntoft T, Ponz De Leon M, Rosty C, Rodriguez-Bigas M, Ruschoff J, Ruszkiewicz A, Sabourin J, Salovaara R, Moslein G (2001) The reliability of immunohistochemistry as a prescreening method for the diagnosis of hereditary nonpolyposis colorectal cancer (HNPCC)—results of an international collaborative study. Fam Cancer 1:87–92
45. Peltomaki P (2003) Role of DNA mismatch repair defects in the pathogenesis of human cancer. J Clin Oncol 21:1174–1179
46. Peltomaki P, Vasen HF (1997) Mutations predisposing to hereditary nonpolyposis colorectal cancer: database and results of a collaborative study. The International Collaborative Group on Hereditary Nonpolyposis Colorectal Cancer. Gastroenterology 113:1146–1158
47. Potocnik U, Glavac D, Golouh R, Ravnik-Glavac M (2001) Causes of microsatellite instability in colorectal tumors: implications for hereditary non-polyposis colorectal cancer screening. Cancer Genet Cytogenet 126:85–96
48. Ribic CM, Sargent DJ, Moore MJ, Thibodeau SN, French AJ, Goldberg RM, Hamilton SR, Laurent-Puig P, Gryfe R, Shepherd LE, Tu D, Redston M, Gallinger S (2003) Tumor microsatellite-instability status as a predictor of benefit from fluorouracil-based adjuvant chemotherapy for colon cancer. N Engl J Med 349:247–257
49. Rigau V, Sebbagh N, Olschwang S, Paraf F, Mourra N, Parc Y, Flejou JF (2003) Microsatellite instability in colorectal carcinoma. The comparison of immunohistochemistry and molecular biology suggests a role for hMSH6 [correction of hMLH6] immunostaining. Arch Pathol Lab Med 127:694–700
50. Ruszkiewicz A, Bennett G, Moore J, Manavis J, Rudzki B, Shen L, Suthers G (2002) Correlation of mismatch repair genes immunohistochemistry and microsatellite instability status in HNPCC-associated tumours. Pathology 34:541–547
51. Salahshor S, Koelble K, Rubio C, Lindblom A (2001) Microsatellite Instability and hMLH1 and hMSH2 expression analysis in familial and sporadic colorectal cancer. Lab Invest 81:535–541
52. Scartozzi M, Bianchi F, Rosati S, Galizia E, Antolini A, Loretelli C, Piga A, Bearzi I, Cellerino R, Porfiri E (2002) Mutations of hMLH1 and hMSH2 in patients with suspected hereditary nonpolyposis colorectal cancer: correlation with microsatellite instability and abnormalities of mismatch repair protein expression. J Clin Oncol 20:1203–1208
53. Shia J, Ellis NA, Paty PB, Nash GM, Qin J, Offit K, Zhang XM, Markowitz AJ, Nafa K, Guillem JG, Wong WD, Gerald WL, Klimstra DS (2003) Value of histopathology in predicting microsatellite instability in hereditary nonpolyposis colorectal cancer and sporadic colorectal cancer. Am J Surg Pathol 27:1407–1417
54. Stone JG, Robertson D, Houlston RS (2001) Immunohistochemistry for MSH2 and MHL1: a method for identifying mismatch repair deficient colorectal cancer. J Clin Pathol 54:484–487
55. Terdiman JP, Gum JR Jr, Conrad PG, Miller GA, Weinberg V, Crawley SC, Levin TR, Reeves C, Schmitt A, Hepburn M, Sleisenger MH, Kim YS (2001) Efficient detection of hereditary nonpolyposis colorectal cancer gene carriers by screening for tumor microsatellite instability before germline genetic testing. Gastroenterology 120:21–30
56. Thibodeau SN, French AJ, Cunningham JM, Tester D, Burgart LJ, Roche PC, McDonnell SK, Schaid DJ, Vockley CW, Michels VV, Farr GH Jr, O'Connell MJ (1998) Microsatellite instability in colorectal cancer: different mutator phenotypes and the principal involvement of hMLH1. Cancer Res 58:1713–1718
57. Umar A, Boland CR, Terdiman JP, Syngal S, de la Chapelle A, Ruschoff J, Fishel R, Lindor NM, Burgart LJ, Hamelin R, Hamilton SR, Hiatt RA, Jass J, Lindblom A, Lynch HT, Peltomaki P, Ramsey SD, Rodriguez-Bigas MA, Vasen HF, Hawk ET, Barrett JC, Freedman AN, Srivastava S (2004) Revised Bethesda Guidelines for hereditary nonpolyposis colorectal cancer (Lynch syndrome) and microsatellite instability. J Natl Cancer Inst 96:261–268
58. Van Rijnsoever M, Elsaleh H, Joseph D, McCaul K, Iacopetta B (2003) CpG island methylator phenotype is an independent predictor of survival benefit from 5-fluorouracil in stage III colorectal cancer. Clin Cancer Res 9:2898–2903
59. Vasen HF, Wijnen JT, Menko FH, Kleibeuker JH, Taal BG, Griffioen G, Nagengast FM, Meijers-Heijboer EH, Bertario L, Varesco L, Bisgaard ML, Mohr J, Fodde R, Khan PM (1996) Cancer risk in families with hereditary nonpolyposis colorectal cancer diagnosed by mutation analysis. Gastroenterology 110: 1020–1027
60. Wagner A, Barrows A, Wijnen JT, van der Klift H, Franken PF, Verkuijlen P, Nakagawa H, Geugien M, Jaghmohan-Changur S, Breukel C, Meijers-Heijboer H, Morreau H, van Puijenbroek M, Burn J, Coronel S, Kinarski Y, Okimoto R, Watson P, Lynch JF, de la Chapelle A, Lynch HT, Fodde R (2003) Molecular analysis of hereditary nonpolyposis colorectal cancer in the United States: high mutation detection rate among clinically selected families and characterization of an American founder genomic deletion of the MSH2 gene. Am J Hum Genet 72:1088–1100
61. Wahlberg SS, Schmeits J, Thomas G, Loda M, Garber J, Syngal S, Kolodner RD, Fox E (2002) Evaluation of microsatellite instability and immunohistochemistry for the prediction of germ-line MSH2 and MLH1 mutations in hereditary nonpolyposis colon cancer families. Cancer Res 62:3485–3492
62. Ward R, Meagher A, Tomlinson I, O'Connor T, Norrie M, Wu R, Hawkins N (2001) Microsatellite instability and the clinicopathological features of sporadic colorectal cancer. Gut 48:821–829
63. Wheeler JM, Loukola A, Aaltonen LA, Mortensen NJ, Bodmer WF (2000) The role of hypermethylation of the hMLH1 promoter region in HNPCC versus MSI+ sporadic colorectal cancers. J Med Genet 37:588–592
64. Yan H, Papadopoulos N, Marra G, Perrera C, Jiricny J, Boland CR, Lynch HT, Chadwick RB, de la Chapelle A, Berg K, Eshleman JR, Yuan W, Markowitz S, Laken SJ, Lengauer C, Kinzler KW, Vogelstein B (2000) Conversion of diploidy to haploidy. Nature 403:723–724
65. Young J, Simms LA, Biden KG, Wynter C, Whitehall V, Karamatic R, George J, Goldblatt J, Walpole I, Robin SA, Borten MM, Stitz R, Searle J, McKeone D, Fraser L, Purdie DR, Podger K, Price R, Buttenshaw R, Walsh MD, Barker M, Leggett BA, Jass JR (2001) Features of colorectal cancers with high-level microsatellite instability occurring in familial and sporadic settings: parallel pathways of tumorigenesis. Am J Pathol 159:2107–2116

Virchows Arch (2004) 445:442–448
DOI 10.1007/s00428-004-1088-z

ORIGINAL ARTICLE

Cord Langner · Beate J. Wegscheider · Peter Rehak · Manfred Ratschek · Richard Zigeuner

Prognostic value of keratin subtyping in transitional cell carcinoma of the upper urinary tract

Received: 27 April 2004 / Accepted: 11 July 2004 / Published online: 18 September 2004
© Springer-Verlag 2004

Abstract To investigate the prognostic value of keratin subtyping in invasive transitional cell carcinomas (TCCs), we performed a systematic study applying 15 different monoclonal keratin antibodies on 53 upper urinary tract TCCs using a tissue microarray technique. Immunoreactivity was correlated with pT stages and tumour grades using the Fisher's exact test. Impact on disease-free survival was analysed using the Kaplan-Meier method and compared by the log-rank test. Immunoreactivity for keratins 5/6, 6, 7, 8, 13, 14, 17, 18, 19, 20, low molecular weight (LMW) keratins (8, 18) and high molecular weight (HMW) keratins (1, 5, 10, 14) was detected in varying quantities. Regarding semi-quantitative assessment, a prognostic impact was found for keratins 5/6, 7, 8, 13, 17, 20 and HMW keratins, with reduced expression or loss of immunoreactivity being significantly associated with disease progression. With respect to analysis of staining patterns, the retention of a basally accentuated labelling for keratin 5/6 and HMW keratin as well as a superficially accentuated labelling for keratin 20 was significantly associated with a favourable outcome. In conclusion, this investigation is the first to demonstrate a possible prognostic value for keratin subtyping in invasive (upper urinary tract) TCCs with respect to metastasis-free survival. Further studies, however, are needed to substantiate our results.

C. Langner (✉) · B. J. Wegscheider · M. Ratschek
Institute of Pathology, Medical University of Graz,
Auenbruggerplatz 25, 8036 Graz, Austria
e-mail: cord.langner@meduni-graz.at
Tel.: +43-316-38583665
Fax: +43-316-384329

P. Rehak
Department of Surgery,
Division of Biomedical Engineering & Computing,
Medical University of Graz,
Auenbruggerplatz 29, 8036 Graz, Austria

R. Zigeuner
Department of Urology, Medical University of Graz,
Auenbruggerplatz 7, 8036 Graz, Austria

Keywords Transitional cell carcinoma · Upper urinary tract · Keratin · Immunohistochemistry · Prognosis

Introduction

Upper urinary tract transitional cell carcinomas (TCC) account for approximately 5% of all urothelial tumours and for 10% of all renal tumours [11, 13]. Only 2–4% of mucosally confined tumours (pTa) are likely to progress. In contrast, 30–50% of tumours invading the lamina propria (pT1) have this potential [20]. Tumour node metastasis (TNM) stage and tumour grade are known prognostic factors in TCCs [13, 14]. Assessment of tumour grade, however, may show considerable variation owing to low intra- and inter-individual consistency [14]. Therefore, new additional ("objective") biomarkers are needed to predict disease progression, thus aiding both adjuvant therapy and surveillance strategies.

Keratins are intermediate filament proteins that are constituents of the mammalian epithelial cytoskeleton. Normal adult urothelium is known to express keratin subtypes characteristic of "simple" epithelia (K7, K8, K18, K19 and K20) as well as subtypes associated with stratified epithelia, predominantly K13. Some studies have also detected small amounts of K4, K5 and K17 in normal urothelium [37]. K7, K8, K18 and K19 are retained by all TCCs, whereas the expression patterns of the other keratins can vary. Moreover, additional expression of K14 has been reported as an indicator of squamous differentiation [37].

Keratin immunoreactivity has been related to tumour progression in breast, colorectal and non-small cell lung cancer as well as oral, pharyngeal, oesophageal and cervical squamous cell carcinoma [2, 3, 8, 9, 10, 32, 35, 38]. In urothelial cancers, keratin subtyping has thus far only been investigated with respect to the prediction of local tumour recurrence in superficial bladder tumours [1, 16, 17, 18, 31]. However, studies relating the differential expression of keratin subtypes in invasive TCCs with metastasis-free survival are currently lacking. Therefore,

we decided to apply a high-throughput tissue microarray technique using 15 different mouse monoclonal antibodies to evaluate the keratin expression profile of upper urinary tract TCC and to correlate immunohistochemical data with clinical follow-up.

Materials and methods

Formalin-fixed and paraffin-embedded specimens of 53 upper urinary tract TCCs from consecutive patients (32 males, 21 females) operated on between January1988 and August 2002 were chosen for analysis. The mean and median age of patients at surgery was 69.5 years and 70.3 years (range 39–87 years, ±SD 9.8 years), respectively. All patients underwent nephroureterectomy and did not receive additional therapy. All tumour specimens were independently re-evaluated with respect to pT stage and grade by two pathologists (C.L. and M.R). pT stages were adjusted according to the International Union Against Cancer (UICC) 2002 issue of the TNM system [36], nuclear grading was performed according to the World Health Organisation guidelines [25]. Stage pT1 was present in 22 (42%), pT2 in 9 (17%) and pT3 in 22 (42%) cases, respectively. Tumour grades were G2 in 31 (58%) and G3 in 22 (42%) cases, respectively. Neither stage pTa nor G1 tumours were included in our studies, since no prognostic information could be expected from these cases. Neither institutional review board approval nor informed consent is required for retrospective studies dealing with archival material at our institution.

For immunohistochemical evaluation, a tissue microarray (TMA) technique was used. At least three cylindrical core biopsies, 0.6 mm in diameter, were taken from different areas of each tumour and arrayed in a recipient paraffin TMA block. The details of this technique have been described previously [23]. The immunohistochemical staining procedure applied in the current investigation was identical to that reported in our previous study [24]. Briefly, TMA sections were deparaffinised, rehydrated in graded alcohols and treated for 5 min with 1% H_2O_2. Thereafter, sections were subjected to antigen retrieval using either microwave treatment (30 min 160 W in 0.01 M sodium citrate buffer pH 7.3), protease digestion (10 min room temperature 0.1% protease type XXIV, Sigma-Aldrich, Steinheim, Germany), or Epitope Retrieval Solution (Dako, Code No. K 5205, 40 min 98°C) and subsequently incubated for 30 min with the different mouse monoclonal anti-human keratin antibodies. For specificity, dilution, antigen retrieval method and source as well as positive control of the 15 different mouse monoclonal anti-human keratin antibodies used, see Table 1. Binding of the primary antibody was assessed using the Dako LSAB2 System HRP (AEC) Detection kit. Negative controls were performed by substitution of the primary antibody using the Dako ChemMate Antibody Diluent Code No. S2022. A distinct cytoplasmic and/or membranous staining was defined as positive reaction, and immunoreactivity was assessed considering the average positivity of the core biopsies and documented in a semi-quantitative fashion (0%, 1–10%, 11–25%, 26–50%, 51–75%, 76–90%, >90%) independently by two pathologists (C.L. and M.R.). A keratin immunostaining of less than or equal to 50% of cancer cells was assessed as "low", and an immunoreactivity of greater than 50% of cancer cells was assessed as "high" expression. Discrepancies were resolved by simultaneous re-examination of the slides by both investigators using a double-headed microscope.

Subgroups arranged according to pT-stage and tumour grade were compared with respect to possible differences in keratin immunostaining using the Fisher's exact test. Metastasis-free survival was related to keratin immunoreactivity using the Kaplan-Meier method and compared by the log-rank test. Owing to small sample size, multivariate testing could not be performed.

Results

Tumour tissue sufficient for a reliable evaluation of immunoreactivity was present in all cases. The keratin expression profile of upper urinary tract TCCs is summarised in Table 2. Regarding analysis of metastasis-free survival, follow-up data were available for all patients. After mean and median follow-up of 38 months and 26 months (range 1–148 months, ±SD 35 months), respectively, metastatic disease was observed in 14 of 53 (26%) patients. Mean time to progression was 19 months. Progression to metastatic disease was strongly associated with stage and grade: 13 of 14 (93%) cases were stage pT3; 1 case (7%) was stage pT2 (P <0.001); 12 of 14 (86%) cases were grade 3; 2 of 14 (14%) cases were grade 2 (P <0.001).

Keratin 5/6

K5/6 immunoreactivity prevailed in low-stage [22/22 (100%) pT1 versus 18/31 (58%) pT2/pT3; P =0.0003] and

Table 1 List of antibodies used. *MW*, microwave treatment 30 min 160 W in 0.01 M sodium citrate buffer pH 7.3, *P* protease digestion 10 min at room temperature (0.1% protease type XXIV, Sigma-Aldrich, Steinheim, Germany), *ER* Epitope Retrieval Solution (Dako, Glostrup, Denmark, Code No. K 5205) 40 min at 98°C, *HMW* high molecular weight, *LMW* low molecular weight

Antibody specificity	Dilution, antigen retrieval	Positive control	Source
K 4 (Clone 6B10)	1:5, MW	Cervix	Monosan, Uden, The Netherlands
K 5/6 (Clone D5/16 B4)	1:50, MW	Breast	Dako, Glostrup, Denmark
K 6 (Clone Ks6.KA12)	Ready to use, MW	Cervix	Progen, Heidelberg, Germany
K 7 (Clone OV-TL 12/30)	1:100, P	Breast	Dako
K 8 (Clone RCK 102)	1:10, P	Breast	ICN, Aurora, USA
K 8/18, LMW (Clone 5D3)	1:50, P	Skin	Novocastra, Newcastle upon Tyne, UK
K 10 (Clone DE-K 10)	1:100 (no retrieval)	Skin	Dako
K 13 (Clone DE-K 13)	1:50, MW	Cervix	Dako
K 14 (Clone LL002)	1:50, MW	Skin	Novocastra
K 16 (Clone LL025)	1:10, MW	Cervix	Novocastra
K 17 (Clone E3)	1:20, MW	Breast	Dako
K 18 (Clone DC 10)	1:10, MW	Breast	Dako
K 19 (Clone RCK 108)	1:100, P	Breast	Dako
K 20 (Clone K_S 20.8)	1:100, P	Colon	Dako
HMW (Clone 34βE12, K 1, 5, 10, 14)	1:50, ER	Prostate	Dako

Table 2 Keratin expression profile (+ : overall immunoreactivity; ++ : immunostaining of more than 50% of tumour cells) of upper urinary transitional cell carcinomas (TCCs) related to pT stages and tumour grades. *HMW* high molecular weight, *LMW* low molecular weight

Antibody specificity	TCC (*n*=53)		pT1 (*n*=22)		pT2 (*n*=9)		pT3 (*n*=22)		G2 (n=31)		G3 (n=22)	
	+ (%)	++ (%)	+ (%)	++ (%)	+ (%)	++ (%)	+ (%)	++ (%)	+ (%)	++ (%)	+ (%)	++ (%)
K 4	0	0	0	0	0	0	0	0	0	0	0	0
K 5/6	40 (75)	16 (30)	22 (100)	10 (45)	6 (67)	1 (11)	12 (55)	5 (23)	27 (87)	12 (39)	13 (59)	4 (18)
K 6	12 (23)	7 (13)	7 (32)	3 (14)	2 (22)	1 (11)	3 (14)	3 (14)	8 (26)	3 (10)	4 (18)	4 (18)
K 7	53 (100)	51 (96)	22 (100)	22 (100)	9 (100)	9 (100)	22 (100)	20 (91)	31 (100)	30 (97)	22 (100)	21 (95)
K 8	51 (96)	39 (74)	22 (100)	20 (91)	8 (89)	7 (78)	21 (95)	13 (55)	30 (97)	24 (77)	21 (95)	15 (68)
K 10	0	0	0	0	0	0	0	0	0	0	0	0
K 13	39 (74)	21 (40)	21 (95)	14 (64)	8 (89)	4 (44)	10 (45)	3 (14)	27 (87)	15 (48)	12 (55)	6 (27)
K 14	11 (21)	1 (2)	2 (9)	0	3 (33)	0	6 (27)	1 (5)	5 (16)	0	6 (27)	1 (5)
K 16	0	0	0	0	0	0	0	0	0	0	0	0
K 17	42 (79)	21 (40)	18 (86)	10 (45)	8 (89)	5 (56)	15 (68)	6 (27)	26 (84)	12 (39)	16 (73)	9 (41)
K 18	53 (100)	47 (89)	22 (100)	19 (86)	9 (100)	9 (100)	22 (100)	19 (86)	31 (100)	28 (90)	22 (100)	19 (86)
K 19	50 (94)	44 (83)	22 (100)	20 (91)	9 (100)	8 (89)	19 (86)	16 (73)	31 (100)	27 (87)	19 (86)	17 (77)
K 20	33 (62)	11 (21)	14 (64)	6 (27)	5 (56)	2 (22)	14 (64)	3 (14)	20 (65)	5 (16)	13 (59)	6 (27)
LMW	53 (100)	51 (96)	22 (100)	21 (95)	9 (100)	9 (100)	22 (100)	21 (95)	31 (100)	30 (97)	22 (100)	21 (95)
HMW	41 (64)	19 (36)	22 (100)	11 (50)	7 (78)	3 (33)	12 (55)	5 (23)	28 (90)	13 (42)	13 (59)	6 (27)

low-grade tumours [27/31 (87%) G2 versus 13/22 (59%) G3; P =0.03]. Moreover, a basal staining pattern, showing accentuation of immunostaining at the periphery of tumour cell nests with a decreasing gradient to the central zone (Fig. 1A), was predominantly seen in low-stage [15/22 (68%) pT1 versus 9/31 (29%) pT2/pT3; P =0.006] and low-grade tumours [19/31 (61%) G2 versus 5/22 (23%) G3; P =0.01]. Regarding prognosis, 8 of 13 (62%) K5/6 negative tumours, 5 of 16 (31%) cases with diffuse K5/6 staining (Fig. 1B) and 1 of 24 (4%) cases with basal K5/6 staining pattern developed metastatic disease (P =0.001; log-rank test; Fig. 2).

Keratin 7

K7 expression was not associated with either tumour stage or grade. However, regarding metastasis-free survival, 5 of 8 (63%) patients with tumours showing less than or equal to 90% K7 immunoreactivity developed disease progression compared with 9 of 45 (20%) patients with tumours showing immunoreactivity of greater than 90% of cancer cells (P =0.01; log-rank test).

Keratin 8

Overall, K8 expression was not associated with either tumour stage or grade. Using a cut-off value of 90%, however, immunostaining was stronger in low-stage [13/22 (59%) pT1 versus 6/31 (19%) pT2/pT3; P =0.004] and low-grade tumours [16/31 (52%) G2 versus 3/22 (14%) G3; P =0.008]. Regarding prognosis, only 1 of 19 (5%) patients with a tumour showing K8 immunoreactivity of greater than 90% of cancer cells developed metastatic disease compared with 13 of 34 (38%) patients with tumours showing less than or equal to 90% K8 immunoreactivity (P =0.03; log-rank test).

Keratin 13

K13 immunoreactivity prevailed in low-stage [21/22 (95%) pT1 versus 18/31 (58%) pT2/pT3; P =0.003] and low-grade tumours [27/31 (87%) G2 versus 12/22 (55%) G3; P =0.01]. Regarding prognosis, 8 of 14 (57%) patients with K13-negative tumours, 5 of 18 (28%) patients with tumours showing low K13 expression and 1 of 21 (5%) patients with a tumour showing high K13 expression developed metastatic disease (P =0.004; log-rank test; Fig. 3).

Keratin 17

K17 expression was not associated with either tumour stage or grade. However, regarding metastasis-free survival 6 of 11 (55%) patients with K17-negative TCCs showed disease progression compared with 8 of 42 (19%) patients with K17-positive TCCs (P =0.04; log-rank test).

Keratin 20

Overall, K20 expression was not associated with either tumour stage or grade. However, a predominantly superficial staining pattern (Fig. 1C) prevailed in low-stage [12/22 (55%) pT1 versus 5/31 (16%) pT2/pT3; P =0.006] and low-grade tumours [15/31 (48%) G2 vs. 2/22 (9%) G3; P =0.003], whereas diffuse immunostaining (Fig. 1D) was predominantly seen in high-stage [2/22 (9%) pT1 versus 14/31 (45%) pT2/pT3; P =0.006] and high-grade tumours [5/31 (16%) G2 versus 11/22 (50%) G3; P =0.01]. Regarding prognosis, only the diffuse staining pattern was significantly associated with metastasis-free survival (P =0.02; log-rank test): 8 of 16 (50%) patients with diffuse K20 immunostaining developed metastatic disease compared with 6 of 37 (16%) patients with tumours showing either superficial immunostaining (3/17, 18%) or lacking any K20 immunostaining (3/20, 15%).

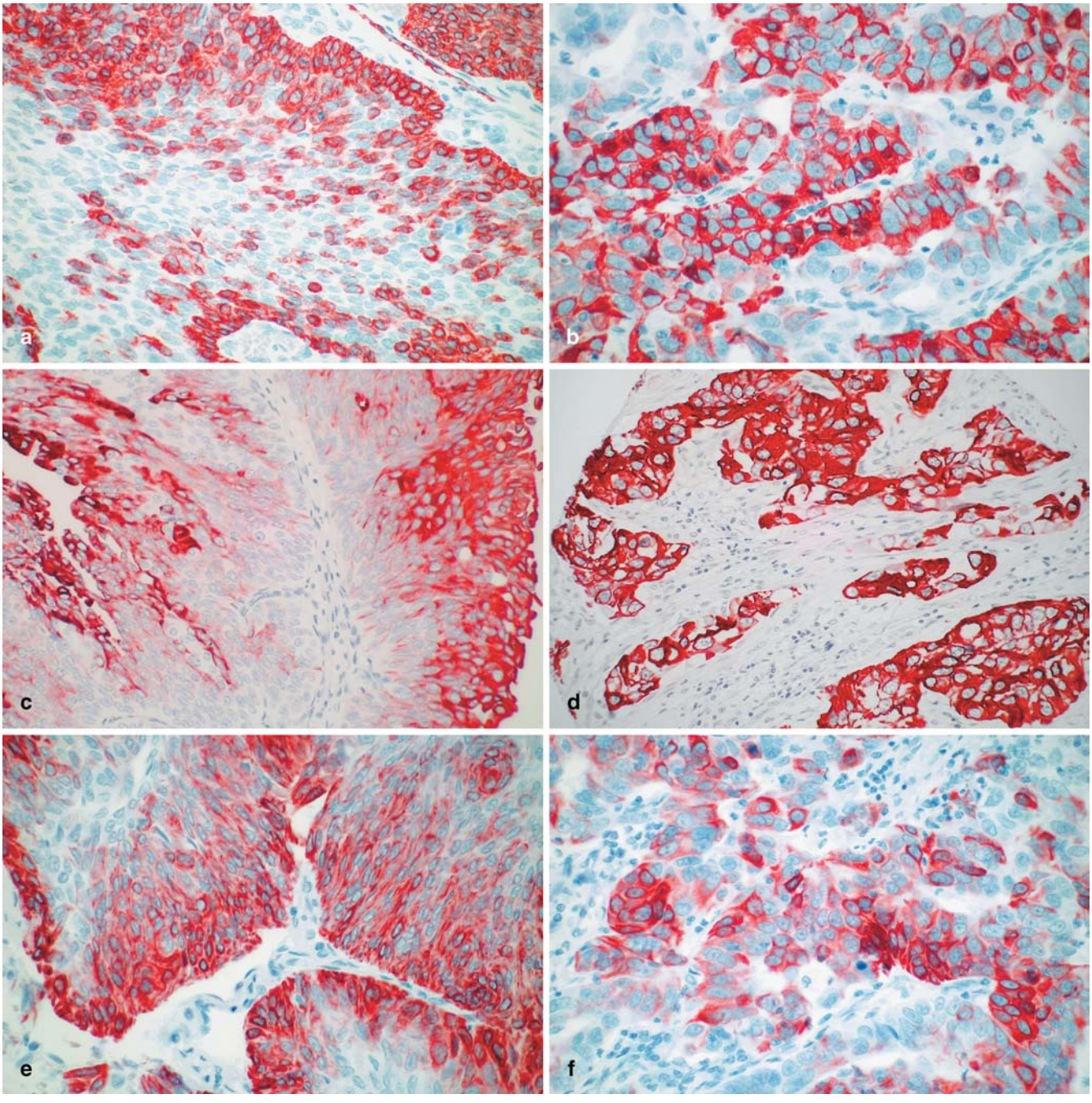


Fig. 1 Keratin immunohistochemistry in upper urinary tract transitional cell carcinomas (TCCs). Zonal staining pattern for K5/6 (**A**) and high molecular weight (HMW) keratins (**E**) with accentuation of immunoreactivity at the periphery of tumour cell nests and decreasing reactivity in suprabasal cell layers in a moderately differentiated TCC (identical case). In contrast, distinct heterogeneous staining for K5/6 (**B**) and for HMW keratins (**F**) without a zonal pattern in a poorly differentiated TCC (identical case). Zonal K20 immunostaining in a moderately differentiated TCC with lack of staining at the periphery of tumour cell nests and an increasing gradient to the surface and/or outer aspect of papillary tumour projections (**C**). However, note strong diffuse K20 staining in a poorly differentiated TCC (**D**)

HMW keratins (K1, K5, K10 and K14)

Immunoreactivity prevailed in low-stage [22/22 (100%) pT1 versus 19/31 (61%) pT2/pT3; P =0.0006] and low-grade tumours [28/31 (90%) G2 versus 13/22 (59%) G3; P =0.01]. Comparable to K5/6, a basal staining pattern (Fig. 1E) was predominantly seen in low-stage [12/22 (55%) pT1 versus 7/31 (23%) pT2/pT3; P =0.02] and low-grade tumours [16/31 (52%) G2 versus 3/22 (14%) G3; P =0.008]. Regarding prognosis, 8 of 12 (75%) patients with tumours negative for high molecular weight (HMW) keratins, 4 of 22 (18%) patients with low HMW

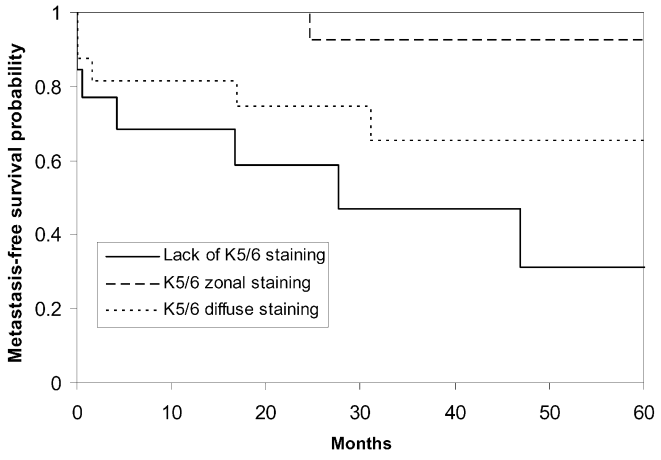


Fig. 2 Disease-free survival (months) in patients with upper urinary tract transitional cell carcinoma (TCC) related to K5/6 immunostaining. Favourable outcome of patients with TCCs showing a zonal, basally accentuated staining pattern compared with diffuse staining and/or lack of K5/6 immunoreactivity (P =0.001; log-rank test)

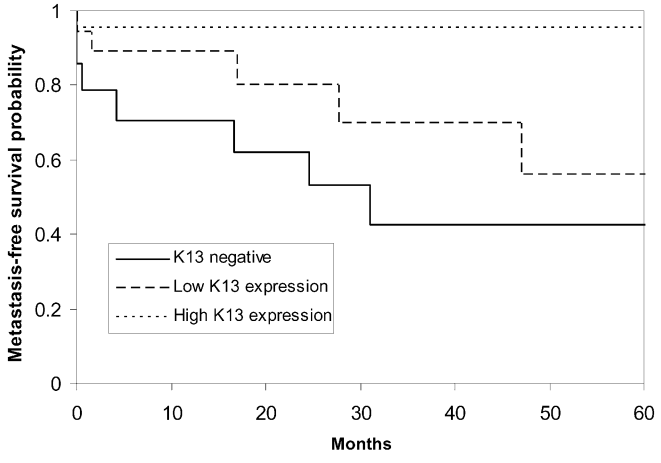


Fig. 3 Disease-free survival (months) in patients with upper urinary tract transitional cell carcinoma (TCC) showing high K13 expression (>50% of tumour cells), low K13 expression (≤50% of tumour cells) or lack of K13 immunostaining (P =0.004; log-rank test)

keratin expression and 2 of 19 (11%) patients with high HMW keratin expression developed metastatic disease (P =0.005; log-rank-test; Fig. 4). Moreover, metastasis-free survival was found to be associated with staining patterns, since only 1 of 19 (5%) tumours showing a basal staining pattern developed metastatic disease compared with 5 of 22 (23%) patients with tumours showing a diffuse staining pattern (Fig. 1F; P =0.004; log-rank test).

Other keratins

Regarding the keratin subtypes 6, 14, 18 and 19 as well as the low molecular weight (LMW) keratin (K8 and K18)

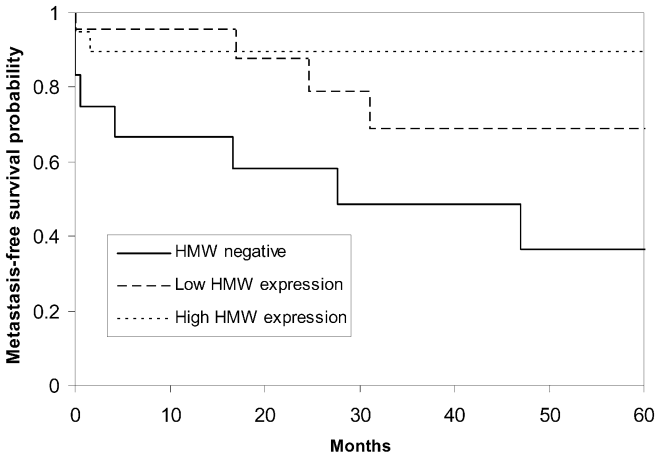


Fig. 4 Disease-free survival (months) in patients with upper urinary tract transitional cell carcinoma (TCC) showing high high molecular weight (HMW) expression (>50% of tumour cells), low HMW expression (≤50% of tumour cells) or lack of HMW immunostaining (P =0.005; log-rank test)

antibody preparation, no associations with either tumour stage, grade or patient's outcome were detected.

Discussion

Keratins are intermediate filament proteins, which are constituents of the mammalian epithelial cytoskeleton. At least 20 different types have been discriminated in various tissues on the basis of molecular weight and isoelectric pH values. Different subsets of keratins are expressed by different epithelia, and these patterns are largely retained during neoplastic transformation. Hence, both epithelia and epithelial tumours can be classified on the basis of keratin protein expression [5, 27].

The keratin expression profile of upper urinary tract TCCs presented in our study is comparable with data reported by others who, however, mainly concentrated on single keratin subtypes and/or TCCs obtained from the urinary bladder [4, 5, 6, 7, 12, 21, 22, 26, 28, 29, 30, 33, 34, 37, 39]. This expression profile, together with that recently reported by our group for renal cell carcinomas and renal oncocytomas [24], may be used by the surgical pathologist as a basis for the immunohistochemical differentiation of selected renal neoplasms whose classification is difficult in standard haematoxylin & eosin sections.

In the current study, however, we concentrated on the use of keratin subtyping as a means to predict disease progression in patients with invasive TCCs. With regard to K5/6 and HMW keratins, a luminal shift up to diffuse immunostaining of all cell layers with increasing stage and grade is known from exophytic superficially invasive (pT1) and non-invasive (pTa) low-grade bladder carcinomas [18, 19]. Moreover, the occurrence of a diffuse labelling pattern has been related to local tumour recurrence [18, 31]. According to our results, K5/6 and HMW

keratin immunostaining may additionally be used to predict disease progression, since patients with TCCs showing diffuse labelling were at a significantly higher risk to develop metastatic disease. The same holds true for patients with TCCs lacking K5/6 or HMW keratin immunoreactivity. The loss of these markers is supposed to reflect progressive tumour cell dedifferentiation, and this may indicate a particularly unfavourable outcome, since disease progression occurred in approximately two-thirds of patients, respectively.

K17 is another keratin mainly expressed in basal urothelial cells [37]. In our investigation, lack of K17 immunoreactivity was associated with poor prognosis in more than 50% of patients. This finding is related to the work by Guelstein et al. [12], who noted a highly variable K17 staining pattern in G3 and anaplastic TCCs ranging from completely negative to completely positive tumours with several intermediate phenotypes, whereas all G1 and G2 tumours were immunoreactive.

K20 is known to label superficial umbrella and occasional intermediate cells in non-neoplastic urothelium [37], and this "normal" pattern in low-grade non-invasive papillary urothelial neoplasms has been related to tumour non-recurrence in the urinary bladder [1, 16, 17, 31]. Moreover, Parker et al. [30] noted K20 immunostaining throughout all cell layers in high-grade and invasive bladder cancer as well as metastatic urothelial tumour tissue, whereas in non-invasive and low-grade TCCs, mainly superficial tumour cells were stained. Follow-up data were not included. According to our results, however, the diffuse K20 staining pattern may be used as an additional marker to predict disease progression, since again patients with TCCs showing diffuse keratin labelling were at a significantly higher risk to develop metastatic disease.

The majority of tumours in our series expressed keratin subtypes characteristic of "simple" epithelia (K7, K8, K18 and K19) as well as subtypes associated with stratified epithelia, predominantly K13. Reduced expression or lack of expression of K7, K8 and K13 (but not of K18 and K19) was found to be associated with the occurrence of metastatic disease and may represent secondary changes related to dysregulation of the urothelial differentiation programme [37]. Similar observations were made by others [28, 33], who noted greatly reduced or absent levels of K13 and other stratification-related keratins in high-stage and high-grade urothelial cancers, although an extensive proportion of K13-positive tumour cells was still found in some TCCs, even in metastases [34].

K14 immunostaining in TCCs has been related to squamous differentiation [7, 15]. According to Schaafsma et al. [33], increasing K14 expression is related to increasing degree of malignancy in bladder cancer, with some tumours showing accentuation of K14 labelling in the infiltrating tumour components. In our series of upper urinary tract TCCs, however, no association with either pT stage, grade or prognosis was found.

In conclusion, this study is the first to show that keratin subtyping (overall immunoreactivity and staining patterns) in invasive (upper urinary tract) TCCs may have prognostic value. However, our results should be substantiated by further investigations, since multivariate testing could not be performed due to small sample size.

Acknowledgements The authors are grateful to Mrs. M. Gogg-Kamerer, Ms. M. Lindbauer, Ms. A. Sommersacher, Mr. M. Al-Effah and Mr. R. Christof for excellent technical assistance.

References

1. Alsheikh A, Mohamedali Z, Jones E, Masterson J, Gilks CB (2001) Comparison of the WHO/ISUP classification and cytokeratin 20 expression in predicting the behaviour of low-grade papillary urothelial tumors. Mod Pathol 14:267–272
2. Bhatavdekar JM, Patel DD, Chikhlikar PR, Shah NG, Vora HH, Ghosh N, Trivedi TI (2001) Molecular markers are predictors of recurrence and survival in patients with Dukes B and Dukes C colorectal adenocarcinoma. Dis Colon Rectum 44:523–533
3. Bommel van PF, Kenemans P, Helmerhorst TJM, Gallee MPW, Ivanyi D (1994) Expression of cytokeratin 10, 13, and in involucrin as prognostic factors in low stage squamous cell carcinoma of the uterine cervix. Cancer 74:2314–2320
4. Chu PG, Weiss LM (2002) Expression of cytokeratin 5/6 in epithelial neoplasms: an immunohistochemical study of 509 cases. Mod Pathol 15:6–10
5. Chu PG, Weiss LM (2002) Keratin expression in human tissues and neoplasms. Histopathology 40:403–439
6. Chu PG, Wu E, Weiss LM (2000) Cytokeratin 7 and cytokeratin 20 expression in epithelial neoplasms: a survey of 435 cases. Mod Pathol 13:962–972
7. Chu PG, Lyda MH, Weiss LM (2001) Cytokeratin 14 expression in epithelial neoplasms: a survey of 435 cases with emphasis on its value in differentiating squamous cell carcinomas from other epithelial tumours. Histopathology 39:9–16
8. Cintorino M, Tripod SA, Santopietro R, Antonio P, Lutfi A, Chang F, Syrjanen S, Shen Q, Tosi P, Syrjanen K (2001) Cytokeratin expression patterns as an indicator of tumour progression in oesophageal squamous cell carcinoma. Anticancer Res 21:4195–4201
9. Cohen R, Guber A, Siegal A, Brudermamn I, Huszar M, Yellin A, Marom Z, Geiger B (1997) The prognostic application of cytokeratin typing of nonsmall cell ling carcinoma. A retrospective study. Cancer 79:468–473
10. Depondt J, Shabana AH, Sawaf H, Gehanno P, Forest N (1999) Cytokeratin alterations as diagnostic and prognostic markers of oral and pharyngeal carcinomas. A prospective study. Eur J Oral Sci 107:442–454
11. Genega EM, Porter CR (2002) Urothelial neoplasm of the kidney and ureter. An epidemiologic, pathologic, and clinical review. Am J Clin Pathol 117[Suppl]:S36–S48
12. Guelstein VI, Tchipysheva TA, Ermilova VD, Troyanovsky SM (1993) Immunohistochemical localization of cytokeratin 17 in transitional cell carcinomas of the human urinary tract. Virchows Arch 64:1–5
13. Hall MC, Womack S, Sagalowsky AI (1998) Prognostic factors, recurrence, and survival in transitional cell carcinoma of the upper urinary tract: a 30-year experience in 252 patients. Urology 52:594–601
14. Harnden P, Parkinson MC (1996) Transitional cell carcinoma of the bladder: diagnosis and prognosis. Curr Diagn Pathol 3:109–121
15. Harnden P, Southgate J (1997) Cytoketain 14 as a marker of squamous differentiation in transitional cell carcinomas. J Clin Pathol 50:1032–1033
16. Harnden P, Allam A, Joyce AD, Patel A, Selby P, Southgate J (1995) Cytokeratin 20 expression by non-invasive transitional

cell carcinomas: potential for distinguishing recurrent from non-recurrent disease. Histopathology 27:169–174
17. Harnden P, Mahmood N, Southgate J (1999) Expression of cytokeratin 20 redefines urothelial papillomas of the bladder. Lancet 353:974–977
18. Helpap B, Köllermann J (1999) Proliferative pattern of exophytic and superficially invasive and non-invasive low-grade urothelial carcinomas. Hum Pathol 30:145–150
19. Helpap B, Köllermann J (2000) Assessment of basal cell status and proliferative in flat and papillary urothelial lesions: a contribution to the new WHO classification of urothelial tumors of the bladder. Hum Pathol 31:745–750
20. Helpap B, Schmitz-Dräger BJ, Hamilton PW, Muzzonigro G, Galosi AB, Kurth KH, Lubaroff D, Waters DJ, Droller MJ (2003) Molecular pathology of non-invasive urothelial carcinoma (part I). Virchows Arch 442:309–316
21. Kaufmann O, Fietze E, Mengs J, Dietel M (2001) Value of p63 and cytokeratin 5/6 as immunohsitochemical markers for the differential diagnosis of poorly differentiated and undifferentiated carcinomas. Am J Clin Pathol 116:823–830
22. Kim K, Kim S (2002) Immunohistochemical profile of common epithelial neoplasms arising in the kidney. Appl Immunohistochem Mol Morphol 10:332–338
23. Kononen J, Bubendorf L, Kallioniemi A, Barlund M, Schraml P, Leighton S, Torhorst J, Mihatsch MJ, Sauter G, Kallioniemi OP (1998) Tissue microarrays for high-throughput molecular profiling of tumor specimens. Nat Med 4:844–847
24. Langner C, Wegscheider BJ, Ratschek M, Schips L, Zigeuner R (2004) Keratin immunohistochemistry in renal cell carcinoma subtypes and renal oncocytomas: a systematic analysis of 233 tumors. Virchows Arch 444:127–134
25. Lopez-Beltran A, Sauter G, Gasser T, Hartmann A, Schmitz-Dräger BJ, Helpap B, Ayala AG, Tamboli P, Knwles MA, Sidransky D, Cordon-Cardo C, Jones PA, Cairns P, Simon R, Amin MB, Tyczynski JE (2004) Tumours of the urinary system. Infiltrating urothelial carcinoma. In: Eble JN, Sauter G, Epstein JI, Sesterhenn IA (eds) World Health Organization classification of tumours. Pathology and genetics. Tumours of the urinary system and male genital organs. IARC Press, Lyon pp 93–109
26. Miettinen M (1995) Keratin 20: immunohistochemical marker for gastrointestinal, urothelial, and Merkel cell carcinomas. Mod Pathol 8:384–388
27. Moll R (1998) Cytokeratins as markers of differentiation in the diagnosis of epithelial tumors. Subcell Biochem 31:205–262
28. Moll R, Achtstätter T, Becht E, Balcarova-Ständer J, Ittensohn M, Franke WW (1988) Cytokeratins in normal and malignant transitional epithelium. Maintenance of expression of urothelial differentiation features in transitional cell carcinomas and bladder carcinomas and bladder carcinoma cell culture lines. Am J Pathol 132:123–144
29. Moll R, Löwe A, Laufer J, Franke WW (1992) Cytokeratin 20 in human carcinomas. A new histodiagnostic marker detected by monoclonal antibodies. Am J Pathol 140:427–447
30. Parker DC, Folpe AL, Bell J, Oliva E, Young RH, Cohen C, Amin MB (2003) Potential utility of uroplakin III, thrombomodulin, high molecular weight cytokeratin and cytokeratin 20 in non-invasive, invasive, and metastatic urothelial (transitional cell) carcinomas. Am J Surg Pathol 27:1–10
31. Ramos D, Navarro S, Villamon R, Gil-Salom M, Llombart-Bosch A (2003) Cytokeratin expression patterns in low-grade papillary urothelial neoplasms of the urinary bladder. Cancer 97:1876–1883
32. Rijn van de M, Perou CM, Tibshirani R, Haas P, Kallioniemi O, Kononen J, Torhorst J, Sauter G, Zuber M, Köchli OR, Mross F, Dieterich H, Seitz R, Ross D, Botstein D, Brown P (2002) Expression of cytokeratins 17 and 5 identifies a group of breast carcinomas with poor clinical outcome. Am J Pathol 161:1991–1996
33. Schaafsma HE, Ramaekers FCS, Muijen van GNP, Lane EB, Leigh IM, Robben H, Huijsmans A, Ooms ECM, Ruiter DJ (1990) Distribution of cytokeratin polypeptides in human transitional cell carcinomas, with special emphasis on changing patterns during tumour progression. Am J Pathol 136:329–343
34. Schaafsma HE, Ramaekers FCS, Muijen van GNP, Robben H, Lane EB, Leigh IM, Ooms ECM, Schalken JA, Morselaar van RJA, Ruiter DJ (1991) Cytokeratin expression patterns in metastatic transitional cell carcinoma of the urinary tract. An immunohistochemical study comparing local tumor and autologous metastases. Am J Pathol 139:1389–1400
35. Schaller G, Fuchs I, Pritze W, Ebert A, Herbst H, Pantel K, Weitzel H, Lengyel E (1996) Elevated keratin 18 protein expression indicates a favourable prognosis in patients with breast cancer. Clin Cancer Res 2:1879–1885
36. Sobin LH, Wittekind C (eds) (2002) TNM classification of malignant tumors, 6th edn. Wiley-Liss, Inc., New York
37. Southgate J, Harnden P, Trejdosiewicz LK (1999) Cytokeratin expression patterns in normal and malignant urothelium: a review of the biological and diagnostic implications. Histol Histopathol 14:657–664
38. Takei H, Iino Y, Horiguchi J, Kanoh T, Takao Y, Oyama T, Morishita Y (1995) Immunohistochemical analysis of cytokeratin 8 as a prognostic factor in invasive breast carcinoma. Anticancer Res 15:1101–1105
39. Wang NP, Zee S, Zarbo RJ, Bacchi CE, Gown AM (1995) Coordinate expression of cytokeratins 7 and 20 defines unique subsets of carcinomas. Appl Immunohistochem 3:99–107

Virchows Arch (2004) 445:449–455
DOI 10.1007/s00428-004-1106-1

ORIGINAL ARTICLE

Giuseppe Pelosi · Michele Masullo · Maria Elena Leon · Giulia Veronesi · Lorenzo Spaggiari · Felice Pasini · Angelica Sonzogni · Antonio Iannucci · Enrica Bresaola · Giuseppe Viale

CD117 immunoreactivity in high-grade neuroendocrine tumors of the lung: a comparative study of 39 large-cell neuroendocrine carcinomas and 27 surgically resected small-cell carcinomas

Received: 9 June 2004 / Accepted: 22 July 2004 / Published online: 16 September 2004
© Springer-Verlag 2004

Abstract Little is known about CD117 prevalence and clinicopathological implications in pulmonary large-cell neuroendocrine carcinoma. We studied CD117 immunoreactivity in surgical specimens from 39 large-cell neuroendocrine carcinomas of stages I–III and 27 limited-disease small-cell carcinomas, 56 typical and atypical carcinoids of the lung, and 10 neuroendocrine tumorlets, including the membrane and cytoplasmic immunostaining patterns. Membrane CD117 immunoreactivity in 5% or more tumor cells was documented in 30 (77%) large-cell neuroendocrine carcinomas and 18 (67%) small-cell carcinomas and 4 (7%) carcinoids, whereas cytoplasmic labeling was seen in 17 (44%) large-cell neuroendocrine carcinomas, 19 (70%) small-cell carcinomas, and 3 (5%) carcinoids. None of the neuroendocrine cells of the normal bronchial epithelium and of 10 tumorlets showed any CD117 immunoreactivity. Cytoplasmic immunostaining was more prevalent in small-cell carcinomas, whereas membrane labeling did not differ between the two types of high-grade carcinomas. Downregulation of CD117 by neoadjuvant chemotherapy was seen in large-cell neuroendocrine carcinomas but not small-cell carcinomas. Multiple linear regression analysis demonstrated a marginal association between cytoplasmic CD117 immunoreactivity and regional lymph node metastasis in small-cell carcinomas but not large-cell neuroendocrine carcinomas. There was no association between CD117 immunoreactivity and survival in either small-cell carcinoma or large-cell neuroendocrine carcinoma patients.

Keywords CD117 · Large-cell · Small-cell · Neuroendocrine · Carcinoma

G. Pelosi (✉) · M. Masullo · A. Sonzogni · E. Bresaola
Division of Pathology and Laboratory Medicine,
European Institute of Oncology,
Via G. Ripamonti 435, 20141 Milan, Italy
e-mail: giuseppe.pelosi@ieo.it
Tel.: +39-02-57489414
Fax: +39-02-57489417

G. Pelosi · M. Masullo · A. Sonzogni · E. Bresaola · G. Viale
School of Medicine,
University of Milan,
Milan, Italy

M. E. Leon
Division of Statistics and Epidemiology,
European Institute of Oncology,
Via G. Ripamonti 435, 20141 Milan, Italy

G. Veronesi · L. Spaggiari
Division of Thoracic Surgery,
European Institute of Oncology,
Via G. Ripamonti 435, 20141 Milan, Italy

F. Pasini
Institute of Medical Oncology,
University of Verona,
Verona, Italy

A. Iannucci
Division of Pathology,
City Major Hospital,
Verona, Italy

Introduction

Approximately one-fourth to one-third of lung neoplasms are neuroendocrine tumors. These are classified along a continuum from low-grade tumors to intermediate-grade tumors with longer life expectancy (e.g., typical and atypical carcinoids) to very aggressive neoplasms with dismal prognosis (e.g., small-cell carcinomas and large-cell neuroendocrine carcinomas) [5, 30, 31]. Large-cell neuroendocrine carcinomas share most of the epidemiological and clinical features of small-cell lung carcinomas, including the highest association with a male prevalence, the highest incidence of regional lymph node and distant metastases at the time of the diagnosis, and the shortest survival; however, they reportedly differ in both morphological and genetic characteristics [9, 11, 28, 32,

33]. In particular, recent molecular data support the view that large-cell neuroendocrine carcinomas are much more akin to non-neuroendocrine large-cell carcinomas than to small-cell carcinomas or the other types of pulmonary neuroendocrine tumors [32], and therefore they have been included in the most recent World Health Organization classification of lung cancer.

Cell receptors with tyrosine kinase activity are important regulators of cell proliferation, differentiation, and survival and are thought to play a central role in the development and progression of several human malignancies, including lung cancer [19]. The proto-oncogene c-*Kit*, mapping to the chromosome 4q11-q12, encodes for a 145- to 160-kDa type 3 transmembrane tyrosine kinase receptor (CD117) that may undergo activation upon binding to its specific ligand [4, 35, 36] or through somatic intragenic mutations [13]. In neuroendocrine tumors of the lung CD117 immunoreactivity is commonly reported in small-cell carcinoma cell lines and in excised primary tumors, and some studies have reported it to be associated with adverse prognosis [14, 16, 20, 22, 29, 34]. Very few data, however, are available on the prevalence and clinicopathological implications of CD117 immunoreactivity in large-cell neuroendocrine carcinomas of the lung, with only two reports published in the English literature, to our knowledge [2, 8].

The aim of the present study was to compare the prevalence of CD117 immunoreactivity in (a) 39 stage I-III surgically resected large-cell neuroendocrine carcinomas of the lung and (b) 27 radically operated limited-disease small-cell carcinomas and 56 stage I-III typical and atypical carcinoids. We also investigated any change in CD117 immunoreactivity following neoadjuvant chemotherapy and its prognostic implications.

Materials and methods

Patients

The study included 122 consecutive patients who underwent radical resection at the participating institutions between 1987 and 2002. The population consisted of 79 men and 43 women with stage I–III neuroendocrine tumors [21]: 34 typical carcinoids, 22 atypical carcinoids, 39 large-cell neuroendocrine carcinomas, 27 small-cell carcinomas. All paraffin blocks were retrieved in each case, and the original hematoxylin and eosin-stained sections were reviewed. The diagnosis and the typing of tumors followed the 1999 WHO classification of lung and pleural tumors and adopted previously refined immunohistochemical criteria (immunoreactivity for synaptophysin, chromogranin A, and a variety of respiratory tract related hormones including gastrin-related peptide, calcitonin, adrenocorticotropic hormone, serotonin, and α-subunit of human chorionic gonadotropin) [24]. To ensure accurate staging all tumors had been removed by radical surgery, including an extensive mediastinal lymph node dissection (median: nine excised lymph nodes per patient). Two sections from each regional lymph node were examined histologically as previously reported [24].

Table 1 presents clinicopathological characteristics of the 122 neuroendocrine patients. All patients with small-cell carcinoma patients had limited disease according to the Veterans Administration Lung Cancer Study Group classification [15] (i.e., tumors restricted to one hemithorax without bulky regional metastases to hilar, ipsilateral, or contralateral mediastinal lymph nodes, or to supraclavicolar lymph nodes, or without ipsilateral pleural effusion). Among the patients undergoing neoadjuvant combination chemotherapy by the protocol of cyclophosphamide, doxorubicin, vincristine, and etoposide, including 5 with large-cell neuroendocrine carcinomas and 12 with small-cell carcinomas, there was a prevalence of more advanced-stage disease than among untreated patients (P=0.002). Detailed information on the cigarette smoking history was unavailable at the time of the present study, but most patients with high-grade tumors were known to be heavy smokers, consuming at least 20 cigarettes per day.

Immunohistochemistry

Formalin-fixed and paraffin-embedded tissue samples obtained at surgery were investigated. Tumors up to 2 cm in size were entirely

Table 1 Clinicopathological data in 122 neuroendocrine tumors (*TC* typical carcinoids, *ATC* atypical carcinoids, *LCNEC* large-cell neuroendocrine carcinomas, *SCLC* small-cell lung cancer)

	TC vs. ATC			LCNEC vs. SCLC		
	TC (n=34)	ATC (n=22)	P	LCNEC (n=39)	SCLC (n=27)	P
Age, median (years)	54	60	NS	64	64	NS
Gender: F/M	18/6	13/9	NS	5/34	7/20	NS
Stage: I/II, III	28/6	9/13	0.004	21/18	9/18	NS
Neoadjuvant chemotherapy: yes/no	3/31	3/19	NS	5/34	12/15	0.009
Lymph node metastases: no/yes	28/6	9/13	0.003	23/16	9/18	0.048
pN class: 0/1/2	28/5/1	9/7/6	0.003	23/10/6	9/9/9	NS
Positive lymph nodes, median[a]	0	1.5	<0.001	0	2	0.036
Size, median (cm)	2.4	3.0	NS	4	2.5	0.024
Ki-67, median (%)	2.9	9.3	<0.001	49	63	<0.001
Follow-up, mean ±SD (months)[b]	40±19	38±38	NS	36±36	29±25	NS
Follow-up, median (range; months)[b]	37 (9–77)	30 (2–184)		21 (2–135)	20 (5–92)	
Relapses: yes/no[b]	4/30	5/17	NS	23/16	15/5	NS
Vital status: dead/ alive[b]	0/34	2/20	NS	20/16	10/10	NS

[a] Number of regional positive lymph nodes per tumor
[b] n=36 for LCNEC, n=20 SCLC

embedded and immunostained; at least two representative tissue blocks were investigated in larger neoplasms. Ten samples of normal bronchial tree taken at different levels from patients with nonmalignant lung diseases, and ten samples of pulmonary neuroendocrine tumorlets and nonneoplastic peritumoral tissue from the study patients were used as control groups. Scattered neuroendocrine cells of the bronchial epithelium and tumorlets were identified with after chromogranin A immunostaining as previously described [23].

After blocking endogenous peroxidase activity with 5% hydrogen peroxide for 12 min, the tissue sections were reacted with the primary antibody to CD117 (a polyclonal antiserum raised against the C-terminal region of the human p145 KDa c-*kit* gene product encompassing the 963–976 amino acid residues; Dako-Cytomation, Glostrup, Denmark) for 30 min at room temperature using an automatic immunostainer (Autostainer, Dako) with no retrieval antigen procedure at the dilution of 10 µg/ml and then incubated with a high-sensitivity detection kit (Dako EnVision Plus-HRP) according to the manufacturer's instructions. Peroxidase activity was then developed with 3–3′diaminobenzidine-copper sulfate (Sigma, St. Louis, Mo., USA) to obtain a bright brown-black end product. The specificity of all immunoreactions was double-checked by replacing the primary antibody by a nonrelated isotypic mouse immunoglobulin at a comparable dilution a nonrelated or by normal serum alone [7]. Appropriate internal positive controls of tumor-infiltrating mast cells were also checked in all reactions. The proliferative fraction was evaluated by Ki-67 immunostaining as previously reported [23].

Scoring method

Immunostaining reactions were evaluated without knowledge of the patient's identity or clinical outcome. The proportion of immunoreactive tumor cells (labeling index) was assessed by scanning at least 1,000 neoplastic cells in representative fields of immunostaining. The CD117 immunostaining pattern was recorded as either predominantly membranous, if staining was primarily confined to the tumor cell membrane, or predominantly cytoplasmic, if a granular dotting reaction was identified in the cytoplasm of tumor cells with uneven membrane reinforcement. Tumors were considered negative for CD117 if staining was either completely absent or observed in only 5% or fewer of the neoplastic cells.

Statistical analysis

The significance of differences was evaluated using the χ^2 or Fisher's exact test. The medians of continuous data (e.g., age, tumor size) were compared by the Mann-Whitney or the Kruskal-Wallis test. To identify factors associated with the occurrence of regional lymph node metastases (yes/no) multiple logistic regression models included variables that emerged as significant in univariate regression analyses. Logistic regression results are expressed as odds ratios (OR) and corresponding 95% confidence intervals (CI). The overall and disease-free survival of patients classified in accordance with CD117 immunoreactivity were calculated by the Kaplan-Maier method and compared by the log-rank test. Cox's proportional regression models of survival data were calculated including patient age and gender, tumor stage, Ki-67 labeling index, neoadjuvant chemotherapy, and three different cutoff thresholds (5%, 10%, and 30%) for cytoplasmic and membrane CD117 immunostaining. Hazard ratios (HR) and 95% CI were calculated. All analyses used SAS (SAS Institute, Cary, N.C., USA). All *P* values reported here are two-tailed.

Results

CD117 immunoreactivity is lacking in normal and hyperplastic neuroendocrine cells of the lung

The scattered neuroendocrine cells and the neuroepithelial bodies of the normal respiratory mucosa, highlighted by chromogranin A immunostaining on adjacent sections, were consistently nonreactive for CD117, both in the nonneoplastic peritumoral lung tissue of the patients under investigation and in the bronchial tree taken at different levels from patients with nonmalignant lung diseases. Likewise, the hyperplastic neuroendocrine cells of tumorlets were always devoid of any CD117 immunoreactivity. Mast cells in the tumor tissue and the stroma of all examined samples were the only cells consistently and strongly immunoreactive for this marker.

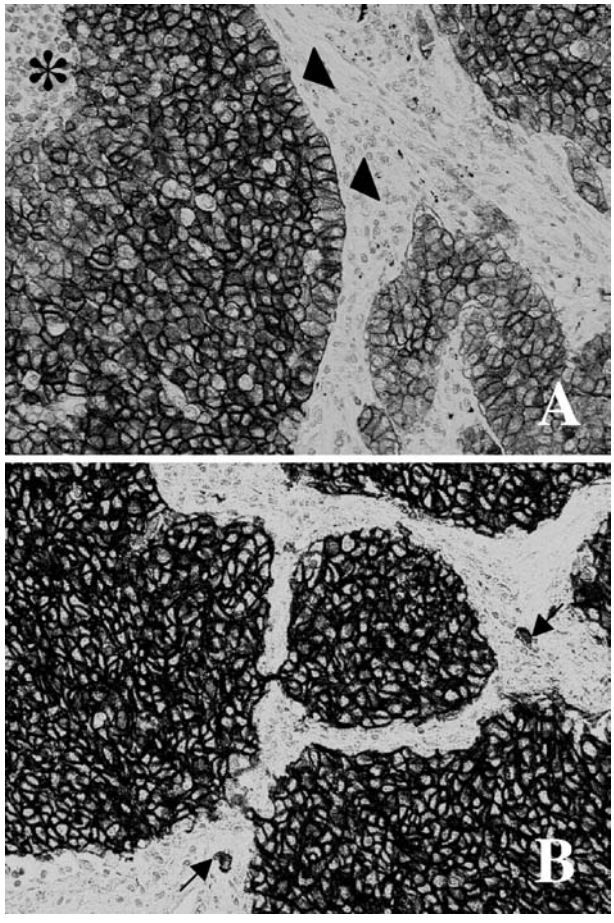


Fig. 1 CD117 immunoreactivity in high-grade neuroendocrine carcinomas of the lung. A membrane and cytoplasmic decoration is present in a case of large-cell neuroendocrine carcinoma with peripheral palisading of tumor cells (*arrowheads*) and focal necrosis (*asterisk*; **A**), whereas a predominantly cytoplasmic accumulation of immunostaining product is found in a case of small-cell carcinoma (**B**). Stromal mast cells are strongly decorated for CD117 and act as an internal positive control (**B**, *arrows*). All immunoperoxidase staining was performed with diaminobenzidine-copper sulfate, and counterstained with hematoxylin; ×250

Table 2 Relationship between CD117 and biopathological variables in 39 large-cell neuroendocrine carcinomas (*LCNEC*) and 27 surgically resected small-cell lung carcinomas (*SCLC*)

	Membrane labeling			Cytoplasmic labeling		
	<5%	≥5%	*P*	<5%	≥5%	*P*
LCNEC						
n	9	30	–	22	17	–
Age, median (years)	55	67	NS	64	67	NS
Gender: F/M	1/8	4/26	NS	2/13	3/8	NS
Stage I/II, III	5/4	16/14	NS	13/9	8/9	NS
Neoadjuvant chemotherapy: yes/no	4/5	1/29	0.007	2/20	3/14	NS
Lymph node metastases: no/yes	5/4	18/12	NS	15/7	8/9	NS
pN class: 0/1/2	5/2/2	18/8/4		15/3/4	8/7/2	
Positive lymph nodes, median[a]	0	0	NS	0	2	NS
Size, median (cm)	3.5	4.0	NS	3.8	4.0	NS
Ki-67, median (%)	53	48	NS	47	51	NS
SCLC						
n	9	8	–	8	19	–
Age, median (years)	59	69	0.018	61	68	NS
Gender: F/M	6/3	14/4	NS	3/5	4/15	NS
Stage: I/II, III	3/6	6/12	NS	4/4	5/14	NS
Neoadjuvant chemotherapy: yes/no	6/3	6/12	0.127	2/20	3/14	NS
Lymph node metastases: no/yes	3/6	6/12	NS	4/4	5/14	NS
pN class: 0/1/2	3/1/5	6/8/4	NS	4/2/2	5/7/7	NS
Positive lymph nodes, median[a]	3	1.5		1.5	2	NS
Size, median (cm)	2.5	2.8	NS	2.8	2.5	NS
Ki-67, median (%)	53	47.5	NS	47	51	NS

[a] Number of regional positive lymph nodes per tumor

CD117 immunoreactivity was correlated with high-grade neuroendocrine carcinomas and lymph node metastases

Overall the CD117 membrane labeling of 5% or more tumor cells was observed in 52 (43%) neuroendocrine tumors, and prominent cytoplasmic decoration in 39 (32%). Membrane immunoreactivity was documented in 30 (77%) large-cell neuroendocrine carcinomas, 18 (67%) small-cell carcinomas, and 4 (7%) carcinoids, whereas cytoplasmic labeling was seen in 17 (44%) large-cell neuroendocrine carcinomas, 19 (70%) small-cell carcinomas, and 3 (5%) carcinoids ($P<0.001$). Figure 1 shows representative features of membrane and cytoplasmic immunostaining in both large-cell neuroendocrine carcinomas and small-cell carcinomas.

Cytoplasmic immunostaining was more common in small-cell carcinomas than large-cell neuroendocrine carcinomas (median 5% vs. 0%, respectively; $P=0.014$), whereas membrane labeling did not differ between the various histotypes (median 0% in carcinoids, 10% in large-cell neuroendocrine carcinomas, 30% in small-cell carcinomas). Therefore a trend for membrane-positive/cytoplasm-negative tumors was seen in large-cell neuroendocrine carcinomas (80%) compared with small-cell carcinomas (20%), whereas the membrane-negative/cytoplasm-positive tumors were more likely to be small-cell carcinomas (63%) than large-cell neuroendocrine carcinomas (37%; $P=0.096$). In large-cell neuroendocrine carcinomas downregulation of CD117 membrane immunoreactivity was seen following neoadjuvant chemotherapy (Table 2), while in small-cell carcinomas only the patient's age was associated with increased membrane labeling of tumor cells (Table 2).

Overall, regional lymph node metastases were identified in 34 (52%) high-grade carcinoma patients (Table 1). Factors associated with the occurrence of regional lymph node metastases were female gender ($P=0.059$) and the presence of adjuvant chemotherapy ($P=0.019$) in small-cell but not large-cell neuroendocrine carcinomas; no significant correlations were found with age, tumor size, or proliferative activity. Multiple linear regression analysis for regional lymph node involvement revealed only neoadjuvant chemotherapy (HR=25.3, CI=1.3–501.3, $P=0.034$) and, marginally, CD117 cytoplasmic immunoreactivity (HR=10.9, CI=0.7–181.0, $P=0.093$) in the model based on a cutoff of 5% or more immunoreactive tumor cells was correlated independently with the occurrence of regional lymph node metastases in small-cell carcinomas but not large-cell neuroendocrine carcinoma.

CD117 immunoreactivity and survival in high-grade neuroendocrine carcinomas

In the present series either disease-free or overall survival was similar for large-cell neuroendocrine carcinoma and small-cell carcinoma (Fig. 2). Using the cutoff level of 5% immunoreactive cells, in small-cell carcinoma but not large-cell neuroendocrine carcinomas there was a trend for predominantly cytoplasm, not membrane-immunoreactive, tumors to take a more aggressive course, with shorter time to progression and overall survival (Fig. 3) Similar results were obtained the cutoff thresholds of 10% and 30%, with a trend for more aggressive clinical course in small-cell carcinoma only (data not shown). Multivariate Cox's analysis identified only neoadjuvant therapy (HR=3.9, CI=1.1–14.7, $P=0.038$) in large-cell neuroendocrine carcinoma and tumor stage (HR=19.9, CI=1.6–248.1, $P=0.021$) in small-cell carcinoma as independent predictor of shorter overall survival, and Ki-67 la-

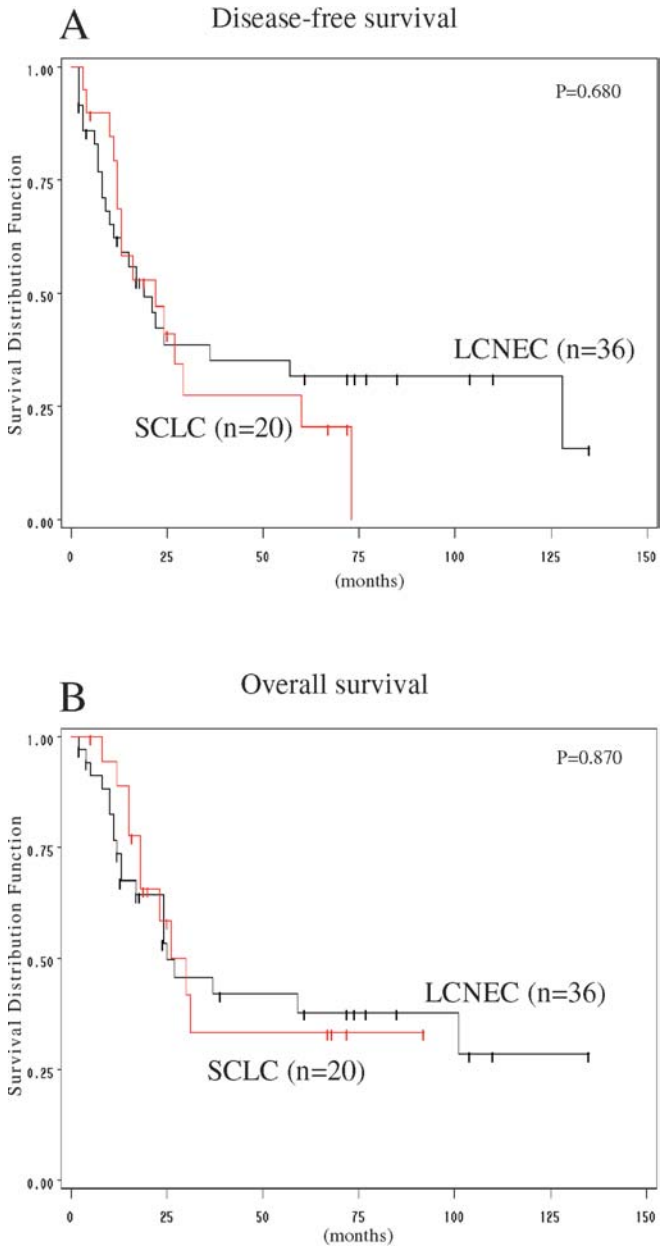


Fig. 2 Disease-free (**A**) and overall (**B**) survival curves according to histological typing of 56 high-grade neuroenodocrine tumors of the lung (36 large-cell and 20 small-cell neuroendocrine carcinomas), for which complete follow-up information was available at the time of the study. No significant differences in survival were seen between the two histologies. *Brackets* Number of patients for each survival curve

beling index (HR=1.1, CI=1.0–1.1, *P*=0.048) in large-cell neuroendocrine carcinoma and tumor stage (HR=19.8, CI=1.7–234.2, *P*=0.018) in small-cell carcinoma as independent indicator of reduced disease-free survival in the model of based on a cutoff of 5% or more immunoreactive tumor cells for CD117.

Discussion

This study identified a subset of pulmonary high-grade neuroendocrine carcinomas that consistently exhibit either membranous or cytoplasmic CD117 immunoreactivity. Membrane immunostaining is downregulated in large-cell neuroendocrine carcinoma patients treated with neoadjuvant chemotherapy, whereas there is a trend for predominantly cytoplasmic decoration to be associated with regional lymph node metastasis in small-cell carcinomas. Although CD117 is not an independent predictor of survival in either large-cell neuroendocrine carcinoma or small-cell carcinomas of the lung, a predominantly cytoplasmic pattern of immunostaining is marginally associated with shorter disease-free and overall survival in patients with limited-disease small-cell carcinoma.

The high prevalence of CD117 immunoreactivity in pulmonary high-grade neuroendocrine tumors (as opposed to the lack of staining in normal and hyperplastic neuroendocrine cells of the lower respiratory tract and to the occasional immunoreactivity in low- to intermediate-grade neuroendocrine tumors) emphasizes the possible involvement of this molecule in the development of most large-cell neuroendocrine carcinoma and small-cell carcinomas. The mechanisms responsible for CD117 overexpression/activation in high-grade neuroendocrine tumors of the lung are largely unknown, although the possibility of an autocrine growth loop has been suggested for small-cell carcinoma cell lines [12]. The actual prevalence of small-cell carcinomas coexpressing CD117 and its cognate ligand and/or bearing activating gene mutations, however, is unknown, but this has not thus far been fully assessed [12].

The prevalence of CD117 immunoreactivity in high-grade neuroendocrine tumors of the lung that we observed (77% in large-cell neuroendocrine carcinoma, 70% in small-cell carcinomas) is higher than previously reported in (from 39% [8] to 55% [2] in cell lines or tumor specimens of large-cell carcinomas and 25–70% in small-cell carcinomas [12]). We believe that this may be explained at least in part by the different selection crietria for assessing immunoreactivity. Standardized criteria for evaluating CD117 immunoreactivity in tumors other then gastrointestinal stromal tumors are lacking [6]. We used a cutoff threshold of 5% immunostained tumor cells for evaluating immunoreactivity, in contrast to the 10% threshold used by Araki et al. [2] and the 50% threshold used by Casali et al. [8] for large-cell neuroendocrine carcinomas to ensure inclusion of all cases with valuable immunoreactivity. We excluded from the analysis all positive tumors showing less than 5% immunoreactive cells because these findings are less reproducibile and may be biologically negligible. Variable cutoff levels have previously been used to assess immunoreactivity in small-cell carcinomas, with threshold values ranging from 10% to 50% [17, 20, 26, 27]. In our series, cytoplasmic CD117 immunoreactivity in even 5% or more tumor cells was marginally correlated with the occurrence of regional lymph node metastases in small-cell carcinomas but not

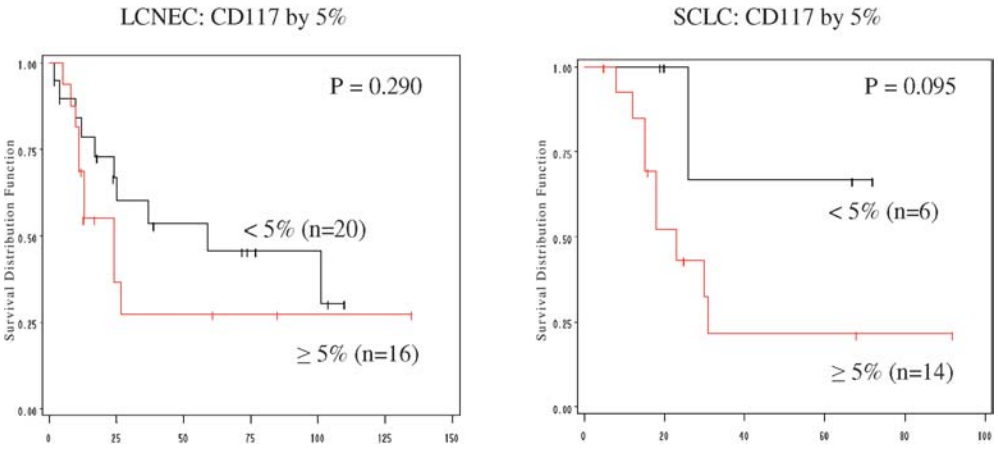


Fig. 3 Overall survival curve according to histological typing and 5% cutoff threshold of predominantly cytoplasmic immunoreactivity for CD117. In small-cell carcinomas but not large-cell neuroendocrine carcinomas there was a trend for cytoplasm—but not membrane—immunoreactive tumors to take a more aggressive course and entail a shorter life expectancy. *Brackets* Number of patients for each survival curve

in large-cell neuroeendocrine carcinomas. This suggests that CD117 expression plays different roles in the progression of the various types of high-grade pulmonary neuroendocrine carcinomas, and that it may be biologically relevant to the clinical behavior of small-cell lung carcinomas.

Moreover, we report for the first time that neoadjuvant therapy is effective in downregulating membrane CD117 labeling even in large-cell neuroendocrine carcinoma, as recently reported for small-cell carcinoma of the lung [27]. The possible downregulation of CD117 induced by chemotherapy may be relevant in the selection of candidate patients for second-line treatments targeting CD117. The lack of CD117 downregulation following induction chemotherapy among small-cell carcinoma patients of the present series may be due to the inclusion of patients showing only very limited disease and amenable to complete surgical resection. However, there was a trend for patients not undergoing chemotherapy to show more immunoreactive tumor cells in the membrane (Table 2).

This study examined both membrane and cytoplasmic CD117 immunoreactivity, at variance with previous investigations, although the biological implications of the cytoplasmic accumulation of CD117 are currently unknown. A cytoplasmic labeling for this molecule, however, has been reported by others in several tumor types, including small-cell carcinomas [17, 20, 27], large-cell neuroendocrine carcinomas [8], non-small-cell carcinomas of the lung [3, 25], colorectal neuroendocrine carcinoma [1], and gastrointestinal stromal tumors [10]. Moreover, definite paranuclear, dotlike, cytoplasmic immunoreactivity for CD117 is also common in gastrointestinal tumor cells [10], and a definite nuclear immunolocalization was reported [18] in both normal and neoplastic medullary cells of the adrenal gland, suggesting that CD117 differs in compartmentalization between the various normal and neoplastic cells.

The prognostic implications of CD117 immunoreactivity in pulmonary neuroendocrine carcinomas are still under debate. Using a 5% cutoff for immunoreactivity we found no effect of CD117 on survival of patients with large-cell neuroendocrine carcinomas, thus confirming previous data using a 10% cutoff [2]. Other authors reported a reduction in both overall survival and time to progression in 33 large-cell neuroendocrine carcinomas by increasing the threshold level up to 50% immunoreactive tumor cells [8]. In the our study, however, increasing the cutoff levels (up to 30% of CD117 immunoreactive tumor cells) was ineffective in reaching any prognostic value for CD117 in large-cell carcinomas, although a marginal influence on overall survival and time to progression was found in limited-disease small-cell carcinoma patients. In multivariate analysis only neoadjuvant therapy and Ki-67 labeling index for large-cell neuroendocrine carcinomas and tumor stage in small-cell carcinomas emerged as significant risk factors for death and time to progression. These findings again emphasize that CD117 is relevant to the development of high-grade neuroendocrine tumors of the lung and probably is an early event considering the high prevalence of immunoreactivity within these tumors, but that it is less important as a prognosticator of prognosis.

In conclusion, we observed CD117 immunoreactivity in most high-grade neuroendocrine carcinomas, with differential expression of predominantly cytoplasmic labeling in small-cell carcinomas and chemotherapy-related downregulation of membrane staining in large-cell neuroendocrine carcinomas. Its effect on prognosis is marginal.

References

1. Akintola-Ogunremi O, Pfeifer JD, Tan BR, Yan Y, Zhu X, Hart J, Goldblum JR, Burgart L, Lauwers GY, Montgomery E, Lewin D, Washington K, Bronner M, Xiao SY, Greenson JK, Lamps L, Lazenby A, Wang HL (2003) Analysis of protein expression and gene mutation of c-kit in colorectal neuroendocrine carcinomas. Am J Surg Pathol 27:1551–1558

2. Araki K, Ishii G, Yokose T, Nagai K, Funai K, Kodama K, Nishiwaki Y, Ochiai A (2003) Frequent overexpression of the c-kit protein in large cell neuroendocrine carcinoma of the lung. Lung Cancer 40:173–180
3. Arber DA, Tamayo R, Weiss LM (1998) Paraffin section detection of the c-kit gene product (CD117) in human tissues: value in the diagnosis of mast cell disorders. Hum Pathol 29:498–504
4. Ashman LK (1999) The biology of stem cell factor and its receptor C-kit. Int J Biochem Cell Biol 31:1037–1051
5. Axiotis CA (2002) The neuroendocrine lung. In: Li Volsi V, Asa SL (eds) Endocrine pathology. Churchill Livingstone, Edinburgh, pp 261–296
6. Berman J, O'Leary TJ (2001) Gastrointestinal stromal tumor workshop. Hum Pathol 49:786–798
7. Burry RW (2000) Specificity controls for immunocytochemical methods. J Histochem Cytochem 48:163–166
8. Casali C, Stefani A, Rossi G, Migaldi M, Bettelli S, Parise A, Morandi U (2004) The prognostic role of c-kit protein expression in resected large cell neuroendocrine carcinoma of the lung. Ann Thorac Surg 77:247–252
9. Debelenko LV, Swalwell JI, Kelley MJ, Brambilla E, Manickam P, Baibakov G, Agarwal SK, Spiegel AM, Marx SJ, Chandrasekharappa SC, Collins FS, Travis WD, Emmert-Buck MR (2000) MEN1 gene mutation analysis of high-grade neuroendocrine lung carcinoma. Genes Chromosomes Cancer 28: 58–65
10. Fletcher CD, Berman JJ, Corless C, Gorstein F, Lasota J, Longley BJ, Miettinen M, O'Leary TJ, Remotti H, Rubin BP, Shmookler B, Sobin LH, Weiss SW (2002) Diagnosis of gastrointestinal stromal tumors: a consensus approach. Hum Pathol 33:459–465
11. Haruki N, Yatabe Y, Travis WD, Nomoto S, Osada H, Nakamura S, Nakao A, Fujii Y, Takahashi T (2000) Characterization of high-grade neuroendocrine tumors of the lung in relation to menin mutations. Jpn J Cancer Res 91:317–323
12. Heinrich MC (2003) Is KIT an important therapeutic target in small cell lung cancer? Clin Cancer Res 9:5825–5828
13. Heinrich MC, Rubin BP, Longley BJ, Fletcher JA (2002) Biology and genetic aspoects of gastrointestinal stromal tumors: KIT activation and cytogenetic alterations. Hum Pathol 33: 486–495
14. Hida T, Ueda R, Sekido Y, Hibi K, Matsuda R, Ariyoshi Y, Sugiura T, Takahashi T, Takahashi T (1994) Ectopic expression of c-kit in small-cell lung cancer. Int J Cancer Suppl 8:108–109
15. Hyde L, Yee J, Wilson R (1965) Cell type and the natural history of lung cancer. JAMA 193:52–54
16. Krystal GW, Hines SJ, Organ CP (1996) Autocrine growth of small cell lung cancer mediated by coexpression of c-kit and stem cell factor. Cancer Res 56:370–376
17. Lonardo F, Pass HI, Lucas DR (2003) Immunohistochemistry frequently detects c-Kit expression in pulmonary small cell carcinoma and may help select clinical subsets for a novel form of chemotherapy. Appl Immunohistochem Mol Morphol 11:51–55
18. Matsuda R, Takahashi T, Nakamura S, Sekido Y, Nishida K, Seto M, Seito T, Sugiura T, Ariyoshi Y, Takahashi T, Ueda R (1993) Expression of the c-kit protein in human solid tumors and in corresponding fetal and adult normal tissues. Am J Pathol 142:339–346
19. Maulik G, Kijima T, Salgia R (2003) Role of receptor tyrosine kinases in lung cancer. Methods Mol Med 74:113–125
20. Micke P, Basrai M, Faldum A, Bittinger F, Ronnstrand L, Blaukat A, Beeh KM, Oesch F, Fischer B, Buhl R, Hengstler JG (2003) Characterization of c-kit expression in small cell lung cancer: prognostic and therapeutic implications. Clin Cancer Res 9:188–194
21. Mountain CF (1997) Revisions in the international system for staging for lung cancer. Chest 111:1710–1717
22. Naeem M, Dahiya M, Clark JI, Creech SD, Alkan S (2002) Analysis of c-kit protein expression in small-cell lung carcinoma and its implication for prognosis. Hum Pathol 33:1182–1187
23. Pelosi G, Pasini F, Olsen Stenholm C, Pastorino U, Maisonneuve P, Sonzogni A, Maffini F, Pruneri G, Fraggetta F, Cavallon A, Roz E, Iannucci A, Bresaola E, Viale G (2002) p63 immunoreactivity in lung cancer: yet another player in the development of squamous cell carcinomas? J Pathol 198:100–109
24. Pelosi G, Pasini F, Fraggetta F, Pastorino U, Iannucci A, Maisonneuve P, Arrigoni G, De Manzoni G, Bresaola E, Viale G (2003) Independent value of fascin immunoreactivity for predicting lymph node metastases in typical and atypical pulmonary carcinoids. Lung Cancer 42:203–213
25. Pelosi G, Barisella M, Pasini F, Leon ME, Veronesi G, Spaggiari L, Fraggetta F, Iannucci A, Masullo M, Sonzogni A, Maffini F, Viale G (2004) CD117 immunoreactivity in stage I adenocarcinoma and squamous cell carcinoma of the lung: relevance to prognosis in a subset of adenocarcinoma patients. Mod Pathol 17:711–721
26. Potti A, Moazzam N, Ramar K, Hanekom DS, Kargas S, Koch M (2003) CD117 (c-Kit) overexpression in patients with extensive-stage small-cell lung carcinoma. Ann Oncol 14:894–897
27. Rossi G, Cavazza A, Marchioni A, Milgaldi M, Bavieri M, Facciolongo N, Petruzzelli S, Longo L, Tamberi S, Crino L (2003) KIT expression in small cell carcinomas of the lung: effects of chemotherapy. Mod Pathol 16:1041–1047
28. Sampietro G, Tomasic G, Collini P, Biganzoli E, Boracchi P, Bidoli P, Pilotti S (2000) Gene product immunophenotyping of neuroendocrine lung tumors. No linking evidence between carcinoids and small-cell lung carcinomas suggested by multivariate statistical analysis. Appl Immunohistochem Mol Morphol 8:49–56
29. Sekido Y, Obata Y, Ueda R, Hida T, Suyama M, Shimokata K, Ariyoshi Y, Takahashi T (1991) Preferential expression of c-kit protooncogene transcripts in small cell lung cancer. Cancer Res 51:2416–2419
30. Travis WD, Gal AA, Colby TV, Klimstra DS, Falk R, Koss MN (1998) Reproducibility of neuroendocrine lung tumor classification. Hum Pathol 29:272–279
31. Travis WD, Rush W, Flieder DB, Falk R, Fleming MV, Gal AA, Koss MN (1998) Survival analysis of 200 pulmonary neuroendocrine tumors with clarification of criteria for atypical carcinoid and its separation from typical carcinoid. Am J Surg Pathol 22:934–944
32. Ullmann R, Petzmann S, Sharma A, Cagle PT, Popper HH (2001) Chromosomal aberrations in a series of large-cell neuroendocrine carcinomas: unexpected divergence from small-cell carcinoma of the lung. Hum Pathol 32:1059–1063
33. Ullmann R, Petzmann S, Klemen H, Fraire AE, Hasleton P, Popper HH (2002) The position of pulmonary carcinoids within the spectrum of neuroendocrine tumors of the lung and other tissues. Genes Chromosomes Cancer 34:78–85
34. Wang WL, Healy ME, Sattler M, Verma S, Lin J, Maulik G, Stiles CD, Griffin JD, Johnson BE, Salgia R (2000) Growth inhibition and modulation of kinase pathways of small cell lung cancer cell lines by the novel tyrosine kinase inhibitor STI 571. Oncogene 19:3521–3528
35. Witte O (1990) Steel locus defines new multipotent growth factor. Cell 63:5–6
36. Yarden Y, Kuang WJ, Yang-Feng T, Coussens L, Munemitsu S, Dull JT, Chen E, Schlessinger J, Francke U, Ullrich A (1987) Human proto-oncogene *c-kit*: a new cell surface receptor tyrosine kinase for an undefinited ligand. EMBO J 6:3341–3351

Virchows Arch (2004) 445:456–464
DOI 10.1007/s00428-004-1095-0

ORIGINAL ARTICLE

Martin Köbel · Wilko Weichert · Katharina Crüwell · Wolfgang D. Schmitt · Christine Lautenschläger · Steffen Hauptmann

Epithelial hyaluronic acid and CD44v6 are mutually involved in invasion of colorectal adenocarcinomas and linked to patient prognosis

Received: 12 April 2004 / Accepted: 7 July 2004 / Published online: 16 September 2004
© Springer-Verlag 2004

Abstract Desmoplastic stroma of colorectal adenocarcinomas contains a variety of extracellular matrix molecules, including hyaluronic acid (HA). Overexpression of the HA receptor CD44 and, in particular, its splicing variant CD44v6 has been described as a prognostic factor for patients with colorectal adenocarcinomas in some studies, but converse reports also exist. Our hypothesis is that these divergent results may be related to the fact that the function of CD44v6 depends on the HA content of cell-surrounding matrix. Therefore, we studied the expression of HA and CD44v6 in tissue samples of 145 patients suffering from colorectal adenocarcinomas using immunohistochemistry. Expression of HA was separately evaluated in tumor epithelium and stroma. We additionally examined the influence of HA on invasion and adhesion of colorectal adenocarcinoma cells in vitro. The results show that epithelial HA expression was not correlated with tumor stage but with lymph-node or distant metastasis. Patients with tumors expressing epithelial HA had a decreased overall survival (P=0.017) as well as tumors with coexpression of epithelial HA and CD44v6 (P=0.011). The latter issue remained an independent prognostic factor in multivariate analysis (relative risk 5.06; 95% confidence interval, 1.18–21.57; P=0.028). HA exclusively stimulated in vitro invasion of CD44v6-expressing cells. This stimulation was partly reversed by an anti-CD44v6 antibody. Our findings suggest that the adverse prognostic effect of CD44v6 in colorectal adenocarcinoma might be restricted to those tumors that have pericellular HA.

Keywords Colorectal adenocarcinoma · CD44v6 · Hyaluronic acid · Invasion · Prognosis

M. Köbel (✉) · K. Crüwell · W. D. Schmitt · S. Hauptmann
Institute of Pathology,
Martin-Luther-University Halle-Wittenberg,
Magdeburger Strasse 14, 06097 Halle, Germany
e-mail: martin.koebel@medizin.uni-halle.de
Tel.: +49-345-5571532
Fax: +49-345-5571295

W. Weichert
Institute of Pathology,
Charité University Hospital,
Berlin, Germany

C. Lautenschläger
Institute of Biostatistics,
Martin-Luther-University Halle-Wittenberg,
Germany

Introduction

The desmoplastic stroma of colorectal adenocarcinomas contains a variety of extracellular matrix components, e.g., collagens (type I, III, and V), glycoproteins (fibronectin and tenascin), and glycosaminoglycans such as hyaluronic acid [1, 2]. The functional importance of these different stromal components has not yet been adequately examined. However, this seems to be necessary, since changes in the expression of some of the extracellular matrix receptors are associated with patient's prognosis. This is particularly true for the HA receptor CD44. In normal colorectal mucosa, CD44 standard form (CD44s) and isoforms (CD44v6–10) are weakly expressed in the lower parts of crypts [3]. In colorectal adenocarcinomas, however, there is an overexpression of CD44 isoforms, which has been interpreted as a defect of the splicing machinery [4]. One isoform, CD44v6, became of special interest after a study by Gunthert et al. [5], who showed that overexpression of CD44v6 confers metastatic capacity to pancreatic carcinoma cell line. High expression levels of CD44v6 have been described in 42% and 57% of colorectal carcinomas [6, 7]. However, the prognostic relevance of CD44v6 in colorectal cancer has been considered controversial. Several studies have shown that overexpression of CD44v6 indicates poor prognosis [8, 9, 10, 11], whereas other studies could not confirm those findings [5, 12, 13, 14, 15]. Our hypothesis is that these discrepancies are related to the fact that the function of CD44v6 depends on the HA content of the cell-surrounding matrix. This supposal seems to be justified, since the amount of HA has already been identified as a prognostic

factor in colorectal adenocarcinomas [16]. Thereby, we investigated the expression of HA and CD44v6 in identical tissue samples of 145 colorectal adenocarcinomas and studied the role of HA in invasion and adhesion of three colorectal adenocarcinoma cell lines in vitro.

Materials and methods

Study population

Immunohistochemical examination of colorectal adenocarcinomas was retrospectively performed on tissue samples taken from 145 patients undergoing surgery between 1996 and 1999 at the department of surgery at Charité University Hospital, Berlin, Germany. The cases were selected based on the availability of tissue and were not stratified for known preoperative or pathological prognostic factors. None of the patients had received any treatment before surgery. All patients agreed that their tissue, which was removed for diagnostic or therapeutic purposes, could be used for scientific studies by signing the treatment contract of the Charité hospital.

Immunohistochemistry

Immunohistochemical staining was performed according to standard procedures as described previously for COX-2 [17]. For CD44v6 immunohistochemistry, we used the monoclonal antihuman CD44v6 antibody (clone VFF-7, 1:1000; Bender Medical Systems, Vienna, Austria) with antigen retrieval in citrate buffer in a pressure cooker for 5 min. HA detection was performed using biotinylated HA-binding protein (1:2000; Medac, Wedel, Germany). To evaluate the specificity of the biotinylated HA-binding protein, we predigested sections with 0.1 M hyaluronidase from Streptomyces (Sigma, Deisenhofen, Germany) for 3 h. No staining was observed in the hyaluronidase-treated controls (data not shown).

Evaluation of immunohistochemical tissue staining

Staining of all slides was independently evaluated by two pathologists (M.K. and W.W.), who were blinded to the patients' characteristics and outcomes. For semi-quantitative evaluation, the Dako scoring system was applied. In tumor epithelium, the staining intensity was designated as either not existent (0), weak (1), moderate (2), or strong (3). The number of cells stained was scored as either no cells stained (0), less than 10% (1), 10–50% (2), 50–80% (3), or more than 80% of cells stained (4). Dako score was calculated by multiplication of these two variables. For statistical analysis, patients were grouped as either CD44v6 negative (score 0–5) or CD44v6 positive (score 6–12); thus, a case with strong staining intensity in at least 10% of tumor cells was considered as CD44v6 positive. We separately evaluated HA expression in tumor epithelium and stroma. Epithelial HA expression was much weaker than CD44v6; thus, patients were grouped as either epithelial HA negative (score 0–2) or epithelial HA positive (score 3–12). Interobserver reproducibility for grouping CD44v6 and epithelial HA either as positive or negative was 97%. In cases with different interpretation, grouping agreement was achieved by discussing at a multiheaded microscope. Subsequent statistical analysis was performed, comparing positive and negative cases. Regarding the stroma, the cases were split into three groups: weaker than (1), equal to (2), or stronger than (3) adjacent normal stroma.

Statistical analysis

Statistical correlation among several clinicopathological factors and expression of HA and CD44v6 was assessed by use of the chi-square test for trends. The probability of differences in overall survival as a function of time was determined by use of a Kaplan–Meier test, with probing for significance by applying a log-rank test. We used multivariate regression analysis based on the Cox's proportional hazard model to test the independence of these parameters in the prediction of overall survival. Generally, P values smaller than 0.05 were considered as significant. For all statistic procedures, SPSS version 11.0 software was used.

Cells and cell culture

The human colon adenocarcinoma cell lines HRT-18 and CX-2 were obtained from the German Cancer Research Center (Heidelberg, Germany). HT-29 was obtained from the American Type Culture Collection (Rockville, MD, USA). Cells were cultured in RPMI 1640 supplemented with 10% fetal calf serum and 1% L-glutamine.

Flow cytometry

Confluent monolayers were harvested from 75-cm^2 tissue culture flasks by gentle treatment with 0.02% ethylenediaminetetraacetate (EDTA), 0.5% bovine serum albumin (BSA), and 0.1% NaN_3 in phosphate-buffered saline (PBS). Cells were rinsed with 0.1% NaN_3 in PBS, collected by centrifugation (1100×g for 5 min), and fixed with 1% paraformaldehyde in PBS for 10 min. Next, 2×10^5 cells per sample were incubated with either monoclonal anti-CD44s (clone SFF-2; Bender Medical Systems, Vienna, Austria) or monoclonal anti-CD44v6 (clone VFF-7) for 30 min on ice, washed with 5% fetal calf serum/0.1% NaN_3 in PBS twice, and finally incubated with fluorescein isothiocyanate (FITC)-conjugated rabbit anti mouse antibody (Dako, Copenhagen, Denmark) diluted 1:300 in PBS for 30 min on ice. Cells were then washed twice and analyzed on a Becton Dickinson FACStar plus flow cytometer (Heidelberg, Germany) at a wavelength of 488 nm.

Reverse-transcription polymerase chain reaction

Subconfluent colorectal carcinoma cells were harvested, and total RNA was prepared with RNAeasy kit (Qiagen, Hilden, Germany) and reverse transcribed. Polymerase chain reaction (PCR) cycling conditions for CD44s/CD44v6 were 30 cycles of denaturation, annealing, and extension (95°C for 60 s, 55°C for 60 s, and 72°C for 60 s). The primers used were: CD44 sense 5′-GAC ACA TAT TGC TTC AAT GCT TCA GC-3′, antisense 5′-GAT GCC AAG ATG ATC AGC CAT TCT GGA-3′; CD44v6 sense 5′-CAG CTG TCC CTG TTG -3′ [18]; GAPDH sense 5′-ACC ACA GTC CAT GCC ATC AC- 3′, antisense 5′-TCC ACC ACC CTG TTG CTG TA-3′.

Immunofluorescence histochemistry

Subconfluent cells grown on Labtec chamber slides were fixed with 3% paraformaldehyde (4°C) for 20 min. Afterward, cells were incubated with either the monoclonal anti-CD44s or monoclonal anti-CD44v6, each diluted in PBS containing 0.5% BSA for 60 min at room temperature and subsequently washed three times with PBS. Cells were incubated with FITC-conjugated secondary antibody for 30 min. Images were taken with a confocal laser scan microscope (Leica, Benzheim, Germany).

Radioimmunoassay for HA

Next, 2.5×10^4/ml human colorectal carcinoma cells were subcultured in 6-well plates under serum-free conditions for 24 h. Supernatants were collected and stored at −20°C. By use of a HA radiometric system (Pharmacia, Peapack, NJ, USA), analysis for hyaluronic acid was performed according to the manufacturer's instructions.

Matrigel invasion assay

Transwells chambers with polycarbonate membranes (8-μm pores in 6-well tissue culture plates (Costar, Cambridge, MA) were coated with matrigel (Becton Dickinson, Heidelberg, Germany) diluted in RPMI (1 mg/ml, 675 μl per 4.7 cm^2) and incubated for 60 min at 37°C. In some experiments, HA diluted in 0.1 M NA_2HPO_4 (3 mg/ml, 675 μl per 4.7 cm^2) was added. For inhibition, cells were preincubated with either 10 μg/ml CD44 blocking antibody (clone 2C5, R&D Systems, Wiesbaden, Germany) or monoclonal anti-CD44v6 (clone VFF-7) for 60 min. Then, 2×10^5 cells/ml in serum-free RPMI were added to the upper compartment of the transwell inserts for 72 h. Finally, cultures were incubated with 0.5 mg/ml MTT [3-(4,5- dimethylthiazol-2-yl)-2,5-diphenyltetrazolium bromide] (Sigma, Deisenhofen, Germany). Living cells convert the yellowish MTT to an insoluble purple formazan, which was used for colorimetric assay at a wavelength of 560 nm [19]. After incubating for 4 h, the cells on the upper and lower surface of the transwell insert were removed separately and then lysed, and the formazan was solubilized with dimethylsulfoxide.

Adhesion assay

Microtiter plates (96 wells, Costar, Cambridge, MA) were coated with a thin layer of Matrigel diluted in RPMI (10 μg/ml). In some experiments, HA was added at a concentration of 3 mg/ml in 0.1 M Na_2HPO_4. Nonspecific binding was blocked by 1% BSA/PBS for 2 h. Cells were harvested with 0.1% collagenase I (Worthington, Freehold, NJ) in EDTA. For blocking experiments, cells were pretreated with antibodies for 60 min parallel to the invasion assays, then cells were plated at a density of 2×10^4 cells/100 μl in each well for 90 min. Unbound cells were removed by aspirating the medium, whereas attached cells were fixed with 70% ethanol at 20°C for 10 min and stained by use of crystal violet (0.1% in H_2O). After washing plates with distilled water, 0.2%Triton-X 100 was added to lyse the cells, and the absorbance of the solution was measured at 590 nm on a plate reader.

Results

Clinical and pathological characteristics of patients with colorectal adenocarcinomas

Samples from a total of 145 patients were investigated for CD44v6 and HA immunoreactivity. The mean age of patients at surgery was 65 years (ranging from 31 years to 86 years). The clinicopathological data for the patients with colorectal adenocarcinomas are shown in Table 1. The median follow-up time was 44 months. Data on survival were available for all 145 patients. Of the patients, 32 died of disease (78% 3-year survival rate).

Table 1 Relationship between CD44v6 and epithelial hyaluronic acid (HA) expression and various clinicopathological parameters as well as between CD44v6 and epithelial HA expression in colorectal adenocarcinomas

Characteristic	All cases	CD44v6 negative	CD44v6 positive	*P* value	Epithelial HA negative	Epithelial HA positive	*P* value
		(Score 0–5)	(Score 6–12)		(Score 0–2)	(Score 3–12)	
All cases							
	145	83 (57.2%)	62 (42.8%)		83 (57.2%)	62 (42.8%)	
Age				0.108			0.943
<65 years	73 (50.3%)	37 (44.6%)	36 (58.1%)		42 (50.6%)	31 (50.0%)	
≥65 years	72 (49.7%)	46 (55.4%)	26 (41.9%)		41 (49.4%)	31 (50.0%)	
Duke's stage				0.643			0.201
A	32 (22.1%)	20 (24.1%)	12 (19.6%)		22 (26.5%)	10 (16.1%)	
B	52 (35.8%)	29 (34.9%)	23 (36.6%)		30 (36.1%)	22 (35.5%)	
C	49 (33.8%)	29 (34.9%)	20 (32.4%)		27 (32.6%)	22 (35.5%)	
D	12 (8.3%)	5 (6.1%)	7 (11.4%)		4 (4.8%)	8 (12.9%)	
Tumor stage				0.435			0.219
T1	9 (6.2%)	7 (8.4%)	2 (3.2%)		8 (9.6%)	1 (1.6%)	
T2	33 (22.8%)	21 (25.3%)	12 (22.8%)		18 (21.7%)	15 (24.2%)	
T3	92 (63.4%)	49 (59.1%)	43 (63.4%)		52 (62.7%)	40 (64.5%)	
T4	11 (7.6%)	6 (7.2%)	5 (7.6%)		5 (6.0%)	6 (9.7%)	
Nodal status				0.681			0.034
N0	87 (60.0%)	51 (61.4%)	36 (58.1%)		56 (67.5%)	31 (50.0%)	
N1	58 (40.0%)	32 (38.6%)	26 (41.9%)		27 (32.5%)	31 (50.0%)	
Metastasis				0.151			0.043
M0	132 (91.0%)	78 (94.0%)	54 (87.1%)		79 (95.2%)	53 (85.5%)	
M1	13 (9%)	5 (6.0%)	8 (12.9%)		4 (4.8%)	9 (14.5%)	
Grade				0.473			0.814
G1	6 (4.1%)	2 (2.4%)	4 (6.5%)		4 (4.8%)	2 (3.2%)	
G2	116 (80%)	68 (81.9%)	48 (77.4%)		65 (78.4%)	51 (82.3%)	
G3	23 (15.9%)	13 (15.7%)	10 (16.1%)		14 (16.8%)	9 (14.5%)	
Epithelial HA				0.128			
Negative	83 (57.2%)	52 (62.7%)	31 (50.0%)				
Positive	62 (42.8%)	31 (37.3%)	31 (50.0%)				

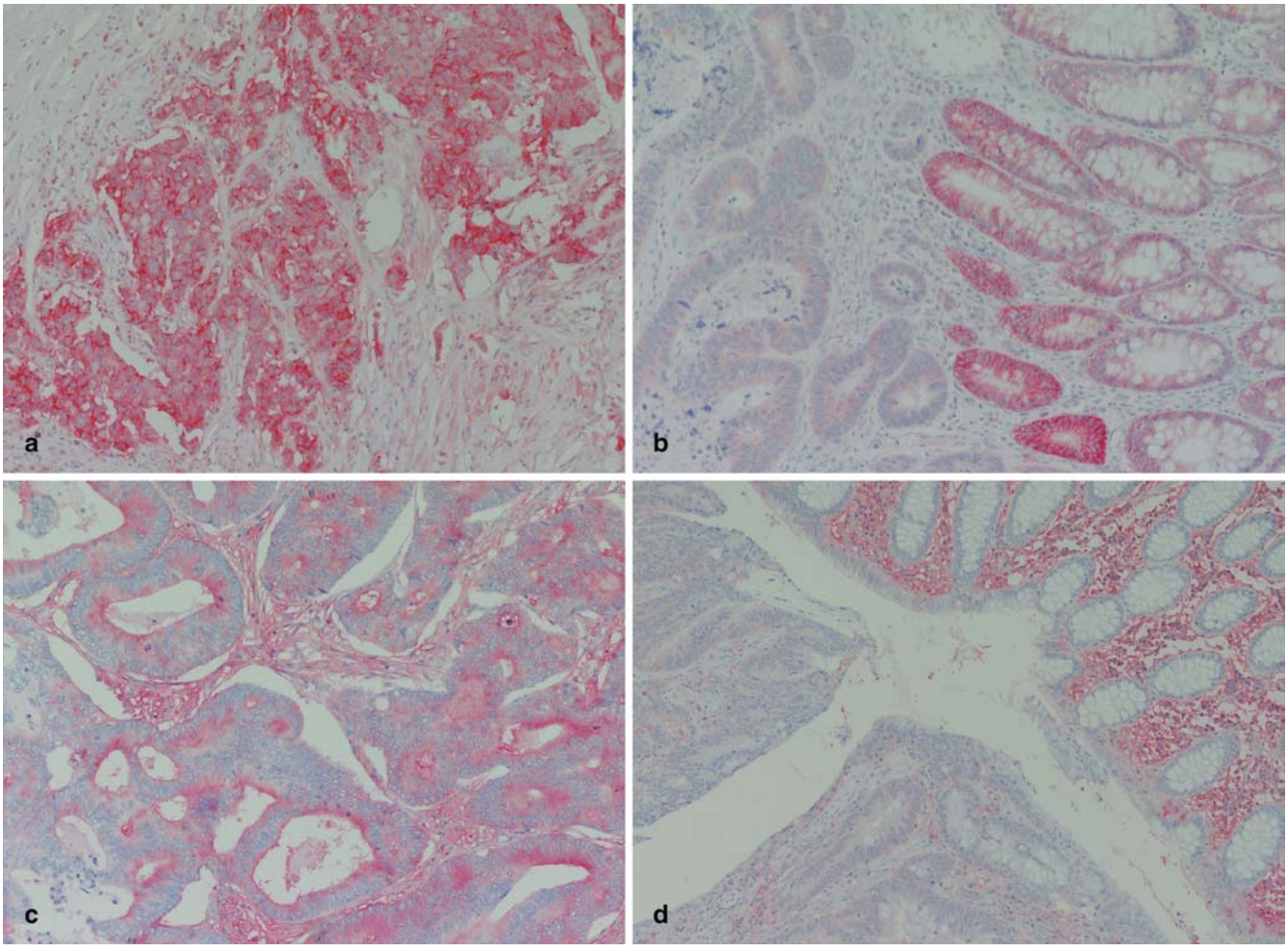


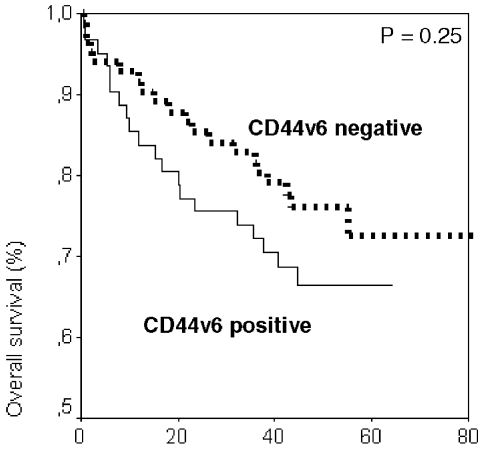
Fig. 1 CD44v6 (**A**, **B**) and hyaluronic acid (HA) (**C**, **D**) immunohistochemical staining of colorectal adenocarcinomas. **A** CD44v6-positive tumor. **B** *Left* CD44v6-negative tumor, *right* CD44v6 expression in basal normal crypts. **C** Epithelial and stromal HA-positive tumor. **D** *Left* HA-negative tumor, *right* HA-positive adjacent normal stroma

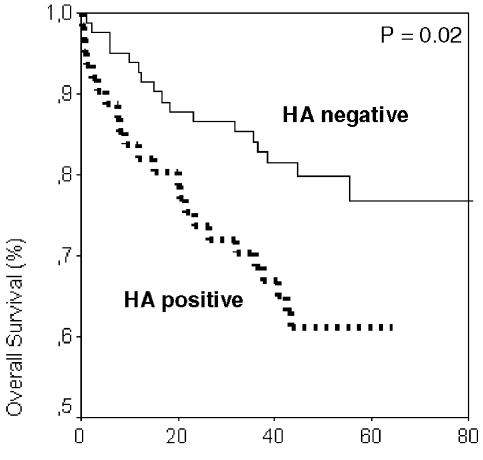
CD44v6 and HA immunostaining in colorectal adenocarcinomas

The different expression pattern of CD44v6 and HA is shown in Fig. 1. In a subgroup of 42.8% of colorectal adenocarcinomas, overexpression of CD44v6 was observed as membranous staining. The majority of tumors expressed low levels of CD44v6, and some tumors were completely negative. Adjacent normal mucosa showed CD44v6 expression in the basal crypts. HA staining was not only observed in tumor and adjacent normal stroma, but there was a subgroup of tumors where a cytoplasmic HA expression was remarkable as well. The latter we called epithelial HA expression. Table 1 depicts the distribution of CD44v6 and epithelial HA expression (positive versus negative) in colorectal adenocarcinomas in relation to age, Duke's stage, tumor stage and nodal status, state of metastasis, and histopathological tumor grade. No significant correlations were found for CD44v6 with any of these parameters. In contrast, epithelial HA was correlated with positive nodal status and distant metastasis (P=0.034 and P=0.043, respectively). Interestingly, there was no correlation between CD44v6 and epithelial HA expression.

Epithelial HA and CD44v6 coexpression are prognostic factors in univariate and multivariate survival analysis

We compared the survival rate of our patients suffering from colorectal cancer according to the expression status of CD44v6 and epithelial HA as well as stromal HA (Fig. 2, Table 2). The 3-year survival rate of the 62 patients positive for CD44v6 (77.2%) was not significantly lower than that of the 83 patients with negative tumors (82.3%). Stromal expression of HA did not exert an association with patient survival. In contrast, epithelial HA expression was associated with a diminished 3-year survival rate (68.6% positive for epithelial HA versus 84.1% negative for epithelial HA, P=0.0176). In addition, patients with coexpression of CD44v6 and epithelial HA showed a 3-year survival rate of 61.7%, whereas 97.1 % of patients with neither expression of CD44v6 nor epithelial HA were still alive after 3 years (P=0.0113). Other





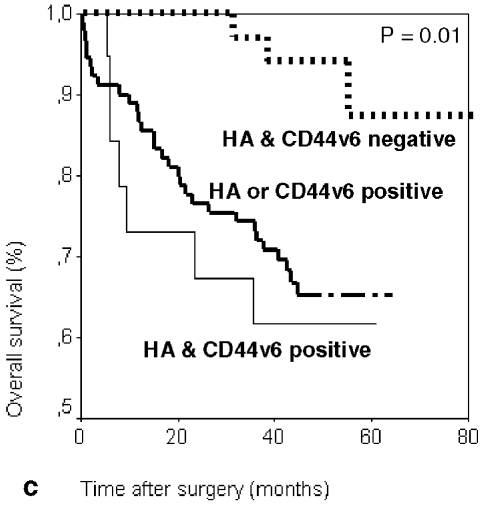


Fig. 2 Univariate survival analysis (Kaplan–Meier) of all 145 patients with colorectal adenocarcinoma. **A** Patients with tumors negative for CD44v6 have a 3-year survival (82.7%, *n*=83) compared with patients with positive tumors for CD44v6 (72.2%, *n*=62) (log-rank test; *P*=0.2564). **B** Patients with tumors negative for epithelial hyaluronic acid (HA) have a 3-year survival (84.1%, *n*=83) compared with patients with positive tumors for epithelial HA (68.5%, *n*=62) (log-rank test; *P*=0.0176). **C** Patients with tumors negative for both epithelial HA and CD44v6 have a 3-year survival (97.0%, *n*=36) compared with patients with positive tumors for epithelial HA or CD44v6 (74%, *n*=90) or patients positive for both epithelial HA and CD44v6 (61.7%, *n*=19) (log-rank test; *P*=0.0113)

significant prognostic parameters in univariate analysis were patient's age (*P*=0.0132), Duke's stage (*P*<0.0001), tumor stage (*P*=0.0005), nodal status (*P*<0.001), state of metastasis (*P*<0.001), and histopathological tumor grade (*P*=0.0026). The variables included in multivariate COX regression analysis were patient's age, Duke's stage, and histopathological tumor grade (Table 3). Tumor node and metastasis parameters were not included, since they are already part of the Duke's system. As a result, we found that coexpression of CD44v6 and epithelial HA was an independent prognostic factor for poor patient's survival (relative risk, 5.06; 95% confidence interval 1.18–21.57; *P*=0.028). Other independent risk factors were Duke's stage and age.

CD44 expression in vitro

In the three cell lines used here, CD44v6 expression was exclusively detected in HT-29, which also expressed high levels of CD44s using flow cytometry (Fig. 3). HRT-18 showed a moderate CD44s expression in approximately 50% of cells. CX-2 was completely negative for CD44. Reverse-transcription PCR confirmed the expression pattern of CD44s and CD44v6 (Fig. 4). If CD44 expression was observed, the protein was always continuously membranous located, as shown using immunofluorescence histochemistry (Fig. 5).

HA synthesis

To obtain information on the capacity of the cell lines to secrete the primary CD44 ligand, we performed a HA-specific radioimmunoassay. All three tumor cell lines synthesized HA but differed widely in quantity. The largest amounts of HA were detected in the supernatants of CX-2 cells, with 1700 ng/10^6 cells after 3 days (Fig. 6).

Matrigel invasion assay

HT-29 and HRT-18 were able to invade Matrigel, whereas CX-2 was not invasive (Fig. 7). Thereby, no inhibitory experiments were performed with this cell line. To study the in vitro role of CD44 in invasion of human colorectal cancer cells, HT-29 and HRT-18 cells were preincubated with either a monoclonal antibody against the HA-binding region of CD44 or a monoclonal antibody against the variable region encoded by exon 6. In the CD44v6-expressing cell line HT-29, the anti-CD44v6 antibody sig-

Table 2 Univariate survival analysis (Kaplan–Meier): 3-year survival rate of all patients with colorectal adenocarcinomas according to clinicopathological factors and CD44v6, epithelial or stromal hyaluronic acid (HA) expression

		Cases	Events	3-Year survival %	Standard error	Log-rank test (*P* value)
Age at diagnosis	<65 years	73	12	82.89	4.50	0.0132
	≥65 years	72	20	72.22	5.28	
Duke's stage	A	32	1	96.88	3.08	<0.0001
	B	52	4	92.07	3.81	
	C	49	17	64.64	6.90	
	D	12	10	16.67	10.76	
Tumor stage	pT1	8	0	100		
	pT2	33	3	90.91	5.00	0.0005
	pT3	92	21	76.65	4.47	
	pT4	11	7	36.36	14.50	
Nodal status	pN0	87	5	94.13	2.55	<0.0001
	pN1	58	26	54.44	6.60	
Metastasis	M0	132	22	83.76	3.25	<0.0001
	pM1	13	10	23.08	11.96	
Grade	G1	5	0	100		
	G2	116	20	82.36	3.58	0.0026
	G3	23	11	52.17	10.42	
CD44v6	Negative	83	14	82.76	4.20	0.2564
	Positive	62	17	72.22	5.73	
Epithelial HA	Negative	83	13	84.10	4.04	0.0176
	Positive	63	19	68.56	5.98	
Stromal HA	Weaker	24	8	66.67	9.88	0.5244
	Equal	120	24	79.55	3.73	
	Stronger	1	0	100		
Coexpression of CD44v6 and epithelial HA	Both negative	36	1	97.06	2.90	0.0113
	One positive	90	23	74.24	4.63	
	Both positive	19	7	61.75	11.41	

Table 3 Multivariate survival analysis (Cox regression model). *RR* relative risk

		Overall survival		
		RR	95% confidence interval	*P* value
Age	<65 years	1.000		
	≥65 years	3.045	1.51–6.12	0.002
Duke's stage	A	1.000		
	B	0.800	0.18–3.41	0.764
	C	5.572	1.63–18.94	0.006
	D	14.435	3.75–55.55	<0.0001
Grading	G1/G2	1.000		
	G3	1.777	0.84–3.76	0.132
Epithelial HA	Negative	1.000		
	Positive	1.139	0.67–2.66	0.406
Coexpression of CD44v6 and epithelial HA	Both negative	1.000		
	One positive	3.405	1.51–6.12	0.063
	Both positive	5.060	1.18–21.57	0.028

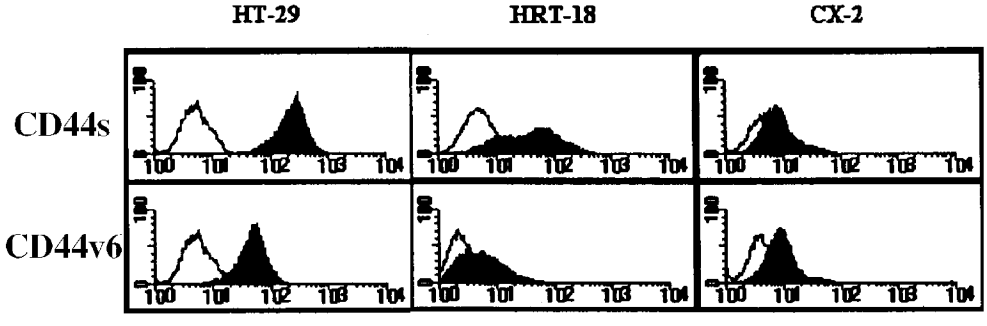


Fig. 3 Expression of CD44s and CD44v6 in three different human colon cancer cell lines investigated by flow cytometry. *Black and white peaks* represent the fluorescence of tumor cells treated with the CD44s (*upper row*) or CD44v6 (*lower row*) antibody and the control antibody

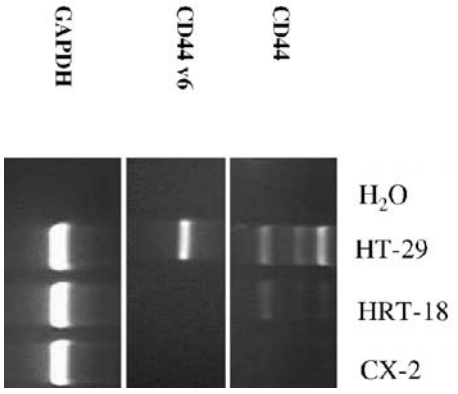


Fig. 4 Reverse-transcription polymerase chain reaction detection of CD44 and CD44v6 in HT-29, HRT-18, and CX-2

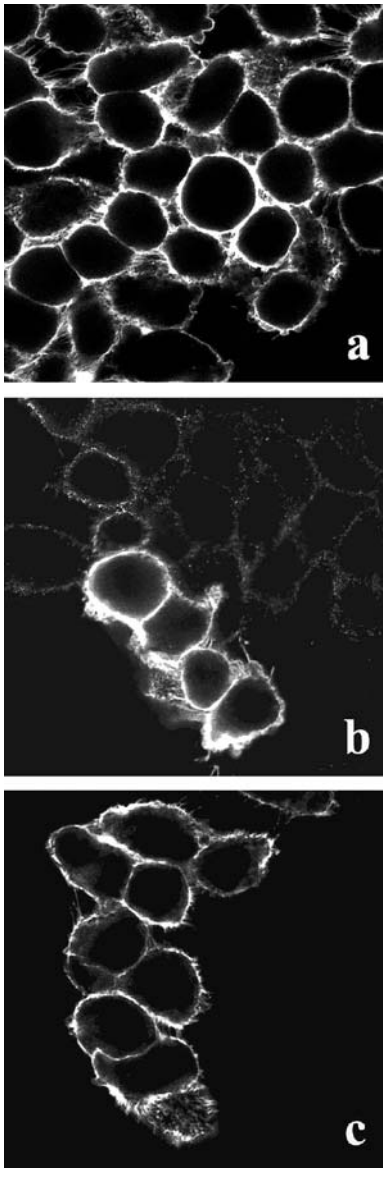


Fig. 5 Fluorescence micrograph of CD44s in HT-29 (**A**), HRT-18 (**B**), and CD44v6 in HT-29 (**C**)

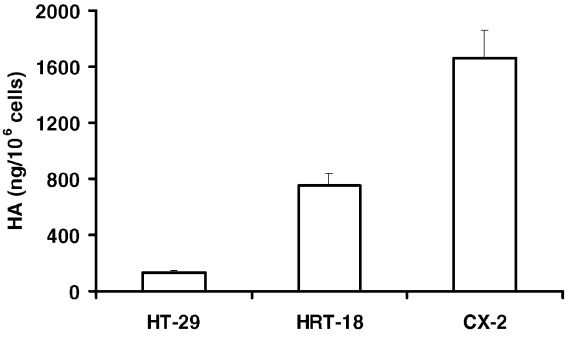


Fig. 6 Hyaluronic acid synthesis in HT29, HRT-18, and CX-2 cells detected in the supernatants

nificantly inhibited invasion by 32%, whereas the CD44-blocking antibody did not. Both antibodies had no effect on the invasive ability of HRT-18.

For further experiments, HA was mixed with Matrigel and coated to the polycarbonate membranes. The addition of HA resulted in a significant 76% increase of invasion of HT-29 cells but did not change invasion of the HRT-18 and CX-2 cells. Incubation with anti-CD44v6 antibody partly reversed the increased invasion of HT-29 in HA-enriched Matrigel.

Adhesion assay

To investigate whether this effect could be explained by changes in cell adhesion, we performed adhesion assays in a parallel manner to the invasion assays. All cell lines showed strong adhesion to Matrigel when compared with BSA control (Fig. 8). Addition of HA to Matrigel or antibodies had different effects on adhesion of these cell lines. Both antibodies significantly reduced adhesion of HT-29, whereas adhesion of HRT-18 and CX-2 was not affected and vice versa—Matrigel reduced adhesion of HRT-18 and CX-2 but not of HT-29.

Discussion

In this study, we evaluated the expression of CD44v6 as well as the epithelial and stromal HA content of colorectal adenocarcinomas. CD44v6 was expressed in 62 (43%) of 145 tissue samples of patients with colorectal adenocarcinomas, which is within the range (42–57%) described in the literature [6, 7]. In cell culture, one of three colorectal adenocarcinoma cell lines expressed CD44v6. The CD44 ligand, HA, was detectable in the stroma of all colorectal adenocarcinomas without significant correlations to any clinicopathological parameters. The most probable origin of stromal HA was the local fibroblasts, but we showed that some tumors were also able to synthesize HA, which was demonstrated by in vitro detection of HA in the three investigated cell lines as well as epithelial HA expression in a subset of tumor samples. Epithelial expression of HA showed a correlation with positive nodal status and state

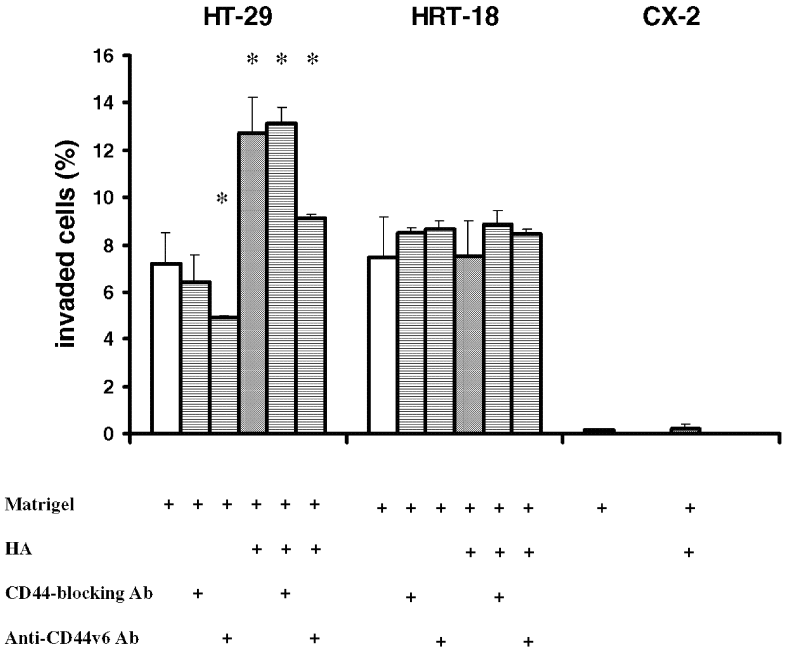


Fig. 7 Boyden chamber assay of colorectal cancer cells with CD44-blocking antibody, anti-CD44v6 antibody, and hyaluronic acid. Columns represent percentages of invasive cells (n=3, mean and SD). *Asterisk* indicates significant results

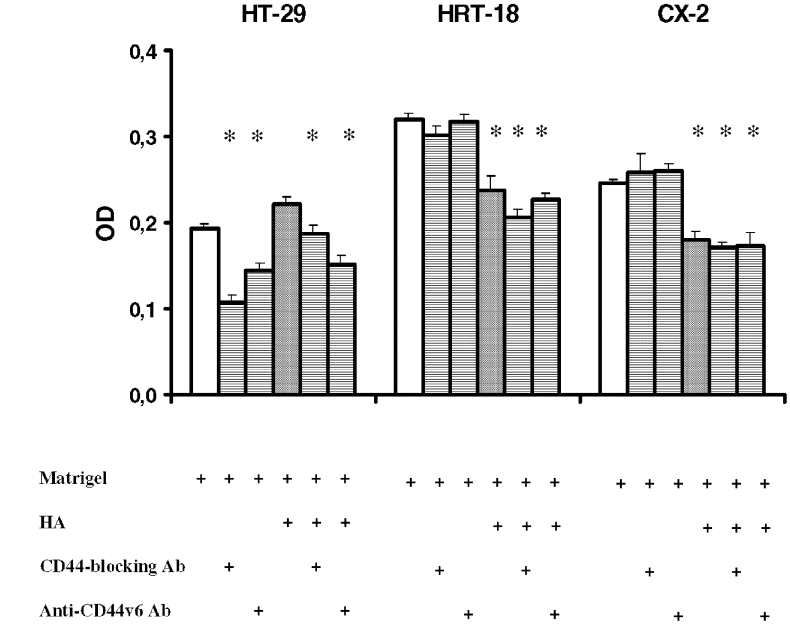


Fig. 8 Adhesion assay to Matrigel of colorectal cancer cells with CD44-blocking antibody, anti-CD44v6 antibody, and hyaluronic acid. *Columns* represent optical density of adhesive cells (n=3, mean and SD). *Asterisk* indicates significant results

of metastasis and was a significant prognostic factor for worse 3-year survival (68.5% versus 84.1%) in univariate but not in multivariate analysis. In a study by Ropponen et al. [16], epithelial HA expression was described as a predictor of survival in univariate and multivariate analysis as well. Since prognosis is clearly related to metastasis, the different findings regarding the multivariate analysis might be due to correlation of epithelial HA expression with metastasis in our study. Interestingly, coexpression of epithelial HA with CD44v6 was a significant prognostic parameter in multivariate analysis, independently of age, Duke's stage, and grading. To evaluate a mutual effect of HA and CD44v6 on tumor progression, we further studied the effect of exogenous HA and anti-CD44v6 antibodies on invasion and adhesion in vitro. Our supposal was sustained by the finding that mixing of Matrigel with exogenous HA exclusively escalated invasion of the CD44v6-expressing cell line and that this effect could partly be reversed by an anti-CD44v6 antibody. Since this blocking was only partial, it is conceivable that other mechanisms contribute to increased tumor cell invasion, e.g., hydration of the extracellular matrix. Moreover, HA may act via other HA receptors, which we are currently investigating. To address

a possible role of adhesion, we performed parallel adhesion experiments, but changes in adhesion did not explain changes in invasion. This is in line with studies by Reeder et al. [20] and Yakushijin et al. [21], who showed that a gain of metastatic capacity in CD44v6-expressing human tumor cells of colorectal and lymphoid origin was not associated with a change in adhesion to HA.

Thus, we conclude that HA and CD44v6 mutually enhance colorectal cancer invasion. To illuminate the molecular mechanism of this interaction was not within the scope of this study. But we believe that the epithelial HA might be secreted via exocytosis to form a pericellular coat by linking with CD44v6. Our attempts to verify such a susceptible pericellular coat using an immunofluorescence technique have not been prosperous thus far. Although to date there is no evidence, our hypothesis is that of a direct outside-in signaling pathway for HA via CD44v6, as signal transmitters to the cytoskeleton could serve the submembranal linking proteins of the ERM (Ezrin, Radixin, Moesin) family, which bind to CD44v6 on the inner membrane [22]. Another molecular explanation might be that the pericellular coat of HA could act as a reservoir for cytokines such as HGF/SF. It has been recently shown that HGF/SF built up a complex with c-Met and CD44v6. This formation can be inhibited by an anti-CD44v6 antibody, thus, abrogating the promigratory signaling via HGF/SF [23].

Taken together, our experimental data suggest that coexpression of epithelial HA and CD44v6 enhances tumor progression, presumably by increasing invasion and not affecting adhesion. Further elucidation of a molecular mechanism, e.g., CD44v6 outside-in signaling pathways induced by HA binding, might provide insight into the regulation of tumor invasion.

References

1. Miura S, Kodaira S, Hosoda Y (1993) Immunohistologic analysis of the extracellular matrix components of the fibrous stroma of human colon cancer. J Surg Oncol 53:36–42
2. Hauptmann S, Zardi L, Siri A, Carnemolla B, Borsi L, Castellucci M, Klosterhalfen B, Hartung P, Weis J, Stocker G (1995) Extracellular matrix proteins in colorectal carcinomas. Expression of tenascin and fibronectin isoforms. Lab Invest 73:172–182
3. Furuta K, Zahurak M, Yang XL, Rosada C, Goodman SN, August JT, Hamilton SR (1996) Relationship between CD44 expression and cell proliferation in epithelium and stroma of colorectal neoplasms. Am J Pathol 149:1147–1155
4. Givehchian M, Worner S, Strater J, Zoller M, Heuschen U, Heuschen G, Lehnert T, Herfarth C, von Knebel Doeberitz M (1998) No evidence for cancer-related CD44 splice variants in primary and metastatic colorectal cancer. Eur J Cancer 34: 1099–1104
5. Gunthert U, Hofmann M, Rudy W, Reber S, Zoller M, Haussmann I, Matzku S, Wenzel A, Ponta H, Herrlich P (1991) A new variant of glycoprotein CD44 confers metastatic potential to rat carcinoma cells. Cell 65:13–24
6. Weg-Remers S, Anders M, von Lampe B, Riecken EO, Schuder G, Feifel G, Zeitz M, Stallmach A (1998) Decreased expression of CD44 splicing variants in advanced colorectal carcinomas. Eur J Cancer 34:1607–1611
7. Ishida T (2000) Immunohistochemical expression of the CD44 variant 6 in colorectal adenocarcinoma. Surg Today 30:28–32
8. Mulder JW, Kruyt PM, Sewnath M, Oosting J, Seldenrijk CA, Weidema WF, Offerhaus GJ, Pals ST (1994) Colorectal cancer prognosis and expression of exon-v6-containing CD44 proteins. Lancet 344:1470–1472
9. Nihei Z, Ichikawa W, Kojima K, Togo S, Miyanaga T, Hirayama R, Mishima Y (1996) The positive relationship between the expression of CD44 variant 6 and prognosis in colorectal cancer. Surg Today 26:760–761
10. Ropponen KM, Eskelinen MJ, Lipponen PK, Alhava E, Kosma VM (1998) Expression of CD44 and variant proteins in human colorectal cancer and its relevance for prognosis. Scand J Gastroenterol 33:301–309
11. Wielenga VJ, van der Voort R, Mulder JW, Kruyt PM, Weidema WF, Oosting J, Seldenrijk CA, van Krimpen C, Offerhaus GJ, Pals ST (1998) CD44 splice variants as prognostic markers in colorectal cancer. Scand J Gastroenterol 33:82–87
12. Koretz K, Moller P, Lehnert T, Hinz U, Otto HF, Herfarth C (1995) Effect of CD44v6 on survival in colorectal carcinoma. Lancet 345:327–328
13. Gotley DC, Fawcett J, Walsh MD, Reeder JA, Simmons DL, Antalis TM (1996) Alternatively spliced variants of the cell adhesion molecule CD44 and tumour progression in colorectal cancer. Br J Cancer 74:342–351
14. Coppola D, Hyacinthe M, Fu L, Cantor AB, Karl R, Marcet J, Cooper DL, Nicosia SV, Cooper HS (1998) CD44V6 expression in human colorectal carcinoma. Hum Pathol 29:627–635
15. Jungling B, Menges M, Goebel R, Wittig BM, Weg-Remers S, Pistorius G, Schilling M, Bauer M, Konig J, Zeitz M, Stallmach A (2002) Expression of CD44v6 has no prognostic value in patients with colorectal cancer. Z Gastroenterol 40:229–233
16. Ropponen K, Tammi M, Parkkinen J, Eskelinen M, Tammi R, Lipponen P, Agren U, Alhava E, Kosma VM (1998) Tumor cell-associated hyaluronan as an unfavorable prognostic factor in colorectal cancer. Cancer Res 58:342–347
17. Denkert C, Kobel M, Pest S, Koch I, Berger S, Schwabe M, Siegert A, Reles A, Klosterhalfen B, Hauptmann S (2002) Expression of cyclooxygenase 2 is an independent prognostic factor in human ovarian carcinoma. Am J Pathol 160:893–903
18. Akisik E, Bavbek S, Dalay N (2002) CD44 variant exons in leukemia and lymphoma. Pathol Oncol Res 8:36–40
19. Imamura H, Takao S, Aikou T (1994) A modified invasion-3-(4,5-dimethylthiazole-2-yl)-2,5-diphenyltetrazolium bromide assay for quantitating tumor cell invasion. Cancer Res 54: 3620–3624
20. Reeder JA, Gotley DC, Walsh MD, Fawcett J, Antalis TM (1998) Expression of antisense CD44 variant 6 inhibits colorectal tumor metastasis and tumor growth in a wound environment. Cancer Res 58:3719–3726
21. Yakushijin Y, Steckel J, Kharbanda S, Hasserjian R, Neuberg D, Jiang W, Anderson I, Shipp MA (1998) A directly spliced exon 10-containing CD44 variant promotes the metastasis and homotypic aggregation of aggressive non-Hodgkin's lymphoma. Blood 91:4282–4291
22. Orian-Rousseau V, Chen L, Sleeman JP, Herrlich P, Ponta H (2002) CD44 is required for two consecutive steps in HGF/c-Met signaling. Genes Dev 16:3074–3086
23. Ponta H, Sherman L, Herrlich P (2003) The CD44: from adhesion molecules to signaling regulators. Natl Cancer Rev 4:33–46

Virchows Arch (2004) 445:465–471
DOI 10.1007/s00428-004-1116-z

ORIGINAL ARTICLE

Jy-Ming Chiang · Yah-Huei Wu Chou · Shih-Chieh Ma · Jim-Ray Chen

Influence of age on adenomatous polyposis coli and p53 mutation frequency in sporadic colorectal cancer—rarity of co-occurrence of mutations in APC, K-ras, and p53 genes

Received: 26 January 2004 / Accepted: 2 August 2004 / Published online: 24 September 2004
© Springer-Verlag 2004

Abstract *Introduction:* Previous studies have investigated the possibility that specific mutations may be related to specific clinicopathological features. However, most previous investigations included only an average age (40–80 years) group of sporadic colorectal cancers and, moreover, studied only a single gene in isolation. Therefore, the influence of age on these mutation frequencies remains unclear, despite age being considered a risk factor for genetic mutation. *Materials and methods:* This study included 122 sporadic colorectal cancers from three different age groups and analyzed mutation frequencies of adenomatous polyposis coli (APC), K-ras, and p53 genes and microsatellite instability to determine their mutation frequencies and relationships with clinicopathological features. *Results:* Significantly lower p53 mutation frequencies were observed among young (32 years old or younger) and old (86 years old or older) patient groups compared with an average age (39–85 years old) patient group (14.3% and 19.2% versus 51.5%, $P<0.001$). APC mutation frequency (11.8%) was significantly lower in highly aggressive (Dukes' stage D) tumors ($P=0.003$) than in the other stage tumors (Dukes' stage A, B, and C). Additionally, simultaneous occurrence of all three genetic alterations in an individual tumor was rare (below 5%). Statistical analysis further confirmed that mutation number in Dukes' D tumors occurred less frequently than expected in other stage tumors ($P=0.008$). *Conclusions:* Genetic alterations of sporadic colorectal cancers have different relationships with age or tumor stage. Additionally, most sporadic colorectal tumors do not necessarily require following the widely accepted genetic model, because the three key genetic mutations, APC, K-ras, and p53, rarely occur simultaneously.

Keywords Carcinogenesis · Age · Metastases · Colorectal cancer

J.-M. Chiang (✉)
Division of Colon and Rectal Surgery,
Chang Gung Memorial Hospital,
5 Fu-Hsing St., Kuei-Shan, Tao-Yuan, Taiwan
e-mail: jmjiang@adm.cgmh.org.tw
Tel.: +886-3-3281200
Fax: +886-3-3278355

J.-M. Chiang · Y.-H. Wu Chou · S.-C. Ma
Human Molecular Genetic Laboratory,
Chang Gung Memorial Hospital, Taipei, Taiwan

J.-R. Chen
Department of Pathology,
Chang Gung Memorial Hospital, Taipei, Taiwan

Introduction

During the past two decades, colorectal carcinogenesis has been widely studied at the genetic level. Most colorectal cancers (CRCs) are currently thought to evolve through genomic instability, including two distinct pathways, namely the chromosomal instability pathway or the microsatellite instability (MSI) pathway. A popular molecular genetic model based on the adenoma to adenocarcinoma sequence has been proposed and described—that successive accumulation of multiple genetic alterations drives the transition from normal colonic epithelia through increasing dysplastic adenoma to malignant cancer [40]. Of the genes characterized in this model, inactivation of tumor-suppressor gene adenomatous polyposis coli (APC) and activation of oncogene K-ras are considered important determinants of early carcinogenesis, while inactivation of tumor-suppressor gene p53 and DCC is thought to occur during late carcinogenesis. However, it has been further suggested that accumulation is more critical than the specific nature and temporal order of the mutation [13].

Regarding the origins of these genetic mutations, epidemiological and experimental studies demonstrated that environmental and dietary factors are the major causes of these genetic alterations in sporadic CRC [24]. Age, thus, is considered as a risk factor for carcinogenesis, because age not only prolongs exposure to both exogenous and endogenous carcinogens, but susceptibility to neoplasia also increases in older organisms [4]. Both of these phe-

nomena lead the genetic alterations to accumulate. The incidence of sporadic CRC increases with age and is highest in the age range 60–80 years old. Nevertheless, age of onset of CRC has a wide distribution from very young to very old, with 1–3% of all patients younger than 30 years and 5% older than 85 years [10, 23]. The molecular features responsible for both early and late onset of CRC are not well understood, although MSI is considered the major underlying molecular mechanism for young-onset CRC [25].

Since the proposal of the molecular genetic model of CRC [13, 40], many studies have investigated the relationships among the key genetic alterations described in this model and clinicopathological features of sporadic CRC, and these studies have indicated that specific genetic mutations may be preferentially related to specific clinicopathological features. Of these genes, K-ras and p53 mutations probably were the most exhaustively studied previously. In these studies, K-ras mutation is preferentially involved in carcinoma developing from adenoma, which preserves differentiation [7, 19], and codon 12 of K-ras mutation may have a role in the mucinous differentiation pathway [5, 18]. Studies also suggest that CRCs harboring p53 mutations are more aggressive, have a higher propensity for lymphatic and hematogenous spread, and have a worse prognosis than those without p53 mutation [15, 34]. However, the majority of these previous studies investigated only a single gene in isolation. Therefore, understanding of the frequencies of co-occurrence of these three genes is poor, as is understanding of whether these key mutations exist in the same tumor in a synergistic fashion or whether they occur independently.

This study, thus, comprehensively analyzed genetic alterations, including APC, K-ras, and p53, which are most commonly studied in multi-step CRC carcinogenesis, and MSI among patients in different age groups and also related these genetic alterations to different clinicopathological features.

Materials and methods

This study sampled 122 primary CRC patients undergoing colectomy at Chang Gung Memorial Hospital from January 2000 to December 2001. Tissues from tumor part and normal mucosa situated 8–10 cm from the tumor were removed together immediately after resection. All samples were stored in a freezer at −80°C until use. The specimens had the histopathological characteristics of adenocarcinoma. Patients with family histories of familial adenomatous polyposis or hereditary nonpolyposis colonic cancer were excluded. Patients' details, including age, sex, tumor location, tumor differentiation, mucin content of tumor, and Dukes' staging, also were collected from the medical records.

All tumors were classified with a modified Dukes' staging system in which Dukes' A tumors were limited to the bowel wall, Dukes' B tumors involved extramural spread, Dukes' C tumors involved the lymph nodes and Dukes' D tumors involved distant metastasis [2]. Regarding location, tumors were classified as belonging to one of three anatomical sites, namely: right colon (from cecum to transverse colon), left colon (from splenic flexure to sigmoid colon), and rectum.

DNA extraction

Genomic DNA was isolated from 300 mg of tumor and normal mucosa using standard proteinase K digestion and phenol/chloroform extraction procedure. The DNA was precipitated with ethanol and dissolved in 500 μl H_2O. After photometric evaluation, genomic DNA was diluted to a final concentration of 0.2 μg/μl in diethlpyrocarbonate-treated water and stored at −20°C.

466Analysis of K-ras mutations

Mutations of K-ras (codons 12 and 13 of exon 1) were screened using mismatched primer-mediated polymerase chain reaction (PCR) amplification, followed by restriction fragment-length polymorphism analysis in accordance with the method modified by Levi et al. [21]. PCR products were cleaved with BstNI at one site of normal codon 12 and Mph I for codon 13, respectively. Mutations of K-ras then were detected by NuSieve 3:1 agarose gel electrophoresis and ethidium bromide after digestion [22].

Analysis of APC gene mutation

The region between codon 686 and codon 1701 of the APC gene was analyzed for mutation using the protein truncation test (PTT) assay and/or single-strand conformation polymorphism (SSCP). For PTT assay, briefly, two overlapping segments of the APC gene (segment 1 from codon 686 to codon 1283 and segment 2 from codon 1099 to codon 1701) were amplified using PCR as described previously [32, 39]. For the PCR reaction mixture, 8 μl was used without purification as a template in 40 μl in a linked transcription-translation system, (TNT T7 Quick Coupled transcription/translation system, Promega, Madison, USA) containing 20 μCi of [35S]-methionine for 90 min (transcription/translation) at 30°C. Samples were diluted in sodium dodecylsulfate denature buffer, denatured for 5 min at 95°C, and analyzed on 10% sodium dodecylsulfate-polyacrylamide gel. Finally proteins were visualized using autoradiography at room temperature overnight.

Analysis of p53 point mutation

Using a PCR-SSCP approach, this study analyzed all 122 CRCs for mutations in exons 5, 6, 7, and 8 of the p53 gene. The 10-μl PCR mixture contained 50 ng each of the labeled primers listed previously [9], as well as 10 nmol each of the four deoxynucleotides, 0.1 μg of genomic sample DNA, and 0.5 unit of *Taq* polymerase in 10× PCR buffer specified in the GeneAmp Kit (Perkin-Elmer Cetus). Next, 30 reaction cycles at 95°C for 1 min, 95°C for 30 s, 68°C for 30 s, and 72°C for 1 min were run in a thermocycler (Perkin-Elmer/cetus). The reaction mixture then was topped off with an equal amount (12 μl) of loading dye, and electrophoresis using a GiniGel Excel 12.5/24 kit (Pharmacia Biotech, Uppsala, Sweden) was performed at 15 W for 90 min with a constant temperature system (Gene Phor Electrophoresis Unit; Pharmacia Biotech). Additionally, gels were stained using a Silver Staining Kit (Pharmacia Biotech, Uppsala, Sweden) according to the manufacturer's guidelines.

MSI analysis

A standard panel of five microsatellite markers (BAT26, BAT40, D2S123, D5S346, and D17S250) was used as markers for MSI [6]. The panel comprised two mononucleotide and three dinucleotide repeats. The sequences of the microsatellite PCR primers were described previously. Using genomic DNA derived from tissue specimens, the five microsatellite sequences were amplified using PCR. MSI-positive tumors were characterized by the presence of one or more bands in the corresponding constitutional DNA. In each case, the MSI-positive status was confirmed by a second analysis that included a new PCR amplification. Tumors were defined as MSI positive when information that was available from at least two of the markers revealed PCR fragments not found in the normal tissue of the same patient.

Statistical analysis

Categorical variables were compared using the Chi-square test. For evaluation of the difference in percentage of numbers of mutation, statistical analysis using the Mann-Whitney U test and Kruskal-Wallis test were performed. Statistical significance was assumed when $P<0.05$. All statistical analyses were conducted using the SPSS 8.0 software package (SPSS, Chicago, IL).

Results

Table 1 summarizes comparisons of the clinicopathological findings of the colorectal adenocarcinomas among young (age of 32 years or younger), average (age ranging from 39 years to 85 years), and old age (age older than 85 years) groups. A significant gender difference ($P=0.001$) of female predominance was found in young age colorectal adenocarcinoma. Young age patients were more likely to have tumors with poor differentiation (25% versus 2.9% and 0%, $P=0.001$) and to have significantly more mucinous-type tumors (32.1% versus 11.8% and 7.7%, $P=0.02$). However, the tumor stage and the distribution of tumor location were similar among varied age groups.

The overall frequencies of mutation of APC, K-ras, p53, and MSI in this study were 46.7%, 33.6%, 36.1%, and 10.7%, respectively (Table 2). Table 2 compares the genetic alterations of colorectal adenocarcinoma, according for different ages, tumor histologies, stages, differentiations, and locations.

Incidence of p53 was significantly lower in the young and old age groups (14.3% and 19.2%) than in the average age group (51.5%, $P<0.001$). Moreover, the young age group also showed a higher frequency of MSI (28.6%) than the average and old age groups (5.9% and 3.8%, $P=0.002$). K-ras mutation rates ($P=0.133$) and APC mutation rates ($P=0.062$) did not differ significantly among the different age groups.

Table 1 Clinicopathological variables for different patient age groups

	Young age group	Average age group	Old age group	*P* value
Patient number	28	68	26	
Age, median (range)	29 (23–32) years	63 (39–85) years	89 (86–94) years	
Sex, male/female	10/18	44/24	15/11	0.001
Tumor stage				0.319
A	2 (7.1%)	6 (8.8%)	2 (7.7%)	
B	8 (28.6%)	36 (52.9%)	13 (50%)	
C	13 (46.4%)	19 (27.9%)	6 (23.1%)	
D	5 (17.9%)	7 (10.3%)	5 (19.2%)	
Tumor differentiation				0.001
Well	4 (14.3%)	18 (26.5%)	5 (19.2%)	
Moderate	17 (60.7%)	48 (70.6%)	21 (80.8%)	
Poor	7 (25%)	2 (2.9%)	0 (0%)	
Tumor histology				0.02
Mucinous	9 (32.1%)	8 (11.8%)	2 (7.7%)	
Non-mucinous	19 (67.9%)	60 (88.2%)	24 (92.3%)	
Tumor location				0.706
Right colon	7 (25%)	10 (14.7%)	4 (15.4%)	
Left colon	9 (32.1%)	20 (29.4%)	7 (26.9%)	
Rectum	12 (42.9%)	38 (55.9%)	15 (57.7%)	

Table 2 Molecular alterations related to clinicopathological features among 122 patients. *MSI* microsatellite instability, *APC* adenomatous polyposis coli

	K-ras mutation	P53 mutation	APC mutation	MSI
Overall mutation rate	41 (33.6%)	44 (36.1%)	57 (46.7%)	13 (10.7%)
Age groups				
Young (n=28)	5 (17.9%)	4 (14.3%)	11 (39.3%)	8 (28.6%)
Average (n=68)	26 (38.2%)	35 (51.5%)	38 (55.9%)	4 (5.9%)
Old (n=26)	10 (38.5%)	5 (19.2%)	8 (30.8%)	1 (3.8%)
	P=0.133	P=0.000	P=0.062	P=0.002
Tumor histology				
Mucinous (n=19)	7 (36.8%)	5 (26.3%)	7 (36.8%)	4 (21.1%)
Non-mucinous (n=103)	34 (33.0%)	39 (37.9%)	50 (48.5%)	9 (8.7%)
	P=0.540	P=0.498	P=0.567	P=0.074
Differentiation				
Well (n=27)	9 (33.3%)	7 (25.9%)	15 (55.6%)	1 (3.7%)
Moderate (n=86)	29 (33.7%)	34 (39.5%)	41 (47.7%)	11 (12.8%)
Poor (n=9)	3 (33.3%)	3 (33.3%)	1 (11.1%)	1 (11.1%)
	P=0.999	P=0.431	P=0.065	P=0.410
Tumor stage				
A (n=10)	5 (50%)	1 (10%)	7 (70%)	0 (0%)
B (n=57)	19 (33.3%)	21 (36.8%)	33 (57.9%)	6 (10.5%)
C (n=38)	13 (34.2%)	17 (44.7%)	15 (39.5%)	7 (18.4%)
D (n=17)	4 (23.5%)	5 (29.4%)	2 (11.8%)	0 (0%)
	P=0.575	P=0.210	P=0.003	P=0.131

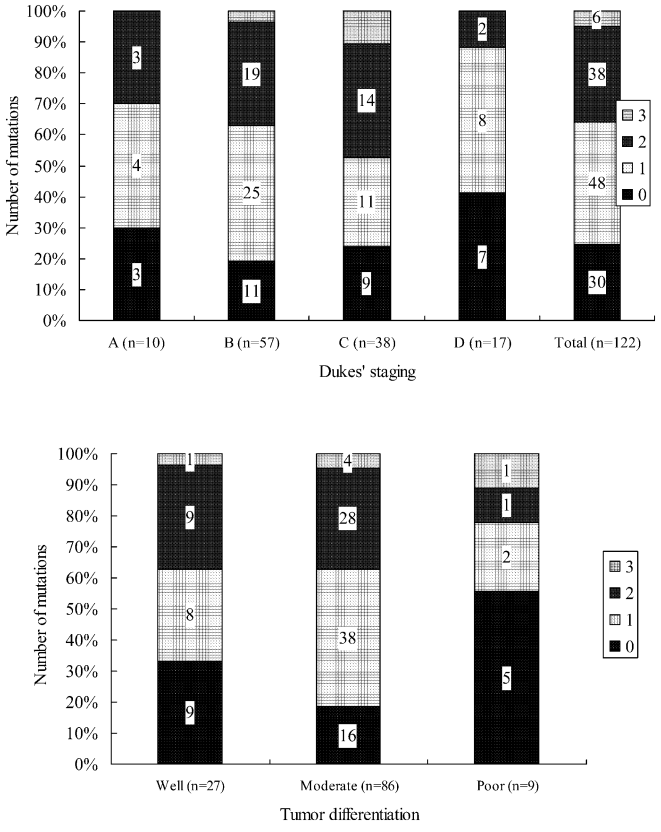


Fig. 1 Number of mutations related to Dukes' staging and tumor differentiation

Regarding the relationship between genetic mutations and other clinicopathological factors, Dukes' stage-D patients (P=0.003) displayed significantly lower frequencies of APC mutation rate. No other significant differences in mutation rates were noted among different histological types in terms of APC, K-ras, p53, and MSI, respectively.

Regarding numbers of mutations in individual tumors, only six tumors (4.9% of all tumors analyzed) contained alterations in all three (APC, K-ras, and p53) genes, whereas 30 tumors (24.6%) had none of such alterations. The percentages of tumors containing mutations in only one of these genes was 39.3% (48 cases), and 31.1% (38 cases) had two mutations. The percentage of combination of these mutations was 33.3% (14/42) for p53 and APC and 42.9% (18/42) for APC and K-ras, whereas the percentage of tumors with mutations in both p53 and K-ras was 23.8% (10/42). The average numbers of mutations for Dukes' stage A, B, and C tumors were 1.10±0.7379, 1.26±0.7683, 1.3684±0.9704, significantly exceeding that for Dukes' D tumors (0.7059±0.6860). Statistical analysis confirmed that mutation number in Dukes' D tumors was lower than that which could be expected among the other stage tumors (P=0.008). In addition, a significant difference of mutation numbers of these genes (APC, K-ras, and p53) was also found among different age groups (0.71±0.659 for the young age group, 1.46±0.854 for the average age group, and 0.88±0.766 for the old age group, P=0.006). However, no significant difference of mutation numbers was found for tumor differentiations (P=0.206) and mucinous-type tumor (P=0.091) (Fig. 1).

Discussion

Although age-related influences on molecular genetic changes of sporadic CRC are seldom reported, this study found that in addition to a significantly higher frequency of MSI in the young age group patients, which is similar to previous studies [25], significantly lower incidences of p53 gene mutation (P<0.001) and marginal significance of APC gene mutation (P=0.062) were found in the young patients (32 years of age or younger) and in old patients (85 years of age and older) compared with the average age patients.

Regarding the criteria used to stratify the series in the three age groups, no strict criteria for age definitions exist in CRC studies, although most studies define young age as 40 years, while other studies defined it as 35, 45, or 50 years. Our previous clinical study [8] indicated that the influence of age on tumor characteristics appeared continuous rather than categorical, because significant decreasing or increasing trends were observed with the analysis of different tumor characteristics. This study aimed to determine the differences in genetic alteration among different age groups with CRC and postulated that the differences in measured variables would increase with the age gap between the study and control groups. Therefore, this study chose the very young (younger than 35 years) and very old patients (older than 85 years) and compared them with the average age group. Interestingly, when we change the age criteria to younger than 45 years old, 45–75 years old, and older than 75 years old, significantly lower incidences of p53 mutation (P=0.023) and MSI (P=0.004) in relation to young and old age group patients were also observed, as well as a marginal significant difference of APC gene mutation (P=0.055). These findings are similar to those for the stratification of age as younger than 35 years old, 45–85 years old, and over than 85 years old. These findings, thus, suggested that the influence of age on genetic alteration might be a continuum, though this needs to be further confirmed by a population-based or a large-series study.

P53 gene mutations are believed to be a mutation induced by either endogenous or exogenous carcinogens [13, 24, 29]. For older age group patients, who are at risk of long-term carcinogen exposure and have a lower incidence of p53 mutation than patients in the other two groups, their conditions may be attributable to different dietary or lifestyle factors, since previous molecular epidemiological studies have indicated a protection of p53 alteration with a high intake of cruciferous vegetables, fiber, and vitamin E [13, 14, 29]. Some other possibilities may result from certain specific carcinogens that are reported to be less involved in p53 mutations [26] or geographic differences, as reported in some European regions [30]. Another possibility of lower incidence of p53 gene

mutation observed in the younger and older age groups compared with the average age group may be related to an alternative pathway independent of p53 gene mutation, such as the MSI pathway, showing an inverse relationship to p53 mutation for sporadic CRC [11, 33, 38]. This association has further been explained by p14 methylation in human colon cancer [36]. However, our data did not show a significant correlation between MSI and genetic mutations, although lower p53 mutation incidence (15.4% for MSI versus 38.5% for MSS, P=0.1) was found. These may be due to small sample size of MSI cases or due to the inclusion of distinct sample groups, such as very young and very old patients. A correlation between young age and reduced incidence of p53 gene mutation was also reported in malignant glioma in childhood [31]. These data may imply that the etiological mechanisms underlying CRC development differ among patient age groups.

Mutation frequencies for each gene in this study were entirely consistent with previous reports in CRC [1, 12, 17, 27, 28, 34]. For the genes studied, this study focused on areas that were considered hot-spots and studied in detail previously, that is, the region between exon 5 and exon 8 of the p53 gene, the region between codon 686 and codon 1693, including the mutation cluster of APC exon 15 and K-ras codons 12 and 13. This study then observed that mutation frequency of APC was 46.7%, comparable with previous reports on sporadic CRC [12, 28]. Moreover, the frequency of K-ras mutation was 33.6%, similar to 37.7% in the RASCAL study of 2721 colorectal carcinomas [17] and within the range reported in other reports, ranging from 30% to 50% [1, 18, 34]. Additionally, that the p53 mutation rate was 36.1%, which was slightly lower than in other reports from Western countries [27, 34], which ranged from 37% to 55%, may be best explained by the low frequencies of young and old age CRC tumors in this study, because the frequency was 51.1% if only the average age group of patients was included. However, the incidence of co-occurrence of all specific APC, K-ras and p53 gene mutations is small (only 4.9%), and 39.3% of all patients had only one type of mutation, while 24.6% of patients had none of these mutations. The present data, thus, are comparable to a recent report indicating that progressive accumulation of multiple mutations in these genes is not a prerequisite for tumor development of most sporadic CRC [37]. In combination, these results differ from the widely accepted genetic model of CRC carcinogenesis, in which the APC gene is considered as an early molecular event occurring in the initiation stage, K-ras gene in the intermediate stage, and p53 mutation as a late molecular event in the carcinoma transformation stage [13, 40]. Our previous study [10] and other studies [35, 40] comparing synchronous adenoma and adenocarcinoma in the same patient have also demonstrated that at least one-third of CRC do not follow this linear model. Furthermore, the average number of mutations (APC, K-ras, and p53) is significantly fewer in young and old age groups than that in an average age group. Considering the heterogeneous combination of these genes shown in this study and elsewhere, most sporadic CRC might follow a non-linear or chaodynamic model during cancer development [35, 41]. The data in this study remain insufficient to confirm that multiple alternative genetic pathways in CRC carcinogenesis exist, as suggested in some reports [1, 35, 41]. However, data from this study clearly demonstrated that the existing model described by Fearon and Vogelstein only rationalizes tumor formation in a very small number (5%) of CRCs. Accumulations of genetic alterations during carcinogenesis may remain to be true, although other chromosomal abnormalities, such as 8q and 13q gain and 18q loss and 20q gain, may be also equally important during genetic progression suggested by others [16]. A recent study indicating that mutations of APC, K-ras, and p53 are associated with specific chromosomal aberrations in colorectal adenocarcinomas [3] further refines the relationships between genetic abnormalities. Nevertheless, an important question following from this is whether viewing molecular events as represented by APC, K-ras, or p53 as specific pathway rather than as specific gene mutations would provide more complete unifying principles than the specific genes.

Previous studies have identified the presence of mutations in K-ras and p53 as prognostic factors of tumor behavior and survival in patients with CRC [1, 5, 7, 15, 17, 18, 22, 34]. However, the literature contains only sporadic data about the prognostic significance of APC gene alterations [12], and APC mutations are considered as the initiating events in tumorigenesis. The data presented here further specifically associated lowest frequencies of APC mutation with Dukes' stage-D tumors, consistent with a previous report [12] indicating that highly aggressive Dukes' stage-D tumors develop metastasis through an unknown mechanism independent of APC mutations. The data presented here also revealed that these three key genes had significantly fewer mutations in the highly aggressive (synchronous distant metastasis) Dukes' stage-D tumors than in the other stage tumors, providing further evidence that it may develop in a distinct pathway [12]. In general, Dukes' D CRCs are significantly higher in younger patients, something that has been reported in many series and cannot be simply attributed to delays in diagnosis [8]. The molecular mechanism underlying this phenomenon and the biological interpretation of the lowest mutation rates in Dukes' D tumors remain unclear. Because we only tested the mutation cluster region of the APC gene and hot-spots of p53 and K-ras genes, the possibility that these tumors may display mutations occurring in the non-hot-spots of these genes cannot be excluded, meaning the mutation would be related to its aggressive behavior, though very few papers have supported this possibility. Various other known oncogenes or tumor-suppressor genes that have been reported are related to the metastatic potential of CRCs, such as NM23 and S100A4 genes. However, both genes occurring in the late stage of colorectal carcinogenesis and the present study showed the lowest rate of APC mutations (an early mutation in chromosomal instability) and MSI to be associated with Dukes' D tumor,

which suggests that Dukes' D tumor might follow a distinct molecular pathway rather than the conventional chromosomal instability or MSI pathways.

Tumor heterogeneity is another factor that may affect the results in this study in two ways. First, because of trying to check the tumor content more than 80% under microscopic examination and remove non-malignant tissue such as the normal mucosa, necrotic, or inflammation parts, this type of error should be minimized in this study, even in the cases of advanced Dukes' D tumor. However, the intratumor heterogeneity may derive from coexisting different subclones of tumor cells in the same tumor specimens. Unfortunately, this problem initially appeared unavoidable because of the large number of samples required to solve the problem, which are difficult to obtain for the very young and very old age patients. Intratumor heterogeneity for genetic alteration was proposed in some human malignancies, including colorectal carcinomas with 20% difference in relation to sampling using the mutation detection method [20]. Previous studies also demonstrated the differences between genotypes in the primary tumor and in metastatic tumors. These data force the reconsideration of the use of molecular genetic markers for prognosis management and to predict tumor behavior. However, we totally agree with that the issue of intratumor heterogeneity should be further clarified in the future studies using molecular genetic markers to predict tumor behavior.

In summary, this study showed that p53 gene mutations are significantly lower in young and old age patients compared with average age group patients, and APC gene mutations are lower in highly aggressive CRC tumors compared with the other tumors. These heterogeneous patterns of genetic alterations among different subgroups of sporadic CRC indicate the possible existence of multiple alternative genetic pathways. Although individual APC, K-ras, and p53 genes have been found to be important and frequent in colorectal carcinogenesis, data presented in this study further demonstrated that combinations of these three genetic alterations in sporadic CRC are rare. Considering that over 60% of CRC tumors in this study harbored none or only one mutation of these three key genes, this study, therefore, infers that most sporadic CRCs may not follow the popular lineal model of CRC carcinogenesis. Consequently, considerable care is required to predict clinicopathological features by combined use of these three genes as universal molecular genetic markers.

Acknowledgement Supported by the National Science Council of the Republic of China, Taiwan (NSC89-2314-B-182A-171).

References

1. Al-Mulla F, Going JJ, Sowden ET, Winter A, Pickford IR, Birnie GD (1998) Heterogeneity of mutant versus wild-type Ki-ras in primary and metastatic colorectal carcinomas, and association of codon-12 valine with early mortality. J Pathol 185:130–138
2. Astler VB, Coller FA (1954) The prognostic significance of direct extension of carcinoma of the colon and rectum. Ann Surg 139:846–848
3. Baisse B, Bouzourene H, Saraga E, Bosman FT, Benhattar J (2001) Intratumor genetic heterogeneity in advanced human colorectal adenocarcinoma. Int J Cancer 93:346–352
4. Balducci L, Beghe C (2001) Cancer and age in the USA. Crit Rev Oncol Hematol 37:137–145
5. Bazan V, Migliavacca M, Zanna I, Tubiolo C, Grassi N, Latteri MA, La Farina M, Albanese I, Dardanoni G, Salerno S, Tomasino RM, Labianca R, Gebbia N, Russo A (2002) Specific codon 13 K-ras mutations are predictive of clinical outcome in colorectal cancer patients, whereas codon 12 K-ras mutations are associated with mucinous histotype. Ann Oncol 13:1438–1446
6. Boland CR, Thibodeau SN, Hamilton SR, Sidransky D, Eshleman JR, Burt RW, Meltzer SJ, Rodriguez-Bigas MA, Fodde R, Ranzani GN, Srivastava SA (1998) National Cancer Institute Workshop on Microsatellite Instability for cancer detection and familial predisposition: development of international criteria for the determination of microsatellite instability in colorectal cancer. Cancer Res 58:5248–5257
7. Breivik J, Meling GI, Spurkland A, Rognum TO, Gaudernack G (1994) K-ras mutation in colorectal cancer: relations to patient age, sex and tumour location. Br J Cancer 69:367–371
8. Chiang JM, Chou-Wu YH, Wang JY (2000) Synchronous colorectal carcinoma and adenoma may arise from independent neoplastic colonal expansion. JS CRS ROC 11:1–7
9. Chiang JM, Chou YH, Chen TC, Ng KF, Lin JL (2002) Nuclear beta-catenin expression is closely related to ulcerative growth of colorectal carcinoma. Br J Cancer 86:1124–1129
10. Chiang JM, Chen MC, Changchien CR, Chen JS, Tang R, Wang JY, Yeh CY, Fan CW, Tsai WS (2003) Favorable influence of age on clinicopathological features of sporadic colorectal cancer. Dis Colon Rectum 46:904–910
11. Cottu PH, Muzeau F, Estreicher A, Flejou JF, Iggo R, Thomas G, Hamelin R (1996) Inverse correlation between RER+ status and p53 mutation in colorectal cancer cell lines. Oncogene 13:2727–2730
12. De Filippo C, Luceri C, Caderni G, Pacini M, Messerini L, Biggeri A, Mini E, Tonelli F, Cianchi F, Dolara P (2002) Mutations of the APC gene in human sporadic colorectal cancer Scand J Gastroenterol 9:1048–1053
13. Fearon ER, Vogelstein B (1990) A genetic model for colorectal tumorigenesis. Cell 61:759–767
14. Freedman AN, Michalek AM, Marshall JR, Mettlin CJ, Petrelli NJ, Black JD, Zhang ZF, Satchidanand S, Asirwatham JE (1996) Familial and nutritional risk factors for p53 overexpression in colorectal cancer. Cancer Epidemiol Biomarkers Prev 5:285–291
15. Goh HS, Chan CS, Khine K, Smith DR (1994) P53 and behavior of colorectal cancer. Lancet 344:233–234
16. Hermsen M, Postma C, Baak J, Weiss M, Rapallo A, Sciutto A, Roemen G, Arends JW, Williams R, Giaretti W, De Goeij A, Meijer G (2002) Colorectal adenoma to carcinoma progression follows multiple pathways of chromosomal instability. Gastroenterology 123:1109–1119
17. Jervoise H, Andreyev N, Norman AR, Cunningham D, Oates JR, Clarke PA (1998) Kirsten ras mutations in patients with colorectal cancer: the multicenter 'RASCAL' study. J Natl Cancer Inst 90:675–684
18. Kastrinakis WV, Ramchurren N, Rieger KM, Hess DT, Loda M, Steele G, Summerhayes IC (1995) Increased incidence of p53 mutations is associated with hepatic of metastasis in colorectal neoplastic progression. Oncogene 11:647–652
19. Laurent-Puig P, Olschwang S, Delattre O, Validire P, Melot T, Mosseri V, Salmon RJ, Thomas G (1991) Association of Ki-ras mutation with differentiation and tumor-formation pathways in colorectal carcinoma. Int J Cancer 49:220–223
20. Leslie A, Pratt NR, Gillespie K, Sales M, Kernohan NM, Smith G, Wolf R, Carey FA, Steele RJC (2003)**M**utations of APC, K-ras, and p53 are associated with specific chromosomal

aberrations in colorectal adenocarcinomas. Cancer Res 63:4656–4661
21. Levi S, Urbano-Ispizua A, Gill R, Thomas DM, Gilbertson J, Foster C, Marshall CJ (1991) Multiple K-ras codon 12 mutations in cholangiocarcinomas demonstrated with a sensitive polymerase chain reaction technique. Cancer Res 51:3497–3502
22. Liang JT, Cheng YM, Chang KJ, Chien CT, Hsu HC (1999) Reappraisal of K-ras and p53 gene mutations in the recurrence of Dukes'B2 rectal cancer after curative resection. Hepatogastrointerology 46:830–837
23. Liang JT, Huang KC, Cheng AL, Jeng YM, Wu MS, Wang SM (2003) Clinicopathological and molecular biological features of colorectal cancer in patients less than 40 years of age. Br J Surg 90:205–214
24. Lichtenstein P, Holm NV, Verkasalo PK, Iliadou A, Kaprio J, Koskenvuo M, Pukkala E, Skytthe A, Hemminki K (2000) Environmental and heritable factors in the causation of cancer—analyses of cohorts of twins from Sweden, Denmark, and Finland. N Engl J Med 343:78–85
25. Liu B, Farrington SM, Petersen GM, Hamilton SR, Parsons R, Papadopoulos N, Fujiwara T, Jen J, Kinzler KW, Wyllie AH (1995) Genetic instability occurs in the majority of young patients with colorectal cancer. Nat Med 1:348–352
26. Makino H, Ushijima T, Kakiuchi H, Onda M, Ito N, Sugimura T, Nagao M (1994) Absence of p53 mutations in rat colon tumors induced by 2-amino-6- methyldipyrido [1, 2-a:3', 2'-d] imidazole, 2-amino-3-methylimidazo [4, 5-f] quinoline, or 2-amino-1-methyl-6-phenylimidazo [4, 5-b] pyridine. Jpn J Cancer Res 85:510–514
27. Miyki M, Iijima T, Yasuno M, Kita Y, Hishima T, Kuroki T, Mori T (2002) High incidence of protein-truncating mutations of the p53 gene in liver metastases of colorectal carcinoma. Oncogene 21:6689–6693
28. Nakamura Y (1993) The role of the adenomatous polyposis coli (APC) gene in human cancer. Adv Cancer Res 62:65–87
29. Obrador A, Moreno V, Bautista D, Cabeza E, Canet R (1998) Colorectal cancer, diet, and p53 Gastroenterology, 114[Suppl 4]:G2705, part 2
30. Pauly M, Schmitz M, Kayser I, Tureci O, Tureci O, Lagoda P, Seitz G, Dicato M (1997) Ki-ras oncogene and p53 tumor suppressor gene mutations in colorectal carcinomas from the European Saar-Luxembourg region are less frequent than predicted by the classic adenoma-carcinoma sequence model. Eur J Cancer 33:2265–2272
31. Pollack IF, Finkelstein SD, Burnham J, Holmes EJ, Hamilton RL, Yates AJ, Finlay JL, Sposto R (2001) Children's Cancer Group. Age and TP53 mutation frequency in childhood malignant gliomas: results in a multi-institutional cohort. Cancer Res 61:7404–7407
32. Prosser J, Condie A, Wright M, Horn JM, Fantes JA, Wyllie AH, Dunlop MG (1994) APC mutation analysis by chemical cleavage of mismatch and a protein truncation assay in familial adenomatous polyposis. Br J Cancer 70:841–846
33. Samowitz WS, Holden JA, Curtin K, Edwards SL, Walker AR, Lin HA, Robertson MA, Nichols MF, Gruenthal KM, Lynch BJ, Leppert MF, Slattery ML (2001) Inverse relationship between microsatellite instability and K-ras and p53 gene alterations in colon cancer. Am J Pathol 158:1517–1524
34. Samowitz WS, Curtin K, Ma KN, Edwards S, Schaffer D, Leppert MF, Slattery ML (2002) Prognostic significance of p53 mutations in colon cancer at the population level. Int J Cancer 99:597–602
35. Sedivy R, Wolf B, Kalipciyan M, Steger GG, Karver-Hanusch J, Moder RM (2000) Genetic analysis of multiple synchronous lesions of the colon adenoma-carcinoma sequence, Br J Cancer 82:1276–1282
36. Shen L, Kondo Y, Hamilton SR, Rashid A, Issa JP (2003) P14 methylation in human colon cancer is associated with microsatellite instability and wild-type p53. Gastroenterology 124:626–633
37. Smith G, Carey FA, Beattie J, Wilkie MJ, Lightfoot TJ, Coxhead J, Garner RC, Steele RJ, Wolf CR (2002) Mutations in APC, Kirsten-ras, and p53—alternative genetic pathways to colorectal cancer. PNAS 99:9433–9438
38. Suh JH, Lim SD, Kim JC, Hong SH, Kang GH (2002) Comparison of clinicopathologic characteristics and genetic alterations between microsatellite instability-positive and microsatellite instability-negative sporadic colorectal carcinomas in patients younger than 40 years old. Dis Colon Rectum 45:219–228
39. van der Luijt R, Khan PM, Vasen H, van Leeuwen C, Tops C, Roest P, den Dunnen J, Fodde R (1994) Rapid detection of translation-terminating mutations at the adenomatous polyposis coli (APC) gene by direct protein truncation test. Genomics 20:1–4
40. Vogelstein B, Fearon ER, Hamilton SR, Kern SE, Preisinger AC, Leppert M, Nakamura Y, White R, Smits AM, Bos JL (1988) Genetic alterations during colorectal-tumor development. N Engl J Med 319:525–532
41. Zauber NP, Sabbath-Solitare M, Marotta SP, Zauber AG, Bishop DT (2001) Molecular changes in the Ki-ras and APC genes in colorectal adenomas and carcinomas arising in the same patient. J Pathol 93:303–309

Virchows Arch (2004) 445:472–476
DOI 10.1007/s00428-004-1054-9

ORIGINAL ARTICLE

Hirotoshi Tobioka · Yuichi Tokunaga · Hiroshi Isomura · Yasuo Kokai · Jun Yamaguchi · Norimasa Sawada

Expression of occludin, a tight-junction-associated protein, in human lung carcinomas

Received: 19 January 2004 / Accepted: 17 April 2004 / Published online: 30 June 2004
© Springer-Verlag 2004

Abstract Occludin is a tight-junction-associated transmembrane protein, and previous observations suggested that occludin might play a crucial role in the formation and maintenance of organized tubular structures. Based on these observations, we explored the possible role of occludin immunostaining in the diagnosis of lung carcinomas. A total of 68 lung carcinomas and surrounding normal lung tissues were studied. A formalin-fixed, paraffin-embedded section from each tumor was stained with a new anti-occludin monoclonal antibody raised in our laboratory. In normal lung tissues, the anti-occludin antibody strongly stained the apicoluminal borders of the bronchial/bronchiolar epithelia and bronchial glands as a dot or short line. The antibody also stained the intercellular borders of alveolar epithelia. In cancer cells that faced lumina of all adenocarcinomas, regardless of grade, including bronchioloalveolar carcinomas, occludin showed an expression pattern identical to that of the normal bronchial and alveolar epithelia. Occludin reactivity was not noted in any cases of squamous cell carcinoma, large cell carcinoma, small cell carcinoma, or large cell neuroendocrine carcinoma. The results of the present study suggest that occludin can serve as an immunohistochemical indicator of the "true" glandular differentiation that forms tubulo-papillary structures in human lung carcinoma tissues.

H. Tobioka (✉) · Y. Tokunaga · H. Isomura · N. Sawada
Department of Pathology,
Sapporo Medical University School of Medicine,
S. 1, W.17, Chuo-ku, 060-8556 Sapporo, Japan
e-mail: tobioka@sapmed.ac.jp
Tel.: +81-11-6112111
Fax: +81-11-6135665

Y. Kokai
Department of Biomedical Engineering,
Sapporo Medical University School of Medicine,
Sapporo, Japan

J. Yamaguchi
Department of Pathology,
Obihiro Kosei General Hospital,
Obihiro, Japan

Keywords Lung carcinoma · Tight junction · Occludin · Immunohistochemistry

Introduction

In polarized epithelial cells, the tight junctions are positioned at the boundary of the apical and basolateral plasma membrane domains. The tight junctions contribute to the transepithelial barrier that controls the transport of electrolytes and small molecules through the paracellular pathway referred to as the "barrier" function [8]. They are also crucial for the organization of epithelial cell polarity by separating the plasma membrane into apical and basolateral domains [9, 11, 22] and are, thus, responsible for the polarized localization of ion channels, receptors, and enzymes to proper membrane domains to form structurally and functionally developed epithelia. This function of the tight junctions is referred to as the "fence" function [1, 8]. In glandular epithelia, the tight junctional "fence" function is crucial for the formation and maintenance of organized tubular structures. Occludin was the first identified tight-junction-associated transmembrane protein [10]. Previous immunohistochemical studies of various neoplastic and non-neoplastic glandular epithelia have suggested that occludin is crucial for the formation of glandular structures [5, 14].

The tight junctions of pulmonary epithelia provide the structural basis for the so-called air–blood barrier that prevents invasion by inhaled pathogenic organisms, while at the same time preventing non-selective leakage of fluid into air spaces. In addition, the tight junctional fence function may play key roles for pulmonary epithelia transporting electrolytes [7] and in secreting mucus [17] and surfactants [15] into the airspace in a polarized fashion. Tight junctions are also important for maintaining the organized structure of pulmonary airways. Although the ultrastructural morphology of human pulmonary tight junctions has been described in detail [4], studies related to the expression and localization of tight-junction-associated proteins in human lung tumors have

been hampered by the lack of antibodies suitable for immunohistochemical studies of formalin-fixed, paraffin-embedded tissue sections.

In this study, we investigated the expression of occludin in human lung carcinomas as well as corresponding normal lung tissue immunohistochemically, using a new anti-occludin monoclonal antibody raised in our laboratory [24]. In this investigation, formalin-fixed, paraffin-embedded tissue sections of 68 primary lung carcinomas were analyzed. The results suggest that occludin can be an immunohistochemical marker of differentiation for glandular epithelia, which form tubulo-papillary structures in lung carcinomas.

Materials and methods

Case selection

A total of 68 cases, including adenocarcinoma (n=24), squamous cell carcinoma (n=12), large cell carcinoma (n=12), small cell carcinoma (n=15), large cell neuroendocrine carcinoma (n=4), and adenoid cystic carcinoma (n=1), were identified by examining conventional hematoxylin and eosin-stained sections. The large cell neuroendocrine carcinomas were immunoreactive for at least one neuroendocrine marker. The adenocarcinomas included 12 acinar/papillary adenocarcinomas and 12 bronchioloalveolar carcinomas. Two acinar/papillary adenocarcinomas were associated with poorly differentiated solid components focally. Normal lung tissue included in the surgical specimens was evaluated in all cases. All patients had undergone surgical operation at our hospitals between 1998 and 2002. The patients had not received preoperative radiotherapy or chemotherapy. The tissues were fixed in 10% formalin and embedded in paraffin.

Antibodies and immunohistochemistry

To examine the immunohistochemical localization of occludin in formalin-fixed, paraffin-embedded tissue sections, we utilized anti-occludin monoclonal antibody 1A8, which was raised in our laboratory [24]. Briefly, 5-μm-thick sections of the representative blocks were deparaffinized with xylene and rehydrated with gradient alcohol. Before blocking endogenous peroxidase, sections treated for heat-induced epitope retrieval were immersed in citrate buffer (pH 6.0) and autoclaved at 121°C for 20 min. After rinsing in phosphate-buffered saline (PBS) containing 10% skim milk, the sections were incubated with the 1A8 for 3 h. The sections were then washed three times with PBS and incubated with Dako EnVision Labeled Polymer (Dako Japan, Kyoto, Japan) for 1 h. Following another wash in PBS, after development of the diaminobenzidine chromogen for 20 min, the slides were washed with distilled water for 3 min and counterstained for 2 min with hematoxylin. As a negative control, each sample was stained with the second antibody with omission of the first antibody.

Results

Expression of occludin in normal human lung tissue

Histologically normal structures present in the lung tumor specimens were studied. The anti-occludin antibody strongly stained the apicoluminal borders of the bronchial/bronchiolar epithelial cells lining the airways, regardless of the cell type, as a dot or short line (Fig. 1A). In addition, occludin reactivity was also detected in endothelial cells of blood vessels within the tissue. The antibody also stained the apicoluminal borders of bronchial

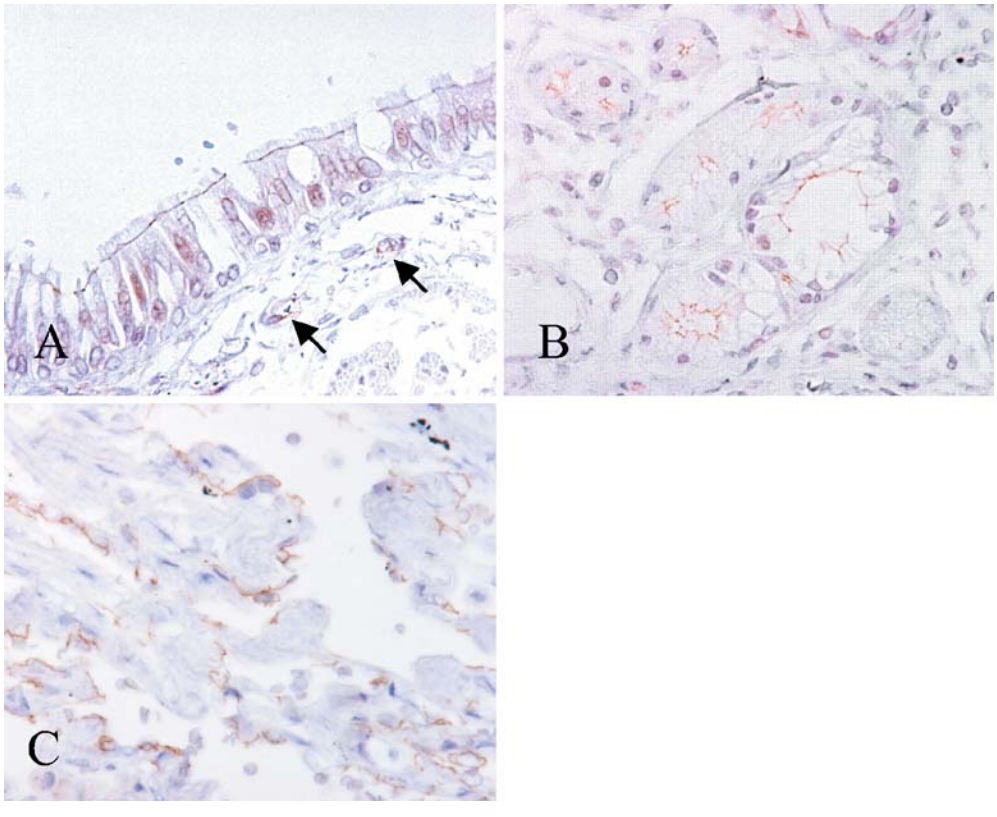


Fig. 1 Expression of occludin in normal lung tissue. **A** Occludin was detected at the apical cell borders of bronchial epithelia. Occludin reactivity was also detected in endothelial cells of blood vessels (*arrows*). **B** In bronchial glands, occludin was detected at the apicoluminal borders of glandular cells as a *short line*. **C** Occludin was expressed in the intercellular borders of alveolar epithelia. ×400

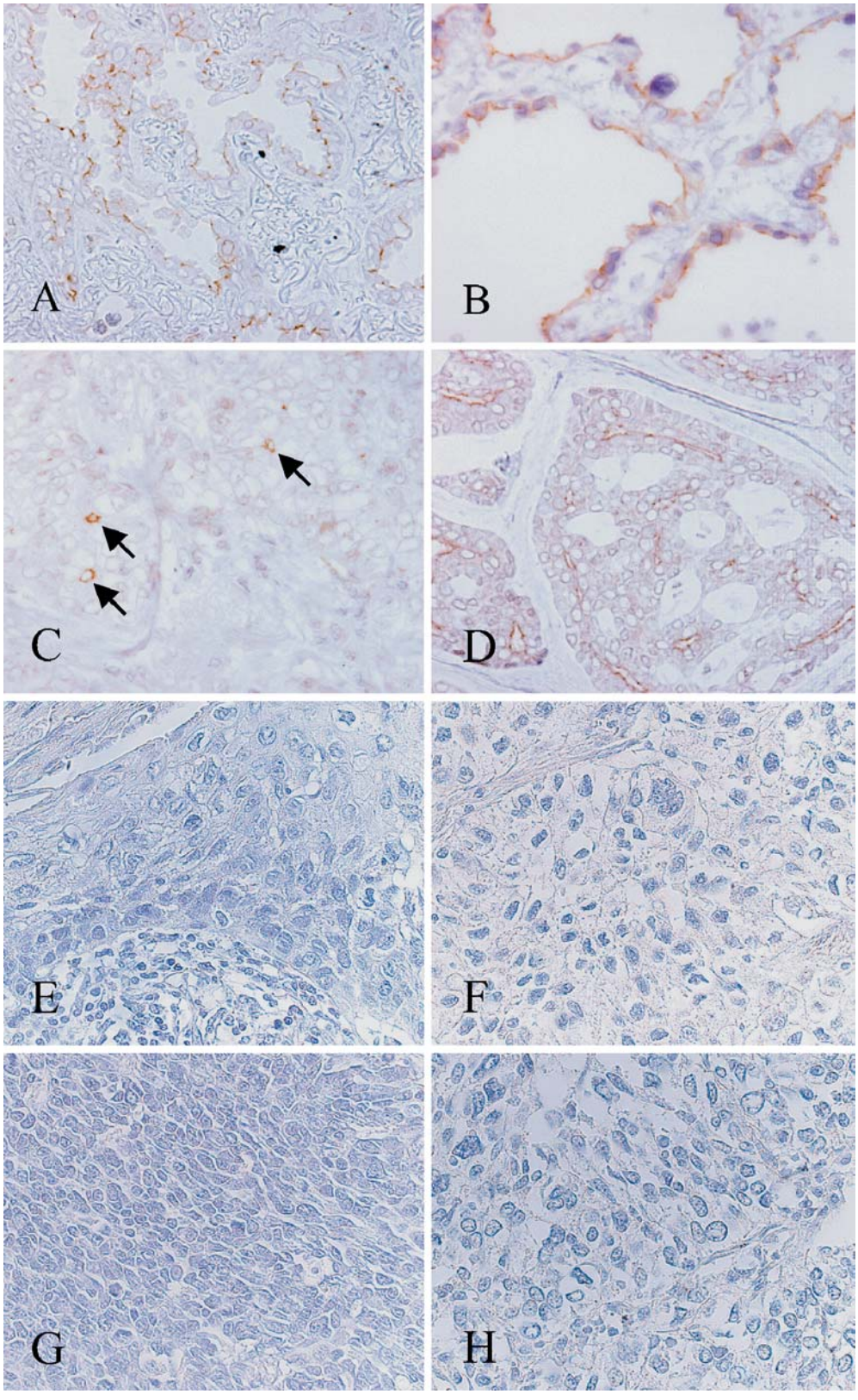


Fig. 2 Expression of occludin in lung carcinomas. **A** Occludin was detected in the cancer cells that faced lumina of adenocarcinomas. **B** In bronchioloalveolar carcinomas, occludin showed an expression pattern identical to the normal alveolar epithelia. **C** In small tubular structures in poorly differentiated solid components of adenocarcinomas, the expression of occludin was detected (*arrows*). **D** In adenoid cystic carcinoma, occludin reactivity was detected in the luminal surfaces of some tubular structures, but not in the pseudocystic structures. All squamous cell carcinomas (**E**), large cell carcinomas (**F**), small cell carcinomas (**G**), and large cell neuroendocrine carcinomas (**H**) were occludin negative. ×400

glands (Fig. 1B) and the intercellular borders of alveolar epithelia (Fig. 1C).

Expression of occludin in lung carcinomas

In cancer cells that faced a lumen of all adenocarcinomas, regardless of grade, including bronchioloalveolar carcinomas, occludin showed an expression pattern identical to the normal bronchial and alveolar epithelia (Fig. 2A, B). In small tubular structures in poorly differentiated solid component of adenocarcinomas, the expression of occludin was detected (Fig. 2C). In adenoid cystic carcinoma (Fig. 2D), occludin was detected on the luminal surfaces of some tubular structures. However, occludin was not detected in the pseudocystic structures. In squamous cell carcinomas (Fig. 2E), large cell carcinomas (Fig. 2F), small cell carcinomas (Fig. 2G), and large cell neuroendocrine carcinomas (Fig. 2H), occludin expression was not detected. In particular, occludin reactivity was not detected in gland-like structures of small cell carcinomas or large cell neuroendocrine carcinomas.

Discussion

The tight junction is one of the most characteristic structural markers of the polarized epithelial phenotype. In polarized epithelial cells, it is positioned at the boundary of the apical and basolateral plasma membrane domains. Occludin is an integral membrane protein that was the first component of tight-junction strands to be identified [10]. Occludin comprises four transmembrane domains, a long carboxyl-terminal cytoplasmic domain, two extracellular loops, and one intracellular turn. It is distributed in tight junctions more ubiquitously than the other integral membrane proteins, the claudin family, which are involved in tight-junction strands in a tissue-specific manner [16]. The level of occludin expression in various types of cells generally correlates well with the number of tight-junction strands [19]. Changes in the expression and localization of occludin have been shown to correlate with changes in the physiological functions of tight junctions [3, 12]. Thus, occludin is considered to be a reliable immunohistochemical marker of tight junctions. Recently, we raised an anti-occludin monoclonal antibody that can be used for formalin-fixed, paraffin-embedded tissue sections, so it can be a powerful tool for the study of tight junctions in surgically resected human materials [24].

In the present study, we immunohistochemically analyzed the expression and localization of occludin in 68 human lung carcinomas as well as in corresponding normal lung tissue. In normal lung tissue surrounding carcinoma, occludin was detected in the apicoluminal borders of all kinds of bronchial/bronchiolar epithelial cells and alveolar pneumocytes as a dot or short line. These findings are in agreement with previous physiological and ultrastructural tracer studies of the air–blood barrier [20, 21]. Occludin in all cases of adenocarcinoma and adenoid cystic carcinoma showed an expression pattern identical with that of the normal bronchial and alveolar epithelia in cancer cells facing the luminal surface. In squamous cell carcinomas, large cell carcinomas, small cell carcinomas, and large cell neuroendocrine carcinomas, no occludin expression was noted.

The structure and function of tight junctions in normal and neoplastic glandular tissues were reported [5, 6, 13, 14, 18, 19, 23]. Recently, we have shown that the expression of occludin progressively decreases in parallel with the progress in the grade of human endometrial adenocarcinoma [25]. In glandular epithelia, it is highly plausible that loss of tight junctions during carcinogenesis is closely related to the loss of the functionally organized tubular structures and possibly to neoplastic growth of the epithelia. We also reported that polarized distribution of carcinoembryonic antigen (CEA) in well-differentiated colonic adenocarcinoma was closely associated with expression of occludin immunohistochemically [24]. Occludin appeared to prevent lateral diffusion of CEA on the cell surface in the well-differentiated components of colonic adenocarcinomas. However, the expression of occludin was completely lost in poorly differentiated solid components of the same tumors. Kimura et al. [14] investigated occludin and ZO-1 expression in adenocarcinomas of the stomach and colon. Their expression, observed at the apical cell border, where gland-like structures were formed, appeared to be similar to that in normal epithelia. They suggested that occludin and ZO-1 molecules play important roles in formation of gland-like structures and the maintenance of simple polarized epithelial structures. Busch et al. [5] investigated the expression of occludin in prostate cancers and reported that occludin showed very consistent expression in all cancer cells that faced a glandular lumen, regardless of grade. The expression pattern of occludin was identical to that in normal counterparts. However, basal cells and cells without polarity in solid cancerous nests showed no occludin expression. Thus, they reported that occludin had a role in maintenance of glandular structures and cellular polarity of epithelial cells. From these findings, it is suggested that tight junctions play a crucial role in the formation of organized tubular structures in normal and neoplastic glandular epithelia.

Occludin expression was not found in gland-like structures (rosettes) of small cell carcinomas and large cell neuroendocrine carcinomas in our series. In our recent study investigating the occludin expression in 40 colorectal typical carcinoid tumors, occludin expression was not detected in most rosette-like structures [26]. However, a small number of glandular structures outlined by occludin expression were detected in 8% of carcinoid tumors in our series. This result was in accordance with previous histochemical and ultrastructural analyses of glandular differentiation in colorectal typical carcinoid tumors [2]. Occludin can also be a useful marker for distinguishing true glands from rosettes in neuroendocrine tumors. Occludin can detect divergent adenocarcinoma-

tous differentiation in high-grade neuroendocrine tumors (small cell and large cell neuroendocrine carcinomas).

It is often not easy to distinguish the "true" glandular structures from the glandular mimics, such as rosette structures in neuroendocrine tumors and gland-like tissue defects in tumors with non-glandular differentiation in human lung carcinoma tissues. The results of the present study suggest that occludin can serve as an immunohistochemical indicator of the "true" glandular differentiation that forms tubulo-papillary structures in human lung carcinomas.

Acknowledgements This study was supported by grants-in-aids from the Ministry of Health, Labour and Welfare, from the Ministry of Education, Culture, Sports, Science, and Technology of Japan, and from the Smoking Research Foundation.

References

1. Anderson JM, Balda MS, Fanning AS (1993) The structure and regulation of tight junctions. Curr Opin Cell Biol 5:772–778
2. Arai T, Kino I (1994) Histochemical and ultrastructural analyses of glandular differentiation in typical carcinoid tumor of the hindgut. Pathol Int 44:49–56
3. Balda MS, Whitney JA, Flores C, Gonzalez S, Cereijido M, Matter K (1996) Functional dissociation of paracellular permeability and transepithelial electrical resistance and disruption of the apical-basolateral intramembrane diffusion barrier by expression of a mutant tight junction membrane protein. J Cell Biol 134:1031–1049
4. Bartels H (1979) The air–blood barrier in the human lung. A freeze-fracture study. Cell Tissue Res 198:269–285
5. Busch C, Hanssen TA, Wagener C, OBrink B (2002) Down-regulation of CEACAM1 in human prostate cancer: correlation with loss of cell polarity, increased proliferation rate, and Gleason grade 3 to 4 transition. Hum Pathol 33:290–298
6. Citi S, Amorosi A, Franconi F, Giotti A, Zampi G (1991) Cingulin, a specific protein component of tight junctions, is expressed in normal and neoplastic human epithelial tissues. Am J Pathol 138:781–789
7. Cott GR, Sugahara K, Mason RJ (1986) Stimulation of net active ion transport across alveolar type II cell monolayers. Am J Physiol 250:222–227
8. Diamond JM (1977) The epithelial junction: bridge, gate, and fence. Physiologist 20:10–18
9. Eaton S, Simons K (1995) Apical, basal, and lateral cues for epithelial polarization. Cell 82:5–8
10. Furuse M, Hirase T, Itoh M, Nagafuchi A, Yonemura S, Tsukita S, Tsukita S (1993) Occludin: a novel integral membrane protein localizing at tight junctions. J Cell Biol 123:1777–1788
11. Gumbiner B, Louvard D (1985) Localized barriers in the plasma membrane: a common way to form domains. Trends Biochem Sci 10:435–438
12. Hirase T, Staddon JM, Saitou M, Ando-Akatsuka Y, Itoh M, Furuse M, Fujimoto K, Tsukita S, Rubin LL (1997) Occludin as a possible determinant of tight junction permeability in endothelial cells. J Cell Sci 110:1603–1613
13. Hoover KB, Liao SY, Bryant PJ (1998) Loss of the tight junction MAGUK ZO-1 in breast cancer: relationship to glandular differentiation and loss of heterozygosity. Am J Pathol 153:1767–1773
14. Kimura Y, Shiozaki H, Hirao M, Maeno Y, Doki Y, Inoue M, Monden T, Ando-Akatsuka Y, Furuse M, Tsukita S, Monden M (1997) Expression of occludin, tight-junction-associated protein, in human digestive tract. Am J Pathol 151:45–54
15. King RJ (1982) Pulmonary surfactant. J Appl Physiol 53:1–8
16. Morita K, Furuse M, Fujimoto K, Tsukita S (1999) Claudin multigene family encoding four-transmembrane domain protein components of tight junction strands. Proc Natl Acad Sci U S A 96:511–516
17. Nadel JA, Davis B, Phipps RJ (1979) Control of mucus secretion and ion transport in airways. Annu Rev Physiol 41:369–381
18. Polak-Charcon S, Shoham J, Ben-Shaul Y (1980) Tight junctions in epithelial cells of human fetal hindgut, normal colon, and colon adenocarcinoma. J Natl Cancer Inst 65:53–62
19. Saitou M, Ando-Akatsuka Y, Itoh M, Furuse M, Inazawa J, Fujimoto K, Tsukita S (1997) Mammalian occludin in epithelial cells: its expression and subcellular distribution. Eur J Cell Biol 73:222–231
20. Schneeberger EE, Karnovsky MJ (1976) Substructure of intercellular junctions in freeze-fractured alveolar-capillary membranes of mouse lung. Circ Res 38:404–411
21. Schneeberger EE, McCormack JM (1984) Intercellular junctions in upper airway submucosal glands of the rat: a tracer and freeze fracture study. Anat Rec 210:421–433
22. Simons K, Fuller SD (1985) Cell surface polarity in epithelia. Ann Rev Cell Biol 1:289–315
23. Soler AP, Miller RD, Laughlin KV, Carp NZ, Klurfeld DM, Mullin JM (1999) Increased tight junctional permeability is associated with the development of colon cancer. Carcinogenesis 20:1425–1431
24. Tobioka H, Isomura H, Kokai Y, Sawada N (2002) Polarized distribution of carcinoembryonic antigen is associated with a tight junction molecule in human colorectal adenocarcinoma. J Pathol 198:207–212
25. Tobioka H, Isomura H, Kokai Y, Tokunaga Y, Yamaguchi J, Sawada N (2004) Occludin expression decreases with the progression of human endometrial carcinoma. Hum Pathol 35:159–164
26. Tokunaga Y, Tobioka H, Isomura H, Kokai Y, Sawada N (2004) Expression of occludin in human rectal carcinoid tumours as a possible marker of glandular differentiation. Histopathology 44:247–250

Virchows Arch (2004) 445:477–484
DOI 10.1007/s00428-004-1107-0

ORIGINAL ARTICLE

Shigeki Shimizu · Takeo Yoshinouchi · Taio Naniwa · Mikae Nakamura · Shigeki Sato · Yuji Ohtsuki · Jiro Fujita · Ichiro Yamadori · Tadaaki Eimoto · Ryuzo Ueda

Distribution of CXCR3- or CCR4-positive cells in interstitial pneumonia associated with primary Sjögren's syndrome

Received: 10 May 2004 / Accepted: 27 July 2004 / Published online: 10 September 2004
© Springer-Verlag 2004

Abstract Patients with primary Sjögren's syndrome (SS) occasionally develop interstitial pneumonia (SS-IP), the prognosis of which is less grave compared with that of idiopathic pulmonary fibrosis (IPF). We examined distribution of helper T-cell subsets in open lung biopsy specimens from seven patients with SS-IP and, for comparison, ten patients with IPF. The expression of CXCR3 and CCR4, chemokine receptors associated in vitro with Th1 and Th2 cells, respectively, was analyzed in the mononuclear infiltrate using immunohistochemistry. The expression of CD4, CD8, and CD20 in the infiltrate was similarly examined. The positive cells were semiquantified in fibrosing areas and lymphoid clusters of both SS-IP and IPF. In fibrosing areas, CXCR3-positive cells were dominant over CCR4-positive cells in all cases of SS-IP, whereas the two types of cells showed no such difference in cases of IPF. Each of the CXCR3/CD4 and CXCR3/CCR4 ratios was significantly higher in SS-IP than in IPF ($P<0.05$ and $P<0.05$, respectively). The CCR4/CD4 ratio showed a significantly lower value in SS-IP than in IPF ($P<0.05$). In lymphoid clusters, prominent in SS-IP and few and small in IPF, CXCR3-positive cells predominated over CCR4-positive cells in both lung lesions. There was no significant difference of CXCR3/CCR4 ratio in lymphoid clusters between SS-IP and IPF ($P=0.33$). These findings in SS-IP are in accordance with those reported in previous studies of the salivary glands of SS patients, where most of the infiltrating lymphocytes expressed CXCR3, and the expression of interferon-gamma was upregulated. In contrast, the Th2 cell dominance was reported in IPF in the previous studies. The present findings suggest that the pathogenesis of interstitial pneumonia is different between SS-IP and IPF in regard to the roles of helper T-cell subsets.

Keywords Sjögren's syndrome · Interstitial pneumonia · Chemokine receptor · CXCR3 · CCR4

S. Shimizu (✉) · T. Eimoto
Department of Pathology,
Nagoya City University Medical School,
Mizuho-ku, 467-8601 Nagoya, Japan
e-mail: shimizsh@med.nagoya-cu.ac.jp
Tel.: +81-52-853-8161
Fax: +81-52-851-4166

S. Shimizu · T. Yoshinouchi · T. Naniwa · S. Sato · R. Ueda
Department of Internal Medicine,
Nagoya City University Medical School,
Aichi, Japan

M. Nakamura
Division of Internal Medicine,
Respiratory Disease Center, Seirei Mikatabara General Hospital,
Hamamatsu, Japan

Y. Ohtsuki
Department of Tumor Pathology,
Kochi Medical School,
Kochi, Japan

J. Fujita
Department of Internal Medicine,
Faculty of Medicine, Kagawa University,
Kagawa, Japan

I. Yamadori
Department of Pathology,
National Okayama Medical Center,
Okayama, Japan

Introduction

Sjögren's syndrome (SS) is a chronic inflammatory autoimmune disease characterized pathologically by lymphocytic infiltration, primarily in the lacrimal and salivary glands. SS can be categorized as primary or secondary. The latter form occurs in association with other autoimmune diseases, such as rheumatoid arthritis, systemic lupus erythematosus, and progressive systemic sclerosis. Differences between primary and secondary SS in terms of pulmonary involvement have been described [26, 37]. Primary SS patients who are anti-Ro antibody positive often develop more systemic manifestations, with lung disease being commonly reported [6, 9, 15, 29, 33]. The most frequent pulmonary abnormalities are interstitial

lung disease with interstitial pneumonia (SS-IP) and small airways disease. A long-term follow-up of primary SS patients suggests that the disease occurs early, and most patients do not develop progressive lung disease [6]. Since idiopathic pulmonary fibrosis (IPF) shows poorer prognosis [18], the mechanism of interstitial pneumonia may be different between SS-IP and IPF.

Studies of lymphocyte signaling indicate a complex series of regulatory interactions between lymphocyte subsets. Localization of the subsets is regulated by expression of chemokine receptors and ligands, and these molecules are recognized as useful markers for identifying the cell types [3, 5, 16, 20, 28]. Clones of CD4+ cells show divergence into Th1 and Th2 subpopulations. It is reported that Th1 cells and Th2 cells express chemokine receptors, CXCR3 and CCR4, respectively [5, 16, 20, 28]. CXCR3 ligands, such as IP-10, MIG and I-TAC, and CCR4 ligands, such as MDC and TARC, are expressed by a number of cell types and are widely associated with sites of inflammation [1, 4, 21, 35]. These studies primarily relied on in vitro regimens to induce T-cell polarization, and the significance of Th1- and Th2-cell differentiation in physiological and pathological settings is controversial [17, 24]. However, each of the many chemoattractant receptors expressed on leukocyte surfaces may contribute to the versatility and efficiency of leukocyte targeting in vivo [13]. Thus, it is worthwhile that the pathogenesis of SS-IP may be assessed in association with the chemokine receptor expression in infiltrating lymphocytes. To our knowledge, no such study has been reported yet in relation to SS-IP.

In this report, we have immunohistochemically studied open-lung biopsy specimens from patients with SS-IP to examine distribution and subpopulation of T-cell subsets in comparison with those of IPF.

Materials and methods

Patients

The study included seven patients with SS-IP and ten patients with IPF, the pathological diagnosis of which was made by open-lung biopsy. Seven cases with IP-SS were diagnosed as primary Sjögren's syndrome based on the criteria as previously reported [36]. These patients consisted of six women and one man, with a median age of 60 years (Table 1). All biopsy specimens were pathologically analyzed according to the criteria described by the American Thoracic Society, with attention to usual interstitial pneumonia (UIP) and non-specific interstitial pneumonia (NSIP) [2]. Five cases showed features of a UIP pattern, and two showed those of a NSIP pattern of fibrosis. However, UIP and NSIP patterns in all cases of SS-IP were associated with more prominent chronic inflammation and lymphoid hyperplasia than IPF. In one case (case 7) of SS-IP, the upper lobe showed a UIP pattern with patchy subpleural fibrosis and remodeling of the lung architecture, alternating with areas of normal lung. However, the lower lobe showed a cellular NSIP pattern with interstitial fibrosis and some lymphoid aggregates and with fibrosis of approximately the same age and relatively preserved lung architecture. This case was classified into a case of SS-IP with UIP pattern according to the previous report [10]. The ten patients with IPF were all men, with a median age of 62 years. All the biopsy specimens showed UIP histology with the fibrosing area containing variable lymphocytes and forming a few lymphoid clusters. No patients with SS-IP or IPF had histories of occupational dust inhalation. None of the patients had received immunosuppressive treatment, such as corticosteroid or cyclophosphamide, at the time of the biopsy.

Immunohistochemical staining

The immunohistological staining was performed using a SS MultiLink Detection Kit, horseradish peroxidase/diaminobenzidine (BioGenex Laboratories, San Ramon, CA, USA) for formalin-fixed, paraffin-embedded sections as previously described [32]. The antibodies used were for CD20 (L20; Dako), CD4 (clone IF6; Novocastra, Benton, UK), CD8 (clone 4B11; Novacastra), CXCR3 (BD Bioscience, Fronklin, Lakes, NJ), and CCR4 (Kyowahakko, Tokyo, Japan). In our preliminary study, both anti-CXCR3 and anti-CCR4 antibodies gave a positive staining in lymphocytes of synovial tissues from patients with rheumatoid arthritis and in skin biopsy specimens from patients with atopic dermatitis. Reactivity of these antibodies was approximately similar between formalin-fixed, paraffin-embedded cell blocks and flow cytometry specimens of peripheral blood mononuclear cells [14]. As for anti-CCR4 antibody, immunoabsorption using CCR4 antigen resulted in negative stains of these specimens [14].

Mirror section methods

To evaluate the relationship among CD4-, CXCR3-, and CCR4-positive cells, the mirror section method was performed on a similarly fixed paraffin block of inflammatory locus around the lung cancer specimen. Two consecutive 3-μm-thick sections were obtained with the cut surfaces facing each other. Each section was then individually reacted with antibodies to CXCR3, CCR4, or CD4.

Semiquantitative assessment of B cells and T-cell subsets

The infiltrating mononuclear cells that stained positively for CD20, CD4, CD8, CXCR3, and CCR4 were separately evaluated in fibrosing areas and lymphoid clusters of SS-IP and IPF cases. The positive cells were counted in 20 random high-power (×400) fields (HPFs) of fibrosing areas and in 5 HPFs of lymphoid clusters. In case 7, the positive cells in the upper lobe with a UIP pattern were counted.

Table 1 Clinical features of patients. *UIP* usual interstitial pneumonia, *NSIP* non-specific interstitial pneumonia, *LH* lymphoid hyperplasia

Patient	Age (years)	Sex	Autoantibodies	Pathological diagnosis
1	65	Female	SS-A	UIP pattern, LH
2	71	Female	SS-A	NSIP (cellular) pattern, LH
3	50	Male	ANA	NSIP (fibrotic) pattern, LH
4	69	Female	ANA	UIP pattern, LH
5	59	Female	SS-A	UIP pattern, LH
6	52	Female	ANA, SS-A, SS-B	UIP pattern, LH
7	52	Female	SS-A	UIP pattern, LH

Statistical analysis

We compared the two groups of SS-IP and IPF in terms of CXCR3/CCR4 ratio, CXCR3/CD4 ratio, and numbers of CXCR3- or CCR4-positive cells using Mann-Whitney tests. For the difference between lymphoid clusters and fibrosing areas, Wilcoxon's signed-rank test was used in terms of CXCR3/CCR4 ratio, CXCR3/CD4 ratio, and numbers of CXCR3- or CCR4-positive cells.

Results

Mirror section method

In the mirror sections stained for CD4 and CXCR3, most CXCR3-positive cells were also positive for CD4 (Fig. 1a, b). As for CD4 and CCR4 in the same manner, most CCR4-positive cells were also positive for CD4. The mirror sections stained each for CXCR3, and CCR4 showed that most CCR4-positive cells were negative for CXCR3 and vice versa (Fig. 1c, d).

Distribution of CD20-, CD4-, CD8-, CXCR3-, and CCR4-positive cells

CD20-positive cells were seen only in lymphoid clusters (Fig. 2a) and were few in fibrosing areas of both SS-IP and IPF. CD4- or CD8-positive cells infiltrated in fibrosing areas and lymphoid clusters of both SS-IP and IPF, more prominent in the latter than the former areas (Fig. 2b, c). Many CD8-positive lymphocytes but only a few CD4-positive cells infiltrated the loci of alveolitis in SS-IP and IPF (Fig. 2d).

In fibrosing areas and lymphoid clusters of SS-IP lung tissues, CXCR3-positive cells infiltrated in dominance over CCR4-positive cells in all cases (Table 2, Table 3). The CXCR3-positive cells were particularly prominent in lymphoid clusters (Fig. 3c; Table 3). Comparatively less CXCR3-positive cells were seen in fibrosing areas, but CXCR3-positive cells were also more numerous than CCR4-positive cells in all cases (Fig. 3a; Table 2). However, CCR4-positive cells were detected in only a small number in fibrosing areas and lymphoid clusters of SS-IP (Fig. 3, Fig. 4) but were detected significantly more

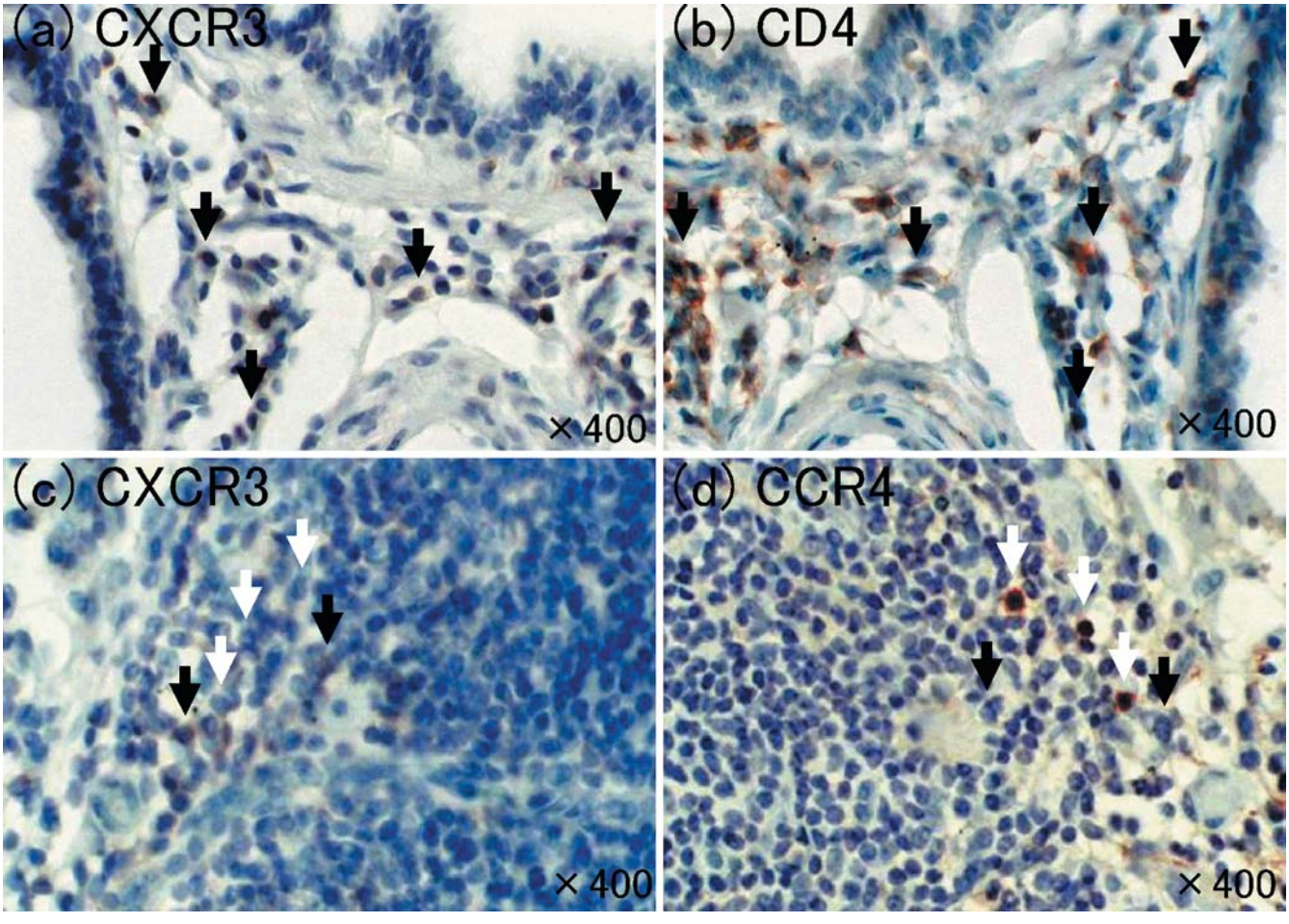


Fig. 1 Immunohistochemical staining with anti-CXCR3 (**a**), CD4 (**b**), anti-CXCR3 (**c**), and anti-CCR4 (**d**) antibodies using the mirror-section method. Most CXCR3-positive lymphocytes are also CD4 positive (**a**, **b**, *arrows*). Most CXCR3-positive lymphocytes are CCR4 negative (**c**, **d**, *black arrows*), and most CCR4-positive lymphocytes are CXCR3 negative (**c**, **d**, *white arrows*)

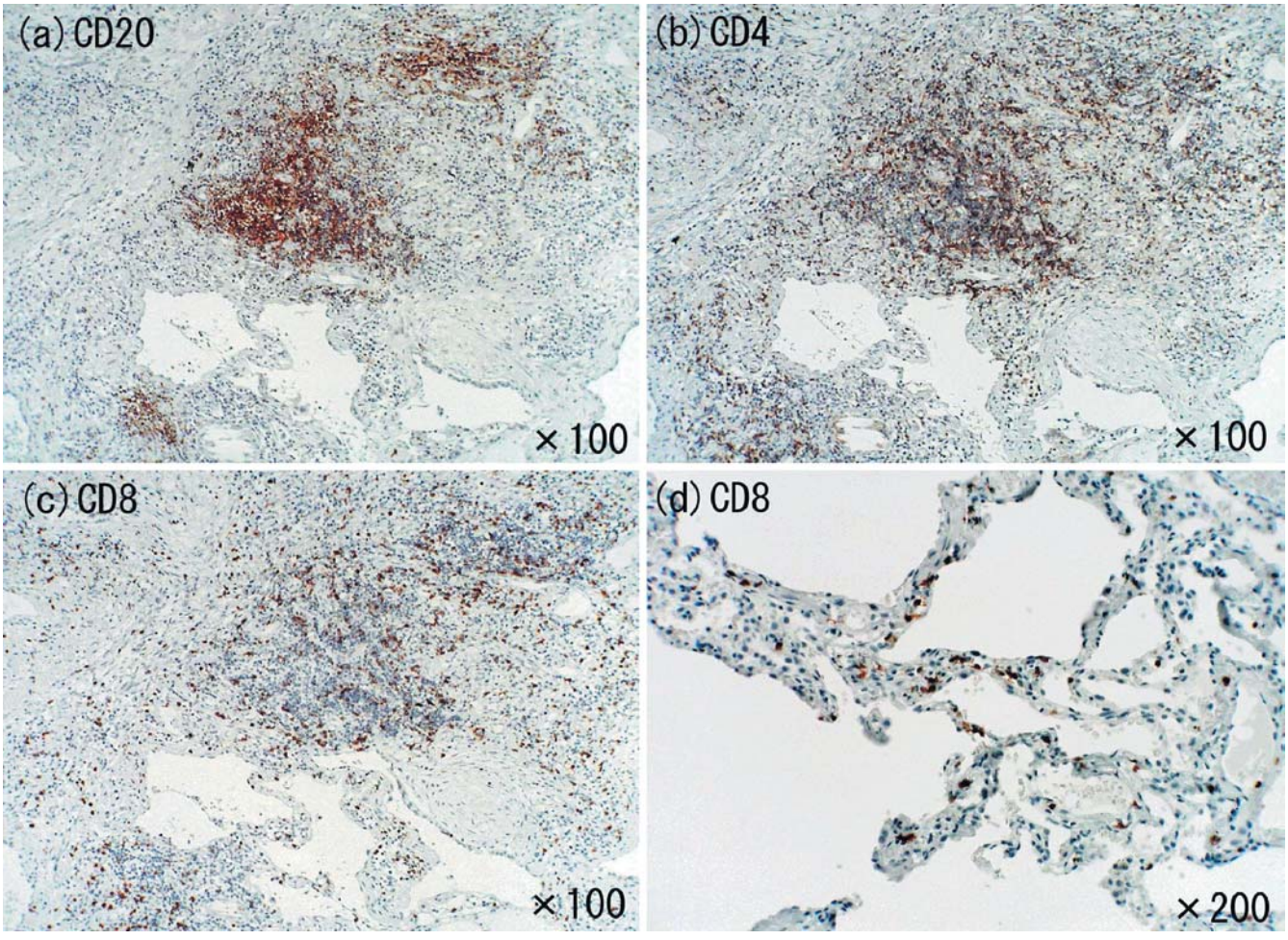


Fig. 2 Immunohistochemical staining with CD20, CD4, and CD8 antibodies in Sjögren's syndrome with interstitial pneumonia. CD20-positive B lymphocytes (**a**), CD4-positive T lymphocytes (**b**), and CD8-positive T lymphocytes (**c**) are prominent in lymphoid clusters. CD8-positive T lymphocytes are seen in the loci of alveolitis (**d**)

Table 2 Lymphocyte subsets in fibrosing areas of interstitial pneumonia associated with primary Sjogren's syndrome (SS-IP) and idiopathic pulmonary fibrosis (IPF). *HPF* high-power field

Patient no.	Diagnosis	CD4+cells (cells/20 HPF)	CXCR3+cells (cells/20 HPF)	CCR4+cells (cells/20 HPF)	CXCR3/CD4	CCR4/CD4	CXCR3/CCR4
1	SS-IP	365	353	30	0.97	0.08	11.77
2	SS-IP	42	40	3	0.95	0.07	13.33
3	SS-IP	34	27	14	0.79	0.41	1.93
4	SS-IP	345	225	25	0.65	0.07	9.00
5	SS-IP	76	75	4	0.99	0.05	18.75
6	SS-IP	70	45	14	0.64	0.20	3.21
7	SS-IP	87	105	34	1.21	0.39	3.09
8	IPF	62	34	30	0.55	0.48	1.13
9	IPF	125	63	82	0.50	0.66	0.77
10	IPF	83	29	51	0.35	0.61	0.57
11	IPF	57	48	26	0.84	0.46	1.85
12	IPF	92	47	41	0.51	0.45	1.15
13	IPF	154	64	87	0.42	0.56	0.74
14	IPF	149	71	74	0.48	0.50	0.96
15	IPF	177	97	74	0.55	0.42	1.31
16	IPF	250	122	115	0.49	0.46	1.06
17	IPF	126	74	46	0.59	0.37	1.61

Table 3 Lymphocyte subsets in lymphoid clusters of Sjogren's syndrome with interstitial pneumonia (SS-IP) and idiopathic pulmonary fibrosis (IPF) lungs. *HPF* high-power field

Patient no.	Diagnosis	CD4+cells (cells/5HPF)	CXCR3+cells (cells/5HPF)	CCR4+cells (cells/5HPF)	CXCR3/CD4	CCR4/CD4	CXCR3/CCR4
1	SS-IP	820	718	118	0.88	0.14	6.08
2	SS-IP	302	290	10	0.96	0.03	29.00
3	SS-IP	175	152	8	0.87	0.05	19.00
4	SS-IP	610	601	156	0.99	0.26	3.85
5	SS-IP	251	298	6	1.19	0.02	49.67
6	SS-IP	378	383	10	1.01	0.03	38.30
7	SS-IP	422	382	86	0.91	0.20	4.44
8	IPF	176	148	12	0.84	0.07	12.33
9	IPF	112	111	9	0.99	0.08	12.33
10	IPF	188	157	18	0.84	0.10	8.72
11	IPF	421	358	32	0.85	0.08	11.19
12	IPF	178	176	18	0.99	0.10	9.78
13	IPF	191	159	23	0.83	0.12	6.91
14	IPF	297	210	71	0.71	0.24	2.96
15	IPF	281	245	52	0.87	0.19	4.71
16	IPF	187	168	27	0.90	0.14	6.22
17	IPF	804	680	133	0.85	0.17	5.11

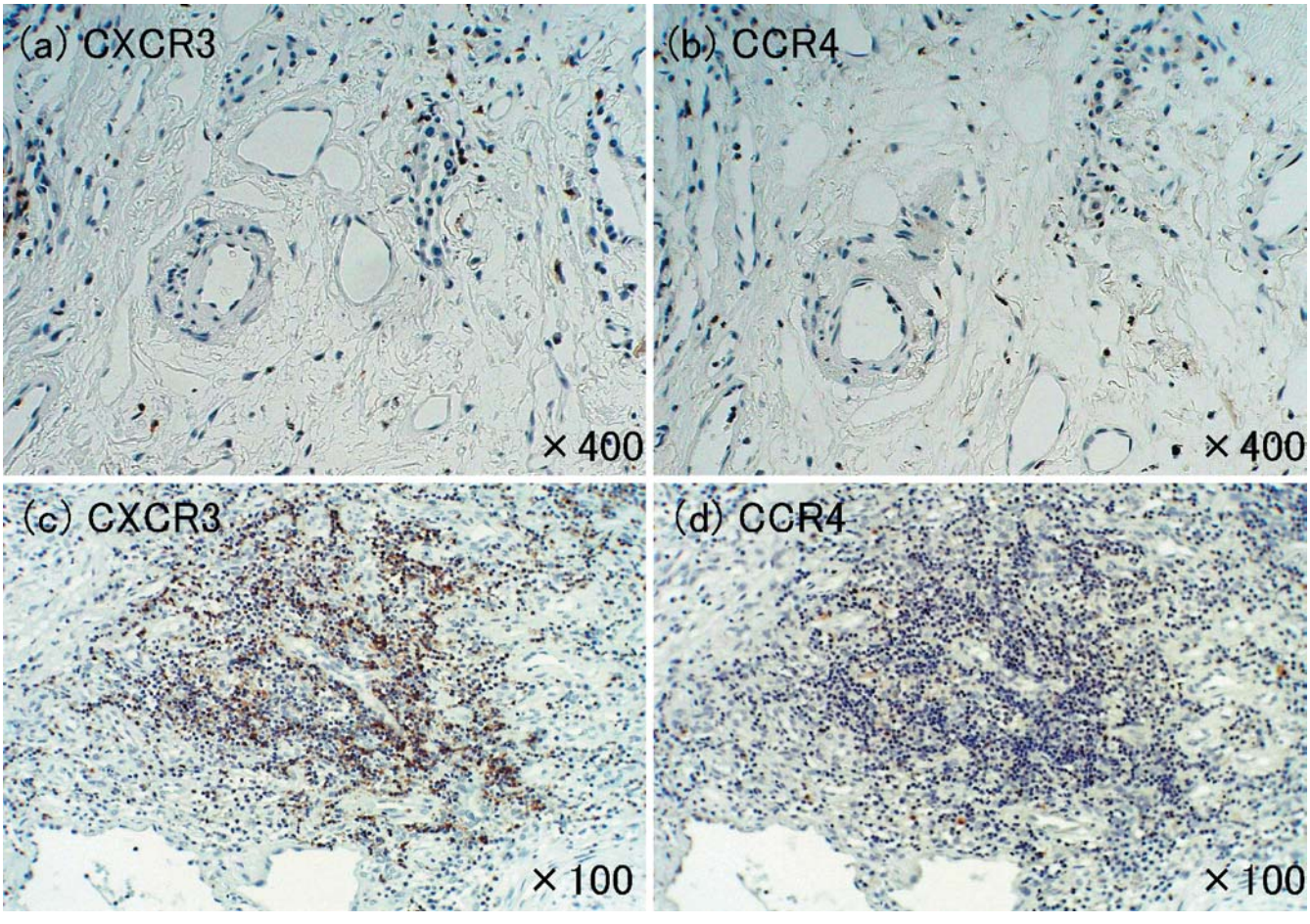


Fig. 3 Immunohistochemical staining with anti-CXCR3 and anti-CCR4 antibodies in fibrosing areas (**a**, **b**) and anti-CXCR3 and anti-CCR4 antibodies in lymphoid clusters (**c**, **d**) in Sjögren's syndrome with interstitial pneumonia. Serial sections show that CXCR3-positive cells (**a**) are more numerous than CCR4-positive cells (**b**). CXCR3-positive cells (**c**) are more numerous than CCR4-positive cells (**d**)

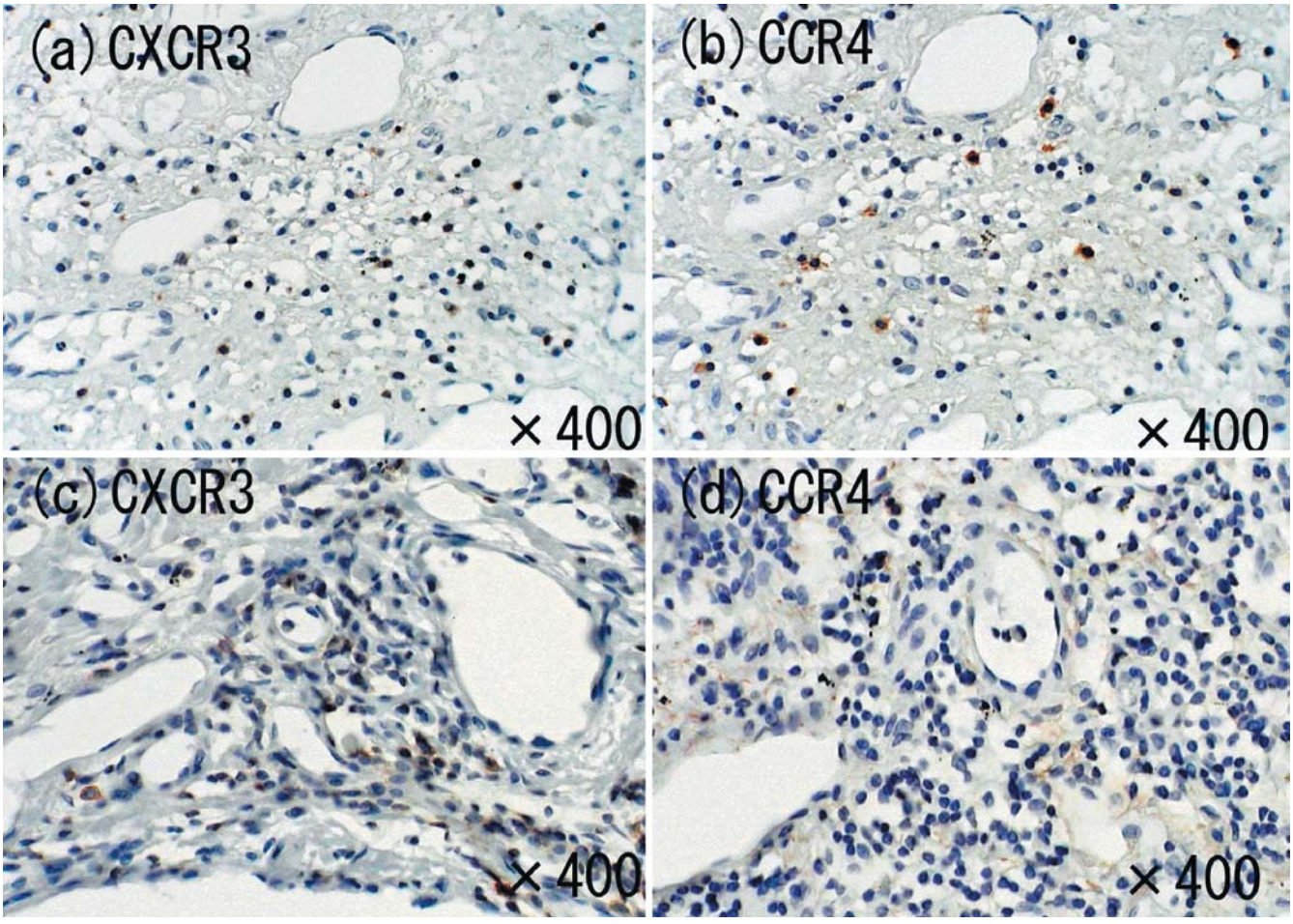


Fig. 4 Immunohistochemical staining with anti-CXCR3 and CCR4 antibodies in fibrosing areas and lymphoid clusters in idiopathic pulmonary fibrosis. CXCR3-positive cells (**a**) are slightly less than CCR4-positive cells (**b**) in fibrosing areas. However, CXCR3-positive cells (**c**) are more numerous than CCR4-positive cells (**d**) in lymphoid clusters

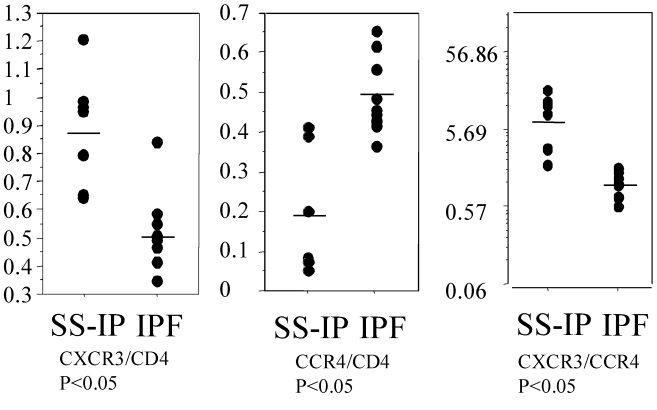


Fig. 5 Comparison of CXCR3-positive or CCR-4-positive cell ratios between Sjögren's syndrome with interstitial pneumonia and idiopathic pulmonary fibrosis in fibrosing areas

in the fibrosing areas of IPF by Mann-Whitney tests (P<0.05) (Table 2).

In fibrosing areas of IPF, the difference between the number of CXCR3-positive or CCR4-positive cells is generally subtle, but the former cells were more numerous in two cases (case 11, case 17) and the latter in three cases (case 9, case 10, case 13) (Fig. 4; Table 2). The CXCR3/CD4 ratio was significantly higher in SS-IP than in IPF (P<0.05), while the CCR4/CD4 ratio was significantly lower in SS-IP than IPF (P<0.05) (Fig. 5). The CXCR3/CCR4 ratio was significantly higher in SS-IP than IPF (P<0.05). There were a few lymphoid clusters in IPF, and CXCR3-positive cells were more prominent in these foci. There was no significant difference of CXCR3/CCR4 ratio between SS-IP and IPF as far as the lymphoid clus-ters were concerned (P=0.33).

There was no significant difference of CXCR3/CCR4 ratio between fibrosing areas and lymphoid clusters in SS-IP (P=0.13). The CXCR3/CCR4 ratio was significantly higher in lymphoid clusters than fibrosing areas in IPF (P<0.05) by means of Wilcoxon's signed-rank test. The result showed that, in IPF, lymphoid subtypes were different between patchy fibrosing areas, with some chronic inflammation and a few small lymphoid clusters.

Discussion

Clones of CD4-positive cells diverge into Th1 and Th2 subpopulations. The recent in vitro studies indicate that Th1 cells express chemokine receptors CXCR3 and CCR5, and Th2 cells express CCR3, CCR4, and CCR8 [3, 5, 16, 20, 28], although controversy exists as to the relationship between the receptors and T-helper subsets in vivo [24]. Kim et al. [17] described that 88% of Th1 cells in blood are $CXCR3^{+}CCR4^{-}$, 90% of Th2 cells are $CXCR3^{-}CCR4^{+}$, and synovial CD4-positive T cells in arthritis differ from blood T cells. Thus, it is suspected that the infiltration patterns of CD4-positive T-cell subtypes vary according to organs and diseases. We have performed the mirror section method to evaluate the relationship among CD4-, CXCR3-, and CCR4-positive cells. Most CXCR3-positive or CCR4-positive cells were positive for CD4, and double-positive cells for CXCR3 and CCR4 were rare. Thus, we have confirmed that the CXCR3-positive or CCR4-positive cells in our study belong to helper T cells and represent their different subtypes.

The Th1 cells produce cytokines IL-2 and IFN-γ, and the Th2 cells produce IL-4, IL-5, IL-6, and IL-10. The perturbation of cytokine homeostasis seems to be evident in several connective tissue diseases [7, 19, 23]. Several groups have noted that IFN-γ has an inhibitory effect of fibroblast proliferation and collagen production [8, 27]. Sempowski et al. [31] have identified a subset of murine fibroblasts for which IL-4 promotes proliferation and production of both collagenous and non-collagenous extracellular-matrix proteins. These findings suggest that IL-4 stimulates and INF-γ downregulates the development of fibrosis. In our study, the difference between the numbers of CXCR3-positive and CCR4-positive cells is generally subtle in fibrotic areas of IPF, whereas CXCR3-positive cells infiltrated in dominance over CCR4-positive cells in those of SS-IP, even with a UIP pattern in histology. These results could suggest that, in fibrotic areas, Th1 cells are predominant over Th2 cells in SS-IP but not in IPF. Wallace et al. [38] reported that the Th2 pattern of cytokines appears to predominate in IPF and that the IL-4, IL-5, IL-6, and IL-10 produced by Th2 cells stimulate humoral immune responses with an antibody-mediated response and play a role in fibrosis formation of interstitial pneumonia [38]. Therefore, it may be possible that a higher Th1/Th2 cell ratio in SS-IP causes less fibroblast proliferation and less collagen deposition compared with IPF, resulting in a different prognosis between SS-IP and IPF.

It has been recognized that SS is a unique autoimmune and lymphoproliferative disorder in which the salivary and lacrimal glands are the major targets for autoimmune tissue damage, and IFN-γ is a major cytokine in salivary glands of SS patients [11, 34]. Mononuclear cell infiltrates containing a predominance of activated T cells develop around the ducts in salivary glands as a result of autoimmune reactions between epithelium and lymphocytes [22, 30]. Fox et al. [12] reported that salivary gland epithelial cells in SS produced over 40-fold more IL-1α, IL-2, IL-6, IL-10, and IFN-γ mRNA than normal controls, and the salivary gland CD4-positive T cells produced little IL-4 and IL-5 mRNA immediately after elution from the salivary gland. Ogawa et al. [25] showed that IFN-γ stimulated the production of IP-10 and MIG (CXCR3 ligands) in the SS salivary glands and that the dense periductal infiltrates contained many CXCR3-positive lymphocytes. In the present study, CXCR3-positive cells infiltrated significantly more than CCR4-positive cells in the fibrotic areas and lymphoid clusters of SS-IP, reflecting a similarity to those that occurred in the salivary glands with SS [12, 25].

The CXCR3/CCR4 ratio was significantly higher in lymphoid clusters than fibrosing areas in IPF. In IPF, the infiltration of T-cell subsets may be different between areas with patchy fibrosis and those with prominent chronic inflammation forming a few lymphoid aggregates. It may be suggested that the lower rate of CXCR3/CCR4 indicates that Th2 cells infiltrate more in the fibrosing areas of IPF, in accordance with in vitro studies [3, 5, 16, 20, 28]. So, while Th2 cells and Th2 cytokines may stimulate fibroblasts and deposit collagen in fibrosing areas, Th1 cells and Th1 cytokines may stimulate persistence of inflammation in areas with prominent interstitial chronic inflammation. This heterogeneous infiltration of T-cell subsets may have a connection with fibrosis of UIP pattern, of which the histological hallmark is patchy interstitial inflammation and fibrosis, alternating with areas of normal lung.

In conclusion, we have demonstrated that CXCR3-positive and CD4-positive T cells dominantly infiltrate in SS-IP compared with IPF. The difference of T helper cell subsets may affect the fibrogenesis of these interstitial pneumonias, resulting in a better prognosis of SS-IP than IPF.

Acknowledgements We gratefully acknowledge Kyowahakko, Tokyo, Japan, and Dr. Masamichi Koike, who supplied CCR4 antibody. We also thank Mr. Seizo Nagaya, Department of Pathology, Nagoya City University Medical School, for excellent technical assistance.

References

1. Agostini C, Facco M, Siviero M, Carollo D, Galvan S, Cattelan AM, Zambello R, Trentin L, Semenzato G (2000) CXC chemokines IP-10 and mig expression and direct migration of pulmonary CD8+/CXCR3+ T cells in the lungs of patients with HIV infection and T-cell alveolitis. Am J Respir Crit Care Med 162:1466–1473
2. American Thoracic Society (2002) American Thoracic Society/European Respiratory Society International Multidisciplinary Consensus Classification of Idiopathic Interstitial Pneumonia. Am J Respir Crit Care Med 165:277–304
3. Annunziato F, Galli G, Cosmi L, Romagnani P, Manetti R, Maggi E, Romagnani S (1998) Molecules associated with human Th1 or Th2 cells. Eur Cytokine Netw 9:12–16
4. Berin MC, Eckmann L, Broide DH, Kagnoff MF (2001) Regulated production of the T helper 2-type T-cell chemoattractant TARC by human bronchial epithelial cells in vitro and in human lung xenografts. Am J Respir Cell Mol Biol 24:382–389

5. Bonecchi R, Bianchi G, Bordignon PP, D'Ambrosio D, Lang R, Borsatti A, Sozzani S, Allavena P, Gray PA, Mantovani A, Sinigaglia F (1998) Differential expression of chemokine receptors and chemotactic responsiveness of type 1 T helper cells (Th1s) and Th2s. J Exp Med 187:129–134
6. Davidson BK, Kelly CA, Griffiths ID (2000) Ten year follow up of pulmonary function in patients with primary Sjögren's syndrome. Ann Rheum Dis 59:709–712
7. Del Prete G (1998) The concept of type-1 and type-2 helper T cells and their cytokines in humans. Int Rev Immunol 16:427–455
8. Duncan MR, Berman B (1985) Gamma interferon is the lymphokine and beta interferon the monokine responsible for inhibition of fibroblast collagen production and late but not early fibroblast proliferation. J Exp Med 162:516–527
9. Fairfax AJ, Haslam PL, Pavia D, Sheahan NF, Bateman JR, Agnew JE, Clarke SW, Turner-Warwick M (1981) Pulmonary disorders associated with Sjögren's syndrome. Q J Med 50: 279–295
10. Flaherty KR, Travis WD, Colby TV, Toews GB, Kazerooni EA, Gross BH, Jain A, Strawderman RL, Flint A, Lynch JP, Martinez FJ (2001) Histopathologic variability in usual and nonspecific interstitial pneumonias. Am J Respir Crit Care Med 164:1722–1727
11. Fox RI, Bumol T, Fantozzi R, Bone R, Schreiber R (1986) Expression of histocompatibility antigen HLA-DR by salivary gland epithelial cells in Sjögren's syndrome. Arthritis Rheum 29:1105–1111
12. Fox RI, Kang HI, Ando D, Abrams J, Pisa E (1994) Cytokine mRNA expression in salivary gland biopsies of Sjögren's syndrome. J Immunol 152:5532–5539
13. Foxman EF, Campbell JJ, Butcher EC (1997) Multistep navigation and the combinatorial control of leukocyte chemotaxis. J Cell Biol 139:1349–1360
14. Ishida T, Utsunomiya A, Iida S, Inagaki H, Takatsuka Y, Kusumoto S, Takeuchi G, Shimizu S, Ito M, Komatsu H, Wakita A, Eimoto T, Matsushima K, Ueda R (2003) Clinical significance of CCR4 expression in adult T-cell leukemia/lymphoma: its close association with skin involvement and unfavorable outcome. Clin Cancer Res 9:3625–3634
15. Kelly CA, Foster H, Pal B, Gardiner P, Malcolm AJ, Charles P, Blair GS, Howe J, Dick WC, Griffiths ID (1991) Primary Sjögren's syndrome in north east England—a longitudinal study. Br J Rheumatol 30:437–442
16. Kim CH, Kunkel EJ, Boisvert J, Johnston B, Campbell JJ, Genovese MC, Greenberg HB, Butcher EC (2001) Bonzo/CXCR6 expression defines type 1-polarized T-cell subsets with extralymphoid tissue homing potential. J Clin Invest 107:595–601
17. Kim CH, Rott L, Kunkel EJ, Genovese MC, Andrew DP, Wu L, Butcher EC (2001) Rules of chemokine receptor association with T cell polarization in vivo. J Clin Invest 108:1331–1339
18. King TE, Jr., Schwarz MI, Brown K, Tooze JA, Colby TV, Waldron JA, Jr., Flint A, Thurlbeck W, Cherniack RM (2001) Idiopathic pulmonary fibrosis: relationship between histopathologic features and mortality. Am J Respir Crit Care Med 164:1025–1032
19. Kusaba M, Honda J, Fukuda T, Oizumi K (1998) Analysis of type 1 and type 2 T cells in synovial fluid and peripheral blood of patients with rheumatoid arthritis. J Rheumatol 25:1466–1471
21. Loetscher P, Pellegrino A, Gong JH, Mattioli I, Loetscher M, Bardi G, Baggiolini M, Clark-Lewis I (2001) The ligands of CXC chemokine receptor 3, I-TAC, Mig, and IP10, are natural antagonists for CCR3. J Biol Chem 276:2986–2991
20. Loetscher P, Uguccioni M, Bordoli L, Baggiolini M, Moser B, Chizzolini C, Dayer JM (1998) CCR5 is characteristic of Th1 lymphocytes. Nature 391:344–345
22. Matthews JB, Deacon EM, Kitas GD, Salmon M, Potts AJ, Hamburger J, Bacon PA (1991) Primed and naive helper T cells in labial glands from patients with Sjögren's syndrome. Virchows Arch 419:191–197
23. Miossec P, van den Berg W (1997) Th1/Th2 cytokine balance in arthritis. Arthritis Rheum 40:2105–2115
24. Nanki T, Lipsky PE (2000) Lack of correlation between chemokine receptor and T(h)1/T(h)2 cytokine expression by individual memory T cells. Int Immunol 12:1659–1667
25. Ogawa N, Ping L, Zhenjun L, Takada Y, Sugai S (2002) Involvement of the interferon-gamma-induced T cell-attracting chemokines, interferon-gamma-inducible 10-kd protein (CXCL10) and monokine induced by interferon-gamma (CXCL9), in the salivary gland lesions of patients with Sjögren's syndrome. Arthritis Rheum 46:2730–2741
26. Papathanasiou MP, Constantopoulos SH, Tsampoulas C, Drosos AA, Moutsopoulos HM (1986) Reappraisal of respiratory abnormalities in primary and secondary Sjögren's syndrome. A controlled study. Chest 90:370–374
27. Pfeffer LM, Murphy JS, Tamm I (1979) Interferon effects on the growth and division of human fibroblasts. Exp Cell Res 121:111–120
28. Sallusto F, Lenig D, Mackay CR, Lanzavecchia A (1998) Flexible programs of chemokine receptor expression on human polarized T helper 1 and 2 lymphocytes. J Exp Med 187:875–883
29. Segal I, Fink G, Machtey I, Gura V, Spitzer SA (1981) Pulmonary function abnormalities in Sjögren's syndrome and the sicca complex. Thorax 36:286–289
30. Segerberg-Konttinen M, Bergroth V, Jungell P, Malmstrom M, Nordstrom D, Sane J, Immonen I, Konttinen YT (1987) T lymphocyte activation state in the minor salivary glands of patients with Sjögren's syndrome. Ann Rheum Dis 46:649–653
31. Sempowski GD, Beckmann MP, Derdak S, Phipps RP (1994) Subsets of murine lung fibroblasts express membrane-bound and soluble IL-4 receptors. Role of IL-4 in enhancing fibroblast proliferation and collagen synthesis. J Immunol 152:3606–3614
32. Shimizu S, Yoshinouchi T, Ohtsuki Y, Fujita J, Sugiura Y, Banno S, Yamadori I, Eimoto T, Ueda R (2002) The appearance of S-100 protein-positive dendritic cells and the distribution of lymphocyte subsets in idiopathic nonspecific interstitial pneumonia. Respir Med 96:770–776
33. Strimlan CV (1986) Pulmonary involvement in Sjögren's syndrome. Chest 89:901–902
34. Sun D, Emmert-Buck MR, Fox PC (1998) Differential cytokine mRNA expression in human labial minor salivary glands in primary Sjögren's syndrome. Autoimmunity 28:125–137
35. Vestergaard C, Kirstejn N, Gesser B, Mortensen JT, Matsushima K, Larsen CG (2001) IL-10 augments the IFN-gamma and TNF-alpha induced TARC production in HaCaT cells: a possible mechanism in the inflammatory reaction of atopic dermatitis. J Dermatol Sci 26: 46–54
36. Vitali C (2003) Classification criteria for Sjoren's syndrome. Ann Rheum Dis 62:94–95
37. Vitali C, Tavoni A, Viegi G, Begliomini E, Agnesi A, Bombardieri S (1985) Lung involvement in Sjögren's syndrome: a comparison between patients with primary and with secondary syndrome. Ann Rheum Dis 44:455–461
38. Wallace WA, Ramage EA, Lamb D, Howie SE (1995) A type 2 (Th2-like) pattern of immune response predominates in the pulmonary interstitium of patients with cryptogenic fibrosing alveolitis (CFA). Clin Exp Immunol 101:436–441

Virchows Arch (2004) 445:485–490
DOI 10.1007/s00428-004-1109-y

ORIGINAL ARTICLE

Lynne C. Tetlow · David E. Woolley

Effect of histamine on the production of matrix metalloproteinases-1, -3, -8 and -13, and TNFα and PGE_2 by human articular chondrocytes and synovial fibroblasts in vitro: a comparative study

Received: 18 February 2004 / Accepted: 5 July 2004 / Published online: 17 September 2004
© Springer-Verlag 2004

Abstract Histamine has many regulatory activities and is well recognised for its importance in allergic and inflammatory disorders. Recently, histamine has been implicated in the pathophysiological processes of both rheumatoid and osteoarthritis, where human articular chondrocytes (HACs) and rheumatoid synovial fibroblasts (RSFs) are reported to express histamine receptors. This study has demonstrated H_1 and H_2 histamine receptors using immunohistochemistry on HACs and RSFs in vitro and has compared the effects of histamine (20 μM) on both cell types with regard to the production of matrix metalloproteinases (MMPs-1, -3, -8 and -13), the proinflammatory cytokine tumour necrosis factor α (TNFα) and prostaglandin E_2 (PGE_2). On incubation with histamine, HACs showed increased production of MMP-3, MMP-13, TNFα and PGE_2 (statistical significance P=0.02, 0.005, 0.008 and 0.03, respectively, student's t-test), but MMP-1 expression was unaffected. In contrast, the RSF showed a histamine-induced increase in MMP-1 (P=0.028) and an approximate 10-fold level of MMP-3 and PGE_2 release over that of HACs, each being stimulated by histamine (P=0.02 and 0.032, respectively, student's t-test). However, MMP-8, MMP-13 and TNFα were not detected for RSF cultures. Our results show that histamine modifies the behaviour of both HACs and RSFs in vitro, but different effects were observed for the production of specific MMPs and TNFα by the two cell types.

Keywords Histamine · Articular chondrocytes · Synovial fibroblasts · Metalloproteinases · Arthritis

L. C. Tetlow (✉) · D. E. Woolley
University Department of Medicine,
Manchester Royal Infirmary,
Oxford Road, Manchester, M13 9WL, UK
e-mail: lynne.c.tetlow@man.ac.uk
Tel.: +44-161-2768668
Fax: +44-161-2768668

Introduction

Rheumatoid arthritis is a disease characterised by chronic inflammation and cartilage destruction, with activated synoviocytes strongly implicated in chondrolytic processes [15, 28]. Osteoarthritis is characterised by degeneration and loss of articular cartilage, with matrix depletion and cell clusters reflecting the aberrant behaviour of the resident chondrocytes [5, 14]. As of yet, the pathogenesis of both these crippling diseases remains to be elucidated. However, common to both is the probable involvement of proinflammatory cytokines and matrix metalloproteinases (MMPs) in the breakdown of cartilage matrix [5, 14, 15, 28].

Mast cells are the prime source of histamine in vivo and are found in increased numbers in arthritic joints, with measurable levels of histamine reported in a significant proportion of synovial fluids [2, 12]. Histamine is a well-recognised mediator in allergic and inflammatory reactions and is reported to affect numerous cell types, such as macrophages, epithelial cells, eosinophils and various subsets of T cells [27]. Our earlier work has shown that human articular chondrocytes (HACs) possess both H_1 and H_2 histamine receptors, whilst rheumatoid synovial fibroblasts (RSFs) possess H_1 receptors [18, 19]; histamine stimulates both cell types in vitro to increase prostanoid production and proliferative rate [20, 24, 29].

In addition to evidence for mast cell activation in the rheumatoid lesion [21], the recent observation that HACs express histamine and histidine decarboxylase in vitro, as well as in degenerative zones of osteoarthritic cartilage [25], strongly suggested that the local production of histamine in arthritic joints could promote several catabolic processes. This hypothesis was supported by recent reports of histamine-induced MMP production [23] and increased proliferative rate by HACs in vitro [24]. Chondrocytes and synovial fibroblasts are crucial for the homeostatic integrity of normal cartilage and adjacent connective tissues, respectively; but, in arthritic disorders, it is likely that they become potential targets for histamine and other factors that modify their behaviour/phenotype.

The present study was designed to compare the effects of histamine on HACs and RSFs with regard to their production of MMPs, tumour necrosis factor α (TNFα) and prostaglandin E_2 (PGE_2).

Materials and methods

HAC cultures

Human articular cartilage from osteoarthritis knee specimens (n=6), obtained with ethics approval and informed patient consent, was enzymically digested to provide chondrocyte cultures as previously described [26]. Primary HAC cultures were grown to confluence in Dulbecco's Modified Eagles Medium (DMEM)+10% foetal calf serum (FCS), harvested and re-seeded into 12-well culture dishes (NUNC, Gibco, UK). Triplicate wells of sub-confluent HAC (passage 2) in DMEM+2% FCS were treated with histamine (20 μM) and incubated for 24 h at 37°C. The histamine concentration of 20 μM was shown to be optimal for maximal stimulation of HAC proliferation [24] and MMP-3 production (data not shown). The conditioned culture medium from wells +/- histamine was collected and assayed for MMPs-1, -3, -8 and -13, TNFα and PGE_2 using enzyme-linked immunosorbent assay (ELISA) methodology. Chondrocytes from each preparation were also seeded onto 8-well chamber slides (NUNC, UK) and immunostained for S100 protein and type-II collagen to confirm a chondrocytic phenotype [22]. The antibodies used for those studies were as follows: rabbit anti-cow S100 (crossreacts with human) from Dako, catalogue number Z311, diluted 1:400 in Tris-buffered saline (TBS) and mouse monoclonal antibody to type-II collagen from Chemicon, Chandlers Ford, Hampshire, UK, MAB1330, lot 20040499, diluted 1:10 in TBS for immunohistochemistry (IHC).

RSF cultures

Rheumatoid synovial tissue obtained from remedial arthroplasties (n=5), with ethics approval and patient consent, was enzymically dissociated to provide synovial fibroblast cultures [20]. At passage 2, the cells were grown to confluence in DMEM+10% (FCS), harvested and seeded into 12-well culture dishes. Triplicate wells of sub-confluent RSF in DMEM+2% FCS were treated with histamine (20 μM) and incubated for 24 h at 37°C. The conditioned culture medium from wells +/- histamine was collected, suitably diluted and assayed as described for the HAC cultures.

For both HAC and RSF cultures, the cell numbers were counted at the end of each experiment following 70% ethanol fixation and toluidine blue staining (six fields of 1 mm^2, total area 6 mm^2).

Immunolocalisation of H_1 and H_2 histamine receptors

HACs and RSFs were seeded into 4-well chamber slides and immunostained for H_1 and H_2 histamine receptors. The cells were fixed in 4% buffered formalin for 5 min, washed, pre-incubated with 10% (v/v) swine serum as a blocking step and then incubated with rabbit polyclonal antibody to either the H_1 or H_2 histamine receptors (H_1R, cat no. AB5654P, lot 22030577 and H_2R cat no. AB5658P, lot 22020282 Chemicon, Hampshire, UK) at 5 μg/ml for 2 h at 20°C. After washing, biotinylated swine anti-rabbit IgG (Dako, UK) diluted 1:300 in TBS was applied for 45 min at 20°C, followed, after further washing, by alkaline phosphatase-conjugated avidin/biotin detection agent (Dako, UK) and development with New Fuchsin to give a red colour [26]. Controls included the use of non-immune rabbit IgG or TBS in place of the primary antibody; all showed negative staining (Fig. 1). Photomicrographs were taken on a Nachet Nomarski microscope using Kodak Ektachrome T160 film.

MMP measurement

Conditioned culture medium from HAC and RSF was diluted 1:20 and assayed for MMP-1 and MMP-3 using ELISA assay kits with sensitivities of 0.025–32 ng/ml and 0.8–25 ng/ml, respectively, purchased from The Binding Site, Birmingham, UK.

MMP-8 and MMP-13 were measured using ELISA assay kits with sensitivities 0.125–4 ng/ml and 0.094–3 ng/ml, respectively, purchased from Amersham UK Ltd.

PGE_2 and TNFα measurement

Undiluted conditioned medium from the cell cultures was assayed for prostaglandin E_2 using an ELISA assay kit from R&D Systems, UK (sensitivity 39–5000 pg/ml) and for TNFα using an ELISA assay kit supplied by IDS, Newcastle, UK (sensitivity 12.5–800 pg/ml).

Results

Both HACs and RSFs were positively stained for H_1 and H_2 receptors (Fig. 1). The intensity of staining varied between individual cells, and the proportion of cells staining positive in any one culture was also variable. In general 20–80% of HACs were positive for the H_1 receptor (Fig. 1A); and, whilst staining for the H_2 receptor tended to be stronger, a similar proportion of cells was positive (Fig. 1B). For RSFs, positive H_1 receptor staining is shown in Fig. 1D and that for the H_2 receptor in Fig. 1E. The staining intensity also varied from cell to cell as described for HAC cultures.

For HAC cultures, the addition of 20 μM was shown to increase the production of MMP-3, MMP-13, TNFα and PGE_2 relative to untreated controls, as shown in Fig. 2A, B, C, D, respectively. Averaged data for each parameter and statistical significance are given in the figure legend.

For RSF cultures, the addition of 20 μM histamine increased MMP-1 production as shown in Fig. 3A. Averaged values from three different RSF cultures showed a significant increase (P=0.028) in MMP-1 production by histamine treatment (Fig. 3B). Similarly, histamine treatment increased MMP-3 production in all RSF cultures—this representing an approximate 1.5-fold stimulation (P=0.02, Fig. 3C, D). PGE_2 production was also increased following histamine treatment—this representing an approximate 2.5-fold enhancement, (P=0.032, Fig. 3E, F). As a positive control, the addition of interleukin-1β (0.5 ng/ml) to both HAC and RSF cultures (n=6) produced a marked increase in MMP-1, MMP-3 and PGE_2 production from both cell types (data not shown).

For RSF cultures, MMP-8, MMP-13 and TNFα were not detected by the ELISA assay employed, either before or after histamine additions; and, similarly, MMP-8 was not detected in HAC cultures. A summary of data for the effects of histamine on both HAC and RSF cultures is provided by Table 1 for comparison.

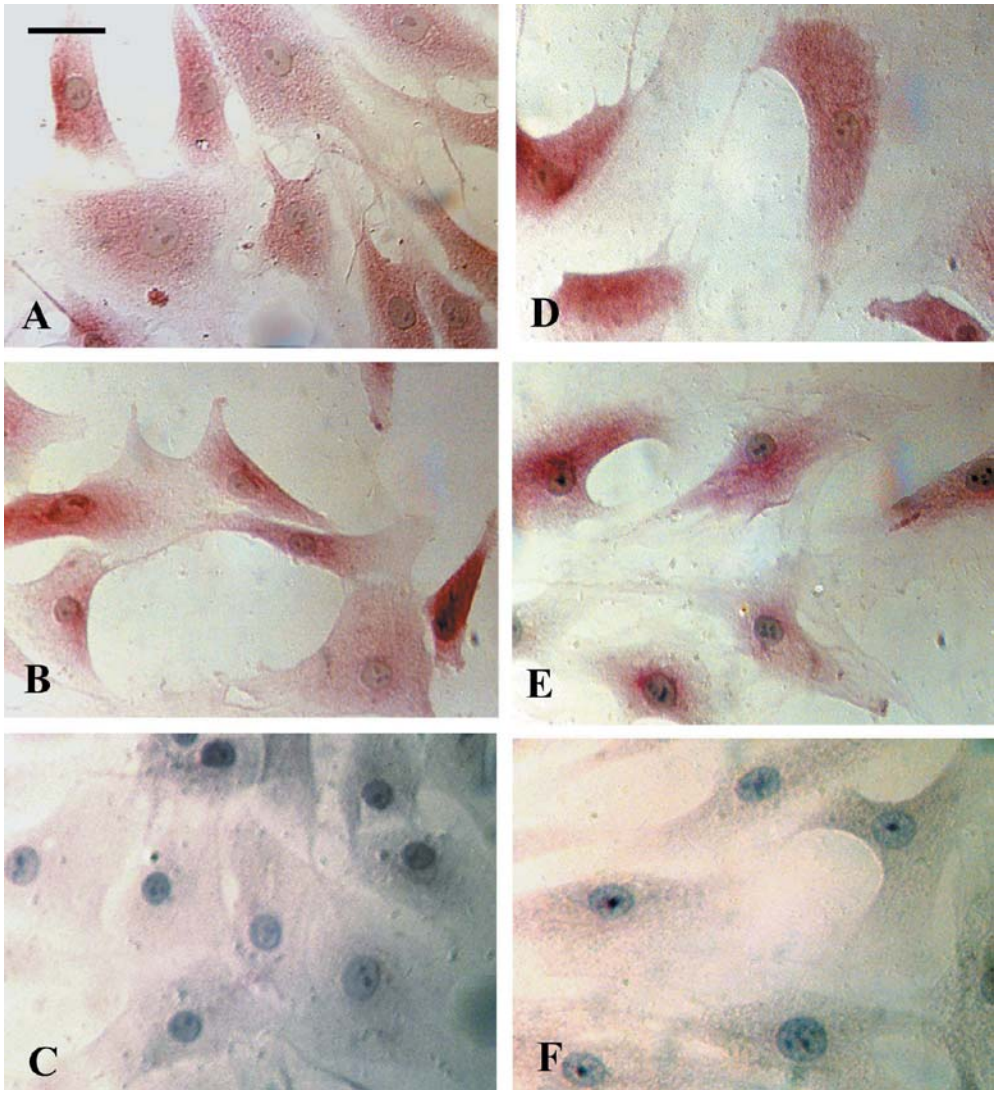


Fig. 1 Immunolocalisation of H_1 and H_2 histamine receptors in human articular chondrocytes (HACs) and rheumatoid synovial fibroblasts (RSFs) in vitro. **A** Immunostaining of H_1 histamine receptors of HACs in vitro (*red stain*). **B** Immunostaining of H_2 histamine receptors of HACs in vitro (*red stain*). **C** Negatively stained control HAC culture treated with non-immune rabbit IgG for comparison with **A** and **B**. **D** Immunostaining of H_1 histamine receptors of RSFs in vitro (*red stain*). **E** Immunostaining of H_2 histamine receptors of RSFs in vitro (*red stain*). **F** Negatively stained control RSF culture treated with non-immune rabbit IgG for comparison with **E** and **F**. *Bar* 30 μm for all micrographs

Discussion

Cartilage degradation in either rheumatoid or osteoarthritis reflects multifactorial processes, including complex interactions among cytokines, proteinases, prostanoids and other factors [15, 28]. Several mediators are purported to act on both immune and resident stromal cells and various cell types have been proposed as key players in the pathogenesis of joint destruction. Recent studies have implicated the mast cell in both arthritic disorders, with mast-cell activation releasing a broad range of potent effector molecules, especially histamine [8, 12].

Elevated levels of histamine have been reported in the synovial fluids of arthritic joints [12], and, more recently, chondrocytes have been shown to produce histamine and the enzyme responsible for its synthesis, histidine decarboxylase [25]. Histamine is known to induce localised tissue oedema and to participate in both allergic and inflammatory processes via its interaction with histamine receptors [27]. Evidence for histamine receptor expression has been reported for several cell types, usually determined by the use of receptor antagonists, agonists or in situ hybridisation studies [6]. The immunohistochemical observations presented here suggest that the expression of these receptors in vitro is not necessarily a common feature for all cells within a culture, but a major proportion of either HAC or RSF was shown to express both H_1 and H_2 histamine receptors. This variance in H receptor staining may have several explanations, including variations between different cell cultures, mitotic cell cycles and the clinical states of the tissues available. It is recognised that culture conditions can markedly affect chondrocyte phenotype, and, for this reason, only early cultures (passage #2) were used, each of which was shown using IHC to be positive for the chondrocyte markers S100 and type-II collagen synthesis [22]. Earlier studies with chondrocytes in vitro have demonstrated that histamine increases MMP production [23], increases their rate of proliferation [24], increases cytosolic calcium levels [7] and modifies proteoglycan and keratan sulphate synthesis via changes in intracellular cAMP levels [4].

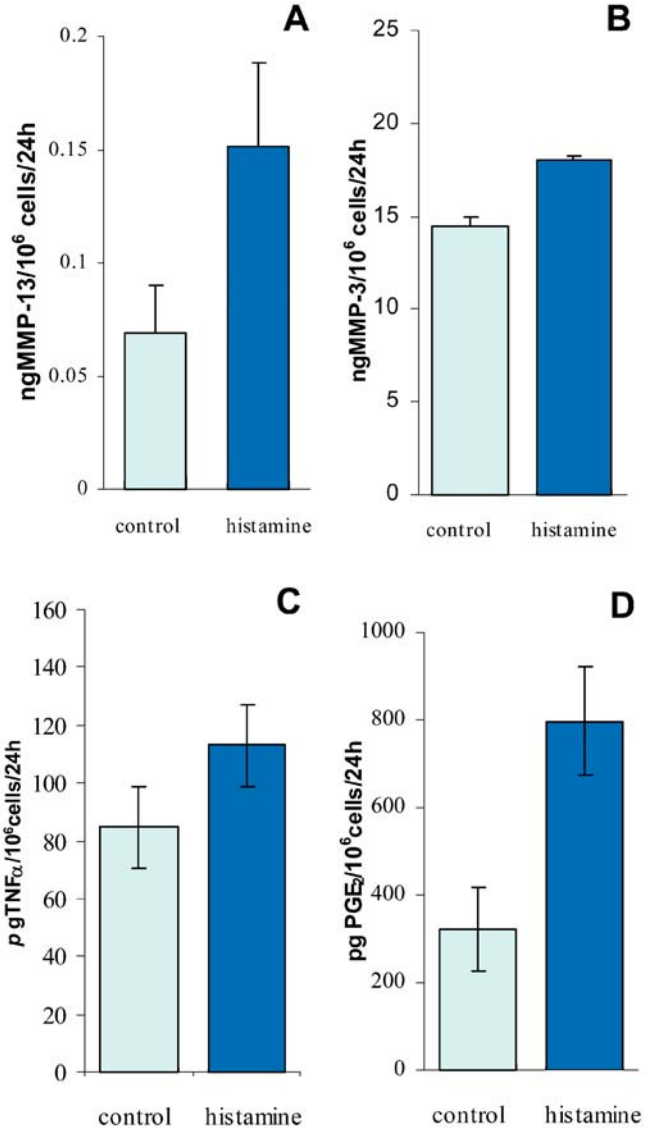


Fig. 2 Effects of 20 μM histamine on matrix metalloproteinases (MMP)-13, MMP-3, tumour necrosis factor α (TNFα) and prostaglandin E_2 (PGE_2) production by human articular chondrocytes in vitro. **A** MMP-13. Control 68.8±20.1 $pg/10^6$ cells/24 h; +histamine 150.9±37.4 $pg/10^6$ cells/24 h (P=0.0049, student's t-test). **B** MMP-3. Control 14.4±0.5 $ng/10^6$ cells/24 h; +histamine 18.0±0.3 $ng/10^6$ cells/24 h (P=0.02, student's t-test). **C** TNFα. Control 84.8±9.5 $pg/10^6$ cells/24 h; +histamine 113.2±13.2 $pg/10^6$ cells/24 h (P=0.008, student's t-test). **D** PGE_2. Control 323.3±95.6 $pg/10^6$ cells/24 h; +histamine 797.7±122.4 $pg/10^6$ cells/24 h (P=0.03, student's t-test). Data presented are average values for at least three different cultures

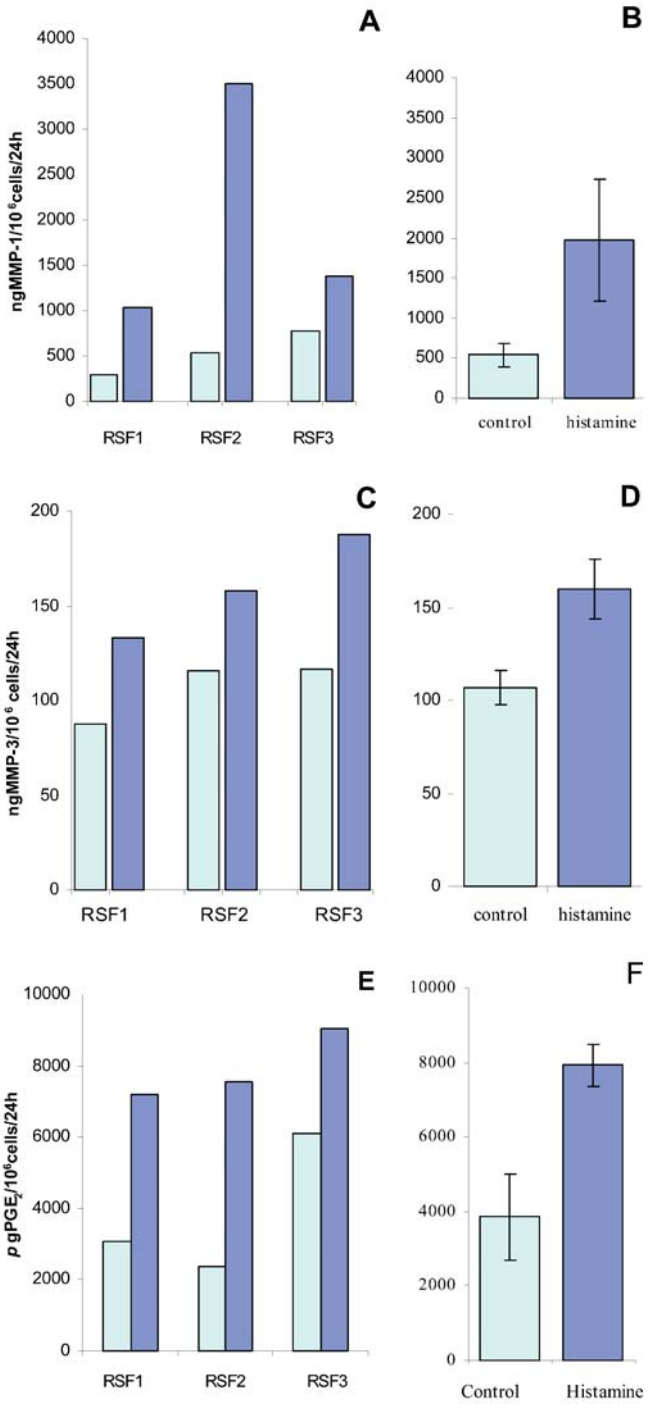


Fig. 3 Effects of 20 μM histamine on matrix metalloproteinases (MMP)-1, MMP-3 and prostaglandin E_2 (PGE_2) production by rheumatoid synovial fibroblasts in vitro. **A**, **B** MMP-1 control=537±142 $ng/10^6$ cells/24 h; +histamine 20 μM=1970±768 $ng/10^6$ cells/24 h (P=0.02, student's t-test). **C**, **D** MMP-3 control=106±10 $ng/10^6$ cells/24 h; +histamine 20 μm=159.60±15 $ng/10^6$ cells/24 h (P=0.028, student's t-test). **E**, **F** PGE_2 control=3846±1141 $pg/10^6$ cells/24 h; +histamine 20 μM=7922±565 $pg/10^6$ cells/24 h (P=0.032, student's t-test). Data presented are average values for at least three different cultures

The effect of histamine on RSFs in vitro has demonstrated H_1 receptor-mediated responses resulting in increased cell proliferation, MMP-1 and PGE_2 production, phosphoinositide metabolism and intracellular Ca^{++} concentration [29]. Zenmyo et al. [29] also reported a histamine-induced upregulation of H_1 receptor expression by RSFs, together with an increase in intracellular cAMP. The latter suggested a typical H_2 receptor-mediated response, an observation supported by the IHC reported

Table 1 Summary of the effects of 20 μM histamine on human articular chondrocytes (HAC) and rheumatoid synovial fibroblasts (RSFs) in vitro. Results are tabulated as fold increase produced by 10^6 cells over a 24 h incubation period. *TNFα* tumour necrosis factor, *PGE_2* prostaglandin E_2, *MMP* matrix metalloproteinases

	HAC (fold increase)	RSFs (fold increase)
MMP-1	No effect	↑ (×2.0)
MMP-3	↑ (×1.2)	↑ (×1.5)
MMP-8	Not detected	Not detected
MMP-13	↑ (×2.4)	Not detected
TNFα	↑ (×1.3)	Not detected
PGE_2	↑ (×3)	↑ (×2.5)

here. Similar studies of histamine on primary and immortalised human corneal epithelial cells also reported increased phosphoinositide turnover and mobilisation of intracellular Ca^{++}, this effect possibly being related to the increased production of interleukin-6, IL-8 and GMCSF, responses shown to be H_1 receptor mediated [17]. Human conjunctival fibroblasts in vitro also responded to histamine with increased production of IL-1, IL-6, IL-8 and ICAM-1 expression [9], and a similar histamine-induced increase in IL-6 and IL-8 production was reported for human coronary artery endothelial cells [11]. In addition, histamine was reported to induce eotaxin production [1] and to increase hyaluronic acid secretion in normal synovial fibroblasts [13]. Such reports demonstrate a plethora of histamine-induced responses by various mesenchymal cells, with many relating to specific cellular functions and tissue origin.

The 2.5- and 3-fold upregulation of PGE_2 for RSFs and HACs, respectively, over 24 h, shows that histamine significantly influences prostanoid metabolism. It is known that PGE_2 contributes to several regulatory processes, including proteinase and cytokine expression by cells. The addition of indomethacin (14 μM) to these HAC and RSF cultures (to block PGE_2 expression) did not prevent the H-induced increase in MMP-13 production by HACs nor MMP-3 production by RSFs, suggesting a direct histamine effect. Whether or not PGE_2 contributes to some other histamine-induced responses remains to be elucidated.

Although the histamine effects observed here for human chondrocytes and synovial fibroblasts in vitro were similar for increased MMP-3 and PGE_2 production, differences were observed for MMP-1, MMP-13 and TNFα expression. Whether such effects occur in vivo remains uncertain, but there the potential synergy with other mediators, such as specific cytokines and growth factors, would seem more likely. For example, histamine synergises with IL-1 to stimulate PGE_2 production from both human chondrocytes and synoviocytes [20] and histamine potentiated an increase in MMP-1 production induced by IL-4 on synovial fibroblasts [30]. Since histamine is known to modulate the production of many cytokines and the expression of their receptors [3], it would seem that this potent amine could potentially initiate a cascade of pro-inflammatory events. As of yet, it remains unclear which histamine receptors, designated H_1, H_2, H_3 and H_4 [10, 16], are expressed by the two cell types in situ and where precisely histamine expression relates to the sequence of pathophysiological events that characterise joint disease. With the recognised advance in treatments of atopic disorders with "anti-histamines", it would seem that the availability of specific histamine receptor antagonists would help to elucidate further the relative importance of histamine in the modified phenotypes of chondrocytes and synoviocytes in vitro, possibly with therapeutic benefits for the arthritides.

Acknowledgements This study was supported by The Health Foundation (formerly The PPP Foundation). The authors would also like to thank orthopaedic surgeons T. Dunningham (Tameside Hospital, Manchester) and D.S. Johnson (Stepping Hill Hospital, Stockport) for the supply of joint tissues.

References

1. Bae SJ, Tanaka Y, Ogawa F, Takenaka M, Hamazaki Y, Shimizu K et al (2002) Inhibitory effect of cetrizine in histamine-induced eotaxin production in normal human fibroblasts. Curr Ther Res Clin Exp 63:128–140
2. Buckley MG, Walters C, Wong WM, Cawley MID, Ren S, Schwartz LB et al (1997) Mast cell activation in arthritis; detection of alpha- and beta-tryptase, histamine and eosinophilic cationic protein in synovial fluid. Clin Sci 93:363–370
3. Falus A, Meretey K (1992) Histamine- an early messenger in inflammatory and immune reactions. Immunol Today 13:154–156
4. Fukuda K, Matsumura F Tanaka S (1993) Histamine H2 receptor mediates keratin sulphate secretion in rabbit chondrocytes. Am J Physiol 265:1653–1657
5. Goldring MB (2000) The role of the chondrocyte in osteoarthritis. Arthritis Rheum 43:1916–1926
6. Hill SJ, Ganellin CR, Timmerman H, Schwartz JC, Shankley NP, Young JM et al (1997) International Union of Pharmacology. XIII. Classification of histamine receptors. Pharmacol Rev 49:253–278
7. Horowitz ER, Higgins TM, Harvey BJ (1996) Histamine-induced cytosolic increase in porcine articular chondrocytyes. Biochim Biophys Acta 1313:95–100
8. Lee DM, Friend DS Gurish MF, Benoist C, Mathis D, Brenner MB (2002) Mast cells: a cellular link between autoantibodies and inflammatory arthritis. Science 297:1689–1692
9. Leonardi A, DeFranchis G, De Paoli M, Fregona I, Plebani M, Secchi AG (2002) Histamine induced cytokine production and ICAM-1 expression in human conjunctival fibroblasts. Curr Eye Res 25:189–196
10. Leurs R, Smit MJ, Timmerman H (1995) Molecular pharmacological aspects of histamine receptors. Pharmacol Therapeut 66:413–463
11. Li Y, Chi L, Stechschulte DJ, Dileepan KN (2001) Histamine-induced production of interleukin-6 and interleukin-8 by human coronary artery endothelial cells is enhanced by endotoxin and tumor necrosis factor-α. Microvasc Res 61:253–262
12. Malone AM, Schwartz LB, Barrett KE, Metcalfe DD (1986) Mast cell numbers and histamine levels in synovial-fluids from patients with diverse arthritides. Arthritis Rheum 29:956–963
13. Nagata Y, Matsumura F, Motoyoshi H, Yamasaki H, Fukuda K, Tanaka S (1992) Secretion of a hyaluronic acid from synovial fibroblasts is enhanced by histamine—a newly observed metabolic effect of histamine. J Lab Clin Med 120:707–712
14. Pelletier J-P, Martel-Pelletier J, Abramson SB (2001) Osteoarthritis, an inflammatory disease. Potential implication for the selection of new therapeutic targets. Arthritis Rheum 44:1237–1247

15. Poole AR (1993) Cartilage in health and disease. In: McCarty DJ, Koopman WJ (eds) Arthritis and allied conditions: a textbook of rheumatology, vol. 2, 12th edn. Lea & Febiger, Philadelphia, pp 279–333
16. Schneider E, Rolli-Derkinderen M, Arock M, Dy M (2002). Trends in histamine research: new functions during immune responses and hematopoiesis. Trends Immunol 23:255–263
17. Sharif NA, Wiernas TK, Griffin BW, Davis TL (1998) Pharmacology of [^{3}H]-pyrilamine binding and of the histamine-induced inositol phosphates generation, intracellular Ca^{2+}-mobilization and cytokine release from human corneal epithelial cells. Br J Pharmacol 125:1336–1344
18. Taylor DJ, Woolley DE (1987) Evidence for both histamine H-1 and H-2 receptors on human articular chondrocytes. Ann Rheum Dis 46:431–435
19. Taylor DJ, Woolley DE (1987) Histamine H1 receptors on adherent rheumatoid synovial cells in culture: demonstration by radioligand binding and inhibition of histamine-stimulated prostaglandin E production by histamine H1 antagonists. Ann Rheum Dis 46:425–430
20. Taylor DJ, Yoffe JR, Brown DM, Woolley DE (1986) Histamine stimulates prostaglandin-E production by rheumatoid synovial cells and human articular chondrocytes in culture. Arthritis Rheum 29:160–166
21. Tetlow LC, Woolley DE (1995) Mast cells cytokines and metalloproteinases at the rheumatoid lesion—dual immunolocalisation studies. Ann Rheum Dis 54: 896–903
22. Tetlow LC, Woolley DE (2001) Expression of vitamin D receptors and matrix metalloproteinases in osteoarthritic cartilage and human articular chondrocytes in vitro. Osteoarthritis Cart 9:423–443
23. Tetlow LC, Woolley DE (2002) Histamine stimulates matrix metalloproteinase-3 and -13 production by human articular chondrocytes in vitro. Ann Rheum Dis 61:737–740
24. Tetlow LC, Woolley DE (2003) Histamine stimulates the proliferation of human articular chondrocytes in vitro and is expressed by chondrocytes in human articular cartilage. Ann Rheum Dis 62:991–994
25. Tetlow LC, Woolley DE (2004) Immunolocalisation of histamine and histidine decarboxylase in chondrocytes of arthritic cartilage. Inflamm Res 53:S21–S22
26. Tetlow LC, Adlam DJ, Woolley DE (2001) Matrix metalloproteinases and proinflammatory cytokine production by chondrocytes of human osteoarthritic cartilage. Arthritis Rheum 44: 585–594
27. White MV, Kaliner MA (1988) Histamine. In: Gallin JR, Goldstein IM, Snyderman R (eds) Inflammation: basic principles and clinical correlates. Raven Press, New York, pp 169–193
28. Woolley DE, Tetlow LC (1997) Observations on the microenvironmental nature of cartilage degradation in rheumatoid arthritis. Ann Rheum Dis 56:1–11
29. Zenmyo M, Hiraoka K, Komiya S, Morimatsu M, Sasaguri Y (1995) Histamine stimulated production of matrix metalloproteinase 1 by human rheumatoid fibroblasts is mediated by H1 receptors. Virchows Archiv 427:437–444
30. Zenmyo M, Hiraoka K, Sasaguri T, Komiya S, Inoue A, Morimatsu M et al (1996) Interleukin-4 stimulates rheumatoid synovial fibroblasts to express matrix metalloproteinase-1 (tissue collagenase) and histamine H1 receptor mRNA. Biochem Mol Biol Int 40:1253–1260

Virchows Arch (2004) 445:491–497
DOI 10.1007/s00428-004-1049-6

ORIGINAL ARTICLE

Christian Woenckhaus · Irina Fenic · Jürgen Giebel · Sebastian Hauser · Klaus Failing · Joachim Woenckhaus · Thomas Dittberner · Micaela Poetsch

Loss of heterozygosity at 12p13 and loss of p27KIP1 protein expression contribute to melanoma progression

Received: 9 March 2004 / Accepted: 17 May 2004 / Published online: 17 June 2004
© Springer-Verlag 2004

Abstract Little is known about the mechanisms causing p27KIP1 decrease in melanomas. Therefore, we performed loss of heterozygosity (LOH) analysis with polymerase chain reaction at seven different loci surrounding the *p27KIP1/CDKN1B* gene at 12p13 and direct DNA sequencing analysis of all exons. Furthermore, the immunohistochemical expression of p27KIP1 and Ki-67 was investigated. Only two mutations in the sequence of *p27KIP1/CDKN1B* were detected, but the number of tumours showing LOH at 12p13 increased significantly with the parameters of tumour progression (pT level, P=0.018; Breslow index, P=0.01; Clark level, P<0.001), with a more aggressive tumour growth (radial versus vertical growth, P=0.018) and tumour subtype (superficial spreading melanomas versus nodular melanomas versus metastases, P<0.001). p27KIP1 protein expression decreased with the Clark level (P=0.026) and the pT level (P=0.045). No correlation between LOH affecting 12p13 and p27KIP1 protein decrease in melanomas was stated. This does not exclude the participation of *p27KIP1/CDKN1B* in p27KIP1 protein decrease, since protein expression is regulated at various cellular levels; but it could also suggest that other tumour suppressors are situated in the same region as *p27KIP1/CDKN1B*. Taken together, our data shows that loss of p27KIP1 protein expression and LOH at 12p13 contribute to tumour progression in melanoma.

Keywords Melanoma · LOH · 12p13 · p27KIP1 · RGP · VGP

Part of this work was presented at the XXIVth International Congress of the International Academy of Pathology, Amsterdam, The Netherlands, October 2002 and published in abstract form (Histopathology 2002 41[Suppl 1]:144–145). This work is part of S.H.'s doctoral thesis

C. Woenckhaus (✉) · S. Hauser
Institute of Pathology,
University of Greifswald,
Fr. Loeffler Strasse 23e, 17489 Greifswald, Germany
e-mail: woenck@uni-greifswald.de
Tel.: +49-3834-865721

I. Fenic
Institute of Veterinary Pathology,
Justus Liebig University of Gießen,
Gießen, Germany

J. Giebel
Institute of Anatomy,
University of Greifswald,
Greifswald, Germany

K. Failing
Institute of Veterinary Physiology,
Department of Biomathematics,
Justus Liebig University of Gießen,
Gießen, Germany

J. Woenckhaus
Institute of Pathology,
Justus Liebig University of Gießen,
Gießen, Germany

T. Dittberner
Consultant Committee of the Health Insurance,
Stralsund, Germany

M. Poetsch
Institute of Forensic Medicine,
University of Greifswald,
Greifswald, Germany

Introduction

Tumour progression in malignant melanoma is characterised by the shift from the radial growth phase (RGP), which is exhibited by superficial spreading melanomas (SSM) in early stages, to the vertical growth phase (VGP), encountered in nodular melanomas (NM) and advanced forms of SSM. In contrast to RGP, VGP melanomas are coupled with a high risk for developing metastases (M) [5]. G1/S cell-cycle abnormalities seem to be one of the most important factors for the development and progression of melanoma [21].

Normal cell-cycle progression is ruled by cyclins (A, B, D and E), cyclin-dependent kinases and cyclin-de-

pendent kinase inhibitors (CDK-Is) of the INK4 family and the KIP family. The passage from G1 to S phase relies on stimulation by extracellular mitogens and is mostly affected in malignant transformation [22]. Oncogenic factors determine uncontrolled cell proliferation by targeting particular regulators of the G1 phase progression and G1/S checkpoint, thus interrupting the relationship between mitogenic stimuli and the potentially autonomous cell-cycle machinery [22]. Failure to arrest proliferation, for example by loss of CDK-Is, will release cells with highly unstable genomes, which could evolve into cancer cells [22].

From all CDK-Is, p27KIP1 provides a central signal, which co-ordinates various inputs from the extracellular environment and serves as a threshold for progression to the S phase or for exiting the cell cycle [18, 23]. Experiments on cultured melanoma cells revealed the implication of p27KIP1 as an inhibitor in several intracellular growth pathways [10, 24]. Moreover, it was shown that progression from primary to metastatic status was accompanied by reduction of p27KIP1 protein expression [29]. However, another study failed to find a reduction of p27KIP1 expression in melanoma compared with compound and Spitz naevi (N) [14]. Finally, p27KIP1 was found elevated in even primary melanomas in connection with an increased Breslow index [1]. Still, no information is available to date about the status of the p27 gene (*p27KIP1/CDKN1B*, located on12p13) in melanoma.

To gain insights into the mechanism regulating the p27KIP1 expression in melanoma, we performed polymerase chain reaction (PCR)-based loss of heterozygosity (LOH) analysis at seven different micro-satellite loci surrounding the *p27KIP1/CDKN1B* gene and direct DNA sequencing of all exons of the *p27KIP1/CDKN1B* gene and compared the immunohistochemical expression of p27KIP1 and Ki-67 (for assessment of proliferative status) in N, primary melanomas and M.

Materials and methods

Patients and tumours

Tissue and patient data were obtained and used after advice of the medical ethics committee of the University of Greifswald in accordance with the declaration of Helsinki and the International Conference of Harmonisation—Good Clinical Practice. The anonymity of the patients investigated was preserved corresponding to rules of data protection of the Human Medical Faculty Greifswald and the county Mecklenburg-Vorpommern.

Melanomas were classified as stated elsewhere [19]. For evaluation of tumour extension, the latest tumour node metastasis classification was used [24], and, for statistical analysis, no distinction was made between ulcerated and non-ulcerated tumours. In all, 85 melanocytic tumours were investigated: 15 N (3 epidermal, 6 compound and 6 dermal N), 46 primary melanomas and 24 M, including 21 lymph-node and 3 dermal and subcutaneous skin M. The primary tumours were subgrouped into SSM and NM or RGP and VGP melanomas (Table 1, Table 2, Table 3). No hereditary or acral melanomas were studied. Due to limited tissue on the paraffin blocks, not all samples could be analysed with all methods available: 72 tumours were investigated using immunohistochemistry, including 40 tumours additionally investigated for LOH at 12p13. Of tumours, 13 were solely investigated for LOH. All 53 tumours with LOH analysis yielded sufficient DNA for sequencing (for details see Table 1 and Table 3).

Patient data regarding clinical follow-up was available for 26 patients with malignant melanoma (ranging from 12 months to 96 months, mean: 43 months) (Table 1, Table 2, Table 3).

Table 1 Immunoreactive score (IRS) for p27KIP1 and Ki-67 and loss of heterozygosity (LOH) at microsatellite loci surrounding the *p27KIP1/CDKN1B* gene in superficial spreading melanomas (SSM), nodular melanomas (NM) and metastases (M). *RGP* radial growth phase melanomas, *VGP* vertical growth phase melanomas. *Breslow* tumour thickness in millimetres (mean value). *pT* tumour extension according to the latest tumour node metastasis classification [12]. *LTF* lost to follow-up, *NED* no evidence of disease, *AWD* alive with disease, *DOD* dead of disease. *Number in parentheses* number of tumours. IRS for p27KIP1 and Ki-67 is expressed as mean value when multiple tumours are listed. *1 loc* LOH at one microsatellite locus, *>1 loc* LOH at more than one microsatellite locus

Tumour	Breslow	Clark level	pT	Follow-up (months)	p27KIP1	Ki-67	LOH 0 loc	LOH 1 loc	LOH >1 loc
RGP									
SSM 1	0.02	I	Is	NED 60	6.4	4.6	-	1	-
SSM 2–6	0.42	II	1a	LTF (2), NED 12, 18, 72	8.7	8.0	5	-	-
VGP									
SSM 7, 9	1.3	III	1a	LTF	2.2	15.3	1	-	1
SSM 8,10–12; 15, 16	1.5	III	2a	LTF (5), NED 60	4.9	10.9	4	1	1
SSM 13	1.1	III	2b	AWD 24	2.6	17.1	1	-	-
SSM 14	1.6	III	3a	NED 48	6.2	7.9	-	1	-
NM 1	0.77	III	1a	NED 72	4.1	10.1	-	-	
NM 3, 4	2	IV	2a	LTF, AWD 96	6.0	5.3	1	-	1
NM 2, 6, 8	3.3	IV	3a	LTF, DOD 13, 16	5.6	11.2	1	-	2
NM 5, 7	3.4	IV	3b	LTF, DOD 48	1.3	10.0	1	-	1
NM 9–13	5.1	V	4a	LTF (3), AWD 24, DOD 60	3.4	13.7	1	2	2
Metastases									
M 1–11				LTF (3), AWD 16, DOD 13 (2), 48 (2), 60 (3)	3.4	23.9	4	3	4

Table 2 Immunoreactive score (IRS) for p27KIP1 and Ki-67 in naevi (N), superficial spreading melanomas (SSM), nodular melanomas (NM) and metastases (M) without DNA analysis. *RGP* radial growth phase melanomas, *VGP* vertical growth phase melanomas. *Breslow* tumour thickness in millimetres (mean value). *pT* tumour extension according to the latest tumour node metastasis classification [12]. *LTF* lost to follow-up, *NED* no evidence of disease, *AWD* alive with disease, *DOD* dead of disease. *Number in bracelets* number of tumours. IRS for p27KIP1 and Ki-67 is expressed as mean value when multiple tumours are listed

Tumour	pT	Breslow	Clark level	Follow-up (months)	p27KIP1	Ki-67
N 1–15					14.3	1.5
RGP						
SSM 17–19	Is	0.02	I	NED 12, 96, LTF	5.4	11.8
VGP						
SSM 20	1a	0.6	III	LTF	10.8	15.3
NM 14–16	2a	1.5	III	LTF	5.2	6.8
NM 17	3a	3.1	IV	DOD 48	5.0	17.2
NM18	4a	6.5	V	DOD 17	3.6	32.2
Metastases						
M 12–19				LTF, DOD 17 (3), 48, 60 (3)	3.4	18.4

Table 3 Loss of heterozygosity (LOH) at microsatellite loci surrounding the *p27KIP1/CDKN1B* gene in superficial spreading melanomas (SSM), nodular melanomas (NM) and metastases (M) without immunohistochemical analysis. *RGP* radial growth phase melanomas, *VGP* vertical growth phase melanomas. *Breslow* tumour thickness in millimetres (mean value). *pT* tumour extension according to the latest tumor node metastasis classification [12]. *LTF* lost to follow-up, *NED* no evidence of disease, *AWD* alive with disease, *DOD* dead of disease. *Number in bracelets* number of tumours. *1 loc* LOH at one microsatellite locus, *>1 loc* LOH at more than one microsatellite locus

Tumour	Breslow	Clark level	pT	Follow-up (month)	LOH 0 loc	LOH 1 loc	LOH >1 loc
RGP							
SSM 22, 23	0.05	I	Is	LTF	2	-	-
SSM 24	1	II	Ia	NED 36	1	-	-
VGP							
NM 20	2	IV	2b	LTF	-	1	-
NM 19, 22, 23	2.5	IV	3a	LTF	1	2	-
NM 21	10	V	4a	LTF	-	1	-
Metastases							
M 20–24				LTF (2), DOD 24 (2), 38	-	1	4

Immunohistochemistry and staining interpretation

Of melanocytic tumours, 72 (15 N, 20 SSM, 18 NM, 19 M) yielded sufficient tissue to carry out immunohistochemistry (Table 1 and Table 3). First, 4-μm serial sections were subjected to heat (30 min in TEC buffer pH 7.8) for p27KIP1 and to heat pressure epitope retrieval for Ki-67 (1.5 min in TEC buffer pH 7.8). Staining was carried out with an automated immunostainer, Ventana NexES (Ventana Medical Systems, Frankfurt/M, Germany), with a DAB (3,3′-diaminobenzidine) detection system (Ventana Medical Systems) using monoclonal antibodies against p27KIP1 (1:20, incubation for 60 min at room temperature; Novocastra, New Castle upon Tyne, UK) and Ki-67 (1:50, incubation for 32 min at room temperature; DakoCytomation, Hamburg, Germany). Controls were carried out by omitting primary antibodies. Nuclear counter-staining was achieved using DAPI (4′, 6-diamidino-2′-phenylindole-dihydrochloride, direct immunofluorescence, wavelength 330 nm) 0.5 μg/ml in citrate buffer pH 6.0. Quantitative evaluation was carried out using a morphometry system consisting of a Zeiss microscope (Axioskop, Jena, Germany), a digital video camera (C4742–95, Hamamatsu, Japan) and a Macintosh computer (Macintosh Power G3, Apple Computer Inc., U.S.A.) using Openlab software (Improvision, Conventry, U.K.). For each marker, at least 300 melanocytes were assessed. The cells showing nuclear signals were expressed as a percentage of the total number of tumour cells, which were stained with DAPI. All samples were evaluated in a blinded fashion by two investigators. When the difference of each immunoreactive score measurement was below 10%, the mean value was used and when above 10%, the measurements were repeated for two times, and the mean values were employed.

DNA isolation from peripheral blood and paraffin-embedded tissue

From 53 melanocytic tumours (19 SSM, 18 NM and 16 M), tumoural and corresponding non-lesional DNA could be isolated by a mechanical micro-dissection as previously described (Table 1 and Table 3) [20, 27]. DNA isolation from paraffin-embedded tissue was done with the High Pure PCR Template Preparation Kit (Roche Molecular Biochemicals, Mannheim, Germany) according to the manufacturer's instructions with proteinase K digestion overnight. DNA isolation from peripheral blood cells was also performed as previously described [20] with the Blood Extraction Kit (Qiagen, Hilden, Germany).

Microsatellite analysis

Of tumours investigated using immunohistochemistry, 40 yielded sufficient DNA for microsatellite analysis (Table 1). For13 tumours, only microsatellite analysis was performed (Table 3).

The following seven microsatellite loci were studied: D12S1615, D12S1088, D12S1652, D12S1626, D12S1664, D12S314 and D12S99 at chromosome 12p, surrounding the *p27KIP1/CDKN1B* gene. The primer sequences were obtained from Genome Data Base (http://gdbwww.gdb.org), and cytogenetic location was obtained from the Sanger Centre Human Chromosome 1 Page (http://www.sanger.ac.uk/chr12). PCR amplification was performed in 12.5-ml sample volumes with 20–30 ng of genomic tumour or normal DNA as template in 15 mM Tris/HCl, 50 mM KCl, with 200 μM dNTPs, 1.5 mM $MgCl_2$, 0.3 nM primers, 5% formamide and 1 Unit HotStart *Taq* Polymerase (Qiagen, Hilden, Germany). An initial denaturation and activation step of 12 min at 95°C was followed by 30–35 cycles

of 1 min at 95°C, 1 min at 55°C and 3 min at 72°C, as well as a 30-min final elongation step at 72°C. PCR products were electrophoresed on denaturing (8 M urea) 10% polyacrylamide gels and visualised using silver staining. The band patterns produced from each normal and tumour tissue pair were visually assessed for allelic imbalances in the tumour DNA. In case of suspected LOH, the PCR of the respective normal/tumour pair at this locus was repeated twice with fluorochrome-labeled primers (6-FAM, HEX or TAMRA) and analysed on an ABI310 genetic analyser (Applied Biosystems, Weiterstadt, Germany) with a ROX-labelled internal lane standard, mostly in multiplex analyses. LOH was determined as described previously [3]. The decrease of one allele varied predominantly between 60% and 95%.

Sequencing analysis of p27KIP1/CDKN1B

All 53 tumours analysed for LOH were additionally submitted to DNA sequencing. For the analysis of both exons of the *p27KIP1/CDKN1B* gene, we used three PCR assays because exon 1 has to be subdivided into two parts due to the investigation of paraffin-embedded material. The following primer sequences were used: exon 1–1: 5′ ACCCGGGAGAAAGATGTCAA and 5′ ACCTCTTGCCACTCGTACTTG; exon 1–2: 5′ AAGTACGAGTGGCAAGAGGTG and 5′ ATTCTATGGTTGGGAAAGGG; exon 2:5′ AAAAATTTCCCCTGCGCT and 5′ TTCCAGTGCGTGCTCCTTTA. In the PCR, 30–50 ng of template DNA were amplified in a 25-µl reaction volume containing 200 µM dNTPs, 1.5 mM $MgCl_2$, 15 mM Tris/HCl, 50 mM KCl, 0.3 nM primers and 1 Unit HotStartTaq (Qiagen, Hilden, Germany) by denaturing at 95°C for 10 min, followed by 30 cycles of 95°C for 30 s, 55°C for 90 s, 72°C for 120 s and an additional 30 min at 72°C with the Trio Thermocycler (Biometra, Göttingen, Germany). Primers were designed using the internet program at http://genome-www2.stanford.edu/cgi-bin/SGD/web-primer.

For the sequencing PCR, the BigDye Ready Reaction Kit (Applied Biosystems, Weiterstadt, Germany) was used with the same primers according to the manufacturer's instructions. PCR conditions were: 25 cycles at 95°C for 30 s, 60°C for 4 min. The PCR products were sequenced with the ABI 310 DNA sequencer (Applied Biosystems). Each polymorphism or mutation was verified by a second sequencing reaction of an independent amplification product.

Statistical analysis

Statistical evaluation was performed using the statistical software package BMDP/Dynamic release 7.0 (BMDP Statistical Software Inc, Los Angeles, CA, USA). For description of data, two-dimensional frequency tables were formed (BMDP4F). Here, the cases were grouped as N, primary tumours and M. The primary tumours were sub-grouped as SSM and NM, respectively, in RGP and VGP. The differences between groups concerning the expression of p27KIP1 and Ki-67 were assessed by one-way analysis of variance (ANOVA) (BMDP7D). All variables were logarithmically transformed before the analysis because their statistical distributions were skewed to the right. The differences between groups concerning the occurrence of microsatellite LOH surrounding *p27KIP1/CDN1B* locus were assessed by the exact Kruskal-Wallis-test and the exact Wilcoxon-Mann-Whitney test, respectively, because the variables were discrete. For the exact tests, the software TESTIMATE was used (Idv-Datenanalyse und Versuchsplanung, Munich, Germany). The correlation between markers to each other and between each marker and Breslow index was evaluated by correlation analysis (BMDP6D). The Spearman-rank correlation coefficient was used for assessing the correlation between each marker and pT level, respectively, and Clark level, as well for assessing the correlation between microsatellite LOH surrounding the *p27K1P1/CDN1B* locus and Breslow index, pT level, Clark level and p27KIP1, respectively (BMDP3S). The analysis of the follow-up was done by the Mantel-Cox test (BMDP1L) or by the Cox-regression in the presence of covariates (BMDP2L), respectively.

Results

Microsatellite analysis

From 53 melanocytic tumours (19 SSM, 18 NM and 16 M), seven microsatellite loci surrounding the *p27KIP1/CDKN1B* gene could be amplified using PCR (Table 1 and Table 3). Due to lack of space and for better survey, the data concerning single microsatellite loci are not listed in the tables, but are available from the authors on request. A total of 371 microsatellite loci were studied; 21 were non informative, and, in 8, no confident result could be obtained. LOH was not shown in 15 SSM, 5NM and 3M at any locus investigated. Tumours with LOH at more than one locus were mostly NM (7/18) (Fig. 1) and M (9/16) and only one SSM (Table 1 and Table 3). The most frequent deleted region was D12S1088, demonstrating LOH in nine tumours (2 SSM, 2 NM, 5 M). Deletions at D12S1664 and D12S99 were exclusively detected in NM and M, while deletions of all other loci

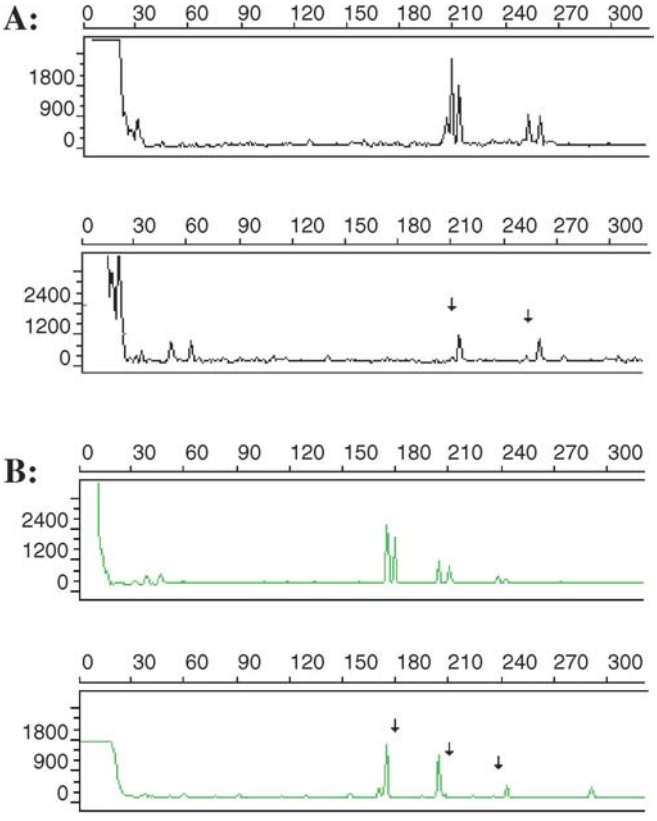


Fig. 1 Electropherograms of five investigated loci with the *y axis* representing the peak height in fluorescence units (normal tissue *above*, tumour tissue *below*). **A** Loss of heterozygosity (LOH) at D12S99 and D12S314 in a nodular melanoma. The *arrows* mark the lost alleles. **B** LOH at D12S1626, D12S1615 and D12S1664 (in this order) in a nodular melanoma. The *arrows* mark the lost alleles

were distributed over all tumours. LOH at loci surrounding *p27KIP1/CDKN1B* gene significantly increased in VGP compared with RGP melanomas (P=0.018) and when compared with the SSM, NM and M (Kruskal-Wallis-analysis, P<0.001). There was a significant correlation between LOH at microsatellite loci surrounding *p27KIP1/CDKN1B* gene and pT level (r_s=0.38, P=0.018) (Fig. 2C), Clark level (r_s=0.28, P=0.0009) and Breslow index (r_s=0.32, P=0.01).

Sequencing analysis of p27KIP/CDKN1B gene

One common polymorphism in exon 1 (G326T) and two heterozygous mutations in two different tumours could be detected: A68G in SSM9 resulted in an amino acid change (histidine to glutamine), and C93T in M20 was silent.

Immunohistochemistry

In all samples where p27KIP1 was immunohistochemically detected in the nuclei of melanocytes or keratinocytes, a cytoplasmic reaction was not evident. Single melanocytes in the basal epidermis presented a nuclear stain for p27KIP1. In the epidermis, p27KIP1 was present in apical keratinocytes (Fig. 3A, B, C).

p27KIP1 was positive in 6.2–30.1% of the cells in N (mean:14.3%, SD: 6.34%), in 1.2–20.3% of the cells in primaries (mean: 5.2%, SD: 3.5%) and in 1.2–8.4% of the cells in M (mean: 3.4%, SD: 2.04%) (Fig. 2A and Fig. 3A, B, C, D). The proliferation marker Ki-67 was present in 0.5–4.5% of the cells in N (mean 1.5%, SD: 1%), in 3.5–32.2% of the cells in primaries (mean: 11.3%, SD: 6.55%) and in 6.9–42.8% of the cells in M (mean: 21.6%, SD: 12.43%) (Fig. 2C and Fig. 3A, B, C, D).

The expression of p27KIP1 significantly decreased, whereas that of Ki-67 significantly increased from N over primary melanomas to M (one way ANOVA, both P<0.001). No significant difference concerning any marker was stated when comparing RGP with VGP melanomas or SSM with NM. p27KIP1 significantly decreased with increasing pT levels (r_s= −0.32, P=0.045) and Clark levels (r_s= −0.36, P=0.026) (Fig. 2A), whereas the variation of Ki-67 showed no correlation with pT and Clark levels.

The survival time after diagnosis inversely correlated with the expression of Ki-67 (P=0.0019), with the pT level (P=0.0076), Breslow index (P=0.033) and Clark

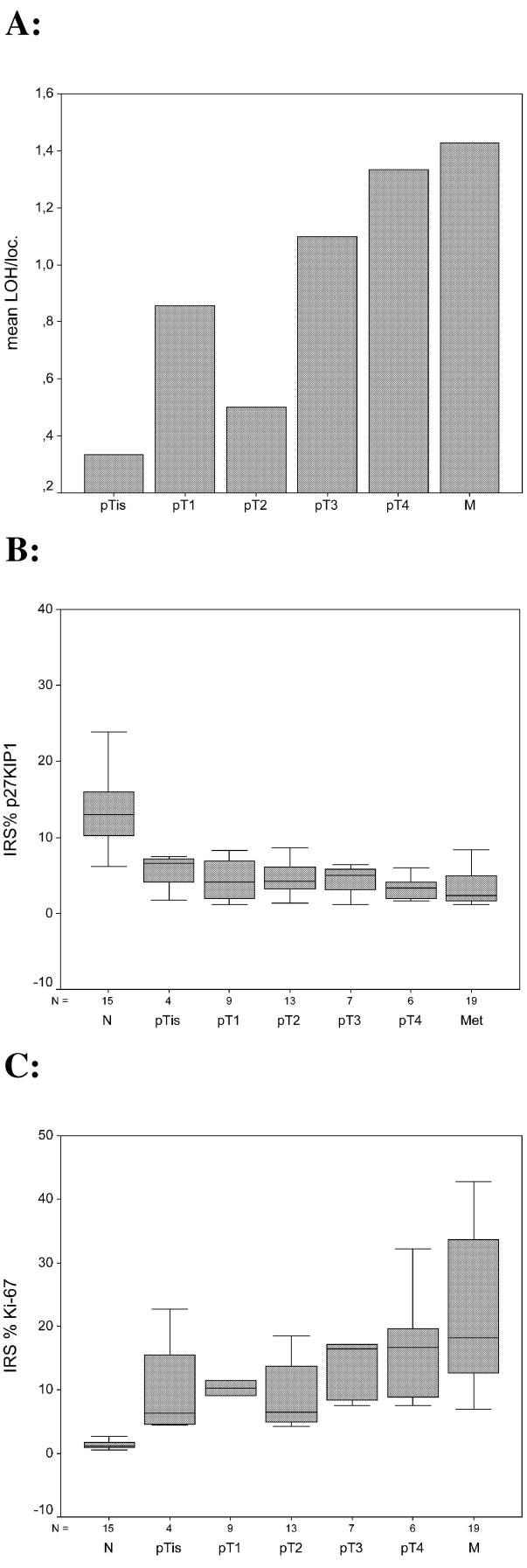


Fig. 2 Loss of heterozygosity (LOH) at different microsatellite loci surrounding the *p27KIP1/CDKN1B* gene (**A**). Quantitative analysis of p27KIP1 and Ki-67 expression in naevi (N), malignant melanomas and metastases (**B** and **C**). Primary melanomas are grouped according to the pT level (*x-axis*). Quantity of samples (*N*). **A** Frequency of LOH at different microsatellite loci (*y-axis*) in relation to primary melanomas (grouped according to the pT level) and metastases (*M*). Immunoreactivity is given as percentage of stained tumour cells (*y-axis*). Quantitative expression of p27KIP1 (**B**) and of Ki-67 (**C**)

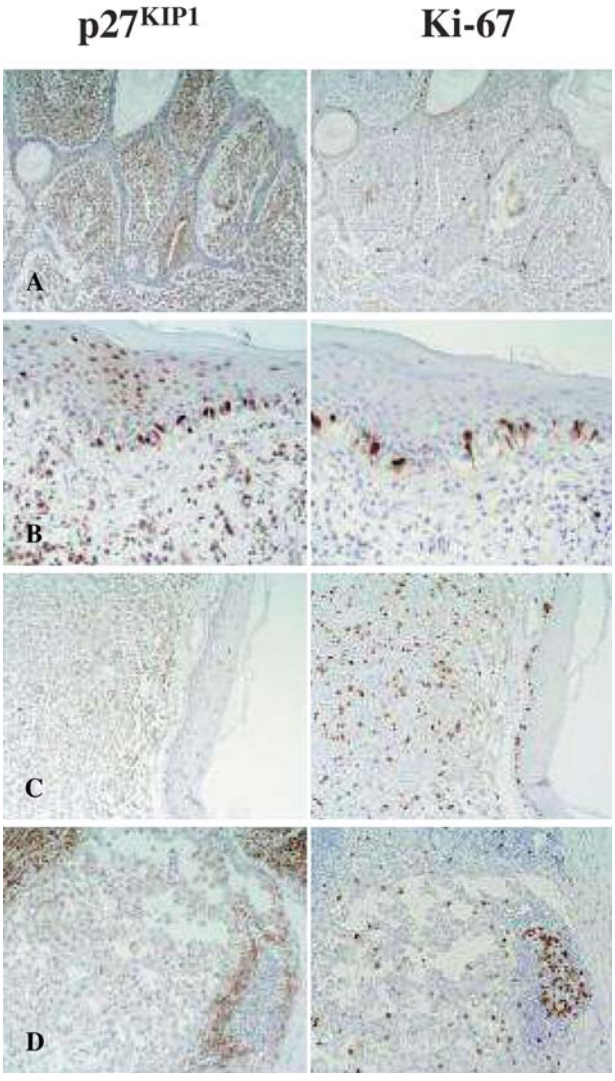


Fig. 3 Immunohistochemistry for p27KIP1 and Ki-67 in a naevus, melanomas and a lymph-node metastasis. Counter-staining with haematoxylin instead of 4′, 6-diamidino-2′-phenylindole-dihydrochloride, direct immunofluorescence. From the left to the right: immunohistochemical expression of p27KIP1 and Ki-67: dermal naevus (**A**), superficial spreading melanoma in situ (**B**), nodular melanoma (**C**) and lymph-node metastasis of malignant melanoma (**D**). Note positive staining for p27KIP1 in apical keratinocytes (**A**, **B** and **C**)

level (P=0.0048). The histogenetic subtypes of melanoma (SSM versus NM versus M) and, to a lesser extent, the tumour growth (RGP versus VGP) influenced the survival time (P=0.0035, respectively P=0.07).

Discussion

In this study, LOH at 12p13 significantly correlated with all parameters of tumour progression; however, only two heterozygous mutations were found in the *p27KIP1/CDKN1B* gene. p27KIP1 expression declined in melanomas compared with N, and the p27KIP1 decrease correlated with increasing pT and Clark levels.

Haploinsufficiency (inactivation of one allele without alteration of the remaining allele) of *p27KIP1/CDKN1B* has been previously reported in human cancers such as acute myeloid leukaemia, acute lymphoblastic leukaemia, ovarian and prostate cancer. However, only rare somatic mutations affecting *p27/CDKN1B* are described and seem to be restricted to a small percentage of haematological malignancies [18]. Our results concerning the status of *p27KIP1/CDKN1B* in melanomas are similar to those found in other solid tumours. In melanoma, *p27KIP1/CDKN1B* does not follow the trait of a classical tumour-suppressor gene—inactivation of both alleles through LOH and/or somatic mutations in the remaining allele [13]. Even though clinical outcome did not correlate to a decrease of p27KIP1 protein or LOH at 12p13, we found a strong association between the occurrence of LOH and markers of tumour progression (Clark and pT levels, Breslow index). This is in agreement with previous results in prostate cancer [11] and may reflect (1) the implication of the *p27KIP1/CDKN1B* gene as a haploinsufficient tumour suppressor in melanoma or (2) the existence of other tumour suppressors with significance in melanoma situated in this region.

Concerning the first hypothesis, animal experiments have shown that loss of one *p27KIP1/CDKN1B* gene copy made mice more susceptible to tumorigenesis induced by DNA-damaging agents than wild-type animals [18]. Fur-thermore, quantitative immunoblotting revealed an approximately 50% decrease of p27KIP1 protein in certain organs of these mice, indicating that hemizygosity could contribute to a reduced p27KIP1 level [7]. These data suggest that, in some malignancies, loss of a single *p27KIP1/CDKN1B* allele may exert a latent tumour-triggering effect. Haploinsufficiency of *p27KIP1/CDKN1B* may, in fact, be more favourable for tumorigenesis than a total inactivation of the gene, as shown in mouse mammary epithelium. The expression of the Erb2 oncogene in $p27^{+/-}$ mouse mammary epithelium induced more aggressive breast tumours than in $p27^{-/-}$ genotypes [15]. This may be explained by the complex role played by p27KIP1 in the cell cycle: inhibiting the activity of cyclin E/A-CDK2 and, at the same time, facilitating the assembly of D-type cyclins with CDK4/6 [23]. It is possible that elevated p27KIP1 expression restrains the cell cycle by inhibiting cyclinE/A-CDK2; whereas, low p27KIP1 levels could still lead to cyclinD-CDK4/6 assembly and G1 progression under mitogenic stimulation, but might be insufficient to inhibit the succeeding cell-cycle kinases.

The fact that we could not find a correlation between the occurrence of LOH affecting the 12p13 locus and p27KIP1 protein decrease in melanomas supports the second hypothesis, although p27KIP1 protein expression significantly diminished from N over primary melanomas to M and negatively correlated to progression markers such as Clark and pT levels. This does not exclude that LOH at 12p13 contributes to the observed p27KIP1 protein decrease, since protein expression is regulated at

different cellular levels, but could also indicate the existence of other tumour suppressors with significance in melanoma situated in the same region as *p27KIP1/CDKN1B*. Possible candidates could be *ETV6/TEL*, a member of the ets-like transcription factor and possible tumour suppressor gene in leukaemias [17] and solid tumours [26], *LRP6*, a member of the LDL receptor [25], and *BCL-G*, a pro-apoptotic gene [8].

The reduction of p27KIP1 protein expression in melanoma could also be due to post-transcriptional down-regulation. p27KIP1 could be cleaved by caspases [6], since the expression of activated caspases has been demonstrated in melanomas and was associated with tumour progression [27]. Promoter methylation might be an additional mechanism causing reduced p27KIP1 expression. Although in lymphoid malignancies promoter methylation could cause loss of p27KIP1 protein [16], it is not of relevance in prostate carcinoma [12] and was present in melanoma at a very low frequency [28]. In vitro and in vivo experiments showed a reduction of p27KIP1 protein by increased proteasomal degradation through Skp2 (S-phase kinase-associated protein 2)-mediated ubiquitination [2]. Additionally, other mechanisms contributing to p27KIP1 degradation independent of Skp2 have been described recently [9].

In conclusion, this work sustains the implication of p27KIP1 protein in melanoma progression and extends previous studies by demonstrating that an increase of LOH surrounding the *p27KIP1/CDKN1B* gene significantly contributes to tumour progression in melanoma.

Acknowledgements We thank S. Seefeldt and M. Maschke (Institute of Forensic Medicine), A. Wolter, S. Uffmann, C. Mueller and M. Richter (Institute of Pathology) for their excellent technical assistance.

References

1. Bales ES, Dietrich C, Bandyopadhyay D, Schwahn DJ, Xu W, Didenko V, Leiss P, Conrad N, Pereira-Smith O, Orengo I, Medrano EE (1999) High levels of expression of p27KIP1 and cyclin E in invasive primary malignant melanomas. J Invest Dermatol 113:1039–1046
2. Bloom J, Pagano M (2003) Deregulated degradation of the cdk inhibitor p27 and malignant transformation. Semin Cancer Biol 13:41–47
3. Canzian F, Salovaara R, Hemminki A, Kristo P, Chadwick RB, Aaltonen LA, de la Chapelle A (1996) Semiautomated assessment of loss of heterozygosity and replication error in tumors. Cancer Res 56:3331–3337
4. D'Agnano I, Valentini A, Fornari C, Bucci B, Starace G, Felsani A, Citro G (2001) Myc down-regulation induces apoptosis in M14 melanoma cells by increasing p27(kip1) levels. Oncogene 20:2814–2825
5. Elder DE, Murphy GF (1991) Melanocytic tumors of the skin. 3rd series edn. Armed Forces Institute of Pathology, Washington DC
6. Eymin B, Sordet O, Droin N, Munsch B, Haugg M, Van de Craen M, Vandenabeele P, Solary E (1999) Caspase-induced proteolysis of the cyclin-dependent kinase inhibitor p27Kip1 mediates its anti-apoptotic activity. Oncogene 18:4839–4847
7. Fero ML, Randel E, Gurley KE, Roberts JM, Kemp CJ (1998) The murine gene p27Kip1 is haplo-insufficient for tumour suppression. Nature 396:177–180
8. Guo B, Godzik A, Reed JC (2001) Bcl-G, a novel pro-apoptotic member of the Bcl-2 family. J Biol Chem 276:2780–2785
9. Hara T, Kamura T, Nakayama K, Oshikawa K, Hatakeyama S (2001) Degradation of p27(Kip1) at the G(0)-G(1) transition mediated by a Skp2-independent ubiquitination pathway. J Biol Chem 276:48937–48943
10. Henriet P, Zhong ZD, Brooks PC, Weinberg KI, DeClerck YA (2000) Contact with fibrillar collagen inhibits melanoma cell proliferation by up-regulating p27KIP1. Proc Natl Acad Sci U S A 97:10026–10031
11. Kibel AS, Faith DA, Bova GS, Isaacs WB (2000) Loss of heterozygosity at 12P12–13 in primary and metastatic prostate adenocarcinoma. J Urol 164:192–196
12. Kibel AS, Christopher M, Faith DA, Bova GS, Goodfellow PJ, Isaacs WB (2001) Methylation and mutational analysis of p27(kip1) in prostate carcinoma. Prostate 48:248–253
13. Knudson AG Jr (1991) Mutation and cancer: statistical study of retinoblastoma. Proc Natl Acad Sci U S A 68:820–823
14. Morgan MB, Cowper SE (1999) Expression of p-27 (kip1) in nevi and melanomas. Am J Dermatopathol 21:121–124
15. Muraoka RS, Lenferink AE, Law B, Hamilton E, Brantley DM, Roebuck LR, Arteaga, CL (2002) ErbB2/Neu-induced, cyclin D1-dependent transformation is accelerated in p27-haploinsufficient mammary epithelial cells but impaired in p27-null cells. Mol Cell Biol 22:2204–2219
16. Nakatsuka S, Liu A, Yao M, Takakuwa T, Tomita Y, Hoshida Y, Nishiu M, Aozasa, K (2003) Methylation of promoter region in p27 gene plays a role in the development of lymphoid malignancies. Int J Oncol 22:561–568
17. Patel N, Goff LK, Clark T, Ford AM, Foot N, Lillington D, Hing S, Pritchard-Jones K, Jones LK, Saha V (2003) Expression profile of wild-type ETV6 in childhood acute leukaemia. Br J Haematol 122:94–98
18. Philipp-Staheli J, Payne SR, Kemp CJ (2001) p27(Kip1): regulation and function of a haploinsufficient tumor suppressor and its misregulation in cancer. Exp Cell Res 264:148–168
19. Poetsch M, Woenckhaus C, Dittberner T, Pambor M, Lorenz G, Herrmann FH (1998) Differences in chromosomal aberrations between nodular and superficial spreading malignant melanoma detected by interphase cytogenetics. Lab Invest 78:883–888
20. Poetsch M, Dittberner T, Woenckhaus C (2001) PTEN/MMAC1 in malignant melanoma and its importance for tumor progression. Cancer Genet Cytogenet 125:21–26
21. Sauroja I, Smeds J, Vlaykova T, Kumar R, Talve L, Hahka-Kemppinen M, Punnonen K, Jansen CT, Hemminki K, Pyrhonen S (2000) Analysis of G(1)/S checkpoint regulators in metastatic melanoma. Genes Chromosomes Cancer 28:404–414
22. Sherr CJ (1996) Cancer cell cycles. Science 274:1672–1677
23. Sherr CJ, Roberts JM (1999) CDK inhibitors: positive and negative regulators of G1-phase progression. Genes Dev 13: 1501–1512
24. Sobin LH, Wittekind C (2002) TNM classification of malignant tumours, 6th edn. John Wiley & Sons Ltd., New York
25. Tamai K, Semenov M, Kato Y, Spokony R, Liu C, Katsuyama Y, Hess F, Saint-Jeannet JP, He X (2000) LDL-receptor-related proteins in Wnt signal transduction. Nature 407:530–535
26. Wang L, Hiebert SW (2001) TEL contacts multiple co-repressors and specifically associates with histone deacetylase-3. Oncogene 20:3716–3725
27. Woenckhaus C, Giebel J, Failing K, Fenic I, Dittberner T, Poetsch M (2003) Expression of AP-2alpha, c-kit, and cleaved caspase-6 and -3 in naevi and malignant melanomas of the skin. A possible role for caspases in melanoma progression? J Pathol 201:278–287
28. Worm J, Bartkova J, Kirkin AF, Straten P, Zeuthen J, Bartek J, Guldberg P (2000) Aberrant p27Kip1 promoter methylation in malignant melanoma. Oncogene 19:5111–5115
29. Zhang H, Schneider J, Rosdahl I (2002) Expression of p16, p27, p53, p73 and Nup88 proteins in matched primary and metastatic melanoma cells. Int J Oncol 21:43–48

Virchows Arch (2004) 445:498–505
DOI 10.1007/s00428-004-1040-2

ORIGINAL ARTICLE

Domenico Corradi · Sergio Callegari · Stefano Benussi · Simona Nascimbene · Paolo Pastori · Simone Calvi · Roberta Maestri · Ettore Astorri · Carlo Pappone · Ottavio Alfieri

Regional left atrial interstitial remodeling in patients with chronic atrial fibrillation undergoing mitral-valve surgery

Received: 22 January 2004 / Accepted: 23 April 2004 / Published online: 19 June 2004
© Springer-Verlag 2004

Abstract Ablation of the left atrial free wall around the pulmonary vein ostia (LAFW) may be effective in the treatment of chronic atrial fibrillation associated with mitral disease (CAF-MVD). Using light and conventional electron microscopy analyses, we wanted to evaluate, in CAF-MVD, the interstitial remodeling in the LAFW as well as in a more remote region, such as the left atrial appendage (LAA). LAFW and LAA samples were obtained from 33 CAF-MVD patients during combined mitral surgery and radiofrequency ablation and from 16 autoptic controls. Interstitial fibrosis (IF) and perivascular fibrosis (PF), capillary densities and the maximal oxygen diffusion distance were morphometrically determined. In CAF-MVD patients, the LAFW, compared with the LAA, showed a higher percentage of IF (7.16±3.23% versus 2.51±1.40%, respectively), a lower myocardial capillary density per mm^2 (830±106 versus 989±173) and an increased oxygen maximal diffusion distance (19.70± 1.27 μm versus 18.13±1.58 μm). All these values were also significantly different than controls. No differences were found in evaluating PF. At variance with the LAA, in CAF-MVD patients, the LAFW around the pulmonary vein ostia is a region characterized by a marked interstitial remodeling such that it may be morphologically indicated as an appropriate target for ablation treatment aimed at sinus rhythm restoration.

Keywords Atrial fibrillation · Fibrosis · Capillaries · Remodeling · Ablation

D. Corradi (✉) · R. Maestri
Department of Pathology and Laboratory Medicine,
Pathology Section, University of Parma,
Via Gramsci 14, 43100 Parma, Italy
e-mail: dcorrad8@unipr.it
Tel.: +39-0521-702011
Fax: +39-0521-292710

S. Callegari · P. Pastori
Division of Cardiology,
Fidenza Hospital,
Fidenza (Parma), Italy

S. Benussi · S. Nascimbene · S. Calvi · O. Alfieri
Cardiothoracic Surgery Unit, Department of Cardiology,
San Raffaele University Hospital,
Milan, Italy

E. Astorri
Department of Clinical Sciences,
University of Parma,
Parma, Italy

C. Pappone
Clinical Cardiac Electrophysiology and Pacing Unit,
Department of Cardiology,
San Raffaele University Hospital,
Milan, Italy

Introduction

Atrial fibrillation (AF), the most common sustained cardiac arrhythmia, is characterized by simultaneous reentrant wavelets with loss of organized atrial depolarization and efficient atrial contraction [1]. Its incidence increases with age and with associated structural heart diseases [16]. In fact, about 50% of patients undergoing mitral-valve surgery have chronic atrial fibrillation (CAF) [8]. However, the likelihood of sinus rhythm recovery after a conventional mitral-valve operation in the presence of CAF is less than 10% [15].

Ablation is a successful technique for restoring sinus rhythm in patients with chronic atrial fibrillation and structural heart disease. This approach is based on the assumption that without a large myocardial mass in which to operate, re-entrant circuits sufficient in number to perpetuate AF are unable to coexist [24]. Therefore, by causing lines of muscular tissue destruction, the purpose of this procedure is to reduce the myocardial atrial mass into areas electrically isolated from each other and too small to sustain AF. The swift development of several ablation methods using different energy sources to create lesions in different atrial locations, with or without left atrial appendage (LAA) exclusion, increased interest in the anatomic substrate that favors the onset and mainte-

nance of the AF. Recent studies indicate that ablation of limited left atrial areas may be effective in the treatment of CAF associated with mitral-valve disease (CAF-MVD) [5, 9, 11, 21, 28]. In particular, the left atrial free wall near the pulmonary vein ostia (LAFW) seems to be a critical area for the maintenance of AF in patients with mitral-valve disease [28].

The aim of this study was to verify whether, in patients with CAF-MVD, this high-risk arrhythmogenic zone, located near the pulmonary veins, develops greater myocardial interstitial damage than a more remote left atrial area, such as the LAA.

Materials and methods

A total number of 49 cases was studied. LAFW and LAA were sampled from 33 patients with CAF during combined mitral-valve surgery and radiofrequency ablation at the Cardiothoracic Surgery Unit of the S. Raffaele Hospital, Milan, Italy, and from 16 control autopsies performed at the Department of Pathology and Laboratory Medicine of the University of Parma, Parma, Italy. All specimens were collected during the period between February 2003 and June 2003.

CAF-MVD patients

In conformity with clinical, echocardiographical [29] and Doppler criteria [22], 33 CAF-MVD patients were separated into three groups: 9 with mitral-valve stenosis (CAF-MVS), 13 with mitral-valve insufficiency (CAF-MVI) and 11 with mitral-valve steno-insufficiency (CAF-MVSI).

All patients underwent radiofrequency ablation and mitral-valve repair surgery as previously described in detail by Benussi et al. [5, 6]. Briefly, two encircling lesions around the ostia of the pulmonary veins were carried out epicardially, using a temperature-controlled multipolar radiofrequency catheter (Therma Line, Boston Scientific). After a conventional left atriotomy, the treatment was completed, with two ablative endocardial lesions connecting the two encirclings between them and connecting to the mitral-valve annulus. Subsequently, mitral-valve repair or replacement was performed, and the LAA was sutured.

The subjects enrolled in the present study signed an informed written consent to the procedure in accordance with a protocol approved by the Institutional Human Research Committee and the principles outlined in the Declaration of Helsinki.

Control patients

All the autopsies were performed within 24 h after death, in accordance with ongoing Italian laws. The criteria for exclusion [23] from the control group were: medical record of any type of arrhythmia, atherosclerosis of the major coronary arteries with greater than 30% of reduction of the lumen, valvular abnormalities, acute or healed myocardial infarction, heart hypertrophy (>400 g for women and >450 g for men), neoplasms with metastasis, multiple myocardial focuses of the replacement fibrosis with a diameter greater than 2 mm, inflammatory cells in the myocardial interstitium, amyloidosis, sarcoidosis, chronic inflammatory processes of the respiratory system and connective tissue disorders.

Tissue sampling for morphological and morphometric evaluations

Two left atrial samples were taken from each pathological and control heart: a strip of LAFW myocardium (adjacent to the atriotomy in the CAF-MVD patients) between the interatrial groove and the orifices of the left pulmonary veins and a portion of the LAA. The LAFW and LAA fragments measured 5×10 mm. After the excision, these specimens were fixed in 10% buffered formalin solution for 24–48 h and embedded in paraffin. Tissue blocks were sectioned at a thickness of 5 μm and stained with hematoxylin-eosin and Van Gieson method for the collagen. Additional 5-μm histological sections were stained with Picosirius Red (43665, Direct Red 80, Fluka, Buchs, CH) [26]. The Picosirius Red-stained sections were observed using a polarization light microscope to highlight the birefringence of the collagen fibers and, on the basis of the color, the type of collagen.

Immunohistochemical methods

Immunohistochemical staining of the endothelial cells was performed on 5-μm-thick paraffin-embedded sections using an anti-CD31 primary antibody (M0823, 1:20; Dako, Glostrup, Denmark). Briefly, sections were dewaxed in xylene, rehydrated through graded alcohols and xylene, and, after quenching of endogenous peroxidase with a 3% H_2O_2 water solution, the specimens were incubated with a protein block (Ready to Use Dako Biotin Blocking System, Carpenteria, CA). Slides were then incubated with the primary antibody for 30 min. The reaction was revealed using, in order, the streptavidin-HRP Dako LSAB2 System, (K0675, Dako, Carpenteria, CA) and a 0.25% solution of 3–3′-diaminobenzidine tetrahydrochloride. Finally, histological sections were counterstained with Mayer hematoxylin, mounted and coverslipped.

Ultrastructural examination

Ultrastructural examination was conducted in ten pathological and five control LAPW and LAA. A small myocardial fragment (2×1 mm) was cut out from the samples for the light microscopy analysis and immediately fixed in a mixture of 4% paraformaldehyde and 5% glutaraldehyde in 0.1 M phosphate buffer (pH 7.3) for 3 h at room temperature, post-fixed in 1% osmium tetroxide, dehydrated and embedded in araldite. A 1-μm section was stained with methylene blue and safranin. Thin sections of selected fields were collected on a 300-mesh copper grid and, after staining with uranyl acetate and lead citrate, were qualitatively examined under a transmission electron microscope (Philips, EM 208S, Eindhoven, NL).

Morphometric analysis

The percentages of myocardium occupied by myocytes and normal interstitium and replaced by interstitial fibrosis (IF) and perivascular fibrosis (PF) were evaluated using a light microscope (Olympus BX 51, Tokyo, Japan) with an ocular reticule containing 42 sampling points (No. 105844, Wild Heerbrugg Instruments, Inc.). Morphometric sampling was performed at a magnification of ×400 in Van Gieson method-stained histological sections and consisted of counting the fraction of ocular reticule points overlying the myocytes, the normal interstitium and the interstitial and perivascular sclerotic tissue (red color) [20]. Microscopic fields from the LAA (n=35) and from the LAPW (n=35) of each heart were measured.

Morphometric evaluation of the capillary density was performed on CD31-labeled tissue sections of 11 controls and 15 pathological atria. For each sample, 20 different histological images were taken, using a digital photocamera (Olympus DP11, Tokyo, Japan) at a magnification of ×400 and in fields in which cardiac muscle fibers and capillaries were transversely sectioned.

The capillary density (CD) per mm^2 of myocardium was calculated by counting the number of transverse capillary sections (Nc) in the picture field area. Each image consisted of a square

tissue area equal to 34,630 μm^2, measured using the Image-Pro Plus, 4.5 software (Media Cybernetics, Silver Spring, MD).

$$CD = Nc/0.03463$$

The capillary density per myocyte area (*CDm*) was obtained by relating the number of transverse capillary sections to the myocyte-cell tissue fraction (*m*%).

$$CDm = (CD \cdot 100)/m\%$$

The tissue cylinder radius (R_t), related to the maximal oxygen diffusion distance from the center of the capillary, was finally calculated using the Krogh's formula [17].

$$R_t = \sqrt{1/(\pi \times CD)}$$

Statistical analysis

Data are expressed as mean±standard deviation. A normal distribution of the morphometric values was verified using the Kolmogorov-Smirnov test, and the differences among groups were assessed with a one-way analysis of variance and Student's *t* test for paired and unpaired data. Linear regression analysis between morphometric results and patient population and control data was carried out using the Pearson correlation coefficient. All tests were performed using SPSS version 10.0 software (SPDD Inc., Chicago, IL). *P* values less than 0.05 were considered as statistically significant.

Results

CAF-MVD patients

The patients enrolled in the study included 33 with CAF (9 males and 24 females), who were scheduled for mitral-valve surgery. They were characterized by 9 CAF-MVS (5 severe mitral stenosis and 4 severe mitral stenosis associated with mild mitral regurgitation), 13 CAF-MVI (severe mitral regurgitation) and 11 CAF-MVSI (5 severe mitral stenosis associated with moderate or severe mitral regurgitation, 6 moderate mitral stenosis associated with severe mitral regurgitation). Patient characteristics and main echocardiographical data are detailed in Table 1. Patients' ages and body surface areas were not statistically different among the three groups, and they were comparable with the controls. Of the patients, 23 (69.7%) had an underlying rheumatic disease and 10 (30.1%) had a degenerative mitral-valve disease.

Before heart surgery, 3 patients were in the New York Heart Association class I, 19 in class II and 11 in class III. CAF duration ranged from 6 months to 120 months (mean 30±27 months in the CAF-MVS, 53±41 months in the CAF-MVSI and 57±50 months in the CAF-MVI).

Control patients

Control heart samples were collected from 16 autopsies: 7 males and 9 females. Ages varied from 40 years to 83 years, averaging 61±15 years; body surface areas ranged from 1.58 m^2 to 1.86 m^2 and averaged 1.71±0.16 m^2. Inclusion criteria in the control group were based on clinical, autoptical and histological data. Death in control patients was a consequence of cerebral hemorrhage (five cases), traumatic injury (four cases), septic shock (two cases), abdominal hemorrhage with hypovolemic shock (three cases), ketoacidosic coma (one case) and acute pyogenic meningitis (one case). Heart weight averaged 388±41 g. The macroscopic and histological examination of the other organs excluded all the pathologies listed in the exclusion criteria.

Quantitative and qualitative fibrosis analysis

IF and PF percentages are detailed in Table 2. In pathological atria, the percentage of IF was significantly higher in LAFW samples than in the LAA (8.52±4.32 versus 3.03±1.71, respectively, $P<0.005$ in patients with CAF-MVS; 6.75±2.95 versus 2.21±1.68, $P<0.0005$ in CAF-MVSI and 6.57±2.50 versus 2.42±0.83, $P<0.0001$ in CAF-MVI). No differences were found among the three groups of patients. In addition, all pathological LAWF and LAA showed a conspicuous increase of IF compared with cor-

Table 1 Patient characteristics and echocardiographic data. *CAF* chronic atrial fibrillation, *CAF-MVS* CAF with mitral-valve stenosis, *CAF-MVI* CAF with mitral-valve insufficiency, *CAF-MVS* CAF with mitral-valve steno-insufficiency, *CAF-MVD* CAF with mitral-valve disease, *LVEDD* left ventricle end–diastolic diameter, *LVESD* left ventricle end–systolic diameter, *LVEF* left ventricle ejection fraction, *LA-SID* left atrial superior–inferior dimension, *LA-MLD* left atrial medial–lateral dimension, *LAA-NW* left atrial appendage neck width, *LAA* left atrial appendage, *PAPs* pulmonary artery systolic pressure. Data are expressed as mean±standard deviation; range values are shown in parentheses

	CAF-MVS (*n*=9)	CAF-MVSI (*n*=11)	CAF-MVI (*n*=13)	Total CAF-MVD (*n*=33)
Age (years)	57±6 (45–64)	59±12 (34–75)	61±7 (50–72)	59±9 (34–75)
Sex, (male–female)	1–8	0–11	8–5	9–24
Body-surface area (m^2)	1.70±0.15 (1.50–1.97)	1.62±0.15 (1.35–1.85)	1.78±0.18 (1.50–2.00)	1.70±0.17 (1.35–2.00)
CAF duration (months)	30±27 (6–84)	53±41 (6–120)	57±50 (4–120)	48±42 (6–120)
LVEDD (mm)	50±2 (47–53)	52±3 (47–58)	60±5 (50–70)	55±6 (47–70)
LVESD (mm)	34±5 (28–42)	34±6 (21–46)	38±8 (26–49)	36±7 (21–49)
LVEF (%)	58±7 (40–62)	59±7 (42–65)	57±8 (40–65)	58±7 (40–65)
LA-SID (mm)	71±9 (60–83)	60±14 (52–77)	63±9 (51–75)	66±10 (51–83)
LA-MLD (mm)	61±9 (46–72)	57±6 (53–59)	64±10 (53–82)	62±9 (46–82)
LAA-NW (mm)	22±2 (18–24)	25±4 (22–31)	24±5 (18–32)	23±4 (18–32)
LAA length (mm)	33±5 (26–40)	38±5 (34–44)	43±8 (30–50)	38±7 (26–50)
PAPs (mmHg)	48±12 (35–70)	49±10 (33–70)	46±15 (30–70)	48±12 (30–70)

Table 2 Myocardial fibrosis. Data are expressed as mean±standard deviation; range values are shown in parenthesis. *LAFW* left atrial free wall around the pulmonary vein ostia, *LAA* left atrial appendage, *CAF* chronic atrial fibrillation, *CAF-MVS* CAF with mitral-valve stenosis, *CAF-MVI* CAF with mitral-valve insufficiency, *CAF-MVS* CAF with mitral-valve steno-insufficiency, *CAF-MVD* CAF with mitral-valve disease

	CAF-MVS (n=9)		CAF-MVSI (n=11)		CAF-MVI (n=13)		Total CAF-MVD (n=33)		Controls (n=16)	
	LAA	LAFW	LAA	LAFW	LAA	LAFW	LAA	LAFW	LAA	LAFW
Interstitial Fibrosis (%)	3.03±1.71§ (0.64–6.53)	8.52±4.32*¶ (3.66–14.69)	2.21±1.68‡ (0.11–6.18)	6.75±2.95*# (3.19–12.40)	2.42±0.83† (1.12–3.88)	6.57±2.50†‖ (2.33–10.62)	2.51±1.40* (0.11–6.53)	7.16±3.23†‖ (2.33–14.69)	0.74±0.68 (0.00–2.32)	1.23±0.75 (0.35–2.75)
Perivascular Fibrosis (%)	0.13±0.19 (0.00–0.60)	0.21±0.17 (0.00–0.48)	0.27±0.22 (0.00–0.55)	0.37±0.21 (0.08–0.74)	0.23±0.26 (0.00–0.80)	0.29±0.24 (0.00–0.81)	0.26±0.28 (0.00–1.00)	0.32±0.25 (0.00–0.97)	0.33±0.35 (0.00–1.00)	0.37±0.30 (0.08–0.97)

Statistical results. Pathological atria values compared with those of corresponding controls:
†=P<0.0001
*=P<0.001
§=P<0.005
‡=P<0.05
LAFW values compared with those of LAA of the same group:
‖=P<0.0001
#=P<0.0005
¶=P<0.005

Fig. 1 Photomicrographs from a patient with chronic atrial fibrillation associated with mitral disease. Histological appearance of the myocardial interstitial fibrosis (IF) (*arrows*) and the perivascular fibrosis (*arrowheads*) in the left atrial free wall around the pulmonary vein ostia (LAFW) (*panel A*) and left atrial appendage (LAA) (*panel B*). The LAFW shows a more intense IF than the correspondent LAA. Van Gieson stain. Bar is 100 μm, ×10

responding controls. In the control left atria, the percentage of IF was similar in the LAFW and the LAA (1.23±0.75 versus 0.74±0.68, respectively, P=n.s.). In pathological hearts, independently from groups, the LAFW and LAA IF percentages showed a statistically significant correlation (Pearson coefficient r=0.4, P<0.01).

No significant differences resulted from the comparison of the PF among the three pathological groups and the controls. Furthermore, no correlations were found between patients' age and CAF duration when related to the percentages of IF and PF and to the echocardiographical measurements.

All histological samples were examined using hematoxylin and eosin staining to confirm the sample preservation and the Van Gieson method for collagen to reveal IF and PF (Fig. 1). Interstitial focuses of fibrosis sur-

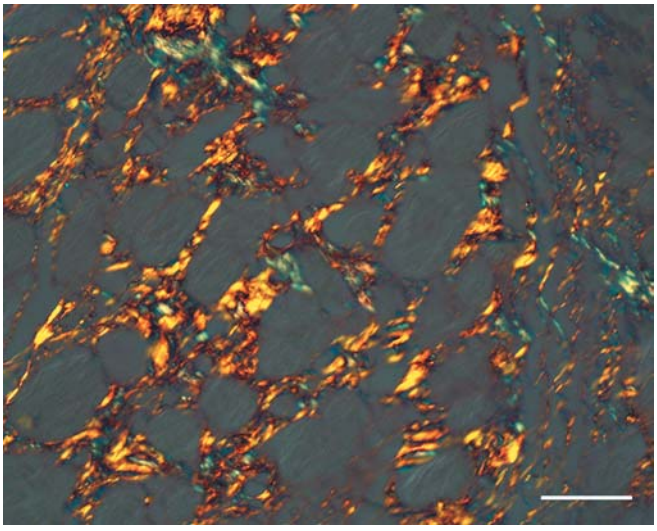


Fig. 2 Left atrial free wall around the pulmonary vein ostia histological appearance in a patient with chronic atrial fibrillation associated with mitral disease. The atrial myocytes are diffusely surrounded by a marked collagen network (orange stain). Picosirius Red stain, observed by polarization light microscopy. Bar is 30 μm, ×40

rounded the myocytes in a fine network that often distorted the architecture of the tissue. Some samples, in which the IF was more evident, also showed a conspicuous thickening of the subendocardial soft tissues. Furthermore, polarization light microscopy on Picosirius Red-stained sections suggested the presence, as orange color, of type-I collagen in the interstitial, perivascular or subendocardial sclerotic tissue (Fig. 2).

At discharge, 29 patients (87.9%) were in stable sinus rhythm, while in 4 (12.1%, 1 with mitral-valve stenosis and 3 with mitral-valve insufficiency), AF recurred. These 4 patients showed an LAFW IF far greater than the average value of their group: 14.69% with respect to an average of 8.52% in the CAF-MVS; 8.20%, 10.62% and 9.88% with respect to an average of 6.57% in the CAF-MVI. In addition, 2 of these CAF-MVI subjects showed a percentage of LAA IF more extensive than the average value of its group (3.02% and 3.56% with respect to an average of 2.42%).

Quantitative capillary network analysis

Endothelial cells were immunohistochemically revealed using an anti-CD31 primary antibody (Fig. 3). Quantitative capillary network analysis was performed in 11 controls and in 15 pathological left atria (3 with CAF-MVS, 4 with CAF-MVI and 8 with CAF-MVSI) and without separation into groups. Control atria showed a higher capillary density and a more regular microvascular architecture than the pathological hearts.

Capillary network characteristics expressed as myocardial capillary density, capillary density related to the myocyte area and the maximal oxygen diffusion distance

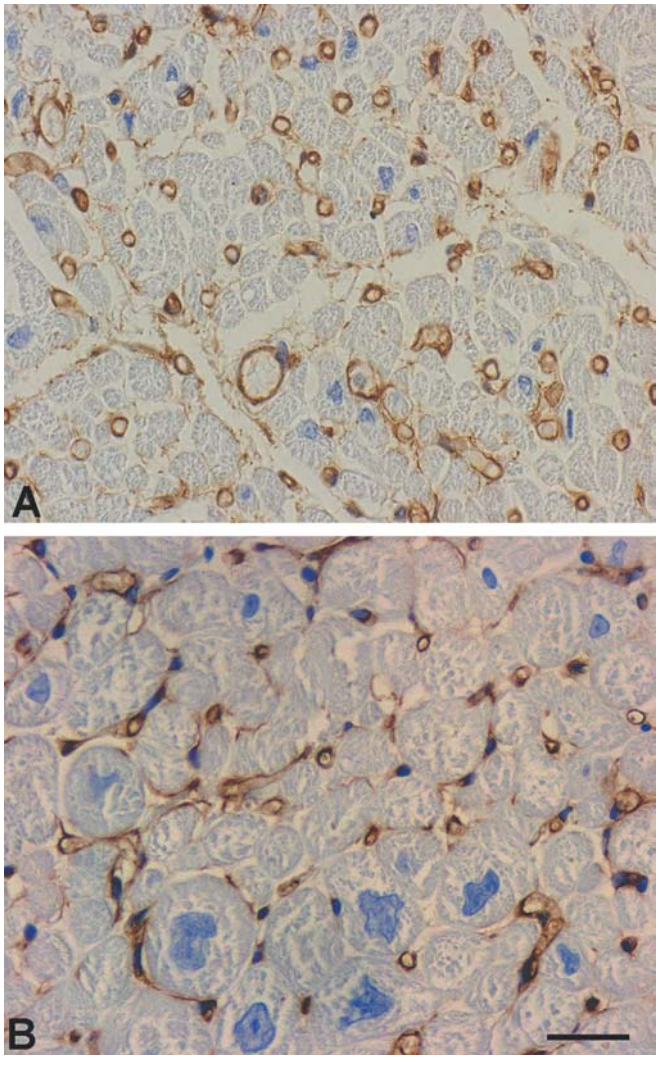


Fig. 3 Photomicrographs from left atrial free wall around the pulmonary vein ostia. Immunohistochemical staining (*brown color*) for CD31 endothelial antigen in a control (*panel A*) and in a patient with chronic atrial fibrillation associated with mitral disease (*panel B*) showing a significantly lower capillary density in the pathological subject. Counterstained with Mayer hematoxylin. Bar is 30 μm, ×40

[17, 19] (Krogh's tissue cylinder radius, R_t) are listed in Table 3. CAF-MVD atria showed a significant reduction of the myocardial capillary density (−29.0%, $P<0.0001$ in the LAA and −39.8%, $P<0.0001$ in the LAFW) and of the capillary density corrected for the myocyte area (−32.3%, $P<0.0001$ in the LAA and −40.9%, $P<0.0001$ in the LAFW), compared with controls. In parallel, the maximal oxygen diffusion distance increased in pathological atria (+15.9%, $P<0.0001$ in the LAA and +22.7%, $P<0.0001$ in the LAFW). In pathological LAFW, the myocardial capillary density and the oxygen maximal diffusion distance were statistically different when compared with the LAA (−16.1%, $P<0.05$ and +8.0%, $P<0.05$ respectively, in the LAFW). In control atria, no differences were found between LAA and LAFW capillary network parameters.

Table 3 Myocardial capillary network. Data are expressed as mean±standard deviation; range values are shown in parenthesis. *LAFW* left atrial free wall around the pulmonary vein ostia. *LAA* left atrial appendage, *CAF-MVD* chronic atrial fibrillation with mitral-valve disease

	Total CAF-MVD (n=15)		Controls (n=11)	
	LAA	LAFW	LAA	LAFW
Capillary density (no./mm^2 of myocardium)	989±173* (736–1291)	830±106*† (670–1020)	1392±107 (1215–1522)	1379±57 (1276–1459)
Capillary density per myocyte area (no./mm^2 of myocytes)	1052±179* (785–1383)	951±123* (8788–1201)	1554±140 (1329–1707)	1609±89 (1474–1714)
Maximal O_2 diffusion distance (μm)	18.13±1.58* (15.71–20.80)	19.70±1.27*† (17.67–21.81)	15.16±0.60 (14.47–16.19)	15.21±0.32 (14.78–15.80)

*P<0.0001 compared with corresponding control
†P<0.05 compared with CAF-MVD LAA

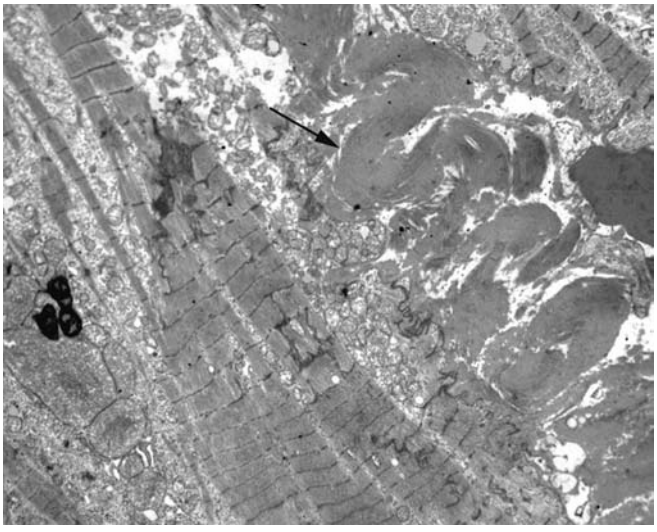


Fig. 4 Ultrastructural appearance of the left atrial free wall around the pulmonary vein ostia interstitial fibrosis in a patient with chronic atrial fibrillation associated with mitral disease. Bands of collagen (*arrow*) between two myocytes. Original magnification ×2800

Ultrastructural examination

The myocardial collagen deposition and the distortion of the intercellular space of the CAF-MVD specimens were confirmed using ultrastructural analysis. Among myocytes showing characteristics of cellular dedifferentiation [2], bands of collagen enlarged the interstitial spaces, thus modifying the normal myocardial architecture (Fig. 4). Fibroblasts and adipocytes were found in some IF areas, particularly near the blood vessels. The extent of the interstitial damage was always greater in the LAFW than in the LAA specimens.

Discussion

The present study shows that CAF-MVD patients present several modifications in the atrial interstitium with significant differences between LAFW and LAA. In the LAFW, this remodeling was mainly characterized by a higher degree of IF and a lower capillary density.

The CAF-MVD patients showed, on average, an IF of 7.16% in the LAFW and 2.51% in the LAA (2.85-times greater), without differences among the three pathological groups. No statistical differences for PF were found in examining pathological and control atria.

IF plays a role as a reparative process and can interfere with myocardial electrical activity. In the 1980s, Boyden et al. [7] studied the structure of left atrial enlargement and its effects on electrophysiological properties in dogs with mitral-valve disease. Extensive IF was found in the atria between enlarged myocytes. These atria were highly susceptible to the initiation and perpetuation of atrial arrhythmias, while the resting and action potentials did not differ from the non-enlarged right atrium or in the control atria. In fact, atrial dilation would permit the co-existence of many re-entrant circuits, and structural interstitial remodeling would alter anisotropic properties (leading to slow, zig-zag conduction, unidirectional block) and would also increase the dispersion of refractoriness favoring reentry circuits [2, 18, 27].

Furthermore, in atria with severe IF, sympathetic and parasympathetic fibers may be interrupted, causing regional supersensitivity to catecholamines and acetylcholine and dishomogeneities in refractoriness [14]. Thus, a highly sclerotic region can be a local source for AF.

In our patient population, the recurrence, after radiofrequency treatment, of AF in four subjects with extensive LAFW IF supports the role of the myocardiosclerosis as a structural factor in the pathogenesis of the AF in subjects with MVD. In these patients, a great amount of IF, usually found around the pulmonary vein ostia, could also be present in the atrial myocardium interposed between LAPW and LAA, thereby explaining the ineffectiveness of the ablative approach. In fact, two patients also showed a noteworthy IF in the LAA myocardium.

IF percentages in LAA and LAFW were different and statistically correlated. An explanation of this asymmetric and parallel myocardial injury could be the close anatomical position of the investigated atrial area to the pulmonary vein orifices, a region subjected to an intense stress. Furthermore, the fact that the internal diameter of the left atrium is greater than the LAA diameter [12, 30]—even though the internal left atrial and LAA pressures are similar—determines a higher tension in the atrial free wall than in the LAA (according to Laplace's

law). In addition, considering that the LAFW and the LAA have different embryological origins—the trabecular LAA is the only remnant part of the original embryonic left atrium, while the left atrial smooth wall develops from the outgrowth of the pulmonary veins—we suggest that a different embryological origin of the two areas may contribute to a different reaction to stress factors [25].

Differences in regional distensibility and function exist between the left atrial body and the LAA. The LAA appears more compliant than the remaining left atrium, and it may play a crucial role in maintaining hemodynamic function when filling pressures are elevated [10, 13]. Extracellular matrix remodeling of the left atrium in patients with hemodynamically overloaded and with dilated atria, favors the occurrence and the perpetuation of AF as well as the reduction of left atrial compliance. Therefore, in the light of our results, differences in regional distensibility and function existing between LAFW and LAA may highlight the role of the LAA in maintaining the hemodynamic function in patients with elevated filling pressures.

In our study, we evaluated three microvascular morphological parameters, within the myocardial interstitial remodeling: the myocardial capillary density, the myocardial capillary density related to the myocyte area and the maximal oxygen diffusion distance. These parameters were significantly different than the controls. In the interstitial remodeling, capillary densities and maximal oxygen diffusion distance, not being statistically correlated with the IF and PF percentages, behaved as independent variables. Myocyte hypertrophy, myocyte-cell loss with reparative fibrosis and stretching-induced atrial enlargement could induce a reduction of the capillary density as well as an increase in the maximal oxygen diffusion distance [4] (+15.9% in the LAA and +22.7% in the LAFW). Additionally, the maximal oxygen diffusion distance and the myocardial capillary density were more altered in the LAFW when compared with the LAA in CAF-MVD patients (+8.0% and −16.1%, respectively, in the LAFW). These modifications can expose the myocardium to a higher risk of damage in cases of increased need for oxygen [3, 4]. Thus, we suggest that this smaller capillary network may contribute to sustaining arrhythmogenic focuses.

In conclusion, in patients with CAF-MVD, the interstitial remodeling process is quantitatively different in the LAFW than in LAA. The LAFW myocardium, located near the pulmonary vein ostia, shows a higher percentage of IF and a reduced capillary density. These features could represent an aspect of the anatomic substrate for the CAF in this subset of patients and may actually have some implications regarding the treatment strategy. The kind of interstitial damage occurring in the perivenous LAFW indicates this anatomic area as an appropriate target for ablations aimed at restoring sinus rhythm in patients with CAF-MVD. However, based on the finding that the LAA appears to be more heavily protected in interstitial remodeling, systematic LAA exclusion in patients with AF and mitral-valve disease who are undergoing surgery should be reconsidered.

References

1. Alessie MA (1994) Reentrant mechanisms underlying atrial fibrillation. In: Zipes DP, Jalife J (eds) Cardiac electrophysiology: from cell to bedside. WB Saunders, Philadelphia, pp 562–566
2. Allessie M, Ausma J, Schotten U (2002) Electrical, contractile and structural remodeling during atrial fibrillation. Cardiovasc Res 54:230–246
3. Anversa P, Sonnenblick EH (1990) Ischemic cardiomyopathy: pathophysiologic mechanisms. Prog Cardiovasc Dis 33:49–70
4. Bache RJ (1988) Effects of hypertrophy on the coronary circulation. Prog Cardiovasc Dis 30:403–440
5. Benussi S, Pappone C, Nascimbene S, Oreto G, Caldarola A, Stefano PL, Casati V, Alfieri O (2000) A simple way to treat chronic atrial fibrillation during mitral valve surgery: the epicardial radiofrequency approach. Eur J Cardiothorac Surg 17:524–529
6. Benussi S, Nascimbene S, Agricola E, Calori G, Calvi S, Caldarola A, Oppizzi M, Casati V, Pappone C, Alfieri O (2002) Surgical ablation of atrial fibrillation using the epicardial radiofrequency approach: mid-term results and risk analysis. Ann Thorac Surg 74:1050–1056
7. Boyden PA, Tilley LP, Pham TD, Liu SK, Fenoglic JJ Jr, Wit AL (1982) Effects of left atrial enlargement on atrial transmembrane potentials and structure in dogs with mitral valve fibrosis. Am J Cardiol 49:1896–1908
8. Chua YL, Schaff HV, Orszulak TA, Morris JJ (1994) Outcome of mitral valve repair in patients with preoperative atrial fibrillation. Should the maze procedure be combined with mitral valvuloplasty? J Thorac Cardiovasc Surg 107:408–415
9. Cox JL, Boineau JP, Schuessler RB, Ferguson TB Jr, Cain ME, Lindsay BD, Corr PB, Kater KM, Lappas DG (1991) Successful surgical treatment of atrial fibrillation. Review and clinical update. JAMA 266:1976–1980
10. Davis CA 3rd, Rembert JC, Greenfield JC Jr (1990) Compliance of left atrium with and without left atrium appendage. Am J Physiol 259:1006–1008
11. Gaita F, Gallotti R, Calo L, Manasse E, Riccardi R, Garberoglio L, Nicolini F, Scaglione M, Di Donna P, Caponi D, Franciosi G (2000) Limited posterior left atrial cryoablation in patients with chronic atrial fibrillation undergoing valvular heart surgery. J Am Coll Cardiol 36:159–166
12. Ho SY, Sanchez-Quintana D, Cabrera JA, Anderson RH (1999) Anatomy of the left atrium: implications for radiofrequency ablation of atrial fibrillation. J Cardiovasc Electrophysiol 10:1525–1533
13. Hoit BD, Walsh RA (1992) Regional atrial distensibility. Am J Physiol 262:1356–1360
14. Inoue H, Zipes DP (1987) Results of sympathetic denervation in the canine heart: supersensitivity that may be arrhythmogenic. Circulation 75:877–887
15. Jessurun ER, van Hemel NM, Kelder JC, Elbers S, de la Rivi AB, Defauw JJ, Ernst JM (2000) Mitral valve surgery and atrial fibrillation: is atrial fibrillation surgery also needed? Eur J Cardiothorac Surg 17:530–537
16. Kannel WB, Abbott RD, Savage DD, McNamara PM (1982) Epidemiologic features of chronic atrial fibrillation: the Framingham study. N Engl J Med 306:1018–1022
17. Krogh A (1919) The number and distribution of capillaries in muscles with calculation of the oxygen pressure head necessary for supplying the tissue. J Physiol (London) 52:409–415
18. Li D, Fareh S, Leung TK, Nattel S (1999) Promotion of atrial fibrillation by heart failure in dogs: atrial remodeling of a different sort. Circulation 100:87–95
19. Londraville RL, Sidell BD (1990) Maximal diffusion-distance within skeletal muscle can be estimated from mitochondrial distributions. Respir Physiol 81:291–301
20. Loud AV, Anversa P (1984) Morphometric analysis of biologic processes. Lab Invest 50:250–261
21. Melo J, Adragao P, Neves J, Ferreira M, Timoteo A, Santiago T, Ribeiras R, Canada M (2000) Endocardial and epicardial

radiofrequency ablation in the treatment of atrial fibrillation with a new intra-operative device. Eur J Cardiothorac Surg 18:182–186
22. Nichol PM, Gilbert BW, Kisslo JA (1977) Two-dimensional echocardiographic assessment of mitral stenosis. Circulation 55:120–128
23. Olivetti G, Giordano G, Corradi D, Melissari M, Lagrasta C, Gambert SR, Anversa P (1995) Gender differences and aging: effects on the human heart. J Am Coll Cardiol 26:1068–1079
24. Pappone C, Oreto G, Lamberti F, Vicedomini G, Loricchio ML, Shpun S, Rillo M, Calabrò MP, Conversano A, Ben-Haim SA, Cappato R, Chierchia S (1999) Catheter ablation of paroxysmal atrial fibrillation using a 3D mapping system. Circulation 100:1203–1208
25. Sadler TW (1990) Cardiovascular system. In: Langman J (ed) Langman's medical embryology. Williams and Wilkins, Baltimore, pp 179–227
26. Sampson SP, Badalamente MA, Hurst LC, Seidman J (1991) Pathobiology of the human A1 pulley in trigger finger. J Hand Surg 16:714–721
27. Spach MS, Dolber PC (1986) Relating extracellular potentials and their derivatives to anisotropic propagation at a microscopic level in human cardiac muscle. Evidence for electrical uncoupling of side-to-side fiber connections with increasing age. Circ Res 58:356–371
28. Sueda T, Nagata H, Shikata H, Orihashi K, Morita S, Sueshiro M, Okada K, Matsuura Y (1996) Simple left atrial procedure for chronic atrial fibrillation associated with mitral valve disease. Ann Thorac Surg 62:1796–1800
29. Thomas L, Foster E, Hoffman JI, Schiller NB (1999) The mitral regurgitation index: an echocardiographic guide to severity. J Am Coll Cardiol 33:2016–2022
30. Veinot JP, Harrity PJ, Gentile F, Khandheria BK, Bailey KR, Eickholt JT, Seward JB, Tajik AJ, Edwards WD (1997) Anatomy of the normal left atrial appendage: a quantitative study of age-related changes in 500 autopsy hearts: implications for echocardiographic examination. Circulation 96:3112–3115

Virchows Arch (2004) 445:506–514
DOI 10.1007/s00428-004-1096-z

ORIGINAL ARTICLE

Yan-Chin Tai · Jin-Ai Mary Anne Tan · Suat-Cheng Peh

18q21 Rearrangement and trisomy 3 in extranodal B-cell lymphomas: a study using a fluorescent in situ hybridisation technique

Received: 18 April 2004 / Accepted: 6 July 2004 / Published online: 9 September 2004
© Springer-Verlag 2004

Abstract t(11;18)(q21;q21) Translocation and trisomy 3 are the most common chromosomal aberrations reported in low-grade mucosa-associated lymphoid tissue (MALT) lymphoma. The current study aims to investigate the frequency of these chromosomal aberrations in a series of 52 extranodal B-cell lymphomas. The tumours were categorised into three histological grades: grade 1 (low-grade lymphoma of MALT type), grade 2 [diffuse large B-cell lymphoma (DLBCL) with MALT component] and grade 3 (DLBCL without MALT component). Fluorescence in situ hybridisation analyses on paraffin tissue sections were performed using a locus-specific probe for the 18q21 region and a centromeric probe for chromosome 3. The 18q21 rearrangement was detected in 9 of 40 (23%) cases, including 7 of 23 (30%) grade-1 and 2 of 11 (18%) grade-3 tumours. Amplification of the 18q21 region was detected in 10 of 40 (25%) cases, and trisomy 3 was detected in 9 of 34 (26%) cases. Amplification of the 18q21 region may be an important alternative pathogenetic pathway in MALT lymphoma and was found almost exclusively in tumours without 18q21 rearrangement. Our study showed that tumours with 18q21 rearrangement and 18q21 amplification develop along two distinct pathways, and the latter was more likely to transform into high-grade tumours upon acquisition of additional genetic alterations, such as trisomy 3. Trisomy 3 was more frequently found in coexistence with 18q21 abnormalities, suggesting that it was more likely to be a secondary aberration.

Y.-C. Tai · S.-C. Peh (✉)
Department of Pathology,
Faculty of Medicine, University of Malaya,
50603 Kuala Lumpur, Malaysia
e-mail: pehsc@um.edu.my
Tel.: +603-7967-5797
Fax: +603-7955-6845

J.-A. M. A. Tan
Department of Molecular Medicine,
Faculty of Medicine, University of Malaya,
Kuala Lumpur, Malaysia

Keywords 18q21 Rearrangement · 18q21 Amplification · Trisomy 3 · MALT lymphoma

Introduction

Genetic instability, in general, reflects defects in the cellular processes that maintain the integrity of the genome, either as nucleotide sequence alteration, gross chromosomal number alteration, chromosomal translocation or gene amplification [22]. Gastric lymphomas carry more genetic aberrations than other subtypes of non-Hodgkin's lymphoma (NHL), and studies have found that chromosomal translocation and alteration in chromosome number represent important pathogenetic pathways in gastric lymphomas [8, 42, 43]. Chromosomal translocation involving the *API2* gene on chromosome 11q21 and *MALT1* gene on chromosome 18q21 is the most common recurrent genetic aberration in extranodal marginal zone B-cell lymphoma of mucosa-associated lymphoid tissue (MALT lymphoma) [3, 12, 28, 33]. The *API2* gene on chromosome 11q21 belongs to the inhibitor of apoptosis family [10], while the function of the *MALT1* gene has yet to be characterised but is postulated to have an anti-apoptotic function reminiscent of BCL-2 protein [27]. The API2-MALT1 fusion protein co-operates with BCL-10 protein in activating the NFκ-B pathway, which is a transcription factor for other cell cycle-related genes [25]. It was shown that tumours carrying t(11;18)(q21;q21) translocation were resistant to *Helicobacter pylori* antibiotic therapy [1, 24, 46] and were also associated with a more advanced stage of the disease [1, 3].

It was reported that the type of trisomy observed in MALT lymphoma differed from extranodal diffuse large B-cell lymphoma (DLBCL) [7, 14, 36, 42, 49] in that MALT lymphomas were associated with higher frequencies of trisomies 3 and 18, whereas trisomy 12 was more common in extranodal DLBCL [42, 49, 51]. The prognosis of the tumours with chromosomal translocation t(11;18)(q21;q21) did not differ from the tumours with alteration in chromosome number [44]. However, co-ex-

istence of these aberrations in a tumour increases the risk of tumour recurrence and high-grade transformation [44]. Alteration in chromosome number may be an alternative pathogenetic mechanism for MALT lymphoma, as it was found almost exclusively in tumours without t(11;18)(q21;q21) translocation [38, 44].

Fluorescence in situ hybridisation (FISH) is an effective method in detecting genetic aberrations in paraffin-embedded tissue sections [6, 35, 37]. FISH circumvented some common problems in conventional cytogenetic analysis, which are attributed to the low proliferation of the tumours in cell culture and lower sensitivity of karyotyping technique [7, 11, 20, 31]. In addition, FISH analysis targeting the 18q21 region is able to detect other translocations involving the *MALT1* gene, such as t(14;18)(q32;q21) [20, 45]. FISH performed on thin tissue sections (<6 μm) requires less material when compared with FISH technique on isolated nuclei (50–150 μm), and it also retains the histological architecture of the tissue [37, 48, 50]. However, nuclear slicing and overlapping can compromise the accuracy of quantification. Hence, it is necessary to incorporate statistical correction in data interpretation [35, 37].

Studies revealed that Bcl-2 protein is frequently expressed in low-grade MALT lymphoma but not in high-grade tumours [2, 29, 30, 47] and the contrary for Bcl-6 protein [21, 32]. The genes encoding these proteins, *bcl-2* and *bcl-6*, are located on 18q21 and *3q27*, respectively, and thus far there has been no report on whether the expressions of these genes are affected by chromosomal translocation t(11;18)(q21;q21) or alteration of number in chromosome 3, which are aberrations detected in extranodal B-cell lymphomas of MALT type.

This study aimed to determine the frequency of aberrations at the 18q21 region and chromosome 3 using FISH technique in a series of extranodal B-cell lymphomas and to correlate the expression pattern of Bcl-2 and Bcl-6 oncoproteins with the pattern of chromosomal aberrations to elucidate whether these chromosomal aberrations may have an effect on the gene expression.

Materials and methods

Histological classification and grading

Formalin-fixed, paraffin-embedded tissues of previously diagnosed extranodal lymphomas were retrieved from the archives for review and reconfirmation by the pathologist (PSC). The relevant clinical information was extracted from the records volunteered by the clinicians. The diagnosis was based on the criteria of the World Health Organisation classification of tumours of haematopoietic and lymphoid tissues [19] in that tumours occurred exclusively at the extranodal sites, and cases with history of nodal B-cell NHL were excluded from the study. The tumours were categorised according to the histological grades proposed by Isaacson [16]: low-grade MALT lymphoma (grade 1), DLBCL with evidence of MALT component (grade 2), and DLBCL without evidence of MALT component (grade 3).

Immunophenotyping

Immunostaining was performed on 4-μm-thick paraffin sections, and the panel of antibodies used are listed in Table 1. The colour was developed using liquid 4'-6'-diamidino-2-phenylindole $(DAB)^+$ substrate-chromogen system (DakoCytomation). The tissues were then lightly counterstained with haematoxylin.

Bcl-2 and Bcl-6 expressions were categorised as absence and presence when the cytoplasmic and nuclear staining in the tumour cells were less than 10% and greater than or equal to 10% respectively [9].

Fluorescence in situ hybridisation

FISH was performed on 3-μm-thick paraffin tissue sections using LSI MALT1 (18q21) dual colour, break-apart rearrangement probe (Vysis Inc., Downers Grove, IL) and the centromeric α-satellite CEP3 (3p11.1 to 3q11.1) SpectrumOrange probe (Vysis Inc.). The LSI MALT1 probe consists of a mixture of a 460-kb DNA probe labelled in SpectrumOrange, which flanks the 5′ side of the *MALT1* gene, and a 660 kb DNA probe labelled with SpectrumGreen, which flanks the 3′ side of the *MALT1* gene, with a 65-kb gap between the two probes. In addition to the study cases, FISH analysis was also performed on reactive lymphoid hyperplasia and chronic gastritis tissues to establish the baseline cut-off value for correction of errors derived from nuclear splicing and overlapping in thin sections. The sections were pre-treated with 0.2 N hydrochloric acid (HCl) (20 min at room temperature), followed by sodium thiocynate (30 min at 80°C) from a Paraffin Pretreatment Reagent Kit (Vysis Inc.). The sections were then microwaved in citrate buffer (pH 6.0) for 10 min. After the slides had cooled down, the sections were treated with protease solution (Vysis Inc.) at 37°C

Table 1 The panel of antibodies against lymphoid markers used in the study and the putative retrieval method and detection system. *Dako* DakoCytomation, Glostrup, Denmark; *Novocastra* Novocastra, New Castle Upon Tyne, UK; *MW CB* microwave in citrate buffer, pH 6.0; *MW EDTA* microwave in ethylenediaminetetraacetate buffer, pH 8.0; *PC EDTA* pressure cook in ethylenediaminetetraacetate buffer, pH 8.0; *PC Tris-EDTA* pressure cook in Tris-ethylenediaminetetraacetate buffer, pH 9.0

Antibody	Clone/source	Retrieval method	Detection system
CD20	L26/Dako	MW CB	ABC
CD3	Polyclonal/Dako	MW CB	ABC
CD5	NCL-5/Novocastra	MW EDTA	EnVision+
CD10	NCL-CD10–270/Novocastra	MW high pH	EnVision+
CD21	1F8/Dako	Trypsin digestion	EnVision+
CD23	NCL-Cd23–1B12/Novocastra	MW CB	EnVision+
CD35	NCL-CD35/Novocastra	MW EDTA	ABC
Bcl-2	124/Dako	MW CB	EnVision+
Bcl-6	PG-B6p/Dako	PC EDTA	StrepABC
CyclinD1	NCL-CYCLIN D1-GM/Novocastra	PC Tris-EDTA	StrepABC

for 30 min. The LSI MALT1 and CEP3 probes were diluted (1:50) in *t*DenHyb-2 (Insitus Biotechnologies, Albuquerque, NM) and *t*DenHyb-1 (Insitus Biotechnologies) solution, respectively, and 10–15 μl of the mixture was applied to each slide. It was evenly dispersed by applying coverslips over the section and was sealed with rubber cement. Co-denaturation was carried out at 83°C for 5 min, followed by hybridisation for 20 h in HYBrite Denaturation/Hybridisation System (Vysis Inc.) at 42°C and 37°C for CEP3 and LSI MALT1 probes, respectively. Post-hybridisation wash with 2×SSC/0.1%NP-40 (Vysis Inc.) was carried out at 72°C for 2 min, followed by 1 min at room temperature. The sections were then counterstained with DAPI II (Vysis Inc.), and then the coverslips were sealed with rubber cement. The slides were stored at −20°C prior to viewing.

FISH signal evaluation

The slides were evaluated using a DMLB fluorescence microscope with an HC PL APO 100× objective (Leica Microsystems, Wetzlar, Germany) and Q-FISH software (Leica Microsystem). The filter cube used for evaluation of spectrum green was a green single bandpass filter (Vysis Inc.) and N2.1 (Leica Microsystems) for spectrum orange. The signal from N2.1 appeared as a red signal. Nuclear signals from at least 200 cells with clearly discernible, non-overlapping nuclei were evaluated. Additional slides were supplemented for small biopsies with less than 200 assessable nuclei per slide, and the case was regarded as uninformative if the supplemented slide also yielded poor signals. Tissues with excessive autofluorescence in the background were considered as uninformative.

According to the manufacturer's quality certificate, for a normal cell that lacks 18q21 rearrangement, two fusion (green/red or yellow) signals will be observed reflecting the two intact copies of *MALT1* alleles. Nuclei with more than two fusion signals were scored for amplification of the 18q21 region. Only those cells with nuclear signals consisting of one fusion, one green and one orange signal were regarded as carrying 18q21 rearrangement. The distance between the green and orange signal must be at least two times the diameter of an individual signal to be considered as a discrete signal [5].

In the interphase and metaphase chromosomes of normal cells, the CEP3 probe may generate two, three or possibly four signals, depending on the cell cycle stage, DNA condensation and relative distances between chromatids. In addition, an elevated number of cells exhibiting three signals may be observed due to the configuration of the CEP3 probe. Therefore, a case was only considered as carrying an aberration when the putative signal was above the cut-off value calculated by statistical analysis.

Statistical analysis

The cut-off value for 18q21 rearrangement and trisomy 3 was mean+3SD, which was established by using the mean percentage, and standard deviation obtained from control tissues as recommended by Ott et al. and Banerjee et al. [4, 34]. The control tissues used for evaluation of the cut-off value for LSI MALT1 probe were ten lymphoid tissues, while nine reactive lymphoid tissues and an additional ten chronic gastritis tissue were used for the evaluation of a CEP3 probe. The cut-off value for the signals for FISH was determined and was verified with receiver operating characteristic (ROC) curve analysis. The association of Bcl-2 and Bcl-6 expressions with chromosomal aberrations were evaluated by χ^2 test (SPSS, Windows).

Results

Histological grading and immunophenotyping

A total of 52 biopsies from 48 patients were studied, where 4 patients had 2 biopsies each. The tumours were presented in the gastrointestinal tract (42/52, 81%), orbit (4/52, 7%), thyroid (2/52, 4%), subconjuctiva mass (1/52, 2%), tongue (1/52, 2%), lung (1/52, 2%) and cheek muscle (1/52, 2%). The sites in the gastrointestinal tract included stomach (32), intestine (3), duodenum (2), colon (2), caecum (2) and rectum (1).

The biopsies comprised of 26 (50%) grade-1, 9 (17%) grade-2, and 15 (29%) grade-3 tumours. Of the biopsies, 2 (4%) could not be graded accurately by histology due to limited amount of tissue present. The tumour cells expressed B-cell associated antigen CD20 but not T-cell-associated antigen CD3. Diagnosis of mantle cell and lymphocytic lymphomas were excluded based on the absence of CD5, cyclinD1 and CD23 expression. Bcl-6 was expressed in 14 of 48 (29%) tumours, of which 2 of 26 (8%) were grade-1, 4 of 8 (50%) grade-2 and 8 of 13 (61%) grade-3 tumours. The association with high-grade tumours was found to be statistically significant (P=0.001). Bcl-2 protein was expressed in 30 of 52 (58%) biopsies, comprised of 21 of 26 (81%) grade-1 tumours, 4 of 9 (44%) grade-2 tumours and 3 of 15 (20%) grade-3 tumours. Bcl-2 expression was significantly associated with grade-1 tumours (P=0.001).

LSI MALT1 dual colour probe analysis

The percentage of cells with two fusion signals in the ten reactive lymphoid hyperplasia tissues (Fig. 1a) ranged from 43.9% to 59.2%, with a mean of 51.5% and standard deviation of 4.5. The range, mean percentage and standard deviation for rearrangement and amplification signals for these reactive lymphoid hyperplasia tissues are presented in Table 2. The cut-off value obtained from ROC curve analysis was most specific (1.000) when the percentage of cells with the signal was greater than or equal to 1.10% and 1.45% for rearrangement and amplification signals, respectively. The cut-off values as determined by mean+3SD were 1.2% for rearrangement signal and 2.4% for amplification signal, respectively, and, hence, were above the cut-off values suggested by the ROC curve analysis.

MALT1 FISH analysis was successful in 40 of 52 (77%) cases, and the remaining 12 (23%) cases (three grade-1, four grade-2, four grade-3 tumours and one tumour that was not graded histologically) failed to yield informative signals (Table 3). Most of the unsuccessful cases were small biopsies that yielded poor signals and contained high levels of background autofluorescence. Rearrangement signal was detected in more than 1.2% of the cells in 9 of 40 (23%) cases, consisting of 7 of 23 (30%) grade-1 (Fig. 1b, c) and 2 of 11 (18%) grade-3 tumours (Fig. 1d). None of the grade-2 tumours showed

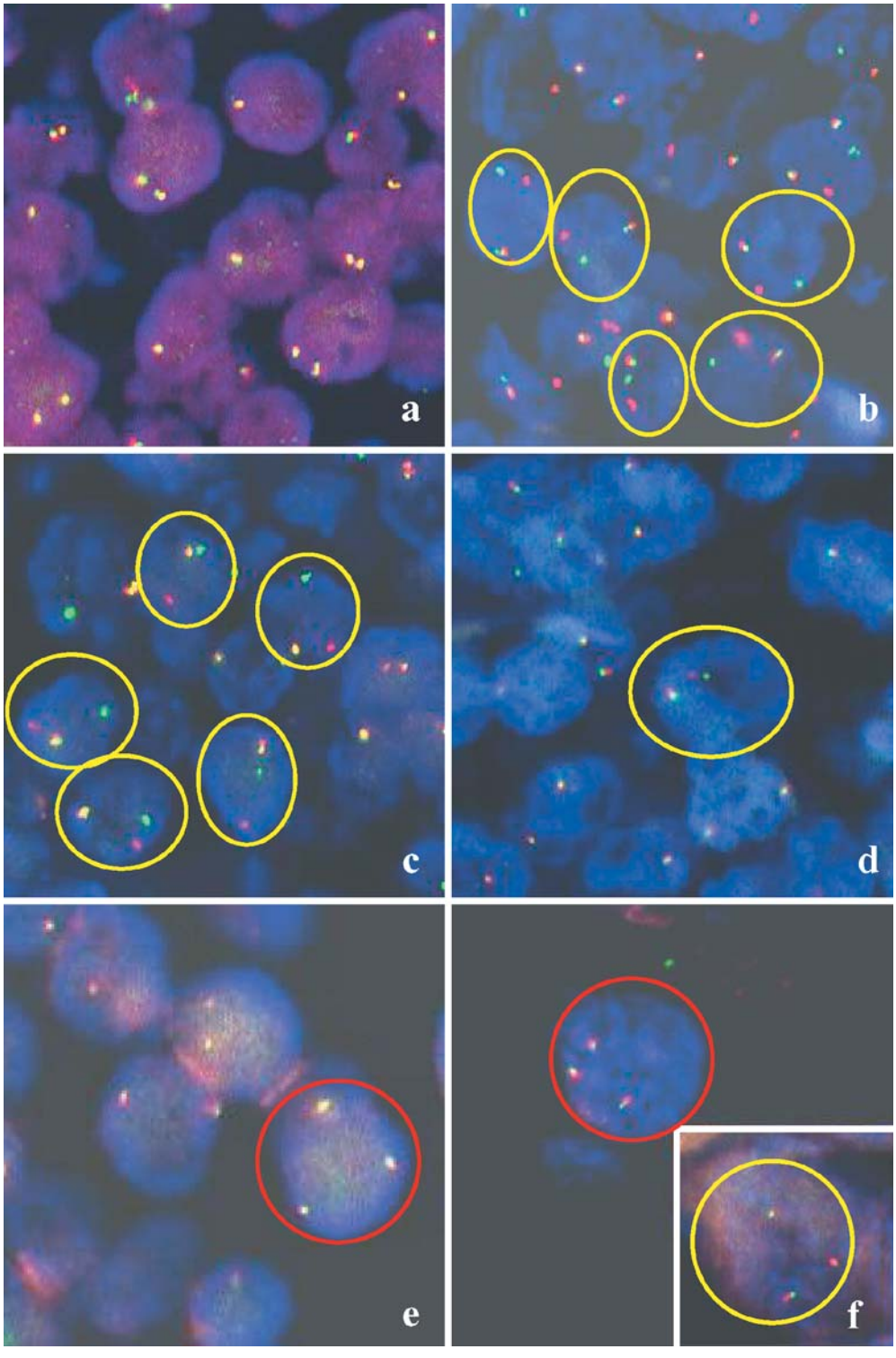


Fig. 1 Fluorescence in situ hybridisation analysis using 18q21 break apart rearrangement probe. The rearrangement and amplification signals are circled in *yellow* and *red*, respectively. **a** A non-neoplastic lymphoid tissue showing two normal alleles and some truncated nuclei showing one normal allele. **b** A gastric low-grade mucosa-associated lymphoid tissue (MALT) lymphoma carrying 18q21 rearrangement. **c** A case of pulmonary low-grade MALT lymphoma carrying 18q21 rearrangement. **d** A case of high-grade diffuse large B-cell lymphoma (DLBCL) with 18q21 rearrangement in minority of the tumour cells. **e** A case of orbital low-grade MALT lymphoma showing 18q21 amplification. **f** A case of high-grade DLBCL carrying 18q21 rearrangement and amplification in two separate clones of tumour cells

rearrangement signals in more than 1.2% of the cells. One of the grade-3 tumours that carried 18q21 rearrangement signal also expressed CD10. Amplification of 18q21 region was detected in 10 of 40 (25%) cases (Fig. 1e), including one grade-3 tumour that carried rearrangement signal (Fig. 1f). This case showed a mix pattern of aberrations, with the majority carrying three copies of 18q21 region (5.4%) and a minor clone carrying 18q21 rearrangement (1.3%). 18q21 rearrangement and 18q21 amplification were not significantly associated with tumour grades (P=0.259). The expression of Bcl-2 protein was not significantly associated with amplification of 18q21 region, where the *bcl-2* gene is located (P=0.194). The occurrence of 18q21 abnormalities was not associated with site of biopsy of the tumours (P=0.210). 18q21 rearrangement was found in biopsies from stomach (6/32,

Table 2 Mean percentage and standard deviation for the signals evaluated on a panel of lymphoid hyperplasia and chronic gastritis tissues for the establishment of cut-off value (mean+3SD) for LSI MALT1 (18q21) and CEP3 probes

	LSI MALT1 18q21		CEP3	
	Rearrangement	Amplification	Monosomy	Trisomy
Range (%)	0.0–0.9	0.0–1.3	25.2–52.4	0.0–10.1
Mean percentage (%)	0.3	0.6	38.6	4.3
Standard deviation	0.3	0.6	7.3	2.7
Cut-off value (%)	1.2	2.4	60.6	12.5

Table 3 Genetic aberrations detected using fluorescence in situ hybridisation (FISH) in a series of extranodal B-cell lymphomas. *NA* not assessable histologically, *NR* not reactive

Case no.	Histological grades	Site of biopsy	Bcl-2	Bcl-6	FISH analysis	
					18q21	Chromosome 3
Case 2	1	Stomach	+	–	Rearrangement	Normal
Case 4	1	Colon	+	–	Normal	Trisomy
Case 8	1	Orbit	+	–	Amplification	Trisomy
Case 9	1	Orbit	+	–	Amplification	Trisomy
Case 11	1	Check mass	+	–	Amplification	Normal
Case 15	1	Stomach	–	–	Rearrangement	Normal
Case 17	1	Stomach	+	–	Rearrangement	Normal
Case 20	1	Duodenum	+	–	Amplification	Normal
Case 21	1	Stomach	+	–	Amplification	Trisomy
Case 23*	1	Stomach	+	–	Rearrangement	Normal
Case 24*	1	Lung	+	–	Rearrangement	Normal
Case 25†	1	Stomach	+	–	Rearrangement	Trisomy
Case 26†	1	Stomach	+	–	Rearrangement	Trisomy
Case 30	2	Stomach	–	+	Normal	Monosomy
Case 36	3	Stomach	–	–	Normal	Trisomy
Case 37	3	Caecum	–	NR	Amplification & rearrangement	Normal
Case 40	3	Intestine	–	–	Rearrangement	Normal
Case 41	3	Duodenum	–	+	Amplification	Normal
Case 42	3	Intestine	–	+	Amplification	Trisomy
Case 45	3	Stomach	–	+	Normal	Trisomy
Case 48	3	Stomach	+	+	Amplification	Normal
Case 52	NA	Stomach	+	–	Amplification	Normal

*Case 23 and case 24 were biopsies from the same patient
†Case 25 and case 26 were biopsies from the same patient

19%), intestine (1/3, 33%), caecum (1/2, 50%) and lung (1/1, 100%). 18q21 amplification was found in biopsies from stomach (3/32, 9%), duodenum (2/2, 100%), intestine (1/3, 33%), orbit (2/4, 50%) and check muscle (1/1, 100%).

CEP3 FISH analysis

The percentage of cells with normal alleles in reactive lymphoid hyperplasia tissues (Fig. 2a) ranged from 51.3% to 62.0%, with a mean of 57.0% and standard deviation of 7.9. The normal alleles in chronic gastritis tissues (Fig. 2b) ranged from 47.6% to 61.2%, with a mean of 54.0% and standard deviation of 5.9. The range, mean percentage and standard deviation for trisomy 3 and monosomy 3 of these control tissues are presented in Table 2. The cut-off value for trisomy 3 and monosomy 3 at mean+3SD were 12.5% and 60.6%, respectively. ROC curve analysis showed that the highest specificity (1.000) was achieved when the cut-off value was greater than or equal to 10.5% and 53.2%, respectively, for trisomy 3 and monosomy 3. Therefore, the cut-off value of 12.5% and 60.6% was stringent for the determination of trisomy 3 and monosomy 3, respectively.

By applying the calculated cut-off value, 24 of 34 (71%) cases did not show trisomy 3 signals in a significant proportion of the cells (Fig. 2c). In the remaining cases, 9 of 34 (26%) showed trisomy, and 1 of 34 (3%) showed monosomy 3 (Table 3). Of the biopsies, 18 (34.6%) were not successful for analysis, as the biopsy materials were mostly small and old blocks, which yielded high autofluorescence, rendering non-informative signals. Of the tumours with trisomy 3, 6 were grade-1 (Fig. 2d) tumours, and the other 3 were grade-3 (Fig. 2e, f) tumours. The presence of trisomy 3 was not significantly associated with histological grades (P=0.133). The only case with monosomy 3 was a grade-2 tumour. There was no significant association between aneuploidy of chromosome 3 and the expression of Bcl-6 protein (P=0.072). Only 2 of 9 (22%) cases that showed trisomy 3 expressed Bcl-6 protein (one of the cases co-expressed CD10), and the only case with monosomy 3 expressed Bcl-6 protein (CD10).

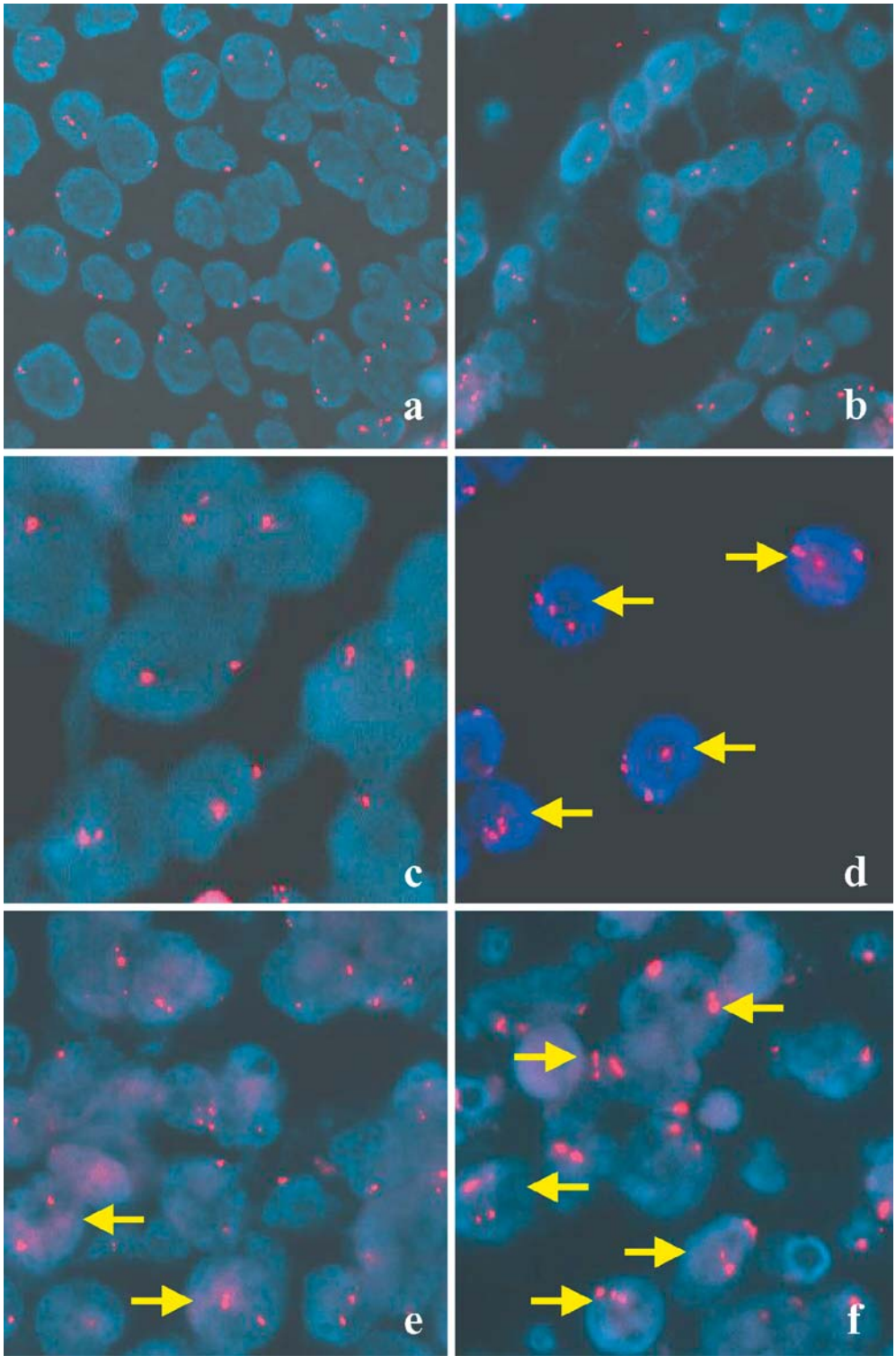


Fig. 2 Fluorescence in situ hybridisation analysis of CEP3 probe and the nuclei with trisomy 3 are indicated with *yellow arrows*. Reactive hyperplastic lymphoid tissue (**a**) and chronic gastritis tissue (**b**) were used for establishing a cut-off value. **c** A grade-2 tumour that carried two chromosome 3. **d** A grade-1 tumour that showed trisomy 3. **e** and **f** Grade-3 tumours that carried trisomy 3

Genetic aberrations by FISH analyses

The overall frequency of chromosomal aberration in this series of extranodal lymphomas was 22 of 40 (55%), which included 9 (23%) with 18q21 rearrangement, 10 (25%) with amplification of 18q21 region and 9 (17.3%) carrying trisomy 3. The results were summarised in Table 3. Rearrangement of the 18q21 region was the sole chromosomal aberration in six of nine (67%) biopsies (five grade-1 and one grade-3 tumours). In the remaining three tumours, two grade-1 tumours (from a single patient) carried additional trisomy 3, and one grade-3 tumour carried additional amplification of 18q21 region. Amplification of the 18q21 region and trisomy 3 was

found exclusively in five of ten (50%) and three of nine (33%) tumours, respectively. Four tumours (three grade-1 and one grade-3 tumours) carried both trisomy 3 and amplification of 18q21 region. Four patients that had two biopsies each showed similar cytogenetic patterns in their tumours. One patient with one biopsy each from the stomach and lung (cases 23 and 24) had 18q21 rearrangement as the sole aberration in both the samples, and another patient with two gastric biopsies (cases 25 and 26) revealed 18q21 rearrangement and trisomy 3 in both these samples. The other biopsies from the remaining two patients did not show aberration of 18q21 region and chromosome 3.

Discussion

A recent study reported the presence of t(14;18)(q32;q21) translocation, which involves translocation of immunoglobulin heavy chain (IGH) gene and MALT1 gene [45]. In contrast to t(11;18)(q21;q21) translocation, which usually appears as the sole genetic alteration in gastric and lung MALT lymphoma [33, 38, 39, 44], tumours with t(14;18)(q32;q32) usually carry other genetic alterations and originate from sites such as liver, ocular adnexa, skin and salivary gland [45]. It is interesting to note that the two grade-1 tumours with 18q21 rearrangement and trisomy 3 both originate from the stomach. However, due to the nature of the FISH probe, we could not ascertain whether the 18q21 rearrangement was t(11;18)(q21;q21) or t(14;18)(q32;q21) translocation. Remstein et al. [38] reported a case of low-grade MALT lymphoma that transformed into large-cell lymphoma with the acquisition of additional trisomy 3. The authors suggested that the presence of t(11;18)(q21;q21) and trisomy 3 may represent a karyotypic progression that could contribute to increased tendency for transformation [38]. It was suggested that subsequent acquisition of trisomy 3 in tumours with t(11;18)(q21;q21) translocation might abrogate the dependency of the tumour cells on growth stimulation from the antigen, thereby conferring the tumour cells the ability to proliferate without the antigenic stimulation [17].

In the current series, two grade-3 tumours had 18q21 rearrangement, in which one also showed 18q21 amplification. t(11;18)(q21;q21) translocation was rarely detected in high-grade tumours [13, 15, 38], and most investigators agree that t(11;18)(q21;q21) translocation does not lead to high-grade transformation [33, 38, 39, 44]. However, there is another suggestion that the low frequency of 18q21 rearrangement in high-grade tumours was thought to be the result of loss of the aberration during high-grade transformation [17, 18, 44]. It is interesting to note that the percentage of tumour cells carrying 18q21 rearrangement in grade-3 tumours was much lower than grade-1 tumours. However, we could not confirm whether this phenomenon was due to the loss of tumours carrying 18q21 rearrangement in the course of high-grade transformation.

Aneuploidy may play a role in lymphomagenesis of extranodal B-cell lymphoma. In the current series, amplification of the 18q21 region was the most common chromosomal aberration, found in 40% and 36% of grade-1 and grade-3 tumours, respectively, and was found almost exclusively in tumours without 18q21 rearrangement. Remstein et al. [38] also reported a similar finding, in that complete and partial trisomy 18 was the most frequent chromosomal abnormality in MALT lymphoma. Therefore, 18q21 amplification may represent an important alternative pathogenetic pathway in MALT lymphoma. Furthermore, a recent study showed that the expression of MALT1 protein can be deregulated by both chromosomal translocation and amplification of the gene [40]. It is interesting to observe that 40% of the tumours with 18q21 amplification in the current series also carried trisomy 3. Previous studies showed that tumours with aneuploidy tend to involve more than one chromosome [38, 44]. Since the same finding was found in grade-1 and grade-3 tumours, it suggests that low-grade tumours with aneuploidy may transform into high-grade tumours upon acquisition of secondary genetic alterations [44]. Our results agree with the proposal that tumours with and without 18q21 rearrangement could develop along two different distinct pathways [38, 41, 44], and tumours with 18q21 rearrangement as the sole genetic alteration were less likely to transform into high-grade tumours [23, 38, 39, 41, 44]. On the other hand, tumours with aneuploidy may develop into high-grade tumours upon acquisition of additional genetic alterations [38, 41].

However, the exact role of chromosomal aneuploidy in the pathogenesis of MALT lymphoma is not well understood. Chromosomal aneuploidy can affect the dosage of the expression of the genes of that particular chromosome, resulting in over-expression of certain oncoproteins. However, the expressions of the two oncogenes, bcl-2 and bcl-6, were not significantly affected by the presence of trisomy 18 and trisomy 3. This may suggest that these oncogenes were not directly involved in the pathogenesis of MALT lymphoma, rather this may only reflect the physiological state of the tumour cells. In cases of human trisomy 21 leading to Down syndrome and trisomy 2 in Arabidopsis, genes that were most severely affected were not located on the trisomic chromosome but rather on normal chromosome [26]. The expression of genes on normal chromosome was modified by the aneuploidy by linking of an unknown chromosomal segment [26].

FISH analysis on paraffin tissue sections had successfully detected genetic aberrations in 55% of the current series of extranodal B-cell lymphomas. The frequency of 18q21 rearrangement in the grade-1 tumours (30%) of the current series was comparable with previous studies. Amplification of 18q21 region may represent an important alternative pathogenetic pathway, as it was the most common genetic aberration detected and was found almost exclusively in tumours without 18q21 rearrangement. This finding concurred with previous study that MALT1 protein could be deregulated by both gene rear-

rangement and amplification. Trisomy 3 was more commonly observed in grade-1 tumours and was often found in coexistence with 18q21 rearrangement or amplification. Although the role of trisomy 3 in the development of MALT lymphoma is not immediately clear, it appears likely to be a secondary aberration. The significance of the coexistence of 18q21 amplification and trisomy 3 in a substantial number of the cases requires further investigation. The current series noted that genetic aberrations associated with grade-1 tumours are also present in grade-3 tumours, which supports the postulation of transformation of low-grade to high-grade tumour. The reason for the lack of these genetic aberrations in grade-2 tumours may be attributed to the small sample size.

Acknowledgements This study was supported by the Ministry of Science, Technology and Environment, Malaysia (IRPA 06–02–03–1014 EA166), and Malaysian Toray Science Foundation (Science and Technology Research Grant). The equipment was purchased under Top-Down Biotechnology 26–02–03-0586.

References

1. Alpen B, Neubauer A, Dierlamm J et al (2000) Translocation t(11;18) absent in early gastric marginal zone B-cell lymphoma of MALT type responding to eradication of *Helicobacter pylori* infection. Blood 95:4014–4015
2. Ashton-Key M, Biddolph SC, Stein H, Gatter KC, Mason DY (1995) Heterogeneity of bcl-2 expression in MALT lymphoma. Histopathology 26:75–78
3. Auer IA, Gascoyne RD, Connors JM, et al (1997) t(11;18)(q21;q21) is the most common translocation in MALT lymphomas. Ann Oncol 8:979–985
4. Banerjee SK, Weston AP, Persons DL, Campbell DR (1997) Non-random loss of chromosome 3 during transition of *Helicobacter pylori*-associated gastric MALT to B-cell MALT lymphoma revealed by fluorescence in situ hybridization. Cancer Lett 121:83–90
5. Blanco R, Lyda M, Davis B, Kraus M, Fenoglio-Preiser C (1999) Trisomy 3 in gastric lymphoma of extranodal marginal zone B-cell (mucosa-associated lymphoid tissue) origin demonstrated by FISH in intact paraffin tissue sections. Hum Pathol 30:706–711
6. Blough RI, Smolarek TA, Ulbright TM, Heerema NA (1997) Bicolor fluorescence in situ hybridizaton on nuclei from formalin-fixed, paraffin-embedded testicular germ cell tumors: comparison with standard metaphase analysis. Cancer Genet Cytogenet 94:79–84
7. Brynes RK, Almaguer PD, Leathery KE et al (1996) Numerical cytogenetic abnormalities of chromosomes 3, 7, and 12 in marginal zone B-cell lymphomas. Mod Pathol 9:995–1000
8. Chong J-M, Fukayama M, Hayashi Y et al (1997) Microsatellite instability and loss of heterozygosity in gastric lymphoma. Lab Invest 77:639–645
9. de Leval L, Harris NL (2003) Variability in immunophenotype in diffuse large B-cell lymphoma and its clinical relevance. Histopathology 43:509–528
10. Deveraux QL, Reed JC (1999) IAP family proteins–suppressors of apoptosis. Genes Dev 13:239–252
11. Dierlamm J, Michaux L, Wlodarska I et al (1996) Trisomy 3 in marginal zone B-cell lymphoma: a study based on cytogenetic analysis and fluorescent in situ hybridization. Br J Haematol 93:242–249
12. Dierlamm J, Baens M, Wlodarska I et al (1999) The apoptosis inhibitor gene API2 and a novel 18q gene, MLT, are recurrently rearranged in the t(11;18)(q21;q21) associated with mucosa-associated lymphoid tissue lymphomas. Blood 93:3601–3609
13. Griffin CA, Zehnbauer BA, Beschorner WE, Ambinder R, Mann R (1992) t(11;18)(q21;q21) is a recurrent chromosome abnormality in small lymphocytic lymphoma. Genes Chromosomes Cancer 4:183–187
14. Hoeve MA, Gisbertz IAM, Schouten HC et al (1999) Gastric low-grade MALT lymphoma, high-grade MALT lymphoma and diffuse large B-cell lymphoma show different frequencies of trisomy. Leukemia 13:799–807
15. Hosaka S, Akamatsu T, Nakamura S et al (1999) Mucosa-associated lymphoid tissue (MALT) lymphoma of the rectum with chromosomal translocation of the t(11;18)(q21;q21) and an additional aberration of trisomy 3. Am J Gastroenterol 94:1951–1954
16. Isaacson PG (1994) Gastrointestinal lymphoma. Hum Pathol 25:1020–1029
17. Isaacson PG (1996) Recent developments in our understanding of gastric lymphomas. Am J Surg Pathol 20:S1–S7
18. Isaacson PG (1999) Gastric MALT lymphoma: from concept to cure. Ann Oncol 10:637–645
19. Jaffe ES, Harris NL, Stein H, Vardiman JW (eds) (2001) World Health Organization classification of tumours: pathology and genetics of tumours of haematopoietic and lymphoid tissues. IARC Press, Lyon
20. Kobayashi Y, Nakata M, Maekawa M et al (2001) Detection of t(11;18) in MALT-type lymphoma with dual-color fluorescence in situ hybridization and reverse transcriptase-polymerase chain reaction analysis. Diagn Mol Pathol 10:207–213
21. Kwon MS, Go JH, Choi JS et al (2003) Critical evaluation of Bcl-6 protein expression in diffuse large B-cell lymphoma of the stomach and small intestine. Am J Surg Pathol 27:790–798
22. Lengauer C, Kinzler KW, Vogelstein B (1998) Genetic instabilities in human cancers. Nature 396:643–649
23. Liu H, Ye H, Dogan A et al (2001) T(11;18)(q21;q21) is associated with advanced mucosa-associated lymphoid tissue lymphoma that expresses nuclear BCL10. Blood 98:1182–1187
24. Liu H, Ye H, Ruskone Fourmestraux A (2002) T(11;18) is a marker for all stage gastric MALT lymphomas that will not respond to *H. pylori* eradication. Gastroenterology 122:1286–1294
25. Lucas PC, Yonezumi M, Inohara N et al (2001) Bcl10 and MALT1, independent targets of chromosomal translocation in MALT lymphoma, cooperate in a novel NF-kappa B signaling pathway. J Biol Chem 276:19012–19019
26. Matzke MA, Mette MF, Kanno T, Matzke AJM (2003) Does the intrinsic instability of aneuploid genomes have a causal role in cancer? Trends Genet 19:253–256
27. Morgan JA, Yin Y, Borowsky AD et al (1999) Breakpoints of the t(11;18)(q21;q21) in mucosa-associated lymphoid tissue (MALT) lymphoma lie within or near the previously undescribed gene *MALT1* in chromosome 18. Cancer Res 59:6205–6213
28. Motegi M, Yonezumi M, Suzuki H et al (2000) API2-MALT1 chimeric transcripts involved in mucosa-associated lymphoid tissue type lymphoma predict heterogeneous products. Am J Pathol 156:807–812
29. Nakamura S, Akazawa K, Kinukawa N, Yao T, Tsuneyoshi M (1996) Inverse correlation between the expression of *bcl*-2 and p53 proteins in primary gastric lymphoma. Hum Pathol 27:225–233
30. Navratil E, Gaulard P, Kanavaros P et al (1995) Expression of the bcl-2 protein in B cell lymphomas arising from mucosa associated lymphoid tissue. J Clin Pathol 48:18–21
31. Nomura K, Yoshino T, Nakamura S et al (2003) Detection of t(11;18)(q21;q21) in marginal zone lymphoma of mucosa-associated lymphocytic tissue type on paraffin-embedded tissue sections by using fluorescence in situ hybridization. Cancer Genet Cytogenet 140:49–54
32. Omonishi K, Yoshino T, Sakuma I, Kobayashi K, Moriyama M, Akagi T (1998) Bcl-6 protein is identified in high-grade but not low-grade mucosa-associated lymphoid tissue lymphomas of the stomach. Mod Pathol 11:181–185

33. Ott G, Katzenberger T, Greiner A et al (1997) The t(11;18)(q21;q21) chromosome translocation is a frequent and specific aberration in low-grade but not high-grade malignant non-Hodgkin's lymphomas of the mucosa-associated lymphoid tissue (MALT-) type. Cancer Res 57:3944–3948
34. Ott G, Kalla J, Steinhoff A, Rosenwald A, Ott MM, Muller-Hermelink HK (1998) Trisomy 3 is not a common feature in malignant lymphomas of mucosa-associated lymphoid tissue type. Am J Pathol 153:689–694
35. Pauletti G, Dandekar S, Rong H et al (2000) Assessment of methods for tissue-based detection of the HER-2/neu alteration in human breast cancer: a direct comparison of fluorescence in situ hybridization and immunohistochemistry. J Clin Oncol 18:3651–3664
36. Peters K, Zetti A, Starostik P et al (2000) Genetic imbalances in primary gastric diffuse large B-cell lymphomas: comparison of comparative genomic hybridization, microsatellite, and cytogenetic analysis. Diagn Mol Pathol 9:58–65
37. Qian J, Bostwick DG, Takahashi S et al (1996) Comparison of fluorescence in situ hybridization analysis of isolated nuclei and routine histological sections from paraffin-embedded prostatic adenocarcinoma specimens. Am J Pathol 149:1193–1199
38. Remstein ED, Kurtin PJ, James CD, Wang X-Y, Meyer RG, Dewald GW (2002) Mucosa-associated lymphoid tissue lymphomas with t(11;18)(q21;q21) and mucosa-associated lymphoid tissue lymphomas with aneuploidy develop along different pathogenetic pathways. Am J Pathol 161:63–71
39. Rosenwald A, Ott G, Stilgenbauer S et al (1999) Exclusive detection of the t(11;18)(q21;q21) in extranodal marginal zone B cell lymphomas (MZBL) of MALT type in contrast to other MZBL and extranodal large B cell lymphomas. Am J Pathol 155:1817–1821
40. Sanchez-Izquierdo D, Buchonnet G, Siebert R et al (2003) MALT1 is deregulated by both chromosomal translocation and amplification in B-cell non-Hodgkin's lymphoma. Blood 101:4539–4546
41. Schreuder MI, Hoeve MA, Hebeda KM et al (2003) Mutual exclusion of t(11;18)(q21;q21) and numerical chromosomal aberrations in the development of different types of primary gastric lymphomas. Br J Haematol 123:590–599
42. Starostik P, Greiner A, Schultz A et al (2000) Genetic aberrations common in gastric high-grade B-cell lymphoma. Blood 95:1180–1187
43. Starostik P, Greiner A, Schwarz S, Patzner J, Schultz A, Muller-Hermelink HK (2000) The role of microsatellite instability in gastric low- and high-grade lymphoma development. Am J Pathol 157:1129–1136
44. Starostik P, Patzner J, Greiner A et al (2002) Gastric marginal zone B-cell lymphomas of MALT type develop along 2 distinct pathogenetic pathways. Blood 99:3–9
45. Streubel B, Lamprect A, Dierlamm J et al (2003) T(14;18)(q32;q21) involving IGH and MALT1 is a frequent chromosomal aberration in MALT lymphoma. Blood 101:2335–2339
46. Sugiyama T, Asaka M, Nakamura T, Nakamura S, Yonezumi M, Seto M (2001) API2-MALT1 chimeric transcript is a predictive marker for the responsiveness of *H. pylori* eradication treatment in low-grade gastric MALT lymphoma. Gastroenterology 120:1884–1885
47. Villuendas R, Piris MA, Orradre JL, Mollejo M, Rodriguez R, Morente M (1991) Different *bcl-2* protein expression in high-grade B-cell lymphomas derived from lymph node or mucosa-associated lymphoid tissue. Am J Pathol 139:989–993
48. Visakorpi T, Hyytinen E, Kallioniemi A, Isola J, Kallioniemi OP (1994) Sensitive detection of chromosome copy number aberrations in prostate cancer by fluorescence in situ hybridization. Am J Pathol 145:624–630
49. Watanobe I, Takamori S, Kojima K et al (2002) Numerical chromosomal abnormality in gastric MALT lymphoma and diffuse large B-cell lymphoma. J Gastroenterol 37:691–696
50. Werner M, Wilkens L, Aubele M, Nolte M, Zitzelsberger H, Komminoth P (1997) Interphase cytogenetics in pathology: principles, methods, and applications of fluorescence in situ hybridization (FISH). Histochem Cell Biol 108:381–390
51. Wotherspoon AC, Finn TM, Isaacson PG (1995) Trisomy 3 in low-grade B-cell lymphomas of mucosa-associated lymphoid tissue. Blood 85:2000–2004

Virchows Arch (2004) 445:515–520
DOI 10.1007/s00428-004-1099-9

ORIGINAL ARTICLE

Michael G. Haase · Anke Klawitter · Gustavo B. Baretton

IκBγ is expressed in mast cells

Received: 11 July 2003 / Accepted: 12 July 2004 / Published online: 17 September 2004
© Springer-Verlag 2004

Abstract IκBγ (IkappaBgamma) is a 70-kDa protein that is encoded by the C-terminal part of the NF-κB p105 gene and acts as an inhibitor of the transcription factor NF-κB. Until now, IκBγ expression has only been described in cell-culture models of B-lymphocytes and enterocytes but not in tissues. In a model of radiation-induced pulmonary damage, we found that mast cells accumulating after irradiation are the only cells in the rat lung that are positive for IκBγ. The mast cells were characterised by their metachromatic staining with toluidine blue and by double immunofluorescence labelling with mast-cell tryptase. Western blotting revealed that the lung mast cells expressed the 70-kDa form of IκBγ cytoplasmatically and that no alternative splicing variants were expressed. In addition, we studied 11 cases of systemic mastocytosis, as well as 5 cases of mast-cell hyperplasia. In all cases, the mast cells stained strongly with IκBγ. Rat peritoneal mast cells also contained high levels of IκBγ. Since NF-κB is an important regulator of mast-cell functions, IκBγ is likely to play a central role in the maintenance of the mast-cell phenotype and possibly in the modification of mast-cell-dependent immune responses.

Keywords IκBγ · Mast cells · NF-κB · Systemic mastocytosis

Introduction

IκBγ [17] is a 70-kDa protein that is encoded by the C-terminal 607 amino acids of the NF-κB p105 gene [8]. In B-lymphocytes, it has been described that IκBγ is generated from the C-terminal part of p105 precursor protein by proteasomes after ubiquitin ligation [3, 6, 27], whereas NF-κB p50 is generated from the N-terminal part. A glycine-rich region in the C-terminal part of p50 is essential for processing [21] and probably serves as a processing stop signal for the 26S proteasome [26]. Lys 441 and 442 serve as ubiquitination targets, whereas residues 446–454 may serve as a ligase recognition motif [3]. The C-terminal part of p105, from which IκBγ is generated, contains seven ankyrin repeats [16]. Inhibition of p105 cleavage is due to binding of NF-κB to the ankyrin repeat domain, whereas phosphorylation of the C-terminal region of p105 (residues 918–934) by the I-kappa kinase (IKK) complex alleviates binding of NF-κB proteins and allows cleavage by the proteasome [3, 14]. IKKβ-induced degradation of p105 is dependent on the ubiquitin ligase SCF$^{\beta\text{-TrCF}}$ (Skp-Cullin 1(Cdec53)-F-box-protein, β-transducin repeat-containing factor), whereas processing of p105 is β-TrCF independent [4].

IκBγ p70 is an inhibitor of p50, p65 and c-Rel, which are members of the NF-κB transcription factor family [9]. Two alternative splicing forms of 63 kDa and 55 kDa have been described, which only inhibit p50 [11]. P70 is expressed only in the cytoplasm, whereas p63 is expressed in both the cytoplasm and the nucleus, and p55 is expressed only in the nucleus [11]. As mentioned above, IκBγ has been described in B-cell lines; one study describes IκBγ in the human colonic adenocarcinoma cell line DLD-1 [33]. In several studies, IκBγ has not been found in other cell types in vivo [6, 15, 17, 23]. This may be explained by the extreme instability of the protein in the living cells studied [10].

We have found that IκBγ is expressed in mast cells, which are important effector cells in the IgE-mediated immune response, including anaphylactic reactions. Mast cells derive from haematopoietic progenitor cells, but do not ordinarily circulate in mature form. Major steps in the differentiation and maturation of the mast-cell lineage occur in peripheral non-haematopoietic tissues. The major growth factors for mast cells are IL-3 and stem-cell factor (SCF), also called kit ligand, mast-cell growth factor or steel factor [7]. SCF acts on the receptor tyrosine kinase c-kit [2, 18, 19]. Activation of mast cells can be induced

M. G. Haase (✉) · A. Klawitter · G. B. Baretton
Department of Pathology,
Dresden University of Technology,
Fetscherstrasse 74, 01307 Dresden, Germany
e-mail: michael.haase@mailbox.tu-dresden.de
Tel.: +49-351-4583020
Fax: +49-351-4584328

by various mediators, such as SCF, IgE or TNFα. All those factors induce an activation of NF-κB in mast cells [5, 22]. Theophylline exerts its anti-inflammatory effect on allergic inflammation through NF-κB inactivation in mast cells [30]. Apart from their role in IgE-mediated immune response, mast cells proliferate in tissues as a consequence of a number of other inflammatory reactions, including the chronic phase of radiation damage [1, 32] or proliferate autonomously, as in systemic mastocytosis (SM) [31].

Materials and methods

Experimental design

Specific pathogen-free female fisher rats weighing 200–250 g (Charles River, Sulzfeld, Germany) were used for selective γ-irradiation of the right lung [9, 12] with 20 Gy (9 MV photons, 3.5 Gy/min). The irradiation procedure was performed under anaesthesia (3 mg/kg xylazine hydrochloride, 66 mg/kg ketamine and 200 µg/ml medetomidine hydrochloride applied into the muscle of the lower extremity). Animals (four animals each time point, including control animals) were sacrificed with an overdose of thiopental (250 mg/kg intraperitoneally) 8 weeks and 12 weeks after irradiation. The lungs were removed and immediately snap-frozen in liquid nitrogen. For immunohistochemistry, lungs were perfused over the bronchi with 4% buffered formaldehyde (pH 8.0), fixed for 24 h and paraffin embedded. Rat peritoneal macrophages were obtained by rinsing the peritoneum of rats with 10 ml phosphate-buffered saline (PBS) and aspirating the fluid with a syringe. Cells were washed by centrifugation and fixed in 4% neutrally buffered formaldehyde for 24 h, embedded in a fibrin clot and finally embedded in paraffin. Animal housing and experiments were approved according to German animal welfare regulations and the ethics committee of the Dresden University of Technology.

Immunohistochemistry

Deparaffinised sections were microwaved for 4×5 min at 750 W in 10 mM citric acid, pH 6.0, blocked with normal serum and incubated at room temperature for 1 h with an 1:10 dilution of the polyclonal antibody 5177C to IκBγ (Santa Cruz Biotech.). The washed sections were incubated with peroxidase-labelled goat anti-rabbit antibody (dilution 1:400) and developed with diaminobenzidine followed by counterstaining with haematoxylin.

Immunofluorescence double labelling

Sections were pre-treated as above. Incubation with the rabbit polyclonal primary antibody 5177C to IκBγ (dilution 1:5) and monoclonal anti-mast cell tryptase antibody AA1 (dilution 1:10) was for 45 min at room temperature. After washing in PBS (10 min), slides were incubated with Texas Red conjugated anti-mouse antibody (dilution 1:80) and dichlorotriazinylaminofluorescein (DTAF)-conjugated anti-rabbit antibody (dilution 1:40). For the rat peritoneal macrophages, secondary antibodies were DTAF-conjugated goat anti-mouse (dilution 1:40) and Texas red conjugated goat anti-rabbit (dilution 1:40). For negative controls, primary antibodies were omitted or replaced by non-immune rabbit or mouse IgG. Slides were finally mounted in PBS-glycerol (1:9 v/v) [28].

Western blotting

Nuclear and cytoplasmic protein extracts were essentially prepared as previously described [29]. Briefly, lung tissue was pulverised in liquid nitrogen, immediately transferred to ice-cold lysis buffer (10 mM Hepes, pH 7.9, 10 mM KCl, 0.1 mM ethyleneglycol tetraacetic acid (EGTA), 0.1 mM ethylenediamine tetraacetic acid (EDTA), 1 mM dithiothreitol (DTT), 0.5 mM phenylmethylsulfonyl fluoride (PMSF) supplemented with Complete protease-inhibitor mix (Roche, Mannheim, Germany) according to the manufacturer's instructions and homogenized. All the following steps were done on ice. Cellular debris was pelleted by centrifugation at 400 *g* for 30 s. The supernatant was adjusted to 0.5% NP-40 and vortexed for 10 s. Nuclei were pelleted by centrifugation at 22600 *g* for 30 s. The supernatant that contained the cytoplasmic proteins was snap-frozen in liquid nitrogen and stored at −80°C. The nuclear pellet was suspended in nuclear lysis buffer (20 mM Hepes, pH 7.9, 400 mM NaCl, 1 mM EGTA, 1 mM EDTA, 1 mM DTT, 0.5 mM PMSF and Complete protease-inhibitor mix as above). The suspension was incubated for 20 min with continuous shaking and centrifuged at 22600 *g* for 5 min. The supernatant that contained the nuclear proteins was snap-frozen in liquid nitrogen and stored at −80°C. For the preparation of total protein extracts, the tissue was immediately lysed in nuclear lysis buffer. The protein concentration was determined with the bicinchoninic acid protein assay (Pierce-KMF, Sankt-Augustin, Germany). Protein (50 µg) was denatured in Laemmli-buffer [20] at 95°C for 5 min and separated on a 10% sodium dodecyl sulfate-polyacrylamide gel. Proteins were transferred to an enhanced chemiluminescence (ECL) nitrocellulose membrane (Amersham Biotech, Freiburg, Germany). The membrane was blocked with PBS containing 0.5% Tween 20 (PBS-T) [28] and 5% non-fat dry milk at 4°C overnight. Rabbit polyclonal IκBγ (antibody 5177C) was diluted 250-fold in 0.5% non-fat dry milk/PBS-T and incubated for 4 h at room temperature. Peroxidase-labelled donkey anti-rabbit secondary antibody was employed at 1000-fold dilution. Incubation time was 30 min at room temperature. Blots were developed with SuperSignal ULTRA horseradish peroxidase substrate (Pierce-KMF, Sankt-Augustin, Germany) and exposed to Hyperfilm-ECL (Amersham Biotech, Freiburg, Germany) for 5–30 s.

Results

Rat lungs

The normal rat lung (Fig. 1A) contained virtually no IκBγ, with the exception of a few peribronchiolar or perivascular cells positive for IκBγ that have been identified as mast cells (data not shown). In contrast, the irradiated rat lung contains many round-to-oval-shaped cells with strong cytoplasmic positivity for IκBγ (Fig. 1B). These cells can be detected in the rat lung starting from about 6 weeks after irradiation. At the same time, mast cells can be detected in the lung with the help of toluidine blue or Giemsa staining (data not shown). To prove the hypothesis that mast cells are the cells that express IκBγ, we performed immunofluorescence double staining with a monoclonal antibody against mast-cell tryptase. The cells that were positive for IκBγ (Fig. 1C) directly co-localised with the cells that were positive for mast-cell tryptase (Fig. 1D). Only very few mast-cell tryptase-positive cells contained low amounts of IκBγ. The staining for IκBγ was strictly cytoplasmic. Mast cells contained only low amounts of NF-κB p50 [13], a protein that is derived from the same pro-protein (p105) as IκBγ.

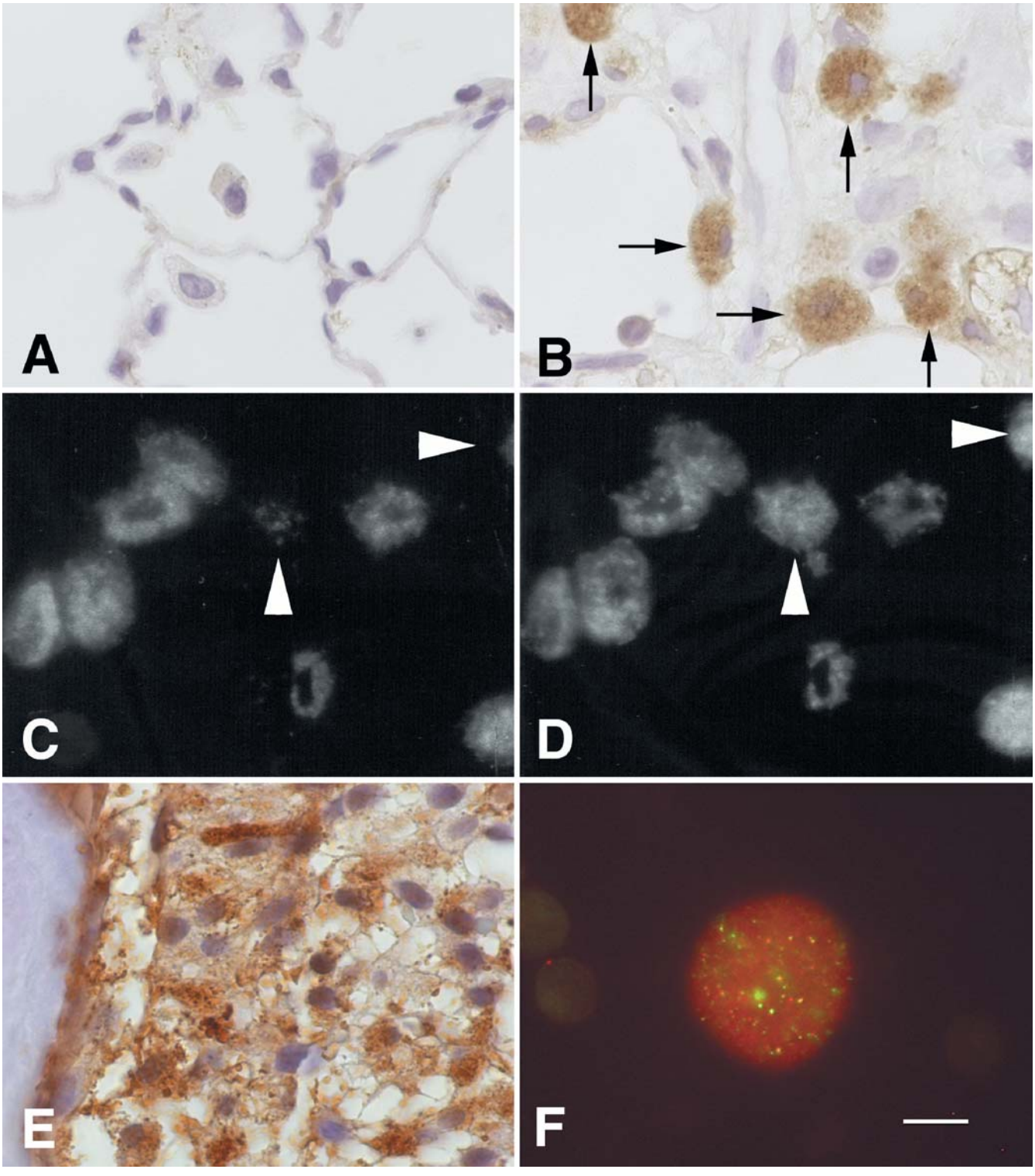


Fig. 1 Immunohistological characterisation of IκBγ expression in mast cells using peroxidase-based immunohistochemistry and immunofluorescence double labelling on paraffin sections. Normal rat lung contained virtually no IκBγ-positive cells (**A**), with the exception of a few peribronchiolar or perivascular mast cells (not shown). In the irradiated lung 2 months after irradiation, many quite uniform round-to-oval cells showed cytoplasmic positivity for IκBγ (**B**, *arrows*). Immunofluorescent double staining of these IκBγ positive cells (**C**) with an antibody to mast-cell tryptase (**D**) identifies the IκBγ positive cells as mast cells. Only two mast-cell tryptase-positive cells contained low amounts of IκBγ (*arrowheads*). In a bone marrow manifestation of systemic mastocytosis, mast cells adjacent to a bone trabecula were positive for IκBγ (**E**). Rat peritoneal mast cells (**F**) were also positive for IκBγ as shown using immunofluorescence double labelling with IκBγ (*red*) and mast-cell tryptase (*green*). The bar is 10 μm in **A**–**E** and 5.5 μm in **F**

Western blotting

To verify the immunohistochemical data of the rat lungs and to test the specificity of the antibody, we performed protein blots (Western blots) with the rat lung tissue. Because a selective cytoplasmic expression of IκBγ had been described for B-lymphocytes, we prepared cytoplasmic and nuclear extracts of the cells and used them for denaturing electrophoresis and blotting. Control rat lungs (0 months after irradiation) contained no IκBγ, neither in the cytoplasm (Fig. 2) nor in the nucleus (Fig. 2). Lungs from animals that had been irradiated 3 months previously contained the characteristic 70-kDa (p70) IκBγ protein in the cytoplasm (Fig. 2). In contrast, nuclei of irradiated lungs contained no IκBγ (Fig. 2). Except for a very weak band (slightly above background), only the 70 kDa band could be detected in the cytoplasm of the irradiated lung.

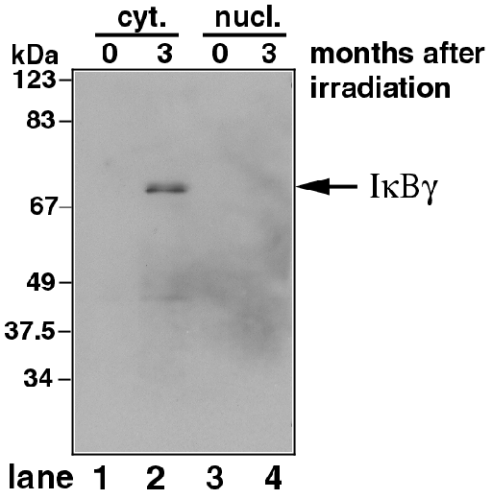


Fig. 2 Western blot of the rat lung stained with IκBγ. Nuclear and cytoplasmic proteins were isolated from normal and irradiated rat lungs (at 2 months after irradiation) and fractionated on a denaturing polyacrylamide gel. Proteins were blotted on a nitrocellulose membrane, incubated with an IκBγ antibody and detected with a luminol-based detection system. Normal rat lung (*lanes 1 and 3*) contained no IκBγ, neither in the cytoplasm (*cyt., lane 1*) nor in the nucleus (*nucl., lane 3*). Irradiated rat lungs also contained no nuclear IκBγ (*lane 4*), but the cytoplasmic extracts contained the characteristic 70-kDa form of IκBγ (*lane 2*)

Mast-cell-associated lesions

To test the expression of IκBγ in human mast cells, we studied 15 cases of mast-cell proliferations in archival histological samples (Table 1). In all the cases, mast cells stained strongly with the antibody to IκBγ. The cases included 13 samples of SM from 11 different patients. The staining intensity did not change with the morphology of the mast cells, since mast cells with spindle-cell type (data not shown) also stained strongly with IκBγ. One patient with SM had an associated refractory anaemia-type of myelodysplastic syndrome, classified as systemic mastocytosis with associated clonal haematological non-mast-cell lineage disease (SM-AHNMD) according to the current World Health Organisation classification [31]. Five cases with reactive mast-cell hyperplasia also showed a strong staining of the mast cells with the IκBγ antibody. The mast cells in all histological samples have been verified by Giemsa staining and using immunohistological staining with an antibody to mast-cell tryptase.

Table 1 Histological data of 13 samples (11 patients) of systemic mastocytosis (SM), including 1 case of associated clonal haematological non-mast cell lineage disease (AHNMD) and 5 cases with reactive mast cell hyperplasia (MH). *BM* bone marrow, *CM* cutaneous mastocytosis, *LN* lymph node, *MDS-RA* myelodysplastic syndrome-refractory anemia, *St* stomach, B-CLL *B-cell chronic lymphocytic leukaemia*

Case no.	Year	Gender	Age (years)	Staining intensity for IκBγ	Spindle cell morphology (%)	Involvement (%)	Organ	Diagnosis
1	1992	Female	83	3+	50	50	BM	SM
1	1993	Female	84	3+	50	60	BM	SM
2	1996	Female	50	2+	10	20	BM	SM
3	1999	Male	62	3+	60	30	BM	SM
4	1999	Male	64	3+	30	40	BM	SM, MDS-RA (=SM-AHNMD)
4	2000	Male	65	3+	25	100	LN	SM
5	2000	Male	69	3+	50	70	BM	SM
6	2000	Male	48	3+	70	60	BM	SM
7	1900	Male	67	3+	80	40	BM	SM
8	2000	Male	69	3+	80	90	BM	SM
9	2001	Male	39	3+	70	40	BM	SM, CM
9	2001	Male	39	3+	0	5	St	MH
10	2001	Male	44	3+	90	40	BM	SM
11	2001	Male	42	3+	80	50	BM	SM
12	1996	Female	72	3+	0	5	LN	Diffuse lymphadenitis and MH
13	1997	Female	56	3+	0	3	BM	MH
14	1998	Female	88	3+	0	1	BM	B-CLL, MH
15	2001	Female	86	3+	0	<1	BM	MH

IκBγ in rat peritoneal macrophages

Thus far, we had studied only mast cells in pathological conditions. To find out whether normal resident (non-activated) mast cells also contain IκBγ, we obtained mast cells from the peritoneal cavity of untreated rats. These mast cells were characterised by haematoxylin as well as Giemsa staining (data not shown). In addition, they were stained in a double immunofluorescence reaction with IκBγ and mast-cell tryptase (Fig. 1F), which proves that IκBγ is actually expressed in all peritoneal mast cells.

Discussion

In a model of radiation-induced lung damage, we found that the mast cells in the irradiated lung express IκBγ, an inhibitor of the transcription factor NF-κB. Western blotting experiments revealed that the characteristic p70 protein of IκBγ is expressed in the cytoplasm of the cells. No p63 or p55 splice variants can be detected. While these splice variants only inhibit NF-κB p50, IκBγ p70 also inhibits NF-κB p65 and c-rel [11]. This might be of functional importance, since only low amounts of p50 could be detected in mast cells [13]. The low expression of NF-κB p50 in contrast to IκBγ was surprising, since both IκBγ and NF-κB p50 are generated from the same precursor protein called p105. In B-lymphocytes, it has been described that p105 is ubiquitinylated and subsequently cleaved by the proteasome [27]. Theoretically, similar amounts of p50 and IκBγ should be generated after cleavage. The low amount of p50 compared with IκBγ seems to be even more surprising in light of the fact that IκBγ has been described as a very unstable protein in B-lymphocytes [6]. These facts raise the question of how the considerable difference in the expression of IκBγ and p50 is generated. Theoretically, three possible mechanisms might be responsible alone or in concert: (1) stabilisation of IκBγ protein, (2) instability of p50, (3) generation of IκBγ from a separate reading frame. Further studies are needed to clarify the mechanism. We also performed in situ hybridisations with an mRNA probe for IκBγ (data not shown). These experiments revealed a positivity of many lung cells, including type-II pneumocytes, alveolar macrophages and bronchial epithelial cells, which was not surprising because there is a common mRNA (p105 mRNA) for both NF-κB p50 and IκBγ. Therefore, the IκBγ antisense probe detects p105 mRNA that also encodes for p50 protein, a protein that is strongly expressed in type-II pneumocytes and alveolar macrophages [13]. Mast cells also contain the mRNA detected by the IκBγ probe. However, the amount of this mRNA is comparatively low in relation to type-II pneumocytes and alveolar macrophages. Since there is plenty of IκBγ protein in mast cells, part of the regulation of IκBγ production seems to be post-transcriptional.

Activation of NF-κB is associated with mast-cell activation. Since IκBγ belongs to the family of NF-κB inhibitors, its presence in mast cells should theoretically inhibit mast-cell function. However, it has been shown that IκB proteins can activate transcription under certain circumstances [24]. The activation domain of IκBγ can behave as a genuine acidic activator of transcription from promoters containing GAL4-binding sites in avian, mammalian and yeast cells [25]. Therefore, it is possible that IκBγ acts both as a transcriptional activator and repressor in mast cells, activating sets of genes that are important and repressing genes that are dispensable for mast-cell function.

Mast cells are the first type of cells described to contain IκBγ in vivo. In the cell-culture system, IκBγ has been described in B-lymphocytes and in an enterocytic cell line. Further studies should address the distribution of IκBγ in other cells of the body in physiological and pathological conditions.

In conclusion, the mast cells examined in this study show a strong expression of IκBγ, an inhibitor of NF-κB. Since NF-κB is a strong mediator of several mast-cell functions, IκBγ is likely to play an important role in maintaining the mast-cell phenotype and possibly in the modulation of mast-cell functions in various diseases.

Acknowledgements This work was supported by the Deutsche Forschungsgemeinschaft (DFG, MU 1299/1–1) and the BMBF (01ZZ9604), as well as a grant of the Faculty of Medicine of the Technical University of Dresden to M.H. We thank Peter Geyer and Dr. Rainer Kumpf for skilful assistance during the radiation treatment. Last but not least, we wish to thank R. Hahn, B. Liebschner, Silke Langer and H. Seidel for excellent technical assistance.

References

1. Adawi A, Zhang Y, Baggs R, Rubin P, Williams J, Finkelstein J et al (1998) Blockade of CD40–CD40 ligand interactions protects against radiation-induced pulmonary inflammation and fibrosis. Clin Immunol Immunopathol 89:222–230
2. Chabot B, Stephenson DA, Chapman VM, Besmer P, Bernstein A (1988) The proto-oncogene c-kit encoding a transmembrane tyrosine kinase receptor maps to the mouse W locus. Nature 335:88–89
3. Ciechanover A, Gonen H, Bercovich B, Cohen S, Fajerman I, Israel A et al (2001) Mechanisms of ubiquitin-mediated, limited processing of the NF-kappaB1 precursor protein p105. Biochimie 83:341–349
4. Cohen S, Achbert-Weiner H, Ciechanover A (2004) Dual effects of IkappaB kinase beta-mediated phosphorylation on p105 Fate: SCF(beta-TrCP)-dependent degradation and SCF(beta-TrCP)-independent processing. Mol Cell Biol 24:475–486
5. Coward WR, Okayama Y, Sagara H, Wilson SJ, Holgate ST, Church MK (2002) NF-kappaB and TNF-alpha: a positive autocrine loop in human lung mast cells? J Immunol 169:5287–5293
6. Fan CM, Maniatis T (1991) Generation of p50 subunit of NF-kappa B by processing of p105 through an ATP-dependent pathway. Nature 354:395–398
7. Flanagan JG, Leder P (1990) The kit ligand: a cell surface molecule altered in steel mutant fibroblasts. Cell 63:185–194
8. Gerondakis S, Morrice N, Richardson IB, Wettenhall R, Fecondo J, Grumont RJ (1993) The activity of a 70 kilodalton I kappa B molecule identical to the carboxyl terminus of the p105 NF-kappa B precursor is modulated by protein kinase A. Cell Growth Differ 4:617–627

9. Geyer P (1993) An irradiation technique for the right half of the rat lung using 9 MV photons from a linear accelerator. Strahlenther Onkol 169:734–739
10. Grimm S, Baeuerle PA (1993) The inducible transcription factor NF-kappa B: structure-function relationship of its protein subunits. Biochem J 290:297–308
11. Grumont RJ, Gerondakis S (1994) Alternative splicing of RNA transcripts encoded by the murine p105 NF- kappa B gene generates I kappa B gamma isoforms with different inhibitory activities. Proc Natl Acad Sci U S A 91:4367–4371
12. Haase M, Geyer P, Appold S, Schuh D, Kasper M, Muller M (2000) Down-regulation of SP1 DNA binding activity in the process of radiation-induced pulmonary fibrosis. Int J Radiat Biol 76:487–492
13. Haase MG, Klawitter A, Geyer P, Alheit H, Baumann M, Kriegel TM et al (2003) Sustained elevation of NF-KappaB DNA binding activity in radiation-induced lung damage in rats. Int J Radiat Biol 79:863–877
14. Heissmeyer V, Krappmann D, Hatada EN, Scheidereit C (2001) Shared pathways of IkappaB kinase-induced SCF(betaTrCP)-mediated ubiquitination and degradation for the NF-kappaB precursor p105 and I kappa B alpha. Mol Cell Biol 21:1024–1035
15. Henkel T, Zabel U, van-Zee K, Muller JM, Fanning E, Baeuerle PA (1992) Intramolecular masking of the nuclear location signal and dimerization domain in the precursor for the p50 NF-kappa B subunit. Cell 68:1121–1133
16. Heron E, Deloukas P, van Loon AP (1995) The complete exon-intron structure of the 156-kb human gene NFKB1, which encodes the p105 and p50 proteins of transcription factors NF-kappa B and I kappa B-gamma: implications for NF-kappa B-mediated signal transduction. Genomics 30:493–505
17. Inoue J, Kerr LD, Kakizuka A, Verma IM (1992) I kappa B gamma, a 70 kd protein identical to the C-terminal half of p110 NF-kappa B: a new member of the I kappa B family. Cell 68:1109–1120
18. Kitamura Y, Go S (1979) Decreased production of mast cells in S1/S1d anemic mice. Blood 53:492–497
19. Kitamura Y, Go S, Hatanaka K (1978) Decrease of mast cells in W/Wv mice and their increase by bone marrow transplantation. Blood 52:447–452
20. Laemmli UK (1970) Cleavage of structural proteins during the assembly of the head of bacteriophage T4. Nature 227:680–685
21. Lin L, Ghosh S (1996) A glycine-rich region in NF-kappaB p105 functions as a processing signal for the generation of the p50 subunit. Mol Cell Biol 16:2248–2254
22. Marquardt DL, Walker LL (2000) Dependence of mast cell IgE-mediated cytokine production on nuclear factor-kappaB activity. J Allergy Clin Immunol 105:500–505
23. Moine P, McIntyre R, Schwartz MD, Kaneko D, Shenkar R, Le Tulzo Y et al (2000) NF-kappaB regulatory mechanisms in alveolar macrophages from patients with acute respiratory distress syndrome. Shock 13:85–91
24. Morin PJ, Gilmore TD (1992) The C terminus of the NF-kappa B p50 precursor and an I kappa B isoform contain transcription activation domains. Nucleic Acids Res 20:2453–2458
25. Morin PJ, Subramanian GS, Gilmore TD (1993) GAL4-I kappa B alpha and GAL4-I kappa B gamma activate transcription by different mechanisms. Nucleic Acids Res 21:2157–2163
26. Orian A, Schwartz AL, Israel A, Whiteside S, Kahana C, Ciechanover A (1999) Structural motifs involved in ubiquitin-mediated processing of the NF-kappaB precursor p105: roles of the glycine-rich region and a downstream ubiquitination domain. Mol Cell Biol 19:3664–3673
27. Palombella VJ, Rando OJ, Goldberg AL, Maniatis T (1994) The ubiquitin-proteasome pathway is required for processing the NF-kappa B1 precursor protein and the activation of NF-kappa B. Cell 78:773–785
28. Sambrook J, Fritsch EF, Maniatis T (1989) Molecular cloning. A laboratory manual. Cold Spring Harbor Laboratory Press, Woodbury, NY
29. Schreiber E, Matthias P, Muller MM, Schaffner W (1989) Rapid detection of octamer binding proteins with 'mini-extracts', prepared from a small number of cells. Nucleic Acids Res 17:6419
30. Umeda M, Ichiyama T, Hasegawa S, Kaneko M, Matsubara T, Furukawa S (2002) Theophylline inhibits NF-kappaB activation in human peripheral blood mononuclear cells. Int Arch Allergy Immunol 128:130–135
31. Valent P, Horny HP, Li CY, Longley BJ, Metcalfe DD, Parwaresch RM et al (2001) Mastocytosis (Mast cell disease). In: Jaffe ES, Harris NL, Stein H, Vardiman JW (eds) World Health Organization classification of tumours. Pathology of tumours of haematopoietic and lymhoid tissues. IARC Press, Lyon, pp 293–302
32. Ward WF, Solliday NH, Molteni A, Port CD (1983) Radiation injury in rat lung. II. Angiotensin-converting enzyme activity. Radiat Res 96:294–300
33. Wilson L, Szabo C, Salzman AL (1999) Protein kinase C-dependent activation of NF-kappaB in enterocytes is independent of IkappaB degradation. Gastroenterology 117:106–114

Virchows Arch (2004) 445:521–526
DOI 10.1007/s00428-004-1089-y

ORIGINAL ARTICLE

A. Giatromanolaki · E. Sivridis · P. Tsikouras · I. Manavis · G. Maroulis · M. I. Koukourakis

Angiogenesis and vascular survival ability in ovarian adenocarcinomas

Received: 28 April 2004 / Accepted: 6 July 2004 / Published online: 9 September 2004
© Springer-Verlag 2004

Abstract This study was designed to investigate the prognostic relevance of ovarian tumour angiogenesis in terms of tumour angiogenic activity (TAA) and vascular survival ability (VSA), i.e. the ability of newly formed vessels to survive once incorporated into the main tumour mass. TAA was assessed at the edge of the invading tumour, while VSA was evaluated in inner tumour areas, always in comparison with the invading edge. A series of 46 ovarian grade-1 adenocarcinomas of the endometrioid and the serous cell type was assessed. Endothelial cells were revealed after using a standard immunohistochemical technique and the CD31 antibody. Vascular density was, in general, higher at the periphery of the tumour than in the inner tumour areas, although in both cases, a rich vascular supply was associated with a poor survival. By combining counts at the tumour edge versus inner tumour areas (edvin), four groups of tumour vascularity emerged: edvin type 1 (low TAA/low VSA), edvin type 2 (low TAA/high VSA), edvin type 3 (high TAA/low VSA) and edvin type 4 (high TAA/high VSA). Edvin type-4 tumours were related to the most unfavourable prognosis. It is concluded that VSA and TAA are complementary procedures in assessing ovarian tumour vasculature and, therefore, prognosis, and by combining the two parameters, a more precise impression of the state of vascularisation in the ovary is obtained, which may prove useful in designing anti-angiogenic therapies.

Keywords Angiogenesis · Tumour angiogenic ability · Vascular survival ability · Ovarian adenocarcinomas

A. Giatromanolaki (✉) · E. Sivridis
Department of Pathology,
Democritus University of Thrace,
P.O. Box 12, 68100 Alexandroupolis, Greece
e-mail: targ@her.forthnet.gr
Tel.: +30-25510-75118
Fax: +30-25510-30440

P. Tsikouras · G. Maroulis
Department of Obstetrics and Gynaecology,
Democritus University of Thrace,
Alexandroupolis, Greece

I. Manavis
Department of Radiology,
Democritus University of Thrace,
Alexandroupolis, Greece

M. I. Koukourakis
Department of Radiotherapy,
Democritus University of Thrace,
Alexandroupolis, Greece

Introduction

Malignant epithelial tumours stimulate new blood vessel formation and, in doing so, facilitate metastasis [25], although, need for oxygen and nutriments can also activate the angiogenic process [4]. Tumours with high angiogenic activity have been associated with aggressiveness and poor patient survival in a variety of human malignancies, including endometrium, breast, lung, gastric and bladder carcinoma [7, 17, 21, 24, 26].

We have previously shown that vascular density (VD) is high at the tumour periphery and low in the inner tumour areas, with a tendency of decreasing gradually from the invading tumour edge to the heart of the tumour [9, 10, 11, 20]. Such an observation is, however, by no means novel as Thompson et al. reached the same conclusion 20 years earlier after investigating angiogenesis in experimental mammary carcinomas [28]. The highest angiogenic activity was noted in the tumour/host interaction area. That endothelial cell proliferation occurs mainly, if not exclusively, at the edge of a tumour was indicated clearly by Fox et al. [5] after intravenous administration of BrdURD to breast cancer patients. They stated that angiogenesis occurs primarily in the tumour edge, while remodelling of the newly formed vessels takes place in inner tumour areas [5]. Giatromanolaki et al. [8] succeeded in giving further support to Thompson's et al. original view [28] using a standard immunohistochemical technique; they found single endothelial cells in excess in the tumour/normal tissue interface, while endothelial cell migration was negligible in the main tumour mass.

It is generally thought that vascular depletion in inner tumour areas is a consequence of unfavourable intratumoral conditions, i.e. hypoxia, acidity, lack of nutrients, failure of waste removal [12, 13, 27], adversely affecting the proliferation/apoptosis balance of the newly formed endothelial cells [18, 23]. The ability of tumours to maintain a relatively high VD in areas away from the tumour periphery (vascular survival ability, VSA) [21] varies considerably among tumours of similar or different histological type and is independent of tumours' ability to form new blood vessels (tumour angiogenic activity, TAA). Quantitative and qualitative differences in the secretion of factors inhibiting endothelial cell apoptosis by both cancer and stromal cells may be responsible for such differences in vascular viability [14, 22, 29]. Patients harbouring tumours with high VSA have also been associated with poor prognosis, and the VSA statistical value was shown to be stronger than and independent of TAA [9, 11, 17, 26]. It is postulated that excessive formation of blood vessels not complemented by sufficient viability would be of little service to tumour progression.

In this study, both TAA and VSA were investigated in a series of primary G1 ovarian adenocarcinomas of the endometrioid and serous cell type, and their prognostic significance was assessed.

Materials and methods

Formalin-fixed, paraffin-embedded tissues from 46 patients with primary ovarian carcinomas were retrieved from the files of the Department of Pathology, Democritus University of Thrace Medical School, Alexandroupolis, Greece. All cases were well-differentiated endometrioid and serous ovarian adenocarcinomas. The patients had been treated with surgery. The original haematoxylin and eosin slides were reviewed, and sections containing the tumour/normal tissue interface and inner tumour areas were selected for the study. The immunohistochemical staining was assessed by two pathologists [AG, ES] independently, and discrepancies were resolved on the conference microscope.

The patients in the series and their disease characteristics are presented in Table 1. Patients who died within 30 days after surgery were not included in this study to avoid bias from peri-operative mortality. The follow-up of the patients ranged from 12 months to 90 months (median 50 months). For patients alive at the time of analysis, the follow-up ranged from 36 months to 90 months (median 80 months). Precise data regarding the administration of chemotherapy in these patients were lacking.

Table 1 Patients and tumor characteristics. *FIGO* International Federation of Gynecology and Obstetrics

No. of patients	46
Age	
Range	23–76 years
Median	60 years
Mean	57.7 years
FIGO stage	
I	7
II	24
III	15
Histological type	
Endometrioid adenocarcinomas	26
Grade 1	26
Serous adenocarcinomas	20
Grade 1	20

Immunohistochemical staining

The JC70 monoclonal antibody (Dako) recognising CD31 (platelet/endothelial cell adhesion molecule; PECAM-1) was used for microvessel staining on 3-μm paraffin-embedded sections using the alkaline phosphatase/anti-alkaline phosphatase (APAAP) procedure. Sections were dewaxed, rehydrated and pre-digested with protease type XXIV for 20 min at 37°C. JC70 was applied 1:20 at room temperature for 30 min and washed in Tris-buffered saline (TBS). Rabbit anti-mouse antibody 1 in 25 was applied for 30 min, followed by application of APAAP complex 1 in 25 for 30 min. After washing in TBS, the last two steps were repeated for 10 min each. The colour was developed after 20 min incubation with New Fuchsin solution.

Assessment of the tumour angiogenic activity

TAA activity was assessed at the edge of the tumour. Three areas of maximum vascular density ("hot spots") were identified at low-power magnification (×40 and ×100), but vascular counting was performed at ×200 field. Vessels adjacent to necrotic areas were excluded from the appraisal. The final VD, i.e. the TAA of the tumour, was the mean of the vessel counts obtained in these fields. The median VD value was used as a cut-off point to define tumours of low and high TAA.

Assessment of the vascular survival ability

The VSA was assessed in inner tumour areas, as previously described [9, 10, 11, 20]. Briefly, three areas of highest tumour vascularisation adjacent to normal ovary were identified per case. Vessel counting was performed in three consecutive fields at ×200 magnification, starting from the tumour area adjacent to the normal tissue (t_1 field; tumour periphery) and heading to the tumour centre by moving twice the optical field (t_2 and t_3 fields; inner and innermost tumour areas, respectively). These three fields were estimated to cover a course of approximately 6 mm (2 mm each) from the periphery to the centre. The mean VD in peripheral, inner and innermost tumour areas were the mean value obtained from the assessed t_1, t_2 and t_3 areas (VD_{t1}, VD_{t2} and VD_{t3}), respectively. Cases were divided into two groups according to their ability to maintain a relatively rich or otherwise VD in t_2 and t_3 areas. Specifically, tumours were considered as having a high VSA when the mean VD in t_2+t_3 areas was higher than the 50% of the VD in the t_1 area

Edvin vascular types

On the basis of the results obtained from TAA and VSA, four edvin vascular types could be identified [7, 8, 12, 18]: tumours with low TAA and low VSA designated as edvin type 1; tumours with high TAA and high VSA designated as edvin type 4; tumours with low TAA and high VSA defined as edvin type 2 and tumours with high TAA and low VSA corresponding to edvin type 3. Typical cases of edvin 1 and edvin 2 are shown in Fig. 1.

Ultrasonographic imaging of tumour vasculature

All colour doppler examinations were performed with Kontron S40 using a high-frequency linear probe 7.5 MHz, sector 7.5 MHz and 3 MHz. Starting with setting optimised to detect weak and low velocity signals (highest frequency transducer, minimum filter and grey/colour thresholding; lowest maximum velocity range; gain set at a level where colour noise just disappears), slow searches

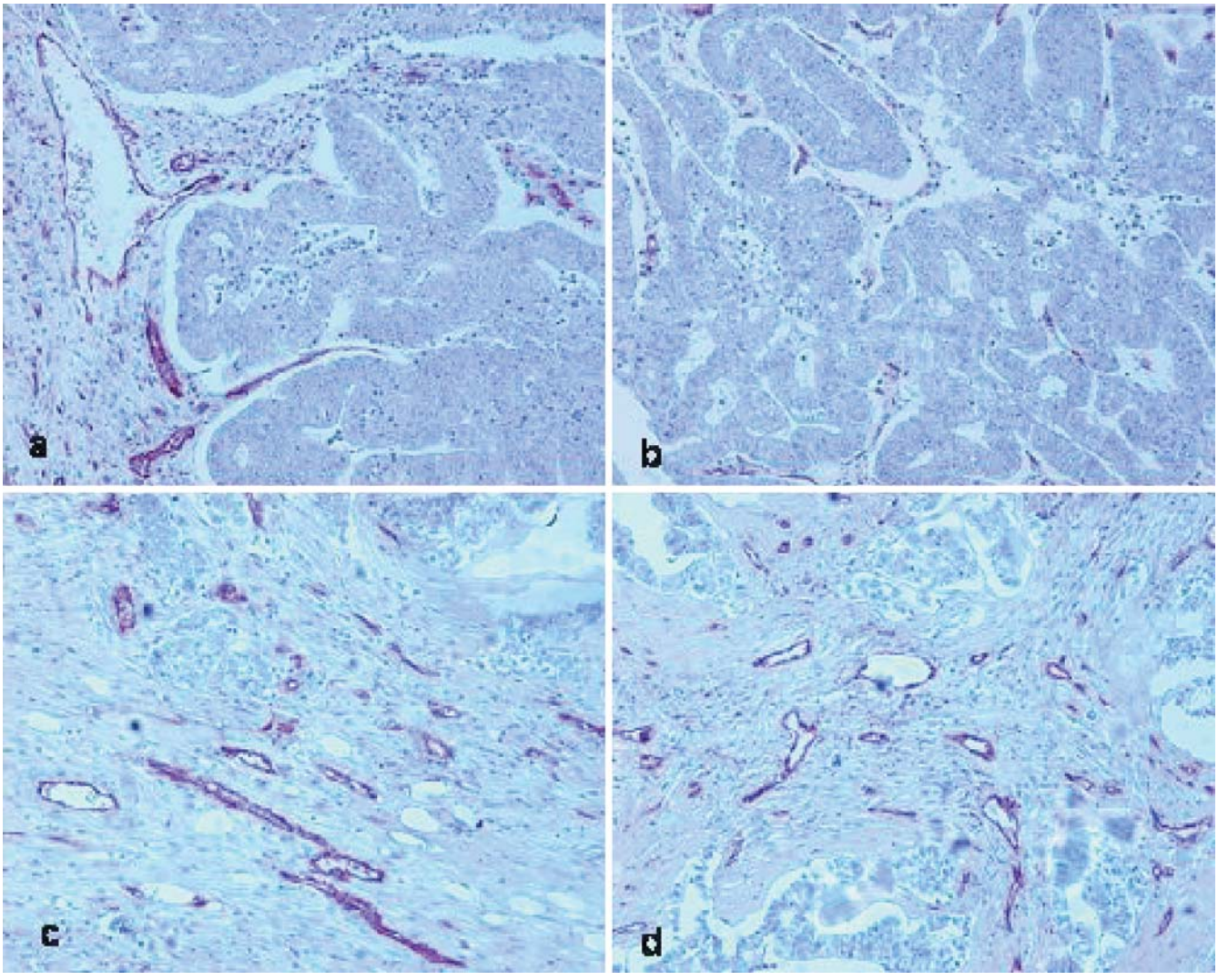


Fig. 1 Tumour vascularity edge versus inner (edvin) tumour areas type 3, characterised by high tumour angiogenic activity (TAA) (**a**) and low vascular survival ability (VSA) (**b**); tumour vascularity edvin type 4, characterised by high TAA (**c**) and high VSA (**d**)

sweeping through the region of interest were used. Changing the interrogation angle was used to help blood flowing parallel to the skin, which otherwise fails to give a doppler shift signal because there is no flow component in the direction of the beam.

According to the blood flow at colour imaging, ovarian tumours were grouped somewhat subjectively in three categories: (1) no vessels detected, (2) vessels in the periphery of the tumour and (3) vessels in the periphery and the inner tumour areas [3].

Statistical analysis

Statistical analysis and graphs were performed using the Graph Pad Prism 2.01 package. Survival curves were plotted using the method of Kaplan and Meier, and the log-rank test was used to determine statistical differences among life tables. A Fisher's exact test or a chi-square two-tailed *t*-test was used for testing relationships among categorical tumour variables, as appropriate. A Cox proportional hazard model was used to assess the effects of patient and tumour variables on overall survival. A P value <0.05 was required for significance.

Results

TAA, VSA and histological variables

The VD in t_1, t_2 and t_3 areas stratified for histological subtype are shown in Table 2. A statistically significant difference was noted between t_1/t_2 and t_3 areas and between t_2 and t_3 areas.

Using the median VD in t_1 areas (40 vessels), cases were grouped into two categories, the low (VD 10–40, 24 patients) and the high TAA (VD 41–116, 22 patients). Using the criteria mentioned in the methods, 20 of 46 cases were classified as bearing high and 26 of 46 low VSA.

There was no association between VSA and TAA. High VSA was associated with advanced T-stage, while TAA was significantly higher in serous carcinomas (Table 3). There was no association of TAA or VSA with the ages of patients at diagnosis.

Table 2 Vascular density (median, range) in tumour periphery and inner tumour areas

	t_1	t_2	t_3	*P* value
All tumours	40 (10–116)	27 (5–52)	15 (2–54)	1 versus 2; $P<0.0001$ 1 versus 3; $P<0.0001$ 2 versus 3; $P=0.001$
Endometrioid adenocarcinomas	32 (13–105)	23 (8–52)	14 (2–54)	1 versus 2; $P=0.03$ 1 versus 3; $P=0.001$ 2 versus 3; $P=0.07$
Serous adenocarcinomas	45 (10–116)	27 (5–47)	15 (2–29)	1 versus 2; $P=0.0006$ 1 versus 3; $P<0.0001$ 2 versus 3; $P=0.007$

Table 3 Association of vascular parameters with histology and stage of disease. *Edvin* edge versus inner tumour areas score

	Histological type of ovarian carcinoma			Stage			
	Serous	Endometrioid	*P* value	1	2	3	*P* value
TAA							
Low	14	10	0.03	3	16	5	0.11
High	6	16		4	8	10	
VSA							
Low	10	16	0.43	7	13	6	0.02
High	10	10		0	11	9	
Edvin							
1	6	6		3	7	2	
2	8	4	0.15	0	9	3	0.03
3	4	10		4	6	4	
4	2	6		0	2	6	

TAA, VSA, edvin and prognosis

Kaplan–Meier survival curves showed that stage of disease but not histological type or age of patients at diagnosis was an important predictor of prognosis. TAA and VSA were also related to survival (Fig. 2a, b). Analysis according to the edvin types revealed that patients with edvin-1 tumours had the most favourable prognosis, in contrast to those harbouring edvin-4 tumours, who experienced the worst prognosis. Patients with edvin type-2 and type-3 tumours showed an intermediate prognosis (Fig. 2c).

In multivariate analysis, International Federation of Gynecology and Obstetrics (FIGO) stage of disease and edvin-type vascularity were significant and independent predictors of prognosis (Table 4).

Ultrasonographic findings

Colour Doppler ultrasonographic imaging of the blood flow was performed in 12 adenocarcinomas: 7 of endometrioid and 5 serous types. In 2 of 12 cases, vessel detection was not possible. In 3 of 12, vessels were detected mainly in the tumour periphery, and in 7 of 12, there were vessels recognised in both peripheral and inner tumour areas.

Analysis of the ultrasonographic features according to the edvin type is shown in Table 5. Despite the small number of cases analysed, the majority of cases with

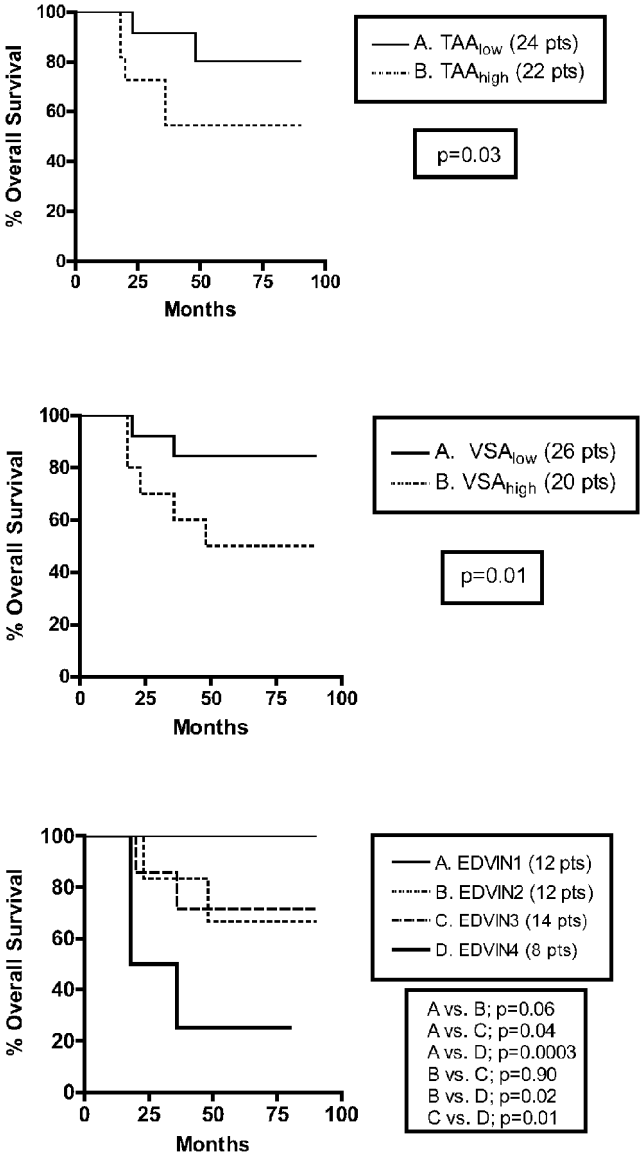


Fig. 2 Kaplan-Meier curves of overall survival stratified for tumour angiogenic activity (**a**), vascular survival ability (**b**), and edvin (edge versus inner tumour areas) types of tumour vascularity (**c**)

Table 4 Multivariate (MV) analysis including the standard histological parameters (stage and histology) together with vascular parameters [tumour angiogenic activity (TAA), vascular survival ability (VSA) edge versus inner (edvin) tumour areas score]. *FIGO* International Federation of Gynecology and Obstetrics

Variable	MV model 1		MV model 2		MV model 3	
	t-ratio	*P* value	t-ratio	*P* value	t-ratio	*P* value
FIGO stage	5.09	<0.0001	5.57	<0.0001	5.36	0.0001
Histology	1.64	0.10	1.49	0.14	–	–
TAA	1.83	0.07	–	–	–	–
VSA	1.89	0.06	–	–	–	–
Edvin	–	–	2.23	0.03	2.69	0.01

Table 5 Association between colour Doppler ultrasonographic detection of vessels and immunohistochemical edge versus inner tumour areas (edvin) vascular types

	Edvin types				
	1	2	3	4	*P* value
Ultrasound distribution of vessels					
No vessel detection	2	0	0	0	
Peripheral	0	0	2	1	0.01
Peripheral and central	0	2	1	4	

peripheral and central vessels were of edvin type 2 and type 4, while both cases without detectable vessels on ultrasound were of edvin 1.

Discussion

There have been a number of reports on the prognostic significance of angiogenesis in ovarian neoplasms. Hollingsworth et al. in 1995, when investigating advanced stage ovarian carcinomas, found that patients with low VD had an improved overall survival compared with those with high VD [16]. Gasparini et al. in 1996 related high VD with response to chemotherapy and poor overall prognosis [6]. Abulafia et al. in 2000 noted that high angiogenesis at sites of omental metastasis was associated with increased tumour aggressiveness and decreased overall survival [1]. Several other reports followed which were along these lines [2, 15, 19].

In this study, we were able to reach similar conclusions after approaching the issue by two different, although complementary, procedures. First, it was shown that angiogenesis is, indeed, important to prognosis in ovarian adenocarcinomas by counting blood vessels at the edge of the tumour, i.e. by assessing the TAA, and, second, by counting blood vessels in the inner and innermost tumour areas, i.e. by assessing the tumour's VSA. A rich vascular network, evaluated by both procedures, was associated with poor survival, although the two parameters were unrelated. In addition, VSA but not TAA was associated with advanced stage of disease, and TAA but not VSA was related to ovarian serous adenocarinomas.

This double approach of assessing tumour vasculature was considered necessary, for it would give a more precise picture of the angiogenic state in ovarian neoplasms; it illustrates the rate of production but also the ability of survival of the newly-formed blood vessels under unfavourable conditions. For, indeed, new blood vessels are formed in the tumour/normal tissue interface but, as the malignant tumour advances, are gradually engulfed and incorporated within the main tumour mass. At the inner tumour areas, unfavourable environmental conditions prevail (hypoxia, acidity, etc.) [13, 27], and the neo-vascularisation undergoes regressive changes, the magnitude of which depends on the adequacy of factors antagonising endothelial cell apoptosis [18, 23].

Furthermore, by combining the results of TAA and VSA counts, four distinct patterns of tumour vascularisation emerged—the edvin types 1 to 4, with specific biological behaviour. Tumours with low TAA and low VSA (edvin 1) showed the most favourable prognosis, while those with high TAA and high VSA (edvin 4) had the most unfavourable outcome. The remaining groups, i.e. low TAA/high VSA (edvin 2) and high TAA/low VSA (edvin 3), were associated with an intermediate prognosis.

It becomes apparent, therefore, that the aggressiveness or otherwise of an ovarian tumour does not only depend on its potential to form new blood vessels at the invading tumour edge but also on its ability to maintain a reasonably good blood supply into inner tumour areas, once the newly formed blood vessels have been incorporated into the main tumour mass. This assertion has been born out in carcinomas of the breast, lung, colon and urinary bladder [9, 10, 11, 20].

Interestingly, a comparable distribution of vessels into tumour periphery and tumour centre was also noted prior to surgery into the admittedly few cases studied using Doppler ultrasonographic method. This distinction of tumour vessels into central and peripheral was first proposed by Brown et al. [3], and it is most fascinating that a direct association between ultrasonographic findings and immunohistochemical/edvin types was noted in our study, suggesting that the pre-operative visual detection of vessels at the tumour periphery and the inner tumour areas correspond with high TAA and high VSA counts. This, however, should be confirmed in large prospective studies.

It is concluded that VSA is an important, complementary to TAA prognostic marker and, by combining the two procedures, a more precise topography of tumour vasculature is obtained. More importantly, the recognition of different vascularisation edvin patterns may prove useful for the stratification of patients into different anti-angiogenic regimens. High TAA/low VSA tumours could

be targeted by angiostatic therapies, while high VSA tumours may well be treated with angiotoxic strategies.

References

1. Abulafia O, Ruiz JE, Holcomb K, Dimaio TM, Lee YC, Sherer DM (2000) Angiogenesis in early-invasive and low-malignant-potential epithelial ovarian carcinoma. Obstet Gynecol 95:548–552
2. Alvarez AA, Krigman HR, Whitaker RS, Dodge RK, Rodriguez GC (1999) The prognostic significance of angiogenesis in epithelial ovarian carcinoma. Clin Cancer Res 5:587–591
3. Brown DL, Doubilet PM, Miller FH, Frates MC, Laing FC, DiSalvo DN, Benson CB, Lerner MH (1998) Benign and malignant ovarian masses: selection of the most discriminating gray-scale and Doppler sonographic features. Radiology 208: 103–110
4. Folkman J (1985) Tumor angiogenesis. Adv Cancer Res 43: 175–203
5. Fox SB, Gatter KC, Bicknell R, Going JJ, Stanton P, Cooke TG, Harris AL (1993) Relationship of endothelial cell proliferation to tumour vascularity in human breast cancer. Cancer Res 53:4161–4163
6. Gasparini G, Bonoldi E, Viale G, Verderio P, Boracchi P, Panizzoni GA, Radaelli U, Di Bacco A, Guglielmi RB, Bevilacqua P (1996) Prognostic and predictive value of tumour angiogenesis in ovarian carcinomas. Int J Cancer 69:205–211
7. Giatromanolaki A (2001) Prognostic role of angiogenesis in non-small cell lung cancer. Anticancer Res 21:4373–4382
8. Giatromanolaki A, Koukourakis MI, Theodossiou D, Barbatis K, O'Byrne K, Harris AL, Gatter KC (1997) Comparative evaluation of angiogenesis assessment with anti-factor-VIII and anti-CD31 immunostaining in non-small cell lung cancer. Clin Cancer Res 3:2485–2492
9. Giatromanolaki A, Koukourakis MI, Sivridis E, O'Byrne K, Gatter KC, Harris AL (2000) 'Invading edge vs. inner' (edvin) patterns of vascularization: an interplay between angiogenic and vascular survival factors defines the clinical behaviour of non-small cell lung cancer. J Pathol 192:140–149
10. Giatromanolaki A, Sivridis E, Minopoulos G, Polychronidis A, Manolas C, Simopoulos C, Koukourakis MI (2002) Differential assessment of vascular survival ability and tumor angiogenic activity in colorectal cancer. Clin Cancer Res 8:1185–1191
11. Giatromanolaki A, Sivridis E, Simopoulos C, Polychronidis A, Gatter KC, Harris AL, Koukourakis MI (2002) Differential assessment of angiogenic activity and of vascular survival ability (VSA) in breast cancer. Clin Exp Metastasis 19:673–679
12. Giatromanolaki A, Sivridis E, Koukourakis MI (2004) Tumour angiogenesis: vascular growth and survival. Acta Pathol Micro Immunol Scan (in press)
13. Griffiths JR, McIntyre DJ, Howe FA, Stubbs M (2001) Why are cancers acidic? A carrier-mediated diffusion model for H+ transport in the interstitial fluid. Novartis Found Symp 240:46–62
14. Harfouche R, Hassessian HM, Guo Y, Faivre V, Srikant CB, Yancopoulos GD, Hussain SN (2002) Mechanisms which mediate the antiapoptotic effects of angiopoietin-1 on endothelial cells. Microvasc Res 64:135–147
15. Heimburg S, Oehler MK, Papadopoulos T, Caffier H, Kristen P, Dietl J (1999) Prognostic relevance of the endothelial marker CD34 in ovarian cancer. Anticancer Res 19:2527–2529
16. Hollingsworth HC, Kohn EC, Steinberg SM, Rothenberg ML, Merino MJ (1995) Tumor angiogenesis in advanced stage ovarian carcinoma. Am J Pathol 147:33–41
17. Leek RD (2001) The prognostic role of angiogenesis in breast cancer. Anticancer Res 21:4325–4331
18. Liu W, Davis DW, Ramirez K, McConkey DJ, Ellis LM (2201) Endothelial cell apoptosis is inhibited by a soluble factor secreted by human colon cancer cells. Int J Cancer 92:26–30
19. Obermair A, Wasicky R, Kaider A, Preyer O, Losch A, Leodolter S, Kolbl H (1999) Prognostic significance of tumor angiogenesis in epithelial ovarian cancer. Cancer Lett 138:175–182
20. Papadopoulos I, Giatromanolaki A, Koukourakis MI, Sivridis E (2004) Tumour angiogenic activity (TAA) and vascular survival ability (VSA) in bladder carcinoma. J Clin Pathol 57:250–255
21. Saito H, Tsujitani S (2001) Angiogenesis, angiogenic factor expression and prognosis of gastric carcinoma. Anticancer Res 21:4365–4372
22. Sata M, Kakoki M, Nagata D, Nishimatsu H, Suzuki E, Aoyagi T, Sugiura S, Kojima H, Nagano T, Kangawa K, Matsuo H, Omata M, Nagai R, Hirata Y (2000) Adrenomedullin and nitric oxide inhibit human endothelial cell apoptosis via a cyclic GMP-independent mechanism. Hypertension 36:83–88
23. Scott PA, Gleadle JM, Bicknell R, Harris AL (1998) Role of the hypoxia sensing system, acidity and reproductive hormones in the variability of vascular endothelial growth factor induction in human breast carcinoma cell lines. Int J Cancer 75:706–712
24. Sivridis E (2001) Angiogenesis and endometrial cancer. Anticancer Res 21:4383–4388
25. Sivridis E, Giatromanolaki A, Koukourakis MI (2003) The vascular network of tumours—what is it not for? J Pathol. 201:173–180
26. Streeter EH, Crew JP (2001) Angiogenesis, angiogenic factor expression and prognosis of bladder cancer. Anticancer Res 21:4355–4363
27. Subarsky P, Hill RP (2003) The hypoxic tumour microenvironment and metastatic progression. Clin Exp Metastasis 20:237–250
28. Thompson WD, Shiach KJ, Fraser RA, McIntosh LC, Simpson JG (1987) Tumour acquire their vasculature by vessel incorporation, not vessel ingrowth. J Pathol 151:323–332
29. Zachary I (2001) Signaling mechanisms mediating vascular protective actions of vascular endothelial growth factor. Am J Physiol Cell Physiol 280:1375–1386

Virchows Arch (2004) 445:527–530
DOI 10.1007/s00428-004-1100-7

CASE REPORT

Rathi Ramakrishnan · Richard Young · Barry Powell · M. G. Cook

Features of sentinel lymph nodes for melanoma may lead to re-diagnosis of the cutaneous primary: an unusual case and review of literature

Received: 18 February 2004 / Accepted: 14 June 2004 / Published online: 9 September 2004
© Springer-Verlag 2004

Abstract Although sentinel lymph-node biopsy is accepted as a reliable method of staging of melanoma, it is not without problems to the pathologist. It has been re-emphasised that aggregates of benign naevus cells are not uncommon. Usually these are easily identified by a combination of their benign cytology and location in the fibrous skeleton of lymph nodes. This case represents a combination of an unusual pseudo-malignant pattern in the primary lesion with unusual morphology of the sentinel lymph node. The latter prompted reassessment of the cutaneous lesion as a benign naevus. Confirmation of the diagnosis as cutaneous melanoma by a positive sentinel-node biopsy was averted only by a careful comparison of unusual features of the putative primary and the sentinel lymph node. This case illustrates the need for a rigorous protocol for pathological assessment of sentinel lymph nodes for melanomas to assure detection of all metastases but also to avoid misdiagnosis and over-treatment. It also supports "benign metastases" as the mechanism underlying at least some melanocytes in regional lymph nodes.

Keywords Atypical dermal nodule · Sentinel lymph node · Benign naevus cells · Immunohistochemistry

Introduction

Sentinel lymph-node biopsy has required the establishment of a reliable protocol for the detection of as many as possible of any metastases [1, 2, 3, 4, 5, 6, 7, 8, 9, 10]. By the detailed assessment of large numbers of lymph nodes, the existence of benign naevus cells in lymph nodes has been re-emphasised [11, 12, 13, 14, 15, 16]. Aggregates of naevus cells occurring in lymph nodes are common and can be mistaken for metastatic melanomas. These aggregates of cytologically benign cells are found either within the capsule, around afferent lymphatics or in trabeculae. Since sentinel lymphadenectomy is becoming a routine procedure in the staging of patients with melanoma, pathological assessment of these specimens will become more commonplace and, hence, the need for careful evaluation to prevent misdiagnosis and over-treatment. Although the site and cytology of the naevus cells in the lymph node usually allows a confident recognition, occasionally cases are more problematic.

We describe here a case that posed a diagnostic dilemma because of peculiar histological and immunohistochemical features of both the cutaneous and nodal lesions, illustrating an extreme form of this difficulty. It also raises the consideration of the underlying biology of the nodal naevus cells and metastasis.

R. Ramakrishnan · M. G. Cook (✉)
Department of Histopathology,
The Royal Surrey County Hospital,
Egerton Road, Guildford, Surrey, GU2 5XX, UK
e-mail: mgcook@globalnet.co.uk
Tel.: +44-1483-571122
Fax: +44-1483-452718

R. Young · B. Powell
Department of Plastic Surgery,
St. George's Hospital,
London, UK

Clinical history

A 32-year-old female patient presented with a pigmented lesion in her left lower eyelid. This had been present for approximately 4 years but had shown a recent increase in size and change in colour. There was no history of previous excessive sun exposure or sunburn. A shave biopsy of this lesion was performed and was interpreted at an outside centre as an invasive malignant melanoma, Breslow's thickness 1.5 mm [17] and a Clark's level of at least three with incomplete excision margins arising in the background of an intradermal melanocytic naevus. Based on this diagnosis, a sentinel lymph-node biopsy was performed with wide local excision of the eyelid lesion. Sentinel lymph-node biopsy was done using lymphoscintigraphy with technetium nanocolloid and 2.5% blue dye. Three sentinel nodes were identified in the parotid gland. One of the nodes contained three nests of melanocytes; these had slightly enlarged nuclei and abundant cytoplasm and were noted in the trabecula and focally within the paratrabecula (Fig. 1). The signs of atypia within these cells raised a suspicion for metastasis of melanoma. But the features were unusual, and a review of the primary cutaneous lesion was requested. Upon review, the primary lesion was regarded confidently as a benign intradermal naevus

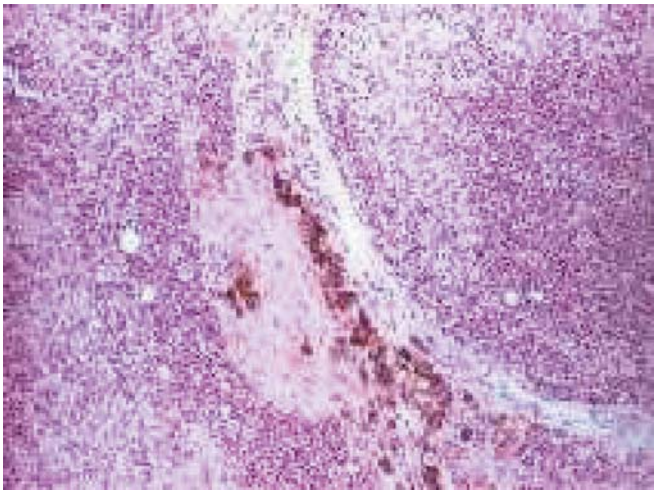


Fig. 1 Nests of large melanocytes within the trabecula of a sentinel lymph node. Haematoxylin and eosin ×200

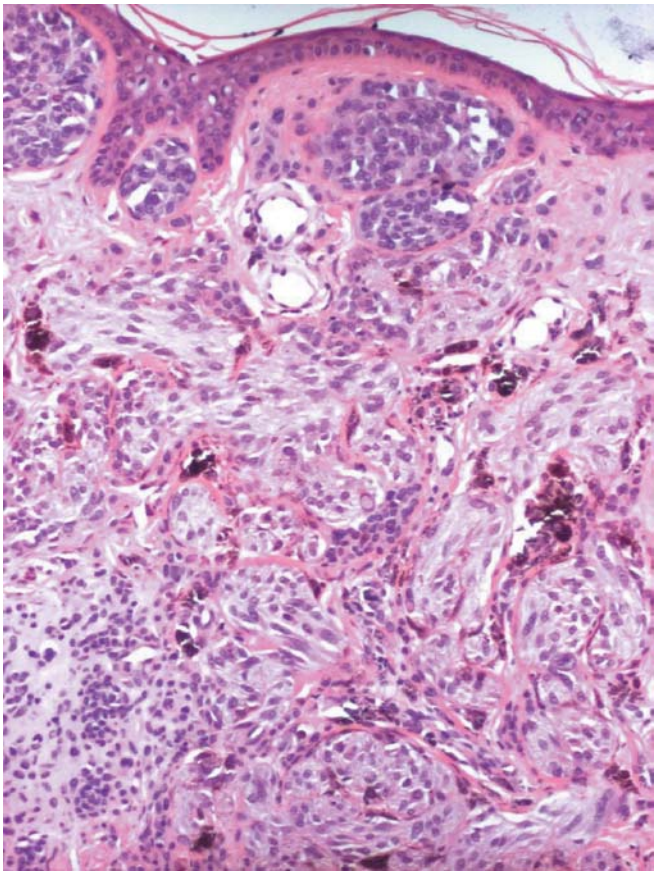


Fig. 2 Cutaneous benign intradermal naevus with a component of "atypical dermal nodule" adjacent to usual type-B naevus cells. Haematoxylin and eosin ×200

with a benign atypical dermal nodule (Fig. 2) [18]. In light of this revised diagnosis of the eyelid lesion, the melanocytes within the sentinel lymph node were assessed as trabecular naevus cells. MIB-1 in the sentinel lymph node showed no activity within the melanocytic component (Fig. 3) [19, 20]. Since the eyelid lesion was confidently diagnosed as benign, the cells in the sentinel lymph node were more easily classified as trabecular (and paratrabecular) naevus cells albeit showing unusual cytological features. These conclusions were supported by Dr. Alistair Cochran, who saw the slides in consultation.

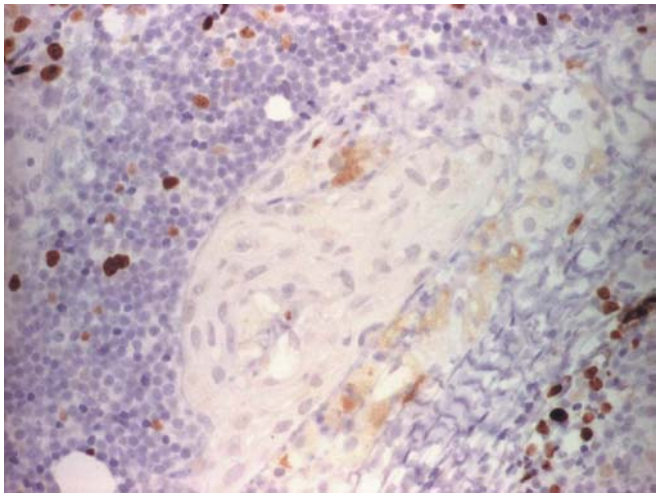


Fig. 3 The melanocytic component in the sentinel lymph node showing no MIB-1 reactivity. Immunohistochemistry (MIB-1) ×400

The patient was counselled, and her earlier planned surgery was cancelled. Follow-up for 18 months has been uneventful in keeping with the revised benign pathological diagnosis.

Discussion

We report this case to illustrate the diagnostic difficulties we encountered in evaluation of this cutaneous lesion and the nodal deposits. The primary lesion as suggested by the gross appearance and histology was recognised on review as a compound melanocytic proliferation showing some divergent differentiation sometimes referred to as "melanocytic naevi with focal atypical epithelioid cell component" [21] or inverted type-A naevus [22], more recently described as atypical dermal nodule in benign naevi [18]. They are a source of confusion with nodular melanoma arising in benign naevi. The presence of large pigmented cells predominantly within the trabeculae of the node with a small component appearing to be in the paratrabecular tissue was unusual and prompted reassessment of the primary lesion. A parenchymal site for the melanocytes is usually indicative of melanoma, but an extension from the deposits in the capsular or trabecular fibrous tissue can be seen [13, 14, 15, 23] and that was considered to be the explanation in this case. In addition, the histology of the cells in the sentinel lymph nodes was identical to those seen in the benign "atypical nodule" of the eyelid lesion.

Immunohistochemistry is of particular relevance in the evaluation of these lesions, particularly the antibody to Ki-67 (MIB-1) antigen, which is helpful in demonstrating the cells, which are in a proliferative cycle. Although immunoreactivity for S-100 was present indicating a melanocytic origin of the tumour cells, reactivity for

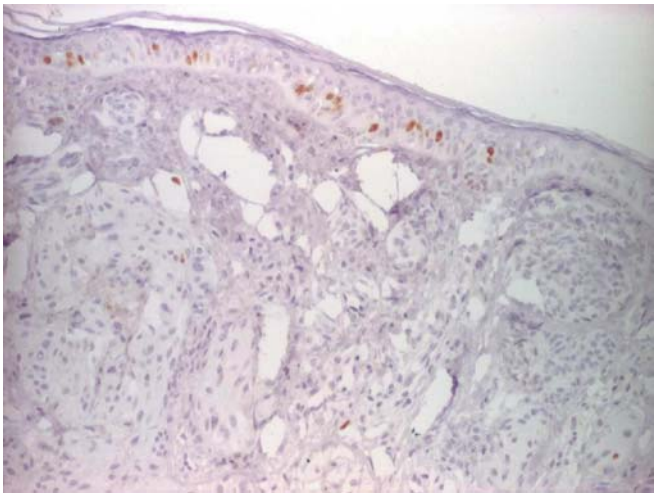


Fig. 4 Both components of the intradermal naevus with an atypical dermal nodule show a negative MIB-1 reaction. Immunohistochemistry ×200

MIB-1 was virtually absent in the melanocytes within the sentinel lymph node. Melanomas show a higher rate of MIB-1 positivity than naevus cells [19, 20], and this is also reflected in the nodal deposits of melanoma. In the present case, the MIB-1 reactivity in the lesion (Fig. 4) and its nodal deposits was negligible (<1%) supporting the benign nature of the melanocytic proliferation.

The mechanism by which nevus cells are deposited in lymph nodes has been a source of interest and controversy. One explanation, as proposed by Von Albertini, was that the cutaneous naevus cells enter the dermal lymphatics and travel through the lymphatics to reach the regional lymph nodes [24]. Since the sentinel nodes are the first nodes draining the region, one would expect to find a higher incidence of these "benign metastases" within the sentinel nodes than in the non-sentinel nodes. This has been supported by histological evidence of invasion of dermal lymphatics by cells of pigmented naevus [25, 26]. Theories in this regard also include an aberration in the embryological migration of melanocytes [27] and arrested migration of naevus cells during embryogenesis and benign spread of these naevus cells [28]. The concept of "benign metastasis" is contradicted by the lack of cutaneous naevi in some cases with intranodal inclusions [29, 30]. Moreover, why most aggregates are found within the capsule or trabeculae rather than intraprenchymal sinuses is not easily explained.

The purpose of this report is to emphasise the difficulty in evaluating many atypical melanocytic lesions and the need for a more structured review for problematic lesions. The performance of a sentinel-node biopsy can be justified in problematic diagnostic cases [11, 13, 14]. In this case, the unusual features of the sentinel lymph node led to the reassessment of the cutaneous lesion, which otherwise could have remained classified as a melanoma with a positive sentinel node. Although immunohistochemistry aids in the identification and categorisation of melanocytic cells in the nodes [31], it should only be complementary to a careful morphological assessment. Histology of the primary tumour should always be compared with the nodal counterparts, and, therefore, there is an argument for a review of all cutaneous melanomas before sentinel-node biopsy. Although extremely sensitive techniques such as reverse-transcription polymerase chain reaction have been described for the identification of metastatic cells in sentinel nodes [32, 33, 34, 35], these have not been reliable in the distinction between naevi and melanomas and do not yet provide any diagnostic advantage over a thorough assessment of the sentinel lymph node using immunohistochemistry [36]. The presence of identical cells in the sentinel lymph node and in the "atypical" nodule part of the skin lesion supports the concept of benign metastasis as the mechanism for the occurrence of naevus cells in the lymph nodes rather than some form of heterotopia.

Acknowledgements Dr. Alistair Cochran (Head, Department of Pathology and Laboratory Medicine, David Geffen School of Medicine at UCLA, Los Angeles, USA) for his opinion on the case

References

1. Cochran AJ, Roberts AA, Saida T (2003) The place of lymphatic mapping and sentinel node biopsy in oncology. Int J Clin Oncol 8:139–150
2. Nowecki ZI, Rutkowski P, Nasierowska-Guttmejer A, Ruka W (2003) Sentinel lymph node biopsy in melanoma patients with clinically negative regional lymph nodes—one institution's experience. Melanoma Res 13:35–43
3. Mahmood MN, Lee MW, Linden MD, Nathanson SD, Hornyak TJ, Zarbo RJ (2002) Diagnostic value of HMB-45 and anti-Melan A staining of sentinel lymph nodes with isolated positive cells. Mod Pathol 15:1288–1293
4. Carcoforo P, Soliani G, Bergossi L, Basaglia E, Virgili AR, Pagani W, Pozza E, Feggi LM (2002) Reliability and accuracy of sentinel node biopsy in cutaneous malignant melanoma. Tumori 88:S14–S16
5. Doting MH, Hoekstra HJ, Plukker JT, Piers DA, Jager PL, Tiebosch AT, Vermey A, Schraffordt Koops H (2002) Is sentinel node biopsy beneficial in melanoma patients? A report on 200 patients with cutaneous melanoma. Eur J Surg Oncol 28:673–678
6. Pizzocaro C, Rossini PL, Magri GC, Manca G, Caglioni C, Manganoni MA, Giubbini R (2000) Sentinel node biopsy in melanoma: the experience of Brescia Civic Hospital. Tumori 86:349–350
7. Hettiaratchy SP, Kang N, O'Toole G, Allan R, Cook MG, Powell BW (2000) Sentinel lymph node biopsy in malignant melanoma: a series of 100 consecutive patients. Br J Plast Surg 53:559–562
8. Jansen L, Nieweg OE, Peterse JL, Hoefnagel CA, Olmos RA, Kroon BB (2000) Reliability of sentinel lymph node biopsy for staging melanoma. Br J Surg 87:484–489
9. Karakousis CP, Grigoropoulos P (1999) Sentinel node biopsy before and after wide excision of the primary melanoma. Ann Surg Oncol 6:785–789
10. Jacobs IA, Chevinsky AH, Swayne LC, Magidson JG, Britto EJ, Smith TJ (2001) Gamma probe-directed lymphatic mapping and sentinel lymphadenectomy in primary melanoma: reliability of the procedure and analysis of failures after long-term follow-up. J Surg Oncol 77:157–164
11. Cook MG, Green MA, Anderson B, Eggermont AM, Ruiter DJ, Spatz A, Kissin MW, Powell BW, EORTC Melanoma group

(2003) The development of the optimal pathological assessment of sentinel lymph nodes for melanoma. J Pathol 300:314–319
12. Rutty GN. Benign lymph node inclusions (1994) J Pathol 173:301–302
13. Bautista NC, Cohen S, Anders KH (1994) Benign melanocytic naevus cells in axillary lymph nodes. A prospective incidence and immunohistochemical study with literature review. Am J Clin Pathol 102:102–108
14. Biddle DA, Evans HL, Kemp BL, El-Naggar AK, Harvell JD, White WL, Iskandar SS, Prieto VG (2003) Intraparenchymal naevus cell aggregates in lymph nodes: a possible diagnostic pitfall with malignant melanoma and carcinoma. Am J Surg Pathol 27:673–681
15. Fisher CJ, Hill S, Millis RR (1994) Benign lymph node inclusions mimicking metastatic carcinoma. J Clin Pathol 47: 245–247
16. Pantanowitz L, Upton MP (2003) Benign axillary lymph node inclusions. Breast J 9:56–57
17. Blaheta HJ, Paul T, Sotlar K, Maczey E, Schittek B, Paul A, Moehrle M, Breuninger H, Bueltmann B, Rassner G, Garbe C (2001) Detection of melanoma cells in sentinel lymph nodes, bone marrow and peripheral blood by a reverse transcription-polymerase chain reaction assay in patients with primary cutaneous melanoma: association with Breslow's tumour thickness. Br J Dermatol 145:195–202
18. Collina G, Deen S, Cliff S, Jackson P, Cook MG (1997) Atypical dermal nodules in benign melanocytic naevi. Histopathology 31:97–101
19. Lohmann CM, Iversen K, Jungbluth AA, Berwick M, Busam KJ (2002) Expression of melanocyte differentiation antigens and ki-67 in nodal naevi and comparison of ki-67 expression with metastatic melanoma. Am J Surg Pathol 26:1351–1357
20. Li LX, Crotty KA, McCarthy SW et al (2000) A zonal comparison of MIB-1-ki67 immunoreactivity in benign and malignant melanocytic lesions. Am J Dermatopathol 22:489–495
21. Ball NJ, Golitz LE (1994) Melanocytic naevi with focal atypical epithelioid cell components: a review of seventy-three cases. J Am Acad Dermatol 30:724–729
22. Mihm MC, Googe PB (1990) Variations on the common acquired naevus. (Problematic pigmented lesions) Lee & Farber, Philadelphia, p 75
23. Hruban RH, Eckert F, Baricevic B (1990) Melanocytes of a melanocytic naevus in a patient with primary cutaneous melanoma associated with a small congenital naevus. Am J Dermatopathol 12:402–407
24. Von Albertini M (1935) Sur un cas de neuro-naevus avec metastase ganglionnaiere de meme caractere. Bull Soc Franc Derm Syph 42:1273–1278
25. Bell ME, Hill DP, Bhargava MK (1979) Lymphatic invasion in pigmented naevi. Am J Clin Pathol 72:97–100
26. Bichel P, Ornsholt J (1988) Benign nevus cells in lymph nodes: an immunohistochemical study. APMIS 96:117–122
27. Fontaine D, Parkhill W, Greer W, Walsh N (2002) Nevus cells in lymph nodes: an association with congenital cutaneous naevi. Am J Dermatopathol 24:1–5
28. Hara K (1993) Melanocytic lesions in lymph nodes associated with congenital naevi. Histopathology 23:445–451
29. Hart WR (1971) Primary nevus of a lymph node. Am J Clin Pathol 55:88–92
30. Shenoy BV, Fort L 3rd, Benjamin SP (1987) Malignant melanoma primary in the lymph node: the case of the missing link. Am J Surg Pathol 11:140–146
31. Preito VG, Clark SH (2002) Processing of sentinel lymph nodes for the detection of metastatic melanoma. Ann Diagn Pathol 6:257–264
32. Starz H, Haas CJ, Schulz GM, Balda BR (2003) Tyrosinase RT-PCR as a supplement to histology for detecting melanoma and naevus cells in paraffin sections of sentinel lymph nodes. Mod Pathol 16:920–929
33. Goydos JS, Patel KN, Shih WJ, Lu SE, Yudd AP, Kempf JS, Bancila E, Germino FJ (2003) Patterns of recurrence in patients with melanoma and histologically negative but RT-PCR-positive sentinel lymph nodes. J Am Coll Surg 196:196–204
34. Kuo CT, Hoon DS, Takeuchi H, Turner R, Wang HJ, Morton DL, Taback B (2003) Prediction of disease outcome in melanoma patients by molecular analysis of paraffin-embedded sentinel lymph nodes. J Clin Oncol 21:3566–3572
35. Rimoldi D, Lemoine R, Kurt AM, Salvi S, Berset M, Matter M, Roche B, Cerottini JP, Guggisberg D, Krischer J, Braun R, Willi JP, Antonescu C, Slosman D, Lejeune FJ, Lienard D (2003) Groupe Melanome Lemanique. Detection of micrometastases in sentinel lymph nodes from melanoma patients: direct comparison of multimarker molecular and immunopathological methods. Melanoma Res 13:511–520
36. Eudy GE, Carlson GW, Murray DR, Waldrop SM, Lawson D, Cohen C (2003) Rapid immunohistochemistry of sentinel lymph nodes for metastatic melanoma. Hum Pathol 34:797–802

Virchows Arch (2004) 445:531–536
DOI 10.1007/s00428-004-1084-3

CASE REPORT

Evariste Gafumbegete · Susann Richter · Ludwig Jonas · Horst Nizze · Josef Makovitzky

Nonsecretory multiple myeloma with amyloidosis. A case report and review of the literature

Received: 7 August 2003 / Accepted: 28 June 2004 / Published online: 29 July 2004
© Springer-Verlag 2004

Abstract We report a case concerning a 49-year-old female patient with thoracic pain. X-rays showed a single osteolytic lesion on the right seventh rib. The excision of the rib disclosed a plasmocytic plasmocytoma with extensive amyloidosis. Serum and urine protein electrophoresis were both negative for monoclonal gammopathy. Bone marrow biopsy showed that 80% of the marrow had been replaced by plasma cells. A diagnosis of nonsecretory multiple myeloma was made. Immunohistochemistry revealed amyloid light (AL) amyloidosis of κ-light chain origin. The relationship between nonsecretory multiple myeloma and amyloidosis is discussed.

Keywords Nonsecretory · Multiple myeloma · AL amyloidosis · Electron microscopy

Introduction

Nonsecretory multiple myeloma (NSMM) is characterized by the absence of monoclonal immunoglobulins in serum and urine. The reported incidence is 1–5% of all multiple myeloma (MM) cases. The following case is of interest because of the rare association between nonsecretory myeloma and amyloidosis as soon as the presence of only one single bone lesion. There is very little knowledge about pathogenesis and therapy of this disorder. Treatment of MM and NSMM is the same, including conventional chemotherapy with melphalan and prednisone, steroids, interferon α, high-dose melphalan or hematopoietic stem cell transplantation. The aim of this report was to emphasize the presence of NSMM with steady production of amyloid. An attempt is made to explain the lack of monoclonal immunoglobulins in serum and urine, although massive tumorous amyloid deposits were found. The assumption is that the neoplastic plasmocytic plasma cells possess an excretory mechanism, which allows the pathological immunoglobulins to be secreted either as amyloid proteins polymerizing into amyloid fibrils or as immunoglobulin fragments falling in degradation as soon as they are excreted out of the tumor cells.

E. Gafumbegete · H. Nizze
Department of Pathology,
University of Rostock,
Germany

S. Richter · J. Makovitzky (✉)
Clinic of Gynecology and Obstetrics,
Laboratory of Gynecopathology,
University of Rostock,
PO Box 10 08 88, 18055 Rostock, Germany
e-mail: josef.makovitzky@med.uni-rostock.de
Tel.: +49-381-4948193
Fax: +49-381-4948102

L. Jonas
Department of Pathology,
Electron Microscopic Centre, University of Rostock,
Germany

Clinical history

A 49-year-old female patient was investigated in our clinic because of severe progressive bone pain involving the right thorax. On clinical examination, the patient expressed painful limitation of movement and presented with progressive weakness and weight loss. A fractured rib was presumed. Her past history included a carpal tunnel syndrome (CTS) on both sides with following surgical procedure. Laboratory data were registered as follows; reference values are given in parentheses: IgG 4.75 g/l (8–18 g/l), IgA 0.14 g/l (0.9–4.5 g/l), IgM 0.18 g/l (0.45–2.5 g/l), Ig/light chain kappa type 1.19 g/l (6.29–13.5 g/l); Ig/light chain lambda type 0.36 g/l (3.13–7.23 g/l), β_2-microglobulin 1.63 µg/ml (1–2.5 µg/ml), hemoglobin (Hb) 6.9 mmol/l (7.4–9.9 mmol/l), leucocytes 5400/µl (3800–10,500/µl), thrombocytes 306,000/µl (140,000–345,000/µl). Electrolyte, creatinine and liver parameters were normal. Serum and urine protein electrophoresis were both negative for monoclonal gammopathy; however, immunoelectrophoresis failed to demonstrate light chains. X-ray, computed tomography and magnet resonance imaging showed a single osteolytic lesion on the seventh right rib. Bone marrow aspiration and costectomy showed the same histopathological feature: a massive infiltration (80%) of mature small plasma cells corresponding to MM (Fig. 1). Amyloidosis was found around the tumor of the rib. A pulmonary biopsy and biopsy of the left breast revealed an extensive amyloidosis 4 years after the diagnosis of NSMM was made. Congo Red staining showed an anisotropy and green polarization color. Treatment consisted of melphalan and prednisone. The patient responded favorably. The

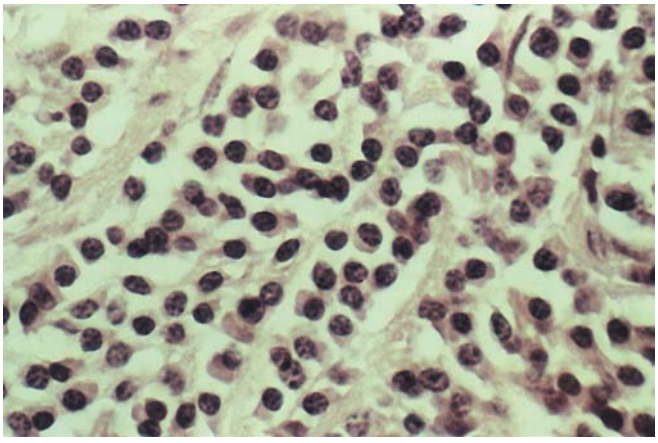


Fig. 1 Dense infiltrates of atypical plasmocytic plasma cells in the bone marrow. Staining was performed using hematoxylin and eosin. ×250

tumor mass was reduced from formerly 80% to 25% of the total of the plasma cells. This therapy was followed by interferon-α and finally by the combination of idarubicin (Zavedos) and dexamethasone. Therapy was completed with allogenic bone marrow transplantation of a HLA-identical sister of the patient. The patient is doing well 5 years after the diagnosis; neither clinical changes nor radiological or biological disturbances have been noted.

Materials and methods

Electrophoresis and immunofixation

Serum electrophoresis of the proteins was performed in 1% agarose gel according to Johansson [12]. Immunofixation was carried out using a concentration of fresh morning urine samples with the same procedures as for serum.

Histochemistry

Investigations were performed on tissue samples of the rib tumor, lung and mamma containing high quantities of amyloid. The specimens were fixed in phosphate-buffered saline-buffered formalin (pH 7.2), embedded in paraffin and sectioned at 2–4 μm. Before staining the birefringent paraffin was carefully removed from the sections in xylene at 70°C for 24 h. The polarization optical investigations were performed with a Carl Zeiss Jena Axioskop 2. Deparaffinized slides were stained with Congo red, according to Romhányi [24], without alcoholic differentiation and sealed with gum arabic (Kristall-Gummi, Fa. Gutenberg Werk, Mainz). The amyloid deposits were determined and histochemically characterized by Congo red staining after performic acid pretreatment (8 ml 90% HCOOH; 3 ml 33% H_2O_2; 0.22 ml concentrated H_2SO_4) according to Romhányi [26] and potassium permanganate oxidation according to Wright et al. [29].

Immunohistochemistry

The immunohistochemistry was directed at the deparaffinized tissues using the conventional alkaline phosphatase–antialkaline phosphatase method. After pretreatment with the microwave oven technique (3×5 min, 450 W) [18], the immunostaining was performed with the monoclonal antibody VS38 (1:50; Dako, Hamburg), the monoclonal antibodies IgA (1:10), IgG (1:100) and IgM (1:100) as well as the antibodies against the light chains kappa (1:500) and lambda (1:3000). All the preceding antibodies (from Dako, Hamburg) were pretreated 10 min with protease (Sigma-Aldrich, Munich). The stains were accompanied with positive and negative controls.

Two different antisera were used for the identification of the amyloid fibril proteins. These were directed against amyloid of lambda light chain (Aλ [HAR]; dilution 1:10,000) and kappa light chain origin (Aκ [SIN]; dilution 1:50,000). The avidin-biotin-method was used to visualize immunostaining with anti-Aλ and anti-Aκ, and 3′3-diaaminobenzidine tetrahydrochloride served as chromogen.

Electron microscopy

For electron microscopy, small pieces less than 2 mm^3 were cut out of the paraffin block by a razor blade, deparaffinized in xylene, rehydrated with alcohol/buffer and postfixed with phosphate-buffered 4% glutaraldehyde. A further fixation and contrast of the tissue was performed with 1% OSO_4 for 1 h. The material was dehydrated in acetone and embedded in Araldite M (Fluka, Buchs, Swiss). After polymerization, ultrathin sections were prepared with an ultramicrotome Ultracut SWS (Leica) and studied under a transmission electron microscope (TEM) EM 902 A (Zeiss).

Results

Electrophoresis and immunofixation

Agarose gel electrophoresis of the plasma and concentrated urine failed to show any monoclonal immunoglobulins (M-component). Also, immunoelectrophoresis was negative for monoclonal gammopathy. However, immunofixation as the most sensitive routine technique detects light chains of κ type in the concentrated urine. The only abnormalities found in serum protein electrophoresis were the depressed plasma levels in following immunoglobulin classes: IgG 4.75 g/l (8–18 g/l), IgA 0.14 g/l (0.9–4.5 g/l) and IgM 0.18 g/l (0.45–2.5 g/l).

Histochemistry

Staining with Congo red induces congophilia and strong birefringence of amyloid with the typical green polarization color. A bone-destructive tumor of plasmocytic plasmocytoma with large amounts of amyloid is presented in Fig. 2. After Congo red staining according to Romhányi with gum arabic as mounting medium, one can differentiate between the linear positively birefringent amyloid (green) and the weakly linear negatively birefringent collagen fibers (gray). The resistance of amyloid deposits in the lung parenchyma to preoxydation with potassium permanganate is illustrated in Fig. 3. The lung tissue was extensively replaced by masses of amyloid (Fig. 3A). Amyloid deposits were also located within the walls of blood vessels (Fig. 3B).

Immunohistochemistry

The plasma cell infiltrates were immunoreactive with the antibody VS38, against the 64kDalton protein, specific

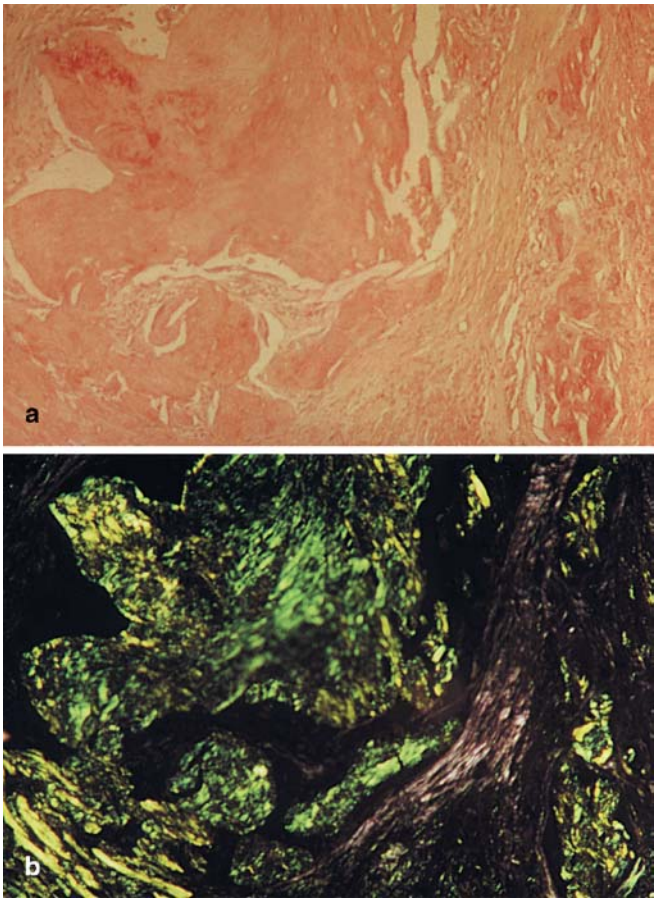


Fig. 2 Plasmocytic plasmocytoma with large amounts of amyloid. **A** Amyloid deposits showing congophilia in the light microscope. **B** Strong positive birefringence of Congo red-stained amyloid deposits with the typical green polarization color. Collagen fibers appear linear negatively birefringent. Staining was performed using Congo red. ×40

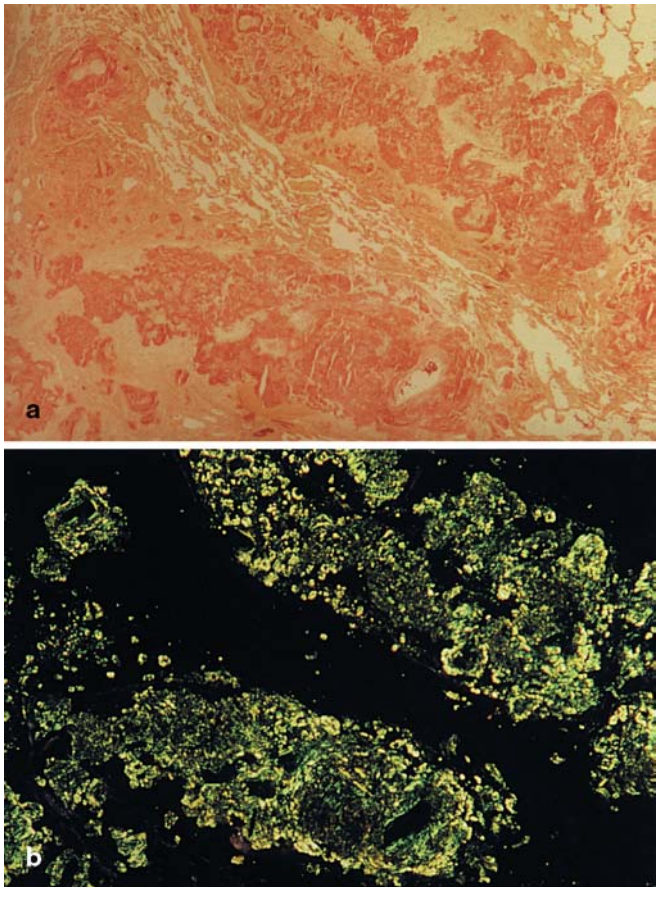


Fig. 3 Lung tissue with extensive amyloidosis. **A** Amyloid deposits showing strong congophilia in the light microcope. **B** Amyloidosis with green polarization color involving blood vessels. The amyloid deposits are resistant to pretreatment with potassium permanganate. The green polarization color is not abolished by this agent. Staining was performed using Congo red after potassium permanganate preoxydation. ×10

for the plasma cells (according to the manufacturer). The antibodies IgA, IgG, IgM as well as the antibodies against the light chains kappa and lambda were repeatedly negative for the plasma cell infiltrates. The amyloid deposits in the rib tumor (Fig. 4) and the lung reacted positively with anti-amyloid kappa (Aκ).

Electron microscopy

Ultrastructurally, the myeloma cells showed normal morphology with the typical wheel-spoke nuclei, strongly condensed prominent heterochromatin on the inner surface of the nuclear membrane and around the central nucleolus (Fig. 5A). A myeloma cell at higher magnification with a wheel-spoke nucleus and vesiculated rough endoplasmic reticulum containing granular material is demonstrated in Fig. 5B. Furthermore, electron-dense inclusions with a fibrillar content limited by a membrane are visible in the cytoplasm of the plasma cell, indicating that it is amyloid. These inclusions are composed of tightly packed fine fibrils oriented parallel to the long

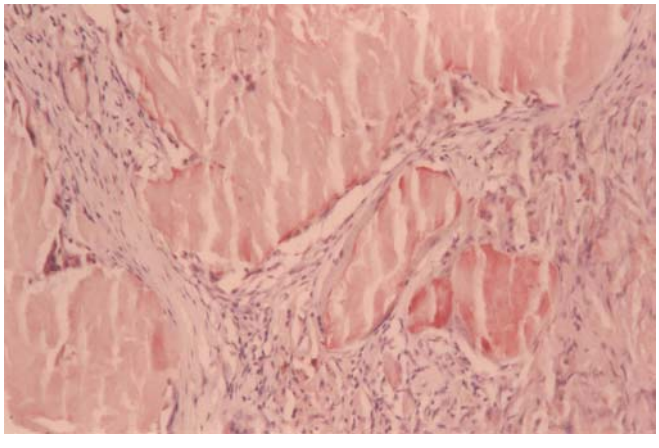


Fig. 4 Immunohistochemistry of the rib tumor. Amyloid deposits display a positive reaction with anti-amyloid kappa (Aκ). ×80

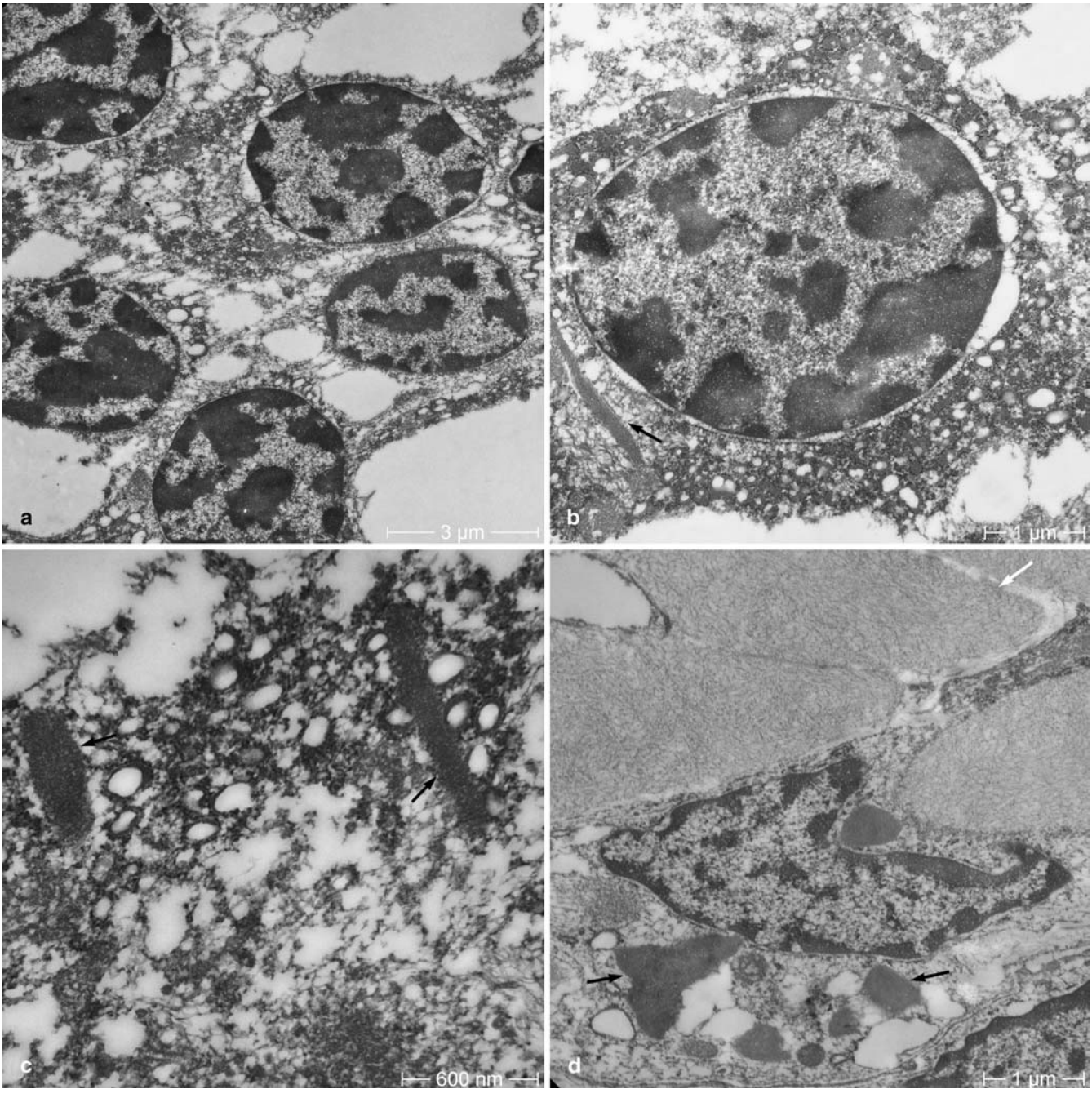


Fig. 5 **A** Myeloma cells with wheel-spoke nuclei, strongly condensed heterochromatin on the inner surface of the nuclear membrane and central located nucleoli. **B** Stronger magnification of a myeloma cell with a wheel-spoke nucleus, vesiculated endoplasmic reticulum containing proteinous material and ribosomes on the outer surface of the cisternal membrane. An elongated membrane-bordered inclusion filled with amyloid fibrils, arranged parallel to the longitudinal axis (*black arrow*). The mitochondria are inadequate preserved by formaldehyde fixation. **C** Numerous vesiculated elements of the endoplasmic reticulum and two elongated membrane-bordered inclusions containing amyloid fibrils (*black arrows*). The dilated nearly empty cisternae possess a protein coat on the inner surface and numerous ribosomes on the outer surface of the membrane. **D** Myeloma cell with intracellular accumulation of amyloid (*black arrows*) in close contact to extracellular amyloid deposits (*white arrow*)

axis. In cross section, the content of these membrane-bordered organelles is of granular structure. The plasma cells show a well-developed endoplasmic reticulum, mostly dispersed as vesicles, presumably because of the inadequate preservation after formaldehyde fixation (Fig. 5B, C). The rough endoplasmic reticulum, including dilated nearly empty cisternae with a protein coat on the inner surface and numerous ribosomes on the outer surface of the cisternal membrane, are demonstrated in Fig. 5C. Electron microscopic examination revealed intracellular and extracellular amyloid deposits in the interstitium. Extracellular amyloid fibrils are in close con-

tact to the plasma cell. These features are illustrated in Fig. 5D.

Discussion

MM is a neoplastic disorder characterized by proliferation of a single clone of plasma cells derived from B cells. This clone of plasma cells proliferates in the bone marrow, frequently invades the adjacent bone and produces skeletal destruction, resulting in bone pain and fractures. NSMM is a rare variant of the classic MM. The reported incidence is 1–5%. The diagnosis of NSMM should be considered in patients with signs and symptoms similar to those of MM but who have no evidence of monoclonal gammopathy by serum or urine electrophoresis [1].

Two types of NSMM have been described: the "producer type", which is characterized by producing immunoglobulins but not secreting them out of the cell, and the "nonproducer type", in which the plasma cells are unable to produce immunoglobulins. There are several hypotheses regarding the pathogenesis of the producer form of NSMM. Preud'homme et al. suggested that the inability to detect serum or urinary immunoglobulin may be due to a chain defect that confers a susceptibility to rapid extracellular enzymatic breakdown of the immunoglobulin [22]. The occurrence of amyloid deposits in some rare cases of NSMM, including ours, and the detection of intermittent urinary output of minute quantities of Bence Jones proteins described by some authors [3] favor such a hypothesis. The cause of nonproducer MM may be a very rapid intracellular degradation of immunoglobulins, the lost capacity to synthesize immunoglobulins [6], lack of normal intracellular immunoglobulin transport and processing or release of antigenically unrecognizable products [7].

In our case study, serum and urine electrophoresis were both negative for monoclonal gammopathy. Additionally, serum immunoelectrophoresis was entirely normal. Concentrated urinary immunofixation demonstrated light chains of κ type. There were no detectable Bence Jones proteins in the urine. It has been previously reported that there are myelomas in which the quantity of light chains in serum or urine is very small. These cases should be regarded as oligosecretory rather than nonsecretory [5]. The use of immunofixation as the most sensitive routine technique shows that 85–90% of all AL amyloid deposits are associated with circulating monoclonal immunoglobulins [9, 15]. Blade et al. observed that in low secretory MM, the light chain is of κ type in 75% [5]. In a series of six patients with NSMM, four cases with trace amounts of monoclonal κ chains were detected in the urine [28].

Hypogammaglobulinemia has been a constant finding in previous reports. Osserman and Takatsuki described as the only difference between MM and NSMM a decrease in serum gamma globulin concentration found in each case of NSMM [21]. The depression of immunoglobulin levels in this case is in comparison with findings of Turesson and Grubb: all patients had depressed plasma levels of at least one immunoglobulin class, and most patients had low plasma levels of all immunoglobulin classes including IgG, IgA and IgM [28].

On the basis of our ultrastructural study, we assume that the patient described in this article represents the "producer type" of NSMM. Azar et al. pointed out that cells that are able to synthesize large amounts of protein intended for export are characterized by a well-developed endoplasmic reticulum [3]. As described above, we found an abundance of rough endoplasmic reticulum with cisternal dilatation as an indirect sign of secretion. The cisternae were filled with granular material. The recognition of amyloid deposits either in the cytoplasm of plasma cells or extracellularly led to the hypothesis that plasma cells may also be able to excrete immunoglobulins, which are then accumulated into amyloid fibrils. The presence of amyloid deposits in the lung and the left breast provides further indication for this proposal.

Staining with Congo red induces strong birefringence of amyloid with a green polarization color between crossed polars. We used Romhányi's staining method because histological sections stained with Congo red according to Eastwood and Cole [8] or Puchtler et al. [23] may show birefringence in non-amyloid structures, such as cellulose and collagen [4, 13, 17, 24].

Congo red staining reaction after pretreatment with potassium permanganate and/or performic acid is useful to differentiate secondary amyloid deposits from primary, senile, localized amyloidosis. Secondary amyloid deposits are sensitive to potassium permanganate and/or performic acid pretreatment. The Congo red-induced birefringence, and green polarization color is abolished by these agents. Primary (AL), local and senile types of amyloid are resistant to potassium permanganate and performic acid. After Congo red staining, they have the same induced birefringence and green polarization color. Also, myeloma-associated amyloidosis has a performic acid resistant ultrastructure and resistance to permanganate pretreatment [25, 26, 27]. The simplicity of the proposed staining reactions suggests performing them first, indicating the special subtype of amyloidosis, followed by immunohistochemistry to confirm these findings.

AL amyloidosis as described in our case is a disease caused by deposition of immunoglobulin light chains in a fibrillar form. Amyloidosis is the end result of a dynamic process in which normally soluble proteins form insoluble fibrils [20]. Glenner et al. demonstrated that amyloid fibrils in a patient with amyloidosis were identical to the variable segment of a monoclonal light chain. This variable portion of a fragment or a complete light chain constitutes the typical fibril of AL [10]. The light chain could be of κ- or λ type. AL amyloidosis should be suspected in nephrotic-range proteinuria with or without renal insufficiency, heart failure resulting from restrictive cardiomyopathy, unexplained hepatomegaly and peripheral neuropathy [9]. CTS is present in 40% of the cases [11]. The patient described in this article had a CTS on

both sides with following surgical procedure in her anamnesis.

Kyle et al. showed in a review of 1027 patients with MM from 1985 to 1998 that only 3% of these patients had no M-protein in the serum or urine and were designated as having nonsecretory myeloma [14]. Development of amyloidosis in NSMM has been only occasionally reported in the literature. Preud'homme et al. described 25 patients with NSMM, only one of whom developed amyloidosis [22]. Another case of amyloidosis complicating NSMM has been pointed out by Lugassy [16], Nores [19] and Ajana [2]. Azar et al. observed that in 123 cases of MM, only 7 patients had a NSMM, and occurrence of amyloidosis has been pointed out in only 1 patient [3]. The finding of amyloidosis in this and previous publications of NSMM favors the hypothesis that many cases are not truly nonsecretory but low secretory.

Acknowledgements The authors wish to express their special regards to Mrs. Epper from the Institute of Pathology (University of Basel) for her help in performing the immunohistochemistry.

References

1. Abdalla IA, Tabbara IA (2002) Nonsecretory multiple myeloma. South Med J 95:761–764
2. Ajana FA (1998) Amylose osseuse et ganglionnaire associée à un myélome non excrétant. Ann Med Interne 149:311–312
3. Azar HA, Zaino EC, Pham TD, Yannopoulos K (1972) "Nonsecretory" plasma cell myeloma: observations on seven cases with electron microscopic studies. Am J Clin Pathol 58:618–629
4. Bély M, Apáthy A (2000) Histochemical and immunohistochemical differential diagnosis of amyloidosis—a brief illustrated essay and personal experience with Romhányi's method. Amyloid Int J Exp Clin Invest 7:212–217
5. Bladé J, Kyle RA (1999) Nonsecretory myeloma, immunoglobulin D myeloma, and plasma cell leukemia. Hematol Oncol Clin North Am 13:1259–1272
6. Bourantas K (1996) Nonsecretory multiple myeloma. Eur J Haematol 56:109–111
7. Doster DR, Folds J, Gabriel DA (1988) Nonsecretory multiple myeloma. Arch Pathol Lab Med 112:147–150
8. Eastwood H, Cole KR (1971) Staining of amyloid by buffered Congo red in 50% ethanol. Stain Technol 46:208–209
9. Gertz MA, Lacy MQ, Dispenzieri A (1999) Amyloidosis. Hematol Oncol Clin North Am 13:1211–1233
10. Glenner GG, Ein D, Eanes ED, Bladen HA, Terry W, Page DL (1971) Creation of "amyloid" fibrils from Bence Jones proteins in vitro. Science 174:712–714
11. Hawkins PN, Pepys MB (1998) Amyloidosis. Myeloma: biology and management. Oxford University Press, Oxford
12. Johansson BG (1972) Agarose gel electrophoresis. Scand J Clin Lab Invest 124[Suppl]:7–19
13. Klatskin G (1969) Nonspecific green birefringence in Congo red stained tissues. Am J Pathol 56:1–13
14. Kyle RA, Gertz MA, Witzig TE, Lust JA, Lacy MQ, Dispenzieri A, Fonseca R, Rajkumar SV et al (2003) Review of 1027 patients with newly diagnosed multiple myeloma. Mayo Clin Proc 78:21–33
15. Linke RP (2002) Amyloidosen bei monoklonaler Gammopathie. Tumorzentrum München
16. Lugassy G, Ducach A, Yossefi C, Michal J (1993) Unusual case of amyloidosis complicating nonsecretory multiple myeloma. Am J Hematol 43:332–333
17. Makovitzky J, Tanka D (1979) Das Vorkommen von Amyloid bei rheumatoider Arthritis. In 9th European Rheumatology Meeting, Wiesbaden (FRG) Abstr W-18:422
18. Malisius R, Merz H, Heinz B, Gafumbegete E, Koch BU, Feller AC (1997) Constant detection of CD2, CD3, CD4, and CD5 in fixed and paraffin-embedded tissue using the peroxidase-mediated deposition of biotin-tyramide. J Histochem Cytochem 45:1665–1672
19. Nores JM, Remy JM, Nenna AD, Dalayeun J (1990) Twelve-year profile of a non-secretory myeloma with amyloidosis. Br J Clin Pract 44:529–530
20. Omtvedt LA, Bailey D, Renouf DV et al (2000) Glycosylation of immunoglobulin light chains associated with amyloidosis. Amyloid 7:227–244
21. Osserman EF, Takatsuki K (1963) Plasma cell myeloma: gamma globulin synthesis and structure. Medicine 42:357–384
22. Preud'homme JL, Hurez D, Danon F, Brouet JC, Seligmann M (1976) Intracytoplasmic and surface-bound immunoglobulins in nonsecretory and Bence–Jones myeloma. Clin Exp Immunol 25:428–436
23. Puchtler H, Sweat F, Levine M (1962) On the binding of Congo red by amyloid. J Histochem Cytochem 10:355–364
24. Romhányi G (1971) Selective differentiation between amyloid and connective tissue structures based on the collagen specific topo-optical staining reaction with congo red. Virchows Arch 354:209–222
25. Romhányi G (1972) Differences in ultrastructural organization of amyloid as revealed by sensitivity or resistance to induced proteolysis. Virchows Arch 357:29–52
26. Romhányi G (1979) Selective demonstration of amyloid deposits and methodical possibilities of analysis of their ultrastructural differences (author's transl). Zentralbl Allg Pathol 123:9–16
27. Romhányi G, Deák G (1974) Topo-optical studies on age pigment, corpora amylacea and senile amyloid-like substances of the brain. Proceedings of VIIth International Congress of Neuropathology, Budapest 2:123–126
28. Turesson I, Grubb A (1978) Nonsecretory or low secretory myeloma with intracellular kappa chains. Report of six cases and review of the literature. Acta Med Scand 204:445–451
29. Wright JR, Calkins E, Humphrey RL (1977) Potassium permanganate reaction in amyloidosis. A histologic method to assist in differentiating forms of this disease. Lab Invest 36:274–281

Virchows Arch (2004) 445:537–540
DOI 10.1007/s00428-004-1097-y

CASE REPORT

Nicolas Sirvent · Christophe Perrin · Jean-Philippe Lacour · Georges Maire · Rita Attias · Florence Pedeutour

Monosomy 9q and trisomy 16q in a case of congenital solitary infantile myofibromatosis

Received: 8 July 2004 / Accepted: 12 July 2004 / Published online: 9 September 2004
© Springer-Verlag 2004

Abstract Although infantile myofibromatosis (IM) is the most common fibrous proliferation of infancy, many aspects of this benign lesion have not been explored. IM histogenesis is still poorly understood, despite immunohistochemical staining and ultrastructural features that suggest a myofibroblastic origin. IM diagnosis is often made difficult by the predominance of small primitive spindle cells over myofibrobasts and the presence of intravascular growth. Genetic information is scarce, with only one karyotyped case. Here we describe a case of solitary IM discovered at birth in an otherwise healthy girl. The tumor was well circumscribed, arranged in nodules and made up of ovoid cells without atypia, in a myxoid background. Immunohistochemical evaluation indicated a myofibroblastic differentiation. The cytogenetic and fluorescence in situ hybridization analyses revealed an abnormal chromosome 9, derived from an unbalanced whole-arm translocation between chromosomes 9 and 16. On both chromosomes, the breakpoints were located in the pericentric heterochromatic region. This clonal abnormality has not been reported in other tumors and is different from the chromosome 6q deletion reported in the single previous reported IM karyotype.

Keywords Soft tissue neoplasms · Infantile myofibromatosis · Children · Cytogenetics · Translocation · FISH

N. Sirvent
Service de Pédiatrie,
CHU de Nice,
France

C. Perrin
Laboratoire d'Anatomie Pathologique,
CHU de Nice,
France

J.-P. Lacour
Service de Dermatologie,
CHU de Nice,
France

G. Maire · R. Attias · F. Pedeutour (✉)
Laboratoire de Génétique,
Hôpital de l'Archet, CHU de Nice,
151 route de Saint-Antoine de Ginestière,
06202 Nice cedex 3, France
e-mail: pedeutou@unice.fr
Tel.: +33-4-92036456
Fax: +33-4-92036465

Introduction

Benign neoplasms, such as fibromatoses, are the most frequent neonatal soft-tissue tumors [8]. Among them, infantile myofibromatosis (IM), first described in 1951 by Williams and Schrum, who designated the lesion "congenital fibrosarcoma," is the most common fibrous proliferation in infancy, usually detected at birth or within the first 2 years of life [14]. Two IM types can be distinguished: the solitary IM, also called myofibroma, a single lesion arising in the cutaneous or subcutaneous tissues, skeletal muscles, aponeuroses, or bones and the multicentric IM, which involves both soft tissue and bones, including visceral locations in 25–35% of cases [9]. IM can be either sporadic or familial, and there is now a consensus for an autosomal dominant inheritance of the familial cases [1, 15]. Because IM usually tends to regress spontaneously, the assessment of a correct and precise diagnosis is of great importance to avoid unnecessary aggressive treatments. Such a diagnosis is often difficult and, as for many other soft tissue tumors, might be improved by the discovery of specific genetic features. The single previous cytogenetic report of IM showed deletion of chromosome 6: del (6)(q12q15) [11]. We report here the second cytogenetic description of a solitary IM that revealed another type of chromosomal alteration.

Clinical history

A 3500-g baby girl was born at term to a healthy 28-year-old mother. The pregnancy was uneventful, and the familial history showed no specific features. At birth, physical examination of the patient was normal except for a firm, subcutaneous non-tender

nodule, measuring 1 cm in diameter, located behind the left ear. Cranial magnetic resonance images demonstrated a subcutaneous soft-tissue mass. Intravenous gadolinium administration did not detect bone erosion or peripheral enhancement. Surgical resection of the nodule was performed at the age of 2 months. Chest X-ray, skeletal survey, and abdominal ultrasound did not detect any visceral lesions. At the age of 2 years, the patient was in excellent condition without clinical signs of recurrence.

Materials and methods

Histology and immunohistochemistry

Tumor material was fixed in formalin. Paraffin-embedded tissue was examined by standard histopathological techniques. Immunohistochemistry was carried out with antibodies against vimentin (1:100; Immunotech, Marseille, France), smooth-muscle actin (prediluted; Immunotech), epithelial membrane antigen (1:50; Dako, Glostrup, Denmark), S-100 protein (1:200; Immunotech) and cytokeratin KL1 (1:50; Immunotech).

Cytogenetic and FISH analysis

A fresh fragment of the tumor was prepared for cytogenetic analysis. Cells from short-term (4 days) and long-term (10–20 days) cultures were used for metaphase chromosome preparations according to established procedures [3]. Metaphase cells (n=20) were analyzed by reverse banding using heat and Giemsa (RHG) banding. Preparation of metaphase cells for fluorescence in situ hybridization (FISH) analyses, labeling of probes, and evaluation of results were done as described previously [10]. Individual whole chromosome painting (WCP) probes for chromosomes 6, 9, and 16 (Q-Biogene, Illkirch, France) and a set of multi-color WCP probes for the 24 human chromosomes (Spectra Vysion Assay, Abbott, Rungis, France), the subtelomeric probes for 9pter and 9qter (D9S17 and D9S1838, Q-Biogene), the arm-specific painting probe for chromosome 16p (American Laboratory Technology, Arlington, VA), the centromeric probes for chromosomes 9 and 16 (Q-Biogene), and the LSI *CBFB* dual color probe that hybridizes to 16q22 (Vysis, Downers Grove, IL) were used according to the supplier's recommendations. Slides were visualized on a Zeiss Axioplan 2 fluorescence microscope and analyzed with an image processor (Imstar, Paris, France). Multi-color FISH slides were analyzed by using a Q-FISH software (Leica, Rueil-Malmaison, France).

Results

Histopathological features

The histological evaluation showed well-circumscribed monomorphous proliferation composed of ovoid cells without atypia, in a myxoid background and arranged in nodules (Fig. 1A). Some peripheral nodules were made up of cells arranged around a typical hemangiopericytoma-like vascular pattern. The immunohistochemical staining was positive for vimentin and smooth-muscle actin (Fig. 1B) and negative for epithelial membrane antigen, S 100 protein, and cytokeratin, consistent with a myofibroblastic differentiation. According to these features, a diagnosis of IM was made.

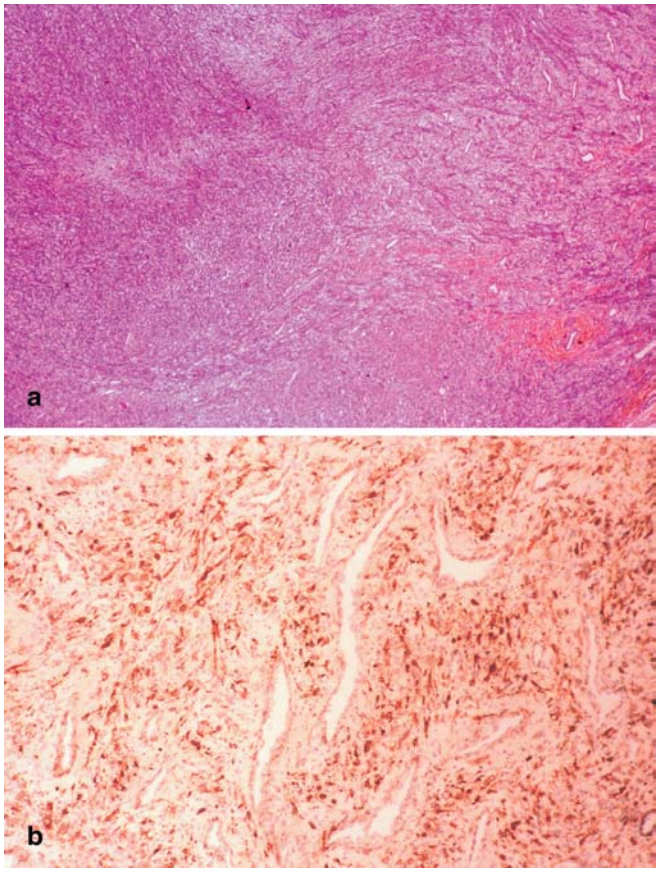


Fig. 1 **A** Nodule composed of bundles of plump spindle shaped myofibroblasts surrounding more immature appearing areas (hematoxylin and eosin ×25). **B** Strong expression for alpha-smooth muscle actin in immature rounded cells with hemangiopericytoma-like pattern (×100 magnification)

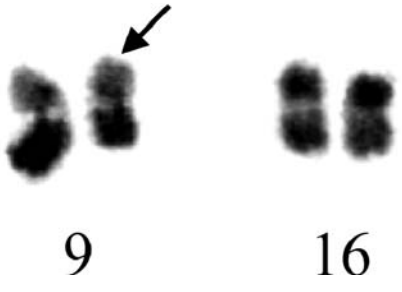


Fig. 2 Partial R-banded karyotype showing the der(9;16)(q10;q10) (*arrow*). This abnormality results in a monosomy 9q and trisomy 16q but was first interpreted as a partial deletion of the chromosome 9 long arm. Both chromosomes 16 are normal

Cytogenetic and FISH analysis

All RHG-banded metaphase cells from short-term cultures showed an abnormal karyotype with a structural rearrangement of chromosome 9, first interpreted as a partial deletion of the long arm (Fig. 2). However, the FISH analysis with the 24-color set of WCP probes as well as the individual WCP 9 and WCP 16 probes indicated that only the short arm of this abnormal chromo-

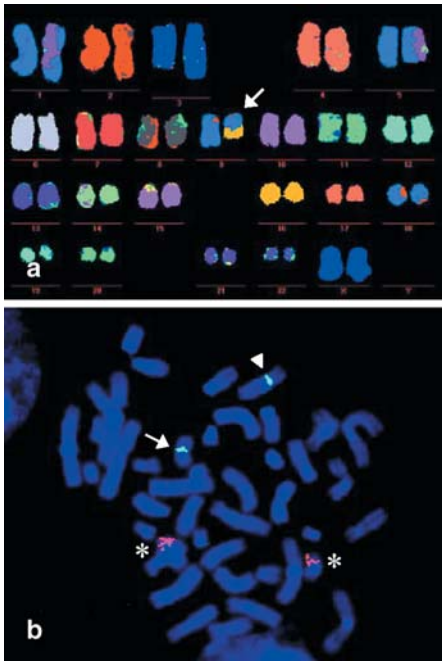


Fig. 3 A Multi-fluorescence in situ hybridization (FISH) analysis of a metaphase cell showing the der(9;16)(q10;q10) as the sole chromosomal abnormality (*arrow*). **B** Partial (arm-specific) chromosome painting with a probe for chromosome 16p and centromere labeling with a probe for chromosome 9: both normal (*arrowhead*) and der(9)t(9;16) (*arrow*) contain chromosome 9 centromere. The two normal chromosomes 16 (*asterisks*), but not the der(9), contain chromosomes 16p sequences, indicating that the chromosome 16 sequences on the der(9) are originating from 16q

some was made up of chromosome 9 sequences, whereas the long arm was originating from chromosome 16 (Fig. 3A). No other abnormality was detected. Complementary FISH analysis with a WCP probe for chromosome 6 confirmed the absence of chromosome 6 rearrangement. In addition, positive signals were detected on the abnormal chromosome with the centromeric chromosome 9 (Fig. 3B), telomere 9p, whereas no signal was detected with the telomere 9q probe. A positive signal, weaker than the signals observed on the two normal chromosomes 16, was observed by using the centromeric chromosome 16 probes, indicating that the breakpoint was localized within the chromosome 16 alpha-satellite centromeric sequences and that only a part of these sequences were retained on the abnormal chromosome. A positive signal was also observed on the derivative chromosome with the *CBFB* probe, located onto chromosome 16 long arm (16q22), whereas no signal was observed with the short arm-specific painting probes for chromosome 16 (Fig. 3B), indicating the 16q origin of the chromosome 16 sequences. We concluded that the abnormal chromosome 9 was, therefore, derived from an unbalanced whole-arm translocation between chromosome 9 and chromosome 16, the result of which consisted in a complete 9q monosomy and a 16q trisomy. According to the international nomenclature [5], the karyotype was: 46,XX,der(9;16)(q10;q10),+16. The metaphase cells from long-term cultures did not show any abnormality (46,XX), indicating that the constitutional karyotype was normal, in accordance to the normal phenotype, mental status, and development of the child.

Discussion

Despite the fact that IM is the most common fibrous proliferation in infancy, many of its biological aspects remain unclear. In particular, IM histogenesis is still not fully understood, although immunohistochemical staining and ultrastructural features suggest a myofibroblastic origin [13]. IM diagnosis is often made difficult by the predominance of primitive small spindle-shaped cells over myofibrobasts. Differential diagnosis mainly includes nodular fasciitis, neurofibroma, fibrous histiocytoma, infantile fibromatosis, infantile fibrosarcoma, and infantile hemangiopericytoma (IH) [9]. It has been suggested that IM and IH, which also present as solitary and multicentric lesions, might, in fact, represent different stages of maturation of a same entity [4]. Both are present at birth or occur early in life, may spontaneously regress, and share the same anatomical distribution. As observed in the present case, the immature areas of IM are sometimes histologically indistinguishable from those of IH. Some clues for a more precise identification of IM and IH might be given by cytogenetic and molecular studies. Dramatic improvements have been made during the last decade in the genetic characterization of pediatric soft-tissue tumors. Malignant tumors, such as Ewing sarcomas and peripheral neuroectodermal tumors, alveolar rhabdomyosarcomas, congenital fibrosarcomas, as well as benign tumors, such as inflammatory myofibroblastic tumors or lipoblastomas, show specific chromosomal patterns, the detection of which has been widely used as a tool for diagnosis [2, 9]. In contrast, the karyotypic picture of IM is still obscure. In the sole cytogenetic analysis of a solitary IM, an interstitial deletion of the long arm of chromosome 6 was reported [11]. Here, we describe a second case with chromosomal analysis and show the presence of an unbalanced whole-arm translocation involving the chromosome 9 and 16 long arms. This rearrangement, which results in the loss of chromosome 9q and a gain of chromosome 16q material, has not been described in other type of tumors [6]. On both chromosomes, the breakpoint was located in the pericentromeric heterochromatin region. Chromosomes 1, 9, and 16 have large pericentromeric heterochromatin regions, the size of which are variable among individuals and are composed of satellite repeat sequences. Breakpoints in pericentromeric heterochromatin region of chromosomes 1 and 16 have been reported in myelomas, B-cell lymphomas, breast cancers, and Ewing sarcomas [6, 7]. Instability and breakages within the pericentromeric heterochromatin might be caused by hypomethylation of the satellite sequences [12]. Further investigations will be required to assess whether alterations of chromosome 9 and 16 are of

any significance in the pathogenesis of IM and to elucidate the possible common link between IM and IH.

Acknowledgements The authors thank Christiane Brahimi-Horn for careful reading of the text. This work was supported by grants from the Programme Hospitalier de Recherche Clinique régional (CHU de Nice n°01–04), the Association pour la Recherche sur le Cancer (ARC grant no. 3386) and the Canceropôle Provence-Alpes-Côte d'Azur.

References

1. Ikediobi NI, Iyengar V, Hwang L, Collins WE, Metry DW (2003) Infantile myofibromatosis: support for autosomal dominant inheritance. J Am Acad Dermatol 49:148–150
2. Lawrence BD, Perez-Atayde A, Hibbard MK, Rubin BP, Dal Cin P, Pinkus JL, Pinkus GS, Xiao S, Yi ES, Fletcher CD, Fletcher JA (2000) TPM3-ALK and TPM4-ALK oncogenes in inflammatory myofibroblastic tumor. Am J Pathol 23:305–312
3. Limon J, Dal Cin P, Sandberg AA (1986) Application of long term collagenase disaggregation for the cytogenetic analysis of human solid tumors. Cancer Genet Cytogenet 23:305–312
4. Mentzel T, Calonje E, Nascimento AG, Fletcher CD (1994) Infantile hemangiopericytoma versus infantile myofibromatosis. Study of a series suggesting a continuous spectrum of infantile myofibroblastic lesions. Am J Surg Pathol 18:922–930
5. Mitelman F (ed) (1995) ISCN: an international system for human cytogenetic nomenclature. Karger, Basel
6. Mitelman F, Johansson B, Mertens F (eds) (2003) Mitelman database of chromosome aberrations in cancer.http://cgap.nci.nih.gov/Chromosomes/Mitelman
7. Mugneret F, Lizard S, Aurias A, Turc-Carel C (1988) Chromosomes in Ewing's sarcoma. II. Nonrandom additional changes, trisomy 8 and der(16)t(1;16). Cancer Genet Cytogenet 32:239–245
8. Parkes SE, Muir KR, Southern L, Cameron AH, Darbyshire PJ, Stevens MC (1994) Neonatal tumours: a thirty-year population-based study. Med Pediatr Oncol 22:309–317
9. Rubin BP, Bridge JA (2002) Myofibroma/myofibromatosis. In: Fletcher CDM, Unni KK, Mertens F (eds) World Health Organization classification of tumours. Pathology and genetics of tumours of soft tissue and bones. IARC press, Lyon, pp 59–61
10. Sirvent N, Forus A, Lescaut W, Burel F, Benzaken S, Chazal M, Bourgeon A, Vermeesch JR, Myklebost O, Turc-Carel C, Ayraud N, Coindre J-M, Pedeutour F (2000) Characterization of centromere alterations in liposarcomas. Genes Chromosomes Cancer 29:117–129
11. Stenman G, Nadal N, Persson S, Gunterberg B, Angervall L (1999) del (6)(q12q15) as the sole cytogenetic anomaly in case of solitary infantile myofibromatosis. Oncology Reports 6:1101–1104
12. Tsuda H, Takarabe T, Kanai Y, Fukutomi T, Hirohashi S. (2002) Correlation of DNA hypomethylation at pericentromeric heterochromatin regions of chromosome 16 and 1 with histological features and chromosomal abnormalities of human breast carcinomas. Am J Pathol 161:859–866
13. Weiss SW (2001) Fibrous tumors of infancy and childhood. In: Weiss SW, Goldblum JR (eds) Enzinger and Weiss's soft tissue tumors. Mosby, Inc., St. Louis, pp 357–363
14. Williams JO, Schrum D (1951) Congenital fibrosarcoma: report of a case in a newborn infant. AMA Arch Pathol 51:548
15. Zand DJ, Huff D, Everman D, Russell K, Sattia S, McDonal-McGinn D, Zackai EH (2004) Autosomal inheritance of infantile myofibromatosis. Am J Med Genet 3:261–266

Virchows Arch (2004) 445:541–543
DOI 10.1007/s00428-004-1086-1

LETTER TO THE EDITOR

Tadashi Terada · Shinobu Ikeuchi · Chie Inomoto · Kazuo Shimamura

Mucoepidermoid carcinoma of the palate composed exclusively of clear cells (clear cell variant)

Received: 25 November 2003 / Accepted: 7 July 2004 / Published online: 29 July 2004
© Springer-Verlag 2004

To the Editor, Mucoepidermoid carcinoma (MC) of the salivary glands is a malignant epithelial tumor that is composed of varying proportions of mucus, epidermoid, intermediate, columnar, and clear cells [2]. It is classified into low-, intermediate-, and high-grade types on the basis of morphologic and cytologic features [2, 6]. Although mucous, intermediate, and epidermoid cells are predominant in most MCs, it is well known that clear cells very infrequently predominate over other cell types [1, 2, 3, 4, 5]. Such cases are called clear cell variant of MC [1, 2, 3, 4, 5]. The authors here report a rare case of MC of the palate composed exclusively of clear cells.

A 42-year-old Japanese man presented a palate mass measuring approximately 2 cm in diameter. The mass in the palate was whitish pink and relatively hard in consistency. The overlying mucosa showed mild hyperemia. A needle biopsy was performed, and it showed clear cells that were arranged in a medullary, solid pattern (Fig. 1). The clear cells had small hyperchromatic nuclei and abundant clear cytoplasm. A low-grade malignant tumor was suspected pathologically, and the tumor was excised with wide margins. Scrutiny of visceral organs including kidneys showed no remarkable changes. The patient is now free of disease 11 months after the operation.

Grossly, the resected tumor measured 20×20×12 mm and was whitish tan in color and relatively hard in consistency. The mucosal surface showed mild erosion. Histologically, the tumor was composed exclusively of clear tumor cells (Fig. 2A). They were arranged in a medullary, sheet-like, and solid pattern separated by thin fibrous septae (Fig. 2B). Invasions into the surrounding mucosa and minor salivary glands were recognized. Clusters of non-clear cells having small hyperchromatic nuclei and small acidophilic cytoplasm were noted in a very few areas (Fig. 2C). They were regarded as intermediate cells. These cells appeared to merge with the clear cells (Fig. 2C). Relatively large cells with mucus in the cytoplasm were scattered in a very small number (Fig. 2D). These cells were considered as mucous cells. The proportions of clear cells, intermediate cells, and mucous cells were approximately 95%, 4%, and less than 1%, respectively. The surgical margins were negative for tumor cells. Cytologically, the clear cells showed small hyperchromatic nuclei that were centrally located in the cytoplasm (Fig. 2B). The cytoplasm was clear, and cell membranes were clearly recognized. Neither keratinization nor intercellular bridges were recognized. The intermediate cells showed small hyperchromatic nuclei and small acidophilic cytoplasm (Fig. 2C). The mucous cells show acidophilic mucin-like materials in the cytoplasm

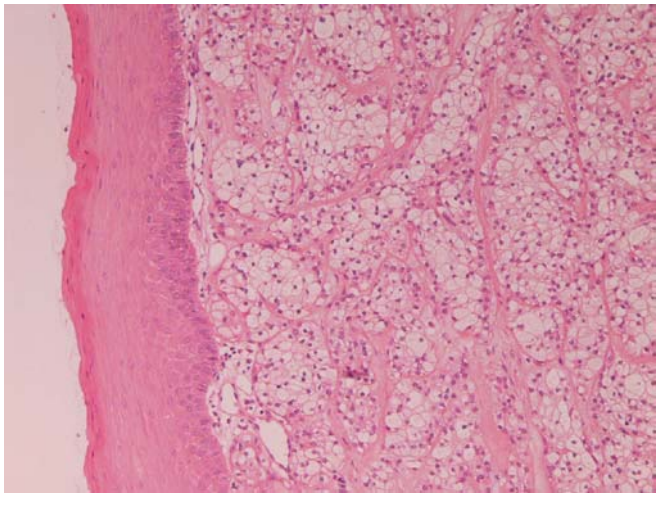


Fig. 1 A needle biopsy of the palate tumor. Clear cells arranged in a medullary, solid nests pattern are seen under the squamous epithelial layer of the palate mucosa. Hematoxylin and eosin, ×40

T. Terada (✉) · S. Ikeuchi
Departments of Pathology and Oral Surgery,
Shizuoka Municipal Shimizu Hospital,
Shimizu-Miyakami 1231, 424-8636 Shizuoka, Japan
Tel.: +81-543-361111
Fax: +81-543-361315

C. Inomoto · K. Shimamura
Department of Pathology,
Tokai University School of Medicine,
Isehara, Japan

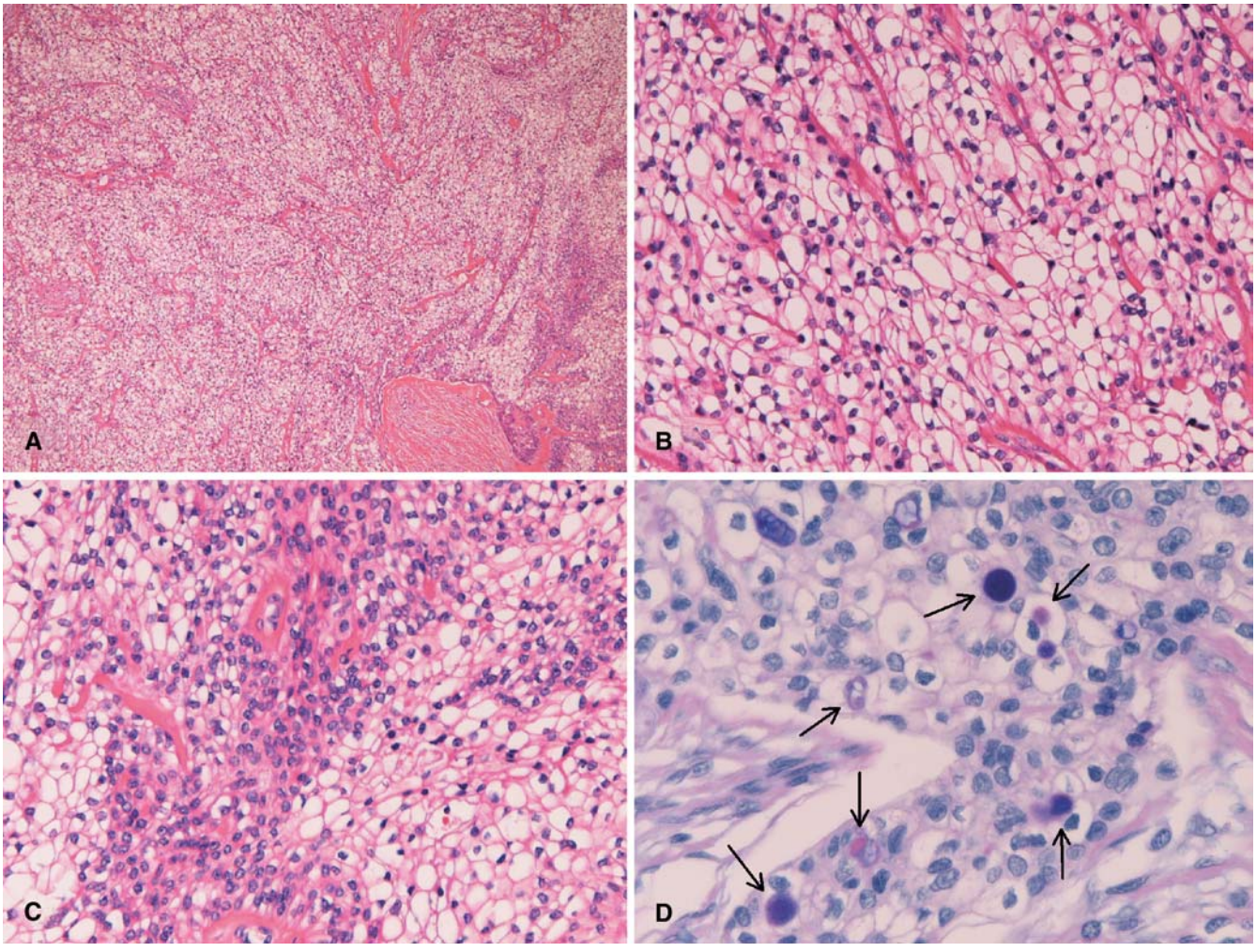


Fig. 2 **A** Low-power view of the palate tumor. The tumor is composed exclusively of clear cells arranged in a medullary sheet-like pattern. Hematoxylin and eosin (HE), ×20. **B** High-power view of the tumor. The tumor cells have clear cytoplasm, small hyperchromatic nuclei, and clear cell boundaries. HE, ×200. **C** High-power view of one part of the tumor. Some of the tumor cells show relatively small acidophilic cytoplasm regarded as intermediate cells. There is a gradual transition between clear cells and intermediate cells. HE, ×200. **D** High-power view of a part of the tumor. A few cells with mucins (*arrows*) are seen among clear tumor cells. Combined alcian blue at pH 2.5 and periodic acid–Schiff after diastase digestion stain, ×400

(Fig. 2D). No mitotic figures were recognized in tumor cells.

Histochemically, periodic acid–Schiff (PAS) stain showed reaction products focally in the clear and intermediate cells and showed positive reaction products in the mucous cells. Mucin stains including PAS after diastase digestion, alcian blue at pH 2.5, mucicarmine, and combined PAS after diastase digestion and alcian blue at pH 2.5 stains did not label the clear and intermediate cells, but showed positive reaction products in the mucous cells (Fig. 2D). Immunohistochemically, tumor cells were positive for epithelial markers (epithelial membrane antigen and cytokeratins using various antibodies). Tumor cells were negative for a mesenchymal marker (vimentin), an adenocarcinoma marker (carcinoembryonic antigen), myoepithelial markers (S-100 protein, alpha-smooth muscle actin, desmin, smooth muscle actin, and CD10), an acinic cell marker (salivary alpha-amylase), and tumor oncogene and anti-oncogene products (C-erbB-2/neu and p53 protein). The Ki-67 labeling was approximately 8%.

The present tumor was composed exclusively of clear cells (approximately 95%) without apparent differentiation. A very small amount of intermediate (approximately 4%) and mucous cells (approximately less than 1%) were also recognized. Since the tumor cells showed mild atypia and few mitotic figures and were seen to invade into the surrounding tissue, the present tumor is a low-grade malignant tumor. Although no epidermoid and columnar cells were noted, the present case appears to be a clear cell variant of MC (low-grade malignancy).

Differential diagnosis includes malignant salivary gland tumors with clear cells and metastatic renal cell carcinoma. Clear tumor cells are seen in several malignant salivary gland tumors including MC, acinic cell carcinoma, clear cell oncocytoma, clear cell adenocarcinoma, epithelial-myoepithelial carcinoma, and myoepi-

thelial carcinoma [1, 2]. The present case did not fit these neoplasms except for MC in terms of histology, histochemistry, and immunohistochemistry. Metastatic renal cell carcinoma is also unlikely because no lesions were seen in the kidneys and also because CD10 that is positive in most of renal clear cell carcinoma was negative in the present case.

Clear cells may be due to the cytoplasmic accumulation of glycogen, fat, or mucins. The clear cells of the present case showed focal PAS-positive materials (glycogen). Neither keratinization nor intercellular bridges were recognized. Therefore, the histogenesis of the clear cells of the present case is unclear. The clear cells in the present case, however, showed a gradual transition into the intermediate cells, suggesting a close relationship between clear cells and intermediate cells in the present case. The focal PAS-positive glycogens in the clear and intermediate cells may suggest epidermoid nature in this case. However, clear cells in MC may show PAS-positive glycogen and mucins, and there may be a gradual transition between epidermoid cells and clear cells [3, 4, 5]. In addition, they may show desmosomes and tonofilaments [3, 4, 5], suggesting that the origin of the clear cells in MC is epidermoid cells in certain cases.

In summary, the authors reported a rare case of clear cell variant of MC which was composed exclusively of clear cells. No apparent differentiation was noted in the clear cells.

References

1. Ellis GL (1998) Clear cell neoplasm in salivary glands: clearly a diagnostic challenge. Ann Diagn Pathol 2:61–78
2. Ellis GL, Auclaire PL (1996) Tumors of the salivary glands. In: Atlas of tumor pathology, third series, fascicle 17. AFIP, Washington
3. Miura K, Ishimaru Y, Yoshiomura T (1986) Light and electron microscopic study of mucoepidermoid tumor of clear cell type. Acta Pathol Jpn 36:1419–1427
4. Ogawa I, Nikai H, Takata T, Yasui R (1992) Clear-cell variant of mucoepidermoid carcinoma: report of a case with immunohistochemical and ultrastructural observations. J Oral Maxillofac Surg 50:906–910
5. Peison B, Benisch B, Schwarz IS, Gordon RE (1988) Clear-cell mucoepidermoid carcinoma arising in the nasal cavity: case report with ultrastructural observations. Mt Sinai J Med 55:417–420
6. Tommaso LD, Foschini MP, Ragazzini T, Magrini E, Fornelli A, Ellis IO, Eusebi V (2004) Mucoepidermoid carcinoma of the breast. Virchows Arch 444:13–19

Virchows Arch (2004) 445:544
DOI 10.1007/s00428-004-1150-x
© Springer-Verlag 2004

ANNOUNCEMENTS

19–24 April 2005
10th International Congress on Oral Cancer
Crete, Greece

Creta Maris Conference Centre

- The 10th International Congress on Oral Cancer is supported by the World Health Organization, the International Union Against Cancer, the International Congress on Oral Cancer, the Hellenic Association for the Research and Treatment of Oral Cancer, and the Hellenic Cancer Society
- The Congress theme is *The Oral Cancer Patient: the anthropocentric approach to a multidisciplinary problem*
- A number of Keynote Lectures will be delivered by international leaders in their specialties
- Limited attendance Courses will be provided for interested participants
- Deadline for abstract submission: November 30th, 2004
- Accepted abstracts for oral and poster presentations will be published as a supplement to the journal Oral Oncology. Details at www.harcourt-international.com/journals/oron
- Social events include Presidents Reception, Cretan Night and Gala Dinner

Further details at www.icooc-2005.org or from the Congress President at rapidis@icooc-2005.org

13–24 June 2005
International course on Laboratory Animal Science
Utrecht, The Netherlands

A two week intensive course on laboratory animal science will be organized at the Division of Laboratory Animal Science – Utrecht, The Netherlands in June 2005. This course is organized once a year since 1993.
The objective of this course is to present basic facts and principles that are essential for the humane use and care of animals and for the quality of research.
The contents of the course are in line with recommendations of the Federation of European Laboratory Animal Science Associations (FELASA) regarding the training of the young scientist whose research involves the use of vertebrate animals.
The course may also be of interest for those who intend to set up a similar course at their location. For this purpose, during the course the acquisition of teaching materials can be discussed with the course committee.

For information and application forms please contact:
Mr. Stephan van Meulebrouck, MA
Division of Laboratory Animal Science
Faculty of Veterinary Medicine
P.O. Box 80.166
3508 TD Utrecht
The Netherlands
Tel.: +31-30-2532033
Fax: +31-30-2537997
E-mail: pdk@las.vet.uu.nl
Internet: http://las.vet.uu.nl>Education and Training>International Course

Virchows Arch (2004) 445:545–551
DOI 10.1007/s00428-004-1129-7

REVIEW ARTICLE

Bettina Fabiani · Alain Delmer · Eric Lepage · Catherine Guettier · Tony Petrella · Josette Brière · Anne-Marie Penny · Marie-Christine Copin · Jacques Diebold · Felix Reyes · Philippe Gaulard · Thierry J. Molina · Groupe d'Etudes des Lymphomes de l'Adulte

CD10 expression in diffuse large B-cell lymphomas does not influence survival

Received: 2 August 2004 / Accepted: 24 August 2004 / Published online: 27 October 2004
© Springer-Verlag 2004

B. Fabiani
Département de Pathologie,
Hôpital Saint-Antoine, AP-HP,
Paris, France

A. Delmer
Service d'Hématologie clinique,
Hôpital Hôtel-Dieu, AP-HP,
Paris, France

E. Lepage
Département de Biostatistiques et Informatique Médicale,
Hôpital Henri-Mondor, AP-HP,
Créteil, France

C. Guettier
Département de Pathologie,
Hôpital Paul Brousse, AP-HP,
Villejuif, France

T. Petrella
Département de Pathologie,
Faculté de Médecine,
Dijon, France

J. Brière
Département de Pathologie,
Hôpital Saint-Louis, AP-HP,
Paris, France

A.-M. Penny
Service d'Hématologie Clinique,
Centre François Baclesse, Caen, France

M.-C. Copin
Département de Pathologie,
Hôpital Calmette, Lille, France

J. Diebold · T. J. Molina (✉)
Department of Pathology,
Hôtel-Dieu, AP-HP,
1 place du Parvis Notre-dame, 75181 Paris Cedex 04, France
e-mail: thierry.molina@htd.ap-hop-paris.fr
Tel.: +33-1-42348282
Fax: +33-1-42348641

F. Reyes
Service d'Hématologie Clinique,
Hôpital Henri Mondor, AP-HP,
Créteil, France

P. Gaulard
Département de Pathologie,
Hôpital Henri Mondor, AP-HP,
Créteil, France

Abstract CD10 expression is considered as a marker of centrofollicular-derived diffuse large B-cell lymphomas (DLBCL). The aim of our study was to determine retrospectively among 98 patients with DLBCL, enrolled in the LNH93 trial of the Groupe d'Etude des Lymphomes de l'Adulte (GELA) and homogeneously treated with high-dose cyclophosphamide, doxorubicin, vincristine and prednisone (CHOP)-like regimen [doxorubicin, cyclophosphamide, vindesine, bleomycin and prednisone (ACVBP)], the expression of CD10 using immunohistochemistry and its correlation with morphological features and clinical parameters. Of the 98 patients studied, 33 (34%) expressed CD10. There was no correlation among clinical parameters, International Prognostic Index risk groups and CD10 expression, with the exception of lactic dehydrogenase levels, which were lower in CD10-negative cases (P=0.005). There was no significant correlation between CD10 expression and morphological subtyping of DLBCL. Indeed, centrofollicular-derived DLBCL may present with numerous immunoblasts or as an immunoblastic lymphoma. Overall survival rate and event-free survival were not significantly different according to CD10 expression (P=0.44 and P=0.34 respectively). Therefore, it appears that CD10 expression does not influence survival or event-free survival in DLBCL.

Keywords Lymphoma · Tumor marker · Clinical pathology

Introduction

Diffuse large B-cell lymphomas (DLCBL) represent the most frequent type of non-Hodgkin's lymphoma in adults, diagnosed on morphology and immunophenotype [18]. They represent a heterogeneous group of diseases in terms of phenotype, cytogenetics abnormalities and clinical behavior. Overall, 50–60% of these patients can be cured with anthracycline-based chemotherapy [3, 7, 26], while others will die from lymphoma due to primary or secondary treatment refractoriness. The formulation of an International Prognostic Index (IPI) has provided a widely accepted set of criteria to predict the evolution of aggressive lymphomas and, thus, to design appropriate treatment strategies. Molecular abnormalities of cell death–cell viability balance as reflected in bcl-2 overexpression [11, 15], p53 mutations [17, 20, 21] or survivin expression [1] have emerged as important adverse prognostic indicators of DLBCL. Moreover, studies from gene-expression profiles have identified cell of origin as of prognostic significance. The germinal center B-cell-like profile has been associated with a good outcome, whereas the activated B-cell-like profile, resembling activated blood B cells, was associated with a poor outcome. Moreover, centroblastic monomorphic subtype and immunoblastic subtype appear to be significantly more represented in the germinal center B-cell-like group and in activated B-cell-like groups, respectively [25]. Nevertheless, factors other than cell of origin signature, related to proliferation markers or microenvironment-related genes have been included in a new gene-based predictor [25]. However, microarray technologies still require important molecular platforms and to find out molecular predictors based on paraffin immunohistochemistry staining could be of high interest in daily practice. Among these potential markers, the prognostic value of CD10 is controversial. CD10 is a human membrane-associated neutral endopeptidase, and antibodies working on paraffin-embedded sections are available. In peripheral B-cell differentiation, CD10 is considered as a highly specific marker of normal centrofollicular B cells, whereas approximately 70% of follicular lymphomas stained for CD10 [9]. It is widely accepted as a marker of centrofollicular origin of B cells, although it underestimates the real numbers of centrofollicular-derived cases. The aim of our study was to determine among 98 patients enrolled in the LNH93 protocol of the Groupe d'Etude des Lymphomes de l'Adulte (GELA) group and all treated with the same high-dose cyclophosphamide, doxorubicin, vincristine and prednisone (CHOP)-like regimen [doxorubicin, cyclophosphamide, vindesine, bleomycin and prednisone (ACVBP)] the expression of CD10 using immunohistochemistry and to correlate the results with clinical presentation and morphological features.

Materials and methods

Patient selection

The LNH93 trial, conducted by GELA, recruited patients from 50 participating French and Belgian centers who were at least 15 years old, presenting with DLBCL or peripheral T-cell lymphoma from 22 April 1993 until 29 November 1999. The non-Hodgkin's lymphoma series of the present study included retrospectively a subset of patients registered in the LNH93 trial with a diagnosis of diffuse large B-cell lymphomas confirmed by pathological review and treated with the same reference arm of the GELA, ACVBP. Moreover, the availability of routinely processed paraffin-embedded unstained slides was necessary for inclusion in that study.

In the LNH93 trial, patients were stratified in seven groups from 1993 to 1998 according to age and the presence of the following adverse prognostic factors: performance status greater than 1, lactic dehydrogenase (LDH) elevated, stage III or stage IV. Details of the chemotherapy regimens have been reported elsewhere [12]. Patients were randomized between arm A and arm B. ACVBP treatment was given only in the arm A of 93–1, 93–2, 93–3 and 93–5 groups. Patients 15–60 years were randomized in 93–1 (none of the three adverse prognostic factors), 93–2 (one of the three adverse prognostic factors) or 93–3 groups (two or three of the three adverse prognostic factors). Patients 61–69 years with one to three adverse prognostic factors were randomized in the 93–5 group. Briefly, arm A consisted of four cycles of ACVBP (doxorubicin 75 mg/m^2 on day 1, cyclophosphamide 1200 mg/m^2 on day 1, vindesine 2 mg/m^2 and bleomycin 10 mg on day 1 and day 5, prednisone 60 mg/m^2 from day 1 to day 5 and intrathecal methotrexate 15 mg on day 2) at 2-week intervals followed by outpatient consolidation that lasted 4 months. Patients then received consolidation at 2-week intervals, with two cycles of methotrexate (3 g/m2) plus leucovorin rescue, four cycles of etoposide (300 mg/m^2) and ifosfamide (1500 mg/m^2) and two cycles of cytarabine (100 mg/m^2) subcutaneously for 4 days.

Among the 1247 patients included in the LNH93–1, 2, 3, 5, arms A, 100 were randomly selected. Because of lack of unstained slides for some of them, cases were added to gather overall 98 patients. Disease dissemination was evaluated prior to treatment by physical examination, bone marrow biopsy and computed tomography scan of the chest and abdomen. Patients were staged according to the Ann Arbor system. The number of extranodal sites and larger tumor mass diameter were also determined. Performance status was assessed according to the Eastern Cooperative Oncology Group scale.

Tumor responses were assessed at the end of treatment and were classified as complete response (CR), unconfirmed complete response (CRu), partial response, stable disease or progressive disease according to the International Workshop criteria [6]. CR was defined as the disappearance of all lesions and of radiological or biological abnormalities observed at diagnosis and the absence of new lesions.

Histological study

The histological diagnosis of diffuse large B-cell lymphoma of patients enrolled in the LNH93 protocol was made independently by three pathologists according to the updated Kiel classification and to the morphological variants of the World Health Organization classification as centroblastic, immunoblastic and anaplastic large cell. The anaplastic variant was excluded from this study. The diagnosis was based on morphological examination of slides from routinely paraffin-embedded samples stained with hematoxylin–eosin, Giemsa and on immunophenotyping results. In all cases, immunophenotyping was performed by panel review with antibodies targeting CD20 (L26) and CD3 (Dako, Glostrup, Denmark) to determine the B- or T-cell lineage, respectively, using an indirect immunoperoxidase or alkaline phosphatase anti-alkaline phosphatase method.

For the purpose of this study, two hematopathologists (J.D. and T.J.M.) independently reviewed the morphology of tumor cells among the selected cases for CD10 staining when the Giemsa stain

allowed good morphological analysis (91 of the 98 selected for CD10). The presence (more or less than 50%) or absence of immunoblasts as well as multilobated cells (more or less than 30%) were evaluated semi-quantitatively. Cases were also classified according to the updated Kiel classification. According to the Kiel classification, immunoblastic lymphoma comprises immunoblastic cases with less than 10% of centroblasts and at least 90% of immunoblasts. In a few discordant cases, a consensus was reached at the two-head microscope.

CD10 expression

Immunostains were performed using the streptavidin-biotin-peroxidase technique. Sections were dewaxed and rehydrated, and endogeneous peroxidase activity was blocked with hydrogen peroxide. Antigen retrieval was carried out in ethylenediaminetetraacetate buffer (1 mM, pH 8) by microwaving for 20 min. Sections were incubated with the primary antibody (CD10, clone 56C6, Novocastra, Newcastle Upon Tyne, IK, dilution 1/50) for 2 h. Thereafter, tissue sections were sequentially incubated with biotinylated goat anti-mouse antiserum and streptavidin peroxidase and developed with diaminobenzidine. Sections were subsequently counterstained with hematoxylin and mounted in glycergel (Dako). On lymphoma tissue sections, stromal cell staining often provided an internal control for CD10. In some lymphomas, the presence of adjacent reactive germinal centers staining for CD10 served as internal controls.

Cases were classified independently by two pathologists (B.F., P.G.) as CD10 positive if more than 10% of tumor cells exhibited a distinct membranous staining. In doubtful cases, immunostains were performed twice. They were interpreted without knowledge of the clinical data.

Statistical analysis

Patient characteristics and CR rates were compared using the chi-square test. Event-free survival (EFS) was measured from the date of randomization to that of disease progression, relapse or death from any cause or to the stopping date (1 August 2001). Overall survival (OS) was calculated from the date of randomization until death or last follow-up examination. When the stopping date was not reached, the data were censored at the date of the last follow-up evaluation. Survival curves were estimated using the product-limit method of Kaplan–Meier [19] and were compared using the log-rank test. Univariate analyses were made using the chi-square test and the log-rank test. $P<0.05$ was considered to indicate statistical significance. All calculations were performed on SAS software, version 6.10 (SAS Institute, Cary, NYC).

Results

CD10 expression was found in 34% of the patients examined using immunohistochemistry (33/98) (Fig. 1). The median age of the population was 56 years and the sex ratio male/female was 52/46. Of the patients, 55% have

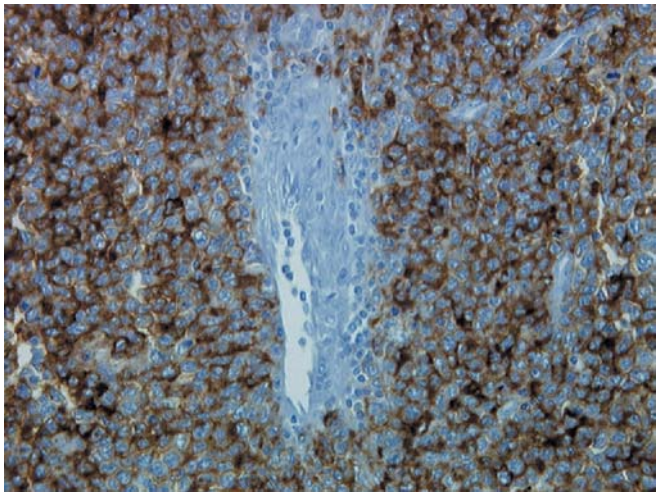


Fig. 1 Strong membranous staining of CD10 by tumor cells (anti-CD10 antibody ×400)

Table 1 Clinical characteristics of the 98 patients according to CD10 expression. *PS* Performance status; *ECOG* Eastern Cooperative Oncology Group, *IPI* International Prognostic index

	CD10-positive group	CD10-negative group	*P* value
Number of patients (%)	33 (34)	65 (66)	
Clinical stage			0.95
Stage I, II	14 (42)	28 (43)	
Stage III, IV	19 (58)	37 (57)	
PS (ECOG)			0.58
0–1	27 (82)	48 (74)	
More than 1	6 (18)	15 (23)	
Lactate dehydrogenase			0.005
Normal	21 (64)	22 (34)	
>100%	12 (36)	43 (66)	
Extranodal sites			0.38
0–1	27 (82)	48 (74)	
More than 1 site	6 (18)	17 (26)	
Bone marrow involvement			0.74
No	30 (91)	55 (89)	
Yes	3 (9)	7 (11)	
IPI score			0.62
0–1	16 (49)	21 (32)	
2	8 (24)	17(26)	
3	4 (12)	15 (23)	
4–5	5 (15)	12 (18)	
Evolution			0.29
Complete remission	28 (85)	46 (75)	
No complete remission	5 (15)	15 (25)	

Table 2 Morphological characteristics of the 91 cases according to CD10 expression

	CD10-positive group	CD10-negative group	*P* value
Number of patients (%)	31 (34)	60 (66)	
Kiel classification			0.74
Immunoblastic	5 (16)	15 (25)	
Centroblastic (Cb)	26 (84)	45 (75)	
Cb monomorphic	8 (26)	13 (22)	
Cb polymorphic	11 (35)	17 (29)	
Cb multilobated (>30%)	7 (23)	15 (25)	
Immunoblasts			0.25
No. immunoblast	8 (26)	8 (13)	
Minority of immunoblast	18 (58)	36 (60)	
Majority of immunoblast (>50%)	5 (16)	16 (27)	

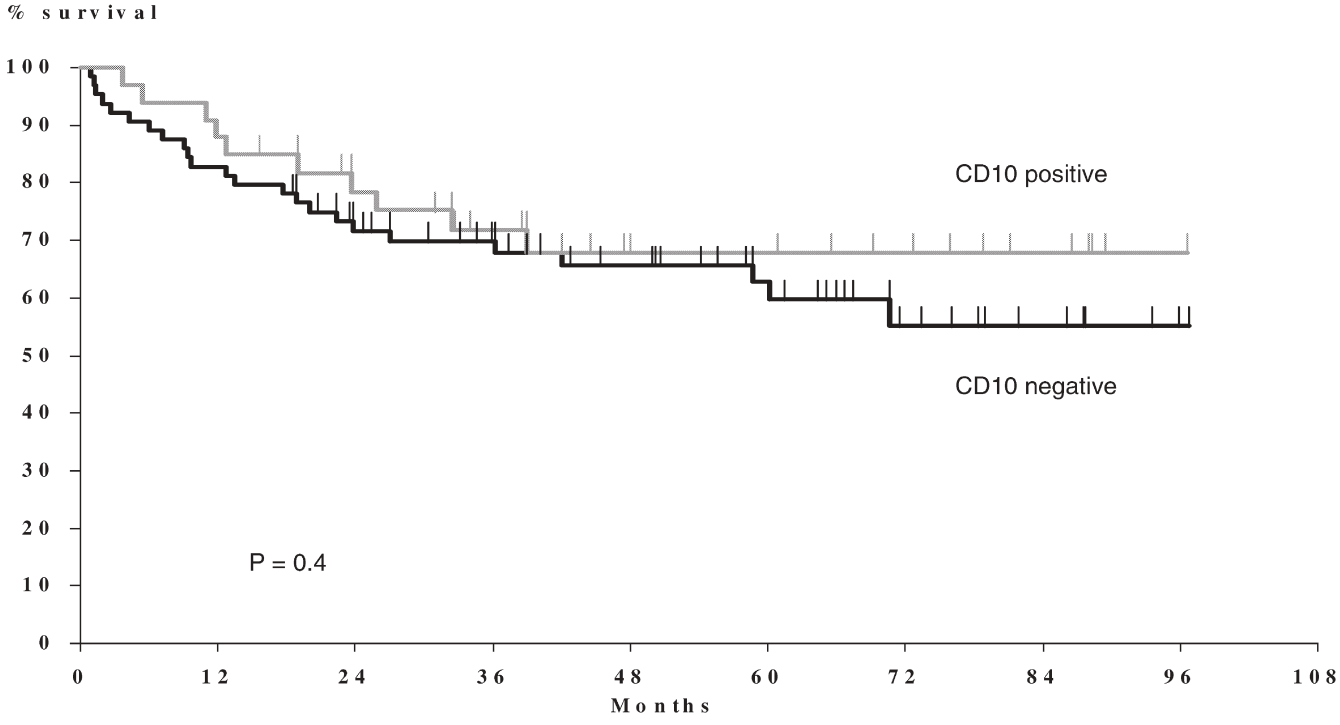


Fig. 2 Kaplan–Meier curves of overall survival of 98 patients according to CD10 expression (CD10-positive cases *n*=33, CD10-negative cases *n*=65)

elevated LDH levels, 56% were stage III–IV, 21% had a PS more than one and 23% presented with more than one extranodal site. There was no correlation among clinical parameters, IPI risk groups and CD10 expression, with the exception of LDH levels, which were lower in CD10-positive patients (Table 1). Among the 91 cases evaluable for the morphological analysis, according to Kiel classification, 22% were immunoblastic lymphomas and 78% were centroblastic lymphomas (monomorphic 23%, polymorphic 31%, multilobated 24%). No immunoblasts were present in 17% of the cases, and 60% of the patients had between 1% and 50% immunoblasts. There was no difference in the repartition of immunoblastic and centroblastic lymphomas among the CD10-positive and -negative groups. There were also no significant differences considering the percentage of immunoblasts (Table 2). However, there was a trend for rare CD10 expression among the cases with a majority of immunoblasts (5/21) compared with cases without any immunoblasts (8/16), but this was not significant (*P*=0.1).

With a median follow-up of 58 months, OS and EFS were not significantly different according to CD10 expression (Fig. 2, Fig. 3). Analysis of OS and EFS among low- and high-risk IPI did not show statistically significant differences among CD10-positive and CD10-negative patients (data not shown).

Discussion

In this series of 98 patients with diffuse large B-cell lymphomas treated with the same anthracycline-containing regimen, CD10 was expressed in 33 patients (34%). Detection of CD10 in most of the studies was performed using immunohistochemistry. CD10 was detected by flow cytometric analysis in four studies [2, 10, 14, 28] and by

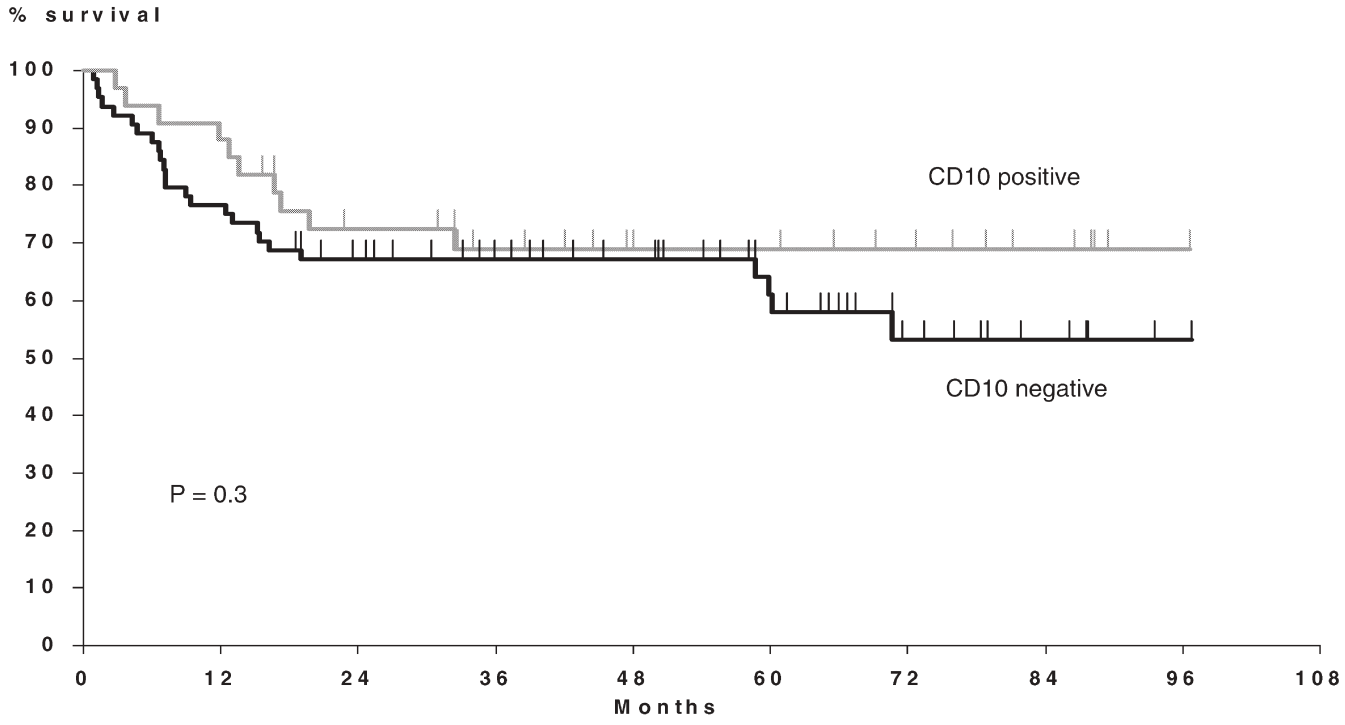


Fig. 3 Kaplan-Meier curves of event-free survival of 98 patients according to CD10 expression (CD10-positive cases *n*=33, CD10-negative cases *n*=65)

both methods in one study [5]. Xu et al. [29] showed 75% sensitivity and 100% specificity of CD10 expression using immunohistochemistry compared with multi-parameter flow cytometry. CD10 positivity in DLBCL has been previously reported in several studies, varying from 16% to 43% [2, 4, 5, 8, 9, 10, 13, 14, 16, 22, 23, 24, 27, 28, 29]. However, the level of positivity in our study fit well with the largest and recent study [13] published using tissue microarray of 152 cases (28% of CD10 expression using a 30% threshold). This observation suggests that the threshold of CD10 expression to assess positivity (between 10% and 30% in most studies) does not play a major role to explain variation of CD10 expression among the series. Indeed, the heterogeneous number of cases evaluated (from 28 [27] to 152 [13]) might play a major role in explaining differences of CD10 expression among the studies. We did not find any correlation between CD10 expression and the morphological subtyping of the lymphomas. However, there is a tendency for the cases without any immunoblasts to be CD10+ and for the cases with numerous immunoblasts to be CD10–. However, as indicated by Colomo [8] and Rosenwald [25], centrofollicular-derived cases may present as an immunoblastic lymphoma and activated-derived cases as centroblastic monomorphic. Indeed, some cases might be difficult to classify morphologically between immunoblastic with plasma cell differentiation and centroblasts with large cytoplasm, and further morphological analysis on standardized–fixed cases might be useful. Few studies evaluated CD10 expression as a prognostic factor. However, the prognostic value of CD10 on tissue sections is still a controversial issue, with studies reporting no prognostic value of CD10 expression [8, 14, 28], whereas others found CD10 expression as a good prognostic indicator [13, 23] or, even in a small series, as a worse prognostic factor [27]. In our series, CD10 expression does not appear as a prognostic factor in DLBCL, even in low-risk IPI. The selection of patients might account for the differences among series. Overall, clinical presentation does not seem to explain differences among good prognosis series [13, 23] and series with no influence of CD10 expression, such as ours and that of Colomo et al. [8]. Indeed, in our series, only 22% of patients had bad Performance Status compared with 40% in other series [8, 13]. However, 57% were stage III–IV, compared with 49% [13] and 51% [8] in other series. Comparing IPI repartition, 36% of patients presented with high-risk IPI compared with 34% [13], 39% [23] and 47% [8]. The heterogeneity of the results might be due also to the fact that the treatments in these series were not always reported [5, 23] or were heterogeneous [4, 8, 13, 14, 27], sometimes including radiotherapy [14, 18, 27]. In our series, all patients received the same treatment and were all enrolled in a prospective trial. Our findings might indicate that the cell of origin signature is not a powerful prognostic indicator, even if we might have underestimated a part of centrofollicular cases that did not express CD10. Nevertheless, the recent study of Colomo [8] found that even in addition with bcl-6, mum-1 and CD138 staining, the cell of origin signature based on immunohistochemistry does not appear as a prognostic predictor. This apparent discrepancy with the cell of origin concept

based on microarrays might be due to posttranscriptional regulation, although tissue microarrays phenotyping performed on samples evaluated using cDNA microarrays suggest that CD10 protein expression is associated with better OS but not EFS [13]. As suggested using the microarray studies, it is probably difficult to rely only on a single factor to predict prognosis in the large subset of DLBCL. Therefore, from our study, CD10 does not appear as a good prognostic marker to be tested using tissue microarray in large clinical series of DLBCL.

Acknowledgements We thank Nicolas Nio, who performed the statistical analysis, Pauline Brice, Karen Leroy-Viard and Gilles Salles for critical review of the manuscript and Chafika Copeaux for technical help. Acknowledgements of source of support: this study was supported by grants from the Ministère de la Santé (PHRC AOM 95061), and from Amgen-Roche, Neuilly sur Seine, France.

Appendix

The following investigators participated in the study: N. Albin, C. Allard, M. Aoudjane, D. Assouline, M. Attal, B. Audhuy, M.Azagury, J.C. Barats, C. Beaumont, E. Baumelou, P. Biron, M. Blanc, D. Bordessoule, A. Bosly, K. Bouabdallah, C. Bouleuc, P. Bourquard, P. Bourquelot, F. Boué, O. Boulat, P. Brice, J. Brière, G. Brun, D. Caillot, O. Casasnovas, P. Carde, S. Castaigne, S. Chèze, B. Christian, B. Coiffier, P. Colin, C. Collet, T. Conroy, T. Cosnard, B. Corront, H. Curé, V. Delwail, L. Detourmignies, A. Devidas, H. Dombret, J.F. Dor, C. Doyen, F. Dreyfus, S. Dront, G. Dupont, B. Dupriez, J.C. Eisenmann, M. Fabbro, C. Fermé, G. Fillet, M. Flesch, C. Fruchart, J. Gabarre, C. Haioun, R. Herbrecht, O. Hermine, A. Huyn, F. Huguet, M. Janvier, E. Jourdan, J.M. Karsenti, Y. Kerneis, F. Kohser, V. Leblond, P. Lederlin, S. Lefort, P. Lenain, G. Lepeu, S. Lepretre, X. Levaltier, A. Le Rol, G. Marit, C. Martin, F. Mayer, C. Nouvel, P.Morel, M. Moriceau, J.N. Munck, G. Nedellec, F. Offner, J.M. Pavlovitch, I. Plantier, P.Y. Péaud, A.M. Peny, J. Pico, C. Platini, J.P. Pollet, B. Quesnel, O. Reman, B. Richard, R. Riou, P. Rodon, B. Salles, G. Salles, C. Sarazin, D. Schlaifer, C. Sebban, M. Simon, P. Solal-Céligny, J.J. Sotto, A. Stamatoullas, C. Soussain, G. Tertian, A. Thyss, H. Tilly, J.D. Tigaud, G. Tobelem, P. Travade, A. Van Hoof, B. Varet, A. Zaniboni and J.M. Zini.

The following pathologists actively participated to the trial and provided the slides: R. Angonin, I. Abd Alsamad, A. C. Baglin, F. Berger, N. Brousse, J.-P. Brouland, P. Brousset, D. Canioni, O. Casiraghi, D. Cazals-Hatem, A. M. Chesneau, F. Charlotte, M.-P. Chenard-Neu, C. Copie-Bergman, M.-C. Copin, M. Delos, C. Duval, G. Delsol, J. Diebold, C. Fromentin, F. Galateau, B. Gasser, B. Gosselin, C. Guettier, J. Hamels, N. Horschowski, R. Jeandel, J. P. Knopf, E. Labouyrie, C. Legendre, A. Letourneau, A. de Mascarel, V. Meignin, M. Parrens, B. Petit, M. Raphael, M. C. Raymond-Gelle, P. Straub, Y. Theate, S. Thiebaut, M. Tulliez and L. Xerri.

References

1. Adida C, Haioun C, Gaulard P, Lepage E, Morel P, Briere J, Dombret H, Reyes F, Diebold J, Gisselbrecht C, Salles G, Altieri DC, Molina TJ (2000) Prognostic significance of survivin expression in diffuse large B-cell lymphomas. Blood 96:1921–1925
2. Almasri NM, Iturraspe JA, Braylan RC (1998) CD10 expression in follicular lymphoma and large cell lymphoma is different from that of reactive lymph node follicles. Arch Pathol Lab Med 122:539–544
3. Andre M, Mounier N, Leleu X, Sonet A, Brice P, Henry-Amar M, Tilly H, Coiffier B, Bosly A, Morel P, Haioun C, Gaulard P, Reyes F, Gisselbrecht C (2004) Second cancers and late toxicities after treatment of aggressive non-Hodgkin lymphoma with the ACVBP regimen. A GELA cohort study on 2837 patients. Blood 103:1222–1228
4. Barrans SL, Carter I, Owen RG, Davies FE, Patmore RD, Haynes AP, Morgan GJ, Jack A (2002) Germinal center phenotype and bcl-2 expression combined with the International Prognostic Index improves patient risk stratification in diffuse large B-cell lymphoma. Blood 99:1136–1143
5. Chang CC, Cleveland RP, Perkins SL (2002) CD10 expression and survival. Am J Clin Pathol 117:660–661
6. Cheson BD, Horning SJ, Coiffier B, Shipp MA, Fisher RI, Connors JM, Lister TA, Vose J, Grillo-Lopez A, Hagenbeek A, Cabanillas F, Klippensten D, Hiddemann W, Castellino R, Harris NL, Armitage JO, Carter W, Hoppe R, Canellos GP (1999) Report of an international workshop to standardize response criteria for non-Hodgkin's lymphomas. NCI Sponsored International Working Group. J Clin Oncol 17:1244
7. Coiffier B (2001) Diffuse large cell lymphoma. Curr Opin Oncol 13:325–334
8. Colomo L, Lopez-Guillermo A, Perales M, Rives S, Martinez A, Bosch F, Colomer D, Falini B, Montserrat E, Campo E (2003) Clinical impact of the differentiation profile assessed by immunophenotyping in patients with diffuse large B-cell lymphoma. Blood 101:78–84
9. Dogan A, Bagdi E, Munson P, Isaacson PG (2000) CD10 and BCL-6 expression in paraffin sections of normal lymphoid tissue and B-cell lymphomas. Am J Surg Pathol 24:846–852
10. Fang JM, Finn WG, Hussong JW, Goolsby CL, Cubbon AR, Variakojis D (1999) CD10 antigen expression correlates with the t(14;18)(q32;q21) major breakpoint region in diffuse large B-cell lymphoma. Mod Pathol 12:295–300
11. Gascoyne RD, Adomat SA, Krajewski S, Krajewska M, Horsman DE, Tolcher AW, O'Reilly SE, Hoskins P, Coldman AJ, Reed JC, Connors JM (1997) Prognostic significance of Bcl-2 protein expression and Bcl-2 gene rearrangement in diffuse aggressive non-Hodgkin's lymphoma. Blood 90:244–251
12. Gisselbrecht C, Lepage E, Molina T, Quesnel B, Fillet G, Lederlin P, Coiffier B, Tilly H, Gabarre J, Guilmin F, Hermine O, Reyes F (2002) Shortened first-line high-dose chemotherapy for patients with poor-prognosis aggressive lymphoma. J Clin Oncol 20:2472–2479
13. Hans CP, Weisenburger DD, Greiner TC, Gascoyne RD, Delabie J, Ott G, Muller- Hermelink HK, Campo E, Braziel RM, Jaffe ES, Pan Z, Farinha P, Smith LM, Falini B, Banham AH, Rosenwald A, Staudt LM, Connors JM, Armitage JO, Chan WC (2004) Confirmation of the molecular classification of diffuse large B-cell lymphoma by immunohistochemistry using a tissue microarray. Blood 103:275–282
14. Harada S, Suzuki R, Uehira K, Yatabe Y, Kagami Y, Ogura M, Suzuki H, Oyama A, Kodera Y, Ueda R, Morishima Y, Naka-mura S, Seto M (1999) Molecular and immunological dissection of diffuse large B cell lymphoma: CD5+, and CD5– with CD10+ groups may constitute clinically relevant subtypes. Leukemia 13:1441–1447
15. Hermine O, Haioun C, Lepage E, d'Agay MF, Briere J, Lavignac C, Fillet G, Salles G, Marolleau JP, Diebold J, Reyas F, Gaulard P (1996) Prognostic significance of bcl-2 protein expression in aggressive non-Hodgkin's lymphoma. Groupe d'Etude des Lymphomes de l'Adulte (GELA). Blood 87:265–272

16. Hojo H, Kuze T, Nakamura N, Hashimoto Y, Sasaki Y, Sato M, Shirakawa A, Abe M (2002) Analysis of immunoglobulin VH genes in CD10-positive diffuse large B-cell lymphoma. Pathol Int 52:586–594
17. Ichikawa A, Kinoshita T, Watanabe T, Kato H, Nagai H, Tsushita K, Saito H, Hotta T (1997) Mutations of the p53 gene as a prognostic factor in aggressive B-cell lymphoma. N Engl J Med 337:529–534
18. Jaffee ES, Harris NL, Stein H, Vardiman JW (eds) (2001) World Health Organization classification of tumors. Pathology and genetics of tumours of haematopoietic and lymphoid tissues. IARC Press, Lyon
19. Kaplan EMP (1958) Non-parametric estimation from incomplete observations. J Am Stat Assoc 53:457
20. Koduru PR, Raju K, Vadmal V, Menezes G, Shah S, Susin M, Kolitz J, Broome JD (1997) Correlation between mutation in p53, p53 expression, cytogenetics, histologic type, and survival in patients with B-cell non-Hodgkin's lymphoma. Blood 90:4078–4091
21. Leroy K, Haioun C, Lepage E, Le Metayer N, Berger F, Labouyrie E, Meignin V, Petit B, Bastard C, Salles G, Gisselbrecht C, Reyes F, Gaulard P (2002) p53 gene mutations are associated with poor survival in low and low-intermediate risk diffuse large B-cell lymphomas. Ann Oncol 13:1108–1115
22. McCluggage WG, Catherwood M, Alexander HD, McBride HA, Smith ME, Morris TC (2002) Immunohistochemical expression of CD10 and t(14;18) chromosomal translocation may be indicators of follicle centre cell origin in nodal diffuse large B-cell lymphoma. Histopathology 41:414–420
23. Ohshima K, Kawasaki C, Muta H, Muta K, Deyev V, Haraoka S, Suzumiya J, Podack ER, Kikuchi M (2001) CD10 and Bcl10 expression in diffuse large B-cell lymphoma: CD10 is a marker of improved prognosis. Histopathology 39:156–162
24. Ree HJ, Yang WI, Kim CW, Huh J, Lee SS, Cho EY, Ko YH, Charney D (2001) Coexpression of Bcl-6 and CD10 in diffuse large B-cell lymphomas: significance of Bcl-6 expression patterns in identifying germinal center B-cell lymphoma. Hum Pathol 32:954–962
25. Rosenwald A, Wright G, Chan WC, Connors JM, Campo E, Fisher RI, Gascoyne RD, Muller-Hermelink HK, Smeland EB, Giltnane JM, Hurt EM, Zhao H, Averett L, Yang L, Wilson WH, Jaffe ES, Simon R, Klausner RD, Powell J, Duffey PL, Longo DL, Greiner TC, Weisenburger DD, Sanger WG, Dave BJ, Lynch JC, Vose J, Armitage JO, Montserrat E, Lopez-Guillermo A, Grogan TM, Miller TP, LeBlanc M, Ott G, Kvaloy S, Delabie J, Holte H, Krajci P, Stokke T, Staudt LM (2002) The use of molecular profiling to predict survival after chemotherapy for diffuse large-B-cell lymphoma. N Engl J Med 346:1937–1947
26. Tilly H, Lepage E, Coiffier B, Blanc M, Herbrecht R, Bosly A, Attal M, Fillet G, Guettier C, Molina TJ, Gisselbrecht C, Reyes F (2003) Intensive conventional chemotherapy (ACVBP regimen) compared with standard CHOP for poor-prognosis aggressive non-Hodgkin's lymphoma. Blood 102:4284–4289
27. Uherova P, Ross CW, Schnitzer B, Singleton TP, Finn WG (2001) The clinical significance of CD10 antigen expression in diffuse large B-cell lymphoma. Am J Clin Pathol 115:582–588
28. Xu Y, McKenna RW, Molberg KH, Kroft SH (2001) Clinicopathologic analysis of CD10+ and CD10– diffuse large B-cell lymphoma. Identification of a high-risk subset with coexpression of CD10 and bcl-2. Am J Clin Pathol 116:183–190
29. Xu Y, McKenna RW, Kroft SH (2002) Comparison of multiparameter flow cytometry with cluster analysis and immunohistochemistry for the detection of CD10 in diffuse large B-Cell lymphomas. Mod Pathol 15:413–419

Virchows Arch (2004) 445:552–563
DOI 10.1007/s00428-004-1140-z

ORIGINAL ARTICLE

Giuseppe Zamboni · Jutta Lüttges · Paola Capelli · Luca Frulloni · Giorgio Cavallini · Paolo Pederzoli · Alexander Leins · Daniel Longnecker · Günter Klöppel

Histopathological features of diagnostic and clinical relevance in autoimmune pancreatitis: a study on 53 resection specimens and 9 biopsy specimens

Received: 29 July 2004 / Accepted: 21 September 2004 / Published online: 27 October 2004
© Springer-Verlag 2004

Abstract *Background and Aims:* Autoimmune pancreatitis seems to be a disease with a heterogeneous appearance. Our intention was to establish key diagnostic criteria, define grades of severity and activity, identify features of potential subtypes and evaluate the diagnostic relevance of biopsy specimens. *Methods:* Histopathological criteria and clinical features were recorded in pancreatic resection specimens from 53 patients who were found to have chronic pancreatitis lacking pseudocysts, calculi, irregular duct dilatations, pancreas divisum and/or duodenal wall inflammation. The severity of the chronic inflammation was graded, and the activity of the acute inflammatory component and the granulocytic epithelial lesion (GEL) were determined. Additionally, pancreatic biopsy specimens from 9 patients with suspected AIP were assessed. *Results:* Periductal lymphoplasmacytic infiltration was identified in all cases, followed in order of frequency by periductal fibrosis and venulitis. These changes were absent in 147 pancreatic specimens that showed chronic pancreatitis associated with pseudocysts, calculi, pancreas divisum and/or duodenal wall inflammation. In 90% of the cases, these chronic changes were graded as 3 or 4. In 81%, the inflammatory process resided in the head of the pancreas and involved the common bile duct. GELs were present in 42% of the patients, who had a mean age of 40.5 years, an almost equal male–female ratio and a high coincidence of ulcerative colitis or Crohn's disease. Patients without GELs were older (mean age 64 years), showed a male preponderance, commonly had Sjögren's syndrome and often developed recurrent bile-duct stenosis. Diagnostically relevant lesions were present in two of five wedge biopsy specimens and three of four fine-needle specimens. *Conclusions:* Periductal lymphoplasmacytic infiltration and fibrosis, preferential occurrence in the pancreatic head and venulitis characterize autoimmune pancreatitis. GELs predominantly occur in a subset of patients who are younger, more commonly have ulcerative colitis and Crohn's disease and seem to have fewer recurrences than patients without GELs. Pancreatic biopsy material proved to be a very helpful adjunct for establishing the diagnosis.

Keywords Autoimmune pancreatitis · Duct destructive chronic pancreatitis · Histopathology · Grading · Biopsy

G. Zamboni · P. Capelli
Department of Pathology,
University of Verona,
Verona, Italy

J. Lüttges · G. Klöppel (✉)
Department of Pathology,
University of Kiel,
Michaelisstrasse 11, 24105 Kiel, Germany
e-mail: gkloeppel@path.uni-kiel.de
Tel.: +49-431-5973400
Fax: +49-431-5973462

L. Frulloni · G. Cavallini · P. Pederzoli
Department of Surgical and Gastroenterological Sciences,
University of Verona,
Verona, Italy

A. Leins
Department of Surgery,
University of Kiel,
Kiel, Germany

D. Longnecker
Department of Pathology,
Dartmouth-Hitchcock Medical Center,
Lebanon, NH, USA

Introduction

In recent years, a special type of chronic pancreatitis has increasingly been recognized, the clinicopathological features of which suggest an autoimmune etiology [19, 26, 32, 43]. The disease has been referred to by various names, depending on whether it was studied by pathologists, clinicians or radiologists. The most widely used names are chronic sclerosing pancreatitis [37], lymphoplasmacytic sclerosing pancreatitis [18], duct-destructive

chronic pancreatitis [9] and autoimmune pancreatitis (AIP) [43]. Here, we will use the term AIP, although the evidence for an autoimmune pathogenesis is, so far, only circumstantial [19, 26, 28].

Recent reviews have described the currently available clinical, immunological, radiological and morphological features [19, 26, 28, 30]. Clinically, it is a heterogeneous disease that can present with either the classical symptoms of acute or severe pancreatitis or with obstructive jaundice due to a mass in the head of the pancreas mimicking pancreatic ductal carcinoma [6, 16, 28]. Immunologically, some patients show elevated levels of serum gamma globulin and particularly IgG_4 [12]. IgG positive plasma cells were also demonstrated in the pancreatic inflammatory infiltrate of patients with AIP [17]. Morphologically, AIP displays a lymphoplasmacellular and sclerosing inflammation that is particularly associated with the pancreatic ducts and may also involve the common bile duct as well as the gallbladder [1, 18, 34]. These features and the lack of calculi, pseudocysts and focal autodigestive necrosis distinguish it from alcoholic chronic pancreatitis, the most frequent type of chronic pancreatitis seen in western countries [9].

Recently, a number of articles have appeared that emphasized AIP as a mimicker of pancreatic ductal carcinoma [3, 14, 25, 41]. It was also reported that some cases show a conspicuous eosinophilic component [2]. Moreover, in a study performed by a group at the Mayo Clinic, it was demonstrated that there may be two morphological types of AIP, which were called lymphoplasmacytic sclerosing pancreatitis (LPSP) and idiopathic duct-centric chronic pancreatitis (IDCP) [25]. Finally, the disease seems to unevenly involve the pancreas with preferential occurrence in the head or tail [9]. So far, it is not known whether these variable changes are all part of the spectrum of one disease, depending on its duration and progression, or whether they reflect subtypes of AIP with different etiologies, different clinical courses and different associations with other autoimmune diseases.

Because AIP is responsive to steroid therapy [15, 21], surgical treatment may be required in only a minority of cases. The decision to give steroid therapy, however, requires a precise tissue diagnosis based on a pancreatic biopsy [28]. Yet little information is available about the value of this method for establishing the diagnosis of AIP [41].

In this study, we investigated the histopathology of a series of cases of chronic pancreatitis that were treated surgically and were lacking pseudocysts, calculi, irregular duct dilatations, pancreas divisum and duodenal wall inflammation. On the basis of this selection process, we were able to identify 53 cases in which we suspected AIP. In addition, we studied 9 biopsy specimens from patients whose clinical, radiological and laboratory features were suggestive of AIP. Our special aims were (1) to identify histopathological features that distinguish AIP, (2) to grade the severity and activity of the inflammatory changes, in order to characterize AIP in the individual patient, (3) to search for biologically relevant morphological subgroups of AIP, and (4) to study the diagnostic value of pancreatic biopsy.

Materials and methods

Patients

We reviewed the pancreatic pathology of a series of 200 surgically treated patients with chronic pancreatitis and retained those cases that had neither pseudocysts, calculi, irregular duct dilatation, pancreas divisum, duodenal wall cysts with associated pancreatitis nor a history of alcohol abuse, cholelithiasis or choledocholithiasis. We identified 53 patients who met these criteria. Clinical information was obtained from each patient's medical and surgical records and by direct consultation with the clinician in charge. The presence of autoimmune antibodies was recorded in a few cases; they failed to show a consistent pattern. Hypergammaglobulinemia and IgG_4 levels were not available for this retrospective study. Particular attention was paid to whether the patient had evidence of autoimmune or autoimmune-related diseases, such as Sjögren's syndrome, ulcerative colitis, Crohn's disease, primary sclerosing cholangitis, primary biliary cirrhosis, retroperitoneal fibrosis, rheumatoid arthritis, Hashimoto's thyroiditis and asthma. Follow-up data was available in 22 patients. It ranged from 6 months to 23 years (mean 3 years). Pancreatic biopsy specimens were available from 9 patients with strong evidence of AIP and detailed clinical and follow-up data. These patients met the same selection criteria as the above cohort of 53 patients.

Tissues

The histopathological material from the 53 selected cases was obtained from 43 pancreaticoduodenectomy specimens, 8 distal pancreatectomy and 2 total pancreatectomy specimens. The pancreatic biopsies consisted of 5 intraoperative biopsy specimens and 4 ultrasound (US)-guided percutaneous fine-needle core specimens, including cytological material. Tissue blocks were retrieved from the files and consultation files of the Department of Pathology of the University of Kiel, Germany (patients 1–38), the Department of Pathology of Dartmouth-Hitchcock Medical Center, Lebanon, New Hampshire, USA (patients 39, 40) and the Department of Pathology of the University of Verona, Italy (patients 41–62). Eight patients included in the series (patients 1, 2, 5–9, 11) had been reported on previously [9]. Additional histopathological material, retrieved from the files of the Department of Pathology, Kiel, was obtained from 147 resection specimens showing chronic pancreatitis characterized by one or more of the following criteria: presence of pseudocysts, calculi, irregular duct dilatation, pancreas divisum and duodenal wall inflammation associated heterotopic pancreatic tissue.

All tissue samples were routinely fixed in formalin or Bouin's fixative and embedded in paraffin. Multiple samples were obtained from the surgical specimens. The number of blocks available in each case ranged from 2 to 18. In the group of biopsied patients, only a single block was available in each case. Deparaffinized sections 4-μm thick were stained with hematoxylin and eosin and periodic acid-Schiff, both with and without diastase pretreatment.

Immunohistochemical analysis was carried out on serial sections in 20 of the 53 selected cases and 10 of the remaining 147 cases, using the alkaline phosphatase-anti-alkaline phosphatase (APAAP) or peroxidase-anti-peroxidase (PAP) method. The antibodies used for the immunohistochemical stains included CD3 (Dako, Glostrup, Denmark, polyclonal), CD4 (Novocastra, Newcastle, UK, 1F6), CD8 (Dako, C8/144B), CD20 (Dako, clone 26), CD57 (Immunotech, Marseille, France, polyclonal), CD79α (Dako, JCB117), kappa and lambda chains (Dako, A8B5, N10/2), CD68 (Dako, 3MA134), S100 (Dako, polyclonal), HLA-DR (Biotest-Seralc, Brussels, Belgium, Tu34), vimentin (Dako, V9) and smooth muscle actin (Dako, 1A4).

Table 1 Grading of severity of autoimmune pancreatitis

Grade 1	Scattered periductal lymphoplasmacytic infiltrates; mild duct narrowing; almost no interlobular and acinar involvement
Grade 2	Multiple periductal lymphoplasmacytic infiltrates; mild periductal fibrosis and duct narrowing; mild interlobular and acinar involvement; focal inflammatory storiform fibrosis; occasional, mild venulitis
Grade 3	Diffuse periductal lymphoplasmacytic infiltrates; marked periductal fibrosis and duct obstruction; moderate interlobular and acinar involvement; moderate focal inflammatory storiform fibrosis; frequent venulitis; scattered lymphoid follicles
Grade 4	Diffuse periductal lymphoplasmacytic infiltrates; severe periductal fibrosis and duct obstruction/disappearance; severe interlobular and acinar involvement; severe inflammatory storiform fibrosis and diffuse sclerosis; frequent venulitis and occasional arteritis; scattered and occasionally prominent lymphoid follicles

Grading of severity and activity index

The detailed histopathological features of AIP were assessed according to a standardized protocol. Briefly, the following features were considered: focal involvement (i.e. if the sections contained affected and unaffected pancreatic tissue next to each other) and diffuse involvement (i.e. if the sections contained only affected tissue); periductal lymphoplasmacytic infiltration, ductal narrowing and obstruction, periductal fibrosis, "granulocytic epithelial lesions" [GELs (i.e. granulocytic periductal and ductal infiltration with or without rupture and destruction of ductal epithelium)], acinar lymphoplasmacytic infiltration, acinar granulocytic infiltration, periacinar fibrosis and acinar atrophy, inflammatory storiform fibrosis (myofibroblastic cells intermingled with some lymphocytes, plasma cells, macrophages and collagen bundles), venulitis, obliterative arteritis, presence of lymphoid follicles, bile-duct involvement, and involvement of the major and/or minor papilla. All features were graded according to their severity and extent as mild/moderate or severe. On the basis of this evaluation, the grade of severity of the entire inflammatory process was determined, as outlined in Table 1. Since the "GELs" were only found in a limited number of cases and appeared to be active changes, differing in severity from patient to patient, an activity index was determined in every affected patient. The activity was considered low if there were only sparse GELs affecting one or multiple ducts and sometimes associated with a few intralobular granulocytes. High activity, in contrast, was characterized by prominent GELs affecting one or multiple ducts, forming "duct abscesses," occasionally leading to duct destruction and commonly associated with inter- and intralobular granulocytes.

Results

Surgically treated patients

Clinical features

Table 2 summarizes the detailed clinical features of the 53 selected patients. They included 35 men and 18 women ranging in age from 14 years to 77 years (mean 56 years; men 56 years; women 55.5 years). Of the patients, 40 (75%) presented with jaundice. Abdominal discomfort and pain were the main symptoms in 16 patients. Since, radiologically, 51 patients were found to have either a mass-forming lesion, the preoperative diagnosis in these patients was pancreatic carcinoma. In two patients the radiological findings were suggestive of chronic pancreatitis, but a carcinoma could not be excluded. Of the patients, 43 were treated by pancreaticoduodenectomy, 8 by distal pancreatectomy and 2 patients by total pancreatectomy. At the time of diagnosis, 10 of the 53 patients (19%) had associated autoimmune or autoimmune-related diseases (Table 2), Sjögren's syndrome being most frequent (4 of 53 patients). During follow-up, 4 other patients also developed autoimmune diseases. Apart from these diseases, one patient had had Hodgkin's disease, another suffered from bronchial asthma and a third patient had diabetes which was already present before the symptoms of pancreatitis started. In all patients, the short-term postoperative course was uneventful. Among 22 of 53 (41%) patients who were followed for a mean of 3 years (range 6 months to 23 years), 5 (24%) developed an inflammatory stenosis of the bile-duct remnant at an average of 2.5 years (range 1–4 years) after pancreaticoduodenectomy. Of these patients, 2 were treated by liver transplantation, the others by stenting the bile-duct stenosis. One of the transplant patients died of sepsis. Histopathological examination of the explanted livers revealed a stenosing fibroinflammatory process showing many lymphocytes and plasma cells and surrounding the common hepatic duct and its hilar branches. The portal tracts were expanded by periportal and periductal fibrosis and contained scattered lymphocytes, findings consistent with a diagnosis of unspecific chronic cholangitis and excluding primary sclerosing cholangitis. Another patient suffered from relapsing pancreatitis and additionally developed Sjögren's syndrome after 8 years. None of the patients received steroid treatment for the pancreatic disease before or after pancreatic resection.

Histopathological findings

The frequency of occurrence of the investigated criteria is summarized in Fig. 1. The most significant and frequent finding was an intense inflammatory cell infiltration around medium-sized and large interlobular ducts (Fig. 2). Smaller ducts were also involved, but usually only in advanced cases. The periductal infiltrates were composed mainly of lymphocytes and plasma cells, but also contained some macrophages. Mast cells were detected in almost all cases, but were only occasionally abundant. The affected ducts were narrowed by an infolding of their epithelium, often giving their lumen a slit-like or star-like appearance. In most cases, the infiltrated duct walls were further thickened by cuff-like fibrosis and this change was usually accompanied by an extension of the inflammatory infiltrate and fibrosis into the interlobular and often also the intralobular areas. The intralobular fibrosis showed a periacinar pattern and was associated with atrophy of the acinar cells and encasement of the islets. In about half of the patients, a special type of fi-

Table 2 Clinical features of patients with diagnosis of autoimmune pancreatitis on surgical specimens. *CA* carcinoma, *CP* chronic pancreatitis, *PD* pancreaticoduodenectomy, *DP* distal pancreatectomy, *TP* total pancreatectomy, *SS* Sjögren's syndrome, *UC* ulcerative colitis, *CD* Crohn's disease, *RA* rheumatoid arthritis, *RF* retroperitoneal fibrosis, *TH* thyroiditis, *NED* no evidence of disease, *NA* not available, *A* alive, *CBD* common bile duct, *DOD* dead of disease

Case no.	Age (years)	Sex	Jaundice	Pain	Autoimmune disease	Site	Clinical diagnosis	Surgical procedure	Follow-up (years)
1	29	Male	+	−	SS	Head	CA	PD	
2	17	Female	−	+		Tail	CA	DP	
3	50	Male	+	−		Head	CA	PD	
4	69	Male	+	−		Head	CA	PD	
5	77	Male	+	−		Head	CA	PD	A, 2, CBD stenosis
6	59	Male	+	−	CD and RA	Head	CA	PD	
7	20	Female	+	−		Diffuse	CA	TP	
8	59	Male	+	−	CD	Head	CA/CP	PD	
9	67	Female	+	−		Head	CP	PD	
10	28	Male	+	−		Head	CA	PD	
11	76	Male	+	−		Head	CA	PD	NED, 7
12	71	Male	−	+		Tail	CA	DP	
13	24	Female	−	+		Tail	CA/CP	DP	
14	64	Male	+	−		Head	CA	PD	
15	73	Male	+	−		Head	CA	PD	A, 4, CBD stenosis
16	62	Male	+	−		Head	CA	PD	DOD, 1, CBD stenosis
17	56	Male	+	−		Head	CA	PD	
18	24	Female	+	−		Head	CA	PD	
19	70	Male	+	−		Head	CA	PD	
20	64	Female	+	−		Head	CA	PD	NED, 3
21	69	Female	+	−		Head	CA	PD	
22	60	Male	+	−		Head	CA	PD	
23	71	Female	+	−		Head	CA	PD	
24	66	Male	+	−		Head	CA	PD	NED, 9
25	36	Male	−	+	SS and TH	Tail	CA	DP	A, 1, CBD stenosis
26	69	Male	+	−	SS and RF	Head	CA	PD	A, 3, recurrence
27	40	Female	−	+		Tail	CA	DP	
28	40	Male	−	+		Tail	CA	DP	
29	66	Female	+	−		Head	CA	PD	
30	56	Male	+	−		Head	CA	PD	A, 3, CBD stenosis
31	65	Female	+	+		Head	CA	PD	NED, 2
32	59	Male	+	−		Head	CA	PD	
33	52	Male	+	−		Head	CA	PD	
34	67	Male	+	−		Head	CA	PD	
35	41	Female	+	−		Head	CA	PD	
36	30	Male	+	−		Head	CA	PD	
37	40	Male	+	−		Head	CA	PD	
38	62	Male	+	−		Head	CA	PD	NED, 7
39	64	Female	−	+		Diffuse	CA	TP	NED, 11
40	14	Female	−	+		Head	CA	PD	
41	36	Male	−	+	CD	Head	CA	PD	NED, 8
42	56	Male	+	−	UC	Head	CA	PD	NED, 16
43	52	Male	−	+		Tail	CA	DP	
44	62	Female	+	+	UC	Head	CA	PD	NED, 1
45	66	Male	+	−		Head	CA	PD	NED, 3
46	32	Male	+	−	UC	Head	CA	PD	NED, 6
47	41	Male	−	+		Head	CA	PD	
48	46	Female	+	−		Head	CA	PD	NED, 2
49	54	Female	−	+		Tail	CA	DP	NED, 23
50	26	Male	+	−		Head	CA	PD	NED, 3
51	49	Male	+	−	SS	Head	CA	PD	A, 8, recurrence
52	48	Male	−	+		Head	CA	PD	
53	57	Female	+	+		Head	CA	PD	NED, 0.5

brotic changes was encountered, characterized by the presence of inflammatory cells and plump myofibroblasts intermingled with collagen bundles, some of which were arranged in a storiform pattern (Fig. 3). In 10% of the cases, this type of fibrosis occupied a large area, giving it a tumorous appearance. Scattered lymphoid follicles, mainly located at the periphery of the fibrotic areas, were found in two-thirds of the cases. In 7 cases, however, they were restricted to periductal areas (Fig. 4). Another frequent finding was venulitis, which was mainly present in fibrotic areas (Fig. 5). Obliterative arteritis was less common and was usually seen together with advanced fibrosis. Focal involvement of the resected tissue (i.e. involvement of a small group of lobes, leaving the adja-

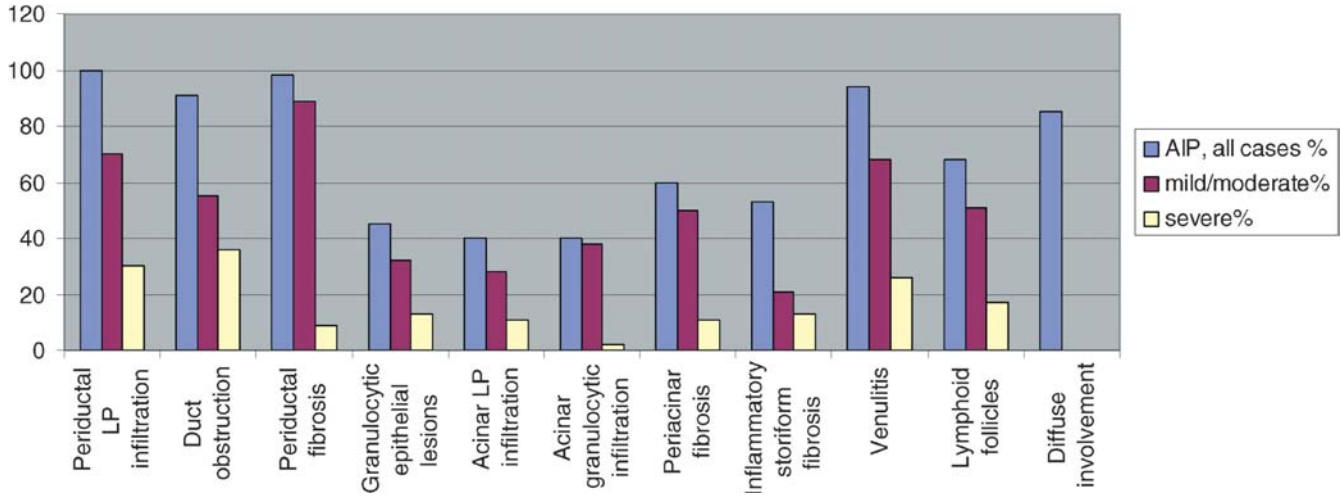


Fig. 1 Frequency (%) of histopathological features in 53 resected pancreatic specimens from patients with autoimmune pancreatitis (AIP)

cent ones unaffected) was seen in 8 patients (15%). The granulocytic infiltrate consisted mainly of neutrophils in

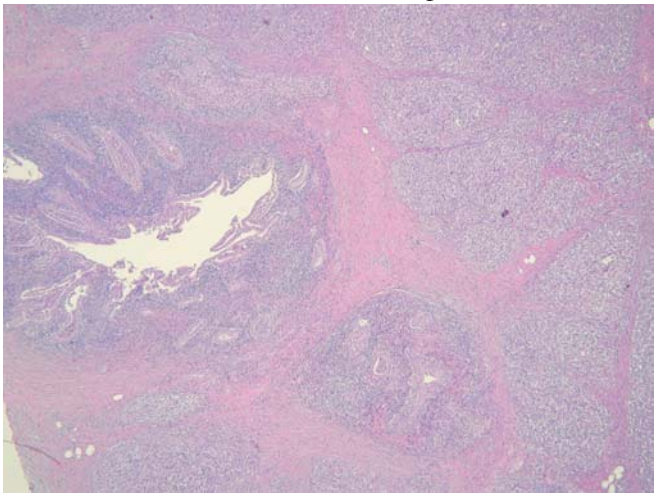


Fig. 2 Autoimmune pancreatitis showing periductal lymphoplasmacytic infiltration and fibrosis leading to duct narrowing (H&E ×120)

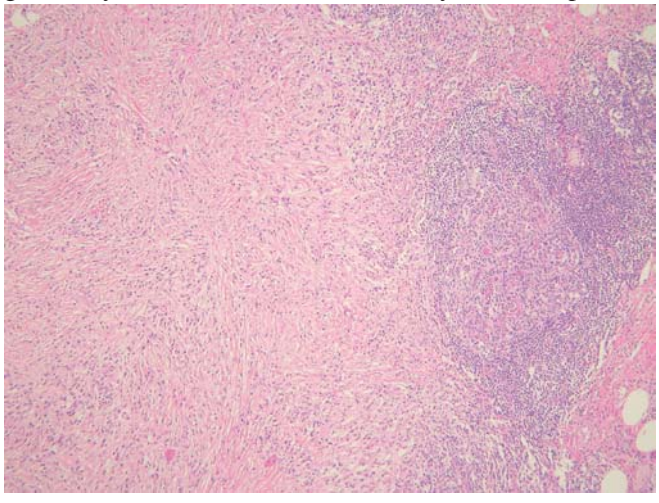


Fig. 3 Autoimmune pancreatitis showing complete replacement of acinar tissue by storiform fibrosis (H&E ×200)

distal bile duct was affected by the inflammatory process in 25 patients (47%) (Fig. 6). However, this figure is not representative, because it only refers to the cases with histologically documented involvement of the distal bile duct. If all patients with jaundice because of a bile-duct stenosis are considered, 75% of the patients were affected. In 18 of 53 (34%) patients, the inflammatory process involved the major papilla and in 6 of 53 (11%) the minor papilla was also involved. In 16 patients (30%), both the distal bile duct and the major and/or minor papilla were affected. When the severity of the disease was graded on the basis of the above findings (Table 1), only 4 cases proved to be in grades 1 (1 of 53) or 2 (3 of 53), while the majority (92%) showed grades 3 (25 of 53) and 4 (24 of 53).

In addition to the described chronic changes, GELs (Fig. 7) were observed in 24 of 53 (45%) patients. The all cases. In 21 of 53 cases, it extended into the small intralobular ducts and the acini. The granulocytic infiltration was considered an acute inflammatory process and was classified into two grades of activity. In 17 of 24 (71%) patients, the activity was classified as low and in 7 of 24 (29%) patients as high. A predominantly eosinophilic infiltration that barely affected the ductal epithelium was observed in 3 cases.

When the activity index of the GELs was related to the severity grade of the chronic inflammatory process, it was found that high activity was mainly associated with grade 4 (4 of 7 patients, 57%), whereas low activity was mainly noted in grade 3 (12 of 17 patients, 70%).

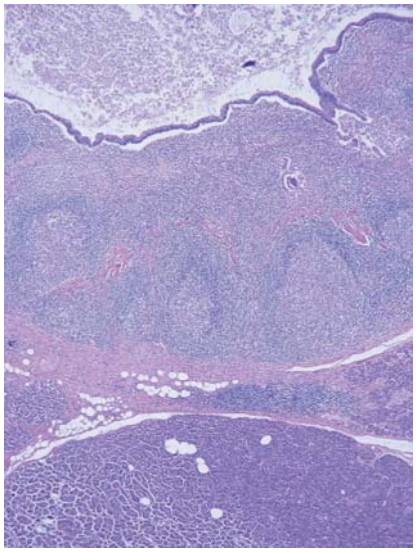


Fig. 4 Autoimmune pancreatitis showing lymphoid follicles within a dense mononuclear cell infiltration surrounding a large duct (H&E ×120)

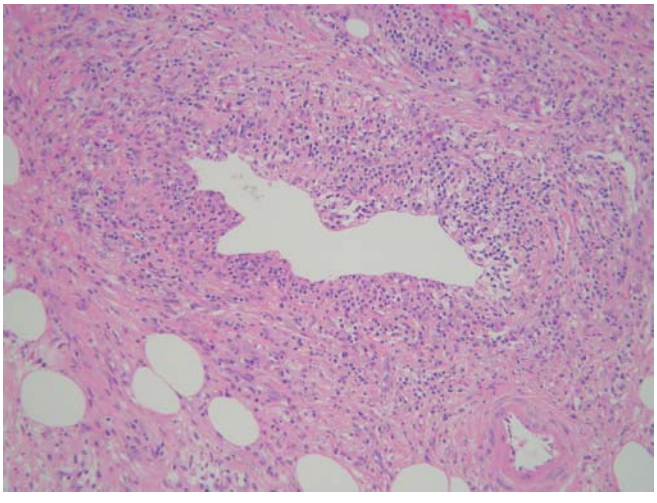


Fig. 5 Autoimmune pancreatitis showing an area with intense venulitis (H&E ×200)

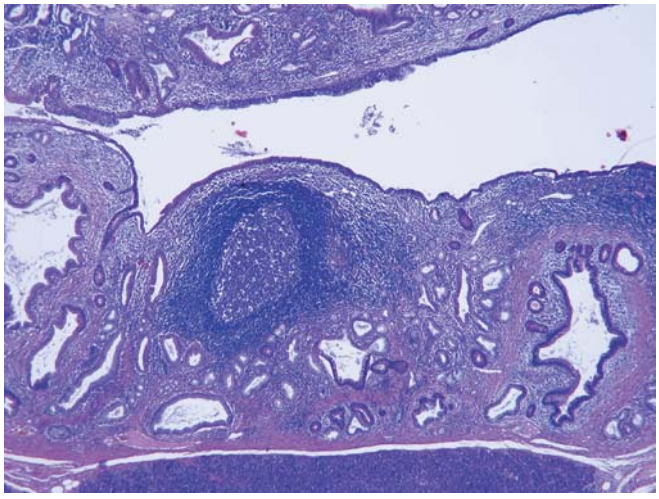


Fig. 6 Autoimmune pancreatitis with common bile duct involvement (H&E ×120)

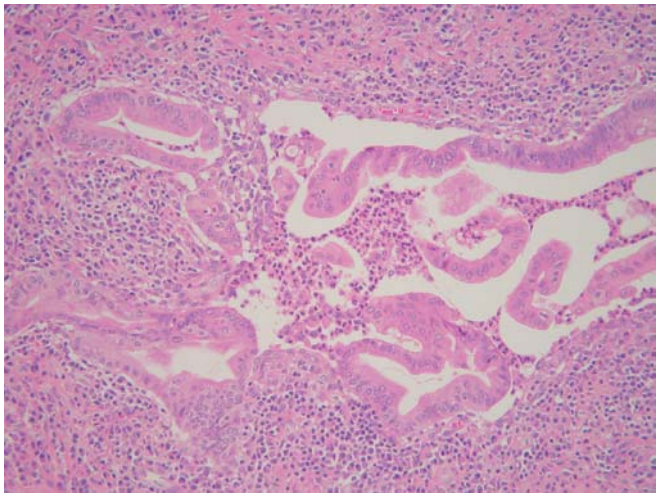


Fig. 7 Autoimmune pancreatitis showing granulocytic infiltration and destruction of the ductal epithelium (H&E ×200)

Immunohistochemical findings

Immunohistochemical staining in the 20 selected cases revealed a predominance of CD3+, CD4+ and CD8+ T lymphocytes in the inflammatory infiltrates surrounding the medium-sized and large interlobular ducts. In addition, the infiltrates contained CD20+ B lymphocytes and CD68+ macrophages. The plasma cells showed a polyclonal pattern, expressing either kappa or lambda chains. T lymphocytes (CD4+>CD8+) occasionally invaded the duct epithelium. The lymphoid follicles that were found either scattered in sclerotic tissue or around ducts consisted mainly of B lymphocytes.

Analysis of the spindle cells that were found in areas with inflammatory storiform fibrosis revealed the expression of smooth muscle actin and vimentin, whereas most of the intermingled mononuclear cells stained with CD68, characterizing them as macrophages. In addition, T lymphocytes and CD79+ plasma cells were identified. Scattered HLA-DR expression was found in duct cells, endothelial cells, inflammatory cells and myofibroblastic cells.

Comparison of histopathological and immunohistochemical features

The most significant findings, i.e. periductal lymphoplasmacytic infiltration, cuff-like periductal fibrosis and venulitis, which were found in all or most of the 53 selected specimens (Fig. 1), were not detected in any of the other 147 pancreatic specimens showing chronic pancre-

Table 3 Clinical and radiological features in patients with suspected autoimmune pancreatitis who underwent pancreatic biopsy. *UC* ulcerative colitis, *BD* before diagnosis, *AD* after diagnosis, *NED* no evidence of disease

Case no.	Age (years)	Sex	Signs and symptoms	Radiological findings	Site	Autoimmune disease	Steroid therapy	Follow-up (years)
1	47	Male	Jaundice	Mass	Head	UC (3 years BD)		NED, 10
2	25	Female	Jaundice	Mass	Head	UC (1 week AD)		NED, 8
3	55	Male	Abdominal pain	Mass	Head	UC (10 years BD)		NED, 8
4	50	Male	Jaundice	Mass	Head	UC (4 years BD)		NED, 9
5	18	Male	Jaundice	Mass	Head	UC (3 years AD)		NED, 3
6	50	Male	Jaundice	Enlargement	Head-body	UC, sialadenitis	Yes	Recurrence, 6
7	60	Male	Jaundice	Enlargement	Head-body	Retroperitoneal fibrosis		NED, 6
8	29	Male	Abdominal pain	Mass	Body	UC (2 years BD)	Yes	Recurrence, 2
9	32	Female	Abdominal pain	Mass	Head	No	Yes	NED, 1

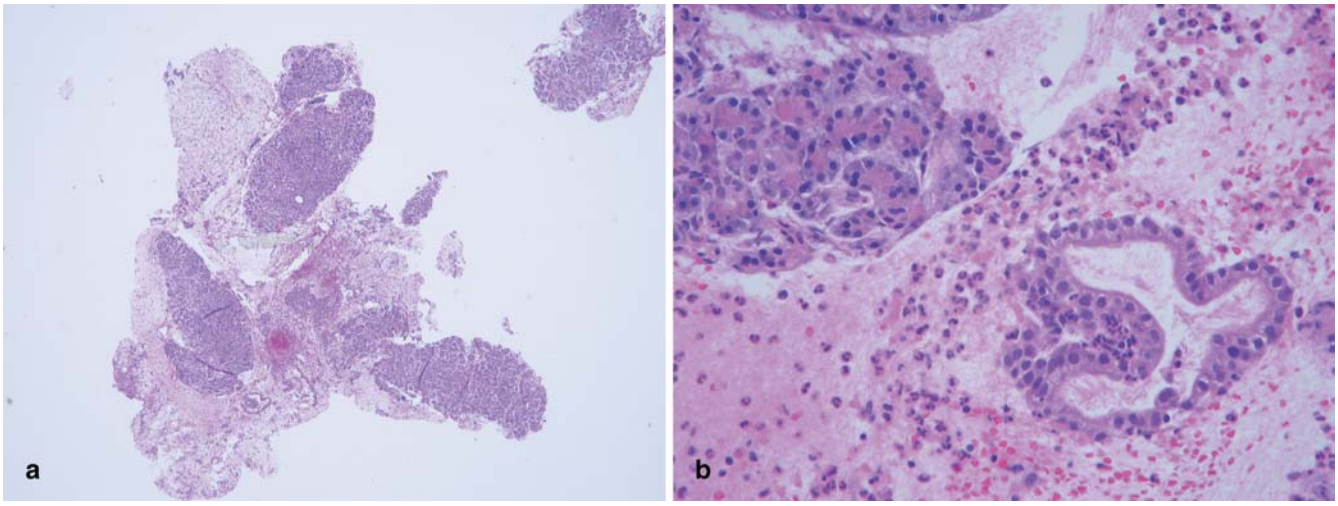


Fig. 8 Biopsy specimen from a patient (no. 9, Table 5) with suspected autoimmune pancreatitis. **a** Low-power view showing perilobular fibrosis and lymphoplasmacytic infiltration. **b** High-power view showing a granulocytic epithelial lesion (H&E ×40 and ×240)

atitis associated with pseudocysts, calculi, irregular duct dilatation, pancreas divisum and/or duodenal wall inflammation. The immunohistochemical staining identified sparse T cell infiltrates and a few scattered B cells and macrophages. Plasma cells were very rare. Smooth muscle actin positive myofibroblasts were abundant in the fibrotic areas close to pseudocysts as well as in interlobular areas with high cellularity.

Biopsied patients

Clinical features

Table 3 summarizes the clinical features of 9 patients who were diagnosed on the basis of biopsy and radiological findings. They included 7 men and 2 women, whose mean age was 47 years (range 18–60 years). Of these patients, 6 had jaundice in association with pain; 3 patients had pain only. Ulcerative colitis had developed in 4 patients before the diagnosis of AIP and in 3 after or at the time of diagnosis of AIP; 1 patient had retroperitoneal fibrosis and another chronic sialadenitis. Radiologically, US and computed tomography (CT) scans revealed a mass or enlargement in the pancreatic head in 8 patients and 1 had a mass in the body. All patients were followed up (mean period 6 years; range 1–10 years); 6 patients are alive and well without steroid treatment. Steroid treatment was given to 3 patients, starting with 50–75 mg tapered by 2.5–5 mg/week. Of these 3 patients, 2 are still on therapy because abdominal pain recurred when they reached a dose of 10–15 mg; 1 patient is doing well after withdrawal of the initial steroid therapy.

Histopathological findings

Intraoperative wedge biopsy was performed in 5 patients who had an explorative laparotomy to rule out malignancy. The biopsy specimens did not show any signs of any type of pancreatic malignancy. In 1 patient, the biopsy findings were diagnostic of AIP (Fig. 8 and Table 4). In another patient, the findings were suggestive of AIP, while in the remaining patients they were inconclusive. In 4 patients, a percutaneous US-guided, fine-needle-core biopsy was performed. Both the histological and the cy-

Table 4 Histopathological features of pancreatic biopsy specimens from patients with suspected autoimmune pancreatitis. *FNCB* fine-needle-core biopsy, *IWB* intraoperative wedge biopsy, *LP* lymphoplasmacytic, *GEL* granulocytic epithelial lesion

Case no.	Biopsy	LP infiltrate	Periductal LP infiltrate	GEL	Acinar granulocytic infiltrate	Venulitis	Storiform proliferation	Histopathology
1	IWB	++	++	+	+	+	−	Diagnostic
2	IWB	++	−	+	+	+	+	Suggestive
3	IWB	−	−	−	−	−	−	Inconclusive
4	IWB	−	−	−	−	−	−	Inconclusive
5	IWB	−	−	−	−	−	−	Inconclusive
6	FNCB	+	−	−	+	−	−	Suggestive
7	FNCB	++	−	−	−	+	+++	Suggestive
8	FNCB	−	−	−	+	−	−	Inconclusive
9	FNCB	+	+	+++	++	−	+	Diagnostic

Table 5 Patients with associated autoimmune diseases, distinguished by the absence or presence of granulocytic epithelial lesions (GELs). *CBD* common bile duct, *NED* no evidence of disease

Case no.	Age (years)	Sex	Site	Disorders	Follow-up	Recurrence (years)
AIP/GEL-neg						
1	29	Male	Head	Sjögren's syndrome	/	/
2	59	Male	Head	Crohn's disease, rheumatoid arthritis (before)	/	/
3	36	Male	Head	Sjögren's syndrome, thyroiditis (+1 yr)	1 year, CBD stenosis	1, CBD stenosis
4	69	Male	Head	Sjögren's syndrome, retroperitonal fibrosis (+3 yrs)	3 years, recurrence	3, recurrence
5	49	Male	Head	Sjögren's syndrome (+2 yrs)	8 years, recurrence	8, recurrence
6	50	Male	Head-body	Ulcerative colitis (simultaneously), sialadenitis (+1 yr)	6 years, recurrence	6, recurrence
7	60	Male	Head-body	Retroperitoneal fibrosis (simultaneously)	6 years, NED	No
AIP/GEL-pos						
1	59	Male	Head	Crohn's disease (before)	/	/
2	36	Male	Head	Crohn's disease (before)	8 years, NED	No
3	56	Male	Head	Ulcerative colitis (−12 years)	16 years, NED	No
4	62	Female	Head	Ulcerative colitis (−1 year)	1 year, NED	No
5	32	Male	Head	Ulcerative colitis (+2 years)	6 years, NED	No
6	47	Male	Head	Ulcerative colitis (−3 years)	10 years, NED	No
7	25	Female	Head	Ulcerative colitis (+1 week)	8 years, NED	No

tological evaluation excluded a malignant pancreatic tumor and allowed the diagnosis of AIP in 1 patient, while it was suggestive in 2 others and inconclusive in 1 (Table 4).

Clinicopathological correlations

Clinicopathological correlation was only performed in the selected 53 surgically treated patients. When the 24 patients with GELs were compared with the 29 patients without this finding, it was found that the sex distribution was almost equal (57% men) in the AIP/GEL-positive group, whereas males predominated (77%) in the AIP/GEL-negative group. Moreover, the AIP/GEL-positive patients were considerably younger (mean age 40.5 years versus 64 years), had no Sjögren's syndrome and only ulcerative colitis or Crohn's disease and, finally, showed no recurrence of AIP (Table 5). In contrast, the AIP/GEL-negative group showed a strong association with Sjögren's syndrome and retroperitoneal fibrosis and were all males. In addition, all recurrent bile-duct stenoses were observed in the latter group of patients (Table 5), who in general also had more advanced AIP than the AIP/GEL-negative patients. There was no significant difference between the two groups of patients regarding the main localization of the disease (i.e. pancreatic head versus body-tail).

Discussion

Periductal lymphoplasmacytic infiltration, cuff-like periductal fibrosis and venulitis were identified as the most characteristic histological lesions in pancreatic specimens that showed chronic pancreatitis lacking pseudocysts, calculi, irregular duct dilatations, pancreas divisum and/or duodenal wall inflammation associated with heterotopic pancreatic tissue. This spectrum of findings seems to define the pathology of AIP, since all chronic pancreatitis specimens in our series that showed one or more of the above-mentioned changes, such as pseudocysts or calculi, lacked lymphoplasmacytic duct changes and venulitis. Recent reports on the occurrence of calculi in otherwise typical cases of AIP do not contradict our findings, since the calculi obviously only appeared late in the course of AIP and were not present at the time of diagnosis [13]. Further help in distinguishing AIP from chronic pancreatitis of other causes is provided by the frequent occurrence of AIP in the head of the pancreas combined with

bile-duct stenosis and the abundant occurrence of plasma cells and CD4 and CD8 T lymphocytes around the ducts.

Reports of chronic interstitial pancreatitis and primary inflammatory sclerosis by Ball [5] and Sarles [32], respectively, were probably the first recorded cases of AIP. However, their histological descriptions are only suggestive of AIP—not conclusive. The first description that we regard as diagnostic of AIP was by Kawaguchi [18] and included prominent infiltration of the pancreas by lymphocytes and plasma cells combined with marked interstitial fibrosis, acinar atrophy and obliterating phlebitis. Subsequently, it became obvious that the lymphoplasmacytic infiltration concentrated around narrowed pancreatic ducts and was frequently associated with a "cuff" of periductal fibrosis. Moreover, it was noted that there were often granulocytes (some of them eosinophils), lymph follicles and an occasionally distinct patchy involvement [2, 3, 9, 14, 25, 41, 44]. Analysis of our 53 patients, none of them previously treated with steroids, revealed that periductal lymphoplasmacytic infiltration was present in each case, followed in order of frequency by periductal fibrosis and venulitis. In 80% of the patients, these changes were seen throughout the pancreatic tissue that was available for review. In the remaining patients, the involvement of the pancreatic tissue was patchy. Less frequent histopathological features, present in only 40–60% of cases, included involvement of the acinar tissue, fibrotic areas rich in myofibroblasts where acinar cells, ducts and islets were replaced by collagen bundles partly arranged in a storiform pattern, and inflammatory cells such as lymphocytes, plasma cells, neutrophils and occasionally also eosinophils. An impressive acute inflammatory component that we called GEL was detected in 42% of cases. This change, first described by Ectors [9] and later by Scully [33], was characterized by focal detachment, disruption and destruction of the epithelium of interlobular ducts due to invading neutrophilic and occasionally eosinophilic granulocytes, which were also in the duct wall, particularly under the duct epithelium, and in the duct lumen (duct abscesses). In the cases with the most severe GELs, the acute inflammatory infiltrate extended into the ductules, acini and interstitial spaces. Notohara [25] recently reported this finding in 31% of 35 AIP cases, a proportion similar to ours. Their diagnosis in these cases was IDCP, and they differentiated it from LPSP. Although we believe that the GEL is a distinctive biologically important finding, we refrain from using Notohara's terminology since, in our study, the GELs were superimposed on the periductal lymphoplasmacytic infiltration and fibrosis and did not occur independently of these basic changes. We, therefore, prefer "AIP with GEL" to identify pancreases exhibiting this acute inflammatory component.

The severity of the chronic inflammatory process and the activity of the GELs varied from case to case. To quantify these differences in individual patients, we developed a grading system and an activity index, distinguishing four grades of severity and two levels of activity, respectively. Grading of the chronic inflammatory process revealed that 92% of the cases were grades 3 and 4. We had only one grade-1 and three grade-2 cases. Grade-1 and grade-2 AIP may only rarely cause clinical symptoms (e.g. pain and jaundice) of such intensity that they become an indication for resection. Looking at the acute inflammatory component of AIP represented by the GELs, we noted that the grade of severity of AIP paralleled the activity index in 60–70% of the patients, suggesting that the two processes are to some extent interrelated.

Fibrosis of the pancreas in AIP predominantly shows a periductal and interlobular pattern [20], features that are characteristic of grade-3 AIP. If the fibrosis extended into the lobules, grade-4 AIP was assigned. In grade 4, there were also fibroinflammatory areas that share histological features with those described in inflammatory pseudotumors of the pancreas and the common bile duct [7, 8, 10, 11, 24, 27, 31, 38, 40, 42]. These features include smooth muscle actin-positive myofibroblasts admixed with lymphocytes and plasma cells and embedded between bundles of dense collagen with storiform foci. Additionally, venulitis and obliterative arteritis have also been mentioned in several cases [8, 40, 42]. Since the clinical features of patients with inflammatory pseudotumors are very similar, the possibility that inflammatory pseudotumors of the pancreas might represent grade-4 AIP in which the fibroinflammatory storiform fibrosis has acquired a tumor-like appearance should be considered [10].

Because most of our patients presented with jaundice, pancreatic head resection specimens comprised almost 80% of the resected material. Although the inflammatory lesions in the resected tissue often extended up to the resection margin, it appeared that the major involvement was in the head of the pancreas since the corresponding CT images from these cases showed a mass-forming enlargement of the head. In 15% of our patients, the disease obviously focused on the tail of the pancreas, which was resected because of a mass. Primary involvement of the tail was supported by a disease-free pancreatic margin in these cases. These findings suggest that in most instances AIP is a focally accentuated disease that involves the head of the pancreas, including the distal common bile duct, four times more often than the remainder of the gland. However, the patchy pattern of involvement in some cases suggests that non-resected parenchyma may be involved even if the resection margins appear to be normal. Moreover, our series included two patients whose pancreases were totally removed because of suspected malignancies. In each of these patients, the entire pancreatic tissue was found to be affected by AIP, although unevenly. Similar conclusions can be drawn from ERCP images [15]. AIP, therefore, may involve the entire pancreas, but is usually focal, with strong preference for the head. Here, the fibroinflammatory process, if it shows grade-3 and grade-4 severity, affects the common bile duct and may also spread to the gallbladder, as has been noted in a number of reports [1, 18], and was also seen in some of our patients (data not shown).

Autoimmune diseases, notably autoimmune sialadenitis (Sjögren's syndrome) [22, 36, 37, 39], Crohn's disease

and ulcerative colitis [4, 23, 29, 35] and retroperitoneal fibrosis [31], have been reported in [38] between 8% and 25% of patients with AIP [3, 9, 14, 25, 41]. The incidence is higher if diseases such as Hashimoto thyroiditis, rheumatoid arthritis or asthma are added. The real incidence of autoimmune diseases in AIP, however, will only be ascertained if we consider not only the diseases that are present at the time of diagnosis, but also those that develop subsequently. Two of our patients developed Sjögren's syndrome or rheumatoid arthritis only after follow-up of several years. Autoimmune diseases occurred in 19% of our patients, Sjögren's syndrome being most frequent.

Notohara [25] noted that the two patients with Sjögren's syndrome in their series were among those who had LPSP, whereas the two patients with ulcerative colitis or Crohn's disease showed IDCP, what we call AIP with GELs. In addition, they found those in the group of patients with LPSP were older, on average (63.4 years), and contained more males than the group with IDCP (average age 48 years, male:female ratio 5:7). Our findings confirm and extend these observations. Our AIP patients without GELs were also considerably older (mean age 64 years), included relatively more men and had a stronger association with Sjögren's syndrome than the AIP patients with GELs, who were younger (mean age 40.5 years) and had an almost equal sex distribution and a strong association with inflammatory bowel disease. These observations suggest that AIP is a heterogeneous disease with two biologically different types, morphologically characterized by the presence or absence of GELs and clinically by the association either with sclerosing autoimmune disease (e.g. Sjögren) or with inflammatory bowel disease. The biological relevance of these observations is further underlined by the fact that all recurrent bile-duct stenoses and AIP recurrences, which were noted in 5 of 22 patients whose follow-up data were available to us, occurred in AIP patients without GELs. It seems, therefore, that these patients may have a higher risk of recurrent AIP after resection, either in the common bile duct or in the pancreas, than AIP patients with GELs. Whether this dichotomy also applies to the response of AIP patients to steroid therapy [26], which has an approximate response rate of 80% [15], is not yet known. It is of interest to note that the GELs in AIP share a number of histological features with ulcerative colitis, a disease that is known to respond to steroid treatment.

In view of the high success rate of corticosteroid therapy in AIP, it can be anticipated that, in the future, the AIP patients who will be treated surgically will be those who prove refractory to steroids and suspect for carcinoma. It is therefore essential to improve our ability to recognize AIP on the basis of clinical data, biopsy, imaging and laboratory findings [28]. Among five wedge biopsy specimens obtained during exploratory laparotomy and four percutaneous fine-needle-core biopsy specimens, the histological findings were diagnostic or suggestive of AIP in about half of the patients. More importantly, malignancy was excluded in all cases. The diagnosis of AIP relied on its specific features discussed above. In the other half of the patients, the biopsy specimens showed inconclusive changes, such as perilobular fibrosis, that may also be seen in other types of pancreatitis. As a consequence of the biopsy results, which were supplemented by clinical, laboratory and radiological findings [28], none of the patients underwent pancreatic resection. Clearly, these preliminary results concerning the value of biopsies in AIP need to be confirmed in a prospective study, but we are more optimistic in this respect than other authors who, on the basis of the risk of complications and inconclusive results in preoperative fine-needle aspirations from six patients, did not recommend pancreatic biopsy [41].

In summary, we have shown that AIP is characterized by a spectrum of morphological features. These include the absence of pseudocysts and calculi, the preferential occurrence in the head of the pancreas, with frequent involvement of the distal bile duct, and the presence of a cuff-like lymphoplasmacytic infiltration and fibrosis and venulitis. Although these features are very distinctive, it should be kept in mind that, in individual cases of AIP, calculi or other alterations that are more characteristic of other types of pancreatitis may develop [13]. The histopathological features of AIP allow a diagnosis to be made on biopsy specimens but, because of the occasional focal accentuation of the disease, we have to expect some biopsies to be inconclusive. If the pancreatic changes that we considered as grade 1 are interpreted as the initial alteration in AIP, the disease starts as a duct-associated lymphoplasmacytic inflammation that may progress to duct narrowing, periductal fibrosis and finally duct obliteration and diffuse fibrosis, the hallmarks of grade-4 AIP. In addition to this chronic fibroinflammatory process, there may be an acute inflammatory component characterized by GELs that may cause rapid duct destruction. The initiating event(s) of this obviously heterogeneous disease, which is primarily oriented toward the duct system including the distal common bile duct, is totally unclear. However, the predominance of CD4- and CD8-positive lymphocytes, the selective demonstration of IgG_4-positive plasma cells [17], the oligoclonal pattern of T-cell receptor γ gene rearrangement [10] and the morphological features of the disease point to a specific immune process directed against antigens related to the pancreatic duct system, but also to the biliary duct system. Infectious agents that could trigger the disease and could explain its focality and often rapid onset have not yet been detected.

Acknowledgements Sincere thanks are due to the many pathologists who sent in cases for consultation. Specifically, we would like to thank Drs. Anita Goossens and Franz Borchert. We are grateful to M. Pacena and A. Paulus for their excellent technical assistance and K. Dege for editing the manuscript.

References

1. Abraham SC, Cruz-Correa M, Argani P, Furth EE, Hruban RH, Boitnott JK (2003) Lymphoplasmacytic chronic cholecystitis and biliary tract disease in patients with lymphoplasmacytic sclerosing pancreatitis. Am J Surg Pathol 27:441–451
2. Abraham SC, Leach S, Yeo CJ, Cameron JL, Murakata LA, Boitnott JK, Albores-Saavedra J, Hruban RH (2003) Eosinophilic pancreatitis and increased eosinophils in the pancreas. Am J Surg Pathol 27:334–342
3. Abraham SC, Wilentz RE, Yeo CJ, Sohn TA, Cameron JL, Boitnott JK, Hruban RH (2003) Pancreaticoduodenectomy (Whipple resections) in patients without malignancy. Are they all "chronic pancreatitis"? Am J Surg Pathol 27:110–120
4. Axon ATR, Ashton MG, Lintott DJ (1979) Chronic pancreatitis and inflammatory bowel disease. Clin Radiol 30:179–182
5. Ball WP, Baggenstoss AH, Bargen JA (1950) Pancreatic lesions associated with chronic ulcerative colitis. Arch Pathol 50:347–358
6. Cavallini G, Frulloni L (2001) Autoimmunity and chronic pancreatitis: a concealed relationship. J O P 2:61–68
7. Chutaputti A, Burrell MI, Boyer JL (1995) Pseudotumor of the pancreas associated with retroperitoneal fibrosis: a dramatic response to corticosteroid therapy. Am J Gastroenterol 90:1155–1158
8. Clark A, Zeman RK, Choyke PL, White EM, Burrell MI, Grant EG, Jaffe MH (1988) Pancreatic pseudotumors associated with multifocal idiopathic fibrosclerosis. Gastrointest Radiol 13:30–32
9. Ectors N, Maillet B, Aerts R, Geboes K, Donner A, Borchard F, Lankisch P, Stolte M, Lüttges J, Kremer B, Klöppel G (1997) Non-alcoholic duct destructive chronic pancreatitis. Gut 41:263–268
10. Esposito I, Bergmann F, Penzel R, di Mola FF, Shrikhande S, Büchler MW, Friess H, Otto HF (2004) Oligoclonal T-cell populations in an inflammatory pseudotumor of the pancreas possibly related to autoimmune pancreatitis: an immunohistochemical and molecular analysis. Virchows Arch 444:119–126
11. Fukushima N, Suzuki M, Abe T, Fukayama M (1997) A case of inflammatory pseudotumour of the common bile duct. Virchows Arch 431:219–224
12. Hamano H, Kawa S, Horiuchi A, Unno H, Furuya N, Akamatsu T, Fukushima M, Nikaido T, Nakayama K, Usuda N, Kiyosawa K (2001) High serum IgG4 concentrations in patients with sclerosing pancreatitis. N Engl J Med 344:732–738
13. Hamano H, Kawa S, Ochi Y, Takayama M, Komatsu K, Muraki T, Kiyosawa K (2004) Recurrent attacks of autoimmune pancreatitis result in pancreatic stone formation. Pancreatology 4:297
14. Hardacre JM, Iacobuzio-Donahue CA, Sohn TA, Abraham SC, Yeo CJ, Lillemoe KD, Choti MA, Campbell KA, Schulick RD, Hruban RH, Cameron JL, Leach SD (2003) Results of pancreaticoduodenectomy for lymphoplasmacytic sclerosing pancreatitis. Ann Surg 237:853–859
15. Horiuchi A, Kawa S, Hamano H, Hayama M, Ota H, Kiyosawa K (2002) ERCP features in 27 patients with autoimmune pancreatitis. Gastrointest Endosc 55:494–499
16. Kamisawa T, Egawa N, Nakajima H, Tsuruta K, Okamoto A, Kamata N (2003) Clinical difficulties in the differentiation of autoimmune pancreatitis and pancreatic carcinoma. Am J Gastroenterol 98:2694–2699
17. Kamisawa T, Funata N, Hayashi Y, Tsuruta K, Okamoto A, Amemiya K, Egawa N, Nakajima H (2003) Close relationship between autoimmune pancreatitis and multifocal fibrosclerosis. Gut 52:683–687
18. Kawaguchi K, Koike M, Tsuruta K, Okamoto A, Tabata I, Fujita N (1991) Lymphoplasmacytic sclerosing pancreatitis with cholangitis: variant of primary sclerosing cholangitis extensively involving pancreas. Hum Pathol 22:387–395
19. Klöppel G, Lüttges J, Löhr M, Zamboni G, Longnecker D (2003) Autoimmune pancreatitis: pathological, clinical, and immunological features. Pancreas 27:14–19
20. Klöppel G, Detlefsen S, Feyerabend B (2004) Fibrosis of the pancreas: the initial tissue damage and the resulting pattern. Virchows Arch 445:1–8
21. Kojima E, Kimura K, Noda Y, Kobayashi G, Itoh K, Fujita N (2003) Autoimmune pancreatitis and multiple bile duct strictures treated effectively with steroid. J Gastroenterol 38:603–607
22. Lindström E, Lindström F, Von Schenck H, Ihse I (1991) Pancreatic ductal morphology and function in primary Sjogren's syndrome. Int J Pancreatol 8:141–149
23. Lysy J, Goldin E (1992) Pancreatitis in ulcerative colitis. J Clin Gastroenterol 15:336–339
24. Nonomura A, Minato H, Shimizu K, Kadoya M, Matsui O (1997) Hepatic hilar inflammatory pseudotumor mimicking cholangiocarcinoma with cholangitis and phlebitis—a variant of primary sclerosing cholangitis? Pathol Res Pract 193:519–525
25. Notohara K, Burgart LJ, Yadav D, Chari S, Smyrk TC (2003) Idiopathic chronic pancreatitis with periductal lymphoplasmacytic infiltration: clinicopathologic features of 35 cases. Am J Surg Pathol 27:1119–1127
26. Okazaki K, Chiba T (2002) Autoimmune related pancreatitis. Gut 51:1–4
27. Palazzo JP, Chang CD (1993) Inflammatory pseudotumour of the pancreas. Histopathology 23:475–477
28. Pearson RK, Longnecker DS, Chari ST, Smyrk TC, Okazaki K, Frulloni L, Cavallini G (2003) Controversies in clinical pancreatology: autoimmune pancreatitis: does it exist? Pancreas 27:1–13
29. Potamianos S, Koutroubakis IE, Chatzicostas C, Rolles K, Burroughs AK, Kouroumalis EA (2000) Idiopathic fibrosing pancreatitis and Crohn's disease: an interesting association. Eur J Gastroenterol Hepatol 12:1021–1024
30. Procacci C, Carbonin G, Biasiutti C, Frulloni L, Bicego E, Spoto E, El-Khaldi M, Bassi C, Pagnotta N, Talamini G (2001) Autoimmune pancreatitis: possibilities of CT characterization. Pancreatology 1:246–253
31. Renner IG, Ponto GC, Savage WT3, Boswell WD (1980) Idiopathic retroperitoneal fibrosis producing common bile duct and pancreatic duct obstruction. Gastroenterology 79:348–351
32. Sarles H, Sarles JC, Muratore R, Guien C (1961) Chronic inflammatory sclerosis of the pancreas—an autoimmune pancreatic disease? Am J Dig Dis 6:688–698
33. Scully KA, Li SC, Hebert JC, Trainer TD (2000) The characteristic appearance of non-alcoholic duct destructive chronic pancreatitis. A report of 2 cases. Arch Pathol Lab Med 124:1535–1538
34. Scully RE, Mark EJ, McNeely BU (1982) Weekly clinicopathological exercises—case 6–1982. N Engl J Med 306:349–358
35. Seyrig JA, Jian R, Modigliani R, Golfain D, Florent C, Messing B, Bitoun A (1985) Idiopathic pancreatitis associated with inflammatory bowel disease. Dig Dis Sci 30:1121–1126
36. Sjögren I, Wengle B, Korsgren M (1979) Primary sclerosing cholangitis associated with fibrosis of the submandibular glands and the pancreas. Acta Med Scand 205:139–141
37. Sood S, Fossard DP, Shorrock K (1995) Chronic sclerosing pancreatitis in Sjögren's syndrome: a case report. Pancreas 10:419–421
38. Uchida K, Okazaki K, Asada M, Yazumi S, Ohana M, Chiba T (2003) Case of chronic pancreatitis involving an autoimmune mechanism that extended to retroperitoneal fibrosis. Pancreas 26:92–94
39. Waldram R, Kopelman H, Tsantoulas D, Williams R (1975) Chronic pancreatitis, sclerosing cholangitis, and sicca complex in two siblings. Lancet 550–552
40. Walsh SV, Evangelista F, Khettry U (1998) Inflammatory myofibroblastic tumor of the pancreaticobiliary region. Morphologic and immunocytochemical study of three cases. Am J Surg Pathol 22:412–418
41. Weber SM, Cubukcu-Dimopulo O, Palesty JA, Suriawinata A, Klimstra D, Brennan MF, Conlon K (2003) Lymphoplasma-

cytic sclerosing pancreatitis: inflammatory mimic of pancreatic carcinoma. J Gastrointest Surg 7:129–139
42. Wreesmann V, van Eijck CHJ, Naus DCWH, van Velthuysen MLF, Jeekel J, Mooi WJ (2001) Inflammatory pseudotumour (inflammatory myofibroblastic tumour) of the pancreas: a report of six cases associated with obliterative phlebitis. Histopathology 38:105–110
43. Yoshida K, Toki F, Takeuchi T, Watanabe S, Shiratori K, Hayashi N (1995) Chronic pancreatitis caused by an autoimmune abnormality. Proposal of the concept of autoimmune pancreatitis. Dig Dis Sci 40:1561–1568
44. Youssef N, Petitjean B, Bonte H, Terris B, de Saint Maur PP, Fléjou JF (2004) Non-alcoholic duct destructive chronic pancreatitis: a histological, immunohistochemical and in-situ apoptosis study of 18 cases. Histopathology 44:453–461

Virchows Arch (2004) 445:564–571
DOI 10.1007/s00428-004-1104-3

ORIGINAL ARTICLE

Tae Jung Jang

Expression of proteins related to prostaglandin E_2 biosynthesis is increased in human gastric cancer and during gastric carcinogenesis

Received: 20 May 2004 / Accepted: 21 June 2004 / Published online: 14 September 2004
© Springer-Verlag 2004

Abstract Prostaglandin E_2 (PGE_2) is related to carcinogenesis. Cyclooxygenase (COX) and prostaglandin E synthase (PGES) are involved in PGE_2 synthesis. However, overall situation of COX and microsomal PGES (mPGES) expression in gastric cancer has not been studied in detail. The expression of COX and mPGES was evaluated in 45 cases of gastric cancer (22 intestinal type and 23 diffuse type), 13 gastric dysplasia, 15 intestinal metaplasia, 18 *Helicobacter pylori* associated gastritis, and 10 normal gastric tissues by performing immunohistochemistry and Western blot analysis. COX-1 expression was higher in intestinal type cancers than diffuse ones. COX-2 and mPGES-1 were expressed more in cancers than in paired nonneoplastic adjacent tissues, and intestinal type cancers showed higher expression of COX-2 than diffuse ones. The expression of COX and mPGES was gradually increased with progression of gastric lesions and the highest in dysplasia. mPGES-1 was expressed not only in epithelial cells but also in stromal cells, whose phenotype was myofibroblast, endothelial cells and others. In conclusion, proteins related to PGE_2 biosynthesis affect both histogenesis and the carcinogenesis of human gastric cancer.

Keywords Gastric cancer · Cyclooxygenase · Microsomal prostaglandin E synthase

Introduction

Prostaglandin (PG) E_2 is a major prostanoid in gastric tissue and involved in various physiological and pathological functions of gastric mucosal cells [5]. Gastric cancer tissues release higher levels of PGE_2 than non-neoplastic mucosa [38]. PGE_2 is related to carcinogenesis through immunosuppression, inhibiting apoptosis, increasing metastatic potential of epithelial cells, and promoting angiogenesis [4, 12, 34, 35, 36]. PGE_2 mediates its effects, in part through G protein coupled PGE receptors, designated EP_1, EP_2, EP_3, and EP_4 [1]. EP_1 and EP_4 knockout mice show a reduction in the number of aberrant crypt foci that develop in mice following azoxymethane treatment [20, 40].

Cyclooxygenase (COX) catalyzes the conversion of arachidonic acid to PGG_2 and PGH_2. PGH_2 is subsequently converted to a variety of prostaglandins that include PGE_2, PGD_2, $PGF_{2\alpha}$, PGI_2, and thromboxane A_2 by each prostaglandin synthase. Prostaglandin E synthase (PGES), which is the terminal isomerase involved in the synthesis of PGE_2, occurs in multiple forms in mammalian cells [17]. Among these, cytosolic PGES (cPGES) is ubiquitously and constitutively expressed in cells and converts COX-1 derived PGH_2 to PGE_2 in cooperation with heat shock protein 90 [33]. Microsomal PGES-1 (mPGES-1) is functionally coupled with COX-2, and therefore its expression is induced in various pathophysiological events in which COX-2 derived PGE_2 has been implicated, such as rheumatoid arthritis, febrile response, reproduction, bone metabolism, and Alzheimer's disease [6, 16, 27, 28, 41]. A recent study suggests that aberrant expression of mPGES-1 in combination with COX-2 contribute to tumorigenesis [13]. Several studies have reported overexpression of mPGES-1 in colorectal cancers, non-small-cell lung cancers, and endometrial cancers [9, 42, 43]. Recently two reports have demonstrated overexpression of mPGES-1 in intestinal type gastric cancer [21, 24]. A third PGES, mPGES-2, was initially purified from the microsomal fraction of bovine heart, and the whole sequences of human and monkey were determined [32, 39]. Murakami et al. [18] reported that this enzyme was functionally coupled with both COX-1 and COX-2 and was expressed in cells and tissues relatively constitutively with exception of marked elevation in colorectal cancer.

T. J. Jang (✉)
Department of Pathology,
Dongguk University College of Medicine,
Suek-jang Dong 707, Kyongju, 780-714 Kyongbuk, Korea
e-mail: taejung@mail.dongguk.ac.kr
Tel.: +82-54-7702410
Fax: +82-54-7702431

The overall situation of COX and mPGES expression in gastric carcinoma has not yet been studied in detail. In addition, there have not been reports regarding as the expression of mPGES-2 in human gastric cancer. The aim of this study was to evaluate the expression of COX-1, COX-2, mPGES-1, and mPGES-2 in gastric cancer and during human gastric carcinogenesis.

Materials and methods

Tissue samples

Forty-five cases of gastric cancer (22 intestinal type and 23 diffuse type), 13 gastric dysplasia, 15 intestinal metaplasia, 18 *Helicobacter pylori* associated gastritis, and 10 normal gastric tissues were retrieved from the files of Pathology Department. Each group showed similar distribution of sex distinction and age range (49 men, 52 women; age range 35–60 years). The *H. pylori* infection was assessed by rapid urease test and immunohistochemical staining, using anti-*H. pylori* polyclonal antibody. Patients were considered to be *H. pylori*-positive if the result of one or both diagnostic methods was positive and *H. pylori*-negative if both methods had negative results. Eight gastric cancers and adjacent nonneoplastic tissues were obtained immediately after surgical resection and stored in liquid nitrogen until protein extraction. Pathological features were analyzed using hematoxylin and eosin-stained sections. The depth of tumor invasion, Lauren classification, and nodal metastasis were examined in gastric cancers.

Immunohistochemistry

Gastric sections of 4 μm thickness were made and spread on poly-L-lysine coated slides. Paraffin sections were immersed in three changes of xylene and hydrated using a graded series of alcohol. Antigen retrieval was performed routinely by immersing the sections in 0.01 M citrate buffer (pH 6.0) in a pressure cooker by autoclaving for 15 min. Endogenous peroxidase activity was blocked with 3% hydrogen peroxide for 15 min and then incubated with primary antibody for 2 h in room temperature. Primary antibodies were rabbit polyclonal anti-COX-1 (Cayman Chemical, Ann Arbor, Mich., USA, dilution 1:1000), anti-COX-2 antibody (Cayman Chemical, dilution 1:500), anti-mPGES-1 antibody (Cayman Chemical, dilution 1:500), and anti-mPGES-2 (Cayman Chemical, dilution 1:750). In addition, immunohistochemical staining was performed in the biopsy tissues using mouse monoclonal anti-Ki-67 antibody (Zymed Laboratories, South San Franciso, Calif., USA, dilution 1:200) to determine topographic distribution between cell proliferation and COX-2 expression. Staining was achieved with a Dako LSAB+kit labeled with peroxidase (Dako, Santa Barbara, Calif., USA) and developed with 3, 3′-diaminobenzidine tetrahydrochloride (Zymed) as a chromogen. Sections were counterstained for 3 min with Meyer's hematoxylin and then mounted. As a negative control, rabbit and mouse IgG isotypes were used instead of primary antibody. Immunoreactivity was evaluated by assessing the proportion of positive cells and graded as absence (no staining), mild (1–30%), moderate (31–60%), or severe (>60%).

Double-staining immunohistochemistry and in situ apoptosis detection

To evaluate the nature of stromal cells with positive signal for mPGES-1 double-staining immunohistochemistry was performed with anti-mPGES-1 antibody and a mouse monoclonal antibody for CD68, vimentin, CD34 or α-smooth muscle actin (all Dako). After finishing immunohistochemical staining for mPGES-1 according to procedure described above, a second one was performed from the step of antibody incubation. Second staining was achieved with a Dako LSAB+kit labeled with alkaline phosphatase (Dako) and developed with Fast Blue (Sigma, St. Louis, Mo., USA) as a chromogen.

To assess the topographical distribution between apoptosis and COX-2 expression we performed terminal deoxynucleotidyl transferase mediated deoxyuridine triphosphate nick-end labeling was performed and then immunohistochemical staining for COX-2 as described above. Briefly, the deparaffinized slides were treated with proteinase K for 15 min and endogenous peroxidase activity was blocked by 5 min of incubation in 3% H_2O_2 in methanol. Cleaved DNA fragments were labeled with bromodeoxyuridine at the 3′ ends using terminal deoxynucleotidyl transferase and detected with biotinylated anti-bromodeoxyuridine antibody and streptavidin-horseradish peroxidase. Diaminobenzidine was used as a chromogen.

Western blot

Tissues were suspended in a lysis buffer [10 mM Tris-HCl (pH 7.4), 1 mM EDTA, and 0.25 M sucrose, 1% Triton X-100] supplemented with Complete mini protease inhibitor mixture tablets (Boehringer-Mannheim, Mannheim, Germany) on ice for 1 h. After removal of cell debris by centrifugation the protein concentration in cell lysates was determined by BCA protein assay reagent (Pierce, Rockford, Ill., USA) with bovine serum albumin as a standard. We separated 40 μg protein by 12% sodium dodecyl sulfate polyacrylamide gel electrophoresis and transferred it to a nitrocellulose membrane. The membranes were blocked with 5% skim milk in Tris-buffered saline for 1 h at room temperature and probed with antibodies overnight at 4°C. The antibodies used were described above. After washing with Tris-buffered saline 0.05% Tween 20 the blots were treated with horseradish peroxidase-conjugated anti-rabbit IgG antibody (1:3000; Zymed) for 1 h at room temperature. Enhanced chemiluminescence (Pierce) and autoradiography were used for detection.

Statistical analysis

Four immunohistochemical staining grades were divided into positive (moderate and severe) and negative one (absent and mild) for statistical analysis. Fisher's exact test and the χ^2 test were used. Statistical significance was accepted for differences with a P value less than 0.05.

Results

Higher expression of COX-2 and mPGES-1 in cancers than in corresponding nonneoplastic adjacent tissues

Positive expression of COX-2 and mPGES-1 was observed in 27% (12/45) and 33.3% (15/45) of cancers, respectively (Table 1). In contrast, positive rates in corresponding adjacent tissues were negligible ($P<0.05$). Therefore COX-2 and mPGES-1 expressed higher in cancers than in adjacent tissues (Fig. 1). On Western blot analysis (Fig. 2) COX-2 and mPGES-1 expression was higher in cancers than adjacent nonneoplastic tissue, whereas mPGES-2 expression was nearly similar between cancers and nonneoplastic adjacent tissue.

Table 1 Expression of COX and mPGES in cancers and adjacent nonneoplastic tissues

Grade	Cancer	Adjacent tissue
COX-1		
Absent	0	0
Mild	12	12
Moderate	22	28
Severe	11	5
COX-2*		
Absent	7	30
Mild	26	15
Moderate	10	0
Severe	2	0
mPGES-1*		
Absent	14	19
Mild	16	25
Moderate	15	1
Severe	0	0
mPGES-2		
Absent	4	4
Mild	7	13
Moderate	25	22
Severe	9	6

* $P<0.05$ negative (absent and mild) vs. positive (moderate and severe)

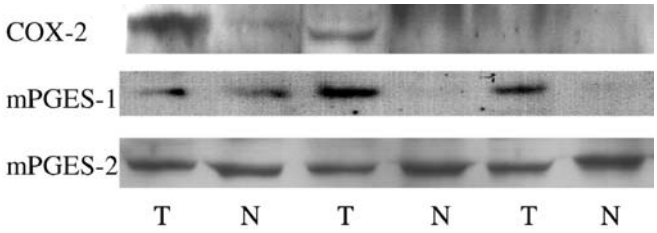


Fig. 2 Western blot analysis of COX-2, mPGES-1, and mPGES-2 in gastric cancers (*T*) and corresponding non-neoplastic tissues (*N*). Forty micrograms of protein was separated by 12% sodium dodecyl sulfate polyacrylamide gel electrophoresis and transferred to a nitrocellulose membrane

Higher expression of COX-1 and COX-2 in intestinal type cancers than in diffuse type

Positive expression of COX-1 and COX-2 was observed in 91% (20/22) and 45% (10/22) of intestinal type cancers, respectively (in Table 2, Fig. 1). In contrast, in diffuse type the COX-1 positive rate was 57% (13/23), and COX-2 was 9% (2/23) ($P<0.05$). mPGES expression was

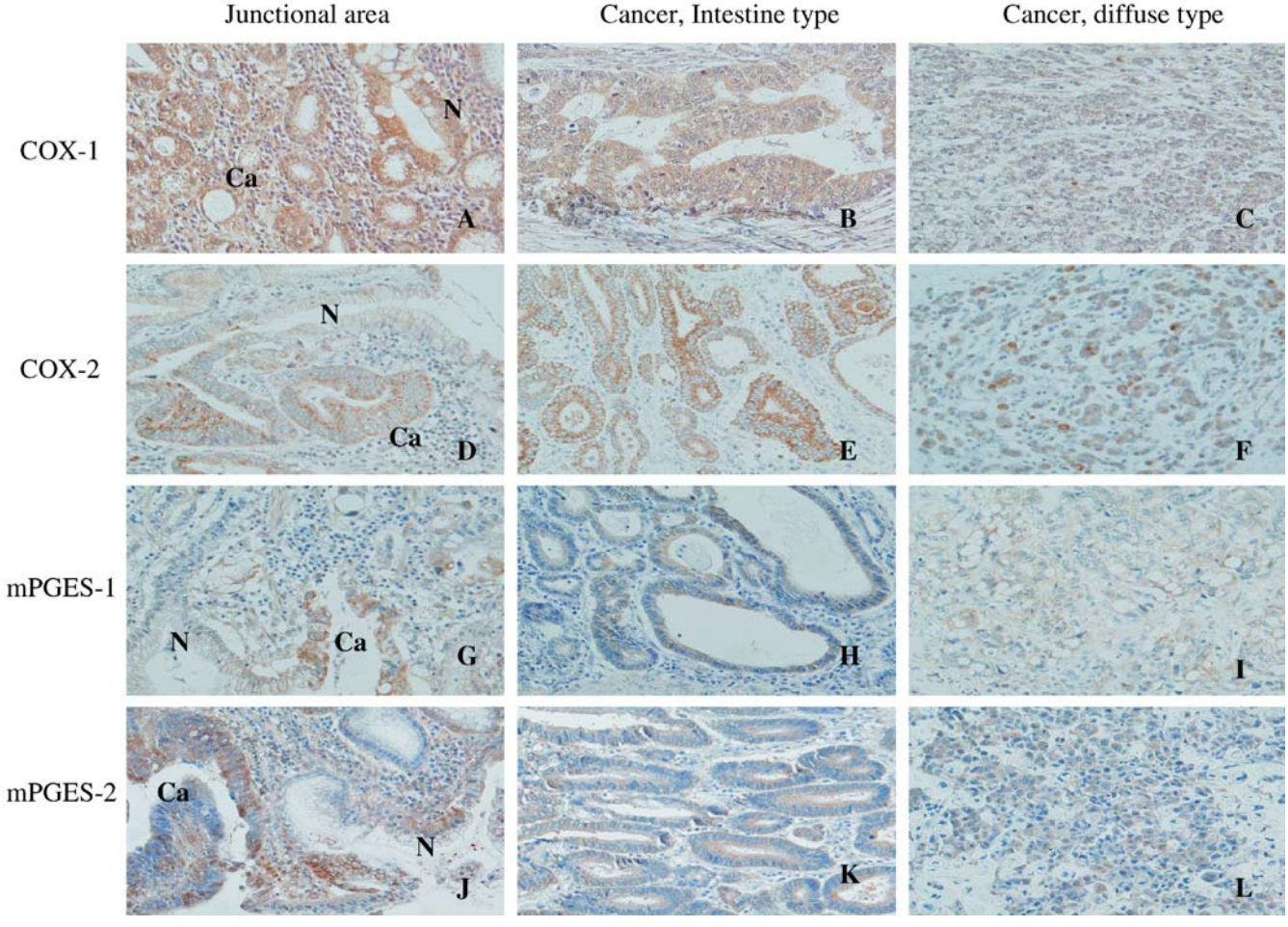


Fig. 1 Immunohistochemical staining of COX and mPGES in gastric cancers (*Ca*) and adjacent non-neoplastic tissues (*N*). Gastric cancers showed stronger immunoreactivity for COX-2 and mPGES-1 than paired nonneoplastic tissues. Intestinal type gastric cancers displayed more intense signal for COX-1 and COX-2 than diffuse ones. Junctional area means junction between cancer and adjacent non-neoplastic tissue. **B**, **D**, **G**, **J**, ×400; **A**, **C**, **E**, **F**, **H**, **I**, **K**, **L**, ×200

Table 2 Expression of COX and mPGES in intestinal type and diffuse type of gastric cancers

Grade	Intestinal type	Diffuse type
COX-1*		
Absent	0	0
Mild	2	10
Moderate	13	9
Severe	7	4
COX-2*		
Absent	0	7
Mild	12	14
Moderate	8	2
Severe	2	0
mPGES-1		
Absent	5	9
Mild	8	8
Moderate	9	6
Severe	0	0
mPGES-2		
Absent	1	3
Mild	5	2
Moderate	9	16
Severe	7	2

* $P<0.05$ negative (absent and mild) vs. positive (moderate and severe

also increased in intestinal type, but not to a statistically significant extent. Clinicopathological characteristics and the expression of COX and mPGES in gastric cancers were compared and analyzed. The depth and nodal metastasis, age, and sex showed no relationship, but distant metastasis was correlated with expression of mPGES-1. The positive expression of mPGES-1 was observed in 70% (7/10) of gastric cancers with distant metastasis and 20% (7/35) of cancers without it.

The highest expression of COX and mPGES in gastric dysplasia

The expression level of these proteins was significantly lower in normal stomach than the other lesions ($P<0.05$; Figs. 3, 4). COX-1 expression level was significantly higher in intestinal metaplasia and dysplasia than in *H. pylori* associated gastritis ($P<0.05$). COX-2 and mPGES-1 were similarly expressed between *H. pylori* associated gastritis and intestinal metaplasia and showed the highest expression level in dysplasia ($P<0.05$). mPGES-2 expres-

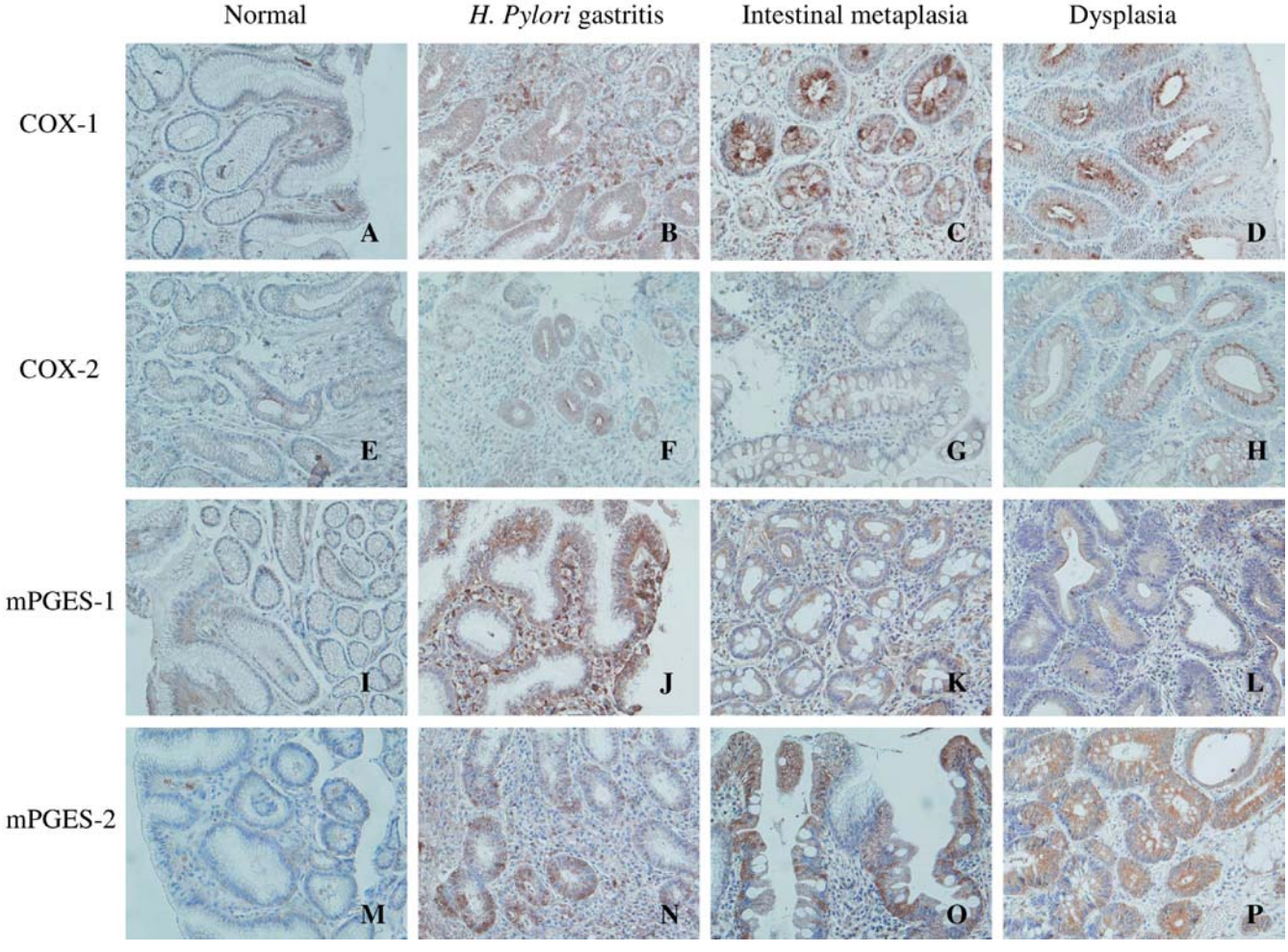


Fig. 3 Immunohistochemical staining of COX and mPGES in biopsied gastric tissues according to pathological diagnosis. Immunoreactivity of COX and mPGES was insignificant in normal stomach. In contrast, their expression was gradually increased with progression of gastric lesions. **O**, ×400; **A**–**N**, **P**, ×200

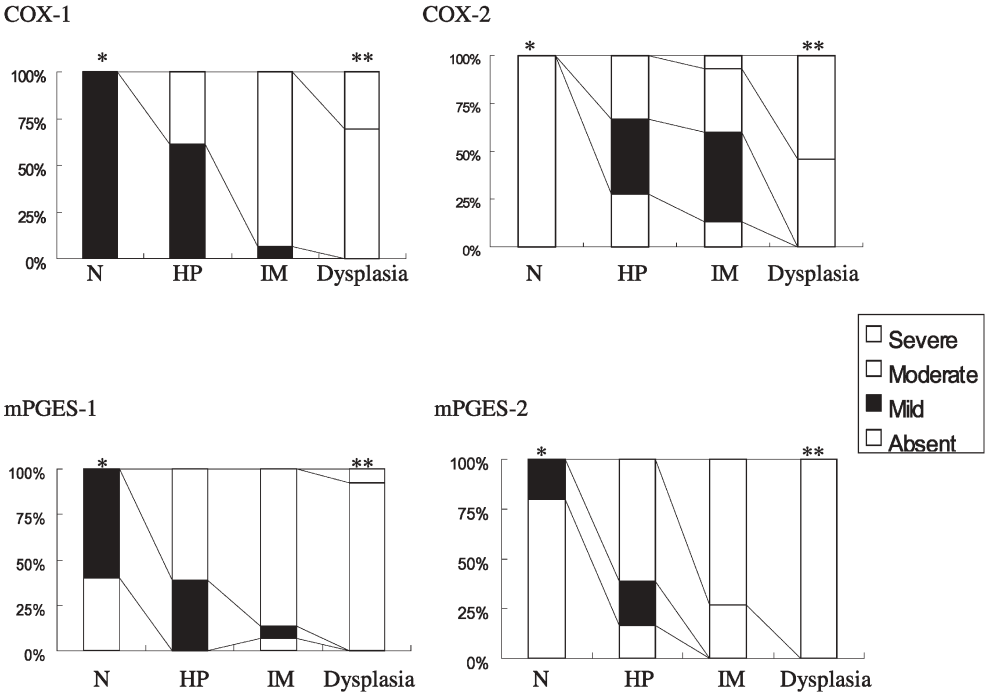


Fig. 4 Expression level of COX and mPGES in normal stomach, *H. pylori* associated gastritis, intestinal metaplasia and dysplasia. *Single asterisk* The lowest expression level of all groups ($P<0.05$); *double asterisk* the highest of all groups ($P<0.05$). *N* Normal stomach tissue; *IM* intestinal metaplasia; *HP H. pylori* associated gastritis

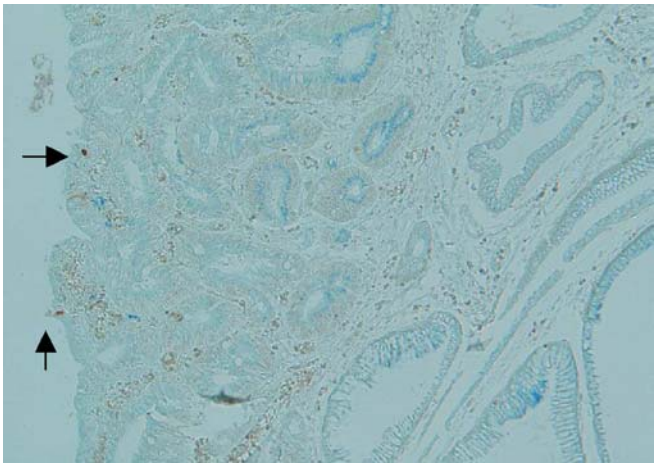


Fig. 5 In situ apoptosis detection on tissue with immunoreactivity for COX-2. Terminal deoxynucleotidyl transferase mediated deoxyuridine triphosphate nick-end labeling was carried out and then immunohistochemical staining for COX-2. Apoptotic cells (*arrow*, *brown*) were not observed at the area with immune signal for COX-2 (*granular blue*). ×200

sion was significantly increased with the progression of gastric lesions ($P<0.05$).

Apoptosis and cell proliferation are related to COX-2 expression

Forced COX-2 expression has been shown to confer resistance to apoptosis [34]. Therefore immunohistochemical staining for COX-2 and terminal deoxynucleotidyl transferase mediated nick-end labeling was performed at the same time in the tissue of gastric dysplasia. Dysplastic cells with COX-2 expression did not display apoptotic signal (Fig. 5). The COX-2 positive area was nearly identical to the proliferation zone with immunoreactiviy for Ki-67 (data not shown).

Phenotype of mPGES-1 positive stromal cells

Strong immunoreactivity for mPGES-1 was always present in stromal cells around erosion, beneath epithelial cells or within tumor cells. I attempted to characterize the mPGES-1 positive cells by using double-staining immunohistochemistry in the tissue sample of *H. pylori* associated gastritis. Colocalization of mPGES-1 positive stromal cells was seen with vimentin, α-smooth muscle actin, and CD34 (Fig. 6).

Discussion

Gastric cancer is one of the world's most common cancers and represents a major clinical challenge [8]. The cancer tissues are reported to release higher levels of PGE_2 than nonneoplastic mucosa [38]. PGE_2 has been shown to involve in carcinogenesis [4, 12, 34, 35, 36]. A number of studies have reported upregulation of COX-2 in gastric cancers and during gastric carcinogenesis [15, 19, 25, 30, 37], but the overall situation of COX and mPGES expression in gastric cancer has not been studied in detail.

In this study COX-1 expression was more elevated in various gastric lesions than normal stomach and the highest in dysplasia. It was expressed higher in intestinal type cancer than diffuse type. *COX-1* knockout *APC*^{min}

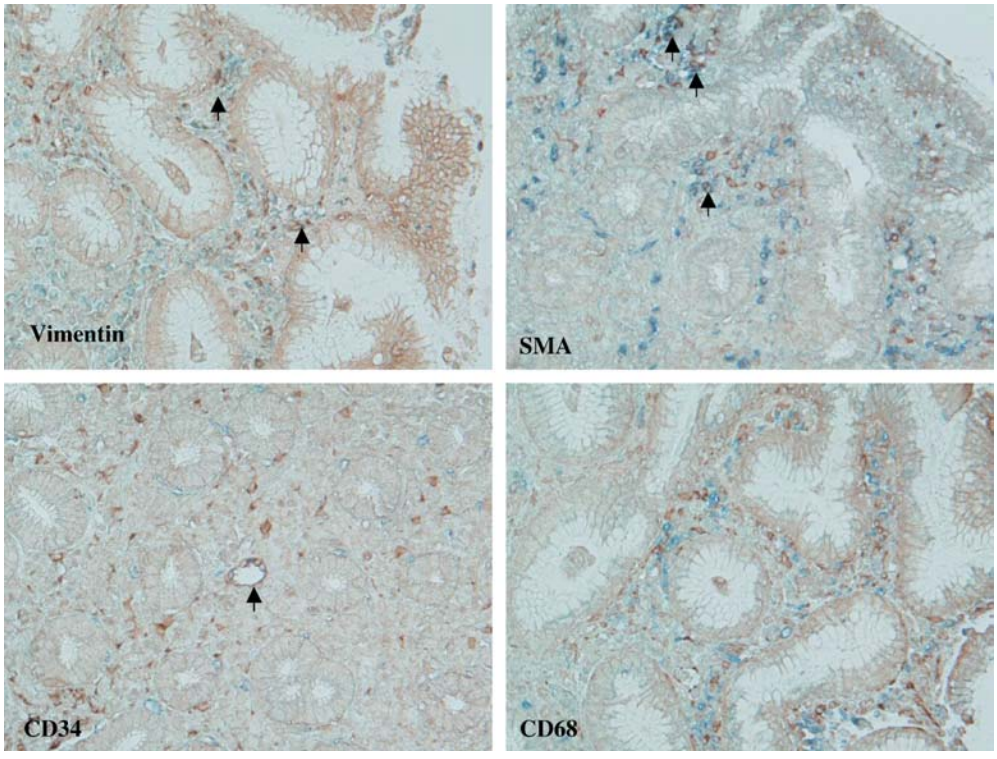


Fig. 6 Double-staining immunohistochemistry with anti-mPGES-1 antibody (*brown*) and a mouse monoclonal antibody (*blue*) for either CD68, vimentin, CD34, or α-smooth muscle actin, in *H. pylori* associated gastritis. Stromal cells expressing mPGES-1 sometimes displayed immunoreactivity for vimentin, α-smooth muscle actin and CD34 (*arrows*). ×200

mice indicate that deletion of *COX-1*, in addition to *COX-2*, reduces the number of intestinal polyps in these mice [3]. A COX-1 specific inhibitor was effective at inhibiting the number of aberrant crypt foci in rats fed azoxymethane and reduced the number of colorectal polyp in *APC* gene knockout mice (*APC1309*) [14]. SC-560, COX-1 specific inhibitor, showed chemopreventive effect in human colorectal cancer cells by altering gene expression [2]. COX-1 expression was also overexpressed in human ovarian cancers and rat mammary tumors induced by 7,12-dimethylbenz[a]anthracene (DMBA) compared to normal tissue [7, 10]. Therefore the possibility that COX-1 plays a role in the carcinogenesis of intestinal type gastric cancer cannot be excluded.

COX-2 and mPGES-1 were more expressed in cancers than in paired nonneoplastic adjacent tissues and revealed higher expression in intestinal type than diffuse type. The present work also confirmed that their expressions were related to gastric carcinogenesis. It is well known that COX-2 expression is closely related to gastric carcinogenesis [15, 19, 23, 25, 30, 37]. Two recent studies have reported that mPGES-1 expression is more elevated in gastric cancers and is closely associated with intestinal type [21, 24]. mPGES-1 is functionally coupled with COX-2 and can contribute to tumorigenesis in combination with COX-2 [13, 16]. However, tumor cells expressing COX-2 did not always show immunoreactivity for mPGES-1 in the present work. A recent study demonstrated that interleukin 1β and phorbol 12-myristate 13-acetate induce COX-2 but not mPGES-1 in gastric cancer cells [24]. It suggested that COX-2 and mPGES-1 expression may become regulated via separate pathways in gastric cancer cells. Apoptotic inhibition has been reported to be associated with carcinogenesis [22]. COX-2 overexpression reduces apoptotic susceptibility by inhibiting the cytochrome *c* dependent apoptotic pathway as well as DR5 expression [29, 31]. A recent study has reported that the expression of COX-2 and mPGES-1 is significantly correlated with that of bcl-x_L in the human model of *H. pyori* related gastric carcinogenesis [21]. In the present study the cells expressing COX-2 did not show apoptotic signal. *H. pylori* infection is the most important environmental factor implicated in the etiology of gastric cancer and directly induces COX-2 mRNA expression and PGE_2 production [26]. A recent study has reported that mPGES-1 was also induced in the gastric tissue samples with *H. pylori* infection [21]. In the present study the expression of COX-2 and mPGES-1 was higher in tissue samples with *H. pylori* associated gastritis than in normal stomach tissue.

We have found that subepithelial stromal cells in surgically induced rat Barret's esophagus express mPGES-1 [11]. In the present work mPGES-1 was expressed not only in epithelial cells but also in stromal cells, whose phenotype appeared to be myofibroblast, endothelial cells, or others. mPGES-1 expression in stromal cells could possibly stimulate (pre)neoplastic epithelium in a paracrine fashion and contribute to the neoplastic process. However, it may be merely an inflammatory response to mucosal injury unrelated to carcinogenesis itself. I perform primary culture for fibroblasts obtained from the patients of gastric cancer, peptic ulcer, chronic gastritis, and normal stomach in order to investigate the role of stromal cells expressing mPGES-1 on gastric carcinogenesis.

mPGES-2 expression was negligible in normal stomach tissues and significantly elevated with progression of gastric lesions. This present work reports the expression of mPGES-2 in gastric cancer and carcinogenesis for the first time. mPGES-2 that can be coupled with both COX is constitutively expressed in various tissues to involve in homeostasis [18]. The expression of mPGES-2 was more elevated in colon cancer than in corresponding nonneoplastic tissue [18]. Therefore mPGES-2 can promote PGE_2 production in some gastric cancers devoid of COX-2 expression via COX-1.

In summary, the expression of COX-2 and mPGES-1 is higher in gastric cancers than nonneoplastic adjacent tissue. Overall expression of COX and mPGES is greater in intestinal type gastric cancers than in diffuse type. Compared to normal stomach, the expression of COX and mPGES is increased during progression of gastric lesions, from *H. pylori* associated gastritis to gastric dysplasia. These data suggest that proteins related to PGE_2 biosynthesis exert influence on the histogenesis as well as carcinogenesis of human gastric cancer.

Acknowledgements This work was supported by the Dongguk University research fund. I thank Ka Hyuen Cho for immunohistochemical staining.

References

1. Ashby B (1998) Co-expression of prostaglandin receptors with opposite effects: a model for homeostatic control of autocrine and paracrine signaling. Biochem Pharmacol 55:239–246
2. Bottone FG Jr, Martinez JM, Alston-Mills B, Eling TE (2004) Gene modulation by Cox-1 and Cox-2 specific inhibitors in human colorectal carcinoma cancer cells. Carcinogenesis 25:349–357
3. Chulada PC, Thompson MB, Mahler JF, Doyle CM, Gaul BW, Lee C, Tiano HF, Morham SG, Smithies O, Langenbach R (2000) Genetic disruption of Ptgs-1, as well as Ptgs-2, reduces intestinal tumorigenesis in Min mice. Cancer Res 60:4705–4708
4. DeWitt DL (1991) Prostaglandin endoperoxide synthase: regulation of enzyme expression. Biochim Biophys Acta 1083: 121–134
5. Eberhart CE, DuBois RN (1995) Eicosanoids and gastrointestinal tract. Gastroenterology 109:285–301
6. Filion F, Bouchard N, Goff AK, Lussier JG, Sirois J (2001) Molecular cloning and induction of bovine prostaglandin E synthase by gonadotropins in ovarian follicles prior to ovulation in vivo. J Biol Chem 276:34323–34330
7. Gupta RA, Tejada LV, Tong BJ, Das SK, Morrow JD, Dey SK, DuBois RN (2003) Cyclooxygenase-1 is overexpressed and promotes angiogenic growth factor production in ovarian cancer. Cancer Res 63:906–911
8. Hanahan D, Weinberg RA (2000) Hallmarks of cancer. Cell 100:57–70
9. Jabbour HN, Milne SA, Williams AR, Anderson RA, Boddy SC (2001) Expression of COX-2 and PGE synthase and synthesis of PGE2 in endometrial adenocarcinoma: a possible autocrine/paracrine regulation of neoplastic cell function via EP_2/EP_4 receptors. Br J Cancer 85:1023–1031
10. Jang TJ, Jung HG, Jung KH, O MK (2002) Chemopreventive effect of celecoxib and expression of cyclooxygenase-1 and cyclooxygenase-2 on chemically-induced rat mammary tumours. Int J Exp Pathol 83:173–182
11. Jang TJ, Min SK, Bae JD, Jung KH, Lee JI, Kim JR, Ahn WS (2004) Expression of cyclooxygenase 2, microsomal prostaglandin E synthase 1, and EP receptors is increased in rat oesophageal squamous cell dysplasia and Barrett's metaplasia induced by duodenal contents reflux. Gut 53:27–33
12. Jones MK, Wang H, Peskar BM, Levin E, Itani RM, Sarfeh IJ, Tarnawski AS (1999) Inhibition of angiogenesis by nonsteroidal anti-inflammatory drugs: insight into mechanisms and implications for cancer growth and ulcer healing. Nat Med 5:1418–1423
13. Kamei D, Murakami M, Nakatani Y, Ishikawa Y, Ishii T, Kudo I (2003) Potential role of microsomal prostaglandin E synthase-1 in tumorigenesis. J Biol Chem 278:19396–19405
14. Kitamura T, Kawamori T, Uchiya N, Itoh M, Noda T, Matsuura M, Sugimura T, Wakabayashi K (2002) Inhibitory effects of mofezolac, a cyclooxygenase-1 selective inhibitor, on intestinal carcinogenesis. Carcinogenesis 23:1463–1466
15. Lim HY, Joo HJ, Choi JH, Yang MS, Cho DY, Kim HS, Nam DK, Lee KB, Kim HC (2000) Increased expression of cyclooxygenase-2 protein in human gastric carcinoma. Clin Cancer Res 6:519–525
16. Murakami M, Naraba H, Tanioka T, Semmyo N, Nakatani Y, Kojima F, Ikeda T, Fueki M, Ueno A, Oh S, Kudo I (2000) Regulation of prostaglandin E_2 biosynthesis by inducible membrane-associated prostaglandin E_2 synthase that acts in concert with cyclooxygenase-2. J Biol Chem 275:32783–32792
17. Murakami M, Nakatani Y, Tanioka T, Kudo I (2002) Prostaglandin E synthase. Prostaglandins Other Lipid Mediat 68-69:383–399
18. Murakami M, Nakashima K, Kamei D, Masuda S, Ishikawa Y, Ishii T, Ohmiya Y, Watanabe K, Kudo I (2003) Cellular prostaglandin E2 production by membrane-bound prostaglandin E synthase-2 via both cyclooxygenase-1 and–2. J Biol Chem 278:37937–37947
19. Murata H, Kawano S, Tsuji S, Tsuji M, Sawaoka H, Kimura Y, Shiozaki H, Hori M (1999) Cyclooxygenase-2 overexpression enhances lymphatic invasion and metastasis in human gastric carcinoma. Am J Gastroenterol 94:451–455
20. Mutoh M, Watanabe K, Kitamura T, Shoji Y, Takahashi M, Kawamori T, Tani K, Kobayashi M, Maruyama T, Kobayashi K, Ohuchida S, Sugimoto Y, Narumiya S, Sugimura T, Wakabayashi K (2002) Involvement of prostaglandin E receptor subtype EP_4 in colon carcinogenesis. Cancer Res 62:28–32
21. Nardone G, Rocco A, Vaira D, Staibano S, Budillon A, Tatangelo F, Sciulli MG, Perna F, Salvatore G, Di Benedetto M, De Rosa G, Patrignani P (2004) Expression of COX-2, mPGE-synthase1, MDR-1 (P-gp), and Bcl-xL: a molecular pathway of *H pylori*-related gastric carcinogenesis. J Pathol 202:305–312
22. Que FG, Gores J (1996) Cell death by apoptosis: basic concept and disease relevance for the gastroenterologist. Gastroenterology 110:1238–1243
23. Rees BP van, Saukkonen K, Ristimaki A (2002) Cyclooxygenase-2 expression during carcinogenesis in human stomach. J Pathol 196:171–179
24. Rees BP van, Sivula A, Thoren S, Yokozaki H, Jakobsson PJ, Offerhaus GJ, Ristimaki A (2003) Expression of microsomal prostaglandin E synthase-1 in intestinal type gastric adenocarcinoma and in gastric cancer cell lines. Int J Cancer 107:551–556
25. Ristimäki A, Honkanen N, Jänkala H, Sipponen P, Härkönen M (1997) Expression of cyclooxygenase-2 in human gastric carcinoma. Cancer Res 57:1276–1280
26. Romano M, Ricci V, Memoli A, Tuccillo C, Di Popolo A, Sommi P, Acquaviva AM, Del Vecchio Blanco C, Bruni CB, Zarrilli R (1998) *Helicobacter pylori* upregulates cyclooxygenase-2 mRNA expression and prostaglandin E2 synthesis in MKN 28 gastric mucosal cells in vitro. J Biol Chem 273: 28560–28563
27. Satoh K, Nagano Y, Shimomura C, Suzuki N, Saeki Y, Yokota H (2000) Expression of prostaglandin E synthase mRNA is

induced in beta-amyloid treated rat astrocytes. Neurosci Lett 283:221–223
28. Stichtenoth DO, Thoren S, Bian H, Peters-Golden M, Jakobsson PJ, Crofford LJ (2001) Microsomal prostaglandin E synthase is regulated by proinflammatory cytokines and glucocorticoids in primary rheumatoid synovial cells. J Immunol 167:469–474. 14
29. Sun Y, Tang XM, Half E, Kuo MT, Sinicrope FA (2002) Cyclooxygenase-2 overexpression reduces apoptotic susceptibility by inhibiting the cytochrome c-dependent apoptotic pathway in human colon cancer cells. Cancer Res 62:6323–6328
30. Sung JJ, Leung WK, Go MY, To KF, Cheng AS, Ng EK, Chan FK (2000) Cyclooxygenase-2 expression in *Helicobacter pylori*-associated premalignant and malignant gastric lesions. Am J Pathol 157:729–735
31. Tang X, Sun YJ, Half E, Kuo MT, Sinicrope FA (2002) Cyclooxygenase-2 overexpression inhibits death receptor 5 expression and confers resistance to tumor necrosis factor-related apoptosis-inducing ligand-induced apoptosis in human colon cancer cells. Cancer Res 62:4903–4908
32. Tanikawa N, Ohmiya Y, Ohkubo H, Hashimoto K, Kangawa K, Kojima M, Ito S, Watanabe K (2002) Identification and characterization of a novel type of membrane-associated prostaglandin E synthase. Biochem Biophys Res Commun 291:884–889
33. Tanioka T, Nakatani Y, Semmyo N, Murakami M, Kudo I (2000) Molecular identification of cytosolic prostaglandin E2 synthase that is functionally coupled with cyclooxygenase-1 in immediate prostaglandin E2 biosynthesis. J Biol Chem 275: 32775–32782
34. Tsujii M, DuBois RN (1995) Alterations in cellular adhesion and apoptosis in epithelial cells overexpressing prostaglandin endoperoxide synthase 2. Cell 83:493–501
35. Tsujii M, Kawano S, DuBois RN (1997) Cyclooxyenase-2 expression in human colon cancer cells increases metastatic potential. Proc Natl Acad Sci USA 94:3336–3340
36. Tsujii M, Kawano S, Tsuji S, Sawaoka H, Hori M, DuBois RN (1998) Cyclooxygenase regulates angiogenesis induced by colon cancer cells. Cell 93:705–716
37. Uefuji K, Ichikura T, Mochizuki H, Shinomiya N (1998) Expression of cyclooxygenase-2 protein in gastric adenocarcinoma. J Surg Oncol 69:168–172
38. Uefuji K, Ichikura T, Mochizuki H (2000) Cyclooxygenase-2 expression is related to prostaglandin biosynthesis and angiogenesis in human gastric cancer. Clin Cancer Res 6:135–138
39. Watanabe K, Kurihara K, Suzuki T (1999) Purification and characterization of membrane-bound prostaglandin E synthase from bovine heart. Biochim Biophys Acta 1439:406–414
40. Watanabe K, Kawamori T, Nakatsugi S, Ohta T, Ohuchida S, Yamamoto H, Maruyama T, Kondo K, Ushikubi F, Narumiya S, Sugimura T, Wakabayashi K (1999) Role of the prostaglandin E receptor subtype EP_1 in colon carcinogenesis. Cancer Res 59:5093–5096
41. Yamagata K, Matsumura K, Inoue W, Shiraki T, Suzuki K, Yasuda S, Sugiura H, Cao C, Watanabe Y, Kobayashi S (2001) Coexpression of microsomal-type prostaglandin E synthase with cyclooxygenase-2 in brain endothelial cells of rats during endotoxin-induced fever. J Neurosci 21:2669–2677
42. Yoshimatsu K, Altorki NK, Golijanin D (2001) Inducible prostaglandin E synthase is overexpressed in non-small cell lung cancer. Clin Cancer Res 7:2669–2674
43. Yoshimatsu K, Golijanin D, Paty PB, Soslow RA, Jakobsson PJ, DeLellis RA, Subbaramaiah K, Dannenberg AJ (2001) Inducible microsomal prostaglandin E synthase is overexpressed in colorectal adenomas and cancer. Clin Cancer Res 7:3971–3976

Virchows Arch (2004) 445:572–579
DOI 10.1007/s00428-004-1130-1

ORIGINAL ARTICLE

Enrico Solcia · Ombretta Luinetti · Francesca Tava · Catherine Klersy · Federica Grillo · Nicola Pandolfo · Roberto Fiocca

Identification of a lower grade muconodular subtype of gastric mucinous cancer

Received: 18 August 2004 / Accepted: 25 August 2004 / Published online: 28 October 2004
© Springer-Verlag 2004

Abstract Until now, survival analysis of gastric mucinous cancers showed either no difference or an even worse prognosis than stage-adjusted non-mucinous tumours. In the pancreas and breast, mucinous cancers showing well-demarcated mucin deposits (muconodular pattern), expansile growth and predominance of MUC2 mucin are known to have a more favourable prognosis. In this study, an attempt was made to separate, among 41 gastric mucinous cancers, a subgroup of tumours with muconodular expansile pattern, possibly predictive of a more favourable outcome. A group of 15 tumours was identified, which were characterised by overwhelming (80–100%) mucinous component, predominance of mucus over tumour cells inside muconodules, moderately aggressive growth of their epithelial component (reduced proliferative rate, moderate anaplasia, lack of angioinvasion and limited lymphoinvasion) and dominant expression of intestinal goblet cell markers, with special reference to MUC2 mucin. Univariate and multivariate survival analysis showed a significantly improved outcome of these lower grade muconodular tumours compared with the remaining mucinous cancers as well as with non-mucinous cancers of cohesive, diffuse (signet-ring cell included) and undifferentiated high-grade types.

E. Solcia (✉) · O. Luinetti · F. Tava
Department of Human Pathology and Genetics,
University of Pavia and IRCCS Policlinico San Matteo,
Via Forlanini 16, 27100 Pavia, Italy
e-mail: solciae@smatteo.pv.it
Tel.: +39-038-2503451
Fax: +39-038-2502505

C. Klersy
Medical Statistics Unit,
IRCCS Policlinico San Matteo,
Piazzale Golgi 1, 27100 Pavia, Italy

F. Grillo · N. Pandolfo · R. Fiocca
Department of Surgical and Morphological Sciences,
University of Genova,
via De Toni 14, 16132 Genova, Italy

Keywords Gastric mucinous cancer · Muconodular type · Lower grade · MUC2 mucin · MUC5AC and MUC6 mucin · Survival analysis

Introduction

Mucinous cancers are characterised by extensive extracellular accumulation of mucus forming gelatinous lakes into which more or less aggregated tumour cells are immersed. The tumours represent a minor proportion of neoplasms arising in various organs, such as colon, pancreas and breast [16, 18, 26, 30]. In the stomach, mucinous tumours may account for 2–5% of all cancers [17] and are considered separately from more common signet-ring cell cancers, whose mucin is essentially intracellular.

Common phenotypic and genetic patterns may be shared by mucinous cancers from different sites, among which preferential expression of the gel-forming mucin MUC2, uncommon p53 gene mutation and frequent K-ras gene mutation [15, 16]. However, marked prognostic differences have been reported, with generally poor survival for mucinous cancers arising in the colon and stomach [1, 17, 26, 33] and much better outcome of those found in the pancreas and breast, even compared with non-mucinous tumours of the same organs [3, 18].

In the past, attempts were made to separate, among gastric mucinous cancers, a well- from a poorly differentiated subtype, according to the presence of well-formed glandular epithelium or dispersed signet-ring cells, respectively, in mucin lakes [1, 19]. On histopathological grounds, a less aggressive behaviour was attributed to the former subtype. Surprisingly, at survival analysis, this tumour turned out to show either no prognostic difference or even a worse outcome than its "poorly differentiated" counterpart [2, 28, 33], despite the indolent course shown by a few "well-differentiated mucinous cancers" reported in an early study [7]. It seems of interest that the latter authors noticed a "rounded or pushing" type of advancing tumour edge and a large predominance of mucus over tumour cells in their indo-

lent gastric tumours. A similarly expansile pattern of growth has been also shown to be a powerful independent predictor of better survival in pancreatic, breast and colorectal mucinous cancers [3, 18, 22].

The above findings raise the interesting possibility that, among gastric mucinous tumours, a low-grade subtype with well-demarcated mucin deposits (muconodular pattern) and expansile overall growth could be separated on histopathological grounds from more aggressive tumours. In this study, a group of 41 mucinous tumours identified retrospectively among gastric cancers that had already undergone clinico-pathological, histochemical and molecular study [8, 20] were reinvestigated for histopathological patterns of potential prognostic value, including amount and type of mucin deposits, expansile or infiltrative type of growth, lympho- or angioinvasion, as well as phenotype, aggregation status, proliferative rate and anaplasia of tumour cells. A small group (15 cases) of histologically lower grade tumours was identified, which at follow-up investigation showed significantly better outcome than the remaining mucinous tumours as well as non-mucinous cancers.

Materials and methods

Archival histological material from 282 gastric cancers, 238 operated at San Matteo General Hospital in Pavia from 1985 to 1998 and 44 operated at San Martino General Hospital in Genova during 1998 and 1999, was reinvestigated for the presence of prominent extracellular mucin deposits. Only tumours with extensive tissue sampling, accurately assessed stage by the tumour node metastasis (TNM) system [29] and adequate patient follow-up available from clinical studies were considered [9, 20].

Tumours (n=41), including 0 of 48 intramucosal or superficially submucosal, 4 of 35 deeply submucosal and 37 of 199 advanced cancers, showed mucinous areas in at least 40% of their growth and were classified as mucinous. The 162 non-mucinous advanced cancers were further classified, according to the main histological structure of their locally invasive component [9], as cohesive (97 cases), diffuse (46 cases) or undifferentiated high grade (19 cases; 8 small cell and 11 large cell). Among the diffuse tumours, 18 signet-ring cell cancers were identified.

From each paraffin block of the 41 mucinous and 18 signet-ring cell tumours, new sections were stained with haematoxylin-eosin, alcian blue-periodic acid-Schiff (PAS), high iron diamine (HID) method for sulfomucins and the periodic acid-concanavalin A test for mucopeptic cell mucin [11]. In addition, the immunoperoxidase method was applied with specific antibodies directed against gastrointestinal mucins [25, 31], including MUC2 (Ccp mAb, Santa Cruz Biotech, USA) and M3 [23, 27] for goblet cell mucin, CAR5 mucin-like antigen for colorectal columnar and goblet cells [12], CD10 (56C6 mAb, Novocastra, UK) and MUC4 (H300 pAb, Santa Cruz Biotech) for columnar enterocytes, MUC5AC (CLH2 mAb, Novocastra) and M1 [5, 13] for gastric foveolar cell mucin and MUC6 (CLH5 mAb, Novocastra) for mucopeptic cell mucin. Only reactivities involving more than 5% of cells were considered for the assessment of tumour cell phenotype. The Ki67 nuclear proliferative index (% of positive tumours cells) was also investigated with the immunoperoxidase method using MIB1 antibodies (Dako, Denmark).

Survival analysis and statistics

For most survivors, the follow-up extended to 2003 so as to reach a median of 130 months (25–75th percentiles: 67–151 months) for survivors with early cancer and 62 months (41–104 months) for survivors with advanced cancer. The cause of death was reconstructed from clinical and anatomic pathology records for those who died during hospitalisation. Tumour registry records and family doctors' interviews were added for those who died at home.

Data were described as mean and standard deviation or median and 25–75th percentiles, if skewed, and absolute and relative frequencies for continuous and categorical variables, respectively. Distribution of tumour characteristics was assessed by means of cross-tabulations and compared with the Fisher exact test.

Survival rates were calculated per 100 person year. Cox models were used to assess the prognostic role of a series of risk factors. Stata 8.0 (College Station, TX) was used for computation. A P value <0.05 was considered as statistically significant.

Results

Histology

The 41 tumours entering the investigation were characterised by extensive deposition of extracellular mucin admixed with more or less abundant tumour cells (Fig. 1, Fig. 2, Fig. 3). In 24 cases, the mucinous areas accounted for 40–70% of the invasive (submucosal or beyond) tumour (score-1 mucinous carcinomas), while, in the remaining 17 cases, they formed 80–100% of the invasive growth (score-2 mucinous carcinomas). In their more juxtaluminal part, corresponding topographically to adjacent non-tumour mucosa, the mucinous component was usually less prominent.

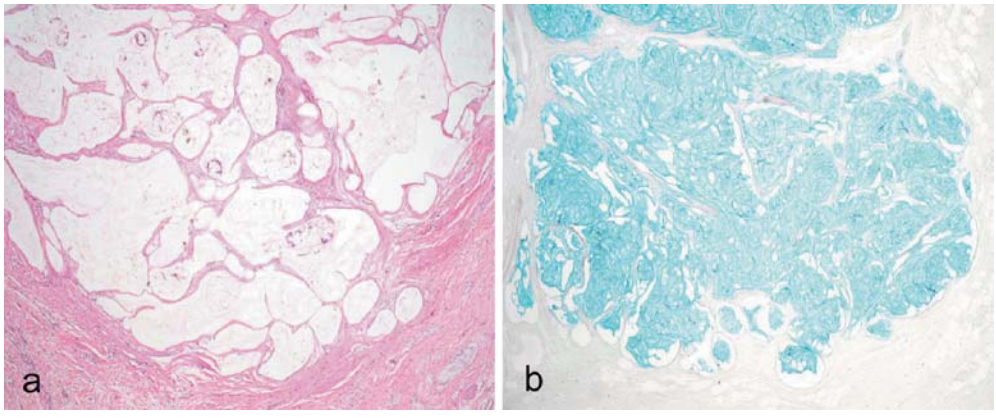


Fig. 1a, b Muconodular, low-grade cancer with mucin lakes, containing very few tumour cells, separated by thin stromal septae. Note expansile type of growth. Haematoxylin-eosin (**a**); alcian blue staining (**b**)

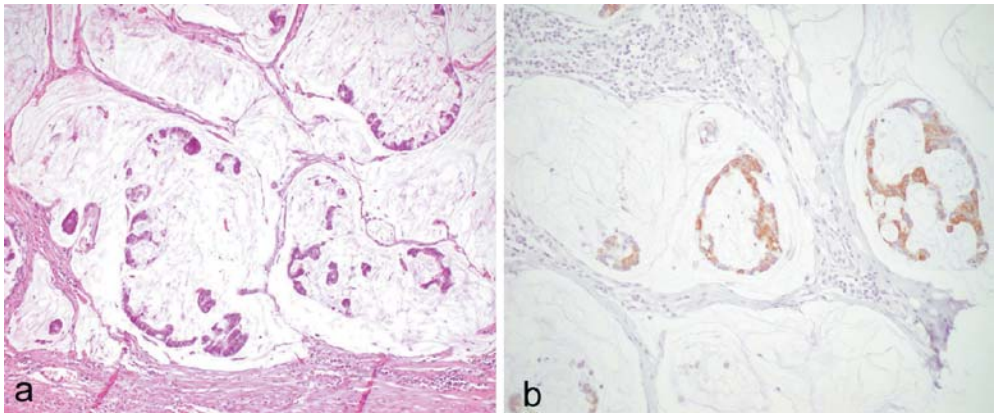


Fig. 2a, b Muconodular, expansile, low-grade cancer with cohesive tumour cells floating inside mucin lakes. Haematoxylin-eosin (**a**); MUC2 immunostaining (**b**)

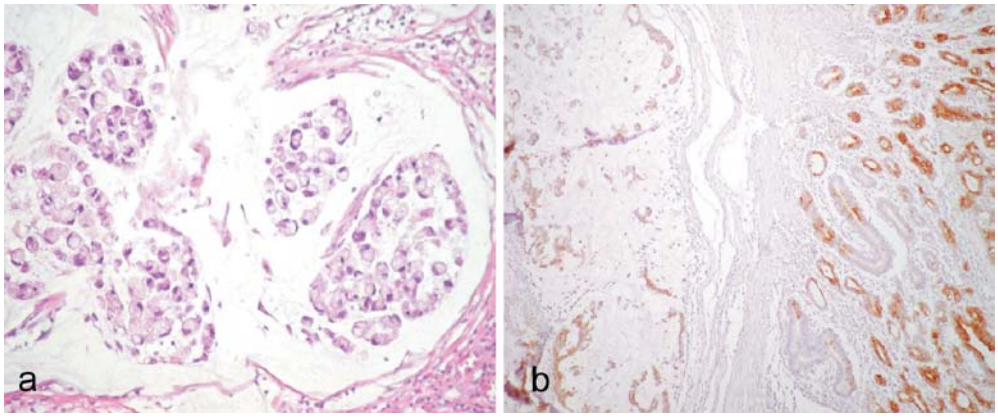


Fig. 3 a Muconodular, low-grade cancer with poorly aggregated signet-ring tumour cells, floating inside a well-demarcated mucin lake. Haematoxylin-eosin. **b** Topographic correlation between a MUC2-positive muconodular tumour (*left*) growing in the submucosa and intestinal metaplasia (*right*) in the overlying mucosa. MUC2 immunostaining

Inside the mucinous areas, tumour cells were mostly dispersed in the mucus as single elements, small aggregates or minor epithelial fragments in 27 of 41 tumours (66%), corresponding to "poorly differentiated" mucinous tumours of previous investigations [1, 2, 19]. In the remaining 14 cases, corresponding to "well-differentiated" mucinous tumours of previous studies, well-formed glands, epithelial cords or solid aggregates were a dominant component, with mucin deposits both inside glandular lumina and interposed between epithelia and the surrounding stroma. Of the 14 tumours, 2 showed a very well-differentiated tubulo-cystic pattern formed by regular, monostratified epithelium with limited cytological atypia, sometimes with intercalated goblet cells, bordering or floating inside score-2 mucin deposits. One of these tumours (Fig. 4) was contiguous with extensive, complete-type intestinal metaplasia in the adjacent and overlying mucosa, thus resembling closely the low-grade tumours recently reported by Endoh et al. [10] as "complete intestinal metaplasia cancer". Two histologically similar cases (apart from scarce and purely endoluminal mucin deposits) were also observed among the non-mucinous tumours investigated.

Of the 17 (76%) score-2 and 24 score-1 cancers, 13 and 0, respectively, showed an overall expansile type of growth with well-demarcated mucin nodules (muconodular pattern), predominance of mucin deposits over enclosed tumour cells and no signs of aggressive growth (such as severe nuclear atypia, extensive/multifocal necrosis, angioinvasion or prominent lympho-invasion) in their mucinous or non-mucinous areas (Fig. 1, Fig. 2, Fig. 3). A typical muconodular pattern with mucin nodules directly contacting the stroma, owing to apparent atrophy, fragmentation and desquamation of the epithelium, was also found in the deeper, growing part of the two well-differentiated tubulocystic cases (Fig. 4). This finding, coupled with low-grade histology in the rest of the tumour, suggested their inclusion among muconodular/lower grade mucinous tumours. These encompassed 15 cases as a whole, all with score-2 mucin deposits.

Among the 24 score-1 tumours, 12 (though showing well-circumscribed nodules in their mucinous areas) had an infiltrative, more or less aggressive pattern in their prominent non-mucinous component (Fig. 5). In addition, 12 score-1 and 2 score-2 tumours showed an essentially infiltrative growth pattern in both mucinous and non-mucinous components. The histopathological profile of the 15 lower grade and the remaining 26 (higher grade) mucinous tumours is outlined in Table 1, where the lower

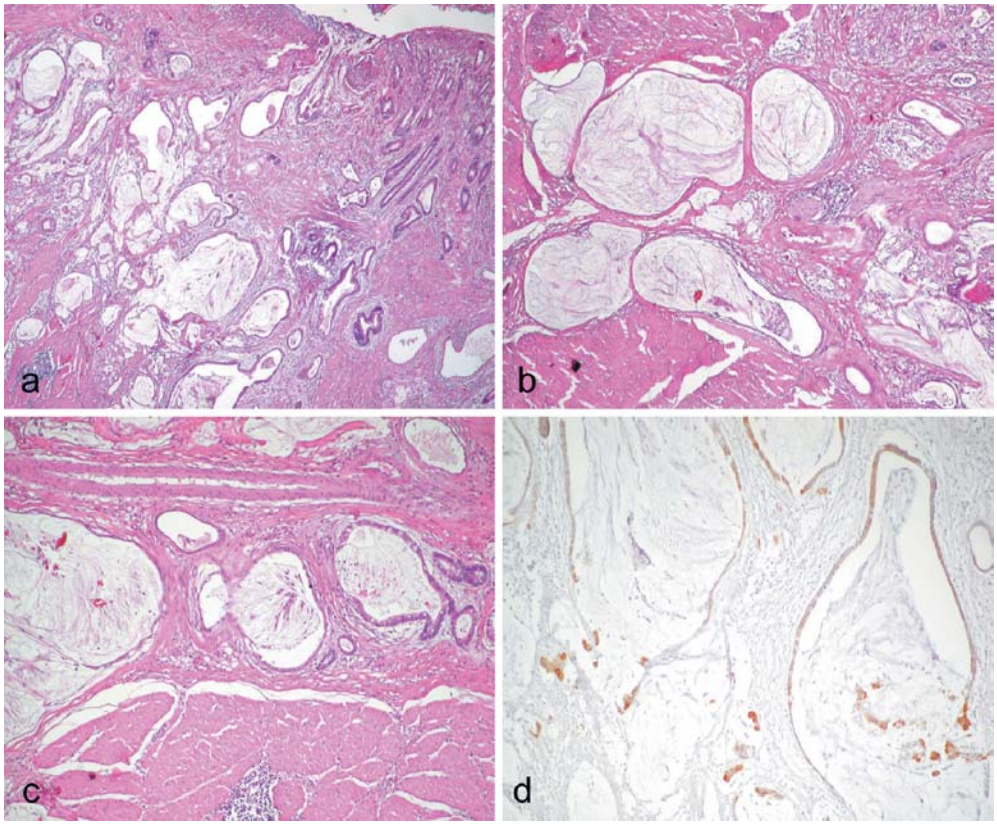


Fig. 4a–d Well-differentiated, mucin-producing tubulocystic carcinoma. **a** Origin from complete-type intestinal metaplasia (*upper right corner*). Haematoxylin-eosin. **b** Muconodular pattern in the deeper (*left*) part of the tumour. Haematoxylin–eosin. **c** and **d** Progressive attenuation and desquamation, up to complete disappearance, of the epithelium lining the cysts, from upper (*left*) to deeper (*right*) muscularis propria (**c**) (haematoxylin–eosin), and from upper (top) to deeper (bottom) submucosa in (**d**) (MUC2 immunostaining)

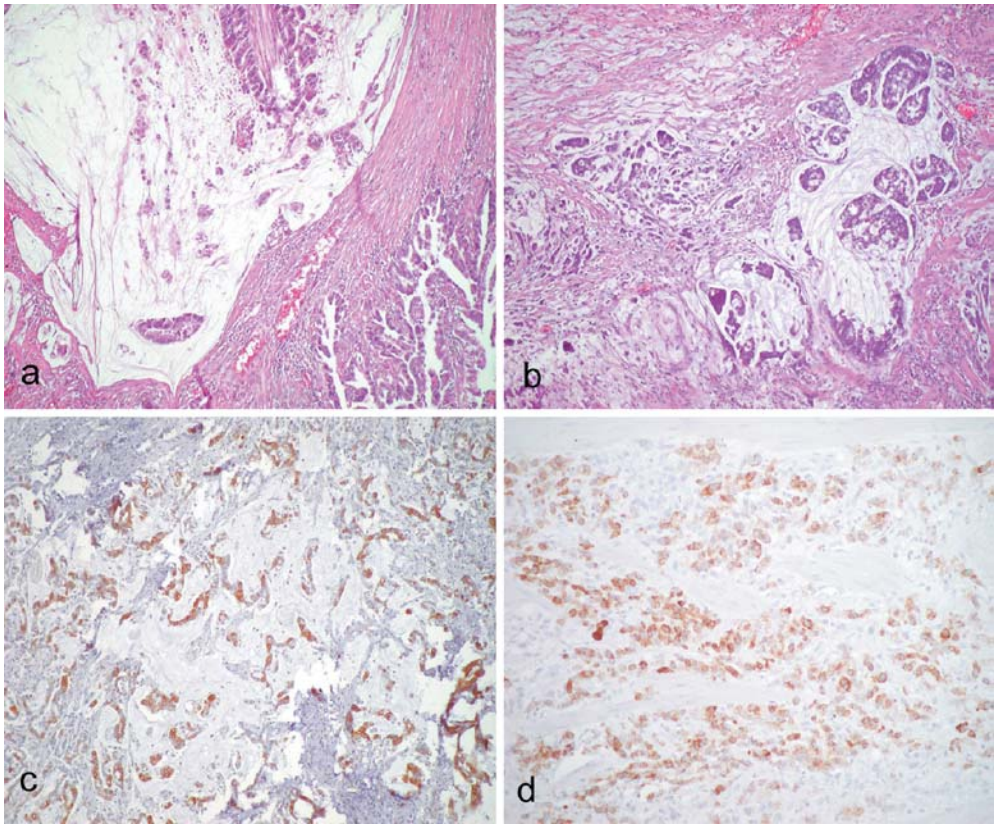


Fig. 5 Higher grade mucinous cancer. **a** An infiltrative glandular component (*left lower corner*) is found, in addition to a muconodular component. Haematoxylin–eosin. **b** A diffuse infiltrative component (*left*) is associated with the mucinous tumour. Haematoxylin–eosin. **c** MUC5AC-positive small epithelial cords and cell aggregates are scattered inside as well as outside the mucinous deposits. MUC5AC immunostaining. **d** Diffuse infiltration of round and signet-ring cells in the non-mucinous part of a mucinous cancer. MUC5AC immunostaining

Table 1 Histopathological profile of lower and higher grade mucinous cancers

	Lower grade (15 cases)	Higher grade (26 cases)	*P* value
Mucin score:			
1 (40–70%)	0	24	
2 (80–100%)	15	2	<0.001
Epithelial structure:			
Well differentiated	5	9	
Poorly differentiated	10	17	1.000
Invasion level:			
Within subserosa	12	8	
Serosa perigastric tissues and organs	3	18	0.004
Lymph-node involvement:			
No	7	3	No versus N+=0.022
N1 (1–6)	3	11	
N2 (7–15)	4	8	No versus N1 versus N2+3 =0.043
N3 (>15)	1	4	
Distant metastases	1	3	1.000
Phenotype:			
Intestinal only, all with goblet cells	10	6	<0.009*
Intestinal + gastric,	5	20	
with goblet cells	5	15	
with faveolar cells	5	20	
Gastric only	0	0	

* Intestinal only versus intestinal + gastric

grade group shows significantly less proneness to deep local invasion and lymph-node metastases.

In their non-mucinous areas, the mucinous carcinomas showed various cohesive or diffuse structures, partly recalling the histological pattern shown by the neoplastic epithelium in the mucinous areas. As a rule, the mucinous component showed a lower proportion of Ki67-reactive cells than non-mucinous areas of the same tumour. This was especially true for the deeper invasive part of expansile-muconodular cases, where usually less than 10% of tumour cells reacted for the proliferative marker.

In the adjacent gastric mucosa, intestinal metaplasia (IM) was found in 31 of 41 (76%) mucinous and 2 of 16 (12%) signet-ring cell cancers ($P<0.001$). Although no significant difference was ascertained between lower and higher grade mucinous tumours, a trend for more extensive and direct association of IM (especially of complete, goblet + columnar cell type) with the former tumour subtype was observed (Fig. 3b and Fig. 4a).

Tumour phenotype

Most intracellular and intercellular mucin deposits of mucinous tumours proved alcian blue positive (acidic) and often also HID positive (sulfated), with a limited, if any, PAS-positive neutral component. Both mucin deposits and cell cytoplasms reacted for the goblet cell mucin M3 antigen, the gastric faveolar cell mucin M1 antigen or the periodic acid-concanavalin A test for gastric mucopeptic (mucous-neck, pyloric and cardial gland) cells. Tumour cell cytoplasms (but not well-formed mucin deposits) reacted for MUC2, MUC4, CAR5, MUC5AC or MUC6 mucin (Fig. 2b, Fig. 4d, Fig. 5c, d). Hybrid MUC2/MUC5-positive cells were observed in a few tumours, especially in their superficial/intramucosal part. This finding, already reported in hyperplastic polyps and serrated adenomas of the colon [6], suggested to focus mucin phenotype investigations on the invasive component of tumours to identify more distinctive and prognostically relevant patterns.

The results obtained are outlined in Table 1. While no marker or cell phenotype was exclusive of lower or higher grade mucinous tumours, a trend for the presence of more gastric-type markers among higher grade cases, especially in their non-mucinous component, was observed (20/26, 77%, versus 5/15, 33%, of lower grade cases). An equally high (75%) prevalence of gastric (especially foveolar cell) markers was found in signet-ring cell cancers. These, however, differed from mucinous cancers, both higher and lower grade, in showing scarce reactivity for the goblet cell markers MUC2 and M3 (2/18, 17%), which were closely associated with mucinous tumours only (36/41, 88%; $P<0.001$ versus signet-ring cell tumours).

Follow-up

Survival analysis of the 41 patients with mucinous cancer showed no significant difference compared with the 193 patients with non-mucinous tumours of corresponding invasion level (deep submucosa or beyond). No difference was found even when the 37 advanced (T2 or beyond) mucinous cases were compared with 162 advanced non-mucinous tumours, either as a whole or as individual histological groups, with the only exception of undifferentiated high-grade cancers, which had worse survival (Table 2). However, when analysed separately, the 15 submucosal or advanced, muconodular and lower grade tumours showed obviously better survival than the re-

Table 2 Univariate survival analysis of 199 advanced gastric cancers: comparison of mucinous and non-mucinous types

Histological type	Deaths	Rate	95% confidence interval	*P* value
Mucinous[1]	21/37 (56.8)	18.58	12.12–28.50	NS versus 4, 5, 6; <0.001 versus 7
Lower grade[2]	2/11 (18.2)	3.34	0.83–13.34	0.005 versus 3; 0.03 versus 4
Higher grade[3]	19/26 (73.1)	35.82	22.85–56.16	0.050 versus 4; NS versus 5
Cohesive[4]	62/97 (63.9)	18.99	14.80–24.35	NS versus 5
Diffuse[5]	31/46 (67.4)	20.83	14.65–29.61	0.025 versus 2
Signet ring[6]	13/18 (72.2)	30.60	17.77–52.70	0.012 versus 2; 0.008 versus 7; NS versus 3, 4
Undifferentiated high grade[7]	18/19 (94.7)	103.21	65.03–163.82	0.015 versus 3; <0.001 versus 2, 4, 5

With models 3, 4, 5 and 7 versus 2, likelihood ratio (LR) χ^2 (4): 31.48, $P<0.0001$

Table 3 Multivariate survival analysis of 199 advanced gastric cancers

	Hazard ratio	*P* value	95% confidence interval
Age	1.017	0.039	1.001–1.034
Sex	1.224	0.330	0.835–1.792
Stage (Ib+II versus III+IV)	5.516	<0.001	3.682–8.266
Histology*		<0.001	
3 versus 2	11.054	<0.001	2.528–48.341
4+5 versus 2	7.559	0.005	1.839–31.066
7 versus 2	21.856	<0.001	4.949–96.517

* See Table 2 for corresponding histological groups
LR χ^2 (6): 115.76, $P<0.0001$; Model explained variation: .4411; Shrinkage coefficient: .9482

maining 26 mucinous ($P=0.001$) and the corresponding 193 non-mucinous tumours ($P=0.008$)—a difference that was confirmed when only advanced tumours were considered (Table 2). No tumour-related death was observed among the 4 patients with submucosal mucinous cancers (all of the muconodular subtype) compared with 6 patients who died of disease among the 31 corresponding non-mucinous cases. The 26 higher grade mucinous cancers, all of advanced invasion level, showed a survival slightly worse than that of corresponding cohesive cancers, though better than that of undifferentiated high-grade cancers and more akin to that of diffuse cancers, with special reference to its signet-ring subtype (Table 2).

A multivariate analysis inclusive of age, sex and TNM stage (Ib+II versus III+IV) confirmed the independent predictor power of lower grade muconodular histology versus higher grade mucinous, cohesive and diffuse (grouped together) or undifferentiated high-grade types, in addition to the well-known power of stage (Table 3).

Discussion

This study provides evidence of a histologically lower grade, muconodular subset of gastric mucinous cancer showing limited aggressiveness and a relatively favourable prognosis. The tumour is characterised by an overwhelming (80% or more) mucinous component in the form of well-demarcated mucin lakes with tumour cells floating inside, predominance of extracellular mucin over tumour cells, an overall expansile pattern of growth, moderate cellular anaplasia and proliferative rate, no or limited lymphoinvasion and absence of angioinvasion.

Histologically similar low-grade tumours have been reported in the pancreas [3, 27] and breast [18]. In both sites, MUC2 was the dominant mucin [16]. This gel-forming mucin has been suggested to prevent active infiltration of surrounding tissues by interposing itself between tumour cells and stroma, thus contributing to the favourable tumour behaviour [3, 4]. Alternatively, a tumour suppressive role of MUC2 may be considered, as suggested by the occurrence in MUC2 genetically deficient mice of colorectal cancers associated with increased cell proliferation and decreased apoptosis of non-tumour intestinal epithelia [32].

In keeping with previous findings [14, 24], we found MUC2 to also be the main mucin in gastric mucinous cancers. This was especially true for muconodular tumours, where goblet cell mucin was largely represented in all cases, although in 5 of 15 (33%) of these, an appreciable MUC5AC mucin content, with or without associated MUC6, was also detected. The latter, gastric-type mucins were significantly more represented among non-muconodular tumours, with special reference to their non-mucinous component. In general, no mucin type and no gastric or intestinal cell phenotype proved by itself diagnostic for muconodular versus non-muconodular, or for lower versus higher grade tumour subsets, although they proved contributive when coupled with histological pattern.

It should be outlined that a well-formed glandular structure of the cellular component floating in or bordering the nodules was only found in a minority (5 of 15) of our low-grade cases. Most of these tumours showed predominance of isolated cells or small cellular groups and epithelial fragments freely floating inside mucin

lakes, a pattern of epithelial growth recalling that of signet-ring cells in tumour stroma of non-mucinous cancers. In fact, in both previous [2, 28, 33] and present investigations, separation among mucinous cases of tumours with well-differentiated from poorly differentiated epithelial structure failed to identify prognostically different groups. For this purpose, other criteria must be considered, such as the ratio between mucinous and non-mucinous components, the expansile or infiltrative type of overall tumour growth, the type (MUC2/M3 versus MUC5AC/M1) of mucin produced and the degree of tumour anaplasia and aggressiveness. Some of these have been already shown to characterise low-grade mucinous tumours of other sites [3, 16, 18, 21].

A likely equivalent of the previously described "well-differentiated mucoid carcinoma with indolent behaviour" [7] were two tubulo-cystic cancers closely mimicking intestinal crypts epithelium. They showed CD10-, MUC4- and/or CAR5-positive, regular, monostratified epithelium with intercalated MUC2-positive goblet cells, with or without well-defined mucin thecae, and a muconodular pattern in their deeply invasive part. One such case also showed continuity with complete-type intestinal metaplasia in the overlying mucosa, thus resembling closely, mucin deposits apart, the "extremely well-differentiated intestinal type adenocarcinomas" recently described by Endoh et al. [10]. Two non-mucinous tumours showing a similar histological pattern were also observed.

In general, association with intestinal metaplasia was a common finding in mucinous tumours, especially in the case of lower grade tumours, where complete type metaplasia, with goblet- as well as columnar intestinal-type cells, was mostly found. On the contrary, diffuse signet-ring cell cancers consistently lacked association with intestinal metaplasia. Although occasionally we found a phenotypically intestinal cancer to arise "de novo" in non-metaplastic gastric mucosa, as a whole, the above findings support a histogenetic link between lower grade muconodular tumours and intestinal metaplasia, especially of complete type, in keeping with the predominance of goblet cells and MUC2 in these tumours. However, a link between most signet-ring cell cancers and gastric foveolar cells is supported by the predominance of MUC5AC/M1 mucin and the poor reactivity for MUC2/M3 markers found in such tumours as well as by their lack of association with intestinal metaplasia. Intermediate patterns were found in higher grade mucinous tumours, where often both intestinal- and gastric-type cells were substantially represented, while the association with complete-type intestinal metaplasia was less prominent.

In accordance with previous findings [9, 24], survival analysis of 41 mucinous cancers showed no difference from most other gastric cancers. However, 15 histologically low-grade mucinous tumours showed an obviously better outcome than the remaining 26 mucinous cancers, thus confirming their less ominous nature. This was partly due to their lower infiltration level, possibly reflecting a more effective resistance of the gastric wall towards their pushing-type invasion (to be compared with the infiltrative, more aggressive invasion of most higher grade mucinous tumours). However, multivariate analysis inclusive of stage showed a stage-independent improved survival of muconodular cancers, suggesting an intrinsically lower malignant potential of such tumours. It seems of interest that among the 199 advanced cancers investigated, the 26 higher grade mucinous tumours showed a death rate significantly worse than that of non-mucinous tumours with cohesive pattern and more akin to that of diffuse cancers of the signet-ring cell subtype. This behaviour may be in keeping with the histological and histochemical similarities, among which is MUC5AC expression [14, 24, present investigation], observed between the signet-ring tumours and the non-mucinous component of several higher grade mucinous cancers.

In conclusion, separation on histological grounds of a lower grade muconodular group among gastric mucinous cancers may improve substantially our clinico-pathological understanding of such tumours and may help in reconstructing their natural history.

Acknowledgements The study was supported in part by grants from the Italian Ministry of Health to IRCCS Policlinico San Matteo and from the Italian Ministry of Education, University and Research to E.S. and R.F. The experiments reported in this paper comply with current Italian laws.

References

1. Adachi Y, Mori M, Kido A, Shimono R, Maehara Y, Sugimachi K (1992) A clinicopathologic study of mucinous gastric carcinoma. Cancer 69:866–871
2. Adachi Y, Yasuda K, Inomata M, Sato K, Shiraishi N, Kitano S (2000) Pathology and prognosis of gastric carcinoma: well versus poorly differentiated type. Cancer 89:1418–1424
3. Adsay NV, Pierson C, Sarkar F, Abrams J, Weaver D, Conlon KC, Brennan MF, Klimstra DS (2001) Colloid (mucinous noncystic) carcinoma of the pancreas. Am J Surg Pathol 25:26–42
4. Adsay NV, Merati K, Nassar H, Shia J, Sarkar F, Pierson CR, Cheng JD, Visscher DW, Hruban RH, Klimstra DS (2003) Pathogenesis of colloid (pure mucinous) carcinoma of exocrine organs: coupling of gel-forming mucin (MUC2) production with altered cell polarity and abnormal cell-stroma interaction may be the key factor in the morphogenesis and indolent behavior of colloid carcinoma in the breast and pancreas. Am J Surg Pathol 27:571–578
5. Bara J, Chastre E, Mahiou J, Singh RL, Forgue-Lafitte ME, Hollande E, Godeau F (1998) Gastric M1 mucin, an early oncofetal marker of colon carcinogenesis, is encoded by the MUC5AC gene. Int J Cancer 75:767–773
6. Biemer-Huttmann AE, Walsh MD, McGuckin MA, Ajioka Y, Watanabe H, Leggett BA, Jass JR (1999) Immunohistochemical staining patterns of MUC1, MUC2, MUC4, and MUC5AC mucins in hyperplastic polyps, serrated adenomas, and traditional adenomas of the colorectum. J Histochem Cytochem 47:1039–1047
7. Brander L, Needham PR, Morgan AD (1974) Indolent mucoid carcinoma of stomach. J Clin Pathol 27:536–541
8. Candusso ME, Luinetti O, Villani L, Alberizzi P, Klersy C, Fiocca R, Ranzani GN, Solcia E (2002) Loss of heterozygosity at 18q21 region in gastric cancer involves a number of cancer-related genes and correlates with stage and histology, but lacks independent prognostic value. J Pathol 197:44–50

9. Chiaravalli AM, Cornaggia M, Furlan D, Capella C, Fiocca R, Tagliabue G, Klersy C, Solcia E (2001) The role of histological investigation in prognostic evaluation of advanced gastric cancer. Analysis of histological structure and molecular changes compared with invasive pattern and stage. Virchows Arch 439:158–169
10. Endoh Y, Tamura G, Motoyama T, Ajioka Y, Watanabe H (1999) Well-differentiated adenocarcinoma mimicking complete-type intestinal metaplasia in the stomach. Hum Pathol 30:826–832
11. Fiocca R, Villani L, Tenti P, Solcia E, Cornaggia M, Frigerio B, Capella C (1987) Characterization of four main cell types in gastric cancer: foveolar, mucopeptic, intestinal columnar and goblet cells. An histopathologic, histochemical and ultrastructural study of "early" and "advanced" tumours. Pathol Res Pract 182:308–325
12. Fiocca R, Villani L, Tenti P, Cornaggia M, Finzi G, Capella C, Prat M, Bussolati G, Solcia E (1988) Widespread expression of intestinal markers in gastric carcinoma: a light and electron microscopic study using BD-5 monoclonal antibody. J Clin Pathol 41:178–187
13. Fiocca R, Villani L, Tenti P, Cornaggia M, Finzi G, Riva C, Capella C, Bara J, Samloff IM, Solcia E (1990) The foveolar cell component of gastric cancer. Hum Pathol 21:260–270
14. Gürbüz Y, Kahlke V, Kloppel G (2002) How do gastric carcinoma classification systems relate to mucin expression patterns? An immunohistochemical analysis in a series of advanced gastric carcinomas. Virchows Arch 440:505–511
15. Hanski C (1995) Is mucinous carcinoma of the colorectum a distinct genetic entity? Br J Cancer 72:1350–1356
16. Hanski C, Hofmeier M, Schmitt-Graff A, Riede E, Hanski ML, Borchard F, Sieber E, Niedobitek F, Foss HD, Stein H, Riecken EO (1997) Overexpression or ectopic expression of MUC2 is the common property of mucinous carcinomas of the colon, pancreas, breast, and ovary. J Pathol 182:385–391
17. Kawamura H, Kondo Y, Osawa S, Nisida Y, Okada K, Isizu H, Uebayasi T, Takahasi M, Hata T (2001) A clinicopathologic study of mucinous adenocarcinoma of the stomach. Gastric Cancer 4:83–86
18. Komaki K, Sakamoto G, Sugano H, Morimoto T, Monden Y (1988) Mucinous carcinoma of the breast in Japan. A prognostic analysis based on morphologic features. Cancer 61:989–996
19. Kubo T (1971) Histologic appearance of gastric carcinoma in high and low mortality countries: comparison between Kyushu, Japan and Minnesota, USA. Cancer 28:726–734
20. Luinetti O, Fiocca R, Villani L, Alberizzi P, Ranzani GN, Solcia E (1998) Genetic pattern, histological structure, and cellular phenotype in early and advanced gastric cancers: evidence for structure-related genetic subsets and for loss of glandular structure during progression of some tumours. Hum Pathol 29:702–709
21. Luttges J, Zamboni G, Longnecker D, Kloppel G (2001) The immunohistochemical mucin expression pattern distinguishes different types of intraductal papillary mucinous neoplasms of the pancreas and determines their relationship to mucinous noncystic carcinoma and ductal adenocarcinoma. Am J Surg Pathol 25:942–948
22. Messerini L, Ciantelli M, Baglioni S, Palomba A, Zampi G, Papi L (1999) Prognostic significance of microsatellite instability in sporadic mucinous colorectal cancers. Hum Pathol 30:629–634
23. Nardelli J, Bara J, Rosa B, Burtin P (1983) Intestinal metaplasia and carcinomas of the human stomach: an immunohistological study. J Histochem Cytochem 31:366–375
24. Pinto-de-Sousa J, David L, Reis CA, Gomes R, Silva L, Pimenta A (2002) Mucins MUC1, MUC2, MUC5AC and MUC6 expression in the evaluation of differentiation and clinico-biological behaviour of gastric carcinoma. Virchows Arch 440:304–310
25. Reis CA, David L, Carvalho F, Mandel U, de Bolos C, Mirgorodskaya E, Clausen H, Sobrinho-Simões M (2000) Immunohistochemical study of the expression of MUC6 mucin and co-expression of other secreted mucins (MUC5AC and MUC2) in human gastric carcinomas. J Histochem Cytochem 48:377–388
26. Secco GB, Fardelli R, Campora E, Lapertosa G, Gentile R, Zoli S, Prior C (1994) Primary mucinous adenocarcinomas and signet-ring cell carcinomas of colon and rectum. Oncology 51:30–34
27. Sessa F, Solcia E, Capella C, Bonato M, Scarpa A, Zamboni G, Pellegata NS, Ranzani GN, Rickaert F, Kloppel G (1994) Intraductal papillary-mucinous tumours represent a distinct group of pancreatic neoplasms: an investigation of tumour cell differentiation and K-ras, p53 and c-erbB-2 abnormalities in 26 patients. Virchows Arch 425:357–367
28. Shibuya H, Nishida R, Koide S, Kurokawa J, Okita K (2000) Clinicopathological study of mucinous gastric carcinoma. Ann Chir Gynaecol 89:273–276
29. Sobin LH, Wittekind C (1997) TNM classification of malignant tumours, 5th edn. Wiley-Liss, New York, pp 59–62
30. Solcia E, Capella C, Kloppel G (1997) Tumors of the pancreas. Armed Forces Institute Pathology. Atlas of Tumor Pathology, vol. 20. American Registry of Pathology, Washington, DC
31. Tsukashita S, Kushima R, Bamba M, Sugihara H, Hattori T (2001) MUC gene expression and histogenesis of adenocarcinoma of the stomach. Int J Cancer 94:166–170
32. Velcich A, Yang W, Heyer J, Fragale A, Nicholas C, Viani S, Kucherlapati R, Lipkin M, Yang K, Augenlicht L (2002) Colorectal cancer in mice genetically deficient in the mucin Muc2. Science 295:1726–1729
33. Wu CY, Yeh HZ, Shih RT, Chen GH (1998) A clinicopathologic study of mucinous gastric carcinoma including multivariate analysis. Cancer 83:1312–1318

Virchows Arch (2004) 445:580–588
DOI 10.1007/s00428-004-1134-x

ORIGINAL ARTICLE

Ryoko Nagaike · Akira Sawaguchi · Jun-ichi Kawano · Fumiyo Aoyama · Tsutomu Oinuma · Tatsuo Suganuma

Regeneration of gastric mucosa during ulcer healing follows pathways that correspond to the ontogenetic course of rat fundic glands

Received: 20 May 2004 / Accepted: 2 September 2004 / Published online: 28 October 2004
© Springer-Verlag 2004

Abstract Gastric ulcers in humans are notoriously chronic and recurring lesions. Although the average individual who undergoes no treatments requires many years for healing, most studies on the healing process of the experimentally induced ulcers have mainly focused on the early stages. Natural history of the ulcer healing has not been completely revealed. We have undertaken long-term investigation up to the 150th day after the cryo-injury to shed light on the natural history of the ulcer healing process compared with developmental changes of postnatal fundic glands. By the 30th day, restitutive gastric glands were mostly seen to cover the ulcer lesions, where well-developed gland-type mucous cells, showing *Griffonia simplicifolia* agglutinin (GSA)-II labeling, appeared to occupy the basal portion. Most of the bromodeoxyuridine-labeled cells were superimposed on the GSA-II-positive cell zone, forming the proliferative zone. By the 150th day, the restitutive glands were complete, with all epithelial components and topology of the normal fundic glands. The process of the ulcer healing was quite compatible with the developmental changes of the postnatal fundic glands. These results imply that the regeneration of gastric epithelium during the ulcer healing follows pathways linked to the ontogenetic course of the fundic gland.

Keywords Stomach · Ulcer · Regeneration · Bromodeoxyuridine · Immunohistochemistry

Introduction

Gastric ulcers in humans are notoriously chronic, recurring lesions. They more often impair the quality of life. When untreated, the average individual requires many years for the healing of either a gastric or duodenal ulcer. It has been well documented that mucins secreted from the pit and neck regions play a physiologically important role in the mucosal defense of the gastrointestinal tract [2, 9, 10]. Although there are several reports focusing on the changes in the gastric mucins of the regenerating mucosa during the ulcer healing [4, 6, 30], the ulcer healing process, both in humans and experimental ulcer models, is a complex process, requiring the collaborative efforts of many different tissues and cell lineages. The behavior of each contributing cell type during the phases of proliferation, migration, matrix synthesis, and contraction, as well as the presence of various growth factors, including matrix signals present at a ulcer site, are now roughly understood [1, 12, 21, 22, 28, 29, 31, 32], as most of the attention has been paid to the early stage of the healing process of the gastric ulcer.

To our knowledge, there is no other report investigating the morphological dynamics of the ulcer healing for a long period except the studies conducted by Hayashida et al. [10] and Helap et al. [13]. They described that the lower part of the regenerating epithelia was occupied with HIK 1083-positive mucous cells on the 50th day. HIK 1083 monoclonal antibody specifically reacts with the gland-cell-type mucin of stomach [9, 10]. Therefore, they designated this type of change as the pseudopyloro-cardiac gland, which was formerly referred to as the pseudopyloric gland or pyloric metaplasia [10, 13, 20]. However, our preliminary experiments, including electron microscopy, revealed that the regenerating mucosa on the 50th day after ulceration consisted of not only surface mucous cells and gland-type mucous cells but also parietal cells, arguing that the only involvement of pseudopyloric gland-type change was taking place at the time of the healing process of the corpus mucosa. Therefore, we undertook a long-term (up to the 150th day) histological and histochemical investigation to shed light on the regenerating process to the complete healing of the experimentally induced ulcer.

R. Nagaike · A. Sawaguchi · J.-i. Kawano · F. Aoyama · T. Oinuma · T. Suganuma (✉)
Department of Anatomy,
Miyazaki Medical College, University of Miyazaki,
5200 Kihara, Kiyotake, 889-1692 Miyazaki, Japan
e-mail: suganumat@med.miyazaki-u.ac.jp
Tel.: +81-985-851784
Fax: +81-985-858406

There are several methods of ulcer induction to the stomach, such as surgical resection of the mucosa, acetic acid injection, and cryoprobe treatment. Gastric ulcers induced by cryoprobe application are easily obtained and reproducible. Moreover, they have an advantage of being an experimental model more closely resembling human peptic ulcers [1, 13]. In addition, we reexamined the normal developmental changes of rat fundic glands [5, 14, 17, 34, 35] during the postnatal period to compare with the healing process of cryoprobe-induced gastric ulcers. Based on our findings, we propose that the healing process of gastric ulcer follows pathways that correspond to the ontogenetic course of the fundic gland.

Materials and methods

Animals

Adult male Wistar rats (Charles River, Yokohama, Japan) (n=61) approximately 8–12 weeks old were used. They were starved for 24 h (water ad libitum) prior to ulcer induction. After ulcer induction, they were allowed to access water and rat chow. Postnatal Wistar rats (n=21) were used to investigate the normal development of rat fundic glands for comparison with the healing process of the gastric ulcer.

Reagents

Bromodeoxyuridine (BrdU) was purchased from Sigma Chemical Co. (St Louis, MO, USA). Monoclonal mouse anti-BrdU antibody was from Beckton Dickinson Inc. (San Jose, CA, USA). Biotinylated *Griffonia simplicifolia* agglutinin (GSA) II was from Vector Laboratories (Burlingame, CA, USA). GSA-II specifically recognizes *N*-acetylglucosamine residues and labels the mucin derived from the gland-type mucous cells, such as mucous neck cells, cardiac gland, and pyloric gland cells of the gastric mucosa [14]. Biotinylated horse anti-mouse IgG antibody and avidin-biotin-horseradish peroxidase complex (ABC) kit were from Vector Laboratories.

Induction of gastric ulcer

Induction of gastric ulcer was performed according to the method of Alison et al. [1]. Briefly, under anesthesia with diethylether and intraperitoneal application of sodium pentobarbital, stomachs were exposed through a 3-cm laparotomy incision. Gastric ulcers were induced by applying a 6-mm diameter Pb cryoprobe, cooled to equilibrium in liquid nitrogen, to the serosal surface of stomachs for 25 s. After the recovery, animals were allowed free access to water and rat chow. Simple laparotomy was carried out as a sham operation. This study was performed according to the guidelines for the care and use of laboratory animals, approved by the Animal Research Committee of Miyazaki Medical College, and following the "Principles of laboratory animal care" (NIH publication no. 85-23, revised 1985).

Tissue preparations

Rats were sacrificed by lapse of time after the ulcer induction (on the 3rd, 7th, 30th, 60th, 90th, and 150th days). We also used stomachs of postnatal rats on the day of the birth, 3rd, 7th, 10th, 14th, 21st, 28th, and 35th days after birth for the ontogenetic study of the fundic gland. Under deep anesthesia, stomachs were removed, immersed in 10% buffered formalin for 24 h, and then embedded in paraffin for light microscopy. For electron microscopy, some of the ulcer-induced rats were perfused with a mixture of 4% paraformaldehyde and 0.2% glutaraldehyde in 0.1 M phosphate buffer (PB), pH 7.4, and small pieces of the stomachs were immersed in the same fixative for a further 1 h at 4°C. After rinsing with 0.1 M PB, they were postfixed with 1%OsO_4 in 0.1 M PB, pH 7.4, for 1 h, dehydrated through a graded series of ethanols, and then embedded in Epon/Alardite. Ultrathin sections mounted on cupper grids were contrasted with uranyl acetate for 3 min and lead citrate for 30 s and then observed with a JEOL 1200EX electron microscope.

Glycoconjugate histochemistry

Paraffin sections (4-μm thickness) were stained by each of the following methods for histology and mucin histochemistry [33]: hematoxylin-eosin, alcian blue (AB) at pH 2.5 followed by periodic acid-Schiff (PAS) [19], high iron-diamine (HID) followed by AB at pH 2.5 [23].

For GSA-II staining, paraffin sections were deparaffinized, immersed in 0.3% hydrogen peroxide in methanol for 20 min for blocking the endogenous peroxidase, and incubated with 1% bovine serum albumin (BSA) in phosphate-buffered saline (PBS) for 5 min. Then, the sections were incubated with biotinylated GSA-II (20 μg/ml of 1% BSA/PBS) for 60 min. After rinsing with PBS, the sections stained with GSA-II were immersed in the freshly prepared ABC solution for 30 min. Peroxidase reaction was developed by incubating sections in 0.05% 3-3′diaminobenzidine tetrahydrochloride in 0.05 M Tris buffer, pH 7.6, containing 0.001% H_20_2. Sections were counterstained with hematoxylin. As a control, the lectin preincubated with haptenic sugar (0.2 M *N*-acetyl-D-galactosamine) and then applied to sections. All procedures were carried out at room temperature.

BrdU immunohistochemistry and labeling index

Rats (15 ulcer-induced and 21 postnatal) were injected with BrdU (50 mg/kg) intraperitoneally 1 h prior to sacrifice. After quenching for endogenous peroxidase, sections were treated with 2 M HCl for 20 min and digested with 0.1% trypsin (Gibco, Detroit, MI, USA) in 0.05 M Tris-HCl, pH 7.6, containing 0.1% $CaCl_2$ for 20 min. After rinsing with PBS, they were immersed in 5% normal horse serum/1% BSA/PBS for 60 min and treated with anti-BrdU monoclonal antibody (at a dilution of 1:150) at 4°C overnight. They were rinsed with PBS and treated with biotin-labeled horse anti-mouse IgG antibody (at a dilution of 1:100) for 60 min. After PBS wash, they were incubated with the freshly prepared ABC solution for 30 min. Peroxidase reaction was performed as mentioned above. Sections were lightly counterstained with hematoxylin. As a control, sections were treated with normal mouse IgG instead of anti-BrdU antibody.

Some specimens (3rd, 7th, 30th, 90th, and 150th days) were used for the analysis of the labeling index. Three different areas, including the regenerating glands (A), the residual glands adjacent to A (B), and the residual glands in the distal region from the ulcers (C) were selected, and the labeling index of BrdU was calculated. For calculating of the labeling index, more than 1000 epithelial cells and BrdU-labeled epithelial cells were counted, and the percentages of BrdU-labeled epithelial cells were estimated. As a control, the sham-operated rats on the 7th day were used.

Results

General histology of cryoprobe-induced gastric ulcer

As expected, the cryoprobe application easily and reproducibly produced ulcer lesions, morphologically re-

sembling human peptic ulcers. On the 3rd day, the mucosa was disrupted with ongoing necrosis penetrating from the epithelial lining through the muscularis. There was little evidence of any regenerative response, although the residual fundic glands existed on the ulcer margin (Fig. 1A, B).

On the 7th day, the ulcer base was completely composed of granulation tissue. Though the central part of the ulcer base was still covered with necrotic tissue and a nonspecific inflammatory infiltrate, the regenerative mucosa began to appear at the ulcer margin. Two different kinds of epithelial tissues were discernible: a thin layer of the regenerating epithelium composed of flat to cuboidal cells, which extended toward the denuded area of the ulcer base, and the foveolate glands, mainly composed of the mucous cells compatible with gastric surface mucous cells, presenting a fan-like arrangement. It was notable that a few immature parietal cells with less eosinophilic cytoplasm and round nuclei were already observed in the middle portion of the regenerating foveolate glands adjacent to the ulcer base (Fig. 1C, D). The presence of these immature parietal cells was confirmed by electron microscopy with a number of mitochondria as well as free ribosomes in their cytoplasm, even though a tubulovesicular system could not be detected (Fig. 2A, B). However, parietal cells with a well-developed tubulovesicular system were noticed in the regenerating foveolate gland adjacent to the residual epithelium (Fig. 2C).

On the 30th day to the 90th day, most of the ulcer lesions appeared to be covered with the regenerating mucosa, consisting of surface mucous cells (pit cells), parietal cells, and gland-type mucous cells at the bottom of the glands, but without discernible chief cell at this stage (Fig. 1E, F).

On the 150th day, components of the restitutive glands were quite similar to those of normal fundic glands with an exception of slightly elongated gastric pits. The chief cells finally appeared at the bottom of the glands at this stage (Fig. 1G, H). Electron microscopy of this group revealed emergence of mature chief cells with zymogen granules and abundant rough-surfaced endoplasmic reticula (Fig. 3) and also existence of intermediate cells between mucous neck cells and chief cells [14, 15, 16, 25, 26].

Glycoconjugate histochemistry

Conventional histochemistry (AB-PAS, HID-AB) and lectin staining (GSA-II) were performed to clarify the topological alteration of mucous cells during the healing process. The fundic glands of the sham-operated rats showed the same histochemical results as those of a previous report [24]. Namely, PAS stained all the pit cells strongly and the mucous neck cells moderately. AB at pH 2.5 showed the positive reaction on both pit cells and some of the mucous neck cells in the upper part of the neck region. HID presented the strong reaction on the mid to low pit cells. GSA-II specifically labeled the mucous neck cells [14].

On the 7th day, the foveolate mucous glands of the regenerating mucosa were intensely stained with AB-PAS as well as HID-AB. The HID-positive mucous cells in this region remarkably increased in number (Fig. 4A). However, gland-type mucous cells extending toward the basal portion of the residual fundic glands were vividly labeled with GSA-II (Fig. 4B).

On the 30th day, well-developed gland-type mucous cells that appeared at the basal portion of the restitutive glands were intensely labeled with GSA-II (Fig. 4C). The same distribution pattern of GSA-II-positive cells was also confirmed at the 60th day. After the 90th day, these GSA-II-reactive cells appeared to be located in the mid-portion of the glands (Fig. 4D), which became very similar to the normal fundic glands (Fig. 7I). Preincubation of the lectin with haptenic sugar completely abolished the staining (data not shown).

BrdU immunohistochemistry and labeling index

BrdU immunostaining of the 7th day group demonstrated the more intense labeling in the mid to basal region of the regenerating foveolate glands (Fig. 5A, B). There was no BrdU-positive cell in the thin layer of the regenerating epithelium extending toward the denuded area of the ulcer base on the 7th day (not shown). The fundic glands of sham-operated rats revealed the presence of BrdU-labeled cells in the isthmus and the lower gastric pit (Fig. 5C) [8]. The labeling pattern of BrdU was quite compatible with that of normal fundic glands. Interestingly, the restitutive glands at the 30th day demonstrated the superimposed BrdU-labeled cells on the gland-type mucous cells present in the basal portion of the glands, forming the proliferative zone (Fig. 5D).

The BrdU-labeling indexes are summarized in Fig. 6. Although there was no regenerating gland, the residual glands adjacent to the ulcer region showed high labeling intensity on the 3rd day, as much as the regenerating glands on the 7th day and 30th day. After the 30th day, the BrdU-labeling intensity in the regenerating glands gradually decreased. No distinguishable labeling index could be detected between the glands on the 90th day and 150th day. However, the labeling index on the 150th day still remained higher than that of the fundic glands 7 days after the sham operation.

Ontogeny of the normal rat fundic gland

Figure 7 demonstrates normal developmental changes of the fundic glands during the postnatal days. The 3rd day preparation revealed immature fundic glands and the first appearance of parietal cells at this stage (Fig. 7A). Proliferative cells labeled with BrdU were scattered throughout the immature glands, while GSA-II-reactive cells were localized at the bottom of the glands (Fig. 7B, C). In the 14th day preparation, fundic glands were growing, and the BrdU-labeled cells were mainly ob-

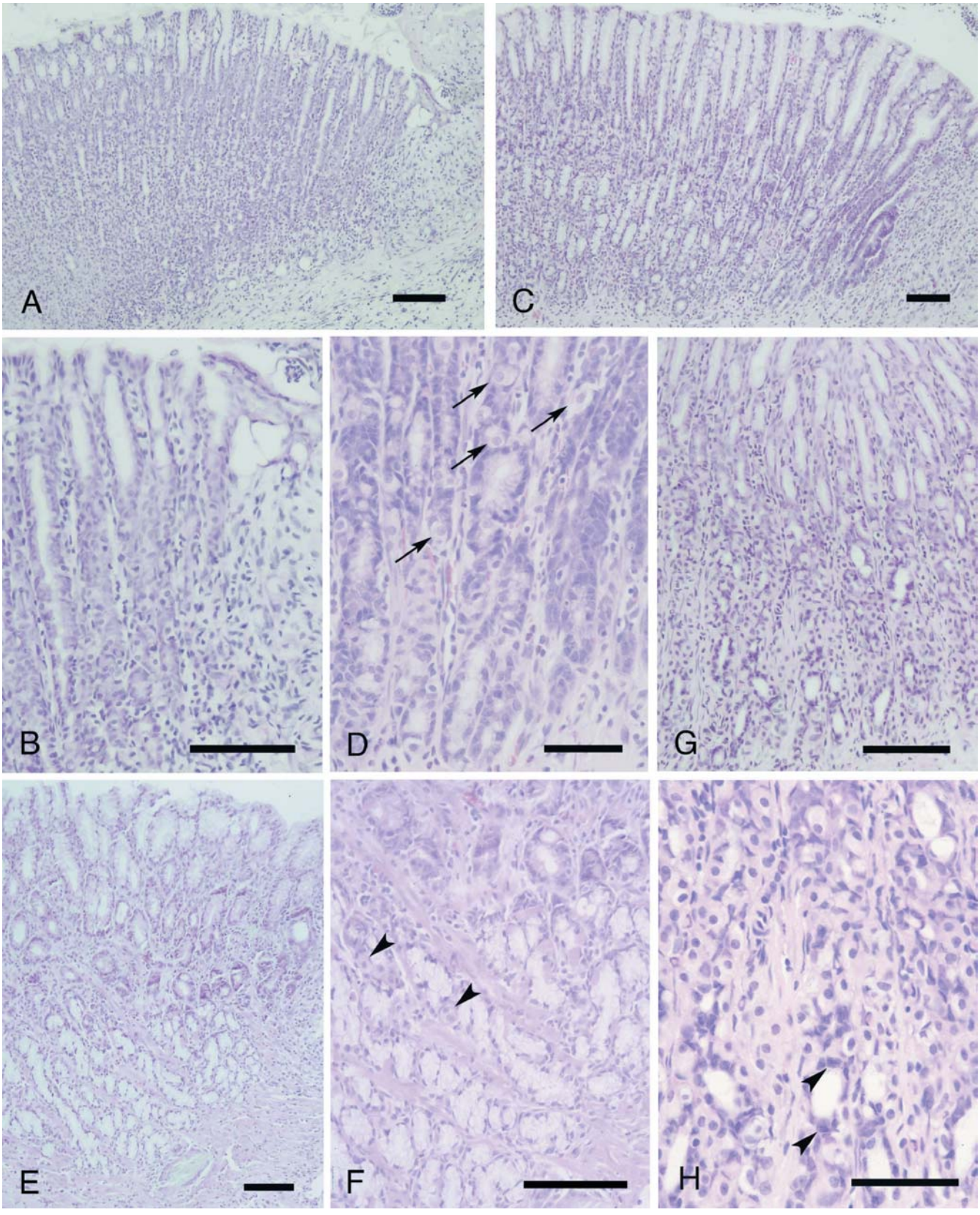


Fig. 1 General histology of the cryoprobe-induced gastric ulcer. **A** The 3rd day after ulcer induction. Complete necrosis is caused by the cryoprobe application. **B** Higher magnification of **A**. No regenerative epithelium appears at the ulcer margin. **C** The 7th day after ulcer induction. Some regenerating foveolate glands are arising at the ulcer margin. **D** Higher magnification of **C**. Immature parietal cells are observed in the regenerating foveolate glands (*arrows*). **E** The 30th day after ulcer induction. Note that gland-type

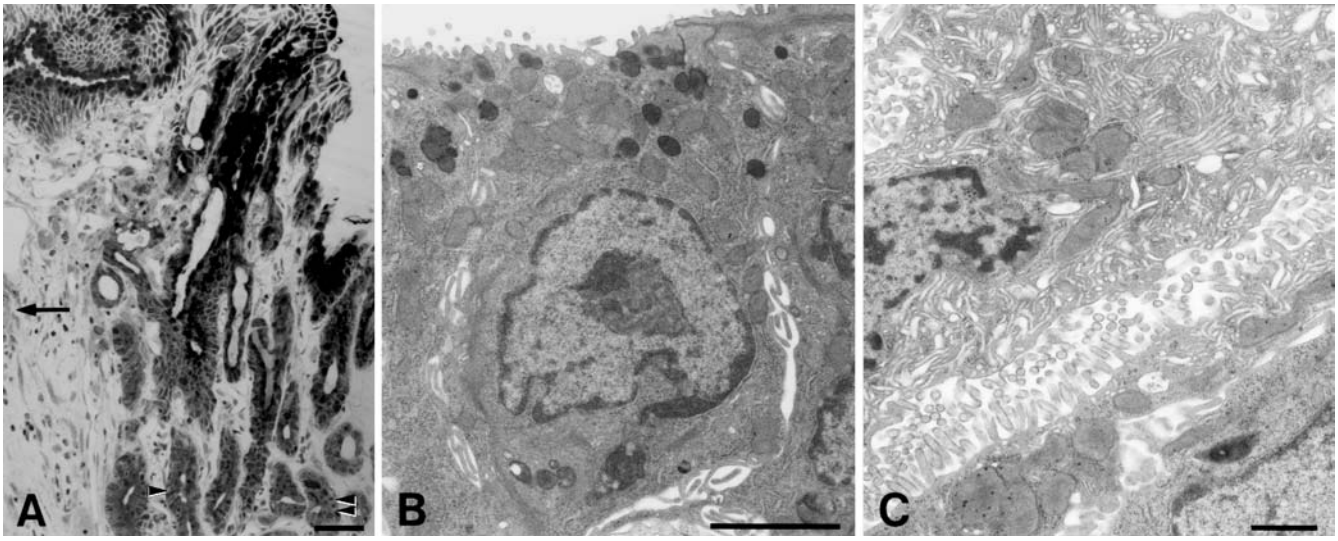


Fig. 2 The regenerating foveolate glands on the 7th day after the cryo-injury. **A** Toluidine blue staining of a semi-thin section. An *arrow* indicates the direction of the ulcer base. Electron micrographs are provided from the spots indicated by *arrowheads*; *single arrowhead* refers to **B**, *double arrowheads* to **C**. **B** Electron microphotograph of the regenerating gland adjacent to the ulcer base (*single arrowhead* in **A**). Immature epithelial cell contains a number of free ribosomes, mitochondria, and a few mucous granules. **C** Higher magnification of the regenerating gland close to the residual glands (*double arrowheads* in **A**). Regenerated parietal cell reveals the tubulovesicular system and many mitochondria in its cytoplasm. *Bars* **A**=50 μm, **B**=2 μm, **C**=1 μm

served in the upper portion of the glands (Fig. 7D, E). GSA-II-labeled cells were still located at the basal portion of the growing fundic glands (Fig. 7F). By the 21st day after birth, fundic glands became quite similar to the adult ones, where chief cells with basophilic cytoplasm appeared at the basal portion of the glands (Fig. 7G). BrdU-labeled cells mostly situated within the isthmus portion of fundic glands were forming the proliferative zone (Fig. 7H), and the majority of GSA-II-reactive cells were located at the neck portion, beneath the proliferative zone (Fig. 7I).

Discussion

The brief application of a liquid nitrogen-chilled cryoprobe to the external wall of the stomach adequately produces a distinct gastric ulcer that heals over several weeks [1]. This cryoprobe model, therefore, is suitable for histological investigation of the ulcer healing process. The results obtained from this study are in accordance with those of former findings, especially during the early stage of the healing process [3, 11, 27, 30]. We provide a new insight from our long-term study that the complete replacement of the injured mucosa with normal fundic glands is finally observable at day 150 following cryo-injury.

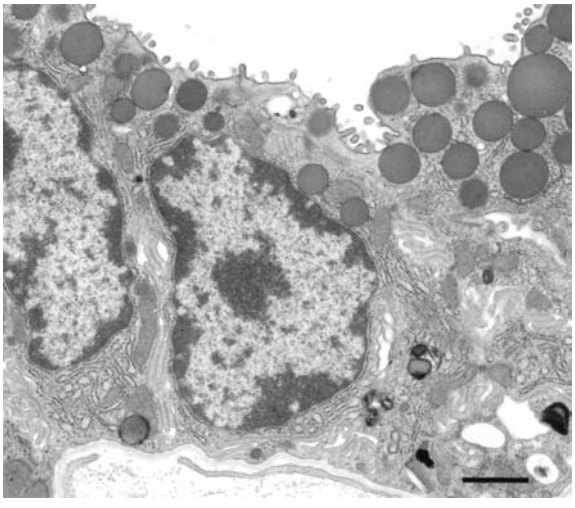


Fig. 3 Electron microphotograph of the restitutive gland at the 150th day after the cryo-injury. Note a typical chief cell with zymogen granules as well as well-developed rough-surfaced endoplasmic reticula. *Bar*=1 μm

Early stages of the ulcer healing

During the earlier stages of the healing process of the gastric ulcer, the regenerating mucosa appeared at the ulcer margin, showing the foveolate gland structure to be mainly composed of surface-type mucous cells, where the appearance of immature parietal cells preceded other epithelial cells, with an exception of surface-type mucous

mucous cells are present at the basal portion of the restitutive glands. **F** Higher magnification of **E**. Several parietal cells can be clearly seen in the middle portion of the regenerating glands (*arrowheads*). **G** The 150th day after ulcer induction. The restitutive glands closely resemble the normal fundic glands. **H** Higher magnification of **G**. The chief cells with the basophilic cytoplasm are discernible at the basal portion of the restitutive glands (*arrowheads*). *Bars* **A**–**C** and **E**–**G**=100 μm, **D** and **H**=50 μm

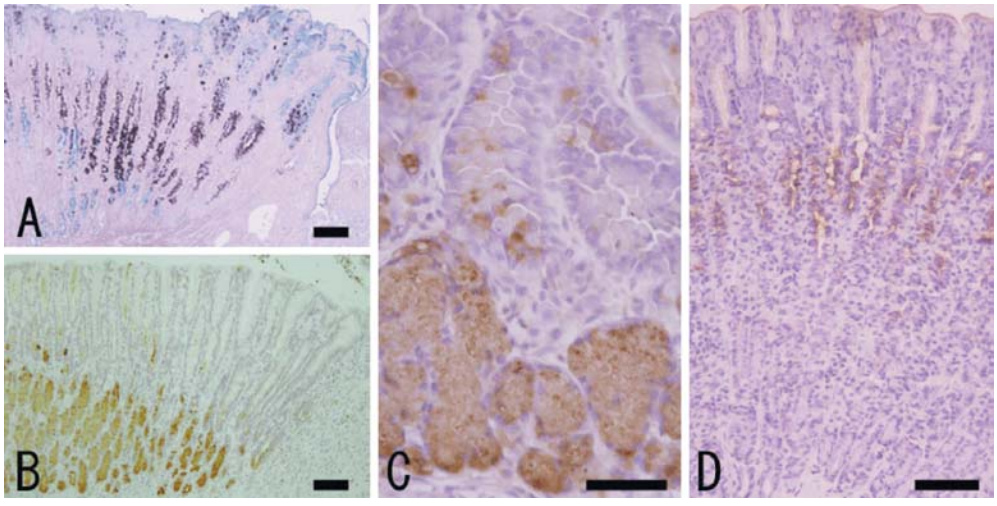
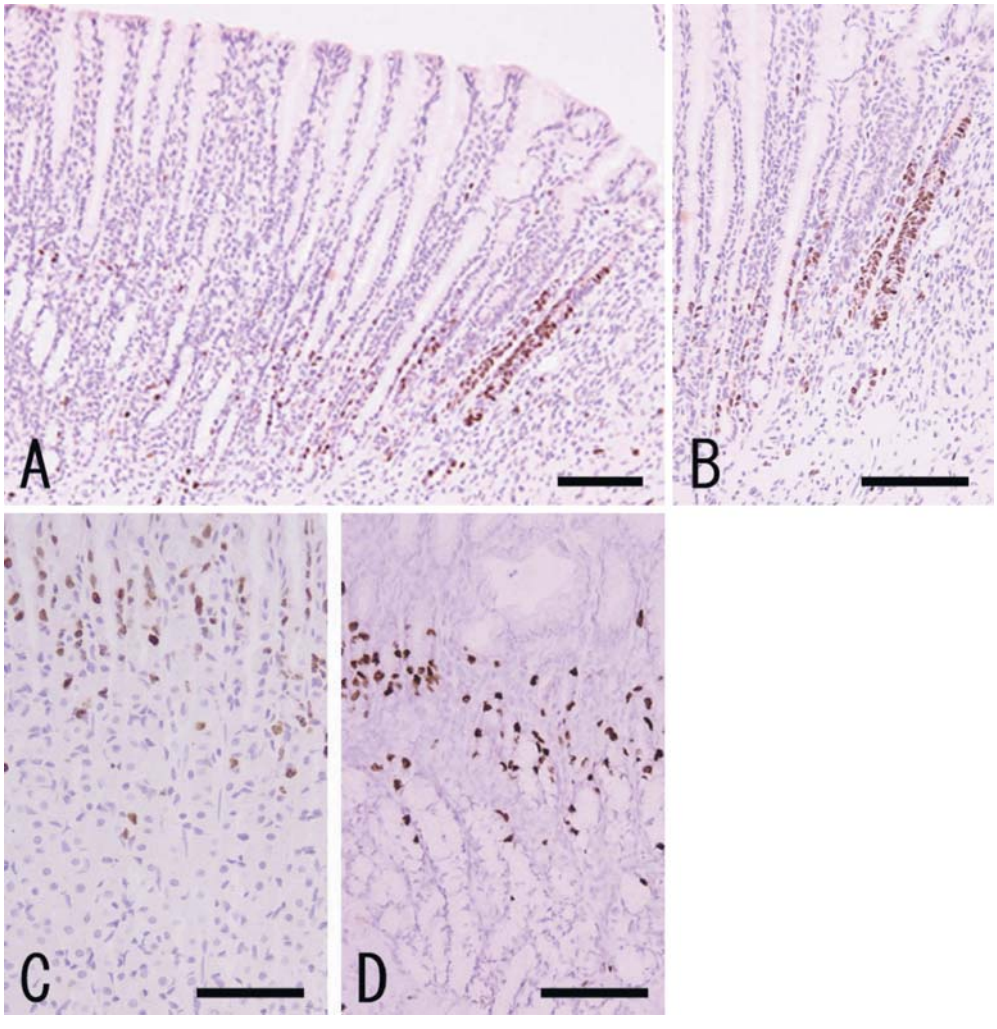


Fig. 4 Glycoconjugate histochemistry. The 7th day after the cryo-injury (**A**, **B**) the 30th day (**C**) and the 150th day (**D**). **A** high iron-diamine (HID)-Alcian blue at pH 2.5. A number of HID-positive mucous cells are observed in the regenerating foveolate glands as well as the residual glands. **B** *Griffonia simplicifolia* agglutinin (GSA)-II staining. The mucous cells at the bottom of the regenerating foveolate glands are intensely stained with GSA-II. **C** Well-developed gland-type mucous cells appeared at the basal portion of the restitutive glands are obviously labeled with GSA-II. **D** GSA-II-labeled mucous cells are localized in the neck portion of the restitutive fundic glands on the 150th day. *Bars* **A** and **B**=100 μm, **C** and **D**=50 μm

Fig. 5 BrdU immunohistochemistry. **A** At the 7th day after the cryo-injury, BrdU-positive cells are present in the middle to basal portion of the regenerating foveolate glands, especially in adjacent area to the ulcer base. **B** Higher magnification of **A**. **C** Sham-operated group at the 7th day after the laparotomy. **D** The 30th day after the cryo-injury. BrdU-positive cells are localized just above the gland-type mucous cells in the restitutive glands. *Bars*=100 μm



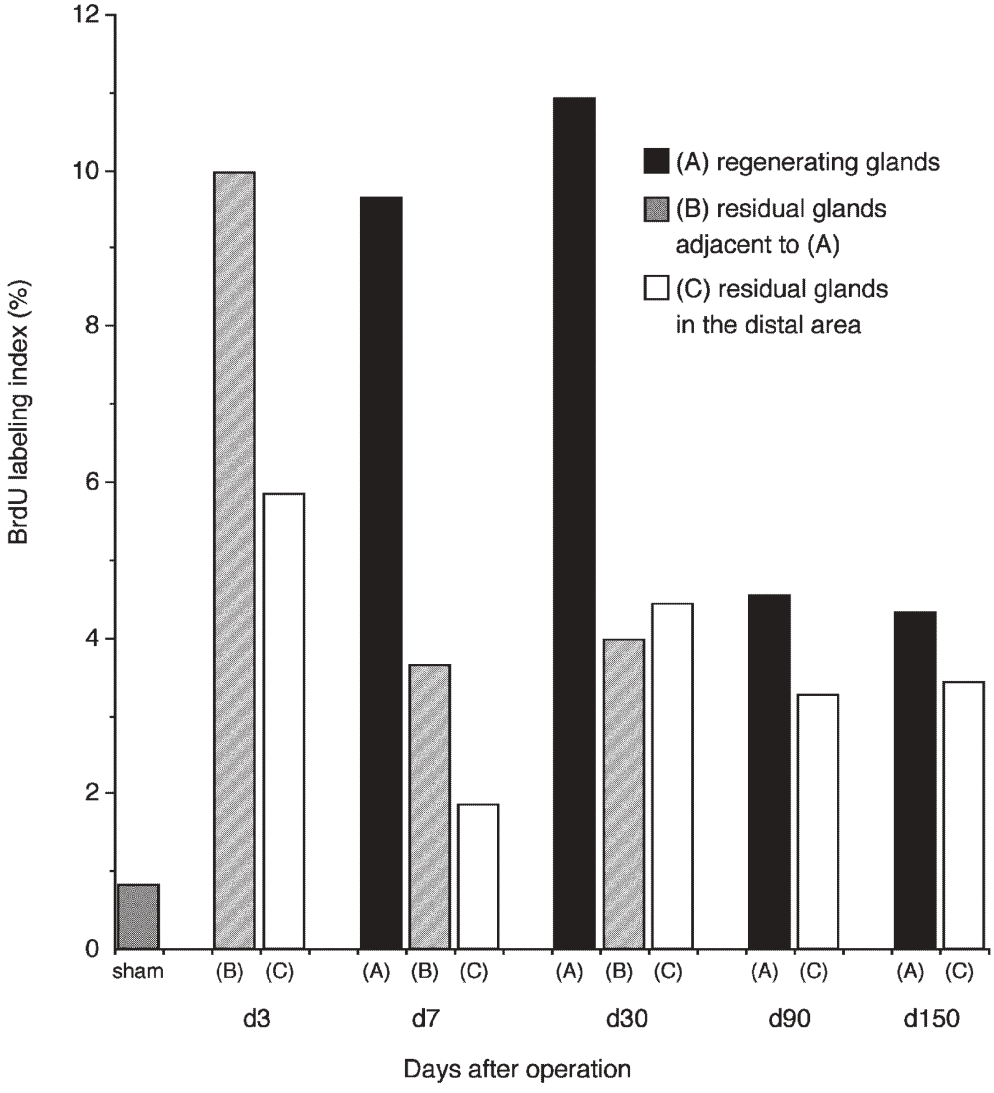


Fig. 6 BrdU-labeling indexes of the ulcerated mucosa. Labeling index of the residual glands increases at the 3rd day after the cryo-injury, while that of the regenerating glands reaches the peak at the 30th day after the ulcer induction

cells, composing the fundic gland at the 7th day after the ulcer induction. This notion of the earlier appearance of parietal cells in the regenerating mucosa also supports previous observations [4, 6, 27, 30]. These results might be linked to the recent findings using the transgenic mice—that the parietal cells might contribute to ontogenesis and the maintenance of the gastric epithelium [7, 18].

Late stages of the ulcer healing

During the late stages of the ulcer healing, the ulcer lesion was replaced by the characteristic restitutive mucosa. In the basal part of the regenerating epithelium, gland-type mucous cells were apparent at the 30th day. BrdU immunohistochemistry on the 30th day group demonstrated that most of the BrdU-labeled proliferative cells appeared at the middle portion of the restitutive glands overlying the gland-type mucous cells. This type of change of the fundic area during the ulcer healing or chronic gastritis was formerly considered as the pseudopyloric mucosa, due to the lack of evidence regarding existence of parietal cell or chief cell [10, 13, 20]. Here, we demonstrated reappearance of not only gland-type mucous cells but also parietal cells in the restitutive gland during the ulcer healing. The characteristic topology of restitutive glands, mainly consisting of pit cells in the upper portion, parietal cells in the upper to middle, and gland-type mucous cells at the bottom of the glands, was maintained until the 90th day. GSA-II staining could intensely label these gland-type mucous cells at the basal portion of the restitutive gastric glands. This is quite coincident with that of HIK1083 [11]. Finally, the shifting of the proliferating cell zone from the lower to the neck portion of the regenerating epithelium was perfected along with complete restoration of the restitutive glands associated with epithelial components, including chief cells by the 150th day.

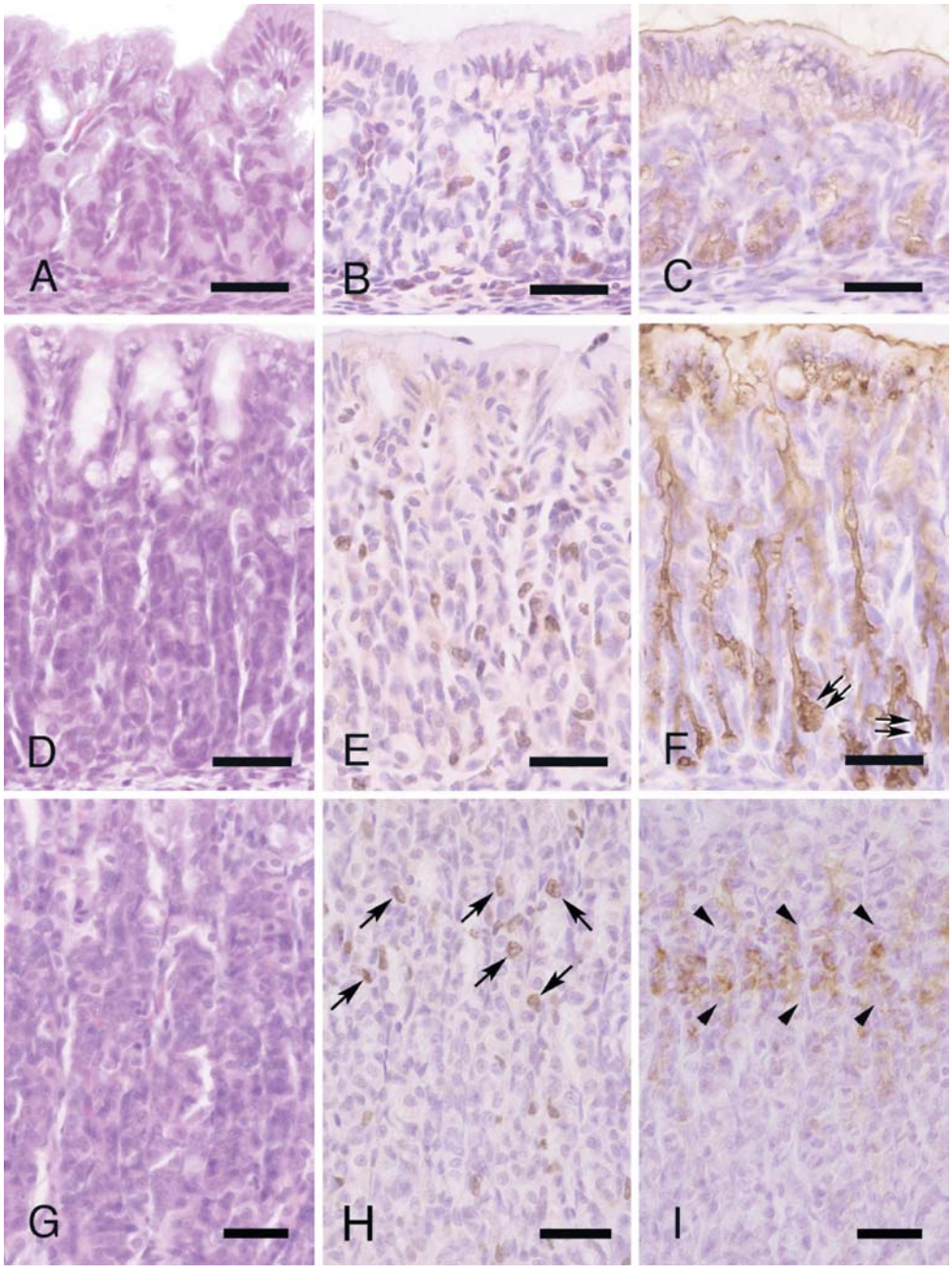


Fig. 7 The normal development of postnatal rat fundic gland. **A–C** 3rd day after birth. **D–F** 14th day after birth. **G–I** 21st day after birth. **A**, **D**, **G** Hematoxylin and eosin staining. **B**, **E**, **H** BrdU immunohistochemistry. **C**, **F**, **I** *Griffonia simplicifolia* agglutinin (GSA)-II staining. In the 3rd day preparation, the first appearance of parietal cells is noticed in the immature fundic glands (**A**). Proliferative cells labeled with BrdU are scattered throughout the glands (**B**). GSA-II-labeled cells are located at the base of the immature glands (**C**). By the 14th day after birth, fundic glands are vividly growing (**D**), and the distribution of BrdU-labeled cells appears to shift to the mid-portion of the glands (**E**). GSA-II reactive cells increase in number and are situated at the basal portion of the growing fundic glands (*double arrows*) (**F**). By the 21st day after birth, fundic glands become quite similar to the adult ones. Chief cells with basophilic cytoplasm appear at the basal portion of the fundic glands (**G**). BrdU-labeled cells (*arrows*) mostly situated within the isthmus portion of the glands are forming the proliferative zone (**H**), and the majority of GSA-II-reactive cells are located at the neck portion, beneath the proliferative zone (**I**). *Bars*=30 μm

Comparison of the ulcer healing process with the normal developmental changes of fundic glands

Postnatal 3rd day preparation revealed that immature fundic glands consisted mainly of surface mucous cells, parietal cells, and gland-type mucous cells at the bottom portion of it. Proliferative cells were seen to be scattered throughout the glands. Topological cellular distribution of the immature fundic glands was quite compatible with that of the regenerating foveolate glands observed at the ulcer margin at day 7 following cryo-injury. Postnatal 14th day preparation showed the growing fundic glands, where BrdU-labeled proliferative cells appeared to shift to the mid-portion of the glands [35], but GSA-II-reactive gland-type mucous cells were still localized at the basal portion [14]. These patterns of cellular distribution characteristically resembled those of the regenerating fundic glands found on the 30th day to 90th day after the cryo-injury.

Taken together, we propose that the natural history of the gastric ulcer healing follows pathways that correspond to normal development of fundic glands, because the transient change of regenerating mucosa in the fundic area is not likely to be referred to as the pseudopyloric gland. It will be interesting to define further characteristics of the regenerating mucosa of human stomach.

Acknowledgements We are grateful to Soyuki Ide, Eiko Matsuura (Department of Anatomy, Miyazaki Medical College, University of Miyazaki) and Yoshiteru Goto (Division of Electron Microscopy, Central Research Laboratories, Miyazaki Medical College, University of Miyazaki) for their expert assistance and to Mr. H. K. Barman for his editorial reading. This research was supported by Grants-in-Aid for 21st Century COE Program (Life Science) from the Ministry of Education, Culture, Sports, Science and Technology (MEXT) of Japan, for Scientific Research from the MEXT of Japan (08670024), and from the Japan Society for the Promotion of Science (1370019).

References

1. Alison MR, Chinery R, Poulsom R, Ashwood P, Longcroft JM, Wright NA (1995) Experimental ulceration leads to sequential expression of spasmolytic polypeptide, intestinal trefoil factor, epidermal growth factor and transforming growth factor alpha mRNAs in rat stomach. J Pathol 175:405–414
2. Allen A, Flemstrom G, Garner A, Kivilaakso E (1993) Gastroduodenal mucosal protection. Physiol Rev 73:823–857
3. Blom H (1985) The structure of normal and regenerating rat oxyntic mucosa. Scand J Gastroenterol 110[Suppl]:73–80
4. Blom H, Helander HF (1981) Quantitative ultrastructural studies on parietal cell regeneration in experimental ulcers in rat gastric mucosa. Gastroenterology 80:334–343
5. Falk P, Roth KA, Gordon JI (1994) Lectins are sensitive tools for defining the differentiation programs of mouse gut epithelial cell lineages. Am J Physiol 266:G987–G1003
6. Ferguson AN (1928) A cytological study of the regeneration of gastric glands following the areas of mucosa. Am J Anat 42: 403–441
7. Goldenring JR, Ray GS, Coffey RJ, Meunier PC, Haley PJ, Barnes TB, Car BD (2000) Reversible drug-induced oxyntic atrophy in rats. Gastroenterology 118:1080–1093
8. Hattori T, Fujita S (1976) Tritiated thymidine autoradiographic study on cellular migration in the gastric gland of the golden hamster. Cell Tissue Res 172:171–184
9. Hayashida H, Ishihara K, Ichikawa T, Kurihara M, Saigenji K, Hotta K (2000) Alteration of mucins in rat gastric mucosa healing from acetic acid-induced ulcer: an immunohistochemical study using monoclonal antibodies against gastric mucins. Biomed Res 21:95–103
10. Hayashida H, Ishihara K, Ichikawa T, Okayasu I, Kurihara M, Saigenji K, Hotta K (2001) Expression of a specific mucin type recognized by monoclonal antibodies in the rat gastric mucosa regenerating from acetic acid-induced ulcer. Scand J Gastroenterol 36:467–473
11. Helander HF (1983) Morphological studies on the margin of gastric corpus wounds in the rat. J Submicrosc Cytol 15:627–643
12. Helander HF, Weijdegard B, Bamberg K (1996) The expression of pepsinogen C mRNA in normal gastroduodenal mucosa and the gastric ulcer margin of the rat. Histochem Cell Biol 105:163–169
13. Helpap B, Hattori T, Gedigk P (1981) Repair of gastric ulcer. A cell kinetic study. Virchows Arch 392:159–170
14. Ihida K, Suganuma T, Tsuyama S, Murata F (1988) Glycoconjugate histochemistry of the rat fundic gland using *Griffonia simplicifolia* agglutinin-II during the development. Am J Anat 182:250–256
15. Karam SM, Leblond CP (1993) Dynamics of epithelial cells in the corpus of the mouse stomach. I. Identification of proliferative cell types and pinpointing of the stem cell. Anat Rec 236:259–279
16. Karam SM, Leblond CP (1993) Dynamics of epithelial cells in the corpus of the mouse stomach. III. Inward migration of neck cells followed by progressive transformation into zymogenic cells. Anat Rec 236:297–313
17. Kasamo H, Yang DH, Tsuyama S, Ge YB, Murata F (1996) Ontogeny of proliferative cells in the rat fundic gland. Acta Anat Nippon 71:20–29
18. Li Q, Karam SM, Gordon JI (1996) Diphtheria toxin-mediated ablation of parietal cells in the stomach of transgenic mice. J Biol Chem 271:3671–3676
19. Mowry RW (1963) The special value of methods that color both acidic and vicinal hydroxyl groups in the histochemical study of mucins with revised directions for the colloidal iron stain, the use of alcian blue 8GX and their combinations with the periodic acid-Schiff reaction. Ann N Y Acad Sci 106:402–423
20. Owen DA (1997) Stomach. In: Sternberg SS (ed) Histology for pathologists. Lippincott–Raven, Philadelphia, pp 481–493
21. Schmassmann A, Reubi JC (2000) Cholecystokinin-B/gastrin receptors enhance wound healing in the rat gastric mucosa. J Clin Invest 106:1021–1029
22. Schmassmann A, Stettler C, Poulsom R, Tarasova N, Hirschi C, Flogerzi B, Matsumoto K, Nakamura T, Halter F (1977) Roles of hepatocyte growth factor and its receptor Met during gastric ulcer healing in rats. Gastroenterology 113:1858–1872
23. Spicer SS (1965) Diamine methods for differentiating mucosubstances histochemistry. J Histochem Cytochem 13:211–234
24. Suganuma T, Suzuki S, Tsuyama S, Murata F (1981) Mucosubstances of the rat gastric mucosa studied by means of several histochemical methods. Acta Histochem Cytochem 14: 534–548
25. Suganuma T, Tsuyama S, Murata F (1985) Glycoconjugate cytochemistry of the rat fundic gland using lectin/colloidal gold conjugates and Lowicryl K4 M. *Helix pomatia* lectin is a specific marker for mucous neck cells in fundic glands of the rat gastric mucosa. Histochemistry 83:489–495
26. Suzuki S, Tsuyama S, Murata F (1983) Cells intermediate between mucous neck cells and chief cells in rat stomach. Cell Tissue Res 233:475–484
27. Tahara E (1971) Regeneration of the gastric epithelia in mice; an electron microscopic study. Hiroshima J Med Sci 20:65–99
28. Tanabe H, Yokota K, Kohgo Y (1999) Localization of syndecan-1 in human gastric mucosa associated with ulceration. J Pathol 187: 338–344
29. Tarnawski A, Szabo IL, Husain SS, Soreghan B (2001) Regeneration of gastric mucosa during ulcer healing is triggered by growth factors and signal transduction pathways. J Physiol Paris 95:337–344
30. Townsend SF (1961) Regeneration of gastric mucosa in rats. Am J Anat 109:133–147
31. Wong WM, Playford RJ, Wright NA (2000) Peptide gene expression in gastrointestinal mucosal ulceration: ordered sequence or redundancy? Gut 46:286–292
32. Wright NA, Pike C, Elia G (1990) Induction of a novel epidermal growth factor-secreting cell lineage by mucosal ulceration in human gastrointestinal stem cells. Nature 343:82–85
33. Yamada K (1972) Dual staining methods for the light microscopic histochemistry of mucosaccharides. Connect Tissue 5: 1–8
34. Yang DH, Tsuyama S, Ge YB, Wakamatsu D, Ohmori J, Murata F (1997) Proliferation and migration kinetics of stem cells in the rat fundic gland. Histol Histopathol 12:719–727
35. Yeomans ND, Trier JS (1976) Epithelial cell proliferation and migration in the developing rat gastric mucosa. Dev Biol 53:206–216

Virchows Arch (2004) 445:589–596
DOI 10.1007/s00428-004-1118-x

ORIGINAL ARTICLE

Thomas Longerich · Kai Breuhahn · Margarete Odenthal · Katharina Petmecky · Peter Schirmacher

Factors of transforming growth factor β signalling are co-regulated in human hepatocellular carcinoma

Received: 3 August 2004 / Accepted: 4 August 2004 / Published online: 29 September 2004
© Springer-Verlag 2004

Abstract Transforming growth factor β (TGFβ) is a central mitoinhibitory factor for epithelial cells, and alterations of TGFβ signalling have been demonstrated in many different human cancers. We have analysed human hepatocellular carcinomas (HCCs) for potential pro-tumourigenic alterations in regard to expression of Smad4 and mutations and expression changes of the pro-oncogenic transcriptional co-repressors Ski and SnoN, as well as mRNA levels of matrix metalloproteinase-2 (MMP2), which is transcriptionally regulated by TGFβ. Smad4 mRNA was detected in all HCCs; while, using immunohistology, loss of Smad4 expression was found in 10% of HCCs. Neither mutations in the transformation-relevant sequences nor significant pro-tumourigenic expression changes of the Ski and SnoN genes were detected. In HCC cell lines, expression of both genes was regulated, potentially involving phosphorylation. Ski showed a distinct nuclear speckled pattern, indicating recruitment to active transcription complexes. MMP2 mRNA levels were increased in 19% of HCCs, whereas MMP2 mRNA was not detectable in HCC cell lines, suggesting that MMP2 was derived only from tumour stroma cells. Transcript levels of Smad4, Ski, SnoN and MMP2 correlated well. These data argue against a significant role of Ski and SnoN in human hepatocarcinogenesis and suggest that, in the majority of HCCs, the analysed factors are co-regulated by an upstream mechanism, potentially by TGFβ itself.

Keywords HCC · TGF-beta · Ski · SnoN · Smad4

T. Longerich · K. Breuhahn · M. Odenthal · K. Petmecky · P. Schirmacher
Institute of Pathology,
University of Cologne,
Joseph-Stelzmann-Strasse 9, 50931 Cologne, Germany

P. Schirmacher
Center for Molecular Medicine Cologne,
University of Cologne,
Joseph-Stelzmann-Strasse 9, 50931 Cologne, Germany

T. Longerich · K. Breuhahn · P. Schirmacher (✉)
Institute of Pathology, Department of General Pathology,
University of Heidelberg,
Im Neuenheimer Feld 220, 69120 Heidelberg, Germany
e-mail: peter.schirmacher@med.uni-heidelberg.de
Tel.: +49-6221-562601
Fax: +49-6221-56-5251

Introduction

Alterations of transforming growth factor (TGF)β signalling are frequent pro-tumourigenic molecular changes and have been documented in a wide variety of human malignancies [32]. For example, TGFβ type-II receptor mutations are frequently found in colon cancer [17], and Smad4-inactivating mutations are often present in carcinomas of the exocrine pancreas [8, 33]. Since TGFβ is a central mitoinhibitory factor for non-neoplastic hepatocytes, inactivation of TGFβ signalling may also support hepatocarcinogenesis. Surprisingly, TGFβ type-II receptor mutations are rare in human hepatocellular carcinomas (HCCs), and Smad4 mutations have been found only in approximately 10% of HCCs [10, 35]. Recently, several co-factors important for regulation of TGFβ-induced transcription, such as the oncogenes Ski and SnoN, have been identified, some of them acting as negative-feedback regulators [21, 28, 29]. The *v-ski* gene is a retroviral oncogene, which transforms chicken embryonic fibroblasts [13]. The human *ski* gene is located on chromosome $1p_{36.2–36.3}$ and codes for a 95-kDa protein, consisting of 728 amino acids [6, 22, 30]. Ski is expressed in rhabdomyosarcomas and neuroblastoma cell lines, as well as in carcinomas of the stomach, thyroid, lung, prostate, chorionepithelium and vulva [4, 22]. In malignant melanomas, Ski is overexpressed [7, 24]. The *sno* gene represents another human member of the *ski* gene family, consists of 684 amino acids and has a molecular weight of 77 kDa [22, 23]. High SnoN levels have been reported in carcinoma cells of the stomach, thyroid and lung [22]. In squamous cell carcinomas of the oesophagus, the locus 3q26, the position of the SnoN gene, is frequently amplified [9]. The sequences governing the transforming

potential of both proteins are mainly represented by exon 1 of both genes [37]. Matrix metalloproteinase-2 (MMP2) is involved in remodelling of basement membranes and supports the invasive and metastatic behaviour of tumour cells [14, 26]. Increased expression levels of MMP2 have been described in human HCCs [19]. In non-neoplastic liver, MMP2 is mainly localised in hepatic stellate cells and fibroblasts of fibrotic tissues [20, 36]. Although the exact mode of MMP2 activation is still unclear, it is transcriptionally regulated by TGFβ in a delayed fashion [31].

We have analysed human HCCs for alterations in central TGFβ signalling and effector molecules, including Smad4, the transcriptional co-repressors Ski and SnoN and the transcriptional target gene MMP2. Ski and SnoN lacked transformation-relevant changes, but all analysed factors were co-regulated, which may be due to upstream regulation, potentially by TGFβ itself.

Materials and methods

Tissue samples and cell lines

Snap-frozen tissue samples for mRNA analyses were obtained from 32 HCCs, 4 peri-tumourous liver tissues and 3 normal adult liver tissues. The panel included HCCs induced by hepatitis B virus (n=3), hepatitis C virus (n=9), chronic alcohol abuse (n=5), genetic haemochromatosis (n=1) and 14 HCCs of unknown aetiology. RNA extraction was performed using Rneasy Mini-Kit (Qiagen, Hilden, Germany) according to the manufacturer's guidelines and controlled spectrophotometrically.

For protein analyses, total cellular protein was extracted using ice-cold RIPA-buffer (1×phosphate-buffered saline, 1% Ipegal CA-630; Sigma, Deisenhofen, Germany) with 20 μl of a proteinase-inhibitor cocktail (Sigma). After incubation on ice for 1 h, lysates were centrifuged, and the supernatants were collected. The analysed panel consisted of 11 HCCs, 4 peri-tumourous liver tissues, 4 human liver cancer cell lines and 1 normal adult control. Cell lines HepG2, HuH7 and SK-Hep1 were cultured in RPMI 1640-medium (Biochrom, Berlin, Germany) supplemented with 10% foetal calf serum (Sigma) and 1% penicillin-streptomycin (10 mg/ml, Sigma). Hep3B cells were cultured in MEM-Earle (Biochrom) with the same supplements. Cells were cultured at 37°C (5% CO_2) and were passaged every 3–4 days.

Reverse-transcription polymerase chain reaction, sequencing and real-time polymerase chain reaction

From total RNA, 1 μg was reverse transcribed using random primers. Afterwards, 1 μl of the product was used as a template for further analyses. For amplification of exons 1 of the Ski and SnoN genes, two overlapping primer sets were generated, respectively. The analysed segments spanned positions 210–1029 of the Ski gene (Genebank accession number X15218) and positions 721–1829 of the SnoN gene (number X15219). The following primer pairs were used: *ski* 1-forward 5′-CTACAAGAAGGAGAGCGCCAAG–3′ and reverse 5′-gatgcc-catgactttgaggatc-3′, *ski* 2-forward 5′-GATCCTCAAAGTCATGGGCATC-3′ and reverse 5′-ccgcttgtacttgttgccatag-3′, *snoN* 1-forward 5′-CCAGAC-AAATTTCTCCTTGGTTCAG-3′ and reverse 5′-TCGGAGAACAGAATTTAAGAC-TTGGG-3′ and *snoN* 2-forward 5′-CCCATTGCTCATCCCTTCAGATAGCT-3′ and reverse 5′-CCATTCCTGATGGTGCATCTGTCTTG-3′.

The following temperature profiles were used: *ski* 94°C for 1 min followed by 56°C for 1 min and 72°C for 1 min, *snoN* 94°C for 1 min followed by 58°C (*snoN* 1) or 64°C (*snoN* 2). The amplicons were bi-directionally sequenced after 5′-IRD800-labelling (MWG, Ebersberg, Germany) using the following primer pairs: *ski* 1-forward 5′-CTACAAGAAGGAGAGCGCC-3′ and reverse 5′-TGACTT-TGAGGATCTCCAGC-3′, *ski* 2-forward 5′-CAAAGTCATGGGCATCCT-3′ and reverse 5′-GTACTTGTTGCCATAGTCGA-3′, *snoN* 1-forward 5′-AATTTCTCC-TTGGTTCAGGG-3′ and reverse 5′-ATTCCCCTTCCAACACAGTC-3′, *snoN* 2-forward 5′-CATCCCTTCAGATAGCTCCA-3′ and reverse 5′-TGGTGCATCTGTCTTGGAT-3′.

The temperature profile chosen was 95°C for 30 s followed by 60°C for 30 s and 72°C for 45 s for 30 cycles. Sequence analyses were performed using 1 μl of 5′-IRD800-labelled amplicon by a LiCOR Biotech Analyser Gene Reader 4200 (MWG) under the following conditions: 1500 V, 37 mA, 50 W and 50°C. Gels were first analysed visually, followed by computer-assisted analyses using DNasis version 2.1 (Hitachi, Tokyo, Japan).

Semi-quantitative real-time polymerase chain reaction (PCR) was performed with 18 s rRNA as the housekeeping gene by a ABI PRISM 7700 Sequence Detection System (software version 1.7; PE Biosystems, Foster City, CA, USA) according to the manufacturer's guidelines, using the following primer and probe combinations: *ski* forward (2347–2365) 5′-GCAGCCCACACAGCACAAC-3′, probe (2368–2400) 5′-CTTACCGTGCCTATTACCAAGCGAGTGTTTGTA-3′ and reverse (2467–2448) 5′-GGACGCGGCTTACTCACTTG-3′, *snoN* forward (1355–1375) 5′-CCATCCTGTGGGCTGATTACA-3′, probe (1394–1423) 5′-TTATGTAATGCTTTATTGCGG-CCACGAACT-3′ and reverse (1496–1477) 5′-CAAAGGCACTGCCAGTTTCC-3′, *smad4* (#NM_005359) forward (1064–1085) 5′-ACCTAATTTGCCTCACCACCAA-3′, probe (1129–1157) 5′-GACATTACTGGCCTGTTCACAATGAGCTT-3′ and reverse (1193–1172) 5′-AGGAGCAGGATGATTGGAAATG-3′, *mmp2* (#NM_004530) forward (1084–1103) 5′-TGAGAAGGATGGCAAGTACG-3′, probe (1149–1173) 5′-AAGGACAGCCCTGCAAGTTTCCATT-3′ and reverse (1212–1193) 5′-TCAGTG-GTGCAGCTGTCATA-3′, *18 s* rRNA (#X03205) forward (447–466) 5′-AAACGGCTA-CCACATCCAAG-3′, probe (473–492) 5′-AGCAGGCGCGCAAAT-TACCC-3′ and reverse (601–582) 5′-CCTCCAATGGATCCTCGTTA-3′. The respective thresholds (0.15 for Ski and SnoN, 0.02 for Smad4 and MMP2 and 0.01 for 18 s rRNA) were set in the linear amplification phase of the PCR reaction. The values for comparison were obtained by first normalising against 18 s rRNA and afterwards against a human adult liver tissue sample.

Immunohistology

Immunostaining was performed on 6-μm sections of snap-frozen liver tissues or cytospins of cell lines, respectively. For the detection of Ski, a monoclonal mouse anti-human Ski antibody (clone G8, Alexis Biochemicals, Grünberg, Germany; dilution 1:100) was used. After incubation at 4°C overnight, immunohistology was carried out using the labelled streptavidin biotin method (Dako, Glostrup, Denmark) according to the manufacturer's guidelines. Counterstaining was performed using hemalum.

Tissue microarray design and analyses

Overall, 128 samples were included in this study, including 5 normal control livers, 13 cirrhotic liver tissues, 30 dysplastic nodules (DNs, 21 low and 9 high grade) from 10 patients, 9 peritumourous and 71 different HCCs (Grading: 25 G1, 37 G2, and 9 G3) from 52 patients. All cases were surgically resected at the University of Cologne and histologically graded by two pathologists, independently.

For tissue microarray analysis (TMA), design samples were fixed in 10% neutral-buffered formalin and embedded in paraffin, followed by conventional preparation of 3-µm sections and haematoxylin/eosin staining. Vital and representative tumour regions were selected for punch cylinder (0.6 mm diameter) transfer from

donor to recipient paraffin blocks using a tissue-arraying instrument (Beecher Instruments, Silver Spring, MD, USA). Two different and representative regions of each tissue sample were punched and analysed separately to minimise staining artefacts and to control for intratumoural variability. Consecutive 5-μm sections of the recipient blocks were made with a conventional microtome and processed according to the manufacturer's instructions. Monoclonal mouse anti-human Smad4 antibody (clone B8, Santa Cruz Biotechnology, Santa Cruz, USA) was diluted 1:50. After overnight incubation at 4°C, immunohistochemical detection was carried out using the EnVision method (Dako) according to the manufacturer's guidelines. Counterstaining was performed using hemalum. The immunohistological reaction was evaluated separately for cytoplasmic and nuclear localisation. Cytoplasmic staining was scored semi-quantitatively by subdividing mild, moderate, intensive or no staining, whereas nuclear staining was scored according to the percentage of positive nuclei (0=no staining, + <35%, ++ 35–65%, +++ >65%).

Western immunoblot analyses

Western immunoblot analyses were performed by 6% sodium dodecyl sulphate polyacrylamide gel electrophoresis (SDS-PAGE) [2.6 ml H_2O, 1 ml 30% acrylamide-mix (Serva, Heidelberg, Germany), 1.3 ml 1.5 M Tris (pH 8.8), 50 μl 10% SDS, 50 $(NH_4)_2S_2O_8$ and 4 μl TEMED] for Ski and 8% SDS-PAGE for Sno. Protein concentrations were determined by Bradford assay after Coomassie blue staining (Biorad, Munich, Germany). Each slot was loaded with 20 μg of protein extract. Specific protein detection was achieved with anti-human Ski (clone H-329, Santa Cruz) or Sno antibodies (Upstate Biotechnology, Waltham, MA, USA) followed by detection with horseradish peroxidase-conjugated secondary antibodies. After intense washing, visualisation was performed with specific luminescence [9 ml water, 500 μl 20× H_2O_2, 500 μl 20× LumiGlo (Cell Signaling Technology, Beverly, MA, USA)] and recorded with Kodak-BioMax-ML film. For control purposes, the filters were reincubated with anti-β-actin antibodies.

Statistical analyses

Statistical analyses were performed by Spearman's correlation or *t*-test (paired/unpaired) using SPSS 11.0 software (SPSS 11.0, Chicago, Illinois, USA), depending on the groups to be tested. $P<0.05$ was considered significant.

Table 1 Smad4, Ski, SnoN and matrix metalloproteinase-2 (MMP2) mRNA expression in human hepatocellular carcinomas (HCCs) and liver tumor cell lines. *TU* tumor sample, *PT* peritumourous sample of the same case, *NA* not analysed

Samples	Smad4	Ski	SnoN	MMP2
Normal liver	1.000	1.000	1.000	1.000
A	0.298	0.701	0.478	7.744*
B-TU	0.118	0.323	0.398	0.683
B-PT	0.278	0.357	0.630	0.593
C-TU	0.062	0.002	0.001	0.158
C-PT	0.021	0.003	0.001	0.105
D-TU	0.373	0.229	0.754	0.893
D-PT	0.437	0.246	0.796	0.450
3	0.298	0.330	0.190	0.291
4	0.524	0.162	0.525	0.214
6	1.441	1.309	2.000*	4.493*
7	0.144	0.315	0.211	0.098
9	0.445	NA	NA	1.670
10	0.130	0.190	0.226	4.990*
11	0.329	0.225	0.114	0.540
13	0.601	1.407	0.919	0.282
15	0.639	3.701*	1.656	12.270*
30	0.455	0.489	0.447	0.993
35	0.283	0.132	0.179	0.335
39	0.228	0.387	0.394	0.309
40	0.316	0.451	0.719	2.800*
42	0.328	0.923	0.432	1.762
46	0.390	0.334	0.429	0.150
49	0.285	0.322	0.313	0.502
50	0.213	0.100	0.133	1.133
51	0.457	0.258	0.279	0.184
53	0.172	0.170	0.052	0.192
60	0.043	0.057	0.081	0.284
61	0.773	NA	NA	8.469*
62	0.102	0.085	0.049	0.072
63	0.242	0.183	0.189	0.226
65	0.107	0.624	0.467	0.250
66	0.102	0.048	0.111	0.197
69	0.098	0.048	0.029	0.473
70	0.036	0.101	0.017	0.009
73	0.122	0.178	0.137	0.169
Hep3B	0.071	0.147	0.211	0.000
HepG2	0.087	0.168	0.041	0.003
HuH7	0.046	4.157*	1.391	0.000

* Increased expression

Results

Smad4 expression in human HCCs

To analyse the expression of the Smad4 gene in human HCCs, we performed semi-quantitative TaqMan reverse transcription (RT)-PCR and immunohistology. Semi-quantitative TaqMan RT-PCR was normalised for 18S rRNA and showed that all 32 HCCs expressed *smad4* mRNA (Table 1). Interestingly, in 84% of HCCs, *smad4* mRNA levels were reduced to less than 50% of the expression in normal human liver. Only 16% of HCCs showed *smad4* mRNA levels comparable with normal control livers. Overexpression of *smad4* was not observed (Fig. 1). In conclusion, *smad4* mRNA was present in all HCCs, but levels were significantly reduced in the majority of HCCs.

Smad4 protein expression was determined immunohistologically using TMA. Of HCCs, 90.1% (64/71) showed Smad4 reactivity in tumour cells, whereas 7 HCCs (9.9%) were completely negative for Smad4 (Fig. 2). Smad4 positivity was detected in hepatocytes of all normal control livers, cirrhotic livers and peri-tumourous liver tissues. In HCCs, cytoplasmic Smad4 staining was predominantly mild (+=73.2%, ++=14.1%, +++=11.3%). Nuclear Smad4 signals were present in 46.5% (33/71) of HCCs (+=28.2%, ++=7%, +++= 11.3%). All cytoplasmic-negative cases also lacked nuclear Smad4 expression. Using unpaired *t*-test, there was no statistical significant difference in Smad4 expression among benign, premalignant and malignant liver tissue samples. Whereas complete loss of Smad4 reactivity was not observed in non-tumourous liver tissue samples, 3.3% of DNs (1/30), 4% of G1 (1/25), 10.8% of G2 (4/37) and 22.2% (2/9) of G3 HCCs were completely negative for Smad4. Although the frequency increased with dedifferentiation, the difference did not reach statistical significance ($P>0.05$). In summary, complete loss of

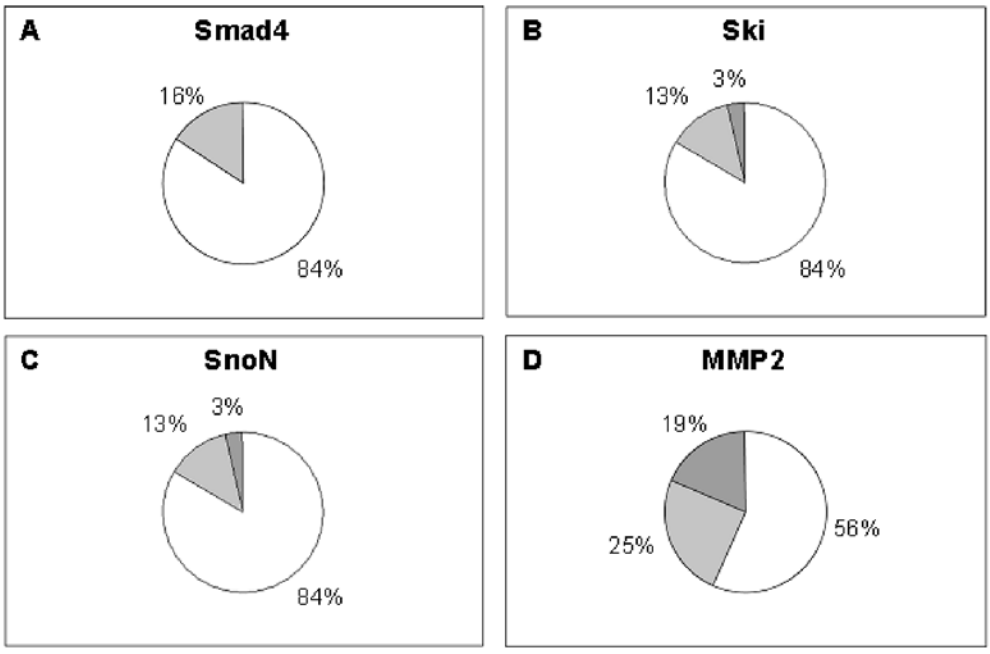


Fig. 1 Distribution of expression levels of Smad4 (**A**), Ski (**B**), SnoN (**C**) and MMP2 (**D**) in human hepatocellular carcinomas. *White* represents reduced expression, *pale grey* represents expression comparable with normal human liver and *grey* represents increased expression

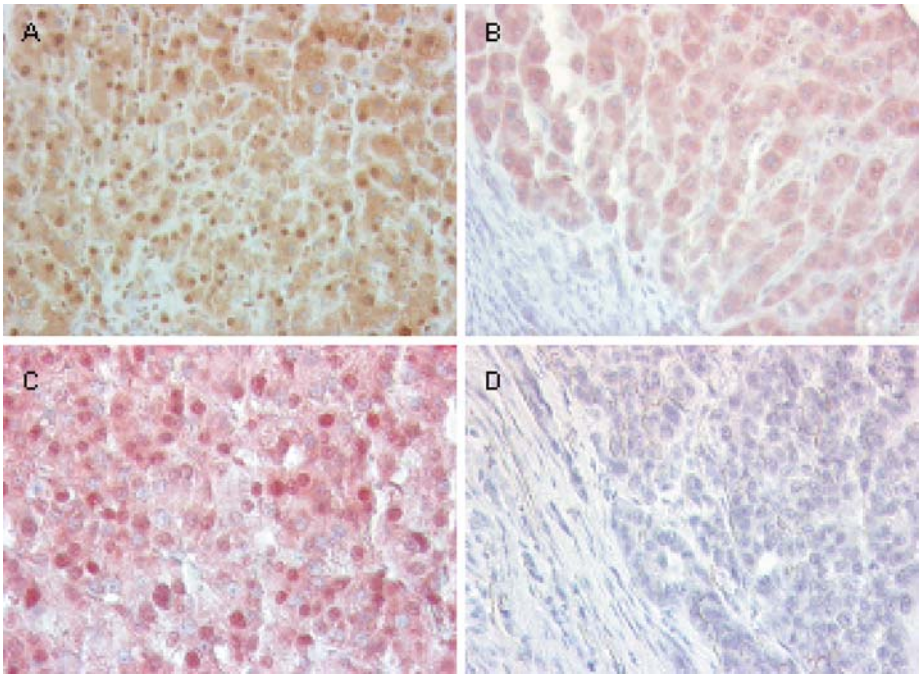


Fig. 2 Smad4 expression in human hepatocellular carcinomas (HCCs). **A** Normal liver with weak cytoplasmic and strong nuclear Smad4 reactivity. **B** Cirrhotic liver with moderate cytoplasmic and weak nuclear Smad4 expression. **C** HCC with strong nuclear and moderate cytoplasmic Smad4 signal. **D** Smad4-negative HCC (original magnification ×250)

Smad4 protein expression in tumour cells was infrequent but showed a tendency to increase in frequency with dedifferentiation.

Expression of *ski* and *snoN* in human HCCs

We determined *Ski* and *SnoN* mRNA levels using semi-quantitative TaqMan real-time PCR. *Ski* and *SnoN* mRNAs were expressed in all samples. Overall, we did not detect significant (more than two-fold) upregulation of *ski* and *snoN* mRNA levels in human HCCs and HCC cell lines, with the exception of one case for each gene, which expressed moderately increased Ski and SnoN mRNA levels (2- and 3.7-fold, respectively) and the HCC cell line HuH7, which showed somewhat higher Ski mRNA levels (Table 1). Most HCCs (84%) showed reduced levels of Ski or SnoN mRNA. In all cases, mRNA levels of tumourous and the respective peri-tumourous liver tissues were comparable (Fig. 3). There was no correlation between the mRNA levels and HCC aetiology or grading (data not shown), but a significant correlation between *smad4* and *ski* mRNA levels (Spearman's rho (r)=0.686, $P<0.001$) and *smad4* and *snoN* expression (r=0.779, $P<0.001$), as

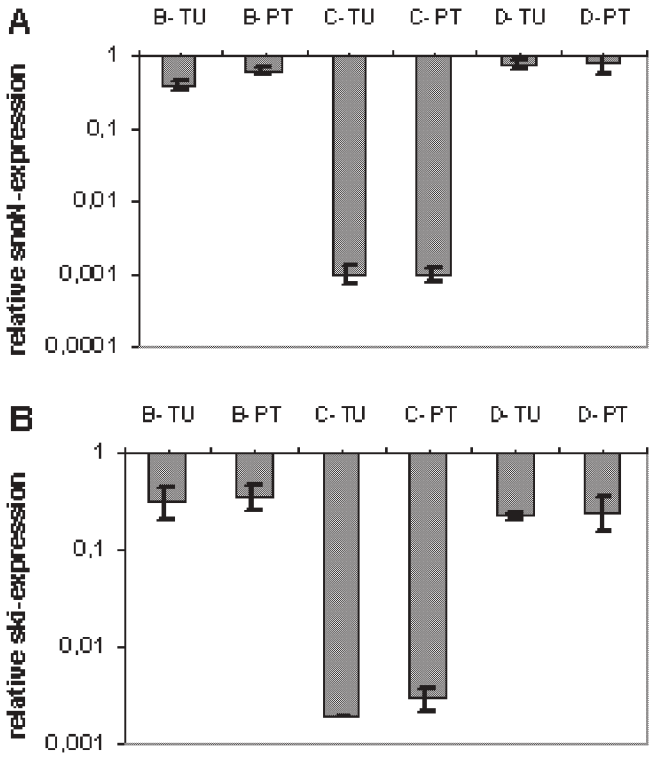


Fig. 3 Ski (**A**) and SnoN (**B**) mRNA expression in tumourous and peri-tumourous liver tissue. Because of very low expression levels in tissue **C**, a logarithmic scale was used for illustration. There was no significant difference between tumourous and peri-tumourous tissues ($P>0.05$)

well as *ski* and *snoN* expression, was observed (r=0.850, $P<0.001$).

Ski and SnoN proteins were found in all HCC cell lines. Ski protein was detected at approximately 100 kDa using Western immunoblots (Fig. 4) and immunohistology in tumour cell nuclei showing a speckled pattern (Fig. 5). Using Western immunoblot, Sno protein was found at 90 kDa, sometimes with an additional band at 80 kDa (Fig. 4). Expression differed among the cell lines and in regard to cell growth. Although differences in expression levels were obvious, there was no general correlation with cell growth.

Mutational analysis of *ski* and *snoN* genes

To detect potential tumour-associated mutations in the *ski* and *snoN* genes, we analysed the regions that have previously been shown to be relevant for malignant transformation in 32 HCCs. They have been mapped to the N-terminal of 300 amino acids, which are represented by the exons 1 of the *ski* and *snoN* genes, respectively [37].

In none of the HCC tissues the analysis of the *ski* gene revealed any difference when compared with the published sequence (Table 2). Frequently, *snoN* sequences showed a substitution of thymidine instead of cytosine at base position 822, which represents a previously described sequence polymorphism [22] and leads to a conservative amino acid substitution from valine to alanine on position 38 of the SnoN protein. This alteration was observed in normal adult liver (2/3), one HCC cell line and 32% of the analysed HCCs (6/19). When tumourous and non-tumourous tissues were compared, the respective sequences were always concordant.

MMP2 mRNA expression in human HCCs

Expression of *mmp2* mRNA in human HCCs was analysed semi-quantitatively in 32 HCCs. It was present in all cases. Of HCCs, 25% (8/32) did not show altered mRNA levels of *mmp2* (Fig. 1), whereas 56% (18/32) of HCCs showed reduced *mmp2* mRNA-concentration, and 19% (6/32) showed increased expression. There was a significant correlation among *mmp2*, *smad4*, *ski* and *snoN* mRNA levels (r=0.488, $P=0.05$; r=0.495, $P=0.005$, and

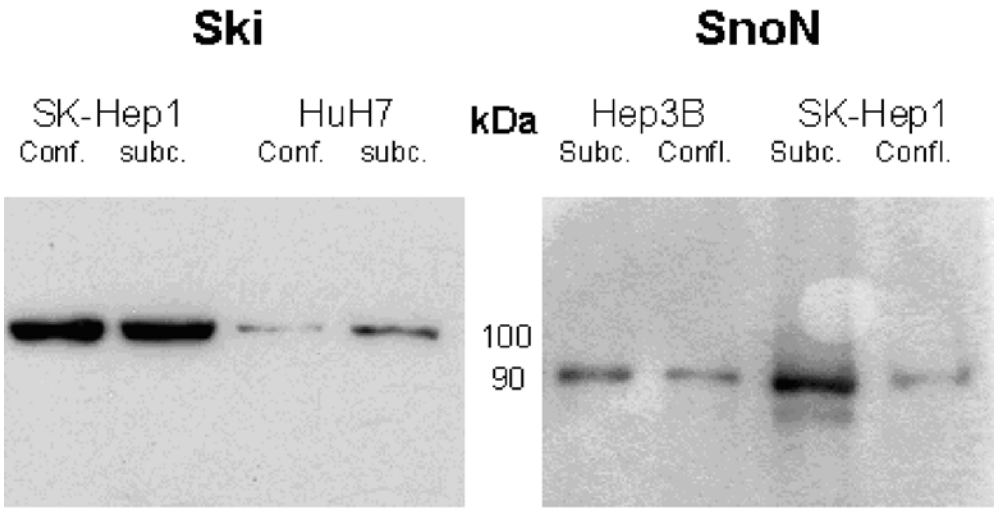


Fig. 4 Western immunoblot analysis of Ski and SnoN protein in human liver tumour cell lines

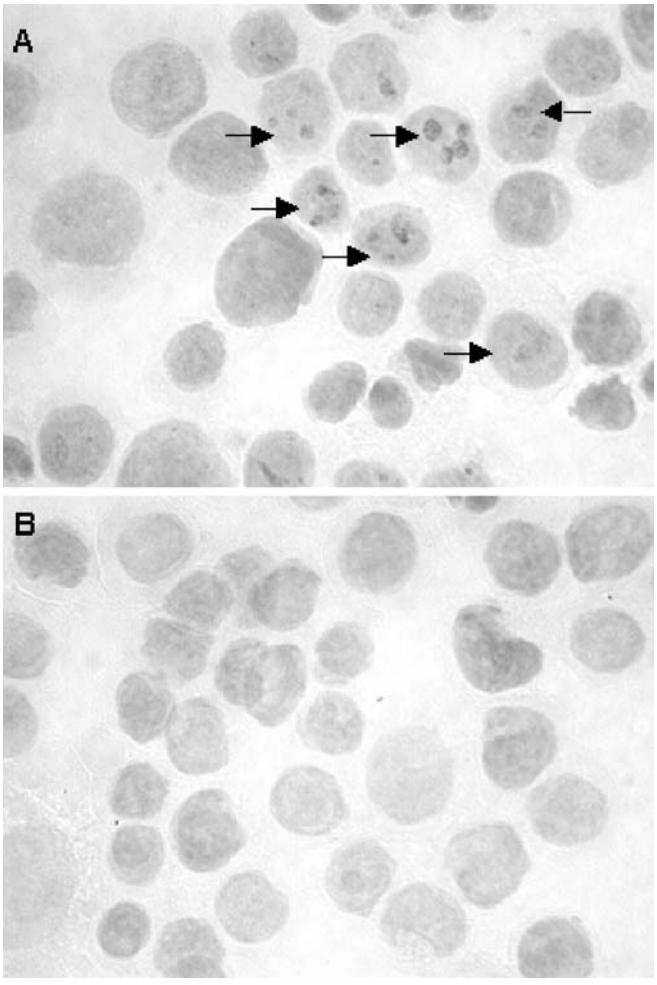


Fig. 5 Immunohistology for Ski (**A**) in the human hepatocellular carcinoma cell line HuH7. Ski is localised in distinct nuclear speckles (*arrows*). Negative control (**B**) (original magnification ×1000)

Table 2 Mutation analysis of *Ski* and *SnoN* genes in human hepatocellular carcinomas (HCCs) and liver tumor cell lines

Sample	Tissue	Ski/SnoN mutations	SnoN polymorphism T 822 C
a	Normal adult liver	∅	∅
b	Normal adult liver	∅	Heterozygous
c	Normal adult liver	∅	Heterozygous
1	HCC	∅	∅
1	Peri-tumourous liver tissue	∅	∅
2	HCC	∅	∅
2	Peri-tumourous liver tissue	∅	∅
3	HCC	∅	Heterozygous
3	Peri-tumourous liver tissue	∅	Heterozygous
4	HCC	∅	Heterozygous
4	Peri-tumourous liver tissue	∅	Heterozygous
5	HCC	∅	∅
6	HCC	∅	∅
7	HCC	∅	∅
8	HCC	∅	∅
9	HCC	∅	∅
10	HCC	∅	Homozygous
11	HCC	∅	Heterozygous
12	HCC	∅	∅
13	HCC	∅	Heterozygous
14	HCC	∅	∅
15	HCC	∅	∅
16	HCC	∅	∅
17	HCC	∅	∅
18	HCC	∅	∅
19	HCC	∅	Homozygous
Hep3B	HCC-cell line	∅	Heterozygous
HepG2	Hepatoblastoma-cell line	∅	∅
HuH7	HCC-cell line	∅	∅
SK-Hep1	Liver adenocarcinoma cell line	∅	∅

r=0.547, P=0.002, respectively). In HCC cell lines, *mmp2* mRNA was not detectable by TaqMan (data not shown).

Discussion

TGFβ may be tumour suppressive due to its anti-proliferative and differentiation-inducing potential. In contrast, during malignant progression, tumours may become resistant to this suppressive effect, and TGFβ may act pro-tumourigenic, especially by promoting tumour-associated neo-angiogenesis and invasion [12, 25]. Thus, it is tempting to hypothesise that inactivation of TGFβ-mediated growth inhibition may be a common pro-tumourigenic event. In accordance, alterations of TGFβ signalling are frequent in pancreatic adenocarcinoma, where Smad4 is inactivated in about 50% of cases [8]. Thus far, several alterations in TGFβ signalling have been identified in human hepatocarcinogenesis, but their frequency is low [10, 35]. Loss of Smad4 immunoreactivity reflects loss of function of the *smad4* gene with high sensitivity and specificity [34] and has been established as a useful marker in different tumour entities [3, 16, 18]. We found complete loss (nuclear and cytoplasmic) of Smad4 immunoreactivity in about 10% of HCCs, which was comparable with the data of Yakicier et al. [35], who found inactivating Smad4 mutations in less than 10% of HCCs. There was a tendency for loss of Smad4 immunoreactivity to occur more frequently in less-differentiated HCCs, although the changes did not reach statistical significance. All other cases with detectable Smad4 expression did not show any significant differences in regard to subcellular localisation, suggesting largely intact nuclear-cytoplasmic shuttling of Smad4. The fact that *smad4* mRNA was detectable in all cases analysed was most likely due to the expression of *smad4* mRNA by non-neoplastic stroma cells.

Ski and SnoN are negative-feedback regulators of TGFβ signalling [2, 27, 28], and their overexpression may induce malignant transformation [5]. In both genes, the transformation-relevant domains are coded by exon 1 [37]. We did not detect any mutation in these regions, suggesting the structural potential for intact Ski/SnoN–

Smad4 interaction. The known polymorphism T822C of the *snoN* gene [22], which results in a conservative amino acid substitution, was found in 36% of the samples. There is no indication for its pro-tumourigenic role: the sequences of tumourous and corresponding peri-tumourous tissues were always concordant, and the alteration was detectable in different non-tumourous control tissues. Ski and SnoN mRNA levels in HCCs tended to be lower than in normal adult liver, and there were no significant expression differences between tumourous and peri-tumourous tissues. Thus, mutations or expression changes of *ski* or *snoN* are unlikely to contribute significantly to human hepatocarcinogenesis.

In liver tumour cell lines, Ski protein was present at a size of 100 kDa, which was likely to represent a hyperphosphorylated form resulting from phosphorylation at three serine residues coded by exon 6 (aa 633, 664, 720) [22, 30]. There was regulation of Ski expression, since Ski protein concentrations differed significantly between subconfluent and confluent cultures of HCC cell lines, although no uniform tendency was present. Since we did not work with synchronised cell lines, this result may be explained by the data of Macdonald et al. [15], who were able to show that Ski protein levels are controlled post-translationally by cell cycle-dependent proteolysis, indicating intact feedback regulation of TGFβ signalling at least in HCC cell lines. The distinct sub-nuclear, speckled pattern of Ski in liver tumour cells was comparable with that observed in transformed, Ski-overexpressing fibroblasts [30], which corresponded to subnuclear structures in interchromatin regions of the nucleoplasm that are likely to include active transcription sites [11]. SnoN was detectable in cell lines at about 90 kDa, which was most likely a phosphorylated form (aa 563–565, 567, 584, 619). Additionally, a sometimes found 80-kDa form was most likely non-phosphorylated SnoN [23]. Thus, SnoN may experience differential post-translational phosphorylation in liver tumour cells. Although there is a general tendency for reduced Ski and SnoN expression, apparently both factors are regulated, and at least Ski remains involved in transcriptional regulation. Since overexpression of TGFβ_{1-3} has been described in human HCCs [1], and Ski and SnoN are known to be transcriptionally regulated by TGFβ, a likely candidate responsible for Ski and SnoN downregulation in human HCCs is TGFβ.

MMP2 mRNA, which is derived from non-parenchymal cells of HCCs [20] and was completely absent in liver tumour cell lines, was expressed by all HCCs at varying levels. Different expression levels may indicate differences in non-parenchymal cell content of the tumours, although stroma content is relatively low in HCCs in general and was also low in our HCCs, as judged by histology.

Positive correlation of mRNA levels for *mmp2*, *smad4*, *ski* and *snoN* indicates that all four genes may be transcriptionally regulated by a common (upstream) mechanism. Since expression is derived from different cell types (tumour versus stroma cells), a diffusible factor may act in a paracrine manner, further supporting the hypothesis that TGFβ, which is known to regulate transcription of all four genes, may be responsible.

Although these data do not allow one to conclude about the functional consequences, such as tumour growth, they suggest that central TGFβ-signalling molecules and cofactors (*smad4*, *ski*, *snoN*) are not or are only infrequently inactivated in HCCs and may still react to external stimulation and feedback regulation. Furthermore, Ski appears to become recruited to transcription complexes. Correlation of *smad4*, *ski*, *snoN* and *mmp2* mRNA levels argues for a common upstream regulation, potentially by TGFβ.

Acknowledgements The study was supported by grants from the Dr. Mildred-Scheel-Stiftung (10–1631-Schi I) and the Deutsche Forschungs-Gemeinschaft (Schi 273/4–1/2). We thank D. Lohfink for support in sequence analyses.

References

1. Abou-Shady M, Baer HU, Friess H, Berberat P, Zimmermann A, Graber H, Gold LI, Korc M, Buchler MW (1999) Transforming growth factor betas and their signaling receptors in human hepatocellular carcinoma. Am J Surg 177:209–215
2. Akiyoshi S, Inoue H, Hanai J, Kusanagi K, Nemoto N, Miyazono K, Kawabata M (1999) c-Ski acts as a transcriptional corepressor in transforming growth factor-beta signaling through interaction with smads. J Biol Chem 274:35269–35277
3. Argani P, Shaukat A, Kaushal M, Wilentz RE, Su GH, Sohn TA, Yeo CJ, Cameron JL, Kern SE, Hruban RH (2001) Differing rates of loss of DPC4 expression and of p53 overexpression among carcinomas of the proximal and distal bile ducts. Cancer 91:1332–1341
4. Colmenares C, Stavnezer E (1990) Structure and activities of the ski oncogene. Semin Cancer Biol 1:383–387
5. Colmenares C, Sutrave P, Hughes SH, Stavnezer E (1991) Activation of the c-ski oncogene by overexpression. J Virol 65:4929–4935
6. Colmenares C, Heilstedt HA, Shaffer LG, Schwartz S, Berk M, Murray JC, Stavnezer E (2002) Loss of the SKI proto-oncogene in individuals affected with 1p36 deletion syndrome is predicted by strain-dependent defects in Ski–/– mice. Nat Genet 30:106–109
7. Fumagalli S, Doneda L, Nomura N, Larizza L (1993) Expression of the c-ski proto-oncogene in human melanoma cell lines. Melanoma Res 3:23–27
8. Hahn SA, Schutte M, Hoque AT, Moskaluk CA, da Costa LT, Rozenblum E, Weinstein CL, Fischer A, Yeo CJ, Hruban RH, Kern SE (1996) DPC4, a candidate tumor suppressor gene at human chromosome 18q21.1. Science 271:350–353
9. Imoto I, Pimkhaokham A, Fukuda Y, Yang ZQ, Shimada Y, Nomura N, Hirai H, Imamura M, Inazawa J (2001) SNO is a probable target for gene amplification at 3q26 in squamous-cell carcinomas of the esophagus. Biochem Biophys Res Commun 286:559–565
10. Kawate S, Takenoshita S, Ohwada S, Mogi A, Fukusato T, Makita F, Kuwano H, Morishita Y (1999) Mutation analysis of transforming growth factor beta type II receptor, Smad2, and Smad4 in hepatocellular carcinoma. Int J Oncol 14:127–131
11. Lamond AI, Spector DL (2003) Nuclear speckles: a model for nuclear organelles. Nat Rev Mol Cell Biol 4:605–612
12. Letterio JJ, Roberts AB (1997) TGF-beta: a critical modulator of immune cell function. Clin Immunol Immunopathol 84:244–250
13. Li Y, Turck CM, Teumer JK, Stavnezer E (1986) Unique sequence, ski, in Sloan-Kettering avian retroviruses with properties of a new cell-derived oncogene. J Virol 57:1065–1072

14. Lin SW, Lee MT, Ke FC, Lee PP, Huang CJ, Ip MM, Chen L, Hwang JJ (2000) TGFbeta1 stimulates the secretion of matrix metalloproteinase 2 (MMP2) and the invasive behavior in human ovarian cancer cells, which is suppressed by MMP inhibitor BB3103. Clin Exp Metastasis 18:493–499
15. Macdonald M, Wan Y, Wang W, Roberts E, Cheung TH, Erickson R, Knuesel MT, Liu X (2004) Control of cell cycle-dependent degradation of c-Ski proto-oncoprotein by Cdc34. Oncogene 23: 5643–5653
16. Maitra A, Molberg K, Albores-Saavedra J, Lindberg G (2000) Loss of Dpc4 expression in colonic adenocarcinomas correlates with the presence of metastatic disease. Am J Pathol 157:1105–1111
17. Markowitz S, Wang J, Myeroff L, Parsons R, Sun L, Lutterbaugh J, Fan RS, Zborowska E, Kinzler KW, Vogelstein B et al (1995) Inactivation of the type II TGF-beta receptor in colon cancer cells with microsatellite instability. Science 268:1336–1338
18. McCarthy DM, Hruban RH, Argani P, Howe JR, Conlon KC, Brennan MF, Zahurak M, Wilentz RE, Cameron JL, Yeo CJ, Kern SE, Klimstra DS (2003) Role of the DPC4 tumor suppressor gene in adenocarcinoma of the ampulla of vater: analysis of 140 cases. Mod Pathol 16:272–278
19. McKenna GJ, Chen Y, Smith RM, Meneghetti A, Ong C, McMaster R, Scudamore CH, Chung SW (2002) A role for matrix metalloproteinases and tumor host interaction in hepatocellular carcinomas. Am J Surg 183:588–594
20. Musso O, Theret N, Campion JP, Turlin B, Milani S, Grappone C, Clement B (1997) In situ detection of matrix metalloproteinase-2 (MMP2) and the metalloproteinase inhibitor TIMP2 transcripts in human primary hepatocellular carcinoma and in liver metastasis. J Hepatol 26:593–605
21. Nakao A, Afrakhte M, Moren A, Nakayama T, Christian JL, Heuchel R, Itoh S, Kawabata M, Heldin NE, Heldin CH, ten Dijke P (1997) Identification of Smad7, a TGFbeta-inducible antagonist of TGF-beta signalling. Nature 389:631–635
22. Nomura N, Sasamoto S, Ishii S, Date T, Matsui M, Ishizaki R (1989) Isolation of human cDNA clones of ski and the ski-related gene, sno. Nucleic Acids Res 17:5489–5500
23. Pearson-White S, Crittenden R (1997) Proto-oncogene Sno expression, alternative isoforms and immediate early serum response. Nucleic Acids Res 25:2930–2937
24. Reed JA, Bales E, Xu W, Okan NA, Bandyopadhyay D, Medrano EE (2001) Cytoplasmic localization of the oncogenic protein Ski in human cutaneous melanomas in vivo: functional implications for transforming growth factor beta signaling. Cancer Res 61:8074–8078
25. Reiss M (1999) TGF-beta and cancer. Microbes Infect 1:1327–1347
26. Stetler-Stevenson WG, Aznavoorian S, Liotta LA (1993) Tumor cell interactions with the extracellular matrix during invasion and metastasis. Annu Rev Cell Biol 9:541–573
27. Stroschein SL, Wang W, Zhou S, Zhou Q, Luo K (1999) Negative feedback regulation of TGF-beta signaling by the SnoN oncoprotein. Science 286:771–774
28. Sun Y, Liu X, Eaton EN, Lane WS, Lodish HF, Weinberg RA (1999) Interaction of the Ski oncoprotein with Smad3 regulates TGF-beta signaling. Mol Cell 4:499–509
29. Sun Y, Liu X, Ng-Eaton E, Lodish HF, Weinberg RA (1999) SnoN and Ski protooncoproteins are rapidly degraded in response to transforming growth factor beta signaling. Proc Natl Acad Sci U S A 96:12442–12447
30. Sutrave P, Copeland TD, Showalter SD, Hughes SH (1990) Characterization of chicken c-ski oncogene products expressed by retrovirus vectors. Mol Cell Biol 10:3137–3144
31. Verrecchia F, Chu ML, Mauviel A (2001) Identification of novel TGF-beta/Smad gene targets in dermal fibroblasts using a combined cDNA microarray/promoter transactivation approach. J Biol Chem 276:17058–17062
32. Wieser R (2001) The transforming growth factor-beta signaling pathway in tumorigenesis. Curr Opin Oncol 13:70–77
33. Wilentz RE, Iacobuzio-Donahue CA, Argani P, McCarthy DM, Parsons JL, Yeo CJ, Kern SE, Hruban RH (2000) Loss of expression of Dpc4 in pancreatic intraepithelial neoplasia: evidence that DPC4 inactivation occurs late in neoplastic progression. Cancer Res 60:2002–2006
34. Wilentz RE, Su GH, Dai JL, Sparks AB, Argani P, Sohn TA, Yeo CJ, Kern SE, Hruban RH (2000) Immunohistochemical labeling for dpc4 mirrors genetic status in pancreatic adenocarcinomas: a new marker of DPC4 inactivation. Am J Pathol 156:37–43
35. Yakicier MC, Irmak MB, Romano A, Kew M, Ozturk M (1999) Smad2 and Smad4 gene mutations in hepatocellular carcinoma. Oncogene 18:4879–4883
36. Yamamoto H, Itoh F, Adachi Y, Sakamoto H, Adachi M, Hinoda Y, Imai K (1997) Relation of enhanced secretion of active matrix metalloproteinases with tumor spread in human hepatocellular carcinoma. Gastroenterology 112:1290–1296
37. Zheng G, Teumer J, Colmenares C, Richmond C, Stavnezer E (1997) Identification of a core functional and structural domain of the v-Ski oncoprotein responsible for both transformation and myogenesis. Oncogene 15:459–471

Virchows Arch (2004) 445:597–602
DOI 10.1007/s00428-004-1110-5

ORIGINAL ARTICLE

Victor Piana de Andrade · Helenice Gobbi

Accuracy of typing and grading invasive mammary carcinomas on core needle biopsy compared with the excisional specimen

Received: 25 November 2003 / Accepted: 21 July 2004 / Published online: 8 October 2004
© Springer-Verlag 2004

Abstract *Introduction* Breast core needle biopsy (CNB) allows evaluation of histological, prognostic, and predictive factors in invasive mammary carcinomas (IMC). We tested the CNB accuracy on typing and grading of invasive breast carcinomas. *Materials and methods* A histological review of 120 CNBs and their related surgical specimens was carried out in a double-blind fashion. Tumor type and grade were assigned according to the World Health Organization classification and the Nottingham grading system. *Results* The sum of CNB fragment lengths varied from 4 mm to 38 mm (mean 16.7 mm), and tumor sample size varied from 1 mm to 26 mm (mean 11.1 mm). Histological type matched surgical specimen evaluation in 80 of 120 cases (66.6%). Of the cases, 17 (14.2%) were changed to a different prognostic category. Histological grade comparison was accurate in 56 of 95 cases (59.0%, kappa=0.35). Histological grade components (tubule formation, nuclear grade, and mitotic index) agreed, respectively, in 54.7%, 58.9%, and 62.1% (kappa index 0.30, 0.36, and 0.28). *Discussion* Typing IMC on CNB can be routinely assessed based on good correlation with surgical specimens, especially considering prognostic categories for IMC. Grading IMC based on CNB is not as accurate, and its evaluation should be delayed until the surgical specimen examination. Tumor heterogeneity seems to be the most important factor for disagreement.

This paper was presented as a poster presentation during the 24th International Congress of the International Academy of Pathology, Amsterdam, Netherlands, 5–11 October 2002, and the abstract was published in Histopathology 2002; 41[Suppl 4]:74–75.

V. P. de Andrade · H. Gobbi
Departamento de Anatomia Patológica,
Faculdade de Medicina da UFMG,
Belo Horizonte, Minas Gerais, Brazil

V. P. de Andrade (✉)
FLEURY—Centro de Medicina Diagnóstica,
Av. General Waldomiro de Lima 508, Jabaquara-CEP 04344-070,
São Paulo, Brazil
e-mail: victor.andrade@fleury.com.br
Tel.: +55-11-50147664
Fax: +55-11-50147651

Keywords Breast cancer · Prognostic factors · Core needle biopsy · Histological type · Histological grade

Introduction

Definitive pre-operative diagnosis of breast lesions avoids uncertainty and anxiety for the patient, more precise planning of the treatment and, in great part, avoids the need for frozen section assessment. [8, 9] Core needle biopsies (CNBs) have been used increasingly with the development of core biopsy devices [21, 22, 27, 38]. It is an alternative to excisional biopsy for the initial evaluation in women with mammographically and clinically identified lesions [31, 38, 39]. CNB is a simple and low-cost procedure, which can be performed in an outpatient setting with a low complication rate and reduction in scarring, allowing for better mammographic follow-up of the lesions [9, 31]. The use of CNB also results in cost savings, because it reduces the need for excisional biopsy in patients with benign lesions [31, 38]. CNB has been shown to be highly specific and sensitive in establishing a diagnosis of breast cancer [8, 9, 21]. Because of the increasing use of neoadjuvant chemotherapy, many oncologists are interested in obtaining as much prognostic information as possible from CNB [31]. Tumor type and histological grade have been included among the most important prognostic indicators of breast cancer, along with tumor size and axillary and distant metastases [7, 10, 11, 12, 13, 16, 23, 25, 26, 29, 34, 35]. However, there are few studies assessing classical prognostic factors in CNB, such as histological classification and grade [1, 5, 17, 24, 31]. In this study, we tested the CNB accuracy of typing and grading breast carcinomas compared with the subsequent excisional specimens.

Materials and methods

This was a retrospective study using CNB slides with a diagnosis of invasive mammary carcinoma (IMC) and the subsequent excisional specimens. Patients had the ultrasound-guided CNB performed from

1995 to 2000, by the same mastologist at the Clinical Hospital of Federal University of Minas Gerais, using a 14-gauge needle, three to five passes each (the number of passes for each patient was not recorded). Patients without excisional specimen material on files and those who received neoadjuvant chemotherapy or radiotherapy between the time of the CNB and excisional specimens were excluded. Hematoxylin/eosin slides from CNB and excisional specimens were reviewed by the same pathologist (VPN). Discordant cases were reviewed by a second pathologist (HG). The CNB and excisional specimen slides were reviewed independently at different times of the study. Tumor type was assigned using the World Health Organization classification [37] with the recommendations suggested by Simpson and Page [34] and the College of American Pathologists Consensus Conference on prognostic factors in breast cancer [12, 13]. Tumor grade was assigned using the Nottingham grading system [11]. CNB cases with tumors occupying less than ten high power fields were not considered for tumor grade evaluation. CNB sample size and tumor sample size were assessed on light microscope using a glass disk marked with a millimeter scale over CNB or excisional specimen slides. For tumors over 2.0 cm, the gross measurement of the tumor was recorded. Prognostic categories for IMC were also considered for purposes of accuracy [9, 28].

Statistical analysis was performed using raw concordance between the information from the CNB and subsequent excisional specimen and kappa statistic with calculated 95% confidence interval. The kappa statistic takes into account the level of concordance that might be expected by chance alone [5, 21, 33]. A kappa statistic of "0" indicates the same level of agreement as expected by chance; "1" indicates perfect agreement. The kappa benchmarks used in this study were less than 0.20 (slight), 0.21–0.40 (fair), 0.41–0.60 (moderate), 0.61–0.80 (substantial), and 0.81–1.00 (almost perfect) [20, 33].

Results

We identified 120 cases containing the CNB and excisional specimen slides for review on our files. Histological grade comparison was possible in 95 of 120 cases. In 25 cases, there were less than ten high power fields to evaluate mitotic counting, and the tumors were not graded.

Tumor size

The sum of CNB fragment size varied from 4 mm to 38 mm (mean 16.7 mm; 90% smaller than 30 mm). The sum of tumor representation on CNB ranged from 1 mm to 26 mm (mean 11.1 mm; 90% smaller than 23 mm). The tumor size of surgical specimens measured from 10 mm to 181 mm (mean 35.1 mm; 90% smaller than 70 mm). The proportion of tumor on CNB fragments ranged from 3% to 100% (mean 66.2%; 50% with tumor in 100% of the sample size). There was no correlation between CNB sample size and tumor size based on categories: T1 (<2 cm), T2 (2–5 cm) and T3 (>5 cm) (Pearson's coefficient=0.06) (Fig. 1).

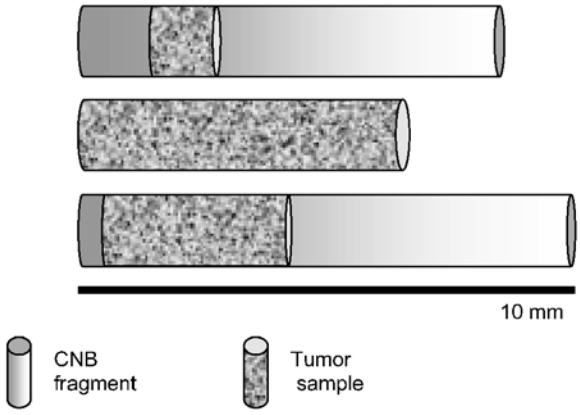


Fig. 1 CNB specimen and its tumor sample were sized in a scaled device in order to analyze its influence on typing and grading disagreement rates

Histological type

The most common tumor type was invasive ductal carcinoma not otherwise specified (IDC-NOS), diagnosed in the majority of both CNB and surgical specimens. Histological type on CNB correlated exactly with excisional specimen in 80 of 120 cases (Table 1). Of the cases, 17 (14.2%) were changed to a different category based on prognostic categories for IMC [9, 28]. Typing disagreements were not influenced by CNB size or tumor

Table 1 Frequency of invasive mammary carcinoma types on core needle biopsy and excisional specimens (ES). *IDC-NOS* invasive ductal carcinoma not otherwise specified

		Core needle biopsy									
		IDC-NOS	Lobular	Mucinous	Medullary	Tubular	Apocrine	Micro-papillary	Lobular variants	Mucinous variant	Medullary variant
ES	IDC-NOS	64	0	2	0	2	0	2	4	2	1
	Lobular	2	4	0	0	0	0	2	1	0	0
	Mucinous	3	0	4	0	0	0	0	1	0	0
	Medullary	1	0	0	1	0	0	0	0	0	0
	Tubular	1	0	0	0	2	0	0	0	0	0
	Apocrine	1	0	0	0	0	0	0	1	0	0
	Micropapillary	5	0	0	0	0	0	2	1	0	0
	Lobular variants[a]	5	2	0	0	0	0	0	2	0	0
	Mucinous variants[b]	0	0	0	0	0	0	0	0	0	0
	Medullary variants[c]	1	0	0	0	0	0	0	0	0	1

[a] Includes alveolar, pleomorphic, and solid variants of lobular carcinoma
[b] Hypercelular variant of mucinous carcinoma
[c] Atypical medullary carcinoma

Table 2 Comparison between original and reviewed invasive mammary carcinoma histological types from excisional specimen. *RHT* reviewed histological type, *IDC-NOS* invasive ductal carcinoma not otherwise specified

		Original histological type									
		IDC-NOS	Lobular	Mucinous	Medullary	Tubular	Apocrine	Micro-papillary	Lobular Variants	Mucinous Variant	Cribri-form
RHT	IDC-NOS	72	1	2	0	2	0	0	0	0	1
	Lobular	2	6	0	0	0	0	0	1	0	0
	Mucinous	4	0	4	0	0	0	0	0	0	0
	Medullary	2	0	0	0	0	0	0	0	0	0
	Tubular	2	0	0	0	1	0	0	0	0	0
	Apocrine	2	0	0	0	0	0	0	0	0	0
	Micropapilary	8	0	0	0	0	0	0	0	0	0
	Lobular variants[a]	7	1	0	0	0	0	0	1	0	0
	Mucinous variant[b]	0	0	0	0	0	0	0	0	0	0
	Medullary variant[c]	1	0	0	0	0	0	0	0	0	0

[a] Includes alveolar, pleomorphic, and solid variants of lobular carcinoma
[b] Hypercelular variant of mucinous carcinoma
[c] Atypical medullary carcinoma

sample size (P=0.65). The excisional specimen confirmed four of six cases diagnosed by CNB as pure mucinous carcinoma. Two of them were IDC-NOS with a small focus of mucinous features. The two examples of carcinoma with mucinous features (hypercellular variant) diagnosed on CNB showed more than 90% of areas with classical mucinous characteristics (hypocellular) in the excisional specimen and were classified as IMC. Four cases were diagnosed as invasive tubular carcinoma on CBN. One of them showed large areas of invasive ductal carcinoma with solid nests in the excisional specimen. There were eight pure invasive micropapillary carcinomas diagnosed on excisional specimens. On CNB typing, two of them were correctly diagnosed, five were assigned as invasive ductal carcinomas, and one was diagnosed as the alveolar variant of lobular carcinoma due to CNB artifacts and small tumor representation. The micropapillary pattern, when present in mixed tumors, occurred as a minor component in combination with ductal, lobular, and mucinous carcinomas. In the original diagnosis made by different pathologists, the IDC-NOS category was even larger (83.3%). The absolute concordance rate between the original and the reviewed diagnoses was obtained in 84 of 120 (70%) cases (Table 2). Pure special types and variants of IMC (n=28) were not recognized in the original evaluation CNB or excisional specimen (Fig. 2).

Table 3 Histological grade comparison between core needle biopsy (CNB) and excisional specimen

CNB histological grade	Surgical specimen histological grade			
	I	II	III	Total
I	33	13	2	48
II	8	13	7	28
III	0	9	10	19
Total	41	35	19	95

Histological grade

Histological grade comparison (Table 3) was accurate in 56 of 95 cases (59.0%, kappa=0.35). The evaluation of histological grade components showed concordance in 54.7% for tubule formation, 58.9% for nuclear grade, and 62.1% for mitotic index; the kappa indices were 0.30, 0.36, and 0.28, respectively (Table 4). Grading disagreements were not influenced by CNB size or tumor sample size (P=0.15).

Discussion

We evaluated the accuracy of typing and grading IMC on CNB compared with the excisional specimen. Histological type of CNB correlated exactly with that of excision in 80 of 120 cases (66.6%). In 17 cases, the histological type disagreement led to a change in prognostic category (5 of them led to a worse prognosis). Shariff et al. [31] obtained

Table 4 Agreement and disagreement between histological grade and its components, when compared for core needle biopsy and surgical specimen, and the Kappa index for comparison. Tumors graded according to the Nottingham modification of Bloom & Richardson scoring system

	Histological grade	Tubular formation	Nuclear grade	Mitotic index
Kappa index	0.35	0.30	0.36	0.28
Total agreement	59.0%	54.7%	58.9%	62.1%
One-level disagreement	38.9%	41.1%	36.8%	26.3%
Two-level disagreement	2.1%	4.2%	4.2%	13.7%

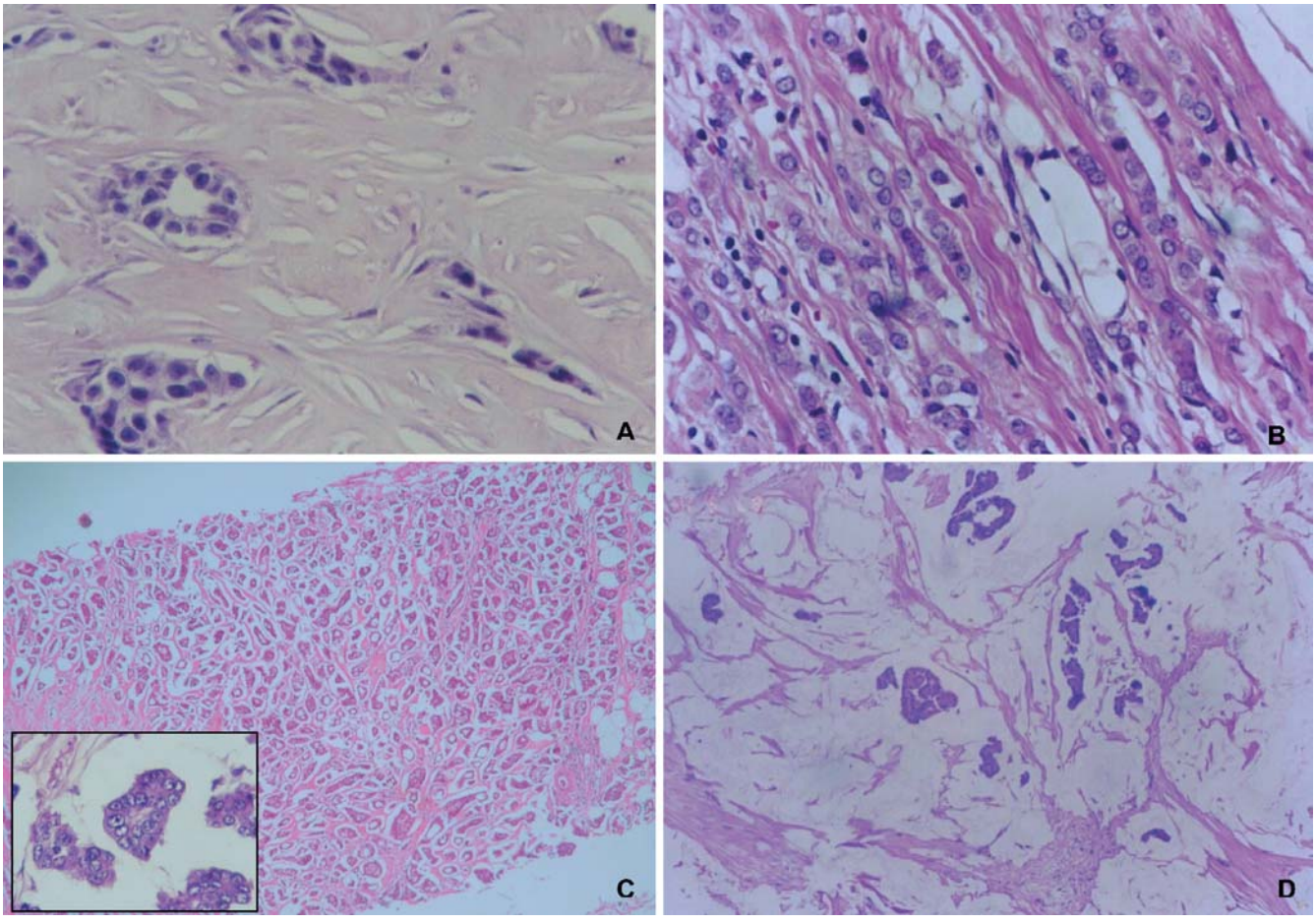


Fig. 2 **A** CNB; Tubular carcinoma. A well-differentiated carcinoma composed by grade one nuclei cells with tubule formation in a densely desmoplastic stroma. H&E, 400×. **B** Excisional specimen; classic invasive lobular carcinoma. Grade one nuclei cells in cords and targetoid distribution composes this special type of breast carcinoma. H&E, 400×. **C** CNB; Invasive micropapillary carcinoma. Small nests of cells with variable nuclear grade seem to be flooting, mimicking lymphatic invasion. H&E, 40×; inset: 400×. **D** Excisional specimen, classic invasive colloid carcinoma. More than 90% of the tumor was composed of small islands of grade one nuclei cells in a mucinous background. H&E, 100×

81% (n=79 cases) and Harris et al. [17] obtained 74% (n=500 cases) correlation comparing the histological tumor type on CNB with the excisional specimen of breast cancers. Breast tumor heterogeneity and the sample size seem to be the most important factors for disagreement of typing breast tumors on CNB. However, our results did not relate tumor sample size to disagreement rates. Studies for validation of tissue microarray technology have shown that it is possible to achieve a 98% concordance rate for immunohistochemical markers in breast cancer using three samples, sizing 0.6 mm each [3]. To construct tissue microarrays using such small samples, pathologists choose the most informative areas to overcome tumor heterogeneity. Instead of this, on CNB, the tumor is randomly biopsied, and the most informative areas are not always sampled.

Our series included special types and variants of IMC (Table 1), and not only the pure lobular, tubular, and mucinous types. This would explain the worse correlation obtained for tumor typing on CNB when compared with the results of Shariff et al. [31] and Harris et al. [17].

Tumor type has been considered one of the most powerful prognostic factors in breast cancer. The College of American Pathologists Consensus Conference included tumor type among the category-I prognostic factors [13]. They also proposed that an adequate tumor classification should follow rigid criteria and training [13]. There are important clinical implications of tumor typing, because breast tumors can be assigned prognostic categories that influence adjuvant treatment decisions [10, 16, 25, 28, 32, 36]. In our series, the original diagnosis, made by different pathologists, had overdiagnosed the IDC-NOS type. Thus, 28 special type and variants of IMC, including 8 invasive micropapillary carcinomas, had been originally recognized. One can note that typing breast carcinomas is not easy and should be done by pathologists with special interest and training in breast pathology.

We also evaluated the histological grade of CNB compared with the excisional specimen in our study. Defining whether a carcinoma diagnosed by CNB can be definitively categorized as either low grade (grade I) or high grade (grade III) has implications in clinical practice,

especially for patients eligible for neoadjuvant chemotherapy. Therapeutic decisions could be based on the histological grade information obtained from the CNB in addition to tumor size and other clinical parameters. In our study, the histological grade comparison was accurate in 56 of 95 cases (59.0%) with a fair kappa (0.35). Even when histological grade was categorized by grouping tumors into two grades (high-grade and not high-grade tumors), kappa index was fair (0.40). Harris et al. [17] obtained comparable results: 67% concordance rate (kappa=0.48). However, Shariff et al. [31] obtained a 75% concordance rate in a similar study comparing histological grades, with a higher kappa statistic (0.62). Concordant and discordant cases in our study had similar mean size and tumor sample size measured in the CNB. We also assessed the histological grade components (tubule formation, nuclear grade, and mitotic index), and our data showed concordance in 54.7%, 58.9%, and 62.1%, and kappa indices of 0.30, 0.36, and 0.28, respectively (Table 3). Previous studies showed 76–82%, 67–73%, and 58–68% for tubule formation, nuclear grade, and mitotic index, respectively, indicating that each of these factors is subject to some degree of sampling error [17, 31]. Our data indicate that CNB was not highly accurate in grading breast tumors, probably because the mitotic hot spot and the most pleomorphic nuclei are not represented in the same sample. Additionally, in only a few cases did we get a true idea of tubule formation on CNB. This can explain why a grade-III tumor on CNB changed to a grade II on excisional specimen evaluation.

The disagreement rates can be influenced by intraobserver variation. Many authors have assessed histological grade and its components in a large series of surgical specimens to evaluate intraobserver and interobserver agreement and reproducibility of grading systems [2, 4, 6, 14]. Factors such as sample size, adequate technical processing conditions, and pathologist training influenced the results [5, 10, 15]. Variations on the adequate evaluation of each component of the grading system may influence the final histological grade [18, 19, 30, 36].

The results of our study were based on the evaluation of CNB, which was obtained using standard 14-gauge needles, without vacuum assistance. Recent studies have indicated that the use of directional vacuum-assisted biopsy device (mammotome) results in the acquisition of larger specimens and shows that discrepancies between larger CNB and excisional specimens are less frequent than with the standard 14-gauge devices [1, 27, 31]. It is possible that the accuracy of assessing pathological prognostic factors in CNB may be improved with the use of larger biopsy devices, thereby reducing the level of sampling error inherent in needle biopsy procedures [31]. Nevertheless, the mammotome device can make tumor size assessment difficult. The lack of this important prognostic information has led some authors to argue against its use when a malignant lesion is suspected [38].

In conclusion, our data indicate that histological typing of breast carcinomas by CNB could be routinely assessed based on good correlation with an excisional specimen, especially considering prognostic categories for IMC. In contrast, grading of breast carcinomas based on 14-gauge standard CNB is not so accurate, and its definitive evaluation should be delayed until the examination of the excisional specimen.

Acknowledgements Supported by grants from Fundação de Amparo à Pesquisa de Minas Gerais (CDS-560/01) and Conselho Nacional de Desenvolvimento Científico e Tecnológico (520117/00–0), Brazil. We are thankful to Ms. Sandra J. Olson, Vanderbilt University, USA, for revising the English manuscript.

References

1. Astall EC, Bobrow LG (1998) Assessment of the accuracy of diagnostic and prognostic information provided by core biopsy in breast carcinoma. J Pathol 186:ssPA6
2. Boiesen P, Bendahl P, Anagnostaki L, Domanski H, Holm E, Idvall I, Johansson S, Ljungberg O, Ringberg A, Östberg G, Fernö M (2000) Histological grading in breast cancer. Reproducibility between seven pathologic departments. Acta Oncologica 39:41–45
3. Camp RL, Charaette LA, Rimm DL (2000) Validation of tissue microarray technology in breast carcinoma. Lab Invest 80: 1943–1949
4. Cross SS (1998) Grading and scoring in histopathology. Histopathology 33:99–106
5. Cross SS (2000) Correspondence Re: Sharifi S, Peterson MK, Baum JK, Raza S, Schnitt SJ. Assessment of pathological prognostic factors in breast core needle biopsies. Mod Pathol 1999,12(10):941–945. Mod Pathol 13:1332
6. Dalton LW, Page DL, Dupont WD (1994) Histologic grading of breast cancer. A reproducibility study. Cancer 73:2765–2770
7. Dalton, LW, Pinder SE, Elston CW, Ellis IO, Page DL, Dupont WD, Blamey RW (2000) Histologic grading of breast cancer: linkage of patient outcome with level of pathologist agreement. Mod Pathol 13:730–735
8. Denley H, Pinder SE, Elston CW, Lee AHS, Ellis IO (2000) Needle core biopsy of the breast. Curr Diag Pathol 6:200–205
9. Ellis IO, Pinder S (2001) Pitfalls and problems in breast pathology. USCAP 2001 Syllabus. Short Course #10. Handout
10. Ellis IO, Galea M, Broughton N, Locker A, Blamey RW, Elston CW (1992) Pathological prognostic factors in breast cancer. II. Histologic type. Relationship with survival in a large study with long-term follow-up. Histopathology 20:479–489
11. Elston CW, Ellis IO (1991) Pathological prognostic factors in breast cancer. 1. The value of histological grade in breast cancer—experience from a large study with long-term follow-up. Histopathology 19:403–410
12. Fitzgibbons PL, Page DL, Weaver D, Thor AD, Allred DC, Clark GM, Ruby SG, O'Malley F, Simpson JF, Connolly JL, Hayes DF, Edge SB, Lichter A, Schnitt SJ (2000) Updated protocol for the examination of specimens from patients with carcinomas of the breast. A basis for checklists. Arch Pathol Lab Med 124:1026–1033
13. Fitzgibbons PL, Weaver D, Thor AD, Allred DC, Clark GM, Ruby SG, O'Malley F, Simpson JF, Connolly JL, Hayes DF, Edge SB, Lichter A, Schnitt SJ (2000) Prognostic factors in breast cancer. College of American Pathology consensus statement 1999. Arch Pathol Lab Med 124:966–978
14. Frierson HF, Wolber RA, Berean KW, Franquemont DW, Gaffey MJ, Boye JC, Wilbur DC (1995) Interobserver reproducibility of Nottingham modification of the Bloom and Richardson histologic grading scheme for infiltrating ductal carcinoma. Am J Clin Pathol 103:195–198
15. Goldhirsch A, Glick JH, Gelber RD, Coates AS, Senn HJ (1998) Meeting highlights: international consensus panel on the treatment of primary breast cancer. J Natl Cancer Inst 90:1601–1608

16. Greene FL, Page DL, Fleming ID, Fritz A, Balch CM, Haller DG, Morrow M (2002) AJCC cancer staging manual, 6th edn. Springer, Berlin Heidelberg New York
17. Harris GC, Denley HE, Pinder SE, Lee AH, Ellis IO, Elston CW, Evans A (2003) Correlation of histologic prognostic factors in core biopsies and therapeutics excisions of invasive breast carcinoma. Am J Surg Pathol 27:11–15
18. Jannink I, Risberg B, Van Diest PJ, Baak JP (1996) Heterogeneity of mitotic activity in breast cancer. Histopathology 29:421–428
19. Kronqvist P, Kuopio T, Collan Y (2000) Morphometric grading of breast cancer: thresholds for tubular differentiation. Br J Cancer 82:1656–1661
20. Landis RJ, Koch GG (1977) The measurement of observer agreement for categorical data. Biometrics 33:159–174
21. Liberman L (1999) Impact of percutaneous imaging-guided core biopsy on the clinical management of breast disease. In: Rosen PP (ed) Breast pathology: diagnosis by needle core biopsy. Lipincott Williams & Wilkins, Philadelphia, pp 291–300
22. Lind DS, Minter R, Steinbach B, Abbitt P, Lanier L, Haigh L, Vauthey JN, Russin M, Hackett R, Copeland EM (1998) Stereotactic core biopsy reduces the reexcision rate and the cost of mammographically detected cancer. J Surg Res 78:23–26
23. Lundin, J, Lundin M, Holli K, Kataja V, Elomaa L, Pylkkänen L, Turpeenniemi-Hujanen T, Joensuu H (2001) Omission of histologic grading from clinical decision making may result in overuse of adjuvant therapies in breast cancer: results from a nationwide study. J Clin Oncol 19:28–36
24. Mcllehenny C, Doughty JC, George WD, Mallon EA (2002) Optimal number of core biopsies for accurate assessment of histological grade in breast cancer. Br J Surg 89:84–85
25. Page DL, Simpson JF (2000) Pathology of preinvasive and excellent-prognosis breast cancer Curr Opin Oncol 12:526–531
26. Page DL, Jensen RA, Simpson JF (1998) Routinely available indicators of prognosis in breast cancer. Breast Cancer Res Treat 51:195–208
27. Parker SH, Jobe WE, Dennis MA, Stavros AT, Johnson KK, Yakes WF, Truell JE, Price JG, Kortz AB, Clark DG (1993) US-guided automated large-core breast biopsy. Radiology 187: 507–511
28. Pereira H, Pinder SE, Sibbering DM, Galea MH, Elston CW, Blamey RW, Robertson JFR, Ellis IO (1995) Pathological prognostic factors in breast cancer. IV: Should we be a typer or a grader? A comparative study of two histological prognostic features in operable breast carcinoma. Histopathology 27:219–226
29. Rampaul RS, Pinder SE, Elston CW, Ellis IO (2001) Prognostic and predictive factors in primary breast cancer and their role in patient management: the Nottingham breast team. Eur J Surg Oncol 27:229–238
30. Robbins P, Pinder SE, de Klerk N, Dawkins H, Harvey J, Sterrett G, Ellis IO, Elston CW (1995) Histological grading of breast carcinomas. A study of interobserver agreement. Hum Pathol 26:873–879
31. Sharifi S, Peterson MK, Baum JK, Raza S, Schnitt SJ (1999) Assessment of pathological prognostic factors in breast core needle biopsies. Mod Pathol 12:941–945
32. Shosua S (2000) Reporting breast biopsies. Curr Diagn Pathol 6:140–145
33. Simon R, Altman G (1994) Statistical aspects of prognostic factor studies in oncology. Br J Cancer 69:979–985
34. Simpson JF, Page DL (1994) Status of breast cancer prognostication based on histopathologic data. Am J Clin Pathol 102[Suppl 1]:S3–S8
35. Simpson JF, Gray O, Dressler LG, Cobau CD, Falkson CI, Gilchrist KW, Pandya KJ, Page DL, Robert NJ (2000) Prognostic value of histologic grade and proliferative activity in axillary node-positive breast cancer: results from the Eastern Cooperative Oncology Group companion study, EST 4189. J Clin Oncol 18:2059–2069
36. Sloane JP, Amendoeira I, Apostolikas N, Bellocq JP, Bianchi S, Boecker W, Bussolati G, Coleman D, Connollu CE, Eusebi V, De Miguel C, Dervan P, Drijkoningen R, Elston CW, Faverly D, Gad A, Jacquemier J, Lacerda M, Martinez-Penuela J, Munt C, Peterse JL, Rank F, Sylvan M, Tsakraklides V, Zafrani B (1999) Consistency achieved by 23 European pathologists from 12 countries in diagnosing disease and reporting prognostic features in carcinomas. Virchows Arch 434:3–10
37. Tavassoli FA, Devilee P (2003) Pathology and genetics of tumors of the breast and female genital organs. IARC WHO Classification of tumors
38. Wong AY, Salisbury E, Bilous M (2000) Recent developments in stereotactic breast biopsy methodologies: an update for the surgical pathologist. Adv Anat Pathol 7:26–35
39. Yim JH, Barton P, Weber B, Radford D, Levy J, Monsees B, Flanagan F, Norton JA, Doherty GM (1996) Mammographically detected breast cancer. Benefits of setereotactic core versus wire localization biopsy. Ann Surg 223:688–700

Virchows Arch (2004) 445:603–609
DOI 10.1007/s00428-004-1117-y

ORIGINAL ARTICLE

Catherine Uzan · Annie Cortez · Charlotte Dufournet · Raffaèle Fauvet · Jean-Pierre Siffroi · Emile Daraï

Eutopic endometrium and peritoneal, ovarian and bowel endometriotic tissues express a different profile of matrix metalloproteinases-2, -3 and -11, and of tissue inhibitor metalloproteinases-1 and -2

Received: 3 June 2004 / Accepted: 5 August 2004 / Published online: 28 September 2004
© Springer-Verlag 2004

Abstract Endometriosis is subsequent to the ability of endometrial glands to invade normal tissues. Matrix metalloproteinases (MMPs)—enzymes that mediate normal tissue turnover, including endometrial breakdown during menstruation—appear to be involved in this invasive process. Here, we examined the immunohistochemical expression of MMP-2, MMP-3, MMP-11, tissue inhibitor metalloproteinase (TIMP)-1 and TIMP-2 in endometrium from women with (n=9) or without endometriosis (n=18) in comparison with peritoneal (n=20), ovarian (n=20) and colorectal endometriosis (n=20). Women with endometriosis showed decreased endometrial MMP-2 expression compared with women without endometriosis (mean±SD positive cells: 24.3±28.3% and 69.3±12.1%), together with loss of MMP-3 expression (0 versus 17.5%±20.2). MMP-11, TIMP-1 and TIMP-2 expression was similar in the two groups. Endometrial MMP-2, -3 and -11 expression and TIMP-1 and -2 expression were similar in women with endometriosis and in those with peritoneal endometriosis. MMP-2, -3 and -11 expression was higher in colorectal endometriosis than in ovarian and peritoneal endometriosis. TIMP-2 expression was lower in colorectal endometriosis (P=0.0002) and ovarian endometriotic cysts (P=0.003) than in peritoneal endometriosis. TIMP-1 expression did not vary according to the location of endometriotic lesions. These results suggest that MMP-2 and -3 and TIMP-2 may be involved in the pathogenesis of endometriosis. Interestingly, MMP-2 and -3 overexpression was related to the infiltrative nature of endometriotic lesions, with possible sequential expression from peritoneal to colorectal endometriosis.

Keywords Matrix metalloproteinase · Endometriosis · Colorectal endometriosis · Ovarian endometriosis · Endometrium · Immunohistochemistry

C. Uzan · A. Cortez
Service d'Anatomie Pathologie,
Hôpital Tenon, AP-HP,
France

C. Uzan
UPRESS EA 1533 UFR Saint-Antoine,
Université Paris VI,
Paris, France

C. Dufournet · R. Fauvet · E. Daraï (✉)
Service de Gynécologie,
Hôpital Tenon,
4 rue de la Chine, 75020 Paris, France
e-mail: emile.darai@tnn.ap-hop-paris.fr
Tel.: +33-1-567318
Fax: +33-1-56017317

J.-P. Siffroi
Laboratoire de cytogénétique,
Hôpital Tenon, AP-HP,
France

Introduction

Matrix metalloproteinases (MMPs) and their natural inhibitors, tissue inhibitor metalloproteinases (TIMPs), act in concert to control extracellular-matrix turnover [1]. MMP and TIMP have multiple functions during embryogenesis, organogenesis, angiogenesis and wound healing [1, 20]. MMP and TIMP expression is altered in both benign and malignant tumoural disease. Presence of active MMPs and correlations of their expressions with increasing tumour grade and invasion have been demonstrated in endometrial carcinoma and endometrial stromal tumours [9, 18]. Particularly in endometrial stromal tumours, MMP-3 and MMP-9 were more diffusely expressed in high-grade tumours [18]. It was recently demonstrated that MMP and TIMP are involved in reproductive function and in regulating the dynamic structural changes that occur in the endometrium during the menstrual cycle [16]. Several MMPs are cyclically expressed in normal endometrium, apparently under the control of oestrogen and progesterone [22]. Progesterone inhibition of endometrial MMPs during the secretory phase appears to be deficient in women with endometriosis [2].

Endometriosis is defined as the presence of ectopic endometrial glands and stroma outside the uterus. The incidence of endometriosis in the general female popu-

lation ranges from 5% to 15% but can reach 50% in infertile women [28, 31, 33]. Endometriosis has been tentatively explained on the basis of the metaplasia and transplantation theories [27, 29]. The metaplasia theory, based on the concept that the peritoneum has the potential to differentiate into Mullerian-type epithelium, postulates that invasive mechanisms assist in the establishment of endometriotic lesions beneath the peritoneal surfaces. The transplantation theory infers that endometrial cells have the ability to detach from the endometrium, reattach to the peritoneum after passive transport through the Fallopian tubes and invade target tissues. Previous studies have shown that endometrium from women with endometriosis have altered expression of apoptosis-related proteins [10], adhesion molecules [8, 11, 25, 32] and MMP and TIMP [23]. Kokorine et al. found that peritoneal and ovarian endometriotic tissue strongly expressed MMP-1, possibly explaining its invasive potential [16]. Chung et al. obtained evidence that eutopic endometrium from women with endometriosis was more invasive and prone to peritoneal implantation, owing to strong expression of MMP-2 and membranous type-1 MMP [6]. Few data are available on MMP and TIMP expression according to the location of endometriotic tissue. In a preliminary qualitative study, Mizumoto et al. observed differential expression of MMP-1, -2, -3, -7, -9 and TIMP-1 in normal endometrium during the menstrual cycle but found no differences relative to endometriotic ovarian cysts [19]

The aims of this study were to examine MMP-2, -3 and -11 expression and TIMP-1 and -2 expression in eutopic endometrium from women with and without endometriosis, and to compare their expression in peritoneal, ovarian and colorectal endometriotic tissue.

Materials and methods

Between 2001 and 2003, tissue samples were obtained from 77 women undergoing surgery or endometrial biopsy in the Gynaecology Department of Tenon Hospital, Paris. The samples consisted of 27 endometrial tissues (9 and 18 from women with and without endometriosis, respectively), 20 ovarian endometriotic cysts, 20 peritoneal endometriotic tissues and 20 colorectal endometriotic tissues.

Normal endometrial samples were obtained from women undergoing hysterectomy or endometrial biopsy for reasons other than endometrial disorders. No macroscopic feature on behalf of endometriosis was found during laparoscopy for patients included in the group of normal endometrium. All the patients were premenopausal. Samples from women without endometriosis were obtained during the proliferative phase of the menstrual cycle in ten cases and the secretory phase in eight cases. Samples from women with endometriosis were obtained in the proliferative phase in six cases and in the secretory phase in three cases. None of the women had hormonal treatment prior to biopsy.

Antibodies

We used mouse monoclonal antibodies against MMP-2 (gelatinase-A, Ab-3, IM33L, Oncogene Research Products, Cambridge, MA, England), MMP-3 (stromelysin 1, Ab1, IM36L, Oncogene Research Products), MMP-11 (stromelysin 3, Ab-2, IM86, Oncogene Research Products), TIMP-1 (Ab-4, IM63, Oncogene Research Products) and TIMP-2 (Ab-2, IM56L, Oncogene Research Products). All of them were purified antibodies. Immunogen used was a synthetic peptide corresponding to amino acid residue 468–483 of human MMP-2 for anti-MMP-2, human pro-MMP-3 purified from the conditioned media of rheumatoid synovial fibroblasts for anti-MMP-3, human recombinant active MMP-11 for anti-MMP-11, recombinant TIMP-1 protein for TIMP-1 and a synthetic peptide corresponding to amino-acid residues 178–193 in the C-terminal region human TIMP-2 for anti-TIMP-2. The anti-MMP-2 recognises both latent and active MMP-2. The anti-MMP-3 recognises both latent and active MMP-3 and can react with MMP-3/TIMP-1 complexes. The anti-MMP-11 recognises both latent and active form and also two degradated products of MMP-11.

Immunohistochemistry

Tissues were fixed immediately in formalin (10%) and then processed as paraffin blocks. Sections 4-μm thick of formalin-fixed tissues were deparaffinated in xylene and rehydrated through a graded series of ethanol solutions. Sections were immunostained using the Ventana Nexes automated immunohistochemistry system (Ventana Medical Systems, Tucson, AZ). Prior to MMP-2, TIMP-1 and TIMP-2 staining, an antigen retrieval step was used (Dako Target Retrieval Solution; 98°C, 20 min). The automated procedure is based on an indirect biotin-avidin system with a universal biotinylated immunoglobulin as secondary antibody, diaminobenzidine as substrate and haematoxylin as counterstain. For MMP-3 and TIMP-2, in addition to the automated procedure, a Ventana amplification kit was used (Ventana Medical Systems). Anti-MMP-2, MMP-3 and TIMP-2 antibodies were used at a dilution of 1/10 (10 µg/ml for anti-MMP-2 and 20 µg/ml for anti MMP-3 and TIMP-2), and anti-MMP-11 and anti-TIMP-1 were used at 1/75 (1.3 µg/ml) and 1/50 (4 µg/ml), respectively.

Positive controls were sections of invasive ductal breast carcinoma. The primary antibody was replaced by an irrelevant antibody of the same IgG subtype for negative controls.

Analysis of immunohistochemical results

For qualitative analysis, samples were considered negative when no labelled cells were observed on the tissue section and positive in all other cases. For semi-quantitative analysis, positive cells were counted in the most characteristic areas, and the percentage of labelled cells among 500 cells was calculated by two independent observers. Variations between the two observers were below 5% (not shown).

Statistical analysis

We used the Chi-square test for categorical variables and the Kruskal–Wallis and Mann–Whitney tests for continuous variables. Correlations between MMP and TIMP expression were evaluated using Spearman's test. P values below 0.05 were considered significant.

Results

MMP and TIMP expression in endometrium

The expression of endometrial MMP-2, -3 and -11 and TIMP-1 and -2 in women with and without endometriosis is summarised in Table 1. In glandular cells, MMP and TIMP immunostaining was restricted to the cytoplasm (Fig. 1A). Semi-quantitative MMP-2 and MMP-3 expression differed between the two groups. MMP-2 ex-

Table 1 Expression of matrix metalloproteinase-(MMP)-2, -3, and -11 and tissue inhibitor metalloproteinase (TIMP)-1 and -2 in endometrium from women with and without endometriosis (mean±SD percentage of positive cells). *NS* not significant

	Endometrium from women without endometriosis	Endometrium from women with endometriosis	*P* value
	(*n*=18)	(*n*=9)	
MMP-2	69.3±12.1	24.3±28.3	0.0004
MMP-3	17.5±20.2	0	0.04
MMP-11	38.2±25.3	32.8±26.0	NS
TIMP-1	5.8±6.6	7.2±18.2	NS
TIMP-2	24.7±18.4	26.1±20.4	NS

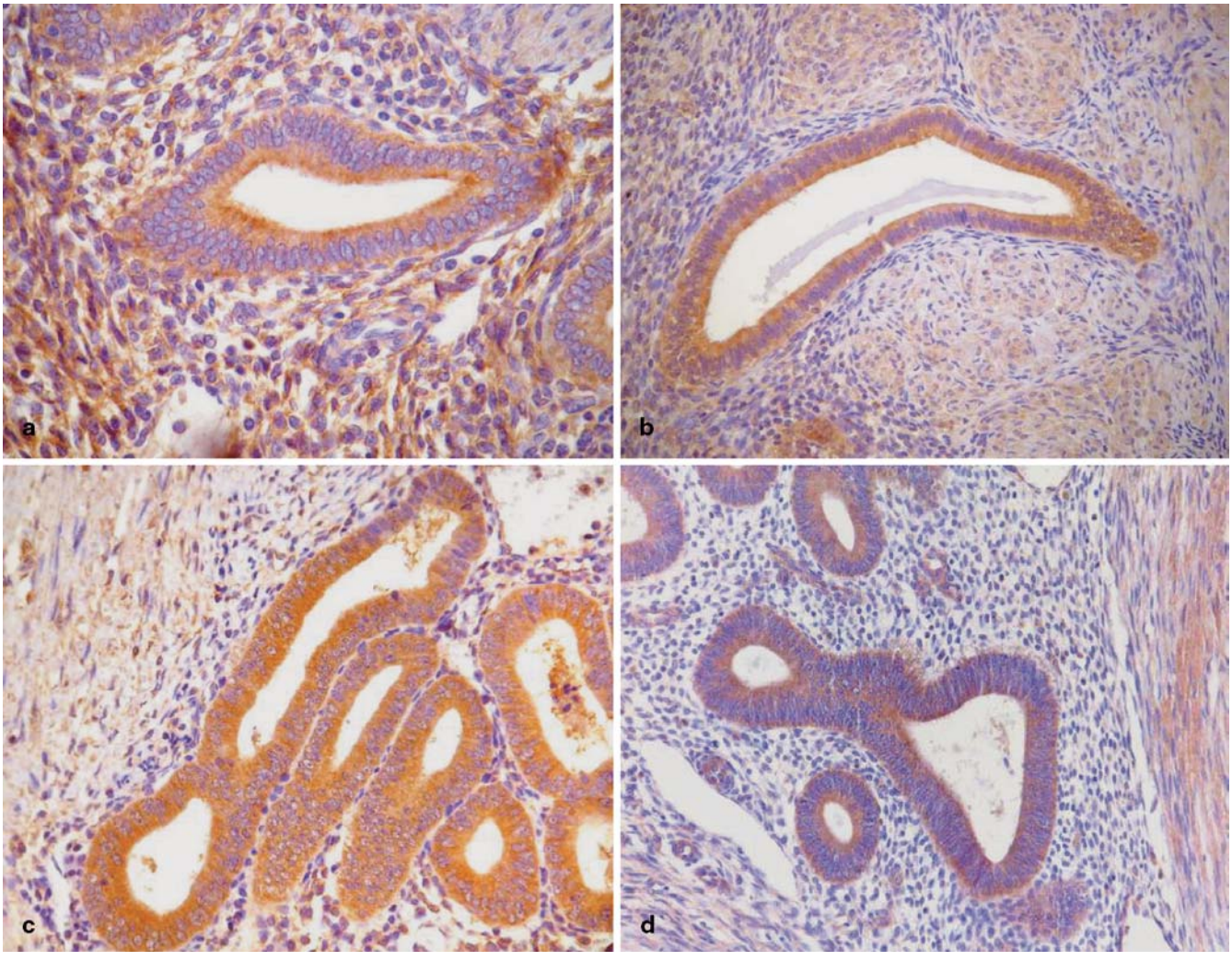


Fig. 1 Immunoperoxidase staining with diaminobenzidine as chromogen and nuclear counterstaining with Harris' haematoxylin. Representative examples of matrix metalloproteinase-2 expression in endometrium from women with endometriosis (**A**), peritoneal endometriosis (**B**) and colorectal endometriosis (**C**, **D**) detected in cytoplasm of glandular cells

pression was lower in women with endometriosis than in those without endometriosis. MMP-3 expression was present in women without endometriosis and absent in women with endometriosis. MMP-11, TIMP-1 and TIMP-2 expression did not differ between the two groups.

In women without endometriosis, MMP-3 expression (mean±SD positive cells) in the proliferative and secretory phases was 26.5%±18.0 and 0%+0, respectively (*P*=0.0008). In women with endometriosis, MMP-3 expression was absent in both phases. MMP-2 expression did not differ between the proliferative and secretory phases in women with or without endometriosis. MMP-11 expression during the proliferative phase was 51.0%±23.3 and 22.3%±18.5 in women without endometriosis and women with endometriosis, respectively (*P*=0.01); the respective values during the secretory phase were 48.0%±

Table 2 Expression of matrix metalloproteinase (MMP)-2, -3, and -11 and tissue inhibitor metalloproteinase (TIMP)-1 and -2 in ovarian endometriotic cysts, peritoneal endometriosis and colorectal endometriosis (mean±SD percentage of positive cells). *NS* not significant

	Peritoneal endometriosis	Ovarian endometriotic cyst	Colorectal endometriosis	*P* value
	(*n*=20)	(*n*=20)	(*n*=20)	
MMP-2	28.8±27.5	60.0±16.1	83.9±19.5	<0.0001
MMP-3	1.2±2.4	0.8±3.4	30.4±24.9	0.0002
MMP-11	33.2±22.7	19.9±14.2	55.9±26.3	<0.0001
TIMP-1	4.6±7.5	6.7±16.8	0.6±2.5	NS
TIMP-2	44.6±27.1	23.8±10.9	16.6±14.1	0.001

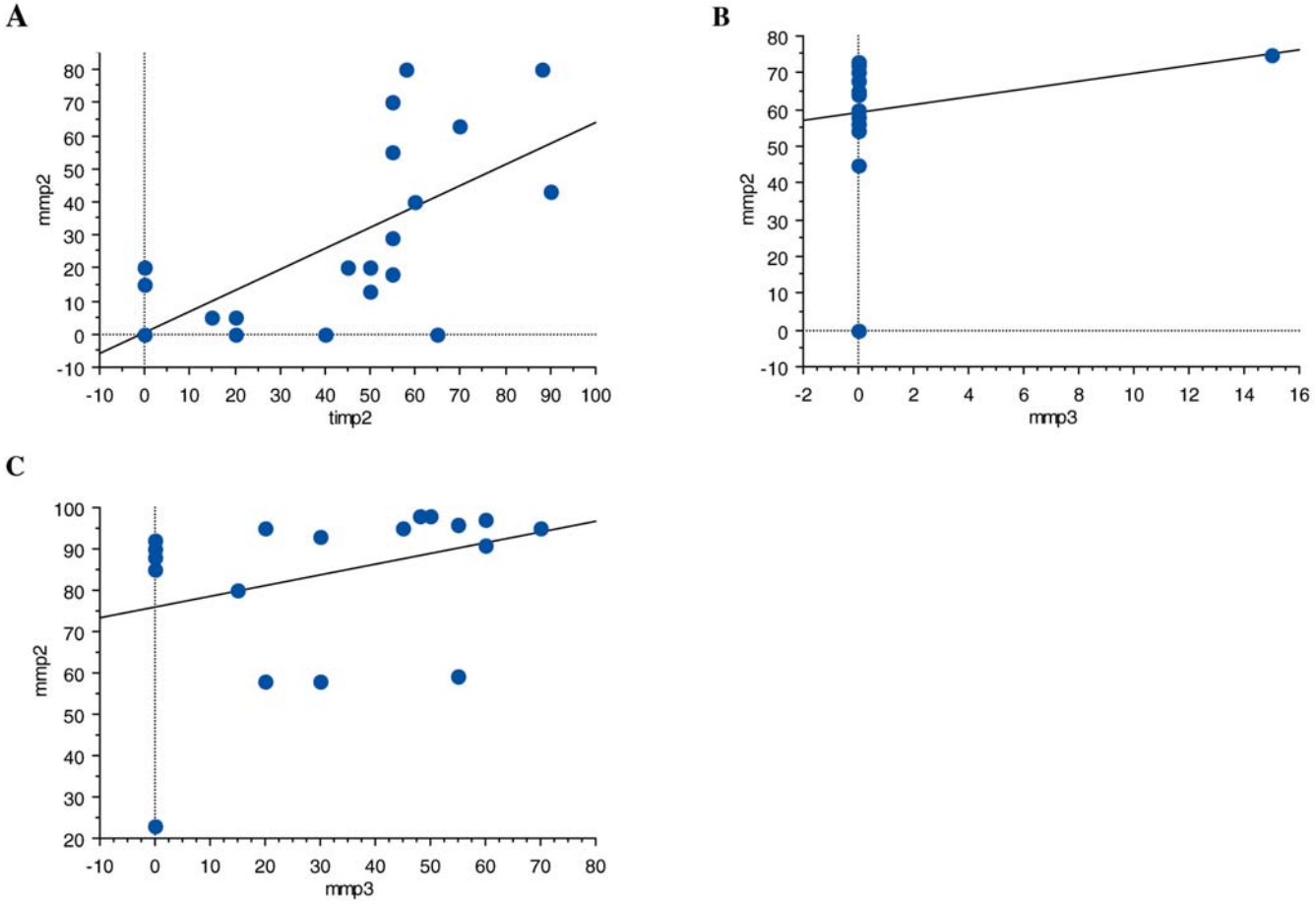


Fig. 2 *Dot plots* showing a negative correlation between matrix metalloproteinase (MMP)-2 and tissue inhibitor metalloproteinase-2 expression in peritoneal endometriosis (*P*=0.005, Rho=0.638) (**A**) and a positive correlation between MMP-2 and MMP-3 expression in ovarian endometriotic cysts (*P*=0.01, Rho=0.576) (**B**) and in colorectal endometriosis (*P*=0.02, Rho=0.538) (**C**)

22.0 and 13.8%±17.0 (*P*=0.04). No correlation was found between MMP-2 and MMP-3 expression in women with or without endometriosis.

MMP and TIMP expression in endometriotic lesions

Expression of MMP-2, -3 and -11 and TIMP-1 and -2 in peritoneal endometriosis, ovarian endometriotic cysts and colorectal endometriosis is summarised in Table 2. In glandular cells, MMP and TIMP expression was restricted to the cytoplasm (Fig. 1B, C, D).

MMP-2 expression differed according to the location of endometriotic lesions (*P*<0.0001). MMP-2 expression was higher in colorectal endometriosis than in ovarian endometriotic cysts (*P*=0.0001) and in peritoneal endometriosis (*P*<0.0001). MMP-2 expression was also higher in ovarian endometriotic cysts than in peritoneal endometriosis (*P*<0.0001).

MMP-3 expression also differed according to the location of endometriotic lesions (*P*=0.0002). Like MMP-2, MMP-3 expression was higher in colorectal endometriosis than in ovarian endometriotic cysts (*P*<0.0001) and in peritoneal endometriosis (*P*<0.0001). However, MMP-3

expression did not differ between peritoneal endometriosis and ovarian cysts. Successive alterations in MMP expression were observed from peritoneal to colorectal endometriosis: in addition to the altered MMP-2 expression also found in peritoneal and ovarian endometriosis, colorectal lesions exhibited MMP-3 overexpression.

MMP-11 expression also differed according to the location of endometriotic lesions ($P<0.0001$). MMP-11 expression was higher in colorectal endometriosis than in ovarian endometriotic cysts ($P<0.0001$) and in peritoneal endometriosis ($P=0.006$). MMP-11 expression was also higher in peritoneal endometriosis than in ovarian cysts ($P=0.03$).

TIMP-1 expression did not differ according to the location of endometriotic lesions. TIMP-2 expression differed according to the location of endometriotic lesions ($P<0.001$). TIMP-2 expression was higher in peritoneal endometriosis than in ovarian endometriotic cysts ($P=0.003$) and in colorectal endometriosis ($P=0.0002$). TIMP-2 expression tended to be higher in ovarian endometriotic cysts than in colorectal endometriosis ($P=0.08$).

In peritoneal endometriosis, a negative correlation was found between MMP-2 and TIMP-2 expression ($P=0.005$, Rho=0.638) (Fig. 2A) and between MMP-3 and TIMP-2 expression ($P=0.04$, Rho=0.471). In ovarian endometriotic cysts, there was a positive correlation between MMP-2 and MMP-3 expression ($P=0.01$, Rho=0.576) (Fig. 2B) and a negative correlation between MMP-3 and TIMP-2 expression ($P=0.02$, Rho=0.517).

In colorectal endometriosis, there was a positive correlation between MMP-2 and MMP-3 expression ($P=0.02$, Rho=0.538) (Fig. 2C) and a negative correlation between MMP-11 and TIMP-2 expression ($P=0.04$, Rho=0.464).

Comparison of MMP and TIMP expression between eutopic endometrium and endometriotic lesions

MMP-2 ($P<0.0001$), -3 ($P=0.0002$), -11 ($P=0.0002$) and TIMP-1 ($P=0.02$) and -2 ($P=0.002$) expression differed between endometriotic tissue and normal endometrium from women without endometriosis. Relative to peritoneal endometriotic tissue, endometrium from women without endometriosis showed higher expression of MMP-2 ($P<0.0001$) and MMP-3 ($P=0.0009$) and lower expression of TIMP-2 ($P=0.01$). No difference in MMP-11 and TIMP-1 expression was found between peritoneal endometriosis and endometrium from women without endometriosis. No difference in MMP-2, -3, -11 and TIMP-1 and -2 expression was found between peritoneal endometriosis and endometrium from women with endometriosis.

Discussion

This study shows that endometrial tissues from women with and without endometriosis have different MMP expression profiles. Moreover, MMP and TIMP expression profiles differed in peritoneal, ovarian and colorectal endometriosis. Endometrium from women without endometriosis expressed MMP-2, TIMP-1 and -2 throughout the menstrual cycle, whereas MMP-3 was expressed during the proliferative but not the secretory phase. These patterns of MMP and TIMP expression are in keeping with those previously reported during proliferative and secretory phases of normal endometrium, supporting the view that progesterone regulates MMP-3 but not MMP-2, TIMP-1 and -2 expression [7]. However, Goffin et al. have suggested that MMP-3 is expressed only in the menstrual phase [14].

Our most striking result was the complete loss of endometrial MMP-3 expression during the proliferative phase in women with endometriosis. Conflicting results for endometrial MMP-3 expression have been reported. Sillem et al. found no difference in MMP-3 expression between women with and without endometriosis [30]. In an in vivo study, Cox et al. detected no MMP-3 mRNA in eutopic endometrium [5]. In contrast, previous studies showed MMP-3 overexpression in women with endometriosis, with no cyclic variations, suggesting either a loss of progesterone regulation or inadequate progesterone secretion [2, 13]. It should be noted that none of the women included in our study was receiving progesterone therapy prior to tissue sampling. There is no clear explanation for the loss of MMP-3 expression in proliferative-phase samples from women with endometriosis [19]. It is conceivable that changes in paracrine factors, including transforming factors, could be involved. Bruner-Tran et al. suggested that endometrial MMP-3 expression required local TGFα and retinoid acid production by stromal cells, which is altered in endometriotic women [2]. However, mRNA levels do not necessarily correspond to protein levels, and the latent proenzyme zymogen must also be taken into account [14]. The changes in MMP and TIMP expression in women with endometriosis recall those observed by Gagne et al., showing altered proportions of leukocyte subsets [12]. These latter authors suggested that these alterations, when combined with CA125 serum assay, could serve as a novel diagnostic tool for endometriosis [12]. Further studies are required to determine the diagnostic value of the loss of proliferative-phase MMP-3 expression for endometriosis.

Whatever the phase of the menstrual cycle, we found that MMP-2 expression was reduced in endometriotic tissue compared with normal endometrium. In contrast, Wenzl and Heinzl found no difference in qualitative MMP-2 expression according to the presence or absence of endometriosis [34]. We found that endometrial MMP-2 expression did not correlate with MMP-3 expression in women with or without endometriosis.

MMP and TIMP expression profiles were similar in normal endometrium and peritoneal endometriotic tissue. The study population was too small to identify a possible correlation with macroscopic features, such as red, black or white lesions. The similar MMP and TIMP expression profiles in eutopic endometrium from women with en-

dometriosis and peritoneal endometriotic tissue supports the concept that endometrial changes play a major pathophysiological role in endometriosis [3, 15, 21, 35].

MMP-2 expression was significantly higher in colorectal endometriosis than in ovarian endometriotic cysts and peritoneal endometriosis. This is in keeping with previous in vivo and in vitro studies suggesting that MMP-2 overexpression is linked to the development and aggressiveness of endometriotic lesions [6, 26]. Only one previous study has analysed MMP-1 expression in colorectal endometriosis, the most aggressive clinical form of deep infiltrating endometriosis [17]. Our results are in keeping with those of Ria et al., who reported that MMP-2 overexpression was more pronounced in women with stage-IV endometriosis than in women with less severe forms [26]. Interestingly, TIMP-2 expression tended to show a downwards gradient from peritoneal to colorectal endometriosis. We also found a negative correlation between MMP-2 and TIMP-2 expression in endometriotic lesions, in keeping with the classical regulatory pathway involving MMP-2, TIMP-2 and MT1-MMP [7]. Although only a trend towards lower TIMP-2 expression was observed from ovarian to colorectal endometriosis, probably owing to the small sample size, our results suggest that TIMP-2 expression falls gradually with the extent of endometriotic lesions.

MMP-3 was overexpressed in colorectal endometriosis compared with peritoneal and ovarian endometriosis, while the latter two locations did not differ in this respect. This again points to sequential MMP expression according to the aggressiveness of endometriotic lesions, with the most infiltrative lesions exhibiting both high MMP-2 and high MMP-3 expression. In contrast to glandular component, we were able to evaluate MMPs and TIMPs in the stromal component of endometriotic tissues. Previous studies have shown a correlation between high cytokine levels in peritoneal fluid or serum and the extent of endometriotic lesions and also between cytokine overexpression and MMP expression [22, 30]. Other studies have reported potential roles in endometriosis of MMPs not used in this work, such as MMP-1, MMP-9, MT1-MMP [24, 26]. We focused on MMP-1, -2, -3, TIMP-1 and -2 because of available data on both endometrium and endometriotic tissues, which allowed for an adequate comparison. Moreover, previous studies using the enzyme-linked immunosorbent assay technique have demonstrated a high correlation with those obtained using immunohistochemistry in endometrium and endometriotic tissues [4, 19, 26, 30]. The data of this study, combined with reports of a relationship between MMP and adhesion molecule expression [32], confirm that MMPs and TIMPs not only regulate the extracellular matrix but also mediate cross-talk between endometriotic tissue and the stroma.

In conclusion, our results show MMP-2 and -3 underexpression in endometriotic tissue compared with endometrium from women without endometriosis. MMP-2 and -3 overexpression was related to the infiltrative nature of the endometriotic lesions, pointing to an expression gradient related to the potential to invade adjacent anatomic structures.

Acknowledgement We want to thank the "Ligue contre le cancer" for the grant.

References

1. Birkedal-Hansen H, Moore WG, Bodden MK et al (1993) Matrix metalloproteinases: a review. Crit Rev Oral Biol Med 4:197–250
2. Bruner-Tran KL, Eisenberg E, Yeaman GR, Anderson TA, McBean J, Osteen KG (2002) Steroid and cytokine regulation of matrix metalloproteinase expression in endometriosis and the establishment of experimental endometriosis in nude mice. J Clin Endocrinol Metab 87:4782–4791
3. Bruse C, Bergqvist A, Carlstrom K, Fianu-Jonasson A, Lecander I, Astedt B (1998) Fibrinolytic factors in endometriotic tissue, endometrium, peritoneal fluid, and plasma from women with endometriosis and in endometrium and peritoneal fluid from healthy women. Fertil Steril 70:821–826
4. Collette T, Bellehumeur C, Kats R, Maheux R, Mailloux J, Villeneuve M, Atloum A (2004) Evidence for an increase release of proteolytic activity by eutopic endometrial tissue in women with endometriosis and for involvement of MMP-9. Human Reprod 19:1257–1264
5. Cox KE, Piva M, Sharpe-Timms KL (2001) Differential regulation of matrix metalloproteinase-3 gene expression in endometriotic lesions compared with endometrium. Biol Reprod 65:1297–1303
6. Chung HW, Lee JY, Moon HS et al (2002) Matrix metalloproteinase-2, membranous type 1 matrix metalloproteinase, and tissue inhibitor of metalloproteinase-2 expression in ectopic and eutopic endometrium. Fertil Steril 78:787–795
7. Curry TE Jr, Osteen KG (2001) Cyclic changes in the matrix metalloproteinase system in the ovary and uterus. Biol Reprod 64:1285–1296
8. Darai E, Leblanc M, Walker-Combrouze F, Bringuier AF, Madelenat P, Scoazec JY (1998) Expression of cadherins and CD44 isoforms in ovarian endometrial cysts. Hum Reprod 13:1346–1352
9. di Nezza LA, Misajon A, Zhang J et al (2002) Presence of active gelatinases in endometrial carcinoma and correlation of matrix metalloproteinase expression with increasing tumor grade and invasion. Cancer 94:1466–1475
10. Fauvet R, Poncelet C, Hugol D, Lavaur A, Feldmann G, Darai E (2003) Expression of apoptosis-related proteins in endometriomas and benign and malignant ovarian tumours. Virchows Arch 443:38–43
11. Gaetje R, Kotzian S, Herrmann G, Baumann R, Starzinski-Powitz A (1995) Invasiveness of endometriotic cells in vitro. Lancet 346:1463–1464
12. Gagne D, Rivard M, Page M et al (2003) Development of a nonsurgical diagnostic tool for endometriosis based on the detection of endometrial leukocyte subsets and serum CA-125 levels. Fertil Steril 80:876–885
13. Gilabert-Estelles J, Estelles A, Gilabert J et al (2003) Expression of several components of the plasminogen activator and matrix metalloproteinase systems in endometriosis. Hum Reprod 18:1516–1522
14. Goffin F, Frankenne F, Beliard A et al (2002) Human endometrial epithelial cells modulate the activation of gelatinase a by stromal cells. Gynecol Obstet Invest 53:105–111
15. Jolicoeur C, Boutouil M, Drouin R, Paradis I, Lemay A, Akoum A (1998) Increased expression of monocyte chemotactic protein-1 in the endometrium of women with endometriosis. Am J Pathol 152:125–133
16. Kokorine I, Marbaix E, Henriet P et al (1996) Focal cellular origin and regulation of interstitial collagenase (matrix metal-

loproteinase-1) are related to menstrual breakdown in the human endometrium. J Cell Sci 109:2151–2160
17. Kokorine I, Nisolle M, Donnez J, Eeckhout Y, Courtoy PJ, Marbaix E (1997) Expression of interstitial collagenase (matrix metalloproteinase-1) is related to the activity of human endometriotic lesions. Fertil Steril 68:246–251
18. Liokumovich P, Goldberg I, Davidson B, Gotlieb WH, Zahavi T, Ben Baruch G (1999) Expression of metalloproteinases endometrial stromal sarcoma: immunohistochemical study using image analysis. J Clin Pathol 52:198–202
19. Mizumoto H, Saito T, Ashihara K et al (2002) Expression of matrix metalloproteinases in ovarian endometriomas: immunohistochemical study and enzyme immunoassay. Life Sci 71:259–273
20. Nagase H, Woessner JF Jr (1999) Matrix metalloproteinases. J Biol Chem 274:21491–2149
21. Noble LS, Simpson ER, Johns A, Bulun SE (1996) Aromatase expression in endometriosis. J Clin Endocrinol Metab 81:174–179
22. Osteen KG, Keller NR, Feltus FA, Melner MH (1999) Paracrine regulation of matrix metalloproteinase expression in the normal human endometrium. Gynecol Obstet Invest 48 [Suppl 1]: 2–13
23. Osteen KG, Igarashi TM, Bruner-Tran KL (2003) Progesterone action in the human endometrium: induction of a unique tissue environment which limits matrix metalloproteinase (MMP) expression. Front Biosci 8:78–86
24. Osteen KG, Yeaman GR, Bruner-Tran KL (2003) Matrix metalloproteinases and endometriosis. Semin Reprod Med 21:155–164
25. Poncelet C, Leblanc M, Walker-Combrouze F et al (2002) Expression of cadherins and CD44 isoforms in human endometrium and peritoneal endometriosis. Acta Obstet Gynecol Scand 81:195–203
26. Ria R, Loverro G, Vacca A et al (2002) Angiogenesis extent and expression of matrix metalloproteinase-2 and -9 agree with progression of ovarian endometriomas. Eur J Clin Invest 32:199–206
27. Ridley JH (1981) Coelomic metaplasia. Am J Obstet Gynecol 140:233–234
28. Ryan IP, Taylor RN (1997) Endometriosis and infertility: new concepts. Obstet Gynecol Surv 52:365–371
29. Sampson JA (1927) Peritoneal endometriosis due to menstrual dissemination of endometrial tissue into the peritoneal cavity. Am J Obstet Gynecol 14:422–469
30. Sillem M, Prifti S, Koch A, Neher M, Jauckus J, Runnebaum B (2001) Regulation of matrix metalloproteinases and their inhibitors in uterine endometrial cells of patients with and without endometriosis. Eur J Obstet Gynecol Reprod Biol 95:167–174
31. Stovall DW, Bowser LM, Archer DF, Guzick DS (1997) Endometriosis-associated pelvic pain: evidence for an association between the stage of disease and a history of chronic pelvic pain. Fertil Steril 68:13–18
32. Ueda M, Yamashita Y, Takehara M et al (2002) Gene expression of adhesion molecules and matrix metalloproteinases in endometriosis. Gynecol Endocrinol 16:391–402
33. Vercellini P, Trespidi L, De Giorgi O, Cortesi I, Parazzini F, Crosignani PG (1996) Endometriosis and pelvic pain: relation to disease stage and localization. Fertil Steril 65:299–304
34. Wenzl RJ, Heinzl H (1998) Localization of matrix metalloproteinase-2 in uterine endometrium and ectopic implants. Gynecol Obstet Invest 45:253–257
35. Wingfield M, Macpherson A, Healy DL, Rogers PA (1995) Cell proliferation is increased in the endometrium of women with endometriosis. Fertil Steril 64:340–346

Virchows Arch (2004) 445:610–615
DOI 10.1007/s00428-004-1111-4

ORIGINAL ARTICLE

N. Murphy · C. C. B. B. Heffron · B. King · U. G. Ganuguapati · M. Ring · E. McGuinness · O. Sheils · J. J. O'Leary

P16^{INK4A} positivity in benign, premalignant and malignant cervical glandular lesions: a potential diagnostic problem

Received: 19 July 2004 / Accepted: 30 July 2004 / Published online: 18 September 2004
© Springer-Verlag 2004

Abstract A wide array of immunohistochemical markers have been evaluated with respect to their specificity in staining dysplastic cervical cells in cervical biopsies and cervical cytological smears. However, there is still a significant demand for better biomarkers to identify neoplastic cervical glandular and squamous epithelial cells precisely. The CDKN2A gene, located on chromosome 9p21, encodes the tumour suppressor protein, p16^{INK4A}, which decelerates the cell cycle by inactivating CDK4 and CDK6. The aim of this study was to compare and contrast the expression pattern of p16^{INK4A} in benign and neoplastic glandular lesions and tubo-endometrioid metaplasia. All cases in each category displayed some p16^{INK4A} expression. Adenocarcinoma and in situ cases showed a combination of intense nuclear and cytoplasmic staining. It was observed that all cases of tubo-endometrioid metaplasia showed occasional nuclear positivity and definite cytoplasmic staining. These findings may have important implications for the potential utility of p16^{INK4A} as a biomarker for glandular dysplastic lesions. While p16^{INK4A} has been demonstrated to be an excellent marker of cervical dysplasia in squamous neoplastic lesions of the cervix, it has potential pitfalls in cervical glandular lesions that may limit the utility of this biomarker in resolving the nature of suspicious glandular lesions, particularly in cytopathology.

Keywords Adenocarcinoma in situ · Cervical glandular intraepithelial neoplasia · p16^{INK4A}

N. Murphy and C.C.B.B. Heffron contributed equally to the work.

N. Murphy · C. C. B. B. Heffron · B. King · U. G. Ganuguapati · M. Ring · J. J. O'Leary (✉)
Department of Pathology, Coombe Women's Hospital, Dublin 8, Ireland
e-mail: oleary@tcd.ie
Tel.: +353-1-4085326
Fax: +353-1-4085608

N. Murphy · M. Ring · E. McGuinness · O. Sheils · J. J. O'Leary
Trinity College, Dublin, Ireland

Introduction

P16^{INK4A} is a cell-cycle regulatory protein encoded on chromosome 9p21, which inhibits the cyclin-dependent kinase inhibitors CDK4 and CDK6 [43, 44]. CDK4 and CDK6 complex with cyclin D, thereby phosphorylating pRb and rendering it inactive. This allows the cell to progress through the G1-S checkpoint and complete the cell cycle. Thus, p16^{INK4A} acts to prevent such progression and inhibit the cell cycle. P16^{INK4A} mutations and inactivation of p16^{INK4A} by overexpression of CDK4 or cyclin D have been shown in many cancers. Loss of heterozygosity [10] and homozygous deletions [6] at the 9p21 locus, called MLM encoding p16^{INK4A}, have been shown in malignant melanoma [14]. CDK 4 mutations resulting in ineffective p16^{INK4A} action have also been shown [38]. Similar mutations have been reported to be associated with prognosis and response to chemotherapy in ovarian cancer [9, 18, 32].

P16^{INK4A} has received much attention as a biomarker of dysplasia in the diagnosis of cervical squamous lesions [15, 24, 41, 42], with the potential to be used as an additional screening tool. However, cervical glandular lesions, such as adenocarcinoma and its precursors adenocarcinoma in situ (AIS) or cervical glandular intraepithelial neoplasia (cGIN), are less amenable to accurate screening than their squamous counterpart, implying that screening cytology is both less specific and sensitive for the identification of glandular lesions of the cervix [29]. This may be related to the difficulty in sufficiently sampling the entire endocervical canal, where the majority of glandular lesions occur. In 1985, Saigo et al. [33] regarded screening as an unreliable method of identification of glandular abnormalities. Similarly, in 2001, Krane et al. [17] reported the sensitivity of the Papanicolaou smear for the detection of adenocarcinoma to be only between 45% and 76%. Thus, there is a strong demand for a more specific method to improve the detection of glandular lesions and their precursors in cervical screening programs. Some studies have reported p16^{INK4A} as a useful marker in the diagnosis of adenocarcinoma of the cervix

and its precursors in a similar manner to cervical squamous lesions [25]. Others recommend its use in a panel of immunohistochemical markers, including MIB1 and BCL2 [3, 23]. Indeed, a wide array of immunohistochemical markers has been evaluated with respect to their specificity in staining dysplastic cervical cells in biopsies and cytological smears. These include: MN, a transmembrane glycoprotein [19]; the proliferation marker, Ki-67/MIB1 [3, 4, 15, 27]; bcl2 [3, 23]; a cell-cycle protein, cyclin E [15]; the tumour suppressor protein, p53 [4]; CEA, carcinoembryonic antigen [4, 21]; and mucin gene expression, MUC2 and MUC5AC [30]. However, the sensitivity and specificity of these markers are only of limited clinical utility and are only useful when used in a wide panel of markers. Thus, there is still a significant demand for better biomarkers to identify both squamous and glandular dysplastic or neoplastic cervical epithelial cells precisely in biopsy samples and cervical smears.

In addition to this, there are many mimics of endocervical adenocarcinoma and its precursors, which may cause diagnostic difficulties both histologically and cytologically [22, 46]. The body's normal response mechanisms, such as inflammation and response to irradiation, can also result in glandular atypia [46]. Other mimics include tunnel clusters [36], microglandular hyperplasia [37, 45] and, commonly, tubal or tubo-endometrioid metaplasia (TEM) [12, 37, 46].

TEM is considered a benign lesion in which endometrial- or fallopian tube-type cells are present in the endocervical glands due to metaplasia. This condition is characterised histologically by endocervical glands containing clear or ciliated cells, non-ciliated cells and intercalated or peg cells [5, 20, 28, 39, 40]. This lesion was originally diagnosed in women treated for cervical squamous intraepithelial neoplasia and may commonly be found in cone and hysterectomy specimens [5, 13]. It is vital that TEM is correctly recognised, as it may often mimic cGIN or AIS of the uterine cervix [28, 29, 37].

Our study highlights a potential pitfall in the use of $p16^{INK4A}$ as a marker of cervical glandular dysplasia. We used an anti-$p16^{INK4A}$ monoclonal antibody to stain cervical adenocarcinoma, its precursors and benign mimics, specifically TEM, to compare and contrast their immunohistochemical expression of $p16^{INK4A}$.

Materials and methods

Tissues and cytology samples

Cervical biopsy samples were selected from the pathology files of the Coombe Women's Hospital, Dublin. Samples were formalin fixed and paraffin embedded by conventional techniques [1]. To select the most appropriate sections for immunohistochemical examination, the original haematoxylin and eosin-stained slides of all samples were reviewed by a certified pathologist and classified according to standard criteria. Invasive cervical squamous cell carcinoma and ThinPreps of HeLa invasive squamous carcinoma cells and Caski cells were employed as a positive control to evaluate the specificity of each staining run. A total of 12 cervical glandular intraepithelial neoplasia (6 high grade and 6 low grade) cases and 11 cervical adenocarcinoma cases were selected for analysis. A total of 12 cases of TEM, 12 cases of normal cervical squamous epithelium and endocervical glands, 12 cases of endometrium (6 proliferative and 6 secretory phase endometrium) and 12 cases of normal fallopian tube were also examined for $p16^{INK4A}$ expression.

Immunohistochemistry for $p16^{INK4A}$

Sections 4-μm thick were cut from formalin-fixed and paraffin wax-embedded biopsy samples and mounted on APES (3 aminopropyltriethoxysilane)-coated glass slides. Sections were dewaxed by passage through two xylene baths and rehydrated through graded alcohols (100%, 80%, 60%, 40%). Slides were incubated in 0.3% hydrogen peroxide (H_2O_2) in methanol (Sigma) for 30 min to block endogenous peroxidase. Antigen retrieval was achieved by pressure-cooking in 0.01 M citrate buffer, pH 6, for 90 s. The slides were cooled and then transferred to Tris-buffered saline (TBS). Samples were then incubated in 0.1% bovine serum albumin (BSA) in TBS for 30 min. The BSA was decanted, and the slides were incubated for 1 h at room temperature with a purified anti-human $p16^{INK4A}$ monoclonal antibody (Pharmingen, Becton Dickinson) (1:75 dilution was made using 0.1% BSA in TBS). Slides were rinsed and incubated in the biotinylated secondary antibody (Vectastain Universal–Elite ABC Kit, Vector Laboratories) for 30 min. Excess antibody was removed by a 10-min wash in TBS. The slides were incubated in the avidin/biotin complex (Vectastain Universal–Elite ABC Kit, Vector laboratories) for 30 min and washed in TBS for a final 10 min. The slides were then incubated in approximately 200 μl of diaminobezaminidine solution (Vector Laboratories DAB substrate Kit for peroxidase) for approximately 1 min. The slides were washed in running water and counterstained briefly in Harris haematoxylin (BDH). The slides were differentiated, dehydrated, cleared and mounted in DPX (BDH).

Interpretation of $p16^{INK4A}$ expression in biopsy tissues

All formalin-fixed, paraffin wax-embedded sections that showed either strong nuclear or cytoplasmic staining were considered positive. Staining was graded qualitatively into three categories: negative, focal and diffuse staining.

Results

Immunohistochemical staining for $p16^{INK4A}$ in histologically normal tissues

Negative staining with anti-$p16^{INK4A}$ antibody was observed in normal squamous and glandular cervical epithelium. Figure 1a illustrates negative staining for $p16^{INK4A}$ normal endocervical glands. Normal endocervical stromal cells and inflammatory cells also stained negatively for $p16^{INK4A}$.

Immunohistochemical staining for $p16^{INK4A}$ in premalignant and malignant cervical glandular lesions

Diffuse cytoplasmic and nuclear staining was observed in 12 cases (6 cGIN, 6 adenocarcinoma) (Fig. 1b, c, Fig. 2a, b, c, d, Fig. 3a, b, c, d). In 2 cases (1 cGIN, 1 adenocarcinoma), there was an exclusive cytoplasmic pattern of staining. Of the cases, 7 (3 cGIN, 4 adenocarcinoma) showed strong cytoplasmic and only occasional nuclear

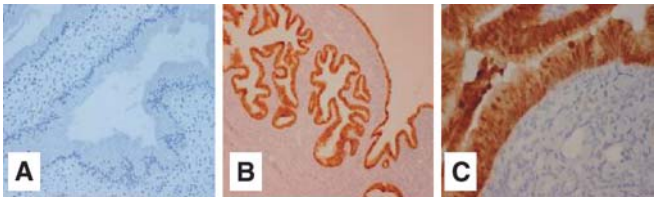


Fig. 1 **A** Normal endocervical glands. **B** Cervical adenocarcinoma, low power, p16. **C** Cervical adenocarcinoma, high power, p16

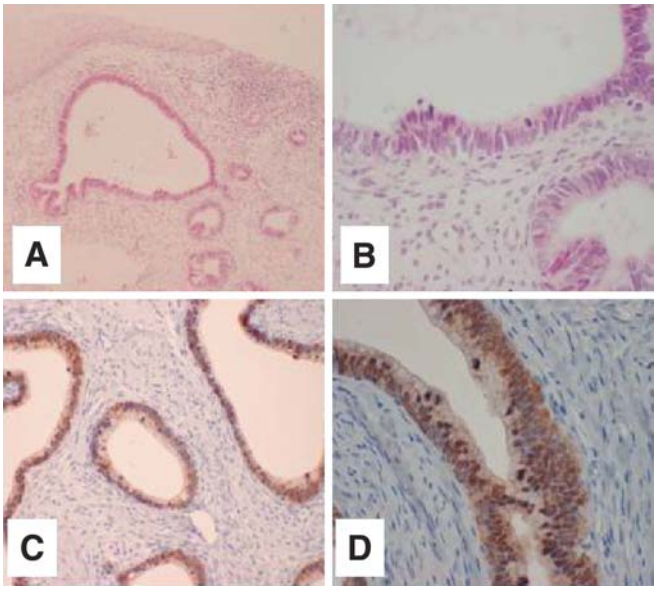


Fig. 2 Low-grade cervical glandular intraepithelial neoplasia. **A** Low power, haematoxylin and eosin (H&E). **B** High power, H&E. **C** Low power, p16. **D** High power, p16

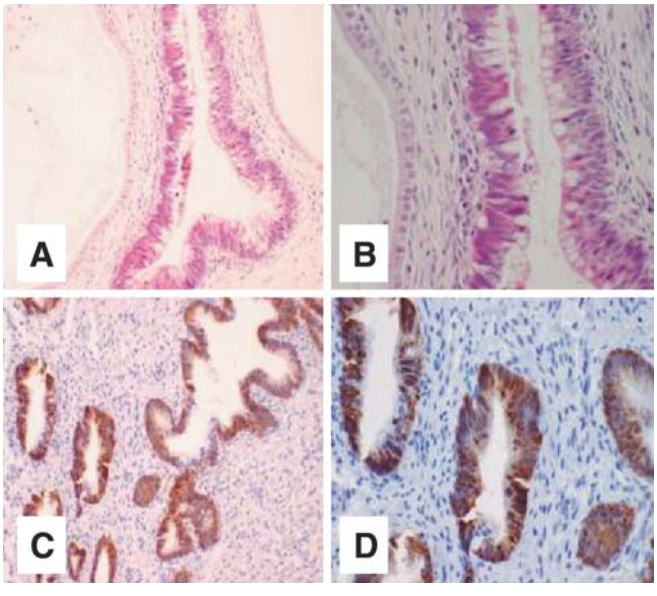


Fig. 3 High-grade cervical glandular intraepithelial neoplasia . **A** Low power, haematoxylin and eosin (H&E). **B** High power, H&E. **C** Low power, p16. **D** High power, p16

Table 1 Results of immunohistochemical analysis of $p16^{INK4A}$. *cGIN* cervical glandular intraepithelial neoplasia, *LGcGIN* low-grade cervical glandular intraepithelial neoplasia, *HGcGIN* high-grade cervical glandular intraepithelial neoplasia, *TEM* tubal or tubo-endometrioid metaplasia

	No.	Negative	Focal	Diffuse
CGIN (total)	12	0 (0%)	3 (25%)	9 (75%)
LGcGIN	6	0	3	3
HGcGIN	6	0	0	6
Cervical adenocarcinoma	11	0 (0%)	0 (0%)	11 (100%)
TEM	12	2 (16.7%)	10 (83.3%)	0 (0%)

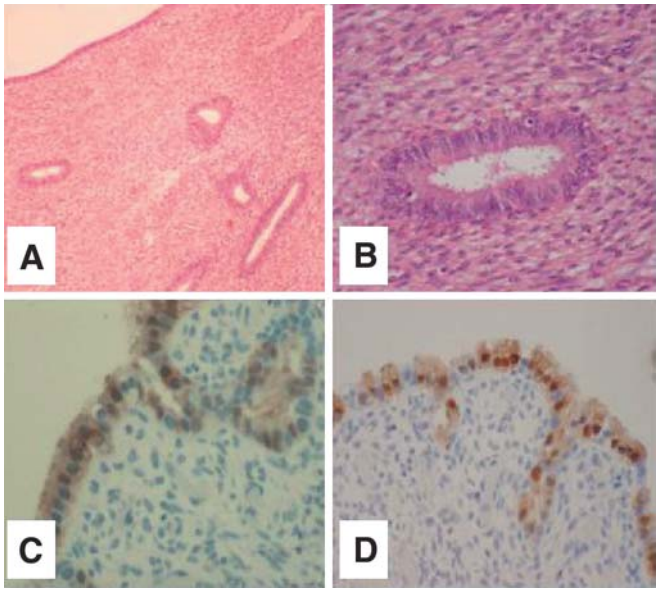


Fig. 4 Tubo-endometrioid metaplasia. **A** Low power, haematoxylin and eosin (H&E). **B** High power, H&E. **C**, **D** High power, p16

staining. Strong nuclear but weak cytoplasmic staining was noted in 2 cases of cGIN. A nuclear signal alone was not detected in any case examined (Table 1).

Immunohistochemical staining for $p16^{INK4A}$ in TEM

TEM exhibited cytoplasmic staining with occasional nuclear positivity. Normal fallopian tubes exhibited focal positive cytoplasmic staining. No staining was observed in the intercalating/peg cells (Fig. 4a, b, c, d).

Immunohistochemical staining for $p16^{INK4A}$ in the endometrium

Normal endometrial glands showed a variety of staining patterns from negative to intense positive cytoplasmic staining with occasional nuclear positivity (Fig. 5a, b). The endometrial stromal cells displayed sporadic nuclear immunopositivity (Fig. 5c).

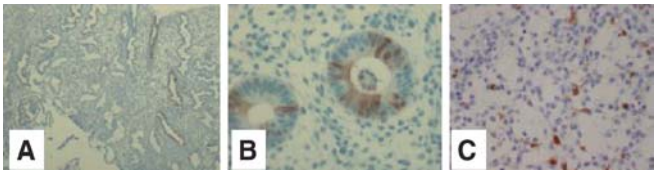


Fig. 5 Endometrium, p16. **A** Low power. **B** Endometrial glands. **C** Endometrial stroma

Discussion

In recent years, the immunohistochemical expression of $p16^{INK4A}$ in normal and squamous pre-neoplastic and neoplastic tissues of the cervix has been extensively investigated. It has been successfully demonstrated to be a reliable marker of the squamous dyskaryotic phenotype [16, 24], due to its integral relationship with the human papilloma virus proteins E6 and E7. Indeed, $p16^{INK4A}$ immunohistochemistry is performed widely to identify dysplasia in the setting of cervical intraepithelial neoplasia and invasive squamous cell carcinoma and may be a potential adjunct in automated screening programmes in the future.

Cervical adenocarcinomas now represent 15–25% of all cervical carcinomas, and evidence is accumulating that the incidence is rising [11, 35, 46]. This may be due to an increased interest in potential precursors of cervical adenocarcinomas [8] as well as a better understanding and ability of histopathologists and cytopathologists in recognising these lesions. Terminology within the area of premalignant cervical glandular lesions also varies with differences between the UK terminology and the widely used World Health Organisation classification, thus leaving the distinguishing morphological features of these lesions unsettled. Atypical glandular lesions were first identified in 1953 by Friedell and McKay [7], who described endocervical glands that showed features of cellular atypia comparable with those seen in squamous cervical intraepithelial neoplasia. These features include nuclear stratification, mitotic activity, nuclear pleomorphism and irregularity of gland structure. These lesions have been collectively described as cGIN and were categorised in 1986 by Brown and Wells [2] into low grade and high grade. AIS is equivalent to high-grade cGIN. Thus, these lesions give rise to much controversy in their diagnosis, classification and accurate detection.

In addition to this, there are many mimics of endocervical adenocarcinoma and its precursors, which may cause diagnostic difficulties both histologically and cytologically [21, 46]. The body's normal response mechanisms, such as inflammation and response to irradiation, can also result in glandular atypia [46]. Other mimics include tunnel clusters [36], microglandular hyperplasia [37, 45] and, commonly, TEM [12, 37, 46]. In this study, glands with TEM were analysed for their $p16^{INK4A}$ expression. Normal fallopian tube epithelium and normal endometrium at various stages of the menstrual cycle as well as normal squamous epithelium, normal endocervical epithelium, cGIN and cervical adenocarcinoma were also studied.

In the 12 cGIN and 11 adenocarcinoma cases obtained for analysis, $p16^{INK4A}$ overexpression was exhibited in all cases. Interestingly, the majority of cases in this study showed a combination of both nuclear and cytoplasmic staining. These findings correlate with the results of a number of other previously published studies [3, 16, 31, 34]. Sano et al. [34] reported strong immunoreactivity in both nuclei and in the cytoplasm of dysplastic glandular epithelial cells in the cervix, as did Cameron et al. [3]. Riethdorf et al. [31] and Klaes et al. [16] reported a predominantly cytoplasmic staining pattern. It is important to mention here that Klaes et al. [16] utilised a different clone of $p16^{INK4A}$ antibody from that incorporated in this study. Sano et al. [34] used the JC8 clone, while Klaes et al. [16] used E6H4, a clone derived from a hybridoma generated in their own laboratory. Presence of $p16^{INK4A}$ in the cytoplasm may be an example of post-transcriptional modification, and currently our laboratory is examining this phenomenon.

All pure histologically normal cervical tissues in this study did not show any immunohistochemical detectable $p16^{INK4A}$ expression, except in one isolated condition, i.e. TEM. This immunonegativity in normal tissue was also seen in 22 normal cases previously examined by our group. An interesting study by Nielsen et al. [26], who documented $p16^{INK4A}$ expression in normal human tissues, reported $p16^{INK4A}$ immunopositivity in some scattered normal glandular epithelial cells of the endocervix. In most normal cells, $p16^{INK4A}$ expression is known to be low at both mRNA and protein level [34]. In this regard, expression of $p16^{INK4A}$ may be immunohistochemically detectable only when $p16^{INK4A}$ is physiologically upregulated, especially in cervical neoplastic lesions.

Although $p16^{INK4A}$ has been demonstrated to be a good marker of glandular dyskaryosis in neoplastic lesions, it has one potential pitfall that may limit the utility of this biomarker in resolving the discrimination of benign from dyskaryotic cervical glandular cells—potentially limiting its diagnostic use. In this study, $p16^{INK4A}$ immunopositivity was detected in TEM, which is not associated with a dyskaryotic phenotype and, thus, may have important implications for cervical cytology and histology. Previous studies reported metaplastic cells to be $p16^{INK4A}$ immunonegative [16, 24]. Interestingly, in line with our observations, Nielsen et al. [26], who documented $p16^{INK4A}$ expression in normal human tissues, reported intense $p16^{INK4A}$ immunopositivity in TEM epithelia. They also noted that squamous metaplasia in some cervical transitional zones showed strong $p16^{INK4A}$ expression. They commented on predominantly nuclear staining, in contrast to our finding of diffuse cytoplasmic staining and occasional nuclear staining, supported by similar findings in other studies [3, 31]. However, Nielsen et al. [26] used the JC8 $p16^{INK4A}$ antibody, which may explain the different staining pattern. Riethdorf et al. [31] described a heterogeneous pattern of staining with $p16^{INK4A}$ in both tubal metaplasia and normal fallopian

tube epithelium with weak to moderate cytoplasmic staining.

$P16^{INK4A}$ immunopositivity in TEM glands may be due to resemblance with their cells of origin—endometrial cells and fallopian tube cells, which both exhibited $p16^{INK4A}$ immunostaining as demonstrated in this study, possibly related to their common origin from the Mullerian system. Normal endometrial tissue, both proliferative and secretory, has been analysed in a number of studies. Nielsen et al. [26] observed intense staining in the proliferative endometrial tissue and both positive and negative staining in the secretory type. Our studies of normal endometrial glands revealed a variety of staining patterns—from negative to intense positive cytoplasmic staining with occasional nuclear positivity. Similar findings are described by Riethdorf et al. [31].

This study highlights $p16^{INK4A}$ immunopositivity in TEM and endometrium and suggests it may be a potential pitfall in routine clinical practice. The findings of $p16^{INK4A}$ immunostaining have significant implications for the use of $p16^{INK4A}$ as a biomarker in cervical glandular dyskaryosis. In particular, the use of $p16^{INK4A}$ in conventional and Thin prep cytology samples may be limited by the potential pitfall of $p16^{INK4A}$ staining in TEM as well as cGIN and cervical adenocarcinoma. The recommendation coming from the literature is that a wide panel of immunohistochemical markers, of which $p16^{INK4A}$ is but one, should be used in differentiating benign cervical glandular lesions from dysplastic lesions [3, 4, 22].

In summary, these findings have significant implications for the analysis of glandular lesions using histopathology and cytopathology but may potentially shed new light on the underlying pathobiology of TEM and related reactive glandular lesions of the uterine cervix.

Acknowledgements Health research board, Irish Cancer Society, Royal City of Dublin Hospital Trust.

References

1. Anderson G, Gordon KC (1996) Tissue processing, microtomy and paraffin sections. In: Bancroft JD, Stevens A (eds) Theory and practice of histological techniques, 4th edn. Churchill & Livingstone, New York
2. Brown LJ, Wells M (1986) Cervical glandular atypia associated with squamous intraepithelial neoplasia: a premalignant lesion? J Clin Pathol 39:22–28
3. Cameron, RI, Maxwell, P, Jenkins D, McCluggage WG (2002) Immunohistochemical staining with MIB1, bcl2 and p16INK4A assists in the distinction of cervical glandular intraepithelial neoplasia from tubo-endometrial metaplasia, endometriosis and microglandular hyperplasia. Histopathology 41:313–321
4. Cina SJ, Richardson MS (1997) Immunohistochemical staining for Ki-67 antigen, carcinoembryonic antigen, and p53 in the differential diagnosis of glandular lesions of the cervix. Mod Pathol 10:176–180
5. Ducatman BS, Wang HH (1993) Tubal metaplasia: a cytologic study with comparison to other neoplastic and non-neoplastic conditions of the endocervix. Diagn Cytopathol 9:98–103
6. Fountain JW, Karayiorgou M, Ernstoff MS, Kirkwood JM, Volck DR, Titus-Ernstoff L, Bouchard B, Vijayasaradhi S, Houghton AN, Lahti J et al (1992) Homozygous deletions within human chromosome band 9p21 in melanoma. Proc Natl Acad Sci U S A 89:10557
7. Friedell G, McKay D (1953) Adenocarcinoma in situ of the endocervix. Cancer 6:887–897
8. Goldstein NS, Ahmad E (1998) Endocervical glandular atypia: does a preneoplastic lesion of adenocarcinoma in situ exist? Am J Clin Pathol 110:200–209
9. Havrilesky LJ, Alvarez AA, Whitaker RS, Marks JR, Berchuck A (2001) Loss of expression of the p16 tumour suppressor gene is more frequent in advanced ovarian cancers lacking p53 mutations. Gynecol Oncol 83:491–500
10. Healy E, Rehman I, Angus B, Rees JL (1995) Loss of heterozygosity in sporadic primary cutaneous melanoma. Genes Chromosomes Cancer 12:152
11. Hopkins MP, Morley GW (1991) A comparison of adenocarcinoma and squamous cell carcinoma of the cervix. Obstet Gynecol 77:912–917
12. Johnson JE, Rahemtulla A (1999) Endocervical glandular neoplasia and its mimics in ThinPrep Pap tests. A descriptive study. Acta Cytol 43:369–375
13. Jonasson JG, Wang HH (1992) Tubal metaplasia of the uterine cervix: a prevalence study in patients with gynaecological pathologic findings. Int J Gynecol Pathol 11: 89–95
14. Kamb A, Shattuck-Eidens D, Eeles R, Liu Q, Gruis NA, Ding W, Hussey C, Tran T, Miki Y, Weaver-Feldhaus J, McClure M, Aitken JF, Anderson DE, Bergman W, Frants R, Goldgar DE, Green A, MacLennan R, Martin NG, Meyer LJ, Youl P, Zone JJ, Skolnick MH, Cannon-Albright LA. (1994) Analysis of the p16 gene (CDKN2) as a candidate for the chromosome 9p melanoma susceptibility locus. Nat Genet 8:22
15. Keating JT, Cviko A, Riethdorf S, Riethdorf L, Quade BJ, Sun D, Duensing S, Sheets EE, Munger K, Crum CP (2001) Ki-67, Cyclin E, and p16 are complimentary surrogate biomarkers for human papilloma virus-related cervical neoplasia. Am J Surg Pathol 25:884–891
16. Klaes R, Friedrich T (2001) Overexpression of p16 as a specific marker for dysplastic and neoplastic epithelial cells of the cervix uteri. Int J Cancer 92:276–284
17. Krane JF, Granter SR (2001) Papanicolaou smear sensitivity for the detection of adenocarcinoma of the cervix: a study of 49 cases. Cancer 93:8–15
18. Kudoh K, Ichikawa Y, Yoshida S, Hirai M, Kikuchi Y, Nagata I, Miwa M, Uchida K (2002) Inactivation of p16/CDKN2 and p15/MTS2 is associated with prognosis and response to chemotherapy in ovarian cancer. Int J Cancer 99:579–582
19. Liao SY, Brewer C (1994) Identification of MN antigen as a marker of cervical intraepithelial squamous and glandular neoplasia and cervical carcinoma. Am J Pathol 145:598–609
20. Marques T, Andrade LA (1997) Endocervical tubal metaplasia: morphological concepts and practical importance. Rev Assoc Med Bras 43:21–24
21. McCluggage WG (2002) Recent advances in immunohistochemistry in gynaecological pathology. Histopathology 40:309–326
22. McCluggage WG (2003) Endocervical glandular lesions: controversial aspects and ancillary techniques. J Clin Pathol 56:164–173
23. McCluggage WG, Maxwell P, McBride HA, Hamilton PW, Bharucha H (1995) Monoclonal antibodies Ki67 and MIB1 in the distinction of tuboendometrial metaplasia from endocervical adenocarcinoma and adenocarcinoma in situ in formalin-fixed material. Int J Gynecol Pathol 14:209–216
24. Murphy N, Ring M, Killalea AG, Uhlmann V, O'Donovan M, Mulcahy F, McGuinness E, Griffin, Martin C, Sheils O, O'Leary JJ (2003) P16INK4A as a marker for cervical dyskaryosis: CIN and cGIN in cervical biopsies and ThinPrep smears. J Clin Pathol 56:56–63
25. Negri G, Egarter-Vigl E, Kasal A, Roman F, Haitel A, Mian C (2003) p16INK4A is a useful marker for the diagnosis of ad-

enocarcinoma of the cervix uteri and its precursors. Am J Surg Pathol 27:187–193
26. Nielsen GP, Stemmer-Rachaminov AO (1999) Immunohistochemical survey of p16 expression in normal human adult and infant tissues. Lab Invest 79:1137–1141
27. Novotny DB, Maygarden S (1992) Tubal metaplasia—a frequent potential pitfall in the cytologic diagnosis of endocervical glandular dysplasia on cervical smears. Acta Cytol 36:1–10
28. Olivia E, Clement PB (1995) Tubal and tubo-endometrioid metaplasia of the uterine cervix. Unemphasized features that may cause problems in differential diagnosis: a report of 25 cases. Am J Clin Pathol 103:618–623
29. Pacey F, Ayer B, Greenberg M (1988) The cytologic diagnosis of adenocarcinoma in situ of the cervix uteri and related lesions. III. Pitfalls in diagnosis. Acta Cytol 32:325–330
30. Riethdorf L, O'Connell JT (2000) Differential expression of MUC2 and MUC5AC in benign and malignant glandular lesions of the cervix uteri. Virchows Arch 437:365–371
31. Riethdorf L, Riethdorf S (2002) Human papillomaviruses, expression of p16 and early endocervical glandular neoplasia. Hum Pathol 33:899–904
32. Saegusa M, Machida BD, Okayasu I (2001) Possible associations among expression of p14 (ARF), p16 (INK4A), p21 (WAF1/CIP1), p27 (KIP1) and p53 accumulation and the balance of apoptosis and cell proliferation in ovarian carcinomas. Cancer 92:1177–1189
33. Saigo PE, Wolinska WH (1985) The role of cytology in the diagnosis and follow up of patients with cervical adenocarcinoma. Acta Cytol 29:785–794
34. Sano T, Oyama T (1998) Expression status of p16 protein is associated with human papilloma virus oncogenic potential in cervical and genital lesions. Am J Pathol 153:1741–1748
35. Schwartz S, Weiss N (1986) Increased incidence of adenocarcinoma of the cervix in young women in the United States. Am J Epidemiol 124:1045–1047
36. Segal GH, Hart WR (1990) Cystic endocervical tunnel clusters: a clinicopathologic study of 29 cases of so-called adenomatous hyperplasia. Am J Surg Pathol 14:895–903
37. Selvaggi SM, Haefner HK (1997) Microglandular endocervical hyperplasia and tubal metaplasia: pitfalls in the diagnosis of adenocarcinoma on cervical smears. Diagn Cytopathol 16:168–173
38. Serrano M, Lee H, Chin L, Cordon-Cardo C, Beach D, DePinho RA (1996) Role of the INK4a locus in tumour suppression and cell mortality Cell 85:27
39. Suh KS, Silverberg SG (1990) Tubal metaplasia of the uterine cervix. Int J Gynecol Pathol 9:122–128
40. Umezaki K, Sanezumi M (1998) Immunohistochemical demonstration of aberrant glycosylation and epidermal growth factor receptor in tubal metaplasia of the uterine cervix. Gynecol Oncol 70:40–44
41. Von Knebel Doeberitz M (2001) New molecular tools for efficient screening of cervical cancer. Dis Markers 17:123–128
42. Williams GH, Romanowski P, Morris L, Madine M, Mills AD, Stoeber K, Marr J, Laskey RA, Coleman N (1998) Improved cervical smear assessment using antibodies against proteins that regulate DNA replication. Proc Natl Acad Sci U S A 95:14932–14937
43. Wong YF, Chung TK (1999) Methylation of p16 in primary gynaecologic malignancy. Cancer Lett 136:231–235
44. Yoshinouchi M, Hongo A (2000) Alteration of the CDKN2/P16 gene is not required for HPV-positive uterine cervical cell lines. Int J Oncol 16:537–541
45. Young RH, Scully RE (1989) Atypical forms of microglandular hyperplasia of the cervix simulating carcinoma: a report of 5 cases and a review of the literature. Am J Surg Pathol 13:50–56
46. Zaino RJ (2000) Glandular lesions of the uterine cervix. Mod Pathol 13:261–274

Virchows Arch (2004) 445:616–620
DOI 10.1007/s00428-004-1127-9

ORIGINAL ARTICLE

Giovanni Negri · Fabio Vittadello · Fabio Romano · Armin Kasal · Francesco Rivasi · Salvatore Girlando · Christine Mian · Eduard Egarter-Vigl

P16^{INK4a} expression and progression risk of low-grade intraepithelial neoplasia of the cervix uteri

Received: 11 June 2004 / Accepted: 13 August 2004 / Published online: 9 October 2004
© Springer-Verlag 2004

Abstract The aim of the study was to evaluate the immunohistochemical expression of p16^{INK4a} as a marker of progression risk in low-grade dysplastic lesions of the cervix uteri. p16^{INK4a} immunohistochemistry was performed on 32 CIN1 with proven spontaneous regression of the lesion in the follow-up (group A), 31 (group B) with progression to CIN3 and 33 (group C) that were randomly chosen irrespective of the natural history of the lesion. p16^{INK4a} staining pattern was scored as negative (less than 5% cells in the lower third of dysplastic epithelium stained), as focally positive ($\leq$25%) and as diffuse positive (>25%). A diffuse staining pattern was detected in 43.8% of CIN1 of group A, 74.2% of group B and 56.3% of group C. No p16^{INK4a} staining was detected in 31.3% and 12.9% CIN1 lesions of groups A and B, respectively. Overall, 71.4% and 37.8% of p16^{INK4a}-negative and diffusely positive CIN1 had regressed at follow-up, whereas 28.6% and 62.2% negative and diffusely positive CIN1 were progressed to CIN3, respectively (P<0.05). All CIN3 lesions analyzed during follow-up of group B were diffusely stained for p16^{INK4a}. Although p16^{INK4a} may be expressed in low-grade squamous lesions that undergo spontaneous regression, in this study, CIN1 cases with diffuse p16^{INK4a} staining had a significantly higher tendency to progress to a high-grade lesion than p16^{INK4a}-negative cases. p16^{INK4a} may have the potential to support the interpretation of low-grade dysplastic lesions of the cervix uteri.

Keywords p16 · Immunohistochemistry · Human papilloma virus · Cervical intraepithelial neoplasia · Progression · Regression

G. Negri (✉) · F. Vittadello · F. Romano · A. Kasal · C. Mian · E. Egarter-Vigl
Department of Pathology, General Hospital Bolzano,
Via Boehler 5, 39100 Bolzano, Italy
e-mail: gneg@iol.it
Tel.: +39-0471-908156
Fax: +39-0471-908175

F. Rivasi
Department of Pathologic Anatomy and Forensic Medicine,
Section of Pathology,
University of Modena and Reggio Emilia,
Modena, Italy

S. Girlando
Department of Surgical Pathology,
S. Chiara Hospital,
Trento, Italy

Introduction

The value of p16^{INK4a} as a diagnostic marker of cervical dysplasia and carcinomas of the cervix uteri has already been demonstrated. A diffuse p16^{INK4a} staining is immunohistochemically detected in almost all high-grade precanceroses and carcinomas of squamous and glandular epithelia of the cervix, whereas reactive conditions such as squamous metaplasia and microglandular hyperplasia are, in most cases, negative or show only sporadic staining [11, 14, 16]. Conversely, p16^{INK4a} is diffusely overexpressed only in 50–60% of the low-grade lesions of the squamous epithelia (CIN1) and is typically associated with high-risk human papillomavirus (HR-HPV) infection, although HR-HPV was also demonstrated in a fraction of p16^{INK4a}-negative lesions [1, 11, 18, 24]. In fact, the incidence of HR-HPV in young women is very high, and the large majority of HPV infections are transient and regress spontaneously [7, 19, 24]. However, overexpression of p16^{INK4a} has been shown to indicate already advanced interference of the viral oncoproteins with cellular proteins involved in cell-cycle regulation [6, 17, 24]. Thus, p16^{INK4a} may serve as a surrogate marker for the oncogenic activities of HPV in replication-competent cells of cervical epithelia. This raises the question whether immunohistochemical p16^{INK4a} overexpression could also be used as a marker of progression tendency in early lesions of the cervix uteri. The possibility of finding cases with a higher tendency to progress to high-grade lesions could be of value in clinical practice [20]. Unfortunately, morphological criteria alone are not useful in distinguishing lesions that will regress from those that

will persist or progress. Several studies have already approached this issue and have evaluated the significance of HPV types [3, 9], HPV integration [5, 10], clonality [4, 23] and immunohistochemical markers on cervical lesions [8, 13, 16, 25]. However, at present, none of the techniques used in these studies seems to be able to combine simplicity, low cost and high reliability. To evaluate the overexpression of $p16^{INK4a}$ as a possible marker of progression risk of cervical precancerosis, we performed $p16^{INK4a}$ immunohistochemistry on low-grade dysplasias of the cervix uteri and compared the results with the natural history of the lesions.

Materials and methods

Overall, for this study, 127 histological samples from 96 women were stained with $p16^{INK4a}$. Specimens were reviewed by three pathologists (GN, FR, EE-V); only biopsies with a morphologically clear dysplastic lesion were chosen. All CIN1 cases had a typical abnormal enlargement of the basal third of the epithelium, associated with viral changes in the upper layers. All CIN3 cases showed a complete replacement of the epithelium by atypical cells with obvious mitotic activity. Group A included 32 CIN1 punch biopsy specimens from women with cytologically proven regression of the lesion and a negative cytological follow-up of at least 4 years (mean 9.50 years). All punch biopsies were preceded by an atypical squamous cells of undetermined significance (ASCUS) or low-grade squamous intraepithelial lesion (LSIL) cytology. Surgical or non-invasive treatment was excluded by interviewing the clinicians. Group B comprised 31 CIN1 punch biopsy specimens of women who developed a histologically proven severe dysplasia or carcinoma in situ (CIN3) in the follow-up (at least 18 months, mean 3.34 years). All CIN1 punch biopsies were preceded by an ASC-US or LSIL cytology, all CIN3 by a high-grade squamous intraepithelial lesion (HSIL) cytology. Both CIN 1 and CIN3 lesions were analyzed for $p16^{INK4a}$ expression. The mean age was 32.28 years and 33.61 years for the groups A and B, respectively. Group C consisted of an additional 33 CIN1 punch biopsy specimens, which were randomly chosen irrespective of the clinical history of the women.

For immunohistochemical analysis, a $p16^{INK4a}$ monoclonal antibody (clone E6H4, CINtec $p16^{INK4a}$ Histology Kit, DakoCytomation A/S, Glostrup, Denmark) was used. Tissue sections were cut at 2–4 μm and deparaffinized. After antigen unmasking for 40±1 min at 97.5°C in citrate buffer, pH 6.0, slides were cooled down in the solution for 20±1 min to room temperature. Endogenous peroxidase blocking was performed in 3% hydrogen peroxide for 5±1 min. The slides were then first stained with the primary antibody (1:25 for 30 min at room temperature) and then with the visualization reagent provided with the kit for 30±1 min at room temperature. After development with substrate-chromogene solution (diaminobenzidine) for 10±1 min (provided with the kit), they were finally counterstained with hematoxylin (DakoCytomation).

By the evaluation of the immunohistochemically stained slides, both nuclear and cytoplasmic staining were evaluated. CIN1 specimens with less than 5%, 5–25% and over 25% of $p16^{INK4a}$-stained cells in the lower third of the dysplastic epithelia were classified as negative, focally positive and diffuse positive, respectively. In CIN3, the whole thickness of the dysplastic epithelium was evaluated. Statistical analysis was performed using the Pearsons chi-square test. A value of $P<0.05$ was considered as statistically significant.

Results

The pattern of $p16^{INK4a}$ staining in CIN1 lesions is summarized in Table 1. Overall, $p16^{INK4a}$ was expressed in 71 of 96 CIN1 cases (74.7%). The expression pattern was typical for low-grade lesions, being particularly evident in nuclei and cytoplasm of the lower third of the dysplastic epithelia. In detail, 55 (57.9%) of the cases showed a diffuse staining pattern (>25% of cells, Fig. 1). In 16 (16.8%) specimens, the expression was only focal, albeit clearly positive (≤25% of cells, Fig. 2), and 25 (26.3%) specimens were judged as negative (<5% of cells, Fig. 3).

In group A, $p16^{INK4a}$ was expressed in 22 of 32 specimens (68.8%). The staining pattern was diffuse in 14 (43.8%), focal in 8 (25.0%) and negative in 10 (31.3%) cases, respectively.

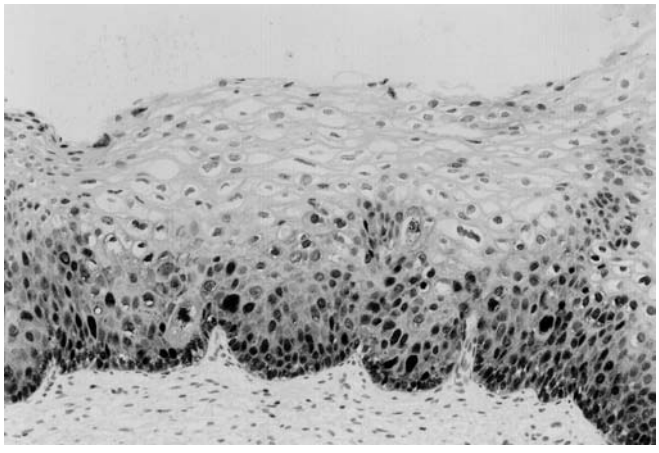


Fig. 1 CIN1 with diffuse $p16^{INK4a}$ staining in the lower third of the dysplastic epithelium

Table 1 $p16^{INK4a}$ staining in CIN1 lesions. *Group A* CIN1 with spontaneous regression of the lesion. *Group B* CIN1 with progression of the lesion to CIN3. *Group C* control group, randomly chosen CIN1 irrespective of follow-up. *Diffuse positivity* >25% of dysplastic cells in the lower third of epithelium stained, *focal positivity* ≥5%≤25%, *negative* <5%

$p16^{INK4a}$ staining	Group A (n=32)		Group B (n=31)		Group C (n=33)		All CIN1 (n=96)	
	No. cases	%	No. cases	%	No. cases	%	No. cases	%
Any positivity	22	68.8	27	87.1	22	66.7	71	74.7
Diffuse positivity	14	43.8	23	74.2	18	56.3	55	57.9
Focal positivity	8	25.0	4	12.9	4	12.5	16	16.8
Negative	10	31.3	4	12.9	11	37.4	25	26.3

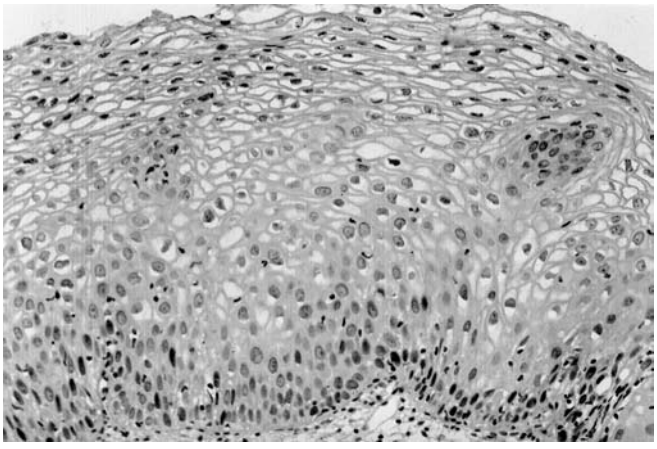


Fig. 2 CIN1 with focal p16^{INK4a} staining in the lower third of the dysplastic epithelium

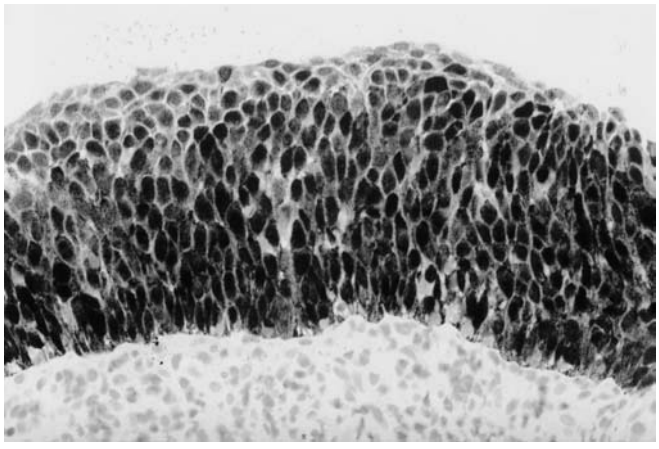


Fig. 4 CIN3 with diffuse p16^{INK4a} staining throughout all of the thickness of the epithelium

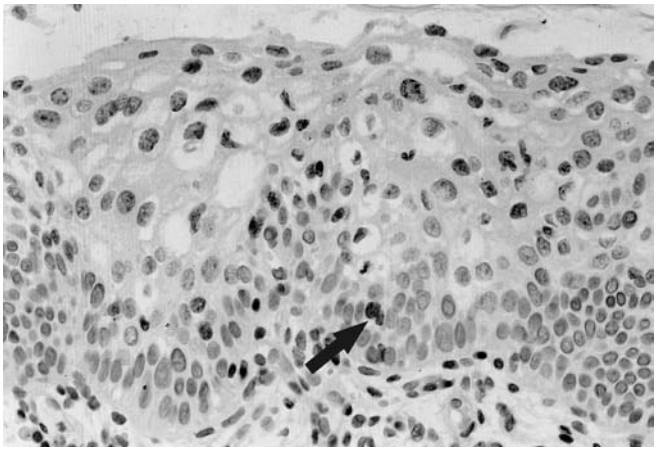


Fig. 3 CIN1 with p16^{INK4a} staining in only isolated cells (*arrow*). This case was judged as negative

Group B showed a positive p16^{INK4a} staining in 27 of 31 specimens (87.1%). The staining pattern was diffuse in 23 (74.2%), focal in 4 (12.9%) and negative in 4 (12.9%) cases, respectively. All CIN3 cases of this group stained diffusely positive (Fig. 4).

In group C, p16^{INK4a} was expressed in 22 of 33 specimens (66.7%). The staining pattern was diffuse in 18 (56.3%), focal in 4 (12.5%) and completely negative in 11 (34.4%) of the cases.

Overall, as shown in Table 2, 71.4% and 37.8% of p16^{INK4a}-negative and diffusely positive CIN1 cases regressed at follow-up, respectively, whereas 28.6% and 62.2% negative and diffusely positive CIN1, respectively, progressed to CIN3.

Statistical analysis showed a significant association between diffuse p16^{INK4a} staining and progression to CIN3, as well as between p16^{INK4a} negativity and regression at follow-up ($P<0.05$). Putting together group A and B, no significant difference in p16^{INK4a} expression was observed when compared with group C.

Discussion

The high sensitivity and specificity of p16^{INK4a} in high-grade cervical lesions is a consequence of the oncogenic mechanism of HPV. The oncogenic influence of HPV depends on the interaction of viral gene products, particularly E6 and E7, with specific host proteins. While E6 inactivates p53, E7 binds and thus inactivates the tumor suppressor protein pRB. As the transcription of the cyclin-dependent kinase inhibitor p16^{INK4a} underlies a negative feedback control by pRB, an inactivation of pRB due to HPV results in an overexpression of p16^{INK4a} in replication-competent epithelial cells [11, 24]. Immunohistochemically detected p16^{INK4a} overexpression is mostly associated with high-risk HPV types [11]. However, even if HR-HPV persistence is required for progression, not all HR-HPV-associated CIN1 are p16^{INK4a} positive, and regression of HR-HPV-associated lesions is still possible [2, 7]. Indeed, although over 80% of CIN1 are associated with HR-HPV [21], and p16^{INK4a} overexpression is detected in 50–60% of these lesions [1, 11, 18], the overall likelihood of regression of CIN1 is about 60% [15].

Table 2 p16^{INK4a} staining and progression risk of CIN1. *FU* follow-up. *Diffuse positivity* >25% of dysplastic cells in the lower third of epithelium stained, *focal positivity* ≥5%≤25%, *negative* <5%

p16^{INK4a} staining on CIN1	No. cases	Regression in FU	Progression in FU
All positive	49	22 (44.9%)	27 (55.1%)
Diffusely positive	37	14 (37.8%)	23 (62.2%)
Focally positive	12	8 (66.7%)	4 (33.3%)
Negative	14	10 (71.4%)	4 (28.6%)
Negative and focally positive	26	18 (69.2%)	8 (30.8%)

pRB inactivation by E7 is an early but necessary event in the oncogenesis of cervical carcinoma. However, it may require further molecular events, such as, for example, the induction of chromosomsal instability and the accumulation of mutations to fully develop the potential for a malignant progression of a cervical lesion [24]. Furthermore, the current status of the individual host's immune system may have a significant influence on the probability of whether an HPV infection and the lesions derived thereof are eliminated over time. Thus, it is comprehensible that despite a strong and diffuse $p16^{INK4a}$ overexpression, early lesions are still capable of regressing spontaneously.

Indeed, in the present study, $p16^{INK4a}$ was expressed in a substantial fraction of CIN1 lesions that underwent spontaneous regression. Altogether, 68.8% of these lesions stained at least focally with $p16^{INK4a}$. However, a significant difference between group A and group B was observed when considering only cases with diffuse or negative staining patterns. Overall, 71.4% and 37.8% of $p16^{INK4a}$-negative and diffusely positive CIN1 regressed at follow-up, respectively, whereas 28.6% and 62.2% negative and diffusely positive CIN1 lesions progressed to CIN3, respectively. Conversely, focally positive lesions showed a tendency to regression rather than to progression. Statistical analysis revealed a significant association between diffuse $p16^{INK4a}$ staining and progression to CIN3, as well as between $p16^{INK4a}$ negativity and regression at follow-up. The probability of a progression of the lesion in this study was therefore significantly higher for the CIN1 cases characterized by a diffuse $p16^{INK4a}$ staining. However, $p16^{INK4a}$-negative lesions can also progress to CIN3, even though these cases are significantly more rare than negative lesions, which regress at follow-up.

Previous studies describe a correlation between degree of atypia of CIN1 and $p16^{INK4a}$ expression [11, 22]. However, because of the already low reproducibility of the CIN1 diagnosis [12], it may be questionable whether a further distinction of different degrees of atypia would be practicable. In the present study, only cases with clear dysplastic changes were included, and although CIN1 cases with particularly evident atypia in the lower third of the epithelium were mostly diffusely stained with $p16^{INK4a}$, it was not possible to draw a definite correlation between $p16^{INK4a}$ staining intensity and morphology.

Apart from this, the results of our study confirm that $p16^{INK4a}$ is a specific marker for high-grade lesions of the cervix uteri. The cyclin-dependent kinase inhibitor $p16^{INK4a}$ was diffusely expressed in all CIN3 cases, whereas adjacent reactive or normal epithelia were consistently negative.

There are some limitations in this study. Unfortunately, no HPV data were available for the CIN1 cases enrolled in this evaluation study. Thus, any potential correlation between the $p16^{INK4a}$ staining pattern, the type of HPV infection(s) underlying the low-grade lesions and the progression rate of the CIN1 lesions could not be assessed. However, based on Hybrid Capture II (Digene, Gaithersburg, MD) testing, in general, an HR-HPV infection is detected in 88% of liquid-based cervical cytology specimens with a LSIL diagnosis in our institution. This observation agrees with data of previously performed studies, which describe that more than 80% of CIN1 lesions are associated with HR-HPV [21]. Conversely, only 50–60% of CIN1 are $p16^{INK4a}$ positive, and HR-HPV may also be detected in a number of $p16^{INK4a}$-negative cases [11]. Thus, although it cannot be excluded that in this study some $p16^{INK4a}$-negative CIN1 lesions that regressed were associated with a low-risk HPV, this should be a sporadic event. Obviously, whereas regression of $p16^{INK4a}$-positive lesions is relatively easy to demonstrate, evaluation of progression tendency of CIN1 lesions is more difficult. CIN1 lesions may coexist with high-grade dysplasias, and, in some cases, only the low-grade, $p16^{INK4a}$-negative lesion may be bioptically detected due to a sampling error. However, in this study, all CIN1 punch biopsies were preceded only by an ASC-US or LSIL cytology, and all progressive cases developed a cytological HSIL prior to the histological diagnosis of CIN3.

Finally, it is possible that $p16^{INK4a}$-negative lesions become positive only after the time of biopsy. This is a general limitation in studies assessing the progression risk on small bioptical specimens, independently of the used marker, and it may be avoided only by prospective studies with close follow-up using cytology, immunocytochemistry and HPV typing.

In summary, although $p16^{INK4a}$ may be expressed in low-grade squamous lesions that undergo spontaneous regression, in this study, CIN1 cases with diffuse $p16^{INK4a}$ staining had a significantly higher tendency to progress to a high-grade lesion than $p16^{INK4a}$-negative cases. Thus, $p16^{INK4a}$ immunohistochemistry could help to clarify the still somewhat confusing definition of low-grade dysplastic lesion and to distinguish true dysplastic lesions with higher progression risk from those which could rather be defined with the more general term of "HPV-induced cytopathic effect."

Acknowledgements This study was only possible thanks to the cooperation of over 30 clinicians—too many to be acknowledged individually—which was essential for assessing the follow-up of the cases. We are grateful to Dr. Ruediger Ridder, Heidelberg, for helpful scientific discussions.

References

1. Agoff NS, Lin P, Morihara J, Mao C, Kiviat NB, Koutsky LA (2003) $p16^{INK4a}$ expression correlates with degree of cervical neoplasia: a comparison with Ki-67 expression and detection of high-risk HPV types. Mod Pathol 16:665–673
2. Chan JK, Monk BJ, Brewer C Keefe KA, Osann K, McMeekin S, Rose GS, Youssef M, Wilczynski SP, Meyskens FL, Berman ML (2003) HPV infection and number of lifetime sexual partners are strong predictors for "natural" regression of CIN2 and 3. Br J Cancer 15:1062–1066
3. Dalstein V, Riethmuller D, Pretet JL Le Bail Carval K, Sautiere JL, Carbillet JP, Kantelip B, Schaal JP, Mougin C (2003) Persistence and load of high-risk HPV are predictors for de-

velopment of cervical lesions: a longitudinal French cohort study. Int J Cancer 106:396–403
4. El Hamidi A, Kocjan G, Du M-Q (2003) Clonality analysis of archival cervical smears. Correlation of monoclonality with grade and clinical behaviour of cervical intraepithelial neoplasia. Acta Cytol 47:117–123
5. Gallo G, Bibbo M, Bagella L Zamparelli A, Sanseverino F, Giovagnoli MR, Vecchione A, Giordano A (2003) Study of viral integration of HPV-16 in young patients with LSIL. J Clin Pathol 56:532–536
6. Giarre M, Caldeira S, Malanchi I Ciccolini F, Leao MJ, Tommasino M (2001) Induction of pRb degradation by the human papillomavirus type 16 E7 protein is essential to efficiently overcome p16INK4a-imposed G1 cell cycle arrest. J Virol 75:4705–4712
7. Ho GYF, Bierman R, Beardsley L, Chang CJ, Burk RD (1998) Natural history of cervicovaginal papillomavirus infection in young women. N Engl J Med 338:423–428
8. Huang LW, Chao SL, Chen TJ (2003) Reduced Fhit expression in cervical carcinoma: correlation with tumor progression and poor prognosis. Gynecol Oncol 90:331–337
9. Kjaer SK, van den Brule AJ, Paull G Svare EI, Sherman ME, Thomsen BL, Suntum M, Bock JE, Poll PA, Meijer CJ (2002) Type specific persistence of high risk human papillomavirus (HPV) as indicator of high grade cervical squamous intraepithelial lesions in young women: population based prospective follow up study. BMJ 325:572
10. Klaes R, Woerner SM, Ridder R Wentzensen N, Duerst M, Schneider A, Lotz B, Melsheimer P, von Knebel Doeberitz M (1999) Detection of high-risk cervical intraepithelial neoplasia and cervical cancer by amplification of transcripts derived from integrated papillomavirus oncogenes. Cancer Res 59:6132–6136
11. Klaes R, Friedrich T, Spitkowsky D, Ridder R, Rudy W, Petry U, Dallenbach-Hellweg G, Schmidt D, von Knebel Doeberitz M (2001) Overexpression of p16INK4a as a specific marker for dysplastic and neoplastic epithelial cells of the cervix uteri. Int J Cancer 92:276–284
12. Klaes R, Benner A, Friedrich T, Ridder R, Herrington S, Jenkins D, Kurman RJ, Schmidt D, Stoler M, von Knebel Doeberitz M (2002) p16INK4a immunohistochemistry improves interobserver agreement in the diagnosis of cervical intraepithelial neoplasia. Am J Surg Pathol 26:1389–1399
13. Kruse AJ, Baak JP, Janssen EA Bol MG, Kjellevold KH, Fianne B, Lovslett K, Bergh J (2003) Low- and high-risk CIN 1 and 2 lesions: prospective predictive value of grade, HPV, and Ki-67 immuno-quantitative variables. J Pathol 199:462–470
14. Negri G, Egarter-Vigl E, Kasal A, Romano F, Haitel A, Mian C (2003) $p16^{INK4a}$ is a useful marker for the diagnosis of adenocarcinoma of the cervix uteri and its precursors. An immunohistochemical study with immunocytochemical correlations. Am J Surg Pathol 27:187–193
15. Ostor AG (1993) Natural history of cervical intraepithelial neoplasia: a critical review. Int J Gynecol Pathol 12:186–192
16. Ozalp SS, Yalcin OT, Tanir HM Dundar E, Yildirim S (2002) Bcl-2 expression in preinvasive and invasive cervical lesions. Eur J Gynaecol Oncol 23:419–422
17. Sano T, Oyama T, Kashiwabara K, Fukuda T, Nakajima T (1998) Expression status of p16 protein is associated with human papilloma virus oncogenic potential in cervical and genital lesions. Am J Pathol 153:1741–1748
18. Sano T, Oyama T, Kashiwabara K, Fukuda T, Nakajima T (1998) Immunohistochemical overexpression of p16 protein associated with intact retinoblastoma protein expression in cervical cancer and cervical intraepithelial neoplasia. Pathol Int 48:580–585
19. Schlecht NF, Platt RW, Duarte-Franco E Costa MC, Sobrinho JP, Prado JC, Ferenczy A, Rohan TE, Villa LL, Franco EL (2003) Human papillomavirus infection and time to progression and regression of cervical intraepithelial neoplasia. J Natl Cancer Inst 95:1336–1343
20. Schneider V (2003) CIN prognostication: will molecular techniques do the trick? Acta Cytol 47:115–116
21. The Atypical Squamous Cells of Undetermined Significance/Low-Grade Squamous Intraepithelial Lesions Triage Study (ALTS) Group (2000) Human papillomavirus testing for triage of women with cytologic evidence of low-grade squamous intraepithelial lesions: baseline data from a randomized trial. J Natl Cancer Inst 92:397–402
22. Tringler B, Gup CJ, Singh M, Groshong S, Shroyer AL, Heinz DE, Shroyer KR (2004) Evaluation of p16INK4a and pRb expression in cervical squamous and glandular neoplasia. Hum Pathol 35:689–696
23. Ueda J, Enomoto T, Miyatake T Ozaki K, Yoshizaki T, Kanao H, Ueno Y, Nakashima R, Shroyer KR, Murata Y (2003) Monoclonal expansion with integration of high-risk human papillomavirus is an initial step for cervical carcinogenesis: association of clonal status and human papillomavirus infection with clinical outcome in cervical intraepithelial neoplasia. Lab Invest 83:1517–1527
24. von Knebel Doeberitz M (2002) New markers for cervical dysplasia to visualise the genomic chaos created by aberrant oncogenic papillomavirus infections. Eur J Cancer 38:2229–2242
25. Wollscheid V, Kuhne-Heid R, Stein I Jansen L, Kollner S, Schneider A, Durst M (2002) Identification of a new proliferation-associated protein NET-1C4.8 characteristic for a subset of high-grade cervical intraepithelial neoplasia and cervical carcinomas. Int J Cancer 99:771–775

Virchows Arch (2004) 445:621–630
DOI 10.1007/s00428-004-1113-2

ORIGINAL ARTICLE

M. Wuelling · G. Delling · E. Kaiser

Differential gene expression in stromal cells of human giant cell tumor of bone

Received: 8 June 2004 / Accepted: 2 August 2004 / Published online: 23 September 2004
© Springer-Verlag 2004

Abstract Giant cell tumor (GCT) offers a unique model for the hematopoietic–stromal cell interaction in human bone marrow. Evidence has been presented that GCT stromal cells (GCTSCs) promote accumulation, size and activity of the giant cells. Although GCTSCs are considered the neoplastic component of GCT, little is known about their genetic basis and, to date, a tumor-specific gene expression pattern has not been characterized. Mesenchymal stem cells (MSCs) have been identified as the origin of the GCT neoplastic stromal cell. Using state of the art array technology, expression profiling was applied to enriched stromal cell populations from five different GCTs and two primary MSCs as controls. Of the 29 differentially expressed genes found, 25 showed an increased expression. Differential mRNA expression was verified by real-time polymerase chain reaction analysis of 10 selected genes, supporting the validity of cDNA arrays as a tool to identify tumor-related genes in GCTSCs. Increased expression of two oncogenes, JUN and NME2, was substantiated at the protein level, utilizing immunohistochemical evaluation of GCT sections and Western-blot analysis. Increased phosphorylation of JUN Ser-63 was also found.

Keywords Bone tumor · c-DNA array · Mesenchymal stem cells · mRNA expression

Introduction

The giant cell tumor (GCT) is comprised of three cell types: the characteristic multinucleated giant cells, CD68-positive monocytes, and mononucleated fibroblast-like stromal cells [6]. The neoplastic component of GCT appears to be the stromal cells (GCTSCs), as has been confirmed by the expression of the proliferation markers MDM 2 and Ki67 [1] and the finding that only the stromal cells survive cell culturing [29]. It is assumed that through the secretion of a variety of cytokines, GCTSCs promote the migration of monocytes and their fusion into multinucleated giant cells, thus supporting the hypothesis that monocytes and giant cells are reactive tumor components [22, 29]. A recent study [28] demonstrated that GCTSCs most likely derive from undifferentiated mesenchymal stem cells (MSCs), substantiating the hypothesis of Robinson et al. [8, 22].

Very few studies have investigated the genetic profile of GCTs [1, 29]. In this study, we aimed to trace the transformation process leading to neoplastic stromal cells through determination of differentially expressed genes in GCTSCs. It was assumed that if cancer-related gene expression could be observed, then GCTSCs could be presumed to be decisive in the development and maintenance of GCTs. In addition, functional analysis of the differentially expressed genes could convey new insights into stromal–hematopoietic cell interaction in GCTs. Normal MSCs were chosen as control cells not only because they display a GCTSC-like phenotype but, moreover, because recent evidence has suggested that GCTSCs originate from MSCs [8, 28].

M. Wuelling · G. Delling · E. Kaiser (✉)
Department of Bone Pathology,
Center of Biomechanics, University Hospital Hamburg-Eppendorf,
Lottestrasse 59, 22529 Hamburg, Germany
e-mail: ekaiser@uke.uni-hamburg.de
Tel.: +49-40-428036364
Fax: +49-40-428039636

Materials and methods

Cell culture

Tumor samples from 16 different GCTs were surgically obtained (Table 1). Tumor tissue was mechanically dissected and digested with 200 U/ml collagenase (GibcoBRL, Karlsruhe, Germany) for 1 h at 37°C. The cells were collected by centrifugation and plated in culture flasks with complete α-MEM (1% Penicillin/Streptomycin (Pen/Strep), 10% fetal calf serum, 1% glutamine) at 37°C, 5% CO_2. Confluent monolayers were passaged by incubation in 1% trypsin-ethylenediaminetetraacetate (GibcoBRL) for 5 min. After the third passage, the GCT cell culture consisted of homogeneous fibroblast-like GCTSCs. As determined using immunohistochemistry, described in Wuelling et al. [28], the cell culture no longer contained giant cells or their monocytic precursors. The specific antibodies

Table 1 Patient age, tumor, localization and analysis method of 16 analyzed giant cell tumors (GCTs). Diagnosis of tumor was confirmed by two independent pathologists. *a* cDNA array, *b* real-time PCR, *c* immunohistochemistry, *d* Western-blot analysis

GCT sample	Age (years)	Localization	Methods
1	57	Left pelvis	a
2	63	Right distal radius epiphysis	a
3	42	Right distal femur epiphysis	a, b, d
4	24	Left distal femur epiphysis	a
5	46	OS sacrum	a, b
6	41	Right proximal tibia epiphysis	b
7	24	Right distal femur epiphysis	b
8	39	Right proximal tibia epiphysis	b
9	20	Right distal tibia epiphysis	b
10	18	Right distal femur epiphysis	d
11	17	Right distal femur epiphysis	d
12	25	Left proximal tibia epiphysis	c, d
13	33	OS metacarpus, left thumb	d
14	64	Right proximal tibia epiphysis	d
15	57	Left OS ishium	d
16	26	Right distal femur epiphysis	d

utilized have been previously described in Wuelling et al. [28]. Protein extracts from GCT-derived cryo-preserved GCTSCs (Table 1: GCT 10–15) and extracts from re-cultured GCTSCs (Table 1: GCTs 11r and 16r) were analyzed using Western-blot analysis. GCTSC cultures from up to six passages were used for RNA isolation. Normal MSCs were obtained from BioWhittaker (Verviers, Belgium) and propagated in Poietics MSCGM–Mesenchymal Stem Cell Medium.

RNA isolation and cDNA arrays

Total RNA was extracted from five GCTSC samples (Table 1: GCTs 1–5) and two MSC cultures using Trizol (GibcoBRL) according to the manufacturer's instructions. Total RNA (25 µg) was used for the mRNA isolation with the "Atlas Pure RNA Isolation System" as recommended by the manufacturer's protocol. Probe mixture synthesis was performed by reverse transcribing the isolated mRNAs, utilizing the array-specific cDNA Synthesis Primer Mix and 3000 Ci/mmol α^{32}-dATP (Amersham-Pharmacia, Freiburg, Germany). Unincorporated α^{32}-dATP was removed with the "NucleoSpin Kit" (Clontech, Heidelberg, Germany). The activity of each labeled cDNA sample was tested in a scintillation counter, and samples with an activity over 5×10^6 cpm/ml were used to hybridize the "Atlas Human Cancer 1.2 cDNA Arrays" (Clontech, Heidelberg, Germany) according to the manufacturer's protocol with 1176 tumor-relevant genes. Following high-stringency washing, the hybridization pattern was quantified on a phosphorimager and evaluated with "Atlas Image 2.0 software" (Clontech).

Due to the limited amount of primary tumor samples available, Clontech blots were utilized, as they require much less RNA for probe preparation than other microarrays. Although RNA amplification procedures have been developed, these techniques may result in a biased amplification of certain RNA subpopulations. Also, other recent publications acknowledge the value of Atlas Human cancer 1.2 cDNA Expression Arrays as an inexpensive and practical methodology that provides manageable numbers of differentially expressed genes within a particular area of research interest [25, 31].

Computational analysis

To obtain a patient-independent expression pattern, five GCTSC samples and both MSC samples were aligned and the obtained data averaged for each cell type. This reduced patient-specific gene expression and ensured the selection of expressed tumor genes. The expression pattern of all arrays was normalized to the glyceraldehyde-3-phosphate-dehydrogenase (GAPDH) expression spotted on the array. Genes with a signal intensity ratio above 1.5 and an intensity difference of 1500 were detected as differentially expressed. Signal intensity ratio greater than or equal to 1.5 meant that the background-adjusted GAPDH-normalized intensity of the combined GCTSC mRNAs expression levels showed at least a 1.5-fold difference in signal intensity compared with the background-adjusted intensity of the combined MSC control mRNAs expression levels. Intensity differences greater than or equal to 1500 meant that the background-adjusted GAPDH-normalized intensity of the combined GCTSC mRNA expression levels compared with the background-adjusted intensity of the combined MSC control mRNAs expression levels was at least 1500. If both gene signals were above background level, both parameters had to be met. If the ratio could not be determined because a gene signal was less than or equal to the background level, an intensity difference of greater than 1500 was required. Applying this strategy excluded genes that demonstrated adjusted intensity ratios of 1.5 with small adjusted intensity differences (smaller than 1500). It also excluded those genes that were upregulated, compared with their unexpressed counterparts, but that only demonstrated adjusted intensity differences less than 1500. Applying this approach, signals that were barely above background levels were more critically evaluated.

Real-time polymerase chain reaction

Ten genes were selected as candidate genes associated with GCT development based on previous studies (Table 2). The oligonucleotide sequences of the ten differentially expressed genes were obtained from Clontech, and specific primer pairs were ordered from Invitrogen (Groningen, Netherlands). The mRNA of the GCTSCs (Table 1: GCTs 3, 5–9) and MSCs were transcribed into cDNA with the "Ready to Go You Prime First-Strand Beads" (Amersham-Pharmacia, Freiburg, Germany) with random primers (GibcoBRL) for 60 min at 37°C. Real-time polymerase chain reaction (PCR) was performed with the "Light Cycler Fast Start DNA Master SYBR Green I Kit" (Roche, Mannheim, Germany) in a "Roche Light Cycler System". The analyzed mRNA expression was normalized to the GAPDH expression of each sample. The mean mRNA expression value of all GCTSCs and MSCs was calculated to illustrate the differences between the cell types and included in Table 2. Also, the median and the range (minimum and maximum) was determined and depicted in Fig. 1.

Immunohistochemical studies

Sections 4 µm thick of paraffin-embedded tumor samples were prepared. Antigen retrieval was accomplished through microwaving (15 min with intervals until boiling, 800 Watt) in Antigen Retrieval Solution (Dako, Hamburg) followed by 20 min cooling. GCT sections were then screened with primary antibodies (1:100) for the expression of NME2 (BD Transduction Laboratories, Heidelberg), JUN (H-79) (Santa Cruz, Heidelberg), pJUN (1:20, KM-1, sc-822, Santa Cruz, Heidelberg, Germany), and CD68 (Dako) antigens, utilizing the alkaline phosphatase anti-alkaline phosphatase technique (Dako) according to the manufacturer's instructions.

Western-blot analysis

GCTSCs and MSCs were lysed using Laemmli buffer supplemented with Complete Mini Protease Inhibitor (Roche, Mannheim, Germany) and Phosphatase Inhibitor Cocktail II (Sigma, Munich, Germany) as described elsewhere [21]. Total protein extracts were separated on sodium dodecyl sulfate-polyacrylamide gels (15% resolving/4% stacking), transferred to 0.45-mm nitrocellulose membranes, and blocked with 5% bovine serum albumin and 2% normal swine serum (NSS) in 10 mM Tris-HCl pH 8, 150 mM

Table 2 The "ratio array" is determined by the comparison of the mean gene expression values from array evaluation of five different giant cell tumor stromal cells (GCTSC) (Table 1: GCTs 1–5) and two mesenchymal stem cell (MSC) populations applying the "Atlas Image 2.0 software" (Clontech). Bold script marks genes verified by real-time polymerase chain reaction (PCR). The "ratio PCR" is determined by the comparison of the mean gene expression values from the real-time PCR evaluation of six different GCTSC (Table 1: GCTs 3, 5–9) and three MSC populations. – represents reduced expression in GCTSC compared with MSC mRNA. *ND* not determined. The direction of genetic regulation observed in real-time PCR mRNA expression always corresponded with the genetic regulation in the specific cDNA arrays. *GO* annotations were obtained from http://www.geneontology.org

Name of gene	Gene symbol	Ratio array	Ratio PCR	Gen-bank number	GO biological process description	GO molecular function description	GO cellular component description
Protein (NM23B) expressed in non-metastatic cells 2	*NME2*	1.57	1.83	L16785	Nucleoside triphosphate biosynthesis /// UTP biosynthesis /// negative regulation of cell cycle /// CTP biosynthesis /// regulation of transcription, DNA-dependent /// GTP biosynthesis /// negative regulation of cell proliferation	Transferase activity /// ATP binding /// nucleoside-diphosphate kinase activity /// kinase activity /// transcription factor activity	Nucleus
v-jun sarcoma virus 17 oncogene homolog (avian)	*JUN*	2.46	3.85	J04111	Cell growth and/or maintenance /// regulation of transcription, DNA-dependent	Transcription factor activity /// RNA polymerase II transcription factor activity	Nuclear chromosome
Low density lipoprotein receptor-related protein associated protein 1	*LRPAP1, α2-MRaP*	4.83	3.15	M63959	Cell proliferation /// vesicle-mediated transport /// protein folding	Asialoglycoprotein receptor activity /// calcium ion binding /// heparin binding /// lipoprotein binding /// chaperone activity	Integral to membrane /// plasma membrane
Calmodulin 1 (phosphorylase kinase, delta)	*CALM1*	1.53	2.51	D45887	G-protein coupled receptor protein signaling pathway	Calcium ion binding /// protein binding	Plasma membrane /// cytoplasm
Cathepsin L	*CTSL*	1.52	4.35	X12451	Proteolysis and peptidolysis	Hydrolase activity /// cathepsin L activity /// Peptidase_C1;cysteine-type peptidase activity	Lysosome
Decorin	*DCN*	1.55	4.04	M14219	Histogenesis and organogenesis	–	Extracellular matrix
Interleukin 6 (interferon, beta 2)	*IL6*	1.67	2.88	X04602	–	IL6; cytokine activity	–
Prostate differentiation factor	*PLAB*	2.45	15.27	AF019770	–	–	–
Tissue inhibitor of metalloproteinase 3 (Sorsby fundus dystrophy, pseudoinflammatory)	*TIMP3*	–6.43	–3.55	Z30183	Proteolysis and peptidolysis	Metalloendopeptidase inhibitor activity	–
Fibronectin 1	*FN1*	–8.67	–2.85	X02761	Signal transduction /// cell adhesion /// cell motility	Cell adhesion molecule activity	fn1; extracellular /// extracellular space /// soluble fraction /// extracellular matrix

Table 2 (continued)

Name of gene	Gene symbol	Ratio array	Ratio PCR	Gen-bank number	GO biological process description	GO molecular function description	GO cellular component description
Insulin-like growth factor-binding protein 3	*IGFBP3*	4.10	ND	M31159	Signal transduction /// regulation of cell growth	Insulin-like growth factor binding	Extracellular space
Growth arrest-specific 6	*GAS6*	1.54	ND	L13720	Cell proliferation /// signal transduction	Calcium ion binding /// receptor binding	Extracellular
Eukaryotic translation elongation factor 1 alpha 1	*EEF1A1*	2.17	ND	M27364	Oncogenesis /// translational elongation /// regulation of cell shape /// regulation of translation	GTP_EFTU; translation elongation factor activity /// GTP binding	Cytoplasm /// eukaryotic translation elongation factor 1 complex
Eukaryotic translation elongation factor 2	*EEF2*	5.78	ND	X51466	Translational elongation	GTP binding /// translation elongation factor activity	–
Transmembrane trafficking protein	*TMP21*	2.91	ND	X97442	Intracellular protein transport /// ER to Golgi transport	Protein transporter activity /// protein carrier activity	Microsome /// Golgi apparatus /// membrane fraction /// integral to plasma membrane
TRAM	*TRAM1*	1.92	ND	X63679	Protein targeting /// cotranslational membrane targeting	Endoplasmic reticulum receptor activity	Integral to membrane /// endoplasmic reticulum
Low density lipoprotein-related protein 1 (alpha-2-macroglobulin receptor)	*LRP1*	6.04	ND	X13916	Endocytosis /// cell proliferation /// lipid metabolism /// pathogenesis	Receptor activity /// calcium ion binding /// lipid transporter activity /// lipoprotein binding	Membrane fraction /// coated pit /// integral to plasma membrane
Likely ortholog of mouse plexin 3	PLXN3	1.87	ND	X87852	–	–	–
Integrin, alpha E (antigen CD103, human mucosal lymphocyte antigen 1; alpha polypeptide)	*ITGAE*	1.63	ND	L25851	Leukocyte cell adhesion /// cell-matrix adhesion /// integrin-mediated signaling pathway	Cell adhesion receptor activity /// receptor activity /// magnesium ion binding	Integrin complex /// integral to membrane
Insulin-like growth factor-binding protein 4	*IGFBP4*	2.59	ND	M62403	Regulation of cell growth /// signal transduction /// DNA metabolism /// cell proliferation /// skeletal development	Insulin-like growth factor binding	Extracellular
Superoxide dismutase 1, soluble [amyotrophic lateral sclerosis 1 (adult)]	*SOD1*	2.56	ND	K00065	Neurogenesis /// response to oxidative stress /// superoxide metabolism	Iron superoxide dismutase activity /// oxidoreductase activity /// copper, zinc superoxide dismutase activity /// nickel superoxide dismutase activity /// metal ion binding /// antioxidant activity /// manganese superoxide dismutase activity	Cytoplasm

Table 2 (continued)

Name of gene	Gene symbol	Ratio array	Ratio PCR	Gen-bank number	GO biological process description	GO molecular function description	GO cellular component description
Vimentin	*VIM*	5.83	ND	X56134	–	–	–
A kinase (PRKA) anchor protein (gravin) 12	*AKAP12*	1.86	ND	M96322	–	PkinA_anch; protein transporter activity	–
Ribonuclease 6 Precursor	*RNASE6PL*	3.14	ND	U85625	RNA catabolism	Ribonuclease_T2; RNA binding /// ribonuclease activity	Extracellular
Transforming growth factor, beta-induced, 68 kDa	*TGFBI*	4.64	ND	M77349	Fasciclin; cell adhesion	–	–
Regulator of G protein signaling 4	*RGS4*	–2.37	ND	U27768	Inactivation of MAPK /// signal transduction /// regulation of G-protein coupled receptor protein signaling pathway	Signal transducer activity /// calmodulin binding /// GTPase activator activity	–
Ribosomal protein S5	*RPS5*	2.06	ND	U14970	Protein biosynthesis	RNA binding /// structural constituent of ribosome	Intracellular /// ribosome /// cytosolic small ribosomal subunit (sensu Eukarya)
Ribosomal protein S16	*RPS16*	–1.95	ND	M60854	Protein biosynthesis	RNA binding /// structural constituent of ribosome	Intracellular /// ribosome /// cytosolic small ribosomal subunit (sensu Eukarya)
Fatty acid synthase	*FASN*	1.56	ND	S80437	Biosynthesis /// fatty acid biosynthesis	[Acyl-carrier protein] hydrolase activity /// lauroyl-[acyl-carrier protein] hydrolase activity /// enoyl-[acyl-carrier protein] reductase (NADPH, B-specific) activity /// oleoyl-[acyl-carrier protein] hydrolase activity /// 3-oxoacyl-[acyl-carrier protein] synthase activity /// alcohol dehydrogenase activity, zinc-dependent /// 3-oxoacyl-[acyl-carrier protein] reductase activity /// zinc ion binding /// ketoacyl-synt;catalytic activity /// [acyl-carrier protein] S-malonyltransferase activity /// lyase activity /// palmitoyl-[acyl-carrier protein] hydrolase activity /// S-adenosyl-methionine-dependent methyltransferase activity /// oxidoreductase activity /// hydrolase activity, acting on ester bonds /// myristoyl-[acyl-carrier protein] hydrolase activity /// transferase activity	–

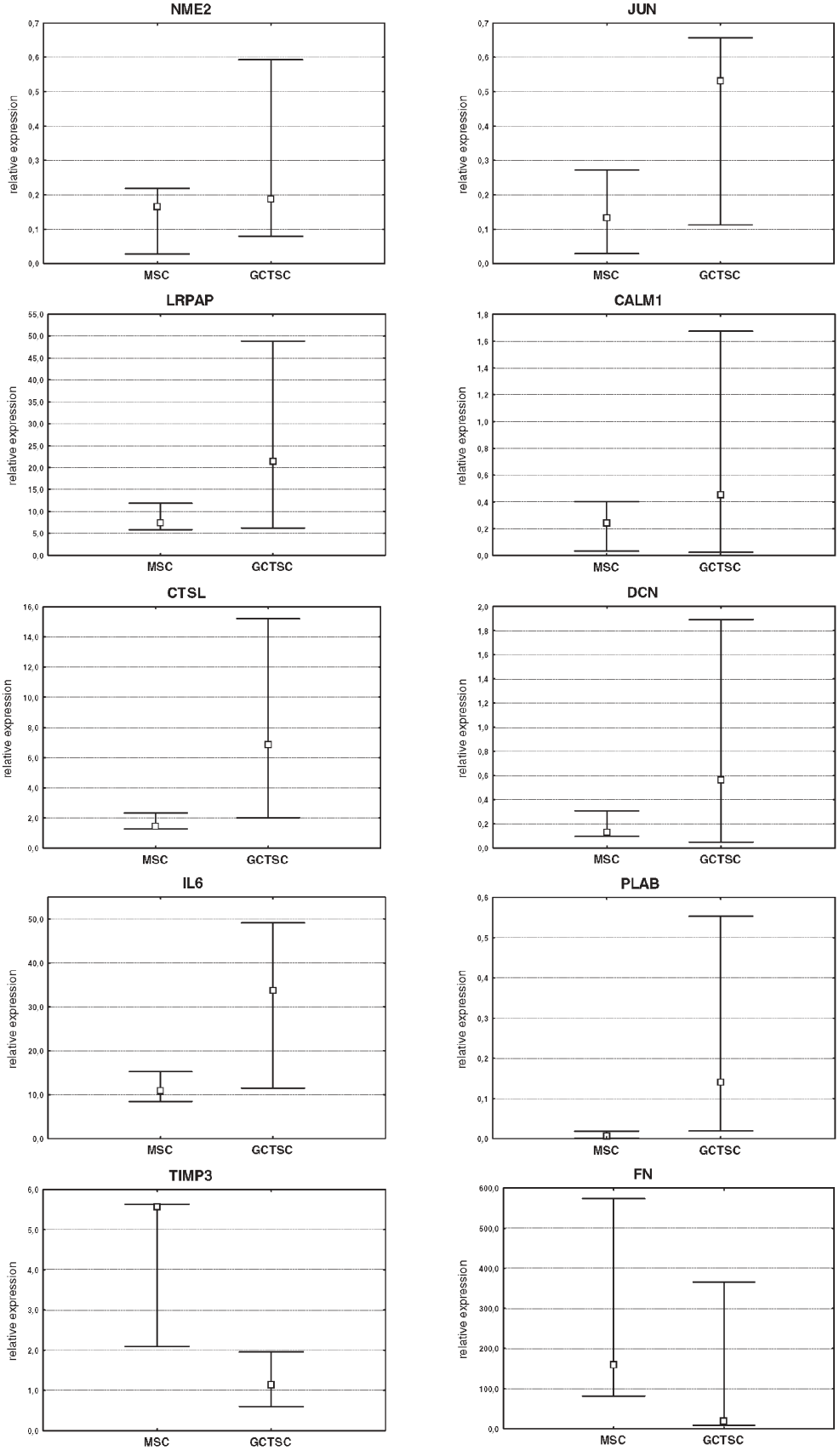


Fig. 1 Whisker blots of real-time polymerase chain reaction analysis from ten differentially expressed mRNAs depicting median (*open square*) and range (*minimum and maximum*) of six different giant cell tumor (GCT) stromal cells (Table 1: GCT 3, 5–9) and three different mesenchymal stem cell populations

NaCl with 0.1% Tween20 (TBST) for 1 h at room temperature. The primary rabbit JUN antibody (1:1,000) was added for 1 h at room temperature in 2% bovine serum albumin, 1% NSS in TBST, then incubated with horseradish peroxidase (HRP)-conjugated secondary anti-rabbit antibody (1:10,000; Promega, Mannheim, Germany) for 1 h at room temperature. The immunoreactive bands were visualized on an X-ray film using the ECL detection system (Amersham, Freiburg, Germany). Normalization for total amount of protein was achieved through the assessment of Actin [anti-Actin antibody (Abcam, Acris, Hiddenhausen, Germany 1:5,000; HRP-conjugated secondary anti-mouse antibody, 1:10,000; Amersham-Pharmacia, Freiburg, Germany) after stripping with Restore Western Blot Stripping Buffer (Pierce, Bonn, Germany) for 30 min at 37°C and extensive washing. The same procedure was applied to assess the relative amount of phosphorylated JUN/total JUN, utilizing the mouse primary phospho-specific p-jun (Ser63) antibody (1:100). The appreciable protein size difference of NME2 (19 kDa) and Actin (38 kDa) allowed the consecutive incubation with the two primary antibodies NME2 (1:2000; Transduction Laboratories) and Actin (1:5000). The protein bands were quantified by densitometric scanning of the x-ray film using the SoftMax Analysis software (BioRad). The fold changes in NME2, JUN, and pJUN protein expression levels in GCTSCs are shown relative to control MSCs.

Results

The comparison of the mRNA expression profiles of in vitro-propagated GCTSCs and MSCs identified a set of 29 genes differentially regulated in GCTSCs (Table 2). Of the genes, 4 displayed a decreased expression, while the mRNA of 25 genes was increased. Expression ratios are depicted in Table 2 (ratio array).

The differential expression of ten selected genes was verified with real-time PCR analysis (Table 2). Consistent with the array data, an increased mRNA expression was found in *v-jun sarcoma virus 17 oncogene homolog* (*JUN*), *non-metastatic cells 2 protein* (*NME2*), *interleukin-6* (*IL6*), *prostate differentiation factor* (*PLAB*), *decorin* (*DCN*), *cathepsin L* (*CTSL*), *calmodulin* (*CALM1*)

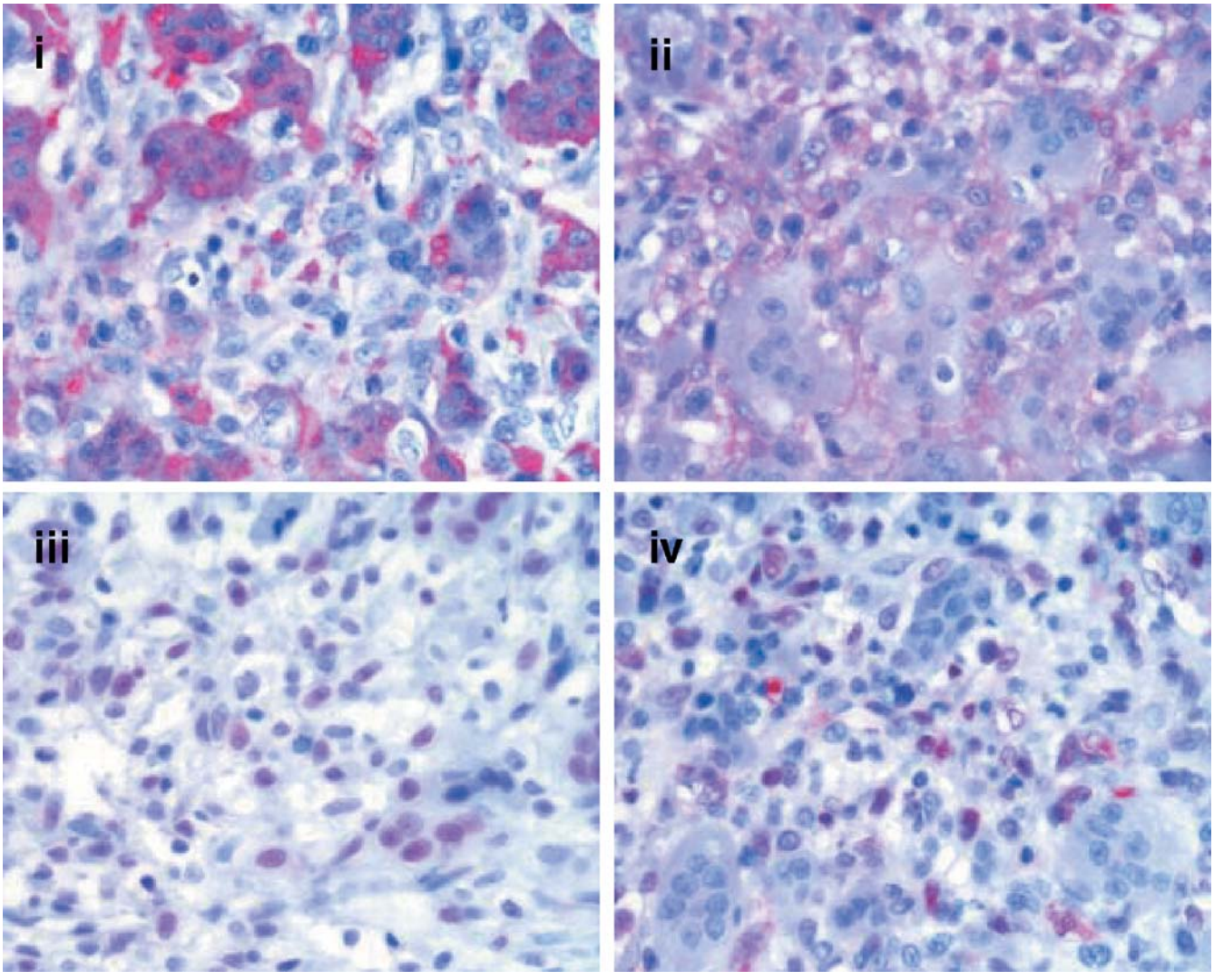


Fig. 2 Exemplary paraffin sections of giant cell tumor. Immunohistochemical protein expression patterns for CD68 (**i**) NME2 (**ii**) JUN (**iii**), and pJUN (**iv**). Magnification of **i**, **ii**, **iii**, **iv** ×400

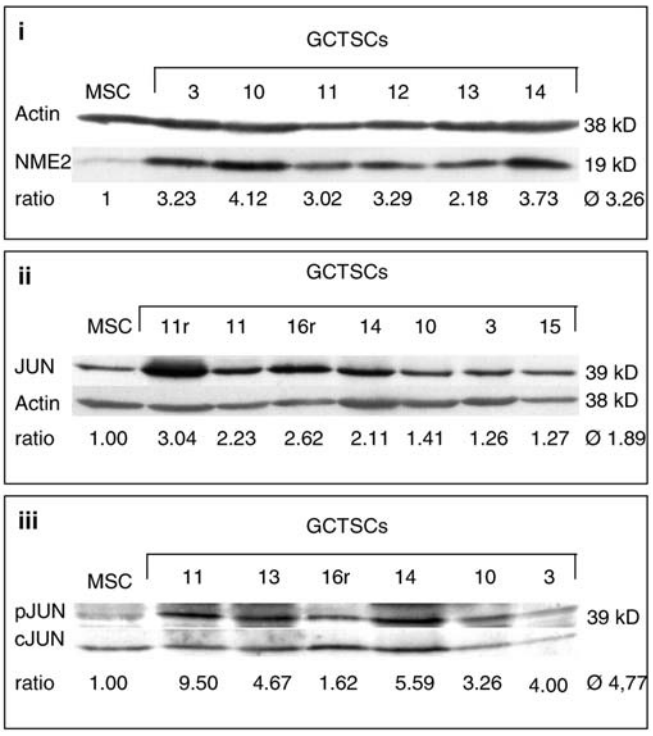


Fig. 3 Western-blot analysis of NME2 (**i**), JUN (**ii**), and pJUN (**iii**) in mesenchymal stem cells (MSCs) and cryopreserved [Table 1: giant cell tumors (GCTs) 10–15] and re-cultured (*r*) GCTSCs (Table 1: GCTs 11, 16). Ratios of NME2/Actin, JUN/Actin and pJUN/JUN (normalized expression) were utilized for the comparison of MSC and giant cell tumor stroma cell (GCTSC) lysates. The fold changes in NME2, JUN, and pJUN protein expression levels in GCTSCs are shown relative to control MSCs. *Ø* is average of NME2, JUN, and pJUN ratios in depicted GCTSCs

and *low density lipoprotein receptor-related protein-associated protein 1* (*LRPAP1*) (Fig. 1). A decreased mRNA expression was observed in the *tissue inhibitor of metalloproteinase 3* (*TIMP3*) and in the extracellular matrix protein *fibronectin* (*FN1*) (Fig. 1). The direction of genetic regulation always corresponded with the direction of the expression of differences in the specific cDNA arrays (Table 2). Reasons for the differences observed in the mean values of c-DNA array and real-time PCR (Table 2) could be due to the large expressional differences observed among the mRNAs due to the use of primary material and its intrinsic patient-specific variations in mRNA expression, as well as the use of different GCTSC mRNAs (Fig. 1).

To substantiate NME2 or JUN mRNA expression at the protein level, GCT sections were immunohistologically stained with antibodies against NME2, JUN, or pJUN. CD68-positive monocytes and giant cells demonstrated a typical histological GCT appearance with an abundance of giant cells intermediated with mononuclear GCTSCs and cells of monocytic origin (Fig. 2i). NME2 (Fig. 2ii) stained the cytoplasma of giant cells, monocytes, and GCTSCs in a great number of cells. JUN (Fig. 2iii) and pJUN (Fig. 2iv) staining was localized to the nucleus of quite a few mononuclear and giant cells within the tumor tissue.

To quantify changes in protein expression of NME2, JUN, and pJUN, Western-blot analysis was conducted with directly lysed cryopreserved GCTSCs (Table 1, 10–15), re-cultured GCTSCs (Table 1, 11, 16), and first-passage MSCs. Of the GCTSCs tested, 50% showed an average elevated NME2 expression of 3.26 compared with MSCs (Fig. 3i). Of the GCTSCs tested, 60% showed an average elevated JUN protein expression of 1.89 compared with MSCs (Fig. 3ii). Also, an average 4.77 increase of JUN Ser63 phosphorylation was observed (Fig. 3iii) in these GCTSCs relative to MSCs.

In conclusion, Western-blot analysis substantiated the changes observed in mRNA expression exhibited by array and real-time analysis. In addition, immunohistochemistry identified a substantial number of mononucleated cells expressing NME2, JUN, and pJUN, supporting future analysis of NME and JUN as candidate GCT cancer-related genes. Increased JUN phosphorylation in GCTSCs points to a functional level of GCT-related changes, which may have an impact on gene regulation.

Discussion

The comparison of GCTSC gene expression with the expression of the corresponding non-transformed MSC on human cancer cDNA arrays has resulted in the identification of a set of 29 genes. The overall similar expression pattern of these two cell types affirms the selection of MSCs as non-transformed control cells [22, 28]. Noteworthy is that this study confirms the increased expression of *interleukin-6* (*IL6*) in GCTs, as has been previously observed [5, 15], demonstrating the utility and reliability of this cDNA array data. The role of the other 28 genes in different steps of GCT development will be examined in more detail in future studies. Only genes whose regulation at the protein level has been verified (IL6, [5, 15] and JUN, NME2, in this study) are discussed in terms of neoplastic transformation and tumor phenotype, angiogenesis, or the recruitment and fusion of monocytes into giant cells.

The cytokine IL6 is important for osteoclastogenesis in certain pathological states. In these cases, both the cytokine and its soluble IL6 receptor (sIL6R) are probably upregulated in a variety of bone marrow cells [2]. Our finding of an increased *IL6* mRNA level in GCTSCs is in accordance with findings of other groups, demonstrating IL6 as the crucial factor for giant cell formation, osteolysis, and aggressiveness in GCT [5, 15]. The expression of IL6 has been suggested to contribute not only to monocyte and giant cell development, as well as their increased resorbing activity, but also to affect the commitment of mesenchymal progenitor cells [12]. The increased *IL6* expression may be induced by JUN through an activator protein-1 (AP-1) binding site in the *IL6* promoter [3].

The finding of an increased mRNA level of the well-known proto-oncogene *JUN* expressed in our tumor samples might also offer a clue toward understanding GCT development from the initiation of cell proliferation to induction of osteolysis. Immunohistochemical analysis proved JUN protein expression and its phosphorylation in mononuclear cells of GCT. Increased expression of JUN protein in Western-blot analysis (average 1.89-fold) was observed in 60% of the GCTSCs (Fig. 3ii), and an increased activation of JUN as assessed by an increased phosphorylation (Fig. 3iii) (pJUN, average 4.77-fold) signified its relevance for GCT development and maintenance. Induced expression or activity of JUN through activated oncogenes resulting in the transcriptional deregulation of JUN-responsive target genes might contribute to the ability of GCTSCs to proliferate in an autocrine fashion and, thus, lead to their neoplastic transformation, as has been shown for other cell systems [17, 26, 27]. Three lines of argumentation must be considered. First, after dimerization with any one of a number of other leucine-zipper proteins, JUN is the DNA-binding component of AP-1 transcription factor [27]. Overexpression of JUN results in a change in the make-up of AP-1 dimer composition within a cell. Alterations in AP-1 composition can have dramatic effects on gene expression. An increased level of JUN drives dimerization equilibrium to the formation of homodimers. JUN homodimer stabilization in specific promoter contexts might contribute to oncogenesis [17, 26].

Second, a significant involvement of AP-1 in the regulation of extracellular matrix protein (ECM) components has been established. Proteolytic enzymes and inhibitors, such as cathepsin L and TIMP-3, which were differentially expressed in our tumor samples, could be preferred targets for JUN transcriptional control [9, 19]. JUN may also be involved in the upregulation of matrix-metalloproteinases in GCT. The matrix-metalloproteinases MMP-2 and MMP-9 have been shown to be expressed in GCT tissues [20, 24]. Interestingly, both MMP-2 and MMP-9 display several AP-1 consensus sequences within their promoter regions and may be directly upregulated by JUN [30]. Possible target genes of JUN that encode ECM components include fibronectin and decorin, which were also identified in the present screen. Thus, JUN could influence normal ECM physiology, thereby promoting growth and destructiveness of GCT.

Third, GCTSCs retain an undifferentiated MSC-like phenotype without evidence of in vivo differentiation into expected cell types [28, 29]. Increased expression of the transcription factor JUN may restrain GCTSC differentiation as has been described in other mesenchymal cells, such as chondroblasts and myoblasts [27]. In myoblasts, JUN interacts with the muscle-specific transcription factor MyoD to inhibit myoblastic differentiation through direct protein–protein interaction [27]. The mechanism by which JUN perturbs chondroblast differentiation is not known [27]. In the osteoblastic lineage, the expression of JUN is restricted to the proliferating progenitor cells [13]. The transcription of the osteoblast-specific genes osteocalcin and alkaline phosphatase is inhibited through the binding of AP-1 to consensus sequences in the promoters, thereby restricting gene expression in the mature osteoblasts [13]. An interaction study of JUN with several osteoblastic and chondroblastic transcription factors [7] would help discover its function as an antagonist of mesenchymal differentiation. The expression and activity of JUN protein is regulated by several inhibitors, so that increased *Jun* mRNA expression does not inevitably result in an increased JUN activity [26]. However, in the present study, an increase in Ser-63 phosphorylation, which is one of the phosphorylation sites required for JUN activation and JUN-mediated augmentation of transformation [10], suggests that there is an increase in active JUN protein in GCTSCs. Still the question remains: why do GCTSCs over-express *Jun* as compared with proliferated MSCs? Future analysis of AP-1 composition and interaction with other regulatory proteins in GCTSCs is of critical importance, since this dramatically influences transcriptional activity and the selection of target genes. Upstream signal transduction pathways must also be elucidated to determine the potential induction of increased JUN expression.

The increased expression of the tumor suppressor gene *NME2* and abundant detection of NME2 protein in GTCSCs, detected using immunohistochemistry and Western-blot analysis, might be involved in the first steps of tumorigenesis. The *NME2* gene codes for nucleoside-diphosphate kinase B and is also referred to as the c-myc activating transcription factor PuF [18]. The increased expression of *NME2* mRNA has been observed after immortalization of normal human fibroblasts as well as in a variety of benign neoplasms and solid tumors [11]. *NME2* overexpression corresponds with an increased proliferation capacity during the initial stages of tumor development [11]. It may, therefore, influence the neoplastic transformation of MSCs to GCTSCs. The increased levels of *MYC* expression in GCTs, as described by Gamberi et al. [4], may also be explained by a transcriptional induction of the *MYC* gene by NME2 [18]. However, *NME* has been suggested to be a direct target of the transcription factor c-myc, potentially forming an auto-regulatory loop in GCT gene expression [23]. The involvement of NME2 in differentiation and metastatic potential appears to be cell-type dependent. An increased NME2 concentration can either be associated with a decreased metastatic potential without altering tumor proliferation or with an adverse outcome [16]. The present study, showing an expression of NME2 protein in all GCTSC tested and an increased expression (3.26-fold) in 50% of the GCTSCs is in contrast to former results from Oda et al. [14], who detected NME2 protein in only 4 of 13 GCTs. Functional analysis of these gene products in later research should help define their contribution to GCT development.

Acknowledgements This work was supported by the Deutsche Forschungsgemeinschaft, Graduiertenkolleg 476 and the Rudolf Bartling Stiftung. The authors thank Dr. S. Marotzki for technical

help with the Light Cycler System, S. Loges for her contribution of GAPDH plasmid DNA, Dr. T. Steichert for the support with the geneontology database, Dr. J. Knispel for his language advice, and Dr. S. Johnsen for proofreading. All experiments comply with the current laws of Germany.

References

1. de Souza PE, Paim JF, Carvalhais JN, Gomez RS (1999) Immunohistochemical expression of p53, MDM 2, Ki-67 and PCNA in central giant cell granuloma and giant cell tumor. J Oral Pathol Med 28:54–58
2. Devlin RD, Reddy SV, Savino R, Ciliberto G, Roodman GD (1998) IL-6 mediates the effects of IL-1 or TNF, but not PTHrP or 1,25(OH)2D3, on osteoclast-like cell formation in normal human bone marrow cultures. J Bone Miner Res 13:393–399
3. Franchimont N, Durant D, Rydziel S, Canalis E (1999) Platelet-derived growth factor induces interleukin-6 transcription in osteoblasts through the activator protein-1 complex and activating transcription factor-2. J Biol Chem 274:6783–6789
4. Gamberi G, Benassi MS, Bohling T, Ragazzini P, Molendini L, Sollazzo MR, Merli M, Ferrari C, Magagnoli G, Bertoni F, Picci P (1998) Prognostic relevance of C-myc gene expression in giant-cell tumor of bone. J Orthop Res 16:1–7
5. Gamberi G, Benassi MS, Ragazzini P, Pazzaglia L, Ponticelli F, Ferrari C, Balladelli A, Mercuri M, Gigli M, Bertoni F, Picci P (2004) Proteases and interleukin-6 gene analysis in 92 giant cell tumors of bone. Ann Oncol 15:498–503
6. Goldring SR, Roelke MS, Petrison KK, Bhan AK (1987) Human giant cell tumors of bone identification and characterization of cell types. J Clin Invest 79:483–491
7. Hess J, Porte D, Munz C, Angel P (2001) AP-1 and Cbfa/runt physically interact and regulate parathyroid hormone- dependent MMP13 expression in osteoblasts through a new osteoblast-specific element 2/AP-1 composite element. J Biol Chem 276:20029–20038
8. Huang L, Teng XY, Cheng YY, Lee KM, Kumta SM (2004) Expression of preosteoblast markers and Cbfa-1 and Osterix gene transcripts in stromal tumour cells of giant cell tumour of bone. Bone 34:393–401
9. Janulis M, Silberman S, Ambegaokar A, Gutkind JS, Schultz RM (1999) Role of mitogen-activated protein kinases and c-Jun/AP-1 trans-activating activity in the regulation of protease mRNAs and the malignant phenotype in NIH 3T3 fibroblasts. J Biol Chem 274:801–813
10. Jochum W, Passegue E, Wagner EF (2001) AP-1 in mouse development and tumorigenesis. Oncogene 20:2401–2412
11. Kimura N, Shimada N, Ishijima Y, Fukuda M, Takagi Y, Ishikawa N (2003) Nucleoside diphosphate kinases in mammalian signal transduction systems: recent development and perspective. J Bioenerg Biomembr 35:41–47
12. Manolagas SC (1998) The role of IL-6 type cytokines and their receptors in bone. Ann N Y Acad Sci 840:194–204
13. McCabe LR, Banerjee C, Kundu R, Harrison RJ, Dobner PR, Stein JL, Lian JB, Stein GS (1996) Developmental expression and activities of specific fos and jun proteins are functionally related to osteoblast maturation: role of Fra-2 and Jun D during differentiation. Endocrinology 137:4398–4408
14. Oda Y, Walter H, Radig K, Rose I, Neumann W, Roessner A (1995) Immunohistochemical analysis of nm23 protein expression in malignant bone tumors. J Cancer Res Clin Oncol 121:667–673
15. Ohsaki Y, Takahashi S, Scarcez T, Demulder A, Nishihara T, Williams R, Roodman GD (1992) Evidence for an autocrine/paracrine role for interleukin-6 in bone resorption by giant cells from giant cell tumors of bone. Endocrinology 131:2229–2234
16. Ouatas T, Salerno M, Palmieri D, Steeg PS (2003) Basic and translational advances in cancer metastasis: Nm23. J Bioenerg Biomembr 35:73–79
17. Papachristou DJ, Batistatou A, Sykiotis GP, Varakis I, Papavassiliou AG (2003) Activation of the JNK-AP-1 signal transduction pathway is associated with pathogenesis and progression of human osteosarcomas. Bone 32:364–371
18. Postel EH (2003) Multiple biochemical activities of NM23/NDP kinase in gene regulation. J Bioenerg Biomembr 35:31–40
19. Puyraimond A, Weitzman JB, Babiole E, Menashi S (1999) Examining the relationship between the gelatinolytic balance and the invasive capacity of endothelial cells. J Cell Sci 112:1283–1290
20. Rao VH, Singh RK, Delimont DC, Schaefer GB, Bridge JA, Neff JR, Sanger WG, Sappenfield JW, Buehler BA, Finnell RH (1999) Interleukin-1beta upregulates MMP-9 expression in stromal cells of human giant cell tumor of bone. J Interferon Cytokine Res 19:1207–1217
21. Rennefahrt UE, Illert B, Kerkhoff E, Troppmair J, Rapp UR (2002) Constitutive JNK activation in NIH 3T3 fibroblasts induces a partially transformed phenotype. J Biol Chem 277: 29510–29518
22. Robinson D, Segal M, Nevo Z (2002) Giant cell tumor of bone. The role of fibroblast growth factor 3 positive mesenchymal stem cells in its pathogenesis. Pathobiology 70:333–342
23. Schuldiner O, Shor S, Benvenisty N (2002) A computerized database-scan to identify c-MYC targets. Gene 292:91–99
24. Teti A, Farina AR, Villanova I, Tiberio A, Tacconelli A, Sciortino G, Chambers AF, Gulino A, Mackay AR (1998) Activation of MMP-2 by human GCT23 giant cell tumour cells induced by osteopontin, bone sialoprotein and GRGDSP peptides is RGD and cell shape change dependent. Int J Cancer 77:82–93
25. Udtha M, Lee SJ, Alam R, Coombes K, Huff V (2003) Up-regulation of c-MYC in WT1-mutant tumors: assessment of WT1 putative transcriptional targets using cDNA microarray expression profiling of genetically defined Wilms' tumors. Oncogene 22:3821–3826
26. van Dam H, Castellazzi M (2001) Distinct roles of Jun:Fos and Jun:ATF dimers in oncogenesis. Oncogene 20:2453–2464
27. Vogt PK (2001) Jun, the oncoprotein. Oncogene 20:2365–2377
28. Wuelling M, Delling G, Kaiser E (2003) Characterization of the neoplastic stromal cell in giant cell tumor of bone. Hum Pathol 34:983–993
29. Wulling M, Engels C, Jesse N, Werner M, Delling G, Kaiser E (2001) The nature of giant cell tumor of bone. J Cancer Res Clin Oncol 127:467–474
30. Yoon SO, Park SJ, Yun CH, Chung AS (2003) Roles of matrix metalloproteinases in tumor metastasis and angiogenesis. J Biochem Mol Biol 36:128–137
31. Zhu G, Reynolds L, Crnogorac-Jurcevic T, Gillett CE, Dublin EA, Marshall JF, Barnes D, D'Arrigo C, Van Trappen PO, Lemoine NR, Hart IR (2003) Combination of microdissection and microarray analysis to identify gene expression changes between differentially located tumour cells in breast cancer. Oncogene 22:3742–3748

Virchows Arch (2004) 445:631–636
DOI 10.1007/s00428-004-1121-2

ORIGINAL ARTICLE

Cord Langner · Reinhard von Wasielewski · Manfred Ratschek · Peter Rehak · Richard Zigeuner

Biological significance of p27 and Skp2 expression in renal cell carcinoma. A systematic analysis of primary and metastatic tumour tissues using a tissue microarray technique

Received: 13 July 2004 / Accepted: 18 August 2004 / Published online: 28 October 2004
© Springer-Verlag 2004

Abstract p27 (p27/kip1) is involved in cell-cycle control, and loss of p27 expression may result in tumour development and/or progression. Association with Skp2 targets p27 for degradation. Using a tissue microarray technique, 171 primary renal cell carcinomas (RCCs) and 58 RCC metastases were immunostained for p27 and Skp2. p27 Immunoreactivity was noted in 83 of 129 (64%) clear cell, 6 of 22 (27%) chromophobe and 15 of 20 (75%) papillary tumours as well as 44 of 58 (76%) metastases. In clear cell cancers, high p27 expression ($\geq$50% of tumour cells) decreased with rising tumour stage (50% pT1/pT2 versus 20% pT3; $P<0.001$) and grade (44% G1/G2 versus 21% G3/G4; $P=0.008$). None of 22 chromophobe cancers showed high expression in contrast to 46 of 129 (36%) clear cell tumours ($P<0.001$). Skp2 expression was noted in 8 of 129 (6%) clear cell cancers and 11 of 55 (20%) metastases ($P=0.008$). Immunoreactivity increased with rising tumour stage (1% pT1/pT2 versus 11% pT3; $P=0.03$) and grade (1% G1/G2 versus 15% G3/G4; $P=0.004$) and was associated with sarcomatoid morphology ($P<0.001$). In multivariate analysis, patients with low p27 expression and Skp2 immunoreactivity in clear cell cancers had a less favourable outcome. In conclusion, p27 and Skp2 proved to be additional biomarkers in renal cancer pathology with both prognostic and diagnostic impact.

Keywords Renal cell carcinoma · p27 · Skp2 · Tissue microarray · Prognosis

C. Langner (✉) · M. Ratschek
Institute of Pathology,
Medical University of Graz,
Auenbruggerplatz 25, 8036 Graz, Austria
e-mail: cord.langner@meduni-graz.at
Tel.: +43-316-38583665
Fax: +43-316-384329

R. von Wasielewski
Institute of Pathology,
Medical School Hannover,
Carl-Neuberg-Straße 1, 30625 Hannover, Germany

P. Rehak
Department of Surgery,
Division of Biomedical Engineering and Computing,
Medical University of Graz,
Auenbruggerplatz 29, 8036 Graz, Austria

R. Zigeuner
Department of Urology,
Medical University of Graz,
Auenbruggerplatz 7, 8036 Graz, Austria

Introduction

Renal cell carcinoma (RCC) accounts for approximately 2–3% of annual new cancer cases in the United States, with men having a higher risk than women (male to female ratio=1.5:1). Moreover, the incidence of RCC is still increasing in North America and northern Europe, with rates of approximately 3% per year in the United States [21]. RCCs exhibit a variety of distinct histological patterns with different prognoses [4]. However, the principal prognostic factors are tumour stage at presentation and histological grade [22].

Cyclins and cyclin-dependent kinase (CDK) complexes have important regulatory roles during cell-cycle progression. They are, in turn, regulated by CDK inhibitors, which generally inhibit cell-cycle progression and can be separated, based on structural and functional properties, into the INK4 group and the Cip/Kip family [18]. p27 is a member of the latter (p27/kip1) and has been shown to induce G1 arrest by inhibition of cyclin E-CDK2. p27 protein levels are increased in quiescent cells and rapidly decrease after stimulation with mitogens, thus reflecting the role of p27 in the connection of mitogenic signals to the cell cycle [18]. In addition, p27 is a putative tumour suppressor, regulator of drug resistance in solid tumours and promoter of apoptosis. Loss of p27 protein expression may result in tumour development and/or progression [18]. p27 Expression is regulated by cell-contact inhibition and by specific growth factors, such as transforming growth factor-β. Decrease in p27 expression commonly occurs at the post-translational level, due to

increased protein degradation by the ubiquitin–proteasome pathway. Transfer of ubiquitin to a substrate requires at least the collaboration of ubiquitin-activating enzyme (E1), ubiquitin-conjugating enzyme (E2) and ubiquitin-protein ligase (E3). The E3 ligase activity in the ubiquitination of p27 is provided by the SCF complex, composed of S-phase kinase-associated protein 1 (Skp1), Cul-1, Roc-1/Rbx-1 and the F-box protein Skp2, which acts as the specific substrate-recognition subunit. The association with Skp2 targets p27 for degradation by the multicatalytic 26S proteasome [3]. Hence, Skp2 indirectly promotes the S-phase, and its overexpression leads to adhesion-dependent and -independent cell-cycle progression. Furthermore, direct oncogenic properties have been attributed to Skp2 by mediating malignant transformation [8, 16] and modulating invasion and motility of cancer cells independent of p27 degradation [19].

Reports on p27 expression in RCCs are limited, sometimes even contradictory, and have mainly focused on the clear cell subtype [9, 11, 12, 23]. Skp2 expression has been reported in a variety of neoplasms, including breast [27], gastric [19], colorectal [13] and prostate adenocarcinomas [1, 29] as well as non-small-cell lung cancer [30]. Data concerning the expression and possible clinical significance of Skp2 in RCCs are currently lacking. The objective of our study was to evaluate the expression of both p27 and Skp2 among all histological subtypes of RCC, including metastatic tumour tissue, with respect to prognostic as well as diagnostic significance.

Materials and methods

Case selection

Formalin-fixed and paraffin-embedded specimens of primary (n=171) and metastatic (n=58) RCCs operated on consecutive patients between June 1987 and October 2002 were chosen for analysis; clinical data are summarised in Table 1. All tumours were re-evaluated with respect to pT stage, grade and histological subtype by two pathologists (C.L. and M.R.): pT stages were adjusted according to the International Union Against Cancer 2002 issue of the tumour node metastases (TNM) system [28], nuclear grading was performed according to the Fuhrman grading system [7] and RCC histological subtypes were classified according to the recently published World Health Organization criteria [6]. Details regarding pT stages and tumour grades of primary tumour specimens are presented in Table 2. Clear cell primary RCCs included 9 tumours with small foci of sarcomatoid change and 4 tumours with predominant sarcomatoid morphology showing only small residual foci of pre-existing clear cell carcinoma. Papillary primary RCCs comprised 12 type-1 and 8 type-2 tumours. Among the RCC metastases, 55 (95%) were of clear cell (including 7 tumours with sarcomatoid change), 2 (3%) of papillary and 1 (2%) of chromophobe type. Sites of metastases were as follows: bone (n=12), brain (n=11), thyroid gland (n=9), skin (n=6), lung (n=5), adrenal gland (n=4), pancreas (n=3), soft tissue (n=3), gastrointestinal tract (n=3) and bladder (n=2). Two specimens of non-neoplastic renal tissue were analysed for comparison.

Table 1 Clinical data of the patients with primary and metastatic renal cell carcinoma (RCC)

	Primary RCCs	Metastatic RCCs
n	171	58
Sex (male:female)	1.5:1	1.4:1
Mean age (years)	62.3	63.6
Median age (years)	63.1	65.0
Age range (years)	28–85	39–82

Table 2 Tumour stage and grade related to histological subtypes of renal cell carcinoma

Stage/grade	Clear cell		Chromophobe		Papillary	
	n=129		n=22		n=20	
	n	%	*n*	%	*n*	%
pT1a	43	33	5	23	7	35
pT1b	20	16	3	14	4	20
pT2	5	4	3	14	3	15
pT3a	27	21	6	27	4	20
pT3b	34	26	5	23	2	10
G1	15	12	0	0	1	5
G2	66	51	13	59	13	65
G3	44	34	9	41	6	30
G4	4	3	0	0	0	0

Immunohistochemistry

For immunohistochemical evaluation, a tissue microarray technique was used. The details of this technique have been described previously [14]. Tissue microarrays were constructed using a manual tissue-arraying instrument (Beecher, Silver Spring, MD). With respect to the well-known histological heterogeneity of RCCs, at least three cylindrical core biopsies, 0.6 mm in diameter, were taken from different sites of each tumour and arrayed in a recipient paraffin tissue microarray block. Briefly, 4-μm tissue microarray sections were deparaffinised by xylene, rehydrated in graded alcohols, treated for 5 min with 1% H_2O_2 and submitted to microwave epitope retrieval (30 min 160 W in 0.01 M sodium citrate buffer, pH 6.0). For the detection of p27, sections were incubated for 30 min with the monoclonal mouse antibody NCL-p27 (1:20; Novocastra, Newcastle upon Tyne, UK) using an automated immunostainer (Dako-Autostainer, Universal Staining System, Dako, Glostrup, Denmark). Binding of the primary antibody was assessed using the Dako LSAB2 System detection kit. For the detection of Skp2, sections were incubated for 60 min with the monoclonal mouse antibody SKP2 (1:100; Zymed, San Francisco, CA) using the Shandon coverplate system in a Tecan Genesis Autostainer (ThermoShandon, Frankfurt, Germany; Tecan, Deisenhofen, Germany). A biotinylated secondary antibody was used for the catalysed signal amplification technique (CSA, Dako). New fuchsin served as chromogen, haematoxylin served as counterstain.

Immunohistochemical evaluation and controls

Immunoreactivity was independently assessed in a semi-quantitative fashion by two pathologists (C.L. and M.R.), who were blinded to clinicopathological data. Discrepancies were resolved by simultaneous re-examination of the slides by both investigators using a double-headed microscope. All tumour cell nuclei that exhibited a distinct strong staining were considered positive, and immunoreactivity was documented in categories as follows: 0, no reactivity; 1, less than 10% of cancer cells positive; 2, 10–25% positive; 3, 25–50% positive; 4, 50–75% positive; 5, 75–90% positive and 6, more than 90% of cancer cells positive. According to the practice used in a previous study [23], immunoreactivity of p27 was further classified as "high expression" ($\geq$50% of tumour cell nuclei) and "low expression" (<50% of tumour cell nuclei). A normal tonsil was

used as a positive control for both p27 and Skp2. Negative controls included omission of the primary antibody and incubation with Dako ChemMate Antibody Diluent (Code No. S 2022).

Statistical analysis

Subgroups according to histological subtypes, tumour grade and pT stage, respectively, were compared with respect to possible differences in immunoreactivity using the Fisher's exact test. Tumour-specific and disease-free survivals were investigated using the Kaplan–Meier method and compared using the log-rank test. For multivariate testing, a Cox's proportional hazards regression model, including tumour stage and grade as well as p27 and Skp2 expression, was performed. Analysis of prognostic impact had to be restricted to the clear cell subtype because sample sizes of the other histological subtypes were too small to permit a separate analysis.

Results

Non-neoplastic renal tissue showed strong nuclear p27 immunoreactivity in tubule and collecting-duct epithelium, glomerular cells and pelvic urothelium but lacked immunoreactivity for Skp2. In the primary RCC group, p27 expression was noted in 83 of 129 (64%) clear cell, 6 of 22 (27%) chromophobe and 15 of 20 (75%) papillary tumours. Regarding the potential value of p27 as a differential diagnostic tool, none of the chromophobe tumours showed high p27 expression, in contrast to 46 of 129 (36%) clear cell tumours ($P<0.001$; Table 3). In clear cell RCCs, high p27 expression decreased with rising stage [34/68 (50%) pT1/pT2 versus 12/61 (20%) pT3; $P<0.001$] and grade [36/81 (44%) G1/G2 versus 10/48 (21%) G3/G4; $P=0.008$; Fig. 1A, B; Table 3] but was not found to be associated with the presence of sarcomatoid morphology. In papillary RCCs, both histological types showed comparable staining results [8/12 (67%) type 1 versus 7/8 (88%) type 2]. Regarding metastatic RCC tissue, p27 immunoreactivity was seen in 44 of 58 (76%) cases with 32 of 58 (55%) cases showing high expression (Fig. 1C).

Skp2 expression was noted only in clear cell cancers, with 8 of 129 (6%) primary and 11 of 55 (20%) metastatic tumours ($P=0.008$) being stained. All but 2 cases showed immunoreactivity of less than 10% of cancer cells (Fig. 1D). Skp2 expression in primary tumours increased with rising stage [1/68 (1%) pT1/pT2 versus 7/61 (11%) pT3; $P=0.03$] and rising grade [1/81 (1%) G1/G2 versus 7/48 (15%) G3/G4; $P=0.004$; Table 3]. In addition, 5 of 13 (38%) clear cell RCCs with sarcomatoid morphology (including 9 RCCs with focal sarcomatoid change and 4 predominantly sarcomatoid RCCs) showed Skp2 expression, compared with 3 of 116 (3%) clear cell RCCs without sarcomatoid transformation ($P<0.001$). Moreover, 4 of 7 (57%) metastatic RCCs of clear cell type with sarcomatoid change showed Skp2 expression. No correlation between p27 and Skp2 immunoreactivities was found: 3 of 8 (38%) Skp2-positive primary (clear cell) RCCs showed low p27 expression; 5 of 8 (63%) showed high p27 expression.

Table 3 p27 and Skp2 expression in primary renal cell carcinomas in relation to histological subtypes, tumour stages and tumour grades

Stage/grade	p27 Immunoreactivity			p27 High expression			Skp2 Immunoreactivity		
	n (%)			*n* (%)			*n* (%)		
	Clear cell	Chromophobe	Papillary	Clear cell	Chromophobe	Papillary	Clear cell	Chromophobe	Papillary
pT1a	34/43 (79)	2/5 (40)	7/7 (100)	27/43 (63)	0/5 (0)	3/7 (43)	1/43 (2)	0/5 (0)	0/7 (0)
pT1b	10/20 (50)	2/3 (67)	3/4 (75)	5/20 (25)	0/3 (0)	3/4 (75)	0/20 (0)	0/3 (0)	0/4 (0)
pT2	3/5 (60)	0/3 (0)	1/3 (33)	2/5 (40)	0/3 (0)	1/3 (33)	0/5 (0)	0/3 (0)	0/3 (0)
pT3a	17/27 (63)	2/6 (33)	2/4 (50)	7/27 (26)	0/6 (0)	2/4 (50)	5/27 (19)	0/6 (0)	0/4 (0)
pT3b	19/34 (56)	0/5 (0)	2/2 (100)	5/34 (15)	0/5 (0)	1/2 (50)	2/34 (6)	0/5 (0)	0/2 (0)
G1	13/15 (87)	-	1/1 (100)	11/15 (73)	-	0/1 (0)	0/15 (0)	-	0/1 (0)
G2	46/66 (70)	4/13 (31)	9/13 (69)	25/66 (38)	0/13 (0)	6/13 (46)	1/66 (2)	0/13 (0)	0/13 (0)
G3	21/44 (48)	2/9 (22)	5/6 (83)	10/44 (23)	0/9 (0)	4/6 (67)	4/44 (9)	0/9 (0)	0/6 (0)
G4	3/4 (75)	-	-	0/4 (0)	-	-	3/4 (75)	-	-
Total	83/129 (64)	6/22 (27)	15/20 (75)	46/129 (36)	0/22 (0)	10/20 (50)	8/129 (6)	0/22 (0)	0/20 (0)

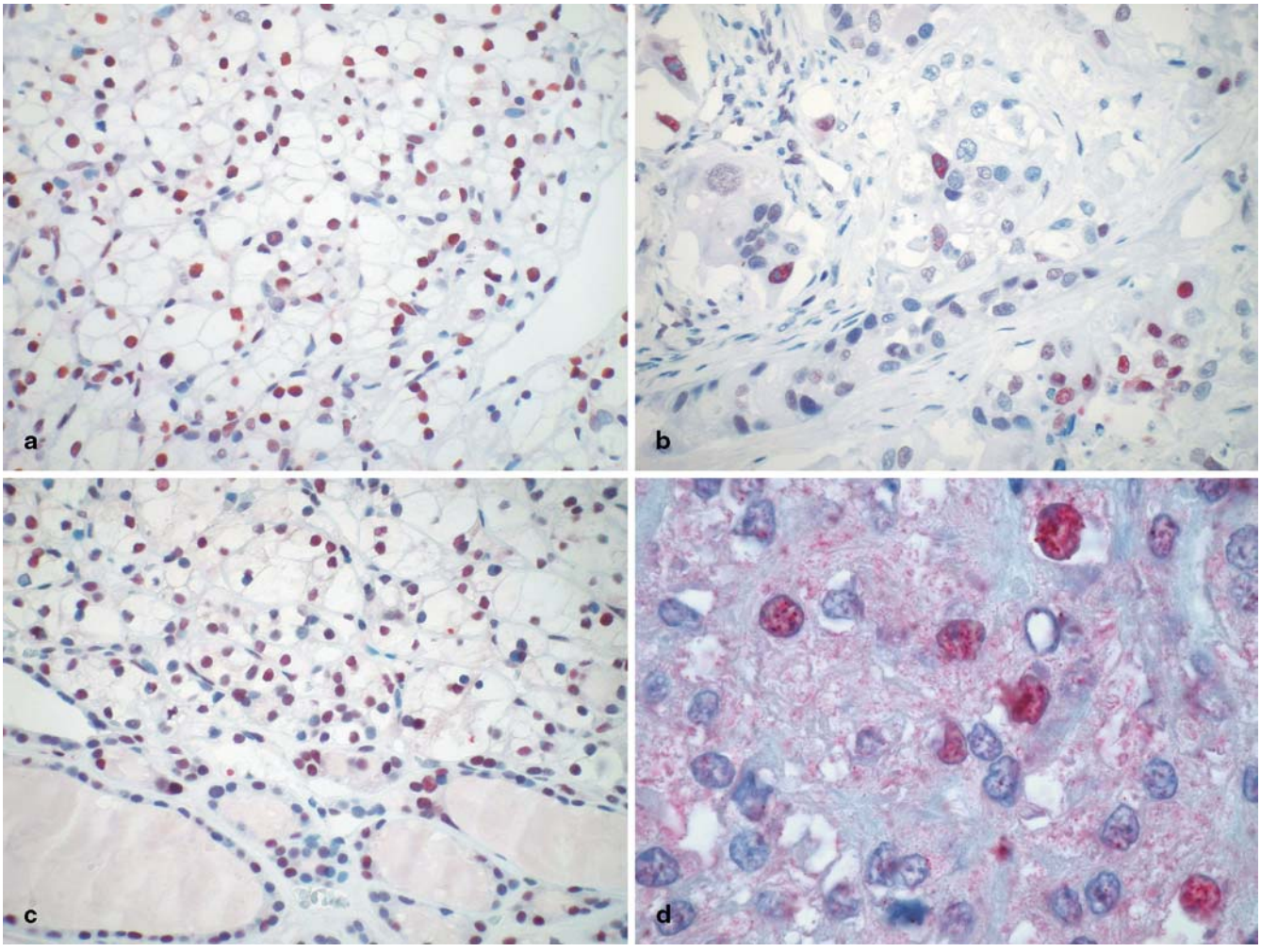


Fig. 1 High nuclear p27 expression in a well-differentiated (**A**) and low nuclear p27 expression in a poorly differentiated (**B**) clear cell renal cell carcinoma (RCC). High nuclear p27 expression in metastatic clear cell RCC in the thyroid gland (**C**). Strong though focal nuclear Skp2 expression in metastatic poorly differentiated clear cell RCC (**D**)

Follow-up data were available in 124 of 129 (96%) patients with clear cell primary RCCs. After a mean follow-up of 26 months and a median follow-up of 24 months, progressive disease was observed in 29 of 124 (23%) patients, including 15 patients who died from cancer and 14 patients who currently are alive with metastatic disease. Three patients died from causes not related to RCC. Progressive disease was noted in 26 of 79 (33%) cases either lacking p27 immunoreactivity or showing only low p27 expression, compared with 3 of 45 (7%) with high p27 expression (P=0.002; Fig. 2). Regarding Skp2, 6 of 8 (75%) patients with positive tumours developed progressive disease, compared with 23 of 116 (20%) with negative tumours (P<0.001, Fig. 3). The Cox's proportional hazards regression model proved tumour stage greater than 2 [risk ratio (RR) 3.26, 95% confidence interval (CI) 1.04–10.19; P=0.04], tumour grade greater than 2 (RR 13.0, CI 3.68–45.87; P<0.001), low p27 expression or lack of p27 immunoreactivity (RR 3.55, CI 1.01–12.49; P=0.049) and Skp2 immunoreactivity (RR 4.69, CI 1.7–12.92; P=0.003) as independent

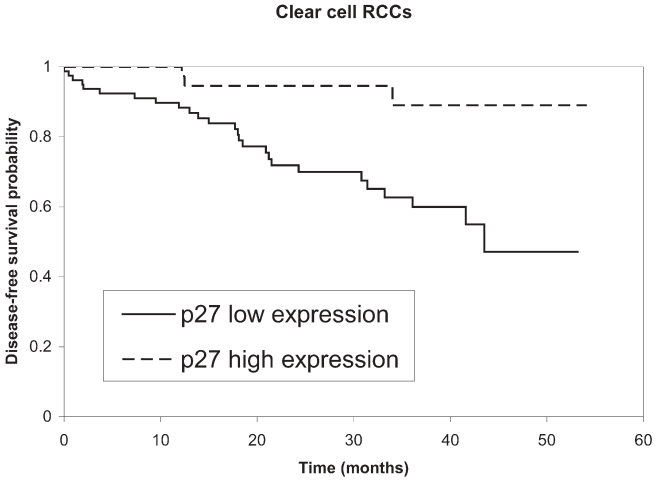


Fig. 2 Disease-free survival (months) in patients with clear cell renal cell carcinoma (RCC) showing high (≥50% of tumour cell nuclei) and low (<50% of tumour cell nuclei) p27 expression (P=0.002; log-rank test)

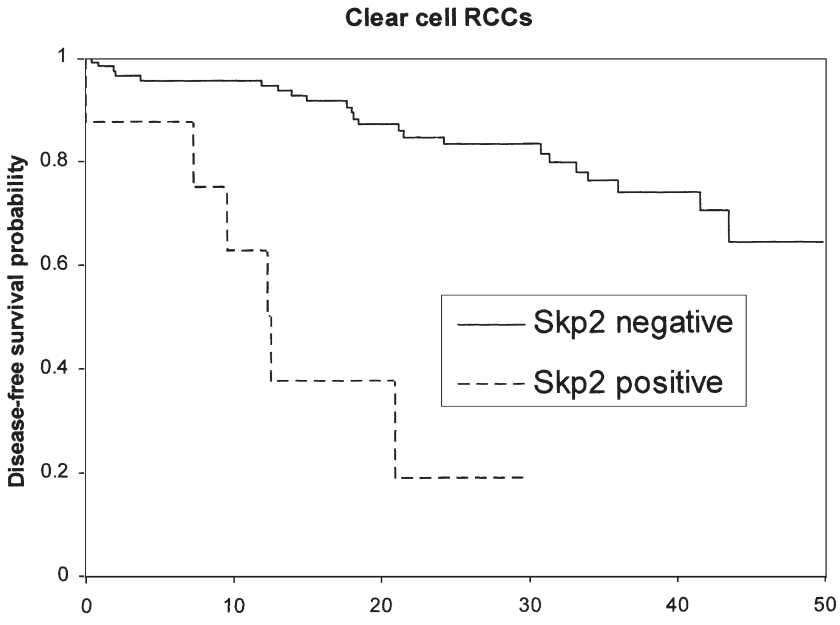


Fig. 3 Disease-free survival (months) in patients with clear cell renal cell carcinoma (RCC) with or without Skp2 expression ($P<0.001$; log-rank test)

prognostic factors regarding disease-free survival, respectively.

Discussion

The current study is one of the largest investigating p27 expression and the first to analyse Skp2 expression in renal cancer with respect to possible associations with histological subtype, tumour stage and grade as well as patients' outcome. Moreover, for the first time, Skp2 expression was compared in primary and metastatic tissues of any type of cancer.

The significant association between low p27 expression and high-stage and high-grade clear cell RCCs found in our study confirms the results by Hedberg et al. [11, 12], while others have reported an association only with the TNM stage [23] or no associations at all [9]. All of these studies, however, mainly concentrated on the clear cell subtype of RCC and did not analyse metastatic tumour tissues. Hence, only Hedberg et al. [12] noticed the diagnostic value of p27 as a marker to separate the chromophobe from the clear cell subtype. However, we could not reproduce their finding of a general lack of p27 immunoreactivity in the chromophobe subtype, since 6 of 22 (27%) chromophobe tumours in our series showed, albeit low, p27 expression.

Thus far, possible differences in p27 expression between primary and metastatic tumours have only rarely been investigated. The high p27 protein expression (resembling primary RCC tissue) in metastatic renal cancer tissue in our series suggests a lack of direct involvement of p27 in the metastatic process, as has already been proposed previously by McKay et al. [20] for colorectal carcinomas and corresponding metastases.

Our data regarding Skp2 expression in RCCs are in agreement with the results reported from other types of cancer. The association of Skp2 immunoreactivity with increasing tumour stage or increasing tumour grade has already been shown in breast [27], colorectal [13] and prostate adenocarcinomas [1, 29], as well as non-small-cell lung cancer [30]. However, the significant association between Skp2 expression and a morphological feature of aggressive tumour growth, such as sarcomatoid change in RCC, has never been previously reported. The significantly higher expression of Skp2 in metastatic compared with primary cancer (with unaltered expression of p27 as shown above) in our study may be explained by in vitro results, which indicate that Skp2 overexpression may facilitate the metastatic process due to tumourigenic properties independent of p27 proteolysis: first, Skp2-transfected gastric cancer cells were shown to be resistant to induction of apoptosis and exhibited a higher potential of invasion and motility than control cells [19], and, second, overexpression of Skp2 allows cell division in the absence of cell adhesion [2].

In contrast to other studies [1, 8, 13, 27, 29], we did not detect an inverse relationship between p27 and Skp2. Similar results have recently been reported for soft tissue sarcomas [24] and a subset of malignant lymphomas [5, 17]. The observation may be explained by alternative molecular events involving p27 downregulation, such as decreased transcription or translation and abnormal localisation or sequestration [5]. Moreover, p27 degradation may occur by Skp2- or even ubiquitin-independent processing [10, 26].

With regard to prognostic significance of p27 expression in clear cell RCCs, our results confirm the studies mentioned above, reporting a significant association between low p27 expression and unfavourable outcome [9, 11, 12, 23]. The poor prognosis of patients with expression of Skp2 in our series is in accordance with the results obtained from other types of cancer [1, 15, 25, 30]. The low overall rate of Skp2 immunoreactivity in RCCs,

however, limits its practical use in the evaluation of patients with this tumour entity.

In conclusion, p27 and Skp2 proved to be useful additional biomarkers with both prognostic and diagnostic impact in renal cancer pathology. The significant association of Skp2 expression with high-grade tumours, sarcomatoid morphology and metastatic tumours as well as the lack of expression in non-neoplastic tissue suggest Skp2 as a promising target of future cancer therapy strategies.

Acknowledgements The authors are grateful to Mrs. M. Gogg-Kamerer, Mrs. M. Lindbauer, Mrs. A. Sommersacher, Mr. M. Al-Effah and Mr. R. Christof for excellent technical assistance.

References

1. Ben-Izhak O, Lahaz-Baratz S, Meretyk S, Ben-Eliezer S, Sabo E, Dirnfeld M, Cohen S, Ciechanover A (2003) Inverse relationship between Skp2 ubiquitin ligase and the cyclin dependent kinase inhibitor p27kip1 in prostate cancer. J Urol 170:241–245
2. Carrano AC, Pagano M (2001) Role of the F-box protein Skp2 in adhesion-dependent cell cycle progression. J Cell Biol 153:1381–1389
3. Carrano AC, Eytan E, Hershko A, Pagano M (1999) Skp2 is required for ubiquitin-mediated degradation of the CDK inhibitor p27. Nat Cell Biol 1:193–199
4. Cheville JC, Lohse CM, Zincke H, Weaver AL, Blute ML (2003) Comparison of outcome and prognostic features among histologic subtypes of renal cell carcinoma. Am J Surg Pathol 27:612–624
5. Chiarle R, Fan Y, Piva R, Boggino H, Skolnik J, Novero D, Palestro G, De Wolf-Peeters C, Chilosi M, Pagano M, Inghirami G (2002) S-phase kinase-associated protein 2 expression in non-Hodgkin' lymphoma inversely correlates with p27 expression and defines cells in S phase. Am J Pathol 160:1457–1466
6. Eble JN, Togashi K, Pisani P (2004) Renal cell carcinoma. In: Eble JN, Sauter G, Epstein JI, Sesterhenn IA (eds) World Health Organization classification of tumours. Pathology & genetics, tumours of the urinary system and male genital organs. IARC Press, Lyon, pp 12–43
7. Fuhrman SA, Lasky LC, Limas C (1982) Prognostic significance of morphologic parameters in renal cell carcinoma. Am J Surg Pathol 6:655–663
8. Gstaiger M, Jordan R, Lim M, Catzavelos C, Mestan J, Slingerland J, Krek W (2001) Skp2 is oncogenic and overexpressed in human cancers. Proc Natl Acad Sci U S A 98:5043–5048
9. Haitel A, Wiener HG, Neudert B, Marberger M, Susani M (2001) Expression of the cell cycle proteins p21, p27, and pRb in clear cell renal cell carcinoma and their prognostic significance. Urology 58:477–481
10. Hara T, Kamura T, Nakayama K, Oshikawa K, Hatekeyama S, Nakayama K (2001) Degradation of p27kip1 at the G0–G1 transition mediated by a skp2-independent ubiquitination pathway. J Biol Chem 276:48937–48943
11. Hedberg Y, Davoodi E, Ljungberg B, Roos G, Landberg G (2002) Cyclin E and p27 protein content in human renal cell carcinoma: Clinical outcome and associations with cyclin D. Int J Cancer 102:601–607
12. Hedberg Y, Ljungberg B, Roos G, Landberg G (2003) Expression of cyclin D1, D3, E, and p27 in human renal cell carcinoma analysed by tissue microarray. Br J Cancer 88:1417–1423
13. Hershko D, Bornstein G, Ben-Izhak O, Carrano A, Pagano M, Krausz MM, Hershko A (2001) Inverse relation between levels of p27kip1 and of its ubiquitin ligase subunit Skp2 in colorectal carcinomas. Cancer 91:1745–1751
14. Kononen J, Bubendorf L, Kallioniemi A, Barlund M, Schraml P, Leighton S, Torhorst J, Mihatsch MJ, Sauter G, Kallioniemi OP (1998) Tissue microarrays for high-throughput molecular profiling of tumor specimens. Nat Med 4:844–847
15. Kudo Y, Kitajima S, Sato S, Miyauchi M, Ogawa I, Takata T (2001) High expression of S-phase kinase-interacting protein 2, human F-box protein, correlates with poor prognosis in oral squamous cell carcinomas. Cancer Res 61:7044–7047
16. Latres E, Chiarle R, Schulman BA, Pavletich NP, Pellicer A, Inghirami G, Pagamo M (2001) Role of the F-box protein Skp2 in lymphomagenesis. Proc Natl Acad Sci U S A 98:2515–2520
17. Lim MS, Adamson A, Lin Z, Perez-Ordonez B, Jordan RC, Tripp S, Perkins SL, Elenitoba-Johnson KS (2002) Expression of Skp2, a p27 (Kip1) ubiqitin ligase, in malignant lymphoma: correlation with p27 (Kip1) and proliferation index. Blood 100:2950–2956
18. Lloyd RV, Erickson LA, Jin L, Kulig E, Qian X, Cheville JC, Scheithauer BW (1999) p27kip1: a multifunctional cyclin-dependent kinase inhibitor with prognostic significance in human cancers. Am J Pathol 154:313–323
19. Masuda TA, Inoue H, Sonoda H, Mine S, Yoshikawa Y, Nakayama T, Nakayama T, Mori M (2002) Clinical and biological significance of S-phase kinase-associated protein 2 (Skp2) gene expression in gastric carcinoma: modulation of malignant phenotype by Skp2 overexpression, possibly via p27 proteolysis. Cancer Res 62:3819–3825
20. McKay JA, Douglas JJ, Ross VG, Curran S, Ahmed FY, Loane JF, Murray GI, McLeod HL (2000) Expression of cell cycle control proteins in primary colorectal tumors does not always predict expression in lymph node metastases. Clin Cancer Res 6:1113–1118
21. McLaughlin JK, Lipworth L (2000) Epidemiologic aspects of renal cell cancer. Semin Oncol 27:115–123
22. Méjean A, Oudard S, Thiounn N (2003) Prognostic factors of renal cell carcinoma. J Urol 169:821–827
23. Migita T, Oda Y, Naito S, Tsuneyoshi M (2002) Low expression of p27kip1 is associated with tumor size and poor prognosis in patients with renal cell carcinoma. Cancer 94:973–979
24. Oliveira AM, Okuno SH, Nascimento AG, Lloyd RV (2003) Skp2 protein expression in soft tissue sarcomas. J Clin Oncol 21:722–727
25. Shigemasa K, Gu L, O'Brien TJ, Ohama K (2003) Skp2 overexpression is a prognostic factor in patients with ovarian adenocarcinoma. Clin Cancer Res 9:1756–1763
26. Shirane M, Harumiya Y, Ishida N, Hirai A, Miyamoto C, Hatakeyama S, Nakayama K, Kitagawa M (1999) Down-regulation of p27kip1 by two mechanisms, ubiquitin-mediated degradation and proteolytic processing. J Biol Chem 274:13886–13893
27. Signoretti S, Di Marcotullio L, Richardson A, Ramaswamy S, Isaac B, Rue M, Monti F, Loda M, Pagano M (2002) Oncogenic role of the ubiquitin ligase subunit Skp2 in human breast cancer. J Clin Invest 110:633–641
28. Sobin LH, Wittekind C (eds) (2002) TNM classification of malignant tumors, 6th edn. Wiley–Liss, Inc., New York
29. Yang G, Ayala G, De Marzo A, Tian W, FrolovA, Wheeler TM, Thompson TC, Harper JW (2002) Elevated Skp2 protein expression in human prostate cancer: association with loss of cyclin-dependent kinase inhibitor p27 and PTEN and with reduced recurrence-free survival. Clin Cancer Res 8:3419–3426
30. Yokoi S, Yasui K, Mori M, Iizasa T, Fujisawa T, Inazawa J (2004) Amplification and overexpression of Skp2 are associated with metastasis of non-small-cell lung cancers to lymph nodes. Am J Pathol 165:175–180

Virchows Arch (2004) 445:637–640
DOI 10.1007/s00428-004-1124-z

ORIGINAL ARTICLE

Hélène Kafé · Jean-Marc Verbavatz · Béatrix Cochand-Priollet · Patrice Castagnet · Annick Vieillefond

Collecting duct carcinoma: an entity to be redefined?

Received: 14 April 2004 / Accepted: 23 August 2004 / Published online: 8 October 2004
© Springer-Verlag 2004

Abstract Collecting duct carcinomas (CDCs) are highly aggressive tumors with poor survival at 1 year and are often metastatic at the time of diagnosis. It has been shown that patients may have better survival when treated with a chemotherapy regimen used for urothelial carcinoma. Such tumors must therefore be recognized, but their pathological diagnosis remains difficult. The two main differential diagnoses are renal pelvis urothelial carcinoma with infiltration of the kidney and/or high-grade and high-stage papillary renal cell carcinoma. The aim of our study was to compare the immunophenotype of 14 CDCs with 6 renal pelvis urothelial carcinomas (RPUC) infiltrating the medulla. The following markers were evaluated: ulex europeus aglutinin (UEA), peanuts aglutinin, vimentin and aquaporin 3 (AQP-3), a membrane component of normal collecting duct and urothelial cells. We were able to define a reproductive urothelial phenotype AQP-3+, vimentin– and UEA+. Among the 14 CDCs, 10 cases demonstrated this immunophenotype. It coincided with an urothelial-like trabecular and tubular pattern. In contrast, the 4 remaining papillary CDCs had the inverse pattern, AQP-3–, vimentin+ and UEA–. These results suggest that: (1) the trabecular and tubular variant of CDC with the urothelial AQP-3+, vimentin– phenotype can be included in the spectrum of urothelial diseases; (2) the papillary variant probably does not belong to the same entity; (3) AQP-3 is a marker of interest for improving the histological classification of CDC and unclassified aggressive renal tumors.

Keywords Kidney · Collecting duct carcinoma · Aquaporin · Urothelial carcinoma

H. Kafé (✉) · B. Cochand-Priollet · P. Castagnet
Service d'Anatomie pathologique,
Hôpital Lariboisière,
2 rue Ambroise Paré, 75475 Paris Cedex 10, France
e-mail: kafe@caramail.com

J.-M. Verbavatz
Service de Biologie cellulaire,
CEA/Saclay,
91191 Gif sur Yvette Cedex, France

A. Vieillefond
Service d'Anatomie pathologique,
Hôpital Cochin,
75679 Paris Cedex 14, France

Introduction

Within the renal medulla, three subtypes of high-grade carcinomas may be discussed: collecting duct carcinoma (CDC), renal pelvis urothelial carcinoma (RPUC) with renal infiltration or high-grade papillary carcinoma. The differential diagnosis of these entities relies on imperfect criteria. These tumors may have a similar histological tubular and tubulopapillar pattern, while tumors other than RPUC may protrude into the renal pelvis. In this study, we focused on the immunophenotype of CDC and RPUC with renal infiltration to determine whether there exists a marker enabling us to distinguish between them. We compared the immunophenotype of 14 CDC and 6 renal-infiltrating RPUC. We used two classical collecting-duct markers (*Ulex europeus* and *peanuts aglutinin* lectins) and also tested the expression of vimentin, which is variable in the different CDC series in the literature [2, 10].

In addition, we felt it relevant to test the expression of the aquaporin-3 (AQP-3) protein, which is present in the urothelium and also constitutively highly expressed in the normal collecting duct [1, 11]. This protein belongs to a family of ten isoforms, acting as membrane water channels and playing a major role in fluid homeostasis. Aquaporins have been demonstrated in various species (plants, mammalians, bacteria, etc.) and tissues (skin, liver, kidney, brain, etc.) [7, 13]. In the normal kidney (Fig. 1), AQP-1 protein is a major component of the proximal tubule and the descending thin limb, whereas AQP-2, AQP-3 and AQP-4 are located on collecting duct principal cell membranes [4].

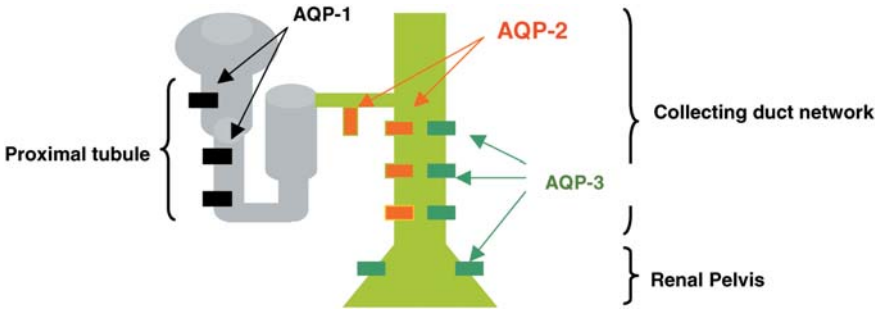


Fig. 1 Distribution of aquaporin-1, -2 and -3 proteins in the normal kidney

Table 1 Clinical data and lectin histochemistry and immunohistochemistry results. *CDC* Collecting-duct carcinoma, *AQP* aquaporin, *UEA* ulex europeus aglutinin, *PNA* peanuts aglutinin, *CK* cytokeratin, *ND* non-determined

Cases (n=20)	Age (years)	Sex	Architecture	AQP-3	UEA-1	Vimentin	CK7	PNA
CDC (n=14)								
Case 1	71	Male	Trabecular & tubular	+	+	−	+	+
Case 2*	79	Female	Trabecular & tubular	+	+	−	+	+
Case 3	75	Male	Trabecular & tubular	+	+	−	+	+
Case 4	56	Male	Trabecular & tubular	+	+	−	+	+
Case 5	77	Male	Trabecular & tubular	+	+	−	+	+
Case 6	65	Male	Trabecular & tubular	+	+	−	ND	−
Case 7*[a]	45	Male	Trabecular	+	+	−	+	+
Case 8*[a]	25	Female	Trabecular	+	+	−	+	+
Case 9*	56	Male	Trabecular	ND	+	−	−	+
Case 10*	56	Male	Trabecular & tubular	+	+	+	+	−
Case 11	ND	Male	Tubular & papillary	−	−	+	−	−
Case 12*	55	Male	Tubular & papillary	−	+	+	+	+
Case 13*	70	Male	Tubular & papillary	−	−	+	ND	−
Case 14*	63	Male	Trabecular & cystic	−	−	+	ND	−
Urothelial carcinoma (n=6)								
Case 15	77	Male	Trabecular & tubular	+	+	−	ND	+
Case 16	77	Female	Trabecular & tubular	+	+	−	ND	+
Case 17	63	Male	Trabecular & tubular	+	+	−	+	+
Case 18	68	Male	Trabecular	+	+	−	+	+
Case 19	69	Male	Trabecular	+	ND	−	+	+
Case 20	80	Male	Trabecular	+	+	−	+	ND

[a] Patients with sickle trait anemia
* Patients with lymph nodes and/or visceral metastases

Materials and methods

We reviewed 14 CDC and 6 renal infiltrating RPUC. The majority of the CDC cases were "consultation cases." Other cases were retrieved from a nephrectomy series performed at two surgical centers during the period of 1993–2003. All cases were similarly processed. After short fixation in 10% neutral buffered formalin, sections 5-μm thick were cut from the paraffin-embedded blocks. We performed routine histological stains (hematoxylin & eosin), lectin histochemistry using *Ulex europeus* agglutinin (UEA-1, Vector) and *Arachis hypogaea* (PNA, Dako) and immunochemical studies, using the following primary antibodies: anti-vimentin (Immunotech), anti-CK7 (Dako) and anti-AQP-3. AQP-3 antibodies were obtained as described previously from the Commissariat à l'Energie Atomique/Saclay, France [8]. They included polyclonal rabbit antibodies raised against a peptide corresponding to the rat AQP-3 carboxyl terminus. Blocking of endogenous peroxidase activity was performed by treatment with 10% H_2O_2 in methanol for 30 min. Non-specific protein binding was inhibited by a 30-min incubation in clear powder skimmed milk (5%). When using the AQP-3 antibody (1:200 dilution), sections were placed in ethylenediaminetetraacetate buffer solution, pH 7 (Speci) and incubated in a microwave 3×5 min at 700 W to enhance immunostaining. The staining reaction was performed using the avidin-biotin complex method (PK 4000, Vector). The final reaction was developed via a diaminobenzidine–H_2O_2 reaction (Chromogen kit, Immunotech).

Results

The clinical and pathological data are summarized in Table 1. The 14 patients with CDC ranged in age from 25 years to 79 years (mean age of 61 years). Two were female, and 12 were male. Two had sickle cell trait. All tumors were larger than 6 cm and extended into the perirenal fat (stage T3). Of 14 cases, 8 were metastatic at the time of the diagnosis. The 6 patients with renal infiltrating RPUC ranged in age from 63 years to 80 years (mean age of 72 years). Of these patients, 1 was female, and 5 were male. Their grades were G2–G3.

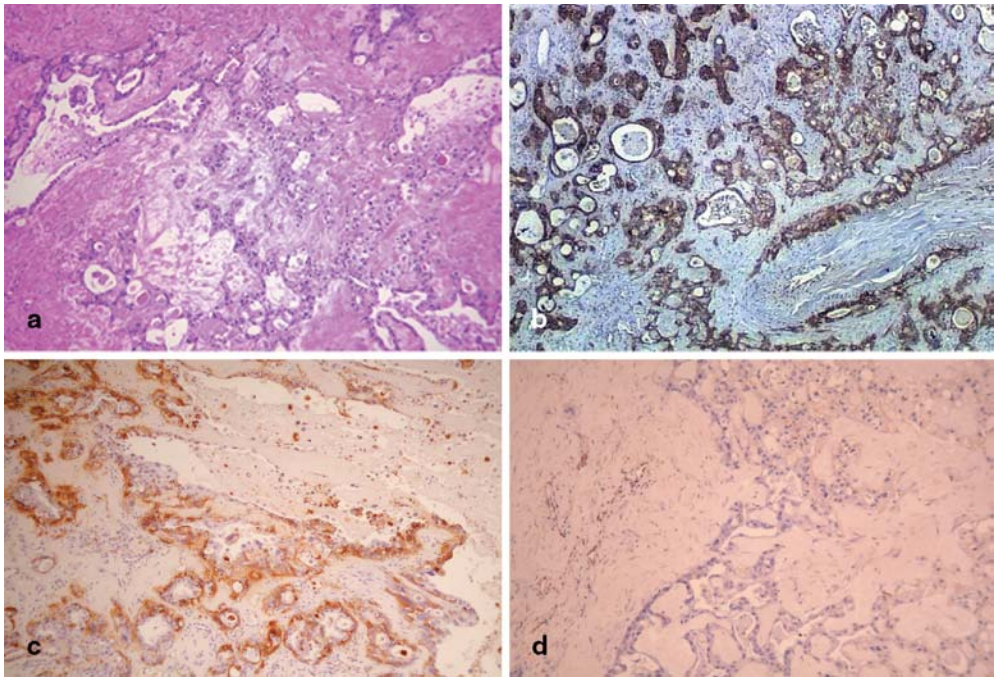


Fig. 2 Histological and phenotypic pattern of trabecular and/or tubular variant of collecting duct carcinoma. **a** Hematoxylin and eosin ×25: a poorly delimited trabecular and/or tubular infiltrating proliferation. **b** Strong aquaporin-3 membranous expression revealing an urothelial-like pattern. **c** Reaction with ulex europeus aglutinin. **d** no expression of vimentin

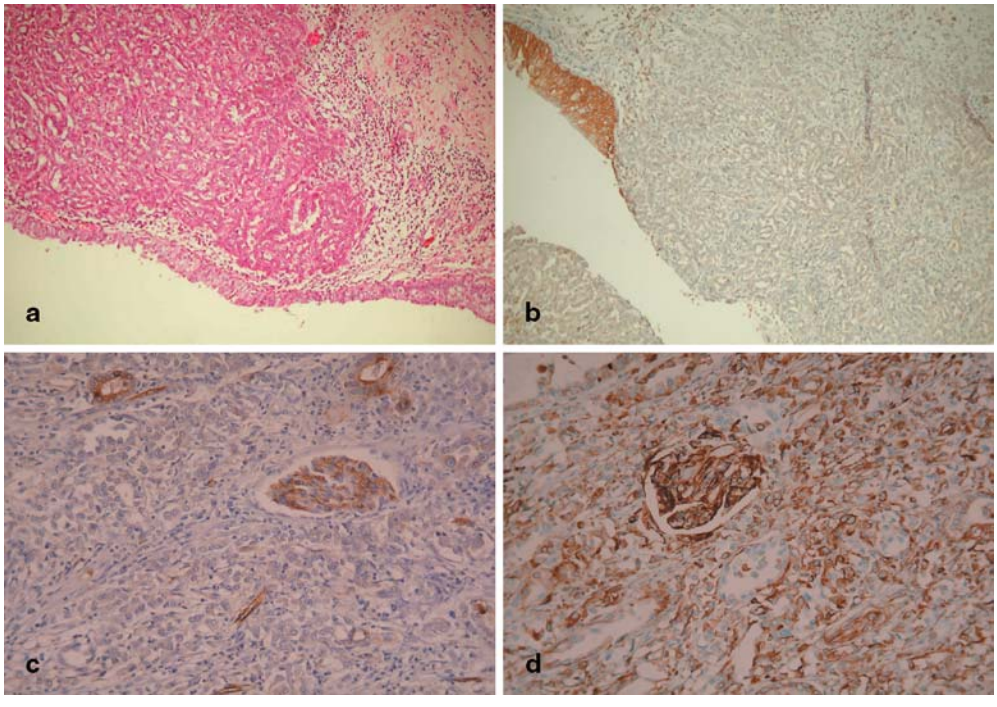


Fig. 3 Histological and phenotypic pattern of papillary variant of collecting duct carcinoma. **a** Hematoxylin and eosin ×25: a nodular and compact pattern. **b** No tumor aquaporin-3 expression. **c** No reaction with UEA-1. **d** Expression of vimentin

Pathology

CDC group

After re-examination of our 14 cases, we were able to delineate two subtypes of CDC. The most frequent pattern (A) (10 cases) consisted of a poorly delimited trabecular and/or tubular infiltrating proliferation of medium-size and large cells within a desmoplastic stroma, with inconsistent solid "urothelial-like" areas (Fig. 2). Typical urothelial carcinoma was never observed in renal pelvis. The second pattern (B) (4 cases) displayed a more compact architecture, with a mixture of tubular and papillary structures organized into nodules (Fig. 3). In contrast to group A, the tumor component was not imbricate with normal renal structures and was more clearly defined.

Renal pelvis urothelial carcinoma group

In all six cases, the renal pelvis component showed a typical urothelial papillary pattern, whereas the renal component infiltrated the medulla with trabecular and tubular structures, mimicking the CDC group A.

Lectin histochemistry and immunohistochemistry

CDC group

Among the14 cases, 11 reacted with UEA-1 (78%), 9 with anti-AQP-3 antibodies (64%), 9 with PNA (64%), 5 with anti-vimentin antibodies (35%) and 14 with anti-CK7 antibodies. When positive, AQP-3 labeling was strong and membranous. Normal control collecting ducts were marked. Within each of our two variants of CDC, the pattern was homogeneous. The trabecular and/or tubular subtype (group A) displayed an association of AQP-3+, vimentin− and UEA-1+ in 80% (8/10 cases) (Fig. 2). In contrast, 75% (3/4 cases) of the tubular and papillary cases (group B) had the inverse phenotype AQP-3−, vimentin+, UEA-1− (Fig. 3).

Urothelial carcinoma group

The group of urothelial carcinomas demonstrated the same pattern as variant A of CDC, reacting with AQP-3 antibodies in six cases (100%), UEA-1 in five (83%) and PNA in four (66%). As expected, tumor cells consistently expressed CK7 and were vimentin negative.

Discussion

Primary renal carcinomas group together different clinico-pathological entities, depending on the renal segment at the origin of the malignant proliferation. Papillary tumors originate from the proximal tubule, whereas CDC, chromophobe renal cell carcinomas and oncocytomas arise from collecting duct epithelium (principal cells for CDC and intercalated cells for chromophobe renal cell carcinoma and oncocytomas) [2, 10]. CDCs usually recapitulate the immunostaining pattern of normal collecting ducts and react with antibodies to high-molecular-weight keratin (CK-19, 34 β E12), CK7, epithelial membrane antigen and with the lectins *Arachis hypogaea* and *Ulex europeus* [2, 9, 12]. UEA-1 has even become the CDC emblematic marker [3]. However, our study clearly demonstrates the following: (a) This lectin has no discriminative value for the differential diagnosis between CDC and RPUC with renal infiltration. (b) It is possible to isolate an urothelial-like variant of CDC with a few markers. In our series, the most significant ones were vimentin and AQP-3 protein, and their association led to obtaining reproductible results. (c) Trabecular and/or tubular CDC with a pertinent phenotype (AQP-3+, vimentine−) belong to the spectrum of urothelial diseases and should be regarded as high-grade urothelial carcinomas. Not surprisingly, it has recently been shown that patients with CDC may have better survival when treated with a chemotherapy regimen used for urothelial carcinomas [5, 6]. Our results reinforce this data. (d) Conversely, our second variant of CDC, which displayed an inverse phenotype and a different morphology, probably does not belong to the same entity. Indeed, it may be closer to high-grade papillary renal cell carcinoma than to CDC. (e) The discovery of the aquaporin water channels family has opened up the perspective of finally understanding renal physiology. It will also undoubtedly help in the future classification of renal tumors.

Acknowledgment The authors thank The Société Française de Pathologie for its financial support.

References

1. Ecelbarger CA, Terris J, Frindt G et al (1995) Aquaporin-3 water channel localization and regulation in rat kidney. Am J Physiol 269:663–672
2. Kennedy SM, Merino MJ, Linehan WM et al (1990) Collecting duct carcinoma of the kidney. Hum Pathol 21:449–456
3. Kovacs G, Akhtar M, Beckwith BJ et al (1997) The Heidelberg classification of renal cell tumours. J Pathol 183:131–133
4. Marples D, Frokiaer J, Nielsen S (1999) Long-term regulation of aquaporins in the kidney. Am J Physiol Renal Physiol 276:331–339
5. Milowsky MI, Rosmarin A, Tickoo SK, Papanicolaou N, Nanus DM (2002) Active chemotherapy for collecting duct carcinoma of the kidney. Cancer 94:111–116
6. Peyromaure M, Thiounn N, Scotté F, Vieillefond A, Debré B, Oudard S (2003) Collecting duct carcinoma of the kidney: a clinicopathological study of nine cases. J Urol 170:1138–1140
7. Preston GM, Carroll TP, Guggino WB, Agre P (1992) Appearance of water channels in Xenopus oocytes expressing red cell CHIP28 protein. Science 256:385–387
8. Roudier N, Verbavatz JM, Maurel C et al (1998) Evidence for the presence of aquaporin-3 in human reed blood cells. J Biol Chem 273:8407–8412
9. Rumpelt HJ, Storkel S, Moll R et al (1991) Bellini duct carcinoma: further evidence for this rare variant of renal cell carcinoma. Histopathology 18:115–122
10. Srigley J, Eble JN (1998) Collecting duct carcinoma of kidney. Semin Diagn Pathol 15:54–67
11. Terris J, Ecelbarger CA, Nielsen S, Knepper MA (1996) Long-term regulation of four renal aquaporins in rats. Am J Physiol Renal Physiol 271:414–422
12. Ulrich W, Horvat R, Krisch K (1985) Lectin histochemistry of kidney tumours and its pathomorphological relevance. Histopathology 9:1037–1050
13. Verkman AS, Mitra AK (2000) Structure and function of aquaporin water channels. Am J Physiol Renal Physiol 278:13–28

Virchows Arch (2004) 445:641–646
DOI 10.1007/s00428-004-1091-4

CASE REPORT

Masayuki Shimoda · Kaori Kameyama · Shojiroh Morinaga · Youichi Tanaka · Kazuhiro Hashiguchi · Megumi Shimada · Yasunori Okada

Malignant transformation of sialadenoma papilliferum of the palate: a case report

Received: 5 May 2004 / Accepted: 6 July 2004 / Published online: 29 September 2004
© Springer-Verlag 2004

Abstract We report a case of a 79-year-old woman with an unusual salivary gland tumor that developed at the junction between the soft and hard palates. The tumor consisted of sialadenoma papilliferum (SP) with areas of an epithelial–myoepithelial carcinoma (EMC) component and a high-grade carcinoma component. There were also transitional regions among the SP, the EMC and the high-grade carcinoma components. The high-grade carcinoma component, which was similar to invasive micropapillary carcinoma of the breast, infiltrated into the right parapharyngeal space and metastasized to the lungs and cervical vertebrae. The high-grade carcinoma cells were positively immunostained for p53 protein. SP has been considered to be a benign tumor with exceptionally good prognosis, and, to the best of our knowledge, there has never been a confirmed case of malignant SP. This is the first report of SP with a definite malignant component.

Keywords Sialadenoma papilliferum · Epithelial–myoepithelial carcinoma · High-grade carcinoma · p53

M. Shimoda · Y. Okada (✉)
Department of Pathology,
School of Medicine, Keio University,
35 Shinanomachi, Shinjuku-ku, 160-0016 Tokyo, Japan
e-mail: okada@sc.itc.keio.ac.jp
Tel.: +81-3-53633763
Fax: +81-3-33533290

K. Kameyama
Division of Diagnostic Pathology,
Keio University Hospital,
35 Shinanomachi, Shinjuku-ku, 160-8582 Tokyo, Japan

S. Morinaga
Division of Diagnostic Pathology,
Kitasato Institute Hospital,
5-9-1, Shirokane, Minato-ku, 108-8642 Tokyo, Japan

Y. Tanaka
Division of Surgical Pathology,
Tokyo Dental College Ichikawa General Hospital,
5-11-13, Sugano, Ichikawa City, 272-8513 Chiba, Japan

K. Hashiguchi
Division of Otorhinolaryngology,
Kitasato Institute Hospital,
5-9-1, Shirokane, Minato-ku, 108-8642 Tokyo, Japan

M. Shimada
Division of Internal Medicine,
Kitasato Institute Hospital,
5-9-1, Shirokane, Minato-ku, 108-8642 Tokyo, Japan

Introduction

Sialadenoma papilliferum (SP) is a rare salivary gland tumor that was first described by Abrams and Flinck [1] in 1969. They coined the term "sialadenoma papilliferum" because of the histological similarity between this type of salivary gland tumor and the syringocystadenoma papilliferum of cutaneous adnexal origin. The histogenesis of SP is still unclear. Some authors have proposed intercalated salivary ducts as the origin of SP [21, 25], while others have suggested excretory duct cells or pluripotential basal cells as the cells of origin [11, 16]. Typical SP is a slowly growing exophytic small tumor. The majority of SP occurs on the palate, and nearly two-thirds of the palatal lesion involves the hard palate. Patients' age ranges from 2 years to 87 years, and the average age is 56 years. Histologically, it is characterized by both exophytic and endophytic proliferation of ductal epithelium composed of a double layer of cells [9, 29]. The surface of the tumor is covered by acanthotic stratified squamous epithelium, which merges into the papillary fronds formed by the ductal proliferation in the deep areas. According to the approximately 50 reported cases, SP is considered to be a benign tumor with an exceptionally good prognosis, although post-operative recurrence was observed in two cases [23, 24]. Solomon et al. [27] reported an intra-oral malignant neoplasm as a possible malignant SP, but subsequent studies have discounted their interpretation [3, 9]. There has never been a confirmed case of malignancy associated with SP. To the

best of our knowledge, we report the first case of SP with a definite malignant component.

Clinical history

A 79-year-old Japanese woman was admitted to the Division of Otorhinolaryngology, Kitasato Institute Hospital, Tokyo, because of appetite loss. She had been followed up for diabetes mellitus, hypertension and postoperative rectal carcinoma. The family history was non-contributory. Oral examination revealed an exophytic pink-white papillary mass, measuring 3.0×4.0×1.0 cm, at the junction between the hard and soft palates. A computed tomographic (CT) scan showed a high density mass in the soft palate that infiltrated the right parapharyngeal space (Fig. 1). There was no evidence of metastatic lesions on the chest X-rays. Biopsy specimens from the exophytic mass revealed SP of salivary gland origin with no evidence of malignancy. At the patient's request, the palate was not resected, and she was conservatively treated with intravenous hyperalimentation. The patient's respiratory status gradually deteriorated, and 1 month after her admission she died of asphyxia secondary to hemorrhage from the tumor. An autopsy was performed 3 h postmortem.

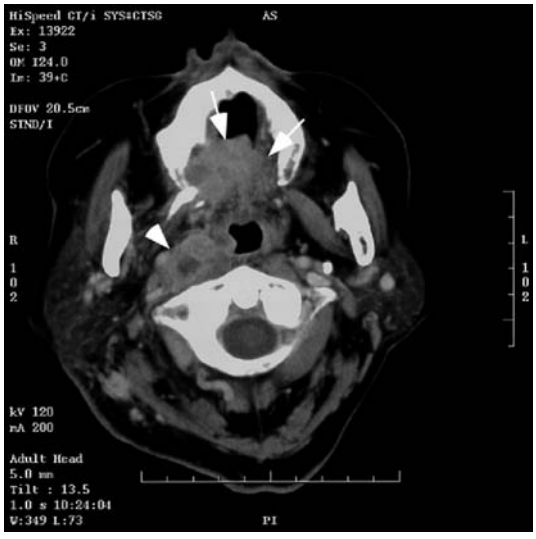


Fig. 1 Computed tomographic (CT) scan. A CT shows a high density mass in the soft palate (*arrows*) and infiltration into the right parapharyngeal space (*arrowhead*)

Materials and methods

For light microscopic evaluation, the specimen was fixed in 10% buffered formalin, and 5-mm-thick tissue slices were embedded in paraffin. Paraffin sections were stained with hematoxylin-eosin, and some sections were subjected to immunohistochemistry by the indirect method or the labeled streptavidin-biotin peroxidase complex method on the Ventana automated immunostainer (Ventana medical systems, Japan), using the primary antibodies listed in Table 1. In the examination of p53 protein expression, only tumor cells with distinct nuclear immunostaining were regarded as positive.

Results

At autopsy, a papillary exophytic lesion (3.0×4.0×1.0 cm) invading the palate was observed in the oral cavity (Fig. 2). Since the trachea was filled with a clot of blood,

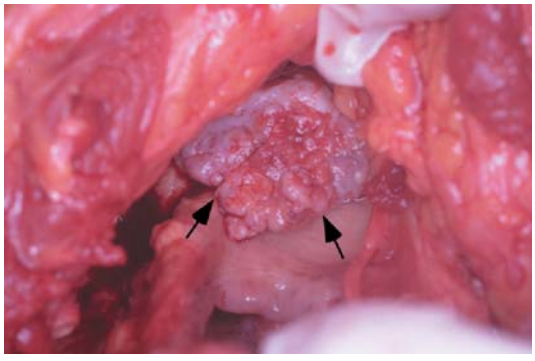


Fig. 2 Macroscopic observation of the tumor. The mass shows a papillary exophytic lesion covered with mucosa (*arrows*)

Table 1 Primary antibodies and staining methods used in this study. *Indirect* indirect method, *LSAB* labeled streptavidin-biotin peroxidase complex method, *Dako* Dako A/S, Glostrup, Denmark, *Nichirei* Nichirei corporation, Japan, *Ventana* Ventana medical systems, Japan, *Novacastra* Novocastra Laboratories, Newcastle, UK

Antibody	Clone	Dilution	Method	Antigen retrieval method	Source
Cytokeratin	AE1/AE3	1:50	Indirect	Trypsin	Dako
S-100 protein	Polyclonal	1:50	Indirect	Trypsin	Nichirei
Alpha-Smooth Muscle Actin (SMA)	1A4	1:100	Indirect	Microwave heating	Dako
Vimentin	V9	1:25	Indirect	Microwave heating	Dako
Carcinoembryonic antigen (CEA)	2–7	1:1	LSAB	Trypsin	Ventana
Epithelial membrane antigen (EMA)	E29	1:25	Indirect	Microwave heating	Dako
Glial fibrillary acidic protein	Polyclonal	1:1000	Indirect	Microwave heating	Dako
Gross cystic disease fluid protein-15	23A3	1:100	Indirect	Microwave heating	Novocastra
Estrogen receptor	1D5	1:200	LSAB	None	Dako
Androgen receptor	AR27	1:200	LSAB	None	Novocastra
Progesterone receptor	PgR636	1:400	LSAB	None	Dako
Prostate-specific antigen	Polyclonal	1:1000	Indirect	None	Dako
c-erbB-2 oncoprotein	CB11	1:1	LSAB	None	Novocastra
P53 protein	DO-7	1:400	Indirect	Microwave heating	Dako

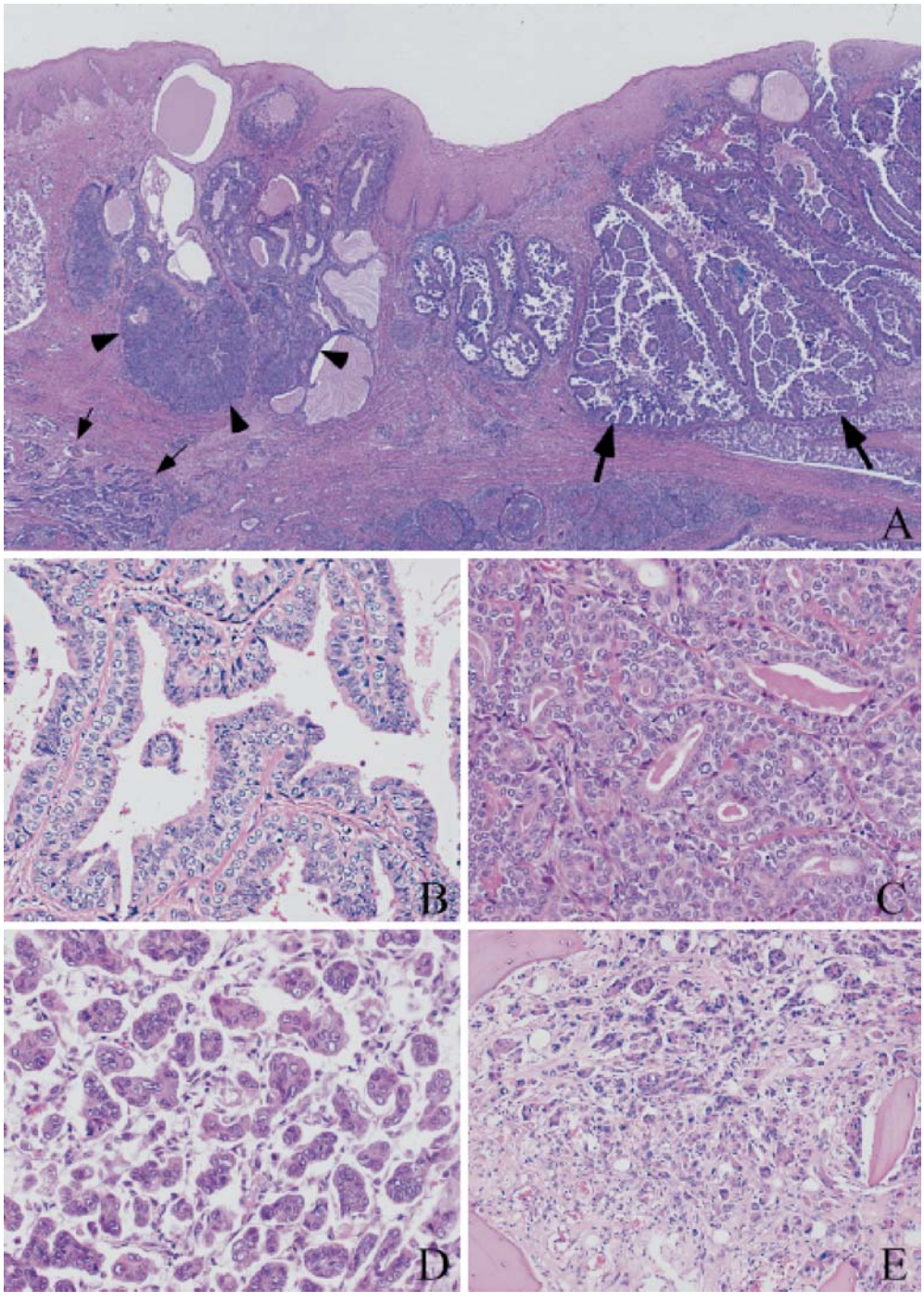


Fig. 3 Microscopic findings of the tumor. **A** The tumor consisting of three distinct histological types, sialadenoma papilliferum (SP) (*large arrows*), epithelial–myoepithelial carcinoma (EMC) (*arrowheads*) and high-grade carcinoma (*small arrows*) components. Original magnification ×20. **B** SP component showing ductal proliferation with papillary fronds. Note a double epithelium: cuboidal or columnar cells luminally and cuboidal cells basally. Original magnification ×200. **C** EMC component showing a biphasic pattern, composed of eosinophilic cuboidal cells and clear cells. Original magnification ×200. **D** High-grade carcinoma component arranged in micropapillae surrounded by clear spaces. Original magnification ×200. **E** Metastasis of the high-grade carcinoma component to the cervical vertebra. Original magnification ×100

the patient was considered to have died of asphyxia. Microscopic examination revealed that the tumor consisted of SP with areas of an epithelial–myoepithelial carcinoma (EMC) component and a high-grade carcinoma component. The SP and EMC components were located mainly in the upper layer of the submucosa, and high-grade carcinoma was observed in deeper portions of the tumor (Fig. 3A). The SP component showed ductal proliferation with papillary fronds covered with squamous epithelium (Fig. 3A). The papillae were lined with a double layer of epithelium: cuboidal or columnar cells luminally and cuboidal cells basally (Fig. 3B). The stratified squamous epithelium in the exophytic portion was slightly acanthotic and exhibited parakeratosis, although some areas of the epithelium were ulcerated. The ductal structures of the SP component were continuous with the overlying squamous epithelium. The immunohistochemical studies indicated intense reactivity for cytokeratin AE1/AE3, epithelial membrane antigen (EMA) and carcinoembryonic antigen (CEA) in the luminally located cells of the ductal structure, while the basally located cells were positive for alpha-smooth muscle actin (SMA),

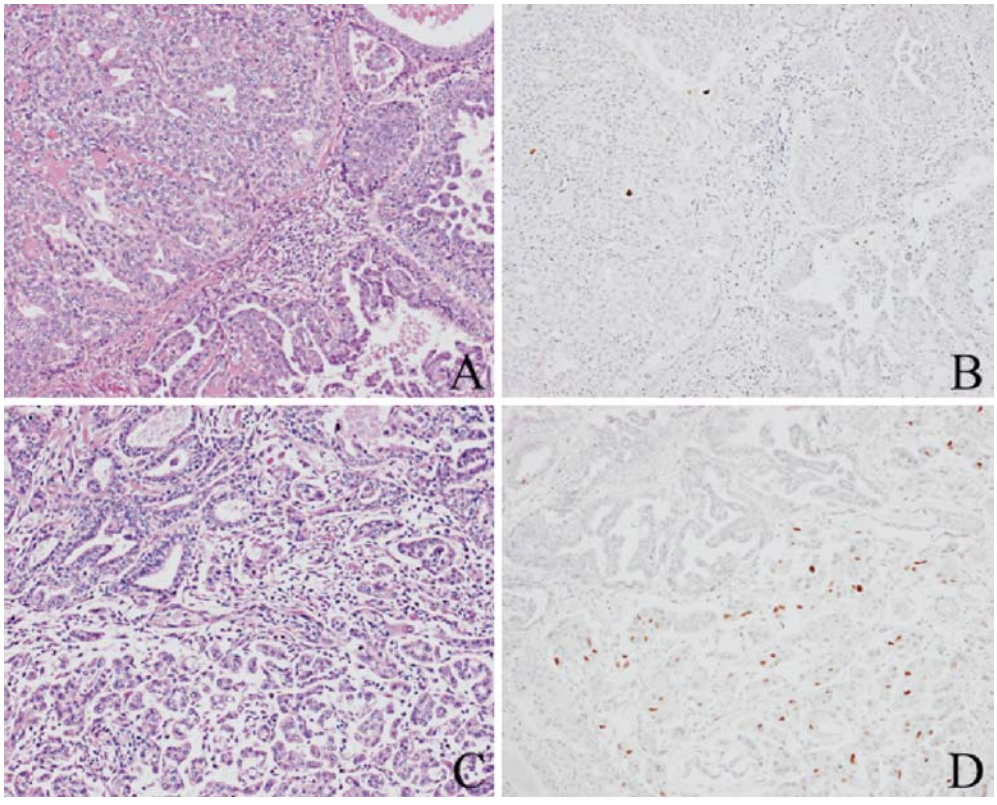


Fig. 4 Immunostaining of p53 protein in the transitional regions among the sialadenoma papilliferum (SP), epithelial–myoepithelial carcinoma (EMC) and high-grade carcinoma components. **A** Transitional region between the SP component (*right*) and the EMC component (*left*). Hematoxylin–eosin (HE) staining. **B** Immunohistochemistry for p53 protein, showing negligible staining. **C** Transitional region between the EMC component (*upper left*) and the high-grade carcinoma component (*lower right*). HE staining. **D** Immunohistochemistry for p53 protein. Note that the high-grade carcinoma cells accumulate p53 protein, while the EMC is almost negative. Original magnification ×100

S-100 protein and vimentin (data not shown). There were transitional regions between the SP component and the EMC component, the latter of which showed a multinodular growth pattern with islands of tumor separated by fibrous connective tissue septa. Small ducts exhibited a biphasic pattern and were lined with cuboidal epithelium and surrounded by clear cells (Fig. 3C). Mitotic figures were almost absent. Using immunohistochemistry, diffuse positivity of the cuboidal cells in the ductal structure was obtained for cytokeratin AE1/AE3, EMA and CEA, while the clear cells showed the characteristic phenotype of myoepithelial cells, being positive for SMA and S-100 protein and focally positive for vimentin (data not shown).

Importantly, we identified a high-grade carcinoma component in the present tumor. The high-grade carcinoma, which was continuous to the EMC component (Fig. 4C), showed more infiltrative growth. The carcinoma cells were composed of randomly arranged epithelial elements separated by fibrous stroma without myoepithelial cells and showed significant nuclear atypia. Tufts of the carcinoma cells with micropapillary arrangement surrounded by clear spaces devoid of any mucoid secretory content were observed (Fig. 3D). The high-grade carcinoma component invaded the right parapharyngeal space and microscopically metastasized to the lungs and cervical vertebrae (Fig. 3E). Immunohistochemically, the cells were positive for cytokeratin AE1/AE3, EMA, S-100 protein and CEA but showed no expression of SMA (data not shown). Some areas of the high-grade carcinoma resembled salivary duct carcinoma, but they were not positive for glial fibrillary acidic protein, gross cystic disease fluid protein-15, estrogen receptor, androgen receptor, c-erbB-2 oncoprotein, progesterone receptor or prostate-specific antigen.

When p53 protein was immunostained with the transitional regions among the SP, EMC and high-grade carcinoma components, only the high-grade carcinoma component showed accumulation of p53 protein. Approximately 15% of the carcinoma cells were positive, whereas the SP and EMC components showed almost negligible or no staining (Fig. 4A, B, C, D).

Discussion

In the present case, the tumor consisted of SP with areas of an EMC component and a high-grade carcinoma component. Since there were the transitional zones among three components, it is reasonable to postulate that all three components may have the same origin but not a collision tumor. Regarding papillary proliferation of the SP component, we have to consider papillary EMC or low-grade papillary adenocarcinoma in the differential diagnosis. EMCs that exhibit papillary growth are called papillary EMCs [9]. Although there were transitional regions between the SP and EMC components, to the best of our knowledge, no EMCs with papillary growth as marked as in the present tumor have ever been described. Low-grade papillary adenocarcinoma tends to occur in the palate [19, 20]. However, the papillary fronds of the present tumor were lined with a double layer of epithe-

lium and continuous with the overlying squamous epithelium, unlike typical low-grade papillary adenocarcinoma. Thus, it is more reasonable to diagnose this area as SP than as other papillary salivary gland neoplasms. The high-grade carcinoma was similar to invasive micropapillary carcinoma of the breast. Michal et al. [18] have reported a case of micropapillary carcinoma of the parotid gland arising in mucinous cystadenoma. Since the histological and immunohistochemical features of the high-grade carcinoma component of the present tumor appeared to be similar to those of the micropapillary carcinoma, the high-grade carcinoma component might belong to the category of micropapillary carcinoma. All histological studies on salivary duct carcinoma have noted the strong morphological resemblance to ductal carcinoma of the breast [26]. Some areas of the high-grade carcinoma also resembled salivary duct carcinoma, but the results of immunohistochemical studies were contrary to the usual findings associated with salivary duct carcinoma.

Since the present tumor contained low-grade malignant component (EMC component) and high-grade malignant component (high-grade carcinoma component), it might belong to the category of "dedifferentiated" tumors, which indicate the morphological co-existence of low-grade and high-grade malignancy. Although the term "dedifferentiation" was originally used in osteoskeletal pathology, its application has been broadened to soft tissue [6, 10, 17] and salivary gland pathology. Among salivary gland tumors, acinic cell carcinomas are known to be able to dedifferentiate [15, 22, 28], but dedifferentiation of EMCs is very rare [2, 12, 13].

The development and progression of cancer are regulated by the expression of various oncogenes and tumor suppressor genes. Recent molecular studies have demonstrated that tumor suppressor gene p53 is involved in various cancer types. However, among salivary gland tumors, the molecular events leading to dedifferentiation of salivary gland tumors have been disputed [4, 5, 7, 8, 14]. In the present case, the high-grade carcinoma cells showed accumulation of p53 protein, although the SP and EMC cells were negative. SP has been considered to be a benign tumor, but the present case suggests the possibility that malignant components may develop from SP, once aberration of p53 gene is added during the tumorigenesis of SP. We have to take into consideration the possibility of SP with a malignant potential.

References

1. Abrams AM, Flinck FM (1969) Sialadenoma papilliferum. A previously unreported salivary gland tumor. Cancer 24:1057–1063
2. Alos L, Carrilo R, Ramos J, Baez JM, Mallofre C, Fernandez PL, Cardesa A (1999) High-grade carcinoma component in epithelial-myoepithelial carcinoma of salivary glands clinicopathological, immunohistochemical and flow-cytometric study of three cases. Virchows Arch 434:291–299
3. Asahina I, Abe M (1997) Sialadenoma papilliferum of the hard palate: a case report and review of literature. J Oral Maxillofac Surg 55:1000–1003
4. Chau Y, Hongyo T, Aozasa K, Chan JK (2001) Dedifferentiation of adenoid cystic carcinoma: report of a case implicating p53 gene mutation. Hum Pathol 32:1403–1407
5. Cheuk W, Chan J, Ngan RKC (1999) Dedifferentiation in adenoid cystic carcinoma of salivary gland. A common complication associated with an accelerated clinical course. Am J Surg Pathol 23:465–472
6. Dahlin DC, Beabout JW (1971) Dedifferentiation in low-grade chondrosarcoma. Cancer 28:461–466
7. Di Palma S, Corletto V, Lovarino C Birindelli S, Pilotti S (1999) Unilateral aneuploid dedifferentiated acinic cell carcinoma associated with bilateral low-grade diploid acinic cell carcinoma of the parotid gland. Virchows Arch 434:361–365
8. Di Palma S, Corletto V, Lovarino C, Birindelli, Pilotti S (2000) Dedifferentiation in salivary gland carcinoma. Am J Surg Pathol 24:1439–1440
9. Ellis GL, Auclair PL (1995) Tumors of the salivary glands. Armed Forced Institute of Pathology, Washington, DC
10. Evans HL (1979) Liposarcoma: a study of 55 cases with a reassessment of its classification. Am J Surg Pathol 3:507–523
11. Fantasia JE, Nocco CE, Lally ET (1986) Ultrastructure of sialadenoma papilliferum. Arch Pathol Lab Med 110:523–527
12. Fonseca I, Felix A, Soarses J (2000) Dedifferentiation in salivary gland carcinoma. Am J Surg Pathol 24:469–471
13. Foschini MP, Eusebi V (1998) Carcinomas of the breast showing myoepithelial cell differentiation. A review of the literature. Virchows Arch 432:303–310
14. Gallo O, Franchi A, Bianchi S, Boddi V, Giannelli E, Alajmo E (1995) p53 oncoprotein expression in parotid gland carcinoma is associated with clinical outcome. Cancer 75:2037–2044
15. Henley JD, Geary WA, Jackson CL, Wu CD, Gnepp DR (1997) Dedifferentiated acinic cell carcinoma of the parotid gland: a distinct rarely described entity. Hum Pathol 28:869–873
16. Maiorano E, Favia G, Ricco R (1996) Sialadenoma papilliferum: an immunohistochemical study of five cases. J Oral Pathol Med 25:336–342
17. Meis JM (1991) "Dedifferentiation" in bone and soft tissue tumors: a histological indicator of tumor progression. Pathol Annu 26:37–62
18. Michal M, Skalova A, Mukensnabl P (2000) Micropapillary carcinoma of the parotid gland arising in mucinous cystadenoma. Virchows Arch 437:465–468
19. Mills SE, Garland TA, Allen MS (1984) Low-grade papillary adenocarcinoma of palatal salivary gland origin. Am J Surg Pathol 8:367–374
20. Mostofi R, Wood RS, Christison W, Talerman A (1992) Low-grade papillary adenocarcinoma of minor salivary glands. Case report and literature review. Oral Surg Oral Med Oral Pathol 73:591–595
21. Nakahata A, Deguchi H, Yanagawa T, Yoshida H, Sato M, Hayashi Y (1990) Coexpression of intermediate-sized filaments in sialadenoma papilliferum and other salivary gland neoplasms. J Oral Pathol Med 19:313–318
22. Piana S, Cavazza A, Pedroni C, Scotti R, Serra L, Gardini G (2002) Dedifferentiated acinic cell carcinoma of the parotid gland with myoepithelial features. Arch Pathol Lab Med 126:1104–1105
23. Pimentel MT, Lopez Amado M, Garcia Sarandeses (1995) A Recurrent sialadenoma papilliferum of the buccal mucosa. J Laryngol Otol 109:787–790
24. Rennie JS, MacDonald DG, Critchlow HA (1984) Sialadenoma papilliferum. A case report and review of the literature. Int J Oral Surg 13:452–454
25. Shirasuna K, Watatani K, Miyazaki T (1984) Ultrastructure of a sialadenoma papilliferum. Cancer 53:468–474
26. Simpson RH, Prasad AR, Lewis JE, Skalova A, David L (2003) Mucin-rich variant of salivary duct carcinoma: a clinicopathologic and immunohistochemical study of four cases. Am J Surg Pathol 27:1070–1079

27. Solomon MP, Rosen Y, Alfonso A (1978) Intraoral papillary squamous cell tumor of the soft palate with features of sialadenoma papilliferum-? malignant sialadenoma papilliferum. Cancer 42:1859–1869
28. Stanley RJ, Weiland LH, Olsen KD, Pearson BW (1988) Dedifferentiated acinic cell (acinous) carcinoma of the parotid gland. Otolaryngol Head Neck Surg 98:155–161
29. Ubaidat MA, Robinson RA, Belding PJ, Merryman DJ (2001) Sialadenoma papilliferum of the hard palate: report of 2 cases and immunohistochemical evaluation. Arch Pathol Lab Med 125:1595–1597

Virchows Arch (2004) 445:647–650
DOI 10.1007/s00428-004-1094-1

CASE REPORT

R. Ciranni · G. Fornaciari

Juvenile cirrhosis in a 16th century Italian mummy. Current technologies in pathology and ancient human tissues

Received: 7 April 2004 / Accepted: 9 July 2004 / Published online: 16 September 2004
© Springer-Verlag 2004

Abstract The natural headless mummy of a young man from the Basilica of Saint Domenico Maggiore in Naples (16th century) showed at autopsy a well-preserved fibrous liver with a nodular surface, suggesting a case of cirrhosis. Stereo and light microscope study confirmed this diagnosis. To identify the possible etiology of this cirrhosis, additional techniques currently used in pathology were performed. Hemochromatosis and alpha1-antitrypsin deficiency were investigated without results. Investigation regarding Wilson's disease gave positive results, since the use of rhodamine staining, which is specific to detect the presence of copper in tissues, resulted in red-brown grains at light microscopy. The positive rhodamine test was invalidated by atomic absorption spectroscopy (AAS), which revealed normal copper levels in the tissues. These negative results and the clear and diffuse macronodularity of the liver suggest a case of post-necrotic cirrhosis.

Keywords Paleopathology · Liver · Cirrhosis · Histology · Histochemistry · AAS

Introduction

The Abbey of Saint Domenico Maggiore dates back to the beginning of the 14th century and is one of the most important churches in Naples. In the monumental Sacristy, on a suspended 5-m-high gateway, 37 wooden coffins contain the well-preserved bodies of ten Aragonese kings, princes and other Neapolitan nobles who died between the 15th and 17th centuries [11]. These mummies are unique in Italy, not only for their antiquity and for the excellent state of preservation of the bodies but also for the historical importance of the individuals [3].

Therefore, the study of various diseases affecting these people, their dietary habits and lifestyles make it extremely interesting to compare the paleopathological with the historical data. The analysis of particular pathological conditions and a better understanding of the pathocenosis (the whole of pathologies characterizing a human society) can provide important and useful information on the environment and social habits of the upper classes of those times [4].

In regard to the case in question, autopsy of mummy NaSD 29 showed clear features of cirrhosis. Our paleopathological target was to confirm the macroscopic diagnosis using standard histology and to investigate some of the possible causes of the disease. The conditions investigated were: hemochromatosis, α_1-antitrypsin deficiency (α_1-AT) and Wilson's disease.

Materials and methods

NaSD 29 is a well-preserved headless natural mummy of an adult male aged 24±2 years [10] and approximately 175 cm tall (Fig. 1). Autopsy, carried out by anterior opening of the thorax and abdomen, allowed the macroscopic examination of the internal organs. Fragments of tissues (0.8×0.8×0.8 cm) belonging to different organs were collected and rehydrated using Sandison's method [8] and were submitted to routine histological processes. Thin sections were fixed on clean slides previously treated with an 8% solution of $KCr(SO_4)_2$ to avoid dispersion. The slides were stained with hematoxylin-eosin to evaluate the preservation of the tissue, and Masson's trichrome was applied for the connective tissue. Hemochromatosis, α_1-AT deficiency and Wilson's disease were investigated using histochemistry.

Hemochromatosis was detected by Perls' Prussian blue method using a 2% $K_4Fe(CN)$ solution in HCl 2% for 10 min. The reaction with iron ions was evidenced by blue grains at light microscope.

For α_1-AT deficiency diagnosis, the periodic acid of Schiff's (PAS) method was applied using a 1% periodic acid solution for 5 min and the Schiff reagent for 5–10 min. In α_1-AT deficiency, the liver is characterized by the presence of PAS-positive dark red grains, which are diastase resistant.

Wilson's disease was detected staining selected sections of liver tissue with a solution of rhodanine 0.2% in ethanol, which is specific to detect copper, resulting in red-brown grains at light mi-

R. Ciranni (✉) · G. Fornaciari
Department of Oncology,
Transplants and Advanced Technologies in Medicine,
Division of Pathology, Section of History of Medicine,
University of Pisa,
Via Roma 56, 56126 Pisa, Italy
e-mail: r.ciranni@do.med.unipi.it
Tel.: +39-50-992894
Fax: +39-50-992706



Fig. 1 The headless mummified body of NaSD 29

croscopy. Lung tissue sections from the same individual and liver tissue from the NaSD 14 mummy were used as negative controls.

Atomic absorption spectroscopy (AAS) [9] was performed to detect copper concentration in six different samples of tissue: three were from different organs of NASD 29 (left and right lobes of the liver and pectoral muscle); two of the samples belonged to the liver of other mummies of the same group (NASD 1 and NASD 14); the latter, used as negative control, was from modern liver biopsy. Dry tissue (500 mg) enveloped in muffle and diluted in 1:5 distilled water was placed in an open oven at 250°C for 30 min. After this time, temperature was adjusted at 450°C, and the oven was closed 30 min later. The material was maintained at 450°C overnight. At the end of the procedure, the residual concentration (μg/ml) of copper was evaluated for each sample.

Results

Autopsy revealed well-preserved thoracic and abdominal organs, dried and partially collapsed on the posterior wall. The mediastinum and the diaphragm were clearly identified as well as the bronchial tree and lungs. The pericardial sac contained the heart, wrinkled (7×4 cm) and flattened. The liver—reduced in size (18×9cm) but of typical shape, with sickle-like ligament and easily recognizable hepatic lobes—showed a granular surface with many single or clumped 0.5- to 1.5-cm nodules (Fig. 2a). The kidneys were typically shaped (7×3 cm) and appeared flattened up to 0.5 cm.

Histology, using hematoxylin-eosin and Masson's trichromic staining, showed excellent preservation of the tissues, making it possible to identify some pathological conditions, such as pulmonary apical fibrosis and severe anthracosis.

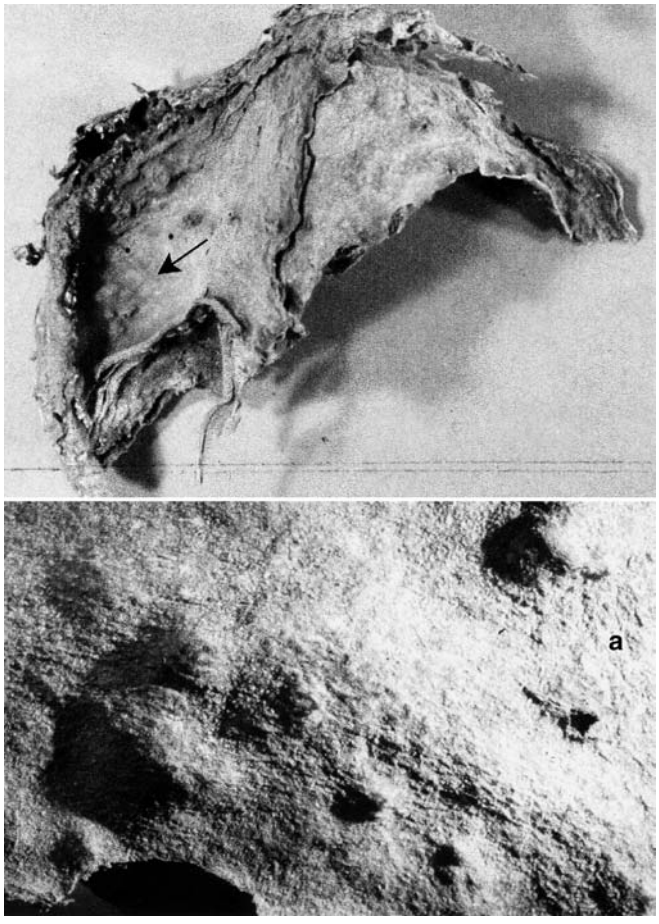


Fig. 2 The NaSD 29 liver appears reduced in size but of typical shape. The sickle-like ligament, the hepatic lobes and the nodular surface (*arrow*). Stereoscopic image (4×) showing some of the hepatic nodules (*a*)

Liver histology evidenced coarse bands of fibrous tissue dissecting and surrounding areas of homogeneous, brown and granular material representing residual hepatic parenchyma, which resulted in a sort of pseudo-lobular organization (Fig. 3). Some nodular formations, with multi-layered fibrous connective bands, surrounding regions of degenerated parenchyma, were well evident (Fig. 3a). Therefore, the macroscopic and microscopic picture clearly revealed a picture of micro-macronodular cirrhosis.

The histochemical results, specific for iron, were positive in the liver and in lungs, where light microscopy revealed massive deposits of the metal. PAS staining was negative for α_1-AT hepatic accumulation, owing to the absence of the typical grains. Positive results were also obtained using differential rhodamine staining, specific for copper: this result, suggestive of Wilson's disease, was not confirmed by AAS, which revealed normal copper levels in the tissues.

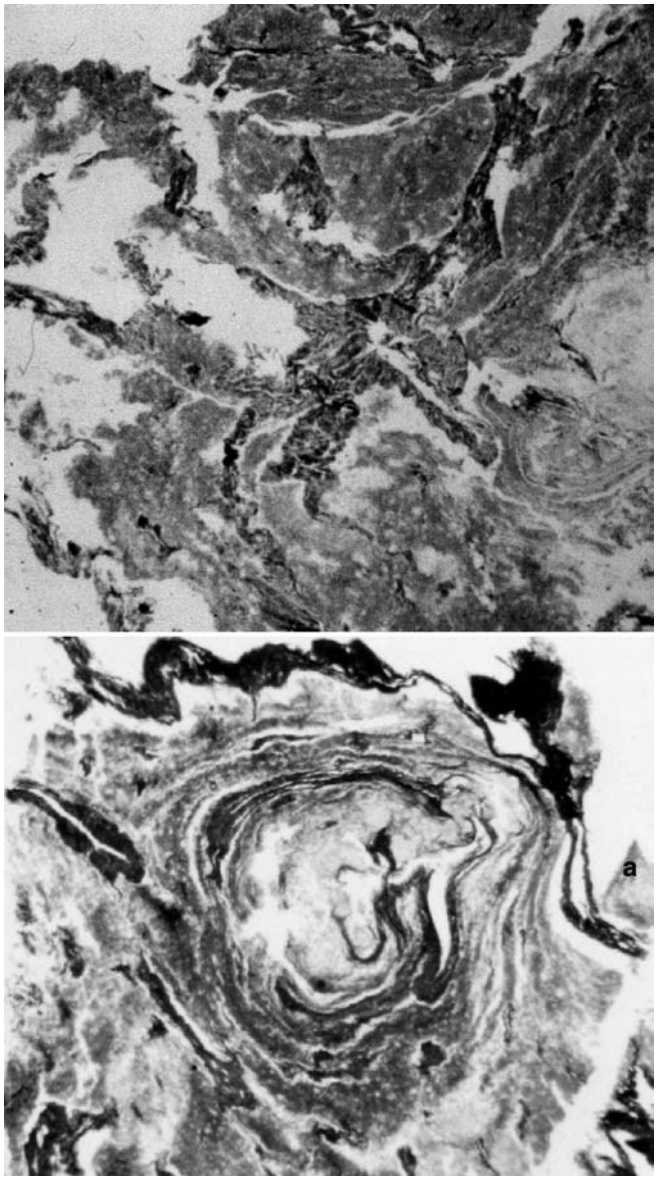


Fig. 3 Coarse bands of fibrous tissue dissecting and surrounding the hepatic parenchyma, resulting in a sort of pseudo-lobular organization (hematoxylin-eosin staining 10×). *a* Nodular formations, with multi-layered fibrous connective scars, surrounding degenerate parenchyma (Masson's trichrome staining 10×)

Discussion

Cirrhosis is currently a very common pathological condition in Western countries. Even though it is well documented in the ancient medical texts [1], the paleopathological diagnoses are rare. Overview of the literature has shown some cases of mummies with cirrhotic livers, clearly caused by parasitic infections. In the Egyptian Nakht case (first half of the12th century B.C.), for example, schistosomal ova were found in the liver, suggesting cirrhosis caused by hepatic schistosomiasis [5]. Another parasitic cirrhosis, due to clonorchiasis and Schistosoma japonicum, was also described in a Jiangling male body, a very well-preserved Chinese mummy dated back to 167 B.C. [7]. The only case of cirrhosis not dependent on parasites has been described recently by Zimmerman in a frozen body belonging to a young Eskimo girl (800–1000 A.D.), who died of pulmonary edema and severe emphysema [12]. This condition was a complication of genetic α_1-AT deficiency, as histologically evidenced by the author using PAS and diastase methods.

Alcoholism, at present the most frequent cause (70–80%) of cirrhosis, was initially attributed to NaSD 29. However, several decades of alcohol abuse are necessary to generate cirrhosis [2], and this strongly contrasts with the young age (24±2 years) of the man.

Histochemistry was strongly positive for iron in both the liver and lung of the mummy. These results could be consistent with a diagnosis of hemochromatosis, but the significance of its massive presence in the lung remains unclear. Forensic medicine provides a simple explanation for iron accumulation, for colliquative post-mortem events: hemoglobin present in the erythrocytes supports severe degradation, releasing high levels of iron throughout the whole body, but particularly in the lungs and liver, through their rich venous and capillary net [6].

During macroscopic examination, our attention, supported by the finding of pulmonary fibrosis and by the young age of the individual, was firstly focused on α_1-AT deficiency. Since the test results for α_1-AT deficiency were negative, this hypothesis was abandoned. Lung fibrosis was considered an independent condition, probably depending on apical tuberculosis, very common in the past.

Because of its rarity, Wilson's cirrhosis was the last hypothesis we considered. At present, the incidence of Wilson's disease is very low (0.005%) [2].

The positive results obtained with rhodamine method made this diagnosis seem possible, but the elemental analysis using AAS revealed normal levels of copper. Therefore, the positive rhodamine reaction could be referred to the normal copper concentration in a mummified and shrunken organ such as cirrhotic liver.

In conclusion, despite its very typical macroscopic and histological picture and the different modern tests, the real etiology of this juvenile cirrhosis is still unclear, but macroscopic and histological picture and, in particular, presence of large nodules (macronodules) is peculiar of post-necrotic cirrhosis.

Acknowledgements We would like to thank Mrs. Debora Barraco and Mr. Marcello Gambini (Santa Chiara Hospital) for their precious technical support.

References

1. Brothwell DR, Sandison AT(1967) Disease in antiquity. Charles C. Thomas Publisher, Springfield
2. Cotran RS, Kumar V, Robbins SL (1994) Pathologic basis of disease. W.B. Saunders Company, Philadelphia

3. Fornaciari G (1998) Italian mummies. In: Cockburn A, Cockburn E, Reyman TA (eds) Mummies, disease and ancient culture. Cambridge University Press, 2nd edn. Cambridge, pp 266–281
4. Grmek MD (1983) Les maladies à l'aube de la civilisation Occidentale. Payot, Paris
5. Hart GD, Cockburn TA, Millet NB, Scott JW (1977) Editorial: autopsy of an Egyptian mummy. Can Med Assoc J 117:461
6. Janssen W (1984) Forensic histopatology. Springer, Berlin Heidelberg New York
7. Peng L, Wu Z (1998) China: the Mawangtui-type cadavers in China. In: Cockburn A, Cockburn E, Reyman TA (eds) Mummies, disease and ancient culture, 2nd edn. Cambridge University Press, Cambridge, pp 328–335
8. Sandison AT (1955) The histological examination of mummified material. Stain Technology 30:277–283
9. Szpunar CB, Lambert JB, Buikstra JE (1978) Analysis of excavated bone by atomic absorption. Am J Phys Anthropol 48:199–202
10. Todd TW (1920) Age changes in the pubic bone: I. The male white pubis. Am J Phys Anthropol 3:285–334
11. Valle R, Minichini B (eds) (1854) Descrizione storica, artistica e letteraria della chiesa di San Domenico Maggiore. Napoli
12. Zimmerman MR (1998) Alaskan and Aleutian mummies. In: Cockburn A, Cockburn E, Reyman TA (eds) Mummies, disease and ancient culture, 2nd edn. Cambridge University Press, Cambridge, pp 138–153

Virchows Arch (2004) 445:651–654
DOI 10.1007/s00428-004-1112-3

CASE REPORT

Katharina Pauls · Eva Wardelmann · Sabine Merkelbach-Bruse · Reinhard Büttner · Hui Zhou

c-KIT codon 816 mutation in a recurrent and metastatic dysgerminoma of a 14-year-old girl: case study

Received: 22 June 2004 / Accepted: 30 July 2004 / Published online: 29 September 2004
© Springer-Verlag 2004

Abstract Dysgerminomas are rare female germ-cell tumors that correspond histologically and immunohistochemically to seminomas. Analogous to seminomas, most dysgerminomas respond very well to cisplatin- or carboplatin-based chemotherapy and to radiotherapy. KIT tyrosine kinase is crucial for normal germ-cell development, and its expression is observed in the majority of seminomas and dysgerminomas. Recently, activating KIT mutations were described in a panel of male germ-cell tumors [5, 10]. All mutations were localized in exon 17, encoding the second tyrosine kinase domain. Because receptor tyrosine kinase KIT might also be involved in the pathogenesis of dysgerminomas, we studied the expression and mutational status of a pure dysgerminoma, which was sent to our department for diagnostic reasons. The tumor revealed an exon 17 D816 V mutation in the *c-KIT* gene and strong KIT expression was found immunohistochemically. Clinically, the tumor was highly aggressive and resistant to carboplatin-based chemotherapy. Our case raises the question of whether exon 17 *c-KIT* mutations might be involved in the pathogenesis of dysgerminoma and whether exon 17 KIT mutations may predict aggressive and chemotherapy-resistant behavior of dysgerminomas.

Keywords c-KIT-mutation · Germ cells · Immunohistochemistry

K. Pauls · E. Wardelmann · S. Merkelbach-Bruse · R. Büttner · H. Zhou
Department of Pathology,
University of Bonn,
Germany

K. Pauls (✉)
Institut für Pathologie,
Sigmund-Freud-Strasse 25, 53127 Bonn, Germany
e-mail: katharina.pauls@ukb.uni-bonn.de
Tel.: +49-228-2879245
Fax: +49-641-2875030

Introduction

The transmembrane tyrosine kinase receptor (KIT), encoded by the *c-KIT* proto-oncogene, is crucial for normal development and survival of germ cells and is expressed in germ-cell tumors (GCTs) and intratubular carcinoma in situ of the testis [15, 16]. Activation of KIT is naturally induced by the ligand stem-cell factor and initiates the phosphorylation of downstream substrates involved in receptor signaling. Gene mutations causing constitutive phosphorylation of KIT, independent of ligand binding, are common in gastrointestinal stromal tumors (GISTs) and also occur in mastocytosis and in acute myeloid leukemia [1, 2, 4, 8]. GISTs, formerly resistant to any chemotherapy, respond well to inhibition of KIT with imatinib mesylate (Glivec, formerly known as STI571). Activating *c-KIT* mutations were recently found in a subset of testicular GCTs [5, 10]. Dysgerminoma is the female counterpart of a seminoma, exhibiting the same histology and similar excellent prognosis due to the good response to platinum-based chemotherapy.

However, the prevalence of *c-KIT* mutations in female GCTs and their effect on the clinical response and prognosis is not yet known. Here we provide for the first time clinico-pathological data of a 14-year-old girl with an aggressive *c-KIT*-mutated dysgerminoma, which relapsed soon after carboplatin-based chemotherapy and extensively metastasized to the lymph nodes and bones. We also present a *c-KIT* mutation analysis of the primary tumor of this patient.

Materials and methods

For immunohistochemistry using aviditin-biotin peroxidase complex technique, antibodies to PLAP (BioGenex, Hamburg, Germany) and KIT (Dako, Hamburg, Germany) were applied on dewaxed and microwave-pretreated tissue sections as has been published in detail [9, 14]. The fraction of proliferating cells was assessed using the monoclonal Ki-67antibody Mib-1 (Dianova, Hamburg, Germany). DNA extraction, polymerase chain reaction (PCR) and sequencing exon 17 of c-KIT were performed as previously described [14]. In short, total DNA was extracted after

pretreatment with proteinase K according to the manufacturer's protocol (Qiagen, Hilden, Germany). PCR reaction and cycle sequencing were carried out using exon 17 forward primer 5′-ATGGTTTTCTTTTCTCCTCC-3′ and exon 17 reverse primer 5′-TACATTATGAAAGTCACACG-3′, platinum *Taq* polymerase (Invitrogen, Karlsruhe, Germany) and ABI PRISM Dye Terminator Sequencing KIT (Applied Biosystems, Weiterstadt, Germany) on a TC 9600 thermocycler (Perkin Elmer, Rodgau-Jügesheim, Germany) with 20 ng of PCR products. The mutation was confirmed by a second independent round of DNA extraction, PCR and cycle sequencing.

Case report

A 14-year-old girl complained about severe abdominal pain and had a visible and palpable abdominal mass. The diagnostic laparoscopy at the first day of admission revealed a 10-cm large retroperitoneal tumor, which was located in the space from the left adrenal gland to the pelvis minor (Fig. 1). The uterus was displaced to the front wall of the pelvis by the tumor mass and the colon sigmoideum to the right side. The mesosigma was completely infiltrated by the tumor, which also enclosed big retroperitoneal vessels. While the right ovary was of normal size and form, the left ovary was not visible, and the left fallopian tube was adjacent to the tumor nodules. After histological examination, final diagnosis was unilateral pure dysgerminoma arising from the left ovary, which had spread to the pelvis minor, grossly infiltrated the retroperitoneum and the sigma and had metastasized to the retroperitoneal lymph nodes.

To induce tumor reduction and facilitate surgical resection, treatment was initiated by percutane ethanol injection (PEI)-chemotherapy. After surgical extirpation of the tumor masses, chemotherapy of three cycles of carboplatin and etoposide was performed. Then, 3 months after combined chemotherapy and 18 months after primary diagnosis, the tumor within the pelvis minor recurred and also infiltrated the vertebral spine in the region L4 to S3. The tumor penetrated the gluteal musculature, and the tumor masses restricted the rectum, both ureters and peripheral crural veins. Numerous skeletal metastases within the pelvis, from the third to sixth rib on the right side and on both scapulae were present. Neoadjuvant chemotherapy with carboplatin, etoposide and ifosfamide was performed, followed by local PEI. Subsequently, abdominal surgery was carried out again for tumor extirpation and adhesiolysis of small bowel loops. Radiological investigations 9 months later, including magnetic resonance imaging and bone scanning, revealed very good remission, reduced tumor size in the pelvis minor and decreased uptake of ^{99m}Tc-tracer in the thorax. To achieve further regression of residual tumor mass, low-dose radiation therapy was performed. Currently, 6 months after radiation and 3 years after her first admission to hospital, the patient is alive with no evidence of tumor progress.



Fig. 1 Computed tomography scan at the time of the primary diagnosis reveals a large tumor in the pelvis minor, which displaces sigma and the retroperitoneal vessels (*arrow*)

Results

Pathological examination and mutation analysis of the KIT gene

The primary tumor was soft, yellowish-white on the cut surface and partially necrotic. Histological examination revealed a tumor with typical characteristics for dysgerminoma, which infiltrated the left fallopian tube. The tumor cells were dispersed in sheets and cords separated by scant fibrous stroma with some lymphocytes (Fig. 2). No other differentiation (embryonal carcinoma, chorioncarcinoma, etc.) or normal ovarian tissue was found. Immunohistochemically, the tumor cells showed strong membranous expression of PLAP and KIT (Fig. 2). The

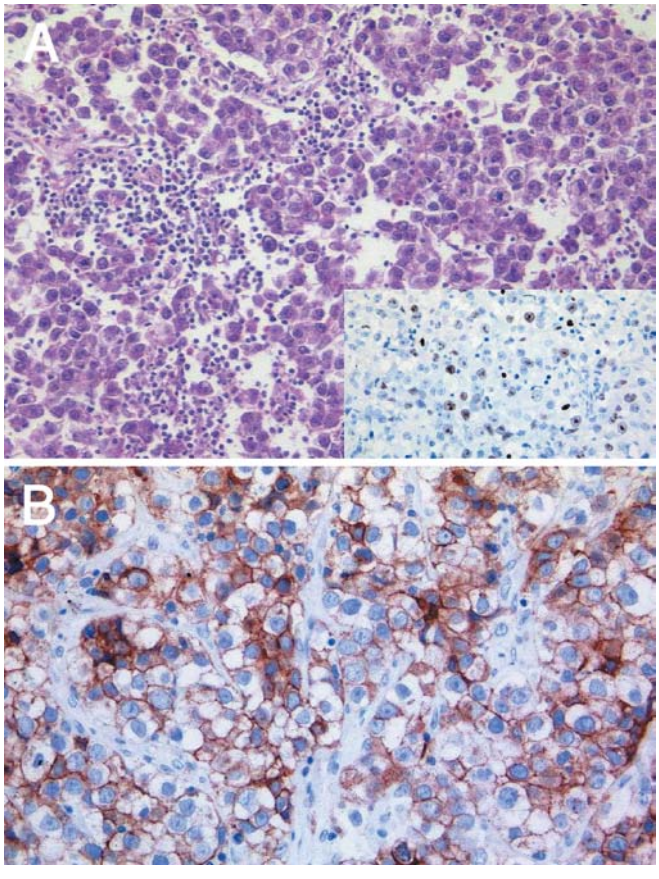


Fig. 2 A Dysgerminoma displays a typical morphology (hematoxylin and eosin staining, ×100) and a high proliferation rate, estimated by Ki-67-index (*insert*) (Mib-1 antibody, ×100). **B** Immunohistochemistry using anti-CD117 antibody. Strong membranous Kit expression on tumor cells (×200)

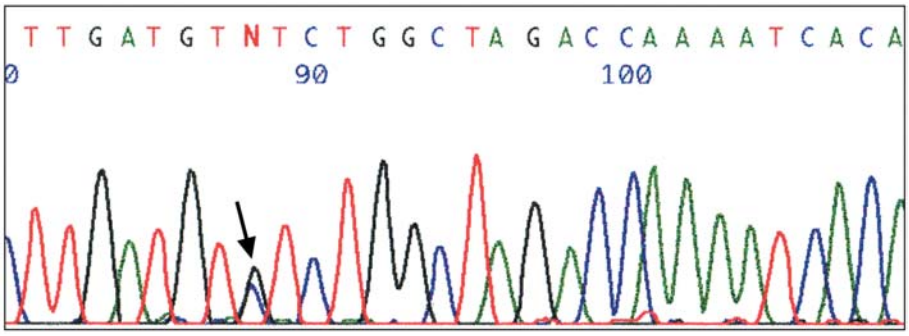


Fig. 3 Sequencing of exon 17 of *c-KIT* displays heterozygous point mutation with G-to-C nucleotide substitution in codon 816, causing the amino acid change from aspartate to histidine

growth fraction measured by Ki-67 antigen immunostaining was between 40% and 50% (Fig. 2). Sequencing exon 17 of the c-KIT gene revealed a point mutation in codon 816 in two of two tested tumor specimens. Here, a G-to-C nucleotide substitution caused the exchange from aspartate to histidine (D816H) (Fig. 3). No DNA mutations were observed in exon 11 of the *c-KIT* gene.

The histology from the recurred tumor obtained after the second operation, as described above, revealed tissue with severe scaring and fibrotic inflammation but no vital tumor cells. Herein, no immunohistochemically KIT- or PLAP-positive cells were observed.

Discussion

Dysgerminoma is a rare female tumor, accounting for approximately 1–2% of all primary ovarian malignancies and presenting with a mean patient age between late teens and early 20s [6]. Due to the good response to chemotherapy, the prognosis of most patients with dysgerminoma is considered to be very favorable. For dysgerminoma confined to the ovary, less than 10 cm in size, with an intact, smooth capsule unattached to other organs and without ascites, the 10-year survival following conservative surgery was 88.6% [12]. A report of 35 cases of GCTs, half of which were in advanced stage or recurrent or progressive disease, demonstrated a sustained remission rate 10–54 months after chemotherapy in 97% of cases [3]. Thus, our case demonstrates an uncommonly aggressive course of a dysgerminoma, with an early onset at the age of 14, rapid growth, poor response to the platinum-based chemotherapy and an extensive metastatic spread. Partial response with currently stable disease was finally achieved after 3 years of treatment by repeated combination chemotherapy, PEIs, surgical resection and radiotherapy.

The identification of a D816H mutation within the codon 816 of *c-KIT* in this dysgerminoma led us to speculate about its significance concerning aggressive tumor biology. At present, the frequency of *c-KIT* mutations among dysgerminomas and the role of these mutations in tumorigenesis are not known. Tian and colleagues detected 2 exon 17 codon 816 point mutations among 33 ovarian and testicular GCTs, including 1 mutation in 9 analyzed dysgerminomas [13]. Another recent study was able to detect activating *c-KIT* mutations in 14 of 57 testicular seminomas (25.9%). All mutations were localized in exon 17 of *c-KIT*, including D816 V (6 cases), D816H (3 cases), Y823D (2 cases) and single examples of Y823C, N822 K and T801I [5]. Moreover, biochemical evidence of KIT activation in D816H mutants was provided by cell-transfection assays and by analysis of tumor-cell lysates, which contained an increased level of phosphorylated KIT protein and KIT-associated phosphatidylinositol 3-kinase [5, 13]. Thus, KIT activation in *c-KIT*-mutated dysgerminomas and seminomas might contribute to tumorigenesis. Our report supports this theory and raises the question of whether mutations of *c-KIT* exon 17 predict a subset of aggressive and chemotherapy-refractory dysgerminomas. KIT inhibitors may stop the growth of seminomas/dysgerminomas by blocking the KIT kinase, which is necessary for tumor cell growth. To test the value of imatinib mesylate, which is already effectively adopted in the therapy of GISTs, a clinical trial in phase II of Cancer and Leukemia Group B is currently carried out in cisplatin-refractory testicular and ovarian cancer in stages II and III (http://www.clinicaltrials.gov). Interestingly, recent in vitro studies indicate that seminomas and mastocytosis with D816V mutation are resistant to imatinib in vivo [1, 7]. In contrast, the new KIT kinase inhibitor PP1 was shown to inhibit KIT activity in mutant and constitutively active forms D816 V and D816H in cell lines [11]. Thus, given the possibility of a new clinical approach to high-stage GCTs via inhibition of KIT kinase, more data are needed to evaluate the influence of genomic *c-KIT* mutation on the clinical progress, particularly in metastatic and recurrent seminomas/dysgerminomas.

Acknowledgements We thank Inge Losen, Ellen Paggen, Susanne Steiner and Barbara Reddemann for their technical assistance.

References

1. Akin C, Fumo G, Yavuz AS, Lipsky PE, Neckers L, Metcalfe DD (2004) A novel form of mastocytosis associated with a transmembrane c-KIT mutation and response to imatinib. Blood 103:3222–3225
2. Gari M, Goodeve A, Wilson G, Winship P, Langabeer S, Linch D, Vandenberghe E, Peake I, Reilly J (1999) c-KIT proto-on-

cogene exon 8 in-frame deletion plus insertion mutations in acute myeloid leukaemia. Br J Haematol 105:894–900
3. Gershenson DM (1993) Update on malignant ovarian germ cell tumors. Cancer 71:1581–1590
4. Hirota S, Isozaki K, Moriyama Y, Hashimoto K, Nishida T, Ishiguro S, Kawano K, Hanada M, Kurata A, Takeda M, Tunio GM, Matsuzawa Y, Kanakura Y, Shinomura Y, Kitamura Y (1998) Gain-of-function mutations of c-KIT in human gastrointestinal stromal tumors. Science 279:577–580
5. Kemmer K, Corless CL, Fletcher JA, McGreevey L, Haley A, Griffith D, Cummings OW, Wait C, Town A, Heinrich MC (2004) KIT mutations are common in testicular seminomas. Am J Pathol 164:305–313
6. LaPolla JP, Benda J, Vigliotti AP, Anderson B (1987) Dysgerminoma of the ovary. Obstet Gynecol 69:859–864
7. Ma Y, Zeng S, Metcalfe DD, Akin C, Dimitrijevic S, Butterfield JH, McMahon G, Longley BJ (2002) The c-KIT mutation causing human mastocytosis is resistant to STI571 and other KIT kinase inhibitors; kinases with enzymatic site mutations show different inhibitor sensitivity profiles than wild-type kinases and those with regulatory-type mutations. Blood 99: 1741–1744
8. Pardanani A, Reeder TL, Kimlinger TK, Baek JY, Li CY, Butterfield JH, Tefferi A (2003) Flt-3 and c-KIT mutation studies in a spectrum of chronic myeloid disorders including systemic mast cell disease. Leuk Res 27:739–742
9. Pauls K, Fink L, Franke FE (1999) Angiotensin-converting enzyme (CD143) in neoplastic germ cells. Lab Invest 79:1425–1435
10. Sakuma Y, Sakurai S, Oguni S, Hironaka M, Saito K (2003) Alterations of the c-KIT gene in testicular germ cell tumors. Cancer Sci 94:486–491
11. Tatton L, Morley GM, Chopra R, Khwaja A (2003) The Src-selective kinase inhibitor PP1 also inhibits KIT and Bcr-Abl tyrosine kinases. J Biol Chem 278:4847–4853
12. Thomas GM, Dembo AJ, Hacker NF, DePetrillo AD (1987) Current therapy for dysgerminoma of the ovary. Obstet Gynecol 70:268–275
13. Tian Q, Frierson HF JR, Krystal GW, Moskaluk CA (1999) Activating c-KIT gene mutations in human germ cell tumors. Am J Pathol 154:1643–1647
14. Wardelmann E, Neidt I, Bierhoff E, Speidel N, Manegold C, Fischer HP, Pfeifer U, Pietsch T (2002) c-kit mutations in gastrointestinal stromal tumors occur preferentially in the spindle rather than in the epithelioid cell variant. Mod Pathol 15:125–136
15. Yan W, Suominen J, Toppari J (2000) Stem cell factor protects germ cells from apoptosis in vitro. J Cell Sci 113:161–168
16. Yoshinaga K, Nishikawa S, Ogawa M, Hayashi S, Kunisada T, Fujimoto T, Nishikawa S (1991) Role of c-KIT in mouse spermatogenesis: identification of spermatogonia as a specific site of c-KIT expression and function. Development 113:689–699

Virchows Arch (2004) 445:655–658
DOI 10.1007/s00428-004-1115-0

CASE REPORT

Matthias Evert · Albert Roessner · Christoph Röcken

Synchronous granulomatous cholecystitis and fibroelastosis of the gallbladder

Received: 18 June 2004 / Accepted: 3 August 2004 / Published online: 23 September 2004
© Springer-Verlag 2004

Abstract We describe an unusual form of xanthogranulomatous cholecystitis in a 69-year-old man, with abundant intramural concrement formation and a local fibroelastosis of the adjacent interstitium and arteries. The gallbladder was obtained following resection of an adenocarcinoma of the gastro-esophageal junction without evidence of metastases. Only two cases of fibroelastosis of the gallbladder have previously been reported, and its pathogenesis is unknown. The influence of bile that leaked into the interstitium or a specific local tissue response to cytokines secreted by histiocytes are among the possible explanations for its development in our case.

Keywords Granulomatous cholecystitis · Fibroelastosis · Gallbladder

Introduction

Chronic cholecystitis (CC) is a frequent cause of morbidity in Western countries, and approximately 90% of the cases are associated with gall stones [13]. Histologically, it is mainly characterized by infiltration of the gallbladder (GB) wall by lymphocytes, mast cells, and plasma cells, leading to hyperplasia of the muscle layer and often finally to fibrosis. The development of Rokitansky–Aschoff sinus (RAS), regarded as pseudo-diverticula of the mucosa penetrating deep into the adventitia, is a peculiar phenomenon of CC [10]. Some cases of CC show an infiltrate of foamy histiocytes in connection with cholegranulomas. If this pattern predominates, the lesion is also referred to as xanthogranulomatous cholecystitis [8, 11].

M. Evert (✉) · A. Roessner · C. Röcken
Institute of Pathology,
Otto-von-Guericke-University Magdeburg,
Leipziger Strasse 44, 39120 Magdeburg, Germany
e-mail: matthias.evert@medizin.uni-magdeburg.de
Tel.: +49-391-6713182
Fax: +49-391-6715818

Here, we report on a patient with a distinct variant of granulomatous cholecystitis that had developed numerous foreign body granulomas surrounding encrustrated bile. To the best of our knowledge, such a variant has not yet been reported in the literature. Moreover, this case constitutes a peculiarity, as it is associated with severe fibroelastosis of the GB wall.

Clinical history

The patient, a 69-year-old man, underwent tumor resection of the distal esophagus. The surgical procedure consisted of partial esophago-gastrectomy. Surgical pathological examination led to the diagnosis of a high-grade adenocarcinoma of the gastro-esophageal junction with infiltration of the subserosa and without lymph-node metastases. The GB was also removed, because cholecystolithiasis was suspected.

Materials and methods

All tissue specimens were fixed in 10% buffered formalin and embedded in paraffin. Deparaffinized sections were stained with hematoxylin and eosin (H&E), periodic acid-Schiff with and without Diastase-pretreatment, Congo red according to Puchtler, and Elastica-van Gieson (EvG). Immunostaining was done with an antibody directed against the amyloid P component (clone A0203, Dako, Denmark; dilution: 1:1600) following antigen retrieval by microwave pretreatment (10 min, ethylenediaminetetraacetate). Immunoreactions were visualized with the avidin-biotin-complex method, applying a Vectastain ABC-alkaline phosphatase-kit. Neufuchsin served as a chromogen. Specimens were counterstained with hematoxylin. A positive control was used for monitoring the specificity of immunostaining.

Results

The gallbladder measured 6×4×3 cm and was filled with gelatinous pale yellow-green bile. No concrements were found in the lumen. However, on the cut surfaces, particularly near the neck of the GB, we noted depositions of brown-colored calculi in the exterior part of the wall and in the adventitial connective tissue (Fig. 1A). These cal-

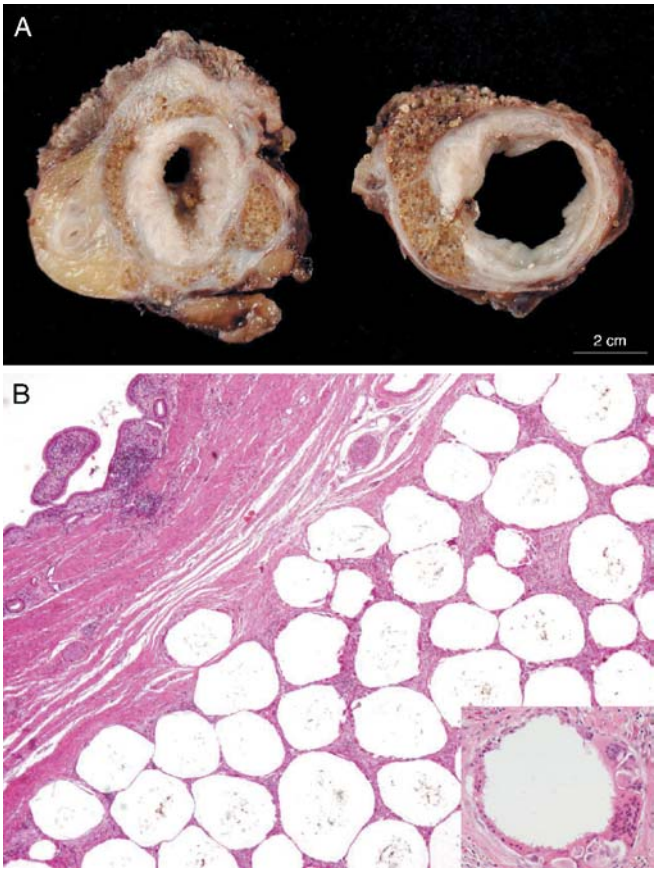


Fig. 1 Granulomatous cholecystitis: macroscopic aspect of the gallbladder (**A**). The wall is fibrous thickened, and there are depositions of multiple minute concrements in the exterior wall and the adventitia. Histologically (**B**), there are numerous honeycomb-like spaces in the outer wall after removal of the concrements, while the mucosa in this area shows only a mild chronic inflammatory infiltrate. The spaces are surrounded by macrophages and histiocytic giant cells (*inset*). Hematoxylin and eosin stain

culi presented as tiny concrements of approximately 1 mm in diameter. In the remaining part, we found thickening of the GB wall, measuring up to 6 mm (Fig. 1A).

Histologically, in the concrement-free segments of the GB wall, we noted a typical CC with predominantly lymphocytic inflammatory infiltrates, a moderate fibrosis, and numerous, frequently ectatic RAS. Removal of the concrements resulted in a honeycomb-like pattern of cavities (Fig. 1B). These were surrounded by concentrically closed rings of histiocytes, most often forming giant cells of the foreign-body type, occasionally interspersed with Touton-type giant cells (Fig. 1B). Under a polarizing microscope, the sparse remnants of the concrements showed no birefringence.

These areas bordered on large areas of connective tissue of the GB wall. H&E staining revealed slight basophilia and a rather fibrillar network of fibers, which resembled actinic elastosis of the skin at low magnification (Fig. 2A). EvG stain disclosed abundant elastic fibers (Fig. 2B, C), which also stained immunohistochemically for amyloid P component (Fig. 2D). The presence of amyloid was excluded by Congo red staining and polarization microscopy. In the immediate vicinity of the fibroelastosis of the GB wall, we noted arteries that were conspicuous for a remarkable, lumen-stenosing highly elastoid intima fibrosis (Fig. 2E). Interestingly, this fibroelastoid arteriopathy was noted only in areas adjacent to elastosis. Arteries located further away were morphologically unremarkable.

Discussion

A morphologically distinct inflammatory reaction of the GB in conjunction with a synchronously occurring fibroelastosis, which also involves local arteries, has not yet been described in this form in the GB. The occasional occurrence of cholegranulomas in CC is a common finding, whereas a primarily granulomatous cholecystitis is rare. In two studies, xanthogranulomatous cholecystitis has been reported to occur in 1.2% and 1.46% of all surgically removed GBs, respectively [9, 16]. Owing to nodular thickening of the wall, it has often been misinterpreted clinically and macroscopically as a tumor [6, 15]. Histomorphologically, the inflammatory infiltrate consists mainly of bile-, lipofuscin- or ceroid-pigment-laden foam cells and histiocytic giant cells [4, 16]. We presume that our case is a special variant of xanthogranulomatous cholecystitis. Analogous to a hypothesis explaining the development of xanthogranulomatous cholecystitis [8], we presume that our lesion developed as a result of a rupture of one or more RAS and that leaking bile subsequently underwent calcification. The calcification was probably not only a result of its chemical composition but might also have been a consequence of a specific interaction with the surrounding tissue compartment, as no concrements were present in the GB lumen. Unlike an ordinary xanthogranulomatous inflammation, the encrustrated bile was not able to be absorbed by the histiocytes, leading to the development of foreign body granulomas.

A literature search in Medline gives only two descriptions of GB elastosis [5, 7]. As in other anatomical sites, elastosis of the GB also enclosed amyloid P component, which is a structural component of elastic microfibrils [2], but the origin of elastosis is still not understood. Formerly, it was attributed to a degeneration of collagen fibers, but, currently, it is believed that actinic elastosis of the skin results from hyperplasia of elastic fibers with secondary degeneration due to ultraviolet exposure [12]. This cannot account for elastosis of the GB. Rather, in our case, the macrophage-rich inflammatory milieu may have stimulated the development of elastic fibers. Regarding the fibroelastosis in adjacent arteries, with far-distant arteries being morphologically unremarkable, a local effect is most likely. The connection of elastosis with either local elastoid arteriopathy or local atherosclerosis has already been described in a case report on elastosis in the prostate [1]. Moreover, in actinic elastosis of the skin, fibroelastosis of the intima of su-

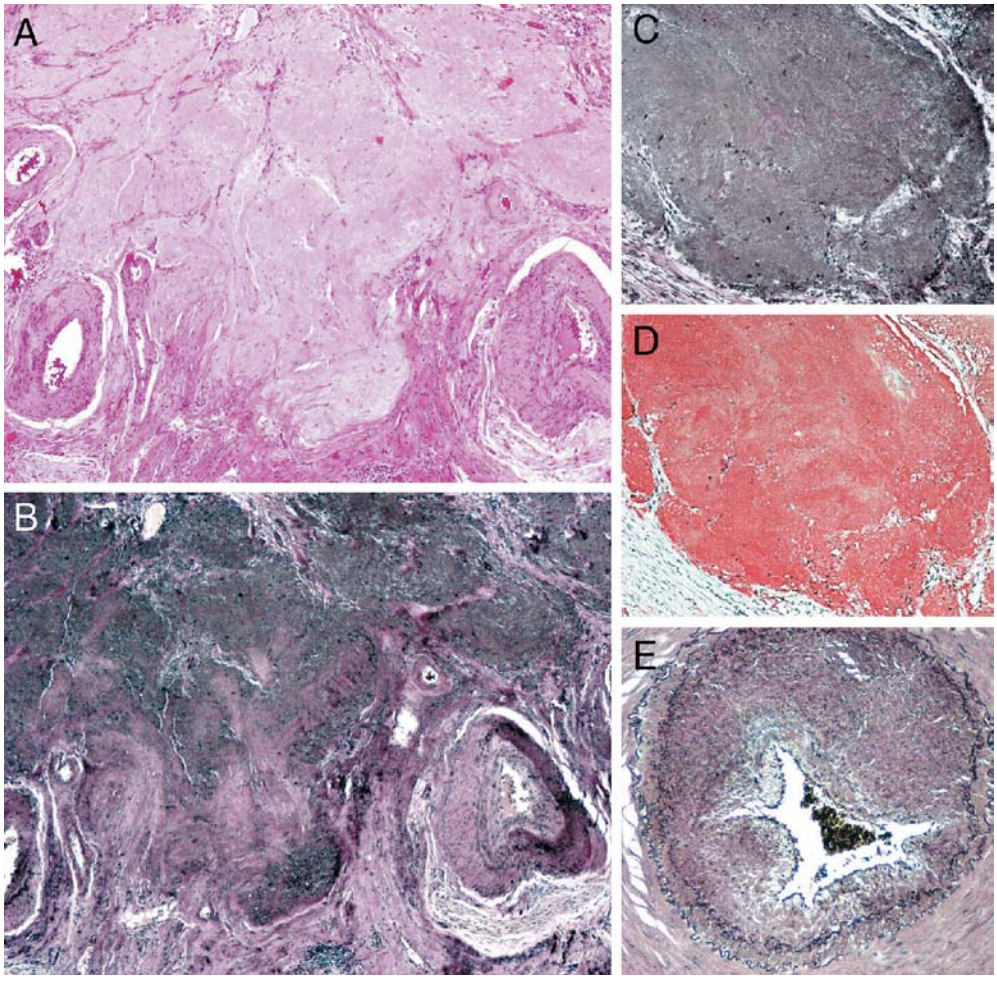


Fig. 2 Fibroelastosis: serial sections of the thickened gallbladder wall (**A**, **B**). Deposition of homogenous material, which is slightly basophilic in the hematoxylin and eosin stain (**A**) and represents largely elastic fibers as revealed by Elastica-van Gieson (EvG) stain (**B**). Another area of elastosis (**C**, EvG stain) and the serial section (**D**), showing strong immunoreactivity of the fibroelastosis for amyloid P component. Elastosis-adjacent arteries show a fibroelastoid arteriopathy (**E**, EvG stain) which can already be assumed at the *right bottom* of pictures (**A**) and (**B**)

perficial dermal arteries, particularly in the exterior (sunny side) half of the circumference, may occur, further supporting the hypothesis of a common mechanism triggering the development of vascular and interstitial elastosis [12]. Periductal and stromal elastosis of the mammary gland is repeatedly found in association with benign breast diseases, such as complex sclerosing lesions, and also with invasive breast carcinoma [14]. Moreover, elastosis has been reported to occur in salivary gland tumors [3]. One of the two documented cases of elastosis in the GB was associated with a synchronous neurofibroma [5], the other with a pseudotumorous fibroangiomyomatous hyperplasia [7]. However, we found neither a primary tumor nor metastases from the adenocarcinoma of the gastro-esophageal junction in the GB of our patient, excluding a local "paraneoplastic" tissue response, e.g., induced by tumor-born growth factors or cytokines.

In summary, we describe an unusual presentation of xanthogranulomatous cholecystitis with abundant intramural concrement formation and a local fibroelastosis of the adjacent interstitium and arteries. One might speculate that the inflammatory milieu in the present case may have triggered fibroelastosis of the GB in our patient.

References

1. Billis A, Magna LA (2000) Prostate elastosis: a microscopic feature useful for the diagnosis of postatrophic hyperplasia. Arch Pathol Lab Med 124:1306–1309
2. Breathnach SM, Pepys MB, Hintner H (1989) Tissue amyloid P component in normal human dermis is non-covalently associated with elastic fiber microfibrils. J Invest Dermatol 92:53–58
3. David R, Buchner A (1980) Elastosis in benign and malignant salivary gland tumors. A histochemical and ultrastructural study. Cancer 45:2301–2310
4. Duarte Z, Guevara U, Vuong PN (1994) Ceroid granulomas of the gallbladder. A clinicopathologic study of nine cases. Arch Anat Cytol Pathol 42:5–9
5. Eggleston JF, Goldman RL (1982) Neurofibroma and elastosis of the gallbladder. Report of an unusual case. Am J Gastroenterol 77:335–337
6. Enomoto T, Todoroki T, Koike N, Kawamoto T, Matsumoto H (2003) Xanthogranulomatous cholecystitis mimicking stage IV gallbladder cancer. Hepatogastroenterology 50:1255–1258
7. Furugaki K, Satoh H, Shinohara M, Saimura M, Nagai E, Yonemasu H, Kishikawa H (2001) Benign pseudotumorous lesion (fibroangiomyomatous hyperplasia with elastosis) in the gallbladder. J Gastroenterol 36:504–507
8. Goodman ZD, Ishak KG (1981) Xanthogranulomatous cholecystitis. Am J Surg Pathol 5:653–659
9. Guzman-Valdivia G (2004) Xanthogranulomatous cholecystitis: 15 years' experience. World J Surg 28:254–257
10. Halpert B (1961) Significance of the Rokitansky–Aschoff sinuses. Am J Gastroenterol 36:534–539

11. Ladefoged C, Lorentzen M (1993) Xanthogranulomatous cholecystitis. A clinicopathological study of 20 cases and review of the literature. APMIS 101:869–875
12. O'Brien JP, Regan W (1991) A study of elastic tissue and actinic radiation in "aging," temporal arteritis, polymyalgia rheumatica, and atherosclerosis. The actinic storm in the modern world. J Am Acad Dermatol 24:765–776
13. Palayew MJ (1976) Chronic cholecystitis and cholelithiasis. Semin Roentgenol 11:249–257
14. Parfrey NA, Doyle CT (1985) Elastosis in benign and malignant breast disease. Hum Pathol 16:674–676
15. Pinocy J, Lange A, Konig C, Kaiserling E, Becker HD, Krober SM (2003) Xanthogranulomatous cholecystitis resembling carcinoma with extensive tumorous infiltration of the liver and colon. Langenbecks Arch Surg 388:48–51
16. Takahashi K, Oka K, Hakozaki H, Kojima M (1976) Ceroid-like histiocytic granuloma of gall-bladder—a previously undescribed lesion. Acta Pathol Jpn 26:25–46

Virchows Arch (2004) 445:659–660
DOI 10.1007/s00428-004-1098-x

LETTER TO THE EDITOR

Gaetano Magro · Piero Gangemi · Loredana Villari · Paolo Greco

Deciduoid-like stromal cells in a diabetic patient with bilateral gynecomastia: a potential diagnostic pitfall

Received: 3 June 2004 / Accepted: 12 July 2004 / Published online: 17 September 2004
© Springer-Verlag 2004

Sir, Epithelioid stromal cells (ESCs) were originally described as a typical feature of diabetic mastopathy, along with lymphocytic mastitis [5]. As these cells have also been reported in the breast stroma of patients with hypothyroidism and systemic lupus erythematous, it has been postulated that they may represent a reliable morphological marker of autoimmune disorders [1]. Diabetic mastopathy may be clinically and histologically confused with carcinoma [2], especially in those cases where there is a presence of large-sized ESCs [1].

We report the first case of gynecomastia with extensive deciduoid-like stromal changes in a patient affected by long-standing insulin-dependent diabetes mellitus (IDDM). A 44-year-old man presented with a retro-areolar nodule in the left breast. Ultrasound analysis revealed an irregular outlined, non-homogeneous hypoechoic mass. The lesion was surgically excised. After a 1-year clinical follow-up, a similar lesion was noted and excised from the contralateral breast. The patient referred to had a 31-year history of IDDM, and he had been undergoing hemodialysis for diabetic nephropathy for 2 years. Grossly, both surgical samples consisted of unencapsulated fibrous nodular masses, measuring 3 cm and 4 cm in greatest diameter, respectively, with a firm, grayish-white cut surface. Histologically, both lesions exhibited the typical features of florid gynecomastia: increased number of ducts with epithelial proliferation and periductal myxoid stroma containing slight lymphocytic infiltration (Fig. 1A). An unexpected feature was the presence in the interlobular stroma of numerous, large cells with deciduoid-like features, arranged in solid sheets and embedded in fibrous tissue (Fig. 1A, B). These cells were round, ovoid, or polygonal in shape, with an abundant pale-to-eosinophilic cytoplasm, well-defined cellular borders and large, round vesicular nuclei containing one or more prominent nucleoli (Fig. 1B). A low number of cells were binucleate and showed a granular eosinophilic cytoplasm. A mild nuclear pleomorphism was focally seen. Mitotic figures were seen infrequently (2–3×50 high-power field). No atypical mitosis or necrosis was identified. A moderate stromal perivascular lymphocytic infiltrate was observed. Immunohistochemical analyses, revealing reactivity for vimentin, α-smooth-muscle actin (20–30% of cells) (Fig. 1C) and no staining with pancytokeratins, epithelial membrane antigen, desmin, h-caldesmon, calponin, CD34, S100 protein, HMB45, CD68 and p63 were consistent with a fibro/myofibroblastic nature of deciduoid-like stromal cells.

The association of diabetes mellitus with gynecomastia has only rarely been reported [3]. As plump stromal cells are lacking in common gynecomastia [3], we think that the deciduoid-like stromal cells of the present case represent a morphological variant of ESCs, typically occurring in diabetic mastopathy [1, 5]. It is likely that the deciduoid-like morphology is the result of reactive stromal changes to a hormonally related proliferative disease (gynecomastia) and to hemodialytic treatment, which may play a role through tissue micro-environmental modifications. In a large series of lymphocytic mastitis due to different basic diseases, the two most florid examples of epithelioid stromal changes were seen in the only diabetic male patient and in a woman undergoing hemodialysis by systemic lupus erythematosus [1]. Interestingly, our patient was a diabetic man undergoing hemodialysis.

Awareness of deciduoid-like stromal changes in patients with the association diabetes mellitus/gynecomastia is crucial for pathologist to avoid confusion with benign and malignant tumors. Differential diagnosis mainly re-

G. Magro (✉)
Dipartimento G.F. Ingrassia, Anatomia Patologica,
Università di Catania,
Via S. Sofia 87, 95123 Catania, Italia
e-mail: g.magro@unict.it
Tel.: +39-95-3782024
Fax: +39-95-3782023

P. Gangemi · L. Villari
Servizio Anatomia Patologica,
Azienda Ospedaliera Vittorio Emanuele, Catania, Italia

P. Greco
Servizio Anatomia Patologica,
Azienda Ospedaliera Garibladi, S. Luigi S. Currò, Ascoli Tomaselli, Italia

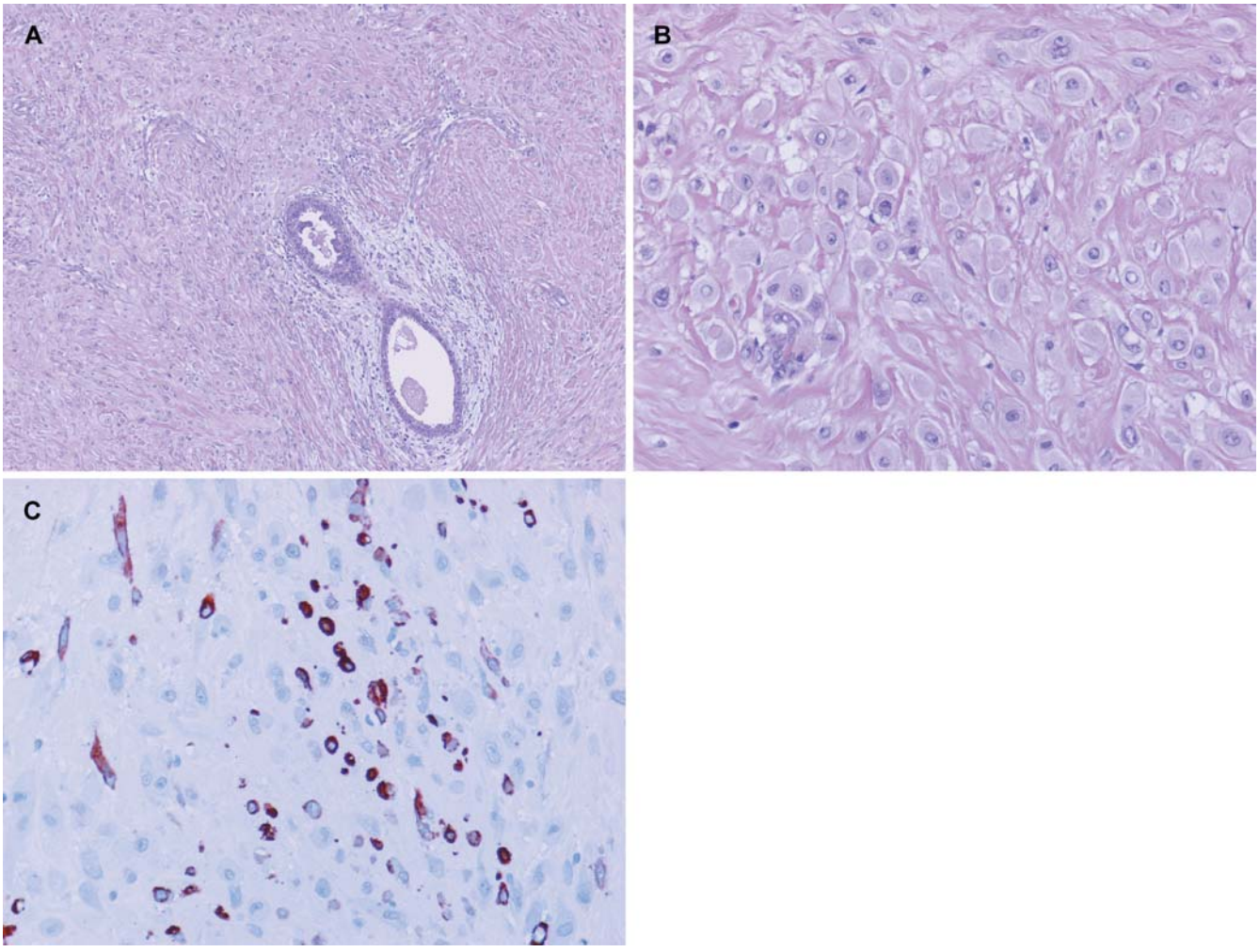


Fig. 1 The interlobular stroma of florid gynecomastia is completely occupied by large round-to-ovoid cells (**A**) showing deciduoid-like features such as large size, abundant cytoplasm, defined cellular borders, and large vesicular nuclei with prominent nucleoli (**B**). Some cells are stained with α-smooth-muscle actin (**C**)

volves around epithelioid myofibroblastoma, granular cell tumor, invasive carcinoma—especially with apocrine or oncocytic features—and metastatic deciduoid mesothelioma [6]. Although myofibroblastoma may be composed largely of epithelioid cells and occurs in association with gynecomastia, it is by definition a pure mesenchymal tumor lacking any epithelial component and grows as a well-circumscribed tumor nodule [4]. Granular cell tumor, invasive carcinoma and deciduoid mesothelioma are easily ruled out using immunohistochemical analysis showing no reactivity to S-100 protein, cytokeratins and calretinin, respectively.

References

1. Ashton MA, Lefkowitz M, Tavassoli FA (1994) Epithelioid cells in lymphocytic mastitis-a source of confusion with invasive carcinoma. Mod Pathol 7:49–53
2. Foschini MP, Cavazza A, Pinto IMM, Eusebi V (1990) Diabetic fibrous mastopathy. Virchows Arch 417:529–532
3. Hunfeld KP, Bassler R, Kronsbein H (1997) Diabetic mastopathy in the male breast-a special type of gynecomastia. Pathol Res Prac 193:197–205
4. Magro G, Bisceglia M, Michal M, Eusebi V (2002) Spindle cell lipoma-like tumor, solitary fibrous tumor and myofibroblastoma of the breast: a clinico-pathological analysis of 13 cases in favor of a unifying histogenetic concept. Virchows Arch 440:249–260
5. Tomnsezewaki JE, Brooks JJ, Hicks D, Li Volsi VA (1992) Diabetic mastopathy: a distinctive clinicopathologic entity. Hum Pathol 23:780–786
6. Shia J, Erlandson RA, Klimstra DS (2002) Deciduoid mesothelioma: a report of 5 cases and literature review. Ultrastruct Pathol 26:355–363

Virchows Arch (2004) 445:661
DOI 10.1007/s00428-004-1108-z

BOOK REVIEW

M. Oehmichen

Book review on "Forensic Pathology Reviews (Book Series, Vol. 1)" by M. Tsokos

Received: 23 July 2004 / Accepted: 27 July 2004 / Published online: 8 October 2004
© Springer-Verlag 2004

Forensic Pathology Reviews (Book Series, Vol. 1)

This new book series intends to provide up-to-date knowledge on special topics in the field of forensic pathology. This intention—beyond any doubt—is to be appreciated. This new concept is reflected by two corresponding papers with a special emphasis on neuropathology of drug abuse (A. Büttner and S. Weis, Munich, Germany) as well as the systematic review on sudden cardiac death (V. Fineschi and C. Pomara, Foggia, Italy). The paper on drug abuse encompasses a reference list of 550 state-of-the-art entries. The review not only provides a very good synopsis of the pathomorphology, supported by characteristic figures, but it also gives information on the pathophysiological process, which needs to be discussed as the cause for the neuropathological changes. The paper on sudden cardiac death offers a brief summary of the methods of assessing morphological changes of the heart, with the results predominantly complemented by figures, which are apparently, at least in part, derived from slides/power point presentations. These figures are extremely small in size and, thus, do not convey the desired information. The remaining 13 papers do not—or only marginally—meet the intentions of the editor. There are papers that repeat well-known, already published knowledge, papers dealing with primary problems in clinical pathology, and papers with forensic case reports.

In summary, it can be noted: a book series with the intention of compiling reviews has to be highly recommended. Yet, such a series should consider those reviews that actually provide recent information. Moreover, the question arises: who is the board behind this very young, enthusiastic yet unavoidably inexperienced editor? Who can guarantee the validity of statements made by the mainly young authors? I hope this new book series will meet international standards; yet, some things need to be changed.

M. Oehmichen (✉)
Universitätsklinikum S-H,
Campus Kiel,
Arnold-Heller-Strasse 12, 24105 Kiel, Germany
e-mail: oehmich@rechtsmedizin.uni-kiel.de
Tel.: +49-431-5973600
Fax: +49-431-5973612

Virchows Arch (2004) 445:662
DOI 10.1007/s00428-004-1172-4
© Springer-Verlag 2004

ANNOUNCEMENTS

26–28 January 2005
Gynecological Pathology Course
A three-day course will take place in Barcelona, Spain.

Hospital del Mar.
This course will be given in English and Spanish
by Dr.E.Oliva (Boston), Dr.D.Bell (Boston) Dr.M.Nucci (Boston)
Prof.J.Prat (Barcelona), and Dr.X.Matias-Guiu (Barcelona)
It will consist of several lectures combined with with slide review on multiple headed microscope or videoprojeccion.
In addition, there will be a slide seminar during the meeting, with a discussion at the end.
The audience will be limited to 75 participants.
Course Fee: 300 euros for staff, and 180 Euros for pathologists in training.

For further information, please contact:
F.Alameda MD
Dept of Pathology
Hospital del Mar
Passeig Maritim 25-28 08003 Barcelona, Spain
Tel.: 932483031
E-mail: 86780@imas.imim.es

19–24 April 2005
10th International Congress on Oral Cancer
Crete, Greece

Creta Maris Conference Centre

- The 10th International Congress on Oral Cancer is supported by the World Health Organization, the International Union Against Cancer, the International Congress on Oral Cancer, the Hellenic Association for the Research and Treatment of Oral Cancer, and the Hellenic Cancer Society
- The Congress theme is *The Oral Cancer Patient: the anthropocentric approach to a multidisciplinary problem*
- A number of Keynote Lectures will be delivered by international leaders in their specialties
- Limited attendance Courses will be provided for interested participants
- Deadline for abstract submission: November 30th, 2004
- Accepted abstracts for oral and poster presentations will be published as a supplement to the journal Oral Oncology. Details at www.harcourt-international.com/journals/oron
- Social events include Presidents Reception, Cretan Night and Gala Dinner

Further details at www.icooc-2005.org or from the Congress President at rapidis@icooc-2005.org

13–24 June 2005
International course on Laboratory Animal Science
Utrecht, The Netherlands

A two week intensive course on laboratory animal science will be organized at the Division of Laboratory Animal Science – Utrecht, The Netherlands in June 2005. This course is organized once a year since 1993.
The objective of this course is to present basic facts and principles that are essential for the humane use and care of animals and for the quality of research.
The contents of the course are in line with recommendations of the Federation of European Laboratory Animal Science Associations (FELASA) regarding the training of the young scientist whose research involves the use of vertebrate animals.
The course may also be of interest for those who intend to set up a similar course at their location. For this purpose, during the course the acquisition of teaching materials can be discussed with the course committee.

For information and application forms please contact:
Mr. Stephan van Meulebrouck, MA
Division of Laboratory Animal Science
Faculty of Veterinary Medicine
P.O. Box 80.166
3508 TD Utrecht
The Netherlands
Tel.: +31-30-2532033
Fax: +31-30-2537997
E-mail: pdk@las.vet.uu.nl
Internet: http://las.vet.uu.nl>Education and Training>International Course